frontiers | Research Topics

Adaptation mechanisms of grass and forage plants to stressful environments

Edited by
Jing Zhang, Maofeng Chai, Sergey Shabala, Kehua Wang and Jin-Lin Zhang

Published in
Frontiers in Plant Science

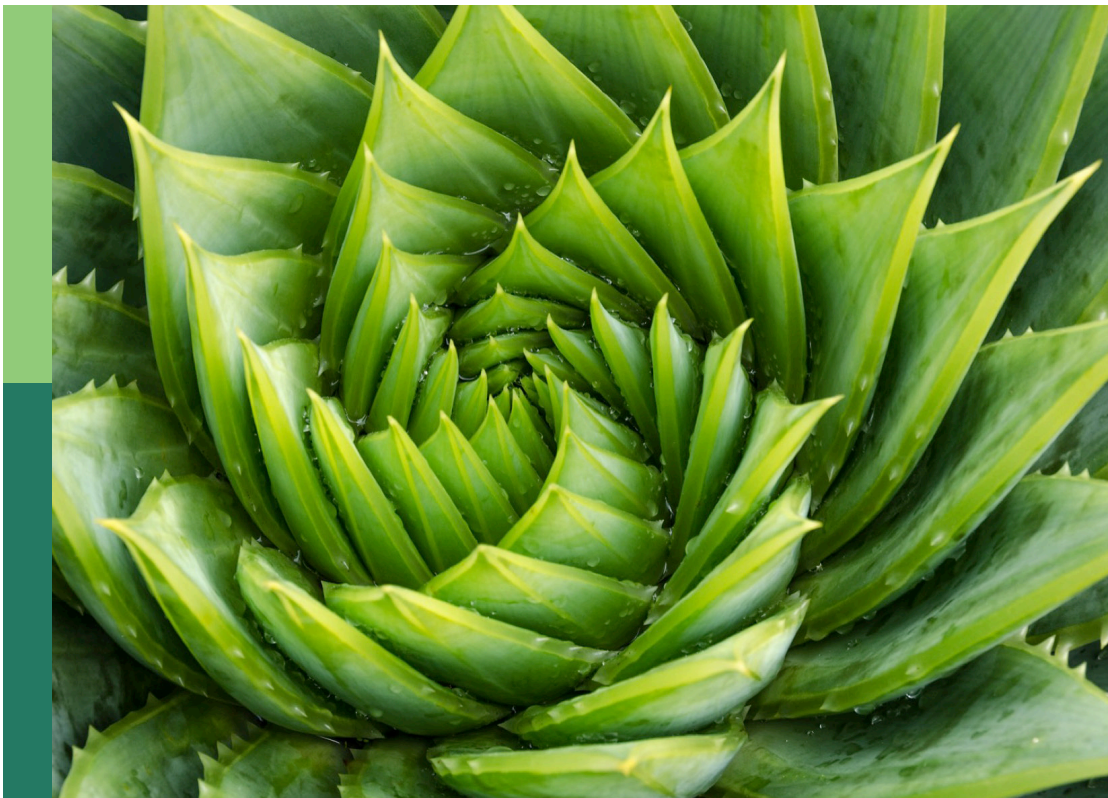

ISSN 1664-8714
ISBN 978-2-83251-728-4
DOI 10.3389/978-2-83251-728-4

About Frontiers

Frontiers is more than just an open access publisher of scholarly articles: it is a pioneering approach to the world of academia, radically improving the way scholarly research is managed. The grand vision of Frontiers is a world where all people have an equal opportunity to seek, share and generate knowledge. Frontiers provides immediate and permanent online open access to all its publications, but this alone is not enough to realize our grand goals.

Frontiers journal series

The Frontiers journal series is a multi-tier and interdisciplinary set of open-access, online journals, promising a paradigm shift from the current review, selection and dissemination processes in academic publishing. All Frontiers journals are driven by researchers for researchers; therefore, they constitute a service to the scholarly community. At the same time, the *Frontiers journal series* operates on a revolutionary invention, the tiered publishing system, initially addressing specific communities of scholars, and gradually climbing up to broader public understanding, thus serving the interests of the lay society, too.

Dedication to quality

Each Frontiers article is a landmark of the highest quality, thanks to genuinely collaborative interactions between authors and review editors, who include some of the world's best academicians. Research must be certified by peers before entering a stream of knowledge that may eventually reach the public - and shape society; therefore, Frontiers only applies the most rigorous and unbiased reviews. Frontiers revolutionizes research publishing by freely delivering the most outstanding research, evaluated with no bias from both the academic and social point of view. By applying the most advanced information technologies, Frontiers is catapulting scholarly publishing into a new generation.

What are Frontiers Research Topics?

Frontiers Research Topics are very popular trademarks of the *Frontiers journals series*: they are collections of at least ten articles, all centered on a particular subject. With their unique mix of varied contributions from Original Research to Review Articles, Frontiers Research Topics unify the most influential researchers, the latest key findings and historical advances in a hot research area.

Find out more on how to host your own Frontiers Research Topic or contribute to one as an author by contacting the Frontiers editorial office: frontiersin.org/about/contact

Adaptation mechanisms of grass and forage plants to stressful environments

Topic editors

Jing Zhang — Nanjing Agricultural University, China
Maofeng Chai — Qingdao Agricultural University, China
Sergey Shabala — University of Tasmania, Australia
Kehua Wang — China Agricultural University, China
Jin-Lin Zhang — Lanzhou University, China

Citation

Zhang, J., Chai, M., Shabala, S., Wang, K., Zhang, J.-L., eds. (2023). *Adaptation mechanisms of grass and forage plants to stressful environments*. Lausanne: Frontiers Media SA. doi: 10.3389/978-2-83251-728-4

Table of contents

frontiers | Frontiers in Plant Science

TYPE Editorial
PUBLISHED 07 February 2023
DOI 10.3389/fpls.2023.1132198

OPEN ACCESS

EDITED AND REVIEWED BY
Ravi Valluru,
University of Lincoln, United Kingdom

*CORRESPONDENCE
Jin-Lin Zhang
jlzhang@lzu.edu.cn

SPECIALTY SECTION
This article was submitted to Plant Abiotic Stress, a section of the journal Frontiers in Plant Science

RECEIVED 27 December 2022
ACCEPTED 27 January 2023
PUBLISHED 07 February 2023

CITATION
Zhang J, Chai M-F, Shabala S, Wang K-H and Zhang J-L (2023) Editorial: Adaptation mechanisms of grass and forage plants to stressful environments.
Front. Plant Sci. 14:1132198.
doi: 10.3389/fpls.2023.1132198

Editorial: Adaptation mechanisms of grass and forage plants to stressful environments

Jing Zhang[1], Mao-Feng Chai[2], Sergey Shabala[3], Ke-Hua Wang[4] and Jin-Lin Zhang[5]*

[1]College of Agro-grassland Science, Nanjing Agricultural University, Nanjing, China, [2]Key Laboratory of National Forestry and Grassland Administration on Grassland Resources and Ecology in the Yellow River Delta, College of Grassland Science, Qingdao Agricultural University, Qingdao, China, [3]Tasmanian Institute of Agriculture, University of Tasmania, Hobart, TAS, Australia, [4]Department of Turfgrass Science and Engineering, College of Grassland Science and Technology, China Agricultural University, Beijing, China, [5]State Key Laboratory of Herbage Improvement and Grassland Agro-ecosystems; Key Laboratory of Grassland Livestock Industry Innovation, Ministry of Agriculture and Rural Affairs; College of Pastoral Agriculture Science and Technology, Lanzhou University, Lanzhou, China

KEYWORDS

grass and forage plants, stress tolerance, natural metabolites, synthetic chemicals, host-microbe interactions, gene functional characterization, molecular breeding

Editorial on the Research Topic
Adaptation mechanisms of grass and forage plants to stressful environments

Environments determine plant distribution and productivity in the world (Bailey-Serres et al., 2019). In nature, plants are constantly challenged by stressful environments, such as drought, heat, cold, nutrient deficiency, flooding, salinity and toxic heavy metals in the soil, insufficient or excessive light, and pathogens and pests, etc. (Zhang et al., 2022). These abiotic stresses limit the world-wide utilization of arable lands and negatively affect crop productivity (Bailey-Serres et al., 2019). There are growing concerns about continued global warming and increasing extreme weather events, which subsequently lead to frequent natural disasters and environmental problems for agricultural practice worldwide (Zandalinas et al., 2021; Verslues et al., 2023). Global population rose from 5 billion inhabitants in 1990 to more than 7.5 billion presently and will rise to 9.7 billion to 10 billion by 2050 (Gupta et al., 2020). The current pace of crop yield increase cannot meet the demand for future population (Hickey et al., 2019). Therefore, understanding the mechanisms on how plants adapt to stressful environments is critical for global ecological protection and food security.

Grasslands dominate terrestrial ecosystem on the earth, producing food, feed, fiber and fuel, and serving as weather amelioration, carbon sequestration, biodiversity enhancement, soil conservation, recreation, and the maintenance of the atmospheric composition (Bai and Cotrufo, 2022; Strömberg and Staver, 2022). Grass and forage plants serve multiple functions and benefits to humans and animals, such as beautifying landscapes, protecting the environments, improving human recreational activities, and providing feed for livestock and wild animals (Kopecký and Studer, 2014; Simeão et al., 2021) More importantly, grass and forage plants with rich biodiversity, especially including many wild species, have evolved multiple mechanisms to adapt to various stressful environments as described above at physiological, biochemical, molecular, cellular, and subcellular levels, compared to crop plants (Pardo and VanBuren, 2021; McSteen and Kellogg, 2022). Hence, it is urgently

10.3389/fpls.2023.1132198

necessary to explore these mechanisms and the underlying strategies that will facilitate grass and forage plant breeding and crop plant breeding for improved stress tolerance. In this topic, recent research advances in adaptation mechanisms of grass and forage plants to stressful environments are presented in 40 research articles and one review article, contributed by 273 authors. The 40 research articles covered 23 plant genera and 30 species, 10 of which is about *Medicago*, including five in *Medicago sativa*, three in *Medicago truncatula*, one in *Medicago falcate* and another one in *Medicago ruthenica*, indicating that alfalfa as "the king of forage plants" still arouses the greatest concern of scientists in the field (Figure 1).

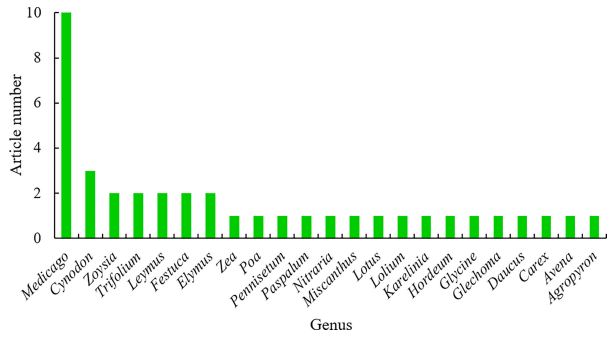

FIGURE 1
Genus distribution of 41 articles published in this topic.

Functional characterization of genes relevant to stress tolerance

The processes of plant adaptation to stressful environments are controlled and regulated by multiple genes (Pardo and VanBuren, 2021; Zhang et al., 2022). Functional characterization of these genes is helpful to understand how grass and forage plants adapt to stressful environments and selected genes can be used for breeding grass, forage and crop plant cultivars with improved stress tolerance. Jiang et al. characterized a novel transcriptional regulator HbERF6 that regulates the HbCIPK2-coordinated pathway conferring salt tolerance in a halophytic grass *Hordeum brevisubulatum*. Zhou et al. constructed a high-density genetic map and localized grazing-tolerant QTLs in *Medicago falcata* L. Wang et al. identified *LjHDZ7* encoding a 40 HD-Zip transcription factor from *Lotus japonicas* and the overexpression of *LjHDZ7* increased plant salt tolerance. The overexpression of abscisic acid-insensitive gene (*ABI4*) from *Medicago truncatula* by Li et al. enhanced the content of endogenous ABA in plants and improved plant cold tolerance. Guan et al. found that *Zoysia japonica* ZjNOL promotes chlorophyll degradation and senescence and negatively affects the integrity and function of the photosystem.

Regulations of stress tolerance by natural metabolites or synthetic chemicals

Numerous structurally different metabolites are produced in plants in response to various stressful environments (Kim et al., 2007; Kim et al., 2017). Li et al. found that caffeic acid O-methyltransferase gene *CrCOMT* from *Carex rigescens* conferred melatonin-mediated drought tolerance in plants. Differential responses of four white clover genotypes to salt stress associated with root growth, endogenous polyamines metabolism, and sodium/potassium accumulation and transport were identified by Li et al. Yu et al. identified 90 uridine diphosphate glycosyltransferase (UGT) members in ten evolutionary groups that are likely related to secondary metabolites in alfalfa (*Medicago sativa* L.). Li et al. found that the flexible response of a large number of genes and metabolites endows *Poa crymophila* with robust cold and drought tolerance. Yang et al. demonstrated that genotypic-specific reprogramming and crosstalk of various plant hormones are crucial for root growth and salt tolerance of bermudagrass (*Cynodon dactylon*). Lin et al. found that *Leymus chinensis* adapts to degraded soil environments by changing its metabolic pathways and root exudate components. Overexpression of *Pennisetum purpureum* CCoAOMT encoding caffeoyl-CoA O-methyltransferase by Song et al. contributes to lignin deposition and drought tolerance by promoting the accumulation of flavonoids in transgenic plants.

Roles of host-microbe interactions in stress responses

Root-associated microbes can improve plant growth, and offer the potential to increase plant tolerance to stressful environments (Saijo and Loo, 2020; Vries et al., 2020). Mei et al. found that the planting of alfalfa can promote the proliferation of specific beneficial microbiota groups in the soil. Wang et al. demonstrated that *Bacillus amyloliquefaciens* GB03 augmented tall fescue growth by regulating phytohormone and nutrient homeostasis under nitrogen deficiency condition. Hou et al. found that *Bacillus atrophaeus* WZYH01 and *Planococcus soli* WZYH02 improved salt tolerance of maize (*Zea mays* L.). Zhang et al. demonstrated that inoculation of *Elymus nutans* with arbuscular mycorrhizal fungi *Funneliformis mosseae* improved the uptake of nutrients and induced the resistance to grasshopper attack. Pan et al. found that root exudates and rhizosphere soil bacterial relationships of *Nitraria tangutorum* are linked to k-strategist bacterial community under salt stress. Wei et al. demonstrated that salt-tolerant endophytic bacterium *Enterobacter ludwigii* B30 enhance bermudagrass growth under salt stress by modulating plant physiology and changing rhizosphere and root bacterial community.

Omics-related studies in stress tolerance of grass and forage plants

Recent significant progress in omics techniques (transcriptomics, genomics, proteomics, and metabolomics) have helped to deeply understand the molecular insights into multiple stress tolerance of plants (Singhal et al., 2021). Salt tolerance in alfalfa is associated with regulation of ionic homeostasis, antioxidative enzymes and fatty acid metabolism at both transcriptional and physiological level (Li et al.). Transcriptomic profiling by Chen et al. showed the role of 24-epibrassinolide in alleviating salt stress damage in tall fescue (*Festuca arundinacea*). A transcriptome analysis by Dong et al. revealed the molecular regulatory mechanisms of leaf senescence in *Medicago truncatula* under alkaline stress. Another transcriptome analysis by Li et al. revealed the molecular response mechanism of high-resistant and low-resistant alfalfa varieties to *Verticillium alfalfa*. A combined analysis of the transcriptome and proteome by Ming et al. revealed the mechanisms underlying the enhanced salt tolerance by the protein disulfide isomerase gene (*ZmPDI*) in *Zoysia matrella* [L.] Merr. An integrated analysis of small RNAs, transcriptome and degradome sequencing by Fan et al. revealed the drought stress network in *Agropyron mongolicum*. A series integrated analyses in *Medicago truncatula* in response to salt stress by An et al. revealed multiple differentially expressed coding and non-coding RNAs, including mRNAs, lncRNAs, circRNAs, and miRNAs, and they identified multiple DEmRNA and ceRNA interaction pairs that function in many pathways of salt stress responses.

Overall, the articles collected on this Research Topic represent a substantial contribution to fill gaps in knowledge of the roles of complex signaling transduction pathways in grass and forage plants in response to various stressful environments. Moreover, the stress tolerance-related genes, beneficial natural metabolites, and root-associated microbes identified are valuable resources not only for grass and forage plants, but also for other crops. Jiuxin and Liebao reviewed the research progress of turfgrass resistance breeding, analyzed the bottlenecks of turfgrass resistance breeding, and put forward the strategies to cope with the bottlenecks, which will be useful to guide turfgrass breeding for stress tolerance.

Author contributions

J-LZ and JZ prepared the draft. JZ, M-FC, SG, K-HW and J-LZ revised the manuscript. All authors approved the final version of the manuscript and approved it for publication.

Funding

This work was financially supported by National Natural Science Foundation of China (32071875), the Fundamental Research Funds for the Central Universities (XUEKEN2022020), and Jiangsu Agricultural Science and Technology Innovation Fund (CX(21)3004).

Acknowledgments

We greatly appreciate all authors and reviewers for their contribution to this Research Topic as well as the editorial office of *Frontiers in Plant Science* for persistent support

Conflict of interest

The authors declare that the work was conducted in the absence of any commercial or financial relationships that could be construed as a potential conflict of interest.

Publisher's note

References

Bai, Y., and Cotrufo, M. F. (2022). Grassland soil carbon sequestration: Current understanding, challenges, and solutions. *Science* 377, 603–608. doi: 10.1126/science.abo2380

Bailey-Serres, J., Parker, J. E., Ainsworth, E. A., Oldroyd, G. E. D., and Schroeder, J. I. (2019). Genetic strategies for improving crop yields. *Nature* 575, 109–118. doi: 10.1038/s41586-019-1679-0

Gupta, A., Rico-Medina, A., and Cao-Delgado, A. I. (2020). The physiology of plant responses to drought. *Science* 368, 266–269. doi: 10.1126/science.aaz7614

Hickey, L. T., Hafeez, A. N., Robinson, H., Jackson, S. A., Leal-Bertioli, S. C. M., Tester, M., et al. (2019). Breeding crops to feed 10 billion. *Nat. Biotechnol.* 37, 744–754. doi: 10.1038/s41587-019-0152-9

Kim, J. K., Bamba, T., Harada, K., Fukusaki, E., and Kobayashi, A. (2007). Time-course metabolic profiling in *Arabidopsis thaliana* cell cultures after salt stress treatment. *J. Exp. Bot.* 58, 415–424. doi: 10.1093/jxb/erl216

Kim, J. M., To, T. K., Matsui, A., Tanoi, K., Kobayashi, N. I., Matsuda, F., et al. (2017). Acetate-mediated novel survival strategy against drought in plants. *Nat. Plants* 3, 17097. doi: 10.1038/nplants.2017.97

Kopecký, D., and Studer, B. (2014). Emerging technologies advancing forage and turf grass genomics. *Biotechnol. Adv.* 32, 190–199. doi: 10.1016/j.biotechadv.2013.11.010

McSteen, P., and Kellogg, E. A. (2022). Molecular, cellular, and developmental foundations of grass diversity. *Science* 377, 599–602. doi: 10.1126/science.abo5035

Pardo, J., and VanBuren, R. (2021). Evolutionary innovations driving abiotic stress tolerance in C4 grasses and cereals. *Plant Cell* 33, 3391–3401. doi: 10.1093/plcell/koab205

Saijo, Y., and Loo, E. P. (2020). Plant immunity in signal integration between biotic and abiotic stress responses. *New Phytol.* 225, 87–104. doi: 10.1111/nph.15989

Simeão, R. M., Resende, M. D. V., Alves, R. S., Pessoa-Filho, M., Azevedo, A. L. S., Jones, C. S., et al. (2021). Genomic selection in tropical forage grasses: current status and future applications. *Front. Plant Sci.* 12. doi: 10.3389/fpls.2021.665195

Singhal, R. K., Saha, D., Skalicky, M., Mishra, U. N., Chauhan, J., Behera, L. P., et al. (2021). Crucial cell signaling compounds crosstalk and integrative multi-omics techniques for salinity stress tolerance in plants. *Front. Plant Sci.* 12. doi: 10.3389/fpls.2021.670369

Strömberg, C. A. E., and Staver, A. C. (2022). The history and challenge of grassy biomes. *Science* 377, 592–593. doi: 10.1126/science.add1347

Verslues, P. E., Bailey-Serres, J., Brodersen, C., Buckley, T. N., Conti, L., Christmann, A., et al. (2023). Burning questions for a warming and changing world: 15 unknowns in plant abiotic stress. *Plant Cell* 35, 67–108. doi: 10.1093/plcell/koac263

Vries, F., Griffiths, R. I., Knight, C. G., Nicolitch, O., and Williams, A. (2020). Harnessing rhizosphere microbiomes for drought-resilient crop production. *Science* 368, 270–274. doi: 10.1126/science.aaz5192

Zandalinas, S. I., Fritschi, F. B., and Mittler, R. (2021). Global warming, climate change, and environmental pollution: Recipe for a multifactorial stress combination disaster. *Trends Plant Sci.* 26, 588–599. doi: 10.1016/j.tplants.2021.02.011

Zhang, H., Zhu, J., Gong, Z., and Zhu, J. K. (2022). Abiotic stress responses in plants. *Nat. Rev. Genet.* 23, 104–119. doi: 10.1038/s41576-021-00413-0

frontiers | Frontiers in Plant Science

ORIGINAL RESEARCH
published: 18 April 2022
doi: 10.3389/fpls.2022.891361

Integrated Analysis of Coding and Non-coding RNAs Reveals the Molecular Mechanism Underlying Salt Stress Response in *Medicago truncatula*

*Yixin An, Haotian Su, Qichen Niu and Shuxia Yin**

School of Grassland Science, Beijing Forestry University, Beijing, China

Salt stress is among the most severe abiotic stresses in plants worldwide. *Medicago truncatula* is a model plant for legumes and analysis of its response to salt stress is helpful for providing valuable insights into breeding. However, few studies have focused on illustrating the whole-transcriptome molecular mechanism underlying salt stress response in *Medicago truncatula*. Herein, we sampled the leaves of *Medicago truncatula* treated with water or NaCl and analyzed the characteristics of its coding and non-coding RNAs. We identified a total of 4,693 differentially expressed mRNAs (DEmRNAs), 505 DElncRNAs, 21 DEcircRNAs, and 55 DEmiRNAs. Gene ontology and Kyoto Encyclopedia of Genes and Genomes pathway enrichment analyses revealed that their functions were mostly associated with metabolic processes. We classified the lncRNAs and circRNAs into different types and analyzed their genomic distributions. Furthermore, we predicted the interactions between different RNAs based on the competing endogenous RNA (ceRNA) theory and identified multiple correlation networks, including 27 DEmiRNAs, 43 DEmRNAs, 19 lncRNAs, and 5 DEcircRNAs. In addition, we comprehensively analyzed the candidate DEmRNAs and ceRNAs and found that they were involved in Ca^{+} signaling, starch and sucrose biosynthesis, phenylpropanoid and lignin metabolism, auxin and jasmonate biosynthesis, and transduction pathways. Our integrated analyses in salt stress response in *Medicago truncatula* revealed multiple differentially expressed coding and non-coding RNAs, including mRNAs, lncRNAs, circRNAs, and miRNAs, and identified multiple DEmRNA and ceRNA interaction pairs that function in many pathways, providing insights into salt stress response in leguminous plants.

Keywords: *Medicago truncatula*, legume, whole-transcriptome RNA sequencing, salt stress, non-coding RNAs (ncRNAs)

OPEN ACCESS

Edited by:
Maofeng Chai,
Qingdao Agricultural University, China

Reviewed by:
Hao Lin,
Biotechnology Research Institute (CAAS), China
Shuxin Zhang,
Shandong Agricultural University, China

****Correspondence:***
Shuxia Yin
yinsx369@bjfu.edu.cn

Specialty section:
This article was submitted to Plant Abiotic Stress, a section of the journal Frontiers in Plant Science

Received: *07 March 2022*
Accepted: *28 March 2022*
Published: *18 April 2022*

Citation:
An Y, Su H, Niu Q and Yin S (2022) Integrated Analysis of Coding and Non-coding RNAs Reveals the Molecular Mechanism Underlying Salt Stress Response in Medicago truncatula. Front. Plant Sci. 13:891361. doi: 10.3389/fpls.2022.891361

Abbreviations: DEmRNA, differentially expressed mRNA; lncRNA, long non-coding RNA; circRNA, circular RNA; miRNA, microRNA; FPKM, fragments per kilobase per million reads; RPM, back-spliced reads per million mapped reads; FDR, false discovery rate; GO, Gene Ontology; KEGG, Kyoto Encyclopedia of Genes and Genomes; qRT-PCR, quantitative real-time reverse transcription-polymerase chain reaction.

INTRODUCTION

Soil salinity is an increasingly severe global problem that threatens more than 100 countries and approximately 831 million hectares of land (Rengasamy, 2006; Butcher et al., 2016). It is projected that salinization will impact 50% of all arable land by 2050 (Wang et al., 2003; Butcher et al., 2016). The increase in soil salinity will cause ionic, osmotic, secondary, and oxidative stresses in plants and severely limit their growth and productivity (Yang and Guo, 2018a).

To effectively improve the salt tolerance of plants, we need to identify genes and signaling pathways that are important in salt resistance. Over the past two decades, multiple elements of salt tolerance and their regulatory mechanisms have been explored through genetic and biochemical analyses (Yang and Guo, 2018b; Zelm et al., 2020). The salt overly sensitive (SOS) pathway, which comprises SOS1 (Na^+/H^+ antiporter), SOS2/CIPK24 (CBL-interacting protein kinase 24), and SOS3/CBL4 (calcineurin B-like protein), represents the best-characterized CBL-CIPK pathway for regulating sodium concentration in the cytosol under salt stress condition (Ji et al., 2013; Manishankar et al., 2018). Different members in mitogen-activated protein kinase (MAPK) cascades function in regulating ionic and reactive oxygen species (ROS) homeostasis by phosphorylating and activating SOS1 and controlling the scavenging of ROS, respectively (Pitzschke et al., 2009; Yu et al., 2010; Pérez-Salamó et al., 2014). In response to osmotic stress induced by salinization, abscisic acid (ABA)-independent sucrose non-fermenting1-related protein kinase 2 (SnRK2s) and ABA-dependent SnRK2s play important roles in transcriptional and post-transcriptional regulation (Kulik et al., 2011; Zelm et al., 2020). In addition, the biosynthesis and transport of auxin and ABA are responsible for salt tolerance (Duan et al., 2013; He et al., 2018; Korver et al., 2018).

With the advancement of next-generation sequencing technologies, whole-transcriptome RNA sequencing has revealed that protein-coding RNAs, as well as non-coding RNAs (ncRNAs), play essential regulatory roles in plants' response to salt stress (Wang et al., 2017). MicroRNAs (miRNAs) form an extensive class of ncRNA molecules with 20–24 nucleotides; they negatively regulate target mRNA expressions (Zhang, 2015). Previous studies have demonstrated that miRNAs are involved in plants' response to salt stress. For instance, overexpressing *osa-miR171c* decreased salt stress tolerance in rice (Yang et al., 2017). Also, overexpressing *osa-miR396c* reduced salt stress tolerance in *Arabidopsis thaliana* and rice (Gao et al., 2010). Transgenic *Arabidopsis* overexpressing *miR399f* showed tolerance to salt stress (Baek et al., 2016) and overexpression of *miR156* conferred salt tolerance in alfalfa (Arshad et al., 2017). Long non-coding RNAs (lncRNAs) are defined as a group of ncRNAs with more than 200 nucleotides, which provide an important perspective on the centrality of RNA in gene regulation (Rinn and Chang, 2012). LncRNAs are often grouped into sense, antisense, intronic, bidirectional, and intergenic lncRNAs depending on their location relative to nearby protein-coding genes. They can regulate gene expression *via cis*-acting or *trans*-acting (Ponting et al., 2009). Using whole-transcriptome RNA sequencing, Wang et al. (2015) and Deng et al. (2018) identified and characterized the lncRNAs involved in salt stress in *Medicago truncatula* and *Gossypium hirsutum*. Circular RNAs (circRNAs) are endogenous covalently closed RNAs generated by alternative circularization (Li et al., 2017; Fu et al., 2019). Emerging evidence has demonstrated that plant circRNAs are differentially expressed (DE) under various stress conditions (Li et al., 2017).

Recently, a competing endogenous RNA (ceRNA) theory has been widely accepted as a novel type of gene regulatory model (Salmena et al., 2011). LncRNAs and circRNAs act as ceRNAs to interact with common miRNA response elements and ultimately de-repress the transcriptional or/and translational limitations on miRNA target genes (Ala et al., 2013; Li et al., 2019). Based on this theory, a number of studies have analyzed the ceRNA-miRNA-target gene regulatory networks based on lncRNA/miRNA, circRNA/miRNA, and miRNA/mRNA interactions in plants (Xu et al., 2016; Li et al., 2019; He et al., 2020). However, to the best of our knowledge, the comprehensive studies of the mRNA, miRNA, lncRNA, circRNA, and ceRNA networks in salt stress response in *Medicago truncatula* are lacking. In addition, the functions of these networks have not been extensively clarified.

Medicago truncatula, a close relative of alfalfa, is a model plant widely used in the study of legumes due to its simple genomic ploidy, small genome size, and short growth cycle (Tang et al., 2014). Considering the severe trend of soil salinization, there is a need to unravel the molecular mechanisms underlying salt stress responses in *Medicago truncatula* to provide important instructions in breeding practice for legumes. Therefore, in this study, we used whole-transcriptome RNA sequencing to identify and characterize coding and non-coding RNAs, and the ceRNA networks in *Medicago truncatula* treated with NaCl or water. Our results extend the current view on non-coding RNAs as ubiquitous regulators under salt stress and further deepen our understanding of the molecular mechanisms underlying salt stress response in *Medicago truncatula*.

MATERIALS AND METHODS

Plant Growth Conditions and Salt Treatment

Sterilized seeds of Jemalong A17, an ecotype of *Medicago truncatula*, were kept at 4°C for 2 days. After vernalization, the seeds were placed in the Murashige and Skoog medium to germinate at 25°C. Afterward, the sprouted seedlings were transplanted into plastic pots filled with vermiculite and nutrient soil in a ratio of 1:1. The seedlings were cultured at 25°C with a 16 h light/8 h dark cycle and a relative humidity of 75%. After 3 weeks, the control group (CK) was continuously watered with neutral water, whereas the experimental group (Salt) was watered with a solution of 300 mmol/L NaCl. After 1 week, leaves of the CK and Salt groups were collected for whole-transcriptome RNA sequencing (with 3 biological repetitions) in Gene *Denovo* Biotechnology Co., Ltd (Guangzhou, China).

RNA Extraction and Sequencing

Leaves of the CK and Salt groups were collected (with three biological repetitions) and frozen in liquid nitrogen. Total RNA extraction was performed from 6 samples using TRIzol reagent (Invitrogen). RNA quality was estimated using a NanoDrop 2,000 spectrophotometer (Thermo Fisher Scientific). After ribosomal RNA (rRNA) removal, template RNA fragmentation (200–500 nucleotides), cDNA synthesis, and PCR amplification, we used Illumina HiSeq^{TM} 4000 for total RNA sequencing. The raw reads were first quality-controlled with FASTQ by filtering low-quality reads (Chen et al., 2018). Afterward, clean reads were aligned to the *Medicago truncatula* genome (MedtrA17_4.0) using the HISAT2 software (Kim et al., 2015).

mRNA Identification and Analysis

Based on the genomic mapping results, we reconstructed transcripts using Stringtie to identify protein-coding genes (Pertea et al., 2015). The fragments per kilobase per million reads (FPKM) values were obtained to estimate the expression level of mRNAs after correction for sequencing depth and transcript length. Differentially expressed mRNAs (DEmRNAs) were defined with a cutoff of $\log_2$FC > 1 and FDR < 0.05. The heat map based on Z-score was drawn for the DEmRNAs. Gene ontology (GO) annotation and functional enrichment analyses of DEmRNAs were performed using an online database.[1]

Long Non-coding RNA Identification and Analysis

After reconstruction, we retained the transcripts with length $\geq$200 bp and exon number $\geq$1. To improve the reliability in identifying true lncRNAs, we selected the transcripts with no coding potential predicted by both coding potential calculator 2 (CPC2) and coding-non-coding index (CNCI) for further analysis (Sun et al., 2013; Kang et al., 2017). According to the positions of the lncRNAs relative to the protein-coding genes in the genome, we divided the lncRNAs into 5 types, including sense lncRNAs, antisense lncRNAs, intronic lncRNAs, bidirectional lncRNAs, and intergenic lncRNAs. Their genomic distributions were shown by Circos plots using an online platform.[2] The FPKM values of the lncRNAs were calculated, and DESeq2 was used for the DE analysis (Love et al., 2014). The DElncRNAs were selected with the criteria of $\log_2$FC >1 and FDR < 0.05. We used RNAplex to predict the complementary relationship between antisense lncRNAs and mRNAs (Tafer and Hofacker, 2008). A prediction of *cis*-acting interactions was made if the location of the lncRNA was upstream or downstream of a gene within 10 kb. On the other hand, a prediction of *trans*-acting interactions was made based on Pearson's correlation coefficients between lncRNAs and protein-coding genes. Genes with an absolute correlation greater than 0.95 was considered the *trans*-acting target genes. Pathway enrichment analysis of these genes was performed using the Kyoto Encyclopedia of Genes and Genomes (KEGG) (Kanehisa et al., 2008).

[1]http://www.geneontology.org/

[2]https://yimingyu.shinyapps.io/shinycircos/

Circular RNA Identification and Analysis

For circRNA identification, we extracted the unmapped reads from the genome alignment. Afterward, the reads (about 20 bp) at both terminals of these unmapped reads were aligned again to the reference genome using bowtie2 and the mapped reads were referred to as anchor reads (Langmead and Salzberg, 2012). All mapped anchor reads in 6 samples were submitted to the find_circ module in bowtie2 to identify circRNAs (Memczak et al., 2013). Expression levels of circRNAs were calculated by back-spliced reads per million mapped reads (RPM). GO annotation and functional enrichment analysis of the identified circRNAs were performed using an online database (see text footnote 1).

MicroRNA Identification and Analysis

The total RNA was subjected to agarose gel electrophoresis and small RNAs with 18–30 nucleotides were extracted. Afterward, 3′ and 5′ adapters were added to the small RNAs and reverse transcription and PCR amplification were performed. We extracted and purified the PCR products with a length of 140–160 bp to construct the cDNA library for miRNA and Illumina HiSeq^{TM} 4000 was used for the sequencing. To obtain the clean tags (sequences of miRNA), we filtered low-quality reads (reads containing more than one base with quality value less than 20 or reads containing N), reads with 5′ adapters, reads with long polyA tails (more than 70% of the bases in reads were A), and reads without 3′ adapters. All the clean tags were aligned in GenBank and Rfam databases to remove rRNAs, scRNAs, snoRNAs, snRNAs, and tRNAs. The screened clean tags were searched against the miRBase database to identify known miRNAs in *Medicago truncatula*. Afterward, the unannotated tags were aligned to the reference genome and predicted hairpin structures to identify novel miRNAs. The expression of the miRNAs was represented as TPM (tags per million). DEmiRNAs were identified using edgeR, with dispersion set to 0.01 and other parameters set to default (Robinson et al., 2010).

Construction and Analysis of the Competing Endogenous RNAs Regulatory Network

Based on the ceRNA theory, we predicted the interaction pairs, DEmiRNAs-DEmRNAs, DEmiRNAs-DElncRNAs, and DEmiRNAs-DEcircRNAs, using Patmatch_v1.2.[3] Pairwise correlations were calculated using the Spearman correlation coefficient (SCC) and the interaction networks were built using gene pairs with SCC < -0.5. Cytoscape software was used to display the visual models (Shannon et al., 2003).

Quantitative Real-Time Reverse Transcription-Polymerase Chain Reaction Validation

To validate the accuracy of the whole-transcriptome RNA sequencing, we performed quantitative real-time reverse transcription-polymerase chain reaction (qRT-PCR) for some

[3]https://www.arabidopsis.org/cgi-bin/patmatch/nph-patmatch.pl

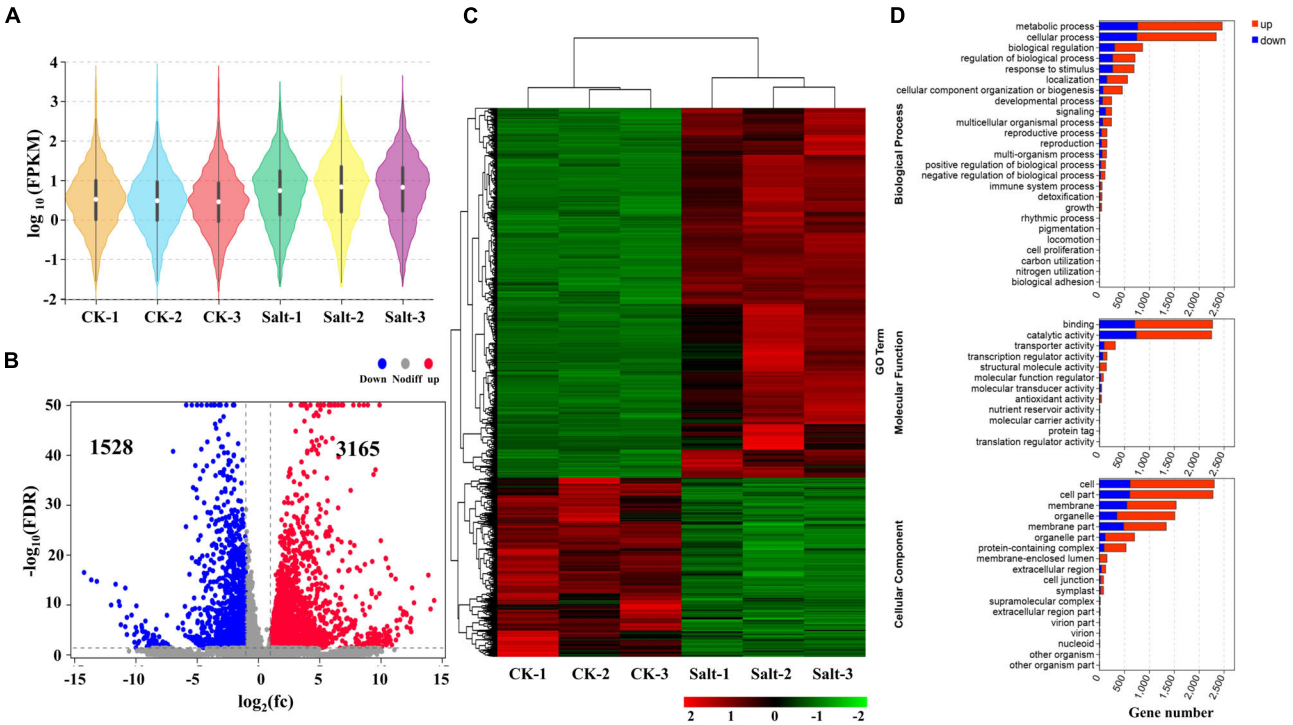

FIGURE 1 | Identification and analysis of mRNAs and DEmRNAs in *Medicago truncatula* leaf under salt stress. **(A)** FPKM distribution of mRNAs in six samples. **(B)** DEmRNAs statistics after salt treatment. **(C)** Heat map of all DEmRNAs. **(D)** GO enrichment of all DEmRNAs.

randomly selected DEmRNAs. *MtActin* served as the internal reference gene. The primers were designed using the Primer 5.0 software and are listed in **Supplementary Table 1**. First-strand cDNA was synthesized from 1 μg total RNA using TransScript-Uni One-Step gDNA Removal and cDNA Synthesis SuperMix (TransGen Biotech, Beijing, China). The SYBR Premix Ex Taq (Takara, Japan) was used for quantitative detection on the 7,500 Real-Time PCR System (Applied Biosystems, CA, United States). A 20-μl PCR system containing 10 μl 2 × SYBR Premix Ex Taq (Takara, Japan), 8 μl ddH_2O, 0.8 μl cDNA, 0.4 μl Dye II, and 0.8 μl primers, was used. The qPCR process included the holding stage (95°C for 30 s), cycling stage (95°C for 5 s and 60°C for 34 s), and melt curve stage (95°C for 15 s, 60°C for 1 min, 95°C for 30 s, and 60°C for 15 s). All samples analyses were repeated thrice and the relative expressions of DEmRNAs were calculated using the $2^{-\Delta\Delta Ct}$ method (Livak and Schmittgen, 2001).

RESULTS

Analysis of mRNAs Characteristics in Response to Salt Stress

From the whole-transcriptome RNA sequencing data, we obtained the FPKM values of protein-coding genes. According to the distribution of the expression abundance of the transcripts from the 6 different samples, we found that the overall gene expression levels could be distinctly divided into two groups: the control group treated with water (CK-1, CK-2, and CK-3) and the experimental group treated with salt (Salt-1, Salt-2, and Salt-3) (**Figure 1A**). This result indicated that the salt treatment used in this study was effective. We identified a total of 4,693 (3,165 up-regulated and 1,528 down-regulated) DEmRNAs (**Figure 1B** and **Supplementary Table 2**). A heat map presented the expression profiles of the DEmRNAs and showed that three repeats of each treatment clustered together, while the Salt-treated group and the CK group were clustered separately (**Figure 1C**). Cluster analysis also revealed that most genes were up-regulated after the salt treatment, while a relatively few genes were down-regulated (**Figure 1C**). To explore the functions of the DEmRNAs, we performed a GO enrichment analysis. Based on the GO enrichment analysis, we found that, in terms of biological process, most of the DEmRNAs were annotated to metabolic and cellular processes, and in terms of molecular function, the two largest categories were annotated to binding and catalytic activities. In addition, two major terms (cell and cell part of cellular component) were also enriched (**Figure 1D** and **Supplementary Table 3**). These enrichment analyses suggested that these GO terms might be involved in the salt stress response of *Medicago truncatula*. KEGG pathway analysis showed that the metabolic pathways were the most enriched (**Supplementary Figure 1**).

Subsequently, we identified 12 transcription factor families from the DEmRNAs (**Figure 2**). By comparing the expression levels of the transcription factors (TFs) among the 6 different samples, we divided them into 4 groups. First, the core-binding

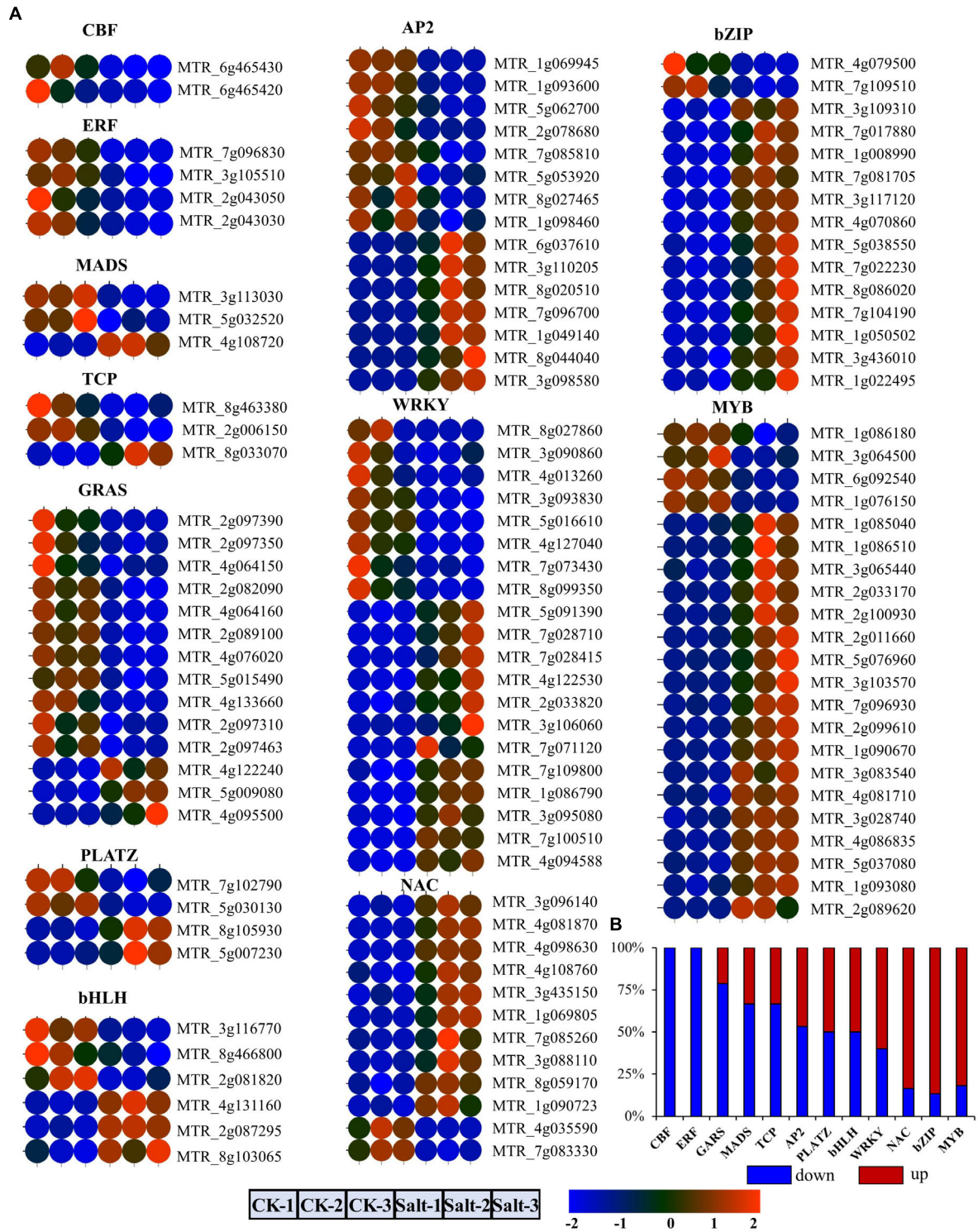

FIGURE 2 | Identification and analysis of differentially expressed TFs under salt stress. **(A)** The expression level of 12 TFs in six samples. **(B)** Histogram of up-regulated and down-regulated genes in 12 TF families.

factor (CBF) and ethylene-responsive factor (ERF) TF families, including 2 and 4 differentially expressed TFs, respectively, were all down-regulated after salt stress (**Figure 2A**). Second, more than 50% of the DEmRNAs belonging to the GRAS, MADS, and TCP TF families were down-regulated (**Figure 2A**). Third, 50% of the DEmRNAs in the bHLH, PLATA, WRKY, and AP2

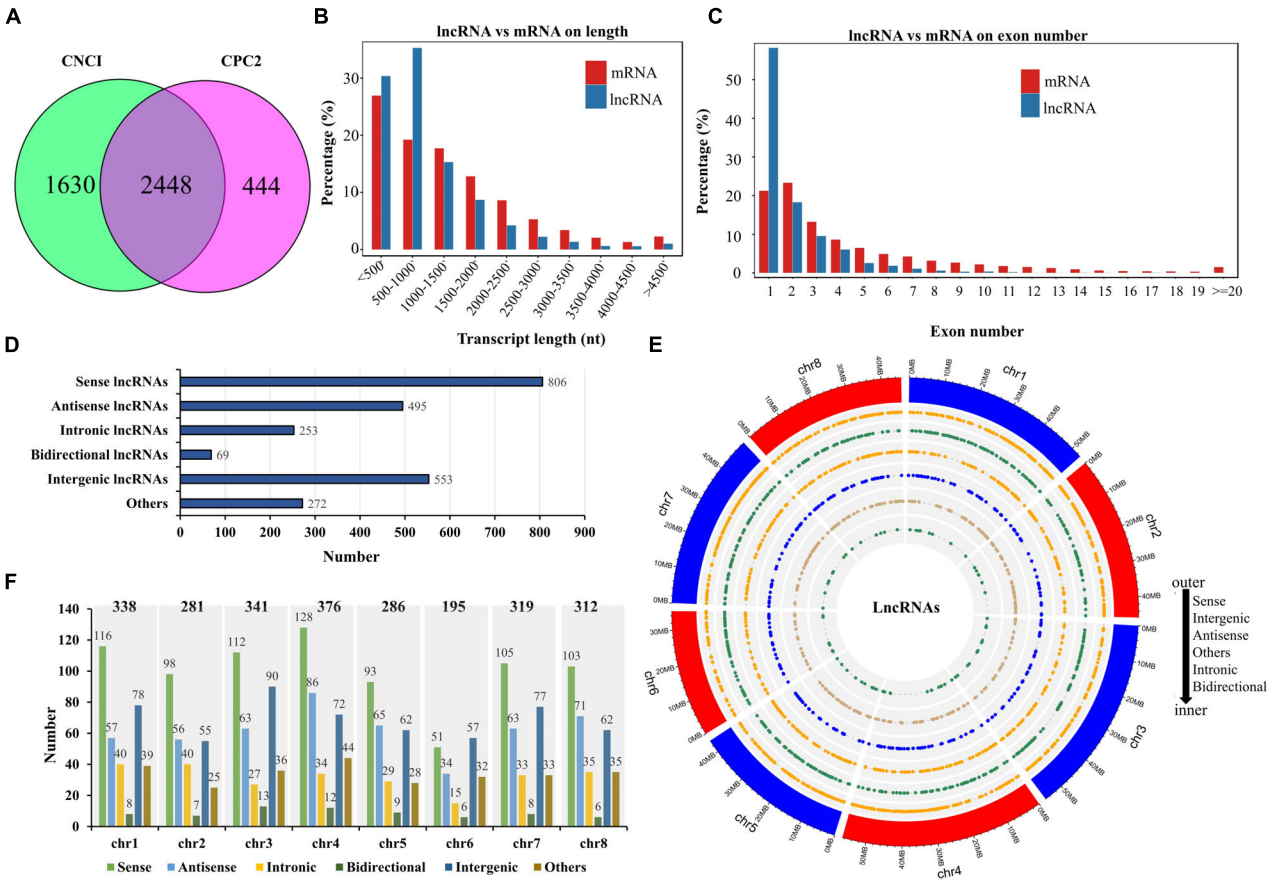

FIGURE 3 | Identification and distribution of lncRNAs. **(A)** The number of lncRNAs identified by the CNCI and CPC2 methods. **(B)** Comparison of lncRNA with mRNA in terms of transcript length. **(C)** Comparison of lncRNA with mRNA in terms of exon number. **(D)** Number statistics of different lncRNAs types. **(E)** Genomic distribution of different lncRNAs types. **(F)** Number statistics of different lncRNAs types on eight chromosomes.

transcription factor families were down-regulated under salt stress (**Figure 2B**). Fourth, most differentially expressed TFs in the MYB, bZIP, and NAC TF families were up-regulated in response to salt stress (**Figure 2B**).

Analysis of Long Non-coding RNAs Characteristics in Response to Salt Stress

To improve the accuracy of lncRNA identification before salt stress, we used the CNCI and CPC2 software to predict the coding potential of transcripts and selected the common transcripts without coding potential as reliable lncRNAs. Therefore, we obtained a total of 2,448 lncRNAs (**Figure 3A** and **Supplementary Table 4**). Comparing the length between the lncRNA and mRNA, we found that their length distributions were similar (most transcripts were less than 1,500 nucleotides), except that ratio of lncRNAs with 500–1,000 nucleotides was higher than that of mRNAs with the same nucleotide length (**Figure 3B**). The exon number in the mRNAs was more widely distributed than that of the lncRNAs, mostly ranging from 1 to 4, and the percentage of the lncRNAs with one exon was much higher than that of the mRNAs (**Figure 3C**). According to the position of the lncRNAs relative to the protein-coding genes in the genome, we identified 806 sense lncRNAs, 495 antisense lncRNAs, 253 intronic lncRNAs, 69 bidirectional lncRNAs, 553 intergenic lncRNAs, and 272 other lncRNAs (**Figure 3D**). The genomic location and number distribution on 8 chromosomes of these different types of lncRNAs are shown in **Figures 3E,F**, respectively.

Subsequently, we performed lncRNA expression analysis and, based on the FPKM values, we found that lncRNA expression was significantly different from that of mRNA either in the CK group or the Salt group (**Figure 4A**). Compared with the CK group, the overall expression levels of lncRNAs were more similar within the Salt group, which was consistent with those of mRNAs (**Figures 1A**, **4B**). The expression levels of lncRNA in the CK and Salt groups and their fold changes are shown in **Figure 4C**. We obtained a total of 293 up-regulated lncRNAs and 212 down-regulated lncRNAs (**Figures 4C,D** and **Supplementary Table 5**). A heat map of these DElncRNAs showed that three repeats of each treatment clustered together (**Figure 4D**).

According to complementary base pairing, we predicted antisense lncRNAs. The result showed that 496 lncRNAs

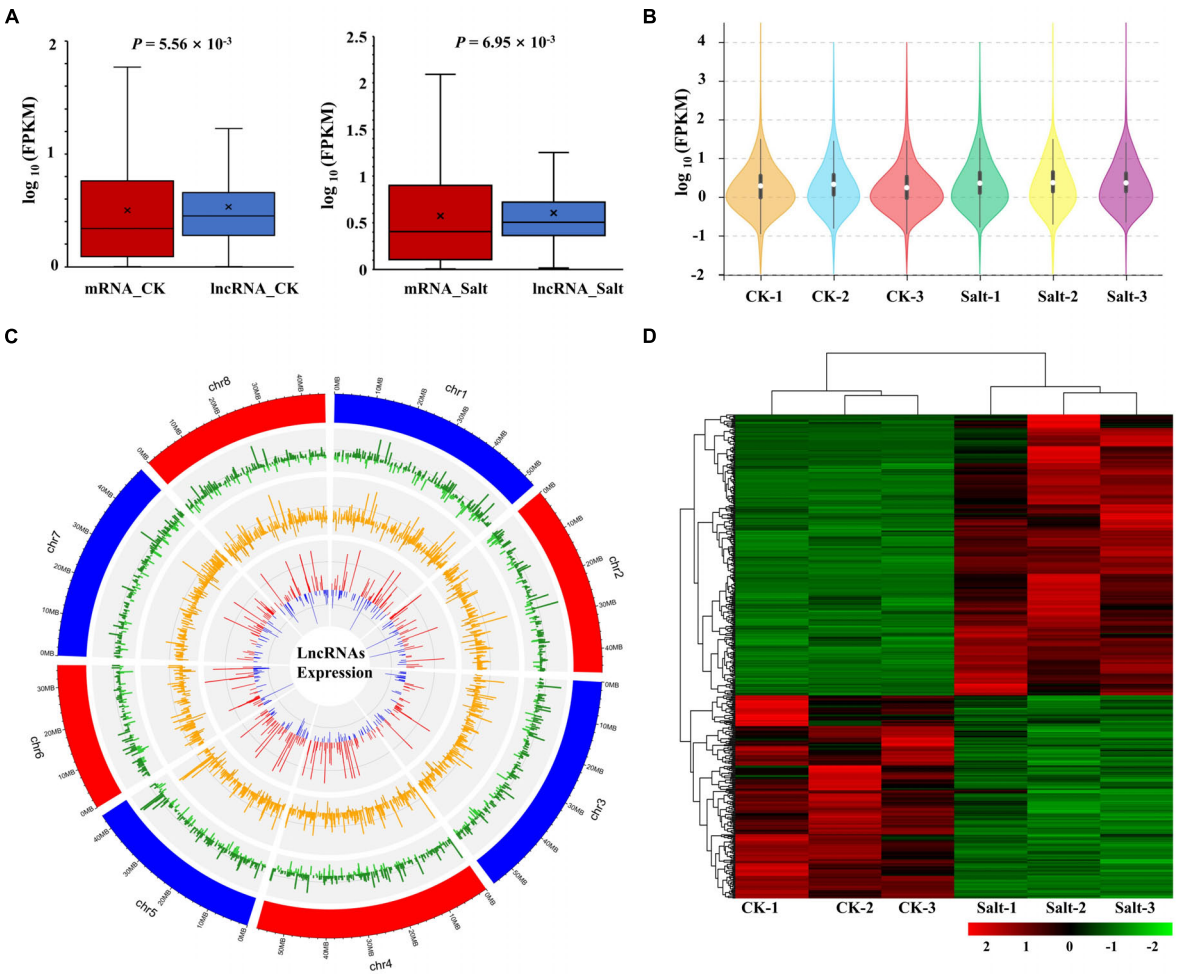

FIGURE 4 | Expression analysis of lncRNAs. **(A)** Comparison of the expression levels between lncRNAs and mRNAs in the CK and Salt groups. **(B)** FPKM distribution of lncRNAs in six samples. **(C)** Genomic distribution of lncRNAs. The three circles (from outer to inner) represented the expression levels (log_{10}FPKM) of lncRNA in the CK group, lncRNA in the Salt group, and fold change of the expression levels, respectively. **(D)** The heat map of all DElncRNAs.

and 488 mRNAs formed 541 antisense pairs, while between DElncRNAs and DEmRNAs, only 31 pairs were identified (**Table 1** and **Supplementary Table 6**). Afterward, the KEGG pathway analysis was performed on the antisense-targeted DEmRNAs and metabolic pathways were enriched with the most gene numbers (**Figure 5A**). We used a 10-kb window upstream or downstream of the lncRNA to identify *cis*-interactions and identified 191 DElncRNA-DEmRNA pairs (**Table 1** and **Supplementary Table 7**). The *cis*-targeted DEmRNAs were enriched in photosynthetic pathways with a minimum *q*-value (**Figure 5B**). Correlation analysis revealed 419,734 *trans*-interactions between DElncRNAs and DEmRNAs (**Table 1**). KEGG pathway analysis showed that the metabolic pathway and biosynthesis of secondary metabolites pathway were the most enriched (**Figure 5C**). The results of the GO enrichment analysis of antisense, *cis*, and *trans* lncRNAs are shown in **Supplementary Figure 2**.

TABLE 1 | Association analysis between lncRNA and mRNA.

Association	List	lncRNA	mRNA	Pair
Antisense	All	496	488	541
	Diff	31	30	31
Cis	All	2,328	5,554	6,842
	Diff	160	168	191
Trans	All	2,448	48,179	1.18 E^{08}
	Diff	505	4,675	419,734

Analysis of Circular RNAs Characteristics in Response to Salt Stress

In this study, we identified a total of 546 circRNAs that could be classified into 6 types (**Figure 6A** and **Supplementary Table 8**). The genomic distribution of the different types of circRNAs is presented in **Figure 6A**. In terms of length, most circRNAs were shorter than 400 bp (**Figure 6B**). Different chromosomes

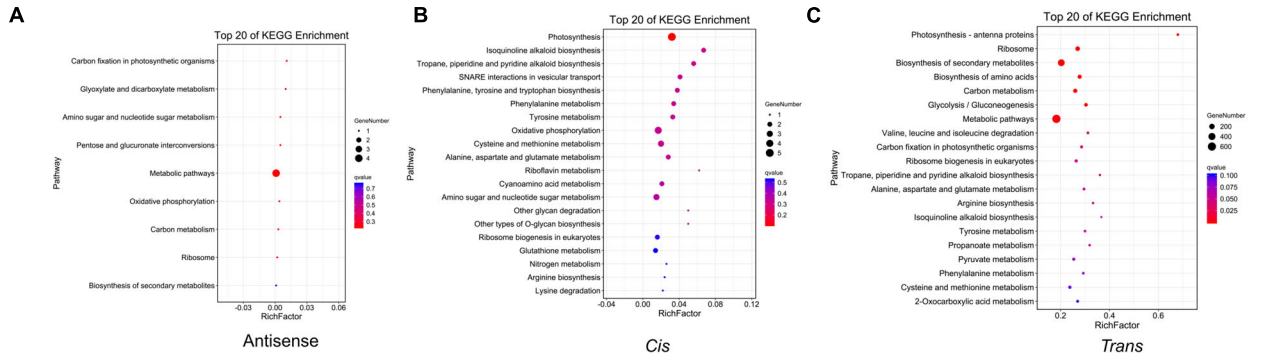

FIGURE 5 | The KEGG pathway analysis of the target genes of DElncRNAs. **(A)** The KEGG pathway analysis of the antisense-targeted genes of DElncRNAs. **(B)** The KEGG pathway analysis of *cis*-targeted genes of DElncRNAs. **(C)** The KEGG pathway analysis of *trans*-targeted genes of DElncRNAs.

included different numbers of circRNAs. Chromosome 1 (Chr. 1) had the most circRNAs (**Figure 6C**). GO annotation of the circRNA genes showed that, in terms of biological process, they were enriched in cellular process, metabolic process, and biological regulation; in terms of molecular function, there were enriched in binding, catalytic, and transport activities; whereas, in terms of cellular component, they were enriched in cell, cell part, and organelle (**Figure 6D**).

The expression levels of circRNAs in the 6 samples were visualized in a violin plot (**Figure 7A**). We identified a total of 21 DEcircRNAs (12 up-regulated and 9 down-regulated, **Figure 7B** and **Supplementary Table 9**). Their IDs and expressions in six samples are shown in **Figure 7C** and **Supplementary Table 9**, respectively. Novel_circ_000001 is one of the DEcircRNAs and MTR_1g116947 is its source gene. In the CK group, novel_circ_000001 was not expressed. However, after salt treatment, the second exon of MTR_1g116947 formed a circRNA, which resulted in a significantly higher expression of novel_circ_000001 (**Figure 7D**). We performed the GO enrichment analysis on all the source genes of DEcircRNAs and found that membranes under the cellular components, binding activities under the molecular functions, and cellular processes under the biological process contained the largest number of source genes (**Figure 7E**).

Analysis of MicroRNAs Characteristics in Response to Salt Stress

Through whole-transcriptome RNA sequencing and reads alignment, we identified multiple known and novel miRNAs (**Supplementary Table 10**). The top 10 known and novel miRNAs in the CK and Salt groups are shown in **Figures 8A,B**, respectively. Of note, mtr-miR166 and novel-m0001-3p were most highly expressed. For novel miRNAs, 19 DEmiRNAs (12 up-regulated and 7 down-regulated) were identified (**Figure 8C**). Their expression levels in the 6 samples (3 for both the CK and Salt groups) are shown in **Figure 8D**. For the known miRNAs, 36 DEmiRNAs (10 up-regulated and 26 down-regulated) were identified (**Figure 8C**). For these miRNAs, 8 miRNAs belonging to the miR2111 family, 2 miRNAs belonging to the miR2592 family, 2 miRNAs belonging to the miR5205 family, and 2 miRNAs belonging to the miR5285 family were down-regulated; in contrast, 2 miRNAs belonging to the miR398 family were up-regulated (**Figure 8E**).

Construction of the Competing Endogenous RNA Regulatory Network in Response to Salt Stress

To explore the relationship between protein-coding RNAs and ncRNAs under salt stress, we constructed the ceRNA regulatory networks based on the ceRNA theory. Between DEmiRNAs and mRNAs, we found a total of 524 pairs of interactions (**Supplementary Table 11**). There were 10 pairs between DEmiRNAs and DEcircRNAs and 46 pairs between DEmiRNAs and lncRNAs (**Supplementary Tables 13**, **14**). A total of 42 DEmRNAs were predicted as targets of 27 DEmiRNAs (**Figure 9** and **Supplementary Table 12**). Moreover, 19 lncRNAs and 5 DEcircRNAs were predicted as DEmiRNA sponges in salt stress response in leaves of *Medicago truncatula* (**Figure 9**). In the up-regulated miRNAs, we found 4 DEmiRNAs formed 7 DEmiRNA-DEmRNA, 8 DEmiRNA-lncRNA, and 3 DEmiRNA-DEcircRNA interactions (**Figure 9A**). Most of the down-regulated miRNAs were involved in multiple pairs with DEmRNAs and DEceRNAs (**Figure 9B**). Novel-m0018-5p and novel-m0019-5p interacted with the same DEmRNAs and lncRNAs. The mtr-miR2111 family included 8 DEmiRNAs, targeted MTR_3g085050 (**Figure 9B**). These DEceRNA, DEmiRNA, and DEmRNA might act as important regulators for salt stress response in *Medicago truncatula*.

Analysis of Key Pathways in Response to Salt Stress

According to the results of whole-transcriptome RNA sequencing, we analyzed genes and pathways that are important in response to salt stress in *Medicago truncatula*. In the nucleus, TFs act as important regulators for gene expression. In this study, we identified TFs, including 2 CBFs (MTR_6g465430 and MRT-6g465420) and 4 ERFs (MTR_7g096830, MTR_3g105510, MTR_2g043050, and MTR_2g043030), were down-regulated

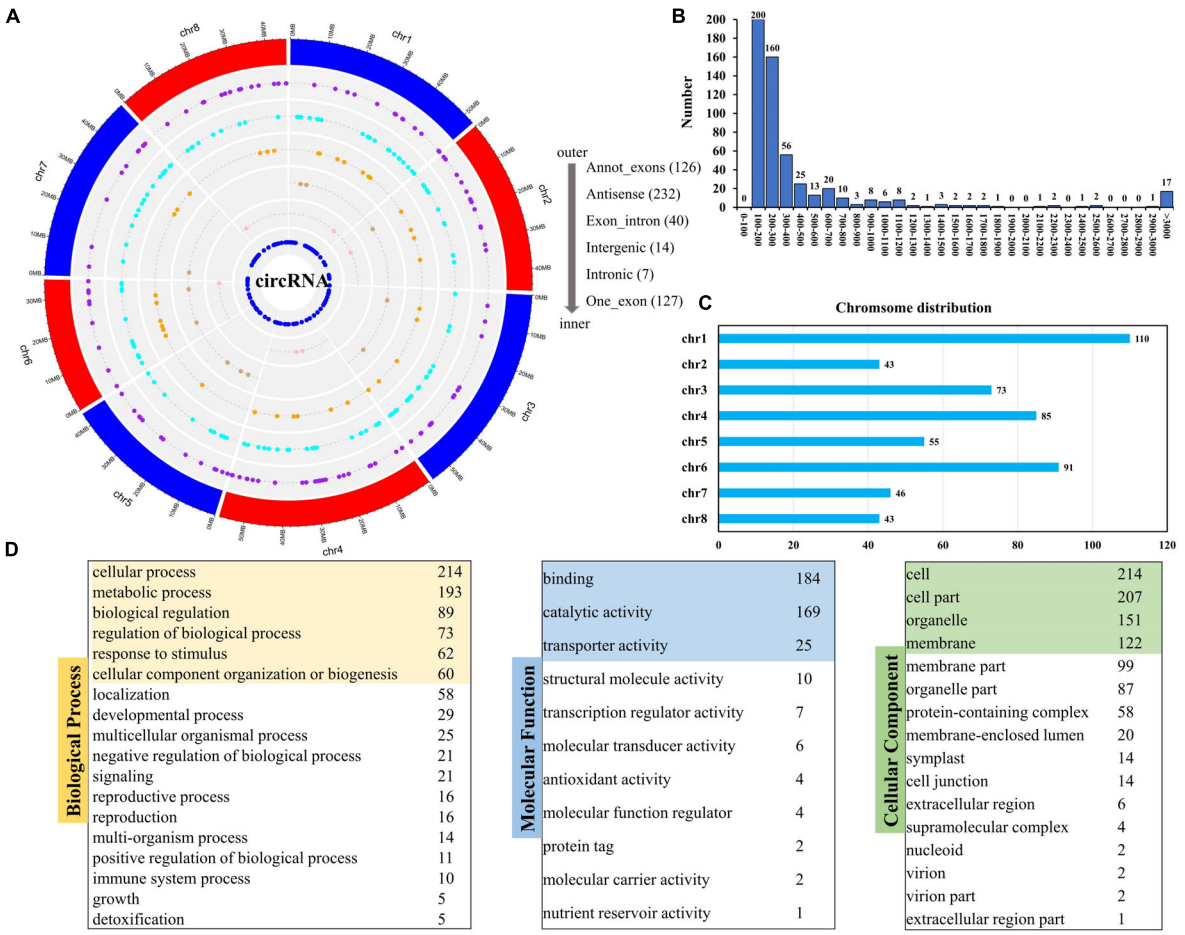

FIGURE 6 | Distribution of circRNAs and GO analysis of source genes. **(A)** Genomic distribution of different circRNAs types. **(B)** Number statistics of different circRNAs in length. **(C)** Chromosome distribution of circRNAs. **(D)** GO enrichment of all source genes of circRNAs.

after salt treatment, whereas most genes in the NAC, bZIP, and MYB family were up-regulated (**Figures 2**, **10**). SPL transcription factors were negatively regulated by novel-m0037-5p and novel-m0037-5p interaction with the lncRNA MSTRG.15691.1 (**Figures 9B**, **10**). These results suggested that TFs themselves or TFs in relationship with non-coding RNAs play important roles in salt stress response in *Medicago truncatula*.

In this study, we found that 8 genes related to calmodulin (CaM) were up-regulated, including MTR_3g085050, which was negatively regulated by miR2111. The 8 members belonging to the miR2111 family were down-regulated, thus resulting in the up-regulation of MTR_3g085050, which encodes a calmodulin-binding protein (**Figures 9B**, **10** and **Supplementary Table 15**). We simultaneously identified 7 down-regulated *CaM* genes. The significant changes in the expression levels of the *CaM* genes indicated that Ca^{+} signal transduction was essential for salt stress response in *Medicago truncatula* and that different *CaM* genes functioned differently to regulate Ca^{+} concentration balance and downstream signals.

Genes involved in carbohydrate metabolism in the chloroplast also responded to salt stress (**Figure 10**). 1 gene (MTR_4g131760) related to starch synthesis (in the first step) was down-regulated and 2 genes (MTR_1g019440 and MTR_2g020240) related to starch degradation were up-regulated. In addition, eight differentially expressed genes related to sucrose metabolism were up-regulated (**Figure 10** and **Supplementary Table 15**).

In the plant hormones pathway, 6 genes related to auxin transport were down-regulated, while 2 genes were up-regulated after salt treatment. In addition, 8 auxin response factors were up-regulated, while 10 related factors were down-regulated (**Figure 10** and **Supplementary Table 15**). In the jasmonate pathway, 4 genes participating in the process from linolenic acid to hydroperoxylinolenic acid were down-regulated, while 2 genes were up-regulated. 2 12-oxo-PDA-reductases genes were down-regulated, while 3 genes were up-regulated (**Figure 10** and **Supplementary Table 15**).

In the phenylpropanoid metabolism, we found that 12 genes related to phenylpropanoid biosynthesis were up-regulated, while only 4 genes were down-regulated (**Figure 10** and **Supplementary Table 15**). In the secondary metabolism, only 2 genes (MTR_5g031300 and MTR_5g031360) related to cinnamyl-alcohol dehydrogenase (CAD) were down-regulated,

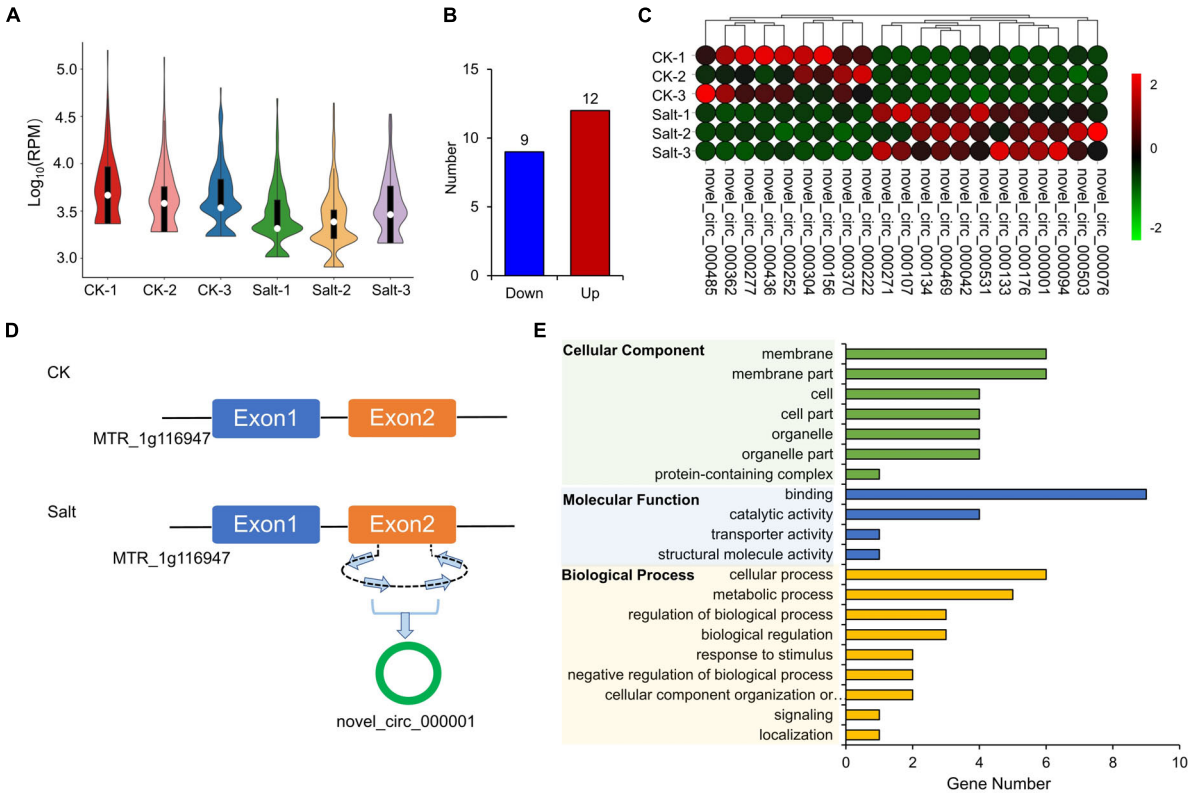

FIGURE 7 | Expression analysis of circRNAs. **(A)** FPKM distribution of cirsRNAs in six samples. **(B)** Statistics of down-regulated and up-regulated DEcircRNAs. **(C)** Expression visualization of DEcircRNAs in six samples. **(D)** MTR_1g116947 formed novel_circ_000001. **(E)** GO enrichment of source genes of DEcircRNAs.

while other 11 genes related to lignin biosynthesis were all up-regulated (**Figure 10** and **Supplementary Table 15**). Further analyses of the lignin content are necessary to explore the relationship between lignin genes and salt tolerance in *Medicago truncatula*.

In the mitochondrion, genes related to 4 electron transport protein complexes, tricarboxylic acid cycle (TCA), and alternative oxidase (AOX) were up-regulated (**Figure 10** and **Supplementary Table 15**). This revealed that the salt stress affected the reactions in the mitochondrion.

Based on the candidate genes involved in the key pathways implicated in response to salt stress, we further analyzed their regulatory relationship with lncRNAs. The result revealed that 6 and 81 genes may be *cis*- and *trans*-regulated by lncRNAs, respectively (**Supplementary Table 15**). This suggested that complex mechanisms, including interactions between mRNAs and lncRNAs, might respond to salt stress and that the fine control module worth further study.

Validation of the Expression of RNA by Quantitative Real-Time Reverse Transcription-Polymerase Chain Reaction

To confirm the results of the whole-transcriptome RNA sequencing, we used qRT-PCR to verify the expressions of randomly selected DERNAs, DEmiRNAs and lncRNAs. As shown in **Supplementary Figure 3**, the qRT-PCR results were consistent with the RNA-seq data. MTR_8g059170 was up-regulated, while the other 5 genes were significantly down-regulated after the salt treatment. And, we also found the miRNAs and its target genes had an opposite expression patterns (mtr-miR2088-5p and MTR_4g044297, novel-m0148-5p, and MTR_8g464450). These results demonstrate the accuracy of the RNA-seq data in this study.

DISCUSSION

Salt stress is among the most severe abiotic stresses that threaten plant growth (Butcher et al., 2016). With the expansion of saline land, there is a need to broaden the current knowledge on plant responses to salt stress. To date, an immense amount of research has been performed to assess different plants' responses to salinity; however, there are still many unknown regulatory elements and processes, including transcription and post-transcriptional regulation. In this study, we identified multiple key salt stress response factors through whole-transcriptome sequencing on the leaves of *Medicago truncatula*, a legume model crop, by comparing salt and water treated groups.

Based on the results of the whole-transcriptome sequencing, we first analyzed the protein-coding mRNA characteristics in

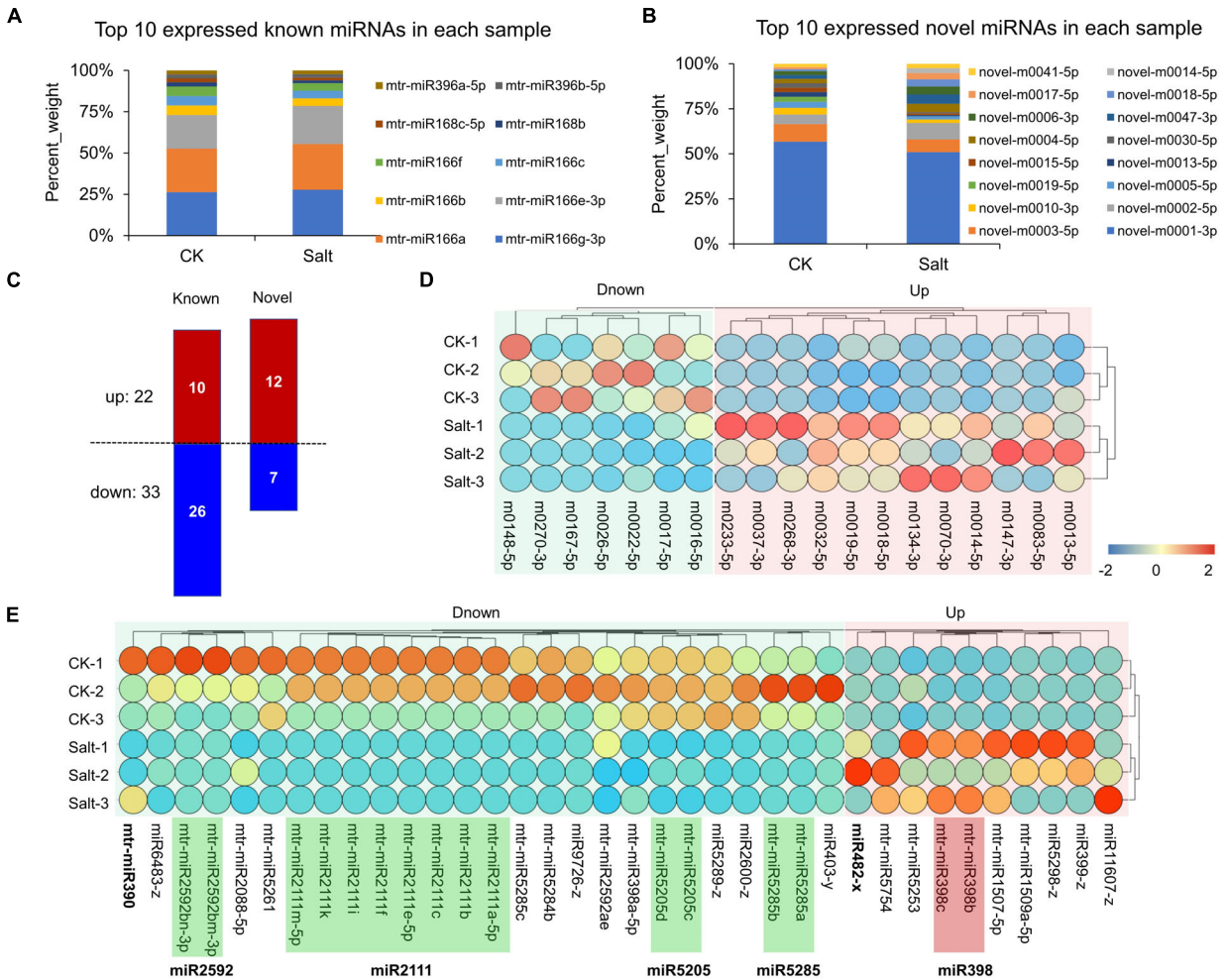

FIGURE 8 | Expression analysis of miRNAs. **(A)** Top 10 expressions of known miRNAs in the CK and Salt groups. **(B)** Top 10 expressions of novel miRNAs in the CK and Salt groups. **(C)** Statistics of down-regulated and up-regulated DEmiRNAs. **(D)** Expression visualization of novel DEmiRNAs in six samples. **(E)** Expression visualization of known DEmiRNAs in six samples.

response to salt stress in *Medicago truncatula* leaves. It has been recognized that many TFs have an important role in stress-responsive transcription, such as bZIP, AP2/ERF, MYB, NAC, and WAKY (Golldack et al., 2011). Yang et al. (2009) reported that *AtbZIP24* was induced by salt stress in *Arabidopsis thaliana* but suppressed in the salt-tolerant relative *Lobularia maritima*. Liu et al. (2007) reported that salt stress in *Arabidopsis thaliana* induced a signaling cascade involving the processing of *AtbZIP17*. Among the differentially expressed TFs in this study, 15 bZIP TFs (13 were highly induced) were induced by salt stress in *Medicago truncatula* leaves and their functions worth further study. We also found that 4 ERFs were down-regulated after salt treatment, suggesting that ERFs may be involved in the salt response. Cheng et al. (2013) reported that *ERF1* was highly induced by high salinity in *Arabidopsis* and that *ERF1*-overexpressing *Arabidopsis* lines were more tolerant to salt stress. It has been demonstrated that the overexpression of *WAKY25* and *WAKY33* could improve salt tolerance in *Arabidopsis* and that other WRKY-type TFs involved in salt response were also supported in rice and halotolerant grass *Festuca rubra* ssp. *litoralis* (Diédhiou et al., 2009a,b; Jiang and Deyholos, 2009). We identified 20 differentially expressed WRKY TFs; however, there was no consistent expression change in them, which may due to different functions in response to saline stress. Moreover, members in the MYB and bHLH families were also reported in response to ABA and ROS signaling related to salt adaptation (Lippold et al., 2009; Golldack et al., 2011). Our study also found some differentially expressed MYB and bHLH TFs. These results suggest that the differentially expressed TFs identified in *Medicago truncatula* might be involved in the complex regulatory systems in salt response as seen in other plants. Also, our results provide potential opportunities for improving salt tolerance in *Medicago truncatula* and *Medicago sativa*.

Recently, non-coding RNAs, including lncRNAs, circRNAs, and miRNAs, have been shown to play crucial regulatory roles in diverse biological processes involving complex mechanisms.

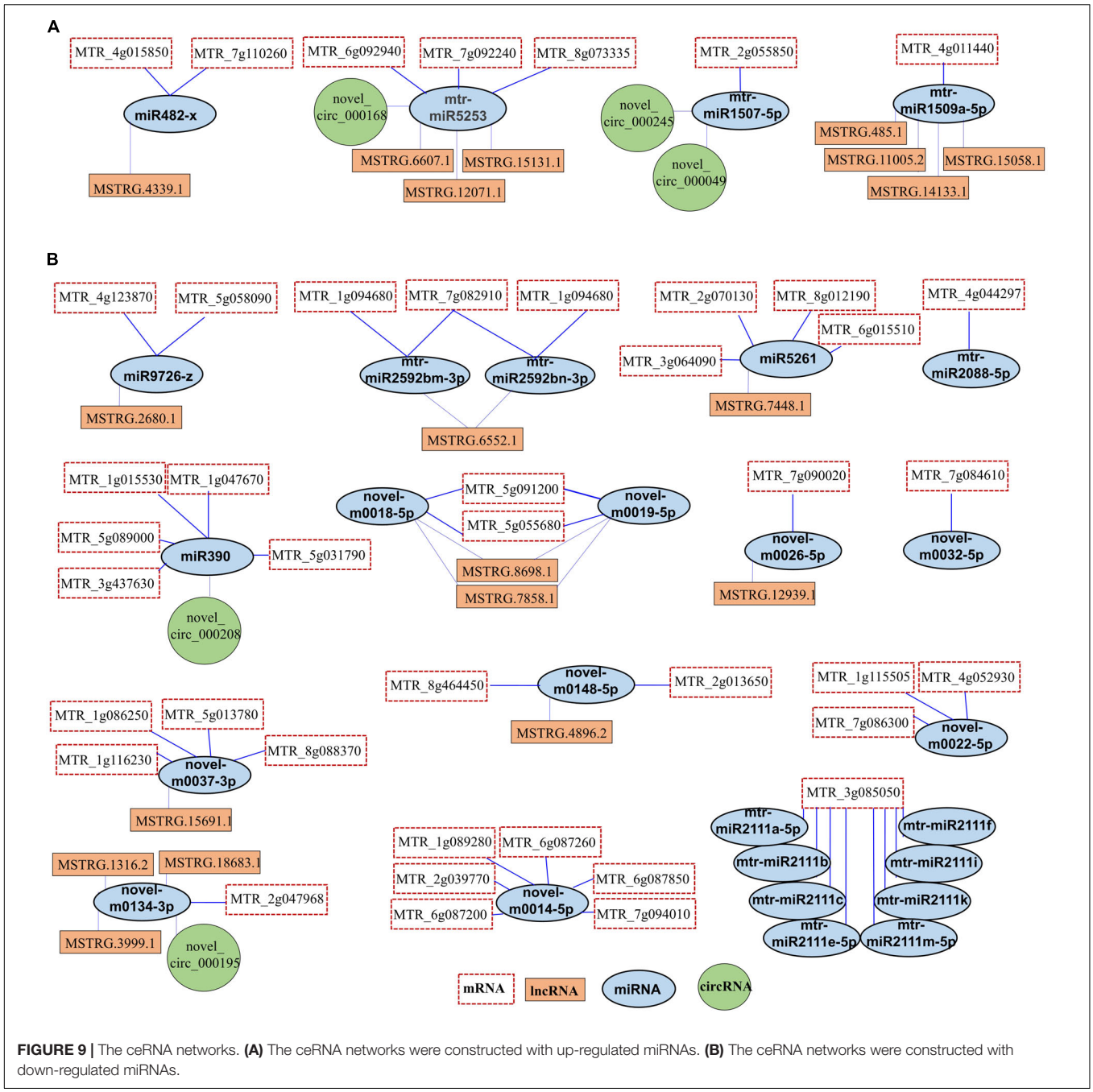

FIGURE 9 | The ceRNA networks. **(A)** The ceRNA networks were constructed with up-regulated miRNAs. **(B)** The ceRNA networks were constructed with down-regulated miRNAs.

Wang et al. (2015) identified the lncRNAs involved in salt stress in *Medicago truncatula* and predicted the interaction networks among the lncRNAs and protein-coding RNAs. In this study, a total of 2,448 lncRNAs were identified, which is quite different from the previous identification results (Wang et al., 2015). This phenomenon may be caused by different analysis methods in different studies. Zhang et al. (2021) identified lncRNA354 and found that its expression was reduced in salt-treated cotton. Silencing lncRNA354 enhanced the resistance to salt stress in cotton. The lncRNA DRIR could be significantly activated by drought and salt stress; moreover, its overexpression in *Arabidopsis* increased tolerance to salt stress (Qin et al., 2017). For circRNAs, Li et al. (2021) analyzed their expression patterns and functions between salt-sensitive and salt-tolerant poplars and concluded that circRNAs might regulate the gene expression of woody poplars efficiently in the salt tolerance of different poplars. Based on a previous transcriptome-wide analysis of circRNAs in rice (Lu et al., 2015), Zhou et al. (2021) used a multiplexed CRISPR-Cas9 strategy to efficiently acquire individual null mutants for 4 circRNAs (Os02circ25329, Os06circ02797, Os03circ00204, and Os05circ02465) in rice and revealed that they all participated

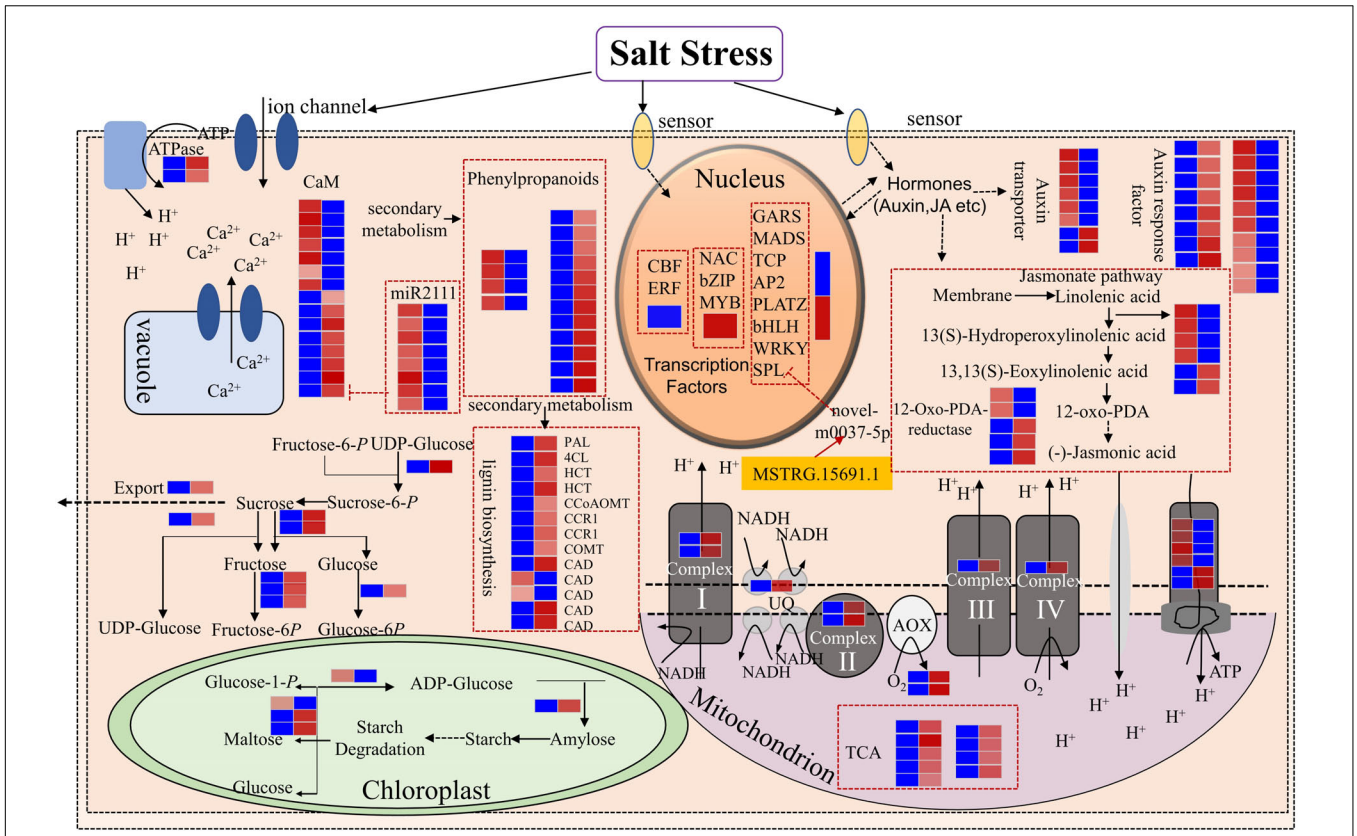

FIGURE 10 | The important pathways of *Medicago truncatula*'s response to salt stress and the relationship between DEmRNAs and ceRNAs. Blue boxes represent lower expression lever and red boxes represent higher expression level.

in salt stress response during seed germination. Furthermore, through molecular and computational analyses, a previous study demonstrated that Os06circ02797 could bind and sequester OsMIR408. Long et al. (2015) analyzed salt-stress-regulated miRNAs from roots of *Medicago* and found that different expression levels of some miRNAs were perhaps a consequence of the long-term adaptive evolution. In maize, miR169q was found to respond to stress-induced ROS signals and negatively regulate seedling salt tolerance. MiR169q repressed the transcript abundance of its target *NUCLEAR FACTOR YA8* (*ZmNF-YA8*), whose high expression improved salt tolerance in maize (Xing et al., 2021). In poplar, He et al. (2018) found that miR390 overexpression stimulated lateral root development and increased salt tolerance. The miR390/ARFs (auxin response factors) module is a key regulator subjected to salt stress by modulating the auxin pathway. In this study, we found that miRNA390 was significantly down-regulated in *Medicago truncatula* leaves after salt stress (**Figure 8E**). We also identified some ARFs, whose expression levels changed significantly (**Figure 10**). These results suggest that the miR390/ARFs module may play a role in *Medicago truncatula* leaves in response to salinity stress. MiRNA482 was reported to be involved in immune and drought response in plants (Tang and Chu, 2017; Song et al., 2019; Waititu et al., 2020). In this study, we found that miRNA482 was induced by salt stress (**Figure 8E**). This discovery may broaden the current knowledge on the function of miRNA482. MiR398 is directly related to the plant stress regulation network, including those regulating plants' responses to salt (Tang and Chu, 2017; Song et al., 2019; Chen et al., 2020; Waititu et al., 2020), which was consistent with our results (**Figure 8E**). The miR2111, which was reported to be related to legume susceptibility to rhizobial infection and root competence for nodulation (Tsikou et al., 2018), was found to be down-regulated under salt stress in *Medicago truncatula*. Compared with other plant studies, we also identified many new RNAs. This difference might be due to the fact that different studies used different salt concentrations at different periods to simulate salt stress.

CONCLUSION

In summary, it is known that protein-coding and non-coding RNAs and their interactions are essential for plant response to salt stress. However, the molecular mechanisms underlying the ceRNA network remain unknown. Our study comprehensively analyzed the coding and non-coding RNAs in *Medicago truncatula* after salt or water treatments and showed the interactions between them are important for regulating the salt stress response. Furthermore, we identified the DERNAs as

salt response factors and displayed the intracellular pathways implicated in response to salt stress. Our results provide helpful information for further molecular function studies and breeding practices in *Medicago*.

DATA AVAILABILITY STATEMENT

The datasets presented in this study can be found in online repositories. The names of the repository/repositories and accession number(s) can be found below: National Center for Biotechnology Information (NCBI) BioProject database under accession number PRJNA813502.

AUTHOR CONTRIBUTIONS

YA: samples collection, data analysis, and original draft preparation. HS: figures and tables preparation. QN: data validation and analysis. SY: manuscript review and editing. All authors contributed to the article and approved the submitted version.

FUNDING

This work was financially supported by the Joint Funds of the National Natural Science Foundation of China (Grant No. U20A2005) and the China Postdoctoral Science Foundation (2021M700452).

ACKNOWLEDGMENTS

We thank the sequencing platform and bioinformatic analysis of Gene *Denovo* Biotechnology Co., Ltd. (Guangzhou, China).

SUPPLEMENTARY MATERIAL

The Supplementary Material for this article can be found online at: https://www.frontiersin.org/articles/10.3389/fpls.2022.891361/full#supplementary-material

Supplementary Figure 1 | The KEGG pathway analysis of DEmRNAs.

Supplementary Figure 2 | GO enrichment of the target genes of antisense, *cis*-acting, and *trans*-acting DElncRNAs. Green: Molecular Function; Purple: Cellular Component; blue: Biological Process.

Supplementary Figure 3 | qRT-PCR validation of the expression levels of RNAsin the CK and Salt groups.

Supplementary Table 1 | The primers used in qRT-PCR validation.

Supplementary Table 2 | The list of DEmRNAs.

Supplementary Table 3 | GO enrichment of DEmRNAs.

Supplementary Table 4 | The list of lncRNAs.

Supplementary Table 5 | The list of DElncRNAs.

Supplementary Table 6 | The list of antisense pairs between DElncRNAs and DEmRNAs.

Supplementary Table 7 | The list of *cis*-acting between DElncRNAs and DEmRNAs.

Supplementary Table 8 | The list of circRNAs.

Supplementary Table 9 | The list of DEcircRNAs.

Supplementary Table 10 | The list of DEmiRNAs.

Supplementary Table 11 | The list of DEmiRNA-mRNA interactions.

Supplementary Table 12 | The list of DEmiRNA-DEmRNA interactions.

Supplementary Table 13 | The list of DEmiRNA-DEcircRNA interactions.

Supplementary Table 14 | The list of DEmiRNA-lncRNA interactions.

Supplementary Table 15 | The list of differentially expressed genes involved in important pathways implicated in response to salt stress in *Medicago truncatula*.

REFERENCES

Ala, U., Karreth, F. A., Bosia, C., Pagnani, A., Taulli, R., Léopold, V., et al. (2013). Integrated transcriptional and competitive endogenous RNA networks are cross-regulated in permissive molecular environments. *Proc. Natl. Acad. Sci. U.S.A.* 110, 7154–7159. doi: 10.1073/pnas.1222509110

Arshad, M., Gruber, M. Y., Wall, K., and Hannoufa, A. (2017). An insight into microRNA156 role in salinity stress responses of alfalfa. *Front. Plant Sci.* 8:356. doi: 10.3389/fpls.2017.00356

Baek, D., Chun, H. J., Kang, S., Shin, G., Park, S. J., Hong, H., et al. (2016). A role for *Arabidopsis miR399f* in salt, drought, and ABA signaling. *Mol. Cells* 39, 111–118. doi: 10.14348/molcells.2016.2188

Butcher, K., Wick, A. F., DeSutter, T., Chatterjee, A., and Harmon, J. (2016). Soil salinity: a threat to global food security. *Agron. J.* 108, 2189–2200. doi: 10.2134/agronj2016.06.0368

Chen, P., Chen, J., Sun, M., Yan, H., Feng, G., Wu, B., et al. (2020). Comparative transcriptome study of switchgrass (*Panicum virgatum* L.) homologous autopolyploid and its parental amphidiploid responding to consistent drought stress. *Biotechnol. Biofuels* 13:170. doi: 10.1186/s13068-020-01810-z

Chen, S., Zhou, Y., Chen, Y., and Gu, J. (2018). fastp: an ultra-fast all-in-one FASTQ preprocessor. *Bioinformatics* 34, i884–i890. doi: 10.1093/bioinformatics/bty560

Cheng, M. C., Liao, P. M., Kuo, W. W., and Lin, T. P. (2013). The *Arabidopsis* ETHYLENE RESPONSE FACTOR1 regulates abiotic stress-responsive gene expression by binding to different cis-acting elements in response to different stress signals. *Plant Physiol.* 162, 1566–1582. doi: 10.1104/pp.113.221911

Deng, F., Zhang, X., Wang, W., Yuan, R., and Shen, F. (2018). Identification of *Gossypium hirsutum* long non-coding RNAs (lncRNAs) under salt stress. *BMC Plant Biol.* 18:23. doi: 10.1186/s12870-018-1238-0

Diédhiou, C. J., Poppva, O. V., and Golldack, D. (2009a). Comparison of salt-responsive gene regulation in rice and in the salt-tolerant *Festuca rubra ssp. litoralis*. *Plant Signal. Behav.* 4, 533–535. doi: 10.4161/psb.4.6.8589

Diédhiou, C. J., Poppva, O. V., and Golldack, D. (2009b). Transcript profiling of the salt-tolerant *Festuca rubra ssp. litoralis* reveals a regulatory network controlling salt acclimatization. *J. Plant Physiol.* 166, 697–711. doi: 10.1016/j.jplph.2008.09.015

Duan, L., Dietrich, D., Ng, C. H., Chan, P. M., Bhalerao, R., Bennett, M. J., et al. (2013). Endodermal ABA signaling promotes lateral root quiescence during salt stress in *Arabidopsis* seedlings. *Plant Cell* 25, 324–341. doi: 10.1105/tpc.112.107227

Fu, X. Z., Zhang, X. Y., Qiu, J. Y., Zhou, X., Yuan, M., He, Y. Z., et al. (2019). Whole-transcriptome RNA sequencing reveals the global molecular responses and ceRNA regulatory network of mRNAs, lncRNAs, miRNAs and circRNAs in response to copper toxicity in Ziyang Xiangcheng (*Citrus junos* Sieb. Ex Tanaka). *BMC Plant Biol.* 19:509. doi: 10.1186/s12870-019-2087-1

Gao, P., Bai, X., Yang, L., Lv, D., Li, Y., Cai, H., et al. (2010). Over-expression of *osa-MIR396c* decreases salt and alkali stress tolerance. *Planta* 231, 991–1001. doi: 10.1007/s00425-010-1104-2

Golldack, D., Lüking, I., and Yang, O. (2011). Plant tolerance to drought and salinity: stress regulating transcription factors and their functional significance in the cellular transcriptional network. *Plant Cell Rep.* 30, 1383–1391. doi: 10.1007/s00299-011-1068-0

He, F., Xu, C., Fu, X., Shen, Y., Guo, L., Leng, M., et al. (2018). The *microRNA390/trans-acting short interfering RNA3* module mediates lateral root growth under salt stress *via* the auxin pathway. *Plant Physiol.* 177, 775–791. doi: 10.1104/pp.17.01559

He, X., Guo, S., Wang, Y., Wang, L., Shu, S., and Sun, J. (2020). Systematic identification and analysis of heat-stress-responsive lncRNAs, circRNAs and miRNAs with associated co-expression and ceRNA networks in cucumber (*Cucumis sativus* L.). *Physiol. Plant.* 168, 736–754. doi: 10.1111/ppl.12997

Ji, H., Pardo, J. M., Batelli, G., Van Oosten, M. J., Bressan, R. A., and Li, X. (2013). The salt overly sensitive (SOS) pathway: established and emerging roles. *Mol. Plant* 6, 275–286. doi: 10.1093/mp/sst017

Jiang, Y., and Deyholos, M. K. (2009). Functional characterization of *Arabidopsis* NaCl-inducible *WRKY25* and *WRKY33* transcription factors in abiotic stresses. *Plant Mol. Biol.* 69, 91–105. doi: 10.1007/s11103-008-9408-3

Kanehisa, M., Araki, M., Goto, S., Hattori, M., Hirakawa, M., Itoh, M., et al. (2008). KEGG for linking genomes to life and the environment. *Nucleic Acids.Res.* 36, 480–484. doi: 10.1093/nar/gkm882

Kang, Y. J., Yang, D. C., Kong, L., Hou, M., Meng, Y. Q., Wei, L., et al. (2017). CPC2: a fast and accurate coding potential calculator based on sequence intrinsic features. *Nucleic Acids Res.* 45, W12–W16. doi: 10.1093/nar/gkx428

Kim, D., Langmead, B., and Salzberg, S. L. (2015). HISAT: a fast spliced aligner with low memory requirements. *Nat. Methods* 12, 357–360. doi: 10.1038/nmeth.3317

Korver, R. A., Koevoets, I. T., and Testerink, C. (2018). Out of shape during stress: a key role for auxin. *Trends Plant Sci.* 23, 783–793. doi: 10.1016/j.tplants.2018.05.011

Kulik, A., Wawer, I., Krzywinska, E., Bucholc, M., and Dobrowolska, G. (2011). SnRK2 protein kinases-key regulators of plant response to abiotic stresses. *OMICS* 15, 859–872. doi: 10.1089/omi.2011.0091

Langmead, B., and Salzberg, S. L. (2012). Fast gapped-read alignment with Bowtie 2. *Nat. Methods* 9, 357–359. doi: 10.1038/nmeth.1923

Li, G. T., Niu, Z. M., Zheng, Z. Y., Lv, J. J., Chen, Q. Y., Liu, J. Q., et al. (2021). Contrasting origins, expression patterns and functions of circRNAs between salt-sensitive and salt-tolerant poplars. *Environ. Exp. Bot.* 185:104403. doi: 10.1016/j.envexpbot.2021.104403

Li, Q. F., Zhang, Y. C., Chen, Y. Q., and Yu, Y. (2017). Circular RNAs roll into the regulatory network of plants. *Biochem. Biophys. Res. Commun.* 488, 382–386. doi: 10.1016/j.bbrc.2017.05.061

Li, Z., An, X., Zhu, T., Yan, T., Wu, S., Tian, Y., et al. (2019). Discovering and constructing ceRNA-miRNA-target gene regulatory networks during anther development in maize. *Int. J. Mol. Sci.* 20:3480. doi: 10.3390/ijms20143480

Lippold, F., Sanchez, D. H., Musialak, M., Schlereth, A., Scheible, W. R., Hincha, D. K., et al. (2009). AtMyb41 regulates transcriptional and metabolic responses to osmotic stress in *Arabidopsis*. *Plant Physiol.* 149, 1761–1772. doi: 10.1104/pp.108.134874

Liu, J. X., Srivastava, R., Che, P., and Howell, S. H. (2007). Salt stress responses in *Arabidopsis* utilize a signal transduction pathway related to endoplasmic reticulum stress signaling. *Plant J.* 51, 897–909. doi: 10.1111/j.1365-313X.2007.03195.x

Livak, K. J., and Schmittgen, T. D. (2001). Analysis of relative gene expression data using real-time quantitative PCR and the 2(-Delta Delta C(T)) Method. *Methods* 25, 402–408. doi: 10.1006/meth.2001.1262

Long, R. C., Li, M. N., Kang, J. M., Zhang, T. J., Sun, Y., and Yang, Q. C. (2015). Small RNA deep sequencing identifies novel and salt-stress-regulated microRNAs from roots of *Medicago sativa* and *Medicago truncatula*. *Physiol. Plant.* 154, 13–27. doi: 10.1111/ppl.12266

Love, M. I., Huber, W., and Anders, S. (2014). Moderated estimation of fold change and dispersion for RNA-seq data with DESeq2. *Genome Biol.* 15:550. doi: 10.1186/s13059-014-0550-8

Lu, T., Cui, L., Zhou, Y., Zhu, C., Fan, D., Gong, H., et al. (2015). Transcriptome-wide investigation of circular RNAs in rice. *RNA* 21, 2076–2087. doi: 10.1261/rna.052282.115

Manishankar, P., Wang, N., Köster, P., Alatar, A. A., and Kudla, J. (2018). Calcium signaling during salt stress and in the regulation of ion homeostasis. *J. Exp. Bot.* 69, 4215–4226. doi: 10.1093/jxb/ery201

Memczak, S., Jens, M., Elefsinioti, A., Torti, F., Krueger, J., Rybak, A., et al. (2013). Circular RNAs are a large class of animal RNAs with regulatory potency, circular RNAs are a large class of animal RNAs with regulatory potency. *Nature* 495, 333–338. doi: 10.1038/nature11928

Pérez-Salamó, I., Papdi, C., Rigó, G., Zsigmond, L., Vilela, B., Lumbreras, V., et al. (2014). The heat shock factor A4A confers salt tolerance and is regulated by oxidative stress and the mitogen-activated protein kinases MPK3 and MPK6. *Plant Physiol.* 165, 319–334. doi: 10.1104/pp.114.237891

Pertea, M., Pertea, G. M., Antonescu, C. M., Chang, T. C., Mendell, J. T., and Salzberg, S. L. (2015). StringTie enables improved reconstruction of a transcriptome from RNA-seq reads. *Nat. Biotechnol.* 33, 290–295. doi: 10.1038/nbt.3122

Pitzschke, A., Djamei, A., Bitton, F., and Hirt, H. (2009). A major role of the MEKK1-MKK1/2-MPK4 pathway in ROS signaling. *Mol. Plant* 2, 120–137. doi: 10.1093/mp/ssn079

Ponting, C. P., Oliver, P. L., and Reik, W. (2009). Evolution and functions of long non-coding RNAs. *Cell* 136, 629–641. doi: 10.1016/j.cell.2009.02.006

Qin, T., Zhao, H., Cui, P., Albesher, N., and Xiong, L. (2017). A nucleus-localized long non-coding RNA enhances drought and salt stress tolerance. *Plant Physiol.* 175, 1321–1336. doi: 10.1104/pp.17.00574

Rengasamy, P. (2006). World salinization with emphasis on Australia. *J. Exp. Bot.* 57, 1017–1023. doi: 10.1093/jxb/erj108

Rinn, J. L., and Chang, H. Y. (2012). Genome regulation by long non-coding RNAs. *Annu. Rev. Biochem.* 81, 145–146. doi: 10.1146/annurev-biochem-051410-092902

Robinson, M. D., McCarthy, D. J., and Smyth, G. K. (2010). edgeR: a bioconductor package for differential expression analysis of digital gene expression data. *Bioinformatics* 26, 139–140. doi: 10.1093/bioinformatics/btp616

Salmena, L., Poliseno, L., Tay, Y., Kats, L., and Pandolfi, P. P. (2011). A ceRNA hypothesis: the Rosetta Stone of a hidden RNA language? *Cell* 146, 353–358. doi: 10.1016/j.cell.2011.07.014

Shannon, P., Markiel, A., Ozier, O., Baliga, N. S., Wang, J. T., Ramage, D., et al. (2003). Cytoscape: a software environment for integrated models of biomolecular interaction networks. *Genome Res.* 13, 2498–2504. doi: 10.1101/gr.1239303

Song, X., Li, Y., Cao, X., and Qi, Y. (2019). MicroRNAs and their regulatory roles in plant-environment interactions. *Annu. Rev. Plant Biol.* 70, 489–525. doi: 10.1146/annurev-arplant-050718-100334

Sun, L., Luo, H., Bu, D., Zhao, G., Yu, K., Zhang, C., et al. (2013). Utilizing sequence intrinsic composition to classify protein-coding and long non-coding transcripts. *Nucleic Acids Res.* 41:e166. doi: 10.1093/nar/gkt646

Tafer, H., and Hofacker, I. L. (2008). RNAplex: a fast tool for RNA-RNA interaction search. *Bioinformatics* 24, 2657–2663. doi: 10.1093/bioinformatics/btn193

Tang, H., Krishnakumar, V., Bidwell, S., Rosen, B., Chan, A., Zhou, S., et al. (2014). An improved genome release (version Mt4.0) for the model legume *Medicago truncatula*. *BMC Genomics* 15:312. doi: 10.1186/1471-2164-15-312

Tang, J., and Chu, C. (2017). MicroRNAs in crop improvement: fine-tuners for complex traits. *Nat. Plants* 3:17077. doi: 10.1038/nplants.2017.77

Tsikou, D., Yan, Z., Holt, D. B., Abel, N. B., Reid, D. E., Madsen, L. H., et al. (2018). Systemic control of legume susceptibility to rhizobial infection by a mobile microRNA. *Science* 362, 233–236. doi: 10.1126/science.aat6907

Waititu, J. K., Zhang, C., Liu, J., and Wang, H. (2020). Plant non-coding RNAs: origin, biogenesis, mode of action and their roles in abiotic stress. *Int. J. Mol. Sci.* 21:8401. doi: 10.3390/ijms21218401

Wang, J., Meng, X., Dobrovolskaya, O. B., Orlov, Y. L., and Chen, M. (2017). Non-coding RNAs and their roles in stress response in plants. *Genom. Proteom. Bioinf.* 15, 301–312. doi: 10.1016/j.gpb.2017.01.007

Wang, T. Z., Liu, M., Zhao, M. G., Chen, R., and Zhang, W. H. (2015). Identification and characterization of long non-coding RNAs involved in osmotic and salt stress in *Medicago truncatula* using genome-wide high-throughput sequencing. *BMC Plant Biol.* 15:131. doi: 10.1186/s12870-015-0530-5

Wang, W., Vinocur, B., and Altman, A. (2003). Plant responses to drought, salinity and extreme temperatures: towards genetic engineering for stress tolerance. *Planta* 218, 1–14. doi: 10.1007/s00425-003-1105-5

Xing, L., Zhu, M., Luan, M., Zhang, M., Jin, L., Liu, Y., et al. (2021). *miR169q* and *NUCLEAR FACTOR YA8* enhance salt tolerance by activating PEROXIDASE1 expression in response to ROS. *Plant Physiol.* 188, 608–623. doi: 10.1093/plphys/kiab498

Xu, X. W., Zhou, X. H., Wang, R. R., Peng, W. L., An, Y., and Chen, L. L. (2016). Functional analysis of long intergenic non-coding RNAs in phosphate-starved rice using competing endogenous RNA network. *Sci. Rep.* 6:20715. doi: 10.1038/srep20715

Yang, O., Popova, O. V., Süthoff, U., Lüking, I., Dietz, K. J., and Golldack, D. (2009). The *Arabidopsis* basic leucine zipper transcription factor *AtbZIP24* regulates complex transcriptional networks involved in abiotic stress resistance. *Gene* 436, 45–55. doi: 10.1016/j.gene.2009.02.010

Yang, W., Fan, T., Hu, X., Cheng, T., and Zhang, M. (2017). Overexpressing *osa-miR171c* decreases salt stress tolerance in rice. *J. Plant Biol.* 60, 485–492. doi: 10.1007/s12374-017-0093-0

Yang, Y., and Guo, Y. (2018a). Elucidating the molecular mechanisms mediating plant salt-stress responses. *New Phytol.* 217, 523–539. doi: 10.1111/nph.14920

Yang, Y., and Guo, Y. (2018b). Unraveling salt stress signaling in plants. *J. Integr. Plant Biol.* 60, 796–804. doi: 10.1111/jipb.12689

Yu, L., Nie, J., Cao, C., Jin, Y., Yan, M., Wang, F., et al. (2010). Phosphatidic acid mediates salt stress response by regulation of MPK6 in *Arabidopsis thaliana*. *New Phytol.* 188, 762–773. doi: 10.1111/j.1469-8137.2010.03422.x

Zelm, E., Zhang, Y., and Testerink, C. (2020). Salt tolerance mechanisms of plants. *Annu. Rev. Plant Biol.* 71, 403–433. doi: 10.1146/annurev-arplant-050718-100005

Zhang, B. (2015). MicroRNA: a new target for improving plant tolerance to abiotic stress. *J. Exp. Bot.* 66, 1749–1761. doi: 10.1093/jxb/erv013

Zhang, X., Shen, J., Xu, Q., Dong, J., Song, L., Wang, W., et al. (2021). Long non-coding RNA lncRNA354 functions as a competing endogenous RNA of miR160b to regulate *ARF* genes in response to salt stress in upland cotton. *Plant Cell Environ.* 44, 3302–3321. doi: 10.1111/pce.14133

Zhou, J., Yuan, M., Zhao, Y., Quan, Q., Yu, D., Yang, H., et al. (2021). Efficient deletion of multiple circle RNA loci by CRISPR-Cas9 reveals *Os06circ02797* as a putative sponge for *OsMIR408* in rice. *Plant Biotechnol. J.* 19, 1240–1252. doi: 10.1111/pbi.13544

Conflict of Interest: The authors declare that the research was conducted in the absence of any commercial or financial relationships that could be construed as a potential conflict of interest.

Publisher's Note: All claims expressed in this article are solely those of the authors and do not necessarily represent those of their affiliated organizations, or those of the publisher, the editors and the reviewers. Any product that may be evaluated in this article, or claim that may be made by its manufacturer, is not guaranteed or endorsed by the publisher.

frontiers | Frontiers in Plant Science

ORIGINAL RESEARCH
published: 28 April 2022
doi: 10.3389/fpls.2022.881456

Transcriptome Analysis of Leaf Senescence Regulation Under Alkaline Stress in *Medicago truncatula*

Shuwei Dong, Wenhui Pang, Zhe Liu, He Li, Kangning Zhang, Lili Cong, Guofeng Yang, Zeng-Yu Wang and Hongli Xie*

Key Laboratory of National Forestry and Grassland Administration on Grassland Resources and Ecology in the Yellow River Delta, College of Grassland Science, Qingdao Agricultural University, Qingdao, China

OPEN ACCESS

Edited by:
Jing Zhang,
Nanjing Agricultural University, China

Reviewed by:
Naichong Chen,
Oklahoma State University, United States
Bin Xu,
Nanjing Agricultural University, China

***Correspondence:**
Hongli Xie
hlxie08@126.com
orcid.org/0000-0001-6392-0494

Specialty section:
This article was submitted to Plant Abiotic Stress, a section of the journal Frontiers in Plant Science

Received: *22 February 2022*
Accepted: *01 April 2022*
Published: *28 April 2022*

Citation:
Dong S, Pang W, Liu Z, Li H, Zhang K, Cong L, Yang G, Wang Z-Y and Xie H (2022) Transcriptome Analysis of Leaf Senescence Regulation Under Alkaline Stress in Medicago truncatula. Front. Plant Sci. 13:881456. doi: 10.3389/fpls.2022.881456

In plants, the leaf is an essential photosynthetic organ, and is the primary harvest in forage crops such as alfalfa (*Medicago sativa*). Premature leaf senescence caused by environmental stress can result in significant yield loss and quality reduction. Therefore, the stay-green trait is important for improving the economic value of forage crops. Alkaline stress can severely damage leaf cells and, consequently, cause leaf senescence. To understand the molecular regulatory mechanisms and identify vital senescence-associated genes under alkaline stress, we used high-throughput sequencing to study transcriptional changes in *Medicago truncatula*, a model plant for forage crops. We identified 2,165 differentially expressed genes, 985 of which were identical to those in the dark-induced leaf senescence group. Gene ontology (GO) and Kyoto Encyclopedia of Genes and Genomes (KEGG) pathway enrichment analyses showed that the 985 genes were mainly enriched in nutrient cycling processes such as cellular amino acid metabolic processes and organic substance catabolic processes, indicating nutrient redistribution. The other 1,180 differentially expressed genes were significantly enriched in the oxidoreductase complex, aerobic respiration, and ion transport. Our analysis showed the two gene sets guiding the coupled physiological and biochemical alterations play different roles under alkaline stress with a coordinated and integrated way. Many transcription factor families were identified from these differentially expressed genes, including *MYB*, *WRKY*, *bHLH*, and *NAC* which have particular preference involved in stress resistance and regulation of senescence. Our results contribute to the exploration of the molecular regulatory mechanisms of leaf senescence in *M. truncatula* under alkaline stress and provide new candidate genes for future breeding to improve the biomass and quality of forage crops.

Keywords: alkaline stress, *Medicago truncatula*, leaf senescence, transcriptome analysis, senescence-associated genes (SAGs)

INTRODUCTION

Senescence occurs when the photosynthetic efficiency in a leaf is constantly decreasing; its stages include a color change from green to yellow, wilting, and death. During senescence, the nutrients in the leaf are transferred to new buds, developing flowers, maturing seeds, or other plant development, thus directly enhancing plant adaptability and reproductive success in the face of stress (Uauy et al., 2006; Lim et al., 2007). Therefore, the timing of leaf senescence is of biological significance. Premature senescence caused by environmental stressors can result in significant yield loss and quality reduction. Such stressors include darkness, drought, saline, and alkaline conditions (Guo and Gan, 2012; He et al., 2018; Guo et al., 2021). Saline-alkaline stress is a common abiotic stress that limits plant growth and development, and has become a serious problem restricting crop production as well as ecological environment construction (Zhu, 2016; Wei et al., 2021). High salinity accelerates leaf senescence, thereby reducing plant biomass (Balazadeh et al., 2010; Allu et al., 2014; Yang and Guo, 2018b). We confirmed this phenomenon in our previous study, and preliminarily investigated the associated molecular mechanisms (Dong et al., 2021).

Unlike salt stress, alkaline stress is caused mainly by $NaHCO_3$ and Na_2CO_3. Therefore, Na^+ stress occurs in alkali stress, as well as HCO_3^- and pH stresses (Zhang et al., 2019). It can induce ion toxicity, osmotic stress, and oxidative damage in plants leading to accelerated leaf senescence (Fan et al., 2021). Alkaline stress can significantly disrupt ion balance and interfere with the uptake of mineral elements, resulting in excessive Na^+ accumulation in leaf cytoplasm, thereby producing ion toxicity and inducing leaf senescence (Ghanem et al., 2008; Guo et al., 2009; Yang and Guo, 2018b). The decreasing K^+/Na^+ ratio disrupts the ultrastructure of chloroplasts, leading to chlorophyll degradation, a reduced photosynthetic rate, and accelerated leaf senescence (Zhao et al., 2001; Wang et al., 2019). Excess ions produce osmotic stress and lead to dehydration in leaves, followed by rapid leaf senescence (Yang and Guo, 2018a; Zhang P. et al., 2021).

The effect of oxidative damage on leaf senescence requires investigation. High pH stress results in increased permeability of the cell membrane in leaves by inducing the accumulation of malondialdehyde (MDA) and reactive oxygen species (ROS), allowing penetration by small molecules of organic substances and electrolytes into the cell. The intracellular molecular structures and functions are in turn damaged, accelerating leaf senescence (An et al., 2016; Zou et al., 2020). Plants have developed a series of regulatory adaptive mechanisms to resist senescence, such as alleviation of osmotic stress, modulation of ion homeostasis, and antioxidant protection (Yang and Guo, 2018b; Wei et al., 2020). It has been reported that with leaf senescence, numerous leaf senescence-associated genes (SAGs) are expressed and associated transcription factors (TFs) are involved in regulation (Buchanan-Wollaston, 1997; Guo and Gan, 2005). TF families (such as NAC, MYB, WRKY, and bZIP) have been shown to participate, often critically, in the regulation of senescence in plants (Hao et al., 2010; Mao et al., 2017; Woo et al., 2019; Xu et al., 2020; Dong et al., 2021). During leaf senescence, a large number of SAGs and TFs are expressed at high levels, and these genes constitute several complex senescence regulatory networks that are interlinked and regulated by each other to control leaf senescence. However, there is little understanding of the relationship between SAGs and alkaline stress.

In recent years, significant progress has been made in elucidating the relationship between SAGs and abiotic stresses in *Arabidopsis thaliana* (Breeze et al., 2011), tobacco (Pageau et al., 2006) and rice (Lee et al., 2001). At present, few reports have been published on the mechanism of leaf senescence in leguminous forage species (Chao et al., 2018; Yuan et al., 2020). However, the key regulators of leaf senescence induced by alkaline stress remain unclear. Alfalfa (*Medicago sativa* L.) is considered to be one of the most important forages in the world because of its high yield, high quality, and wide range of adaptations (Bouton, 2007; Wang et al., 2016). Most of nutrients in alfalfa are stored in the leaves, and leaf senescence can greatly affect the nutritional quality of the plant, especially when affected by environmental factors such as saline and alkaline stress. Therefore, preventing premature senescence or delaying senescence appropriately to increase biomass accumulation is important for improving alfalfa quality and increasing agricultural economic efficiency (Zhou et al., 2011). *Medicago truncatula* has been adopted as a suitable model for studying forage crop improvements and leaf senescence (Barker et al., 1990; Zhang et al., 2014). The highly controlled repeatable detached leaves are widely used to evaluate leaf senescence in different plant species (Mao et al., 2017; He et al., 2018; Sakuraba et al., 2018).

In a previous study, we investigated salt- and dark-induced leaf senescence in *M. truncatula* by collecting transcriptional data over the course of leaf senescence. In this study, we investigated the relationship between leaf senescence and alkaline stress by analyzing detailed expression profiles and annotating the SAGs. The purpose of this study was to identify the genes involved in alkali-induced leaf senescence so as to provide new candidate genes for breeding management strategies.

MATERIALS AND METHODS

Plant Material and Alkaline Stress Treatments

The *M. truncatula* ecotype R108 was used in this study. Seeds that had already been vernalized for 2 days were sown in dishes with moistened filter paper and grown in a light incubator for 7 days. They were then transferred into Hoagland's nutrient solution for hydroponic growth cultivation, and the culture medium was changed every 3 days. Plants were placed in a light incubator with a 16 h photoperiod, day/night temperatures of 25°C/22°C, and a relative humidity of 60–70%.

After 5 weeks, the third compound leaf of each plant was removed and immediately transferred into Petri dishes containing 0, 10, 20, and 40 mM $NaHCO_3$ solution [prepared with half Murashige–Skoog medium, 3 mM MES (2-morpholine ethyl sulfonic acid) buffer, adjusted to pH 5.8]. The Petri dishes were then placed under light or dark conditions, with the growth

conditions: 16 h light (25)/8 h darkness (22°C), relative humidity of 60–70%, and light intensity of 300 mol/m^2·s.

Individual samples were harvested at 0, 2, 4, and 6 days post-alkaline salt stress treatment and briefly immersed in liquid nitrogen before being stored at −80°C. The sampled materials were used to measure physiological indicators [chlorophyll, MDA, H_2O_2, and abscisic acid (ABA)] and for transcriptomic sequencing.

Three biological replicates were analyzed for each sample group. All data were subjected to one-way analysis of variance (ANOVA) using SPSS 26 (IBM Corp., Armonk, NY, United States). Mean differences were analyzed using Duncan's multiple range test, and statistical significance was set at $P < 0.05$. All charts were created using Microsoft Excel 2019 (Microsoft Corp., Redmond, WA, United States).

A dark treatment group (dark) was established as a positive control to better screen the SAGs (Sobieszczuk-Nowicka et al., 2018). In addition, a light control group (control-light) was established to remove background effects, so as to acquire SAGs involved in senescence upon alkaline stress, not just the genes reacting to alkaline stress.

RNA Quantification and Qualification

Total RNA extraction and quality control were conducted as per the method in an earlier study (Dong et al., 2021). Only high-quality RNA samples ($OD_{260/280}$ = 1.8–2.2, ≥ 50 ng/μL, > 1 μg) were used for sequence library constructions.

Library Preparation and Transcriptome Sequencing

RNA libraries were prepared using the TruSeq™ RNA sample preparation kit from Illumina (San Diego, CA, United States) using 1 μg of RNA. Messenger RNA (mRNA) was enriched and randomly fragmented into small fragments of approximately 200 bp, and cDNA synthesized using a SuperScript double-stranded cDNA synthesis kit (Invitrogen, CA, United States). The synthesized cDNAs were subjected to end-repair, phosphorylation, and "A" base addition according to Illumina's library construction protocol. Libraries were size selected for 200–300 bp cDNA target fragments using 2% Low Range Ultra Agarose electrophoresis followed by enrichment of PCR (sample preparation kit; Illumina, San Diego, CA). After quantification using TBS380 (Turner BioSystems, Sunnyvale, CA, United States), the paired-end RNA-seq sequencing library was constructed on an Illumina HiSeq xten/NovaSeq 6000 platform, and 150 bp paired-end reads were generated.

Raw reads were trimmed, and their quality controlled by Fastp (Version: 0.19.5)[1] to acquire clean reads. All downstream analyses were based on clean data.

All obtained high-quality and clean reads were separately aligned to the reference genome of *M. truncatula* (reference genome version MedtrA17_4.0; reference genome source can be accessed via http://plants.ensembl.org/Medicago_truncatula/Info/Index with orientation mode using hisat2 (Version 2.1.0)[2] software. The mapped reads of each sample were assembled using StringTie (version 1.3.3 b).[3]

Quantification of Gene and Differential Expression Analysis

StringTie was used to count the number of reads mapped to each gene. The transcripts per million reads (TPM) of each gene were calculated from gene length and the read count mapped to it. RNA-Seq by Expectation-Maximization (RSEM, Version 1.3.1)[4] was applied to quantify gene abundance for each group and time point.

Differential expression analysis was performed using R statistical package software (EdgeR, Version 3.24.3).[5] The resulting *P*-values were adjusted using Benjamini and Hochberg's approach in order to control the false discovery rate. Genes with adjust < 0.05, $|\log_2 FC| \geq 1$ by EdgeR were defined as significantly different.

Gene Ontology and Kyoto Encyclopedia of Genes and Genomes Pathway Enrichment Analysis of Differentially Expressed Genes

Gene Ontology (GO)[6] functional enrichment was conducted using Goatools (Version 0.6.5)[7] and Fisher's precision tests. GO terms with BH-corrected P adjustment (<0.05) were considered significantly enriched by DEGs.

We used KOBAS (Version 2.1.1)[8] and Fisher's precision test for DEGs in the Kyoto Encyclopedia of Genes and Genomes (KEGG)[9] pathways. The metabolic pathways were considered significantly enriched by DEGs at a BH-corrected value of $P < 0.05$.

Transcription Factor Analysis

TFs are a class of proteins that bind to specific DNA sequences and are widely found in living organisms. They have an activating or blocking effect on gene expression. TF analysis was undertaken using PlantTFDB 4.0 (Version 4.0).[10] A threshold of less than e^{-5} was used for the Hmmscan search.

Time-Course Senescence-Associated Gene Analysis

Time-series SAG analysis based on the microarray Significant Profiles (maSigPro, Version 1.56.0)[11] was performed to obtain genes with different expression profiles throughout the series of sampling time nodes.

A short time-series expression miner (STEM, Version 1.3.11) with a $P < 0.05$ threshold was used for temporal pattern analysis.

[1] https://github.com/OpenGene/fastp

[2] http://ccb.jhu.edu/software/hisat2/index.shtml

[3] https://ccb.jhu.edu/software/stringtie/

[4] http://deweylab.biostat.wisc.edu/rsem/

[5] http://bioconductor.org/packages/stats/bioc/edgeR/

[6] http://www.geneontology.org/

[7] https://github.com/tanghaibao/Goatools

[8] http://kobas.cbi.pku.edu.cn/home.do

[9] http://www.genome.jp/kegg/

[10] http://planttfdb.cbi.pku.edu.cn/

[11] http://www.bioconductor.org/packages/release/bioc/html/maSigPro.html

Quantitative Real-Time PCR Analysis

Quantitative real-time PCR (qRT-PCR) was used to verify the reliability of RNA-seq data. The RNAs were reverse transcribed using the M5 Super Plus qPCR RT kit with gRNA remover (mei5 Biotech Co., Ltd., Beijing, China) and then subjected to qRT-PCR using ChamQ SYBR color qPCR Master Mix (Vazyme Biotech Co., Ltd., Nanjing, China). Three replicates were performed for each reaction. Twenty-five genes were chosen for qRT-PCR with the following criteria: TFs (**Supplementary Table 5**), 15 upregulated genes and 9 downregulated genes, belonging to profiles 21 and 4 of 985 SAGs, and differential expression in different groups. Mt UBC Q-2 served as the reference gene.

Gene-specific primers were designed using Primer 5.0 and are shown in **Supplementary Table 1**.

RESULTS

Phenotypic and Physiological Responses of Detached Leaves to Alkaline Stress

The detached leaves showed different phenotypic changes across different groups (**Figure 1A**). In the control light group, leaves remained green throughout 6 days; in the dark group, leaves showed progressive yellowing from days 4 to 6; in the alkaline-stress groups, leaves treated with concentrations of 10 and 20 mM $NaHCO_3$ turned yellow on day 2 and formed eroded lesions; over time, the leaves slowly turned transparent from necrosis. There was a significant correlation between the concentration of $NaHCO_3$ and leaf phenotypic change.

The physiological response of detached leaves treated with 20 mM $NaHCO_3$ was investigated through measuring chlorophyll, H_2O_2, MDA, and ABA contents. These four physiological and biochemical indicators are commonly used to evaluate the leaf senescence process. The chlorophyll content in both the alkaline-stress and dark groups decreased distinctly from days 2 to 6 in comparison to the slight reduction in the control-light group. Moreover, the chlorophyll content was even undetectable in the 20 mM $NaHCO_3$ group on day 6 (**Figure 1B**). As expected, H_2O_2 levels in the alkaline-stress group increased progressively from days 2 to 6 during leaf senescence; those in the dark-induced group followed the same trend, steadily increasing from days 2 to 4, and decreasing at day 6, as found in an earlier study (Dong et al., 2021; **Figure 1C**). MDA content in the alkaline stress and dark groups significantly increased to a maximum on day 4 and then dropped slightly on day 6 compared to the mild increase in the control-light group (**Figure 1D**). ABA content in both the treatment and control groups peaked on day 4, and then decreased, remaining above the initial value (**Figure 1E**).

Transcriptome Sequencing

The detached leaves were treated under the conditions of control-light, dark, 10 mM, and 20 mM $NaHCO_3$ for 0, 2, 4, and 6 days; a total of 13 groups with three biological replicates in each group (in total 39 samples) were sampled for library construction and subsequent sequencing. A total of 283.60 Gb high-quality clean data were obtained. The clean reads from each sample exceeded 7.27 Gb, and the matching to the reference genomic sequence was 81.78–89.05%. The GC content was above 42.60% and the percentage of Q30 bases was at least 92.82% (**Supplementary Table 2**). Principal component analysis (PCA) showed higher similarity among biological replicates of the same group and higher variability among different groups under different conditions (**Figure 2A**). The high Pearson correlation values of the biological replicates for the 39 samples achieved the expectation of the experimental design (**Supplementary Figure 1**). The specific gene expression profiles obtained by qRT-PCR analysis were used for the validation of RNA-Seq data, and the results showed similar expression profiles between RNA-Seq and qRT-PCR analysis (**Figure 2B** and **Supplementary Figure 2**).

Identification of Differentially Expressed Senescence-Associated Genes

Compared with day 0 levels, the upregulated and downregulated genes in both the control-dark and 20 mM $NaHCO_3$ treatment groups ranged from 8,700 to 11,910, while the number of DEGs in the control-light group was much smaller than that in the treatment group, ranging between 3,800 and 5,300 DEGs (**Figure 3A** and **Supplementary Table 3**). The number of upregulated and downregulated genes in the alkaline stress group decreased with extended treatment time, while there was an opposite trend in both control groups.

Venn diagrams at three time points based on all DEGs from both the 10 and 20 mM $NaHCO_3$ treatments groups compared with the DEGs from the control-light group were constructed to obtain SAGs in order to identify genes associated with leaf senescence (**Figure 3B**). We identified 2,165 unique genes in the 10 and 20 mM $NaHCO_3$ treatment groups compared with the control group. These genes were then divided into two parts after taking the intersection with the set of SAGs obtained from the dark-induced groups: 985 SAGs and 1,180 genes (**Supplementary Table 4**). STEM temporal pattern analysis showed genes with the same expression type were grouped into the same profile (**Figure 3C**). The 985 SAGs were divided into four significant gene expression profiles ($P < 0.05$), including one upregulated profile (red; profile 21; 340 genes), two downregulated profiles (green; profiles 3 and 4; 71 and 394 genes), and one other profile (gray; profile 6; 60 genes). The 1,180 genes were divided into six significant gene expression profiles: three being upregulated (profiles 21, 23, and 24; with 461, 42, and 127 genes, respectively), two downregulated (profiles 3 and 4; with 106 and 219 genes, respectively), and one other profile (profile 6; 30 genes).

Gene Ontology and Kyoto Encyclopedia of Genes and Genomes Pathway Enrichment Analysis

GO enrichment analysis characterizes the gene function and relations in three categories: biological processes (BP), molecular functions (MF), and cellular components (CC). As shown in **Table 1**, the GO terms with the top 10 highest enrichment degree were all went to BP category for 985 SAGs, while for 1,180 DEGs the top 10 highest enrichments were classified into CC and BP categories. For the 985 SAGs, the top GO terms

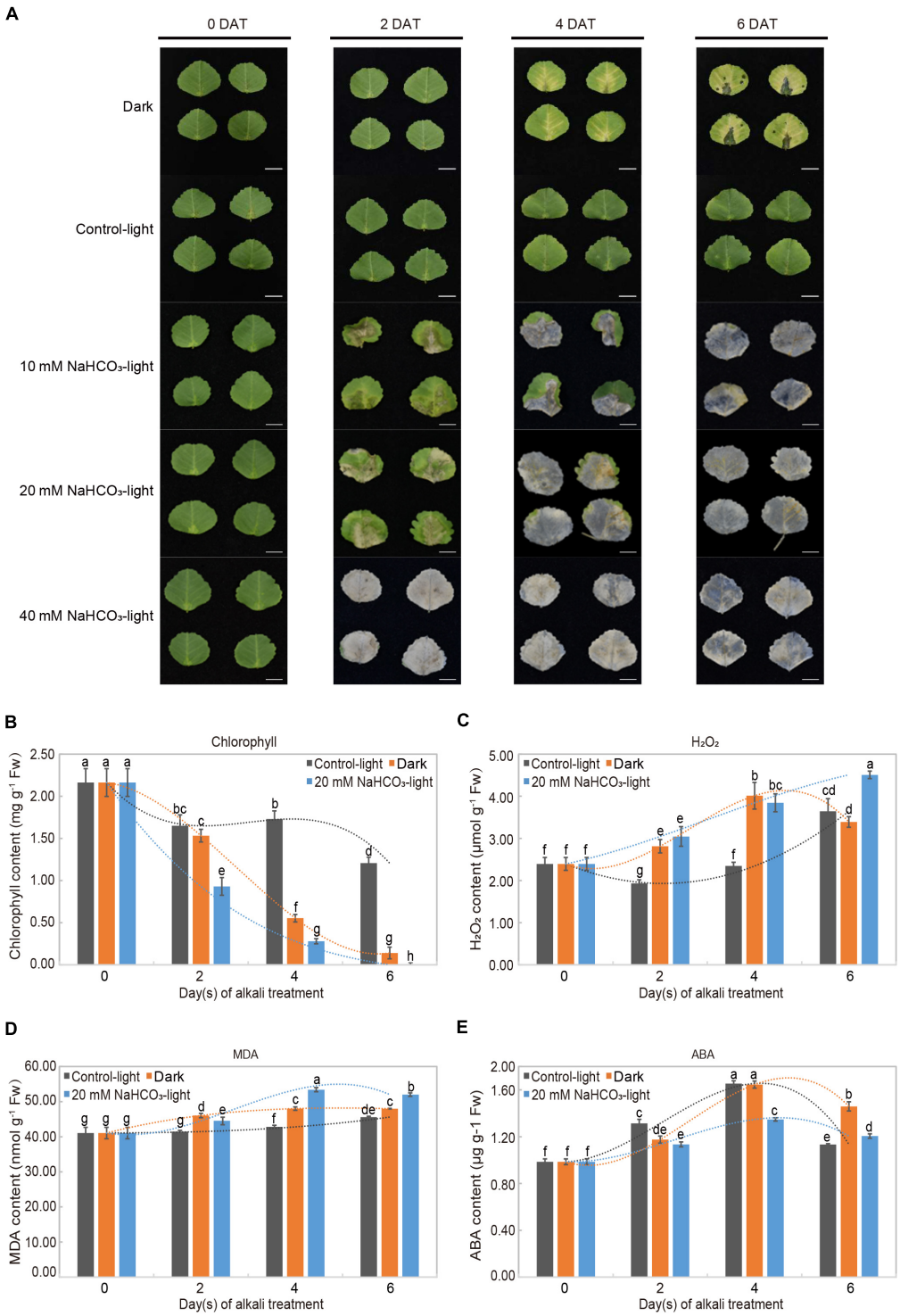

FIGURE 1 | Alkali stress-induced leaf senescence and physiological analysis in *Medicago truncatula*. **(A)** Leaf senescence progression and color change of detached *M. truncatula* leaves under dark (Dark), normal light (Control-light), and 10, 20, 40 mM $NaHCO_3$ (10 mM $NaHCO_3$-light, 20 mM $NaHCO_3$-light and 40 mM $NaHCO_3$-light) conditions for 0, 2, 4, and 6 days. DAT: days after treatment. Scale bar = 1 cm. **(B)** Chlorophyll (a + b), **(C)** H_2O_2, **(D)** malondialdehyde (MDA), and **(E)** abscisic acid (ABA) in detached *M. truncatula* leaves exposed to different conditions during senescence. Values are presented as mean ± SE of three independent biological replicates per time point. Different letters indicate significant differences among treatments according to the analysis of variance (ANOVA, $P < 0.05$). Error bars correspond to standard error. FW, fresh weight.

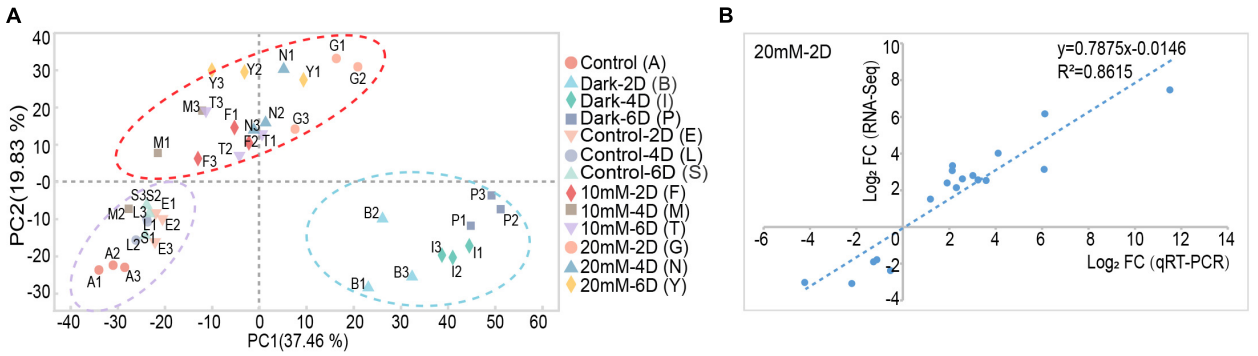

FIGURE 2 | The PCA analysis and qRT-PCR validation of transcriptome data derived from alkali stress-induced detached leaf senescence in *M. truncatula*. **(A)** Principal component analysis (PCA) plot of transcriptome profiles from different conditions. **(B)** Validation of RNA-seq data by qRT-PCR analysis. Correlation of expression changes observed by RNA-seq (*Y*-axis) and qRT-PCR (*X*-axis) relative expression levels from $\log_2$ fold change of 25 genes in 20 mM $NaHCO_3$-light-2 day; data for other groups are shown in **Supplementary Figure 2**.

were mainly involved in "small molecule catabolic and metabolic process," "cellular amino acid metabolic processes," "carboxylic acid catabolic and metabolic process," and "organic acid and substance catabolic process" of BP category; while among the 1,180 DEGs, the top GO terms in BP category were "aerobic respiration," "aerobic electron transport chain," "ion transport," and "cation transport"; also in CC category, "mitochondrion," "oxidoreductase complex," "NADH dehydrogenase complex," and "Membrane-bounded organelle" were significantly enriched. In all, the enrichment of GO terms with higher degrees from the two gene sets (985 SAGs and 1,180 DEGs) was remarkably significantly different, indicating that the genes of the two gene sets play different roles under alkaline stress.

KEGG enrichment analysis showed that the most significantly enriched pathways in 985 genes were related to "glyoxylate and dicarboxylate metabolism," "valine, leucine, and isoleucine degradation," "tyrosine metabolism," and "arginine and proline metabolism." On the contrary, thermogenesis, and oxidative phosphorylation were the enriched KEGG pathway terms for the 1,180 genes.

It is reported that regulation of plasma membrane (PM) H^+-ATPase activity is important for plant adaptation to alkali stress and enhancement of higher leaf photosynthesis (Fuglsang et al., 2007; Yang et al., 2010, 2019; Zhang M. et al., 2021). Four key genes related to PM H^+-ATPase are up-regulated expression, and phylogenetic analysis indicated that MTR_5g009720, MTR_6g011310, MTR_7g117500, and MTR_1g064540 are orthologs of Arabidopsis PM H^+-ATPase (**Figure 4**).

Transcription Factor Analysis

TFs play an important role in regulating leaf senescence; the PlantTFDB 4.0 match analysis was used for predicting TFs. We identified 101 and 173 TFs in 985 SAGs and 1,180 DEGs, belonging to 16 and 26 TF families, respectively (**Supplementary Table 5**). The most typical representative TF families in 985 SAGs included *bHLH* (seven genes), *MYB* (four genes), and *WRKY* (three genes), while *B3* (seven genes), *MYB* (seven genes), and *HB-other* (six genes) were the most representatives in 1,180 DEGs (**Table 2**). As shown in **Table 2** for the representatives from 1,180 DEGs, most *B3*, *HB-other*, and *ARF* TFs were downregulated, whereas the *MYB* and *WRKY* TF families were upregulated.

The families and numbers of TFs have big differences in the two gene sets. The *NAC* and *bZIP* TF families belong to 985 SAGs, and these TF families are widely reported in the regulation of senescence. The *B3*, *HB-other*, and *ARF* TF families in the 1,180 DEGs play an important role in abiotic stress defense responses. The *MYB*, *WRKY*, and *bHLH* families are multifunctional but essentially regulate plant senescence directly or indirectly.

Time-Course Senescence-Associated Gene Analysis

Time-course gene expression analysis found that 985 SAGs and 1,180 DEGs (**Figure 3B**) were divided into eight clusters, each of which included certain genes with the same expression patterns. The gene expression trend differences between the control and treated groups are illustrated in **Figure 5**. Among the 985 SAGs, the 106 genes were upregulated in clusters 1, 2, 5, 6, and 8, and the 108 downregulated genes (50.5%) were enriched in clusters 3, 4, and 7 (**Figure 5A**). In clusters 1, 2, 4, 6, 7, and 8 of 1,180 DEGs, 81 genes were upregulated, while in clusters 3 and 5, 34 genes (29.6%) were downregulated (**Figure 5B**). The expression patterns of all genes are shown in **Supplementary Figure 3**.

To elucidate the expression pattern and function of genes in different clusters of 985 SAGs and 1,180 DEGs, we performed KEGG pathway enrichment analysis. Among the 985 SAGs, the genes related to nutrient cycling are enriched in the clusters of upregulated genes, including clusters 1, 2, and 8 with strikingly expressed amino acid metabolism-related genes. The genes related to photosynthesis are enriched in clusters 3, 4, and 7 with downregulated expression patterns. There was a strong difference of enriched genes' function between 985 SAGs and 1,180 DEGs. Among the 1,180 DEGs, the genes related to oxidative phosphorylation and thermogenesis are enriched in clusters of upregulated genes, especially in clusters 1 and 5. It

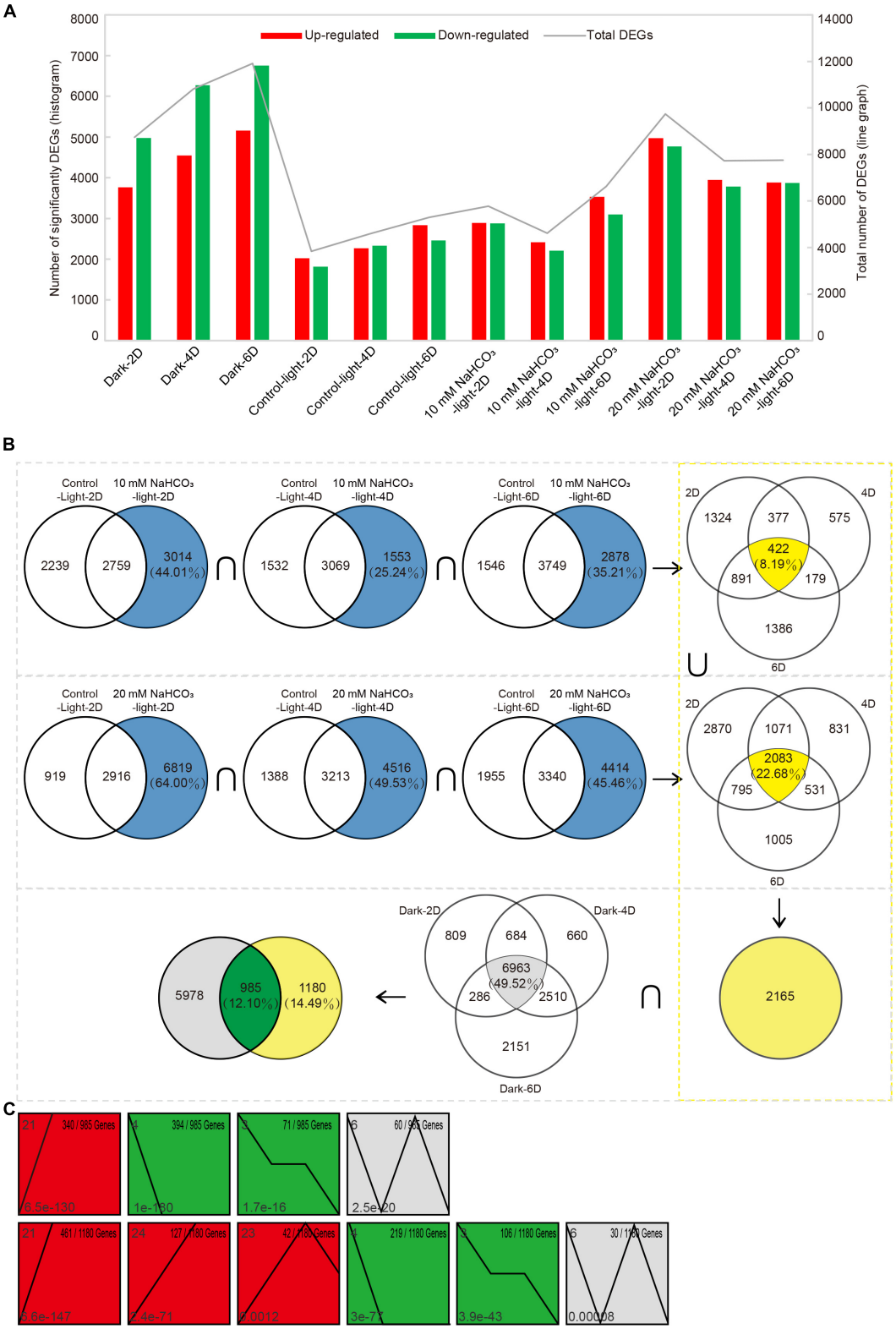

FIGURE 3 | Analysis of differentially expressed senescence-associated genes (SAGs) under alkali stress. **(A)** The number of differentially expressed genes that were upregulated or downregulated during leaf senescence compared with 0 day control prior to treatment, as assessed using the difference analysis software edgeR at thresholds of $|\log_2 FC| \geq 1$ and $P < 0.05$. **(B)** Venn diagram of DEGs ($|\log_2 FC| \geq 1$ and $P < 0.05$) in the 10 mM, 20 mM $NaHCO_3$ treatments and darkness on day 2, 4, and 6 compared with control-light condition. There were 985 SAGs shared by darkness and $NaHCO_3$ treatments across three time points. **(C)** Short time-series expression miner (STEM) analysis of 985 and 1,180 genes across three time points. Each square box indicates a type of expression profile, with the profile order on the upper left and the *P*-value on the bottom left. Only significantly enriched cluster profiles with a $P < 0.05$ threshold are shown.

TABLE 1 | Gene ontology (GO) and Kyoto Encyclopedia of genes and genomes (KEGG) pathways enrichment analysis of DEGs (**Figure 3B**, 985 SAGs and 1,180 genes) shared by darkness and alkaline-induced leaf senescence at three time points.

From	No.	GO/KEGG pathway id	GO/KEGG pathway term	Category	Sample gene number			Background gene number	Rich factor	P-adjust
					Total	Up	Down			
985 SAGs	1	GO:0010027	Thylakoid membrane organization	Biological process	17	0	17	104	0.16346	0.00076
	2	GO:0044282	Small molecule catabolic process	Biological process	23	18	5	224	0.10268	0.00076
	3	GO:0006520	Cellular amino acid metabolic process	Biological process	32	15	17	569	0.05624	0.00076
	4	GO:0019752	Carboxylic acid metabolic process	Biological process	51	28	23	1160	0.04397	0.00076
	5	GO:0016054	Organic acid catabolic process	Biological process	14	12	2	150	0.09333	0.00076
	6	GO:0046395	Carboxylic acid catabolic process	Biological process	14	12	2	150	0.09333	0.00076
	7	GO:1901575	Organic substance catabolic process	Biological process	68	42	26	1670	0.04072	0.00076
	8	GO:0044281	Small molecule metabolic process	Biological process	82	39	43	2000	0.04100	0.00076
	9	GO:0019252	Starch biosynthetic process	Biological process	10	2	8	75	0.13333	0.00076
	10	GO:0043436	Oxoacid metabolic process	Biological process	54	28	26	1248	0.04327	0.00076
	1	GO:0005739	Mitochondrion	Cellular component	49	42	7	747	0.06560	0.00107
1180 Genes	2	GO:1990204	Oxidoreductase complex	Cellular component	12	12	0	92	0.13043	0.00107
	3	GO:0009060	Aerobic respiration	Biological process	7	7	0	29	0.24138	0.00127
	4	GO:0030964	NADH dehydrogenase complex	Cellular component	7	7	0	31	0.22581	0.00160
	5	GO:0019646	Aerobic electron transport chain	Biological process	5	5	0	13	0.38462	0.00185
	6	GO:0006811	Ion transport	Biological process	51	37	14	1136	0.04489	0.00315
	7	GO:0006812	Cation transport	Biological process	35	24	11	690	0.05072	0.00616
	8	GO:0043227	Membrane-bounded organelle	Cellular component	236	156	80	7800	0.03026	0.00746
	9	GO:0055085	Transmembrane transport	Biological process	64	52	12	1608	0.03980	0.01016
	10	GO:1902600	Proton transmembrane transport	Biological process	15	14	1	227	0.06608	0.04282
	1	Map00630	Glyoxylate and dicarboxylate metabolism	Carbohydrate metabolism	10	4	6	112	0.08929	0.029559
985 SAGs	2	Map00280	Valine, leucine and isoleucine degradation	Amino acid metabolism	8	6	2	68	0.11765	0.033328
	3	Map00350	Tyrosine metabolism	Amino acid metabolism	7	6	1	65	0.10769	0.033824
	4	Map00330	Arginine and proline metabolism	Amino acid metabolism	9	5	4	103	0.08738	0.043300
1180 Genes	1	Map04714	Thermogenesis	Environmental adaptation	22	21	1	256	0.08594	0.00056
	2	Map00190	Oxidative phosphorylation	Energy metabolism	22	22	0	291	0.075601	0.00207

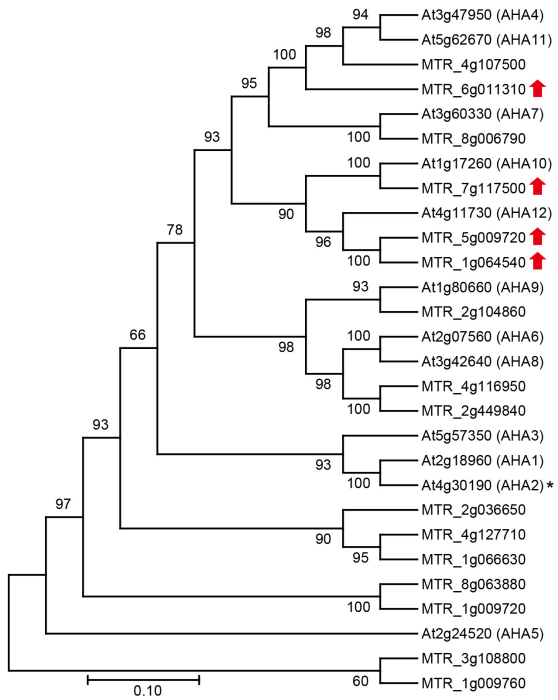

FIGURE 4 | Phylogenetic analysis of PM H^+-ATPase gene family members in *M. truncatula* and *Arabidopsis thaliana*. The upward red arrows indicates that the genes are up-regulated in the alkali stress-induced detached leaf senescence in *M. truncatula*; and the asterisk shows the alkaline-stress-regulated PM H^+-ATPase gene in Arabidopsis. The scale bar indicates the sequence divergence is 0.10 per unit bar.

is worth noting that there are arginine and proline metabolism-related genes present in clusters 7 and 8, and these genes are acting to relieve osmotic stress (**Supplementary Table 6**).

Integration Analysis of the Physiological Data and Transcriptome

Physiological indicators were closely linked to the transcriptome during plant leaf senescence (**Table 3**). A large number of genes related to nutrient metabolism were differentially expressed, such as 59 DEGs involved in amino acid metabolism, which could be expected to rapidly loose and shift nutrients during leaf senescence; and 76 chloroplast and thylakoid metabolism-related genes were observed, consistent with leaf yellowing and chlorophyll breakdown. Alkaline stress induced ROS production and accelerated leaf senescence; 178 genes related to oxidation activity were differentially expressed, in alignment with the increased H_2O_2 and MDA contents observed. Furthermore, the accumulation of ROS increased the permeability of the cell membrane in leaves, causing 169 genes related to ion transport to be differentially expressed (**Supplementary Table 7**).

The enrichment network map for GO terms described in **Table 3** is displayed in **Figure 6**, and highlights the relationships between GO terms and GO terms, and between GO terms and genes. Functionally related GO terms were highly correlated.

Responses of Detached Leaves to Salt Stress and Alkali Stress

The transcription profiles of salt stress have been analyzed in our previous study (Dong et al., 2021). Combined with the previous data, analysis showed that 1,463 DEGs were induced by both salt and alkali stresses, and these genes were mostly associated with nutrient cycling metabolism. The 702 DEGs were induced by alkali stress and enriched in thermogenic and oxidative phosphorylation pathways; 1,518 DEGs were induced by salt stress and enriched in porphyrin and chlorophyll metabolism, the citrate cycle (TCA cycle), and photosynthesis (**Figure 7A** and **Supplementary Table 8**). On this basis, we focused on the differential expression of senescence-associated genes in the two stresses; 792 SAGs were induced under both salt and alkali stresses (**Figure 7B**).

DISCUSSION

We obtained high-precision RNA-seq data from highly controlled and detached leaves from individual *M. truncatula* plants at four time points; and analyzed data through standard procedures. In addition, we compared the data from this study (alkali stress-induced leaf senescence) with data from a

TABLE 2 | Transcription factors (TFs) predicted from 985 SAGs and 1,180 DEGs (**Figure 3B**).

No.	TF family	985 SAGs Gene number	Up	Down	TF family	1180 DEGs Gene number	Up	Down
1	bHLH	7	3	4	B3	7	1	6
2	MYB	4	2	2	MYB	7	6	1
3	WRKY	3	1	2	HB-other	6	0	6
4	CO-like	3	0	3	ARF	5	0	5
5	Dof	3	2	1	GRAS	5	2	3
6	DBB	2	0	2	WRKY	5	4	1
7	MYB-related	2	2	0	ERF	3	3	0
8	NAC	2	2	0	MIKC	3	2	1
9	bZIP	2	2	0	M-type	3	2	1
10	ERF	2	0	2	bHLH	3	1	2

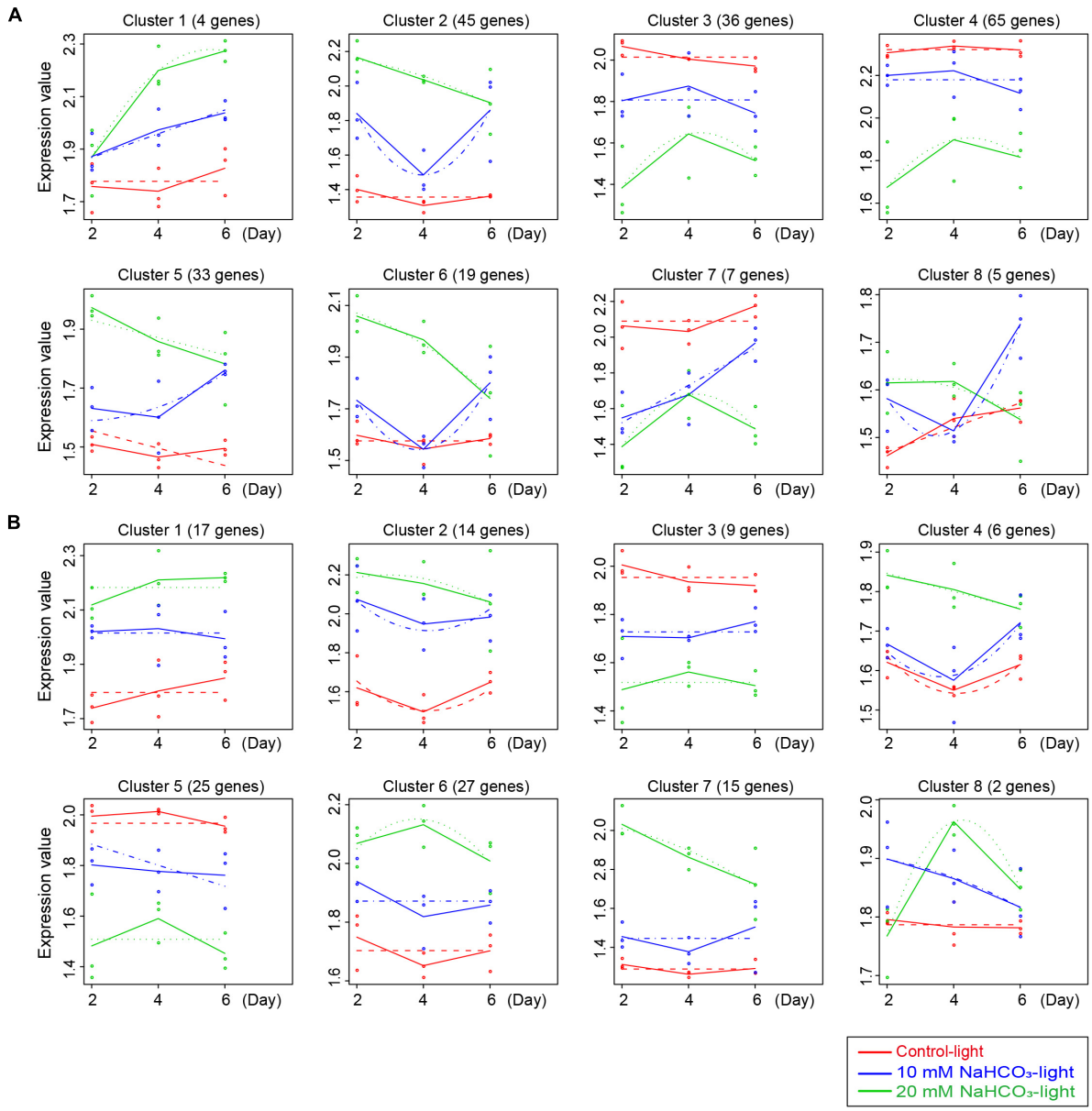

FIGURE 5 | Data visualization according to the cluster analysis. Each map shows the average expression profiles of the gene clusters from all samples. The horizontal coordinates represent different time points, and the vertical coordinates represent the treated expression values. Different colored lines represent different groups (red, blue, and green lines represent the control light, 10 mM $NaHCO_3$-light, and 20 mM $NaHCO_3$-light groups, respectively) and show the actual average value of gene expression at each time point. Different points represent the actual average expression levels for specific individual samples. The dotted lines represent the fitted curves of gene expression at each time point. **(A,B)** Are the cluster analysis for 985 SAGs and 1,180 DEGs, respectively.

previous study (salt stress-induced leaf senescence) to construct a complete and rigorous experimental design strategy.

Salinity and alkaline conditions are widely recognized as abiotic stresses which restrict crop production as well as ecological environment construction. High salinity can affect the growth and development of plants by accelerating leaf senescence and plant death (Guo et al., 2021). In this process, chlorophyll degrades, and leaf color changes from green to yellow (Xue et al., 2021). Our physiological data confirmed this phenomenon (**Figures 1A,B**). We found that alkaline stress was more toxic than salt stress because of more rapid chlorophyll breakdown and more severely eroded leaves. Transcriptome data also showed that the molecular mechanisms of leaf senescence induced by the two stresses were not the same (**Figure 7** and **Supplementary Table 8**), and many studies have reached similar conclusions (Guo et al., 2009; Yang et al., 2009; Li et al., 2010). Salt stress (mainly NaCl) and alkali stress (mainly Na_2CO_3 and $NaHCO_3$) can accelerate leaf senescence through

TABLE 3 | Gene ontology (GO) enrichment analysis of DEGs (**Figure 3B**, 2,165 genes) that regulation of physiological activity.

Function	No.	GO id	GO term	Category	Sample gene number	Background gene number	Rich factor	P-adjust
Oxidation activity	1	GO:0055114	Oxidation-reduction process	Biological process	178	2739	0.06499	0.00069
	2	GO:0015980	Energy derivation by oxidation of organic compounds	Biological process	11	61	0.18033	0.00382
	3	GO:0034440	Lipid oxidation	Biological process	8	40	0.20000	0.01422
	4	GO:0019395	Fatty acid oxidation	Biological process	7	35	0.20000	0.02858
Amino acid metabolism	1	GO:1901605	Alpha-amino acid metabolic process	Biological process	41	364	0.11264	0.00069
	2	GO:0006520	Cellular amino acid metabolic process	Biological process	59	569	0.10369	0.00069
	3	GO:0009064	Glutamine family amino acid metabolic process	Biological process	17	106	0.16038	0.00069
	4	GO:1901606	Alpha-amino acid catabolic process	Biological process	13	84	0.15476	0.00435
	5	GO:0008652	Cellular amino acid biosynthetic process	Biological process	26	259	0.10039	0.00516
	6	GO:1901607	Alpha-amino acid biosynthetic process	Biological process	24	230	0.10435	0.00641
	7	GO:0009063	Cellular amino acid catabolic process	Biological process	13	89	0.14607	0.00704
	8	GO:0003333	Amino acid transmembrane transport	Biological process	10	73	0.13699	0.04495
Chloroplast and thylakoid metabolism	1	GO:0044434	Chloroplast part	Cellular component	87	1114	0.07810	0.00069
	2	GO:0009570	Chloroplast stroma	Cellular component	36	399	0.09023	0.00378
	3	GO:0009507	Chloroplast	Cellular component	76	1139	0.06673	0.01457
	4	GO:0010027	Thylakoid membrane organization	Biological process	17	104	0.16346	0.00069

ion toxicity, osmotic stress, and oxidative stress. However, alkali stress causes more damage to leaves in less time, and the molecular mechanism is more complex (Guo et al., 2015). We propose a model of the physiological activities and molecular mechanisms of *M. truncatula* leaf responding to alkali stress. As shown in **Figure 8**, in the early stage of leaves upon to alkali stress, plant mainly faces to resist the stress. The corresponding physiological activities included ion transport, alleviation of osmotic stress, pH rebalance, hormone regulation, ROS protection; In molecular mechanisms, more changes focus on: (1) signal Transduction Pathways; (2) expression of alkali resistance-associated genes; (3) Ca^{2+} signaling system; (4) transcription factors; (5) epigenetic Changes. In the late stage of leaves under alkali stress, plant mainly shift to nutrient transport. The corresponding physiological activities included chlorophyll degradation, protein degradation and nutrient recycling. This strategy adjustment means that plant is about to give up the leaves that suffer from alkali stress.

Alkaline stress greatly disrupts the ionic dynamic balance in plants and interferes with the uptake of mineral elements, leading to excessive accumulation of Na^+ in the leaf cytoplasm, causing ion toxicity which damages cell organelles (Yang et al., 2008; Ruiz et al., 2016). In our assay, enrichment of DEGs related to ion transport and transmembrane transport was detected, with most being upregulated (**Table 1**). It has been reported that alkali stress can affect the distribution of ions in plant organs; for example, a large amount of Na^+ and Cl^- accumulates in old leaves, and the content of Na^+ and Cl^- in new leaves is lower (Foolad, 2004; Wang et al., 2012). The Na^+ content in the leaves also increases significantly with increasing alkali stress (Dai et al., 2014; Abdel Latef and Tran, 2016). Plants maintain ion balance through ion metabolism, an important mechanism for adaptation to alkali stress (Blumwald et al., 2000).

Alkali stress can lead to massive water shortages in the leaves and accelerate leaf senescence (Zhang P. et al., 2021). In our study, genes related to metabolic intermediates, such as organic acid catabolic process and proline metabolism, were found to be significantly enriched; these metabolic intermediates act to relieve osmotic stress and contribute to the maintenance of normal water content in the leaves (Ali et al., 2008).

The effect of oxidative damage on leaf senescence is notable. High salinity can induce superoxide radicals, resulting in membrane lipid peroxidation and disruption of membrane integrity, which is a direct and important cause of leaf senescence. MDA is one of the main products of membrane lipid peroxidation (Bao et al., 2009), and we found that MDA content accumulated during leaf senescence (**Figure 1D**), suggesting that leaves suffered oxidative damage under alkaline stress. Similar results have been reported elsewhere (Zou et al., 2020; Wei et al., 2021; Wu et al., 2021). H_2O_2 is a common ROS involved in plant senescence. It can oxidize macromolecules and damage cell membranes, causing senescence (Halliwell, 1984; Chen et al., 2012). The H_2O_2 content increased during alkaline-induced senescence (**Figure 1C**). Transcriptional profile analysis also confirmed this result, with a large number of DEGs enriched in the oxidation-reduction process, energy derivation by oxidation of organic compounds, lipid oxidation,

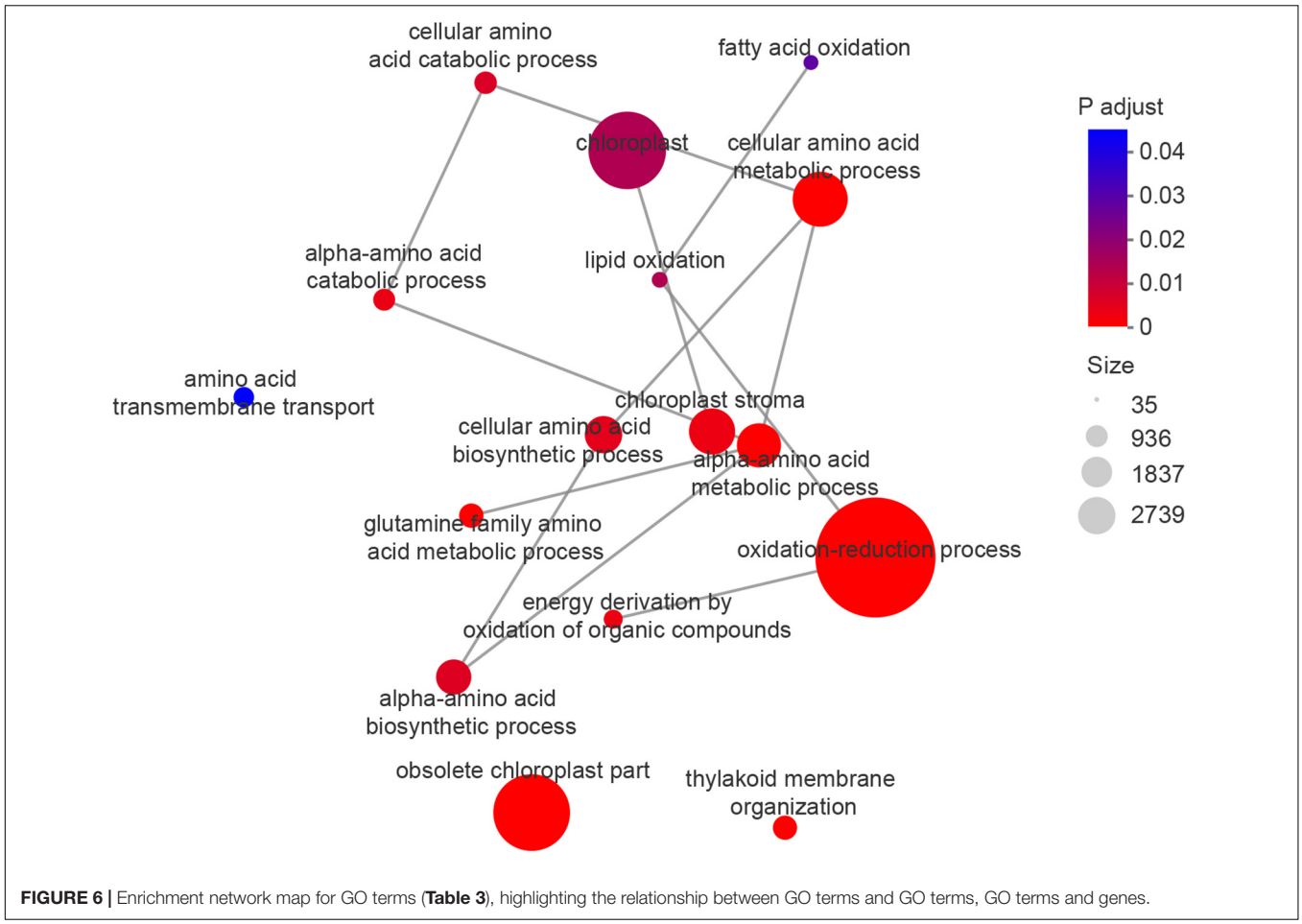

FIGURE 6 | Enrichment network map for GO terms (**Table 3**), highlighting the relationship between GO terms and GO terms, GO terms and genes.

and fatty acid oxidation (**Table 3**). The levels of MDA and H_2O_2, as markers of oxidative stress-induced cellular damage, are widely used to assess the degree of plant senescence in *Arabidopsis* (Cui et al., 2013), alfalfa (Wei et al., 2021), rice (Chen et al., 2018), and adzuki bean (Li et al., 2020). Plants have ROS scavenging systems, including secondary metabolites and antioxidant enzymes, to reduce accumulated ROS and defend against oxidative damage (Gong et al., 2013; Wu et al., 2021). Secondary metabolites act as antioxidants to help plants scavenge ROS, such as ASA, carotenoids, glutathione, and certain low-molecular-weight compounds (Fan et al., 2021; Fang et al., 2021). Our transcriptome analysis showed that DEGs were enriched in KEGG pathways of secondary metabolites, such as carotenoid biosynthesis and glutathione metabolism (**Supplementary Figure 4** and **Supplementary Table 9**). These DEGs may be involved in ROS elimination. Antioxidant enzymes play the most important role in the ROS scavenging system, and mainly include superoxide dismutase, peroxidase, and catalase, which catalyze H_2O_2 into O_2 and H_2O (Sun et al., 2019), and ascorbic acid peroxidase, which reduces membrane lipid peroxidation by scavenging MDA (Fang et al., 2021). It has been reported that overexpression of Cu/Zn-superoxide dismutase can increase the degree of tolerance to H_2O_2, thus reducing the damage caused by alkaline stress in plants (Wu et al., 2016). Additionally, antioxidant enzymes and antioxidants work together to effectively scavenge ROS and alleviate oxidative stress (Fu et al., 2017). Although plants have developed a series of regulatory adaptive mechanisms to resist alkali stress-induced senescence, the regulatory adaptive mechanisms of plants lose their effect if the concentration of alkali stress exceeds a threshold, leading to senescence and death.

In our assay, 2,165 DEGs were identified through transcriptomics of alkali-induced detached leaves. For further analysis, we divided the 2,165 DEGs into two parts: 985 SAGs and 1,180 DEGs; 985 genes were identical to the SAGs of the dark treatment group, which we believe are directly involved in the leaf senescence process. The remaining 1,180 genes may indirectly regulate leaf senescence (**Figure 3B**). GO and KEGG pathway enrichment analysis confirmed our conjecture that the genes of the two gene sets play different roles in leaf senescence: 985 SAGs were mainly enriched in nutrient cycling processes, such as cellular amino acid metabolic processes and organic substance catabolic processes, indicating nutrient redistribution. The 1,180 SAGs were significantly enriched in oxidoreductase complex, aerobic respiration, and ion transport (**Table 1**), most of which were upregulated during senescence (**Figure 5**).

TFs are the most significant components in the regulation of leaf senescence (Guo et al., 2004; Balazadeh et al., 2008). In

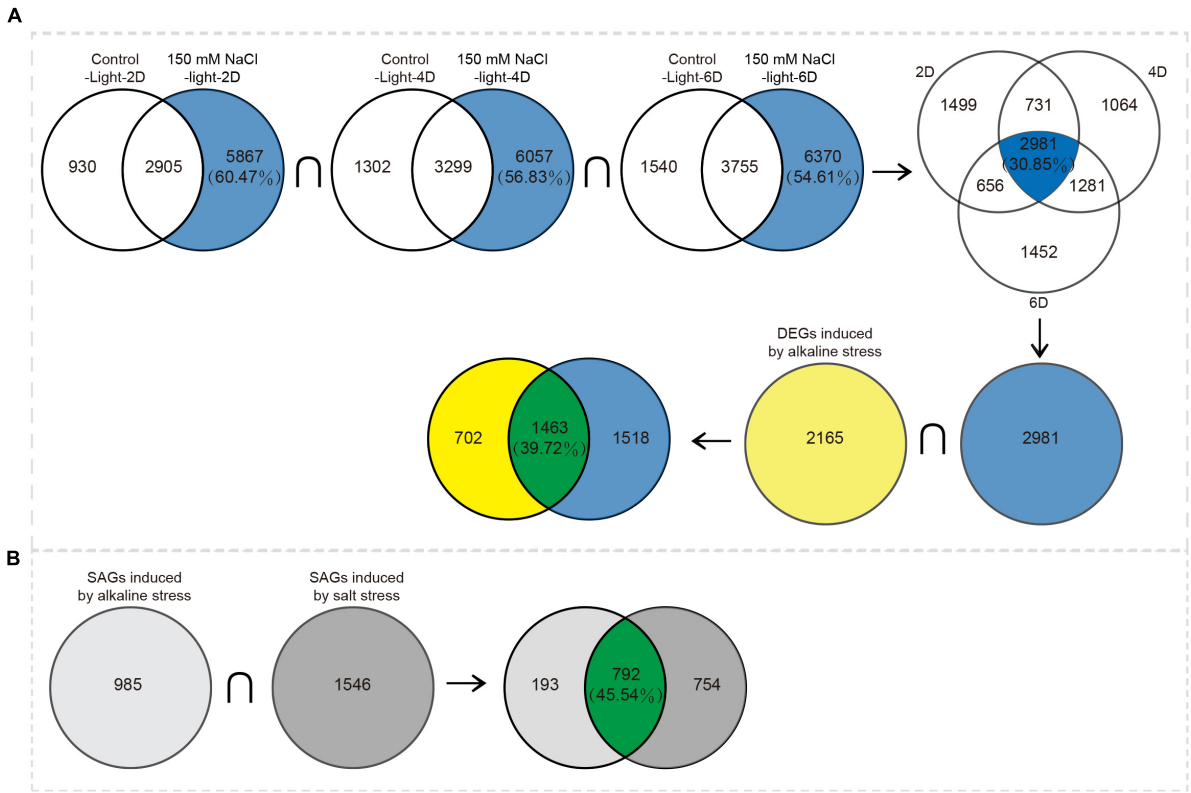

FIGURE 7 | Venn diagram analysis of DEGs induced by alkaline stress and by salt stress. **(A)** Differences between DEGs induced by alkaline stress and by salt stress. **(B)** Differences between SAGs induced by alkaline stress and by salt stress.

Health	Resist response	Senescence	Nutrient transport	Death
Physiological activity	**Ion transport:** Na^+, Cl^-, K^+ **Alleviation of osmotic stress:** inorganic ions (K^+, Cl^-, NO_3^-); organic solutes (Pro, Betaine, MA, D-Mannose) **pH rebalance:** organic acids, inorganic anion, H^+-ATPase **Hormones regulate:** ABA, ET, JA, SA **ROS protection:** secondary metabolites (ASA, CAR, GSH); antioxidant enzymes (SOD, POD, CAT, APX)		**Chlorophyll degradation:** chloroplast structure is changed, Mg^{2+} precipitation and chlorophyll synthesis is blocked **Protein degradation:** cessation of protein synthesis **Autophagy:** eliminates proteins and organelles **Nutrient recycling:** nutrients from senescent leaves to new leaves, seeds and storage organs	
Molecular mechanism	**Signal Transduction Pathways:** SOS pathway, protein kinase pathway, ABA pathway **Expression of alkali resistance-associated genes:** *MsGSTU8, MsMYB4, MsSiR, OsLOL5, OsIRO3, OsALT1, OsCu /Zn-SOD* **Ca^{2+} signaling system:** DREPP, CRTs; SOS pathway , ROS pathway **Transcription factors:** AP2/ERF, MYB, WRKY, NAC **Epigenetic Changes:** DNA methylation, histone modification, miRNA		**GO term:** Cellular amino acid metabolic process Organic substance catabolic process Small molecule catabolic process Carboxylic acid metabolic process **KEGG pathway:** Glyoxylate and dicarboxylate metabolism Valine, leucine and isoleucine degradation Tyrosine metabolism Arginine and proline metabolism	

FIGURE 8 | A model of leaf senescence regulation under alkaline stress in *M. truncatula*.

our study, we identified 101 and 173 TFs among the 985 SAGs and 1,180 DEGs, respectively. The *MYB*, *WRKY*, *NAC,* and *bZIP* TF families belonged to the 985 SAGs, which are known to be involved in the regulation of senescence (Guo et al., 2004; Ay et al., 2010; Guo and Gan, 2011). The *B3*, *HB-other*, and *ARF* TF families in the 1,180 DEGs play an important role in abiotic stress defense responses. *MYB*, *WRKY*, and *bHLH* are multifunctional but essentially regulate plant senescence directly or indirectly.

The leaf is an important site for photosynthesis in plants and is sensitive to senescence. Premature leaf senescence caused by numerous environmental stresses (such as darkness, drought, salt, and alkali stress) can result in significant yield loss and quality reduction, especially in plants that focus on harvesting leaves, such as alfalfa. Therefore, the regulation of appropriate senescence time under abiotic stress needs investigation, with the aim to obtain varieties with an ideal senescence time. Alfalfa is considered a major forage crop worldwide, due to its high yield, high nutrient quality, and wide range of adaptation; however, premature leaf senescence caused by stress affects the quality and yield of alfalfa.

In summary, this study described detailed expression profiles of leaf senescence induced by alkali stress in *M. truncatula*, and annotated many SAGs. New candidate genes have been identified for further senescence resistance breeding, in order to improve the biomass and quality of forage crops under alkaline stress.

DATA AVAILABILITY STATEMENT

The datasets presented in this study can be found in online repositories. The names of the repository/repositories and accession number(s) can be found below: National Center for Biotechnology Information (NCBI) BioProject database under accession number PRJNA805030.

AUTHOR CONTRIBUTIONS

HX, Z-YW, and SD conceived and designed the experiments. SD, WP, HL, and KZ performed the experiments. SD, ZL, LC, and GY analyzed the data. SD wrote the manuscript. HX and Z-YW revised the manuscript. All authors read, revised and approved the final manuscript.

FUNDING

This work was supported by the Start Up Funds for High Level Talents of Qingdao Agricultural University (663-1120001), the National Natural Science Foundation of China (U1906201), and the First Class Grassland Science Discipline Program of Shandong Province, China.

SUPPLEMENTARY MATERIAL

The Supplementary Material for this article can be found online at: https://www.frontiersin.org/articles/10.3389/fpls.2022.881456/full#supplementary-material

Supplementary Figure 1 | Correlation analysis showed the direct association between samples in the same treatment.

Supplementary Figure 2 | Validation of RNA-seq data by the qRT-PCR analysis. Correlation of expression changes observed by RNA-seq (*Y*-axis) and qRT-PCR (*X*-axis) relative expression levels from $\log_2$ Fold Change of 25 genes in different groups.

Supplementary Figure 3 | Data visualization according to cluster analysis. The horizontal coordinates represent specific samples, the vertical coordinates represent the expression values after treatment $\log_{10}(x + 1)$ and the different colored lines represent the trend of different genes in all samples.

Supplementary Figure 4 | Pathview analysis of the Carotenoid (CAR) biosynthesis and Glutathione (GSH) metabolism pathway. The genes in the red rectangle are up-regulated.

Supplementary Table 1 | Primers of genes used for real-time quantitative PCR in this study.

Supplementary Table 2 | Project sample information, raw data, quality control data and comparison data.

Supplementary Table 3 | Differentially expressed genes (DEGs) at days 2, 4, and 6.

Supplementary Table 4 | 985 SAGs and 1,180 genes are obtained using the Venn diagram.

Supplementary Table 5 | TF family analysis data.

Supplementary Table 6 | KEGG pathway enrichment analysis in individual cluster.

Supplementary Table 7 | 169 DEGs related to ion transport.

Supplementary Table 8 | Responses of detached leaves to salt stress and alkali stress.

Supplementary Table 9 | Carotenoid biosynthesis and glutathione metabolism.

REFERENCES

Abdel Latef, A. A., and Tran, L. S. (2016). Impacts of priming with silicon on the growth and tolerance of maize plants to alkaline stress. *Front. Plant Sci.* 7:243. doi: 10.3389/fpls.2016.00243

Ali, Q., Athar, H.-U.-R., and Ashraf, M. (2008). Modulation of growth, photosynthetic capacity and water relations in salt stressed wheat plants by exogenously applied 24-epibrassinolide. *Plant Growth Regul.* 56, 107–116. doi: 10.1007/s10725-008-9290-7

Allu, A. D., Soja, A. M., Wu, A., Szymanski, J., and Balazadeh, S. (2014). Salt stress and senescence: identification of cross-talk regulatory components. *J. Exp. Bot.* 65, 3993–4008. doi: 10.1093/jxb/eru173

An, Y. M., Song, L. L., Liu, Y. R., Shu, Y. J., and Guo, C. H. (2016). De novo transcriptional analysis of alfalfa in response to saline-alkaline stress. *Front. Plant Sci.* 7:931. doi: 10.3389/fpls.2016.00931

Ay, N., Irmler, K., Fischer, A., Uhlemann, R., Reuter, G., and Humbeck, K. (2010). Epigenetic programming via histone methylation at WRKY53 controls leaf senescence in *Arabidopsis thaliana*. *Plant J. Cell Mol. Biol.* 58, 333–346. doi: 10.1111/j.1365-313X.2008.03782.x

Balazadeh, S., Riano-Pachon, D. M., and Mueller-Roeber, B. (2008). Transcription factors regulating leaf senescence in *Arabidopsis thaliana*. *Plant Biol.* 10(Suppl. 1), 63–75. doi: 10.1111/j.1438-8677.2008.00088.x

Balazadeh, S., Wu, A., and Mueller-Roeber, B. (2010). Salt-triggered expression of the ANAC092-dependent senescence regulon in *Arabidopsis thaliana*. *Plant Signal. Behav.* 5, 733–735. doi: 10.4161/psb.5.6.11694

Bao, A.-K., Wang, S.-M., Wu, G.-Q., Xi, J.-J., Zhang, J.-L., and Wang, C.-M. (2009). Overexpression of the *Arabidopsis* H^+-PPase enhanced resistance to salt and drought stress in transgenic alfalfa (*Medicago sativa* L.). *Plant Sci.* 176, 232–240. doi: 10.1016/j.plantsci.2008.10.009

Barker, D. G., Bianchi, S., Blondon, F., Dattée, Y., Duc, G., Essad, S., et al. (1990). Medicago truncatula, a model plant for studying the molecular genetics of the *Rhizobium*-legume symbiosis. *Plant Mol. Biol. Rep.* 8, 40–49. doi: 10.1007/BF02668879

Blumwald, E., Aharon, G. S., and Apse, M. P. (2000). Sodium transport in plant cells. *Biochim. Biophys. Acta* 1465, 140–151. doi: 10.1016/S0005-2736(00)00135-8

Bouton, J. (2007). The economic benefits of forage improvement in the United States. *Euphytica* 154, 263–270. doi: 10.1007/s10681-006-9220-6

Breeze, E., Harrison, E., Mchattie, S., Hughes, L., Hickman, R., Hill, C., et al. (2011). High-resolution temporal profiling of transcripts during *Arabidopsis* leaf senescence reveals a distinct chronology of processes and regulation. *Plant Cell* 23, 873–894. doi: 10.1105/tpc.111.083345

Buchanan-Wollaston, V. (1997). The molecular biology of leaf senescence. *J. Exp. Bot.* 48, 181–199. doi: 10.1093/jxb/48.2.181

Chao, Y., Xie, L., Yuan, J., Guo, T., Li, Y., Liu, F., et al. (2018). Transcriptome analysis of leaf senescence in red clover (*Trifolium pratense* L.). *Physiol. Mol. Biol. Plants* 24, 753–765. doi: 10.1007/s12298-018-0562-z

Chen, G., Wu, C., He, L., Qiu, Z., Zhang, S., Zhang, Y., et al. (2018). Knocking out the gene RLS1 induces hypersensitivity to oxidative stress and premature leaf senescence in rice. *Int. J. Mol. Sci.* 19:2853. doi: 10.3390/ijms19102853

Chen, H. J., Lin, Z. W., Huang, G. J., and Lin, Y. H. (2012). Sweet potato calmodulin SPCAM is involved in salt stress-mediated leaf senescence, H_2O_2 elevation and senescence-associated gene expression. *J. Plant Physiol.* 169, 1892–1902. doi: 10.1016/j.jplph.2012.08.004

Cui, M. H., Ok, S. H., Yoo, K. S., Jung, K. W., Yoo, S. D., and Shin, J. S. (2013). An Arabidopsis cell growth defect factor-related protein, CRS, promotes plant senescence by increasing the production of hydrogen peroxide. *Plant Cell Physiol.* 54, 155–167. doi: 10.1093/pcp/pcs161

Dai, L. Y., Zhang, L. J., Jiang, S. J., and Yin, K. D. (2014). Saline and alkaline stress genotypic tolerance in sweet sorghum is linked to sodium distribution. *Acta Agric. Scand. B Soil Plant Sci.* 64, 471–481. doi: 10.1080/09064710.2014.925574

Dong, S., Sang, L., Xie, H., Chai, M., and Wang, Z. Y. (2021). Comparative transcriptome analysis of salt stress-induced leaf senescence in *Medicago truncatula*. *Front. Plant Sci.* 12:666660. doi: 10.3389/fpls.2021.666660

Fan, Y., Lu, X., Chen, X., Wang, J., Wang, D., Wang, S., et al. (2021). Cotton transcriptome analysis reveals novel biological pathways that eliminate reactive oxygen species (ROS) under sodium bicarbonate ($NaHCO_3$) alkaline stress. *Genomics* 113, 1157–1169. doi: 10.1016/j.ygeno.2021.02.022

Fang, S., Hou, X., and Liang, X. (2021). Response mechanisms of plants under saline-alkali stress. *Front. Plant Sci.* 12:667458. doi: 10.3389/fpls.2021.667458

Foolad, M. (2004). Recent advances in genetics of salt tolerance in tomato. *Plant Cell Tissue Organ Cult.* 76, 101–119. doi: 10.1023/B:TICU.0000007308.47608.88

Fu, J., Liu, Z., Li, Z., Wang, Y., and Yang, K. (2017). Alleviation of the effects of saline-alkaline stress on maize seedlings by regulation of active oxygen metabolism by *Trichoderma asperellum*. *PLoS One* 12:e0179617. doi: 10.1371/journal.pone.0179617

Fuglsang, A. T., Guo, Y., Cuin, T. A., Qiu, Q., Song, C., Kristiansen, K. A., et al. (2007). Arabidopsis protein kinase PKS5 inhibits the plasma membrane H^+-ATPase by preventing interaction with 14-3-3 protein. *Plant Cell* 19, 1617–1634. doi: 10.1105/tpc.105.035626

Ghanem, M. E., Albacete, A., Martinez-Andujar, C., Acosta, M., Romero-Aranda, R., Dodd, I. C., et al. (2008). Hormonal changes during salinity-induced leaf senescence in tomato (*Solanum lycopersicum* L.). *J. Exp. Bot.* 59, 3039–3050. doi: 10.1093/jxb/ern153

Gong, B., Wen, D., Vandenlangenberg, K., Wei, M., Yang, F., Shi, Q., et al. (2013). Comparative effects of NaCl and $NaHCO_3$ stress on photosynthetic parameters, nutrient metabolism, and the antioxidant system in tomato leaves. *Sci. Hortic.* 157, 1–12. doi: 10.1016/j.scienta.2013.03.032

Guo, R., Shi, L., and Yang, Y. (2009). Germination, growth, osmotic adjustment and ionic balance of wheat in response to saline and alkaline stresses. *Soil Sci. Plant Nutr.* 55, 667–679. doi: 10.1111/j.1747-0765.2009.00406.x

Guo, R., Yang, Z., Li, F., Yan, C., Zhong, X., Liu, Q., et al. (2015). Comparative metabolic responses and adaptive strategies of wheat (*Triticum aestivum*) to salt and alkali stress. *BMC plant biology* 15:170. doi: 10.1186/s12870-015-0546-x

Guo, Y., Cai, Z., and Gan, S. (2004). Transcriptome of *Arabidopsis* leaf senescence. *Plant Cell Environ.* 27, 521–549. doi: 10.1111/j.1365-3040.2003.01158.x

Guo, Y., and Gan, S. (2005). Leaf senescence: signals, execution, and regulation. *Curr. Top. Dev. Biol.* 71, 83–112. doi: 10.1016/S0070-2153(05)71003-6

Guo, Y., and Gan, S. (2011). AtMYB2 regulates whole plant senescence by inhibiting cytokinin-mediated branching at late stages of development in *Arabidopsis*. *Plant Physiol.* 156, 1612–1619. doi: 10.1104/pp.111.177022

Guo, Y., and Gan, S. S. (2012). Convergence and divergence in gene expression profiles induced by leaf senescence and 27 senescence-promoting hormonal, pathological and environmental stress treatments. *Plant Cell Environ.* 35, 644–655. doi: 10.1111/j.1365-3040.2011.02442.x

Guo, Y., Ren, G., Zhang, K., Li, Z., Miao, Y., and Guo, H. (2021). Leaf senescence: progression, regulation, and application. *Mol. Hortic.* 1, 1–25. doi: 10.1186/s43897-021-00006-9

Halliwell, B. (1984). *Chloroplast Metabolism: The Structure and Function of Chloroplasts in Green Leaf Cells*. Oxford: Clarendon Press.

Hao, Y. J., Song, Q. X., Chen, H. W., Zou, H. F., Wei, W., Kang, X. S., et al. (2010). Plant NAC-type transcription factor proteins contain a NARD domain for repression of transcriptional activation. *Planta* 232, 1033–1043. doi: 10.1007/s00425-010-1238-2

He, L., Wu, W., Zinta, G., Yang, L., Wang, D., Liu, R., et al. (2018). A naturally occurring epiallele associates with leaf senescence and local climate adaptation in *Arabidopsis* accessions. *Nat. Commun.* 9:460. doi: 10.1038/s41467-018-02839-3

Lee, R. H., Wang, C. H., Huang, L. T., and Chen, S. C. (2001). Leaf senescence in rice plants: cloning and characterization of senescence up-regulated genes. *J. Exp. Bot.* 52, 1117–1121. doi: 10.1093/jexbot/52.358.1117

Li, R., Shi, F., Fukuda, K., and Yang, Y. (2010). Effects of salt and alkali stresses on germination, growth, photosynthesis and ion accumulation in alfalfa (*Medicago sativa* L.). *Soil Sci. Plant Nutr.* 56, 725–733. doi: 10.1111/j.1747-0765.2010.00506.x

Li, W. Y., Wang, C., Shi, H. H., Wang, B., Wang, J. X., Liu, Y. S., et al. (2020). Genome-wide analysis of ethylene-response factor family in adzuki bean and functional determination of VaERF3 under saline-alkaline stress. *Plant Physiol. Biochem.* 147, 215–222. doi: 10.1016/j.plaphy.2019.12.019

Lim, P. O., Kim, H. J., and Gil Nam, H. (2007). Leaf senescence. *Annu. Rev. Plant Biol.* 58, 115–136. doi: 10.1146/annurev.arplant.57.032905.105316

Mao, C., Lu, S., Lv, B., Zhang, B., and Ming, F. (2017). A rice NAC transcription factor promotes leaf senescence via ABA biosynthesis. *Plant Physiology* 174, 1747–1763. doi: 10.1104/pp.17.00542

Pageau, K., Reisdorf-Cren, M., Morot-Gaudry, J. F., and Masclaux-Daubresse, C. (2006). The two senescence-related markers, GS1 (cytosolic glutamine synthetase) and GDH (glutamate dehydrogenase), involved in nitrogen mobilization, are differentially regulated during pathogen attack and by stress hormones and reactive oxygen species in *Nicotiana tabacum* L. leaves. *J. Exp. Bot.* 57, 547–557. doi: 10.1093/jxb/erj035

Ruiz, K., Biondi, S., Martínez, E., Orsini, F., Antognoni, F., and Jacobsen, S.-E. (2016). Quinoa–a model crop for understanding salt-tolerance mechanisms in halophytes. *Plant Biosyst.* 150, 357–371. doi: 10.1080/11263504.2015.1027317

Sakuraba, Y., Kim, D., and Paek, N.-C. (2018). *Plant Senescence*. Berlin: Springer, 141–149.

Sobieszczuk-Nowicka, E., Wrzesiński, T., Bagniewska-Zadworna, A., Kubala, S., Rucińska-Sobkowiak, R., Polcyn, W., et al. (2018). Physio-genetic dissection of dark-induced leaf senescence and timing its reversal in barley. *Plant Physiol.* 178, 654–671. doi: 10.1104/pp.18.00516

Sun, J., He, L., and Li, T. (2019). Response of seedling growth and physiology of *Sorghum bicolor* (L.) moench to saline-alkali stress. *PLoS One* 14:e0220340. doi: 10.1371/journal.pone.0220340

Uauy, C., Distelfeld, A., Fahima, T., Blechl, A., and Dubcovsky, J. (2006). A NAC Gene regulating senescence improves grain protein, zinc, and iron content in wheat. *Science* 314, 1298–1301. doi: 10.1126/science.1133649

Wang, H., Wu, Z., Han, J., Zheng, W., and Yang, C. (2012). Comparison of ion balance and nitrogen metabolism in old and young leaves of alkali-stressed rice plants. *PLoS One* 7:e37817. doi: 10.1371/journal.pone.0037817

Wang, J., Zhao, Y., Ray, I., and Song, M. (2016). Transcriptome responses in alfalfa associated with tolerance to intensive animal grazing. *Sci Rep* 6:19438. doi: 10.1038/srep19438

Wang, N., Wang, X., Shi, J., Liu, X., Xu, Q., Zhou, H., et al. (2019). Mepiquat chloride-priming induced salt tolerance during seed germination of cotton (*Gossypium hirsutum* L.) through regulating water transport and K^+/Na^+ homeostasis. *Environ. Exp. Bot.* 159, 168–178. doi: 10.1016/j.envexpbot.2018.12.024

Wei, T., Wang, Y., and Liu, J. H. (2020). Comparative transcriptome analysis reveals synergistic and disparate defense pathways in the leaves and roots of trifoliate orange (*Poncirus trifoliata*) autotetraploids with enhanced salt tolerance. *Hortic. Res.* 7:88. doi: 10.1038/s41438-020-0311-7

Wei, T.-J., Wang, M.-M., Jin, Y.-Y., Zhang, G.-H., Liu, M., Yang, H.-Y., et al. (2021). Abscisic acid priming creates alkaline tolerance in alfalfa seedlings (*Medicago sativa* L.). *Agriculture* 11:608. doi: 10.3390/agriculture11070608

Woo, H. R., Kim, H. J., Lim, P. O., and Nam, H. G. (2019). Leaf senescence: systems and dynamics aspects. *Annu. Rev. Plant Biol.* 70, 347–376. doi: 10.1146/annurev-arplant-050718-095859

Wu, G.-Q., Li, H., Zhu, Y.-H., and Li, S.-J. (2021). Comparative physiological response of sainfoin (*Onobrychis viciaefolia*) seedlings to alkaline and saline-alkaline stress. *J. Anim. Plant Sci.* 31, 1028–1035. doi: 10.36899/JAPS.2021.4.0299

Wu, J., Zhang, J., Li, X., Xu, J., and Wang, L. (2016). Identification and characterization of a PutCu/Zn-SOD gene from Puccinellia tenuiflora (Turcz.) Scribn. et Merr. *Plant Growth Regul.* 79, 55–64. doi: 10.1007/s10725-015-0110-6

Xu, P., Chen, H., and Cai, W. (2020). Transcription factor CDF4 promotes leaf senescence and floral organ abscission by regulating abscisic acid and reactive oxygen species pathways in *Arabidopsis*. *EMBO Rep.* 21:e48967. doi: 10.15252/embr.201948967

Xue, J., Lu, D., Wang, S., Lu, Z., Liu, W., Wang, X., et al. (2021). Integrated transcriptomic and metabolomic analysis provides insight into the regulation of leaf senescence in rice. *Sci. Rep.* 11:14083. doi: 10.1038/s41598-021-93532-x

Yang, C., Shi, D., and Wang, D. (2008). Comparative effects of salt and alkali stresses on growth, osmotic adjustment and ionic balance of an alkali-resistant halophyte *Suaeda glauca* (Bge.). *Plant Growth Regul.* 56, 179–190. doi: 10.1007/s10725-008-9299-y

Yang, C.-W., Xu, H.-H., Wang, L.-L., Liu, J., Shi, D.-C., and Wang, D.-L. (2009). Comparative effects of salt-stress and alkali-stress on the growth, photosynthesis, solute accumulation, and ion balance of barley plants. *Photosynthetica* 47, 79–86. doi: 10.1007/s11099-009-0013-8

Yang, Y., and Guo, Y. (2018a). Elucidating the molecular mechanisms mediating plant salt-stress responses. *New Phytol.* 217, 523–539. doi: 10.1111/nph.14920

Yang, Y., and Guo, Y. (2018b). Unraveling salt stress signaling in plants. *J. Integr. Plant Biol.* 60, 796–804. doi: 10.1111/jipb.12689

Yang, Y., Qin, Y., Xie, C., Zhao, F., Zhao, J., Liu, D., et al. (2010). The *Arabidopsis* chaperone J3 regulates the plasma membrane H^+-ATPase through interaction with the PKS5 kinase. *Plant Cell* 22, 1313–1332. doi: 10.1105/tpc.109.069609

Yang, Y., Wu, Y., Ma, L., Yang, Z., Dong, Q., Li, Q., et al. (2019). The Ca^{2+} sensor SCaBP3/CBL7 modulates plasma membrane H^+-ATPase activity and promotes alkali tolerance in *Arabidopsis*. *Plant Cell* 31, 1367–1384. doi: 10.1105/tpc.18.00568

Yuan, J., Sun, X., Guo, T., Chao, Y., and Han, L. (2020). Global transcriptome analysis of alfalfa reveals six key biological processes of senescent leaves. *PeerJ* 8:e8426. doi: 10.7717/peerj.8426

Zhang, J. Y., Cruz De Carvalho, M. H., Torres-Jerez, I., Kang, Y., Allen, S. N., Huhman, D. V., et al. (2014). Global reprogramming of transcription and metabolism in *Medicago truncatula* during progressive drought and after rewatering. *Plant Cell Environ.* 37, 2553–2576. doi: 10.1111/pce.12328

Zhang, M., Wang, Y., Chen, X., Xu, F., Ding, M., Ye, W., et al. (2021). Plasma membrane H^+ -ATPase overexpression increases rice yield via simultaneous enhancement of nutrient uptake and photosynthesis. *Nat. Commun.* 12:735. doi: 10.1038/s41467-021-20964-4

Zhang, P., Duo, T., Wang, F., Zhang, X., Yang, Z., and Hu, G. (2021). De novo transcriptome in roots of switchgrass (*Panicum virgatum* L.) reveals gene expression dynamic and act network under alkaline salt stress. *BMC Genomics* 22:82. doi: 10.1186/s12864-021-07368-w

Zhang, Z., He, K., Zhang, T., Tang, D., Li, R., and Jia, S. (2019). Physiological responses of Goji berry (*Lycium barbarum* L.) to saline-alkaline soil from Qinghai region, China. *Sci. Rep.* 9:12057. doi: 10.1038/s41598-019-48514-5

Zhao, D., Oosterhuis, D., and Bednarz, C. (2001). Influence of potassium deficiency on photosynthesis, chlorophyll content, and chloroplast ultrastructure of cotton plants. *Photosynthetica* 39, 103–109. doi: 10.1023/A:1012404204910

Zhou, C., Han, L., Pislariu, C., Jin, N., and Fu, C. (2011). From model to crop: functional analysis of a STAY-GREEN gene in the model legume *Medicago truncatula* and effective use of the gene for alfalfa improvement. *Plant Physiol.* 157, 1483–1496. doi: 10.1104/pp.111.185140

Zhu, J. K. (2016). Abiotic stress signaling and responses in plants. *Cell* 167, 313–324. doi: 10.1016/j.cell.2016.08.029

Zou, C., Liu, D., Wu, P., Wang, Y., Gai, Z., Liu, L., et al. (2020). Transcriptome analysis of sugar beet (*Beta vulgaris* L.) in response to alkaline stress. *Plant Mol. Biol.* 102, 645–657. doi: 10.1007/s11103-020-00971-7

Conflict of Interest: The authors declare that the research was conducted in the absence of any commercial or financial relationships that could be construed as a potential conflict of interest.

Publisher's Note: All claims expressed in this article are solely those of the authors and do not necessarily represent those of their affiliated organizations, or those of the publisher, the editors and the reviewers. Any product that may be evaluated in this article, or claim that may be made by its manufacturer, is not guaranteed or endorsed by the publisher.

frontiers | Frontiers in Plant Science

ORIGINAL RESEARCH
published: 29 April 2022
doi: 10.3389/fpls.2022.896358

Moderately Reducing Nitrogen Application Ameliorates Salt-Induced Growth and Physiological Damage on Forage Bermudagrass

*An Shao†, Hongli Wang†, Xiao Xu, Xiaoning Li, Erick Amombo and Jinmin Fu**

Coastal Salinity Tolerant Grass Engineering and Technology Research Center, Ludong University, Yantai, China

Nitrogen (N) application is one of the most effective methods to alleviate salt-induced damage on plants. Forage bermudagrass has higher utilization potential on saline soil, but whether its N requirement changed under high salt stress has not been studied. Through examining plant growth-related traits, salt-stress-responsive physiological traits, photosynthesis, N metabolism, and forage quality supplied with different N concentrations under high salt stress (200 mM NaCl), we noticed that the optimum N requirement of forage bermudagrass reduced. When supplied with 10 mM N under higher salt stress, plants had a similar biomass, turf color, and chlorophyll content with plants supplied with 15 mM N, accompanied by a lower firing rate and Na^+ content of leaves. The N content, crude protein, crude fat content, the expression of *AMTs* (ammonium transporters), *NR* (nitrate reductase), *GS* (glutamine synthetase), and *GOGAT* (glutamate synthetase), the chlorophyll fluorescence curve, and parameters of leaves (e.g., PI_{ABS}; PI_{CS}; ABS/RC; TRo/RC; ETo/RC) all peaked under 10 mM N under high salt stress instead of 15 mM N. Through exploring the proper N application under higher salt stress and its alleviation mechanisms, our results indicated that moderate reduction in N application under high salt level had a maximum promotion effect on the salt tolerance of forage bermudagrass without growth or forage quality inhibition. These response mechanisms obtained can provide a useful reference for N application in moderation rather than in excess on forage bermudagrass, especially in higher salinity areas.

Keywords: forage bermudagrass, salt stress, nitrogen application, physiological response, forage quality

OPEN ACCESS

Edited by:
Jin-Lin Zhang,
Lanzhou University, China

Reviewed by:
Jingjin Yu,
Nanjing Agricultural University, China
Juanjuan Sun,
Institute of Grassland Research (CAAS), China

***Correspondence:**
Jinmin Fu
turfcn@qq.com

†These authors have contributed equally to this work

Specialty section:
This article was submitted to Plant Abiotic Stress, a section of the journal Frontiers in Plant Science

Received: *15 March 2022*
Accepted: *04 April 2022*
Published: *29 April 2022*

Citation:
Shao A, Wang H, Xu X, Li X, Amombo E and Fu J (2022) Moderately Reducing Nitrogen Application Ameliorates Salt-Induced Growth and Physiological Damage on Forage Bermudagrass. Front. Plant Sci. 13:896358. doi: 10.3389/fpls.2022.896358

INTRODUCTION

Bermudagrass [*Cynodon dactylon* (L.) Pers.] is one of the most widely used grass species as forage and turfgrass in warm climatic regions. Bermudagrass was also considered to be a salt-tolerant grass species (Maas and Hoffman, 1977; Chen and Liu, 2012). However, the growth, forage quality, and turf quality of bermudagrass could be seriously inhibited by salt stress (Marcum and Pessarakli, 2006), greatly limiting its wide application in salinity areas. Salt stress generally disrupts the osmotic and ionic equilibrium in bermudagrass cells, which would lead to ionic toxicity, osmotic stress, and secondary stresses (Ahanger et al., 2019; Maksup et al., 2020; Amin et al., 2021),

including nutritional imbalance, inhibition of photosynthesis, and membrane disorganization (Munns and Tester, 2008). Like other plants, bermudagrass has established corresponding response mechanism in acclimation to external salt stress to reduce their damage (Deinlein et al., 2014; Zhao et al., 2020), such as the induction of antioxidant enzymes (Baby and Jini, 2010; Ahmad et al., 2019), ion transport and compartmentation, compatible solutes synthesis, and accumulation (Zhao et al., 2020).

Nitrogen (N) fertilizer plays a critical role in alleviating salt-induced damage in plants (Mansour, 2000; Villa et al., 2003; Esmaili et al., 2005; Jia et al., 2017). As the most important macro-nutrient of plants, N is an important constituent of the nucleic acids, proteins, chlorophyll, and many other N metabolites (Kishorekumar et al., 2020). N also mediates the utilization of potassium, phosphorus, and other elements and serves as an important component of proteins involved in a series of metabolic processes to coordinate plant growth and development (Zubillaga et al., 2002). Two primary inorganic N sources ammonium (NH_4^+) and nitrate (NO_3^-) from soil can be directly absorbed by roots and are transported to plants by their respective transporters ammonium transporters (AMTs) and nitrate transporters (NRT) (Giagnoni et al., 2016; Dechorgnat et al., 2019). The NH_4^+ absorbed must be transformed into NO_3^- under the catalyst of nitrate reductase (NR). Then, NO_3^- can be further assimilated and converted into amino acid through glutamine synthetase (GS) and glutamate synthase (GOGAT) metabolic pathway, which was considered to be the main pathway for N assimilation in plants (Xu et al., 2012).

However, reduced N uptake of plants always occurs due to the high Na^+ and Cl^- content in the saline soil (Akram et al., 2011). Salinity results in significantly decreased activities of NR, GS, and GOGAT in many plants species, such as maize and rice (Khan and Srivastava, 1998; Wang et al., 2012), and further inhibits the N use efficiency in plants (Murtaza et al., 2013; Singh et al., 2016; Teh et al., 2016). Moreover, several N-containing compounds could be induced by salt stress and contributed to salt tolerance of plants (Hoai et al., 2003; Dluzniewska et al., 2007; Sudmalis et al., 2018) through participating in osmotic adjustment, the promotion of photosynthetic capacity, and mitigation of oxidative stress caused by excessive ROS (Homaee et al., 2002; Song et al., 2006). Therefore, N application is considered to be one of the most effective methods of improving plant growth in salinity regions where N content is lower than that in non-salinity land.

Related research also showed that, rather than N alone, plant growth was significantly affected by the interaction between soil salinity and N. Some reports showed that the alleviation effects of N fertilizer supplied might associate with its concentrations supplied. For instance, low-to-moderate N application could mitigate the adverse effects from salt stress, while excessive N could aggravate the negative effects of salt stress on cotton (Chen et al., 2010). Moreover, excessive application or inefficient use of N fertilizer will lead to secondary salinization, which in turn adversely inhibits plant growth (Soussi et al., 1998; Chen et al., 2010; Lacerda et al., 2016). In ryegrass, moderately reducing N application has the maximum alleviation effect, especially under mild salt stress (Shao et al., 2020). To sum up, the N requirement of plants might be changed (demand goes up or down) under a certain level of salt stress (higher and lower). However, there were no consistent regular changes in the N requirement under different salt concentrations or among different species.

Although bermudagrass has higher utilization potential on saline soil, excessive N application on higher levels of saline soil that cannot be fully utilized by bermudagrass might contribute to N leaching and lead to groundwater pollution. To this end, we attempt to reveal the physiological response mechanism of bermudagrass to salt stress after moderate N application by synthetically analyzing the growth rate, physiological indicators, quality-related traits, and the metabolism of N under control and salt stress treatment with different N supplied levels. The response mechanism obtained will be important for the agricultural practice to guide rational N fertilization application on forage bermudagrass cultures to further improve their salt stress resistance, maintain their growth and quality, and promote their utilization, especially under severe salt stress.

MATERIALS AND METHODS

Plant Materials and Growth Conditions

A common tetraploid bermudagrass cultivar "Wrangle" was used in this experiment. The experimental materials used for treatment were generated by asexual propagation using the cuttings at the top of each branch from the original bermudagrass plants cultured in the greenhouse. The cuttings were planted in a solid medium (sand applied with Hoagland solution) for 1 week, and then, the same number of uniform stolons (about 20 stolons per pot) in each pot was retained in the solid medium. After 1 month, the plants of each pot were then removed from the solid medium and washed clean with water. Before the treatments were initiated, the plants were cultured in Hoagland solution to acclimate for 1 week. Subsequently, the plants were cut to the same height and transferred into different treatments in a hydroponic culture using a modified Hoagland solution. Each treatment contains four replicates. The treatments used NH_4NO_3 as an N source. The other components included 0.2 mM KH_2PO_4, 1 mM $MgSO_4$, 1.5 mM KCl, 2.5 mM $CaCl_2$, 1×10^{-3} mM H_3BO_3, 5×10^{-5} mM $(NH_4)_6Mo_7O_{24}$, 5×10^{-4} mM $CuSO_4$, 1×10^{-3} mM $ZnSO_4$, 1×10^{-3} mM $MnSO_4$, and 0.1 mM Fe(III)-EDTA. The hydroponic culture media were processed in a growth chamber under the following conditions: 22/18°C (day/night), 60% relative humidity, 450 $\mu mol\ m^{-2}\ s^{-1}$ photons, and a 16-h day/8-h night cycle. The culture solution was refreshed every 2 days.

Experimental Design

The salt treatment condition of bermudagrass was determined based on previous studies (Dudeck et al., 1983; Adavi et al., 2006) through a simple and fast short-term salt treatment experiment (Marcum and Pessarakli, 2006; Chen et al., 2008). A pre-experiment (experiment 1) was conducted to observe the salt-induced damage of bermudagrass supplied with different N levels (2, 5, 10, and 15 mM) grown under different NaCl levels (a

single step—up to 0, 50, 100, and 200 mM, respectively). After 1 month of treatment, the plant growth rate and leaf Na^+ content were detected. According to the results of pre-experiment, 2 mM (deficiency), 10 mM (moderate), and 15 mM (excessive) N levels were chosen to explore the underlying alleviation mechanism of the reduction in N demand under high salt stress (a single step—up to 200 mM NaCl) in the subsequent experiment (experiment 2). After 1-month treatment of experiment 2, the plant growth-related trait (plant height, biomass, turf color, and leaf firing rate), salt-stress-responsive physiological traits (ion content and antioxidant enzyme activities), nitrogen content, chlorophyll content, chlorophyll a fluorescence transient, and quality-related traits of samples were measured and the gene expression involved in N metabolism was analyzed.

Measurements

Plant Growth-Related Trait

Before treatment of experiments 1 and 2, the plant height and biomass of each sample were recorded. After treatment for 1 month, the plant height and the relative increment of biomass were determined according to the method described by Hu et al. (2013). The leaf color (based on a scale of 1–9, with 9 being best) and leaf firing rate were valued based on visual inspection (Fu and Huang, 2001).

Ion Content

After treatment, the plant samples were dried at 130°C for half an hour and then placed at 75°C for 3 days to further determine ion contents. 0.1 g dried sample was finely ground and then digested with 10 mL sulfuric acid using graphite digestion apparatus (SH220N; Hanon, Jinan, Shandong, China) with a temperature of 420°C for 2 h. After digestion, the supernatant was diluted 5–10 times. Na^+ and K^+ contents of each sample were measured by a flame spectrophotometer (F-500; Shanghai, China) based on the method as previously described (Fu and Huang, 2001).

Antioxidant Enzyme Activity

Fully expanded fresh leaves (0.3 g) were ground into powder with liquid nitrogen. Ice-cold phosphate buffer (4 mL; 50 mM, pH 7.8) was added to the powder. All the samples were centrifuged at 12,000 rpm for 20 min at 4°C. The supernatant was collected to measure the activity of antioxidant enzyme based on the method as previously described (Fu and Huang, 2001).

Nitrogen Content and Quality-Related Traits

After the samples were dried, green leaves, old leaves, stems, and roots were separated and ground into powder using a grinder (DFT40; Jiuping, Wuxi, Jiangsu, China). Then, the samples were digested with 10 mL sulfuric acid using graphite digestion apparatus under the temperature of 420°C for 2 h. The nitrogen content and crude protein content of samples were determined by the Kjeldahl apparatus. The Soxhlet extraction method was used to determine the crude fat content. The crude fiber content was measured according to a protocol by the International Standard Organization (2000) intermediate filtration method. The weighed samples were boiled by adding H_2SO_4 followed by NaOH. The extracted residue was dried at 130°C for 2 h (KSL-1200X; KeJing, Hefei, Anhui, China). Then, the dried sample was weighed and put in a furnace (500°C for 3 h). Finally, the crude fiber content of each sample was weighed. The crude ash content was determined by the high-temperature burning method. Samples were weighed and put into the muffle furnace. The temperature of the muffle furnace was set to 580°C for 5 h, and then, the crude ash of each sample was weighed. The quality-related traits were determined according to the AOAC method.

Chlorophyll Content and Chlorophyll a Fluorescence Transient

After treatment, leaves (fresh weight: 0.1 g) were chopped and placed into centrifuge tubes containing 4 mL dimethyl sulfoxide for 3 days. One milliliter of extract and 2 mL of dimethyl sulfoxide were mixed. The UV absorbance of each mixture was measured at 663 and 645 nm wavelengths by a UV spectrophotometer (UV-1700; Meixi, Shanghai, China). Chlorophyll fluorescence transient (OJIP curve) was determined using a pulse-amplitude modulation fluorimeter (PAM 2500, Heinz Walz GmbH). Before measurement, the plants were pre-processed in the dark for half an hour and then exposed to 3,000 μmol photons m^{-2} s^{-1} red light condition. Each treatment was repeated three times. The chlorophyll fluorescence parameters were further determined according to the calculation method described previously (Yusuf et al., 2010).

Gene Expression Analysis

Fresh leaves of each sample were quickly ground into powder with liquid nitrogen. RNA was extracted using RNA pure Plant Kit (Tiangen Biotech, Beijing, China) and then reverse-transcribed using ReverTra Ace qPCR RT Kit (Applied Biosystems, Foster City, CA). Quantitative real-time RT-PCR analysis was performed using SYBR Green real-time PCR master mix (YeSen, Shanghai, China) and ABI real-time PCR system (Applied Biosystems, Foster City, CA) as described before (Hu et al., 2013). The relative expression level of each gene was determined according to the $2^{-\Delta Ct}$ method (Vandesompele et al., 2002). The technical requirement of RT-qPCR fitted MIQE Guidelines (Bustin et al., 2009). Specific primers of selected genes are listed in **Supplementary Table 6**.

Statistical Analysis

Two-way analysis of variance (ANOVA) was used with "N" and "Salt" as two main factors and "N*Salt" as one interaction term. The significance level was set at $P < 0.05$ as a threshold to analyze the significant affection of individual factors and their interactions with detected variables in this study. Histogram results were expressed as mean ± *SD* of four replicates. Tukey's test was used to evaluate the effects of N and Salt application.

RESULTS

Plant Growth and Na^+ Content Under Different Nitrogen and Salt Levels

We first made a pre-experiment to observe the salt-induced damage of bermudagrass supplied with different N levels (2,

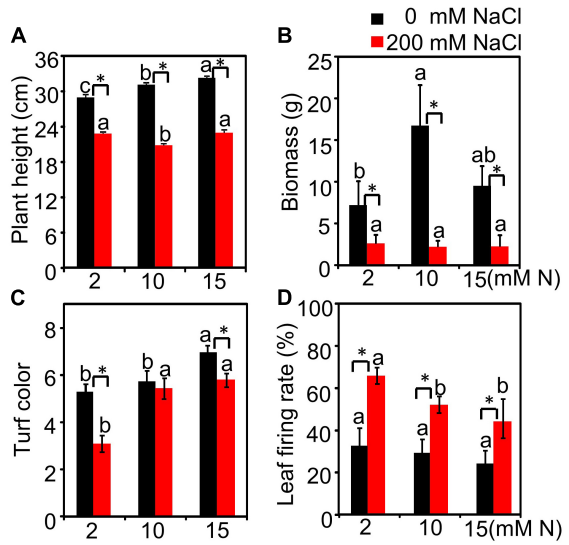

FIGURE 1 | Morphological parameters of bermudagrass grown under different treatments. The plants were cut to the same height and then transferred into different nitrogen levels (2, 10, and 15 mM) under NaCl (0 and 200 mM) treatment in hydroponic culture. After treatment, the plant height **(A)**, biomass **(B)**, leaf color **(C)**, and firing rate **(D)** were measured. Different letters above the columns indicate statistically significant differences at $P < 0.05$ under different N levels with the same NaCl level by Tukey's test. * Shows significant differences ($P < 0.05$) under 200 mM NaCl treatment and 0 mM NaCl condition with the same N level by Tukey's test.

5, 10, and 15 mM) grown under different NaCl levels (0, 50, 100, and 200 mM) (**Supplementary Figure 1**). Under control (0 mM NaCl) and low salt conditions (50 and 100 mM NaCl), the plant height peaked at 15 mM N (**Supplementary Figure 1A**). After a higher NaCl exposure (200 mM NaCl), the plant height showed no significant difference among different N levels (**Supplementary Figures 1A,C**). Moreover, plants grown under 10 mM N had the lowest leaf Na^+ content under 200 mM NaCl treatment (**Figure 1B**). We then chose 2 mM N (deficiency), 10 mM N (moderate), and 15 mM N (excessive) and did a separate experiment to focus on the alleviation mechanism of moderate N application at high salt levels (200 mM NaCl). The results showed a similar tendency to the pre-experiment. Without NaCl treatment, the plant height increased with the increase in N concentration and peaked under 15 mM N, while the biomass peaked under 10 mM N and then declined under 15 mM N. When exposed to 200 mM NaCl, the biomass of plants had no significant alteration among different N levels (**Figure 1B**). Besides, both N and salt significantly affected plant height (**Supplementary Table 1** and **Figures 1A,B**). Plant biomass was significantly affected by salt, but not by N (**Supplementary Table 1** and **Figure 1B**). The interactive effect of N by salt was significant for both plant height and biomass (**Supplementary Table 1**). Moreover, the plants supplied with 10 mM N under salt stress had a similar turf color (**Figure 1C**) and a lower leaf firing rate (**Figure 1D**) compared with the plants supplied with 15 mM N.

Na^+ Content Affected by Nitrogen Levels Under High Salt Stress

The Na^+ and Na^+/K^+ of different tissues detected from different treatments were further measured. The results showed that salt had a significant effect on Na^+ and Na^+/K^+ of all detected tissues, while N had no significant effect on roots Na^+ and Na^+/K^+ of green leaves and roots. The interactive effect of N by salt was significant for Na^+ of green leaves, stems, old leaves, and roots and the Na^+/K^+ of green leaves, old leaves, and roots (**Supplementary Table 2**). Under the high salt condition, the Na^+ contents of green leaves and stems had the lowest values when plants were grown with 10 mM N (**Figures 2A,B**). Moreover, the Na^+ content of old leaves grown under 10 mM N had a significantly lower value compared with that grown under 15 mM N (**Figure 2C**). However, the content of Na^+ of roots showed no significant difference among different N levels (**Figure 2D**). When grown with 10 or 15 mM N, the Na^+/K^+ of green leaves significantly declined compared with 2 mM N under salt stress. However, the Na^+/K^+ of plants grown with 10 or 15 mM N showed no significant difference (**Figure 2E**). Moreover, in the stems, the value of Na^+/K^+ showed no significant difference among different N levels under high salt stress (**Figure 2F**). When grown under 10 mM N, the Na^+/K^+ of old leaves had a significantly lower value compared with that grown under 15 mM N (**Figure 2G**), while the Na^+/K^+ of roots had no significant difference among N levels (**Figure 2H**).

Antioxidant Enzyme Activities Affected by Nitrogen Levels Under High Salt Stress

The antioxidant enzyme activities in the leaves of plants grown under different treatments were also determined. The results showed that, with the increase in N application level, the peroxidase (POD) enzyme activity showed an upward trend and peaked at 10 mM N level followed by a downward trend under both control and salt conditions (**Figure 3A**). Under control conditions, the catalase (CAT) enzyme activity had a higher value when the plants were supplied with 15 mM N compared with 10 mM N (**Figure 3B**). After 200 mM NaCl exposure, the CAT and superoxide dismutase (SOD) enzyme activity of leaves increased slightly when the plants were grown under 10 mM N condition compared with 2 and 15 mM N conditions, but the difference was not significant (**Figures 3B,C**).

Nitrogen and Protein Content Affected by Nitrogen Levels Under High Salt Stress

We then measured the N content and crude protein of green leaves and the residual N and crude protein content in old leaves and stems from different treatments. The results showed that N had a significant effect on N content or crude protein of green leaves and stems but had no significant effect on N content or crude protein content of old leaves. The effect of salt and the interactive effect of N by salt were significant for these variables measured (**Supplementary Table 3**). Without salt treatment, the N content of green leaves increased with the increase in N

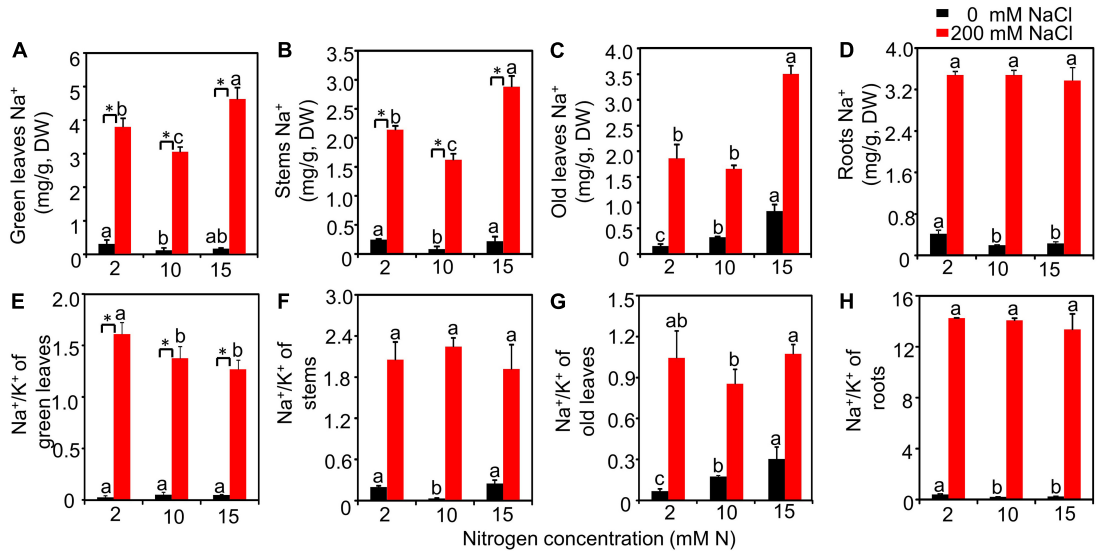

FIGURE 2 | The Na^+ content and Na^+/K^+ of the bermudagrass under different treatments. Na^+ content of green leaves **(A)**, stems **(B)**, old leaves **(C)**, and roots **(D)** and Na^+/K^+ of green leaves **(E)**, stems **(F)**, old leaves **(G)**, and roots **(H)** of plants grown with different nitrogen concentrations exposed to different NaCl levels, respectively. Different letters above the columns indicate statistically significant differences at $P < 0.05$ under different N levels with the same NaCl level by Tukey's test. * Shows significant differences ($P < 0.05$) under 200 mM NaCl treatment and 0 mM NaCl condition with the same N level by Tukey's test.

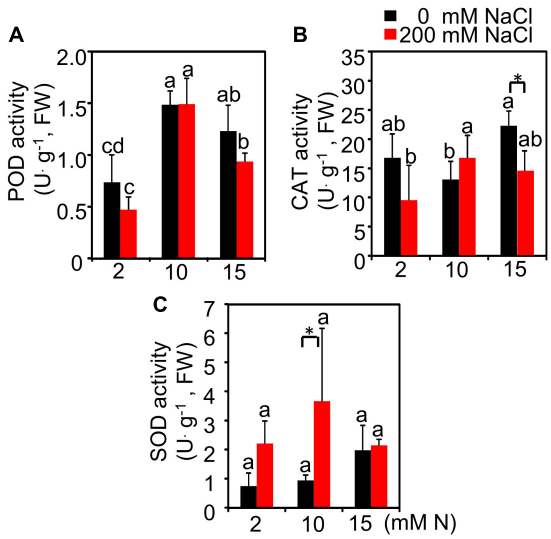

FIGURE 3 | Effect of nitrogen application on the antioxidant enzyme activities of bermudagrass under control and salt treatment. POD activity **(A)**, CAT activity **(B)**, and SOD activity **(C)** in the leaves of plants grown with different nitrogen concentrations (2, 10, and 15 mM N) exposed to control (0 mM NaCl) and salt treatment (200 mM NaCl), respectively. Different letters above the columns indicate statistically significant differences at $P < 0.05$ under different N levels with the same NaCl level by Tukey's test. * Shows significant differences ($P < 0.05$) under 200 mM NaCl treatment and 0 mM NaCl condition with the same N level by Tukey's test.

concentration and peaked under 15 mM N. After 200 mM NaCl exposure, the N content of green leaves peaked under 10 mM N and then declined under 15 mM N (**Figure 4A**). Without NaCl treatment, the residual N content in stems of plants grown with 2 mM N had a significantly lower value than those grown with 10 or 15 mM N. When 200 mM NaCl was added, the residual N content in stems of plants had the lowest value under 10 mM N (**Figure 4B**). Under high salt conditions, the residual N content in old leaves significantly increased under all three N levels. In addition, the residual N content in the stems of plants grown with 2 mM N was lower than those grown with 10 or 15 mM N (**Figure 4C**). The crude protein content of green leaves grown under control conditions peaked under 15 mM N, while it peaked under 10 mM N when the plants were grown under high salt conditions. This trend was consistent with that of the N content of green leaves (**Figure 4D**). The crude protein of stems and old leaves showed a significant increase under a high level of N application (15 or 10 mM) compared with a low level of N application (2 mM). After 200 mM NaCl exposure, although the crude protein of old leaves decreased when plants were grown under higher N levels (10 or 15 mM), the residual crude protein of stems has no significant difference among all three N levels (**Figures 4E,F**).

Nitrogen Metabolism-Related Gene Expression Affected by Nitrogen Levels Under High Salt Stress

The N content and crude protein of green leaves and the residual N and crude protein content in old leaves and stems from different treatments were further determined. N had a significant effect on *NR*, *AMT*, and *GOGAT* expression, while salt only had a significant effect on *NR* expression. The interactive effect of N by salt was significant for the expression of all genes detected (**Supplementary Table 4**). Without NaCl treatment, the

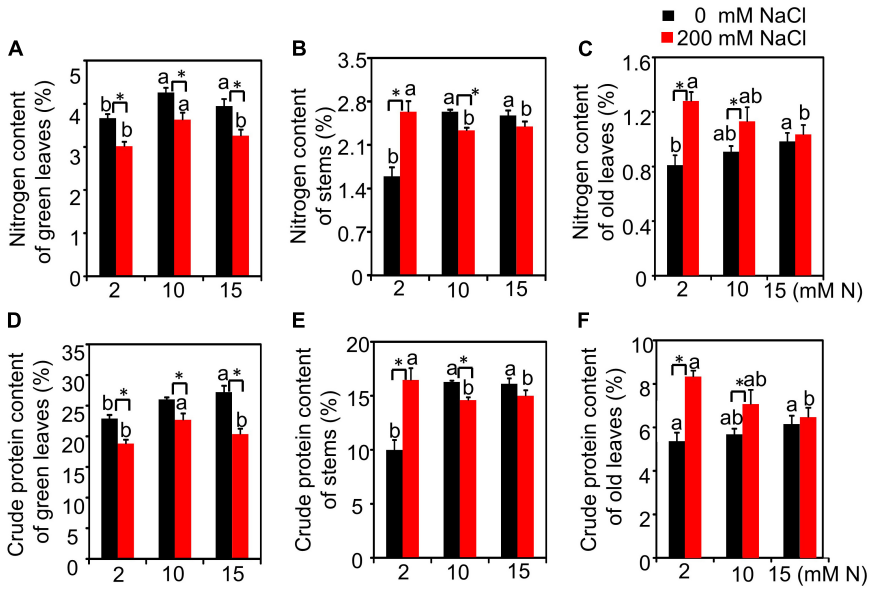

FIGURE 4 | The nitrogen content and crude protein content of bermudagrass under different treatments. Nitrogen content of green leaves **(A)**, stems **(B)**, and old leaves **(C)**. Crude protein of green leaves **(D)**, stems **(E)**, and old leaves **(F)**. Different letters above the columns indicate statistically significant differences at $P < 0.05$ under different N levels with the same NaCl level by Tukey's test. * Shows significant differences ($P < 0.05$) under 200 mM NaCl treatment and 0 mM NaCl condition with the same N level by Tukey's test.

expression of *NR* increased with the increase in N concentration and peaked at 15 mM N. After 200 mM NaCl exposure, although *NR* expression was inhibited by salt, there was no significant difference among different N concentrations (**Figure 5A**). *AMT* gene expression showed no significant difference among plants grown with different N concentrations under control conditions. Under high salt stress, the expression level of *AMT* showed an increased trend compared with the control condition when plants were grown with 10 mM N and the expression level was significantly higher than the other two N concentrations. On the contrary, the expression level of *AMT* decreased under 2 or 15 mM N (**Figure 5B**) after 200 mM NaCl exposure. Under control conditions, the expression of *GS* and *GOGAT* both peaked under 15 mM N. Salt stress significantly induced the expression of GS when supplied with 10 mM N, while the expression of *GS* was reduced significantly by salt when the plants were supplied with 15 mM N (**Figure 5C**). Moreover, under high salt stress conditions, the expression of *GS* and *GOGAT* both peaked under 10 mM N and then significantly declined under 15 mM N (**Figures 5C,D**).

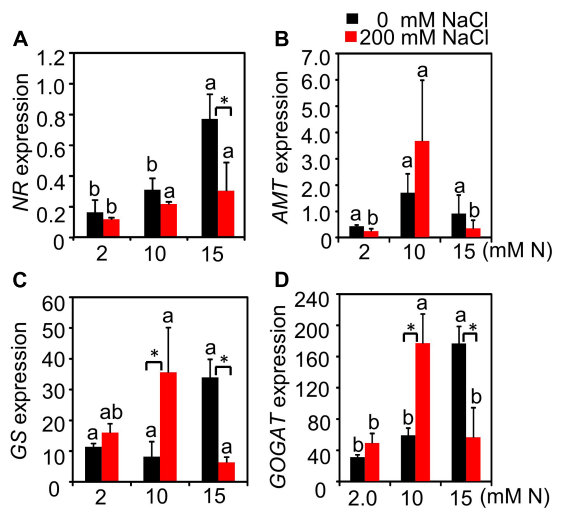

FIGURE 5 | Relative expression level of N metabolism-related genes of bermudagrass under different treatments. The expression level of *NR* **(A)**, *AMT* **(B)**, *GS* **(C)**, and *GOGAT* **(D)** in the leaves of bermudagrass grown under different nitrogen concentrations exposed to different NaCl levels (0 and 200 mM NaCl), respectively. Different letters above the columns indicate statistically significant differences at $P < 0.05$ under different N levels with the same NaCl level by Tukey's test. * Shows significant differences ($P < 0.05$) under 200 mM NaCl treatment and 0 mM NaCl condition with the same N level by Tukey's test.

Chlorophyll Fluorescence Affected by Nitrogen Levels Under High Salt Stress

The total chlorophyll content of leaves grown with different treatments was measured. Both N and salt significantly affected total chlorophyll content. The interactive effect of N by salt was not significant on total chlorophyll content (**Supplementary Table 1**). NaCl exposure did not significantly affect chlorophyll content as compared to the control condition (**Figures 6A,B**). However, the chlorophyll a and total chlorophyll content of leaves reached the highest level when the plants were grown under 10 mM N and then decreased slightly under 15 mM N with or without NaCl treatment (**Figures 6A,B**).

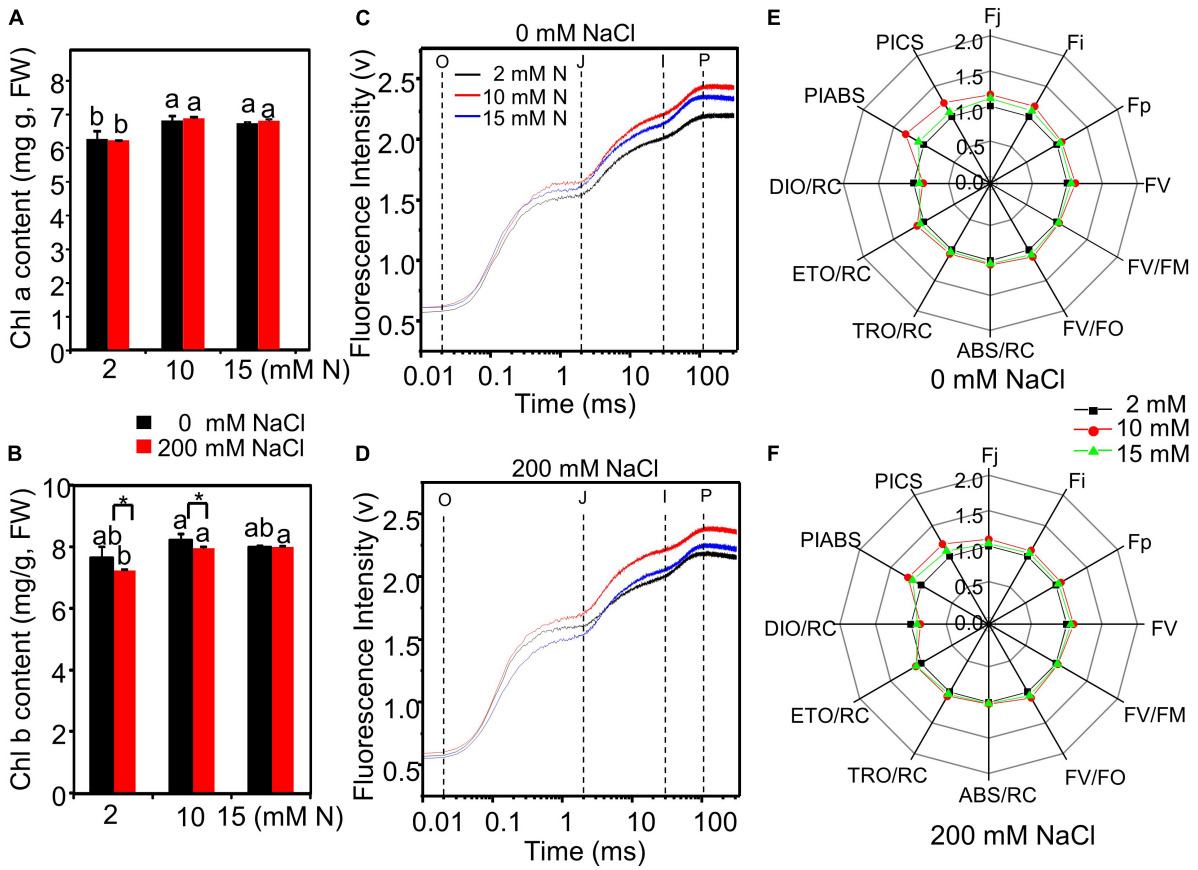

FIGURE 6 | Chlorophyll fluorescence in the leaves of bermudagrass grown with different nitrogen levels under control and salt treatment. Chlorophyll a content **(A)** and total chlorophyll content **(B)** and OJIP curve in the leaves of bermudagrass grown with different nitrogen levels (2, 10, and 15 mM) under 0 mM **(C)** and 200 mM NaCl **(D)** concentrations, respectively (O: at 0.2 ms; J: at 2 ms; I: at 30 ms; P: at maximum fluorescence position). "Radar plots" of picked parameters characterizing the influence of nitrogen concentration on PS II of bermudagrass grown under 0 mM **(E)** and 200 mM NaCl **(F)**, respectively. The parameters of plants grown under 2 mM N were set as control. Control = 1. * Shows significant differences ($P < 0.05$) under 200 mM NaCl treatment and 0 mM NaCl condition with the same N level by Tukey's test.

Then, the impact of N levels on the photochemistry of photosystem II (PS II) of NaCl-treated bermudagrass was determined through chlorophyll a fluorescence transient–JIP test. Under control or salt condition, the fluorescence of the I and P phases of leaves grown with 10 mM N was stronger than those grown with 15 mM N, respectively (**Figure 6**). In particular, the OJIP curve was much higher when plants were exposed to salt under 10 mM N compared with plants grown with 15 mM N under control conditions (**Figures 6C,D**). The chlorophyll fluorescence parameters were further determined. Under control and salt conditions, the PI_{ABS} and PI_{CS} values, representing the overall activity of PSII, peaked under 10 mM N (**Figures 6E,F** and **Supplementary Figures 2A,B**). The absorption flux per RC (QA-reducing PSII reaction center) (ABS/RC) (**Figure 6** and **Supplementary Figure 2C**), trapped energy flux per RC (TRo/RC) (**Figure 6** and **Supplementary Figure 2D**), and electron transport flux per RC (ETo/RC) (**Figure 6** and **Supplementary Figure 2E**) of plants grown with 10 mM N had a higher level or were similar to the levels of those grown with 2 or 15 mM N under control and salt conditions. On the contrary, dissipated energy flux per RC (DIo/RC) had a lower level under 10 mM N compared with other N levels under control and salt conditions (**Figures 6E,F** and **Supplementary Figure 2F**).

Quality-Related Traits Affected by Nitrogen Levels Under High Salt Stress

Salt had a significant effect on crude fat, crude fiber, and crude ash content, while N had a significant effect on crude fiber and crude ash content, but not crude fat. The interactive effect of N by salt was significant for all quality-related traits detected (**Supplementary Table 5**). Without salt treatment, the increased N application significantly decreased the crude fat content. The crude fat content had the highest value when plants were grown under 2 mM N compared with 10 or 15 mM N. After 200 mM NaCl exposure, the crude fat content significantly declined under 2 mM N, while the crude fat content was not obviously affected under 10 or 15 mM N (**Figure 7A**). Under 0 mM NaCl condition, the crude fiber content had the lowest value under 10 mM N.

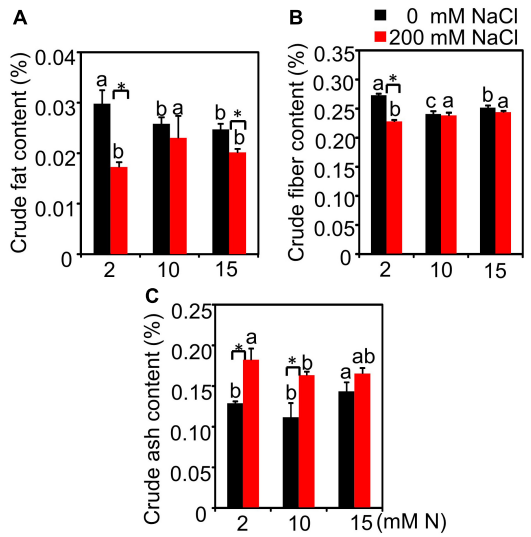

FIGURE 7 | The quality-related traits of bermudagrass under different treatments. Crude fat content **(A)**, crude fiber content **(B)**, and crude ash content **(C)** in the leaves of plants grown with different nitrogen concentrations (2, 10, and 15 mM N) exposed to different NaCl levels (0 and 200 mM NaCl), respectively. Different letters above the columns indicate statistically significant differences at $P < 0.05$ under different N levels with the same NaCl level by Tukey's test. * Shows significant differences ($P < 0.05$) under 200 mM NaCl treatment and 0 mM NaCl condition with the same N level by Tukey's test.

When exposed to NaCl, the crude fiber content of plants grown under 10 mM N was higher than those grown under 2 mM N. However, the value showed no significant difference with plants grown under 15 mM N (**Figure 7B**). Moreover, the ash content had the lowest value when plants were grown with 10 mM N under both control and salt treatment conditions (**Figure 7C**).

DISCUSSION

Salt-induced inhibition, such as ion toxicity, osmotic effects, and nutrient imbalance, can be alleviated by the moderate use of N fertilizer (Chen et al., 2010; Fan et al., 2013; Duan and Chang, 2017). In forage, such as pasture grass, moderate N application has a positive effect on plant growth and yield production (Irshad et al., 2009; Shao et al., 2020). Due to possible reduction in the N requirement under higher salt stress in forage bermudagrass (10 mM N under high salt stress compared with 15 mM N under control condition) according to the plant growth rate, Na^+ content, and antioxidant enzyme activity alteration, we mainly focused on exploring the underlying mitigation mechanism after moderate N application under high salt stress.

Salt stress can affect N uptake in plants (Murtaza et al., 2013). The ammonium N (NH_4^+) transported by AMT can be directly assimilated by plants (Giagnoni et al., 2016). In forage bermudagrass, after a high level of NaCl exposure, the expression of *AMT* had the highest value when plants were grown with 10 mM N compared with other N levels (**Figure 5B**). Previous studies reported that *AMT* gene expression was downregulated by salt in *Brassica juncea* (Goel and Singh, 2015), while most *AMT*s were upregulated in the moderate salt-treated roots of *Populus simonii* (Zhang et al., 2014). The different expression alteration of *AMT*s in different species might be due to the differential interaction of N and salt levels. In forage bermudagrass, N application could promote the expression of *AMT* within a certain range, suggesting that excessive NH_4^+ application had no positive effect on N absorption by upregulating the *AMT* expression under high salt conditions. Moreover, moderate N application without excess under high salt stress could help forage bermudagrass maintain or promote the expression level of N assimilation-related enzymes, such as NR, GS, and GOGAT, which can be affected by salt (Wang et al., 2012; Parul et al., 2015; **Figure 5**). Moreover, the green leaves N content also had the highest value when plants were supplied with 10 mM N, but not 15 mM N (**Figures 4A,B**) after NaCl exposure, which was consistent with the trend of N metabolism-related gene expression. Besides, the highest value of green leaves N content and lowest value of stems N content supplied with 10 mM N suggested that the moderate N application might promote the N accumulation in green leaves and reduce the residual N in stems or old leaves, which played a critical role in the rational distribution of N under salt stress.

N is a structural element of chlorophyll, affecting the formation of chloroplasts and the accumulation of chlorophyll in plants (Xu et al., 2012). In this study, N application significantly increased the chlorophyll a and total chlorophyll content of bermudagrass (**Figures 6A,B** and **Supplementary Table 1**). However, the chlorophyll content could not increase in proportion when N was applied over 10 mM, which was consistent with previous studies (Zhang et al., 2013; Yang et al., 2015; Shao et al., 2020). N deficiencies can also decrease leaf area and intensity of photosynthesis (Zhang et al., 2013). Previous studies reported that N application significantly improved physiological parameters and elevated the photosynthetic capacity of leaves in some plant species (Siddiqui et al., 2010; Zhang et al., 2013). However, other studies showed that the promotion of N application on photosynthetic characteristics might also have concentration effects. For instance, N fertilizer can improve the photosynthetic characteristics of soybeans and ryegrass, but their effects were gradually inhibited or decreased with the increase in N fertilization application level (Zhang et al., 2013; Shao et al., 2020). In our study, the chlorophyll fluorescence intensity of bermudagrass leaves grown under moderate N (10 mM) was highest compared with 15 or 2 mM N, especially under high salt conditions (**Figure 6**). Under salt stress, excessive application of N could not promote but weaken the fluorescent transients of bermudagrass, especially the J (2 ms) and P (30 ms) steps, suggesting that N over application under salt stress might lead to the photosynthetic electron transport traffic jam, especially beyond Q_A^- (**Figure 6**). Moreover, the optimum amount of N might promote primary photochemical reactions of PSII under high salt stress. The PI_{ABS} and PICS value, which could accurately reflect the state of plant photosynthetic apparatus, peaked under 10 mM N (**Figure 6E**), indicating that N could promote the primary photochemical reactions of PSII in the waterside. Changes in various quantum efficiencies per reaction

center reflected the elevated absorption and transformation of light energy and the reduction in heat dissipation of leaves after appropriate N application (**Figures 6E,F**; Yusuf et al., 2010).

For forage bermudagrass, the yield and forage quality maintenance should be taken into consideration when evaluating the optimal N application under salt stress. We noticed that different N application levels had no significantly different effects on biomass under NaCl treatment, which is consistent with the previous study in other plants (Jia et al., 2017). However, the plant height had a lower value when plants were grown with 10 mM N compared with 15 mM N. The reason might be because those effectors contributing to the biomass, such as the decrease in firing rate (**Figure 1D**), might make up for the possible biomass reduction. Nitrogen application has critical effects on forage quality traits (e.g., crude protein, crude fat, and crude fiber) (Collins, 1991). In this study, under salt stress, when 10 mM N was added, the crude protein of green leaves had the highest value compared with 15 mM N (**Figure 4D**). The similar tendency of N content and crude protein content suggested that N might be redistributed among different tissues under salt stress and more N might be transferred into the green leaves to synthesize crude protein after being supplied with moderate N in bermudagrass. The constituents of crude fiber and crude cash are both the most remarkable factors to evaluate forage quality, which can limit forage intake and digestibility (Bruun et al., 2010; Shaer, 2010; Wolf et al., 2012). In this study, 10 mM N application could maintain crude fiber content at a lower level with the lowest crude ash content under high salt conditions, suggesting better maintenance of forage quality when supplied with moderate N.

Together with the previous studies, N requirements for plants in a saline environment might be inconsistent with those in the normal environment and salt stress might lead to the reduction in nutrients absorbed from the surrounding environment (Shenker et al., 2003; Ramos et al., 2012; Zhang et al., 2012). For forage bermudagrass, the optimal N application under salt stress should be considered in terms of plant growth, salt-stress-responsive physiological parameters, and nutrient value maintenance. Moderate reduction in N application had the optimal effect on alleviating the damage of high salt stress to forage bermudagrass through regulating numerous interconnected physico-chemical activities. These results obtained in this study are important for the agricultural practice to guide rational N fertilization application rather than in excess on bermudagrass, especially under severe salinity environment to reduce N leaching and environmental burden.

DATA AVAILABILITY STATEMENT

The original contributions presented in the study are included in the article/**Supplementary Material**, further inquiries can be directed to the corresponding author/s.

AUTHOR CONTRIBUTIONS

AS and HW performed the experimental design and data analysis. AS wrote the first draft of the manuscript. XX and XL performed the experiments. EA modified the manuscript draft. JF supervised all the experiments. All authors contributed to seen and the study conception and design and approved the manuscript.

FUNDING

This work was supported by the National Key R&D Program of China (2019YFD0900702) and the Agricultural Variety Improvement Project of Shandong (2019LZGC010).

ACKNOWLEDGMENTS

We thank the National Key R&D Program of China and the Agricultural Variety Improvement Project of Shandong for the financial support.

SUPPLEMENTARY MATERIAL

The Supplementary Material for this article can be found online at: https://www.frontiersin.org/articles/10.3389/fpls.2022.896358/full#supplementary-material

REFERENCES

Adavi, Z., Razmjoo, K., and Mobli, M. (2006). Salinity tolerance of bermudagrass (*Cynodon spp*. L. C. Rich) cultivars and shoot Na, K and Cl concentration under a high saline environment. *J. Hortic. Sci. Biotech.* 81, 1074–1078. doi: 10.1080/14620316.2006.11512174

Ahanger, M. A., Aziz, U., Alsahli, A. A., Alyemeni, M. N., and Ahmad, P. (2019). Influence of exogenous salicylic acid and nitric oxide on growth, photosynthesis, and Ascorbate-Glutathione Cycle in salt stressed *Vigna angularis*. *Biomolecules* 10:42. doi: 10.3390/biom10010042

Ahmad, P., Tripathi, D. K., Deshmukh, R., Singh, V. P., and Corpas, F. J. (2019). Revisiting the role of ROS and RNS in plants under changing environment. *Environ. Exp. Bot.* 161, 1–3. doi: 10.1016/j.envexpbot.2019.02.017

Akram, M., Ashraf, M. Y., Jamil, M., Iqbal, R. M., Nafees, M., and Khan, M. A. (2011). Nitrogen application improves gas exchange characteristics and chlorophyll fluorescence in maize hybrids under salinity conditions. *Russ. J. Plant Physl.* 58, 394–401. doi: 10.1134/s1021443711030022

Amin, I., Rasool, S., Mir, M. A., Wani, W., Masoodi, K. Z., and Ahmad, P. (2021). Ion homeostasis for salinity tolerance in plants: a molecular approach. *Physiol. Plant.* 171, 578–594. doi: 10.1111/ppl.13185

Baby, J., and Jini, D. (2010). Insight into the role of antioxidant enzymes for salt tolerance in plants. *Int. J. Plant Sci.* 6, 456–464. doi: 10.3923/ijb.2010.456.464

Bruun, S., Jensen, J. W., Magid, J., Lindedam, J., and Engelsen, S. R. B. (2010). Prediction of the degradability and ash content of wheat straw from different cultivars using near infrared spectroscopy. *Ind. Crop. Prod.* 31, 321–326. doi: 10.1016/j.indcrop.2009.11.011

Bustin, S. A., Benes, V., Garson, J. A., Hellemans, J., Huggett, J., Kubista, M., et al. (2009). The MIQE guidelines: minimum information for publication of quantitative realtime PCR experiments. *Clin. Chem.* 55, 611–622. doi: 10.1373/clinchem.2008.112797

Chen, J. B., and Liu, J. X. (2012). Salinity tolerance evaluation and mechanisms in bermudagrass (*Cynodon* spp.). *Acta Pratacul. Turae Sin.* 21, 302–310.

Chen, J. B., Yan, J., Zhang, T. T., and Liu, J. X. (2008). Growth responses of four warm season turfgrasses to long-term salt stress. *Acta Pratacul. Turae Sin.* 17, 30–36.

Chen, W., Hou, Z., Wu, L., Liang, Y., and Wei, C. (2010). Effects of salinity and nitrogen on cotton growth in arid environment. *Plant Soil* 326, 61–73. doi: 10.13227/j.hjkx.201910137

Collins, M. (1991). Nitrogen effects on yield and forage quality of perennial ryegrass and tall fescue. *Agron. J.* 83, 588–595. doi: 10.2134/agronj1991.00021962008300030017x

Dechorgnat, J., Francis, K. L., Dhugga, K. S., Rafalski, J. A., Tyerman, S. D., and Kaiser, B. N. (2019). Tissue and nitrogen-linked expression profiles of ammonium and nitrate transporters in maize. *BMC Plant Biol.* 19:206. doi: 10.1186/s12870-019-1768-0

Deinlein, U., Stephan, A. B., Horie, T., Luo, W., Xu, G., and Schroeder, J. I. (2014). Plant salt-tolerance mechanisms. *Trends Plant Sci.* 19, 371–379.

Dluzniewska, P., Geßler, A., Dietrich, H., Schnitzler, J. P., and Rennenberg, H. (2007). Nitrogen uptake and metabolism in *Populus* × *canescens* as affected by salinity. *New Phytol.* 173, 279–293. doi: 10.1111/j.1469-8137.2006.01908.x

Duan, M., and Chang, S. X. (2017). Nitrogen fertilization improves the growth of lodgepole pine and white spruce seedlings under low salt stress through enhancing photosynthesis and plant nutrition. *For. Ecol. Manag.* 404, 197–204. doi: 10.1016/j.foreco.2017.08.045

Dudeck, A. E., Singh, S., Giordano, C. E., and Nell, T. (1983). Effects of sodium chloride on *Cynodon turfgrasses*. *Agron. J.* 75, 927–930. doi: 10.2134/agronj1983.00021962007500060017x

Esmaili, E., Kapourchal, S., Malakouti, M., and Homaee, M. (2005). Interactive effect of salinity and two nitrogen fertilizers on growth and composition of sorghum. *Plant Soil Environ.* 54, 537–546. doi: 10.17221/425-pse

Fan, H., Meng, G. H., Cheng, R. R., Li, L., Yun, X., and Wang, B. S. (2013). Effect of different nitrogen levels on the photosynthesis and growth of sweet *Sorghum* seedlings under salt stress. *Adv. Mat. Res.* 72, 4352–4357. doi: 10.4028/www.scientific.net/amr.726-731.4352

Fu, J., and Huang, B. (2001). Involvement of antioxidant and lipid peroxidation in the adaptation of two cool-season grasses to localized drought stress. *Environ. Exp. Bot.* 45, 105–114. doi: 10.1016/s0098-8472(00)00084-8

Giagnoni, L., Pastorelli, R., Mocali, S., Arenella, M., and Renella, G. (2016). Availability of different nitrogen forms changes the microbial communities and enzyme activities in the rhizosphere of maize lines with different nitrogen use efficiency. *Appl. Soil Ecol.* 98, 30–38. doi: 10.1016/j.apsoil.2015.09.004

Goel, P., and Singh, A. K. (2015). Abiotic stresses downregulate key genes involved in nitrogen uptake and assimilation in *Brassica juncea* L. *PLoS One* 10:e0143645.

Hoai, N. T. T., Shim, I. S., Kobayashi, K., and Kenji, U. (2003). Accumulation of some nitrogen compounds in response to salt stress and their relationships with salt tolerance in rice (*Oryza sativa* L.) seedlings. *Plant Growth Regul.* 41, 159–164.

Homaee, M., Feddes, R. A., and Dirksen, C. (2002). A macroscopic water extraction model for nonuniform transient salinity and water stress. *Soil Sci. Soc. Am. J.* 66, 1764–1772. doi: 10.2136/sssaj2002.1764

Hu, T., Hu, L., Zhang, X., Zhang, P., Zhao, Z., and Fu, J. (2013). Differential responses of CO2 assimilation, carbohydrate allocation and gene expression to NaCl stress in perennial ryegrass with different salt tolerance. *PLoS One* 8:e66090. doi: 10.1371/journal.pone.0066090

International Standard Organization (2000). *Animal Feeding Stuffs – Determination of Crude Fiber Content. Method With Intermediate Filtration. ISO 6865:2000.* Geneva: ISA.

Irshad, M., Eneji, A. E., Khattak, R. A., and Khan, A. (2009). Influence of nitrogen and saline water on the growth and partitioning of mineral content in maize. *J. Plant Nutr.* 32, 458–469. doi: 10.1080/01904160802660768

Jia, J., Huang, C., Bai, J., Zhang, G., Zhao, Q., and Wen, X. (2017). Effects of drought and salt stresses on growth characteristics of euhalophyte *Suaeda salsa* in coastal wetlands. *Phys. Chem. Earth.* 103, 68–74. doi: 10.1016/j.pce.2017.01.002

Khan, M. G., and Srivastava, H. S. (1998). Changes in growth and nitrogen assimilation in maize plants induced by NaCl and growth regulators. *Biol. Plant.* 41, 93–99. doi: 10.1023/a:1001768601359

Kishorekumar, R., Bulle, M., Wany, A., and Gupta, K. J. (2020). "An overview of important enzymes involved in nitrogen assimilation of plants," in *Methods in Molecular Biology*, Vol. 2057, ed. K. Gupta (New York, NY: Humana). doi: 10.1007/978-1-4939-9790-9_1

Lacerda, C. F., Ferreira, J. F. S., Liu, X., and Suarez, D. L. (2016). Evapotranspiration as a criterion to estimate nitrogen requirement of maize under salt stress. *J. Agro. Crop Sci.* 202, 192–202. doi: 10.1111/jac.12145

Maksup, S., Sengsai, S., Laosuntisuk, K., Asayot, J., and Pongprayoon, W. (2020). Physiological responses and the expression of cellulose and lignin associated genes in *Napier grass* hybrids exposed to salt stress. *Acta Physiol. Plant.* 42:109.

Mansour, M. M. F. (2000). Nitrogen containing compounds and adaptation of plants to salinity stress. *Biol. Plant.* 43, 491–500. doi: 10.1023/a:1002873531707

Marcum, K. B., and Pessarakli, M. (2006). Salinity tolerance and salt gland excretion efficiency of bermudagrass turf cultivar. *Crop Sci.* 46, 2571–2574. doi: 10.2135/cropsci2006.01.0027

Maas, E. V., and Hoffman, G. J. (1977). Crop salt tolerance–current assessment. *J. Irrig. Drain. Div.* 103, 115–134. doi: 10.1061/JRCEA4.0001137

Munns, R., and Tester, M. (2008). Mechanisms of salinity tolerance. *Annu. Rev. Plant Biol.* 59, 651–681.

Murtaza, B., Usman, Y., and Saqib, M. (2013). "Nitrogen-Use-Efficiency (NUE) in plants under NaCl stress," in *Salt stress in plants*, eds P. Ahmad, M. M. Azooz, and M. N. V. Prasad (New York, NY: Springer), 415–437. doi: 10.1080/15592324.2017.1297000

Parul, G., Kumar, S. A., and Kumar, T. P. (2015). Abiotic stresses downregulate key genes involved in nitrogen uptake and assimilation in *Brassica juncea* L. *PLoS One* 10:e0143645.

Ramos, T. B., Šimùnek, J., Gonçalves, M. C., Martins, J. C., Prazeres, A., and Pereira, L. S. (2012). Two-dimensional modeling of water and nitrogen fate from sweet sorghum irrigated with fresh and blended saline waters. *Agr. Water Manage.* 111, 87–104. doi: 10.1016/j.agwat.2012.05.007

Shaer, H. M. E. (2010). Halophytes and salt-tolerant plants as potential forage for ruminants in the Near East region. *Small Ruminant Res.* 91, 3–12. doi: 10.1016/j.smallrumres.2010.01.010

Shao, A., Sun, Z. C., Fan, S. G., Xu, X., Wang, W., Amombo, E., et al. (2020). Moderately low nitrogen application mitigates the negative effects of salt stress on annual ryegrass seedlings. *PeerJ* 8:e10427. doi: 10.7717/peerj.10427

Shenker, M., Ben-Gal, A., and Shani, U. (2003). Sweet corn response to combined nitrogen and salinity environmental stresses. *Plant Soil* 256, 139–147. doi: 10.1023/a:1026274015858

Siddiqui, M. H., Mohammad, F., Khan, M. N., Ha-Whaibi, M., and Bahkali, A. (2010). Nitrogen in relation to photosynthetic capacity and accumulation of osmoprotectant and nutrients in *Brassica* genotypes grown under salt stress. *Agr. Sci. China* 9, 671–680. doi: 10.1016/s1671-2927(09)60142-5

Singh, M., Singh, V. P., and Prasad, S. M. (2016). Responses of photosynthesis, nitrogen and proline metabolism to salinity stress in *Solanum lycopersicum* under different levels of nitrogen supplementation. *Plant Physiol. Bioch.* 109, 72–83. doi: 10.1016/j.plaphy.2016.08.021

Song, J., Ding, X., Feng, G., and Zhang, F. (2006). Nutritional and osmotic roles of nitrate in a euhalophyte and a xerophyte in saline conditions. *New Phytol.* 171, 357–366. doi: 10.1111/j.1469-8137.2006.01748.x

Soussi, M., Ocaña, A., and Lluch, C. (1998). Effects of salt stress on growth, photosynthesis and nitrogen fixation in chick-pea (L.). *J. Exp. Bot.* 49, 1329–1337. doi: 10.1093/jxb/49.325.1329

Sudmalis, D., Silva, P., Temmink, H., Bijmans, M. M., and Pereira, M. A. (2018). Biological treatment of produced water coupled with recovery of neutral lipids. *Water Res.* 147, 33–42. doi: 10.1016/j.watres.2018.09.050

Teh, C. Y., Shaharuddin, N. A., Ho, C. L., and Mahmood, M. (2016). Exogenous proline significantly affects the plant growth and nitrogen assimilation enzymes activities in rice (*Oryza sativa*) under salt stress. *Acta. Physiol. Plant* 38, 1–10.

Vandesompele, J., Preter, K. D., Pattyn, F., Poppe, B., Roy, N. V., Paepe, A. D., et al. (2002). Accurate normalization of real-time quantitative RT-PCR data by geometric averaging of multiple internal control genes. *Genome Biol.* 3:research0034.1. doi: 10.1186/gb-2002-3-7-research0034

Villa, M., Ulery, A., Catalan-Valencia, E., and Remmenga, M. (2003). Salinity and nitrogen rate effects on the growth and yield of Chile Pepper plants. *Soil Sci. Soc. Amer. J.* 6, 1781–1789. doi: 10.2136/sssaj2003.1781

Wang, H., Zhang, M., Guo, R., Shi, D., Liu, B., Lin, X., et al. (2012). Effects of salt stress on ion balance and nitrogen metabolism of old and young leaves in rice (*Oryza sativa* L.). *BMC Plant Biol.* 12:194. doi: 10.1186/1471-2229-12-194

Wolf, S., Hématy, K., and Höfte, H. (2012). Growth control and cell wall signaling in plants. *Annu. Rev. Plant Biol.* 63, 381–407. doi: 10.1146/annurev-arplant-042811-105449

Xu, G., Fan, X., and Miller, A. J. (2012). Plant nitrogen assimilation and use efficiency. *Annu. Revi Plant Biol.* 63, 153–182. doi: 10.1146/annurev-arplant-042811-105532

Yang, J., Shi, S., Gong, W., Du, L., Ma, Y. Y., Zhu, B., et al. (2015). Application of fluorescence spectrum to precisely inverse paddy rice nitrogen content. *Plant Soil Environ.* 61, 182–188. doi: 10.17221/7/2015-pse

Yusuf, M. A., Kumar, D., Rajwanshi, R., Strasser, R. J., Tsimilli-Michael, M., Govindjee et al. (2010). Overexpression of γ- tocopherol methyl transferase gene in transgenic *Brassica juncea* plants alleviates abiotic stress: physiological and chlorophyll a fluorescence measurements. *Biochim. Biophys. Acta* 1797, 1428–1438. doi: 10.1016/j.bbabio.2010.02.002

Zhang, C., Meng, S., Li, Y., and Zhao, Z. (2014). Net NH_4^+ and NO_3^- fluxes, and expression of NH_4^+ and NO_3^- transporter genes in roots of *Populus simonii* after acclimation to moderate salinity. *Trees* 28, 1813–1821. doi: 10.1007/s00468-014-1088-9

Zhang, D., Li, W., Xin, C., Tang, W., Eneji, A. E., and Dong, H. (2012). Lint yield and nitrogen use efficiency of field-grown cotton vary with soil salinity and nitrogen application rate. *Field Crop. Res.* 138, 63–70. doi: 10.1016/j.fcr.2012.09.013

Zhang, X., Huang, G., Bian, X., and Zhao, Q. (2013). Effects of root interaction and nitrogen fertilization on the chlorophyll content, root activity, photosynthetic characteristics of intercropped soybean and microbial quantity in the rhizosphere. *Plant Soil Environ.* 59, 80–88. doi: 10.17221/613/2012-pse

Zhao, C., Zhang, H., Song, C., Zhu, J. K., and Shabala, S. (2020). Mechanisms of plant responses and adaptation to soil salinity. *Innovation* 1:100017. doi: 10.1016/j.xinn.2020.100017

Zubillaga, M. M., Aristi, P. J., and Lavado, S. R. (2002). Effect of phosphorus and nitrogen fertilization on sunflower (*Helianthus annus* L.) nitrogen uptake and yield. *J. Agron. Crop Sci.* 188, 267–274. doi: 10.1046/j.1439-037x.2002.00570.x

Conflict of Interest: The authors declare that the research was conducted in the absence of any commercial or financial relationships that could be construed as a potential conflict of interest.

Publisher's Note: All claims expressed in this article are solely those of the authors and do not necessarily represent those of their affiliated organizations, or those of the publisher, the editors and the reviewers. Any product that may be evaluated in this article, or claim that may be made by its manufacturer, is not guaranteed or endorsed by the publisher.

frontiers | Frontiers in Plant Science

ORIGINAL RESEARCH
published: 06 May 2022
doi: 10.3389/fpls.2022.906018

Zoysia japonica Chlorophyll *b* Reductase Gene *NOL* Participates in Chlorophyll Degradation and Photosynthesis

Jin Guan[1], Ke Teng[2], Yuesen Yue[2], Yidi Guo[1], Lingyun Liu[1], Shuxia Yin[1] and Liebao Han[1]**

[1]College of Grassland Science, Beijing Forestry University, Beijing, China, [2]Institute of Grassland, Flowers, and Ecology, Beijing Academy of Agriculture and Forestry Sciences, Beijing, China

The degradation of chlorophyll is of great significance to plant growth. The chlorophyll *b* reductase NOL (NYC1-like) is in charge of catalyzing the degradation of chlorophyll *b* and maintaining the stability of the photosystem. However, the molecular mechanisms of NOL-mediated chlorophyll degradation, senescence, and photosynthesis and its functions in other metabolic pathways remain unclear, especially in warm-season turfgrass. In this study, *ZjNOL* was cloned from *Zoysia japonica*. It is highly expressed in senescent leaves. Subcellular localization investigation showed ZjNOL is localized in the chloroplast and the bimolecular fluorescence complementation (BiFC) results proved ZjNOL interacts with ZjNYC1 *in vivo*. *ZjNOL* promoted the accumulation of abscisic acid (ABA) and carbohydrates, and the increase of *SAG14* at the transcriptional level. *ZjNOL* simultaneously led to the excessive accumulation of reactive oxygen species (ROS), the activation of antioxidant enzymes, and the generation of oxidative stress, which in turn accelerated senescence. Chlorophyll fluorescence assay (JIP-test) analysis showed that *ZjNOL* inhibited photosynthetic efficiency mainly through damage to the oxygen-evolving complex. In total, these results suggest that *ZjNOL* promotes chlorophyll degradation and senescence and negatively affects the integrity and functionality of the photosystem. It could be a valuable candidate gene for genome editing to cultivate *Z. japonica* germplasm with prolonged green period and improved photosynthesis efficiency.

Keywords: chlorophyll *b* reductase, chlorophyll degradation, photosynthesis, chlorophyll fluorescence, *Zoysia japonica*

OPEN ACCESS

Edited by:
Jing Zhang,
Nanjing Agricultural University, China

Reviewed by:
Xunzhong Zhang,
Virginia Tech, United States
Guohui Yu,
Nanjing Agricultural University, China
David Jespersen,
University of Georgia, United States

***Correspondence:**
Shuxia Yin
yinsx369@bjfu.edu.cn
Liebao Han
hanliebao@163.com

Specialty section:
This article was submitted to Plant Abiotic Stress, a section of the journal Frontiers in Plant Science

Received: *28 March 2022*
Accepted: *20 April 2022*
Published: *06 May 2022*

Citation:
Guan J, Teng K, Yue Y, Guo Y, Liu L, Yin S and Han L (2022) Zoysia japonica Chlorophyll b Reductase Gene NOL Participates in Chlorophyll Degradation and Photosynthesis. Front. Plant Sci. 13:906018. doi: 10.3389/fpls.2022.906018

INTRODUCTION

Commonly known as a warm-season turfgrass, *Zoysia japonica* (2n = 4x = 40) has many remarkable characteristics, including minimal maintenance, excellent tolerance to drought, salinity, and freezing, good ability to conserve water and soil, and excellent traffic tolerance (Patton and Reicher, 2007; Teng et al., 2017, 2018). Nevertheless, the short green period and unaesthetic appearance during senescence hamper its further popularization and utilization (Teng et al., 2016, 2021b). Therefore, it is critical to interpret the molecular regulation mechanism of chlorophyll degradation and photosynthesis with the help of molecular biology.

In the process of plant senescence and maturation, efficient chlorophyll degradation can lead to rapid chlorosis of plants and the emergence of carotenoids and anthocyanins to form various leaf and flower colors (Hebbar et al., 2014). Chlorophyll degradation is a crucial part of the aging and maturation process, facilitating the transport of nutrients from aging tissues and organs to reproductive and storage organs (Lim et al., 2007; Hebbar et al., 2014; Zhang et al., 2022). The nitrogen in chloroplasts accounts for 75% of the total nitrogen content of the entire photosynthetic system, and 95% of the nitrogen in seeds comes from nitrogen degraded in leaves (Taylor et al., 2010). Chlorophyll degradation removes toxic substances produced during photosynthesis, maintaining cell viability and efficient nutrient redistribution. Chlorophyll degradation is also a prerequisite for the degradation of light-harvesting complexes (LHCs) in senescent leaves, which is crucial for fully utilizing nitrogen in chloroplasts (Hörtensteiner and Feller, 2002). Therefore, the degradation of chlorophyll has significance for the growth of plants and must be strictly regulated.

The chlorophyll of green plants consists of two components, chlorophyll *a* and chlorophyll *b*. Chlorophyll degradation is a complex process that requires the participation of multiple enzymes (Kuai et al., 2018). The degradation of chlorophyll first occurs through the process of converting chlorophyll *b* to chlorophyll *a*, which is the chlorophyll cycle (Shimoda et al., 2012). Non-Yellow Coloring 1 (NYC1) and NYC1-like (NOL) are two key enzymes that catalyze the initial step in chlorophyll *b* degradation to 7-hydroxymethyl-chlorophyll *a* (Shimoda et al., 2012). In many green plants, NYC1 and NOL physically interact and may function as an enzymatic complex to co-catalyze the degradation of chlorophyll *b* (Sato et al., 2010; Sakuraba et al., 2012; Yu et al., 2017; Teng et al., 2021b). In addition, functional differentiation was found between *NOL* and *NYC1* in *Oryza sativar*, *Arabidopsis thaliana*, and *Lolium perenne* (Kusaba et al., 2007; Sato et al., 2010; Yu et al., 2021).

In our previous study, we cloned *ZjNYC1* in *Z. japonica* and found *ZjNYC1* accelerates chlorophyll degradation and leaf senescence (Teng et al., 2021b). *ZjNOL* shows 42.78% amino acid identity to *ZjNYC1*. However, despite the knowledge of NOL's roles in chlorophyll *b* degradation, the molecular mechanisms underlying NOL-mediated chlorophyll degradation and photosynthesis in *Z. japonica*, and whether its functions differ with *ZjNYC1* are unclear. Leaf senescence induced the expression of *NYC1* and *NOL*, and a close similarity between the phenotypes of *nol* and *nyc1* mutants suggested that *NYC1* and *NOL* have similar functions in leaf senescence (Kusaba et al., 2007; Sato et al., 2010). In Arabidopsis, *NOL* mainly plays a role in the vegetative growth stage and does not significantly promote the leaf senescence process (Sakuraba et al., 2012). These results suggest that the functions of *NYC1* and *NOL* in regulating leaf senescence may be different depending on the plant. However, the mechanisms underlying why the same enzyme performs different functions in mode and non-mode plants remain unknown.

The objectives of this study were to characterize the function and determine the molecular mechanisms of *ZjNOL* in photosynthesis, chlorophyll degradation, and senescence. In addition, clarifying the functional differences in photosynthesis between *ZjNOL* and *ZjNYC1* also was our concern. The information will contribute to the genetic improvement and breeding projects for *Z. japonica* in the future.

MATERIALS AND METHODS

Plant Materials and Growth Conditions

We purchased *Z. japonica* seeds (cv. Zenith) from Patten Seed Company (Lakeland, GA, United States). We sowed them in Klasmann TS1 peat substrate (Klasmann-Deilmann GmbH, Geeste, Germany). Plants were cultivated in climate chambers at 28/25°C (day/night), with a 14-h photoperiod and an average photosynthetic active radiation (PAR) of 400 $\mu mol\, m^{-2}\, s^{-1}$. The plants were watered once a week with Hoagland nutrition solution.

ZjNOL and Its Promoter Cloning

Total RNA was extracted from *Z. japonica* leaves using the Plant RNA Kit (Omega, Georgia, United States). Next, cDNA was generated using the PrimeScriptTM RT reagent Kit (TaKaRa, Dalian, China). We used the CTAB method to obtain genomic DNA. Then, *ZjNOL* and its promoter sequence were amplified using the *Z. japonica* genome database information. The PCR products were purified by the Cycle-Pure Kit (Omega, Georgia, United States) and connected to the pMD-19T cloning vector (TaKaRa, Dalian, China). The plasmids pMD-ZjNOL and pMD-*ZjNOL*pro were obtained after sequencing verification and stored at −80°C.

Plasmid Construction

The primers used for gene cloning, expression analysis, and plasmid construction in this experiment are listed in **Supplementary Table 1**. To generate the *ZjNOL*pro::GUS constructs for GUS staining analysis, we inserted the *ZjNOL* promoter sequence into the pCambia1391Z vector. To observe subcellular localization, we constructed the plasmid 3302Y3-ZjNOL, encoding a ZjNOL-YFP fusion protein and driven by a CaMV 35S promoter. The vectors 35S-pSPYCE-YFP and 35S-pSPYNE-YFP were used for bimolecular fluorescence complementation (BiFC). For yeast two-hybrid analysis, we constructed the vectors pGBKT7 and pGADT7. Coding sequences of *ZjNOL* were recombined into the pTA7002 vector to generate *ZjNOL*-overexpressing Arabidopsis lines. The control plants (CK) were using the pTA7002 empty vector.

Bioinformatic Analysis of *ZjNOL* and Its Promoter Sequence

We performed the BLAST analysis on the NCBI database to search for homologs. The neighbor-joining method was used to construct a phylogenetic tree using the MEGA 11 software (Tamura et al., 2021). To further confirm the evolutionary selection types of these *NOL* genes, we calculated the Ks/Ka ratio using DnaSP6 software (Rozas et al., 2017). The PlantCARE database was used to predict the *cis*-elements in the promoter sequence (Lescot et al., 2002). The compute pI/Mw tool was used to calculate the molecular weight (MW) and theoretical isoelectric point (PI).[1] ProtComp 9.0[2]

[1]https://web.expasy.org/computepi/
[2]http://www.softberry.com

and TargetP 1.1[3] were used to predict subcellular localization characteristics.

Quantitative Real-Time PCR

To analyze the expression pattern of the *ZjNOL*, we extracted total RNA from various tissues (roots, stolons, stems, and leaves) and three different development stages (young, mature, and senescent) of leaves. In addition, we treated 3-month-old plants after 12 h induction with hormones, such as 10 μmol GA, 10 μmol methyl jasmonate (MeJA), 10 μmol ABA, and dark. We collected the tissues after induced 0, 0.5, 1, 3, 6, and 12 h. We used four different RNA templates in each study. Each set came with three technical replicates. The qRT-PCR evaluation and data analysis were carried out in accordance with the ΔΔCt method (Teng et al., 2017). *Zoysia japonica β-actin* (GenBank accession no. GU290546) was selected as the housekeeping gene.

Subcellular Localization and Protein Interaction Analysis

Plasmid 3302Y3-ZjNOL was transformed into *Z. japonica* protoplasts to investigate subcellular localization. The transient gene expression system of *Z. japonica* protoplasts was modified by a previously reported protocol (Yoo et al., 2007). For BiFC analysis, we cloned *ZjNOL* and *ZjNYC1* and fused them with split YFP^N and YFP^C fragments to co-transform. The yeast two-hybrid experiment, which examined the interaction between ZjNOL and ZjNYC1, was repeated three times according to the instructions of Clontech. We used an SP8 laser confocal scanning microscope for fluorescence observation of protein subcellular localization and BiFC analysis (Leica, Mannheim, Germany).

Development and Characterization of Transgenic *Arabidopsis thaliana* Lines

Using the floral dip method, *A. tumefaciens* GV3101 transformed with the pTA7002-ZjNOL plasmid was used to generate transgenic *A. thaliana* lines. The harvested seeds were tested on MS medium containing 30 mg/L hygromycin. Following PCR confirmation, only T3 lines with 100% hygromycin resistance were harvested for further morphological analysis. The 3-week-old lines were transferred from MS medium to filter paper soaked in ddH_2O with 30 M dexamethasone (DEX; Sigma-Aldrich, Munich, Germany) and 0.01% Tween-20. We photographed the seedlings after 4 days of induction.

The chlorophyll content was determined using a previously published protocol (Teng et al., 2016). ELISA kit (H251), H_2O_2 assay kit (A064-1-1), and inhibition superoxide anion assay kit (A052-1-1), obtained from Nanjing Jiancheng Bioengineering Institute, Nanjing, China, were used to assay ABA content, H_2O_2 content, and inhibit superoxide anion activity, respectively. The plant soluble sugar content test kit (A145-2-1), starch content kit (A148-1-1), and malondialdehyde (MDA) assay kit (MDA-2-Y), purchased from the Jiancheng Bioengineering Institute, Nanjing, China, were used to determine the content of soluble sugars, starch, and MDA. According to the manufacturer's instructions, we measured superoxide dismutase (SOD), peroxidase (POD), catalase (CAT), and ascorbate peroxidase (APX) activity using reactive oxygen species (ROS) assay kits (Jiancheng Bioengineering Institute, Nanjing, China). All experiments in this study included at least three biological replicates.

To determine chlorophyll fluorescence parameters, we used the Handy PEA analyzer (Hansatech, Kings Lynn, United Kingdom) according to the instructions provided by the manufacturer. After 30 min of dark adaption, leaves were exposed to 2 s saturation light pulses of 3,500 mol photons m^{-2} s^{-1} to measure chlorophyll fluorescence. Ten replicants were used for the CK, line-10, and line-31. We calculated the photosynthetic parameters and the average values of the same group, and a Student *t*-test was used to differentiate the different parameters by comparison to the control. To visualize the data, we used Origin Pro v.2019b (OriginLab Corporation, Northampton, MA, United States).

Statistical Analysis

We used SPSS version 18.0 (IBM, Chicago, IL, United States) to analyze variance and verify it by a Student *t*-test at a significance level of 0.05 to determine the effect of *ZjNOL*-overexpressing on leaf physiology and transcription level. We used Fisher's protected least significant difference (LSD) test at the 0.05 probability level to analyze the expression characteristics of *ZjNOL*. All data were presented as means ± SD ($n \geq 3$).

RESULTS

Cloning and Bioinformatic Analysis of *ZjNOL*

Using the *Z. japonica* genome and the full-length transcriptome databases as references, we designed the primers and cloned the *ZjNOL* (accession number: OL581613) using RT-PCR. The sequencing results showed that the CDS sequence of the *ZjNOL* was 1,035 bp in length and encoded a total of 344 amino acids. Analysis of homologous sequences revealed that *ZjNOL* contains an SDR domain (**Figure 1A**), with theoretical isoelectric points and molecular weights of 9.76 and 37.39 kD, respectively. Furthermore, the results of the phylogenetic analysis showed that *ZjNOL* is more closely related to NOL of sorghum (*Sorghum bicolor*; **Figure 1B**). We calculated the synonymous and non-synonymous substitution rates (Ka/Ks) to further confirm the evolutionary selection types of these *NOL* genes, and the results showed that some *NOL* homologous genes were under diversifying selection (Ka/Ks > 1; **Figure 1C**).

Isolation of *ZjNOL* Promoter and GUS Staining Assay

Using *Z. japonica* genomic DNA as a reference, we amplified a 712 bp nucleotide promoter sequence. Furthermore, we predicted and analyzed the *cis*-acting elements of the *ZjNOL* promoter using the PlantCARE website. In addition to the basic functional elements of the promoter, it also contains an ABRE element that responds to ABA induction, five MYB transcription factor binding sites, and three light-responsive elements (**Table 1**). To further clarify the activity characteristics of the *ZjNOL* promoter, the *ZjNOL*pro::GUS expression vector was constructed and transformed into Arabidopsis. GUS histochemical staining of

[3]http://www.cbs.dtu.dk/services/TargetP-1.1/index.php

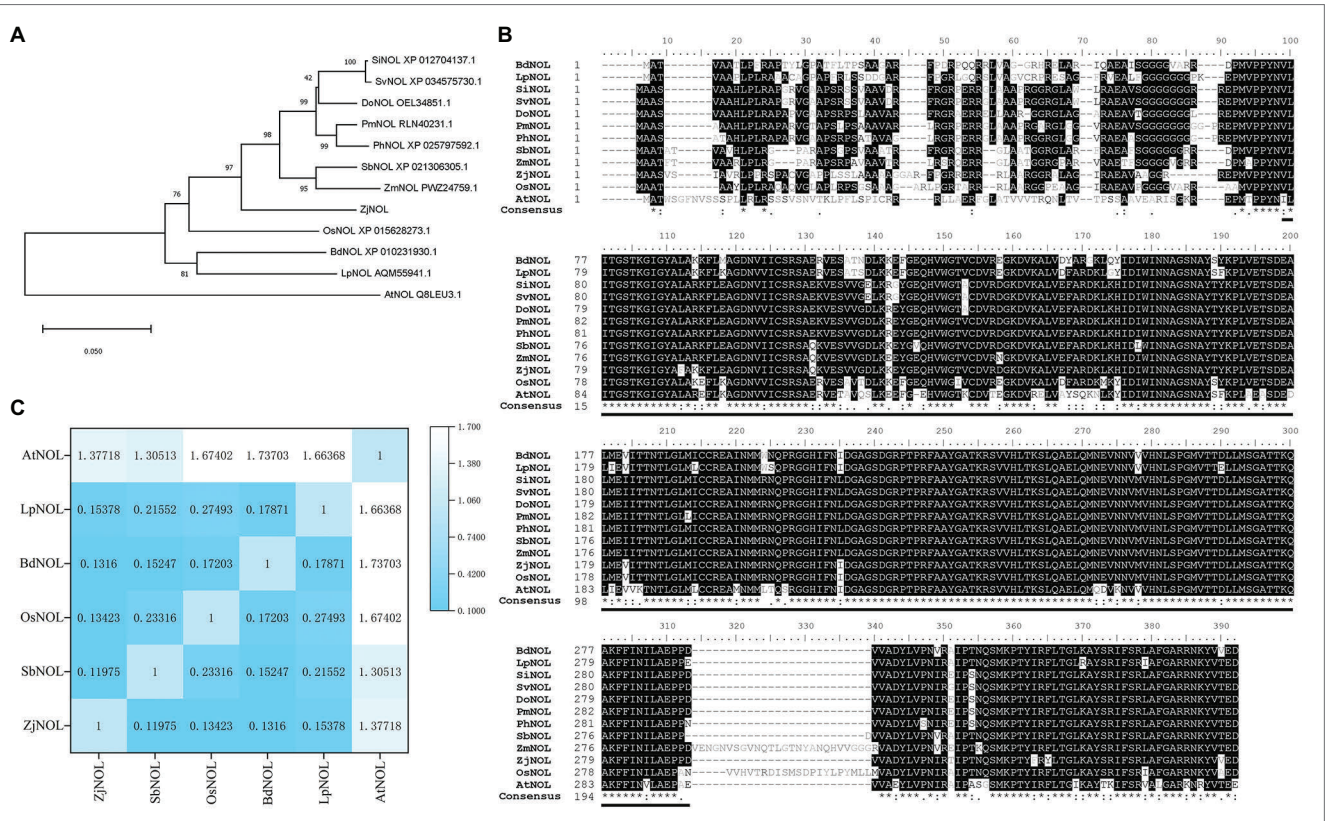

FIGURE 1 | Bioinformatic analysis of *ZjNOL*. **(A)** Phylogenetic tree. The neighbor-joining tree was constructed using MEGA 11, orthologous proteins in *Setaria italica* (SiNOL), *Setaria viridis* (SvNOL), *Dichanthelium oligosanthes* (DoNOL), *Panicum miliaceum* (PmNOL), *Panicum hallii* (PhNOL), *Sorghum bicolor* (SbNOL), *Zea mays* (ZmNOL), *Zoysia japonica* (ZjNOL), *Oryza sativa* (OsNOL), Brachypodium distachyon (BdNOL), *Lolium perenne* (LpNOL), and *Arabidopsis thaliana* (AtNOL) were used for analysis. **(B)** Multiple sequences alignment and conserved domain prediction. **(C)** Calculation of the Ka/Ks.

TABLE 1 | *cis*-elements prediction in the *ZjNOL* promoter.

cis-element	Sequences	Amount	Function
ARE	AAACCA	2	Anaerobic inducible
AAGAA-motif	GAAAGAA	1	Unknown
CAAT-box	C(C)A(A)AT	8	Promoter structure
G-Box	CACGTT	1	Light response
MYC	CATG/TTG	5	MYB binding site
GT1-motif	GGTTAA	1	Light response
Sp1	GGGCGG	1	Light response
ABRE	ACGTG	1	ABA response
TATA-box	TATA(A)(A)(A)	19	Promoter core element

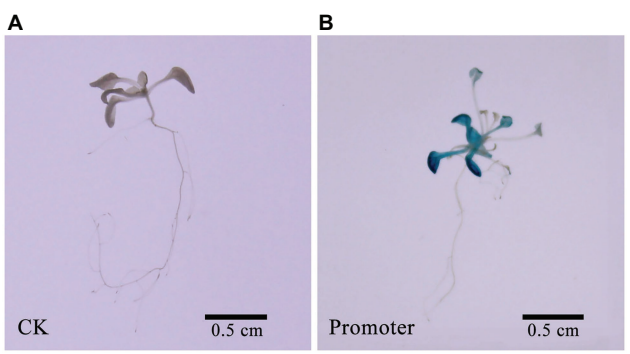

FIGURE 2 | GUS staining results of promoter. **(A)** CK. **(B)** Promoter.

transgenic seedlings showed that the promoter could drive GUS gene expression in transgenic *Arabidopsis thaliana*, and a large amount of blue was found in the leaves (**Figure 2**).

Expression Characters of *ZjNOL*

We analyzed the expression pattern of the *ZjNOL* gene using qRT-PCR. The results showed that all the tissues could detect the *ZjNOL* gene expression (**Figure 3A**). Nevertheless, its expression in leaves was significantly higher than that in other tissues ($p < 0.05$), and its expression in stems was also significantly higher than roots and stolons ($p < 0.05$). This result indicates that the expression of the *ZjNOL* is correlated with the content of chlorophyll positively. To determine whether the *ZjNOL* is involved in chlorophyll degradation during leaf senescence, we analyzed the *ZjNOL* gene expression in young, mature, and senescent leaves for qRT-PCR. The results showed that the *ZjNOL* was more actively expressed in senescent leaves, indicating that the *ZjNOL* was involved in the senescence process (**Figure 3B**).

The *ZjNOL* gene promoter contains *cis*-elements involved in ABA, JA, and light response. Therefore, we analyzed the expression pattern of *ZjNOL* under these treatments. Under

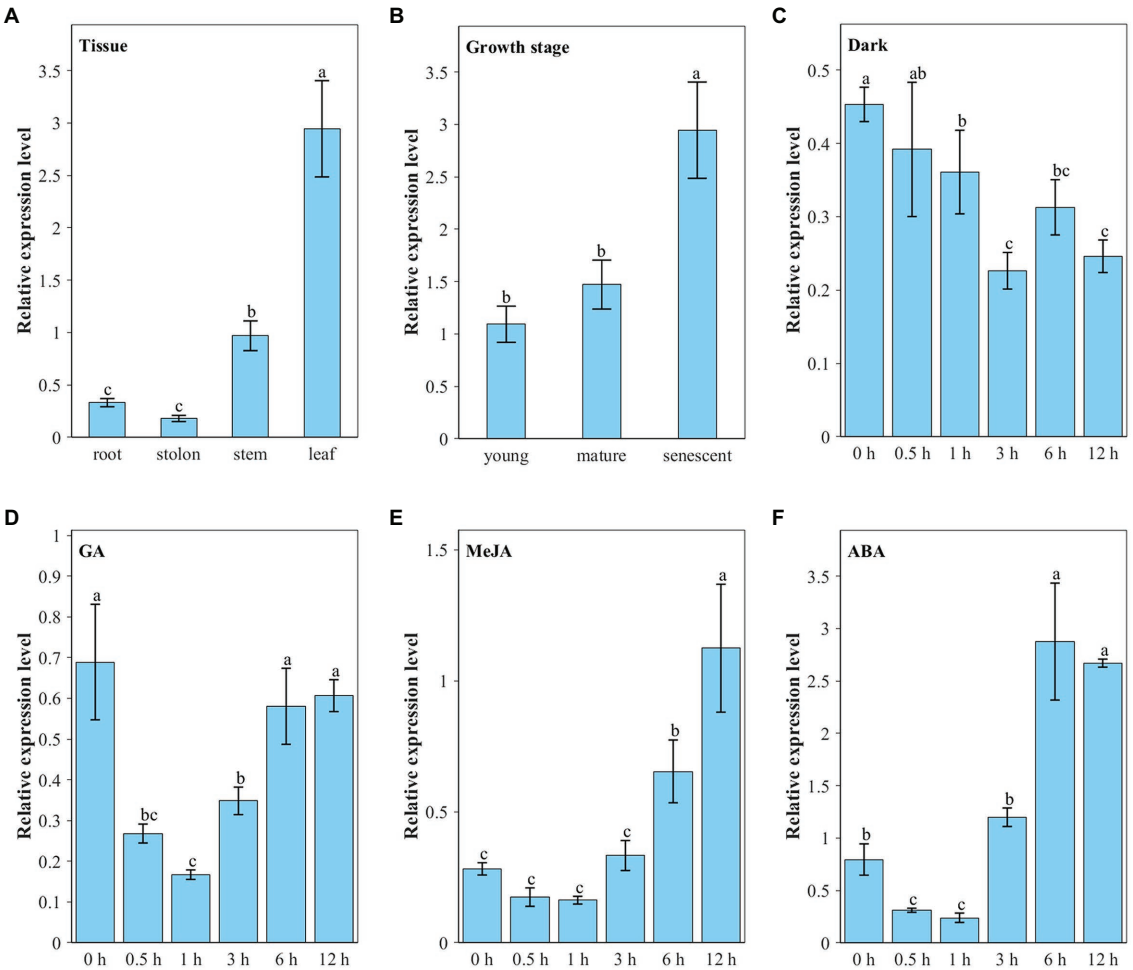

FIGURE 3 | Transcriptional expression characters of *ZjNOL*. **(A)** Different tissues; **(B)** leaves at different growth stages; continuous expression tendency under different treatments: dark **(C)**, GA **(D)**, MeJA **(E)**, and ABA **(F)**. Data were expressed as mean ± SD ($n = 4$). Different letters indicate significant differences at $p \leq 0.05$ based on Fisher's protected least significant difference (LSD) test.

dark treatment, the expression of *ZjNOL* showed a slow downward trend (**Figure 3C**). Ten-micromole GA treatment significantly inhibited the expression of *ZjNOL* within 0–3 h and recovered to the initial level after 6 h (**Figure 3D**). Ten-micromole MeJA treatment had a significant inducing effect on *ZjNOL*, and the expression level at 12 h was four times higher than that at 0 h (**Figure 3E**). Ten-micromole ABA treatment showed a trend of first inhibiting and then promoting the expression of *ZjNOL*, and the expression level was the lowest at the 1st hour, 0.4 times that of the 0 h; it reached the highest level at the 6th hour, which was 3.6 times that of the 0 h (**Figure 3F**).

Subcellular Localization of ZjNOL

We further used the *Z. japonica* protoplast transient expression system to observe the subcellular localization of ZjNOL, and the results showed that the YFP signal was detected in chloroplasts (**Figure 4**). Theoretically, NOL can interact with NYC1 in plants such as Arabidopsis, rice, and ryegrass. We performed BiFC analysis on ZjNOL and ZjNYC1 to clarify whether NOL and NYC1 proteins in *Z. japonica* can interact. The results indicate that ZjNOL and ZjNYC1 can interact with each other in *Z. japonica* chloroplasts (**Figure 5**). In the yeast system, however, ZjNOL and ZjNYC1 did not interact with each other (**Supplementary Figure 1**).

Overexpression of *ZjNOL* Accelerated Chlorophyll Degradation and Senescence

With the inflorescence infection method, we obtained transgenic Arabidopsis lines to determine the function of the *ZjNOL* gene. After 4 days of induction with 30 μM DEX under normal lighting conditions, the control plants remained green, but the transgenic lines turned yellow (**Figure 6A**). The total chlorophyll content and the chlorophyll *b* levels in line-10 and line-31 were lower than that of CK significantly ($p < 0.05$), and the ratio of chlorophyll *a*/chlorophyll *b* of the transgenic plants was 12 times higher than that of the control plant ($p < 0.05$). The above results indicated that *ZjNOL* catalyzed the conversion of chlorophyll *b* to chlorophyll *a* and promoted chlorophyll degradation (**Figures 6B–D**). ABA content and H_2O_2 content in the transgenic line were significantly higher than those of the control (**Figures 6E,F**; $p < 0.05$). The inhibition of superoxide

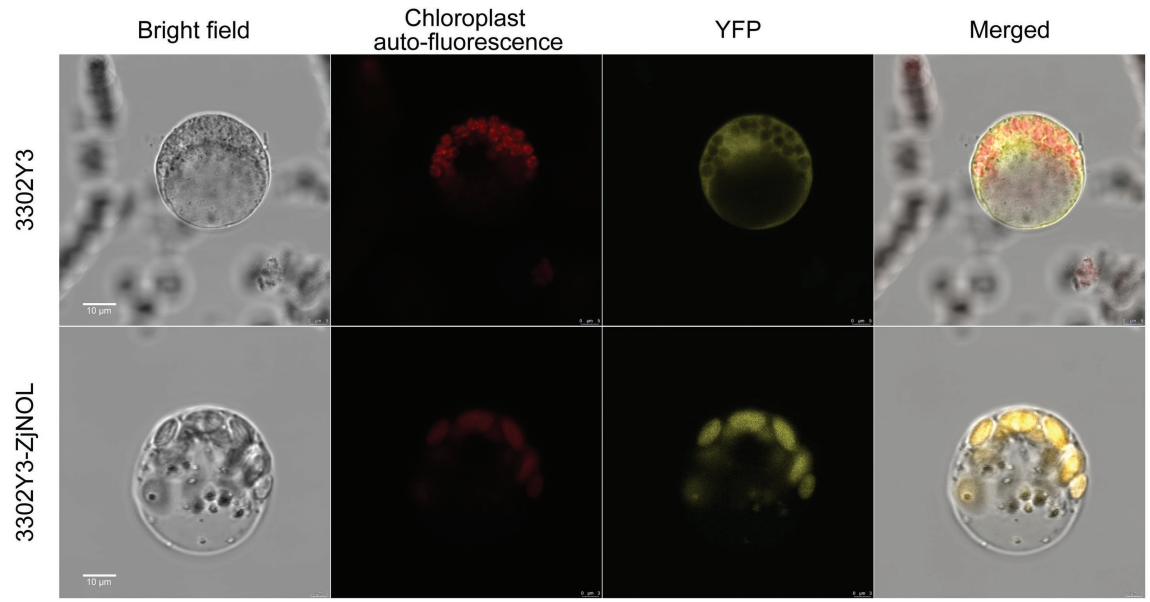

FIGURE 4 | Subcellular localization of ZjNOL in *Zoysia japonica* protoplast. The results showed that ZjNOL was localized in the chloroplast.

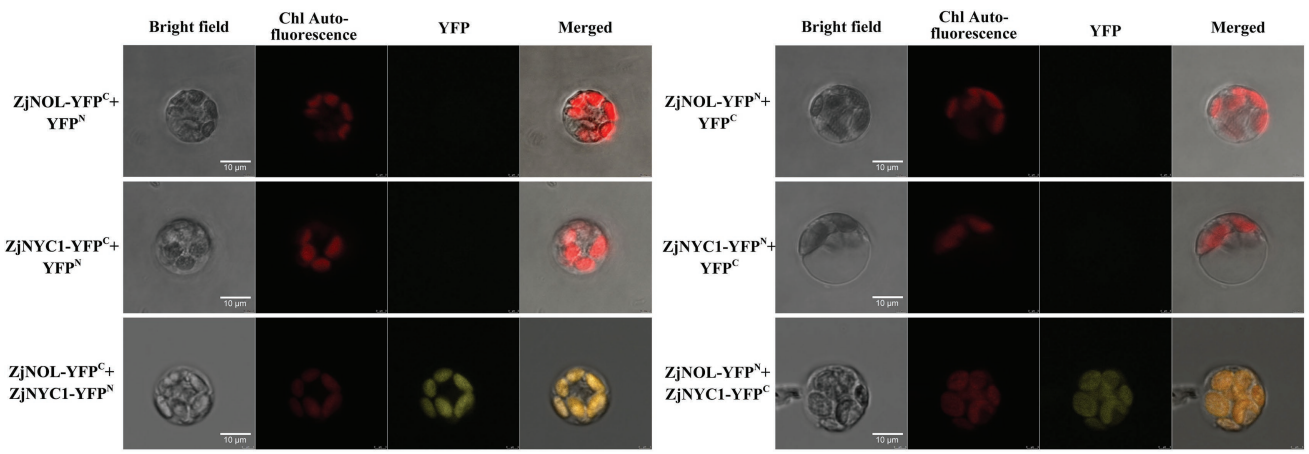

FIGURE 5 | BiFC analysis of the interaction between ZjNYC1 and ZjNOL.

anion activity in transgenic lines was decreased compared to the control plant (**Figure 6G**; $p < 0.05$). In addition, the content of soluble sugar, starch, and MDA was also markedly higher than that of the CK (**Figure 6H**; $p < 0.05$). The changes in the antioxidant enzyme system of the transgenic lines showed that POD, CAT, APX, and SOD in the transgenic lines were significantly higher than those in the CK (**Figure 6H**; $p < 0.05$). The above physiological indicators show (**Figure 6**) that *ZjNOL* promotes chlorophyll degradation and accelerates the senescence process.

Transcriptional Characteristics Analysis of *ZjNOL*-Overexpressing Lines

We analyzed the effect of overexpression of *ZjNOL* in transgenic lines utilizing qRT-PCR. The results showed that *ZjNOL* was expressed efficiently in the transgenic lines (**Figure 7A**). *SAG14* is a marker gene for senescence. This study found that the overexpression of *ZjNOL* significantly increased the expression of *SAG14*, indicating that it promoted the senescence process of transgenic lines (**Figure 7B**). Four photosynthetic efficiency marker genes were selected to assess the impact of *ZjNOL* on photosynthesis. The results showed that the expression of *CAB1*, *rbcL*, *RCA*, and *PsaF* significantly downregulated in transgenic lines, reflecting that *ZjNOL* inhibited the photosynthetic efficiency (**Figures 7C–F**).

Chlorophyll Fluorescence Induction Curves Analysis of *ZjNOL*-Overexpressing Lines

We carried out a standard OJIP analysis of the fluorescence induction curves to evaluate the photosynthetic activity in *ZjNOL* transgenic lines. The results showed that typical O, J, I, and P characteristic steps appeared, as well as an obvious K-step.

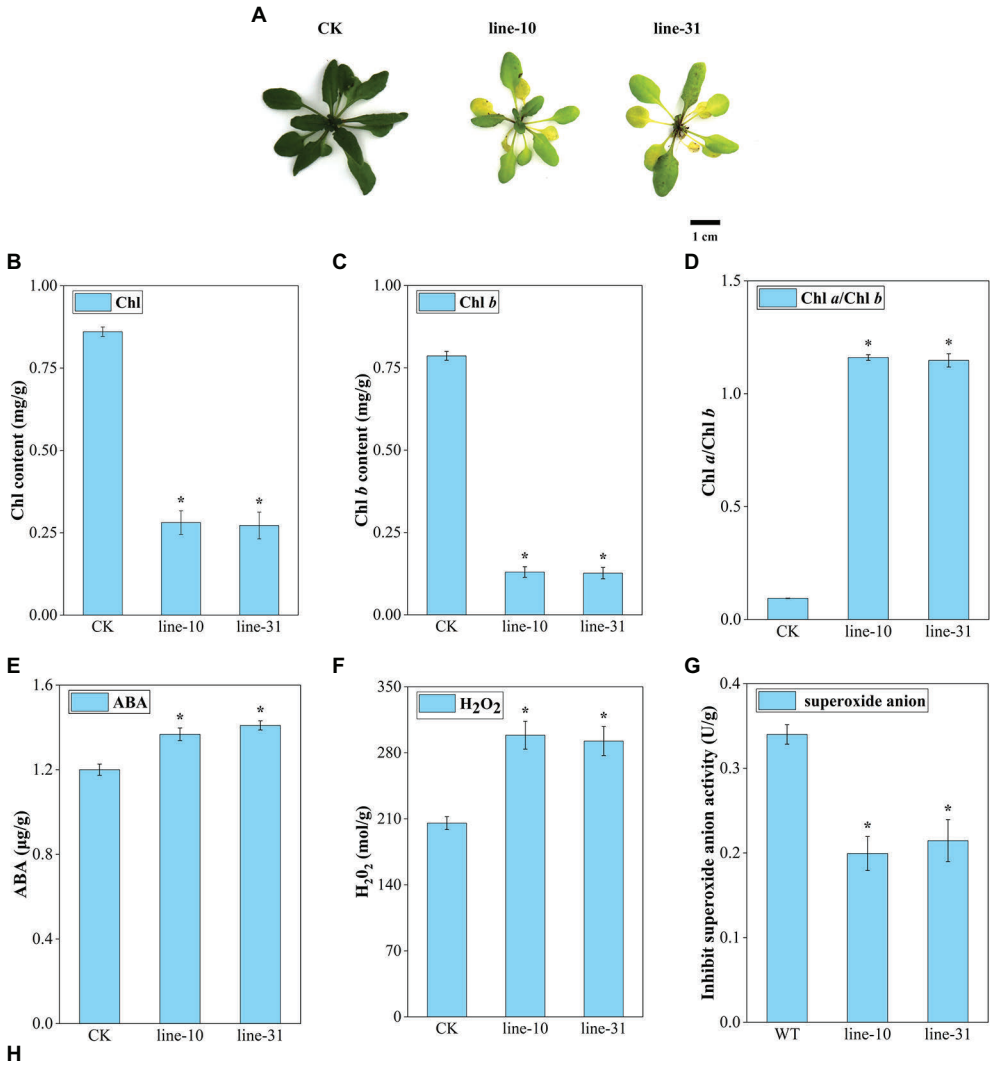

H

	SOD (U/g)	POD (U/mg)	CAT (nmol/min/g)	APX (U/g)	Sugar (mg/g)	Starch (mg/g)	MDA (nmol/g)
CK	13.40±1.72	16.48±0.08	18.76±0.39	0.040±0.001	2.96±0.08	1.51±0.03	9.12±0.79
line-10	83.04±4.71*	26.83±1.55*	37.98±1.79*	0.369±0.040*	3.85±0.36*	3.39±0.17*	12.04±1.19*
line-31	80.53±2.98*	29.14±1.63*	37.97±2.35*	0.365±0.042*	4.43±0.64*	3.50±0.34*	13.24±1.19*

FIGURE 6 | Morphological and physiological assessment of *ZjNOL*-overexpressing lines. **(A)** Photographs of transgenic plants compared with control. **(B)** Chlorophyll (Chl) contents. **(C)** Chlorophyll *b* (Chl *b*) content. **(D)** Chlorophyll *a*/Chlorophyll *b* (Chl *a*/Chl *b*) ratio. **(E)** ABA content. **(F)** H_2O_2 content. **(G)** Inhibit superoxide anion activity. **(H)** Physiological changes of enzyme activities (SOD, POD, CAT, and APX) and carbohydrate content (sugar, starch, and MDA). Results are means of three replicates ± SDs. Asterisks indicate significant differences at $p \leq 0.05$ based on Student *t*-test.

The expression of *ZjNOL* decreased the minimal fluorescence level (F_o) and maximal fluorescence level (F_m), and the maximal variable fluorescence (F_v) changed little (**Figure 8A**). We compared the double normalized curves in the O-P transient of chlorophyll fluorescence and found that values of the L-band, K-band were positive, whereas G-band was negative. The positive values of the K-band and the negative values of the G-band in the transgenic lines were significantly higher than those of the control ($p < 0.05$; **Figure 8B**; **Supplementary Figure 2**).

The other fluorescence parameters of the JIP-test were further analyzed. We found that some parameters were decreased significantly in the transgenic lines compared to the control and constructed a radar plot to show the detailed parameters (**Figure 8C**). PI_{ABS} in transgenic lines was significantly lower than that of the control ($p < 0.05$), demonstrating the distributed energy performance index of electron acceptors from the absorption of light energy by PSII to photosynthetic systems (**Figure 8C**). We drew a phenomenological energy pipeline model to study

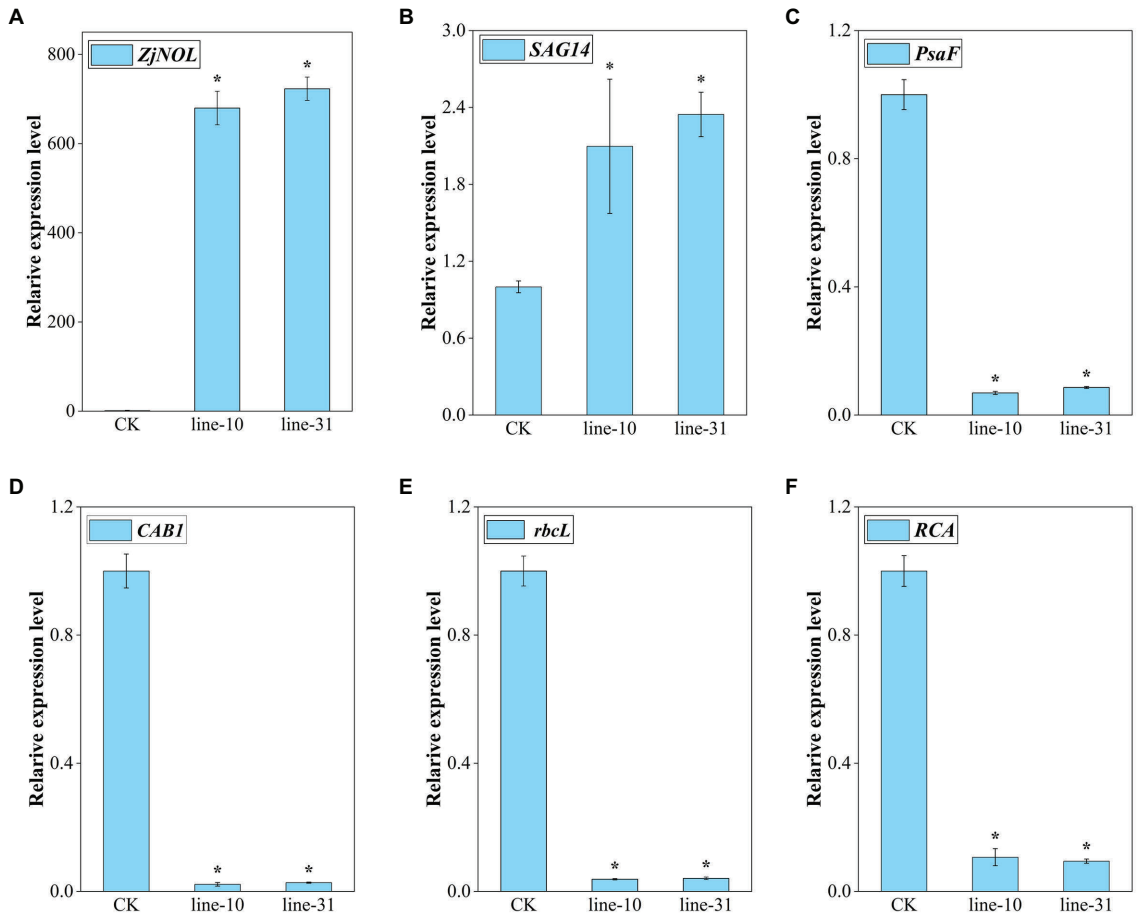

FIGURE 7 | Expression analysis of senescence markers and photosynthesis-related genes. **(A)** *ZjNOL*. **(B)** *SAG14*. **(C)** *PsaF*. **(D)** *CAB1*. **(E)** *rbcL*. **(F)** *RCA*. Data were expressed as mean ± SD ($n = 4$). Asterisks indicate significant differences at $p \leq 0.05$ based on Student *t*-test.

the influence of *ZjNOL* overexpression (**Supplementary Figure 3**). It showed that the specific flux membrane model parameters, including ABS/RC, TRo/RC, of the transgenic lines increased, while ETo/RC and DIo/RC did not change much. At the same time, the phenomenological flux leaf model and the radar plot all indicated that parameters of the transgenic lines, including ABS/CSm, TRo/CSm, ETo/CSm, and DIo/CSm, were reduced ($p < 0.05$; **Figure 8C**; **Supplementary Figure 3**). In addition, the inactive reaction centers of the transgenic lines increased.

DISCUSSION

In this study, the full-length *ZjNOL* sequence was cloned. We found that *ZjNOL* was phylogenetically close to its orthologs of *Sorghum bicolor* and shared conserved sequence features as well as similar expression patterns and subcellular localization in chloroplasts. To judge the "purifying selection" and "diversifying selection" in the process of plant evolution, we analysis the synonymous and non-synonymous substitution rates of homologous genes (Gaut et al., 1996). Most chlorophyll catabolism genes, such as *NYC1* and *PPH*, are under purifying selection (Ka/Ks < 1; Teng et al., 2021a,b). However, some *NOL* homologous genes were under diversifying selection (Ka/Ks > 1; **Figure 1C**). This result is consistent with the reports of perennial ryegrass, indicating that *NOL* has functional diversity in different species (Yu et al., 2021). Therefore, it inspired us to investigate the function of ZjNOL in the typical warm-season turfgrass, *Z. japonica*.

Chlorophyll *b* reductase enzymes, *NYC1* and NYC1-like (*NOL*), play critical roles in the chlorophyll cycle. The BiFC and yeast two-hybrid analysis showed that ZjNOL and ZjNYC1 could interact *in vivo* but not in the Clontech yeast two-hybrid system. This result is consistent with the previous reports in *Z. japonica* (Teng et al., 2021b) but different from rice and Arabidopsis (Sato et al., 2010; Sakuraba et al., 2012). We speculate that there are some differences in the functions of *ZjNOL* and *ZjNYC1* among species. At the same time, there might be some substances in *Z. japonica* that regulate the interaction between ZjNOL and ZjNYC1. SGR is required for protein interactions with the chlorophyll catabolic enzyme (CCE; Sakuraba et al., 2012). Therefore, it is necessary to deeply explore the external factors of the interaction between ZjNOL and ZjNYC1 in future research.

Consistent with the findings in rice (Kusaba et al., 2007), Arabidopsis (Horie et al., 2009), and perennial ryegrass

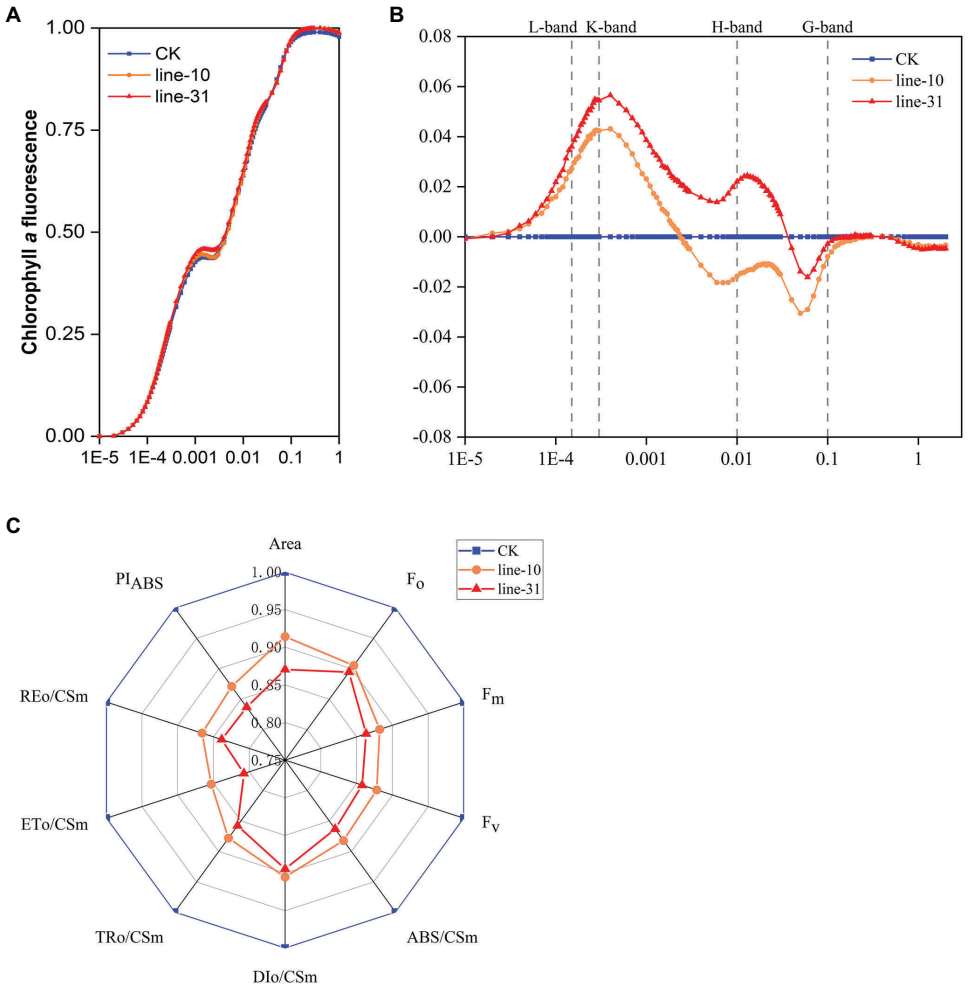

FIGURE 8 | Chlorophyll fluorescence induction curves analysis of *ZjNOL*-overexpressing transgenic lines. **(A)** The standard OJIP curves. **(B)** The relative variable fluorescence V_t of the transient chlorophyll *a* fluorescence. **(C)** Radar plot of the fluorescence parameters. The fluorescence parameters were displayed as means of 10 replicates. The K-band and G-band between the transgenic lines and control were significantly different at $p \leq 0.05$ based on Student *t*-test.

(Yu et al., 2021), the expression of *ZjNOL* was positively correlated with senescence. In *A. thaliana*, overexpression of *AtNOL* resulted in accelerated leaf senescence and chlorophyll *b* degradation in *A. thaliana* (Jia et al., 2015). In *N. benthamian*, the transient overexpression of *LpNOL* accelerated leaf senescence and chlorophyll *b* degradation. Perennial ryegrass *LpNOL* RNA interference (*NOLi*) delays leaf senescence (Yu et al., 2021). In this study, the overexpression of *ZjNOL* accelerated total chlorophyll and chlorophyll *b* degradation, demonstrating that *ZjNOL* is the functional orthologous *NOL* in *Z. japonica*.

The accumulation of ABA plays a positive role in the promotion of senescence (Schippers et al., 2015). *SAG14* is a commonly accepted senescence marker (Wan et al., 2018). Overexpression of *ZjNOL* significantly increased the expression of *SAG14* and the content of ABA, indicating the accelerated senescence process in the *ZjNOL*-overexpressing lines. Carbohydrates, such as soluble sugar and starch, act as energy reserves and are essential for plant growth (Taiz and Zeiger, 2002). Sugar and starch levels are high in senescent Arabidopsis and tobacco leaves (Pourtau et al., 2006; Gan, 2010). Sucrose and starch accumulation can hasten leaf senescence (Lim et al., 2007). The balance of SOD, POD, and APX or CAT activities is crucial for determining superoxide radicals and H_2O_2 steady-state levels (Mittler, 2002; Zhang et al., 2021). One of the products of lipid degradation is malondialdehyde (MDA). Thus, increased MDA levels correlated with oxidative stress levels in plants (Bouazizi et al., 2010; Rusinowski et al., 2019). Sugar, starch, and MDA play roles in plant senescence regulation (Wingler et al., 2009; Gan, 2010). In this study, the content of MDA, sucrose, and starch in *ZjNOL*-overexpressing lines was increased significantly higher than in control lines ($p < 0.05$). *ZjNOL* reduced their ability to scavenge H_2O_2 and superoxide anion, resulting in excessive accumulation of ROS, activation of antioxidant enzymes, and production of oxidative stress. Consequently, it proved that *ZjNOL* accelerated leaf senescence.

PsaF, *CAB1*, *rbcL*, and *RCA* were photosynthetic efficiency markers (Teng et al., 2021a). The expression levels of all four photosynthetic efficiency genes were decreased significantly in this study. Transgenic lines also had lower chlorophyll *b* content

and higher chlorophyll *a*/*b* ratio. Overexpression of *ZjNOL* resulted in chlorophyll degradation and destruction of photosynthetic activity in *Z. japonica*. This result is consistent with reports of perennial ryegrass (Yu et al., 2021).

"JIP-test" analysis was widely used to plant gene function studies due to their simplicity, rapidity, ease of reproducibility, and the ability to obtain large amounts of reliable data (Zhang et al., 2020; Bi et al., 2021; Wang et al., 2021). The transient induction curves and JIP-test parameters provide us with information to understand the changes in structural and functional efficiency of photosynthetic apparatus (Baker, 2008; Bussotti et al., 2010; Kalaji et al., 2014; Sitko et al., 2017). The positive K-band was due to slower electron transport from the donor side because of the oxygen-evolving complex (OEC) inactivation and/or faster electron-withdrawal from the acceptor side (Zagorchev et al., 2020). It indicated that *ZjNOL* inhibits the function of PSII by damaging the oxygen-evolving complex. A positive G-band value reveals that the PSI terminal electron acceptor pool is relatively large (Yusuf et al., 2010). We speculated that *ZjNOL* inhibited PSI activity. The negative G-band and significantly lower REo/CSm values support this hypothesis.

The performance index provides comprehensive information on overall photosynthetic efficiency and performance simultaneously (Bussotti et al., 2010). The reduction in the area of the induction curves indicates that the redox state of the electron transport chain or the stoichiometric ratio of the acceptor sides of PSII and PSI has changed (Kalaji et al., 2016). The initial fluorescence (F_o) represents fluorescence yield when all reaction centers are open or oxidized (Szopiński et al., 2019). The overexpression of *ZjNOL* promoted chlorophyll degradation and led to a decrease in F_o. ABS/RC and ABS/CSm are two key indicators that indicate the efficiency of the antenna complex (Szopiński et al., 2019). The reduction in the efficiency of the antenna complex further limited photosynthesis. The decrease in ABS/CSm, TRo/CSm, and ETo/CSm was associated with an increase in the density of inactive reactive centers and the ineffectiveness of PSII (Kalaji et al., 2011; Faseela et al., 2019). In detail, the increase in ABS/RC indicated the rise of absorption flux per reaction center. The enhanced TRo/RC reflected the increase of trapped energy flux per reaction center. The above results indicated that the expression of *ZjNOL* inhibited the utilization of light energy in plants. To sum up, we concluded that the effect of *ZjNOL* inhibited photosynthetic efficiency mainly through damage to the oxygen-evolving complex. It is different from the influence of *ZjNYC1* on photosynthesis, which negatively affects the integrity and functionality of PSII, PSI, and the intermedia electron transport chain (Teng et al., 2021b). Taken together, it is reasonable to assume that *ZjNOL* and *ZjNYC1* function differently in photosynthesis.

CONCLUSION

In conclusion, we proposed a working model of the molecular mechanism of *ZjNOL* in regulating senescence and photosynthesis (**Figure 9**). *ZjNOL* was highly expressed in senescent leaves. ABA and MeJA induced the expression of *ZjNOL*. ZjNOL is

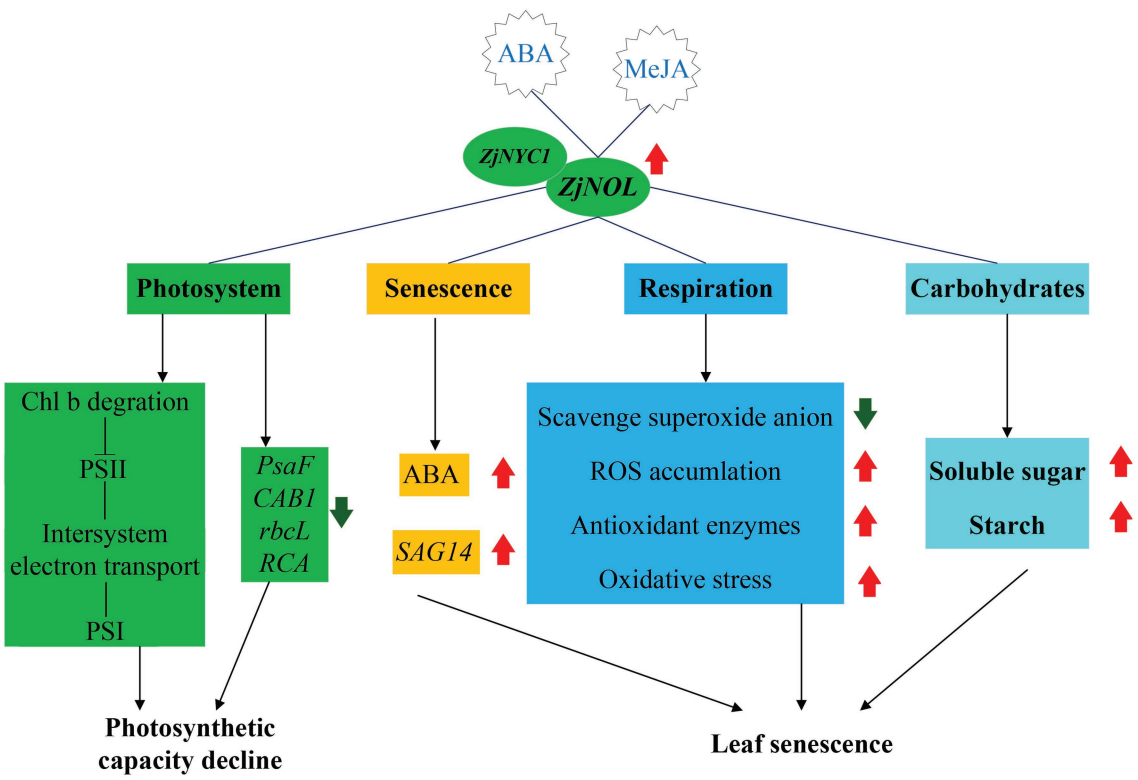

FIGURE 9 | A proposed working model of *ZjNOL* in regulating photosynthesis and senescence.

localized in the chloroplast and can interact with ZjNYC1 *in vivo*. *ZjNOL* promoted the accumulation of ABA and carbohydrates and the increase of *SAG14* at the transcriptional level. *ZjNOL* simultaneously led to the excessive accumulation of ROS, the activation of antioxidant enzymes, and the generation of oxidative stress, which in turn accelerated senescence. *ZjNOL* decreased the transcriptional level of photosynthetic efficiency related marker genes and promoted chlorophyll degradation. The JIP-test analysis showed that *ZjNOL* inhibited photosynthetic efficiency mainly through damage to oxygen-evolving complex, which is different from the influence of *ZjNYC1* on photosynthesis. In total, these results suggest that *ZjNOL* promotes chlorophyll degradation and senescence and negatively affects the integrity and functionality of the photosystem. This gene has valuable genetic editing value for cultivating new varieties with stay-green characteristics and improved photosynthesis efficiency.

DATA AVAILABILITY STATEMENT

The original contributions presented in the study are included in the article/**Supplementary Material**, and further inquiries can be directed to the corresponding authors.

AUTHOR CONTRIBUTIONS

SY and LH conceived the study and designed the experiments. JG performed the experiment, analyzed data, and wrote the manuscript. KT, YY, YG, and LL provided suggestions. All authors contributed to the article and approved the submitted version.

FUNDING

This study was supported by the National Natural Science Foundation of China (nos. 31971770 and 31901397), and the Scientific Funds of Beijing Academy of Agriculture and Forestry Sciences (KJCX20210431, CZZJ202210, and KJCX20220103).

ACKNOWLEDGMENTS

The authors would like to thank Kai Wang from the Hansha Scientific Instruments Ltd. for the Handy PEA parameter analysis. The authors would like to thank Prof. Duowei Li from Northwest University for providing the pTA7002 vector.

SUPPLEMENTARY MATERIAL

The Supplementary Material for this article can be found online at: https://www.frontiersin.org/articles/10.3389/fpls.2022.906018/full#supplementary-material

Supplementary Figure 1 | Yeast two-hybrid analysis of ZjNOL and ZjNYC1.

Supplementary Figure 2 | The OJIP curves, K-band, and G-band. **(A)** The OJIP curves. **(B)** K-band. **(C)** G-band.

Supplementary Figure 3 | The proportion of phenomenological energy flux parameters of the transgenic lines and the control displayed by the leaf pipeline model. The fluorescence parameters were displayed as means of ten replicates. The width of the arrow represents the relative values of the associated parameters; dark circle represents non-active reaction centers.

REFERENCES

Baker, N. R. (2008). Chlorophyll fluorescence: a probe of photosynthesis *in vivo*. *Annu. Rev. Plant Biol.* 59, 89–113. doi: 10.1146/annurev.arplant.59.032607.092759

Bi, A., Wang, T., Wang, G., Zhang, L., Wassie, M., Amee, M., et al. (2021). Stress memory gene FaHSP17. 8-CII controls thermotolerance via remodeling PSII and ROS signaling in tall fescue. *Plant Physiol.* 187, 1163–1176. doi: 10.1093/plphys/kiab205

Bouazizi, H., Jouili, H., Geitmann, A., and El Ferjani, E. (2010). Copper toxicity in expanding leaves of *Phaseolus vulgaris* L.: antioxidant enzyme response and nutrient element uptake. *Ecotoxicol. Environ. Saf.* 73, 1304–1308. doi: 10.1016/j.ecoenv.2010.05.014

Bussotti, F., Desotgiu, R., Pollastrini, M., and Cascio, C. (2010). The JIP test: a tool to screen the capacity of plant adaptation to climate change. *Scand. J. For. Res.* 25(sup8), 43–50. doi: 10.1080/02827581.2010.485777

Faseela, P., Sinisha, A., Brestič, M., and Puthur, J. (2019). Chlorophyll *a* fluorescence parameters as indicators of a particular abiotic stress in rice. *Photosynthetica* 57, 108–115. doi: 10.32615/ps.2019.147

Gan, S. (2010). "The hormonal regulation of senescence," in *Plant Hormones: Biosynthesis, Signal Transduction, Action!* ed. P. J. Davies (Dordrecht; Springer Netherlands), 597–617.

Gaut, B. S., Morton, B. R., McCaig, B. C., and Clegg, M. T. (1996). Substitution rate comparisons between grasses and palms: synonymous rate differences at the nuclear gene *Adh* parallel rate differences at the plastid gene *rbcL*. *Proc. Natl. Acad. Sci.* 93, 10274–10279. doi: 10.1073/pnas.93.19.10274

Hebbar, K. B., Rane, J., Ramana, S., Panwar, N. R., Ajay, S., Rao, A. S., et al. (2014). Natural variation in the regulation of leaf senescence and relation to N and root traits in wheat. *Plant Soil* 378, 99–112. doi: 10.1007/s11104-013-2012-6

Horie, Y., Ito, H., Kusaba, M., Tanaka, R., and Tanaka, A. (2009). Participation of chlorophyll *b* Reductase in the initial step of the degradation of light-harvesting chlorophyll *a*/*b*-protein complexes in *Arabidopsis*. *J. Biol. Chem.* 284, 17449–17456. doi: 10.1074/jbc.M109.008912

Hörtensteiner, S., and Feller, U. (2002). Nitrogen metabolism and remobilization during senescence. *J. Exp. Bot.* 53, 927–937. doi: 10.1093/jexbot/53.370.927

Jia, T., Ito, H., and Tanaka, A. (2015). The chlorophyll *b* reductase NOL participates in regulating the antenna size of photosystem II in *Arabidopsis thaliana*. *Procedia Chem.* 14, 422–427. doi: 10.1016/j.proche.2015.03.057

Kalaji, H. M., Bosa, K., Kościelniak, J., and Żuk-Gołaszewska, K. (2011). Effects of salt stress on photosystem II efficiency and CO_2 assimilation of two Syrian barley landraces. *Environ. Exp. Bot.* 73, 64–72. doi: 10.1016/j.envexpbot.2010.10.009

Kalaji, H. M., Jajoo, A., Oukarroum, A., Brestic, M., Zivcak, M., Samborska, I. A., et al. (2016). Chlorophyll *a* fluorescence as a tool to monitor physiological status of plants under abiotic stress conditions. *Acta Physiol. Plant.* 38, 1–11. doi: 10.1007/s11738-016-2113-y

Kalaji, H. M., Oukarroum, A., Alexandrov, V., Kouzmanova, M., Brestic, M., Zivcak, M., et al. (2014). Identification of nutrient deficiency in maize and tomato plants by in vivo chlorophyll a fluorescence measurements. *Plant Physiol. Biochem.* 81, 16–25. doi: 10.1016/j.plaphy.2014.03.029

Kusaba, M., Ito, H., Morita, R., and Tanaka, H. H. M. N. A. (2007). Rice NON-YELLOW COLORING1 is involved in light-harvesting complex II and grana degradation during leaf senescence. *Plant Cell* 19, 1362–1375. doi: 10.1105/tpc.106.042911

Kuai, B., Chen, J., and Hörtensteiner, S. (2018). The biochemistry and molecular biology of chlorophyll breakdown. *Narnia* 69, 751–767. doi: 10.1093/jxb/erx322

Lescot, M., Déhais, P., Thijs, G., Marchal, K., Moreau, Y., Van de Peer, Y., et al. (2002). PlantCARE, a database of plant *cis*-acting regulatory elements

and a portal to tools for *in silico* analysis of promoter sequences. *Nucleic Acids Res.* 30, 325–327. doi: 10.1093/nar/30.1.325

Lim, P. O., Kim, H. J., and Nam, H. G. (2007). Leaf senescence. *Annu. Rev. Plant Biol.* 58, 115–136. doi: 10.1146/annurev.arplant.57.032905.105316

Mittler, R. (2002). Oxidative stress, antioxidants and stress tolerance. *Trends Plant Sci.* 7, 405–410. doi: 10.1016/S1360-1385(02)02312-9

Patton, A. J., and Reicher, Z. J. (2007). Zoysiagrass species and genotypes differ in their winter injury and freeze tolerance. *Crop Sci.* 47, 1619–1627. doi: 10.2135/cropsci2006.11.0737

Pourtau, N., Jennings, R., Pelzer, E., Pallas, J., and Wingler, A. (2006). Effect of sugar-induced senescence on gene expression and implications for the regulation of senescence in *Arabidopsis*. *Planta* 224, 556–568. doi: 10.1007/s00425-006-0243-y

Rozas, J., Ferrer-Mata, A., Sánchez-DelBarrio, J. C., Guirao-Rico, S., Librado, P., Ramos-Onsins, S. E., et al. (2017). DnaSP 6: DNA sequence polymorphism analysis of large data sets. *Mol. Biol. Evol.* 34, 3299–3302. doi: 10.1093/molbev/msx248

Rusinowski, S., Szada-Borzyszkowska, A., Zieleźnik-Rusinowska, P., Małkowski, E., Krzyżak, J., Woźniak, G., et al. (2019). How autochthonous microorganisms influence physiological status of *Zea mays* L. cultivated on heavy metal contaminated soils? *Environ. Sci. Pollut. Res.* 26, 4746–4763. doi: 10.1007/s11356-018-3923-9

Sakuraba, Y., Schelbert, S., Park, S.-Y., Han, S.-H., Lee, B.-D., Andrès, C. B., et al. (2012). STAY-GREEN and chlorophyll catabolic enzymes interact at light-harvesting complex II for chlorophyll detoxification during leaf senescence in *Arabidopsis*. *Plant Cell* 24, 507–518. doi: 10.1105/tpc.111.089474

Sato, Y., Morita, R., and Kusaba, S. K. M. N. A. T. M. (2010). Two short-chain dehydrogenase/reductases, NON-YELLOW COLORING 1 and NYC1-LIKE, are required for chlorophyll *b* and light-harvesting complex II degradation during senescence in rice. *Plant J.* 57, 120–131. doi: 10.1111/j.1365-313X.2008.03670.x

Schippers, J. H. M., Schmidt, R., Wagstaff, C., and Jing, H.-C. (2015). Living to die and dying to live: the survival strategy behind leaf senescence. *Plant Physiol.* 169, 914–930. doi: 10.1104/pp.15.00498

Shimoda, Y., Ito, H., and Tanaka, A. (2012). Conversion of chlorophyll *b* to chlorophyll *a* precedes magnesium dechelation for protection against necrosis in Arabidopsis. *Plant J.* 72, 501–511. doi: 10.1111/j.1365-313X.2012.05095.x

Sitko, K., Rusinowski, S., Kalaji, H. M., Szopiński, M., and Małkowski, E. (2017). Photosynthetic efficiency as bioindicator of environmental pressure in *A. halleri*. *Plant Physiol.* 175, 290–302. doi: 10.1104/pp.17.00212

Szopiński, M., Sitko, K., Gieroń, Ż., Rusinowski, S., Corso, M., Hermans, C., et al. (2019). Toxic effects of cd and Zn on the photosynthetic apparatus of the *Arabidopsis halleri* and *Arabidopsis arenosa* pseudo-metallophytes. *Front. Plant Sci.* 10:748. doi: 10.3389/fpls.2019.00748

Taiz, L., and Zeiger, E. (2002). Photosynthesis: physiological and ecological considerations. *Plant Physiol.* 9, 172–174. doi: 10.1093/aob/mcg079

Tamura, K., Stecher, G., and Kumar, S. (2021). MEGA11: molecular evolutionary genetics analysis version 11. *Mol. Biol. Evol.* 38, 3022–3027. doi: 10.1093/molbev/msab120

Taylor, L., Nunes-Nesi, A., Parsley, K., Leiss, A., Leach, G., Coates, S., et al. (2010). Cytosolic pyruvate, orthophosphate dikinase functions in nitrogen remobilization during leaf senescence and limits individual seed growth and nitrogen content. *Plant J.* 62, 641–652. doi: 10.1111/j.1365-313X.2010.04179.x

Teng, K., Chang, Z., Li, X., Sun, X., Liang, X., Xu, L., et al. (2016). Functional and RNA-sequencing analysis revealed expression of a novel stay-green gene from *Zoysia japonica* (*ZjSGR*) caused chlorophyll degradation and accelerated senescence in Arabidopsis. *Front. Plant Sci.* 7:1894. doi: 10.3389/fpls.2016.01894

Teng, K., Han, C., Yue, Y., Xu, L., Li, H., Wu, J., et al. (2021a). Functional characterization of the pheophytinase gene, *ZjPPH*, from *Zoysia japonica* in regulating chlorophyll degradation and photosynthesis. *Front. Plant Sci.* 12:786570. doi: 10.3389/fpls.2021.786570

Teng, K., Tan, P., Guan, J., Dong, D., Liu, L., Guo, Y., et al. (2021b). Functional characterization of the chlorophyll b reductase gene *NYC1* associated with chlorophyll degradation and photosynthesis in *Zoysia japonica*. *Environ. Exp. Bot.* 191:104607. doi: 10.1016/j.envexpbot.2021.104607

Teng, K., Tan, P., Guo, W., Yue, Y., Fan, X., and Wu, J. (2018). Heterologous expression of a novel *Zoysia japonica* C2H2 zinc finger gene, *ZjZFN1*, improved salt tolerance in Arabidopsis. *Front. Plant Sci.* 9:1159. doi: 10.3389/fpls.2018.01159

Teng, K., Tan, P., Xiao, G., Han, L., Chang, Z., and Chao, Y. (2017). Heterologous expression of a novel *Zoysia japonica* salt-induced glycine-rich RNA-binding protein gene, ZjGRP, caused salt sensitivity in Arabidopsis. *Plant Cell Rep.* 36, 179–191. doi: 10.1007/s00299-016-2068-x

Wan, Y., Mao, M., Wan, D., Yang, Q., Yang, F., Li, G., et al. (2018). Identification of the *WRKY* gene family and functional analysis of two genes in *Caragana intermedia*. *BMC Plant Biol.* 18, 1–16. doi: 10.1186/s12870-018-1235-3

Wang, T., Amee, M., Wang, G., Xie, Y., Hu, T., and Xu, H. (2021). FaHSP17.8-CII orchestrates lead tolerance and accumulation in shoots via enhancing antioxidant enzymatic response and PSII activity in tall fescue. *Ecotoxicol. Environ. Saf.* 223:112568. doi: 10.1016/j.ecoenv.2021.112568

Wingler, A., Masclaux-Daubresse, C., and Fischer, A. M. (2009). Sugars, senescence, and ageing in plants and heterotrophic organisms. *J. Exp. Bot.* 60, 1063–1066. doi: 10.1093/jxb/erp067

Yoo, S., Cho, Y., and Sheen, J. (2007). *Arabidopsis* mesophyll protoplasts: a versatile cell system for transient gene expression analysis. *Nat. Protoc.* 2, 1565–1572. doi: 10.1038/nprot.2007.199

Yu, G., Cheng, Q., Xie, Z., Xu, B., Huang, B., and Zhao, B. (2017). An efficient protocol for perennial ryegrass mesophyll protoplast isolation and transformation, and its application on interaction study between LpNOL and LpNYC1. *Plant Methods* 13:46. doi: 10.1186/s13007-017-0196-0

Yu, G., Xie, Z., Zhang, J., Lei, S., Lin, W., Xu, B., et al. (2021). NOL-mediated functional stay-green traits in perennial ryegrass (*Lolium perenne* L.) involving multifaceted molecular factors and metabolic pathways regulating leaf senescence. *Plant J.* 106, 1219–1232. doi: 10.1111/tpj.15204

Yusuf, M. A., Kumar, D., Rajwanshi, R., Strasser, R. J., Tsimilli-Michael, M., and Sarin, N. B. (2010). Overexpression of γ-tocopherol methyl transferase gene in transgenic *Brassica juncea* plants alleviates abiotic stress: physiological and chlorophyll a fluorescence measurements. *Biochim. Biophys. Acta Bioenerg.* 1797, 1428–1438. doi: 10.1016/j.bbabio.2010.02.002

Zagorchev, L., Traianova, A., Teofanova, D., Li, J., Kouzmanova, M., and Goltsev, V. (2020). Influence of Cuscuta campestris Yunck. On the photosynthetic activity of Ipomoea tricolor Cav.–in vivo chlorophyll a fluorescence assessment. *Photosynthetica* 58, 422–432. doi: 10.32615/ps.2020.004

Zhang, J., Li, H., Huang, X., Xing, J., Yao, J., Yin, T., et al. (2022). STAYGREEN-mediated chlorophyll a catabolism is critical for photosystem stability during heat-induced leaf senescence in perennial ryegrass. *Plant Cell Environ.* 45, 1412–1427. doi: 10.1111/pce.14296

Zhang, H., Xu, Z., Huo, Y., Guo, K., Wang, Y., He, G., et al. (2020). Overexpression of Trx CDSP32 gene promotes chlorophyll synthesis and photosynthetic electron transfer and alleviates cadmium-induced photoinhibition of PSII and PSI in tobacco leaves. *J. Hazard. Mater.* 398:122899. doi: 10.1016/j.jhazmat.2020.122899

Zhang, J., Zhang, Q., Xing, J., Li, H., Miao, J., and Xu, B. (2021). Acetic acid mitigated salt stress by alleviating ionic and oxidative damages and regulating hormone metabolism in perennial ryegrass (*Lolium perenne* L.). *Grass Research* 1, 1–10. doi: 10.48130/GR-2021-0003

Conflict of Interest: The authors declare that the research was conducted in the absence of any commercial or financial relationships that could be construed as a potential conflict of interest.

Publisher's Note: All claims expressed in this article are solely those of the authors and do not necessarily represent those of their affiliated organizations, or those of the publisher, the editors and the reviewers. Any product that may be evaluated in this article, or claim that may be made by its manufacturer, is not guaranteed or endorsed by the publisher.

frontiers | Frontiers in Plant Science

ORIGINAL RESEARCH
published: 06 May 2022
doi: 10.3389/fpls.2022.891372

Bacillus atrophaeus WZYH01 and *Planococcus soli* WZYH02 Improve Salt Tolerance of Maize (*Zea mays* L.) in Saline Soil

Yaling Hou[1], Wenzhi Zeng[1], Chang Ao[1]*, Ying Luo[1], Zhao Wang[2], Menglu Hou[2] and Jiesheng Huang[1]*

[1] State Key Laboratory of Water Resources and Hydropower Engineering Science, Wuhan University, Wuhan, China, [2] State Key Laboratory of Hybrid Rice, Institute for Advanced Studies, Wuhan University, Wuhan, China

With the increasing shortage of land resources and people's attention to the ecological environment, the application of microbial fertilizer with natural soil microorganisms as the main component has attracted increasing attention in saline agriculture. In this study, two salt-tolerant strains, YL07 (*Bacillus atrophaeus*) and YL10 (*Planococcus soli*), were isolated from maize (*Zea mays* L.) rhizosphere soil with a saturated conductivity (EC_e) of 6.13 dS/m and pH of 8.32 (Xinjiang, China). The effects of *B. atrophaeus* WZYH01 (YL07) and *Planococcus soli* WZYH02 (YL10) on the growth and development of maize (*Zea mays* L.) under salt stress (EC_e = 5.9 dS/m) were further studied. The results showed that compared with uninoculation, inoculation with *B. atrophaeus* WZYH01 and *Planococcus soli* WZYH02 significantly improved maize growth performance, biomass yield, and antioxidant levels under salt stress, and the effect of *Planococcus soli* WZYH02 was more prominent than the effect of *B. atrophaeus* WZYH01. Moreover, inoculation with *B. atrophaeus* WZYH01 and *Planococcus soli* WZYH02 protected maize from salt stress by regulating plant hormone [IAA and abscisic acid (ABA)] levels and increasing nutrient acquisition. In addition, the tested strains were most efficient for maize growth and health, increasing the content of K^+ accompanied by an effective decrease in Na^+ in maize tissues. The transcription levels of salt tolerance genes (*ZMNHX1*, *ZMNHX2*, *ZMHKT*, *ZMWRKY58,* and *ZMDREB2A*) in inoculated maize were also dramatically higher than the transcription levels of the specified salt tolerance genes in uninoculated maize. In conclusion, *B. atrophaeus* WZYH01 and *Planococcus soli* WZYH02 can alleviate the harmful effects of salt stress on crop growth, thereby promoting sustainable agricultural development.

Keywords: maize, PGPR, soil salinity, plant growth promotion, antioxidant

OPEN ACCESS

Edited by:
Jin-Lin Zhang,
Lanzhou University, China

Reviewed by:
Manoj Kumar Solanki,
University of Silesia in Katowice, Poland
Honghong Wu,
Huazhong Agricultural University, China

****Correspondence:***
Wenzhi Zeng
zengwenzhi1989@whu.edu.cn
Chang Ao
aochang@whu.edu.cn

Specialty section:
This article was submitted to Plant Abiotic Stress, a section of the journal Frontiers in Plant Science

Received: *07 March 2022*
Accepted: *08 April 2022*
Published: *06 May 2022*

Citation:
Hou Y, Zeng W, Ao C, Luo Y, Wang Z, Hou M and Huang J (2022) Bacillus atrophaeus WZYH01 and Planococcus soli WZYH02 Improve Salt Tolerance of Maize (Zea mays L.) in Saline Soil. Front. Plant Sci. 13:891372. doi: 10.3389/fpls.2022.891372

INTRODUCTION

Currently, approximately 1,125 million hectares of land worldwide are affected by salinization (Wicke et al., 2011; Dong et al., 2022). In China, approximately 3.67 million hectares of soil, which represents 4.88% of the total available land across the country, is threatened by salt (Zeng et al., 2016; Liu et al., 2020). To increase crop yield in salinized land, a large amount of chemical

fertilizer is applied to the soil (Wang L. L. et al., 2018), but the increase in chemical input is not directly proportional to the increase in crop yield (Hawkesford, 2014). Meanwhile, this behavior has also brought serious soil ecological and environmental problems such as secondary salinization, soil consolidation, soil acidification, and microecological imbalance (Hawkesford, 2014; Ma et al., 2021). In addition, the Ministry of Agriculture and Rural Affairs of the People's Republic of China (2015)[1] stated that the use of chemical fertilizer should be greatly reduced and that resource-saving and environmentally friendly modern agricultural development roads should be actively explored. Therefore, it is imperative to reduce the use of chemical fertilizer in agricultural production in saline land.

To overcome this issue, a new biocontrol approach has been developed to protect plants from salt stress in soil by utilizing beneficial microorganisms to achieve eco-friendly sustainable agriculture (Etesami and Maheshwari, 2018; Moreira et al., 2019). Plant growth-promoting rhizobacteria (PGPR) are an important microbial community that has a beneficial impact on plant growth and development. PGPR extensively colonizes plant roots, increases their growth, and reduces plant diseases (Shameer and Prasad, 2018). When combined with roots and other tissues, PGPR improves the nutritional supply of crop plants through several mechanisms. PGPR has direct effects, including nitrogen fixation, phosphorus solubilization, production of NH_3, indole acetic acid (IAA), and siderophores, and indirect effects, including antioxidant defense, volatile organic compounds (VOCs), exopolysaccharides (EPS), and osmotic balance mechanisms for improving plant growth and enhancing tolerance against salt stress (Moreira et al., 2016; Abbas et al., 2019; Kumar et al., 2019). Therefore, for decades, people have been studying how soil microorganisms play a role in plant growth to provide an alternative way to reduce the amount of fertilizer.

The application of PGPR to alleviate salinity-induced plant stress has become a promising approach. PGPR-mediated tolerance has been demonstrated in different plant–microbe interactions (Goswami et al., 2014; Li et al., 2020; Tirry et al., 2021). However, the efficiency of PGPR is affected by environmental factors such as climate, weather conditions, soil characteristics (e.g., texture, pH, temperature, and water content), and interaction with soil indigenous microbial flora (Siddikee et al., 2010; Qiu et al., 2019; Khalilpour et al., 2021). van Elsas et al. (1986) also reported that the numbers of *Bacillus subtilis* decreased rapidly in loamy sand and silt loam, while *Pseudomonas fluorescens* survived better in silty sand than in loamy loam. In addition, Habibi et al. (2019) found that PGPR isolated from Bala Doshi rice cultivars could promote Bala Doshi rice plant growth more than other rice cultivars, which might be due to the host specificity of Bala Doshi rice cultivars to the obtained strains. Simultaneously, recent studies have increasingly emphasized the benefits of using local microorganisms to enhance plant resistance to biological and abiotic stresses (Marulanda et al., 2009; Banerjee et al., 2017), suggesting that the activities of strains already adapted to the plant environment may increase the chances of inoculum survival and confer a positive effect on plant development under stress (Qiu et al., 2019). Therefore, we suggest screening of PGPR suitable for local soil and climate conditions.

Xinjiang is one of the most important agricultural production areas in the arid and semiarid regions of China (Wang et al., 2012), but 31.1% of the existing arable land in Xinjiang has suffered soil salinization (Liang et al., 2021; Liu Y. et al., 2021). The Statistical Yearbook of Xinjiang (2015) has shown that the annual yields of these three crops (grain, vegetables, and fruits) are approximately 1.50×10^7, 1.93×10^7, and 0.96×10^7 tons, respectively (Liu W. G. et al., 2021). At present, many studies on screening indigenous PGPR have also been carried out in these crops. Han et al. (2021) indicated that *Pseudomonas* SCPG-7 inoculated from pepper (*Capsicum annuum* L.) seeds had the ability to promote plant growth by secreting organic acids, alkaline phosphatase, siderophore, and IAA under salt stress in Shihezi, Xinjiang Province. The bacterial strain *Klebsiella oxytoca* Rs-5 was screened from the salinized soil of cotton in Xinjiang Province and could relieve salt stress and promote cotton seedling growth (Yue et al., 2007). *Pseudomonas putida* Rs-198 isolated from a cotton alkaline soil in Xinjiang mitigated osmotic stress in cotton seedlings, which led to an improved germination rate, healthy stands, and growth parameters (Yao et al., 2010). Liu et al. (2011) also reported that *Bacillus subtilis* SL-13 obtained from tomato field soil in Xinjiang Province was proven to promote sprouting and seedling growth in tomatoes. However, in the saline soils of Xinjiang, relatively few studies have been carried out on the screening of maize rhizosphere growth-promoting bacteria, which requires attention from the scientific community.

Compared with PGPR isolated from other soils, PGPR isolated from plants grown under chronically stressful salinity conditions have a stronger ability to survive due to their adaptation to the local environment (Kumar et al., 2017). However, knowledge of the potential of native PGPR isolates and their effects in maize plant growth and physiological characteristics under salt stress is still gravely limited. Therefore, the purpose of this study was to screen indigenous stress-tolerant PGPR with growth-promoting traits and evaluate the effects of PGPR isolates on the growth, physiology, and expression levels of stress-tolerant genes in maize seedlings under salt stress.

MATERIALS AND METHODS

Plant Material, Growing Conditions, and Treatments

Two strains (YL07 and YL10) were screened from maize rhizosphere soil in Yanqi, Xinjiang province, China (41°91' N, 86°49' E, elevation 1,061 m). The screening method is described in detail in the Supplementary Material. Maize seeds were treated with 75% ethanol for 30 s, sterilized with 10% sodium hypochlorite solution for 15 min, and then washed with sterile water 5–6 times. Sterilized seeds were soaked in sterile water for 12 h and then dipped in strain inoculum for 2 h. All the above experiments were carried out in a sterile environment. Thereafter, the treated maize seeds were cultivated in the seedling tray for 7 days, and then, maize seedlings with consistent growth were selected and transplanted into pots containing 1.2 kg

[1] http://english.moa.gov.cn

sterilized soil (120°C, 30 min, 100 kPa, and sterilized twice) in each pot. Three maize plants were maintained in each pot. The three treatments were as follows: uninoculated strain exposed to 5.9 dS/m salt stress (CK); YL07 strain exposed to 5.9 dS/m salt (YL07); and YL10 strain exposed to 5.9 dS/m salt stress (YL10). Each treatment had five repetitions. The maize was harvested after 31 days of growth.

Growth, Biomass Yield, Physiological Indicators, and Plant Hormones

After 31 days of cultivation, the plants were collected, and the roots were rinsed with sterile water. Plant height was measured and recorded. To obtain plant dry biomass, the plants were dried at 105°C for 30 min and kept at 75 ± 2°C for 24 h to achieve a constant dry weight (DW). The leaf superoxide dismutase (SOD), catalase (CAT), peroxidase (POD), ascorbate peroxidase (APX), glutathione reductase (GR) and reduced glutathione (GSH), soluble sugar, proline, IAA, and abscisic acid (ABA) contents were measured by Qingdao Sci-tech Innovation Quality Testing Co., Ltd[2].

Determination of N, K^+, Na^+, and K^+/Na^+

After 31 days of cultivation, the maize roots were washed and wiped dry to determine the content of nutrients and ions. Briefly, the maize leaves and roots were ground into fine powder, and then, 0.2 g samples were weighed into digestive tubes with 1 ml of distilled water. Then, 5 ml of H_2SO_4 was added to the mixture, and 2 ml of hydrogen peroxide was added twice. After the fierce reaction, the mixtures were put on the digestion furnace for digestion, and heating was stopped when the solution turned brown. After cooling slightly, 10 drops of H_2O_2 were added, heating was continued until the solution was colorless or clear, and heating continued for 5 min to remove excess H_2O_2. Nutrient nitrogen (N) was determined by the Kjeldahl method as indicated previously (Bremner, 2009). K^+ and Na^+ were determined by flame photometry according to Wolf (2008). The K^+/Na^+ ratio was calculated in line with the K^+ and Na^+ concentrations.

Transcription Analysis

The expression levels of related genes in maize seedlings inoculated with YL07, YL10, and the control treatment under salt stress were determined by quantitative real-time polymerase chain reaction (qRT-PCR). Total RNA was extracted from each maize seedling using TRIzol reagent following the manufacturer's instructions. The transcription levels of the ion balance-related genes *ZmNHX1* and *ZmNHX2* and *ZmHKT*, key transcription factor genes linked to the plant response to abiotic stress *ZmDREB2A* and *ZmWRKY58,* and key genes associated with ABA synthesis *ZmNCED* were measured. The sequences of primers used in qRT-PCR to study the relative expression of genes in maize lines are presented in the **Supplementary Table 1**. All PCR experiments were performed with SYBR Green Master Mix on a CFX Connect Real-Time PCR Detection System (1855201) with 40 cycles, and an annealing temperature of 55°C was used (in a final volume of 20 μl). The constitutively expressed β-actin gene was used as an internal control. The relative expression levels of the target genes were calculated using the $2^{-\Delta\Delta Ct}$ method. Five mRNA samples from five independent leaf samples (biological replicates) were analyzed.

Data and Statistical Analysis

All the data were statistically analyzed using RStudio (version 4.0.3). The significance of the differences between the control and treated groups was analyzed using one-way ANOVA followed by LSD *post hoc* comparison tests. Different letters indicate significant differences at the $P < 0.05$ level. Means and standard errors for all parameters were calculated from at least three replicates. Hierarchical clustering was performed using the "pheatmap" package based on Euclidean distance. Principal component analysis (PCA) was conducted using the "FactoMineR" package. All results were visualized using the "ggplot2" package in RStudio.

RESULTS

Growth and Biomass Yield

In the pot experiments, we recorded the maize growth index, such as plant height and dry biomass, under salt stress. The results showed that the plant height ($F = 1.93$, $P < 0.05$) and dry weight ($F = 6.33$, $P < 0.01$) were increased significantly by inoculating strains YL07 and YL10 under salt stress conditions. Compared with control plants, the plant height of inoculated strains YL07 and YL10 increased by 12.48 and 21.71%, respectively (**Figure 1A**), and the dry weight increased by 12.56 and 21.67%, respectively (**Figure 1B**).

The Contents of N, K^+, Na^+, and K^+/Na^+

To determine the absorption of nutrients and main ions in inoculated YL07 and YL10, the contents of N, K^+, and Na^+ in maize seedlings were measured. As shown in **Table 1**, the contents of nutrient N and K^+ in roots and shoots increased significantly ($P < 0.05$) in inoculated with YL07 and YL10, and the contents of shoots were higher than the contents of roots. Nevertheless, the content of Na^+ in roots and shoots inoculated with YL07 and YL10 decreased significantly ($P < 0.05$) in comparison with the control treatment. These results showed that the inoculated YL07 and YL10 strains could promote the absorption of N and K^+ and prevent the absorption of Na^+. Moreover, the K^+/Na^+ ratio is an indicator of ion balance in maize plants. As shown in **Table 1**, after inoculating the YL07 and YL10 strains, the K^+/Na^+ ratio in maize roots and shoots increased significantly ($P < 0.05$) compared with the K^+/Na^+ ratio in the control treatment. This result further reveals that inoculated YL07 and YL10 strains could promote the absorption of K^+ and inhibit the absorption of Na^+ in maize plants.

Antioxidant Enzymes, GSH, Soluble Sugar, and Proline Content

Salt stress mainly triggers the production of reactive oxygen species (ROS), and a large amount of ROS will cause serious

[2]http://www.kcscin.com

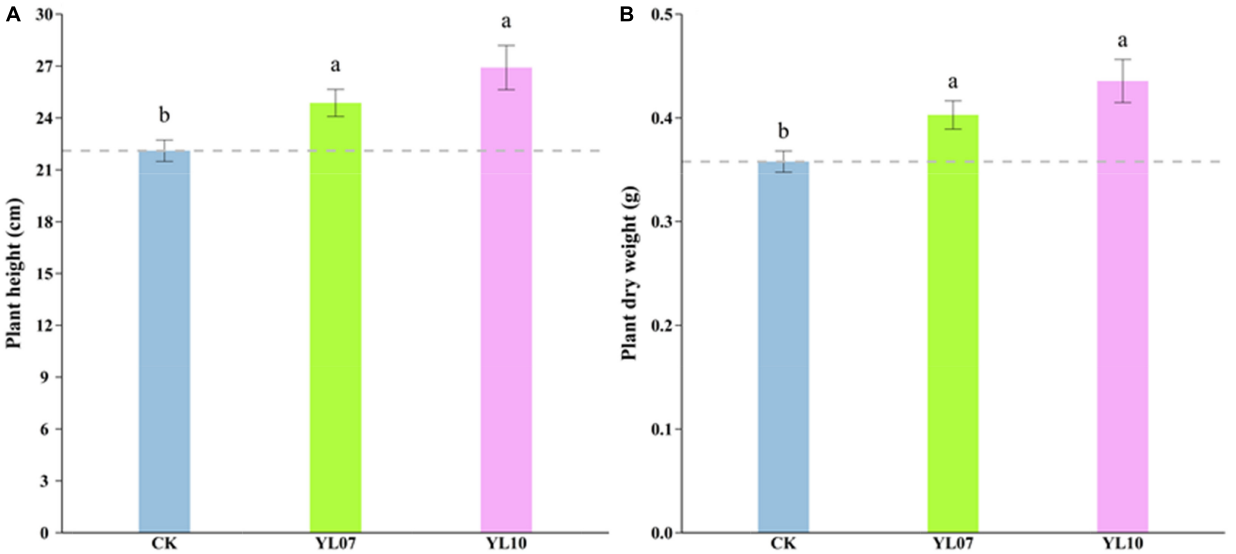

FIGURE 1 | Effect of strains YL07 and YL10 on the plant height **(A)** and dry weight **(B)** of maize under NaCl stress. Different letters indicate significant differences at the $P < 0.05$ level among the different treatments, as determined by LSD *post hoc* comparison tests.

TABLE 1 | Effects of YL07 and YL10 strain inoculation on nutrient elements and essential ion absorption by maize seedlings grown in pots under NaCl stress.

Groups	N content (mg g^{-1} DW)		K^+ (mg g^{-1} DW)		Na^+ (mg g^{-1} DW)		K^+/Na^+ ratio	
	Shoot	Root	Shoot	Root	Shoot	Root	Shoot	Root
CK3	30.03 ± 2.61b	14.95 ± 0.76b	30.66 ± 3.54b	12.92 ± 0.28c	5.47 ± 0.19a	8.99 ± 0.62a	5.68 ± 0.84b	1.45 ± 0.08b
YL	36.47 ± 1.57a	22.31 ± 1.61a	51.79 ± 1.76a	14.31 ± 0.34b	2.13 ± 0.28b	5.58 ± 0.21b	25.19 ± 3.03a	2.68 ± 0.33a
YL	35.46 ± 0.75ab	23.65 ± 1.76a	56.92 ± 4.43a	16.83 ± 0.56a	2.67 ± 0.28b	5.57 ± 0.32b	21.82 ± 1.56a	3.04 ± 0.17a

Different letters indicate significant differences at the $P < 0.05$ level among the different treatments based on one-way ANOVA.

damage to plant cells. Antioxidant enzymes such as SOD, CAT, POD, APX, and GR can remove excess ROS to maintain normal plant physiological activities. As shown in **Figure 2**, the contents of SOD, CAT, POD, APX, and GR in leaves inoculated with the YL07 and YL10 strains dramatically increased compared to the control treatment, in which SOD, YL07 and YL10 increased by 11.13 and 10.42% ($F = 96.08$, $P < 0.001$), respectively; CAT, YL07 and YL10 increased by 17.88 and 21.49% ($F = 279.60$, $P < 0.001$); POD, YL07 and YL10 increased by 26.65 and 25.11% ($F = 132.10$, $P < 0.001$); APX, YL07 and YL10 increased by 18.07 and 22.10% ($F = 153.10$, $P < 0.001$); GR, YL07 and YL10 increased by 23.15 and 25.73% ($F = 127.60$, $P < 0.001$), respectively. Similarly, the GSH content of YL07 and YL10 was significantly enhanced by 13.31 and 20.94%, respectively ($F = 223.80$, $P < 0.001$), compared to the control treatment (**Figure 2F**). As shown in **Figures 2G,H**, soluble sugars and proline showed the same results. The inoculated YL07 and YL10 were also considerably increased compared to the control treatment, in which soluble sugar, YL07 and YL10 increased by 5.24 and 9.26%, respectively ($F = 81.51$, $P < 0.001$); proline, YL07 and YL10 increased by 3.07 and 6.71%, respectively ($F = 11.96$, $P < 0.001$).

Under salt stress, the content of plant endogenous hormones regulates a series of physiological and biochemical reactions. As shown in **Figure 3**, the production of IAA was dramatically enhanced and the level of ABA was reduced in inoculated YL07 and YL10 under NaCl stress. Under inoculation with YL07 and YL10, the IAA content in the leaves of inoculated maize seedlings was significantly ($F = 447.40$, $P < 0.001$) increased by 18.46 and 22.96%, respectively, compared to the IAA content in the leaves of uninoculated control seedlings (**Figure 3A**). In contrast, the ABA content in maize leaves was significantly ($F = 158.30$, $P < 0.001$) decreased by 2.55 and 13.67%, respectively, under inoculation with the YL07 and YL10 treatments compared to the control treatments (**Figure 3B**).

Expression of Related Genes in Maize Seedlings

As shown in **Figures 4A–C**, the transcription levels of the ion balance-related genes *ZmNHX1* and *ZmNHX2* and *ZmHKT* in inoculated YL07 and YL10 under NaCl stress were upregulated in comparison with the control treatments, in which *ZmNHX1*, YL07 and YL10 increased by 465.04 and 742.80% ($F = 76.90$, $P < 0.001$), respectively; *ZmNHX2*, YL07, and YL10 increased by 385.20 and 602.87% ($F = 150.60$, $P < 0.001$), respectively; and *ZmHKT*, YL07, and YL10 increased by 442.57 and 673.70% ($F = 68.13$, $P < 0.001$), respectively. Similarly, key transcription gene *ZmDREB2A* and *ZmWRKY58* levels linked

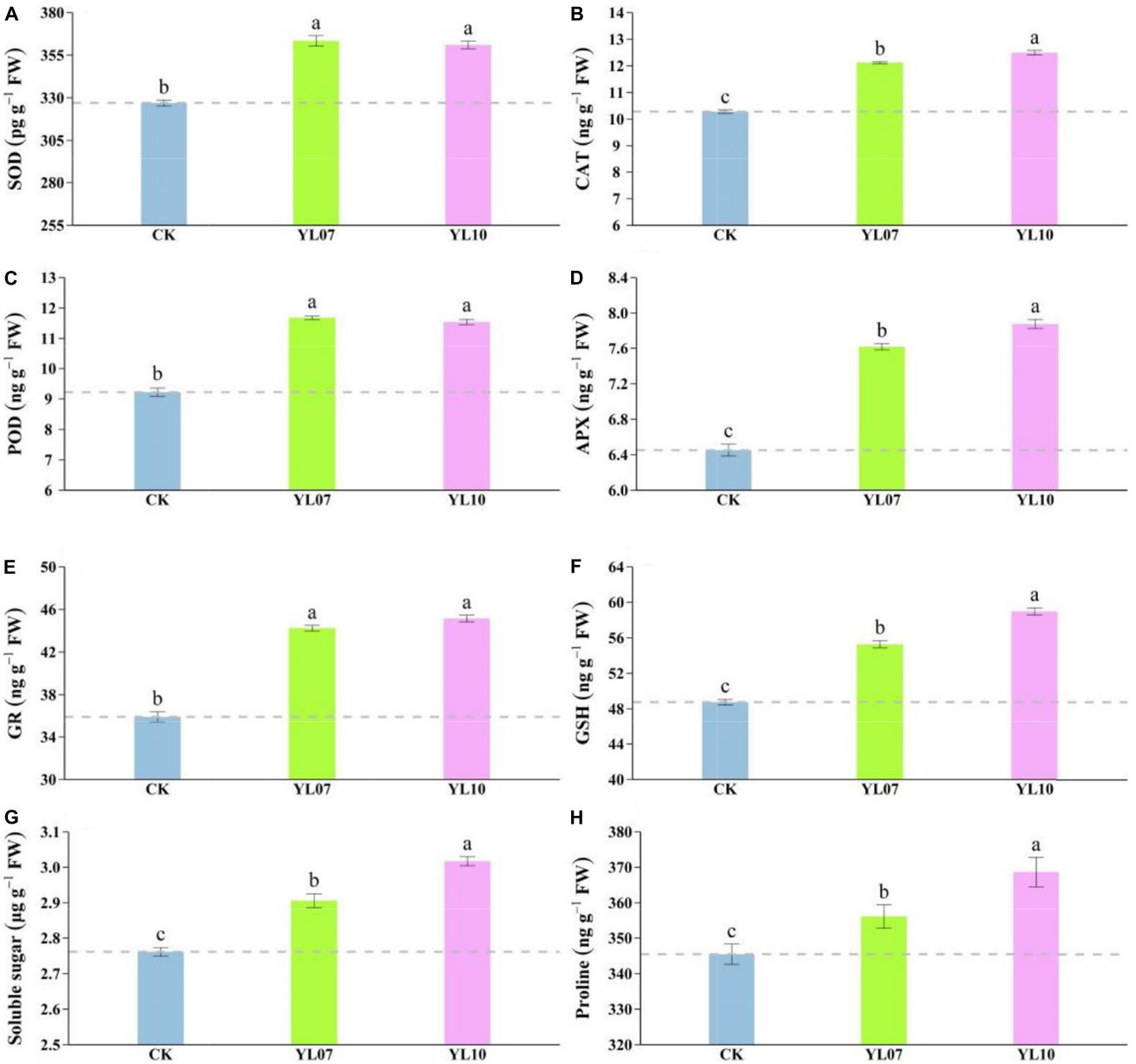

FIGURE 2 | Effect of strains YL07 and YL10 on antioxidant enzymes, including SOD **(A)**, CAT **(B)**, POD **(C)**, APX **(D)**, and GR **(E)** activities of maize under NaCl stress. Effects of YL07 and YL10 inoculation on GSH **(F)**, soluble sugar **(G)**, and proline **(H)** contents of maize grown in pots for 31 days under NaCl stress. Different letters indicate significant differences at the $P < 0.05$ level among the different treatments, as determined by LSD *post hoc* comparison tests. The content of IAA and ABA in plants.

to plant response to abiotic stress were also upregulated inoculated with YL07 and YL10 in which *ZmDREB2A*, YL07 and YL10 increased by 232.13 and 497.66% ($F = 82.28$, $P < 0.001$), respectively (**Figure 4D**); *ZmWRKY58*, YL07 and YL10 increased by 305.60 and 441.68% ($F = 57.79$, $P < 0.001$), respectively (**Figure 4E**). Moreover, the expression level of the key gene *ZmNCED*, which is associated with the ABA biosynthesis pathway, indicated that the YL07 and YL10 strains dramatically reduced the ABA content (**Figure 4F**). Analogously, the expression levels of *ZmNCED* were significantly decreased by 41.96 and 69.77% ($F = 51.92$, $P < 0.001$) under inoculated YL07 and YL10, respectively, compared to the control treatments.

Correlation Analysis Between the Studied Parameters

Cluster analysis of all studied parameters revealed that all samples clustered into two major clusters (**Figure 5**). The changes in the parameters were further observed in the heatmap and indicated

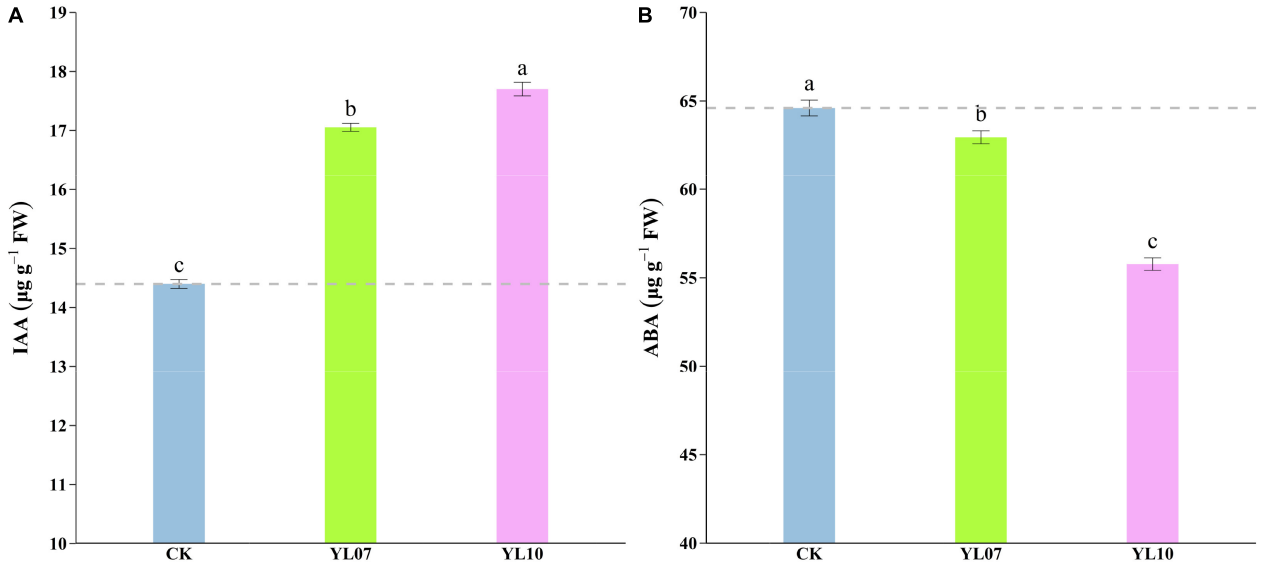

FIGURE 3 | Effect of inoculating with strains YL07 and YL10 on endogenous phytohormone IAA content **(A)** and ABA content **(B)** of maize seedlings grown in pots for 31 days under NaCl stress conditions. Different letters indicate significant differences at the $P < 0.05$ level among the different treatments, as determined by LSD *post hoc* comparison tests.

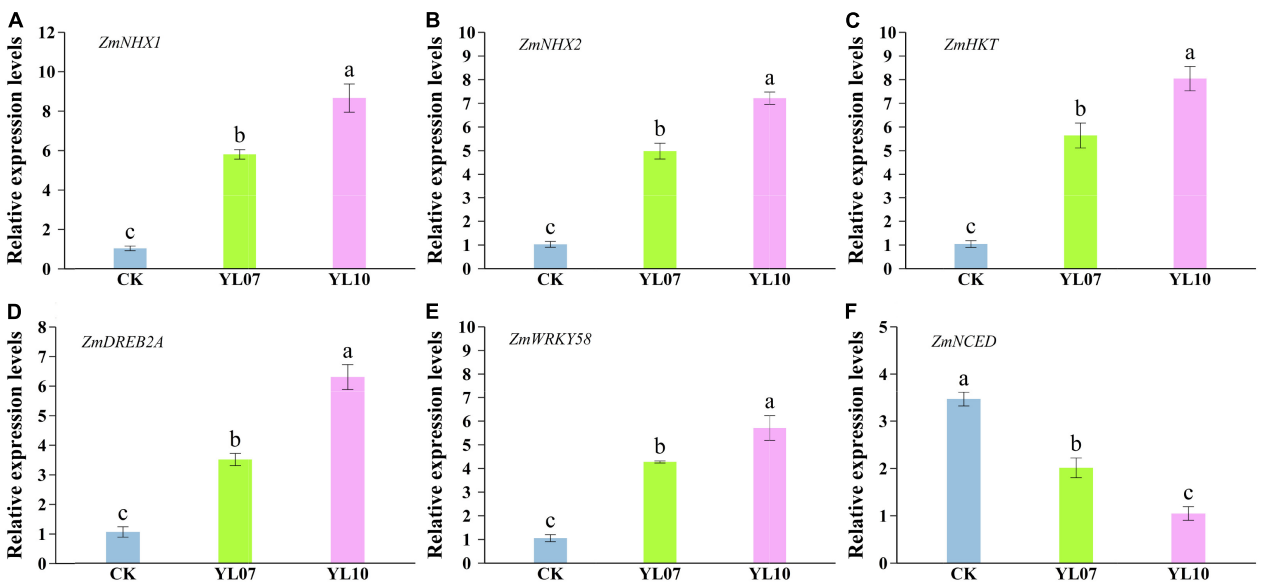

FIGURE 4 | Effect of inoculating with strains YL07 and YL10 on the expression of genes including ZmNHX1 **(A)**, ZmNHX2 **(B)**, ZmHKT **(C)**, ZmDREB2A **(D)**, ZmWRKY58 **(E)**, and ZmNCED **(F)** related to salt tolerance in maize seedlings under NaCl stress conditions. Different letters indicate significant differences at the $P < 0.05$ level among the different treatments, as determined by LSD post hoc comparison tests.

that the different treatment groups could be separated based on these parameters. The PCA of all parameters revealed the effects of uninoculated CK and inoculation YL07 and YL10 on maize plants under salt stress (**Figure 6**). PC1 accounted for 80.1% of the variance, and PC2 accounted for 6.1% of the variance. The CK treatment group was differentiated from the YL07 and YL10 groups, which might be attributed mainly to changes in parameters, including Na^+ content, ABA level, and *ZmNCED* expression level.

DISCUSSION

In previous studies, we found that fungi were more vulnerable to salt than bacteria in Xinjiang saline–alkali land (Hou et al., 2021). Therefore, in this screening of plant growth-promoting rhizobacteria, we focused on bacteria. Second, the previous screening methods were first based on the secretion characteristics of bacteria (Arruda et al., 2013; Pandey and Gupta, 2020; Sultana et al., 2021), but we first started from

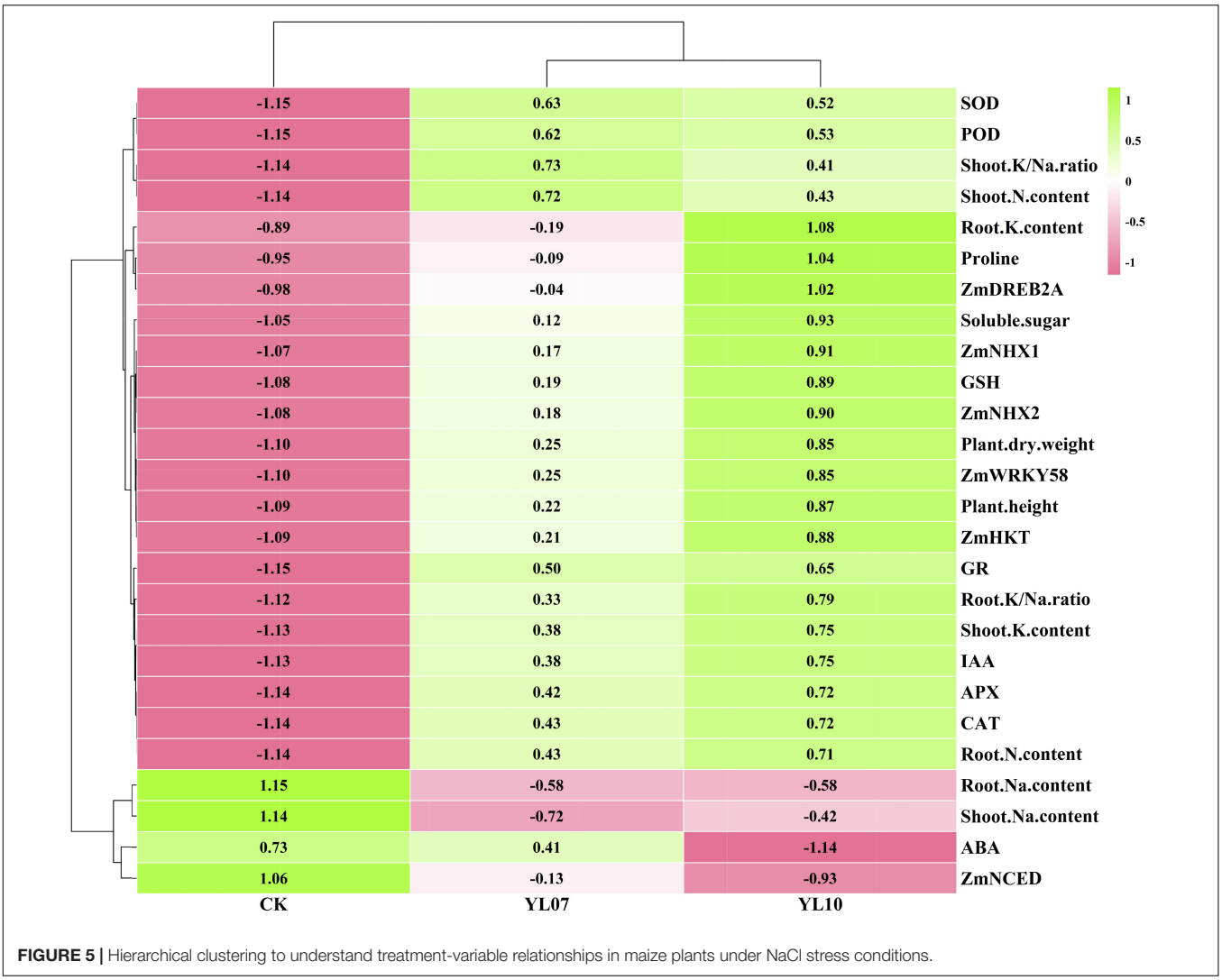

FIGURE 5 | Hierarchical clustering to understand treatment-variable relationships in maize plants under NaCl stress conditions.

the germination rate experiment of maize by bacteria. On the one hand, our procedure was more instructive from the perspective of production practice. On the other hand, we found that bacteria secreting promoting substances (such as indole acetic acid, solubilized phosphates, siderophores, and extracellular polysaccharides) might not necessarily promote the growth of crops (Arruda et al., 2013; Wang W. F. et al., 2018). Based on these reasons, combined with the results of the germination experiment and salt tolerance results by bacteria, we comprehensively selected the two kinds of dominant strains, precisely measured the growth-promoting substance secreted by bacteria, and finally thoroughly explained the growth-promoting function of bacteria on maize at the mechanistic level.

Characterization of Plant Growth-Promoting Rhizobacteria Traits Under Salt Stress

In this study, we isolated culturable rhizosphere bacteria from maize rhizosphere soil in saline–alkali land of Xinjiang for the first time and studied their ability *in vitro*. Two PGPR strains, *Bacillus atrophaeus* WZYH01 (YL07) and *Planococcus soli* WZYH02 (YL10), were capable of producing IAA and EPS and solubilizing phosphate effectively (**Supplementary Figure 3**). *Bacillus atrophaeus* belongs to the *Bacillus* genus, which is a gram-positive, aerobic, spore-forming bacterium phenotypically (Nakamura, 1989). *Bacillus atrophaeus* includes many strains that play an important role in the production of a range of products, including fermented food, bioinsecticides, antibiotics, and other products with commercial applications (Schallmey et al., 2004). A study showed that *B. atrophaeus* was remarkably resistant to extreme environments (i.e., heat, radiation, toxic chemicals, and pH extremes) (Moir, 2006). Ma et al. (2018) reported that *B. atrophaeus* strain GQJK17, as a kind of PGPR, had significant effects on inhibiting some soil-borne diseases and promoting the growth of some plants. *Bacillus atrophaeus* was verified to promote the growth of *Zea mays* L. and *Solanum lycopersicum* and had extraordinary activity in root colonization (Huang et al., 2015). The genus *Planococcus* was first proposed by Migula to adapt to accommodate gram-positive, aerobic

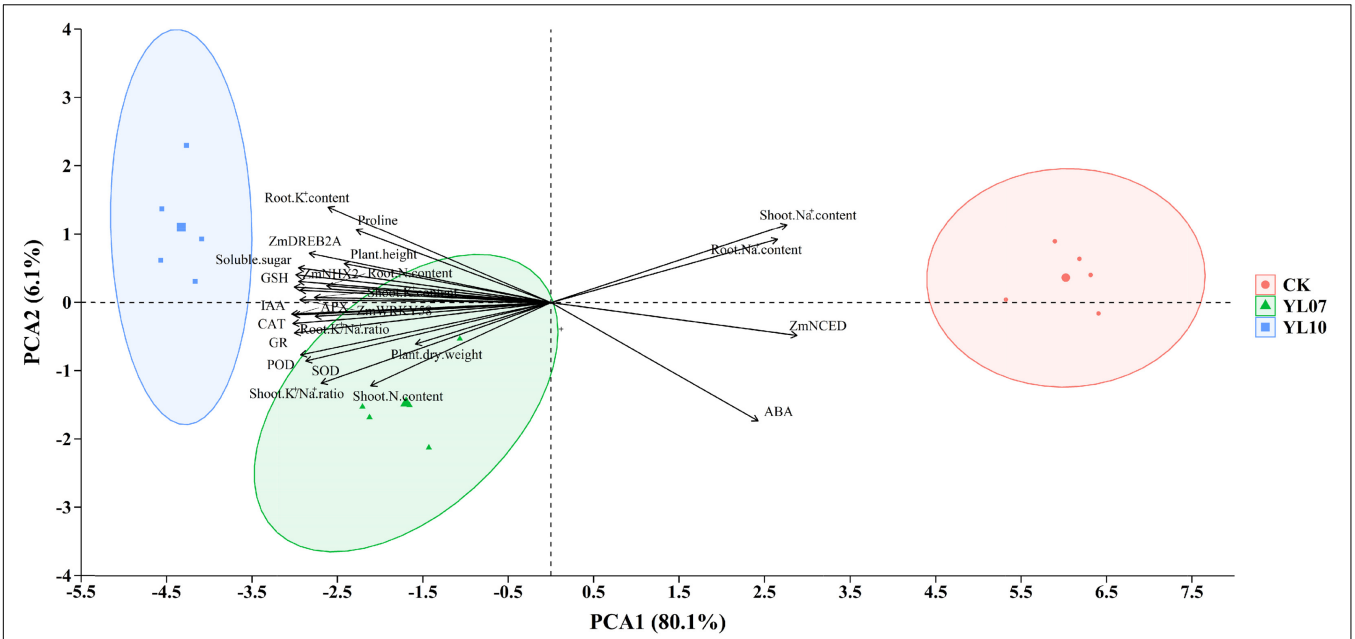

FIGURE 6 | Principal component analysis of all indicators in maize plants under salt stress.

bacteria of the family Planococcaceae (Yang et al., 2020). Many *Planococcus* species have been isolated from a variety of natural environments, including soil samples, marine samples, and extreme environments (Yang et al., 2020). They were highly resistant to the environment, usually salt-tolerant, and could grow at lower temperatures; some special strains could even grow at −15°C (Zhang et al., 2021). For example, *Planococcus* has also shown the ability to degrade and treat various pollutants, such as phenols and heavy metals (Sun et al., 2014). *Planococcus rifietoensis* M8^T is a salt-tolerant bacterium with potential plant growth-promoting properties that can promote the growth of the wheat by converting ammonia into nitrogen (See-Too et al., 2016). Although the above literature evidence indicates that some species belonging to the *Bacillus* and *Planococcus* genera have appropriate potential as PGPR, to our knowledge, this is the first report that *B. atrophaeus* and *Planococcus soli* can produce IAA, EPS, and solubilized phosphate under salt stress, which can be used as PGPR to promote maize plant growth under salt stress.

Plant growth-promoting rhizobacteria can effectively improve the tolerance of plants to abiotic stress and then promote plant growth and yield. In our results, we observed that maize inoculated with *B. atrophaeus* WZYH01 and *Planococcus soli* WZYH02 showed better growth prospects under salt stress. For example, in the germination experiment, the strains *B. atrophaeus* WZYH01 and *Planococcus soli* WZYH02 reduced the adverse effect of salt stress on the maize germination rate compared with the control (**Supplementary Figure 1A**). Inoculation with *B. atrophaeus* WZYH01 and *Planococcus soli* WZYH02 also increased maize root length compared with the root length in the uninoculated treatment (**Supplementary Figure 1B**). Our research was consistent with a previous study showing that the application of PGPR strains significantly improved the percentage of seed germination under saline conditions (Kaymak et al., 2009).

In the pot experiment, we also found that the strains *B. atrophaeus* WZYH01 and *Planococcus soli* WZYH02 had a certain alleviating effect on the growth of maize under salt stress. Compared with the uninoculated control, inoculating strains markedly increased the maize plant height and dry weight (**Figure 1**). Consistently, Mayak et al. (2004) indicated that salt-tolerant PGPR bacteria could improve the salt tolerance and yield of tomato, corn, and pepper crops in saline soil land.

Plant growth-promoting rhizobacteria traits, such as hormone production, phosphate solubilization, EPS secretion, ACC deaminase synthesis, siderophore production, and nitrogen fixation, had positive effects on promoting plant growth (Etesami and Maheshwari, 2018). This study clearly stated that both *B. atrophaeus* WZYH01 and *Planococcus soli* WZYH02, which produce hormone IAA, solubilize phosphorus, and secrete EPS, could improve the maize germination rate, root length, and growth conditions. Therefore, with the inoculation of these two strains, the promoting effect of maize under salt stress might be mediated by these growth-promoting characteristics. The hormone IAA secreted by bacteria was suggested to play an important role in promoting the growth of maize. Kumari et al. (2015) indicated that the higher root length of the inoculated plants might be due to the existence of the IAA hormone secreted by bacteria. Several studies also reported that PGPR strains showed IAA activity, and the interaction between IAA and plants helped to increase root growth under salt stress, which might be an adaptive response to salt stress (Albacete et al., 2008).

Bacterial polysaccharides synthesized and secreted into the external environment may be referred to as exopolysaccharides (Nwodo et al., 2012). EPS produced by PGPR contributed to soil aggregation, water retention, and chelation of metal ions in plants under salinity (Upadhyay et al., 2011). Under salt stress, EPS produced by PGPR could combine with Na^+ ions, reduce Na^+ content, and help to maintain ion balance in the root zone (Mishra et al., 2021). Liu et al. (2017) found that EPS produced by *B. amyloliquefaciens* FZB42 could finally reduce the Na^+ concentration in plants owing to binding to Na^+ content and inhibiting the absorption of Na^+. In the current study, *B. atrophaeus* WZYH01 and *Planococcus soli* WZYH02 produced a large number of EPS (**Supplementary Figure 3**), which could help maize plants resist salt stress. A previous study indicated that the formation of EPS and biofilms produced by the PGPR *Pseudomonas anguilliseptica* SAW 24 significantly improved the growth of *Vicia faba* L. under salt stress (Mohammed, 2018).

Phosphorus is the second most important key plant nutrient after nitrogen (Nanthakumar and Panneerselvam, 2017). Phosphorus participates in the important functions of plant energy metabolism, structural function, and signal transduction function and is necessary for plant growth and development (Lobo et al., 2019). Most of the phosphorus in the soil was fixed. Therefore, although the soil was rich in inorganic phosphorus and organic phosphorus, plant-available phosphorus was rarely effective. Phosphate solubilizing bacteria (PSB) have the ability to mobilize insoluble phosphate in soil and improve the tolerance of plants to various stresses (Kumar et al., 2018). The available phosphorus is dissolved by phosphate-dissolving microorganisms by producing acids (Alori et al., 2017). In this investigation, *B. atrophaeus* WZYH01 and *Planococcus soli* WZYH02 were solubilized phosphorus strains, which could help maize overcome nutrient deficiency and hormone imbalance under salt conditions (**Supplementary Figure 3**). Consistently, PSB could increase the content of soluble phosphorus in soil solution, promote the root growth of rice seedlings, and increase plant biomass (Panhwar et al., 2013). In addition, cucumber plants inoculated with *Cucumis sativus* also exhibited a higher P content than uninoculated plants under salinity stress (Kang et al., 2014a).

Effect of Plant Growth-Promoting Rhizobacteria Inoculation on Maize Tolerance to NaCl Stress

Salt stress inhibited plant growth due to the increase in Na^+ concentration and the decrease in the K^+/Na^+ ratio. Na^+ exclusion and K^+ influx are the most important strategies for plants to alleviate salt stress (Rojas-Tapias et al., 2012). PGPR could increase intracellular K^+ levels and maintain the K^+/Na^+ ratio by removing excess Na^+ in plant cells under salt stress (Mishra et al., 2021). We observed that high levels of Na^+ in maize roots and shoots were negatively correlated with maize biomass and plant height. In contrast, the K^+ content was positively correlated with plant biomass and plant height (**Figure 6**). Similarly, the results showed that inoculation with the two bacteria resulted in a decrease in Na^+ and a significant increase in K^+, which led to an increase in the K^+/Na^+ ratio (**Table 1**). Consistently, under salt stress, inoculation of PGPR has been reported to be able to avoid excessive accumulation of Na^+ in plants and maintain ion homeostasis (Kang et al., 2014b). Moreover, PGPR *Azospirillum lipoferum* and *Azotobacter chroococcum* increased the K^+ level of maize plants under salt stress, maintained the K^+/Na^+ ratio, and reduced the Na^+ level (Latef et al., 2020).

The main aspects of PGPR-mediated plant salt tolerance include generating reaction mechanisms to concentrate toxicity and establish osmotic equilibrium to avoid plant cell desiccation and flaccidity. As part of this regulatory pathway, Na^+/H^+ antiporters of tonoplast are encoded by the *NHX* genes. This progress in understanding the signal transduction pathway for the ion homeostasis and salt resistance of higher plants opens possibilities to establish salt-resistant crop plants (Zorb et al., 2005). PGPR inhibits the absorption of Na^+ by changing the composition of the cell wall or cell membrane, increases the electrogenic Na^+/H^+ ion transporters in plants, and increases the expression of *NHX* transporters (Kumar Arora et al., 2020). In this study, inoculating two strains, *B. atrophaeus* WZYH01 and *Planococcus soli* WZYH02, significantly reduced the level of Na^+ and upregulated the expression of *ZmNHX* and *ZmHKT* genes in maize under salt stress, indicating that inoculated strains might reduce the content of Na^+ in maize by isolating Na^+ into vacuoles and excreting Na^+ from cells to improve Na^+ toxicity and salt tolerance (**Figures 4A–C**). A previous study indicated that *Bacillus* promoted the growth of maize under salt stress by upregulating the expression of the plant ion homeostasis-related genes *NHX1* and *HKT1*. Furthermore, *Bacillus subtilis* reduced Na^+ uptake by *Arabidopsis thaliana* roots by downregulating the high-affinity K^+ transporter (*HKT1*) under salt stress (Zhang et al., 2008). Our results substantiate that the two PGPRs could improve maize salt tolerance by the upregulation of *ZmNHX* and *ZmHKT* genes with increased inclusion of Na^+ in vacuoles to avoid the accumulation of Na^+.

Mechanism of Plant Growth-Promoting Rhizobacteria in Promoting Maize Growth

The plant responds to salt stress conditions by generating reactive oxygen species (ROS), which generate oxidative stain in plants and impair chlorophyll, DNA, protein, and membrane functions (Kaushal and Wani, 2016). Salinity also causes the deleterious effect of osmotic pressure, deterioration of metabolic functions, decreased energy requirements, and disruption of cell divisions as well (Desoky et al., 2019). Whenever possible, plants are developing and/or adopting an antioxidant system to mitigate the destructive effects caused by salinity-induced ROS (Desoky et al., 2020). This system contains many enzymatic and non-enzymatic antioxidants with low molecular weights (Mishra et al., 2021). In the current study, inoculation with *B. atrophaeus* WZYH01 and *Planococcus soli* WZYH02 significantly increased the activity of

enzymatic antioxidants (SOD, CAT, POD, APX, and GR) and the content of the non-enzymatic antioxidant GSH in maize under salt stress (**Figures 2A–F**). The above results showed that the two strains could stimulate the defense response of plants to reactive oxygen species detoxification and promote the growth of maize seedlings. Enzymatic and non-enzymatic antioxidant activities may be reduced as PGPR detoxifies ROS through a variety of plant protection mechanisms, such as K^+ accumulation and phytohormones secreted by PGPR.

Plant growth-promoting rhizobacteria treatment resulted in a significant increase in proline and soluble sugars contents in salt stress, which acted as an osmoprotectant mechanism (**Figures 2G,H**). Proline, as a non-enzymatic antioxidant, increases with PGPR inoculation to improve the plant antioxidant system and restore energy compensation in plants. Proline reduces ROS damage and enhances plant tolerance by reducing the detoxification of ROS resulting from salinity stress (Howladar, 2014). Likewise, the accumulation of soluble sugars maintains the harmony between the osmotic quality of the cytosol and the vacuole. However, Desoky et al. (2020) indicated that proline and soluble sugars were significantly reduced by inoculation with PGPRs, which was not consistent with our research. In the present study, *B. atrophaeus* WZYH01 and *Planococcus soli* WZYH02 could increase proline and soluble sugar accumulation under salt stress. This also suggested the existence of other osmoprotectants to improve plant resistance to salt stress.

Plant growth-promoting rhizobacteria have been reported to stimulate the plant's nutrient acquisition machinery by activating nutrient-deficiency-induced transcription factors in addition to auxins and cytokinin secretion (Li et al., 2020). ABA is involved in various physiological processes of plants, including stomatal conductance, seedling growth, and plant responses to environmental stress (Li et al., 2020). Mishra et al. (2021) indicated that inoculation with PGPR could change the expression of ABA and the related gene *NCED* in plants. PGPR *P. fluorescence* and *P. putida* could downregulate the NCED gene of ABA biosynthesis in salt-stressed barley (Zaib et al., 2020). This study was consistent with our research. *Bacillus atrophaeus* WZYH01 and *Planococcus soli* WZYH02 showed a lower ABA content and *ZmNCED* expression (**Figures 3B**, **4F**). *DREBs* and *WRKY* transcript factors also play a critical role in enhancing plant salt tolerance (Li et al., 2020). Similar to the situation in wheat, the expression of a *DREB2* homolog in maize was found to be activated also by cold despite its induction by drought and salt stress (Nguyen et al., 2009). This study showed an increase in *ZmDREB2A* and *ZmWRKY58* gene expression in *B. atrophaeus* WZYH01 and *Planococcus soli* WZYH02-inoculated maize under saline conditions compared to non-inoculated control plants (**Figures 4D,E**). Therefore, under salt stress, *B. atrophaeus* WZYH01 and *Planococcus soli* WZYH02 are involved in changes in plant hormone-related gene expression, which may be involved in the improvement of salt stress and the regulation of plant development.

CONCLUSION

In this study, two salt-tolerant strains, *B. atrophaeus* WZYH01 and *Planococcus soli* WZYH02, were isolated from maize rhizosphere soil in Xinjiang, China. Two strains could tolerate up to 1197 mM NaCl and exhibited three growth-promoting traits: IAA, exopolysaccharide production, and phosphate solubilization. *Bacillus atrophaeus* WZYH01 and *Planococcus soli* WZYH02 could protect maize from salt stress, which could be considered the integration of multiple physiological processes, including improving plant mineral nutrition and increasing plant antioxidant capacity through plant hormones (IAA and ABA), and the expression of transporter genes, increasing the K^+/Na^+ ratio in maize plants. In general, the effect of *Planococcus soli* WZYH02 was more prominent in the growth index and gene expression than the effect of *B. atrophaeus* WZYH01. In conclusion, this study showed that *B. atrophaeus* WZYH01 and *Planococcus soli* WZYH02 could be used as eco-friendly PGPR based on their potential in promoting and protecting maize plant growth under saline conditions.

DATA AVAILABILITY STATEMENT

The datasets presented in this study can be found in online repositories. The names of the repository/repositories and accession number(s) can be found below: National Center for Biotechnology Information (NCBI) BioProject database under accession numbers MZ919348 and MZ919345.

AUTHOR CONTRIBUTIONS

YH involved in investigation, data curation, writing—original draft preparation, and visualization. WZ involved in conceptualization, methodology, writing—review and editing, funding acquisition, and supervision. CA took a leading role in writing—review and editing. YL involved in investigation, validation, and formal analysis. ZW and MH designed the methodology and formal analysis. JH involved in funding acquisition and supervision. All authors contributed to the article and approved the submitted version.

FUNDING

We are grateful for the financial support from the Program of the National Natural Science Foundation of China (NSFC) (grant numbers 51790533, 51879196, and 52179039).

SUPPLEMENTARY MATERIAL

The Supplementary Material for this article can be found online at: https://www.frontiersin.org/articles/10.3389/fpls.2022.891372/full#supplementary-material

REFERENCES

Abbas, R., Rasul, S., Aslam, K., Baber, M., Shahid, M., Mubeen, F., et al. (2019). Halotolerant PGPR: a hope for cultivation of saline soils. *J. King Saud Univ. Sci.* 31, 1195–1201. doi: 10.1016/j.jksus.2019.02.019

Albacete, A., Ghanem, M. E., Martinez-Andujar, C., Acosta, M., Sanchez-Bravo, J., Martinez, V., et al. (2008). Hormonal changes in relation to biomass partitioning and shoot growth impairment in salinized tomato (*Solanum lycopersicum* L.) plants. *J. Exp. Bot.* 59, 4119–4131. doi: 10.1093/jxb/ern251

Alori, E. T., Glick, B. R., and Babalola, O. O. (2017). Microbial phosphorus solubilization and its potential for use in sustainable agriculture. *Front. Microbiol.* 8:971. doi: 10.3389/fmicb.2017.00971

Arruda, L., Beneduzi, A., Martins, A., Lisboa, B., Lopes, C., Bertolo, F., et al. (2013). Screening of rhizobacteria isolated from maize (*Zea mays* L.) in Rio Grande do Sul State (South Brazil) and analysis of their potential to improve plant growth. *Appl. Soil Ecol.* 63, 15–22. doi: 10.1016/j.apsoil.2012.09.001

Banerjee, A., Bareh, D. A., and Joshi, S. R. (2017). Native microorganisms as potent bioinoculants for plant growth promotion in shifting agriculture (Jhum) systems. *J. Soil Sci. Plant Nutr.* 17, 127–140. doi: 10.4067/s0718-95162017005000010

Bremner, J. M. (2009). Determination of nitrogen in soil by the Kjeldahl method. *J. Agric. Sci.* 55, 11–33. doi: 10.1017/s0021859600021572

Desoky, E. M., Elrys, A. S., and Rady, M. M. (2019). Integrative moringa and licorice extracts application improves *Capsicum annuum* fruit yield and declines its contaminant contents on a heavy metals-contaminated saline soil. *Ecotoxicol. Environ. Saf.* 169, 50–60.

Desoky, E.-S. M., Saad, A. M., El-Saadony, M. T., Merwad, A.-R. M., and Rady, M. M. (2020). Plant growth-promoting rhizobacteria: potential improvement in antioxidant defense system and suppression of oxidative stress for alleviating salinity stress in *Triticum aestivum* (L.) plants. *Biocatal. Agric. Biotechnol.* 30:101878.

Dong, Y., Chen, R., Petropoulos, E., Yu, B., Zhang, J., Lin, X., et al. (2022). Interactive effects of salinity and SOM on the ecoenzymatic activities across coastal soils subjected to a saline gradient. *Geoderma* 406:115519. doi: 10.1016/j.geoderma.2021.115519

Etesami, H., and Maheshwari, D. K. (2018). Use of plant growth promoting rhizobacteria (PGPRs) with multiple plant growth promoting traits in stress agriculture: action mechanisms and future prospects. *Ecotox. Environ. Saf.* 156, 225–246. doi: 10.1016/j.ecoenv.2018.03.013

Goswami, D., Dhandhukia, P., Patel, P., and Thakker, J. N. (2014). Screening of PGPR from saline desert of Kutch: growth promotion in *Arachis hypogea* by *Bacillus licheniformis* A2. *Microbiol. Res.* 169, 66–75. doi: 10.1016/j.micres.2013.07.004

Habibi, S., Djedidi, S., Ohkama-Ohtsu, N., Sarhadi, W. A., Kojima, K., Rallos, R. V., et al. (2019). Isolation and screening of indigenous plant growth-promoting rhizobacteria from different rice cultivars in afghanistan soils. *Microbes Environ.* 34, 347–355. doi: 10.1264/jsme2.ME18168

Han, Y. J., Liu, S. X., Chen, F. L., Deng, X. L., Miao, Z., Wu, Z. S., et al. (2021). Characteristics of plant growth-promoting rhizobacteria SCPG-7 and its effect on the growth of *Capsicum annuum* L. *Environ. Sci. Pollut. Res.* 28, 11323–11332. doi: 10.1007/s11356-020-11388-6

Hawkesford, M. J. (2014). Reducing the reliance on nitrogen fertilizer for wheat production. *J. Cereal Sci.* 59, 276–283. doi: 10.1016/j.jcs.2013.12.001

Hou, Y. L., Zeng, W. Z., Hou, M. L., Wang, Z., Luo, Y., Lei, G. Q., et al. (2021). Responses of the soil microbial community to salinity stress in maize fields. *Biol. Basel* 10:1114. doi: 10.3390/biology10111114

Howladar, S. M. (2014). A novel *Moringa oleifera* leaf extract can mitigate the stress effects of salinity and cadmium in bean (*Phaseolus vulgaris* L.) plants. *Ecotoxicol. Environ. Saf.* 100, 69–75.

Huang, X. F., Zhou, D., Guo, J., Manter, D. K., Reardon, K. F., and Vivanco, J. M. (2015). Bacillus spp. from rainforest soil promote plant growth under limited nitrogen conditions. *J. Appl. Microbiol.* 118, 672–684. doi: 10.1016/10.1111/jam.1272

Kang, S. M., Khan, A. L., Waqas, M., You, Y. H., Kim, J. H., Kim, J. G., et al. (2014a). Plant growth-promoting rhizobacteria reduce adverse effects of salinity and osmotic stress by regulating phytohormones and antioxidants in *Cucumis sativus*. *J. Plant Interact.* 9, 673–682. doi: 10.1080/17429145.2014.894587

Kang, S. M., Radhakrishnan, R., Khan, A. L., Kim, M. J., Park, J. M., Kim, B. R., et al. (2014b). Gibberellin secreting rhizobacterium, *Pseudomonas* putida H-2-3 modulates the hormonal and stress physiology of soybean to improve the plant growth under saline and drought conditions. *Plant Physiol. Biochem.* 84, 115–124. doi: 10.1016/j.plaphy.2014.09.001

Kaushal, M., and Wani, S. P. (2016). Rhizobacterial-plant interactions: strategies ensuring plant growth promotion under drought and salinity stress. *Agric. Ecosyst. Environ.* 231, 68–78. doi: 10.1016/j.agee.2016.06.031

Kaymak, H. C., Guvenc, I., Yarali, F., and Donmez, M. F. (2009). The effects of bio-priming with PGPR on germination of radish (*Raphanus sativus* L.) seeds under saline conditions. *Turk. J. Agric. For.* 33, 173–179. doi: 10.3906/tar-0806-30

Khalilpour, M., Mozafari, V., and Abbaszadeh-Dahaji, P. (2021). Tolerance to salinity and drought stresses in pistachio (*Pistacia vera* L.) seedlings inoculated with indigenous stress-tolerant PGPR isolates. *Sci. Hortic.* 289:110440. doi: 10.1016/j.scienta.2021.110440

Kumar, A., Kumar, A., and Patel, H. (2018). Role of microbes in phosphorus availability and acquisition by plants. *Int. J. Curr. Microbiol. App. Sci.* 7, 1344–1347. doi: 10.20546/ijcmas.2018.705.161

Kumar, A., Patel, J. S., Meena, V. S., and Srivastava, R. (2019). Recent advances of PGPR based approaches for stress tolerance in plants for sustainable agriculture. *Biocatal. Agric. Biotechnol.* 20:101271. doi: 10.1016/j.bcab.2019.101271

Kumar, K., Amaresan, N., and Madhuri, K. (2017). Alleviation of the adverse effect of salinity stress by inoculation of plant growth promoting rhizobacteria isolated from hot humid tropical climate. *Ecol. Eng.* 102, 361–366. doi: 10.1016/j.ecoleng.2017.02.023

Kumar Arora, N., Fatima, T., Mishra, J., Mishra, I., Verma, S., Verma, R., et al. (2020). Halo-tolerant plant growth promoting rhizobacteria for improving productivity and remediation of saline soils. *J. Adv. Res.* 26, 69–82. doi: 10.1016/j.jare.2020.07.003

Kumari, S., Vaishnav, A., Jain, S., Varma, A., and Choudhary, D. K. (2015). Bacterial-mediated induction of systemic tolerance to salinity with expression of stress alleviating enzymes in soybean (*Glycine max* L. Merrill). *J. Plant Growth Regul.* 34, 558–573. doi: 10.1007/s00344-015-9490-0

Latef, A. A. H. A., Abu Alhmad, M. F., Kordrostami, M., Abo-Baker, A. B. A., and Zakir, A. (2020). Inoculation with *Azospirillum lipoferum* or *Azotobacter chroococcum* reinforces maize growth by improving physiological activities under saline conditions. *J. Plant Growth Regul.* 39, 1293–1306. doi: 10.1007/s00344-020-10065-9

Li, X. Z., Sun, P., Zhang, Y. N., Jin, C., and Guan, C. F. (2020). A novel PGPR strain *Kocuria rhizophila* Y1 enhances salt stress tolerance in maize by regulating phytohormone levels, nutrient acquisition, redox potential, ion homeostasis, photosynthetic capacity and stress-responsive genes expression. *Environ. Exp. Bot.* 174:104023. doi: 10.1016/j.envexpbot.2020.104023

Liang, J. P., Li, Y., Si, B. C., Wang, Y. Z., Chen, X. G., Wang, X. F., et al. (2021). Optimizing biochar application to improve soil physical and hydraulic properties in saline-alkali soils. *Sci. Total Environ.* 771:144802. doi: 10.1016/j.scitotenv.2020.144802

Liu, M. L., Wang, C., Liu, X. L., Lu, Y. C., and Wang, Y. F. (2020). Saline-alkali soil applied with vermicompost and humic acid fertilizer improved macroaggregate microstructure to enhance salt leaching and inhibit nitrogen losses. *Appl. Soil Ecol.* 156:103705. doi: 10.1016/j.apsoil.2020.103705

Liu, S. F., Hao, H. T., Lu, X., Zhao, X., Wang, Y., Zhang, Y. B., et al. (2017). Transcriptome profiling of genes involved in induced systemic salt tolerance conferred by Bacillus amyloliquefaciens FZB42 in *Arabidopsis thaliana*. *Sci. Rep.* 7:10795. doi: 10.1038/s41598-017-11308-8

Liu, W. G., Yang, X. D., Duan, L. C., Naidu, R., Yan, K. H., Liu, Y. J., et al. (2021). Variability in plant trace element uptake across different crops, soil contamination levels and soil properties in the Xinjiang Uygur Autonomous Region of northwest China. *Sci. Rep.* 11:2064. doi: 10.1038/s41598-021-81764-w

Liu, Y., Ao, C., Zeng, W. Z., Srivastava, A. K., Gaiser, T., Wu, J. W., et al. (2021). Simulating water and salt transport in subsurface pipe drainage systems with HYDRUS-2D. *J. Hydrol.* 592:125823. doi: 10.1016/j.jhydrol.2020.125823

Liu, Y., Tao, J., Yan, Y. J., Li, B., Li, H., and Li, C. (2011). Biocontrol efficiency of *Bacillus subtilis* SL-13 and characterization of an antifungal chitinase. *Chin. J. Chem. Eng.* 19, 128–134. doi: 10.1016/S1004-9541(09)60188-9

Lobo, C. B., Juarez Tomas, M. S., Viruel, E., Ferrero, M. A., and Lucca, M. E. (2019). Development of low-cost formulations of plant growth-promoting bacteria to be used as inoculants in beneficial agricultural technologies. *Microbiol. Res.* 219, 12–25. doi: 10.1016/j.micres.2018.10.012

Ma, J. J., Wang, C. Q., Wang, H. D., Liu, K., Zhang, T. R., Yao, L. T., et al. (2018). Analysis of the complete genome sequence of *Bacillus atrophaeus* GQJK17 reveals its biocontrol characteristics as a plant growth-promoting rhizobacterium. *Biomed. Res. Int.* 2018:9473542. doi: 10.1155/2018/9473542

Ma, T., Zeng, W. Z., Lei, G. Q., Wu, J. W., and Huang, J. S. (2021). Predicting the rooting depth, dynamic root distribution and the yield of sunflower under different soil salinity and nitrogen applications. *Ind. Crop Prod.* 170:113749. doi: 10.1016/j.indcrop.2021.113749

Marulanda, A., Barea, J. M., and Azcon, R. (2009). Stimulation of plant growth and drought tolerance by native microorganisms (AM Fungi and Bacteria) from dry environments: mechanisms related to bacterial effectiveness. *J. Plant Growth Regul.* 28, 115–124. doi: 10.1007/s00344-009-9079-6

Mayak, S., Tirosh, T., and Glick, B. R. (2004). Plant growth-promoting bacteria confer resistance in tomato plants to salt stress. *Plant Physiol. Biochem.* 42, 565–572. doi: 10.1016/j.plaphy.2004.05.009

Mishra, P., Mishra, J., and Arora, N. K. (2021). Plant growth promoting bacteria for combating salinity stress in plants - Recent developments and prospects: a review. *Microbiol. Res.* 252:126861. doi: 10.1016/j.micres.2021.126861

Mohammed, A. F. (2018). Effectiveness of exopolysaccharides and biofilm forming plant growth promoting rhizobacteria on salinity tolerance of faba bean (*Vicia faba* L.). *Afr. J. Microbiol. Res.* 12, 399–404. doi: 10.5897/ajmr2018.8822

Moir, A. (2006). How do spores germinate? *J. Appl. Microbiol.* 101, 526–530. doi: 10.1111/j.1365-2672.2006.02885.x

Moreira, H., Pereira, S. I. A., Marques, A. P. G. C., Rangel, A. O. S. S., and Castro, P. M. L. (2016). Selection of metal resistant plant growth promoting rhizobacteria for the growth and metal accumulation of energy maize in a mine soil — Effect of the inoculum size. *Geoderma* 278, 1–11. doi: 10.1016/j.geoderma.2016.05.003

Moreira, H., Pereira, S. I. A., Marques, A. P. G. C., Rangel, A. O. S. S., and Castro, P. M. L. (2019). Effects of soil sterilization and metal spiking in plant growth promoting rhizobacteria selection for phytotechnology purposes. *Geoderma* 334, 72–81. doi: 10.1016/j.geoderma.2018.07.025

Nakamura, L. K. (1989). Taxonomic relationship of black-pigmented Bacillus subtilis strains and a proposal for *Bacillus atrophaeus* sp. nov. *Int. J. Syst. Bacteriol.* 39, 295–300. doi: 10.1099/00207713-39-3-295

Nanthakumar, S., and Panneerselvam, P. (2017). Phosphorus and sulphur releasing pattern and their availability for maize cultivation. *J. Cer. Oil.* 8, 10–13. doi: 10.5897/jco2016.0152

Nguyen, H. T., Leipner, J., Stamp, P., and Guerra-Peraza, O. (2009). Low temperature stress in maize (*Zea mays* L.) induces genes involved in photosynthesis and signal transduction as studied by suppression subtractive hybridization. *Plant Physiol. Biochem.* 47, 116–122.

Nwodo, U. U., Green, E., and Okoh, A. I. (2012). Bacterial exopolysaccharides: functionality and prospects. *Int. J. Mol. Sci.* 13, 14002–14015. doi: 10.3390/ijms131114002

Pandey, S., and Gupta, S. (2020). Diversity analysis of ACC deaminase producing bacteria associated with rhizosphere of coconut tree (*Cocos nucifera* L.) grown in Lakshadweep islands of India and their ability to promote plant growth under saline conditions. *J. Biotechnol.* 324, 183–197. doi: 10.1016/j.jbiotec.2020.10.024

Panhwar, Q. A., Jusop, S., Naher, U. A., Othman, R., and Razi, M. I. (2013). Application of potential phosphate-solubilizing bacteria and organic acids on phosphate solubilization from phosphate rock in aerobic rice. *Sci. World J.* 2013:272409. doi: 10.1155/2013/272409

Qiu, Z., Egidi, E., Liu, H., Kaur, S., and Singh, B. K. (2019). New frontiers in agriculture productivity: optimised microbial inoculants and in situ microbiome engineering. *Biotechnol. Adv.* 37:107371. doi: 10.1016/j.biotechadv.2019.03.010

Rojas-Tapias, D., Moreno-Galvan, A., Pardo-Diaz, S., Obando, M., Rivera, D., and Bonilla, R. (2012). Effect of inoculation with plant growth-promoting bacteria (PGPB) on amelioration of saline stress in maize (*Zea mays*). *Appl. Soil Ecol.* 61, 264–272. doi: 10.1016/j.apsoil.2012.01.006

Schallmey, M., Singh, A., and Ward, O. P. (2004). Developments in the use of *Bacillus* species for industrial production. *Can. J. Microbiol.* 50, 1–17. doi: 10.1139/w03-076

See-Too, W. S., Convey, P., Pearce, D. A., Lim, Y. L., Ee, R., Yin, W. F., et al. (2016). Complete genome of *Planococcus rifietoensis* M8T, a halotolerant and potentially plant growth promoting bacterium. *J. Biotechnol.* 221, 114–115. doi: 10.1016/j.jbiotec.2016.01.026

Shameer, S., and Prasad, T. N. V. K. V. (2018). Plant growth promoting rhizobacteria for sustainable agricultural practices with special reference to biotic and abiotic stresses. *Plant Growth Regul.* 84, 603–615. doi: 10.1007/s10725-017-0365-1

Siddikee, M. A., Chauhan, P. S., Anandham, R., Han, G. H., and Sa, T. (2010). Isolation, characterization, and use for plant growth promotion under salt stress, of ACC deaminase-producing halotolerant bacteria derived from coastal soil. *J. Microbiol. Biotechnol.* 20, 1577–1584. doi: 10.4014/jmb.1007.07011

Sultana, S., Alam, S., and Karim, M. M. (2021). Screening of siderophore-producing salt-tolerant rhizobacteria suitable for supporting plant growth in saline soils with iron limitation. *J. Agric. Food Res.* 4:100150. doi: 10.1016/j.jafr.2021.100150

Sun, J. Q., Xu, L., Zhang, Z., Li, Y., Tang, Y. Q., and Wu, X. L. (2014). Diverse bacteria isolated from microtherm oil-production water. *Antonie Van Leeuwenhoek* 105, 401–411. doi: 10.1007/s10482-013-0088-x

Tirry, N., Kouchou, A., Laghmari, G., Lemjereb, M., Hnadi, H., Amrani, K., et al. (2021). Improved salinity tolerance of *Medicago sativa* and soil enzyme activities by PGPR. *Biocatal. Agric. Biotechnol.* 31:101914. doi: 10.1016/j.bcab.2021.101914

Upadhyay, S. K., Singh, J. S., and Singh, D. P. (2011). Exopolysaccharide-producing plant growth-promoting rhizobacteria under salinity condition. *Pedosphere* 21, 214–222. doi: 10.1016/s1002-0160(11)60120-3

van Elsas, J. D., Dijkstra, A. F., Govaert, J. M., and van Veen, J. A. (1986). Survival of *Pseudomonas* fluorescens and *Bacillus subtilis* introduced into two soils of different texture in field microplots. *FEMS Microbiol. Ecol.* 2, 151–160. doi: 10.1111/j.1574-6968.1986.tb01724.x

Wang, L. L., Palta, J. A., Chen, W., Chen, Y. L., and Deng, X. P. (2018). Nitrogen fertilization improved water-use efficiency of winter wheat through increasing water use during vegetative rather than grain filling. *Agric. Water Manage.* 197, 41–53. doi: 10.1016/j.agwat.2017.11.010

Wang, R. S., Kang, Y. H., Wan, S. Q., Hu, W., Liu, S. P., Jiang, S. F., et al. (2012). Influence of different amounts of irrigation water on salt leaching and cotton growth under drip irrigation in an arid and saline area. *Agric. Water Manage.* 110, 109–117. doi: 10.1016/j.agwat.2012.04.005

Wang, W. F., Wu, Z. S., He, Y. H., Huang, Y. Y., Li, X., and Ye, B. C. (2018). Plant growth promotion and alleviation of salinity stress in *Capsicum annuum* L. by *Bacillus* isolated from saline soil in Xinjiang. *Ecotoxicol. Environ. Saf.* 164, 520–529. doi: 10.1016/j.ecoenv.2018.08.070

Wicke, B., Smeets, E., Dornburg, V., Vashev, B., Gaiser, T., Turkenburg, W., et al. (2011). The global technical and economic potential of bioenergy from salt-affected soils. *Energy Environ. Sci.* 4, 2669–2681. doi: 10.1039/c1ee01029h

Wolf, B. (2008). A comprehensive system of leaf analyses and its use for diagnosing crop nutrient status. *Commun. Soil Sci. Plant Anal.* 13, 1035–1059. doi: 10.1080/00103628209367332

Yang, R. Q., Zhang, B. L., Wang, J. C., Tai, X. S., Sun, H. L., Zhang, G. S., et al. (2020). *Planococcus lenghuensis* sp. nov., an oil-degrading bacterium isolated from petroleum-contaminated soil. *Antonie van Leeuwenhoek* 113, 839–850. doi: 10.1007/s10482-020-01394-6

Yao, L. X., Wu, Z. S., Zheng, Y. Y., Kaleem, I., and Li, C. (2010). Growth promotion and protection against salt stress by *Pseudomonas* putida Rs-198 on cotton. *Eur. J. Soil Biol.* 46, 49–54. doi: 10.1016/j.ejsobi.2009.11.002

Yue, H. T., Mo, W. P., Li, C., Zheng, Y. Y., and Li, H. (2007). The salt stress relief and growth promotion effect of Rs-5 on cotton. *Plant Soil* 297, 139–145. doi: 10.1007/s11104-007-9327-0

Zaib, S., Ahmad, I., and Shakeel, S. N. (2020). Modulation of barley (*Hordeum vulgare*) defense and hormonal pathways by *Pseudomonas* species accounted for salinity tolerance. *Pak. J. Agric. Sci.* 57, 1469–1481. doi: 10.21162/PAKJAS/20.9373

Zeng, W. Z., Xu, C., Wu, J. W., and Huang, J. S. (2016). Sunflower seed yield estimation under the interaction of soil salinity and nitrogen application. *Field Crop. Res.* 198, 1–15. doi: 10.1016/j.fcr.2016.08.007

Zhang, H., Kim, M. S., Sun, Y., Dowd, S. E., Shi, H., and Pare, P. W. (2008). Soil bacteria confer plant salt tolerance by tissue-specific regulation of the sodium transporter HKT1. *Mol. Plant Microbe Interact.* 21, 737–744. doi: 10.1094/MPMI-21-6-0737

Zhang, S. Y., Ping, W. W., Xin, Y. H., Xin, D., and Zhang, J. L. (2021). *Planococcus soli* sp. nov., isolated from antarctic soil. *Antonie Van Leeuwenhoek* 114, 1107–1115. doi: 10.1007/s10482-021-01581-z

Zorb, C., Noll, A., Karl, S., Leib, K., Yan, F., and Schubert, S. (2005). Molecular characterization of Na+/H+ antiporters (ZmNHX) of maize (*Zea mays* L.) and their expression under salt stress. *J. Plant Physiol.* 162, 55–66.

Conflict of Interest: The authors declare that the research was conducted in the absence of any commercial or financial relationships that could be construed as a potential conflict of interest.

Publisher's Note: All claims expressed in this article are solely those of the authors and do not necessarily represent those of their affiliated organizations, or those of the publisher, the editors and the reviewers. Any product that may be evaluated in this article, or claim that may be made by its manufacturer, is not guaranteed or endorsed by the publisher.

frontiers | Frontiers in Plant Science

ORIGINAL RESEARCH
published: 10 May 2022
doi: 10.3389/fpls.2022.884456

Overexpression of *Pennisetum purpureum CCoAOMT* Contributes to Lignin Deposition and Drought Tolerance by Promoting the Accumulation of Flavonoids in Transgenic Tobacco

Jian-Ling Song[1†], Ze-Yu Wang[2,3†], Yin-Hua Wang[2,3], Juan Du[4], Chen-Yu Wang[2], Xiang-Qian Zhang[2,3], Shu Chen[2,3], Xiao-Ling Huang[2], Xin-Ming Xie[2,3] and Tian-Xiu Zhong[2,3]**

[1] Office of Academic Research, Xingyi Normal University for Nationalities, Xingyi, China, [2] Department of Grassland Science, College of Forestry and Landscape Architecture, South China Agricultural University, Guangzhou, China, [3] Guangdong Engineering Research Center for Grassland Science, Guangzhou, China, [4] Institute for Agricultural Biosciences, Oklahoma State University, Ardmore, OK, United States

Elephant grass (*Pennisetum purpureum*) is a fast-growing and low-nutrient demand plant that is widely used as a forage grass and potential energy crop in tropical and subtropical regions of Asia, Africa, and the United States. Transgenic tobacco with the *PpCCoAOMT* gene from *Pennisetum purpureum* produces high lignin content that is associated with drought tolerance in relation to lower accumulation of reactive oxygen species (ROS), along with higher antioxidant enzyme activities and osmotic adjustment. In this study, transgenic tobacco plants revealed no obvious cost to plant growth when expressing the *PpCCoAOMT* gene. Metabolomic studies demonstrated that tobacco plants tolerant to drought stress accumulated flavonoids under normal and drought conditions, which likely explains the observed tolerance phenotype in wild-type tobacco. Our results suggest that plants overexpressing *PpCCoAOMT* were better able to cope with water deficit than were wild-type controls; metabolic flux was redirected within primary and specialized metabolism to induce metabolites related to defense to drought stress. These results could help to develop drought-resistant plants for agriculture in the future.

Keywords: elephant grass, drought tolerance, *PpCCoAOMT*, lignin, flavonoids

KEY MESSAGE

- The *PpCCoAOMT* gene contributes to lignin deposition and flavonoid accumulation; it plays important roles in controlling drought tolerance, stomatal number, and aperture size without any plant growth cost.

OPEN ACCESS

Edited by:
Jing Zhang,
Nanjing Agricultural University, China

Reviewed by:
Gang Nie,
Sichuan Agricultural University, China
Mingna Li,
Chinese Academy of Agricultural Sciences (CAAS), China

****Correspondence:***
Xin-Ming Xie
xiexmbs@scau.edu.cn
Tian-Xiu Zhong
zhongxinbi@163.com

† These authors have contributed equally to this work

Specialty section:
This article was submitted to Plant Abiotic Stress, a section of the journal Frontiers in Plant Science

Received: *26 February 2022*
Accepted: *25 March 2022*
Published: *10 May 2022*

Citation:
Song J-L, Wang Z-Y, Wang Y-H, Du J, Wang C-Y, Zhang X-Q, Chen S, Huang X-L, Xie X-M and Zhong T-X (2022) Overexpression of Pennisetum purpureum CCoAOMT Contributes to Lignin Deposition and Drought Tolerance by Promoting the Accumulation of Flavonoids in Transgenic Tobacco. Front. Plant Sci. 13:884456. doi: 10.3389/fpls.2022.884456

INTRODUCTION

The plant cell wall is the first barrier against external hazards, such as biotic and abiotic stressors; lignin is one of the most important functional components of the cell wall for multiple cells in plant tissues (Barros et al., 2015). As a major secondary metabolite, lignin is produced by the phenylpropanoid pathway. Lignin metabolism involves lignin biosynthesis, transport, and polymerization enzymes. Among the synthetic network of lignin monomers in the cytoplasm, caffeoyl-CoA O-methyltransferase (CCoAOMT) is a key enzyme that participates in the first methylation step required to produce G units, which are the three structural units (p-hydroxyphenyl, guaiacyl, and sinapyl moieties) from monolignols (Xia et al., 2018). In addition, CCoAOMT provides feruloyl-CoA for other biosynthetic pathways (Kai et al., 2008). The downregulation of *CCoAOMT* results in a decrease in lignin content (Wagner et al., 2011; Li et al., 2013), while the overexpression of *CCoAOMT* results in an increase in lignin content (Zhang et al., 2014; Zhao et al., 2021), indicating an essential role for CCoAOMT in lignin biosynthesis.

Lignin has many biological functions, such as water transport, mechanical support, and resistance to various stressors. Notably, low molecular weight lignin monomers derived from H and G units have antioxidant capacity; thus, lignin has some biological activity. Oxidative stress includes excessive production of reactive oxygen species (ROS), such as superoxide radicals (O_2^-) and hydrogen peroxide (H_2O_2), which are produced under adverse environmental conditions. H_2O_2 has an important regulatory role in lignin biosynthesis (Kováčik et al., 2010; Liu et al., 2015; Rui et al., 2016), indicating that the lignin biosynthetic pathway and the abiotic response may participate in crosstalk (Guo et al., 2017). A previous study demonstrated that *CCoAOMT* expression is enhanced under drought stress in the root elongation region of soybean (Yamaguchi et al., 2010), in grape berries (Giordano et al., 2016), and in the stem and leaf tissues of switchgrass (Liu et al., 2016). Many studies have shown that lignin biosynthesis is enhanced under drought stress and in response to other abiotic stressors. Lignin content significantly increases in the stem when plants are exposed to drought stress (Hu et al., 2009; Moura-Sobczak et al., 2011; Geng et al., 2018; Li et al., 2022). Moreover, an increase in lignin deposition is required for drought tolerance (Hu et al., 2009; Srivastava et al., 2015; Geng et al., 2018; Zhou et al., 2020) and the metal ion response (Xia et al., 2018; Su et al., 2020) *via* overexpression of lignin biosynthesis-related genes. For example, increased lignin content and improved drought tolerance are caused by the overexpression of genes such as *PoCCoAOMT* in *Nicotiana tabacum* (Zhao et al., 2021), *Gh4CL7* in *Arabidopsis thaliana* (Sun S. C. et al., 2020), *PtoMYB170* in *Populus tomentosa* (Xu et al., 2017), and *PuC3H35* in *Populus ussuriensis* (Li et al., 2022).

Elephant grass (*Pennisetum purpureum*) is a fast-growing low nutrient demand plant that has potential for use in bio-oil production (Strezov et al., 2008) and for the alleviation of feed shortage because it is drought-resistant which could endure 5 mm monthly precipitation (Gomide et al., 2011) and produces high biomass (Rusdy, 2016). Elephant grass is a species of perennial C_4 deep-rooted bunchgrass that inhabits tropical and subtropical regions of Asia, Africa, and the United States (Yan et al., 2021). The modulation of lignin deposition *via CCoAOMT* has been implicated in environmental stress responses in several species (Xia et al., 2018; Su et al., 2020; Zhao et al., 2021). However, few studies have explored the crosstalk between the lignin biosynthetic pathway and other biosynthetic pathways involved in drought tolerance. In the present study, we report that the overexpression of *PpCCoAOMT* in tobacco plants led to lignin accumulation but exhibited a contrasting effect on leaf area under transient drought conditions. The full-length cDNA of *P. purpureum CCoAOMT* was cloned and an overexpression construct of *CCoAOMT* (OE-*PpCCoAOM*T) was produced in transgenic tobacco plants by *Agrobacterium*-mediated transformation. The growth and development phenotypes of OE-*PpCCoAOMT* transgenic tobacco were evaluated and compared to wild-type (WT) plants. OE-*PpCCoAOMT* transgenic tobacco had higher drought stress tolerance because of ROS scavenging and higher maintenance of relative water content (RWC). Metabolomics analyses showed that *PpCCoAOMT* conferred transgenic tobacco with primary metabolites, resulting in more flavonoids that exhibited high antioxidant activities. These results will provide insights concerning the *CCoAOMT* lignin biosynthesis gene and the regulation of drought tolerance.

MATERIALS AND METHODS

Isolation and *PpCCoAOMT* Bioinformatics Analysis

Total RNA of elephant grass (*P. purpureum*) was extracted from leaves and immediately reverse transcribed to obtain cDNA; the cDNA was used as a template to amplify the coding sequence of the *PpCCoAOMT* gene *via* 3′ random amplification of DNA ends (RACE) technology. Genomic DNA was used to amplify the 5′ end of the *PpCCoAOMT* gene using the high-efficiency thermal asymmetric interlaced polymerase chain reaction (hiTAIL-PCR). The PCR product was subjected to agarose gel electrophoresis and verified by sequencing. The homology of the PpCCoAOMT protein was analyzed by BLASTP. The amino acid sequences were aligned with DNAMAN software; conserved domains were identified using Red hollow boxes. Forty-one experimentally proven or putative CCoAOMT sequences from various species were used to construct a neighbor-joining phylogenetic tree in MEGA 6.0 software; 500 bootstrap replicates were used to estimate branch support.

Verification of *PpCCoAOMT* Overexpressing Transgenic Tobacco Plants

Agrobacterium strain *LBA4404* harboring pBA002/3HA-*PpCCoAOMT* was transformed into tobacco (*N. tabacum* cultivar Wisconsin 38) using a leaf disc transformation method; regenerated shoots were rooted in the presence of 5 mg/L Basta before the plants were transferred to pots. The T0-generation of

the transformed plants was identified by both PCR and RT-PCR. Total genomic DNA from all transgenic plants was extracted using the sodium dodecyl sulfate method. PCR was performed to confirm positive transformants using primers for the selectable marker gene BASTA (Bar: 5′-CGACTGCCAGAAACCCACGT-3′, 5′-CTGCACCATCGTCAACCACT-3′); the tobacco actin gene served as the internal control. After the removal of negatively transformed plants, the remaining plants were confirmed by specific primers. Total RNA was extracted from different OE plants and used for RT-PCR performed with a pair of primers (*PpCCoAOMT*: 5′-GGACATCAACCGCGAGAACT-3′, 5′-AGGTAGTTGTCCTTGTCGGC-3′) specific to the *PpCCoAOMT* gene. The tobacco actin gene was used as the internal control to normalize RNA expression (Cen et al., 2020).

Stomatal Observations and Lignin Quantification

The adaxial side of the same position on the leaf was used for analyses of stomatal number, stomatal area, stomatal length, and stomatal width by means of the Scotch tape method. Photographs of stomata were captured using an advanced optical microscope (BX51) with a DP70 charge-coupled device camera (Olympus, Tokyo, Japan). Image-Pro Plus 6.0 software (Media Cybernetics, Silver Spring, MD, United States) was used to determine stomatal area, length, and width; a microscopic ruler (Olympus, Tokyo, Japan) was used to calibrate size.

The upper and middle internodes of the tobacco plants were embedded in 10% agarose (Sigma-Aldrich, St. Louis, MO, United States) and sectioned using a VT1000 vibratome (Leica, Sollentuna, Sweden). Transverse cross-sections were stained with Wiesner reagent and photographed using an Olympus BX51 microscope (Blaschek et al., 2020). The dye width was calculated using Image-Pro Plus 6.0 software. The lignin contents of the upper and middle internodes of tobacco were quantified in accordance with the method established by Li et al. (2011), which comprised a modified Klason method with three biological replicates. Statistical analyses were conducted using independent samples *t*-tests in SPSS 26.0 software (IBM Corp., Armonk, NY, United States).

Drought Stress Treatment and Physiological Parameters

Six-week-old tobacco plants were grown in 1-gallon pots containing a mixture of potting soil and vermiculite (4:1, V/V) under natural conditions at the South China Agricultural University. During the experiment, daily maximum and minimum temperatures were 36 and 24℃. Daily maximum and minimum relative humidity was 82 and 78%. Moreover, a random block design was adopted using three replicates of each of the WT and OE plants. When the plants reached a height of 35 cm, they were subjected to drought stress *via* cessation of irrigation. The plant height, stem diameter, internode number, leaf area, leaf blade length, and leaf blade width were analyzed using Image-Pro Plus software. Leaf relative water content (RWC), proline content, malondialdehyde (MDA) content, and antioxidant enzyme activities were determined in accordance with methods described in our previous study (Zhong et al., 2014). H_2O_2 and O_2 were detected using the 3,3-diaminobenzidine (DAB) and nitro blue tetrazolium (NBT) staining methods established by Wang et al. (2007). Analysis of variance was carried out on all data using SPSS software. *P*-values < 0.05 were considered statistically significant.

Widely Targeted Metabolomics Analysis

Plant materials used for the metabolomics analysis were identical to the materials used for measurement of physiological indices after 0 and 17 days of drought treatment. Approximately 1.5 g of fresh sample were collected from all OE and WT plants, immediately frozen in liquid nitrogen, and stored at −80°C. Subsequently, these samples were sent to Wuhan Metware Biotechnology Co., Ltd. (Wuhan, China) for widely targeted metabolomics analysis. The sample extracts were analyzed using an ultrahigh performance liquid chromatography-electrospray ionization-tandem mass spectroscopy system (SHIMADZU Nexera X2[1]; Applied Biosystems 4500 Q TRAP).[2]

Unsupervised principal component analysis (PCA), hierarchical cluster analysis, and other multivariate statistical analysis methods were applied. The identified metabolites were annotated using the KEGG Compound database[3]; the annotated metabolites were mapped to the KEGG Pathway database.[4] Pathways with significantly regulated metabolites were then fed into a metabolite set enrichment analysis; their significances were determined by hypergeometric test *p*-values.

RESULTS

PpCCoAOMT Isolation and Genetic Analysis

The coding sequence of the *PpCCoAOMT* cDNA measured 801 bp, encoding a protein of 266 amino acid residues with a molecular weight of 29.7 KDa and a theoretical isoelectric point of 5.15; the length of the corresponding genomic sequence was 1,272 bp. Based on 3′ RACE and hiTAIL-PCR methods, the elephant grass genomic DNA template was amplified to obtain a sequence of 1,804 bp (Nucleotide Accession No. KJ9957361); the numbers of exons and introns, along with their lengths, were analyzed using Genescan software. The results showed that the *PpCCoAOMT* gene has five exons and four introns when applying the "GT-AG" rule, as well as a promoter region of 349 bp and a 3′ untranslated region (UTR) of 184 bp (**Supplementary Figure 1**).

A BLASTP search showed that the PpCCoAOMT amino acid sequence shared 97% identity with a query cover of 92% from *Zea mays* (AAQ89900), 95% identity with a query cover of 100% from *Panicum virgatum* (AFY17068), and 90% identity with a query cover of 92% from *Bambusa oldhamii* (ABO26812). Subsequently, the neighbor-joining phylogenetic

[1]www.shimadzu.com.cn/

[2]www.appliedbiosystems.com.cn/

[3]http://www.kegg.jp/kegg/compound/

[4]http://www.kegg.jp/kegg/pathway.html

tree involving 41 orthologs was constructed using MEGA 6.0 after multiple alignments of the protein sequences using Clustal X, which demonstrated that PpCCoAOMT was closely grouped with monocot plant species; the highest homology was with the predicted protein of *Panicum virgatum* (**Supplementary Figure 2**). Seven amino acid sequences of known CCoAOMTs were selected based on evolutionary relationships and alignments with PpCCoAOMT. Although the length varied, eight conserved motifs were found in which A, B, and C methyl donor domains were ubiquitous characteristic elements; the D, E, F, G, and H domains represented specific conserved motifs for Mg^{2+} and substrate binding (Zhang Y. et al., 2019) in the CCoAOMT family (**Figure 1**).

Overexpression of *PpCCoAOMT* Increases Lignin Content

The recombinant vector was prepared in pBA002/3HA under control of the CaMV35S promoter to upregulate *PpCCoAOMT* gene expression, then mobilized into *A. tumefaciens* strain *LBA4404* for genetic transformation of tobacco. PCR and RT-PCR were used together to identify the transgenic tobacco plants. PCR analysis demonstrated that all tobacco plants detected the NtActin product; one expected band of the selectable marker gene BASTA (Bar, 438 bp) was observed in the transgenic lines, whereas it was not observed in WT plants (**Supplementary Figure 3A**). Furthermore, RT-PCR results showed that the *PpCCoAOMT* gene was expressed in most transgenic plants, but the WT tobacco plants did not show any amplification (**Supplementary Figure 3B**).

To evaluate the growth status of transgenic tobacco, we measured plant height, stem diameter, and the number of internodes under the normal watered and drought treatments. The transgenic tobacco plants and the WT controls after recovery treatment are shown in **Figures 2A,B**. The plant height, stem diameter, and number of nodes were not significantly different after the 21-day drought (**Figures 2C–E**). Despite the lack of significant differences in plant growth between the WT and OE lines, the leaf area was significantly smaller in OE plants than in WT plants after 6 days without irrigation. In addition, the leaf area of the OE tobacco plants rapidly increased after 13 days of drought, in contrast to leaf area in WT plants (**Figure 2F**). The leaf area is proportional to the leaf length and leaf width, but the decreased leaf area was not accompanied by a significant decrease in leaf length or leaf width compared to WT plants (**Figures 2G,H**). It has been widely reported that smaller leaves of transgenic plants maintain reduced transpiration because of smaller stomata with reduced stomatal pores (Nir et al., 2014; Zhong et al., 2014; Illouz-Eliaz et al., 2020). We examined the abaxial leaf epidermal tissues *via* microscopy. The number of stomata in the OE transgenic tobacco significantly decreased to 60.88% of the number in WT plants (**Figures 3A,C**). Additionally, microscopy analyses revealed larger stomata in OE plants (**Figure 3B**). The stomatal area, length, and aperture in the OE lines under normal conditions increased by 171.61, 129.10, and 132.54%, respectively, compared to values in WT plants (**Figures 3D–F**). Taken together, the overexpression of *PpCCoAOMT* decreased leaf area and reduced the number of stomata after cessation of watering for 6 days, but increased stomatal area, length, and aperture under normal conditions.

Lignin staining and content were examined because CCoAOMT is an important enzyme that participates in lignin monomer synthesis (Yang et al., 2017; Xiao et al., 2020; Zhao et al., 2021). The dye width in the OE line significantly increased (**Figures 4A,B**), such that it was 28.18 and 124.24% wider than in WT plants at the upper and middle internodes, respectively (**Figure 4C**). Moreover, quantitative analysis of lignin content showed a similar trend in which the OE line increased to 128.46 and 118.43% of the content in WT plants (**Figure 4D**). These results demonstrated that the upregulation of *PpCCoAOMT* promotes lignin biosynthesis.

Overexpression of *PpCCoAOMT* Increases Drought Stress Tolerance

The production of H_2O_2 was monitored by DAB staining, which yields a brown precipitate produced by the peroxidase-catalyzed reaction of the dye with H_2O_2. WT plants accumulated more H_2O_2 in leaves under normal and drought treatments. O_2^- accumulation was demonstrated by a blue NBT precipitate, with a substantially decreased extent of NBT staining in the OE transgenic tobacco leaves, indicating that overexpression of the PpCCoAOMT gene led to less impairment under drought stress (**Figures 5A,B**). Related physiological indices were measured to further evaluate the growth statuses of WT and OE lines under drought. The leaf RWC was significantly higher in OE plants than in WT plants under normal conditions (**Figure 5C**). Thus, we speculate that the number of stomata was a major factor affecting transpiration. Eleven days into the drought treatment, leaf RWC decreased in the OE lines but remained significantly higher than in WT plants (**Figure 5C**). Proline content showed a similar pattern, such that OE plants were significantly different from WT plants on days 0 and 11. When measured at day 17, proline content was 14.98% greater in OE plants than in WT plants. Although proline content decreased after 3 days of rehydration, the OE tobacco plants retained more proline than did the WT plants (**Figure 5D**). The MDA content, an essential indicator of membrane injury, exhibited greater accumulation in WT plants than in OE plants during the drought stress (**Figure 5E**).

Antioxidant enzyme activities were determined, including superoxide dismutase (SOD), catalase (CAT), ascorbate peroxidase (APX), and peroxidase (POD). SOD activity was initially lower in OE plants than in WT plants, but its was greater in OE plants on day 17 and 3 days of recovery (**Figure 5F**). CAT, APX, and POD activities were higher in the OE line than in WT plants at all sampling times. CAT activity was significantly greater (by 86.75%) in the OE line than in WT plants after 11 days without irrigation (**Figure 5G**). Because SOD and CAT were the first two responding antioxidant enzymes, they managed severe ROS damage during the prolonged water deficit. APX and POD activities significantly increased in the OE transgenic plants in response to 17 days of drought stress; they were 64.71 and 137.33% greater than activities in WT plants. APX and POD activities in OE lines were also higher during recovery, such that

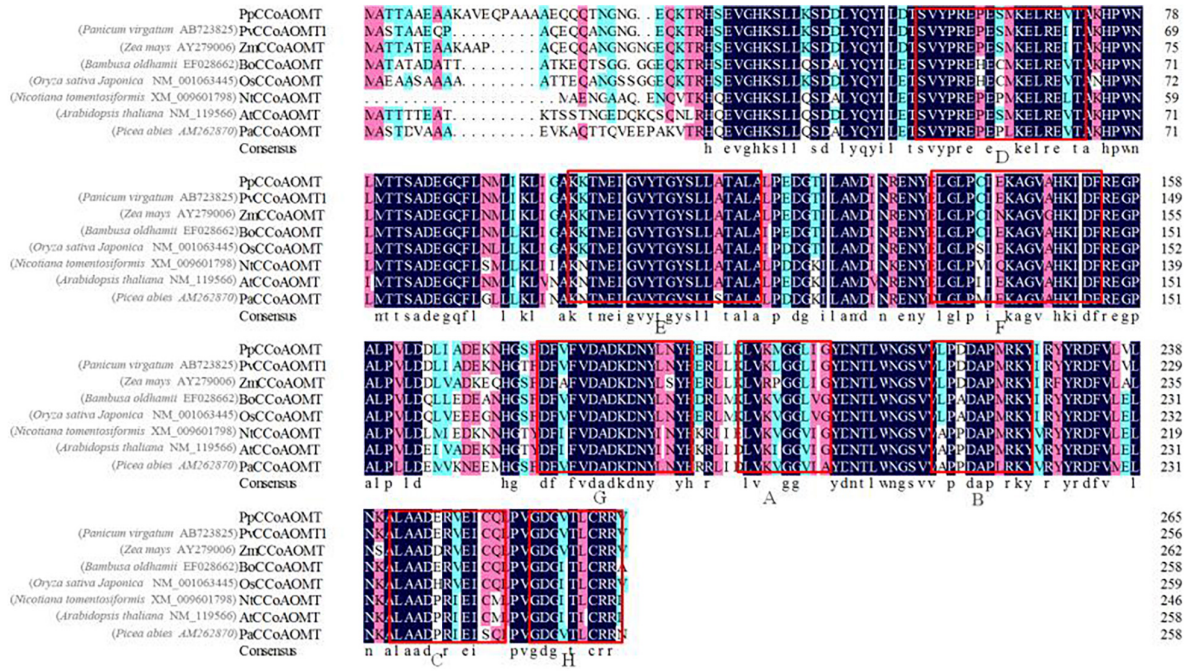

FIGURE 1 | Multiple sequence alignment indicated that the CCoAOMT amino acid sequence of elephant grass (*Pennisetum purpureum*) contained motifs that were highly conserved in other species. Red hollow boxes indicate conserved motif patterns.

they increased by approximately 1.4- and 1.5-fold, respectively, compared with the WT (**Figures 5H,I**). These results indicated that OE-*PpCCoAOMT* plants were more resistant to drought stress because of higher RWC, lower MDA, and the accumulation of proline and antioxidant enzyme activities.

Comparison of Metabolite Profiles Between Wild-Type and OE-*PpCCoAOMT* Plants

We performed ultrahigh performance liquid chromatography-electrospray ionization-tandem mass spectroscopy to gain insight into the underlying metabolite profiles of OE-*PpCCoAOMT* and WT plants. Mass spectral data were processed using Analyst 1.6.3 software. The data were subjected to PCA; the score plot showed strong and significant separation between the OE and WT plants along the first component (**Figure 6A**). To identify differentially expressed metabolites in OE and WT plants, metabolites were selected with a fold-change ≥ 2 (upregulated) or ≤ 0.5 (downregulated), and a variable importance of projection value ≥ 1 from the orthogonal projections to latent structures discriminant analysis model. In this study, 87 differentially expressed metabolites were identified including 77 upregulated (red scatter points) and 10 downregulated (green scatter points) (**Figure 6B**). These 87 metabolites were categorized into 10 classes, including 28 alkaloids, 23 amino acids, and derivatives, 10 flavonoids, 10 organic acids, 5 phenolic acids, 5 terpenoids, 2 nucleotides and derivatives, 2 quinones, 1 lipid, and 1 other; unit variance scaling of peak areas was then applied to perform hierarchical cluster analysis (**Supplementary Table 1** and **Figure 6C**). Among all metabolites, the top 10 upregulated metabolites were alkaloids, organic acids, and flavonoids, while the top 10 downregulated metabolites were flavonoids and amino acids and derivatives (**Figure 6D**).

Complex metabolic reactions and regulation in living organisms usually involve different genes and proteins that form complex pathways and networks, which interact with and regulate each other; these exchanges result in systematic changes in the metabolome (Töpfer et al., 2015). Accordingly, we obtained the detailed pathways of the differentially expressed metabolites based on the KEGG database (**Supplementary Table 2**). In total, 51 pathways were involved in WT plants vs. OE plants; the top 20 most significantly enriched pathways are presented in a bubble plot (**Figure 6E**). Considering the DA score, *P*-value, and the number of enriched metabolites, the top 5 pathways were "Glucosinolate biosynthesis," "Cyanoamino acid metabolism," "Aminoacyl-tRNA biosynthesis," "Phenylalanine, tyrosine, and tryptophan biosynthesis," and "2-Oxocarboxylic acid metabolism." All of these metabolic pathways showed a *P*-value < 0.01 in the enrichment analysis and were upregulated (**Figure 6E**).

Variations in the Metabolites From the Wild-Type and OE-*PpCCoAOMT* Plants Under Drought Stress

To further explore the major physiological changes caused by water deficit in the WT and OE lines, the metabolic profiles were compared to verify metabolite fluctuations during drought treatment. PCA plots showed that the cumulative

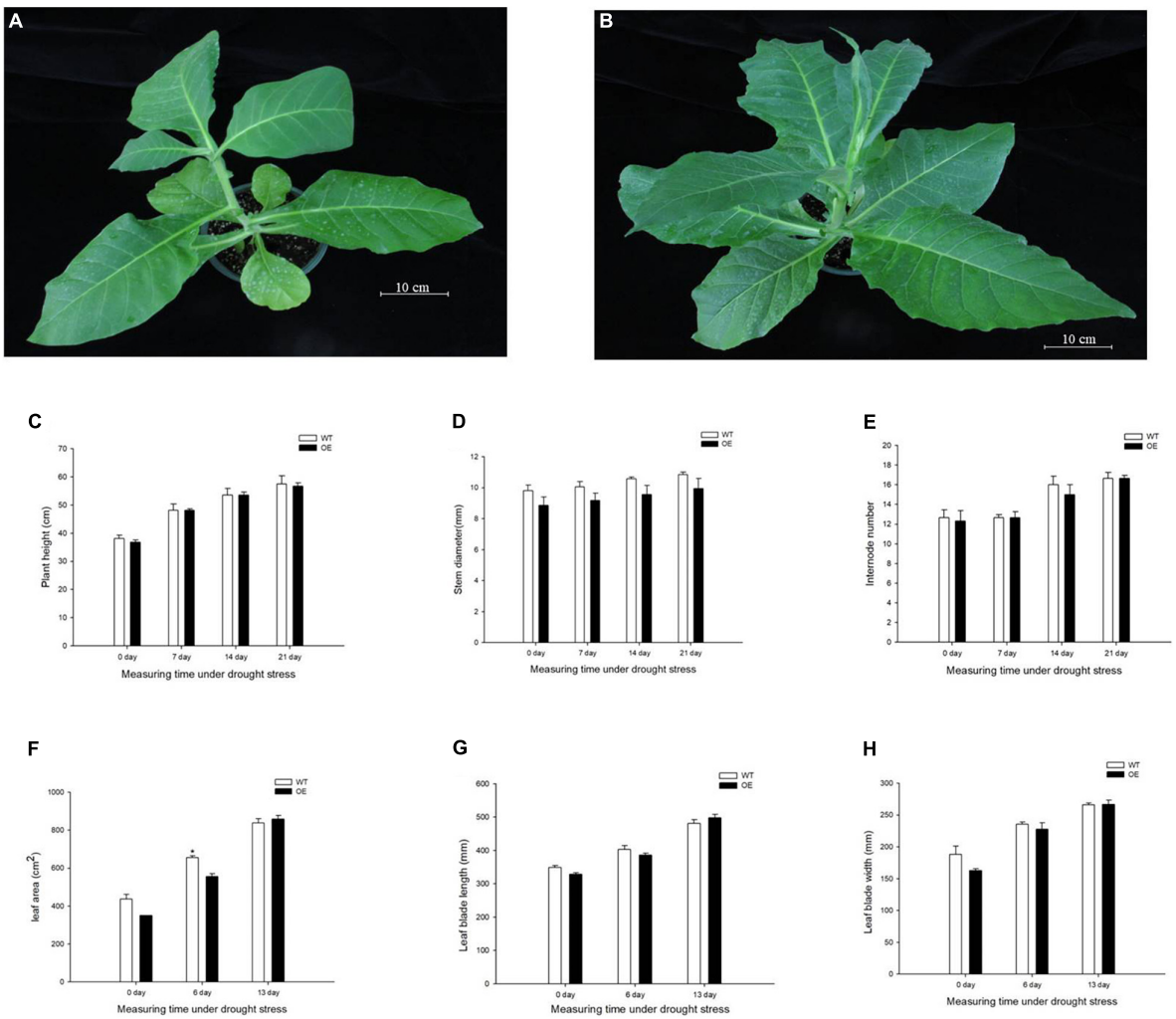

FIGURE 2 | *PpCCoAOMT* did not affect plant height, stem diameter, or the number of internodes, although it decreased leaf growth in transgenic tobacco plants under transient drought. **(A)** Phenotype of the WT line after recovery treatment. **(B)** Phenotype of the *PpCCoAOMT*-overexpressing (OE) line after recovery treatment. **(C)** Plant height, **(D)** stem diameter, **(E)** internode number, **(F)** leaf area, **(G)** leaf length, and **(H)** leaf width of the WT and OE lines under drought stress. Data are means (± SDs) of three replicates. Significant differences between WT and OE lines were determined using independent samples *t*-tests. $^{*}P < 0.05$, $^{**}P < 0.01$.

contribution rates reached 84.4 and 81.0% from the intra-group comparison of the WT-CK vs. the WT-Drought and the OE-CK vs. OE-Drought samples, respectively. In total, WT-CK, WT-Drought, OE-CK, and OE-Drought were significantly separated, whereas the repeated samples from each group were clustered together (**Figures 7A**, **8A**). The metabolites were screened by combining the variable importance of projection value and the fold-change value. We identified 307 and 302 differentially expressed metabolites in the WT and OE groups. Overall, 208 metabolites increased and 99 decreased in the WT-CK compared with their counterparts in WT-Drought plants. There were 183 upregulated and 119 downregulated metabolites between the OE-CK and OE-Drought plants (**Figures 7B**, **8B**). According to the results of hierarchical cluster analysis, the differentially expressed metabolites of each group were visualized in thermogram format; flavonoids constituted the largest class in the WT group, whereas alkaloids constituted the largest class in the OE group (**Figures 7C**, **8C**). In the WT group, 64 of 65 (98.46%) flavonoids were upregulated, whereas 49 of 54 (90.74%) flavonoids were upregulated in the OE group. For alkaloids, 36 of 56 were upregulated (64.29%) and 20 of 56 (35.71%) were downregulated in the WT group. In comparison, 38 of 58 (65.52%) increased and 20 of 58 (34.48%) decreased in the OE-CK vs. OE-Drought comparison. Notably, 90% (45 of 50) and 86.84% (33 of 38) of lipids were downregulated in the OE and WT groups, respectively (**Supplementary Tables 3**, **5**). We then investigated the top 10 differentially expressed metabolites. Alkaloids and flavonoids exhibited the greatest increases. Unexpectedly, alkaloids also exhibited the greatest increase in the WT-CK vs. WT-Drought group comparison. Most differentially expressed metabolites in the OE-CK vs. OE-Drought samples were alkaloids (**Figures 7D**, **8D**).

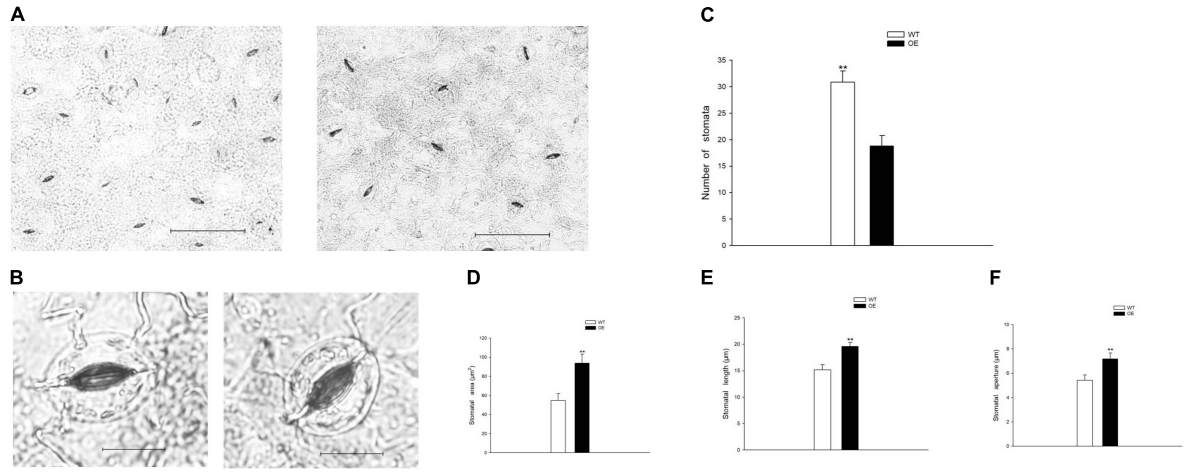

FIGURE 3 | *PpCCoAOMT* overexpression reduces stomatal number but increases stomatal area, length, and aperture under normal conditions. **(A)** Advanced upright optical microscopic images of the WT and OE lines. Bars = 100 μm. **(B)** Image of a single stoma from the WT and OE transgenic lines. Bars = 20 μm. Images were acquired using a BX51 bright-field microscope with a DP70 charge-coupled device camera (Olympus, Tokyo, Japan). **(C)** The number of stomata was calculated for each line using Image-Pro Plus 6.0 software. Data are means (± SDs) of 25 replicates. **(D)** Stomatal area, **(E)** stomatal length, and **(F)** stomatal aperture of the WT and OE transgenic tobacco lines were determined using Image-Pro Plus 6.0 software. Data are means (± SDs) of 35 replicates. A microscopic ruler (Olympus) was used to calibrate size. Significant differences between WT and OE lines were determined using independent samples *t*-tests. $^{*}P < 0.05$, $^{**}P < 0.01$.

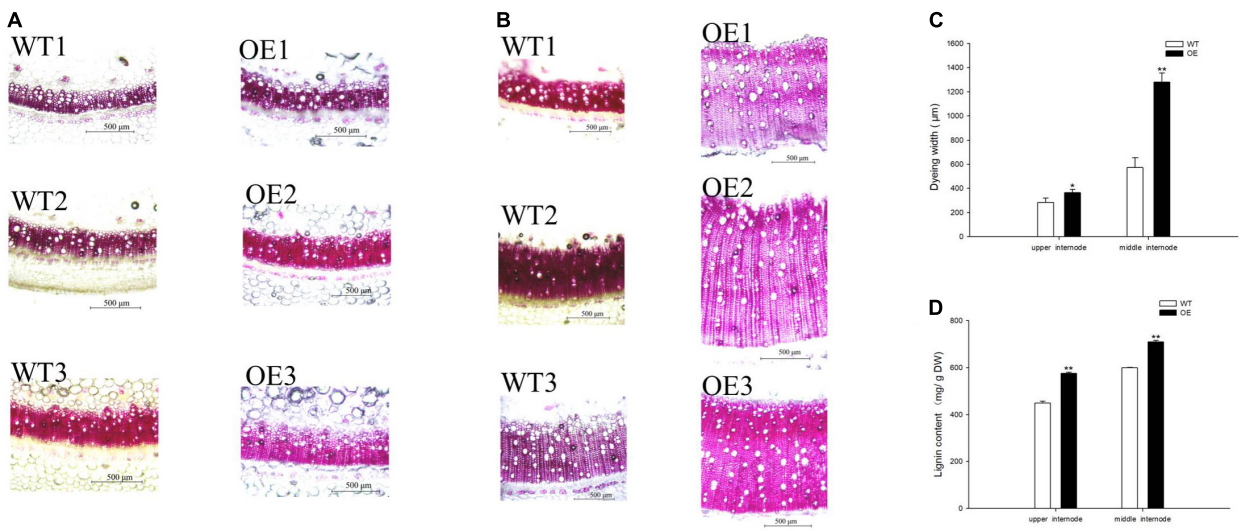

FIGURE 4 | *PpCCoAOMT* overexpression increases xylem vessel proliferation and expansion. **(A)** Representative upper internode cross-sections of WT and OE plants stained with Wiesner stain. Bars = 500 μm. **(B)** Representative middle internode cross-sections of WT and OE plants stained with Wiesner stain. Bars = 500 μm. **(C)** The dye widths of the WT and OE transgenic tobacco lines were determined using Image-Pro Plus 6.0 software. Data are means (± SDs) of nine replicates. Each replicate was measured three times at different angles. **(D)** Lignin content in WT and OE plants. Data are means (± SDs) of triplicates Significant differences between WT and OE lines were determined using independent samples *t*-tests. $^{*}P < 0.05$, $^{**}P < 0.01$.

Moreover, we mapped the differentially expressed metabolites to the KEGG database and analyzed the pathway information. The results showed that the WT group involved 67 pathways, whereas the OE-CK and OE-Drought plants involved 74 pathways (**Supplementary Tables 4**, **6**). The major pathways are presented in bubble plots. The top 5 pathways in the WT-CK vs. WT-Drought comparison (**Figure 7E**) were "Arachidonic acid metabolism," "Flavonoid biosynthesis," "Flavone and flavonol biosynthesis," "Tryptophan metabolism," and "Phenylalanine, tyrosine, and tryptophan biosynthesis." The top 5 pathways in the OE-CK vs. OE-Drought group comparison (**Figure 8E**) were "Arachidonic acid metabolism," "Flavonoid biosynthesis," "Tryptophan metabolism," "Arginine and proline metabolism," and "Flavone and flavonol biosynthesis." In addition, "Flavonoid biosynthesis" and "Flavone and flavonol biosynthesis" were two specialized pathways that were enriched and significantly

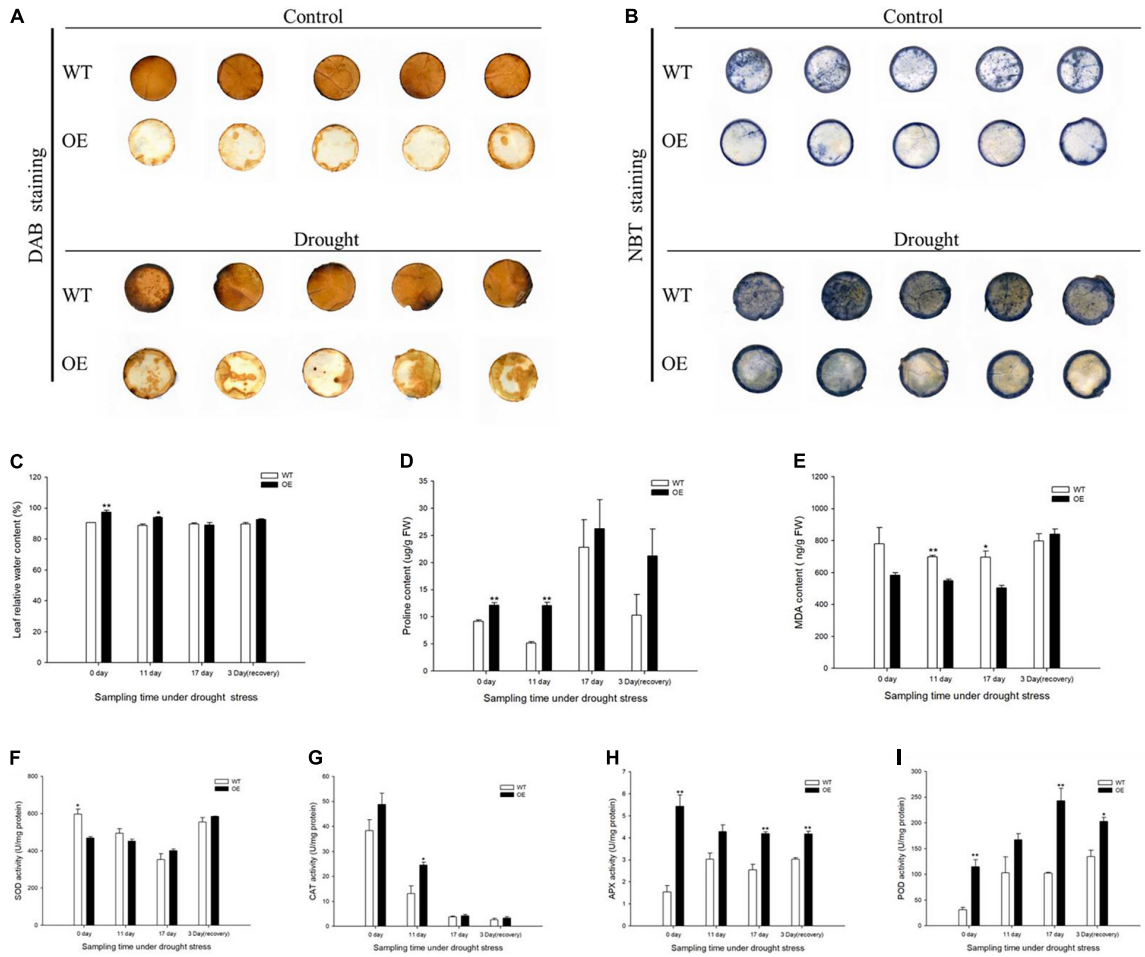

FIGURE 5 | Overexpression of *PpCCoAOMT* promotes tolerance to drought stress. **(A)** Diaminobenzidine (DAB) (displaying H_2O_2) staining of leaves from WT and OE seedlings under normal and drought stress treatment. **(B)** Nitro blue tetrazolium (NBT) (displaying O_2^-) staining of WT and OE leaves under normal and drought conditions. **(C)** Mean leaf relative water content (RWC), **(D)** proline content, **(E)** malondialdehyde (MDA) content, and **(F)** superoxide dismutase (SOD), **(G)** catalase (CAT), **(H)** ascorbate peroxidase (APX), and **(I)** peroxidase (POD) activities in WT and OE plants during drought stress and recovery periods. Data are means (± SDs) of triplicates. Significant differences between WT and OE lines were determined using independent samples *t*-tests. $^*P < 0.05$, $^{**}P < 0.01$.

different ($P < 0.05$) in the two groups, indicating that flavonoids may be closely related to drought tolerance.

Unique and Common Drought-Responsive Differential Accumulated Metabolites Between Wild-Type and OE-*PpCCoAOMT* Plants

A Venn diagram was constructed to examine the unique and common differentially expressed metabolites between the drought treatment and unstressed control and between the WT and OE plants after drought treatment. Large numbers of differential accumulated metabolites (DAMs) were identified in WT and OE plants. In total, 307 and 302 were DAMs in WT and OE plants, respectively, among which 210 DAMs were common drought-responsive metabolites. Moreover, 139 of the 210 metabolites were upregulated and 69 were downregulated in WT and OE plants under the drought treatment (**Figure 9A** and **Supplementary Table 7**). In addition, among the top 20 DAMs responding to drought in WT and OE plants, 11 metabolites were shared, demonstrating a shared drought response mechanism (**Figure 9C**). Sixty-four and 41 DAMs were specifically found in WT vs. OE plants under normal and drought conditions. Overall, 23 DAMs were common compounds, indicating that the essential difference between the WT and OE lines was unrelated to drought. Seventeen of the 23 metabolites were upregulated, while only one was downregulated in WT vs. OE plants regardless of the drought treatment (**Figure 9B** and **Supplementary Table 8**).

The total number of metabolites in the plant kingdom is estimated to exceed 200,000 (Schauer and Fernie, 2006; Le Roy et al., 2016). To cope with abiotic stress, plants have evolved mechanisms to regulate the levels of metabolites, such as phenylpropanoids and alkaloids. The DAMs between WT and OE plants under normal and drought treatments were annotated in the metabolic pathways (**Figure 10**). In total, 69 DAMs related to 10 pathways (including core and

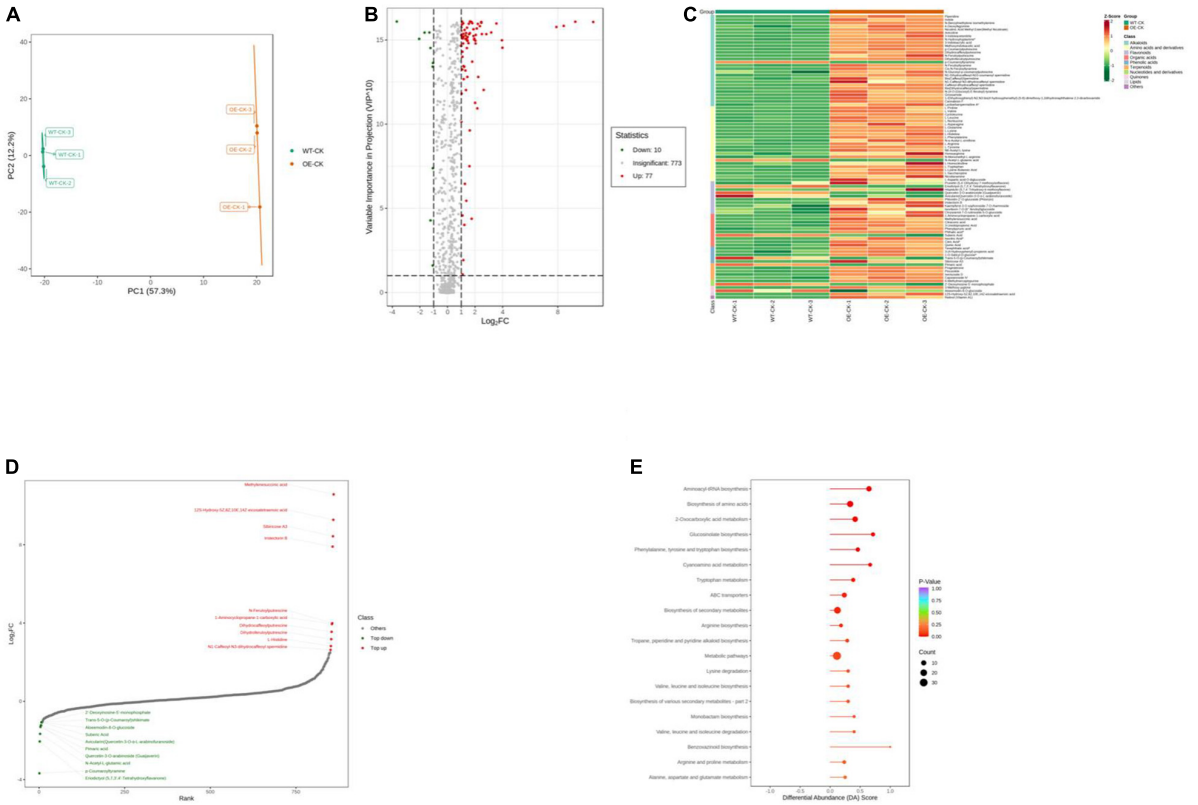

FIGURE 6 | Qualitative and quantitative analyses of differentially expressed metabolites in WT and OE plants. **(A)** PCA score plots for the mass spectra data of WT and OE samples. The abscissa represents the first principal component (PC1), while the ordinate represents the second principal component (PC2). **(B)** Volcano plot of differentially expressed metabolites between WT and OE plants. The abscissa represents the contents of differentially expressed metabolites between the two samples; a greater absolute value of the abscissa indicates a greater difference in relative content. A larger ordinate value indicates a more credible difference. Red scatter indicates metabolites that were significantly upregulated; green scatter indicates metabolites that were significantly downregulated; gray scatter indicates metabolites with no significant difference. **(C)** Clustering analysis of the metabolome data from WT and OE plants. Heatmap representation of the levels of differentially expressed metabolites and the color indicated low (green) to high (red). Each line in the heatmap represents a metabolite. Ten classes were evident after the clustering analysis. **(D)** The top 10 upregulated and downregulated metabolites between WT and OE plants. Red dots represent upregulated metabolites; green dots represent downregulated metabolites. **(E)** KEGG enrichment analysis of differentially accumulating metabolites between WT and OE samples. DA score represents the overall changes in all metabolites in the metabolic pathways; a score of 1 indicates upregulated trend, while a score of –1 indicates a downregulated trend. Each bubble in the plot represents the number of associated metabolites; *P*-values are indicated by colors.

specialized metabolism) were shared, demonstrating a role for the *PpCCoAOMT* response pathway in the drought metabolome. The results of KEGG enrichment analysis showed that most DAMs were annotated in flavonoid biosynthesis; flavone and flavonol biosynthesis were upregulated, while phenylpropanoid biosynthesis was downregulated, after drought treatment in WT and OE plants. Notably, the arginine and proline metabolic pathway increased in OE-Drought plants.

DISCUSSION

PpCCoAOMT Contributes to Drought Tolerance in Transgenic Tobacco

In this study, we demonstrated that transgenic tobacco plants overexpressing the *PpCCoAOMT* gene, which codes for lignin biosynthesis, were better able to cope with drought stress than were non-transformed control plants. This conclusion was supported by the positive RWC, proline content, and antioxidant enzyme values, as well as the decreases in MDA and ROS contents, including O_2^- and H_2O_2, observed in the leaves of transgenic plants after 17 days of water deficit. A plant's first response, when subjected to a water shortage, is to avoid low water potential by decreasing stomatal conductance; it also prevents water loss by hardening the cell wall or promoting water influx through osmotic adjustments. The presence of significantly higher leaf RWC on days 0 and 11 after the drought treatment in transgenic tobacco (**Figure 5C**) may have occurred because of smaller leaf area (**Figure 2F**) and lower stomatal number (**Figures 3A,C**), despite increased stomatal area (**Figures 3B,D**). Stomatal density reportedly exhibits a negative correlation with stomatal size (Yu et al., 2013; Wang et al., 2020). We also detected this correlation in our study, such that stomatal length, aperture, and area were significantly higher in the OE tobacco lines than in WT plants, whereas the number of stomata was lower in the OE

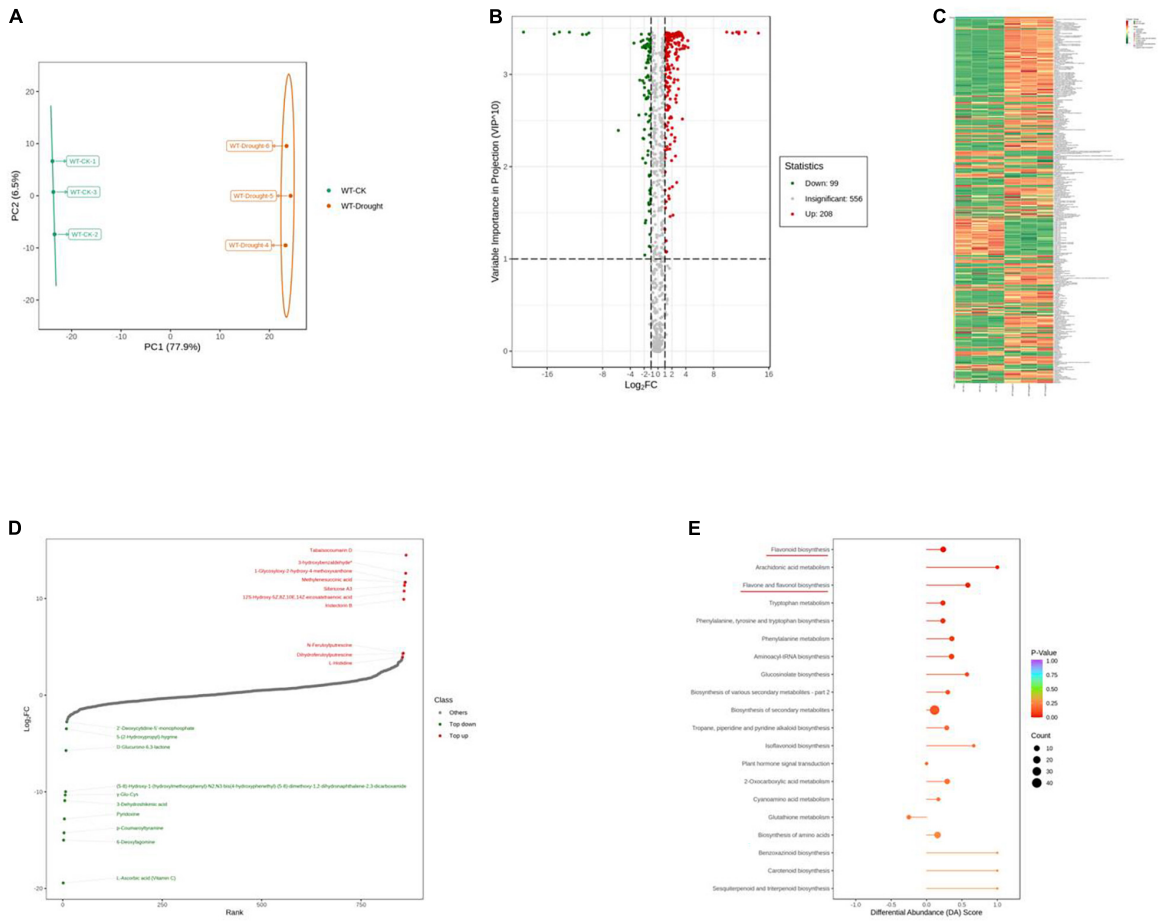

FIGURE 7 | Qualitative and quantitative analyses of differentially expressed metabolites in WT plants after drought stress. **(A)** PCA score plots for the mass spectra data of WT and OE samples. The abscissa represents the first principal component (PC1), while the ordinate represents the second principal component (PC2). **(B)** Volcano plot of differentially expressed metabolites between WT and OE plants. The abscissa represents the contents of differentially expressed metabolites between the two samples; a greater absolute value of the abscissa indicates a greater difference in relative content. A larger ordinate value indicates a more credible difference. Red scatter indicates metabolites that were significantly upregulated; green scatter indicates metabolites that were significantly downregulated; gray scatter indicates metabolites with no significant difference. **(C)** Clustering analysis of the metabolome data from WT and OE plants. Heatmap representation of the levels of differentially expressed metabolites and the color indicated low (green) to high (red). Each line in the heatmap represents a metabolite. Ten classes were evident after the clustering analysis. **(D)** The top 10 upregulated and downregulated metabolites between WT and OE plants. Red dots represent upregulated metabolites; green dots represent downregulated metabolites. **(E)** KEGG enrichment analysis of differentially accumulating metabolites between WT and OE samples. DA score represents the overall changes in all metabolites in the metabolic pathways; a score of 1 indicates upregulated trend, while a score of –1 indicates a downregulated trend. Each bubble in the plot represents the number of associated metabolites; *P*-values are indicated by colors.

plants. Therefore, we propose that the total number of stomata was the major factor that affected stomatal conductance, which brought higher leaf RWC in the OE line under the transient drought condition. Moreover, with the prolonged drought period, additional tolerance mechanisms (e.g., hardening of the cell wall and osmotic adjustment) confer protection against low water potential and help to avoid cell dehydration (Verslues et al., 2006). Thus far, many studies have reported that regulation of the *PpCCoAOMT* gene alters lignin composition and content. The downregulation (Pinçon et al., 2001; Boerjan et al., 2003; Wagner et al., 2011; Li et al., 2013; Pang et al., 2014; Wang et al., 2017) or upregulation (Zhang et al., 2014; Zhang Y. et al., 2019; Yang et al., 2017; Fu et al., 2019, 2020; Zhao et al., 2021) of *CCoAOMT* leads to a decrease or increase of lignin content in transgenic plants, respectively. In this study, the OE lines had significantly accumulated lignin deposits under normal conditions (**Figures 4A,C**), a conclusion supported by a higher lignin content in the upper and middle internodes (**Figure 4D**). Because lignin is covalently linked to non-cellulosic polysaccharides, the reinforcement of plant walls facilitates defense against abiotic assaults (Boudet, 2007). With a strengthened plant cell wall, plants can maintain water resistance to prolonged drought. Osmotic adjustments are another method to maintain osmolality; proline is an osmotic adjustment mediator (Zhang et al., 1999) and a ROS scavenger that stabilizes DNA, proteins, and membranes (Alia et al., 2001). The accumulation of proline was confirmed in OE-*PpCCoAOMT* plants under normal and drought conditions (**Figure 5D**),

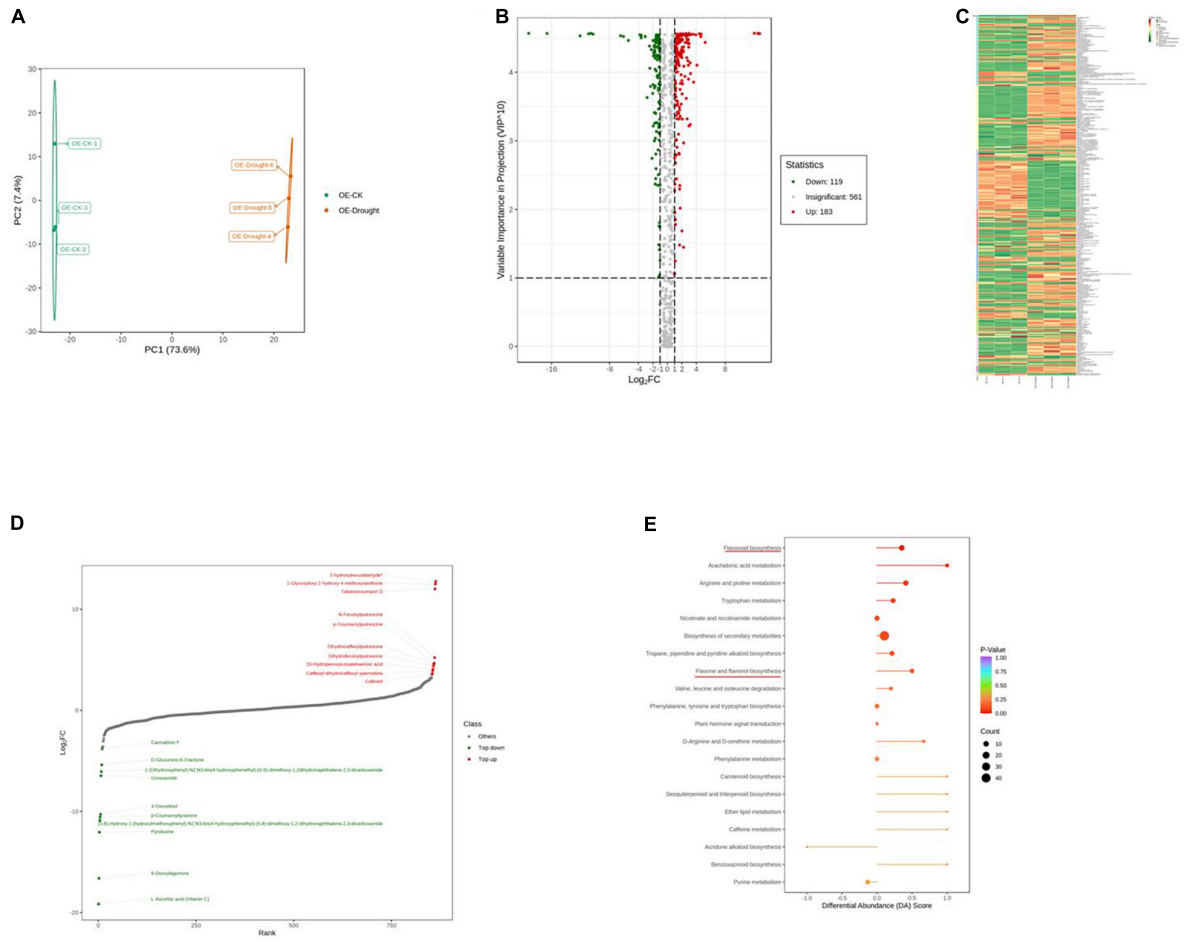

FIGURE 8 | Qualitative and quantitative analyses of differentially expressed metabolites in OE plants after drought stress. **(A)** PCA score plots for the mass spectra data of WT and OE samples. The abscissa represents the first principal component (PC1), while the ordinate represents the second principal component (PC2). **(B)** Volcano plot of differentially expressed metabolites between WT and OE plants. The abscissa represents the contents of differentially expressed metabolites between the two samples; a greater absolute value of the abscissa indicates a greater difference in relative content. A larger ordinate value indicates a more credible difference. Red scatter indicates metabolites that were significantly upregulated; green scatter indicates metabolites that were significantly downregulated; gray scatter indicates metabolites with no significant difference. **(C)** Clustering analysis of the metabolome data from WT and OE plants. Heatmap representation of the levels of differentially expressed metabolites and the color indicated low (green) to high (red). Each line in the heatmap represents a metabolite. Ten classes were evident after the clustering analysis. **(D)** The top 10 upregulated and downregulated metabolites between WT and OE plants. Red dots represent upregulated metabolites; green dots represent downregulated metabolites. **(E)** KEGG enrichment analysis of differentially accumulating metabolites between WT and OE samples. DA score represents the overall changes in all metabolites in the metabolic pathways; a score of 1 indicates upregulated trend, while a score of –1 indicates a downregulated trend. Each bubble in the plot represents the number of associated metabolites; *P*-values are indicated by colors.

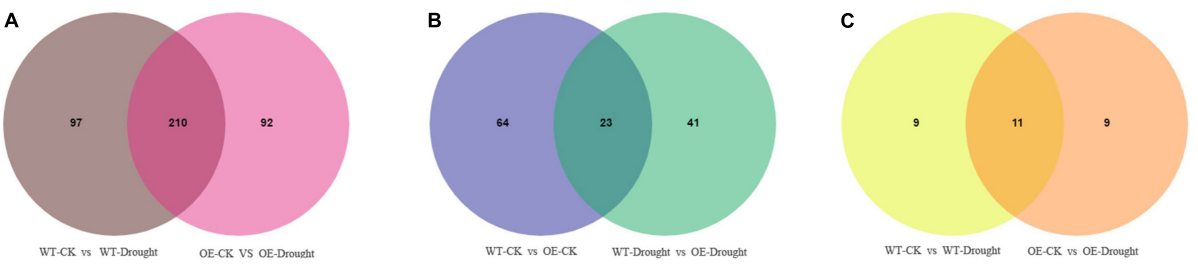

FIGURE 9 | Venn diagrams of differentially accumulated metabolites (DAMs). **(A)** Venn diagram showing common DAMs between normal and drought conditions in WT and OE plants. **(B)** Venn diagram showing unique and common DAMs between WT and OE plants under normal and drought conditions. **(C)** Venn diagram showing common DAMs in the top 20 differentially expressed metabolites in WT and OE plants after drought stress.

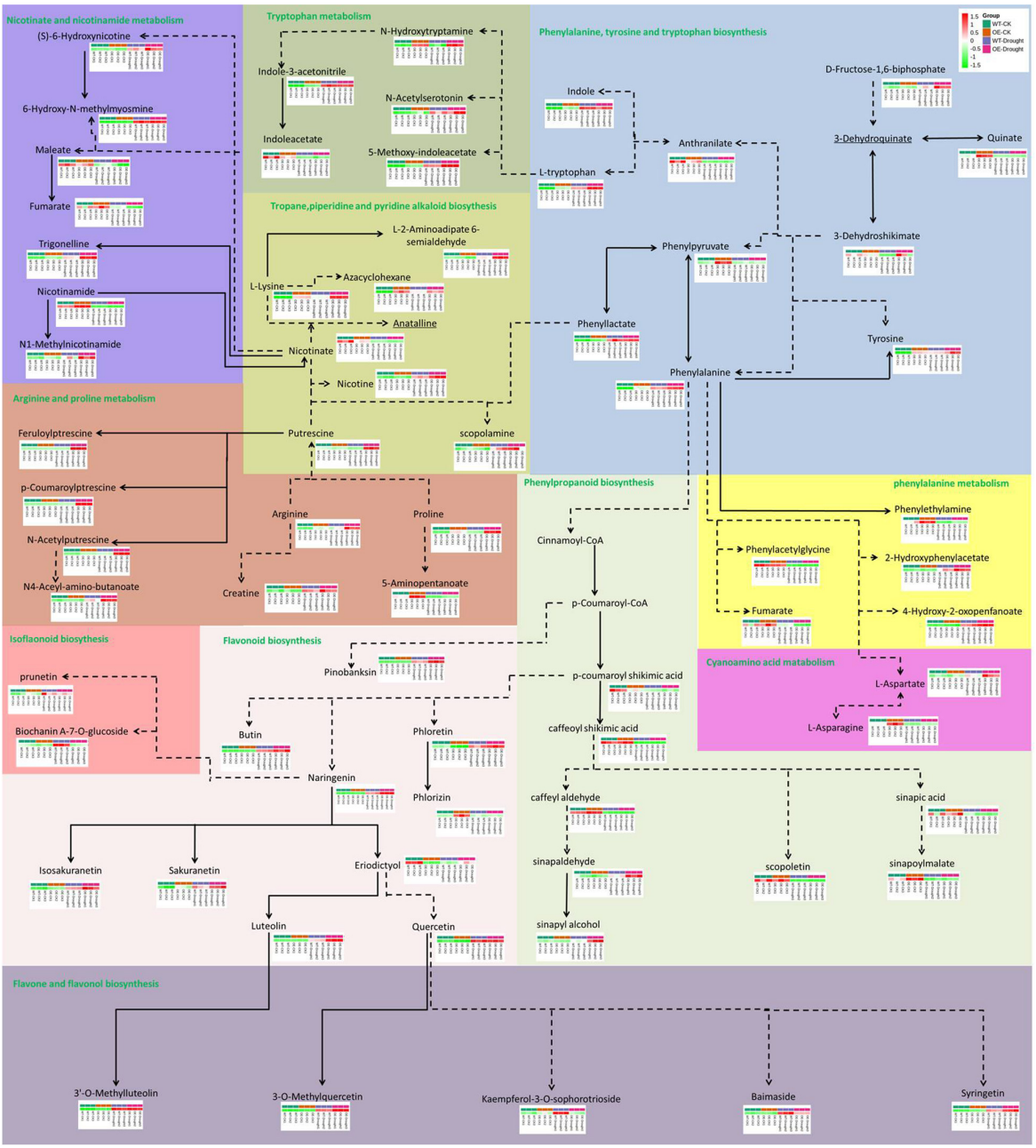

FIGURE 10 | Analysis of pathway metabolite changes between WT and OE plants under normal and drought treatments. Dashed arrows represent multiple enzymatic steps. Red represents upregulated metabolites, while green represents downregulated metabolites.

indicating that the overexpression of *PpCCoAOMT* in transgenic plants contributed to drought tolerance.

Stomatal closure is one of the earliest responses to drought; it has an important role in water loss control in plants (Chaves et al., 2003; Wang et al., 2020), which subsequently downregulates CO_2 uptake and causes a decline in photosynthesis. Thus, the electron transport chain becomes over-reduced and favors excess ROS production. In plants, MDA is an indicator of cell membrane damage caused by ROS-induced lipid peroxidation (Zhong et al., 2014). The OE plants had significantly lower MDA content than did the WT plants (**Figure 5E**). Moreover, H_2O_2 and O_2^- staining (**Figures 5A,B**) revealed that *PpCCoAOMT* mitigated the effects of the water deficit. These observations suggested activation of the antioxidant system. The activities of the four enzymes evaluated in this study were higher because of the high free proline concentration present in the leaves of transgenic plants. However, the APX and POD (**Figures 5H,I**) activities significantly increased in OE tobacco, even under

the control treatment, possibly because POD is a key enzyme involved in monolignol polymerization in the secondary cell wall (Bonawitz and Chapple, 2010; Miao and Liu, 2010; Liu et al., 2011; Alejandro et al., 2012). Because of higher lignin content in OE-*PpCCoAOMT* plants, it is perhaps unsurprising that POD activity was approximately 3.6-fold greater in OE plants than in WT plants on day 0. APX enhances the tolerance of transgenic Arabidopsis by increasing the accumulation of lignin and maintaining the level of H_2O_2 (Shafi et al., 2015). APX, POD, and CAT are involved in scavenging H_2O_2 to H_2O and O_2 (Mittler, 2002). Thus, the decrease in CAT (**Figure 5G**) activity during drought stress may orchestrate the regulation of these three enzymes to ensure balance with other metabolic processes. This balancing also occurs in *P5CSF129A*-overexpressing "Swingle" citrumelos and *P5CR*-overexpressing soybeans (Kocsy et al., 2005; de Campos et al., 2011).

PpCCoAOMT Affects Primary and Specialized Metabolism, Leading to Flavonoid Accumulation Under Normal and Drought Conditions

In general, H_2O_2 is both a stress-induced ROS and an important regulatory component in lignin biosynthesis (Kováčik et al., 2010; Liu et al., 2015; Xia et al., 2018). It is unknown whether *PpCCoAOMT* contributes to crosstalk between the lignin biosynthetic pathway and the abiotic stress response. Thus, we used OE-*PpCCoAOMT* transgenic tobacco plants to analyze widely targeted metabolomes under normal and drought conditions. Among the top 10 ranked DAMs for the WT-CK vs. OE-CK group comparison (**Figure 6D** and **Supplementary Table 1**), two upregulated and three downregulated metabolites were flavonoids, three upregulated and one downregulated metabolite were alkaloids, and two upregulated and one downregulated metabolite were organic acids. In the WT-CK vs. WT-Drought group comparison (**Figure 7D** and **Supplementary Table 3**), two upregulated and four downregulated metabolites were alkaloids, two upregulated metabolites were flavonoids, and one upregulated and one downregulated metabolite were organic acids. In the OE-CK vs. OE-Drought group comparison (**Figure 8D** and **Supplementary Table 5**), four upregulated and four downregulated metabolites were alkaloids. These results indicate that flavonoids and organic acids changed in OE-*PpCCoAOMT* transgenic tobacco plants under normal conditions, which may have begun acting in ROS scavenging during the initial stages of water deprivation (Nakabayashi and Saito, 2015; Jiang et al., 2016; Khan et al., 2020); this may have prevented further cell damage during prolonged stress. As mentioned above, hierarchical cluster analysis (**Figure 6C**) results supported the conclusion that *PpCCoAOMT* modulated flavonoids and organic acids in the watered plants.

Metabolic pathway analysis of the DAMs revealed that the top 5 pathways for the WT-CK vs. OE-CK group comparison were mostly involved in primary metabolism (**Figure 6E**). However, in WT (**Figure 7E**) and OE (**Figure 8E**) plants, the drought treatment affected the KEGG pathways that were enriched in primary and specialized metabolism, in which WT plants showed more secondary metabolism. This observation is consistent with the hierarchical cluster analysis of the WT (**Figure 7C**) and OE (**Figure 8C**) plants, whereby 65 flavonoids and 56 alkaloids differentially accumulated in WT samples after drought treatment compared to 58 flavonoids and 54 alkaloids in the OE-*PpCCoAOMT* transgenic tobacco.

CCoAOMT is a key enzyme involved in the first methylation step required to produce lignin monomers in the phenylpropanoid metabolic pathway. The phenylpropanoid metabolic pathway is on the boundary of core metabolism (traditionally known as "primary metabolism") and specialized metabolism (traditionally known as "secondary metabolism") and directs the metabolic flux from the core to specialized metabolism (Fraser and Chapple, 2011; Dong and Lin, 2021). In OE-*PpCCoAOMT* transgenic tobacco plants, metabolic flux redirection within the primary metabolism (**Figure 10**) led to large quantities of proline accumulation in plant tissues in response to different abiotic stressors during experiments involving exogenous application (Hoque et al., 2007a,b, 2008; Ozden et al., 2009) or genetic manipulation (Kocsy et al., 2005; Molinari et al., 2007); this redirection also caused decreases in the contents of nicotinate involved in drought tolerance and biomass (Ahmad et al., 2021). The metabolic fluxes of the WT and OE plants were redirected to the flavonoid biosynthetic pathway with significantly different concentrations after drought treatment (**Figure 10**). In particular, quercetin has an important role in the drought tolerance of tea plants (Sun J. et al., 2020), *Holcus lanatus*, and *Alopecurus pratensis* (Gargallo-Garriga et al., 2015). Luteolin may have antioxidant activity at low concentrations (Singh et al., 2014). Treatment with naringenin reduces oxidative damage and enhances tolerance to osmotic stress (Yildiztugay et al., 2020).

CONCLUSION

In conclusion, we have characterized the lignin biosynthetic gene, *PpCCoAOMT*, which contributes to lignin deposition and flavonoid accumulation; it has important roles in controlling drought tolerance, stomatal number, and aperture size. There was no cost to the growth of transgenic plants (Zhang Y. et al., 2019) based on leaf size (**Figures 2A,B,F**), plant height (**Figure 2C**), or stem diameter (**Figure 2D**), which highlights the importance of the *PpCCoAOMT* gene in future attempts to breed drought-resistant plants.

DATA AVAILABILITY STATEMENT

The datasets presented in this study can be found in online repositories. The names of the repository/repositories and accession number(s) can be found in the article/**Supplementary Material**.

AUTHOR CONTRIBUTIONS

J-LS and Z-YW completed most research experiments. Y-HW, JD, and C-YW contributed to data analysis. X-QZ, SC, and X-LH

helped with manuscript reviewing. X-MX and T-XZ revised the manuscript. All authors read and approved the final manuscript.

FUNDING

This study was supported by the National Natural Science Foundation of China (No. 31802116) and the Technology Foundation of the Guizhou Provincial Science and Technology Department (No. LH20177027).

SUPPLEMENTARY MATERIAL

The Supplementary Material for this article can be found online at: https://www.frontiersin.org/articles/10.3389/fpls.2022.884456/full#supplementary-material

REFERENCES

Ahmad, Z., Bashir, K., Matsui, A., Tanaka, M., Sasaki, R., Oikawa, A., et al. (2021). Overexpression of nicotinamidase 3 (NIC3) gene and the exogenous application of nicotinic acid (NA) enhance drought tolerance and increase biomass in *Arabidopsis*. *Plant Mol. Biol.* 107, 63–84. doi: 10.1007/s11103-021-01179-z

Alejandro, S., Lee, Y., Tohge, T., Sudre, D., Osorio, S., Park, J., et al. (2012). AtABCG29 is a monolignol transporter involved in lignin biosynthesis. *Curr. Biol.* 22, 1207–1212. doi: 10.1016/j.cub.2012.04.064

Alia, Mohanty, P., and Matysik, J. (2001). Effect of proline on the production of singlet oxygen. *Amino Acids* 21, 195–200. doi: 10.1007/s007260170026

Barros, J., Serk, H., Granlund, I., and Pesquet, E. (2015). The cell biology of lignification in higher plants. *Ann. Bot.* 115, 1053–1074. doi: 10.1093/aob/mcv046

Blaschek, L., Champagne, A., Dimotakis, C., Decou, R., Hishiyama, S., Kratzer, S., et al. (2020). Cellular and genetic regulation of coniferaldehyde incorporation in lignin of herbaceous and woody plants by quantitative wiesner staining. *Front. Plant Sci.* 11:109. doi: 10.3389/fpls.2020.00109

Boerjan, W., Ralph, J., and Baucher, M. (2003). Lignin biosynthesis. *Annu. Rev. Plant Biol.* 54, 519–546.

Bonawitz, N. D., and Chapple, C. (2010). The genetics of lignin biosynthesis: connecting genotype to phenotype. *Annu. Rev. Genet.* 44, 337–363. doi: 10.1146/annurev-genet-102209-163508

Boudet, A. M. (2007). Evolution and current status of research in phenolic compounds. *Phytochemistry* 68, 2722–2735. doi: 10.1016/j.phytochem.2007.06.012

Cen, H., Wang, T., Liu, H., Wang, H., Tian, D., Li, X., et al. (2020). Overexpression of MsASMT1 promotes plant growth and decreases flavonoids biosynthesis in transgenic alfalfa (*Medicago sativa* L.). *Front. Plant Sci.* 11:489. doi: 10.3389/fpls.2020.00489

Chaves, M. M., Maroco, J. P., and Pereira, J. S. (2003). Understanding plant responses to drought—from genes to the whole plant. *Funct. Plant Biol.* 30, 239–264. doi: 10.1071/FP02076

de Campos, M. K. F., de Carvalho, K., de Souza, F. S., Marur, C. J., Pereira, L. F. P., Bespalhok Filho, J. C., et al. (2011). Drought tolerance and antioxidant enzymatic activity in transgenic 'Swingle'citrumelo plants over-accumulating proline. *Environ. Exp. Bot.* 72, 242–250. doi: 10.1016/j.envexpbot.2011.03.009

Dong, N. Q., and Lin, H. X. (2021). Contribution of phenylpropanoid metabolism to plant development and plant–environment interactions. *J. Integr. Plant Biol.* 63, 180–209. doi: 10.1111/jipb.13054

Fraser, C. M., and Chapple, C. (2011). The phenylpropanoid pathway in *Arabidopsis*. *Am. Soc. Plant Biol.* 9:0152.

Fu, Y., Win, P., Zhang, H., Li, C., Shen, Y., He, F., et al. (2019). PtrARF2. 1 is involved in regulation of leaf development and lignin biosynthesis in poplar trees. *Int. J. Mol. Sci.* 20:4141. doi: 10.3390/ijms20174141

Fu, Y., Zhu, Y., Yang, W., Xu, W., Li, Q., Chen, M., et al. (2020). Isolation and functional identification of a *Botrytis cinerea*-responsive caffeoyl-CoA O-methyltransferase gene from *Lilium regale* Wilson. *Plant Physiol. Biochem.* 157, 379–389. doi: 10.1016/j.plaphy.2020.10.030

Gargallo-Garriga, A., Sardans, J., Pérez-Trujillo, M., Oravec, M., Urban, O., Jentsch, A., et al. (2015). Warming differentially influences the effects of drought on stoichiometry and metabolomics in shoots and roots. *New Phytol.* 207, 591–603. doi: 10.1111/nph.13377

Geng, D., Chen, P., Shen, X., Zhang, Y., Li, X., Jiang, L., et al. (2018). MdMYB88 and MdMYB124 enhance drought tolerance by modulating root vessels and cell walls in apple. *Plant Physiol.* 178, 1296–1309. doi: 10.1104/pp.18.00502

Giordano, D., Provenzano, S., Ferrandino, A., Vitali, M., Pagliarani, C., Roman, F., et al. (2016). Characterization of a multifunctional caffeoyl-CoA O-methyltransferase activated in grape berries upon drought stress. *Plant Physiol. Biochem.* 101, 23–32. doi: 10.1016/j.plaphy.2016.01.015

Gomide, C. A. D. M., Paciullo, D. S. C., Costa, I. D. A., Lima, A. M., Castro, C. R. T. D., and Lédo, F. J. D. S. (2011). Morphogenesis of dwarf elephant grass clones in response to intensity and frequency of defoliation in dry and rainy seasons. *Rev. Brasil. Zootec.* 40, 1445–1451. doi: 10.1590/s1516-35982011000700007

Guo, H., Wang, Y., Wang, L., Hu, P., Wang, Y., Jia, Y., et al. (2017). Expression of the MYB transcription factor gene Bpl MYB 46 affects abiotic stress tolerance and secondary cell wall deposition in *Betula platyphylla*. *Plant Biotechnol. J.* 15, 107–121. doi: 10.1111/pbi.12595

Hoque, M. A., Banu, M. N. A., Nakamura, Y., Shimoishi, Y., and Murata, Y. (2008). Proline and glycinebetaine enhance antioxidant defense and methylglyoxal detoxification systems and reduce NaCl-induced damage in cultured tobacco cells. *J. Plant Physiol.* 165, 813–824. doi: 10.1016/j.jplph.2007.07.013

Hoque, M. A., Banu, M. N. A., Okuma, E., Amako, K., Nakamura, Y., Shimoishi, Y., et al. (2007a). Exogenous proline and glycinebetaine increase NaCl-induced ascorbate–glutathione cycle enzyme activities, and proline improves salt tolerance more than glycinebetaine in tobacco bright yellow-2 suspension-cultured cells. *J. Plant Physiol.* 164, 1457–1468. doi: 10.1016/j.jplph.2006.10.004

Hoque, M. A., Okuma, E., Banu, M. N. A., Nakamura, Y., Shimoishi, Y., and Murata, Y. (2007b). Exogenous proline mitigates the detrimental effects of salt stress more than exogenous betaine by increasing antioxidant enzyme activities. *J. Plant Physiol.* 164, 553–561. doi: 10.1016/j.jplph.2006.03.010

Hu, Y., Li, W. C., Xu, Y. Q., Li, G. J., Liao, Y., and Fu, F. L. (2009). Differential expression of candidate genes for lignin biosynthesis under drought stress in maize leaves. *J. Appl. Genet.* 50, 213–223. doi: 10.1007/BF03195675

Illouz-Eliaz, N., Nissan, I., Nir, I., Ramon, U., Shohat, H., and Weiss, D. (2020). Mutations in the tomato gibberellin receptors suppress xylem proliferation and reduce water loss under water-deficit conditions. *J. Exp. Bot.* 71, 3603–3612. doi: 10.1093/jxb/eraa137

Jiang, N., Doseff, A. I., and Grotewold, E. (2016). Flavones: from biosynthesis to health benefits. *Plants* 5:27. doi: 10.3390/plants5020027

Kai, K., Mizutani, M., Kawamura, N., Yamamoto, R., Tamai, M., Yamaguchi, H., et al. (2008). Scopoletin is biosynthesized *via* ortho-hydroxylation of feruloyl CoA by a 2-oxoglutarate-dependent dioxygenase in *Arabidopsis thaliana*. *Plant J.* 55, 989–999. doi: 10.1111/j.1365-313X.2008.03568.x

Khan, N., Ali, S., Zandi, P., Mehmood, A., Ullah, S., Ikram, M., et al. (2020). Role of sugars, amino acids and organic acids in improving plant abiotic stress tolerance. *Pak. J. Bot.* 52, 355–363.

Kocsy, G., Laurie, R., Szalai, G., Szilágyi, V., Simon-Sarkadi, L., Galiba, G., et al. (2005). Genetic manipulation of proline levels affects antioxidants in soybean subjected to simultaneous drought and heat stresses. *Physiol. Plant.* 124, 227–235. doi: 10.1111/j.1399-3054.2005.00504.x

Kováčik, J., Grúz, J., Klejdus, B., Štork, F., Marchiosi, R., and Ferrarese-Filho, O. (2010). Lignification and related parameters in copper-exposed *Matricaria chamomilla* roots: role of H_2O_2 and NO in this process. *Plant Sci.* 179, 383–389. doi: 10.1016/j.plantsci.2010.06.014

Le Roy, J., Huss, B., Creach, A., Hawkins, S., and Neutelings, G. (2016). Glycosylation is a major regulator of phenylpropanoid availability and biological activity in plants. *Front. Plant Sci.* 7:735. doi: 10.3389/fpls.2016.00735

Li, D., Yang, J., Pak, S., Zeng, M., Sun, J., Yu, S., et al. (2022). PuC3H35 confers drought tolerance by enhancing lignin and proanthocyanidin biosynthesis in the roots of *Populus ussuriensis*. *New Phytol.* 233, 390–408. doi: 10.1111/nph.17799

Li, Q., Min, D., Wang, J. P. Y., Peszlen, I., Horvath, L., Horvath, B., et al. (2011). Down-regulation of glycosyltransferase 8D genes in *Populus trichocarpa* caused reduced mechanical strength and xylan content in wood. *Tree Physiol.* 31, 226–236. doi: 10.1093/treephys/tpr008

Li, X., Chen, W., Zhao, Y., Xiang, Y., Jiang, H., Zhu, S., et al. (2013). Downregulation of caffeoyl-CoA O-methyltransferase (CCoAOMT) by RNA interference leads to reduced lignin production in maize straw. *Genet. Mol. Biol.* 36, 540–546. doi: 10.1590/S1415-47572013005000039

Liu, C. J., Miao, Y. C., and Zhang, K. W. (2011). Sequestration and transport of lignin monomeric precursors. *Molecules* 16, 710–727. doi: 10.3390/molecules16010710

Liu, Q., Zheng, L., He, F., Zhao, F. J., Shen, Z., and Zheng, L. (2015). Transcriptional and physiological analyses identify a regulatory role for hydrogen peroxide in the lignin biosynthesis of copper-stressed rice roots. *Plant Soil* 387, 323–336. doi: 10.1007/s11104-014-2290-7

Liu, S. J., Huang, Y. H., He, C. J., Cheng, F. A. N. G., and Zhang, Y. W. (2016). Cloning, bioinformatics and transcriptional analysis of caffeoyl-coenzyme A 3-O-methyltransferase in switchgrass under abiotic stress. *J. Integr. Agric.* 15, 636–649. doi: 10.1016/s2095-3119(16)61363-1

Miao, Y. C., and Liu, C. J. (2010). ATP-binding cassette-like transporters are involved in the transport of lignin precursors across plasma and vacuolar membranes. *Proc. Natl. Acad. Sci.U.S.A.* 107, 22728–22733. doi: 10.1073/pnas.1007747108

Mittler, R. (2002). Oxidative stress, antioxidants and stress tolerance. *Trends Plant Sci.* 7, 405–410. doi: 10.1016/s1360-1385(02)02312-9

Molinari, H. B. C., Marur, C. J., Daros, E., De Campos, M. K. F., De Carvalho, J. F. R. P., Filho, J. C. B., et al. (2007). Evaluation of the stress-inducible production of proline in transgenic sugarcane (*Saccharum* spp.): osmotic adjustment, chlorophyll fluorescence and oxidative stress. *Physiol. Plant.* 130, 218–229. doi: 10.1111/j.1399-3054.2007.00909.x

Moura-Sobczak, J., Souza, U., and Mazzafera, P. (2011). Drought stress and changes in the lignin content and composition in *Eucalyptus*. *BMC Proc.* 5:103. doi: 10.1186/1753-6561-5-S7-P103

Nakabayashi, R., and Saito, K. (2015). Integrated metabolomics for abiotic stress responses in plants. *Curr. Opin. Plant Biol.* 24, 10–16. doi: 10.1016/j.pbi.2015.01.003

Nir, I. D. O., Moshelion, M., and Weiss, D. (2014). The *Arabidopsis* GIBBERELLIN METHYL TRANSFERASE 1 suppresses gibberellin activity, reduces whole-plant transpiration and promotes drought tolerance in transgenic tomato. *Plant Cell Environ.* 37, 113–123. doi: 10.1111/pce.12135

Ozden, M., Demirel, U., and Kahraman, A. (2009). Effects of proline on antioxidant system in leaves of grapevine (*Vitis vinifera* L.) exposed to oxidative stress by H_2O_2. *Sci. Horticult.* 119, 163–168. doi: 10.1016/j.scienta.2008.07.031

Pang, S. L., Ong, S. S., Lee, H. H., Zamri, Z., Kandasamy, K. I., Choong, C. Y., et al. (2014). Isolation and characterization of CCoAOMT in interspecific hybrid of *Acacia auriculiformis* x *Acacia mangium*—a key gene in lignin biosynthesis. *Genet. Mol. Res.* 13, 7217–7238. doi: 10.4238/2014.September.5.7

Pinçon, G., Maury, S., Hoffmann, L., Geoffroy, P., Lapierre, C., Pollet, B., et al. (2001). Repression of O-methyltransferase genes in transgenic tobacco affects lignin synthesis and plant growth. *Phytochemistry* 57, 1167–1176. doi: 10.1016/s0031-9422(01)00098-x

Rui, H., Chen, C., Zhang, X., Shen, Z., and Zhang, F. (2016). Cd-induced oxidative stress and lignification in the roots of two *Vicia sativa* L. varieties with different Cd tolerances. *J. Hazard. Mater.* 301, 304–313. doi: 10.1016/j.jhazmat.2015.08.052

Rusdy, M. (2016). Elephant grass as forage for ruminant animals. *Livestock Res. Rural Dev.* 28, 1–6.

Schauer, N., and Fernie, A. R. (2006). Plant metabolomics: towards biological function and mechanism. *Trends Plant Sci.* 11, 508–516. doi: 10.1016/j.tplants.2006.08.007

Shafi, A., Chauhan, R., Gill, T., Swarnkar, M. K., Sreenivasulu, Y., and Kumar, S. (2015). Expression of SOD and APX genes positively regulates secondary cell wall biosynthesis and promotes plant growth and yield in *Arabidopsis* under salt stress. *Plant Mol. Biol.* 87, 615–631. doi: 10.1007/s11103-015-0301-6

Singh, M., Kaur, M., and Silakari, O. (2014). Flavones: an important scaffold for medicinal chemistry. *Eur. J. Med. Chem.* 84, 206–239. doi: 10.1016/j.ejmech.2014.07.013

Srivastava, S., Vishwakarma, R. K., Arafat, Y. A., Gupta, S. K., and Khan, B. M. (2015). Abiotic stress induces change in cinnamoyl CoA reductase (CCR) protein abundance and lignin deposition in developing seedlings of *Leucaena leucocephala*. *Physiol. Mol. Biol. Plants* 21, 197–205. doi: 10.1007/s12298-015-0289-z

Strezov, V., Evans, T. J., and Hayman, C. (2008). Thermal conversion of elephant grass (*Pennisetum Purpureum Schum*) to bio-gas, bio-oil and charcoal. *Bioresour. Technol.* 99, 8394–8399. doi: 10.1016/j.biortech.2008.02.039

Su, N., Ling, F., Xing, A., Zhao, H., Zhu, Y., Wang, Y., et al. (2020). Lignin synthesis mediated by CCoAOMT enzymes is required for the tolerance against excess Cu in *Oryza sativa*. *Environ. Exp. Bot.* 175:104059. doi: 10.1016/j.envexpbot.2020.104059

Sun, J., Qiu, C., Ding, Y., Wang, Y., Sun, L., Fan, K., et al. (2020). Fulvic acid ameliorates drought stress-induced damage in tea plants by regulating the ascorbate metabolism and flavonoids biosynthesis. *BMC Genomics* 21:411. doi: 10.1186/s12864-020-06815-4

Sun, S. C., Xiong, X. P., Zhang, X. L., Feng, H. J., Zhu, Q. H., Sun, J., et al. (2020). Characterization of the Gh4CL gene family reveals a role of Gh4CL7 in drought tolerance. *BMC Plant Biol.* 20:125. doi: 10.1186/s12870-020-2329-2

Töpfer, N., Kleessen, S., and Nikoloski, Z. (2015). Integration of metabolomics data into metabolic networks. *Front. Plant Sci.* 6:49. doi: 10.3389/fpls.2015.00049

Verslues, P. E., Agarwal, M., Katiyar-Agarwal, S., Zhu, J., and Zhu, J. K. (2006). Methods and concepts in quantifying resistance to drought, salt and freezing, abiotic stresses that affect plant water status. *Plant J.* 45, 523–539. doi: 10.1111/j.1365-313X.2005.02593.x

Wagner, A., Tobimatsu, Y., Phillips, L., Flint, H., Torr, K., Donaldson, L., et al. (2011). CCoAOMT suppression modifies lignin composition in *Pinus radiata*. *Plant J.* 67, 119–129. doi: 10.1111/j.1365-313X.2011.04580.x

Wang, C., Chen, S., Dong, Y., Ren, R., Chen, D., and Chen, X. (2020). Chloroplastic Os3BGlu6 contributes significantly to cellular ABA pools and impacts drought tolerance and photosynthesis in rice. *New Phytol.* 226, 1042–1054. doi: 10.1111/nph.16416

Wang, C. F., Huang, L. L., Buchenauer, H., Han, Q. M., Zhang, H. C., and Kang, Z. S. (2007). Histochemical studies on the accumulation of reactive oxygen species (O_2^- and H_2O_2) in the incompatible and compatible interaction of wheat—*Puccinia striiformis* f. sp. tritici. *Physiol. Mol. Plant Pathol.* 71, 230–239. doi: 10.1016/j.pmpp.2008.02.006

Wang, Z., Ge, Q., Chen, C., Jin, X., Cao, X., and Wang, Z. (2017). Function analysis of caffeoyl-COA O-methyltransferase for biosynthesis of lignin and phenolic acid in *Salvia miltiorrhiza*. *Appl. Biochem. Biotechnol.* 181, 562–572. doi: 10.1007/s12010-016-2231-4

Xia, Y., Liu, J., Wang, Y., Zhang, X., Shen, Z., and Hu, Z. (2018). Ectopic expression of *Vicia sativa* caffeoyl-CoA O-methyltransferase (VsCCoAOMT) increases the uptake and tolerance of cadmium in *Arabidopsis*. *Environ. Exp. Bot.* 145, 47–53. doi: 10.1016/j.envexpbot.2017.10.019

Xiao, Y., Li, J., Liu, H., Zhang, Y., Zhang, X., Qin, Z., et al. (2020). The effect of co-transforming *Eucalyptus urophylla* catechol-O-methyltransferase and caffeoyl-CoA O-methyltransferase on the biosynthesis of lignin monomers in transgenic tobacco. *Rus. J. Plant Physiol.* 67, 879–887. doi: 10.1134/s1021443720050180

Xu, C., Fu, X., Liu, R., Guo, L., Ran, L., Li, C., et al. (2017). PtoMYB170 positively regulates lignin deposition during wood formation in poplar and confers drought tolerance in transgenic *Arabidopsis*. *Tree Physiol.* 37, 1713–1726. doi: 10.1093/treephys/tpx093

Yamaguchi, M., Valliyodan, B., Zhang, J., Lenoble, M. E., Yu, O., Rogers, E. E., et al. (2010). Regulation of growth response to water stress in the soybean primary root. I. Proteomic analysis reveals region-specific regulation of phenylpropanoid metabolism and control of free iron in the elongation zone. *Plant Cell Environ.* 33, 223–243. doi: 10.1111/j.1365-3040.2009.02073.x

Yan, Q., Wu, F., Xu, P., Sun, Z., Li, J., Gao, L., et al. (2021). The elephant grass (*Cenchrus purpureus*) genome provides insights into anthocyanidin

accumulation and fast growth. *Mol. Ecol. Resour.* 21, 526–542. doi: 10.1111/1755-0998.13271

Yang, Q., He, Y., Kabahuma, M., Chaya, T., Kelly, A., Borrego, E., et al. (2017). A gene encoding maize caffeoyl-CoA O-methyltransferase confers quantitative resistance to multiple pathogens. *Nat. Genet.* 49, 1364–1372. doi: 10.1038/ng.3919

Yildiztugay, E., Ozfidan-Konakci, C., Kucukoduk, M., and Turkan, I. (2020). *Flavonoid naringenin* alleviates short-term osmotic and salinity stresses through regulating photosynthetic machinery and chloroplastic antioxidant metabolism in *Phaseolus vulgaris*. *Front. Plant Sci.* 11:682. doi: 10.3389/fpls.2020.00682

Yu, L., Chen, X., Wang, Z., Wang, S., Wang, Y., Zhu, Q., et al. (2013). *Arabidopsis* enhanced drought tolerance1/HOMEODOMAIN GLABROUS11 confers drought tolerance in transgenic rice without yield penalty. *Plant Physiol.* 162, 1378–1391. doi: 10.1104/pp.113.217596

Zhang, G., Zhang, Y., Xu, J., Niu, X., Qi, J., Tao, A., et al. (2014). The CCoAOMT1 gene from jute (*Corchorus capsularis* L.) is involved in lignin biosynthesis in *Arabidopsis thaliana*. *Gene* 546, 398–402. doi: 10.1016/j.gene.2014.05.011

Zhang, J., Nguyen, H. T., and Blum, A. (1999). Genetic analysis of osmotic adjustment in crop plants. *J. Exp. Bot.* 50, 291–302. doi: 10.1093/jxb/50.332.291

Zhang, X. S., Ni, R., Wang, P. Y., Zhu, T. T., Sun, C. J., Lou, H. X., et al. (2019). Isolation and functional characterization of two caffeoyl coenzyme A 3-O-methyltransferases from the fern species *Polypodiodes amoena*. *Plant Physiol. Biochem.* 136, 169–177. doi: 10.1016/j.plaphy.2019.01.021

Zhang, Y., Hu, X., Zheng, Y., and Liu, X. (2019). Ectopic expression of an antisense BpCCoAOMT gene from *Betula platyphylla* Suk. affects growth and development of tobacco due to lignin content reduction. *J. Plant Biochem. Biotechnol.* 29, 266–275. doi: 10.1007/s13562-019-00533-z

Zhao, D., Luan, Y., Shi, W., Zhang, X., Meng, J., and Tao, J. (2021). A *Paeonia ostii* caffeoyl-CoA O-methyltransferase confers drought stress tolerance by promoting lignin synthesis and ROS scavenging. *Plant Sci.* 303:110765. doi: 10.1016/j.plantsci.2020.110765

Zhong, T., Zhang, L., Sun, S., Zeng, H., and Han, L. (2014). Effect of localized reduction of gibberellins in different tobacco organs on drought stress tolerance and recovery. *Plant Biotechnol. Rep.* 8, 399–408. doi: 10.1007/s11816-014-0330-7

Zhou, Y., Zhang, Y., Wang, X., Han, X., An, Y., Lin, S., et al. (2020). Root-specific NF-Y family transcription factor, PdNF-YB21, positively regulates root growth and drought resistance by abscisic acid-mediated indoylacetic acid transport in *Populus*. *New Phytol.* 227, 407–426. doi: 10.1111/nph.16524

Conflict of Interest: The authors declare that the research was conducted in the absence of any commercial or financial relationships that could be construed as a potential conflict of interest.

Publisher's Note: All claims expressed in this article are solely those of the authors and do not necessarily represent those of their affiliated organizations, or those of the publisher, the editors and the reviewers. Any product that may be evaluated in this article, or claim that may be made by its manufacturer, is not guaranteed or endorsed by the publisher.

frontiers | Frontiers in Plant Science

ORIGINAL RESEARCH
published: 26 May 2022
doi: 10.3389/fpls.2022.894346

Leymus chinensis Adapts to Degraded Soil Environments by Changing Metabolic Pathways and Root Exudate Components

*Yulong Lin[1†], Pan Zhang[1†], Qingying Wu[1], Ying Zhang[2], Qianhao Wei[1], Yihang Sun[1], Yuchen Wu[1], Shixuan Sun[1] and Guowen Cui[1]**

[1] School of Animal Science and Technology, Northeast Agricultural University, Harbin, China, [2] School of Resources and Environment, Northeast Agricultural University, Harbin, China*

OPEN ACCESS

Edited by:
Jing Zhang,
Nanjing Agricultural University, China

Reviewed by:
Gao Yingzhi,
Northeast Normal University, China
Peizhi Yang,
Northwest A&F University, China

***Correspondence:**
Guowen Cui
cgw603@163.com

† These authors have contributed equally to this work

Specialty section:
This article was submitted to Plant Abiotic Stress, a section of the journal Frontiers in Plant Science

Received: *11 March 2022*
Accepted: *01 April 2022*
Published: *26 May 2022*

Citation:
Lin Y, Zhang P, Wu Q, Zhang Y, Wei Q, Sun Y, Wu Y, Sun S and Cui G (2022) Leymus chinensis Adapts to Degraded Soil Environments by Changing Metabolic Pathways and Root Exudate Components. Front. Plant Sci. 13:894346. doi: 10.3389/fpls.2022.894346

Phytoremediation is a promising remediation strategy for degraded soil restoration. Root exudates are the main carrier substances for information communication and energy transfer between plant roots and soil, which play non-negligible roles in the restoration process. This work investigated the adaptation of *Leymus chinensis* root exudates to different degraded levels of soil and the mechanism of rhizosphere restoration in a 3-year degraded soil field study. We found that the soil quality at each degradation level significantly increased, with the soil organic matter (SOM) content slightly increasing by 1.82%, moderately increasing by 3.27%, and severely increasing by 3.59%, and there were significant increases in the contents of available nutrients such as available phosphorus (AP), ammonia nitrogen (AN), and nitrate nitrogen (NN). The physiological activities indicated that root tissue cells also mobilize oxidative stress to respond to the soil environment pressure. A total of 473 main components were obtained from root exudates by gas chromatography–time-of-flight mass spectrometry (GC–TOFMS), including acids, alcohols, carbohydrates, and other major primary metabolites. OPLS-DA revealed that soil degradation exerted an important influence on the metabolic characteristics of root exudates, and the numbers of both up- and downregulated metabolic characteristic peaks increased with the increase in the degree of degradation. Forty-three metabolites underwent clear changes, including some defense-related metabolites and osmotic adjustment substances that were significantly changed. These changes mainly mobilized a series of lipid metabolism pathways to maintain the fluidity of membrane function and help plants adapt to unfavorable soil environmental conditions. The PPP energy metabolism pathway was mobilized in response to slight degradation, and TCA energy pathways responded to the environmental pressure of severe soil degradation.

Keywords: phytoremediation, metabolomics, root exudates (RE), soil degradation, feed crop

INTRODUCTION

Soil degradation leads to salinization, soil organic matter (SOM) loss, decreased fertility, unbalanced elements, reduced aggregate stability, and deterioration of soil structure (Tamene et al., 2019; Jin et al., 2022). It has severely affected crop growth and economic productivity and has become a worldwide disaster. Phytoremediation is an environmentally friendly, economical, and effective method to remediate degraded soils (Liu et al., 2018). As an important microhabitat surrounding the plant root surface, the rhizosphere links the bulk soil and living roots, which are generally involved in the phytoremediation process. In the local area, root exudates play an important role in the soil remediation process (Zhang et al., 2021).

Roots can continuously secrete a large amount of root exudates into the rhizosphere during plant growth. These exudates are mainly composed of organic acids, amino acids, lipids, phenols, alcohols, and other low-molecular-weight organic metabolites, high-molecular-weight substances such as mucus and protein, and other special metabolites (Rohrbacher and St-Arnaud, 2016). Although the biological functions of these compounds have not been confirmed, some low-molecular-weight organic compounds (LMWOA) have been considered carrier substances for energy transfer media and communication signals between plants, soil, and rhizosphere microorganisms (Hu et al., 2018). The main components and abundance of root exudates vary with plant species, environmental conditions, soil nutrients, soil types, and other factors. Plants will adjust their nutrition, cells, physiology, and biochemistry when encountering extreme soil environments and enhance their adaptability to reduce the negative effects of adverse environmental conditions (Rodriguez-Garrido et al., 2020). For example, plants increase the root exudate rate by altering root morphological characteristics and associated changes in underground C allocation to cope with elevated temperatures (Yin et al., 2013). Shen et al. (2020) studied how plants respond to long-term overgrazing soil degradation by enhancing species-specific enhancements to the root exudation rate and changing the formation and stability of grassland SOC by releasing root exudates.

It is important to explore the ecological and physiological responses and mechanisms of plant root exudates in the process of soil restoration. Recently, different scholars have conducted research on root exudates and their ecological applications. A few studies have found that the intercropping system of *Moso bamboo* and *Sedum plumbizincicola* increased the organic acids in root exudates and facilitated the absorption of heavy metals by *Moso bamboo* (Bian et al., 2021). Peizataifeng rice increased the contents of oxalic acid, critic acid, and malonic acid in root exudates and promoted DBP and DEHP desorption in the soil (Du et al., 2020). *Sonchus asper* L. and *Vicia faba* L. have been reported to adapt to cadmium stress by regulating LMWOA in root exudates (Zhan et al., 2016). However, current phytoremediation research mainly focuses on pollutants and heavy metals, and the actual *in situ* soil rhizosphere process has not been fully demonstrated beyond idealized laboratory research. There have been few studies on the total components of plant root exudate analysis and differential metabolite identification. The composition of metabolites secreted by plant roots in degraded soil environments has changed, which indicates that the metabolic pathways involved have also changed. There have been few studies on the *Leymus chinensis* root exudate characteristics and metabolic pathways in degraded soil restoration. The emergence and development of metabolomics provide new ideas for this research. Metabolomics is derived from systems biology and identifies significant differences in key biomarkers and has been widely used in defining the tolerance response of plants under external circumstances, which has an increasingly important role in revealing the basic activities and laws of life (Li X. et al., 2021).

In this study, a 3-year phytoremediation experiment was conducted at different soil degradation levels to investigate how *L. chinensis* remediates the degraded soil environment by altering root exudate components and metabolism pathways. We evaluated the enhancement effect of root exudates on degraded soil nutrients. Root exudate component changes were detected by untargeted metabolomics based on gas chromatography–time-of-flight mass spectrometry (GC–TOFMS). Metabolic pathway analysis during the restoration process was performed according to the identified differential metabolic markers. In addition, the effects on physiological activities in root tissues were also analyzed. The obtained research findings provide new insights for defining the phytoremediation mechanism in degraded soils.

MATERIALS AND METHODS

Experimental Area and Setup

The experimental area was located at the demonstration base (126°26′04″E, 45°57′87″N) around Harbin, China (**Figure 1**). This site experiences a humid temperate continental monsoon climate, with an average annual precipitation of 350 mm and an annual average temperature of −5 to 4°C. More than 80% of the total precipitation occurs during the growing period, and the highest average temperature is 23°C. According to the land use survey results, three typical soil degradation levels were selected for experimental sites: slightly (SL), moderately (MO), and severely (SE) degraded soils. *L. chinensis* was planted on 20 July 2017. Each site used a land area of 5 m × 5 m, and the adjacent plot was untreated as a buffer to minimize the crossover effect. Each treatment was performed in triplicate according to a randomized block design.

Effects of Root Exudate Release on Soil Remediation

The soil samples were harvested on 3 September 2020. The root systems in different degraded plots were collected randomly and shaken gently to remove the loose soil. The closely attached soil on the root surface (<3 mm from the root surface) was collected and defined as the rhizosphere soil (the three rhizosphere soils were marked as RSL, RMO, and RSE), and the soil without plants was bulk soil (Solá et al., 2019). The soil samples were mixed evenly, air-dried at 25°C, and passed through a 2-mm sieve to determine the soil's physical and chemical properties. EC meters (Rex) and pH meters (Rex) were used to measure the electrical

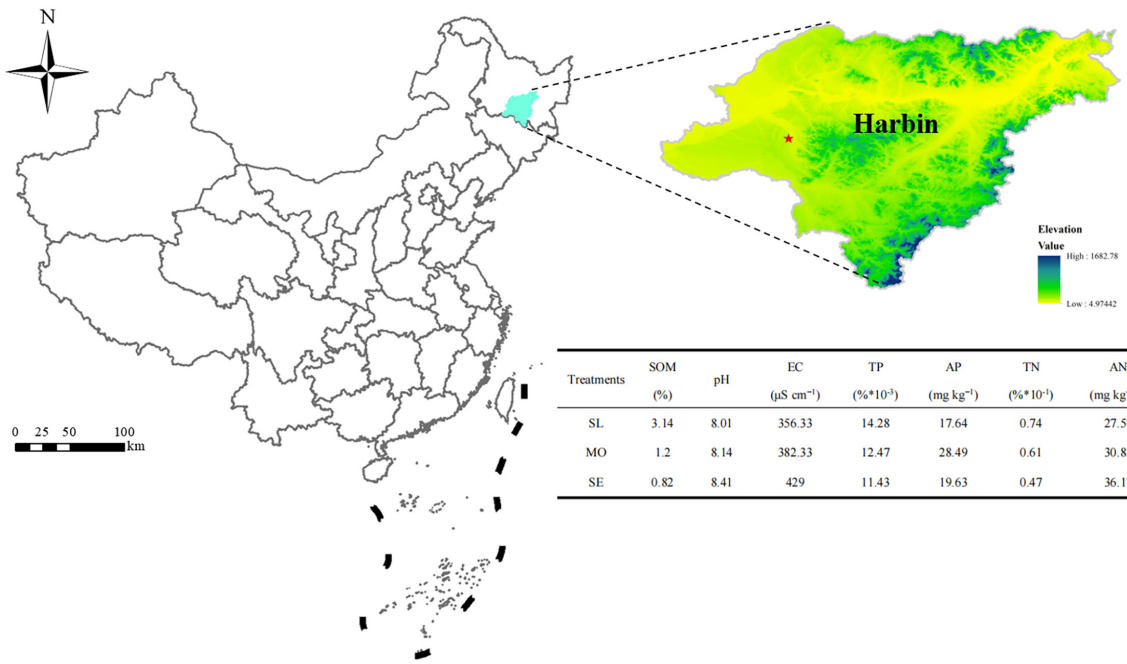

Treatments	SOM (%)	pH	EC (μS cm^{-1})	TP (%*10^{-3})	AP (mg kg^{-1})	TN (%*10^{-1})	AN (mg kg^{-1})	NN (mg kg^{-1})
SL	3.14	8.01	356.33	14.28	17.64	0.74	27.57	3.9
MO	1.2	8.14	382.33	12.47	28.49	0.61	30.81	3.13
SE	0.82	8.41	429	11.43	19.63	0.47	36.17	1.02

FIGURE 1 | Location of the experimental area.

conductivity (EC) and pH, respectively (1:5 soil/water ratio, m/V). The potassium dichromate method was used to analyze SOM (Bao, 2010). Soil total phosphorus (TP), total nitrogen (TN), available phosphorus (AP), ammonia nitrogen (AN), and nitrate nitrogen (NN) were all detected by a continuous segmented flow analyzer (SEAL AutoAnalyzer 3 HR).

Physiological Activities of Root Samples

The physiological activities of root samples were determined by malondialdehyde (MDA), proline (Pro), enzyme activity (POD), superoxide dismutase (SOD), catalase (CAT), and protein (Nanjing Jiancheng Bioengineering Institute, Inc., China) kits. MDA, Pro, POD, SOD, and CAT test kits were provided by Suzhou Keming Biotechnology Co., Ltd. (Suzhou, China). Fresh root samples (0.5 g) were homogenized with normal saline at a ratio of 1:9 w/v under low-temperature conditions and then centrifuged at 3,500 rpm/min for 10 min to obtain the supernatant liquid, and the sample absorbances of MDA, protein, POD, SOD, and CAT were detected at 532, 595, 420, 550, and 240 nm according to the test kit instructions. Root tissue (0.5 g) was shaken at 96°C for 10 min, and the supernatant was extracted according to the instructions. Then, the absorbance of Pro was read at 520 nm.

Root Exudate Sample Collection and Detection

The roots were carefully collected, and any attached soil was carefully removed with Milli-Q water. Then, the roots were transferred to a glass conical flask containing 200 mL sterilized Milli-Q water and covered with aluminum foil to protect the roots from light. The plants were removed after 2 h to collect the liquid, and the process was repeated until the required amount of root exudates was obtained and filtered with glass fiber filters. Finally, a 10-mL methanol and dichloromethane mixture (50:50) was used to elute the SPE cartridges for the next step of derivatization (Lin et al., 2019). Forty milliliters of root solution was freeze-dried and transferred to 2-mL Eppendorf tubes, and 1,000 μL precooled extraction solution was added. Then, 10 μL ribitol (adonitol, 0.5 mg/mL stock) was added as the internal standard and vortexed for 30 s to mix the solution well. The samples were homogenized at 35 Hz for 4 min in a grinder, posttreated in ice water for 5 min, and then centrifuged at 12,000 rpm at 4°C for 15 min. The supernatant was pipetted into 1.5-mL Eppendorf tubes and dried. At this stage, 100 μL supernatant of each sample was mixed as a quality control sample (QC). Then, 20 μL methoxyamine hydrochloride (in pyridine 20 mg mL^{-1}) was added and incubated for 30 min at 80°C, followed by derivatization with 30 μL BSTFA reagent (1% TMCS, v/v) for 1.5 h at 70°C. After cooling to room temperature, 5 μL of FAMEs (in chloroform) was added to complete the derivatization process for analysis.

Metabolite Analytical Methodology

An Agilent 7890 gas chromatograph coupled with a Pegasus HT time-of-flight mass spectrometer was used to analyze root exudate-derived extracts, and a DB-5MS capillary column (30 m × 250 μm × 0.25 μm, J&W Scientific, Folsom, CA, United States) was used for separation. Then, 1 μL of the derivatized sample was injected in split mode, the purge flow rate of helium was 3 mL min^{-1}, and the gas flow rate passing through the column was 1 mL min^{-1}. The GC oven column

temperature was set as 50°C for 1 min, increased to 310°C at a rate of 10°C min^{-1}, and finally held for 8 min. The TOFMS injection, transfer line, and ion source temperatures were set as 280, 280, and 250°C, respectively. Ionization was achieved by a −70 eV collision energy electron collision. After a solvent delay of 6.30 min, the mass spectrometry data were collected in full-scan mode with an m/z range of 50–500, and TOFMS data were acquired at a rate of 12.5 spectra per second. The quality of the data was checked, and the deviation value was filtered to remove noise by the single data interquartile range method. Single peaks were filtered, and the low-mass ions that were more than 50% missing in the QC sample and more than 80% missing in the actual sample were removed. The data were normalized by the internal standard method based on the total ion current of each sample, and the missing values in the original data were simulated and filled using the minimum-half method. More than 30% of the relatively fluctuating relative standard deviation (RSD) ions with large fluctuations were filtered out in all QC samples.

Data Analysis

Raw peak extraction, baseline correction, deconvolution analysis, peak integration, and alignment analysis of mass spectrometry data were allowed by the Chroma TOF package (V 4.3x, LECO). The calculated variable important for the projection (VIP) of the first principal component was used to measure the impact strength of differences between groups, and VIP scores over 1.0 were selected for further interpretation of metabolic markers. Finally, Student's *t*-test ($P < 0.05$) was used to evaluate and filter the remaining variables. The mass spectra and retention times of the differential metabolic markers were matched by searching the LECO-Fiehn Rtx5 database. Finally, based on the Kyoto Encyclopedia of Genes and Genomes (KEGG) metabolic database, the metabolic pathway was constructed. The soil physical and chemical property data and physiological data of plant tissues were analyzed by Origin Pro 9.0 and SPSS 19.0. In addition, one-way ANOVAs followed by Duncan's multiple range tests ($P \leq 0.05$) were performed to check for differences in data.

RESULTS

Leymus chinensis Root Exudates Significantly Improved Soil Nutrients

According to our data (**Figure 2**), the SOM contents in SL, MO, and SE increased by 1.82, 3.27, and 3.59%, respectively, in a 3-year phytoremediation; due to root exudates, the contents increased by 1.50, 1.64, and 1.19% compared with the bulk soil. Phytoremediation increased the N content significantly, and root exudates also increased AN in RSL, RMO, and RSE by 40.52, 15.30, and 24.46%, NN by 57.14, 47.93, and 70.03%, and TN by 2.37, 2.94, and 3.17%, respectively, compared with bulk soil. There was a certain difference between the P and N contents; phytoremediation increased the TP content slightly, but the AP content increased significantly, and the TP content in the rhizosphere soil increased by 30.38, 34.75, and 24.62%, respectively. The pH values of RSL, RMO, and RSE were reduced by 0.24, 0.39, and 0.25 U, respectively, and EC levels were reduced by 15.92, 8.49, and 14.61%, respectively. The above results indicated that 3 years of phytoremediation improved the degraded soil nutrients well, indicating that the interaction between root exudates and soil cannot be ignored.

Effects of Plant Physiological Activities

We analyzed the activities of POD, SOD, and CAT, the three important enzymes of root tissues, in different degraded soil levels due to the crucial role of antioxidant enzymes in ROS removal. As shown in **Figure 3A**, the activities of all three enzymes showed increasing trends with increasing soil degradation level, and the SE root system showed 1. 74-, 1. 62-, and 1.21-fold higher POD, SOD, and CAT activities than SL and MO, respectively. These results suggest that *L. chinensis* enhanced the activities of antioxidant enzymes to maintain a low level of ROS to cope with soil degradation by scavenging excess H_2O_2 and O_2 in roots. The MDA level in H was 0.83 U/mg prot, which was enhanced by 14.78% compared with SL, but there was no significant difference between MO and SL. The levels of Pro, MO, and SE were enhanced by 22.82 and 31.31%, respectively, compared with those in SL roots, but there was no significant difference between MO and SE. In addition, the protein level in root tissues of SE and MO was significantly decreased compared with SL. These findings indicated that *L. chinensis* could adapt to soil degradation by changing the osmotic pressure of root cells, the cell membrane fluidity, and the protein content in plant tissues.

Analysis of the *Leymus chinensis* Root Exudate Composition

We identified the main components of root exudates of *L. chinensis* based on GC–TOFMS metabolic profiling, which is a sensitive analysis. The overall pattern of metabolite changes after exposure to stressors can be monitored and has gradually been applied to study plant tolerance to abiotic stress. The GC–TOFMS molecular characteristic peaks were compared based on the HDMB, PubChem, and METLIN databases by retention time and similarity. The *L. chinensis* root exudate composition was complex, with a total of 473 peaks detected, of which 293 were unknown metabolites and 180 were named metabolites. The exudate contained 60.22% acids, alcohols, and carbohydrates, each 8.84%, with amines 5.52%, ketones 3.31%, esters 2.20%, and phenols 1.66%; metabolites <1.10% were classified as other substances, which comprised a total quantity of 9.41% (**Figure 3B**). Of the most important acids in root exudates, organic acids had the most types, accounting for 51.38%, followed by amino acids, fatty acids, and phenolic acids, accounting for 19.27, 15.60, and 13.75%, respectively (**Figure 3B**). In addition, *L. chinensis* root exudates also contain a variety of secondary metabolites, such as pyrimidines, pyridines, purines, terpenes, and diterpenes, which have been commonly detected in most plant root exudates, and some allelochemicals, such as benzoic acid and hydrocarbons.

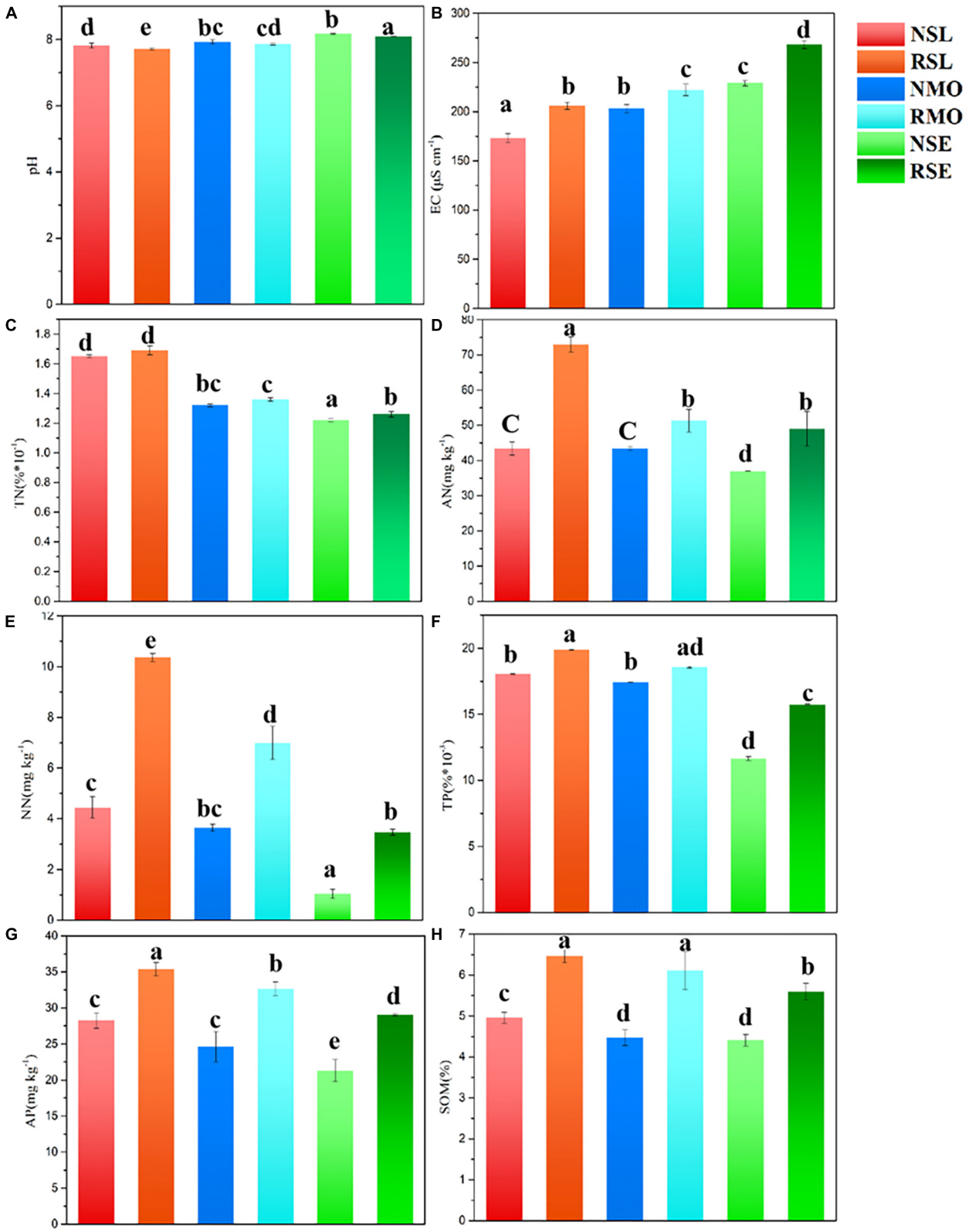

FIGURE 2 | Effect of 3 years of phytoremediation on soil physical and chemical parameters, including pH **(A)**, EC **(B)**, TN **(C)**, AN **(D)**, NN **(E)**, TP **(F)**, AP **(G)**, and SOM **(H)**. The bars with different letters are significantly different ($P < 0.05$), and the results were obtained from one-way ANOVA. The first letter of the sample ID indicates the root compartment (R, rhizosphere soil; N, bulk soil).

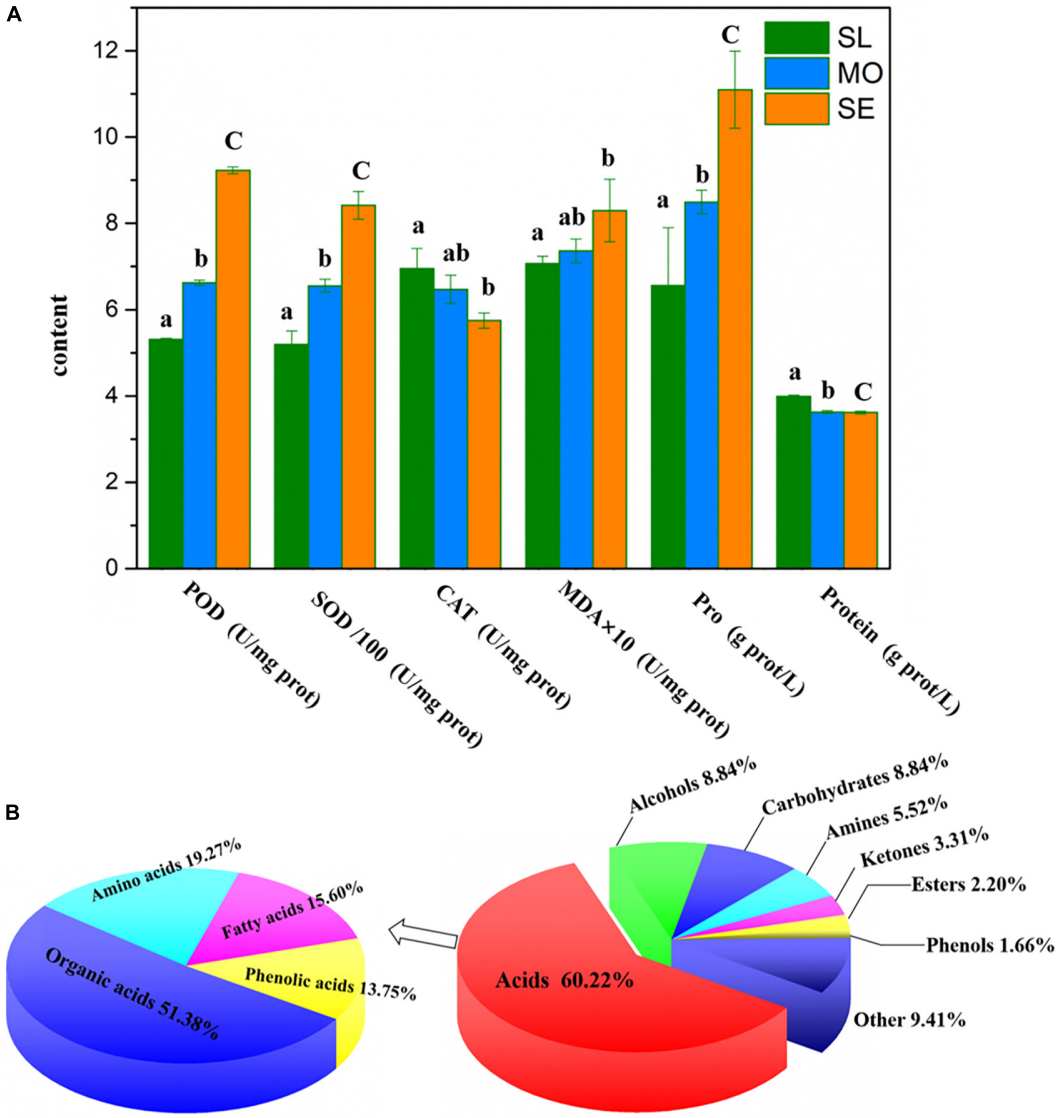

FIGURE 3 | (A) Effect of soil degradation on physiological activities in plant tissues. The bars of different letters are significantly different ($P < 0.05$). **(B)** Classification of known metabolites and acids.

Changes in the *Leymus chinensis* Root Exudates Upon Growth With Soil Degradation Level

OPLS-DA was used to compare the influence of degraded soil on root exudates to distinguish metabolic changes under slightly, moderately, and severely degraded soil levels. OPLS-DA (**Figure 4A**) within the 95% confidence interval (Hotelling's T-squared ellipse) showed that the sample points in the same treatment clearly clustered and showed small differences. A clear separation was observed in the MO degradation level from SL along PC1, and SE, with more severe degradation, was significantly separated from the MO and SL degradation levels along PC1. These results indicated that the soil degradation markedly changed the *L. chinensis* root exudates, and its components were dependent on the degradation level, indicating that it might adapt and restore different degradation levels in soil by adjusting its own metabolic system.

The differential metabolites of each treatment were determined by selecting MS peaks with Student's *t*-test ($P \leq 0.05$) and VIP scores. A total of 0.56 and 2.82% of the total MS peaks in the MO level group were significantly downregulated and upregulated, respectively, in comparison with the SL group (**Figure 4B**). In the SE degradation group, in comparison with the MO group, 2.20 and 13.54% of the total MS peaks were significantly downregulated and upregulated, respectively (**Figure 4C**). The numbers of upregulated and downregulated MS peaks increased with increasing soil degradation level. A total of 43 significantly different metabolites in comparison were identified according to the HDMB, PubChem, and METLIN

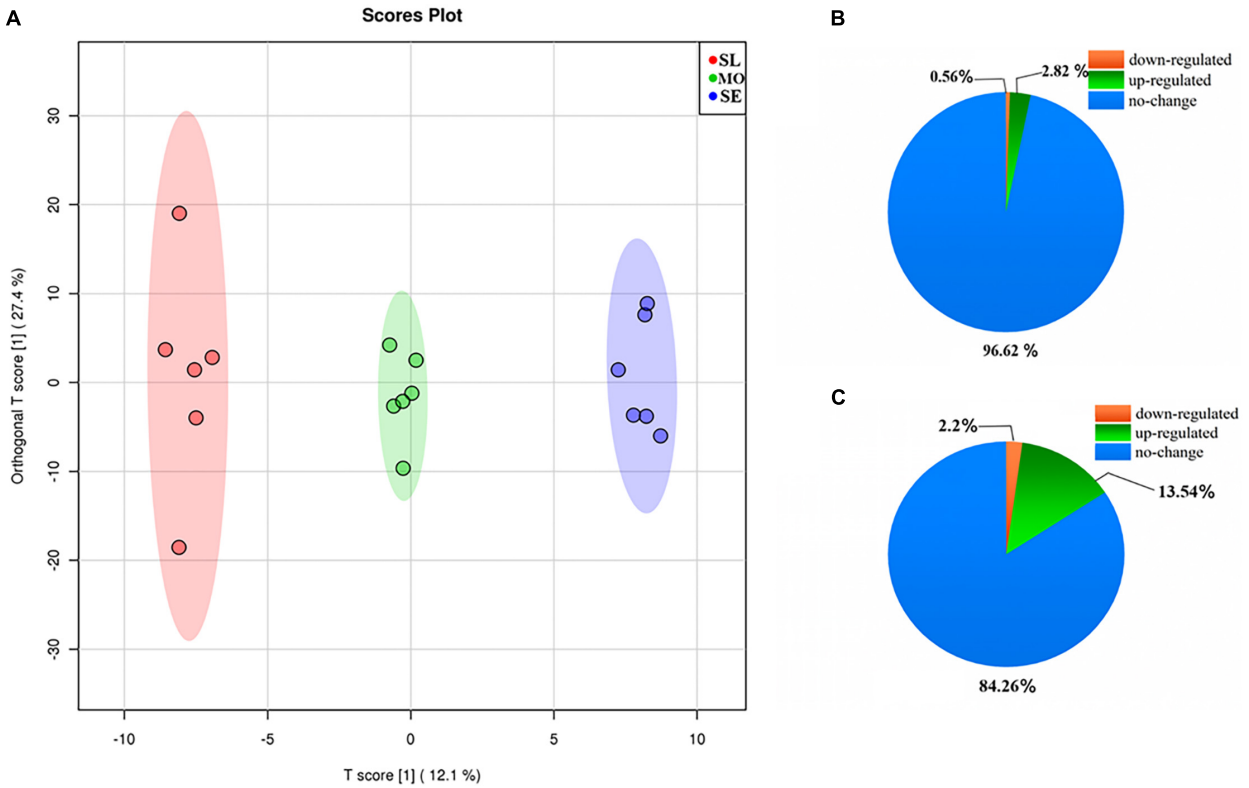

FIGURE 4 | (A) OPLS-DA analysis of soil samples at different degradation levels. Percentages of MS peaks with no change, upregulation, and downregulation in SL/MO **(B)** and MO/SE **(C)**.

databases, and hierarchical cluster analysis was used to visualize the relationships between these metabolites (**Figure 5**). The differential metabolites in root exudates included eight fatty acids, seven organic acids, six amino acids, three phenolic acids, four alcohols, three esters, three ketones, three sugars, two phenols, two amines, one fluorene, and one nucleoside. Two metabolites were downregulated, and 10 metabolites were upregulated in the comparison of the B and A groups. Among these identified compounds, eight and 49 metabolites were downregulated and upregulated, and 12 metabolites were upregulated and downregulated in the comparison between Group C and Group B. In summary, the above results indicated that the differential expression of primary and secondary metabolites in root exudates might be one of the reasons for plants adapting to or changing degraded soil.

Combination of Metabolites in Root Exudates and Biological Endpoints

The metabolites with significant differences were used to check the changes in metabolic pathways in the KEGG database. The enrichment pathway analysis revealed that there were six significantly enriched metabolic pathways in the MO/SL group ($P < 0.05$). In detail, these pathways included the pentose phosphate (ath00030), fatty acid biosynthesis (ath00061), fatty acid elongation (ath00062), fatty acid degradation (ath00071), phenylpropanoid biosynthesis (ath00940), and unsaturated fatty acid biosynthesis (ath01040) metabolic pathways (**Figure 6A**). The SE/SL group showed 10 significantly enriched metabolic pathways ($P < 0.05$). **Figure 6B** shows the citric acid cycle (TCA cycle) (ath00020), fatty acid biosynthesis (ath00061), fatty acid elongation (ath00062), fatty acid degradation (ath00071), phenylalanine, alanine, aspartate, and glutamate (ath00250), arginine and proline metabolism (ath00330), tyrosine metabolism (ath00350), glycerolipid metabolism (ath00561), phenylpropanoid biosynthesis (ath00940), and unsaturated fatty acid biosynthesis (ath01040). Taken together, the above results indicated that the abnormal expression of these primary and secondary metabolites by roots might be one of the reasons for plant adaptation or remediation of degraded soil.

The different metabolites of *L. chinensis* root exudates in different degraded soil levels were mapped to plant metabolic pathways, and the results are shown in **Figure 7**. In the primary metabolic networks, carbohydrates, amino acids, and lipid metabolites were usually significantly upregulated in the MO/SL and SE/SL groups. Many expression patterns were the same in the two groups. For example, metabolites such as lauric acid, stearic acid, oleic acid, and palmitic acid showed significant upregulation trends in lipid biosynthesis and metabolism-related pathways compared with the SL group. *L. chinensis* adapted to different degraded levels of soil environments by mobilizing different pathways in energy metabolism-related pathways. For example,

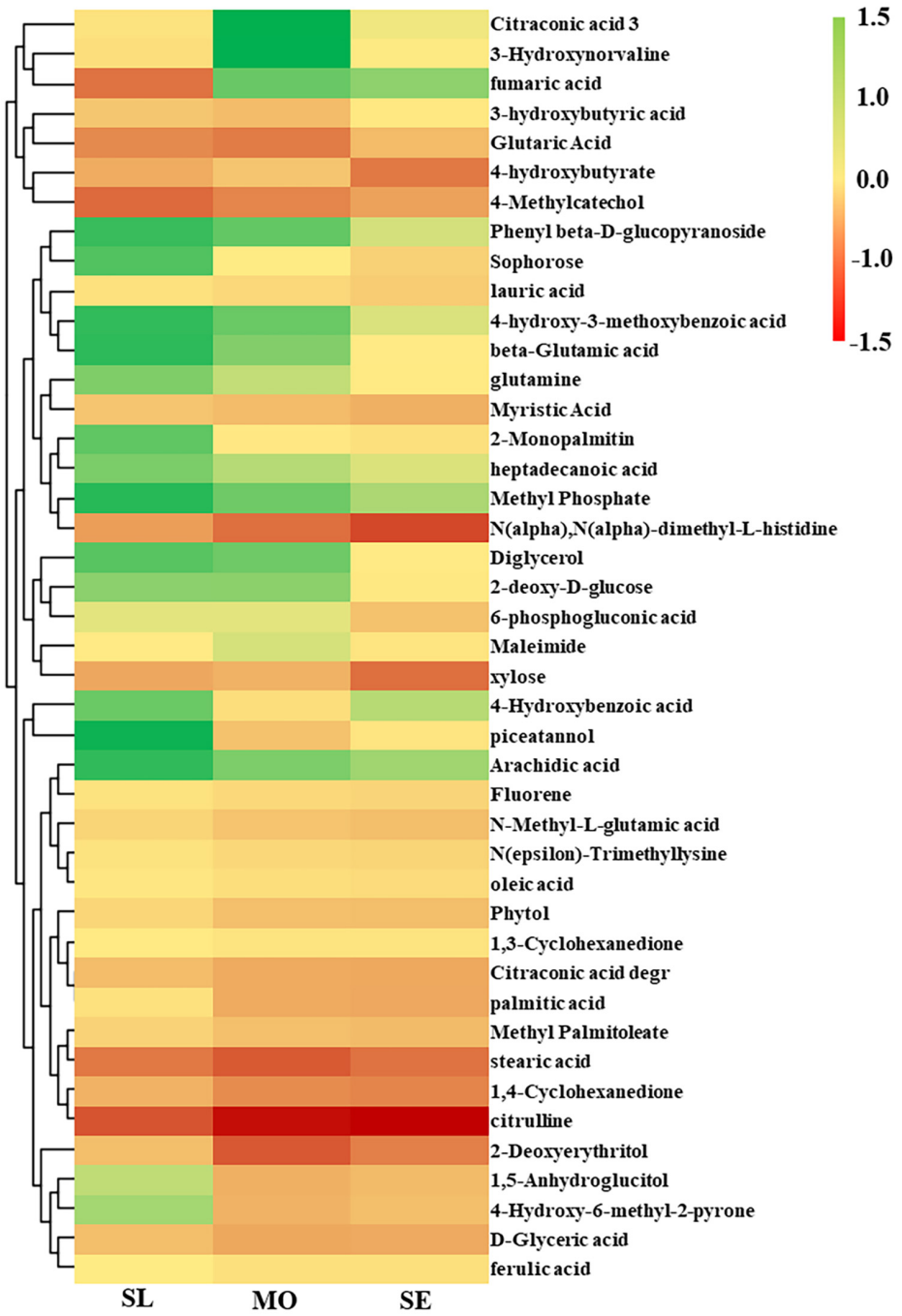

FIGURE 5 | Heatmap analysis for the identified *L. chinensis* metabolites with significant differences (VIP > 1.0, $P \leq 0.05$).

it mobilized the pentose phosphate pathway (PPP) to adapt to the rhizosphere soil environment by upregulating the expression level of 6-phosphogluconate in MO/SL. Severely degraded soils upregulated the expression level of fumaric acid to mobilize the TCA cycle and amino acid biosynthesis and amino acid biosynthesis metabolic pathways *via* metabolite expression levels, such as glutamine, manganese–trimethyllysine, and ferulate, to adapt to the soil environment.

DISCUSSION

Soil quality is the primary determinant of food production or regional ecosystem resource regulation in the agricultural value chain, and a healthy soil environment is the key to human survival (Greiner et al., 2017). Food problems caused by unreasonable development and overutilization of agricultural soils around the world not only cause catastrophic economic

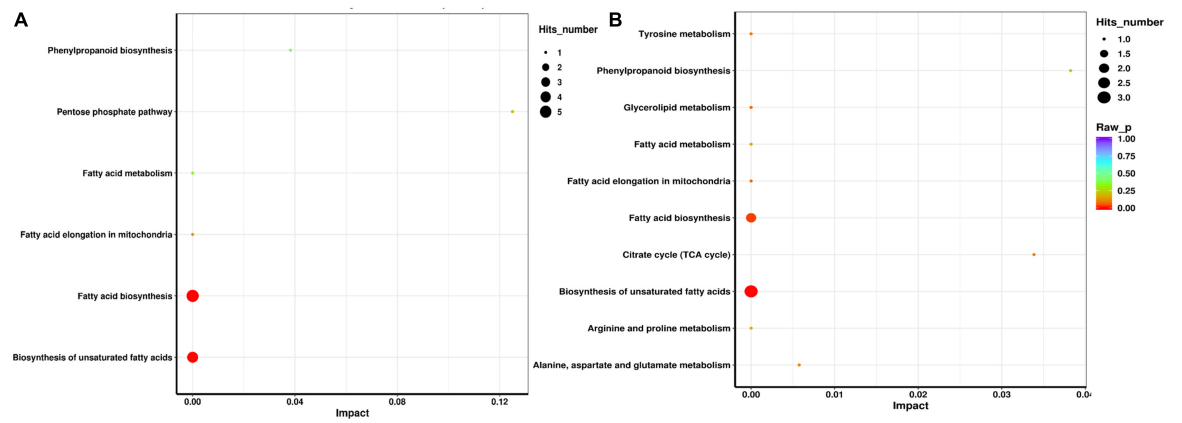

FIGURE 6 | Pathway analysis of identified metabolites with significant differences in SL/MO **(A)** and MO/SE **(B)**.

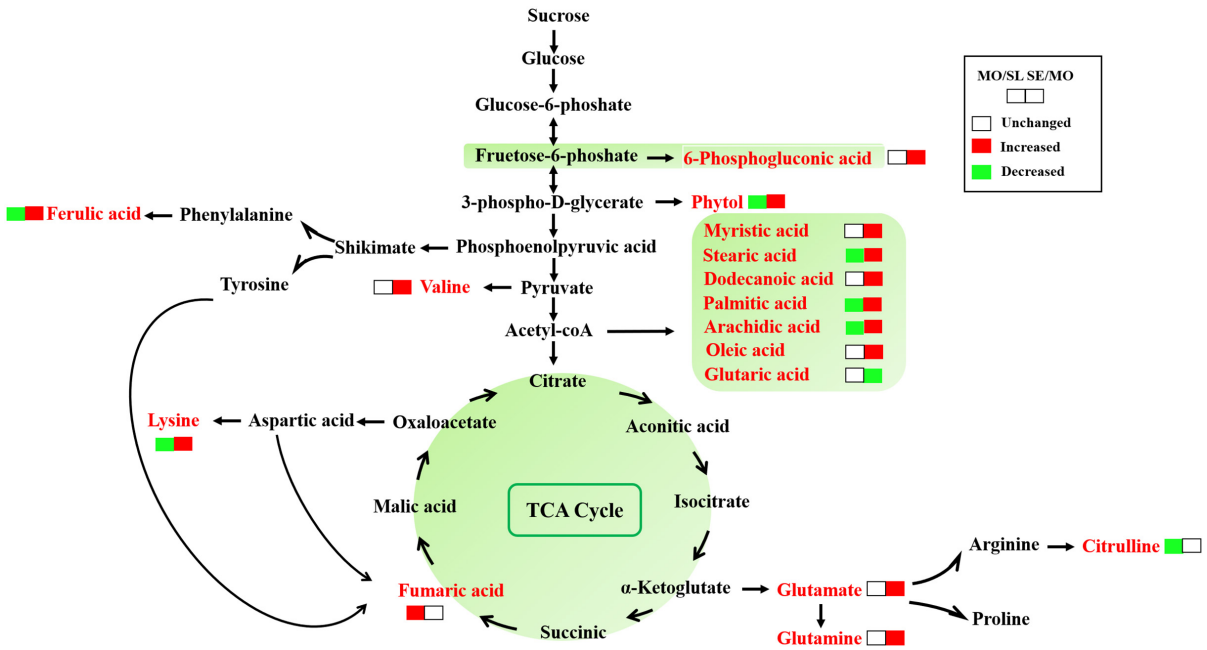

FIGURE 7 | Alteration of related metabolic pathways of *L. chinensis* root exudates to adapt to soil degradation. The metabolites in red text are the differential metabolites. The red, green, and boxes indicate the metabolites with upregulation, downregulation, and no change, respectively.

losses for farmers and agricultural development restrictions but also reduce soil productivity continuously and even lead to soil desertification, which severely threatens ecological security (Ronchi et al., 2019; Kik et al., 2021). Currently, different soil remediation methods promote soil quality in countries around the world to maintain long-term soil sustainability (FAO, 2017). Phytoremediation, as a promising environmentally friendly soil remediation technology, has become a hot research topic for scholars worldwide. Non-food crop forage is not only simple field management but also provides strong support for animal husbandry and generates considerable economic benefits. Phytoremediation can fix carbon by photosynthesis, rhizodeposition below-ground, and litter materials above-ground to ensure the long-term sustainability of soil quality (Rasse et al., 2005). Root litters and plant shoots have been well studied, though living roots such as root exudates are still less well known.

Recent studies have shown that bioactive compounds released from root systems, namely, root exudates, play important roles in soil improvement and restoration issues (Xiong et al., 2019). Plants can adjust and even improve the environment by adjusting the main components of root exudates when confronted with external adverse factors. In this research, we investigated the rhizosphere ecological mechanism of *L. chinensis* phytoremediation of degraded soil by analyzing root tissue physiological activities and the root exudate metabolic profile. ROS have emerged as the main signaling molecules

in plants in response to stress conditions (Chen and Yang, 2020). Soil degradation induces the accumulation of ROS in plants and gradually destroys cell lipids, proteins, and DNA. Then, plants mobilize complex antioxidant defense systems to synthesize antioxidant substances and enhance antioxidant enzyme activities to maintain the intracellular ROS metabolic balance and resist the plant cell oxidative damage suffered by degraded soil environments. POD, SOD, and CAT are the most important antioxidant enzymes in this process and coordinate with each other (Hu et al., 2021). SOD converts superoxide anions into H_2O_2 *via* disproportionation; subsequently, POD and CAT convert H_2O_2 into H_2O and O_2. The activities of SOD, POD, and CAT in plant root tissues seem to increase with the soil degradation level, indicating that ROS metabolism might play an important role in the resistance of *L. chinensis* to soil degradation and that plants mobilize antioxidant POD to remove excess ROS. MDA is produced in the lipid peroxidation process caused by free radical oxidation and is an important indicator of lipid peroxidation (Sadauskiene et al., 2018). The MDA contents in SL and SE plant root tissues seemed to increase with increasing soil degradation levels, indicating that *L. chinensis* might respond to soil degradation by increasing membrane lipid peroxidation. However, the difference in MDA between SE and MO was not significant, which might indicate that it has a strong resistance to soil degradation. Protein content was related to plant growth, with the lowest content in SE, indicating that soil degradation had a certain negative impact on protein synthesis (Gao et al., 2019). The above data indicated that *L. chinensis* might adapt to degraded soil environments by mobilizing different physiological activities.

The *L. chinensis* root exudates were complex, and the main components were acids, alcohols, carbohydrates, and other primary metabolites, which have been commonly detected in most plant root exudates (Zhang et al., 2014; Wu et al., 2015). Acid had great effects on soil formation and nutrient and pollutant conversion, and the root system could adjust these substances to cope with differences in hydraulic conditions and nutrient concentrations. A previous study showed that plants increased organic acid exudation under P-limited conditions (Edayilam et al., 2018). This was due to organic acids lowering the rhizosphere soil pH, mobilizing the activity of P, K, Ca, and other soluble mineral nutrients in the rhizosphere, and enhancing the absorption rate of plant nutrients. This was confirmed by our results showing that the rhizosphere soil pH was lower than that of bulk soil and that the contents of AP, AN, and NN in rhizosphere soil were also significantly higher than in bulk soil. The presence of acetic acid could also increase the accessibility of microorganisms to mineral-protected SOM by a non-biological dissolution reaction (Keiluweit et al., 2015). Root exudates provide vital nutrients and energy substances for soil microorganism growth and reproduction and have a selective effect on the microbial community, which has a certain ability to shape the rhizosphere microbiota. The presence of citric acid might increase the number of functional bacteria and improve the microbial community structure (Ma et al., 2020). Malic acid promoted the growth and colonization of *Paenibacillus polymyxa* and *Bacillus amyloliquefaciens*, which induce plant systemic resistance (Martins et al., 2018). Succinic acid and oxalic acid are considered to be the main C sources of denitrification microorganisms (Liu et al., 2016), and some phenolic substances have been shown to promote organic matter in soil decomposition by stimulating changes in microbial community composition (Huang et al., 2019). Plant roots can release amino acids and exert a variety of biological effects by passive diffusion; for example, the osmotic adjustment substance proline can protect cell membranes from oxidative stresses and stabilize protein structure (Li et al., 2019). In addition, some substances such as benzoic acid, hydrocarbons, and others detected were allelopathic substances, which could affect seed germination and microbial growth and possibly interfere with the growth of other plants. In addition to the primary metabolites, several secondary metabolites were detected, including atropine, polyphenols (cinnamic acid), terpenes, and diterpenes such as cuminic alcohol and phytol, ethanolamine, and 1,3-propylene diamine, which might be beneficial for slow-growing microorganisms that rely on low concentrations of secondary plant metabolites.

The release of root exudates is a dynamic process and may be greatly influenced by various environmental stress factors; it affects not only the soil ecosystem structure and resilience but also plant–soil feedback and long-term ecosystem maintenance, soil function, and stability (including nitrification) (Williams and de Vries, 2020; Li Y. et al., 2021). Plant metabolites are diverse and have complex metabolic pathways; therefore, differential metabolite detection and metabolic pathway analysis may reflect the state during plant growth. In our data, the contents of most fatty acids in root exudates were upregulated under exposure to the degraded soil, and *L. chinensis* mobilized fatty acid metabolism to promote the lipid composition in root cells and the adjustment of the membrane fatty acids. Lipids are the most compliant biomolecules; they are important parts of biofilms and protect cells from oxidative stress responses (Zhou et al., 2012). As a sensory device for contact with external signals, cell membranes mediate various reactions caused by external factors to cells, which is the target of harmful components of toxicity in the degrading soil. ROS in degraded soil attack root cells, and to adapt to the pressure of external factors, they increase saturated unsaturated fatty acid metabolism, such as palmitic acid, stearic acid, and arachidic acid, to maintain the fluidity and stability of biofilms and protect plant cell membranes from reactive oxygen species attack, which is also consistent with the physiological and biochemical indicator results (Wang et al., 2019). Therefore, the increase in fatty acid levels in root exudates in degraded soil may be an indicator of the root membrane resisting external environmental pressure. Zhao et al. (2018) also observed increased levels of fatty acid content in cucumber leaves under low copper stress, which suggested that it helps maintain the fluidity necessary for proper membrane function. Jung et al. (2015) also found that unsaturated fatty acids increased when burdock roots were exposed to copper. In short, degraded grassland might change the root exudate composition by upregulating fatty acid metabolism pathways of *L. chinensis* and changing the fluidity of root cell membranes.

Our results showed that 6-phosphogluconic acid was significantly affected by slightly degraded soils, indicating that

the glucose produced by *L. chinensis* was phosphorylated rapidly and fueled the PPP preferentially. The PPP communicates with lipid, protein, nucleic acid, and secondary biomass metabolism. It provides building blocks for nucleotide biosynthesis and reducing power. It can also be routed to glycolysis intermediates to generate ATP, which provides the material basis for plant growth (de Tredern et al., 2021). A main function of the PPP is to produce NADPH, which is necessary to participate in photosynthesis and readily relieves the oxidative stress induced by ROS that provokes cell damage (Bolaños and Almeida, 2010). Therefore, *L. chinensis* supported the participation of non-oxidative glucose consumption to regulate antioxidant levels in the slightly degraded soil and, thus, the ROS concentration within rhizosphere cells. The influence of severely degraded soil on energy metabolism was more inclined to the TCA cycle. We found that intermediate metabolites such as citric acid and fumaric acid in the TCA cycle were upregulated. The TCA cycle provides substrates and energy for the synthesis of other metabolites and is a major part of plant aerobic respiration (Niehaus, 2021). For severely degraded soil, the results indicated that the TCA cycle pathway was greatly affected, and *L. chinensis* may adjust root cell respiration metabolism to adapt to severely degraded soil, which was confirmed by metabolic pathway analysis (**Figure 7**). In addition, severe degradation data showed that the metabolism of a variety of amino acids was clearly affected, indicating that *L. chinensis* also mobilizes protein breakdown to adapt to stress. Protein interactions are the basis of cells in the plant growth and development process, and protein interactions can produce a variety of effects. Thus, it can be considered that severely degraded soil environmental pressure has a certain role in promoting photosynthesis and maintaining energy balance.

CONCLUSION

This investigation is a preliminary observation of the role of *L. chinensis* root exudates in the soil remediation process. The results showed that root exudates significantly improved soil nutrients, and the root cell tissue also mobilized oxidative stress to respond to the soil environment pressure. Some osmotic regulators and defense-related metabolites were significantly upregulated in root exudates to remediate degraded soils, and they mainly mobilized a series of fatty acid metabolic pathways to maintain the fluidity for membrane function to help plants adapt to adverse conditions. The PPP and TCA energy metabolism pathways were mobilized in response to slight and severe degradation environmental pressures, respectively. This study defines *L. chinensis* metabolic pathways and root exudate components related to the degraded soil response and offers valuable insights into the phytoremediation mechanism in degraded soils.

DATA AVAILABILITY STATEMENT

The raw data supporting the conclusions of this article will be made available by the authors, without undue reservation.

AUTHOR CONTRIBUTIONS

YL and PZ performed the data analyses and wrote the manuscript. QWu and YZ contributed significantly to analysis and manuscript preparation. QWe helped to perform the analysis with constructive discussions. YS and SS performed the experiment. GC contributed to the conception of the study. All authors contributed to the article and approved the submitted version.

FUNDING

This work was financially supported by the Heilongjiang Provincial Natural Science Foundation of China (LH2020C021), National Key R&D Program of China (2016YFC0500607), Heilongjiang Postdoctoral Fund to pursue scientific research (LBH-Z20003), the Young Talents Project of Northeast Agricultural University (19QC21), and Heilongjiang Provincial Natural Science Foundation of China (YQ2021C019).

REFERENCES

Bao, S. D. (2010). *Soil Agrochemical Analysis Method*, 3rd Edn. Beijing: China Agricultural.

Bian, F., Zhong, Z., Li, C., Zhang, X., Gu, L., Huang, Z., et al. (2021). Intercropping improves heavy metal phytoremediation efficiency through changing properties of rhizosphere soil in bamboo plantation. *J. Hazard. Mater.* 416:125898. doi: 10.1016/j.jhazmat.2021.125898

Bolaños, J., and Almeida, A. (2010). The pentose-phosphate pathway in neuronal survival against nitrosative stress. *Iubmb Life* 62, 14–18. doi: 10.1002/iub.280

Chen, Q., and Yang, G. (2020). Signal function studies of ROS, especially RBOH-dependent ROS, in plant growth, development and environmental stress. *J. Plant Growth Regul.* 39, 157–171. doi: 10.1007/s00344-019-09971-4

de Tredern, E., Rabah, Y., Pasquer, L., Minatchy, J., Placais, P.-Y., and Preat, T. (2021). Glial glucose fuels the neuronal pentose phosphate pathway for long-term memory. *Cell Rep.* 36:109620. doi: 10.1016/j.celrep.2021.109620

Du, P., Huang, Y., Lu, H., Xiang, L., Li, Y., Li, H., et al. (2020). Rice root exudates enhance desorption and bioavailability of phthalic acid esters (PAEs) in soil associating with cultivar variation in PAE accumulation. *Environ. Res.* 186:109611. doi: 10.1016/j.envres.2020.109611

Edayilam, N., Montgomery, D., Ferguson, B., Maroli, A. S., Martinez, N., Powell, B. A., et al. (2018). Phosphorus stress-induced changes in plant root exudation could potentially facilitate uranium mobilization from stable mineral forms. *Environ. Sci. Technol.* 52, 7652–7662. doi: 10.1021/acs.est.7b05836

FAO (2017). *Voluntary Guidelines for Sustainable Soil Management*. Rome: Food and Agriculture Organization of the United Nations.

Gao, M., Guo, Z., Dong, Y., and Song, Z. (2019). Effects of di-n-butyl phthalate on photosynthetic performance and oxidative damage in different growth stages of wheat in cinnamon soils. *Environ. Pollut.* 250, 357–365. doi: 10.1016/j.envpol.2019.04.022

Greiner, L., Keller, A., Gret-Regamey, A., and Papritz, A. (2017). Soil function assessment: review of methods for quantifying the contributions of soils to ecosystem services. *Land Use Policy* 69, 224–237.

Hu, L., Robert, C. A. M., Cadot, S., Zhang, X., Ye, M., Li, B., et al. (2018). Root exudate metabolites drive plant-soil feedbacks on growth and defense by shaping the rhizosphere microbiota. *Nat. Commun.* 9:2738. doi: 10.1038/s41467-018-05122-7

Hu, T., Wang, T., Wang, G., Bi, A., Wassie, M., Xie, Y., et al. (2021). Overexpression of FaHSP17.8-CII improves cadmium accumulation and tolerance in tall fescue shoots by promoting chloroplast stability and photosynthetic electron transfer of PSII. *J. Hazard. Mater.* 417:125932. doi: 10.1016/j.jhazmat.2021.125932

Huang, A., Jiang, T., Liu, Y., Bai, Y., Reed, J., Qu, B., et al. (2019). A specialized metabolic network selectively modulates *Arabidopsis* root microbiota. *Science* 364:eaau6389. doi: 10.1126/science.aau6389

Jin, Q., Wang, C., Sardans, J., Vancov, T., Fang, Y. Y., Wu, L. Q., et al. (2022). Effect of soil degradation on the carbon concentration and retention of nitrogen and phosphorus across Chinese rice paddy fields. *Catena* 209:105810. doi: 10.1016/j.catena.2021.105810

Jung, Y., Ha, M., Lee, J., Ahn, Y., Kwak, J., Ryu, D., et al. (2015). Metabolite profiling of the response of burdock roots to copper stress. *J. Agric. Food Chem.* 63, 1309–1317. doi: 10.1021/jf503193c

Keiluweit, M., Bougoure, J. J., Nico, P. S., Pett-Ridge, J., Weber, P. K., and Kleber, M. (2015). Mineral protection of soil carbon counteracted by root exudates. *Nat. Clim. Chang.* 5, 588–595. doi: 10.1038/nclimate2580

Kik, M. C., Claassen, G. D. H., Meuwissen, M. P. M., Smit, A. B., and Saatkamp, H. W. (2021). Actor analysis for sustainable soil management-A case study from the Netherlands. *Land Use Policy* 107:105491. doi: 10.1016/j.landusepol.2021.105491

Li, X., Zhang, M., Li, Y., Yu, X., and Nie, J. (2021). Effect of neonicotinoid dinotefuran on root exudates of *Brassica rapa* var. *chinensis*. *Chemosphere* 266:129020. doi: 10.1016/j.chemosphere.2020.129020

Li, Y., Long, L., Ge, J., Li, H., Zhang, M., Wan, Q., et al. (2019). Effect of imidacloprid uptake from contaminated soils on vegetable growth. *J. Agric. Food Chem.* 67, 7232–7242. doi: 10.1021/acs.jafc.9b00747

Li, Y., Yuan, L., Xue, S., Liu, B., and Jin, G. (2021). Artificial root exudates excite bacterial nitrogen fixation in the subsurface of mine soils. *Appl. Soil Ecol.* 157:103774. doi: 10.1016/j.apsoil.2020.103774

Lin, Y., Zhang, Y., Zhang, F., Li, R., Hu, Y., Yu, H., et al. (2019). Effects of bok choy on the dissipation of dibutyl phthalate (DBP) in mollisol and its possible mechanisms of biochemistry and microorganisms. *Ecotoxicol. Environ. Saf.* 181, 284–291. doi: 10.1016/j.ecoenv.2019.05.073

Liu, L., Li, W., Song, W., and Guo, M. (2018). Remediation techniques for heavy metal-contaminated soils: principles and applicability. *Sci. Total Environ.* 633, 206–219. doi: 10.1016/j.scitotenv.2018.03.161

Liu, Y., Chen, L., Zhang, N., Li, Z., Zhang, G., Xu, Y., et al. (2016). Plant-microbe communication enhances auxin biosynthesis by a root-associated bacterium, *Bacillus amyloliquefaciens* SQR9. *Mol. Plant Microbe Interact.* 29, 324–330. doi: 10.1094/MPMI-10-15-0239-R

Ma, H., Li, X., Wei, M., Zeng, G., Hou, S., Li, D., et al. (2020). Elucidation of the mechanisms into effects of organic acids on soil fertility, cadmium speciation and ecotoxicity in contaminated soil. *Chemosphere* 239:124706. doi: 10.1016/j.chemosphere.2019.124706

Martins, S. J., Medeiros, F. H. V., Lakshmanan, V., and Bais, H. P. (2018). Impact of seed exudates on growth and biofilm formation of *Bacillus amyloliquefaciens* ALB629 in common bean. *Front. Microbiol.* 8:2631. doi: 10.3389/fmicb.2017.02631

Niehaus, T. D. (2021). Phosphatases are involved in modulating the TCA cycle in plants. *Mol. Plant* 14, 1036–1037. doi: 10.1016/j.molp.2021.05.019

Rasse, D. P., Rumpel, C., and Dignac, M. F. (2005). Is soil carbon mostly root carbon? Mechanisms for a specific stabilisation. *Plant Soil* 269, 341–356. doi: 10.1071/FP05117

Rodriguez-Garrido, B., Balseiro-Romero, M., Kidd, P. S., and Monterroso, C. (2020). Effect of plant root exudates on the desorption of hexachlorocyclohexane isomers from contaminated soils. *Chemosphere* 241:124920. doi: 10.1016/j.chemosphere.2019.124920

Rohrbacher, F., and St-Arnaud, M. (2016). Root exudation: the ecological driver of hydrocarbon rhizoremediation. *Agronomy* 6:19. doi: 10.3390/agronomy6010019

Ronchi, S., Salata, S., Arcidiacono, A., Piroli, E., and Montanarella, L. (2019). Policy instruments for soil protection among the EU member states: a comparative analysis. *Land Use Policy* 82, 763–780. doi: 10.1016/j.landusepol.2019.01.017

Sadauskiene, I., Liekis, A., Bernotiene, R., Sulinskiene, J., Kasauskas, A., and Zekonis, G. (2018). The effects of buckwheat leaf and flower extracts on antioxidant status in mouse organs. *Oxid. Med. Cell. Long.* 2018:6712407. doi: 10.1155/2018/6712407

Shen, X., Yang, F., Xiao, C., and Zhou, Y. (2020). Increased contribution of root exudates to soil carbon input during grassland degradation. *Soil Biol. Biochem.* 146, 107817. doi: 10.1016/j.soilbio.2020.107817

Solá, M., Lovaisa, N., Costa, J., Benimeli, C., Polti, M., and Alvarez, A. (2019). Multi-resistant plant growth-promoting actinobacteria and plant root exudates influence Cr (VI) and lindane dissipation. *Chemosphere* 222, 679–687. doi: 10.1016/j.chemosphere.2019.01.197

Tamene, L., Sileshi, G. W., Ndengu, G., Mponela, P., Kihara, J., Sila, A., et al. (2019). Soil structural degradation and nutrient limitations across land use categories and climatic zones in Southern Africa. *Land Degrad. Dev.* 30, 1288–1299. doi: 10.1002/ldr.3302

Wang, Y., Ren, W., Li, Y., Xu, Y., Teng, Y., Christie, P., et al. (2019). Nontargeted metabolomic analysis to unravel the impact of di (2-ethylhexyl) phthalate stress on root exudates of alfalfa (*Medicago sativa*). *Sci. Total Environ.* 646, 212–219. doi: 10.1016/j.scitotenv.2018.07.247

Williams, A., and de Vries, F. T. (2020). Plant root exudation under drought: implications for ecosystem functioning. *New Phytol.* 225, 1899–1905. doi: 10.1111/nph.16223

Wu, K., Yuan, S., Xun, G., Shi, W., Pan, B., Guan, H., et al. (2015). Root exudates from two tobacco cultivars affect colonization of *Ralstonia solanacearum* and the disease index. *Eur. J. Plant Pathol.* 141, 667–677. doi: 10.1007/s10658-014-0569-4

Xiong, L., Liu, X., Vinci, G., Spaccini, R., Drososa, M., Li, L., et al. (2019). Molecular changes of soil organic matter induced by root exudates in a rice paddy under CO_2 enrichment and warming of canopy air. *Soil Biol. Biochem.* 137:107544. doi: 10.1016/j.soilbio.2019.107544

Yin, H., Li, Y., Xiao, J., Xu, Z., Cheng, X., and Liu, Q. (2013). Enhanced root exudation stimulates soil nitrogen transformations in a subalpine coniferous forest under experimental warming. *Glob. Chang. Biol.* 19, 2158–2167. doi: 10.1111/gcb.12161

Zhan, F., Qin, L., Guo, X., Tan, J., Liu, N., Zu, Y., et al. (2016). Cadmium and lead accumulation and low-molecular-weight organic acids secreted by roots in an intercropping of a cadmium accumulator *Sonchus asper* L. with *Vicia faba* L. *Rsc Adv.* 6, 33240–33248. doi: 10.1039/c5ra26601g

Zhang, M., Cai, Z., Zhang, G., Zhang, D., and Pan, X. (2021). Abiotic mechanism changing tetracycline resistance in root mucus layer of floating plant: the role of antibiotic-exudate complexation. *J. Hazard. Mater.* 416:125728. doi: 10.1016/j.jhazmat.2021.125728

Zhang, N., Wang, D., Liu, Y., Li, S., Shen, Q., and Zhang, R. (2014). Effects of different plant root exudates and their organic acid components on chemotaxis, biofilm formation and colonization by beneficial rhizosphere-associated bacterial strains. *Plant Soil* 374, 689–700. doi: 10.1007/s11104-013-1915-6

Zhao, L., Huang, Y., Paglia, K., Vaniya, A., Wancewicz, B., and Keller, A. A. (2018). Metabolomics reveals the molecular mechanisms of copper induced cucumber leaf (*Cucumis sativus*) senescence. *Environ. Sci. Technol.* 52, 7092–7100. doi: 10.1021/acs.est.8b00742

Zhou, J., Zhang, L., Chang, Y., Lu, X., Zhu, Z., and Xu, G. (2012). Alteration of leaf metabolism in Bt-Transgenic rice (*Oryza sativa* L.) and its wild type under insecticide stress. *J. Proteome Res.* 11, 4351–4360. doi: 10.1021/pr300495x

Conflict of Interest: The authors declare that the research was conducted in the absence of any commercial or financial relationships that could be construed as a potential conflict of interest.

frontiers | Frontiers in Plant Science

ORIGINAL RESEARCH
published: 31 May 2022
doi: 10.3389/fpls.2022.898969

Mycorrhizal Inoculation Enhances Nutrient Absorption and Induces Insect-Resistant Defense of *Elymus nutans*

Wantong Zhang, Lu Yu, Bing Han, Kesi Liu and Xinqing Shao**

Department of Grassland Resources and Ecology, College of Grassland Science and Technology, China Agricultural University, Beijing, China

The majority of terrestrial plants can form symbiotic associations on their roots with arbuscular mycorrhizal fungi (AMF) in the soil to stimulate the growth and nutrient uptake of the host plant and to improve plant resistance to insects and disease. However, the use of AMF for insect control on gramineous forages requires further study. Here, we evaluated the effects of AMF (*Funneliformis mosseae*) inoculation on the defense against *Locusta migratoria* attack in *Elymus nutans*. Inoculation assays showed that mycorrhizal plants had a higher resistance than non-inoculated plants, as evidenced by plants having more plant biomass, a higher nitrogen and phosphorus content, and greater lipoxygenase (LOX) activity. The results of insect damage showed that in addition to a decrease in the enzyme phenylalanine-ammonia-lyase, the activities of other plant defense-related enzymes (including polyphenol oxidase and β-1,3-glucanase) were increased. A key enzyme, LOX, belonging to the jasmonic acid (JA) signaling pathway was notably increased in mycorrhizal treatment. Volatile organic compounds (VOCs) were identified using gas chromatography mass spectrometry and the results showed that several metabolites with insect-resistant properties, including D-Limonene, p-Xylene, 1,3-Diethylbenzene were detected in mycorrhizal plants. These findings suggest that mycorrhizal inoculation has potential applications in insect management on forage grasses and demonstrates that the JA signaling pathway is essential for insect resistance in *Elymus nutans*.

Keywords: arbuscular mycorrhizal fungi, *Elymus nutans*, plants defense, volatile organic compounds, *Locusta migratoria*, *Funneliformis mosseae*

OPEN ACCESS

Edited by:
Jin-Lin Zhang,
Lanzhou University, China

Reviewed by:
Yinglong Chen,
University of Western Australia, Australia
Kai Xue,
University of Chinese Academy of Sciences, China

****Correspondence:***
Kesi Liu
kliu@cau.edu.cn
Xinqing Shao
shaoxinqing@163.com

Specialty section:
This article was submitted to Plant Abiotic Stress, a section of the journal Frontiers in Plant Science

Received: *18 March 2022*
Accepted: *10 May 2022*
Published: *31 May 2022*

Citation:
Zhang W, Yu L, Han B, Liu K and Shao X (2022) Mycorrhizal Inoculation Enhances Nutrient Absorption and Induces Insect-Resistant Defense of Elymus nutans. Front. Plant Sci. 13:898969. doi: 10.3389/fpls.2022.898969

INTRODUCTION

Plants have evolved a series of complex, protective strategies in order to enhance their fitness and survival under herbivore attack and biotic stresses (Sharma et al., 2017; Frew et al., 2022). One important strategy is the formation of symbiotic relationships between plant roots and some specific fungi, such as arbuscular mycorrhiza (Begum et al., 2019; Dowarah et al., 2021).

Arbuscular mycorrhizal fungi (AMF) belong to the subphylum Glomeromycotina of the phylum Mucoromycota (Spatafora et al., 2016). They are important beneficial fungi that form

symbiotic relationships with over 90% of plant roots including ferns, herbaceous plants, and some economically important crop species (Begum et al., 2019; Selvaraj et al., 2020). AMF are obligate biotrophs that ingest plant photosynthetic products (Dowarah et al., 2021) and lipids to support their life cycle (Jiang et al., 2017). AMF symbiosis can help plants to obtain essential nutrients from the soil, such as nitrogen, phosphorus, and potassium, absorb other trace nutrients from resource-deficient soils, and assist plant roots to take-up more water from the soil (Kayama and Yamanaka, 2014; Bhantana et al., 2021; Jiang et al., 2021). In return, plants supply AMF with carbohydrates and lipids that can be used to develop extensive mycelial networks (Bernaola et al., 2018). These mycelial networks act as conduits for carbon and mineral nutrient transmission (Jiang et al., 2017; Luginbuehl et al., 2017); they also signal transmission channels between plants to initiate an early warning for disease and herbivore attack (Basu et al., 2018; Begum et al., 2019).

Arbuscular mycorrhizal fungi confer benefits to their host plant in many ways, including enhancement in nutrient uptake and protection against stressors (Dowarah et al., 2021). Most importantly, AMF inoculation is known to induce the activation of plant resistance and protect plants from phytopathogenic fungi, bacteria, viruses, and herbivores (Hao et al., 2019; Miozzi et al., 2019; Jiang et al., 2021). Mycorrhizal symbiosis have been reported to respond variably to above-ground insect damage, including positive (Babikova et al., 2013; Meier and Hunter, 2018), negative (Bernaola et al., 2018; Bolin et al., 2018), and neutral (Gehring and Bennett, 2009) effects on plant defense. In addition, the defense response of mycorrhizal plants to herbivorous insects has been found to vary with the species involved and the growth stage of the plant (Malik et al., 2018) and the AMF (Selvaraj et al., 2020). Specifically, mycorrhizal inoculation improves plant resistance to generalist herbivores and insects that are sensitive to jasmonic acid (JA)-associated defenses (Frew et al., 2022).

Plants can release distinct blends of volatile organic compounds (VOCs) following an external attack, including alkenes, terpenes, and aldehydes (Sharma et al., 2017; Ye et al., 2018). VOCs can be classified according to their metabolic pathway: terpenoids [mevalonate/2-methyl-D-erythritol-4-phosphate (MVA/MEP) pathway], volatile fatty acid derivatives [lipoxygenase (LOX) pathway], and benzenic compounds and amino acid derivatives [shikimate (SK) pathway] (Dudareva et al., 2004; Velásquez et al., 2020a). Plants can communicate with both distant plants (Heil and Ton, 2008), and neighboring plants (Karban et al., 2016) *via* VOCs, and this airborne signal allows receptor plants to invoke defense systems prior to the threat. Specifically, VOCs can induce the expression and production of defense-related enzymes (polyphenol oxidase, PPO; β-1,3-glucanase, phenylalanine-ammonia-lyase, PAL; and lipoxygenase, LOX), hormones (JA, and salicylic acid, SA), protease inhibitor I and II genes (PI-I and PI-II) and other related secondary metabolites in recipient plants, activating the defense system (Jung et al., 2012; Song et al., 2013). Recent studies have found that plant volatile emissions are strongly influenced by environmental stimuli, including plant-microorganism interaction which plays a key role in plant development (Valenzuela et al., 2019; Velásquez et al., 2020a). For one thing, the impact of mycorrhizal symbiosis extends beyond plant growth, enhancing plant defenses by promoting the synthesis of secondary metabolites such as VOC. For example, milkweeds inoculated with AMF release more VOC after being fed on by insects (Meier and Hunter, 2019). For another, AMF affect the diversity of plant primary and secondary metabolites by altering plant nutrient uptake and defensive signaling pathways (Schweiger et al., 2014; Begum et al., 2019), including the SA and JA pathways (Frew et al., 2022), which are essential defense systems to herbivore feeding (Meier and Hunter, 2019; Dowarah et al., 2021). Song Y. Y. et al. (2015) showed that JA-related genes and defense enzymes (LOX and PPO) are notably up-regulated in receptor tomato plants through common mycorrhizal networks, when neighboring plants are eaten by herbivores. However, these mycorrhiza-related studies mainly focused on cultivated crops (Babikova et al., 2013; Song Y. Y. et al., 2015; Selvaraj et al., 2020) and less information is available regarding the tripartite interactions among AM fungi, gramineous forage, and phytophagous insects.

Elymus nutans (*Elymus nutans* Griseb.) is a perennial gramineous grass that grows in alpine regions (Xu et al., 2018). It is highly resistant to drought, cold, and salt, and has become a preferred forage species for planting in high altitude areas (Tan et al., 2020; Quan et al., 2021). As the forage livestock industry expands at high altitudes, the areas of cultivated grasslands growing *E. nutans* will continue to increase; therefore, the stability of *E. nutans* swards in alpine regions needs to be addressed. Grasshopper feeding can cause necrotic spots or even plant mortality, thus reducing the palatability of *E. nutans* and affecting livestock grazing (Hao H. et al., 2019). Furthermore, *E. nutans* can form a symbiotic relationship with AMF (Gai et al., 2009). However, whether this symbiosis enhances *E. nutans* resistance to grasshopper attack and what types of signaling substances are induced by AMF inoculation with *Elymus* spp., transduction pathways, physiological effects, and mechanisms of action have not been systematically explored. Therefore, we selected *E. nutans* in an alpine meadow as host plants to investigate the response of inoculation with *F. mosseae* to insect attack. We sought to (i) determine the response and main defense pathways of *E. nutans* to grasshopper feeding and (ii) elucidate the role of AMF on plant growth and defense against insects. The hypotheses were (i) *E. nutans* will produce large amounts of defense-related enzymes to activate relevant defense pathways. (ii) AMF-colonized plants will have higher nutrient content, increased defense enzyme activity, and will release more VOCs.

MATERIALS AND METHODS

Plant, Fungal, and Insect Materials

Elymus nutans seeds were collected from natural alpine meadows in Haiyan County, Haibei Tibetan Autonomous Prefecture, Qinghai Province, China (36°55′ N, 100°57′ E, 3029 m a.s.l.) in August 2021.

The mycorrhizal fungus *Funneliformis mosseae* (BGCYN05), isolated from white clover and maize, was obtained from the Beijing Academy of Agricultural and Forestry Sciences and propagated by the Guizhou Academy of Agricultural Sciences. These AMF inocula contained root fragments, rhizosphere soil, and 133 spores per gram of dry soil.

The grasshoppers *Locusta migratoria* (Orthoptera, Locusta Linnaeus) were collected from a Qinghai Haibei alpine meadow. As the dominant locust species, the density of *L. migratoria* was 10 grasshopper/m^2 (Hao et al., 2019). They were reared on gramineous plants in the laboratory (28 ± 2°C; 18 h day:8 h night; 30–50% relative humidity) (Babikova et al., 2013; Veenstra et al., 2021).

Growth Medium

Field soil was obtained from natural alpine grassland in Haiyan County, Haibei Tibetan Autonomous Prefecture, Qinghai Province, China (36°55′ N, 100°57′ E, 3029 m a.s.l.). All soils were sieved with a 2-mm sieve, autoclaved at 121°C for 1 h twice within 3 days and dried at 110°C for 36 h (Li et al., 2021). The physical and chemical properties were: 4.1 g·kg^{-1} total nitrogen, 48 g·kg^{-1} total carbon, 0.69 g·kg^{-1} total phosphorus, and pH 8.2. Each pot was filled with 2.5 kg of sterilized soil.

Experimental Design

The pot trials took place in a greenhouse at the China Agricultural University from December 2020 to April 2021. *F. mosseae* was used for mycorrhizal inoculation of *E. nutans*, and the grasshopper *L. migratoria* was used for insect feeding. Experiment designs consisted of one AMF inoculation factor (inoculate with *F. mosseae*, F), one insect feeding factor (attack by grasshopper *L. migratoria*, L) and their interaction. The whole experiment had four treatments with five replications each to exclude possible effects of sole AMF inoculation and grasshopper feeding; CK (plants without AMF inoculation and grasshopper feeding), Fm (plants only inoculated with *F. mosseae*), Lm (non-inoculated plants with grasshopper feeding), and Fm + Lm (plants inoculated with AMF plus grasshopper feeding). There were 20 experimental pots, and each pot was placed randomly.

Seeds were surface sterilized with 10% H_2O_2 and rinsed five times with sterile distilled water before sowing in autoclaved soil (121°C; 2 h). Forty to fifty plants from the original 80 were chosen randomly per pot and watered regularly four times a week to maintain soil moisture. One week after germination, 40 healthy seedlings with good growth were kept.

Thirty grams of AMF inoculum (fungal: soil mixture) were spread on the soil to a depth of 2 cm. For non-AMF treatments, an equal amount of soil containing autoclaved fungi was added (121°C; 2 h). Insect feeding treatments took place when *E. nutans* plants were 14 weeks old. Before the formal experiment, all plants were placed in polyethylene terephthalate (PET) bags to prevent plant-to-plant communication *via* aerial volatiles, and grasshoppers were starved for 2 h. Subsequently, 12 fifth-instar grasshoppers were placed in each pot of Lm and Fm + Lm treatments to feed on the plants.

After 24 h of grasshopper feeding, we collected VOCs and removed the insects (all grasshoppers were alive). The plants continued growing for 48 h and were then harvested for the measurement of plant nutrient content, biomass, and AMF colonization of roots.

Mycorrhizal Colonization Analysis

Mycorrhizal colonization was examined following the procedure of Koske and Gemma (1989). After harvesting of plant roots, they were washed with distilled water to remove soil particles, and approximately 0.5–1.0 g of roots were cut into 1 cm segments. Root segments were soaked in KOH (10%, w/v) and boiled until the roots were transparent. Then root segments were acidified in HCl (2%, v/v), and stained with trypan blue (0.05%, w/v). After 30 min, these roots were immersed in destaining solution (glycerol: lactic = 1:1). Finally, stained roots were mounted on slides and AMF colonization was calculated using the magnified gridline intersect method (McGonigle et al., 1990) with a compound microscope under 40× magnification. A root intersection was considered colonized if hyphae, arbuscules, or vesicles were present.

Enzyme Assays

The kits for assaying the PPO, PAL, β-1,3-glucanase, and LOX were obtained from Solarbio Science & Technology Co., Ltd. (Beijing, China). All the chemicals used were analytical (Li et al., 2019). Leaf samples (0.1 g) were ground in liquid nitrogen with different 1 ml extractive solutions; they were then centrifuged and homogenated, and the supernatants were used for enzyme assays. A Microplate reader (SpectraMax iD5, Molecular Devices, San Jose, CA, United States) and 96-well plates were used. PPO enzyme absorbance was recorded at 410 nm for the measurement and control tubes; a change in absorbance at 410 nm of 0.005/min was defined as a unit of enzyme activity. PAL enzyme absorbance was read at 290 nm; a change in absorbance at 290 nm of 0.05/min was defined as a unit of enzyme activity. β-1,3-glucanase enzyme was measured at 540 nm for the measurement and control tubes, then a standard curve was built to calculate enzyme activity. LOX enzyme catalyzed the oxidation of linolenic acid, and the oxidation product had a characteristic absorption peak at 234 nm; a change in absorbance at 234 nm of 0.0006/min was defined as a unit of enzyme activity.

Collection of Plant Volatile Organic Compounds

Plants and grasshoppers were placed in PET bags (100 cm × 111 cm, low volatility at high temperatures and high light intensities). After 24 h of insect feeding, volatiles were collected using an aerated kit (Babikova et al., 2013). The air was purified by activated carbon through a dry glass sorbent tube (0.5 cm diameter, 8.0 cm long) and the ends of this tube were plugged with clean glass fiber, containing 50 mg of sorbent (Porapak Q, 80–100 mesh, Waters Corporation, Ireland). After the air had been extracted from the bag for a short time, sampling began after 30 min. During this process, the gas in the bag was adsorbed by the sorbent. The flow rate was 300 ml min^{-1} and the extraction was continuous for 6 h. The sorbent was eluted with 4 ml of chromatographic n-hexane into 2 ml sample bottles and the samples were then stored at −20 °C in a deep freezer for later use.

GC-MS Analysis of Plant VOCs We analyzed a 2 μl aliquot of a VOC sample by gas chromatography mass spectrometry (GC-MS, Agilent Technologies, Santa Clara, CA, United States) using the following GC method: Injector maintained at 220°C, initial column temperature maintained at 50°C for 10 min, ramped to 200°C at 5°C min^{-1}, and held for 10 min, with a helium carrier gas flow rate of 1 ml min^{-1}. We used a DB-5MS column (30 m × 0.25 mm × 0.25 μm film; J&W Scientific, Folsom, CA, United States) with a 0.25-μm film thickness (Velásquez et al., 2020b). Then VOCs were initially identified by using the mass spectra with a library of authentic standards or databases (NIST 08, National Institute of Standards and Technology, Gaithersburg, MD, United States, 2008). The relative concentrations of VOCs were determined by comparing each peak area with the total peak area in each treatment.

We selected random harvested plant material (roots, stems, and leaves) to measure nutrient content. They were dried at 65 °C for 24 h and milled with a ball mill (Retsch MM400, Retsch, Haan, Germany) Samples of 0.15-g sieved plant material were weighed and placed into tin cups. Plant total nitrogen and total carbon contents were determined using an elemental analyzer (Elementar, Hanau, Germany); total phosphorus was determined by the $HClO_4$-H_2SO_4 method (Han et al., 2021).

Statistical Analysis

All available data were analyzed by SPSS 19.0 (Inc., Armonk, NY, United States). Two-way analysis of variance (ANOVA) was used to examine the effects of inoculation and insect feeding on plant biomass, defense-related enzyme activities and plant nutrient content. Differences among treatments were performed at $P < 0.05$ by Duncan's multiple range test (DMRT). The results were given as means with standard errors (mean ± SE). Origin2018 (OriginLab, United States) was used for plotting.

RESULTS

Mycorrhizal Colonization Rate and Plant Biomass

Mycorrhizal colonization structures such as vesicles and mycelium were observed in all inoculation treatments, which indicated successful inoculation with AMF (**Figure 1A**). Mycorrhizal colonization rates were similar between the two inoculation treatments (**Figure 1B**). Grasshopper feeding resulted in a small amount of aboveground biomass (**Supplementary Figure 1**). Mycorrhizal inoculation and insect feeding significantly affected plant biomass ($P < 0.05$). The Fm treatment had the greatest aboveground biomass, 53.53% higher than non-inoculated CK treatment ($F = 13.82$; $P < 0.05$). Insect attack caused a decrease in the aboveground biomass of plants, the Fm + Lm treatment was still higher than that of the Lm treatment, similar to the aboveground biomass of plants that were not inoculated (**Figure 2A**). The belowground biomass of Fm treatment was significantly higher than other treatments (**Figure 2B**). After the plants were attacked by insects, inoculated plants showed higher belowground biomass, at 43.46% higher in Fm + Lm than in the Lm treatment ($F = 96.64$; $P < 0.05$).

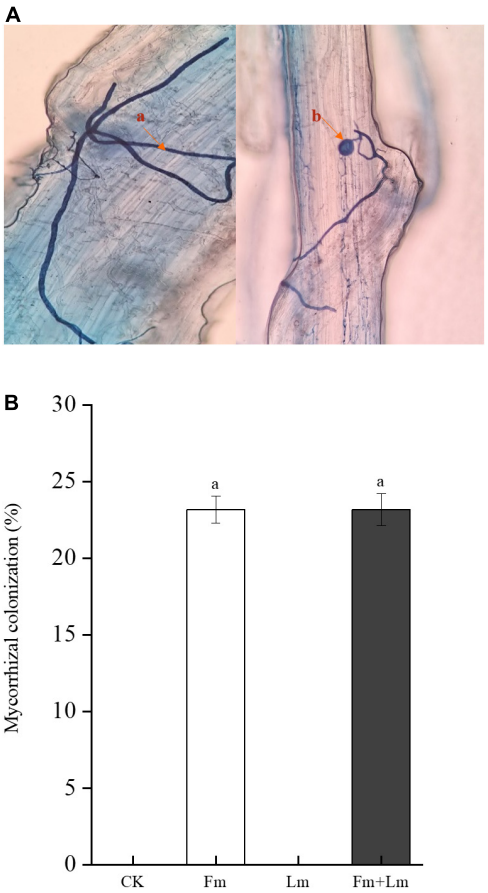

FIGURE 1 | The mycorrhizal colonization structure of AMF observed under 40× magnification after **(A)** the root segments of *E. nutans* were stained with trypan blue **(B)** (0.05%, w/v) and the percentage of root mycorrhizal colonization in plants. The four treatments were (1) CK: no inoculation; (2) Fm: inoculated with *F. mosseae* only; (3) Lm: feeding with *L. migratoria* only; (4) Fm + Lm: inoculated with *F. mosseae* and *L. migratoria* feeding. (a) Internal hyphae; (b) Vesicles.

Plant Nutrient Content

Arbuscular mycorrhizal fungi inoculation promoted the uptake of nutrients by *E. nutans*, the inoculated plants contained more nitrogen and phosphorus than non-inoculated plants (**Supplementary Table 1**). Total nitrogen content in Fm plants was 16.07 g·kg^{-1} (**Figure 3A**), a significant increase of 30.11% compared to CK ($F = 102.42$; $P < 0.05$); But, insect attack significantly affected plant nutrient content ($P < 0.001$). After grasshopper feeding, all insect treatments showed a reduced nutrient content (**Figure 3B** and **Supplementary Table 1**). Plant total phosphorus content decreased by 26.70% in Fm + Lm and 18.57% in Lm compared to Fm and CK treatments, respectively. Plant carbon content decreased after AMF inoculation, the total carbon content of CK treatment was 395.98 g·kg^{-1}, which was notably higher than that of Fm (**Figure 3C**). Insect feeding further

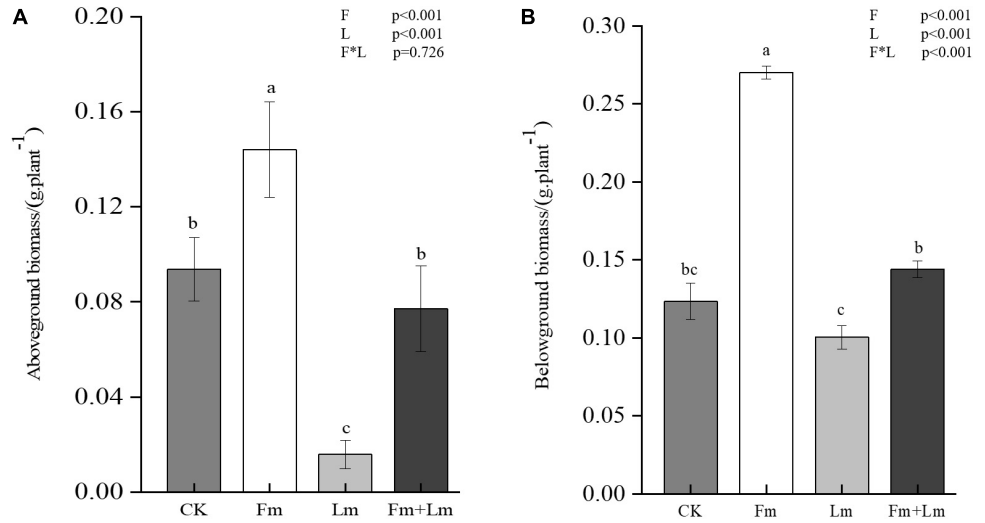

FIGURE 2 | Plant aboveground biomass **(A)** and belowground biomass **(B)** under different treatments. The four treatments were (1) CK: no inoculation; (2) Fm: inoculated with *F. mosseae* only; (3) Lm: feeding with *L. migratoria* only; (4) Fm + Lm: inoculated with *F. mosseae* and *L. migratoria* feeding. Values are means ± standard error. *P*-values for inoculation and insect feeding effects were based on two-way ANOVA, F: inoculated AMF; L: insect feeding. Mean values followed by the same letter do not differ significantly at $P \leq 0.05$ by DMRT.

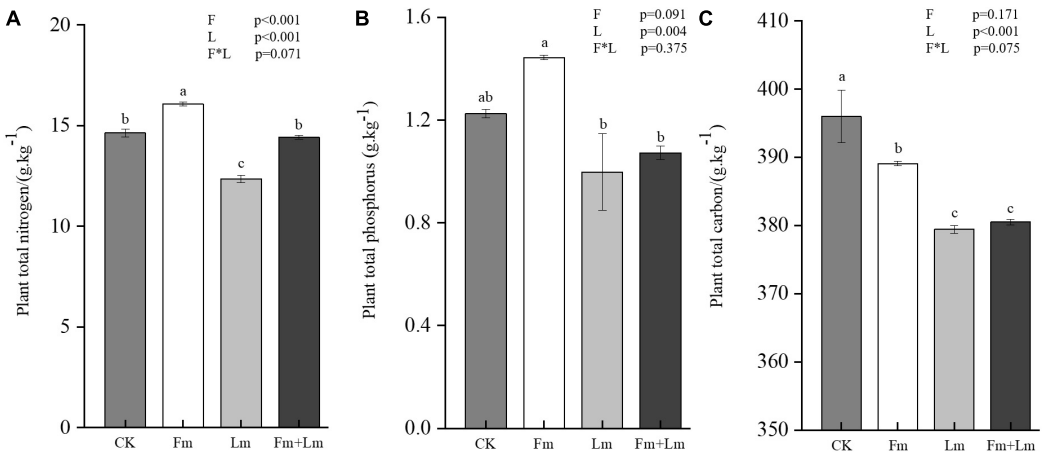

FIGURE 3 | The effects of different treatments on plant nutrition. Total nitrogen, **(A)** total phosphorus, **(B)** and total carbon **(C)** of plant leaves. Four treatments (CK, Fm, Lm, and Fm + Lm) were established as described in **Figure 2**. Values are means ± standard error. *P*-values for inoculation and insect feeding effects were based on two-way ANOVA. Mean values followed by the same letter do not differ significantly at $P \leq 0.05$ by DMRT.

reduced the total carbon content of plants; Fm + Lm decreased by 2.22% compared to Fm and Lm treatments, which decreased by 4.17% ($F = 15.932$; $P < 0.05$).

Induction of Defense-Related Enzymes by Mycorrhizal Inoculation

Both inoculation and insect feeding significantly influenced the expression of plant defense-related enzyme activities ($P < 0.05$) (**Table 1**). PPO and β-1,3-glucanase enzyme activities were significantly lower in the Fm treatment compared to the CK treatment ($P < 0.05$). The two enzyme activities were increased in Fm + Lm and Lm treatments after insect attack, with 65.79 and 19.83% increase in Lm treatment compared to CK treatment, respectively. However, mycorrhizal inoculation decreased the expression of the two enzyme activities in insect treatments (Fm + Lm, Lm), PPO, β-1,3-glucanase enzyme activities in the Fm + Lm treatment were decreased by 54.38 and 17.92% compared to the Lm treatment, respectively. No matter inoculation or insect attack, PAL enzyme activity was decreased, but there was no significant differences among treatments.

After plants were inoculated with AMF, the LOX enzyme activity of mycorrhizal plants was significantly higher compared to CK treatment (**Table 1**). And grasshopper feeding caused an increase in LOX enzyme activity in the Lm treatment, which

TABLE 1 | The activity of four defense-related enzymes in leaves of *Elymus nutans* plants in response to mycorrhizal colonization by *F. mosseae* and herbivorous feeding by fifth-instar grasshoppers *L. migratoria*.

Treatment	PPO (U/g FW)		PAL (U/g FW)		β-1,3-Glucanase (U/g FW)		LOX (U/g FW)	
CK	74.84 ± 0.35b		42.69 ± 7.32a		18.86 ± 0.77ab		481.08 ± 97.12c	
Fm	11.25 ± 2.07d		27.54 ± 4.33a		14.34 ± 0.77c		1846.54 ± 324.47b	
Lm	124.08 ± 0.44a		26.17 ± 5.39a		22.60 ± 2.60a		1277.18 ± 2.83bc	
Fm + Lm	56.60 ± 3.24c		25.02 ± 3.36a		18.55 ± 1.52ab		2903.68 ± 396.47a	
Variables	***F***	***P***	***F***	***P***	***F***	***P***	***F***	***P***
F	1137.507	0.000	2.355	0.163	7.138	0.028	32.922	0.000
L	592.560	0.000	3.217	0.111	6.134	0.038	12.631	0.007
F*L	0.998	0.347	1.742	0.223	0.022	0.887	0.251	0.630

We employed two-way ANOVA to determine the effect of inoculated AMF (F) and insect feeding (L) on four defense-related enzymes. Means with different letters (a, b, c, d) indicate significant differences among four treatments by using DMRT at $P \leq 0.05$ level. Five replications per treatment. Values are means ± standard error. (1) CK: non-inoculate plants; (2) Fm: plants inoculated with F. mosseae only; (3) Lm: non-inoculate plants eaten by L. migratoria; (4) Fm + Lm: plants inoculated with F. mosseae and L. migratoria feeding.

was about 2.5 times higher than that in CK treatment, but still lower than that in the Fm treatment. Moreover, inoculation further increased the expression of LOX enzyme activity in plants, and the LOX enzyme activity in the Fm + Lm treatment was significantly increased by 57.25% ($F = 15.268$; $P < 0.01$) compared with Fm treatment, which was about twice as much as that in the Lm treatment. Two-way ANOVA showed no significant effects of the interaction between inoculation and insect feeding on LOX enzyme activity expression.

Composition and Concentration of Volatile Organic Compounds

Grasshopper feeding resulted in VOCs released from *E. nutans*. A total of 24 VOCs were produced after plants were attacked by insect, and these metabolites include ketones, aldehydes and benzenic compounds (**Table 2**). The Lm treatment detected 18 VOCs, of which were "benzenic compounds" (6) (1-methylpropyl Benzene, p-ethyl-Cumene, 4-Ethyltoluene, 1,2,3-Trimethylbenzene, 1,4-Diethylbenzene, Cumene), "ketones" (4) (2′-Methylacetophenone, 2,4-Dimethylacetophenone, 2,5-Dimethylacetophenone, 4′-Ethylacetophenone), "alkenes" (2), "alkanes" (2), "aldehydes" (2), "alcohols" (1), and ethyl acetate. The VOCs with high relative concentrations in the Lm treatment were 2,4-Dimethylacetophenone, β-Cymene, and 1,4-Diethylbenzene. Ethyl acetate was only released from non-AMF plants after grasshopper feeding. There were 19 VOCs detected in Fm + Lm treatment, including "benzenic compounds" (9), "ketones" (3), "alkenes" (3), "alkanes" (2), "aldehydes" (1), "alcohols" (1). Mycorrhizal inoculation led plants to release some different, insect-resistant compounds, like 1,3-Diethylbenzene, D-Limonene, p-Xylene, p-Methylcumene. The VOCs with high relative concentrations in the Fm + Lm treatment were 2,4-dimethylacetophenone, D-Limonene and p-Xylene. Regardless of whether AMF was inoculated or not, 13 common VOCs were detected in *E. nutans* after the insect feeding and the relative concentration of 2,4-dimethylacetophenone was the greatest; however, mycorrhiza slightly reduced emissions.

DISCUSSION

Mycorrhizal symbiosis as a potential pest control strategy may be an effective alternative to some chemical pesticides in contemporary agriculture (Jiang et al., 2021). However, the applicability of this insect resistance mechanism in alpine forage plants is unknown. In the present study, we investigated the results of insect–plant–microbe interactions, the first report of a tripartite interaction between *Elymus nutans*, AMF, and a chewing insect.

It has been commonly reported in both laboratory and field experiments that plant inoculation with AMF promote growth and increase biomass, a phenomenon considered as the positive mycorrhizal growth response (MGR) (Bernaola et al., 2018; Zhang et al., 2019). Positive MGR was previously found to be due to the improved uptake and transfer of nutrients (usually phosphorus and nitrogen) (Jiang et al., 2021), which is consistent with the findings of this study. *E. nutans* inoculated with *F. mosseae* significantly increased plant biomass compared to the non-inoculated treatment, in addition to increasing the uptake of nitrogen and phosphorus. This improvement is probably because a common mycorrhizal network can greatly improve the efficiency of use of soil nutrients by increasing the contact area between the root system and soil *via* a greater number of extraradical hyphae (Begum et al., 2019). There is a consequent increase in concentration of various macro-nutrients and micro-nutrients in plants, which increases the production of photosynthetic products, and leads to greater biomass accumulation (Balliu et al., 2015; Chen et al., 2017). Therefore, AMF assist plant development under normal as well as stressful circumstances and improve plant tolerance to biotic and abiotic factors (Plassard and Dell, 2010; Begum et al., 2019).

The soil used in this study was native soil from alpine meadows where the *F. mosseae* had a good symbiotic relationship with *E. nutans* (Gai et al., 2009), but we used commercial AMF inocula whose host plants were maize and clover, the experiment results revealed a low mycorrhizal colonization rate (Jin et al., 2011; Xu et al., 2018). The reason may be explained

TABLE 2 | The composition and concentration of volatile organic compounds (VOCs) collected from plants through GC-MS analysis, included four treatments.

Compound	Relative concentration (%)				CAS
	CK	Fm	Lm	Fm + Lm	
Cumene	—	—	0.71 ± 0.32	0.90 ± 0.40	98-82-8
1-methylpropyl Benzene	—	—	0.52 ± 0.23	0.47 ± 0.21	135-98-8
Hydrindene	—	—	—	0.41 ± 0.18	496-11-7
p-Methylcumene	—	—	—	6.51 ± 1.78	99-87-6
para-Ethylstyrene	—	—	1.10 ± 0.22	0.72 ± 0.24	3454-07-07
p-ethyl-Cumene	—	—	1.16 ± 0.34	1.54 ± 0.42	4218-48-8
Ethyl-benzaldehyde	—	—	0.94 ± 0.26	1.32 ± 0.24	4748-78-1
4′-Ethylacetophenone	—	—	2.13 ± 0.95	5.46 ± 2.44	937-30-4
2,4-Dimethylacetophenone	—	—	36.4 ± 4.97	30.08 ± 4.44	89-74-7
4-Ethyltoluene	—	—	2.12 ± 0.58	2.22 ± 0.48	622-96-8
p-Propyltoluene	—	—	—	0.45 ± 0.20	1074-55-1
β-Cymene	—	—	11.55 ± 1.50	4.37 ± 1.43	535-77-3
Isobutenylbenzene	—	—	0.50 ± 0.22	0.54 ± 0.247	768-49-0
2,5-Dimethylacetophenone	—	—	10.72 ± 3.32	5.64 ± 2.52	2142-73-6
1,3-Diethylbenzene	—	—	—	6.44 ± 2.88	141-93-5
D-Limonene	—	—	—	6.90 ± 3.09	7705-14-8
p-Xylene	—	—	—	6.66 ± 2.98	106-42-3
Phenethyl alcohol	—	—	0.96 ± 0.26	0.41 ± 0.19	1123-85-9
2-methylcyclopropyl benzene	—	—	0.53 ± 0.24	0.52 ± 0.23	3145-76-4
2-Phenyl-1-propanal	—	—	0.49 ± 0.22	—	93-53-8
ethyl acetate	—	—	9.86 ± 4.40		141-78-6
1,2,3-Trimethylbenzene	—	—	0.39 ± 0.17	—	526-73-8
1,4-Diethylbenzene	—	—	15.26 ± 6.82	—	105-05-5
2′-Methylacetophenone	—	—	0.31 ± 0.14	—	577-16-2

Five replications per treatment. Data are expressed as mean ± standard deviation. (1) CK (non-inoculate plants); (2) Fm: (plants inoculated with F. mosseae only); (3) Lm (non-inoculated plants with L. migratoria feeding); (4) Fm + Lm (plants with inoculated F. mosseae plus L. migratoria feeding); (3) CAS (Chemical abstracts service).

by the fact when *E. nutans* inoculated with AMF from the other plants rhizosphere soil, the other plants produced secondary metabolites which cause negative effects on plant growth (Wang et al., 2019), and possibly because of the lignification of plant roots intensified—it was not favorable for AMF colonization (Xu et al., 2018). However, AMF could still promote the nutrient uptake and utilization of *E. nutans*, probably because the small amount of AMF inocula diluted the potential allelopathy effects of the host plant (Wang et al., 2019). As Bati et al. (2015) showed, irrespective of mycorrhizal inoculation (commercial or native), AMF promoted nutrient uptake and plant growth. Therefore, the low colonization rate of *E. nutans* in the current experiment was acceptable. The total carbon in plants is an important physiological parameter reflecting their carbon metabolism and an important indicator of a plant's physiological condition, growth, vitality, and disease resistance (Jiang et al., 2017; Charters et al., 2020). Extra disturbance will affect the carbon allocation of plants and could then influence AMF activity (Walder and van der Heijden, 2015; Charters et al., 2020). We found that after AMF inoculation, the total carbon content of plants (Fm, Fm + Lm) decreased compared with the non-inoculated treatment (CK), while AMF inoculation (Fm) increased the phosphorus content of plants. However, after grasshopper feeding, the total carbon and phosphorus content decreased in the Fm + Lm treatment. These results suggested that the insects reduced belowground plant carbon allocation and ultimately aboveground phosphorus, possibly as AMF resulted in a lower transfer of phosphorus to the host plant (Frew, 2021). Girousse et al. (2005) found that aphid feeding had a profound effect on plant carbon allocation, which was detrimental to mycorrhizal fungi. The result indicated that herbivore insects could drive asymmetry in the nutrient exchange between mycorrhizal symbionts (Walder and van der Heijden, 2015). We therefore speculated that short-term changes in external biological carbon sinks may have altered the nutrient supply of *E. nutans* to AMF; this finding was similar to that of Charters et al. (2020), but there was insufficient evidence to prove this. Greater attention could be paid to this point in future experiments.

Mycorrhizal inoculation enhances direct and indirect plant defense systems (Jung et al., 2012; Velásquez et al., 2020b). When inoculated plants are eaten by herbivores, mycorrhizal symbionts increase the release of defense metabolites, through interactions with phytohormone signaling pathways (Meier and Hunter, 2018). Study have demonstrated that the JA signaling pathway plays a critical role in mediating plant defense in response to herbivorous insects (Frew et al., 2022). Therefore, we tested defense-related enzyme activities including PPO, which

catalyzes the formation of lignin and other oxidative phenols (Song et al., 2010). PAL is involved in the biosynthesis of SA signal molecules and phytoalexin or phenolic compounds (Selvaraj et al., 2020). LOX, a key enzyme of the JA signaling pathway, catalyzes the initial reaction in the JA biosynthesis pathway, and β-1,3-glucanase is able to degrade fungal cell walls, causing lysis of fungal cells to participate in the SA defense pathway (Zhao et al., 2009; Song Y. Y. et al., 2015). Song et al. (2013) found that mycorrhizal colonization could initiate the JA signaling defense pathway in tomatoes and upregulate the expression of genes that synthesize LOX enzymes in response to caterpillar feeding. This could explain our result that LOX was significantly increased in mycorrhizal treatments. The LOX enzyme activity of Fm + Lm was approximately double that of the non-inoculated Lm treatment. Thus, despite the low levels of colonization in our experiments, we could still detect significant impacts of AMF on insect attack (Bernaola et al., 2018). However, the activities of PAL and β-1,3-glucanase decreased after AMF inoculation and grasshopper feeding did not notably increase these plant enzyme activities, suggesting that *E. nutans* may be predominantly protected against adverse external factors through the JA pathway and that the SA pathway does not play a dominant role. Previous studies found that once the JA defense pathway was up-regulated, the SA pathway was inhibited (Song Y. Y. et al., 2015; Schoenherr et al., 2019).

Previous research has also demonstrated that AMF could change the concentration and composition of VOCs (Sharma et al., 2017; Meier and Hunter, 2018), which alter plant attractiveness to insect behavior (Babikova et al., 2014; Meier and Hunter, 2019). The genus *Glomus* can be seen as a potent AMF in imparting biotic stress tolerance in a wide range of plants that are eaten by herbivores (Dowarah et al., 2021). Our results, in addition to findings from previous studies, clearly show that some of the genus *Glomus* fungi could induce plants to produce large amounts of volatile compounds, and these VOCs included terpenes, alcohols, esters, and small amounts of alkanes (Roger et al., 2013). In the present study, insect feeding led *E. nutans* to produce more terpenoids such as 2,4-Dimethylacetophenone and 2,5-Dimethylacetophenon, which have been shown to deter herbivores (Sharma et al., 2017). Ethyl acetate was only detected in the non-inoculated treatment, with low relative concentrations of other VOCs. The Fm + Lm treatment produced a greater variety of VOCs and metabolites with insect-repelling properties. AMF-inoculated plants increased the relative concentration of benzenic compounds compared to non-AMF plants. Benzenic compounds are the main components of various essential oils and

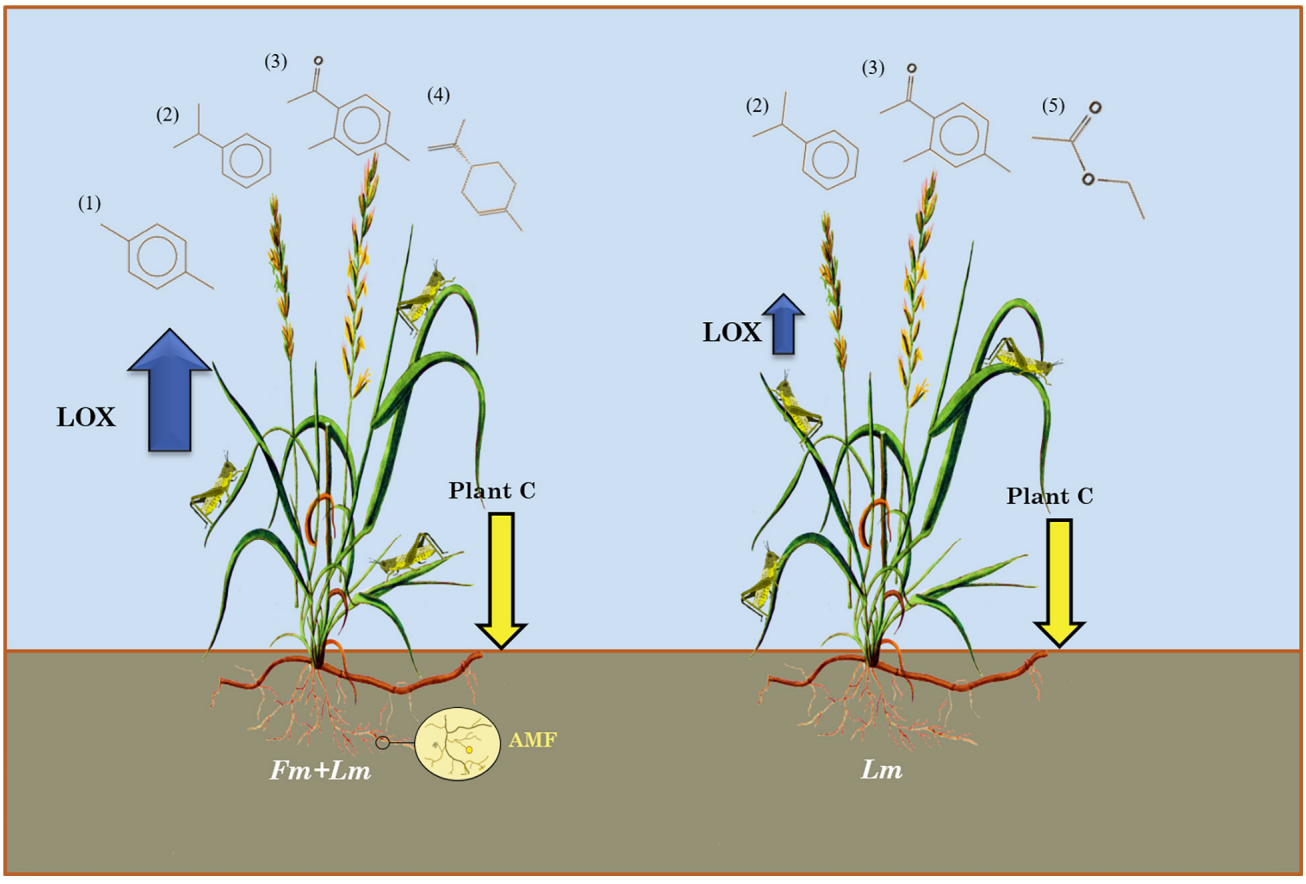

FIGURE 4 | Diagrammatic representation of the various means of *E. nutans* defense response induction by AMF. (1) p-Xylene, (2) Cumene, (3) 2,4-dimethylacetophenone, (4) D-Limonene, and (5) ethyl acetate.

are involved in plant reproduction and defense (Dudareva et al., 2004; Velásquez et al., 2020a). D-limonene and 1,3-diethylbenzene could be produced in other insect-infested plants and it has an important role in improving plant defenses and the repellence of insects (Agut et al., 2015; Kigathi et al., 2019; Mitra et al., 2021). p-Xylene mainly acts as an attractant to natural enemies of the feeding insect (Li et al., 2022). Taken together, these results suggest that AMF *F. mosseae* colonization can improve the chemical defense of *E. nutans*.

In conclusion, inoculation of *E. nutans* with *F. mosseae* improved the uptake of nutrients and induced resistance to grasshopper attack. AMF promote the expression of defense-related enzymes and the types of insect-resistant VOCs increased (**Figure 4**). The JA pathway was also found to be the main insect resistance pathway in *E. nutans*, with mycorrhizal colonization further inducing to strength the defense response. Furthermore, insect feeding could reduce the nutrient content of plants. Thus, the initiation of defense by common symbiotic organisms may be an important evolutionary strategy for plant defense against herbivores and other biotic stresses. Nevertheless, additional experiments are needed to assess whether *E. nutans* under AMF colonization in the field will initiate the same defense pathways and produce similar VOCs. This will help to clarify the mode and mechanism of AMF-grasshopper interactions and analyze the complex relationship of AMF-plant-herbivore interaction.

DATA AVAILABILITY STATEMENT

The original contributions presented in the study are included in the article/**Supplementary Material**, further inquiries can be directed to the corresponding author.

AUTHOR CONTRIBUTIONS

XS and KL conceived the study, supervised the writing, and revised the manuscript. WZ led the writing. LY and BH contributed sections to the manuscript. All authors read and approved the final submission.

FUNDING

This work was supported by the National Natural Science Foundation of China (Grant Nos. 31971746 and 32171685) and Qilian Mountain National Park Qinghai Area Biodiversity Conservation Project (QHTX-2021-009).

SUPPLEMENTARY MATERIAL

The Supplementary Material for this article can be found online at: https://www.frontiersin.org/articles/10.3389/fpls.2022.898969/full#supplementary-material

REFERENCES

Agut, B., Gamir, J., Jaques, J. A., and Flors, V. (2015). *Tetranychus urticae*-triggered responses promote genotype-dependent conspecific repellence or attractiveness in citrus. *N. Phytol.* 207, 790–804. doi: 10.1111/nph.13357

Babikova, Z., Gilbert, L., Bruce, T. J. A., Birkett, M., Caulfield, J. C., Woodcock, C., et al. (2013). Underground signals carried through common mycelial networks warn neighbouring plants of aphid attack. *Ecol. Lett.* 16, 835–843. doi: 10.1111/ele.12115

Babikova, Z., Gilbert, L., Randall, K. C., Bruce, T. J. A., and Pickett, J. A. (2014). Increasing phosphorus supply is not the mechanism by which arbuscular mycorrhiza increase attractiveness of bean (*Vicia faba*) to aphids. *J. Exp. Bot.* 65, 5231–5241. doi: 10.1093/jxb/eru283

Balliu, A., Sallaku, G., and Rewald, B. (2015). AMF inoculation enhances growth and improves the nutrient uptake rates of transplanted, salt-stressed tomato seedlings. *Sustainability* 7, 15967–15981. doi: 10.3390/su71215799

Basu, S., Rabara, R. C., and Negi, S. (2018). Amf: the future prospect for sustainable agriculture. *Physiol. Mol. Plant Pathol.* 102, 36–45. doi: 10.1016/j.pmpp.2017.11.007

Bati, C. B., Santilli, E., and Lombardo, L. (2015). Effect of arbuscular mycorrhizal fungi on growth and on micronutrient and macronutrient uptake and allocation in olive plantlets growing under high total Mn levels. *Mycorrhiza* 25, 97–108. doi: 10.1007/s00572-014-0589-0

Begum, N., Qin, C., Ahanger, M. A., Raza, S., and Khan, M. I. (2019). Role of arbuscular mycorrhizal fungi in plant growth regulation: implications in abiotic stress tolerance. *Front. Plant Sci.* 10:1068. doi: 10.3389/fpls.2019.01068

Bernaola, L., Cosme, M., Schneider, R. W., and Stout, M. (2018). Belowground inoculation with arbuscular mycorrhizal fungi increases local and systemic susceptibility of rice plants to different pest organisms. *Front. Plant Sci.* 9:747. doi: 10.3389/fpls.2018.00747

Bhantana, P., Rana, M. S., Sun, X., Moussa, M. G., and Saleem, M. H. (2021). Arbuscular mycorrhizal fungi and its major role in plant growth, zinc nutrition, phosphorous regulation and phytoremediation. *Symbiosis* 84, 19–37. doi: 10.1007/s13199-021-00756-6

Bolin, L. G., Benning, J. W., and Moeller, D. A. (2018). Mycorrhizal interactions do not influence plant–herbivore interactions in populations of *Clarkia xantiana* ssp.xantiana spanning from center to margin of the geographic range. *Ecol. Evol.* 8, 10743–10753. doi: 10.1002/ece3.4523

Charters, M. D., Sait, S. M., and Field, K. J. (2020). Aphid herbivory drives asymmetry in carbon for nutrient exchange between plants and an arbuscular mycorrhizal fungus. *Curr. Biol.* 30, 1801–1808. doi: 10.1016/j.cub.2020.02.087

Chen, S., Zhao, H., Zou, C., Li, Y., and Chen, Y. (2017). Combined inoculation with multiple arbuscular mycorrhizal fungi improves growth, nutrient uptake and photosynthesis in cucumber seedlings. *Front. Microbiol.* 8:2516. doi: 10.3389/fmicb.2017.02516

Dowarah, B., Gill, S. S., and Agarwala, N. (2021). Arbuscular mycorrhizal fungi in conferring tolerance to biotic stresses in plants. *J. Plant Growth Regul.* 110:999. doi: 10.1007/s00344-021-10392-5

Dudareva, N., Pichersky, E., and Gershenzon, J. (2004). Biochemistry of plant volatiles. *Plant Physiol.* 135, 1893–1902. doi: 10.1104/pp.104.049981

Frew, A. (2021). Aboveground herbivory suppresses the arbuscular mycorrhizal symbiosis, reducing plant phosphorus uptake. *Appl. Soil Ecol.* 168:104133. doi: 10.1016/j.apsoil.2021.104133

Frew, A., Antunes, P. M., Cameron, D. D., Hartley, S. E., and Johnson, S. N. (2022). Plant herbivore protection by arbuscular mycorrhizas: a role for fungal diversity? *N. Phytol.* 233, 1022–1031. doi: 10.1111/nph.17781

Gai, J. P., Christie, P., Cai, X. B., Fan, J. Q., and Zhang, J. L. (2009). Occurrence and distribution of arbuscular mycorrhizal fungal species in three types of grassland community of the Tibetan Plateau. *Ecol. Res.* 24, 1345–1350. doi: 10.1007/s11284-009-0618-1

Gehring, C., and Bennett, A. (2009). Mycorrhizal fungal-plant-insect interactions: the importance of a community approach. *Environ. Entomol.* 38, 93–102. doi: 10.1603/022.038.0111

Girousse, C., Moulia, B., Silk, W., and Bonnemain, J. (2005). Aphid infestation causes different changes in carbon and nitrogen allocation in alfalfa stems as

well as different inhibitions of longitudinal and radial expansion. *Plant Physiol.* 137, 1474–1484. doi: 10.1104/pp.104.057430

Han, B., Li, J., Liu, K., Zhang, H., and Wei, X. (2021). Variations in soil properties rather than functional gene abundances dominate soil phosphorus dynamics under short-term nitrogen input. *Plant Soil* 469, 227–241. doi: 10.1007/s11104-021-05143-0

Hao, H., Bao, M., Ke, J., Li, L., and Ma, C. (2019). Fauna elements and eco-geographical distribution of locus in Qinghai province. *J. Biol.* 36, 62–68.

Hao, Z., Xie, W., and Chen, B. (2019). Arbuscular mycorrhizal symbiosis affects plant immunity to viral infection and accumulation. *Viruses* 11:534. doi: 10.3390/v11060534

Heil, M., and Ton, J. (2008). Long-distance signalling in plant defence. *Trends Plant Sci.* 13, 264–272. doi: 10.1016/j.tplants.2008.03.005

Jiang, D., Tan, M., Wu, S., Zheng, L., and Wang, Q. (2021). Defense responses of arbuscular mycorrhizal fungus-colonized poplar seedlings against gypsy moth larvae: a multiomics study. *Hortic. Res.* 8:245. doi: 10.1038/s41438-021-00671-3

Jiang, Y., Wang, W., Xie, Q., Liu, N., and Liu, L. (2017). Plants transfer lipids to sustain colonization by mutualistic mycorrhizal and parasitic fungi. *Science* 356, 1172–1175. doi: 10.1126/science.aam9970

Jin, L., Zhang, G., Wang, X., Dou, C., and Chen, M. (2011). Arbuscular mycorrhiza regulate inter-specific competition between a poisonous plant, *Ligularia virgaurea*, and a co-existing grazing grass, *Elymus nutans*, in Tibetan Plateau Alpine meadow ecosystem. *Symbiosis* 55, 29–38. doi: 10.1007/s13199-011-0141-3

Jung, S. C., Martinez-Medina, A., Lopez-Raez, J. A., and Pozo, M. J. (2012). Mycorrhiza-induced resistance and priming of plant defenses. *J. Chem. Ecol.* 38, 651–664. doi: 10.1007/s10886-012-0134-6

Karban, R., Wetzel, W. C., Shiojiri, K., Pezzola, E., and Blande, J. D. (2016). Geographic dialects in volatile communication between sagebrush individuals. *Ecology* 97, 2917–2924. doi: 10.1002/ecy.1573

Kayama, M., and Yamanaka, T. (2014). Growth characteristics of ectomycorrhizal seedlings of *Quercus glauca*, *Quercus salicina*, and *Castanopsis cuspidata* planted on acidic soil. *Trees* 28, 569–583. doi: 10.1007/s00468-013-0973-y

Kigathi, R. N., Weisser, W. W., Reichelt, M., Gershenzon, J., and Unsicker, S. B. (2019). Plant volatile emission depends on the species composition of the neighboring plant community. *BMC Plant Biol.* 19:58. doi: 10.1186/s12870-018-1541-9

Koske, R. E., and Gemma, J. N. (1989). A modified procedure for staining roots to detect VA mycorrhizas. *Mycol. Res.* 92, 486–488. doi: 10.1016/S0953-7562(89)80195-9

Li, B., Ding, Y., Tang, X., Wang, G., and Wu, S. (2019). Effect of L-arginine on maintaining storage quality of the white button mushroom (*Agaricus bisporus*). *Food Bioproc. Technol.* 12, 563–574. doi: 10.1007/s11947-018-2232-0

Li, M., Xia, S., Zhang, T., Williams, R. L., and Xiao, H. (2022). Volatiles from cotton plants infested by *Agrotis segetum* (Lep.: Noctuidae) attract the larval parasitoid *Microplitis* mediator (Hym.: Braconidae). *Plants (Basel)* 11:863. doi: 10.3390/plants11070863

Li, Y., Duan, T., Nan, Z., and Li, Y. (2021). Arbuscular mycorrhizal fungus alleviates alfalfa leaf spots caused by *Phoma medicaginis* revealed by RNA-seq analysis. *J. Appl. Microbiol.* 130, 547–560. doi: 10.1111/jam.14387

Luginbuehl, L. H., Menard, G. N., Kurup, S., Van Erp, H., and Radhakrishnan, G. V. (2017). Fatty acids in arbuscular mycorrhizal fungi are synthesized by the host plant. *Science* 356, 1175–1178. doi: 10.1126/science.aan0081

Malik, R. J., Ali, J. G., and Bever, J. D. (2018). Mycorrhizal composition influences plant anatomical defense and impacts herbivore growth and survival in a life-stage dependent manner. *Pedobiologia* 66, 29–35. doi: 10.1016/j.pedobi.2017.12.004

McGonigle, T. P., Miller, M. H., Evans, D. G., Fairchild, G. L., and Swan, J. A. (1990). A new method which gives an objective measure of colonization of roots by vesicular-arbuscular mycorrhizal fungi. *N. Phytol.* 115, 495–501. doi: 10.1111/j.1469-8137.1990.tb00476.x

Meier, A. R., and Hunter, M. D. (2018). Arbuscular mycorrhizal fungi mediate herbivore-induction of plant defenses differently above and belowground. *Oikos* 127, 1759–1775. doi: 10.1111/oik.05402

Meier, A. R., and Hunter, M. D. (2019). Mycorrhizae alter constitutive and Herbivore-Induced volatile emissions by milkweeds. *J. Chem. Ecol.* 45, 610–625. doi: 10.1007/s10886-019-01080-6

Miozzi, L., Vaira, A. M., Catoni, M., Fiorilli, V., and Accotto, G. P. (2019). Arbuscular mycorrhizal symbiosis: plant friend or foe in the fight against viruses? *Front. Microbiol.* 10:1238. doi: 10.3389/fmicb.2019.01238

Mitra, P., Das, S., Debnath, R., Mobarak, S. H., and Barik, A. (2021). Identification of *Lathyrus sativus* plant volatiles causing behavioral preference of *Aphis craccivora*. *Pest Manag. Sci.* 77, 285–299. doi: 10.1002/ps.6018

Plassard, C., and Dell, B. (2010). Phosphorus nutrition of mycorrhizal trees. *Tree Physiol.* 30, 1129–1139. doi: 10.1093/treephys/tpq063

Quan, X., Qiao, Y., Chen, M., Duan, Z., and Shi, H. (2021). Comprehensive evaluation of the allelopathic potential of *Elymus nutans*. *Ecol. Evol.* 11, 12389–12400. doi: 10.1002/ece3.7982

Roger, A., Gétaz, M., Rasmann, S., and Sanders, I. R. (2013). Identity and combinations of arbuscular mycorrhizal fungal isolates influence plant resistance and insect preference. *Ecol. Entomol.* 38, 330–338. doi: 10.1111/een.12022

Schoenherr, A. P., Rizzo, E., Jackson, N., Manosalva, P., and Gomez, S. K. (2019). Mycorrhiza-induced resistance in potato involves priming of defense responses against cabbage looper (Noctuidae: Lepidoptera). *Environ. Entomol.* 48, 370–381. doi: 10.1093/ee/nvy195

Schweiger, R., Baier, M. C., Persicke, M., and Müller, C. (2014). High specificity in plant leaf metabolic responses to arbuscular mycorrhiza. *Nat. Commun.* 5, 3886. doi: 10.1038/ncomms4886

Selvaraj, A., Thangavel, K., and Uthandi, S. (2020). Arbuscular mycorrhizal fungi (*Glomus intraradices*) and diazotrophic bacterium (Rhizobium BMBS) primed defense in blackgram against herbivorous insect (*Spodoptera litura*) infestation. *Microbiol. Res.* 231:126355. doi: 10.1016/j.micres.2019.126355

Sharma, E., Anand, G., and Kapoor, R. (2017). Terpenoids in plant and arbuscular mycorrhiza-reinforced defence against herbivorous insects. *Ann. Bot.* 119, 791–801. doi: 10.1093/aob/mcw263

Song, Y., Chen, D., Lu, K., Sun, Z., and Zeng, R. (2015). Enhanced tomato disease resistance primed by arbuscular mycorrhizal fungus. *Front. Plant Sci.* 6:786. doi: 10.3389/fpls.2015.00786

Song, Y. Y., Ye, M., Li, C., He, X., and Zhu-Salzman, K. (2015). Hijacking common mycorrhizal networks for herbivore-induced defence signal transfer between tomato plants. *Sci. Rep.* 4:3915. doi: 10.1038/srep03915

Song, Y. Y., Ye, M., Li, C. Y., Wang, R. L., and Wei, X. C. (2013). Priming of anti-herbivore defense in tomato by arbuscular mycorrhizal fungus and involvement of the jasmonate pathway. *J. Chem. Ecol.* 39, 1036–1044. doi: 10.1007/s10886-013-0312-1

Song, Y. Y., Zeng, R. S., Xu, J. F., Li, J., and Shen, X. (2010). Interplant communication of tomato plants through underground common mycorrhizal networks. *PLoS One* 5:e13324. doi: 10.1371/journal.pone.0013324

Spatafora, J. W., Chang, Y., Benny, G. L., Lazarus, K., and Smith, M. E. (2016). A phylum-level phylogenetic classification of zygomycete fungi based on genome-scale data. *Mycologia* 108, 1028–1046. doi: 10.3852/16-042

Tan, X., Huang, Y., Xiong, D., Lv, K., and Chen, F. (2020). The effect of Elymus nutans sowing density on soil reinforcement and slope stabilization properties of vegetation–concrete structures. *Sci. Rep.* 10, 20462. doi: 10.1038/s41598-020-77407-1

Valenzuela, M., Méndez, V., Montenegro, I., Besoain, X., and Seeger, M. (2019). Streptomycin resistance in *Clavibacter michiganensis* subsp. michiganensis strains from Chile is related to anrpsL gene mutation. *Plant Pathol.* 68, 426–433. doi: 10.1111/ppa.12971

Veenstra, J. A., Leyria, J., Orchard, I., and Lange, A. B. (2021). Identification of gonadulin and insulin-like growth factor from migratory locusts and their importance in reproduction in *Locusta migratoria*. *Front. Endocrinol.* 12:693068. doi: 10.3389/fendo.2021.693068

Velásquez, A., Valenzuela, M., Carvajal, M., Fiaschi, G., and Avio, L. (2020a). The arbuscular mycorrhizal fungus *Funneliformis mosseae* induces changes and increases the concentration of volatile organic compounds in *Vitis vinifera* cv. Sangiovese leaf tissue. *Plant Physiol. Biochem.* 155, 437–443. doi: 10.1016/j.plaphy.2020.06.048

Velásquez, A., Vega-Celedón, P., Fiaschi, G., Agnolucci, M., and Avio, L. (2020b). Responses of *Vitis vinifera* cv. Cabernet Sauvignon roots to the arbuscular mycorrhizal fungus *Funneliformis mosseae* and the plant growth-promoting rhizobacterium *Ensifer meliloti* include changes in volatile organic compounds. *Mycorrhiza* 30, 161–170. doi: 10.1007/s00572-020-00933-3

Walder, F., and van der Heijden, M. G. A. (2015). Regulation of resource exchange in the arbuscular mycorrhizal symbiosis. *Nat. Plants* 1:15159. doi: 10.1038/nplants.2015.159

Wang, X., Wang, Q., Jin, L., Sun, L., and Wang, Q. (2019). Arbuscular mycorrhizal fungi in the rhizosphere soil of poisonous plants depressed the growth of pasture grasses in the Tibetan Plateau Alpine meadow. *Ecosyst. Health Sustain.* 5, 226–236.

Xu, Y. F., Chu, X. T., Zhang, X. H., Liu, Q., and Miao, Y. J. (2018). The forms of nitrogen source influence the interaction between *Elymus nutans* Griseb and arbuscular mycorrhizal fungi. *S. Afr. J. Bot.* 119, 37–44. doi: 10.1016/j.sajb.2018.08.007

Ye, M., Veyrat, N., Xu, H., Hu, L., and Turlings, T. (2018). An herbivore-induced plant volatile reduces parasitoid attraction by changing the smell of caterpillars. *Sci. Adv.* 4, r4767. doi: 10.1126/sciadv.aar4767

Zhang, S., Lehmann, A., Zheng, W., You, Z., and Rillig, M. C. (2019). Arbuscular mycorrhizal fungi increase grain yields: a meta-analysis. *N. Phytol.* 222, 543–555. doi: 10.1111/nph.15570

Zhao, L. Y., Chen, J. L., Cheng, D. F., Sun, J. R., and Liu, Y. (2009). Biochemical and molecular characterizations of *Sitobion avenae*-induced wheat defense responses. *Crop Prot.* 28, 435–442. doi: 10.1016/j.cropro.2009.01.005

Conflict of Interest: The authors declare that the research was conducted in the absence of any commercial or financial relationships that could be construed as a potential conflict of interest.

Publisher's Note: All claims expressed in this article are solely those of the authors and do not necessarily represent those of their affiliated organizations, or those of the publisher, the editors and the reviewers. Any product that may be evaluated in this article, or claim that may be made by its manufacturer, is not guaranteed or endorsed by the publisher.

frontiers | Frontiers in Plant Science

ORIGINAL RESEARCH
published: 02 June 2022
doi: 10.3389/fpls.2022.896436

Differential Responses to Salt Stress in Four White Clover Genotypes Associated With Root Growth, Endogenous Polyamines Metabolism, and Sodium/Potassium Accumulation and Transport

Zhou Li[1†], Wan Geng[1†], Meng Tan[1], Yao Ling[1], Yan Zhang[1], Liquan Zhang[2] and Yan Peng[1*]*

[1] College of Grassland Science and Technology, Sichuan Agricultural University, Chengdu, China, [2] Key Laboratory of Forage and Endemic Crop Biology, Ministry of Education, Inner Mongolia University, Hohhot, China

OPEN ACCESS

Edited by:
Jin-Lin Zhang,
Lanzhou University, China

Reviewed by:
Mohamed Magdy F. Mansour,
Ain Shams University, Egypt
Zhaolong Wang,
Shanghai Jiao Tong University, China

***Correspondence:**
Liquan Zhang
zhangliquan430@126.com
Yan Peng
pengyanlee@163.com

[†] These authors have contributed equally to this work

Specialty section:
This article was submitted to Plant Abiotic Stress, a section of the journal Frontiers in Plant Science

Received: 15 March 2022
Accepted: 09 May 2022
Published: 02 June 2022

Citation:
Li Z, Geng W, Tan M, Ling Y, Zhang Y, Zhang L and Peng Y (2022) Differential Responses to Salt Stress in Four White Clover Genotypes Associated With Root Growth, Endogenous Polyamines Metabolism, and Sodium/Potassium Accumulation and Transport. Front. Plant Sci. 13:896436. doi: 10.3389/fpls.2022.896436

Selection and utilization of salt-tolerant crops are essential strategies for mitigating salinity damage to crop productivity with increasing soil salinization worldwide. This study was conducted to identify salt-tolerant white clover (*Trifolium repens*) genotypes among 37 materials based on a comprehensive evaluation of five physiological parameters, namely, chlorophyll (Chl) content, photochemical efficiency of PS II (Fv/Fm), performance index on an absorption basis (PIABS), and leaf relative water content (RWC), and to further analyze the potential mechanism of salt tolerance associated with changes in growth, photosynthetic performance, endogenous polyamine metabolism, and Na^+/K^+ uptake and transport. The results showed that significant variations in salt tolerance were identified among 37 genotypes, as PI237292 and Tr005 were the top two genotypes with the highest salt tolerance, and PI251432 and Korla were the most salt-sensitive genotypes compared to other materials. The salt-tolerant PI237292 and Tr005 not only maintained significantly lower EL but also showed significantly better photosynthetic performance, higher leaf RWC, underground dry weight, and the root to shoot ratio than the salt-sensitive PI251432 and Korla under salt stress. Increases in endogenous PAs, putrescine (Put), and spermidine (Spd) contents could be key adaptive responses to salt stress in the PI237292 and the Tr005 through upregulating genes encoding Put and Spd biosynthesis (*NCA*, *ADC*, *SAMDC*, and *SPDS2*). For Na^+ and K^+ accumulation and transport, higher salt tolerance of the PI237292 could be associated with the maintenance of Na^+ and Ca^+ homeostasis associated with upregulations of *NCLX* and *BTB/POZ*. The K^+ homeostasis-related genes (*KEA2*, *HAK25*, *SKOR*, *POT2/8/11*, *TPK3/5*, and *AKT1/5*) *are* differentially expressed among four genotypes under salt stress. However, the K^+ level and K^+/Na^+ ratio were not completely consistent with the salt tolerance of the four genotypes. The regulatory

function of these differentially expressed genes (DEGs) on salt tolerance in the white clover and other leguminous plants needs to be investigated further. The current findings also provide basic genotypes for molecular-based breeding for salt tolerance in white clover species.

Keywords: ion transport, root to shoot ratio, plant growth regulator, salinization, differentially expressed genes, water use efficiency

INTRODUCTION

Soil salinity has been decreasing global agricultural productivity, which poses a threat to agriculture and food security since more than 20% of agricultural land worldwide is negatively affected by soil salinization (Mickelbart et al., 2015). Identification or development of salt-tolerant germplasms or cultivars is one of the most effective strategies for mitigating salinity damage to crop productivity because genetic variation is often found within one particular species, especially for those widely distributed across the world (Munns, 2005). It has been reported that abundant genetic diversity and variation in salt tolerance among 552 sunflower (*Helianthus annuus*) germplasms and 30 materials with different genetic backgrounds were identified as salt-tolerant genotypes (Li et al., 2020a). A genome-wide association scan in 174 barley (*Hordeum vulgare*) accessions found that salt-tolerant germplasms exhibited stronger antioxidant capacity in response to salt stress (Thabet et al., 2021). A significant variation in salt tolerance was also observed among rice (*Oryza sativa*) germplasms (Yuan et al., 2020; Lar et al., 2021; Rasel et al., 2021). The salt tolerance of 15 basil (*Ocimum* spp.) genotypes varied with morphological parameters, growth, and photosynthetic performance (Shirahmadi et al., 2022). The white clover (*Trifolium repens*) is a vital legume component of the temperate pasture, which is cultivated widely as forage due to its high nutrient value. Improvement or maintenance of white clover productivity is essential for livestock husbandry under environmental stress (Egan et al., 2018). However, the white clover is often recognized as a salt-sensitive species. Salt stress is considered the main limitation to its production and quality in arid and semi-arid regions (Rogers et al., 1997; Wang et al., 2010). It is important to identify white clover genotypes with superior salt tolerance and productivity under salt stress.

Salt stress causes damage to plants mainly involved in osmotic stress, ion toxicity, and secondary stress, since high concentrations of salt ions in soil hinder water uptake, and the overaccumulation of Na^+ in cells causes ion toxicity, physiological disturbance, nutritional imbalance, and oxidative damage (Motos et al., 2017). Intracellular ion homeostasis is a fundamental mechanism by which plants survive salt stress. However, the K^+ uptake and transport are significantly inhibited by Na^+ in plants, resulting in K^+ deficiency under high salt conditions (Abbasi et al., 2016). K^+ content has been considered to be a key indicator of salt tolerance because of its vital role in stress signaling, ion homeostasis, and nutrition (Wu et al., 2018). A previous study demonstrated that the maintenance of a higher K^+/Na^+ ratio was positively correlated with salt tolerance in different plant species. For example, salt-tolerant rice genotypes (Ghunsi, Nonabokra, and BINA dhan-10) exhibited a significantly higher K^+/Na^+ ratio than salt-sensitive BINA dhan-17, indicating that the K^+/Na^+ ratio could be used as an essential indicator of salt tolerance (Rasel et al., 2021). It has been found that the decrease in the in Na^+/K^+ ratio regulated by exogenous alpha-lipoic acid or transcription factor *OsSTAP1* through a transgenic approach was related to enhanced salt tolerance in plants (Wang Y. et al., 2020; Youssef et al., 2021). A study by Yan et al. (2020) found that melatonin application increased the K^+/Na^+ ratio and endogenous PAs accumulation, contributing to enhanced salt tolerance in rice. However, no significant differences in Na^+ content, K^+ content, and the Na^+/K^+ ratio were identified between salt-tolerant rice cultivar Zhegeng 78 and salt-sensitive cultivar Zhegeng 99 at post-germination and seedling stages under salt stress (Ye et al., 2021). In response to salt stress, salt-tolerant rice cultivar Pokkali exhibited significantly higher Na^+ content and Na^+/K^+ ratio than salt-sensitive IR29, along with a significant upregulation of *OsNHX1,* which was responsible for the compartmentation of Na^+ into vacuoles to maintain growth and photosynthetic performance under salt stress (Theerawitaya et al., 2020). These findings indicated that salt tolerance mechanism is related to the K^+/Na^+ ratio and that their contents could vary in different plant species.

In addition to Na^+/K^+ accumulation and transportation, salt tolerance is also involved in many other mechanisms such as osmotic adjustment, oxidation-reduction equilibrium, hormonal regulation, and metabolic homeostasis (Yu et al., 2020). It has been found that polyamine (PA) metabolic pathways were closely related to salt tolerance in plants (Pottosin et al., 2021). Putrescine (Put), spermidine (Spd), and spermine (Spm) are abundant PAs in plants exhibiting various roles in mediating stress tolerance as compatible solutes for osmotic adjustment, scavengers of reactive oxygen species for antioxidant defense, signal molecules for stress signal transduction, and regulators of ion channels for ion homeostasis (Minocha et al., 2014). Improvement in salt tolerance *via* enhanced PA biosynthesis and metabolism has been reported in many plant species such as wheat (Talaat, 2021) and switchgrass (*Panicum virgatum*) (Guan et al., 2020), and rice (Islam et al., 2020; Das et al., 2021). For the PA metabolism, arginine decarboxylase (ADC) catalyzes the decarboxylation of arginine into agmatine, which is used for the Put biosynthesis. Spd is produced from the Put by spermidine synthase (SPDS), and spermine synthase (SPMS) catalyzes Spm synthesis by using Spd. Two processes (from Put to Spd and from Spd to Spm) need the sequential addition of decarboxylated *S*-adenosyl-methionine synthesized by *S*-adenosylmethionine decarboxylase proenzyme (SAMDC). Polyamine oxidase (PAO) catalyzes the degradation

of Spd and Spm in cells (Miller-Fleming et al., 2015). A previous study showed that overexpression of *SAMDC* or *ADC* could significantly improve salt tolerance in plants (Espasandin et al., 2018; Islam et al., 2020).

Enhanced salt tolerance in transgenic tobacco (*Nicotiana tabacum*) or apple (*Malus pumila*) plants *via* ectopic expression of a *CsTGase* or *MdATG8i* was associated with PA accumulation and Na^+/K^+ homeostasis (Huo et al., 2020; Zhong et al., 2020). However, different types of PAs may exhibit different responses to salt stress. For example, salt stress significantly increased Put content in salt-sensitive sorghum (*Sorghum bicolor*) plants, but a significant decline in Put content and significant increases in Spd and Spm contents in salt-tolerant plants (de Oliveira et al., 2020). It is worth further investigating the potential mechanism of salt tolerance associated with variations in endogenous PA metabolism and Na^+/K^+ transport in leguminous plants.

Salt tolerance is a complex trait and possesses species-specific regulatory effects and mechanisms in the plant kingdom (Van Zelm et al., 2020). Natural variations in PA metabolism and Na^+/K^+ accumulation and transport remain to be identified in white clover species. The aims of the current study were to screen and evaluate salt tolerance of 37 white clover germplasms and to elucidate the potential mechanism of salt tolerance among different genotypes associated with changes in growth, photosynthetic performance, endogenous PAs, and Na^+/K^+ accumulation. Transcriptional profiling further identified key genes involved in PAs metabolism and Na^+/K^+ transportation in four white clover genotypes with varying degrees of salt tolerance. The research results will help us gain an understanding of salt tolerance in leguminous plant species and provide basic materials for the salt tolerance breeding of the white clover.

MATERIALS AND METHODS

Plant Material and Treatments

A total of 37 white clover genotypes were used for the evaluation of salt tolerance and subsequent research about the potential mechanism of genotypes differing in salt tolerance. Among them, 19 genotypes were provided by the National Plant Germplasm System of the United States. The 10 genotypes were commercial cultivars. The eight genotypes were wild resources collected from Sichuan in China (**Supplementary Table 1**). The seeds were germinated in petri dishes containing two layers of filter paper and 20 ml of deionized water for 8 days. The seedlings were then transplanted into polyvinyl chloride tubes (12 cm in diameter and 20 cm in length) filled with sand and loam (1: 1). Each tube contained five seedlings, and all tubes were placed in the greenhouse for 40 days for cultivation (average day/night temperatures of 24/17°C, 12 h photoperiod at 750 mmol m^{-2} s^{-1} photosynthetically active radiation, and 65% relative humidity). A 250 ml of Hoagland's nutrient solution was irrigated in each tube weekly (Hoagland and Arnon, 1950). For salt stress, all materials were divided into two groups: one group was cultivated under normal conditions without salt stress for 16 days, and the other group was irrigated with 200 ml of 150 mM NaCl for 3 days, 200 ml of 200 mM NaCl for 3 days, and 200 ml of 250 mM NaCl for 10 days (a total of 16 days of salt stress). The NaCl was dissolved in the Hoagland solution. Leaf and root samples were taken on the 16th day of normal cultivation and salt stress. Four independent replicates were used to determine the growth (fresh and dry weight) and physiological parameters, and three independent replicates were used to detect the transcriptome.

Determinations of Growth Parameters and Water Status

The aboveground and underground fresh tissues of all plants in each tube were collected and weighed immediately to get a fresh weight. Then, these tissues were put into an oven at 105°C for 30 min and 75°C for 3 days until constant dry weight. Then, the dry to fresh weight ratio was calculated. The root to shoot ratio was calculated as the ratio of underground dry weight to aboveground dry weight. Relative water content (RWC) was evaluated according to the formula RWC = [(FW-DW)/(TW-DW)] × 100%. The FW, DW, or TW indicated fresh, dry, or turgid weight, respectively (Barrs and Weatherley, 1962).

Determinations of Photosynthetic Parameters and Cell Membrane Stability

Cell membrane stability was evaluated by changing electrolyte leakage (EL) (Blum and Ebercon, 1981). Fresh leaves (0.15 g) were cleaned and immersed in 35 ml of deionized water for 24 h at 20°C in a 50 ml centrifuge tube. The initial conductivity (C1) of the solution was identified by using a conductivity meter (YSI Model 32, Yellow Springs Instrument Co., Yellow Spring, OH, United States). The centrifuge tube was autoclaved at 105°C for 15 min. After being cooled down to room temperature, the final conductivity (C2) was determined. Then, EL was calculated based on the formula EL (%) = C1/C2 × 100%. Chlorophyll (Chl) content was determined based on the method of Amnon (1949). For determination of photochemical efficiency of PS II (Fv/Fm) and performance index on an absorption basis (PIABS), a Chl fluorescence system (Pocket PEA, Hansatech, Norfolk, United Kingdom) was used. The PIABS, a key indicator of maximum photochemical efficiency and total numbers of activated photochemical reaction centers of PS II, reflects the health status of chloroplasts under stress conditions. A single layer of leaves was put into the leaf chamber for 20 min dark adaptation before the Fv/Fm and PI_{ABS} were recorded. Net photosynthetic rate (Pn), transpiration rate (Tr), stomatal conductance (Gs), intercellular CO_2 concentration (Ci), and water use efficiency (WUE) were identified by using a portable photosynthesis system (CIRAS-3, PP Systems, Amesbury, MA, United States) that provided stable 400 μl L^{-1} CO_2 and 800 μmol photon m^{-2} red and blue light.

Determinations of Polyamines, Sodium/Potassium Contents, and Transcriptome

Endogenous PAs, Put, Spd, and Spm were identified by high-performance liquid chromatography (HPLC, Agilent-1200, Agilent Technologies, Santa Clara, CA, United States) with some modifications based on the method of Duan et al. (2008),

which was demonstrated in our previous study (Li et al., 2016). To determine Na^+ and K^+ contents, an inductively coupled plasma-mass spectrometry (ICP-MS, ICAP6300, Thermo Fisher Scientific, MA, United States) was used, and the assay method in detail has been recorded in the study by Geng et al. (2021). The transcriptome was used to detect differentially expressed genes (DEGs) in the leaves of the white clover in response to salt stress. RNA extraction, library construction, and sequencing have also been demonstrated in our previous study (Li et al., 2017). The gene function was annotated by using databases including Nr (NCBI non-redundant protein sequences), NCBI non-redundant nucleotide sequences (Nt), clusters of orthologous groups of proteins (KOG/COG), a manually annotated and reviewed protein sequence database (Swiss-Prot), KEGG Ortholog database (KO), and gene ontology (GO). The p-value < 0.05 and fold change of gene ≥ 1.5 were set as the threshold for DEGs.

Statistical Analysis

For statistical analysis of growth and physiological parameters, differences among treatment means were tested using Fisher's protected least significance (LSD) test at the $P \leq 0.05$ probability level. For a comprehensive evaluation of salt tolerance, subordinate function value analysis (SFVA) of five physiological parameters (EL, Chl, Fv/Fm, PIABS, and RWC) was performed. Then, the D value was calculated using the SFV ($D = \Sigma U(X_i)/n$). The bigger the D value, the higher salt tolerance (Li Z. et al., 2021). A heat map of physiological parameters was created using the R statistical software (R3.5.2 by the R Development Core Team).

RESULTS

Evaluation of Salt Tolerance Among 37 White Clover Genotypes

The heat map showed physiological parameters: EL, Chl, Fv/Fm, PIABS, and RWC; they were changed by salt stress in 37 materials (**Supplementary Figure 1A**). These materials could be mainly divided into three subclusters based on the hierarchical clustering, as subcluster a included 19 materials, subcluster b included 11 materials, and subcluster c contained seven materials (**Supplementary Figure 1A**). The salt tolerance of 37 materials was ranked according to the SFVA and D values (**Supplementary Figure 1B**). As shown in **Supplementary Figure 1B**, the top five materials with higher salt tolerance than other materials in the sequences were PI237292, Tr005, Sulky, Tr002, and Tr037. Korla (least) and PI251432 (the last but one) exhibited less salt tolerance than other materials (**Supplementary Figure 1B**).

Water Status and Photosynthetic Parameters Affected by Salt Stress Among Four White Clover Genotypes

Phenotypic changes showed that salt stress caused leaf wilting and chlorosis, and PI251432 and Korla suffered from severer damage than PI237292 and Tr005 in response to salt stress (**Figure 1A**). EL increased significantly, whereas RWC decreased greatly in the leaves of PI237292, Tr005, PI251432, and Korla under salt stress (**Supplementary Figures 2A,B**). PI237292 and Tr005 maintained significantly lower EL and higher RWC than PI251432 and Korla after 16 days of salt stress (**Supplementary Figures 2A,B**). No significant differences in Fv/Fm and PIABS were observed among the four materials under normal conditions (**Supplementary Figures 2C,D**). Salt stress caused a significant decline in Fv/Fm in the leaves of PI237292, PI251432, or Korla, but not in Tr005 (**Supplementary Figure 2C**). Under salt stress, PI237292 and Tr005 exhibited more than 3 or 16 times higher PIABS than PI251432 or Korla, respectively (**Supplementary Figure 2D**). Chl content was maintained at an average level in PI237292 and Tr005 when subjected to salt stress but significantly declined in PI251432 or Korla (**Figure 1B**). Pn, Tr, and Gs were reduced significantly in four materials under salt stress (**Figures 1C–E**). Ci significantly decreased in PI237292 and Tr005 but increased in PI251432 or Korla under salt stress (**Figure 1F**). A prolonged period of salt stress did not affect WUE significantly in the leaves of PI237292 and Tr005 but caused a significant decline in WUE in the leaves of PI251432 or Korla (**Figure 1G**).

Growth Affected by Salt Stress Among Four White Clover Genotypes

PI237292 had the highest aboveground fresh weight of the three materials under normal conditions and salt stress (**Figure 2A**). Tr005 increased its aboveground fresh weight by 25% more than PI251432 or Korla under salt stress (**Figure 2A**). Salt stress led to a significant decline in the underground fresh weight of PI237292, PI251432, or Korla but did not affect the underground fresh weight of Tr005 (**Figure 2B**). PI237292 had more than a 30% increase in aboveground dry weight than the other three materials under normal conditions but did not maintain the superiority under salt stress (**Figure 2C**). Significant declines in aboveground dry weight were caused by salt stress in PI237292, PI251432, and Korla, but not in Tr005 (**Figure 2C**). There was no significant difference in the underground dry weight of PI237232 under normal conditions and salt stress (**Figure 2D**). Salt stress significantly improved underground dry weight in Tr005 but decreased underground dry weight in PI251432 and Korla (**Figure 2D**). Salt-caused increase in dry to fresh weight ratio was more pronounced in Korla than in other materials (**Figure 2E**). Under salt stress, the root to shoot ratio was highest in Tr005, second highest in PI237292, third highest in PI251432, and lowest in Korla (**Figure 2F**). In addition, a significant decline in the root to shoot ratio was only observed in Korla under salt stress (**Figure 2F**).

Endogenous Polyamines, Sodium, and Potassium Content Were Affected by Salt Stress Among Four White Clover Genotypes

Endogenous PAs content was highest in PI251432 than in the other three materials under normal conditions (**Figure 3A**). Salt stress caused a significant increase in PAs content in PI237292 and Tr005 but a significant decrease in PI251432 and Korla (**Figure 3A**). PI251432 and Korla maintained significantly higher Put content than PI237292 and Tr005 under normal conditions; on the contrary, PI237292 and Tr005 showed

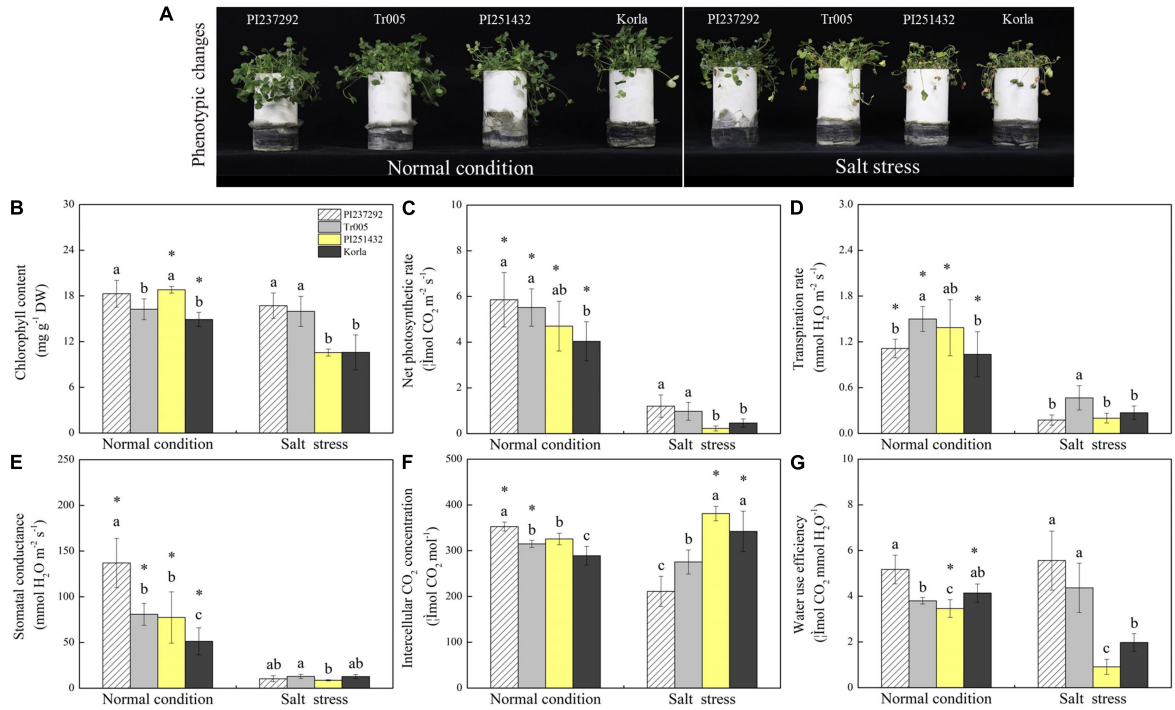

FIGURE 1 | Changes in **(A)** phenotypic changes, **(B)** chlorophyll content, **(C)** net photosynthetic rate, **(D)** transpiration rate, **(E)** stomatal conductance, **(F)** intercellular CO2 concentration, and **(G)** water use efficiency in the leaves of four white clover materials (PI237292, Tr005, PI251432, and Korla) under normal and salt stress conditions. Vertical bars indicate ± standard error (SE) of the mean (n = 4), and different letters above the column indicate significant differences ($P \leq 0.05$) under normal conditions or salt stress. The "*" represents the significant difference between normal conditions and salt stress for a specific genotype (PI237292, Tr005, PI251432, or Korla).

significantly higher Put content than PI251432 and Korla did in response to salt stress (**Figure 3B**). No significant differences were observed in Spd and Spm contents among four materials under the normal condition as well as in Spm content between four materials under salt stress (**Figures 3C,D**). PI251432 and Korla exhibited a 17% increase in Spd content compared to PI251432 and Korla under salt stress (**Figure 3C**). A significant rise in Na^+ content was caused by salt stress in the leaves of four materials, as demonstrated by the highest content in Korla, the second highest content in PI251432, the third highest in Tr005, and the lowest in PI237292 (**Figure 4A**). Under normal conditions, Tr005 and PI251432 exhibited significantly higher K^+ content than PI237292 and Korla, and PI251432 had the highest K^+ content than other materials under salt stress (**Figure 4B**). Salt stress resulted in a significant K^+ to Na^+ ratio decline in four materials (**Figure 4C**). PI237292 or Korla maintained the highest or the lowest K^+ to Na^+ ratio than other materials under salt stress, respectively (**Figure 4C**).

Differentially Expressed Genes Affected by Salt Stress Among Four White Clover Genotypes

Supplementary Table 2 shows basic information about the transcriptome data, namely, samples, replicates, clean reads, clean bases, GC content, and % ≥ Q30. Transcriptome identified abundant genes in the four materials (PI237292, Tr005, PI251432, and Korla) in response to salt stress, and analyses of the GO, KEGG, and KOG of these identified genes involved in gene function and metabolic processes are depicted in **Supplementary Figures 3–5**. The heat map of DEGs demonstrated different comparable groups, including PI237292 vs. PI251432, PI237292 vs. Korla, Tr005 vs. PI251432, and Tr005 vs. Korla, and had differential DEGs profiling (**Figure 5A**). The most abundant or least DEGs were identified in PI237292 vs. PI251432 or Tr005 vs. Korla, respectively (**Figure 5B**). The Venn diagram of DEGs showed total numbers of common and differential DEGs in four comparable groups (**Figure 5C**).

For DEGs involved in PAs metabolism, four DEGs (*ADC*, *NCA*, *SAMDC*, and *SPDS2*) were significantly upregulated, and two DEGs (*PAO2* and *PAO4*) were significantly downregulated in the PI237292 vs. PI251432 (**Figure 6A**). *SPDS2*, *PAO2*, and *PAO5* were upregulated, but *SPMS* was downregulated in the PI237292 vs. Korla (**Figure 6A**). In the Tr005 vs. PI251432, two DEGs (*SAMDC* and *PAT*) were upregulated, and two (*PAO2* and *PAO4*) were downregulated, and *SPMS* or *PAO2* was downregulated or upregulated in the Tr005 vs. Korla, respectively (**Figure 6B**). For DEGs involved in Na^+ and K^+ transportation, three DEGs (*NCLX*, *KEA2*, and *BTB/POZ*) or two DEGs (*NHX2* and *BASS5*) were upregulated or downregulated in PI237292 vs. PI251432, respectively (**Figure 7A**). PI237292 exhibited significantly higher

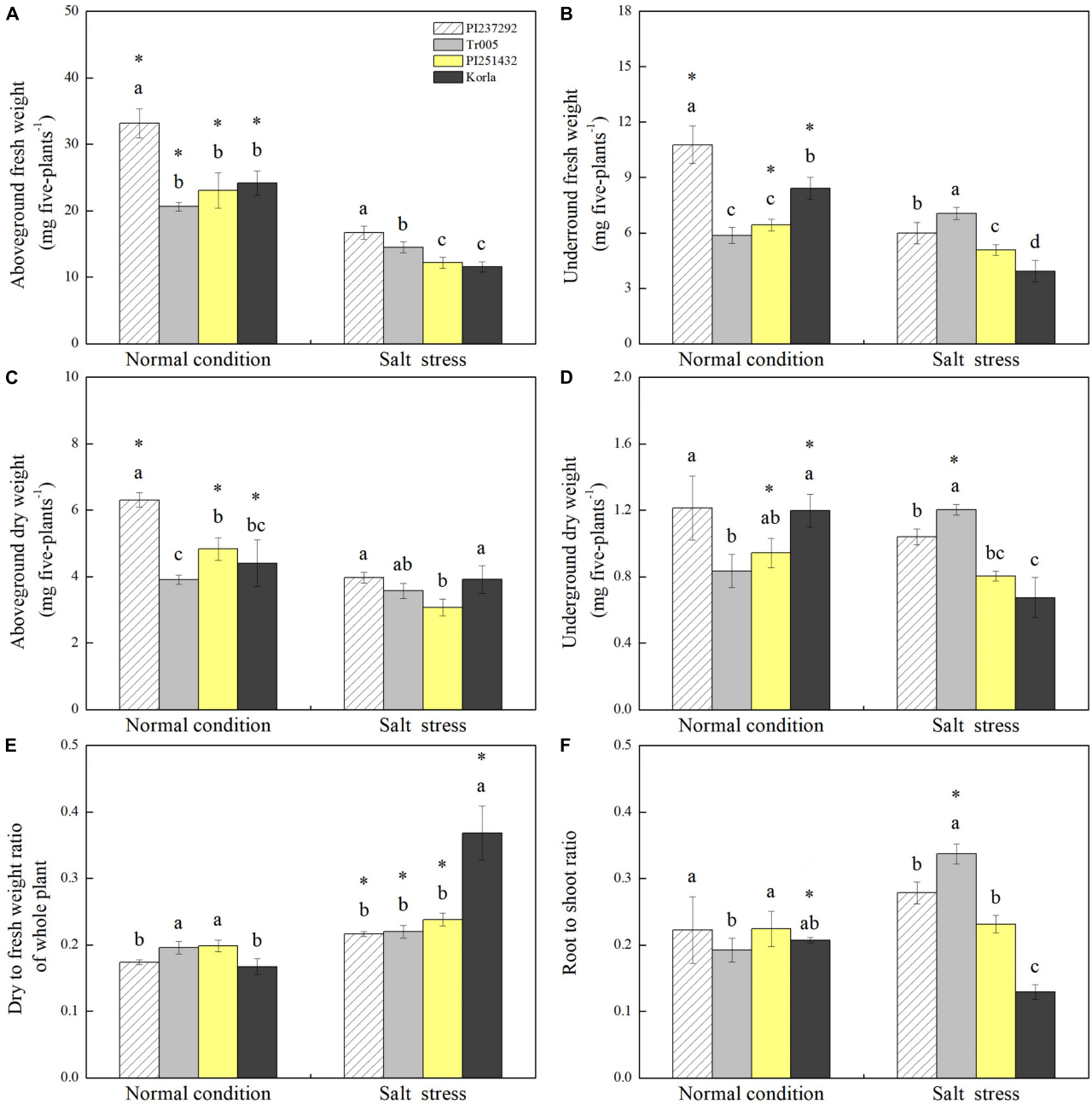

FIGURE 2 | Changes in **(A)** aboveground fresh weight, **(B)** underground fresh weight, **(C)** aboveground dry weight, **(D)** underground dry weight, **(E)** dry to fresh weight ratio, and **(F)** root to shoot ratio in the leaves of four white clover materials (PI237292, Tr005, PI251432, and Korla) under normal and salt stress conditions. Vertical bars indicate ± standard error (SE) of the mean (n = 4), and different letters above the column indicate significant differences ($P \leq 0.05$) under normal conditions or salt stress. The "*" represents the significant difference for a specific genotype (PI237292, Tr005, PI251432, or Korla) between normal conditions and salt stress.

NCLX and *BTB/POZ* as well as lower *TPK5* and *AKT5* under salt stress (**Figure 7A**). Significant upregulation in four DEGs (*NCLX*, *SKOR*, *POT2*, and *HAK25*) was identified in the Tr005 vs. PI251432, and another four DEGs (*POT8*, *AKT1*, *AKT5*, and *TPK3*) were downregulated (**Figure 7B**). Under salt stress, Tr005 significantly upregulated *SKOR*, *POT8*, and *POT11* while downregulating *NHX2* compared to Korla (**Figure 7B**).

DISCUSSION

Increasing soil salinization yearly at a rate of 10% accelerates the demand for salt-tolerant crop germplasms to maintain agricultural yield worldwide (Shrivastava and Kumar, 2015). For the evaluation of salt tolerance in white clover species, the study by Rogers et al. (1994) found that cv. Haifa and cv.

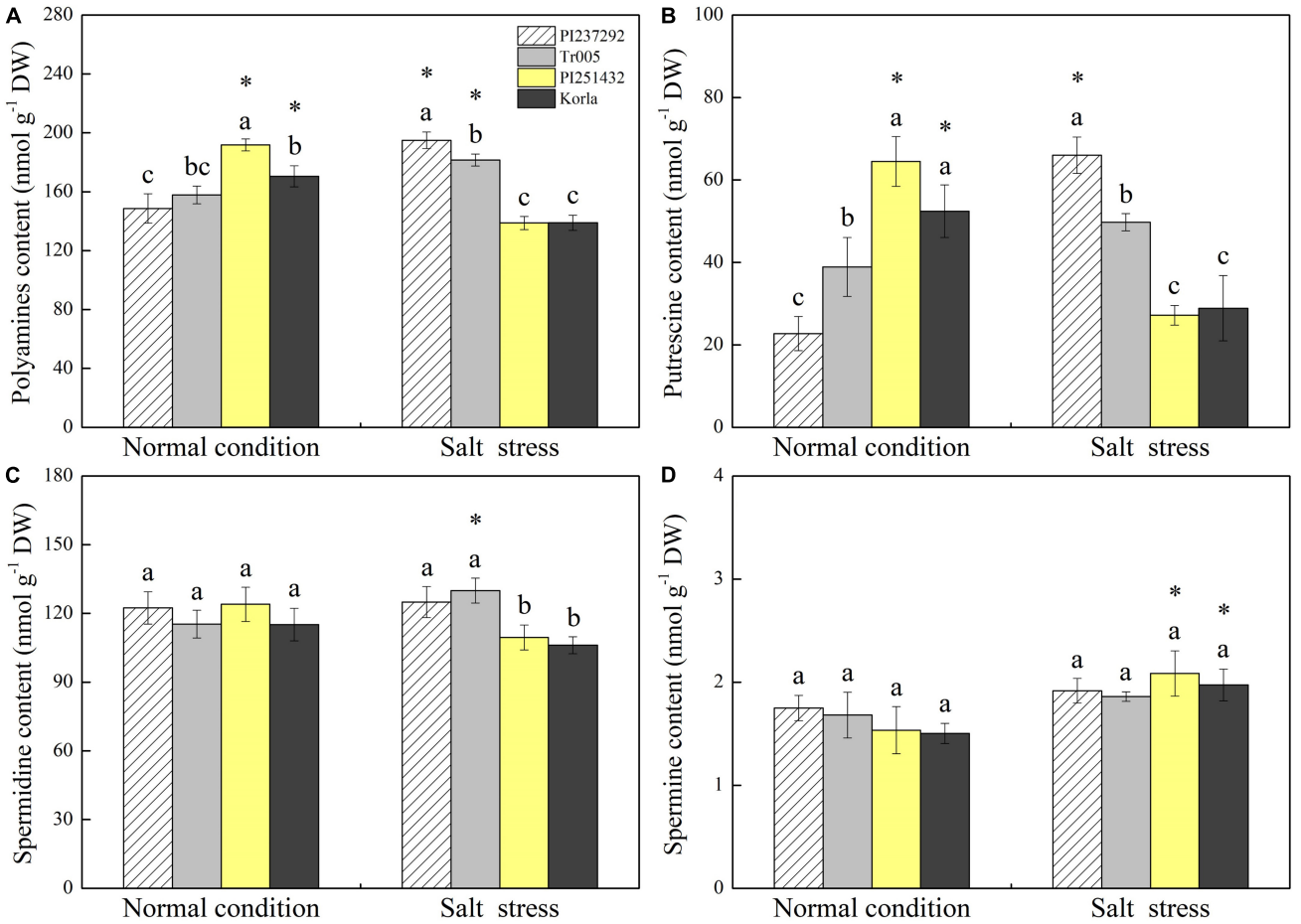

FIGURE 3 | Changes in **(A)** polyamine content, **(B)** putrescine content, **(C)** spermidine content, and **(D)** spermine content in the leaves of four white clover materials (PI237292, Tr005, PI251432, and Korla) under normal and salt stress conditions. Vertical bars indicate ± standard error (SE) of the mean (n = 4), and different letters above the column indicate significant differences ($P \leq 0.05$) under normal conditions or salt stress. The "*" represents the significant difference for a specific genotype (PI237292, Tr005, PI251432, or Korla) between normal conditions and salt stress.

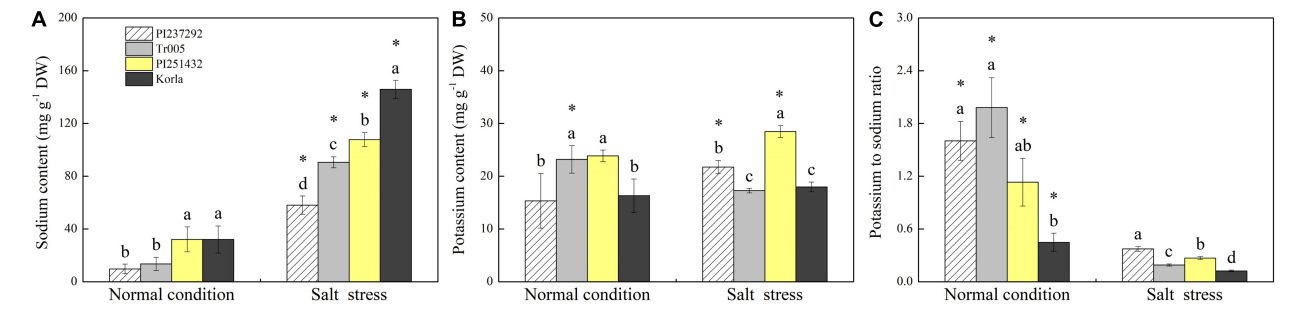

FIGURE 4 | Changes in **(A)** sodium content, **(B)** potassium content, and **(C)** potassium to sodium ratio in the leaves of four white clover materials (PI237292, Tr005, PI251432, and Korla) under normal and salt stress conditions. Vertical bars indicate ± standard error (SE) of the mean (n = 4), and different letters above the column indicate significant differences ($P \leq 0.05$) under normal conditions or salt stress. The "*" represents the significant difference for a specific genotype (PI237292, Tr005, PI251432, or Korla) between normal conditions and salt stress.

Irrigation exhibited superior salt tolerance to the other four cultivars, Aran, Kopu, Pitau, and Tamar. Wang et al. (2010) identified quantitative trait loci for salinity tolerance in the white clover population comprising 232 progenies. However, salt tolerance often varies depending on plant species and cultivars. The primary symptoms of salt damage include tip burning, leaf

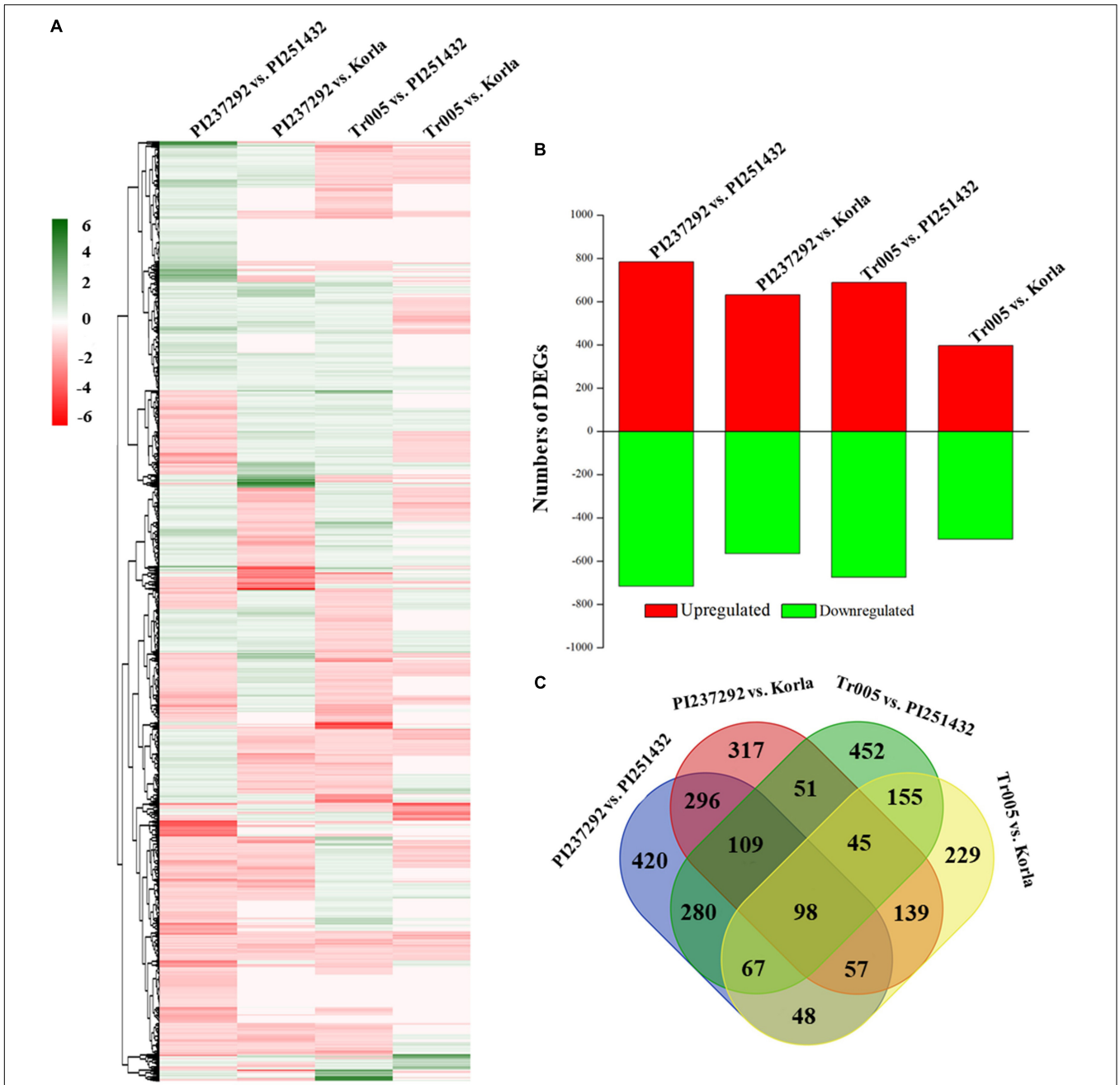

FIGURE 5 | Changes in the **(A)** heat map of differentially expressed genes (DEGs), **(B)** the total number of DEGs, and **(C)** the Venn diagram of DEGs of each comparable group based on the transcriptome analysis.

yellowing and rolling, plant wilting, and stunted plant growth (Acosta-Motos et al., 2017). EL, Chl, or Fv/Fm have been widely used to identify tolerance to environmental stress in various plant species, such as heat stress in creeping bentgrass (Li Z. et al., 2021), drought tolerance in common bean (*Phaseolus vulgaris*) genotypes (Munyasa, 2013), and salt tolerance in blue panicgrass (*Panicum antidotale*) (Javed et al., 2021), basil (Shirahmadi et al., 2022), and tomato (*Lycopersicon esculentum*) (Sivakumar et al., 2020). Recently, PIABS has been regarded as a potential indicator of stress tolerance since it synthetically reflects the maximum photochemical efficiency of PSII and is more sensitive than the Fv/Fm in response to diverse abiotic stresses (Dai et al., 2019; Liang et al., 2021; Shirahmadi et al., 2022). Our current study demonstrated physiological variations in 37 white clover materials under salt stress. PI237292 and Tr005 exhibited superior salt tolerance with high levels of RWC, Fv/Fm, and PIABS, as well as lower EL levels than other white clover materials. On the contrary, PI251432 and Korla were

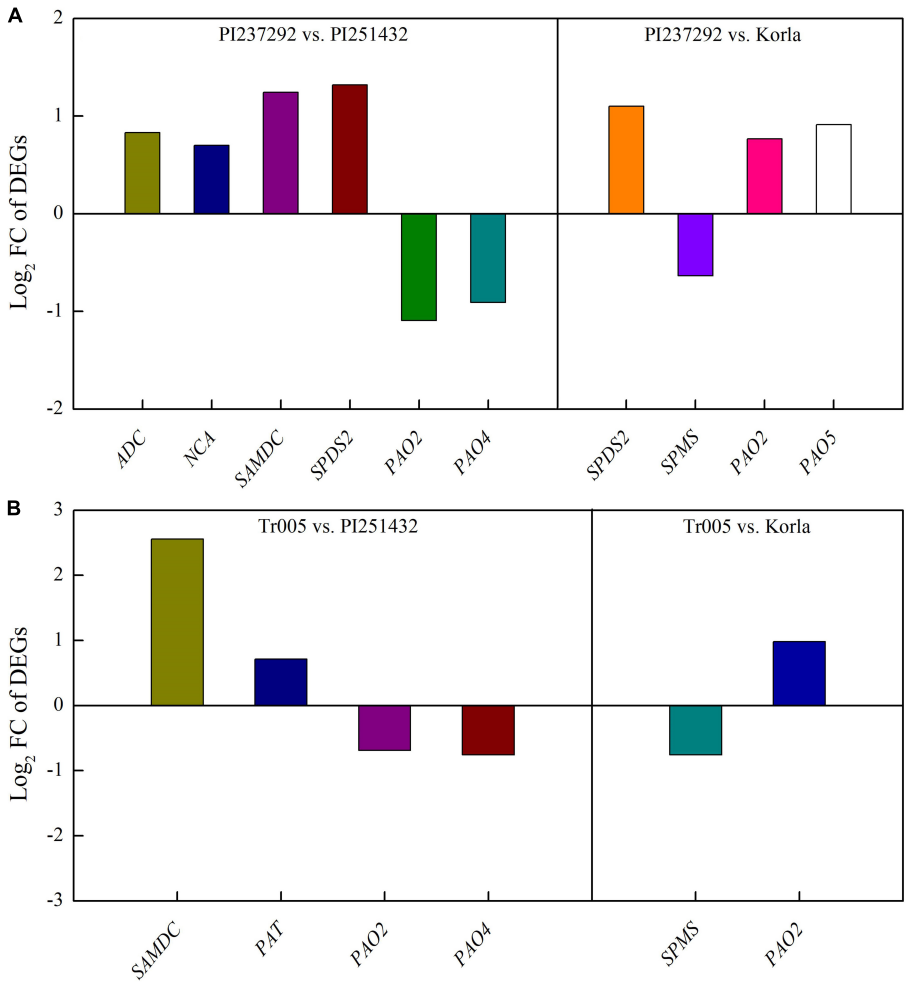

FIGURE 6 | Changes in key differentially expressed genes in **(A)** PI237292 vs. PI251432 and PI237292 vs. Korla and **(B)** Tr005 vs. PI251432 and Tr005 vs. Korla involved in polyamine metabolism in the leaves of white clover under salt stress. *ADC*, arginine decarboxylase; *NCA*, *N*-carbamoylputrescine amidase; *SAMDC*, *S*-adenosylmethionine decarboxylase proenzyme; *SPDS2*, spermidine synthase 2; *PAO2*, polyamine oxidase 2; *PAO4*, polyamine oxidase 4; *PAO5*, polyamine oxidase 5; SPMS, spermine synthase; *PAT*, polyamine transporter.

the most susceptible to salt stress. These salt-tolerant and salt-sensitive white clovers provide potential materials for breeding, cultivation, and utilization and further studies on the mechanism of salt tolerance in leguminous plants.

One of the harmful effects caused by salt stress is photosynthetic inhibition due to limited water supply, weakened gaseous interchange, and accelerated chloroplast degradation (Acosta-Motos et al., 2017). In general, the limitation of photosynthesis could be caused by the stomata factor, mainly owing to reduced stomatal conductance and limited intercellular CO_2 supply and non-stomatal factor as a result of chloroplast degradation and impaired photobiochemistry under stressful conditions (Pan et al., 2021). A previous study demonstrated that photosynthesis in sunflower (*H. annuus*) was not affected by non-stomatal limitation under mild salt stress (Steduto et al., 2000). The salt-caused decline in Pn was ascribed to the stomatal limitation in sorghum (Yan et al., 2012). Significant decreases in Pn, Gs, and Ci were observed in PI237292 and Tr005 in response to salt stress, but Chl contents were not significantly affected by salt stress in these two white clover materials, which implied that stomatal limitation dominated the main limiting factor to photosynthesis in the current study. However, salt stress caused significant decreases in Chl content, Pn, and Gs while significantly increasing Ci in PI251432 and Korla, indicating that PI251432 and Korla have already not effectively used intercellular CO_2 for chloroplast degradation and impaired photobiochemistry, as mainly affected by non-stomatal limitation. In addition, WUE is an essential indicator of energy conversion efficiency, reflecting homeostasis between Pn and Tr (Lavergne et al., 2019). Maintenance of better WUE could be attributed to better water utilization and growth associated with enhanced salt tolerance in plants (Lugassi et al., 2019; Oljira et al., 2020). Therefore, PI237292 and Tr005 exhibited significantly higher WUE than PI251432 and Korla under salt stress, which could be a critical reason for survival.

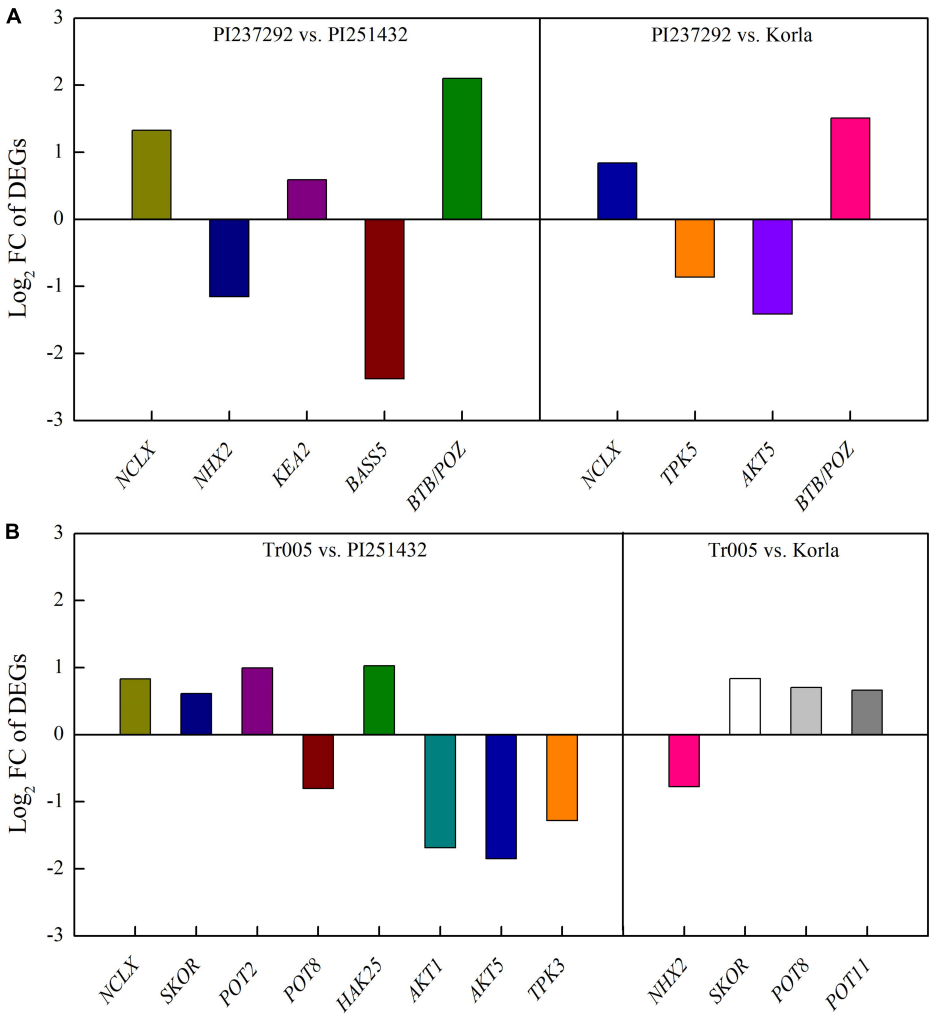

FIGURE 7 | Changes in key differentially expressed genes in **(A)** PI237292 vs. PI251432 and PI237292 vs. Korla and **(B)** Tr005 vs. PI251432 and Tr005 vs. Korla involved in sodium and potassium transport in the leaves of white clover under salt stress. *NCLX*, sodium/calcium exchanger; *NHX2*, sodium/hydrogen exchanger 2; *KEA2*, potassium efflux antiporter 2; *BASS5*, probable sodium/metabolite cotransporter; *BTB/POZ*, BTB/POZ domain-containing protein; *TPK3*, two-pore potassium channel 3; *TPK5*, two-pore potassium channel 5; *AKT1*, potassium channel 1; *AKT5*, potassium channel 5; *SKOR*, potassium channel SKOR; *POT2*, potassium transporter 2; *POT8*, potassium transporter 8; *POT11*, potassium transporter 11; *HAK25*, high affinity potassium transporter 25.

Salt stress inhibits plant photosynthetic rate, resulting in reduced biomass accumulation. Maintenance of yield stability is a major challenge for many mesophytes, including white clover, under salt stress conditions (Rogers et al., 1994; Guo et al., 2013; Javed et al., 2021). The previous study showed that salt stress significantly caused declines in chlorophyll content and biomass of white clover (Han et al., 2014). Salt-tolerant rice genotypes grew better than salt-sensitive plants under salt stress (Rasel et al., 2021). When plants suffer from salt stress, alteration in root to shoot ratio indicates allocation strategy of biomass. Increased root to shoot ratio is attributed to salt tolerance since roots are in close contact with salt ions and are responsible for water uptake and nutrient absorption (Maggio et al., 2007; da Silva et al., 2008). An earlier study showed that tomato cultivars Arka Samrat and Arka Pakshak, with stronger salt tolerance, had longer root length and higher root dry weight than salt-sensitive PKM-OP (Sivakumar et al., 2020). Rice genotypes exhibited higher salt tolerance, as evidenced by the alleviation of growth limitation of roots and shoots under salt stress (Rasel et al., 2021). Denser root systems caused by arbuscular mycorrhizal in two maize genotypes (salt-tolerant JD52 with a large root system and salt-sensitive FSY1 with a small root system) were propitious for the amelioration of salinity damage (Wang et al., 2021). This present study found that PI237292 and Tr005 grown in salt conditions maintained significantly higher underground dry weight and root to shoot ratio than PI251432 and Korla, indicating that the mediation of root growth and root to shoot ratio could confer better tolerance to salt stress. An increase in the root to shoot ratio regulated by paclobutrazol was also reported in barley cultivars associated with enhanced salt tolerance (Özmen et al., 2003). These findings further proved that enhanced root growth and allocation could be

beneficial for the improvement of salt tolerance associated with moisture and nutrition absorption.

Plants develop various adaptive strategies against salt stress, such as alterations in defense-associated compounds and PAs (Gupta et al., 2013). It has been well documented that regulation of PA accumulation and metabolism improved tolerance against various types of environmental stresses, including salt stress, by triggering many biochemical reactions in white clover and other plant species (Li et al., 2020b,d; Geng et al., 2021). In response to salt stress, total PAs and Put significantly accumulated in salt-tolerant PI237232 and Tr005 but significantly declined in salt-sensitive PI251432 and Korla compared to normal conditions. PI237232 and Tr005 also exhibited significantly higher endogenous Spd content than PI251432 and Korla, but no significant difference in Spm content was observed among the four materials under salt stress. These findings were consistent with the results from the transcriptome, as PI237232 and Tr005 significantly upregulated genes encoding Put and Spd biosynthesis (*NCA*, *ADC*, *SAMDC*, and *SPDS2*) and PAs transport (*PAT*) but downregulated Spm biosynthesis-related gene *SPMS* relative to PI251432 and Korla. It has been reported that transgenic plants overexpressing *SAMDC*, *ADC*, and *SPDS* improved salt tolerance in different plant species by increasing endogenous PA content (He et al., 2008; Espasandin et al., 2018; Islam et al., 2020; Jia et al., 2021). NCA is an enzyme involved in the degradation of N-carbamoylputrescine into Put (Takahashi and Tong, 2015). Increased Put biosynthesis through inducing NCA accumulation could mitigate detrimental effects of oxidative damage (Wang et al., 2022). PAT is responsible for PA transport (Fujita et al., 2012; Mulangi et al., 2012). Although PAT was involved in modulating heat tolerance in *Arabidopsis* by enhancing mRNA stability (Shen et al., 2016), its role in regulating salt tolerance remains unclear and requires further investigation in plants. However, expression levels of PAs degradation-related genes (*PAO2*, *PAO4*, and *PAO5*) differed between PI237292/Tr005 vs. PI251432 and PI237292/Tr005 vs. Korla in response to salt stress. The current findings highlight the significant roles of endogenous Put and Spd as key adaptive regulators in white clover suffering from salt stress.

The PAs were also involved in the regulation of Na^+ homeostasis, contributing to enhanced salt tolerance in plants. For example, PAs mitigated salt-caused damage owing to their biological functions in improving the K^+/Na^+ ratio and Na^+ compartmentalization in creeping bentgrass (Geng et al., 2021). A previous study also found that causative variation in the Na^+/K^+ ratio had a dominant position on salt tolerance in 369 tomato accessions (Wang Z. et al., 2020). Significant variations in Na^+/K^+ content and ratio were observed in six wheat (*Triticum aestivum*) genotypes (Iqra et al., 2020). An increase in the K^+/Na^+ ratio through exogenous application of *Azospirillum brasilense* or silicon contributing to enhanced salt tolerance has been reported in the white clover (Guo et al., 2013; Khalid et al., 2017). Our current findings demonstrated that salt-tolerant PI237292 maintained a significantly higher K^+/Na^+ ratio than salt-tolerant Tr005 and salt-sensitive PI251432 and Korla in response to salt stress; however, a significantly higher K^+/Na^+ ratio was identified in salt-sensitive PI251432 than in salt-tolerant Tr005 and salt-sensitive Korla, which indicated that salt tolerance in white clover genotypes not only depended on K^+/Na^+ ratio but also involved other mechanisms.

Transcriptional profiling identified many DEGs related to Na^+ transport and compartmentalization. Among these DEGs, the BTB/POZ domain-containing protein family has diverse functions of stress-defensive protection, namely, transcriptional regulation, ion transportation, and protein degradation (Tazuke et al., 2015; Li et al., 2018; Zhang et al., 2021). Transgenic *Arabidopsis* overexpressing a novel BTB domain-containing protein gene *AtSIBP1* enhanced tolerance to salt stress (Wan et al., 2019). *NCLX* encoding Na^+/Ca^{2+} exchanger protein plays an important role in Ca^{2+} homeostasis in plants under stress conditions (Singh et al., 2015). Higher salt tolerance in the PI237292 could be associated with the maintenance of Na^+ and Ca^+ homeostasis through the activation of *NCLX* and *BTB/POZ* under salt stress. The NHXs family is recognized as Na^+/H^+ exchangers to sequestrate cytoplasmic Na^+ into the vacuole, which is a critical regulatory pathway for plants to decrease Na^+ concentration in the cytosol (Long et al., 2020). Enhanced Na^+ compartmentalization by upregulating *NHXs* was related to higher salt tolerance in plants (Geng et al., 2020; Geng et al., 2021). Our previous study found that γ-aminobutyric acid improved salt tolerance of creeping bentgrass by decreasing Na^+ accumulation in the leaves along with significant inhibition of *AsNHX1*, *AsNHX2*, *AsNHX4*, and *AsNHX6* expression (Li et al., 2020c). Similar findings were presented in our present results. The PI237232 and the Tr005 accumulated significantly lower Na^+ content and *NHX2* expression level than the PI251432 and Korla under salt stress. The "the more Na^+ accumulation, the higher *NHX2* expression level in cells" could be an important adaptive response when plants suffer from salt stress since the transportation of Na^+ from the cytosol to the vacuole is an effective approach to decreasing Na^+ toxicity to plant cells. It has been proved that Na^+ accumulation in vacuoles could act as a cheap strategy for osmotic adjustment in plants under high salinity stress (Glenn and Brown, 1998; Wang et al., 2004). *BASS* serves as a Na^+/metabolite cotransporter, which could be significantly caused by salt stress (Huang et al., 2018; Şahin-Çevik et al., 2020). However, there is only limited information available about the function and regulatory mechanism of salt tolerance in plants.

Many DEGs involved in K^+ homeostasis were identified in four white clover genotypes under salt stress, including *KEA2*, *HAK25*, *SKOR*, *POT2/8/11*, *TPK3/5*, and *AKT1/5*. The KEAs family regulates intracellular K^+ homeostasis for ameliorating salt toxicity in plants. It has been reported that the inhibition of *GhKEA4* and *GhKEA12* expression led to salt sensitivity in cotton (*Gossypium*) plants (Li Y. et al., 2021). *Arabidopsis KEA2* overexpression conferred salt tolerance in yeast (*Saccharomyces cerevisiae*) cells (Aranda-Sicilia et al., 2012). HAKs serve as high-affinity K^+ transporters involved in K^+ uptake and K^+/Na^+ homeostasis in plants under salt stress (Chen et al., 2015; Shen et al., 2015). SKORs are involved in the uptake and transport of K^+ from roots to leaves, conferring salt tolerance in plants (Long-Tang et al., 2018). *POTs* encode K^+ transporter proteins

in plants (Shabala and Cuin, 2008). TPKs are vacuolar two-pore K^+ channel proteins and are responsible for the release of vacuolar K^+ to the cytosol, which plays a critical role in K^+ homeostasis (Gobert et al., 2007). An earlier study found that enhanced salt tolerance in transgenic tobacco with *PaTPK1* overexpression could be associated with the improvement in K^+ transfer from the vacuole to the cytosol, thereby maintaining cytosolic K^+ homeostasis (Wang et al., 2013). AKTs are known as inward-rectifying K^+ channels, and their expression affects K^+ uptake and nutrition (Hirsch et al., 1998; Ahmad et al., 2016). Salt stress significantly inhibited *OsAKT1* expression in the salt-tolerant rice variety Pokkali with less Na^+ accumulation but not in the salt-sensitive variety IR29 with extremely high Na^+ accumulation. However, there was no significant difference in K^+ content between these two varieties under salt stress (Golldack et al., 2003). The study of Ahmad et al. (2016) also found that either loss of *OsAKT1* function rice mutant or transgenic rice overexpressing the *OsAKT1* did not show the difference in salt tolerance as compared to wild type, but *OsAKT1* expression increased Na^+ accumulation and Na^+/K^+ ratio suggesting its role in Na^+ uptake under salt stress. In the current study, the K^+ homeostasis-related genes (*KEA2*, *HAK25*, *SKOR*, *POT2*/*8*/*11*, *TPK3*/*5*, and *AKT1*/*5*) were differentially expressed among four white clover genotypes. The K^+ level and K^+/Na^+ ratio were not completely consistent with the salt tolerance of four white clover genotypes. Therefore, the regulatory function and mechanism of these DEGs associated with salt tolerance in the white clover and other leguminous plants need to be investigated further.

CONCLUSION

Salt-tolerant and salt-sensitive white clover genotypes were identified among 37 genotypes based on the evaluation of physiological traits (EL, Chl, Fv/Fm, PIABS, and RWC), as PI237232 and Tr005 were the top two genotypes with the highest salt tolerance, and PI251432 and Korla were the most salt-sensitive genotypes compare to other materials. In response to salt stress, the salt-tolerant PI237232 and Tr005 not only maintained significantly lower EL but also showed significantly better photosynthetic performance, higher leaf RWC, underground dry weight, and root to shoot ratio than the salt-sensitive PI251432 and Korla. Increases in endogenous PAs, Put, and Spd contents could be key adaptive responses to salt stress in the PI237232 and the Tr005 through upregulating genes encoding Put and Spd biosynthesis (*NCA*, *ADC*, *SAMDC*, and *SPDS2*). For Na^+ and K^+ accumulation and transport, higher salt tolerance of the PI237292 could be associated with the maintenance of Na^+ and Ca^+ homeostasis through the activation of *NCLX* and *BTB/POZ*. The K^+ homeostasis-related genes (*KEA2*, *HAK25*, *SKOR*, *POT2*/*8*/*11*, *TPK3*/*5*, and *AKT1*/*5*) are differentially expressed among four genotypes under salt stress. However, the salt tolerance of four genotypes was not completely consistent with the higher K^+ level and K^+/Na^+ ratio. The regulatory function of these DEGs on salt tolerance in the white clover and other leguminous plants needs to be investigated further.

DATA AVAILABILITY STATEMENT

The datasets presented in this study can be found in online repositories. The names of the repository/repositories and accession number(s) can be found in the article/ **Supplementary Material**.

AUTHOR CONTRIBUTIONS

ZL, YP, and LZ conceived and designed the experiments. ZL and YP provided different chemical reagents and experimental materials. WG, MT, and ZL performed the experiment, analyzed the data, and wrote the manuscript. YL, YZ, LZ, and YP reviewed and improved the manuscript. All authors have read and approved the published version of the manuscript.

FUNDING

This research was supported by the Opening Fund of the Key Laboratory of Forage and Endemic Crop Biology, Ministry of Education (No. FECBOF2021008) and the Sichuan Forage Innovation Team Project of the Industrial System Construction of Modern Agriculture of China (sccxtd-2020-16).

SUPPLEMENTARY MATERIAL

The Supplementary Material for this article can be found online at: https://www.frontiersin.org/articles/10.3389/fpls.2022.896436/full#supplementary-material

REFERENCES

Abbasi, H., Jamil, M., Haq, A., Ali, S., Ahmad, R., and Malik, Z. (2016). Salt stress manifestation on plants, mechanism of salt tolerance and potassium role in alleviating it: a review. *Zemdirbyste Agric.* 103, 229–238.

Acosta-Motos, J. R., Ortuño, M. F., Bernal-Vicente, A., Diaz-Vivancos, P., Sanchez-Blanco, M. J., and Hernandez, J. A. (2017). Plant responses to salt stress: adaptive mechanisms. *Agronomy* 7:18.

Ahmad, I., Mian, A., and Maathuis, F. J. M. (2016). Overexpression of the rice *AKT1* potassium channel affects potassium nutrition and rice drought tolerance. *J. Exp. Bot.* 67, 2689–2698. doi: 10.1093/jxb/erw103

Amnon, D. (1949). Copper enzymes in isolated chloroplasts. Polyphenoloxidase in *Beta vulgaris*. *Plant Physiol.* 24, 1–15. doi: 10.1104/pp.24.1.1

Aranda-Sicilia, M. N., Cagnac, O., Chanroj, S., Sze, H., Rodríguez-Rosales, M. P., and Venema, K. (2012). Arabidopsis *KEA2*, a homolog of bacterial *KefC*, encodes a K^+/H^+ antiporter with a chloroplast transit peptide. *Biochim. Biophys. Acta (BBA) Biomembranes* 1818, 2362–2371. doi: 10.1016/j.bbamem.2012.04.011

Barrs, H., and Weatherley, P. (1962). A re-examination of the relative turgidity technique for estimating water deficits in leaves. *Aust. J. Biol. Sci.* 15, 413–428.

Blum, A., and Ebercon, A. (1981). Cell membrane stability as a measure of drought and heat tolerance in wheat. *Crop Sci.* 21, 43–47.

Chen, G., Hu, Q., Luo, L., Yang, T., Zhang, S., Hu, Y., et al. (2015). Rice potassium transporter OsHAK1 is essential for maintaining potassium-mediated growth and functions in salt tolerance over low and high potassium concentration ranges. *Plant Cell Environ.* 38, 2747–2765. doi: 10.1111/pce.12585

da Silva, E. C., Nogueira, R. J. M. C., de Araújo, F. P., de Melo, N. F., and de Azevedo Neto, A. D. (2008). Physiological responses to salt stress in young umbu plants. *Environ. Exp. Bot.* 63, 147–157. doi: 10.1016/j.envexpbot.2007.11.010

Dai, Y., Yuan, L., Zhang, S., Wang, J., Xie, S., Zhao, M., et al. (2019). Comprehensive evaluation for cold tolerance in wucai (*Brassica campestris* L.) by the performance index on an Absorption Basis (PIabs). *Agronomy* 9:61.

Das, P., Manna, I., Sil, P., Bandyopadhyay, M., and Biswas, A. K. (2021). Silicon augments salt tolerance through modulation of polyamine and GABA metabolism in two indica rice (*Oryza sativa* L.) cultivars. *Plant Physiol. Biochem.* 166, 41–52. doi: 10.1016/j.plaphy.2021.05.030

de Oliveira, D. F., Lopes, L. S., and Gomes-Filho, E. (2020). Metabolic changes associated with differential salt tolerance in sorghum genotypes. *Planta* 252:34. doi: 10.1007/s00425-020-03437-8

Duan, J., Li, J., Guo, S., and Kang, Y. (2008). Exogenous spermidine affects polyamine metabolism in salinity-stressed *Cucumis sativus* roots and enhances short-term salinity tolerance. *J. Plant Physiol.* 165, 1620–1635. doi: 10.1016/j.jplph.2007.11.006

Egan, M., Galvin, N., and Hennessy, D. (2018). Incorporating white clover (*Trifolium repens* L.) into perennial ryegrass (*Lolium perenne* L.) swards receiving varying levels of nitrogen fertilizer: effects on milk and herbage production. *J. Dairy Sci.* 101, 3412–3427. doi: 10.3168/jds.2017-13233

Espasandin, F. D., Calzadilla, P. I., Maiale, S. J., Ruiz, O. A., and Sansberro, P. A. (2018). Overexpression of the arginine decarboxylase gene improves tolerance to salt stress in *Lotus tenuis* plants. *J. Plant Growth Regul.* 37, 156–165.

Fujita, M., Fujita, Y., Iuchi, S., Yamada, K., Kobayashi, Y., Urano, K., et al. (2012). Natural variation in a polyamine transporter determines paraquat tolerance in *Arabidopsis*. *Proc. Natl. Acad. Sci. U.S.A.* 109, 6343–6347. doi: 10.1073/pnas.1121406109

Geng, W., Li, Z., Hassan, M. J., and Peng, Y. (2020). Chitosan regulates metabolic balance, polyamine accumulation, and Na^+ transport contributing to salt tolerance in creeping bentgrass. *BMC Plant Biol.* 20:506. doi: 10.1186/s12870-020-02720-w

Geng, W., Qiu, Y., Peng, Y., Zhang, Y., and Li, Z. (2021). Water and oxidative homeostasis, Na^+/K^+ transport, and stress-defensive proteins associated with spermine-induced salt tolerance in creeping bentgrass. *Environ. Exp. Bot.* 192:104659. doi: 10.1016/j.envexpbot.2021.104659

Glenn, E. P., and Brown, J. J. (1998). Effects of soil salt levels on the growth and water use efficiency of *Atriplex canescens* (Chenopodiaceae) varieties in drying soil. *Am. J. Bot.* 85, 10–16.

Gobert, A., Isayenkov, S., Voelker, C., Czempinski, K., and Maathuis, F. J. (2007). The two-pore channel *TPK1* gene encodes the vacuolar K^+ conductance and plays a role in K^+ homeostasis. *Proc. Natl. Acad. Sci. U.S.A.* 104, 10726–10731. doi: 10.1073/pnas.0702595104

Golldack, D., Quigley, F., Michalowski, C. B., Kamasani, U. R., and Bohnert, H. J. (2003). Salinity stress-tolerant and -sensitive rice (*Oryza sativa* L.) regulate AKT1-type potassium channel transcripts differently. *Plant Mol. Biol.* 51, 71–81. doi: 10.1023/a:1020763218045

Guan, C., Cui, X., Liu, H, Li, X., Li, M, and Zhang, Y (2020). Proline biosynthesis enzyme genes confer salt tolerance to switchgrass (*Panicum virgatum* L.) in cooperation with polyamines metabolism. *Front. Plant Sci.* 11:46. doi: 10.3389/fpls.2020.00046

Guo, Q., Meng, L., Mao, P., and Tian, X. (2013). Role of silicon in alleviating salt-induced toxicity in white clover. *Bull. Environ. Contamination Toxicol.* 91, 213–216. doi: 10.1007/s00128-013-1034-3

Gupta, K., Dey, A., and Gupta, B. (2013). Plant polyamines in abiotic stress responses. *Acta Physiol. Plant.* 35, 2015–2036. doi: 10.1007/s11738-013-1239-4

Han, Q.-Q., Lü, X.-P., Bai, J.-P., Qiao, Y., Paré, P. W., Wang, S.-M., et al. (2014). Beneficial soil bacterium *Bacillus subtilis* (GB03) augments salt tolerance of white clover. *Front. Plant Sci.* 5:525. doi: 10.3389/fpls.2014.00525

He, L., Ban, Y., Inoue, H., Matsuda, N., Liu, J., and Moriguchi, T. (2008). Enhancement of spermidine content and antioxidant capacity in transgenic pear shoots overexpressing apple spermidine synthase in response to salinity and hyperosmosis. *Phytochemistry* 69, 2133–2141. doi: 10.1016/j.phytochem.2008.05.015

Hirsch, R. E., Lewis, B. D., Spalding, E. P., and Sussman, M. R. (1998). A role for the AKT1 potassium channel in plant nutrition. *Science* 280, 918–921. doi: 10.1126/science.280.5365.918

Hoagland, D. R., and Arnon, D. I. (1950). *The Water Culture Method for Growing Plants Without Soil*. Berkeley, CA: California Agricultural Experiment Station Circular.

Huang, L., Kuang, L., Li, X., Wu, L., Wu, D., and Zhang, G. (2018). Metabolomic and transcriptomic analyses reveal the reasons why *Hordeum marinum* has higher salt tolerance than *Hordeum vulgare*. *Environ. Exp. Bot.* 156, 48–61. doi: 10.1016/j.envexpbot.2018.08.019

Huo, L., Guo, Z., Wang, P., Zhang, Z., Jia, X., Sun, Y., et al. (2020). *MdATG8i* functions positively in apple salt tolerance by maintaining photosynthetic ability and increasing the accumulation of arginine and polyamines. *Environ. Exp. Bot.* 172:103989. doi: 10.1016/j.envexpbot.2020.103989

Iqra, L., Rashid, M. S., Ali, Q., Latif, I., and Mailk, A. (2020). Evaluation for Na^+/K^+ ratio under salt stress condition in wheat. *Life Sci. J.* 17, 43–47.

Islam, M. A., Pang, J., Meng, F., Li, Y., Xu, N., Yang, C., et al. (2020). Putrescine, spermidine, and spermine play distinct roles in rice salt tolerance. *J. Integr. Agric.* 19, 643–655. doi: 10.1016/S2095-3119(19)62705-X

Javed, M., Ashraf, M., Iqbal, M., Farooq, M. A., Zafar, Z. U., and Athar, H-u-R (2021). Chlorophyll fluorescence, ion uptake, and osmoregulation are potential indicators for detecting ecotypic variation in salt tolerance of *Panicum antidotale* Retz. *Arid Land Res. Manage.* 36, 84–108.

Jia, T., Hou, J., Iqbal, M. Z., Zhang, Y., Cheng, B., Feng, H., et al. (2021). Overexpression of the white clover *TrSAMDC1* gene enhanced salt and drought resistance in *Arabidopsis thaliana*. *Plant Physiol. Biochem.* 165, 147–160. doi: 10.1016/j.plaphy.2021.05.018

Khalid, M., Bilal, M., Hassani, D., Iqbal, H. M., Wang, H., and Huang, D. (2017). Mitigation of salt stress in white clover (*Trifolium repens*) by *Azospirillum brasilense* and its inoculation effect. *Bot. Stud.* 58, 1–7. doi: 10.1186/s40529-016-0160-8

Lar, S. M., Seo, J., Jang, S., Zhang, H., Lee, A., Cao, F., et al. (2021). Genome-wide association study for detecting salt-tolerance loci and candidate genes in rice. *Agriculture* 11:1174.

Lavergne, A., Graven, H., De Kauwe, M. G., Keenan, T. F., Medlyn, B. E., and Prentice, I. C. (2019). Observed and modelled historical trends in the water-use efficiency of plants and ecosystems. *Glob. Chang. Biol.* 25, 2242–2257. doi: 10.1111/gcb.14634

Li, J., Su, X., Wang, Y., Yang, W., Pan, Y., Su, C., et al. (2018). Genome-wide identification and expression analysis of the BTB domain-containing protein gene family in tomato. *Genes Genomics* 40, 1–15. doi: 10.1007/s13258-017-0604-x

Li, W., Zhang, H., Zeng, Y., Xiang, L., Lei, Z., Huang, Q., et al. (2020a). A salt tolerance evaluation method for sunflower (*Helianthus annuus* L.) at the seed germination stage. *Sci. Rep.* 10:10626. doi: 10.1038/s41598-020-67210-3

Li, Y., Feng, Z., Wei, H., Cheng, S., Hao, P., Yu, S., et al. (2021). Silencing of *GhKEA4* and *GhKEA12* revealed their potential functions under salt and potassium stresses in upland cotton. *Front. Plant Sci.* 12:789775. doi: 10.3389/fpls.2021.789775

Li, Z., Cheng, B., Peng, Y., and Zhang, Y. (2020b). Adaptability to abiotic stress regulated by γ-aminobutyric acid in relation to alterations of endogenous polyamines and organic metabolites in creeping bentgrass. *Plant Physiol. Biochem.* 157, 185–194. doi: 10.1016/j.plaphy.2020.10.025

Li, Z., Hou, J., Zhang, Y., Zeng, W., Cheng, B., Hassan, M., et al. (2020d). Spermine regulates water balance associated with $Ca2^+$-dependent aquaporin (TrTIP2-1, TrTIP2-2 and TrPIP2-7) expression in plants under water stress. *Plant Cell Physiol.* 61, 1576–1589. doi: 10.1093/pcp/pcaa080

Li, Z., Cheng, B., Zeng, W., Zhang, X., and Peng, Y. (2020c). Proteomic and metabolomic profilings reveal crucial function of γ-aminobutyric acid (GABA) on regulating ionic, water, and metabolic homeostasis in creeping bentgrass under salt stress. *J. Proteome Res.* 19, 769–780. doi: 10.1021/acs.jproteome.9b00627

Li, Z., Tang, M., Hassan, M. J., Zhang, Y., Han, L., and Peng, Y. (2021). Adaptability to high temperature and stay-green genotypes associated with variations in antioxidant, chlorophyll metabolism, and γ-aminobutyric acid accumulation in

creeping bentgrass species. *Front. Plant Sci.* 12:750728. doi: 10.3389/fpls.2021.750728

Li, Z., Zhang, Y., Zhang, X., Merewitz, E., Peng, Y., Ma, X., et al. (2017). Metabolic pathways regulated by chitosan contributing to drought resistance in white clover. *J. Proteome Res.* 16, 3039–3052. doi: 10.1021/acs.jproteome.7b00334

Li, Z., Zhang, Y., Zhang, X., Peng, Y., Merewitz, E., Ma, X., et al. (2016). The alterations of endogenous polyamines and phytohormones induced by exogenous application of spermidine regulate antioxidant metabolism, metallothionein and relevant genes conferring drought tolerance in white clover. *Environ. Exp. Bot.* 124, 22–38.

Liang, L. L., Cao, Y. Q., Wang, D., Peng, Y., Zhang, Y., and Li, Z. (2021). Spermine alleviates heat-induced senescence in creeping bentgrass by regulating water and oxidative balance, photosynthesis, and heat shock proteins. *Biol. Plant.* 65, 184–192. doi: 10.32615/bp.2021.008

Long-Tang, H., Li-Na, Z., Li-Wei, G., Anne-Aliénor, V., Hervé, S., and Yi-Dong, Z. (2018). Constitutive expression of *CmSKOR*, an outward K^+ channel gene from melon, in *Arabidopsis thaliana* involved in saline tolerance. *Plant Sci.* 274, 492–502.

Long, L., Zhao, J., Guo, D., Ma, X., Xu, F., Yang, W., et al. (2020). Identification of *NHXs* in *Gossypium* species and the positive role of *GhNHX1* in salt tolerance. *BMC Plant Biol.* 20:147. doi: 10.1186/s12870-020-02345-z

Lugassi, N., Yadav, B. S., Egbaria, A., Wolf, D., Kelly, G., Neuhaus, E., et al. (2019). Expression of *Arabidopsis* hexokinase in tobacco guard cells increases water-use efficiency and confers tolerance to drought and salt stress. *Plants* 8:613. doi: 10.3390/plants8120613

Maggio, A., Raimondi, G., Martino, A., and De Pascale, S. (2007). Salt stress response in tomato beyond the salinity tolerance threshold. *Environ. Exp. Bot.* 59, 276–282. doi: 10.1016/j.envexpbot.2006.02.002

Mickelbart, M. V., Hasegawa, P. M., and Bailey-Serres, J. (2015). Genetic mechanisms of abiotic stress tolerance that translate to crop yield stability. *Nat. Rev. Genet.* 16, 237–251. doi: 10.1038/nrg3901

Miller-Fleming, L., Olin-Sandoval, V., Campbell, K., and Ralser, M. (2015). Remaining mysteries of molecular biology: the role of polyamines in the cell. *J. Mol. Biol.* 427, 3389–3406. doi: 10.1016/j.jmb.2015.06.020

Minocha, R., Majumdar, R., and Minocha, S. (2014). Polyamines and abiotic stress in plants: a complex relationship. *Front. Plant Sci.* 5:175. doi: 10.3389/fpls.2014.00175

Motos, J. R., Ortuño, M., Bernal-Vicente, A., Díaz-Vivancos, P., Sánchez-Blanco, M. J., and Hernandez, J. (2017). Plant responses to salt stress: adaptive mechanisms. *Agronomy* 7:18. doi: 10.20944/preprints201702.0083.v2

Mulangi, V., Phuntumart, V., Aouida, M., Ramotar, D., and Morris, P. (2012). Functional analysis of *OsPUT1*, a rice polyamine uptake transporter. *Planta* 235, 1–11. doi: 10.1007/s00425-011-1486-9

Munns, R. (2005). Genes and salt tolerance: bringing them together. *New Phytol.* 167, 645–663. doi: 10.1111/j.1469-8137.2005.01487.x

Munyasa, A. J. (2013). *Evaluation of Drought Tolerance Mechanisms in Mesoamerican dry Bean Genotypes*. Nairobi: University of Nairobi.

Oljira, A. M., Hussain, T., Waghmode, T. R., Zhao, H., Sun, H., Liu, X., et al. (2020). Trichoderma enhances net photosynthesis, water use efficiency, and growth of wheat (*Triticum aestivum* L.) under salt stress. *Microorganisms* 8:1565. doi: 10.3390/microorganisms8101565

Özmen, A. D., Özdemír, F., and Türkan, I. (2003). Effects of paclobutrazol on response of two barley cultivars to salt stress. *Biol. Plant.* 46, 263–268. doi: 10.1023/a:1022862929881

Pan, T., Liu, M., Kreslavski, V. D., Zharmukhamedov, S. K., Nie, C., Yu, M., et al. (2021). Non-stomatal limitation of photosynthesis by soil salinity. *Crit. Rev. Environ. Sci. Technol.* 51, 791–825.

Pottosin, I., Olivas-Aguirre, M., Dobrovinskaya, O., Zepeda-Jazo, I., and Shabala, S. (2021). Modulation of Ion transport across plant membranes by polyamines: understanding specific modes of action under stress. *Front. Plant Sci.* 11:616077. doi: 10.3389/fpls.2020.616077

Rasel, M., Tahjib-Ul-Arif, M., Hossain, M. A., Hassan, L., Farzana, S., and Brestic, M. (2021). Screening of salt-tolerant rice landraces by seedling stage phenotyping and dissecting biochemical determinants of tolerance mechanism. *J. Plant Growth Regul.* 40, 1853–1868. doi: 10.1007/s00344-020-10235-9

Rogers, M., Noble, C., Nicolas, M., and Halloran, G. (1994). Leaf, stolon and root growth of white clover (*Trifolium repens* L.) in response to irrigation with saline water. *Irrigation Sci.* 15, 183–194.

Rogers, M. E., Noble, C. L., Halloran, G. M., and Nicolas, M. E. (1997). Selecting for salt tolerance in white clover (*Trifolium repens*): chloride ion exclusion and its heritability. *New Phytol.* 135, 645–654.

Şahin-Çevik, M., Çevik, B., and Coşkan, A. (2020). Identification and expression analysis of salinity-induced genes in rangpur lime (*Citrus limonia*). *Horticult. Plant J.* 6, 267–276. doi: 10.1016/j.hpj.2020.07.005

Shabala, S., and Cuin, T. (2008). Potassium transport and plant salt tolerance. *Physiol. Plant.* 133, 651–669. doi: 10.1111/j.1399-3054.2007.01008.x

Shen, Y., Ruan, Q., Chai, H., Yuan, Y., Yang, W., Chen, J., et al. (2016). The *Arabidopsis* polyamine transporter LHR1/PUT3 modulates heat responsive gene expression by enhancing mRNA stability. *Plant J.* 88, 1006–1021. doi: 10.1111/tpj.13310

Shen, Y., Shen, L., Shen, Z., Jing, W., Ge, H., Zhao, J., et al. (2015). The potassium transporter OsHAK21 functions in the maintenance of ion homeostasis and tolerance to salt stress in rice. *Plant Cell Environ.* 38, 2766–2779. doi: 10.1111/pce.12586

Shirahmadi, S., Esna-Ashari, M., Aliniaeifard, S., and Abbas Akbari, G. (2022). Natural variation for salt tolerance among basil accessions from iran based on fluorescence transient and morphological and growth characteristics. *J. Agric. Sci. Technol.* 24, 183–198.

Shrivastava, P., and Kumar, R. (2015). Soil salinity: a serious environmental issue and plant growth promoting bacteria as one of the tools for its alleviation. *Saudi J. Biol. Sci.* 22, 123–131. doi: 10.1016/j.sjbs.2014.12.001

Singh, A. K., Kumar, R., Tripathi, A. K., Gupta, B. K., Pareek, A., and Singla-Pareek, S. L. (2015). Genome-wide investigation and expression analysis of Sodium/Calcium exchanger gene family in rice and *Arabidopsis*. *Rice* 8:21. doi: 10.1186/s12284-015-0054-5

Sivakumar, J., Prashanth, J. E. P., Rajesh, N., Reddy, S. M., and Pinjari, O. B. (2020). Principal component analysis approach for comprehensive screening of salt stress-tolerant tomato germplasm at the seedling stage. *Jo. Biosci.* 45:141. doi: 10.1007/s12038-020-00111-9

Steduto, P., Albrizio, R., Giorio, P., and Sorrentino, G. (2000). Gas-exchange response and stomatal and non-stomatal limitations to carbon assimilation of sunflower under salinity. *Environ. Exp. Bot.* 44, 243–255. doi: 10.1016/S0098-8472(00)00071-X

Takahashi, T., and Tong, W. (2015). "Regulation and diversity of polyamine biosynthesis in plants," in *Polyamines*, eds T. Kusano and H. Suzuki (Tokyo: Springer), 27–44.

Talaat, N. B. (2021). Polyamine and nitrogen metabolism regulation by melatonin and salicylic acid combined treatment as a repressor for salt toxicity in wheat (*Triticum aestivum* L.) plants. *Plant Growth Regul.* 95, 315–329.

Tazuke, A., Kinoshita, T., and Asayama, M. (2015). Expression of the BTB/POZ domain-containing protein At1g63850-like gene *CsFDI1* is enhanced by sugar starvation in cucumber fruit. *Acta Physiol. Plant.* 37:15. doi: 10.1007/s11738-014-1766-7

Thabet, S. G., Alomari, D. Z., and Alqudah, A. M. (2021). Exploring natural diversity reveals alleles to enhance antioxidant system in barley under salt stress. *Plant Physiol. Biochem.* 166, 789–798. doi: 10.1016/j.plaphy.2021.06.030

Theerawitaya, C., Tisarum, R., Samphumphuang, T., Takabe, T., and Cha-Um, S. (2020). Expression levels of the Na^+/K^+ transporter *OsHKT2*; 1 and vacuolar Na^+/H^+ exchanger *OsNHX1*, Na enrichment, maintaining the photosynthetic abilities and growth performances of indica rice seedlings under salt stress. *Physiol. Mol. Biol. Plants* 26, 513–523. doi: 10.1007/s12298-020-00769-3

Van Zelm, E., Zhang, Y., and Testerink, C. (2020). Salt tolerance mechanisms of plants. *Annu. Rev. Plant Biol.* 71, 403–433.

Wan, X., Peng, L., Xiong, J., Li, X., Wang, J., Li, X., et al. (2019). AtSIBP1, a novel BTB domain-containing protein, positively regulates salt signaling in *Arabidopsis thaliana*. *Plants* 8:573. doi: 10.3390/plants8120573

Wang, F., Deng, S., Ding, M., Sun, J., Wang, M., Zhu, H., et al. (2013). Overexpression of a poplar two-pore K^+ channel enhances salinity tolerance in tobacco cells. *Plant Cell Tissue Organ Cult.* 112, 19–31. doi: 10.1007/s11240-012-0207-9

Wang, H., An, T., Huang, D., Liu, R., Xu, B., Zhang, S., et al. (2021). Arbuscular mycorrhizal symbioses alleviating salt stress in maize is associated with a decline in root-to-leaf gradient of Na^+/K^+ ratio. *BMC Plant Biol.* 21:457. doi: 10.1186/s12870-021-03237-6

Wang, J., Drayton, M. C., George, J., Cogan, N. O. I., Baillie, R. C., Hand, M. L., et al. (2010). Identification of genetic factors influencing salt stress tolerance in white

clover (*Trifolium repens* L.) by QTL analysis. *Theor. Appl. Genet.* 120, 607–619. doi: 10.1007/s00122-009-1179-y

Wang, L., Yang, M., Dong, Y., Reiter, R. J., Xu, Y., Lin, X., et al. (2022). Melatonin confers enhanced polyamine metabolism and cell tolerance in *Vitis vinifera* against oxidative damage: quantitative proteomic evidence. *Postharv. Biol. Technol.* 184:111756.

Wang, S., Wan, C., Wang, Y., Chen, H., Zhou, Z., Fu, H., et al. (2004). The characteristics of Na^+, K^+ and free proline distribution in several drought-resistant plants of the Alxa Desert, China. *J. Arid Environ.* 56, 525–539.

Wang, Y., Wang, J., Zhao, X., Yang, S., Huang, L., Du, F., et al. (2020). Overexpression of the transcription factor gene *OsSTAP1* increases salt tolerance in rice. *Rice* 13, 1–12. doi: 10.1186/s12284-020-00405-4

Wang, Z., Hong, Y., Zhu, G., Li, Y., Niu, Q., Yao, J., et al. (2020). Loss of salt tolerance during tomato domestication conferred by variation in a Na^+/K^+ transporter. *EMBO J.* 39:e103256. doi: 10.15252/embj.2019103256

Wu, H., Zhang, X., Giraldo, J. P., and Shabala, S. (2018). It is not all about sodium: revealing tissue specificity and signalling roles of potassium in plant responses to salt stress. *Plant Soil* 431, 1–17. doi: 10.1007/s11104-018-3770-y

Yan, F., Wei, H., Li, W., Liu, Z., Tang, S., Chen, L., et al. (2020). Melatonin improves K^+ and Na^+ homeostasis in rice under salt stress by mediated nitric oxide. *Ecotoxicol. Environ. Saf.* 206:111358. doi: 10.1016/j.ecoenv.2020.111358

Yan, K., Chen, P., Shao, H., Zhao, S., Zhang, L., Xu, G., et al. (2012). Responses of photosynthesis and photosystem ii to higher temperature and salt stress in Sorghum. *J. Agron. Crop Sci.* 198, 218–225. doi: 10.1111/j.1439-037X.2011.00498.x

Ye, S., Huang, Z., Zhao, G., Zhai, R., Ye, J., Wu, M., et al. (2021). Differential physiological responses to salt stress between salt-sensitive and salt-tolerant japonica rice cultivars at the post-germination and seedling stages. *Plants* 10:2433. doi: 10.3390/plants10112433

Youssef, M. H. M., Raafat, A., El-Yazied, A. A., Selim, S., Azab, E., Khojah, E., et al. (2021). Exogenous application of alpha-lipoic acid mitigates salt-induced oxidative damage in sorghum plants through regulation growth, leaf pigments, ionic homeostasis, antioxidant enzymes, and expression of salt stress responsive genes. *Plants* 10:2519. doi: 10.3390/plants10112519

Yu, Z., Duan, X., Luo, L., Dai, S., Ding, Z., and Xia, G. (2020). How plant hormones mediate salt stress responses. *Trends Plant Sci.* 25, 1117–1130. doi: 10.1016/j.tplants.2020.06.008

Yuan, J., Wang, X., Zhao, Y., Khan, N. U., Zhao, Z., Zhang, Y., et al. (2020). Genetic basis and identification of candidate genes for salt tolerance in rice by GWAS. *Sci. Rep.* 10:9958. doi: 10.1038/s41598-020-66604-7

Zhang, C., Gao, H., Sun, Y., Jiang, L., He, S., Song, B., et al. (2021). The BTB/POZ domain protein GmBTB/POZ promotes the ubiquitination and degradation of the soybean AP2/ERF-like transcription factor GmAP2 to regulate the defense response to *Phytophthora sojae*. *J. Exp. Bot.* 72, 7891–7908. doi: 10.1093/jxb/erab363

Zhong, M., Wang, Y., Shu, S., Sun, J., and Guo, S. (2020). Ectopic expression of *CsTGase* enhances salt tolerance by regulating polyamine biosynthesis, antioxidant activities and $Na+^+/K^+$ homeostasis in transgenic tobacco. *Plant Sci.* 296:110492. doi: 10.1016/j.plantsci.2020.110492

Conflict of Interest: The authors declare that the research was conducted in the absence of any commercial or financial relationships that could be construed as a potential conflict of interest.

Publisher's Note: All claims expressed in this article are solely those of the authors and do not necessarily represent those of their affiliated organizations, or those of the publisher, the editors and the reviewers. Any product that may be evaluated in this article, or claim that may be made by its manufacturer, is not guaranteed or endorsed by the publisher.

frontiers | Frontiers in Plant Science

ORIGINAL RESEARCH
published: 02 June 2022
doi: 10.3389/fpls.2022.917354

Growth-Defense Trade-Offs Induced by Long-term Overgrazing Could Act as a Stress Memory

Kairi Qu[1], *Yunxiang Cheng*[1], *Kairu Gao*[1], *Weibo Ren*[1]*, *Ellen L. Fry*[2], *Jingjing Yin*[1] and *Yaling Liu*[3]

[1] School of Ecology and Environment, Inner Mongolia University, Hohhot, China, [2] Department of Biology, Edge Hill University, Ormskirk, United Kingdom, [3] Inner Mongolia Mongolian Grass Seed Industry Science and Technology Research Institute Co., Ltd., Hohhot, China

Long-term overgrazing (OG) is one of the key drivers of global grassland degradation with severe loss of productivity and ecosystem functions, which may result in stress memory such as smaller stature of grassland plants. However, how the OG-induced stress memory could be regulated by phytohormones is unknown. In this study, we investigated the changes of four phytohormones of cloned offspring of *Leymus chinensis* that were developed from no-grazing (NG) plants and OG plants with a grazing history of 30 years. The concentrations of auxin (IAA) and gibberellic acid (GA) in OG plant leaves were 45% and 20% lower than control, respectively. Meanwhile, the level of abscisic acid (ABA) in OG leaves nearly doubled compared with that in NG leaves. The situation was quite similar in roots. Unexpectedly, no significant changes in the jasmonic acid (JA) level were observed between OG and NG plants. The changes in gene expression patterns between OG and NG plants were also investigated by transcriptomic analysis. In total, 302 differentially expressed genes (DEGs) were identified between OG and NG plants, which were mainly classified into the functions of synthesis, receptor, and signal transduction processes of phytohormones. The expression of 24 key genes related to the biosynthesis and signal transduction of IAA and GA was downregulated in OG plants. Among them, *OASA1* and *AO1* (regulating the biosynthesis of IAA and ABA, respectively) were reduced significantly by 88 and 92%, respectively. In addition, the content of secondary metabolites related to plant defense such as flavonoids and phenols was also increased in leaves. Taken together, the decrease of positive plant growth-related hormones (IAA and GA) together with the increase of plant stress-related hormones or factors (ABA, flavonoids, and phenols) induced the growth-defense trade-offs for *L. chinensis* adaptation to long-term OG stress. The findings reported in this study shed new light on the mechanism of plant–animal interaction in the grassland ecosystem and provide a deeper insight into optimizing grazing management and sustainable utilization of grassland.

Keywords: phytohormone, stress memory, overgrazing, *Leymus chinensis*, growth-defense

OPEN ACCESS

Edited by:
Jin-Lin Zhang,
Lanzhou University, China

Reviewed by:
Yanjun Guo,
Southwest University, China
Xiangyang Hou,
Shanxi Agricultural University, China

***Correspondence:**
Weibo Ren
rppcaucau@163.com

Specialty section:
This article was submitted to Plant Abiotic Stress, a section of the journal Frontiers in Plant Science

Received: *11 April 2022*
Accepted: *26 April 2022*
Published: *02 June 2022*

Citation:
Qu K, Cheng Y, Gao K, Ren W, Fry EL, Yin J and Liu Y (2022) Growth-Defense Trade-Offs Induced by Long-term Overgrazing Could Act as a Stress Memory. Front. Plant Sci. 13:917354. doi: 10.3389/fpls.2022.917354

INTRODUCTION

Serving as a global reservoir of biodiversity and a provider of direct and indirect benefits to humans, grassland is one of the most important terrestrial ecosystems, covering 40% of the Earth's surface (Bardgett et al., 2021). However, it is subject to widespread degradation, with overgrazing (OG) as one of the key drivers, inducing desertification (Ibáñez et al., 2007). In the 2000s, approximately 90% of grassland had been degraded to some extent in China (Liu et al., 2019), which can be characterized by a decrease in grassland productivity. Recently, it has been suggested that long-term OG can lead to stunting of grassland plants over multiple generations, and this dwarfism could persist even after stress was removed (Li et al., 2015).

Leymus chinensis, a perennial rhizome plant, is the dominant and most important fodder species of the typical steppe. Reports show a consistent trait shift including dwarfed height, shorter and narrower leaves, smaller cluster width, and shallow root distribution under long-term OG (Wang, 2004). Stress memory, when plants store and retain information of previous stress cues and exhibit a much stronger and faster response to recurring events, is regulated by different mechanisms (Saqlain et al., 2021). Stress such as drought, cold, and insect invasion can induce stress memory which can help plants cope with these stresses (Rasmann et al., 2012; Walter et al., 2013; Mantoan et al., 2020). Many phytohormones such as ABA and JA were found to play a key role in the maintenance of stress memory (Avramova, 2019). Recent reports showed that long-term OG could also produce stress memory such as smaller plant size and leaves and increased secondary metabolites such as flavonoids (Ren et al., 2017; Liu et al., 2019a). However, stress memory can help plants defend against animal grazing, but how this grazing-induced stress memory works still unclear. We have found that there was stress memory induced by long-term OG in the offspring of *L. chinensis* (Ren et al., 2017), but the regulatory mechanism is still being explored. Phytohormones are characterized as messengers, which act to regulate different plant traits (Koepfli et al., 1938; Sharma et al., 2021). Recent studies have shown that abscisic acid (ABA), auxin (IAA), gibberellin (GA), cytokinin (CTK), jasmonic acid (JA), salicylic acid (SA), brassinosteroids (BR), and peptide hormones are involved in plant defense signaling pathways, which are likely to be key agents in response to OG (Bari and Jones, 2009; Urano et al., 2017; Tzipilevich and Benfey, 2021). Hormones not only respond to abiotic stress but also contribute greatly to mitigate biotic stress. For biotic stress, ABA and JA pathways synergistically mediate responses of defense-related genes to repeated herbivore stresses (Avramova, 2019). These changes may influence the responses of plants to recurring stress and form a memory to cope with the next threat. We expect that long-term OG also causes *L. chinensis* to develop stress memory which is expressed as dwarfed plants with smaller leaves, as a result of upregulation of specific phytohormones such as ABA or JA. Additionally, OG stress in the wild can lead to the activation of some genes in ABA and JA signaling pathways in *L. chinensis*, thus enhancing its defense ability through modulating metabolism and development such as stomatal closure and secondary metabolite content (Zhang et al., 2020).

Dwarf forms of long-term grazed *L. chinensis* may be an adaptation to long-term grazing by large herbivores (Li et al., 2015). At the transcriptome and proteome level, the expression of the genes involved in defense and immune responses, pathogenic resistance, and cell development was changed, which collectively inhibited the growth of clonal *L. chinensis* (Ren et al., 2018a). Furthermore, the proteins associated with dwarfism induced by OG were also altered, including upregulated ATPB_DIOEL and downregulated DNAK_GRATL, as well as proteins that interact with them, such as RPOB2_LEPTE, A0A023H9M8_9STRA, and RBL_AMOTI, (Ren et al., 2018b). Interestingly, it was found that clonal transgenerational effects in *L. chinensis* phenotypic traits heavily involve photosynthetic plasticity (Ren et al., 2017). Phytohormones such as IAA can regulate growth and development by controlling photosynthesis (Malkowski et al., 2020). Do phytohormones also play an important role in dwarf forms induced by long-term OG?

The aim of this research was to explore how phytohormones changed and regulated after plants experienced long-term OG. We questioned the following: (1) Which phytohormones related to growth and defense pathways play roles in the maintenance of stress memory induced by long-term OG? (2) How are these phytohormones regulated by key genes? (3) How does the downstream defense system of secondary metabolites respond? The findings will expand our knowledge of the mechanism of how plants respond to long-term OG.

MATERIALS AND METHODS

Field Site and Plant Material

Our experimental materials were taken from Baiyinxile Pasture in Xilingol League, Inner Mongolia which belongs to the Inner Mongolia Grassland Ecosystem Research Station (IMGERS, 43°38′N, 116°42′E, 1,211 m). The research site is in a northern temperate semiarid climate, with an average annual temperature of 0.3°C (lowest monthly average temperature of −21.6°C in January and the highest of 19.0°C in July) and annual precipitation of 270.78 mm. Precipitation is concentrated from May to September when the temperature and moisture are best for plant growth. Dominant vegetation species are *L. chinensis* and *Stipa grandis* (Ren et al., 2017).

We sampled from two plots: one grazing exclosure plot that has been fenced since 1983, while the outside of the exclosure has been subjected to long-term OG, with a stocking rate of three sheep units per hectare for more than 50 years. We collected rhizomes of *L. chinensis* from the exclosure plot (no grazing, NG) and outside of the exclosure plot (long-term OG) in September 2020. In each plot, six lines were set parallel to the fence, and a point was set every 20 m on each plotline to collect five samples of *L. chinensis* rhizomes. To avoid cross-area interference between the NG and OG plots, all lines were more than 30 m away from the fence. Then we brought them back for potted culture in the greenhouse.

Greenhouse Experiment

We replanted rhizome buds selected randomly from NG and OG individuals before the start of the *L. chinensis* growing season, in

May 2021. Different parent plants were cut to 2–3 cm lengths and each rhizome with a bud, and then the materials were planted into 18 cm depth pots after the pots were filled with nutritional soil. Each treatment (NG and OG) was replicated 30 times across a total of 60 pots (2 treatments × 30 replicates). The average temperature was 25°C during the day and 15°C at night. Samples were measured when the seedlings had grown for 6 weeks.

Morphological Traits

We measured the morphological traits of *L. chinensis* at harvest including height, leaf number, tiller number, leaf width, leaf length, leaf area, aboveground biomass, belowground biomass, and total biomass. The height was measured as the vertical height of the plant. Leaf morphological traits were measured using the second leaf from the top of the materials using a leaf area meter (LI-3000 Portable Area meter Produced by LI-COR Lincoln, NE, USA). For the biomass, we divided the individuals into aboveground and belowground, then cleaned and dried them at 65°C for 24 h, and weighed them to 0.01 accuracy.

Phytohormone Content

Phytohormone analyses were carried out according to Yilamujiang et al. (2016) with some modifications. Plants were separated into leaves and roots and then the tissue samples were ground to powder with liquid nitrogen. After grinding, the samples were put into a 2 ml centrifuge tube, followed by adding methanol-acetonitrile-aqueous solution (40:40:20, v/v), shaken, mixed for 2 min, and then extracted at 4°C for 12 h under light protection, and centrifuged at 14,000 r/min for 10 min. The supernatant was taken and dried with nitrogen. Methanol-aqueous solution (50:50, v/v) was centrifuged at 14,000 r/min for 10 min at constant volume, and the supernatant was taken for sample analysis.

The chromatographic conditions were as follows: mobile phase, liquid A was 0.04% formic acid-aqueous solution, liquid B was 0.04% formic acid-acetonitrile solution, column temperature was 45°C, the flow rate was 400 μl, min^{-1}, and sample volume was 4 μl. Chromatographic column, Waters, ACQUITY UPLCBEHC18 (2.1 mm × 100 mm, I.D. 1.7 μm); electrospray electric ion source (ESI), ion source temperature 500°C. The detection equipment was the Agilent 1290 HPLC-MS System.

Secondary Metabolite Content

The roots and leaves of the plant samples were separated prior to the quantification of secondary metabolites. The tissue samples were dried to a constant weight, crushed, and sifted through 40 mesh.

Tannins

Tannin content was determined based on the study by Kabir et al. (2015). Briefly, the volume of distilled water (ml) was 1:5-10 (approximately 0.1 g of tissue was weighed and 1 ml of distilled water was added). After full homogenization, the liquid was transferred to an EP tube, extracted in a water bath at 80°C for 30 min and centrifuged at 8,000 *g* at 25°C for 10 min. The supernatant was taken and tested. Notably, 0.5 ml of supernatant was mixed with 3 ml of 4% vanillin methanol solution and 1.5 ml of pure hydrochloric acid, and the absorbance was measured at 510 nm using a microplate reader (Multiskan GO 1510, Thermo). Tannin content was measured using the standard curve of the spectrometer.

Total Phenols

Approximately 0.1 g of each sample was weighed, 2.5 ml of 60% ethanol was added, and then shaken for 2 h at 60°C. The supernatant was centrifuged at 10,000 *g* for 10 min at 25°C, and the volume of the extract to be tested was fixed to 2.5 ml. Of note, 0.5 ml of supernatant was mixed with 5 ml of distilled water and 0.5 ml of Folin-Ciocalteu reagent (Al-Saeedi and Hossain, 2015). Notably, 2 ml of 20% Na_2CO_3 was then added, and the mixture was kept in water at 50°C for 30 min. The absorbance was measured at 750 nm using a microplate reader (Multiskan GO 1510, Thermo).

Flavonoids

Flavonoids were measured according to the aluminum nitrate colorimetric method (Xiang N. et al., 2021). Approximately 0.02 g was weighed, and 2 ml of the anhydrous ethanol was added. The sample was shaken for 2 h at 60°C and then centrifuged for 10 min at 25°C. Notably, 1 ml of supernatant was mixed with 1 ml of 70% methanol and 0.3 ml of 5% sodium nitrate, stored at room temperature for 6 min, and then 0.3 ml of aluminum nitrate was added to each tube. After 6 min, 3 ml of 4% sodium hydroxide was added to dissolve the mixed solution. The absorbance of the solution was measured at 510 nm using a microplate reader (Multiskan GO 1510, Thermo). The established standard curve was used to calculate the content of total flavonoids in the samples.

RNA Extraction

RNA was extracted from roots and leaves separately using the factory protocol (TIANGEN Company, DP419 total RNA Extraction Kit). RNA purity, concentration, and integrity were measured using spectrophotometers (NanoDrop, Qubit 2.0, and Agilent 2100).

Transcriptome Sequencing

The samples were from the RNA extraction. The eukaryotic mRNA with a polyA tail was enriched by magnetic beads with Oligo(dT), and the mRNA was interrupted by ultrasound. The first cDNA strand was synthesized in the m-Mulv reverse transcriptase system using fragment mRNA as a template and random oligonucleotide as a primer. Subsequently, the RNA strand was degraded by RNaseH, and the second cDNA strand was synthesized by dNTPs in the DNA Polymerase I system. The purified double-stranded cDNA was repaired at the end, an A tail was added, and sequencing joints were connected. Approximately 200 bp cDNA was screened with AMPure XP Beads for PCR amplification. The PCR products were purified again with AMPure XP Beads to obtain the library. Analysis was carried out using the EdgeR and DESeq2 software, including standardization of read counts and calculation of *P* and FDR values.

Quantitative Real-Time PCR Analysis

National Center for Biotechnology Information (https://www.ncbi.nlm.nih.gov) was used to design primer sequences. The corresponding real-time PCR primers (**Supplementary Table S1**) were designed using the sequence information obtained by sequencing, and then the extracted RNA was reverse-transcribed into cDNA, which was diluted to a certain multiple according to its concentration. A real-time PCR reaction was performed on an ABI real-time PCR machine (QuantStudio 3, Thermofisher), and each cDNA sample was repeated three times. ΔCT = CTtreatment-CTreference and $\Delta\Delta CT$= ΔCTgrazing-ΔCTnograzing relative to normal grazing were calculated for relative gene expression differences. After internal homogenization, the relative expression differences of target genes were expressed as a 2-$\Delta\Delta CT$ value, indicating the differential expression multiple of overgrazed *L. chinensis* relative to enclosure *L. chinensis*.

Statistical Analysis

We reported the results as means ± SE for all the above indicators. The SPSS statistical software version 26.0 (SPSS, Chicago, Illinois, USA) was used for ANOVA, significant difference ($P < 0.05$) detection, and graphical representations. Read count data obtained from the gene expression level analysis were analyzed using the edgeR and Deseq2 software, including the standardization of read counts and calculation of *P* and FDR values. Statistical test FDR value and differential multiple log2FC were used to screen differential genes. The default threshold was FDR < 0.05.

RESULTS

The Phenotype of Grazing Plants Showed Dwarfism

All measured morphological traits were reduced in OG plants compared with NG (**Figure 1**). Three traits were significantly lower (**Figure 1A**: plant height, **Figure 1B**: leaf number, and **Figure 1G**: aboveground biomass), with the height of the OG plants on average 50% lower than that of the NG plants ($P < 0.001$). Compared with the NG control, the leaf number of the OG plant decreased by approximately 30% ($P = 0.023$), while the aboveground biomass of OG plants was only half as much as the NG plants ($P = 0.018$). Besides, other trait as tiller number (**Figure 1C**), leaf length (**Figure 1D**), leaf width (**Figure 1E**), leaf area (**Figure 1F**), underground biomass (**Figure 1H**) and total biomass (**Figure 1I**) reduced with no significance.

Hormone Content Response to Grazing

The IAA concentration was significantly reduced in both roots and leaves in the OG plants compared with the NG (**Figure 2A**). GA was also lower in the leaves of *L. chinensis*, but there was no significant effect of grazing on GA in the roots (**Figure 2B**). Moreover, the concentration of IAA and GA in leaves and roots also decreased after plants experienced long-term OG (**Figures 2A,B**). Compared with NG plants, the content of IAA in OG plants reduced to 45% ($P < 0.001$) in leaves and 65% in the roots ($P = 0.001$). As to GA, there was a 20% reduction in OG leaves ($P = 0.03$). The situation of ABA was quite different. The content of ABA of OG plants increased 1.2-fold in roots and 1.1-fold in leaves ($P < 0.001$) (**Figure 2C**). The content of JA in OG plants shows slight decreases relative to that of NG plants, but with no significant difference (**Figure 2D**).

Analysis of Hormone Biosynthesis or Metabolism-Related Genes Under OG Stress Memory

There were 1,001 differentially expressed genes (DEGs) in leaves, where 499 were upregulated and 502 were downregulated (**Figure 3B**). There were 636 DEGs in the roots, 251 of which were upregulated and 385 were downregulated. In total, 1,646 DEGs were found between the leaf and root (**Figure 3C**), which were enriched in metabolism, environmental information processing, and genetic information processing based on gene ontology (GO) enrichment analysis (**Figure 3A**). In addition, the Kyoto Encyclopedia of Genes and Genomes (KEGG) analysis indicated that most DEGs were enriched in genetic information processing, metabolism, environmental information processing, and cellular processing (**Figure 3D**).

Among the DEGs, 302 genes in leaves were identified to be related to biosynthesis pathways and signal transduction of auxin, ABA, and gibberellin. Compared with NG plants, the expression level of nine genes related to IAA biosynthesis and signal transduction was downregulated in OG plants (**Figure 4A**). The expression level of four genes related to GA biosynthesis and signal transduction was also downregulated in OG plants (**Figure 4B**). As to ABA, the situation was quite different. The expression level of four genes related to ABA biosynthesis and signal transduction was upregulated in OG plants compared with NG plants (**Figure 4C**).

Among them, six genes were selected, and their expression levels were verified by RT-PCR testing (**Supplementary Figure S1**). The expression of two genes related to IAA and GA biosynthesis and signal transduction was significantly downregulated by OG, among which the expression of *OASA1* reduced by 88% ($P = 0.023$) and *GID* lowered approximately 671% compared to NG ($P = 0.017$). Meanwhile, there was a 92% increase in expression of the ABA-related gene *AO1* ($P < 0.05$), while *PP2C53* rose five times ($P < 0.05$).

Secondary Metabolite Concentration

To further explore the changes in defense-related secondary metabolites, we measured the content of tannins (**Figure 5A**), total phenols (**Figure 5B**), and flavonoids (**Figure 5C**) in leaves and roots. As to the leaves, both the content of total phenols and flavonoids in OG plants increased 110% ($P = 0.004$) and 15% ($P = 0.043$) compared with NG plants. The content of tannins in OG plants decreased slightly than that in NG plants ($P > 0.05$). As to roots, the content of total phenols in OG plants decreased by approximately 17% ($P = 0.026$) compared with NG plants. Moreover, the activity of peroxidase (POD) and superoxide

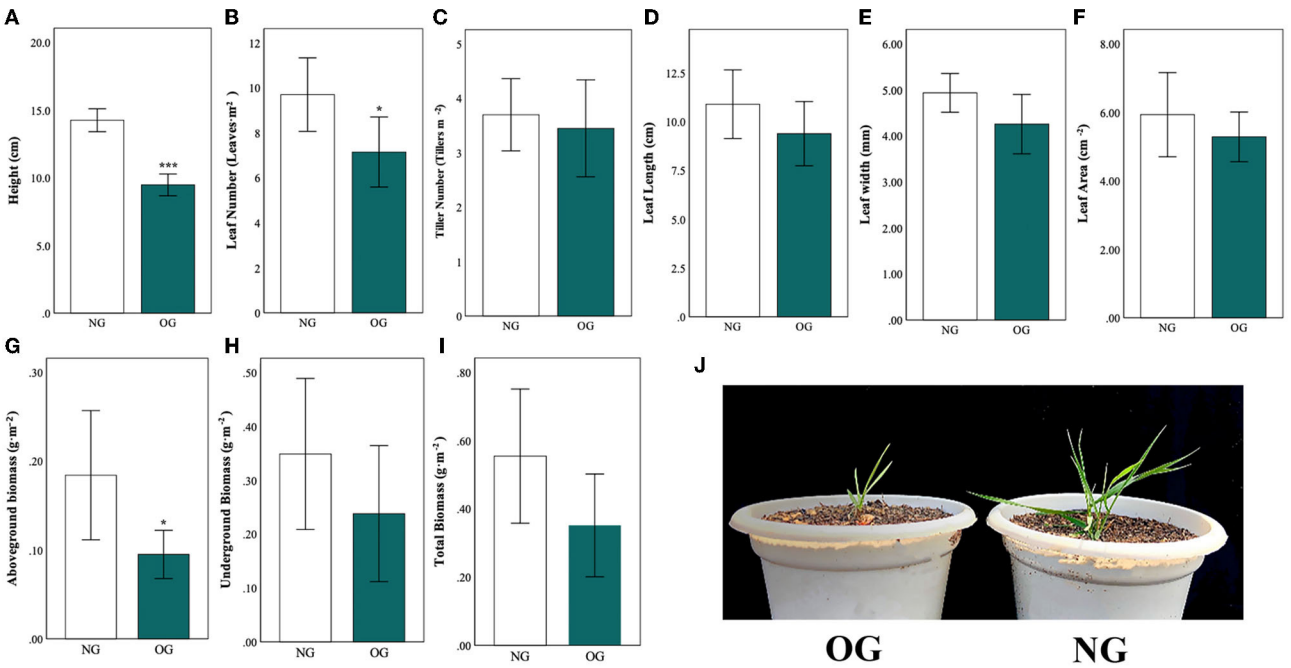

FIGURE 1 | Differences in plant morphological traits in *Leymus chinensis* in response to no-grazing (NG) and overgrazing (OG) conditions. **(A–I)** show different morphological traits, **(J)** comparison of early growth stage. Statistical significance is denoted by ***$P < 0.001$; **$P < 0.01$; *$P < 0.05$. Error bars denote standard error of the mean.

dismutase (SOD) in the roots was significantly reduced by 56% and 49%, respectively (**Supplementary Figure S2**).

DISCUSSION

Plants of *L. Chinensis* Tend to Be Small Due to Stress Memory

As one of the main natural enemies of plants, herbivores can damage plants by chewing, trampling, and saliva deposition (Chen et al., 2021). Under such biotic stress, plants develop multiple defense mechanisms to address these stresses, and many of them can be passed on to their offspring. In this study, we found that plants tend to be much smaller with decreased plant height and aboveground biomass (**Figure 1J**). This finding is quite similar to previous reports (Li et al., 2015). This can be explained by plant grazing avoidance mechanisms (Suzuki and Suzuki, 2011) induced by stress memory, in which morphological plasticity of clones of grassland plants caused a significant reduction in plant biomass which directly led to the decline of grassland productivity (Li et al., 2014), in order to avoid herbivores.

Stunting May Be Regulated by the Phytohormones IAA, GA, and ABA

In our study, ABA was found to play an important role in long-term grazing stress. In the meanwhile, plant growth-enhancing factors such as IAA and GA were also involved to cope with long-term OG stress. Contrary to our expectations, we did not find a significant effect of OG on JA concentration in root or leaf tissue. Previous reports indicated that JA can often be used as a signal to trigger herbivore-induced defense (Li et al., 2002; Koo and Howe, 2009; Qi et al., 2016; Hu et al., 2021). The content of JA in leaves was significantly higher in the extremely heavy grazing plot than that in the NG treatment under field conditions (Liu et al., 2019). One of the possible reasons is that plants may choose different phytohormone responses to OG with a different grazing history. As to short-term OG stress, JA is often used as a signal to activate the defense system against biotic stress (Liu et al., 2019). Some researchers have observed that the accumulation of JA isoleucine was one necessary condition for ABA synthesis under abiotic stress, so it can be postulated that JA regulation is upstream of ABA biosynthesis (Teng et al., 2014). In contrast, ABA can inhibit the expression of JA pathway-related genes, which suppress the resistance to pathogen infection mediated by JA (Xie et al., 2018). We considered that when exposed to long-term OG, plants tend to use ABA instead of JA as signals enhancing their tolerance. In total, the interaction of these hormones regulates the growth-defense trade-off to affect plant growth under grazing stress (Wang and Irving, 2011).

Phytohormones Are Regulated at the Gene Level

To explore how these key phytohormones are regulated after long-term OG stress, the gene expression pattern between OG and NG was investigated. DEGs in the leaves were nearly doubled than that in the roots. This can be explained by

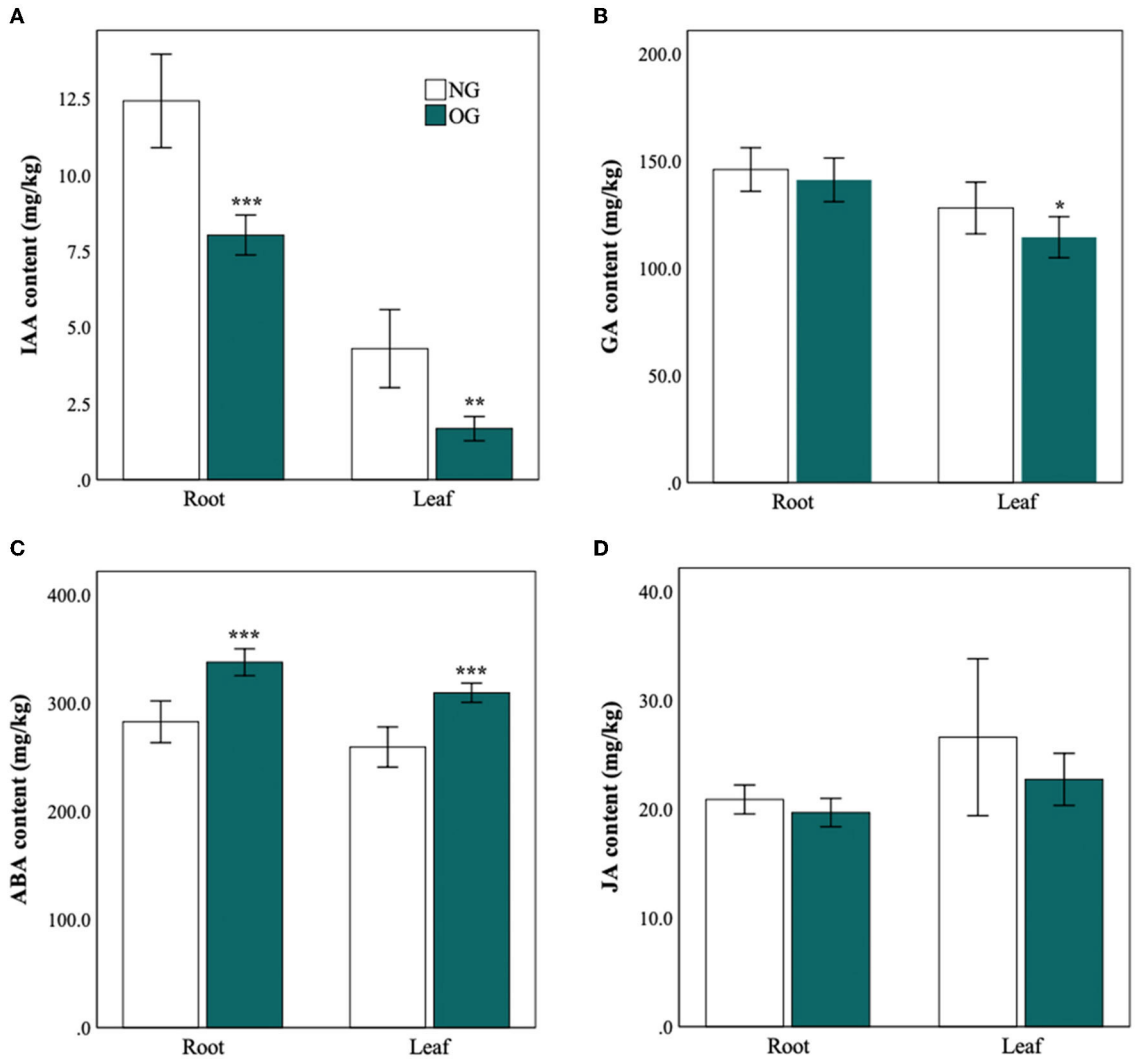

FIGURE 2 | Different hormone levels in roots and leaves of *L. chinensis* in response to NG and OG. **(A)** Auxin (IAA) concentration; **(B)** gibberellic acid (GA) concentration; **(C)** abscisic acid (ABA) concentration; and **(D)** jasmonic acid (JA) concentration. Statistical significance is denoted by ***$P < 0.001$; **$P < 0.01$; *$P < 0.05$. Error bars denote standard error of the mean.

the fact that the leaves were more sensitive to OG than roots. Then, we found genes involved in hormone synthesis, metabolism, and signal transduction in leaves of *L. chinensis*. The *YUC* family has been proposed as crucial genes that act in the common IAA biosynthetic pathway (Mashiguchi et al., 2011), and the anthranilate synthase (AS) gene encodes a key enzyme in the synthesis of tryptophan (Trp) (Tozawa, 2001). The expression levels of *YUC11*, *YUCCA4*, and *OASA1* were strongly downregulated (**Figure 4A**) which regulates auxin synthesis (Du et al., 2013). IAA plays an essential role in lateral organ initiation at the shoot apical meristem, patterning, and vascular development, maintaining stem cell fate at the root apical meristem, as well as promoting branching in the root (Wolters and Jurgens, 2009). This means that the content of IAA in the plant is restricted, which affects the growth of *L. chinensis*.

Similarly, several key genes that participated in the biosynthesis of GA including *GID1*, *GID4*, *GID8*, *GA20OX3,* and *GA20ox1B* were induced by OG stresses. *GID1* is a key gene of the GA receptor, and *G20ox* is a GA synthesis gene. GA is essential for determining plant height by regulating stem elongation (Zhang et al., 2016), so it is likely that GA is involved in the dwarfing of *L. chinensis*.

Additionally, genes such as *AO1*, *SDIR1*, *ABA2*, and *NCED5* related to ABA synthesis were significantly upregulated in OG plants. ABA helps plants respond to abiotic stress, especially in water-deficit responses (Vickers et al., 2009). In addition, ABA regulates the stomatal aperture by changing the volume of guard cells that control gas exchange (Chen et al., 2021). Our previous study found that stomatal conductance of overgrazed *L. chinensis* significantly decreased (Yin et al., 2020), which may be related to ABA content changes.

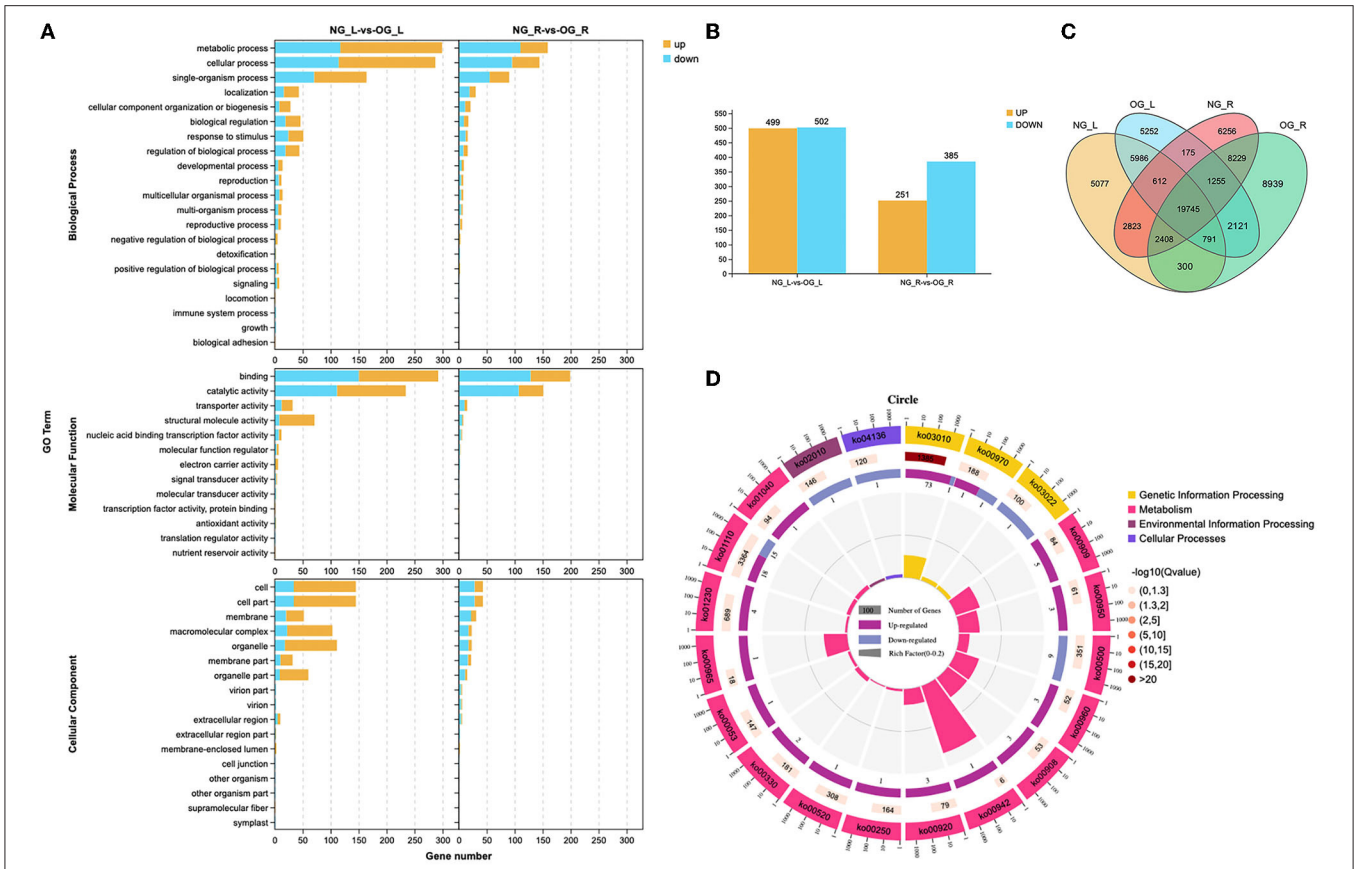

FIGURE 3 | Differences between the NG and OG plants at the transcriptome level. **(A)** Gene ontology (GO) enrichment maps of differentially expressed genes (DEGs). **(B)** Number of DEGs between NG and OG plants. **(C)** Venn diagram of all genes between the leaf and root. **(D)** Kyoto Encyclopedia of Genes and Genomes (KEGG) enrichment maps of DEGs. NG_L, leaf of no-grazing plants; NG_R, root of no-grazing plants; OG_L, leaf of overgrazing plants; OG_R, root of overgrazing plants.

The Secondary Metabolites of *L. Chinensis* Were Changed After Long-Term OG

Plants can protect themselves from biotic or abiotic stress through the synthesis of secondary metabolites. It has been revealed by phytochemical studies that the secondary metabolites contain alkaloids, terpenoids, flavonoids, and phenols (Mutuku et al., 2020). Under the wild condition, grazing can cause changes in the content of secondary metabolites (Liu et al., 2019b). The secondary metabolites, especially flavonoids, exist widely in plants and are involved in responses to biotic and abiotic stresses (Baozhu et al., 2022), which play the role of a defensive weapon. The change in hormone content may cause a difference in flavonoid synthesis (Nik and Durkin, 2018). For example, ABA has been used to induce the biosynthesis of secondary metabolites such as phenol, flavonoid, anthocyanin, and carotenoid production in *Dracocephalum moldavica L.* (Khaleghnezhad et al., 2019). Plants often enhanced their defense induced by animals or insects by the increase of some specific secondary metabolites such as alkaloids, flavanols, and phenols. Among them, many phenols were reported to inhibit herbivore growth and reproduction, even by direct toxicity (Huitu et al., 2014). Similarly, flavanols have digestibility-reducing effects in herbivores (Tohge et al., 2017), which is a relatively cheap defense due to its low biosynthetic costs (Scogings et al., 2021). Interestingly, in this research, GA content did not change significantly in roots, while the concentration of tannins and phenols declined. At the same time, the activity of POD and SOD in the roots was significantly reduced (**Supplementary Figure S1**), which may facilitate endophytic colonization by suppressing plant-produced reactive oxygen species (Trivedi et al., 2020). Successful colonization of fungus can improve the adaptive of grassland plant response to grazing stress by enhancing nutrition acquisition (Xu et al., 2018). Interestingly, Xie et al. (2018) also confirmed that ABA treatment inhibited the accumulation of ROS by inducing the expression of enzymes such as SOD.

The most obvious finding to emerge from this research is that the stress memory of plants induced by long-term OG may be regulated by the elevated level of ABA and activation of defense weapons such as phenolics and flavonoids, as well as the inhibition of the biosynthesis of IAA and GA and their reception and signal transduction process (**Figure 6**). Moreover, the root tends to maintain growth by lowering its defense with decreased secondary metabolites and enzymes. These changes

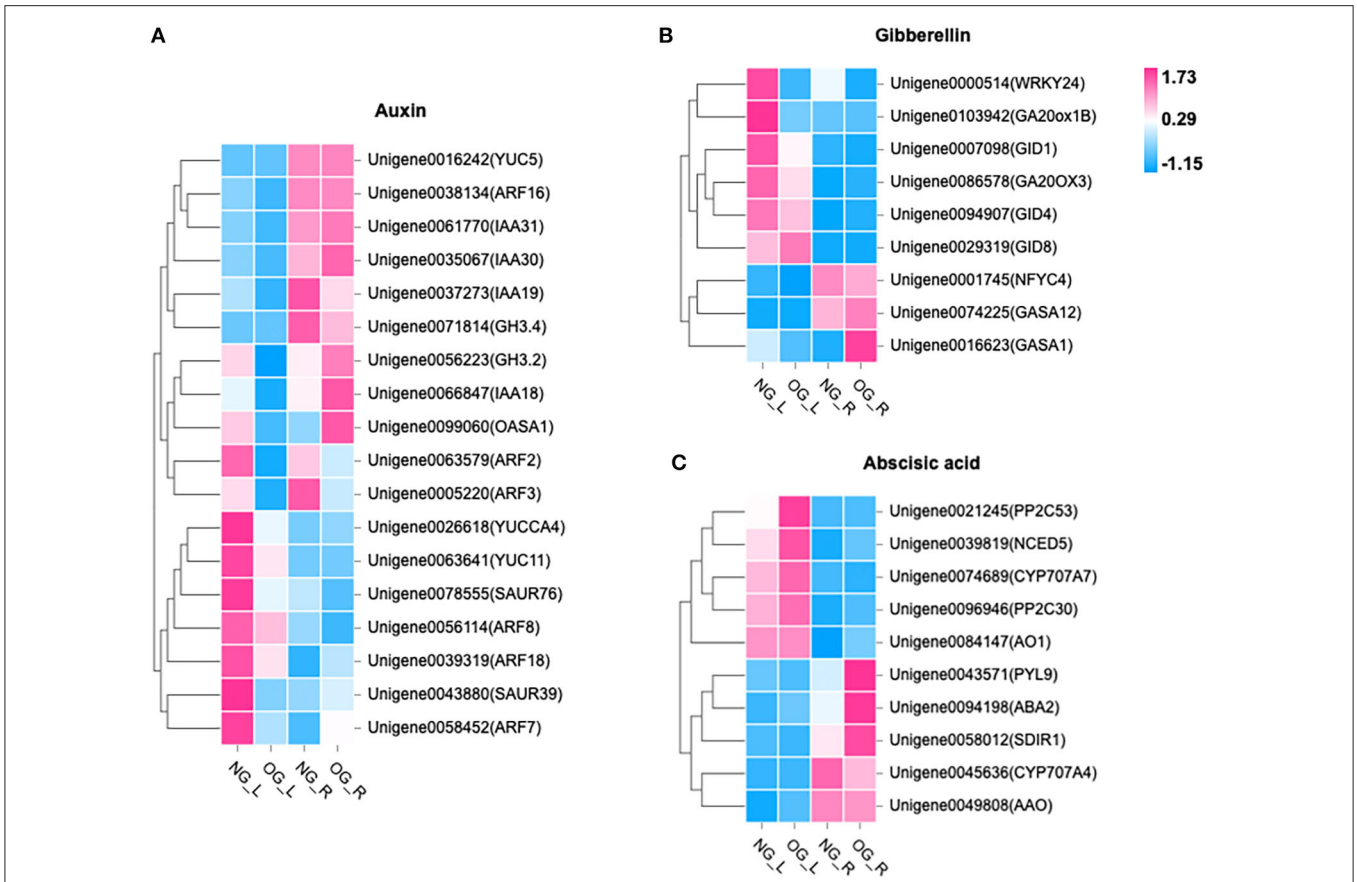

FIGURE 4 | Changes in the expression of genes in response to long-term OG stress. The heat map shows the relative transcript levels of selected biosynthetic, metabolic, and signaling genes for **(A)** IAA, **(B)** ABA, and **(C)** GA. NG_L, leaf of no-grazing; NG_R, root of no-grazing; OG_L, leaf of overgrazing; OG_R, root of overgrazing.

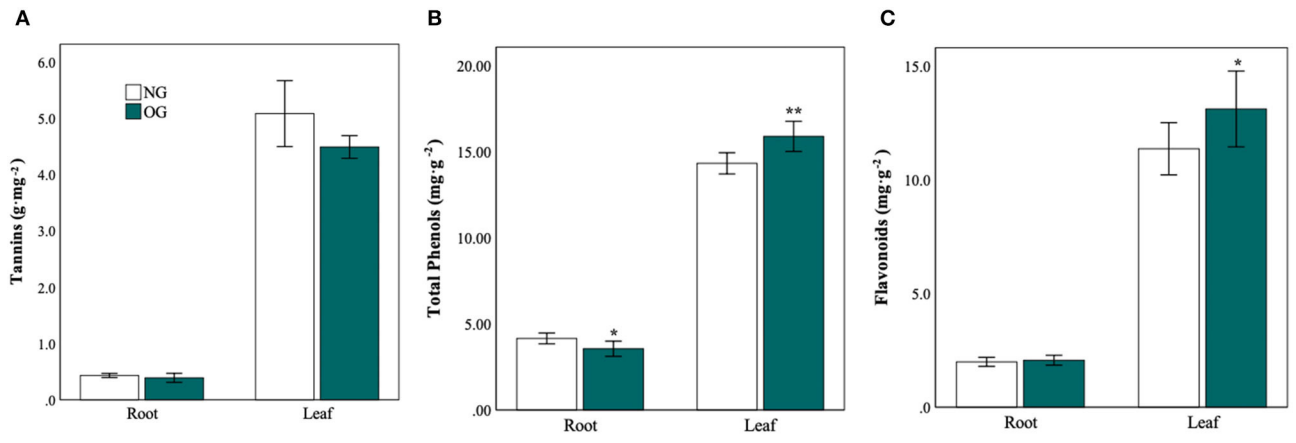

FIGURE 5 | Plant defense compounds in roots and leaves in response to a legacy of OG metabolism. **(A)** Tannins, **(B)** flavonoids, and **(C)** total phenols in roots and leaves in response to two conditions. Statistical significance is denoted by $^{***}P < 0.001$; $^{**}P < 0.01$; $^{*}P < 0.05$. Error bars denote the standard error of the mean.

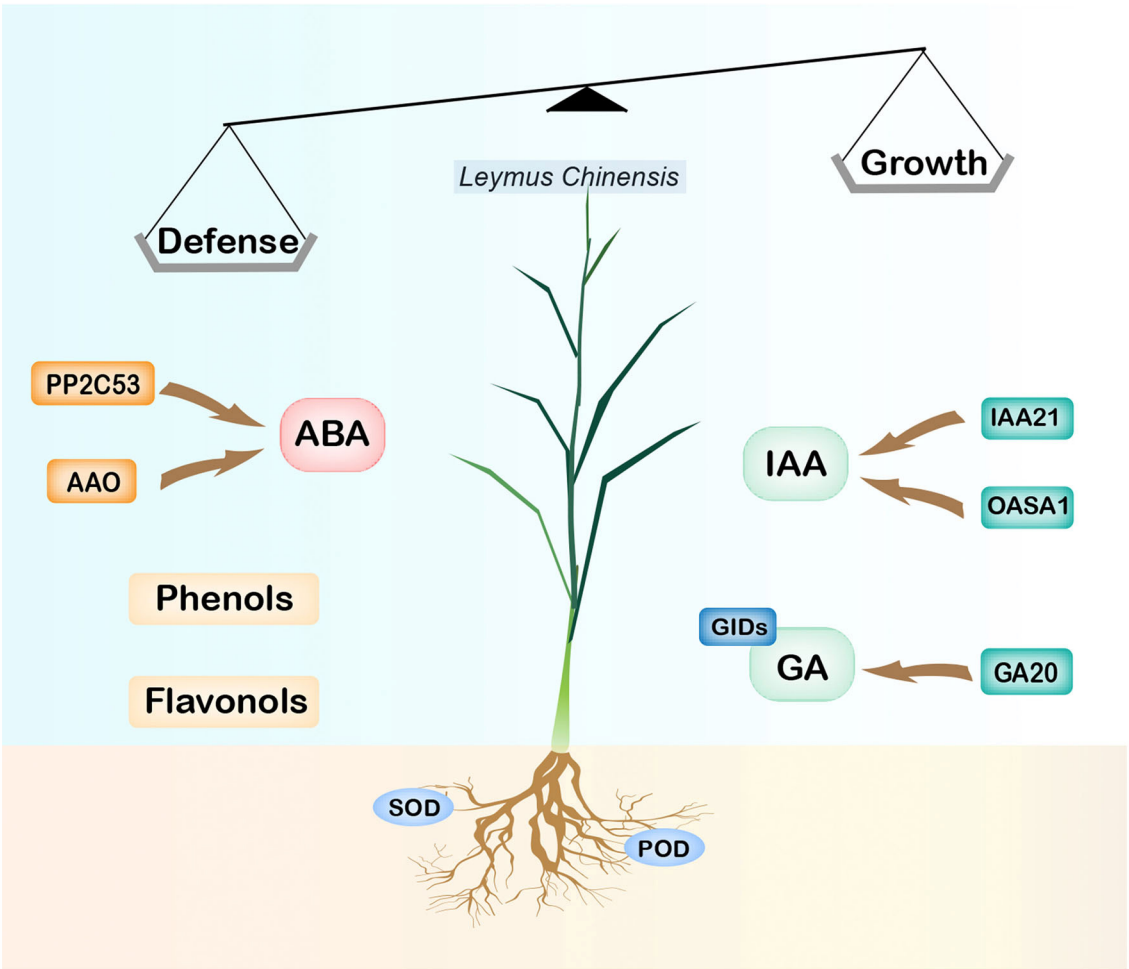

FIGURE 6 | A model for the mechanisms under long-term OG stresses. For the downregulation of synthetic genes OASAs, G20, and receptor protein genes GIDs, the contents of IAA and GA are reduced, thus limiting plant growth; the increase of the ABA level induced individual defense and further inhibited plant growth. The contents of flavonoids and phenols in leaves increased, while the activities of superoxide dismutase (SOD) and peroxidase (POD) in roots decreased.

in phytohormones were modulated by several key genes such as *YUCs*, *OASAs*, *G20s*, *AAO*, and *NCEDs* which were key players in the biosynthesis of ABA, IAA, and GA. These findings will expand our knowledge of how grassland plants regulate their phenotype by phytohormones after experiencing long-term OG. Several questions remain unanswered at present. Does the situation change under different development stages? How many generations can the grazing-induced stress memory pass down? Further investigation is needed for us to establish a greater degree of accuracy on this matter, which could also be conducted to determine the effectiveness of the recovery procedure and mechanism of grassland degeneration.

DATA AVAILABILITY STATEMENT

Our data is publicly available by providing a valid accession number BioProject ID: PRJNA830275.

AUTHOR CONTRIBUTIONS

WR communicated with all authors as corresponding author. KQ, WR, YC, and YL contributed to conception and design of the study. KQ, KG, and JY prepared the experimental materials and performed the statistical analysis. KQ wrote the first draft of the manuscript. WR and EF read and revised the manuscript. All authors contributed to manuscript, read, and approved the submitted version.

FUNDING

We are sincerely grateful for funding from the National Natural Science Foundation of China (Nos. 32060407 and 31872407), the National Natural Science Foundation of Inner Mongolia (No. 2020MS03029), and the Major Science and Technology Projects of Inner Mongolia (Nos. 2020GG0063, 2021ZD0008, and 2020ZD0020).

SUPPLEMENTARY MATERIAL

The Supplementary Material for this article can be found online at: https://www.frontiersin.org/articles/10.3389/fpls.2022.917354/full#supplementary-material

Supplementary Figure S1 | Expression levels of auxin (IAA), gibberellic acid (GA), and abscisic acid (ABA)-related genes.

Supplementary Figure S2 | The activity of peroxidase (POD) and superoxide dismutase (SOD) in roots and leaves in response to two conditions. $^{***}P < 0.001$; $0.001 < ^{**}P < 0.05$; $^{*}P < 0.05$.

REFERENCES

Al-Saeedi, A. H., and Hossain, M. A. (2015). Total phenols, total flavonoids contents and free radical scavenging activity of seeds crude extracts of pigeon pea traditionally used in Oman for the treatment of several chronic diseases. *Asian Pac. J. Trop. Dis.* 5, 316–321. doi: 10.1016/S2222-1808(14)60790-8

Avramova, Z. (2019). Defence-related priming and responses to recurring drought: Two manifestations of plant transcriptional memory mediated by the ABA and JA signalling pathways. *Plant Cell Environ.* 42 983–997. doi: 10.1111/pce.13458

Baozhu, L., Ruonan, F., Yanting, L., Runan, Z., Hui, C., Tingting, L., et al. (2022). The flavonoid biosynthesis regulator PFG3 confers drought stress tolerance in plants by promoting flavonoid accumulation. *Environ. Exp. Bot.* 196, 104792. doi: 10.1016/j.envexpbot.2022.104792

Bardgett, R. D., Bullock, J. M., Lavorel, S., Manning, P., and Shi, H. (2021). Combatting global grassland degradation. *Nat. Rev. Earth Environ.* 15, 720–735. doi: 10.1038/s43017-021-00207-2

Bari, R., and Jones, J. (2009). Role of plant hormones in plant defence responses. *Plant Mol. Biol.* 69, 473–488. doi: 10.1007/s11103-008-9435-0

Chen, D. L., He, M., Lin, Y., Jing, C., Liang, H., and Liu, J., et al. (2021). A ras-related small GTP-binding protein, RabE1c, regulates stomatal movements and drought stress responses by mediating the interaction with ABA receptors. *Plant Sci.* 306, 110858. doi: 10.1016/j.plantsci.2021.110858

Du, H., Liu, H., and Xiong, L. (2013). Endogenous auxin and jasmonic acid levels are differentially modulated by abiotic stresses in rice. *Front. Plant Sci.* 4, 397. doi: 10.3389/fpls.2013.00397

Hu, C. C., Wei, Q., Ma, H., Dong, K., Shi, Y., Zhou, C. H., et al. (2021). Ethylene response factors 15 and 16 trigger jasmonate biosynthesis in tomato during herbivore resistance. *Plant Physiol.* 185, 1182–1197. doi: 10.1093/plphys/kiaa089

Huitu, O., Forbes, K. M., Helander, M., Julkunen-Tiitto, R., Lambin, X., Saikkonen, K., et al. (2014). Silicon, endophytes and secondary metabolites as grass defenses against mammalian herbivores. *Front. Plant Sci.* 5, 478. doi: 10.3389/fpls.2014.00478

Ibáñez, J., Martínez, J., and Schnabel, S. (2007). Desertification due to overgrazing in a dynamic commercial livestock–grass–soil system. *Ecol. Model.* 205, 277–288. doi: 10.1016/j.ecolmodel.2007.02.024

Kabir, M., Ahmad, S., Mahamoud, M. S., Masum, M., and Adnan, M. (2015). Evaluation of total condensed tannin content and anthelmintic activities of organic extracts of four Bangladeshi plants on Tubifex tubifex worm using in vitro method. *Int. J. Pharm.* 5, 903–910.

Khaleghnezhad, V., Yousefi, A. R., Tavakoli, A., and Farajmand, B. (2019). Interactive effects of abscisic acid and temperature on rosmarinic acid, total phenolic compounds, anthocyanin, carotenoid and flavonoid content of dragonhead (*Dracocephalum moldavica L.*). *Sci. Hortic.* 250, 302–309. doi: 10.1016/j.scienta.2019.02.057

Koepfli, J., Thimann, K., and Went, F. W. (1938). Phytohormones: structure and physiological activity. *J. Biol. Chem.* 122, 763–780. doi: 10.2307/2332015

Koo, A. J., and Howe, G. A. (2009). The wound hormone jasmonate. *Phytochemistry* 70, 1571–1580. doi: 10.1016/j.phytochem.2009.07.018

Li, L., Li, C., Lee, G. I., and Howe, G. A. (2002). Distinct roles for jasmonate synthesis and action in the systemic wound response of tomato. *Proc. Natl. Acad. Sci. U. S. Am.* 99, 6416–6421. doi: 10.1073/pnas.072072599

Li, R., Li, Y., Zhang, Y. L., Sheng, J., Zhu, H., and Shen, L. (2021). Transcriptome analysis reveals that SlNPR1 mediates tomato fruit resistance against *Botrytis cinerea* by modulating phenylpropanoid metabolism and balancing ROS homeostasis. *Postharvest Biol. Technol.* 172, 11382. doi: 10.1016/j.postharvbio.2020.111382

Li, X., Hou, X., Wu, X., Sarula, J. L., Chen, H., Liu, Z., et al. (2014). Plastic responses of stem and leaf f unctional traits in *Leymus chinensis* to long-term grazing in a meadow steppe. *Chin. J. Plant Ecol.* 38, 440–451. doi: 10.3724/SP.J.1258.2014.00040

Li, X., and Wu, Z., Liu, Z., Hou, X., Badgery, W., Guo, H., et al.(2015). Contrasting Effects of Long-Term Grazing and Clipping on Plant Morphological Plasticity: evidence from a Rhizomatous Grass. *Plos ONE* 10, e0141055. doi: 10.1371/journal.pone.0141055

Liu, M., Dries, L., Heijman, W., Zhu, X., Deng, X., and Huang, J. (2019a). Land tenure reform and grassland degradation in Inner Mongolia, China. *China Econ. Rev.* 55, 181–198. doi: 10.1016/j.chieco.2019.04.006

Liu, M., Gong, J., Li, Y., Li, X., Yang, B., Zhang, Z., et al. (2019b). Growth-defense trade-off regulated by hormones in grass plants growing under different grazing intensities. *Physiol. Plant.* 166, 553–569. doi: 10.1111/ppl.12802

Malkowski, E., Sitko, K., Szopinski, M., Gieron, Z., Pogrzeba, M., Kalaji, H. M., et al. (2020). Hormesis in Plants: The Role of Oxidative Stress, Auxins and Photosynthesis in Corn Treated with Cd or Pb. *Int. J. Mol. Sci.* 21, 2099. doi: 10.3390/ijms21062099

Mantoan, L., Corrêa, C., Rainho, C. A., and Almeida, L. (2020). Rapid dehydration induces long-term water deficit memory in sorghum seedlings: advantages and consequences. *Environ. Exp. Bot.* 180, 104252. doi: 10.1016/j.envexpbot.2020.104252

Mashiguchi, K., Tanaka, K., Sakai, T., Sugawara, S., Kawaide, H., Natsume, M., et al. (2011). The main auxin biosynthesis pathway in Arabidopsis. *Proc. Natl. Acad. Sci.* 108, 18512–18517. doi: 10.1073/pnas.1108434108

Mutuku, A., Mwamburi, L., Keter, L., Ondicho, J., Korir, R., Kuria, J., et al. (2020). Evaluation of the antimicrobial activity and safety of Rhus vulgaris (Anacardiaceae) extracts. *BMC Complement. Med. Therap.* 20, 272. doi: 10.1186/s12906-020-03063-7

Nik, K., and Durkin, P. (2018). Hormone deficient mutants have distinct flavonoid proportion fingerprints in response to abiotic stress. *Plant Signal. Behav.* 13, e1542241. doi: 10.1080/15592324.2018.1542241

Qi, J., Sun, G., Wang, L., Zhao, C., Hettenhausen, C., and Schuman, M. C. (2016). Oral secretions from *Mythimna separata* insects specifically induce defense responses in maize as revealed by high-dimensional biological data. *Plant Cell Environ.* 39, 1749–1766. doi: 10.1111/pce.12735

Rasmann, S., De Vos, M., Casteel, C. L., Tian, D., Halitschke, R., and Sun, J. Y. (2012). Herbivory in the previous generation primes plants for enhanced insect resistance. *Plant Physiol.* 158, 854–863. doi: 10.1104/pp.111.187831

Ren, W., Hou, X., Wu, Z., Kong, L., Guo, H., Hu, N., et al. (2018a). De novo transcriptomic profiling of the clonal *Leymus chinensis* response to long-term overgrazing-induced memory. *Sci. Rep.* 8, 17912. doi: 10.1038/s41598-018-35605-y

Ren, W., Hu, N., Hou, X., Zhang, J., Guo, H., Liu, Z., et al. (2017). Long-term overgrazing-induced memory decreases photosynthesis of clonal offspring in a perennial grassland plant. *Front. Plant Sci.* 8, 419. doi: 10.3389/fpls.2017.00419

Ren, W., Xie, J., Hou, X., Li, X., Guo, H., Hu, N., et al. (2018b). Potential molecular mechanisms of overgrazing-induced dwarfism in sheepgrass (*Leymus chinensis*) analyzed using proteomic data. *BMC Plant Biol.* 18, 81. doi: 10.1186/s12870-018-1304-7

Saqlain, H., Iqbal, J., Shaukat, M., Naseer, S., and Mahmood, T. (2021). The epigenetic chromatin-based regulation of somatic heat stress memory in plants. *Plant Gene* 27, 100318. doi: 10.1016/j.plgene.2021.100318

Scogings, P. F., Demmer, S., and Hattas, D. (2021). Spinescence and Total Phenolic Content Do Not Influence Diet Preference of a Critically Endangered Megaherbivore, but the Mix of Compounds Does. *J. Chem. Ecol.* 47, 322–333. doi: 10.1007/s10886-021-01258-x

Sharma, M., Singh, D., Saksena, H. B., Sharma, M., Tiwari, A., Awasthi, P., et al. (2021). Understanding the Intricate Web of Phytohormone

Signalling in Modulating Root System Architecture. *Int. J. Mol. Sci.* 22, 5508. doi: 10.3390/ijms22115508

Suzuki, R. O., and Suzuki, S. N. (2011). Facilitative and competitive effects of a large species with defensive traits on a grazing-adapted, small species in a long-term deer grazing habitat. *Plant Ecol.* 212, 343–351. doi: 10.1007/s11258-010-9826-6

Teng, K., Li, J., and Liu, L. (2014). Exogenous ABA induces drought tolerance in upland rice: the role of chloroplast and ABA biosynthesis-related gene expression on photosystem II during PEG stress. *Acta Physiol. Plant.* 36, 2219–2227. doi: 10.1007/s11738-014-1599-4

Tohge, T., de Souza, L. P., and Fernie, A. R. (2017). Current understanding of the pathways of flavonoid biosynthesis in model and crop plants. *J. Exp. Bot.* 68, 4013–4028. doi: 10.1093/jxb/erx177

Tozawa, Y. (2001). Characterization of rice anthranilate synthase alpha-subunit genes *OASA1* and *OASA2*. Tryptophan accumulation in transgenic rice expressing a feedback-insensitive mutant of *OASA1*. *Plant Physiol.* 126,1493–1506. doi: 10.1104/pp.126.4.1493

Trivedi, P., Leach, J. E., Tringe, S. G., Sa, T., and Singh, B. K. (2020). Plant-microbiome interactions: from community assembly to plant health. *Nat. Rev. Microbiol.* 18, 607–621. doi: 10.1038/s41579-020-0412-1

Tzipilevich, E., and Benfey, P.. (2021). Plant immune system activation is necessary for efficient interaction with auxin secreting beneficial bacteria. *Cell Host Microbe* 29, 1507–1520. doi: 10.1016/j.chom.2021.09.005

Urano, K., Maruyama, K., Jikumaru, Y., Kamiya, Y., Yamaguchi-Shinozaki, K., and Shinozaki, K. (2017). Analysis of plant hormone profiles in response to moderate dehydration stress. *Plant J.* 90, 17–36. doi: 10.1111/tpj.13460

Vickers, C. E., Gershenzon, J., Lerdau, M. T., and Loreto, F. (2009). A unified mechanism of action for volatile isoprenoids in plant abiotic stress. *Nat. Chem. Biol.* 5, 283–291. doi: 10.1038/nchembio.158

Walter, J., Beierkuhnlein, C., Jentsch, A., and Kreyling, J. (2013). Ecological stress memory and cross stress tolerance in plants in the face of climate extremes. *Environ. Exp. Bot.* 94, 3–8. doi: 10.1016/j.envexpbot.2012.02.009

Wang, R. Z. (2004). Response of Leymus chinensis to long-term grazing disturbance in the Songnen grasslands of north-eastern China. *Grass Forage Sci.* 59, 191–195. doi: 10.1111/j.1365-2494.2004.00417.x

Wang, Y. H., and Irving, H. R. (2011). Developing a model of plant hormone interactions. *Plant Signal. Behav.* 6, 494–500. doi: 10.4161/psb.6.4.14558

Wolters, H., and Jurgens, G. (2009). Survival of the flexible: hormonal growth control and adaptation in plant development. *Nat. Rev. Gene.* 10, 305–317. doi: 10.1038/nrg2558

Xiang, N., Hu, J. G., Yan, S., and Guo, X. (2021). Plant Hormones and Volatiles Response to Temperature Stress in Sweet Corn (*Zea mays L.*) Seedlings. *J. Agric. Food Chem.* 69, 6779–6790. doi: 10.1021/acs.jafc.1c02275

Xie, K., Li, L., Zhang, H., Wang, R., Tan, X., He, Y., et al. (2018). Abscisic acid negatively modulates plant defence against rice black-streaked dwarf virus infection by suppressing the jasmonate pathway and regulating reactive oxygen species levels in rice. *Plant Cell Environ.* 41, 2504–2514. doi: 10.1111/pce.13372

Xu, J., Zhang, Y., Zhang, P., Trivedi, P., Riera, N., Wang, Y., et al. (2018). The structure and function of the global citrus rhizosphere microbiome. *Nat. Commun.* 9, 4894. doi: 10.1038/s41467-018-07343-2

Yilamujiang, A., Reichelt, M., and Mithofer, A. (2016). Slow food: insect prey and chitin induce phytohormone accumulation and gene expression in carnivorous Nepenthes plants. *Ann. Bot.* 118, 369–375. doi: 10.1093/aob/mcw110

Yin, J., Li, X., Guo, H., Zhang, J., Kong, L., and Ren, W. (2020). Legacy effects of historical grazing alter leaf stomatal characteristics in progeny plants. *PeerJ* 8, e9266. doi: 10.7717/peerj.9266

Zhang, N., Xie, Y. D., Guo, H. J., Zhao, L. S., Xiong, H. C., Gu, J. Y., et al. (2016). Gibberellins regulate the stem elongation rate without affecting the mature plant height of a quick development mutant of winter wheat (*Triticum aestivum L.*). *Plant Physiol. Biochem.* 107, 228–236. doi: 10.1016/j.plaphy.2016.06.008

Zhang, Z., Gong, J., Wang, B., Li, X., Ding, Y., and Yang, B., et al. (2020). Regrowth strategies of *Leymus chinensis* in response to different grazing intensities. *Ecol. Appl.* 30, e02113. doi: 10.1002/eap.2113

Conflict of Interest: YL was employed by Inner Mongolia Mongolian Grass Seed Industry Science and Technology Research Institute Co., Ltd..

The remaining authors declare that the research was conducted in the absence of any commercial or financial relationships that could be construed as a potential conflict of interest.

Publisher's Note: All claims expressed in this article are solely those of the authors and do not necessarily represent those of their affiliated organizations, or those of the publisher, the editors and the reviewers. Any product that may be evaluated in this article, or claim that may be made by its manufacturer, is not guaranteed or endorsed by the publisher.

frontiers | Frontiers in Plant Science

ORIGINAL RESEARCH
published: 09 June 2022
doi: 10.3389/fpls.2022.919912

Effects of a Furrow-Bed Seeding System on Stand Establishment, Soil Bacterial Diversity, and the Yield and Quality of Alfalfa Under Saline Condition

*Juanjuan Sun[1,2], Jinmei Zhao[1,2], Tengwei Zhang[1,2], Linqing Yu[1] and Ke Jin[1,2]**

[1]Institute of Grassland Research of Chinese Academy of Agricultural Sciences, Hohhot, China, [2]Inner Mongolia Academy of Grassland Science, Hohhot, China

OPEN ACCESS

Edited by:
Jin-Lin Zhang,
Lanzhou University, China

Reviewed by:
Junmei Kang,
Institute of Animal Sciences (CAS), China
Zhijian Jiang,
South China Sea Institute of Oceanology (CAS), China
Everlon Cid Rigobelo,
São Paulo State University, Brazil

***Correspondence:**
Ke Jin
jinke@caas.cn

Specialty section:
This article was submitted to Plant Abiotic Stress, a section of the journal Frontiers in Plant Science

Received: 14 April 2022
Accepted: 19 May 2022
Published: 09 June 2022

Citation:
Sun J, Zhao J, Zhang T, Yu L and Jin K (2022) Effects of a Furrow-Bed Seeding System on Stand Establishment, Soil Bacterial Diversity, and the Yield and Quality of Alfalfa Under Saline Condition. Front. Plant Sci. 13:919912. doi: 10.3389/fpls.2022.919912

Salt stress account for large decreases in crop yield all over the world. Furrow-bed system is an efficient practice to promote plant growth in saline soil. However, the effects of Furrow-bed system on the soil environment and the growth of alfalfa (*Medicago sativa* L.) in salinity are not clear. For a wider and more detail evaluation, alfalfa were planted in saline sandy loam soil in fall, the effects of two plant systems (FU, furrow-bed seeding system; FL, flat-bed seeding system) on soil moisture, root zone salinity, soil microbial community structure, seedling emergence number in the early stage of the growth period and soil nutrient contents, alfalfa production characteristics in the second growth year were determined in a 2-year field experiment. The result showed that, compared with FL, FU resulted in increased soil moisture content and seedling emergence, and significantly reduced relative abundance of Actinobacteria and Choroflexi in soil, but it did not affect root zone salinity at the seedling stage. In April of second growth year, the soil salinity was lower, and the soil available phosphorus, potassium, nitrogen, and soil organic matter contents of the root zone were higher in FU than in FL. Compared with FL, FU resulted in increased yield (by 37.5%), protein content (by 3.6%), and potassium concentration (by 33.2%), and decreased ash content (by 7.7%), and sodium concentration (by 19.0%) in alfalfa plants. Pearson's correlation analysis indicated that the increased yield was positively correlated with seedling emergence, soil available potassium, total nitrogen, and organic matter contents, and shoot potassium content and negatively correlated with shoot sodium content. The relative abundance of Actinobacteria was negatively correlated with alfalfa ash, calcium, and sodium concentrations, and positively correlated with shoot potassium content. Taken together, the results indicate that Furrow-bed seeding in early fall alleviated salt stress of alfalfa and have the potential to enhance the yield and quality of alfalfa cultivated in saline soils by improving the soil environment and regulating the growth and physiology of alfalfa.

HIGHLIGHTS

1. Furrow-bed seeding system increased soil moisture content and alfalfa seedling emergence number in the seedling stage.
2. Seeding pattern derived soil microbial community change in seedling stage in saline soil.
3. Furrow-bed seeding system decreased root zone salinity in spring.
4. Alfalfa shoot Na^+ concentration was decreased and yield was enhanced by furrow-bed seeding system.

Keywords: ***Medicago sativa*** **L., furrow-bed seeding, soil bacterial diversity, Na^+ concentration, yield, soil moisture**

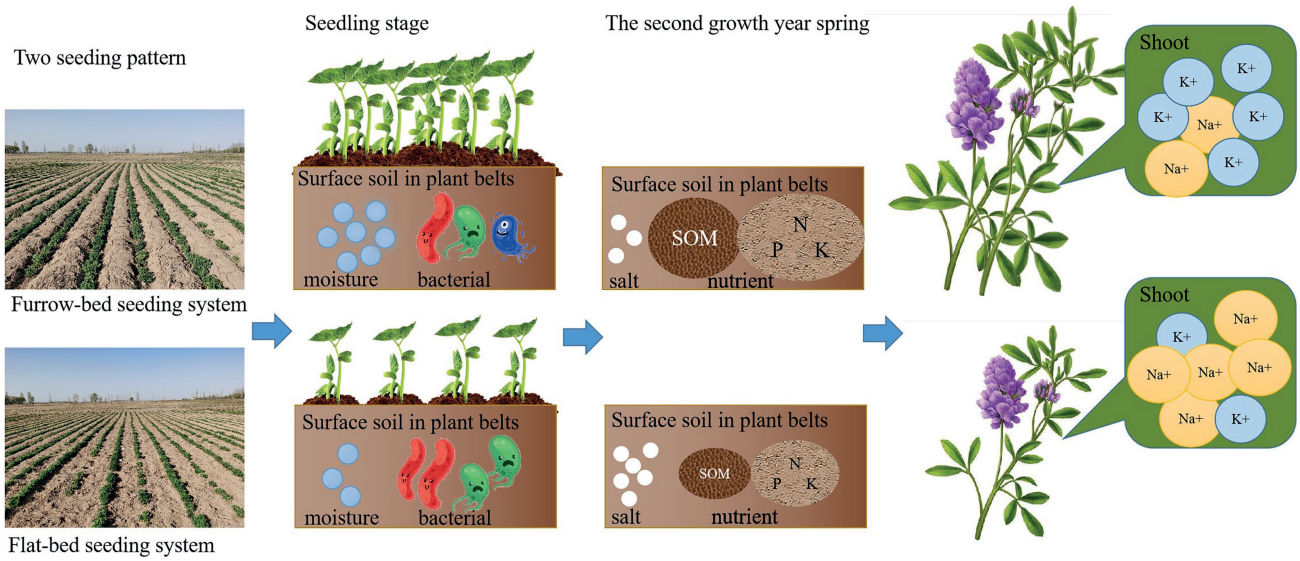

GRAPHICAL ABSTRACT |

INTRODUCTION

Soil salinization is a growing problem for agriculture worldwide (Deinlein et al., 2014), more than 6% of the world's total land area are salt affected, especially in arid and semiarid regions (Munns and Tester, 2008). Gansu, Inner Mongolia, Xinjiang, Ningxia, Heilongjiang, and Hebei provinces are the major alfalfa-growing areas in China. Although these six provinces produce 89.9% of Chinese high-quality alfalfa, they have almost two-thirds (65.7%) of the area of saline soil in China (Fan et al., 2001). Soil salinity, limited rainfall in spring, high evapotranspiration rates, and poor water management are among the main challenges for agricultural production in this area.

Alfalfa is the most important forage crop and extensively cultivated in the world, and large alfalfa-growing area are known to be subjected to salt stress (Anower et al., 2013). Although it is classified as moderately salt tolerant (Noble et al., 1984), it has been well documented that salt stress inhibits alfalfa shoot growth and increases the shoot sodium (Na^+) concentration (Sun et al., 2016). Salinity negatively affects alfalfa growth when the electrical conductivity of soil is above 2–3.5 dSm^{-1}, and its effects also vary depending on the stage plant growth and development. Alfalfa is very sensitive to salt stress during germination (Allen et al., 1985), at the seedling stage (Ashraf et al., 1987; Esechie et al., 2002), and at the pre-flowering stage (Noble et al., 1984). The accumulated salt in the soil inhibits seed germination, seedling emergence, and plant growth and development through osmotic effects, by causing nutritional imbalances, or by toxicity of salt ions (Na^+ and Cl^-). This leads to sparse germination, stunted plants, and/or reduced crop yield and quality (Latrach et al., 2014). Low soil moisture also negatively affects alfalfa seedling emergence and crop establishment. In fact, soil moisture is one of the most important factors affecting crop productivity (Liu et al., 2010a).

Planting patterns affect water and salt transport by controlling evaporation and distributing rainfall, and they are inexpensive and do not pollute the soil. Thus, the use of suitable planting patterns is an environmentally friendly way to moderate soil salinity (Devkota et al., 2015). In arid and semiarid areas, the soils are highly saline with a low moisture content. Consequently, crop productivity in such areas is low, and it cannot meet

local food demands. Controlling salinity in the root zone so that it is below harmful levels (reducing root zone salinity) is one beneficial strategy to improve crop emergence and stand establishment in saline fields (Meiri and Plaut, 1985). Previous studies have shown that a furrow-bed seeding system (FU) can efficiently collect rainfall and leach salt from the root zone (Dong et al., 2009; Sun et al., 2017a), so it may be a promising planting pattern for agricultural reclamation in saline–alkaline areas around the world. Dong et al. (2010) found that over-irrigation before planting in an FU system consisting of alternate parallel ridges and furrows on flat land after leaching improved stand establishment and yield (Dong et al., 2010). This was because salts moved upward by capillary action under an evaporation gradient, and accumulated on the soil surface after planting (Dong et al., 2009). The FU system results in the unequal distribution of salts in the surface soil layers (Meiri and Plaut, 1985). Unequal salt distribution under controlled conditions has been shown to affect the physiological characteristics of alfalfa and improve its growth (Sun et al., 2016, 2017b; Xiong et al., 2020). However, it is unknown whether the use of an FU system can improve the growth and yield of alfalfa and the properties of soil in saline soil environments.

The plastic-covered ridge and furrow rainwater harvesting system (PRRFHS) is a well-known soil–water conservation practice used in crop production (Liu et al., 2014; Cuello et al., 2015), and it is one of the most efficient technical applications for maximizing rainfall use. The PRRFHS can improve soil moisture availability in the crop root zone by collecting water from light rain, and this can significantly increase crop yield and water-use efficiency (Liu et al., 2014). It also reduces evaporation and promotes rainfall infiltration and has been widely used in maize and cotton production (Li et al., 2000). However, mulching with plastic also has some negative effects, including plastic waste, greenhouse gas emissions associated with the production of the film (Cuello et al., 2015), and increased planting costs. To date, there have been no studies on the effects of growing alfalfa in a ridge-furrow crop system with no mulch and with a narrow planting belt under saline conditions.

In the soil microbial community, bacteria are one of the richest and most diverse microbial groups, and they play important roles in many soil processes. They participate in soil nutrient cycling, the decomposition of organic matter and waste, the degradation of pesticides and contaminants, and soil aggregation and humus formation. In addition, they affect the soil structure and the growth and health of plants (Jurburg et al., 2018). Soil microbial populations and community composition are affected by a range of edaphic factors, such as soil physicochemical properties (Wakelin et al., 2007) and soil management practices (Chen et al., 2014). Nutrient substrates (Ling et al., 2017), soil pH (Bainard et al., 2016), moisture (Battin et al., 2003; Nguyen et al., 2018; Yang et al., 2019; Chi et al., 2021), and plant community cover (Bainard et al., 2016) are the main ecological drivers of soil bacterial abundance, diversity, and community composition. Soil carbon (C) and nitrogen (N) contents strongly affect soil bacteria, because they decompose soil organic C and N to obtain energy (Yang et al., 2018). For example, Chloroflexi, Nitrospirae, and Planctomycetes tend to be abundant in nutrient-poor soil where they show slow growth rates and use recalcitrant C substrates (Nie et al., 2018). In contrast, Proteobacteria and Bacteroidetes favor nutrient-rich conditions and utilize labile C materials (Philippot et al., 2013). In addition, soil salinity is a critical factor that influence soil microbial community structure and diversity (Guo et al., 2018; Zhao et al., 2020; Cheng et al., 2021; Li et al., 2021). A previous study found that soil salinity negatively affects the abundance of most bacterial groups, but has little effect on bacterial diversity (Gao et al., 2015). Consequently, determining the effects of different planting systems on the soil bacterial community can shed light on how such planting systems affect plant growth.

Soil ridging with plastic film has been shown to improve rainwater utilization and improve alfalfa yield in semiarid areas where alfalfa production is largely rainfed (Li et al., 2007; Gu et al., 2018), However the width of bare soil between planting belts is increased from 30 to 60 cm (Li et al., 2007), the wider planting belts cause higher evaporation. Numerous field studies have explored the effects of the FU system on soil properties, especially soil moisture content, and plant yield. However, few have explored the effects of the narrow plant row FU system on alfalfa grown in saline soils. In addition, the effects of FU on soil bacterial diversity at the seedling stage and the relationships among soil microbes, soil properties, crop yield, and crop quality need further study. We hypothesize that FU system will decrease soil salinity of root zone and improve alfalfa growth in the salinity soil and also have positive impact on the soil microbial and soil properties. Therefore, the objectives of this study were as follows: (1) to evaluate the effects of the FU seeding system with a narrow plant belt on soil properties (especially salinity), soil bacterial diversity at the seedling stage, and alfalfa yield and quality in the second growth year; and (2) investigate the relationships among soil moisture content, soil microbes, soil nutrient contents, soil salinity, and the growth and physiology of alfalfa plants. Therefore, a 2-year field experiment was conducted to explore these topics in detail.

MATERIALS AND METHODS

Experimental Site

A field experiment was conducted in an area with saline sandy loam soil in the Hohhot district (111°45′E, 40°36′N) on the Tumochuan plain, China, during two consecutive alfalfa-growing seasons: 2019 and 2020. The site has a typical continental climate with mean annual air temperature of 7.6°C and mean annual maximum and minimum air temperatures of 23.3°C (July) and −11.0°C (January), respectively. The mean annual precipitation is 392.6 mm (average values for 1981–2010), and around 74.8% of the precipitation occurs between July and September. The potential annual evaporation is about 1757.1 mm. Mean annual sunshine exceeds 2829.8 h, and the frost-free period is about 137 days (range, 99 to 183 days). The distribution of precipitation in 2019 and 2020 is shown in **Figure 1**.

The properties of the background surface soil (0–15 cm) were as follows: 15.9 g kg^{-1} soil organic matter (SOM), 930 mg kg^{-1}

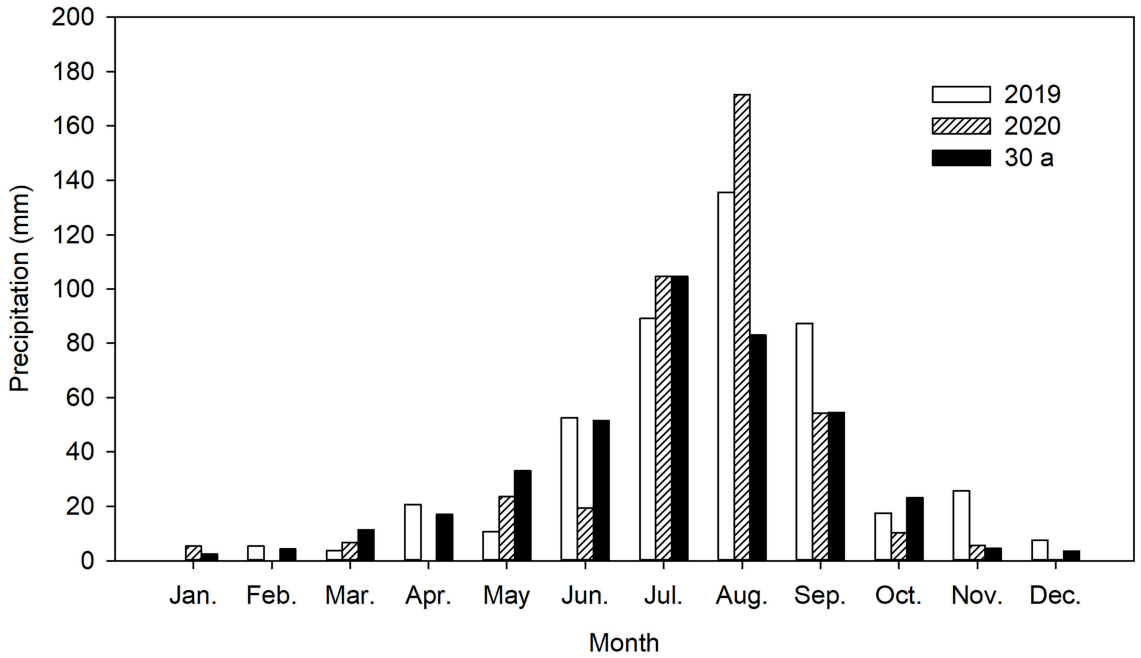

FIGURE 1 | Precipitation distribution from 2019 to 2020 and 30-year average (30 a) at the experimental site.

total N, 14 mg kg^{-1} available phosphorus (P), and 225 mg kg^{-1} available potassium (K), with an ECe (electrical conductivity of a saturated soil extract) of 15.8 dSm^{-1} in spring and with an ECp (electrical conductivity of pore water) of 1.1dSm^{-1} in early fall. Alfalfa seeds were sown in early August (fall) in 2019.

Experimental Design and Field Management

The cold-tolerant alfalfa cultivar *M. sativa* L. cv. "Zhongcao NO.3," bred by Linqing Yu, Chinese Academy of Agricultural Sciences, was selected for this study, as it is widely cultivated on the Inner Mongolia plateau in China. The experiment comprised two cultivation systems: furrow-bed seeding (FU; cultivation with ridges and furrows) and flat-bed seeding (FL; conventional flat cultivation without ridges). The experiment had a completely randomized block design with four replicates. Each plot was 20.0-m long and 3.2-m wide. Alfalfa seeds were planted on 8th August 2019 using the drill planting method with a hand-pushed vegetable planter. For the FU treatment, the width of the ridges and the furrows was 35 and 5 cm, respectively, and the ridge height was 15 cm. The furrows were leveled as planting belts (**Figure 2**). The ridge and furrow were made using a tiny furrow machine and the ridges were compacted using a roller. Alfalfa seeds were drill-sown in the furrows in the FU system and then covered with 1 cm soil. All the planting rows in both FU and FL systems had a north–south orientation with 40-cm spacing between adjacent rows. Weeds were controlled manually, with care taken not to destroy the ridge soil crust. Alfalfa plants were harvested manually in 2020.

The alfalfa plants in the plots were not irrigated in 2019 because rainfall was sufficient that year, but were irrigated three times at key stages of growth in 2020. Other field management was conducted according to local agronomic practices.

Data Collection

Data were collected for rainfall, soil temperature, soil salinity, soil moisture content, seedling emergence number, soil bacterial diversity, soil properties, plant height, plant yield, shoot sodium (Na^+) concentration, shoot potassium (K^+) concentration, shoot calcium (Ca^{2+}) concentration, and plant nutritional components.

Rainfall at the experimental site was measured using an automatic weather station (WSSTD1, Campbell Scientific, Loughborough, United Kingdom). The number of emerged seedlings (number of alfalfa seedlings at the cotyledon stage) was counted in five 100-cm-long seed row sections and the average number per 100-cm-long seed row in each plot at 4, 6, and 9 days after sowing (DAS) was calculated. The soil moisture content, salinity, and temperature during the seedling stage at 4, 6, and 9 DAS were determined by analyzing 10 surface (0–10 cm) soil samples with a HH2 Moisture Meter and a WET-2 sensor (Delta-T Devices Ltd. Cambridge, United Kingdom; Kargas et al., 2011). For analyses of the soil bacterial community, five surface (0–15 cm) soil samples were collected from random positions along the crop row from each plot in both systems on 9 DAS. The soil samples from each plot were homogenized to form a composite sample and sieved through a 2 mm sieve to remove rocks and roots. A subsample was immediately stored at −80°C until use in molecular analyses.

For determination of the properties of the soil before the experiments started, 10 soil cores were collected from random positions in the experimental field. For determination of soil

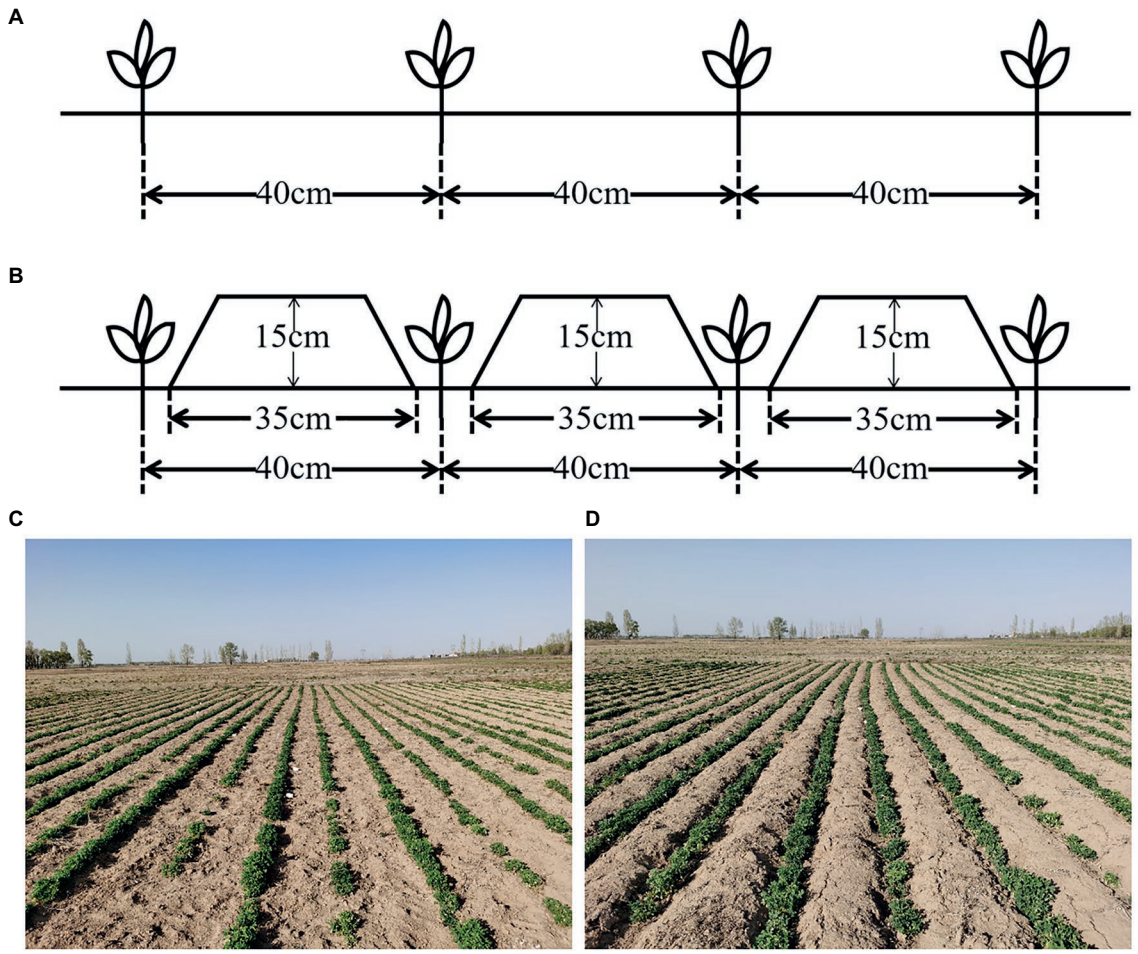

FIGURE 2 | Schematic diagram of **(A)** flat-bed seeding (FL) or **(B)** furrow-bed seeding (FU) systems and the pictures of field experiment in the seedling stage of FL **(C)** or FU **(D)**.

salinity and the contents of SOM, total N, available P, and available K during the experiment, five soil cores were collected from random positions along the crop row to a depth of 15 cm from both the FU and FL treatment in the spring of 2020 when the alfalfa plants had just turned green. The soil samples from each plot were homogenized to form a composite sample. Subsamples were air-dried, ground, and passed through a 2-mm sieve, then used for analyses of soil salinity, SOM, available K, available P, and total N. Soil was mixed with water (1:5 soil to water ratio) to determine soil salinity. Soil chemical characteristics were tested following the method described by Bao (2018).

Plant Characteristics

Plant height was measured five times from 17 October 2019 to 3 July 2020. At each measurement time, 20 plants were selected from each plot and the height was measured and the average height of alfalfa were used. In 2020, the yield of the first cut of alfalfa was measured. Alfalfa plants were cut in a 1-m long part of the row, with three replicates per plot. The average yield from plants in 1 m was calculated and used to estimate the yield per hectare. The harvested material was dried at 65°C for 48 h and then weighed to determine dry matter content. Then, the dried samples were ground to pass through 1-mm screen using a laboratory knife mill (FW100, Taisite Instruments, Tianjin, China) for later analysis. Neutral detergent fiber (NDF; Van Soest et al., 1991) and acid detergent fiber (ADF; Robertson and Van Soest, 1981) were measured using an ANKOM fiber analyzer (ANKOM2000; Macedon, NY, United States). Crude ash (ash) content was determined by burning samples in a muffle furnace at 500°C for 5 h and then weighing the residue. Total nitrogen (total N) content was determined by the Kjeldahl procedure (Krishnamoorthy et al., 1982); crude protein (CP) was determined by multiplying the total N by 6.25. Ions were extracted by shaking ground leaf samples in 0.5 M HNO_3 in vials for 48 h. Then, the diluted extracts were analyzed to determine their Na^+, K^+, and Ca^{2+} contents using an M410 flame photometer (Sherwood, Cambridge, United Kingdom).

DNA Extraction

DNA was extracted from 0.25-g soil using an E.Z.N.A.®Soil DNA Kit (Omega Biotek, Norcross, GA, United States) according to the manufacturer's instructions. The reagents in this kit

were designed to isolate DNA from trace amounts of sample, and are effective for isolating DNA from most bacteria. Nucleic acid-free water was used as the blank. The total DNA was eluted in 50-μl elution buffer and stored at −80°C until PCR analyses by the LC-Bio Technology Co., Ltd. (Hang Zhou, Zhejiang Province, China).

PCR Amplification and 16S rDNA Sequencing

The V3–V4 region of the prokaryotic (bacterial and archaeal) small-subunit 16S rDNA gene was amplified with slightly modified versions of the primers 338F (5′-ACTCCTACGGG AGGCAGCAG-3′) and 806R (5′-GGACTACHVGGGTWT CTAAT-3′). The 5′ ends of the primers were tagged with specific barcodes for each sample and universal sequencing primers (Logue et al., 2016).

Each PCR amplification reaction mixture contained 25-ng template DNA, 12.5-μl PCR premix, 2.5 μl each primer, and PCR-grade water to complete the volume to 25 μl. The thermal cycling conditions to amplify the prokaryotic 16S fragments were as follows: initial denaturation at 98°C for 30 s; 35 cycles of denaturation at 98°C for 10 s, annealing at 54°C/52°C for 30 s, and extension at 72°C for 45 s; and then final extension at 72°C for 10 min. The PCR products were confirmed by 2% agarose gel electrophoresis. Throughout the DNA extraction process, ultrapure water, instead of a sample solution, was used to exclude the possibility of false-positive PCR results as a negative control. The PCR products were purified using AMPure XT beads (Beckman Coulter Genomics, Danvers, MA, United States) and quantified by Qubit (Invitrogen, Carlsbad, CA, United States). The amplicons were prepared for sequencing using a Library Quantification Kit for Illumina (Kapa Biosciences, Woburn, MA, United States), and the size and quantity of the amplicon library were assessed using an Agilent 2100 Bioanalyzer (Agilent, Palo Alto, CA, United States). The PhiX Control library (v3; Illumina) was combined with the amplicon library (expected at 30%). The libraries were sequenced with 300PE MiSeq runs. One library was sequenced with both protocols using standard Illumina sequencing primers, eliminating the need for a third (or fourth) index read. The sequencing data were submitted to the NCBI Sequence Read Archive database (accession number: PRJNA826619).

Data Analysis

Samples were sequenced on the Illumina MiSeq platform according to the manufacturer's recommendations (LC-Bio). Paired-end reads were assigned to samples based on their unique barcode and truncated by cutting off the barcode and primer sequences. Paired-end reads were merged using FLASH. Quality filtering of the raw tags was performed under specific filtering conditions to obtain high-quality clean tags according to FastQC (V 0.10.1). Chimeric sequences were filtered using Verseach software (v 2.2.4). Sequences with ≥97% similarity were assigned to each representative sequence using the RDP (Ribosomal Database Project) classifier. Differences in dominant species among different groups were detected and multiple sequence alignments were conducted using PyNAST software, which revealed the phylogenetic relationships among different operational taxonomic units (OTUs). Abundance information for OTUs was normalized using a standard sequence number corresponding to the sample with the least sequences. Alpha diversity was determined by calculating four indices (Chao 1, Shannon's, Simpson's, and Observed species) using QIIME (V 1.8.0). Differences in beta diversity (species complexity) among samples were detected by a principle co-ordinates analysis (PCoA) conducted using QIIME (V 1.8.0).

Statistical Analysis

One-way analysis of variance (ANOVA) was used to evaluate statistical significance of the effects of the two seeding patterns on soil properties, plant properties, relative abundance of dominant bacterial phyla, classes, and genera; bacterial community richness, diversity indices, and OTUs. T-test were conducted to ascertain any significant difference between two seeding patterns at the 0.05 probability level. Proc GlM procedure was used for analysis of variance. Levene's test were used for homogeneity of variance. All above data analysis was performed using SAS version 8.02 (SAS Institute, Cary, NC, United States). SigmaPlot was used to generate bar graphs. Spearman correlation analysis was performed to detect relationships among soil and plant properties and soil fungal abundance, diversity, and relative abundance of dominant bacteria phyla and classes using the package stats of the software R version 3.6.3. Pearson's correlation analysis was performed to detect relationships between alfalfa yield and soil and plant properties ($n = 4$) in two crop systems using Systat version 12.0 (Systat Software Inc., Chicago, IL, United States). The relationships between the soil bacterial community composition, at both phylum and class level, with soil and plant properties were analyzed with redundancy analysis (RDA) using the package vegan of the software R version 3.6.3.

RESULTS

Soil Moisture Content, Soil Salinity, Soil Temperature, and Seedling Emergence

The seeding pattern significantly affected the soil moisture content, soil temperature, and number of emerged seedlings, but not soil EC (**Figure 3**). At 4, 6, and 9 DAS, compared with the FL system, the FU system increased soil moisture content by 12.5%, 10.2%, and 15.6%, respectively; increased the number of emerged seedlings by 194.1%, 63.8%, and 75.7%, respectively; and decreased the soil temperature by 1.6°C, 1.1°C, and 0.3°C, respectively.

Inter-Row and Inner-Row Soil Moisture Content During the Vegetative Growth Stage

The seeding pattern significantly affected the inter-row soil moisture content, but not the inner-row moisture content (**Figure 4**). At 14, 28, and 42 DAS, the inter-row soil moisture

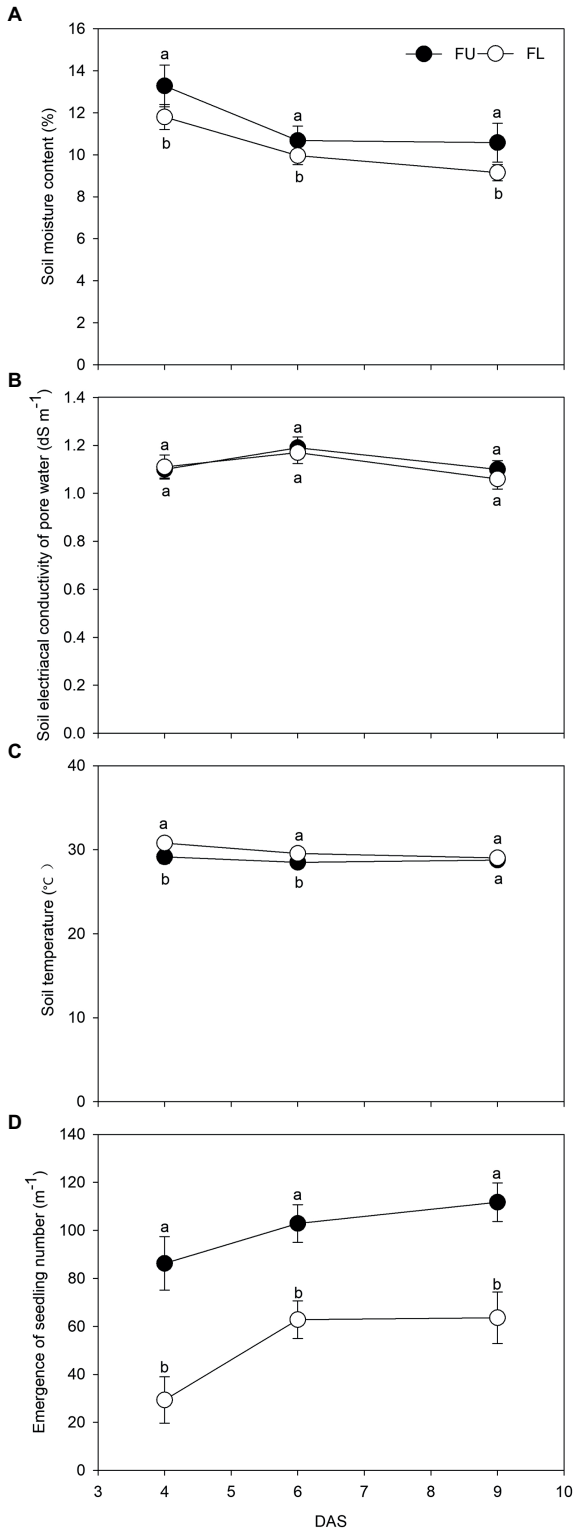

FIGURE 3 | Effects of FU and FL on Soil moisture content **(A)**, soil electrical conductivity of pore water **(B)**, soil temperature **(C)**, and number of emerged seedlings **(D)** of alfalfa 4, 6, and 9 days after sowing (DAS). During the seedling stage. Solid circles show FU treatment; hollow circles show FL treatment. Values are means ($n = 4$) ± SE. Same lowercase capital letters indicate no significant difference between two seeding patterns at $p \leq 0.05$.

content was 35.11% higher, 33.44% higher, and 22.37% higher, respectively, than the inner-row soil moisture content in FU. However, the inter-row and inner-row soil moisture contents were not significantly different in FL. The seeding pattern significantly affected the inter-row soil moisture content. At 2, 4, and 6 weeks after sowing, the soil moisture content in FU was 24.38% higher, 56.77% higher, and 44.18% higher, respectively, in FU than in FL.

Soil Bacterial Alpha Diversity and Beta Diversity Analysis

The seeding pattern had no significant effect on OTU richness, species richness (Chao1 index), and diversity (Shannon's index). However, the values of OTU richness, Chao1's, and Shannon's indices were higher in FU than in FL (**Table 1**).

A PCoA was used to analyze beta diversity, to identify the differences in soil bacterial community composition between FU and FL (**Figure 5**). At the OTU level, PCoA analyses showed that the FU soil samples clustered together, and were distinct from FL soil samples, indicating that their bacterial community compositions were dissimilar.

Taxonomic Composition of Soil Bacterial Communities

Proteobacteria (relative abundance, 25.97%–32.28%), Actinobacteria (22.76%–31.60%), Acidobacteria (16.92%–18.06%), Gemmatimonadetes (6.54%–8.57%), and Chloroflexi (3.77%–5.38%), were the main bacteria phyla (**Figures 6A-E**). Latescibacteria was a minor phylum, with relative abundance ranging from 0.021% to 0.028% (**Figure 6P**). Proteobacteria was the dominant bacterial phylum in FU, but Actinobacteria was the dominant bacterial phylum in FL. The relative abundance of Actinobacteria and Chloroflexi was significantly lower in FU than in FL. The relative abundance of other bacteria groups showed no significant difference between the two seeding patterns (**Figure 6**).

The main bacterial classes were Actinobacteria (relative abundance, 21.78%–29.85%), Alphaproteobacteria (14.07%–14.34%), Acidobacteria (15.90%–16.73%), Betaproteobacteria (4.58%–6.06%), Gemmatimonadetes (4.57%–5.59%), and Deltaproteobacteria (4.18%–5.77%; **Figures 7A-F**). Thermomicrobia was a minor class, with relative abundance ranging from 0.63% to 1.13% (**Figure 7N**). Actinobacteria was the dominant bacterial class in FU and FL. The relative abundance of Actinobacteria and Thermoleophilia was significantly lower in FU than in FL, while that of Deltaproteobacteria and Gammaproteobacteria was significantly higher in FU than in FL. The relative abundance of other bacterial classes did not differ significantly between the two seeding patterns (**Figure 7**).

At the genus level, the relative abundance of unclassified Actinobacteria (*Actinobacteria-unclassified*) and unclassified Actinomycetales (*Actinomycetales_unclassified*) were lower in FU soil than in FL soil, while that of unclassified Betaproteobacteria (*Betaproteobacteria_unclassified*) was higher in FU than in FL (**Supplementary Figure S1**).

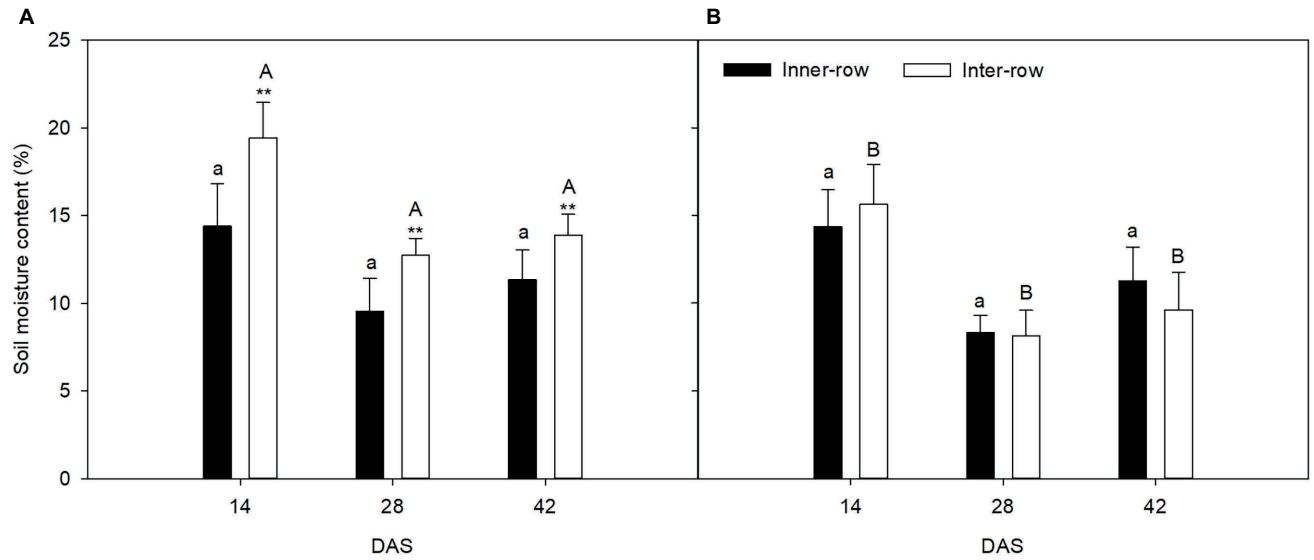

FIGURE 4 | Effects of FU **(A)** and FL **(B)** on soil moisture content of ridge/inter-row and furrow/inner-row at 14, 28, and 42 days after sowing (DAS). Solid bars show furrow/inner-row soil moisture content; hollow bars show ridge/inter-row soil moisture content. Values are means ($n = 4$) ± SE. Asterisks above symbols indicate significant differences in soil moisture content between inter-row and inner-row at $p \leq 0.05$. Same capital letters indicate no significant difference in inter-row soil moisture content between two seeding patterns at $p \leq 0.05$. Same lowercase capital letters indicate no significant difference in inner-row soil moisture content between two seeding patterns at $p \leq 0.05$.

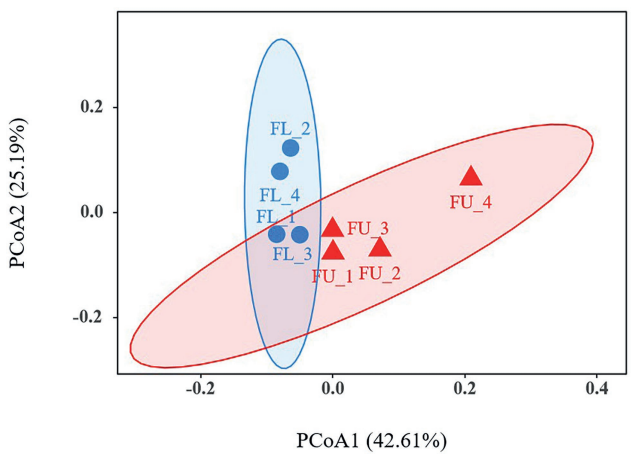

FIGURE 5 | Principal co-ordinates analysis (PCoA) at operational taxonomic unit (OTU) level. The red triangles represent FU soil samples, and the blue circles represent FL soil samples.

TABLE 1 | Number of sequences analyzed and observed bacterial community richness and diversity indexes of two seeding patterns obtained for clustering at 97% similarity levels.

Seeding pattern	OTU richness	Observed species	Shannon	Chao 1
FU	6,870 ± 199	6,418 ± 87	11.29 ± 0.07	8,096 ± 115
FL	6,808 ± 29	6,082 ± 126	11.11 ± 0.11	7,681 ± 113

Values are mean (n = 4) ± SE.

Plant Height at Different Growth Stages

The seeding pattern significantly affected alfalfa height in both 2019 and 2020 (**Figure 8**). In 2019, plant height was 17.12% higher in FU than in FL. In 2020, the plant height at the four measurement times was 30.79%, 27.59%, 16.89%, and 14.82% higher in the FU system than in the FL system.

Soil Properties in April 2020

The soil available K, soil total N, and SOM were significantly higher in FU than in FL, while the ECe was lower in FU than in FL (**Table 2**). Soil available K, total N, and SOM were 18.3%, 23.8%, and 28.8% higher, respectively, in FU than in FL. The ECe was 25.7% lower in FU than in FL.

Yield and Nutrient Contents of First-Cut Alfalfa in 2020

The seeding pattern significantly affected alfalfa yield, and the contents of CP, NDF, ADF, ash, and ions in alfalfa plants (**Table 3**). Compared with FL, FU resulted in increased alfalfa yield, CP content, K^+ concentration, and Ca^{2+} concentration (by 37.4%, 3.56%, 33.2%, and 17.8%, respectively), and decreased contents of ash and Na^+ (by 7.71% and 19.01%, respectively).

Relationships Between Soil Bacterial Communities and Soil and Plant Properties

Spearman correlation analysis indicated that the Observed species index was positively correlated with soil available K, soil total N, SOM, and soil moisture content (**Figure 9**). The Chao1 species richness index was positively correlated with

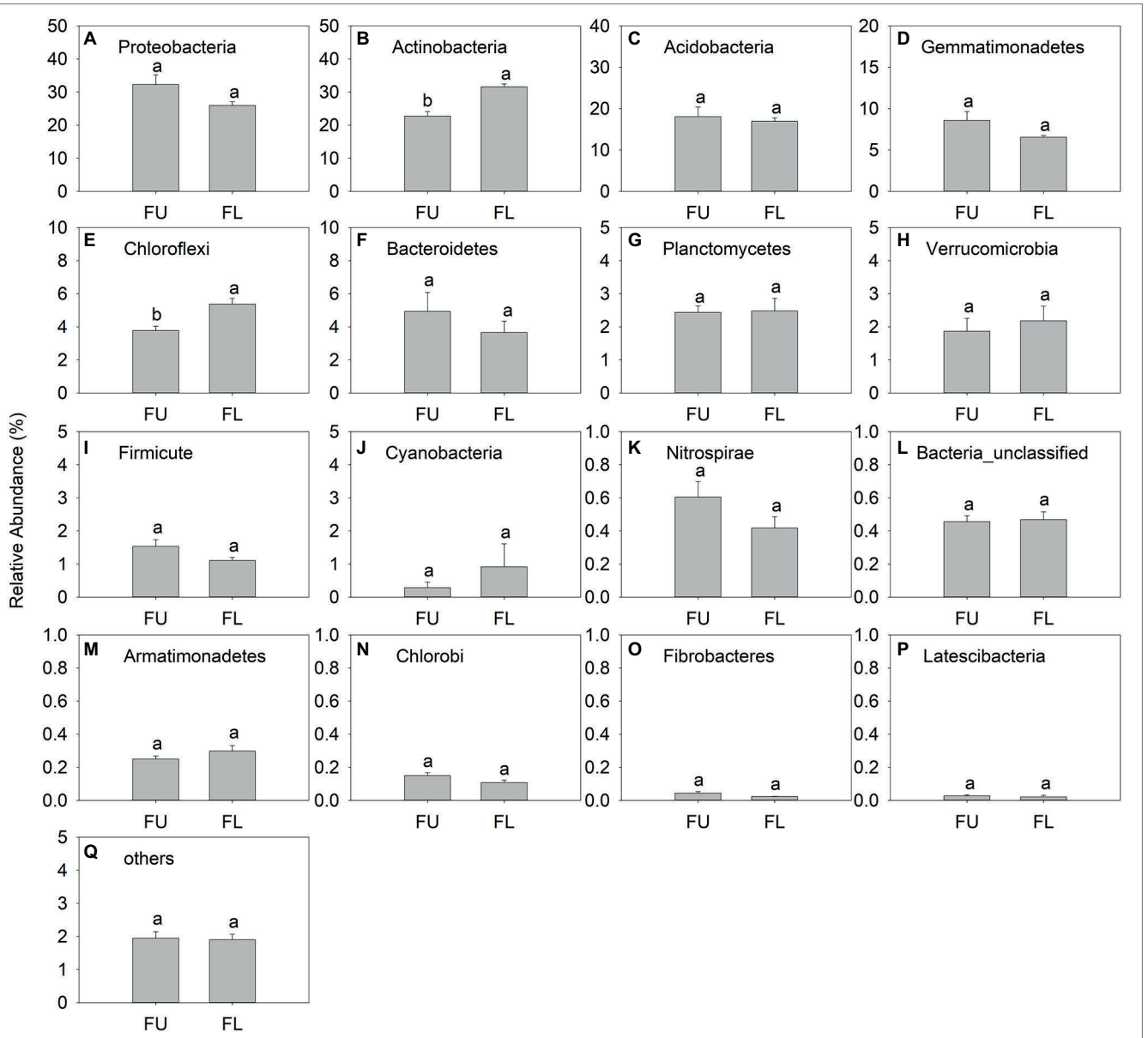

FIGURE 6 | Relative abundance (% of individual taxonomic group) of dominant bacteria phyla (mean ± SE, $n = 4$) in microbial communities following FU and FL of alfalfa. **(A-Q)** represented different soil bacterial at phylum level. Different lowercase capital letters indicate statistically significant difference among communities at $p = 0.05$.

soil available K, soil total N, and SOM, and negatively correlated with the shoot Na^+ concentration (**Figure 9**). The relative abundance of Actinobacteria was highly correlated with alfalfa ash content, shoot Ca^{2+} concentration, and shoot Na^+ concentration and negatively correlated with shoot K^+ concentration. The relative abundance of Chloroflexi was positively correlated with the shoot Ca^{2+} and Na^+ concentrations and negatively correlated with the soil available P concentration. The relative abundance of Deltaproteobacteria was positively correlated with soil total N, SOM, and alfalfa CP content. The relative abundance of Gammaproteobacteria was positively correlated with soil available K, soil total N, SOM, alfalfa CP content, and shoot K^+ concentration, and negatively correlated with shoot Ca^{2+} and Na^+ concentrations. The relative abundance of Thermoleophilia was positively correlated with shoot Ca^{2+} concentration and negatively correlated with shoot K^+ concentration.

Relationships Between Alfalfa Yield and Soil and Plant Properties in the Second Growth Year

Pearson's correlation analysis indicated that alfalfa yield was positively correlated with the number of emerged seedlings, and the contents of soil available K, soil total N, and SOM. In addition, alfalfa yield was positively correlated with the shoot K^+ concentration and negatively correlated with the shoot Na^+ concentration (**Table 4**).

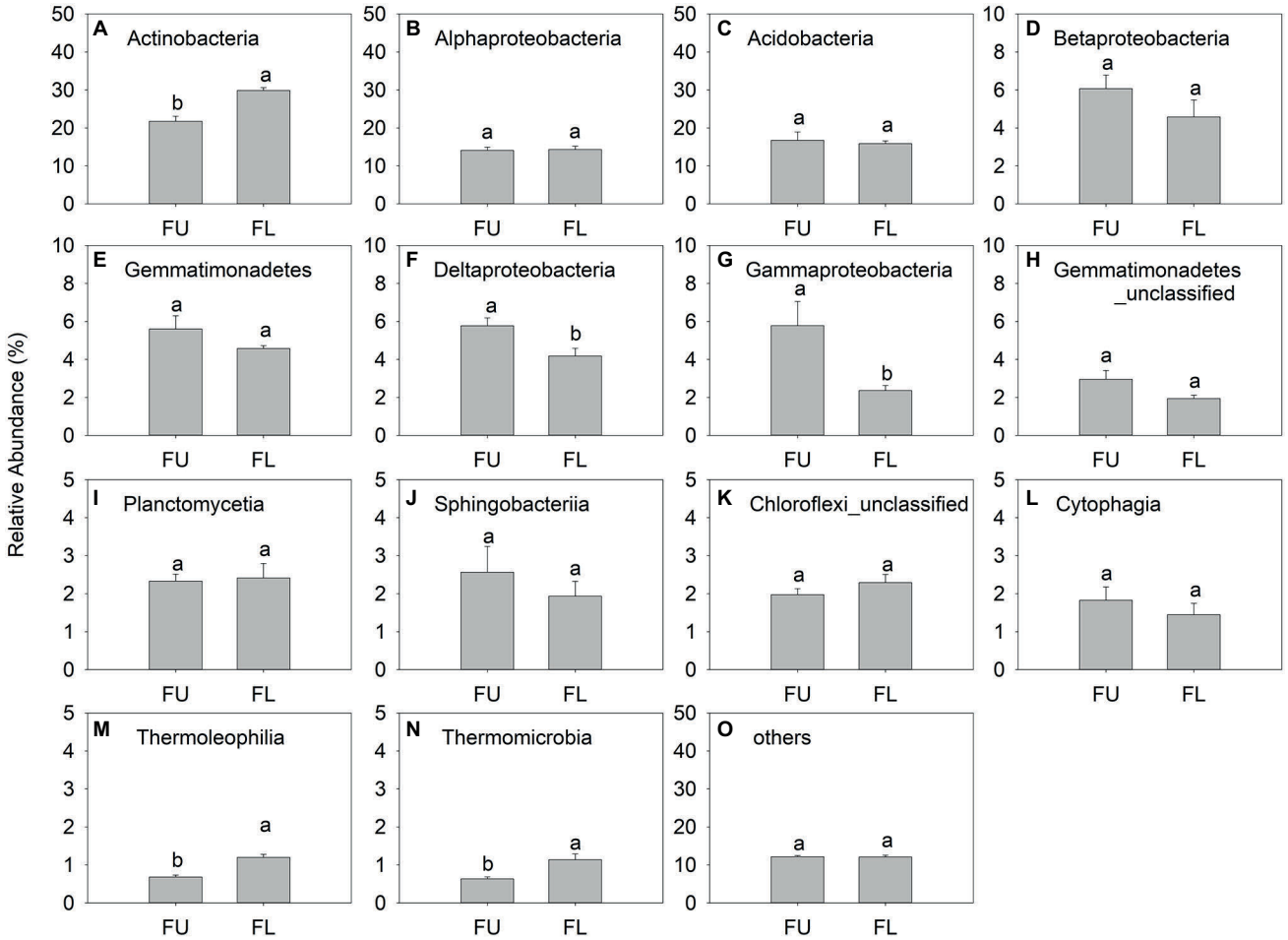

FIGURE 7 | Relative abundance (% of individual taxonomic group) of dominant bacteria classes (mean ± SE, $n = 4$) in microbial communities following FU and FL. **(A-O)** represented different soil bacterial at class level. Different lowercase capital letters indicate statistically significant difference among communities at $p = 0.05$.

DISCUSSION

Effects of FU on Seedling Emergence and Soil Properties at the Seedling Stage

Seedling emergence and establishment are key processes in alfalfa production (Kunzova and Hejcman, 2009). In our study, FU significantly increased the number of emerged seedlings, and this was positively correlated with alfalfa yield (**Table 4**). Soil moisture is one of the main factors affecting seed emergence and plant growth and development (Silvente et al., 2012; Liao et al., 2021). Even a small change in soil water storage can affect crop productivity (Liu et al., 2010a,b). The higher seedling emergence in the FU system than in the FL system was mainly due to the higher soil moisture content in the FU system. Ridge-furrow cropping is a well-known soil–water conservation practice used in crop production. In our study, the water content in the furrow during the seed germination stage was increased in the FU system, consistent with the results of previous studies (Li et al., 2007; Zhang et al., 2011; Zribi et al., 2015; Liao et al., 2019; Suo et al., 2019). The higher soil moisture content in the furrow was mainly because the soil moisture content was higher in the top 15-cm soil layer (the ridge height was 15 cm) than in the surface soil after the rainy season in early fall. It was not due to rainwater harvesting, because there was no rainfall during the seedling period in our experiment. In our study, the FU system reduced the soil temperature at the seedling stage, because the higher soil moisture in the FU treatment reduced the thermal conductivity compared with that of soil in FL. The lower soil temperature did not inhibit seed germination, because alfalfa seeds begin germinating shortly after planting, when soil temperatures are above 18°C and adequate moisture is present (Summers and Putna, 2008). In our study, FU did not significantly affect the soil salinity at the seedling stage, probably because alfalfa seeds were planted after the rainy season in early fall. At this time, the salt had been leached from the soil by rain, so that the salinity levels in topsoil were low both in FU and FL.

Effects of FU on Soil Bacterial Diversity

The PCoA plots show that the bacterial community composition was significantly different between FU and FL (**Figure 5**), indicating that the FU system affected the bacterial

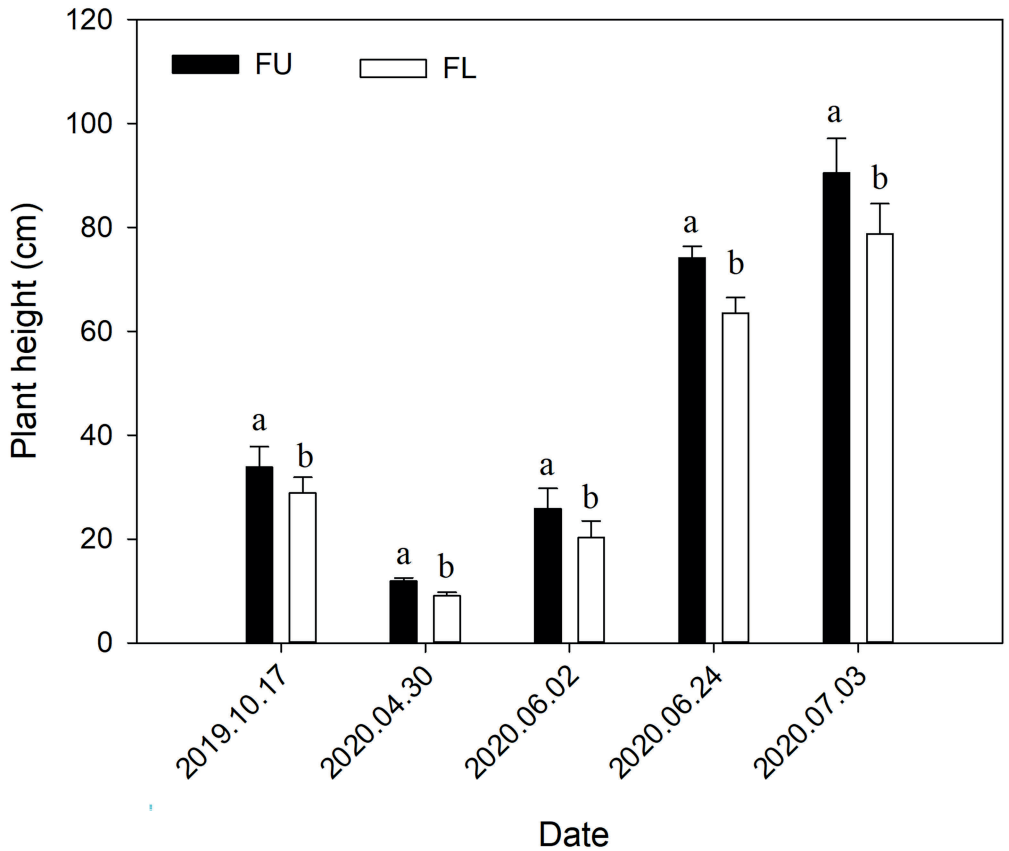

FIGURE 8 | Effects of seeding pattern on alfalfa plant height in 2019 and 2020. Values are means ($n = 4$) ± SE. Different lowercase letters indicate significant difference in plant height between FU and FL at each measurement time ($p \leq 0.05$).

TABLE 2 | Soil properties (0–15 cm depth) under two seeding pattern treatments in April 2020.

Seeding pattern	Ava_P (mg kg^{-1})	Ava_K (mg kg^{-1})	Total N (g kg^{-1})	ECe (dSm^{-1})	SOM (g kg^{-1})
FU	21.7 ± 0.73a	280.7 ± 8.6a	1.05 ± 0.009a	12.8 ± 0.61b	18.8 ± 0.10a
FL	18.0 ± 3.76a	237.3 ± 5.8b	0.8 ± 0.047b	17.3 ± 1.43a	14.6 ± 0.90b

Values are mean (n = 4) ± SE. ava_P, available P; ava_K, available K; ECe, electrical conductivity of a saturated soil extract; SOM, soil organic matter. Different lowercase letters within each column indicate statistically significant differences at p = 0.05.

abundance and diversity at the seedling stage. As indicated by the higher Chao1 value, the FU system increased the bacterial richness compared with that in the FL system (**Table 1**). Consistent with this, a previous study found that agricultural management influences the soil microbial community and composition (Chen et al., 2014). In the present study, the higher bacterial richness in the FU system may have resulted from the higher soil moisture content. Previous studies have shown that soil moisture strongly affects soil bacteria (Bainard et al., 2016; Nguyen et al., 2018) and that higher soil moisture content can favor bacterial growth (Nakamura et al., 2003). Interestingly, neither our study nor a previous study (Yang et al., 2019) detected a strong relationship between soil salinity and soil bacterial abundance. This might be because there were only small variations in salinity at the seedling stage, since alfalfa seeds were sown after the rainy season when much of the salt had been leached from the soil.

In the present study, high-throughput sequencing revealed that the dominant bacterial phyla in saline soils were Proteobacteria, Actinobacteria, Acidobacteria, Gemmatimonadetes, and Chloroflexi (**Figure 6**). These five phyla accounted for an average 85.45% and 86.41% of total bacterial sequences in FU and FL, respectively. This soil bacterial community composition differs from that detected in other agro-ecosystems (Chen et al., 2014). Among these taxa, Chloroflexi, a representative oligotrophic taxa that favors nutrient-poor conditions, was less abundant in FU than in FL. In contrast, the relative abundance of copiotrophic taxa, including Proteobacteria, was higher in FU than in FL. Proteobacteria, especially Betaproteobacteria, are

TABLE 3 | Alfalfa characteristics under two seeding pattern treatments at the first cut in 2020.

Seeding pattern	Yield(DM kg/hm²)	CP (g kg^{-1} DM)	NDF (g kg^{-1} DM)	ADF (g kg^{-1} DM)	Ash (g kg^{-1} DM)	K^+ (g kg^{-1} DM)	Ca^{2+} (g kg^{-1} DM)	Na^+ (g kg^{-1} DM)
FU	7,590 ± 566a	181 ± 1.8a	629 ± 10.9	456 ± 25.4	83.8 ± 2.3b	14.0 ± 0.2a	4.5 ± 0.1a	2.3 ± 0.11b
FL	5,520 ± 405b	174 ± 1.7b	631 ± 26.9	464 ± 21.5	90.8 ± 1.0a	10.5 ± 0.7b	3.8 ± 0.7b	2.8 ± 0.04a

DM, dry matter; CP, crude protein; NDF, Neutral detergent fiber; ADF, acid detergent fiber. Values are mean (n = 4) ± SE. Different lowercase letters within each column indicate statistically significant differences at p = 0.05.

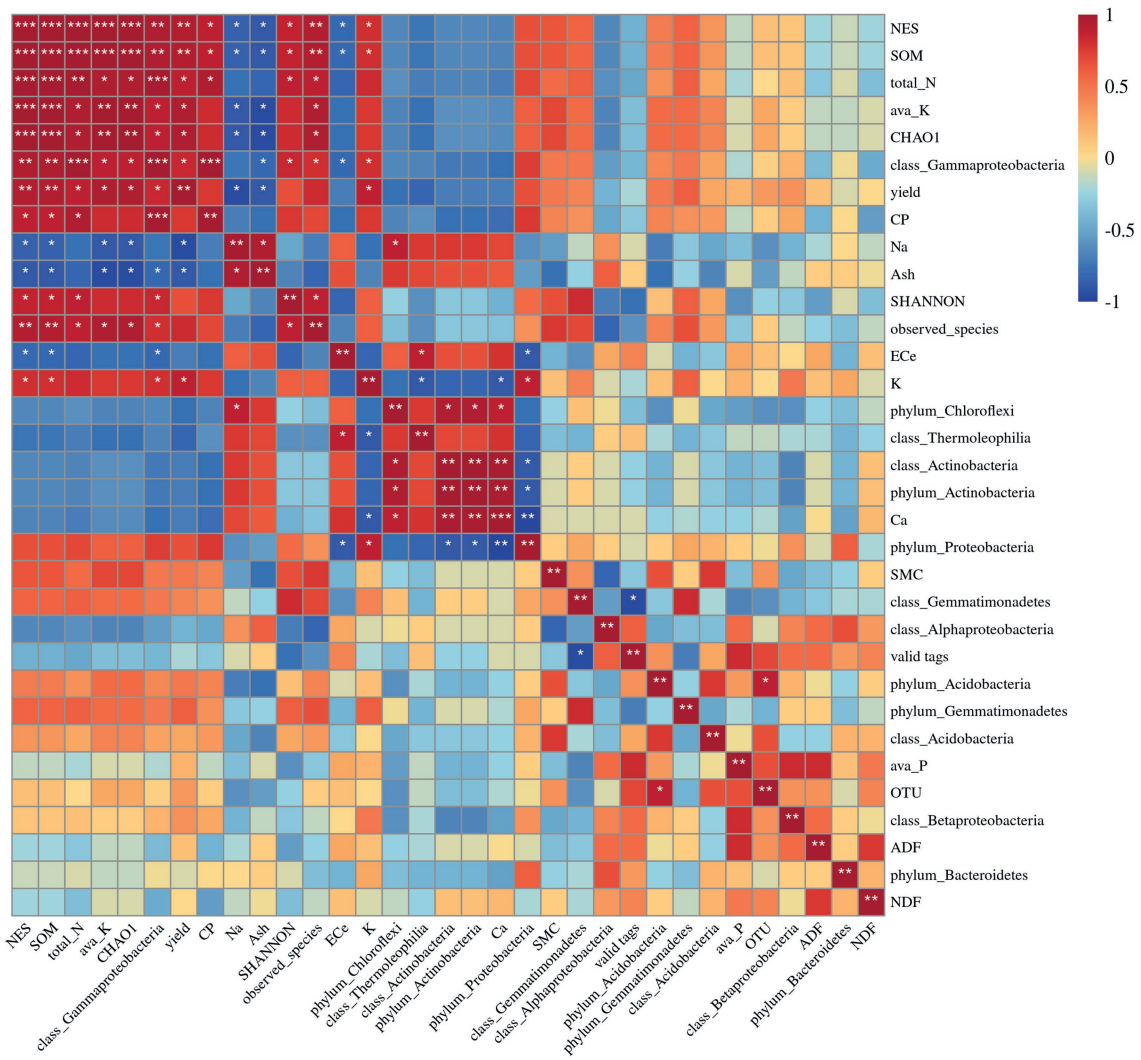

FIGURE 9 | Spearman correlation analysis among soil and plant properties and soil fungal abundance, diversity, and relative abundance of dominant bacteria phyla and classes. NES, number of emergence seedling; SMC, soil moisture content; ava_K, available K; ava_P, available P. The values presented by colors in the heat map correspond to the Spearman correlation coefficient r, which ranged between −1 and 1, where $r < 0$ indicates a negative correlation (blue), $r > 0$ indicates a positive correlation (red), "*" represents $p < 0.05$, "**" represents $p < 0.01$, "***" represents $p < 0.001$.

copiotrophic and favor nutrient-rich conditions with a high C content (Fierer et al., 2007; Newton and McMahon, 2011; Philippot et al., 2013; Wang et al., 2017). Unfortunately, we only analyzed the background surface soil, rather than soil samples collected from plant rows in the FU and FU treatments during the seedling period. Thus, the increased abundance of Proteobacteria in FU may be because of the increased supply of nutrient substrates that improved their growth. Bacteroidetes are copiotrophic and saprophytic bacteria (Fierer et al., 2007) that live in anaerobic environments (Xu et al., 2017). In our study, the abundance of Bacteroidetes was increased in FU. This may have been because of the higher SOM in FU than in FL. In addition, increased soil moisture favors the growth of Bacteroidetes (Xu et al., 2017).

TABLE 4 | Pearson correlations coefficients between alfalfa yield and soil and plant properties ($n = 4$) under two seeding pattern treatments.

	Ava_P	Ava_K	Total N	ECe	SOM	K^+	Ca^{2+}	Na^+	NES
Yield	0.239	0.974**	0.892*	0.106	0.883*	0.888*	−0.689	−0.891*	0.953**

Ava_P, available P; Ava_K, available K; ECe, electrical conductivity of a saturated soil extract; SOM, soil organic matter; NES, number of emergence seedling.
*$p < 0.05$, **$p < 0.05$ (Pearson's correlation coefficient test).*

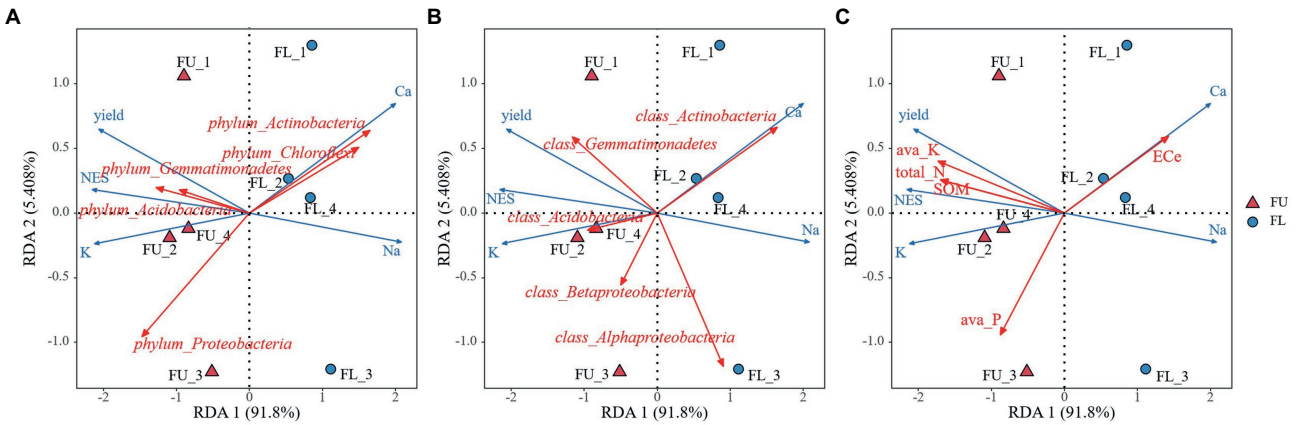

FIGURE 10 | Redundancy analysis (RDA) diagram illustrating the relationship between the plant characteristics between soil bacterial community composition at phylum-level **(A)** class-level **(B)** and soil properties **(C)** from two seeding patterns.

Effects of FU on Soil Properties in the Second Year

Compared with FL, FU reduced the soil salinity in plant belts in the second growth year spring, consistent with the results of a previous study (Dong et al., 2010). The salinity level was lower in furrows in FU than in seeding rows in FL. This is because salinity moves upwards along a capillary gradient in the spring when there is little rainfall, and accumulates on the surface of the soil ridges. A previous study showed that FU can lead to a heterogeneous distribution of salts in the plant root zone (Dong et al., 2010), and our previous study showed that alfalfa plants grow better with heterogeneous salinity than with uniform salinity in the root zone (Sun et al., 2016). The results of the present study show that FU alleviated salt stress in alfalfa in the second growth year.

In this study, the FU system significantly affected the soil physico-chemical properties and enhanced the contents of available nutrients in soil (**Table 2**), similar to the results of a previous study (Sun et al., 2017a). Our results showed that soil available K, total N, and SOM were significantly correlated with observed species and richness (Chao 1) indexes of soil bacterial communities. In our study, the observed species and Chao 1 index values were higher in FU than in FL. Previous studies have indicated that soil moisture content and other physicochemical properties affect microbial populations and community composition (Li and Sarah, 2003; Nguyen et al., 2018), which in turn enhances the formation and decomposition of organic matter (Nair and Ngouajio, 2012; Jing et al., 2013). In our study, the FU system enhanced the SOM, soil total N, and soil available K in the second growth year, possibly as a result of changes in soil microbial populations and community composition.

Effects of FU on Alfalfa Yield and Quality

The FU system increased alfalfa yield compared with the traditional FL system. The yield of alfalfa in the first cut of the second growth year was 37.4% higher in FU than in FL. Previous studies have also reported that FU systems can improve plant production (Li et al., 2001, 2013). In our study, Pearson's correlation analyses showed that alfalfa yield was positively correlated with seedling emergence, soil available K, soil total N, SOM, and shoot K^+ concentration, and negatively correlated with shoot Na^+ concentration (**Table 4**), similarly result were found using RDA analysis (**Figure 10**), indicating that the increased yield was due to high emergence during the seedling stage, and greater nutrient availability for alfalfa uptake. Pearson's correlation analyses showed that there was no significant relationship between soil ECe and yield (**Table 4**), however, RDA analysis shown soil ECe was negatively correlated with alfalfa yield ($p < 0.05$) (**Figure 10C**). In our experiment soil salinity was lower in FU than in FL, and that the alfalfa shoot Na^+ concentration was lower in FU than in FL, suggesting that FU alleviated salinity and improved alfalfa production. Similar results were found in a previous study (Dong et al., 2010). During the whole plant growth period in our study, plant height was higher in FU than in FL in the second growth year spring, and this is an important yield component for alfalfa.

Notably, FU improved alfalfa quality compared with FL. For the first cut of alfalfa, the CP content was higher and NDF, ADF, and ash contents in alfalfa plants were lower in FU than in FL in the second year. The results of the Spearman correlation analyses revealed that the alfalfa CP content was positively correlated with soil total N and SOM (**Figure 9**). Thus, the increased alfalfa CP in FU was related to the increased soil total

N and SOM in the FU system, while the decreased ash content in FU was due to higher soil available K, total N, and SOM. Another important aspect of the improved alfalfa quality in FU was the higher left-stem height, because the CP was lower and NDF, ADF, and ash contents were higher at the basal part of stem. In our experiment, we only compared the responses of alfalfa to the two seeding pattern at the first and second growth year. Response of alfalfa to FU pattern in the other growth year and over longer exposure to salinity soil need further study.

In conclusion, compared with FL, FU increased the soil moisture content and seedling emergence and altered the soil bacterial community during the seedling stage. The FU system also increased the available soil nutrient contents and decreased soil salinity at the returning green stage in the second growth year. Compared with FL, the FU system resulted in significant improvements in alfalfa plant height, yield, and quality, and decreased salt injury. The improved yield was due to higher soil moisture content, higher seedling emergence, higher contents of soil available nutrients and SOM, and lower salt content in the plant rows in spring of the second growth year. Enhanced K^+ and reduced Na^+ accumulation in shoots may be mechanisms to avoid salinity stress. Overall, our results show that specific cultural practices, such as FU, with sowing in early fall have immense potential for alleviating salt stress and improving alfalfa productivity and quality in saline fields. Additionally, FU with sowing in early fall with no need for mulching with plastic, it is inexpensive and do not pollute the soil. Therefore, FU is the effective way of sustaining the alfalfa productivity in saline soil.

DATA AVAILABILITY STATEMENT

The datasets presented in this study can be found in online repositories. The names of the repository/repositories and accession number(s) can be found at: https://www.ncbi.nlm.nih.gov/, PRJNA826619.

AUTHOR CONTRIBUTIONS

KJ and JS conceived and designed the research. JS, JZ, LY, and TZ conducted the experiment and collected the field data. JS and JZ analyzed the data. KJ and JS wrote the manuscript. All authors reviewed and edited the manuscript. All authors contributed to the article and approved the submitted version.

FUNDING

This work was supported by Key Projects in Science and Technology of Inner Mongolia (2021ZD0031), Natural Science Foundation of Inner Mongolia (2018MS03028), Agricultural Science and Technology Innovation Program of CAAS (27-GRI-01), and Science and Technology Project from Inner Mongolia (2021GG0068 and 2019GG260).

ACKNOWLEDGMENTS

We thank Gao Feixiang for providing us weather date. We also thank Jennifer Smith, from Liwen Bianji (Edanz; www.liwenbianji.cn/) for editing the English text of a draft of this manuscript.

SUPPLEMENTARY MATERIAL

The Supplementary Material for this article can be found online at: https://www.frontiersin.org/articles/10.3389/fpls.2022.919912/full#supplementary-material

Supplementary Figure S1 | Relative abundance (% of individual taxonomic group) of dominant bacteria genera (mean ± SE, $n = 4$) in microbial communities following FU and FL. Different lowercase capital letters indicate statistically significant difference among communities at $p = 0.05$.

REFERENCES

Allen, S. G., Dobrenz, A. K., Schonhorst, M. H., and Stoner, J. E. (1985). Heritability of Nacl tolerance in germinating alfalfa seeds. *Aoron. J.* 77, 99–101. doi: 10.2134/agronj1985.00021962007700010023x

Anower, M. R., Mott, I. W., Peel, M. D., and Wu, Y. (2013). Characterization of physiological responses of two alfalfa half-sib families with improved salt tolerance. *Plant Physiol. Biochem.* 71, 103–111. doi: 10.1016/j.plaphy.2013.06.026

Ashraf, M., Mcneilly, T., and Bradshaw, A. D. (1987). Selection and heritability of tolerance to sodium-chloride in four forage species. *Crop. Sci.* 27, 232–234. doi: 10.2135/cropsci1987.0011183X002700020021x

Bainard, L. D., Hamel, C., and Gan, Y. (2016). Edaphic properties override the influence of crops on the composition of the soil bacterial community in a semiarid agroecosystem. *Appl. Soil Ecol.* 105, 160–168. doi: 10.1016/j.apsoil.2016.03.013

Bao, S. D. (2018). *Soil and Agricultural Chemistry Analysis*. Beijing: China Agriculture Press.

Battin, T. J., Kaplan, L. A., Newbold, J. D., and Hansen, C. M. E. (2003). Contributions of microbial biofilms to ecosystem processes in stream mesocosms. *Nature* 426, 439–442. doi: 10.1038/nature02152

Chen, Y., Wen, X., Sun, Y., Zhang, J., Wu, W., and Liao, Y. (2014). Mulching practices altered soil bacterial community structure and improved orchard productivity and apple quality after five growing seasons. *Sci. Hortic.* 172, 248–257. doi: 10.1016/j.scienta.2014.04.010

Cheng, Q., Chang, H., Yang, X., Wang, D., and Wang, W. (2021). Salinity and nutrient modulate soil bacterial communities in the coastal wetland of the Yellow River Delta, China. *Environ. Sci. Pollut. Res.* 28, 14621–14631. doi: 10.1007/s11356-020-11626-x

Chi, Z., Wang, W., Li, H., Wu, H., and Yan, B. (2021). Soil organic matter and salinity as critical factors affecting the bacterial community and function of *Phragmites australis* dominated riparian and coastal wetlands. *Sci. Total Environ.* 762:143156. doi: 10.1016/j.scitotenv.2020.143156

Cuello, J. P., Hwang, H. Y., Gutierrez, J., Kim, S. Y., and Kim, P. J. (2015). Impact of plastic film mulching on increasing greenhouse gas emissions in temperate upland soil during maize cultivation. *Appl. Soil Ecol.* 91, 48–57. doi: 10.1016/j.apsoil.2015.02.007

Deinlein, U., Stephan, A. B., Horie, T., Luo, W., Xu, G., and Schroeder, J. I. (2014). Plant salt-tolerance mechanisms. *Trends Plant Sci.* 19, 371–379. doi: 10.1016/j.tplants.2014.02.001

Devkota, M., Martius, C., Gupta, R. K., Devkota, K. P., Mcdonald, A. J., and Lamers, J. P. A. (2015). Managing soil salinity with permanent bed planting in irrigated production systems in Central Asia. *Agric. Ecosyst. Environ.* 202, 90–97. doi: 10.1016/j.agee.2014.12.006

Dong, H., Kong, X., Luo, Z., Li, W., and Xin, C. (2010). Unequal salt distribution in the root zone increases growth and yield of cotton. *Eur. J. Agron.* 33, 285–292. doi: 10.1016/j.eja.2010.08.002

Dong, H., Li, W., Tang, W., and Zhang, D. (2009). Early plastic mulching increases stand establishment and lint yield of cotton in saline fields. *Field Crop Res* 111, 269–275. doi: 10.1016/j.fcr.2009.01.001

Esechie, H. A., Al-Barhi, B., Al-Gheity, S., and Al-Khanjari, S. (2002). Root and shoot growth in salinity-stressed alfalfa in response to nitrogen source. *J. Plant Nutr.* 25, 2559–2569. doi: 10.1081/PLN-120014713

Fan, Z. L., Ma, Y. J., and Ma, Y. J. (2001). Salinized soils and their improvement and utilization in West China. *Arid Zone Res.* 18, 1–6. doi: 10.13866/j.azr.2001.03.001

Fierer, N., Bradford, M. A., and Jackson, R. B. (2007). Toward an ecological classification of soil bacteria. *Ecology* 88, 1354–1364. doi: 10.1890/05-1839

Gao, Y., Wang, J., Guo, S., Hu, Y., Li, T., Mao, R., et al. (2015). Effects of salinization and crude oil contamination on soil bacterial community structure in the Yellow River Delta region, China. *Appl. Soil Ecol.* 86, 165–173. doi: 10.1016/j.apsoil.2014.10.011

Gu, Y. J., Han, C. L., Kong, M., Shi, X. Y., Zdruli, P., and Li, F. M. (2018). Plastic film mulch promotes high alfalfa production with phosphorus-saving and low risk of soil nitrogen loss. *Field Crop Res* 229, 44–54. doi: 10.1016/j.fcr.2018.09.011

Guo, X. P., Lu, D. P., Niu, Z. S., Feng, J. N., Chen, Y. R., Tou, F. Y., et al. (2018). Bacterial community structure in response to environmental impacts in the intertidal sediments along the Yangtze estuary, China. *Mar. Pollut. Bull.* 126, 141–149. doi: 10.1016/j.marpolbul.2017.11.003

Jing, T., Lu, S., Fan, M., Li, X., and Kuzyakov, Y. (2013). Labile soil organic matter fractions as influenced by non-flooded mulching cultivation and cropping season in rice-wheat rotation. *Eur. J. Soil Biol.* 56, 19–25. doi: 10.1016/j.ejsobi.2013.02.001

Jurburg, S. D., Natal-da-Luz, T., Raimundo, J., Morais, P. V., Sousa, J. P., van Elsas, J. D., et al. (2018). Bacterial communities in soil become sensitive to drought under intensive grazing. *Sci. Total Environ.* 618, 1638–1646. doi: 10.1016/j.scitotenv.2017.10.012

Kargas, G., Kerkides, P., Seyfried, M., and Sgoumbopoulou, A. (2011). WET sensor performance in organic and inorganic media with heterogeneous moisture distribution. *Soil Sci. Soc. Am. J.* 75, 1244–1252. doi: 10.2136/sssaj2010.0238

Krishnamoorthy, U., Muscato, T. V., Sniffen, C. J., and Van Soest, P. J. (1982). Nitrogen fractions in selected feedstuffs. *J. Dairy Sci.* 65, 217–225. doi: 10.3168/jds.S0022-0302(82)82180-2

Kunzova, E., and Hejcman, M. (2009). Yield development of winter wheat over 50 years of FYM, N, P and K fertilizer application on black earth soil in the Czech Republic. *Field Crop Res* 111, 226–234. doi: 10.1016/j.fcr.2008.12.008

Latrach, L., Farissi, M., Mouradi, M., Makoudi, B., Bouizgaren, A., and Ghoulam, C. (2014). Growth and nodulation of alfalfa-rhizobia symbiosis under salinity: electrolyte leakage, stomatal conductance, and chlorophyll fluorescence. *Turk. J. Agric. For.* 38, 320–326. doi: 10.3906/tar-1305-52

Li, X. Y., Gong, J. D., Gao, Q. Z., and Li, F. R. (2001). Incorporation of ridge and furrow method of rainfall harvesting with mulching for crop production under semiarid conditions. *Agric Water Manag* 50, 173–183. doi: 10.1016/S0378-3774(01)00105-6

Li, X. Y., Gong, J. D., and Wei, X. H. (2000). In-situ rainwater harvesting and gravel mulch combination for corn production in the dry semi-arid region of China. *J. Arid Environ.* 46, 371–382. doi: 10.1006/jare.2000.0705

Li, R., Hou, X., Jia, Z., Han, Q., Ren, X., and Yang, B. (2013). Effects on soil temperature, moisture, and maize yield of cultivation with ridge and furrow mulching in the rainfed area of the loess plateau, China. *Agric Water Manag* 116, 101–109. doi: 10.1016/j.agwat.2012.10.001

Li, Y., Kang, Z., Song, B., Wang, J., Zhang, X., Wang, J., et al. (2021). Soil salinity and nutrients availability drive patterns in bacterial community and diversity along succession gradient in the Yellow River Delta. *Estuar. Coast. Shelf Sci.* 262:107621. doi: 10.1016/j.ecss.2021.107621

Li, X., and Sarah, P. (2003). Enzyme activities along a climatic transect in the Judean Desert. *Catena* 53, 349–363. doi: 10.1016/S0341-8162(03)00087-0

Li, X., Su, D., and Yuan, Q. (2007). Ridge-furrow planting of alfalfa (*Medicago sativa* L.) for improved rainwater harvest in rainfed semiarid areas in Northwest China. *Soil Tillage Res.* 93, 117–125. doi: 10.1016/j.still.2006.03.022

Liao, Y., Cao, H. X., Xue, W. K., and Liu, X. (2021). Effects of the combination of mulching and deficit irrigation on the soil water and heat, growth and productivity of apples. *Agric Water Manag* 243:106482. doi: 10.1016/j.agwat.2020.106482

Liao, R., Wu, Y., Hu, Y., Xu, D., Huang, Q., and Wang, S. (2019). Micro-irrigation strategies to improve water-use of cherry trees in Northern China. *Agric. Water Manage.* 221, 388–396. doi: 10.1016/j.agwat.2019.05.017

Ling, N., Chen, D., Guo, H., Wei, J., Bai, Y., Shen, Q., et al. (2017). Differential responses of soil bacterial communities to long-term N and P inputs in a semi-arid steppe. *Geoderma* 292, 25–33. doi: 10.1016/j.geoderma.2017.01.013

Liu, Y., Li, S., Chen, F., Yang, S., and Chen, X. (2010a). Soil water dynamics and water use efficiency in spring maize (*Zea mays* L.) fields subjected to different water management practices on the loess plateau. *China Agric. Water Manag.* 97, 769–775. doi: 10.1016/j.agwat.2010.01.010

Liu, X. E., Li, X. G., Hai, L., Wang, Y. P., and Li, F. M. (2014). How efficient is film fully-mulched ridge-furrow cropping to conserve rainfall in soil at a rainfed site? *Field Crop Res* 169, 107–115. doi: 10.1016/j.fcr.2014.09.014

Liu, Y., Yang, S., Li, S., Chen, X., and Chen, F. (2010b). Growth and development of maize (*Zea mays* L.) in response to different field water management practices: resource capture and use efficiency. *Agric. For. Meteorol.* 150, 606–613. doi: 10.1016/j.agrformet.2010.02.003

Logue, J., Stedmon, C., Kellerman, A., Nielsen, N., Andersson, A., Laudon, H., et al. (2016). Experimental insights into the importance of aquatic bacterial community composition to the degradation of dissolved organic matter. *ISME J.* 10, 533–545. doi: 10.1038/ismej.2015.131

Meiri, A., and Plaut, Z. (1985). Crop production and management under saline conditions. *Plant and Soil* 89, 253–271. doi: 10.1007/bf02182246

Munns, R., and Tester, M. (2008). Mechanisms of salinity tolerance. *Annu. Rev. Plant Biol.* 59, 651–681. doi: 10.1146/annurev.arplant.59.032607.092911

Nair, A., and Ngouajio, M. (2012). Soil microbial biomass, functional microbial diversity, and nematode community structure as affected by cover crops and compost in an organic vegetable production system. *Appl. Soil Ecol.* 58, 45–55. doi: 10.1016/j.apsoil.2012.03.008

Nakamura, A., Tun, C. C., Asakawa, S., and Kimura, M. (2003). Microbial community responsible for the decomposition of rice straw in a paddy field: estimation by phospholipid fatty acid analysis. *Biol. Fertil. Soils* 38, 288–295. doi: 10.1007/s00374-003-0658-6

Newton, R. J., and McMahon, K. D. (2011). Seasonal differences in bacterial community composition following nutrient additions in a eutrophic lake. *Environ. Microbiol.* 13, 887–899. doi: 10.1111/j.1462-2920.2010.02387.x

Nguyen, L. T. T., Osanai, Y., Lai, K., Anderson, I. C., Bange, M. P., Tissue, D. T., et al. (2018). Responses of the soil microbial community to nitrogen fertilizer regimes and historical exposure to extreme weather events: flooding or prolonged-drought. *Soil Biol. Biochem.* 118, 227–236. doi: 10.1016/j.soilbio.2017.12.016

Nie, Y., Wang, M., Zhang, W., Ni, Z., Hashidoko, Y., and Shen, W. (2018). Ammonium nitrogen content is a dominant predictor of bacterial community composition in an acidic forest soil with exogenous nitrogen enrichment. *Sci. Total Environ.* 624, 407–415. doi: 10.1016/j.scitotenv.2017.12.142

Noble, C. L., Halloran, G. M., and West, D. W. (1984). Identification and selection for salt tolerance in lucerne (*Medicago sativa* L.). *Aust. J. Agr. Res.* 35, 239–252. doi: 10.1071/ar9840239

Philippot, L., Raaijmakers, J. M., Lemanceau, P., and van der Putten, W. H. (2013). Going back to the roots: the microbial ecology of the rhizosphere. *Nat. Rev. Microbiol.* 11, 789–799. doi: 10.1038/nrmicro3109

Robertson, J. B., and Van Soest, P. J. (1981). "The detergent system of analysis and its application to human foods," in *The Analysis of Dietary Fiber in Food*. eds. W. P. T. James and O. Theander (New York, NY, USA: Marcel Dekker), 123–158.

Silvente, S., Sobolev, A. P., and Lara, M. (2012). Metabolite adjustments in drought tolerant and sensitive soybean genotypes in response to water stress. *PLoS One* 7:e38554. doi: 10.1371/journal.pone.0038554

Summers, CG, and Putna, DH. (2008). *Irrigated Alfalfa Management for Mediterranean and Desert Zones*. University of California Agriculture and Natural Resources, California

Sun, C. T., Feng, D., Mi, Z. R., Li, C. X., Zhang, J. P., Gao, Y., et al. (2017a). Impacts of ridge-furrow planting on salt stress and cotton yield under drip irrigation. *Watermark* 9:49. doi: 10.3390/w9010049

Sun, J., Yang, G., Zhang, W., and Zhang, Y. (2016). Effects of heterogeneous salinity on growth, water uptake, and tissue ion concentrations of alfalfa. *Plant and Soil* 408, 211–226. doi: 10.1007/s11104-016-2922-1

Sun, J., Yu, L., Zhao, J., Liu, H., and Zhang, Y. (2017b). Effects of heterogeneous root zone salinity on plant growth and ion characteristic in alfalfa. *Sci. Agric. Sin.* 50, 4329–4306. doi: 10.3864/j.issn.0578-1752.2017.22.006

Suo, G. D., Xie, Y. S., Zhang, Y., and Luo, H. (2019). Long-term effects of different surface mulching techniques on soil water and fruit yield in an apple orchard on the loess plateau of China. *Sci. Hortic.* 246, 643–651. doi: 10.1016/j.scienta.2018.11.028

Van Soest, P. J., Robertson, J. B., and Lewis, B. A. (1991). Methods for dietary fiber, neutral detergent fiber, and nonstarch polysaccharides in relation to animal nutrition. *J. Dairy Sci.* 74, 3583–3597. doi: 10.3168/jds.S0022-0302(91)78551-2

Wakelin, S. A., Colloff, M. J., Harvey, P. R., Marschner, P., Gregg, A. L., and Rogers, S. L. (2007). The effects of stubble retention and nitrogen application on soil microbial community structure and functional gene abundance under irrigated maize. *FEMS Microbiol. Ecol.* 59, 661–670. doi: 10.1111/j.1574-6941.2006.00235.x

Wang, J., Song, Y., Ma, T., Raza, W., Li, J., Howland, J. G., et al. (2017). Impacts of inorganic and organic fertilization treatments on bacterial and fungal communities in a paddy soil. *Appl. Soil Ecol.* 112, 42–50. doi: 10.1016/j.apsoil.2017.01.005

Xiong, X., Wei, Y.-q., Chen, J.-h., Liu, N., and Zhang, Y.-j. (2020). Transcriptome analysis of genes and pathways associated with salt tolerance in alfalfa under non-uniform salt stress. *Plant Physiol. Biochem.* 151, 323–333. doi: 10.1016/j.plaphy.2020.03.035

Xu, S., Lu, W., Liu, Y., Ming, Z., Liu, Y., Meng, R., et al. (2017). Structure and diversity of bacterial communities in two large sanitary landfills in China as revealed by high-throughput sequencing (MiSeq). *Waste Manag.* 63, 41–48. doi: 10.1016/j.wasman.2016.07.047

Yang, Y., Dou, Y., and An, S. (2018). Testing association between soil bacterial diversity and soil carbon storage on the loess plateau. *Sci. Total Environ.* 626, 48–58. doi: 10.1016/j.scitotenv.2018.01.081

Yang, W., Jeelani, N., Zhu, Z. H., Luo, Y. Q., Cheng, X. L., and An, S. Q. (2019). Alterations in soil bacterial community in relation to *Spartina alterniflora* Loisel. Invasion chronosequence in the eastern Chinese coastal wetlands. *Appl. Soil Ecol.* 135, 38–43. doi: 10.1016/j.apsoil.2018.11.009

Zhang, S., Li, P., Yang, X., Wang, Z., and Chen, X. (2011). Effects of tillage and plastic mulch on soil water, growth and yield of spring-sown maize. *Soil Tillage Res.* 112, 92–97. doi: 10.1016/j.still.2010.11.006

Zhao, Q., Bai, J., Gao, Y., Zhao, H., Zhang, G., and Cui, B. (2020). Shifts in the soil bacterial community along a salinity gradient in the Yellow River Delta. *Land Degrad. Dev.* 31, 2255–2267. doi: 10.1002/ldr.3594

Zribi, W., Aragues, R., Medina, E., and Faci, J. M. (2015). Efficiency of inorganic and organic mulching materials for soil evaporation control. *Soil Tillage Res.* 148, 40–45. doi: 10.1016/j.still.2014.12.003

Conflict of interest: The authors declare that the research was conducted in the absence of any commercial or financial relationships that could be construed as a potential conflict of interest.

Publisher's Note: All claims expressed in this article are solely those of the authors and do not necessarily represent those of their affiliated organizations, or those of the publisher, the editors and the reviewers. Any product that may be evaluated in this article, or claim that may be made by its manufacturer, is not guaranteed or endorsed by the publisher.

frontiers | Frontiers in Plant Science

ORIGINAL RESEARCH
published: 09 June 2022
doi: 10.3389/fpls.2022.931619

Comparative Physiological and Transcriptome Profiles Uncover Salt Tolerance Mechanisms in Alfalfa

*Jiali Li, Maosen Ma, Yanmei Sun, Ping Lu, Haifan Shi, Zhenfei Guo and Haifeng Zhu**

College of Grassland Science, Nanjing Agricultural University, Nanjing, China

Salinity is a major limiting factor that affects crop production. Understanding of the mechanisms of plant salt tolerance is critical for improving crop yield on saline land. Alfalfa (*Medicago sativa* L.) is the most important forage crop, while its salt tolerance mechanisms are largely unknown. The physiological and transcriptomic responses in two contrasting salt tolerant cultivars to salinity stress were investigated in the present study. "Magnum Salt" showed higher salt tolerance than "Adrenalin," with higher relative germination rate, survival rate, biomass and K^+/Na^+ ratio after salt treatment. Activities of antioxidant enzymes SOD, CAT and GR, and proline concentrations were upregulated to higher levels in roots and shoots in Magnum Salt than in Adrenalin after salinity stress, except for no difference in GR activity in shoots, and lower levels of $O_2^{\cdot -}$ and H_2O_2 were accumulated in leaves. It was interesting to find that salinity caused a decrease in total unsaturated fatty acid in Adrenalin other than Magnum Salt, C18:2 was increased significantly after salinity in Magnum Salt, while it was unaltered in Adrenalin. High quality RNA sequencing (RNA-seq) data was obtained from samples of Magnum Salt and Adrenalin at different time points (0, 2, and 26 h). Generally, "phagosome," "TCA cycle" and "oxidative phosphorylation" pathways were inhibited by salinity stress. Upregulated DEGs in Magnum Salt were specifically enriched in "fatty acid metabolism," "MAPK signaling" and "hormone signal transduction" pathways. The DEGs involved in ionic homeostasis, reactive oxygen species (ROS) scavenging and fatty acid metabolism could partially explain the difference in salt tolerance between two cultivars. It is suggested that salt tolerance in alfalfa is associated with regulation of ionic homeostasis, antioxidative enzymes and fatty acid metabolism at both transcriptional and physiological level.

Keywords: alfalfa, salt tolerance, transcriptome, ionic homeostasis, antioxidant defense system, unsaturated fatty acids

OPEN ACCESS

Edited by:
Maofeng Chai,
Qingdao Agricultural University, China

Reviewed by:
Jinlong Liu,
Northwest A&F University, China
Wenxian Liu,
Lanzhou University, China

***Correspondence:**
Haifeng Zhu
zhuhaifeng@njau.edu.cn

Specialty section:
This article was submitted to Plant Abiotic Stress, a section of the journal Frontiers in Plant Science

Received: *29 April 2022*
Accepted: *19 May 2022*
Published: *09 June 2022*

Citation:
Li J, Ma M, Sun Y, Lu P, Shi H, Guo Z and Zhu H (2022) Comparative Physiological and Transcriptome Profiles Uncover Salt Tolerance Mechanisms in Alfalfa. Front. Plant Sci. 13:931619. doi: 10.3389/fpls.2022.931619

INTRODUCTION

Salinity is one of the most important abiotic stresses affecting agricultural productions. Over 800 million hectares of arable lands are facing the problem of salinity in the world (Liu and Wang, 2021). Salt stress can cause growth inhibition even senescence and death in plants. Hyperosmosis is the primary transient effect of salinization to plants that lead to water absorption inhibition and dehydration. As exposure prolong, ionic equilibrium is interrupted with Na^+ hyperaccumulation and K^+ and Ca^{2+} influx hinder, followed by secondary injury such as photosynthesis inhibition,

oxidative injury and metabolic disorder. Cultivation of salt-tolerant plants is a sustainable strategy to make better use of saline land, contributing to carbon neutral at mean time. The identification of salt tolerant plant germplasm resources and understanding their salt tolerance mechanisms are significant for new salt tolerant plant breeding and saline soil utilization.

Alfalfa (*Medicago sativa* L.) is the world's most extensively cultivated forage legume. Improving salt tolerance is an important goal in alfalfa breeding. Different genotypes of alfalfa exhibit wide variations in salt tolerance. Yu et al. (2021) evaluated salt tolerance of 20 alfalfa cultivars at seedling stage and divided them into highly salt-tolerant, salt-tolerant, moderately salt-tolerant and salt-sensitive groups. Cornacchione and Suarez (2017) identified "SISA14" and "SW 8421S" populations as the most salt tolerant out of 15 alfalfa populations with high production in salt condition. In our research, salt-tolerance of 8 alfalfa cultivars was studied and one salt tolerant cultivar "Magnum Salt" and one salt sensitive cultivar "Adrenalin" were identified for further study.

Plants utilize multiple strategies to alleviate salt stress damage. Thus, salt tolerance is a complex trait controlled by multiple genes involving in salt perception, signaling transduction, osmotic regulation, ion transport, hormones synthesis, photosynthesis and metabolization (Deinlein et al., 2014). A few genes involved in salt resistance have been reported in alfalfa. For example, *MsCBL4* enhances calcium metabolism but not sodium transport in transgenic tobacco under salt stress (An et al., 2020); *MsPP2CA1* gene confers enhanced salt tolerance in *Arabidopsis*, which may due to osmolytes accumulation other than protecting the cell membrane from the damage by superoxide anion radicals (Guo et al., 2018). Besides, gene function of *MsGRP* (Long et al., 2013), *MsWRKY11* (Wang et al., 2018), *MsERF11* (Chen et al., 2012), *MsGME* (Ma et al., 2014), *MsRCI2A/B/C* (Li et al., 2021) and *MsZEP* (Zhang et al., 2016) in salt resistance have been reported.

RNA sequencing allows for analysis of the transcript levels as well as alternative splicing and novel transcript identification, showing great potential in tolerance mechanism studying and salt tolerant genes identification. Gruber et al. (2017) compared the transcriptome profiles of two salinity-tolerant alfalfa breeding populations and a more salinity-sensitive population, found that both saline-tolerant populations showed more substantial up-regulation in redox-related genes and B-ZIP transcripts. Time course full-length transcriptome database for alfalfa root tips under NaCl was constructed by Luo et al. (2019). Total of 8861 NaCl-regulated differentially expressed genes were identified, in which continuously up-regulated genes were mainly involved in "ion homeostasis," "antiporter activity," "trehalose biosynthetic process," "thiamine pyrophosphate binding," and "ethylene-activated signaling pathway." By analyzing the transcriptome of salt tolerant "Halo" and salt intolerant "Vernal," Bhattarai et al. (2021) found out that ion binding was the key molecular activity for salt tolerance in alfalfa. Furthermore, they identified 28 (leaf) and 31 (root) salt responsive candidate genes involved in transmembrane protein function, photosynthesis, carbohydrate metabolism, defense against oxidative damage, cell wall modification and protection against lipid peroxidation.

In our research, time course transcriptome database of roots from salt tolerant cultivar "Magnum Salt" and salt sensitive "Adrenalin" was conducted to understand the salt resistance mechanism of alfalfa. It was found that regulation of genes involved in K^+, Na^+, and Ca^{2+} homeostasis, reactive oxygen species (ROS) scavenging, as well as fatty acid metabolization, especially unsaturated fatty acid linoleic acid (C18:2) metabolization, might play important roles in salt resistance in alfalfa.

MATERIALS AND METHODS

Evaluation of Germination Rate Under Salt Solution

A germination test was carried out using eight alfalfa cultivars, and 150 mM NaCl was used as salt treatment according to pre-experiments. Fifty plump seeds per petri dish were treated with 30 mL ddH_2O or 150 mM NaCl solution with three replicates. The criterion of germination is the appearance of a 2 mm radicle protrusion. The relative germination was calculated as 100 × germination rate within 7 days in salt treatment group divided by germination rate in control group.

Evaluation of Survival Rate Under Salt Treatment

Survival rates were evaluated according to Sun et al. (2020) with modification. The four-week old seedings planted in 50-pots tray were treated with 1 L Hoagland nutrient solution with or without 500 mM NaCl (pH 5.8) weekly for 3 weeks. The surviving plants with turgid and green leaves and dead plants were counted for calculation of survival rate after 1 week of recovery by washing NaCl solution with water.

Evaluation of Biomass and $K^+/Na^+/Ca^{2+}$ Concentration by Hydroponic Culture

Two-week old Magnum Salt and Adrenalin seedlings grown in soil with a mixture of pearlite, vermiculite and perlite (1:1:2) were transferred to a plate filled with 1/2 Hoagland nutrient solution (pH 5.8) for 1 week recovery growth. After that, seedlings were treated with 1/2 Hoagland nutrient solution containing 0 or 150 mM NaCl for 7 days, which was determined according to pre-experiments. Biomass were analyzed with 10 replicates, and $K^+/Na^+/Ca^{2+}$ concentrations were measured as described by Dai et al. (2022).

ROS, Antioxidant Enzyme Activities and Proline Content Analysis

Four-week old Magnum Salt and Adrenalin seedlings grown in soil (pearlite: vermiculite: perlite 1:1:2) were treated with ddH_2O or 500 mM NaCl every 3 days, which was modified with reference to method of Dai et al. (2022). Six days later, DAB (3,3′-Diaminobenzidine) and NBT (ρ-nitro blue tetrazolium chloride) staining for H_2O_2 and $O_2^{\cdot-}$ were performed as below. Leaves of the same position were collected followed by submerging into 0.1% DAB or NBT solution for 24 h. After decolorizing with

95% alcohol, photographs of the leaves were taken under an optical microscope. Antioxidant enzyme activity and free proline content were analyzed according to Zhuo et al. (2018).

Fatty Acids Content Analysis

Roots from seedlings treated with 500 mM NaCl solution for 3 and 6 days were collected for fatty acid content analysis. Gas chromatographic analysis was used and the procedure was as described previous (Huang et al., 2017). DBI (Double-bond index) was used to measure the degree of lipid total unsaturation. DBI = [1 × (% 18:1) + 2 × (% 18:2) + 3 × (% 18:3)]/100, as described by De Vos et al. (1993).

RNA Extraction, Library Construction, and Sequencing

Two-week old seedlings grown in soil with a mixture of pearlite, vermiculite and perlite (1:1:2) were transferred to a plate filled with 1/2 Hoagland nutrient solution (pH 5.8) for 1 week recovery growth. After that, seedlings were treated with 1/2 Hoagland nutrient solution containing 150 mM NaCl, roots were sampled at 0, 2, and 26 h. Total RNA of roots were extracted using a RNAprep pure Plant Kit (Tiangen Inc., Beijing, China). mRNAs were purified using Dynabeads Oligo$(dT)_{25}$ (Life Technologies). Ribo-Zero^{TM} Magnetic Kit (Epicentre) was used to remove rRNA. The derived mRNAs were fragmented and reverse transcribed into cDNAs with random hexamer. The cDNAs were purified and ligated to adaptors for Illumina paired-end sequencing. The cDNA library was sequenced using the Illumina HiSeq^{TM}4000 system by Gene Denovo Biotechnology Co. (Guangzhou, China). The sequencing data has all been archived in the NCBI Sequence Read Archive (SRA) database under accession number PRJNA830977.

Unigene *de novo* Assembly and Annotation

Raw reads were initially cleaned by removing adaptor sequences and low quality reads to get clean reads. The Trinity program was carried out to assemble the clean reads to obtain nonredundant unigenes. The assembly unigenes functional annotations were obtained using NCBI nucleotide sequence database (Nt), nonredundant protein database, Swiss-Prot database, Clusters of Orthologous Groups of proteins (COG) database, Gene Ontology (GO) annotation and Kyoto Encyclopedia of Genes and Genomes (KEGG) annotation database.

Identification of Differentially Expressed Genes

Differentially expressed genes (DEGs) was analyzed by a DESeq R package[1] with the thresholds of false discovery rate (FDR) < 0.05 and $|\text{Log2Fold-Change}| > 4$. Then DEGs GO enrichment and KEGG analysis were performed with agriGO 2.0[2] and KOBAS 3.0[3], respectively.

[1]http://www.r-project.org/

[2]http://systemsbiology.cau.edu.cn/agriGOv2/

[3]http://kobas.cbi.pku.edu.cn/

Differentially Expressed Genes Temporal Expression Patterns Analysis

To achieve the temporal expression patterns, the DEGs of at 2 and 26 h after salt treatment were analyzed with the Short Time-series Expression Miner (STEM) software (v1.3.11; Ernst and Bar-Joseph, 2006). The potential function annotations and enrichments of DEGs identified in STEM analysis were explored with KEGG analysis.

Heatmap Analysis

FPKM was used for representing the expression abundance of genes. The clustered heatmap was portrayed after normalized with zero-to-one scale method using the TBtools software (Chen et al., 2020).

Quantitative Real-Time PCR Analysis

cDNA synthesis was performed with HiScript III RT SuperMix for qPCR (+gDNA wiper) reagent kit with gDNA Eraser (Vazyme, China). qRT-PCR reaction was performed following the instructions of ChamQ Universal SYBR qPCR Master Mix (Vazyme, China). All primer sequences are shown in **Supplementary Table 5**. The relative gene expression level was calculated with $2^{-\Delta\Delta Ct}$ method.

Statistical Analysis

All data were subjected to analysis of variances according to the model for completely randomized design using an SPSS program (SPSS Inc., Chicago, United States). Significant differences among means of cultivars in **Figure 1** were evaluated by one-way ANOVA at 0.05 probability level. Significant differences among means of both treatments and cultivars were evaluated by LSD test at 0.05 probability level.

RESULTS

Identification of Salt-Tolerant and Salt-Sensitive Cultivars

Salt tolerance of eight commonly planted cultivars was evaluated based on relative germination rate and survival rate in response to salt treatment. The relative germination rate decreased in "Magnum Salt," "Magnum 601," "Magnum II," "Magnum 5010," "Zhongmu No.1," "Sanditi," and "Adrenalin" sequentially (**Figure 1A**). "Magnum Salt," "Magnum 601," "Magnum II," "Magnum 5010," and "Zhongmu No.1" had significantly higher survival rate than "Sanditi" and "Adrenalin" after the seedling were irrigated with 500 mM NaCl solution for 3 weeks (**Figures 1B,C**). The data indicated that "Magnum Salt" and "Adrenalin" showed the highest and lowest salt tolerance, respectively.

Growth performance of Magnum Salt and Adrenalin was further evaluated by hydroponic culture experiment (**Figure 2**). Treatment with 150 mM NaCl caused obvious inhibition of root growth and yellowing of leaves in both cultivars (**Figure 2A**). Dry weight of roots or shoots showed no significant difference between Magnum Salt and Adrenalin under control condition

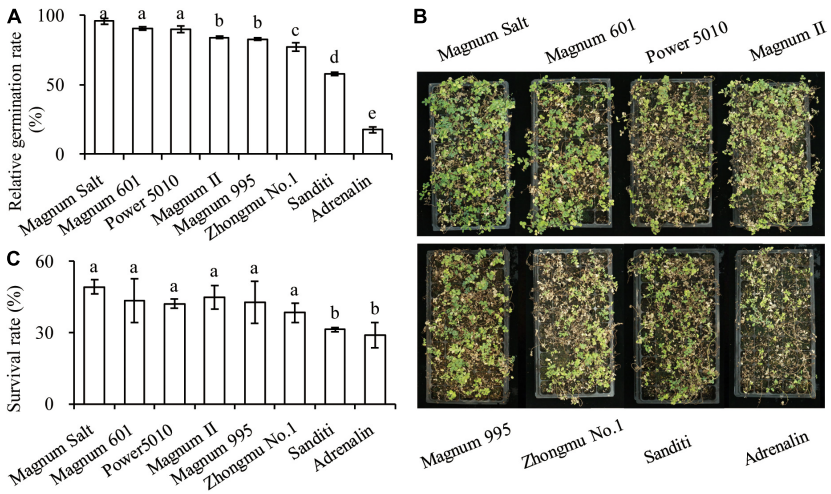

FIGURE 1 | Evaluation of salt tolerance of 8 alfalfa cultivars by analyzing relative germination rate and survival rate under salt condition. Alfalfa seeds were treated with 0 or 150 mM NaCl solution, and relative germination rate **(A)** were calculated within 7 days. Four-week old seedlings treated with Hoagland nutrient solution with 500 mM NaCl (pH 5.8) weekly. Three weeks later, photographs **(B)** were taken and survival rates **(C)** were analyzed. Values are mean ± SE (n = 3 replicates). Different letters ($P < 0.05$, one-way ANOVA) compare different cultivars.

(**Figures 2B,C**). It was decreased after salt treatment in both cultivars, while that was higher in Magnum Salt than that in Adrenalin (**Figures 2B,C**).

Analysis of Na^+, K^+ and Ca^{2+} Concentrations

The Na^+ concentration was increased in both roots and shoots after 7 d of salt treatment, with higher level in Adrenalin than in Magnum Salt (**Figures 3A,B**). K^+ and Ca^{2+} concentrations were decreased in both cultivars, with higher levels in Magnum Salt than in Adrenalin after salt treatment (**Figures 3C–F**). As a consequence, the Na^+/K^+ ratio in roots and shoots were higher in Adrenalin than in Magnum Salt (**Figures 3G,H**).

Analysis of Antioxidants, Proline and ROS Accumulation

Antioxidant enzyme activities and proline concentrations were measured after plants were treated with NaCl. SOD, CAT, GR, and APX activities showed no difference between two cultivars under control condition. SOD, CAT, and GR were increased after salt treatment, and higher levels were observed in roots and shoots in Magnum Salt than that in Adrenalin, except for no difference in GR activity in shoots (**Figures 4A–F**). APX activity was increased in both cultivars after salt treatment and showed no difference in roots, but higher level was maintained in shoots in Adrenalin than in Magnum Salt (**Figures 4G,H**). No significant difference in proline concentration was observed between two cultivars under control condition. It was increased greatly in roots and shoots in both cultivars, while higher levels were maintained in both roots and shoots in Magnum Salt than in Adrenalin after salt treatment (**Figures 4I,J**).

Leaves were sampled for detection of ROS accumulation using NBT and DAB staining. Compared to the control leaves, $O_2^{\cdot-}$ and H_2O_2 accumulation was observed in leaves in both cultivar after salt treatment, while lower levels were maintained in Magnum Salt than in Adrenalin (**Figure 5**).

Analysis of Fatty Acids Content

Nearly 90% of total fatty acids were C16 and C18 fatty acids in alfalfa roots under control condition, among them were major C18:2 (40%), C18:3 (20%) and C16:0 (20%). The portion of C18:2 increased significantly after 6 d of salt stress in Magnum Salt, but it was slightly decreased after 3 d of salt treatment, followed by a recovery at 6 d in Adrenalin. C18:3 content continuously decreased after salinity treatment, with no significant difference between two cultivars. C16:0 fatty acid was higher in Magnum Salt than in Adrenalin under control condition, and it showed no significant difference between two cultivars under salt stress (**Figure 6A**). Both saturated fatty acid (SFA) and unsaturated fatty acid (UFA) abundance were not altered in Magnum Salt after salinity treatment, while SFA was slightly increased but UFA was decreased in Adrenalin (**Figure 6B**). The monounsaturated fatty acids (MUFA) abundance was increased under salt stress, while polyunsaturated fatty acid (PUFA) was decreased, with lower level in Adrenalin. Double bond index (DBI; number of double bonds per mole) showed no difference between two cultivars under control condition, but it was decreased after salinity treatment with higher level in Magnum Salt than in Adrenalin (**Figure 6C**).

Identification and Functional Annotation of Differentially Expressed Genes

In order to study the expression profiles of genes in response to salinity, cDNA libraries representing samples of two cultivars (S-Adrenalin; T-Magnum Salt) at different time points (0, 2, and

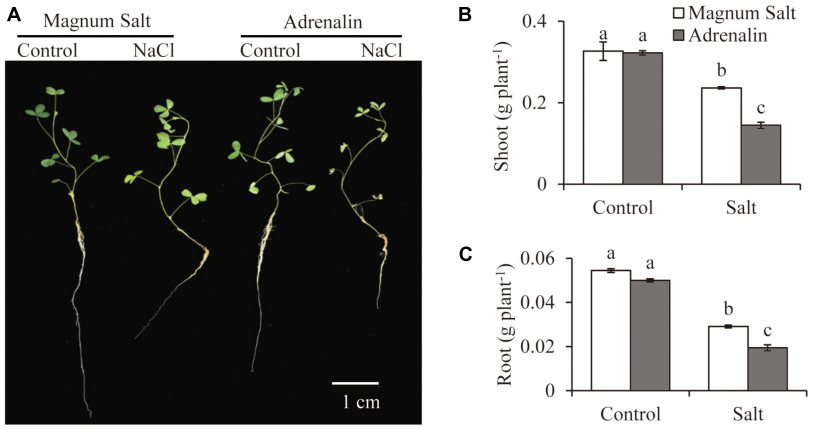

FIGURE 2 | Effect of salt treatment on the biomass of Magnum Salt and Adrenalin. Three-week old seedlings were treated with 1/2 Hoagland solution containing 0 or 150 mM NaCl for 1 week. Photographs **(A)** were taken and biomass of shoot **(B)** and root **(C)** were analyzed. Values are mean ± SE (n = 10 replicates). Different letters indicate the significant differences (P < 0.05, LSD) between two cultivars or treatments.

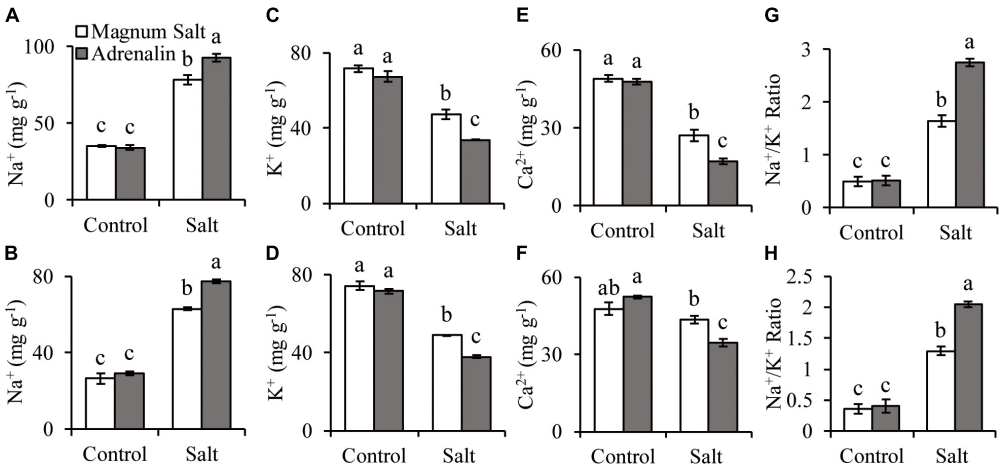

FIGURE 3 | Effect of salt treatment on the Na^+, K^+ and Ca^{2+} accumulation in Magnum Salt and Adrenalin. Three-week old seedlings were treated with 1/2 Hoagland solution containing 0 or 150 mM NaCl for 1 week. Na^+, K^+, Ca^{2+} content and Na^+/K^+ ratio in roots **(A,C,E,G)** and shoots **(B,D,F,H)** were analyzed. Values are mean ± SE (n = 3 replicates). Different letters indicate the significant differences (P < 0.05, LSD) between two cultivars or treatments.

26 h) were constructed for high-throughput RNA-Seq. A total of 740,274,514 raw reads were obtained (**Supplementary Table 1**).

A total of 735,954,286 clean reads remained after removing the adaptor sequences and low-quality sequences. Then, 79,712 unigenes with average GC content of 40.71% and N50 value of 1260 bp were obtained (**Supplementary Table 1**). By searching against four databases (Nr, Swiss-Prot, KOG and KEGG), 53171 unigenes were annotated (**Supplementary Table 2**). A total of 47365 DEGs matching the thresholds of false discovery rate (FDR) < 0.05 and | Log2Fold-Change| > 4 were identified (**Figure 7**). At 2 h, 12558 and 7399 DEGs were detected in Adrenalin and Magnum Salt, with 1684 DEGs in common. After 26 h treatment, 12227 and 15181 DEGs were identified in Adrenalin and Magnum Salt, with 6664 DEGs in common. There were 1684 and 6664 genes that differently expressed in both cultivars at 2 and 26 h.

Differentially Expressed Genes Temporal Expression Patterns Analysis

Temporal expression patterns of the DEGs at 2 and 26 h after salt treatment were analyzed with the Short Time-series Expression Miner (STEM) software (v1.3.11). Eight different profiles of DEGs identified in STEM analysis were explored and enriched with KEGG analysis (**Supplementary Table 3**). Profile 0, exhibited a consistent decreasing trend, contains 6464 DEGs enriched in "phagosome," "endocytosis," "TCA cycle," "carbon metabolism," "glyoxylate and dicarboxylate metabolism," "steroid biosynthesis," "tryptophan metabolism," "oxidative phosphorylation," "arginine and proline metabolism" in Magnum Salt, and 2845 DEGs enriched in "phagosome," "oxidative phosphorylation," "isoquinoline alkaloid biosynthesis," "cysteine and methionine metabolism," "ribosome biogenesis," "TCA cycle," "steroid biosynthesis," "cutin, suberine and wax

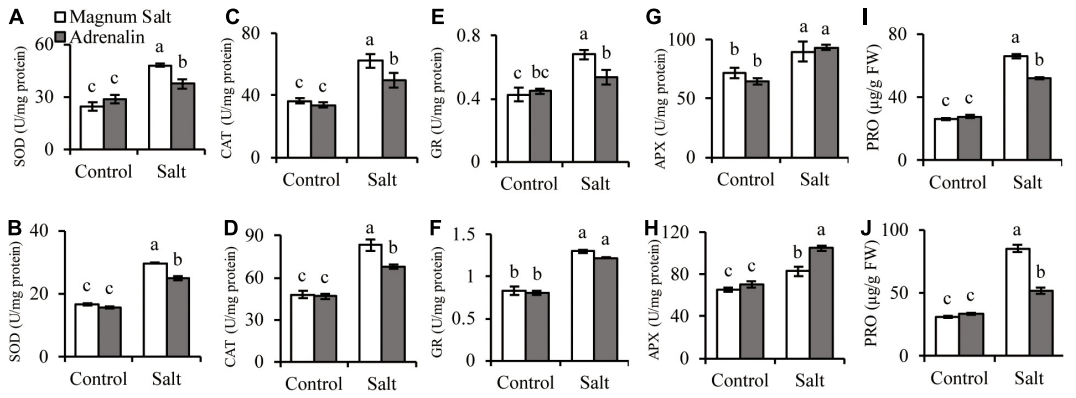

FIGURE 4 | Effect of salt treatment on the antioxidant enzyme activities and proline content in Magnum Salt and Adrenalin. Four-week old seedlings grown in soil with a mixture of pearlite, vermiculite and perlite (1:1:2) were treated with 0 or 500 mM NaCl for 6 days. SOD, CAT, GR, and APX activities and proline contents were analyzed in both root **(A,C,E,G,I)** and shoot **(B,D,F,H,J)**. Values are mean ± SE (n = 3 replicates). Different letters indicate the significant differences ($P < 0.05$, LSD) between two cultivars or treatments.

biosynthesis," "sesquiterpenoid and triterpenoid biosynthesis" in Adrenalin. Profile 7 exhibited an opposite trend. In Magnum Salt, 912 continuously upregulated DEGs were contained in Profile 7, and were enriched mainly in "linoleic acid metabolism," "MAPK signaling pathway" and "hormone signal transduction" and so on. However, 393 DEGs in Adrenalin were contained in Profile 7, and were enriched mainly in "pyruvate metabolism," "endocytosis," "glycolysis." Notably, "phagosome," "TCA cycle" and "oxidative phosphorylation" pathways were frequently present in enrichment results of profile 0, 1, and 3, indicating that vesicle transport and aerobic metabolism were inhibited under salinity stress. The DEGs in profile 4, 6, and 7 in Magnum Salt were frequently enriched in "fatty acid metabolism," "MAPK signaling pathway" and "hormone signal transduction" pathways, implying that fatty acid metabolization and signal transduction played an important role in coping with salt in alfalfa.

Differentially Expressed Genes Involved in Na^+, K^+ and Ca^{2+} Transport, ROS Scavenging, and Fatty Acid Metabolization

DEGs involved in $K^+/Na^+/Ca^{2+}$ transport were investigated in our research (**Figure 8A** and **Supplementary Table 4**). The levels of *AKT1*, *NHX2*, *HKT1* and *HKT6* that involved in sodium/potassium homeostasis were higher in Magnum Salt after 26 h salinity, nevertheless, *NHX7*, *AKT2*, *HAK23* and *KAT3* always had higher expression in Adrenalin. Six unigenes annotated as *CNGC3* and *CNGC20* were expressed at higher levels in Magnum Salt than in Adrenalin at 2 h. At 26 h, *ACA2*, *ACA8* and *ACA12* involved in Ca^{2+} influx or efflux pathways were upregulated and both *ACA2* and *ACA12* were expressed at higher levels in Magnum Salt.

Differentially expressed genes encoding SOD, CAT, APX and GR were analyzed. Most of them were upregulated after 2 or 26 h of salt treatment in Magnum Salt, while less genes were upregulated in Adrenalin (**Figure 8B** and **Supplementary Table 5**).

DEGs involved in fatty acid metabolization pathway were highly enriched in profile 7 in Magnum Salt (**Supplementary Table 3**). *KCS2*, *ACAA1*, *ACAA1B*, *LACS4*, *FAD2* and *FAD7* were upregulated to higher levels in Magnum Salt by NaCl. Nevertheless, the expression levels of *GPAT5* and *GPAT6* increased more strongly in Adrenalin following salt stress (**Figure 8C** and **Supplementary Table 6**). The transcript levels of *KCS1*, *LOX1.1* and *LOX1.4* were induced by salinity stress, but they were expressed at higher levels in Adrenalin.

RNA-Seq Results Validation With qRT-PCR Analysis

The relative folder change of eleven randomly selected DEGs were analyzed by qRT-PCR to verify the RNA-Seq results. Primers were listed in **Supplementary Table 7**. A high consistency was detected for these genes between qRT-PCR and RNA-seq results

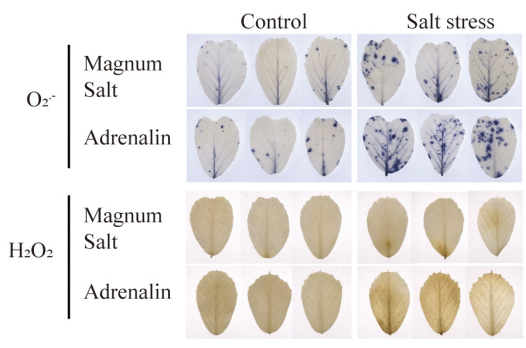

FIGURE 5 | Effect of salt treatment on the ROS content in Magnum Salt and Adrenalin. Four-week old seedlings grown in soil with a mixture of pearlite, vermiculite and perlite (1:1:2) were treated with 0 or 500 mM NaCl for 6 days. Leaves were sampled for NBT and DAB staining.

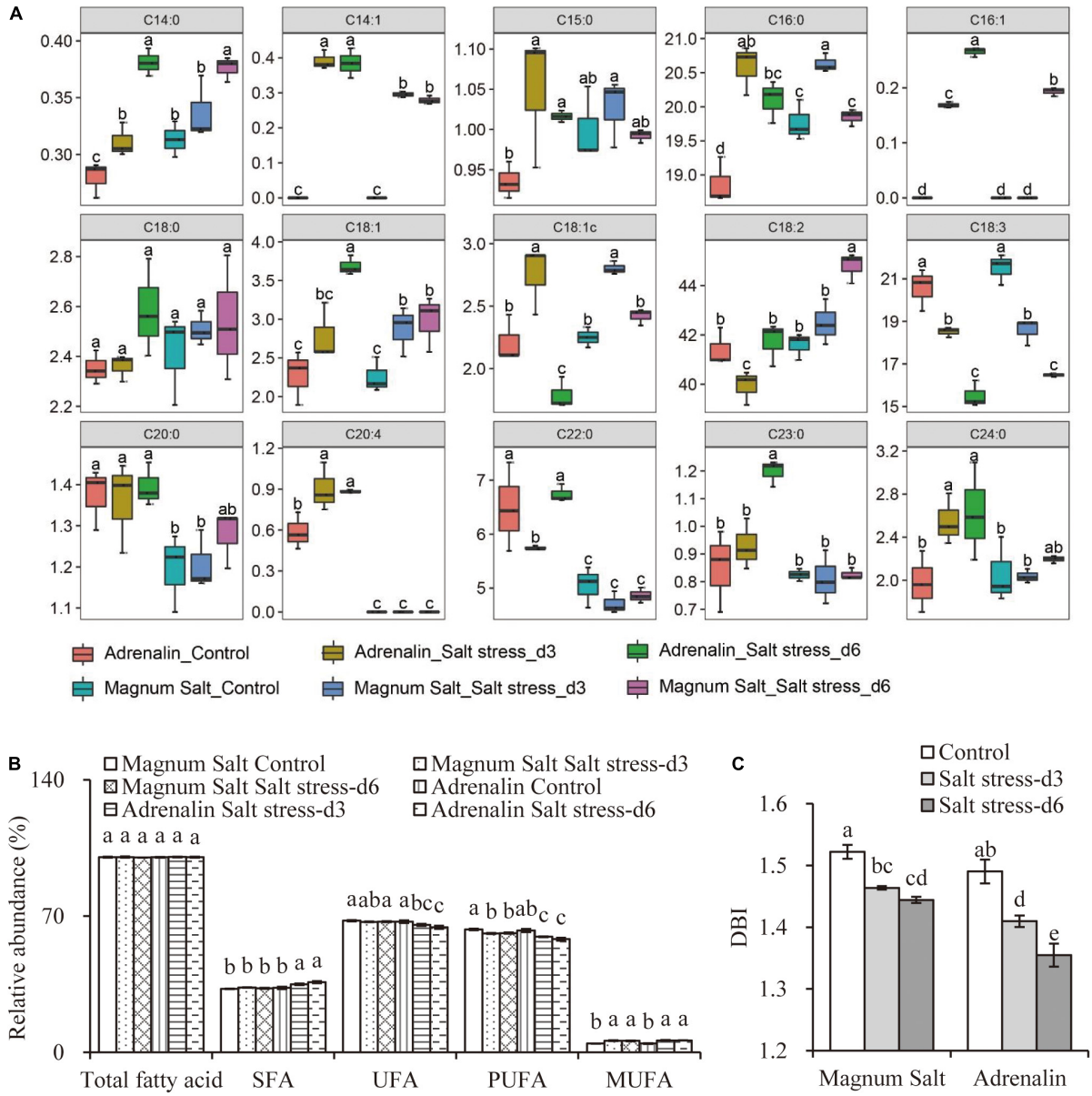

FIGURE 6 | Effect of salt treatment to the Fatty acids content in Magnum Salt and Adrenalin. Four-week old seedlings treated with 0 or 500 mM NaCl. At 0, 3 and 6 days, roots were sampled for fatty acids content analysis **(A)**. The upper and lower edges of the box in the boxplot represent the maximum and minimum values, respectively, and the horizontal line in the middle represents the median values. Relative abundance of saturated fatty acids (SFA), unsaturated fatty acid (UFA), monounsaturated fatty acids (MUFA), polyunsaturated fatty acid (PUFA); **(B)** and double bond index (DBI; number of double bonds per mole) **(C)** were calculated. Values are mean ± SE (n = 3 replicates). Different letters indicate the significant differences ($P < 0.05$, LSD) between two cultivars or treatments.

(**Figures 9A–K**). As shown in **Figure 9L**, a strong positive correlation (R^2 = 0.8917) was obtained by a linear regression analysis, suggesting that our transcriptome data were reliable.

DISCUSSION

By analyzing the germination rates, survival rates and biomass under salt treatment, "Magnum Salt" and "Adrenalin" were identified as salt tolerant and salt sensitive cultivar, respectively (**Figures 1**, **2**). Both physiological and transcriptional responses of these two cultivars to salinity stress were investigated. It was found that regulation of ionic homeostasis, fatty acid metabolization and antioxidative system played important roles in salt tolerance in alfalfa.

Ion Homeostasis

Maintaining ion homeostasis, especially a low cytosolic Na^+/K^+ ratio, is an important adaptive trait of salt-tolerant plants, which was also observed in salt-tolerant cultivar Magnum Salt in

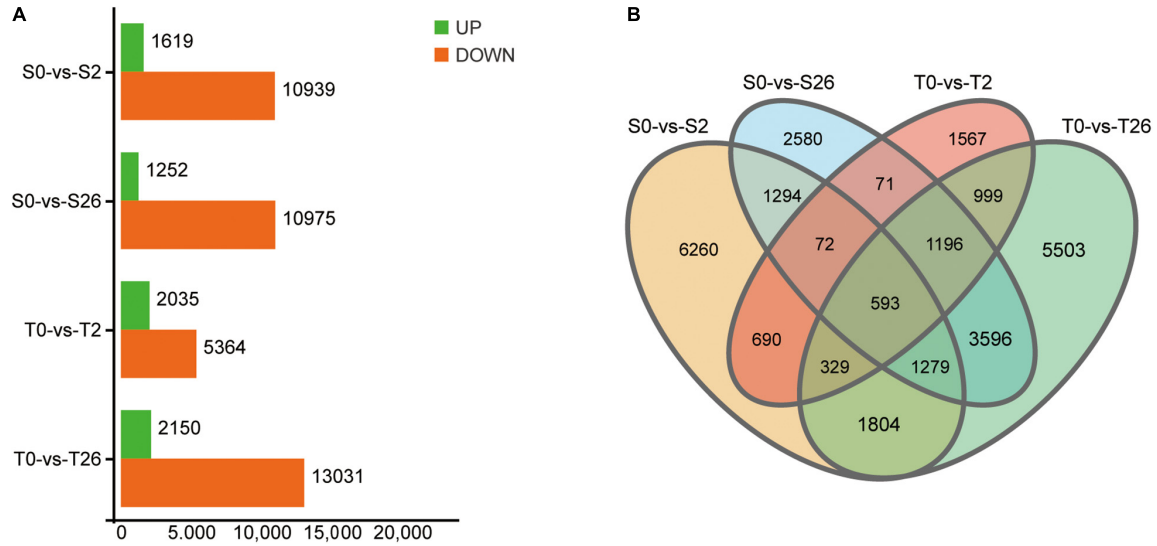

FIGURE 7 | Differentially expressed genes (DEGs) in Magnum Salt (T) and Adrenalin (S) under salt stress. **(A)** Number of upregulated and downregulated DEGs under salt stress. **(B)** Venn diagram analysis of the DEGs in different comparison groups of S0-vs-S2, S0-vs-S26, T0-vs-T2 and T0-vs-T26.

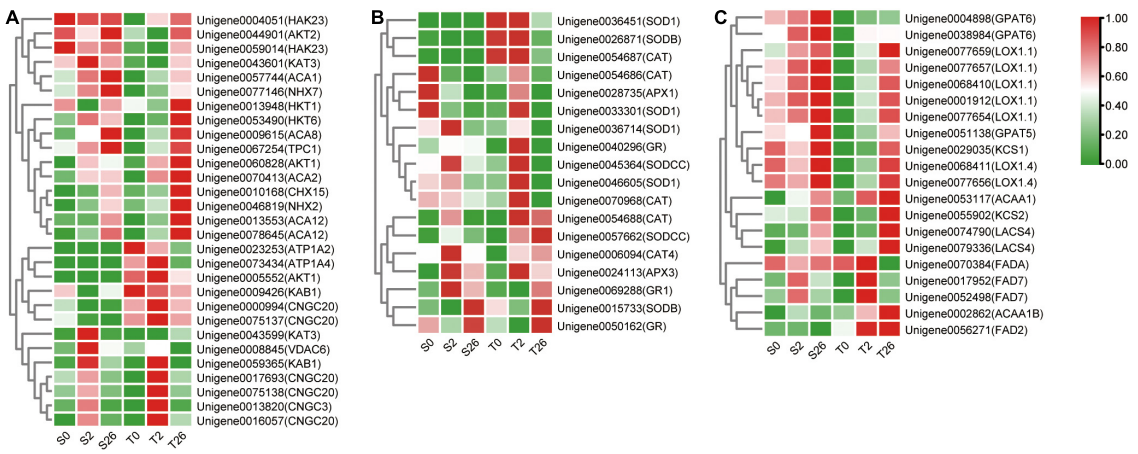

FIGURE 8 | Heatmap of the relative expression of the DEGs involved in Na^+, K^+ and Ca^{2+} transport **(A)**, ROS-scavenging **(B)** and fatty acid metabolization **(C)** in Magnum Salt and Adrenalin under salt stress. FPKM was used for representing the expression abundance of genes. The clustered heatmap was portrayed after normalized with zero-to-one scale method using the TBtools software.

our experiments (**Figures 3G,H**). The transporters or channels involved in Na^+ efflux and K^+ uptake play important roles in salt resistance. NHX-type cation/H^+ transporters in plants have been shown to mediate $Na^+(K^+)/H^+$ exchange for salinity tolerance and K^+ homoeostasis, providing an important strategy for ionic homeostasis in plants under saline conditions (Apse et al., 1999; Zeng et al., 2018). There were two salt-upregulated *NHX* genes identified in DEGs, *NHX2* and *NHX7*. *NHX2* expression abundance was about three times higher than *NHX7* in all samples collected in our research (**Supplementary Table 4**). Notably, *NHX2* increased greater in Magnum Salt than in Adrenalin. High-affinity K^+ channel (HKT) and a low-affinity K^+ channel Arabidopsis K^+ Transporter1 (AKT1) were reported to mediate K^+/Na^+ influx (Ali et al., 2021, Wang et al., 2021). *KAT3* encoded a member of the shaker family of voltage-gated potassium channel subunits and responded to low potassium stress in Arabidopsis, however, its function in salinity response had not been reported (Wang et al., 2016). The expression of *AKT1*, *HKT1* and *HKT6* were significantly higher in Magnum Salt after 26 h salinity, while genes encoding HKT23 or KAT3 were highly expressed in Adrenalin (**Figure 8A**).

Plant response to salt is closely linked to the calcium (Ca^{2+}) channels as well as Ca^{2+} sensing and signaling (Seifikalhor et al., 2019, Feng et al., 2018). A rapid rise in cytosolic Ca^{2+} level can be detected within seconds of exposure to salt stress (Jiang et al., 2019). In another hand, salinity inhibited nutrient uptake, including Ca^{2+}, just as showed in this paper (**Figures 3E,F**). However, Ca^{2+} concentrations were inhibited in a higher degree

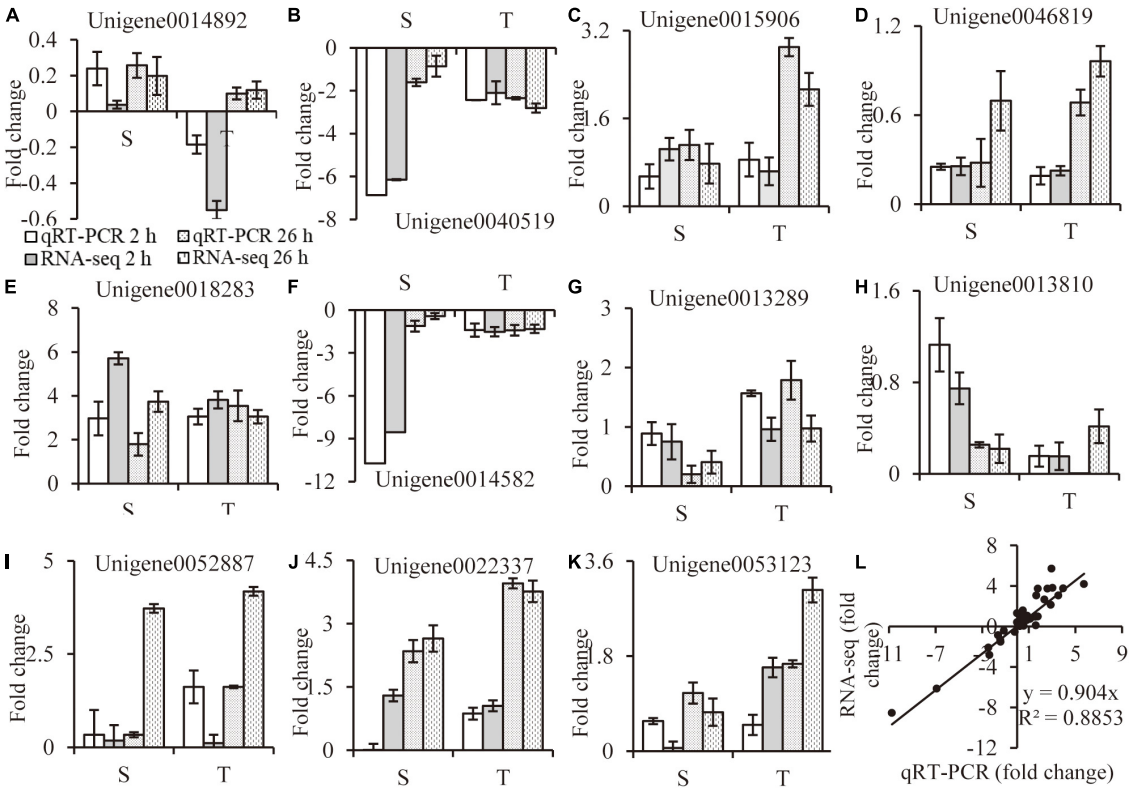

FIGURE 9 | RNA-seq data validation. Random selected genes with different expression patterns were analyzed by qRT-PCR **(A–K)**, correlation between qRT-PCR and RNA-seq data are calculated **(L)**. Values are mean ± SE (n = 3 replicates).

in Adrenalin than Magnum Salt by NaCl. The cyclic nucleotide-gated ion channel (CNGC) family have been implicated in the uptake of cations such as Na^+, K^+ and Ca^{2+}, so that mediate numerous biological processes ranging from plant development to stress tolerance. Among *CNGC* members in Arabidopsis, *AtCNGC3* helps in seed germination and cation transport, whereas *AtCNGC19* and *AtCNGC20* are associated with salt tolerance (Gobert et al., 2006, Kugler et al., 2009. Both *CNGC3* and *CNGC20* were expressed at higher levels in Magnum Salt than in Adrenalin at 2 h. Autoinhibited Ca^{2+}-ATPases (ACAs) can mediate Ca^{2+} efflux to help restore $[Ca^{2+}]_{cyt}$ to resting basal levels, for example, AtACA1, 2, and 7 mediate Ca^{2+} efflux from cytoplasm to endoplasmic reticulum and contribute to growth and pollen fitness in a redundant way (Ishka et al., 2021). There were four ACAs that were upregulated by salt. Among them, *ACA2* and *ACA12* involved in Ca^{2+} homeostasis were expressed at higher levels in Magnum Salt at 26 h. It's interesting to find out whether they are involved in salt tolerance at future.

Antioxidative System

Oxidative injury happened in about all biotic and abiotic stress as a secondary injury. Thus, the ability to scavenge ROS efficiently is vital for tolerance (Nadarajah, 2020). Salt-sensitive XJ had high levels of ROS and elevation of ROS-related enzyme activity in response to salinity stress, whereas the salt-tolerant ZM showed relatively lower levels of ROS production and unaltered activity of ROS-related enzymes (Lei et al., 2018). Bhattarai et al. (2021) found out that salt tolerance in alfalfa appears to be associated with consistent expression of genes for enhancing defense against oxidative damage and protection against lipid peroxidation. In our research, salinity stress caused accumulation of $O_2^{\cdot-}$ and H_2O_2 in alfalfa leaves and upregulation of SOD, CAT, GR and APX activities in both roots and shoots. Magnum Salt accumulated less ROS in leaves than Adrenalin, corresponding with the higher SOD and CAT activities in Magnum Salt than in Adrenalin under salt treatment. Higher levels of SOD, CAT and GR were observed in roots in Magnum Salt than that in Adrenalin (**Figures 4A–H** and **5**). Transcriptional levels of genes encoding antioxidative enzymes were quickly upregulated after salt treatment in Magnum Salt, indicating its fast response to apply antioxidative enzymes to scavenge ROS (**Figure 8B** and **Supplementary Table 5**).

Fatty Acids Metabolization

Membrane fluidity and integrity are largely affected by lipid composition and the degree of fatty acid desaturation in plants (Mikami and Murata, 2003). Alterations in membrane lipids in response to salinity have been observed in a number of plant species including both halophytes and glycophytes (Guo et al., 2019). Membrane fatty acids unsaturation was suggested to affect cell salinity tolerance by affect membrane fluidity so that corelated to Na^+ and Cl^- transport (Lin and Wu, 1996).

In peanut, unsaturated fatty acids improved salt tolerance by alleviating photoinhibition (Liu et al., 2017). It has been reported in buffalograss (*Buchloe dactyloides*; Lin and Wu, 1996), corn (*Zea mays* L.; Hajlaoui et al., 2009) and Fabaceae (Bejaoui et al., 2016) that salt-tolerant clones or species had higher unsaturated fatty acids ratio than salt-sensitive ones after salinity treatment. However, no research has investigated the fatty acids contents under salt stress in alfalfa. In our research, it was found that palmitic (16:0), linoleic (18:2) and linolenic acid (18:3) accounted for the largest proportion of the fatty acid in alfalfa (**Figure 6A**), which was conserved across plant species (Guo et al., 2019). Salinity stress caused a decrease in total unsaturated fatty acids in salt-sensitive Adrenalin, which has been observed in many other plants. However, no significant difference existed in unsaturated fatty acids abundance in Magnum Salt between control or treated group (**Figure 6B**). Among unsaturated fatty acids, linoleic acid in Magnum Salt increased significantly after 6 days' salinity. However, no significant difference existed in Adrenalin (**Figure 6A**).

There are four types of key enzyme in fatty acids synthesis, including fatty acid synthases (FAS), 3-ketoacyl-CoA thiolase (ACAA), β-ketoacyl-coenzyme A (CoA) synthases (KCS) and fatty acid desaturase (FAD). ACAA family members are responsible for the thiolytic cleavage of straight chain 3-oxoacyl-CoAs. KCS mediates the synthesis of very-long-chain fatty acids (VLCFAs) from 22 to 26 carbons in length. Research showed that *KCS1* was salt-inducible, and might play a role in adapting intracellular membrane compartments to function in balancing the external osmotic pressure in extreme halotolerant alga *Dunaliella salina* (Azachi et al., 2002). FAD family members are responsible for fatty acid unsaturation. Endoplasmic reticulum localized FAD2 and FAD6 in plastids convert oleic acid (18:1) to linoleic acid (18:2) by inserting a double bond at the ω-6 position. Whereas FAD3, FAD7, and FAD8 convert linoleic acid (18:2) to linolenic acid (18:3). By investigating the phenotype of mutation materials, FAD2 and FAD6 were proved to be required for salt tolerance probably by maintaining proper function of membrane attached Na^+/H^+ exchangers in *Arabidopsis* (Zhang et al., 2012). Lipoxygenase (LOX) is also involved in fatty acid metabolization by catalyzing the hydroperoxidation of linolenic acid. High lipoxygenase activity and its further upregulation by salt stress are the unique features of salt-sensitive sunflower seedlings (Gogna and Bhatla, 2020). In our result, fatty acid metabolization pathway were highly enriched in profile 0 DEGs in Magnum Salt (**Supplementary Table 3**). Expression levels of *ACAA1*, *ACAA1b*, *KCS1*, *FAD2,* and *FAD7* were upregulated by salinity to higher levels in Magnum Salt than that in Adrenalin, except for *KCS2*, which was highly expressed in Adrenalin. The transcript levels of *LOX1.1* and *LOX1.4* were higher in Adrenalin than Magnum Salt (**Figure 8C** and **Supplementary Table 6**). These results might partially explain the higher content of unsaturated fatty acids in Magnum Salt under salt stress.

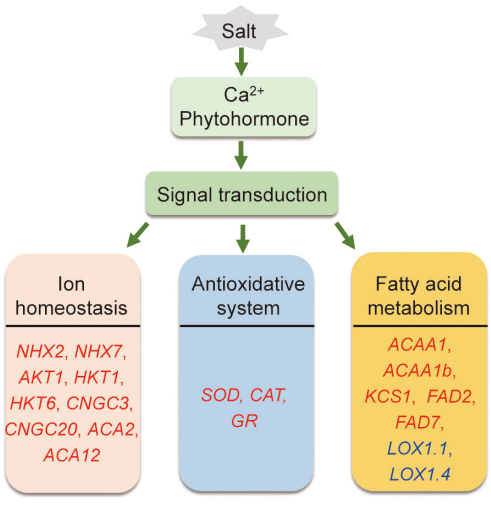

FIGURE 10 | A proposed model showing salt tolerance mechanisms in alfalfa. Salt tolerance in alfalfa is associated with regulation of ionic homeostasis, antioxidative enzymes and fatty acid metabolism. Red and blue genes are proposed positive and negtive regulatory genes in salt tolerance.

CONCLUSION

In conclusion, compared to Adrenalin, salt-tolerant Magnum Salt applied different strategies to cope with salinity condition by regulation of ionic homeostasis, antioxidative enzyme activities and fatty acid metabolization at both transcriptional and physiological level (**Figure 10**).

DATA AVAILABILITY STATEMENT

The datasets presented in this study can be found in online repositories. The names of the repository/repositories and accession number(s) can be found in the article/**Supplementary Material**.

AUTHOR CONTRIBUTIONS

ZG and HZ designed the experiments. JL, MM, YS, and PL performed the experiments. JL, HZ, and HS contributed to the data analysis. HZ and ZG wrote and revised this manuscript. All authors approved the submitted version.

FUNDING

This work was supported by the National Natural Science Foundation of China (Grant numbers 32101439) and the Fundamental Research Funds for the Central Universities (KYQN2022015).

SUPPLEMENTARY MATERIAL

The Supplementary Material for this article can be found online at: https://www.frontiersin.org/articles/10.3389/fpls.2022.931619/full#supplementary-material

REFERENCES

Ali, A., Raddatz, N., Pardo, J. M., and Yun, D. J. (2021). HKT sodium and potassium transporters in *Arabidopsis thaliana* and related halophyte species. *Physiol. Plant.* 171, 546–558. doi: 10.1111/ppl.13166

An, Y. M., Yang, X. X., Zhang, L. S., Zhang, J., Du, B. H., Yao, L., et al. (2020). Alfalfa MsCBL4 enhances calcium metabolism but not sodium transport in transgenic tobacco under salt and saline-alkali stress. *Plant Cell Rep.* 39, 997–1011. doi: 10.1007/s00299-020-02543-x

Apse, M. P., Aharon, G. S., Snedden, W. A., and Blumwald, E. (1999). Salt tolerance conferred by overexpression of a vacuolar Na+/H+ antiport in *Arabidopsis*. *Science* 285, 1256–1258. doi: 10.1126/science.285.5431.1256

Azachi, M., Sadka, A., Fisher, M., Goldshlag, P., Gokhman, I., and Zamir, A. (2002). Salt induction of fatty acid elongase and membrane lipid modifications in the extreme halotolerant alga *Dunaliella salina*. *Plant Physiol.* 129, 1320–1329. doi: 10.1104/pp.001909

Bejaoui, F., Salas, J. J., Nouairi, I., Smaoui, A., Abdelly, C., Martinez-Force, E., et al. (2016). Changes in chloroplast lipid contents and chloroplast ultrastructure in *Sulla carnosa* and Sulla coronaria leaves under salt stress. *J. Plant Physiol.* 198, 32–38. doi: 10.1016/j.jplph.2016.03.018

Bhattarai, S., Fu, Y. B., Coulman, B., Tanino, K., Karunakaran, C., and Biligetu, B. (2021). Transcriptomic analysis of differentially expressed genes in leaves and roots of two alfalfa (*Medicago sativa* L.) cultivars with different salt tolerance. *BMC Plant Biol.* 21:446. doi: 10.1186/s12870-021-03201-4

Chen, C., Chen, H., Zhang, Y., Thomas, H. R., Frank, M. H., He, Y., et al. (2020). TBtools: An integrative toolkit developed for interactive analyses of big biological data. *Mol. Plant.* 13, 1194–1202. doi: 10.1016/j.molp.2020.06.009

Chen, T. T., Yang, Q. C., Zhang, X. Q., Ding, W., and Gruber, M. (2012). An alfalfa (*Medicago sativa* L.) ethylene response factor gene, MsERF11, enhances salt tolerance in transgenic *Arabidopsis*. *Plant Cell Reports* 31, 1737–1746. doi: 10.1007/s00299-012-1287-z

Cornacchione, M. V., and Suarez, D. L. (2017). Evaluation of alfalfa (*Medicago sativa* L.) populations' response to salinity stress. *Crop Sci.* 57, 137–150. doi: 10.2135/cropsci2016.05.0371

Dai, M. T., Huang, R. S., Han, Y. Y., Zhang, Z. Y., Chen, Y. Y., Shi, H. F., et al. (2022). A novel salt responsive PvHAK16 negatively regulates salt tolerance in transgenic *Arabidopsis thaliana*. *Environ. Exp. Bot.* 194:104689. doi: 10.1016/j.envexpbot.2021.104689

De Vos, C. H. R., TenBookum, W. M., Vooijs, R., Schat, H., and De Kok, L. J. (1993). Effect of copper on fatty acid composition and peroxidation of lipids in the roots of copper tolerant and sensitive *Silene-cucubalus*. *Plant Physiol. Biochem.* 31, 151–158. doi: 10.1111/j.1399-3054.1986.tb05073.x

Deinlein, U., Stephan, A. B., Horie, T., Luo, W., Xu, G., and Schroeder, J. I. (2014). Plant salt-tolerance mechanisms. *Trends Plant Sci.* 19, 371–379. doi: 10.1016/j.tplants.2014.02.001

Ernst, J., and Bar-Joseph, Z. (2006). STEM: a tool for the analysis of short time series gene expression data. *BMC Bioinformatics* 7:191. doi: 10.1186/1471-2105-7-191

Feng, W., Kita, D., Peaucelle, A., Cartwright, H. N., Doan, V., Duan, Q. H., et al. (2018). The FERONIA receptor kinase maintains cell-wall integrity during salt stress through Ca2+ signaling. *Curr. Biol.* 28, 666–675 e5. doi: 10.1016/j.cub.2018.01.023

Gobert, A., Park, G., Amtmann, A., Sanders, D., and Maathuis, F. J. M. (2006). Arabidopsis thaliana Cyclic Nucleotide Gated Channel 3 forms a non-selective ion transporter involved in germination and cation transport. *J. Exp. Bot.* 57, 791–800. doi: 10.1093/jxb/erj064

Gogna, M., and Bhatla, S. C. (2020). Salt-tolerant and -sensitive seedlings exhibit noteworthy differences in lipolytic events in response to salt stress. *Plant Signal. Behav.* 15:1737451.

Gruber, M. Y., Xia, J., Yu, M., Steppuhn, H., Wall, K., Messer, D., et al. (2017). Transcript analysis in two alfalfa salt tolerance selected breeding populations relative to a non-tolerant population. *Genome* 60, 104–127. doi: 10.1139/gen-2016-0111

Guo, P., Shi, W. C., Li, L. L., and Bao, Y. J. (2018). MsPP2C, a protein phosphatase 2C gene of alfalfa, confers enhanced salt tolerance in *Arabidopsis*. *Int. J. Agric. Biol.* 20, 62–70. doi: 10.17957/Ijab/15.0362

Guo, Q., Liu, L., and Barkla, B. J. (2019). Membrane lipid remodeling in response to salinity. *Int. J. Mol. Sci.* 20:4264. doi: 10.3390/ijms20174264

Hajlaoui, H., Denden, M., and Ayeb, N. E. (2009). Changes in fatty acids composition, hydrogen peroxide generation and lipid peroxidation of salt-stressed corn (*Zea mays* L.) roots. *Acta Physiol. Plant.* 31, 787–796. doi: 10.1007/s11738-009-0293-4

Huang, J. X., Xue, C. W., Wang, H., Wang, L. S., Schmidt, W., Shen, R. F., et al. (2017). Genes of acyl carrier protein family show different expression profiles and overexpression of acyl carrier protein 5 modulates fatty acid composition and enhances salt stress tolerance in *Arabidopsis*. *Front. Plant Sci.* 8:987. doi: 10.3389/fpls.2017.00987

Ishka, M. R., Brown, E., Rosenberg, A., Romanowsky, S., Davis, J. A., Choi, W. G., et al. (2021). Arabidopsis Ca2+-ATPases 1, 2, and 7 in the endoplasmic reticulum contribute to growth and pollen fitness. *Plant Physiol.* 185, 1966–1985. doi: 10.1093/plphys/kiab021

Jiang, Z. H., Zhou, X. P., Tao, M., Yuan, F., Liu, L. L., Wu, F. H., et al. (2019). Plant cell-surface GIPC sphingolipids sense salt to trigger Ca2+ influx. *Nature* 572, 341–346. doi: 10.1038/s41586-019-1449-z

Kugler, A., Kohler, B., Palme, K., Wolff, P., and Dietrich, P. (2009). Salt-dependent regulation of a CNG channel subfamily in *Arabidopsis*. *BMC Plant Biol.* 9:140. doi: 10.1186/1471-2229-9-140

Lei, Y., Xu, Y., Hettenhausen, C., Lu, C., Shen, G., Zhang, C., et al. (2018). Comparative analysis of alfalfa (*Medicago sativa* L.) leaf transcriptomes reveals genotype-specific salt tolerance mechanisms. *BMC Plant Biol.* 18:35. doi: 10.1186/s12870-018-1250-4

Li, C. X., Song, T. T., Zhan, L. F., Cong, C. L., Xu, H. H., Dong, L., et al. (2021). Overexpression of MsRCI2A, MsRCI2B, and MsRCI2C in alfalfa (*Medicago sativa* L.) provides different extents of enhanced alkali and salt tolerance due to functional specialization of MsRCI2s. *Front. Plant Sci.* 12:1836. doi: 10.3389/fpls.2021.702195

Lin, H., and Wu, L. (1996). Effects of salt stress on root plasma membrane characteristics of salt-tolerant and salt-sensitive buffalograss clones. *Environ. Exp. Bot.* 36, 239–254. doi: 10.1016/0098-8472(96)01025-8

Liu, L. L., and Wang, B. S. (2021). Protection of halophytes and their uses for cultivation of saline-alkali soil in China. *Biology* 10:353. doi: 10.3390/biology10050353

Liu, S. S., Wang, W. Q., Li, M., Wan, S. B., and Sui, N. (2017). Antioxidants and unsaturated fatty acids are involved in salt tolerance in peanut. *Acta Physiol. Plant.* 39, 1–10. doi: 10.1007/s11738-017-2501-y

Long, R. C., Yang, Q. C., Kang, J. M., Zhang, T. J., Wang, H. M., Li, M. N., et al. (2013). Overexpression of a novel salt stress-induced glycine-rich protein gene from alfalfa causes salt and ABA sensitivity in *Arabidopsis*. *Plant Cell Rep.* 32, 1289–1298. doi: 10.1007/s00299-013-1443-0

Luo, D., Zhou, Q., Wu, Y. G., Chai, X. T., Liu, W. X., Wang, Y. R., et al. (2019). Full-length transcript sequencing and comparative transcriptomic analysis to evaluate the contribution of osmotic and ionic stress components towards salinity tolerance in the roots of cultivated alfalfa (*Medicago sativa* L.). *BMC Plant Biol.* 19:32. doi: 10.1186/s12870-019-1630-4

Ma, L. C., Wang, Y. R., Liu, W. X., and Liu, Z. P. (2014). Overexpression of an alfalfa GDP-mannose 3, 5-epimerase gene enhances acid, drought and salt tolerance in transgenic *Arabidopsis* by increasing ascorbate accumulation. *Biotechnol. Lett.* 36, 2331–2341. doi: 10.1007/s10529-014-1598-y

Mikami, K., and Murata, N. (2003). Membrane fluidity and the perception of environmental signals in cyanobacteria and plants. *Prog. Lipid Res.* 42, 527–543. doi: 10.1016/s0163-7827(03)00036-5

Nadarajah, K. K. (2020). ROS homeostasis in abiotic stress tolerance in plants. *Int. J. Mol. Sci.* 21:5208. doi: 10.3390/ijms21155208

Seifikalhor, M., Aliniaeifard, S., Shomali, A., Azad, N., Hassani, B., Lastochkina, O., et al. (2019). Calcium signaling and salt tolerance are diversely entwined in plants. *Plant Signal. Behav.* 14:1665455. doi: 10.1080/15592324.2019.1665455

Sun, G. L., Zhu, H. F., Wen, S. L., Liu, L. S., Gou, L. M., and Guo, Z. F. (2020). Citrate synthesis and exudation confer Al resistance in alfalfa (*Medicago sativa* L.). *Plant Soil* 449, 319–329. doi: 10.1007/s11104-020-04490-8

Wang, X. P., Chen, L. M., Liu, W. X., Shen, L. K., Wang, F. L., Zhou, Y., et al. (2016). AtKC1 and CIPK23 synergistically modulate AKT1-mediated low-potassium stress responses in *Arabidopsis*. *Plant Physiol.* 170, 2264–2277. doi: 10.1104/pp.15.01493

Wang, X. S., Zhao, J. L., Fang, Q. W., Chang, X. C., Sun, M. Y., Li, W. B., et al. (2021). GmAKT1 is involved in K+ uptake and Na+/K+ homeostasis in

Arabidopsis and soybean plants. *Plant Sci.* 304:110736. doi: 10.1016/j.plantsci.2020.110736

Wang, Y. J., Jiang, L., Chen, J. Q., Tao, L., An, Y. M., Cai, H. S., et al. (2018). Overexpression of the alfalfa WRKY11 gene enhances salt tolerance in soybean. *PLoS One* 13:e0192382. doi: 10.1371/journal.pone.0192382

Yu, R. G., Wang, G. L., Yu, X. Y., Li, L. Y., Li, C. X., Song, Y. X., et al. (2021). Assessing alfalfa (*Medicago sativa* L.) tolerance to salinity at seedling stage and screening of the salinity tolerance traits. *Plant Biol.* 23, 664–674. doi: 10.1111/plb.13271

Zeng, Y., Li, Q., Wang, H. Y., Zhang, J. L., Du, J., Feng, H. M., et al. (2018). Two NHX-type transporters from *Helianthus tuberosus* improve the tolerance of rice to salinity and nutrient deficiency stress. *Plant Biotechnol. J.* 16, 310–321. doi: 10.1111/pbi.12773

Zhang, J. T., Liu, H., Sun, J., Li, B., Zhu, Q., Chen, S. L., et al. (2012). Arabidopsis fatty acid desaturase FAD2 is required for salt tolerance during seed germination and early seedling growth. *PLoS One* 7:e30355. doi: 10.1371/journal.pone.0030355

Zhang, Z. Q., Wang, Y. F., Chang, L. Q., Zhang, T., An, J., Liu, Y. S., et al. (2016). MsZEP, a novel zeaxanthin epoxidase gene from alfalfa (*Medicago sativa*), confers drought and salt tolerance in transgenic tobacco. *Plant Cell Reports* 35, 439–453.

Zhuo, C. L., Liang, L., Zhao, Y. Q., Guo, Z. F., and Lu, S. Y. (2018). A cold responsive ethylene responsive factor from *Medicago falcata* confers cold tolerance by up-regulation of polyamine turnover, antioxidant protection, and proline accumulation. *Plant Cell Environ.* 41, 2021–2032. doi: 10.1111/pce.13114

Conflict of Interest: The authors declare that the research was conducted in the absence of any commercial or financial relationships that could be construed as a potential conflict of interest.

Publisher's Note: All claims expressed in this article are solely those of the authors and do not necessarily represent those of their affiliated organizations, or those of the publisher, the editors and the reviewers. Any product that may be evaluated in this article, or claim that may be made by its manufacturer, is not guaranteed or endorsed by the publisher.

frontiers | Frontiers in Plant Science

REVIEW
published: 14 June 2022
doi: 10.3389/fpls.2022.922175

Progress and Challenges in China Turfgrass Abiotic Stress Resistance Research

*Lai Jiuxin and Han Liebao**

School of Grassland Science, Beijing Forestry University, Beijing, China

Turfgrasses are an important vehicle for urban ecology and one of the most important indicators of economy and civilization. The biological characteristics of different turfgrass species affect the productivity and quality of the turf and its potential use in landscapes, slopes, and sports fields. Cultivation and management techniques can assist turfgrasses to meet the challenges of climate change, while the development of molecular breeding will provide a broader platform for the application of turfgrasses. The turfgrass industry of China has developed considerably in the last three decades; however, there is still an objective gap with developed countries. This manuscript reviewed the research progress of turfgrass resistance breeding, analyzed the bottlenecks in the development of turfgrass resistance breeding, and put forward the strategies to cope with the bottlenecks. Our review aims to promote research and utilization of turfgrasses.

Keywords: turfgrass, temperature tolerance, drought tolerance, molecular breeding, industrial development

OPEN ACCESS

Edited by:
Kehua Wang,
China Agricultural University, China

Reviewed by:
Dung Tien Le,
Bayer Crop Science, Vietnam
Dejun Li,
Chinese Academy of Tropical Agricultural Sciences, China

***Correspondence:**
Han Liebao
Hanliebao@163.com

Specialty section:
This article was submitted to Plant Abiotic Stress, a section of the journal Frontiers in Plant Science

Received: *17 April 2022*
Accepted: *24 May 2022*
Published: *14 June 2022*

Citation:
Jiuxin L and Liebao H (2022) Progress and Challenges in China Turfgrass Abiotic Stress Resistance Research. Front. Plant Sci. 13:922175. doi: 10.3389/fpls.2022.922175

INTRODUCTION

Turfs are relatively flat, evenly vegetated grasslands dominated by low perennial herbaceous plants that have been artificially planted or naturally formed and are artificially managed for landscaping, environmental protection, and sports ground. Turfs usually have a specific purpose and strongly intervene while also assuming a unique ecosystem function. China's urban development, especially the goal of developing into a strong sports nation, has led to an increased interest and demand in high quality and resilient sports turfs. However, this momentum provides new challenges and opportunities for the development of the turf industry. This paper reviews the research progress on turfgrasses and proposes a way to develop the turfgrass industry.

Turfgrass is used to grow turf that together with the soil, microorganisms, and the environment, form an organic ecosystem of the lawn. Turfgrass forms a dense even turf if mown and maintained properly. There are many different types of turfgrasses and these are classified according to a classification criterion based on their characteristics. Gramineous plants used to play a major role in the establishment of lawns, but in the recent years non-Gramineous species, such as *Salicaceae*, *Leguminosae*, and *Spiniferae* have also been introduced. They are also classified as thin-leaved and broad-leaved on the basis of the width of the grass leaves or as low and prostrate or tall and robust on the basis of turfgrass height. Moreover, based on their use turfgrasses are classified into ornamental, regular green, soil retaining, and accent turfgrass. However, they are mostly classified as, warm-season and cool-season turfgrasses, based on the climatic conditions of their geographic location. Cool-season turfgrasses, also

known as winter grasses, mainly include *Poa L.*, *Agrostis L.*, *Festuca L.*, and *Lolium L.* and are mostly found in temperate to subtropical regions of the Northern Hemisphere and are suitable for planting in northeast, north, northwest, and southwest China (Han, 1996). Whereas, warm-season turfgrasses, also known as summer grasses, are mainly found in tropical and subtropical regions with warm humid, warm semi-humid, and warm semi-arid climates, as well as in the central temperate regions of China. Warm-season turfgrasses are primarily limited by extremely low temperatures and duration. This type of grass shows high heat resistance with an optimum growth temperature of 25°C–35°C, disease resistant and tolerates rough management. The main species in this group are *Cynodon L.*, *Zoysia L.*, *Axonopus L.*, *Eremochloa L.*, *Buchloe Engelm.*, etc.

China is rich in turfgrass germplasm resources. However, few new turfgrass varieties are being cultivated, most of which have been imported from the U.S. The cultivation of turfgrass in China began in 1950, with the introduction of buffalo grass in Beijing. Additionally, small quantities of seeds of *Poa Annua*, *Agrostis canina*, and *Lolium perenne* were imported in the late 1980s (Gao and Wang, 2000) and in 1984, "Kentucky" and "Wabash," varieties of *P. Annua*, were introduced in Qingdao; these varieties had a long green period, high resistance, excellent lawn quality, and were low maintenance (Shao and Liu, 1995). In 1987, many species of *Agrostis* were first introduced in Henan and after years of cultivation, they have obtained a cool-season turfgrass, *Agrostis stolonifera*, suitable for areas north of the Yellow River. Further, more than 10 grass species suitable for desert planting were obtained in trials conducted by Lv (1995) and Liu et al. (1998) in arid and deserted areas.

Research on native turfgrass germplasm resources started late in China, but the collection and evaluation of germplasm resources have advanced in the recent years. Dong and Gong (2001) collected more than 100 turfgrass resources from different areas in China and Weng (1999) collected 147 accessions of germplasm of the genus *Zoysia* in Taiwan. The Institute of Turfgrass Research, Beijing Forestry University collected 132 accessions of *Zoysia*, which are naturally distributed in China (Wang et al., 2006). The Jiangsu Institute of Botany, Chinese Academy of Sciences, collected 1,227 accessions of eight genera and 20 species of warm-season turfgrasses in China (Liu, 2011). Although the collection of turfgrass germplasms has been on par with foreign countries, breeding of new turfgrass varieties in China is still relatively lagged behind. The registration of grass varieties in China is increasing every year, with 173 varieties registered between 2008 and 2016 (**Figure 1**), of which one-third are being utilized. Most of the registered varieties are types of forage grass or ecological grass. However, turfgrass varieties are still relatively few and the rich germplasm resources of turfgrasses in China are not fully utilized, the distributions of registered varieties were illustrated in **Figure 1**. The development of molecular breeding technology has shortened the plant breeding cycles at an accelerated rate. However, most of the fundamental research materials used in turfgrass molecular biology research are imported varieties. Therefore, our primary task is to strengthen the in-depth research and application of turfgrass resources, actively use molecular methods and clone key genes for resistance breeding, also for accelerating the pace of selection and breeding of new varieties of turfgrass.

CURRENT STATE OF RESEARCH ON THE STRESS TOLERANCE OF TURFGRASSES

Turfgrass is popular for its carpet-like appearance. It is used on sports fields and is an important component of landscaping; it further helps resist flooding and storm erosion. In hot areas, well-maintained turfs can naturally reduce the temperature thereby reducing urban cooling energy consumption. However, there are many challenges to maintain a healthy turf. Most turfgrasses are susceptible to extreme weather, disease, pests, and soil salinity, which can lead to brown spots or turf death (**Figure 2**).

Research on Heat and Cold Tolerance of Turfgrasses

The regulation of heat and cold tolerance in turfgrass is mainly based on their maintenance (fertilization, watering, etc.) or the use of advanced technologies (transgenic for heat and cold tolerance), which can effectively reduce the damage caused by temperature adversity. The underlying principle of turfgrass research is to reduce the accumulation of oxygen radicals and toxic substances in plants, reduce the degree of oxidative stress, prevent lipid membrane peroxidation, reduce protein denaturation, and improve photosynthetic efficiency in turfgrasses. The fundamental purpose of turfgrass research is to promote the orderly functioning of plant physiological metabolism even under extreme conditions.

Under low temperature, many physiological changes occur in turfgrasses, for example, increase in soluble protein concentration, starch and non-structural carbohydrates, sulfur and hydroxyl nitrogen and amino acid contents, as well as photosynthetic efficiency and amylase activity and decrease in hydration levels (Xu et al., 2011). Warm-season turfgrasses are less resistant to cold; low temperatures reduce photosynthesis and respiration in these varieties. The limitations caused by extreme temperature can be compensated for by management techniques such as reseeding. Yan et al. (1998) chased ryegrass on hybrid bermudagrass in autumn to compensate for the withering weakness of hybrid bermudagrass in winter, eventually achieving evergreen landscape turfs in all seasons in Shanghai People's Square. Use of a mixed variety of ryegrass was suggested over direct planting of cool-season grasses to reduce initial construction costs and year-round management costs.

Proper application of nitrogen and potassium fertilizers can help enhance heat or cold tolerance of turfgrass and prolong the green period. Application of phytohormones, such as gibberellin (Hedden and Sponsel, 2015), abscisic acid (Li et al., 2017), exogenous spermine (Pegg, 2014), and ethylene (Hu et al., 2020) can also effectively enhance stress tolerance of turfgrass. Some endophytic fungi increase drought and heat tolerance of turfgrasses by altering antioxidant enzyme activities

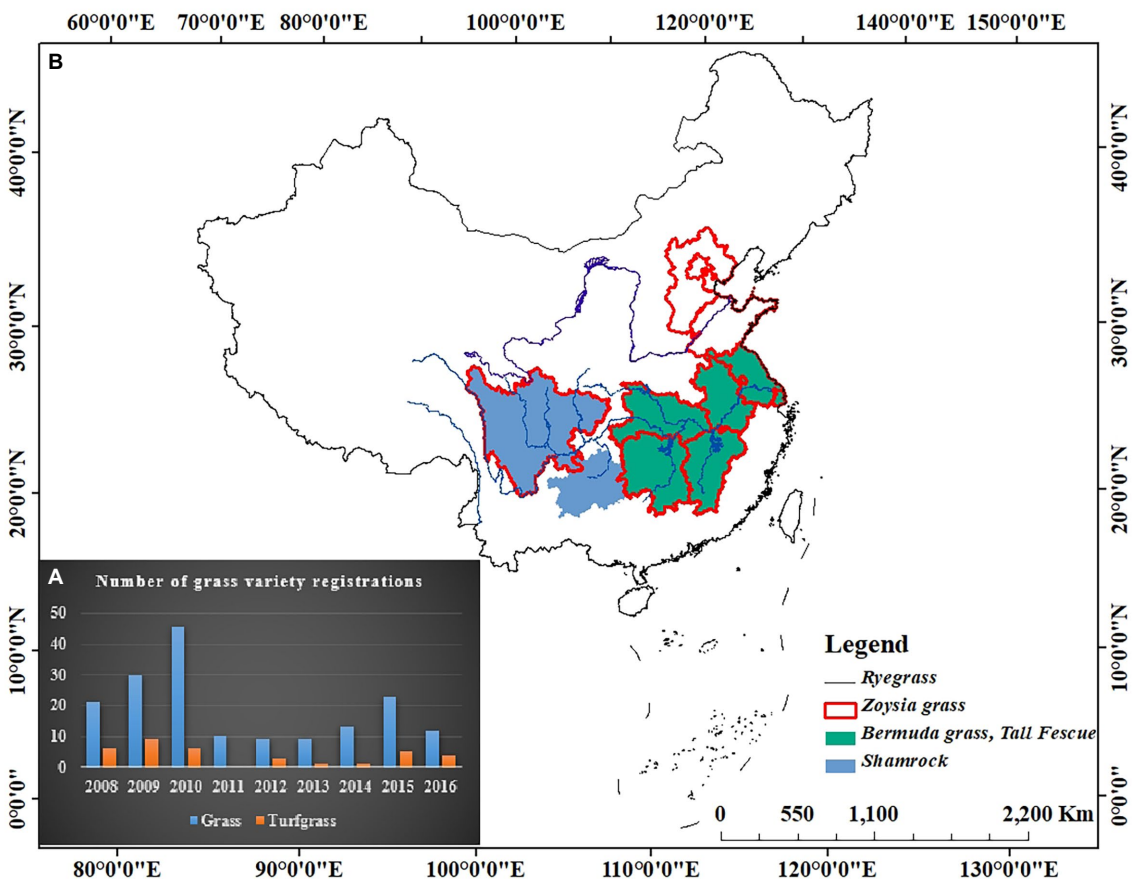

FIGURE 1 | Variety registrations of turfgrass from 2008 to 2016 in China. **(A)** Number of turfgrass variety registrations; **(B)** Distribution of registered varieties.

(Xu et al., 2017a). Temperature tolerance of different grass species varies greatly; the variety "Midiron" has a semi-lethal temperature of −11°C, hybrid bermudagrass 'Brooking' is able to tolerate temperatures as low as −17°C, while the wild bermudagrass in Xinjiang can survive at −32°C. Traditional breeding methods can produce grasses with improved resistance; however, they have long breeding times and disorderly sample selection. The breeding cycle can be accelerated and the target characteristics can be clearly defined using cell and molecular engineering. Somatic cell-induced mutagenesis, or the introduction of functional genes into the tissues or protoplasts of specific plants, can create highly resistant transgenic plants and has been widely reported in crops such as rice and maize. However, successful use of transgenic variety in turfgrass is yet to be achieved.

The scientists from Wuhan Botanical Garden analyzed 106 germplasm resources of bermudagrass for cold tolerance and found 34 loci related to cold tolerance traits using SSR molecular markers. They identified that the *CdERF1* gene was suppressed by low temperature using the virus-induced gene silencing (VIGS) method. RNA-seq analysis in overexpressed transgenic *Arabidopsis* and the roots of VIGS bermudagrass revealed that *CdERF1* might respond to low-temperature stress by transcriptionally regulating the expression of antioxidant genes (POD), lipid transfer protein family genes (LTP) and CBF2 genes (Hu et al., 2020). Exogenous ABA-mimicking ligand treatment can significantly increase cold tolerance by modulation of stress-inducible genes in *Cynodon dactylon* (Cheng et al., 2016).

Alam et al. (2018) characterized *FaHSFA3*, *FaAWPM*, and *FaCYTC2* genes in *Festuca arundinacea* in response to heat stress and improved its thermotolerance using melatonin and 24-epibrassinolide. In addition, Sun et al. (2016) found that small heat shock proteins are involved in abiotic stress response and cloned *AsHSP17* gene from creeping bentgrass to study its role in stress response. *AsHSP17* encodes a 17 kDa protein whose expression is strongly induced by heat in leaves and by salt and abscisic acid (ABA) in roots. *AsHSP17* transgenic *Arabidopsis* plants were strongly sensitive to heat and salt, along with reduced chlorophyll content and reduced photosynthesis compared to the wildtype plants. Overexpression of *AsHSP17* in creeping bentgrass led to high sensitivity to exogenous ABA and salt during germination and growth. Further, *AsHSP17* was shown to act as a protein chaperone that negatively regulates photosynthesis and ABA-dependent independent signaling pathways in response to adverse environmental stress (Sun et al., 2016). To further validate the response of heat shock proteins to stress in *Arabidopsis*, Han's group cloned a novel chloroplast heat shock protein gene,

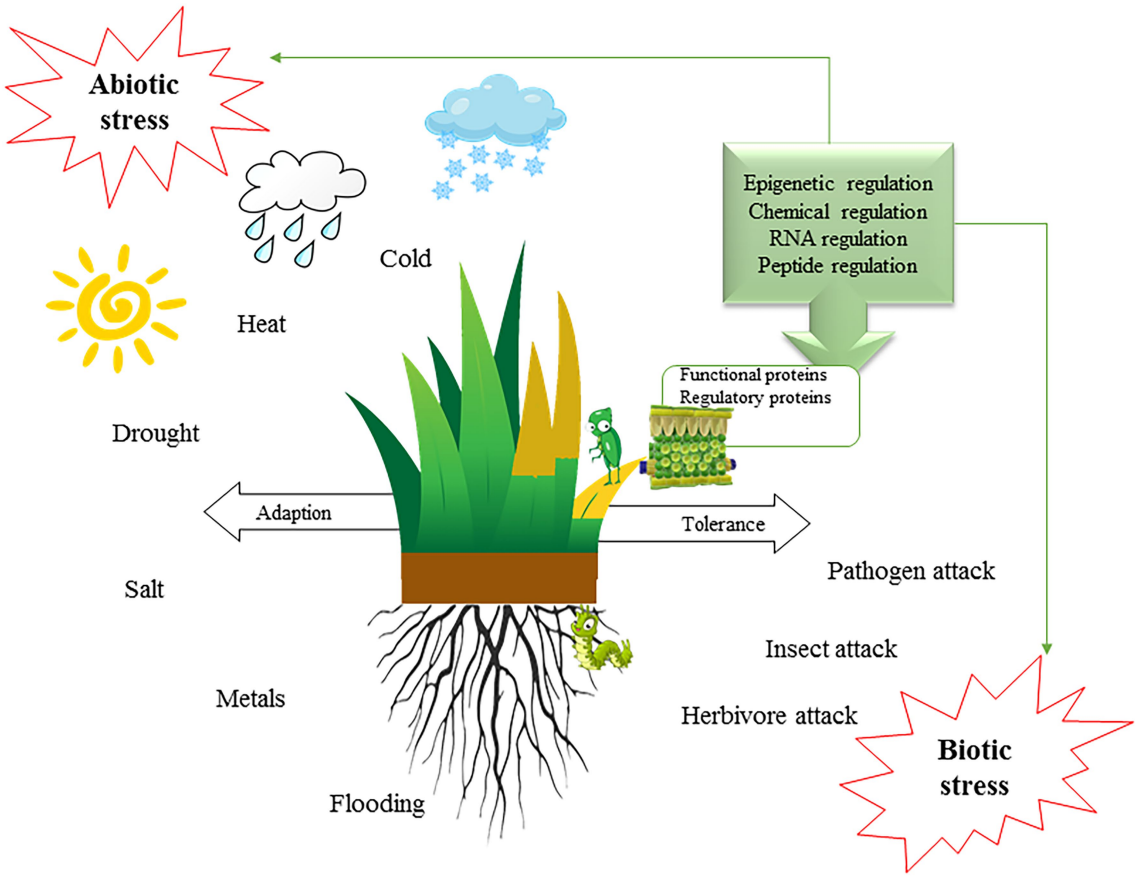

FIGURE 2 | Tolerance and response to environmental stress in turfgrass.

AsHSP26.8a whose expression is strongly induced by heat in both leaves and roots. Transgenic *Arabidopsis* plants overexpressing *AsHSP26.8a* showed reduced tolerance to high temperatures. Whole gene expression analysis revealed that *AsHSP26.8a* regulates the expression of heat stress transcription factors. This result suggests that *AsHSP26.8a* may negatively regulate plant responses to biological stresses by regulating ABA and other signaling pathways (Sun et al., 2020).

Turfgrass Drought Tolerance Study

In the last decade, DNA sequencing technology has developed rapidly and the cost of sequencing is decreasing day after day, with increasing applications on whole genomes, chromosomes, regional genomes, and specific genes. The molecular regulatory mechanisms of plants in response to stress are complex such as for drought stress (**Figure 3**). Many genes have been reported in plants in response to drought stress (Wang et al., 2016; Ma, 2017). However, the identification of each gene from the gene bank is very laborious. Ma (2017) used GWAS combined with RNA-seq approach for differential gene expression analysis in a natural population and screened a total of 46 candidate genes associated with drought stress in plant leaves. Apart from molecular marker development, next-generation sequencing (NGS) technologies can be applied for resequencing and identifying domestication-related genes by comparing crop genomes with their wild relatives (Henry, 2012). Further, NGS can be used in plant breeding by using genome-wide selection studies to predict the reproductive value of traits having high potential to develop economical varieties. Thus, NGS has become a powerful tool for marker-based detection of DNA sequence polymorphisms and is a powerful tool for the next generation of plant breeding. Furthermore, many studies have reported on the response of herbaceous plants to stress such as drought using RNA-seq, WGRS, and GWAS to identify drought-related molecular markers in plants. However, only a few resistance-related molecular markers were discovered in turfgrass. Ontology-based studies on resistance mechanisms have rarely been done on turfgrass. Additionally, most research on resistance mechanisms has identified the target genes in model plants and transformed functional genes in turfgrasses whose metabolic pathways have been revealed in model plants (Evers et al., 2010; Tůmová et al., 2018). The water consumption of turfgrasses has been a major concern for applications in urban landscapes and sports fields. Approximately 26% of changes in environmental factors trigger plants into drought-responsive growth patterns (Obidiegwu et al., 2015). Xu et al. (2011) used drought and rehydration treatments to compare the antioxidant enzyme levels and transcript levels in *P. pratensis* "Midnight" and "Brilliant" varieties. The

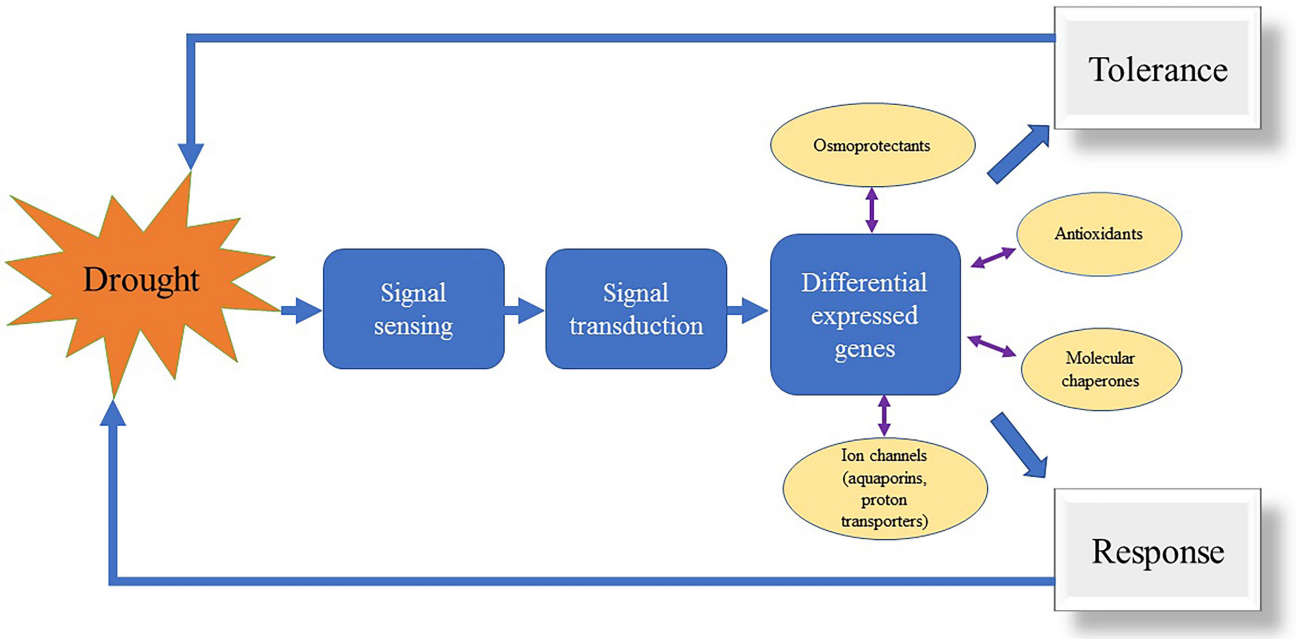

FIGURE 3 | Drought response mechanism in turfgrass.

results revealed that the activities of APX, monodehydroascorbate reductase, glutathione reductase, and dehydroascorbate reductase were significantly increased, and lipid peroxidation levels were reduced. This suggests that the enzymes involved in the ascorbate-glutathione cycle may play a protective role in the antioxidant process, while CAT, POD, and APX may be associated with the excellent recoverability of *P. pratensis* after drought treatment. Alam et al. (2018) showed that drought tolerance was enhanced by using exogenous melatonin in *F. arundinacea*. Moreover, polyamine plays an important role in regulating stress tolerance in plants. Tang et al. (2020) found that γ-Aminobutyric acid induces NO production and could align with the enhancement of antioxidant defense mechanism. Further, Tan et al. (2022) found that spermine enhanced proline metabolism rather than proline accumulation which could be the main regulatory mechanism for drought tolerance in *A. stolonifera*.

Transcriptome analysis (RNA-Seq) is an accurate and effective tool for evaluating gene expression profiles, providing an excellent view for studying the expression and molecular mechanisms of complex characteristics in plants (Deng et al., 2019). In general, gene expression under stress is a complex network involving multiple genes and therefore, poses a major challenge for pinpointing environmentally responsive genes. RNA-seq has many advantages over microarray techniques, such as the ability to identify new genes or new variable spliceosomes without relying on known gene models, identification of RNA editors, and greater detection sensitivity (Rai et al., 2018). Therefore, RNA-seq is often used for the identification of differentially expressed genes (**Figure 3**). When comparing the differences in photosynthetic response, Xu et al. (2013) found that the drought-tolerant cultivar of *P. pratensis* had higher levels of ribulose-1,5-bisphosphate carboxylase (Rubisco) and glyceraldehyde phosphate dehydrogenase (GADPH) transcripts, as well as a high photosynthetic rate. The enzymatic activities and gene transcription levels of ribulose phosphate kinase were not significantly different from those of Rubisco. This result suggests that Rubisco-regulated carboxylation and GAPDH-regulated carbon reduction may be the key metabolic processes responsible for genetic variation under drought stress. Rubisco, GAPDH, and Rubisco-activated enzymes are all involved in the recovery of photosynthetic rate to drought stress in *P. pratensis*. Moreover, Xu et al. (2017b) overexpressed the *AtDREB1A* gene in *P. pratensis* and validated its role under drought stress. They found that increased drought resistance of transgenic grass may be associated with an increased accumulation of organic solutes (WSC, proline, and protein) and altered hormone metabolism. Thereafter, Luo et al. (2020) found that a sort of salt-responsive gene in the healing tissue was regulated by microRNAs in *P. pratensis*.

Xie et al. (2015) used high-throughput sequencing to construct a transcriptome database of *Zoysia japonica* under salt stress. Teng et al. (2016) selected the *ZjGRP* gene which is expressed in the roots, stems, and leaves of *Z. japonica* from a database and cloned it in *Arabidopsis*. The translation products were mainly distributed in the nucleus and cytoplasm, and they found that *ZjGRP* expression was induced by NaCl, ABA, MeJA, and SA treatments. Overexpression of this gene caused salt sensitivity in *Arabidopsis*, probably due to its effect on ion transport, osmosis, and antioxidation.

Response to Heavy Metals

Melatonin can reduce the damage caused by heavy metal ions, chemicals pollutions, extreme temperature or humidity, and high plant oxidative stress. In addition, melatonin can enhance

plant resistance to biotic stress. Considering that N-acetyl-5-hydroxybutylamine is converted to melatonin *via* methyltransferase, Luo et al. (2018) cloned the methyltransferase gene, *ZjOMT* from *Z. japonica* and found that this gene was expressed in leaves and roots and was affected by aluminum (Al) stress. The expression of *ZjOMT* in *Escherichia coli* increased the melatonin content by approximately eight-fold in the recombinant strain compared to the control strain, thereby indicating that heterologous expression of *ZjOMT* could increase resistance to Al stress by increasing melatonin content in *E. coli*. Yuan et al. (2018) performed high-throughput sequencing of *A. stolonifera* under cadmium (Cd) stress and screened four families of Cd stress-related transcripts. Their results provide new ideas for further studies on Cd stress response in turfgrass. Ye et al. (2021) proved that alkali stress has a severely inhibitory effect in *C. dactylon* partially due to combined ionic stress and high pH stress. In conclusion, genetic engineering in turfgrass over the recent years has provided rich genetic materials for breeding industrialization.

Genomic Information and Association Analysis of Turfgrass

In recent years, plant breeding has shifted from phenotypic selection to precise genotypic selection (Varshney et al., 2014). Traditional phenotypic selection methods are expensive and time-consuming (Hajibarat et al., 2015; Saidi et al., 2017). Therefore, determining the molecular mechanisms underlying plant resistance and expression patterns of resistance-associated genes *via* multi-omics studies has become increasingly necessary. The adaptive capacity of plants drives them to escape stresses through physiological and morphological changes. Thus, measuring phenotypic and genotypic changes under different stress treatments can elucidate the molecular mechanisms by which plants respond to stress. The development of sequencing technologies has reduced the cost of high-throughput sequencing, and the widespread demand for scientific research has contributed to the development of NGS which has led to the deposition of millions of sequences in the databank (Nadeem et al., 2018). More and more plants are undergoing whole-genome sequencing, thereby rapidly advancing the process of molecular marker-assisted plant breeding.

Germplasms of turfgrasses are diverse; however, whole genome sequencing was conducted for only a few grasses species owing to their complex genetic background. By December 2021, the whole genomic sequences of *Z. japonica*, *C. transvaalensis, L. perenne* and the model species *Brachypodium distachyon* had been released (International Brachypodium Initiative, 2010; Tanaka et al., 2016; Cui et al., 2021; Frei et al., 2021).

The genus *Zoysia* has 11 species which are mostly tetraploid ($2n = 40$); in general, they are typical warm-season turfgrasses with various morphological and physiological characteristics. Tanaka et al. (2016) used HiSeq and MiSeq platforms to sequence the genome of *Z. japonica* and assembled the whole genomic sequence and predicted 59,271 protein-coding genes. Furthermore, the genome sketches of *Z. matrella* "Wakaba" and *Z. tenuifolia* "Zanpa" were sequenced for comparative genomic analysis (Tanaka et al., 2016). To study the genetic diversity of *Z. japonica*, genome sketches of *Z. japonica* "Kyoto," *Z. japonica* "Miyagi," and *Z. matrella* "Chiba Fair Green" were drafted and compared with "Nagirizaki," "Wakaba," and "Zanpa" varieties. The results indicated that the polymorphisms in the three species were mainly concentrated between *Z. japonica* and *Z. tenuifolia*, and that these loci tended to be heterozygous. Moreover, the result of heterozygosity of the ANAC102, STO/BBX24, and ANS1 genes, as well as population analysis of genome-wide SSR markers, suggest that *Z. matrella* is most likely an interspecific hybrid between *Z. japonica* and *Z. tenuifolia*.

Cui et al. (2021) sequenced and assembled the genome of a diploid *C. transvaalensis* by using Illumina, Nanopore, BioNano, and Hi-C technologies; genome assembly resulted in 282 scaffolds (~423.42 Mb, N50 = 5.37 Mb), covering 93.2% of the predicted genome size (~454.4 Mb). Considering that selective expansion of gene families often facilitates plant environmental adaptation, Cui et al. (2021) examined 193 heat-shock genes of the HSP70 family from seven species (*C. transvaalensis*, *A. thaliana*, *B. distachyon*, *O. sativa*, *S. bicolor*, *S. viridis*, and *Z. japonica*). Their results revealed higher homology between *C. transvaalensis* and *Z. japonica* compared to other species. *C. transvaalensis* genome encodes more species-specific duplicated genes, providing genetic evidence that *C. transvaalensis* has higher heat tolerance.

Frei et al. (2021) assembled the reference genome of *L. perenne* by an optimal sequencing protocol (Oxford Nanopore Technologies) and obtained a highly complete (2.3 of 2.7 Gb), correct (QV 45), and contiguous (contig N50 and N90 11.74 and 3.34 Mb, respectively) genome assembly. They provided the first high-quality haploid reference assembly for perennial ryegrass and revealed the transposable elements' dominance and repeated sequences (81.6% of the assembly), and identified 38,868 protein coding genes. Almost 90% of the bases could be anchored to seven pseudomolecules.

Brachypodium distachyon is a wild Mediterranean and Middle Eastern herb with a small genome size, simple growth conditions, and a short life cycle. Its genome size is approximately 272 Mb, and it is closely related to economically important crops, such as wheat, barley, maize, and sorghum. As *B. distachyon* was first to be sequenced entirely, it is treated as a model plant for functional genomic studies in the Subfamily Pooideae, which contains a large number of economically important crops.

SUGGESTIONS ON RESISTANCE BREEDING IN TURFGRASS

Many countries give equal importance to planting and animal husbandry in the overall development of agriculture. Developed countries are constantly developing in the direction of science and modernization in the management and construction of grassland. Although the rapid development in the grass industry in China has filled the gap in turfgrass research, it is still behind that of the developed countries. In the future, we should focus more on the development of talent in turf, professionals in turf cultivation and management, application of breeding

and biotechnology, as well as pest and disease control, comprehensively and healthily.

However, with the increasing demand for quality and yield in urban turfs, there is an urgent need to produce new varieties with distinctive colors or phenotypes that are adapted to environmental pressures. Therefore, hastened breeding process and genetic research, either *via* traditional techniques or molecular breeding, are necessary to meet these demands. However, there is a misalignment between scientific research and practice, as field workers find suitable mutants but do not know how to utilize them, while laboratory researchers are constrained by the lack of suitable mutants for their research. There is therefore a great need to build a resistance breeding platform of turfgrass to break the barriers between turfgrass research and industry. With advances in sequencing technology and reduced costs, vast amounts of data have been accumulated on genetic variations, in genome, transcriptome, and metabolome. Huge databases will lay the foundation for transgenic breeding and genome editing in turfgrass. Although, many genes associated with target traits can be selected from bioinformatic analyses, it is difficult to speed up the process of identification. It is, therefore, necessary to combine molecular data with breeding and phenotypic data for analysis. Breaking the barriers between industry, academia, and research will help in the advancement of turfgrass research and industry.

Improving Turfgrass Resistance Through Distant Hybridization

Distant hybridization also known as cross-breeding occurs between different species, genera or more distantly related plant species and is a key means of overcoming reproductive isolation. Distant hybridization can combine biological characteristics of distantly related species, break species restrictions, amplify genetic variation, lead to phenotypic and genotypic variations, and create new variants or species (Liu, 2014). Using distant hybridization, genetic resources for commercial characteristics (e.g., disease resistance, insect resistance, high stress resistance, high quality, etc.) from other species can be introduced into the target species. However, some of the limitations of distant hybridization are incompatibility of crosses, hybrid decay or sterility, segregation of hybrid progeny, and time-consuming acquisition of stable genetic material. Regardless, the introduction of exogenous genes through distant hybridization has become an important means of expanding genetic variation among plants (Sharma and Gill, 1983). The cross-border expression of resistance genes often leads to unexpected results. In the 1990s, researchers transferred the antifreeze protein gene (AFP) from *Pseudopleuronectes arnericanus* into tomatoes and found that the transgenic tomatoes not only stably transcribed the AFP mRNA but also expressed AFP, and that tissue extracts from this transgenic tomato were effective in preventing the growth of ice crystals under freezing conditions (Hightower et al., 1991). More notably, the genomes of extreme habitat organisms are more likely to be screened for novel genes or new functional and structural domains imparting environmental adaptation mechanisms. The presence of a species-specific META domain in the salt resistance gene Hal2 of the yeast *Aureobasidium pullulans* improved the salt resistance of the transgenic *Arabidopsis* and greatly increased its drought resistance (Gostinčar et al., 2011). Therefore, the selection of specific functional genes for application in plants is a novel strategy to improve turfgrass stress tolerance.

Isotope marker relative quantification (iTRAQ) and transcriptome techniques can be used to analyze the mechanisms of distant hybrid incompatibility barriers and embryo rescue, and *in vitro* fertilization can be used to overcome pre-fertilization reproductive barriers (He et al., 2020). Polyploidy induction can be used as an intermediate means of breeding, combined with cell fusion techniques, gene editing techniques, chromosome fragment substitution, and other techniques that can be used to overcome hybridization barriers. Cross-breeding with different inbred species, using superior characteristics from different populations, as well as using mutagenesis to create mutants, can create more plants with variations in chromosome structure, such as the cloning of the *Yr28* and *Pm21* genes in wheat (Fu et al., 2009; Zhang et al., 2019). Gene covariance can be verified using the chromosomal interval where the super genes of the model plant have been cloned and the above-mentioned small fragment interval, and then homologous cloning of the genes from closely related plants.

Genomic Data Mining and Exploitation

Most turfgrass species are heterozygous and have a complex genetic background. Therefore, SSR markers are not effective in amplifying allelic fragments in samples at high ploidy levels. The presence of a band or a fragment indicates the presence of an allele on the chromosome forming the homologous cluster, whereas the absence of a fragment indicates that the same allele is not present on any chromosome. SSR markers can be used for GWAS analysis, but it is limited primarily due to the lack of SSRs in microsatellite databases (Gebhardt et al., 2004; Guo et al., 2012). In GWAS analysis, the use of SNP markers is more advantageous as the expected heterozygosity (He) of SNP markers is lower than that of SSR markers and yields better results in population structure evaluation analysis for most crops. In addition, SNPs are distributed throughout the genome and are cheaper than SSRs. Some species, such as chrysanthemum, carnation, pinto bean, chickpea, and potato have already been applied for marker-assisted breeding (Hajibarat et al., 2015; Saidi et al., 2018). One of the most important reasons for using GWAS is that it has high-resolution mapping, a large volume of data, and better identification of rare alleles (Guo et al., 2012). However, this technique is limited by the genomic information availability. Although most species of turfgrass have more complex genetic backgrounds and long durations of population generation, there are only a few reports on GWAS analysis in turfgrass.

Meanwhile, SCoT and CDDP markers have received more attention in recent years, as they do not require genome sequence databases (Andersen and Lubberstedt, 2003), while molecular markers developed based on conserved regions can also be identified across species (Al-qurainy et al., 2015), and markers developed based on functional genes have a stronger

advantage over random markers for trait association (Andersen and Lubberstedt, 2003).

Building a Turfgrass Resilience Breeding Platform

Although there is relatively little genomic data on turfgrass, the increasing accumulation of transcriptomic data will facilitate research on important traits, such as salt tolerance, cold tolerance, and disease resistance. Identification of gene function is a key prerequisite, while a stable genetic transformation system is the foundation. Currently, the Turf Research Institute of Beijing Forestry University has constructed stable genetic transformation systems based on gene gun transformation methods (Qi et al., 2005; Xin et al., 2006) and *Agrobacterium*-mediated methods (Dai, 2013) for major turfgrass species, such as *P. pratensis* and *Z. japonica*, focusing on improving stress resistance in turfgrass. Although research on gene editing and CRISPR/Cas9 is gradually being strengthened, there are some limitations on policy and experimental conditions for field validation and utilization of transgenic strains.

Research on key characteristics, whether by traditional or molecular breeding, is used to obtain superior progeny with the desirable target trait. Each method has its advantages and disadvantages and is unlikely to accelerate the breeding process if applied independently. Therefore, a resistance breeding platform should be constructed to integrate a range of approaches and research ideas, including breeding techniques, herbicide resistance mechanisms, molecular mechanisms underlying stress tolerance and disease resistance, and the development of molecular markers for identifying important characteristics, to facilitate the breeding of new resistant turfgrass varieties.

CONCLUSION

In recent years, the amount of grass species used for turfgrass establishment has increased rapidly and led to an increase in the area under urban landscaping in China. Hundreds of species have been introduced in China and new varieties are available every year. Further, the introduction of good quality turfgrasses has contributed to the development of China's turf industry. The continuous improvement of the molecular breeding system and scientific research has largely stimulated domestic researchers to continue to breed turfgrass species suitable for China's climatic conditions. At present, there is a huge market for grass seeds in China, and with a green space coverage rate of <10% and an urban green space of <1.6 square meters per person, more investment is needed to change the status. In addition, the landscape of large factories, construction of sports grounds, soil and water conservation projects for highways, railways, and river banks, and desertification treatments require large amounts of high-quality grass seeds. These potential markets provide a good opportunity for the development of resistance breeding for turfgrass in China.

AUTHOR CONTRIBUTIONS

LJ wrote the manuscript. HL suggested the concept of the manuscript and worked in the manuscript structure and language and contributed to the overall look of the manuscript. All authors contributed to the article and approved the submitted version.

FUNDING

This research was funded by National Natural Science Foundation of China, grant number 31971770.

ACKNOWLEDGMENTS

The authors would like to thank the people who work at the Turf Research Institute, Beijing Forestry University. The author would also like to thank Xu Lixin, Chao Yuehui, Chan Zhulong, and Luo Yingfeng for providing help during the research and to all those who contributed to this paper.

REFERENCES

Alam, M. N., Zhang, L., Yang, L., Islam, M. R., Liu, Y., Luo, H., et al. (2018). Transcriptomic profiling of tall fescue in response to heat stress and improved thermotolerance by melatonin and 24-epibrassinolide. *BMC Genomics* 19:224. doi: 10.1186/s12864-018-4588-y

Al-qurainy, F., Salim, K., Mohammad, N., and Mohamed, T. (2015). SCoT marker for the assessment of genetic diversity in Saudi Arabian date palm cultivars. *Pak. J. Bot.* 47, 637–643.

Andersen, J. R., and Lubberstedt, T. (2003). Functional markers in plants. *Trends Plant Sci.* 8, 554–560. doi: 10.1016/j.tplants.2003.09.010

Cheng, Z., Jin, R., Cao, M., Liu, X., and Chan, Z. (2016). Exogenous application of ABA mimic 1 (AM1) improves cold stress tolerance in bermudagrass (*Cynodon dactylon*). *Plant Cell Tiss. Org. Cult.* 125, 231–240. doi: 10.1007/s11240-016-0941-5

Cui, F., Taier, G., Li, M., Dai, X., Hang, N., Zhang, X., et al. (2021). The genome of the warm-season turfgrass African bermudagrass (*Cynodon transvaalensis*). *Hort. Res.* 8:93. doi: 10.1038/s41438-021-00519-w

Dai, X. M. (2013). *Study on the Expression Pattern of ZjGA20ox gene of Zoysia japonica Steud. and the genetic Transformation system of RNA Interference Vector*. Beijing: Beijing Forestry University Press.

Deng, T., Liang, A., Liang, S., Ma, X., Lu, X., Duan, A., et al. (2019). Integrative analysis of transcriptome and GWAS data to identify the hub genes associated with milk yield trait in buffalo. *Front. Genet.* 10:36. doi: 10.3389/fgene.2019.00036

Dong, H. D., and Gong, L. J. (2001). *The Ecology of Chinese Knotweed and Its Resource Development and Application*. Beijing: China Forestry Press.

Evers, D., Lefevre, I., Legay, S., Lamoureux, D., Hausman, J. F., Rosales, R. O. G., et al. (2010). Identification of drought-responsive compounds in potato through a combined transcriptomic and targeted metabolite approach. *J. Exp. Bot.* 61, 2327–2343. doi: 10.1093/jxb/erq060

Frei, D., Veekman, E., Grogg, D., Stoffel-Studer, I., Morishima, A., Shimizu-Inatsugi, R., et al. (2021). Ultralong Oxford nanopore reads enable the development of a reference-grade perennial ryegrass genome assembly. *Genome Biol. Evol.* 13:159. doi: 10.1093/gbe/evab159

Fu, D., Uauy, C., Distelfeld, A., Blechl, A., Epstein, L., Chen, X., et al. (2009). A kinase-START gene confers temperature-dependent resistance to wheat stripe rust. *Science* 323, 1357–1360. doi: 10.1126/science.1166289

Gao, Z. M., and Wang, Y. (2000). Current status and problems of lawn grass introduction and cultivation research. *Grassland China* 3:6. doi: 10.3321/j.issn:1673-5021.2000.03.014

Gebhardt, C., Ballvora, A., Walkemeier, B., Oberhagemann, P., and Schüler, K. (2004). Assessing genetic potential in germplasm collections of crop plants by marker-trait association: a case study for potatoes with quantitative variation of resistance to late blight and maturity type. *Mol. Breeding* 13, 93–102. doi: 10.1023/B:MOLB.0000012878.89855.df

Gostinčar, C., Lenassi, M., Gunde-Cimerman, N., and Plemenita, A. (2011). Fungal adaptation to extremely high salt concentrations. *Adv. Appl. Microbiol.* 77, 71–96. doi: 10.1016/B978-0-12-387044-5.00003-0

Guo, J., Xu, L., Fang, J., Su, Y., Fu, H., Que, Y., et al. (2012). A novel dirigent protein gene with highly stem-specific expression from sugarcane, response to drought, salt and oxidative stresses. *Plant Cell Rep.* 31, 1801–1812. doi: 10.1007/s00299-012-1293-1

Hajibarat, Z., Saidi, A., Hajibarat, Z., and Talebi, R. (2015). Characterization of genetic diversity in chickpea using SSR markers, start codon targeted polymorphism (SCoT) and conserved DNA-derived polymorphism (CDDP). *Physiol. Mol. Biol. Plants* 21, 365–373. doi: 10.1007/s12298-015-0306-2

Han, L. B. (1996). *A Study on the Climatic-Ecological Zoning of Turfgrasses and Their Introduction Decisions*. Beijing, China Agricultural University Press.

He, D., Zhang, J. R., He, S. L., Liu, H. L., Wang, Z., and Liu, Y. P. (2020). Cloning and expression analysis of distant hybridization incompatibility PlABCF3 gene from Paeonia. *Acta Agri. Boreali Sinica* 35, 81–89. doi: 10.7668/hbnxb.20191499

Hedden, P., and Sponsel, V. (2015). A century of gibberellin research. *J. Plant Growth Regul.* 34, 740–760. doi: 10.1007/s00344-015-9546-1

Henry, R. J. (2012). Next-generation sequencing for understanding and accelerating crop domestication. *Brief. Funct. Genomics* 11, 51–56. doi: 10.1093/bfgp/elr032

Hightower, R., Baden, C., Penzes, E., Lund, P., and Dunsmuir, P. (1991). Expression of antifreeze proteins in transgenic plants. *Plant Mol. Biol.* 17, 1013–1021. doi: 10.1007/BF00037141

Hu, Z., Huang, X., Amombo, E., Liu, A., and Fu, J. (2020). The ethylene responsive factor CdERF1 from bermudagrass (*Cynodon dactylon*) positively regulates cold tolerance. *Plant Sci.* 294:110432. doi: 10.1016/j.plantsci.2020.110432

International Brachypodium Initiative (2010). Genome sequencing and analysis of the model grass *Brachypodium distachyon*. *Nature* 463, 763–768. doi: 10.1038/nature08747

Li, Z., Yu, J., Peng, Y., and Huang, B. (2017). Metabolic pathways regulated by abscisic acid, salicylic acid and γ-aminobutyric acid in association with improved drought tolerance in creeping bentgrass (*Agrostis stolonifera*). *Physiol. Plant.* 159, 42–58. doi: 10.1111/ppl.12483

Liu, J. X. (2011). *Research and Utilization of Germplasm Resources of Major Warm-Season Turfgrasses in China*. Nanjing: Jiangsu Science and Technology Press.

Liu, S. (2014). *Fish Distant Hybridization*. Beijing: Science Press

Liu, J. X., Wei, X. H., and Liu, X. M. (1998). A preliminary study on the introduction and establishment of lawns in the Ejin Desert oasis. *J. Desert Res.* 15, 45–51. doi: 10.1017/S0266078400010713

Luo, H. S., He, C. Y., and Han, L. B. (2018). Heterologous expression of ZjOMT from *Zoysia japonica* in *Escherichia coli* confers aluminum resistance through melatonin production. *PLoS One* 13:e0196952. doi: 10.1371/journal.pone.0196952

Luo, H., Zhou, Z., and Song, G. (2020). Antioxidant enzyme activity and microRNA are associated with growth of *Poa pratensis* callus under salt stress. *Plant Biotech. Rep.* 14, 429–438. doi: 10.1007/s11816-020-00620-x

Lv, S. H. (1995). A preliminary study on the technology and benefits of direct seeding of lawns in dry and cold climatic zones in northern China. *Grassland China* 3:5.

Ma, Y. M. (2017). *Mechanisms of Polyamine-Induced abiotic Stress Tolerance in Creeping Bentgrass (Agrostis stolonifera)*. Michigan: Michigan State University Press.

Nadeem, M. A., Nawaz, M. A., Shahid, M. Q., Doğan, Y., Comertpay, G., Yıldız, M., et al. (2018). DNA molecular markers in plant breeding: current status and recent advancements in genomic selection and genome editing. *Biotechnol. Biotec. Eq.* 32, 261–285. doi: 10.1080/13102818.2017.1400401

Obidiegwu, J. E., Bryan, G. J., Jones, H. G., and Prashar, A. (2015). Coping with drought: stress and adaptive responses in potato and perspectives for improvement. *Front. Plant Sci.* 6:542. doi: 10.3389/fpls.2015.00542

Pegg, A. E. (2014). The function of spermine. *IUBMB Life* 66, 8–18. doi: 10.1002/iub.1237

Qi, C. H., Liang, X. H., and Han, L. B. (2005). Embryogenic callus induction and plant regeneration of *Zoysia japonica*. *Acta Agrestia Sinica* 28:5. doi: 10.11733/j.issn.1007-0435.2005.03.018

Rai, M. F., Tycksen, E. D., Sandell, L. J., and Brophy, R. H. (2018). Advantages of RNA-seq compared to RNA microarrays for transcriptome profiling of anterior cruciate ligament tears. *J. Orthop. Res.* 36, 484–497. doi: 10.1002/jor.23661

Saidi, A., Eghbalnegad, Y., and Hajibarat, Z. (2017). Study of genetic diversity in local rose varieties (Rosa spp.) using molecular markers. *Banat. J. Biotech* 8, 148–157. doi: 10.7904/2068-4738-VIII(16)-148

Saidi, A., Jabalameli, Z., and Ghalamboran, M. (2018). Evaluation of genetic diversity of carnation cultivars using CDDP and DAMD markers and morphological traits. *Nucleus* 61, 129–135. doi: 10.1007/s13237-018-0238-7

Shao, B. Q., and Liu, W. Z. (1995). Introduction and cultivation of Kentucky grass in the Qingdao area. *Pratacult. Sci.* 12:3.

Sharma, H. C., and Gill, B. S. (1983). Current status of wide hybridization in wheat. *Euphytica* 32, 17–31. doi: 10.1007/BF00036860

Sun, X., Sun, C., Li, Z., Hu, Q., Han, L., and Luo, H. (2016). AsHSP17, a creeping bentgrass small heat shock protein modulates plant photosynthesis and ABA-dependent and independent signalling to attenuate plant response to abiotic stress. *Plant Cell Environ.* 39, 1320–1337. doi: 10.1111/pce.12683

Sun, X., Zhu, J., Li, X., Li, Z., Han, L., and Luo, H. (2020). AsHSP26.8a, a creeping bentgrass small heat shock protein integrates different signaling pathways to modulate plant abiotic stress response. *BMC Plant Biol.* 20:184. doi: 10.1186/s12870-020-02369-5

Tan, M., Hassan, M. J., Peng, Y., Feng, G., Huang, L., Liu, L., et al. (2022). Polyamines metabolism interacts with -Aminobutyric acid, Proline and nitrogen metabolisms to affect drought tolerance of creeping Bentgrass. *Int. J. Mol. Sci.* 23:2779. doi: 10.3390/ijms23052779

Tanaka, H., Hirakawa, H., Kosugi, S., Nakayama, S., Ono, A., Hashiguchi, W., et al. (2016). Sequencing and comparative analyses of the genomes of Zoysia grasses. *DNA Res.* 23, 171–180. doi: 10.1093/dnares/dsw006

Tang, M., Li, Z., Luo, L., Cheng, B., Zhang, Y., Zeng, W., et al. (2020). Nitric oxide signal, nitrogen metabolism, and water balance affected by γ-Aminobutyric acid (GABA) in relation to enhanced tolerance to water stress in creeping Bentgrass. *Int. J. Mol. Sci.* 21:7460. doi: 10.3390/ijms21207460

Teng, K., Tan, P., Xiao, G., Han, L., and Luo, H. (2016). Heterologous expression of a novel *Zoysia japonica* salt-induced glycine-rich RNA-binding protein gene, ZjGRP, caused salt sensitivity in Arabidopsis. *Plant Cell Rep.* 36, 179–191. doi: 10.1007/s00299-016-2068-x

Tůmová, L., Tarkowská, D., Řehořová, K., Marková, H., Kočová, M., Rothová, O., et al. (2018). Drought-tolerant and drought-sensitive genotypes of maize (*Zea mays* L.) differ in contents of endogenous brassinosteroids and their drought-induced changes. *PLoS One* 13:e0197870. doi: 10.1371/journal.pone.0197870

Varshney, R. K., Thudi, M., Nayak, S. N., Gaur, P. M., Kashiwagi, J., Krishnamurthy, L., et al. (2014). Genetic dissection of drought tolerance in chickpea (*Cicer arietinum* L.). *Theor. Appl. Genet.* 127, 445–462. doi: 10.1007/s00122-013-2230-6

Wang, X., Cai, X., Xu, C., Wang, Q., and Dai, S. (2016). Drought-responsive mechanisms in plant leaves revealed by proteomics. *Int. J. Mol. Sci.* 17:1706. doi: 10.3390/ijms17101706

Wang, W. Q., Li, Z. D., and Bai, C. J. (2006). Progress in research on germplasm resources of the genus knotweed and its applications. *Grassland Lawns* 2:6. doi: 10.3969/j.issn.1009-5500.2006.02.001

Weng, R. X. (1999). "Introduction of Zoysia japonica," in *Symposium on Chinese Turf Science and Turf Industry in the 21st Century*. (Beijing, China: China Agricultural University Press), 74–78.

Xie, Q., Niu, J., Xu, L., Zhang, Y., Fan, B., Liang, X., et al. (2015). *De novo* assembly of the Japanese turfgrass (*Zoysia japonica* Steud.) root transcriptome and identification of candidate unigenes related to early responses under salt stress. *Front. Plant Sci.* 6:610. doi: 10.3389/fpls.2015.00610

Xin, J. N., Han, L. B., Liu, J., and Han, X. B. (2006). Transformation of Kentucky bluegrasss (*Poa pratensis* L.) by particle bombardment. *China. J. Biol. Eng.* 26, 10–14. doi: 10.3969/j.issn.1671-8135.2006.08.003

Xu, L. X., Han, L. B., and Huang, B. R. (2011). Membrane fatty acid composition and saturation levels associated with leaf dehydration tolerance and post-drought rehydration in Kentucky bluegrass. *Crop. Sci.* 51, 273–281. doi: 10.2135/cropsci2010.06.0368

Xu, L. X., Han, L. B., and Huang, B. R. (2013). Photosynthetic enzyme activities and gene expression associated with drought tolerance and post-drought recovery in Kentucky bluegrass. *Environ. Exp. Bot.* 89, 28–35. doi: 10.1016/j.envexpbot.2012.12.001

Xu, L. X., Han, L. B., and Song, G. L. (2017a). Epichloe endophyte infection improved drought and heat tolerance of tall fescue through altered antioxidant enzyme activity. *Europ J. Hort. Sci.* 82, 90–97. doi: 10.17660/ejhs.2017/82.2.4

Xu, L., Li, F., Han, L., Song, G., and Zhang, X. (2017b). Overexpression of Arabidopsis DREB1A gene in transgenic: impacts on osmotic adjustment and hormone metabolism under drought. *Int. Turfgrass Soc. Res. J.* 13, 527–530. doi: 10.2134/itsrj2016.06.0508

Yan, Y. R., Zhu, Y. R., and Qian, X. W. (1998). Catch-up sowing of cool-season grasses on warm-season lawns is a practical way to keep lawns green in Shanghai. *Shanghai Constr. Technol.* 6:2.

Ye, T., Wang, Y., Feng, Y. Q., and Chan, Z. (2021). Physiological and metabolomic responses of bermudagrass (*Cynodon dactylon*) to alkali stress. *Physiol. Plant.* 171, 22–33. doi: 10.1111/ppl.13209

Yuan, J., Bai, Y., Chao, Y., Sun, X., He, C., Liang, X., et al. (2018). Genome-wide analysis reveals four key transcription factors associated with cadmium stress in creeping bentgrass (*Agrostis stolonifera* L.). *Peerj* 6:e5191. doi: 10.7717/peerj.5191

Zhang, C., Hang, L., Zhang, H., Hao, Q., Lyu, B., Wang, M., et al. (2019). An ancestral NB-LRR with duplicated 3'UTRs confers stripe rust resistance in wheat and barley. *Nat. Commun.* 10:4023. doi: 10.1038/s41467-019-11872-9

Conflict of Interest: The authors declare that the research was conducted in the absence of any commercial or financial relationships that could be construed as a potential conflict of interest.

frontiers | Frontiers in Plant Science

ORIGINAL RESEARCH
published: 16 June 2022
doi: 10.3389/fpls.2022.931001

Transcriptome Analysis Revealed the Molecular Response Mechanism of High-Resistant and Low-Resistant Alfalfa Varieties to Verticillium Wilt

Fang Li†, Xi Chen†, Bo Yang, Yingjie Guang, Dandan Wu, Zunji Shi and Yanzhong Li**

State Key Laboratory of Grassland Agro-Ecosystems, Center for Grassland Microbiome, Gansu Tech Innovation Center of Western China Grassland Industry, College of Pastoral Agriculture Science and Technology, Lanzhou University, Lanzhou, China

OPEN ACCESS

Edited by:
Jing Zhang, Nanjing Agricultural University, China

Reviewed by:
Muhammad Saad Rehmani, South China Agricultural University, China
Yuxia Guo, Henan Agricultural University, China

***Correspondence:**
Zunji Shi
shizj@lzu.edu.cn
Yanzhong Li
liyzh@lzu.edu.cn

†These authors have contributed equally to this work and share first authorship

Specialty section:
This article was submitted to Plant Abiotic Stress, a section of the journal Frontiers in Plant Science

Received: *28 April 2022*
Accepted: *30 May 2022*
Published: *16 June 2022*

Citation:
Li F, Chen X, Yang B, Guang Y, Wu D, Shi Z and Li Y (2022) Transcriptome Analysis Revealed the Molecular Response Mechanism of High-Resistant and Low-Resistant Alfalfa Varieties to Verticillium Wilt. Front. Plant Sci. 13:931001. doi: 10.3389/fpls.2022.931001

Following infestation by Verticillium wilt, alfalfa (*Medicago sativa* L.) often shows symptoms such as disease spots, leaf loss, stem, and leaf yellowing, resulting in the decline of alfalfa yield and quality and causing significant losses to the alfalfa industry. The popularization and planting of disease-resistant varieties is the most effective method to prevent and control Verticillium wilt of alfalfa. Therefore, it is particularly important to reveal the resistance mechanism of Verticillium wilt resistant varieties of alfalfa. In this study, the physiological and biochemical indexes were measured on days 7, 14, 21, and 28 after inoculation with *Verticillium alfalfae* for investigating the response mechanisms of two alfalfa varieties, high-resistant WL343HQ, and low-resistant Dryland. Transcriptome sequencing of alfalfa samples infected with *V. alfalfae* and uninfected alfalfa samples was performed to analyze the potential functions and signaling pathways of differentially expressed genes (DEGs) by GO classification and KEGG enrichment analysis. Meanwhile, weighted gene co-correlation network analysis (WGCNA) algorithm was used to construct a co-expression network of DEGs. Inoculation with *V. alfalfae* significantly affected net photosynthetic rate, stomatal conductance, chlorophyll content, MDA content, JA and SA concentrations, and NO and H_2O_2 contents in both WL343HQ and Dryland inoculated with *V. alfalfae*. Most of the transcription factors in plants were classified in the WRKY, NAC, and bHLH families. WGCNA analysis showed that the number of transcription factors related to plant growth and disease resistance was higher in the corresponding modules of WL343HQ disease groups on days 7 and 28 (WVa) and (WVd) than in the corresponding modules of Dryland disease groups on days 7 and 21 (HVa) and (HVc). These findings provide data for further gene function validation and also provide a reference for in-depth studies on interactions between plants and pathogens.

Keywords: alfalfa, Verticillium wilt, *Verticillium alfalfae*, resistance mechanism, transcriptomics

INTRODUCTION

Alfalfa (*Medicago sativa* L.) is widely grown in the United States, Canada, China, Argentina and other countries. With the expansion of alfalfa cultivation, diseases have become one of the main limitations to the production and utilization of alfalfa. Among them, the most common alfalfa diseases are caused by fungi. A 35 alfalfa diseases caused by more than 70 pathogenic fungi have been reported all over the world (Samac et al., 2014; Wen et al., 2015). Verticillium wilt caused by *Verticillium alfalfae* is a devastating disease in alfalfa production (Peaden et al., 1985). The disease was first reported in Sweden in 1918, thereafter it spread widely in North America (Grau et al., 1981; Gordon et al., 1989). In 2014, Verticillium wilt was detected in Minle County, Gansu Province, China, and the average incidence rate of the disease in Minle was 45%, with 100% isolation of the pathogen in stem and root of symptomatic plants (Xu et al., 2016).

The invasion of *V. alfalfae* causes a series of physiological and biochemical responses, including the increase of membrane lipid peroxidation products and the decrease of soluble sugar content and nutrient uptake (Gharbi et al., 2016; Bibi et al., 2017). Furthermore, *Verticillium dahliae* is able to cause disease by inducing the expression of related genes and regulating signaling pathways. *GhWRKY70D13* gene was upregulated after inoculation with *V. dahliae*, and knockdown of this gene improved resistance to *V. dahliae* in both resistant and susceptible plants (Xiong et al., 2020). Differentially expressed genes (DEGs) in olive samples of susceptible (Picual) and resistant (Frantoio) varieties were analyzed by transcriptomic techniques after 2 weeks of inoculation with *V. dahliae*, and it was found that the amount of mRNA of *V. dahliae* in susceptible varieties was significantly higher than that in resistant varieties (Jimenez-Ruiz et al., 2019). The transcriptome results of Verticillium wilt of eggplants revealed that DEGs associated with Verticillium wilt were mainly involved in "amino acid transport and metabolism," "cytoskeleton" and "cellular activity" (Yang et al., 2019). Compared to control plants, 111 common DEGs were identified in diseased plants and most of them were enriched in "signal transduction pathway."

The popularization and planting of disease-resistant varieties is the most effective method to prevent and control Verticillium wilt of alfalfa. Therefore, it is particularly important to reveal the resistance mechanism of Verticillium wilt resistant varieties of alfalfa. After infected by *Verticillium alfalfae*, plants produced disease resistance-related enzymes such as phenylpropanoid metabolic enzymes, participating in lignin and salicylic acid synthesis for reinforcing cell wall and building systemic resistance (MauchMani and Slusarenko, 1996; Smit and Dubery, 1997). Signal transduction molecules such as hydrogen peroxide (H_2O_2), salicylic acid (SA), and jasmonic acid (JA) induced resistance responses synergistically or individually (Yao et al., 2011; Dhar et al., 2020). H_2O_2 can effectively resist the invasion of pathogenic bacteria and the expansion of pathogenic mycelium by triggering a series of defense responses such as allergic response and programmed cell death (Dat et al., 2000; Mellersh et al., 2002). SA can improve plant tolerance to *V. alfalfae* (Zhen and Li, 2004). JA was associated with plant resistance, and tomato plants lacking JA were more susceptible to *V. alfalfae* (Thaler et al., 2004; Tjamos et al., 2005). After infected by Verticillium wilt, regulatory genes that induce specific defense responses were upregulated in cells near the point of infection (Hill et al., 1999), for example, *Ve* gene can improve resistance of tomatoes to *V. dahliae* (Nachmias et al., 1987).

In this study, physiological and biochemical indexes and transcriptome sequencing were performed after inoculation with *V. alfalfae* for investigating the resistance mechanism of different alfalfa varieties. These findings provide new insights for in-depth studies on the interactions between plants and pathogenic bacteria.

MATERIALS AND METHODS

Sample Collection

We selected a high resistance variety (WL343HQ) and a low resistance variety (Dryland) for this study. The alfalfa seeds were sterilized and placed on sterilized filter paper of culture dish for germination. The soil used for the experiments was turfy soil, which was collected from a grassland in the same place. Impurities in the soil samples, such as gravel, leaves, and grass roots, were removed during the soil collection. The soil was sterilized by γ-radiation and sealed. Each pot contained 1.0 kg. The pathogenic fungus used in this experiment was the *V. alfalfae* strain LYZ0257 isolated from Minle County. A spore suspension of 1×10^6/ml was prepared with sterile water. Two alfalfa varieties, WL343HQ and Dryland, were divided into disease groups (WL + V and HD + V) and control groups (WL and HD). After 3 days of germination, the well-grown seedlings were transplanted into pots with sterilized soil. Each treatment had 10 pots, 40 pots in total, nine alfalfa plants per pot. The plants were watered every 3 days and maintained in the inoculation room, with a 12 h photoperiod, 22 and 18°C day and night temperatures, and 65–90% relative humidity. Alfalfa was inoculated with *V. alfalfae* after 6 weeks of growth by spray method. The inoculation dose was 10 ml of spore suspension of *V. alfalfae* per pot. The control groups were sprayed with 10 ml of sterile water per pot. The leaves were taken from the same parts of alfalfa on days 7, 14, 21, and 28, respectively, then frozen in liquid nitrogen and stored at −80°C for the determination of physiological and biochemical indicators and transcriptome sequencing. The transcriptome sequencing had three replicates for each treatment.

Determination of Physiological and Biochemical Indicators

The number of diseased plants per pot was counted separately and the incidence rate of disease was the mean of 10 replicates. Disease index, representing both incidence rate and symptom severity of disease, can be calculated as Disease index = disease ratio×disease severity×100%. Small segments were cut from the thickest stalk of each plant, and the stalks were sterilized in 75% alcohol and 1% NaClO for 1 min, respectively, and then rinsed 3–4 times with sterile water. After absorbing the surface water

of the stalks with sterilized filter paper, the stalks were cut into small sections of about 2 mm and placed on PDA medium. The plates were placed in the incubator at 23–25°C and observed daily. The plant carrier rate of *V. alfalfae* was counted on the 4th day. Leaf net photosynthetic rate and stomatal conductance were measured using a GFS-3000 photosynthesizer (Heinz Walz GmbH Co., Ltd., Effeltrich, Germany) from 9: 00 a.m. to 12: 00 p.m. on days 7, 14, 21, and 28, respectively. The chlorophyll content of the plants was determined by the acetone extraction method (Fang et al., 2020). The measurement was performed using ELISA kits of SA and JA (Nanjing Jiancheng Biological Engineering Research Institute Co., Ltd., Nanjing, China). The absorbance value of each well was measured sequentially at 450 nm using an RT-6100 Microplate Reader (Rayto Life and Analytical Sciences Co., Ltd., Shenzhen, China). The ELISA kits for NO and H_2O_2 (Nanjing Jiancheng Biological Engineering Research Institute Co., Ltd., Nanjing, China) were used to detect the amount of NO and H_2O_2 in the samples, and the absorbance values were measured at 550 nm and 405 nm, respectively. The superoxide dismutase (SOD) and peroxidase (POD) activities were measured by the nitrogen blue tetrazolium and guaiacol methods (Shi et al., 2014). The thiobarbituric acid method was used to determine the MDA concentration in plants (Yin et al., 2019).

Transcriptome Sequencing

The leaves from the same parts of WL343HQ and Dryland were collected and sent to Biomarker Technologies Co., Ltd. (Beijing, China) for transcriptome sequencing. Samples were selected on days 7, 14, 21, and 28 for WL343HQ disease groups (WVa, WVb, WVc, and WVd), WL343HQ control groups (Wa, Wb, Wc, and Wd), Dryland disease groups (HVa, HVb, HVc, and HVd), and Dryland control groups (Ha, Hb, Hc, and Hd). Three biological replicates were conducted per group, with a total of 48 samples. RNA extraction from alfalfa leaves was performed using the Tiangen DP441 kit (Tiangen Biotech Co., Ltd., Beijing, China). The obtained RNA extracts were measured for concentration and purity using Nanodrop 2000 (Thermo Fisher Scientific Co., Ltd., Waltham, MA, United States). Agilent 2,100 Bioanalyzer (Agilent Technologies, Inc., Santa Clara, CA, United States) and LabChip GX Nucleic Acid Analyzer (PerkinElmer Instrument Co., Ltd., Shanghai, China) were used to check the integrity testing. Samples with a 260:280 ratio of ≥2.0 and RNA integrity number of ≥8 were subjected to transcriptome sequencing. After the samples were tested, cDNA libraries were constructed and sequenced using the Illumina platform. Fastq format raw data were processed through in-house Perl scripts for quality control. Clean data were obtained by removing adapter containing reads and low-quality raw data reads. At the same time, the Q30, GC-content, and sequence duplication level of the clean reads were calculated. All downstream analyses were performed on high-quality and clean data.

Quantitative Real-Time PCR Analysis

To validate the results of transcriptome analysis, the expression levels of 12 DEGs were detected by quantitative real-time PCR (qPCR) with three independent biological replicates for each sample. The primers were designed using Primer Designer 3.0 software, and 18S ribosomal RNA was chosen as the internal reference (Wang et al., 2015). The primers used in this study were listed in **Supplementary Table 1**. A 1 μg RNA was used to synthesize cDNA by Takara PrimeScript RT reagent Kit (Takara Biomedical Technology Co., Ltd., Beijing, China). qPCR assays were performed on CFX96 Touch Real-Time PCR Detection System (Bio-Rad Laboratories Co., Ltd., Hercules, CA, United States). The qPCR reaction conditions were set: 95°C, 3 min; 95°C for 3 s, 60°C for 30 s, 40 cycles. All treatments were repeated three times technically to reduce experimental errors due to handling and the instrument. Finally, the qPCR data were analyzed based on melting curve analysis using the ΔΔCT method (Livak and Schmittgen, 2001) and the relative gene expression was measured and normalized compared to control expression levels, and the control group was set to 1 for comparison of different groups.

Statistical Analysis

The physiological and biochemical indexes were entered into Microsoft Excel 2020 for collation and calculation. Homogeneity of variance was detected by Levene test in SPSS 20.0 statistical software. Significant differences between treatments were analyzed by Tukey's method ($p < 0.05$). The data of qPCR validation results of the genes were entered into Microsoft Excel 2020 and plotted after calculation by the ΔΔCT method (Livak and Schmittgen, 2001). The analysis of transcriptome sequencing data was mainly performed through Biomarker Cloud platform (Biomarker Technologies Co., Ltd., Beijing, China). The DESeq R package (v1.10.1) was used to perform differential expression analysis between different groups. Fragments per kilobase of transcript per million mapped reads (FPKM) were used to verify the transcriptional expression levels of the samples. The co-expression network was analyzed by weighted gene co-correlation network analysis (WGCNA) and mapped by R 4.1.0 software to describe the modules among genes. In addition, the core gene network was constructed and plotted by Cytoscape v.3.4.0 software.

RESULTS

Physiological and Biochemical Indicators

After inoculation with *Verticillium alfalfae*, typical symptoms of verticillium wilt were seen in WL343HQ inoculated with *V. alfalfae* (WL + V) and Dryland inoculated with *V. alfalfae* (HD + V), and *V. alfalfae* was isolated from the plant stalks of both varieties. On day 7, symptoms of Verticillium wilt were found on the Dryland, which had a 2.78% infection rate, while no obvious symptoms were seen on the WL343HQ. On days 14, 21, and 28, the disease incidence rate of Dryland was 36.11, 63.89, and 80.55%, and the disease incidence rate of WL343HQ was 13.89, 30.55, and 41.66%, respectively (**Figure 1A**). On days 14, 21, and 28, the disease indices of Dryland were 17.78, 45 and 68.33, and the disease indices of WL343HQ were 3.33, 16.67, and 32.78, respectively

(**Figure 1B**). There was no significant difference in disease incidence rate and indices between WL343HQ and Dryland on day 7. On days 14, 21, and 28, the disease incidence rate and indices of WL343HQ were lower than those of Dryland ($p < 0.05$). The net photosynthetic rate and stomatal conductance of the disease groups (WL + V and HD + V) were significantly lower than the control groups (WL and HD; **Figures 1C,D**; $p < 0.05$). Compared with the control, chlorophyll content of the disease groups (WL + V and HD + V) significantly decreased on days 7, 14, 21, and 28 (**Figure 1E**; $p < 0.05$). Chlorophyll content of WL343HQ inoculated with *V. alfalfae* (WL + V) was significantly higher than that of Dryland inoculated with *V. alfalfae* (HD + V; **Figure 1E**; $p < 0.05$). Compared with the control, MDA concentrations of HD + V group significantly increased by 38.87, 131.62, 162.24, and 174.57% on days 7, 14, 21, and 28, respectively (**Figure 1F**; $p < 0.05$). On days 14, 21, and 28, MDA concentration of WL + V group significantly increased by 98.48, 116.26, and 134.66% (**Figure 1F**; $p < 0.05$).

Inoculation of *V. alfalfae* significantly affected the SOD and POD activities of plants. Compared with the control, SOD activity of HD + V group increased by 44.08, 94.41, and 142.90% on days 7, 14, and 21, and decreased by 35.34% on day 28 (**Figure 1G**; $p < 0.05$). POD activity of HD + V group increased by 24.10 and 43.80% on days 7 and 14, and decreased by 28.56% on day 28 (**Figure 1H**; $p < 0.05$). SOD and POD activities of WL + V group increased by 61.67 and 31.36%, 103.24 and 62.70%, 115.56 and 44.79% on days 7, 14, and 21, respectively, and showed a decreasing trend on day 28 (**Figures 1G,H**; $p < 0.05$). SOD and POD activities of WL + V group were significantly higher than those of HD + V group. Compared with the control, JA concentrations of HD + V group significantly increased by 31.92, 65.66 and 47.69% on days 14, 21 and 28, respectively (**Figure 1I**; $p < 0.05$). The SA differences in HD + V group were not significant throughout the period of disease succession (**Figure 1J**). Compared with the control, the concentrations of JA and SA in WL + V group on days 7, 14, 21 and 28 significantly increased by 20.91 and 23.33%, 46.64

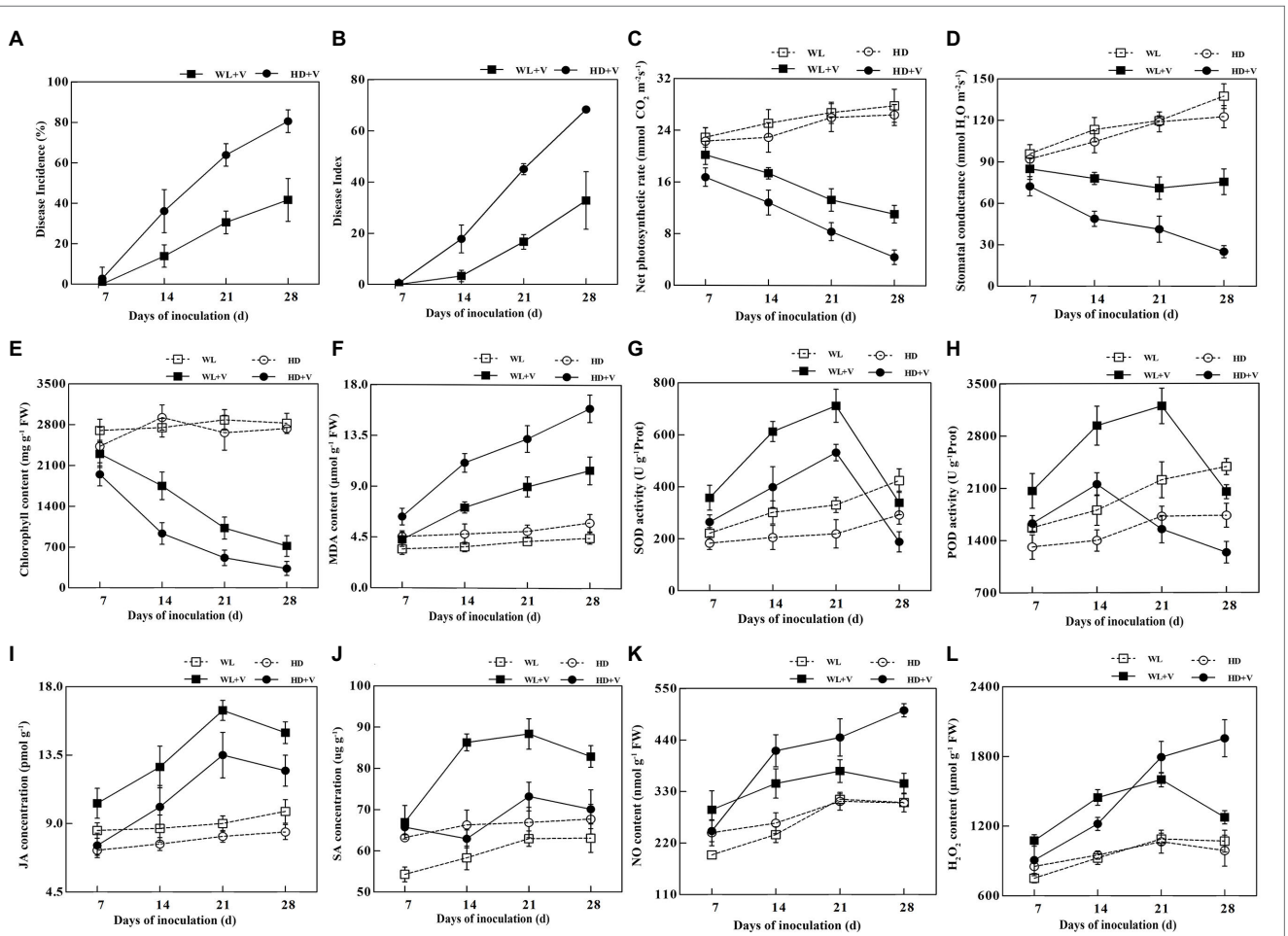

FIGURE 1 | Linear charts of physiological and biochemical indicators of WL343HQ inoculated with *Verticillium alfalfae* (WL + V), Dryland inoculated with *V. alfalfae* (HD + V), and control groups (WL and HD). **(A)** Disease incidence. **(B)** Disease index. **(C)** Net photosynthetic rate. **(D)** Stomatal conductance. **(E)** Chlorophyll content. **(F)** MDA content. **(G)** SOD activity. **(H)** POD activity. **(I)** JA concentration. **(J)** SA concentration. **(K)** NO content. **(L)** H_2O_2 content. Data are presented as mean ± SD; $n = 10$ for each treatment.

and 48.11%, 82.64 and 40.37%, 52.86 and 31.40%, respectively (**Figures 1I,J**; $p < 0.05$). Compared with the control, NO and H_2O_2 contents of HD + V group increased by 58.91 and 28.35%, 44.11 and 68.34%, 64.76 and 97.98% on days 14, 21 and 28, respectively (**Figures 1K,L**; $p < 0.05$). The NO and H_2O_2 contents of WL + V group significantly increased by 49.61 and 43.21%, 45.91 and 56.30%, 19.27 and 47.03%, 13.29 and 19.13% on days 7, 14, 21, and 28, respectively (**Figures 1K,L**; $p < 0.05$).

Analysis of Differentially Expressed Genes in WL343HQ

Compared with the control, the numbers of DEGs of WL343HQ inoculated with *V. alfalfae* (WL + V) on days 7, 14, 21 and 28 were 3,113, 13,526, 21,064, and 18,217, respectively. GO classification, KEGG enrichment analysis and transcription factor prediction were performed for DEGs. GO classification included 3 major categories, such as biological processes, cellular components and molecular functions (**Figures 2A–D**). KEGG enrichment analysis of DEGs on days 7, 14, 21, and 28 (**Figures 2E–H**) revealed that DEGs were mainly enriched in carbon fixation in photosynthetic organisms (ko00710), plant-pathogen interaction (ko04626), MAPK signaling pathway-plant (ko04016), glutathione metabolism (ko00480), photosynthesis-antenna proteins (ko00196) and α-Linolenic acid metabolism (ko00592). By transcription factor prediction, all DEGs were categorized into transcription factor families, and the top 20 transcription factor families with the highest abundance were selected (**Figures 2I–L**). It was found that DEGs of WL + V group on days 7, 14, 21, and 28 were mainly categorized into the following transcription factor families, including WRKY, bHLH, NAC, MYB, C2H2, HSF, bZIP, mTERF, AP2/ERF-ERF, C3H, TCP, GARP-G2-like, HB-HD-ZIP, and AUXIAA. The numbers of transcription factors were the highest in the WRKY, NAC and bHLH families. The numbers of transcription factors in WRKY family on days 7, 14, 21, and 28 were 30, 108, 134, and 118, respectively. The numbers of transcription factors in bHLH family were 13, 55, 88, and 84 on days 7, 14, 21, and 28. The numbers of transcription factors in NAC family were 14, 68, 101, and 77 on days 7, 14, 21, and 28. To investigate the specific changes in genes on days 7, 14, 21, and 28, venn diagrams were performed for the four groups, Wa vs. WVa, Wb vs. WVb, Wc vs. WVc, and Wd vs. WVd (**Supplementary Figure 1A**), the numbers of DEGs specific to the four differential groups were 673, 1954, 6,082 and 3,916, respectively. The number of DEGs co-expressed in the four differential groups was 1,539.

KEGG enrichment analysis were performed for DEGs specific to days 7, 14, 21, and 28, respectively. A 673 DEGs on day 7 were mainly enriched in ribosome (ko03010), biosynthesis of various secondary metabolites-part 2 (ko00998) and starch and sucrose metabolism (ko00500; **Figure 3A**). A 1954 DEGs on day 14 were predominantly enriched in phenylpropanoid biosynthesis (ko00940), linoleic acid metabolism (ko00591), basal transcription factors (ko03022) and caffeine metabolism (ko00232; **Figure 3B**). A 6,082 DEGs on day 21 were mainly enriched in plant hormone signal transduction (ko04075), biosynthesis of amino acids (ko01230), MAPK signaling pathway-plant (ko04016) and plant-pathogen interaction (ko04626; **Figure 3C**). A 3,916 DEGs on day 28 were mainly enriched in the biosynthesis of amino acids (ko01230), carotenoid biosynthesis (ko00906), peroxisome (ko04146) and plant hormone signal transduction (ko04075; **Figure 3D**).

Analysis of Differentially Expressed Genes in Dryland

Compared with the control, the numbers of DEGs of Dryland inoculated with *V. alfalfae* (HD + V) on days 7, 14, 21, and 28 were 14,809, 11,127, 24,460, and 22,295, respectively. GO classification was also mainly in 3 major categories: biological processes, cellular components and molecular functions (**Figures 4A–D**). KEGG enrichment analysis of DEGs on days 7, 14, 21, and 28 (**Figures 4E–H**) revealed that DEGs were mainly enriched in valine, leucine and isoleucine degradation (ko00280), MAPK signaling pathway-plant (ko04016), photosynthesis (ko00195), photosynthesis-antenna proteins (ko00196), and α-Linolenic acid metabolism (ko00592). All DEGs were categorized into transcription factor families, and the top 20 transcription factor families with the highest abundance were selected (**Figures 4I–L**). Consistent with the results of WL343HQ (WL + V), DEGs of HD + V group on days 7, 14, 21, and 28 were mainly categorized into transcription factors of the WRKY, NAC and bHLH families. Venn diagrams were performed for the four groups, including Ha vs. HVa, Hb vs. HVb, Hc vs. HVc, and Hd vs. HVd (**Supplementary Figure 1B**), the numbers of DEGs specific to the four groups were 2,974, 1,437, 6,160, and 4,480, respectively. The number of DEGs co-expressed in the four groups was 5,277. KEGG enrichment analysis were performed for DEGs specific to days 7, 14, 21 and 28, respectively. A 2,974 DEGs on day 7 were mainly enriched in isoflavonoid biosynthesis (ko00943), ribosome (ko03010) and terpenoid backbone biosynthesis (ko00900; **Figure 5A**). A 1,437 DEGs on day 14 were mainly enriched in biosynthesis of amino acids (ko01230), glycine, serine and threonine metabolism (ko00260), RNA polymerase (ko03020) and terpenoid backbone biosynthesis (ko00900; **Figure 5B**). A 6,160 DEGs on day 21 were mainly enriched in ribosome (ko03010), biosynthesis of amino acids (ko01230) and aminoacyl-tRNA biosynthesis (ko00970; **Figure 5C**). A 4,480 DEGs on day 28 were mainly enriched in the circadian rhythm-plant (ko04712), inositol phosphate metabolism (ko00562), pentose phosphate pathway (ko00030) and basal transcription factors (ko03022; **Figure 5D**).

Furthermore, we compared the DEGs between the less resistant HD + V group and the highly resistant WL + V group. The number of DEGs on days 7, 14, 21, 28 were 5,432, 2,202, 2,705 and 1,259, respectively. GO classification and KEGG enrichment analysis were also performed for DEGs. GO classification included 3 major categories, such as biological processes, cellular components and molecular functions (**Supplementary Figures 2A–D**). KEGG enrichment analysis of DEGs on days 7, 14, 21 and 28 (**Supplementary Figures 2E–H**)

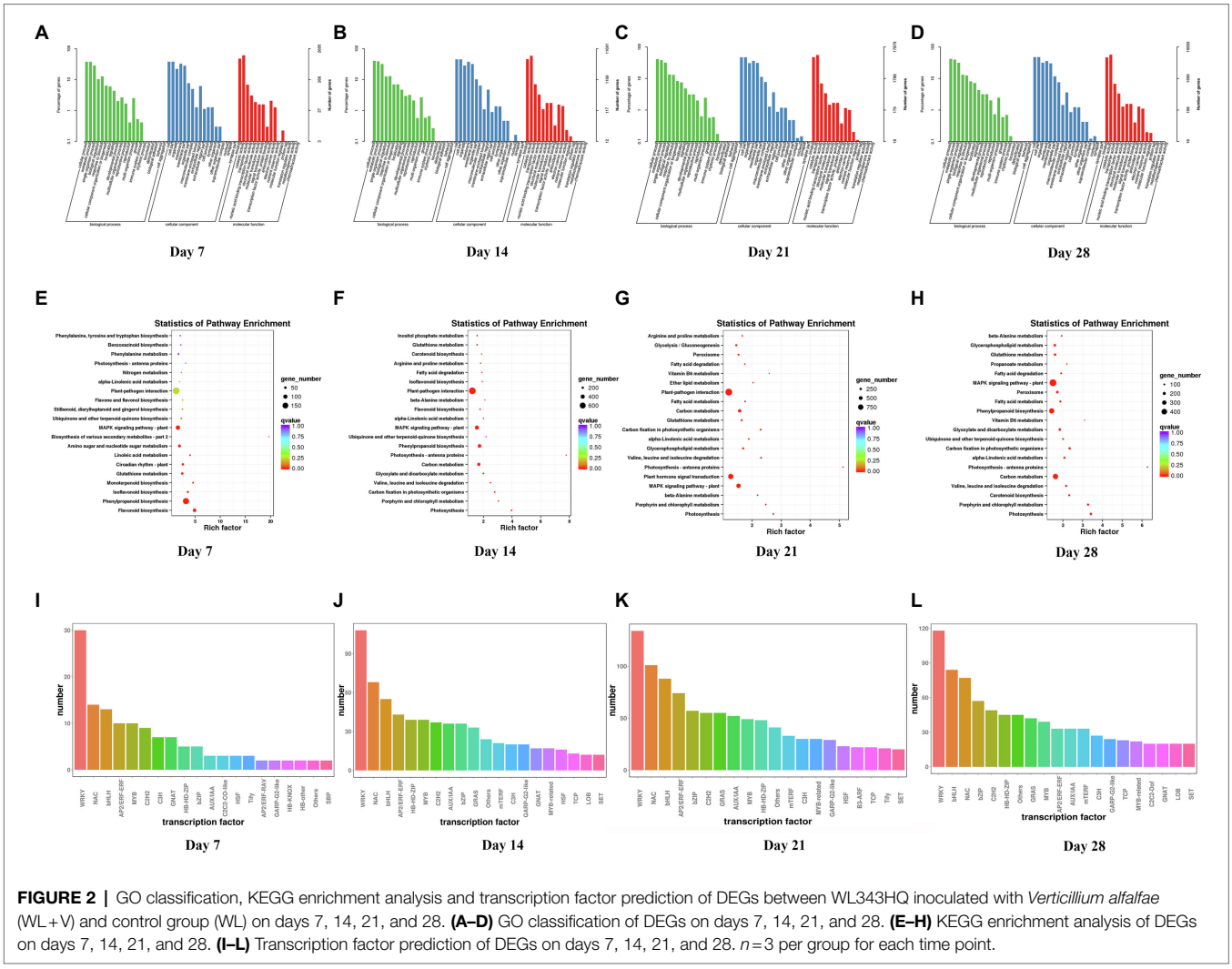

FIGURE 2 | GO classification, KEGG enrichment analysis and transcription factor prediction of DEGs between WL343HQ inoculated with *Verticillium alfalfae* (WL+V) and control group (WL) on days 7, 14, 21, and 28. **(A–D)** GO classification of DEGs on days 7, 14, 21, and 28. **(E–H)** KEGG enrichment analysis of DEGs on days 7, 14, 21, and 28. **(I–L)** Transcription factor prediction of DEGs on days 7, 14, 21, and 28. $n=3$ per group for each time point.

revealed that DEGs were mainly enriched in photosynthesis (ko00195), photosynthesis-antenna proteins (ko00196), MAPK signaling pathway-plant (ko04016), carbon fixation in photosynthetic organisms (ko00710), starch and sucrose metabolism (ko00500) and carbon metabolism (ko01200). To investigate the specific changes in genes on days 7, 14, 21 and 28, venn diagrams were performed for the four groups, HVa vs. WVa, HVb vs. WVb, HVc vs. WVc, and HVd vs. WVd (**Supplementary Figure 1C**), the numbers of DEGs specific to the four differential groups were 4,050, 1,250, 1,695, and 772, respectively. The number of DEGs co-expressed in the four differential groups was 99.

qPCR Validation of Differentially Expressed Genes

To verify the authenticity of the transcriptional data, 12 DEGs were randomly selected for qPCR validation. The results showed that the expressions of 12 DEGs were consistent with the trend of FPKM values of transcriptome sequencing, thus confirming the accuracy of transcriptome analysis (**Supplementary Figure 3**).

Weighted Gene Co-expression Network Analysis

DEGs were screened and 17,414 genes were selected for WGCNA. When the average connectivity tended to 0, a scale-free network could be obtained with a threshold = 11 and $R^2 \geq 0.85$ (**Supplementary Figure 4A,B**). An adjacency matrix was constructed and converted into a topological overlap matrix to reflect the correlation strength in the co-expression network. The clustering of genes was achieved by the dissimilarity. The division of gene modules was realized by dynamic shearing algorithm, and the minimum number of genes in each module was set to 100, then 14 gene co-expression modules were initially obtained by calculating the feature vector of each module and merging similar modules (**Supplementary Figure 4C**). The module eigenvector values were calculated to obtain the dissimilarity between the modules, which was used to get the eigenvector gene proximity heatmap of each module (**Supplementary Figure 4C**). The relationships between the modules can be seen through the heatmap. Moreover, through the module clustering tree, the modules were further reduced in number compared to the pre-merger (**Supplementary Figure 4E**).

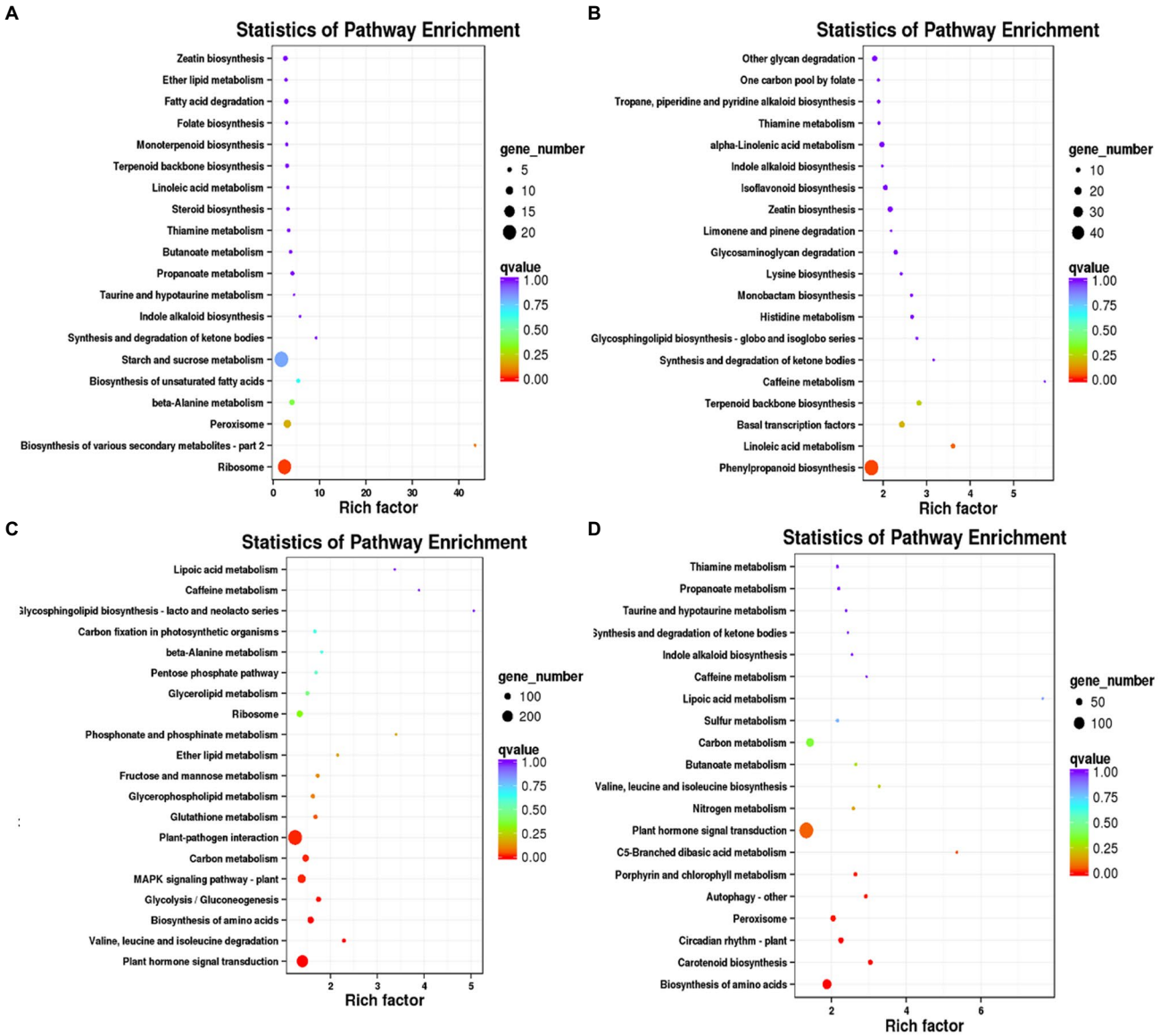

FIGURE 3 | KEGG enrichment analysis of DEGs specific to days 7, 14, 21, and 28 in WL343HQ inoculated with *Verticillium alfalfae* (WL + V). **(A)** KEGG enrichment analysis of DEGs specific to days 7. **(B)** KEGG enrichment analysis of DEGs specific to days 14. **(C)** KEGG enrichment analysis of DEGs specific to days 21. **(D)** KEGG enrichment analysis of DEGs specific to days 28.

After merging the modules, the distribution of gene expression in each module for each sample can be clearly displayed in the heatmap (**Supplementary Figure 4F**).

Among the final 9 gene co-expression modules, genes in four modules, tan, purple, brown and black, showed high correlation with HVa, HVc, WVa and WVd, respectively (**Figure 6A**). The first row in each box was the *R*-value and the second row was the *p*-value. *R*-value represented the correlation coefficient between the co-expression modules and the samples. We primarily screened the core genes of the four corresponding modules by intra-module significance value *R* and intramodular connectivity of the genes, and the screening condition was $R \geq 0.8$ and intramodular connectivity ≥ 0.8. The total number of genes in the tan module corresponding to the HVa was 322, and the number of core genes in this module was 27. The heatmap of tan module genes expression and the barplots of module eigengenes expression values were shown in **Figure 6B**. The expression of module eigengenes in the three replicates of HVa treatment was higher than other treatments, and the visualization result of 27 core genes was shown in **Figure 6B**. The total numbers of genes in the purple, brown and black modules were 398, 2037 and 485, and the numbers of core genes were 25, 36 and 30, respectively (**Figures 6C–E**). In the purple, brown and black modules, the expressions of module eigengenes in the replicates of corresponding HVc, WVa and WVd treatments were higher than other treatments.

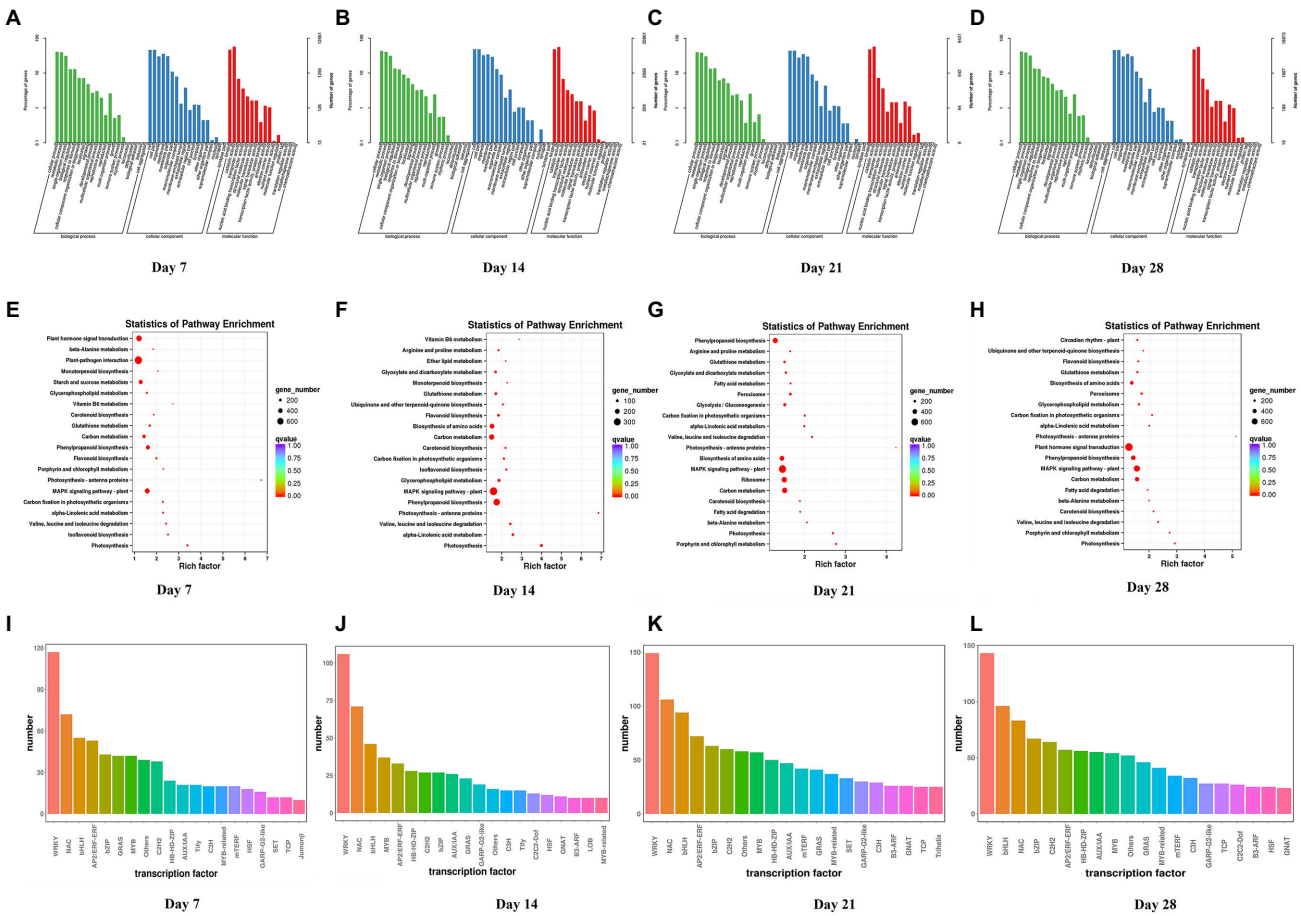

FIGURE 4 | GO classification, KEGG enrichment analysis and transcription factor prediction of DEGs between Dryland inoculated with *Verticillium alfalfae* (HD + V) and control group (HD) on days 7, 14, 21, and 28. **(A–D)** GO classification of DEGs on days 7, 14, 21, and 28. **(E–H)** KEGG enrichment analysis of DEGs on days 7, 14, 21, and 28. **(I–L)** Transcription factor prediction of DEGs on days 7, 14, 21, and 28. $n = 3$ per group for each time point.

DISCUSSION

Pathogen infestation could reduce photosynthesis in plants. The reason is that pathogen infestation restrained acyclic photosynthetic phosphorylation with NADP or ferricyanide as the acceptor, ultimately inhibiting the photochemical reactions in photosynthesis (Labudda et al., 2020). In addition, pathogen infestation damaged pigment proteins involved in photosynthesis (Saleem et al., 2020) and caused chlorophyll breakdown and stomatal closure, blocking plant CO_2 supply and thus limiting photosynthesis (Xia et al., 2016; Gao et al., 2018). It was reported that inoculation with *V. dahliae* decreased photosynthetic rate and stomatal conductance in pepper and reduced plant biomass and yield ultimately (Pascual et al., 2009). In this study, the net photosynthetic rate, stomatal conductance, and chlorophyll content of WL343HQ (WL + V) were higher than those of Dryland (HD + V), which was related to the lower disease incidence and disease index of WL343HQ (WL + V). In the photosynthesis-antenna proteins pathway (ko00196), *MS.gene64487*, *MS.gene018915*, *MS.gene031016* and *MS.gene031989*, which synthesize the light-harvesting chlorophyll protein complexes Lhca1-Lhca4, were downregulated in WL343HQ. Meanwhile, 12 DEGs, such as *MS.gene019953*, *MS.gene025268* and *MS.gene017490*, were downregulated in Dryland, thereby blocking Lhca1-Lhca7 synthesis and further restraining photosynthesis in Dryland. In addition, DEGs in Dryland on days 7, 14, 21, 28 were all enriched in photosynthesis (ko00195). In this pathway, *MS.gene038239*, *MS.gene47675*, *MS.gene47675* and *MS.gene024886*, which are involved in the synthesis of PsbP, PsbB, PsbW and Psb27 in photosystem II, were downregulated in expression. Downregulation of *MS.gene91444*, *MS.gene92305*, *MS.gene038025* and *MS.gene013347* inhibited the synthesis of the subunit proteins PsaD, PsaE, PsaF and PsaK, which are essential components of photosystem I and play important roles in the post-transcription of plastids (Rochaix et al., 2004). Compared with WL + V group, the above reasons led to lower photosynthesis and chlorophyll content of HD + V group.

MDA is the final decomposition product of membrane lipid peroxidation and its level can reflect the degree of stress and tissue peroxidative damage (Del Rio et al., 2005).

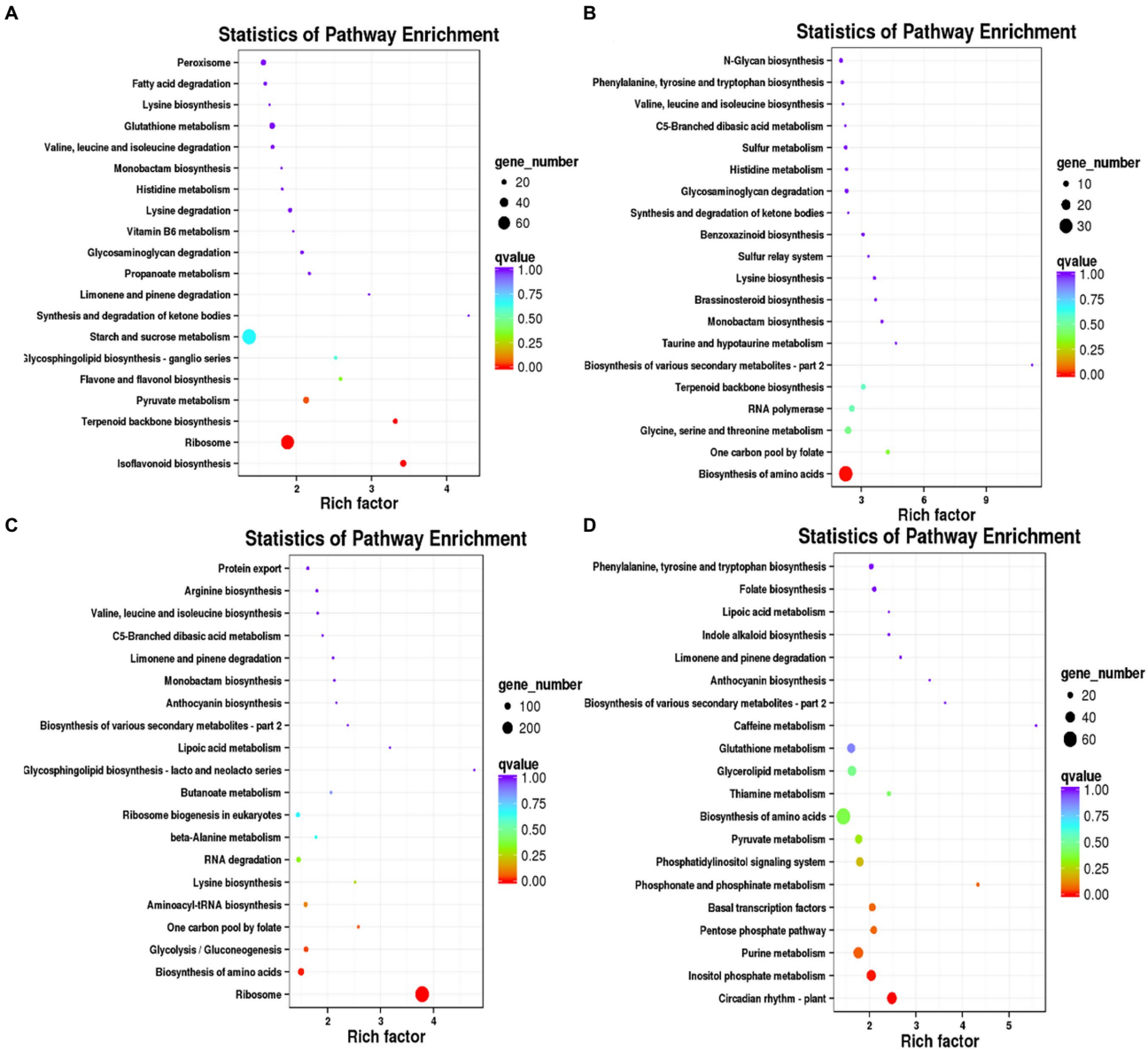

FIGURE 5 | KEGG enrichment analysis of DEGs specific to days 7, 14, 21, and 28 in Dryland inoculated with *Verticillium alfalfae* (HD + V). **(A)** KEGG enrichment analysis of DEGs specific to days 7. **(B)** KEGG enrichment analysis of DEGs specific to days 14. **(C)** KEGG enrichment analysis of DEGs specific to days 21. **(D)** KEGG enrichment analysis of DEGs specific to days 28.

In our study, the lower MDA content of WL + V group indicated that the membrane lipid peroxidation of HD + V group was stronger than that of WL + V group. In the plant-pathogen interaction pathway, upregulated DEGs in WL + V group were more than HD + V group and involved in the biosynthesis of calcium-dependent protein kinases, which were related to plant stress response and disease resistance (Ning et al., 2019). In HD + V group, the majority of DEGs involved in the isoflavone biosynthetic pathway were downregulated, which affected the biosynthesis of UDP-glycosyltransferase and cytochrome P450, thereby reducing the effective response to pathogen infection and resistance to stress of plants (Bolwell et al., 1994; Giovannetti et al., 2015). This is the reason for the lower MDA content in the WL + V group throughout the experiment. The enhanced SOD and POD enzyme activities inhibited the growth and sporulation of mycelium of pathogenic fungi and induced lignification of the host plant (Asthir et al., 2010). By scavenging reactive oxygen species, cell damage was reduced by SOD and POD enzymes (Wang et al., 2012). In the current study, the SOD and POD enzyme activities of HD + V group exhibited a trend of increasing and then decreasing on day 28. The reason for the fall on day 28 may be that the rapid accumulation of reactive oxygen species in the plant exceeded the threshold

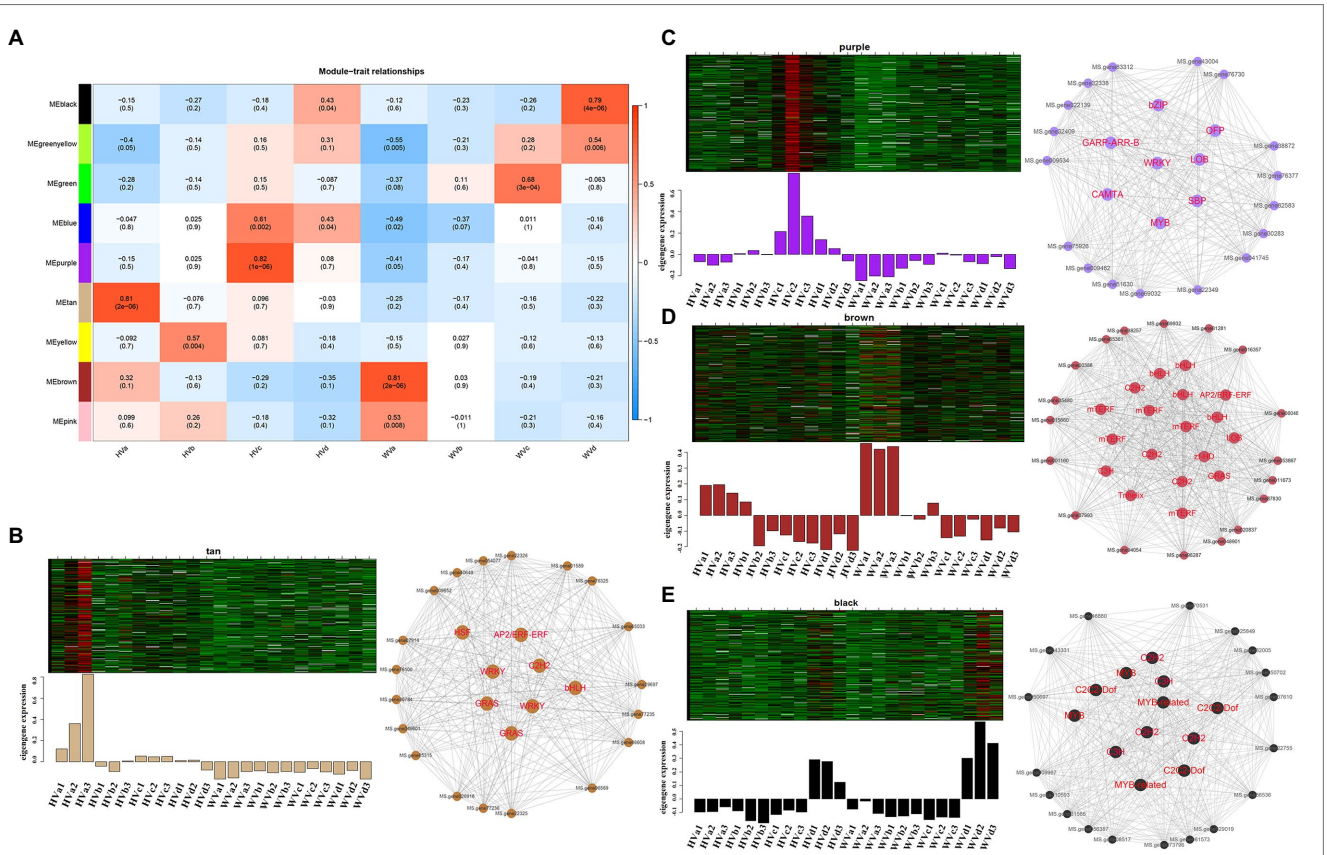

FIGURE 6 | Weighted gene co-expression network analysis (WGCNA) of module eigengenes in corresponding modules. **(A)** Heatmap of correlation between treatment groups and corresponding modules. **(B)** Heatmap and barplots of module eigengenes expression, and visualization of core genes of tan module. **(C)** Heatmap and barplots of module eigengenes expression, and visualization of core genes of purple module. **(D)** Heatmap and barplots of module eigengenes expression, and visualization of core genes of brown module. **(E)** Heatmap and barplots of module eigengenes expression, and visualization of core genes of black module.

value, resulting in the disruption of the normal reactive oxygen scavenging enzyme system and reduction of SOD and POD enzyme activities. DEGs of WL + V and HD + V group on days 7, 14, 21 and 28 were mainly categorized into transcription factors of the WRKY, NAC and bHLH families, which can activate antioxidant enzymes, such as SOD and POD, for enhancing stress response and disease resistance of plants (Varaud et al., 2011; Ishihama and Yoshioka, 2012). Total and upregulated DEGs of the WRKY, NAC and bHLH families were more in WL + V group than in HD + V group, indicating that WL343HQ can produce more antioxidant enzymes against pathogens than Dryland, which was in agreement with our results. The numbers of expressed genes of WRKY, bHLH and NAC transcription factors in both WL + V and HD + V groups were gradually increased on days 7, 14 and 21, and decreased on day 28, indicating that the antioxidant system of plant was gradually retarded on day 28. In addition to WRKY, NAC and bHLH, transcription factor families such as HSF, MYB, SBP, mTERF, zf-HD, C2C2-CO-like, LIM, Trihelix and PLATZ were also involved in plant disease resistance, which was consistent with previous studies (Du et al., 2009a; Scharf et al., 2012).

H_2O_2, NO, JA and SA are common signaling substances that can activate the expression of plant disease-resistant defense genes and induce the defensive responses synergistically or individually (Delledonne et al., 1998; Durner et al., 1998). In addition, H_2O_2 and NO are strongly oxidative and excessive accumulation can cause cell damage. In this study, the H_2O_2 content of WL + V group was significantly higher than that of HD + V group on days 7 and 14. This was related to the role of H_2O_2 as signaling substance against pathogen invasion and mycelium expansion (Zhang et al., 1995; Dat et al., 2000; Mellersh et al., 2002). On day 7 and 14, the majority of DEGs in WL + V group were upregulated in the basal transcription factor pathway and involved in the biosynthesis of receptor-like protein kinase, which was mainly correlated to signal reception and transduction processes in plants (Sakamoto et al., 2019), resulting in higher levels of the signal substances H_2O_2 and NO in WL + V group on days 7 and 14. The following decrease on the days 21 and 24 was mainly due to higher SOD and POD enzyme activities. In the glutathione pathway, there were more DEGs in WL + V group. Among them, *MS.gene019928*, *MS.gene65554*, *MS.gene74672* and *MS.gene063650* involved in glutathione reductase and glutamate-cysteine ligase synthesis

were upregulated in expression. These enzymes can assist SOD and POD in scavenging non-radical reactive oxygen species H_2O_2 in plants (Gill and Tuteja, 2010), which was the reason for lower H_2O_2 in WL + V group. It was reported that infection with *Verticillium longifolium* increased JA content in rape (Ratzinger et al., 2009). The changes of JA and SA concentrations indicated that WL + V group induced JA and SA signaling pathways, while HD + V group only induced JA signaling pathway. DEGs in WL343HQ on days 7, 14, 21, 28 were all enriched in α-linolenic acid metabolism (ko00592). Among them, the upregulated expression of *MS.gene07270*, *MS.gene20792* and *MS.gene20842* promoted the synthesis of triacylglycerol lipase, thus increasing the content of α-linolenic acid. JA was formed by the oxidation process of α-linolenic acid in the chloroplast membrane (Wasternack and Song, 2017). In addition, upregulated *MS.gene031651* was involved in the synthesis of acyl-CoA oxidase, which promoted the synthesis of JA-CoA, an important precursor substance for the synthesis of JA. Compared with HD + V group, the above reasons led to higher JA concentrations in WL + V group. DEGs in WL343HQ on days 7, 14, 21, 28 were all enriched in the phenylpropanoid biosynthesis (ko00940). Phenylalanine ammonia-lyase-mediated phenylalanine pathway is the most important pathway for SA biosynthesis (An and Mou, 2011) and WL + V group had more upregulated genes in this pathway than HD + V group, such as *MS.gene003278*, *MS.gene006350*, *MS.gene062216*, *MS.gene34438* and *MS.gene44482*, resulting in higher SA concentrations in WL + V group.

In addition to the above-mentioned physiological and biochemical changes, alfalfa also resists Verticillium wilt through other mechanisms. In WL + V group, the DEGs specific to day 7, 14, 21 and 28 were mostly upregulated and involved in plant disease defense processes by participating in the biosynthesis of isoflavone reductase homolog in the secondary metabolite biosynthesis pathway (Tee, 2009). In the starch and sucrose metabolism, genes were involved in the biosynthesis of β-1,3 glucanase, which was an enzyme that induced plant resistance to pathogenic invasion and inhibited the growth of pathogenic fungi in plants (Thakur, 2021). In the MAPK signaling pathway-plant, the special DEGs on day 21 were mostly upregulated and associated with the biosynthesis of calmodulin, the most important receptor for Ca^{2+}, which regulated the biosynthesis of SA and thus affected the defense and resistance processes of plants against pathogenic fungi (Du et al., 2009b). In the amino acid biosynthetic pathway, the special DEGs on day 28 were involved in the synthesis of zinc finger proteins, which was associated with plant growth and resistance mechanisms in various biotic and abiotic stresses (Feurtado et al., 2011; Giri et al., 2011). As for the HD + V group, most of the special DEGs were downregulated compared with the control, which led to the reduction of disease resistance in Dryland. The special DEGs on day 14 were mostly downregulated in HD + V group and mainly involved in the biosynthesis of serine acetyltransferase and cysteine synthase, both of which were associated with the biosynthesis of cysteine. Cysteine was important in reversible oxidative modifications, plant development regulation and stress response in plants (Richau et al., 2012). Among the special DEGs on day 21, the downregulated genes were involved in the synthesis of heat shock 70 kDa protein, which protected cells from damage caused by various stressors (Gomez-Pastor et al., 2018). The above results indicated that WL + V group was more resistant to Verticillium wilt compared with HD + V group.

CONCLUSION

Inoculation with *V. alfalfae* significantly affected net photosynthetic rate, stomatal conductance, chlorophyll content, MDA content, JA and SA concentrations, NO and H_2O_2 contents both in WL343HQ and Dryland inoculated with *Verticillium alfalfae*. SOD and POD enzyme activities and JA concentrations of both two disease varieties showed a trend of first increasing and then decreasing. The net photosynthetic rate, stomatal conductance, SOD and POD enzyme activities, and JA and SA concentrations of WL + V group were higher than those of HD + V group, suggesting that the defensive responses of WL + V group were stronger than HD + V group. The number of DEGs between HD + V group and WL + V group on days 7, 14, 21 and 28 were 14,809 and 3,113, 11,127, and 13,526, 24,460 and 21,064, 22,295 and 18,217, respectively. According to KEGG enrichment analysis, most of DEGs were found to be enriched in photosynthesis, photosynthesis-antenna proteins, linoleic acid metabolism, carbon fixation in photosynthetic organisms, MAPK signaling pathway-plant, phenylpropanoid biosynthesis, and glutathione metabolism pathways. Transcription factor prediction revealed a high number of transcription factors in the WRKY, NAC, and bHLH families. WGCNA analysis showed that the number of transcription factors related to plant growth and disease resistance was higher in the corresponding modules of WVa and WVd than in the corresponding modules of HVa and HVc. The number of core genes of the four corresponding modules including HVa, HVc, WVa, and WVd was 27, 25, 36 and 30, respectively. This work provides new insights into the change by which *V. alfalfae* affect physiological indicators and transcriptome at different time after inoculation. In the future, more in-depth studies are required to reveal the molecular mechanisms of the correlation between DEGs and physiological indicators of alfalfa.

DATA AVAILABILITY STATEMENT

The datasets presented in this study can be found in online repositories. The names of the repository/repositories and accession number(s) can be found at: https://www.ncbi.nlm.nih.gov/, PRJNA838389.

AUTHOR CONTRIBUTIONS

YL: project administration, supervision, experimental design, and funding acquisition. ZS: supervision, funding acquisition, validation, visualization, and writing—review and editing. FL: investigation, resources, validation, and data curation. XC: validation, data curation, and writing—original draft. BY:

investigation and resources. YG and DW: methodology and visualization. All authors contributed to the article and approved the submitted version.

FUNDING

This study was financially supported by National Nature Science Foundation of China (32061123004), Gansu Provincial Science and Technology Major Projects (No. 19ZD2NA002), and China Post-doctoral Science Foundation (2019M662893).

ACKNOWLEDGMENTS

The authors are very grateful for the valuable comments on manuscript revisions of the editor and referees.

SUPPLEMENTARY MATERIAL

The Supplementary Material for this article can be found online at: https://www.frontiersin.org/articles/10.3389/fpls.2022.931001/full#supplementary-material

REFERENCES

An, C., and Mou, Z. (2011). Salicylic acid and its function in plant immunity. *J. Integr. Plant Biol.* 53, 412–428. doi: 10.1111/j.1744-7909.2011.01043.x

Asthir, B., Koundal, A., Bains, N. S., and Mann, S. K. (2010). Stimulation of antioxidative enzymes and polyamines during stripe rust disease of wheat. *Biol. Plant.* 54, 329–333. doi: 10.1007/s10535-010-0057-4

Bibi, N., Ahmed, I. M., Fan, K., Dawood, M., Li, F., Yuan, S., et al. (2017). Role of brassinosteroids in alleviating toxin-induced stress of *Verticillium dahliae* on cotton callus growth. *Environ. Sci. Pollut. Res. Int.* 24, 12281–12292. doi: 10.1007/s11356-017-8738-6

Bolwell, G. P., Bozak, K., and Zimmerlin, A. (1994). Plant cytochrome-P450. *Phytochemistry* 37, 1491–1506. doi: 10.1016/S0031-9422(00)89567-9

Dat, J., Vandenabeele, S., Vranova, E., Van Montagu, M., Inze, D., and Van Breusegem, F. (2000). Dual action of the active oxygen species during plant stress responses. *Cell. Mol. Life Sci.* 57, 779–795. doi: 10.1007/s000180050041

Del Rio, D., Stewart, A. J., and Pellegrini, N. (2005). A review of recent studies on malondialdehyde as toxic molecule and biological marker of oxidative stress. *Nutr. Metab. Cardiovasc. Dis.* 15, 316–328. doi: 10.1016/j.numecd.2005.05.003

Delledonne, M., Xia, Y. J., Dixon, R. A., and Lamb, C. (1998). Nitric oxide functions as a signal in plant disease resistance. *Nature* 394, 585–588. doi: 10.1038/29087

Dhar, N., Chen, J. Y., Subbarao, K. V., and Klosterman, S. J. (2020). Hormone signaling and its interplay With development and defense responses in Verticillium-plant interactions. *Front. Plant Sci.* 11:4997. doi: 10.3389/fpls.2020.584997

Du, L., Ali, G. S., Simons, K. A., Hou, J., Yang, T., Reddy, A. S., et al. (2009b). Ca(2+)/calmodulin regulates salicylic-acid-mediated plant immunity. *Nature* 457, 1154–1158. doi: 10.1038/nature07612

Du, H., Zhang, L., Liu, L., Tang, X. F., Yang, W. J., Wu, Y. M., et al. (2009a). Biochemical and molecular characterization of plant MYB transcription factor family. *Biochemistry* 74, 1–11. doi: 10.1134/S0006297909010015

Durner, J., Wendehenne, D., and Klessig, D. F. (1998). Defense gene induction in tobacco by nitric oxide, cyclic GMP, and cyclic ADP-ribose. *Proc. Natl. Acad. Sci. U. S. A.* 95, 10328–10333. doi: 10.1073/pnas.95.17.10328

Fang, L., Ju, W., Yang, C., Jin, X., Liu, D., Li, M., et al. (2020). Exogenous application of signaling molecules to enhance the resistance of legume-rhizobium symbiosis in Pb/Cd-contaminated soils. *Environ. Pollut.* 265:114744. doi: 10.1016/j.envpol.2020.114744

Feurtado, J. A., Huang, D., Wicki-Stordeur, L., Hemstock, L. E., Potentier, M. S., Tsang, E. W., et al. (2011). The Arabidopsis C2H2 zinc finger INDETERMINATE DOMAIN1/ENHYDROUS promotes the transition to germination by regulating light and hormonal signaling during seed maturation. *Plant Cell* 23, 1772–1794. doi: 10.1105/tpc.111.085134

Gao, P., Duan, T. Y., Christensen, M. J., Nan, Z. B., Liu, Q. T., Meng, F. J., et al. (2018). The occurrence of rust disease, and biochemical and physiological responses on Apocynum venetum plants grown at four soil water contents, following inoculation with Melampsora apocyni. *Eur. J. Plant Pathol.* 150, 549–563. doi: 10.1007/s10658-017-1299-1

Gharbi, Y., Barkallah, M., Bouazizi, E., Cheffi, M., Gdoura, R., and Triki, M. A. (2016). Differential fungal colonization and physiological defense responses of new olive cultivars infected by the necrotrophic fungus *Verticillium dahliae*. *Acta Physiol. Plant.* 38, 1–2. doi: 10.1007/s11738-016-2261-0

Gill, S. S., and Tuteja, N. (2010). Reactive oxygen species and antioxidant machinery in abiotic stress tolerance in crop plants. *Plant Physiol. Biochem.* 48, 909–930. doi: 10.1016/j.plaphy.2010.08.016

Giovannetti, M., Mari, A., Novero, M., and Bonfante, P. (2015). Early Lotus japonicus root transcriptomic responses to symbiotic and pathogenic fungal exudates. *Front. Plant Sci.* 6:480. doi: 10.3389/fpls.2015.00480

Giri, J., Vij, S., Dansana, P. K., and Tyagi, A. K. (2011). Rice A20/AN1 zinc-finger containing stress-associated proteins (SAP1/11) and a receptor-like cytoplasmic kinase (OsRLCK253) interact via A20 zinc-finger and confer abiotic stress tolerance in transgenic Arabidopsis plants. *New Phytol.* 191, 721–732. doi: 10.1111/j.1469-8137.2011.03740.x

Gomez-Pastor, R., Burchfiel, E. T., and Thiele, D. J. (2018). Regulation of heat shock transcription factors and their roles in physiology and disease. *Nat. Rev. Mol. Cell Biol.* 19, 4–19. doi: 10.1038/nrm.2017.73

Gordon, T. R., Correll, J. C., Gilchrist, D. G., and Martensen, A. N. (1989). Verticillium wilt of alfalfa in California. *Plant Dis.* 73, 18–20. doi: 10.1094/Pd-73-0018

Grau, C. R., Delwiche, P. A., Norgren, R. L., Oconnell, T. E., and Maxwell, D. P. (1981). Verticillium wilt of alfalfa in Wisconsin. *Plant Dis.* 65, 843–844. doi: 10.1094/Pd-65-843

Hill, M. K., Lyon, K. J., and Lyon, B. R. (1999). Identification of disease response genes expressed in *Gossypium hirsutum* upon infection with the wilt pathogen *Verticillium dahliae*. *Plant Mol. Biol.* 40, 289–296. doi: 10.1023/a:1006146419544

Ishihama, N., and Yoshioka, H. (2012). Post-translational regulation of WRKY transcription factors in plant immunity. *Curr. Opin. Plant Biol.* 15, 431–437. doi: 10.1016/j.pbi.2012.02.003

Jimenez-Ruiz, J., Leyva-Perez, M. D., Cabanas, C. G. L., Barroso, J. B., Luque, F., and Mercado-Blanco, J. (2019). The Transcriptome of *Verticillium dahliae* responds differentially depending on the disease susceptibility level of the olive (*Olea europaea* L.) cultivar. *Gene* 10:251. doi: 10.3390/genes10040251

Labudda, M., Tokarz, K., Tokarz, B., Muszyńska, E., Gietler, M., Górecka, M., et al. (2020). Reactive oxygen species metabolism and photosynthetic performance in leaves of *Hordeum vulgare* plants co-infested with Heterodera filipjevi and Aceria tosichella. *Plant Cell Rep.* 39, 1719–1741. doi: 10.1007/s00299-020-02600-5

Livak, K. J., and Schmittgen, T. D. (2001). Analysis of relative gene expression data using real-time quantitative PCR and the 2(-Delta C(T)) method. *Methods* 25, 402–408. doi: 10.1006/meth.2001.1262

MauchMani, B., and Slusarenko, A. J. (1996). Production of salicylic acid precursors is a major function of phenylalanine ammonia-lyase in the resistance of arabidopsis to Peronospora parasitica. *Plant Cell* 8, 203–212. doi: 10.2307/3870265

Mellersh, D. G., Foulds, I. V., Higgins, V. J., and Heath, M. C. (2002). H_2O_2 plays different roles in determining penetration failure in three diverse plant-fungal interactions. *Plant J.* 29, 257–268. doi: 10.1046/j.0960-7412.2001.01215.x

Nachmias, A., Buchner, V., Tsror, L., Burstein, Y., and Keen, N. (1987). Differential Phytotoxicity of peptides from culture fluids of *Verticillium-Dahliae* races 1 and 2 and their relationship to pathogenicity of the Fungi on tomato. *Phytopathology* 77, 506–510. doi: 10.1094/Phyto-77-506

Ning, M., Tang, F. X., Zhang, Q., Zhao, X. X., Yang, L. P., Cai, W. C., et al. (2019). Effects of Penicillium infection on the expression and activity of CDPK2 in postharvest Hami melon treated with calcium chloride. *Physiol. Mol. Plant Pathol.* 106, 175–181. doi: 10.1016/j.pmpp.2019.02.003

Pascual, I., Azcona, I., Morales, F., Aguirreolea, J., and Sanchez-Diaz, M. (2009). Growth, yield and physiology of Verticillium-inoculated pepper plants treated with ATAD and composted sewage sludge. *Plant Soil* 319, 291–306. doi: 10.1007/s11104-008-9870-3

Peaden, R. N., Gilbert, R. G., and Christen, A. A. (1985). Control of Verticillium-Albo-Atrum on Alfalfa. *Canadian J. Plant Pathology-Revue* 7, 511–514. doi: 10.1080/07060668509501506

Ratzinger, A., Riediger, N., von Tiedemann, A., and Karlovsky, P. (2009). Salicylic acid and salicylic acid glucoside in xylem sap of *Brassica napus* infected with *Verticillium longisporum*. *J. Plant Res.* 122, 571–579. doi: 10.1007/s10265-009-0237-5

Richau, K. H., Kaschani, F., Verdoes, M., Pansuriya, T. C., Niessen, S., Stuber, K., et al. (2012). Subclassification and biochemical analysis of plant papain-like cysteine proteases displays subfamily-specific characteristics. *Plant Physiol.* 158, 1583–1599. doi: 10.1104/pp.112.194001

Rochaix, J. D., Perron, K., Dauvillee, D., Laroche, F., Takahashi, Y., and Goldschmidt-Clermont, M. (2004). Post-transcriptional steps involved in the assembly of photosystem I in *Chlamydomonas*[J]. *Biochem. Soc. Trans.* 32, 567–570. doi: 10.1042/BST0320567

Sakamoto, K., Ogiwara, N., Kaji, T., Sugimoto, Y., Ueno, M., Sonoda, M., et al. (2019). Transcriptome analysis of soybean (*Glycine max*) root genes differentially expressed in rhizobial, arbuscular mycorrhizal, and dual symbiosis. *J. Plant Res.* 132, 541–568. doi: 10.1007/s10265-019-01117-7

Saleem, M., Atta, B. M., Ali, Z., and Bilal, M. (2020). Laser-induced fluorescence spectroscopy for early disease detection in grapefruit plants. *Photochem. Photobiol. Sci.* 19, 713–721. doi: 10.1039/c9pp00368a

Samac, D., Scraber, S., Blosberg, J., and Barclay, S. (2014). A mineral seed treatment for control of seedling diseases of alfalfa suitable for organic production systems. *Phytopathology* 104:103. doi: 10.1094/PDIS-03-14-0240-RE

Scharf, K. D., Berberich, T., Ebersberger, I., and Nover, L. (2012). The plant heat stress transcription factor (Hsf) family: structure, function and evolution. *Biochimica Et Biophysica Acta-Gene Regul. Mechan.* 1819, 104–119. doi: 10.1016/j.bbagrm.2011.10.002

Shi, Y., Zhang, Y., Yao, H., Wu, J., Sun, H., and Gong, H. (2014). Silicon improves seed germination and alleviates oxidative stress of bud seedlings in tomato under water deficit stress. *Plant Physiol. Biochem.* 78, 27–36. doi: 10.1016/j.plaphy.2014.02.009

Smit, F., and Dubery, I. A. (1997). Cell wall reinforcement in cotton hypocotyls in response to a *Verticillium dahliae* elicitor. *Phytochemistry* 44, 811–815. doi: 10.1016/S0031-9422(96)00595-X

Tee, S. S. (2009). Transcriptional changes in response to single and combine inoculation of Mycorrhiza and Ganoderma in Oil Palm (Elaeis Guineensis Jacq.) Roots, Doctoral dissertation, Universiti Putra Malaysia.

Thakur, R. (2021). Use of Trichoderma spp. as biocontrol for disease management.

Thaler, J. S., Owen, B., and Higgins, V. J. (2004). The role of the jasmonate response in plant susceptibility to diverse pathogens with a range of lifestyles. *Plant Physiol.* 135, 530–538. doi: 10.1104/pp.104.041566

Tjamos, S. E., Flemetakis, E., Paplomatas, E. J., and Katinakis, P. (2005). Induction of resistance to *Verticillium dahliae* in *Arabidopsis thaliana* by the biocontrol agent K-165 and pathogenesis-related proteins gene expression. *Mol. Plant-Microbe Interact.* 18, 555–561. doi: 10.1094/MPMI-18-0555

Varaud, E., Brioudes, F., Szecsi, J., Leroux, J., Brown, S., Perrot-Rechenmann, C., et al. (2011). AUXIN RESPONSE FACTOR8 regulates Arabidopsis petal growth by interacting with the bHLH transcription FACTOR BIGPETALp. *Plant Cell* 23, 973–983. doi: 10.1105/tpc.110.081653

Wang, X., Fu, Y., Ban, L., Wang, Z., Feng, G., Li, J., et al. (2015). Selection of reliable reference genes for quantitative real-time RT-PCR in alfalfa. *Genes Genet. Syst.* 90, 175–180. doi: 10.1266/ggs.90.175

Wang, D., Guoqi, L. I., and Dexi, S. U. (2012). Effect of drought stress on osmotic adjustment substances and activity of protective enzymes in two species of Apocynum. *J. Arid Land Res. Env.* 26, 177–181. doi: 10.13448/j.cnki.jalre.2012.12.014

Wasternack, C., and Song, S. (2017). Jasmonates: biosynthesis, metabolism, and signaling by proteins activating and repressing transcription. *J. Exp. Bot.* 68, 1303–1321. doi: 10.1093/jxb/erw443

Wen, Z. H., Duan, T. Y., Christensen, M. J., and Nan, Z. B. (2015). Microdochium tabacinum, confirmed as a pathogen of alfalfa in Gansu Province China. *Plant Dis.* 99, 87–92. doi: 10.1094/Pdis-10-13-1048-Re

Xia, C., Li, N. N., Zhang, X. X., Feng, Y., Christensen, M. J., and Nan, Z. B. (2016). An Epichloe endophyte improves photosynthetic ability and dry matter production of its host Achnatherum inebrians infected by Blumeria graminis under various soil water conditions. *Fungal Ecol.* 22, 26–34. doi: 10.1016/j.funeco.2016.04.002

Xiong, X. P., Sun, S. C., Zhang, X. Y., Li, Y. J., Liu, F., Zhu, Q. H., et al. (2020). GhWRKY70D13 regulates resistance to *Verticillium dahliae* in cotton Through the ethylene and Jasmonic acid signaling pathways (vol 11, 69, 2020). *Front. Plant Sci.* 11:1045. doi: 10.3389/fpls.2020.01045

Xu, S., Li, Y. Z., and Nan, Z. B. (2016). First report of Verticillium wilt of alfalfa caused by *Verticillium alfalfae* in China. *Plant Dis.* 100:220. doi: 10.1094/Pdis-05-15-0496-Pdn

Yang, X., Zhang, Y., Cheng, Y. F., and Chen, X. H. (2019). Transcriptome analysis reveals multiple signal network contributing to the Verticillium wilt resistance in eggplant. *Sci. Hortic.* 256:108576. doi: 10.1016/j.scienta.2019.108576

Yao, L. L., Zhou, Q., Pei, B. L., and Li, Y. Z. (2011). Hydrogen peroxide modulates the dynamic microtubule cytoskeleton during the defence responses to *Verticillium dahliae* toxins in Arabidopsis. *Plant Cell Environ.* 34, 1586–1598. doi: 10.1111/j.1365-3040.2011.02356.x

Yin, J., Jia, J., Lian, Z., Hu, Y., Guo, J., Huo, H., et al. (2019). Silicon enhances the salt tolerance of cucumber through increasing polyamine accumulation and decreasing oxidative damage. *Ecotoxicol. Environ. Saf.* 169, 8–17. doi: 10.1016/j.ecoenv.2018.10.105

Zhang, Z. G., Collinge, D. B., and Thordalchristensen, H. (1995). Germin-Like oxalate oxidase, a H_2O_2-producing enzyme, accumulates in barley attacked by the powdery mildew fungus. *Plant J.* 8, 139–145. doi: 10.1046/j.1365-313X.1995.08010139.x

Zhen, X. H., and Li, Y. Z. (2004). Ultrastructural changes and location of beta-1, 3-glucanase in resistant and susceptible cotton callus cells in response to treatment with toxin of *Verticillium dahliae* and salicylic acid. *J. Plant Physiol.* 161, 1367–1377. doi: 10.1016/j.jplph.2004.04.007

Conflict of Interest: The authors declare that the research was conducted in the absence of any commercial or financial relationships that could be construed as a potential conflict of interest.

Publisher's Note: All claims expressed in this article are solely those of the authors and do not necessarily represent those of their affiliated organizations, or those of the publisher, the editors and the reviewers. Any product that may be evaluated in this article, or claim that may be made by its manufacturer, is not guaranteed or endorsed by the publisher.

frontiers | Frontiers in Plant Science

ORIGINAL RESEARCH
published: 23 June 2022
doi: 10.3389/fpls.2022.926731

Characteristics of Soil Fungal Communities in Soybean Rotations

*Xiuli Song[1], Lei Huang[1], Yanqing Li[1], Chongzhao Zhao[1], Bo Tao[2] and Wu Zhang[1]**

[1] School of Geographical Sciences, Lingnan Normal University, Zhanjiang, China, [2] Agricultural College, Northeast Agricultural University, Harbin, China

Soybean continuous cropping (SC) leads to continuous cropping obstacles, and soil-borne fungal diseases occur frequently. Rotation can alleviate continuous cropping obstacles. However, the long-term effects of continuous cropping and rotation on the structure and function of the fungal community in soil are not clear. In this study, five cropping systems, SC, fallow (CK), fallow-soybean (FS), corn–soybean (CS), and wheat–soybean (WS), were implemented in the long-term continuous cropping area of soybean. After 13 years of planting, high-throughput sequencing was used to evaluate the structure and diversity of soil fungal communities and to study the relationship between fungal communities and soil environmental factors. The results showed that the abundance and diversity of fungal flora in SC soil were the highest. There were significant differences in the formation of soil fungal communities between soybean continuous cropping and the other treatments. There were 355 species of endemic fungi in SC soil. There were 231 and 120 endemic species in WS and CS, respectively. The relative abundance of the potential pathogens *Lectera*, *Gibberella,* and *Fusarium* in the SC treatment soil was significantly high, and the abundance of all potential pathogens in CK was significantly the lowest. The abundance of *Lectera* and *Fusarium* in CS was significantly the lowest. There was a positive correlation between potential pathogens in the soil. The relative abundance of potential pathogens in the soil was significantly positively correlated with the relative abundance of Ascomycetes and negatively correlated with the relative abundance of Basidiomycetes. Potential pathogenic genera had a significant negative correlation with soil OM, available Mn, K and soil pH and a significant positive correlation with the contents of soil available Cu, Fe, and Zn. In general, the fungal communities of SC, FS, WS, and CS were divided into one group, which was significantly different from CK. WS and CS were more similar in fungal community structure. The CK and CS treatments reduced the relative abundance of soil fungi and potential pathogens. Our study shows that SC and FS lead to selective stress on fungi and pathogenic fungi and lead to the development of fungal community abundance and diversity, while CK and CS can reduce this development, which is conducive to plant health.

Keywords: continuous soybean cropping, rotation, fungal community structure and diversity, potential pathogenic genera, soil chemical properties

OPEN ACCESS

Edited by:
Jing Zhang,
Nanjing Agricultural University, China

Reviewed by:
Xingxu Zhang,
Lanzhou University, China
Jianqiang Deng,
Ningxia University, China
Fengge Zhang,
Nanjing Agricultural University, China

***Correspondence:**
Wu Zhang
ldzw1987@163.com

Specialty section:
This article was submitted to Plant Abiotic Stress, a section of the journal Frontiers in Plant Science

Received: *23 April 2022*
Accepted: *23 May 2022*
Published: *23 June 2022*

Citation:
Song X, Huang L, Li Y, Zhao C, Tao B and Zhang W (2022) Characteristics of Soil Fungal Communities in Soybean Rotations. Front. Plant Sci. 13:926731. doi: 10.3389/fpls.2022.926731

INTRODUCTION

China has a great demand for soybeans (Liu et al., 2020). Northeast China is not only an important production base for food security but also a major soybean production area in China. For economic benefit, some farms in Northeast China have been planting soybeans for more than 40 consecutive years (Liu et al., 2020). Continuous planting of soybean leads to continuous cropping obstacles in soil (Liu et al., 2012; Benitez et al., 2017) and aggravation of soil-borne diseases (Yan et al., 2012; Pérez-Brandán et al., 2014; Bai et al., 2015). Studies have shown that these changes are closely related to biological factors in soil (Dias et al., 2015; Liu et al., 2020).

Soil microorganisms play an important role in maintaining ecosystem sustainability and plant health (Avidano et al., 2005). Different cropping systems can significantly change the microbial community structure (Zhou et al., 2018; Liu H. et al., 2019). However, these changes depend on the type of cropping system, soil type and crop type. Xiong et al. (2016) found that continuous cropping significantly increased the proportion of fungi in soil. Rotation can significantly reduce the number of fungal populations (Yu et al., 2011), facilitate the reproduction of plant growth promotion in soil (Baetz and Martinoia, 2014; Pii et al., 2015), and enhance the stability and resilience of soil ecosystems (Clemente et al., 2005; Behera et al., 2007). Understanding how different cropping systems affect the composition of the fungal microbial community is conducive to the regulation of the microbial community through planting and the prevention and treatment of soil-borne diseases in agricultural production.

Soybean continuous cropping (SC) increases the abundance of soil pathogenic fungi and induces crop diseases (Guo et al., 2011; Wang et al., 2013). The change in soil fungal community structure in SC is mainly driven by 14 genera, and *Guehomyces*, *Alternaria*, and *Metacordyceps* contribute more to the change in the fungal community (Liu H. et al., 2019). The pathogenic *Fusarium* sp. in soil is the main pathogen of soybean root rot, which can cause soybean plant wilt at all stages of soybean growth (Liu J. et al., 2019). Crop rotation is an agronomic practice adopted by farmers after the serious outbreak of soil-borne diseases, and it has been proven that they can be successfully controlled (Wright et al., 2015). Studies have shown that crop rotation can maintain the diversity of soil microbial communities and enhance disease inhibition (Peralta et al., 2018). Wheat soybean rotation can reduce the number of *Fusarium* in wheat soil, which may effectively reduce the risk of wheat diseases (Lu et al., 2022). The research results are inconsistent due to the different soil types, rotation systems and continuous cropping years. The related mechanism of continuous cropping obstacles is complex and needs to be explored in many aspects under different conditions.

Soil physical and chemical properties affect the structure and function of the soil microbial community (Xiang et al., 2020). Prior studies have shown that soil total phosphorus and available phosphorus similarly influence the soil fungal community structure and the relative abundance of specific fungi (Yao et al., 2019). Increasing soil organic matter can inhibit fungal pathogens (Saxena et al., 2015). Basic trace elements (TE), such as Zn, Fe, Mn, and Cu, are the main cofactors of various proteins in biological systems and have important biological significance (Pilon et al., 2009). As reported, the fungal community was most correlated with available P, K, and Cu (Song et al., 2018). There have been few studies on the correlation between soil mineral elements and the soil microbial community (Cai et al., 2015).

Long-term unreasonable cultivation makes the soil quality and microecology unbalanced, and crop diseases occur frequently, which seriously affects the quality of crop products and the sustainable development and utilization of cold black soil. Previous studies have mainly focused on the effects of agronomy, cultivation, soil type, fertilizer, and heavy metals on the overall number and diversity of microbial communities or on a certain group of microorganisms under long-term positioning tests (Liu et al., 2010; Hartmann et al., 2015; Li et al., 2018). However, it is not clear how the implementation of rotation cropping systems under long-term continuous cropping will change the structure and function of the fungal community in continuous cropping soil. In this study, the effects of fallow, fallow-soybean (FS), corn–soybean (CS), and wheat–soybean (WS) rotations on the soil fungal community of soybean continuous cropping were studied, and the relationship between cropping systems, soil mineral elements and fungal community structure was explored. We focused on the effects of different cropping systems on harmful and beneficial microbial communities in soil fungal communities. The results enable us to have a clearer understanding of the diversity and composition structure of soil fungal communities under different rotation systems to provide a theoretical basis for formulating an effective rotation cropping system.

MATERIALS AND METHODS

Study Site Description and Soil Sample Collection

The test site is located in Nenjiang County, Heilongjiang Province, China (124°68′ E, 49° N). The soil type belongs to the Vertisol class according to the American soil classification system (Soil Survey Staff, 2014). The annual average temperature is 0.8∼1.4°C, the annual cumulative temperature (greater than or equal to 10°C) is approximately 2,230°C, and the annual rainfall is approximately 480–512 mm. Before the experiment, the experimental site was a soybean continuous cropping area. The long-term positioning experiment was set up in April 2005. The experiment was set up as five treatments: fallow (CK), SC, FS rotation, CS rotation, and WS rotation. Three replications were set for each treatment, and the area of each plot was 666.7 m^2. A randomized block arrangement was used. In the year of the cropping season, wheat was sown from April 1 to April 10, corn was sown from April 30 to May 10, and soybeans were sown from May 10 to May 20. Urea, diammonium phosphate and potassium sulfate were applied once before crop planting. There were 33.1 kg N ha^{-1}, 24.1 kg P ha^{-1} and 21.6 kg K ha^{-1} applied for soybean, 59.0 kg N ha^{-1}, 40.1 kg P ha^{-1} and 43.1 kg K ha^{-1} for maize, and 73.0 kg N ha^{-1}, 30.1 kg P ha^{-1} and 21.6 kg K ha^{-1} for wheat. An addition of 59.0 kg N ha^{-1} was applied at the booting stage of maize. Wheat was harvested from August

1 to August 10, soybeans were harvested from September 20 to October 5, and corn as harvested from October 10 to October 30. On October 30, 2017, soil samples were collected after soybean harvest. According to the aseptic requirements, for each plot, 10 surface soil samples with a depth of 0–20 cm were randomly taken with a soil auger with a diameter of 5 cm and put into a sterile bag for full mixing. This process was repeated three times, and the samples were mixed into one soil sample. A total of 15 soil samples were collected from the five treatments. After returning to the laboratory, the excess parts were removed, and stones, plant roots and animal residues were removed and screened through a 2 mm sterile sieve. Some soil samples in each soil sample were placed in sterilized microcentrifuge tubes and stored at −80°C for DNA extraction. The remaining soil was air dried to measure the chemical properties of the soil.

Analysis of Physical and Chemical Properties of Soil Samples

Soil samples were dried at room temperature and ground into pieces that passed through a 2 mm sieve. The soil micronutrients Fe, Mn, Zn, and Cu were extracted with diethylenetriaminepentaacetic acid followed by atomic absorption spectrophotometry analysis (Lindsay and Norvell, 1978). The available B was determined by potassium imine colorimetry (Malekani and Cresser, 1998), and the pH was measured at a soil-to-water ratio of 2.5:1. Soil organic C was determined following wet digestion (Walkley and Black, 1934), and the values were multiplied by a factor of 1.724 to obtain organic matter (OM) values. A basic N solution was created using the diffusion method (Bremner and Keeney, 1966), and available P was determined using the 0.5 mol·L^{-1} $NaHCO_3$ leaching-molybdenum antimony colorimetric method (Föhse et al., 1991). The available potassium (K) was measured with the 1 mol L^{-1} NH_4OAc extraction-flame photometric method (Petersen and Corey, 1966).

Soil DNA Extraction

Microbial DNA was extracted from 0.5 g samples using an E.Z.N.A.® soil DNA Kit (Omega Bio-Tek, Norcross, GA, United States) according to the manufacturer's instructions. The final DNA concentration and purification were determined using a NanoDrop 2000 ultraviolet–visible (UV–Vis) spectrophotometer (Thermo Scientific, Wilmington, DE, United States), and the DNA quality was checked using 1% agarose gel electrophoresis.

Quantitative Real-Time PCR

The fungal internal transcribed spacer (ITS) region of the rRNA gene copy number for all samples was determined in triplicate using Q-PCR in an ABI 7500 Real-Time PCR System (Applied Biosystems, Carlsbad, CA, United States) with the primer set ITS1F/ITS2R (Adams et al., 2013). Each PCR contained 16.5 μL of AceQ® RSYBR Green quantitative real-time PCR (qPCR) Master Mix (2X), 0.8 μL of 5 μM forward and reverse primers (each) and 2.0 μL of template DNA. The PCR samples were subsequently incubated at 95°C for 5 min, followed by 40 cycles of 5 s at 95°C, 30 s for annealing at 50°C, and 40 s for elongation at 72°C. Negative controls consisted of all the reagents with sterilized water instead of soil DNA. The threshold cycle (Ct) was obtained from triplicate samples and averaged. The copy number of the fungal ITS genes was calculated using a regression equation to convert the cycle threshold (Ct) value to the known number of copies in the standard curves.

Illumina MiSeq Sequencing

The ITS rRNA genes were amplified using the primers ITS1F (5′-CTTGGTCATTTAGAGGAAGTAA-3′) and ITS2R (5′-GCTGCGTTCTTCATCGATGC-3′) (Adams et al., 2013) in a thermocycler PCR system (GeneAmp 9700, ABI, Foster, CA, United States). The PCRs were conducted using the following program: 3 min of denaturation at 95°C; 35 cycles of 30 s at 95°C, 30 s for annealing at 55°C, and 45 s for elongation at 72°C; and a final extension at 72°C for 10 min. The PCR products were purified and then sequenced using the MiSeq Illumina platform (Illumina, United States) at Genesky Biotechnologies Inc. (Shanghai, China). The raw reads were deposited into the National Center for Biotechnology Information (NCBI) Sequence Read Archive (SRA) database (accession number: SRP164820).

Processing of Sequencing Data

After sequencing, the raw FASTQ files were processed using QIIME Pipeline Version 1.19.1. Briefly, all sequence reads were assigned to each sample based on the barcodes. Sequences with low quality (length $<$ 200 bp and average base quality score $<$ 20) were removed before further analysis. The chimeras of trimmed sequences were detected and removed using the UCHIME algorithm (Edgar et al., 2011). After filtering the data, the quality value of the reassembled base Q20 is greater than 99%, and Q30 is greater than 96%. These results fully met the requirements of subsequent data analysis (**Supplementary Tables 1**, **2**). The sequences were phylogenetically assigned according to their best matches to sequences in the Ribosomal Database Project (RDP) database using the RDP classifier (Cole et al., 2009). Operational taxonomic units (OTUs) were classified at 97% sequence similarity using CD-HIT (Li and Godzik, 2015). We rarified the abundance matrix to 110737 (the lowest sequence read depth across the study) sequences per sample to obtain normalized relative abundances. Chao1 richness and Shannon's diversity index were calculated in QIIME. Constrained principal coordinate analysis (CPCoA) and significance tests (Adonis test and Mantel test) were performed in R version 3.5.1 for Windows with the "vegan" package. Mothur (version 1.33.3) was used for alpha diversity analysis [species richness statistics, such as Chao and the abundance-based coverage estimator (ACE), and species diversity statistics, such as Shannon and Simpson], Venn diagrams and beta diversity analysis (PCA). Linear discriminant analysis (LDA) effect size (LEfSe) was used to elucidate the biomarkers in each treatment. Those with an LDA score $\geq$ 2.0 were considered to be important biomarkers in each treatment (Xiang et al., 2020). The cladogram was drawn using the Huttenhower Galaxy web application *via* the LEfSe algorithm (Segata et al., 2011).

Statistical Analysis

The species with significant abundance differences among different groups were detected by the non-parametric Kruskal–Wallis rank sum test. Statistical analyses were performed, and heatmap analysis was performed using the multcomp package in R (3.4.1) (R Development Core Team, 2010) to reveal significant differences in the fungal genera. Additionally, we predicted potentially pathogenic and beneficial fungi using FUNGuild[5] (Nguyen et al., 2016). The pathogenic and beneficial fungi were assigned according to their potential to damage or benefit the plant. The stepwise analysis and correlation test of biological environmental connections were carried out in R (3.4.1) (R Development Core Team, 2010), and the environmental factor with the highest correlation with the community (OTU) was calculated and counted. Pearson correlation analysis was used to test the significance of correlations between fungi. The species with significant abundance differences among different groups were detected by the non-parametric Kruskal–Wallis rank sum test.

RESULTS

Effects of Cropping Systems on the Soil Fungal Community

The number of fungi was quantified by real-time PCR. Compared with CK, SC, FS, WS, and CS significantly increased the abundance of fungi, which were 2.02, 1.78, 1.33, and 1.24 times that of CK, respectively (**Figure 1A**). The PCoA plot and cluster analysis based on the OTU analysis showed clear similarities or differences among the fungal community structures across all the samples. All of the soil samples were separated into two groups. The fungal communities in FS, SC, WS, and CS were grouped together and were clearly separated from CK. WS and CS were grouped together, indicating that WS and CS had similar fungal community structures on PCA (**Figure 1B** and **Supplementary Figure 1**). Venn diagram analysis shows that the number of endemic fungal species in FS planting soil was the largest, 657 species. A total of 472 species of endemic fungi were formed in CK soil. There are 355 species of endemic fungi in SC soil. There were 231 and 120 endemic species in WS and CS, respectively (**Figure 1C**). Continuous cropping of FS and SC increased the fungal community diversity. The Shannon index was significantly higher in FS and SC than in CK and CS. The Chao1 and ACE indexes demonstrated that the upper limits of FS and SC were significantly higher than those of CK and CS. The relative abundance and diversity of fungi in CK soil were the lowest (**Figure 2**). Compared with SC, the abundance and diversity of fungi in CS and WS soil decreased significantly, and CS treatment was the lowest.

Effects of Cropping Systems on the Floristic Composition of the Soil Fungal Community

The soil fungi in the different treatments were mainly distributed in Ascomycota, Basidiomycota and Zygomycota (**Figure 3A** and **Supplementary Table 3**). The relative abundance of Ascomycota was significantly higher in WS, followed by CS, SC, FS, and CK ($p < 0.05$). The relative abundance of Basidiomycota was significantly higher in CK, followed by CS, FS, SC, and WS ($p < 0.05$). The relative abundance of Zygomycota was significantly higher in FS, followed by CK, SC, WS, and CS ($p < 0.05$).

The relative abundance of *Alternaria* in Ascomycota was significantly higher in CS and WS. The relative abundance of *Chaetomium* was significantly higher in CS, WS, and SC. The relative abundance of *Tetraclaudium* was significantly higher in SC. The relative abundance of *Gibberella* was significantly higher in SC and CS. The relative abundance of *Peziza* was significantly high in FS (**Figure 3B** and **Supplementary Table 4**). The relative abundance of *Mortierella* in Zygomycota was significantly higher in FS, followed by CK and SC. The relative abundance of *Cortinarius* and *Amanita* in Basidiomycota was significantly higher in CK. The relative abundance of *Sistotrema* was significantly higher in CS (**Figure 3B** and **Supplementary Table 4**).

Fungal groups significantly different from other treatments were formed in the soils of different cropping systems (**Figure 4A**). Different fungal groups have an important impact on the division of fungal communities in different cropping systems. The relative abundances of *Trichoglossum*, *Paraconiothyrium* and *Unclassified_Lecanorales* and *Eleutheromyces* were more abundant following CK amendment. The relative abundances of *Entorrhiza*, *Unclassified_Corticiaceae*, *Unclassified_Bionectriaceae* and *Udeniomyces* were more abundant following SC amendment. The relative abundances of *Unclassified_Xylariaceae*, *Chaetomidium,* and *Plenodomus* were more abundant following CS amendment. The relative abundances of *Hydropisphaera*, *Ampelomyces,* and *Dioszegia* were higher following WS amendment. The relative abundances of *Eocronartium* and *Peziza* were higher following FS amendment (**Figure 4B**).

The formation of fungal community function was significantly different in different treatments (**Figure 4C**). Compared with SC, the relative abundance of *Cryptococcus* in CK exhibited an extremely significant decline, the relative abundance of T*etraclaudium*, *Alternaria*, *Clonostachys,* and *Chaetomium* decreased significantly, and the relative abundance of *Pseudonymnoascus* increased significantly (**Supplementary Figure 2**). Compared with SC, the relative abundance of *Sarocladium* in FS soil increased significantly, *Vishniacozyma*, *Fusicolla*, *Pseudonymnoascus*, *Solicoccozyma*, *Peziza*, *Paraglomus,* and *Penicillium* increased significantly, and the relative abundance of *Cryptococcus*, *Cladosporium*, *Mrakia*, *Cryptococcus*, *CladosporiumMrakia,* and *Tetraclaudium* decreased significantly. The relative abundance of *Tetraclaudium, Hydropisphaera, Clonostachys, Chaetomium, Metarhizonium, Acremonium,* and *Atractospora* decreased significantly (**Supplementary Figure 3**). Compared with SC, the relative abundance of *Chaetomidium*, *Nectria,* and *Alternaria* in CS increased significantly, and the relative abundance of *Cladosporium*, *Peziza,* and *Cryptococcus* decreased significantly. The relative abundance of *Mrakia*, *Metarhizonium*,

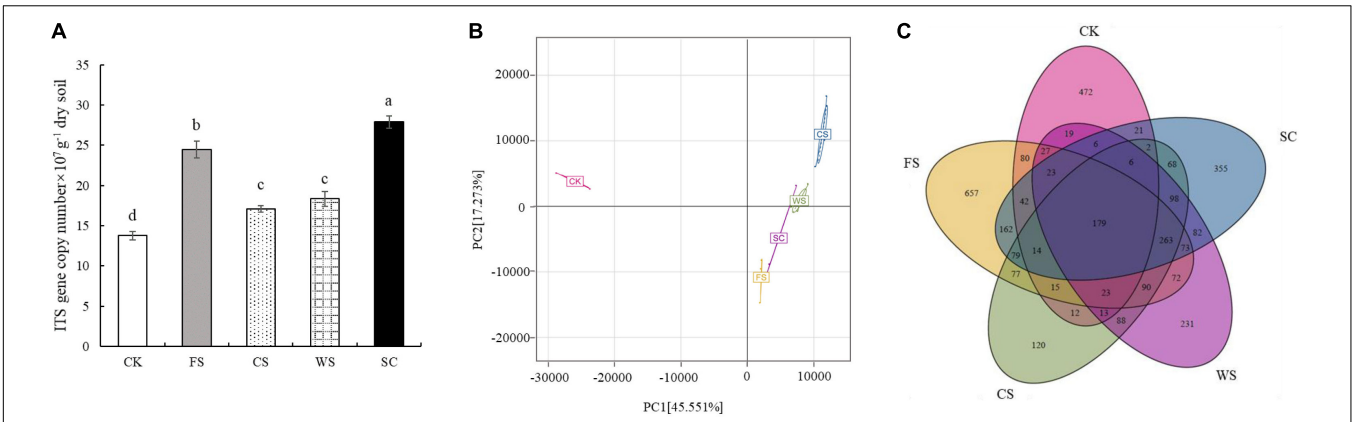

FIGURE 1 | Differences in soil fungal community structure in different cropping systems. **(A)** The abundance of fungal ITS rRNA gene copies assessed by real-time PCR in five soybean cropping systems. Different letters represent significant differences ($P < 0.05$), **(B)** principal coordinate analysis (PCA) plot based on the OTUs for five soybean cropping systems. **(C)** Venn diagram of OTU distribution comparison. The numbers represent the number of species. SC, soybean continuous cropping; CK, fallow; FS, fallow-soybean; CS, corn–soybean; WS, wheat–soybean.

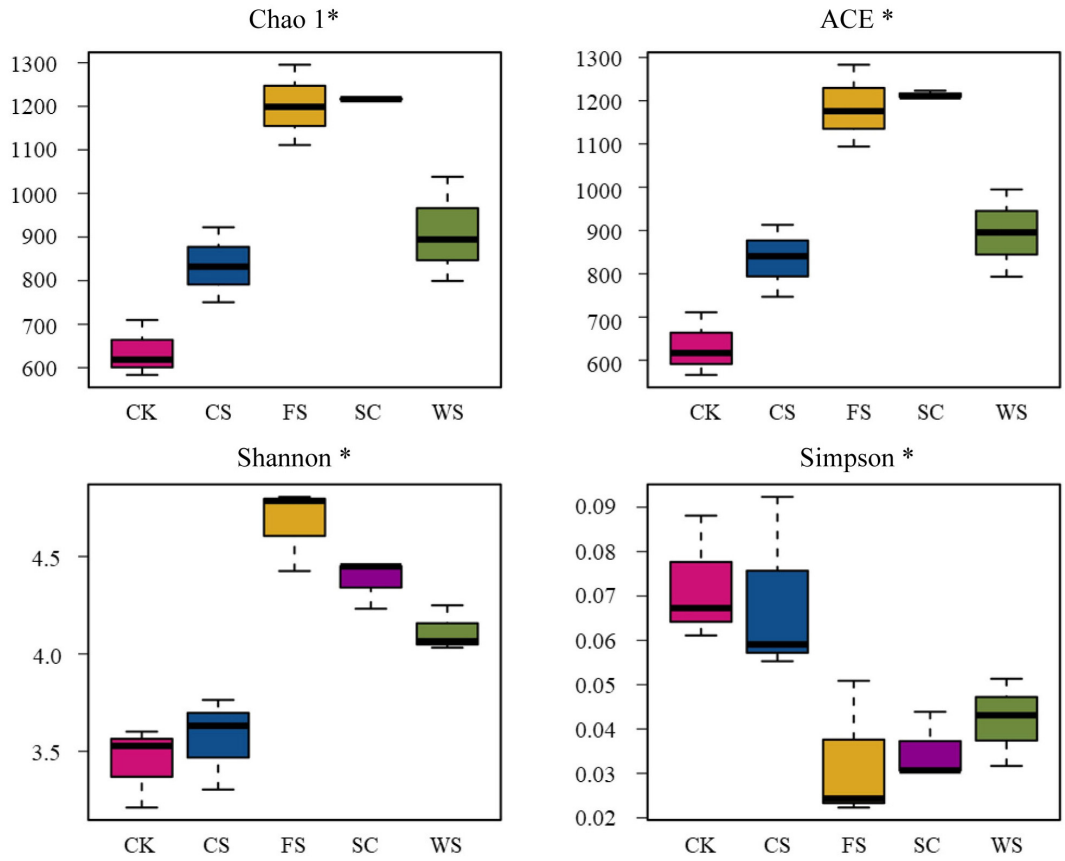

FIGURE 2 | Chao1 index, ACE index, Shannon index, and Simpson index for fungi in five soybean cropping systems with > 97% sequence identity. *Indicates a significant correlation ($P < 0.05$).

Clonostachys, *Nectria,* and *Exophiala* decreased significantly (**Supplementary Figure 4**). Compared with SC, the relative abundance of *Nectria* in WS increased significantly, the relative abundance of *Hydropisphaera*, *Guehomyces*, *Alternaria*, *Humicola, Periconia, Pseudonymnoascus,* and *Atractospora* increased significantly, the relative abundance of *Peziza* and *Cladosporium* decreased significantly, and the relative abundance of *Tetracladium, Moraia, Metarhizium, Exophiala,*

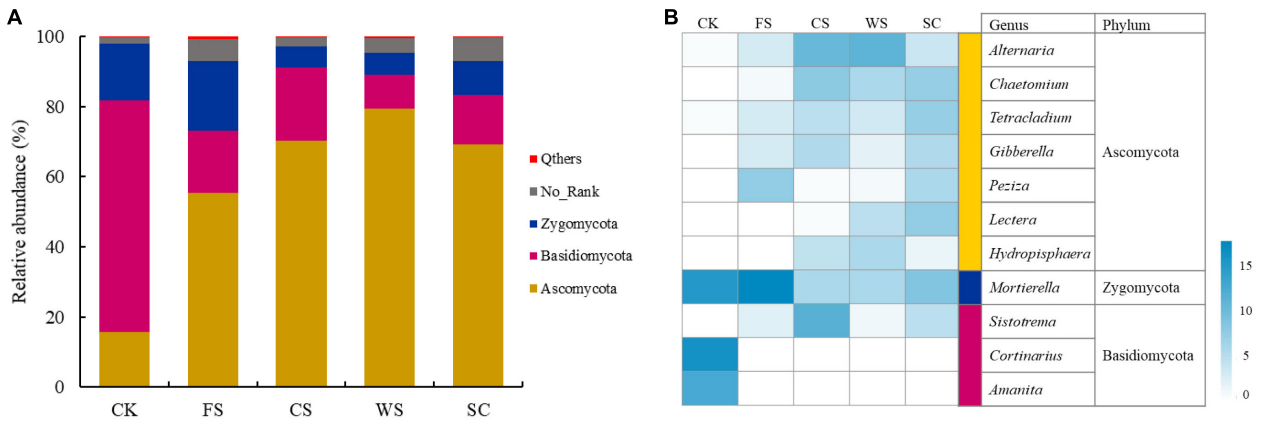

FIGURE 3 | Relative abundance of different fungi at the phylum level **(A)** and heatmap analysis **(B)** of the dominant fungal genera with relative abundance greater than 0.5% in five soybean cropping systems. The color code indicates relative abundance, ranging from white (low abundance) to blue (high abundance).

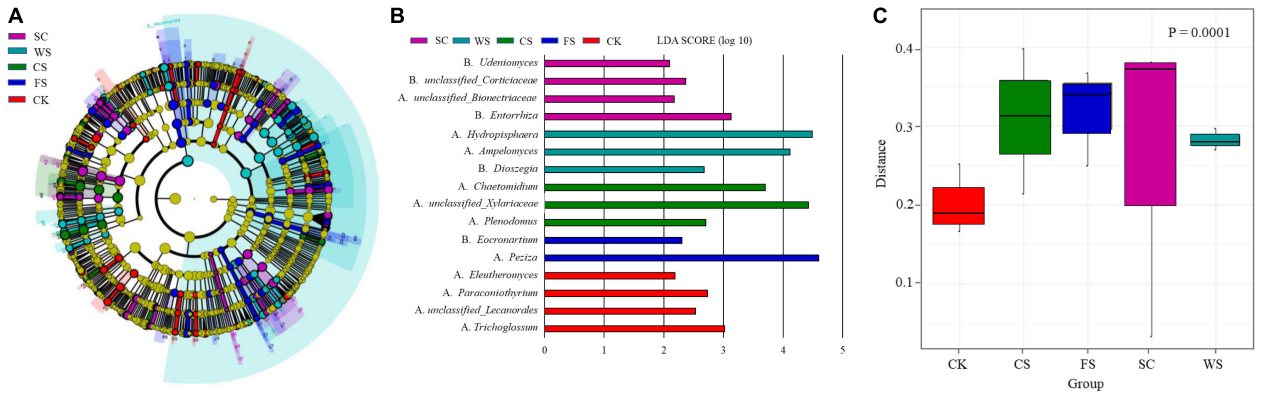

FIGURE 4 | Analysis of species and community functions of fungi with significant differences in soil under different cropping systems. Different color areas represent different groups. **(A)** Taxonomic cladogram produced from LEfSe. The phylum, class, order, family, and genus levels are listed in order from inside to outside of the cladogram. LEfSe diagram. The corresponding color nodes in the diagram represent the groups that play an important role in this grouping (significantly different from other groups), and the yellow nodes represent the microbial groups that do not play an important role. **(B)** Shows the species with significant differences in abundance in different groups, and the length of the histogram represents the influence degree of the species with significant differences. **(C)** The UniFrac distance matrix was used to draw the distance diagram between sample groups. The ordinate represents the sample weighted UniFrac distance, and the *p*-value in the upper right corner represents the test results of the difference between groups.

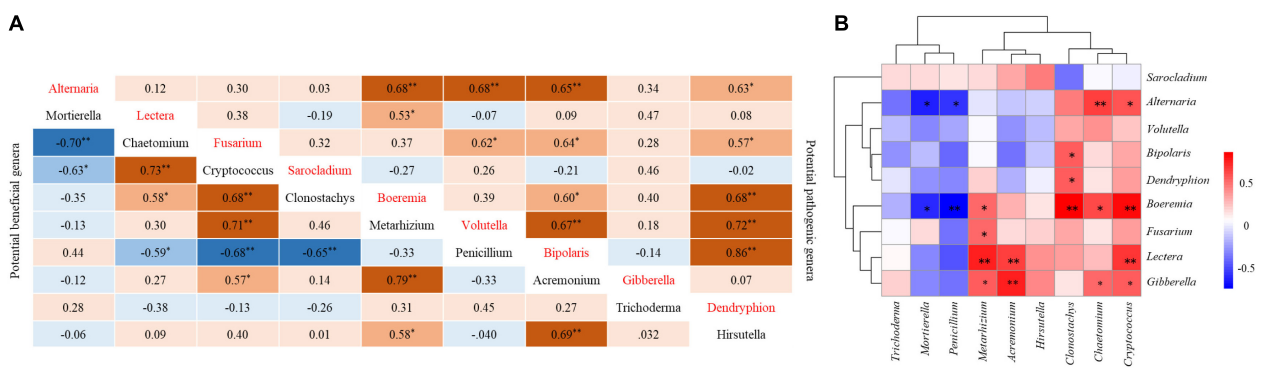

FIGURE 5 | Correlation between potential pathogenic genera in soil and potentially beneficial genera. **(A)** Correlation between potential pathogenic genera and pathogenic genera and between potential beneficial genera and beneficial genera. **(B)** Correlation between potential pathogenic genera and beneficial genera. *Indicates a significant correlation ($P < 0.05$), **indicates an extremely significant correlation ($P < 0.01$).

Unclassified_Halosphaeriaeae, and *Herbotrichia* decreased significantly (**Supplementary Figure 5**).

Potential Pathogenic and Beneficial Fungi

The relative abundances of potential pathogenic *Lectera, Gibberella, and Fusarium* in SC soil were significantly high. The relative abundances of *Fusarium, Sarocladium,* and *Volutella* in FS soil were significantly high. The relative abundances of *Alternaria*, *Lectera*, *Fusarium*, *Boeremia*, *Dendyphion*, *Volutella,* and *Bipolaris* in WS soil were significantly high. The relative abundances of *Alternaria*, *Gibberella,* and *Volutella* in CS soil were significantly high. The relative abundance of all potential pathogens in CK soil was significantly the lowest (**Supplementary Figure 6A**).

The relative abundance of the beneficial fungus *Penicillium* was significantly high in CK. The relative abundances of *Mortierella* and *Penicillium* in FS were significantly higher, and the relative abundance of *Chaetomium* in CS was significantly higher. The relative abundances of *Chaetomium*, *Cryptococcus,* and *Clonostachys* in WS were significantly high. The relative abundances of *Chaetomium*, *Cryptococcus*, *Metarhizonium*, *Acremonium,* and *Hirsutella* in SC were significantly high (**Supplementary Figure 6B**).

There was a significant positive correlation between potential pathogen genera and pathogen genera in soil, and *Alternaria* was very significantly positively correlated with *Boeremia*, *Volutella,* and *Bipolaris*. There was a very significant positive correlation between *Volutella* and *Bipolaris*. *Dendryphion* was significantly positively correlated with *Bipolaris, Volutella, and Boeremia* (**Figure 5A**).

Mortierella was very negatively correlated with *Chaetomium* in beneficial fungi. *Penicillium* was very negatively correlated with *Cryptococcus* and *Clonostachys*. *Chaetomium* was very positively correlated with *Cryptococcus*. *Cryptococcus* was positively correlated with *Clonostachys* and *Metarhizoum*. There was a very significant positive correlation between *Metarhizoum* and *Acremonium*. *Acremonium* was positively correlated with *Hirsutella* (**Figure 5A**).

The beneficial fungus *Mortierella* was significantly negatively correlated with the pathogenic fungi *Alternaria* and *Boeremia*. There was a significant negative correlation between the beneficial fungus *Penicillium* and the pathogenic fungi *Alternaria* and *Boeremi*. Among the beneficial fungi, the relative abundance of *Chaetomium*, *Cryptococcus*, *Clonostachys*, *Acremonium,* and *Metarhizobium* had a significant positive correlation with some pathogens (**Figure 5B**).

The relative abundance of *Fusarium* was significantly positively correlated with the Chao 1 and Shannon indexes of soil fungi, and the correlation coefficients were 0.585 and 0.619, respectively ($p < 0.05$). The relative abundance of *Sarocladium* was significantly positively correlated with the Chao 1 and Shannon indexes of soil fungi, and the correlation coefficients were 0.664 and 0.536, respectively ($p < 0.05$). Other potential pathogens had no significant correlation with the abundance and diversity of soil fungi. The relative abundances of *Alternaria*, *Fusarium*, *Boeremia*, *Volutella*, *Bipolaris*, *Gibberella,* and *Denryphion* were significantly positively correlated with Ascomycota abundances, and the correlation coefficients were 0.759, 0.615, 0.777, 0.684, 0.528, 0.649, and 0.682, respectively ($p < 0.05$). The relative abundances of *Alternaria*, *Fusarium*, *Boeremia*, *Volutella*, *Bipolaris*, *Gibberella,* and *Denryphion* were significantly negatively correlated with the abundances of Basidiomycota, and the correlation coefficients were −0.592, −0.787, −0.655, −0.655, −0.529, −0.637, and −0.615, respectively ($p < 0.05$). The relative abundances of *Alternaria* and *Boeremia* were significantly negatively correlated with the abundance of Zygomycota, and the correlation coefficients were −0.645 and −0.613, respectively ($p < 0.05$). The relative abundance of *Metarhizobium* was positively correlated with the abundance and diversity of the Chao 1 and Shannon indexes ($p < 0.01$). The relative abundance of *Hirsutella* was significantly positively correlated with the Chao 1 and Shannon indexes of fungi ($p < 0.05$). The relative abundance of *Acremonium* was significantly positively correlated with the Chao 1 indexes of fungi ($p < 0.05$). There was no significant correlation between other fungal abundance and diversity. The relative abundance of *Chaetomium*, *Cryptococcus*, *Clonostachys,* and *Metarhizobium* was significantly positively correlated with the abundance of Ascomycota and negatively correlated with the abundance of Basidiomycota ($p < 0.05$). *Mortierella* relative abundance was significantly negatively correlated with Ascomycota abundance and positively correlated with Zygomycota abundance ($p < 0.05$). The relative abundance of *Penicillium* was significantly negatively correlated with the abundance of Ascomycota ($p < 0.05$). The relative abundance of *Chaetomium* and *Cryptococcus* was significantly negatively correlated with the abundance of Zygomycota ($p < 0.05$) (**Table 1**).

Correlation Between Soil Fungi and Soil Chemical Properties

There were significant differences in the correlations between different chemical properties in the soil and soil fungal communities, among which the contents of available Cu, Fe, and Mn were highly correlated with the fungal community (**Figure 6A** and **Supplementary Table 5**). Ascomycota had a very significant positive correlation with the effective content of Cu and a significant negative correlation with the effective content of OM, Mn, and Fe. Basidiomycota had a significant negative correlation with the effective contents of Zn and Fe and a significant positive correlation with the effective content of Mn. Zygomycota was significantly negatively correlated with the effective contents of Cu and P (**Table 2**). The potential pathogens were mainly negatively correlated with the effective contents of OM, Mn, K, and soil pH and positively correlated with the effective contents of Cu, Fe and Zn.

Fusarium was significantly negatively correlated with soil OM, available Mn content and soil pH. *Sarocladium* was very significantly negatively correlated with the effective content of Mn. *Bipolaris, Dendyphion,* and *Volutella* were negatively

TABLE 1 | Correlations between potential pathogenic genera, potentially beneficial genera and the fungal community.

	Fungal diversity				Dominant fungi phylum		
	Chao1	**ACE**	**Shannon**	**Simpson**	**Ascomycota**	**Basidiomycota**	**Zygomycota**
Potential pathogenic genera							
Alternaria	−0.021	−0.025	−0.068	−0.051	0.759**	−0.592*	−0.645**
Lectera	0.300	0.305	0.325	−0.427	0.482	−0.465	−0.281
Fusarium	0.585*	0.574*	0.619*	−0.508	0.615*	−0.787**	0.181
Sarocladium	0.664**	0.668**	0.536*	−0.398	0.273	−0.415	0.219
Boeremia	0.225	0.218	0.150	−0.268	0.777**	−0.655**	−0.613*
Volutella	0.204	0.206	0.281	−0.279	0.684**	−0.655**	−0.293
Bipolaris	0.034	0.009	0.166	−0.160	0.528*	−0.529*	−0.162
Gibberella	0.510	0.521*	0.306	−0.344	0.649**	−0.637*	−0.284
Dendryphion	0.268	0.243	0.373	−0.401	0.628*	−0.615*	−0.259
Potential beneficial genera							
Mortierella	0.112	0.097	0.175	−0.030	−0.555*	0.250	0.998**
Chaetomium	0.154	0.181	−0.020	−0.082	0.716**	−0.549*	−0.701**
Cryptococcus	0.453	0.456	0.315	−0.406	0.837**	−0.737**	−0.622*
Clonostachys	0.203	0.202	0.150	−0.267	0.574*	−0.521*	−0.365
Metarhizium	0.803**	0.805**	0.722**	−0.713**	0.573*	−0.663**	−0.102
Penicillium	−0.069	−0.070	0.169	−0.132	−0.569*	0.467	0.456
Acremonium	0.630*	0.638*	0.445	−0.452	0.393	−0.448	−0.091
Trichoderma	0.338	0.318	0.349	−0.295	−0.135	0.019	0.311
Hirsutella	0.616*	0.617*	0.675**	−0.639*	0.363	−0.451	−0.029

*Indicates a significant correlation ($P < 0.05$), **indicates an extremely significant correlation ($P < 0.01$).

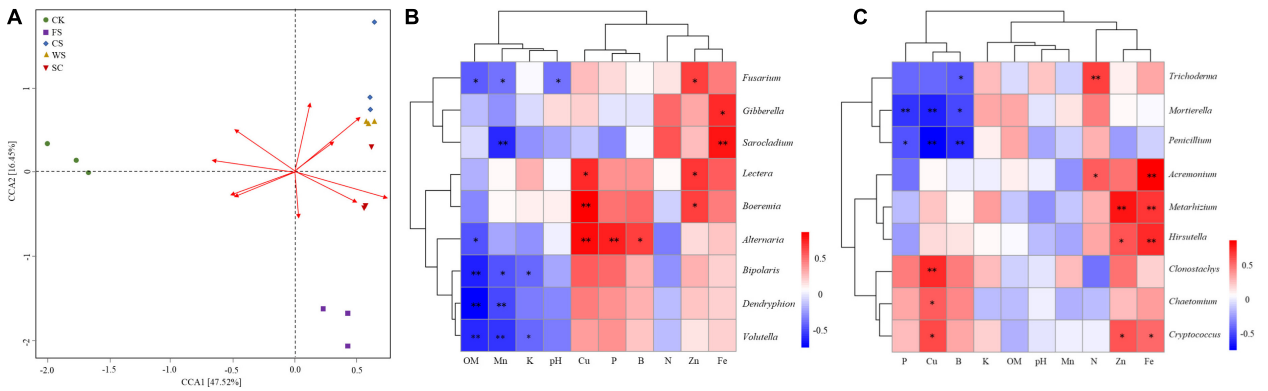

FIGURE 6 | Correlation between soil fungi and soil chemical properties. **(A)** RDA diagram of soil environmental factors and fungi. Arrow rays represent different environmental factors. The longer the ray is, the greater the impact of the environmental factor. The included angle between the sample fungal community central line and the arrow represents the correlation between the fungal and environmental factors (an acute angle indicates a positive correlation, an obtuse angle indicates a negative correlation, and a right angle indicates no correlation); points of different colors represent different samples; **(B)** potentially potential pathogen; **(C)** potentially beneficial fungi. *Indicates a significant correlation ($P < 0.05$), **indicates an extremely significant correlation ($P < 0.01$).

correlated with OM content. *Bipolaris* was significantly negatively correlated with the effective contents of Mn and K. *Dendriphion*, *Volutella,* and Mn effective content were significantly negatively correlated. *Volutella* was negatively correlated with the effective content of K. *Alternaria* was positively correlated with the effective contents of Cu and P.

Boeremia was positively correlated with the effective content of Cu. *Sarocladium* was very significantly positively correlated with the effective content of Fe. *Fusarium*, *Lectera,* and *Boeremia* were significantly positively correlated with the effective content of Zn (**Figure 6B**). The potential beneficial fungus *Trichoderma* was positively correlated with the effective content of N. There was a very significant positive correlation between *Metarhizoum* and the effective contents of Fe and Zn. *Acremonium* and *Hirsutella* were significantly positively correlated with the effective content of Fe. *Clonostachys* was significantly positively correlated with the effective content of Cu. *Mortierella* was negatively correlated with the effective contents of P and Cu. *Penicillium* was significantly negatively correlated with the content of available Cu and B (**Figure 6C**).

TABLE 2 | Correlation coefficients between the main microbial communities (phylum level) and soil physical and chemical properties.

	OM	N	P	K	PH	Cu	Zn	Mn	Fe
Ascomycota	−0.60*	–	–	–	–	0.68**	–	−0.55*	0.58*
Basidiomycota	–	–	–	–	–	–	−0.57*	0.59*	−0.68**
Zygomycota	–	–	−0.64**	–	–	−0.71*	–	–	–

**Indicates a significant correlation ($P < 0.05$), ** indicates an extremely significant correlation ($P < 0.01$).*

DISCUSSION

Effects of Cropping Systems on Fungal Abundance and Community Composition

The species diversity and community structure of soil microorganisms determine the ability of soil to resist pathogens, which is very important for the sustainable development of soil ecosystems (Smith et al., 2008). Continuous cropping will cause an imbalance of soil, a surge of pathogens and an increased probability of crop disease (Meriles et al., 2009). In this study, it was confirmed that there were significant differences in the formation of fungal communities in the soil of the five cropping systems. All of the soil samples were separated into two groups. The fungal communities in FS, SC, WS, and CS were grouped together and were clearly separated from CK, and the similarity of the WS and CS fungal communities was the highest (**Figure 1A**). The soil fungal abundance (Chao1/ACE) and fungal diversity (Shannon) were significantly the highest in FS and SC (**Figure 2**). The relative abundance of Ascomycota in SC was high, and the relative abundance of unknown fungal flora increased significantly (relative abundance of no rank), which may be because SC significantly increased the number of endemic fungi (**Supplementary Table 3**). This study confirmed that SC could increase the relative abundance and diversity of soil fungi. Studies have shown that soybean roots secrete a large number of flavonoids and phenolic acids (Guo et al., 2011), and flavonoids and phenolic acids have a significant impact on fungal pathogens (Wang et al., 2013). Compared with SC, CK, and CS significantly reduced the number and diversity of fungi, and the abundance and diversity of fungi in CK were significantly the lowest. Other studies have shown that there is no difference in the diversity of fungal communities between continuous planting and corresponding rotation systems (Li et al., 2010; Liu et al., 2014a). Research has also shown that soybean maize rotation increases the diversity of fungal communities in rhizosphere and massive soil (Liu J. et al., 2019). This is inconsistent with the results of this study and may be caused by different soil environments and planting management systems. In this study, fungi in the soil samples were mainly distributed among the dominant fungi in the soil, namely, Ascomycota, Basidiomycota, and Zygomycota, which is consistent with previous research results (Xu et al., 2012), and this study confirms that ascomycetes are an important phylum in continuous cropping soybean soil (Li et al., 2010). This study found that different cropping systems changed the composition and structure of Ascomycota significantly. Recent speculation suggests that changes in microbial community composition, such as a decrease in the number of soil-borne pathogens or an increase in the population of beneficial agricultural microorganisms, may be more important in disease suppression than microbial diversity (Peralta et al., 2018). Therefore, enhancing our understanding of microbial composition in different crop rotation systems is very important to determine the classified biological indicators of soil health, which is conducive to the application of effective crop rotation systems.

The Relative Abundance of Potentially Pathogenic and Beneficial Fungi in Different Cropping Systems Was Significantly Different

Studies have shown that short-term continuous soybean cropping leads to an increase in the relative abundance of *Fusarium*, *Humicola,* and *Alternaria*. *Fusarium* and *Alternaria* are the main pathogenic fungi in soybean fields, and their abundance is significantly high during 1 and 2 years of SC (Bai et al., 2015; Cheng et al., 2017). *Humicola* was not detected in the soil samples of this study. However, SC, FS and WS promoted an increase in the relative abundance of *Fusarium* in the soil, and WS and CS promoted an increase in the relative abundance of *Alternaria* in the soil (**Figure 5A**). *Fusarium* is well known to be a pathogenic fungus that leads to soybean *Fusarium* root rot (Chang et al., 2018), and *Alternaria* can infect various crops and cause corresponding diseases, such as soybean Alternaria leaf spot, tomato, and carrot black rots, citrus fruit gray rot and cereal black point (Li and Yang, 2009; Logrieco et al., 2009).

There are also some potential pathogens in the soil. Research reports indicate that *Volutella* can cause diseases of other legumes (Cannon et al., 2012). Some studies have reported that *Boeremia* caused stem rot of Origanum dubium in Cyprus (Origanum dubium Boiss) and black rot of artichoke (Cynara scolymus) in California (Koike et al., 2016; Samouel et al., 2016). *Lectera*, a new genus of Plectosphaerellaceae, is a legume pathogen (Cannon et al., 2012). Studies have proven that *Bipolaris* and *Sarocladium* can cause diseases of gramineous crops (Saravanakumar et al., 2009) and maize smut disease caused by *Bipolaris* (Li et al., 2016).

In this study, FS, CS, and WS promoted an increase *in the* relative abundance of Volutella in the soil. WS promoted an increase in the relative abundance of *Boeremia* and *Bipolaris*, and WS reduced the relative abundance of *Sarocladium* in the soil. The relative abundance of *Bipolaris* in CS and SC soils was significantly low. It was found that CK treatment could reduce the relative abundance of potential pathogens in soil. Therefore, this study demonstrated that different cropping systems can regulate potential pathogens in soil.

Biological control instead of chemical control is considered to be an important method of sustainable agricultural production (Lecomte et al., 2016). In this study, some potentially beneficial fungi formed significant differences under the different treatments. *Mortierella*, *Clonostachys* and Penicillium are antagonists of pathogens. They can inhibit pathogenic *Fusarium* and control banana Fusarium wilt and soybean root rot (Pan et al., 2013; Shen et al., 2018). A previous study reported that

Hirsutella combined with chitosan suppressed the infestation of soybean cyst nematodes in soybean roots (Mwaheb et al., 2017). It was found that *Clonostachys* is abundant in soybean continuous cropping soil (Hamid et al., 2017). This study confirmed this result and found that WS promoted a significant increase in *Clonostachys* in soil. The present results show that the relative abundance of *Penicillium* was significantly lower in CS, WS, and SC. Consistent with previous studies, continuous planting significantly reduced the relative abundance of *Penicillium* (Wu et al., 2016). The relative abundance of the beneficial fungus *Penicillium* was significantly high in CK soil.

To reveal the potential interaction between potential pathogens and beneficial fungi. Pearson correlation analysis showed that the beneficial fungus *Mortierella* was significantly negatively correlated with the potential pathogens *Alternaria* and *Boeremia*. The potentially beneficial fungus *Penicillium* was significantly negatively correlated with the potential pathogen *Alternaria* and extremely significantly negatively correlated with the potential pathogen *Boeremia*. Other potentially beneficial fungi, such as *Metarhizonium*, *Acremonium*, *Chaetomium,* and *Cryptococcus*, were significantly positively correlated with potential pathogens. The potential pathogen *Fusarium* was significantly positively related to the beneficial fungus *Metarhizoum*, which indicated that the potential beneficial fungi will increase with the increase in pathogens. However, how to control pathogens by increasing beneficial fungi in soil through crop rotation needs further research. Therefore, in future research, it is of great significance to pay attention to the interaction between members of the microbiome to regulate the function of soil microorganisms (Jiao et al., 2020).

Fungal Communities Were Significantly Correlated With Soil Chemical Properties

Soil chemical properties were significantly correlated with soil microbial community structure (Liu et al., 2014b). In this study, the soil chemical properties of different cropping systems were significantly different, and the soil chemical properties were significantly correlated with the soil microbial community structure. The relative abundance of Basidiomycota was significantly higher in CK, and Basidiomycota was negatively correlated with the content of available Fe in the soil. The relative abundance of Zygomycota was significantly higher in FS, and there was a very significant negative correlation between Zygomycota and the content of available P in the soil. The relative abundance of Ascomycota increased significantly in WS, which was positively correlated with the content of available Cu in the soil. These results are inconsistent with previous research results (Luo et al., 2016; Cai et al., 2017), which is due to different soil regions, types and cropping systems.

Soil type and environmental factors affect the soil microbial community structure (Luo et al., 2016; Pang et al., 2017). That different cropping systems changed the relative abundance of potential beneficial fungi in the soil. There are many reasons for the change in microbial community composition. An imbalance in soil nutrients, decomposition of soil physical and chemical properties and accumulation of virulence will affect the structure of the fungal community (Wu et al., 2015). Some of them promote the production of some soil-borne pathogenic microorganisms, while others may be conducive to the production of beneficial microorganisms, resulting in changes in the number of relevant microorganisms (Li et al., 2014).

Changes in microbial community structure are related to available nutrients and plant biomass in soil (Bokhorst et al., 2017). Predecessors have shown that organic matter has an important impact on the composition of the soil fungal community (Sun et al., 2016). This study showed that the contents of OM, available Mn, available K and soil pH were significantly negatively correlated with some potential pathogenic fungi. The contents of available Fe and Zn in the soil were significantly positively correlated with potential pathogens and beneficial fungi. In this study, *Fusarium* was significantly negatively correlated with the effective content and pH of soil OM and Mn. *Penicillium* was negatively correlated with the content of available Cu and B in the soil. Predecessors have shown that cropping systems, soil chemical properties and soil microbial community structure are interrelated and interactive (Ofek-Lalzar et al., 2017). This study shows that there is a more significant correlation between soil trace elements and potential pathogens and beneficial fungi in soil. How to regulate the composition of fungal community structure in soil through trace elements and form a stable disease-inhibiting soil needs further research and proof.

CONCLUSION

The fungal communities in FS, SC, WS, and CS were significantly different from those in CK. FS, SC, WS, and CS promoted the formation of fungal abundance and diversity, and different planting methods formed their own unique fungal species. FS and SC showed significantly higher fungal community abundance and species diversity than CK and CS. The abundance of *Fusarium* in FS, SC, and WS in the soil was significantly increased. CK and CS can reduce the relative abundance of *Fusarium* in soil, and CK can significantly reduce the relative abundance of many potential pathogens in soil. The potential pathogens *Alternaria*, *lectera,* and *Gibberella* were significantly positively correlated with the potentially beneficial pathogens *Mortierella*, *Chaetomium,* and *Cryptococcus*. The major potential pathogens *Alternaria*, *lectera*, *Gibberella,* and *Fusarium* in soil were significantly correlated with trace elements, and *Fusarium* was significantly negatively correlated with organic matter and Mn. Cropping system and soil physical and chemical properties are the main factors related to the formation of soil fungal structure. These results provide important significance for the selection of an effective crop rotation system and sustainable agricultural development.

DATA AVAILABILITY STATEMENT

The datasets presented in this study can be found in online repositories. The names of the repository/repositories and

accession number(s) can be found below: https://www.ncbi.nlm.nih.gov/sra/, SRP164820.

AUTHOR CONTRIBUTIONS

XS and BT planned and arranged the entire study. XS performed the main experiments. LH, YL, and CZ assisted in the soil testing. XS and WZ wrote the manuscript together. BT participated in further discussion. All authors discussed and approved the final version of the manuscript.

FUNDING

This study was financially supported by the Youth Fund, the regional joint fund of Guangdong Basic and Applied Basic Research Fund (2019A1515110888) and Research Project Funding of Lingnan Normal University (ZL2044).

ACKNOWLEDGMENTS

We are grateful to the Agriculture College of Northeast Agricultural University, Heilongjiang Academy of Agricultural Sciences, and the numerous staff members who helped protect the test plots and collect the soil samples.

SUPPLEMENTARY MATERIAL

The Supplementary Material for this article can be found online at: https://www.frontiersin.org/articles/10.3389/fpls.2022.926731/full#supplementary-material

REFERENCES

Adams, R. I., Miletto, M., Taylor, J. W., and Bruns, T. D. (2013). Dispersal in microbes: fungi in indoor air are dominated by outdoor air and show dispersal limitation at short distances. *ISME J.* 7, 1262–1273. doi: 10.1038/ismej.2013.28

Avidano, L., Gamalero, E., Cossa, G. P., and Carraro, E. (2005). Characterization of soil health in an Italian polluted site by using microorganisms as bioindicators. *Appl. Soil Ecol.* 30, 21–33. doi: 10.1016/j.apsoil.2005.01.003

Baetz, U., and Martinoia, E. (2014). Root exudates: the hidden part of plant defense. *Trends Plant Sci.* 19, 90–98. doi: 10.1016/j.tplants.2013.11.006

Bai, L., Cui, J., Jie, W., and Cai, B. (2015). Analysis of the community compositions of rhizosphere fungi in soybeans continuous cropping fields. *Microbiol. Res.* 180, 49–56. doi: 10.1016/j.micres.2015.07.007

Behera, U. K., Sharma, A. R., and Mahapatra, I. C. (2007). Crop Diversification for efficient resource management in India: problems, prospects and policy. *J. Sustain. Agric.* 30, 97–127. doi: 10.1300/j064v30n03_08

Benitez, M. S., Osborne, S. L., and Lehman, R. M. (2017). Previous crop and rotation history effects on maize seedling health and associated rhizosphere microbiome. *Sci. Rep.* 7:15709. doi: 10.1038/s41598-017-15955-9

Bokhorst, S., Kardol, P., Bellingham, P. J., Kooyman, R. M., Richardson, S. J., Schmidt, S., et al. (2017). Responses of communities of soil organisms and plants to soil aging at two contrasting long-term chronosequences. *Soil Biol. Biochem.* 106, 69–79. doi: 10.1016/j.soilbio.2016.12.014

Bremner, J. M., and Keeney, D. R. (1966). Determination and isotope-ratio analysis of different forms of nitrogen in soils: 3. Exchangeable ammonium, nitrate, and nitrite by extraction-distillation methods. *Soil Sci. Soc. Am. J.* 30, 577–582. doi: 10.2136/sssaj1966.03615995003000050015x

Cai, F., Chen, W., Wei, Z., Pang, G., Li, R., Ran, W., et al. (2015). Colonization of *Trichoderma harzianum* strain SQR-T037 on tomato roots and its relationship to plant growth, nutrient availability and soil microflora. *Plant Soil* 388, 337–350. doi: 10.1007/s11104-014-2326-z

Cai, F., Pang, G., Miao, Y., Li, R., Li, R., Shen, Q., et al. (2017). The nutrient preference of plants influences their rhizosphere microbiome. *Appl. Soil Ecol.* 110, 146–150. doi: 10.1016/j.apsoil.2016.11.006

Cannon, P., Buddie, A., Bridge, P., de Neergaard, E., Lübeck, M., and Askar, M. (2012). Lectera, a new genus of the *Plectosphaerellaceae* for the legume pathogen *Volutella colletotrichoides*. *MycoKeys* 3, 23–36. doi: 10.3897/mycokeys.3.3065

Chang, X., Dai, H., Wang, D., Zhou, H., He, W., Fu, Y., et al. (2018). Identification of *Fusarium* species associated with soybean root rot in Sichuan Province, China. *Eur. J. Plant Pathol.* 151, 563–577. doi: 10.1007/s10658-017-1410-7

Cheng, P., Gedling, C., Patil, G., Vuong, T., Shannon, J., Dorrance, A., et al. (2017). Genetic mapping and haplotype analysis of a locus for quantitative resistance to Fusarium graminearum in soybean accession PI 567516C. *Theor. Appl. Genet* 130, 999–1010. doi: 10.1007/s00122-017-2866-8

Clemente, R., Walker, D. J., and Bernal, M. P. (2005). Uptake of heavy metals and as by *Brassica juncea* grown in a contaminated soil in Aznalcóllar (Spain): the effect of soil amendments. *Environ. Pollut.* 138, 46–58. doi: 10.1016/j.envpol.2005.02.019

Cole, J. R., Wang, Q., Cardenas, E., Fish, J., Chai, B., Farris, R. J., et al. (2009). The ribosomal database project: improved alignments and new tools for rRNA analysis. *Nucleic Acids Res.* 37, D141–D145. doi: 10.1093/nar/gkn879

Dias, T., Dukes, A., and Antunes, P. M. (2015). Accounting for soil biotic effects on soil health and crop productivity in the design of crop rotations. *J. Sci. Food Agric.* 95, 447–454. doi: 10.1002/jsfa.6565

Edgar, R. C., Haas, B. J., Clemente, J. C., Quince, C., and Knight, R. (2011). UCHIME improves sensitivity and speed of chimera detection. *Bioinformatics* 27, 2194–2200. doi: 10.1093/bioinformatics/btr381

Föhse, D., Claassen, N., and Jungk, A. (1991). Phosphorus efficiency of plants. *Plant Soil* 132, 261–272. doi: 10.1007/bf00010407

Guo, Z. Y., Kong, C. H., Wang, J. G., and Wang, Y. F. (2011). Rhizosphere isoflavones (daidzein and genistein) levels and their relation to the microbial community structure of mono-cropped soybean soil in field and controlled conditions. *Soil Biol. Biochem.* 43, 2257–2264. doi: 10.1016/j.soilbio.2011.07.022

Hamid, M. I., Hussain, M., Wu, Y., Zhang, X., Xiang, M., and Liu, X. (2017). Successive soybean-monoculture cropping assembles rhizosphere microbial communities for the soil suppression of soybean cyst nematode. *FEMS Microbiol. Ecol.* 93:fiw222. doi: 10.1093/femsec/fiw222

Hartmann, M., Frey, B., Mayer, J., Mäder, P., and Widmer, F. (2015). Distinct soil microbial diversity under long-term organic and conventional farming. *ISME J.* 9, 1177–1194. doi: 10.1038/ismej.2014.210

Jiao, S., Yang, Y., Xu, Y., Zhang, J., and Lu, Y. (2020). Balance between community assembly processes mediates species coexistence in agricultural soil microbiomes across eastern China. *ISME J.* 14, 202–216. doi: 10.1038/s41396-019-0522-9

Koike, S. T., Groenewald, J. Z., and Crous, P. W. (2016). First report of black rot caused by *Boeremia exigua var. pseudolilacis* on *Artichoke* in California. *Plant Dis.* 100:524. doi: 10.1094/pdis-07-15-0767-pdn

Lecomte, C., Alabouvette, C., Edel-Hermann, V., Robert, F., and Steinberg, C. (2016). Biological control of ornamental plant diseases caused by *Fusarium oxysporum* : a review. *Biol. Control* 101, 17–30. doi: 10.1016/j.biocontrol.2016.06.004

Li, C., Li, X., Kong, W., Wu, Y., and Wang, J. (2010). Effect of monoculture soybean on soil microbial community in the Northeast China. *Plant Soil* 330, 423–433. doi: 10.1007/s11104-009-0216-6

Li, G. F., Liu, K. X., Xiao, S. Q., Lu, Y. Y., Xue, C. S., and Wang, G. Q. (2016). First report of leaf spot of maize (*Zea mays*) caused by *Bipolaris spicifera* in China. *Plant Dis.* 100:855. doi: 10.1094/pdis-07-15-0750-pdn

Li, J., Wen, Y., Li, X., Li, Y., Yang, X., Lin, Z., et al. (2018). Soil labile organic carbon fractions and soil organic carbon stocks as affected by long-term organic and mineral fertilization regimes in the North China Plain. *Soil Tillage Res.* 175, 281–290. doi: 10.1016/j.still.2017.08.008

Li, W., and Godzik, A. (2015). Cd-hit: a fast program for clustering and comparing large sets of protein or nucleotide sequences. *Bioinformatics* 22, 1658–1659. doi: 10.1093/bioinformatics/btl158

Li, X., and Yang, X. B. (2009). Similarity, pattern, and grouping of soybean fungal diseases in the United States: implications for the risk of soybean rust. *Plant Dis.* 93, 162–169. doi: 10.1094/pdis-93-2-0162

Li, X. G., Ding, C. F., Hua, K., Zhang, T. L., Zhang, Y. N., Zhao, L., et al. (2014). Soil sickness of peanuts is attributable to modifications in soil microbes induced by peanut root exudates rather than to direct allelopathy. *Soil Biol. Biochem.* 78, 149–159. doi: 10.1016/j.soilbio.2014.07.019

Lindsay, W. L., and Norvell, W. A. (1978). Development of a DTPA soil test for zinc, iron, manganese, and copper. *Soil Sci. Soc. Am. J.* 42, 421–428. doi: 10.2136/sssaj1978.03615995004200030009x

Liu, H., Pan, F., Han, X., Song, F., Zhang, Z., Yan, J., et al. (2019). Response of soil fungal community structure to long-term continuous soybean cropping. *Front. Microbiol.* 9:3316. doi: 10.3389/fmicb.2018.03316

Liu, J., Yao, Q., Li, Y., Zhang, W., Mi, G., Chen, X., et al. (2019). Continuous cropping of soybean alters the bulk and rhizospheric soil fungal communities in a Mollisol of Northeast PR China. *Land Degrad. Dev.* 30, 1725–1738. doi: 10.1002/ldr.3378

Liu, X., Li, Y., Han, B., Zhang, Q., Zhou, K., Zhang, X., et al. (2012). Yield response of continuous soybean to one-season crop disturbance in a previous continuous soybean field in Northeast China. *Field Crops Res.* 138, 52–56. doi: 10.1016/j.fcr.2012.09.012

Liu, X., Zhang, J., Gu, T., Zhang, W., Shen, Q., Yin, S., et al. (2014a). Microbial community diversities and taxa abundances in soils along a seven-year gradient of potato monoculture using high throughput pyrosequencing approach. *PLoS One* 9:e86610. doi: 10.1371/journal.pone.0086610

Liu, J., Sui, Y., Yu, Z., Shi, Y., Chu, H., Jin, J., et al. (2014b). High throughput sequencing analysis of biogeographical distribution of bacterial communities in the black soils of Northeast China. *Soil Biol. Biochem.* 70, 113–122. doi: 10.1016/j.soilbio.2013.12.014

Liu, Y. R., Zheng, Y. M., Shen, J. P., Zhang, L. M., and He, J. Z. (2010). Effects of mercury on the activity and community composition of soil ammonia oxidizers. *Environ. Sci. Pollut. Res.* 17, 1237–1244. doi: 10.1007/s11356-010-0302-6

Liu, Z., Liu, J., Yu, Z., Yao, Q., Li, Y., Liang, A., et al. (2020). Long-term continuous cropping of soybean is comparable to crop rotation in mediating microbial abundance, diversity and community composition. *Soil Tillage Res.* 197:104503. doi: 10.1016/j.still.2019.104503

Logrieco, A., Moretti, A., and Solfrizzo, M. (2009). *Alternaria* toxins and plant diseases: an overview of origin, occurrence and risks. *World Mycotoxin J.* 2, 129–140. doi: 10.3920/wmj2009.1145

Lu, J., Li, W., Yang, Y., Ye, F., Lu, H., Chen, X., et al. (2022). The impact of different rotation regime on the soil bacterial and fungal communities in an intensively managed agricultural region. *Arch. Microbiol.* 204:142. doi: 10.1007/s00203-021-02615-w

Luo, S., Yu, L., Liu, Y., Zhang, Y., Yang, W., Li, Z., et al. (2016). Effects of reduced nitrogen input on productivity and N_2O emissions in a sugarcane/soybean intercropping system. *Eur. J. Agron.* 81, 78–85. doi: 10.1016/j.eja.2016.09.002

Malekani, K., and Cresser, M. S. (1998). Comparison of three methods for determining boron in soils, plants, and water samples. *Commun. Soil Sci. Plant Anal.* 29, 285–304. doi: 10.1080/00103629809369946

Meriles, J. M., Vargas Gil, S., Conforto, C., Figoni, G., Lovera, E., March, G. J., et al. (2009). Soil microbial communities under different soybean cropping systems: characterization of microbial population dynamics, soil microbial activity, microbial biomass, and fatty acid profiles. *Soil Tillage Res.* 103, 271–281. doi: 10.1016/j.still.2008.10.008

Mwaheb, M. A. M. A., Hussain, M., Tian, J., Zhang, X., Hamid, M. I., El-Kassim, N. A., et al. (2017). Synergetic suppression of soybean cyst nematodes by chitosan and *Hirsutella minnesotensis* via the assembly of the soybean rhizosphere microbial communities. *Biol. Control* 115, 85–94. doi: 10.1016/j.biocontrol.2017.09.011

Nguyen, N. H., Song, Z., Bates, S. T., Branco, S., Tedersoo, L., Menke, J., et al. (2016). FUNGuild: an open annotation tool for parsing fungal community datasets by ecological guild. *Fungal Ecol.* 20, 241–248. doi: 10.1016/j.funeco.2015.06.006

Ofek-Lalzar, M., Sela, N., Goldman-Voronov, M., Green, S. J., Hadar, Y., and Minz, D. (2017). Niche and host-associated functional signatures of the root surface microbiome. *Nat. Commun.* 5:4950. doi: 10.1038/ncomms5950

Pan, F., Xue, A. G., McLaughlin, N. B., Li, S., Xu, Y., Zhao, D., et al. (2013). Colonization of *Clonostachys rosea* on soybean root grown in media inoculated with *Fusarium graminearum*. *Acta Agric. Scand. B Soil Plant Sci.* 63, 564–569. doi: 10.1080/09064710.2013.816768

Pang, G., Cai, F., Li, R., Zhao, Z., Li, R., Gu, X., et al. (2017). Trichoderma-enriched organic fertilizer can mitigate microbiome degeneration of monocropped soil to maintain better plant growth. *Plant Soil* 416, 181–192. doi: 10.1007/s11104-017-3178-0

Peralta, A., Sun, Y., McDanie, l M, and Lennon, J. (2018). Crop rotational diversity increases disease suppressive capacity of soil microbiomes. *Ecosphere* 9:e2235. doi: 10.1002/ecs2.2235

Pérez-Brandán, C., Huidobro, J., Grümberg, B., Scandiani, M. M., Luque, A. G., Meriles, J. M., et al. (2014). Soybean fungal soil-borne diseases: a parameter for measuring the effect of agricultural intensification on soil health. *Can. J. Microbiol.* 60, 73–84. doi: 10.1139/cjm-2013-0792

Petersen, G. W., and Corey, R. B. (1966). A modified Chang and Jackson procedure for routine fractionation of inorganic soil phosphates. *Soil Sci. Soc. Am. J.* 30, 563–565. doi: 10.2136/sssaj1966.03615995003000050012x

Pii, Y., Mimmo, T., Tomasi, N., Terzano, R., Cesco, S., and Crecchio, C. (2015). Microbial interactions in the rhizosphere: beneficial influences of plant growth-promoting rhizobacteria on nutrient acquisition process. A review. *Biol. Fertil. Soils* 51, 403–415. doi: 10.1007/s00374-015-0996-1

Pilon, M., Cohu, C. M., Ravet, K., Abdel-Ghany, S. E., and Gaymard, F. (2009). Essential transition metal homeostasis in plants. *Curr. Opinion Plant Biol.* 12, 347–357. doi: 10.1016/j.pbi.2009.04.011

R Development Core Team. (2010). *A Language and Environment for Statistical Computing*. Vienna: R Foundation for Statistical Computing.

Samouel, S., Iacovides, T., Evangelides, S., and Kanetis, L. (2016). First report of *Boeremia exigua* var. exigua causing stem rot of *Origanum dubium* in Cyprus. *Plant Dis.* 100:529. doi: 10.1094/pdis-07-15-0808-pdn

Saravanakumar, D., Lavanya, N., Muthumeena, K., Raguchander, T., and Samiyappan, R. (2009). *Fluorescent pseudomonad* mixtures mediate disease resistance in rice plants against sheath rot (*Sarocladium oryzae*) disease. *BioControl* 54, 273–286. doi: 10.1007/s10526-008-9166-9

Saxena, J., Choudhary, S., Pareek, S., Choudhary, A. K., and Iquebal, M. A. (2015). Recycling of organic waste through four different composts for disease suppression and growth enhancement in mung beans. *Clean Soil Air Water* 43, 1066–1071.

Segata, N., Izard, J., Waldron, L., Gevers, D., Miropolsky, L., Garrett, W. S., et al. (2011). Metagenomic biomarker discovery and explanation. *Genome Biol.* 12:R60. doi: 10.1186/gb-2011-12-6-r60

Shen, Z., Penton, C. R., Lv, N., Xue, C., Yuan, X., Ruan, Y., et al. (2018). Banana *Fusarium wilt* disease incidence is influenced by shifts of soil microbial communities under different monoculture spans. *Microb. Ecol.* 75, 739–750. doi: 10.1007/s00248-017-1052-5

Smith, R. G., Gross, K. L., and Robertson, G. P. (2008). Effects of crop diversity on agroecosystem function: crop yield response. *Ecosystems* 11, 355–366. doi: 10.1007/s10021-008-9124-5

Soil Survey Staff. (2014). *Keyto Soil Taxonomy*. Washington, DC: United States Department of Agriculture (USDA).

Song, X., Tao, B., Guo, J., Li, J., and Chen, G. (2018). Changes in the Microbial Community Structure and Soil Chemical Properties of Vertisols Under Different Cropping Systems in Northern China. *Front.Environ.Sci.* 6:132. doi: 10.3389/fenvs.2018.00132

Sun, R. B., Dsouza, M., Gilbert, J. A., Guo, X. S., Wang, D. Z., et al. (2016). Fungal community composition in soils subjected to longterm chemical fertilization is most influenced by the type of organic matter. *Environ.Microbiol.* 18, 5137–5150. doi: 10.1111/1462-2920.13512

Walkley, A., and Black, I. A. (1934). An examination of the degtjareff method for determining soil organic matter, and a proposed modification of the chromic acid titration method. *Soil Sci.* 37, 29–38. doi: 10.1097/00010694-193401000-00003

Wang, J., Li, X., Zhang, J., Yao, T., Wei, D., Wang, Y., et al. (2013). Effect of root exudates on beneficial microorganisms—evidence from a continuous soybean monoculture. *Plant Ecol.* 213, 1883–1892. doi: 10.1007/s11258-012-0088-3

Wright, P., Falloon, R., and Hedderley, D. (2015). Diferent vegetable crop rotations afect soil microbial communities and soilborne diseases of potato and onion: literature review and a long-term feld evaluation. *N.Z.J. Crop Hort* 43, 85–110. 01140671.2014.979839 doi: 10.1080/

Wu, L., Chen, J., Wu, H., Wang, J., Wu, Y., Lin, S., et al. (2016). Effects of consecutive monoculture of *Pseudostellaria heterophylla* on soil fungal community as determined by pyrosequencing. *Sci. Rep.* 6:26601. doi: 10.1038/srep26601

Wu, L., Wang, J., Huang, W., Wu, H., Chen, J., Yang, Y., et al. (2015). Plant-microbe rhizosphere interactions mediated by *Rehmannia glutinosa* root exudates under consecutive monoculture. *Sci. Rep.* 5:15871. doi: 10.1038/srep15871

Xiang, X., Liu, J., Zhang, J., Li, D., and Kuzyakov, Y. (2020). Divergence in fungal abundance and community structure between soils under long-term mineral and organic fertilization. *Soil Tillage Res.* 196:104491.

Xiong, W., Zhao, Q., Xue, C., Xun, W., Zhao, J., Wu, H., et al. (2016). Comparison of fungal community in black pepper-vanilla and vanilla monoculture systems associated with vanilla *Fusarium wilt* disease. *Front. Microbiol.* 7:117. doi: 10.3389/fmicb.2016.00117

Xu, L., Ravnskov, S., Larsen, J., and Nicolaisen, M. (2012). Linking fungal communities in roots, rhizosphere, and soil to the health status of *Pisum sativum*. *FEMS Microbiol. Ecol.* 82, 736–745. doi: 10.1111/j.1574-6941.2012.01445.x

Yan, M. C., Xu, T. T., Song, P. H., and Dai, J. J. (2012). Effects of different cropping patterns of soybean and maize seedlings on soil enzyme activities and MBC and MBN. *J. Northeast Agric. Univ.* 19, 42–47. doi: 10.1016/s1006-8104(13)60049-5

Yao, Q., Xu, Y., Liu, X., Liu, J., Huang, X., Yang, W., et al. (2019). Dynamics of soil properties and fungal community structure in continuous-cropped alfalfa fields in northeast China. *PeerJ.* 7:e7127. doi: 10.7717/peerj.7127

Yu, G. B., Wu, F. Z., and Zhou, X. (2011). Effects of rotations of cucumber with wheat and hairy vetch on soil micro-ecological environment and its yield. *J. Soil* 48, 175–184.

Zhou, X., Wang, Z., Jia, H., Li, L., and Wu, F. (2018). Continuously monocropped Jerusalem artichoke changed soil bacterial community composition and ammonia-oxidizing and denitrifying bacteria abundances. *Front. Microbiol.* 9:705. doi: 10.3389/fmicb.2018.00705

Conflict of Interest: The authors declare that the research was conducted in the absence of any commercial or financial relationships that could be construed as a potential conflict of interest.

Publisher's Note: All claims expressed in this article are solely those of the authors and do not necessarily represent those of their affiliated organizations, or those of the publisher, the editors and the reviewers. Any product that may be evaluated in this article, or claim that may be made by its manufacturer, is not guaranteed or endorsed by the publisher.

frontiers | Frontiers in Plant Science

ORIGINAL RESEARCH
published: 07 July 2022
doi: 10.3389/fpls.2022.927253

A Novel Transcriptional Regulator HbERF6 Regulates the HbCIPK2-Coordinated Pathway Conferring Salt Tolerance in Halophytic *Hordeum brevisubulatum*

*Ying Jiang[1,2], Haiwen Zhang[1,2], Yang Li[1,3], Congcong Chang[1,3], Yunxiao Wang[1,3], Hao Feng[1,2] and Ruifen Li[1,2]**

[1] Agro-Biotechnology Research Institute, Beijing Academy of Agriculture and Forestry Sciences, Beijing, China, [2] Beijing Key Laboratory of Agricultural Genetic Resources and Biotechnology, Beijing, China, [3] College of Life Science, Hebei Normal University, Shijiazhuang, China

Halophytic *Hordeum brevisubulatum* is a perennial grass which has evolved many distinctive salt-adaptive mechanisms. Our previous studies indicated it could thrive under salt stress through maintaining better K^+ and Na^+ homeostasis. Stress-responsive HbCIPK2 can phosphorylate K^+ channel HbVGKC1 and Na^+ transporter HbSOS1L to prevent Na^+ accumulation and K^+ reduction, hence pathway was not detected in glycophytic plants. In this study, we cloned the inducible promoter of *HbCIPK2* by genome-walking, and identified a novel transcriptional regulator HbERF6 through yeast one-hybrid screening. HbERF6 functioned as a transcription factor which can bind to the GCC-box of the *HbCIPK2* promoter to activate its expression. *HbERF6* transgenic lines in *Arabidopsis* improved salt tolerance compared with wild type, and especially induced *AtCIPK24* (*SOS2*) expression, resulting in K^+/Na^+ homeostasis to enhance salt tolerance. All the results confirmed the inducible function of HbERF6 for CIPK genes during salt tolerance. This regulatory network that integrates transcriptional regulation and post-translation modification will unravel a novel salt stress-responsive mechanism, highlighting the value and utilization of the halophytic resource.

Keywords: ***Hordeum brevisubulatum*, salt tolerance, transcription factor, CIPK, halophyte**

OPEN ACCESS

Edited by:
Jin-Lin Zhang,
Lanzhou University, China

Reviewed by:
Liu-Qiang Wang,
Chinese Academy of Forestry, China
Agata Cieśla,
Adam Mickiewicz University, Poland

***Correspondence:**
Ruifen Li
liruifen@aliyun.com

Specialty section:
This article was submitted to Plant Abiotic Stress, a section of the journal Frontiers in Plant Science

Received: *24 April 2022*
Accepted: *30 May 2022*
Published: *07 July 2022*

Citation:
Jiang Y, Zhang H, Li Y, Chang C, Wang Y, Feng H and Li R (2022) A Novel Transcriptional Regulator HbERF6 Regulates the HbCIPK2-Coordinated Pathway Conferring Salt Tolerance in Halophytic Hordeum brevisubulatum. Front. Plant Sci. 13:927253. doi: 10.3389/fpls.2022.927253

INTRODUCTION

Soil salinization is a key environmental factor that adversely affects plant growth and crop productivity (Flowers and Yeo, 1995; Tester and Davenport, 2003). Better understanding of the plant salt tolerance mechanism benefits crop genetic improvement (Mansour et al., 2021). To adapt salt stress, plants develop a large number of physiological, biochemical, and molecular strategies to respond and defend to stress (Chen et al., 2018; Van Zelm et al., 2020). Till present, plenty of studies indicate that many genes are involved in salt stress response (Negrao et al., 2017). From salt sensing to signal transduction and downstream gene response, plants have evolved complex and hierarchical gene regulatory networks (Golldack et al., 2011). Each gene plays a crucial role in these regulatory networks, especially stress-responsive transcription factor networks in plants are attracting more and more attention (Song et al., 2016; Li et al., 2019).

Under stress, the concentration of Ca^{2+} in plant cytoplasm will change specifically with time and space. Calcineurin B-like protein (CBL) is a family of small proteins that can bind Ca^{2+} in plants. CBL and its target protein CBL-interacting protein kinase (CIPK) constitute the CBL-CIPK signal network system and play an important role in multiple abiotic and biotic stresses, such as drought, salt, low temperature, abscisic acid (ABA), nutrient deficiency, and pathogens. CBL-CIPK complexes control membrane transport through phosphorylating transporters and channels in the plasma membrane and tonoplast (Tang et al., 2020). The plasma membrane-localized AtCBL1/AtCBL9-AtCIPK23 complexes exhibit a synergistic effect of potassium and nitrogen nutrition in plants (Verma et al., 2021). AtCBL1/AtCBL9-AtCIPK23 modules phosphorylate the voltage-gated K^+ channel AtAKT1 and promote plant K^+ absorption under low-K^+ condition. The same CBL-CIPK complexes regulate NO_3^- and NH_4^+ uptake separately controlled by AtNRT1.1, a transporter for NO_3^-, and an AMT1-type transporter. AtCIPK3, apple MdCIPK22, TaCIPK27, and so on regulate ABA response (Ma et al., 2017; Sanyal et al., 2017; Wang et al., 2018). AtCIPK26 and SlCIPK6 mediate ROS signaling pathways (Han et al., 2019; Ma et al., 2020). Although CIPKs of model plants and crops have been demonstrated to function in various stress responses, exact functions of other CIPKs in *Hordeum* lack more evidence, in addition to HbCIPK2 contributing to salt tolerance in wild barley (*Hordeum brevisubulatum*) (Li et al., 2012).

Salt response in higher plants occurs in two phases as follows: in the first phase, it responds to higher osmotic potential within an hour, while the second phase occurs mainly due to toxicity of sodium ions from long-term treatment of high salinity (Seifikalhor et al., 2019; Wu et al., 2021). Sodium ions impair potassium uptake and transport, thereby maintaining K^+/Na^+ homeostasis which is one of the elementary mechanisms for plants (Almeida et al., 2017; Zhang et al., 2020a). More obviously, K^+ or Na^+ balance is mainly controlled by respective transporters, whose activities are regulated by CBL-CIPK module-mediated pathways such as classical SOS and CBL-interacting protein kinase 23 (CIPK23) pathways (Qiu et al., 2002; Xu et al., 2006). CIPKs have been confirmed to be the hubs in many pathways and play important roles in plant stress regulatory networks (Ma et al., 2020; Tang et al., 2020). Moreover, some CIPK-encoding genes are responsive to various stresses, and their regulations in the transcriptional level still remain limited.

Transcription factors play a central role in plant response to different stresses, through binding to *cis*-acting elements in the promoters of target genes, or interacting with other transcription factors, which subsequently regulate gene expression (Singh et al., 2002; Wu et al., 2007). The ethylene responsive factor (ERF) is one of the unique transcription factor families, which features the conserved AP2/ERF domain in plants (Rehman and Mahmood, 2015; Xie et al., 2019). The ERFs function in plant stress response and the development process (Licausi et al., 2013; Feng et al., 2020). Previous reports have shown that several ERFs can be phosphorylated by MAPK cascade (Jung et al., 2010; Kishi-Kaboshi et al., 2010). However, it still remains unclear that the ERF transcriptional factor modulates the stress-responsive *CIPK* gene.

Hordeum brevisubulatum is a perennial halophyte in *Triticeae* referring to wild barley. It can grow well in saline-alkaline grassland in northern China as forage grass, and has evolved the salt tolerance mechanism during long-term adaption. Moreover, it is also wildly relative to cultivated barley and wheat, and therefore this wild species is a good resource for crop improvement of stress tolerance (Zhang et al., 2020b). However, less is known about its stress-responsive transcription factor networks. Our previous study indicated that this wild barley maintained K^+/Na^+ balance under salt stress, and stress-responsive HbCIPK2 conferred salt tolerance by preventing Na^+ accumulation and K^+ reduction (Li et al., 2012). Interestingly, a novel coordinated network was verified to link sodium and potassium regulatory pathways for HbCIPK2 as a hub (Zhang et al., 2020a).

In this study, we identified a novel transcriptional regulator of *HbCIPK2* and *HbERF6*, from wild barley through yeast one-hybrid (Y1H) library screening, confirming that HbERF6 can bind to the *cis*-regulatory element of the *HbCIPK2* promoter and activate the expression of *HbCIPK2*. Overexpression of *HbERF6* in *Arabidopsis* can improve the salt tolerance of the transgenic plants. Taken together, we discovered a positive upstream modulator of the *HbCIPK2*-mediated salt responsive network, playing an important role in salt stress.

MATERIALS AND METHODS

Plant Growth Conditions

For *H. brevisubulatum* seedling growth, the procedures were adopted as described previously (Li et al., 2012). Wild-type (WT) and transgenic *Arabidopsis* plants were grown in a greenhouse (21–23°C, 16-h light/8-h dark with 60% relative humidity). For stress treatment, the 4-day-old seedlings grown on Murashige and Skoog media containing 0.5% sucrose and 0.8% agar (pH 5.7) were transferred to MS agar plates with 100 or 125 mM NaCl for another 8 days.

HbCIPK2 Promoter Cloning

The plant genomic DNA of *H. brevisubulatum* was extracted by the CTAB method, and the promoter of *HbCIPK2* was cloned by using the genome-walking kit (Takara). First, two reverse primers, SP1 and SP2, were designed according to the sequence of *HbCIPK2* CDS cloned in our laboratory. According to the operation instructions of the Takara kit, four kinds of restriction enzyme libraries were established with the wild barley genome as the template. The first phase of PCR amplification was performed with the non-specific primer AP1 provided by the kit and specific primer SP1. The second phase of nested amplification was performed with the first phase of PCR products as the template, and AP2 and SP2 as primers. After electrophoresis, the target bands were recovered and connected to the pEASY-Blunt cloning vector (TransGen Biotech) for sequencing. The basic *cis*-elements in the *HbCIPK2* promoter were analyzed using PlantCARE and PLACE online tools.

Yeast One-Hybrid Library Screening

Total RNA was extracted from the shoots and roots of *H. brevisubulatum* seedlings, and subjected to 24 h salt-stress treatment (350 mM NaCl), using the TIANGEN RNA simple total RNA extraction kit. Y1H cDNA library was constructed using the Matchmaker™ Gold Yeast One-Hybrid System (Takara). The *HbCIPK2* promoter was ligated with the bait vector (pAbAi-pHbCIPK2). The bait vector was transferred into the yeast strain Y1HGold to prepare the competent cells, and the minimum inhibitory concentration of Aureobasidin A (AbA) was determined. The library plasmids were transferred into the bait strain which was cultured upside down at 30°C on SD/-Ura-Leu + AbA (300 mg/L) plates at 30°C for 3–5 days. A total of 126 positive yeast colonies were identified by PCR amplification with both T7 forward and AD reverse primers, respectively. After sequencing, the selected insert was amplified and cloned into the prey vector. The prey vector and the pAbAi-pHbCIPK2 vector were co-transformed into the yeast strain Y1HGold, and their growth was observed for further analysis. The full-length cDNA sequence of *HbERF6* was obtained from the positive prey vector mentioned above. Alignment of multiple sequences of the ERF family from different species was analyzed using the DNAMAN software, and the phylogenetic tree was constructed by the neighbor-joining method with the MEGA 7.0 software. The primers applied in this part are listed in **Supplementary Table 3**.

The interaction between the HbERF6 protein and *HbCIPK2* promoter was measured using the pairwise Y1H assay. The two GCC-boxes (box-1, −1086 to −1080; box-2, −232 to −226) of the *HbCIPK2* promoter were separately introduced into the pLacZi vector. The CDS sequence of the *HbERF6* gene was cloned and then inserted to the pB42AD vector. The two vectors of pB42AD-HbERF6 and pLacZi-GCC-box1/2 were co-transformed into yeast cells Y1HGold. The transformed yeast cells were grown on selective medium lacking Leu and Trp with X-gal at 30°C for 2–4 days. The primers applied in this part are listed in **Supplementary Table 3**.

Quantitative Reverse Transcription PCR Analysis

The TRIzol reagent (Takara) was used to extract total RNA from the plant roots or shoots referring to Zhang's paper (Zhang et al., 2020c). The purity (peak shape) and concentration of RNA were detected by using a spectrophotometer (NanoDrop™ 2000c). The sample cDNA was synthesized with the HiScript® II Q Select RT SuperMix reagent Kit (Vazyme). The sample cDNA was diluted five times for real-time PCR (Bio-Rad, United States) with a SYBR mixture system (Vazyme). The gene expression analysis was performed using three biological and three technical replicates. The primers applied in this part are listed in **Supplementary Table 3**.

The effects of salt stress on plants include ion toxicity and osmotic stress. We selected five salt-stress-responsive genes that are related to osmotic adjustment and ion homeostasis, such as *AtCIPK24* (*At5G35410*), *AtCIPK2* (*At5G07070*), *AtCBL4* (*At5G24270*), *AtKIN2* (*At2G02800*), and *AtNHX1* (*At5G27150*). The ROS scavenging and salt-related enzyme-coding genes include *AtPOD* (*At3G49120*), *AtCAT1* (*At1G20630*), *AtP5CS* (*At3G55610*), and *AtADH* (*At1G77120*). In addition, we selected *AtCOR47* (*AT1G20440*) that accumulates in response to osmotic stress and two genes of *AtRD29B* (*At5G52300*) and *AtLEA3* (*At1G02820*) contributing to high salt response, respectively. The seedlings were grown on MS agar plates for 11 days, and then transferred to MS medium containing 100 mM NaCl for 10 days.

Subcellular Localization

The *CaMV35:HbERF6-GFP* plasmid was constructed by amplifying the *HbERF6* CDS and ligating the sequence into the *Bam*HI and *Sal*I sites of the pCAMBIA1307 vector. After sequencing confirmation, *HbERF6-GFP* and *AtCBF1-RFP* (positive control) plasmids were co-transformed into the onion (*Allium cepa*) by micro-particle bombardments or barley protoplast by PEG-mediated transformation, and the plasmid containing only the *GFP* gene was also transformed as the negative control. After 24 h of dark culture at 25°C, the green fluorescent protein (GFP), red fluorescent protein (RFP), and DAPI fluorescence signals were observed using a laser confocal fluorescence microscope. The primers applied in this part are listed in **Supplementary Table 3**.

GUS Stain Analysis

The promoter with a length of 1750 bp and the *GUS* gene was constructed into the pCAMBIA1381 vector, and then transformed into the WT *Arabidopsis* plants by the *Agrobacterium*-mediated floral-dip method. Notably, three T2 transgenic lines were selected, and five plants of each transgenic line were used for GUS staining and the process was repeated for three times. The 18-day-old transgenic *Arabidopsis* seedlings were grown on MS medium at 22°C and treated for 2 days with NaCl (100 mM), PEG (10%), and ABA (20 μM). The treated and untreated (control) seedlings were soaked in the GUS staining solution at 37°C in dark for overnight. The primers applied in this part are listed in **Supplementary Table 3**.

The *HbERF6* promoter (∼2 kb) was cloned using genome-walking mentioned above, and the vector pCAMBIA1381 with *pHbERF6:GUS* was constructed and introduced into *Agrobacterium tumefaciens* strain competent cells (GV3101). The genetic transformation of WT *Arabidopsis thaliana* was carried out through the floral dipping method. T2 transgenic lines were selected, and the 18-day-old transgenic *Arabidopsis* seedlings were grown on MS medium at 22°C and treated for 1 day with NaCl (100 mM). Then, the seedlings were immersed in GUS staining buffer, bleached with ethanol to remove the chlorophyll, and then photographed with a digital camera.

In vivo Imaging and Firefly Luciferase Transient Assay

The promoter of *HbCIPK2* (up to ATG 1750 bp) was inserted to a *LUC* gene expression vector. The coding region of *HbERF6* was amplified and introduced into the pCAMBIA1307 vector as an effector plasmid. The reporter vector of *pHbCIPK2:LUC* and effector vector containing *HbERF6* gene were separately transformed into GV3101, and then the leaves of *Nicotiana*

benthamiana were co-infiltrated. On the third day, after infection, each back blade was dropped in 300 μl of D-luciferin (Promega) with a final concentration of 1 mM, applied evenly, and then placed in dark for 2 min. The treated leaves were scanned and photographed with the plant living imaging system (Night SHADE LV 985), and the promoter activity was compared according to the fluorescence intensity. The primers applied in this part are listed in **Supplementary Table 3**.

Purification of HbERF6 and Electrophoretic Mobility Shift Assays

The *HbERF6* coding fragment was amplified by PCR and inserted into a pET30a expression vector. The sequenced positive clones were used to transform BL21 (DE3) competent cells. The protein expression was examined by adding 0.5 mM isopropyl β-D-1-thiogalactopyranoside (IPTG) in transformed cells followed by incubation at 16°C for 20 h. Ni^{2+}-NTA affinity columns (Cat R901-15, Invitrogen) were used to purify protein.

The GCC-box sequence in the *HbCIPK2* promoter was labeled by biotin at the 3′ end. The LightShift Chemiluminescent EMSA Kit (Thermo Fisher) was used to perform electrophoretic mobility shift assays (EMSAs). To each 20 μl reaction system containing 2 μl of 10× Binding buffer, 1 μl poly (dI.dC), and 2 μl biotin-labeled target DNA, 4 μg purified protein was added to the sample buffer at room temperature after 20 min of reaction. The protein-probe complex was all sampled, separated at 100 V for 40 min, and then transferred to the nylon membrane (380 mA, 40 min). The membrane was cross-linked under ultraviolet (120 mJ/cm^2, 60 s) and then incubated with HRP labeled streptavidin. Finally, the images were exposed using the chemiluminescence imaging system.

Dual-Luciferase Transient Assay

The *HbCIPK2* promoter sequence was inserted upstream of firefly luciferase (LUC) of the pGreenII 0800-LUC vector as a reporter gene. The CDS sequence of *HbERF6* was recombined into the pGreenII 62-SK vector as an effector gene. The negative control was an empty pGreenII 62-SK vector. *Agrobacterium* strain GV3101 carrying the reporter vector together with the effector vector strain was mixed with 1:1 suspension buffer and injected into the back of *N. benthamiana* leaves. The *N. benthamiana* plants were placed in a constant temperature incubator for 3 days. The firefly luciferase (LUC) and Renilla luciferase (REN) activities were measured using a chemiluminescence detector (Promega). Transcriptional regulation activity of HbERF6 on the *HbCIPK2* promoter was calculated using the LUC/REN ratio and normalized to the negative control.

Genetic Transformation and Stress Treatment of *Arabidopsis thaliana*

Agrobacterium strain GV3101 with the *CaMV35:HbERF6* construct was used to infect *A. thaliana* (Ecotype Colombia-0) using the floral-dip method. Notably, three lines (L6, L7, and L13) of *Arabidopsis* T3 transgenic plants were selected to assess salt tolerance. For identification of salt stress tolerance in the transgenic seedlings, the seedlings cultured on MS medium for 4 days were transferred to MS medium supplemented with 100 and 125 mM NaCl for another 8 days. Then, the fresh weight and root length of the seedlings were measured and analyzed. Transgenic lines and WT were seeded in soil to observe salt stress tolerance. When the seedlings were grown at the 6th leaf stage, they were treated with 350 mM NaCl solution once in every 7 days for two times. After normal watering and culturing for 14 days, the survival rates of plants were investigated and photographed.

Sodium and Potassium Ion Content Measurements

The 11-day-old seedlings grown on MS medium were transferred to MS medium plates containing l00 mM NaCl for 10 days. The plants were digested by acid solution and the concentrations of K^+ and Na^+ were analyzed using an inductively coupled plasma atomic emission spectrometer (ICP-AES) according to the methods in the previous study (Li et al., 2012).

Determination of Total Chlorophyll Content

Fresh plant leaves (approximately 0.1 g) were fully ground under dark or low light conditions. According to the description of the plant chlorophyll content detection kit (Solarbio, BC0990), the extract solution (100% ethanol:acetone = 1:2) was added to the grated tissue and reacted for about 3 h, until the color of the tissue residue was close to white. The absorbance was measured with an ultraviolet spectrophotometer (UV-1800PC) at the wavelengths of 645 and 663 nm, respectively. The total chlorophyll content was calculated referring to the kit method.

Data Processing and Analysis

The abovementioned procedures were repeated at least three times. We used the SigmaPlot software for statistical data processing. The data were statistically analyzed using one-way ANOVA ($^*P < 0.05$, $^{**}P < 0.01$, $^{***}P < 0.001$). The results are expressed as mean ± SD.

RESULTS

Discovery and Analysis of the *HbCIPK2* Promoter

Previously, we reported *HbCIPK2* from halophytic *H. brevisubulatum* conferred salt tolerance which was inducible by abiotic stress, which indicates that *HbCIPK2* may be regulated by one type of transcriptional factor. However, the genome-wide sequences of *H. brevisubulatum* are unknown, until then we had to apply the genome-walking procedure to clone the promoter sequence of *HbCIPK2*. Finally, the fragment with a length of 1750 bp was obtained and identified as the target sequence. There are two GCC-box elements (AGCCGCC) at positions −1086 to −1080 and −232 to −226 in the *HbCIPK2* promoter sequence, respectively. A large number of basic *cis*-elements such as CAAT and TATA boxes were found in the promoter using the PlantCARE and PLACE online tools (**Supplementary Table 1**).

In addition, the promoter of *HbCIPK2* also contains several *cis*-acting elements related to abiotic stress, such as salt response element, hormone response element, and dehydration response element (**Figure 1A**). The promoter sequence further suggested that *HbCIPK2* might respond to abiotic stress, and it will provide the possibility for the discovery of the *HbCIPK2* regulatory factor.

To analyze the activity of the *HbCIPK2* promoter, the fusion expression vector of *pHbCIPK2:GUS* was constructed. The transgenic plants were screened for T2 generation and subjected to different stress treatments. GUS staining was almost not observed without treatment, but increased after 10% PEG or 20 μM ABA stress treatment. The transgenic seedlings exhibited maximum GUS staining after 100 mM NaCl treatment (**Figure 1B**). These results showed that the *HbCIPK2* promoter has inducible activities under drought, ABA, and salt stress.

Identification of the Transcription Factor *HbERF6* Through Yeast One-Hybrid Screening

To screen the regulatory factor for *HbCIPK2*, we used the Y1H system and the strategy of the full-length promoter due to uncertain *cis*-element. The 1750 bp promoter of *HbCIPK2* was used as bait to screen the cDNA library from the plants subjected to salt stress (**Figure 1A**). Interestingly, among 126 colonies growing and conferring resistance to higher AbA (**Supplementary Figure 1A**), after PCR amplification, 65 positive yeast colonies with longer than 800-bp fragments were selected to sequence. After sequencing and blast analysis, two prey clones were confirmed to be the homologous gene of transcription factor *ERF6*, which was named as HbERF6. The prey plasmid with *HbERF6* and the bait plasmid with the promoter of *HbCIPK2* were co-transformed into the yeast Y1HGold strain that could grow on the SD/-leu-ura medium containing AbA (**Figure 2A**). This indicated that HbERF6 might be a regulatory factor of the *HbCIPK2* gene.

HbERF6 (GenBank No. MZ935744) contains a 1029 bp intact open reading frame, encoding a polypeptide with 343 amino acids residues. The deduced N-terminus of HbERF6 contains some acidic amino acids as an activation domain, and the C-terminus enriches arginine (R) and lysine (L), showing a nuclear localization signal (**Supplementary Figure 1B**). The HbERF6 protein contains only one conserved AP2/ERF domain as a key element binding to the target DNA, and the 14th and 19th amino acids of which are alanine (A) and aspartic acid (D), respectively, suggesting that it belongs to the ERF family (**Supplementary Figures 1B,D**). The tertiary structure of the HbERF6 AP2/ERF domain (151-213aa) was predicted by online software SWISSMODEL. The AP2/ERF domain contains three β-sheets (β-1-β-3) in the N-terminal and 1 α-helix (α) in the C-terminal (**Supplementary Figure 1C**). The β-3 sheet and α-helix constitute a conserved RAYD element. β-1 and β-2 form a YRG element rich in hydrophilic amino acids (**Supplementary Figure 1E**). The sequenced PCR results using the genomic DNA as the template showed that the *HbERF6* gene has no intron. The analysis of the phylogenetic tree indicated that the HbERF6 protein shows higher homology with HvERF5 (GenBank No. ANA52685), AtERF5 (AT5G47230), ZmERF5 (GenBank No. PWZ220596.1), and OsERF5 (GenBank No. XP015624058), respectively (**Supplementary Figure 1E**).

HbERF6 Can Activate *HbCIPK2*

To identify the regulated function of HbERF6, first, we identified the subcellular localization of HbERF6. The expression vector of HbERF6 fused with GFP was constructed, and the marker protein AtCBF1 fused with RFP acted as a positive control. The construct of *HbERF6-GFP* derived by the *CaMV35* promoter was bombarded into onion epidermal cells. By using confocal microscopy, HbERF6-GFP fusion protein in cells was predominantly co-located at the nucleus, and coincided with marker protein AtCBF1 and DAPI staining (**Figure 2B**), as GFP protein without fusion HbERF6 expressed in the whole cells (**Supplementary Figure 2**).

We next performed a firefly luciferase (LUC) imaging assay to demonstrate that HbERF6 activated the expression of *HbCIPK2 in vivo*. Constructs harboring *LUC* under the control of the *HbCIPK2* promoter and *CaMV35:HbERF6* were co-infiltrated into *N. benthamiana* leaves to transiently detect the LUC activity. We can detect the strong LUC activity in *N. benthamiana* leaves, but no LUC activity was observed in the negative control (**Figure 2C**). Furthermore, we used the effector-reporter system to analyze the LUC transcriptional activity (**Figure 2D**). The LUC activity driven by the promoter of *HbCIPK2* was obviously upregulated in transiently overexpressing *HbERF6 N. benthamiana* leaves, indicating that HbERF6 interacted with the promoter of *HbCIPK2* and positively regulated the expression level of *HbCIPK2* (**Figure 2E**). These results showed that *HbCIPK2* is the downstream target of *HbERF6*.

HbERF6 Binds to the GCC *Cis*-Element

To confirm the binding sites of HbERF6 to the promoter of *HbCIPK2*, we analyzed the sequence of the promoter, and found two GCC-boxes (*pHbCIPK2*GCC-box-1, −2) within 1750 bp before the ATG start codon. The GCC-boxes (sequence: AGCCGCC) were located at positions −230 and −1086, respectively (**Figure 1A**). The two 16-bp repeat fragments of the *HbCIPK2* promoter containing the GCC-box were transformed into yeast cells, respectively, accompanying by *HbERF6*. The result showed that HbERF6 could bind to the GCC-box of the *HbCIPK2* promoter using the Y1H system (**Figure 3A**). Furthermore, we designed two pairs of probes targeting each one of the GCC-boxes according to the 16 bp sequence of Y1H assays. We carried out EMSA experiments to examine the interaction between HbERF6 and the *HbCIPK2* promoter. The recombinant protein His-HbERF6 directly could bind both of the GCC-boxes of *HbCIPK2* promoter *in vitro*, but the mutant probe had no combination with HbERF6 (**Figures 3B,C**). Therefore, all the results confirmed the recognition and interaction between HbERF6 and the GCC-box of the *HbCIPK2* promoter.

HbERF6 Is a Stress-Responsive Gene

To identify the initial response of *HbERF6* to different stresses in *H. brevisubulatum*, we detected the expression of *HbERF6* in shoots and roots during the early stage of salt, drought, and ABA

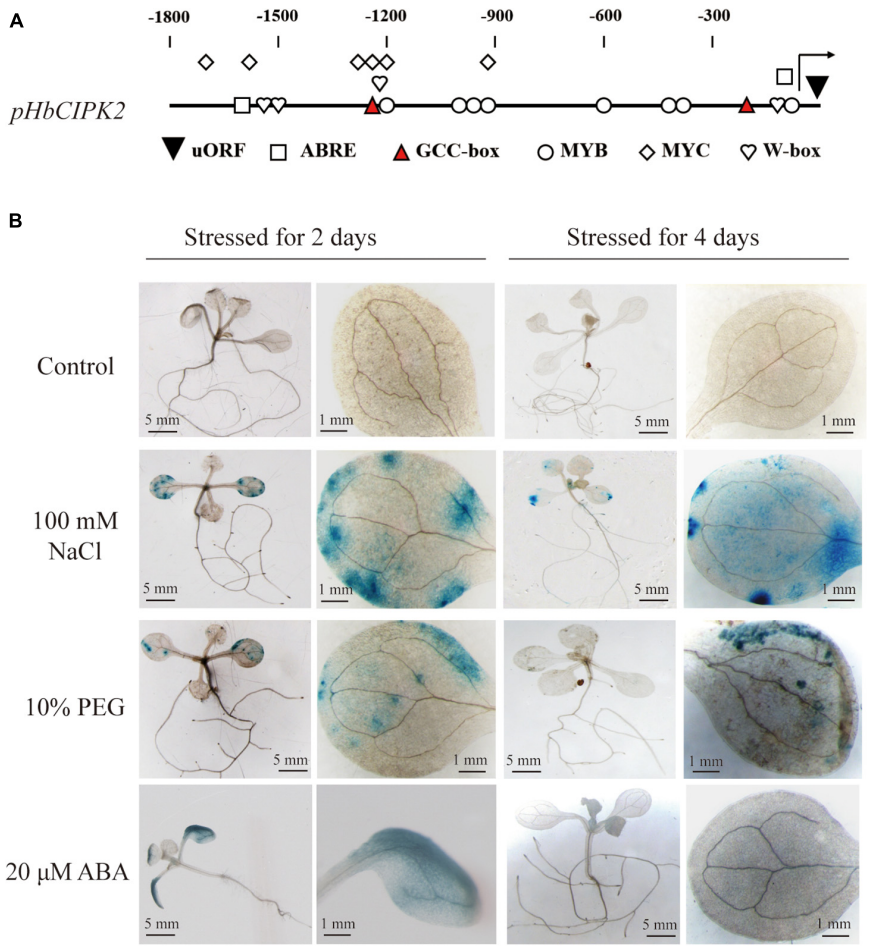

FIGURE 1 | The activity of *HbCIPK2* promoter was induced under different stresses. **(A)** Structural diagram of *HbCIPK2* promoter, *HbCIPK2* promoter contains two GCC-boxes (box-1, –1086 to –1080; box-2, –232 to –226). Different components are represented by different icons. GCC boxes are denoted *via* triangles. **(B)** Histochemical staining of transgenic *Arabidopsis* lines under control and various stress conditions at different times. Scale bars are marked in the figures.

stress. We treated the 3-week-old plants of *H. brevisubulatum* under 350 mM NaCl stress for time series, and then the RNAs of shoots and roots were separately extracted. Using real-time PCR, we found that the transcripts of *HbERF6* were significantly inducible in roots than in shoots under salt treatment. In contrast, *HbERF6* in shoots strongly responded to 10% PEG6000 in shoots than in roots. It showed a similar expression pattern under 350 mM mannitol and 20 μM ABA (**Figure 4A**). In general, *HbERF6* was obviously upregulated under salt treatment, especially in the roots, which was coincident with the reported physiological function of HbCIPK2 (Li et al., 2012).

To establish the tissue-specific expression of HbERF6, transgenic plants in *Arabidopsis* expressing the *GUS* reporter gene driven by the *HbERF6* promoter (∼2 kb upstream from ATG) were detected. Notably, 8 days after imbibition, the strong GUS expression was observed in the shoot apex zone and the vascular bundle of cotyledons (**Figure 4B**). At the reproductive stage, GUS activity was detected mainly in the style and pedicles of inflorescences, and also expressed in the pollen tube of the gynoecium and the stamen filaments (**Figure 4C**). *GUS* expression was also detected in the vasculature of primary roots (**Figure 4D**). Notably, the 15-day-old seedlings showed weak GUS activity in the vascular tissues of the leaves and primary roots as well as in the shoot apex in MS medium (**Figure 4E**). However, when the plants were treated with 100 mM NaCl for 1 day, stronger GUS activity was observed in the vascular tissues of the leaves as well as in the shoot apex, and it was examined in the primary and lateral roots (**Figure 4F**). Obviously, *pHbERF6:GUS* activity of the transformed plants was strongly induced under salt stress.

Overexpression of *HbERF6* Improves Salt Tolerance of *Arabidopsis*

To determine the role of *HbERF6* in plants, transgenic *A. thaliana* lines overexpressing *HbERF6* were analyzed. We compared the growth and development between the *HbERF6* overexpressing lines (L6, L7, and L13) and WT plants subjected to salt stress. Under normal condition (control), the transgenic *Arabidopsis* seedlings had no difference with WT; however, the transgenic

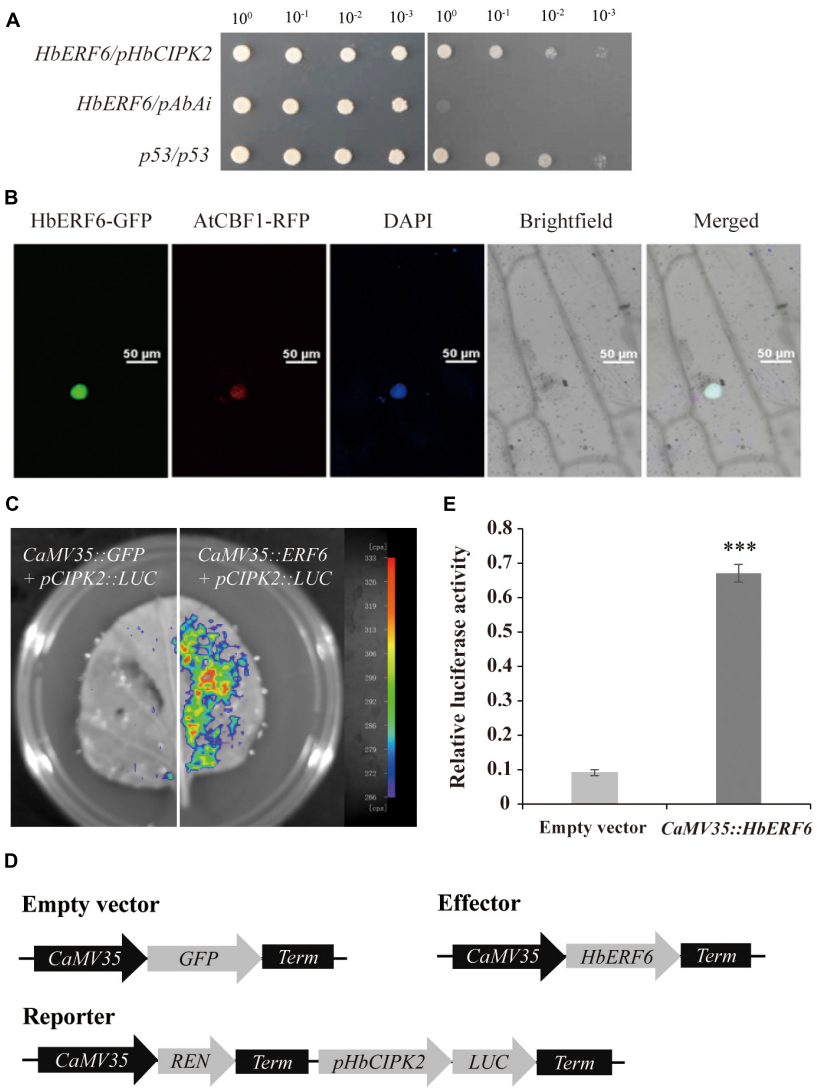

FIGURE 2 | HbERF6 can interact with the *HbCIPK2* promoter in yeast and activate *HbCIPK2* in *N. benthamiana* leaves. **(A)** Interaction of the HbERF6 and *HbCIPK2* promoter was determined based on the ability of transformed yeast to grow on SD/-leu and SD/-Leu/AbA (300 mg/L). **(B)** Nuclear localization of the HbERF6-GFP fusion protein in onion cells. Bar = 50 μm. **(C)** A luciferase imaging assay indicated that HbERF6 can activate the expression of *HbCIPK2*. **(D)** Diagrams of relevant vectors used in the dual luciferase assay. *HbERF6* was cloned into the pGreenII 62-SK vector as an effector, the promoter of *HbCIPK2* was inserted into the pGreenII 0800-LUC vector as a reporter, and each of REN, Renilla luciferase, was used as an internal control. **(E)** The relative LUC activities indicated that HbERF6 can enhance the promoter activity of *HbCIPK2* in *N. benthamiana* leaves. Statistical analysis was performed by one-way ANOVA; asterisks indicate significant variation (***$P < 0.001$).

lines showed longer roots and larger leaves than WT on MS medium containing 100 mM NaCl for 8 days. The WT plants displayed more serious wilting than the transgenic lines following the 125 mM NaCl treatment for 8 days (**Figure 5A**). The fresh weights and root growth rates were significantly greater in the *HbERF6*-overexpressing lines than those in the WT plants treated with 100 or 125 mM NaCl (**Figures 5B,C**).

To further confirm the *HbERF6* function in response to salt tolerance, the phenotype of the transgenic *Arabidopsis* and WT plants in the adult stage was observed. The transgenic lines overexpressing *HbERF6* and WT plants were cultivated until the 6th leaf stage in the greenhouse, and then they were watered with 350 mM NaCl solution once in every 7 days for two times. After treatment, they recovered for 14 days under normal condition for recording their phenotype. The *HbERF6*-overexpressing lines showed better growth than the WT plants during the adult stage (**Figure 5D**). The chlorophyll content of transgenic plants was significantly higher than that of the WT plants (**Figure 5E**). These results indicated that the transgenic plants overexpressing *HbERF6* exhibit enhanced salt tolerance.

To demonstrate the different effect of salt stress on the accumulation of Na^+ and absorption of K^+, the ion content of the 11-day-old transgenic and WT seedlings was examined under normal condition (0 mM NaCl) and salt stress (100 mM

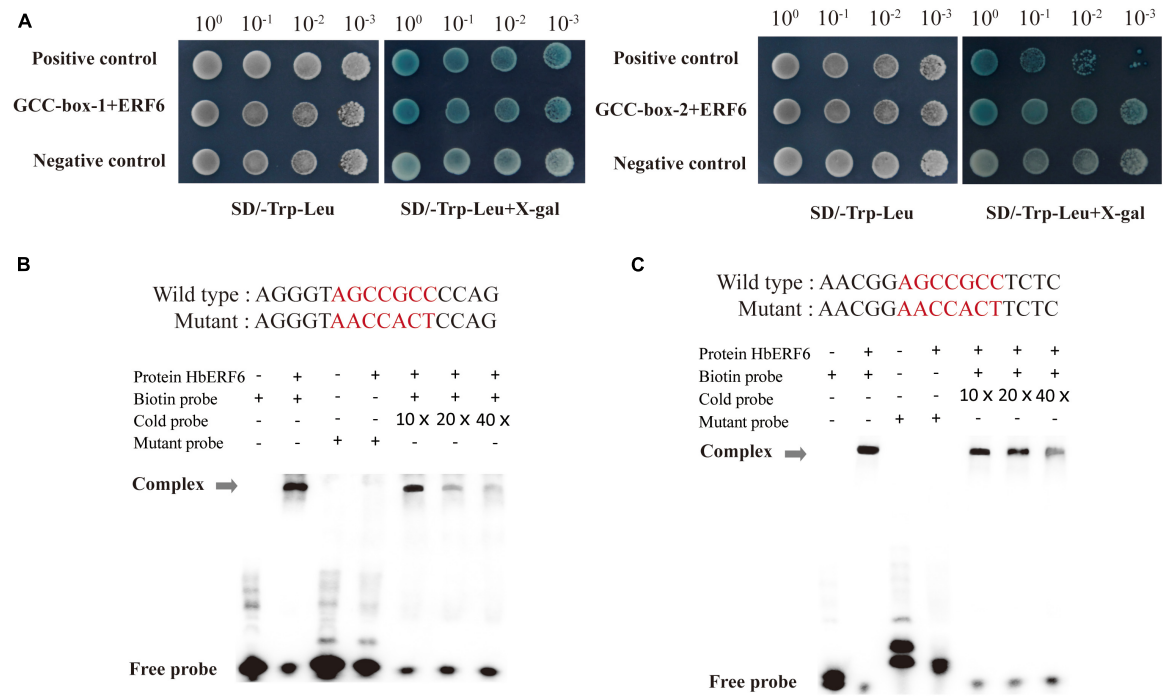

FIGURE 3 | HbERF6 directly binds to GCC-boxes of the *HbCIPK2* promoter. **(A)** Yeast one-hybrid assay showed that HbERF6 binds to the GCC-boxes in the promoter of *HbCIPK2* (GCC-box-1 and GCC-box-2). The transformants were screened by SD/-Trp-Leu and SD/-Trp-Leu + X-gal for 3 days. Electrophoretic mobility shift assays (EMSAs) showed that HbERF6 can, respectively, bind to GCC-box 1 **(B)** and 2 **(C)** of the *HbCIPK2* promoter. A mutant labeled probe with AACCACT to replace the GCC-box (AGCCGCC) was used as a negative control. 10×, 20×, and 40×, respectively, represent the ratio of amounts of non-biotin-labeled probes to biotin-labeled probes. Gray arrows indicate the positions of DNA-protein complexes.

NaCl for 10 days) with ICP-AES. For Na^+ or K^+ content, no significant differences were detected between transgenic and WT plants under normal condition. However, the increase of Na^+ in transgenic *Arabidopsis* was significantly lower than that of WT under salt treatment (**Figure 5F**). The decrease in K^+ of WT plants was significantly higher than that of transgenic seedlings under the same treatment (**Figure 5G**), suggesting that *HbERF6* overexpressing can prevent K^+ reduction and Na^+ accumulation to reach K^+/Na^+ homeostasis in *Arabidopsis*.

HbERF6 Activates the Expression of Stress-Responsive Genes

To know what stress-responsive genes were affected by the overexpression of *HbERF6* in *Arabidopsis*, the expressions of some target genes in whole seedlings were detected using quantitative reverse transcription PCR (qRT-PCR). We analyzed the expression of 12 stress-related genes of interest in *HbERF6*-overexpressing and WT seedlings. According to the qRT-PCR results, the expression levels of *AtCIPK24*, *AtP5CS*, *AtADH*, *AtKIN2*, *AtCOR47*, and *AtRD29B* were upregulated in both of the transgenic and WT seedlings under 100 mM NaCl stress; however, the increase of mRNA abundance of these genes in the transgenic lines was significantly higher than that in WT. Obviously, the expression levels of these genes were not significantly different between transgenic and WT seedlings grown under normal condition (**Figure 6**). The AP2/ERF transcription factor can bind to one or both of GCC-box (AGCCGCC) and DRE (A/GCCGAC) elements to respond to various biotic or abiotic stresses (Cheng et al., 2013; Lee et al., 2015). Interestingly, among six differentially expressed genes, the promoter of *AtP5CS* contains both GCC-box and DRE elements, and that of *AtCIPK24*, *AtCOR47*, *AtRD29B*, and *AtKIN2* contains DRE elements. However, the promoters of other four genes have neither of them resulting in no differential expression (**Supplementary Table 2**). These results indicated that the GCC-box or DRE element of the promoter is important for HbERF6 binding and regulation.

DISCUSSION

Stress-Responsive Promoter of *HbCIPK2*, a Hub of K^+/Na^+ Coordinated Pathways, Was Cloned From Halophytic Wild Barley

Soil salinity substantially impacts plant growth and thus dramatically compromises global agricultural productivity (∼50–80% loss in yield) (Kesten et al., 2019). Discovering novel tolerant genes and unraveling related molecular mechanisms to engineer plants for better stress tolerance are therefore of urgent importance. To date, research on the molecular mechanisms of salt tolerance mainly focuses on the model plants

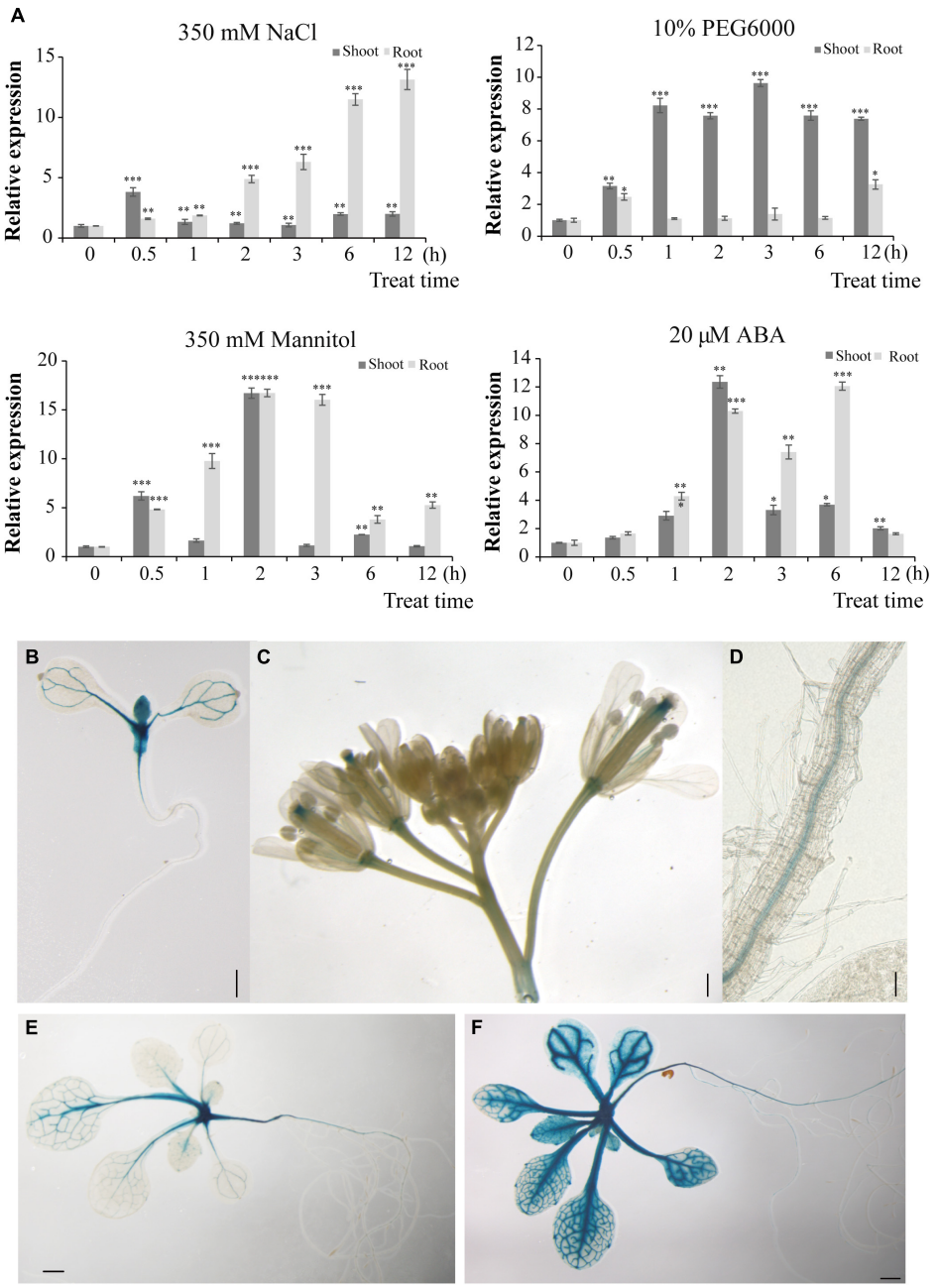

FIGURE 4 | *HbERF6* is inducible under different stress conditions and GUS activity is mediated by the *HbERF6* promoter in transgenic *Arabidopsis* plants. **(A)** Transcript levels of *HbERF6* in roots and shoots of wild barley at two-leaf and one-heart stage suffering from salt (350 mM NaCl), water deficiency (10% PEG6000 and 350 mM mannitol), and ABA (20 μM) using qRT-PCR. *18SrDNA* was used as an internal reference gene. Each value is the average of three biological replicates and error bars mean ± SD. Asterisks indicate significant variation (*$P < 0.05$, *$P < 0.01$ and ***$P < 0.001$). **(B)** The 8-day-old *pHbERF6:GUS* seedlings after imbibition of seeds, **(C)** inflorescence, and **(D)** primary roots, the 15-day-old seedlings after imbibition of seeds in MS medium **(E)** and after 100 mM NaCl treatment for 16 h **(F)**. Scale bars = 2 mm in **(B)**, 1 mm in **(C–E)**, and 400 μm in **(F)**.

or non-halophytic species. Halophytic grass, especially halophyte without specific structures such as salt-gland, has evolved the mechanism adaptive to salt stress, and attracts more attention (Mansour et al., 2021).

Hordeum brevisubulatum is a perennial halophyte relative to cultivated barley, referring to wild barley. Our previous studies indicated that it could maintain higher K^+ content under salt stress, and HbCIPK2 was further identified to prevent K^+ reduction and Na^+ accumulation, and the channel HbVGKC1 and transporter HbSOS1L were coordinated by HbCIPK2 as a hub to maintain K^+/Na^+ homeostasis (Li et al., 2012; Zhang et al., 2020a). HbCIPK2 can phosphorylate the targets to

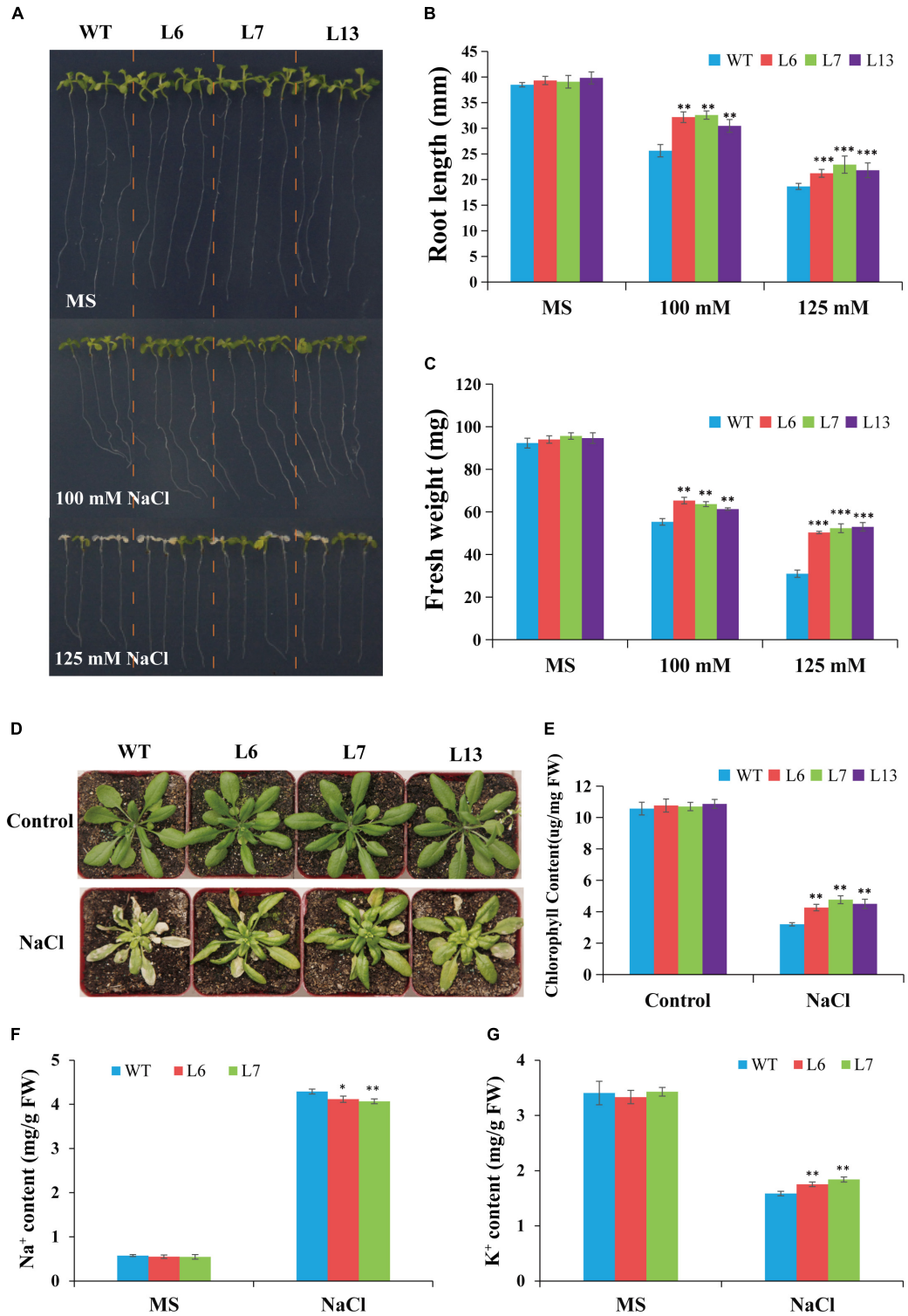

FIGURE 5 | Comparison of salt tolerance between wild type (WT) and transgenic lines. **(A)** Growth and development of the *HbERF6*-overexpressing lines and WT seedlings under NaCl treatment and normal condition. **(B,C)** Root length and fresh weight of the 12-day-old seedlings on MS plates with and without salt were measured, respectively. **(D)** Representative photographs of potted plants of WT and overexpressing *HbERF6* plants at 6th leaf stage which have been treated with 350 mM NaCl solution once in every 7 days for two times. After that, watering and culturing were performed for about 14 days. No treatment was set as control. **(E)** The chlorophyll content of overexpressing lines and WT was measured just after recording the phenotype in **(D)**. The Na^+ **(F)** and K^+ **(G)** contents of the 11-day-old transgenic and WT seedlings were measured under normal condition and salt stress (100 mM NaCl for 10 days). The experiments were repeated three times. Asterisks show that the difference in the values is significant between transgenic lines and the WT (*$P < 0.05$; **$P < 0.01$; ***$P < 0.001$).

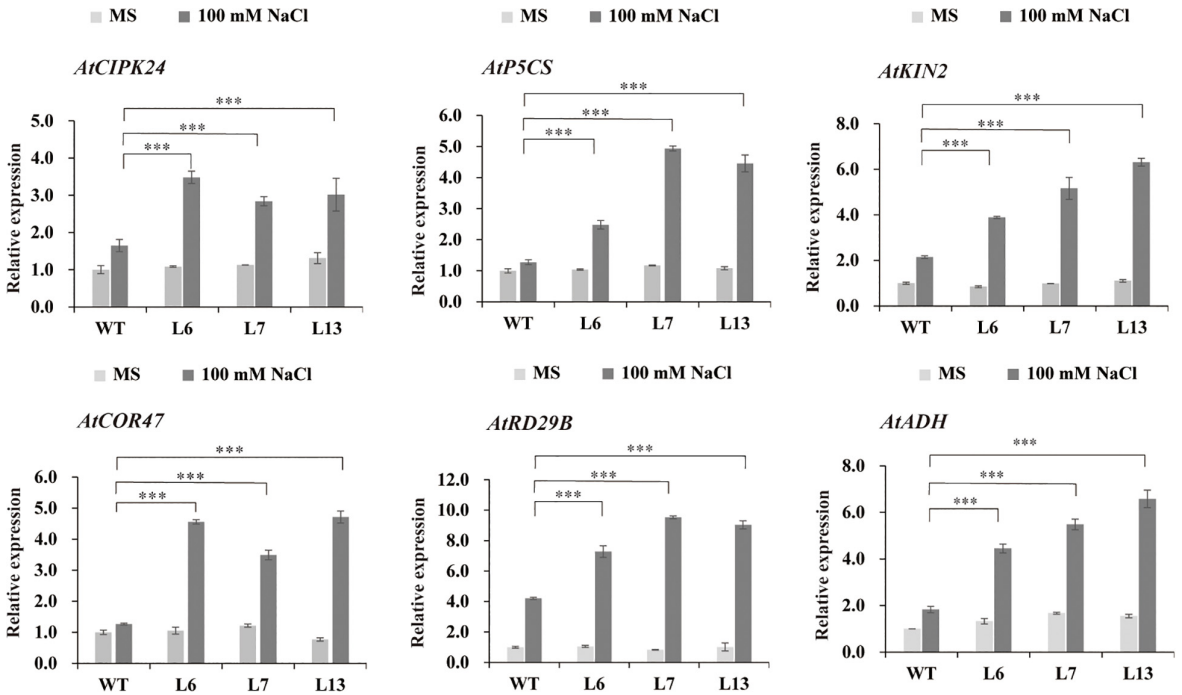

FIGURE 6 | Expression profiles of the six salt stress-responsive genes in WT and *HbERF6*-overexpressing seedlings before and after salt stress using qRT-PCR. The seedlings were grown on MS agar plates for 11 days, and then transferred to MS medium or containing 100 mM NaCl for 10 days. Gene expression was quantified by RT-qPCR and analyzed using the $2^{-\Delta\Delta CT}$ method. *AtACTIN1* was used as an inter-reference gene. The experiments were repeated three times. Asterisks show that the difference in the values is significant between the transgenic lines and WT at the same time point (***$P < 0.001$).

activate their activities, which may determine the coordinated signaling pathways to switch on or off. More importantly, *HbCIPK2* is inducible under NaCl and osmotic stress, and which transcriptional factor may modulate HbCIPK2-mediated pathways is a more interesting question. However, genome information for this species is unknown. Therefore, we have to apply the method of genome-walking to clone the *HbCIPK2* promoter, and then confirm that it is a stress-inducible promoter, which is consistent with the expression of *HbCIPK2*, although the signal of the *GUS* gene driven by the *HbCIPK2* promoter is not strong (**Figure 1B**). This result lays the way for the identification of transcriptional factor for the regulation of HbCIPK2-mediated pathways, especially in halophyte without genome information.

HbERF6 Was Identified *via* Library Screening Using the *HbCIPK2* Promoter as the Bait

The classical method for the identification of the upstream transcriptional regulator is screening Y1H library using the known promoter sequence as the bait. We found that there were several *cis*-acting elements such as ABRE, CRT/DRE, and MYB in the sequence of *HbCIPK2* promoter, but it is not sure which *cis*-element functions (**Figure 1A**). Therefore, the full-length *HbCIPK2* promoter was used as the bait to screen the cDNA library of wild barley. Fortunately, HbERF6 was identified as one of the possible regulators with the strong interaction of the *HbCIPK2* promoter. Subsequently, we performed the assays (EMSA, pairwise Y1H, and dual LUC) to confirm that HbERF6 can specifically bind to the GCC-box of the *HbCIPK2* promoter *in vitro* and *in vivo* (**Figures 2**, **3**). In addition, subcellular localization experiments clearly indicated that the HbERF6 protein localized at the nucleus of the plant cell, suggesting that it may play critical roles in transcriptional regulation (**Figure 2B**). On the other hand, *HbERF6* was also induced by salt, drought, and ABA treatment in wild barley, and the *HbERF6* promoter is also inducible (**Figure 4A**). These results further show that HbERF6 may be a transcriptional regulator of *HbCIPK2*, the hub of K^+/Na^+ homeostasis pathways, in halophytic wild barley.

HbERF6 Regulates HbCIPK2-Mediated Pathways of K^+/Na^+ Homeostasis

The plant-specific AP2/ERF is a large gene family, named after the AP2/ERF domain composed of 60–70 amino acids. Numerous AP2/ERF genes were successfully identified and investigated in plants and have been reported to serve as important regulators in many biological and physiological processes, such as plant morphogenesis, responsive mechanisms to various stresses, hormone signal transduction, and metabolite regulation (Rong et al., 2014; Xie et al., 2019; Girón-Ramírez et al., 2021), and the stress-related downstream genes were regulated by ERFs through direct or indirect binding to the target promoters. However, less is known if the ERF-like transcriptional factor can bind and directly modulate CIPK-like kinase encoding genes. If so, the combination of ERF transcriptional regulation with CIPK

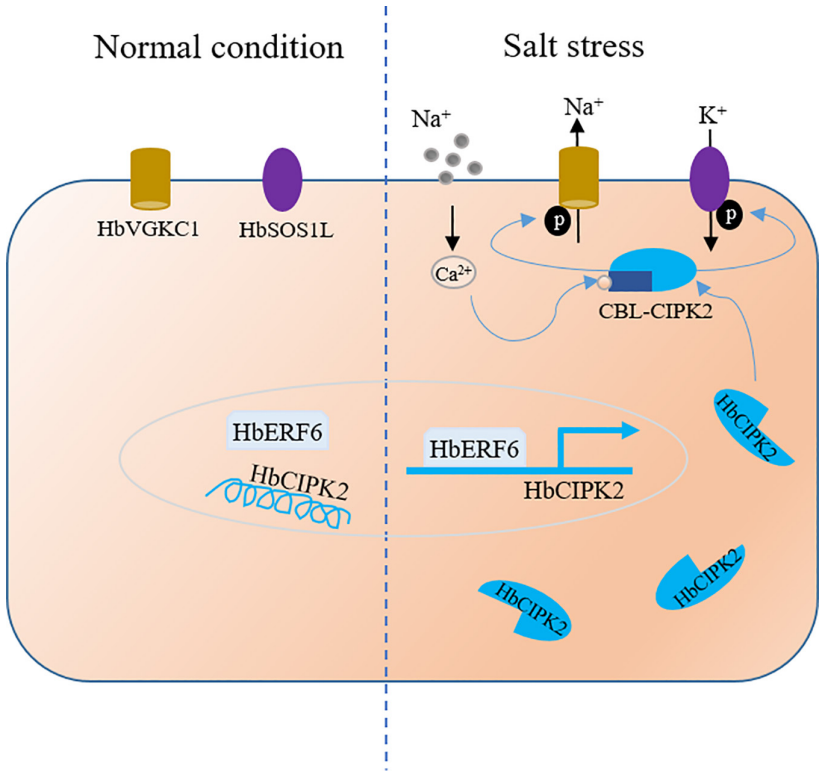

FIGURE 7 | The working model for HbERF6 regulating HbCIPK2-mediated pathways under salt stress. The expression of *HbERF6* is induced by salt conditions. *HbERF6* acts as a transcription factor, binds to the promoter of *HbCIPK2*, and activates the transcription of *HbCIPK2* under salt stress. Then, HbCIPK2 can phosphorylate K^+ channel HbVGKC1 and Na^+ transporter HbSOS1L to coordinate K^+/Na^+ homeostasis.

signaling pathways will highlight stress-responsive transcription factor networks.

In this study, we reported that HbERF6 is a member of the AP2/ERF family which could directly bind to the GCC-box of the *HbCIPK2* promoter, in order to investigate the role of *HbERF6*. It was overexpressed in *Arabidopsis* wild type due to the difficulty of wild barley genetic transformation. The transgenic lines grew well and exhibited longer roots under salt stress (**Figure 5A**). More surprisingly, *HbERF6* overexpressing lines can maintain higher K^+ and reduced Na^+ content (**Figures 5F,G**), which is just speculated. Then, the expression of stress-related genes in the WT and transgenic seedlings under salt stress was checked. Interestingly, among five differentially expressed genes, their promoters contain both or either of GCC-box and DRE elements, which indicates that the GCC-box or DRE element of the promoter is important for HbERF6 binding and regulation. It is worth noting that *AtCIPK24* (*SOS2*) accumulated more in *HbERF6* overexpressing lines, which is a classical salt-tolerant gene controlling Na^+ homeostasis *via* the SOS pathway (Qiu et al., 2002), and its promoter has two DRE elements (A/GCCGAC), which may be so suitable for HbERF6 to bind and activate its higher expression after which K^+/Na^+ homeostasis is eventually promoted contributing to salt tolerance in *Arabidopsis* transgenic plants. Although AtCIPK2 is a homolog of HbCIPK2, the expression of *AtCIPK2* was not as high as that of *AtCIPK24* in HbERF6-overexpressing *Arabidopsis* plants. The possible reasons are that the surrounding sequence of the DRE element in the *AtCIPK2* promoter may affect the binding of HbERF6 and the number of DRE elements in the *AtCIPK2* promoter is less than that in *AtCIPK24* (**Supplementary Table 2**), which needs further investigation.

Above all, we identified the ERF-mediated regulatory network that integrated transcriptional regulation and post-translation modification, which is a novel salt stress-responsive mechanism for halophytic wild barley. Based on our previous studies and results obtained in this study, the working model of HbERF6 regulating *HbCIPK2* is outlined (**Figure 7**). In detail, under normal condition, HbERF6 might bind to the *HbCIPK2* promoter and trans-activate *HbCIPK2*, but salt stress significantly induces more HbERF6 protein to bind to the GCC-box of the *HbCIPK2* promoter to enhance its transcription, then HbCIPK2 interacts with the Ca^{2+}-sensor HbCBL4/10 to phosphorylate the K^+ channel HbVGKC1 and Na^+ transporter HbSOS1L, and finally K^+/Na^+ homeostasis in the cell is maintained.

Soil salinity is becoming more and more serious as population increases and climate changes; it is threatening agricultural production and food security. It will be promising to discover available halophytic resources such as wild barley and to improve crop salt tolerance using important tolerant genes such as the HbERF6-HbCIPK2 signaling pathway.

DATA AVAILABILITY STATEMENT

The original contributions presented in this study are included in the article/**Supplementary Material**, further inquiries can be directed to the corresponding author.

AUTHOR CONTRIBUTIONS

RL, YJ, and HZ planned and designed the experiments. YJ, YL, CC, YW, and HF performed the experiments. YJ wrote the manuscript. RL and HZ revised the manuscript. All authors contributed to the article and approved the submitted version.

FUNDING

This study was supported by the Collaborative Innovation Center of Beijing Academy of Agricultural and Forestry Sciences (grant no. KJCX201907-2); the Young Scientists Fund of Beijing Academy of Agriculture and Forestry Sciences (grant no. QNJJ201832); Science and Technology Innovation Project of Beijing Academy of Agriculture and Forestry Sciences (grant no. KJCX20200112); the Young Scientists Fund of the National Natural Science Foundation of China (grant no. 31801433); and the Outstanding Scientist Development Program of Beijing Academy of Agriculture and Forestry Sciences (grant no. JKZX201901).

ACKNOWLEDGMENTS

We thank Changlong Wen (Vegetable Research Center, Beijing Academy of Agriculture and Forestry Sciences) for kindly providing the plant living imaging system. We also thank Lin Zheng (Agro-Biotechnology Research Center, Beijing Academy of Agriculture and Forestry Sciences) for many good suggestions on experiments.

SUPPLEMENTARY MATERIAL

The Supplementary Material for this article can be found online at: https://www.frontiersin.org/articles/10.3389/fpls.2022.927253/full#supplementary-material

REFERENCES

Almeida, D. M., Oliveira, M. M., and Saibo, N. (2017). Regulation of Na^+ and K^+ homeostasis in plants: towards improved salt stress tolerance in crop plants. *Genet. Mol. Biol.* 40, 326–345. doi: 10.1590/1678-4685-GMB-2016-0106

Chen, H. T., Liu, X. Q., Zhang, H. M., Yuan, X. X., Gu, H., Cui, X., et al. (2018). Advances in salinity tolerance of soybean: genetic diversity, heredity, and gene identification contribute to improving salinity tolerance. *J. Integr. Agric.* 17, 2215–2221. doi: 10.1016/S2095-3119(17)61864-1

Cheng, M. C., Liao, P. M., Kuo, W. W., and Lin, T. P. (2013). The Arabidopsis ETHYLENE RESPONSE FACTOR1 regulates abiotic stress-responsive gene expression by binding to different cis-acting elements in response to different stress signals. *Plant Physiol.* 162, 1566–1582. doi: 10.1104/pp.113.221911

Feng, K., Hou, X. L., Xing, G. M., Liu, J. X., Duan, A. Q., Xu, Z. S., et al. (2020). Advances in AP2/ERF super-family transcription factors in plant. *Crit. Rev. Biotechnol.* 40, 750–776. doi: 10.1080/07388551.2020.1768509

Flowers, T. J., and Yeo, A. R. (1995). Breeding for salinity resistance in crop plants: Where next? *Aust. J. Plant Physiol.* 6, 875–884. doi: 10.1071/PP9950875

Girón- Ramírez, A., Peña-Rodríguez, L. M., Escalante-Erosa, F., Fuentes, G., and Santamaría, J. M. (2021). Identification of the SHINE clade of AP2/ERF domain transcription factors genes in *Carica papaya*; Their gene expression and their possible role in wax accumulation and water deficit stress tolerance in a wild and a commercial papaya genotypes. *Environ. Exp. Bot.* 183:104341. doi: 10.1016/j.envexpbot.2020.104341

Golldack, D., Luking, I., and Yang, O. (2011). Plant tolerance to drought and salinity: stress regulating transcription factors and their functional significance in the cellular transcriptional network. *Plant Cell Rep.* 30, 1383–1391. doi: 10.1007/s00299-011-1068-0

Han, J. P., Koster, P., Drerup, M. M., Scholz, M., Li, S., Edel, K. H., et al. (2019). Fine-tuning of RBOHF activity is achieved by differential phosphorylation and Ca^{2+} binding. *New Phytol.* 221, 1935–1949. doi: 10.1111/nph.15543

Jung, K. H., Cao, P., Seo, Y. S., Dardick, C., and Ronald, P. C. (2010). The Rice Kinase Phylogenomics Database: a guide for systematic analysis of the rice kinase super-family. *Trends Plant Sci.* 15, 595–599. doi: 10.1016/j.tplants.2010.08.004

Kesten, C., Wallmann, A., Schneider, R., McFarlane, H. E., Diehl, A., Khan, G. A., et al. (2019). The companion of cellulose synthase 1 confers salt tolerance through a Tau-like mechanism in plants. *Nat. Commun.* 10:857. doi: 10.1038/s41467-019-08780-3

Kishi-Kaboshi, M., Okada, K., Kurimoto, L., Murakami, S., Umezawa, T., Shibuya, N., et al. (2010). A rice fungal MAMP-responsive MAPK cascade regulates metabolic flow to antimicrobial metabolite synthesis. *Plant J.* 63, 599–612. doi: 10.1111/j.1365-313X.2010.04264.x

Lee, S. Y., Hwang, E. Y., Seok, H. Y., Tarte, V. N., Jeong, M. S., Jang, S. B., et al. (2015). Arabidopsis AtERF71/HRE2 functions as transcriptional activator *via* cis-acting GCC box or DRE/CRT element and is involved in root development through regulation of root cell expansion. *Plant Cell Rep.* 34, 223–231. doi: 10.1007/s00299-014-1701-9

Li, J., Han, G., Sun, C., and Sui, N. (2019). Research advances of MYB transcription factors in plant stress resistance and breeding. *Plant Signal. Behav.* 14:1613131. doi: 10.1080/15592324.2019.1613131

Li, R., Zhang, J., Wu, G., Wang, H., Chen, Y., and Wei, J. (2012). HbCIPK2, a novel CBL-interacting protein kinase from halophyte Hordeum brevisubulatum, confers salt and osmotic stress tolerance. *Plant Cell Environ.* 35, 1582–1600. doi: 10.1111/j.1365-3040.2012.02511.x

Licausi, F., Ohme-Takagi, M., and Perata, P. (2013). APETALA2/Ethylene Responsive Factor (AP2/ERF) transcription factors: mediators of stress responses and developmental programs. *New Phytol.* 199, 639–649. doi: 10.1111/nph.12291

Ma, Q. J., Sun, M. H., Lu, J., Liu, Y. J., You, C. X., and Hao, Y. J. (2017). An apple CIPK protein kinase targets a novel residue of AREB transcription factor for ABA-dependent phosphorylation. *Plant Cell Environ.* 40, 2207–2219. doi: 10.1111/pce.13013

Ma, X., Li, Q. H., Yu, Y. N., Qiao, Y. M., Haq, S. U., and Gong, Z. H. (2020). The CBL-CIPK pathway in plant response to stress signals. *Int. J. Mol. Sci.* 21:5668. doi: 10.3390/ijms21165668

Mansour, M., Emam, M. M., Salama, K., and Morsy, A. A. (2021). Sorghum under saline conditions: responses, tolerance mechanisms, and management strategies. *Planta* 254:24. doi: 10.1007/s00425-021-03671-8

Negrao, S., Schmockel, S. M., and Tester, M. (2017). Evaluating physiological responses of plants to salinity stress. *Ann. Bot.* 119, 1–11. doi: 10.1093/aob/mcw191

Qiu, Q. S., Guo, Y., Dietrich, M. A., Schumaker, K. S., and Zhu, J. K. (2002). Regulation of SOS1, a plasma membrane Na+/H+ exchanger in Arabidopsis thaliana, by SOS2 and SOS3. *Proc. Natl. Acad. Sci. U.S.A.* 99, 8436–8441. doi: 10.1073/pnas.122224699

Rehman, S., and Mahmood, T. (2015). Functional role of DREB and ERF transcription factors: regulating stress-responsive network in plants. *Acta Physiol. Plant* 37:178. doi: 10.1007/s11738-015-1929-1

Rong, W., Qi, L., Wang, A., Ye, X., Du, L., Liang, H., et al. (2014). The ERF transcription factor TaERF3 promotes tolerance to salt and drought stresses in wheat. *Plant Biotechnol. J.* 12, 468–479. doi: 10.1111/pbi.12153

Sanyal, S. K., Kanwar, P., Yadav, A. K., Sharma, C., Kumar, A., and Pandey, G. K. (2017). Arabidopsis CBL interacting protein kinase 3 interacts with ABR1, an APETALA2 domain transcription factor, to regulate ABA responses. *Plant Sci.* 254, 48–59. doi: 10.1016/j.plantsci.2016.11.004

Seifikalhor, M., Aliniaeifard, S., Shomali, A., Azad, N., Hassani, B., Lastochkina, O., et al. (2019). Calcium signaling and salt tolerance are diversely entwined in plants. *Plant Signal. Behav.* 14:1665455. doi: 10.1080/15592324.2019.1665455

Singh, K., Foley, R. C., and Onate-Sanchez, L. (2002). Transcription factors in plant defense and stress responses. *Curr. Opin. Plant Biol.* 5, 430–436. doi: 10.1016/s1369-5266(02)00289-3

Song, L., Huang, S. C., Wise, A., Castanon, R., Nery, J. R., Chen, H., et al. (2016). A transcription factor hierarchy defines an environmental stress response network. *Science* 354:aag1550. doi: 10.1126/science.aag1550

Tang, R. J., Wang, C., Li, K., and Luan, S. (2020). The CBL-CIPK calcium signaling network: unified paradigm from 20 years of discoveries. *Trends Plant Sci.* 25, 604–617. doi: 10.1016/j.tplants.2020.01.009

Tester, M., and Davenport, R. (2003). Na^+ tolerance and Na^+ transport in higher plants. *Ann. Bot.* 91, 503–527. doi: 10.1093/aob/mcg058

Van Zelm, E., Zhang, Y., and Testerink, C. (2020). Salt tolerance mechanisms of plants. *Annu. Rev. Plant Biol.* 71, 403–433. doi: 10.1146/annurev-arplant-050718-100005

Verma, P., Sanyal, S. K., and Pandey, G. K. (2021). Ca^{2+}-CBL-CIPK: a modulator system for efficient nutrient acquisition. *Plant Cell Rep.* 40, 2111–2122. doi: 10.1007/s00299-021-02772-8

Wang, Y., Li, T., John, S. J., Chen, M., Chang, J., Yang, G., et al. (2018). A CBL-interacting protein kinase TaCIPK27 confers drought tolerance and exogenous ABA sensitivity in transgenic Arabidopsis. *Plant Physiol. Biochem.* 123, 103–113. doi: 10.1016/j.plaphy.2017.11.019

Wu, L., Chen, X., Ren, H., Zhang, Z., Zhang, H., Wang, J., et al. (2007). ERF protein JERF1 that transcriptionally modulates the expression of abscisic acid biosynthesis-related gene enhances the tolerance under salinity and cold in tobacco. *Planta* 226, 815–825. doi: 10.1007/s00425-007-0528-9

Wu, T. Y., Goh, H., Azodi, C. B., Krishnamoorthi, S., Liu, M. J., and Urano, D. (2021). Evolutionarily conserved hierarchical gene regulatory networks for plant salt stress response. *Nat. Plants* 7, 787–799. doi: 10.1038/s41477-021-00929-7

Xie, Z., Nolan, T. M., Jiang, H., and Yin, Y. (2019). AP2/ERF transcription factor regulatory networks in hormone and abiotic stress responses in arabidopsis. *Front. Plant Sci.* 10:228. doi: 10.3389/fpls.2019.00228

Xu, J., Li, H. D., Chen, L. Q., Wang, Y., Liu, L. L., He, L., et al. (2006). A protein kinase, interacting with two calcineurin B-like proteins, regulates K^+ transporter AKT1 in Arabidopsis. *Cell* 125, 1347–1360. doi: 10.1016/j.cell.2006.06.011

Zhang, H., Feng, H., Zhang, J., Ge, R., Zhang, L., Wang, Y., et al. (2020a). Emerging crosstalk between two signaling pathways coordinates K^+ and Na^+ homeostasis in the halophyte *Hordeum brevisubulatum*. *J. Exp. Bot.* 71, 4345–4358. doi: 10.1093/jxb/eraa191

Zhang, H., Xiao, W., Yu, W., Jiang, Y., and Li, R. (2020b). Halophytic *hordeum brevisubulatum* HbHAK1 facilitates potassium retention and contributes to salt tolerance. *Int. J. Mol. Sci.* 21:5292. doi: 10.3390/ijms21155292

Zhang, L., Wang, Y., Zhang, Q., Jiang, Y., Zhang, H., Li, R., et al. (2020c). Overexpression of HbMBF1a, encoding multiprotein bridging factor 1 from the halophyte *Hordeum brevisubulatum*, confers salinity tolerance and ABA insensitivity to transgenic Arabidopsis thaliana. *Plant Mol. Biol.* 102, 1–17. doi: 10.1007/s11103-019-00926-7

Conflict of Interest: The authors declare that the research was conducted in the absence of any commercial or financial relationships that could be construed as a potential conflict of interest.

Publisher's Note: All claims expressed in this article are solely those of the authors and do not necessarily represent those of their affiliated organizations, or those of the publisher, the editors and the reviewers. Any product that may be evaluated in this article, or claim that may be made by its manufacturer, is not guaranteed or endorsed by the publisher.

frontiers | Frontiers in Plant Science

TYPE Original Research
PUBLISHED 28 July 2022
DOI 10.3389/fpls.2022.917528

OPEN ACCESS

EDITED BY
Jin-Lin Zhang,
Lanzhou University, China

REVIEWED BY
Ana María Mendez-Espinoza,
Instituto de Investigaciones Agropecuarias (Chile), Chile
Xia Fangshan,
Shanxi Agricultural University, China
Yuying Shen,
Lanzhou University, China

*CORRESPONDENCE
Hui Wang
zzbjwh@163.com

SPECIALTY SECTION
This article was submitted to Plant Abiotic Stress, a section of the journal Frontiers in Plant Science

RECEIVED 11 April 2022
ACCEPTED 12 July 2022
PUBLISHED 28 July 2022

CITATION
Tian H, Zhou Q, Liu W, Zhang J, Chen Y, Jia Z, Shao Y and Wang H (2022) Responses of photosynthetic characteristics of oat flag leaf and spike to drought stress.
Front. Plant Sci. 13:917528.
doi: 10.3389/fpls.2022.917528

Responses of photosynthetic characteristics of oat flag leaf and spike to drought stress

Haoqi Tian[1], Qingping Zhou[1], Wenhui Liu[2], Jing Zhang[3], Youjun Chen[1], Zhifeng Jia[2], Yuqiao Shao[1] and Hui Wang[1]*

[1]Sichuan Zoige Alpine Wetland Ecosystem National Observation and Research Station, Southwest Minzu University, Chengdu, China, [2]Academy of Animal Science and Veterinary Medicine of Qinghai Province, Xining, China, [3]Sichuan Animal Science Academy, Chengdu, China

Raising crops production *via* improving photosynthesis has always been focused. Recently excavating and increasing the photosynthetic capacity of non-leaf organs becomes an important approach to crops yield increase. Here we studied the photosynthetic characteristics of the flag leaf and the non-leaf organs including the sheath, the glume and the lemma under greenhouse. The relative water content (RWC), the stomatal characteristics, the photosynthetic pigment contents, the enzyme activities in C_3 and C_4 pathway and the malate content of the flag leaf and the non-leaf organs on 7, 14, 21, and 28days after anthesis (denoted by 7DAA, 14DAA, 21DAA, and 28DAA) were determined under well-watered (CK) and water-stressed (D) treatments. Drought stress significantly reduced the RWC of the flag leaf and the non-leaf organs, while the variation of RWC in the glume and the lemma was lower than in the flag leaf. The chlorophyll a content, the chlorophyll b content, the total chlorophyll content and the xanthophyll content in the flag leaf were significantly decreased under D. However, drought stress significantly increased the photosynthetic pigment contents in the glume at the late stage (21DAA and 28DAA). In addition, the induced activities of PEPC, NADP-MDH, NADP-ME, NAD-ME, and PPDK in non-leaf organs under drought stress suggested that the C_4 photosynthetic pathway in non-leaf organs compensated the limited C_3 photosynthesis in the flag leaf. Non-leaf organs, in particular the glume, showed the crucial function in maintaining the stable photosynthetic performance of oat.

KEYWORDS

non-leaf organ, C_4 pathway, relative water content, oat, glume

Introduction

Oat is an important crop ranking around sixth in the cereal cultivated area (FAO, 2019), versatilely utilized as grains and forage. Oat grain contains high levels of β-glucan and dietary fiber components and is a source of food, pharmaceutical and industrial products (Zaheri and Bahraminejad, 2012; Marshall et al., 2013; Gorash et al., 2017). In China, oat is grown over a wider area, mainly in the north and southwest, with an annual harvested

area of 0.7 million ha, yielding 8.5 million tons (Diao, 2017; Zhou et al., 2018). The regions cultivating oat in China is characterized by arid and semiarid climate especially in northwest (Li et al., 2019), where water deficit is one of the major constraints for the growth and production of oats (Stevens et al., 2004; Hakala et al., 2020). Drought caused oat grains yield loss of 32%–69% (Varga et al., 2013; Zhao et al., 2021), which was associated with a marked reduction in photosynthesis ability under drought stress (Marcińska et al., 2017). Over 90% of grain yield originated from photosynthetic production, and traditionally, the flag leaf acted as the main assimilation organ for the cereal crops (Evans et al., 1980). Nevertheless, other organs, such as the reproductive structures, were often considered to be the carbon sinks, while were shown to be photosynthetically active (Hu et al., 2014; Sanchez-Bragado et al., 2014; Wang et al., 2020). Recently ear photosynthesis has been focused on its prominent compensation, especially subjected to water deficit (Tambussi et al., 2005; Abebe et al., 2010; Hein et al., 2016; Lou et al., 2018). The reported ear photosynthetic contribution to grain filling ranged from 12% to 65% (Maydup et al., 2010; Sanchez-Bragado et al., 2014; Hu et al., 2019) and the proportion was enhanced with the decrease of water supply (Zhang et al., 2011).

Drought stress inhibited all stages of plant growth and development, especially during the reproductive stage. When subjected to water deficit, the leaves would wilt and senesce due to the water loss (Abebe et al., 2010). Nevertheless, the ear of cereal crops was more resilient, maintaining the stable moisture state under drought stress (Tambussi et al., 2005; Li et al., 2017). In comparison with the leaves, a higher RWC (relative water content) of the non-leaf organs was reported in wheat (Wardlaw, 2002; Tambussi et al., 2005), barley (S'anchez-D'ıaz et al., 2002) and cotton (Hu et al., 2014), which could be explained by the higher osmotic adjustment and the xeromorphic anatomy. The osmotic adjustment was substantially higher in non-leaf organs than in leaves (Tambussi et al., 2005; Hein et al., 2016). In addition, the unique anatomical characteristics, including the thicker wax layer, smaller intercellular spaces and thicker cells, contributed to the higher water use efficiency in the non-leaf organs than in leaves (Blum, 1985; Li et al., 2006). The better photosynthetic performance of non-leaf organs was associated with the ability to maintain a steadier water state under drought stress conditions.

Apart from the higher ability to adjust water state under drought stress, the higher photosynthetic efficiency pathways were considered to sustain grain-filling in the non-leaf organs of C_3 plants. A large body of evidence indicated C_4 pathway, C_4-like pathway or C_3-C_4 intermediate pathway might conduct photosynthesis in non-leaf organs of wheat (Ziegler-Jöns, 1989; Rangan et al., 2016; Balaur et al., 2018), barley (Nutbeam and Duffus, 1976), cucumber (Sui et al., 2017), tobacco and celery (Hibberd and Quick, 2002). Baluar et al. (2018) observed that similar to maize leaf, the glume, the lemma and the awn had the Kranz anatomy with two types of chloroplasts in wheat. In addition, the isotope labeling experiment indicated that most of ^{14}C was detected in malate after assimilating $^{14}CO_2$ by the illuminated ear of wheat (Singal et al., 1986). Some important photosynthetic enzymes in the C_4 pathway exhibited activities in non-leaf organs of C_3 plants. The key enzyme, PEPC, was determined with higher activity in non-leaf organs than in leaves and the activity of PEPC increased under drought stress conditions (Hu et al., 2014; Jia et al., 2015; Wang et al., 2020). Previous studies also reported that photosynthetic enzymes involved in three classical C_4 photosynthesis subtypes, NADP-ME, NAD-ME, and PEPCK, conducted carbon fixation in the non-leaf organs (Singal et al., 1986; Wei et al., 2003; Zhang, 2019). Besides the anatomical and zymologic evidences, the molecular evidence verified that a complete set of C_4 specific genes including *ppc*, *aat*, *mdh*, *me2*, *gpt*, and *ppdk* were up-regulated in caryopsis and NAD-ME type C_4 photosynthesis operated in developing wheat grains (Rangan et al., 2016). The C_4 pathway originated later than the C_3 pathway, while provided enhanced radiation-water-and nitrogen-use efficiency especially in sub-optimal environments (Paulus et al., 2013). Thus, investigating and utilizing the C_4 photosynthetic ability in the non-leaf organs of C_3 plants attracted the attention of plant physiologists and crop breeders.

Materials and methods

Experimental design

Avena sativa cv. Junma seeds were sown in the plastic pots (height 25 cm, diameter 27 cm) in the greenhouse of the Academy of Animal Science and Veterinary Medicine of Qinghai Province in June 2020. Each pot was filled with the field soil (weight 5 kg, maximum field capacity 35.44%) from Huangzhong County in Qinghai Province and 24 pots were used in this study. The field soil was mixed with 0.3 g urea (containing 46% N) and 0.3 g diammonium phosphate (containing 18% N and 46% P_2O_5) per kg soil. Before sowing, 2 L water was added to each pot. When the height of seedlings was around 10 cm, six plants were reserved in each pot. All plants were well-watered (75% of maximum field capacity, CK) till 7 days after anthesis, when half of the pots were started to water with 45% of maximum field capacity, denoted by D. CK and D treatments were controlled till seed maturation by weighing and watering the pot by using an electronic scale at 6:00 p.m. each day. The flag leaf, the sheath, the glume, and the lemma in the plant were collected at 7, 14, 21, and 28 days after anthesis, denoted by 7DAA, 14DAA, 21DAA, and 28DAA, under CK and D treatments with three replicates. All samples were saved in the refrigerator with −80°C for measuring the physiological parameters.

Relative water content

The flag leaf, the sheath, the glume, and the lemma samples were collected, immediately weighed to obtain the fresh weight (w1) and soaked into the distilled water for 30 h. After being weighed again, thus obtaining the saturated weight (w2), the

samples were dried in an oven until constant weight (w3). The relative water content (RWC) was calculated based on the following formula.

$$\mathrm{RWC}(\%) = \left((\mathrm{w1} - \mathrm{w3}) / (\mathrm{w2} - \mathrm{w3})\right) \times 100.$$

Stomata characteristics

The adaxial and abaxial surfaces of the leaf, the interior and exterior surfaces of the sheath, the glume and the exterior surfaces of the lemma on 7DAA were wiped with wet paper. The clear nail polish was smeared on both sides of four organs from 10:00 a.m. to 11:30 a.m. After 20 min, the dried nail polish was peeled away and pressed against the glass slide. The samples were observed under a microscope (DM2000 LED, Leica, Germany) at 40× magnification and the sight area was 272.03 μm × 207.61 μm. From each sample, 10 random sights were selected to record cell numbers, stoma numbers and guard cell length. Stomatal frequency and stomatal index were calculated by the following formula.

$$\text{Stomatal index} = \left(\text{stoma number} / \left(\text{stoma number} + \text{cell number}\right)\right) \times 100\%$$

$$\text{Stomatal frequency} = \text{stoma number} / \text{sight area}$$

Photosynthetic pigment content

The flag leaf, the sheath, the glume, and the lemma samples were snipped into small strips and transferred to the centrifuge tubes with 10 ml of extracting solution. The extracting solution was mixed with acetone and absolute ethyl alcohol by the volume rate of 1:1. Absorbancy of extracting solution at 470, 663, and 645 nm was measured by using the full wavelength microplate analyzer (Multiskan GO, Thermo Fisher, United States). The chlorophyll a content (chla), the chlorophyll b content (chlb), the total chlorophyll content (total chl) and the xanthophyll content (xan) were calculated by the following formula.

$$\mathrm{chla}\left(\mathrm{mg}/\mathrm{g}\right) = \left((12.7 \times \mathrm{D663} - 2.69 \times \mathrm{D645}) \times \mathrm{V}\right) / \left(1000 \times \mathrm{W}\right)$$

$$\mathrm{chla}\left(\mathrm{mg}/\mathrm{g}\right) = \left((22.9 \times \mathrm{D645} - 4.68 \times \mathrm{D663}) \times \mathrm{V}\right) / \left(1000 \times \mathrm{W}\right)$$

$$\mathrm{total\ chl}\left(\mathrm{mg}/\mathrm{g}\right) = \mathrm{chla} + \mathrm{chlb}$$

$$\mathrm{xan}\left(\mathrm{mg}/\mathrm{g}\right) = \left(1000 \times \mathrm{D470} - 3.27 \times \mathrm{chla} - 104 \times \mathrm{chlb}\right) / \left(229 \times \mathrm{V}\right) \times \left(1000 \times \mathrm{W}\right))$$

where, V is the volume of extracting solution, W is the weight of the sample.

Photosynthetic parameters

Pn (net photosynthetic rate) and Gs (stomatal conductance) of the flag leaf, the sheath, the glume, and the lemma were determined by using a portable photosynthesizer (Li-6800, Li-Cor, United States) at 9:00 a.m.–11:30 a.m. We chose the gasket of air chamber with the smallest size of 2 cm^2. The 3 × 3 light source provided independent control of red and blue light intensities.

Photosynthetic enzyme activities

The samples saved in the −80°C refrigerator were used to determine the activities of Rubisco, PEPC, PPDK, NAD-ME, NADP-ME, and NADP-MDH. A 0.1 g sample was ground using a mortar at 4°C and then the grinding media of 1 ml was added. Samples were centrifuged at 8,000 *g* for 10 min at 4°C. The supernatant was used for the activities assays. The grinding media and the reaction mixture solutions were assay kits from the company of Suzhou Comin Biotechnology Co., Ltd. The absorbancy was recorded at 20 s and 5 min 20 s from the starting, respectively, at the wavelength of 340 nm using the full wavelength microplate analyzer (Multiskan GO, Thermo Fisher, United States).

Malate content

An 0.1 g of sample was immediately frozen in liquid N_2, ground thoroughly and soaked in the centrifuge tube with 1 ml of distilled water. The tube was placed in the 4°C refrigerator overnight. Following centrifugation at 8,000 *g* for 10 min at 4°C, the supernatant was filtered with the needle-type filter. The malate content was measured using an HPLC system (High Performance Liquid Chromatography, L3000, RIGOL, China) containing a Rigol C18 reversed-phase column (250 nm × 4.6 nm, 5 μm). The mobile phase was 0.016 M NaH_2PO_4 (pH 4.0) with a flow rate of 0.8 ml/min. The column temperature and the sampling time was 25°C and 30 min, respectively. The injection volume was 10 μl. Samples were detected at 214 nm.

Quantitative real-time PCR (qRT-PCR) analysis

Total RNA was extracted from the samples using the Pure Plant Total RNA Extraction Kit (TSINGKE, Beijing) as described in the manufacturer's instructions. The ratio of absorbancy at 260–280 nm was measured by Nanophotometer of Implen (Implen, Germany). RNA integrity was detected by agarose gel electrophoresis. All samples were stored at-80°C. All

TABLE 1 Sequence of primers used for qRT-PCR.

Primer name	Forward 5′–3′	Reverse 5′–3′
AS-PEPC	TGCGGTTGCGTGAGTCATACATC	TCAGCAGGCTCCTTCTCATCGG
AS-MDH	AACCACTCGTCCAGTCAGTACCC	CGCATTGAGCCATTCATCGTCTTG
AS-ACT	AGCTCGCATATGTGGCTCTTGACT	TCTCATGGATTCCAGCAGCTTCCA

AS, *Avena sativa*.

RNA samples served as templates for the cDNA synthesis by the Goldenstar RT6 cDNA Synthesis Mix(TSINGKE, Beijing). The reverse transcribed products was kept at −20°C.

Quantitative real-time PCR (qRT-PCR) was performed with Step One Plus real-time quantitative PCR instrument (Thermo Fisher, America) and using the SYBR Green I PCR master mix kit (TSINGKE, Beijing) according to the Cmanufacturer's instructions. The relative amount of gene expression was calculated using the expression of actin as internal control gene. qRT-PCR primers were as following (Table 1). The relative quantity of gene expression was calculated using $2^{-\Delta\Delta CT}$ method (Livak and Schmittgen, 2001).

Statistical analysis

The Relative water content, the stomata characteristics, the photosynthetic pigment contents, the photosynthetic parameters, the photosynthetic enzyme activities and the malate content data were subjected to ANOVA. The statistical analysis was conducted with the R software package. Duncan's multiple range test was used to compare mean differences among treatments at the 5% probability level.

Results

Stoma characteristics

Stomata were found on the adaxial and abaxial surface of the flag leaf, the interior and the exterior surface of sheath and the glume and the exterior surface of the lemma in oat (Figure 1). The adaxial surface of the flag leaf had a higher stomatal frequency, stomatal index and guard cell length than of the interior surface of three non-leaf organs (Table 2). Nevertheless, the lower stomatal frequency was found in the abaxial surface of the flag leaf than of the exterior surface of the sheath and the glume, and the exterior surface of the sheath had a higher stomatal index than of the flag leaf.

Relative water content

On 21DAA and 28DAA, the flag leaf showed a significant decrease in the RWC under drought stress (Table 3). In addition, the RWC was significantly reduced under drought stress in the sheath on 14DAA, 21DAA, and 28DAA, in the glume on 21DAA and 28DAA and the lemma on 21DAA. Nevertheless, the variation of the RWC in the glume and the lemma was lower than in the flag leaf and the sheath.

Photosynthetic pigment content

As the growth stage developed, the chla, the chlb, total chl and the xan gradually increased and maximized on 21DAA in the flag leaf under drought stress and CK (Figure 2). In the flag leaf drought stress significantly decreased the chla on 14DAA and 28DAA, the chlb on 14DAA, 21DAA, and 28DAA, total chl on 14DAA and 28DAA and the xan on 14DAA and 28DAA. As the growth stage developed, the chla, the chlb, total chl and the xan gradually increased and maximized on 14DAA under CK and maximized on 21DAA under drought stress in the sheath, the glume and the lemma. Drought stress led to the significant reductions of the chla, the chlb, total chl and the xan on 14DAA in the sheath. The chla on 28DAA, the chlb on 21DAA and 28DAA, total chl on 21DAA and 28DAA and the xan on 28DAA in the glume were increased significantly,while the markedly reduction of chlb was observed in the lemma on 28DAA under drought stress.

Photosynthetic parameters

As the stage developed, Pn was gradually increased and maximized on 14DAA in the flag leaf (Table 4). The significant decreases of Pn were found in the flag leaf on 14DAA, 21DAA, and 28DAA under water stress. Pn was increased significantly on 21DAA, but was decreased significantly on 28DAA in the sheath. In addition, drought stress led to a marked reduction of Pn in the glume on 14DAA, 21DAA, and 28DAA and in the lemma on 14DAA and 28DAA.

Gs was reduced significantly on 14DAA, 21DAA, and 28DAA in the flag leaf. Drought stress significantly increased Gs in the sheath on 14DAA, but decreased on 21DAA, and 28DAA. Gs was decreased significantly in the glume on 14DAA, 21DAA, and 28DAA and in the lemma on 21DAA and 28DAA, but increased on 14DAA in the lemma.

As the stage developed, NPQ was first increased then decreased in the flag leaf under CK, while was decreased under drought stress. NPQ was significantly increased on 21DAA under drought stress, but was decreased on 28DAA in the sheath. Under CK and D treatments, NPQ was higher in sheath, glume and lemma than in flag leaf.

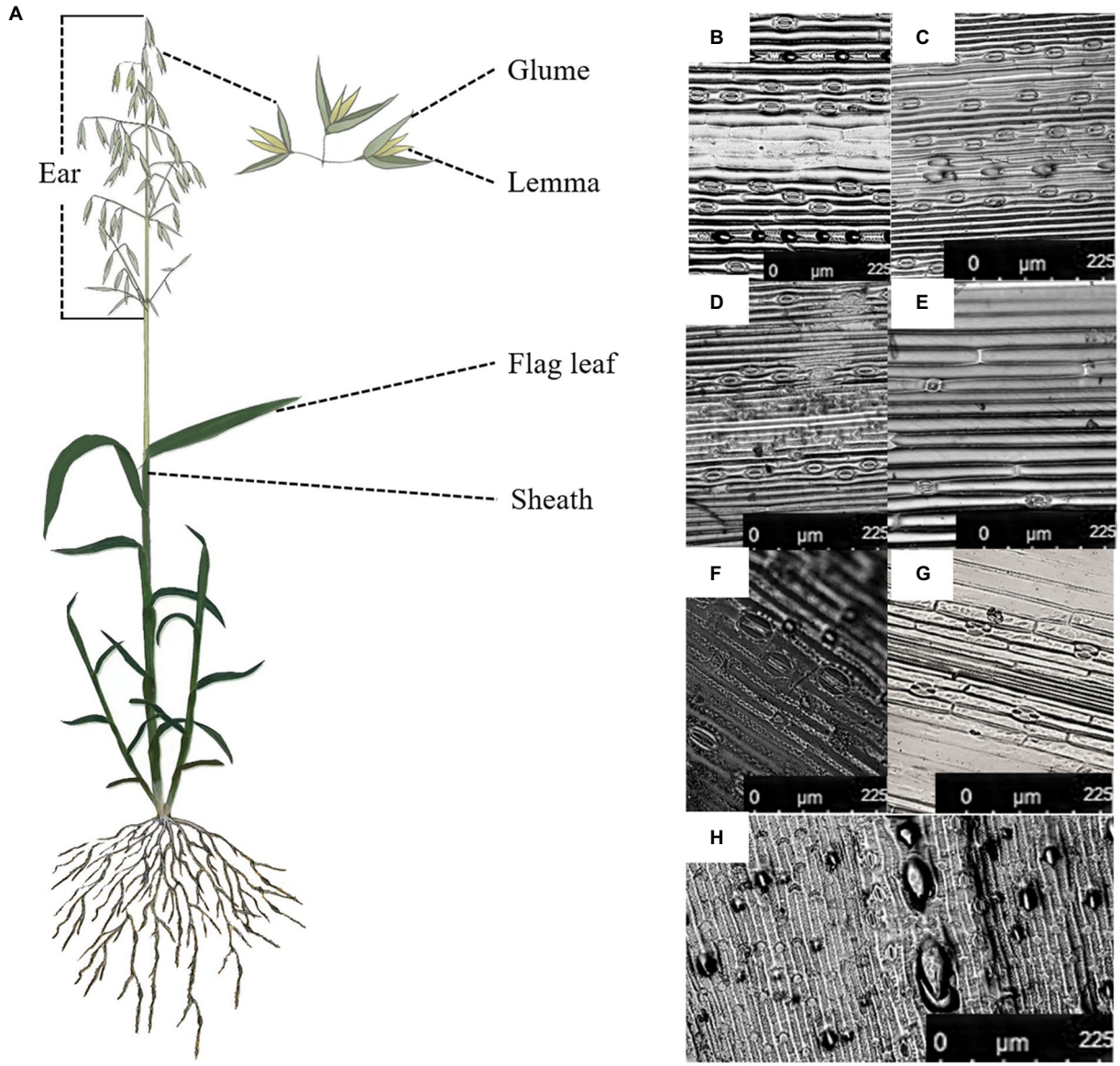

FIGURE 1
Stoma distribution in different green organs of oat on 7DAA. **(A)**, The flag leaf and the non-leaf organs in the oat plant, **(B)**, the adaxial surface of the flag leaf, **(C)**, the abaxial surface of the flag leaf, **(D)**, the exterior surface of the sheath, **(E)**, the interior surface of the sheath, **(F)**, the exterior surface of the glume, **(G)**, the interior surface of the glume, **(H)**, the exterior surface of the lemma.

TABLE 2 Stoma characteristics of the flag leaf, the sheath, the glume and the lemma on 7DAA.

		Stomatal frequency (No. mm^{-2})	Stomatal index	Guard cell length (μm)
Flag leaf	Adaxial surface	90.3a	20.98a	52.39a
	Abaxial surface	47.81c	13.34c	52.76a
Sheath	Interior surface	17.71d	11.35c	37.63c
	Exterior surface	72.60b	16.95b	50.23a
Glume	Interior surface	65.51b	8.03d	33.91d
	Exterior surface	65.51b	10.86c	45.38b
Lemma	Exterior surface	69.05b	12.05c	43.94b

Different small letters within the same column meant a significant difference at the 0.05 probability level.

10.3389/fpls.2022.917528

TABLE 3 The relative water content of the flag leaf, the sheath, the glume and the lemma under drought stress.

		7DAA	14DAA	21DAA	28DAA
Flag leaf	CK	93.95 ± 2.55ab	97.31 ± 1.87a	97.40 ± 0.65a	98.43 ± 0.69a
	D		91.46 ± 5.82ab	88.82 ± 9.19bc	82.38 ± 3.35c
	△		5.85 (6.0%)	8.58 (8.8%)	16.06 (16.3%)
Sheath	CK	85.47 ± 2.24bc	91.09 ± 3.46ab	91.90 ± 0.12a	91.54 ± 1.30a
	D		80.94 ± 4.77c	79.70 ± 2.90c	65.09 ± 5.27d
	△		10.16 (11.1%)	12.20 (13.3%)	26.44 (28.9%)
Glume	CK	93.51 ± 1.67a	94.06 ± 1.56a	94.05 ± 1.36a	92.15 ± 2.05a
	D		91.45 ± 2.14ab	88.67 ± 0.65bc	86.19 ± 2.99c
	△		2.61 (2.8%)	5.38 (5.7%)	5.97 (6.5%)
Lemma	CK	95.43 ± 2.60a	93.45 ± 3.92ab	95.14 ± 0.65a	93.60 ± 0.68ab
	D		94.77 ± 1.46a	90.41 ± 0.96b	93.56 ± 1.66ab
	△		−1.32 (−1.4%)	4.73 (5.0%)	0.04 (0.4%)

Different small letters within the same organ meant a significant difference at the 0.05 probability level.

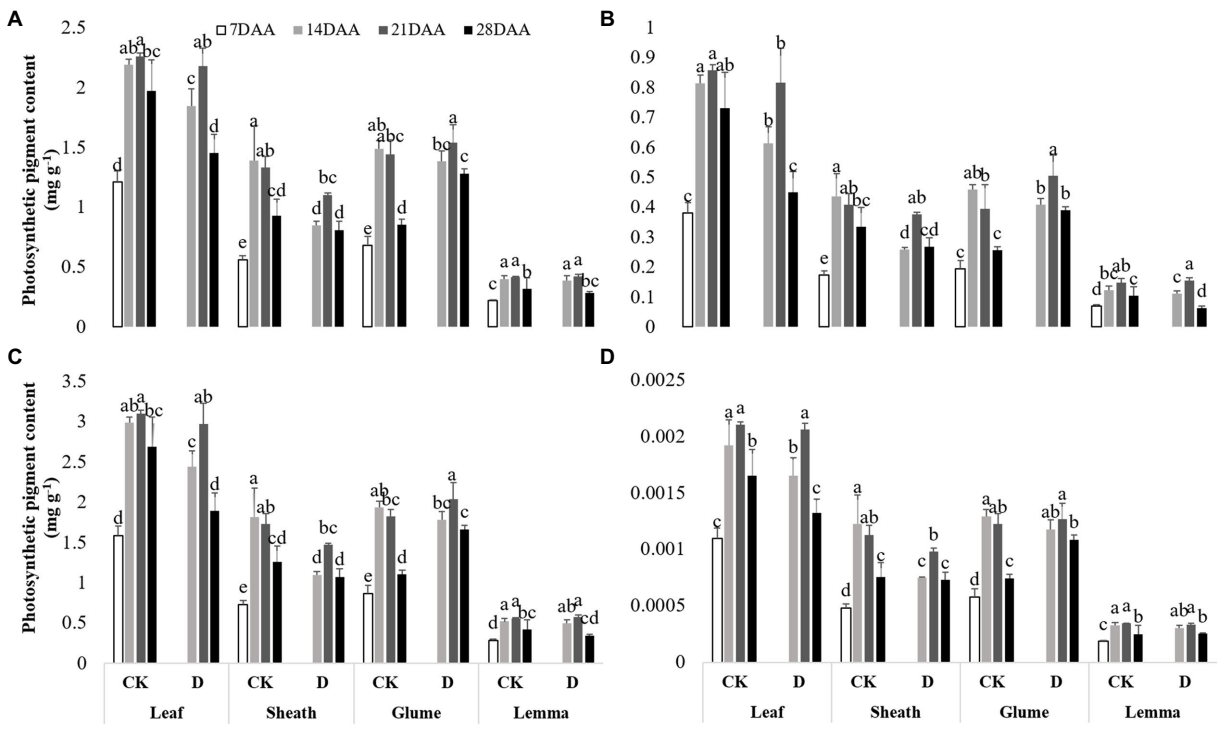

FIGURE 2
Photosynthetic pigment contents in the flag leaf, the sheath, the glume and the lemma under drought stress. **(A)**, chlorophyll a content (chla), **(B)**, chlorophyll b content (chlb), **(C)**, total chlorophyll content (total chl), **(D)**, xanthophyll content (xan). Different small letters within the same organ meant a significant difference at the 0.05 probability level.

Photosynthetic enzyme activities

Drought stress significantly decreased the Rubisco activity in the flag leaf on 14DAA, 21DAA, and 28DAA (Figure 3A-I). In addition, Rubisco activity was significantly declined in the sheath and the glume on 28DAA (Figures 3A-II,III).

A significant reduction of PEPC activity was found in the flag leaf on 28DAA under water stress (Figure 3B-I). Drought stress decreased PEPC activity in the lemma on 14DAA (Figure 3B-IV), but increased significantly in the sheath and the lemma on 28DAA (Figures 3B-II,III).

Under drought stress, NADP-MDH activity was increased significantly in the flag leaf on 14DAA, 21DAA, and 28DAA

10.3389/fpls.2022.917528

TABLE 4 Photosynthetic parameters in the flag leaf, the sheath, the glume and the lemma under drought stress.

Organs	Treatments	Sampling time	Pn	Gs	NPQ
Flag leaf	CK	7DAA	15.596b	0.248d	1.5855abc
		14DAA	18.569a	0.297c	2.1799ab
		21DAA	18.043a	0.387a	2.5695a
		28DAA	11.446c	0.330b	1.2065bc
	D	14DAA	14.618b	0.197e	2.1237ab
		21DAA	14.425b	0.209e	1.6184abc
		28DAA	8.030d	0.092f	0.8127c
Sheath	CK	7DAA	7.861a	0.148a	3.2851bc
		14DAA	3.561cd	0.048d	3.3337bc
		21DAA	3.384d	0.050d	2.9290c
		28DAA	3.509cd	0.111b	2.7648c
	D	14DAA	3.960c	0.057c	3.8778ab
		21DAA	4.597b	0.045d	4.0806a
		28DAA	2.494e	0.036e	1.9966d
Glume	CK	7DAA	3.459c	0.046c	4.5234ab
		14DAA	4.104b	0.055b	——
		21DAA	7.223a	0.134a	4.4632ab
		28DAA	4.185b	0.055b	3.6021b
	D	14DAA	2.245d	0.028d	5.5363a
		21DAA	4.226b	0.058b	3.3079b
		28DAA	1.241e	0.010e	4.2415ab
Lemma	CK	7DAA	1.786a	0.092a	4.4239a
		14DAA	1.786a	0.052 cd	2.3437b
		21DAA	1.317b	0.068b	3.1157ab
		28DAA	0.196c	0.050d	2.4637b
	D	14DAA	1.444b	0.070b	3.5043ab
		21DAA	1.196b	0.055c	2.5838b
		28DAA	−2.050d	0.039e	3.3998ab

Different small letters within the same organ meant a significant difference at the 0.05 probability level.

(Figure 4A-I). In addition, drought stress led to the markedly decreases of NADP-MDH activity in the sheath on 14DAA, 21DAA, and 28DAA (Figure 4A-II). NADP-MDH activity was significantly increased in the glume on 14DAA and in the lemma on 21DAA (Figure 4A-III), but decreased significantly in the lemma on 14DAA (Figure 4A-IV).

NADP-ME activity was significantly increased in the flag leaf on 14DAA and 21DAA under water stress (Figure 4B-I). Drought stress significantly decreased NADP-ME activity in the sheath on 14 DAA (Figure 4B-II), but increased in the glume on 14DAA and 21DAA (Figure 4B-III) and in the lemma on 14DAA (Figure 4B-IV).

NAD-ME activity was significantly decreased in the flag leaf on 14DAA, but increased on 28DAA under drought stress (Figure 4C-I). Drought stress decreased significantly NAD-ME activity in the glume on 14DAA and 21DAA (Figure 4C-III), but increased significantly in the sheath on 14DAA and 21DAA (Figure 4C-II).

PPDK activity was significantly decreased in the flag leaf on 14DAA under water stress (Figure 4D-I). Drought stress significantly reduced PPDK activity in the sheath on 14DAA (Figure 4D-II) and in the glume on 14DAA and 28DAA (Figure 4D-III), but increased in the sheath and the glume on 21DAA (Figures 4D-II,III).

Relative expression of *PEPC* and *MDH*

PEPC was significantly downregulated in the flag leaf on 14DAA and 28 DAA under drought stress and was significantly decreased as the stage developed (Figure 5A). In the glume, *PEPC* was significantly downregulated on 14DAA and in the lemma on 14DAA and 21DAA under drought stress (Figure 5A). *MDH* was significantly upregulated in the leaf at 14DAA and significantly down-regulated in the sheath on 21DAA under drought stress (Figure 5B). In addition, MDH was significantly upregulated in the glume and the lemma on 14DAA, 21DAA, and 28DAA under drought stress (Figure 5B). Under drought stress, the sheath, glume and lemma had the higher relative expression of *PEPC* and *MDH* than flag leaf (Figure 5).

Malate content

Malate content was significantly decreased in the flag leaf and the sheath on 14DAA under drought stress, but increased

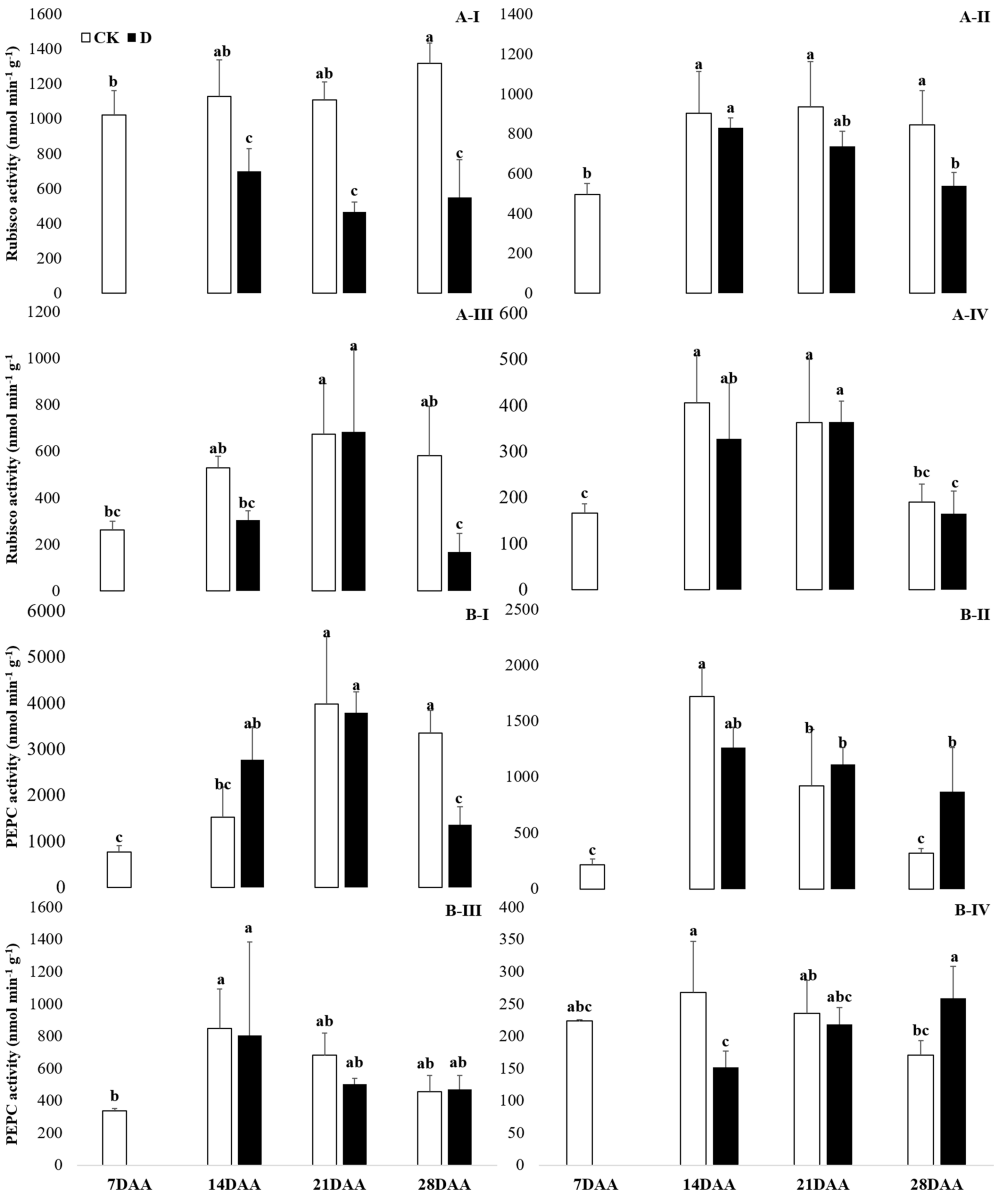

FIGURE 3
Rubisco **(A)** and PEPC **(B)** activity in the flag leaf **(I)**, the sheath **(II)**, the glume **(III)** and the lemma **(IV)** under drought stress. Different small letters within the same organ meant a significant difference at the 0.05 probability level.

significantly in the flag leaf, the sheath and the glume on 28DAA (Figure 6). Drought stress significantly increased malate content in the lemma on 14DAA, but decreased significantly on 28DAA.

Discussion

Drought stress affects the relative water content of non-leaf organs

The greater tolerance of non-leaf organs to drought stress has been previously reported in some studies (Xu and Ishii, 1990; Wardlaw, 2002; Tambussi et al., 2005; Jia et al., 2015; Hein et al., 2016). In this study, the glume and the lemma in oat maintained the higher RWC under drought stress with the lower variation compared to the flag leaf (Table 3). The differences in the capacity to maintain high RWC between leaves and non-leaf organs could be due to the variance in sclerophyllous characteristics (Araus et al., 1986) and the capacity of osmotic adjustment (Hein et al., 2016). Compared to leaves, smaller and denser cells, lower intercellular spaces and thicker cellular walls were observed in non-leaf organs including the glume, the lemma and the awn in cereals, which contributed to reducing the damage resulted from drought

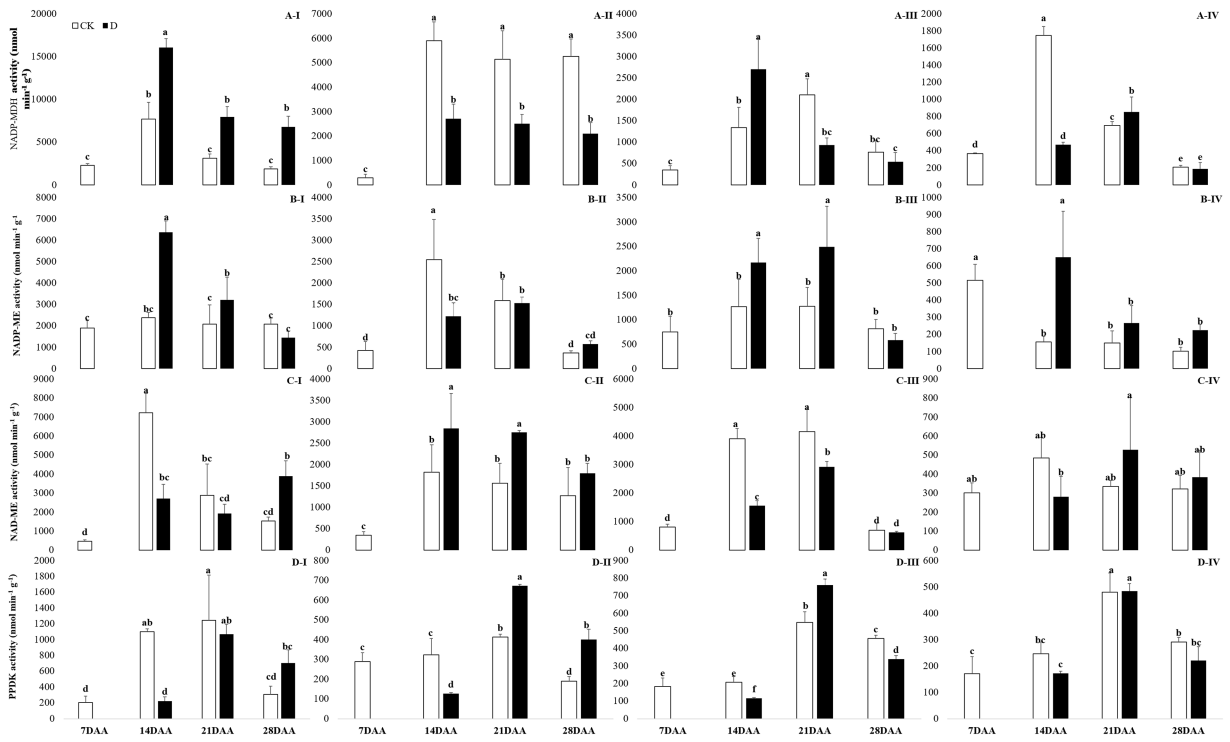

FIGURE 4
NADP-MDH **(A)**, NADP-ME **(B)**, NAD-ME **(C)** and PPDK **(D)** activity in the flag leaf **(I)**, the sheath **(II)**, the glume **(III)** and the lemma **(IV)** under drought stress. Different small letters within the same organ meant a significant difference at the 0.05 probability level.

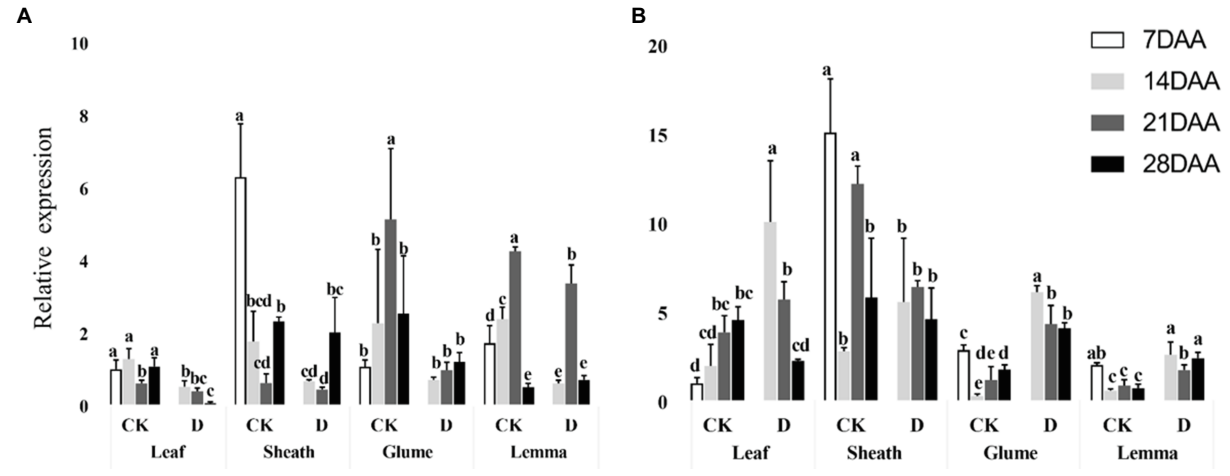

FIGURE 5
Relative expression of *PEPC* gene **(A)** and *MDH* gene **(B)** in different organs under control and drought stress. Different small letters within the same organ meant a significant difference at the 0.05 probability level.

stress (Li et al., 2006; Tambussi et al., 2007). In addition, drought stress could induce the accumulation of osmotic substances including the proline and the raffinose and increase the osmotic potential in ear organs (Tambussi et al., 2005; Li et al., 2006; Abebe et al., 2010; Jia et al., 2015). The non-leaf organs could ensure better physiological performance by maintaining a buffer function under drought conditions, performing better drought adaptation.

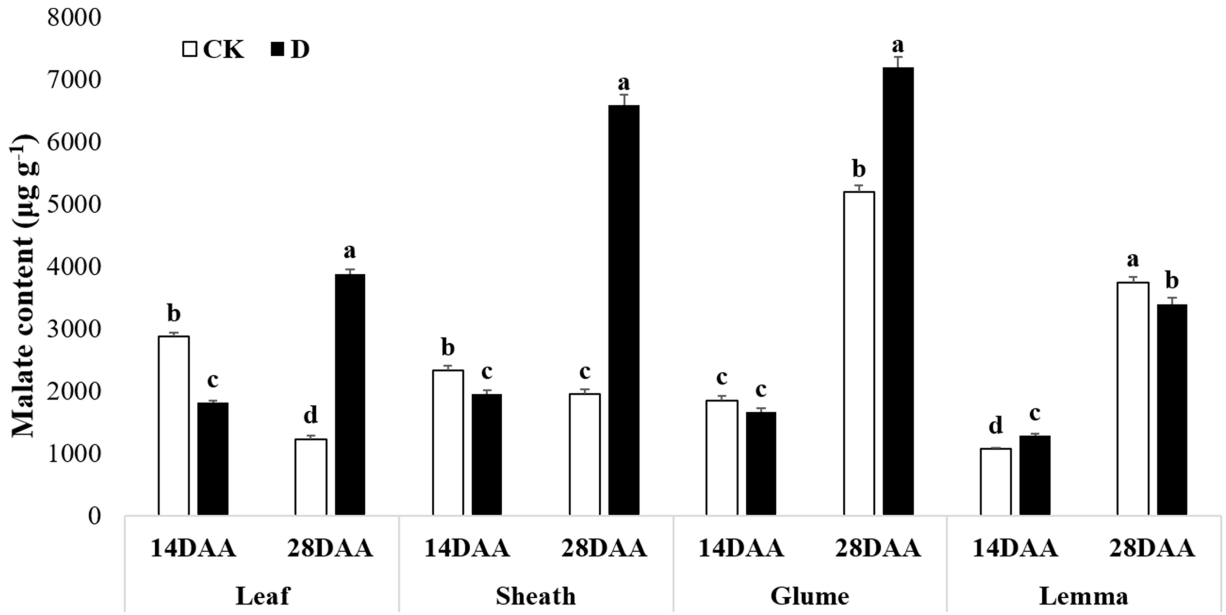

FIGURE 6
Malate content in the flag leaf, the sheath, the glume and the lemma under drought stress. Different small letters within the same organ meant a significant difference at the 0.05 probability level.

Response of photosynthetic parameters in non-leaf organs to drought stress

In addition to the differences of RWC, the non-leaf organs and the flag leaf had different changes in the content of photosynthetic pigments and photosynthetic parameters during the drought treatment. Stable photosynthetic performance implies a strong tolerance to drought stress. Chlorophyll content was lower in non-leaf organs than in leaves, which was found in wheat (Lu and Lu, 2004; Lou et al., 2018), cotton (Zhang et al., 2016) and soybean (Andrews and Svec, 1975). However, the greater photosynthetic activity could be measured per chlorophyll in non-leaf organs than in leaves (Andrews and Svec, 1975; Tambussi et al., 2007). In this study, the drought stress could significantly reduce the chla, chlb, total chl, xan and Pn in the flag leaf at three sampling times, while the photosynthetic pigments content in the glume were increased significantly at the late growth stage (21DAA and 28DAA; Figure 2; Table 4). Similarly, the chlorophyll content in non-leaf organs in cotton and wheat was influenced less by the drought condition, compared with leaves (Zhang et al., 2016; Lou et al., 2018). The regulation effect of the xanthophyll cycle to thermal dissipation was verified in rice and oilseed rape (Zhu et al., 2011). In this study, we found that the higher xan was measured in the glume on 28DAA under drought stress (Figure 2D), which reflected the xanthophyll cycle participated in dissipating excess energy in the glume of oat as well under drought conditions. Among the organs evaluated in this study, drought stress significantly reduced the Pn of the flag leaf, the glume and the lemma, not for the sheath, and even the Pn of the lemma on 28DAA was negative (Table 4). Under the drought condition, the green organs would close the stoma to reduce water evaporation, which attenuated dark reaction (Reddy et al., 2004). In addition, persistent drought stress might cause the degradation of photosynthetic pigments, the damage to membrane system and the reduction of synthetase activity (Ladjal et al., 2000; Jaleel et al., 2009). Previous studies reported that the reduction of Pn in bracts was significantly less than in leaves in cotton under drought stress (Wullschleger et al., 1990; Hu et al., 2014; Zhang et al., 2016). The photosynthesis was less sensitive to water deficit in the non-leaf organs than in leaves, showing a larger contribution to the seed yield (Martinez et al., 2003; Jia et al., 2015). NPQ value represents the ability to protect plants from photodamage by dissipating excess light energy under stress conditions. PSII (Photosynthetic system II) in plants was damaged initially during photosynthesis when confronted stress (Xiao et al., 2019). The higher NPQ value was determined in the glume of wheat than in leaves (Kong et al., 2015), which was consistent to our findings that the non-leaf organs had the higher NPQ value. Under drought stress, as the growth stage developed, the NPQ value in the flag leaf decreased, while the non-leaf maintained stable (Table 4). This suggested higher photosynthetic resistance of the non-leaf organs to the water deficit compared with leaves.

Changes in photosynthetic enzyme activities in non-leaf organs

The results showed that Rubisco activity was markedly influenced by the drought stress in the flag leaf at three growth stages (Figure 3). These findings were in agreement with previous reports for wheat (Guliyev et al., 2008; Simova-Stoilova et al., 2020), rice (Gujjar et al.,

2020), cotton (Carmo-Silva et al., 2012; Hu et al., 2014). Rubisco was regarded as the key enzyme of the Calvin cycle (Lawlor et al., 1989), the reduction of Rubisco activity and content resulted in the decline of photosynthetic ability (Hu et al., 2014). In addition to C_3 pathway enzymes, some C_4 pathway enzymes were activated in non-leaf organs in C_3 plants and water deficit could induce the activities (Wei et al., 2003; Jia et al., 2015; Wang et al., 2020). In the present study, PEPC activity was significantly higher in the sheath and the lemma on 28DAA under drought treatment (Figure 3). The drought stress could significantly induce the activities of NADP-MDH, NADP-ME, NAD-ME, and PPDK in non-leaf organs (Figure 4). The previous studies reported that in non-leaf organs, the PEPC activity was significantly higher than in leaves and was induced under drought stress (Imaizumi et al., 1990; Jia et al., 2015; Zhang, 2019; Wang et al., 2020). The PEP in non-leaf organs was considered to have the possibility to recapture the respired CO_2 in the dark reaction (Singal et al., 1986). Drought stress significantly improved the activities of NADP-MDH, NADP-ME, PPDK and induced the expression of *NADP-MDH-7*, *NADP-ME-1*, *PPDK-1* in the glume of wheat, which was the explanation for the photosynthetic persistence and drought tolerance of non-leaf organs when confronted under water deficit (Jia et al., 2015; Zhang, 2019). In this study, the ear organs had the higher relative expression of *PEPC* and *MDH* than flag leaf under drought stress (Figure 5). Malate is the initial product of photosynthetic CO_2 fixation in C_4 plant leaves and ears in wheat as well (Singal et al., 1986). Photosynthetic enzymes in C_4 cycle played important roles in the anaplerosis of intermediates, such as malate, and supplying carbon skeleton for the amino acids formation (Lea et al., 2001). Therefore, in accordance with the variation of enzyme activities in C_4 cycle, malate content was significantly increased in the glume and the lemma (Zhang, 2019). The increase of malate content likely contributed to improve the osmotic adjustment and supply carbon skeleton. In this study, drought stress significantly increased the malate content in the lemma on 14DAA and in the sheath and the glume on 28DAA (Figure 6).

Conclusion

This study has evaluated the changes of the relative water content, the photosynthetic pigment contents, the photosynthetic parameters, the important enzyme activities in C_3 and C_4 pathway and the malate content in the flag leaf, the sheath, the glume and the lemma of oat under drought stress. These results suggest that C_4 photosynthetic enzymes in non-leaf organs, especially in glume, play crucial functions in improving oat' overall photosynthetic capacity, which contributes to maintaining the stable photosynthetic performance under drought stress conditions.

Data availability statement

The original contributions presented in the study are included in the article/supplementary material, further inquiries can be directed to the corresponding author.

Author contributions

HT and HW prepared the initial draft. QZ, WL, JZ, YC, and ZJ revised the manuscript. YS drew the Figure 1. HW designed the experiment. All authors contributed to the article and approved the submitted version.

Funding

This study was supported by the National Natural Science Foundation of China (32001392), the China Agriculture Research System of MOF and MARA (CARS-34) and "the Fundamental Research Funds for the Central Universities," Southwest Minzu University (2021PTJS30).

Conflict of interest

The authors declare that the research was conducted in the absence of any commercial or financial relationships that could be construed as a potential conflict of interest.

Publisher's note

References

Abebe, T., Melmaiee, K., Berg, V., and Wise, R. P. (2010). Drought response in the spikes of barley: gene expression in the lemma, palea, awn, and seed. *Funct. Integr. Genomics* 10, 191–205. doi: 10.1007/s10142-009-0149-4

Andrews, A. K., and Svec, L. V. (1975). Photosynthetic activity of soybean pods at different growth stages compared to leaves. *Canadian J. Plant Sci.* 55, 501–505. doi: 10.4141/cjps75-076

Araus, J. L., Alegre, L., Tapia, L., and Calafell, R. (1986). Relationship between leaf structure and gas exchange in wheat leaves at different insertion levels. *J. Exp. Bot.* 37, 1323–1333. doi: 10.1093/jxb/37.9.1323

Balaur, N., Badicean, D., Peterhaensel, C., Gardestrom, P., Mereniuc, L., and Vorontsov, V. (2018). The peculiarities of carbon metabolism in the ears of C3 cereals: The carbon metabolism and key genes expression in the photosyn-thetic active components of the ear of cereals. *J. Tissue Cult. Bio.* 1–14. doi: 10.29011/JTCB-102

Blum, A. (1985). Photosynthesis and transpiration in leaves and ears of wheat and barley varieties. *J. Exp. Bot.* 36, 432–440. doi: 10.1093/jxb/36.3.432

Carmo-Silva, A. E., Gore, M. A., Andrade-Sanchez, P., French, A. N., Hunsaker, D. J., and Salvucci, M. E. (2012). Decreased CO2 availability and

inactivation of Rubisco limit photosynthesis in cotton plants under heat and drought stress in the field. *Environ. Exp. Bot.* 83, 1–11. doi: 10.1016/j.envexpbot.2012.04.001

Diao, X. (2017). Production and genetic improvement of minor cereals in China. *Crop J.* 5, 103–114. doi: 10.1016/j.cj.2016.06.004

Evans, L. T., Wardlaw, I. F., and Fischer, R. A. (1980). "Wheat," in *Crop Physiology*. ed. L. T. Evans (Cambridge: Cambridge University Press), 101–149.

FAO. (2019). Available at: http://faostat.fao.org (Accessed on July 9, 2021).

Gorash, A., Armonienė, R., Mitchell, F. J., and Danytė, V. (2017). Aspects in oat breeding: nutrition quality, nakedness and disease resistance, challenges and perspectives. *Ann. Appl. Biol.* 171, 281–302. doi: 10.1111/aab.12375

Gujjar, R. S., Banyen, P., Chuekong, W., Worakan, P., Roytrakul, S., and Supaibulwatana, K. A. (2020). A synthetic cytokinin improves photosynthesis in rice under drought stress by modulating the abundance of proteins related to stomatal conductance, chlorophyll contents, and rubisco activity. *Plan. Theory* 9, 1–21. doi: 10.3390/plants9091106

Guliyev, N., Bayramov, S., and Babayev, H. (2008). Effect of water deficit on RUBISCO and carbonic anhydrase activities in different wheat genotypes. *Photosynthesis. Energy from the Sun*. (Berlin: Springer), 1465–1468.

Hakala, K., Jauhiainen, L., Rajala, A. A., Jalli, M., Kujala, M., and Laine, A. (2020). Different responses to weather events may change the cultivation balance of spring barley and oats in the future. *F. Crop Res.* 259:107956. doi: 10.1016/j.fcr.2020.107956

Hein, J. A., Sherrard, M. E., Manfredi, K. P., and Abebe, T. (2016). The fifth leaf and spike organs of barley (*Hordeum vulgare* L.) display different physiological and metabolic responses to drought stress. *BMC Plant Biol.* 16, 248–212. doi: 10.1186/s12870-016-0922-1

Hibberd, J. M., and Quick, W. P. (2002). Characteristics of C4 photosynthesis in stems and petioles of C3 flowering plants. *Nature* 415, 451–454. doi: 10.1038/415451a

Hu, L., Zhang, Y., Xia, H., Fan, S., Song, J., Lv, X., et al. (2019). Photosynthetic characteristics of non-foliar organs in main C3 cereals. *Physiol. Plant.* 166, 226–239. doi: 10.1111/ppl.12838

Hu, Y. Y., Zhang, Y. L., Yi, X. P., Zhan, D. X., Luo, H. H., Soon, C. W., et al. (2014). The relative contribution of non-foliar organs of cotton to yield and related physiological characteristics under water deficit. *J. Integr. Agric.* 13, 975–989. doi: 10.1016/S2095-3119(13)60568-7

Imaizumi, N., Usuda, H., Nakamoto, H., and Ishihara, K. (1990). Changes in the rate of photosynthesis during grain filling and the enzymatic activities associated with the photosynthetic carbon metabolism in rice panicles. *Plant Cell Physiol.* 31, 835–844. doi: 10.1093/oxfordjournals.pcp.a077986

Jaleel, C. A., Manivannan, P., Wahid, A., Farooq, M., Somasundaram, R., and Panneerselvam, R. (2009). Drought stress in plants: a review on morphological characteristics and pigments composition. *Int. J. Agric. Biol.* 7, 203–216. doi: 10.3763/ijas.2009.0459

Jia, S., Lv, J., Jiang, S., Liang, T., Liu, C., and Jing, Z. (2015). Response of wheat ear photosynthesis and photosynthate carbon distribution to water deficit. *Photosynthetica* 53, 95–109. doi: 10.1007/s11099-015-0087-4

Kong, L., Sun, M., Xie, Y., Wang, F., and Zhao, Z. (2015). Photochemical and antioxidative responses of the glume and flag leaf to seasonal senescence in wheat. *Front. Plant Sci.* 6, 1–10. doi: 10.3389/fpls.2015.00358

Ladjal, M., Epron, D., and Ducrey, M. (2000). Effects of drought preconditioning on thermo tolerance of photosystem II and susceptibility of photosynthesis to heat stress in cedar seedlings. *Tree Physiol.* 20, 1235–1241. doi: 10.1093/treephys/20.18.1235

Lawlor, D. W., Kontturi, M., and Young, A. T. (1989). Photosynthesis by flag leaves of wheat in relation to protein, ribulose Bisphosphate carboxylase activity and nitrogen supply. *J. Exp. Bot.* 40, 43–52. doi: 10.1093/jxb/40.1.43

Lea, P. J., Chen, Z. H., Leegood, R. C., and Walker, R. P. (2001). Does phosphoenolpyruvate carboxykinase have a role in both amino acid and carbohydrate metabolism? *Amino Acids*. 20, 225–241. doi: 10.1007/s007260170041

Li, Y., Li, H., Li, Y., and Zhang, S. (2017). Improving water-use efficiency by decreasing stomatal conductance and transpiration rate to maintain higher ear photosynthetic rate in drought-resistant wheat. *Crop J.* 5, 231–239. doi: 10.1016/j.cj.2017.01.001

Li, X., Wang, H., Li, H., Zhang, L., Teng, N., Lin, Q., et al. (2006). Awns play a dominant role in carbohydrate production during the grain-filling stages in wheat (*Triticum aestivum*). *Physiol. Plant.* 127, 701–709. doi: 10.1111/j.1399-3054.2006.00679.x

Li, X., You, Q., Ren, G., Wang, S., Zhang, Y., Yang, J., et al. (2019). Concurrent droughts and hot extremes in Northwest China from 1961 to 2017. *Int. J. Climatol.* 39, 2186–2196. doi: 10.1002/joc.5944

Livak, K. J., and Schmittgen, T. D. (2001). Analysis of relative gene expression data using real-time quantitative PCR and the $2^{-\Delta\Delta Ct}$ method. *Methods* 25, 402–408. doi: 10.1006/meth.2001.1262

Lou, L., Li, X., Chen, J., Li, Y., Tang, Y., and Lv, J. (2018). Photosynthetic and ascorbate-glutathione metabolism in the flag leaves as compared to spikes under drought stress of winter wheat (*Triticum aestivum* L.). *PLoS One* 13, e0194625–e0194618. doi: 10.1371/journal.pone.0194625

Lu, Q., and Lu, C. (2004). Photosynthetic pigments composition and photosystem II photochemistry of wheat ears. *Plant Physiol. Biochem.* 42, 395–402. doi: 10.1016/j.plaphy.2004.02.008

Marcińska, I., Czyczyło-Mysza, I., Skrzypek, E., Grzesiak, M. T., Popielarska-Konieczna, M., Warchoł, M., et al. (2017). Application of photochemical parameters and several indices based on phenotypical traits to assess intraspecific variation of oat (*Avena sativa* L.) tolerance to drought. *Acta Physiol. Plant.* 39, 1–13. doi: 10.1007/s11738-017-2453-2

Marshall, A., Cowan, S., Edwards, S., Griffiths, I., Howarth, C., Langdon, T., et al. (2013). Crops that feed the world 9. Oats- a cereal crop for human and livestock feed with industrial applications. *Food Secur.* 5, 13–33. doi: 10.1007/s12571-012-0232-x

Martinez, D. E., Luquez, V. M., Bartoli, C. G., and Guiamét, J. J. (2003). Persistence of photosynthetic components and photochemical efficiency in ears of water-stressed wheat (*Triticum aestivum*). *Physiol. Plant.* 119, 519–525. doi: 10.1046/j.1399-3054.2003.00195.x

Maydup, M. L., Antonietta, M., Guiamet, J. J., Graciano, C., López, J. R., and Tambussi, E. A. (2010). The contribution of ear photosynthesis to grain filling in bread wheat (*Triticum aestivum* L.). *F. Crop. Res.* 119, 48–58. doi: 10.1016/j.fcr.2010.06.014

Nutbeam, A. R., and Duffus, C. M. (1976). Evidence for C4 photosynthesis in barley pericarp tissue. *Biochem. Biophys. Res. Commun.* 70, 1198–1203. doi: 10.1016/0006-291X(76)91029-9

Paulus, J. K., Schlieper, D., and Groth, G. (2013). Greater efficiency of photosynthetic carbon fixation due to single amino-acid substitution. *Nat. Commun.* 4, 1518. doi: 10.1038/ncomms2504

Rangan, P., Furtado, A., and Henry, R. J. (2016). New evidence for grain specific C4 photosynthesis in wheat. *Sci. Rep.* 6, 1–12. doi: 10.1038/srep31721

Reddy, A. R., Chaitanya, K. V., and Vivekanandan, M. (2004). Drought-induced responses of photosynthesis and antioxidant metabolism in higher plants. *J. Plant Physiol.* 161, 1189–1202. doi: 10.1016/j.jplph.2004.01.013

S'anchez-D'ıaz, M., Garc'ıa, J. L., Antol'ın, M. C., and Araus, J. L. (2002). Effects of soil drought and atmospheric humidity on yield, gas exchange, and stable carbon composition of barley. *Photosynthetica* 40, 415–421. doi: 10.1023/A:1022683210334

Sanchez-Bragado, R., Molero, G., Reynolds, M. P., and Araus, J. L. (2014). Relative contribution of shoot and ear photosynthesis to grain filling in wheat under good agronomical conditions assessed by differential organ δ13C. *J. Exp. Bot.* 65, 5401–5413. doi: 10.1093/jxb/eru298

Simova-Stoilova, L., Kirova, E., and Pecheva, D. (2020). Drought stress response in winter wheat varieties – changes in leaf proteins and proteolytic activities. *Acta Bot. Croat.* 79, 121–130. doi: 10.37427/BOTCRO-2020-018

Singal, H. R., Sheoran, I. S., and Singh, R. (1986). In vitro enzyme activities and products of $^{14}CO_2$ assimilation in flag leaf and ear parts of wheat (*Triticum aestivum* L.). *Photosynthesis Res.* 8, 113–122. doi: 10.1007/BF00035242

Stevens, E. J., Armstrong, K. W., Bezar, H. J., Griffin, W. B., and Hampton, J. G. (2004). "Fodder oats, an overview," in *Fodder oats, a world overview*. eds. J. M. Suttie and S. G. Reynolds (Rome: Food and Agriculture Organization of the United Nations), 1–9.

Sui, X., Shan, N., Hu, L., Zhang, C., Yu, C., Ren, H., et al. (2017). The complex character of photosynthesis in cucumber fruit. *J. Exp. Bot.* 68, 1625–1637. doi: 10.1093/jxb/erx034

Tambussi, E. A., Bort, J., Guiamet, J. J., Nogués, S., and Araus, J. L. (2007). The photosynthetic role of ears in C3 cereals: metabolism, water use efficiency and contribution to grain yield. *CRC Crit. Rev. Plant Sci.* 26, 1–16. doi: 10.1080/07352680601147901

Tambussi, E. A., Nogués, S., and Araus, J. L. (2005). Ear of durum wheat under water stress: water relations and photosynthetic metabolism. *Planta* 221, 446–458. doi: 10.1007/s00425-004-1455-7

Varga, B., Varga-László, E., Bencze, S., Balla, K., and Veisz, O. (2013). Water use of winter cereals under well-watered and drought-stressed conditions. *Plant Soil Environ.* 59, 150–155. doi: 10.17221/658/2012-pse

Wang, H., Zhou, Q., and Mao, P. (2020). Ultrastructural and photosynthetic responses of pod walls in alfalfa to drought stress. *Int. J. Mol. Sci.* 21, 1–19. doi: 10.3390/ijms21124457

Wardlaw, I. F. (2002). Interaction between drought and chronic high temperature during kernel filling in wheat in a controlled environment. *Ann. Bot.* 90, 469–476. doi: 10.1093/aob/mcf219

Wei, A. L., Wang, Z. M., Zhai, Z. X., and Gong, Y. S. (2003). Effect of soil drought on C_4 photosynthetic enzyme activities of flag leaf and ear in wheat. *Sci. Agric. Sin.* 36, 508–512.

Wullschleger, S. D., Oosterhuis, D. M., and Rutherford, S. A. (1990). Importance of bracts in the carbon economy of cotton. *Arkansas Farm Res.* 39, 4.

Xiao, M., Li, Y., Wang, J., Hu, X., Wang, L., and Miao, Z. (2019). Study on the law of nitrogen transfer and conversion and use of fertilizer nitrogen in paddy fields under water-saving irrigation mode. *Water* 11, 1–13. doi: 10.3390/w11020218

Xu, H. L., and Ishii, R. (1990). Effects of water deficit on photosynthesis in wheat plants: V. Difference among plant parts in water relations. *Japanese J. Crop Sci.* 59, 384–389. doi: 10.1626/jcs.59.384

Zaheri, A., and Bahraminejad, S. (2012). Assessment of drought tolerance in oat (*Avena sativa*) genotypes. *Ann. Biol. Res.* 3, 2194–2201.

Zhang, X. (2019). *Effects of Water Deficit on C_3 and C_4 Photosynthesis Enzymes and Primary Carbon Metabolism in Wheat Flag Leaves and Spikes*. Yangling: Northwest Agriculture and Forestry University.

Zhang, C., Zhan, D. X., Luo, H. H., Zhang, Y. L., and Zhang, W. F. (2016). Photorespiration and photoinhibition in the bracts of cotton under water stress. *Photosynthetica* 54, 12–18. doi: 10.1007/s11099-015-0139-9

Zhang, Y., Zhang, Y., Wang, Z., and Wang, Z. (2011). Characteristics of canopy structure and contributions of non-leaf organs to yield in winter wheat under different irrigated conditions. *F. Crop. Res.* 123, 187–195. doi: 10.1016/j.fcr.2011.04.014

Zhao, B., Ma, B. L., Hu, Y., and Liu, J. (2021). Source–sink adjustment: a mechanistic understanding of the timing and severity of drought stress on photosynthesis and grain yields of two contrasting oat (*Avena sativa* L.) genotypes. *J. Plant Growth Regul.* 40, 263–276. doi: 10.1007/s00344-020-10093-5

Zhou, Q. P., Gou, X. L., Tian, L. H., Chen, Y., Gao, S., Bai, W., et al. (2018). Performances of early and late maturing oat varieties in cold regions. *Chin. Sci. Bull.* 63, 1722–1730. doi: 10.1360/N972018-00343

Zhu, S. Q., Chen, M. W., Ji, B. H., Jiao, D. M., and Liang, J. S. (2011). Roles of xanthophylls and exogenous ABA in protection against NaCl-induced photodamage in rice (*Oryza sativa* L) and cabbage (*Brassica campestris*). *J. Exp. Bot.* 62, 4617–4625. doi: 10.1093/jxb/err170

Ziegler-Jöns, A. (1989). Gas-exchange of ears of cereals in response to carbon dioxide and light. II. Occurrence of a C_3-C_4 intermediate type of photosynthesis. *Planta* 178, 164–175. doi: 10.1007/BF00393191

frontiers | Frontiers in Plant Science

TYPE Original Research
PUBLISHED 02 August 2022
DOI 10.3389/fpls.2022.959427

OPEN ACCESS

EDITED BY
Jing Zhang,
Nanjing Agricultural University, China

REVIEWED BY
Xingxu Zhang,
Lanzhou University, China
Lu Gan,
Yangzhou University, China

*CORRESPONDENCE
Juming Zhang
jimmzh@scau.edu.cn
Tianzeng Liu
liutianzeng@scau.edu.cn

SPECIALTY SECTION
This article was submitted to Plant Abiotic Stress, a section of the journal Frontiers in Plant Science

RECEIVED 01 June 2022
ACCEPTED 01 July 2022
PUBLISHED 02 August 2022

CITATION
Wei H, He W, Li Z, Ge L, Zhang J and Liu T (2022) Salt-tolerant endophytic bacterium *Enterobacter ludwigii* B30 enhance bermudagrass growth under salt stress by modulating plant physiology and changing rhizosphere and root bacterial community. *Front. Plant Sci.* 13:959427. doi: 10.3389/fpls.2022.959427

Salt-tolerant endophytic bacterium *Enterobacter ludwigii* B30 enhance bermudagrass growth under salt stress by modulating plant physiology and changing rhizosphere and root bacterial community

Hongjian Wei[1,2], Wenyuan He[1], Ziji Li[1,2], Liangfa Ge[1,2], Juming Zhang[1,2]* and Tianzeng Liu[1,2]*

[1]College of Forestry and Landscape Architecture, South China Agricultural University, Guangzhou, China, [2]Guangdong Engineering Research Center for Grassland Science, South China Agricultural University, Guangzhou, China

Osmotic and ionic induced salt stress suppresses plant growth. In a previous study, *Enterobacter ludwigii* B30, isolated from *Paspalum vaginatum,* improved seed germination, root length, and seedling length of bermudagrass (*Cynodon dactylon*) under salt stress. In this study, *E. ludwigii* B30 application improved fresh weight and dry weight, carotenoid and chlorophyll levels, catalase and superoxide dismutase activities, indole acetic acid content and K^+ concentration. Without *E. ludwigii* B30 treatment, bermudagrass under salt stress decreased malondialdehyde and proline content, Y(NO) and Y(NPQ), Na^+ concentration, 1-aminocyclopropane-1-carboxylate, and abscisic acid content. After *E. ludwigii* B30 inoculation, bacterial community richness and diversity in the rhizosphere increased compared with the rhizosphere adjacent to roots under salt stress. Turf quality and carotenoid content were positively correlated with the incidence of the phyla Chloroflexi and Fibrobacteres in rhizosphere soil, and indole acetic acid (IAA) level was positively correlated with the phyla Actinobacteria and Chloroflexi in the roots. Our results suggest that *E. ludwigii* B30 can improve the ability of bermudagrass to accumulate biomass, adjust osmosis, improve photosynthetic efficiency and selectively absorb ions for reducing salt stress-induced injury, while changing the bacterial community structure of the rhizosphere and bermudagrass roots. They also provide a foundation for understanding how the bermudagrass rhizosphere and root microorganisms respond to endophyte inoculation.

KEYWORDS

salt stress, endophyte, growth-promoting, bermudagrass, bacterial community

Introduction

Saline-alkali soils are common within terrestrial ecosystems, and salinity affects approximately half of all irrigated land. Typically, salinization increases due to fertilizer overuse and poor water quality (Zhang et al., 2010; Pessarakli, 2014). Plant salt stress (SS) is related to the accumulation of several soluble salts, including calcium chloride, magnesium sulfate, or sodium sulfate, but sodium chloride is the dominant salt-inducing SS within plants (Yu et al., 2013). Soil salinity initially suppresses plant development via osmotic stress, with ionic toxicity appearing later (Liu et al., 2019). SS will produce reactive oxygen species (ROS), thereby inducing oxidative stress (OS) while suppressing plant growth (Essemine et al., 2020). Scorching of leaves and stems, the inhibition of shoot and root developmental, and leaf senescence and abscission, are the major morphological effects induced by SS (Singh and Jha, 2016). In addition, biochemical alterations can involve physiological metabolism, cell oxidation, imbalanced nutritional conditions, and chlorophyll degradation (He et al., 2019; Wang et al., 2022). Many methods such as chemical or fertilizer application, salt-resistant variety development, and plant genetic engineering have been employed for ameliorating such SS-induced impacts (Bui, 2013; Fatma et al., 2014). In recent studies, investigators have paid increasing attention to applying beneficial microbes to mitigate SS (Vaishnav et al., 2019).

Bacterial endophytes are widely distributed in plants, where they colonize intracellular and intercellular spaces. Both fungal and bacterial endophytes typically colonize and live within an individual host plant throughout its life cycle without causing any significant pathological symptoms (Ryan et al., 2008; White et al., 2019). The inoculation of endophytic bacteria into plants promotes the synthesis of compounds such as antioxidants, amino acids (AAs), and sugars and enhances photosynthesis in host plants alleviating SS (Diskit et al., 2018). Phytohormones produced by bacterial endophytes, including jasmonic acid (JA), abscisic acid (ABA), and indole acetic acid (IAA), promote development in their hosts (Singh et al., 2021; Roy Choudhury et al., 2022) while ACC-deaminase reduces ethylene production under SS (Ali et al., 2014). These microorganisms can also reduce plant SS by producing ROS-scavenging enzymes and increasing K^+ absorption for counteracting Na^+ while modulating relevant pathways (Fan et al., 2020). Other studies have reported the role of endophytic bacteria in mitigating plant SS by restoring plant biochemical and physiological states (Kumar et al., 2020). Endophytic bacteria also have important roles in modulating microbial community structures within plant rhizospheres (Cordovez et al., 2019). Due to the growth-promoting effect of endophytic bacteria on plants, more carbon is fixed and transferred to the rhizosphere, where it is released in the form of root exudates (Compant et al., 2010; Li et al., 2021). As a result, more beneficial microorganisms move toward the exudate, colonizing and multiplying within the rhizosphere and root nodules (Lugtenberg and Kamilova, 2009). Galaviz et al. (2018) inoculated mesquite (*Prosopis articulata*) with *B. pumilus* ES4, which improved the relative abundance of the beneficial bacteria *Paenibacillaceae* and *Bacillaceae* in the rhizosphere, thus contributing directly or indirectly to plant growth promotion. In addition, inoculation with the endophytic *Bacillus velezensis* JC-K3 in wheat (*Triticum aestivum* L.) changed bacterial and fungal diversities within the roots and reduced plant salt damage (Ji et al., 2021). *Enterobacter ludwigii* can survive at 15–42°C and pH 5–10 (Hoffmann et al., 2005). Khan et al. (2020) found that *E. ludwigii* generated IAA, gibberellins (GA) and organic acids, thus promoting plant development while enhancing its resistance. Nowadays, little is known about how *Enterobacter ludwigii* alleviates abiotic stress in plants, especially the mechanisms by which changes in microbial communities in the rhizosphere and root of plants regulate plant resistance to abiotic stresses are unclear.

Bermudagrass (*Cynodon dactylon*), a typical warm-season turf grass, is widely used in temperate and tropical regions of the world (Wei et al., 2022a). Turfgrass managers are using reclaimed water as an irrigation resource because of the decreasing availability and increasing cost of fresh water (Xiang et al., 2018). However, reclaimed water contains large amounts of salt ions, and its prolonged use can elevate the salt content of turfs, thereby inhibiting the growth of turfgrass (Liu et al., 2019). Nonetheless, the effect of bacterial endophytes on improving SS resistance of bermudagrass remains unclear. Our previous work isolated endophytic bacterium strain *E. ludwigii* B30 from *Paspalum vaginatum* roots in the salinization experimental site of the Teaching and Research Base in South China Agricultural University, Guangzhou, China (lat.23°30′15″N, long.113°80′21″E). and found that the inoculation of *E. ludwigii* B30 is an effective way to improve seed germination, root length, and seedling length of bermudagrass under salt stress (Zhao et al., 2021). The present work examined the role of *E. ludwigii*. B30 in mitigating high SS-induced unfavorable impacts on Bermudagrass plant development. Additionally, we carried out 16S rDNA amplicon sequencing to determine how *E. ludwigii* B30 affected the bacterial community structure in bermudagrass rhizosphere soils and roots. Understanding the effects of endophytic bacteria on the structures of root and rhizosphere bacterial communities associated with bermudagrass contributes to understanding the complicated interactive network between microbes and their host.

Materials and methods

Plant materials as well as growth conditions

Bermudagrass (*Cynodon dactylon*) seeds were obtained from the International Grass Industry Co. Ltd. in Tianjin, China.

Seeds were immersed in 75% ethanol for 5 min to surface-sterilize them, washed 4 times in sterile distilled water, and planted into plastic pots (diameter 10 cm, height 10 cm; 20 g m^{-2} sowing rate) containing substrate (peat: sand 3:1, V/V). The plastic pots were sterilized at 121°C for 1 h in an autoclave on three successive days prior to setting up the experiment. Potted seedlings were cultured in a growth chamber [controlled at 30/27°C; 60% relative humidity; a 14 h/10 h light/dark cycle; 650 mmol m^{-2} s^{-1} photosynthetic active radiation (PAR)]. Pots were initially watered in the morning and evening to keep the soil moist. After seedling emergence, plants were watered one time a day until water drained from the bottoms of the pots to maintain soil water content and fertilized once weekly with half-strength Hoagland's solution.

Salt-tolerant endophytic bacteria

The salt-tolerant bacteria *Enterobacter ludwigii* B30 was isolated from *Paspalum vaginatum*. A salt tolerance test showed that B30 could grow normally on 500 mM NaCl medium. Before inoculation, 2 ml *E. ludwigii* B30 was activated in beef extract peptone liquid medium and shaking at 30°C for 10 h until OD_{600} reached 0.8.

Bacterial inoculant for bermudagrass growth under salt stress

A randomized complete block experimental design was used, and there were two factors, each with two levels: (1) non-inoculation (E−) and inoculation with *Enterobacter ludwigii* B30 (E +), and (2) NaCl concentration of 0 and 250 mM. Each treatment was replicated three times.

E + treatment was inoculated in 28-days-old bermudagrass seedling roots with 20 mL of *E. ludwigii* B30 bacterial suspension was adjusted with 10 mM $MgSO_4$ to a concentration of 10^9 CFU mL^{-1}. E− treatment was 20 mL of 10 mM $MgSO_4$ solution. Three days after inoculation, all plants were trimmed to a height of 4 cm. To avoid salt shock, NaCl was added to the pots in a stepwise manner by increasing NaCl concentration to 50, 100, 150, 200 and 250 mM daily. Once the 250 mM NaCl content was achieved, it was maintained for 14 days. The day of bacterial inoculation of plants was designated day 0. At 21-days post-stress, root/shoot lengths and fresh/dry plant weights were measured, and plant samples were collected for analysis.

Quantification of photosynthesis-related parameters

Chlorophyll fluorescence parameters were determined in the bermudagrass leaves following *E. ludwigii* B30 inoculation and salt treatments. We used a chlorophyll fluorometer imaging-PAM (Walz, Effeltrich, Germany) to determine chlorophyll fluorescence in the middle part of the first leaf from every seedling, collected at ambient temperature. After a 20 min adaptation in the dark, chlorophyll fluorescence was measured in the plant samples. We set the intensities of saturating and actinic lights at 7200 and 185 μmol m^{-2} s^{-1} PAR, respectively. In line with Murchie and Lawson (2013), quantum yields of regulated and non-regulated energy dissipation of PSII [Y(NPQ), Y(NO) separately] were measured, along with the maximum quantum yield of PSII (Fv/Fm), and the photochemical energy conversion efficiency via PSII Y(II). We calculated parameters qP and qN in equations 1 and 2 below (Rascher et al., 2000). The parameters of chlorophyll fluorescence were determined for 3 leaf sample sets (4 leaf samples from every set) from each pot on the day before harvest.

$$qP = (F'm - Fs)/(F'm - F'0) \quad (1)$$

$$qN = (Fm - F'm)/F'm \quad (2)$$

where Fm and F'0 represent maximum and minimum fluorescence intensities of leaf samples adapted to darkness for a 30-min period; F'm is the maximum fluorescence of the light-adapted leaf sample, and Fs is real-time fluorescence of leaves.

Determination of turf quality, relative water content, antioxidant enzyme activities and photosynthetic pigment content

For evaluating the health as well as the overall performance of bermudagrass, we measured turf quality (TQ) according to color, grass canopy uniformity, and density with a 1–9 point scale, with 1 indicating totally brown and dried plants, 9 indicating a green, dense, turgid canopy, and 6 indicating the minimum acceptable level (**Supplementary Table 1**) (Beard, 1973).

For measuring relative water content (RWC) in leaves, leaf samples were harvested and weighed to determine the fresh weight (FW). The leaf samples were then immersed in deionized water for a 24 h period at 4°C before removing the leaves from the water and determining the turgid weight (TW). Afterward, the leaves were dried for 72 h at 80°C in an oven before recording dry weight (DW). Leaf RWC was calculated using equation 4 (Barrs and Weatherley, 1962):

$$(FW - DW)/(TW - DW) \times 100 \quad (3)$$

Free proline levels were measured using the method of Bates et al. (1973). We homogenized the freshly collected leaves

(500 mg) in sulfosalicylic acid (10 ml, 3% w/v) and filtered it through Whatman No. 2 filter paper. The filtered extract was mixed with glacial acetic acid and acid ninhydrin (2 mL each) and boiled at 100°C for 1 h. After retrieving 2 mL of toluene from the mixture, it was stirred for 15–20 s. Absorbance (OD) was later measured in the toluene blank at 520 nm, followed by isolation of the upper layer from the aqueous phase.

Superoxide dismutase (SOD) activity was measured with a xanthine oxidase T-SOD activity assay kit (Nanjing Jiancheng Bioengineering Institute, Nanjing, China). This determines the inhibitory effect of xanthine in producing superoxide anion free radicals under the catalysis of xanthine oxidase, thereby determining SOD activity. The produced superoxide radicals oxidized hydroxylamine for the generation of nitrite, which served as a developer for creating the purple color. OD values were determined in every reaction mixture at 550 nm. The amount of SOD needed to produce a 50% inhibition of nitrite reduction within the 1 mL reaction system was determined as one SOD activity unit (Beyer and Fridovich, 1987). We utilized an assay kit for detecting CAT activity (Nanjing Jiancheng Bioengineering Institute, Nanjing, China). CAT activity was measured as the reduction in OD value at 240 nm resulting from H_2O_2 decomposition. The enzyme volume inducing 1 mmol H_2O_2 decomposition/second at 25°C in a 1 g tissue protein sample was deemed to be one CAT activity unit. CAT and SOD activities (U/g protein, with U indicating enzymatic activity unit) were determined following manufacturer's protocols (Rady et al., 2019).

Chlorophyll was extracted from freshly collected leaf samples (1 g) through suspension in 80% acetone (5 mL v/v). A spectrophotometer (UV-2800, Unico, Shanghai, China) was utilized to record extract OD values at 470, 646 and 663 nm. Carotenoid and chlorophyll levels were measured using equations in Lichtenthaler and Wellburn (1983).

Determination of ion concentration and membrane stability

K^+ and Na^+ ions content in leaves and roots were measured using the method of Chang et al. (2018). Fresh leaves and roots were dried on filter paper, followed by an additional 2-days drying to constant weight at 70°C. K^+ and Na^+ ions in root and leaf dry matter (0.1 g) were obtained for subsequent analysis. Samples were mixed with an acid mixture (5 mL) containing $HClO_4$ and HNO_3 at a 1:4 ratio, followed by overnight incubation at 60°C and later introduction of 1 mL H_2O_2 and 4 mL HNO_3 for 20 min at 220°C. After 4 h of cooling under ambient temperature, deionized water was added to dilute the extract, followed by injection into an Atomic Absorbance Spectrophotometer [AA-6650, Shimadzu (China) Co., Ltd., JP]. This work obtained ions from 3 plants from every treatment. No plant sample was used in the blank group.

To measure MDA content, 0.2 g of freshly collected leaves were homogenized in 5% trichloroacetic acid (TCA, 1.5 mL), and centrifuged at 14,000 g for 25 min. 0.5 mL aliquots of the supernatant were mixed with 20% TCA (1 mL) containing 0.5% thiobarbituric acid (TBA), heated for 30 min at 100°C, rapidly cooled and then centrifuged at 10,000 g for 10 min. The supernatant was used to measure OD values at 532 and 600 nm. MDA content was measured at the 155 $mM^{-1}cm^{-1}$ extinction coefficient after deducting non-specific absorbance (600 nm) (Heath and Packer, 1968).

Membrane permeability (MP) was measured based on the leaf electrolyte leakage (EL, determined as a percentage). An increase in EL indicates an increased MP value (Wei et al., 2022b). Freshly collected leaf blade samples (300 mg) from several pots were placed in a test tube containing distilled water (30 ml). After 12-h of shaking, electrical conductivity (E1) was measured using a conductivity meter (DDS-307; Zhengyi Technology Co., Guangzhou, China). Samples were then placed into boiling water for 1 h, and electrical conductivity (E2) was again measured at ambient temperature. EL was calculated using the formula:

$$EL = (E1 - E0)/(E2 - E0) \times 100 \quad (4)$$

where E0 indicates the electrical conductivity in distilled water (Lutts et al., 1996).

Endogenous abscisic acid, indole acetic acid, and 1-aminocyclopropane-1-carboxylate measurement

Abscisic acid (ABA) and IAA content was measured by Phytodetek-ABA and Phytodetek-IAA Immunoassay kits (Agdia, Elkhart, IN) (Cluis et al., 2004; Vanderauwera et al., 2007). We determined phytohormone levels following manufacturer's instructions. Shoots were immersed in liquid nitrogen and ground into powder. The powder (0.5 g) was suspended in the extraction solution [8 ml, containing 80% methanol, 0.5 g L^{-1} citric acid monohydrate together with 100 mg L^{-1} butylated hydroxytoluene (BHT)], followed by overnight stirring in the dark at 4°C followed by 20 min centrifugation at 1000 g and 4°C. The resulting supernatant was collected into another tube, vacuum dried, and dissolved in tris-buffered saline (TBS, 900 μL, pH 7.8) and 100% methanol (100 μL). ABA and IAA contents were then measured from the filtrate using the Phytodetek ABA/IAA enzyme immunoassay kit (Agdia Inc., Elkhart, IN).

To measure ACC concentrations in seedling tissues roots (1 g) were immersed in liquid nitrogen and ground to powder.

ACC extraction was then carried out using 2 mg BHT-containing 80% methanol (5 ml) as the antioxidant, followed by 45 min incubation at ambient temperature. After 15 min centrifugation at 2000 g and 20°C, pellets were resuspended in 80% methanol (4 ml), followed by centrifugation. The resulting supernatant was evaporated to dryness with a rotary evaporator. ACC content was measured using the method of Madhaiyan et al. (2007). The residue was resuspended in distilled water (2 ml), and dichloromethane was added. In the upper aqueous phase, 0.5 mL was extracted and mixed with 80 mM $HgCl_2$ (0.1 ml) in a test tube, followed by sealing using rubber septa. Thereafter, each tube had 0.2 ml of sodium hypochlorite solution added, followed by 8 min of incubation in a shaker.

DNA extraction and high-throughput sequencing

Rhizosphere soil and root samples were collected at the end of salt stress treatments. Plants were collected and gently shaken to remove the loosely adhered soil after which rhizosphere soil samples were collected by removing the remnant soil with a fine sterile brush. The root samples were gently rinsed several times with tap water then washed with sterile water, followed by drying on sterilized filter paper. Rhizosphere soil and root samples were stored at −80 °C for DNA extraction. We isolated total DNA from around 0.5 and 0.1 g rhizosphere soils and root separately with the Soil DNA Kit (OMEGA, Shanghai) and plant DNA kit (Tiangen, Beijing) in line with manufacturer's protocols. A Qubit Fluorometer was used to measure DNA quality using the Qubit dsDNA BR Assay kit (Invitrogen, Waltham, MA, USA). 0.1% agarose gel was utilized to test quality. All extracts were stored under 20°C. To conduct PCR amplification, the sequences of primers in the bacterial v3-v4 region (5′-CCGTCAATTCMTTTRAGTTT-3′) and (5′-GTGCCAGCMGCCGCGGTAA-3′) were applied. After amplification, products were subject to recovery and purification, fluorescence intensity was quantified, and a sequencing library was constructed. Finally, we used the Illumina HiSeq platform to conduct sequencing at Guangdong Magigene Biotechnology Co., Ltd. Guangzhou, China.

Bioinformatics analysis

QIIME software (quantitative insights into microbial ecology, v1.8.0[1]) (Caporaso et al., 2010) was used to obtain high-quality clean tags. Typically, this retained sequences whose lengths were ≥ 160 bp, and fuzzy bases were eliminated. Sequences that had > 8 continuous identical bases and those with > 1 5′-primer base mismatches were also ruled out. Usearch (v5.2.236[2]) was utilized for checking and removing chimeric sequences after which the desired sequences were obtained. OTU clustering was carried out at a similarity level of 97%. Afterward, Silva databases (Quast et al., 2013) for bacteria were used to identify OTU classifications following clustering analysis.

Statistical analysis

Data were collated with Microsoft Excel 2019. SPSS22.0 (SPSS Inc., Chicago, IL, United States) was used for the statistical analyses of treatment effects on the bermudagrass plant physiology. We applied one-way and two-way ANOVAs and Fisher's LSD test to test significant differences ($P < 0.05$) between treatments in plant physiology indicators. Origin 8.0 software was employed to plot relative abundance maps showing bacteria whose mean relative abundances were >1%. LEfSe analysis was then conducted to analyze relative general abundances using the Galaxy online analysis platform.[3] The R Project (v4.1.3) ggplot2 package and Bray-Curtis distance metric were used to perform principal coordinate analysis (PCoA), and β-diversity was visualized with the phyloseq package (Oksanen et al., 2007). Redundancy analysis (RDA) was conducted, and RDA diagrams were drawn using the R (v4.1.3) ggplot2 and vegan packages.

Results

Effects of *Enterobacter ludwigii* B30 on the growth of bermudagrass under salt stress

Under SS, *E. ludwigii* B30 (E +) treated plants showed markedly different shoot lengths compared with non-treated control plants. Non-endophyte treated (E−) plants had a 13.40 cm shoot length, while E + plants had a 16.01 cm shoot length (**Table 1**). E + plants also had markedly increased root length ($P < 0.05$) compared with E− treated plants under SS. The fresh weight (FW) of shoot and root biomass increased in plants growing with E + . Under SS, E− plants had fresh weights of shoots and roots of 4.75 g and 1.14 g, whereas those of E + treated plants were 8.78 g and 1.68 g. Similarly, shoot and root dry weights (DW) were improved in plants in the

1 http://qiime.org/

2 http://www.drive5.com/usearch/

3 http://huttenhower.sph.harvard.edu/galaxy/

TABLE 1 Influence of *Enterobacter ludwigii* B30 on shoot length, root length, shoot biomass and root biomass of bermudagrass in the presence and absence of salt stress.

Treatment	Shoot height (cm)	Root length (cm)	Shoot biomass (g FW)	Root biomass (g FW)	Shoot biomass (g DW)	Root biomass (g DW)
Non-stress						
E−	18.33 ± 0.21b	10.68 ± 0.36b	12.31 ± 0.35b	1.69 ± 0.15b	1.43 ± 0.03a	0.21 ± 0.01b
E +	20.11 ± 0.85a	13.33 ± 0.22a	15.94 ± 0.43a	2.06 ± 0.09a	1.66 ± 0.08b	0.26 ± 0.03a
Salt stress						
E−	13.40 ± 0.51d	6.17 ± 0.36d	4.75 ± 0.25d	1.14 ± 0.06c	1.11 ± 0.02c	0.03 ± 0.01d
E +	16.01 ± 0.19c	7.26 ± 0.19c	8.78 ± 0.21c	1.68 ± 0.11b	1.41 ± 0.08a	0.15 ± 0.02c
ANOVA						
E	***	**	***	***	***	***
Salt	***	***	***	***	**	***
E × Salt	***	**	**	***	ns	**

Difference in various growth parameters and comparative analysis. Average ± standard error from three separate replicates. "Non-stress" represents bermudagrass grown without NaCl condition; "Salt stress" represents bermudagrass under 250 mM salt conditions. "E + " represents the infection of *E. ludwigii*, "E−" represents the absence of *E. ludwigii.* Different letters means significantly different based on $P < 0.05$. "**," "***" indicate significant differences at $P < 0.01$, and $P < 0.001$, respectively, and "ns" represents no significant difference.

E + treatment. SS exposure significantly decreased ($P < 0.05$) turf quality (TQ) of E + treated and E− treated bermudagrass. However, the TQ of the E + treated plants was greater than ($P < 0.05$) that of the E− treated plants in SS conditions (Figure 1 and Supplementary Figure 1).

Salt and *E. ludwigii* B30 did not significantly affect shoot dry weight ($P > 0.05$), but affected other plant growth indicators (Table 1).

Physiological response following inoculation of *Enterobacter ludwigii* B30 in salt stress treated plants

Salt stress (SS)-treated plants exposed to E + had increased RWC and decreased proline levels compared with controls. For E-SS treatment plants, the RWC was approximately 83%, and for E + plants, it was approximately 87% (Figure 2A). In E-SS treatment plants, proline levels were approximately 827 μg mg^{-1} FW, while in the E + treatment they were 745 μg mg^{-1} FW (Figure 2D).

Leaf SOD activity under SS significantly increased in E + plants compared with E−plants (726 U g^{-1} and 625 U g^{-1}, respectively; $P < 0.05$; Figure 2B). The leaf CAT activity within plants under SS with E + treatment increased compared with the E− treatment (232 U g^{-1} and 136 U g^{-1}, respectively; $P < 0.05$; Figure 2C).

MDA content and electrolyte leakage under SS decreased in the E + treatment in comparison with plants in the E− treatment (2.43 μmol g^{-1} FW and 1.68 μmol g^{-1} FW, respectively; Figure 2E). For plants under SS, an electrolyte leakage rate of 45% was seen from plants in the E− treatment, compared with 25% in plants in the E + treatment (Figure 2F).

Enterobacter ludwigii B30 enhanced photosynthetic efficiency and protected photosynthetic pigments of bermudagrass under salt stress

The Fv/Fm ratio (maximum quantum yield of PSII), photochemical quenching (qP), and non-photochemical quenching (qN) in bermudagrass plants grown under salt stress with E + increased significantly compared with E− plants (Figures 3A–C; $P < 0.05$). PSII [Y(II)] quantum yield increased dramatically, whereas Y(NPQ) and Y(NO)

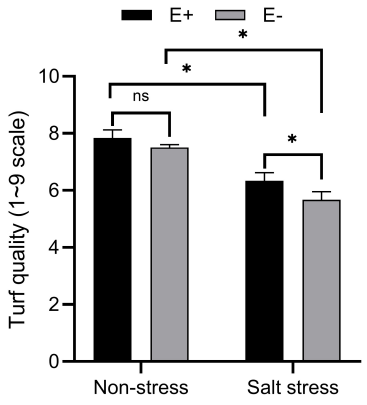

FIGURE 1
Effects of bermudagrass turf quality of inoculated and uninoculated plants under salt stress. Bars denote means ± SE of four treatment. "Non-stress" represents bermudagrass grown without NaCl condition; "Salt stress" represents bermudagrass under 250 mM salt conditions. "E + " represents the infection of *Enterobacter ludwigii*, "E−" represents the absence of *E. ludwigii.* "*" indicate significant differences at $P < 0.05$ and "ns" represents no significant difference.

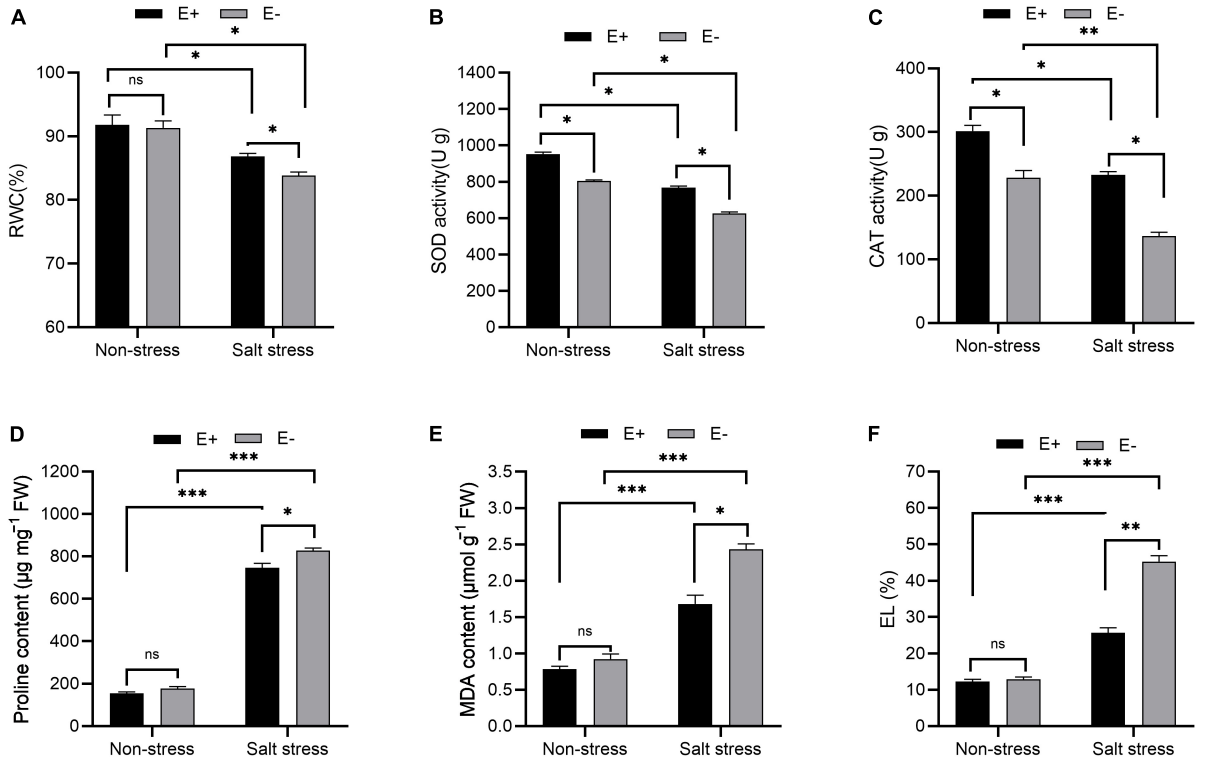

FIGURE 2
Physiological response. Relative water content (RWC) **(A)**, superoxide dismutase (SOD) activity **(B)**, catalase (CAT) activity **(C)**, proline content **(D)**, malonaldehyde (MDA) content **(E)** and electrolyte leakage (EL) **(F)** of bermudagrass with inoculated and uninoculated plants under salt stress. Bars denote means ± SE of four treatment. "Non-stress" represents bermudagrass grown without NaCl condition; "Salt stress" represents bermudagrass under 250 mM salt conditions. "E + " represents the infection of *Enterobacter ludwigii i*, "E−" represents the absence of *E. ludwigii*. "*," "**", "***" indicate significant differences at $P < 0.05$, $P < 0.01$, and $P < 0.001$, respectively, and "ns" represents no significant difference.

decreased significantly in salt-stressed bermudagrass plants grown with E + compared with E− plants (Figures 3D–F; $P < 0.05$).

Chlorophyll and carotenoid content increased under salt stress in E + plants compared with E− plants (Figures 4A,B; $P < 0.05$). The chlorophyll and carotenoid contents were 1.17 and 0.23 mg g^{-1} FW in E− plants compared with 1.36 and 0.32 mg g^{-1} FW in E + plants.

Inoculation of *Enterobacter ludwigii* B30 affected levels of abscisic acid, indole acetic acid, and 1-aminocyclopropane-1-carboxylate under salt stress

Without SS, ABA levels did not significantly change in bermudagrass leaves in E + compared with E− treatments (Figure 5A; $P > 0.05$). Under SS, the E + treatment decreased leaf ABA content by 21.3%, to 617.93 ng g^{-1}. IAA levels in plants exposed to E + under SS were significantly higher than in E− plants (0.51 nmol g^{-1} FW and 0.27 nmol g^{-1} FW, respectively; $P < 0.05$, Figure 5B). ACC content in the leaves of bermudagrass under SS increased by 91.4% in E− plants compared with E + plants ($P < 0.05$), which led to increased ethylene production and inhibition of plant growth. Moreover, the ACC content of E + plants under SS decreased significantly compared with E− plants (12.39 ng g^{-1} FW and 21.48 ng g^{-1} FW, respectively; $P < 0.05$, Figure 5C).

Ion concentration in response to bacterial inoculation under salt stress

In the absence of SS, the E + treatment did not significantly affect Na^+ levels within bermudagrass leaf samples, but it significantly increased K^+ content ($P < 0.05$). The E + treatment significantly reduced Na^+ content in bermudagrass roots but significantly increased the K^+ content ($P < 0.05$). Under SS, the E + treatment reduced the Na^+ content in bermudagrass leaf and root samples while greatly increasing K^+ content ($P < 0.05$). Under salt stress, the E + treatment decreased the Na^+:K^+ ratio within root and leaf samples compared with E− plants (Table 2).

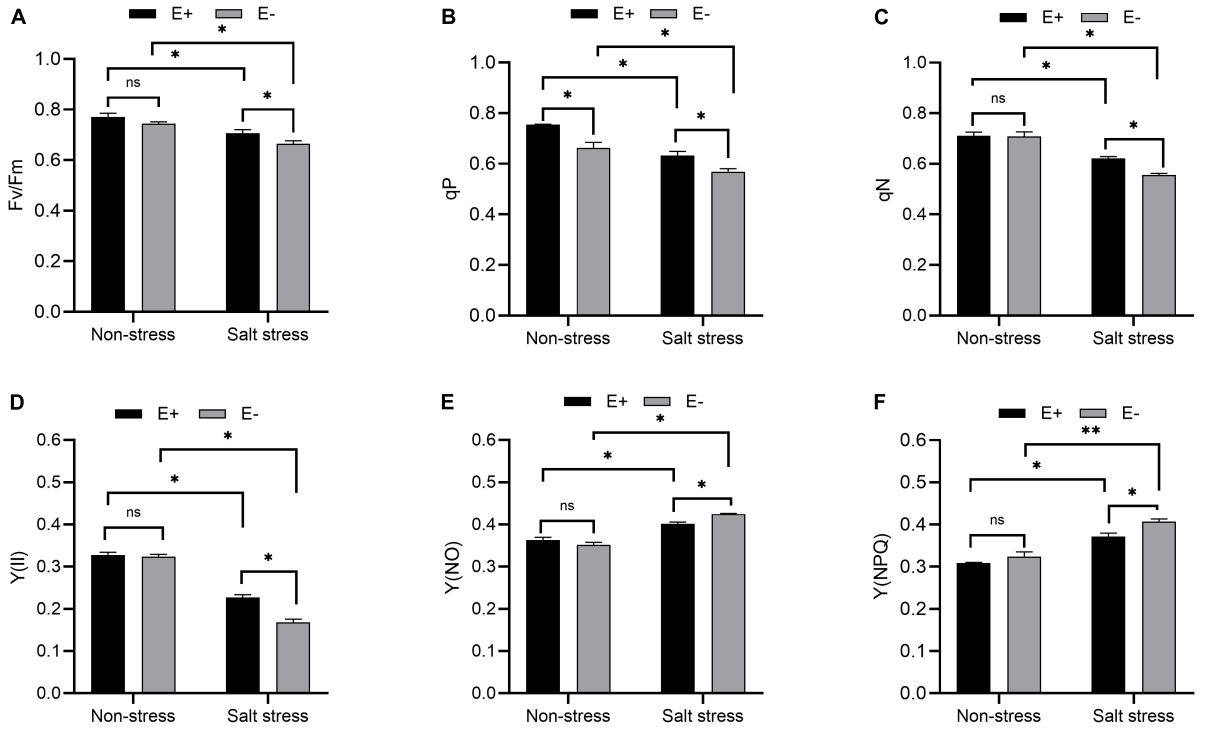

FIGURE 3
Chlorophyll fluorescence parameter. Optimal/maximal quantum yield of PS II [**(A)**; Fv/Fm], photochemical quenching [**(B)**; qP], non-photochemical quenching [**(C)**; qN], quantum yield of PSII [Y(II); **(D)**], Y(NO) **(E)** and Y(NPQ) **(F)** of bermudagrass with inoculated and uninoculated plants under salt stress. Bars denote means ± SE of four treatment. "Non-stress" represents bermudagrass grown without NaCl condition; "Salt stress" represents bermudagrass under 250 mM salt conditions. "E + " represents the infection of *Enterobacter ludwigii*, "E−" represents the absence of *E. ludwigii*. "*," "**," indicate significant differences at $P < 0.05$, and $P < 0.01$, and respectively, and 'ns' represents no significant difference.

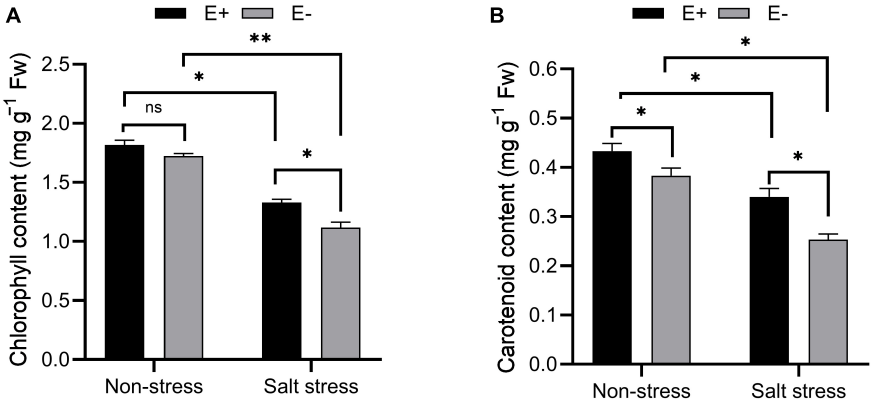

FIGURE 4
Estimation of photosynthetic pigments. Chlorophyll **(A)** and carotenoid **(B)** contents of bermudagrass with inoculated and uninoculated plants under salt stress. Bars denote means ± SE of four treatment. "Non-stress" represents bermudagrass grown without NaCl condition; "Salt stress" represents bermudagrass under 250 mM salt conditions. "E + " represents the infection of *Enterobacter ludwigii*, "E−" represents the absence of *E. ludwigii*. "*," "**," indicate significant differences at $P < 0.05$, and $P < 0.01$, respectively, and 'ns' represents no significant difference.

Changes to the ratio of concentrations of Na^+ (root) and Na^+ (leaf) indicate that Na^+ is translocated from leaves to roots in plants grown with E + under salt stress. However, this ratio was not significantly different among plants grown with E−. Under non-salt stress conditions, the ratio in plants grown with E + was significantly lower than those with E–. Under SS, the K^+

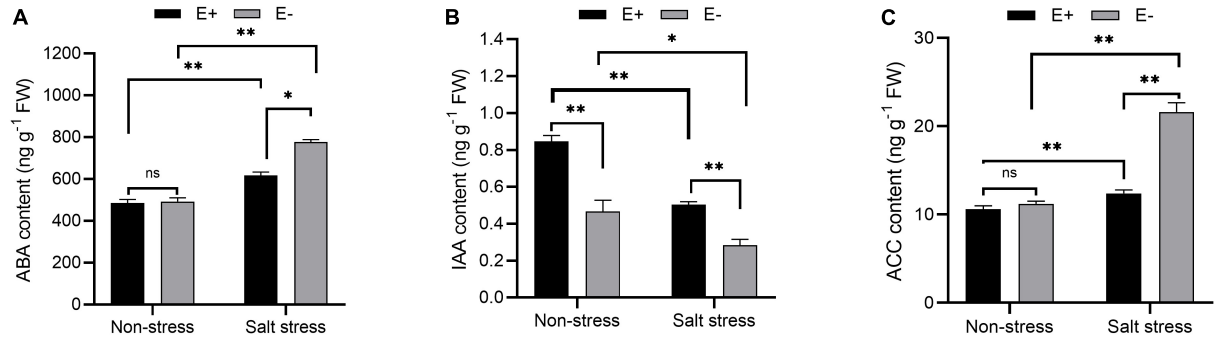

FIGURE 5
Changes in endogenous hormone content. Abscisic acid (ABA) **(A)**, indole acetic acid (IAA) **(B)** and 1-aminocyclopropane-1-carboxylate (ACC) **(C)** contents of bermudagrass with inoculated and uninoculated plants under salt stress. Bars denote means ± SE of four treatment. "Non-stress" represents bermudagrass grown without NaCl condition; "Salt stress" represents bermudagrass under 250 mM salt conditions. "E + " represents the infection of *Enterobacter ludwigii*, "E−" represents the absence of *E. ludwigii*. "*," "**," indicate significant differences at $P < 0.05$, and $P < 0.01$, respectively, and 'ns' represents no significant difference.

TABLE 2 Influence of *Enterobacter ludwigii* B30 on Na^+, K^+, Na^+: K^+ ratio in roots and leaves, Na^+ (root) to Na^+ (leaf) ratio and K^+ (root) to K^+ (leaf) ratio of bermudagrass in the presence and absence of salt stress.

Treatment	Non-stress		Salt stress		ANOVA		
	E +	E−	E +	E−	E	Salt	E × Salt
Root							
Na^+ (mg g^{-1})	1.34 ± 0.04d	2.62 ± 0.06c	24.49 ± 1.12b	32.10 ± 1.59a	***	**	**
K^+ (mg g^{-1})	9.66 ± 1.21b	5.91 ± 1.02d	11.70 ± 0.87a	7.12 ± 0.43c	***	***	***
Na^+/K^+	0.14 ± 0.02d	0.44 ± 0.04c	2.09 ± 0.18b	4.50 ± 0.22a	***	***	***
Leaf							
Na^+ (mg g^{-1})	1.63 ± 0.08c	1.62 ± 0.07c	14.47 ± 0.89b	19.97 ± 1.68a	***	***	***
K^+ (mg g^{-1})	7.89 ± 1.02c	7.40 ± 1.31c	12.66 ± 1.78a	9.91 ± 1.32b	***	***	**
Na^+/K^+	0.21 ± 0.04c	0.22 ± 0.03c	1.14 ± 0.12b	2.02 ± 0.16a	***	***	***
Root/leaf							
Na^+/Na^+	0.82 ± 0.09c	1.62 ± 0.23b	1.70 ± 0.18a	1.61 ± 0.21b	**	**	*
K^+/K^+	1.22 ± 0.21a	0.80 ± 0.11c	0.93 ± 0.18b	0.72 ± 0.22d	**	**	*

Difference in ion uptake analysis. Average ± standard error from three separate replicates. "Non-stress" represents bermudagrass grown without NaCl condition; "Salt stress" represents bermudagrass under 250 mM salt conditions. " E + " represents the infection of *E. ludwigii*, "E-" represents the absence of *E. ludwigii*. Different letters mean significantly different based on $P < 0.05$. "*," "**," "***" indicate significant differences at $P < 0.05$, $P < 0.01$, and $P < 0.001$, respectively, and "ns" represents no significant difference.

(root) to K^+ (leaf) ratio is indicative of K^+ translocation from roots to leaves in plants grown with E + . The ratio in plants grown with E + was significantly higher than in those with E–.

Bacterial community composition within rhizosphere and root

Results of the analysis of rhizosphere soil bacterial phyla showed, under salt stress, that compared with the E− treatment, the E + treatment markedly increased Bacteroidetes ($F = 4.193$, $P = 0.003$), Firmicutes ($F = 5.23$, $P = 0.023$) and Chloroflexi ($F = 3.803$, $P = 0.018$) relative abundances (Figure 6); whereas it significantly decreased the relative abundances of Actinobacteria ($F = 1.282$, $P = 0.005$) and Proteobacteria ($F = 4.186$, $P = 0.041$). The relative abundance of Bacteroidetes (Figure 6A) in the NS + E + treatment increased significantly ($P < 0.05$) compared with the NS + E− treatment, reaching 20.1%. However, the relative abundance of Proteobacteria in the S + E + treatment increased significantly ($P < 0.05$) compared with the NS + E + treatment, reaching 53.6%.

In the analysis of the root bacterial phyla, under salt stress, the *E. ludwigii* B30 treatment (E +) markedly increased Firmicutes ($F = 15.078$, $P = 0.038$) and Spirochetes ($F = 5.124$, $P = 0.029$) relative abundances compared with the SS + E− treatment (Figure 6C) whereas the relative abundances of Actinobacteria ($F = 2.333$, $P = 0.041$) and Planctomycetes ($F = 14.958$, $P = 0.018$) significantly decreased. The relative abundances of Bacteroidetes, Fibrobacteres and Verrucomicrobia in NS + E + increased significantly ($P < 0.05$)

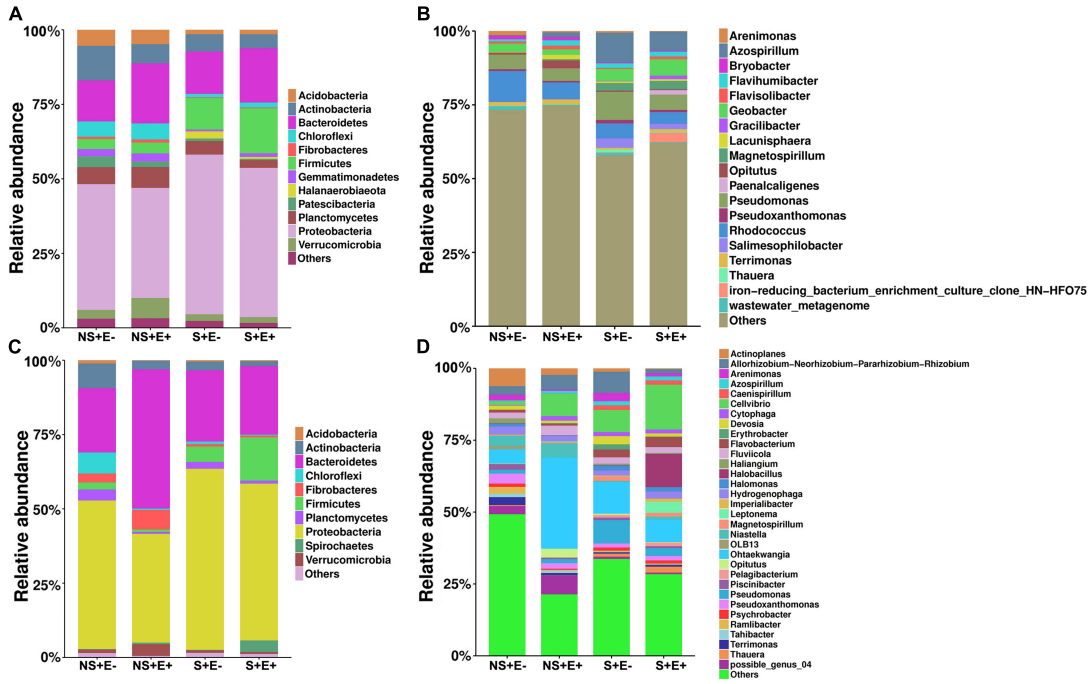

FIGURE 6
The relative abundance (at the phylum and genus level) of rhizosphere soil **(A,B)** and root **(C,D)** bacteria community under *E. ludwigii* B30 infection treatment and salt stress. ($n = 3$; "NS + " represents bermudagrass grown without NaCl condition; "S + " represents bermudagrass under 250 mM salt conditions. "E + " represents the infection of *E. ludwigii* B30, "E−" represents the absence of *E. ludwigii* B30).

compared with the NS + E− treatment. However, the relative abundance of Spirochetes and Firmicutes (Figure 6D) in the S + E + treatment significantly ($P < 0.05$) increased compared with the NS + E + treatment, reaching 3.9% and 14.6%, respectively; whereas the relative abundance of Actinobacteria in the S + E + treatment decreased significantly ($P < 0.05$) compared with the NS + E + treatment, reaching 1.6%.

Bacterial genera relative abundance in rhizosphere soil under SS in plants treated with *E. ludwigii* B30 (E +), compared with plants without *E. ludwigii* B30 (E−), showed increases for *Flavisolibacter* ($F = 4.314$, $P = 0.023$), *Geobacter* ($F = 10.868$, $P = 0.004$), *Gracilibacter* ($F = 8.353$, $P = 0.005$) and *Paenalcaligenes* ($F = 13.939$, $P = 0.001$), and decreases for *Arenimonas* ($F = 11.011$, $P = 0.002$), *Azospirillum* ($F = 1.163$, $P = 0.014$), *Pseudomonas*, *Pseudoxanthomonas* ($F = 0.036$, $P = 0.003$), *Salimesophilobacter* ($F = 2.609$, $P = 0.013$) and *Thauera* ($F = 0.551$, $P = 0.001$) (Figure 6B). The relative abundance of *Flavisolibacter*, *Lacunisphaera*, and *Opitutus* in the NS + E + treatment increased significantly ($P < 0.05$) compared with the NS + E− treatment, reaching 20.1%. However, the relative abundances of *Geobacter*, *Gracilibacter* and *Magnetospirillum* in S + E + treatment markedly ($P < 0.05$) increased compared with the NS + E + treatment.

Bacterial genera relative abundance in roots under SS in *E. ludwigii* B30 (E +) treatment compared with the S + E− treatment increased for *Actinoplanes* ($F = 1.079$, $P = 0.001$), *Cellvibrio* ($F = 0.531$, $P = 0.021$), *Halobacillus* ($F = 15.972$, $P = 0.012$), *Imperialibacter* ($F = 5.031$, $P = 0.025$), and *Pelagibacterium* ($F = 8.071$, $P = 0.006$), and decreased for *Allorhizobium-Neorhizobium-Pararhizobium-Rhizobium* ($F = 4.281$, $P = 0.004$), *Arenimonas* ($F = 1.029$, $P = 0.016$), *Erythrobacter* ($F = 14.119$, $P = 0.022$) and *Ohtaekwangia* ($F = 12.082$, $P = 0.024$) (Figure 3D). *Fluviicola* and *Ohtaekwangia* (Figure 6D) relative abundance in the NS + E + treatment increased significantly ($P < 0.05$) compared with the NS + E− treatment. The relative abundance of *Cellvibrio*, *Flavobacterium*, *Halobacillus*, *Imperialibacter* and *Leptonema* in the S + E + treatment increased significantly ($P < 0.05$) compared with the NS + E + treatment, whereas the relative abundance of *Allorhizobium-Neorhizobium-Pararhizobium-Rhizobium* in S + E + treatment dramatically ($P < 0.05$) decreased relative to NS + S +, reaching 1.5%.

Rhizosphere and root bacterial community richness, diversity and beta diversity analysis

Regardless of the endophyte treatment, salt stress greatly affected bacterial community richness measured by the Chao1 index in bermudagrass rhizosphere ($P < 0.001$, Figure 7A) and roots ($P < 0.05$, Figure 7C). Under Salt stress

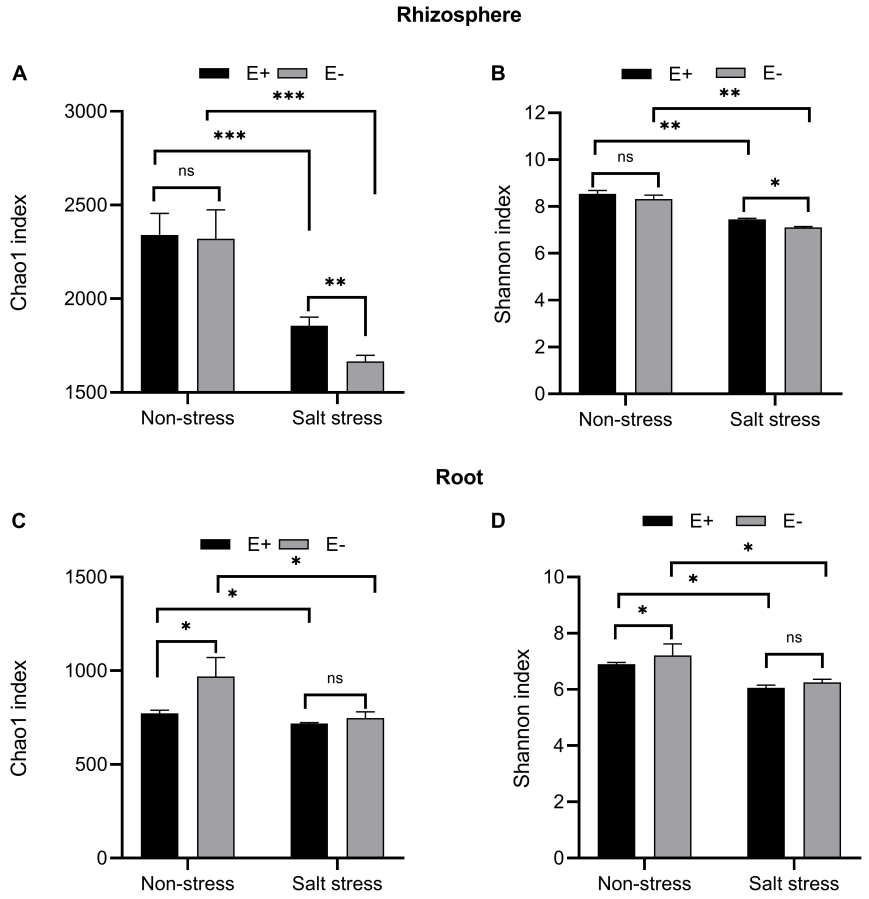

FIGURE 7
Alpha diversity. Bacterial diversity and richness in rhizosphere soil **(A, B)** and root **(C, D)**. Bars denote means ± SE of four treatment. "Non-stress" represents bermudagrass grown without NaCl condition; "Salt stress" represents bermudagrass under 250 mM salt conditions. "E + " represents the infection of *Enterobacter ludwigii*, "E−" represents the absence of *E. ludwigii*. "*," "**," "***" indicate significant differences at $P < 0.05$, $P < 0.01$, and $P < 0.001$, respectively, and 'ns' represents no significant difference.

conditions, inoculation of *E. ludwigii* B30 significantly increased bermudagrass rhizosphere soil bacterial community richness compared with the E− treatment ($P < 0.01$), while the richness of the root bacteria community remained almost unchanged ($P > 0.05$).

Regardless of the endophyte treatment, SS dramatically affected bacterial community diversity, measured by the Shannon index, in bermudagrass rhizosphere soil ($P < 0.01$, Figure 7B) and roots ($P < 0.05$, Figure 7D). Under salt stress conditions, the E + treatment, compared with the E− treatment, significantly increased the bacterial community diversity in the bermudagrass rhizosphere soil ($P < 0.05$) but not in roots ($P > 0.05$).

For rhizosphere soil bacteria, PCoA plots showed different clusters for the E + and E–, salt stress and not salt stress treatments (Supplementary Figure 2A). PCoA1 and PCoA2 (first and second principal components) explained 29.86% and 13.65% of the variance, respectively. The root bacteria PCoA plots (Supplementary Figure 2B) showed separate clusters for E + and E− treatments (PCoA1 and PCoA2 explained 18.38% and 16.16% of the variance, respectively).

LEfSe

We carried out LEfSe analysis to examine how salt stress and *E. ludwigii* B30 treatments affected bacterial taxa. There are Fifty-five bacterial taxa (from phyla to genera) with LDA scores > 4 (Figure 8A), twenty-nine of which were identified from order to genera among plants from the four treatments in bermudagrass rhizosphere soil (Figure 8B). Seven genus clades were found, including *Azospirillum*, *Pseudomonas_stutzeri,* and *Salimesophilobacter* from S + E–; *Geobacter* and *Magnetospirillum* from S + E +; Rhodococcus from NS + E–; and Opitutus from NS + E +.

There are Forty-two bacterial taxa (from phyla to genera) with LDA scores > 4 (Figure 9A), thirty of which were identified from order to genera among

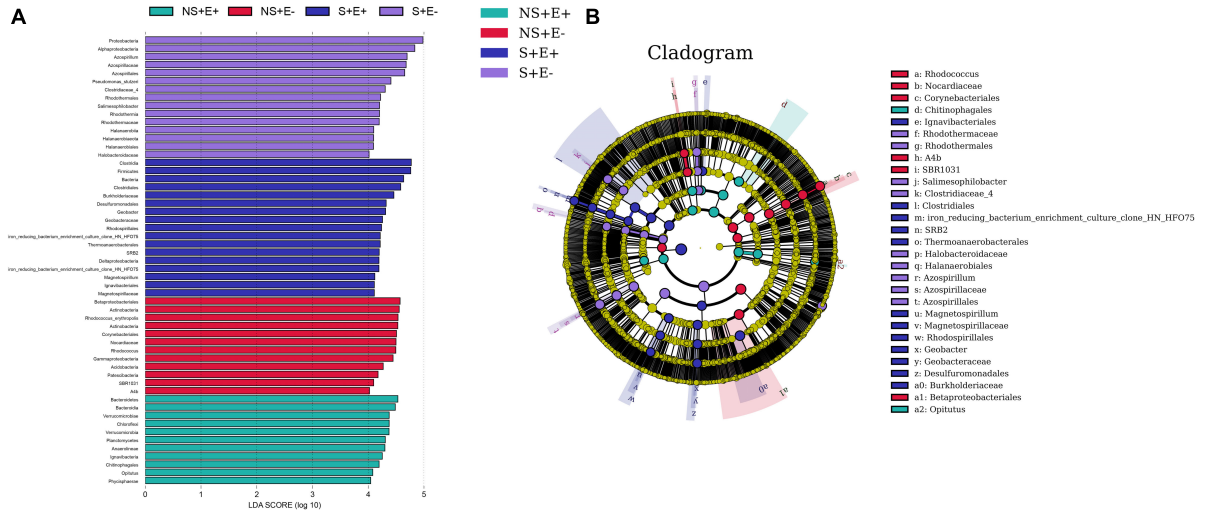

FIGURE 8
The taxonomic differences between treatments based on *E. ludwigii* B30 inoculation and salt stress in bermudagrass. The LEfSe map of bacteria including LDA **(A)** and Cladogram **(B)** in rhizosphere soil. LEfSe map is a linear discriminant analysis based on the composition of sample taxonomy according to different grouping conditions. In the four treatments, $P < 0.05$, LDA > 4 as the standard, communities with significant differences at each classification level are found to be represented by bar chart. Cladogram can intuitively show the difference information of samples at each classification level. "NS + " represents bermudagrass grown without NaCl condition; "S + " represents bermudagrass under 250 mM salt conditions. "E + " represents the infection of *Enterobacter ludwigii* B30, "E−" represents the absence of *E. ludwigii* B30.

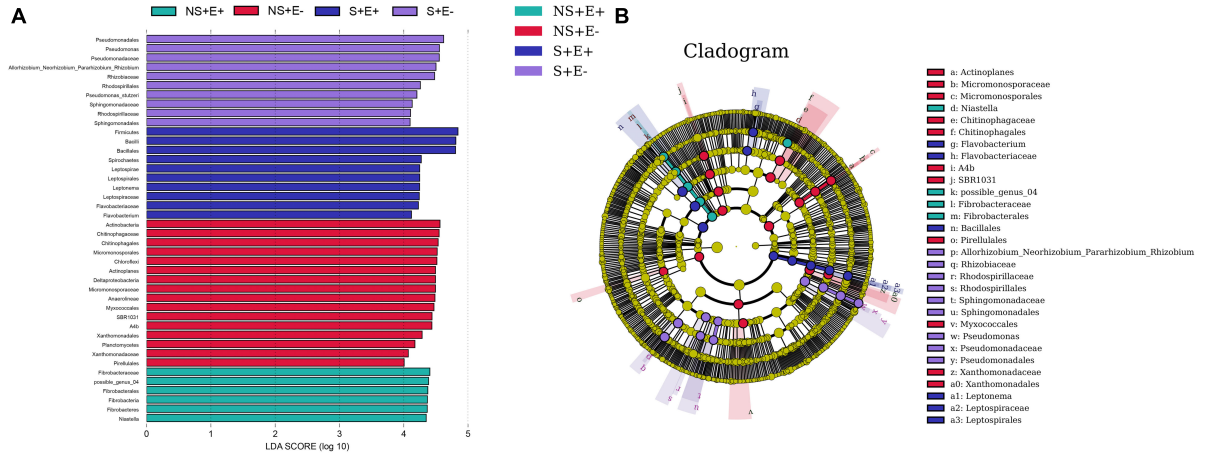

FIGURE 9
The taxonomic differences between treatments based on *E. ludwigii* B30 inoculation and salt stress in bermudagrass. The LEfSe map of bacteria including LDA **(A)** and Cladogram **(B)** in bermudagrass roots. LEfSe map is a linear discriminant analysis based on the composition of sample taxonomy according to different grouping conditions. In the four treatments, $P < 0.05$, LDA > 4 as the standard, communities with significant differences at each classification level are found to be represented by bar chart. Cladogram can intuitively show the difference information of samples at each classification level. "NS + " represents bermudagrass grown without NaCl condition; "S + " represents bermudagrass under 250 mM salt conditions. "E + " represents the infection of *Enterobacter ludwigii* B30, "E−" represents the absence of *E. ludwigii* B30.

plants from the four treatments in bermudagrass roots (Figure 9B). Nine genus clades, including *Pseudomonas*, *Allorhizobium_Neorhizobium_Pararhizobium_Rhizobium*, *Pseudomonas_stutzeri*, and *Erythrobacter* from S + E−; *Spirochetes* and *Flavobacterium* from S + E + ; *Chitinophagales* and *Actinoplanes* from NS + E−; and possible_genus_04 from NS + E + .

Redundancy analysis

The first and second RDA axes among rhizosphere soil bacteria communities and plant indicators contributed 81.55% and 12.71% to the variance (Figure 10A). The plant DW (root + shoot) was positively correlated with phyla Actinobacteria and Patescibacteria. TQ was positively related to

the phyla Chloroflexi, Fibrobacteres, and Planctomycetes. Car content showed positive associations with phyla Chloroflexi, Fibrobacteres, and Gemmatimonadetes. The first and second RDA axes in root bacteria communities and plant indicators explained 59.31% and 35.74% of the variance (**Figure 10B**), respectively. TQ was positively correlated with the phyla Verrucomicrobia, Fibrobacteres, and Bacteroidetes. The IAA content was positively correlated with the phyla Actinobacteria and Chloroflexi.

Discussion

Inoculation of *Enterobacter ludwigii* B30 enhances bermudagrass growth and affects abscisic acid, indole acetic acid, and 1-aminocyclopropane-1-carboxylate levels

Salinity directly affects soil biological and physiochemical characteristics and has adverse impacts on plant growth and yield. The salinity-induced harmful impact on plant development can be ascribed to specific ion toxicity, osmotic stress, nutritional disturbance, or combinations of these factors (Parida and Das, 2005; Ju et al., 2021). Studies have inoculated endophytic bacteria to alleviate SS within numerous plant species (Pal et al., 2021; Sofy et al., 2021). In this study, *E. ludwigii* B30 inoculation enhanced plant development in non-SS and SS conditions, which was manifested by higher shoot height, root length, shoot and root biomass (DW and FW) (**Table 1**) and TQ (**Figure 1**).

Enterobacter ludwigii has been shown to be an ACC deaminase-containing bacteria that can ameliorate drought tolerance in wheat (Gontia-Mishra et al., 2016). Studies have reported applying endophytic bacteria to ameliorate abiotic stresses such as NaCl stress through enhanced ACC deaminase activity (Lu et al., 2021; Sofy et al., 2021). We observed that the ACC content of *E. ludwigii* B30 inoculated bermudagrass was significantly lower than un-inoculated bermudagrass under SS (**Figure 5**). ACC is an immediate precursor of ethylene and under SS, plants characteristically generate increased amounts of ethylene (Barnawal et al., 2017). Ethylene restricts plant growth and proliferation until ethylene levels are reduced, and the SS condition is ameliorated. ABA participates in several physiological processes in plants, such as plant growth, stomatal aperture control, and stress responses to drought or salt stress (Fahad et al., 2015). This effect was evident in the present study as *E. ludwigii* B30 inoculations reduced ABA content within bermudagrass under SS. This may be associated with decreased plant ethylene content as it has been shown to affect plant ABA production (Rowe et al., 2016). Thus, ACC deaminase-containing bacterial inoculation could affect plant ABA levels. The application of *E. ludwigii* B30 reduced ABA levels within stressed plants, indicating that stress levels decreased within these plants. In the present study, ACC deaminase-containing bacteria reduced the adverse effects of harmful stresses by managing ethylene and ABA levels. Some researchers reported that endophytic bacteria inoculation increased ABA content in pea (*Pisum sativum*) under non-stress situations (Sofy et al., 2021). The rise in ABA content induces photosynthesis-influencing stomatal closure (Hamayun et al., 2010). We found that ABA levels did not significantly change in bermudagrass leaves in E + compared with E− treatments under non-stress conditions. We propose that the *E. ludwigii* B30 strains used by us may better balance phytohormones content and promote plant growth, which await further study.

Enterobacter ludwigii B30 inoculation promoted growth while enhancing resistance in NaCl stressed plants, in association with IAA generation and increased ACC deaminase activity. The longer root growth in plants inoculated with *E. ludwigii* B30 under salt stress and in the control plants was partially because of the isolate-generated IAA. The endophytic bacteria-generated phytohormones, in particular IAA are related to root initiation as well as enhanced adventitious and lateral root length, thereby helping nutrient absorption in host plants (Otlewska et al., 2020).

Enterobacter ludwigii B30 modulates plant physiology in bermudagrass under salt stress while mitigating NaCl-mediated ionic disturbance

Decreased RWC is a characteristic osmotic stress response in plants. Our results show that after bacterial inoculation, RWC was elevated under SS. Ahmad et al. (2013) and Abd Allah et al. (2018) reported elevated RWC in chickpea (*Cicer arietinum* Linn.) and mung bean (*Vigna radiata*), respectively, following bacterial inoculation upon SS. Bacterial inoculation can alleviate the SS-induced inhibition of root growth while promoting effective root system development, thus facilitating increased water absorption from deeper in the soil in plants under stress (Marulanda et al., 2010). Abiotic stresses such as SS can induce ROS production within plants. ROS typically react with essential compounds in plants, such as cell membranes, proteins, and lipids, thereby causing oxidative stress (OS) (Wang and Huang, 2019). To combat ROS-induced OS, plants produce a range of antioxidative enzymes such as catalase (CAT) and superoxide dismutase. SOD has been recognized as the first line of defense to resist ROS by enhancing ROS scavenging through the catalysis of O_2^- dismutation into O_2 and H_2O_2 (Wei et al., 2022b). Likewise, CAT can eliminate excess plant superoxide radicals, thereby protecting against OS, promoting the accumulation of dry matter, and improving plant

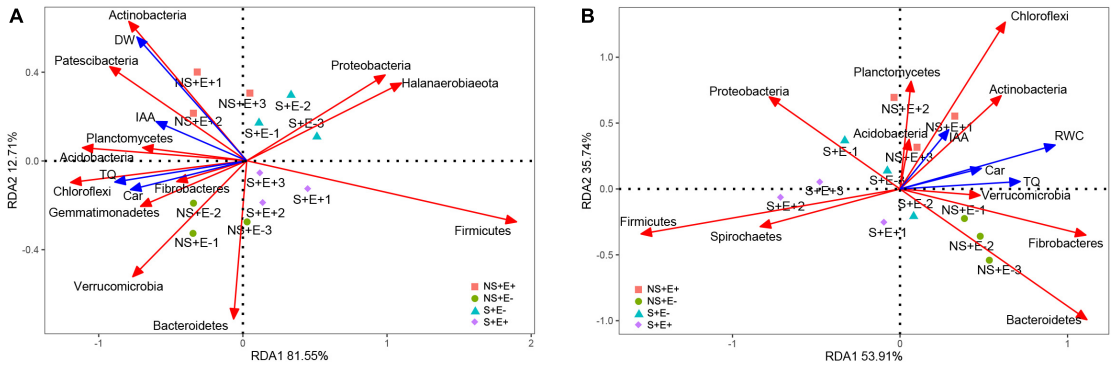

FIGURE 10
Redundancy analysis of relative abundance (phylum level) of rhizosphere soil bacteria and 4 treatments (NS + E−, NS + E + , S + E−, S + E +), and Environmental factors. Environmental factors include Total dry weigh (DW), Turf quality (TQ), indole acetic acid (IAA) and carotenoid (Car) [$n = 3$; **(A)**]. Redundancy analysis of relative abundance (phylum level) of root bacteria and 4 treatments (NS + E−, NS + E + , S + E−, S + E +), and Environmental factors. Environmental factors include Relative water content (RWC), Turf quality (TQ), indole acetic acid (IAA) and carotenoid (Car) [$n = 3$; **(B)**]. "NS + " represents bermudagrass grown without NaCl condition; "S + " represents bermudagrass under 250 mM salt conditions. "E + " represents the infection of *E. ludwigii* B30, "E−" represents the absence of *E. ludwigii* B30.

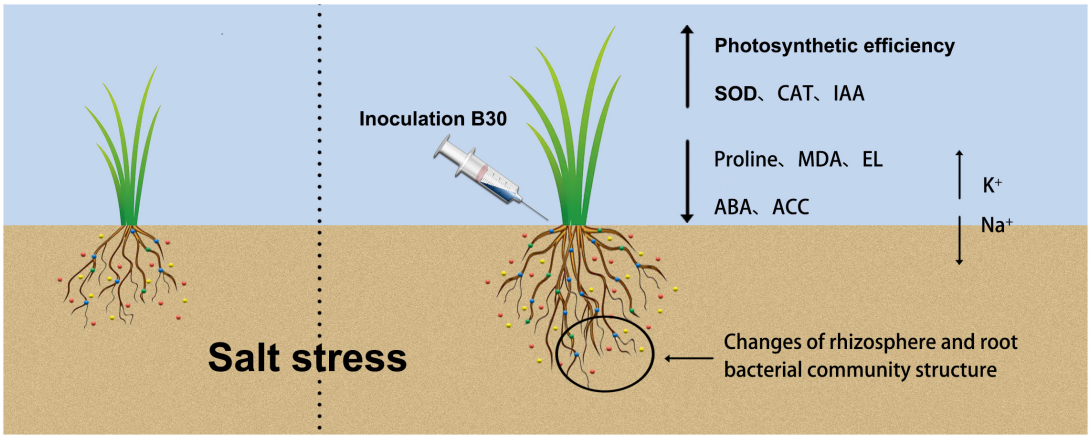

FIGURE 11
A graphical abstract describing the mechanism of endophytic bacterium strain B30 enhancing salt tolerance of bermudagrass we followed to accomplish this work. Under salt stress, B30-associated bermudagrass shows an increase in shoot biomass production as compared to non-B30 bermudagrass. Inoculation of B30 changed rhizosphere and root bacterial community structure, recruited some beneficial bacteria in rhizosphere and root, then enhanced Photosynthetic efficiency, SOD, CAT, and IAA content, also decreased proline, MDA, EL, ABA, and ACC content. Besides, B30 balanced Na^+ and K^+ concentration between shoot and root of bermudagrass to alleviate the damage caused by salt stress.

resistance (Ahmad et al., 2022). Our results show CAT and SOD activities markedly decreased within *E. ludwigii* B30 inoculated bermudagrass compared with non-inoculated bermudagrass under SS (**Figure 3**). These results agree with the study of Masmoudi et al. (2021), where endophytic halotolerant *Bacillus velezensis* FMH2 inoculation reduced the OS-mediated harmful impacts in tomato (*Lycopersicon esculentum*).

Oxidative stress (OS) causes lipid peroxidation damage to cell membranes, thereby altering permeability and increasing cellular electrolyte leakage and malondialdehyde content (Alexander et al., 2020). In this study, EL and MDA content was elevated in SS treatments, indicating damage to cell membranes in saline conditions. *E. ludwigii* B30 inoculation decreased MDA content and EL (**Figure 3**), suggesting that endophytic bacteria helped to resist the harmful NaCl-induced impact on the intact plant cell membrane. Baek et al. (2020) showed similarly that endophytic bacteria inoculation decreased the EL and MDA content in salt-stressed rice (*Oryza sativa* L.).

It is challenging to maintain cellular viscosity and turgidity in plants upon SS. To overcome this, plants produce osmolytes/osmoprotectants, which assist in their survival under harsh conditions while maintaining intracellular water retention (Zulfiqar et al., 2020). As an AA, proline can serve as an osmoprotectant that exerts a range of effects upon different

abiotic stresses and as a scavenger to eliminate hydroxyl free radicals (Chen et al., 2020). Sofy et al. (2021) found that endophytic bacterium *B. subtilis* inoculation increased the proline content in salt-stressed pea, which may be caused by a change in proline-metabolizing enzymes' activity. Additionally, it has been proposed that higher proline concentrations might facilitate the scavenging of ROS to protect proteins and other important biomolecular structures and prevent adverse effects of SS (Abd Allah et al., 2018). However, we noticed that under SS, plants with *E. ludwigii* B30 inoculation exhibited reduced proline contents. However, we observed that bacteria-inoculated plants had low proline content under SS. Decreased in proline content in bacteria-inoculated and salt-stressed plants, indicate that the synthesis of osmotically active substances was not enhanced despite the presence of the salt. This finding has been reported by many scientists and was connected with the alleviation of salt stress (Jha et al., 2011; Rojas-Tapias et al., 2012). We propose that the *E. ludwigii B30* strains we utilized activate a mechanism distinct from the promotion of proline synthesis that is in charge of reducing salt stress. The plant's response to salt stress' osmotic component is proline production. Since bacterial inoculation prevents the rise in proline content, it is possible that bacteria reduce osmotic stress (Szymańska et al., 2020). As a result, the osmotic adjustment is not necessary since the synthesis of osmoprotective chemicals, such as proline, is constrained, which lowers the energy cost of acclimating to salt.

As a photosynthesis parameter, Fv/Fm can be used for detecting plant stress (Maxwell and Johnson, 2000). Fv/Fm measures disturbances in the thylakoid structure at PSII donor sites or photosynthetic electron transport (Zhang et al., 2018). The qP metric, which represents the fraction of PSII open centers, can be used to evaluate energy dissipation by means of PSII electron transport (Rohacek, 2002). Fv/Fm and qP values were higher in *E. ludwigii* B30 inoculated bermudagrass than in non-inoculated bermudagrass under salt stress, indicating that *E. ludwigii* B30 was important for helping the plant maintain optimum photosynthesis. The qN processes associated with heat dissipation can protect photosynthesis when more light energy is absorbed than can be utilized (Müller et al., 2001). qN is measured by decreased PSII antenna efficiency resulting from the great luminal [H +] and xanthophyll cycles, while the latter is related to the proton gradient closely associated with PSII–PSI electron transport (Kramer et al., 2004). In this study, carotenoid levels (**Figure 4**) and qN (**Figure 3**) in bermudagrass increased after inoculation with *E. ludwigii* B30 compared with non-inoculated bermudagrass under salt stress, suggesting that *E. ludwigii* B30 alleviated the SS-induced inhibition of the lutein cycle while significantly increasing photosynthetic protection.

Light energy absorbed by chlorophyll is processed in 3 pathways, namely, photosynthesis (photochemistry), dissipation as heat, and re-emission as light-chlorophyll fluorescence-sometimes referred to as qN (Oxborough and Baker, 1997; Macedo et al., 2008). Following Kramer et al. (2004),

$$Y(II) + Y(NPQ) + Y(NO) = 1$$

Y(II) represents photochemical yield, and the PSII-mediated photochemical energy conversion efficiency, Y(NPQ) is the down-regulation mediated dissipation yield, and Y(NO) is the additional non-photochemical loss yield. Y(NO) measures the non-light-mediated (basal or dark) quenching process. Y(NPQ) is also a measure of chlorophyll, carotenoid, and photoinhibition, and it may just represent changes in those rapidly reversible processes. The above three parameters compete with each other so that an increase in one induces a reduction in the other two. Therefore, by determining chlorophyll fluorescence yield, data regarding changes in heat dissipation and photochemistry efficiency can be acquired. This is determined by the elevation of pH differences in and outside of the thylakoid membrane (ΔpH) occurring, in the case of light saturation, during linear photosynthetic electron transport. In addition, it is related to xanthophyll cycle activation (Crouchman et al., 2006). Our results show Y(II) in *E. ludwigii* B30 inoculated bermudagrass PSII, following SS treatment, decreased compared with non-inoculated bermudagrass; whereas Y(NO) and Y(NPQ) increased compared with non-inoculated bermudagrass (**Figure 3**), suggesting that the *E. ludwigii* B30 application significantly increased the PSII photochemical efficiency under salt stress. Based on alterations of pigment levels (**Figure 4**), we observed that *E. ludwigii* B30 positively affected chlorophyll, carotenoid level, and photosynthetic performance in bermudagrass under SS. Endophytic bacteria are reported to have a similar protective effect on photosynthetic pigments within sugar beet (*Beta vulgaris* L.) under SS (Shi et al., 2010). Such increases in chlorophyll and carotenoid content may suggest that *E. ludwigii* B30 application increased the absorption of light, protected bermudagrass plant photosynthetic systems, and enhanced the capacity of PSII for processing photochemistry under salt stress.

We found that the ratio of Na^+(root) to Na^+(leaf) markedly decreased in un-inoculated bermudagrass compared with *E. ludwigii* B30 inoculated bermudagrass under SS, indicating that *E. ludwigii* B30 inoculation restricted Na^+ translocation from the roots to aerial parts of bermudagrass, thereby restricting toxic Na^+ accumulation within photosynthetic tissues (Porcel et al., 2016). Sahu et al. (2021) showed similarly that endophytic bacteria inoculation restricted Na^+ translocation from the roots to shoot in salt-stressed tomato. Under SS, excess Na^+ ions will compete against K^+ (the other macronutrient), inducing nutritional and metabolic disturbance and exerting adverse impacts on plants. An increased K^+/Na^+ ratio is an indicator of an efficient SS resistance mechanism (Etesami and Glick, 2020). Plants in the present study also exhibited a markedly decreased Na^+ (root, leaf) concentration and increased K^+ (root, leaf) concentration after *E. ludwigii* B30 application under SS, which suggest that endophytic

bacteria help to enhance plant development through altering ion selectivity while maintaining an increased K^+ content in comparison with Na^+. These results agree with the study of Shi et al. (2022), where endophytic strain *B. megaterium* ZS-3 inoculation improved the K^+/Na^+ ratio in *Arabidopsis thaliana* to alleviate SS. We found increased Na^+ and decreased K^+ levels within uninoculated SS-exposed plants compared with controls, whereas there was no such effect in plants inoculated with *E. ludwigii* B30. The decline in Na^+ levels following *E. ludwigii* B30 inoculation could result from bacterial exopolysaccharides binding to cations (in particular Na^+) within roots, preventing cation transfer into leaves and alleviating SS within plants (Ashraf et al., 2004).

Enterobacter ludwigii B30 impacted rhizosphere and root bacterial communities in bermudagrass

Rhizosphere effects (Smalla et al., 2001), the alteration to the composition and number of microbial communities, and their impacts on above-and below-ground plant development were seen within bermudagrass following *E. ludwigii* B30 inoculation. *E. ludwigii* B30 inoculation led to increases in bermudagrass rhizosphere soil bacterial community richness and diversity (**Figure 7**). The inoculation of *E. ludwigii* B30 had a clear impact on bermudagrass rhizosphere bacterial species. These results are similar to studies on *Enterobacter cloacae* HG-1 strains which were shown to affect the rhizobacterial community structure and improve the salt tolerance of wheat (Ji et al., 2020). Our results show that *E. ludwigii* B30 affected the structure of bacterial communities within rhizosphere soils and roots (**Supplementary Figure 2**); however, the rhizosphere soil bacterial community richness and diversity increased more than the root bacterial communities (**Figure 7**). Bacterial community diversity has also been shown to decline from rhizosphere soil to roots within wheat (Donn et al., 2014) and rice (Edwards et al., 2015). This may be linked to the effect of the soil nutrient state affecting bacterial communities in soils. Typically, the root system has an important effect on linking plants with soils. Secondary metabolites can be released into the soil by plant roots, which can provide energy for microbial communities in rhizosphere soils (Vacheron et al., 2013). Bacterial communities closely connected with roots represent the simplest form (Donn et al., 2014). Conversely, other research reports that the root bacterial community richness and diversity dramatically increased within soils in *Ammophila breviligulata*, thriving in sand dunes. It is possible that in sandy soils within dune ecosystems, root exudates supply essential resources to root bacteria (Bell-Dereske et al., 2017).

Endophytic bacteria can construct and maintain the key soil bacterial populations to promote plant growth; additionally, they may change the bacterial community in plant roots, which in turn affects plant growth (Ji et al., 2021). Here, we investigated the abundance of taxa in bermudagrass rhizosphere soils and roots and hypothesized that *E. ludwigii* B30 jointly promote the growth of bermudagrass under salt stress by regulating plant physiology and altering the rhizosphere and root bacterial communities (**Figure 11**). At the phylum level, Proteobacteria, Bacteroidetes, and Firmicutes were the predominant phyla detected within E+ and E− bermudagrass rhizosphere soils. Proteobacteria are known for recycling nutrients and improvement in soil fertility and plant growth (Beckers et al., 2017). Bacteroidetes play crucial roles in recycling organic matter (Fernández-Gómez et al., 2013). Firmicutes are associated with the decomposition of plant organic matter (Pasalari et al., 2020). Additionally, known copiotrophs, such as Bacteroidetes and Chloroflexi, are associated with nutrient concentration (Trivedi et al., 2013). The relative abundance of Bacteroidetes, Firmicutes, and Chloroflexi in *E. ludwigii* B30-inoculated bermudagrass rhizosphere soil significantly increased compared with non-inoculated bermudagrass under salt stress (**Figure 6**). Combined with the RDA result, TQ was positively related to Chloroflexi levels in rhizosphere soil (**Figure 10A**). TQ of bermudagrass in the E + treatment was significantly higher than in the E− treatment, suggesting the possible role of Chloroflexi in increasing rhizosphere soil nutrient content and plant organic matter decomposition. We also noted that Acidobacteria and Actinobacteria levels in rhizosphere soil were positively associated with TQ and DW, and they have been shown elsewhere to be associated with soils with nutrient deficiency (Beckers et al., 2017). The IAA content was positively related to the Actinobacteria in roots (**Figure 10B**). Some genera in the phylum Actinobacteria, such as *Streptomyces* and *Nocardia*, can be used as beneficial bacteria to promote plant growth. *Streptomyces* has been shown to exhibit favorable PGP characteristics, which solubilized phosphates and phytates, and produced siderophores and IAA (Alotaibi et al., 2022). In bermudagrass roots, inoculation of *E. ludwigii* B30 markedly elevated *Actinoplanes*, *Cellvibrio*, *Halobacillus*, *Imperialibacter*, and *Pelagibacterium* under salt stress (**Figure 6**). Of these bacterial genera, *Halobacillus and Pelagibacterium* are genera of bacteria with halophilic properties (Chen et al., 2009; Xu et al., 2011). *Imperialibacter* has the ability to hydrolyze casein and starch (Wang et al., 2013).

Thus, these *E. ludwigii* B30 and salt-induced rhizosphere soil and root beneficial bacteria may enhance bermudagrass growth and improve salt tolerance in some specific mechanisms, such as the improvement of the nitrogen cycle and nutrient uptake and phytohormones production. These await further study. The rhizosphere and root bacterial community might contribute to improving stress tolerance for plants (Dai et al., 2019). In further study, we will propagate and inoculate beneficial endophytic bacteria into plants and analyze the relationship between and soil physi-chemical properties and rhizosphere and root microbial community under salt stress. Managing rhizosphere and root microbes and maintaining the balance of

beneficial and harmful microbes in soil and plant is an important part of improving plant tolerance to abiotic stresses.

Conclusion

This work investigated how an *Enterobacter ludwigii* B30 strain obtained from *Paspalum vaginatum* affected bermudagrass growth under salt stress. *E. ludwigii* B30 improved the osmotic adjustment, biomass accumulation, and photosynthetic efficiency of bermudagrass, as well as selective ion absorption capacities. In addition, *E. ludwigii* B30 markedly altered bacterial community structure in the rhizosphere and roots of bermudagrass. Only limited conclusions can be drawn from the present study because only one endophyte strain and plant host were used; more investigations are warranted to analyze the rhizosphere-root community interactions together with salt tolerance in plants. Our findings help to explain how bermudagrass rhizosphere and root microbiota respond to endophytic bacteria inoculation. Our results suggest that *E. ludwigii* B30 promotes plant development and may serve as an inoculant for reducing SS damage in plants.

Data availability statement

The datasets presented in this study can be found in online repositories. The names of the repository/repositories and accession number(s) can be found below: National Center for Biotechnology Information (NCBI) BioProject database under accession number PRJNA858230. Any queries should be directed to the corresponding author(s).

Author contributions

JZ and TL conceived and initiated the project. HW and WH performed the experiments. ZL and HW performed the material preparation and data collection. LG conducted the bioinformatic analysis. HW wrote the first draft of the manuscript. All authors commented on previous versions of the manuscript, contributed to the study conception and design, and read and agreed to the published version of the manuscript.

Funding

This study was supported by the Natural Science Foundation of Guangdong Province (Grant No. 2020A1515011261) and Key Research and Development Program of Guangzhou (Grant No. 202103000066).

Conflict of interest

The authors declare that the research was conducted in the absence of any commercial or financial relationships that could be construed as a potential conflict of interest.

Publisher's note

All claims expressed in this article are solely those of the authors and do not necessarily represent those of their affiliated organizations, or those of the publisher, the editors and the reviewers. Any product that may be evaluated in this article, or claim that may be made by its manufacturer, is not guaranteed or endorsed by the publisher.

Supplementary material

The Supplementary Material for this article can be found online at: https://www.frontiersin.org/articles/10.3389/fpls.2022.959427/full#supplementary-material

SUPPLEMENTARY FIGURE 1
Morphological difference in different treatments. "NS + " represents bermudagrass grown without NaCl condition; "S +" represents bermudagrass under 250 mM salt conditions. "E +" represents the infection of *E. ludwigii* B30, "E−" represents the absence of *E. ludwigii* B30.

SUPPLEMENTARY FIGURE 2
Principal coordinates analysis (PCoA) of rhizosphere soil **(A)** and root **(B)** bacterial communities at operational taxonomic units (OTUs) level based on the Bray–Curtis dissimilarities under *E. ludwigii* infection treatment and salt stress. ($n = 3$; "NS + " represents bermudagrass grown without NaCl condition; "S + " represents bermudagrass under 250 mM salt conditions. "E + " represents the infection of *E. ludwigii*, "E−" represents the absence of *E. ludwigii* B30).

References

Abd Allah, E. F., Alqarawi, A. A., Hashem, A., Radhakrishnan, R., Al-Huqail, A. A., Al-Otibi, F. O. N., et al. (2018). Endophytic bacterium *Bacillus subtilis* (BERA 71) improves salt tolerance in chickpea plants by regulating the plant defense mechanisms. *J. Plant Interact.* 13, 37–44. doi: 10.1080/17429145.2017.1414321

Ahmad, A., Blasco, B., and Martos, V. (2022). Combating salinity through natural plant extracts based biostimulants: a review. *Front. Plant Sci.* 13:862034. doi: 10.3389/fpls.2022.862034

Ahmad, M., Zahir, Z. A., Khalid, M., Nazli, F., and Arshad, M. (2013). Efficacy of *Rhizobium* and *Pseudomonas* strains to improve physiology, ionic balance and quality of mung bean under salt-affected conditions on farmer's fields. *Plant Physiol. Biochem.* 63, 170–176. doi: 10.1016/j.plaphy.2012.11.024

Alexander, A., Singh, V. K., and Mishra, A. (2020). Halotolerant PGPR *Stenotrophomonas* malto-philia BJ01 induces salt tolerance by modulating physiology and biochemical activities of *Arachis hypogaea*. *Front. Microbiol.* 11:568289. doi: 10.3389/fmicb.2020.568289

Ali, S., Charles, T. C., and Glick, B. R. (2014). Amelioration of high salinity stress damage by plant growth promoting bacterial endophytes that contain ACC deaminase. *Plant Physiol. Biochem.* 80, 160–167. doi: 10.1016/j.plaphy.2014.04.003

Alotaibi, F., St-Arnaud, M., and Hijri, M. (2022). In-depth characterization of plant growth promotion potentials of selected alkanes-degrading plant growth promoting bacterial isolates. *Front. Microbiol.* 13:863702. doi: 10.3389/fmicb.2022.863702

Ashraf, M., Hasnain, S., Berge, O., and Mahmood, T. (2004). Inoculating wheat seedlings with exopolysaccharide-producing bacteria restricts sodium uptake and stimulates plant growth under salt stress. *Biol. Fertil. Soils* 40, 157–162. doi: 10.1007/s00374-004-0766-y

Baek, D., Rokibuzzaman, M., Khan, A., Kim, M. C., Park, H. J., Yun, D., et al. (2020). Plant-growth promoting *Bacillus oryzicola* YC7007 modulates stress-response gene expression and provides protection from salt stress. *Front. Plant Sci.* 10:1646. doi: 10.3389/fpls.2019.01646

Barnawal, D., Pandey, S. S., Bharti, N., Pandey, A., Ray, T., Singh, S., et al. (2017). ACC deami-nase-containing plant growth promoting rhizobacteria protect *Papaver somniferum* from downy mildew. *J. Appl. Microbiol.* 122, 1286–1298. doi: 10.1111/jam.13417

Barrs, H., and Weatherley, P. (1962). A re-examination of the relative turgidity technique for estimating water deficits in leaves. *Austral. J. Biol. Sci.* 15, 413–428. doi: 10.1071/BI9620413

Bates, L. S., Waldren, R. P., and Teare, I. (1973). Rapid determination of free proline for water-stress studies. *Plant Soil* 39, 205–207. doi: 10.1007/BF00018060

Beard, J. B. (1973). *Turfgrass: Science and Culture*. Englewood Cliffs, NJ: Prentice Hall.

Beckers, B., Op De Beeck, M., Weyens, N., Boerjan, W., and Vangronsveld, J. (2017). Structural variability and niche differentiation in the rhizosphere and endosphere bacterial microbiome of field-grown poplar trees. *Microbiome* 5:25. doi: 10.1186/s40168-017-0241-2

Bell-Dereske, L., Takacs-Vesbach, C., Kivlin, S. N., Emery, S. M., and Rudgers, J. A. (2017). Leaf endophytic fungus interacts with precipitation to alter belowground microbial communities in primary successional dunes. *FEMS Microbiol. Ecol.* 93:fix036. doi: 10.1093/femsec/fix036

Beyer, W. F. Jr., and Fridovich, I. (1987). Assaying for superoxide dismutase activity: some large conse-quences of minor changes in conditions. *Anal. Biochem.* 161, 559–566. doi: 10.1016/0003-2697(87)90489-1

Bui, E. (2013). Possible role of soil alkalinity in plant breeding for salt-tolerance. *Biol. Lett.* 9:20130566. doi: 10.1098/rsbl.2013.0566

Caporaso, J. G., Kuczynski, J., Stombaugh, J., Bittinger, K., Bushman, F. D., Costello, E. K., et al. (2010). QIIME allows analysis of high throughput community sequencing data. *Nat. Methods* 7, 335–336. doi: 10.1038/nmeth.f.303

Chang, W., Sui, X., Fan, X.-X., Jia, T.-T., and Song, F.-Q. (2018). Arbuscular mycorrhizal symbiosis modulates antioxidant response and ion distribution in salt-stressed *Elaeagnus angustifolia* seedlings. *Front. Microbiol.* 9:652. doi: 10.3389/fmicb.2018.00652

Chen, S., Huang, H., Chen, J., Fu, C., Zhan, P., Ke, S., et al. (2020). SgRVE6, a LHY-CCA1-like transcription factor from fine-stem stylo, upregulates NB-LRR gene expression and enhances cold tolerance in tobacco. *Front. Plant Sci.* 11:1276. doi: 10.3389/fpls.2020.01276

Chen, Y., Zhang, Y., Liu, Z., Zhuang, D., Klenk, H. P., Tang, S., et al. (2009). *Halobacillus salsuginis* sp. nov., a moderately halophilic bacterium from a subterranean brine. *Int. J. Syst. Evol. Microbiol.* 59, 2505–2509. doi: 10.1099/ijs.0.010801-0

Cluis, C. P., Mouchel, C. F., and Hardtke, C. S. (2004). The *Arabidopsis* transcription factor HY5 inte-grates light and hormone signalling pathways. *Plant J.* 38, 332–347.

Compant, S., Clément, C., and Sessitsch, A. (2010). Plant growth-promoting bacteria in the rhizo- and endosphere of plants: their role, colonization, mechanisms involved and prospects for utilization. *Soil Biol. Biochem.* 42, 669–678. doi: 10.1016/j.soilbio.2009.11.024

Cordovez, V., Dini-Andreote, F., Carrion, V., and Raaijmakers, J. (2019). Ecology and evolution of plant microbiomes. *Annu. Rev. Microbiol.* 73, 69–88. doi: 10.1146/annurev-micro-090817-062524

Crouchman, S., Ruban, A., and Horton, P. (2006). PsbS enhances nonphotochemical fluorescence quenching in the absence of zeaxanthin. *FEBS Lett.* 580, 2053–2058. doi: 10.1016/j.febslet.2006.03.005

Dai, L., Zhang, G., Yu, Z., Ding, H., Xu, Y., and Zhang, Z. (2019). Effect of drought stress and developmental stages on microbial community structure and diversity in peanut rhizosphere soil. *Int. J. Mol. Sci.* 20:2265. doi: 10.3390/ijms20092265

Diskit, D., Phuntsog, D., Stanzin, A., Chaurasia, O. P., and Stobdan, T. (2018). Stress tolerance and plant growth promotion potential of *Enterobacter ludwigii* PS1 isolated from seabuckthorn rhizosphere. *Biocatal. Agric. Biotechnol.* 14, 438–443. doi: 10.1016/j.bcab.2018.04.012

Donn, S., Kirkegaard, J., Perera, G., Richardson, A. E., and Watt, M. (2014). Evolution of bacterial communities in the wheat crop rhizosphere. *Environ. Microbiol.* 17, 610–621. doi: 10.1111/1462-2920.12452

Edwards, J., Johnson, C., Santos-Medellin, C., Lurie, E., Podishetty, N. K., Bhatnagar, S., et al. (2015). Structure, variation, and assembly of the root-associated microbiomes of rice. *Proc. Natl. Acad. Sci. U.S.A.* 112, E911–E920. doi: 10.1073/pnas.1414592112

Essemine, J., Lyu, M.-J. A., Qu, M., Perveen, S., Khan, N., Song, Q., et al. (2020). Contrasting responses of plastid terminal oxidase activity under salt stress in two C4 species with different salt tolerance. *Front. Plant Sci.* 11:1009. doi: 10.3389/fpls.2020.01009

Etesami, H., and Glick, B. R. (2020). Halotolerant plant growth–promoting bacteria: prospects for alleviating salinity stress in plants. *Environ. Exp. Bot.* 178:104124. doi: 10.1016/j.envexpbot.2020.104124

Fahad, S., Hussain, S., Matloob, A., Khan, F. A., Khaliq, A., Saud, S., et al. (2015). Phytohor-mones and plant responses to salinity stress: a review. *Plant Growth Regul.* 75, 391–404. doi: 10.1007/s10725-014-0013-y

Fan, D., Subramanian, S., and Smith, D. L. (2020). Plant endophytes promote growth and alleviate salt stress in *Arabidopsis thaliana*. *Sci. Rep.* 10, 1–18. doi: 10.1038/s41598-020-69713-

Fatma, M., Asgher, M., Masood, A., and Khan, N. A. (2014). Excess sulfur supplementation im-proves photosynthesis and growth in mustard under salt stress through increased production of glutathione. *Environ. Exp. Bot.* 107, 55–63. doi: 10.1016/j.envexpbot.2014.05.008

Fernández-Gómez, B., Richter, M., Schüler, M., Pinhassi, J., Acinas, S. G., González, J. M., et al. (2013). Ecology of marine bacteroidetes: a comparative genomics approach. *ISME J.* 7, 1026–1037. doi: 10.1038/ismej.2012.169

Galaviz, C., Lopez, B. R., de-Bashan, L. E., Hirsch, A. M., Maymon, M., and Bashan, Y. (2018). Root growth improvement of mesquite seedlings and bacterial rhizosphere and soil community changes are induced by inoculation with plant growth-promoting bacteria and promote restoration of eroded desert soil. *Land Degrad. Dev.* 29, 1453–1466. doi: 10.1002/ldr.2904

Gontia-Mishra, I., Sapre, S., Sharma, A., and Tiwari, S. (2016). Amelioration of drought tolerance in wheat by the interaction of plant growth promoting rhizobacteria. *Plant Biol.* 18, 992–1000. doi: 10.1111/plb.12505

Hamayun, M., Khan, S. A., Khan, A. L., Shin, J.-H., Ahmad, B., Shin, D.-H., et al. (2010). Exogenous gibberellic acid reprograms soybean to higher growth and salt stress tolerance. *Agric. Food Chem.* 58, 7226–7232. doi: 10.1021/jf101221t

He, W., Fan, X., Zhou, Z., Zhang, H., Gao, X., Song, F., et al. (2019). The effect of *Rhizophagus irregularis* on salt stress tolerance of *Elaeagnus angustifolia* roots. *J. Forest. Res.* 31, 2063–2073. doi: 10.1007/s11676-019-01053-1

Heath, R. L., and Packer, L. (1968). Photoperoxidation in isolated chloroplasts. I. Kinetics and stoi-chiometry of fatty acid peroxidation. *Arch. Biochem. Biophys.* 125, 189–198. doi: 10.1016/0003-9861(68)90654-1

Hoffmann, H., Stindl, S., Stumpf, A. N., Mehlen, A., Monget, D., Heesemann, J., et al. (2005). Description of *Enterobacter ludwigii* sp. nov., a novel *Enterobacter* species of clinical relevance. *Syst. Appl. Microbiol.* 2, 206–212. doi: 10.1016/J.SYAPM.2004.12.009

Jha, Y., Subramanian, R. B., and Patel, S. (2011). Combination of endophytic and rhizospheric plant growth promoting rhizobacteria in *Oryza sativa* shows higher accumulation of osmoprotect-ant against saline stress. *Acta Physiol. Plant* 33, 797–802.

Ji, C., Liu, Z., Hao, L., Song, X., Wang, C., Liu, Y., et al. (2020). Effects of *Enterobacter cloacae* HG-1 on the nitrogen-fixing community structure of wheat rhizosphere soil and on salt tolerance. *Front. Plant Sci.* 11:1094. doi: 10.3389/fpls.2020.01094

Ji, C., Wang, X., Song, X., Zhou, Q., Li, C., Chen, Z., et al. (2021). Effect of *Bacillus velezensis* JC-K3 on endophytic bacterial and fungal diversity in wheat under salt stress. *Front. Microbiol.* 12:802054. doi: 10.3389/fmicb.2021.802054

Ju, Y., Kou, M., Zhong, R., Christensen, M. J., and Zhang, X. (2021). Alleviating salt stress on seedings using plant growth promoting rhizobacteria isolated from

the rhizosphere soil of *Achnatherum inebrians* infected with *Epichloë gansuensis* endophyte. *Plant Soil* 465, 349–366. doi: 10.1007/s11104-021-05002-y

Khan, M. A., Asaf, S., Khan, A. L., Adhikari, A., Jan, R., Ali, S., et al. (2020). Plant growth promoting endophytic bacteria augment growth and salinity tolerance in rice plants. *Plant Biol.* 22, 850–862. doi: 10.1111/plb.13124

Kramer, D. M., Johnson, G., Kiirats, O., and Edwards, G. E. (2004). New fluorescence parameters for the determination of QA redox state and excitation energy fluxes. *Photosynth. Res.* 79, 209–218. doi: 10.1023/B:PRES.0000015391.99477.0d

Kumar, A., Singh, S., Gaurav, A. K., Srivastava, S., and Verma, J. P. (2020). Plant growth-promoting bacteria: biological tools for the mitigation of salinity stress in plants. *Front. Microbiol.* 11:1216. doi: 10.3389/fmicb.2020.01216

Li, H., La, S., Zhang, X., Gao, L., and Tian, Y. (2021). Salt-induced recruitment of specific root-associated bacterial consortium capable of enhancing plant adaptability to salt stress. *ISME J.* 15, 2865–2882. doi: 10.1038/s41396-021-00974-2

Lichtenthaler, H. K., and Wellburn, A. R. (1983). Determinations of total carotenoids and chloro-phylls a and b of leaf extracts in different solvents. *Biochem. Soc. Transmycol.* 11, 591–593. doi: 10.1042/BST0110591

Liu, T., Zhuang, L., and Huang, B. (2019). Metabolic adjustment and gene expression for root sodium transport and calcium signaling contribute to salt tolerance in *Agrostis* grass species. *Plant Soil* 443, 219–232. doi: 10.1007/s11104-019-04140-8

Lu, L., Chang, M., Han, X., Wang, Q., Wang, J., Yang, H., et al. (2021). Beneficial effects of endophytic *Pantoea ananatis* with ability to promote rice growth under saline stress. *J. Appl. Microbiol.* 131, 1919–1931. doi: 10.1111/jam.15082

Lugtenberg, B., and Kamilova, F. (2009). Plant-growth-promoting rhizobacteria. *Annu. Rev. Microbiol.* 63:541–556.

Lutts, S., Kinet, J. M., and Bouharmont, J. (1996). NaCl-induced senescence in leaves of rice (*Oryza sativa* L.) cultivars differing in salinity resistance. *Ann. Bot.* 78, 389–398. doi: 10.1006/anbo.1996.0134

Macedo, R. S., Lombardi, A. T., Omachi, C. Y., and Rörig, L. R. (2008). Effects of the herbicide bentazon on growth and photosystem II maximum quantum yield of the marine diatom *Skeletonema costatum*. *Toxicol. Vitro* 22, 716–722. doi: 10.1016/j.tiv.2007.11.012

Madhaiyan, M., Poonguzhali, S., and Sa, T. M. (2007). Characterization of 1-aminocyclopropane-1-carboxylate (ACC) deaminase containing *Methylobacterium oryzae* and interactions with auxins and ACC regulation of ethylene in canola (*Brassica campestris*). *Planta* 226, 867–876. doi: 10.1007/s00425-007-0532-0

Marulanda, A., Azcon, R., Chaumont, F., Ruiz-Lozano, J. M., and Aroca, R. (2010). Regulation of plasma membrane aquaporins by inoculation with a *Bacillus megaterium* strain in maize (*Zea mays* L.) plants under unstressed and salt-stressed conditions. *Planta* 232, 533–543. doi: 10.1007/s00425-010-1196-8

Masmoudi, F., Tounsi, S., Dunlap, C. A., and Trigui, M. (2021). Endophytic halotolerant *Bacillus velezensis* FMH2 alleviates salt stress on tomato plants by improving plant growth and altering physiological and antioxidant responses. *Plant Physiol. Biochem.* 165, 217–227. doi: 10.1016/j.plaphy.2021.05.025

Maxwell, K., and Johnson, G.N. (2000). Chlorophyll fluorescence - a practical guide. *J Exp Bot*. 51, 659–668. doi: 10.1093/jxb/ert208

Müller, P., Li, X. P., and Niyogi, K. K. (2001). Non-photochemical quenching: a response to excess light energy. *Plant Physiol.* 125, 1558–1566. doi: 10.1104/pp.125.4.1558

Murchie, E. H., and Lawson, T. (2013). Chlorophyll fluorescence analysis: a guide to good prac-tice and understanding some new applications. *J. Exp. Bot.* 64, 3983–3998. doi: 10.1093/jxb/ert208

Oksanen, J., Kindt, R., Legendre, P., O'Hara, B., Stevens, M. H. H., Oksanen, M. J., et al. (2007). The vegan package. *Commun. Ecol. Pack.* 10:719.

Otlewska, A., Migliore, M., Dybka-Stepien, K., Manfredini, A., Struszczyk-Swita, K., Napoli, R., et al. (2020). When salt meddles between plant, soil, and mi-croorganisms. *Front. Plant Sci* 11:553087. doi: 10.3389/fpls.2020.553087

Oxborough, K., and Baker, N. R. (1997). Resolving chlorophyll a fluorescence images of photo-synthetic efficiency into photochemical and nonphotochemical components-calculation of qP and Fv'/Fm' without measuring Fo'. *Photosynth. Res.* 54, 135–142. doi: 10.1023/A:1005936823310

Pal, K. K., Dey, R., Sherathia, D. N., Devidayal, M. S., Kumar, A., Rupapara, R. B., et al. (2021). Alleviation of salinity stress in peanut by application of endophytic bacteria. *Front. Microbiol.* 12:650771. doi: 10.3389/fmicb.2021.650771

Parida, A. K., and Das, A. B. (2005). Salt tolerance and salinity effects on plants: a review. *Ecotoxicol. Environ. Saf.* 60, 324–349. doi: 10.1016/j.ecoenv.2004.06.010

Pasalari, H., Gholami, M., Rezaee, A., Esrafili, A., and Farzadkia, M. (2020). Perspectives on microbial community in anaerobic digestion with emphasis on environmental parameters: a systematic review. *Chemosphere* 270:128618. doi: 10.1016/j.chemosphere.2020.128618

Pessarakli, M. (2014). *Handbook of Plant and Crop Physiology (2014, Hardcover, Revised, New Edition)*, 3rd Edn. Boca Raton, FL: CRC Press.

Porcel, R., Aroca, R., Azcon, R., and Ruiz-Lozano, J. M. (2016). Regulation of cation transporter genes by the arbuscular mycorrhizal symbiosis in rice plants subjected to salinity suggests improved salt tolerance due to reduced Na+ root-to-shoot distribution. *Mycorrhiza* 26, 673–684. doi: 10.1007/s00572-016-0704-5

Quast, C., Pruesse, E., Yilmaz, P., Gerken, J., Schweer, T., Yarza, P., et al. (2013). The SILVA ribosomal RNA gene database project: improved data processing and web-based tools. *Nucleic Acids Res.* 41, D590–D596. doi: 10.1093/nar/gks1219

Rady, M. M., Kuşvuran, A., Alharby, H. F., Alzahrani, Y., and Kuşvuran, S. (2019). Pretreatment with proline or an organic bio-stimulant induces salt tolerance in wheat plants by improving anti-oxidant redox state and enzymatic activities and reducing the oxidative stress. *J. Plant Growth Regul.* 38, 449–462. doi: 10.1007/s00344-018-9860-5

Rascher, U., Liebig, M., and Lüttge, U. (2000). Evaluation of instant light-response curves of chlorophyll fluorescence parameters obtained with a portable cholrophyll fluorometer on site in the field. *Plant Cell Environ.* 23, 1397–1405.

Rohacek, K. (2002). Chlorophyll fluorescence parameters: the definitions, photosynthetic meaning, and mutual relationships. *Photosynthetica* 40, 13–29. doi: 10.1023/A:1020125719386

Rojas-Tapias, D., Moreno-Galván, A., Pardo-Díaz, S., Obando, M., Rivera, D., and Bonilla, R. (2012). Effect of inoculation with plant growth-promoting bacteria (PGPB) on amelioration of saline stress in maize (*Zea mays*). *Appl. Soil Ecol.* 61, 264–272.

Rowe, J. H., Topping, J. F., Liu, J., and Lindsey, K. (2016). Abscisic acid regulates root growth under osmotic stress conditions via an interacting hormonal network with cytokinin, ethylene and auxin. *New Phytol.* 211, 225–239. doi: 10.1111/nph.13882

Roy Choudhury, A., Roy, S. K., Trivedi, P., Choi, J., Cho, K., Yun, S. H., et al. (2022). Label-free proteomics approach reveals candidate proteins in rice (*Oryza sativa* L.) important for ACC deaminase producing bacteria-mediated tolerance against salt stress. *Environ. Microbiol.* doi: 10.1111/1462-2920.15937

Ryan, R. P., Germaine, K., Franks, A., Ryan, D. J., and Dowling, D. N. (2008). Bacterial endo-phytes: recent developments and applications. *FEMS Microbiol. Lett.* 278, 1–9. doi: 10.1111/j.1574-6968.2007.00918.x

Sahu, P. K., Singh, S., Singh, U. B., Chakdar, H., Sharma, P. K., Sarma, B. K., et al. (2021). Inter-genera colonization of *Ocimum tenuiflorum* endo-phytes in tomato and their complementary effects on Na+/K+ balance, oxidative stress regulation, and root architecture under elevated soil salinity. *Front. Microbiol.* 12:744733. doi: 10.3389/fmicb.2021.744733

Shi, L., Lu, L., Ye, J., and Shi, H. (2022). The endophytic strain ZS-3 enhances salt tolerance in *Arabidopsis thaliana* by regulating photosynthesis, osmotic stress, and ion homeostasis and inducing systemic tolerance. *Front. Plant Sci.* 13:820837. doi: 10.3389/fpls.2022.820837

Shi, Y., Lou, K., and Li, C. (2010). Growth and photosynthetic efficiency promotion of sugar beet (*Beta vulgaris* L.) by endophytic bacteria. *Photosynth. Res.* 105, 5–13. doi: 10.1007/s11120-010-9547-7

Singh, R. P., and Jha, P. N. (2016). A halotolerant bacterium *Bacillus licheniformis* HSW-16 aug-ments induced systemic tolerance to salt stress in wheat plant (*Triticum aestivum*). *Front. Plant Sci.* 7:1890. doi: 10.3389/fpls.2016.01890

Singh, U. B., Malviya, D., Singh, S., Singh, P., Ghatak, A., Imran, M., et al. (2021). Salt-tolerant compatible microbial inoculants modulate physio-biochemical responses enhance plant growth, Zn biofortification and yield of wheat grown in saline-sodic soil. *Int. J. Environ. Res. Public Health* 18:9936. doi: 10.3390/ijerph18189936

Smalla, K., Wieland, G., Buchner, A., Zock, A., Parzy, J., Kaiser, S., et al. (2001). Bulk and rhizosphere soil bacterial communities studied by denaturing gradient gel electrophoresis: plant-dependent enrichment and seasonal shifts revealed. *Appl. Environ. Microbiol.* 67, 4742–4751. doi: 10.1128/AEM.67.10.4742-4751.2001

Sofy, M. R., Aboseidah, A. A., Heneidak, S. A., and Ahmed, H. R. (2021). ACC deaminase containing endophytic bacteria ameliorate salt stress in *Pisum sativum* through reduced oxidative damage and induction of antioxidative defense system. *Environ. Sci. Pollut. Res.* 28, 40971–40991. doi: 10.1007/s11356-021-13585-3

Szymańska, S., Tyburski, J., Piernik, A., Sikora, M., Mazur, J., and Katarzyna, H. (2020). Raising beet tolerance to salinity through bioaugmentation with halotolerant endophytes. *Agronomy* 10:1571. doi: 10.3390/agronomy10101571

Trivedi, P., Anderson, I. C., and Singh, B. K. (2013). Microbial modulators of soil carbon storage: integrating genomic and metabolic knowledge for global prediction. *Trends Microbiol.* 21, 641–651. doi: 10.1016/j.tim.2013.09.005

Vacheron, J., Desbrosses, G., Bouffaud, M., Touraine, B., Moënne-Loccoz, Y., Muller, D., et al. (2013). Plant growth-promoting rhizobacteria and root system functioning. *Front. Plant Sci.* 4:00356. doi: 10.3389/fpls.2013.00356

Vaishnav, A., Shukla, A. K., Sharma, A., Kumar, R., and Choudhary, D. K. (2019). Endophytic bacteria in plant salt stress tolerance: current and future prospects. *J. Plant Growth Regul.* 38, 650–668. doi: 10.1007/s00344-018-9880-1

Vanderauwera, S., De Block, M., Steene, N. V., Cotte, B. V., Metzlaff, M., and Breusegem, F. V. (2007). Silenc-ing of poly (ADP-ribose) polymerase in plants alters abiotic stress signal transduction. *Proc. Natl. Acad. Sci. U.S.A.* 104:38. doi: 10.1073/pnas.0706668104

Wang, H., Li, J., Zheng, T., Hill, R. T., and Hu, X. (2013). Imperialibacter roseus gen. nov., sp. nov., a novel bacterium of the family *Flammeovirgaceae* isolated from Permian groundwater. *Int. J. Syst. Evol. Microbiol.* 63, 4136–4140. doi: 10.1099/ijs.0.052662-0

Wang, J., and Huang, R. (2019). Modulation of ethylene and ascorbic acid on reactive oxygen species scavenging in plant salt response. *Front. Plant Sci.* 10:319. doi: 10.3389/fpls.2019.00319

Wang, Z., Liang, J., Kuang, Y., Li, X., Chen, H., Tang, M., et al. (2022). Cultivation of arbuscular mycorrhizal *Broussonetia papyrifera* seedlings by planting the mycorrhizal nurse plant downwards. *Mycorrhiza* 32, 203–212. doi: 10.1007/s00572-022-01070-9

Wei, H., Wang, Y., Zhang, J., Ge, L., and Liu, T. (2022a). Changes in soil bacterial community structure in bermudagrass turf under short-term traffic stress. *Agriculture* 12:668. doi: 10.3390/agriculture12050668

Wei, H., Yang, W., Wang, Y., Ding, J., Ge, L., Richardson, M., et al. (2022b). Correlations among soil, leaf morphology, and physiological factors with wear tolerance of four warm-season turfgrass species. *Hortscience.* 57, 571–580. doi: 10.21273/HORTSCI16453-21

White, J. F., Kingsley, K. L., Zhang, Q., Verma, R., Obi, N., Dvinskikh, S., et al. (2019). Review: endophytic microbes and their potential applications in crop management. *Pest. Manag. Sci.* 75, 2558–2565. doi: 10.1002/ps.5527

Xiang, M., Moss, J. Q., Martin, D. L., and Wu, Y. (2018). The salinity tolerance of seeded-type common bermudagrass cultivars and experimental selections. *HortTechnology* 28, 276–283. doi: 10.21273/HORTTECH03975-18

Xu, X., Huo, Y., Wang, C., Oren, A., Cui, H. L., Vedler, E., et al. (2011). *Pelagibacterium halotolerans* gen. nov., sp. nov. and *Pelagibacterium luteolum* sp. nov., novel members of the family Hyphomicrobiaceae. *Int. J. Syst. Evol. Microbiol.* 61, 1817–1822. doi: 10.1099/ijs.0.023325-0

Yu, Q., Chang, Z., and Li, D. (2013). Physiological responses of creeping bentgrass cultivars to carbonate, chloride, and sulfate salinity. *Crop Sci.* 53, 1734–1742. doi: 10.2135/cropsci2012.09.0555

Zhang, J. L., Flowers, T. J., and Wang, S. M. (2010). Mechanisms of sodium uptake by roots of higher plants. *Plant Soil.* 326, 45–60. doi: 10.1007/s11104-009-0076-0

Zhang, Y., Kaiser, E., Zhang, Y., Yang, Q., and Li, T. (2018). Short-term salt stress strongly affects dynamic photosynthesis, but not steady-state photosynthesis, in tomato (*Solanum lycopersicum*). *Environ. Exp. Bot.* 149, 109–119. doi: 10.1016/j.envexpbot.2018.02.014

Zhao, X., Chen, X., Li, Z., Zhang, J., and Liu, T. (2021). An evaluation of the effects of the plant endophyte *Enterobacter* on the salt tolerance of bermudagrass. *Acta Prataculturae Silica* 30, 127–136.

Zulfiqar, F., Akram, N. A., and Ashraf, M. (2020). Osmoprotection in plants under abiotic stresses: new insights into a classical phenomenon. *Planta* 251:3. doi: 10.1007/s00425-019-03293-1

frontiers | Frontiers in Plant Science

TYPE Original Research
PUBLISHED 04 August 2022
DOI 10.3389/fpls.2022.956410

OPEN ACCESS

EDITED BY
Jing Zhang,
Nanjing Agricultural University, China

REVIEWED BY
Zhou Li,
Sichuan Agricultural University, China
Jibiao Fan,
Yangzhou University, China
Kun Zhang,
Qingdao Agricultural University, China

*CORRESPONDENCE
Qian Xu
xq20052005@126.com
Long-xing Hu
grass@hunau.edu.cn

†These authors have contributed equally to this work

SPECIALTY SECTION
This article was submitted to Plant Abiotic Stress, a section of the journal Frontiers in Plant Science

RECEIVED 30 May 2022
ACCEPTED 18 July 2022
PUBLISHED 04 August 2022

CITATION
Yang Y, Wassie M, Liu N-f, Deng H, Zeng Y-b, Xu Q and Hu L-x (2022) Genotypic-specific hormonal reprogramming and crosstalk are crucial for root growth and salt tolerance in bermudagrass (*Cynodon dactylon*). *Front. Plant Sci.* 13:956410. doi: 10.3389/fpls.2022.956410

Genotypic-specific hormonal reprogramming and crosstalk are crucial for root growth and salt tolerance in bermudagrass (*Cynodon dactylon*)

Yong Yang[1,2†], Misganaw Wassie[3†], Ning-fang Liu[2], Hui Deng[1], Yi-bing Zeng[1], Qian Xu[2,4*] and Long-xing Hu[2,4*]

[1]College of Physical Education, Changsha University, Changsha, China, [2]Department of Pratacultural Sciences, College of Agronomy, Hunan Agricultural University, Changsha, China, [3]CAS Key Laboratory of Plant Germplasm Enhancement and Specialty Agriculture, Wuhan Botanical Garden, Chinese Academy of Sciences, Wuhan, China, [4]Grassland Research Center of Hunan Province, Changsha, China

Salt stress is one of the major abiotic factors limiting the productivity of bermudagrass (*Cynodon dactylon*). However, the role of hormonal reprogramming and crosstalk in regulating root growth and salt tolerance in bermudagrass was not reported. Here, we examined the physiological and hormonal responses of two contrasting bermudagrass genotypes; 'C43,' salt-tolerant 'C198' salt-sensitive. Under salt stress, 'C43' had better membrane stability and higher photosynthetic activity than the 'C198.' Salt stress promoted root growth and improved root/shoot ratio and root activity in 'C43,' but the root growth of 'C198' was inhibited by salt stress, leading to diminished root activity. The two bermudagrass genotypes also showed critical differences in hormonal responses, especially in the roots. The root contents of indole-3-acetic acid (IAA), cytokinin derivatives, such as *trans*-zeatin riboside (*t*ZR) and dihydrozeatin riboside (DHZR) were increased in 'C43,' but decreased in 'C198' when exposed to salt stress. The root growth rate was positively correlated with the root IAA, tZR and DHZR, indicating their crucial role in root growth under salt stress. The expressions of *TAA*/*YUCCA* and *CYP735A* involved in IAA and tZR biosynthesis were induced by salt stress in 'C43,' but inhibited in 'C198,' leading to reduced hormone accumulations. Salt stress decreased the iP, tZ, and DHZ content in the roots of both genotypes, and no significant difference was observed between the two genotypes. Salt stress reduced the content of GA_3 in both genotypes by inhibiting *GA20ox* and *GA2ox* genes, which could be attributed to the reduced shoot growth in both genotypes. The increased ABA level by salt stress was significantly higher in 'C198' than 'C43.' Furthermore, there were positive and negative correlations between different hormones and

root growth, suggesting that root growth could be regulated by complex hormonal reprogramming and crosstalk. This study provides a foundation for understanding the underlying mechanisms of hormonal-mediated root growth and salt tolerance in bermudagrass.

KEYWORDS

bermudagrass, gene expression, hormone, root growth, salt stress

Introduction

Salt stress is a severe global problem that adversely affects plant growth, development, and productivity (Munns and Tester, 2008; Gupta and Huang, 2014). The primary effects of salt stress are caused by osmotic stress, which results from the accumulation of ions in the rhizosphere (Ismail et al., 2014). The accumulation of ions (mainly Na^+) in the plant cells further causes ion toxicity and inhibits various developmental processes (Munns and Tester, 2008; Deinlein et al., 2014). Salt stress induces the overproduction of reactive oxygen species (ROSs), including H_2O_2 (hydrogen oxide), $^{\cdot}O_2^-$ (superoxide anion radical), $^{\cdot}OH$ (hydroxyl radical) in different organelles and results in oxidative stress (Munns and Tester, 2008), which further disturbs cellular metabolism, and inhibit enzyme activity and photosynthesis, and cause an eventual death of plants (Yu D. et al., 2020).

Roots are the essential organs that absorb water and nutrients from the soil and supply them to the shoots (Zou et al., 2021). Depending on the severity of the stress and plant species, salt stress could impair root development by inhibiting root length and root branching (Gupta and Huang, 2014; Zou et al., 2021). However, root growth can be promoted under salt stress in halophytes (Rahman et al., 2021) and a few salt-tolerant plant species, such as bermudagrass (Hu et al., 2012, 2015). Such responses could be one of the strategies for salt stress acclimation in plants. When exposed to salt stress, plants undergo a dynamic change in the root system architecture to maintain growth and development, thereby enhancing salt tolerance (Zou et al., 2021). Root system architecture modification, such as decreasing lateral root initiation, limiting root growth rates, and redirection of root growth, are crucial mechanisms to cope with osmotic stress and maintain normal root activities under salt stress (Zou et al., 2021). Salt stress-induced increase in root/shoot ratio as a result of improved root growth and inhibition of shoot growth (Albacete et al., 2008) could be an adaptive response to recover the functional equilibrium between below- and above-ground organs, which allows the roots to obtain more water and nutrients from the root zone in saline soils (Pérez-Alfocea et al., 2010).

As a sessile organism, plants develop various complex tolerance mechanisms to cope with the adverse effects of salt stress at the morphological, physiological, biochemical, and molecular levels (Gupta and Huang, 2014). Different metabolites and hormones are produced in different organs to provide stress tolerance mechanisms. Roots are sites for the biosynthesis of various hormones and metabolites involved in salt tolerance (Lu et al., 2019).

Phytohormones regulate plant growth and development and abiotic stress responses (Ryu and Cho, 2015; Yu Z. et al., 2020). The five major plant hormones are ethylene, ABA, gibberellin (GA), auxins such as indole-3-acetic acid (IAA), and cytokinin (CK). These hormones could play vital roles in the salt tolerance of plants individually or collectively through hormonal crosstalk (Ryu and Cho, 2015; Yu Z. et al., 2020). Auxin is a crucial hormone involved in almost all stages of plant development in all organs (Wolters and Jürgens, 2009). IAA is the most active form of auxin that play a crucial role in plant growth and development, including stress response (Cao et al., 2019). ABA is recognized as a stress hormone involved in stress adaptation by inducing stomatal closure and reducing water loss (Mehrotra et al., 2014; Sah et al., 2016). Additionally, ABA could enhance root growth in a dose-dependent manner; a higher concentration inhibits root elongation while promoting root elongation at a moderate concentration (Ghassemian et al., 2000). ABA inhibited the root growth of Arabidopsis by increasing ethylene biosynthesis (Luo et al., 2014).

Cytokinin is another essential plant hormone involved in plant growth and development. CK derivatives, such as tZR and iPA facilitate the responses to delay both stomatal closure and leaf senescence under abiotic stresses, and early CK-induced metabolic disorder may be one of the reasons for the inhibition of shoot growth and leaf senescence under abiotic stress (Ryu and Cho, 2015). CKs can also play positive and negative roles in the stress tolerance of plants (Hai et al., 2020). GA is a critical growth hormone involved in seed germination, stem and root elongation, leaf expansion, flower, and seed development (Ryu and Cho, 2015). GA stimulates root growth and development by monitoring cell proliferation and

Abbreviations: ABA, abscisic acid; DHZ, dihydrozeatin; GA, gibberellic acid; iP, isopentenyl; tZ, *trans*-zeatin; iPA, isopentenyl adenosine; DHZR, dihydrozeatin riboside; IAA, indole acetic acid; tZR, *trans*-zeatin riboside; P_n, net photosynthetic rate.

elongation. The deficiency in endogenous GAs could cause the development of shorter roots and smaller root meristems (Achard et al., 2009).

Hormonal crosstalk is crucial to regulating plant growth and development (Pacifici et al., 2015). For example, ABA plays a role in root growth with auxin crosstalk (Wang et al., 2017; Sun et al., 2018). Auxin could interact with cytokinin and negatively regulate cytokinin accumulation by rapidly inhibiting cytokinin biosynthesis. In contrast, cytokinin overproduction had a slower effect on auxin to regulate plant development (Nordstrom et al., 2004). Despite the role of these hormones have been studied in different plant species (Ryu and Cho, 2015), how these hormones are reprogrammed and the role of their complex interactions in regulating root growth and salt tolerance in bermudagrass was not reported.

Bermudagrass (*Cynodon dactylon* (L). Pers.) is a warm-season turfgrass species widely used to establish sports fields, lawns, and golf courses (Pessarakli, 2015). The growth and development of bermudagrass are affected by different abiotic stresses, including salt stress (Hu et al., 2015). Our previous study showed that improving the root/shoot ratio in plants exposed to salt stress is one of the salt tolerance mechanisms in bermudagrass (Hu et al., 2012). However, the detailed mechanisms associated with the differences in root growth and salt tolerance in bermudagrass, especially at hormonal level, were not reported. Because roots are the sites of hormone synthesis, we hypothesized that the difference in root growth between salt-tolerant and salt-sensitive bermudagrass genotypes could be related to the accumulation of different phytohormones and their specific crosstalk.

In this study, we used liquid chromatography coupled with MS (LC-MS) to characterize the accumulations of different phytohormones in two contrasting bermudagrass genotypes ('C43,' salt-tolerant; 'C198' salt-sensitive) in response to salt stress. Furthermore, to understand how phytohormones are regulated at the molecular level, we investigated the mRNA expression levels of critical genes involved in different phytohormones' metabolism. Overall, this study shed light on how hormonal reprogramming and crosstalk are involved in root growth and salt tolerance in bermudagrass.

Materials and methods

Plant materials and growth conditions

Plant materials were prepared according to our previous studies (Hu et al., 2012, 2015). Briefly, uniform stolons with two nodes (5 cm long) of bermudagrass, 'C43' (salt-tolerant) and 'C198' (salt-sensitive), were planted in solid growth substances (2 peat soil: 1 sand, v/v). Two weeks after planting, an equal amount of plants was transplanted to plastic pots (7 cm diameter and 9 cm tall) filled with coarse silica sand as the plant anchor medium. Pots were suspended over tubs containing 46 L of aerated half-strength Hoagland solution (Hoagland and Arnon, 1950). The tubs were refilled every other day and renewed weekly. The bottom of the pots had a coarse nylon screen to allow the root growth into the solutions. Plants were grown in an environmentally controlled walk-in growth chamber with a temperature regime of 30/25°C (day/night) and photosynthetically active radiation levels of 800 μmol m^{-2} s^{-1} at canopy height for 14 h for 4 weeks. During the establishment period of shoot and root, the shoots were cut weekly at 4-cm height, and roots were clipped back to the bottoms of the pots at the beginning of the salt treatment to allow the plants to reach full maturity and develop uniform and equal size roots and shoots.

Treatment and experiment design

After 4 weeks of cultivation, plants were subjected to 0 mM (control), 180 mM and 300 mM NaCl (salt stress) for 10 days and then canopy height and root length were determined. Roots elongated from nylon screen into nutrient solution were sampled after 4 h light. Plants were removed from the nutrient solution and roots were gently washed for 30 s with distilled water. The root tips, encompassing the meristem and the elongation zone, were excised with a scalpel from the remaining root system and immediately frozen in liquid nitrogen and stored at −80°C for further analysis. Four independent biological replicates, each containing a pool of twenty different plants, were sampled for hormone and qPCR analysis. The salt treatments and grass genotypes were arranged in a randomized complete block design with four replicates.

Measurements

Shoot and root growth rate analysis

Shoot and root growth rates were determined as the difference in growth before and after salt treatment (Hu et al., 2012). The root growth rate was determined only for roots extending from the nylon screen at the pot bottom.

Root viability

The root activity was detected by the TTC method as described previously (Lutts et al., 2004). Briefly, 0.5 g of fresh roots were cut into pieces and quickly rinsed in deionized water containing 0.06% Tween 20 and incubated at 30°C in darkness in tubes containing 6 ml of 0.5% TTC 50 mM K_2HPO_4, pH 7.0 for 20 h. The colored root samples were blotted dry and rinsed in deionized water, then incubated in 10 ml of 95% ethanol at 60°C for 4 h under gentle agitation during the extraction. The absorbance of the extract solution was recorded at 530 nm and

root activity was calculated according to the standard curve with the following equation:

$$\text{Root activity } = D/(W \times t)[\mu g/(g.h)].$$

Where D represents the deoxidizing amount of the TTC (mg); W is the fresh weight of roots (g); t stands for the time of coloration (h).

Cell membrane stability

Cell membrane stability was determined as electrolyte leakage (EL) according to our previous study (Hu et al., 2009). Briefly, about 0.1 g plant tissues were washed with deionized water three times and placed into plastic tubes filled with 15 ml deionized water after being cut to 1 cm long segments and then shaken for 24 h. The initial conductivity (C_i) was determined using a conductivity meter (JENCO-3173, Jenco Instruments, Inc., San Diego, CA, United States). Subsequently, the tubes were autoclaved at 121°C for 20 min, and the second conductivity (C_{max}) was determined after the solution cooled to room temperature. Relative EL was calculated using the formula: EL (%) = (C_i/C_{max}) × 100.

Photosynthetic parameters

Photosynthetic gas exchange measurements were performed in the third fully expanded leaves using a portable infrared gas analyzer (Li-6400, LICOR, Inc., Lincoln, NE, United States) with the controlled atmosphere (400 μmol mol^{-1} CO_2, 500 μmol s^{-1} flow rate) and a Licor 6400 LED external light source providing a photosynthetic photon flux density of 600 μmol $m^{-2}s^{-1}$. Net photosynthetic rate (P_n) and stomatal conductance (G_s) were measured for three subsamples in each pot, with each subsample consisting of five leaves (Hu et al., 2009).

Hormone extraction and fractionation for high performance liquid chromatography-mass spectrometry analysis

Hormones were analyzed as previously described (Albacete et al., 2008). Cytokinins (tZ, ZR, DHZ, DHZR, iP, iPA), auxins (IAA, IBA), gibberellic acid (GA_3), and ABA were extracted and purified according to the method of Dobrev and Kamínek (2002). Briefly, about 0.5 g frozen tissues were ground into a fine powder using a pre-chilled mortar and pestle and then soaked in 5 ml of cold extraction mixture of methanol/water/formic acid (15/4/1, v/v, pH 2.5). After 24 h of extraction at −20°C, solids were separated by centrifugation at 12,000 ×g for 15 min, and re-extracted for 1 h in an additional 2 ml of the same extraction solution at 4°C. After centrifugation, extracts were combined with the first supernatant. Pooled supernatants were passed through a Sep-Pak tC18 cartridge (SepPak Plus, Waters, Milford, MA, United States) on an automated solid-phase extraction system (SPE215; Gilson, Middleton, WI, United States) to remove interfering lipids and plant pigments. The column was washed with 0.3 ml of extraction solvent and then combined with elutes. The combined elute evaporated in a vacuum concentrator at 40°C (MiniVac Beta, LABOGENE, Copenhagen, Denmark) and then reconstituted with 2 ml of 1 M formic acid. The hormone-containing fraction was passed through an Oasis MCX 96-Well Plate 150 mg (Waters) preconditioned with 2 ml of methanol followed by 2 ml of 1 M formic acid. After washing with 1 M formic acid, ABA and auxins were eluted with 2 ml of methanol, and cytokinins were eluted with 2 ml of 0.35 M ammonia in 60% (v/v) methanol as indicated in Dobrev and Kamínek (2002). Each fraction was evaporated to dryness in a vacuum concentrator, and the residues were dissolved in a 500 μl of water/methanol (70/30, v/v) mixture. Before injection, the dissolved fraction was filtered through 13-mm-diameter Millex filters with a 0.22-μm-pore nylon membrane (Millipore, Bedford, MA, United States) and the samples were transferred to 2-ml HPLC vials.

Analyses were carried out on a high-performance liquid chromatography (HPLC)-mass spectrometry (MS) system (Accela; Thermo Fisher Scientific, San Jose, CA, United States) coupled to a triple quadrupole mass spectrometer (TSQ Quantum Access MAX, Thermo Fisher Scientific, San Jose, CA, United States) and equipped with a heated electrospray ionization source (HESI-I). For each sample, 10 μl was injected into a Zorbax SB-C18 HPLC column (3.5 μm, 150 × 2.1 mm, Agilent Technologies) maintained at 35°C and eluted at a flow rate of 200 μl min^{-1}. Mobile phase A consisted of water with 0.1%formic acid, and mobile phase B (methanol), was used for the chromatographic separation. The elution program maintained 70% A, 30% B for 3 min, then a linear gradient from 30 to 70% B in 7 min, followed by another linear gradient from 70 to 95% B in 10 min, and finally 95% B maintained for another 5 min. The column was equilibrated with the starting composition of the mobile phase for 30 min before each analytical run. The eluting ions were subjected to multiple reaction monitoring (MRM). The mass spectrometer was operated in the positive mode for cytokinins and IAA, and negative mode for ABA with a capillary spray voltage of 3500 V and a scan speed of 22,000 (m/z)/s from 50 to 600 m/z. Instrument control, data acquisition and processing were performed with Xcalibur 2.1 software (Thermo Fisher Scientific, San Jose, CA, United States). The level of plant hormones (tZ, t-ZR, DHZ, DHZR, iP, iPA, ABA, GA_3, IBA, and IAA) in the samples were quantified using the calibration curves constructed for each analyzed component (0.5, 1.0, 2.0, 5.0, and 10.0 μg.ml^{-1}) and corrected with the labeled forms of each compounded as internal standards at 0.1 μg.ml^{-1}. The recovery percentages ranged between 90 and 92%.

qRT-PCR analysis of genes involved in hormone biosynthesis

Total RNA was extracted from fresh leaves and roots using the Trizol reagent (Invitrogen, Carlsbad, CA, United States) according to the user's manual. After extraction, the RNA pellet

was dissolved in 100 μl of RNase-free water. RNase-free DNase I was added to the total RNA to remove DNA contamination. The total RNA concentration was then determined by absorbance at 260 nm and RNA quality was evaluated on a 0.8% agarose gel. The first-strand cDNA fragments were synthesized from 2 μg of total RNA using oligo(dT)12-18 primer using a cDNA synthesis kit (Fermentas, Burlington, ON, Canada). The gene-specific primers (**Table 1**) were designed based on the target gene sequences using Primer 5 software (Hu et al., 2015). The actin gene was used as an internal standard. The qRT-PCRs were performed with ABI7500 in a final volume of 20 μl, with each containing 2 μl of cDNA, 10 μl of 2 × SYBR Green qPCR Mix (Takara, Otsu, Shiga, Japan) and 2 μM of the forward and reverse primers. Three independent biological replicates of each sample and two technical replicates of each biological replicate were used for real-time PCR analysis. The thermal cycling conditions were as follows: 40 cycles of 95°C denaturation for 5 s, and 52∼55°C annealing and extension for 20 s. After the PCR, a melting curve was generated by gradually increasing the temperature to 95°C to test the amplicon specificity. The relative expression of genes was calculated using the $2^{-\Delta\Delta Ct}$ method (Livak and Schmittgen, 2001).

Statistical analysis

All data were subjected to two-way ANOVA(analysis of variance) according to the general linear model procedure of SAS (SAS Institute, Cary, NC, United States) to determine the effects of genetypes, salinity and their interactions. Treatment means were separated using the Duncan's multiple range test at the $P = 0.05$ level of probability.

Results

Phenotypic responses of bermudagrass to salinity stress

Salt stress caused severe damage to shoot growth in both bermudagrass genotypes, but the effect was more pronounced in the 'C43' genotype, as evidenced by severe leaf damage and reduced shoot growth (**Figure 1**). Both genotypes showed a higher shoot growth rate than root growth under normal conditions, and the salt-sensitive genotype had significantly higher shoot and root growth rates than the salt-tolerant (**Figure 1**). Interestingly, root growth was promoted in the salt-tolerant genotype 'C43,' but inhibited in the salt-sensitive 'C198' genotype (**Figure 1C**). Although both genotypes exhibited a high root-to-shoot ratio when exposed to salt stress, the tolerant genotype had a significantly higher root/shoot ratio and root activity than the salt-sensitive genotype up on salt stress (**Figures 1D**, **2**).

Physiological responses of bermudagrass to salinity stress

We measured electrolyte leakage in the leaves and roots of the two bermudagrass genotypes to investigate the degree of salt stress-induced membrane damage (**Figure 3**). The two genotypes did not show a significant difference under control conditions. However, salt stress exposure significantly increased ion leakage in the leaves and roots of both genotypes, more pronounced in the salt-sensitive genotype (**Figure 3**). Notably, salt stress-induced electrolyte leakage was lower in the roots than in the leaves in both genotypes (**Figure 3**).

Furthermore, to get insights into the effect of salt stress on the photosynthetic process of bermudagrass, we measured net P_n and G_s in the leaves of both genotypes after salt stress. There were no significant differences in these parameters between the two bermudagrass under normal conditions. But, salt stress significantly reduced P_n (**Figure 4A**) and G_s (**Figure 4B**) in both genotypes compared to the control. The decrease in these photosynthetic parameters was aggravated with increasing salt concentration. Interestingly, the salt-tolerant genotype 'C43' showed significantly higher P_n and G_s than the salt-sensitive bermudagrass, indicating its tolerance to salt stress (**Figures 4A,B**).

Hormonal responses to salinity stress

Given the role of phytohormones in salt tolerance, an HPLC-MS/MS approach was used to quantify the accumulations of various phytohormones in both genotypes after salt exposure. The representative chromatogram of hormone standards and tissue extracts showed that ABA, auxin (IAA, IBA), cytokinins (tZ, tZR, DHZ, DHZR, iP, iPA) and GA_3 had clear separations (**Supplementary Figure 1**). Under the control condition, a significant difference was observed for DHZR between the roots of two genotypes (**Figure 5A**). Salt stress decreased the iP, tZ and DHZ content in the roots of both genotypes compared to the control, and no significant difference was observed between 'C43' and 'C198' under both salt stress levels. Despite salt stress decreased the content of root iPA in both genotypes, 'C43' had significantly higher root iPA content than 'C198' at 180 and 300 mM salt treatments. Interestingly, the root tZR content was significantly increased in the salt-treated 'C43,' but decreased in 'C198' compared to the control (**Figure 5A**).

Both genotype's leaf iP and iPA content showed decreasing trends with increasing NaCl concentrations (**Figure 5B**).

TABLE 1 Primers used for real-time quantitative PCR in this study.

Gene name	Accession		Primers sequences (5′–3′)	Size (bp)	Tm (°C)
NCED	XP_008646127.2	F	CATTCCTCTTCCTCTTGTGT	122	55
		R	GTGTATGCTATGTTGCCTAG		
ZEP	XM_012847662.1	F	ATCTGTCTGTCCGAATAGTG	170	56
		R	CAGTTGGCGATGATGCTA		
IPT	XP_022682330.1	F	GTGGACGAGAGAGTTGGA	226	56
		R	GAACGCCGACAAGATACA		
CKX	XP_004970152.1	F	GTCTCGTCGTCGTAGTTC	232	58
		R	CGCTCTACTCCAACTTCTC		
CYP735A	OQU80479.1	F	CTCGTGGATCACCATCTG	244	58
		R	CAAGAAGAAGAACAGCAACA		
TAA	XP_002455113	F	GGCGACACCTACATTGAG	173	55
		R	GACACCGTGAAGAGCATAA		
YUCCA	PAN21149.1	F	CGAAGATGACAGCATTGAAG	128	52
		R	CGACATTGGAGCACTAACA		
GA2ox	XP_004953177.1	F	CGAAGTAGATGAACGATAGC	199	53
		R	CTCAGGTCCAACTGCATT		
GA20ox	XP_002463483.1	F	ACCACCTTGTCCATCTCC	143	53
		R	GCCTTCGTCGTCAACATC		
Actin		F	TCTGAAGGGTAAGTAGAGTAG		
		R	ACTCAGCACATTCCAGCAGAT		

Relative to the control, the leaf iP content of 'C43' decreased to 91% and 71% and that of 'C198' to 45% and 37% under 180 and 300 mM NaCl, respectively. In 'C43' bermudagrass, 180 and 300 mM NaCl decreased the leaf iPA content to 85% and 71%, but to 44% and 34% l in 'C198,' respectively, relative to the control (Figure 5B). Under control conditions, the leaf tZR and DHZR content were higher in 'C43' than 'C198.' Salt stress caused a significant decline in leaf DHZ content in 'C198' but had no effect in 'C43.' Compared to the control, salt stress significantly increased leaf tZR content in 'C43' by 1.3- and 1.4-fold under 180 and 300 mM NaCl levels, respectively. In contrast, salt stress significantly decreased leaf tZR content in 'C198' to 75% and 37% relative to the control (Figure 5B). Salt stress significantly increased leaf DHZR content in both genotypes, with a higher level in 'C43' than 'C198' bermudagrass.

Salt stress increased the accumulation of ABA in the roots of both genotypes when compared to the control, which was increased by 80% and 267% in 'C43' and by 166% and 412% in 'C198' after exposure to 180 mM and 300 mM NaCl levels, respectively (Figure 6A). Under the control condition, the root GA_3 content was higher in 'C198' than in 'C43.' The root GA_3 content significantly decreased with salt treatments in both genotypes (Figure 6A). Salt stress caused a significant reduction in leaf IAA content in 'C198,' whereas the leaf IAA content significantly increased in 'C43' after salt stress. Relative to the control, the root IAA content was increased by 1.4- and 2.1-fold in 'C43,' but decreased to 67% and 54% in the salt-sensitive bermudagrass under 180 and 300 mM NaCl levels, respectively (Figure 6A). The root IBA content was higher in 'C43' than 'C198' under control conditions and showed an opposite trend in both genotypes under salt stress compared to the IAA content. Increasing the salt stress level decreased root IBA content in 'C43' and significantly increased in 'C198' compared to the control plants (Figure 6A).

Salt stress also induced a remarkable accumulation of ABA in the leaves of both genotypes compared to the control. Exposure of plants to 180 mM and 300 mM NaCl increased ABA content by 2.9- and 5.4-fold in 'C43' and 4.6- and 10.7-fold in 'C198' relative to the control, respectively (Figure 6B). The salt-sensitive bermudagrass exhibited higher leaf GA_3 content than the salt-tolerant under control conditions. The leaf GA_3 content significantly decreased with an increasing salt concentration in both genotypes (Figure 6B). Salt stress caused a significant reduction in leaf IAA content in 'C198' but significantly increased in 'C43' after salt stress exposure. We observed 1.4- and 2.1-fold increase in leaf IAA content in 'C43' under 180 and 300 mM NaCl, respectively. In comparison, leaf IAA content was significantly decreased to 67% and 54% in 'C198' after 180 and 300 mM NaCl, respectively (Figure 6B).

Furthermore, correlation analysis was performed to understand the relationship between different traits. The result showed that leaf and root ABA contents were negatively correlated with the shoot growth rate under salt stress. The shoot growth rate was positively correlated with the leaf IAA, GA_3 and iPA, and root iP and iPA content. The root growth rate

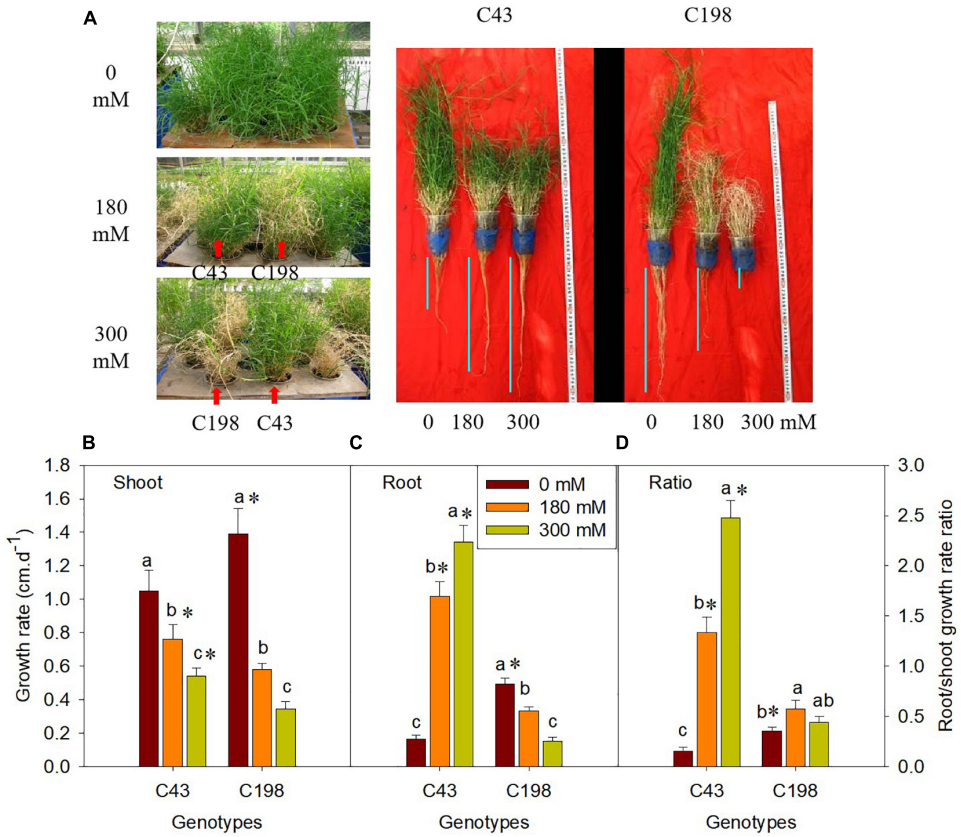

FIGURE 1
Effect of salt stress on phenotype of bermudagrass (**A**; C43, tolerant genotype; C198, sensitive genotype), and on the shoot growth rate **(B)**, root growth rate **(C)** and root/shoot ratio **(D)** in two genotypes of bermudagrass. Bars marked by the same letters are not significant at $P < 0.05$ (Tukey's test) for the comparison of different salt concentrations within a given genotype. Bars marked with star (*) indicate significance at $P < 0.05$ (Tukey's test) between the two genotypes at a given salt concentration. Data represent the mean ± SD of four independent biological replicates.

was positively correlated with the leaf iP, iPA, tZ and tZR, and root IAA, tZR and DHZR content under salt stress (Table 2).

Hormones related gene expressions in bermudagrass

To further examine whether salt regulation of root and shoot growth was associated with hormonal responses at the transcription level, the expression of genes involved in the biosynthesis of ABA, GA, cytokinins, and IAA were measured using quantitative RT-PCR. We investigated the transcription levels of two ABA biosynthesis genes, Zeaxanthin epoxidase (*ZEP*) and 9-*cis*-epoxycarotenoid dioxygenase (*NCED*). Salt stress did not affect the expression of *ZEP* in both genotypes. However, the expression of *NCED* was markedly increased in the roots of the two bermudagrass genotypes, more profoundly in 'C198' than in 'C43' (Figure 7A). We also analyzed the expression levels of the isopentenyl transferase (*IPT*) and *CYP735A* genes, encoding the key enzymes involved in the biosynthesis of tZR. Salt stress did not affect the expression level of *IPT* in the roots of both genotypes. Interestingly, *CYP735A* exhibited contrasting expression between the two bermudagrass in response to salt stress, increased in 'C43' and decreased in 'C198' (Figure 7A). We examined the changes in the expression of genes involved in the degradation of cytokinins (cytokinin oxidase/dehydrogenases, *CKX*). Salt stress caused a remarkable increase in the expression level of *CKX* in 'C198,' particularly under severe salt stress (300 mM). In comparison, only a slight increase in the expression level of CKX was observed in 'C43' under severe salt stress (300 mM) (Figure 7A).

The genes encoding the key enzymes for IAA biosynthesis, *TAA* and *YUCCA*, were up-regulated in 'C43' and down-regulated in 'C198' following salt stress (Figure 7B). The expression level of GA-synthesis genes (*GA20ox*) and GA-degradation genes (*GA2ox*) were significantly down-regulated under salt stress in the roots of the two genotypes (Figure 7B). Salt stress induced the expression of *NCED* in the leaves of the two bermudagrass genotypes, while the *ZEP* was markedly increased in 'C43' but decreased in 'C198' under salt stress

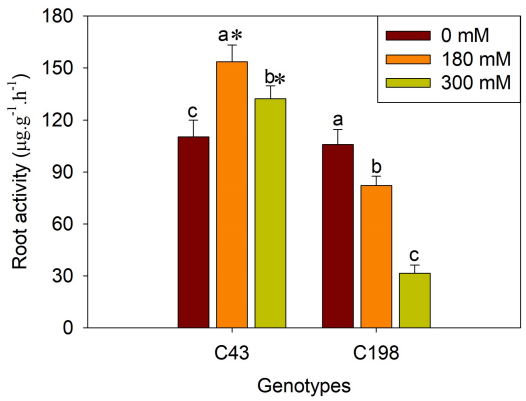

FIGURE 2
Effects of salt stress on root activity in the two bermudagrass genotypes (C43, tolerant; C198, sensitive). Bars marked by the same letters are not significant at $P < 0.05$ (Tukey's test) for the comparison of different salt concentrations within a given genotype. Bars marked with star (*) indicate significance at $P < 0.05$ (Tukey's test) between the two genotypes at a given salt concentration. Data represent the mean ± SD of four independent biological replicates.

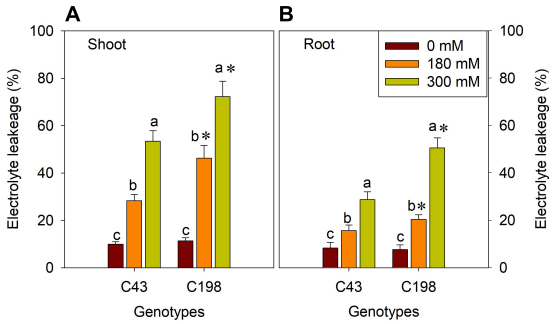

FIGURE 3
Effects of salt stress on shoot **(A)** and root **(B)** membrane stability in the two bermudagrass genotypes (C43, tolerant; C198, sensitive). Bars marked by the same letters are not significant at $P < 0.05$ (Tukey's test) for the comparison of different salt concentrations within a given genotype. Bars marked with star (*) indicate significance at $P < 0.05$ (Tukey's test) between two genotypes at a given salt concentration. Data represent the mean ± SD of four independent biological replicates.

(Figure 8A). Contrastingly, the expression levels of *IPT* and *CYP735A* were increased in the leaves of 'C43' but decreased in 'C198' after salt stress (Figure 8A). Salt stress increased the expression level of *CKX* only in the leaves of 'C198' (Figure 8A). *TAA* and *YUCCA* expression levels were significantly decreased in leaves of both genotypes under salt stress conditions, with a pronounced decrease in 'C198' than in 'C43' compared to the control (Figure 8B). Similarly, the expression levels of *GA20ox* and *GA2ox* involved in GAs metabolism were significantly decreased with an increasing salt concentration in the leaves of both genotypes (Figure 8B).

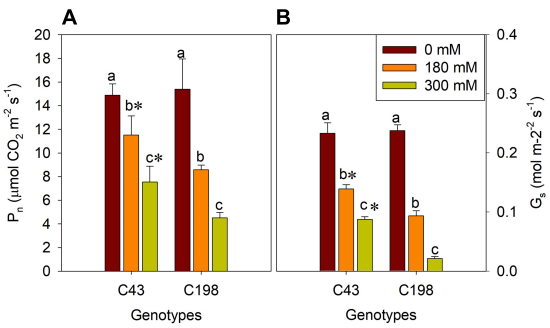

FIGURE 4
Effects of salt stress on leaf net photosynthetic rate (P_n, **A**) and stomatal conductance (G_s, **B**) in the two genotypes of bermudagrass (C43, tolerant; C198, sensitive). Bars marked by the same letters are not significant at $P < 0.05$ (Tukey's test) for the comparison of different salt concentrations within a given genotype. Bars marked with star (*) indicate significance at $P < 0.05$ (Tukey's test) between the two genotypes at a given salt concentration. Data represent the mean ± SD of four independent biological replicates.

Discussion

The adverse impact of salt stress on plant growth and development and related tolerance mechanisms have been widely reported in various plant species (Zelm et al., 2020; Zhao et al., 2021). However, how plants reprogram different phytohormones in response to salt stress and mechanisms associated with phytohormones-mediated root growth and salt tolerance are poorly understood, especially in bermudagrass. This study investigated the morphological, physiological and hormonal responses of two contrasting bermudagrass genotypes; salt-tolerant 'C43' and susceptible 'C43' (Hu et al., 2012, 2015).

The deleterious effect of salt stress is intensely associated with osmotic stress and ion toxicity due to the accumulation of toxic ions in plant cells (Munns and Tester, 2008). Increasing evidences revealed that salt stress reduces membrane integrity, water content, enzyme activity, and photosynthesis (Shahid et al., 2020; Fang et al., 2021). When exposed to moderate and high salt stress levels, the two bermudagrass genotypes showed a clear phenotypic difference. Under salt stress, the salt-tolerant bermudagrass 'C43' showed better green leaves, membrane stability, and photosynthetic activity than the salt-sensitive 'C198.'

Plant roots are a primary organ for nutrient and water uptake from the soil. Thus, the root system could play a key role in plant salt tolerance (Zou et al., 2021). The literature revealed that salt stress harms the growth and development of plant roots. Meanwhile, studies also indicated that salt stress could promote root growth in salt-tolerant grasses/halophytes (Meng et al., 2018; Rahman et al., 2021). In the present study, the two genotypes showed a contrasting root growth under salt

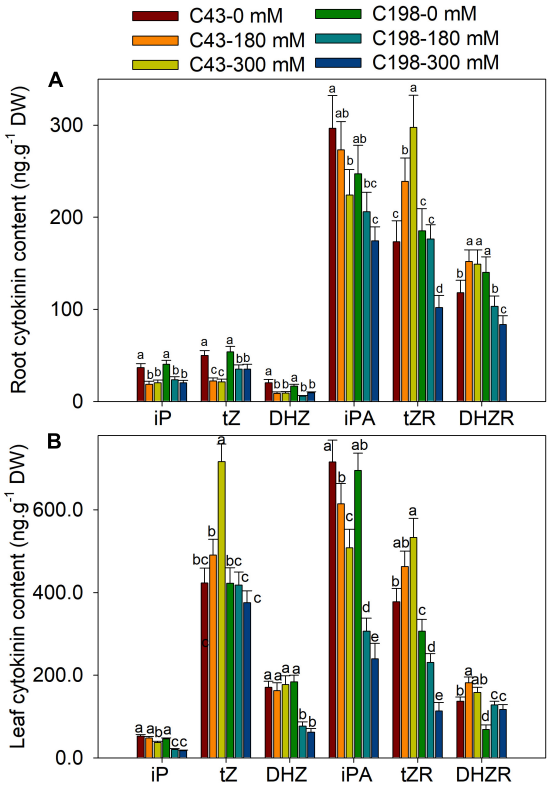

FIGURE 5
Effects of salt stress on root **(A)** and leaf **(B)** cytokinin content in the two genotypes of bermudagrass (C43, tolerant; C198, sensitive). Bars marked by the same letters are not significant at $P < 0.05$ (Tukey's test) for the comparison of different salt concentrations in two genotypes. Data represent the mean ± SD of four independent biological replicates.

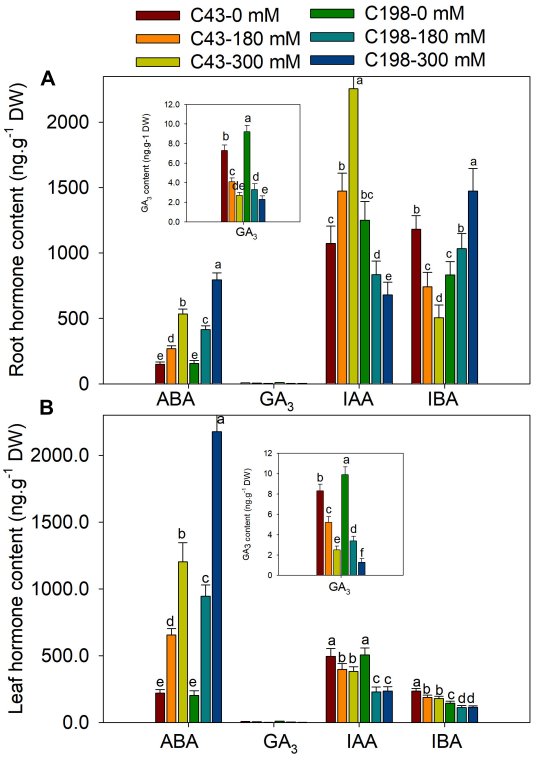

FIGURE 6
Effects of salt stress on root **(A)** and leaf **(B)** cytokinin content in the two genotypes of bermudagrass (C43, tolerant; C198, sensitive). Bars marked by the same letters are not significant at $P < 0.05$ (Tukey's test) for the comparison of different salt concentrations in two genotypes. Data represent the mean ± SD of four independent biological replicates.

stress. The root growth of the salt-tolerant bermudagrass 'C43' was promoted by salt stress, resulting in the higher root/shoot ratio and root activity. Conversely, the root growth of the salt-sensitive bermudagrass was significantly inhibited by salt stress, leading to a lower root/shoot ratio and diminished root activity.

It is well established that an improved root growth under salt stress could retain more toxic ions and prevent translocation to the shoot, providing a crucial mechanism of salt stress tolerance (Cassaniti et al., 2009). Additionally, better root growth could help plants uptake more water and nutrients from the soil under salt-induced osmotic stress conditions (Zou et al., 2021). Here, the salt-tolerant genotype appeared to allocate more energy to root growth, as evidenced by promoted root growth in response to salt stress, which could be an adaptive response to recover the functional equilibrium under new environmental conditions

TABLE 2 Linear correlation coefficients between growth parameters.

Leaf hormones		ABA	IAA	IBA	GA_3	iP	iPA	tZ	tZR	DHZ	DHZR
	Shoot growth rate	−0.92*	**0.77***	0.17	**0.97***	0.035	**0.76***	−0.04	0.14	0.56	−0.27
	Root growth rate	0.48	0.06	0.10	−0.16	**0.74***	**0.85***	**0.84***	**0.61***	0.31	0.19
	Root/shoot growth ratio	0.56	−0.07	−0.05	−0.28	**0.90***	**0.66***	**0.90***	**0.88***	0.12	0.42
Root hormones											
	Shoot growth rate	**−0.95***	0.04	0.46	0.64	**0.82***	**0.62***	0.39	0.12	0.25	0.29
	Root growth rate	0.02	**0.87***	**−0.91***	−0.38	−0.06	0.03	−0.39	**0.87***	−0.15	**0.74***
	Root/shoot growth ratio	0.42	**0.88***	−0.61	−0.59	−0.47	−0.06	**−0.79***	0.55	−0.44	0.27

*Indicate significant correlation at the 0.05 level.
The bold values are also indicating significant correlation at the 0.05 level.

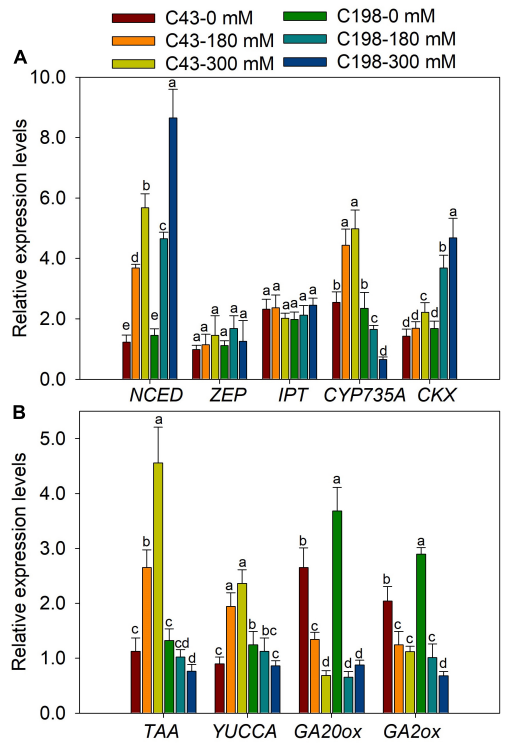

FIGURE 7
Gene expression levels in roots of the two bermudagrass genotypes differing in salt tolerance (C43: tolerant; C198: sensitive). **(A)** genes related to ABA and cytokinin biosynthesis; **(B)** genes relate to auxin and GA biosynthesis. Bars marked by the same letters are not significant at $P < 0.05$ (Tukey's test) for the comparison of different treatments. Data represent the mean ± SD of four independent biological replicates.

(Li and Li, 2017). Overall, the better green leaves, membrane stability, and higher photosynthetic activity in 'C43' could result from improved root growth that retains more toxic ions and/or maintains the water and nutrient supply to the shoots.

Cytokinin is involved in bermudagrass root growth and salt tolerance

Cytokinin is the most crucial hormone that plays a crucial role in the plant cell cycle and various developmental processes, including cell division, cell elongation, transportation of nutrients, root growth, and abiotic stress response (Wu et al., 2021). In this study, the three derivatives of CK, tZ, tZR and DHZR were notably increased in the salt-tolerant genotype but decreased in the salt-sensitive genotype, suggesting that CK may play roles in bermudagrass root growth and salt stress tolerance. Similar results have been reported in *Suaeda salsa* under salinity stress (Guo et al., 2020). *Adenosine phosphate-isopentenyl transferase (IPT)* is a key enzyme that catalyzes the *de novo* synthesis of CKs and the biosynthesis of the major derivatives of CKs, iP- and tZ is catalyzed by *IPT*. Overexpression of *IPT* has enhanced the biosynthesis of CKs (Galichet et al., 2008). In our study, the expression of *IPT* was notably upregulated in the leaves of 'C43' genotype, which could be attributed to the higher accumulation of tZ in 'C43' leaves. But, *IPT* was decreased in 'C198,' resulting in a decrease in tZ content. *CK oxidase/dehydrogenases (CKX)*, an enzyme that catalyzes the degradation of CK, was upregulated by salt stress in both genotypes, but 'C198' had significantly higher expression in both leaves and roots, resulting in lower CK contents in both tissues. The upregulation of *IPT* in the salt-tolerant bermudagrass was responsible for the accumulation of CK, especially tZ, and may be involved in the salt tolerance of bermudagrass (**Figure 9**).

CYP735A is one of the critical enzymes involved in the CK biosynthesis pathway and is required for shoot growth in Arabidopsis (Kiba et al., 2013). Mutation of *CYP735A* significantly reduced the contents of tZ and tZR, leading to a pronounced growth defect in Jatropha plants (Cai et al., 2018). In our study, the concentration of tZR was significantly

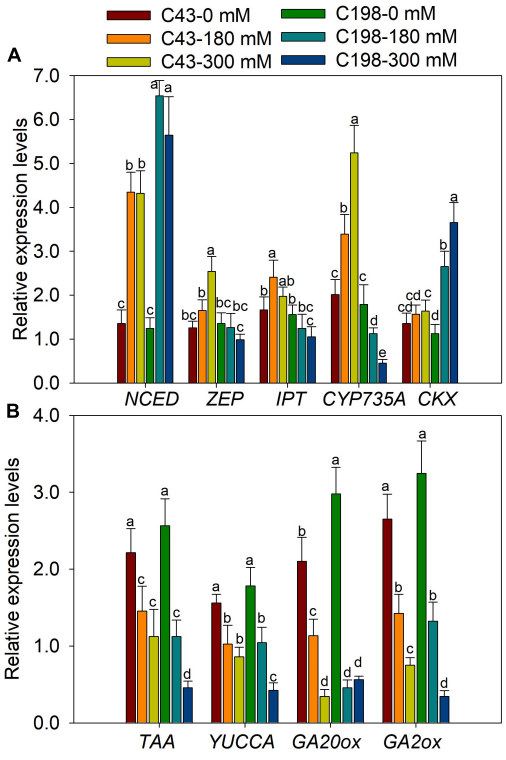

FIGURE 8
Gene expression levels in leaves of the two bermudagrass genotypes differing in salt tolerance (C43: tolerant; C198: sensitive). **(A)** genes related to ABA and cytokinin biosynthesis; **(B)** genes relate to auxin and GA biosynthesis. Bars marked by the same letters are not significant at $P < 0.05$ (Tukey's test) for the comparison of different treatments. Data represent the mean ± SD of four independent biological replicates.

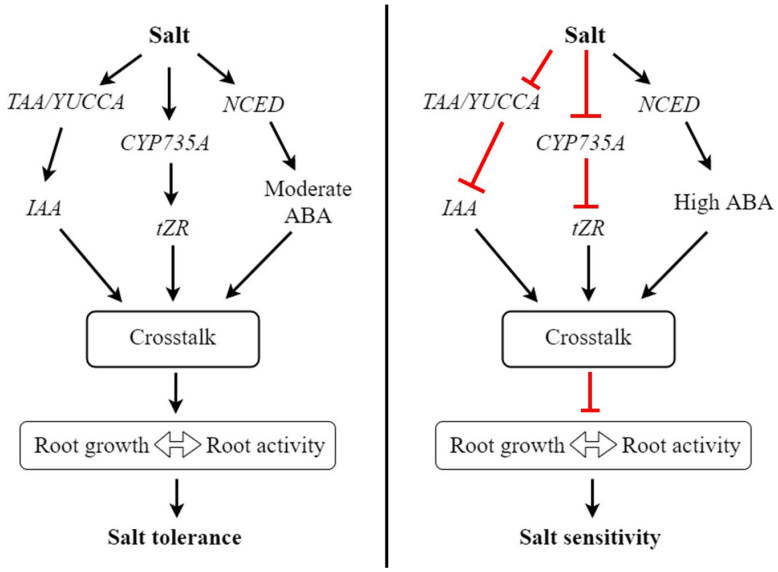

FIGURE 9
A proposed working model of how hormonal reprogramming and crosstalk are involved in root growth and salt tolerance in bermudagrass. In roots, salt stress induces the expression of *TAA/YUCC, CYP735A,* and *NCED* genes involved in auxin, cytokinin, and ABA biosynthesis, respectively. The activation of these genes increases the accumulation of respective hormones in roots. Subsequently, these hormones could work together through hormonal crosstalk and increase root growth and root activity, ultimately improving salt tolerance in bermudagrass. In contrast, salt stress inhibits the expression of *TAA/YUCC* and *CYP735A* genes, leading to reduced auxin and cytokinin levels in roots, respectively. On the other hand, salt stress strongly induces the expression of *NCED*, leading to the accumulation of a high level of ABA in roots. The reduced levels of auxin and cytokinin and high ABA level undergo hormonal crosstalk in roots and inhibit root growth, thus diminishing root activity and increasing salt sensitivity in bermudagrass.

higher in the roots of 'C43' genotype, suggesting that the accumulation of this CK derivative could play a significant role in bermudagrass salt tolerance by promoting root growth. Interestingly, the expression of *CYP735A* was remarkably increased in the roots of 'C43,' but decreased in 'C43' after salt stress. Collectively, these results demonstrate that the upregulation of crucial CK biosynthesis genes could play an invaluable role in salt tolerance by increasing the accumulation of CK derivatives, thereby promoting root growth and salt tolerance in bermudagrass (**Figure 9**).

The role of auxin in root growth and salt tolerance in bermudagrass

Auxin is a critical plant hormone involved in growth, development, and stress response (Zhao, 2018; Blakeslee et al., 2019; Cao et al., 2019). Auxin can be synthesized through the *tryptophan aminotransferase (TAA)* and *YUCCA (YUC)* enzymes-mediated (TAA)/YUCCA (YUC) pathway. In Arabidopsis, the inactivation of several YUC genes dramatically decreased endogenous IAA (Chen et al., 2014). Additionally, the endogenous level of IAA in *yuc1 yuc2 yuc6* triple mutants was decreased, leading to increased drought sensitivity in Arabidopsis (Shi et al., 2014). In this study, the concentration of IAA in the roots of the salt-tolerant bermudagrass 'C43' was significantly higher than that of 'C43' after salt exposure, suggesting that IAA could play a role in root growth. Similarly, salt stress-induced accumulation of IAA has been reported in the roots of a halophyte species, *Prosopis strombulifera* (Llanes et al., 2014).

On the other hand, salt stress reduced the expression of *TAA* and *YUCCA* genes in the leaves of both genotypes. Interestingly, the expression levels of these genes were dramatically increased in the roots of 'C43,' but conversely reduced in 'C198,' which was consistent with the higher accumulation of IAA in 'C43.' It is well established that the higher expression of auxin biosynthesis genes results in higher IAA production in root tips (Brumos et al., 2018). Accumulation of IAA promoted root growth in tea plants exposed to aluminum stress (Gao et al., 2022). Thus, we can speculate that root growth and salt tolerance in bermudagrass could be related to auxin accumulation in the root due to the increased expression of *TAA* and *YUCC* genes by salt stress, as shown in the model (**Figure 9**).

Abscisic acid function in root growth and salt tolerance in bermudagrass

It is well documented that salt-induced osmotic stress could increase the concentration of ABA in both roots and shoots of salt-treated plants, providing a mechanism of salt stress

tolerance (Ryu and Cho, 2015; Yu Z. et al., 2020; Huang et al., 2021). Here, salt stress increased the ABA content in the leaves and roots of both genotypes, more prominently in the salt-sensitive genotype. *Zeaxanthin epoxidase (ZEP)* and *9-cis-epoxycarotenoid dioxygenase (NCED)* are critical enzymes in the biosynthesis of ABA. In this study, salt stress did not affect the expression of ZEP in the roots of both genotypes.

Additionally, the expression of *NCED* was induced by salt stress in bermudagrass. The expression was significantly higher in the roots and leaves of the C198 genotype, consistent with the elevated levels of ABA in both tissues of the salt-sensitive genotype. The accumulation of ABA is primarily associated with the upregulation of *NCED* genes (Leng et al., 2013). Thus, the accumulation of ABA in bermudagrass is related to the pronounced expression of *NCED* by salt stress (**Figure 9**). Because ABA is often recognized as a negative regulator of plant growth (Brookbank et al., 2021), the reduction of shoot growth in the two bermudagrass could have resulted from the increased accumulation of endogenous ABA in the salt-treated leaves.

Interestingly, the increased ABA content was positively correlated with the reduced shoot growth (**Table 2**). More importantly, ABA regulates root growth and lateral root branching in plants (Sah et al., 2016; Wang et al., 2017). ABA was reported to promote root growth at low concentrations, but it could inhibit root formation at high concentrations (Rowe et al., 2016; Li et al., 2017). In the present study, a higher concentration of ABA was observed in the salt-sensitive genotype with retarded root growth and poor root activity. The increased levels of ABA in the roots and leaves of 'C198' could be one reason for the dramatic inhibition of shoot and root growth, increased salt sensitivity.

The role of gibberellin in bermudagrass root growth and salt tolerance

Gibberellin is crucial for plant growth and development, and its deficiency is associated with plant dwarfism (El-Sharkawy et al., 2012; Lee et al., 2014). Stress conditions could inhibit GA biosynthesis and/or increase its degradation, disturbing normal plant metabolism and growth (Llanes et al., 2016). Here, the two bermudagrass genotypes showed a reduced level of GA_3 in response to salt stress, leading to shoot growth reduction. *GA20-oxidase (GA20-ox)* and *GA2-oxidase (GA2ox)* are key enzymes involved in the biosynthesis and degradation of GAs, respectively. Overexpression of *OsGA2ox5* improved rice tolerance to salt stress (Shan et al., 2014).

GA20ox2 was involved in root elongation and root branching by regulating IAA synthesis and transport in Arabidopsis (Lv et al., 2018). Thus, the decrease in GA_3 in bermudagrass could be related to the downregulation of *GA2ox* and *GA20ox* by salt stress. Under normal conditions, the GA_3 content was higher in the salt-sensitive genotype, but relatively 'C43' had significantly higher GA_3 content under salt stress. At optimal concentration, GA_3 is beneficial for the physiology and metabolism of plants under abiotic stresses (Iqbal et al., 2011). These results suggest that the salt-tolerant genotype could produce optimum GA_3 to maintain normal functioning, thus improving root growth and salt tolerance.

Hormonal crosstalk is essential for root growth, shoot source activity and salt tolerance in bermudagrass

When exposed to a stressful condition, plants reprogram the biosynthesis and transport of hormones in a way to cope with the stress. Hormonal crosstalk is a crucial process for the understanding of the role of phytohormones, because hormones may not act independently to regulate plant growth and development (Pacifici et al., 2015). To provide a stress defense mechanism and regulate root development, hormonal crosstalk could occur at multiple levels (Murphy, 2015; Aerts et al., 2020). During lateral root formation, cytokinin has been reported to play antagonistic role with auxin in regulating shoot branching (Shimizu-Sato et al., 2009), and lateral root growth (Durbak et al., 2012).

Studies have shown that the crosstalk and regulation of hormones by each other occurs at the transcription level through regulating biosynthesis and degradation genes. For instance, auxin could inhibit *IPT* expression and conversely increase the expression of *CKX* to inhibit CK biosynthesis (Nordstrom et al., 2004). Despite they work antagonistically at low and moderate concentrations however, they auxin and CK can work synergistically at higher concentration (Kurepa et al., 2019). In our study, the contents of auxin and cytokinin were higher in the salt tolerant genotype, suggesting that these hormones may work together to positively regulate root growth and shoot source activity in bermudagrass under salt stress (**Figures 9**, **10**). Additionally, the expression of *IPT* was higher and CKX was lower in the 'C43,' suggesting that auxin may not antagonistic to CK in bermudagrass.

The negative effect of ABA in seed germination was improved by GAs through antagonistic crosstalk (Verma et al., 2016). In this study, the adverse effect of accumulated ABA in salt tolerant genotype bermudagrass could be masked by accumulation of GAs through hormonal crosstalk, leading to improved growth and salt tolerance (**Figures 9**, **10**). The increase in root growth rate during stress can be regulated by ABA, osmotic stress-induced ABA accumulation could induce auxin transport, thereby improve root elongation under osmotic stress (Xu et al., 2013). Here, the moderately increased level of ABA as a result of salt-induced osmotic stress could be involved in auxin transport to regulate

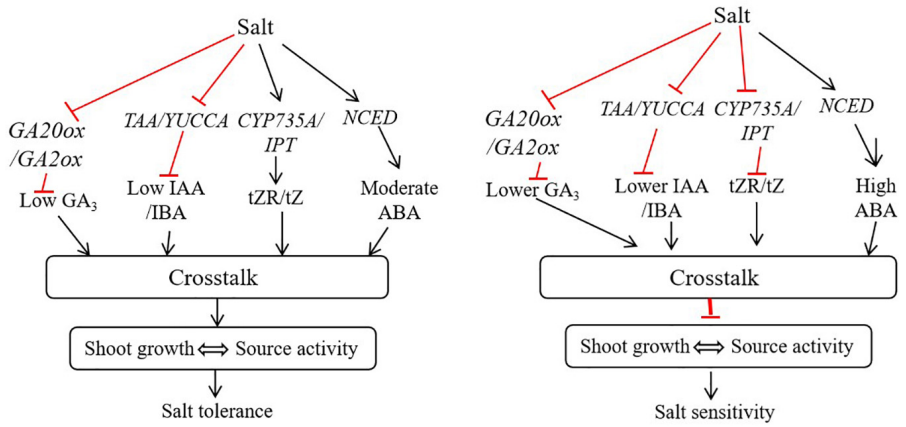

FIGURE 10
A proposed working model of how hormonal reprogramming and crosstalk are involved in shoot growth and salt tolerance in bermudagrass. In shoots, salt stress induces the expression of CYP735A/IPT and *NCED* genes involved in tZR, tZ and ABA biosynthesis. The activation of these genes increases the accumulation of respective hormones in shoots. Subsequently, these hormones could work together through hormonal crosstalk and maintain shoot growth and source activity, ultimately improving salt tolerance in bermudagrass. In contrast, salt stress inhibits the expression of *TAA/YUCC*, *CYP735A/IPT*, and *GA20ox/GA2ox* genes, leading to reduced auxin, cytokinin and gibberellin levels in shoot, respectively. On the other hand, salt stress strongly induces the expression of *NCED*, leading to the accumulation of a high level of ABA in shoot. The reduced levels of auxin, gibberellin and cytokinin and high ABA level undergo hormonal crosstalk in shoot and inhibit shoot growth, thus diminishing source activity and increasing salt sensitivity in bermudagrass.

root growth and shoot source activity in bermudagrass. CKs can interact with other hormones, including auxin (IAA) and ABA, to regulate the growth and development of roots (Nguyen et al., 2018). Treatment of plants with exogenous IAA and GA3 could improve tolerance to salt stress by regulating various physiological and biochemical traits (Khalid and Aftab, 2020).

The contents of IAA, GA3 and IBA were decreased in the leaves of the two bermudagrass in response to salt stress. Interestingly, IAA, GA3 and IBA contents were significantly higher in 'C43.' Moreover, we found a significant positive correlation between the contents of these hormones and shoot growth under control and salt stress conditions (**Table 2**). Thus, the decrease in shoot growth in both genotypes could be attributed to the decrease in these hormones. The negative effect of increased ABA level in the salt-tolerant genotype could be masked by other hormones through hormonal crosstalk, leading to better shoot growth and salt tolerance. Therefore, the crosstalk between different phytohormones could be crucial in bermudagrass root growth and salt tolerance.

Due to the complex nature of plant hormone interactions, integrating physiological and molecular levels to the whole plant response is a key to uncovering the detailed mechanisms of hormonal crosstalk (Ross et al., 2011). It has been suggested that combining experimental and modeling studies is a crucial way to dissect the complexity of hormonal crosstalk in regulating root development (Liu et al., 2014). In maize, a higher level of ABA resulting from salt stress has been shown to disturb auxin transport and distribution and inhibit lateral root growth (Lu et al., 2019). A higher salt level could lead to a higher ABA accumulation, which negatively regulates auxin distribution and root development, while moderate salt stress has the opposite effect (Yu Z. et al., 2020). Therefore, in bermudagrass, the decrease in root growth could be associated with a significantly higher level of ABA caused by salt stress, which further inhibits auxin biosynthesis and distribution.

Conclusion

This study demonstrates the role of hormonal reprogramming and crosstalk in regulating root growth and salt tolerance in bermudagrass. In addition, to the morphological and physiological differences, the two contrasting genotypes showed an apparent hormonal regulation, including biosynthesis and degradation in response to salt stress. With improved root growth and root activity by salt stress, the salt-tolerant genotype 'C43' had a higher accumulation of IAA, CK, and GA_3 in the roots, which are crucial for plant growth and development. The expressions of hormones related genes involved in the biosynthesis of these hormones were induced by salt stress in the salt-tolerant genotype. The antagonistic interaction of two hormones might be affected by the third hormone to synergistically improve root growth and salt tolerance in bermudagrass. Moreover, the crosstalk of hormones and the outcomes depend on the stress condition, the plant species, and the hormones concentration. Thus, further study is necessary to elucidate how hormonal crosstalk

regulates root growth and salt tolerance in bermudagrass at the molecular level.

Data availability statement

The raw data supporting the conclusions of this article will be made available by the authors, without undue reservation.

Author contributions

YY, QX, and L-XH conceived and designed the experiments. YY and MW performed the experiments and wrote the manuscript. YY, MW, and N-FL analyzed the data. HD and Y-BZ helped with manuscript reviewing. QX and L-XH revised the manuscript. All authors read, revised and approved the final manuscript.

Funding

This work was financially supported by the Key Projects of Hunan Provincial Education Department (Grant No. 20A046), the Natural Science Foundation of Hunan Province (Grant No. 2020JJ5245), and Changsha Municipal Science and Technology Project (Grant No. KC1809004).

Conflict of interest

The authors declare that the research was conducted in the absence of any commercial or financial relationships that could be construed as a potential conflict of interest.

Publisher's note

All claims expressed in this article are solely those of the authors and do not necessarily represent those of their affiliated organizations, or those of the publisher, the editors and the reviewers. Any product that may be evaluated in this article, or claim that may be made by its manufacturer, is not guaranteed or endorsed by the publisher.

Supplementary material

The Supplementary Material for this article can be found online at: https://www.frontiersin.org/articles/10.3389/fpls.2022.956410/full#supplementary-material

SUPPLEMENTARY FIGURE 1
Representative chromatogram of hormone standards and tissue extracts of bermudagrass under salt stress **(A)** cytokinin standards; **(B)** cytoinin in tissues; **(C)** ABA, auxin andGA3 standards; **(D)** ABA, auxin and GA3 in tissues.

References

Achard, P., Gusti, A., Cheminant, S., Alioua, M., Dhondt, S., Coppens, F., et al. (2009). Gibberellin signaling controls cell proliferation rate in Arabidopsis. *Curr. Biol.* 19, 1188–1193. doi: 10.1016/j.cub.2009.05.059

Aerts, N., Mendes, M. P., and Van Wees, S. C. M. (2020). Multiple levels of crosstalk in hormone networks regulating plant defense. *Plant J.* 105, 489–504. doi: 10.1111/tpj.15124

Albacete, A., Ghanem, M. E., Martínez-Andújar, C., Acosta, M., Sánchez-Bravo, J., Martínez, V., et al. (2008). Hormonal changes in relation to biomass partitioning and shoot growth impairment in salinised tomato (*Solanum lycopersicum* L.) plants. *J. Exp. Bot.* 59, 4119–4131. doi: 10.1093/jxb/ern251

Blakeslee, J. J., Spatola Rossi, T., and Kriechbaumer, V. (2019). Auxin biosynthesis: Spatial regulation and adaptation to stress. *J. Exp. Bot.* 70, 5041–5049. doi: 10.1093/jxb/erz283

Brookbank, B. P., Patel, J., Gazzarrini, S., and Nambara, E. (2021). Role of basal ABA in plant growth and development. *Genes* 12:1936. doi: 10.3390/genes12121936

Brumos, J., Robles, L. M., Yun, J., Vu, T. C., Jackson, S., Alonso, J. M., et al. (2018). Local auxin biosynthesis is a key regulator of plant development. *Dev. Cell* 47, 306–318.e5. doi: 10.1016/j.devcel.2018.09.022

Cai, L., Zhang, L., Fu, Q., and Xu, Z. F. (2018). Identification and expression analysis of cytokinin metabolic genes *IPTs*, *CYP735A* and *CKXs* in the biofuel plant *Jatropha curcas*. *PeerJ* 6:e4812. doi: 10.3390/ijms20246343

Cao, X., Yang, H., Shang, C., Ma, S., Liu, L., and Cheng, J. (2019). The roles of auxin biosynthesis *YUCCA* gene family in plants. *Int. J. Mol. Sci.* 20:6343. doi: 10.3390/ijms20246343

Cassaniti, C., Leonardi, C., and Flowers, T. J. (2009). The effects of sodium chloride on ornamental shrubs. *Sci. Hort.* 122, 586–593. doi: 10.1016/j.scienta.2009.06.032

Chen, Q., Dai, X., DePaoli, H., Cheng, Y., Takebayashi, Y., Kasahara, H., et al. (2014). Auxin overproduction in shoots cannot rescue auxin deficiencies in Arabidopsis roots. *Plant Cell Physiol.* 55, 1072–1079. doi: 10.1093/pcp/pcu039

Deinlein, U., Stephan, A. B., Horie, T., Luo, W., Xu, G., and Schroeder, J. I. (2014). Plant salt-tolerance mechanisms. *Trends Plant Sci.* 19, 371–379. doi: 10.1016/j.tplants.2014.02.001

Dobrev, P. I., and Kamínek, M. (2002). Fast and efficient separation of cytokinins from auxin and abscisic acid and their purification using mixed-mode solid-phase extraction. *J. Chrom. A.* 950, 21–29. doi: 10.1016/S0021-9673(02)00024-9

Durbak, A., Yao, H., and McSteen, P. (2012). Hormone signaling in plant development. *Curr. Opin. Plant Biol.* 15, 92–99. doi: 10.1016/j.pbi.2011.12.004

El-Sharkawy, I., Kayal, W., Prasath, D., Fernandez, H., Bouzayen, M., Svircev, A. M., et al. (2012). Identification and genetic characterization of a gibberellin 2-oxidase gene that controls tree stature and reproductive growth in plum. *J. Exp. Bot.* 63, 1225–1239. doi: 10.1093/jxb/err345

Fang, S., Hou, X., and Liang, X. (2021). Response mechanisms of plants under saline-alkali stress. *Front. Plant Sci.* 12:667458. doi: 10.3389/fpls.2021.667458

Galichet, A., Hoyerova, K., Kaminek, M., and Gruissem, W. (2008). Farnesylation directs atipt3 subcellular localization and modulates cytokinin biosynthesis in Arabidopsis. *Plant Physiol.* 146, 1155–1164. doi: 10.1104/pp.107.107425

Gao, Y., Wang, M., Shi, Y., Yang, L., Hu, J., and Fan, K. (2022). IAA accumulation promotes the root growth of tea plants under aluminum. *Agronomy* 12:1110. doi: 10.3390/agronomy12051110

Ghassemian, M., Nambara, E., Cutler, S., Kawaide, H., Kamiya, Y., and McCourt, P. (2000). Regulation of abscisic acid signaling by the ethylene response pathway in Arabidopsis. *Plant Cell*. 12, 1117–26.

Guo, J., Lu, C., Zhao, F., Gao, S., and Wang, B. (2020). Improved reproductive growth of euhalophyte *Suaeda salsa* under salinity is correlated with altered phytohormone biosynthesis and signal transduction. *Funct. Plant Biol*. 47, 170–183. doi: 10.1071/FP19215

Gupta, B., and Huang, B. (2014). Mechanism of salinity tolerance in plants: Physiological, biochemical, and molecular characterization. *Int. J. Genom*. 2014:701596. doi: 10.1155/2014/701596

Hai, N. N., Chuong, N. N., Tu, N. H. C., Kisiala, A., Hoang, X. L. T., and Thao, N. P. (2020). Role and regulation of cytokinins in plant response to drought stress. *Plants* 9:422. doi: 10.3390/plants9040422

Hoagland, D. R., and Arnon, D. I. (1950). The water-culture method for growing plants without soil. *Calif. Agr. Expt. Stn. Circ.* 347:32. doi: 10.1016/S0140-6736(00)73482-9

Hu, L., Li, H., Chen, L., Lou, Y. H., Amombo, E., and Fu, J. M. (2015). RNA-seq for gene identification and transcript profiling in relation to root growth of bermudagrass (*Cynodon dactylon*) under salinity stress. *BMC Genom*. 16:575. doi: 10.1186/s12864-015-1799-3

Hu, L. X., Huang, Z. H., Liu, S. Q., and Fu, J. M. (2012). Growth response and gene expression in antioxidant-related enzymes in two bermudagrass genotypes differing in salt tolerance. *J. Am. Soc. Hortic. Sci.* 137, 134–143. doi: 10.21273/JASHS.137.3.134

Hu, L. X., Wang, Z. L., and Huang, B. R. (2009). Photosynthetic responses of bermudagrass to drought stress associated with stomatal and metabolic limitations. *Crop Sci*. 49, 1902–1909. doi: 10.2135/cropsci2008.12.0697

Huang, Y., Zhou, J., Li, Y., Quan, R., Wang, J., Huang, R., et al. (2021). Salt stress promotes abscisic acid accumulation to affect cell proliferation and expansion of primary roots in rice. *Int. J. Mol. Sci*. 22:10892. doi: 10.3390/ijms221910892

Iqbal, N., Nazar, R., Iqbal, M. R. K., Masood, A., and Nafees, A. K. (2011). Role of gibberellins in regulation of source sink relations under optimal and limiting environmental conditions. *Curr. Sci* 100, 998–1007.

Ismail, A., Takeda, S., and Nick, P. (2014). Life and death under salt stress: Same players, different timing? *J. Exp. Bot*. 65, 2963–2979. doi: 10.1093/jxb/eru159

Khalid, A., and Aftab, F. (2020). Effect of exogenous application of IAA and GA_3 on growth, protein content, and antioxidant enzymes of *Solanum tuberosum* L. grown in vitro under salt stress. *In Vitro Cell. Dev. Biol. Plant* 56, 377–389. doi: 10.1007/s11627-019-10047-x

Kiba, T., Takei, K., Kojima, M., and Sakakibara, H. (2013). Side-chain modification of cytokinins controls shoot growth in Arabidopsis. *Dev. Cell* 27, 452–461. doi: 10.1016/j.devce1.2013.10.004

Kurepa, J., Shull, T. E., and Smalle, J. A. (2019). Antagonistic activity of auxin and cytokinin in shoot and root organs. *Plant Direct* 3:e00121. doi: 10.1002/pld3.121

Lee, D. H., Lee, I. C., Kim, K. J., Kim, D. S., Na, H. J., Lee, I. J., et al. (2014). Expression of gibberellin 2-oxidase 4 from Arabidopsis under the control of a senescence-associated promoter results in a dominant semi-dwarf plant with normal flowering. *J. Plant Biol*. 57, 106–116. doi: 10.1007/s12374-013-0528-1

Leng, P., Yuan, B., and Guo, Y. (2013). The role of abscisic acid in fruit ripening and responses to abiotic stress. *J. Exp. Bot*. 65, 4577–4588. doi: 10.1093/jxb/eru204

Li, W., and Li, Q. (2017). Effect of environmental salt stress on plants and the molecular mechanism of salt stress tolerance. *Int. J. Environ. Sci. Nat. Res*. 7:555714. doi: 10.19080/IJESNR.2017.07.555714

Li, X., Chen, L., Forde, B. G., and Davies, W. J. (2017). The biphasic root growth response to abscisic acid in Arabidopsis involves interaction with ethylene and auxin signalling pathways. *Front. Plant Sci*. 8:1493. doi: 10.3389/fpls.2017.01493

Liu, J., Rowe, J., and Lindsey, K. (2014). Hormonal crosstalk for root development: A combined experimental and modeling perspective. *Front. Plant Sci*. 5:116. doi: 10.3389/fpls.2014.00116

Livak, K. J., and Schmittgen, T. D. (2001). Analysis of relative gene expression data using real-time quantitative PCR and the 2(-Delta Delta C(T)) Method. *Methods* 25, 402–408. doi: 10.1006/meth.2001.1262

Llanes, A., Andrade, A., Alemano, S., and Luna, V. (2016). Alterations of endogenous hormonal levels in plants under drought and salinity. *Am. J. Plant Sci*. 7, 1357–1371. doi: 10.4236/ajps.2016.79129

Llanes, A., Masciarelli, O., Ordoñez, R., Isla, M. I., and Luna, V. (2014). Differential growth responses to sodium salts involve different ABA catabolism and transport in the halophyte *Prosopis strombulifera*. *Biol. Plant* 58, 80–88. doi: 10.1007/s10535-013-0365-6

Lu, C., Chen, M. X., Liu, R., Zhang, L., Hou, X., Liu, S., et al. (2019). Abscisic acid regulates auxin distribution to mediate maize lateral root development under salt stress. *Front. Plant Sci*. 10:716. doi: 10.3389/fpls.2019.00716

Luo, X., Chen, Z., Gao, J., and Gong, Z. (2014). Abscisic acid inhibits root growth in Arabidopsis through ethylene biosynthesis. *Plant J*. 79, 44–55. doi: 10.1111/tpj.12534

Lutts, S., Almansouri, M., and Kinet, J. M. (2004). Salinity and water stress have contrasting effects on the relationship between growth and cell viability during and after stress exposure in durum wheat callus. *Plant Sci*. 167, 9–18. doi: 10.1016/j.plantsci.2004.02.014

Lv, S. F., Yu, D. Y., Sun, Q. Q., and Jiang, J. (2018). Activation of gibberellin 20-oxidase 2 undermines auxin-dependent root and root hair growth in NaCl-stressed Arabidopsis seedlings. *Plant Growth Regul*. 84, 225–236. doi: 10.1007/s10725-017-0333-9

Mehrotra, R., Bhalothia, P., Bansal, P., Basantani, M. K., Bharti, V., and Mehrotra, S. (2014). Abscisic acid and abiotic stress tolerance - different tiers of regulation. *J. Plant Physiol*. 171, 486–496. doi: 10.1016/j.jplph.2013.12.007

Meng, X., Zhou, J., and Sui, N. (2018). Mechanisms of salt tolerance in halophytes: Current understanding and recent advances. *Open Life Sci*. 13, 149–154. doi: 10.1515/biol-2018-0020

Munns, R., and Tester, M. (2008). Mechanisms of salinity tolerance. *Annu. Rev. Plant Biol*. 59, 651–681. doi: 10.1146/annurev.arplant.59.032607.092911

Murphy, A. (2015). Hormone crosstalk in plants. *J. Exp. Bot*. 66, 4853–4854. doi: 10.1093/jxb/erv339

Nguyen, T. N., Tuan, P. A., Mukherjee, S., Son, S. H., and Ayele, B. T. (2018). Hormonal regulation in adventitious roots and during their emergence under waterlogged conditions in wheat. *J. Exp. Bot*. 69, 4065–4082. doi: 10.1093/jxb/ery190

Nordstrom, A., Tarkowski, P., Tarkowska, D., Norbaek, R., Astot, C., Dolezal, K., et al. (2004). Auxin regulation of cytokinin biosynthesis in *Arabidopsis thaliana*: A factor pf potential importance for auxin cytokinin regulated development. *Proc. Nat. Acad. Sci. U.S.A.* 101, 8039–8044. doi: 10.1073/pnas.0402504101

Pacifici, E., Polverari, L., and Sabatini, S. (2015). Plant hormone crosstalk: The pivot of root growth. *J. Exp. Bot*. 66, 1113–1121. doi: 10.1093/jxb/eru534

Pérez-Alfocea, F., Albacete, A., Ghanem, M. E., and Dodd, I. C. (2010). Hormonal regulation of source-sink relations to maintain crop productivity under salinity: A case study of root-to-shoot signalling in tomato. *Funct. Plant Biol*. 37, 592–603. doi: 10.1071/FP10012

Pessarakli, M. (2015). Using bermudagrass (*Cynodon dactylon* L.) in urban desert landscaping and as a forage crop for sustainable agriculture in arid regions and combating desertification. *Int. J. Water Resour. Arid Environ*. 4, 8–14.

Rahman, M. M., Mostofa, M. G., Keya, S. S., Siddiqui, M. N., Ansary, M. M. U., Das, A. K., et al. (2021). Adaptive mechanisms of halophytes and their potential in improving salinity tolerance in plants. *Int. J. Mol. Sci*. 22:10733. doi: 10.3390/ijms221910733

Ross, J. J., Weston, D. E., Davidson, S. E., and Reid, J. B. (2011). Plant hormone interactions: How complex are they? *Physiol. Plant* 141, 299–309. doi: 10.1111/j.1399-3054.2011.01444.x

Rowe, J. H., Topping, J. F., Liu, J., and Lindsey, K. (2016). Abscisic acid regulates root growth under osmotic stress conditions via an interacting hormonal network with cytokinin, ethylene and auxin. *New Phytol*. 211, 225–239. doi: 10.1111/nph.13882

Ryu, H., and Cho, Y. G. (2015). Plant hormones in salt stress tolerance. *J. Plant Biol*. 58, 147–155. doi: 10.1007/s12374-015-0103-z

Sah, S. K., Reddy, K. R., and Li, J. (2016). Abscisic acid and abiotic stress tolerance in crop plants. *Front. Plant Sci*. 7:571. doi: 10.3389/fpls.2016.00571

Shahid, M. A., Sarkhosh, A., Khan, N., Balal, R. M., Ali, S., Rossi, L., et al. (2020). Insights into the physiological and biochemical impacts of salt stress on plant growth and development. *Agronomy* 10:938. doi: 10.3390/agronomy10070938

Shan, C., Mei, Z., Duan, J., Chen, H., Feng, H., and Cai, W. (2014). OsGA2ox5, a gibberellin metabolism enzyme, is involved in plant growth, the root gravity response and salt stress. *PLoS One* 9:e87110. doi: 10.1371/journal.pone.0087110

Shi, H., Chen, L., Ye, T., Liu, X., Ding, K., and Chan, Z. (2014). Modulation of auxin content in Arabidopsis confers improved drought stress resistance. *Plant Physiol. Biochem*. 82, 209–217. doi: 10.1016/j.plaphy.2014.06.008

Shimizu-Sato, S., Tanaka, M., and Mori, H. (2009). Auxin–cytokinin interactions in the control of shoot branching. *Plant Mol. Biol*. 69, 429–435. doi: 10.1007/s11103-008-9416-3

Sun, L. R., Wang, Y. B., He, S. B., and Hao, F. S. (2018). Mechanisms for abscisic acid inhibition of primary root growth. *Plant Signal. Behav*. 13:e1500069. doi: 10.1080/15592324.2018.1500069

Verma, V., Ravindran, P., and Kumar, P. P. (2016). Plant hormone-mediated regulation of stress responses. *BMC Plant Biol*. 16:86. doi: 10.1186/s12870-016-0771-y

Wang, T., Li, C., Wu, Z., Jia, Y., Wang, H., Sun, S., et al. (2017). Abscisic acid regulates auxin homeostasis in rice root tips to promote root hair elongation. *Front. Plant Sci*. 8:1121. doi: 10.3389/fpls.2017.01121

Wolters, H., and Jürgens, G. (2009). Survival of the flexible: Hormonal growth control and adaptation in plant development. *Nat. Rev. Genet*. 10, 305–317. doi: 10.1038/nrg2558

Wu, Y., Liu, H., Wang, Q., and Zhang, G. (2021). Roles of cytokinins in root growth and abiotic stress response of *Arabidopsis thaliana*. *Plant Growth Regul*. 94, 151–160. doi: 10.1007/s10725-021-00711-x

Xu, W., Jia, L., Shi, W., Liang, J., Zhou, F., Li, Q., et al. (2013). Abscisic acid accumulation modulates auxin transport in the root tip to enhance proton secretion for maintaining root growth under moderate water stress. *New Phytol*. 197, 139–150. doi: 10.1111/nph.12004

Yu, D., Boughton, B. A., Hill, C. B., Feussner, I., Roessner, U., and Rupasinghe, T. W. T. (2020). Insights into oxidized lipid modification in barley roots as an adaptation mechanism to salinity stress. *Front. Plant Sci*. 11:1. doi: 10.3389/FPLS.2020.00001

Yu, Z., Duan, X., Luo, L., Dai, S., Ding, Z., and Xia, G. (2020). How plant hormones mediate salt stress responses. *Trends Plant Sci*. 25, 1117–1130. doi: 10.1016/j.tplants.2020.06.008

Zelm, E. V., Zhang, Y., and Testerink, C. (2020). Salt tolerance mechanisms of plants. *Ann. Rev. Plant Biol*. 71, 403–433. doi: 10.1146/annurev-arplant-050718-100005

Zhao, S., Zhang, Q., Liu, M., Zhou, H., Ma, C., and Wang, P. (2021). Regulation of plant responses to salt stress. *Int. J. Mol. Sci*. 22:4609. doi: 10.3390/ijms22094609

Zhao, Y. (2018). Essential roles of local auxin biosynthesis in plant development and in adaptation to environmental changes. *Annu. Rev. Plant Biol*. 69, 417–435. doi: 10.1146/annurev-arplant-042817-040226

Zou, Y., Zhang, Y., and Testerink, C. (2021). Root dynamic growth strategies in response to salinity. *Plant Cell Environ*. 45, 695–704. doi: 10.1111/pce.14205

frontiers | Frontiers in Plant Science

TYPE Original Research
PUBLISHED 04 August 2022
DOI 10.3389/fpls.2022.954478

OPEN ACCESS

EDITED BY
Jin-Lin Zhang,
Lanzhou University, China

REVIEWED BY
Julian Mario Peña-Castro,
Universidad del Papaloapan, Mexico
Juan Solomon,
University of Nevada, Reno,
United States
Manuel Esperon-Rodriguez,
Western Sydney University, Australia

*CORRESPONDENCE
Carl A. Frisk
Carl.Frisk@nibio.no
Jon M. Yearsley
Jon.Yearsley@ucd.ie

†PRESENT ADDRESS
Carl A. Frisk,
Department of Urban Greening and Vegetation Ecology, Norwegian Institute of Bioeconomy Research, Ås, Norway

‡These authors share senior authorship

SPECIALTY SECTION
This article was submitted to Plant Abiotic Stress, a section of the journal Frontiers in Plant Science

RECEIVED 27 May 2022
ACCEPTED 11 July 2022
PUBLISHED 04 August 2022

CITATION
Frisk CA, Xistris-Songpanya G, Osborne M, Biswas Y, Melzer R and Yearsley JM (2022) Phenotypic variation from waterlogging in multiple perennial ryegrass varieties under climate change conditions. *Front. Plant Sci.* 13:954478. doi: 10.3389/fpls.2022.954478

Phenotypic variation from waterlogging in multiple perennial ryegrass varieties under climate change conditions

Carl A. Frisk[1,2*†], Georgianna Xistris-Songpanya[1], Matthieu Osborne[1], Yastika Biswas[1], Rainer Melzer[1,2‡] and Jon M. Yearsley[1,2*‡]

[1]School of Biology and Environmental Science, University College Dublin, Dublin, Ireland, [2]Earth Institute, University College Dublin, Dublin, Ireland

Identifying how various components of climate change will influence ecosystems and vegetation subsistence will be fundamental to mitigate negative effects. Climate change-induced waterlogging is understudied in comparison to temperature and CO_2. Grasslands are especially vulnerable through the connection with global food security, with perennial ryegrass dominating many flood-prone pasturelands in North-western Europe. We investigated the effect of long-term waterlogging on phenotypic responses of perennial ryegrass using four common varieties (one diploid and three tetraploid) grown in atmospherically controlled growth chambers during two months of peak growth. The climate treatments compare ambient climatological conditions in North-western Europe to the RCP8.5 climate change scenario in 2050 (+2°C and 550 ppm CO_2). At the end of each month multiple phenotypic plant measurements were made, the plants were harvested and then allowed to grow back. Using image analysis and principal component analysis (PCA) methodologies, we assessed how multiple predictors (phenotypic, environmental, genotypic, and temporal) influenced overall plant performance, productivity and phenotypic responses. Long-term waterlogging was found to reduce leaf-color intensity, with younger plants having purple hues indicative of anthocyanins. Plant performance and yield was lower in waterlogged plants, with tetraploid varieties coping better than the diploid one. The climate change treatment was found to reduce color intensities further. Flooding was found to reduce plant productivity via reductions in color pigments and root proliferation. These effects will have negative consequences for global food security brought on by increased frequency of extreme weather events and flooding. Our imaging analysis approach to estimate effects of waterlogging can be incorporated into plant health diagnostics tools via remote sensing and drone-technology.

KEYWORDS

anthocyanins, chamber experiment, colors, flooding, grasslands, harvest, image analysis, *Lolium perenne*

Introduction

Predicting plant responses caused by climate change is a fundamental challenge that will increasingly impact coming generations (Parmesan and Hanley, 2015). Identifying how the various components of climate change are likely to affect plant responses will inform options of optimal mitigation strategies to minimize any negative effects (Canadell and Raupach, 2008; Pareek et al., 2020). While this is a complex issue affecting all ecosystems, it is especially important for grassland ecosystems due to the unavoidable connection with global food security through agriculture, crop lands and pasture lands (Tester and Langridge, 2010; Kipling et al., 2016a; Lecerf et al., 2019; Raza et al., 2019). There is a growing concern that climate change will result in ecological transformation of grasslands (Kipling et al., 2016b; Wang et al., 2018) which will alter plant phenology (Jentsch et al., 2009; Munson and Long, 2017), biodiversity (Bellocchi and Picon-Cochard, 2021), and productivity (Goliński et al., 2018; Qi et al., 2018).

Grasslands are defined as ecosystems dominated by the Poaceae (grass) taxonomic family, with the ecology varying widely depending on species composition, edaphic factors, topography, management, and climate. Previous studies have suggested that elevated CO_2 levels are likely to increase photosynthetic capability in grasses, increasing Net Primary Production (NPP) and thereby total yield (Ergon et al., 2018; Yiotis et al., 2021). Meanwhile, higher temperatures are likely to extend the length of the growth season, providing longer time for sustained growth (Höglind et al., 2013; Pembleton et al., 2020). While increased ambient temperatures and elevated CO_2 act long-term and are the main components of many climate models (e.g., Thornley and Cannell, 1997; Huntingford et al., 2013), altered precipitation regimes are equally important, and predicted to act both short- and long-term (Dore, 2005; Cullen et al., 2009; Brown et al., 2019). Previous grass research from altered precipitation regimes has focused on the effects of prolonged droughts, reduced water-availability and increased desertification (Farfan-Vignolo and Asard, 2012; Cullen et al., 2014; Bothe et al., 2018; Buttler et al., 2019; Yates et al., 2019), however many areas might see the opposite effect, leading to increased flooding (Kiely, 1999; Rosenzweig et al., 2002).

Climate change-induced alterations to precipitation regimes are expected to contribute to increased frequency of extreme weather events, such as severe storms and extreme flooding (Easterling et al., 2000; Semmler and Jacob, 2004). This is partly due to warmer temperatures increasing evaporation, and warmer air being able to hold more moisture, increasing the total amount of water vapor in atmospheric circulation (Hu et al., 2000; O'Gorman and Muller, 2010). Additionally, predicted changes to the precipitation seasonality are likely to change the frequency and distribution of rain events, potentially enhancing the drought-flooding dichotomy (Feng et al., 2013; Kumar, 2013).

Perennial ryegrass (*Lolium perenne*) is a common cool season pasture grass grown extensively throughout its native Eurasian-range and cultivated worldwide due to its high nutritional quality and palatability for livestock (Hunt and Easton, 1989; Hannaway et al., 1999; Smit et al., 2005; Minneé et al., 2019; Tubritt et al., 2020). Many genetically different varieties of perennial ryegrass are bred and cultivated to match the climatological conditions of specific target regions, which in turn causes differences in plant health and yield depending on local environmental suitability (Grogan and Gilliland, 2011; Helgadóttir et al., 2018). Varieties suitable in current conditions under regular precipitation regimes might prove unsuitable under periods of increased flooding (Mustroph, 2018). Flooding can cause long-term waterlogging, affecting overall plant health and total yield (McFarlane et al., 2003; Striker, 2012) and grassland ecosystem function (Fay et al., 2008). It could also impact plant morphology due to phenotypic plasticity (Münzbergová et al., 2017; Mizutani and Kanaoka, 2018). Previous studies have shown that plants can survive the unfavorable conditions but alters their phenotype in the process as a response, with some varieties of the same species being differentially susceptible to the stressor (Song, 2009; Tong et al., 2021; Stasnik et al., 2022). Decrease in growth due to an altered phenotypic response can have devastating impacts on global food security due to the bottom-up reliance of agricultural system productivity from grassland areas (Hazell and Wood, 2008; Baldos and Hertel, 2014). In addition, economic consequences would be especially severe for countries like Ireland and the United Kingdom with large land areas consisting of ryegrass dominated pasture lands and many rivers currently prone and predicted in the future to flood (Blöschl et al., 2019).

Here, we quantify the effects from waterlogging on perennial ryegrass performance and plant health in the light of climate change. We hypothesized that waterlogging would decrease perennial ryegrass performance and lower plant yield, and that the climate change treated plants would perform better under waterlogging than the ambiently treated plants. We further explored whether waterlogging and climate change impacted the phenotypic plasticity of the plants. We investigated this using atmospherically controlled growth chambers and multiple commercial high-producing perennial ryegrass varieties with varying genetic backgrounds in an image analysis framework.

Materials and methods

Experimental setup

This study used four atmospherically controlled CONVIRON BDW40 walk-in growth chambers located in the PÈAC (Programme for Experimental Atmospheres and Climate) facility in Rosemount Environmental Research Station

belonging to the University College Dublin in Dublin, Ireland. This facility has been used in previous studies to investigate plant responses to elevated CO_2 (Batke et al., 2018; Yiotis et al., 2021) and atmospheric paleoclimatic reconstruction (Evans-Fitz.Gerald et al., 2016; Porter et al., 2017; Yiotis et al., 2017). Two chambers were chosen to represent typical North-western European climatological conditions (CO_2-levels at 415 ppm and ambient temperature conditions) while two chambers were chosen to represent the predicted 2050 combined climate change climatological conditions according to the RCP8.5 scenario [elevated CO_2-levels (550 ppm) and a 2°C increase in temperature (IPCC, 2014)]. The growth chamber climatological baselines (ambient conditions) were constructed from the last thirty years of meteorological data (1989–2018) collated from the meteorological station located at Cork Airport and publicly accessible via the Irish Meteorological Services (Met Éireann). The entire experiment simulated conditions from May to September but only climatological conditions replicating two months of optimal pasture growth (June and July) (McHugh et al., 2020) were used to investigate perennial ryegrass responses to waterlogging (**Table 1**).

Four common internationally grown varieties of perennial ryegrass were used for the experiment: *Aberchoice, Abergain, Carraig*, and *Dunluce* (European Commision, 2019). The varieties vary in heading date and ploidy (**Table 2**), which allowed for an intra-species comparison to identify whether genetic factors might contribute to the response to waterlogging and climate change. At the simulated start of May each chamber was populated with 80 PVC cores (50 cm × 16 cm (ϕ)) filled with John Innes No2 compost (320 cores in total for the four chambers), with the John Innes No2 (Westland) being a loam-mixture compost with peat, horticultural grit, and added nutrients. Each core was sealed inside a plastic bag to allow half of the cores to be waterlogged further on. The 50 cm tall cores allowed for the simulation of largely natural grassland root depth (Wedderburn et al., 2010; Cougnon et al., 2017). Each core was sown with ten seeds from one of the four varieties (DAS 0, Days after sowing) and allowed to germinate. At DAS 43, the most centrally germinated seedling was kept, and the other germinated seeds discarded. The seedlings were then cut to a height of 5 cm to simulate equal growth between all replicates. Waterlogging was initiated in 40 of the 80 cores per chamber on DAS 48, with the additional watering being slowly initiated over three days to reach a stable water level 2 cm above the soil. Non-waterlogged cores continued to be watered normally, once to twice weekly to keep soil moisture around 25%. Waterlogging was actively enforced for one month and then allowed to dissipate naturally. Waterlogging experiments in grasses tend to last around 15 days (e.g., Liu and Jiang, 2015; de la Cruz Jiménez et al., 2017; Ploschuk et al., 2017), with few experiments lasting up to 30 days (McFarlane et al., 2003). The longer duration was implemented due to the increased chance (and consequences) of climate changed-induced extreme flooding events (Dore, 2005; Trenberth, 2011). Chamber treatment, waterlogging, and variety placement were stratified equally among the chambers and then randomized within chambers. The stratification allowed for equal numbers of each variety in each chamber, with half of the 80 cores per chamber being waterlogged for equal comparison for all factors.

Phenotypic data collection

Multiple sets of phenotypic data were collected each month to identify the effects on plant performance from the waterlogging. Soil and Plant Analyzer Development (SPAD) readings were conducted using a SPAD-502 Plus Chlorophyll Meter (Konica Minolta) to sample leaf chlorophyll content (e.g., Bothe et al., 2018; Dong et al., 2019). Three representative leaves were sampled from each plant, with each leaf being sampled at three places and averaged for a reliable measurement. Soil moisture was measured at 10 cm depth using a HH2 Moisture Meter with a calibrated WET sensor type WET-2 attachment (Delta-T Devices). At the end of each month (DAS 72, June and 101, July) the maximum height of the plants were measured. After being measured, the plants were harvested by cutting the grasses using scissors at 5 cm above the soil-level, leaving 5 cm of basal grass tissue intact, simulating natural grazing. The plants were then allowed to recover, grow and then be harvested again the subsequent month. The harvested material from each plant was placed on a flat white background and photographed using a high-resolution LUMIX DC-G9 camera (Panasonic) with an accompanied ColorChecker Classic chart (X-rite). This enabled the harvested material to be processed using color-corrective image analysis techniques to identify differences in leaf color hues (e.g., Hu et al., 2013; Li et al., 2014; Zhang et al., 2014; de la Cruz Jiménez et al., 2017). The leaves were photographed immediately after harvest to prevent structural and color degradation (Løkke et al., 2013; Yamauchi and Watada, 2019). After the photographs all harvest material from each plant was oven dried at 65°C for one week and then weighed to measure dried biomass per plant.

Image analysis

The first stage of image analysis was to convert the color filter array (CFA) in each RAW image from the LUMIX DC-G9 camera into a color-corrected red-green-blue (RGB) image. This was done using a standardized pipeline with the following nine steps: (1) subtract a black value from all pixels in the CFA, (2) set negative pixel values to zero, (3) divide all pixels by the maximum pixel value, (4) correct the white balance by scaling red and blue pixels relative to green pixels in the CFA, (5) convert pixels to unsigned 16-bit integers, demosaiced the

TABLE 1 Experimental Growth Chamber setup for the two ambient and the two climate chambers simulating the months June and July in North-western Europe.

SM	DAS	Length	Treatment	Environmental Conditions					
		Days		CO_2 (ppm)	Light/Dark Hours (h)	Max Light Intensity ($\mu mol \cdot m^{-2} \cdot s^{-1}$)	Day Temp (°C)	Night Temp (°C)	Humidity (%)
June	44–72	28	Ambient	415	17/7	600	14	11	80
	44–72	28	$eCO_2 + 2°C$	550	17/7	600	16	13	80
July	73–101	28	Ambient	415	16/8	600	16	13	80
	73–101	28	$eCO_2 + 2°C$	550	16/8	600	18	15	80

The conditions in the four chambers were changed as each month ended. Dawn and dusk conditions are included in the light hours. SM, simulated months; DAS, days after sowing.

CFA into a true-color image using a gradient-corrected linear interpolation (Malvar et al., 2004), (6) transform the image from the camera's color space to RGB, (7) identify the 24 colors on the X-Rite ColorChecker Classic chart within the image, (8) estimate an affine color-transformation matrix that minimizes the sum of squared deviations between the RGB colors in the image to the known colors of the 24 colored squares, (9) apply the color-transformation matrix to produce a color-correct RGB image. The camera's image metadata was used to obtain values for black level, white-balance correction and camera color space to RGB conversion.

The second stage of the image analysis extracted RGB values from pixels that corresponded to ryegrass leaves. Ryegrass leaves were placed upon a flat, white, rectangular background which enabled the image to be cropped to the white background. The cropped image was then converted into an HSV color-space and an initial mask created with hue values in the range 0.0–0.4 and 0.875–1.0 (corresponding to yellow, green, and red hues), saturation in the range 0.2–1.0 and value in the range 0.0–0.9. Regions of the mask with connected components containing fewer than 100 pixels were removed before the mask was refined using 50 iterations of an active contours region growing algorithm and saturation values retained if they were in the range 0.25–1.0. The final mask was used to extract the position of pixels in the mask and their RGB values. All image processing was performed using MatLAB (version R2021a.) and its image processing toolbox (Mathworks, 2021).

TABLE 2 Perennial ryegrass (*Lolium perenne*) varieties grown and water status for all chambers and variety replicates.

Variety	Heading	Ploidy	Water Status		
			Logged	Normal	Total
Aberchoice	Late	Diploid	40	40	80
Abergain	Late	Tetraploid	40	40	80
Carraig	Intermediate	Tetraploid	40	40	80
Dunluce	Intermediate	Tetraploid	40	40	80

Each water status is equally divided between all four chambers.

Statistical analyses

The ryegrass leaf RGB values from the image analysis were further processed by calculating the median value for each hue from each image of the harvested ryegrass. Median values were used due to their robust statistical properties against outliers and skewed distributions (Chen, 1998; von Hippel, 2005). To dimensionally reduce the three hues into one variable the hues were analyzed using principal component analysis (PCA) from the R package *vegan* (Oksanen et al., 2020). Although variable standardization is normally recommended (Jollife and Cadima, 2016), the hues were analyzed without scaling and centering to preserve the relative values (Lever et al., 2017). We did not expect the removal of scaling to have a detrimental effect on model fitting due to the three bands having similar variances. The principal components (PC) were first tested for normality using the Shapiro-Wilks test (Shapiro and Wilk, 1965) and then analyzed using Kendall's tau rank correlation (Kendall, 1938) and Wilcoxon's signed rank test (Wilcoxon, 1945) to test if there were any correlations and differences in mean values between the harvest groups (DAS 72 and 101) and between each water status. Kendall's tau was used due to the higher robustness and efficiency compared to the otherwise commonly used Spearman's rho (Spearman, 1904; Croux and Dehon, 2010). The first principal component was further used as a response variable to build a linear model to identify relevant covariates responsible for the combined hues. A similar approach has previously been used by Golzarian and Frick (2011) to investigate early growth stages of grasses. Multiple predictor variables were used to build the linear regression model: phenotypic (dried biomass, maximum height and SPAD measurements as a proxy for chlorophyll content), environmental (soil moisture as a proxy for waterlogging and chamber treatment as proxy for ambient and climate change climatological conditions), genetic (variety as a proxy for ploidy and heading date) and temporal (progression of the season and recovery from the waterlogging). Although mixed-models are generally recommended in this type of hierarchical ecological design (Piepho et al., 2003) the estimation of random effects from a low number of levels is

very similar to fitting fixed effects models, and can in some cases cause worse model fits due to zero variance estimates (Harrison et al., 2018). The model terms were subsequently analyzed using a Type II ANOVA (Langsrud, 2003; Smith and Cribbie, 2014). Model selection was then performed to analyze how removing variables in the full model would impact the AIC values and model understanding (Bozdogan, 1987; Aho et al., 2014). All statistical analyses were performed in the statistical software R (version 4.1.3.) (R Core Team, 2022).

Results

Plant appearance

To estimate the effects of long-term waterlogging on perennial ryegrass we grew 320 plants in fully atmospherically controlled growth chambers, simulating typical current climatic conditions in North-western Europe and conditions as predicted in 2050 according to RCP8.5 (550 ppm CO_2 and a mean temperature increase of 2°C). Half of the plants were subjected to waterlogging 48 days after sowing (DAS) for one month. After waterlogging had begun, visible differences were observed between waterlogged and non-waterlogged plants at DAS 72 and continued to be visible at DAS 101 (**Figure 1**). The waterlogged plants by DAS 72 had stunted growth with dark brown leaf hues. The leaf morphology of the waterlogged plants also varied to the non-waterlogged plants, because leaf unfolding was disrupted, causing a concave and folded appearance of many leaves in waterlogged plants (**Figure 2**). By DAS 101 many plants had started to change in leaf color, with many leaves presenting light green shades. This contrasts with the non-waterlogged plants that had darker green shades and a lush appearance. Leaf morphology also differed at DAS 101 between waterlogged and non-waterlogged plants, where the leaves of the waterlogged plants remained concave and light green while the non-waterlogged plants had tall, wide and lush leaves. The median true colors of the harvests at DAS 72 (**Figure 3**) and DAS 101 (**Figure 4**) showed a substantial variation between plants of each water treatment and chamber condition, with darkening of leaves as the growth season progressed. No direct visual difference could be observed between the two climate treatments (ambient vs 2050 RCP8.5 scenario).

FIGURE 1
Perennial Ryegrass (*Lolium perenne*) whole plant appearance examples images for selected harvests and water status. **(A)** DAS 72 non-waterlogged. **(B)** DAS 72 waterlogged. **(C)** DAS 101 non-waterlogged. **(D)** DAS 101 waterlogged. Examples images are not color corrected.

Color quantification through RGB fusion

To quantify the visible differences between the waterlogged and non-waterlogged plants, all plant leaves were harvested at DAS 72 and again at DAS 101, photographed and subjected to a color analysis. The isolated RGB hues from the color analysis were further modeled using a PCA-method. We hypothesized that there would be measurable color differences depending on the water status, with the waterlogging contributing to lighter colors. We also expected color differences between harvest dates, with darker colors as the growth season progressed. The PCA of the three RGB hues isolated from the harvested material from DAS 72 and 101 identified that the greatest variation (97.3%) could be explained by the first PC axis (PC1) (**Figure 5**). All three RGB hues showed a positive increase with the first axis

FIGURE 2
Perennial Ryegrass (*Lolium perenne*) leaf morphology example images for selected harvests and water status. **(A)** DAS 72 non-waterlogged. **(B)** DAS 72 waterlogged. **(C)** DAS 72 waterlogged. **(D)** DAS 101 non-waterlogged. **(E)** DAS 101 waterlogged. Examples images are not color corrected.

(Supplementary Table 1), illustrating that the axis describes a light beige to dark brown hue divergence (Supplementary Figure 1). To simplify this main leaf describing characteristics we classified the axis as overall color intensity. The negative values of PC1 are therefore darker intensities, while the positive values are lighter intensities. The other two minor axes PC2 (1.8%) and PC3 (0.9%) describe pure color hue gradients, a green-purple and an orange-blue hue divergence respectively. Kendall's tau and Wilcoxon's signed rank test showed that the harvested material from the waterlogged plants collected on DAS 72 were not correlated in color to the non-waterlogged plants of the same harvest and were overall lighter ($p < 0.001$) and more purple ($p < 0.001$) (Table 3). The waterlogged plants on DAS 101 were positively correlated in color intensity with the non-waterlogged plants of the same harvest while being darker ($p < 0.001$) and greener ($p < 0.001$). The harvested material from the waterlogged plants were positively correlated in color intensity from DAS 72 to 101 with the plants becoming darker ($p < 0.001$) and greener ($p < 0.001$) as they started to recover from the waterlogging. The non-waterlogged plants were positively correlated in color intensity between the harvests periods and became overall darker ($p < 0.001$) as the growth season progressed. See Supplementary Material for the mean differences in PC axes values between the harvests and water status groupings (Supplementary Table 2).

Phenotypic differentiation

To understand how phenotypic, environmental, genetic and temporal factors contribute to the quantified colors of the harvested leaf material a linear regression model was created and analyzed. The first PC axis (PC1), identified as color intensity, was modeled using three phenotypic variables, two environmental variables, one genetic variable and one temporal variable. The model was analyzed using Type II ANOVA and AIC to see the model performance after subsequently removing each variable individually. We hypothesized that the effects

from the predictor variables would be physiologically connected and cause differences in color intensity. We expected that higher soil moisture would result in lighter colors and cause negative physiological effects on growth by lowering biomass and maximum height. We also expected that the climate change conditions would enhance growth through increased temperature and CO_2, causing darker colors, along with darker colors as the growth season progressed, with variations between varieties caused by inherent genetic differences.

Phenotypically, harvested material from plants with lighter color intensities had significantly lower dried biomass ($F_{1,630} = 232.44$, $p < 0.001$), significantly lower maximum height ($F_{1,630} = 57.92$, $p < 0.001$), and significantly lower SPAD values ($F_{1,630} = 250.01$, $p < 0.001$) (**Table 4** and **Supplementary Figures 2–4**). For the water status, harvested material from cores with lighter color intensities had significantly higher soil moisture ($F_{1,630} = 174.67$, $p < 0.001$) (**Supplementary Figure 5**). The harvested material from plants in chambers in predicted 2050 climate change conditions had significantly lighter intensities than harvested material from plants in ambient conditions ($F_{1,630} = 19.20$, $p < 0.001$) (**Supplementary Figure 6**).

Genetically, there were significant differences in color intensity between the varieties ($F_{3,630} = 33.41$, $p < 0.001$). *Aberchoice*, the only diploid variety, had the lightest color intensities, while the three tetraploid varieties, *Abergain, Dunluce*, and *Carraig* had darker intensities in that order, with *Carraig* having the darkest leaf color intensities (**Supplementary Figure 7**). The harvested material became darker overall as the season progressed ($F_{1,630} = 4.27$, $p = 0.039$), with the leaves in DAS 101 being significantly darker than DAS 72. The AIC revealed that the variables had a differential importance to the model performance. SPAD values ($\Delta AIC = -211.9$), dried biomass ($\Delta AIC = -199.0$), and soil moisture ($\Delta AIC = -154.7$) were the most influential variables able to predict color intensity, while progression of the season ($\Delta AIC = -2.3$), climate treatment ($\Delta AIC = -17.2$) and maximum height ($\Delta AIC = -54.3$) were the least influential. Overall, the linear regression model had a very high accuracy in predicting leaf color intensity, with an adjusted R^2 of 91.8%. See **Supplementary Material** for the linear model estimates (**Supplementary Table 3**).

Discussion

Our aim was to investigate the phenotypic effect of long-term waterlogging on perennial ryegrass. We found that long-term waterlogging reduced perennial ryegrass productivity and changed the plant phenotype. Waterlogged plants were lighter in color than controls, with younger waterlogged plants expressing purple hues, suggestive of anthocyanins. We also found that waterlogged plants had significantly lower dried biomass and maximum height, demonstrating that waterlogging reduced overall plant performance and yield. Our study has experimentally determined the influence of waterlogging and climate change upon plant performance, with the effects of waterlogging largely overshadowing the effects of increased temperature and elevated CO_2. The imaging methods could be developed as remote sensed diagnostics tools in combination with drone-technology to determine the influence of waterlogging on plant health in field environments.

Physiology and anthocyanins

Our results identified substantial variation in leaf coloration in perennial ryegrass caused by long-term waterlogging. This variation was mainly in color intensity, with waterlogging resulting in lighter color intensities. Previous studies have shown that waterlogging can reduce concentrations of plant pigments, mainly chlorophyll, resulting in lighter colors and reduced photosynthetic capability (e.g., Close and Davidson, 2003; Smethurst and Shabala, 2003; Pang et al., 2004; Li et al., 2011; Ou et al., 2011; Simova-Stoilova et al., 2012; Zhang et al., 2015; Barickman et al., 2019; Cotrozzi et al., 2021). Cotrozzi et al. (2021) found that waterlogging damaged the photosynthetic ability of durum wheat but that it depended on the duration, and that longer waterlogging was more detrimental. Li et al. (2011) found that waterlogging previous to anthesis could prevent photosynthetic damage in subsequent waterlogging events after anthesis, enhancing overall tolerance. Pang et al. (2004) found that barley varieties respond differently from waterlogging damage to photosystem II, and that recovery is at least partly genetically determined. We also observed significant variation in hue, with waterlogging resulting in red/blue (purple) shades. This was especially pronounced for the waterlogged plants in DAS 72, with large variation being observed between the plants, showing that varieties but also individual plants respond divergently to the same stimuli. These purple shades are likely caused by an accumulation of secondary anthocyanin metabolites, with multiple compounds having been identified in grasses (Clifford and Harborne, 1967; Fossen et al., 2002; Petrella et al., 2016). This suggests that individual plants respond differently to waterlogging by accumulating anthocyanins of varying degree. This is in agreement with previous research that has suggested that plants accumulate anthocyanins as a response to environmental stressors (Chalker-Scott, 1999), for example water availability as during drought (e.g., Close and Beadle, 2003; Kovinich et al., 2015; Li et al., 2018; Cirillo et al., 2021) and waterlogging (e.g., Close and Davidson, 2003; Smethurst and Shabala, 2003; Hussain et al., 2022). One of the main suggested benefits of increased anthocyanin accumulation is protection against DNA damaging UV-B radiation that can reduce photosynthetic capability (Teramura and Sullivan, 1994; Rozema et al., 1997; Hoch et al., 2001; Steyn et al., 2002).

FIGURE 3
Median color (RGB) of the harvested material for all cores on DAS 72 as identified by the image analysis, sorted on water status, climate treatment and variety. Each cell represents the median true color of the harvested material of a plant. AberC, Aberchoice; AberG, Abergain; Carr, Carraig; Dunl, Dunluce.

Anthocyanin accumulation has also been found as a response to phosphorus deficiency (e.g., Ulrychová and Sosnová, 1970; Shaikh et al., 2008; Sarker and Karmoker, 2011). This is a potential physiological cause of the observed purple shades in our waterlogged plants for two reasons. Firstly, phosphorus has been found to become soluble during excess water availability and migrate down the soil column (Sanyal and De Datta, 1991; Sinaj et al., 2002) and secondly, altered plant nutrient uptake during periods of excess water abundance might make the soil nutrients (e.g., phosphorus) temporarily unavailable (Elzenga and van Veen, 2010). These effects are expected to be especially pronounced for younger plants (Close and Beadle, 2003), as we indicated by our initial results, due to the undeveloped root system occupying only the upper part of the soil column. Additional root growth and reduction in soil moisture would allow the plants to reach the migrated phosphorus and start to recover via normalized nutrient levels, as observed with the reduction in purple hues from the waterlogging in DAS 101. Our results strengthen the consensus of recent studies that phenotypic color variations can effectively be quantified through image analysis and analyzed to detect physiological effects from waterlogging (e.g., de la Cruz Jiménez et al., 2017; Ventura et al., 2020), although detailed soil nutrient analysis would be needed to confirm our findings in connection to phosphorus availability. Future research is needed to validate the soil phosphorus availability in waterlogged scenarios in relation to anthocyanin accumulation in plant tissue and to what extent undeveloped root systems are influenced by this.

Plant performance

Our results showed reductions in dried biomass and height in response to long-term waterlogging for all perennial ryegrass

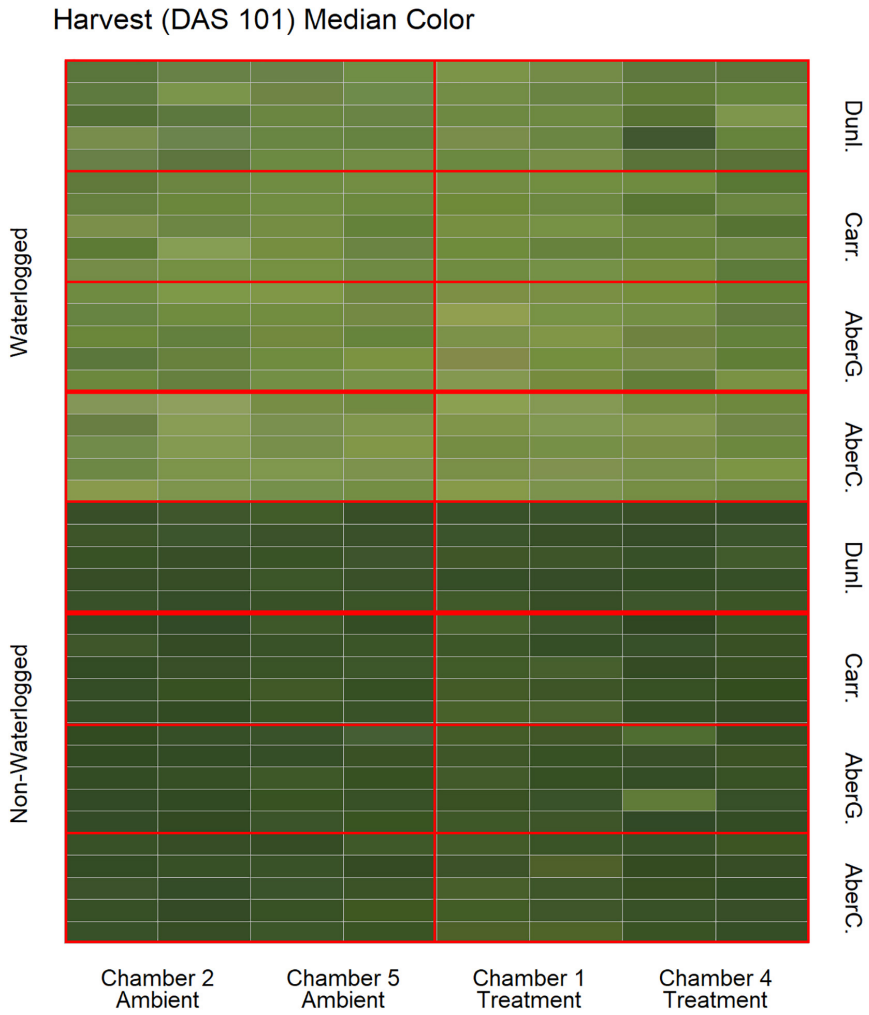

FIGURE 4
Median color (RGB) of the harvested material for all cores on DAS 101 as identified by the image analysis, sorted on water status, climate treatment and variety. Each cell represents the median true color of the harvested material of a plant. AberC, Aberchoice; AberG, Abergain; Carr, Carraig; Dunl, Dunluce.

varieties. These reductions in plant growth likely stems from lower photosynthetic capability caused by a physiological reduction in plant pigments as identified from the SPAD values and color analysis, but also from hindrance to root development. Complex interactions between soil moisture and root proliferation patterns are likely one of the main drivers governing growth performance via soil nutrient absorption (Brugge, 1985; Setter and Belford, 1990; Xu et al., 2013; Medlyn et al., 2016; Cougnon et al., 2017). Previous studies have linked waterlogging to reductions in grass performance caused by altered root development (Malik et al., 2002; Ploschuk et al., 2017). This agrees with our findings, as we observed a clear reduction in root proliferation in the waterlogged cores (visual inspection, results not shown), with long-term waterlogging having previously been shown to reduce root mass in ryegrass (McFarlane et al., 2003). Another potential consequence is reduced root respiration caused by a reduction in soil oxygen levels, which has been shown to have multiple negative feedbacks on grass biomass accumulation and nutrients absorption (Trought and Drew, 1980; Dunbabin et al., 1997; Fukao et al., 2019).

There is also variation in waterlogging tolerance between grass species (e.g., Rubio et al., 1995; Rubio and Lavado, 1999; Xiao and David, 2019) and wheat cultivars (e.g., Ghobadi et al., 2017; Cotrozzi et al., 2021) based on local adaptation and specific genotypes. Genotype specific tolerance to waterlogging has been found between perennial ryegrass varieties (Liu and Jiang, 2015; Byrne et al., 2017). This was expanded upon by Pearson et al. (2011) that found multiple quantitative trait loci (QTLs) that code for morphological traits influencing the tolerance to waterlogging in perennial ryegrass. This is one likely explanation for the differential performance to waterlogging

10.3389/fpls.2022.954478

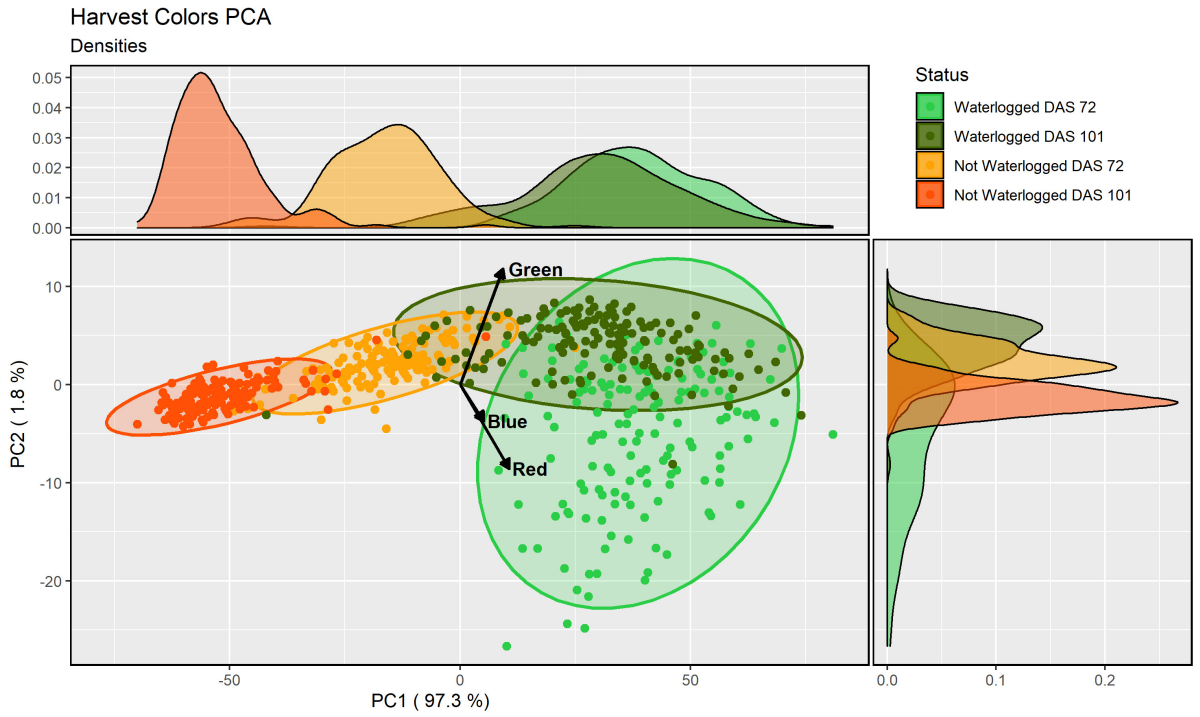

FIGURE 5
Principal component analysis (PCA)-analysis of the three RGB-hues of the harvested material for all cores, water status and harvest (DAS 72 and 101) as identified by the image analysis. Each ellipse represents a 95% confidence ellipse for each group. Side graphs shows the relative densities of each PCA axis and grouping, with the area under each curve representing the entire group distribution.

TABLE 3 Model statistics and significance levels for the comparison of PC axes values for the groupings harvested material (DAS 72 and 101) and water status of the cores in contrast to the other grouping.

PC axis	Water status		Harvest		Model statistics						
	Comparison		Comparison		Kendall's tau Rank Correlation				Wilcoxon Signed-Rank Test		
					z	tau (τ)	*P*-value	Significance	V	*P*-value	Significance
PC1	Logged		DAS 72	DAS 101	9.979	0.532	$<1 \times 10^{-10}$	***	1,967	$<1 \times 10^{-10}$	***
	Normal		DAS 72	DAS 101	2.449	0.131	0.014	*	36	$<1 \times 10^{-10}$	***
PC2	Logged		DAS 72	DAS 101	1.757	0.094	0.079	NS	12,695	$<1 \times 10^{-10}$	***
	Normal		DAS 72	DAS 101	1.732	0.092	0.083	NS	445	$<1 \times 10^{-10}$	***
PC3	Logged		DAS 72	DAS 101	6.007	0.320	1.893×10^{-9}	***	4,232	1.694×10^{-4}	***
	Normal		DAS 72	DAS 101	5.495	0.293	3.907×10^{-8}	***	12,875	$<1 \times 10^{-10}$	***
PC1	Logged	Normal	DAS 72		0.282	0.015	0.778	NS	0	$<1 \times 10^{-10}$	***
	Logged	Normal	DAS 101		3.332	0.178	8.629×10^{-4}	***	2	$<1 \times 10^{-10}$	***
PC2	Logged	Normal	DAS 72		0.285	0.015	0.776	NS	12,053	$<1 \times 10^{-10}$	***
	Logged	Normal	DAS 101		−0.558	−0.030	0.577	NS	323	$<1 \times 10^{-10}$	***
PC3	Logged	Normal	DAS 72		1.374	0.073	0.170	NS	820	$<1 \times 10^{-10}$	***
	Logged	Normal	DAS 101		0.815	0.043	0.415	NS	9,506	1.765×10^{-7}	***

The upper part of the table compares cores within the same water status between harvests. The lower part of the table compares between water status for the same harvest.
DAS, days after sowing.
$^{***}p < 0.001$.
$^{**}p < 0.01$.
$^{*}p < 0.05$.
$^{NS}p > 0.05$.

TABLE 4 Model statistics and significance levels for the linear model in regards to the first PCA axis (Color Intensity) isolated from the color analysis of the harvested perennial ryegrass material.

Variable	Model statistics							
	Df	Sum Sq	RSS	AIC	Δ AIC	F-value	*P*-value	Significance
<none>			79,595	3,106.9				
Weight	1	29,367	108,962	3,305.9	−199.0	232.44	$<1 \times 10^{-10}$	***
Height	1	7,318	86,914	3,161.2	−54.3	57.92	$<1 \times 10^{-10}$	***
SPAD	1	31,587	111,182	3,318.8	−211.9	250.01	$<1 \times 10^{-10}$	***
Soil Moisture	1	22,068	101,663	3,261.5	−154.6	174.67	$<1 \times 10^{-10}$	***
Treatment	1	2,426	82,021	3,124.1	−17.2	19.20	1.379×10^{-5}	***
Variety	3	12,664	92,259	3,195.4	−88.5	33.41	$<1 \times 10^{-10}$	***
Month	1	539	80,134	3,109.2	−2.3	4.27	0.039	*

Df, degrees of freedom; RSS, residual sum of squares.
Model Statistics: Anova (Type II) using the Drop1 function. Model performance: Adjusted $R^2 = 91.8\%$.
$^{***}p < 0.001$.
$^{**}p < 0.01$.
$^{*}p < 0.05$.
$^{NS}p > 0.05$.

amongst our varieties, with the tetraploid varieties generally tolerating waterlogging better than the diploid variety. However, our study only included one diploid variety, introducing a potential risk for bias in evaluating the contribution of ploidy to waterlogging resilience. We did observe substantial variation between the tetraploid varieties, suggesting that other aspects of the genotype could influence the response to the environmental stressors. It is possible that the difference in performance is due to genotypic root development, which has been observed previously between perennial ryegrass varieties (Bonos et al., 2004; Wedderburn et al., 2010; Deru et al., 2014). Although, there is no clear connection between ploidy and stress tolerance to waterlogging or other environmental stressors (Yu et al., 2012; Kemesyte et al., 2017; Tozer et al., 2017; Lee et al., 2019). Future research would benefit from including a wide range of varieties of varying genotypes grown under combinations of environmental stressors coupled with detailed genomics analyses. This could reveal the genetic basis of stress tolerance, and potential genetic trade-offs that occur between phenotypic traits.

Practical implications

We hypothesized that increases in temperature and CO_2 (predicted 2050-levels) would enhance plant performance to climate change-induced waterlogging, but our results showed that perennial ryegrass responded with lighter leaf shades, suggesting reduced photosynthetic capability and reduced yields. This is in contrast to the theory that climate change will generally increase photosynthesis and productivity (Chen et al., 1996; Dusenge et al., 2019; Yiotis et al., 2021). Other studies have suggested that combined stressors brought by climate change could bring further negative effects than each stressor individually (Ahuja et al., 2010; Zandalinas et al., 2021). The developmental period of the grasses could be relevant here, with our study investigating the performance during the first few months including young plants. It is uncertain if these effects are specific to younger plants, or applicable to mature ones as well. Waterlogging has previously been shown to affect grain-crops differently depending on species and development, with wheat being able to sustain growth regardless of the period of waterlogging, while barley being disproportionately affected in later development (Ploschuk et al., 2020, 2021). Daepp et al. (2001) showed that the effects of elevated CO_2 will depend on the developmental stage of the ryegrass, suggesting that some stages are more sensitive to than others. For grasses in general, elevated CO_2 has been suggested to intensify the reproductive period from increases in NPP (Kurganskiy et al., 2021). Climate change will lead to multiple changes in the environment: increased temperature and CO_2 may have positive effects by extending the growing season for certain species while simultaneously flooding or drought may have negative effects on overall plant growth (Richardson et al., 2013). To understand the effects of climate change we need to consider all environmental effects, their relative contribution to the overall impact and possible interactions to different developmental stages (Tubiello et al., 2007; Parmesan and Hanley, 2015; Gray and Brady, 2016; Zhou et al., 2020). In our case, the effect of waterlogging seems to largely overshadow the effects of increased temperature and elevated CO_2.

To our knowledge this is the first study to investigate the combined effects of climate change (both temperature and CO_2) and waterlogging experimentally in any plant. Previous studies have indicated that the interactive effects from elevated CO_2 in isolation with waterlogging are inconclusive. Shimono et al. (2012) observed that soy bean (*Glycine max*) dry weight was

significantly heavier during elevated CO_2 (~580–600 ppm), but did not see an overall interactive effect with waterlogging. Pérez-Jiménez et al. (2018) observed that the stress response of sweet cherry (*Prunus avium*) was significantly reduced after being waterlogged during elevated CO_2 (800 ppm) compared to ambient levels, suggesting that elevated CO_2 can reduce the waterlogging stress response. It is possible that the 200 ppm difference between these two studies is responsible for the difference in response, or that the study species inherently respond differently to the increase. One recent modeling-study has suggested that climate change will reduce waterlogging stress in barley (Liu et al., 2021), but not enough to compensate the reduction in yield (~35% on average) due to high temperatures stress and that the development of resilient varieties to waterlogging will be required. However, increases in flooding due to climate change would cause more severe impacts than from current precipitation regimes (Mirza, 2011; Iglesias et al., 2012). The decrease in overall dried biomass for all varieties as a consequence of waterlogging predicted by our study has implications for global food security. A reduction in overall plant yield due to poor plant growth from flooding would potentially cause increases in fodder prices with follow-up consequences to all agricultural sectors and industries relying on fodder from pasture lands (Hazell and Wood, 2008; Kipling et al., 2016b; Manik et al., 2019). Early detection of waterlogging and identification of varieties resistant to waterlogging, will likely be important to employ mitigation strategies that could minimize reductions in plant health and production yield in pasture lands. Areas prone to current waterlogging are likely to experience increased frequency with climate change, with the utilization of appropriate drainage systems (natural or artificial) have previously been shown to be effective (Singh, 2017; Manik et al., 2019). The identification and breeding of plant lineages resilient to waterlogging damage is likely the most efficient (and cost-effective) approach of mitigating reductions in yield and performance and will be fundamental in a climate change future (Boru et al., 2001; Kole et al., 2015; Rivero et al., 2022).

We demonstrate that image analysis approaches can be used as diagnostic tools to investigate plant performance reductions caused by waterlogging. While most field monitoring would be time consuming and most satellite-based remote sensing products would be low resolution for this type of analysis other more navigable high-resolution options are available, for example drones (Bansod et al., 2017; Cracknell, 2018; Simic Milas et al., 2018). Drones have been shown to be a useful and cost-effective tool for agricultural surveying (Tripicchio et al., 2015; Puri et al., 2017; Kulbacki et al., 2018) and plant ecological investigation (Cruzan et al., 2016; Tay et al., 2018; Zellweger et al., 2019; Sun et al., 2021). The main benefits comes from the use of high-resolution multi- and hyperspectral cameras which capture a wide-range of light wavelengths used to infer plant physiological parameters (e.g., Li et al., 2020; Tao et al., 2020; Papp et al., 2021). Our results showed that differences in color intensity could be observed between perennial ryegrass varieties, suggesting that the imaging analysis method could be developed further to identify closely related varieties or perhaps different grass species using remote-sensed color distributions. Recent studies have also shown the usefulness of drones to monitor the effects of waterlogging on agricultural systems (e.g., Boiarskii et al., 2019; Den Besten et al., 2021; León-Rueda et al., 2021), illustrating that our imaging approaches could be adapted to work as diagnostic tools with drone-technology. Applications using integrated monitoring of plant health will become increasingly important as climate change-induced extreme weather events become more prevalent.

Data availability statement

The data supporting the findings of this study is now publicly available in the general-purpose open-access repository Zenodo developed by the European OpenAIRE program and operated by CERN (doi: 10.5281/zenodo.6334191).

Author contributions

CF: design of the research, performance of the research, data analysis, collection or interpretation, and writing the manuscript. GX-S, MO, and YB: performance of the research and data analysis, collection, or interpretation. RM and JY: design of the research, data analysis, collection or interpretation, and writing the manuscript. All authors contributed to the article and approved the submitted version.

Funding

This project was funded under the EPA Research Programme 2014-2020 (Grant: 2018-CCRP-MS.52). The EPA Research Programme is a Government of Ireland initiative funded by the Department of the Environment, Climate and Communications. It is administered by the Environmental Protection Agency, which has the statutory function of coordinating and promoting environmental research.

Acknowledgments

Thanks goes out to Sónia Negrão for providing assistance with the equipment acquisition. GX-S, MO, and YB acknowledges funding from the Thomas Crawford Hayes Fund administered by the four NUI constituent Universities.

Conflict of interest

The authors declare that the research was conducted in the absence of any commercial or financial relationships that could be construed as a potential conflict of interest.

Publisher's note

All claims expressed in this article are solely those of the authors and do not necessarily represent those of their affiliated organizations, or those of the publisher, the editors and the reviewers. Any product that may be evaluated in this article, or claim that may be made by its manufacturer, is not guaranteed or endorsed by the publisher.

Supplementary material

The Supplementary Material for this article can be found online at: https://www.frontiersin.org/articles/10.3389/fpls.2022.954478/full#supplementary-material

References

Aho, K., Derryberry, D., and Peterson, T. (2014). Model selection for ecologists: the worldviews of AIC and BIC. *Ecology* 95, 631–636. doi: 10.1890/13-1452.1

Ahuja, I., de Vos, R. C. H., Bones, A. M., and Hall, R. D. (2010). Plant molecular stress responses face climate change. *Trends Plant Sci.* 15, 664–674. doi: 10.1016/j.tplants.2010.08.002

Baldos, U. L. C., and Hertel, T. W. (2014). Global food security in 2050: The role of agricultural productivity and climate change. *Aust. J. Agric. Resour. Econ.* 58, 554–570. doi: 10.1111/1467-8489.12048

Bansod, B., Singh, R., Thakur, R., and Singhal, G. (2017). A comparision between satellite based and drone based remote sensing technology to achieve sustainable development: a review. *J. Agric. Environ. Int. Dev.* 111, 383–407. doi: 10.12895/jaeid.20172.690

Barickman, T. C., Simpson, C. R., and Sams, C. E. (2019). Waterlogging Causes early modification in the physiological performance, carotenoids, chlorophylls, proline, and soluble sugars of cucumber plants. *Plants* 160, 1–15. doi: 10.3390/plants8060160

Batke, S., Holohan, A., Hayden, R., Fricke, W., Porter, A. S., and Christiana, C. M. (2018). The pressure is on – Epiphyte water-relations altered under elevated CO2. *Front. Plant Sci.* 871:1758. doi: 10.3389/fpls.2018.01758

Bellocchi, G., and Picon-Cochard, C. (2021). Effects of climate change on grassland biodiversity and productivity. *Agronomy* 11:1047. doi: 10.3390/agronomy11061047

Blöschl, G., Hall, J., Viglione, A., Perdigão, R. A. P., Parajka, J., Merz, B., et al. (2019). Changing climate both increases and decreases European river floods. *Nature* 573, 108–111. doi: 10.1038/s41586-019-1495-6

Boiarskii, B., Hasegawa, H., Muratov, A., and Sudeykin, V. (2019). Application of UAV-derived digital elevation model in agricultural field to determine waterlogged soil areas in Amur region, Russia. *Int. J. Eng. Adv. Technol.* 8, 520–523.

Bonos, S. A., Rush, D., Hignight, K., and Meyer, W. A. (2004). Selection for deep root production in tall fescue and perennial ryegrass. *Crop Sci.* 44, 1770–1775. doi: 10.2135/cropsci2004.1770

Boru, G., Van Ginkel, M., Kronstad, W. E., and Boersma, L. (2001). Expression and inheritance of tolerance to waterlogging stress in wheat. *Euphytica* 117, 91–98. doi: 10.1023/A:1003929803920

Bothe, A., Westermeier, P., Wosnitza, A., Willner, E., Schum, A., Dehmer, K. J., et al. (2018). Drought tolerance in perennial ryegrass (*Lolium perenne* L.) as assessed by two contrasting phenotyping systems. *J. Agron. Crop Sci.* 204, 375–389. doi: 10.1111/jac.12269

Bozdogan, H. (1987). Model selection and akaike's information criterion (AIC): the general theory and its analytical extensions. *Psychometrika* 52, 345–370. doi: 10.1007/BF02294361

Brown, J. N., Ash, A., MacLeod, N., and McIntosh, P. (2019). Diagnosing the weather and climate features that influence pasture growth in Northern Australia. *Clim. Risk Manag.* 24, 1–12. doi: 10.1016/j.crm.2019.01.003

Brugge, R. (1985). A mechanistic model of grass root growth and development dependent upon photosynthesis and nitrogen uptake. *J. Theor. Biol.* 116, 443–467. doi: 10.1016/S0022-5193(85)80281-2

Buttler, A., Mariotte, P., Meisser, M., Guillaume, T., Signarbieux, C., Vitra, A., et al. (2019). Drought-induced decline of productivity in the dominant grassland species *Lolium perenne* L. depends on soil type and prevailing climatic conditions. *Soil Biol. Biochem.* 132, 47–57. doi: 10.1016/j.soilbio.2019.01.026

Byrne, N., Gilliland, T. J., Mchugh, N., Delaby, L., Geoghegan, A., and O'donovan, M. (2017). Establishing phenotypic performance of grass varieties on Irish grassland farms. *J. Agric. Sci.* 155, 1633–1645. doi: 10.1017/S0021859617000740

Canadell, J. G., and Raupach, M. R. (2008). Managing forests for climate change mitigation. *Science* 320, 1456–1457. doi: 10.1126/science.1155458

Chalker-Scott, L. (1999). Environmental significance of anthocyanins in plant stress responses. *Photochem. Photobiol.* 70, 1–9. doi: 10.1111/j.1751-1097.1999.tb01944.x

Chen, D. X., Hunt, H. W., and Morgan, J. A. (1996). Responses of a C3 and C4 perennial grass to CO2 enrichment and climate change: comparison between model predictions and experimental data. *Ecol. Modell.* 87, 11–27. doi: 10.1016/0304-3800(94)00199-5

Chen, Z. (1998). A note on bias robustness of the median. *Stat. Probab. Lett.* 38, 363–368. doi: 10.1016/S0167-7152(98)00049-2

Cirillo, V., D'Amelia, V., Esposito, M., Amitrano, C., Carillo, P., Carputo, D., et al. (2021). Anthocyanins are key regulators of drought stress tolerance in tobacco. *Biology (Basel).* 10, 1–15. doi: 10.3390/biology10020139

Clifford, H. T., and Harborne, J. B. (1967). Anthocyanin composition of and distribution in the Poaceae (Gramineae). *Proc. Linn. Soc. London* 178, 125–127. doi: 10.1111/j.1095-8312.1967.tb00968.x

Close, D. C., and Beadle, C. L. (2003). The ecophysiology of foliar anthocyanin. *Bot. Rev.* 69, 149–161. doi: 10.1016/j.jplph.2020.153161

Close, D. C., and Davidson, N. J. (2003). Long-term waterlogging: Nutrient, gas exchange, photochemical and pigment characteristics of *Eucalyptus nitens* saplings. *Russ. J. Plant Physiol.* 50, 843–847. doi: 10.1023/B:RUPP.0000003284.25827.95

Cotrozzi, L., Lorenzini, G., Nali, C., Pisuttu, C., Pampana, S., and Pellegrini, E. (2021). Transient waterlogging events impair shoot and root physiology and reduce grain yield of durum wheat cultivars. *Plants* 10:2357. doi: 10.3390/plants10112357

Cougnon, M., De Swaef, T., Lootens, P., Baert, J., De Frenne, P., Shahidi, R., et al. (2017). In situ quantification of forage grass root biomass, distribution and diameter classes under two N fertilisation rates. *Plant Soil* 411, 409–422. doi: 10.1007/s11104-016-3034-7

Cracknell, A. P. (2018). The development of remote sensing in the last 40 years. *Int. J. Remote Sens.* 39, 8387–8427. doi: 10.1080/01431161.2018.1550919

Croux, C., and Dehon, C. (2010). Influence functions of the spearman and kendall correlation measures. *Stat. Methods Appl.* 19, 497–515. doi: 10.1007/s10260-010-0142-z

Cruzan, M. B., Weinstein, B. G., Grasty, M. R., Kohrn, B. F., Hendrickson, E. C., Arredondo, T. M., et al. (2016). Small unmanned aerial vehicles (Micro-Uavs, Drones) in plant ecology. *Appl. Plant Sci.* 4, 1–11. doi: 10.3732/apps.1600041

Cullen, B. R., Johnson, I. R., Eckard, R. J., Lodge, G. M., Walker, R. G., Rawnsley, R. P., et al. (2009). Climate change effects on pasture systems in south-eastern Australia. *Crop Pasture Sci.* 60, 933–942. doi: 10.1071/CP09019

Cullen, B. R., Rawnsley, R. P., Eckard, R. J., Christie, K. M., and Bell, M. J. (2014). Use of modelling to identify perennial ryegrass plant traits for future warmer and drier climates. *Crop Pasture Sci.* 65, 758–766. doi: 10.1071/CP13408

Daepp, M., Nösberger, J., and Lüscher, A. (2001). Nitrogen fertilization and developmental stage alter the response of *Lolium perenne* to elevated CO2. *New Phytol.* 150, 347–358. doi: 10.1046/j.1469-8137.2001.00109.x

de la Cruz Jiménez, J., Cardoso, J. A., Leiva, L. F., Gil, J., Forero, M. G., Worthington, M. L., et al. (2017). Non-destructive phenotyping to identify brachiaria hybrids tolerant to waterlogging stress under field conditions. *Front. Plant Sci.* 8:167. doi: 10.3389/fpls.2017.00167

Den Besten, N., Steele-Dunne, S., de Jeu, R., and van der Zaag, P. (2021). Towards monitoring waterlogging with remote sensing for sustainable irrigated agriculture. *Remote Sens.* 13, 1–20. doi: 10.3390/rs13152929

Deru, J., Schilder, H., van der Schoot, J. R., and van Eekeren, N. (2014). Genetic differences in root mass of *Lolium perenne* varieties under field conditions. *Euphytica* 199, 223–232. doi: 10.1007/s10681-014-1129-x

Dong, T., Shang, J., Chen, J. M., Liu, J., Quian, B., Ma, B., et al. (2019). Assessment of portable chlorophyll meters for measuring crop leaf chlorophyll concentrations. *Remote Sens.* 11:2706. doi: 10.3390/rs11222706

Dore, M. H. I. (2005). Climate change and changes in global precipitation patterns: What do we know? *Environ. Int.* 31, 1167–1181. doi: 10.1016/j.envint.2005.03.004

Dunbabin, J. S., Hume, I. H., and Ireson, M. E. (1997). Effects of irrigation frequency and transient waterlogging on the production of a perennial ryegrass-white clover pasture. *Aust. J. Exp. Agric.* 37, 165–171. doi: 10.1071/EA96057

Dusenge, M. E., Duarte, A. G., and Way, D. A. (2019). Plant carbon metabolism and climate change: elevated CO2 and temperature impacts on photosynthesis, photorespiration and respiration. *New Phytol.* 221, 32–49. doi: 10.1111/nph.15283

Easterling, D. R., Meehl, G. A., Parmesan, C., Changnon, S. A., Karl, T. R., and Mearns, L. O. (2000). Climate extremes: observations. *Model Impact. Sci.* 289, 2068–2074. doi: 10.1126/science.289.5487.2068

Elzenga, J. T. M., and van Veen, H. (2010). "Waterlogging and plant nutrient uptake," in *Waterlogging Signalling and Tolerance in Plants*, eds S. Mancuso and S. Shabala (Berlin: Springer), 23–35. doi: 10.1007/978-3-642-10305-6_2

Ergon, A., Seddaiu, G., Korhonen, P., Virkajärvi, P., Bellocchi, G., Jørgensen, M., et al. (2018). How can forage production in nordic and mediterranean europe adapt to the challenges and opportunities arising from climate change? *Eur. J. Agron.* 92, 97–106. doi: 10.1016/j.eja.2017.09.016

European Commision (2019). Common catalogue of varieties of agricultural plant species (Document ID: C2019/013/01). *Off. J. Eur. Union* 37, 1–812.

Evans-Fitz.Gerald, C., Porter, A. S., Yiotis, C., Elliott-Kingston, C., and McElwain, J. C. (2016). Co-ordination in morphological leaf traits of early diverging angiosperms is maintained following exposure to experimental palaeo-atmospheric conditions of sub-ambient O2 and elevated CO2. *Front. Plant Sci.* 7:1368. doi: 10.3389/fpls.2016.01368

Farfan-Vignolo, E. R., and Asard, H. (2012). Effect of elevated CO2 and temperature on the oxidative stress response to drought in *Lolium perenne* L. and *Medicago sativa* L. *Plant Physiol. Biochem.* 59, 55–62. doi: 10.1016/j.plaphy.2012.06.014

Fay, P. A., Kaufman, D. M., Nippert, J. B., Carlisle, J. D., and Harper, C. W. (2008). Changes in grassland ecosystem function due to extreme rainfall events: Implications for responses to climate change. *Glob. Chang. Biol.* 14, 1600–1608. doi: 10.1111/j.1365-2486.2008.01605.x

Feng, X., Porporato, A., and Rodriguez-Iturbe, I. (2013). Changes in rainfall seasonality in the tropics. *Nat. Clim. Chang.* 3, 811–815. doi: 10.1038/nclimate1907

Fossen, T., Slimestad, R., Øvstedal, D. O., and Andersen, ØM. (2002). Anthocyanins of grasses. biochem. *Syst. Ecol.* 30, 855–864. doi: 10.1016/S0305-1978(02)00028-5

Fukao, T., Barrera-Figueroa, B. E., Juntawong, P., and Peña-Castro, J. M. (2019). Submergence and waterlogging stress in plants: a review highlighting research opportunities and understudied aspects. *Front. Plant Sci.* 10:340. doi: 10.3389/fpls.2019.00340

Ghobadi, M. E., Ghobadi, M., and Zebarjadi, A. (2017). Effect of waterlogging at different growth stages on some morphological traits of wheat varieties. *Int. J. Biometeorol.* 61, 635–645. doi: 10.1007/s00484-016-1240-x

Goliński, P., Czerwiński, M., Jørgensen, M., Mølmann, J. A. B., Golińska, B., and Taff, G. (2018). Relationship between climate trends and grassland yield across contrasting European locations. *Open Life Sci.* 13, 589–598. doi: 10.1515/biol-2018-0070

Golzarian, M. R., and Frick, R. A. (2011). Classification of images of wheat, ryegrass and brome grass species at early growth stages using principal component analysis. *Plant Methods* 7:28. doi: 10.1186/1746-4811-7-28

Gray, S. B., and Brady, S. M. (2016). Plant developmental responses to climate change. *Dev. Biol.* 419, 64–77. doi: 10.1016/j.ydbio.2016.07.023

Grogan, D., and Gilliland, T. J. (2011). A review of perennial ryegrass variety evaluation in Ireland. *Irish J. Agric. Food Res.* 50, 65–81.

Hannaway, D., Fransen, S., Cropper, J., Teel, M., Chaney, M., Griggs, T., et al. (1999). *Perennial Ryegrass (Lolium perenne L.). A Pacific Northwest Ext. Publ.* Corvallis: Oregon State University, 1–20.

Harrison, X. A., Donaldson, L., Correa-Cano, M. E., Evans, J., Fisher, D. N., Goodwin, C. E. D., et al. (2018). A brief introduction to mixed effects modelling and multi-model inference in ecology. *PeerJ.* 2018, 1–32. doi: 10.7717/peerj.4794

Hazell, P., and Wood, S. (2008). Drivers of change in global agriculture. *Philos. Trans. R. Soc. B Biol. Sci.* 363, 495–515. doi: 10.1098/rstb.2007.2166

Helgadóttir, A., Aavola, R., Isolahti, M., Marum, P., Persson, C., Aleliūnas, A., et al. (2018). Adaptability and phenotypic stability of *Lolium perenne* L. cultivars of diverse origin grown at the margin of the species distribution. *J. Agron. Crop Sci.* 204, 493–504. doi: 10.1111/jac.12273

Hoch, W. A., Zeldin, E. L., and McCown, B. H. (2001). Physiological significance of anthocyanins during autumnal leaf senescence. *Tree Physiol.* 21, 1–8. doi: 10.1093/treephys/21.1.1

Höglind, M., Thorsen, S. M., and Semenov, M. A. (2013). Assessing uncertainties in impact of climate change on grass production in Northern Europe using ensembles of global climate models. *Agric. For. Meteorol.* 170, 103–113. doi: 10.1016/j.agrformet.2012.02.010

Hu, H., Oglesby, R. J., and Saltzman, B. (2000). The relationship between atmospheric water vapor and temperature in simulations of climate change. *Geophys. Res. Lett.* 27, 3513–3516. doi: 10.1029/2000GL011680

Hu, H., Zhang, J., Sun, X., and Zhang, X. (2013). Estimation of leaf chlorophyll content of rice using image color analysis. *Can. J. Remote Sens.* 39, 185–190. doi: 10.5589/m13-026

Hunt, W. F., and Easton, H. S. (1989). Fifty years of ryegrass research in New Zealand. *Proc. N Z. Grassl. Assoc.* 23, 1–23. doi: 10.33584/jnzg.1989.50.1876

Huntingford, C., Zelazowski, P., Galbraith, D., Mercado, L. M., Sitch, S., Fisher, R., et al. (2013). Simulated resilience of tropical rainforests to CO2 -induced climate change. *Nat. Geosci.* 6, 268–273. doi: 10.1038/ngeo1741

Hussain, S., Mehmood, U., Ashraf, U., and Naseer, M. A. (2022). "Combined salinity and waterlogging stress in plants: limitations and tolerance mechanisms," in *Climate Change and Crop Stress (INC)*, eds A. K. Shanker, C. Shanker, A. Anand, and M. Maheswari (Cambridge, MA: Academic Press), 95–112. doi: 10.1016/b978-0-12-816091-6.00017-1

Iglesias, A., Quiroga, S., Moneo, M., and Garrote, L. (2012). From climate change impacts to the development of adaptation strategies: challenges for agriculture in Europe. *Clim. Change* 112, 143–168. doi: 10.1007/s10584-011-0344-x

IPCC (2014). *Climate Change 2014: Synthesis Report. Contribution of Working Groups I, II and III to the Fifth Assessment Report of the Intergovernmental Panel on Climate Change*. Geneva: IPCC.

Jentsch, A., Kreyling, J., Boettcher-Treschkow, J., and Beierkuhnlein, C. (2009). Beyond gradual warming: extreme weather events alter flower phenology of European grassland and heath species. *Glob. Chang. Biol.* 15, 837–849. doi: 10.1111/j.1365-2486.2008.01690.x

Jollife, I. T., and Cadima, J. (2016). Principal component analysis: a review and recent developments. *Philos. Trans. R. Soc. A Math. Phys. Eng. Sci.* 374, 20150202. doi: 10.1098/rsta.2015.0202

Kemesyte, V., Statkeviciute, G., and Brazauskas, G. (2017). Perennial ryegrass yield performance under abiotic stress. *Crop Sci.* 57, 1935–1940. doi: 10.2135/cropsci2016.10.0864

Kendall, M. G. (1938). A new measure of rank correlation. *Biometrika* 30:81. doi: 10.2307/2332226

Kiely, G. (1999). Climate change in Ireland from precipitation and streamflow observations. *Adv. Water Resour.* 23, 141–151. doi: 10.1016/S0309-1708(99)00018-4

Kipling, R. P., Bannink, A., Bellocchi, G., Dalgaard, T., Fox, N. J., Hutchings, N. J., et al. (2016a). Modeling European ruminant production systems: facing the challenges of climate change. *Agric. Syst.* 147, 24–37. doi: 10.1016/j.agsy.2016.05.007

Kipling, R. P., Virkajärvi, P., Breitsameter, L., Curnel, Y., De Swaef, T., Gustavsson, A. M., et al. (2016b). Key challenges and priorities for modelling European grasslands under climate change. *Sci. Total Environ.* 566–567, 851–864. doi: 10.1016/j.scitotenv.2016.05.144

Kole, C., Muthamilarasan, M., Henry, R., Edwards, D., Sharma, R., Abberton, M., et al. (2015). Application of genomics-assisted breeding for generation of climate resilient crops: progress and prospects. *Front. Plant Sci.* 6:563. doi: 10.3389/fpls.2015.00563

Kovinich, N., Kayanja, G., Chanoca, A., Otegui, M. S., and Grotewold, E. (2015). Abiotic stresses induce different localizations of anthocyanins in *Arabidopsis*. *Plant Signal. Behav.* 10:e1027850. doi: 10.1080/15592324.2015.1027850

Kulbacki, M., Segen, J., Knieć, W., Klempous, R., Kluwak, K., Nikodem, J., et al. (2018). "Survey of drones for agriculture automation from planting to harvest," in *Proceedings of the 2018 IEEE 22nd International Conference on Intelligent Engineering Systems (INES)*, (Las Palmas de Gran Canaria), 21–23. doi: 10.1109/INES.2018.8523943

Kumar, P. (2013). Hydrology: seasonal rain changes. *Nat. Clim. Chang.* 3, 783–784. doi: 10.1038/nclimate1996

Kurganskiy, A., Creer, S., Vere, N., De, Griffith, G. W., Osborne, N. J., et al. (2021). Predicting the severity of the grass pollen season and the effect of climate change in Northwest Europe. *Sci. Adv.* 7:eabd7658. doi: 10.1126/sciadv.abd7658

Langsrud, Ø (2003). ANOVA for unbalanced data: use Type II instead. *Stat. Comput.* 13, 163–167. doi: 10.1023/A:1023260610025

Lecerf, R., Ceglar, A., López-Lozano, R., Van Der Velde, M., and Baruth, B. (2019). Assessing the information in crop model and meteorological indicators to forecast crop yield over Europe. *Agric. Syst.* 168, 191–202. doi: 10.1016/j.agsy.2018.03.002

Lee, M. A., Howard-Andrews, V., and Chester, M. (2019). Resistance of multiple diploid and tetraploid perennial ryegrass (*Lolium perenne* L.) varieties to three projected drought scenarios for the UK in 2080. *Agronomy* 9:159. doi: 10.3390/agronomy9030159

León-Rueda, W. A., León, C., Caro, S. G., and Ramírez-Gil, J. G. (2021). Identification of diseases and physiological disorders in potato via multispectral drone imagery using machine learning tools. *Trop. Plant Pathol.* 47, 152–167. doi: 10.1007/s40858-021-00460-2

Lever, J., Krzywinski, M., and Altman, N. (2017). Points of significance: principal component analysis. *Nat. Methods* 14, 641–642. doi: 10.1038/nmeth.4346

Li, B., Xu, X., Zhang, L., Han, J., Bian, C., Li, G., et al. (2020). Above-ground biomass estimation and yield prediction in potato by using UAV-based RGB and hyperspectral imaging. *ISPRS J. Photogramm. Remote Sens.* 162, 161–172. doi: 10.1016/j.isprsjprs.2020.02.013

Li, C., Jiang, D., Wollenweber, B., Li, Y., Dai, T., and Cao, W. (2011). Waterlogging pretreatment during vegetative growth improves tolerance to waterlogging after anthesis in wheat. *Plant Sci.* 180, 672–678. doi: 10.1016/j.plantsci.2011.01.009

Li, L., Zhang, Q., and Huang, D. (2014). A review of imaging techniques for plant phenotyping. *Sensors (Switzerland)* 14, 20078–20111. doi: 10.3390/s141120078

Li, X., Lv, X., Wang, X., Wang, L., Zhang, M., and Ren, M. (2018). Effects of abiotic stress on anthocyanin accumulation and grain weight in purple wheat. *Crop Pasture Sci.* 69, 1208–1214. doi: 10.1071/CP18341

Liu, K., Harrison, M. T., Archontoulis, S. V., Huth, N., Yang, R., Liu, D. L., et al. (2021). Climate change shifts forward flowering and reduces crop waterlogging stress. *Environ. Res. Lett.* 16:9. doi: 10.1088/1748-9326/ac1b5a

Liu, M., and Jiang, Y. (2015). Genotypic variation in growth and metabolic responses of perennial ryegrass exposed to short-term waterlogging and submergence stress. *Plant Physiol. Biochem.* 95, 57–64. doi: 10.1016/j.plaphy.2015.07.008

Løkke, M. M., Seefeldt, H. F., Skov, T., and Edelenbos, M. (2013). Color and textural quality of packaged wild rocket measured by multispectral imaging. *Postharvest Biol. Technol.* 75, 86–95. doi: 10.1016/j.postharvbio.2012.06.018

Malik, A. I., Colmer, T. D., Lambers, H., Setter, T. L., and Schortemeyer, M. (2002). Short-term waterlogging has long-term effects on the growth and physiology of wheat. *New Phytol.* 153, 225–236. doi: 10.1046/j.0028-646X.2001.00318.x

Malvar, H. S., He, L. W., and Cutler, R. (2004). High-quality linear interpolation for demosaicing of Bayer-patterned color images. *ICASSP, IEEE Int. Conf. Acoust. Speech Signal Proc.* 3, 2–5. doi: 10.1109/icassp.2004.1326587

Manik, S. M. N., Pengilley, G., Dean, G., Field, B., Shabala, S., and Zhou, M. (2019). Soil and crop management practices to minimize the impact of waterlogging on crop productivity. *Front. Plant Sci.* 10:140. doi: 10.3389/fpls.2019.00140

Mathworks (2021). *MATLAB R2021a. The Language for Technical Computing.* Version 9.10.0.1710957. Natick, MA: The MathWorks Inc.

McFarlane, N. M., Ciavarella, T. A., and Smith, K. F. (2003). The effects of waterlogging on growth, photosynthesis and biomass allocation in perennial ryegrass (*Lolium perenne* L.) genotypes with contrasting root development. *J. Agric. Sci.* 141, 241–248. doi: 10.1017/S0021859603003502

McHugh, O., Liu, J., Browne, F., Jordan, P., and McConnell, D. (2020). "Data-driven classifiers for predicting grass growth in northern ireland: a case study," in *Information Processing and Management of Uncertainty in Knowledge-Based Systems Communications in Computer and Information Science*, 1237, (Cham: Springer International), 301–312. doi: 10.1007/978-3-030-50146-4_23

Medlyn, B. E., De Kauwe, M. G., and Duursma, R. A. (2016). New developments in the effort to model ecosystems under water stress. *New Phytol.* 212, 5–7. doi: 10.1111/nph.14082

Minneé, E. M. K., Kuhn-Sherlock, B., Pinxterhuis, I. J. B., and Chapman, D. F. (2019). Meta-analyses comparing the nutritional composition of perennial ryegrass (*Lolium perenne*) and plantain (*Plantago lanceolata*) pastures. *J. N Z. Grasslands* 81, 117–124. doi: 10.33584/jnzg.2019.81.402

Mirza, M. M. Q. (2011). Climate change, flooding in South Asia and implications. *Reg. Environ. Chang.* 11, 95–107. doi: 10.1007/s10113-010-0184-7

Mizutani, M., and Kanaoka, M. M. (2018). Environmental sensing and morphological plasticity in plants. *Semin. Cell Dev. Biol.* 83, 69–77. doi: 10.1016/j.semcdb.2017.10.029

Munson, S. M., and Long, A. L. (2017). Climate drives shifts in grass reproductive phenology across the western USA. *New Phytol.* 213, 1945–1955. doi: 10.1111/nph.14327

Münzbergová, Z., Hadincová, V., Skálová, H., and Vandvik, V. (2017). Genetic differentiation and plasticity interact along temperature and precipitation gradients to determine plant performance under climate change. *J. Ecol.* 105, 1358–1373. doi: 10.1111/1365-2745.12762

Mustroph, A. (2018). Improving flooding tolerance of crop plants. *Agronomy* 8, 1–25. doi: 10.3390/agronomy8090160

O'Gorman, P. A., and Muller, C. J. (2010). How closely do changes in surface and column water vapor follow clausius-clapeyron scaling in climate change simulations? *Environ. Res. Lett.* 5, 1–7. doi: 10.1088/1748-9326/5/2/025207

Oksanen, J., Guillaume Blanchet, F., Friendly, M., Kindt, R., Legendre, P., McGlinn, D., et al. (2020). *Vegan: Community Ecology Package*. Available online at: https://cran.r-project.org/package=vegan.

Ou, L. J., Dai, X. Z., Zhang, Z. Q., and Zou, X. X. (2011). Responses of pepper to waterlogging stress. *Photosynthetica* 49, 339–345. doi: 10.1007/s11099-011-0043-x

Pang, J., Zhou, M., Mendham, N., and Shabala, S. (2004). Growth and physiological responses of six barley genotypes to waterlogging and subsequent recovery. *Aust. J. Agric. Res.* 55, 895–906. doi: 10.1071/AR03097

Papp, L., van Leeuwen, B., Szilassi, P., Tobak, Z., Szatmári, J., Árvai, M., et al. (2021). Monitoring invasive plant species using hyperspectral remote sensing data. *Land* 10:29. doi: 10.3390/land10010029

Pareek, A., Dhankher, O. P., and Foyer, C. H. (2020). Mitigating the impact of climate change on plant productivity and ecosystem sustainability. *J. Exp. Bot.* 71, 451–456. doi: 10.1093/jxb/erz518

Parmesan, C., and Hanley, M. E. (2015). Plants and climate change: complexities and surprises. *Ann. Bot.* 116, 849–864. doi: 10.1093/aob/mcv169

Pearson, A., Cogan, N. O. I., Baillie, R. C., Hand, M. L., Bandaranayake, C. K., Erb, S., et al. (2011). Identification of QTLs for morphological traits influencing waterlogging tolerance in perennial ryegrass (*Lolium perenne* L.). *Theor. Appl. Genet.* 122, 609–622. doi: 10.1007/s00122-010-1473-8

Pembleton, K. G., Cullen, B. R., Rawnsley, R. P., and Ramilan, T. (2020). Climate change effects on pasture-based dairy systems in south-eastern Australia. *Crop Pasture Sci.* 72, 666–677. doi: 10.1071/CP20108

Pérez-Jiménez, M., Hernández-Munuera, M., Piñero, M. C., López-Ortega, G., and del Amor, F. M. (2018). Are commercial sweet cherry rootstocks adapted to climate change? Short-term waterlogging and CO2 effects on sweet cherry cv. 'Burlat.'. *Plant Cell Environ.* 41, 908–918. doi: 10.1111/pce.12920

Petrella, D. P., Metzger, J. D., Blakeslee, J. J., Nangle, E. J., and Gardner, D. S. (2016). Anthocyanin production using rough bluegrass treated with high-intensity light. *HortScience* 51, 1111–1120. doi: 10.21273/HORTSCI10878-16

Piepho, H. P., Büchse, A., and Emrich, K. (2003). A Hitchhiker's guide to mixed models for randomized experiments. *J. Agron. Crop Sci.* 189, 310–322. doi: 10.1046/j.1439-037X.2003.00049.x

Ploschuk, R. A., Grimoldi, A. A., Ploschuk, E. L., and Striker, G. G. (2017). Growth during recovery evidences the waterlogging tolerance of forage grasses. *Crop Pasture Sci.* 68, 574–582. doi: 10.1071/CP17137

Ploschuk, R. A., Miralles, D. J., Colmer, T. D., and Striker, G. G. (2020). Waterlogging differentially affects yield and its components in wheat, barley, rapeseed and field pea depending on the timing of occurrence. *J. Agron. Crop Sci.* 206, 363–375. doi: 10.1111/jac.12396

Ploschuk, R. A., Miralles, D. J., and Striker, G. G. (2021). Early- And late-waterlogging differentially affect the yield of wheat, barley, oilseed rape and field pea through changes in leaf area index, radiation interception and radiation use efficiency. *J. Agron. Crop Sci.* 207, 504–520. doi: 10.1111/jac.12486

Porter, A. S., Yiotis, C., Montañez, I. P., and McElwain, J. C. (2017). Evolutionary differences in Δ13C detected between spore and seed bearing plants following exposure to a range of atmospheric O2:CO2 ratios; implications for paleoatmosphere reconstruction. *Geochim. Cosmochim. Acta* 213, 517–533. doi: 10.1016/j.gca.2017.07.007

Puri, V., Nayyar, A., and Raja, L. (2017). Agriculture drones: a modern breakthrough in precision agriculture. *J. Stat. Manag. Syst.* 20, 507–518. doi: 10.1080/09720510.2017.1395171

Qi, A., Holland, R. A., Taylor, G., and Richter, G. M. (2018). Grassland futures in Great Britain – Productivity assessment and scenarios for land use change opportunities. *Sci. Total Environ.* 634, 1108–1118. doi: 10.1016/j.scitotenv.2018.03.395

Raza, A., Razzaq, A., Mehmood, S. S., Zou, X., Zhang, X., Lv, Y., et al. (2019). Impact of climate change on crops adaptation and strategies to tackle its outcome: A review. *Plants* 8:34. doi: 10.3390/plants8020034

Richardson, A. D., Keenan, T. F., Migliavacca, M., Ryu, Y., Sonnentag, O., and Toomey, M. (2013). Climate change, phenology, and phenological control of vegetation feedbacks to the climate system. *Agric. For. Meteorol.* 169, 156–173. doi: 10.1016/j.agrformet.2012.09.012

Rivero, R. M., Mittler, R., Blumwald, E., and Zandalinas, S. I. (2022). Developing climate-resilient crops: improving plant tolerance to stress combination. *Plant J.* 109, 373–389. doi: 10.1111/tpj.15483

Rosenzweig, C., Tubiello, F. N., Goldberg, R., Mills, E., and Bloomfield, J. (2002). Increased crop damage in the US from excess precipitation under climate change. *Glob. Environ. Chang.* 12, 197–202. doi: 10.1016/S0959-3780(02)00008-0

Rozema, J., Van De Staaij, J., Björn, L. O., and Caldwell, M. (1997). UV-B as an environmental factor in plant life: stress and regulation. *Trends Ecol. Evol.* 12, 22–28. doi: 10.1016/S0169-5347(96)10062-8

Rubio, G., Casasola, G., and Lavado, R. S. (1995). Adaptations and biomass production of two grasses in response to waterlogging and soil nutrient enrichment. *Oecologia* 102, 102–105. doi: 10.1007/BF00333316

Rubio, G., and Lavado, R. S. (1999). Acquisition and allocation of resources in two waterlogging-tolerant grasses. *New Phytol.* 143, 539–546. doi: 10.1046/j.1469-8137.1999.00482.x

Sanyal, S. K., and De Datta, S. K. (1991). "Chemistry of phosphorus transformations in soil," in *Advances in Soil Science. Advances in Soil Science*, 16, ed. B. A. Stewart (New York, NY: Springer), 1–120. doi: 10.1007/978-1-4612-3144-8_1

Sarker, B. C., and Karmoker, J. L. (2011). Effects of phosphorus deficiency on accumulation of biochemical compounds in lentil (*Lens culinaris* Medik). *Bangladesh J. Bot.* 40, 23–27. doi: 10.3329/bjb.v40i1.7992

Semmler, T., and Jacob, D. (2004). Modeling extreme precipitation events - a climate change simulation for Europe. *Glob. Planet. Change* 44, 119–127. doi: 10.1016/j.gloplacha.2004.06.008

Setter, T., and Belford, B. (1990). Waterlogging: how it reduces plant growth and how plants can overcome its effects. *J. Dep. Agric. West. Aust. Ser.* 4, 51–55.

Shaikh, N. P., Adjei, M. B., and Scholberg, J. M. (2008). Interactive effect of phosphorus and nitrogen on leaf anthocyanins, tissue nutrient concentrations, and dry-matter yield of Floralta limpograss during short day length. *Commun. Soil Sci. Plant Anal.* 39, 1006–1015. doi: 10.1080/00103620801925414

Shapiro, S. S., and Wilk, M. B. (1965). An Analysis of variance test for normality (Complete Samples). *Biometrika* 52, 591–611. doi: 10.2307/2333709

Shimono, H., Konno, T., Sakai, H., and Sameshima, R. (2012). Interactive effects of elevated atmospheric CO 2 and waterlogging on vegetative growth of soybean (*Glycine max* (L.) Merr.). *Plant Prod. Sci.* 15, 238–245. doi: 10.1626/pps.15.238

Simic Milas, A., Cracknell, A. P., and Warner, T. A. (2018). Drones–the third generation source of remote sensing data. *Int. J. Remote Sens.* 39, 7125–7137. doi: 10.1080/01431161.2018.1523832

Simova-Stoilova, L., Demirevska, K., Kingston-Smith, A., and Feller, U. (2012). Involvement of the leaf antioxidant system in the response to soil flooding in two Trifolium genotypes differing in their tolerance to waterlogging. *Plant Sci.* 183, 43–49. doi: 10.1016/j.plantsci.2011.11.006

Sinaj, S., Stamm, C., Toor, G. S., Condron, L. M., Hendry, T., Di, H. J., et al. (2002). Phosphorus exchangeability and leaching losses from two grassland soils. *J. Environ. Qual.* 31, 319–330. doi: 10.2134/jeq2002.0319

Singh, A. (2017). Waterlogging and salinity management for sustainable irrigated agriculture. ii: engineering measures and biodrainage. *J. Irrig. Drain. Eng.* 143:04017036. doi: 10.1061/(asce)ir.1943-4774.0001227

Smethurst, C. F., and Shabala, S. (2003). Screening methods for waterlogging tolerance in lucerne: Comparative analysis of waterlogging effects on chlorophyll fluorescence, photosynthesis, biomass and chlorophyll content. *Funct. Plant Biol.* 30, 335–343. doi: 10.1071/FP02192

Smit, H. J., Tas, B. M., Taweel, H. Z., Tamminga, S., and Elgersma, A. (2005). Effects of perennial ryegrass (*Lolium perenne* L.) cultivars on herbage production, nutritional quality and herbage intake of grazing dairy cows. *Grass Forage Sci.* 60, 297–309. doi: 10.1111/j.1365-2494.2005.00480.x

Smith, C. E., and Cribbie, R. (2014). Factorial ANOVA with unbalanced data: a fresh look at the types of sums of squares. *J. Data Sci.* 12, 385–404. doi: 10.6339/jds.201407_12(3).0001

Song, J. (2009). Root morphology is related to the phenotypic variation in waterlogging tolerance of two populations of *Suaeda* salsa under salinity. *Plant Soil* 324, 231–240. doi: 10.1007/s11104-009-9949-5

Spearman, C. (1904). The proof and measurement of association between two things. *Am. J. Psychol.* 15, 72–101.

Stasnik, P., Großkinsky, D. K., and Jonak, C. (2022). Physiological and phenotypic characterization of diverse *Camelina sativa* lines in response to waterlogging. *Plant Physiol. Biochem.* 183, 120–127. doi: 10.1016/j.plaphy.2022.05.007

Steyn, W. J., Wand, S. J. E., Holcroft, D. M., and Jacobs, G. (2002). Anthocyanins in vegetative tissues: a proposed unified function in photoprotection. *New Phytol.* 155, 349–361. doi: 10.1046/j.1469-8137.2002.00482.x

Striker, G. G. (2012). "Flooding stress on plants: anatomical, morphological and physiological responses," in *Botany*, ed. J. K. Mworia (Rijeka: InTechOpen), 3–28.

Sun, Z., Wang, X., Wang, Z., Yang, L., Xie, Y., and Huang, Y. (2021). UAVs as remote sensing platforms in plant ecology: Review of applications and challenges. *J. Plant Ecol.* 14, 1003–1023. doi: 10.1093/jpe/rtab089

Tao, H., Feng, H., Xu, L., Miao, M., Yang, G., Yang, X., et al. (2020). Estimation of the yield and plant height of winter wheat using UAV-based hyperspectral images. *Sensors (Switzerland)* 20, 1–19. doi: 10.3390/s20041231

Tay, J. Y. L., Erfmeier, A., and Kalwij, J. M. (2018). Reaching new heights: can drones replace current methods to study plant population dynamics? *Plant Ecol.* 219, 1139–1150. doi: 10.1007/s11258-018-0865-8

R Core Team (2022). *A Language and Environment for Statistical Computing*. Version 4.1.3. Vienna: R Foundation for Statistical Computing.

Teramura, A. H., and Sullivan, J. H. (1994). Effects of UV-B radiation on photosynthesis and growth of terrestrial plants. *Photosynth. Res.* 39, 463–473. doi: 10.1007/BF00014599

Tester, M., and Langridge, P. (2010). Breeding technologies to increase crop production in a changing world. *Science.* 327, 818–822. doi: 10.1126/science.1183700

Thornley, J. H. M., and Cannell, M. G. R. (1997). Temperate grassland responses to climate change: an analysis using the hurley pasture model. *Ann. Bot.* 80, 205–221. doi: 10.1006/anbo.1997.0430

Tong, C., Hill, C. B., Zhou, G., Zhang, X. Q., Jia, Y., and Li, C. (2021). Opportunities for improving waterlogging tolerance in cereal crops—physiological traits and genetic mechanisms. *Plants* 10, 1–22. doi: 10.3390/plants10081560

Tozer, K. N., Carswell, K., Griffiths, W. M., Crush, J. R., Cameron, C. A., Chapman, D. F., et al. (2017). Growth responses of diploid and tetraploid perennial ryegrass (*Lolium perenne*) to soil-moisture deficit, defoliation and a root-feeding invertebrate. *Crop Pasture Sci.* 68, 632–642. doi: 10.1071/CP17154

Trenberth, K. E. (2011). Changes in precipitation with climate change. *Clim. Res.* 47, 123–138. doi: 10.3354/cr00953

Tripicchio, P., Satler, M., Dabisias, G., Ruffaldi, E., and Avizzano, C. A. (2015). "Towards smart farming and sustainable agriculture with drones," in *Proceedings of the 2015 International Conference on Intelligent Environments*, 2015, (Prague), 140–143. doi: 10.1109/IE.2015.29

Trought, M. C. T., and Drew, M. C. (1980). The development of waterlogging damage in young wheat plants in anaerobic solution cultures. *J. Exp. Bot.* 31, 1573–1585. doi: 10.1093/jxb/31.6.1573

Tubiello, F. N., Soussana, J. F., and Howden, S. M. (2007). Crop and pasture response to climate change. *Proc. Natl. Acad. Sci. U.S.A.* 104, 19686–19690. doi: 10.1073/pnas.0701728104

Tubritt, T., Delaby, L., Gilliland, T. J., and O'Donovan, M. (2020). The relationship between the grazing efficiency and the production, morphology and nutritional traits of perennial ryegrass varieties. *J. Agric. Sci.* 158, 583–593. doi: 10.1017/S0021859620000982

Ulrychová, M., and Sosnová, V. (1970). Effect of phosphorus deficiency on anthocyanin content in tomato plants. *Biol. Plant.* 12, 231–235. doi: 10.1007/bf02920805

Ventura, I., Brunello, L., Iacopino, S., Valeri, M. C., Novi, G., Dornbusch, T., et al. (2020). *Arabidopsis* phenotyping reveals the importance of alcohol dehydrogenase and pyruvate decarboxylase for aerobic plant growth. *Sci. Rep.* 10, 16669. doi: 10.1038/s41598-020-73704-x

von Hippel, P. T. (2005). Mean, median, and skew: Correcting a textbook rule. *J. Stat. Educ.* 13, 1–13. doi: 10.1080/10691898.2005.11910556

Wang, D., Wang, L., Liu, J., Zhu, H., and Zhong, Z. (2018). Grassland ecology in China: Perspectives and challenges. *Front. Agric. Sci. Eng.* 5:24–43. doi: 10.15302/J-FASE-2018205

Wedderburn, M. E., Crush, J. R., Pengelly, W. J., and Walcroft, J. L. (2010). Root growth patterns of perennial ryegrasses under well-watered and drought conditions. *N Z. J. Agric. Res.* 53, 377–388. doi: 10.1080/00288233.2010.514927

Wilcoxon, F. (1945). Individual comparisons by ranking methods. *Biometrics Bull.* 1, 80–83. doi: 10.2307/3001968

Xiao, B., and David, D. (2019). Morphological and physiological responses of seashore paspalum and bermudagrass to waterlogging stress. *J. Am. Soc. Hortic. Sci.* 144, 305–313. doi: 10.21273/JASHS04737-19

Xu, C., Mcdowell, N. G., Sevanto, S., and Fisher, R. A. (2013). Our limited ability to predict vegetation dynamics under water stress. *New Phytol.* 200, 298–300. doi: 10.1111/nph.12450

Yamauchi, N., and Watada, A. E. (2019). Regulated chlorophyll degradation in spinach leaves during storage. *J. Am. Soc. Hortic. Sci.* 116, 58–62. doi: 10.21273/jashs.116.1.58

Yates, S., Jaškūnė, K., Liebisch, F., Nagelmüller, S., Kirchgessner, N., Kölliker, R., et al. (2019). Phenotyping a dynamic trait: leaf growth of perennial ryegrass under water limiting conditions. *Front. Plant Sci.* 10:344. doi: 10.3389/fpls.2019.00344

Yiotis, C., Evans-Fitzgerald, C., and McElwain, J. C. (2017). Differences in the photosynthetic plasticity of ferns and ginkgo grown in experimentally controlled low [o2]:[co2] atmospheres may explain their contrasting ecological fate across the triassic-jurassic mass extinction boundary. *Ann. Bot.* 119, 1385–1395. doi: 10.1093/aob/mcx018

Yiotis, C., Mcelwain, J. C., and Osborne, B. A. (2021). Enhancing the productivity of ryegrass at elevated CO2 is dependent on tillering and leaf area development rather than leaf-level photosynthesis. *J. Exp. Bot.* 72, 1962–1977. doi: 10.1093/jxb/eraa584

Yu, X., Luo, N., Yan, J., Tang, J., Liu, S., and Jiang, Y. (2012). Differential growth response and carbohydrate metabolism of global collection of perennial ryegrass accessions to submergence and recovery following de-submergence. *J. Plant Physiol.* 169, 1040–1049. doi: 10.1016/j.jplph.2012.03.001

Zandalinas, S. I., Sengupta, S., Fritschi, F. B., Azad, R. K., Nechushtai, R., and Mittler, R. (2021). The impact of multifactorial stress combination on plant growth and survival. *New Phytol.* 230, 1034–1048. doi: 10.1111/nph.17232

Zellweger, F., De Frenne, P., Lenoir, J., Rocchini, D., and Coomes, D. (2019). Advances in microclimate ecology arising from remote sensing. *Trends Ecol. Evol.* 34, 327–341. doi: 10.1016/j.tree.2018.12.012

Zhang, Y., Song, X., Yang, G., Li, Z., Lu, H., Kong, X., et al. (2015). Physiological and molecular adjustment of cotton to waterlogging at peak-flowering in relation to growth and yield. *Field. Crop. Res.* 179, 164–172. doi: 10.1016/j.fcr.2015.05.001

Zhang, Y., Tang, L., Liu, X., Liu, L., Cao, W., and Zhu, Y. (2014). Modeling dynamics of leaf color based on RGB value in rice. *J. Integr. Agric.* 13, 749–759. doi: 10.1016/S2095-3119(13)60391-3

Zhou, W., Chen, F., Meng, Y., Chandrasekaran, U., Luo, X., Yang, W., et al. (2020). Plant waterlogging/flooding stress responses: from seed germination to maturation. *Plant Physiol. Biochem.* 148, 228–236. doi: 10.1016/j.plaphy.2020.01.020

frontiers | Frontiers in Plant Science

TYPE Original Research
PUBLISHED 08 August 2022
DOI 10.3389/fpls.2022.970651

OPEN ACCESS

EDITED BY
Kehua Wang,
China Agricultural University, China

REVIEWED BY
Kun Zhang,
Qingdao Agricultural University, China
Jinhui Chen,
Hainan University, China

*CORRESPONDENCE
Jingjing Wang
sherlock47@126.com

†These authors have contributed equally to this work

SPECIALTY SECTION
This article was submitted to Plant Abiotic Stress, a section of the journal Frontiers in Plant Science

RECEIVED 16 June 2022
ACCEPTED 22 July 2022
PUBLISHED 08 August 2022

CITATION
Ming Q, Wang K, Wang J, Liu J, Li X, Wei P, Guo H, Chen J and Zong J (2022) The combination of RNA-seq transcriptomics and data-independent acquisition proteomics reveals the mechanisms underlying enhanced salt tolerance by the *ZmPDI* gene in *Zoysia matrella* [L.] Merr. *Front. Plant Sci.* 13:970651. doi: 10.3389/fpls.2022.970651

The combination of RNA-seq transcriptomics and data-independent acquisition proteomics reveals the mechanisms underlying enhanced salt tolerance by the *ZmPDI* gene in *Zoysia matrella* [L.] Merr.

Qiang Ming[1†], Kai Wang[2†], Jingjing Wang[1*], Jianxiu Liu[1], Xiaohui Li[1], Peipei Wei[1], Hailin Guo[1], Jingbo Chen[1] and Junqin Zong[1]

[1]The National Forestry and Grassland Administration Engineering Research Center for Germplasm Innovation and Utilization of Warm-season Turfgrasses, Institute of Botany, Jiangsu Province and Chinese Academy of Sciences, Nanjing, China, [2]Jiangsu Coastal Area Institute of Agricultural Sciences, Yancheng, China

Zoysia matrella [L.] Merr. is one of the three most economically important *Zoysia* species due to its strong salt tolerance and wide application. However, the molecular mechanisms regulating salt tolerance in *Z. matrella* remain unknown. The protein disulfide isomerase *ZmPDI* of *Z. matrella* was obtained by salt stress screening with yeast cells, and its expression was significantly upregulated after salt stress. Based on the obtained *ZmPDI* overexpression transgenic *Z. matrella* plants, we carried out salt tolerance identification and found that *ZmPDI* can significantly enhance the salt tolerance of *Z. matrella*. Root samples of *OX-ZmPDI* transgenic and wild-type plants were collected at 0 and 24 h after salt treatments for RNA-seq and data-independent acquisition (DIA) proteome sequencing. Combined analysis of the transcriptome and proteome revealed that *ZmPDI* may enhance the salt tolerance of *Z. matrella* by regulating *TUBB2*, *PXG4*, *PLDα2*, *PFK4,* and *4CL1*. This research presents the molecular regulatory mechanism of the *ZmPDI* gene in *Z. matrella* for resistance to salt stress and facilitates the use of molecular breeding to improve the salt tolerance of grasses.

KEYWORDS

***Zoysia matrella*, salt tolerance, PDI, RNA-seq, proteome**

Introduction

Saline-alkali land is widely distributed throughout the world and seriously affects the local ecological environment and economic development. How to efficiently use and improve saline-alkali land resources has become a global research hotspot. Turfgrass plays an important role in ecological and green space construction and is a pioneer plant for ameliorating soil salinization. *Zoysia* grass is an excellent warm-season turfgrass that is famous for its strong tolerance (including salt, cold, and drought tolerance) and wide application (including saline-alkali soil, athletic fields, home lawns, and parks) (Ge et al., 2006). The three most economically important *Zoysia* species are *Zoysia japonica* Steud., *Zoysia matrella* [L.] Merr. and *Zoysia pacifica* (Goudswaard) M. Hotta & Kuroki, and *Z. matrella* has the highest salt tolerance among them (Yamamoto et al., 2016). *Z. matrella* is a perennial warm-season turfgrass belonging to the family Gramineae, subfamily Chloridoideae, *Zoysia* willd (Tanaka et al., 2016a). Although the strong salt tolerance of *Z. matrella* is well known, the molecular mechanism is still unknown.

The current research on the salt tolerance of *Z. matrella* mainly focuses on the evaluation of salt tolerance and the physiological mechanism of salt tolerance. Salt tolerance evaluation shows that *Z. matrella* has strong salt tolerance (Marcum and Murdoch, 1994; Li et al., 2012). The physiological mechanism of salt tolerance showed that *Z. matrella* has large bicellular salt glands on the adaxial side and can secrete excessive Na^+ from the salt glands of leaves to maintain a low Na^+/K^+ ratio to resist salt stress (Chen et al., 2009; Yamamoto et al., 2016). When exposed to salt stress, *Z. matrella* can also synthesize organic matter, such as betaine, glycine, proline, and soluble sugars, to adjust its osmotic potential to alleviate the osmotic stress caused by high salt concentrations (Li et al., 2012). Furthermore, an appropriate concentration of phosphorus under salt stress can promote root growth, increase Na^+ secretion in leaves and inhibit Na^+ transportation from roots to leaves, which is beneficial to the salt resistance of *Z. matrella* (Jiang et al., 2013).

Currently, few molecular mechanism studies on the salt tolerance of *Z. matrella* have been reported. A type I vacuolar H^+-pyrophosphatase (VP) gene, *ZmVP1*, was isolated in *Z. matrella*, and overexpressing this gene in *Arabidopsis thaliana* can promote plant growth with more Na^+ and K^+ in the leaves and higher activities of V-ATPase and V-PPase under salt stress (Chen et al., 2015a). Chen et al. (2015b) constructed a high-quality full-length cDNA expression library in yeast using a Gateway-compatible vector system and screened 16 candidate salt-tolerant genes in *Z. matrella* (Chen et al., 2015b). Yeast validation experiments show that these 16 candidate salt-tolerant genes can improve the salt tolerance of yeast and exhibit different transcription levels under salt stress (Chen et al., 2015b). However, the molecular mechanism of some of these candidate salt-tolerant genes in *Z. matrella*, including a protein disulfide isomerase ZmPDI (NCBI accession number: KM265179), is very limited.

Protein disulfide isomerase (PDI) is a member of the thioredoxin subfamily of redox proteins and has thiol-disulfide oxidoreductase, disulfide isomerase and redox-dependent chaperone catalytic activities (Ali Khan and Mutus, 2014). PDI is mainly distributed throughout the lumen of the endoplasmic reticulum, cell surfaces and cytosol (Ali Khan and Mutus, 2014). It promotes the correct folding of proteins by catalyzing the formation of disulfide bonds and the rearrangement of mismatched disulfide bonds (Okumura et al., 2021). The functions of *PDI* in mammals have been extensively studied, while the functions in plants have less research. Existing studies suggest that, in *Arabidopsis*, *AtPDI11* has been demonstrated to exhibit oxidoreductase activity *in vitro* (Fan et al., 2018). The *AtPDI1* gene has an anti-stress function in *Arabidopsis*, and overexpressing *AtPDI1* can increase the abiotic stress tolerance of seedlings with a higher germination ratio and longer root length (Zhang et al., 2018). Overexpression of the protein disulfide isomerase *AtCYO1* has a negative effect on the initiation of chlorophyll degradation and proteolysis to maintain the functions of chloroplasts (Tominaga et al., 2018). However, studies on the regulatory mechanism of plant salt tolerance by the *PDI* gene have not been reported.

Previous studies showed that the heterologous expression of *ZmPDI* can significantly improve the salt tolerance of yeast, and the expression of *ZmPDI* is significantly upregulated after salt stress in *Z. matrella* (Chen et al., 2015b). Furthermore, *ZmPDI*-overexpressing transgenic *Z. matrella* plants have been successfully obtained (Wang K. et al., 2020). In order to further explore the regulation mechanism of *ZmPDI* in salt tolerance of *Z. matrella*, we evaluated the salt tolerance of *ZmPDI*-overexpressing transgenic *Z. matrella* plants, analyzed the gene ontology (GO) and Kyoto Encyclopedia of Genes and Genomes (KEGG) pathways that *ZmPDI* gene may affect after salt treatment and selected key differentially expressed genes (DEGs) that may be regulated by *ZmPDI* through combined transcriptome and proteome analysis. This study provides new insight into the regulatory mechanism of *ZmPDI* in *Z. matrella* for resistance to salt stress and facilitates the use of molecular breeding to improve the salt tolerance of grasses.

Materials and methods

Plant materials and treatments

The test materials were five *OX-ZmPDI* transgenic lines (Lines 4, 5, 7, 11, and 15) (Wang K. et al., 2020) and wild-type plants of *Z. matrella*, which are conserved by the Grass

Research Center of Institute of Botany, Jiangsu Province and Chinese Academy of Sciences. The callus of *Z. matrella* was supported by Prof. Mingliang Chai from Zhejiang University (China).

Five *OX-ZmPDI* transgenic lines and wild-type plants were cultured in porous PVC tubes (height 40 cm, diameter 10 cm) filled with sand, and each material was cultured in 8 tubes. Water was poured into each tube material once a day, and Hoagland nutrient solution was poured and trimmed once every 5 days. When the growth was consistent, four tubes of each material were treated with NaCl solution, and the other four tubes were treated with water as the control. During salt treatment, 100 mM NaCl was used as the gradient to increase the concentration once every 3 days for progressive treatment with 400 mL each time. When the salt concentration reached 400 mM, the concentration no longer increased. Afterward, the material was treated with 400 mM NaCl every 5 days. The control and salt treatments were irrigated at the same time with 400 mL of water. Phenotypes of treated plants were observed after 30 days, and corresponding physicochemical indices of roots and leaves were determined.

The five *OX-ZmPDI* transgenic lines showed similar phenotypes and corresponding physicochemical index determination results, and transgenic Line 4 was selected for the next treatment and sampling. The stolons with ten nodes of *OX-ZmPDI* transgenic Line 4 and wild-type plants were selected and cut into small pieces with 2 nodes, and 40 small pieces of each material were planted. The hydroponic experiment was performed in the greenhouse. The hydroponic solution was 1/2 Hoagland nutrient solution, which was replaced once a week. When the growth of plants was consistent, 400 mM NaCl solution was added to the 1/2 Hoagland nutrient solution for salt treatment.

Physiological index measurement

The physicochemical indices of *OX-ZmPDI* transgenic lines and wild-type plants in porous PVC tubes were determined after salt treatment for 30 days. The chlorophyll contents of leaves were determined by the acetone extraction method. The free proline contents of roots were determined by the sulfosalicylic acid method. The soluble sugar contents of roots were determined by the anthrone colorimetric method. The SOD activity of roots was determined by a total superoxide dismutase kit (hydroxylamine method) (Nanjing Jiancheng Bioengineering Institute, Nanjing, China). The Na^+ and K^+ contents in roots and leaves were determined according to the method of Wang J. et al. (2020). All data were analyzed for variance by SPSS Statistics v.26.0 (SPSS Inc., Chicago, IL, United States) and plotted by GraphPad Prism v.8 (GraphPad Software, San Diego, CA, United States).

RNA-seq

The roots of *OX-ZmPDI* transgenic Line 4 and wild-type plants were sampled at 0 and 24 h after salt treatment, and three biological replicates were obtained for each sample at each time point. All samples were frozen in liquid nitrogen and stored at −80°C. Total RNA was extracted using a TRIzol reagent kit (Invitrogen, Carlsbad, CA, United States) according to the manufacturer's protocol. A total of 12 cDNA libraries were constructed and sequenced by Gene *Denovo* Biotechnology Co., (Guangzhou, China) using the Illumina HiSeq2500 platform. The datasets are available in the NCBI repository http://www.ncbi.nlm.nih.gov/bioproject/PRJNA848971. *De novo* assembly of the *Z. matrella* transcriptome was accomplished *via* Hisat2 (v2.0.5) (Kim et al., 2015) using the *Z. japonica* genome as a reference (Tanaka et al., 2016b). The mapping reads of each sample were assembled using StringTie v1.3.1 (Pertea et al., 2015), and their expression abundance and variations were calculated by FPKM (fragment per kilobase of transcript per million mapped reads) values (Mortazavi et al., 2008). RNA differential expression analysis was performed by DESeq2 (Love et al., 2014) software and edgeR R package (3.18.1) (Robinson et al., 2010), which were used to analyze significant differences between two groups (determined as a p-value < 0.05 and absolute fold change ≥ 2). The DEGs were selected with a $|\log_2 FC| > 1$ and false discovery rate (FDR) < 0.05.

Data-independent acquisition protein quantification

For data-independent acquisition (DIA) proteomics analysis, proteins from the root samples (the same as RNA-seqsea) were collected from OX-ZmPDI transgenic Line 4 and wild-type plants at 0 and 24 h after salt treatment. Total proteins were extracted using the cold acetone method. After grinding, each sample was dissolved in 2 mL of lysis buffer (8 M urea, 2% SDS, 1 × protease inhibitor cocktail), pyrolyzed by sonication on ice for 30 min and collected by centrifugation at 13,000 rpm for 30 min at 4°C. The supernatant was retained, and prechilled acetone was added to precipitate the proteins at −20°C overnight. After cleaning with acetone three times, the precipitants were dissolved in 8 M urea by sonication on ice. The protein concentration of each sample was determined by a BCA protein assay kit.

For each sample, 50 μg of protein was suspended in 50 μL of solution, and 1 μL of 1 M dithiothreitol (DTT) was added at 55°C for 1 h. Then, 5 μL of 20 mM indoacetamide was used to alkylate the proteins of each sample in the dark at 37°C for 1 h. Then, 300 μL of prechilled acetone was added to each sample to precipitate the proteins at −20°C overnight, and the proteins were washed twice with prechilled acetone. The proteins were resuspended with 50 mM ammonium bicarbonate and digested

with sequence-grade modified trypsin (Promega, Madison, WI, United States) at a substrate/enzyme ratio of 50:1 (w/w) at 37°C for 16 h.

The spectral libraries were generated (Fang et al., 2021), and the spectrophotometer was set up to search the database of *Z. matrella*.[1] After nano-HPLC–MS/MS analysis, the raw DIA data were acquired, processed and analyzed by Spectronaut X (Biognosys AG, Switzerland) with default parameters (Fang et al., 2021). After performing Student's *t*-test, differentially expressed proteins (DEPs) were filtered with a q-value < 0.05 and $|\text{Fold change (FC)}| > 1.5$.

Bioinformatics analysis

The correlation analysis of replicas was performed by R. Correlation to evaluate repeatability between three biological replicate samples. Principal component analysis (PCA) was performed with the R package gmodels[2] to reveal the relationship of all the samples. The correlation analysis of RNA-seq and proteome was performed by R (version 3.5.1), and a nine-quadrant map was drawn based on changes in the expression of the gene in the transcriptome and proteome. All DEP and DEG functions were annotated in the GO database, KEGG database and Clusters of Orthologous Groups of proteins (COG/KOG) database. The significantly enriched GO functions and KEGG pathways were examined within DEGs and DEPs with FDR ≤ 0.05 and q-value ≤ 0.05, respectively.

Quantitative RT-PCR validation

Twelve DEGs were randomly selected from the gene list in **Table 1** for qRT–PCR validation. The primers were designed by Primer Premier 5.0 software and are listed in **Supplementary Table 10**. The *ZjActin* (GenBank: GU290545.1) gene was used as a housekeeping gene. Each sample was analyzed with three biological replicates, and qRT–PCR assays were carried out as described by Xie et al. (2015).

Results

Salt tolerance evaluation of *OX-ZmPDI* transgenic plants of *Zoysia matrella*

To evaluate the salt tolerance of *OX-ZmPDI* transgenic lines, 400 mM NaCl solution was applied for 30 days to treat the *OX-ZmPDI* transgenic lines and wild-type plants. After salt treatment, the wild-type plants were obviously withered and yellowed, while the *OX-ZmPDI* transgenic lines all maintained normal growth, which was not significantly different from the control (CK) treatment (**Figure 1A**). In the wild-type plants, the dry weights of the aboveground and underground biomasses of the salt-treated plants were significantly lower than those of the CK plants (**Figures 1B,C**). However, the dry weights of the aboveground and underground biomasses of the *OX-ZmPDI* transgenic lines were not significantly different between the salt and CK treatments (**Figures 1B,C**).

After salt treatment, the contents of the osmotic adjustment substances, proline and sugars, were detected in *OX-ZmPDI* transgenic lines and wild-type plants. The proline contents of wild-type plants increased after salt treatment, and the proline contents of *OX-ZmPDI* transgenic lines were much higher than those of wild-type plants (**Figure 1D**). However, the soluble sugar contents of *Z. matrella* plants all increased after salt treatment, and the degree of increase in *OX-ZmPDI* transgenic lines was significantly lower than that in wild-type plants (**Figure 1E**). The K^+/Na^+ ratio is also an important index with which to evaluate the salt tolerance of plants. In the CK treatment, the K^+/Na^+ ratios in roots and leaves were not significantly different between the wild-type and *OX-ZmPDI* transgenic plants (**Figures 1F,G**). However, after treatment with 400 mM NaCl, the K^+/Na^+ ratios of *OX-ZmPDI* transgenic lines in roots were all obviously higher than those of wild-type plants, especially *OX-ZmPDI* transgenic line OX-4 (**Figure 1F**). Meanwhile, the K^+/Na^+ ratios in the leaves of *OX-ZmPDI* transgenic line OX-4 were significantly higher than those of the wild-type plants (**Figure 1G**). Furthermore, chlorophyll contents and superoxide dismutase (SOD) activity are also important for assessing salt tolerance. In this study, the chlorophyll content of wild-type plants was obviously lower than that of the CK treatment, while the chlorophyll contents of *OX-ZmPDI* transgenic lines showed no significant difference compared with the CK treatment (**Figure 1H**). After salt treatment, the SOD activity of wild-type plants showed an obviously downward trend, while that of *OX-ZmPDI* transgenic lines showed no significant difference compared with the CK treatment (**Figure 1I**).

Transcriptome and proteome sequencing of *OX-ZmPDI* transgenic plants

Previous studies show that roots may make significant contributions to the salt tolerance in zoysiagrass (Wang J. et al., 2020). In the preliminary physiological index measurement, the K^+/Na^+ ratios were measured both in roots and leaves. The results showed that the K^+/Na^+ ratios in roots of all *OX-ZmPDI* transgenic lines were obviously higher than those of wild-type plants, while only the K^+/Na^+ ratio in leaves of

1 http://zoysia.kazusa.or.jp/

2 http://www.rproject.org/

TABLE 1 Selected differentially expressed genes (DEGs) from transcriptome and proteome association analysis.

GeneID	RNA-seq			Proteome			Gene name	Description
	FC1 (WT24h/0h)	FC2 (ZmPDI24h/0h)	log_2 (FC2/FC1)	FC3 (WT24h/0h)	FC4 (ZmPDI24h/0h)	log_2 (FC4/FC3)		
Zjn_sc00047.1.g03800.1.sm.mk	5.10	11.14	1.13	1.77	1.05	−0.75	\	Hypothetical protein
Zjn_sc00022.1.g04760.1.sm.mk	0.23	0.21	−0.10	1.02	0.22	−2.23	\	WEB family protein At5g16730, chloroplastic
Zjn_sc00015.1.g05160.1.sm.mkhc	0.12	0.09	−0.46	0.98	0.32	−1.62	\	\
Zjn_sc00089.1.g00090.1.am.mk	**0.36**	**0.17**	**−1.11**	**1.00**	**0.42**	**−1.25**	**4CL1**	**4-coumarate-CoA ligase 1**
Zjn_sc00109.1.g00965.1.br	6.83	16.91	1.31	1.74	1.93	0.15	BBE	Berberine bridge enzyme-like Cyn d 4
Zjn_sc00018.1.g01620.1.sm.mkhc	0.16	0.35	1.12	0.70	0.51	−0.46	CCR1	Cinnamoyl-CoA reductase 2
Zjn_sc00090.1.g01530.1.sm.mkhc	2.90	3.10	0.10	0.84	2.93	1.80	CEQORH	Chloroplast envelope quinone oxidoreductase homolog
Zjn_sc00109.1.g00880.1.sm.mk	21.70	22.30	0.04	1.85	0.90	−1.04	CHT2	Chitinase 2-like
Zjn_sc00102.1.g00830.1.am.mk	38.47	16.84	−1.19	2.67	0.80	−1.74	CHT8	Chitinase 8
Zjn_sc00045.1.g00590.1.sm.mk	0.14	0.01	−3.84	0.80	0.56	−0.51	CYP74A4	Allene oxide synthase 4
Zjn_sc00013.1.g09290.1.am.mkhc	0.71	3.73	2.40	0.77	4.19	2.45	ephA	Epoxide hydrolase A-like
Zjn_sc00012.1.g02790.1.am.mkhc	0.31	0.40	0.34	0.86	0.42	−1.04	FPS	Farnesyl pyrophosphate synthase
Zjn_sc00049.1.g01050.1.am.mk	0.23	0.11	−1.06	0.69	0.39	−0.85	GLIP	GDSL esterase/lipase
Zjn_sc00048.1.g00650.1.sm.mkhc	0.43	0.42	−0.05	0.48	1.29	1.42	GSH2	Glutathione synthetase, chloroplastic-like isoform X1
Zjn_sc00003.1.g11520.1.sm.mk	0.33	0.21	−0.62	0.52	1.20	1.19	H2AV	Probable histone H2A variant 1
Zjn_sc00003.1.g07680.1.sm.mkhc	2.91	6.27	1.11	0.98	2.00	1.03	HB2	Non-symbiotic hemoglobin
Zjn_sc00011.1.g02850.1.sm.mkhc	0.22	0.09	−1.25	1.10	0.53	−1.06	LAMP1	Probable glutamate carboxypeptidase LAMP1
Zjn_sc00026.1.g00700.1.sm.mk	104.07	51.72	−1.01	3.53	1.63	−1.11	LEA14-A	Late embryogenesis abundant protein Lea14-A-like
Zjn_sc00075.1.g00370.1.sm.mk	0.43	0.59	0.45	0.54	1.11	1.03	LOX5	Linoleate 9S-lipoxygenase 5
Zjn_sc00034.1.g03480.1.am.mk	0.11	0.13	0.19	0.70	0.32	−1.16	LTP	Protease inhibitor/seed storage/LTP family protein precursor
Zjn_sc00011.1.g06270.1.am.mk	\	0.04	\	0.62	0.15	−2.06	MEE55	Serinc-domain containing serine and sphingolipid biosynthesis protein
Zjn_sc00155.1.g00490.1.am.mk	0.05	0.22	2.12	0.42	0.31	−0.43	NRT2.1	High-affinity nitrate transporter 2.1-like
Zjn_sc00152.1.g00350.1.sm.mk	0.05	0.15	1.43	0.43	0.46	0.08	NRT2.1	High-affinity nitrate transporter 2.1-like
Zjn_sc00052.1.g00190.1.sm.mkhc	0.03	0.09	1.37	0.95	0.57	−0.75	OMT2	O-methyltransferase 2
Zjn_sc00005.1.g03630.1.sm.mkhc	**2.70**	**3.06**	**0.18**	**0.98**	**1.98**	**1.02**	**PFK4**	**ATP-dependent 6-phosphofructokinase 4 chloroplastic**
Zjn_sc00009.1.g08860.1.sm.mkhc	**0.15**	**0.06**	**−1.28**	**0.88**	**0.66**	**−0.42**	**PLDα2**	**Phospholipase D alpha 2**
Zjn_sc00026.1.g02680.1.am.mk	0.45	0.08	−2.46	1.40	0.38	−1.89	PNC1	Cationic peroxidase 1-like
Zjn_sc00143.1.g00490.1.sm.mkhc	1.69	3.15	0.90	0.84	1.83	1.11	pro-resilin	Pro-resilin precursor
Zjn_sc00093.1.g00470.1.sm.mkhc	**0.06**	**0.03**	**−1.13**	**1.29**	**0.59**	**−1.12**	**PXG4**	**Peroxygenase 4**
Zjn_sc00207.1.g00180.1.cf.mkhc	0.29	0.23	−0.33	0.29	0.69	1.25	RPM1	Disease resistance protein RPM1
Zjn_sc00152.1.g00230.1.sm.mk	0.48	0.45	−0.10	0.33	1.25	1.92	RPPR5	Pentatricopeptide repeat-containing protein At2g37230
Zjn_sc00004.1.g14080.1.sm.mkhc	0.09	0.08	−0.08	0.22	0.45	1.06	STY8	Serine/threonine-protein kinase STY8
Zjn_sc00022.1.g06510.1.sm.mkhc	0.19	0.24	0.29	0.99	0.47	−1.06	TIP2-1	Aquaporin TIP2-1
Zjn_sc00007.1.g10230.1.sm.mkhc	0.28	0.35	0.32	0.99	0.47	−1.06	TIP2-1	Aquaporin TIP2-1
Zjn_sc00009.1.g09140.1.sm.mk	**0.20**	**0.07**	**−1.55**	**0.77**	**0.48**	**−0.69**	**TUBB2**	**Tubulin beta-2 chain**
Zjn_sc00096.1.g01880.1.am.mk	54.13	86.21	0.67	4.61	2.25	−1.03	XIP2	Xylanase inhibitor protein 2-like

10.3389/fpls.2022.970651

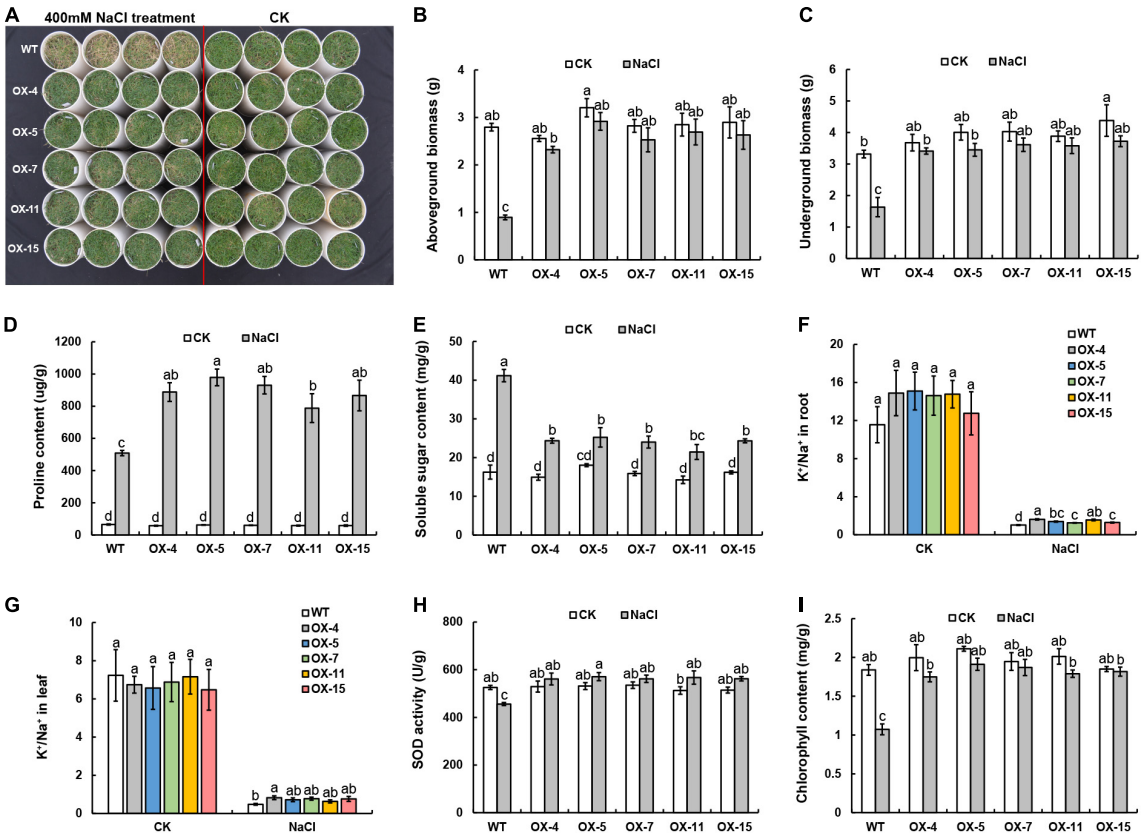

FIGURE 1
Phenotypic and physiological responses to salt stress in *OX-ZmPDI transgenic plants of Z. matrella*. **(A)** *OX-ZmPDI* transgenic lines and wild-type (WT) plants were exposed to 400 mM NaCl and control (CK) treatments for 30 days. **(B)** The aboveground biomasses of *OX-ZmPDI* transgenic and wild-type plants after NaCl and CK treatments for 30 days. **(C)** The underground biomasses of *OX-ZmPDI* transgenic and wild-type plants after NaCl and CK treatments for 30 days. **(D)** The proline contents of *OX-ZmPDI* transgenic and wild-type plants after NaCl and CK treatments for 30 days. **(E)** The soluble sugar contents of *OX-ZmPDI* transgenic and wild-type plants after NaCl and CK treatments for 30 days. **(F)** The K^+/Na^+ ratio in *OX-ZmPDI* transgenic and wild-type plant roots after CK and NaCl treatments. **(G)** The K^+/Na^+ ratio in *OX-ZmPDI* transgenic and wild-type plant leaves after CK and NaCl treatments. **(H)** The chlorophyll contents of *OX-ZmPDI* transgenic and wild-type plants after NaCl and CK treatments for 30 days. **(I)** The SOD activity of *OX-ZmPDI* transgenic and wild-type plants after NaCl and CK treatments for 30 days. Values are presented as the mean ± SE. Letters above the bars indicate significant differences between the respective values ($p < 0.05$).

OX-ZmPDI transgenic line OX-4 was significantly higher than wild-type plants (Figures 1F,G). Therefore, in order to analyze the molecular mechanism by which the *ZmPDI* gene enhances the salt tolerance of *Z. matrella*, root samples of the *OX-ZmPDI* transgenic line OX-4 and wild-type plants were collected at 0 and 24 h after treatment with 400 mM NaCl for transcriptome and proteome sequencing. For RNA-seq, an average of 43.24 million raw reads were obtained, and 97.98% of these reads were confirmed as clean reads (Supplementary Table 1). A total of 69.05–75.64, 15.10—20.39, and 8.65–10.38% of the reads were mapped to exons, introns and intergenic regions in the reference genome, respectively (Supplementary Table 2). In total, 35,197 genes were identified by the RNA-seq assays, including 33,660 unigenes and 1,537 novel genes.

DIA technology was used to perform the comparative analysis of *OX-ZmPDI* transgenic line OX-4 and wild-type plants. More than half of the peptides had lengths between 7 and 18 amino acids (Supplementary Figure 1A). After filtering with FDR $\leq$ 0.05, 36,076 peptides and 6,842 proteins were obtained, and 5,040 (73.66%) proteins had more than one peptide (Supplementary Figures 1B,C). Among the total 6,842 proteins, 6,370 (93.10%) were annotated in at least one of the GO, KEGG and KOG protein libraries (Supplementary Figure 1D). Transcription factor analysis showed that most proteins were in the *bZIP* transcription factor family, followed by the *C3H* and Trihelix transcription factor families (Supplementary Figure 1E).

The correlation values of biological repeat samples for RNA-seq and the proteome were all above 0.866 (Supplementary Figures 2A,B). A total of 4,887, 11, 9, and 6,384 DEGs were identified in the WT24h vs. WT0h, ZmPDI0h vs. WT0h, ZmPDI24h vs. WT24h and ZmPDI24h vs. ZmPDI0h comparisons, respectively (Supplementary Figure 2C). Because the numbers of DEGs in the ZmPDI0h vs. WT0h and

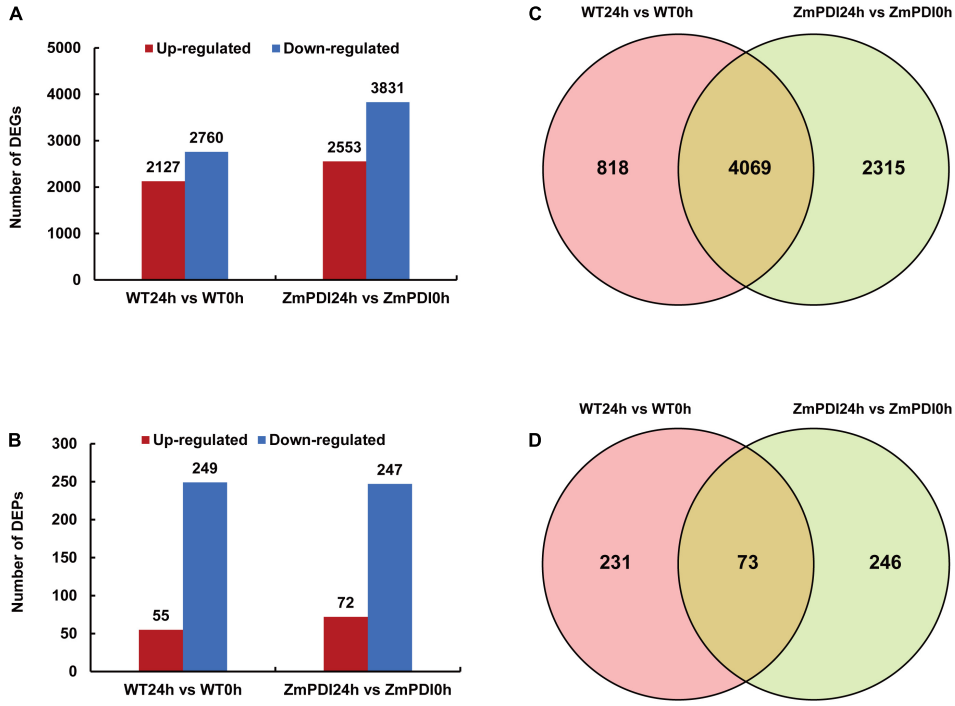

FIGURE 2
Salt tolerance-related transcriptome and proteome expression profiles of *OX-ZmPDI* transgenic and WT plants of *Z. matrella*. **(A)** The number of up- and downregulated DEGs in *OX-ZmPDI* transgenic (ZmPDI24h vs. ZmPDI0h) and wild-type plants (WT24h vs. WT0h). **(B)** The number of up- and downregulated DEPs in *OX-ZmPDI* transgenic (ZmPDI24h vs. ZmPDI0h) and wild-type plants (WT24h vs. WT0h). **(C)** Venn diagram of the number of DEGs in the *OX-ZmPDI* transgenic and wild-type plants after salt treatment. **(D)** Venn diagram of the number of DEPs in the *OX-ZmPDI* transgenic and wild-type plants after salt treatment.

ZmPDI24h vs. WT24h comparisons were very low, we chose WT24h vs. WT0h and ZmPDI24h vs. ZmPDI0h comparisons to continue the further analysis, and found that the downregulation of DEGs in these two comparisons was greater than the upregulation of DEGs (Figure 2A). For proteome sequencing, 304 and 319 DEPs were identified in the WT24h vs. WT0h and ZmPDI24h vs. ZmPDI0h comparisons, respectively, and the number of downregulated DEPs was 4.52 and 3.43 times that of upregulated DEPs in these two comparisons, respectively (Figure 2B). Venn diagrams were constructed and showed that the WT24h vs. WT0h and ZmPDI24h vs. ZmPDI0h comparisons had 4,069 (56.50%) DEGs in common, while only 73 (13.27%) common DEPs were common (Figures 2C,D).

Gene ontology and Kyoto Encyclopedia of Genes and Genomes pathway analysis of differentially expressed genes and differentially expressed proteins

To compare the differences in salt tolerance regulation mechanisms between wild-type and *OX-ZmPDI* transgenic plants, the functional characterization of DEGs and DEPs was classified by GO enrichment analysis. For RNA-seq, the top 20 enriched GO terms were selected in the WT24h vs. WT0h and ZmPDI24h vs. ZmPDI0h comparisons (Supplementary Table 3). A total of 13 GO terms were shared by both the WT24h vs. WT0h and ZmPDI24h vs. ZmPDI0h comparisons, while each comparison had seven unique GO terms (Figures 3A,B). In the ZmPDI24h vs. ZmPDI0h comparison, the unique GO terms included "cytoskeletal protein binding," "polysaccharide metabolic process," "tubulin binding," "plant-type cell wall organization or biogenesis," "external encapsulating structure organization," "cytoskeletal part" and "response to abiotic stimulus," and multiple terms were mainly related to the cytoskeleton (Figure 3B). Furthermore, except for "response to abiotic stimulus," these unique GO terms in the ZmPDI24h vs. ZmPDI0h comparison had more downregulated DEGs (Figure 3B).

For proteome sequencing, the top 20 enriched GO terms were selected in the WT24h vs. WT0h and ZmPDI24h vs. ZmPDI0h comparisons, and only six GO terms were shared by both comparisons (Figures 3C,D and Supplementary Table 4). The WT24h vs. WT0h and ZmPDI24h vs. ZmPDI0h comparisons had 14 unique GO terms, and eight unique GO terms in the ZmPDI24h vs. ZmPDI0h comparison were

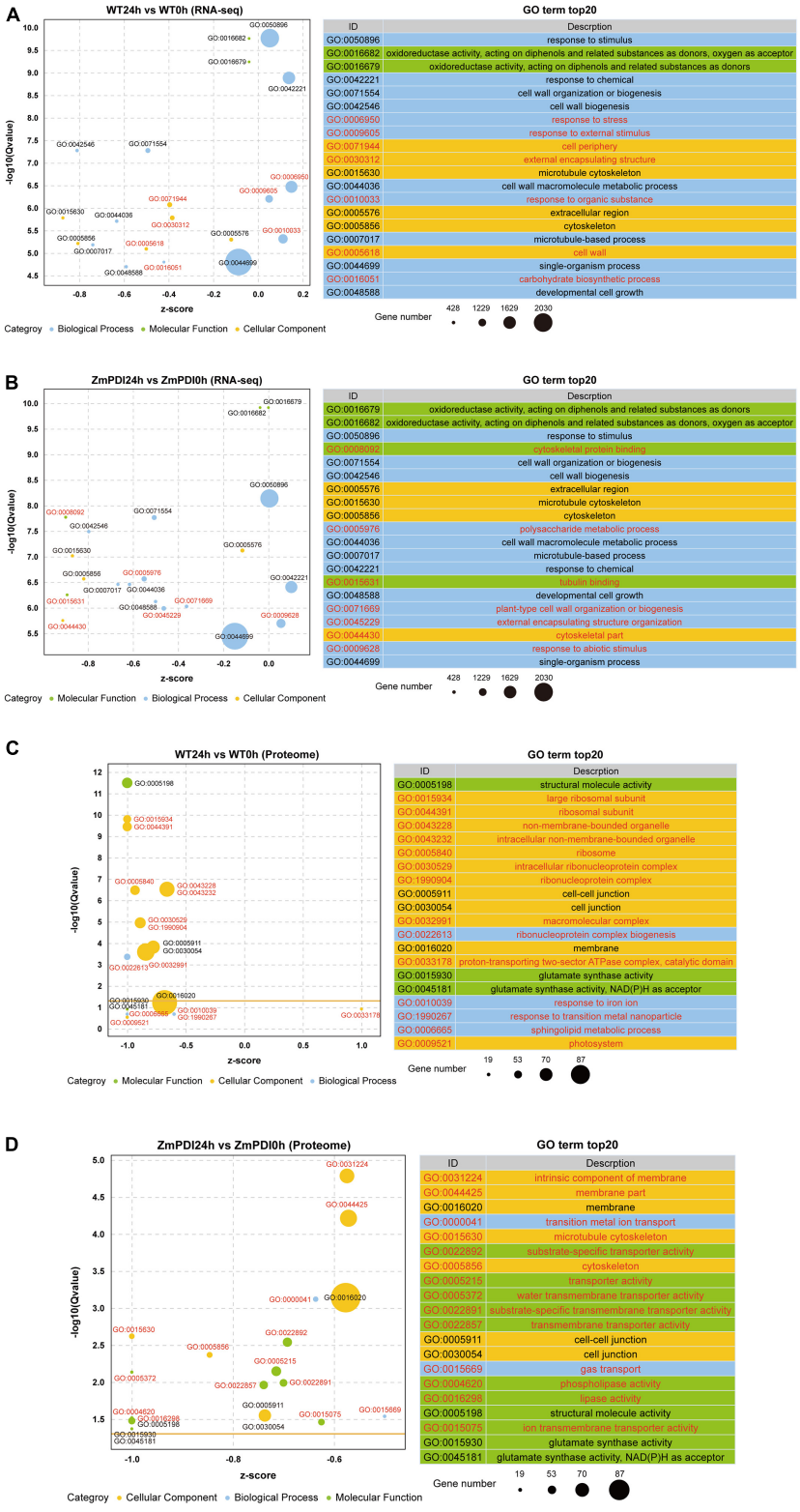

FIGURE 3

Top 20 enriched GO terms of DEGs and DEPs in *OX-ZmPDI* transgenic and WT plants of *Z. matrella*. **(A)** Top 20 enriched GO terms of DEGs in the WT24h vs. WT0h comparison. **(B)** Top 20 enriched GO terms of DEGs in the ZmPDI24h vs. ZmPDI0h comparison. **(C)** Top 20 enriched GO terms of DEPs in the WT24h vs. WT0h comparison. **(D)** Top 20 enriched GO terms of DEPs in the ZmPDI24h vs. ZmPDI0h comparison. The *z*-score value represents the ratio of the difference between the numbers of upregulated and downregulated genes to the total number of differentially expressed genes. The yellow line represents the threshold of *Q*-value = 0.05.

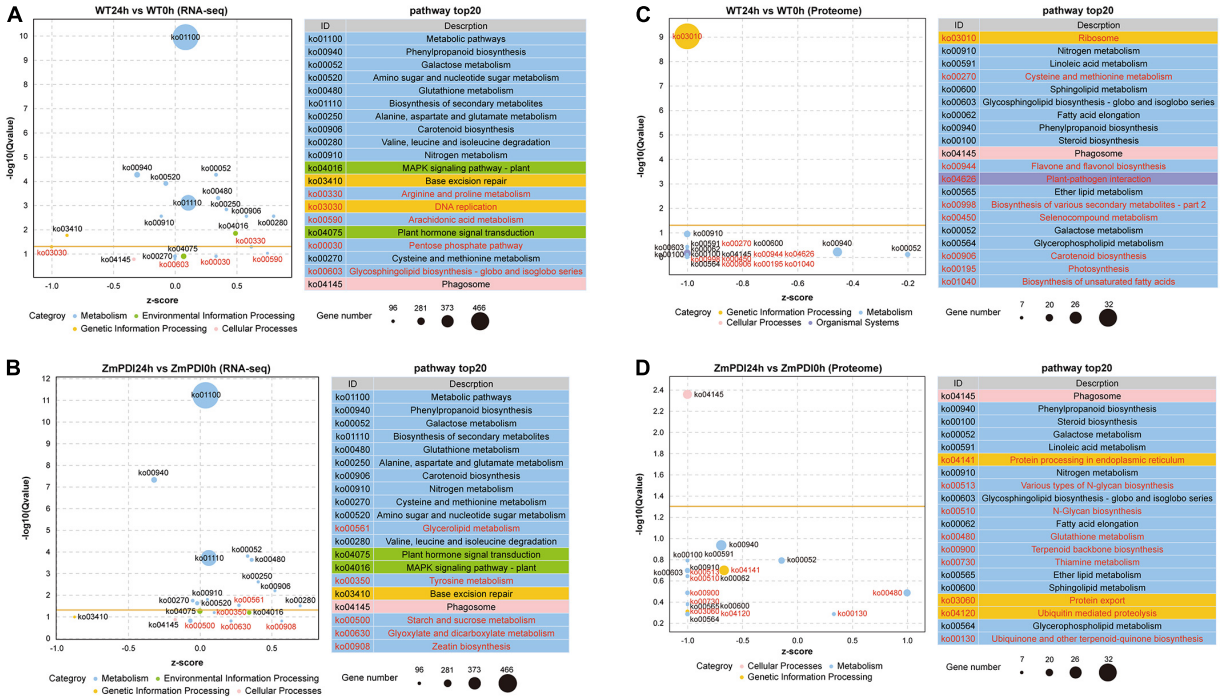

FIGURE 4
Top 20 enriched GO terms of DEGs and DEPs in *OX-ZmPDI* transgenic and WT plants of *Z. matrella*. **(A)** Top 20 enriched KEGG pathways of DEGs in the WT24h vs. WT0h comparison. **(B)** Top 20 enriched KEGG pathways of DEGs in the ZmPDI24h vs. ZmPDI0h comparison. **(C)** Top 20 enriched KEGG pathways of DEPs in the WT24h vs. WT0h comparison. **(D)** Top 20 enriched KEGG pathways of DEPs in the ZmPDI24h vs. ZmPDI0h comparison. The *z*-score value represents the ratio of the difference between the numbers of upregulated and downregulated genes to the total number of differentially expressed genes. The yellow line represents the threshold of *Q*-value = 0.05.

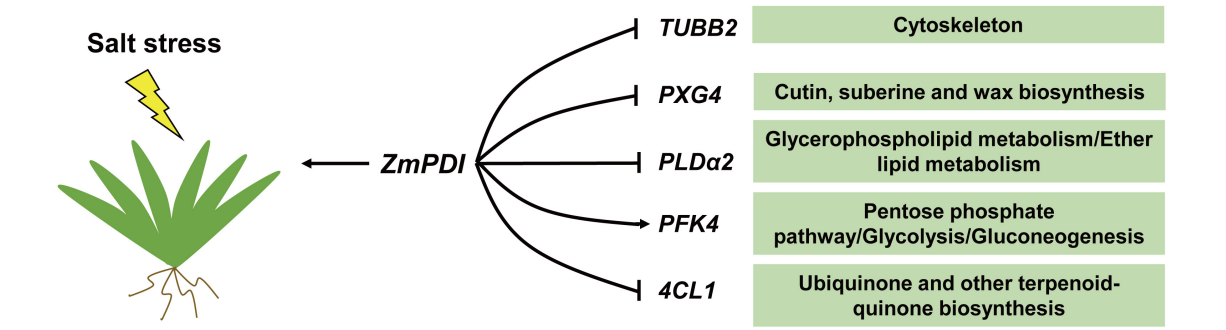

FIGURE 5
A predictive regulatory model of *ZmPDI* enhancing salt tolerance in *Z. matrella*. The contents in the green boxes are the GO term or KEGG pathways of the genes on the left belong.

related to transport or transport activity, including "transition metal ion transport," "substrate-specific transporter activity," "transporter activity," "water transmembrane transporter activity," "substrate-specific transmembrane transporter activity," "transmembrane transporter activity," "gas transport" and "ion transmembrane transporter activity" (Figures 3C,D). Comparing the top 20 enriched GO terms in the ZmPDI24h vs. ZmPDI0h comparison between RNA-seq and proteome sequencing, "microtubule cytoskeleton" and "cytoskeleton" terms were shared, and the DEGs in these two terms were mainly downregulated genes (Figures 3B,D).

The KEGG pathway analysis of DEGs for RNA-seq showed that 15 pathways were shared by both the WT24h vs. WT0h and ZmPDI24h vs. ZmPDI0h comparisons, and each comparison had five unique pathways (Figures 4A,B and Supplementary Table 5). In the ZmPDI24h vs. ZmPDI0h comparison, the five

unique pathways included "Glycerolipid metabolism," "Tyrosine metabolism," "Starch and sucrose metabolism," "Glyoxylate and dicarboxylate metabolism" and "Zeatin biosynthesis" (Figure 4B). Except for "starch and sucrose metabolism," the other four unique pathways had more upregulated DEGs (Figure 4B). KEGG pathway analysis of DEPs for proteome sequencing showed that the top 20 pathways were selected in the WT24h vs. WT0h and ZmPDI24h vs. ZmPDI0h comparisons, and each comparison had nine unique pathways (Figures 4C,D and Supplementary Table 6). In the ZmPDI24h vs. ZmPDI0h comparison, multiple unique pathways were related to proteins, including "Protein processing in endoplasmic reticulum," "Protein export" and "Ubiquitin mediated proteolysis," and DEPs in these pathways were all downregulated (Figure 4D). Comparing the pathways in the ZmPDI24h vs. ZmPDI0h comparison, "phenylpropanoid biosynthesis," "galactose metabolism," "glutathione metabolism," "nitrogen metabolism" and "phagosome" were shared between RNA-seq and proteome sequencing (Figures 4B,D).

Transcriptome and proteome association analysis

To screen the DEGs with the same expression changes in the transcriptome and proteome, we performed an association analysis. In the WT24h vs. WT0h comparison, assessment of the number of genes revealed that there were 104 DEGs upregulated in the transcriptome and proteome, including 78 DEGs that did not meet the *P*-value threshold for significance (Supplementary Table 7). Meanwhile, 276 DEGs were downregulated in the transcriptome and proteome, including 240 DEGs that did not meet the *P*-value threshold (Supplementary Table 7). In the ZmPDI24h vs. ZmPDI0h comparison, the analysis of the number of genes revealed that there were 125 DEGs upregulated in the transcriptome and proteome, with 97 DEGs not meeting the *P*-value threshold (Supplementary Table 7). At the same time, 342 DEGs (including 285 DEGs that did not meet the *P*-value) were downregulated in the transcriptome and proteome (Supplementary Table 7).

The nine quadrant diagrams showed that upregulated and downregulated DEGs in the transcriptome and proteome were in quadrants 3 and 7, respectively, and the DEGs meeting the *P*-value are marked by red dots (Supplementary Figures 2C,D). Then, GO enrichment and KEGG pathway analyses were performed with the DEGs that met the *P*-value in quadrants 3 and 7. The GO enrichment analysis showed that the "cytoskeleton" and "microtubule cytoskeleton" terms were also more significantly enriched in the ZmPDI24h vs. ZmPDI0h comparison than in the WT24h vs. WT0h comparison (Supplementary Figures 3A,B and Supplementary Table 8). Comparing the KEGG pathways in the WT24h vs. WT0h comparison, seven unique metabolic pathways were enriched in the ZmPDI24h vs. ZmPDI0h comparison, including "ether lipid metabolism," "stilbenoid, diarylheptanoid and gingerol biosynthesis," "glycerophospholipid metabolism," "cutin, suberine and wax biosynthesis," "ubiquinone and other terpenoid-quinone biosynthesis," "pentose phosphate pathway" and "glycolysis/gluconeogenesis" (Supplementary Figures 3C,D and Supplementary Table 9).

Differentially expressed gene identification and verification

In total, 119 DEGs that met the *P*-value threshold in quadrants 3 and 7 were selected from the WT24h vs. WT0h and ZmPDI24h vs. ZmPDI0h comparisons (Supplementary Figure 4). Most of these DEGs had similar expression trends between the WT24h vs. WT0h and ZmPDI24h vs. ZmPDI0h comparisons, and the protein levels of most DEGs were consistent with their RNA levels (Supplementary Figure 4). The number of DEGs in the *OX-ZmPDI* transgenic plants was very low compared with the wild-type plants either at the time point of salt treatment at 0h or 24h (Supplementary Figure 2C), which indicating that the degree of change in gene expression induced by salt stress in wild-type and *OX-ZmPDI* transgenic plants may be more important. Therefore, we set a selected condition of $|\log_2[FC(ZmPDI24h/ZmPDI0h)/FC(WT24h/WT0h)]| > 1$ and screened 36 DEGs significantly different between WT24h vs. WT0h and ZmPDI24h vs. ZmPDI0h comparisons at the RNA or proteome levels (Table 1).

Previous GO and KEGG pathway analyses in quadrants 3 and 7 showed that "cytoskeleton," "microtubule cytoskeleton," "ether lipid metabolism," "stilbenoid, diarylheptanoid and gingerol biosynthesis," "glycerophospholipid metabolism," "cutin, suberine and wax biosynthesis," "ubiquinone and other terpenoid-quinone biosynthesis," "pentose phosphate pathway" and "glycolysis/gluconeogenesis" are significantly enriched in the *OX-ZmPDI* transgenic plants (Supplementary Figure 3). According to these GO terms and KEGG pathways, five important DEGs (*TUBB2*, *PXG4*, *PLDα2*, *PFK4*, and *4CL1*) were selected from 36 DEGs, and they belonged to "cytoskeleton," "cutin, suberine and wax biosynthesis," "glycerophospholipid metabolism/ether lipid metabolism," "pentose phosphate pathway/glycolysis/gluconeogenesis" and "ubiquinone and other terpenoid-quinone biosynthesis" respectively (Figure 5). Comparing to wild-type plants, the expression and protein levels of *TUBB2*, *PXG4*, *PLDα2*, and *4CL1* were downregulated and the levels of *PFK4* were upregulated in the *OX-ZmPDI* transgenic plants under salt stress (Figure 5). These results indicated that the *ZmPDI* gene may enhance the salt tolerance of zoysiagrass by affecting the expression level or protein level of these genes. To

confirm the reliability of RNA-seq, 12 genes selected from 36 DEGs (**Table 1**) were validated using qRT–PCR, and the results were largely consistent with the RNA-seq data (**Supplementary Figure 5**).

Discussion

Overexpression of *ZmPDI* can enhance the salt tolerance of *Zoysia matrella*

Previous studies have shown that heterologous expression of *ZmPDI* enhances the salt tolerance of yeast (Chen et al., 2015b), but whether it has the same function in *Z. matrella* remains to be verified. In this study, homologous expression of *ZmPDI* in *Z. matrella* significantly improved salt tolerance while maintaining normal growth and aboveground and underground biomasses (**Figures 1A–C**). Under salinity stress, plant growth and development are inhibited mainly because of osmotic pressure disturbance, ionic imbalance and oxidative stress (Zhao et al., 2020). Plants regulate osmotic pressure mainly through two pathways, namely, the synthesis of organic osmolytes and improved absorption of inorganic ions (Zhao et al., 2020). Proline and sugars are organic osmolytes, and proline plays a dominant role in regulating osmotic pressure under salt stress (Zhao et al., 2020). In the *OX-ZmPDI* transgenic lines, the proline contents were significantly higher than those in the wild-type plants, while the soluble sugar contents were significantly lower (**Figures 1D,E**). These results indicated that *OX-ZmPDI* transgenic plants may synthesize more proline and activate glucose metabolism to adjust osmotic pressure under salinity stress.

Many enzymes involved in primary metabolism are present in the cytosolic compartment, and many of them are controlled by K^+ (Zhao et al., 2020). However, Na^+ is very similar to K^+ and usually replaces K^+ to involve those enzymatic reactions with much less efficiency (Zhao et al., 2020). Therefore, a high concentration of Na^+ can disrupt metabolism and potentially kill the plant (Zhao et al., 2020). In *OX-ZmPDI* transgenic lines, the K^+/Na^+ ratios in roots were all significantly higher than those in wild-type plants after salt treatment (**Figure 1F**), indicating that *ZmPDI* can help plants maintain higher K^+/Na^+ ratios to resist Na^+ damage. Reactive oxygen species (ROS) are rapidly induced by salinity stress and are mainly produced in the apoplast, chloroplasts, mitochondria and peroxisomes (Zhao et al., 2020). SOD can scavenge excess ROS to enhance the salt tolerance of plants (Zhao et al., 2020). Under salt treatment, overexpression of the *ZmPDI* gene significantly maintained normal SOD activity and chlorophyll content in *Z. matrella* (**Figures 1H,I**), indicating that normal SOD activity in chlorophyll may catalyze the scavenging of ROS and maintain the normal function of chloroplasts. These results proved that *ZmPDI* can enhance the salt tolerance of plants by maintaining osmotic pressure and ionic balance and reducing oxidative stress.

ZmPDI may enhance the salt tolerance of *Zoysia matrella* by regulating *TUBB2*, *PXG4*, *PLDα2*, *PFK4*, and *4CL1*

To understand the difference in salt tolerance responses between wild-type and *OX-ZmPDI* transgenic plants, an association analysis of transcriptome and proteome sequencing was performed. The GO enrichment and KEGG pathway analyses of 119 DEGs that met the *P*-value threshold in quadrants 3 and 7 showed that *ZmPDI* may enhance the salt tolerance of *Z. matrella* in five aspects, namely, "cytoskeleton," "cutin, suberine and wax biosynthesis," "glycerophospholipid metabolism/ether lipid metabolism," "pentose phosphate pathway/glycolysis/gluconeogenesis" and "ubiquinone and other terpenoid-quinone biosynthesis" (**Figure 5**). The plant cytoskeleton is mainly composed of microtubules (MTs), microfilaments (MFs) and MT/MF-interacting proteins, and its dynamic organizational changes can enhance plant tolerance through various intracellular activities, including cell morphogenesis and cell signal transduction (Yang and Guo, 2018; Zhao et al., 2021). Salt stress induces the depolymerization and reorganization of MTs, and its destabilization can enhance the salt tolerance of plants (Zhao et al., 2021). However, MF depolymerization is related to cell death under long-term salt stress, and its stabilization can increase the ability of plants to withstand salt stress (Yang and Guo, 2018; Zhao et al., 2021). A cytoskeletal structural component gene, *beta-2-tubulin* (*TUBB2*, *Zjn_sc00009.1.g09140.1.sm.mk*), was screened as a DEG and downregulated in *OX-ZmPDI* transgenic plants at both the transcriptome and proteome levels (**Table 1**). Tubulin is the major constituent of the cytoskeleton, which forms networks of microtubules (Chiolerio et al., 2020). These results indicated that *ZmPDI* may improve the salt tolerance of zoysiagrass by downregulating TUBB2 levels to affect the destabilization of MTs.

Epoxygenated fatty acids are components of cutin and suberin and act as defense molecules (Blee et al., 2012). The caleosin-type peroxygenases catalyze the epoxidation of unsaturated fatty acids in the presence of hydroperoxides to form epoxygenated fatty acids (Blee et al., 2012). *Peroxygenase 4* (*PXG4*, *Zjn_sc00093.1.g00470.1.sm.mkhc*) is a class II caleosin gene that encodes a calcium-binding peroxygenase involved in the degradation of storage lipids (Blee et al., 2012). In *Arabidopsis*, another name of the *PXG4* gene is *AtCLO4*, and previous studies have confirmed that *PXG4* participates in salt tolerance by acting as a negative regulator of abscisic acid (ABA) (Kim et al., 2011; Blee et al., 2012). During salt stress, the *clo4* mutants perform significantly less inhibition of lateral root formation (Rafeh, 2016). After salt treatments, the

"cutin, suberine and wax biosynthesis" and *PXG4* genes were significantly enriched and screened in *OX-ZmPDI* transgenic plants (**Figure 5**). Compared with wild-type plants, the transcript and protein levels of *PXG4* in *OX-ZmPDI* transgenic plants were all decreased (**Table 1**). These results indicated that *ZmPDI* may inhibit *PXG4* expression to decrease this protein level, thereby maintaining lateral root formation to improve the salt tolerance of zoysiagrass.

Phospholipase D (PLD) is a phosphatidyl choline-hydrolyzing enzyme that can generate the lipid second messenger phosphatidic acid (PA) by hydrolyzing membrane phospholipids, and the expression of multiple PLD genes is increased by exposure to various stresses (Bargmann and Munnik, 2006; Ji et al., 2017). PLDs are involved in multiple cellular processes, including membrane composition and microtubule and cytoskeletal dynamics (Faraudo and Travesset, 2007; Zhang et al., 2017). The expression levels of some PLD genes are induced by salt stress, and *pldα1*, *pldα3*, and *pldδ* mutants show salt sensitivity (Hunter et al., 2019). Among them, the molecular mechanism by which *PLDα1* responds to salt stress has been studied in depth. PLDα1 interacts with mitogen-activated protein kinases 3 (MPK3) to enhance salt tolerance and ABA signaling (Vadovič et al., 2019). In addition, Cys-rich receptor-like kinase 2 (CRK2) acts as the downstream target protein of PLDα1 and enhances salt tolerance at the germination stage in *Arabidopsis* (Hunter et al., 2019). Previous studies have shown that *PLDα2* is highly induced by salt and drought stress in rice (Li et al., 2007). However, the transcript and protein levels of *PLDα2* in *OX-ZmPDI* transgenic and wild-type plants all decreased after salt treatments (**Table 1**). The protein alignment of *PLDα2* genes in *Z. matrella* and *Oryza sativa* showed that the amino acid sequences of ZmPLDα2 and OsPLDα2 have an obviously difference (**Supplementary Figure 6A**). These results indicated that *PLDα2* may play a different role in regulating the salt tolerance of zoysiagrass.

In the plant glycolytic pathway, ATP-dependent 6-phosphofructokinase (PFK) catalyzes the phosphorylation of fructose 6-phosphate (F6P), transforming it to fructose-1,6-bisphosphate (F16BP) (Zhong et al., 2016). In previous studies, the expression levels of *PFK* were significantly induced by salt stress in rice, cucumber and tomato (Zhong et al., 2016; Yuenyong et al., 2018; Feng et al., 2019). Soluble sugar is an organic osmolyte that can balance the vacuole solute potential, but the accumulation of sugar in leaves can inhibit photosynthesis (Zhong et al., 2016). In our studies, compared with wild-type plants, the transcript and protein levels of *PFK4* in *OX-ZmPDI* transgenic plants were all increased (**Table 1**). The soluble sugar contents were significantly lower and the chlorophyll contents maintained significant high levels in *OX-ZmPDI* transgenic plant leaves (**Figures 1E,H**). These results indicated that *ZmPDI* may increase *PFK4* expression to accelerate the conversion of F6P into F16BP, thereby enhancing the glycolysis pathway to maintain normal photosynthetic efficiency and chlorophyll content in zoysiagrass.

4-Coumarate-CoA ligase (4CL) is an important branch point involved in phenylpropanoid metabolism that regulates the biosynthesis of flavonoids, lignin and other phenolic secondary metabolites and plays important roles in plant physiology and biotic and abiotic stresses (Lavhale et al., 2018; Chen et al., 2020; Wang et al., 2022). *4CL* genes emerge in response to salt stress in a variety of plants. In desert poplars, the expression of *Pp4CL2, Pp4CL11,* and *Pp4CL12* is increased significantly in response to salt stress compared with salt-sensitive poplar (Zhang et al., 2015). In *Arabidopsis*, higher expression levels of lignin biosynthesis-related genes, including *4CL1* and *4CL2*, are detected in salt-adapted cells with increased lignin content and thickened cell walls relative to normal cells (Chun et al., 2019). In *Sophora alopecuroides*, transcriptomic analysis revealed that *Sa4CL*, which is involved in lignin synthesis, is significantly upregulated under salt stress (Zhu et al., 2021). In our study, a *4CL1* gene was screened between wild-type and *OX-ZmPDI* transgenic plants (**Table 1**). However, the *4CL1* gene was downregulated after salt treatment in transcriptome sequencing, and its downregulation was more obvious in *OX-ZmPDI* transgenic plants (**Table 1**), indicating that *ZmPDI* may influence the expression of *4CL1* to regulate the salt tolerance of zoysiagrass. The protein alignment of *4CL1* genes in *Z. matrella* and *Arabidpsis* showed that the amino acid sequences of Zm4CL1 and At4CL1 have an obviously difference (**Supplementary Figure 6B**). Therefore, the function of 4CL1 in zoysiagrass may be different from that in other plants.

Data availability statement

The datasets presented in this study can be found in online repositories. The names of the repository/repositories and accession number(s) can be found in the article/**Supplementary material**.

Author contributions

QM and KW performed the evaluation experiments. JW, QM, and KW performed the transcriptomic and proteome analyses and verification experiments. JL and JW designed the experiment. XL, PW, HG, JC, and JZ supervised the project. JW and QM participated in writing the manuscript. All authors contributed to the article and approved the submitted version.

Funding

This work was funded by the National Natural Science Foundation of China (Grant Nos. 31672195, 31901383, and 32002081) and the Natural Science Foundation of Jiangsu Province, China (Grant Nos. BK20190274 and BK20200285).

Conflict of interest

The authors declare that the research was conducted in the absence of any commercial or financial relationships that could be construed as a potential conflict of interest.

Publisher's note

All claims expressed in this article are solely those of the authors and do not necessarily represent those of their affiliated organizations, or those of the publisher, the editors and the reviewers. Any product that may be evaluated in this article, or claim that may be made by its manufacturer, is not guaranteed or endorsed by the publisher.

Supplementary material

The Supplementary Material for this article can be found online at: https://www.frontiersin.org/articles/10.3389/fpls.2022.970651/full#supplementary-material

References

Ali Khan, H., and Mutus, B. (2014). Protein disulfide isomerase a multifunctional protein with multiple physiological roles. *Front. Chem.* 2:70. doi: 10.3389/fchem.2014.00070

Bargmann, B. O., and Munnik, T. (2006). The role of phospholipase D in plant stress responses. *Curr. Opin. Plant Biol.* 9, 515–522. doi: 10.1016/j.pbi.2006.07.011

Blee, E., Flenet, M., Boachon, B., and Fauconnier, M. L. (2012). A non-canonical caleosin from A rabidopsis efficiently epoxidizes physiological unsaturated fatty acids with complete stereoselectivity. *FEBS J.* 279, 3981–3995. doi: 10.1111/j.1742-4658.2012.08757.x

Chen, J., Yan, J., Qian, Y., Jiang, Y., Zhang, T., Guo, H., et al. (2009). Growth responses and ion regulation of four warm season turfgrasses to long-term salinity stress. *Sci. Hortic.* 122, 620–625. doi: 10.1016/j.scienta.2009.07.004

Chen, X., Su, W., Zhang, H., Zhan, Y., and Zeng, F. (2020). Fraxinus mandshurica 4-coumarate-CoA ligase 2 enhances drought and osmotic stress tolerance of tobacco by increasing coniferyl alcohol content. *Plant Physiol. Bioch.* 155, 697–708. doi: 10.1016/j.plaphy.2020.08.031

Chen, Y., Li, L., Zong, J., Chen, J., Guo, H., Guo, A., et al. (2015a). Heterologous expression of the halophyte *Zoysia matrella* H^+-pyrophosphatase gene improved salt tolerance in *Arabidopsis thaliana*. *Plant Physiol. Bioch.* 91, 49–55. doi: 10.1016/j.plaphy.2015.04.004

Chen, Y., Zong, J., Tan, Z., Li, L., Hu, B., Chen, C., et al. (2015b). Systematic mining of salt-tolerant genes in halophyte-*Zoysia matrella* through cDNA expression library screening. *Plant Physiol. Bioch.* 89, 44–52. doi: 10.1016/j.plaphy.2015.02.007

Chiolerio, A., Draper, T. C., Mayne, R., and Adamatzky, A. (2020). On resistance switching and oscillations in tubulin microtubule droplets. *J. Colloid Interf. Sci.* 560, 589–595. doi: 10.1016/j.jcis.2019.10.065

Chun, H. J., Baek, D., Cho, H. M., Lee, S. H., Jin, B. J., Yun, D. J., et al. (2019). Lignin biosynthesis genes play critical roles in the adaptation of Arabidopsis plants to high-salt stress. *Plant Signal Behav.* 14:1625697. doi: 10.1080/15592324.2019.1625697

Fan, F., Zhang, Y., Wang, S., Han, Y., Wang, L., and Lu, D. (2018). Characterization of the oxidative protein folding activity of a unique plant oxidoreductase, Arabidopsis protein disulfide isomerase-11. *Biochem. Bioph. Res. Co.* 495, 1041–1047. doi: 10.1016/j.bbrc.2017.11.111

Fang, C., Ye, Z., Gai, T., Lu, K., Dai, F., Lu, C., et al. (2021). DIA-based proteome reveals the involvement of cuticular proteins and lipids in the wing structure construction in the silkworm. *J. Proteomics* 238:104155. doi: 10.1016/j.jprot.2021.104155

Faraudo, J., and Travesset, A. (2007). Phosphatidic acid domains in membranes: Effect of divalent counterions. *Biophys. J.* 92, 2806–2818. doi: 10.1529/biophysj.106.092015

Feng, Y., Chen, X., He, Y., Kou, X., and Xue, Z. (2019). Effects of exogenous trehalose on the metabolism of sugar and abscisic acid in tomato seedlings under salt stress. *Trans. Tianjin Univ.* 25, 451–471. doi: 10.1007/s12209-019-00214-x

Ge, Y. X., Norton, T., and Wang, Z. Y. (2006). Transgenic zoysiagrass (*Zoysia japonica*) plants obtained by Agrobacterium-mediated transformation. *Plant Cell Rep.* 25, 792–798. doi: 10.1007/s00299-006-0123-8

Hunter, K., Kimura, S., Rokka, A., Tran, H. C., Toyota, M., Kukkonen, J. P., et al. (2019). CRK2 enhances salt tolerance by regulating callose deposition in connection with PLDα1. *Plant Physiol.* 180, 2004–2021. doi: 10.1104/pp.19.00560

Ji, T., Li, S., Huang, M., Di, Q., Wang, X., Wei, M., et al. (2017). Overexpression of cucumber phospholipase D alpha gene (CsPLDα) in tobacco enhanced salinity stress tolerance by regulating Na^+-K^+ balance and lipid peroxidation. *Front. Plant Sci.* 8:499. doi: 10.3389/fpls.2017.00499

Jiang, Q., Chen, J., Zong, J., Li, S., Chu, X., Guo, H., et al. (2013). Effect of phosphorus on Na^+ and K^+ concentrations and the growth of *Zoysia matrella* under salt stress. *Acta Pratacult. Sin.* 22, 162–168. doi: 10.11686/cyxb20130321

Kim, D., Langmead, B., and Salzberg, S. L. (2015). HISAT: A fast spliced aligner with low memory requirements. *Nat. Methods* 12, 357–360. doi: 10.1038/nmeth.3317

Kim, Y. Y., Jung, K. W., Yoo, K. S., Jeung, J. U., and Shin, J. S. (2011). A stress-responsive caleosin-like protein, AtCLO4, acts as a negative regulator of ABA responses in Arabidopsis. *Plant Cell Physiol.* 52, 874–884. doi: 10.1093/pcp/pcr039

Lavhale, S. G., Kalunke, R. M., and Giri, A. P. (2018). Structural, functional and evolutionary diversity of 4-coumarate-CoA ligase in plants. *Planta* 248, 1063–1078. doi: 10.1007/s00425-018-2965-z

Li, G., Lin, F., and Xue, H. W. (2007). Genome-wide analysis of the phospholipase D family in Oryza sativa and functional characterization of PLDβ1 in seed germination. *Cell Res.* 17, 881–894. doi: 10.1038/cr.2007.77

Li, S., Chen, J., Guo, H., Zong, J., Zhang, F., Chu, X., et al. (2012). Salinity tolerance evaluation of Zoysia turfgrass germplasm. *Acta Pratacult. Sin.* 21, 43–51.

Love, M. I., Huber, W., and Anders, S. (2014). Moderated estimation of fold change and dispersion for RNA-seq data with DESeq2. *Genome Biol.* 15, 1–21. doi: 10.1186/s13059-014-0550-8

Marcum, K. B., and Murdoch, C. L. (1994). Salinity tolerance mechanisms of six C4 turfgrasses. *J. Am. Soc. Hortic. Sci.* 119, 779–784. doi: 10.21273/JASHS.119.4.779

Mortazavi, A., Williams, B. A., McCue, K., Schaeffer, L., and Wold, B. (2008). Mapping and quantifying mammalian transcriptomes by RNA-Seq. *Nat. Methods* 5, 621–628. doi: 10.1038/nmeth.1226

Okumura, M., Noi, K., and Inaba, K. (2021). Visualization of structural dynamics of protein disulfide isomerase enzymes in catalysis of oxidative folding and reductive unfolding. *Curr. Opin. Struc. Biol.* 66, 49–57. doi: 10.1016/j.sbi.2020.10.004

Pertea, M., Pertea, G. M., Antonescu, C. M., Chang, T. C., Mendell, J. T., and Salzberg, S. L. (2015). StringTie enables improved reconstruction of a transcriptome from RNA-seq reads. *Nat. Biotechnol.* 33, 290–295. doi: 10.1038/nbt.3122

Rafeh, R. (2016). *AtCLO4, a stress responsive calcium binding protein, interacts with the heterotrimeric Gα subunit in Arabidopsis thaliana*. Doctoral dissertation. Montreal: Concordia University.

Robinson, M. D., McCarthy, D. J., and Smyth, G. K. (2010). edgeR: A Bioconductor package for differential expression analysis of digital gene expression data. *Bioinformatics* 26, 139–140. doi: 10.1093/bioinformatics/btp616

Tanaka, H., Hirakawa, H., Muguerza, M., Hashiguchi, M., Tabata, S., Akashi, R., et al. (2016a). The complete chloroplast genome sequence of *Zoysia matrella* (L.) merr. *Crop Sci.* 56, 1206–1212. doi: 10.2135/cropsci2015.08.0517

Tanaka, H., Hirakawa, H., Kosugi, S., Nakayama, S., Ono, A., Watanabe, A., et al. (2016b). Sequencing and comparative analyses of the genomes of zoysiagrasses. *DNA Res.* 23, 171–180. doi: 10.1093/dnares/dsw006

Tominaga, J., Nakahara, Y., Horikawa, D., Tanaka, A., Kondo, M., Kamei, Y., et al. (2018). Overexpression of the protein disulfide isomerase AtCYO1 in chloroplasts slows dark-induced senescence in Arabidopsis. *BMC Plant Biol.* 18:80. doi: 10.1186/s12870-018-1294-5

Vadovič, P., Šamajová, O., Takáč, T., Novák, D., Zapletalová, V., Colcombet, J., et al. (2019). Biochemical and genetic interactions of phospholipase D alpha 1 and mitogen-activated protein kinase 3 affect Arabidopsis stress response. *Front. Plant Sci.* 10:275. doi: 10.3389/fpls.2019.00275

Wang, J., An, C., Guo, H., Yang, X., Chen, J., Zong, J., et al. (2020). Physiological and transcriptomic analyses reveal the mechanisms underlying the salt tolerance of *Zoysia japonica* Steud. *BMC Plant Biol.* 20:114. doi: 10.1186/s12870-020-02330-6

Wang, K., Wang, Y., Qu, A., Wang, R., Guo, H., Li, X., et al. (2020). Establishment of genetic transformation system for *Zoysia matrella*. *Chin. J. Trop. Crops* 41:1566. doi: 10.3969/j.issn.1000-2561.2020.08.009

Wang, Y., Guo, L., Zhao, Y., Zhao, X., and Yuan, Z. (2022). Systematic analysis and expression profiles of the 4-Coumarate: CoA ligase (4CL) gene family in pomegranate (*Punica granatum* L.). *Int. J. Mol. Sci.* 23:3509. doi: 10.3390/ijms23073509

Xie, Q., Niu, J., Xu, X., Xu, L., Zhang, Y., Fan, B., et al. (2015). *De novo* assembly of the Japanese lawngrass (*Zoysia japonica* Steud.) root transcriptome and identification of candidate unigenes related to early responses under salt stress. *Front. Plant Sci.* 6:610. doi: 10.3389/fpls.2015.00610

Yamamoto, A., Hashiguchi, M., Akune, R., Masumoto, T., Muguerza, M., Saeki, Y., et al. (2016). The relationship between salt gland density and sodium accumulation/secretion in a wide selection from three Zoysia species. *Aust. J. Bot.* 64, 277–284. doi: 10.1071/BT15261

Yang, Y., and Guo, Y. (2018). Elucidating the molecular mechanisms mediating plant salt-stress responses. *New Phytol.* 217, 523–539. doi: 10.1111/nph.14920

Yuenyong, W., Chinpongpanich, A., Comai, L., Chadchawan, S., and Buaboocha, T. (2018). Downstream components of the calmodulin signaling pathway in the rice salt stress response revealed by transcriptome profiling and target identification. *BMC Plant Biol.* 18:1–23. doi: 10.1186/s12870-018-1538-4

Zhang, C. H., Ma, T., Luo, W. C., Xu, J. M., Liu, J. Q., and Wan, D. S. (2015). Identification of 4CL genes in desert poplars and their changes in expression in response to salt stress. *Genes* 6, 901–917. doi: 10.3390/genes6030901

Zhang, Q., Qu, Y., Wang, Q., Song, P., Wang, P., Jia, Q., et al. (2017). Arabidopsis phospholipase D alpha 1-derived phosphatidic acid regulates microtubule organization and cell development under microtubule-interacting drugs treatment. *J. Plant Res.* 130, 193–202. doi: 10.1007/s10265-016-0870-8

Zhang, Z., Liu, X., Li, R., Yuan, L., Dai, Y., and Wang, X. (2018). Identification and functional analysis of a protein disulfide isomerase (AtPDI1) in *Arabidopsis thaliana*. *Front. Plant Sci.* 9:913. doi: 10.3389/fpls.2018.00913

Zhao, C., Zhang, H., Song, C., Zhu, J. K., and Shabala, S. (2020). Mechanisms of plant responses and adaptation to soil salinity. *Innovation* 1:100017. doi: 10.1016/j.xinn.2020.100017

Zhao, S., Zhang, Q., Liu, M., Zhou, H., Ma, C., and Wang, P. (2021). Regulation of plant responses to salt stress. *Int. J. Mol. Sci.* 22:4609. doi: 10.3390/ijms22094609

Zhong, M., Yuan, Y., Shu, S., Sun, J., Guo, S., Yuan, R., et al. (2016). Effects of exogenous putrescine on glycolysis and Krebs cycle metabolism in cucumber leaves subjected to salt stress. *Plant Growth Regul.* 79, 319–330. doi: 10.1007/s10725-015-0136-9

Zhu, Y., Wang, Q., Wang, Y., Xu, Y., Li, J., Zhao, S., et al. (2021). Combined transcriptomic and metabolomic analysis reveals the role of phenylpropanoid biosynthesis pathway in the salt tolerance process of *Sophora alopecuroides*. *Int. J. Mol. Sci.* 22:2399. doi: 10.3390/ijms22052399

frontiers | Frontiers in Plant Science

TYPE Original Research
PUBLISHED 10 August 2022
DOI 10.3389/fpls.2022.971431

OPEN ACCESS

EDITED BY
Jing Zhang,
Nanjing Agricultural University, China

REVIEWED BY
Zhou Li,
Sichuan Agricultural University, China
Tianxiu Zhong,
South China Agricultural University, China

*CORRESPONDENCE
Kun Zhang
zk61603@163.com

SPECIALTY SECTION
This article was submitted to Plant Abiotic Stress, a section of the journal Frontiers in Plant Science

RECEIVED 17 June 2022
ACCEPTED 22 July 2022
PUBLISHED 10 August 2022

CITATION
Li Y, Sun Y, Cui H, Li M, Yang G, Wang Z and Zhang K (2022) *Carex rigescens* caffeic acid O-methyltransferase gene *CrCOMT* confer melatonin-mediated drought tolerance in transgenic tobacco.
Front. Plant Sci. 13:971431.
doi: 10.3389/fpls.2022.971431

Carex rigescens caffeic acid O-methyltransferase gene *CrCOMT* confer melatonin-mediated drought tolerance in transgenic tobacco

Yan Li[1], Yan Sun[2], Huiting Cui[2], Mingna Li[3], Guofeng Yang[1], Zengyu Wang[1] and Kun Zhang[1]*

[1]Key Laboratory of National Forestry and Grassland Administration on Grassland Resources and Ecology in the Yellow River Delta, College of Grassland Science, Qingdao Agricultural University, Qingdao, China, [2]College of Grassland Science and Technology, China Agricultural University, Beijing, China, [3]Institute of Animal Sciences, Chinese Academy of Agricultural Sciences (CAAS), Beijing, China

Melatonin is an important, multifunctional protective agent against a variety of abiotic and biotic stressors in plants. Caffeic acid O-methyltransferase (COMT) catalyzes the last step of melatonin synthesis in plants and reportedly participates in the regulation of stress response and tolerance. However, few studies have reported its function in melatonin-mediated drought resistance. In this study, *CrCOMT* was identified and was strongly induced by drought stress in *Carex rigescens*. *CrCOMT* overexpression in transgenic tobacco increased tolerance to drought stress with high levels of seed germination, relative water content, and survival rates. *CrCOMT* overexpression in tobacco improved membrane stability, and plants exhibited lower relative electrolytic leakage and malondialdehyde content, as well as higher photochemical efficiency than the wildtype (WT) under drought stress. The transgenic plants also had higher levels of proline accumulation and antioxidant enzyme activity, which decreased oxidative stress damage due to reactive oxygen species (ROS) hyperaccumulation under drought stress. The transcription of drought stress response and ROS scavenging genes was significantly higher in the *CrCOMT* overexpression plants than in the WT plants. In addition, *CrCOMT* transgenic tobacco plants exhibited higher melatonin content under drought stress conditions. Exogenous melatonin was applied to *C. rigescens* under drought stress to confirm the function of melatonin in mediating drought tolerance; the relative water content and proline content were higher, and the relative electrolytic leakage was lower in melatonin-treated *C. rigescens* than in the untreated plants. In summary, these results show that *CrCOMT* plays a positive role in plant drought stress tolerance by regulating endogenous melatonin content.

KEYWORDS

melatonin, COMT, drought stress, transgenic tobacco, *Carex rigescens*

Introduction

Recently, the effects of global climate change, such as increasing temperatures, have increased pressure on plants to cope with increasingly arid environments (Fahad et al., 2017; Dietz et al., 2021). Water has a great impact throughout the plant growth period, and water deficiency can result in plant withering, impaired development, reduced production, and even death (Anjum et al., 2011). Specifically, drought stress can impede root water absorption and leaf stomatal movement, change plant internal water potential, and affect nutrient transport between the aboveground and underground parts of plants (Ahanger et al., 2021). Under drought stress, a high level of reactive oxygen species (ROS) accumulation in plant tissues leads to oxidative peroxidation of cell membranes and oxidative damage to proteins and nucleic acids (Kar, 2011). At the cellular level, there can be damage to the photosynthetic system, decrease in photochemical efficiency, and multiple effects on plant energy metabolism (Dalal, 2021). Therefore, it is crucial to understand the complicated drought stress tolerance mechanisms in plants, which could contribute to improving plant growth in water-deficient soils and developing water-saving agriculture.

Melatonin (N-acetyl-5-methoxytrytamine) was first identified in vascular plants in 1995, and since then, studies have reported multiple functions for plant growth and development (Hattori et al., 1995; Arnao and Hernández-Ruiz, 2019). In addition, over the last two decades, the multifunctional role of melatonin in plants as a protective agent against different abiotic and biotic stressors has been fully accepted, and it is well known to improve tolerance to salt, drought, high temperatures, cold, and heavy metal stress (Hoque et al., 2021; Sun et al., 2021). As a master regulator, melatonin improves plant tolerance to abiotic stress by regulating the expression of downstream genes, osmolyte accumulation, carbon assimilation, stomatal conductance, and photochemical efficiency of photosystems (Sharma and Zheng, 2019; Moustafa-Farag et al., 2020). The most common mechanism of melatonin-mediated anti-stress regulation is the enhancement of plant antioxidant defense activity, such as peroxidase, superoxide dismutase, and catalase, and key soluble osmolytes, such as proline, soluble protein, and sugars (Alharby and Fahad, 2020). In addition, in studies investigating drought stress improvement functions, it was found that exogenous melatonin confers drought stress tolerance by promoting plant growth, photosynthetic capacity, and antioxidant defense system in the tea plant (*Camellia sinensis*) (Li et al., 2019), lemon verbena (*Lippia citriodora*) (Hosseini et al., 2021), tartary buckwheat (*Fagopyrum tataricum*) (Hossain et al., 2020), and soybean (*Glycine max*) (Imran et al., 2021).

N-acetylserotonin methyltransferase (ASMT) participates in melatonin synthesis from N-acetylserotonin in the cytoplasm, however, *ASMT* homology genes in plants are rare (Byeon et al., 2014b; Zhuang et al., 2020). Caffeic acid O-methyltransferase (COMT), an O-methyltransferase, has enzyme activity similar to that of ASMT, and its catalytic function in the last step of melatonin biosynthesis was recently reported (Byeon et al., 2014a; Lee et al., 2017). Recently, the role of *COMT* in melatonin-mediated physiological mechanism variations has been demonstrated in certain plant species. In herbaceous peony (*Paeonia lactiflora*), manipulating the expression of *COMT1*, which is involved in melatonin biosynthesis, had a significant effect on melatonin, S/G ratio, and stem strength (Zhao et al., 2022). In tomatoes, *COMT1* overexpression resulted in increased melatonin biosynthesis and contributed to the alleviation of carbendazim phytotoxicity and residues (Yan et al., 2019). A previous study also showed that OsCOMT encodes caffeic acid O-methyltransferase in melatonin biosynthesis and increases rice (*Oryza sativa*) grain yield through the dual regulation of leaf senescence and vascular development. In addition, the *COMT* gene has been investigated in melatonin-mediated stress resistance (Huangfu et al., 2022). Overexpression of *SlCOMT* in *Solanum lycopersicum* increased melatonin accumulation and improved tolerance of salt stress (Sun et al., 2020). Watermelon *ClCOMT1* has been reported to play an essential role in melatonin biosynthesis and function in abiotic stress tolerance (Chang et al., 2021). A previous study reported that *COMT* gene expression could be affected by water deficit stress, and a recent study in *Sorghum bicolor* had investigated its role in plant drought stress tolerance (Saluja et al., 2021). However, the function of *COMT* in melatonin-mediated plant drought stress tolerance is not well understood.

Turfgrass growth is severely influenced by limited irrigation and drought stress induced by global climate change (Yu et al., 2019; Wang et al., 2021). *Carex rigescens (Franch.) V. Krecz*, a cool season perennial turfgrass, is widely distributed in northern China, has a strong tolerance to various stresses, and can form turf as an ornamental and lawn plant species even in arid and barren soil (Zhang et al., 2020; Zhang K. et al., 2021). Revealing stress resistance mechanisms, such as drought stress tolerance, may be meaningful not only revealing the molecular mechanisms behind *C. rigescens* drought resistance, but also important for drought tolerance genetic breeding in turfgrass and crop plants which could contribute to water-efficient agriculture. The stress induction (including drought stress) performance of *CrCOMT* expression was verified in our previous study, which led us to hypothesize that *CrCOMT* might play a significant role in drought stress tolerance in *C. rigescens* (Zhang et al., 2019). Further investigation into the specific gene function of *CrCOMT* in drought tolerance regulation in *C. rigescens* is required.

In this study, to verify the specific gene function of *CrCOMT* in response to drought stress, the gene expression patterns of *CrCOMT* in different *C. rigescens* tissues and stress conditions

were analyzed. *CrCOMT* overexpression transgenic tobacco had been generated, and the role of *CrCOMT* in drought stress tolerance was identified. In addition, we compared seed germination, plant growth, physiological response, and stress-responsive gene expression between transgenic and wildtype (WT) tobacco plants response to drought stress. We also assayed endogenous melatonin content and investigated its role in drought stress tolerance in *C. rigescens*. This study reveals the gene functions and regulatory mechanisms of *CrCOMT* under drought stress conditions.

Materials and methods

Plant material and growth conditions

Carex rigescens (of the stress tolerant genotype, 'Huanghua') seeds were sterilized using 75% ethanol for 30 s and 20% NaOH for 30 min then washed ten times with sterilized water. The seeds were sown on wet filter paper and placed in a growth chamber (BDR16, Conviron) under controlled conditions of 25/20°C and 16/8 h (day/night), 1200-1250 μmol $m^{-2}s^{-1}$ light intensity. *C. rigescens* seedlings were then planted in soil (peat soil: roseite = 3:1) for two months in a greenhouse (25/20°C-day and night temperature). Uniform seedlings were then selected and transferred to a container filled with half-strength Hoagland's nutrient solution, and forty-day-old hydroponic *C. rigescens* seedlings were chosen for further gene expression and stress analysis.

Tobacco (*Nicotiana benthamiana*) seeds were sterilized using 75% ethanol for 30 s and 12% NaClO for 10 min and washed ten times with sterilized water. The seeds were sown on 1/2 Murashig and Skoog (MS) medium and kept in the dark at 4°C for two days before being transferred to a growth chamber for germination. After two weeks, robust young seedlings were planted in soil (peat soil: roseite = 3:1) for further analysis.

Expression analysis of *CrCOMT* in *Carex rigescens*

To analyze gene expression in different tissues, forty-day-old *C. rigescens* hydroponic seedlings were used, including old leaves (OL), new generation plants (NGP), rhizomes (R), new leaves (NL), root systems (RS), leaf sheaths (LS), and root crowns (RC). To analyze gene expression under stress conditions, forty-day-old *C. rigescens* hydroponic seedlings were separated into the following treatment groups: salt (300 mM NaCl) and drought (30% Polyethylene glycol (PEG)-6000). Leaves were sampled separately at 0, 1, 3, 6, 9, and 12 h after stress treatment. Samples were harvested, immediately frozen in liquid nitrogen, and stored at –80°C for further RNA isolation and gene expression analysis. Each stress treatment was replicated three times.

Vector construction and tobacco transformation

The *CrCOMT* sequence was acquired based on a previous report (Zhang et al., 2019). First, pCAMBIA3301 was constructed as the expression vector (*Nco*I/*Bgl*II) using In-Fusion® Snap Assembly Master Mix (Takara, China) (Primer: CrCOMT-p3301-S/CrCOMT-p3301-A). The recombinant vector pCAMBIA3301-*CrCOMT* was introduced into *Agrobacterium tumefaciens* strain EHA105. Tobacco agrobacterium-mediated transformation was performed with tobacco leaf disk infiltration, according to the protocol in Gallois and Marinho's study (Gallois and Marinho, 1995). T_0 transgenic tobacco seeds were selected on 1/2 MS medium containing phosphinothricin (50 mg/L). Positive transgenic seedlings were identified using PCR (Primer: 35S-specific-S/CrCOMT-specific-A). Then, qRT-PCR was performed, transgenic tobacco plants with high expression were selected (Primer: qCrCOMT-S/qCrCOMT-A), and homozygous T_3 seeds were used for further experiments. The primers used in PCR and qRT-PCR were designed using Primer 5 software and detailed sequence were shown in **Supplementary Table 1**.

Transgenic tobacco stress tolerance validation

Transgenic and WT tobacco seeds were sterilized and germinated on 1/2 MS with NaCl (100 and 150 mM), mannitol (250 and 275 mM), or no stressor. Germination was recorded based on the emergence of the radicle tip in tobacco seed. Each treatment had three independent replicates and at least 100 tobacco seeds per replicate. For the drought tolerance test, (1) transgenic and WT tobacco plants were grown in soil (peat soil: roseite = 3:1) for four weeks, then tobacco seedlings were treated with 15% PEG-6000 for 3 days. Leaves samples were collected for gene expression analysis. When tobacco plants exhibited lethal effects of dehydration, watering was resumed and the tobacco plants were recovered for 3 days. The photographs were taken after PEG-6000 treatment and rewatering. (2) transgenic and WT tobacco plants were grown in soil (peat soil: roseite = 3:1) for four weeks with sufficient watering. The plants were then subjected to drought stress by withholding irrigation. All pots were placed under the same conditions in a growth chamber, and the position of each pot was randomly changed every day to exclude any positional effects. Photographs were taken at 6 and 12 days after withholding the water treatment, and the survival rate was calculated. Twelve days after the beginning of stress treatment, the leaves were harvested for physiological index analysis. For salt-sensitivity assays in soil, transgenic and WT tobacco plants were grown in soil (peat soil: roseite = 3:1) under long-day conditions for four weeks. Subsequently, the soil was irrigated with NaCl solution every three days. The initial

concentration was 50 mM, which was increased by 50 mM per day to a final concentration of 200 mM. After 21 days of 200 mM NaCl treatment, the tobacco plants were photographed.

Quantitative RT-PCR analysis

Total RNA was isolated using a MiniBEST Plant RNA Extraction Kit (Takara, China), following the manufacturer's instructions. Total RNA (1 μg) was used for cDNA synthesis using the PrimeScriptTM RT Reagent Kit with gDNA Eraser (Takara, China). qRT-PCR was performed on a CFX96 Touch Real-Time PCR Detection System (BIO-RAD, United States) with TB Green® Premix Ex Taq^{TM} (Tli RNaseH Plus; Takara, China) according to the manufacturer's instructions. The primers used in qRT-PCR were designed using Primer 5 software and detailed sequence were shown in **Supplementary Table 1**. The *CreIF-4α* gene was used as a reference control for *CrCOMT* expression patterns in *C. rigescens* according to our previous study (Zhang et al., 2020), and *NtActin* was used as a reference in all tobacco qRT-PCR analyses. Relative gene expression was calculated using the $2^{-\Delta\Delta Ct}$ method (Livak and Schmittgen, 2001) and the results are presented in terms of fold-change.

Melatonin assay

Melatonin content in tobacco plants under normal and drought stress conditions was determined according to a previously described method with an ELISA kit, as described by Zhang (Zhang et al., 2017). To determine the potential effect of exogenous melatonin application on *C. rigescens*, forty-day-old hydroponic *C. rigescens* seedlings were pre-sprayed with 50 μM melatonin before exposure to drought stress. After seven days of melatonin treatment, drought stress treatment was applied by adding 15% PEG-6000 to half-strength Hoagland nutrient solution. Leaf samples were collected after seven days of drought treatment for further relative water content, relative electrolytic leakage, and proline content measurement. Each treatment was replicated three times.

Physiological measurements

To measure leaf photochemical efficiency, leaves were dark-adapted for 30 min before measurement, and variable fluorescence (Fv)/maximal fluorescence (Fm) was measured using a FluorPen FP110 chlorophyll fluorescence meter (PSI, Czechia). To measure relative water content, 0.2 g leaf tissue (W0) was sampled and soaked in a tube containing 30 ml distilled water for 4 h. Leaf surface water was dried with a paper towel and weighed (W1). Following this, the leaf tissues were dried at 80°C and weighed (W2). The relative water content was calculated as (W1-W0/W2-W0) × 100. To examine relative electrical conductivity, 0.2 g leaf tissue (W0) was sampled and soaked in a tube containing 30 ml distilled water for 4 h at 25°C, then conductance (R0) was measured with a conductivity meter (FE38, Mettler Toledo). Afterward, the tubes were autoclaved at 121°C for 20 min. After cooling to 25°C, the final conductance (R1) was measured. Relative electrical conductivity was calculated as R0/R1 × 100. To measure chlorophyll content, 0.1 g leaf tissue was sampled and soaked in a tube containing 10 ml dimethyl sulfoxide for two days, and the extracted chlorophyll was measured at 663 nm and 645 nm using a spectrophotometer (UV-2700, Shimadzu). The chlorophyll content was calculated as described previously (Barnes et al., 1992).

Proline content was measured using an acidic ninhydrin-based method (Ábrahám et al., 2010) with a colorimetric PRO assay kit (BC0290, Solarbio Life Sciences, China), and the absorbance was detected at a wavelength of 520 nm using a spectrophotometer. Malondialdehyde (MDA) content was determined using the thiobarbituric acid (TBA)-based colorimetric method (Wang et al., 2013) with a colorimetric MDA assay kit (BC0020, Solarbio Life Sciences, China), and absorbance was detected at a wavelength of 532 nm. Catalase (CAT) activity was measured using an H_2O_2 -based method (Scebba et al., 2001) colorimetric CAT Kit (BC0200, Solarbio Life Sciences, China), and absorbance was detected at a wavelength of 240 nm. Peroxisome (POD) activity was measured using the guaiacol method (Zhang and Kirkham, 1996) with a colorimetric POD Kit (BC0090, Solarbio Life Sciences, China), and absorbance was detected at a wavelength of 470 nm. Superoxide dismutase (SOD) activity was measured using a nitroblue tetrazolium (Giannopolitis and Ries, 1977) colorimetric SOD Kit (BC0170, Solarbio Life Sciences, China), and absorbance was measured at 560 nm.

Statistical analysis

The data in this study were subjected to statistical analyses using SPSS v20.0 (SPSS Inc., United States). Significant differences were determined using Fisher's protected least significant difference test at a probability level of 0.05. $P < 0.05$ was consider statistically significant.

Results

Expression profile analysis of *CrCOMT* in *Carex rigescens*

Different tissues, as well as salt- and drought-treated leaves of *C. rigescens* seedlings, were harvested to explore

the expression pattern of *CrCOMT*. Specifically, *C. rigescens* different tissues were separately displayed in Figure 1A. *CrCOMT* was expressed at a higher level in new-generation plants (6.20 fold), rhizomes (3.90 fold), new leaves (4.31 fold), root systems (3.34 fold), and leaf sheaths (2.33 fold), and lower levels in old leaves (1.06 fold) and root crowns (1.08 fold; Figure 1B). For the stress treatment, *CrCOMT* was slightly induced within 12 h of NaCl treatment and significantly increased and reached a maximum level at 12 h after treatment (1.70 fold) (Figure 1C); under PEG treatment, *CrCOMT* expression was significantly increased at 6 (3.25 fold), 9 (4.43 fold), and 12 (2.70 fold) h after treatment, with the highest expression level at 9 h (Figure 1D).

Germination rate of *CrCOMT* transgenic tobacco seeds under different stress conditions

To characterize gene function, a *CrCOMT* overexpression vector was constructed (Figure 2A) and different *CrCOMT* overexpression transgenic tobacco plants were generated and detected using PCR and quantitative PCR (Figures 2B–C). Two transgenic tobacco lines (OE1 and OE9) with high expression levels were selected (Figure 2D). Then, OE1, OE9, and WT tobacco T_3 seeds were cultured on 1/2 MS medium with NaCl (100 and 150 mM), mannitol (250 and 275 mM), or no stressor; the germination rates were counted and are shown in Figure 3. Specifically, under the 100 mM NaCl treatment,

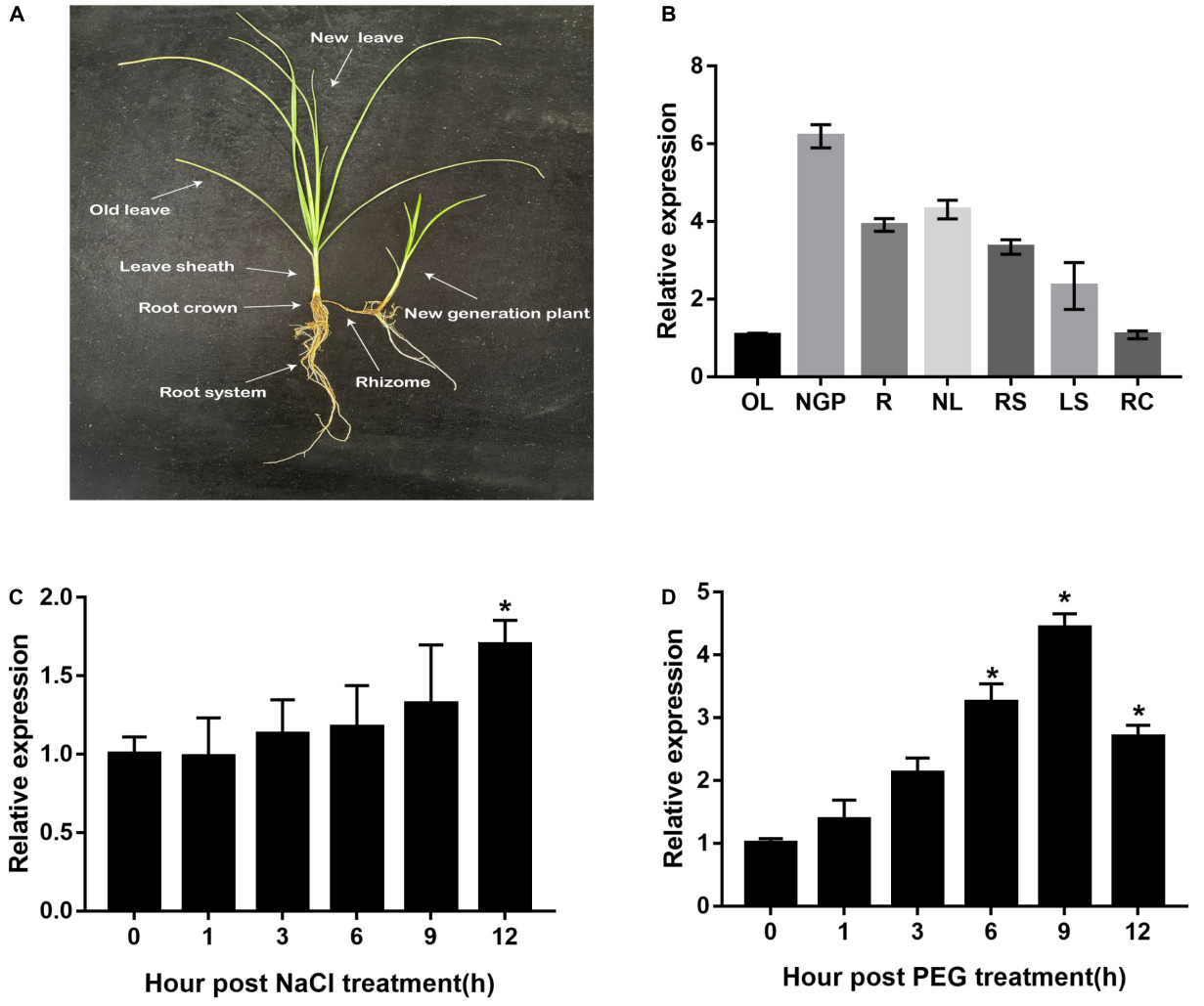

FIGURE 1
CrCOMT expression profile in different tissues and stress conditions in *C. rigescens*. **(A)** *C. rigescens* different tissues including old leave (OL), new generation plant (NGP), rhizome(R), new leave (NL), root system (RS), leave sheath (LS), and root crown (RC). **(B)** *CrCOMT* gene expression in *C. rigescens* different tissues. **(C,D)** Drought stress was used of 30% PEG-6000 and salt stress was used of 300 mM NaCl. *C. rigescens* leaves were harvested separately at different time points after stress treatment for qRT-PCR analysis. *CreIF-4α* gene was used as reference gene. All data are means ± SE for three biological replicates. * Over the bars indicated the significance at $P < 0.05$ among different times points.

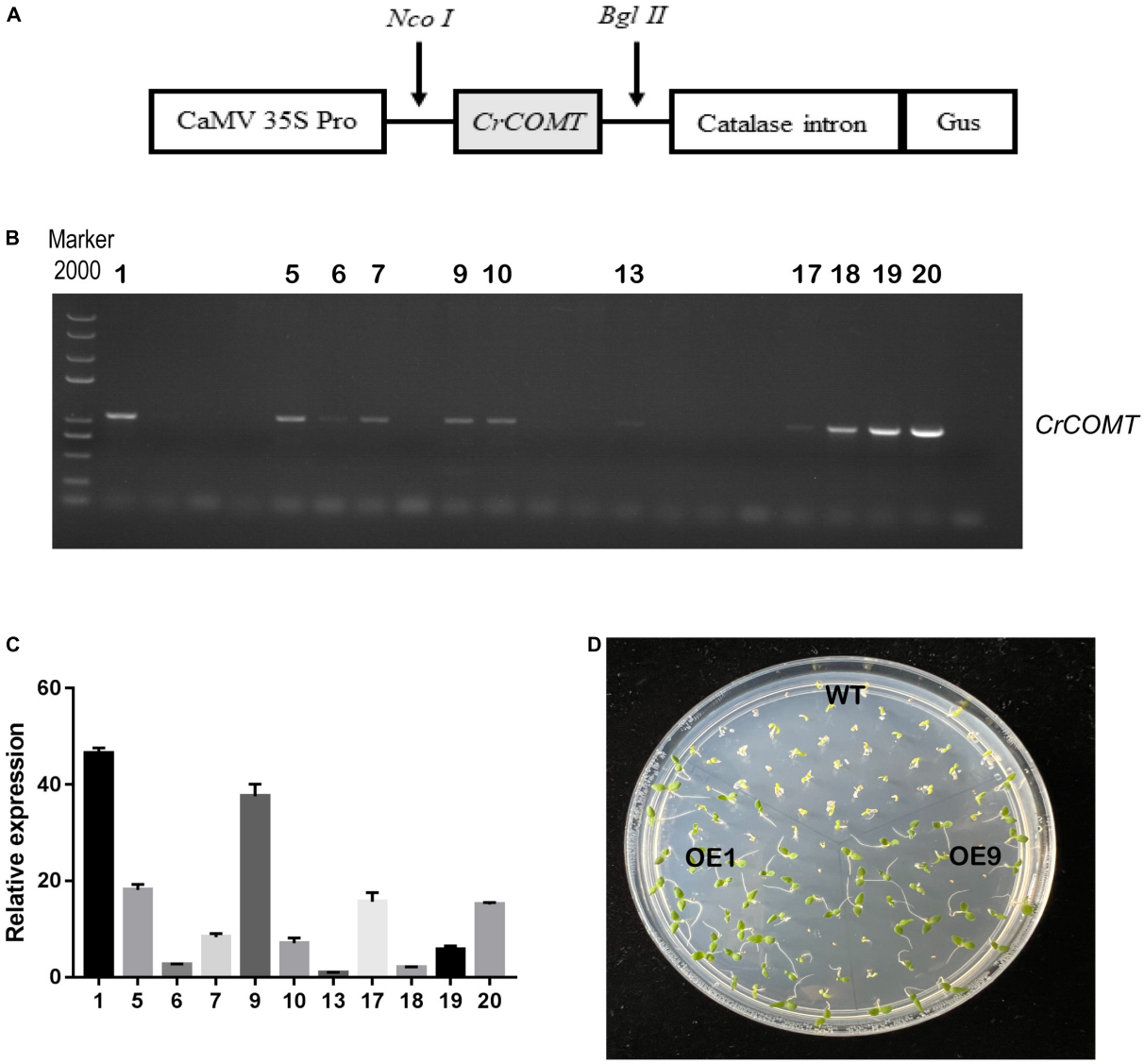

FIGURE 2
CrCOMT overexpression transgenic plants screening and evaluation. **(A)** Expression vector construction of *CrCOMT*. **(B)** Positive transgenic identified by agarose gel electrophoresis. **(C)** Transcription levels of *CrCOMT* in different positive overexpression tobacco plants. **(D)** Transgenic tobacco OE1 and OE9 had highest expression level were choose by antibiotic and homozygous lines were used for further analysis. The *NtActin* gene was used as internal controls. All data are means ± SE for three biological replicates.

there was no significant difference between the transgenic and WT tobacco plant seed germination rates. When treated with 125 mM NaCl, the OE9 germination rate was higher than that of OE1 and WT after ten days of germination (Figures 3A,B). For the drought stress treatment, the seed germination rate of the two transgenic lines was significantly higher than that of the WT after four days of germination under 250 mM mannitol treatment. Additionally, the seed germination rates of the two transgenic tobacco plants were significantly higher than those of the WT plants after seven days of 275 mM mannitol treatment (Figures 3C,D). The seed germination rate of transgenic and WT plants both reached 100% after two days without a stressor (Figure 3E). These results suggest that *CrCOMT* may significantly improve transgenic plant drought resistance; therefore, the gene function in drought tolerance was further studied.

CrCOMT enhanced the drought tolerance of transgenic tobacco plants

To verify whether *CrCOMT* overexpression alters plant drought stress resistance, drought sensitivity and tolerance assays of transgenic and WT tobacco plants were performed.

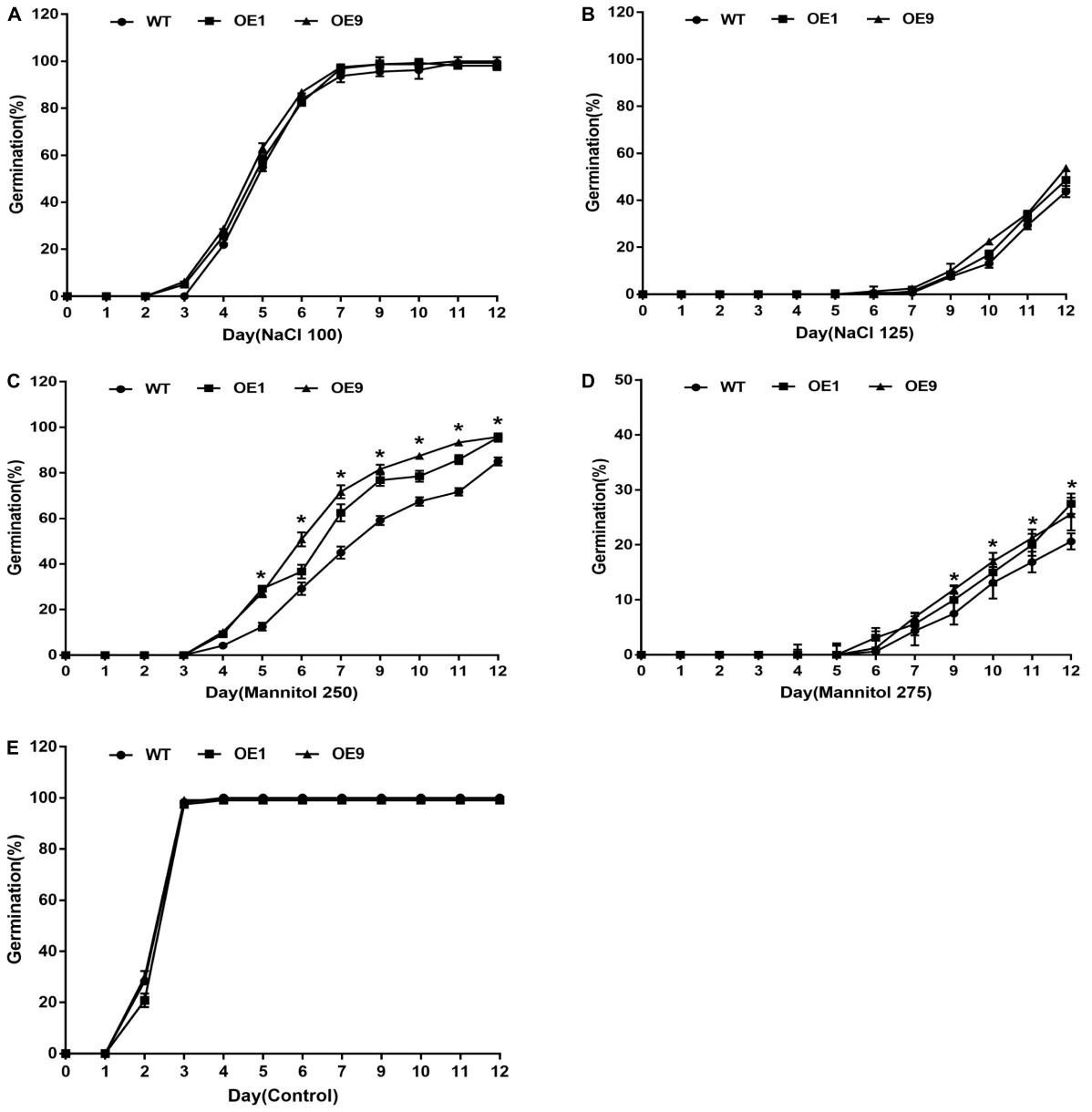

FIGURE 3
Seed germination of transgenic tobacco plants under stress conditions for 12 days. Seed germination rate of OE1, OE9, and WT tobacco plants under **(A)** 100 mM NaCl, **(B)** 125 mM NaCl, **(C)** 250 mM Mannitol, **(D)** 275 mM Mannitol, and **(E)** Control treatment. All data are means ± SE for three biological replicates.

For the drought sensitivity assay, four-week-old transgenic and WT plants were treated with 15% PEG-6000 for seven days and rewatering for three days (Figure 4A). After treatment, both transgenic and WT tobacco displayed a leaf dehydration phenotype after PEG-6000 treatment, but WT tobacco leaves showed more significant withering than transgenic plants. After rewatering, only part of each WT tobacco plant recovered, compared to the majority of transgenic tobacco plants. Following this, the survival rate of drought stress treated tobacco plants was counted, which was higher in both transgenic plants OE1 (98.06%) and OE9 (96.59%) than in the WT plants (65.27%; Figure 4B). For the detached leaf dehydration trial, the water loss of OE1 and OE9 was lower than that of the WT within 7 h after dehydration treatment (Figure 4C), indicating that *CrCOMT* overexpression plants retained more water in detached leaves.

For the natural drought stress experiment, four-week-old transgenic and WT plants were subjected to irrigation. After six days of withholding irrigation, the WT plants started to wither while the transgenic plants remained normal, whereas after

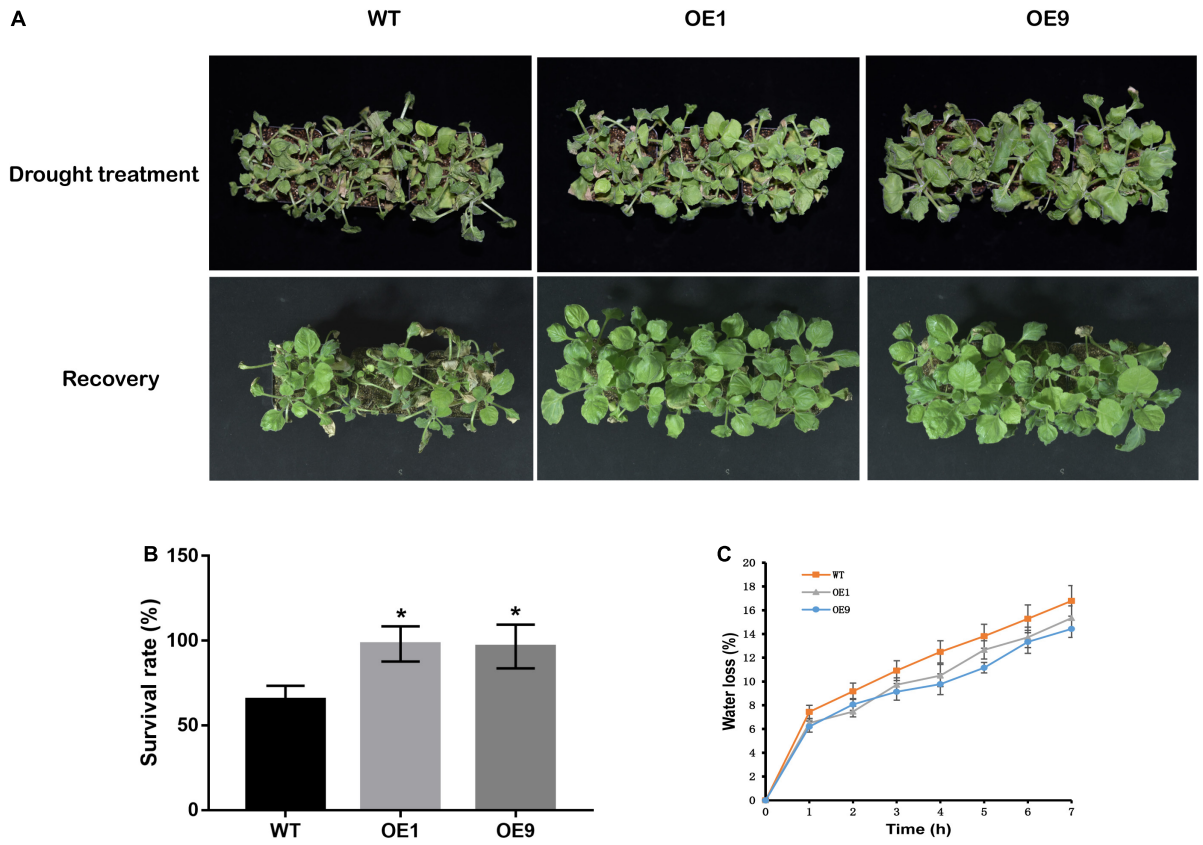

FIGURE 4
Physiological performance of transgenic tobacco plants under drought stress condition. **(A)** The phenotype of tobacco plants after PEG-6000 treatment and rewatering. **(B)** Survival rate of tobacco plants after rewatering. **(C)** For leaves water loss measurement, transgenic and WT tobacco plants were grown in soil (peat soil: roseite = 3:1) for four weeks, then leaves were detached and placed on a filter paper in growth chamber. Leaves were weighed at designated time points, and the loss of fresh weight (percentage) was used to indicate water loss. All data are means ± SE for three biological replicates. * Over the bars indicated the significance at $P < 0.05$ between WT and transgenic tobacco plants.

12 days of withholding irrigation, WT tobacco plants displayed a more significantly withered phenotype than transgenic tobacco plants (Figure 5A). In transgenic tobacco plants, the relative water content and Fv/Fm ratio were significantly higher, and leaf electrolyte leakage was significantly lower than that in WT plants (Figures 5B–D). A non-significant difference in these indices was observed between the transgenic and WT tobacco plants under normal conditions. We also subjected four-week-old transgenic and WT tobacco plants to 200 mM NaCl treatment (Supplementary Figure 1). After 21 days of treatment, there was no significant difference between *CrCOMT* overexpression plants and WT plants, but more old-yellow leaves were observed in the WT plants.

Furthermore, a leaf disk assay was performed using 300 mM NaCl and 300 mM mannitol to assess the stress tolerance of mature transgenic tobacco leaves. The phenotypes of transgenic and WT tobacco leaf disks after stress treatment are shown in Figure 6A. Meanwhile, the chlorophyll content was measured, and transgenic tobacco plants displayed lower levels of degradation than WT plants (Figure 6B). In summary, transgenic tobacco plants showed higher drought tolerance than WT plants based on different drought stress assays.

Stress marker substance and antioxidant enzyme variation in *CrCOMT* transgenic tobacco plants

Stress-related substances, such as MDA and proline, are recognized markers for plant drought stress tolerance evaluation. Under normal conditions, the MDA and proline content of *CrCOMT* overexpression tobacco plants was not significantly different from the WT plants (Figures 7A,B). After drought stress treatment, the *CrCOMT* overexpression plants showed significantly lower MDA and higher proline content than the WT tobacco plant (Figures 7A,B), which indicated better drought resistance performance. Antioxidant enzyme activation is important for improving plant ROS-scavenging and drought stress resistance. CAT, SOD, and POD enzyme activity levels were significantly higher in transgenic tobacco

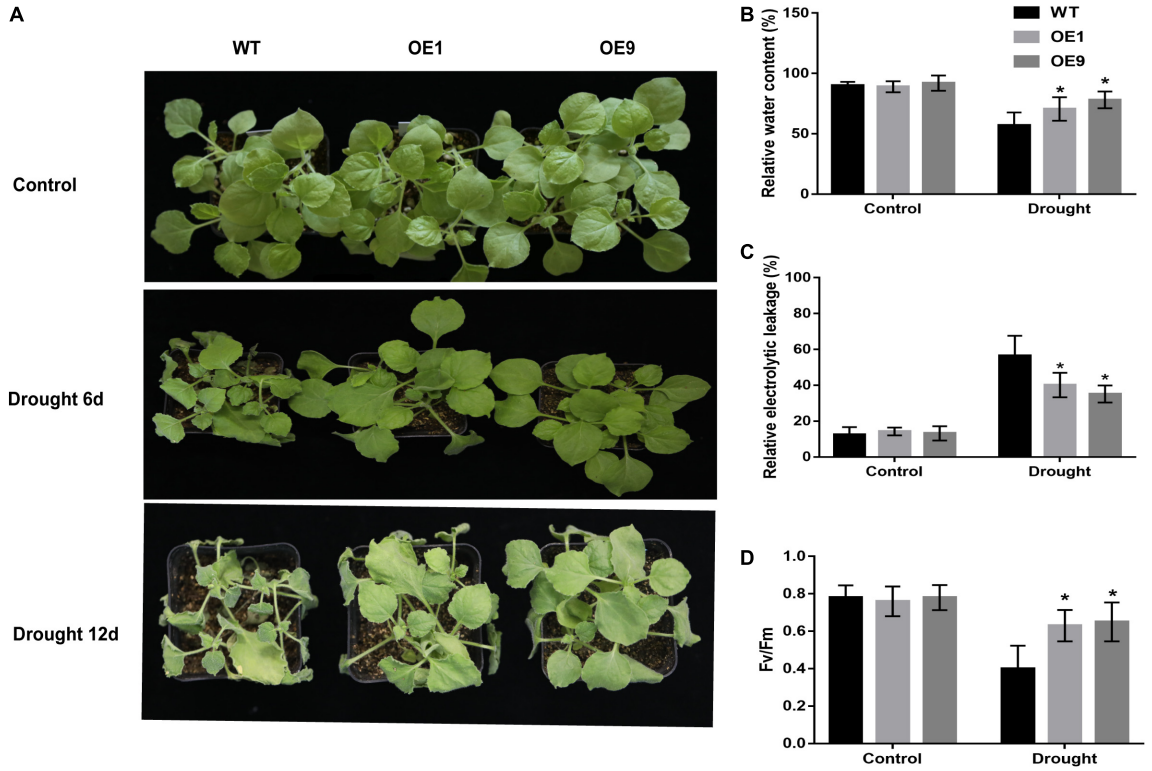

FIGURE 5
Expression of *CrCOMT* enhanced drought tolerance in transgenic tobacco plants. **(A)** The phenotype of four-week-old transgenic and WT tobacco plants under control and drought stress after withholding irrigation. Each experiment had four plant tobacco plants in one plot. The experiment had four replicates. **(B-D)** Relative water content, relative electrical conductivity and Fv/Fm value in transgenic and WT tobacco plants under control and drought stress conditions were measured. All data are means ± SE for three biological replicates. * Over the bars indicated the significance at $P < 0.05$ between WT and transgenic tobacco plants.

plants than in WT plants, but the difference was not significant in the treatment without stressors (Figures 7C–E). In addition, the survival rate of tobacco plants without irrigation was determined (Figure 7F); this was higher in transgenic tobacco plants than in WT plants under the influence of stressors but was not significantly different without stressors. Overexpression of *CrCOMT* could alleviate the damage caused by drought stress via enhancing the ability of osmotic regulation and activity of antioxidant enzymes in tobacco plants.

Analysis of drought stress related genes in *CrCOMT* transgenic tobacco plants

In response to environmental stress, plants modulate the expression of many stress-response genes, constituting an important molecular basis for stress responses and adaptations in plants. To elucidate the molecular regulatory mechanisms of *CrCOMT*-mediated drought stress tolerance, we analyzed the variations in expression of four drought stress response genes (*NtLEA5*, *NtERD10C*, *NtDREB3*, and *NtP5CS*; Figures 8A–D) and two ROS scavenging genes (*NtCAT* and *NtSOD*; Figures 8E,F). Specifically, the drought stress response and ROS scavenging genes were not significantly different between transgenic and WT tobacco in the absence of stressors (Figures 8A–F). Nevertheless, these genes were all highly induced in both transgenic and WT plants and showed significantly higher expression in the *CrCOMT* overexpression plants than in the WT plants after drought stress treatment (Figures 8A–F). These results suggest that *CrCOMT* can increase drought stress tolerance in transgenic tobacco plants by regulating the stress response and ROS scavenging gene expression.

Melatonin content in *CrCOMT* transgenic tobacco plants and validation of its role in improving drought tolerance in *Carex rigescens*

It is well documented that the *COMT* gene plays an important role in the plant melatonin synthesis pathway and

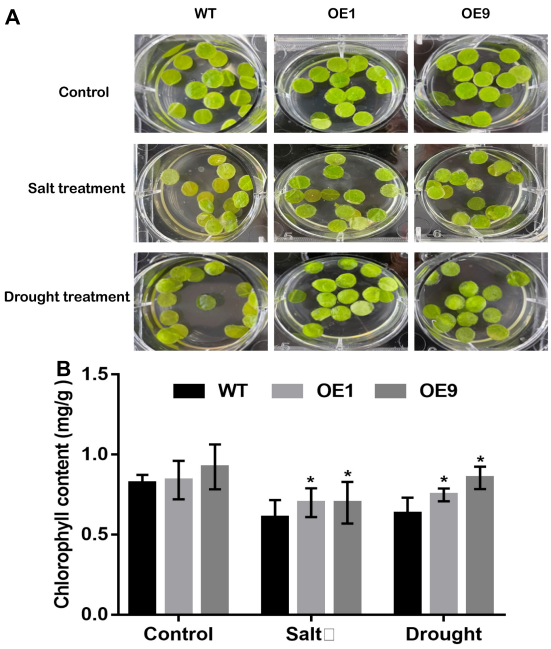

FIGURE 6
Leaf dish phenotype assay of transgenic tobacco plants under stress conditions. **(A)** Leaf disks from five-week-old transgenic and WT tobacco plants were detached and floated on 1/2 MS, 1/2 MS with 300 mM NaCl, and 300 mM Mannitol for 7 days, then the leaf disks was photographed **(B)** Chlorophyll content of OE1, OE9, and WT tobacco plant leaf dish measured. All data are means ± SE for three biological replicates. * Over the bars indicated the significance at $P < 0.05$ between WT and transgenic tobacco plants.

might participate in plant stress tolerance. To verify the function of *CrCOMT* in drought stress tolerance improvement, endogenous melatonin content was measured in transgenic and WT tobacco plants. Under normal conditions, endogenous melatonin levels were not significantly different between the transgenic and WT tobacco plants (**Figure 9A**). However, there was a significant increase in transgenic tobacco plants compared to WT plants under drought stress conditions and the endogenous melatonin content in OE1, OE9 transgenic, and WT tobacco plants were 11.23, 12.16, and 8.4 ng/g, respectively (**Figure 9A**), which indicates that *CrCOMT* overexpression could increase melatonin biosynthesis in transgenic tobacco plants under drought stress conditions.

To evaluate the drought tolerance function of melatonin in *C. rigescens*, *C. rigescens* plants were pretreated with exogenous melatonin and then subject to PEG-6000 treatment. After seven days drought treatment, melatonin treatment slightly decreased relative water content and increased relative electrolytic leakage under non-stress conditions, but the difference was not significant (**Figures 9B,C**). Under drought stress conditions, melatonin treatment resulted a significant increase in the relative water content and proline content compared to the untreated plants (**Figures 9B,D**). In addition, compared to the non-melatonin treatment, the relative electrolytic leakage in the melatonin treatment group was significantly decreased after drought stress (**Figure 9C**). In the absence of stressors, there was no significant difference between the control and melatonin treatments in proline content (**Figure 9D**).

Discussion

Plant O-methyltransferase can transform the methyl group in S-adenosyl-L-methionine to different metabolites, such as flavonoids, alkaloids, and phenols, which play important roles in plant growth, signal transduction, and abiotic and biotic responses (Lam et al., 2007; Struck et al., 2012). Plant O-methyltransferase can be divided into two groups according to their protein molecular weight: class I (23-29 KDa) proteins, which mainly function in lignin synthesis and metabolism, and class II (38-43 KDa) proteins, which mainly affect the metabolism of metabolites, such as flavone, melatonin, and lignin, and participate in plant stress response and tolerance (Gang et al., 2002). CrCOMT is a plant O-methyltransferase class II protein, with a predicted molecular weight of approximately 40.196 KDa (Zhang et al., 2019). Recently, the role of COMT in melatonin biosynthesis has been demonstrated in several species (Byeon et al., 2014a,b), however, few studies have reported the participation of class II O-methyltransferases in plant drought resistance. Based on gene expression under stress conditions, we hypothesized that *CrCOMT* participates in the response of *C. rigescens* to salt and drought stress. To test this, *CrCOMT* was overexpressed in transgenic tobacco and its gene function in response to salt and drought stress was characterized. The transgenic tobacco showed potentially improved drought stress tolerance compared to salt stress, according to a germination trial. Further studies on growth performance and physiological and biochemical reactions to drought stress in transgenic plants suggest *CrCOMT* might play a positive role in dehydration stress tolerance, and this provides a fundamental basis for research on gene regulatory mechanisms.

Drought stress-induced ROS hyperaccumulation results in severe oxidative damage to plant membrane lipids and plant-related electrolytic leakage can be used as a membrane injury indicator to partially reflect cellular membrane lipid peroxidation (Ferreira et al., 2021; Kumar et al., 2021). In this study, transgenic tobacco had a lower lipid peroxidation level than WT plants after drought stress treatment, based on relative electrolytic leakage measurements. The accumulation of MDA reflects the degree of damage suffered by plant cells and the degree of membrane lipid damage (Kumar et al., 2021). After drought stress treatment, the MDA content was lower in the transgenic tobacco plants than in the WT plants, illustrating that *CrCOMT* overexpression could alleviate the degree of

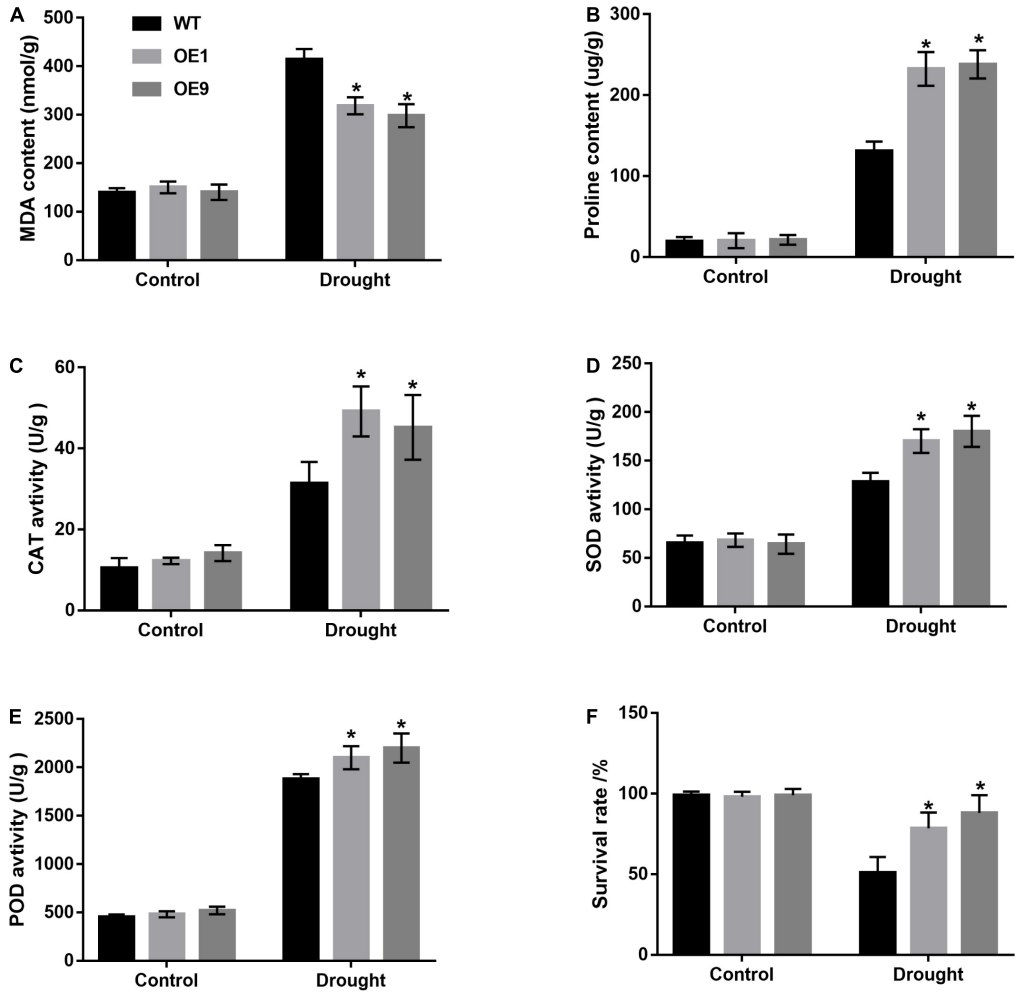

FIGURE 7
Analysis of increased drought tolerance in *CrCOMT* overexpression transgenic tobacco plants. **(A)** MDA content, **(B)** Proline content, the activity of **(C)** CAT enzyme, **(D)** SOD enzyme, **(E)** POD enzyme, and **(F)** survival rate in transgenic and WT tobacco plants as described in **Figure 5A** were measured. All data are means ± SE for three biological replicates. * Over the bars indicated the significance at $P < 0.05$ between WT and transgenic tobacco plants.

membrane lipid damage in tobacco. Plant photosynthetic membrane systems also undergo destruction after drought stress, leading to decreased photochemical efficiency. In the present study, transgenic tobacco plants displayed higher photochemical efficiency and lower degradation than WT plants, according to chlorophyll content measurement and leaf disk observation after drought stress treatment. In summary, *CrCOMT* overexpression may help maintain plant membrane lipid stability under drought stress conditions.

To alleviate oxidative stress damage under drought stress conditions, plant cells simultaneously initiate a series of response mechanisms and stress signals, such as the activation of cellular ROS scavenging mechanisms, which can trigger the production of ROS scavenging enzymes and antioxidants, including SOD, POD, and CAT (Reddy et al., 2004). In this study, there was a marked increase in POD, SOD, and CAT activity levels in transgenic lines compared to WT plants under drought stress treatment, and the corresponding gene expression levels variation of *NtSOD* and *NtCAT* were also consistent with the SOD and CAT activities. Similar ROS scavenging enzyme responses have been reported in *SlCOMT1* overexpression plants, as they significantly enhance antioxidant capabilities, with higher antioxidant enzyme activity observed, including superoxide dismutase, peroxide, and catalase activity, under salt stress conditions (Sun et al., 2020). In addition, overexpression of *COMT1* enhanced antioxidant enzymatic activity and the capacity of tomato plants to reduce MBC phytotoxicity and residues (Yan et al., 2019). Taken together, these results indicate that *CrCOMT* may function to mediate the transcriptional upregulation of ROS-scavenging genes to enhance ROS-scavenging ability and improve drought stress tolerance.

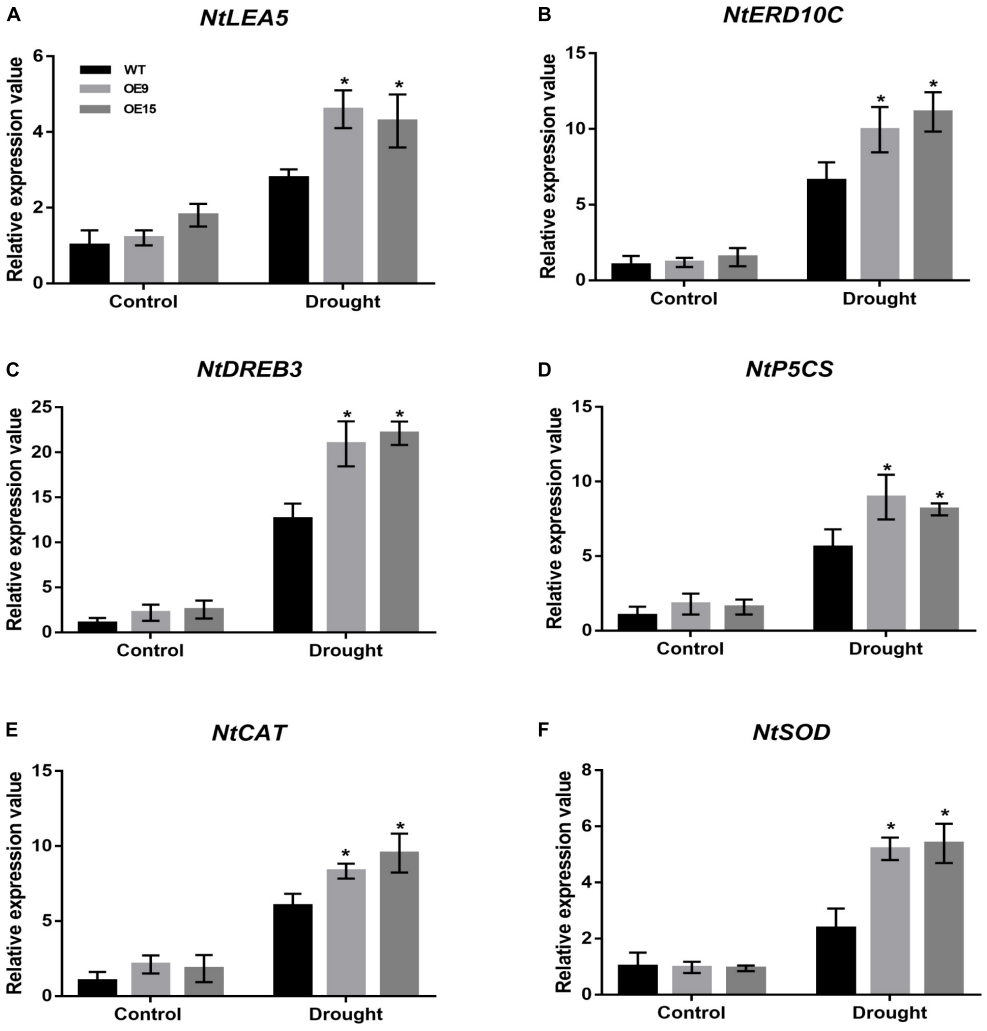

FIGURE 8
Expression of drought stress related genes in transgenic tobacco plants. Transcription levels of stress response and ROS scavenging genes (*NtLEA5*, *NtERD10C*, *NtDREB3*, *NtP5CS*, *NtCAT*, and *NtSOD*) in transgenic and WT tobacco plants as described in as described in **Figure 4A** were determined. Untreated plants were used as controls. Expression of the *NtActin* gene was used as an internal control. All data are means ± SE for three biological replicates. * Over the bars indicated the significance at $P < 0.05$ between WT and transgenic tobacco plants.

Previous studies have shown the involvement of *COMT* in stress tolerance associated with the regulation of stress response gene expression (Vincent et al., 2005; Zhang X. et al., 2021). Molecular chaperones play crucial roles in osmotic adjustment in plants under drought stress, and LEA5 and ERD10C encode late embryogenesis abundant proteins, which partially bind water, help stabilize enzymes and macromolecular structures, and reduce membrane damage (Hundertmark and Hincha, 2008; Magwanga et al., 2018). The dehydration-responsive element-binding protein (DREBs) transcription factor comprises many stress-responsive regulatory genes, and *DREB3* is important for regulating drought stress responses and is used as a marker gene in many plant drought stress tolerance studies (Umezawa et al., 2006). In this study, the transcript abundance of drought-induced protein genes, such as *NtLEA5* and *NtERD10C* and drought stress-responsive gene, such as *NtDREB3* were higher in transgenic tobacco than in the WT after drought stress, suggesting that these genes were upregulated by *CrCOMT* under drought conditions. In addition, 1-pyrroline 5-carboxylate synthetase (P5CS), the rate-limiting enzyme in proline biosynthesis in plants, can control proline levels, which are critical in improving the stress tolerance of plants (Rai and Penna, 2013). The *NtP5CS* gene was found to be more highly induced in *CrCOMT* transgenic tobacco than in WT plants, and its expression was also consistent with the proline content variation. These results highlight the interconnection between *CrCOMT* overexpression and drought stress tolerance, as it results in the increased expression of several stress-responsive genes.

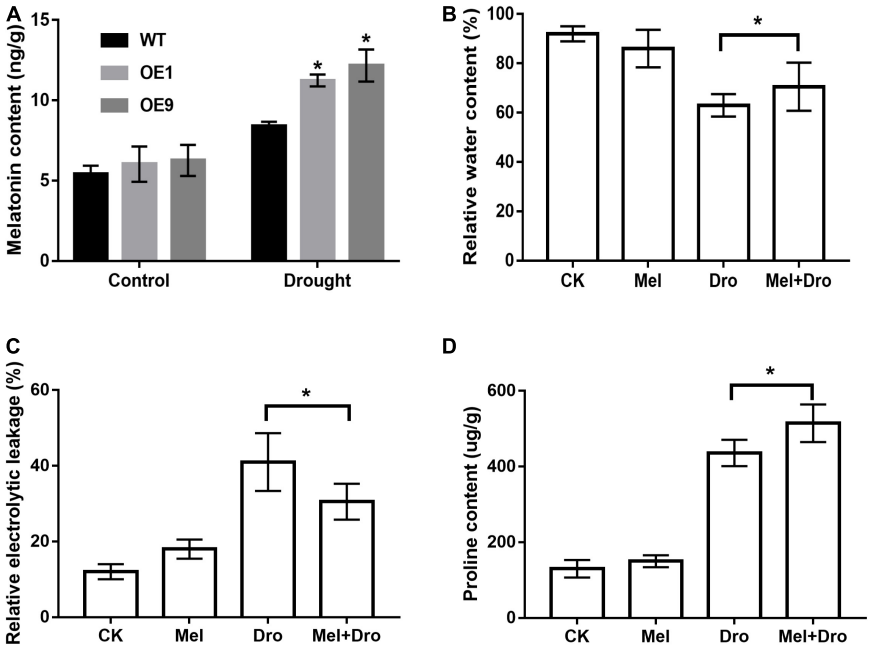

FIGURE 9
CrCOMT affect melatonin synthesis in transgenic tobacco plants and melatonin confers drought tolerance in *C. rigescens*. **(A)** The melatonin content of transgenic and WT tobacco under control and drought treatment. All data are means ± SE for three biological replicates. * Over the bars indicated the significance at $P < 0.05$ between WT and transgenic tobacco plants. **(B)** Relative water content, **(C)** relative electric conductivity and **(D)** proline content was measured after seven days of drought stress in *C. rigescens*. CK, control optimal condition; Mel, melatonin treatment; Dro, drought stress; Mel + Dro, melatonin treatment + drought stress. All data are means ± SE for three biological replicates. * Over the bars indicated the significance at $P < 0.05$ between different melatonin treatment.

Melatonin is a multifunctional regulator in plant response to drought stress. (1) The accumulation of osmolytes, such as free proline, were enhanced in melatonin-treated plants, significantly alleviating adverse effects by facilitating the maintenance of optimum turgor pressure (Zhao et al., 2021). (2) Melatonin induces the expression of transcription factors and modulates the expression of downstream stress-responsive genes, thereby increasing plant drought tolerance (Sharma and Zheng, 2019). (3) Melatonin also could regulate the key genes encoding antioxidative enzymes and activate the activities of these enzymes, which maintain redox balance in cells under stressful conditions. The regulation of transcript levels of key genes encoding antioxidative enzymes has been reported in melatonin-mediated drought stress regulation in chinese hickory (*Carya cathayensis*) (Sharma et al., 2020), maize (*Zea mays*) (Ahmad et al., 2019), and kiwifruit (*Actinidia chinensis*) (Xia et al., 2020). According to the results of the current study, melatonin content variation can partially explain the morphological, physicochemical, and molecular functions in *CrCOMT* overexpression transgenic tobacco under drought stress. To further verify the function of melatonin in mediating drought tolerance, we applied exogenous melatonin to *C. rigescens* under drought stress. The relative water content and proline content were higher, and the relative electrolytic leakage was lower in melatonin-treated *C. rigescens* than in the untreated plants under drought conditions. Therefore, we determined that melatonin may play a positive role in the drought stress tolerance of *C. rigescens*.

In summary, we report a class II O-methyltransferase gene, *COMT,* in *C. rigescens* that plays a positive role in plant drought stress tolerance, which may be associated with its gene function in melatonin synthesis. Genetic functional analysis of *CrCOMT* provides a potential candidate gene for drought tolerance mechanisms. Further analyses of the up- and downstream regulatory genes of *CrCOMT* and its enzyme characteristics in melatonin metabolism will help to enrich the understanding of plant *COMT* gene regulatory mechanisms under drought stress.

Data availability statement

The raw data supporting the conclusions of this article will be made available by the authors, without undue reservation.

Author contributions

KZ and YS carried out the experimental design. YL, KZ, ML, and HC performed the experiments. YL, KZ, and YS prepared the manuscript and coordinated its revision. KZ, GY,

and ZW read and revised the manuscript. All authors provided helpful discussions and approved its final version.

Funding

This work was supported by the First-Class Grassland Science Discipline Program of Shandong Province, China, the National Natural Science Foundation of China (nos. 32101435 and 31872996), the Natural Science Foundation of Shandong Province, China (no. ZR2021QC037), and Start-up Foundation for High Talents of Qingdao Agricultural University (no. 665/1121011).

Conflict of interest

The authors declare that the research was conducted in the absence of any commercial or financial relationships that could be construed as a potential conflict of interest.

Publisher's note

Supplementary material

The Supplementary Material for this article can be found online at: https://www.frontiersin.org/articles/10.3389/fpls.2022.971431/full#supplementary-material

SUPPLEMENTARY FIGURE 1
Phenotype of transgenic and WT tobacco plants under salt stress treatment. Four-week-old transgenic and WT tobacco seedlings were irrigated with 200 mM NaCl solution. The photographs were taken after three weeks salt stress treatment. Six plants were grown in one plot and each experiment had four replicates.

References

Ábrahám, E., Hourton-Cabassa, C., Erdei, L., and Szabados, L. (2010). "Methods for determination of proline in plants," in *Plant Stress Tolerance. Methods in Molecular Biology, vol 639*, ed. R. Sunkar (Totowa, NJ: Humana Press), 317–331.

Ahanger, M. A., Siddique, K. H., and Ahmad, P. (2021). Understanding drought tolerance in plants. *Physiol. Plant* 172, 286–288.

Ahmad, S., Kamran, M., Ding, R., Meng, X., Wang, H., Ahmad, I., et al. (2019). Exogenous melatonin confers drought stress by promoting plant growth, photosynthetic capacity and antioxidant defense system of maize seedlings. *PeerJ* 7:e7793. doi: 10.7717/peerj.7793

Alharby, H. F., and Fahad, S. (2020). Melatonin application enhances biochar efficiency for drought tolerance in maize varieties: Modifications in physio-biochemical machinery. *Agron. J.* 112, 2826–2847.

Anjum, S. A., Xie, X. Y., Wang, L. C., Saleem, M. F., Man, C., and Lei, W. (2011). Morphological, physiological and biochemical responses of plants to drought stress. *Afr. J. Agric. Res.* 6, 2026–2032.

Arnao, M. B., and Hernández-Ruiz, J. (2019). Melatonin: A new plant hormone and/or a plant master regulator?. *Trends Plant Sci.* 24, 38–48.

Barnes, J. D., Balaguer, L., Manrique, E., Elvira, S., and Davison, A. (1992). A reappraisal of the use of DMSO for the extraction and determination of chlorophylls a and b in lichens and higher plants. *Environ. Exp. Bot.* 32, 85–100.

Byeon, Y., Lee, H. Y., Lee, K., Park, S., and Back, K. (2014b). Cellular localization and kinetics of the rice melatonin biosynthetic enzymes SNAT and ASMT. *J. Pineal Res.* 56, 107–114. doi: 10.1111/jpi.12103

Byeon, Y., Lee, H. Y., Lee, K., and Back, K. (2014a). Caffeic acid O-methyltransferase is involved in the synthesis of melatonin by methylating N-acetylserotonin in *Arabidopsis*. *J. Pineal Res.* 57, 219–227. doi: 10.1111/jpi.12160

Chang, J., Guo, Y., Yan, J., Zhang, Z., Yuan, L., Wei, C., et al. (2021). The role of watermelon caffeic acid O-methyltransferase (ClCOMT1) in melatonin biosynthesis and abiotic stress tolerance. *Hort. Res.* 8:210. doi: 10.1038/s41438-021-00645-5

Dalal, V. (2021). Modulation of photosynthesis and other proteins during water–stress. *Mol. Biol. Rep.* 48, 3681–3693.

Dietz, K. J., Zörb, C., and Geilfus, C. M. (2021). Drought and crop yield. *Plant Biol.* 23, 881–893.

Fahad, S., Bajwa, A. A., Nazir, U., Anjum, S. A., Farooq, A., Zohaib, A., et al. (2017). Crop production under drought and heat stress: Plant responses and management options. *Front. Plant Sci.* 8:1147. doi: 10.3389/fpls.2017.01147

Ferreira, D., Figueiredo, J., Laureano, G., Machado, A., Arrabaça, J. D., Duarte, B., et al. (2021). Membrane remodelling and triacylglycerol accumulation in drought stress resistance: The case study of soybean phospholipases A. *Plant Physiol. Biochem.* 169, 9–21. doi: 10.1016/j.plaphy.2021.10.033

Gallois, P., and Marinho, P. (1995). "Leaf disk transformation using *Agrobacterium tumefaciens*-expression of heterologous genes in tobacco," in *Plant Gene Transfer and Expression Protocols. Methods in Molecular Biology™, vol 49*, ed. H. Jones (Totowa, NJ: Springer), 39–48. doi: 10.1385/0-89603-321-X:39

Gang, D. R., Lavid, N., Zubieta, C., Chen, F., Beuerle, T., Lewinsohn, E., et al. (2002). Characterization of phenylpropene O-methyltransferases from sweet basil: Facile change of substrate specificity and convergent evolution within a plant O-methyltransferase family. *Plant Cell* 14, 505–519. doi: 10.1105/tpc.010327

Giannopolitis, C. N., and Ries, S. K. (1977). Superoxide dismutases: II. Purification and quantitative relationship with water-soluble protein in seedlings. *Plant physiol.* 59, 315–318. doi: 10.1104/pp.59.2.315

Hattori, A., Migitaka, H., Iigo, M., Itoh, M., Yamamoto, K., Ohtani-Kaneko, R., et al. (1995). Identification of melatonin in plants and its effects on plasma melatonin levels and binding to melatonin receptors in vertebrates. *Biochem. Mol. Biol. Int.* 35, 627–634.

Hoque, M., Tahjib-Ul-Arif, M., Hannan, A., Sultana, N., Akhter, S., Hasanuzzaman, M., et al. (2021). Melatonin Modulates Plant Tolerance to Heavy Metal Stress: Morphological Responses to Molecular Mechanisms. *Int. J. Mol. Sci.* 22:11445. doi: 10.3390/ijms222111445

Hossain, M., Li, J., Sikdar, A., Hasanuzzaman, M., Uzizerimana, F., Muhammad, I., et al. (2020). Exogenous melatonin modulates the physiological and biochemical mechanisms of drought tolerance in tartary buckwheat (*Fagopyrum tataricum* (L.) Gaertn). *Molecules* 25:2828. doi: 10.3390/molecules25122828

Hosseini, M. S., Samsampour, D., Zahedi, S. M., Zamanian, K., Rahman, M. M., Mostofa, M. G., et al. (2021). Melatonin alleviates drought impact on growth and essential oil yield of lemon verbena by enhancing antioxidant responses, mineral balance, and abscisic acid content. *Physiol. Plant.* 172, 1363–1375. doi: 10.1111/ppl.13335

Huangfu, L., Chen, R., Lu, Y., Zhang, E., Miao, J., Zuo, Z., et al. (2022). OsCOMT, encoding a caffeic acid O-methyltransferase in melatonin biosynthesis, increases rice grain yield through dual regulation of leaf senescence and vascular development. *Plant Biotechnol. J.* 20, 1122–1139. doi: 10.1111/pbi.13794

Hundertmark, M., and Hincha, D. K. (2008). LEA (late embryogenesis abundant) proteins and their encoding genes in *Arabidopsis thaliana*. *BMC Genom.* 9:118. doi: 10.1186/1471-2164-9-118

Imran, M., Latif Khan, A., Shahzad, R., Aaqil Khan, M., Bilal, S., Khan, A., et al. (2021). Exogenous melatonin induces drought stress tolerance by promoting plant growth and antioxidant defence system of soybean plants. *AoB Plants* 13:lab026. doi: 10.1093/aobpla/plab026

Kar, R. K. (2011). Plant responses to water stress: Role of reactive oxygen species. *Plant Signal. Behav.* 6, 1741–1745.

Kumar, M., Patel, M. K., Kumar, N., Bajpai, A. B., and Siddique, K. H. (2021). Metabolomics and molecular approaches reveal drought stress tolerance in plants. *Int. J. Mol. Sci.* 22:9108.

Lam, K. C., Ibrahim, R. K., Behdad, B., and Dayanandan, S. (2007). Structure, function, and evolution of plant O-methyltransferases. *Genome* 50, 1001–1013.

Lee, K., Choi, G. H., and Back, K. (2017). Cadmium-induced melatonin synthesis in rice requires light, hydrogen peroxide, and nitric oxide: Key regulatory roles for tryptophan decarboxylase and caffeic acid O-methyltransferase. *J. Pineal Res.* 63:e12441. doi: 10.1111/jpi.12441

Li, J., Yang, Y., Sun, K., Chen, Y., Chen, X., and Li, X. (2019). Exogenous melatonin enhances cold, salt and drought stress tolerance by improving antioxidant defense in tea plant (*Camellia sinensis* (L.) O. Kuntze). *Molecules* 24:1826. doi: 10.3390/molecules24091826

Livak, K. J., and Schmittgen, T. D. (2001). Analysis of relative gene expression data using real-time quantitative PCR and the 2- ΔΔCT method. *Methods* 25, 402–408.

Magwanga, R. O., Lu, P., Kirungu, J. N., Lu, H., Wang, X., Cai, X., et al. (2018). Characterization of the late embryogenesis abundant (LEA) proteins family and their role in drought stress tolerance in upland cotton. *BMC Genet.* 19:6. doi: 10.1186/s12863-017-0596-1

Moustafa-Farag, M., Mahmoud, A., Arnao, M. B., Sheteiwy, M. S., Dafea, M., Soltan, M., et al. (2020). Melatonin-induced water stress tolerance in plants: Recent advances. *Antioxidants* 9:809. doi: 10.3390/antiox9090809

Rai, A. N., and Penna, S. (2013). Molecular evolution of plant P5CS gene involved in proline biosynthesis. *Mol. Biol. Rep.* 40, 6429–6435.

Reddy, A. R., Chaitanya, K. V., and Vivekanandan, M. (2004). Drought-induced responses of photosynthesis and antioxidant metabolism in higher plants. *J. Plant Physiol.* 161, 1189–1202.

Saluja, M., Zhu, F., Yu, H., Walia, H., and Sattler, S. E. (2021). Loss of COMT activity reduces lateral root formation and alters the response to water limitation in *Sorghum* brown midrib (bmr) 12 mutant. *New Phytol.* 229, 2780–2794. doi: 10.1111/nph.17051

Scebba, F., Sebastiani, L., and Vitagliano, C. (2001). Activities of antioxidant enzymes during senescence of *Prunus armeniaca* leaves. *Biol. Plant.* 44, 41–46.

Sharma, A., and Zheng, B. (2019). Melatonin mediated regulation of drought stress: Physiological and molecular aspects. *Plants* 8:190. doi: 10.3390/plants8070190

Sharma, A., Wang, J., Xu, D., Tao, S., Chong, S., Yan, D., et al. (2020). Melatonin regulates the functional components of photosynthesis, antioxidant system, gene expression, and metabolic pathways to induce drought resistance in grafted *Carya cathayensis* plants. *Sci. Total Environ.* 713:136675. doi: 10.1016/j.scitotenv.2020.136675

Struck, A. W., Thompson, M. L., Wong, L. S., and Micklefield, J. (2012). S-adenosyl-methionine-dependent methyltransferases: Highly versatile enzymes in biocatalysis, biosynthesis and other biotechnological applications. *Chembio. Chem.* 13, 2642–2655. doi: 10.1002/cbic.201200556

Sun, C., Liu, L., Wang, L., Li, B., Jin, C., and Lin, X. (2021). Melatonin: A master regulator of plant development and stress responses. *J. Integr. Plant Biol.* 63, 126–145.

Sun, S., Wen, D., Yang, W., Meng, Q., Shi, Q., and Gong, B. (2020). Overexpression of caffeic acid O-methyltransferase 1 (COMT1) increases melatonin level and salt stress tolerance in tomato plant. *J. Plant Growth Regul.* 39, 1221–1235.

Umezawa, T., Fujita, M., Fujita, Y., Yamaguchi-Shinozaki, K., and Shinozaki, K. (2006). Engineering drought tolerance in plants: Discovering and tailoring genes to unlock the future. *Curr. Opin. Biotechnol.* 17, 113–122. doi: 10.1016/j.copbio.2006.02.002

Vincent, D., Lapierre, C., Pollet, B., Cornic, G., Negroni, L., and Zivy, M. (2005). Water deficits affect caffeate O-methyltransferase, lignification, and related enzymes in maize leaves. A proteomic investigation. *Plant Physiol.* 137, 949–960. doi: 10.1104/pp.104.050815

Wang, D., Ni, Y., Liao, L., Xiao, Y., and Guo, Y. (2021). Poa pratensis ECERIFERUM1 (PpCER1) is involved in wax alkane biosynthesis and plant drought tolerance. *Plant Physiol. Biochem.* 159, 312–321. doi: 10.1016/j.plaphy.2020.12.032

Wang, Y., Ding, M., Gu, X., Wang, J., Pang, Y., Gao, L., et al. (2013). Analysis of interfering substances in the measurement of Malondialdehyde content in plant leaves. *Am. J. Biochem. Biotechnol.* 9, 235–242.

Xia, H., Ni, Z., Hu, R., Lin, L., Deng, H., Wang, J., et al. (2020). Melatonin alleviates drought stress by a non-enzymatic and enzymatic antioxidative system in kiwifruit seedlings. *Int. J. Mol. Sci.* 21:852. doi: 10.3390/ijms21030852

Yan, Y., Sun, S., Zhao, N., Yang, W., Shi, Q., and Gong, B. (2019). COMT1 overexpression resulting in increased melatonin biosynthesis contributes to the alleviation of carbendazim phytotoxicity and residues in tomato plants. *Environ. Pollut.* 252, 51–61. doi: 10.1016/j.envpol.2019.05.052

Yu, X., Brown, J. M., Graham, S. E., Carbajal, E. M., Zuleta, M. C., and Milla-Lewis, S. R. (2019). Detection of quantitative trait loci associated with drought tolerance in St. Augustinegrass. *PLoS One* 14:e0224620. doi: 10.1371/journal.pone.0224620

Zhang, J., and Kirkham, M. (1996). Antioxidant responses to drought in sunflower and *Sorghum* seedlings. *New Phytol.* 132, 361–373. doi: 10.1111/j.1469-8137.1996.tb01856.x

Zhang, J., Shi, Y., Zhang, X., Du, H., Xu, B., and Huang, B. (2017). Melatonin suppression of heat-induced leaf senescence involves changes in abscisic acid and cytokinin biosynthesis and signaling pathways in perennial ryegrass (*Lolium perenne* L.). *Environ. Exp. Bot.* 138, 36–45.

Zhang, K., Cui, H., Cao, S., Yan, L., Li, M., and Sun, Y. (2019). Overexpression of CrCOMT from Carex rigescens increases salt stress and modulates melatonin synthesis in *Arabidopsis thaliana*. *Plant Cell Rep.* 38, 1501–1514. doi: 10.1007/s00299-019-02461-7

Zhang, K., Cui, H., Li, M., Xu, Y., Cao, S., Long, R., et al. (2020). Comparative time-course transcriptome analysis in contrasting Carex rigescens genotypes in response to high environmental salinity. *Ecotoxicol. Environ. Saf.* 194:110435. doi: 10.1016/j.ecoenv.2020.110435

Zhang, K., Sun, Y., Li, M., and Long, R. (2021). CrUGT87A1, a UDP-sugar glycosyltransferases (UGTs) gene from Carex rigescens, increases salt tolerance by accumulating flavonoids for antioxidation in *Arabidopsis thaliana*. *Plant Physiol. Biochem.* 159, 28–36. doi: 10.1016/j.plaphy.2020.12.006

Zhang, X., Chen, B., Wang, L., Ali, S., Guo, Y., Liu, J., et al. (2021). Genome-Wide Identification and Characterization of Caffeic Acid O-Methyltransferase Gene Family in Soybean. *Plants* 10:2816. doi: 10.3390/plants10122816

Zhao, C., Guo, H., Wang, J., Wang, Y., and Zhang, R. (2021). Melatonin Enhances Drought Tolerance by Regulating Leaf Stomatal Behavior, Carbon and Nitrogen Metabolism, and Related Gene Expression in Maize Plants. *Front. Plant Sci.* 12:779382. doi: 10.3389/fpls.2021.779382

Zhao, D., Luan, Y., Shi, W., Tang, Y., Huang, X., and Tao, J. (2022). Melatonin enhances stem strength by increasing the lignin content and secondary cell wall thickness in herbaceous peony. *J. Exp. Bot.* 18:erac165. doi: 10.1093/jxb/erac165 [Epub ahead of print].

Zhuang, W., Liu, T., Shu, X., Wang, H., Wang, Z., Wang, T., et al. (2020). Overexpression of MzASMT 1, a gene from malus zumi mats, enhances salt tolerance in transgenic tobacco. *Front. Plant Sci.* 11:561903. doi: 10.3389/fpls.2020.561903

frontiers | Frontiers in Plant Science

TYPE Original Research
PUBLISHED 17 August 2022
DOI 10.3389/fpls.2022.976684

OPEN ACCESS

EDITED BY
Jing Zhang,
Nanjing Agricultural University, China

REVIEWED BY
Tushar Suhas Khare,
Savitribai Phule Pune University, India
Ke Teng,
Beijing Academy of Agricultural and Forestry Sciences, China

*CORRESPONDENCE
Yanhong Ma
mayanhong80@126.com

SPECIALTY SECTION
This article was submitted to Plant Abiotic Stress, a section of the journal Frontiers in Plant Science

RECEIVED 23 June 2022
ACCEPTED 03 August 2022
PUBLISHED 17 August 2022

CITATION
Fan B, Sun F, Yu Z, Zhang X, Yu X, Wu J, Yan X, Zhao Y, Nie L, Fang Y and Ma Y (2022) Integrated analysis of small RNAs, transcriptome and degradome sequencing reveal the drought stress network in *Agropyron mongolicum* Keng. *Front. Plant Sci.* 13:976684. doi: 10.3389/fpls.2022.976684

Integrated analysis of small RNAs, transcriptome and degradome sequencing reveal the drought stress network in *Agropyron mongolicum* Keng

Bobo Fan[1], Fengcheng Sun[2], Zhuo Yu[1], Xuefeng Zhang[1], Xiaoxia Yu[1], Jing Wu[1], Xiuxiu Yan[1], Yan Zhao[3], Lizhen Nie[2], Yongyu Fang[2] and Yanhong Ma[1]*

[1]Agricultural College, Inner Mongolia Agricultural University, Hohhot, China, [2]Inner Mongolia Academy of Agricultural & Animal Husbandry Sciences, Hohhot, China, [3]College of Grassland, Resources and Environment, Inner Mongolia Agricultural University, Hohhot, China

Agropyron mongolicum (*A. mongolicum*) is an excellent gramineous forage with extreme drought tolerance, which lives in arid and semiarid desert areas. However, the mechanism that underlies the response of microRNAs (miRNAs) and their targets in *A. mongolicum* to drought stress is not well understood. In this study, we analyzed the transcriptome, small RNAome (specifically the miRNAome) and degradome to generate a comprehensive resource that focused on identifying key regulatory miRNA-target circuits under drought stress. The most extended transcript in each collection is known as the UniGene, and a total of 41,792 UniGenes and 1,104 miRNAs were identified, and 99 differentially expressed miRNAs negatively regulated 1,474 differentially expressed target genes. Among them, eight miRNAs were unique to *A. mongolicum*, and there were 36 target genes. A weighted gene co-expression network analysis identified five hub genes. The miRNAs of five hub genes were screened with an integration analysis of the degradome and sRNAs, such as osa-miR444a-3p.2-*MADS47*, bdi-miR408-5p_1ss19TA-*CCX1*, tae-miR9774_L-2R-1_1ss11GT-*carC*, ata-miR169a-3p-*PAO2*, and bdi-miR528-p3_2ss15TG20CA-*HOX24*. The functional annotations revealed that they were involved in mediating the brassinosteroid signal pathway, transporting and exchanging sodium and potassium ions and regulating the oxidation–reduction process, hydrolase activity, plant response to water deprivation, abscisic acid (ABA) and the ABA-activated signaling pathway to regulate drought stress. Five hub genes were discovered, which could play central roles in the regulation of drought-responsive genes. These results show that the combined analysis of miRNA, the transcriptome and degradation group provides a useful platform to investigate the molecular mechanism of drought resistance in *A. mongolicum* and could provide new insights into the genetic engineering of Poaceae crops in the future.

KEYWORDS

Agropyron mongolicum Keng, drought resistance, microRNAs, transcriptome, degradome, integration analysis, co-expression network

Introduction

Global warming increases the environmental stress on crops, making it difficult to fully utilize their genetic potential (Boyer, 1982). The total yield of principal crops decreases by approximately 70% each year owing to ecological pressures (Shubha and Tyagi, 2010; Zurbriggen et al., 2010). Among all the ecological pressures, the impact and restriction of drought on agriculture are particularly prominent (Esfahanian et al., 2017). However, plants that grow in some barren and arid environments have evolved highly effective self-regulatory systems to manage drought. Plants of the *Agropyron* genus are significant pasture resources that have adapted to drought, low temperature and salinity and play essential roles in ecological restoration (Che and Li, 2007; Han et al., 2017). *Agropyron mongolicum* (Poaceae, $2n = 2x = 14$), a representative member of *Agropyron*, is an excellent perennial grazing grass in the arid steppe, which has soft stems and leaves, a highly developed root system, early greening, strong tillering ability, good palatability, adaptability, and is known for its strong drought resistance (Zhao et al., 2010b; Zhang et al., 2019). It can be used for pasture and ecological restoration in cold and arid regions and provides superior gene resources to breed drought resistance and improve forage and wheat (*Triticum aestivum*) crops (Du et al., 2017a). However, the molecular drought resistance mechanism of *A. mongolicum* is still in its infancy and merits more attention and urgent research work.

Drought can cause physiological and morphological changes in plants, which negatively affect their growth and productivity (Chandra et al., 2021). MicroRNAs (miRNAs) play crucial roles in plant-environment interactions (Niu et al., 2016; Song et al., 2019). miRNAs range from 18 to 25 nucleotides (nt) and are a class of endogenous small non-coding RNAs (Carrington and Ambros, 2003; Song et al., 2019). miRBase (miRbase V22.1), a professional research database of miRNA, contains 38,589 mature miRNAs of 271 species, which include 9,168 mature miRNAs of 74 dicotyledonous and monocotyledonous plants. On the basis of sequence complementarity, miRNAs directly target mRNAs to cleave or translationally repress them, thus, completing the regulation of plant function (Frank et al., 2000; Flynt and Lai, 2008). Currently, miRNAs involved in abiotic stress (drought, salinity and temperature) responses have been reported in *Arabidopsis thaliana*, tobacco (*Nicotiana tabacum*), rice (*Oryza sativa*) and other plants. They include miR156, miR159, miR169, miR395 (Ali et al., 2017), miR444 (Jiao et al., 2020; Kannan et al., 2022), miR408 (Hajyzadeh et al., 2015; Taier et al., 2021), and miR528 (Chen et al., 2021; Wang et al., 2021a). miRNAs regulate transcription factors, plant hormones, antioxidant systems and other functional target genes, such as *MYB33*, *OsNAC2*, *ARF22*, *DREB*, *NtCAT1*, *ARF*, *TIR1*, and *OsMADS27* (Reyes and Nam-Hai, 2007; David and Franck, 2011; Hajyzadeh et al., 2015; Yin et al., 2015; Jiang et al., 2018; Qiu et al., 2018; Shi et al., 2018; Kannan et al., 2022) to respond to abiotic stress.

miRNA-led stress regulatory networks are considered novel tools for the development of abiotic stress tolerance in crops (Ali et al., 2017). The integrated miRNAs-target genes interaction network can intuitively reflect the relationship between genes at the global level. The hub genes are the core regulatory genes in the network and play a crucial role in the stability of network. The integrated analysis of miRNA and target mRNAs has been widely used in human medicine, animal growth and development, gene expression regulatory mechanisms and other fields, but research reports on its use in plants are limited. The general workflow for constructing microRNA-mediated gene regulatory network was introduced (Meng et al., 2011). The regulatory network of auxin, miR390, *TAS3* and *ARFs* on the root growth of *Arabidopsis thaliana* (*A. thaliana*) was analyzed (Elena et al., 2010). Floral transcriptomes in woodland strawberries (*Fragaria vesca*) uncovered developing receptacles and anther gene networks and identified the hub genes *FveLOM* and *FveWUS1* (Hollender et al., 2014). A cadmium phytoremediation miRNA-target mRNA network was constructed in hyperaccumulating *Sedum alfredia*, and the hub genes *AAP3* and *ARF4* may play a key regulatory role (Han et al., 2016). Two cold-resistant modules of peanut (*Arachis hypogeae*) were found by a weighted gene co-expression network analysis (WGCNA). They obtained the hub genes involved in soluble sugar, polyamine and the G-lignin biosynthetic pathway at low temperatures (Wang et al., 2021c). A total of 13 hub genes were identified in cotton (*Gossypium hirsutum*) in which the expression of *Gh_A06G1257* was significantly the highest in different tissues, and it was identified as regulating drought stress by a gene silencing technique (Gereziher et al., 2021). The hub gene and regulatory network of cotton were discovered under salt and drought stress (Bano et al., 2022). The research model of gene interaction networks can explore hub genes and the complex regulatory network of drought and salt stress. In this study, the drought-related modules were studied based on the transcriptome data to obtain a comprehensive drought gene regulatory network, which is conducive to the in-depth understanding and analysis of the function of hub genes in complex networks.

The level of tolerance of plants to drought conditions is coordinated by the action of different drought-responsive genes about other stress components, such as high temperature and salt

stress, which stimulate signal transduction pathways and are complex and mutagenic (Oladosu et al., 2019; Gereziher et al., 2021). Exploring the molecular mechanism of drought resistance in *A. mongolicum* requires a comprehensive analytical method, and the current high-throughput sequencing technology provides an effective platform (Mutz et al., 2013; Han et al., 2016). The integrated analysis of transcriptome, sRNAs and degradome offers the feasibility to select and identify the drought stress gene regulatory network and hub genes of *A. mongolicum*.

The regulatory mechanism of drought resistance and hub genes in *A. mongolicum* is still in its early stages. The regulation of drought resistance is complicated, which restricts the development and utilization of gene resources in response to drought stress. By integrating the transcriptome, sRNAs, and degradome analysis, this study aimed to identify the hub genes of drought resistance and establish a co-expression regulatory network of hub genes in *A. mongolicum*. The findings are meaningful to identify drought resistance hub genes and understand the molecular mechanism of drought resistance in *A. mongolicum*, which should promote genetic engineering research on drought resistance in Poaceae crops.

Materials and methods

Plant materials and drought stress treatment

Mature seeds of *A. mongolicum* were collected from the Inner Mongolia Agricultural University's (Hohhot, China) forage test station in the Inner Mongolia Autonomous Region. The lemma was removed from the intact seeds, which were disinfected with a (1,1.3) sodium hypochlorite solution (v/v) for 15 min and then rinsed five times with sterilized distilled water. The seeds were planted in a germination box and cultured in a controlled climate growth chamber at 24°C with 16 h of daylight with an illumination intensity of 30,000 Lx (BIC-300; Boxun, Shanghai, China). Sterilized distilled water was sprayed quantitatively during the seed germination. When the seedlings grew to be 5–8 cm high, they were transplanted into a germination box with 20% Hoagland's nutrient solution and cultured until the three-leaf one heart phase. The seedlings were then exposed to a drought treatment with 25% polyethylene glycol (PEG)-6,000. Their leaves were sampled at 0 h (CK), 12 h (D_12 h), 24 h (D_24 h), 48 h (D_48 h), 3 days (D_3 days), 5 days (D_5 days), and 7 days (D_7 days), and rewatered at 24 h (R_24 h). The sample weight of each biological replicate was 1 g of fresh leaves. The samples were frozen in liquid nitrogen and stored at −80°C.

Total RNA extraction

The total RNA was extracted from the samples using the TRIzol reagent (Invitrogen, Carlsbad, CA, United States). The quantity and purity of RNA were evaluated using a NanoDrop ND-1000 (Thermo Fisher Scientific, Waltham, MA, United States), and the integrity and concentration of RNA were assessed using an Agilent Bioanalyzer 2,100 (Agilent Technology, Santa Clara, CA, United States; RIN number > 7.0, $OD_{260/280} > 1.8$). The total RNA collected from each treatment and control group was utilized to create the library and transcriptome, sRNA and degradome sequencing. The samples were sequenced *de novo* by Hangzhou LC Biology Co., Ltd. (Hangzhou, China).

Transcriptome sequencing and *de novo* assembly analysis

Certified total RNA was purified twice using poly-T oligo linked magnetic beads to obtain poly (A) RNA. Following purification, the mRNA was fragmented into minute fragments under increased temperature using divalent cations. The cleaved RNA fragments were then reverse-transcribed to form the final cDNA library, which was consistent with the manufacturer's instructions for the RNA-Seq sample preparation kit (Illumina, San Diego, CA, United States), with an average insert size of 300 bp (±50 bp) for the paired-end libraries. The paired-end samples were sequenced on an Illumina HiSeq 6,000 at LC Sciences (Houston, TX, United States) according to the manufacturer's instructions.

Cutadapt (Martin, 2011) and in-house Perl scripts were used to delete the reads with adapter contamination, low-quality bases, and uncertain bases. The sequence quality was then confirmed using FastQC,[1] which included the Q20, Q30, N50 and GC content of the clean data. All the downstream analyses relied on high quality clean data. Trinity 2.4.0[2] was used to accomplish *de novo* transcriptome assembly (Grabherr et al., 2011). Trinity groups transcripts into clusters, and the most extended transcript in each collection is known as the UniGene.

All the assembled UniGenes were aligned against the non-redundant (Nr) protein database,[3] Gene Ontology (GO),[4] SwissProt,[5] Kyoto Encyclopedia of Genes and Genomes (KEGG)[6] and eggNOG[7] databases using DIAMOND (Buchfink et al., 2014) with a threshold of *E*-value < 0.00001.

1 http://www.bioinformatics.babraham.ac.uk/projects/fastqc/ (Accessed August 6, 2022).
2 https://github.com/trinityrnaseq/trinityrnaseq/wiki (Accessed August 6, 2022).
3 http://www.ncbi.nlm.nih.gov/ (Accessed August 6, 2022).
4 http://www.geneontology.org (Accessed August 6, 2022).
5 http://www.expasy.ch/sprot/ (Accessed August 6, 2022).
6 http://www.genome.jp/kegg/ (Accessed August 6, 2022).
7 http://eggnogdb.embl.de/ (Accessed August 6, 2022).

Differentially expressed unigene analysis

Salmon (Patro et al., 2017) was used to identify the levels of expression for UniGenes by calculating the transcript per million (TPM; Mortazavi et al., 2008). The differentially expressed unigenes were selected with $\log_2$ (fold change) ≥ 1 or $\log_2$ (fold change) ≤ -1 and with the statistical significance of $p \leq 0.05$ by the R package edgeR (Smyth, 2010). GO and KEGG enrichment analyses were then performed on the differentially expressed genes (DEGs) using in-house Perl scripts.

sRNA sequencing and miRNA basic data analysis

A TruSeq Small RNA Sample Prep Kit (Illumina) was used to create the miRNA library. The experiment was conducted according to the manufacturer's instructions. An Illumina HiSeq 2,500 platform was used to sequence the cDNA library, and single-end (SE50) sequencing was utilized (50 bp). To obtain clean reads, raw reads were submitted to an in-house tool designated ACGT101-miR (LC Sciences), which removed adaptor dimers, repetitions, junk sequences and typical RNA families (rRNA, tRNA, snRNA, and snoRNA). The subsequent use of a BLAST search mapped unique sequences that were 18–25 nt long to miRBase 22.0 to identify the miRNAs. The miRNAs matched to the database are known, while those that do not map to it are unique miRNAs in *A. mongolicum*.

To better understand the overall evolutionary relationship and conservation of miRNA, the family classification of miRNA, the frequency of miRNA in other species, the number of miRNA precursors in different species and the base preference of miRNA were statistically analyzed.

Analysis of the differentially expressed miRNAs

Based on the experimental design, the differential expression of miRNAs was evaluated using a *t*-test. The significance threshold was set at 0.01 and 0.05 in each test. Differentially expressed miRNAs were assigned a *value of* $p \leq 0.05$ and $a|\log_2$ (fold change)$| \geq 1$, and a cluster diagram of the miRNA expression (norm value) was constructed. The up- and downregulated miRNAs were simultaneously enumerated from differentially expressed miRNAs.

Degradome sequencing, target identification and analysis

The total RNA (20 μg) was purified using poly-T oligo-attached magnetic beads (Thermo Fisher Scientific), and the mRNA was collected using poly (A). The captured mRNA was coupled using 5′ adaptor primers (Genewiz, Plainfield, NJ, United States). The attached product was transferred into a new centrifuge tube and supplemented with KAPA Pure Beads (kk8000; Roche Diagnostics Application, Indianapolis, IN, United States). The reverse transcription was amplified with reverse transcriptase (m0368; New England Biolabs, Ipswich, MA, United States). The degradation group sequencing library was built with an NEBNext Ultra II RNA Library Prep Kit (e7770; New England Biolabs). Single-ended sequencing was performed using an Illumina HiSeq 2,500 (Hangzhou LC Biology Co., Ltd.) as previously described (Ma et al., 2010).

The target gene was predicted using the Cleaveland 4.0 algorithm (Addo-Quaye et al., 2009), and oligomap was used to accurately match the mRNAs from different species to the *A. mongolicum* degradation group sequence (Berninger et al., 2008). The redundant sequences were removed from the effective data using norm reads per million (NRPM). The Needle program in EMBoss was used to collect all the sequences that matched the target genes in the miRNA library, and the target genes were scored according to the plant miRNA/target pairing standard (Allen et al., 2005). In addition, the degradome reads were mapped to the *A. mongolicum* transcriptome data as previously described (Xu et al., 2013; Yang et al., 2013). The number of unique genes and the mapping ratio between ideal mRNA and degradation group fragments were counted to assess the degradation group sequencing.

Integrated analysis of transcriptome, miRNA and degradome sequencing

All the miRNAs and their target genes were obtained based on an integrated analysis of the transcriptome, miRNA, and degradome group data. The connection pairs between differential miRNAs and their differential target genes were created using a threshold of $p \leq 0.05$. The miRNAs and their target gene pairings with negative regulatory relationships were chosen. The stats package in the *R package* (version 3.6.1) was used to calculate the cluster data, and the heatmap software (version 1.0.12) was used to create a cluster heat map for the DEGs in negative regulatory mode. The transcription function was annotated.

Construction of the gene co-expression network and screening of the hub gene

A co-expression network analysis was performed based on the transcriptome data using the WGCNA R package (version 1.69). The unigenes of missing values were removed, and the expression data of mRNA was regenerated after filtering. The sample clustering tree was then constructed; the outlier samples were removed, and the appropriate scale-free key parameter β was selected. To ensure a scale-free network, power = 4 was chosen to build a systematic clustering tree between the genes. All the other settings were left at

TABLE 1 A list of primers used for validation in RT-qPCR. RT-qPCR, quantitative reverse transcription PCR.

Primer name	Primer sequence
F-osa-miR444a-3p.2	GTGCTGTTGCTGCCTCATGCTT
F-bdi-miR528-p3_2ss15TG20CA	GGTCTTCCATTCCTGCGGCTAA
F-bdi-miR408-5p_1ss19TA	TTCCCTGCAAGCACTTCACG
F-ata-miR169a-3p	TGGGCATGTCAGCGTCGCTAC
F-tae-miR9774_L-2R-1_1ss11GT	GGGGGCGGACTTATTGTGTATATCTGA
F-MADS47(TRINITY_DN16091_c0_g9)	CAGGCTCGGATTACCACTCTTCAAC
R-MADS47(TRINITY_DN16091_c0_g9)	TATTCAATGCAATGCGCGGTTCAAC
F-HOX24(TRINITY_DN19559_c1_g1)	CCGCCCACGACTTCCATTTCTAC
R-HOX24(TRINITY_DN19559_c1_g1)	CTGCTGCTGGTGCTGCTTGG
F-CCX1(TRINITY_DN29080_c0_g1)	ATCTAGTGACGGAGCAGCAGTACC
R-CCX1(TRINITY_DN29080_c0_g1)	GCAAAGCACCAAATCGTGTCTGTC
F-PAO2(TRINITY_DN28296_c0_g1)	ACAAGTGGCGACAACTCTGTTCTG
R-PAO2(TRINITY_DN28296_c0_g1)	AACTTTAGCAGCCGTCTCCATTGG
F-carC(TRINITY_DN28552_c0_g1)	GTCCAGGGCAATTTAGGTAACATTTCG
R-carC(TRINITY_DN28552_c0_g1)	TCCGACGAGGCGATGATGATATTAAC

TABLE 2 Summary of transcriptome sequencing for *Agropyron mongolicum*.

Index	*A. mongolicum*
Raw reads (Gb)	145.27
Clean reads (Gb)	139.46
Number of unigenes	41,792
GC (%)	50.34
Average Q20 (%)	97.445
Minimum length (bp)	201
Median length (bp)	704
Maximum length (bp)	16,861

the default levels, including the module size of gene modules, the number of modules, computing the feature vector value between modules, and performing module clustering analysis. The webpage of the Horvath lab[8] contains a thorough description of WGCNA that explains the analytical stages (Langfelder and Horvath, 2008).

8 https://horvath.genetics.ucla.edu/coexpression network/ (Accessed August 6, 2022).

The module constructed by WGCNA and drought-related physiological indicators were used for correlation analysis to select specific modules related to drought resistance. The connectivity top 20 in the module were defaulted to be hub genes. The candidate hub genes related to drought resistance were screened from the high connective and specificity genes by GO enrichment analysis. The targeted relationships between the hub genes and miRNAs were confirmed by degradome sequencing data. The drought resistance candidate hub genes of the *A. mongolicum* regulatory network were mapped using Cytoscape (version 3.9.1).

RT-qPCR analysis of miRNA and potential drought resistant candidate hub genes

Quantitative reverse transcription PCR (RT-qPCR) was performed on selected miRNA and candidate hub genes related to drought resistance. Primer Premier 6.0 software was used to design the primers, and the primers were synthesized by Sangon Biotech Co., Ltd. (Shanghai, China; Table 1). An miRcute Plus miRNA qPCR Detection Kit (FP411) and an miRcute Plus miRNA First-Strand cDNA Kit (KR211) from TianGen (Beijing, China) were used for reverse transcription and RT-qPCR of the miRNA. A FastQuant RT Kit (KR106; TianGen) and MonAmp SYBR Green qPCR Mix (MQ10201S; Monad Biotech Co., Ltd.) were used for reverse transcription and RT-qPCR of the candidate hub genes. The relative levels of expression were calculated by the $2^{-\Delta\Delta ct}$ method using U6 as internal standards (Livak and Schmittgen, 2001).

Results

Transcriptome sequencing in *Agropyron mongolicum* under drought treatments

To profile the expression of genes in *A. mongolicum* in response to drought stress, eight libraries were constructed from leaf samples (CK: control, D_12 h, D_24 h, D_48 h, D_3 d, D_5 d, D_7 d: plants under drought stress, R_24 h: plants rewatering after drought stress). More than 145.27 Gb raw reads were generated, and 139.46 Gb clean sRNA reads were obtained. The average Q20 of the sample was 97.445%. Each raw read and clean read of each sample were tallied (Supplementary Table 1A). After quality control, the transcripts were assembled into 41,792 unigenes, and the unigene lengths ranged from 201 bp to 16,861 bp (Table 2; Supplementary Figure 1).

Functional annotation and enrichment analysis of the unigenes

GO functional annotation and enrichment were performed on the transcriptome sequenced UniGenes. A total of 18,259

UniGenes were found to be enriched based on the GO analysis, which accounts for 43.69% of all the UniGenes (Supplementary Table 1B). These terms were primarily involved in biological processes, cell component and molecular function. The GO terms included response to salt stress, response to water deprivation, and response to wounding (Figure 1A) according to the study of GO enrichment in *A. mongolicum*. The enrichment of transcripts was analyzed using KEGG. The transcripts were primarily enriched in five significant pathways, including organic system, metabolism, genetic information processing, environmental information processing and cellular processes. The main pathways involved carbohydrate metabolism, amino acid metabolism and lipid metabolism. In addition, they also participated in translation, folding, sorting and degradation, transcription, replication and repair, signal transduction, membrane transport, transport and catabolism (Figure 1B).

Analysis of the differentially expressed genes

In contrast to the control group, the number of DEGs was screened in each comparison group (Figures 2A,B). A total of 1,166 DEGs were obtained in the seven comparison groups (D_12 h vs. CK, D_24 h vs. CK, D_48 h vs. CK, D_3 d vs. CK, D_5 d vs. CK, D_7 d vs. CK, and R_24 h vs. CK). The number of DEGs generally increased as the drought lasted longer, while the number of DEGs reduced in a comparison group (48 h vs. CK). After 12 h of drought treatment, there were 1,789 upregulated genes and 1,183 downregulated genes compared with the control. There were 3,399 upregulated genes and 2,153 downregulated genes compared with the CK after 24 h of drought treatment. The number of upregulated DEGs was 3,565, 4,270, 5,105, 6,511, and 7,521 compared with the CK at 48 h, 3 d, 5 d, 7 d, and R_24 h under drought treatment, respectively, whereas the number of downregulated DEGs was 1,733, 2,096, 3,052, 5,519, and 7,739, respectively. The information on all the DEGs in seven comparisons is shown in Supplementary Table 2.

Sequencing and identification of the miRNAs

The number of known mature miRNA families of *A. mongolicum* was 71 (Supplementary Figure 2A). In contrast, the pre-miRNA sequences of *A. mongolicum* were highly similar to the known pre-miRNAs in 46 plant species (Supplementary Figure 2B). All the miRNAs were categorized into four groups (gp1, gp2, gp3, and gp4) based on their abundance in the miRNA database and sequencing reads (Supplementary Table 3). miRNA sequences that matched the pre-miRNA sequences in the miRNA database were classified as known miRNAs, whereas those that did not were classified as novel miRNA candidates of *A. mongolicum*. A total of 895 mature miRNAs had been obtained, and the length of known miRNA sequences ranged from 18 to 25 nt, with those that were 21 nt accounting for 49.50%. There were 209 novel miRNAs, and the sizes ranged from 19 to 24 nt, accounting for 77.51% at 21 nt (Supplementary Tables 4, 5A; Supplementary Figures 2C,D). The minimal folding free energy index (MFEI) offers a standard for comparing the MFE of pre-miRNA of different lengths of *A. mongolicum*. The minimal folding energy (MFE) is related to the sequence length of pre-miRNA (Zhang et al., 2006). The MFEI of the novel miRNA in *A. mongolicum* ranged from 0.90 to 2.30 kcal/mol (Supplementary Table 6). It was indicative of the production of a stable hairpin structure.

Differentially expressed miRNAs under drought stress

A total of 101 differentially expressed miRNAs ($p \leq 0.05$) were found among the 24 libraries. The distribution of differential expression miRNAs between the control and treatments was examined (Figure 3A). Compared with the control, the number of upregulated genes (29 miRNAs) was the largest at 7 days under drought stress, and the number of downregulated genes (23 miRNAs) was the largest at 24 h under drought stress. To analyze 101 differentially expressed miRNAs of *A. mongolicum* under drought stress, including 12 novel and 89 known miRNAs (Supplementary Table 7), a clustering diagram was generated based on the normal values of miRNA expression (Figure 3B). The expression of miRNAs in the same family was similar under drought stress treatment. The miR156 family, such as osa-miR156_L+R+1, ata-miR156a-5p, and bdi-miR156b-5p, were significantly upregulated under drought treatment. The expression of miR1137 family was upregulated at 5 days, 7 days, and R_24 h. The expression of miR166 family, including osa-miR166b-5p and gma-miR166a-5p_1ss19AG, was downregulated. Among the 12 differentially expressed novel miRNAs, PC-5p-5881_2,234 was downregulated under drought treatment and upregulated at R_24 h. In general, the level of expression of the four novel miRNAs, which included PC-5p-10048_1508, PC-5p-52255_298, PC-5p-882_11429, and PC-3p-85874_131, were downregulated to different degrees at 12 h to 7 days under drought treatment, and their levels of expression were downregulated at 24 h of rehydration. The levels of expression of four novel miRNAs (PC-3p-93182_112, PC-3p-94625_109, PC-5p-57663_259, and PC-3p-95140_107) were upregulated at 5 and 7 days under drought stress and rehydration at 24 h. Three novel miRNAs (PC-5p-55424_274, PC-5p-41033_410, and PC-5p-77163_159) were downregulated at 24 h under drought stress and upregulated from 3 days under drought stress to 24 h of rehydration (Figure 3B). These data suggest that the expression of miRNAs changes with the prolongation of drought stress and do not always remain up- or downregulated.

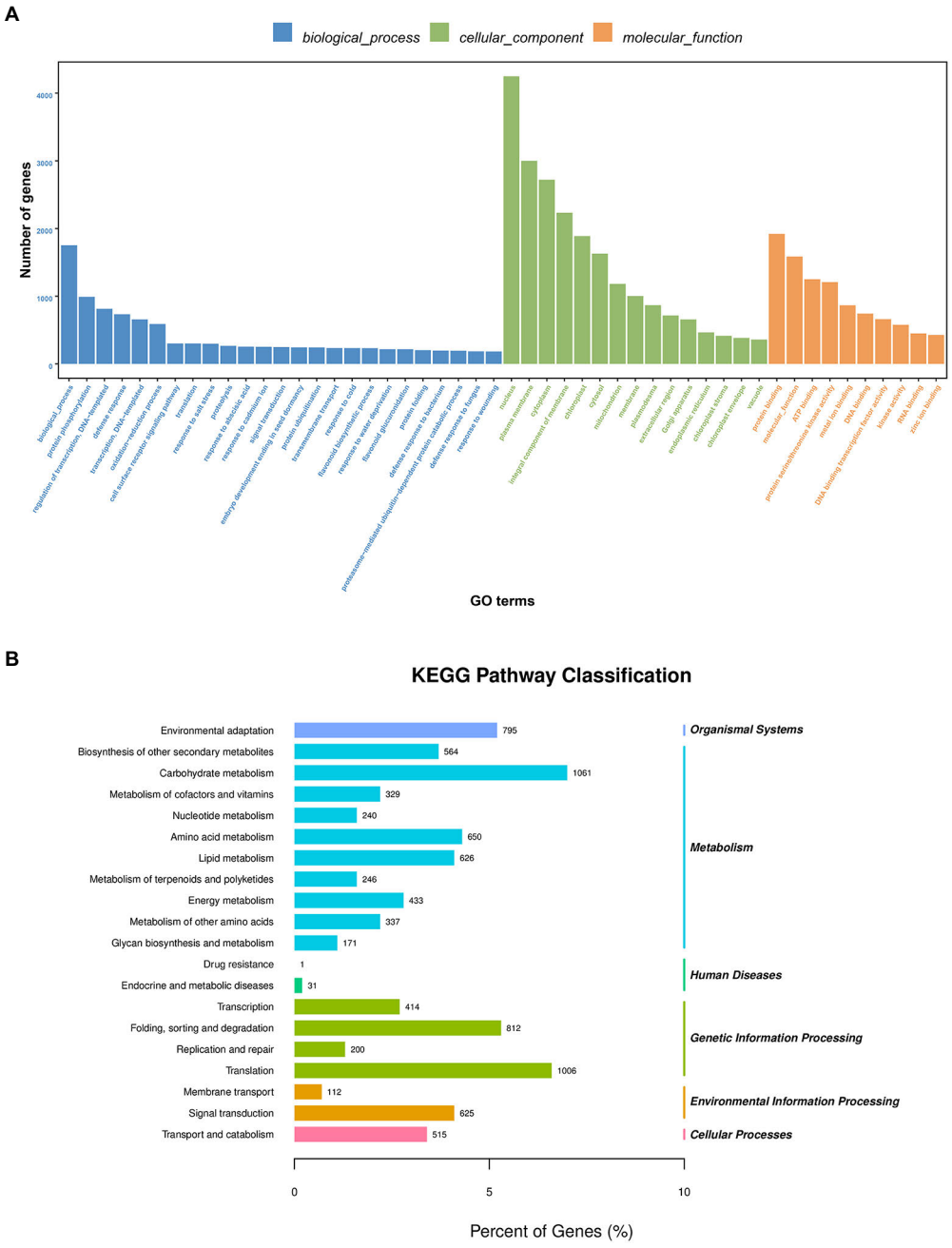

FIGURE 1
GO classification **(A)** and KEGG pathway enrichment **(B)** of UniGenes. GO, Gene Ontology; KEGG, Kyoto Encyclopedia of Genes and Genomes.

Degradome sequencing analysis

After removing the unqualified sequences, 28,885, 26,523, 17,691, 31,196, 28,063, 40,389, 35,357, and 38,874 unique reads were obtained from the CK and each drought treatment group (Supplementary Table 5B), respectively. The ratios of acquired unique mapped reads were 46.83, 53.01, 52.98, 53.63, 53.30, 56.17, 57.03, and 54.35%, respectively (Supplementary Table 5B). The ratios of covered transcripts in the five treatment groups were 80.80, 80.01, 82.18, 81.81, and 81.40%, respectively. The ratios of covered transcripts in the control and drought treatments were 76.52, 77.87, and 71.96% at CK, 12 h, and 24 h of drought stress, respectively. The target genes were separated into five categories (Category 0, 1, 2, 3, and 4; Xu et al., 2013; Yang et al., 2013). A total of 90, 71, 2,591, 2,758, and 3,972 target genes of miRNAs in *A. mongolicum* were in each category (Supplementary Table 5C). A total of 676 miRNAs that regulate 46,456 target genes were identified by degradome sequencing (Supplementary Table 8), and 137

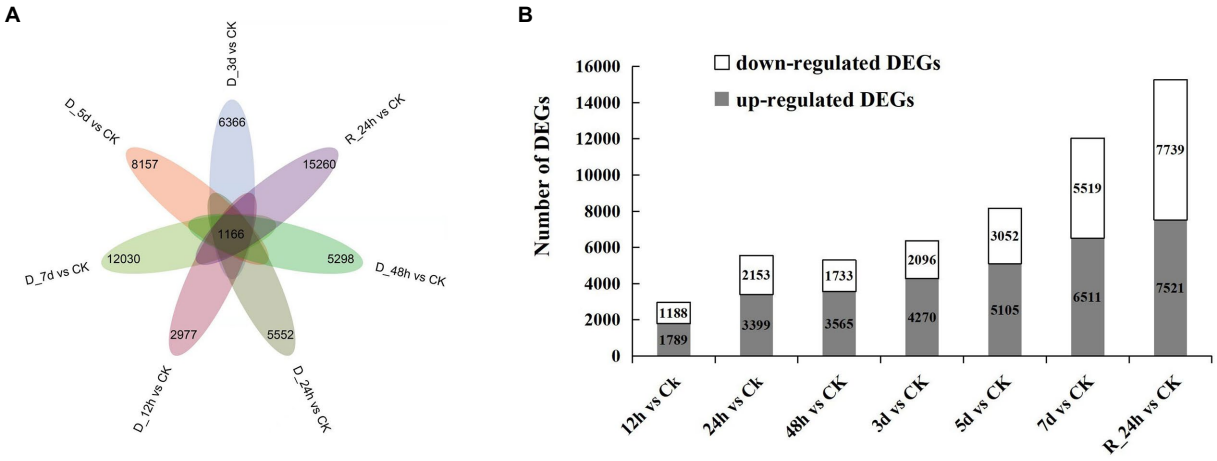

FIGURE 2
Drought responsive genes in *Agropyron mongolicum*. **(A)** Venn diagrams of differentially expressed genes in the treatment and control groups. **(B)** The number of differentially expressed genes under drought stress compared with the control.

novel miRNAs regulated 1,394 target genes (Supplementary Table 9).

Integration analysis of miRNAs and their target genes under drought stress

To investigate the trends of miRNA and mRNA changes in *A. mongolicum* under different stages of drought stress, the differentially expressed miRNAs and DEGs from miRNA were integrated and analyzed based on transcriptome and degradome sequencing data. The miRNAs and their target genes with negative regulatory mode were screened in the control group compared with the seven drought-treated groups based on the general model (cleavage) of the miRNA regulation of target genes in plants (Llave et al., 2002). A total of 91 known miRNAs that belonged to 59 miRNA families were found to negatively regulate 1,438 target genes (Figures 4A,B; Supplementary Table 10), indicating that the miRNAs and target genes are not all regulated one-to-one but are regulated in a network-like radial pattern. One of the target genes (norm value of the highest) was chosen to participate in the heatmap when one miRNA regulated many target genes (Figures 4A,B). Eight differentially expressed novel miRNAs of *A. mongolicum* regulated 36 target genes. Seven upregulated the expression of miRNAs, such as PC-3p-105150_88, PC-3p-68960_194, PC-3p-77094_159, PC-5p-41033_410, PC-5p-77163_159, PC-5p-78312_155, and PC-5p-87000_128, and PC-3p-85874_131 was a downregulated miRNA (Figure 4A; Supplementary Table 11). A total of 36 target genes under drought stress were annotated as uncharacterized oxidoreductase, protein MAK16 homolog, magnesium-chelatase subunit ChlH chloroplastic, NADP-thioredoxin reductase C precursor, chloroplast ferredoxin-dependent glutamate synthase, and heat shock protein (HSP)-interacting protein. All of them were related to drought or adversity stress, and the function of three target genes was annotated as unnamed protein products. The functions of the two target genes were unknown (Table 3).

Gene co-expression network module construction

A WGCNA analysis indicated that genes with similar functions cluster together in the same module (Langfelder and Horvath, 2008). To identify hub genes and their interacting genes of *A. mongolicum* involved in drought resistance, 41,793 genes were used to construct gene co-expression networks and modules, which yielded 39 modules (Figure 5A).The turquoise module was the largest and contained 10,766 genes, while the smallest module was the plum1 module, which included 36 genes (Supplementary Table 12). The module heat map of gene clustering was constructed based on the correlation of expression of feature genes. The gene clusters with highly correlated expression corresponded to a branch of the clustering tree. The clustering heat map drawn by the neighbor relationship was consistent with the clustering results drawn by dynamic shea (Figure 5B). A total of 39 modules of all genes from 24 samples were used to create cluster heatmaps for *A. mongolicum* (Figure 5C). The violet and darkolivegreen modules were highly correlated with drought-treated samples at D_24 h2 and D_24 h3. The red and salmon modules positively correlated with drought-treated samples at D_24 h3; and the turquoise module positively correlated with the drought-treated samples at 5 d, 7 d, and R_24 h. The steelblue module was positively associated with drought-treated samples at 12 h, 5 days, 7 days, and R_24 h. The modules involved in drought stress were initially screened by a module-trait interrelationship heatmap.

10.3389/fpls.2022.976684

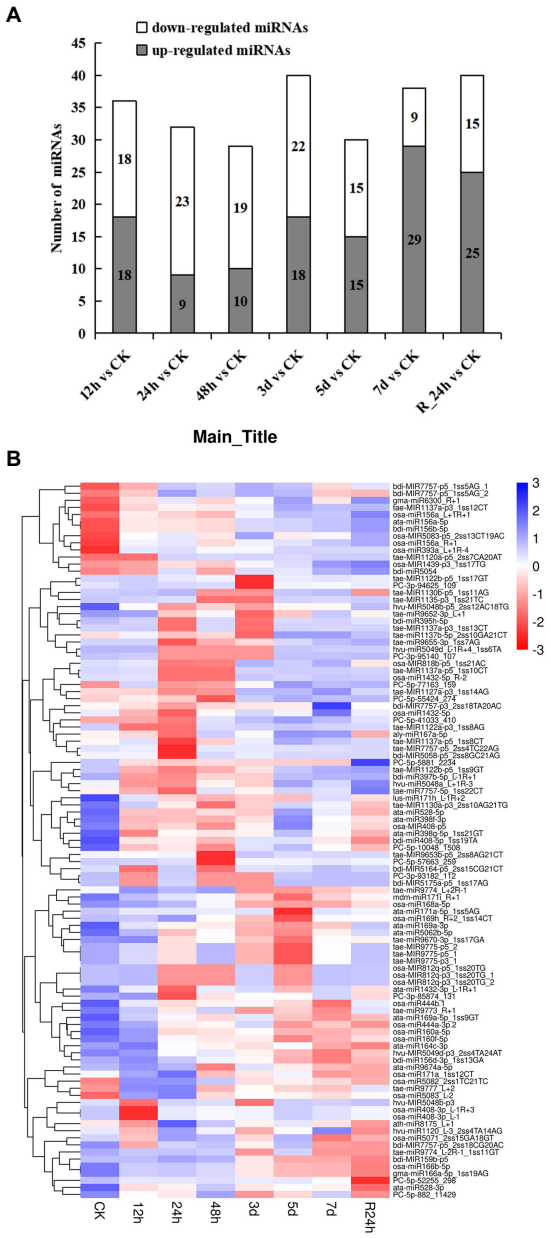

FIGURE 3
Differentially expressed miRNAs under drought stress. **(A)** The number of differentially expressed miRNAs compared with the control. **(B)** Hierarchical clustering of differentially expressed miRNAs in eight different durations of drought treatment [CK (0h), 12h, 24h, 12h, 48h, 3 days, 5 days, 7 days, and R24 h]. Red indicates a lower level of expression of the miRNAs, and blue indicates higher levels of expression of miRNAs. The names of the samples are shown at the bottom, and the name of the differentially expressed gene is shown on the right. The norm expression of miRNA was standardized using a Z-score. The absolute signal intensity ranges from −3 to +3, and the corresponding color changes from red to blue.

Analysis of the drought-related modules

Relative conductivity, proline (Pro) and malondialdehyde (MDA) contents are closely related to the drought tolerance of plants. The use of module-trait correlation analysis facilitates the study of complex drought effects. The relative conductivity, Pro and MDA contents of *A. mongolicum* were measured under 25% PEG-6000 treatment (Supplementary Figure 3). In *A. mongolicum*, a heat map of correlations between the module and trait was created using 39 modules and physiological indices of drought resistance, such as relative conductivity and the contents of MDA and Pro (Figure 6). A correlation analysis showed that the turquoise module positively correlated with relative conductivity and Pro, with correlation coefficients of 0.73 ($p = 5e^{-05}$) and 0.69 ($p = 2e^{-04}$), respectively, and the correlation coefficient of MDA was 0.29 ($p = 0.2$). The steelblue module significantly and positively correlated with relative conductivity, MDA, and Pro, with correlation coefficients of 0.49 ($p = 0.02$), 0.44 ($p = 0.03$), and 0.5 ($p = 0.01$), respectively. The violet module positively correlated with relative conductivity and Pro with correlation coefficients of 0.43 ($p = 0.04$) and 0.44 ($p = 0.03$), respectively, and the correlation coefficient of MDA was 0.36 ($p = 0.08$). The blue module significantly and negatively correlated with relative conductivity, MDA, and Pro with correlation coefficients of −0.65 ($p = 7e^{-04}$), −0.53 ($p = 0.007$), and −0.68 ($p = 3e^{-04}$), respectively.

GO and pathway analysis of genes in specific modules

Under drought treatment, the GO and KEGG analyses showed the functions and pathways of genes in specific modules of *A. mongolicum*. Biological processes, molecular functions, and cellular components were enriched in the GO analysis of turquoise, steelblue, violet, and blue modules (Figures 7A–D). In biological processes, it was primarily enriched for the regulation of transcription, DNA-templated (GO:0006355), protein phosphorylation (GO:0006468), signal transduction (GO:0009737), brassinosteroid-mediated signaling pathway (GO:0009742), abscisic acid (ABA)−activated signaling pathway (GO:0009737, GO:0009788, GO:0009737, GO:0009738), cell surface receptor signaling pathway (GO:0007166), positive regulation of protein ubiquitination (GO:0031398), and response to water deprivation (GO:0009414) processes. The biological processes played an essential role in the mechanism of *A. mongolicum* related to drought resistance. Cellular Component analysis revealed that the four modules were primarily enriched in the nucleus (GO:0005634), plasma membrane (GO:0006351, GO:0005886, and GO:0005829), cytoplasm (GO:0005737), cytosol and chloroplast (GO:0016021 and GO:0009941) components. The results showed that cellular components, such as the nucleus, cytoplasm, plasma membrane and chloroplast, responded to drought stress. Molecular function was primarily enriched to protein binding (GO:0005515), metal ion binding (GO:0046872, GO:0008270), kinase activity (GO:0016301) and other functions, which could play an important role in drought regulation in *A. mongolicum*. The KEGG pathway from four modules of *A. mongolicum* was primarily enriched for transport and

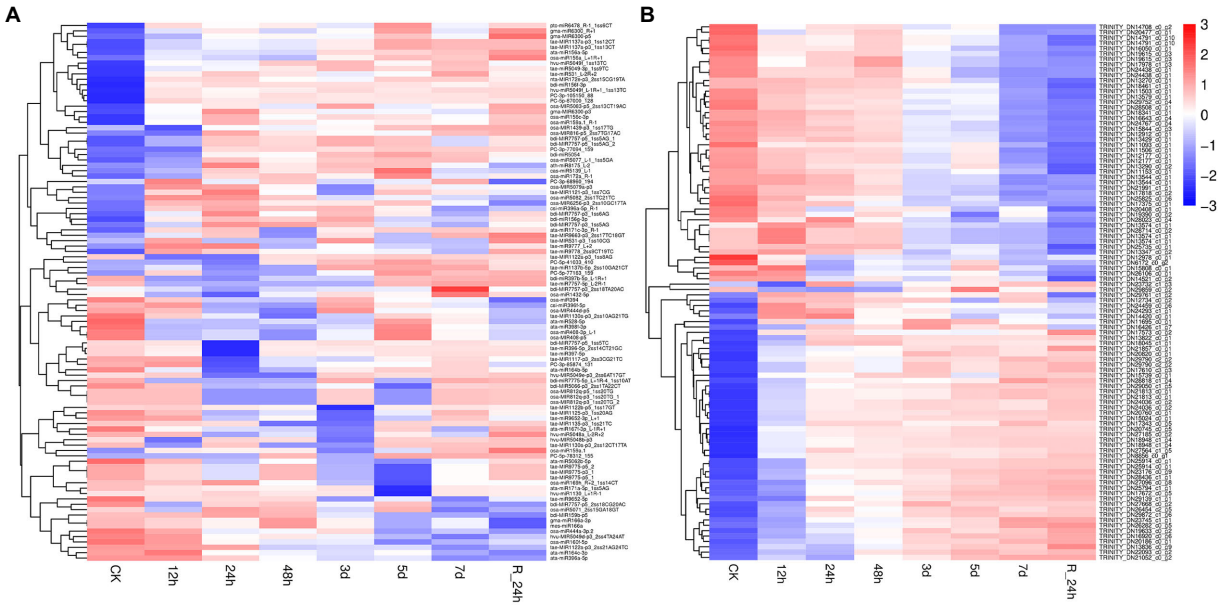

FIGURE 4
A combined view of the levels of expression between differentially expressed miRNAs **(A)** and their target genes **(B)** in *Agropyron mongolicum* in eight different drought treatment durations. The original expression values of miRNAs and their target genes were normalized by Z-score normalization.

catabolism under drought stress, signal transduction, amino acid metabolism, carbohydrate metabolism, and environmental adaptation, indicating that these pathways responded to stimulation in response to drought (Figures 7E–H).

Analysis of drought-resistant hub genes

The top 20 genes in the four modules related to the drought tolerance of *A. mongolicum* with connectivity were used as hub genes, and the genes that interacted with the hub genes were selected (Supplementary Table 12). The differentially expressed miRNAs with a targeted relationship to the hub genes were screened based on the degradome and miRNA sequencing data. The five hub genes that targeted/regulated differentially expressed miRNAs were analyzed, including *MADS47* (TRINITY_DN16091_c0_g9, GO Function annotation: brassinosteroid mediated signaling pathway) targeted/regulated osa-miR444a-3p.2 in the violet module ($p < 0.01$), CCX_1 (TRINITY_DN29080_c0_g1, GO Function annotation: sodium and potassium ion transport) targeted/regulated bdi-miR408-5p_1ss19TA in the turquoise module ($p < 0.05$), steelblue module *PAO2* (TRINITY_DN28296_c0_g1, GO Function annotation: oxidation–reduction process, peroxisome) targeted/regulated ata-miR169a-3p ($p < 0.01$) and *carC* (TRINITY_DN28552_c0_g1, GO Function annotation: hydrolase activity) targeted/regulated tae-miR9774_L-2R-1_1ss11GT in the blue module ($p < 0.01$). The *HOX24* (TRINITY_DN19559_c1_g1) targeted/regulated bdi-miR528-p3_2ss15TG20CA was found in the violet module, and the GO term of the *HOX24* gene was annotated as a signaling pathway in the response to water deprivation and in response to ABA and the ABA–activated signaling pathway, indicating that *HOX24* may play an important role in drought stress resistance. The regulatory network and function of hub genes and interacting genes were deeply explored to better understand the mechanism of drought resistance in *A. mongolicum* (Figure 8). When *A. mongolicum* was subjected to drought stress, *PAO2* controlled the functional genes of water deficit and regulatory proteins (TRINITY_DN18888_c0_g1, TRINITY_DN22628_c0_g2, and TRINITY_DN19796_c0_g3), suggesting that *PAO2* may indirectly controls the enzyme activity-related proteins, ubiquitin-protein transferase activity, MAPK signaling pathway, and other functional genes. This indicates that *PAO2* may play a key role in the gene coexpression regulatory network. *carC* would activate many of the genes that regulate chloroplast functions in response to drought stress and then regulate redox, carbohydrate metabolism, and phosphatase activity. *MADS47* and *HOX24* are the hub genes in the violet module with the connectivity of top1 and top15. These two genes may have direct interactions and co-regulate the downstream functional genes of kinase activity, oxidation–reduction and chloroplast. Secondly, the genes that govern enzyme activity, chloroplast, cytoplasm, protein ubiquitination, and cell components function are activated to achieve drought regulation. *MADS47* is presumed to be the master gene in this module based on gene connectivity. There were 7,993 genes with interactions with *CCX1*, and 905 of the genes were chosen for functions related to water deficiency response, MAPK signaling pathway,

TABLE 3 Differentially expressed novel miRNA and differentially expressed target genes.

Novel miRNA	Regulation	log2 (fold_change)	*p* Value (t_test)	Accession	Annotation	Regulation	Significant
PC-3p-105150_88	Up	inf	0.04	TRINITY_DN15808_c0_g1	Protein ROOT PRIMORDIUM DEFECTIVE 1-like	Down	Yes
PC-3p-105150_88	Up	inf	0.04	TRINITY_DN19688_c0_g2	Uncharacterized oxidoreductase At1g06690, chloroplastic-like	Down	Yes
PC-3p-68960_194	Up	0.87	0.01	TRINITY_DN14521_c0_g2	Protein MAK16 homolog	Down	Yes
PC-3p-77094_159	Up	inf	0.00	TRINITY_DN11948_c0_g1	Unnamed protein product	Down	Yes
PC-3p-77094_159	Up	inf	0.00	TRINITY_DN12469_c0_g1	Unnamed protein product	Down	Yes
PC-3p-77094_159	Up	inf	0.00	TRINITY_DN14567_c0_g1	Uncharacterized protein LOC109765237	Down	Yes
PC-3p-77094_159	Up	inf	0.00	TRINITY_DN17145_c0_g2	Protein TSS isoform X1	Down	Yes
PC-3p-77094_159	Up	inf	0.00	TRINITY_DN17291_c1_g2	RecName: Full = RuBisCO large subunit-binding protein subunit beta, chloroplastic; AltName: Full = 60 kDa chaperonin subunit beta; AltName: Full = CPN-60 beta	Down	Yes
PC-3p-77094_159	Up	inf	0.00	TRINITY_DN18346_c1_g2	Uncharacterized protein LOC109753311	Down	Yes
PC-3p-77094_159	Up	inf	0.00	TRINITY_DN20477_c0_g1	Magnesium-chelatase subunit CHLH, chloroplastic	Down	Yes
PC-3p-77094_159	Up	inf	0.00	TRINITY_DN22992_c0_g1	Predicted protein	Down	Yes
PC-3p-77094_159	Up	inf	0.00	TRINITY_DN25063_c0_g5	Predicted protein	Down	Yes
PC-3p-77094_159	Up	inf	0.00	TRINITY_DN25165_c0_g3	NADP-thioredoxin reductase C precursor, partial	Down	Yes
PC-3p-77094_159	Up	inf	0.00	TRINITY_DN25174_c0_g2	Elongation factor 2	Down	Yes
PC-3p-77094_159	Up	inf	0.00	TRINITY_DN26970_c0_g2	Chloroplast ferredoxin-dependent glutamate synthase	Down	Yes
PC-3p-77094_159	Up	inf	0.00	TRINITY_DN28818_c0_g1	Heat shock factor A6	Down	Yes
PC-3p-77094_159	Up	inf	0.00	TRINITY_DN28919_c0_g1	Isoleucine--tRNA ligase, chloroplastic/mitochondrial-like isoform X1	Down	Yes
PC-3p-77094_159	Up	inf	0.00	TRINITY_DN3290_c0_g1	HSP-interacting protein	Down	Yes
PC-3p-85874_131	Down	−1.32	0.01	TRINITY_DN17343_c0_g5	-	Up	Yes
PC-3p-85874_131	Down	−1.32	0.01	TRINITY_DN17607_c0_g3	Hypothetical protein TRIUR3_23162	Up	Yes
PC-3p-85874_131	Down	−1.32	0.01	TRINITY_DN21478_c1_g5	Predicted protein	Up	Yes
PC-3p-85874_131	Down	−1.32	0.01	TRINITY_DN26358_c3_g4	VQ motif-containing protein 29-like	Up	Yes

(Continued)

TABLE 3 Continued

Novel miRNA	Regulation	log2 (fold_ change)	*p* Value (t_test)	Accession	Annotation	Regulation	Significant
PC-5p-41033_410	Up	1.09	0.05	TRINITY_ DN25475_c1_g1	Unnamed protein product	Down	Yes
PC-5p-41033_410	Up	1.09	0.05	TRINITY_ DN28714_c0_g2	Phosphomethylethanolamine N-methyltransferase-like	Down	Yes
PC-5p-41033_410	Up	1.31	0.02	TRINITY_ DN15316_c2_g6	Chaperone protein ClpD2, chloroplastic	Down	Yes
PC-5p-41033_410	Up	1.31	0.02	TRINITY_ DN28714_c0_g2	Phosphomethylethanolamine N-methyltransferase-like	Down	Yes
PC-5p-77163_159	Up	2.24	0.03	TRINITY_ DN16050_c0_g1	Acetate/butyrate--CoA ligase AAE7, peroxisomal-like	Down	Yes
PC-5p-77163_159	Up	1.97	0.03	TRINITY_ DN16730_c0_g8	Putative ripening-related protein 6	Down	Yes
PC-5p-77163_159	Up	1.97	0.03	TRINITY_ DN19390_c0_g2	-	Down	Yes
PC-5p-77163_159	Up	1.97	0.03	TRINITY_ DN23892_c0_g5	Inositol-tetrakisphosphate 1-kinase 2-like	Down	Yes
PC-5p-77163_159	Up	1.97	0.03	TRINITY_ DN28714_c0_g2	Phosphomethylethanolamine N-methyltransferase-like	Down	Yes
PC-5p-78312_155	Up	inf	0.04	TRINITY_ DN14321_c1_g1	Translation factor GUF1 homolog, chloroplastic	Down	Yes
PC-5p-78312_155	Up	inf	0.04	TRINITY_ DN15829_c0_g2	hypothetical protein	Down	Yes
PC-5p-78312_155	Up	inf	0.04	TRINITY_ DN25857_c0_g2	Hypothetical protein	Down	Yes
PC-5p-78312_155	Up	inf	0.04	TRINITY_ DN28023_c0_g4	Luminal-binding protein 2	Down	Yes
PC-5p-87000_128	Up	inf	0.04	TRINITY_ DN28714_c0_g2	Phosphomethylethanolamine N-methyltransferase-like	Down	Yes

and protein ubiquitination, including 204 genes for ion binding, transport, and exchange; 138 genes for protein ubiquitination; 122 genes for membrane function; and 102 genes for phytohormones, followed by redox regulation (90), chloroplast (82), water deficiency response (49), sugar (42). *CCX1* of *A. mongolicum* would activate the interacting genes under drought stress, which mobilizes drought defense mechanisms to manage drought. The regulatory networks provide important references for subsequent studies of drought resistance mechanisms in *A. mongolicum*.

Correlation analysis of miRNAs and their candidate hub genes for drought resistance

Five miRNAs and their target genes were chosen for RT-qPCR to better understand the connection between the expression of miRNA and its drought-resistant potential hub genes (Figure 9). The patterns of expression of four miRNA-target gene pairings (bid-miR408-5p_1ss19TA-*CCX1*, ata-miR169a-3p-*PAO2*, osa-miR444a-3p.2-*MADS47*, and bdi-miR528-p3_2ss15TG20CA-*HOX24*) were all negatively regulated. The levels of expression of four miRNAs decreased as the drought treatment period increased, but the relative expression of their target genes increased. The levels of expression of target the genes increased after 24 h of rehydration. The relative expression of tae-miR9774_ L-2R-1_1ss11GT and target gene carC decreased overall.

Discussion

Agropyron mongolicum is a vital forage grass and has exceptional drought and cold resistance. It is grown in semiarid and arid desert regions where it is subjected to abiotic stresses, particularly drought stress. *A. mongolicum* has developed a robust set of mature regulatory mechanisms to manage the response to drought stress. The severity of drought is determined by various factors, such as rainfall, the ability of soils to store moisture, and

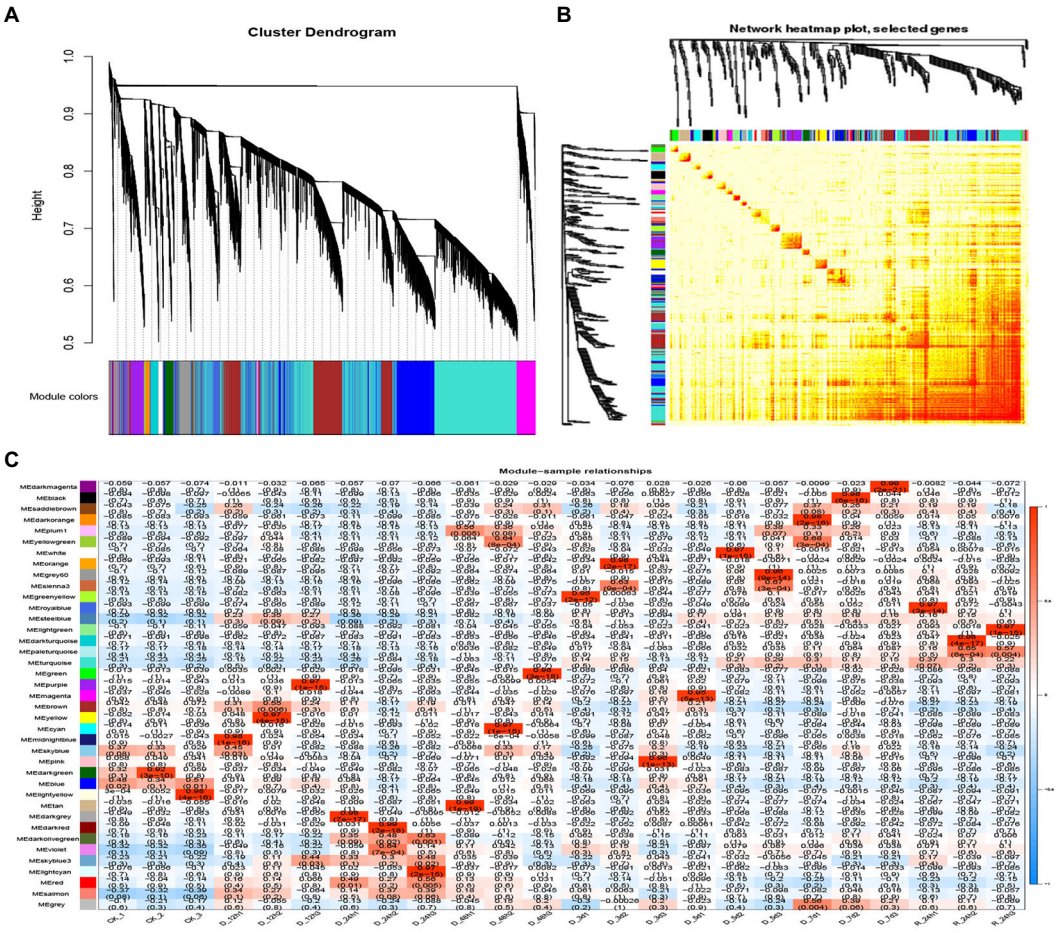

FIGURE 5
Correlation between sample clustering of the modules and genes. **(A)** Clustering dendrograms of the genes. Based on the dynamic hybrid branch cutting method, color strips were used for simple visualization of the module assignment (branch cutting). **(B)** 41,793 gene and module correlation clustering diagrams. **(C)** Heat map of the correlations between the modules and genes of different samples. The colors that range from blue through white to red indicate low through intermediate to high correlations, respectively.

evaporation demand. Drought has many effects on crops and can deleteriously affect metabolism, photosynthesis and defense mechanisms (Andrew et al., 2009). Plants respond to drought through root development, stomatal opening and closing, cell adaptation, ABA and reactive oxygen species (ROS) scavenging (Abid et al., 2017). The genes of exceptional drought resistance in *A. mongolicum* could be beneficial to improving the drought tolerance of gramineous crops, such as wheat and rice. Therefore, it is imperative to study the molecular mechanism of drought resistance in *A. mongolicum*.

Drought stress has been demonstrated to induce the particular expression of drought-related genes in plants (Bano et al., 2022). Three important high-throughput methods, the transcriptome, small RNA, and degradome sequencing, were applied to investigate the mechanism of drought resistance in *A. mongolicum*. In comparison with the miRNAs identified from the other plants, little research has been conducted on the role of miRNAs in *A. mongolicum*. To date, 114 miRNAs that are related to the drought resistance of *A. mongolicum* have been reported in our previous research group, and the functions of amo-miR21, amo-miR5 and amo-miR623 have been correlated with drought resistance (Zhang et al., 2019). The transcriptome dataset of *A. mongolicum* was used as a reference sequence for small RNA and degradome sequencing analyses to identify the miRNAs and their target genes that could be associated with drought stress. A total of 1,104 miRNAs, including 101 highly confident miRNAs (Supplementary Table 7), were identified based on the transcriptome data from *A. mongolicum*. Additionally, the miRNA lengths ranged from 18 to 25 nt, with a peak at 24 nt (Supplementary Figures 2C,D).

The results of the sRNA molecules of *A. mongolicum* match those of most plant miRNAs from prior studies (Zhao et al., 2010a; Niu et al., 2014; Bin et al., 2021). Some miRNAs that responded to drought in previous studies were also detected in our results, including miR156, miR159, miR162, miR171, miR444, and miR408. For example, rice tandem osa-miR156b and osa-miR156c were overexpressed in alfalfa (*Medicago sativa*). The expression of miR156 increased significantly in transgenic alfalfa, and the plants

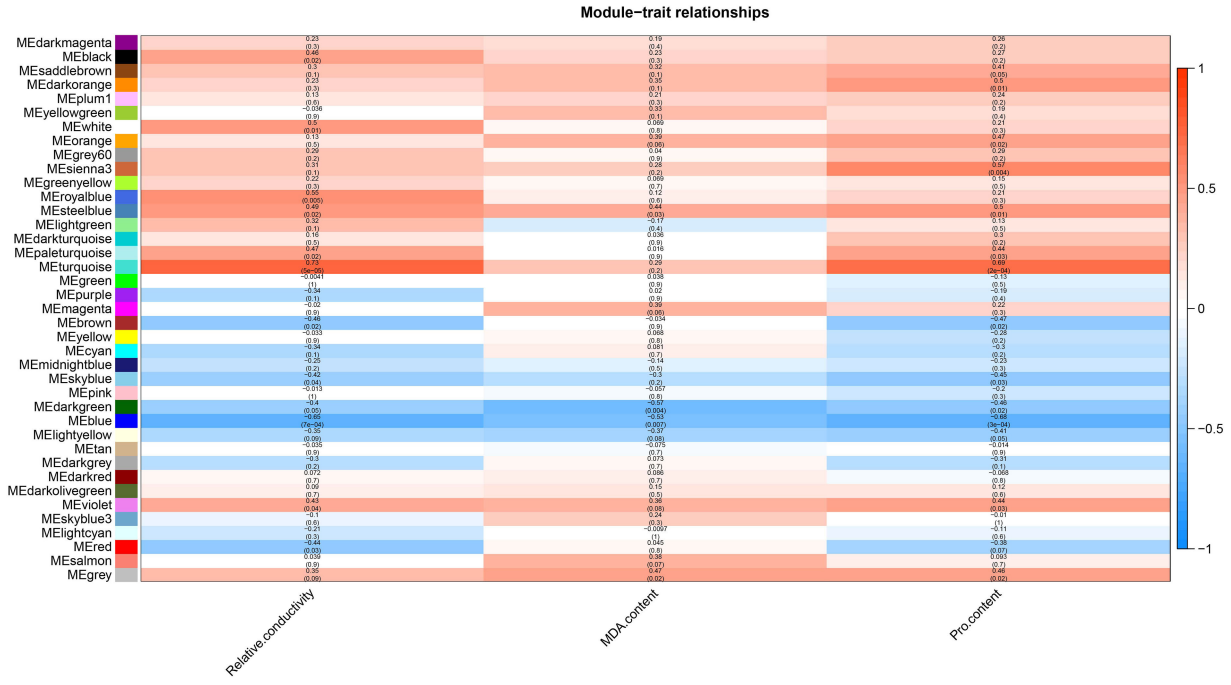

FIGURE 6
Heat map of the correlation between modules and traits.

that overexpressed the gene were better able to tolerate salt and drought resistance (Wang et al., 2021b). The overexpression of miR171f in rice resulted in reduced drought symptoms in transgenic plants compared with the control plants, which were found to play a role in drought tolerance by targeting SCL6-I and SCL6-II (Taeyoung et al., 2022). Sly-miR159 targets *SlMYB33* to regulate the accumulation of proline and putrescine to improve drought resistance (López et al., 2019). The data described above indicate that the sRNA sequencing results of *A. mongolicum* under drought stress are authentic and reliable.

In the WGCNA analysis, the unearthed potential drought-resistant hub genes (*MADS47*, *CCX1*, *carC*, *PAO2*, and *HOX24*) targeted five miRNAs, which were osa-miR444a-3p.2, bdi-miR408-5p_1ss19TA, tae-miR9774_L-2R-1_1ss11GT, ata-miR169a-3p, and bdi-miR528-p3_2ss15TG20CA. Further study of the function of these miRNA targets provides valuable information about the regulatory pathways available for any given gene. The bdi-miR528-p3_2ss15TG20CA expression of *HOX24* may activated the ABA−activated signaling pathway. osa-miR444a-3p.2 was differentially expressed in *A. mongolicum* under drought stress ($p \leq 0.001$) and predicted to regulate *MADS47* target genes. The regulation of *MADS47* by osa-miR444a-3p.2a may affect the brassinosteroid-mediated signaling pathway. Furthermore, the redox process may regulate by ata-miR169a-3p and miR9774, and sodium and potassium ion transport may regulate by bdi-miR408-5p_1ss19TA.

miR444 is specific to monocots and has been confirmed to target four MIKC-type MADS-box genes in rice (*OsMADS23*, *OsMADS27a*, *OsMADS27b*, and *OsMADS57*) (Sunkar et al., 2005; Lu et al., 2008; Wu et al., 2009; Li et al., 2010). Recent research provides evidence of a nitrate-dependent miR444-*OsMADS27* signaling cascade involved in the regulation of root growth in rice, as well as its dramatic role in stress responses (Kannan et al., 2022). The overexpression of miR444 promotes the biosynthesis of brassinosteroids (BRs) and inhibits the elongation of roots in rice (Jiao et al., 2020). In previous research, few studies have reported on miR9774, which is found in the mixed tissues of wheat leaves, stems, roots, and young spikes (Wei et al., 2009). In the low Cd-accumulation of wheat (Chuanyu 17), tae-miR-9,774 downregulated the expression between the group treated with 100 μM $CdCl_2$ and the control group (Zhou et al., 2020). miR408, a conserved and ancient miRNA found widely in plants, is involved in photosynthesis and controls the target genes of copper-binding proteins (Gao et al., 2022), which is vital for leaf growth. miR408 has been linked to drought and water shortage stress in *A. thaliana*, rice (Roseeta et al., 2013; Sonia et al., 2017), wheat (Guray et al., 2016), tomato (*Lycopersicon esculentum*; Bilgin et al., 2016), and perennial ryegrass (*Lolium perenne*; Nan et al., 2020). The antioxidant capability of plants can be improved by miR408, which enhances cellular antioxidants (Gao et al., 2022). In chickpea (*Cicer arietinum*), the expression of *PLC* (a target of miR408) decreased significantly with the overexpression of miR408 to provide drought tolerance (Hajyzadeh et al., 2015). When *A. thaliana* was exposed to drought stress, miR408 was upregulated, while its target genes *PLC* and *LAC3* were downregulated (Chao et al., 2015). miR169 was identified for its involvement in drought stress in *A. thaliana* (Du et al., 2017b), poplar (*Populus* spp.), rape (*Brassica napus*), and potato (*Solanum*

10.3389/fpls.2022.976684

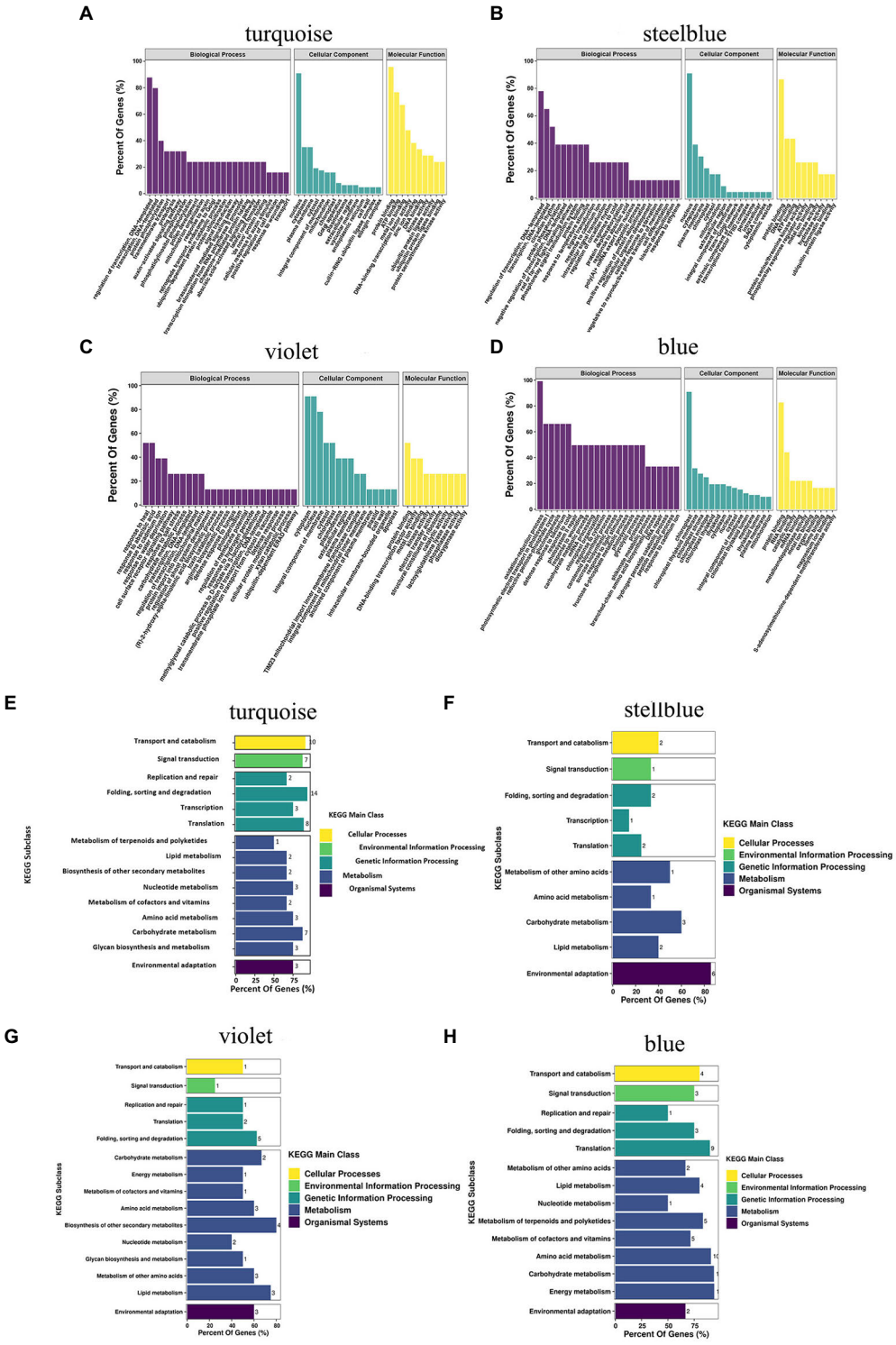

FIGURE 7
GO classification and putative KEGG pathways of specific modules related to drought resistance in *Agropyron mongolicum*. The GO classification and KEGG pathway of turquoise, steelblue, violet, and blue modules are represented by **(A)**, **(B)**, **(C)**, **(D)**, **(E)**, **(F)**, **(G)**, and **(H)**, respectively. GO, Gene Ontology; KEGG, Kyoto Encyclopedia of Genes and Genomes.

tuberosum; Yang et al., 2016) crops. For example, in response to drought and ABA treatment, Bna-miR169n targets *BnaNF-YA9* in *Brassica napus* (Wang et al., 2022). PtmiR169o targets the *PtNF-YA6* gene to regulate drought tolerance in poplar (Jiao et al., 2021). More research into miR169-targeted *PAO2*-regulated drought is required. miR528 is involved in biotic stresses in

10.3389/fpls.2022.976684

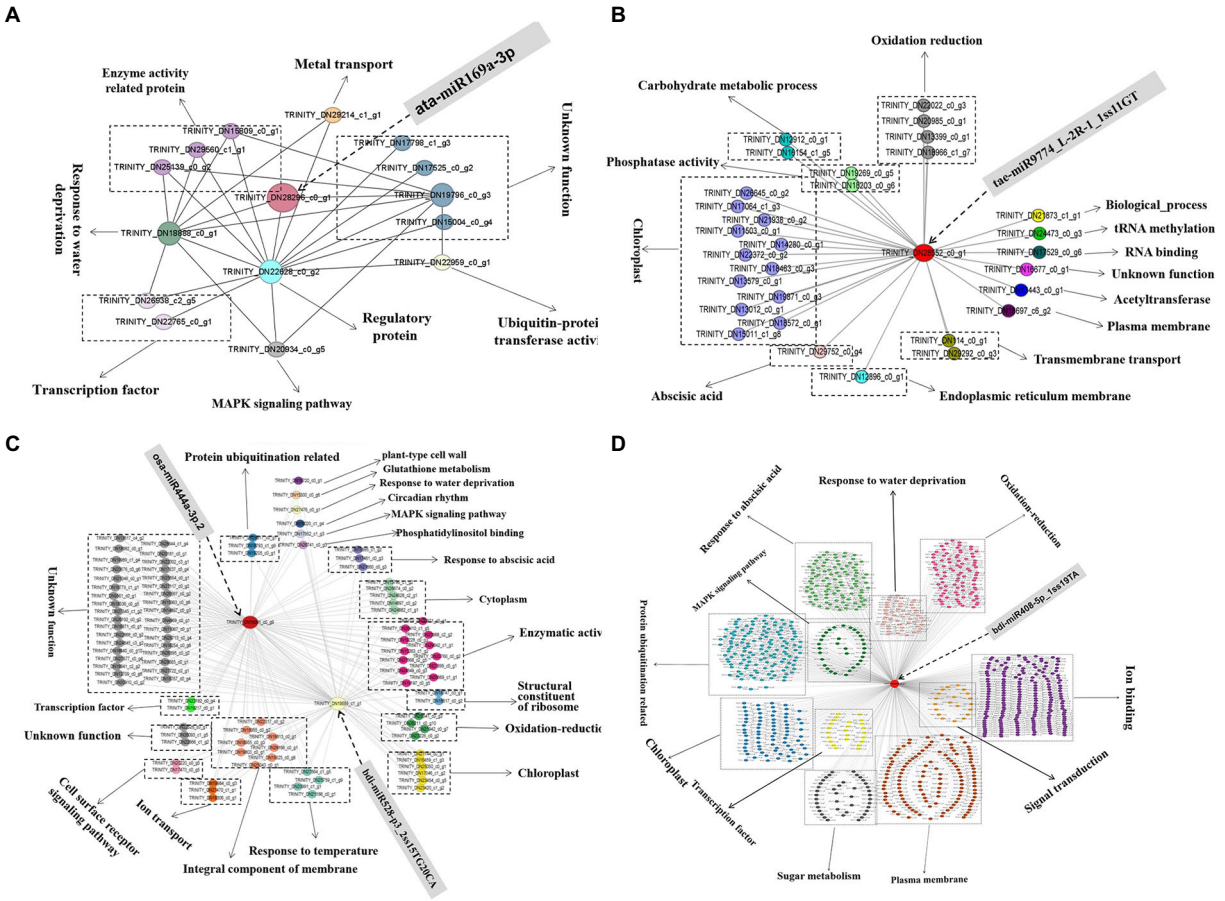

FIGURE 8
The coexpression subnetwork of five hub genes. Red-colored nodes suggest their central role in the network, and other nodes of the same color indicate the same function. **(A)**, **(B)**, **(C)**, and **(D)** represent the coexpression subnetwork of TRINITY_DN28296_c0_g1 (*PAO2*), TRINITY_ DN28552_ c0_g1 (*carC*), TRINITY_DN16091_c0_g9 (MADS47), TRINITY_DN19559_c1 _g1 (*HOX24*), and TRINITY_DN29080_c0_g1 (*CCX1*), respectively. A part of the gene ID corresponds to the gene name: *Os06g0107700* (TRINITY_DN22022_c0_g3), *XB3* (TRINITY_DN22959_c0_g1), *CLPC1* (TRINITY_DN21467_c0_g3), and *BPM2* (TRINITY_DN19691_c0_g7).

plants, such as drought tolerance and salt tolerance stress. In rice, the overexpression of *TCONS_00021861* attenuated the repression of miR528-3p on *YUCCA7*, which, in turn, activated the indole acetic acid (IAA) biosynthetic pathway and conferred resistance to drought stress (Chen et al., 2021). Durum wheat ata-miR528-5p promotes redox homeostasis by targeting the F-box protein and Cu Zn superoxide dismutase (Cu Zn SOD) under stress (Liu et al., 2020). These findings suggest that the known miRNAs are likely to be engaged in cross-adaptation to control plant tolerance to abiotic conditions, such as drought. However, their specific duties and exact functions need to be verified in the future.

It is impossible to extrapolate the complete picture of a complex environmental component, such as drought regulation, from the effects of individual genes. A combination of transcriptome, degradome and miRNAs expression profiles is needed to elucidate the synergistic impact of drought-related genes (Liu et al., 2020). A total of 41,792 UniGenes (Table 2) were detected in the *A. mongolicum* transcriptome. Under specific abiotic stresses, such as drought stress, mRNAs have a particular expression in response to the pressure. Thus, there were 1,166 DEGs in the seven comparison groups under drought stress (Figure 2). The number of up- and downregulated genes also differed among the various comparison groups. The level of gene expression could differ owing to the varying drought treatment times. GO classification to drought-related GO terms include response to salt stress, response to ABA and response to wounding (Figure 1A). The degradome data identified 137 *A. mongolicum*-specific miRNAs that target 1,394 genes (Supplementary Table 9). The integrated analysis of transcriptome, sRNAs and degradome that focused on miRNAs and their target genes in negative regulatory mode, identified 91 miRNAs that negatively regulate 1,438 target genes. Some DEGs were commonly up- or downregulated under drought stress, while others exhibited unique patterns. In *A. mongolicum*, we observed that eight novel miRNAs with different expression

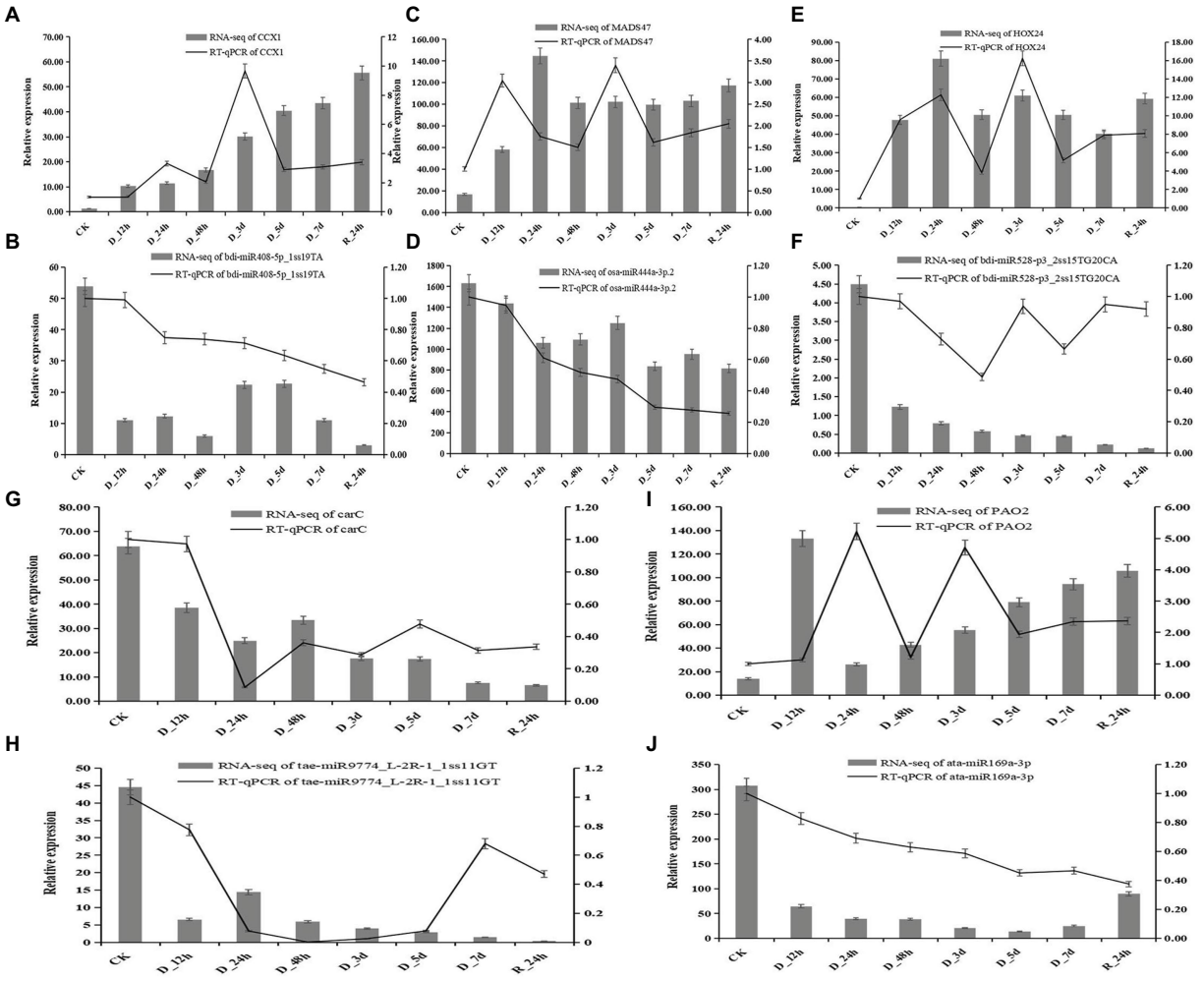

FIGURE 9
Correlation of the expression between miRNAs and the hub genes at eight durations of different drought treatments (25% PEG solution PEG6000). bdi-miR408-5p_1ss19TA target *CCX1* **(A,B)**; osa-miR444a-3p.2 target *MADS47* **(C,D)**; bdi-miR528-p3_2ss15TG20CA target *HOX24* **(E,F)**; tae-miR9774_L-2R-1_1ss11GT target carC **(G,H)**; and ata-miR169a-3p target *PAO2* **(I,J)**.

patterns regulated 36 target genes. The 36 target genes that are controlled (Figure 4; Supplementary Table 10) were annotated under drought stress as uncharacterized oxidoreductase, magnesium-chelatase subunit CHLH chloroplastic, NADP-thioredoxin reductase C precursor, chloroplast ferredoxin-dependent glutamate synthase, and heat shock protein-interacting protein (Table 3). This study showed that all these functional annotations are involved in drought stress regulation. For example, the Chloroplastic, Magnesium Protoporphyrin-IX Chelatase H subunit (CHLH) receptor has been found to bind ABA, and CHLH is a crucial enzyme in chlorophyll production (Wasilewska et al., 2008; Zhang et al., 2019). NADP has been shown to regulate the maintenance of redox homeostasis and respond to environmental stresses in plants (Wang et al., 2020). According to the findings, drought stress is regulated in plants by a variety of pathways, including chlorophyll and ABA regulation. Plants that respond to drought stress could also activate pathways to other stresses, such as salt stress or heat stress, or some of the pathways could be shared by plants that respond to biotic stresses.

To identify the highly putative genes in drought responses in *A. mongolicum*, 41,792 mRNAs were analyzed using WGCNA technology based on transcriptome sequencing data to study the hub genes and co-expression networks in response to drought stress. A total of 39 co-expression modules were constructed, and four modules related to drought resistance were enriched for signal transduction, brassinosteroid mediated signaling pathway, and the ABA−activated signaling pathway (Figure 7). These enriched functions were closely related to drought stress. *MADS47*, *CCX1*, *carC*, *PAO2*, and *HOX24* were five hub genes with putative drought tolerance (Figure 8). *MADS47* is a MADS transcription factor, which plays essential functions in plant growth and development and response to adversity stress (Natalia

et al., 2019; Zhao et al., 2020; Han et al., 2022a). *OsMADS2*, *OsMADS30*, and *OsMADS55* were downregulated in expression under drought and salt stress in rice (Rita et al., 2007). However, the RT-qPCR results of *A. mongolicum* showed that the relative level of expression of *MADS47* was upregulated in drought stress. In rice, *OsMADS26* plays a negative regulatory role and reduces the drought resistance of the plant, which is the same regulatory pattern as *MADS47* in *A. mongolicum*. *MADS47* is a hub gene in the regulatory network and is functionally shown to be associated with the BR-mediated signaling pathway. BRs are plant hormones that promote growth, improve plant stress resistance, and regulate the level of expression of chlorophyll synthase genes (Ryo et al., 2022). BR can promote wound healing by activating reactive oxygen metabolism (Han et al., 2022b).

The *HOX24* annotation information is related to ABA and water deficit regulation. A Homeo-Leucine Zipper (HD-Zip) is a class of transcription factors that is unique to higher plants and involved in stress response and the growth and development of plants. *ATHB-6* is the HD-zip gene of maize (*Zea mays*), and the overexpression of *ATHB-6* in maize activates the expression of critical genes in the ROS signaling pathway and ABA-dependent pathway under drought tolerance (Peng et al., 2022). The annotated function of *HOX24* in sugarcane (*Saccharum officinarum*) under drought stress is related to antioxidants (Peiting et al., 2022). Both *MADS47* and *HOX24* in *A. mongolicum* are hub genes in the violet module, and they are mutually regulated and have genes that act together. Their functions are annotated as enzymatic activity, oxidation–reduction and cell surface receptor signaling pathway. The ABA hormone and BRs are the primary regulatory molecules that respond to drought signals and convey them down to the reciprocal genes that they regulate in the *MADS47*- and *HOX24*-mediated regulatory network, after which they exert drought regulation in the form of a network.

CCX1 is a member of the Cation/Ca^{2+} Exchanger family. The overexpression of *CCX1* in *A. thaliana* increased the sensitivity to hydrogen peroxide (H_2O_2) treatment, suggesting that this gene is involved in ROS homeostasis (Li et al., 2016). Na^+, K^+, and Ca^{2+} can retard the senescence of broccoli (*Brassica oleracea* var. *italica*) buds. The *CCX1* promoter was cloned in broccoli and found to inhibit its senescence. The functional annotation of *CCX1* in *A. mongolicum* under drought stress is sodium-potassium ion transport (Yan et al., 2020). Previous studies have confirmed the regulatory function of *CCX1* from the side. In the co-expression regulatory network of *CCX1*, which regulates genes with functions in oxidation–reduction and ion binding, protein ubiquitination regulation interacts synergistically in response to drought stress.

Polyamines (PA) are key components of plant growth and development and abiotic stress responses (EAlcázar and Tiburcio, 2014; Wimalasekera et al., 2015). Amine oxidases oxidatively catabolize PAs, and polyamine (PAO) oxidase is one of the breakdown products (Angelini et al., 2010). *PAO2* is annotated as regulating the redox process and peroxisome in *A. mongolicum*. In *A. thaliana*, *AtPAO2* is differentially expressed in the interaction of ABA, nitrate and ammonium ions, which can potentially improve the ability to regulate the growth of *A. thaliana* roots (Wimalasekera et al., 2015). *carC* is a regulatory gene and could play an active role in the production of carotene (Revuelta and Eslava, 1983). *CarC* is annotated as hydrolase activity in *A. mongolicum*. The *carC* coexpression network revealed that it primarily regulates chloroplast and redox genes. There are few reports about the role of *carC* gene in plants. As a result, more research is needed on the mechanism of the drought-resistant regulation of the *carC* gene in *A. mongolicum*. In conclusion, these studies show that *MADS47*, *CCX1*, *carC*, *PAO2*, and *HOX24* genes in drought may play an essential role in *A. mongolicum* under drought stress and can be used as suitable hub genes for drought resistance in *A. mongolicum*.

Conclusion

This study provides the first integrated analysis of *A. mongolicum* miRNAs and mRNAs regulated at the transcriptional level in response to drought stress. The multi-layered stress-responsive networks mediated by miRNAs and their hub target genes are no doubt highly complex but are coordinated. Five potential drought tolerance hub genes (*MADS47*, *CCX1*, *carC*, *PAO2*, and *HOX24*) were targeted by the analysis and the regulatory network was mapped. The study provides a theory for the functional validation of drought resistance hub genes in *A. mongolicum*. At the same time, new findings would lay the foundations for improving drought tolerance in gramineous crops *via* molecular breeding strategies.

Data availability statement

The original contributions presented in the study are publicly available. This data can be found at: NCBI, PRJNA742257.

Author contributions

BF conducted the experiments. YM organized and supervised the overall project. BF, FS, ZY, XZ, XY, JW, XY, LN, and YF performed the editing of the manuscript. YZ provided the seeds of *A. mongolicum*. All authors contributed to the article and approved the submitted version.

Funding

This study was funded by the National Natural Science Foundation of China (No. 31860670).

Conflict of interest

The authors declare that the research was conducted in the absence of any commercial or financial relationships that could be construed as a potential conflict of interest.

Publisher's note

All claims expressed in this article are solely those of the authors and do not necessarily represent those of their affiliated organizations, or those of the publisher, the editors and the reviewers. Any product that may be evaluated in this article, or claim that may be made by its manufacturer, is not guaranteed or endorsed by the publisher.

Supplementary material

The Supplementary material for this article can be found online at: https://www.frontiersin.org/articles/10.3389/fpls.2022.976684/full#supplementary-material

References

Abid, U., Heng, S., Xiyan, Y., and Zhang, X. L. (2017). Drought coping strategies in cotton: increased crop per drop. *Plant Biotechnol. J.* 15, 271–284. doi: 10.1111/pbi.12688

Addo-Quaye, C., Snyder, J. A., Park, Y. B., Li, Y.-F., Sunkar, R., and Axtell, M. J. (2009). Sliced microRNA targets and precise loop-first processing of miR319 hairpins revealed by analysis of the physcomitrella patens degradome. *RNA* 15, 2112–2121. doi: 10.1261/rna.1774909

Ali, N., Shah, F., Muhammad, A., Usman, A., Amanullah, , Sumera, A., et al. (2017). miRNAs: major modulators for crop growth and development under abiotic stresses. *Biotechnol. Lett.* 39, 685–700. doi: 10.1007/s10529-017-2302-9

Allen, E., Xie, Z., Gustafson, A. M., and Carrington, J. C. (2005). microRNA-Directed Phasing during Trans-Acting siRNA Biogenesis in Plants. *Cell* 121, 207–221. doi: 10.1016/j.cell.2005.04.004

Andrew, D. B. L., Ainsworth Elizabeth, A., Bernacchi Carl, J., Rogers, A., and Ort Donald, O. D. (2009). Elevated CO_2 effects on plant carbon, nitrogen, and water relations: six important lessons from face. *J. Exp. Bot.* 60, 2859–2876. doi: 10.1093/jxb/erp096

Angelini, R., Cona, A., Federico, R., Fincato, P., Tavladoraki, P., and Tisi, A. (2010). Plant amine oxidases "on the move": an update. *Plant Physiol. Biochem.* 48, 560–564. doi: 10.1016/j.plaphy.2010.02.001

Bano, N., Fakhrah, S., Mohanty, C. S., and Bag, S. K. (2022). Transcriptome meta-analysis associated targeting hub genes and pathways of drought and salt stress responses in cotton (gossypium hirsutum): a network biology approach. *Front. Plant Sci.* 13:818472. doi: 10.3389/FPLS.2022.818472

Berninger, P., Gaidatzis, D., Nimwegen, E. V., and Zavolan, M. (2008). Computational analysis of small RNA cloning data. *Methods* 44, 13–21. doi: 10.1016/j.ymeth.2007.10.002

Bilgin, C. C., Ercan, A., and Baohong, Z. (2016). Small RNA and degradome deep sequencing reveals drought-and tissue-specific micrornas and their important roles in drought-sensitive and drought-tolerant tomato genotypes. *Plant Biotechnol. J.* 14, 1727–1746. doi: 10.1111/pbi.12533

Bin, T., Yusun, S., Aaron, N., Xia, L., Jie, Z., Aiqin, W., et al. (2021). Integration of small RNA and degradome sequencing reveals the regulatory network of al-induced programmed cell death in peanut. *Int. J. Mol. Sci.* 23, 246–264. doi: 10.3390/ijms23010246

Boyer, J. S. (1982). Plant productivity and environment. *Science* 218, 443–448. doi: 10.1126/science.218.4571.443

Buchfink, B., Chao, X., and Daniel, H. H. (2014). Fast and sensitive protein alignment using DIAMOND. *Nat. Methods* 12, 59–60. doi: 10.15496/publikation-1176

Carrington, J. C., and Ambros, V. (2003). Role of microRNAs in plant and animal development. *Science* 301, 336–338. doi: 10.1126/science.1085242

Chandra, P., Wunnava, A., Verma, P., Chandra, A., and Sharma, R. K. (2021). Strategies to mitigate the adverse effect of drought stress on crop plants-influences of soil bacteria: a review. *Pedosphere* 31, 496–509. doi: 10.1016/S1002-0160(20)60092-3

Chao, M., Shaul, B., and Amnon, L. (2015). miR408 is involved in abiotic stress responses in Arabidopsis. *Plant J.* 84, 169–187. doi: 10.1111/tpj.12999

Che, Y. H., and Li, L. H. (2007). Genetic diversity of prolamines in *Agropyron mongolicum* Keng indigenous to northern China. *Genet. Resour. Crop. Evol.* 54, 1145–1151. doi: 10.1007/s10722-006-9006-7

Chen, J., Zhong, Y., and Qi, X. (2021). LncRNA TCONS_00021861 is functionally associated with drought tolerance in rice (*Oryza sativa* L.) via competing endogenous RNA regulation. *BMC Plant Biol.* 21, 410–422. doi: 10.1186/s12870-021-03195-z

David, W., and Franck, V. (2011). miR393: integrator of environmental cues in auxin signaling *plant signaling &. Behavior* 6, 1672–1675. doi: 10.4161/psb.6.11.17900

Du, J., Li, X., Li, T., Yu, D., and Han, B. (2017a). Genome-wide transcriptome profiling provides overwintering mechanism of *Agropyron mongolicum*. *BMC Plant Biol.* 17, 138–151. doi: 10.1186/s12870-017-1086-3

Du, Q., Zhao, M., Gao, W., Sun, S., and Li, W. (2017b). microRNA/microRNA* complementarity is important for the regulation pattern of *NFYA5* by miR169 under dehydration shock in *Arabidopsis*. *Plant J.* 91, 22–33. doi: 10.1111/tpj.13540

EAlcázar, R., and Tiburcio, A. F. (2014). Plant polyamines in stress and development: an emerging area of research in plant sciences. *Front. Plant Sci.* 5:319. doi: 10.3389/fpls.2014.00319

Elena, M., Virginie, J., Aurélie, H., Lokerse, A. S., Dolf, W., Herve, V., et al. (2010). miR390, *Arabidopsis TAS3* tasiRNAs, and their auxin response factor targets define an autoregulatory network quantitatively regulating lateral root growth. *Plant Cell* 22, 1104–1117. doi: 10.1105/tpc.109.072553

Esfahanian, E., Nejadhashemi, A. P., Abouali, M., Adhikari, U., Zhang, Z., Daneshvar, F., et al. (2017). Development and evaluation of a comprehensive drought index. *J. Environ. Manag.* 185, 31–43. doi: 10.1016/j.jenvman.2016.10.050

Flynt, A., and Lai, E. (2008). Biological principles of microRNA-mediated regulation: shared themes amid diversity. *Nat. Rev. Genet.* 9, 831–842. doi: 10.1038/nrg2455

Frank, J. S., Michael, B., Zhongchi, L., Victor, A., Robert, H., and Ruvkun, G. (2000). The lin-41 RBCC gene acts in the C. elegans heterochronic pathway between the let-7 regulatory RNA and the LIN-29 transcription factor. *Mol. Cell* 5, 659–669. doi: 10.1016/S1097-2765(00)80245-2

Gao, Y., Baohua, F., Caixia, G., Huiquan, Z., Fengting, W., Longxing, T., et al. (2022). The evolution and functional roles of miR408 and its targets in plants. *Int. J. Mol. Sci.* 23, 530–555. doi: 10.3390/IJMS23010530

Gereziher, M. T., Yanchao, X., Jawad, U. M., Linyerera, S. M., Yuqing, H., Yuhong, W., et al. (2021). Multi-omics-based identification and functional characterization of *Gh_A06G1257* proves its potential role in drought stress tolerance in gossypium hirsutum&13. *Front. Plant Sci.* 12:746771. doi: 10.3389/FPLS.2021.746771

Grabherr, M. G., Haas, B. J., Yassour, M., Levin, J. Z., Thompson, D. A., Amit, I., et al. (2011). Full-length transcriptome assembly from RNA-Seq data without a reference genome. *Nat. Biotechnol.* 29, 644–652. doi: 10.1038/nbt.1883

Guray, A., Derelli, T. E., Serkan, U., and Turgay, U. (2016). miRNA-based drought regulation in wheat. *Funct. Integr. Genomics* 16, 221–233. doi: 10.1007/s10142-015-0452-1

Hajyzadeh, M., Turktas, M., Khawar, K. M., and Unver, T. (2015). miR408 overexpression causes increased drought tolerance in chickpea. *Gene* 555, 186–193. doi: 10.1016/j.gene.2014.11.002

Han, Y. C., Liu, N., Li, C., Wang, S., Jia, L., Zhang, R., et al. (2022a). *TaMADS2-3D*, a MADS transcription factor gene, regulates phosphate starvation responses in plants. *Crop J.* 10, 243–253. doi: 10.1016/J.CJ.2021.03.020

Han, H., Liu, W., Lu, Y., Zhang, J., Yang, X., Li, X., et al. (2017). Isolation and application of P genome-specific DNA sequences of *Agropyron Gaertn* in Triticeae. *Planta* 245, 425–437. doi: 10.1007/s00425-016-2616-1

Han, Y., Yang, R., Zhang, X., Wang, Q., Wang, B., Zheng, X., et al. (2022b). Brassinosteroid accelerates wound healing of potato tubers by activation of reactive oxygen, metabolism and phenylpropanoid metabolism. *Foods* 11, 906–921. doi: 10.3390/FOODS11070906

Han, X., Yin, H., Song, X., Zhang, Y., Liu, M., Sang, J., et al. (2016). Integration of small RNAs, degradome and transcriptome sequencing in hyperaccumulator sedum

alfredii uncovers a complex regulatory network and provides insights into cadmium phytoremediation. *Plant Biotechnol. J.* 14, 1470–1483. doi: 10.1111/pbi.12512

Hollender, C. A., Chunying, K., Omar, D., Aviva, G., Matthews, B. F., Janet, S., et al. (2014). Floral transcriptomes in woodland strawberry uncover developing receptacle and anther gene networks. *Plant Physiol.* 165, 1062–1075. doi: 10.1104/pp.114.237529

Jiang, D., Chen, W., Dong, J., Li, J., and Fen, Y. (2018). Overexpression of miR164b-resistant *OsNAC2* improves plant architecture and grain yield in rice. *J. Exp. Bot.* 69, 1533–1543. doi: 10.1093/jxb/ery017

Jiao, Z., Lian, C., Han, S., Huang, M., Shen, C., Li, Q., et al. (2021). PtmiR169o plays a positive role in regulating drought tolerance and growth by targeting the *PtNF-YA6* gene in poplar. *Environ. Exp. Bot.* 189, 104549–104563. doi: 10.1016/j.envexpbot.2021.104549

Jiao, X., Wang, H., Yan, J., Kong, X., Liu, Y., Chu, J., et al. (2020). Promotion of BR biosynthesis by miR444 is required for ammonium-triggered inhibition of root growth. *Plant Physiol.* 182, 1454–1466. doi: 10.1104/pp.19.00190

Kannan, P., Vivek, H. S., Anushree, N., Singh, R. R., Soumita, D., Avik Pal, H. C. Y., et al. (2022). Nitrate-dependent regulation of miR444-*OsMADS27* signaling cascade controls root development in rice. *J. Exp. Bot.* 73, 3511–3530. doi: 10.1093/jxb/erac083

Langfelder, P., and Horvath, S. (2008). WGCNA: an R package for weighted correlation network analysis. *BMC Bioinform.* 9, 559–572. doi: 10.1186/1471-2105-9-559

Li, Z., Wang, X., Chen, J., Gao, J., Zhou, X., and Kuai, B. (2016). CCX1, a putative cation/Ca^{2+} exchanger, participates in regulation of reactive oxygen species homeostasis and leaf senescence. *Plant Cell Physiol.* 57, 2611–2619. doi: 10.1093/pcp/pcw175

Li, Y., Zheng, Y., Charles, A., Li, Z., Ajay, S., Guru, J., et al. (2010). Transcriptome-wide identification of microRNA targets in rice. *Plant J.* 62, 742–759. doi: 10.1111/J.1365-313X.2010.04187.X

Liu, H., Amanda, J., and Jason, A. (2020). Integrated analysis of small RNA, transcriptome, and degradome sequencing reveals the water-deficit and heat stress response network in durum wheat. *Int. J. Mol. Sci.* 21, 2260–2285. doi: 10.3390/ijms21176017

Livak, K. J., and Schmittgen, T. D. (2001). Analysis of relative gene expression data using real-time quantitative PCR and the 2(-Delta Delta C(T)) method. *Methods* 25, 402–408. doi: 10.1006/meth.2001.1262

Llave, C., Xie, Z., Kristin, D. K., and James, C. (2002). Cleavage of scarecrow-like mRNA targets directed by a class of Arabidopsis miRNA. *Science* 297, 2053–2056. doi: 10.1126/science.1076311

López, G. M. J., García, R. I., González-Hernández, A. I., Camañes, G., Vicedo, B., Real, M. D., et al. (2019). Expression of miR159 is altered in tomato plants undergoing drought stress. *Plan. Theory* 8, 201–212. doi: 10.3390/plants8070201

Lu, C., Donghoon, J., Karthik, K., Manoj, P., Kan, N., Rana, G., et al. (2008). Genome-wide analysis for discovery of rice microRNAs reveals natural antisense microRNAs (nat-miRNAs). *Proc. Natl. Acad. Sci. U. S. A.* 105, 4951–4956. doi: 10.1073/pnas.0708743105

Ma, Z., Coruh, C., and Axtell, M. J. (2010). Arabidopsis lyrata small RNAs: transient miRNA and small interfering RNA loci within the *Arabidopsis genus*. *Plant Cell* 22, 1090–1103. doi: 10.2307/25680120

Martin, M. (2011). Cut adapt removes adapter sequences from high-throughput sequencing reads. *EMBnet J.* 17, 10–12. doi: 10.14806/ej.17.1.200

Meng, Y., Shao, C., and Chen, M. (2011). Toward microRNA-mediated gene regulatory networks in plants. *Brief. Bioinform.* 12, 645–659. doi: 10.1093/bib/bbq091

Mortazavi, A., Williams, B. A., McCue, K., Schaeffer, L., and Wold, B. (2008). Mapping and quantifying mammalian transcriptomes by RNA-Seq. *Nat. Methods* 5, 621–628. doi: 10.1038/nmeth.1226

Mutz, K., Heilkenbrinker, A., Lönne, M., Walter, J., and Stahl, F. (2013). Transcriptome analysis using next-generation sequencing. *Curr. Opin. Biotechnol.* 24, 22–30. doi: 10.1016/j.copbio.2012.09.004

Nan, H., Tianran, S., Yanrong, L., Wenxin, Y., Geli, T., Yan, S., et al. (2020). Overexpression of Os-microRNA408 enhances drought tolerance in perennial ryegrass. *Physiol. Plant.* 172, 733–747. doi: 10.1111/ppl.13276

Natalia, C.-M., Joel, H., Wendy, C.-S., Maite, A., et al. (2019). MADS-box genes are key components of genetic regulatory networks involved in abiotic stress and plastic developmental responses in plants. *Front. Plant Sci.* 10:853. doi: 10.3389/fpls.2019.00853

Niu, S., Fan, G., Deng, M., Zhao, Z., and Dong, Y. (2014). Transcriptome/degradome-wide discovery of microRNAs and transcript targets in two *Paulownia australis* genotypes. *PLoS One* 9, 106736–106747. doi: 10.1371/journal.pone.0106736

Niu, J., Wang, J., An, J., Liu, L., and Lin, Z. (2016). Integrated mRNA and miRNA transcriptome reveal a cross-talk between developing response and hormone signaling for the seed kernels of *Siberian apricot*. *Sci. Rep.* 6, 35675–33587. doi: 10.1038/srep35675

Oladosu, Y., Rafii, M. Y., Samuel, C., Fatai, A., Magaji, U., Kareem, I., et al. (2019). Drought resistance in rice from conventional to molecular breeding: a review. *Int. J. Mol. Sci.* 20, 3519–3540. doi: 10.3390/ijms20143519

Patro, R., Duggal, G., Love, M. I., Irizarry, R. A., and Kingsford, C. (2017). Salmon provides fast and bias-aware quantification of transcript expression. *Nat. Methods* 14, 417–419. doi: 10.1038/nmeth.4197

Peiting, L., Pingping, L., Zhenli, Z., Zihong, L., Yanming, L., Chaohua, H., et al. (2022). Gene co-expression analysis reveals transcriptome divergence between wild and cultivated sugarcane under drought stress. *Int. J. Mol. Sci.* 23, 569–592. doi: 10.3390/IJMS23010569

Peng, J., Jiang, Z., Wei, X., Liu, S., Qu, J., Guan, S., et al. (2022). Overexpression of the homeobox-leucine zipper protein athb-6 improves the drought tolerance of maize (*Zea mays* L.). *Plant Sci.* 316, 111159–111171. doi: 10.1016/j.plantsci.2021.111159

Qiu, Z., Yan, Y., Zhang, Y., Guo, J., and Li, W. (2018). Characterization of miRNAs and their target genes in he-ne laser pretreated wheat seedlings exposed to drought stress. *Ecotoxicol. Environ. Saf.* 164, 611–617. doi: 10.1016/j.ecoenv.2018.08.077

Revuelta, J. L., and Eslava, A. P. (1983). A new gene (*carC*) involved in the regulation of carotenogenesis in Phycomyces. *Mol. Genet. Genom.* 192, 225–229. doi: 10.1007/BF00327670

Reyes, J. L., and Nam-Hai, C. (2007). ABA induction of miR159 controls transcript levels of two MYB factors during Arabidopsis seed germination. *Plant J.* 49, 592–606. doi: 10.1111/j.1365-313X.2006.02980.x

Rita, A., Pinky, A., Swatismita, R., Ashok, S., Vijay, S., Akhilesh, T., et al. (2007). MADS-box gene family in rice: genome-wide identification, organization and expression profiling during reproductive development and stress. *BMC Genomics* 8, 242–263. doi: 10.1186/1471-2164-8-242

Roseeta, D. M. C. B. S., Shivani, K., Preeti, A., Santosh, K., Mukesh, K., et al. (2013). Evolution of variety-specific regulatory schema for expression of osa-miR408 in indica rice varieties under drought stress. *FEBS J.* 280, 1717–1730. doi: 10.1111/febs.12186

Ryo, T., Ayumi, Y., Shino, M., Miki, N., Minami, M., Masaaki, S., et al. (2022). Brz-insensitive-pale green 1 is encoded by chlorophyll biosynthesis enzyme gene that functions in the downstream of brassinosteroid signaling. *Biosci. Biotechnol. Biochem.* 86, 1041–1048. doi: 10.1093/bbb/zbac071

Shi, G. Q., Jingying, F., Lingjie, R., Peiyue, Z., Chengjin, G., and Kai, X. (2018). TaMIR1119, a miRNA family member of wheat (Triticum aestivum), is essential in the regulation of plant drought tolerance. *J. Integr. Agric.* 17, 2369–2378. doi: 10.1016/S2095-3119(17)61879-3

Shubha, V., and Tyagi, A. K. (2010). Emerging trends in the functional genomics of the abiotic stress response in crop plants. *Plant Biotechnol. J.* 5, 361–380. doi: 10.1111/j.1467-7652.2007.00239.x

Smyth, G. K. (2010). Edge R: a bioconductor package for differential expression analysis of digital gene expression data. *Bioinformatics* 26, 139–140. doi: 10.1093/bioinformatics/btp616

Song, X., Yan, X., and Cao, Y. (2019). MicroRNAs and their regulatory roles in plant-environment interactions. *Annu. Rev. Plant Biol.* 70, 489–525. doi: 10.1146/annurev-arplant-050718-100334

Sonia, B., Mukesh, K., Devi, M. R., Utkarsh, R., Priyanka, A., Saloni, M., et al. (2017). Identification of miRNA-mediated drought responsive multi-tiered regulatory network in drought tolerant rice, Nagina 22. *Sci. Rep.* 7, 15446–15463. doi: 10.1038/s41598-017-15450-1

Sunkar, R., Girke, T., Kumar, J. P., and Zhu, J. K. (2005). Cloning and characterization of microRNAs from rice. *Plant Cell* 17, 1397–1411. doi: 10.1105/tpc.105.031682

Taeyoung, U., Joohee, C., Taehyeon, P., Joong, C. P., Eun, J. S., Sung, S. J., et al. (2022). Rice microRNA171f/*SCL6* module enhances drought tolerance by regulation of flavonoid biosynthesis genes. *Plant Direct.* 6:e374. doi: 10.1002/PLD3.374

Taier, G., Hang, N., Shi, T., Liu, Y., Ye, W., Zhang, W., et al. (2021). Ectopic expression of Os-miR408 improves thermo-tolerance of perennial ryegrass. *Agronomy* 11, 1930–1943. doi: 10.3390/AGRONOMY11101930

Wang, M., Guo, W., Li, J., Pan, X., Pan, L., Zhao, J., et al. (2021b). The miR528-AO module confers enhanced salt tolerance in rice by modulating the ascorbic acid and abscisic acid metabolism and ROS scavenging. *J. Agric. Food Chem.* 69, 8634–8648. doi: 10.1021/ACS.JAFC.1C01096

Wang, X., Li, B., Ma, T., Sun, L., Li, T., Hu, C., et al. (2020). The NAD kinase OsNADK1 affects the intracellular redox balance and enhances the tolerance of rice to drought. *BMC Plant Biol.* 20, 11–30. doi: 10.1186/s12870-019-2234-8

Wang, X., Liu, Y., Han, Z., Chen, Y., Huai, D., Kang, Y., et al. (2021c). Integrated transcriptomics and metabolomics analysis reveal key metabolism pathways

contributing to cold tolerance in Peanut&13. *Front. Plant Sci.* 12:752474. doi: 10.3389/FPLS.2021.752474

Wang, K., Liu, Y., Teng, F., Cen, H., Yan, J., Lin, S., et al. (2021a). Heterogeneous expression of Osa-MIR156bc increases abiotic stress resistance and forage quality of alfalfa. *Crop J.* 9, 1135–1144. doi: 10.1016/j.cj.2020.11.009

Wang, J., Zhou, Z., Tao, Q., Chen, S., Ren, X., Yu, L., et al. (2022). Brassica napus miR169 regulates BnaNF-YA in salinity, drought and ABA responses. *Environ. Exp. Bot.* 199:104882. doi: 10.1016/J.ENVEXPBOT.2022.104882

Wasilewska, A., Vlad, F., Sirichandra, C., Redko, Y., Jammes, F., Valon, C., et al. (2008). An update on abscisic acid signaling in plants and more. *Molecular Plant* 1, 198–217. doi: 10.1093/mp/ssm022

Wei, B., Tao, C., Zhang, R., Li, A., Huo, N., Li, S., et al. (2009). Novel microRNAs uncovered by deep sequencing of small RNA transcriptomes in bread wheat (*Triticum aestivum* L.) and *Brachypodium distachyon* (L.) Beauv. *Funct. Integr. Genomics* 9, 499–511. doi: 10.1007/s10142-009-0128-9

Wimalasekera, R., Schaarschmidt, F., Angelini, R., Cona, A., Tavladoraki, P., and Scherer, G. F. E. (2015). Polyamine oxidase2 of *Arabidopsis* contributes to ABA mediated plant developmental processes. *Plant Physiol. Biochem.* 96, 231–240. doi: 10.1016/j.plaphy.2015.08.003

Wu, L., Zhang, Q., Zhou, H., Ni, F., Wu, X., and Qi, Y. (2009). Rice MicroRNA effector complexes and targets. *Plant Cell* 21, 3421–3435. doi: 10.1105/tpc.109.070938

Xu, X., Yin, L., Ying, Q., Song, H., Xue, D., Lai, T., et al. (2013). High-throughput sequencing and degradome analysis identify miRNAs and their targets involved in fruit senescence of Fragaria ananassa. *PLoS One* 8, e70959–e70969. doi: 10.1371/journal.pone.0070959

Yan, K., Ran, M., Li, S., Zhang, J., Wang, Y., Wang, Z., et al. (2020). The delayed senescence of postharvest buds in salt ions was related to antioxidant activity, *HDA9* and *CCX1* in broccoli (Brassica oleracea L. var. italic planch). *Food Chem.* 324, 126887–126896. doi: 10.1016/j.foodchem.2020.126887

Yang, X., Wang, L., Yuan, D., Lindsey, K., and Zhang, X. (2013). Small RNA and degradome sequencing reveal complex miRNA regulation during cotton somatic embryogenesis. *J. Exp. Bot.* 64, 1521–1536. doi: 10.1093/jxb/ert013

Yang, J., Zhang, N., Zhou, X., Si, H., and Wang, D. (2016). Identification of four novel stu-miR169s and their target genes in Solanum tuberosum and expression profiles response to drought stress. *Plant Syst. Evol.* 302, 55–66. doi: 10.1007/s00606-015-1242-x

Yin, F. Q., Cheng, Q., Gao, J., Liu, M., Luo, X. R., Zhang, W. Y., et al. (2015). Genome-wide identification and analysis of drought-responsive genes and microRNAs in tobacco. *Int. J. Mol. Sci.* 16, 5714–5740. doi: 10.3390/ijms16035714

Zhang, X., Fan, B., Yu, Z., Nie, L., Zhao, Y., Yu, X., et al. (2019). Functional analysis of three miRNAs in *Agropyron mongolicum* Keng under drought stress. *Agronomy* 9, 661–686. doi: 10.3390/agronomy9100661

Zhang, B., Pan, X., Cox, S., Cobb, G., and Anderson, T. (2006). Evidence that miRNAs are different from other RNAs. *Cellular and Molecular Life Sciences* 63, 246–254. doi: 10.1007/s00018-005-5467-7

Zhao, C., Han, X., Taylor, F., Yao, Y., Bi, Y., Li, A., et al. (2010a). Deep sequencing identifies novel and conserved microRNAs in peanuts (*Arachis hypogaea* L.). *BMC Plant Biol.* 10, 3–12. doi: 10.1186/1471-2229-10-3

Zhao, P., Miao, Z., Zhang, J., Chen, S., Liu, Q., and Xiang, C. (2020). MADS-box factor *AGL16* negatively regulates drought resistance via stomatal density and stomatal movement. *J. Exp. Bot.* 71, 6092–6106. doi: 10.1093/jxb/eraa303

Zhao, Y., Yun, J., Shi, F., Wang, J., Yang, Q., and Chao, Y. (2010b). Molecular cloning and characterization of a group 3 *LEA* gene from Agropyron mongolicum Keng. *Afr. J. Biotechnol.* 9, 69–82. doi: 10.1186/1475-2859-9-69

Zhou, M., Zheng, S., Li, Y., Liu, R., Zhang, L., and Wu, Y. (2020). Comparative profiling of roots small RNA expression and corresponding gene ontology and pathway analyses for low- and high-cadmium-accumulating genotypes of wheat in response to cadmium stress. *Funct. Integr. Genomics* 20, 177–190. doi: 10.1007/s10142-019-00710-2

Zurbriggen, M. D., Hajirezaei, M. R., and Carrillo, N. (2010). Engineering the future. Development of transgenic plants with enhanced tolerance to adverse environments. *Biotechnol. Genet. Eng. Rev.* 27, 33–56. doi: 10.1080/02648725.2010.10648144

frontiers | Frontiers in Plant Science

TYPE Original Research
PUBLISHED 17 August 2022
DOI 10.3389/fpls.2022.950758

OPEN ACCESS

EDITED BY
Jin-Lin Zhang,
Lanzhou University, China

REVIEWED BY
Fengming Yan,
Henan Agricultural University, China
Xiaoyun Pan,
Fudan University, China

*CORRESPONDENCE
Ming Yue
yueming@nwu.edu.cn

SPECIALTY SECTION
This article was submitted to Plant Abiotic Stress, a section of the journal Frontiers in Plant Science

RECEIVED 23 May 2022
ACCEPTED 01 August 2022
PUBLISHED 17 August 2022

CITATION
Fan Y, Zhang R, Zhang Y and Yue M (2022) The effects of genetic distance, nutrient conditions, and recognition ways on outcomes of kin recognition in *Glechoma longituba*. *Front. Plant Sci.* 13:950758. doi: 10.3389/fpls.2022.950758

The effects of genetic distance, nutrient conditions, and recognition ways on outcomes of kin recognition in *Glechoma longituba*

Yilei Fan, Ruichang Zhang, Yuanlin Zhang and Ming Yue*

Northwest University, Xi'an, China

Kin recognition might help plants decrease competitive cost and improve inclusive fitness with close genes; thus it might interact with environmental factors to affect communities. Whether and how various factors, such as the genetic distance of neighbors, environmental stressors, or the way a plant recognizes its neighbors, might modify plant growth strategies remains unclear. To answer these questions, we conducted experiments in which ramets of a clonal plant, *Glechoma longituba*, were grown adjacent to different genetically related neighbors (clone kin / close kin / distant kin) in different nutrient conditions (high / medium / low), or with only root exudates from pre-treatment in culture solution. By comparing competitive traits, we found that: (1) kin recognition in *G. longituba* was enhanced with closer genetic distance; (2) the outcomes of kin recognition were influenced by the extent of nutrient shortage; (3) kin recognition helped to alleviate the nutrient shortage effect; (4) kin recognition via root exudates affected only below-ground growth. Our results provide new insights on the potential for manipulating the outcome of kin recognition by altering neighbor genetic distance, nutrient conditions and recognition ways. Moreover, kin recognition can help plants mitigate the effects of nutrient shortage, with potential implications in agricultural research.

KEYWORDS

clonal plant, kin recognition, nutrient shortage, root exudates, genetic distance

Introduction

Kin selection benefits related genes and improves inclusive fitness; this altruism is favored in two ways: kin recognition and viscous populations (Hamilton, 1964). Most plants have limited dispersal, resulting in genetically structured populations within a small spatial scale (Karban et al., 2015; Ehlers et al., 2016; Anten and Chen, 2021),

leading to a high likelihood of interactions with related neighbors, and making kin recognition important (Cheplick, 1992; Queller et al., 2015). Many previous studies provided evidence for kin recognition in plenty of plant species (Dudley and File, 2007; Murphy and Dudley, 2009; Biedrzycki et al., 2010; Masclaux et al., 2010; Bhatt et al., 2011; Biernaskie, 2011; Simonsen et al., 2015; Zhang et al., 2016; Xu et al., 2021), and that showed kin recognition can act as a driver not only always reducing some competitive traits (Dudley and File, 2007; Bhatt et al., 2011; Biernaskie, 2011; Crepy and Casal, 2015), but also sometimes increasing these competitive traits (Milla et al., 2009; Murphy and Dudley, 2009; Masclaux et al., 2010; Mercer and Eppley, 2014). Hence kinship might not be the only determinant in outcome of neighbor recognition, and other factors, e.g., nutrient conditions, water availability and/or other environmental stress, the way plants recognize kinship, or even the plant species, might affect the outcome of kin recognition. Thus more studies of how plants recognize relatedness are needed to understand this process more fully.

Previous studies have examined plant kin recognition among different related neighbors (Dudley and File, 2007; Murphy and Dudley, 2009; Biedrzycki et al., 2010; Bhatt et al., 2011; Mercer and Eppley, 2014; Semchenko et al., 2015; Abakumova et al., 2016), but there have been few studies to test how accurate the recognition might be and how different genetic distance affects kin recognition in specific species (Biedrzycki and Bias, 2010; Kiær et al., 2020). Depending on the dispersal mechanisms of a species, the nearest neighbors of clonal plants would be individuals of different genetic distances from that clone, including identical clones and kins with different degrees of relatedness (Ellstrand and Roose, 1987). Furthermore, crop species with artificially structured populations would have neighbors consisting of different related individuals of the same species (Murphy et al., 2017; Yang et al., 2018). Thus, plant of a given species might be favored by mechanisms that recognize and respond to different related neighbors more accurately (Dudley et al., 2013), so that they might avoid competition with the most closely related genes and so promote the survival of populations (Kiær et al., 2020). Overall, establishing whether plants are able to discriminate multi-level genetic distances and how they respond to different genetic neighbors from a same species might provide insights on how to modulate plant performance by adjusting the genetic structure in artificial plant populations, and suggest useful directions for further studies.

Since nutritional restriction is considered a dominant constraint on plant growth, density, and abundance (Tilman, 1984; Chapin et al., 1986; Ericsson, 1995; Bedford et al., 1999), some previous studies have focused on kin recognition under poor nutrient conditions, but the results have proved controversial. Recent research in *Sorghum vulgare* found that kin-benefit interactions in nutrient-poor soils were less pronounced than in nutrient-rich soil (Li et al., 2018). However, research in *Pisum sativum* showed plant kin selection was stronger in soil of lower fertility (Pezzola et al., 2020). A further study reported that the outcome of kin recognition changed several times when the growing distance from neighbors was altered from far to medium to close (Li et al., 2017). We can surmise that the two soil fertility studies found different consequences because they investigated kin recognition at two levels of fertility and their low fertility settings differed, and the response to kin varied under different degrees of nutrient shortage. Accordingly, we wished to investigate whether, under a range of nutrient decreasing conditions, the response to kin neighbors would remain constant or vary under different nutrient levels.

The capacity of plants to tolerate different constraining circumstances like nutrient shortage both above-ground (Smith, 1995; Anten, 2002; Falster and Westoby, 2003; Wang et al., 2014) and below-ground (Casper and Jackson, 1997; Maina et al., 2002; O' Brien and Joels, 2008; McNickle et al., 2014) is primary for improving fitness, so it would be important if growing adjacent to genetically close neighbors might have benefits under unfavorable conditions. Some previous studies have tested whether plants can integrate both nutrient and neighbor stimuli and respond separately, yet the results were not clear (Gersani et al., 2001; Hess and Kroon, 2007; Cahill et al., 2010; De Kroon et al., 2012; Lamb et al., 2012; Padilla et al., 2013). For example, McNickle et al. (2016) found neighboring plants influenced root foraging performance more than nutrient conditions, which implied that the effect of plant–plant interactions on plant architecture was more important than the effect of nutrients. Because kin recognition always shows positive plant–plant interactions (Hamilton, 1964), we expected it might alleviate plant competition under low nutrient conditions, or mask the effects of small nutrient differences. In summary, the interactions between nutrient conditions and kin recognition remain unclear, and testing whether growing with nearby kins leads to benefits under unfavorable conditions might provide new insight into kin recognition.

Plant have evolved a variety of ways to acquire resources (light, nutrients, water, etc.) and to receive/emit signals from the environment, and root is the major organ of below-ground performance (Lal, 1979; Callaway and Mahall, 2007; Goebel et al., 2011; Depuydt, 2014). Root exudates are widely accepted as one of the most important mechanisms for below-ground interactions, and some previous research has focused on how root exudates mediate kin recognition (Biedrzycki et al., 2010; Mercer and Eppley, 2014; Semchenko et al., 2015; Wang et al., 2020). Previous studies showed that root exudates mediated kin recognition in *Arabidopsis thaliana* (Biedrzycki et al., 2010) and *Distichlis spicata* (Mercer and Eppley, 2014). But after recognition has occurred, the outcomes of kin recognition are different between these two studies. And it remains unclear whether it is root exudates affect the outcome of kin recognition both above and below ground. It has been reported that other factors, such as volatile chemical cues (Karban et al., 2015;

Hussain et al., 2019) and photoreceptors (Crepy and Casal, 2015), were also able to mediate kin recognition. Thus, there might be various mechanisms by which plants can recognize neighbor identity, but there has been little research considering whether the specific outcomes of kin recognition might depend on the ways of recognition. Separating different potential ways of recognition, such as root exudates, would help us better understand how various mechanisms mediate kin recognition and influence its outcomes, and might provide new directions for future research on how responses to neighbors of different relatedness might be modified.

In the current study, we conducted a greenhouse experiment to explore kin recognition in a clonal plant, *Glechoma longituba*, and investigate how factors like neighbor genetic distance, nutrient stress, or ways of recognition affected plant growth. In our experiment, the plants had no initial below-ground parts, and the effects we detected as changes in plant architecture were most pronounced in the below-ground parts. Accordingly, we focused mainly on morphological traits below-ground and the relative growth rate (RGR) index of above-ground plant parts. Specifically, we tested four hypotheses: (1) kin recognition in *G. longituba* is stronger with closer genetic distance; (2) the outcome of kin recognition is influenced by nutrient shortage; (3) kin recognition helps to alleviate the effect of nutrient shortage; (4) kin recognition via root exudates can affect the growth of the whole plant.

Materials and methods

Experiments and plant materials

G. longituba is a normal stoloniferous clonal plant species in China. Each *G. longituba* ramet has two opposite leaves and produces roots when stolons touch the ground.

Genets of *G. longituba* used in our joint experiments were collected from Fenghuangzuigou (33.860 N, 108.825 E) and Hamagou (33.850 N, 108.818 E) in Qinling Mountains, which are 1.3 km apart with a valley between them. There were two different plots (1×1 m^2) in Fenghuangzuigou which were more than 10 m apart and considered plot A_1 and A_2, while only one plot (1×1 m^2) in Hamagou was considered plot B. We calculated the genetic distance of several genet samples collected from plot A_1/A_2 and plot B (**Supplementary Figure 1**). The analysis results showed genets from plot A_1 has a closer genetic distance to genets collected from plot A_2 than plot B, which demonstrates that genets from plot A_2 can be considered as close kin to genets from plot A_1 and genets from plot B can be considered as distant kin. Moreover, for clone species, fragment ramets from a same colon stolon would be same genetic identical but recognized as non-self to each other (Chen et al., 2015). So ramets from a same genet from plot A_1 can be considered as clone kin to each other in our experiment. Then we have three clear genetic distance levels (clone, close, distant) of kin neighbor for genetic distance treatment. All genets were collected on 19th March 2016 and then planted in a greenhouse for 6 months before formal experiments. Ramets chosen in all experiments were seedlings that had not touched culture media so did not have below-ground growth at the beginning of our experiments.

This joint experiment was designed to examine if *G. longituba* discriminates different related kins and how factors like genetic distance, nutrient stress, or the way plant recognizes its neighbor modified outcome of kin recognition (**Figure 1A**).

A control treatment was designed to make sure ramets used in our experiment from different plots (A_1, A_2, B) do not have significant difference in their growth performance (**Figure 1A**). And results showed the differences found in subsequent treatments were not caused simply by preexisting differences among ramets from the three plots (**Supplementary Figure 2**).

Genetic distance treatment * nutrient treatment

These two treatments were designed to verify if *G. longituba* can discriminate 3 levels of genetic distance and how genetic distance and nutrient stress influence appearance of kin recognition. To test this, we planted paired ramets in each pot and designed three different genetic-related levels: clone (the target plant and its neighbor sharing a pot were from a same genet from plot A_1), close (target plant was from genets in plot A_1 and its neighbor was from genets in plot A_2), and distant (target plant was from genets in plot A_1 and its neighbor was from genets in plot B) under a range of decreased nutrient levels (from high to medium to low). Each level had 7 replicates. Paired ramets were in similar size and the planting pots were full of high/medium/low nutrient solution (400 ml 100%/25%/6.25% Hoagland). The two ramets were placed at two diagonally corners of the pot to keep them separate during the experiment and avoid space competition. High/medium/low nutrient solution was added to each pot at the beginning and every 2 days during the experiment to maintain it at 400 ml (**Figure 1A**).

Root exudates treatment

This treatment was designed to examine how root exudates mediate kin recognition in *G. longituba*. The treatment was conducted in parallel with high nutrient condition group in *Genetic distance treatment * nutrient treatment*, kin recognition was supposed to be done after the previous treatment, thus when we removed the paired ramets, there would be liquid solutions left with 3 kinds of root exudates: exudates from target plant and its clone kin neighbor in clone pots, exudates from target plant and its close kin neighbor in close pots and exudates from target plant and its distant kin neighbor in distant pots. Each kind of pot had 7 replicates. Then after the *Genetic distance treatment * nutrient treatment*, we kept the old solution with root exudates

10.3389/fpls.2022.950758

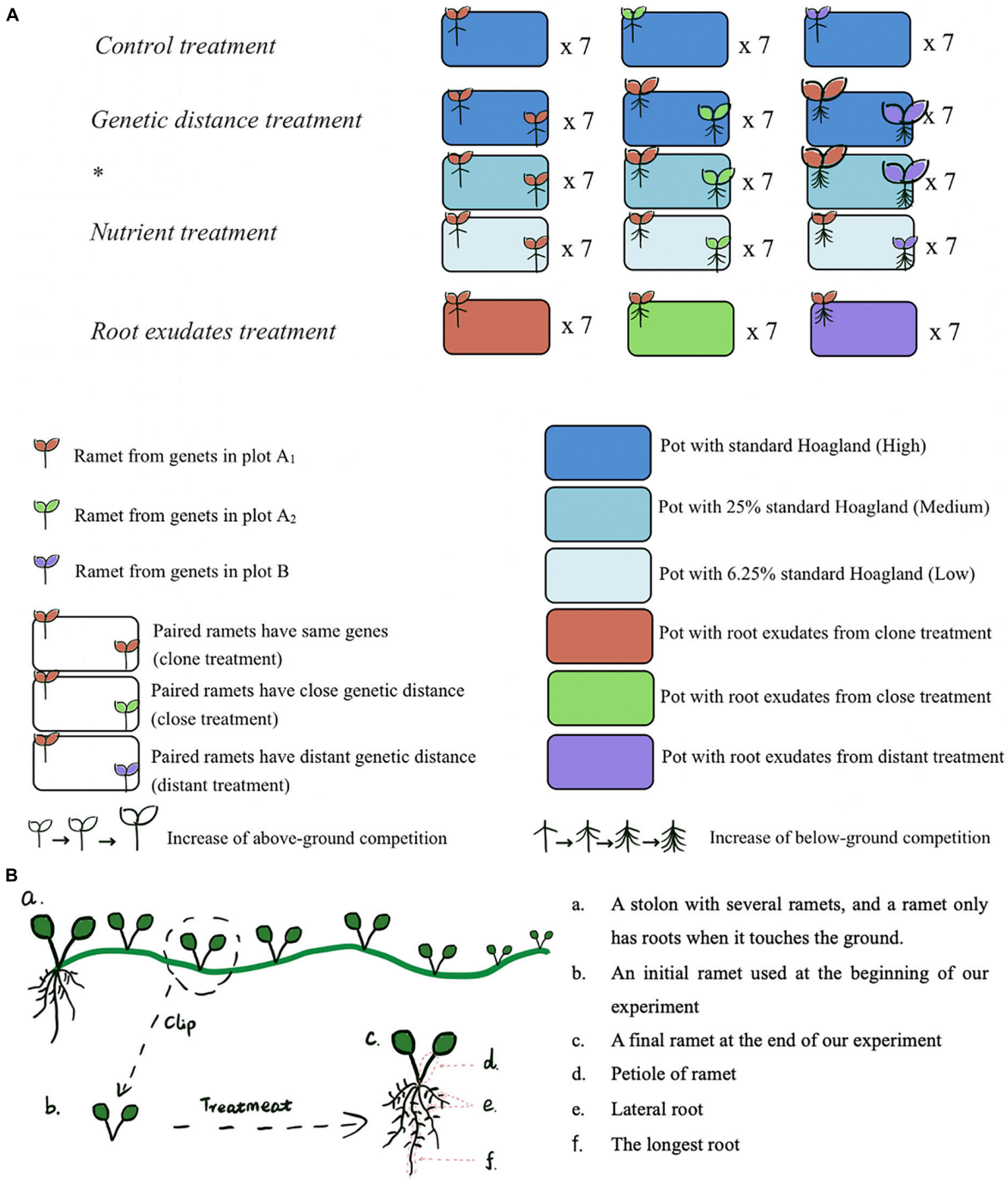

FIGURE 1
(A) Design of experimental units. After the *Genetic distance treatment * Nutrient treatment,* we kept the solution of the high nutrient level, which includes root exudates from ex-target and its neighbor, then put a ramet with the same gene of the ex-target in each pot as the *Root exudates treatment.* **(B)** A plant growth diagram showing the ramet material used in our experiment.

in each pot and put one target plant in each pot. This target plant was from the same genet as the ex-target plant in this pot before. High nutrient solution was added to each pot at the beginning and every 2 days during the experiment to maintain it at 400 ml (Figure 1A).

Growth conditions

The *G. longituba* ramets in our experiment were cultured in a greenhouse at 25°C during the daytime and 20°C during the night in summer 2018. In all experiments, ramets were fostered

in pairs or individually in a pot (150 × 100 × 55 mm) with the corresponding culture solution (400 ml) for 10 days. During this time, the high nutrient solution (medium/low nutrient solution in the other two nutrient level treatments only) would be added in each pot every 2 days to constantly maintain the volume of growth medium at 400 ml.

Measurement and statistical analysis

At the beginning and end of our experiment, fresh biomass, leaf area, and petiole length of each ramet were measured. And after experiments, length of the longest primary root, number of lateral roots were also measured. Then, specimens were separated into root, petiole, and leaf. These organics were dried at 60°C in an oven for 72 h and weighed separately.

Considering there was no initial below-ground of all ramets, we used one-way ANOVA to do multiple comparisons among groups and analyze the effects of neighbor relatedness on below-ground performance in all treatments, including root biomass, length of the longest root, and number of lateral roots (**Figure 1B**).

The ramets in our experiment had initial above-ground part (**Figure 1B**), so to decrease the effect of initial difference, we calculated RGR of fresh ramet biomass, leaf area, and petiole length by the following equation (Lugert et al., 2016).

$$RGR = (Wt\text{-}Wi)/Wi$$

where Wt is the final leaf area/petiole length, Wi is the initial/leaf area/petiole length. Then we used one-way ANOVA to do the *post hoc* test for these variables.

Then we used generalized linear mixed-effects modeling (GLMM) to test main effects of the two factors we focused on in our experiment (nutrient level and neighbor kinship), and their interactive effect on ramet growth performance we mentioned above.

All data were analyzed with SPSS 25.0 software. The data used in figures were all original data.

Results

Genetic distance and nutrient condition

Not only neighbor kinship has significant effects on ramet biomass traits and morphological traits (**Table 1** and **Supplementary Figure 3**), but nutrient level also plays an important role here (**Table 1** and **Supplementary Figure 4**). Moreover, there are significant interactive effects between these two factors on RGR of petiole length/leaf area, root biomass, and length of longest root. The two factors also have non-statistically significant interactive effect on ramet biomass and number of lateral root (**Table 1**).

Under the high nutrient treatment, *G. longituba* showed significant differences in most competitive traits between growing next to clone kin and growing with close or distant kin, while the difference between growing with close kin or distant kin was not statistically significant (**Figure 2**). Moreover, there was a general trend of increased investment in leaf, petiole, and root proliferation and bigger RII of roots when growing with more distant genetic kinship neighbors.

Under the medium nutrient treatment, *G. longituba* showed more obvious discrimination among kinship levels: there were significant differences among growing with clone kin vs. close kin vs. distant kin in all growth traits except root length, and the outcome of kin recognition was stronger than under the high nutrient treatment (**Figure 2**).

Under the low nutrient treatment, *G. longituba* showed little difference among the three types of related kins, and no clear kin discrimination was detected (**Figure 2**).

Nonetheless, *G. longituba* grown with clone kin showed the least change in most traits measured when the nutrient level was decreased, while ramets grown with close kin changed more and those grown with distant kin changed the most (**Figure 2**).

Root exudates treatment

Below-ground architectural traits of ramets in the root exudates treatment showed a similar trend to ramets grown under high/medium nutrient conditions in the genetic distance × nutrient level treatments (**Figure 3**). Both the RGR of petiole length, and leaf areas of target ramets in the root exudates treatment showed no significant difference among the three kinship levels (**Figure 3**), which suggested that *G. longituba* might have multiple ways to recognize neighbor identity, and the responses depended on the ways of recognition.

Discussion

Our results confirmed the first three of our hypotheses, in that the experiments showed that the outcomes of kin recognition were modulated by the genetic distance of neighbors and the nutrient conditions. Specifically, although root exudates were able to mediate kin recognition, the responses depended on multiple factors, and root exudates mediated only below-ground outcomes of kin recognition.

Similar to most previous studies, *G. longituba* showed kin recognition with detectable outcomes both above and below ground under high nutrient conditions (Dudley and File, 2007; Murphy and Dudley, 2009; Biedrzycki et al., 2010; Masclaux et al., 2010; Bhatt et al., 2011; Biernaskie, 2011; Zhang et al., 2016). Moreover, the outcome of kin recognition appeared to be largely dependent on genetic distance. Decreased competitive abilities were correlated with increased relatedness of kin. We

TABLE 1 ANOVA results for effects on neighbor kinship (NK) and nutrient level (NL) on ramet biomass traits and morphological traits of *G. longituba*.

		Ramet biomass		RGR of petiole length		RGR of leaf area		Root biomass		Number of lateral root		Length of the longest root	
	df	*F*	*p*	*F*	*p*	*F*	*p*	*F*	*p*	*F*	*p*	*F*	*p*
NK	2	21.69	**0.000**	13.13	**0.000**	15.36	**0.000**	73.48	**0.000**	5.29	**0.007**	45.50	**0.000**
NL	2	5.46	**0.006**	6.58	**0.002**	7.27	**0.001**	20.40	**0.000**	11.63	**0.000**	7.85	**0.001**
NK*NL	4	2.15	0.084	3.91	**0.006**	5.89	**0.000**	8.87	**0.000**	2.04	0.098	7.26	**0.000**

Values for $p < 0.005$ are in bold.

found *G. longituba* invested less in competitive morphological traits both above and below ground when the genetic distance between neighbors was closer. The lower RGR of leaf area and petiole length indicated less-successful competition for light (Smith, 1995; Gálvez and PeaCcy, 2003), while fewer root branches indicated reduced competitive ability in below-ground nutrient foraging (Biedrzycki et al., 2010; Semchenko et al., 2010; Marler, 2013). Overall, these results indicated reduced investment in resource acquisition and less competition between neighbors when they were closely related (Gersani et al., 2001). We also found that, although *G. longituba* competed less when the genetic distance of kin neighbors was closer, the discrimination between growing next to close kin and distant kin was not statistically significant. This might be because both the target plant and its neighbor were growing under favorable conditions, and the response to kin recognition might exert little effect on promoting population fitness; thus, while the plants might recognize different kins, this led to less-pronounced outcomes.

When the nutrient conditions were reduced from high to medium and even low levels, we found the outcome of kin recognition did not change in a pattern that correlated with nutrient levels. As mentioned above, there was no significant difference between *G. longituba* performance when growing with close kin or distant kin under high nutrient conditions; when the nutrient condition was decreased to medium, *G. longituba* statistically distinguished all clone/close/distant neighboring kins, revealing a stronger expression of kin recognition under the lower nutrient conditions. However, when nutrient levels were decreased to low, the outcome of kin recognition seemed to be masked by nutrient competition. This might explain why two recent studies on kin recognition and soil fertility found different results for plant performance with regard to kinship of neighbors under lower fertility (Li et al., 2018; Pezzola et al., 2020). The different results might be caused by different experimental designs for fertility, because our findings suggested the outcome of kin recognition was influenced by the extent of nutrient shortage. Another report showed similar results to ours, with similar outcomes for changes in kin recognition when the growing distance was altered (Li et al., 2017). Taking into consideration all these results, we speculate that the extent of environmental stress can affect kin recognition expression, and the expression changes from weak to strong to none when the stressor becomes more and more marked.

Because the response of *G. longituba* to kin recognition fluctuated under different nutrient conditions, we wondered whether growing next to closer kins might help plants improve their tolerance for low nutrient conditions. Many studies have shown that plants can synthesize information from their neighbors and nutrients and then respond to this information (Gersani et al., 2001; Novoplansky, 2009; McNickle and Brown, 2012; McNickle et al., 2016). A recent study in four grassland plant species found that information about neighbors exerted a stronger effect than nutrient levels in determining patterns of below-ground growth (McNickle et al., 2016), suggesting that kin recognition might play a dominant role in plant strategies when both neighbor identity and nutrient levels vary. In our research, both neighbor kinship and nutrient condition have significant effects on ramet biomass and morphology. Since these two factors also made significant interactive effects on most morphological traits, and growth of *G. longituba* was affected less by adjacent clone/close kins when grown under low nutrient conditions, indicating that growing with close genetic neighbors might buffer the effects of severe nutrient deficit. This result is similar to a previous study that examined kin selection in inter- and intra-specific competition, and suggested that kinship might influence plant growth (Mercer and Eppley, 2014). Generally, kin recognition is considered as a positive interaction, and kin neighbors are considered as a positive biotic factor by kin selection theory (Hamilton, 1964). Our study shows that kin recognition might play a dominant role in plant performance and help plants to tolerate poor conditions.

Previous studies have shown that root exudates can mediate identity recognition (Biedrzycki et al., 2010; Mercer and Eppley, 2014), and our research found *G. longituba* can recognize different genetic relatedness by ways of root exudates. But the effect was not exerted on the whole plant in our experiment, suggesting that kin recognition responses might be influenced by the method of plant recognition. In the genetic distance experiment, a target plant would not only have physical contact with its neighbor, but might also obtain information from other

10.3389/fpls.2022.950758

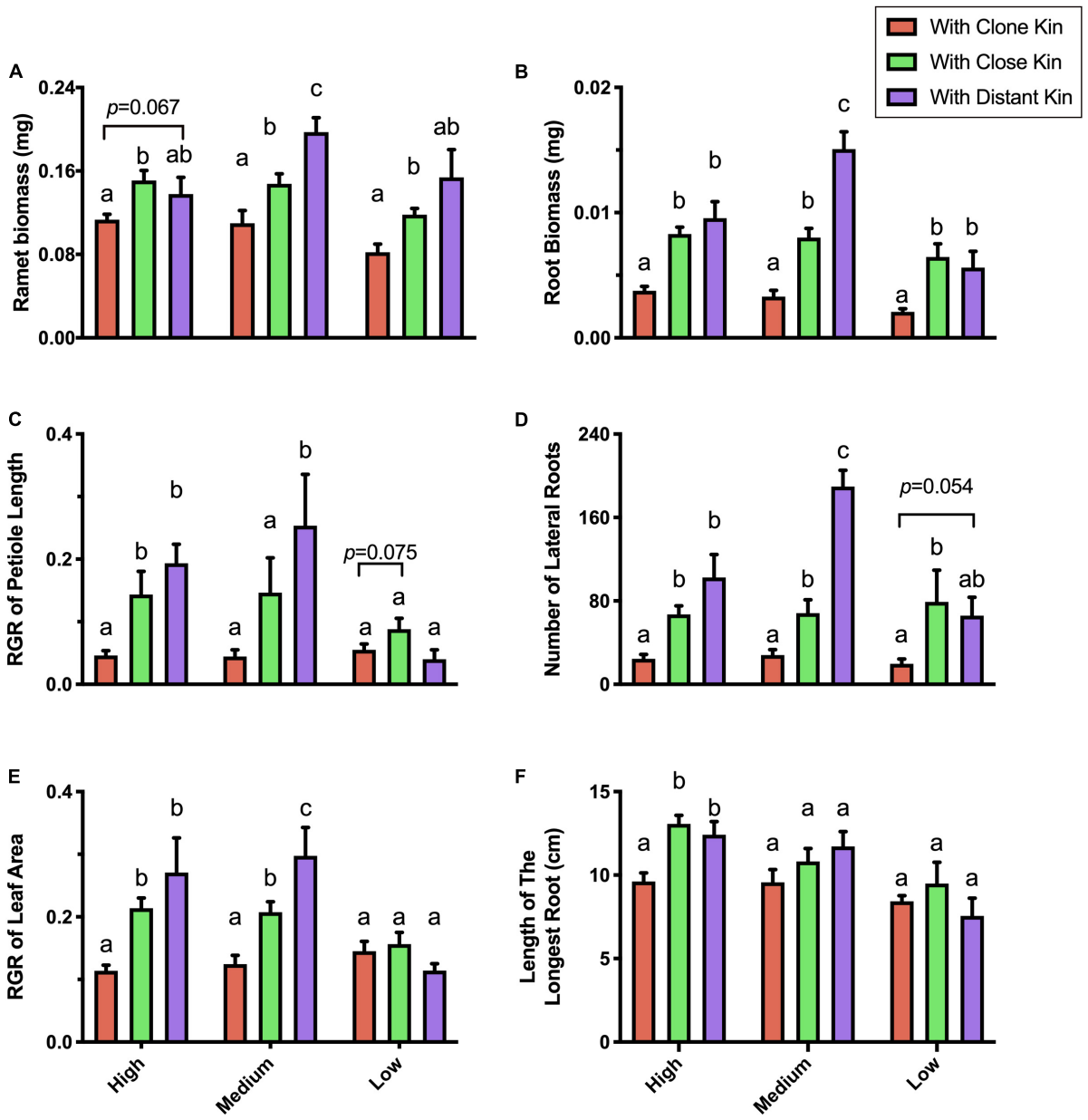

FIGURE 2
Competitive traits of *G. longituba* ramet response to different genetic related kins under different nutrient levels. **(A)** ramet biomass, **(B)** root biomass, **(C)** RGR of petiole length, **(D)** number of lateral roots, **(E)** RGR of leaf area, and **(F)** Length of the longest root. The different genetic related kins are either Clone Kin (target ramet and its neighbor have same genes), Close Kin (target ramet and its neighbor have close genetic distance) or Distant Kin (target ramet and its neighbor have the farthest genetic distance). The nutrient levels are high (100% Hoagland), medium (25% Hoagland), and low (6.25% Hoagland). Bars with different letters mean significant differences at $p < 0.05$.

above-ground signals like volatile chemical cues (Karban et al., 2015; Hussain et al., 2019) and photoreceptors (Crepy and Casal, 2016). By contrast, in the root exudates experiment, there was no distant kin growing simultaneously in the growth chamber, and thus only one mechanism was available for kin recognition, namely the different root exudates from the pre-treatment. Our results showed that *G. longituba* was able to recognize different kins by root exudates alone, but if there were no other kinship signals, the response was exerted weakly only below-ground and not throughout the plant. The different response in above-ground growth between the genetic distance treatment and the root exudates treatment indicates that above-ground and below-ground signals modulated the kin recognition response together, and the overall outcome was the result of integrating multiple ways of recognition. In summary, *G. longituba* can recognize kinship by different mechanisms, and the responses are affected

10.3389/fpls.2022.950758

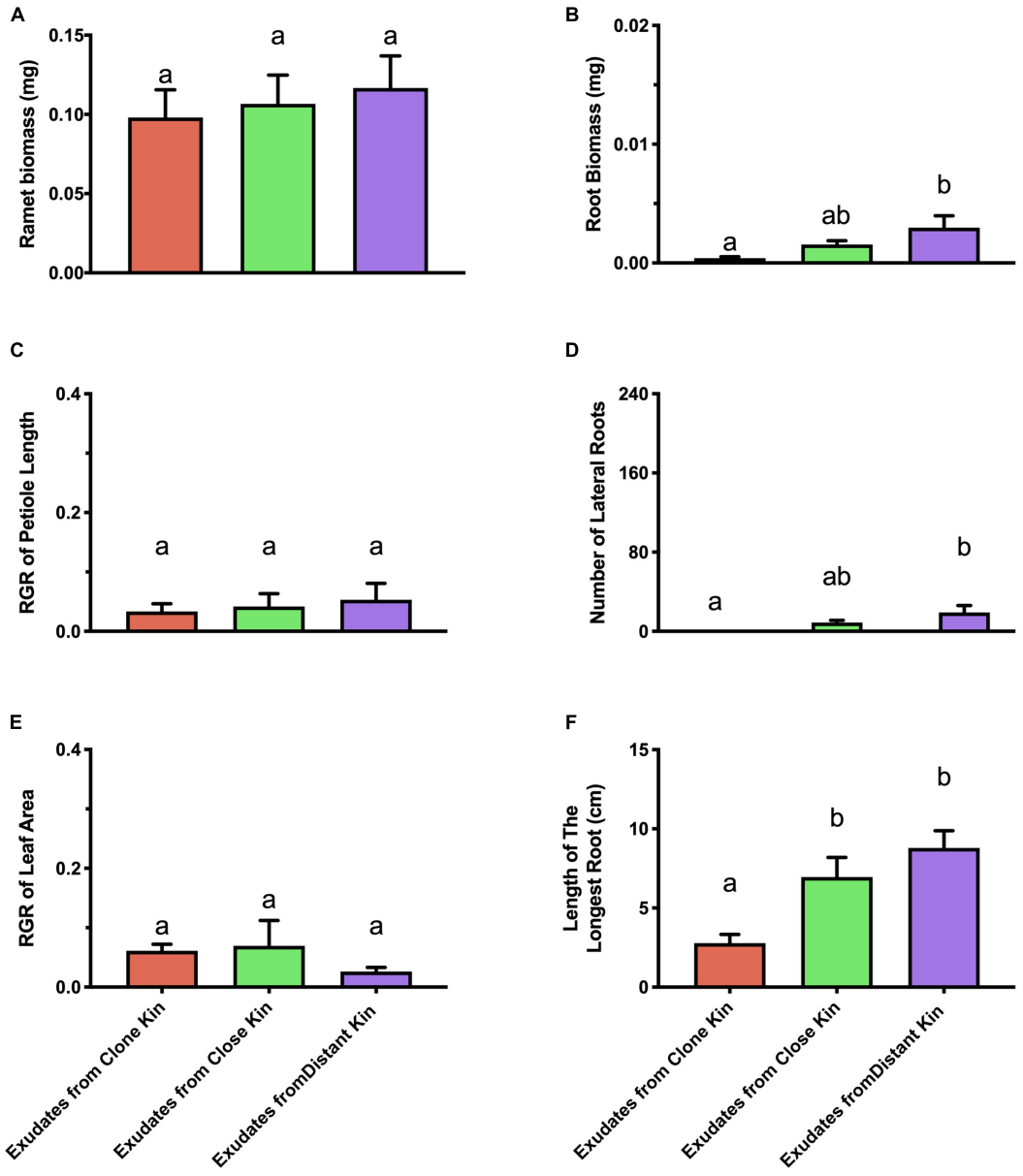

FIGURE 3
Competitive traits of solitary *G. longituba* ramets growing with root exudates from pre-treatment under high nutrient level. **(A)** Ramet biomass, **(B)** Root biomass, **(C)** RGR of petiole length, **(D)** number of lateral roots, **(E)** RGR of leaf area, and **(F)** Length of the longest root. Bars with different letters mean significant differences at $p < 0.05$.

by those mechanisms; thus kin recognition is a complex and sensitive process (File et al., 2012; Crepy and Casal, 2016; Yang et al., 2021). The development of new technologies to monitor biotic/abiotic factors (Depuydt, 2014; Galieni et al., 2021) should enable further exploration of the effect of root exudates and other potential mechanisms of kin recognition.

In conclusion, our investigation of kin recognition in *G. longituba* revealed that individual plants can recognize intra-specific kinship levels more accurately than we thought before, and the outcome of that recognition is strongly influenced by nutrient conditions. Moreover, growing alongside close genetic neighbors might help plants mitigate the effects of nutrient shortages. There are diverse mechanisms by which plants recognize their kin; these mechanisms might also determine the response to kin recognition. Our findings suggest the outcomes of kin recognition could be manipulated in various ways, such as adjusting environmental conditions, selecting the kinship in populations, or controlling the ways plants recognize and respond to their neighbors. By studying kin recognition abilities in specific plant species in crops, ornamental plants, medicinal

herbs, etc., we may make plants improve their investment in seeds, fruits, flowers, leaves, or other organs we need by taking control of different factors mentioned above. And benefits by growing with close kins could even improve plant tolerance under unfavorable conditions. Therefore, further studies on wider ranges of kinships, species, and other factors would help us better understand kin recognition in different plants, and new techniques would enable us to explore more details of kin recognition mechanisms, these relevant studies would provide new potential applications on agriculture, forestry, and environmental protection.

Data availability statement

The raw data supporting the conclusions of this article will be made available by the authors, without undue reservation.

Author contributions

YF performed the experiment and wrote the article. YZ analyzed the data. RZ revised the draft and finalized the manuscript for submission with YF and MY. All authors contributed to the article and approved the submitted version.

Acknowledgments

We thank James Cahill, Ph.D., from University of Alberta, Edmonton, Alberta, Canada for advises of this manuscript. And Huw Tyson, Ph.D., from Liwen Bianji (Edanz) (www.liwenbianji.cn) for editing the English text of a draft of this manuscript. And Altaf Uussain, Ph.D., from University of Alberta, Edmonton, Alberta, Canada for supplying referent article.

Conflict of interest

The authors declare that the research was conducted in the absence of any commercial or financial relationships that could be construed as a potential conflict of interest.

Publisher's note

All claims expressed in this article are solely those of the authors and do not necessarily represent those of their affiliated organizations, or those of the publisher, the editors and the reviewers. Any product that may be evaluated in this article, or claim that may be made by its manufacturer, is not guaranteed or endorsed by the publisher.

Supplementary material

The Supplementary Material for this article can be found online at: https://www.frontiersin.org/articles/10.3389/fpls.2022.950758/full#supplementary-material

References

Abakumova, M., Zobel, K., Lepik, A., and Semchenko, M. (2016). Plasticity in plant. functional traits is shaped by variability in neighbourhood species composition. *New Phytol.* 211, 455–463. doi: 10.1111/nph.13935

Anten, N., and Chen, B. (2021). Detect thy family: Mechanisms, ecology and agricultural. aspects of kin recognition in plants. *Plant Cell Environ.* 2021:14011. doi: 10.1111/pce.14011

Anten, N. P. R. (2002). Evolutionarily stable leaf area production in plant populations. *J. Theor. Biol.* 217, 15–32. doi: 10.1006/jtbi.2002.3022

Bedford, B. L., Walbridge, M. R., and Aldous, A. (1999). Patterns in nutrient availability. and plant diversity of temperate north american wetlands. *Ecology* 80, 2151–2169. doi: 10.2307/176900

Bhatt, M. A., Khandelwal, A., and Dudley, S. A. (2011). Kin recognition, not competitive. Interactions, predicts root allocation in young Cakile edentula seedling pairs. *New Phytol.* 189, 1135–1142. doi: 10.1111/j.1469-8137.2010.03548.x

Biedrzycki, M. L., and Bias, H. P. (2010). Kin recognition in plants: A mysterious. behaviour unsolved. *J. Exp. Bot.* 61, 4123–4128. doi: 10.1093/ietcom/e90-b.11.3004

Biedrzycki, M. L., Jilany, T. A., Dudley, S. A., and Bais, H. P. (2010). Root exudates. Mediate kin recognition in plants. *Commun. Integr. Biol.* 3, 28–35. doi: 10.4161/cib.3.1.10118

Biernaskie, J. M. (2011). Evidence for competition and cooperation among climbing plants. *Proc. Roy. Soc. B Biol. Sci.* 278, 1989–1996. doi: 10.1098/rspb.2010.1771

Cahill, J. F., McNickle, G. G., Haag, J. J., Lamb, E. G., Nyanumba, S. M., and Clair, C. C. S. (2010). Plants integrate information about nutrients and neighbors. *Science* 328:1657. doi: 10.1126/science.1189736

Callaway, R. M., and Mahall, B. E. (2007). Family roots. *Nature* 448, 145–147.

Casper, B. B., and Jackson, R. B. (1997). Plant competition underground. *Annu. Rev. Ecol. Syst.* 28, 545–570. doi: 10.1146/annurev.ecolsys.28.1.545

Chapin, F. S., Vitousek, P. M., and Cleve, K. V. (1986). The nature of nutrient limitation. In plant communities. *Am. Nat.* 127, 48–58.

Chen, B., Vermeulen, P. J., During, H. J., and Anten, N. (2015). Testing for disconnection and distance effects on physiological self-recognition within clonal fragments of potentilla reptans. *Front. Plant Sci.* 6:215. doi: 10.3389/fpls.2015.00215

Cheplick (1992). Sibling competition in plants. *J. Ecol.* 80, 567–575. doi: 10.2307/2260699

Crepy, M. A., and Casal, J. J. (2015). Photoreceptor-mediated kin recognition in plants. *New Phytol.* 205, 329–338. doi: 10.1111/nph.13040

Crepy, M. A., and Casal, J. J. (2016) Kin recognition by self-referent phenotype matching in plants *New Phytol.* 209, 15–16. doi: 10.1111/nph.13638

De Kroon, H., Hendrks, M., Van Ruijven, J., Ravenek, J., Padilla, F. M., Jongejans, E., et al. (2012). Root responses to nutrient and soil biota: Drives of

species coexistence and ecosystem productivity. *J. Ecol.* 100, 6–15. doi: 10.1111/j.1365-2745.2011.01906.x

Depuydt, S. (2014). Arguments for and against self and non - Self root recognition in plants. *Front. Plant Sci.* 2014:614. doi: 10.3389/fpls.2014.00614

Dudley, S. A., and File, A. L. (2007). Kin recognition in an annual plant. *Biol. Lett.* 3, 435–438. doi: 10.1098/rsbl.2007.0232

Dudley, S. A., Murphy, G. P., and File, A. L. (2013). Kin recognition and competition in plants. *Funct. Ecol.* 27, 898–906. doi: 10.1111/1365-2435.12121

Ehlers, B. K., David, P., Damgaard, C. F., and Lenormand, T. (2016). Competitor relatedness, indirect soil effects and plant coexistence. *J. Ecol.* 104, 1126–1135. doi: 10.1111/1365-2745.12568

Ellstrand, N. C., and Roose, M. L. (1987). Patterns of genotypic diversity in clonal plant species. *Am. J. Bot.* 74, 123–131. doi: 10.1002/j.1537-2197.1987.tb08586.x

Ericsson, T. (1995). Growth and shoot: Root ratio of seedlings in relation to nutrient. availability. *Plant Soil.* 169, 205–214. doi: 10.1007/BF00029330

Falster, D. S., and Westoby, M. (2003). Plant height and evolutionary games. *Trends Ecol. Evol.* 18, 337–343. doi: 10.1016/S0169-5347(03)00061-2

File, A. L., Murphy, G. P., and Dudley, S. A. (2012). Fitness consequences of plants growing with siblings: Reconciling kin selection, niche partitioning and competitive ability. *Proc. Roy. Soc. B Biol. Sci.* 279, 209–218. doi: 10.1098/rspb.2011.1995

Galieni, A., D'Ascenzo, N., Stagnari, F., Pagnani, G., and Pisante, M. (2021). Past and future of plant stress detection: An overview from remote sensing to positron emission tomography. *Front. Plant Sci.* 11:609155. doi: 10.3389/fpls.2020.609155

Gálvez, D., and PeaCcy, R. W. (2003). Petiole twisting in the crowns of psychotria limonensis: Implications for light interception and daily carbon gain. *Oecologia* 135, 22–29. doi: 10.1007/s00442-002-1158-3

Gersani, M., Brown, J. S., O'Brien, E. E., Maina, G. M., and Abramsky, Z. (2001). Tragedy of the commons as a result of root competition. *J. Ecol.* 89, 660–669. doi: 10.1046/j.0022-0477.2001.00609.x

Goebel, M., Hobbie, S. E., Bulaj, B., Zadworny, M., Archibald, D. D., Oleksyn, J., et al. (2011). Decomposition of the finest root branching orders: Linking belowground dynamics to fine-root function and structure. *Ecol. Monogr.* 81, 89–102. doi: 10.1890/09-2390.1

Hamilton, W. D. (1964). The genetical evolution of social behavior II. *J. Theor. Biol.* 7, 17–52.

Hess, L., and Kroon, H. D. (2007). Effects of rooting volume and nutrient availability as an alternative explanation for root self/non-self discrimination. *J. Ecol.* 95, 241–251. doi: 10.1111/j.1365-2745.2006.01204.x

Hussain, A., Rodriguez-Ramos, J. C., and Erbilgin, N. (2019). Spatial characteristics of volatile communication in lodgepole pine trees: Evidence of kin recognition and intra-species support. *Sci. Total Environ.* 692, 127–135. doi: 10.1016/j.scitotenv.2019.07.211

Karban, R., Wetzel, W. C., Shiojiri, K., Ishizaki, S., Ramirez, S. R., and Blande, J. D. (2015). Deciphering the language of plant communication: Volatile chemotypes of sagebrush. *New Phytol.* 204, 380–385. doi: 10.1111/nph.12887

Kiær, L. P., Weiner, J., and Rasmussen, C. R. (2020). Effects of kin recognition on root. traits of wheat germplasm over 100 years of breeding. *Plant. Biol.* 2020:243758. doi: 10.1101/2020.09.04.243758

Lal, R. (1979). Plant root systems: Their function and interaction with the soil. *Field Crop Res.* 2, 177–179. doi: 10.1016/0378-4290(79)90020-0

Lamb, E. G., Stewart, A. C., and Cahill, J. F. (2012). Root system size determines plant performance following short-term soil nutrient pulses. *Plant Ecol.* 213, 1803–1812. doi: 10.1007/s11258-012-0135-0

Li, J., Xu, X., and Liang, T. (2017). Kin Interactions of Arabidopsis Based on the Integrated Performance of Plants. *J. Resour. Ecol.* 8 185–190. doi: 10.5814/j.issn.1674-764x.2017.02.009

Li, J., Xu, X., and Feng, R. (2018). Soil fertility and heavy metal pollution (pb and cd) alter kin interaction of sorghum vulgare. *Environ. Exp. Bot.* 155, 368–377. doi: 10.1016/j.envexpbot.2018.05.009

Lugert, V., Thaller, G., Tetens, J., Schulz, C., and Krieter, J. (2016). A review on fish growth calculation: Multiple functions in fish production and their specific application. *Rev. Aquacult* 2016:12071. doi: 10.1111/raq.12071

Maina, G. G., Brown, J. S., and Gersani, M. (2002). Intra-plant versus inter-plant root competition in beans: Avoidance, resource matching or tragedy of the commons. *Plant Ecol.* 160, 235–247. doi: 10.1023/A:1015822003011

Marler, T. (2013). Kin recognition alters root and whole plant growth of split-root cycas edentata seedlings. *HortScience* 48, 1266–1269. doi: 10.21273/HORTSCI.48.10.1266

Masclaux, F., Hammond, R. M., Meunier, J., Gouhier-Darimont, C., Keller, L., and Reymond, P. (2010). Competitive ability not kinship affects growth of *Arabidopsis thaliana* accessions. *New Phytol.* 185, 322–331.

McNickle, G. G., and Brown, J. S. (2012). Evolutionarily stable strategies for nutrient. foraging and below-ground competition in plants. *Evol. Ecol. Res.* 14, 667–687.

McNickle, G. G., Brown, J. S., and Schwinning, S. (2014). An ideal free distribution explains the root production of plants that do not engage in a tragedy of the commons game. *J. Ecol.* 102, 963–971. doi: 10.1111/1365-2745.12259

McNickle, G. G., Deyholos, M. K., and Cahill, J. F. (2016). Nutrient foraging behaviour of four co-occurring perennial grassland plant species alone does not predict behaviour with neighbours. *Func. Ecol.* 30, 420–430. doi: 10.1111/1365-2435.12508

Mercer, C. A., and Eppley, S. M. (2014). Kin and sex recognition in a dioecious grass. *Plant Ecol.* 215, 845–852. doi: 10.1007/s11258-014-0336-9

Milla, R., Forero, D. M., Escudero, A., and Iriondo, J. M. (2009). Growing with siblings: A common ground for cooperation or for fiercer competition among plants? *Proc. Roy. Soc. B Biol. Sci.* 276, 2531–2540. doi: 10.1098/rspb.2009.0369

Murphy, G. P., and Dudley, S. A. (2009). Kin recognition: Competition and cooperation in impatiens (balsaminaceae). *Am. J. Bot.* 96, 1990–1996. doi: 10.3732/ajb.0900006

Murphy, G. P., Swanton, C. J., Van Acker, R. C., and Dudley, S. A. (2017). Kin recognition, multilevel selection and altruism in crop sustainability. *J. Ecol.* 105, 930–934. doi: 10.1111/1365-2745.12787

Novoplansky, A. (2009). Picking battles wisely: Plant behaviour under competition. *Plant Cell Environ.* 32, 726–741. doi: 10.1111/j.1365-3040.2009.01979.x

O' Brien, E. E., and Joels, B. (2008). Games roots play: Effects of soil volume and nutrients. *J. Ecol.* 96, 438–446. doi: 10.1111/j.1365-2745.2008.01354.x

Padilla, F. M., Mommer, L., De, C. H., Smit-Tiekstra, A. E., Wagemaker, C. A., Ouborg, N. J., et al. (2013). Early root overproduction not triggered by nutrients decisive for competitive success belowground. *PLoS One* 8:e55805. doi: 10.1371/journal.pone.0055805

Pezzola, E., Pandolfi, C., and Mancuso, S. (2020). Resource availability affects kin selection in two cultivars of pisum sativum. *Plant Growth Regulation* 90, 321–329. doi: 10.1007/s10725-019-00562-7

Queller, D. C., Rong, S., and Liao, X. (2015). Some agreement on kin selection and eusociality. *PLoS Biol.* 13:e1002133. doi: 10.1371/journal.pbio.1002133

Semchenko, M., John, E. A., and Huchings, M. J. (2010). Effect of physical connection and genetic identity of neighbouring ramets on root - placement patterns in two clonal species. *New Phytol.* 176, 644–654. doi: 10.1111/j.1469-8137.2007.02211.x

Semchenko, M., Saar, S., and Lepik, A. (2015). Plant root exudates mediate neighbour recognition and trigger complex behavioural changes. *New Phytol.* 204, 631–637. doi: 10.1111/nph.12930

Simonsen, A. K., Chow, T., and Stinchcombe, J. R. (2015). Reduced plant competition among kin can be explained by jensen's inequality. *Ecol. Evol.* 4, 4454–4466. doi: 10.1002/ece3.1312

Smith, H. (1995). Physiological and ecological function within the phytochrome family. *Ann. Rev. Plant Physiol. Plant Mol. Biol.* 46, 289–315. doi: 10.1146/annurev.pp.46.060195.001445

Tilman, G. D. (1984). Plant dominance along an experimental nutrient gradient. *Ecology* 65, 1445–1453. doi: 10.2307/1939125

Wang, P., Weiner, J., Cahill, J. F., Zhou, D. W., Bian, H. F., Song, Y. T., et al. (2014). Shoot competition, root competition and reproductive allocation in *Chenopodium acuminatum*. *J. Ecol.* 102, 1688–1696. doi: 10.1111/1365-2745.12313

Wang, Y., Murdock, M., Lai, S., Steele, D. B., and Yoder, J. I. (2020). Kin recognition in the parasitic plant triphysaria versicolor is mediated through root exudates. *Front. Plant Sci.* 11:560682. doi: 10.3389/fpls.2020.560682

Xu, Y., Cheng, H., Kong, C., and Meiners, S. (2021). Intra-specific kin recognition contributes to inter-specific allelopathy: A case study of allelopathic rice interference with paddy weeds. *Plant Cell Environ.* 2021, 1–13. doi: 10.1111/pce.14083

Yang, X. F., Li, L. L., Xu, Y., and Kong, C. H. (2018). Kin recognition in rice (*Oryza sativa*) lines. *New Phytol.* 220, 567–578. doi: 10.1111/nph.15296

Yang, Y., Xiao, C., Wu, X., Long, W., and Liu, G. (2021). Differing trade-off patterns of tree vegetative organs in a tropical cloud forest. *Front. Plant Sci.* 12:680379. doi: 10.3389/fpls.2021.680379

Zhang, L., Liu, Q., Tian, Y., Xu, X., and Ouyang, H. (2016). Kin selection or resource partitioning for growing with siblings: Implications from measurements of nitrogen uptake. *Plant Soil.* 398, 79–86. doi: 10.1007/s11104-015-2641-z

frontiers | Frontiers in Plant Science

TYPE Original Research
PUBLISHED 19 August 2022
DOI 10.3389/fpls.2022.938187

OPEN ACCESS

EDITED BY
Jing Zhang,
Nanjing Agricultural University,
China

REVIEWED BY
Wu Zhang,
Lingnan Normal University,
China
Xiaoping Xin,
Chinese Academy of Agricultural Sciences
(CAAS), China

*CORRESPONDENCE
Guowen Cui
cgw603@163.com

SPECIALTY SECTION
This article was submitted to
Plant Abiotic Stress,
a section of the journal
Frontiers in Plant Science

RECEIVED 07 May 2022
ACCEPTED 29 July 2022
PUBLISHED 19 August 2022

CITATION
Mei L, Zhang N, Wei Q, Cao Y, Li D and
Cui G (2022) Alfalfa modified the effects of
degraded black soil cultivated land on the
soil microbial community.
Front. Plant Sci. 13:938187.
doi: 10.3389/fpls.2022.938187

Alfalfa modified the effects of degraded black soil cultivated land on the soil microbial community

Linlin Mei, Na Zhang, Qianhao Wei, Yuqi Cao, Dandan Li and Guowen Cui*

College of Animal Science and Technology, Northeast Agricultural University, Harbin, Heilongjiang, China

Legume alfalfa (*Medicago sativa* L.) is extensively planted to reduce chemical fertilizer input to the soil and remedy damaged fields. The soil mechanism of these effects is potentially related to the variations in alfalfa-mediated interactions of the soil microbial community. To understand the impact of planting alfalfa on the soil microbial community in degraded black soil cultivated land, a 4-year experiment was conducted in degraded black soil cultivated land. We assessed soil parameters and characterized the functional and compositional diversity of the microbial community by amplicon sequencing that targeted the 16S rDNA gene of bacteria and ITS of fungi in four systems under corn cultivation at the Harbin corn demonstration base (Heilongjiang, China): multiyear corn planting (more than 30years, MC1); 2 years of alfalfa-corn rotation (OC); 3 years of alfalfa planting (TA); and 4 years of alfalfa planting (FA). It was found out that alfalfa led to changes in the alpha diversity of soil bacteria rather than in fungi in the degraded arable land. The abundance of the bacterial groups Gemmatimonadetes, Actinobacteria, Planctomycetes, and Chloroflexi was increased in OC, while Proteobacteria and Acidobacteria and the fungal group Glomeromycota were increased in TA and FA. OC, TA, and FA significantly increased the pH level but reduced soil electrical conductivity, but they had no impact on soil available nitrogen and soil available potassium at the 0–15cm soil depth. However, with the years of alfalfa planting, soil available nitrogen and soil available potassium were reduced at the 15–30cm soil depth. OC, TA, and FA significantly reduced the soil available phosphorus and soil total phosphorus at the 15–30cm soil depth. There was no significant impact made on soil total nitrogen. FA significantly reduced the soil organic matter at the 15–30cm soil depth. Planting alfalfa in degraded black soil cultivated land can reduce the salt content of the soil, and the nutrient content of soil planted with alfalfa without fertilization was equivalent to that of degraded corn cultivated land with annual fertilization. Besides, alfalfa recruited and increased contained taxa with the capacity to improve soil nutrient utilization and inhibit the harmful influences of pathogens for subsequent crops. Meanwhile, the planting of alfalfa can modify soil conditions by promoting the proliferation of specific beneficial microbiota groups.

KEYWORDS

soil degradation, phytoremediation, alfalfa, crop rotation, microbial community

Introduction

Black soil generally refers to Mollisols, which are the fertile soils distributed in four major regions around the world: North America, southeastern Europe, Central Asia, including northeast China, and the Pampas of South America (Durán et al., 2011; Liu et al., 2018a). However, in recent years, the black soil resources have been seriously degraded, the content of soil organic matter has decreased, the soil has hardened, and the degree of salinization has increased (Du et al., 2021; Li et al., 2021). In order to maintain a high grain yield, it is necessary to use a large amount of chemical fertilizers, which results in a large number of residual inorganic salt ions, thus exacerbating the degradation of the soil. The rotation of Gramineae and Leguminosae is a scientific and reasonable combination model for the restoration of degraded black soil.

Previous studies have shown that planting high-quality forage is an important measure to improve the quality and fertility of degraded arable soils (Yu et al., 2021). Meanwhile, a previous study observed improvements in field, pest management, and soil fertility with crop rotations. These improvements are attributed mainly to the soil microbial community (Samaddar et al., 2021).

Alfalfa has long been the preferred forage grass for rotation due to its high perennial persistence, protein content, and biomass production. Alfalfa is a potential "microbial hotspot crop" (Samaddar et al., 2021), as studies have revealed that planting alfalfa increases soil microbial activity (Agnello et al., 2016; Luo et al., 2018), and a large amount of root biomass and lipid root exudates closely related to plant growth and development can be produced (Wang et al., 2017; Bertrand et al., 2020; Zhao et al., 2020). In addition, the soil bacterial population can be introduced into the rhizosphere; for example, the addition of alfalfa in the rotation would increase the abundance of such bacterial groups as Acidobacteria, Actinobacteria, Chloroflexi, Gemmatimonadetes, and the fungal group Glomeromycota that include arbuscular mycorrhizal fungi (Wang et al., 2017; Samaddar et al., 2021). Planting alfalfa significantly improved the soil bacterial population and fungal/bacterial ratio after continuous potato cropping (Qin et al., 2017). A scientific and reasonable rotation mode can be effective in alleviating the deterioration of the soil environment caused by continuous cropping obstacles, enhancing the activity and diversity of microorganisms in soil, and creating a healthy and stable soil ecological environment for subsequent crop growth (Jarecki et al., 2018). Therefore, an improved understanding as to the mechanism of interaction between microorganisms and plants could help improve the remediation of degraded black soil.

Legume alfalfa also has the ability to improve the content of soil organic matter and nutrients (Beimforde et al., 2014; Dong et al., 2016; Luo et al., 2018). However, research suggested a decreasing trend in total nitrogen, total carbon, nitrate nitrogen, and available potassium in alfalfa for up to 10 years after continuous cropping, while the opposite was true for more than 10 years of continuous cropping (Yao et al., 2019). Meanwhile, the changes in the organic matter and nutrient content of the soil after alfalfa cultivation can affect the structure of soil fungal community and the relative abundance of specific fungi (Shen et al., 2013; Bastida et al., 2017; Yao et al., 2019). Research has demonstrated that alfalfa continuous cropping will accelerate the depletion of soil water and phosphorus, thus reducing bacterial diversity (Beauregard et al., 2010; Wang et al., 2021). However, there remain many uncertainties with regard to the impact of alfalfa planting on the soil microbial community and the restoration of degraded black soil.

Herein, our aim is to investigate the impact of planting alfalfa on the soil microbial community in degraded black soil cultivated land. Thus, we drew comparison between multiyear corn planting (more than 30 years), 2 years of alfalfa-corn rotation, 3 years of alfalfa planting, and 4 years of alfalfa planting in all parts of cropping system experiment. It was predicted that (i) alfalfa recruits and increases the microbial community, including taxa with the capacity to improve soil nutrient utilization and promote luxuriant growth for subsequent crops, and (ii) long-term alfalfa planting can modify soil conditions by promoting the proliferation of specific beneficial microbiota groups.

Materials and methods

Experimental design

Conducted at the Harbin corn demonstration base, the research is a long-term agricultural experiment carried out at Wujia Town (126°23′E, 45°31′N) in Heilongjiang Province. The annual average temperature and precipitation are 3.5°C–4.5°C and 400–600 mm, respectively. The soil type of the experimental site is black soil. The cultivars of corn and alfalfa used were "Tiannong 9" and "Dongnong 1," respectively. A potassium sulfate compound fertilizer substrate of 600 kg·hm^{-2} (N 72 kg·hm^{-2}, P 108 kg·hm^{-2}, K 90 kg·hm^{-2}) was applied annually to the corn field. The alfalfa was sown in May 2016 and 2017, respectively. The alfalfa fields were fertilized in the year of sowing with 54 kg·hm^{-2} N and 138 kg·hm^{-2} P. Only a foliar spray was applied 10 days before each crop was mown during the growth of alfalfa.

The four treatments included: multiyear corn planting (more than 30 years, MC1); 2 years of alfalfa corn rotation (OC), where corn was cultivated following two-year alfalfa in 2019; 3 years of alfalfa planting (TA); and 4 years of alfalfa planting (FA). Each treatment was replicated 4 times. The size of each plot was 20 m × 20 m, with 5 m between plots. The topography of the plots was flat, and the soil quality was uniform.

Sampling and laboratory analyses

Soil samples were collected in mid-September 2019 (after crop harvesting). Within each plot, 10 sample points were randomly selected with a 2.5 cm diameter soil auger; then, the soils were mixed into one sample. The root system of alfalfa was a typical taproot system purposed to study the effect of alfalfa on different soil layers for each treatment, with samples collected from two soil

depths: 0–15 cm and 15–30 cm. Within each plot, 10 sample points were randomly selected with a 2.5 cm diameter soil auger. Then, the soils were mixed into one sample. Then, the samples were sieved and divided into two parts. One part was air-dried for soil parameters determination, while the other was reserved at −80°C for microbial analysis.

After the soil surface litter was removed, the soil samples were air-dried at room temperature and then passed through a 2 mm soil sieve for the determination of soil parameters. The soil bulk density (BD) was measured by using the ring knife method. The soil moisture content (MC) was tested by the weight loss of the samples after drying at 105°C. Soil pH and electrical conductivity (EC) were measured using a pH meter and a conductivity meter, respectively (water-soil ratio was 2.5:1; Han et al., 2018). Soil total nitrogen was tested by using the Kjeldahl method. After NaOH melting, soil total nitrogen (TN), soil total phosphorus (TP), and soil total potassium (TK) were tested by means of Kjeldahl nitrogen determination, molybdenum antimony colorimetry, and flame photometry, respectively. Soil available nitrogen (AN) was tested by using the alkaline diffusion method. Soil available phosphorus (AP) was tested by using the $NaHCO_3$ extraction-molybdenum antimony anti-colorimetric method. Soil available potassium (AK) was extracted with neutral ammonium acetate and tested with a flame photometer. Soil organic matter (SOM) was tested by means of oxidation with potassium dichromate-sulfuric acid solution (Sun, 2019).

Amplicon sequencing

The diversity and composition of the soil bacterial and fungal communities were determined by Dene Denovo from Guangzhou. We amplified the V3–V4 region of bacterial 16S rDNA and the ITS2 region of fungal ITS rDNA by using specific primer pairs with barcodes 341F: 5′CCTACGGGNGGCWGCAG3′/806R: 5′ GGACT ACHVGGGTATCTAAT3′ and ITS3_KYO2: 5′ GATGAAGAAC GYAGYRAA3′/ITS4: 5′ TCCTCCGCTTATTGATATGC3′. Each sample was subjected to PCR in a 50 µl mixture. The mixture included 10× Buffer KOD (5 µl), 2 mM dNTPs (5 µl), 25 mM $MgSO_4$ (3 µl), KOD Polymerase (1 µl), 10 µM Primer F (1.5 µl), 10 µM Index Primer (1 µl), 10 µM Primer R (1.5 µl), or 10 µM Universal PCR Primer (1 µl). The reaction conditions for the PCR are as follows: 94°C (2 min), 98°C (10 s), 65°C (30 s), and a final extension at 68°C (10 min). Then, all raw tags were filtered into sequences to obtain high-quality tags. In order to study the compositional diversity information on the species of the samples, all valid tags of all samples were clustered using UPARSE software. Then, the sequences were clustered into OTUs (Operational Taxonomic Units) with 97% agreement by default. The results were calculated and the absolute abundance and relative information of tags in each sample were calculated for each OTU. UPARSE selects representative sequences (the tag sequence with the highest abundance in OTUs) in the process of constructing OTUs. The Naive Bayesian assignment algorithm of RDP Classifier was applied to annotate these representative sequences with the Greengenes database. These representative sequences were then annotated with the Greengenes database using the Naive Bayesian assignment algorithm of RDP Classifier (with a confidence threshold of 0.8~1), so as to obtain the species annotation information of each OTU.

Statistical analysis

Soil parameters, Chao1, Shannon, and Sob were determined by means of one-way ANOVA, PCA, and PERMANOVA tests. The community composition at the OTU level of soil microorganisms was analyzed through PCoA (using Bray–Curtis distances) and PERMANOVA tests. Pearson's correlation analysis was conducted to identify soil physicochemical factors and determine the relative abundance of bacterial and fungal phyla. All data analyses and graphing were performed with the assistance of SPSS 26 and Origin 2019b, respectively. The comparisons between the means were performed through Tukey's test ($p < 0.05$).

Results

Effects on the composition of soil bacterial and fungal communities

The changes in planting practices affected the bacterial and fungal communities. At the 0–15 cm soil depth, the bacterial and fungal communities were generally clustered by sample point (Figures 1A,B). Besides, PERMANOVA showed that the soil bacterial and fungal communities of TA, FA, and OC clearly differed from those of MC1 ($p = 0.004$, $p = 0.001$). At the 15–30 cm soil depth, soil bacterial communities differed significantly between corn and alfalfa plantings, while the closer distance between OC and MC1 along axis 1 indicated the slight differences (Figure 1C). Also, PERMANOVA indicated that they were insignificant ($p = 0.181$). The distance between TA and FA was small, while the two bacterial communities were similar and insignificantly different ($p = 0.543$). The fungal communities were clustered at different sites. The differences in fungal communities between maize and alfalfa plots were observed along axis 1 for years of cultivation, with closer distances between samples from three-year alfalfa and four-year alfalfa plots, indicating that short-term alfalfa cultivation exerted no significant effect on fungal community composition (Figure 1D). PerMANOVA showed that the soil fungal communities differed significantly ($p = 0.005$) between the plantings.

Alpha diversity of soil bacterial and fungal communities

We detected a total of 3,265,694 (94.87% of the total community) effective tags of bacteria from 32 soil samples, with each ranging from 302 to 478 in length. A total of 80,163 OTUs were detected through clustering. Moreover, we detected 3,310,770 (95.95% of the total community) fungal active labels from 32 soil

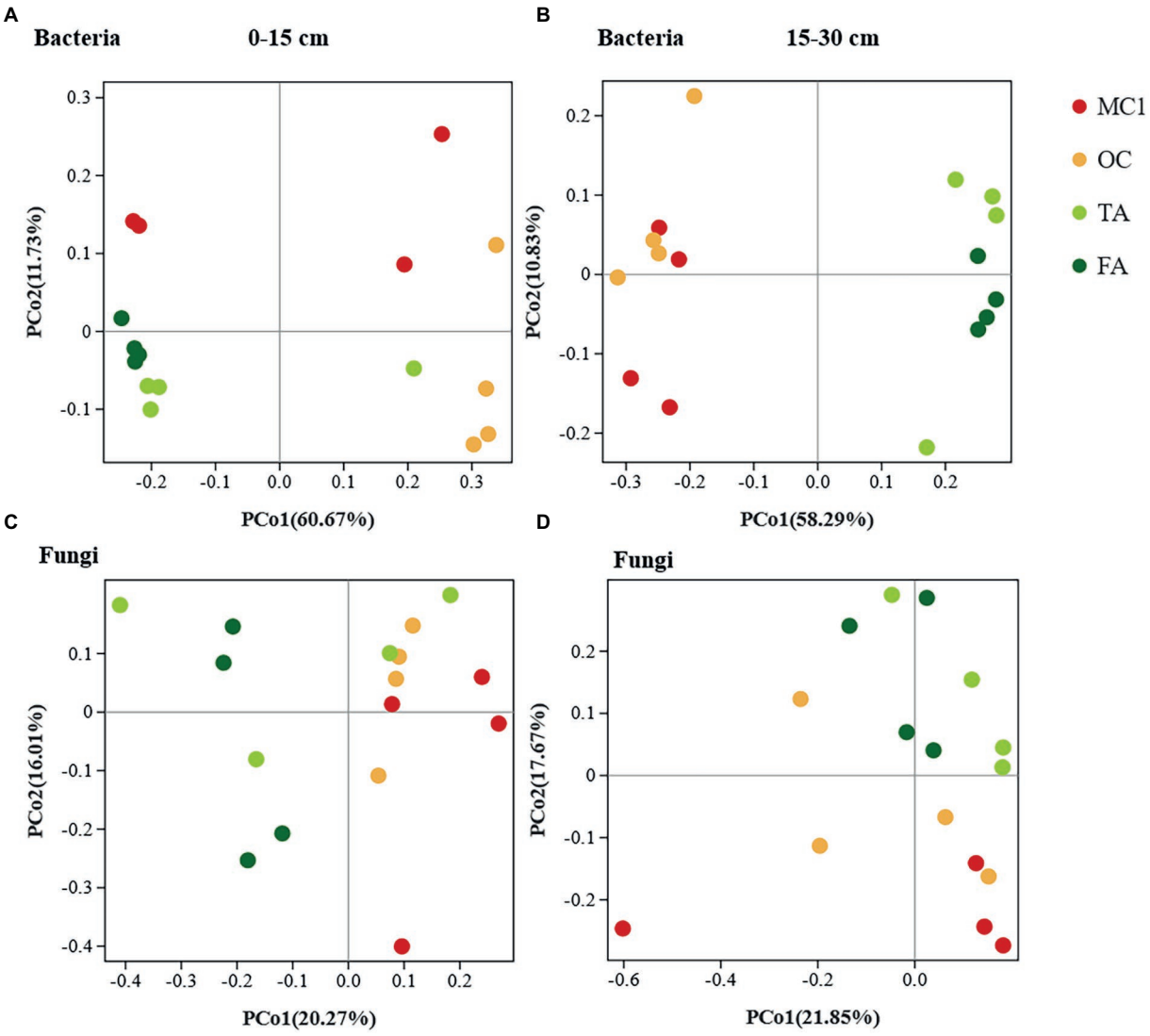

FIGURE 1
The PCoA of soil bacteria and fungals at different soil depths. The PCoA of soil bacteria at the 0-15 cm soil depth (A) and the 15-30 cm soil depth (B). PCoA of soil fungi at the 0-15 cm soil depth (C) and the 15-30 cm soil depth (D).

samples, with each ranging from 206 to 478 in length. These tags were then clustered into 24,894 OTUs.

OC has no significant impact on Chao 1, Shannon, and sobs (Figures 2A–L). TA and FA significantly increased the Chao 1 and Sobs indices of the soil bacterial community at the soil depths of 0–15 cm and 15–30 cm ($p < 0.05$; Figures 2A,C,D,F). FA and TA significantly increased the Shannon index at the 15–30 cm soil depth ($p < 0.05$; Figure 2E). There were no significant impacts made on the Chao 1, Sobs, and Shannon indices of the soil fungal community (Figures 2G–L).

Overall microbial composition patterns

A total of 31 bacterial phyla and 10 fungal phyla were detected (Figure 3). At the 0–15 cm soil depth, OC increased the abundance of Gemmatimonadetes, Actinobacteria, Planctomycetes and Chloroflexi by 62.91%, 16.11%, 52.93%, and 62.03% ($p < 0.05$; Figure 3A), respectively. FA increased the abundance of Proteobacteria by 44.52% ($p < 0.05$). TA and FA increased the abundance of Acidobacteria by 56.83% and 81.06% ($p < 0.05$), respectively, with the abundance of Verrucomicrobia improved by 204.45% and 416.06% ($p < 0.05$), respectively; however, they reduced the abundance of Gemmatimonadetes by 10.17% and 38.70% ($p < 0.05$), respectively, with the abundance of Actinobacteria increased by 31.93% and 35.69% ($p < 0.05$), respectively, with the abundance of Chloroflexi improved by 24.11% and 36.31% at the 0–15 cm soil depth ($p < 0.05$; Figure 3A), respectively. TA and FA increased the abundance of Proteobacteria by 191.38% and 241.87% ($p < 0.05$), respectively, with the abundance of Acidobacteria improved by 149.02% and 168.44% ($p < 0.05$), respectively, with the abundance of Planctomycetes increased by 20.12% and 2.51%

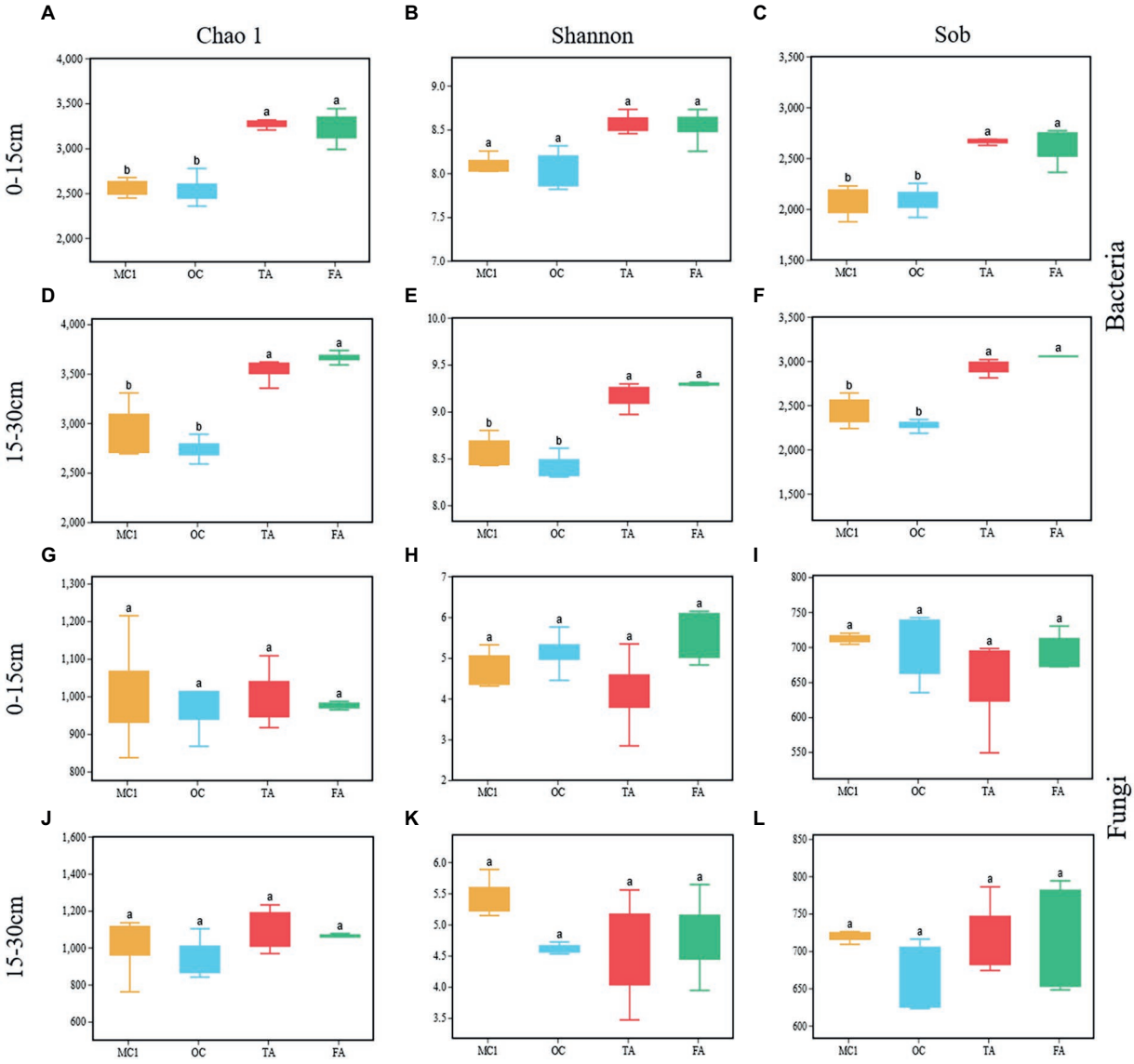

FIGURE 2
Box plots representing soil bacterial (A-F) and soil fungal (G-L) alpha diversity at the soil depths of 0-15 cm and 15-30 cm for different treatments, including Chao1, Shannon and Sob. MC1= multiyear corn planting. OC = two years of alfalfa-corn rotation, TA = three years of alfalfa planting, and FA= four years of alfalfa planting. Different lowercase letters indicate a significant difference between treatments ($p < 0.05$).

($p > 0.05$), respectively; by contrast, the abundance of Actinobacteria was reduced by 52.17% and 52.45% ($p < 0.05$), respectively, with the abundance of Gemmatimonadetes improved by 63.92% and 64.73% ($p < 0.05$), respectively, with the abundance of Chloroflexi reduced by 40.47% and 42.93% at the 15–30 cm soil depth ($p < 0.05$; Figure 3B), respectively.

At the 0–15 cm soil depth, OC, TA, and FA increased the abundance of Mortierellomycota by 126.80%, 216.84%, and 645.29% ($p < 0.05$), respectively, with the abundance of Mucoromycota increased by 130.03%, 107.81%, and 414.69% ($p < 0.05$; Figure 3C). TA and FA increased the abundance of Glomeromycota by 35.78% and 372.35% ($p < 0.05$; Figure 3C), respectively. At the 15–30 cm soil depth, OC, TA, and FA increased the abundance of Ascomycota by 43.75%, 10.22%, and 22.86% ($p < 0.05$; Figure 3D), respectively.

To gain insight into the community differentiation of soil microbial taxa after alfalfa planting, the five most abundant genera were observed at different soil depths. For bacteria, *Gemmatimonas* was dominant at both soil depths. The next most abundant genera were *Sphingomonas* in the 0–15 cm soil depth and *Candidatus_Udaeobacter* and *RB41* in the 15–30 cm soil depth (Figures 4A–H). *Nitrospira* was observed in TA and FA at the 15–30 cm soil depth (Figures 4E,F).

Gemmatimonas was the highest at 0–15 cm and 15–30 cm soil depth in MC1 and OC (Figures 4A,B,E,F). *Sphingomonas* was the highest at 0–15 cm in TA and FA (Figures 4C,D). For fungi, *Penicillium* was the highest at both soil depths under the different treatments. *Fusarium* and *Mortierella* were the dominant species at both soil depths in TA and FA (Figures 4I–P).

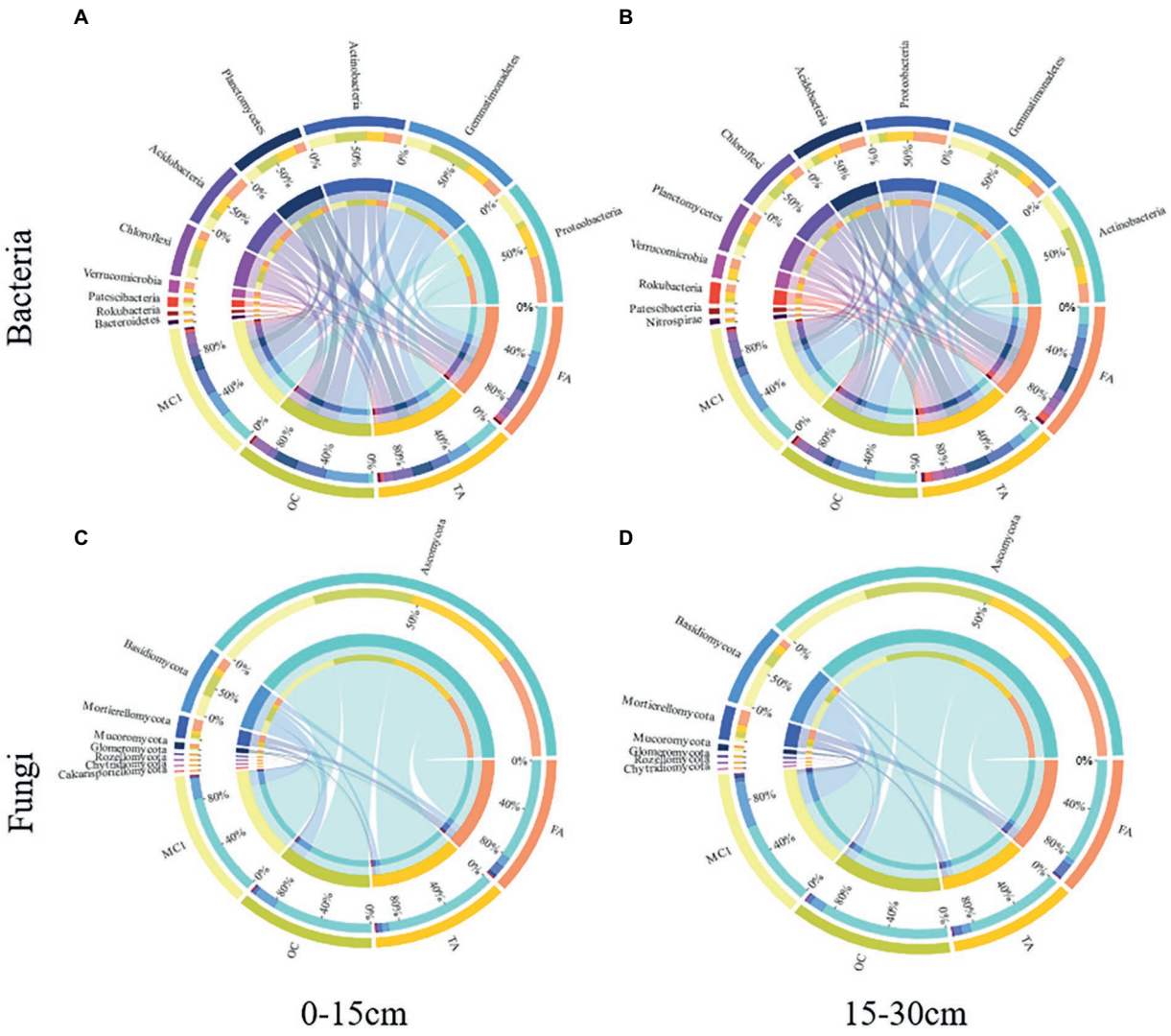

FIGURE 3
Circos plots represent the relative abundance of the top 10 bacterial phyla and the top 8 fungal phyla at different soil depths. The relative abundance of bacteria at the 0-15 cm soil depth (A) and the 15-30 cm soil depth (B) and the relative abundance of fungi at the 0-15 cm soil depth (C) and the 15-30 cm soil depth (D) under different treatments.

Soil parameters

The physicochemical properties of the soil varied considerably when different planting methods were adopted. TA and FA significantly reduced the soil moisture content but increased the soil bulk density at the 0–15 cm soil depth. OC, TA, and FA significantly increased the pH value but reduced soil electrical conductivity at the 0–15 cm soil depth. OC, TA, and FA had no impact on soil available nitrogen and soil available potassium at the 0–15 cm soil depth. However, with the extension of alfalfa planting, soil available nitrogen and soil available potassium were reduced at the 15–30 cm soil depth. OC, TA, and FA significantly reduced the soil available phosphorus and soil total phosphorus at the 15–30 cm soil depth. There was no significant impact on soil total nitrogen. FA significantly reduced the soil organic matter at the 15–30 cm soil depth (Table 1).

At the 0–15 cm soil depth, PC1 explained 45.8% of the variation, and 66.9% of the variation in total with PC2. As shown in the figure, there was a more pronounced separation between the corn and alfalfa plots along the first sorting axis, indicating that the physicochemical properties differed substantially between the OC and TA. Soil pH and soil bulk density were negatively correlated with planting method along the first ranking axis, but positively correlated with soil total phosphorus, soil available phosphorus, and soil electrical conductivity. Soil available potassium, soil organic matter, and soil available nitrogen show shorter arrows, indicating a less significant impact on the sorting plane. The distance between MC1 and OC sample sites was increased, indicating that the change in cropping method (2 years of alfalfa planting followed by maize planting in a multi-year maize field) caused a significant difference in soil physicochemical properties between them. Also, the difference between TA and FA is insignificant (Figure 5A).

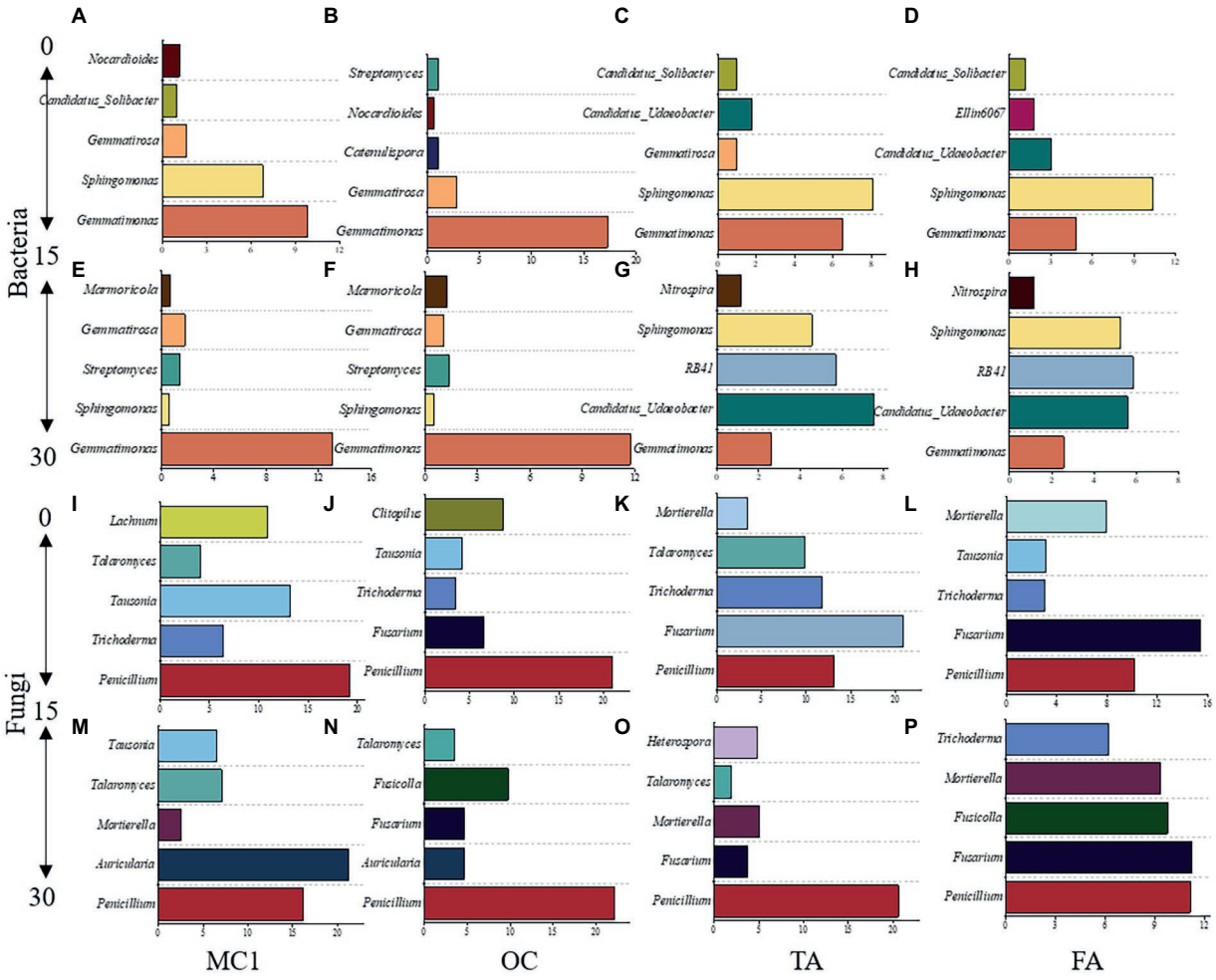

FIGURE 4
The top five dominant genera at the soil depths of 0-15 cm and 15-30 cm under different treatments. The dominant bacterial genera at the 0-15 cm soil depth (A-D) and 15-30 cm soil depth (E-H). The dominant fungal genera at the 0-15 cm soil depth (I-L) and the 15-30 cm soil depth (M-P).

At the 15–30 cm soil depth, PC1 explained 48.2% of the variation, and PC2 explained 13.8% of the variation, according to the principal component analysis. A total of 62% of the variation was explained by the principal component analysis. As can be seen from the figure, the physicochemical properties of the corn field along the first sorting axis were significantly different from those of the alfalfa field. Additionally, the planting method was positively correlated with soil available potassium and soil organic matter. There was a significant separation between MC1 and OC along the second ordination axis, indicating that the soil physicochemical properties differed significantly due to the change in cropping practice. However, the difference between the physicochemical properties of TA and FA was less significant (Figure 5B).

Relationships between soil properties and microbial taxa

At the 0–15 cm soil depth, Proteobacteria and Acidobacteria were negatively correlated with soil electrical conductivity and soil available nitrogen to a significant extent under different planting methods. Actinobacteria and Chloroflexi were positively correlated with soil electrical conductivity and soil available nitrogen to a significant extent. In addition, Acidobacteria and Rokubacteria showed a significant negative correlation with soil total phosphorus. Meanwhile, Acidobacteria ($r = -0.735$) and Verrucaria ($r = -0.6$) were negatively correlated with soil moisture content to a significant extent, and Actinobacteria ($r = 0.716$) showed a significant positive correlation with soil moisture content. Gemmatimonadetes ($r = -0.50$) and Actinobacteria ($r = -0.765$) were negatively correlated with soil bulk density to a significant extent, while Acidobacteria ($r = 0.779$) and Verrucomicrobia ($r = 0.65$) were positively correlated with soil bulk density to a significant extent. Rokubacteria was negatively correlated with soil total phosphorus and soil available phosphorus to a significant extent. The Planctomycetes was positively correlated only with soil organic matter to a significant extent (Figure 6A).

At the 15–30 cm soil depth, Gemmatimonadetes ($r = 0.713$, $r = 0.923$), Actinobacteria ($r = 0.747$, $r = 0.849$), and Chloroflexi

TABLE 1 Effect of planting practices on soil physicochemical properties.

Soil depth cm	Sample	MC%	BD g cm^{-3}	pH	EC μs cm^{-1}	AN mg kg^{-1}	AP mg kg^{-1}	AK mg kg^{-1}	TN g kg^{-1}	TP g kg^{-1}	TK g kg^{-1}	SOM g kg^{-1}
0–15	MCI	26.74 ± 0.40a	1.06 ± 0.03b	5.92 ± 0.06b	81.70 ± 15.52a	111.42 ± 7.88a	89.36 ± 5.30a	103.75 ± 5.79ab	1.35 ± 0.03a	0.66 ± 0.02a	20.48 ± 0.69ab	28.79 ± 2.92a
	OC	26.32 ± 0.40a	1.12 ± 0.06b	6.33 ± 0.06a	45.58±6.98b	120.75 ± 6.64a	34.98 ± 4.70b	100.83 ± 4.90b	1.29 ± 0.04a	0.47 ± 0.05b	24.33 ± 1.46a	27.83 ± 2.48a
	TA	24.84± 0.65bc	1.35 ± 0.05a	6.31 ± 0.01a	34.98 ± 1.65a	102.20 ± 9.611a	34.93 ± 3.92b	127.33 ± 6.31a	1.38 ± 003a	0.39 ± 0.05b	18.26 ± 0.87b	28.32 ± 1.00a
	FA	24.44 ± 0.22b	1.40 ± 0.02a	6.28 ± 0.01a	32.13 ± 0.65b	88.67 ± 7.57a	30.35 ± 1.93b	116.17 ± 6.63ab	1.28 ± 0.02a	0.38 ± 0.05b	19.47 ± 0.32b	27.02 ± 1.31a
15–30	MCI	26.07 ± 0.29a	1.20 ± 0.02b	6.63 ± 0.13a	48.45 ± 7.69a	111.07 ± 6.15ab	30.06 ± 5.27a	133.50 ± 1.79a	1.18 ± 0.02ab	0.44 ± 0.03a	19.78 ± 0.75b	27.46 ± 0.79a
	OC	26.00 ± 0.77a	1.04 ± 0.04c	6.88 ± 0.05a	48.75 ± 5.97a	120.05 ± 3.53a	28.65 ± 6.15a	118.42 ± 1.97b	1.28 ± 0.05a	0.42 ± 0.05a	24.18 ± 1.29a	28.47 ± 1.25a
	TA	25.35 ± 0.54a	1.31 ± 0.02ab	6.76 ± 0.02a	35.23 ± 1.40a	97.71 ± 2.85b	17.87 ± 6.23a	92.58 ± 2.69c	1.23 ± 0.03ab	0.37 ± 0.02a	18.02 ± 1.05b	24.30 ± 1.16ab
	FA	24.72 ± 0.13a	1.39 ± 0.05a	7.00 ± 0.15a	47.43 ± 11.87a	76.42 ± 3.57a	16.57 ± 2.83a	88.17 ± 3.22c	1.10 ± 0.05b	0.31 ± 0.01a	19.34 ± 0.12b	22.22 ± 1.39b

Mean ± standard errors are shown in the table. Different letters indicate significant differences (Tukey's test, $P < 0.05$).

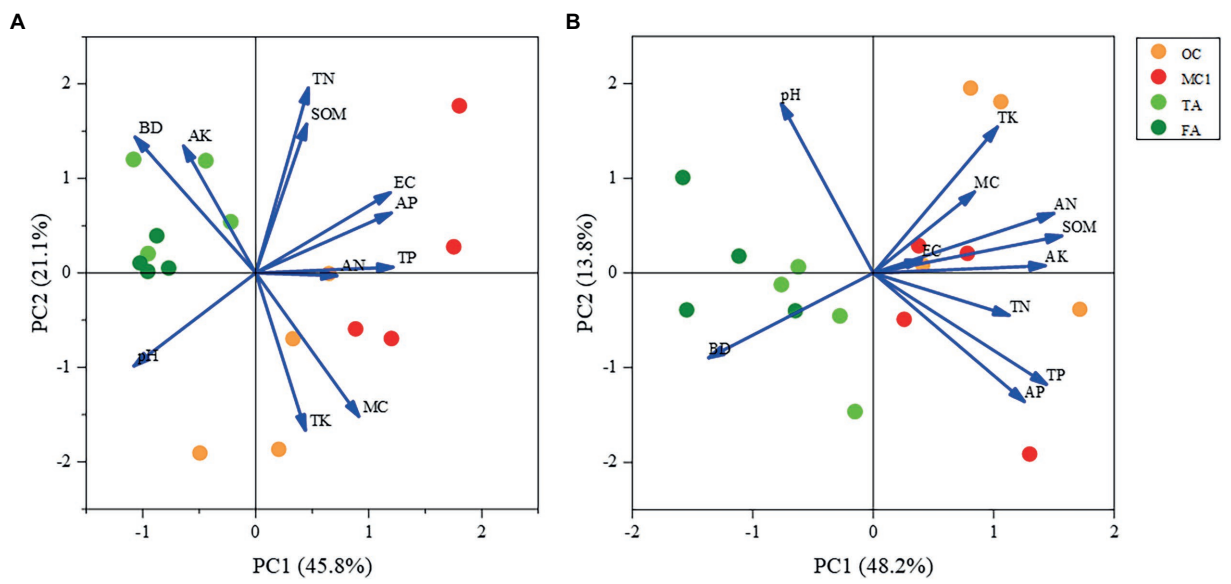

FIGURE 5
PCA of soil physicochemical properties. The PCA of soil physicochemical properties at the 0-15 cm soil depth (A) and soil physicochemical properties at the 15-30 cm soil depth (B).

(r = 0.681, r = 0.818) were positively correlated with soil available nitrogen and soil available potassium to a significant extent. While, Proteobacteria (r = −0.799, r = −0.839), Acidobacteria (r = −0.778, r = −0.854), and *Nitrospira* (r = −0.678, r = −0.721) were negatively correlated with soil available nitrogen and soil available potassium to a significant extent. Gemmatimonadetes (r = −0.694), Actinobacteria (r = −0.802), and Chloroflexi (r = −0.77) were negatively correlated with soil bulk density to a significant extent. Proteobacteria (r = 0.726) and Acidobacteria (r = 0.779) were positively correlated with soil bulk density to a significant extent. Unlike the 0–15 cm soil depth, soil available phosphorus was associated with more bacterial communities. Gemmatimonadetes (r = 0.697) was positively correlated with soil available phosphorus to a significant extent, while Verrucomicrobia (r = −0.660), and Rokubacteria (r = −0.705) were negatively correlated with soil available phosphorus to a significant extent (Figure 6B).

The correlations between fungal community composition and soil factors under different cultivation methods were examined by conducting Pearson's correlation analysis. According to the results, soil physicochemical properties had significant effects on the relative abundance of fungal phylum, and the effects varied by soil depth. At the 0–15 cm soil depth, Mucoromycota was negatively correlated with soil moisture content to a significant extent ($r = -0.610$). Basidiomycota was negatively correlated with soil available potassium to a significant extent ($r = -0.536$). Ascomycota was positively correlated with soil total nitrogen ($r = 0.513$) and soil organic matter ($r = 0.521$) to a significant extent (Figure 6C). It indicates that the dominant soil fungal taxa Ascomycota and Basidiomycota are significantly influenced by environmental factors. At the 15–30 cm soil depth, Basidiomycota and Chytridiomycota were positively correlated with soil available potassium to a significant extent ($r = 0.515$, $r = 0.628$). Mortierellomycota was negatively correlated with soil available nitrogen ($r = -0.515$), soil available potassium ($r = -0.509$), soil total nitrogen ($r = -0.606$), and soil organic matter ($r = -0.626$), showing a significant negative correlation. Rozellomycota was negatively correlated with soil moisture content ($r = -0.547$) and soil available phosphorus ($r = -0.529$) to a significant extent (Figure 6D).

Discussion

Alfalfa led to changes in the alpha diversity of soil bacteria rather than in fungi in the degraded arable land. Adding alfalfa to the rotation recruited and increased the microbial community, including taxa with the capacity to improve soil nutrient utilization and promote luxuriant growth for subsequent crops, such as Gemmatimonadetes, Actinobacteria, Planctomycetes, and Chloroflexi. Long-term alfalfa planting can modify soil conditions by promoting the proliferation of specific beneficial microbiota groups like Proteobacteria and Acidobacteria. Planting alfalfa in degraded black soil cultivated land can help reduce the salt content of the soil, and the nutrient content of soil planted with alfalfa without fertilization was equivalent to that of degraded corn cultivated land with annual fertilization.

Corn and alfalfa rotation makes no significant impact on the alpha diversity of soil bacteria and fungi. However, planting alfalfa for 3 or 4 years led to variations in the alpha diversity of soil bacteria rather than in fungi in the degraded arable land, which is consistent with the outcomes of a previous research (Szoboszlay et al., 2017; Luo et al., 2018). Corn is fertilized twice a year, and the long-term application of chemical fertilizers can cause soil organic matter to accumulate (Tejada and Gonzalez, 2008). The roots of corn stubble remain in the soil after corn harvest, while corn

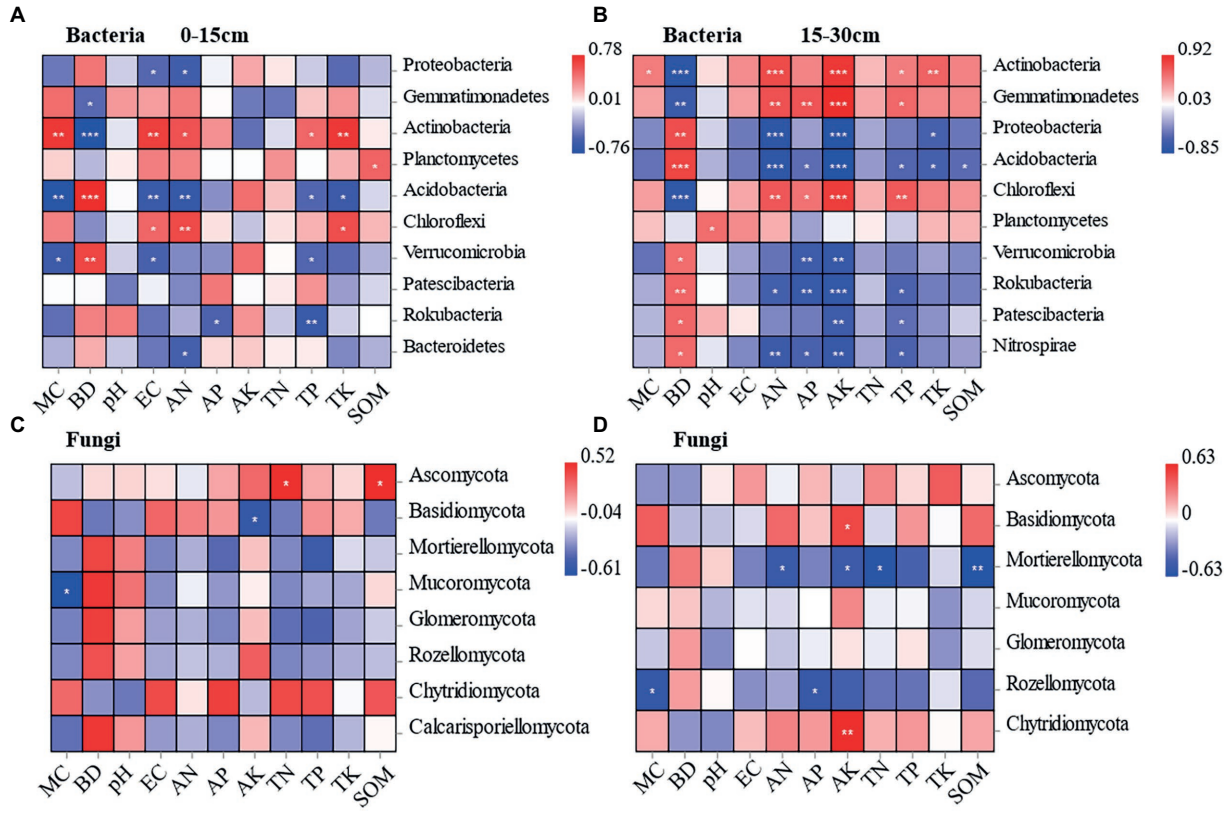

FIGURE 6
Pearson correlation between soil bacteria and soil physicochemical properties at the depths of 0-15 cm and 15-30 cm under different treatments (A, B). Pearson correlation between soil fungal and soil physicochemical properties at the depths of 0-15 cm and 15-30 cm under different treatments (C, D).

residues and secretions can maintain the organic carbon balance (Bajgai et al., 2014). However, due to the destruction of soil aggregates by farming, the microhabitat is lost, which rearranges the spatial environment of the microbial community, promotes soil homogenization, and reduces microbial groups (Lupwayi et al., 2001; Acosta-Martínez et al., 2010). Meanwhile, alfalfa has developed roots, which can go deep into the lower layer of the soil and exert a strong fixation force on the soil, which results in a large rhizosphere area, thus providing nutrients for soil bacteria and increasing the density of bacteria (Solly et al., 2014).

In the present study, the alpha diversity indices of soil fungi remained consistent, and there was no significant difference observed among corn fields, corn alfalfa rotation, and alfalfa planting. In spite of this, at the 15–30 cm soil depth, all diversity indices of the TA and FA fungal communities were found slightly higher than those of MC1. The results demonstrate that planting alfalfa is conducive to the proliferation of fungi under certain conditions, but this process may be a lengthy one. In a study, it has been reported that the long-term continuous cropping of alfalfa (more than 6 years) increased fungal diversity (Yao et al., 2019), which is consistent with our results. In addition, fertilization affects the structure of the soil microbial community and may lead to soil mycosis, such as *Fusarium* (Beauregard et al., 2010). Herein, it was found out that although the alfalfa field is no longer fertilized after planting, its roots can still increase organic matter and nodule nitrogen fixation for the soil, maintain the number of soil fungi and slightly improve the diversity, which is conducive to the survival of fungi. Moreover, corn and alfalfa rotation and planting of alfalfa for 3 and 4 years led to the appearance of plant growth-promoting fungi *Trichoderma* at 0–15 cm soil depth.

In the natural soil, the fungal community in the rhizosphere of maize is similar to that in the original soil, with most of the fungi in the rhizosphere stemming from the soil. There were similar major bacterial phyla after adding alfalfa to the rotation, but the relative abundance of dominant taxa changed significantly. OC increased the abundance of Gemmatimonadetes, Actinobacteria, Planctomycetes, and Chloroflexi, which are contained in nutrient cycling, organic matter turnover, and plant growth-promoting activities, at the 0–15 cm soil depth. Plant microbial interactions and specific groups outside of larger soil communities are recruited by plants (Berendsen et al., 2012). The microorganisms colonizing the alfalfa rhizosphere would be carried over during alfalfa and corn rotation (Samaddar et al., 2021). Adding legume to crop rotation can enrich the genes related to nitrogen cycle in the rhizosphere of subsequent crops, with legume rhizosphere microorganisms left behind.

Meanwhile, the abundance of Proteobacteria and Acidobacteria was increased by TA and FA at the soil depths of 0–15 cm and 15–30 cm. Proteobacteria prefer environments with high effective carbon contents (Ren et al., 2018) and play an important role in saline-alkali soil remediation, pollutant degradation, and plant pest control (Broszat et al., 2014). Alfalfa is a legume forage. The nodule structure can significantly improve biomass accumulation. After the planting of alfalfa, the growth and physiological activity of the root system increase. Root exudates are conducive to promoting the reproduction of soil microorganisms and making Proteobacteria directly related to the rhizosphere effect. Acidobacteria are often more abundant in soils with low resource availability (Liu et al., 2014; Kielak et al., 2016). In the present study, with the extension of alfalfa planting, soil moisture content decreased, which is consistent with the survival strategy of Acidobacteria. Meanwhile, due to the lack of fertilization in alfalfa fields and the reduction in soil nutrients, it provides suitable conditions for its survival series. Therefore, the relative abundance increases. However, the reduced abundance of Gemmatimonadetes, Actinobacteria, and Chloroflexi in the following alfalfa is likely to result from the difference in tillage regimes. In addition, the dominant taxa of soil bacteria were more significantly affected by soil parameters, with Actinobacteria and Chloroflexi being more sensitive to the variations in environmental factors than other dominant taxa.

The relative abundance of Ascomycota also showed no significance but a slightly elevated difference. Fungi are not sensitive to aboveground vegetation changes and farming patterns, and fewer soil physicochemical factors are significantly associated with the relative abundance of the fungal phylum, which is consistent with previous research results (Hibbett et al., 2007). The abundance of Glomeromycota was significantly increased by TA and FA. Glomeromycota has arbuscular mycorrhizal (AM) fungi, which can form a reciprocal symbiosis with plants (Mei et al., 2019). With the extension of alfalfa planting, AM fungi abundance increased, which may be caused by reduced soil disturbance. These results suggest that the long-term planting of alfalfa will improve the colonization and activity of AM fungi in the soil system (Samaddar et al., 2021).

One of the functions performed by planting alfalfa is to accumulate nitrogen reserves for soil, increase the mineralization rate, and improve nitrogen availability under soil microbial activity. In this study, *Nitrospira* was increased, which is an aerobic chemolithoautotrophic nitrite-oxidizing bacteria (Stein, 2019) in the TA and FA. Meanwhile, a greater abundance of S*phingomonas* was observed in TA and FA. *Sphingomonas* has a wide range of metabolic capacities, some strains of which can synthesize valuable extracellular biopolymers and degrade harmful substances in soil. It is thus applicable as a bacterial antagonist of plant pathogenic fungi (Feng et al., 2021). Moreover, the main flora of fungi also changed when different planting methods were applied. As a microbial fertilizer, *Trichoderma* can inhibit most soil-borne pathogens (Bidellaoui et al., 2019) and appear in corn and alfalfa rotation in TA and FA. Plant growth-promoting rhizobacteria *Mortierella* appeared in TA and FA. Our results demonstrate that alfalfa recruits and increases specific symbiotic microbes to adapt and modify degraded black soil cultivated land with the long-term application of chemical fertilizer for a better chance of survival. However, we also detected the pathogenic fungal genus *Fusarium*, which causes plant diseases (Samaddar et al., 2021), but disease incidence was not observed in corn and alfalfa. At present, the reason for alfalfa selective aggregation *Fusarium* remains unclear, which requires verification in the future.

Soil parameters affect plant growth and soil microorganisms. In the present study, TA and FA reduced soil moisture content, soil electrical conductivity, soil available phosphorus, and soil total phosphorus at the 15–30 cm soil depth (Huang et al., 2018; Cao et al., 2021), which is consistent with our finding that TA and FA reduced soil moisture content. Meanwhile, alfalfa increased pH value and reduced soil electrical conductivity. These results show that alfalfa can not only neutralize the pH level of acidic soil and reduce the salt content of soil (Zhao et al., 2016; Liu et al., 2018b), but also promote the development of the soil microbial community and improve soil quality.

Although alfalfa has high requirements for soil phosphorus, the phosphorus in the soil is consumed with the extension of planting, which reduces the contents of soil available phosphorus and soil total phosphorus in the soil after alfalfa planting.

Gramineae corn was a fibrous root system, the root of which is slender and can go deep into the soil layer to absorb nutrients, especially calcium and phosphorus. However, in this process, Gramineae plants lack nitrogen and need to be supplemented by legume plants with deep roots. In this study, corn and alfalfa rotation increased soil available nitrogen and soil total nitrogen. Alfalfa in rotations can improve nitrogen in the soil of subsequent crops. Moreover, planting alfalfa made no difference to soil available nitrogen, soil available potassium, soil total nitrogen, or soil organic matter. Alfalfa nitrogen is derived from the rhizobial nitrogen fixation (Xie et al., 2015) on the degraded black soil cultivated land where corn has been planted for a long time, and the nutrient content of soil (soil total nitrogen, soil total potassium, and soil organic matter) planted with alfalfa without fertilization is equivalent to that of degraded corn cultivated land with annual fertilization. A previous research demonstrated that the reclamation of native sandy grasslands into alfalfa fields significantly increased soil organic carbon, total nitrogen (Beimforde et al., 2014), and available phosphorus contents (Dong et al., 2016). Pot experiments have also shown that planting alfalfa significantly enhanced soil nutrition (Luo et al., 2018). Therefore, planting alfalfa can improve the degraded black soil cultivated land and reduce the use of chemical fertilizer. Compared with the planting of alfalfa for 3 years, soil nutrients decreased slightly after planting alfalfa for 4 years. Besides, with the years of alfalfa planting, soil available nitrogen and soil available potassium were reduced at the 15–30 cm soil depth. Therefore, planting alfalfa for 3 years is more effective in improving soil fertility.

Conclusion

Our results demonstrated that the alfalfa in rotations recruits and increases the contained taxa with the capacity to improve soil nitrogen and inhibit the detrimental impacts of pathogens on subsequent crops. Alfalfa continuous cropping can modify soil conditions by promoting the proliferation of specific beneficial microbiota groups. The nutrient content of soil planted with alfalfa instead of fertilization is equivalent to that of degraded corn cultivated land with annual fertilization. Meanwhile, alfalfa increased the pH level of acid soil, suggesting that alfalfa may have the potential to improve the degraded black soil on cultivated land and reduce the use of chemical fertilizer. However, with the years of alfalfa planting, soil available nitrogen and soil available potassium were reduced at the 15–30 cm soil depth. Planting alfalfa for 3 years exerts a better effect on improving soil fertility. Our study revealed the effects of alfalfa (rotation and continuous cropping) on soil microbial community structure and soil nutrients of degraded black soil cultivated land, thus providing a basis for the in-depth understanding of soil microbial groups and contributing to the restoration of degraded black soil cultivated land. In the future, it is necessary to advance the potential of soil microorganisms and produce potential biological inoculants by conducting an additional research on microbial community functional character through meta-proteome analysis or meta-transcriptome.

Data availability statement

The raw data supporting the conclusions of this article will be made available by the authors, without undue reservation.

Author contributions

LM and NZ performed the data analyses and wrote the manuscript. QW and YC contributed significantly to the analysis and manuscript preparation. DL performed the experiment. GC contributed to the conception of the study. All authors contributed to the article and approved the submitted version.

Funding

This work was financially supported by Forestry Science and Technology Extension Demonstration Project of central Finance (TG 02), the China Postdoctoral Science Foundation (2021M690575), and Young Talents Project of Northeast Agricultural University (20QC17).

Acknowledgments

We would like to thank the reviewers for the helpful comments on the manuscript.

Conflict of interest

The authors declare that the research was conducted in the absence of any commercial or financial relationships that could be construed as a potential conflict of interest.

Publisher's note

References

Acosta-Martínez, V., Dowd, S. E., Bell, C. W., Lascano, R., Booker, J. D., Zobeck, T. M., et al. (2010). Microbial community composition as affected by dryland cropping systems and tillage in a semiarid sandy soil. *Diversity* 2, 910–931. doi: 10.3390/d2060910

Agnello, A. C., Huguenot, D., van Hullebusch, E. D., and Esposito, G. (2016). Citric acid-and tween((R)) 80-assisted phytoremediation of a co-contaminated soil: alfalfa (*Medicago sativa* L.) performance and remediation potential. *Environ. Sci. Pollut. Res. Int.* 23, 9215–9226. doi: 10.1007/s11356-015-5972-7

Bajgai, Y., Kristiansen, P., Hulugalle, N., and McHenry, M. (2014). Changes in soil carbon fractions due to incorporating corn residues in organic and conventional vegetable farming systems. *Soil Res.* 52, 244–252. doi: 10.1071/sr13295

Bastida, F., Torres, I. F., Andres-Abellan, M., Baldrian, P., Lopez-Mondejar, R., Vetrovsky, T., et al. (2017). Differential sensitivity of total and active soil microbial communities to drought and forest management. *Glob. Chang. Biol.* 23, 4185–4203. doi: 10.1111/gcb.13790

Beauregard, M. S., Hamel, C., Atul, N., and St-Arnaud, M. (2010). Long-term phosphorus fertilization impacts soil fungal and bacterial diversity but not AM fungal community in alfalfa. *Microb. Ecol.* 59, 379–389. doi: 10.1007/s00248-009-9583-z

Beimforde, C., Feldberg, K., Nylinder, S., Rikkinen, J., Tuovila, H., Dorfelt, H., et al. (2014). Estimating the phanerozoic history of the ascomycota lineages: combining fossil and molecular data. *Mol. Phylogenet. Evol.* 78, 386–398. doi: 10.1016/j.ympev.2014.04.024

Berendsen, R. L., Pieterse, C. M., and Bakker, P. A. (2012). The rhizosphere microbiome and plant health. *Trends Plant Sci.* 17, 478–486. doi: 10.1016/j.tplants.2012.04.001

Bertrand, A., Gatzke, C., Bipfubusa, M., Lévesque, V., Chalifour, F. P., Claessens, A., et al. (2020). Physiological and biochemical responses to salt stress of alfalfa populations selected for salinity tolerance and grown in symbiosis with salt-tolerant rhizobium. *Agronomy* 10, 569–588. doi: 10.3390/agronomy10040569

Bidellaoui, B., Segarra, G., Hakkou, A., and Isabel Trillas, M. (2019). Beneficial Effects of Rhizophagus irregularis and Trichoderma asperellum strain T34 on growth and fusarium wilt in tomato plants. *J. Plant Pathol.* 101, 121–127. doi: 10.1007/s42161-018-0159-y

Broszat, M., Nacke, H., Blasi, R., Siebe, C., Huebner, J., Daniel, R., et al. (2014). Wastewater irrigation increases the abundance of potentially harmful Gammaproteobacteria in soils in Mezquital Valley. *Mexico. Appl Environ Microbiol.* 80, 5282–5291. doi: 10.1128/AEM.01295-14

Cao, X., Feng, Y., Li, H., Zheng, H., Wang, J., Tong, C., et al. (2021). Effects of subsurface drip irrigation on water consumption and yields of alfalfa under different water and fertilizer conditions. *J. Sens.* 2021, 1–12. doi: 10.1155/2021/6617437

Dong, W.-H., Zhang, S., Rao, X., and Liu, C. A. (2016). Newly-reclaimed alfalfa forage land improved soil properties comparison to farmland in wheat–maize cropping systems at the margins of oases. *Ecol. Eng.* 94, 57–64. doi: 10.1016/j.ecoleng.2016.05.056

Du, Z., Gao, B., Ou, C., Du, Z., Yang, J., Batsaikhan, B., et al. (2021). A quantitative analysis of factors influencing organic matter concentration in the topsoil of black soil in Northeast China based on spatial heterogeneous patterns. *ISPRS Int. J. Geo Inf.* 10, 348–362. doi: 10.3390/ijgi10050348

Durán, A., Morrás, H., Studdert, G., and Liu, X. (2011). Distribution, properties, land use and management of Mollisols in South America. *Chin. Geogr. Sci.* 21, 511–530. doi: 10.1007/s11769-011-0491-z

Feng, F., Zhan, H., Wan, Q., Wang, Y., Li, Y., Ge, J., et al. (2021). Rice recruits Sphingomonas strain HJY-rfp via root exudate regulation to increase chlorpyrifos tolerance and boost residual catabolism. *J. Exp. Bot.* 72, 5673–5686. doi: 10.1093/jxb/erab210

Han, Z., Deng, M., Yuan, A., Wang, J., Li, H., and Ma, J. (2018). Vertical variation of a black soil's properties in response to freeze-thaw cycles and its links to shift of microbial community structure. *Sci. Total Environ.* 625, 106–113. doi: 10.1016/j.scitotenv.2017.12.209

Hibbett, D. S., Binder, M., Bischoff, J. F., Blackwell, M., Cannon, P. F., Eriksson, O. E., et al. (2007). A higher-level phylogenetic classification of the fungi. *Mycol. Res.* 111, 509–547. doi: 10.1016/j.mycres.2007.03.004

Huang, Z., Liu, Y., Cui, Z., Fang, Y., He, H., Liu, B.-R., et al. (2018). Soil water storage deficit of alfalfa (*Medicago sativa*) grasslands along ages in arid area (China). *Field Crop Res* 221, 1–6. doi: 10.1016/j.fcr.2018.02.013

Jarecki, M., Grant, B., Smith, W., Deen, B., Drury, C., Vander Zaag, A., et al. (2018). Long-term trends in corn yields and soil carbon under diversified crop rotations. *J. Environ. Qual.* 47, 635–643. doi: 10.2134/jeq2017.08.0317

Kielak, A. M., Barreto, C. C., Kowalchuk, G. A., van Veen, J. A., and Kuramae, E. E. (2016). The ecology of Acidobacteria: moving beyond genes and genomes. *Front. Microbiol.* 7:744. doi: 10.3389/fmicb.2016.00744

Li, H., Yao, Y., Zhang, X., Zhu, H., and Wei, X. (2021). Changes in soil physical and hydraulic properties following the conversion of forest to cropland in the black soil region of Northeast China. *Catena* 198:104986. doi: 10.1016/j.catena.2020.104986

Liu, S., Hou, X., Yang, M., Cheng, F., Coxixo, A., Wu, X., et al. (2018b). Factors driving the relationships between vegetation and soil properties in the Yellow River delta, China. *Catena* 165, 279–285. doi: 10.1016/j.catena.2018.02.004

Liu, J., Sui, Y., Yu, Z., Shi, Y., Chu, H., Jin, J., et al. (2014). High throughput sequencing analysis of biogeographical distribution of bacterial communities in the black soils of Northeast China. *Soil Biol. Biochem.* 70, 113–122. doi: 10.1016/j.soilbio.2013.12.014

Liu, J., Yu, Z., Yao, Q., Sui, Y., Shi, Y., Chu, H., et al. (2018a). Ammonia-oxidizing archaea show more distinct biogeographic distribution patterns than ammonia-oxidizing bacteria across the black soil zone of Northeast China. *Front. Microbiol.* 9:171. doi: 10.3389/fmicb.2018.00171

Luo, C., Deng, Y., Inubushi, K., Liang, J., Zhu, S., Wei, Z., et al. (2018). Sludge biochar amendment and alfalfa revegetation improve soil physicochemical properties and increase diversity of soil microbes in soils from a rare earth element mining wasteland. *Int. J. Environ. Res. Public Health* 15, 965–986. doi: 10.3390/ijerph15050965

Lupwayi, N. Z., Arshad, M. A., Rice, W. A., and Clayton, G. W. (2001). Bacterial diversity in water-stable aggregates of soils under conventional and zero tillage management. *Appl. Soil Ecol.* 16, 251–261. doi: 10.1016/S0929-1393(00)00123-2

Mei, L., Yang, X., Zhang, S., Zhang, T., and Guo, J. (2019). Arbuscular mycorrhizal fungi alleviate phosphorus limitation by reducing plant N: P ratios under warming and nitrogen addition in a temperate meadow ecosystem. *Sci. Total Environ.* 686, 1129–1139. doi: 10.1016/j.scitotenv.2019.06.035

Qin, S., Yeboah, S., Cao, L., Zhang, J., Shi, S., and Liu, Y. (2017). Breaking continuous potato cropping with legumes improves soil microbial communities, enzyme activities and tuber yield. *PLoS One* 12:e0175934. doi: 10.1371/journal.pone.0175934

Ren, C., Zhang, W., Zhong, Z., Han, X., Yang, G., Feng, Y., et al. (2018). Differential responses of soil microbial biomass, diversity, and compositions to altitudinal gradients depend on plant and soil characteristics. *Sci. Total Environ.* 610-611, 750–758. doi: 10.1016/j.scitotenv.2017.08.110

Samaddar, S., Schmidt, R., Tautges, N. E., and Scow, K. (2021). Adding alfalfa to an annual crop rotation shifts the composition and functional responses of tomato rhizosphere microbial communities. *Appl. Soil Ecol.* 167:104102. doi: 10.1016/j.apsoil.2021.104102

Shen, Z., Zhong, S., Wang, Y., Wang, B., Mei, X., Li, R., et al. (2013). Induced soil microbial suppression of banana fusarium wilt disease using compost and biofertilizers to improve yield and quality. *Eur. J. Soil Biol.* 57, 1–8. doi: 10.1016/j.ejsobi.2013.03.006

Solly, E. F., Schöning, I., Boch, S., Kandeler, E., Marhan, S., Michalzik, B., et al. (2014). Factors controlling decomposition rates of fine root litter in temperate forests and grasslands. *Plant and Soil* 382, 203–218. doi: 10.1007/s11104-014-2151-4

Stein, L. Y. (2019). Insights into the physiology of ammonia-oxidizing microorganisms. *Curr. Opin. Chem. Biol.* 49, 9–15. doi: 10.1016/j.cbpa.2018.09.003

Sun, Y. (2019). Correlation between plant diversity and the physicochemical properties of soil microbes. *Appl. Ecol. Environ. Res.* 17, 10371–10388. doi: 10.15666/aeer/1705_1037110388

Szoboszlay, M., Dohrmann, A. B., Poeplau, C., Don, A., and Tebbe, C. C. (2017). Impact of land-use change and soil organic carbon quality on microbial diversity in soils across Europe. *FEMS Microbiol. Ecol.* 93:fix146. doi: 10.1093/femsec/fix146

Tejada, M., and Gonzalez, J. L. (2008). Influence of two organic amendments on the soil physical properties, soil losses, sediments and runoff water quality. *Geoderma* 145:325. doi: 10.1016/j.geoderma.2008.03.020

Wang, Y., Ji, H., Wang, R., Guo, S., and Gao, C. (2017). Impact of root diversity upon coupling between soil C and N accumulation and bacterial community dynamics and activity: result of a 30 year rotation experiment. *Geoderma* 292, 87–95. doi: 10.1016/j.geoderma.2017.01.014

Wang, L., Xie, J., Luo, Z., Niu, Y., Coulter, J. A., Zhang, R., et al. (2021). Forage yield, water use efficiency, and soil fertility response to alfalfa growing age in the semiarid loess plateau of China. *Agric Water Manag* 243:106415. doi: 10.1016/j.agwat.2020.106415

Xie, K. Y., Li, X.-L., He, F., Zhang, Y.-J., Wan, L.-Q., David, B. H., et al. (2015). Effect of nitrogen fertilization on yield, N content, and nitrogen fixation of alfalfa and smooth bromegrass grown alone or in mixture in greenhouse pots. *J. Integr. Agric.* 14, 1864–1876. doi: 10.1016/s2095-3119(15)61150-9

Yao, Q., Xu, Y., Liu, X., Liu, J., Huang, X., Yang, W., et al. (2019). Dynamics of soil properties and fungal community structure in continuous-cropped alfalfa fields in Northeast China. *Peer J* 7:e7127. doi: 10.7717/peerj.7127

Yu, P., Li, T., Fu, Q., Liu, D., Hou, R., and Zhao, H. (2021). Effect of biochar on soil and water loss on sloping farmland in the black soil region of Northeast China during the spring thawing period. *Sustainability* 13, 1460–1475. doi: 10.3390/su13031460

Zhao, Y., Li, Y., Wang, J., Pang, H., and Li, Y. (2016). Buried straw layer plus plastic mulching reduces soil salinity and increases sunflower yield in saline soils. *Soil Tillage Res.* 155, 363–370. doi: 10.1016/j.still.2015.08.019

Zhao, Y., Liu, X., Tong, C., and Wu, Y. (2020). Effect of root interaction on nodulation and nitrogen fixation ability of alfalfa in the simulated alfalfa/triticale intercropping in pots. *Sci. Rep.* 10, 1008–1010. doi: 10.1038/s41598-020-61234-5

frontiers | Frontiers in Plant Science

TYPE Original Research
PUBLISHED 31 August 2022
DOI 10.3389/fpls.2022.997292

OPEN ACCESS

EDITED BY
Akash Tariq,
Xinjiang Institute of Ecology and Geography (CAS), China

REVIEWED BY
Yanfu Bai,
Sichuan Agricultural University, China
Junhong Zhang,
Zhejiang Agriculture and Forestry University, China

*CORRESPONDENCE
Naiping Song
songnp@163.com
Xinrong Li
lxinrong@lzb.ac.cn

†These authors have contributed equally to this work and share first authorship

SPECIALTY SECTION
This article was submitted to Plant Abiotic Stress, a section of the journal Frontiers in Plant Science

RECEIVED 18 July 2022
ACCEPTED 10 August 2022
PUBLISHED 31 August 2022

CITATION
Pan Y, Kang P, Tan M, Hu J, Zhang Y, Zhang J, Song N and Li X (2022) Root exudates and rhizosphere soil bacterial relationships of *Nitraria tangutorum* are linked to k-strategists bacterial community under salt stress.
Front. Plant Sci. 13:997292.
doi: 10.3389/fpls.2022.997292

Root exudates and rhizosphere soil bacterial relationships of *Nitraria tangutorum* are linked to k-strategists bacterial community under salt stress

Yaqing Pan[1†], Peng Kang[2†], Min Tan[2], Jinpeng Hu[3], Yaqi Zhang[2], Jinlin Zhang[3], Naiping Song[4*] and Xinrong Li[1*]

[1]Shapotou Desert Research and Experiment Station, Northwest Institute of Eco-Environment and Resources, Chinese Academy of Sciences, Lanzhou, China, [2]College of Biological Sciences and Engineering, North Minzu University, Yinchuan, China, [3]College of Pastoral Agriculture Science and Technology, Lanzhou University, Yinchuan, China, [4]Breeding Base for Key Laboratory Land Degradation and Ecological Restoration in Northwest China, Ningxia University, Yinchuan, China

When plants are subjected to various biotic and abiotic stresses, the root system responds actively by secreting different types and amounts of bioactive compounds, while affects the structure of rhizosphere soil bacterial community. Therefore, understanding plant–soil-microbial interactions, especially the strength of microbial interactions, mediated by root exudates is essential. A short-term experiment was conducted under drought and salt stress to investigate the interaction between root exudates and *Nitraria tangutorum* rhizosphere bacterial communities. We found that drought and salt stress increased rhizosphere soil pH (9.32 and 20.6%) and electrical conductivity (1.38 and 11 times), respectively, while decreased organic matter (27.48 and 31.38%), total carbon (34.55 and 29.95%), and total phosphorus (20 and 28.57%) content of *N. tangutorum* rhizosphere soil. Organic acids, growth hormones, and sugars were the main differential metabolites of *N. tangutorum* under drought and salt stress. Salt stress further changed the *N. tangutorum* rhizosphere soil bacterial community structure, markedly decreasing the relative abundance of Bacteroidota as r-strategist while increasing that of Alphaproteobacteria as k-strategists. The co-occurrence network analysis showed that drought and salt stress reduced the connectivity and complexity of the rhizosphere bacterial network. Soil physicochemical properties and root exudates in combination with salt stress affect bacterial strategies and interactions. Our study revealed the mechanism of plant–soil-microbial interactions under the influence of root exudates and provided new insights into the responses of bacterial communities to stressful environments.

KEYWORDS

***Nitraria tangutorum*, drought or salt stress, root exudates, rhizosphere bacteria, co-occurrence network, k-strategists**

Introduction

The plant root system is the interface for material exchange between the plant and soil ecosystem. As the life carrier between plants and the soil environment, root exudates play a prominent role in nutrient absorption and cycling (Mommer et al., 2016; Sokol et al., 2019). Root exudates, mainly including sugars, amino acids, organic acids, phenolic acids, fatty acids, sterols, proteins, and growth factors, can be divided into high and low molecular weight (Baetz and Martinoia, 2014; Wu et al., 2014; Canarini et al., 2019). Plants are often subjected to various biotic and abiotic stresses throughout their life cycle and respond by secreting different bioactive compounds through their roots (Badri and Vivanco, 2009). The composition and quantity of plant root exudates increase considerably under abiotic stress, and their organic acid content markedly increases under water stress (Vives-Peris et al., 2018). Furthermore, salt and other abiotic stressors can induce the synthesis and accumulation of plant secondary metabolites such as polyphenols (Zhou et al., 2018). Previous studies have shown that root exudates serve as the medium for co-evolution between plants and microorganisms and can promote the interaction between them by regulating the plant rhizosphere micro-environment to cope with various biotic and abiotic stresses (Pétriacq et al., 2017; Gargallo-Garriga et al., 2018; Guyonnet et al., 2018; Karlowsky et al., 2018; de Vries et al., 2019).

Soil microbial communities are closely associated with plant roots and participate in biogeochemical cycles, thus shaping the structure and function of terrestrial ecosystems (Bardgett and van der Putten, 2014; Fierer, 2017). The interaction between plant root exudates and rhizosphere microorganisms is an important process. For example, plant roots secrete various secondary metabolites affecting rhizosphere microorganism species, quantity, and distribution (Jenkins et al., 2017). Amino acids, vitamins, and carbohydrates in plant root exudates provide a basis for microbial growth and substrate decomposition (Zhalnina et al., 2018). Furthermore, some allelochemicals in root exudates can inhibit the assembly process of rhizosphere microbial communities (Xia et al., 2016). Soil moisture, vegetation type, and climate shape plant rhizosphere microbial communities through changes in plant rhizosphere metabolites (Kong et al., 2018). Plant root exudates and environmental selection drive the change in rhizosphere microbial community structure (Schleuning et al., 2015). Given the ubiquity, diversity, and plasticity of microorganisms, it is important to explore plant–soil-microorganism interactions mediated by root exudates and to have an in-depth understanding of microbial interactions and functions.

In the past decade, the diversity and complexity of microbial communities have made it urgent to understand the construction and characteristics of microbial communities (Duran et al., 2018; Rottjers and Faust, 2018). With the rapid development of high-throughput sequencing technology, microbial community data have become more accurate. The network of microbial interactions provides a multidimensional and more complete view of ecosystems. These networks are closely related to ecosystem functions and play a key role in maintaining biodiversity (Wardle, 2006). Therefore, the application of microbial network analysis to identify alternative community states and ecological niches has become a common tool for studying the structure of microbial communities (Xiao et al., 2017; Kumar et al., 2019). In microbial co-association networks, nodes represent species and edges represent potential interactions between species (Bahram et al., 2014; Ma et al., 2016). There is growing evidence that the properties of ecological networks, such as soil pH (Banerjee et al., 2019), soil water availability (Ma et al., 2020; Hernandez et al., 2021), and soil nutrients (Shi et al., 2020), may represent interactions between coexisting organisms. A microbial community is a well-constructed complex ecological network in which microorganisms collaborate and interact to maximize their ecological functions (Toju et al., 2018; Banerjee et al., 2019).

Given the large number of soil bacteria, the concept of r-and k-strategists can be applied to the study of soil bacterial ecology to understand bacterial interactions (Fierer et al., 2007; Pascault et al., 2013). R-strategists preferentially consume unstable soil nutrients and maximize their intrinsic growth rate when resources are abundant (Kielak et al., 2009). Contrastingly, k-strategists show a slower growth rate and compete for survival under nutrient deficiency (Meyer, 1994). Studies have shown that in the ecological classification of soil bacteria, Betaproteobacteria, Gammaproteobacteria, Deltaproteobacteria, and Bacteroidota are r-strategists, and Alphaproteobacteria and Acidobacteriota are k-strategists (Klappenbach et al., 2000; Lee et al., 2008; Senechkin et al., 2010; Gu et al., 2018). Microbial communities often respond to environmental stress considering their growth, reproduction, competition, and adaptation strategies. However, there is still a limited understanding of the effects of root exudates on the adaptation strategies of plant rhizosphere bacterial communities under environmental stress.

Soil microorganisms are essential for maintaining the structure and function of terrestrial ecosystems. Many environmental factors (soil pH, moisture, and nutrient availability) and plant root exudates directly or indirectly influence soil microbial communities (Bardgett and van der Putten, 2014; Delgado-Baquerizo et al., 2016; Sayer et al., 2017; Su et al., 2020). However, the mechanisms by which plant root exudates influence rhizosphere microbial communities of the dominant plant species in the desert steppe ecosystems in China are not fully understood. *Nitraria tangutorum* is a typical desert shrub with strong resistance to salinity and drought, and widely distributed in arid areas of Northern China (Luo et al., 2008; Ni et al., 2015; Yan et al., 2018). It is of great significance for sand fixation, soil improvement and has very important ecological functions (Liu et al., 2016). Its fruit is also an important

Abbreviations: CK, Control samples; SWC, Soil water content; EC, Electrical conductivity; TC, Soil total carbon; TN, Total nitrogen; TP, Total phosphorus; TOC, Soil total organic carbon; NMDS, Non-metric multidimensional scale; QC, Quality control; LC–MS, Liquid chromatography-mass spectrometry; SOM, Soil organic matter.

nutritional health food resource with high potential economic value (Kang et al., 2015). In this study, we analyzed the differences in root exudates and microbial communities of *N. tangutorum* under short-term drought and salt stress through controlled experiments. We proposed that there are differences in the root exudates of *N. tangutorum* under short-term drought and salt stress, and that the differences in root exudates affect bacterial survival strategies and interactions.

Materials and methods

Plant materials and treatments

In this study, *N. tangutorum* was obtained from the Lianhuachi Lake in Dingbian County (37°36′20′N, 107°20′25′ E), Shaanxi Province, China, in May 2021. Lianhuachi Lake is 1,310 m above sea level and covers 0.61 km^2. The average annual precipitation is less than 200 mm. *Nitraria tangutorum* with the same growth were transplanted into pots ($\Phi = 33$ cm, height = 20 cm) with sand and vermiculite at a ratio of 4: 1 and placed in a greenhouse. The growth conditions in greenhouse were controlled to maintain a temperature of 26/22°C (day/night), a photoperiod of 16/8 h (light/dark). The plants were watered with 1/2 Hoagland solution and subjected to drought and salt stress after 2 months. In "CK" group, the SWC was maintained at 50% of FWC by irrigated with 1/2 Hoagland solution. In "Drought" group, the SWC was maintained at 30% of FWC by irrigated with 1/2 Hoagland solution. All these values were subsequently maintained constantly by irrigated with corresponding solutions every 5 days for 30 days. In "Salt" group, the SWC was maintained at 50% of FWC by 1/2 Hoagland solution containing 200 mM NaCl, and the treatment solutions were renewed every 5 days to keep constant NaCl concentration (Kang et al., 2016; Pan et al., 2016; Guo et al., 2020).

Sample collections

After 30 days of treatment, *N. tangutorum* were removed from the pots, and the rhizosphere soil was collected; 27 soil samples were collected, including nine CK, nine drought, and nine salt samples. For each treatment, the soil probe was washed with 75% ethanol before collection and gloves were changed before collection. The soil cores were then placed in a sterile centrifuge tube and taken to the laboratory in an ice box (Pan et al., 2021). After sieving and removing surface vegetation and litter, the soil samples were divided into three parts: one for high-throughput sequencing, one for analysis of physicochemical properties, and the other was frozen for metabolite extraction. Soil samples were air-dried for the determination of soil physicochemical properties, and fresh soil samples were used for the determination of soil microorganisms and root exudates. We took 100 g of fresh soil for extraction and collection of root exudate. Firstly, 500 ml deionized water was added, and then centrifuged for 5 min (20°C， 8,000 r/min) after shock extraction for 3 h, and then the supernatant was extracted for filtration. After that, the water was spin-dried at 35°C with the vacuum rotary evaporator, poured on the tin foil until the methanol completely volatilized, and washed repeatedly 2–3 times; and finally stored at −80°C to be tested.

Characterization of physicochemical properties of rhizosphere soil samples

Soil water content (SWC) was measured using the weighing method (Li et al., 2020), soil pH was determined using a pH meter (Mettler S220; Mettler Toledo Solutions, Greifensee, Switzerland), and soil electrical conductivity (EC) was measured using a specific conductivity meter (Leici DDS-307A, Shanghai Leici Instruments, Shanghai, China) with the soil-water ratio of 1:5 (Wang et al., 2019). After the collected soil samples were air-dried, the soil total carbon (TC), total nitrogen (TN), and total phosphorus (TP) were determined using atomic absorption spectrometry with an atomic absorption spectrophotometer (iCE 3,500, Thermo Fisher Scientific, Waltham, MA, United States; Bettinelli et al., 2000; Postma et al., 2016). Soil total organic carbon (TOC) was determined by dichromate oxidation and ammonium ferrous sulfate titration (Gul et al., 2015).

Determination of root metabolites

Nucleic acids were extracted from each sample at the end of the treatment. Plant roots were carefully rinsed with sterile deionized water and soaked in 1,000 ml of sterile deionized water for 8 h, according to Luo et al. (2014). The extract was stored in liquid nitrogen and sent to Novogene Bioinformatics Technology Co. Ltd., Tianjin, China, for the determination of plant root exudates using liquid chromatography-mass spectrometry (LC–MS; Ultimate 3000 LC, Q Exactive; Thermo Fisher Scientific) on a Hyper Gold C18 column [100 mm × 2.1 mm, at 1.9 μm, (Thermo Fisher Scientific)]. Metabolites were detected in positive and negative ion modes. Before sample detection, equal amounts of samples were extracted from 27 root exudates and mixed into a quality control (QC) sample. The total ion flow chromatograms of the QC samples were overlapped to verify the reproducibility of the retention time of the same substance. Compound Discoverer Software (Thermo Fisher Scientific) was used to extract and preprocess the LC–MS detection data, including retention time, molecular weight, sample name, and peak intensity. Subsequently, the ionic characteristics were combined with three predicted components databases (Predicted Compositions, mzCloud Search, and ChemSpider Search) to determine the compound information. Finally, the peak value was converted to the peak value per unit mass using the dry weight of the secretions.

Soil DNA extraction and PCR amplification

The rhizosphere soil bacterial community was examined using Illumina MiSeq sequencing kits (Illumina, San Diego, CA, United States). Total genomic DNA of *N. tangutorum* rhizosphere soil was extracted using the cetyltrimethylammonium bromide/sodium dodecyl sulfate method. The DNA concentration and purity were examined on a 1% agarose gel. Considering the concentration, DNA was diluted to 1 ng/μl using sterile water. All PCR reactions were carried out using 15 μl of Phusion High-Fidelity PCR Master Mix (New England Biolabs, Ipswich, MA, United States), 0.2 μM of forward and reverse primers, and approximately 10 ng template DNA. Illumina MiSeq sequencing libraries (Illumina) for bacteria were prepared *via* PCR amplification of the V3–V4 hypervariable regions of the bacterial 16S rRNA gene using the primers 338F (5′-ACTCCTACGGG AGGCAGCAG-3′) and 806R (5′-GGACTACHVGGGTWT CTAAT-3′) using a GeneAmp 9700 PCR thermocycler (Applied Biosystems, Waltham, MA, United States; Caporaso et al., 2012; Langille et al., 2013). The thermal cycling conditions were as follows: an initial denaturation at 98°C for 1 min, followed by 30 cycles of denaturation at 98°C for 10 s, annealing at 50°C for 30 s, and elongation at 72°C for 30 s, and finally extension at 72°C for 5 min (Haas et al., 2011). The purified amplicons were pooled in equimolar concentrations and paired-end sequenced on an Illumina MiSeq platform (Illumina) according to the standard protocols of Novogene Bioinformatics Technology Co., Ltd. The 16S rRNA gene sequences obtained in this study have been submitted to the NCBI Sequence Read Archive (SRA) database with the serial number PRJNA855333.

Sequence processing and statistical analysis

PE libraries were constructed using a NEXTflex Rapid DNA-SEQ Kit (Bioscience, South San Francisco, CA, United States), and an Illumina MiSeq PE300 platform (Illumina) was used for sequencing. Trimmomatic software (Illumina) was used for quality control of Illumina MiSeq sequencing original sequences. FLASH 1.2.11;[1] software (Illumina) was used for stitching (Magoč and Salzberg, 2011). UPARSE 7.1 software was used for amplicon sequence variants (ASVs) clustering analysis of the sequences (similarity 97%), and UCHIME software was used to remove chimeras (Caporaso et al., 2012). Each sequence was annotated for species classification by the ribosomal database project classifier and compared with the Silva database (SSU128) at a confidence threshold of 0.7 (Quast et al., 2013). All calculations were performed by sub-sampling each sample to an equivalent sequence of 49,556 (Ye et al., 2017).

The QIIME program (2.0) was used to calculate the alpha diversity indices (Shannon and Chao1; Kuczynski et al., 2012). The linkET[2] package in R software (Version 4.1.0) was used to calculate and visualize the correlation between soil physicochemical properties and soil bacterial α-diversity. Canonical correlation analysis (CCA) was applied to distinguish the soil physicochemical properties, differential metabolites community, and bacterial phyla under drought and salt stress (Ramette, 2010). A non-metric multidimensional scale (NMDS) based on the Bray–Curtis distance matrix and ANOSIM test with 9,999 permutations were used to illustrate beta diversity. Differences in community composition between sample groups were analyzed using the vegan package (Pan et al., 2021). The ggalluvial package in R software was used to describe changes in bacteria (top 10 phyla and top 20 genera with the highest abundance). A co-occurrence network was constructed for each treated sample, and coefficients of all possible Spearman correlations among ASVs in all samples were calculated using the psych package (Berry and Widder, 2014; R Core Team, 2020). Cytoscape (3.7.1) was used for network visualization, and the number of ASVs at the phylum level was statistically analyzed. The bacterial phyla or classes for r-and k-strategists were visualized using the ggplot2 package. The psych package was used to calculate the correlation between differential metabolites and soil properties, which was then visualized using the ggplot2 package. We used the fold change value and value of p to screen for significantly upregulated or downregulated differential metabolites and visualized them using the ggplot2 package.

SPSS version 25.0 (SPSS Inc., Chicago, IL, United States) was used for one-way ANOVA of soil physicochemical data, and Duncan's multiple range test was used to identify the significant differences between means at a 5% significance level. All data are presented as the mean ± SE ($n = 9$; Pan et al., 2021).

Results

Relationship between rhizosphere soil bacterial community diversity and physicochemical properties under drought and salt stress

The physicochemical properties of *N. tangutorum* rhizosphere soil were different under drought and salt stress. Salt and drought stress markedly increased rhizosphere soil pH and EC of *N. tangutorum*. Under salt stress, pH and EC were 20.55% and 5.2-fold higher than those of CK, respectively. Conversely, salt and drought stress decreased rhizosphere SOM, TC, and TP contents. Rhizosphere SOM, TC, and TP contents decreased by 38.03, 52.85, and 24.39%, respectively,

1 https://ccb.jhu.edu/software/FLASH/index.shtml

2 https://github.com/Hy4m/linkET

under drought stress, and by 45.62, 42.73, and 39.48%, respectively, under salt stress, compared with that in CK ($p < 0.05$; Supplementary Table 1).

Based on a 97% sequence similarity threshold, 10,535 ASVs were obtained for each sample after normalization. The coverage index of the bacterial ASVs was greater than 0.999, indicating that the sequencing depth was reasonable. Compared with CK, drought decreased the Shannon index in the rhizosphere bacterial community of *N. tangutorum*, while salt stress increased the number of ASVs and the Chao1 index but not significantly (Supplementary Table 2). The rhizosphere soil bacterial community diversity of *N. tangutorum* was significantly correlated with soil SWC, TN, and SOM, and SWC and TN were positively correlated. The correlation between pH and EC was stronger under drought stress, whereas that between SWC and EC was stronger under salt stress. The ASVs and Shannon and Chao1 indices of the rhizosphere soil bacterial community of *N. tangutorum* were correlated with soil pH and EC under salt stress ($p < 0.05$; Figure 1). CCA analysis showed that Firmicutes and Bacteroidetes were correlated with soil SOM under drought stress; while Acidobacteriota, Chloroflexi, Proteobacteria, Actinobacteriota, and Gemmatimonadota were correlated with soil SWC, TS, and Na^+. The analysis explained 27.95 and 14.11% of the variables, respectively (Supplementary Figure 1).

Rhizosphere soil bacterial community composition and r-and k-strategists under drought and salt stress

Non-metric multidimensional scale analysis revealed that the rhizosphere soil bacterial community was clustered under drought stress but dispersed under salt stress. The ASVs of *N. tangutorum* rhizosphere soil bacteria were classified into 50 phyla and 999 genera. The top 10 phyla in relative abundance under drought stress were Firmicutes, Bacteroidota, Proteobacteria, Actinobacteriota, Cyanobacteria, Acidobacteriota, Gemmatimonadota, Fusobacteriota, Chloroflexi, and Myxococcota. Compared with that of CK, the abundance of Proteobacteria (25.44–19.55%) and Actinobacteriota (17.02–11.19%) decreased, whereas that of Firmicutes (24.45–35.44%) and Bacteroidota (16.56–28.78%) increased under drought stress. When considering the relative abundance under salt stress, the top 10 phyla were Proteobacteria, Actinobacteriota, Firmicutes, Bacteroidota, Cyanobacteria, Acidobacteriota, Gemmatimonadota, Chloroflexi, Myxococcota, and Fusobacterium. Under salt stress, the abundance of Proteobacteria (25.44–31.70%) and Actinobacteriota (17.02–32.36%) increased, while Firmicutes (24.45–7.40%) and Bacteroidota decreased (16.56–8.01%) compared with that in CK. The relative abundance of Cyanobacteria decreased under drought and salt stress conditions. Thus, the relative abundance of *Bacteroides*, *Faecalibacterium,* and *Escherichia-Shigella* decreased under drought and salt stress (Figure 2).

There were two r-strategist bacteria (Gammaproteobacteria and Bacteroidota) and two k-strategists (Alphaproteobacteria and Acidobacteriota) in our study. The relative abundance of Gammaproteobacteria (15.65–16.03%) and Bacteroidota (16.56–28.78%) as r-strategists increased, whereas that of Alphaproteobacteria (9.78–3.52%) and Acidobacteriota (2.70–0.76%) as k-strategists decreased under drought stress compared with that of CK. The relative abundance of Gammaproteobacteria (15.65–10.84%) and Bacteroidota (16.56–8.01%) as r-strategists decreased, whereas Alphaproteobacteria (9.78–20.86%) and Acidobacteriota (2.70–3.06%) as k-strategists increased under salt stress (Figures 3A,B). Gammaproteobacteria were significantly negatively correlated with TC under drought stress; furthermore, Gammaproteobacteria, Acidobacteriota, and Bacteroidota were significantly negatively correlated with TC under salt stress. Gammaproteobacteria and Acidobacteriota

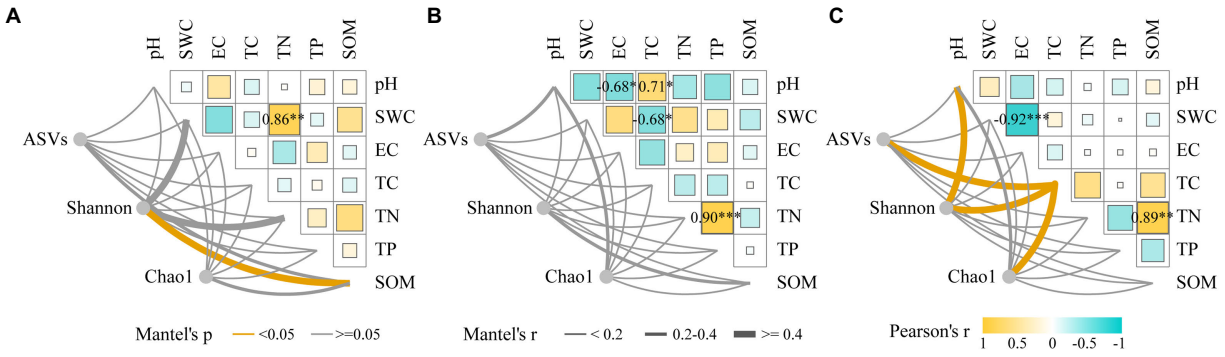

FIGURE 1
Correlation between environmental factors and alpha diversity indices of *Nitraria tangutorum* rhizosphere soil under different stress (**A**: CK; **B**: Drought; and **C**: Salt). Pairwise comparisons of environmental factors are shown with a color gradient denoting Pearson's correlation coefficient. The number of ASVs, Shannon and Chao1 indices were correlated with each environmental factor by Mantel test.

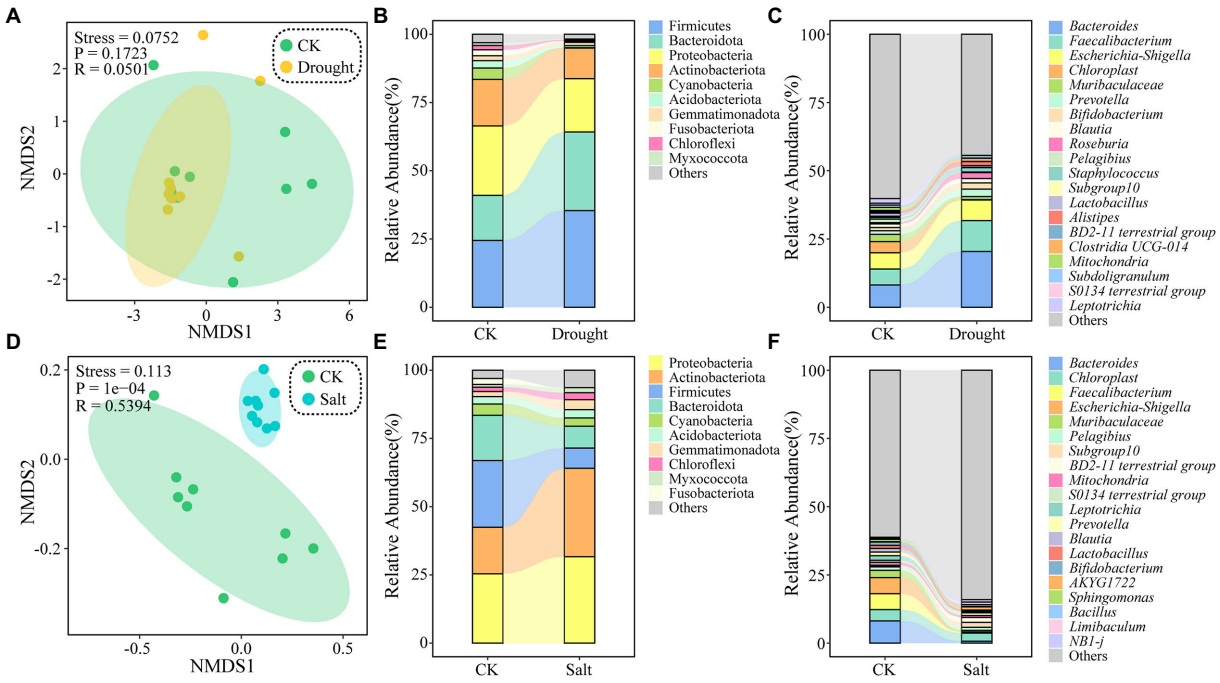

FIGURE 2
Non-metric multidimensional scaling (NMDS) ordination based on Bray Curtis similarities of bacterial communities under drought **(A)** and salt **(D)** stress. Each point represents a replicate, different colors indicate different sample plots. Relative abundance of major taxa (top 10) in the bacterial communities under drought **(B)** and salt **(E)** stress at the phylum level. And relative abundance of major taxa (top 20) in the bacterial communities under drought **(C)** and salt **(F)** stress at the genera level.

were significantly negatively correlated with TN, and Acidobacteriota was significantly negatively correlated with SOM under salt stress ($p < 0.05$; Figure 3).

Rhizosphere soil bacterial network under drought and salt stress

Based on correlation analysis ($p < 0.01$), we constructed bacterial co-occurrence networks of *N. tangutorum* under CK, drought, and salt stress. The co-occurrence network showed that drought and salt stress decreased ASV aggregation in the rhizosphere soil bacterial community of *N. tangutorum*. Under drought stress, the connectivity and complexity of the rhizosphere soil bacterial community network of *N. tangutorum* and the number of edges (47.4%) decreased compared with those of CK. In contrast, salt stress increased the connectivity and complexity of the bacterial community network, and the number of nodes and edges increased by 174.07 and 9.74%, respectively, compared with those of CK (Figure 4). There were 54 nodes and 154 edges, of which 152 were positive and 2 were negative, for CK. Under drought and salt stress, the number of nodes were 61 and 148, number of edges were 81 and 169, respectively, and all were positive. The number of modules was highest (32) under salt stress, followed by those under drought stress (14) and CK (8). Topological features such as graph density, clustering coefficient, betweenness centralization, and degree centralization were the highest in CK, followed by drought stress, and the lowest in salt stress (Supplementary Table 3).

Correlation among root exudates, r-and k-strategists bacteria, and network properties under drought and salt stress

The characteristic peaks of the chromatograms of *N. tangutorum* root exudates under different stress conditions were markedly different. By preprocessing the raw data and comparing the database, 152 and 60 compounds in positive and negative ion modes, respectively, were identified. Root exudates contained various organic acids, amides, esters, sugars, olefins, phenols, growth factors, aromatics, ketones, amino acids and their derivatives, and heterocyclic compounds. Most of the exudates were secondary metabolites. Significant differences in metabolites of *N. tangutorum* root systems under drought and salt stress, with most metabolites correlated with environmental changes (Supplementary Figures 2, 3). Under drought stress, there were 40 differential metabolites in the positive ion mode, of which 14 were upregulated and 26 were downregulated. In addition, there were 13 differential metabolites in the negative

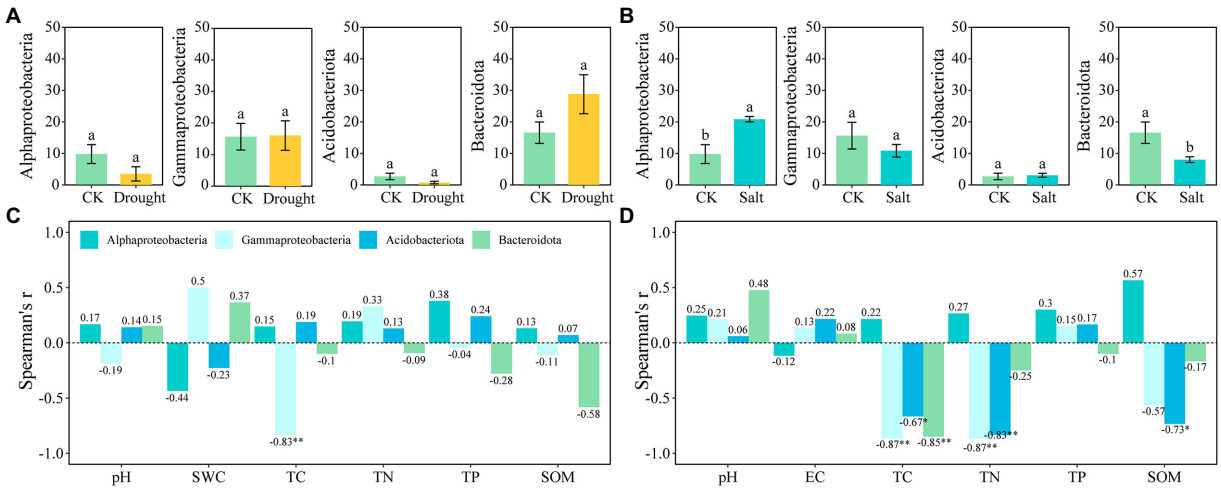

FIGURE 3
The relative abundance of bacteria for r-and k-strategists **(A,B)** and the correlation with rhizosphere soil properties of *N. tangutorum* under different stress **(C,D)**. Drought: **A** and **C**; Salt: **B** and **D**. "*" represents p <0.05, "**" represents p <0.01, and "***" represents p <0.001.

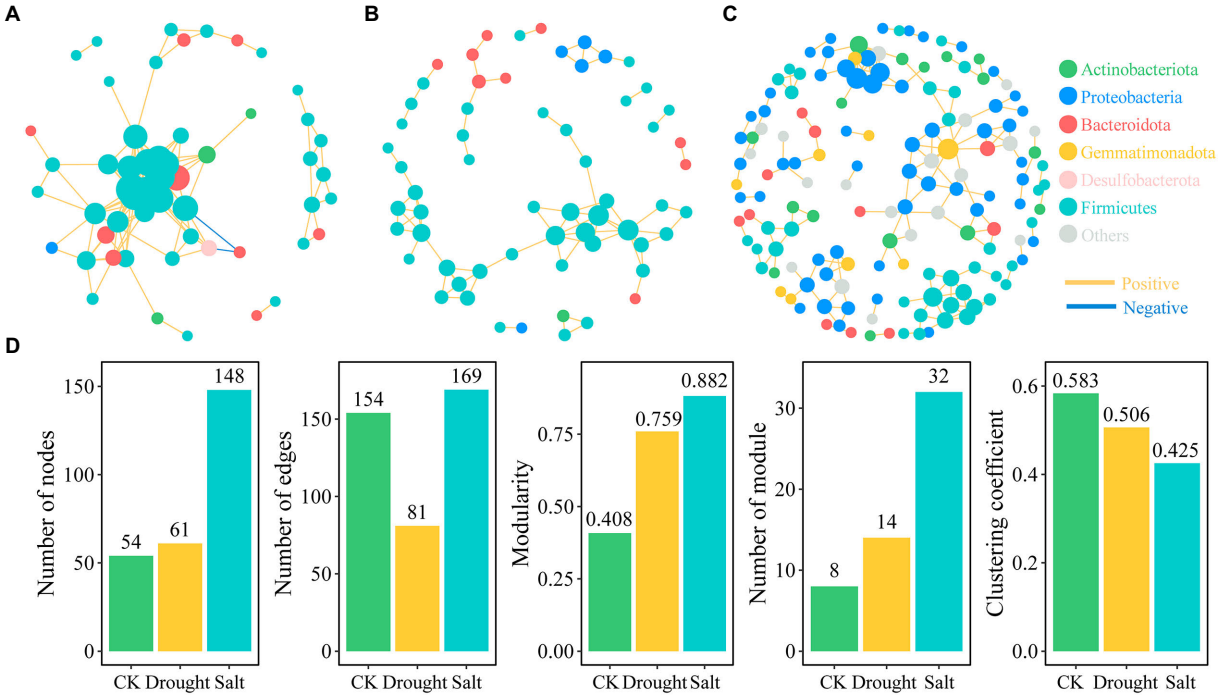

FIGURE 4
Bacterial networks based on correlation analysis of *Nitraria tangutorum* rhizosphere soil under different stress (**A**: CK; **B**: Drought; and **C**: Salt) and the correlation between network properties and soil properties **(D)**. A connection stands for a strong (Spearman's|r|> 0.9) and significant (p <0.01 after FDR correction). Colours of nodes indicate different major phyla while node size is proportional to node degree calculated from each ASV abundance correlation. The yellow lines indicate positive interactions whereas blue lines indicate negative interactions. **(D)** The network topological features of *N.tangutorum* under drought and salt stress.

ion mode, of which three were upregulated and 10 were downregulated. Under salt stress, there were 56 differential metabolites in the positive ion mode, of which 11 were upregulated and 45 were downregulated. However, in the negative ion mode, there were 13 differential metabolites, of which three were upregulated and 10 were downregulated (Figure 5).

Under drought stress, indole-3-acrylic acid and panthenol were negatively correlated with pH; 2-methyl-2,3,4,5-tetrahydro-1,5-benzoxazepin-4-one and thymidine were negatively

correlated with SWC; caffeine, 6-(3-hydroxybutan-2-yl)-5-(hydroxymethyl)-4-methoxy-2H-pyran-2-one, and 7-methylpyrimido [4,5-d]pyrimidin-4-amine were positively correlated with TN; 3-[4-methyl-1-(2-methylpropanoyl)-3-oxocyclohexyl] butanoic acid, TKK, INH, sucrose, and 4-acetamidobutyric acid were positively correlated with TP; caffeine, xanthurenic acid, and maltotetraose were negatively correlated with SOM; and 3-amino-4-methylpentanoic acid and 16-hydroxyhexadecanoic acid were positively correlated with SOM. Under salt stress, (+/−)9-HpODE was negatively correlated with pH; (+/−)9-HpODE and corchorifatty acid F were negatively correlated with EC; palmitoleic acid, 5-OxoETE, and quinoline were positively correlated with TC; 2-amino-1,3,4-octadecanetriol and prostaglandin A3 were negatively correlated with TC; methyl 4-methyl-2-oxo-2H-pyran-6-carboxylate, D-(+)-maltose, quinoline, and L-dopa were positively correlated with TN; prostaglandin A3 was negatively correlated with TN; pyridoxal, carvone, methyl 4-methyl-2-oxo-2H-pyran-6-carboxylate, acetyl-L-carnitine, anthranilic acid, L-dopa, 5,5-dimethyl-3-morpholinocyclohex-2-en-1-one, 3-[4-methyl-1-(2-methylpropanoyl)-3-oxocyclohexyl] butanoic acid, 4-acetyl-4-(ethoxycarbonyl) heptanedioic acid, and phenylacetylglycine were positively correlated with SOM (Figure 6).

Discussion

Drought and salt stress caused significant differences in rhizosphere soil physicochemical properties and root exudates of *Nitraria tangutorum*

Soil water and salt are important factors affecting soil physicochemical properties and plant growth (Flowers et al., 2010). Our study focused on the rhizosphere soil physicochemical characteristics and *N. tangutorum* bacterial community assembly strategies under short-term drought and salt stress conditions in a desert steppe. The results showed that under short-term drought stress, rhizosphere soil pH increased significantly with a decrease in SWC, while EC and pH increased significantly under salt stress. Li et al. (2018) and Pan et al. (2021) concluded that gradient changes in SWC and pH affect soil physicochemical properties, particularly the accumulation of TC content. Although the effect of short-term stress on TOC content was not significant, our study found that drought and salt stress reduced the TOC content of the rhizosphere soil of *N. tangutorum*. Dong et al. (2019) also pointed out that soil TOC is mainly controlled by soil salt concentration, further supporting our conclusions.

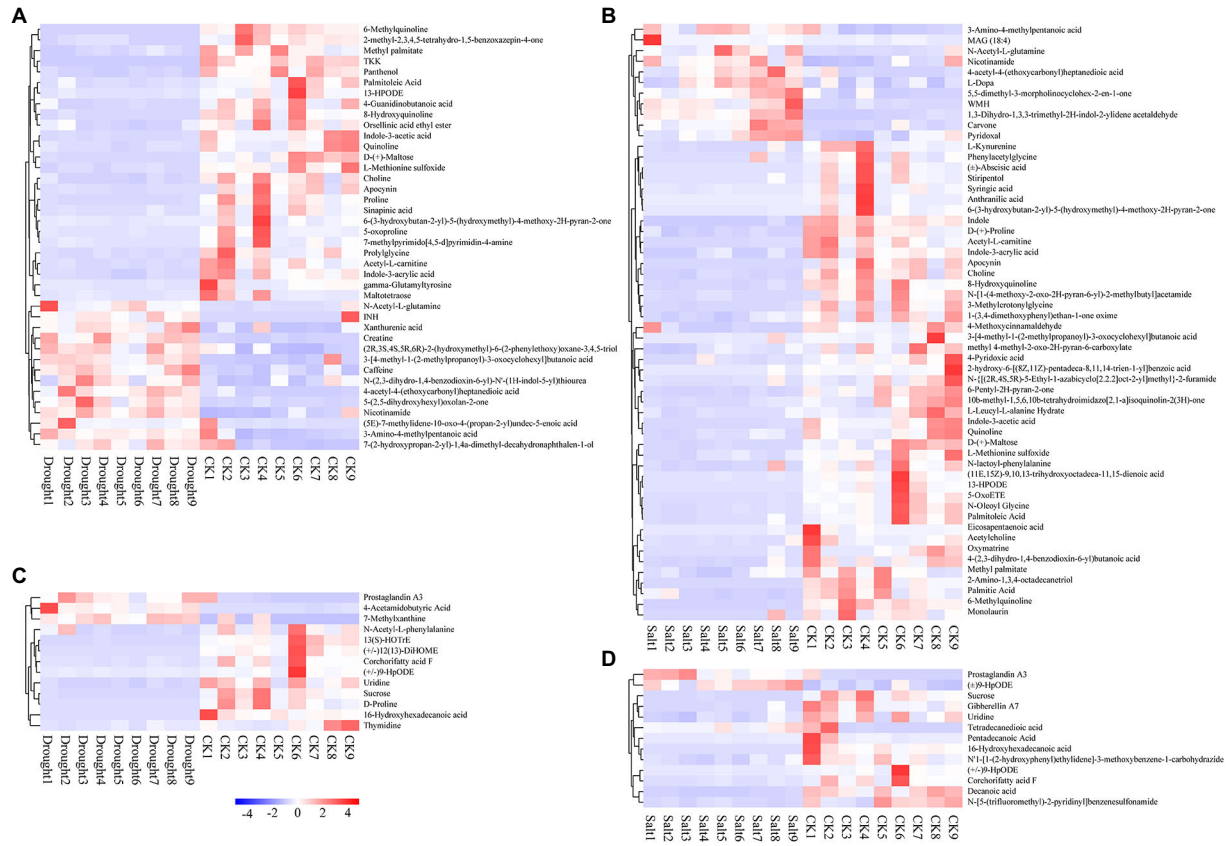

FIGURE 5
Heat map of clustering of differential metabolites of *Nitraria tangutorum* under drought (**A**: pos and **C**: neg) and salt (**B**: pos and **D**: neg) stress.

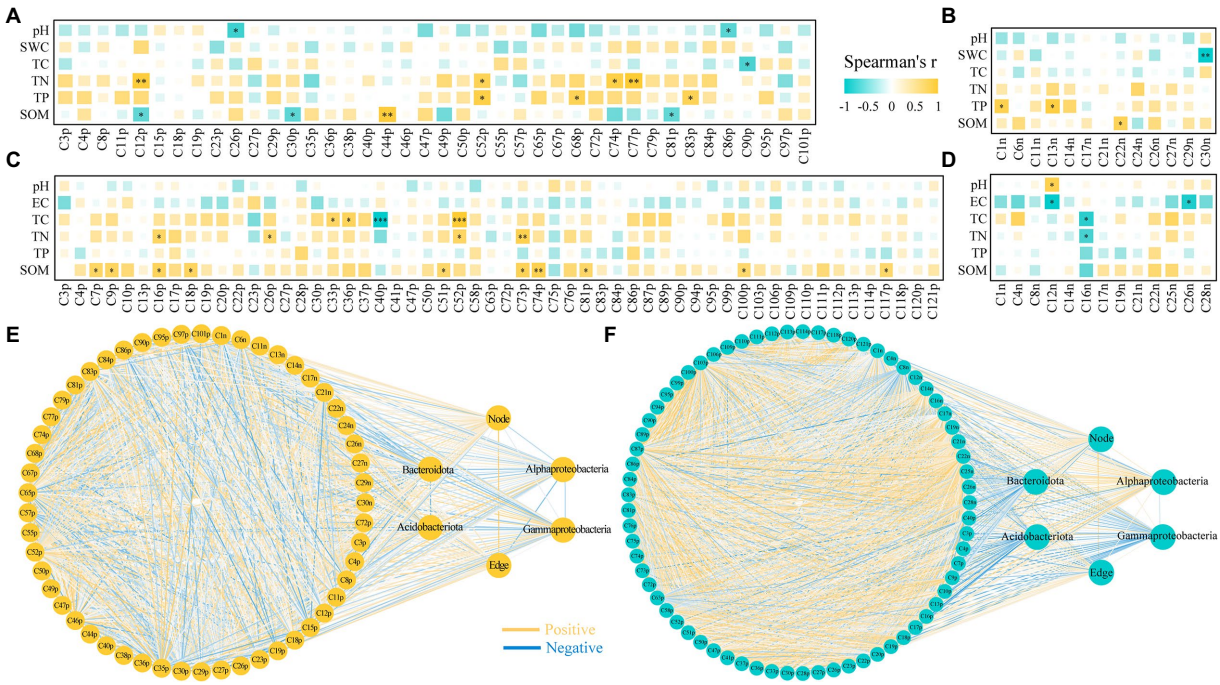

FIGURE 6
Correlation between root exudates and rhizosphere soil properties, bacteria for r-and k-strategists and network properties of *Nitraria tangutorum* under drought and salt stress. **(A)** Spearman correlation coefficients between differential metabolites of positive ion mode and rhizosphere soil physicochemical properties under drought stress. **(B)** Spearman correlation coefficients between differential metabolites of negative ion mode and rhizosphere soil physicochemical properties under drought stress. **(C)** Spearman correlation coefficients between differential metabolites of positive ion mode and rhizosphere soil physicochemical properties under salt stress. **(D)** Spearman correlation coefficients between differential metabolites of negative ion mode and rhizosphere soil physicochemical properties under salt stress. Correlation between differential metabolites of positive and negative ion mode, bacteria for r-and k-strategists and network properties of *N. tangutorum* under drought **(E)** and salt **(F)** stress. The significance of factors and the correlations between factors is marked at the figure, where "*" represents $p<0.05$, "**" represents $p<0.01$, and "***" represents $p<0.001$; yellow lines indicate positive correlations whereas blue lines indicate negative correlations. Name of root exudates under drought stress: C50p: 6-Methylquinoline; C68p: TKK; C3p: Proline; C38p: Creatine; C67p: 8-Hydroxyquinoline; C86p: Panthenol; C19p: Indole-3-acetic acid; C95p: D-(+)-Maltose; C29p: 5-(2,5-dihydroxyhexyl)oxolan-2-one; C27p: Prolylglycine; C4p: Choline; C90p: 2-methyl-2,3,4,5-tetrahydro-1,5-benzoxazepin-4-one; C18p: Acetyl-L-carnitine; C15p: L-Methionine sulfoxide; C26p: Indole-3-acrylic acid; C35p: 4-Guanidinobutanoic acid; C79p: 4-acetyl-4-(ethoxycarbonyl) heptanedioic acid; C55p: Methyl palmitate; C40p: Palmitoleic Acid; C36p: 13-HPODE; C101p: Sinapinic acid; C97p: 5-oxoproline; C77p: 7-methylpyrimido [4,5-d]pyrimidin-4-amine; C47p: Quinoline; C11p: Nicotinamide; C52p: 3-[4-methyl-1-(2-methylpropanoyl)-3-oxocyclohexyl] butanoic acid; C12p: Caffeine; C57p: N-Acetyl-L-glutamine; C65p: gamma-Glutamyltyrosine; C8p: Apocynin; C84p: Orsellinic acid ethyl ester; C83p: INH; C30p: Xanthurenic acid; C72p: (2R,3S,4S,5R,6R)-2-(hydroxymethyl)-6-(2-phenylethoxy)oxane-3,4,5-triol; C46p: (5E)-7-methylidene-10-oxo-4-(propan-2-yl)undec-5-enoic acid; C44p: 3-Amino-4-methylpentanoic acid; C81p: Maltotetraose; C23p: 7-(2-hydroxypropan-2-yl)-1,4a-dimethyl-decahydronaphthalen-1-ol; C49p: N-(2,3-dihydro-1,4-benzodioxin-6-yl)-N′-(1H-indol-5-yl)thiourea; C74p: 6-(3-hydroxybutan-2-yl)-5-(hydroxymethyl)-4-methoxy-2H-pyran-2-one; C1n: Sucrose; C27n: 13(S)-HOTrE; C22n: 16-Hydroxyhexadecanoic acid; C21n: (+/−)12 (13)-DiHOME; C13n: 4-Acetamidobutyric Acid; C14n: D-Proline; C26n: Uridine; C29n: Corchorifatty acid F; C24n: Prostaglandin A3; C17n: (+/−)9-HpODE; C11n: 7-Methylxanthine; C6n: N-Acetyl-L-phenylalanine; and C30n: Thymidine. Name of root exudates under salt stress: C99p: Apocynin; C113p: (+)-Abscisic acid; C40p: 2-Amino-1,3,4-octadecanetriol; C106p: (11E,15Z)-9,10,13-trihydroxyoctadeca-11,15-dienoic acid; C13p: 8-Hydroxyquinoline; C19p: Indole-3-acetic acid; C36p: 5-OxoETE; C90p: 3-Methylcrotonylglycine; C18p: Acetyl-L-carnitine; C26p: D-(+)-Maltose; C120p: Indole; C27p: 6-Methylquinoline; C47p: WMH; C37p: 13-HPODE; C86p: N-Oleoyl Glycine; C3p: Choline; C83p: Oxymatrine; C50p: 6-Pentyl-2H-pyran-2-one; C109p: N-[1-(4-methoxy-2-oxo-2H-pyran-6-yl)-2-methylbutyl]acetamide; C84p: L-Kynurenine; C75p: Eicosapentaenoic acid; C33p: Palmitoleic Acid; C4p: D-(+)-Proline; C114p: 2-hydroxy-6-[(8Z,11Z)-pentadeca-8,11,14-trien-1-yl] benzoic acid; C94p: 4-(2,3-dihydro-1,4-benzodioxin-6-yl) butanoic acid; C20p: Syringic acid; C52p: Quinoline; C23p: Palmitic Acid; C9p: Carvone; C87p: Stiripentol; C89p: 4-Pyridoxic acid; C72p: Monolaurin; C22p: 1,3-Dihydro-1,3,3-trimethyl-2H-indol-2-ylidene acetaldehyde; C110p: 1-(3,4-dimethoxyphenyl)ethan-1-one oxime; C74p: 5,5-dimethyl-3-morpholinocyclohex-2-en-1-one; C17p: L-Methionine sulfoxide; C100p: 4-acetyl-4-(ethoxycarbonyl) heptanedioic acid; C28p: Acetylcholine; C103p: N-lactoyl-phenylalanine; C30p: Indole-3-acrylic acid; C118p: 3-Amino-4-methylpentanoic acid; C51p: Anthranilic acid; C63p: 4-Methoxycinnamaldehyde; C81p: 3-[4-methyl-1-(2-methylpropanoyl)-3-oxocyclohexyl] butanoic acid; C58p: L-Leucyl-L-alanine Hydrate; C117p: Phenylacetylglycine; C76p: N-Acetyl-L-glutamine; C16p: methyl 4-methyl-2-oxo-2H-pyran-6-carboxylate; C112p: 10b-methyl-1,5,6,10b-tetrahydroimidazo [2,1-a] isoquinolin-2(3H)-one; C111p: N-{[(2R,4S,5R)-5-Ethyl-1-azabicyclo [2.2.2] oct-2-yl]methyl}-2-furamide; C10p: Nicotinamide; C95p: 6-(3-hydroxybutan-2-yl)-5-(hydroxymethyl)-4-methoxy-2H-pyran-2-one; C73p: L-Dopa; C41p: Methyl palmitate; C7p: Pyridoxal; C121p: MAG (18: 4); C1n: Sucrose; C4n: Uridine; C8n: N-[5-(trifluoromethyl)-2-pyridinyl]benzenesulfonamide; C12n: (+/−)9-HpODE; C14n: Decanoic acid; C16n: Prostaglandin A3; C17n: N′1-[1-(2-hydroxyphenyl)ethylidene]-3-methoxybenzene-1-carbohydrazide; C19n: 16-Hydroxyhexadecanoic acid; C21n: Tetradecanedioic acid; C22n: (+)9-HpODE; C25n: Pentadecanoic Acid; C26n: Corchorifatty acid F; and C28n: Gibberellin A7.

Plant roots respond to abiotic stress by secreting exudates, including amino acids, carbohydrate peptides, and phenolic compounds (Mercado-Blanco and Bakker, 2007). Under drought stress, 4-acetyl-4-(ethoxycarbonyl) heptanedioic, N-acetyl-L-glutamine, xanthurenic, and 4-acetamidobutyric acids accumulated in the root exudates of *N. tangutorum*. Elevated

phenolic acid content may be a strategy to cope with prolonged plant growth and stress (Henry et al., 2007). As an important metabolite of plant roots, phenolic acids play an important role in regulating their biological functions (Venugopal et al., 2009). We also found that growth factors such as creatine and nicotinamide accumulate during drought stress. These substances are secondary plant metabolites that play a crucial role in plant defense and adaptation to environmental stresses (Fujii et al., 2012). In our study, the D-proline and sucrose contents decreased significantly after 30 days of drought, differing from previous studies (Gong et al., 2005). Plants improve root osmoregulation through changes in sucrose and polyol metabolism under stress (Ruan, 2014). The decrease may be caused by the longer treatment time in our study than in previous studies. However, after 30 days of salt stress, D-proline content in *N. tangutorum* root exudates increased substantially, further proving that the difference in the amount and type of plant root exudates was due to different response strategies under different stressful environments (Per et al., 2017).

In our study, rhizosphere soil pH and EC were mostly negatively correlated with *N. tangutorum* root exudates under drought and salt stress, indicating that the unbalanced absorption and utilization of soil cations and anions by plants under stress resulted in the accumulation of organic and phenolic acids in the root exudates, which in turn had a strong correlation with rhizosphere soil pH (Gregory, 2007). In addition, the root exudates of plants positively correlated with soil TC, TN, TP, and SOM, indicating that root exudates affected plant nutrient uptake, especially in stressful environments. Root exudates have been shown to indirectly affect soil accumulation by secreting carbon-containing organic compounds and low molecular organic acids, which affect the microbial population and enzyme activity related to soil nutrients (Narula et al., 2008). In our study, 3-[4-methyl-1-(2-methylpropanoyl)-3-oxocyclohexyl] butanoic acid, quinoline, L-dopa, and 7-methylpyrimido [4,5-d] pyrimidin-4-amine were strongly correlated with rhizosphere soil TC, TN, and TP content, confirming that root exudates are an important vehicle for material exchange between plant roots and the soil (Santhanam et al., 2015).

Drought and salt stress changed the rhizosphere soil bacterial community structure of *Nitraria tangutorum*

Changes in soil physicochemical properties significantly affect soil bacterial community structure and diversity (Orozco-Aceves et al., 2017; Huang et al., 2019). However, in the present study, there were no significant differences in the abundance and diversity of *N. tangutorum* rhizosphere soil bacteria under drought and salt stress compared with those in CK, indicating that the rhizosphere bacterial community structure was stable, consistent with the results of Liu et al. (2021). NMDS analysis showed that the bacterial community structure of *N. tangutorum* rhizosphere soil was similar under drought and CK (Figure 2), which might be caused by a single species and limited diffusion of the bacterial community. Salt stress changes the composition of the soil bacterial community. Salt induced changes in the *N. tangutorum* rhizosphere bacterial community more than drought, reflecting the response characteristics of plant rhizosphere microorganisms to salt stress (Sarkar et al., 2018; Tiepo et al., 2018). In the current study, Firmicutes, Bacteroidota, Proteobacteria, and Actinobacteriota were the dominant phyla in the *N. tangutorum* rhizosphere. Previous studies have indicated that these bacteria are enriched in the rhizosphere of plants (Filion et al., 2004; Sanguin et al., 2006; Lee et al., 2008; Xu et al., 2009; Gottel et al., 2011;). Under drought stress, the relative abundance of Firmicutes increases, probably because the genera of this phylum are single-skinned bacteria with a thick cell wall that has better resistance to water stress (Lennon et al., 2012; Naylor et al., 2017; Cregger et al., 2018; Xu et al., 2018). However, the relative abundance of Proteobacteria and Actinobacteriota increased under salt stress. The sporogenesis ability of Actinobacteriota has been suggested to enable them to remain stable and quiescent in stressful environments, a strategy that may enable them to survive under adverse conditions (Vanessa et al., 2013; Hacquard et al., 2015; Naylor et al., 2017). Furthermore, a lack of nutrients in the plant rhizosphere soil would increase the abundance of Firmicutes (Singh et al., 2007). In our study, the plants were grown in sandy soils with poor fertility, which was exacerbated by drought. In the present study, drought and salt treatments may have caused drastic changes in soil moisture and pH, affecting the composition of microbial communities. The coexistence of microbial species usually depends on metabolic trade-offs, with each species having an adaptive advantage under specific biotic and abiotic conditions (Xu et al., 2018). *Bacteroides* and *Faecalibacterium* in *N. tangutorum* rhizosphere soil, belonging to phylum Bacteroidota, showed similar changes under drought and salt stress. Studies have shown that the relative abundance of bacteria responding to stress consistently changes for some phyla, classes, orders, families, and genera, which may reflect the common functions and life strategies of specific bacterial lineages (Philippot et al., 2010; Amend et al., 2016). Plants or host species growing in the same environment can attract and aggregate different microbial communities in the root zone and rhizosphere (Aleklett et al., 2015; Samad et al., 2017). Changes in plant rhizosphere soil bacteria observed under drought conditions are usually associated only with changes in drought-sensitive bacterial species but not with changes in the overall plant microflora (Naylor and Coleman-Derr, 2018). Therefore, we hypothesized that the stable rhizosphere soil bacterial diversity of *N. tangutorum* under drought stress is due to the increased abundance of specific bacteria in the rhizosphere soil. Bacterial community network analysis showed that the degree of isolation in the operational taxonomic unit module of the

rhizosphere soil core bacterial community of *N. tangutorum* under drought stress was significantly higher than that in CK (Figure 4).

Salt stress changed the interaction of rhizosphere soil bacteria and the r-and k-strategists of *Nitraria tangutorum*

Under drought and salt stress, plants can influence the species and quantity of bacterial communities in the rhizosphere through changes in root exudates (Mayak et al., 2004). The rhizosphere soil bacterial community structure of *N. tangutorum* under drought and salt stress was significantly different. In stressful environments, plant rhizosphere actively release large amounts of bioactive substances, sugars, and organic acids to attract functional bacteria for colonization, thereby changing the structure of the rhizosphere microbial community to adapt to stress (Fierer, 2017; Keswani et al., 2019). In addition, root exudate composition plays a selective role in establishing rhizosphere microbial communities (Wieland et al., 2001; Kowalchuk et al., 2002). Zwetsloot et al. (2020) found that ubiquitous root phenols could alter soil microbial communities. Changes in soil chemical properties and structure caused by rhizosphere metabolic activities allow growth of specific rhizosphere microbial communities (Haichar et al., 2008; Chaparro et al., 2014; Lareen et al., 2016). Our results further confirmed previous conclusions and also found that the root metabolites of plants under different stresses shaped microbial communities with different ecological functions.

For the ecological functions, microbial taxa are often divided into r-and k-strategists based on their growth, reproduction, competition, and adaptation strategies (Fierer et al., 2007; Li et al., 2021). The observed differences in rhizosphere bacterial populations of r-and k-strategists in *N. tangutorum* under salt stress shed light on the potential microbial mechanism of plant root exudates regulating the interactions among rhizosphere bacteria under stressful environments. Numerous studies have shown that r-strategist bacteria grow and reproduce rapidly in nutrient-rich environments, whereas k-strategist bacteria grow slowly under oligotrophic conditions (Fierer et al., 2007). In the present study, Bacteroidota and Alphaproteobacteria showed r-and k-strategist characteristics, respectively. Under salt stress, plants select suitable bacteria for colonization using different root exudates and then change the bacterial community structure. It has been confirmed that soil bacterial communities are usually limited by the availability of carbon substrates (Raich and Tufekciogul, 2000). In the current study, Bacteroidota and Alphaproteobacteria showed stronger correlations with TC and SOM under salt stress. Therefore, it can be inferred that salt stress reduced soil nutrient availability and inhibited the growth of r-strategist bacteria (Sicardi et al., 2004), whereas the accumulation of unstable carbon sources in low-molecular-weight compounds in *N. tangutorum* root exudates increased the k-strategist bacterial community (Kielak et al., 2009; Zhang et al., 2018).

The high connectivity of soil bacterial network relationships is considered a rapid response to environmental changes (Zhang et al., 2018). Many studies have shown that the stronger the plant-microbe interactions in the soil, the stronger the network relationships (Zhang et al., 2018). We found that rhizosphere soil bacteria had a closer network relationship under CK, whereas drought stress reduced the network connectivity and complexity of *N. tangutorum* rhizosphere soil bacteria. Interactions among the rhizosphere soil bacteria of *N. tangutorum* also decreased under salt stress. Furthermore, Shi et al. (2016) pointed out that the connectivity and complexity of soil microbial networks are important indicators of soil physicochemical properties that determine plant-bacteria interactions (Shi et al., 2016; Li et al., 2018). In our study, the number of nodes and edges in the bacterial network changed with soil moisture and salinity, indicating that these changes were influenced by the soil physicochemical properties. Guan et al. (2021) reported that simple network relationships could negatively affect geochemical functions, especially in salinized soils with unstable bacterial communities. Our study confirms the above conclusion that soil bacterial interactions gradually decrease with increasing soil EC and pH. However, changes in soil physicochemical properties caused by rhizosphere metabolism can shape specific rhizosphere microbial communities (Haichar et al., 2008; Chaparro et al., 2014; Lareen et al., 2016). Our results also confirmed that a change in root exudates caused by soil salinity affects the interaction among rhizosphere soil bacteria.

Conclusion

In conclusion, the rhizosphere soil bacterial community of *N. tangutorum* was highly responsive to environmental changes (drought and salt stress). Drought and salt stress decreased the nutrient content of the rhizosphere soil of *N. tangutorum*, while the differential metabolites such as organic acids, growth hormones, and sugars were the active strategies for the root system in response to stress. Meanwhile, the correlation between bacterial community diversity, richness and soil physicochemical properties was enhanced, which drove the bacterial community towards k-strategists. The network analysis also highlighted the effect of environmental changes on rhizosphere bacterial interactions, while differential root metabolites were important factors influencing the r/k categories of bacterial communities. Our analysis further suggests that root exudates play a prominent role as life carriers between plants and the soil environment in responding to environmental changes and assembling the structure of the rhizosphere microbial communities. This study reveals the mechanism of plant–soil-microbe interactions under the action of root exudates, and provides new ideas for studying the response of bacterial communities to stressful environments.

Data availability statement

The datasets presented in this study can be found in online repositories. The names of the repository/repositories and accession number(s) can be found at: https://www.ncbi.nlm.nih.gov/, PRJNA855333.

Author contributions

PK and NS conceived and designed the study. YP, MT, JH, and YZ did running the experiments and data management. JH and YP performed the data mining, statistical analysis, interpretation, and figure and table preparation of the 16S rRNA amplicon sequencing results. YP, PK, JZ, and XL did the manuscript writing and revising. All authors contributed to the article and approved the submitted version.

Funding

This work was supported financially by the National Natural Science Foundation of China (41621001), Key Research and Development Project of Ningxia (2019BEB04018), Ningxia Natural Science Foundation (2022AAC03227), and Innovation Team for Genetic Improvement of Economic Forests Foundation in Ningxia (2022QCXTD04).

Acknowledgments

We would like to thank Editage (www.editage.cn) for English language editing.

Conflict of interest

The authors declare that the research was conducted in the absence of any commercial or financial relationships that could be construed as a potential conflict of interest.

Publisher's note

All claims expressed in this article are solely those of the authors and do not necessarily represent those of their affiliated organizations, or those of the publisher, the editors and the reviewers. Any product that may be evaluated in this article, or claim that may be made by its manufacturer, is not guaranteed or endorsed by the publisher.

Supplementary material

The Supplementary material for this article can be found online at: https://www.frontiersin.org/articles/10.3389/fpls.2022.997292/full#supplementary-material

References

Aleklett, K., Leff, J. W., Fierer, N., and Hart, M. (2015). Wild plant species growing closely connected in a subalpine meadow host distinct root-associated bacterial communities. *PeerJ.* 3:e804. doi: 10.7717/peerj.804

Amend, A. S., Martiny, A. C., Allison, S. D., Berlemont, R., Goulden, M. L., Lu, Y., et al. (2016). Microbial response to simulated global change is phylogenetically conserved and linked with functional potential. *ISME J.* 10, 109–118. doi: 10.1038/ismej.2015.96

Badri, D. V., and Vivanco, J. M. (2009). Regulation and function of root exudates. *Plant Cell Environ.* 32, 666–681. doi: 10.1111/j.1365-3040.2009.01926.x

Baetz, U., and Martinoia, E. (2014). Root exudates: the hidden part of plant defense. *Trends Plant Sci.* 19, 90–98. doi: 10.1016/j.tplants.2013.11.006

Bahram, M., Harend, H., and Tedersoo, L. (2014). Network perspectives of ectomycorrhizal associations. *Fungal Ecol.* 7, 70–77. doi: 10.1016/j.funeco.2013.10.003

Banerjee, S., Walder, F., Büchi, L., Meyer, M., Held, A. Y., Gattinger, A., et al. (2019). Agricultural intensification reduces microbial network complexity and the abundance of keystone taxa in roots. *ISME J.* 13, 1722–1736. doi: 10.1038/s41396-019-0383-2

Bardgett, R. D., and van der Putten, W. H. (2014). Belowground biodiversity and ecosystem functioning. *Nature* 515, 505–511. doi: 10.1038/nature13855

Berry, D., and Widder, S. (2014). Deciphering microbial interactions and detecting keystone species with co-occurrence networks. *Front. Microbiol.* 5, 219. doi: 10.3389/fmicb.2014.00219

Bettinelli, M., Beone, G. M., Spezia, S., and Baffi, C. (2000). Determination of heavy metals in soils and sediments by microwave-assisted digestion and inductively coupled plasma optical emission spectrometry analysis. *Anal. Chim. Acta* 424, 289–296. doi: 10.1016/S0003-2670(00)01123-5

Canarini, A., Kaiser, C., Merchant, A., Richter, A., and Wanek, W. (2019). Root exudation of primary metabolites: mechanisms and their roles in plant responses to environmental stimuli. *Front. Plant Sci.* 10, 157. doi: 10.3389/fpls.2019.00157

Caporaso, J. G., Lauber, C. L., Walters, W. A., Berg-Lyons, D., Huntley, J., Fierer, N., et al. (2012). Ultra-high-throughput microbial community analysis on the illumina HiSeq and MiSeq platforms. *ISME J.* 6, 1621–1624. doi: 10.1038/ismej.2012.8

Chaparro, J. M., Badri, D. V., and Vivanco, J. M. (2014). Rhizosphere microbiome assemblage is affected by plant development. *ISME J.* 8, 790–803. doi: 10.1038/ismej.2013.196

Cregger, M. A., Veach, A. M., Yang, Z. K., Crouch, M. J., Vilgalys, R., Tuskan, G. A., et al. (2018). The Populus holobiont: dissecting the effects of plant niches and genotype on the microbiome. *Microbiome* 6, 31. doi: 10.1186/s40168-018-0413-8

de Vries, F. T., Williams, A., Stringer, F., Willcocks, R., McEwing, R., Langridge, H., et al. (2019). Changes in root-exudate-induced respiration reveal a novel mechanism through which drought affects ecosystem carbon cycling. *New Phytol.* 224, 132–145. doi: 10.1111/nph.16001

Delgado-Baquerizo, M., Maestre, F. T., Reich, P. B., Trivedi, P., Osanai, Y., Liu, Y. R., et al. (2016). Carbon content and climate variability drive global soil bacterial diversity patterns. *Ecol. Monogr.* 86, 373–390. doi: 10.1002/ecm.1216

Dong, X. L., Li, M. Z., Lin, Q. M., Li, G. T., and Zhao, X. R. (2019). Soil Na^+ concentration controls salt-affected soil organic matter components in Hetao region China. *J. Soils Sediments* 19, 1120–1129. doi: 10.1007/s11368-018-2127-8

Duran, P., Thiergart, T., Garrido-Oter, R., Agler, M., Kemen, E., Schulze-Lefert, P., et al. (2018). Microbial Interkingdom interactions in roots promote Arabidopsis survival. *Cell* 175, 973–983.e14. doi: 10.1016/j.cell.2018.10.020

Fierer, N. (2017). Embracing the unknown: disentangling the complexities of the soil microbiome. *Nat. Rev. Microbiol.* 15, 579–590. doi: 10.1038/nrmicro.2017.87

Fierer, N., Bradford, M. A., and Jackson, R. B. (2007). Toward an ecological classification of soil bacteria. *Ecology* 88, 1354–1364. doi: 10.1890/05-1839

Filion, M., Hamelin, R. C., Bernier, L., and St-Arnaud, M. (2004). Molecular profiling of rhizosphere microbial communities associated with healthy and diseased black spruce (Picea mariana) seedlings grown in a nursery. *Appl. Environ. Microbiol.* 70, 3541–3551. doi: 10.1128/aem.70.6.3541-3551.2004

Flowers, T., Galal, H., and Bromham, L. (2010). Evolution of halophytes: multiple origins of salt tolerance in land plants. *Funct. Plant Biol.* 37, 604–612. doi: 10.1071/FP09269

Fujii, K., Aoki, M., and Kitayama, K. (2012). Biodegradation of low molecular weight organic acids in rhizosphere soils from a tropical montane rain forest. *Soil Biol. Biochem.* 47, 142–148. doi: 10.1016/j.soilbio.2011.12.018

Gargallo-Garriga, A., Preece, C., Sardans, J., Oravec, M., Urban, O., and Peñuelas, J. (2018). Root exudate metabolomes change under drought and show limited capacity for recovery. *Sci. Rep.* 8, 12696. doi: 10.1038/s41598-018-30150-0

Gong, Q., Li, P., Ma, S., Indu Rupassara, S., and Bohnert, H. J. (2005). Salinity stress adaptation competence in the extremophile Thellungiella halophila in comparison with its relative Arabidopsis thaliana. *Plant J.* 44, 826–839. doi: 10.1111/j.1365-313X.2005.02587.x

Gottel, N. R., Castro, H. F., Kerley, M., Yang, Z., Pelletier, D. A., Podar, M., et al. (2011). Distinct microbial communities within the endosphere and rhizosphere of Populus deltoides roots across contrasting soil types. *Appl. Environ. Microbiol.* 77, 5934–5944. doi: 10.1128/aem.05255-11

Gregory, P. J. (2007). "The rhizosphere" in *Plant Roots: Growth, Activity and Interactions with the Soil*. ed. P. J. Gregory (Oxford: Blackwell Publishing), 216–252.

Gu, Y., Bai, Y., Xiang, Q., Yu, X., Zhao, K., Zhang, X., et al. (2018). Degradation shaped bacterial and archaeal communities with predictable taxa and their association patterns in Zoige wetland at Tibet plateau. *Sci. Rep.* 8, 3884. doi: 10.1038/s41598-018-21874-0

Guan, Y. P., Jiang, N. N., Wu, Y. X., Yang, Z. Z., Bello, A., and Yang, W. (2021). Disentangling the role of salinity-sodicity in shaping soil microbiome along a natural saline-sodic gradient. *Sci. Total Environ.* 765:142738. doi: 10.1016/j.scitotenv.2020.142738

Gul, S., Whalen, J. K., Thomas, B. W., Sachdeva, V., and Deng, H. (2015). Physico-chemical properties and microbial responses in biochar-amended soils: mechanisms and future directions. *Agric. Ecosyst. Environ.* 206, 46–59. doi: 10.1016/j.agee.2015.03.015

Guo, H., Cui, Y. N., Pan, Y. Q., Wang, S. M., and Bao, A. K. (2020). Sodium chloride facilitates the Atriplex canescens adaptation to drought stress. *Plant Physiol. Biochem.* 150, 99–108. doi: 10.1016/j.plaphy.2020.02.018

Guyonnet, J. P., Cantarel, A. A. M., Simon, L., and Haichar, F. E. Z. (2018). Root exudation rate as functional trait involved in plant nutrient-use strategy classification. *Ecol. Evol.* 8, 8573–8581. doi: 10.1002/ece3.4383

Haas, B. J., Gevers, D., Earl, A. M., Feldgarden, M., Ward, D. V., Giannoukos, G., et al. (2011). Chimeric 16S rRNA sequence formation and detection in sanger and 454-pyrosequenced PCR amplicons. *Genome Res.* 21, 494–504. doi: 10.1101/gr.112730.110

Hacquard, S., Garrido-Oter, R., González, A., Spaepen, S., Ackermann, G., Lebeis, S., et al. (2015). Microbiota and host nutrition across plant and animal kingdoms. *Cell Host Microbe* 17, 603–616. doi: 10.1016/j.chom.2015.04.009

Haichar, F. Z., Marol, C., Berge, O., Rangel-Castro, J. I., Prosser, J. I., Balesdent, J., et al. (2008). Plant host habitat and root exudates shape soil bacterial community structure. *ISME J.* 2, 1221–1230. doi: 10.1038/ismej.2008.80

Henry, A., Doucette, W., Norton, J., and Bugbee, B. (2007). Changes in crested wheatgrass root exudation caused by flood, drought, and nutrient stress. *J. Environ. Qual.* 36, 904–912. doi: 10.2134/jeq2006.0425sc

Hernandez, D. J., David, A. S., Menges, E. S., Searcy, C. A., and Afkhami, M. E. (2021). Environmental stress destabilizes microbial networks. *ISME J.* 15, 1722–1734. doi: 10.1038/s41396-020-00882-x

Huang, L., Kou, W., Wu, L., Feinstein, L., Kong, Z. Y., and Ge, G. (2019). Microbial composition and activity of natural, restored, and reclaimed wetland soils: a case study of Poyang Lake Basin, China. *Wetlands* 39, S113–S123. doi: 10.1007/s13157-018-1020-y

Jenkins, S., Swenson, T. L., Lau, R., Rocha, A. M., Aaring, A., Hazen, T. C., et al. (2017). Construction of viable soil defined media using quantitative metabolomics analysis of soil metabolites. *Front. Microbiol.* 8, 2618. doi: 10.3389/fmicb.2017.02618

Kang, P., Bao, A. K., Kumar, T., Pan, Y. Q., Bao, Z. L. T., Wang, F., et al. (2016). Assessment of stress tolerance, productivity, and forage quality in T-1 transgenic alfalfa co-overexpressing *ZxNHX* and *ZxVP1-1* from *Zygophyllum xanthoxylum*. *Front. Plant Sci.* 7, 1598. doi: 10.3389/fpls.2016.01598

Kang, J. J., Zhao, W. Z., Zhao, M., Zheng, Y., and Yang, F. (2015). NaCl and Na_2SiO_3 coexistence strengthens growth of the succulent xerophyte Nitraria tangutorum under drought. *Plant Growth Regul.* 77, 223–232. doi: 10.1007/s10725-015-0055-9

Karlowsky, S., Augusti, A., Ingrisch, J., Akanda, M. K. U., Bahn, M., and Gleixner, G. (2018). Drought-induced accumulation of root exudates supports post-drought recovery of microbes in mountain grassland. *Front. Plant Sci.* 9, 1593. doi: 10.3389/fpls.2018.01593

Keswani, C., Prakash, O., Bharti, N., Vílchez, J. I., Sansinenea, E., Lally, R. D., et al. (2019). Re-addressing the biosafety issues of plant growth promoting rhizobacteria. *Sci. Total Environ.* 690, 841–852. doi: 10.1016/j.scitotenv.2019.07.046

Kielak, A., Pijl, A. S., van Veen, J. A., and Kowalchuk, G. A. (2009). Phylogenetic diversity of Acidobacteriota in a former agricultural soil. *ISME J.* 3, 378–382. doi: 10.1038/ismej.2008.113

Klappenbach, J. A., Dunbar, J. M., and Schmidt, T. M. (2000). rRNA operon copy number reflects ecological strategies of bacteria. *Appl. Environ. Microbiol.* 66, 1328–1333. doi: 10.1128/aem.66.4.1328-1333.2000

Kong, C. H., Zhang, S. Z., Li, Y. H., Xia, Z. C., Yang, X. F., Meiners, S. J., et al. (2018). Plant neighbor detection and allelochemical response are driven by root-secreted signaling chemicals. *Nat. Commun.* 9, 3867. doi: 10.1038/s41467-018-06429-1

Kowalchuk, G. A., Buma, D. S., de Boer, W., Klinkhamer, P. G., and van Veen, J. A. (2002). Effects of above-ground plant species composition and diversity on the diversity of soil-borne microorganisms. *Antonie Van Leeuwenhoek* 81, 509–520. doi: 10.1023/a:1020565523615

Kuczynski, J., Stombaugh, J., Walters, W. A., Gonzalez, A., Caporaso, J. G., and Knight, R. (2012). Using QIIME to analyze 16S rRNA gene sequences from microbial communities. *Curr. Protoc. Microbiol.* 1, Unit 1E.5. doi: 10.1002/9780471729259.mc01e05s27

Kumar, M., Ji, B., Zengler, K., and Nielsen, J. (2019). Modelling approaches for studying the microbiome. *Nat. Microbiol.* 4, 1253–1267. doi: 10.1038/s41564-019-0491-9

Langille, M. G., Zaneveld, J., Caporaso, J. G., McDonald, D., Knights, D., Reyes, J. A., et al. (2013). Predictive functional profiling of microbial communities using 16S rRNA marker gene sequences. *Nat. Biotechnol.* 31, 814–821. doi: 10.1038/nbt.2676

Lareen, A., Burton, F., and Schäfer, P. (2016). Plant root-microbe communication in shaping root microbiomes. *Plant Mol. Biol.* 90, 575–587. doi: 10.1007/s11103-015-0417-8

Lee, S. H., Ka, J. O., and Cho, J. C. (2008). Members of the phylum Acidobacteriota are dominant and metabolically active in rhizosphere soil. *FEMS Microbiol. Lett.* 285, 263–269. doi: 10.1111/j.1574-6968.2008.01232.x

Lennon, J. T., Aanderud, Z. T., Lehmkuhl, B. K., and Schoolmaster, D. R. (2012). Mapping the niche space of soil microorganisms using taxonomy and traits. *Ecology* 93, 1867–1879. doi: 10.1890/11-1745.1

Li, J., Li, C., Kou, Y., Yao, M., He, Z., and Li, X. (2020). Distinct mechanisms shape soil bacterial and fungal co-occurrence networks in a mountain ecosystem. *FEMS Microbiol. Ecol.* 96, fiaa030. doi: 10.1093/femsec/fiaa030

Li, J. B., Shen, Z. H., Li, C. N., Kou, Y. P., Wang, Y. S., Tu, B., et al. (2018). Stair-step pattern of soil bacterial diversity mainly driven by pH and vegetation types Along the Elevational gradients of Gongga Mountain, China. *Front. Microbiol.* 9, 569. doi: 10.3389/fmicb.2018.00569

Li, H., Yang, S., Semenov, M., Yao, F., Ye, J., Bu, R., et al. (2021). Temperature sensitivity of SOM decomposition is linked with a K-selected microbial community. *Glob. Chang. Biol.* 27, 2763–2779. doi: 10.1111/gcb.15593

Liu, W., Zhang, Y., Yuan, X., Xuan, Y., Gao, Y., and Yan, Y. (2016). Exogenous salicylic acid improves salinity tolerance of Nitraria tangutorum. *Russ. J. Plant Physiol.* 63, 132–142. doi: 10.1134/S1021443716010118

Liu, Q., Zhao, X., Liu, Y., Xie, S., Xing, Y., Dao, J., et al. (2021). Response of sugarcane Rhizosphere bacterial community to drought stress. *Front. Microbiol.* 12:716196. doi: 10.3389/fmicb.2021.716196

Luo, Q., Sun, L., Hu, X., and Zhou, R. (2014). The variation of root exudates from the hyperaccumulator sedum alfredii under cadmium stress: metabonomics analysis. *PLoS One* 9:e115581. doi: 10.1371/journal.pone.0115581

Luo, G., Zhou, C., Chen, X., and Li, Y. (2008). A methodology of characterizing status and trend of land changes in oases: a case study of Sangong River watershed, Xinjiang. *Chin. J. Environ. Manag.* 88, 775–783. doi: 10.1016/j.jenvman.2007.04.003

Ma, B., Wang, H., Dsouza, M., Lou, J., He, Y., Dai, Z., et al. (2016). Geographic patterns of co-occurrence network topological features for soil microbiota at continental scale in eastern China. *ISME J.* 10, 1891–1901. doi: 10.1038/ismej.2015.261

Ma, B., Wang, Y., Ye, S., Liu, S., Stirling, E., Gilbert, J. A., et al. (2020). Earth microbial co-occurrence network reveals interconnection pattern across microbiomes. *Microbiome* 8, 82. doi: 10.1186/s40168-020-00857-2

Magoč, T., and Salzberg, S. L. (2011). FLASH: fast length adjustment of short reads to improve genome assemblies. *Bioinformatics* 27, 2957–2963. doi: 10.1093/bioinformatics/btr507

Mayak, S., Tirosh, T., and Glick, B. R. (2004). Plant growth-promoting bacteria that confer resistance to water stress in tomatoes and peppers. *Plant Sci.* 166, 525–530. doi: 10.1016/j.plantsci.2003.10.025

Mercado-Blanco, J., and Bakker, P. A. (2007). Interactions between plants and beneficial *Pseudomonas* spp.: exploiting bacterial traits for crop protection. *Antonie Van Leeuwenhoek* 92, 367–389. doi: 10.1007/s10482-007-9167-1

Meyer, O. (1994). Functional groups of microorganisms. *Biodivers. Ecosyst. Funct.* 99, 67–96. doi: 10.1007/978-3-642-58001-7_4

Mommer, L., Hinsinger, P., Prigent-Combaret, C., and Visser, E. J. W. (2016). Advances in the rhizosphere: stretching the interface of life. *Plant Soil* 407, 1–8. doi: 10.1007/s11104-016-3040-9

Narula, N., Kothe, E., and Behl, R. (2008). Role of root exudates in plant-microbe interactions. *J. Appl. Bot. Food Qual.* 82, 122–130. doi: 10.1614/IPSM-08-126.1

Naylor, D., and Coleman-Derr, D. (2018). Drought stress and root-associated bacterial communities. *Front. Plant Sci.* 8, 2223. doi: 10.3389/fpls.2017.02223

Naylor, D., DeGraaf, S., Purdom, E., and Coleman-Derr, D. (2017). Drought and host selection influence bacterial community dynamics in the grass root microbiome. *ISME J.* 11, 2691–2704. doi: 10.1038/ismej.2017.118

Ni, J. W., Yang, X. Y., Zhu, J. F., Liu, Z. X., Ni, Y. Y., Wu, H. W., et al. (2015). Salinity-induced metabolic profile changes in Nitrariatangutorum Bobr. Suspension cells. *Plant Cell Tissue Organ Cult.* 122, 239–248. doi: 10.1007/s11240-015-0744-0

Orozco-Aceves, M., Tibbett, M., and Standish, R. J. (2017). Correlation between soil development and native plant growth in forest restoration after surface mining. *Ecol. Eng.* 106, 209–218. doi: 10.1016/j.ecoleng.2017.06.004

Pan, Y. Q., Guo, H., Wang, S. M., Zhao, B., Zhang, J. L., Ma, Q., et al. (2016). The photosynthesis, Na^+/K^+ homeostasis and osmotic adjustment of *Atriplex canescens* in response to salinity. *Front. Plant Sci.* 7, 848. doi: 10.3389/fpls.2016.00848

Pan, Y. Q., Kang, P., Hu, J. P., and Song, N. P. (2021). Bacterial community demonstrates stronger network connectivity than fungal community in desert-grassland salt marsh. *Sci. Total Environ.* 798:149118. doi: 10.1016/j.scitotenv.2021.149118

Pascault, N., Ranjard, L., Kaisermann, A., Bachar, D., Christen, R., Terrat, S., et al. (2013). Stimulation of different functional groups of bacteria by various plant residues as a driver of soil priming effect. *Ecosystems* 16, 810–822. doi: 10.1007/s10021-013-9650-7

Per, T. S., Khan, N. A., Reddy, P. S., Masood, A., Hasanuzzaman, M., Khan, M. I. R., et al. (2017). Approaches in modulating proline metabolism in plants for salt and drought stress tolerance: Phytohormones, mineral nutrients and transgenics. *Plant Physiol. Biochem.* 115, 126–140. doi: 10.1016/j.plaphy.2017.03.018

Pétriacq, P., Williams, A., Cotton, A., McFarlane, A. E., Rolfe, S. A., and Ton, J. (2017). Metabolite profiling of non-sterile rhizosphere soil. *Plant J.* 92, 147–162. doi: 10.1111/tpj.13639

Philippot, L., Andersson, S. G. E., Battin, T. J., Prosser, J. I., Schimel, J. P., Whitman, W. B., et al. (2010). The ecological coherence of high bacterial taxonomic ranks. *Nat. Rev. Microbiol.* 8, 523–529. doi: 10.1038/nrmicro2367

Postma, A., Slabbert, E., Postma, F., and Jacobs, K. (2016). Soil bacterial communities associated with natural and commercial *Cyclopia* spp. *FEMS Microbiol. Ecol.* 92, fiw016. doi: 10.1093/femsec/fiw016

Quast, C., Pruesse, E., Yilmaz, P., Gerken, J., Schweer, T., Yarza, P., et al. (2013). The SILVA ribosomal RNA gene database project: improved data processing and web-based tools. *Nucleic Acids Res.* 41, D590–D596. doi: 10.1093/nar/gks1219

R Core Team (2020). R: A Language and Environment for Statistical Computing. Vienna: R Foundation for Statistical Computing.

Raich, J. W., and Tufekciogul, A. (2000). Vegetation and soil respiration: correlations and controls. *Biogeochemistry* 48, 71–90. doi: 10.1023/A:1006112000616

Ramette, A. (2010). Multivariate analyses in microbial ecology. *FEMS Microbiol. Ecol.* 62, 142–160. doi: 10.1111/j.1574-6941.2007.00375.x

Rottjers, L., and Faust, K. (2018). From hairballs to hypotheses-biological insights from microbial networks. *FEMS Microbiol. Rev.* 42, 761–780. doi: 10.1093/femsre/fuy030

Ruan, Y. L. (2014). Sucrose metabolism: gateway to diverse carbon use and sugar signaling. *Annu. Rev. Plant Biol.* 65, 33–67. doi: 10.1146/annurev-arplant-050213-040251

Samad, A., Trognitz, F., Compant, S., Antonielli, L., and Sessitsch, A. (2017). Shared and host specific microbiome diversity and functioning of grapevine and accompanying weed plants. *Environ. Microbiol.* 19, 1407–1424. doi: 10.1111/1462-2920.13618

Sanguin, H., Remenant, B., Dechesne, A., Thioulouse, J., Vogel, T. M., Nesme, X., et al. (2006). Potential of a 16S rRNA-based taxonomic microarray for analyzing the rhizosphere effects of maize on agrobacterium spp. and bacterial communities. *Appl. Environ. Microbiol.* 72, 4302–4312. doi: 10.1128/aem.02686-05

Santhanam, R., Luu, V. T., Weinhold, A., Goldberg, J., Oh, Y., and Baldwin, I. T. (2015). Native root-associated bacteria rescue a plant from a sudden-wilt disease that emerged during continuous cropping. *Proc. Natl. Acad. Sci. U. S. A.* 112, E5013–E5020. doi: 10.1073/pnas.1505765112

Sarkar, J., Chakraborty, B., and Chakraborty, U. (2018). Plant growth promoting Rhizobacteria protect wheat plants against temperature stress through antioxidant signalling and reducing chloroplast and membrane injury. *J. Plant Growth Regul.* 37, 1396–1412. doi: 10.1007/s00344-018-9789-8

Sayer, E. J., Oliver, A. E., Fridley, J. D., Askew, A. P., Mills, R. T., and Grime, J. P. (2017). Links between soil microbial communities and plant traits in a species-rich grassland under long-term climate change. *Ecol. Evol.* 7, 855–862. doi: 10.1002/ece3.2700

Schleuning, M., Fründ, J., and García, D. (2015). Predicting ecosystem functions from biodiversity and mutualistic networks: an extension of trait-based concepts to plant-animal interactions. *Ecography* 38, 380–392. doi: 10.1111/ecog.00983

Senechkin, I. V., Speksnijder, A. G., Semenov, A. M., van Bruggen, A. H., and van Overbeek, L. S. (2010). Isolation and partial characterization of bacterial strains on low organic carbon medium from soils fertilized with different organic amendments. *Microb. Ecol.* 60, 829–839. doi: 10.1007/s00248-010-9670-1

Shi, Y., Delgado-Baquerizo, M., Li, Y., Yang, Y., Zhu, Y. G., Peñuelas, J., et al. (2020). Abundance of kinless hubs within soil microbial networks are associated with high functional potential in agricultural ecosystems. *Environ. Int.* 142:105869. doi: 10.1016/j.envint.2020.105869

Shi, S., Nuccio, E. E., Shi, Z. J., He, Z., Zhou, J., and Firestone, M. K. (2016). The interconnected rhizosphere: high network complexity dominates rhizosphere assemblages. *Ecol. Lett.* 19, 926–936. doi: 10.1111/ele.12630

Sicardi, M., Garćia-Préchac, F., and Frioni, L. (2004). Soil microbial indicators sensitive to land use conversion from pastures to commercial Eucalyptus grandis (hill ex maiden) plantations in Uruguay. *Appl. Soil Ecol.* 27, 125–133. doi: 10.1016/j.apsoil.2004.05.004

Singh, B. K., Munro, S., Potts, J. M., and Millard, P. (2007). Influence of grass species and soil type on rhizosphere microbial community structure in grassland soils. *Appl. Soil Ecol.* 36, 147–155. doi: 10.1016/j.apsoil.2007.01.004

Sokol, N. W., Kuebbing, S. E., Karlsen-Ayala, E., and Bradford, M. A. (2019). Evidence for the primacy of living root inputs, not root or shoot litter, in forming soil organic carbon. *New Phytol.* 221, 233–246. doi: 10.1111/nph.15361

Su, X., Su, X., Yang, S., Zhou, G., Ni, M., Wang, C., et al. (2020). Drought changed soil organic carbon composition and bacterial carbon metabolizing patterns in a subtropical evergreen forest. *Sci. Total Environ.* 736:139568. doi: 10.1016/j.scitotenv.2020.139568

Tiepo, A. N., Hertel, M. F., Rocha, S. S., Calzavara, A. K., De Oliveira, A. L. M., Pimenta, J. A., et al. (2018). Enhanced drought tolerance in seedlings of Neotropical tree species inoculated with plant growth-promoting bacteria. *Plant Physiol. Biochem.* 130, 277–288. doi: 10.1016/j.plaphy.2018.07.021

Toju, H., Peay, K. G., Yamamichi, M., Narisawa, K., Hiruma, K., Naito, K., et al. (2018). Core microbiomes for sustainable agroecosystems. *Nat Plants* 4, 247–257. doi: 10.1038/s41477-018-0139-4

Vanessa, N. K., Gouvêa, T. R., Duarte, L. O. M., Dini, A. F., Rodrigo, M., Itamar, S. D. M., et al. (2013). Water regime influences bulk soil and rhizosphere of Cereus jamacaru bacterial communities in the Brazilian Caatinga biome. *PLoS One* 8:e73606. doi: 10.1371/journal.pone.0073606

Venugopal, S. C., Chanda, B., Vaillancourt, L., Kachroo, A., and Kachroo, P. (2009). The common metabolite glycerol-3-phosphate is a novel regulator of plant defense signaling. *Plant Signal. Behav.* 4, 746–749. doi: 10.4161/psb.4.8.9111

Vives-Peris, V., Molina, L., Segura, A., Gómez-Cadenas, A., and Pérez-Clemente, R. M. (2018). Root exudates from citrus plants subjected to abiotic stress conditions have a positive effect on rhizobacteria. *J. Plant Physiol.* 228, 208–217. doi: 10.1016/j.jplph.2018.06.003

Wang, W., Akhtar, K., Ren, G., Yang, G., Feng, Y., and Yuan, L. (2019). Impact of straw management on seasonal soil carbon dioxide emissions, soil water content, and temperature in a semi-arid region of China. *Sci. Total Environ.* 652, 471–482. doi: 10.1016/j.scitotenv.2018.10.207

Wardle, D. A. (2006). The influence of biotic interactions on soil biodiversity. *Ecol. Lett.* 9, 870–886. doi: 10.1111/j.1461-0248.2006.00931.x

Wieland, G., Neumann, R., and Backhaus, H. (2001). Variation of microbial communities in soil, rhizosphere, and rhizoplane in response to crop species, soil type, and crop development. *Appl. Environ. Microbiol.* 67, 5849–5854. doi: 10.1128/aem.67.12.5849-5854.2001

Wu, L. K., Lin, W. X., and Lin, X. M. (2014). Advances and perspective in research on plant-soil-microbe interactions mediated by root exudates. *Chin. J. Plant Ecol.* 38, 298–310. doi: 10.3724/SP.J.1258.2014.00027

Xia, Z. C., Kong, C. H., Chen, L. C., Wang, P., and Wang, S. L. (2016). A broadleaf species enhances an autotoxic conifers growth through belowground chemical interactions. *Ecology* 97, 2283–2292. doi: 10.1002/ecy.1465

Xiao, Y., Angulo, M. T., Friedman, J., Waldor, M. K., Weiss, S. T., and Liu, Y. Y. (2017). Mapping the ecological networks of microbial communities. *Nat. Commun.* 8, 2042. doi: 10.1038/s41467-017-02090-2

Xu, L., Naylor, D., Dong, Z., Simmons, T., Pierroz, G., Hixson, K. K., et al. (2018). Drought delays development of the sorghum root microbiome and enriches for monoderm bacteria. *Proc. Natl. Acad. Sci. U. S. A.* 115, e4284–e4293. doi: 10.1073/pnas.1717308115

Xu, Y., Wang, G., Jin, J., Liu, J., Zhang, Q., and Liu, X. (2009). Bacterial communities in soybean rhizosphere in response to soil type, soybean genotype, and their growth stage. *Soil Biol. Biochem.* 41, 919–925. doi: 10.1016/j.soilbio.2008.10.027

Yan, Y. Q., Pan, C. H., Du, Y. L., Li, D. Y., and Liu, W. (2018). Exogenous salicylic acid regulates reactive oxygen species metabolism and ascorbate-glutathione cycle in Nitrariatangutorum Bobr. Under salinity stress. *Physiol. Mol. Biol.* 24, 577–589. doi: 10.1007/s12298-018-0540-5

Ye, J., Joseph, S. D., Ji, M., Nielsen, S., Mitchell, D. R. G., Donne, S., et al. (2017). Chemolithotrophic processes in the bacterial communities on the surface of mineral-enriched biochars. *ISME J.* 11, 1087–1101. doi: 10.1038/ismej.2016.187

Zhalnina, K., Louie, K. B., Hao, Z., Mansoori, N., da Rocha, U. N., Shi, S., et al. (2018). Dynamic root exudate chemistry and microbial substrate preferences drive patterns in rhizosphere microbial community assembly. *Nat. Microbiol.* 3, 470–480. doi: 10.1038/s41564-018-0129-3

Zhang, X., Liu, S., Huang, Y., Fu, S., Wang, J., Ming, A., et al. (2018). Tree species mixture inhibits soil organic carbon mineralization accompanied by decreased r-selected bacteria. *Plant Soil* 431, 203–216. doi: 10.1007/s11104-018-3755-x

Zhou, Y., Tang, N., Huang, L., Zhao, Y., Tang, X., and Wang, K. (2018). Effects of salt stress on plant growth, antioxidant capacity, glandular Trichome density, and volatile exudates of Schizonepeta tenuifolia Briq. *Int. J. Mol. Sci.* 19, 252. doi: 10.3390/ijms19010252

Zwetsloot, M. J., Ucros, J. M., Wickings, K., Wilhelm, R. C., Sparks, J., Buckley, D. H., et al. (2020). Prevalent root-derived phenolics drive shifts in microbial community composition and prime decomposition in forest soil. *Soil Biol. Biochem.* 145:107797. doi: 10.1016/j.soilbio.2020.107797

frontiers | Frontiers in Plant Science

TYPE Original Research
PUBLISHED 14 September 2022
DOI 10.3389/fpls.2022.955199

OPEN ACCESS

EDITED BY
Jin-Lin Zhang,
Lanzhou University, China

REVIEWED BY
Rahat Sharif,
Yangzhou University, China
Fabrício Almeida-Silva,
Ghent University, Belgium
Meng-fei Li,
Gansu Agricultural University, China

*CORRESPONDENCE
Shuming Nie
nieshuming@163.com

SPECIALTY SECTION
This article was submitted to Plant Abiotic Stress, a section of the journal Frontiers in Plant Science

RECEIVED 28 May 2022
ACCEPTED 12 August 2022
PUBLISHED 14 September 2022

CITATION
Wang D, Gong Y, Li Y and Nie S (2022) Genome-wide analysis of the homeodomain-leucine zipper family in *Lotus japonicus* and the overexpression of *LjHDZ7* in Arabidopsis for salt tolerance. *Front. Plant Sci.* 13:955199. doi: 10.3389/fpls.2022.955199

Genome-wide analysis of the homeodomain-leucine zipper family in *Lotus japonicus* and the overexpression of *LjHDZ7* in Arabidopsis for salt tolerance

Dan Wang, Yuan Gong, Yang Li and Shuming Nie*

Key Laboratory of Southwest China Wildlife Resources Conservation (Ministry of Education), College of Life Science, China West Normal University, Nanchong, China

The homeodomain-leucine zipper (HD-Zip) family participates in plant growth, development, and stress responses. Here, 40 HD-Zip transcription factors of *Lotus japonicus* were identified and gave an overview of the phylogeny and gene structures. The expression pattern of these candidate genes was determined in different organs and their response to abiotic stresses, including cold, heat, polyethylene glycol and salinity. The expression of the *LjHDZ7* was strongly induced by abiotic stress, especially salt stress. Subsequently, *LjHDZ7* gene was overexpressed in Arabidopsis. The transgenic plants grew obviously better than Col-0 plants under salt stress. Furthermore, *LjHDZ7* transgenic lines accumulated higher proline contents and showed lower electrolyte leakage and MDA contents than Col-0 plants under salt stress. Antioxidant activities of the *LjHDZ7* overexpression lines leaf were significantly higher than those of the Col-0 plants under salt stress. The concentration of Na^+ ion in *LjHDZ7* overexpression lines was significantly lower than that of Col-0 in leaf and root parts. The concentration of K^+ ion in *LjHDZ7* overexpression lines was significantly higher than that of Col-0 in the leaf parts. Therefore, these results showed that overexpression of *LjHDZ7* increased resistance to salt stress in transgenic Arabidopsis plants, and certain genes of this family can be used as valuable tools for improving abiotic stresses.

KEYWORDS

HD-ZIP, *Lotus japonicus*, gene expression, *LjHDZ7*, salt stress

Abbreviations: HD-Zip, the homeodomain leucine zipper; TF, transcription factor; Mw, molecular weight; pI, isoelectric point; SA, salicylic acid; JA, jasmonic acid; MeJA, methyl jasmonate; GA, gibberellin; q-PCR, quantitative polymerase chain reaction; ABA, abscisic acid; MDA, malonaldehyde; PEG6000, polyethylene glycol 6000; NCBI, National Center for Biotechnology Information.

Introduction

Homeodomain-leucine zipper (HD-Zip) contains a conserved homology domain (HD) motif and a leucine zipper (LZ) motif (Ariel et al., 2007). HD-Zip is a unique transcription factor (TF) that is present in a variety of plants (Henriksson et al., 2005; Sakuma et al., 2013). HD-Zip is involved in various regulatory processes of plant growth and development and responses to various external environmental signals (Wang et al., 2013; Ribone et al., 2015). HD-Zip is expressed in various tissues and organs of plants and plays an important role in different growth stages (Brant et al., 2014). Excluding the conserved HD-Zip domain, these family members have different amino acid sequence lengths and protein structures (Arce et al., 2011).

The HD-Zip gene family can be divided into four subfamilies, I to IV, according to the amino acid sequence (Capella et al., 2015). Each subfamily member has a unique function and forms a complex interaction network. HD-Zip I positively responds to various environmental stresses, such as drought, salty, pathogens, chilling injury, light signal response and hormone response (Romani et al., 2016). The expression of HD-Zip II genes is affected by light. The TFs of this family play important roles in the development of plant organs, shade avoidance response and hormone response (Turchi et al., 2015; Carabelli et al., 2018; He et al., 2021). HD-Zip III has obvious effects on the development of plant embryos, the formation of microtubule tissue, the differentiation of apical provinces and the polar transport of auxin (Yang S. et al., 2018). HD-Zip IV promotes the differentiation of epidermal cells in plant organs and the formation of anthocyanins (Nakamura et al., 2006; Zalewski et al., 2013).

Plants often face various biological and abiotic stresses during growth and development. Under various stresses, plants form a complex signal transduction network to resist adversity. The HD-Zip gene family has been reported to participate in adversity stress in many species (Zhang J. et al., 2020). HD-Zip genes play a crucial role in plant protection against pathogens and abiotic stresses (Gao et al., 2015). Overexpression of the wheat TaHDZipI-5 gene improved transgenic wheat freezing and drought resistance (Yang et al., 2017). Overexpression of PsnHDZ63 could increase reactive oxygen species scavenging ability and enhanced salt stress tolerance in transgenic *Populus simonii* × *P. nigra* (Guo et al., 2021). Overexpression of the rice HD-Zip I gene *OsHOX24* imparted higher sensitivity to stress hormones, ABA, and abiotic stresses in transgenic Arabidopsis plants than in wild-type plants (Annapurna et al., 2016; Tang et al., 2019). These studies showed that the HD-Zip gene family could play an important role in plant resistance to abiotic stress.

Homeodomain-leucine zipper genes from model plants to higher plants have been identified and analyzed. For example, the model plants *Arabidopsis thaliana* (Nakamura et al., 2006), rice (*Oryza sativa* L.) (Zhang et al., 2012), maize (*Zea mays* L., Gramineae family), moso bamboo (*Phyllostachys edulis*) (Gao et al., 2021), potato (*Solanum tuberosum* L., Solanaceae family) (Li et al., 2019), and pear (*Pyrus pyrifolia*, rose family) (Yang Q. et al., 2018). Many families and genera of the HD-Zip gene family in these species have been identified and analyzed (Yang S. et al., 2022). The functions of a number of HD-Zip genes have been studied (Zhao et al., 2014), and the regulatory mechanisms of certain HD-Zip genes have been clarified (Zhang et al., 2012). However, the evolution of these genes in specific species and groups remains elusive; moreover, limited information is available on the HD-Zip family in *Lotus japonicus*.

Lotus japonicus is an important leguminous forage that is used as a protein feed source, biological nitrogen fixation resource and ecological conservation species. In this study, we identified 40 HD-Zip TFs of *Lotus japonicus*. To provide insights on HD-Zip gene evolution and function, we performed analyses of the phylogeny, proteins, gene structure, promoter *cis*-elements, and tissue and stress expression patterns. We found that the expression of *LjHDZ7* was strongly induced by salt stress. Further studies showed that overexpression of *LjHDZ7* increased the salt resistance of transgenic Arabidopsis plants. Our results will be helpful in understanding the evolutionary relationships, proteins, gene structures, and biological functions of HD-Zip TFs in *Lotus japonicus* and will provide a foundation for further elucidating the salt resistance mechanism of the *LjHDZ7* gene.

Materials and methods

Phylogenetic and physicochemical characteristics of the homeodomain-leucine zipper protein sequence

The protein sequences of the *Lotus japonicus*, *Medicago truncatula*, *Trifolium pretense*, and *Arabidopsis thaliana* HD-Zip family were downloaded from the plant TFDB V4.0 database[1]. The candidate protein sequences were screened and identified using the CDD[2] and SMART[3], and manual elimination was performed to remove redundant sequences and sequences without typical domains. The HD-Zip family was finally determined by the protein sequence of the conserved domain.

To investigate the phylogenetic relationships of the HD-Zip members among different plants, multiple HD-Zip amino acid sequences were aligned via Clustal 2.1 software using the default settings to examine the evolutionary relationships among the sequences. A phylogenetic tree was constructed with

1 http://planttfdb.gao-lab.org/
2 http://www.ncbi.nlm.nih.gov/Structure/cdd/wrpsb.cgi
3 http://smart.embl-heidelberg.de/smart/set_mode.cgi?NORMAL=1

MEGA7.0 software with 1000 bootstrap replicates according to the maximum-likelihood (ML) method (Li et al., 2022).

The *Lotus japonicus* HD-Zip protein structural characteristics, isoelectric point (pI), molecular weight (MW) and Grand average of hydropathicity (GRAVY) values were determined using the ExPASy ProtParam tool[4]. The subcellular localization of HD-Zip genes was predicted using the online tools UniProt[5] and WoLF PSORT[6].

Conserved motif and domain analysis

Conserved protein motifs of the HD-Zip family of *Lotus japonicus* were predicted using MEME Suite[7] with the default settings. The details of the top 10 predicted motifs were obtained from the MEME suite. The conserved domains of the HD-Zip family of *Lotus japonicus* were predicted using NCBI-CDD (see text footnote 2). The distribution of the conserved domain and motif were drawn via the visualization tool in TBtools software. The three-dimensional structure (3D) of LjHD-Zip proteins was predicted in the Phyre2[8] using the default advanced settings.

Gene structure and chromosome localization

The DNA sequences of the HD-Zip gene family of *Lotus japonicus* were obtained from an online transcriptome and genome database[9]. These gene structures were displayed by server GSDS2.0[10], and the intron/exon distribution pattern of each LjHD-Zip is illustrated. These gene chromosome localizations were illustrated using MG2C_V2.1[11].

Promoter sequence analysis

The 2000 bp upstream sequence of the initiation codon of each LjHD-Zip gene was extracted from the corresponding scaffolds (see text footnote 10). Then, the cis-elements in the promoters of each LjHD-Zip gene were predicted using the PlantCARE server[12]. The distribution of the cis-elements in the promoter was drawn via the visualization tool for *cis*-elements in TBtools software.

4 http://web.expasy.org/protparam/
5 https://www.uniprot.org/
6 https://wolfpsort.hgc.jp/
7 http://meme-suite.org/
8 http://www.sbg.bio.ic.ac.uk/$\sim$phyre2/html/page.cgi?id=index
9 http://www.kazusa.or.jp/lotus/
10 http://gsds.cbi.pku.edu.cn/
11 http://mg2c.iask.in/mg2c_v2.1/
12 http://bioinformatics.psb.ugent.be/webtools/plantcare/html/

Plant growth conditions and stress treatments

Lotus japonicus ecotype "MG20" was used in this study. We selected seeds with full grains, planted them in pots with perlite, grew them in a controlled environment with a photoperiod of 16 h/8 h (light/dark) at 24°C and 70% relative humidity in a growth chamber for 60 days, and then started the treatment. For the drought treatment, we removed the original culture solution and then watered the solution with 15% polyethylene glycol (PEG) to simulate drought stress. The leaf sample material was measured at 0, 3, 6, 12, and 24 h. For the salt treatment, the original culture solution was removed and the solution was watered with 250 mM NaCl. The leaf sample material was measured at 0, 3, 6, 12, and 24 h. For the low-temperature treatment, the seedlings were transported to an incubator at 4°C and the leaf sample material was measured at 0, 3, 6, 12, and 24 h. For the high-temperature treatment, the seedlings were transported to an incubator at 42°C and the leaf sample material was measured at 0, 3, 6, 12, and 24 h. Each treatment included three replicates. Each replicate included 10 plants.

Seed germination in the salt stress treatment was evaluated by cultivating seeds of the transgenic Arabidopsis line and Col-0 were grown on MS medium containing 150 mM NaCl for 7 days. Leaf growth and root length were assessed by cultivating the seeds of Col-0 and overexpression *LjHDZ7* transgenic Arabidopsis in MS medium for 7 days, transferring the seedlings to vertical plate culture with MS medium containing 150 mM NaCl, and then cultivating the seedlings for 10 days before investigation. For the salt stress treatments, seeds of Col-0 and overexpression *LjHDZ7* transgenic Arabidopsis were grown in MS medium for 7 days, transplanted into nutrient soil, grown for 35 days, and watered with 300 mM NaCl. Col-0 and transgenic Arabidopsis shoot were harvested and oven dried at 80°C for 24 h to obtain dry weights (DW) (Wu et al., 2018).

Total RNA was extracted from leaves using plant isolation kits (Sangon Biotech, Shanghai, China, Cat. #B518631). cDNA (complementary DNA) was prepared from total RNA with random primers using cDNA synthesis kits (Vazyme, Nanjing, China, Cat. #R312-02) (Nie et al., 2022). The resulting cDNA was used as a template for qPCR (quantitative real-time PCR) analysis using SYBR Green real-time PCR master mix (Vazyme). The qPCR assays were performed in triplicate using a real-time PCR system (Bio-Rad, Hercules, CA, United States) based on the manufacturer's instructions (Wang et al., 2022b). The primers used for the qRT–PCR sets are listed in **Supplementary Table 7**. *Lotus japonicus* LjUbi (*Lotus* ubiquitin gene) was used as a reference gene, and then expression analyses with different treatment times were performed to determine the gene expression under different stress treatments, with 0 h used as a reference. The

relative gene expression was quantified using the $2^{-\Delta\Delta CT}$ method (Livak and Schmittgen, 2001). The PCR program was as follows: 1 cycle of 95°C for 30 s, followed by 40 cycles of 95°C for 10 s, 60°C for 30 s, and 72° for 30 s (Wang et al., 2022a). The resulting clusters were visualized with MeV software.

Interacting protein predictions

The protein interaction network was analyzed and predicted using STRING software[13], using *Arabidopsis* as the background and the default advanced settings. Functional enrichment analysis was performed using STRING.

Electrolyte leakage

Electrolyte leakage was determined by using the conductivity meter method (Su et al., 2015). The leaves were cut into pieces and placed in deionized water in the dark for 12 h, and then the electrical conductivity (EC1) was measured. The sample leaves were boiled for 30 min in water, and after cooling to room temperature, the electrical conductivity (EC2) was measured. Leakage was calculated by the formula:

Relative electrolyte leakage (%) = EC1/EC2 × 100%, where EC1 and EC2 refer to electric conductivity of live leaves and boiled leaves, respectively.

Malondialdehyde content

The malondialdehyde (MDA) contents were determined using the thiobarbituric acid reaction method (He et al., 2018). Fresh leaf samples were powdered in liquid nitrogen and homogenized with trichloroacetic acid (TCA). The supernatant was centrifuged and extracted and then mixed with thiobarbituric acid (TBA). The mixture was boiled and centrifuged, and then the absorbance was measured at wavelengths of 450, 532, and 600 nm. The contents were calculated by the formula:

Malondialdehyde concentration (C) (μmol/L) = 6.45 × (OD532 nm – OD600 nm) – 0.56 OD450 nm. OD450, OD532, and OD600 represented the absorbance value at 450, 532, and 600 nm, respectively. MDA content (μmol/g) = CV/1000 W. C: MDA concentration; V, volume extract; W, fresh weight.

13 https://string-db.org/cgi/input.pl

Proline content

The proline content was determined using the acidic ninhydrin reaction method (Bai et al., 2017). Fresh leaf samples were powdered in liquid nitrogen, homogenized in sulfosalicylic acid and heated in boiling water. The samples were centrifuged, and the supernatant was mixed with acidic ninhydrin and glacial acetic acid. After cooling, the samples were mixed with toluene, the supernatant was collected, and then the absorbance was determined at 520 nm. The content was calculated by the formula:

Proline contents (μg/g) = (C × VT/VS)/W. C: The standard curve for absorbance value at 520 nm (A520), A520 = 0.0512C + 0.001, R^2 = 0.9955; VT, volume extract; VS, supernatant volume; W, fresh weight.

Antioxidant enzyme activities

Superoxide dismutase (SOD), peroxidase (POD) and Catalase (CAT) activity was determined following the protocols proposed by the corresponding assay kit (Geruisi Biotechnology, Suzhou, China), respectively. The homogenate mixed with 0.1 g fresh sample and 1 mL extraction solution was centrifuged at 8,000 *g* for 10 min at 4°C, after which the supernatant was used to assay the activity of antioxidant enzymes. One unit of SOD was defined as the amount of enzyme that caused 50% of NBT photochemical reduction at 450 nm. One unit of POD was the change of 0.01 in a 1 mL reaction mixture at 470 nm per minute and per 1 g tissue. One unit of CAT was the 1 nmol H_2O_2 degradation at 510 nm per minute and per 1 mg tissue (Dong et al., 2021; Lü et al., 2022; Zhang et al., 2022).

Measurements of Na^+ and K^+ concentration

The leaves and roots from Col-0 and *LjHDZ7* overexpression plants were separately harvested, dried for 48 h at 80°C and then ground to powder. The same mass leaves and roots powder was extracted in concentrated (69%, v/v) HNO_3 for 24 h at room temperature (Li et al., 2016). Na^+ and K^+ concentrations were determined by using a flame photometer (Sherwood flame photometer-410, Cambridge, United Kingdom).

Statistical analysis

The data in this paper were analyzed using SPSS version 17.0 and the least significant difference (LSD) test. The three biological replicates were performed. Mean and standard error

values were calculated for the variable comparisons. Values of $p < 0.05$ were considered statistically significant.

Results

Phylogenetic relationship and classification of the homeodomain-leucine zipper family

A phylogenetic tree was constructed using full-length protein sequences obtained for *Lotus japonicus*, *Medicago truncatula*, *Trifolium pretense,* and *Arabidopsis thaliana*. HD-Zip genes were divided into four subfamilies (**Figure 1**). The number of HD-Zip genes in subgroup I was the largest (**Supplementary Figure 1A**), and the subfamily genes accounted for 35.42, 32.69, 36.96, and 32.50% of the whole family in *Arabidopsis thaliana*, *Medicago truncatula*, *Trifolium pretense,* and *Lotus japonicus*, respectively (**Supplementary Figure 2**). Longer amino acid sequences were obtained for HD-Zip III and HD-Zip IV, while shorter sequences were obtained for HD-Zip I and HD-Zip II (**Supplementary Figures 1B–E**).

The physicochemical properties of the amino acids encoded in the three leguminous forage species were analyzed (**Supplementary Tables 1–4**). The largest and smallest proteins were Tp57577_TGAC_v2_mRNA16082 of the HD-Zip III subfamily and Lj4g3v0633410.1 of the HD-Zip II subfamily, respectively, which had peptide chain lengths of 896 aa and 117 aa, respectively. The pI of 70.07% of the HD-Zip family proteins was less than 7, and they were weakly acidic. The pI ranged from 4.44 to 9.80, and the span was very large, indicating that the subfamily members came from different physiological environments. The physicochemical characteristics of *Lotus japonicus* were further predicted. The total average hydropathicity GRAVY values were negative and ranged from −1.186 to −0.116, thus implying their hydrophilic nature (**Supplementary Table 1**). The subcellular localization of *Lotus japonicus* HD-Zip proteins was in the nucleus, as indicated by UniProt software and WoLF PSORT (**Supplementary Tables 1, 5**).

Conservative domain analysis of homeodomain-leucine zipper in *Lotus japonicus*

The structure of HD-Zip proteins was analyzed in *Lotus japonicus* (**Supplementary Figure 3**). The multiple sequence alignment showed that HD-Zip I and HD-Zip II have higher sequence similarity and HD-Zip III and HD-Zip IV have a closer homologous evolution relationship. We examined the LjHD-Zip proteins for discovery motifs using the MEME program, and the top 10 enriched motifs were identified (**Supplementary Table 6**). The structural characteristics of the motif are shown in **Supplementary Figure 4**. From the conservative domain and motif analysis of LjHD-Zip proteins, HD-Zip I and HD-Zip II had the same conservative domain while HD-Zip III and HD-Zip IV had more similar structures. The advanced structure of plant proteins is related to their biological function and activity. The three-dimensional (3D) structure of LjHD-Zip proteins was studied by modeling predictions (**Supplementary Figure 5**). HD-Zip I and HD-Zip II were highly similar in their α-helix and β-sheet structures, while HD-Zip III and HD-Zip IV had complex protein structures.

Gene structure of homeodomain-leucine zipper in *Lotus japonicus*

We analyzed and drew the exon and intron structure diagram of HD-Zip genes in *Lotus japonicus* (**Supplementary Figure 6A**). All LjHD-Zip gene members have introns, and the number of exons in subgroup I and II ranged from 2 to 4, those in subgroup III ranged from 12 to 18 except for one, and those in subgroup IV ranged from 7 to 11 (**Supplementary Figure 6B**). The number of introns in each subgroup was relatively stable, and the gene structure of subgroup III and IV was relatively complex.

All 40 LjHD-Zip gene members were investigated for chromosome localization. They were unevenly distributed on 6 chromosomes (**Supplementary Figure 7A**), and the genes of each subgroup were unevenly distributed on each chromosome (**Supplementary Figure 7B**). The unbalanced distribution of HD-Zip genes on the chromosomes was related to the functional characteristics of the genes over the process of evolution.

Promoter regulatory element of homeodomain-leucine zipper in *Lotus japonicus*

The 2000 bp upstream sequence of the LjHD-Zip gene was intercepted, and the regulatory elements of each gene promoter were obtained by PlantCARE (**Supplementary Figure 8**). The promoter region of the HD-Zip genes had a number of elements involved in different metabolic regulatory elements, and a total of 95 *cis*-elements were detected in *Lotus japonicus*. We classified these elements into 6 categories and analyzed the regulatory elements of each subgroup. All identified cis-elements had stress and hormone response elements, which accounted for 10% and 16% of *Lotus japonicus* HD-Zip I, respectively (**Figure 2A**). The 13-gene promoter of HD-Zip I contained 14 types of stress-related cis-elements, including ABA, GA, MeJA, ETH, SA, drought, temperature, and salt stress cis-elements (**Figure 2B**). The Lj1g3v1037350.1, Lj0g3v0266959.1, Lj2g3v1034880.1,

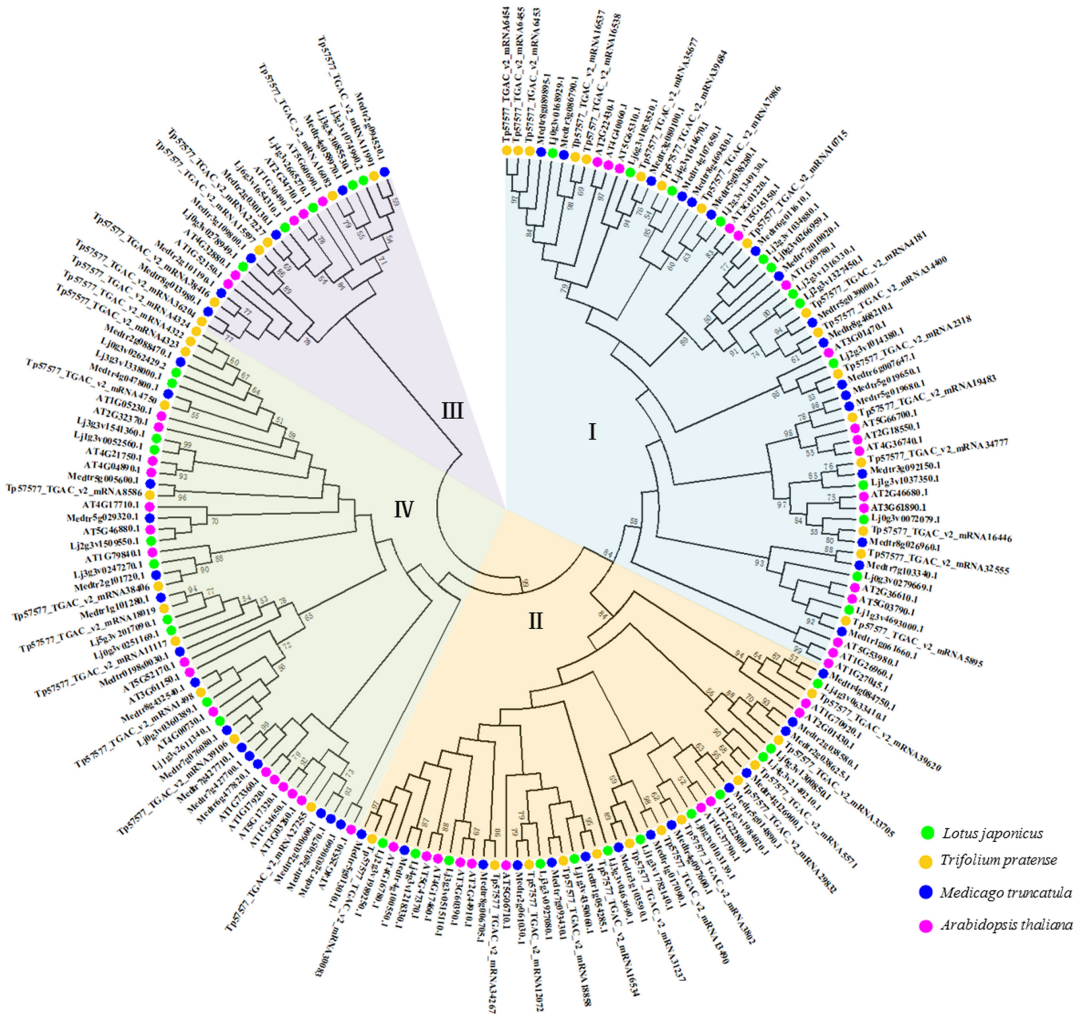

FIGURE 1
Phylogenetic tree of the HD-Zip proteins of three leguminous forage plants and *Arabidopsis thaliana*. Relationship among HD-Zip proteins constructed using the maximum-likelihood method. Different colored branches (blue, yellow, purple, and green) represent different groups (I, II, III, and IV). Labels above the nodes represent HD-Zip proteins from the source species.

Lj2g3v1316330.1, Lj2g3v1327450.1, and Lj0g3v0072079.1 of HD-Zip I were selected for intensive study according to the ABA and salt stress-related *cis*-elements. We further analyzed the regulatory elements of each gene promoter of HD-ZIP II, III, and IV all genes (**Supplementary Figure 9**). Three genes of each HD-Zip family were selected for analysis expression level under different stress types and stress time points.

Gene expression patterns of different tissues and responses to abiotic stress

The expression of 6 HD-Zip I genes in different tissues (root, stem, leaf) was analyzed by qRT–PCR (**Figure 3A**). The relative expression of Lj2g3v1327450.1, Lj2g3v1316330.1, and Lj0g3v0072079.1 was higher than that of the other three genes in the stems. The expression of Lj1g3v1037350.1, Lj0g3v0266959.1, and Lj0g3v0072079.1 was higher than that of the other genes in the roots. After stress treatment for 24 h, these seedlings showed different degrees of wilting and damage (**Figure 3E**). The electrolyte leakage of the 4 and 42°C treatment leaves was significantly higher than that of the control leaves (**Figure 3C**). Our results showed that these six genes had differential expression abundance under different stress types and stress time points (**Figure 3D**). Similarly, nine genes of HD-ZIP II, III, and IV had also differential expression abundance under different stress types and stress time points (**Supplementary Figure 10**). The expression of Lj0g3v0072079.1 was strongly induced by the stress treatments, especially salt stress. The expression of Lj0g3v0072079.1 rapidly increased and then decreased after the 42°C and PEG treatments for 3 h, while it decreased after the 4°C and salt treatments for 6 h (**Figure 3B**).

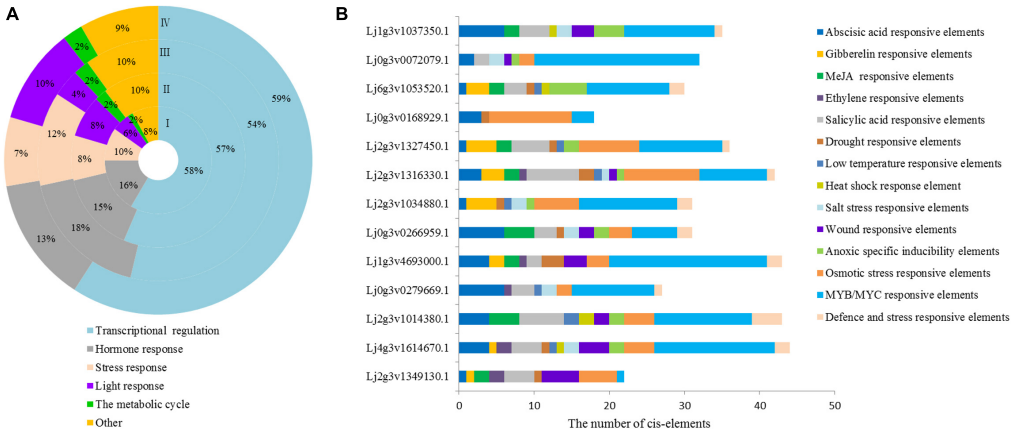

FIGURE 2
Cis-element statistical analysis of HD-Zip promoters of *Lotus japonicus*. **(A)** Different *cis*-element statistical analysis of four subfamilies. **(B)** *Cis*-element statistical analysis of HD-Zip I family gene promoters related to stress and hormone responses. Different *cis*-elements with similar functions are shown in the same color.

Therefore, Lj0g3v0072079.1 may play an important role in stress responses.

Interacting protein predictions

The interacting proteins of Lj0g3v0072079.1 were predicted (**Supplementary Figure 11A**). The red node query protein was interacted with the stress response proteins RD26 and WRKY and ABA signaling-related proteins ABI (ABA-insensitive), HAB (hypersensitive to ABA), PYL (regulatory component of ABA receptors) and PP2C (protein phosphatase 2C). We further predicted the interaction protein networks of Lj0g3v0072079.1, with *Medicago truncatula* as the background, and obtained stress-related proteins (**Supplementary Figure 12**). We performed a Gene Ontology analysis and found that the functional enrichment network of Lj0g3v0072079.1 proteins participated in the ABA-activated signaling pathway (**Supplementary Table 8**). The *Lotus japonicus* PP2C gene families Lj4g3v3044980.2 and Lj6g3v1211810.1 were found through homology comparisons (**Supplementary Figure 13**). The degrees of up- or down-regulation of Lj4g3v3044980.2 and Lj6g3v1211810.1 were different under different stresses (**Supplementary Figure 11B**). These results show that Lj0g3v0072079.1 may be involved in stress responses by regulating the ABA signaling pathway.

Overexpression of *LjHDZ7* improves salt tolerance in transgenic Arabidopsis

Through sequence comparisons, we identified the homology between Lj0g3v0072079.1 and *AtHB7* (**Supplementary Figure 14**); therefore, we named the Lj0g3v0072079.1 gene *LjHDZ7* and subsequently overexpressed *LjHDZ7* in Arabidopsis. Our results showed that the seed germination of the *LjHDZ7* overexpression line was better than that of Col-0 under salt stress (**Figure 4A**). The root growth of the transgenic lines was greater than that of the Col-0 line under salt stress (**Figure 4B**). The leaves of Col-0 gradually turned yellow and died, whereas the leaves of the transgenic lines showed obviously better growth under salt stress (**Figure 4C**). The shoot drought weight (DW) of the transgenic lines was greater than that of the Col-0 line under salt stress (**Figure 5A**). The electrolyte leakage and MDA contents of Col-0 plants leaf were higher than those of the *LjHDZ7* overexpression lines (**Figures 4D,E**). The proline contents of the *LjHDZ7* overexpression lines leaf were higher than those of the Col-0 plants under salt stress (**Figure 4F**). Furthermore, the SOD, peroxidase (POD) and catalase (CAT) activities of the *LjHDZ7* overexpression lines leaf were significantly higher than those of the Col-0 plants under salt stress (**Figures 4G–I**). Similarly, MDA contents of Col-0 plants root was higher than that of the *LjHDZ7* overexpression lines, while proline contents and SOD activities of the *LjHDZ7* overexpression lines root were significantly higher than those of the Col-0 plants under salt stress (**Figures 5B–F**). These results showed that overexpressing *LjHDZ7* could increase the salt resistance of plants.

In this study, the concentrations of Na^+ and K^+ ions in leaves and roots were measured (**Figure 6**). Under 300 mM NaCl treatment, the concentration of Na^+ ions in all plants significantly increased in the leaf and root parts, while the concentration of Na^+ ions in *LjHDZ7* overexpression lines was significantly lower than that of Col-0 in both leaf and root parts (**Figures 6A,C**). Under 300 mM NaCl treatment, the concentration of K^+ ions in all plants was

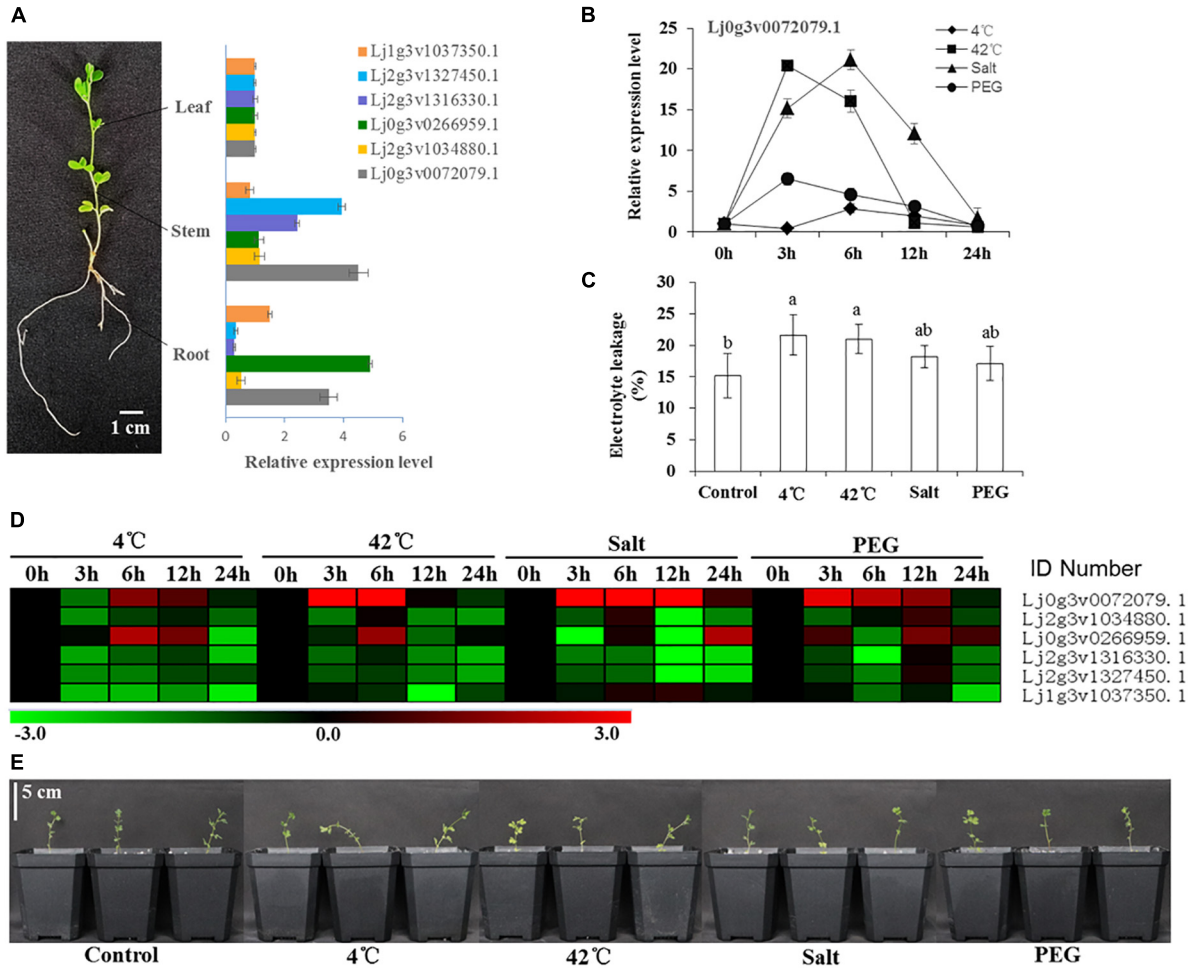

FIGURE 3
Expression levels of six HD-Zip I genes under various stresses in different times. **(A)** Tissue specificity analysis of six HD-Zip I genes and mRNA expression levels in leaves, stems and roots of *Lotus japonicus*. **(B)** Expression level of Lj0g3v0072079.1 during different stresses and times. **(C)** Electrolyte leakage of *Lotus japonicus* under different stresses at 24 h. **(D)** Heatmap of six HD-Zip I genes under 4°C, 42°C, salt and PEG stresses at different times. **(E)** Phenotypes of *Lotus japonicus* seedlings under different stresses at 24 h. Data values are the means ± SD of three independent biological samples. Different letters indicate significance using the LSD test ($p < 0.05$).

significantly decreased in the leaf and root parts, but the concentration of K^+ ions in *LjHDZ7* overexpression lines was significantly higher than that of Col-0 in the leaf parts (**Figures 6B,D**). Under 300 mM NaCl treatment, the expression of the ethylene biosynthesis genes *AtACS5* and *AtACS7* was obviously increased in Col-0 and transgenic plants, while the expression of *AtACS5* was not significantly different between Col-0 and the *LjHDZ7* overexpression lines. The expression of *AtACS7* in the two transgenic lines was significantly lower than that in Col-0 (**Figures 7A,B**). Under 300 mM NaCl treatment, the expression of the auxin biosynthesis genes *AtYUC1* and *AtYUC2* was slightly decreased in Col-0 and transgenic plants, but the expression of *AtYUC1* in *LjHDZ7* overexpression plants was slightly higher than that in Col-0, and one transgenic line reached the level of significance. The expression of *AtYUC2* in the two transgenic lines was significantly higher than that in Col-0 (**Figures 7C,D**).

Discussion

Phylogenetic trees represent an established method for determining evolutionary changes and functional relationships (Li et al., 2015). The HD-Zip protein family has been identified in many species, from mosses to higher plants, such as *Ceratopteris richardii* (Aso et al., 1999), *Physcomitrium patens* (Yip et al., 2016), angiosperms and gymnosperms (Prigge and Clark, 2010). The phylogenetic analysis indicated that the HD-Zip gene family originated before the differentiation of vascular plants and moss lineages (Sakakibara et al., 2001). In our phylogenetic tree, a total of 186 HD-Zip proteins

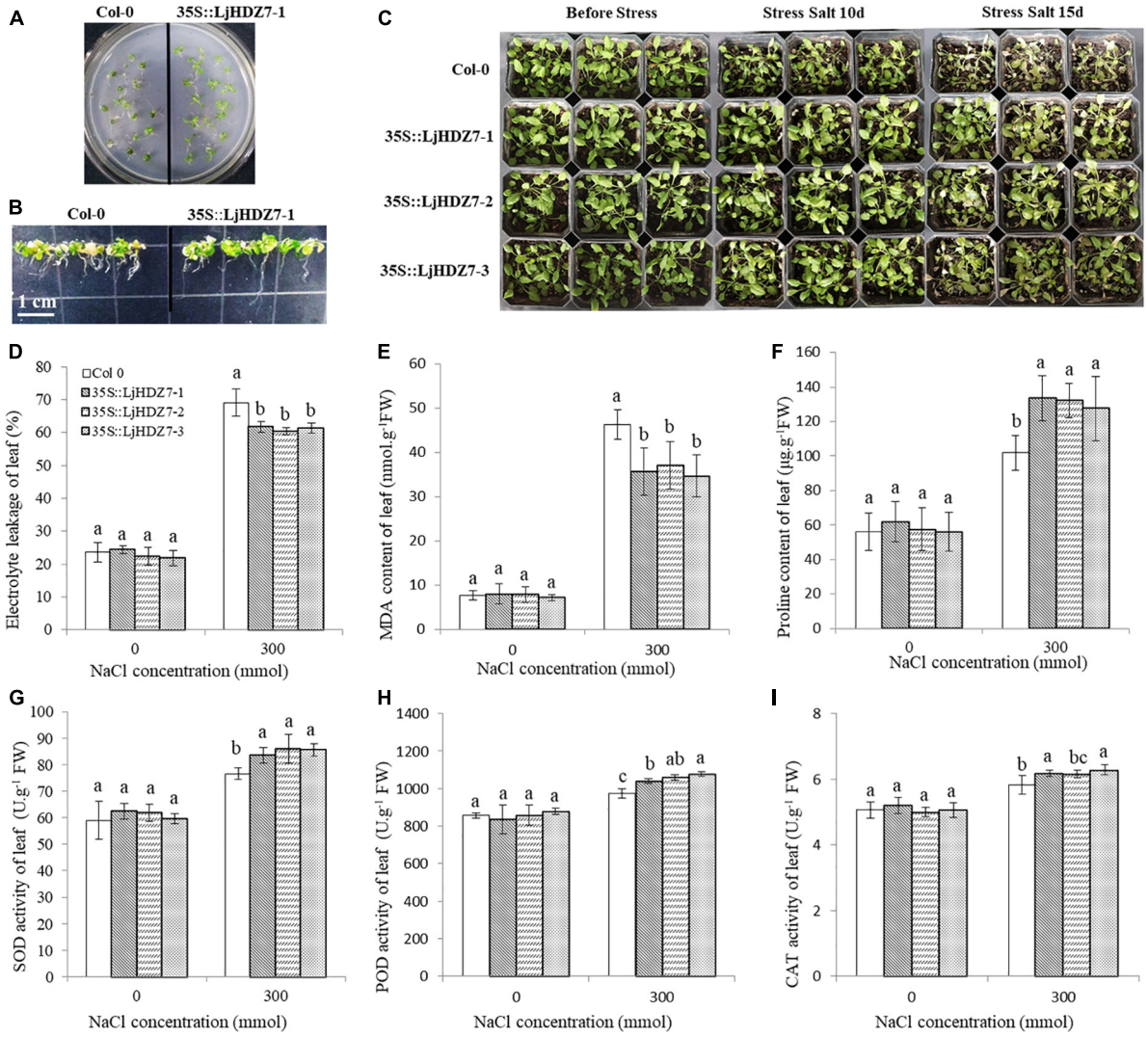

FIGURE 4
Overexpression of *LjHDZ7* in transgenic Arabidopsis improved salt tolerance. **(A)** Seed germination of wild-type (Col-0) and 35S:LjHDZ7-1 transgenic Arabidopsis plants in MS medium containing 150 mM NaCl. **(B)** Seeds of Col-0 and 35S:LjHDZ7-1 transgenic Arabidopsis were planted in MS medium for 7 days, and seedlings were transferred to MS medium containing 150 mM NaCl for 10 days before investigation. **(C)** Phenotypic analysis of Col-0 and 35S:LjHDZ7 transgenic Arabidopsis lines under salt tolerance. **(D)** Electrolyte leakage of leaf. **(E)** MDA content of leaf. **(F)** Proline content of leaf. **(G)** Superoxide dismutase (SOD) activity of leaf. **(H)** Peroxidase (POD) activity of leaf. **(I)** Catalase (CAT) activity of leaf. Data values are the means ± SD of three independent biological samples. Different letters indicate significance differences based on the LSD test ($p < 0.05$).

from three leguminous forage species and Arabidopsis were identified and divided into four subfamilies (**Figure 1**). This result was consistent with research reports on HD-Zip proteins in other species (Turchi et al., 2015). In addition, we also found that the three legumes had different numbers of HD-Zip genes and HD-Zip amino acid sequences (**Supplementary Figure 1**). Following species divergence and in conjunction with genome evolution, some members of the HD-Zip family diverged from their common ancestral genes (Jiang et al., 2015). Earlier findings showed that the exceptional increase in the sizes of TF families in higher plants is often related to WGD (whole-genome duplication) events (Lehti-Shiu et al., 2017). Legumes have undergone two WGDs within their MRCA (the Most Recent Common Ancestor). In particular, a WGD event resulted in major TF family expansions within the legumes (approximately 58 million years ago). Furthermore, TF family expansions occurred at the Glycine genus after a WGD (approximately 13 million years ago), which explains of the increase in most TF families in this genus (Moharana and Venancio, 2020). A study of legume genome evolution through the *Medicago truncatula* and *Lotus japonicus* genomes demonstrated WGD events early in legume evolution

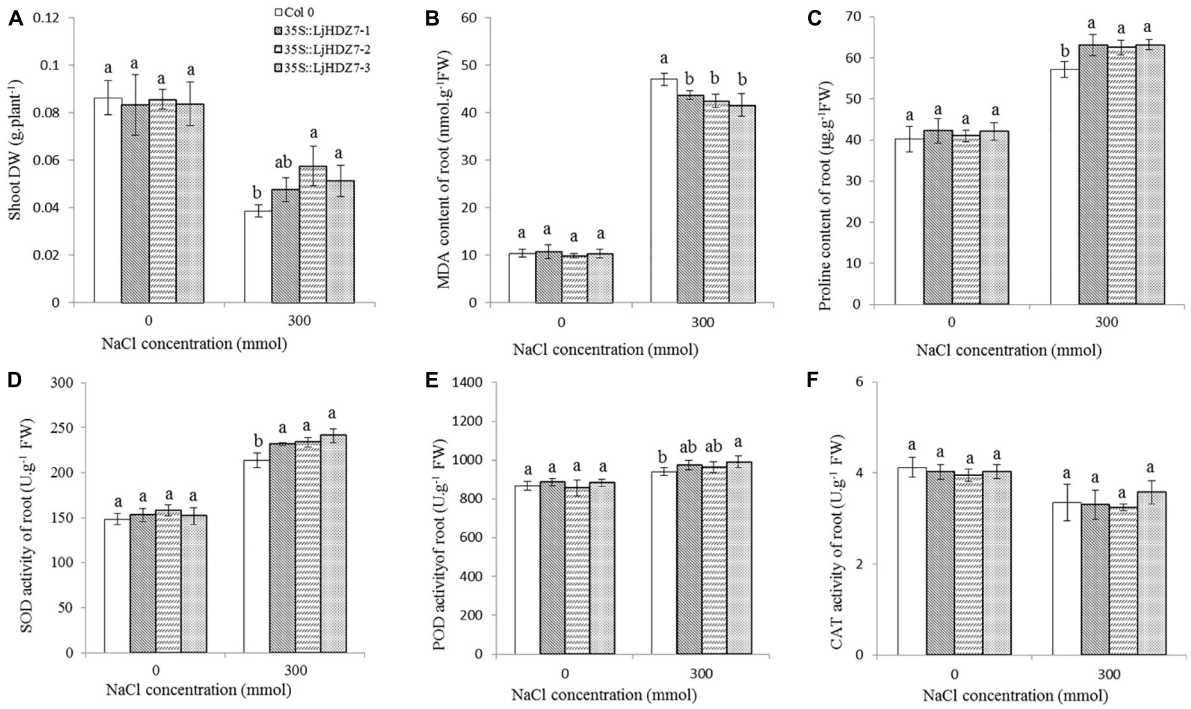

FIGURE 5
The effect of physiological index in Col-0 and *LjHDZ7* overexpression lines. **(A)** The shoot DW of Col-0 and *LjHDZ7* overexpression lines. **(B)** MDA content of root. **(C)** Proline content of root. **(D)** SOD activity of root. **(E)** POD activity of root. **(F)** CAT activity of root. Data values are the means ± SD of three independent biological samples. Different letters indicate significance differences based on the LSD test ($p < 0.05$).

(Cannon et al., 2006). Therefore, the molecular evolution of the HD-Zip gene family in legumes shows that legume genomes have undergone extensive rearrangement, including translocation and inversion (Li et al., 2014).

Previous experiments have proven that the HD-Zip gene family has a variety of motifs and structures in plants that participate in various functions (Capella et al., 2014). Great differences were observed in the number and length of exons in each subgroup, suggesting that different gene structures indicated the different gene functions (Prigge et al., 2005). In our results, *Lotus japonicus* HD-Zip family proteins were all hydrophilic and localized to the nucleus (**Supplementary Table 1**), and they had different motifs, conserved domains, protein 3D structures (**Supplementary Figures 3–5**) and intron and exon numbers (**Supplementary Figure 6**). HD-Zip I and II were highly similar in protein structure, while HD-Zip III and IV had complex protein structures. Furthermore, HD-Zip proteins and the gene structure of each subfamily were very similar. The function of each subfamily was related to their structure. Each subfamily HD-Zip gene may have evolved from the same ancestor. HD-Zip I members have been proven to play critical roles in the regulation of plant developmental processes, signaling networks and responses to environmental stresses (Gong et al., 2019). HD-Zip I gene *LpHOX21* may act as a positive transcriptional regulator for heat tolerance in perennial ryegrass (Wang et al., 2019). Overexpression of the wheat *TaHDZipI-5* gene improved transgenic wheat freezing and drought resistance (Yang et al., 2017).

The response sequence of the gene promoter determines the specific expression pattern of genes and can reflect the function of genes (Butler and Kadonaga, 2002). In this study, a total of 95 *cis*-acting elements were detected in the promoter of *Lotus japonicus* HD-Zip genes (**Supplementary Figure 8**). We further found that 95 *cis*-acting elements contained stress-related elements (MBS, DRE, ERE, etc.) and hormone response elements (TCA-element, ABRE, TGA-element, et al.). Stress- and hormone-related elements are related to the stress function of genes (Zhou et al., 2021). All identified *cis*-elements were classified, and the stress and hormone response elements accounted for 10 and 16% in *Lotus japonicus* HD-Zip I, respectively (**Figure 2A**). The HD-Zip I gene promoters were classified into 14 types of stress-related *cis*-elements, including ABA- and salt stress-related *cis*-elements (**Figure 2B**). Therefore, the *Lotus japonicus* HD-Zip I gene promoter could respond to stress factors and HD-Zip I members could play an important role in plant abiotic stress.

Transcription factor can regulate plant responses to hormones and environmental factors by regulating gene expression (Nath et al., 2019). Studies have shown that the

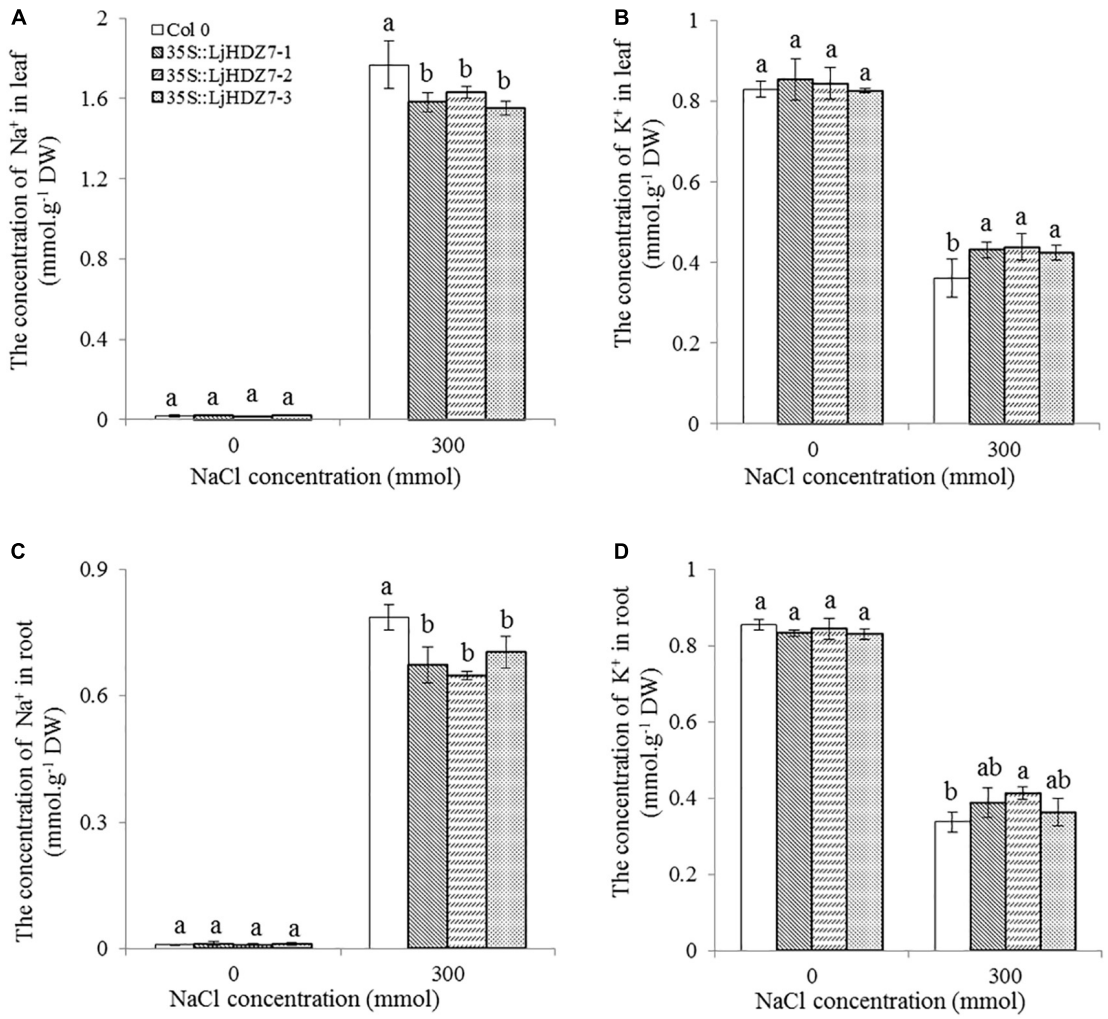

FIGURE 6
The concentrations of Na^+ and K^+ in the leaves and roots of Col-0 and *LjHDZ7*-overexpressing lines. The concentration of Na^+ in leaves **(A)**, the concentration of K^+ in leaves **(B)**, the concentration of Na^+ in roots **(C)** and the concentration of K^+ in roots **(D)** of Col-0 and *LjHDZ7* overexpression lines under control conditions and 300 mM NaCl. Data values are the means ± SD of three independent biological samples. Different letters indicate significant differences based on the LSD test ($p < 0.05$).

expression of HD-Zip subfamily I TFs is induced by drought, high salt, ABA and chilling injury (Manavella et al., 2008). Here, our results showed that the expression of six selected HD-Zip I members was induced by different stresses (**Figure 3D**). These six genes had differential expression abundance in different stress types and stress time points; therefore, they may be involved in different adversity pathways. Expression of the HD-Zip family *HaHB11* was induced by ABA, NaCl and water deficit in sunflower (Cabello et al., 2016). Arabidopsis *AtHB13* was upregulated by low temperatures and played a key role in cold, drought, and salinity stresses (Cabello and Chan, 2012; Cabello et al., 2015). We further found that the expression of the *LjHDZ7* gene was strongly induced by abiotic stress, especially salt stress (**Figure 3B**). Therefore, *LjHDZ7* may play an important role in salt stress.

Homeodomain-leucine zipper genes participate in the hormone signaling pathway and regulate plant cell expansion, division and differentiation by interacting with hormone pathway genes and downstream genes to improve plant stress tolerance (Agalou et al., 2008). In our study, many proteins related to the stress response were predicted to interact with LjHDZ7, such as RD26 (Fujita et al., 2004) and WRKY (Singh et al., 2017), ABA receptor protein, ABA signaling ABI and HAB (**Supplementary Figure 11A**). Furthermore, the homologous family of PP2C was identified and showed different expression levels under different stressors in *Lotus japonicus* (**Supplementary Figure 11B**). PYL and PP2C are key factors in the ABA pathway (Cheng et al., 2017). As previously reported for HD-Zip proteins in *Arabidopsis thaliana, AtHB12* is involved in ABA signaling by regulating PP2C and ABA receptor gene

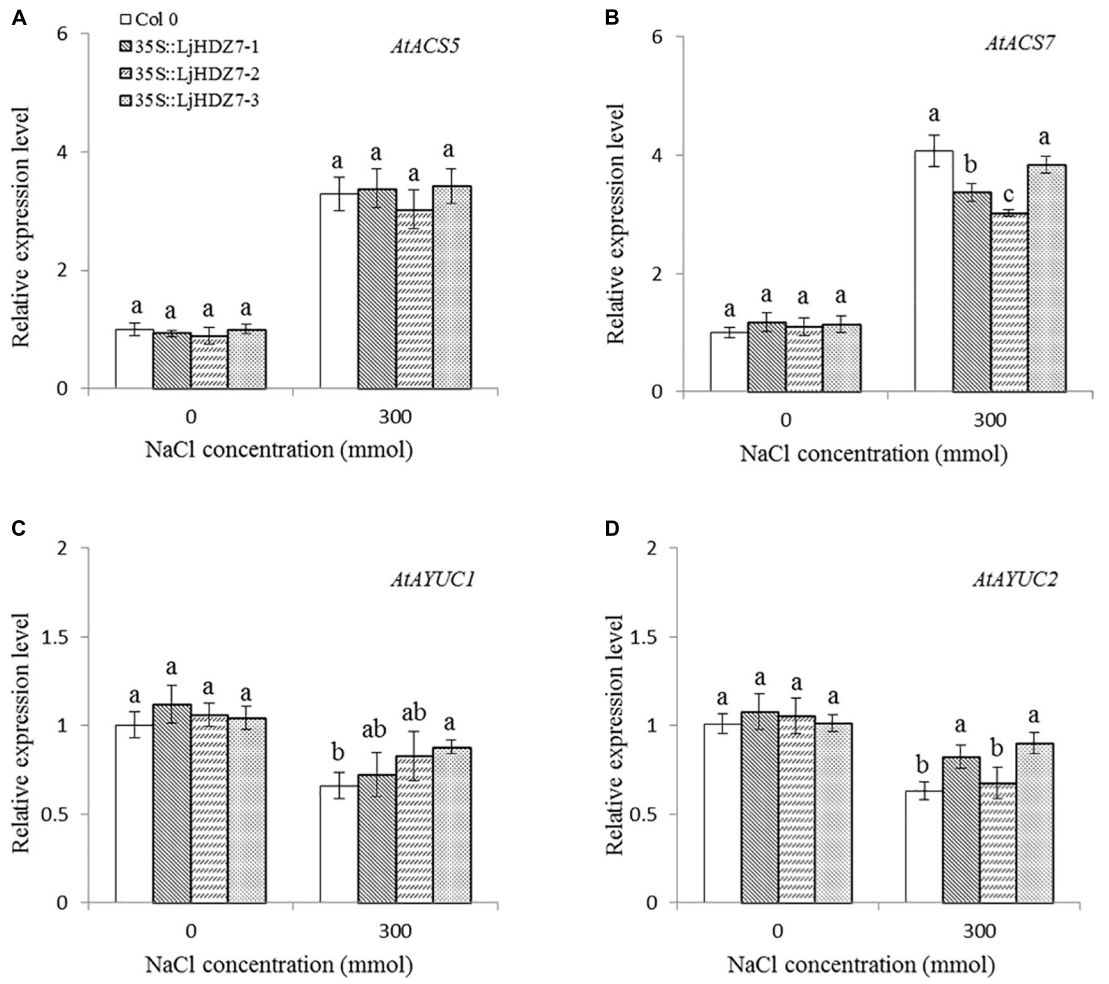

FIGURE 7
The expression levels of auxin and ethylene biosynthesis genes. The expression level of *AtACS5* **(A)**, the expression level of *AtACS7* **(B)**, the expression level of *AtYUC1* **(C)** and the expression level of *AtYUC2* **(D)** in Col-0 and *LjHDZ7* overexpression lines under control conditions and 300 mM NaCl. Data values are the means ± SD of three independent biological samples. Different letters indicate significant differences based on the LSD test ($p < 0.05$).

activities (Valdés et al., 2012). Therefore, our results indicated that *LjHDZ7* may regulate the stress response by the ABA signaling pathway, which needs to be further investigated.

The combination of modern molecular biology and traditional breeding methods can improve breeding efficiency. A drought-induced HD-Zip I gene, *Zmhdz10*, was isolated from maize and positively regulated drought and salt tolerance in both genetically transformed rice and Arabidopsis (Zhao et al., 2014). Overexpression of the wheat *TaHDZipI-5* gene increased transgenic wheat freezing and drought resistance (Yang et al., 2017). We cloned the *LjHDZ7* gene and obtained *LjHDZ7*-overexpressing transgenic Arabidopsis plants. Under salt stress, the growth of the transgenic lines was obviously better than that of the Col-0 line (**Figures 4A–C**). The electrolyte leakage and MDA contents of Col-0 plants were higher than those of the *LjHDZ7* overexpression lines (**Figures 4D,E**, **5B,C**). Furthermore, the proline contents, SOD, POD, and CAT activities of *LjHDZ7* overexpression lines were higher than those of Col-0 plants (**Figures 4F–I**, 5D–F). These results showed that the overexpression of *LjHDZ7* could increase the salt resistance of plants. Overexpression of *PsnHDZ63* resulted in improved reactive oxygen species scavenging ability and enhanced salt stress tolerance in transgenic *Populus simonii* × *P. nigra* (Guo et al., 2021). HD-Zip I gene *BpHOX2* could bind to different cis-acting elements to regulate gene expression, thus improving osmotic tolerance in birch (Tan et al., 2020). Therefore, the HD-Zip gene family may become valuable to improve stress tolerance in molecular breeding methods.

Excessive Na^+ in plants could result in ion toxicity, which causes an imbalance in ion uptake and nutritional disorders and finally leads to growth inhibition and even plant death (Wu et al., 2019; Zhang H. et al., 2020). Maintaining K^+ and Na^+ ion

homeostasis is important for a series of plant physiological and biochemical processes and for resistance to salinity (Ma et al., 2017). In the present study, the concentration of Na^+ ions in *LjHDZ7* overexpression lines was significantly lower than that in Col-0 in both leaf and root parts (**Figures 6A,C**). Furthermore, the concentration of K^+ ions in *LjHDZ7* overexpression lines was significantly higher than that in Col-0 in the leaf parts (**Figures 6B,D**). These results indicated that *LjHDZ7* overexpression lines may have a stronger selective absorption and transportation capacity for K^+ and Na^+ and could maintain a higher concentration of K^+ under saline conditions.

The phytohormone ethylene plays essential roles in plant abiotic stress adaptation. ACS (ACC synthase) is the key enzyme in ethylene biosynthesis. A previous study showed that the expression of *AtACS7* was regulated by salt stress (Dong et al., 2011). In this study, under 300 mM NaCl treatment, the expression of the ethylene biosynthesis genes *AtACS5* and *AtACS7* was obviously increased in both Col-0 and *LjHDZ7* overexpression lines, while there was no significant difference between Col-0 and *LjHDZ7* overexpression lines (**Figures 7A,B**). There may be differences in the expression of other *AtACS* genes between Col-0 and *LjHDZ7* overexpression lines. Auxin regulates many of the key processes in plant growth and stress responses. The YUCCA (YUC) family is the key limiting enzyme in the auxin biosynthetic pathway (Liu et al., 2015). A previous study showed that plant IAA levels were significantly decreased under salt stress (Hofmann, 2011). Our study showed that the expression of the *AtYUC1* and *AtYUC2* genes was downregulated in Col-0 and *LjHDZ7* overexpression plants under salt treatment. The expression of *AtYUC2* in two transgenic lines was significantly higher than that in Col-0 plants (**Figures 7C,D**). These results showed that *LjHDZ7* could change endogenous ethylene and auxin levels by regulating the expression of ethylene and auxin biosynthesis genes under salt treatment.

Conclusion

We performed an evolutionary analysis of the HD-Zip family in three leguminous forage species to obtain comprehensive information on this family, including the protein features and phylogenetic relationships. Furthermore, the motifs and domains of the proteins, gene structures, promoter *cis*-elements and stress expression patterns of HD-Zip genes were analyzed in *Lotus japonicus*. We further found that the expression of the *LjHDZ7* gene was strongly induced by abiotic stress, especially salt stress. Furthermore, our results showed that overexpression of *LjHDZ7* could increase salt resistance in transgenic Arabidopsis plants. Our results are important because they provide a theoretical basis for further functional studies of the HD-Zip gene family in *Lotus japonicus* and resources for prospective applications for stress-resistant breeding.

Data availability statement

The datasets presented in this study can be found in online repositories. The names of the repository/repositories and accession number(s) can be found in the article/**Supplementary material**.

Author contributions

DW and SN wrote the main manuscript text and contributed to the conception of the study. DW, YG, YL, and SN performed the experiments and the data analyses. All authors have read and agreed to the published version of the manuscript.

Funding

This research was funded the Fundamental Research Funds of China West Normal University (19E052). The funding bodies played no role in the design of the study and collection, analysis, and interpretation of data and in writing the manuscript.

Conflict of interest

The authors declare that the research was conducted in the absence of any commercial or financial relationships that could be construed as a potential conflict of interest.

Publisher's note

Supplementary material

The Supplementary Material for this article can be found online at: https://www.frontiersin.org/articles/10.3389/fpls.2022.955199/full#supplementary-material

SUPPLEMENTARY FIGURE S1
Statistical analysis of the HD-Zip subfamily in each plant species. **(A)** Number of HD-Zip genes found in each subfamily of *Lotus japonicus*, *Medicago truncatula*, *Trifolium pratense,* and *Arabidopsis thaliana*. **(B–E)** Amino acid sequences of HD-Zip genes in *Arabidopsis thaliana*, *Medicago truncatula*, *Trifolium pretense,* and *Lotus japonicus*, respectively. Genes corresponding to **(B–E)** X-axis NO were in Supplementary Tables S1–S4, respectively.

SUPPLEMENTARY FIGURE S2
Distribution of HD-Zip subfamilies within four plant species.

SUPPLEMENTARY FIGURE S3
Conserved motif and domain analysis of HD-Zip proteins from *Lotus japonicus*. The phylogenetic tree was generated based on the protein sequences of HD-Zip proteins. Different colored boxes represent different types of motifs and domains.

SUPPLEMENTARY FIGURE S4
Sequence information for Motif 1- Motif 10.

SUPPLEMENTARY FIGURE S5
Three-dimensional modeling structure of HD-Zip proteins in *Lotus japonicus*.

SUPPLEMENTARY FIGURE S6
(A) Chromosome localization of HD-Zip in *Lotus japonicus*. Location of HD-Zip genes in *Lotus japonicus*. **(B)** Number of four distinct HD-Zip subfamilies per chromosome.

SUPPLEMENTARY FIGURE S7
Gene structure of the HD-Zip family of *Lotus japonicus*. **(A)** Exon/intron structures of HD-Zip genes of *Lotus japonicus*. Exons and introns are represented by yellow bones and gray lines, respectively. **(B)** Exon and gene numbers of four HD-Zip subfamilies of *Lotus japonicus*.

SUPPLEMENTARY FIGURE S8
Cis-element identification in the promoters of HD-Zip from *Lotus japonicus*.

SUPPLEMENTARY FIGURE S9
Promoters *cis*-element analysis of HD-Zip of *Lotus japonicus*. *Cis*-element statistical analysis of **(A)** HD-Zip II, **(B)** HD-Zip III, and **(C)** HD-Zip IV family gene promoters related to stress and hormone responses. Different *cis*-elements with similar functions are shown in the same color.

SUPPLEMENTARY FIGURE S10
Expression levels of nine HD-Zip II, III and HD-Zip IV genes under various stresses in different times. **(A)** Expression level of Lj4g3v2140210.1 during different stresses and times. **(B)** Lj2g3v1989250.1. **(C)** Lj3g3v0463690.1. **(D)** Lj4g3v2665270.1. **(E)** Lj3g3v1074990.2. **(F)** Lj0g3v0278949.1. **(G)** Lj1g3v2611340.1. **(H)** Lj0g3v0251169.1. **(I)** Lj0g3v0262429.2.

SUPPLEMENTARY FIGURE S11
Predicted protein interaction networks of Lj0g3v0072079.1. **(A)** Protein interaction network of Lj0g3v0072079.1 was generated using the STRING online database, with *Arabidopsis thaliana* as the background. Edges represent protein–protein associations. The nodes represent proteins, and red nodes represent query proteins. The black, green, blue, light sky blue and purple lines represent co-expression, text mining, gene co-occurrence, protein homology, and experimental determination, respectively. **(B)** Relative expression levels of Lj4g3v3044980.2 and Lj6g3v1211810.1 under different stresses at 24 h.

SUPPLEMENTARY FIGURE S12
Predicted protein interaction networks of Lj0g3v0072079.1, with *Medicago truncatula* as the background.

SUPPLEMENTARY FIGURE S13
Amino acid sequence alignment of the protein phosphatase 2C (PP2C) family. Including Lj4g3v3044980.2 and Lj6g3v1211810.1 from *Lotus japonicus* and ATABI1, ATABI2, ATHAB1, and ATHAB2 from *Arabidopsis thaliana*.

SUPPLEMENTARY FIGURE S14
Amino acid sequence alignment of LjHDZ7, ATHB-7, and AET01987.

SUPPLEMENTARY TABLE S2
Basic physicochemical properties of the HD-Zip family in *Arabidopsis thaliana*.

SUPPLEMENTARY TABLE S3
Basic physicochemical properties of the HD-Zip family in *Medicago truncatula*.

SUPPLEMENTARY TABLE S4
Basic physicochemical properties of the HD-Zip family in *Trifolium pratense*.

References

Agalou, A., Purwantomo, S., OVernaS, E., Johannesson, H., Zhu, X., Estiati, A., et al. (2008). A genome-wide survey of HD-Zip genes in rice and analysis of drought-responsive family members. *Plant Mol. Biol.* 66, 87–103. doi: 10.1007/s11103-007-9255-7

Annapurna, B., Khurana, J. P., and Mukesh, J. (2016). Characterization of Rice Homeobox Genes, *OsHOX22* and *OsHOX24*, and Over-expression of *OsHOX24* in Transgenic *Arabidopsis* Suggest Their Role in Abiotic Stress Response. *Front. Plant Sci.* 7:627. doi: 10.3389/fpls.2016.00627

Arce, A., Raineri, J., Capella, M., Cabello, J., and Chan, R. (2011). Uncharacterized conserved motifs outside the HD-Zip domain in HD-Zip subfamily I transcription factors; a potential source of functional diversity. *BMC Plant Biol.* 11:42. doi: 10.1186/1471-2229-11-42

Ariel, F. D., Manavella, P. A., Dezar, C. A., and Chan, R. (2007). The true story of the HD-Zip family. *Trends Plant Sci.* 12, 419–426. doi: 10.1016/j.tplants.2007.08.003

Aso, K., Kato, M., Banks, J. A., and Hasebe, M. (1999). Characterization of homeodomain-leucine zipper genes in the fern Ceratopteris richardii and the evolution of the homeodomain-leucine zipper gene family in vascular plants. *Mol. Biol. Evol.* 16, 544–552. doi: 10.1093/oxfordjournals.molbev.a026135

Bai, J., Mao, J., Yang, H., Khan, A., Fan, A., Liu, S., et al. (2017). Sucrose non-ferment 1 related protein kinase 2 (SnRK2) genes could mediate the stress responses in potato (*Solanum tuberosum* L.). *BMC Genet.* 18:41. doi: 10.1186/s12863-017-0506-6

Brant, R., Cabedo, M., Xie, Y., and Wenkel, S. (2014). Homeodomain leucine-zipper proteins and their role in synchronizing growth and development with the environment. *J. Integr. Plant Biol.* 56, 518–526. doi: 10.1111/jipb.12185

Butler, J. E., and Kadonaga, J. T. (2002). The RNA polymerase II core promoter: A key component in the regulation of gene expression. *Genes. Dev.* 16, 2583–2592. doi: 10.1101/gad.1026202

Cabello, J. V., Arce, A. L., and Chan, R. (2015). The homologous HD-Zip I transcription factors *HaHB1* and *AtHB13* confer cold tolerance via the induction of pathogenesis-related and glucanase proteins. *Plant J.* 69, 141–153. doi: 10.1111/j.1365-313X.2011.04778.x

Cabello, J. V., and Chan, R. L. (2012). The homologous homeodomain-leucine zipper transcription factors *HaHB1* and *AtHB13* confer tolerance to drought and salinity stresses via the induction of proteins that stabilize membranes. *Plant Biotechnol. J.* 10, 815–825. doi: 10.1111/j.1467-7652.2012.00701.x

Cabello, J. V., Giacomelli, J. I., Piattoni, G. V., Iglesias, A. A., and Chan, R. L. (2016). The sunflower transcription factor HaHB11 improves yield, biomass and tolerance to flooding in transgenic *Arabidopsis* plants. *J. Biotec.* 222, 73–83. doi: 10.1016/j.jbiotec.2016.02.015

Cannon, S. B., Sterck, L., Rombauts, S., Sato, S., Cheung, F., Gouzyf, J., et al. (2006). Legume genome evolution viewed through the *Medicago truncatula* and *Lotus japonicus* genomes. *Proc. Natl. Acad. Sci. U.S.A.* 103, 14959–14964. doi: 10.1073/pnas.0603228103

Capella, M., Ré, D., Arce, A. L., and Chan, R. L. (2014). Plant homeodomain-leucine zipper I transcription factors exhibit different functional AHA motifs that selectively interact with TBP or/and TFIIB. *Plant Cell Rep*. 33, 955–967. doi: 10.1007/s00299-014-1576-9

Capella, M., Ribone, P. A., Arce, A. L., and Chan, R. L. (2015). *Arabidopsis thaliana* HomeoBox 1 (*AtHB1*), a Homedomain-Leucine Zipper I (HD-Zip I) transcription factor, is regulated by PHYTOCHROME-INTERACTING FACTOR 1 to promote hypocotyl elongation. *New Phytol.* 207, 669–682. doi: 10.1111/nph.13401

Carabelli, M., Possenti, M., Sessa, G., Ruzza, V., Morelli, G., and Ruberti, I. (2018). *Arabidopsis* HD-Zip II proteins regulate the exit from proliferation during leaf development in canopy shade. *J. Exp. Bot.* 69, 5419–5431. doi: 10.1093/jxb/ery331

Cheng, C., Wang, Z., Ren, Z., Zhi, L., Yao, B., Su, C., et al. (2017). SCFAtPP2-B11 modulates ABA signaling by facilitating SnRK2.3 degradation in *Arabidopsis thaliana*. *PLoS Genet*. 13:e1006947. doi: 10.1371/journal.pgen.1006947

Dong, H., Zhen, Z., Peng, J., Chang, L., Gong, Q., and Wang, N. (2011). Loss of ACS7 confers abiotic stress tolerance by modulating ABA sensitivity and accumulation in *Arabidopsis*. *J. Exp. Bot.* 62, 4875–4887. doi: 10.1093/jxb/err143

Dong, T., Zhang, R., Liu, J., Fowler, J., Miller, T., and Xu, X. (2021). Warming alters sex-specific responses in leaf defense against insect herbivory in Populus cathayana. *Environ. Exp. Bot.* 189:104557. doi: 10.1016/j.envexpbot.2021.104557

Fujita, M., Fujita, Y., Maruyama, K., Seki, M., Hiratsu, K., Ohme-Takagi, M., et al. (2004). A dehydration-induced NAC protein, RD26, is involved in a novel ABA-dependent stress-signaling pathway. *Plant J.* 39, 863–876. doi: 10.1111/j.1365-313X.2004.02171.x

Gao, Y., Gao, S., Xiong, C., Yu, G., Chang, J., Ye, Z., et al. (2015). Comprehensive analysis and expression profile of the homeodomain leucine zipper IV transcription factor family in tomato. *Plant Physiol. Biochem*. 96, 141–153. doi: 10.1016/j.plaphy.2015.07.025

Gao, Y., Liu, H., Zhang, K., Li, F., Wu, M., and Xiang, Y. (2021). A moso bamboo transcription factor, Phehdz1, positively regulates the drought stress response of transgenic rice. *Plant Cell Rep.* 40, 187–204. doi: 10.1007/s00299-020-02625-w

Gong, S., Ding, Y., Hu, S., Ding, L., Chen, Z., and Zhu, C. (2019). The role of HD-Zip class I transcription factors in plant response to abiotic stresses. *Physiol. Plant* 167, 516–525. doi: 10.1111/ppl.12965

Guo, Q., Jiang, J., Yao, W., Li, L., Zhao, K., Cheng, Z., et al. (2021). Genome-wide analysis of poplar HD-Zip family and over-expression of PsnHDZ63 confers salt tolerance in transgenic Populus simonii×P.nigra. *Plant Sci.* 311:111021. doi: 10.1016/j.plantsci.2021.111021

He, A., Niu, S., Zhao, Q., Li, Y., Gou, J., Gao, H., et al. (2018). Induced Salt Tolerance of Perennial Ryegrass by a Novel Bacterium Strain from the Rhizosphere of a Desert Shrub Haloxylon ammodendron. *Int. J. Mol. Sci*. 19:469. doi: 10.3390/ijms19020469

He, G., Liu, P., Zhao, H., and Sun, J. (2021). The HD-ZIP II Transcription Factors Regulate Plant Architecture through the Auxin Pathway. *Int. J. Mol. Sci*. 21:3205. doi: 10.3390/ijms21093250

Henriksson, E., Olsson, A., Johannesson, H., Johansson, H., Hanson, J., Engström, P., et al. (2005). Homeodomain Leucine Zipper Class I Genes in *Arabidopsis*. Expression Patterns and Phylogenetic Relationships. *Plant Physiol.* 139, 509–518. doi: 10.1104/pp.105.063461

Hofmann, N. (2011). YUC and TAA1/TAR proteins function in the same pathway for auxin biosynthesis. *Plant Cell* 23:3869. doi: 10.1105/tpc.111.231112

Jiang, H., Jing, J., Liu, H., Dong, Q., Yan, H., and Gan, D. (2015). Genome-wide analysis of HD-Zip genes in grape (Vitis vinifera). *Tree Genet. Genom.* 11:827. doi: 10.1007/s11295-014-0827-9

Lehti-Shiu, M. D., Panchy, N., Wang, P., Uygun, S., and Shiu, S. H. (2017). Diversity, expansion, and evolutionary novelty of plant DNA-bindingtranscription factor families. *Biochim. Biophys. Acta Gene. Regul. Mech*. 1860, 3–20. doi: 10.1016/j.bbagrm.2016.08.005

Li, H., Gan, Y., Yue, L., Han, Q., Chen, J., Liu, Q., et al. (2022). Newly Isolated Paenibacillus monticola sp. nov., a Novel Plant Growth-Promoting Rhizobacteria Strain From High-Altitude Spruce Forests in the Qilian Mountains. China. *Front. Microbiol*. 13:833313. doi: 10.3389/fmicb.2022.833313

Li, P., Huang, J., Yu, S., Li, Y., Sun, P., Wu, C., et al. (2016). *Arabidopsis*YL1/BPG2 Is Involved in Seedling Shoot Response to Salt Stress through ABI4. *Sci. Rep*. 6:30163. doi: 10.1038/srep30163

Li, Q., Cao, C., Zhang, C., Zheng, S., Wang, Z., and Wang, L. (2015). The identification of Cucumis sativus Glabrous 1 (CsGL1) required for the formation of trichomes uncovers a novel function for the homeodomain-leucine zipper I gene. *J. Exp. Bot*. 66, 2515–2526. doi: 10.1093/jxb/erv046

Li, W., Dong, J., Cao, M., Gao, X., Wang, D., Liu, B., et al. (2019). Genome-wide identification and characterization of HD-ZIP genes in potato. *Gene* 697, 103–117. doi: 10.1016/j.gene.2019.02.024

Li, Z., Jiang, H., Zhou, L., Deng, L., Lin, Y., Peng, X., et al. (2014). Molecular evolution of the HD-ZIP I gene family in legume genomes. *Gene* 533, 218–228. doi: 10.1016/j.gene.2013.09.084

Liu, W., Li, R., Han, T., Cai, W., Fu, Z., and Lu, Y. (2015). Salt stress reduces root meristem size by nitric oxide-mediated modulation of auxin accumulation and signaling in *Arabidopsis*. *Plant Physiol.* 168, 343–356. doi: 10.1104/pp.15.00030

Livak, K. J., and Schmittgen, T. D. (2001). Analysis of relative gene expression data using real-time quantitative PCR and the $2^{-\Delta\Delta}$ CT method. *Methods* 25, 402–408. doi: 10.1006/meth.2001.1262

Lü, X., Shao, K., Xu, J., Li, J., Ren, W., Chen, J., et al. (2022). A heat shock transcription factor gene (*HaHSFA1*) from a desert shrub, Haloxylon ammodendron, elevates salt tolerance in *Arabidopsis thaliana*. *Environ. Exp. Bot*. 201:104954. doi: 10.1016/j.envexpbot.2022.104954

Ma, Q., Hu, J., Zhou, X. R., Yuan, H. J., Kumar, T., Luan, S., et al. (2017). ZxAKT1 is essential for K^+ uptake and K^+/Na^+ homeostasis in the succulent xerophyte Zygophyllum xanthoxylum. *Plant J.* 90, 48–60. doi: 10.1111/tpj.13465

Manavella, P. A., Dezar, C. A., Ariel, F. D., Drincovich, M. F., and Chan, R. L. (2008). The sunflower HD-Zip transcription factor HAHB4 is up-regulated in darkness, reducing the transcription of photosynthesis-related genes. *J. Exp. Bot*. 59:3143. doi: 10.1093/jxb/ern170

Moharana, K. C., and Venancio, T. M. (2020). Polyploidization events shaped the transcription factor repertoires in legumes (*Fabaceae*). *Plant J.* 103, 726–741. doi: 10.1111/tpj.14765

Nakamura, M., Katsumata, H., Abe, M., Yabe, N., Komeda, Y., Yamamoto, K. T., et al. (2006). Characterization of the class IV homeodomain-Leucine Zipper gene family in *Arabidopsis*. *Plant Physiol.* 141, 1363–1375. doi: 10.1104/pp.106.077388

Nath, V. S., Mishra, A. K., Kumar, A., Matoušek, J., and Jakše, J. (2019). Revisiting the Role of Transcription Factors in Coordinating the Defense Response Against Citrus Bark Cracking Viroid Infection in Commercial Hop (*Humulus Lupulus* L.). *Viruses* 11:419. doi: 10.3390/v11050419

Nie, S., Yang, Z., Xiao, C., Yang, R., and Wang, D. (2022). Physiological and Transcriptomic Analyses of the Effects of SlBRI1 Expression Levels on the Drought Tolerance of Tomato Seedlings. *J. Plant Growth. Regul.* doi: 10.1007/s00344-022-10587-4

Prigge, M. J., and Clark, S. E. (2010). Evolution of the class III HD-Zip gene family in land plants. *Evol. Dev.* 8, 350–361. doi: 10.1111/j.1525-142X.2006.00107.x

Prigge, M. J., Otsuga, D., Alonso, J. M., Ecker, J. R., Drews, G. N., and Clark, S. E. (2005). Class III Homeodomain-Leucine Zipper Gene Family Members Have Overlapping, Antagonistic, and Distinct Roles in *Arabidopsis* Development. *Plant Cell* 17, 61–76. doi: 10.1105/tpc.104.026161

Ribone, P. A., Capella, M., and Chan, R. L. (2015). Functional characterization of the homeodomain leucine zipper I transcription factor AtHB13 reveals a crucial role in *Arabidopsis* development. *J. Exp. Bot*. 66, 5929–5943. doi: 10.1093/jxb/erv302

Romani, F., Ribone, P. A., Capella, M., Miguel, V. N., and Chan, R. L. (2016). A matter of quantity: Common features in the drought response of transgenic plants overexpressing HD-Zip I transcription factors. *Plant Sci*. 251, 139–154. doi: 10.1016/j.plantsci.2016.03.004

Sakakibara, K., Nishiyama, T., Kato, M., and Hasebe, M. (2001). Isolation of Homeodomain–Leucine Zipper Genes from the Moss Physcomitrella patens and the Evolution of Homeodomain–Leucine Zipper Genes in Land Plants. *Mol. Biol. Evol*. 18, 491–502. doi: 10.1093/oxfordjournals.molbev.a003828

Sakuma, S., Pourkheirandish, M., Hensel, G., Kumlehn, J., Stein, N., Tagiri, K., et al. (2013). Divergence of expression pattern contributed to neofunctionalization of duplicated HD-Zip I transcription factor in barley. *New Phytol.* 197, 939–948. doi: 10.1111/nph.12068

Singh, K. A., Kumar, R. S., Dwivedi, V., Rai, A., Pal, S., Shasany, A., et al. (2017). A WRKY transcription factor from Withania somnifera regulates triterpenoid withanolide accumulation and biotic stress tolerance through modulation of phytosterol and defense pathways. *New Phytol*. 215, 1115–1131. doi: 10.1111/nph.14663

Su, L., Dai, Z., Li, S., and Xin, H. (2015). A novel system for evaluating drought–cold tolerance of grapevines using chlorophyll fluorescence. *BMC Plant Biol*. 15:82. doi: 10.1186/s12870-015-0459-8

Tan, Z., Wen, X., and Wang, Y. (2020). Betula platyphylla *BpHOX2* transcription factor binds to different cis-acting elements and confers osmotic tolerance. *J. Integr. Plant Biol.* 62, 1762–1779. doi: 10.1111/jipb.12994

Tang, Y., Bao, X., Wang, S., Liu, Y., Tan, J., Yang, M., et al. (2019). A Physic Nut Stress-Responsive HD-Zip Transcription Factor, *JcHDZ07*, Confers Enhanced

Sensitivity to Salinity Stress in Transgenic *Arabidopsis*. *Front. Plant Sci.* 10:942. doi: 10.3389/fpls.2019.00942

Turchi, L., Baima, S., Morelli, G., and Ruberti, I. (2015). Interplay of HD-Zip II and III transcription factors in auxin-regulated plant development. *J. Exp. Bot.* 66, 5043–5053. doi: 10.1093/jxb/erv174

Valdés, A., Overnäs, E., Johansson, H., Rada-Iglesias, A., and Engström, P. (2012). The homeodomain-leucine zipper (HD-Zip) class I transcription factors ATHB7 and ATHB12 modulate abscisic acid signalling by regulating protein phosphatase 2C and abscisic acid receptor gene activities. *Plant Mol. Biol.* 80, 405–418. doi: 10.1007/s11103-012-9956-4

Wang, D., Cui, B., Guo, H., Liu, Y., and Nie, S. (2022a). Genome-wide identification and expression analysis of the CBF transcription factor family in *Lolium perenne* under abiotic stress. *Plant Signal. Behav.* 17:2086733. doi: 10.1080/15592324.2022.2086733

Wang, D., Yang, Z., Wu, M., Wang, W., Wang, Y., and Nie, S. (2022b). Enhanced brassinosteroid signaling via the overexpression of SlBRI1 positively regulates the chilling stress tolerance of tomato. *Plant Sci.* 320:111281. doi: 10.1016/j.plantsci.2022.111281

Wang, H., Li, G., Zhang, D., Lin, J., Sheng, B., Han, J., et al. (2013). Biological functions of HD-Zip transcription factors. *Hereditas* 35:1179. doi: 10.3724/SP.J.1005.2013.01179

Wang, J., Zhuang, L., Zhang, J., Yu, J., Yang, Z., and Huang, B. (2019). Identification and characterization of novel homeodomain leucine zipper (HD-Zip) transcription factors associated with heat tolerance in perennial ryegrass. *Environ. Exp. Bot.* 160, 1–11. doi: 10.1016/j.envexpbot.2018.12.023

Wu, H., Shabala, L., Zhou, M., Su, N., Wu, Q., Ul-Haq, T., et al. (2019). Root vacuolar Na+ sequestration but not exclusion from uptake correlates with barley salt tolerance. *Plant J.* 100, 55–67. doi: 10.1111/tpj.14424

Wu, Q., Tang, Y., Dong, T., Liao, Y., Li, D., He, X., et al. (2018). Additional AM fungi inoculation increase Populus cathayana intersexual competition. *Front. Plant Sci.* 9:607. doi: 10.3389/fpls.2018.00607

Yang, Q., Niu, Q., Li, J., Zheng, X., Ma, Y., Bai, S., et al. (2018). PpHB22, a member of HD-Zip proteins, activates PpDAM1 to regulate bud dormancy transition in 'Suli' pear (Pyrus pyrifolia White Pear Group). *Plant Physiol. Biochem.* 127, 355–365. doi: 10.1016/j.plaphy.2018.04.002

Yang, S., Olena, P., and Tobias, S. (2018). ALTERED MERISTEM PROGRAM1 restricts shoot meristem proliferation and regeneration by limiting HD-ZIP III-mediated expression of RAP2.6L. *Plant Physiol.* 177, 1580–1594. doi: 10.1104/pp.18.00252

Yang, S., Wang, Y., Zhu, H., Zhang, M., Wang, D., Xie, K., et al. (2022). A novel HD-Zip I/C2H2-ZFP/WD-repeat complex regulates the size of spine base in cucumber. *New Phytol.* 233, 2643–2658. doi: 10.1111/nph.17967

Yang, Y., Luang, S., Harris, J., Riboni, M., Li, Y., Bazanova, N., et al. (2017). Overexpression of the class I homeodomain transcription factor *TaHDZipI-5* increases drought and frost tolerance in transgenic wheat. *Plant Biotechnol. J.* 16, 1227–1240. doi: 10.1111/pbi.12865

Yip, H. K., Floyd, S. K., Sakakibara, K., and Bowman, J. L. (2016). Class III HD-Zip activity coordinates leaf development in Physcomitrella patens. *Dev. Biol.* 419, 184–197. doi: 10.1016/j.ydbio.2016.01.012

Zalewski, C. S., Floyd, S. K., Furumizu, C., Sakakibara, K., and Bowman, J. L. (2013). Evolution of the Class IV HD-Zip Gene Family in Streptophytes. *Mol. Biol. Evol.* 30, 2347–2365. doi: 10.1093/molbev/mst132

Zhang, H., Feng, H., Zhang, J., Ge, R., Zhang, L., Wang, Y., et al. (2020). Emerging crosstalk between two signaling pathways coordinates K^+ and Na^+ homeostasis in the halophyte Hordeum brevisubulatum. *J. Exp. Bot.* 71, 4345–4358. doi: 10.1093/jxb/eraa191

Zhang, J., Wu, J., Guo, M., Aslam, M., and Cao, S. (2020). Genome-wide characterization and expression profiling of Eucalyptus grandis HD-Zip gene family in response to salt and temperature stress. *BMC Plant Biol.* 20:451. doi: 10.1186/s12870-020-02677-w

Zhang, M., Bai, R., Nan, M., Ren, W., Wang, C., Shabala, S., et al. (2022). Evaluation of salt tolerance of oat cultivars and the mechanism of adaptation to salinity. *J. Plant Physiol.* 273:153708. doi: 10.1016/j.jplph.2022.153708

Zhang, S., Haider, I., Kohlen, W., Li, J., and Ouwerkerk, P. (2012). Function of the HD-Zip I gene *OsHOX22* in ABA-mediated drought and salt tolerances in rice. *Plant Mol. Biol.* 80, 571–585. doi: 10.1007/s11103-012-9967-1

Zhao, Y., Ma, Q., Jin, X., Peng, X., Liu, J., Deng, L., et al. (2014). A novel maize homeodomain-leucine zipper (HD-Zip) I gene, Zmhdz10, positively regulates drought and salt tolerance in both rice and *Arabidopsis*. *Plant Cell Physiol.* 55, 1142–1156. doi: 10.1093/pcp/pcu054

Zhou, Q., Liu, L., Cheng, H., Li, Z., Wai, M. H., Luo, T., et al. (2021). Genome-wide Identification and Expression Pattern Analysis of the HD-Zip Transcription Factor Family in Pineapple (*Ananas Comosus*). *Trop. Plant Biol.* 14, 120–131. doi: 10.1007/s12042-020-09279-8

frontiers | Frontiers in Plant Science

TYPE Original Research
PUBLISHED 22 September 2022
DOI 10.3389/fpls.2022.976341

OPEN ACCESS

EDITED BY
Maofeng Chai,
Qingdao Agricultural University, China

REVIEWED BY
Tao Hu,
Lanzhou University, China
Liwen Cao,
Wuhan Botanical Garden (CAS), China

*CORRESPONDENCE
Xuebing Yan
yxbbjzz@163.com
Jibiao Fan
fanjibiao11@126.com

SPECIALTY SECTION
This article was submitted to Plant Abiotic Stress, a section of the journal Frontiers in Plant Science

RECEIVED 23 June 2022
ACCEPTED 29 August 2022
PUBLISHED 22 September 2022

CITATION
Chen Y, Xiang Y, Hu Z, Gao Y, Zhang Y, Chen M, Khaldun ABM, Yan X and Fan J (2022) Transcriptomic profiling revealed the role of 24-epibrassinolide in alleviating salt stress damage in tall fescue (*Festuca arundinacea*). *Front. Plant Sci.* 13:976341. doi: 10.3389/fpls.2022.976341

Transcriptomic profiling revealed the role of 24-epibrassinolide in alleviating salt stress damage in tall fescue (*Festuca arundinacea*)

Yao Chen[1], Yuanhang Xiang[1], Zhengrong Hu[2], Yang Gao[1], Youxin Zhang[1], Minghui Chen[1], A. B. M. Khaldun[3], Xuebing Yan[1]* and Jibiao Fan[1]*

[1]College of Animal Science and Technology, Yangzhou University, Yangzhou, China, [2]Hunan Tobacco Research Institute, Changsha, China, [3]Bangladesh Agricultural Research Institute, Dhaka, Bangladesh

Soil salinization is a major problem all over the world. The accumulation of salt in soil reduces the root water uptake and directly affects plant growth and metabolic activities. Brassinosteroid is a plant hormone that plays an important role in regulation of plant growth and physiological process, including promotion of cell expansion and elongation, signal transduction and stress response. Exogenous 24-epibrassinolide (EBL) has been proved to alleviate various environmental stress in plants. However, the role that EBL plays in salt stress response is still unknown in tall fescue (*Festuca arundinacea*). In this study, the physiology and molecular mechanisms regulated by exogenous EBL of salt stress response in tall fescue was investigated. Tall fescue plants were divided into four groups, including control (CK), NaCl solution (SALT), 24-epibrassinolide (EBL), NaCl solution + 24-epibrassinolide (SE). During the growth period of tall fescue, we found that electrolyte leakage (EL) and malondialdehyde (MDA) were decreased, chlorophyll (Chl) content and antioxidant enzyme activity were increased in leaves of tall fescue in SE group compared with SALT group, indicating that EBL improved the salt tolerance in grasses. Transcriptomic profiling analysis showed that after 12 h of treatments, 10,265, 13,830 and 10,537 differential genes were expressed in EBL, SALT, and SE groups compared with control, respectively. These differentially expressed genes (DEGs) mainly focused on binding, catalytic activity, cellular process, metabolic process, cellular anatomical entity. Moreover, most of the differential genes were expressed in the plant hormone signal transduction pathway. These results helped us to better understand the mechanism of exogenous 24-epibrassinolide to improve the salt tolerance of tall fescue.

KEYWORDS

24-epibrassinolide, salt stress, tall fescue, physiological responses, transcriptomic analysis, gene expression

Introduction

Soil salinization is a major problem worldwide. Around 1 billion hectares of land throughout the world are affected by salinity, and these soils are distributed in more than 100 countries (Food and Agriculture Organization of the United Nations, 2015). Soil salinity is induced by natural causes and human behaviors such as improper irrigation (Munns and Tester, 2008). And the accumulation of salt in the soil can seriously affect growth and yield of the plant (Zelm et al., 2020). Soil salinization makes it difficult for roots to absorb water and further disrupt the water potential and ion balance within plant cells. The accumulation of salt in the aerial parts will reduce the photosynthetic capacity of plants and destroy the antioxidant enzyme system, which resulting in a large increase in oxygen free radicals and continuous reduction in growth. And with the extension of time, the damage caused by salt stress is more and more severe, which eventually leads to the stagnation of plant growth or even death (Zhu, 2001; Munns and Tester, 2008; Zelm et al., 2020). The extent and severity of salt-affected lands will worsen due to issues such as global warming (Munns and Gilliham, 2015).

To defense salt stress, plants have developed various strategies to optimize growth conditions under salinity. In addition to regulating plant growth and development, phytohormones also participate in various environmental stresses to improve stress resistance (Yu et al., 2020). Brassinosteroids (BRs) are a new class of plant hormones that are essential for plant growth and development (Kim et al., 2009). Furthermore, it exhibits excellent growth-promoting activity at very low concentrations (Avalbaev et al., 2021). 24-Epibrassinolide (EBL), an active by-product of brassinolide biosynthesis, can stimulate plant metabolic processes such as protein and nucleic acid biosynthesis (Bajguz, 2000). It can significantly improve the ability of plants to resist abiotic stresses, including salt, heavy metal, drought, and low-temperature (Arora et al., 2012; Wu et al., 2017; Anwar et al., 2018; Tanveer et al., 2019).

Tall fescue (*Festuca arundinacea* Schreb) is a broad-leaved outbreeding allohexaploid grass (Hand et al., 2010). As one of the most important cool-season grass species in the world, tall fescue is widely used as turfgrass and forage (Wang et al., 2004). On account of its strong adaptability, tall fescue can grow in temperate and subtropical regions (Cao et al., 2009). Nonetheless, regional salinization limits the growth of tall fescue, which in turn affects turf persistence and forage yield (Wang et al., 2017).

Salinity can cause the increase of reactive oxygen species (ROS) and the content of malondialdehyde (MDA) (Miller et al., 2010; Hu et al., 2012). Plants have a complex antioxidant defense system to alleviate this oxidative damage, including catalase (CAT), peroxidase (POD), superoxide dismutase (SOD) (Lou et al., 2017). In addition, transcriptome analysis is also an available method to study salt stress responses and has been applied to many plants such as Arabidopsis, rice, alfalfa, bermudagrass (Shen et al., 2014; Shi et al., 2015; Wang et al., 2016; Bhattarai et al., 2021). However, there are few studies on the transcriptomic data on the effects of exogenous 24-epibrassinolide in tall fescue under salt stress. Therefore, this study elucidates the mechanism of action of 24-epibrassinolide in alleviating salt stress from both the physiological and transcriptomic levels.

Materials and methods

Plant material and growth conditions

Tall fescue (*F. arundinacea*) cultivar Houndog 6 was used for this study and quartz sand was used as growth material. All materials were grown in a climatic chamber (ROX-1000CH, Changzhou, China) at 25°C temperature, 14/10 h (light/dark), 60% relative humidity.

Treatments

All plants were divided into four groups: control (CK), 1 μmol/L 24-epibrassinolide (EBL), 300 mmol/L NaCl solution (SALT), 300 mmol/L NaCl solution + 1 μmol/L 24-epibrassinolide (SE). Three repetitions were set up for each group, and 100 seeds were evenly sown in each pot. The plants were watered daily until all seeds germinated, then irrigated with 50 ml 1/2 Hoagland nutrient solution per pot. After the plants had grown for 20 days, NaCl and 24-epibrassinolide treatments were conducted. The salt treatment was increased by daily increments of 100 mmol/L NaCl until a final salinity level (300 mmol/L) was reached. Plants were watered with NaCl solution until the liquid flowed from the drain holes at the bottom of the pot. The leaves of plants in the EBL and SE treatments were sprayed with 24-epibrassinolide evenly every day.

Measurement of chlorophyll content

0.1 g of fresh leaves were immersed in a 15 ml centrifuge tube containing 10 ml of dimethylsulfoxide and were placed in the dark for 48 h. Then, the absorbance of the extraction was measured at 645 and 663 nm with an ultraviolet spectrophotometer (Hiscox and Israelstam, 1979).

Chlorophyll content was calculated with the following formula:

$$\text{Chltotal content } (\text{mg} \cdot \text{L}^{-1}) = 20.2 \times \text{OD645} + 8.02 \times \text{OD663}. \quad (1)$$

OD645 and OD663 indicate the absorbance of the extraction at 645 and 663 nm, respectively.

Measurement of electrolyte leakage

The determination of electrolyte leakage (EL) referred to the method of Feng et al. (2021) with slight modifications. In detail, 0.1 g of fresh leaves were chopped and placed in a 50 ml centrifuge tube containing 25 ml of deionized water. The tubes were shaken at room temperature for 24 h at 200 rpm. The initial conductivity (Ci) was measured with a conductivity meter (DDS-11A conductivity Meter, Hangzhou, China). Then, the leaf tissue in the tube was autoclaved at 121°C for 20 min to release the electrolytes completely. The conductivity (Cmax) was measured again after the solution had been cooled to room temperature. The EL was calculated by the formula:

$$\mathrm{EL}\ (\%) = \frac{\mathrm{Ci}}{\mathrm{Cmax}} \times 100\%$$

Crude enzyme extraction

0.2 g of fresh leaves were quickly ground into powder with liquid nitrogen. 4 mL of pre-chilled sodium phosphate buffer (pH 7.8) was added to the powder and the homogenate was transferred to a 15 mL centrifuge tube. After centrifugation at 4°C at 12,000 rpm for 15 min, the supernatant was extracted as crude enzyme solution.

Measurement of malonaldehyde content

Malonaldehyde (MDA) content was determined by thiobarbituric acid (TBA) method (Fan et al., 2015). Add 1 ml of crude enzyme solution to 2 ml of MDA reaction buffer containing 0.5% (v/v) TBA and 20% (v/v) trichloroacetic acid. The mixed solution was water-bathed at 95°C for 30 min and then rapidly cooled to room temperature in ice. Then the tubes were centrifuged for 10 min at 25°C with 12,000 rpm. The solution was measured at 532 and 600 nm with an ultraviolet spectrophotometer. MDA content was calculated with following formula:

$$\mathrm{MDA}(\mathrm{molg}^{-1}\mathrm{FW}) = \frac{[(\mathrm{OD532} - \mathrm{OD600}) \times \mathrm{L}]}{(\mathrm{l} \times \varepsilon \times \mathrm{FW})}.$$

Where L is the volume of the extraction, l is the thickness of the cuvette, ε is the molar absorption coefficient of 155 mM^{-1} cm^{-1}, and FW is the fresh weight of the leaves.

Quantification of antioxidant enzymes

To determine CAT activity, 0.1 ml of crude enzyme solution was added to a mixed solution containing 2 ml phosphate buffer (100 mM, pH 7.0), 0.5 ml 100 mM hydrogen peroxide (H_2O_2). Absorbance at 240 nm was measured three times with an ultraviolet spectrophotometer and the values were recorded per minute. A reduction of one unit of the absorbance per minute was defined as one unit CAT activity.

To determine POD activity, 20 μL of crude enzyme solution was added to a mixed solution containing 2.5 mL phosphate buffer (100 mM, pH 6.0), 1.4 μL guaiacol, 0.95 μL 30% hydrogen peroxide (30% H_2O_2). Absorbance at 470 nm was measured three times with an ultraviolet spectrophotometer and the values were recorded per minute. Increment of one unit of the absorbance per minute was defined as one unit POD activity.

To determine SOD activity, 0.1 mL of crude enzyme solution was added to a mixed solution containing 1.5 ml phosphate buffer (50 mM, pH 7.8), 0.3 ml 130 mM methionine (Met), 0.3 ml 750 μM nitroblue tetrazolium (NBT), 0.3 ml 100 μM disodium ethylenediamine tetraacetic acid (EDTA-Na_2), and 0.3 mL 20 μM riboflavin. Take the mixed solution without crude enzyme solution as control. Another new tube was regarded as blank, in which phosphate buffer (50 mM, pH 7.8) was used instead of the crude enzyme solution. The control and the experimental groups were placed under the condition of 4,000 Lux for 30 min, and the blank was placed in the dark for 30 min. Absorbance at 560 nm was measured with an ultraviolet spectrophotometer and the blank was used as zero adjustment. Taking NBT photoreduction by 50% as one unit of SOD activity.

RNA extraction and library construction

Total RNA was extracted from plant tissues using the ethanol precipitation protocol and CTAB-PBIOZOL reagent according to the manufacturer's instructions. The concentration and purity of RNA were tested by the Agilent 2100 Bioanalyzer (Thermo Fisher Scientific, MA, USA) and NanoDrop. Use DNase I to digest the DNA fragments presenting in total RNA samples. The magnetic beads were purified to recover the reaction products. RNase H (Illumina, CA, USA) was used to remove the rRNA. Purified mRNA from previous steps was fragmented into small pieces with fragment buffer at appropriate temperature. Then, First-strand cDNA was generated in First Strand Reaction System by PCR, and the second-strand cDNA was generated as well. The reaction product was purified by magnetic beads. A-Tailing Mix and RNA Index Adapters were added by incubating to carry out end repair. The cDNA fragments with adapters were amplified by PCR. The PCR products were heat denatured into single-stranded DNA, and a single-stranded circular DNA library was obtained by circularizing the single-stranded DNA with a bridge primer.

Sequencing data filtering and *de novo* assembly

Raw reads were filtered via SOAPnuke (v1.4.0) (Chen et al., 2018) by removing reads containing adaptors, poly-N or low quality, and then clean reads were obtained. Trinity (v2.0.6) (Grabherr et al., 2011) was used to assemble the clean reads and Tgicl (v2.0.6) (Pertea et al., 2003) to perform clustering and eliminate redundant data in the assembled transcripts to obtain unique genes. Unigenes were divided into two parts. One part were clusters, which were the results of further de-redundancy. And there were several unigenes with high similarity (greater than 70%) in the same cluster, starting with CL, followed by the number of the gene family. The rest were singletons, starting with Unigene, referring to a single unigene without clustering.

Coding DNA sequence forecast and unigene annotation

The candidate coding regions in Unigene were identified using TransDecoder (v3.0.1) (Kim et al., 2015), the longest open reading frame was extracted. Based on sequence similarity, Diamond Blastp was used to align to SwissProt database, and then Hmmscan (v3.0) was used to screen the Blast results in the Pfam database. Trans Decoder. Predict was used to predict coding regions finally. The assembled unigenes were annotated with seven functional databases (KEGG, GO, NR, NT, SwissProt, Pfam, and KOG).

Gene expression analysis

Gene expression levels in each sample were calculated by RSEM (v1.2.8) (Li and Dewey, 2011) and expression analysis of differential genes was performed by the DESeq2 with Qvalue (adjusted p-value) ≤ 0.05 (Anders and Huber, 2010; Love et al., 2014).

Quantitative real-time PCR

cDNA was synthesized using the HiScript® III RT SuperMix for qPCR (+ gDNA wiper) (Vazyme, Nanjing, China). Quantitative real-time PCR (qRT-pCR) reactions were performed on QuantStudio™ 3 Real-Time PCR System (Thermo Fisher Scientific, MA, USA) using the AceQ® Universal SYBR qPCR Master Mix (Vazyme, Nanjing, China). The thermal cycle program was as following: 95°C for 5 min, 40 cycles of 95°C for 10 s and 60°C for 30 s; 95°C for 15 s, 60°C for 1 min, 95°C for 15 s. The information of primers for the genes for qRT-PCR are listed in **Supplementary Table 1**. The expression data were calculated by the $2^{-\Delta\Delta Ct}$ method (Pfaffl, 2001).

Results

Effects of exogenous 24-epibrassinolide on growth and physiological responses under salt stress

In order to investigate whether exogenous 24-epibrassinolide could improve the growth of tall fescue under salt stress, the plant height was measured. The results showed that the plant height of the four groups increased at 10 days after different treatments. Among them, the two groups (SALT and SE) treated with NaCl solution were significantly lower than the CK and the EBL. After application of 24-epibrassinolide, the plant heights of EBL and SE groups were increased by 4.5% and 5.2% compared with the CK and SALT, respectively (**Figure 1A** and **Supplementary Figure 1**). These results indicated that 24-epibrassinolide can enhance the growth of tall fescue under salt stress remarkably.

To investigate the effect of 24-epibrassinolide on the chlorophyll of the leaves under salt stress, the chlorophyll content was determined. After 10 days of treatment, the chlorophyll content in the leaves after SE treatment was the highest, followed by SALT and EBL, and the content of CK was the lowest. With the application of 24-epibrassinolide, the chlorophyll content in the leaves after EBL and SE treatments increased by 9.9% and 6.1%, respectively compared with CK and SALT (**Figure 1B**). These results implied that exogenous 24-epibrassinolide could maintain the chlorophyll stability of tall fescue under salt stress.

To investigate whether the exogenous 24-epibrassinolide played a positive role in maintaining cell membrane stability of tall fescue under salt stress, MDA content and EL alterations were determined. The contents of MDA and EL in tall fescue after 10 days of salt treatment were much higher than those of the CK. However, there were no significant differences observed in MDA and EL contents between CK and EBL groups. After exogenous application of 24-epibrassinolide, MDA and EL contents of SE treatment decreased by 1.09% and 27.8% compared with the SALT, respectively (**Figures 1C,D**). These results suggested that exogenous 24-epibrassinolide could maintain cell membrane stability.

To investigate the effects of 24-epibrassinolide on antioxidant enzymes, activities of SOD, POD and CAT were determined (**Figures 1E–G**). After 10 days of salt treatment, the activities of SOD and POD were enhanced, but CAT had no significant difference compared with control. After the application of 24-epibrassinolide, activities of SOD, POD and CAT increased by 10.7, 5.5, and 3.4% in the leaves of EBL treatment compared with the CK. The SOD, POD, and CAT activities in plants of SE treatment were 34.6, 2.5, and 7.5% higher than those of SALT, respectively. These results

10.3389/fpls.2022.976341

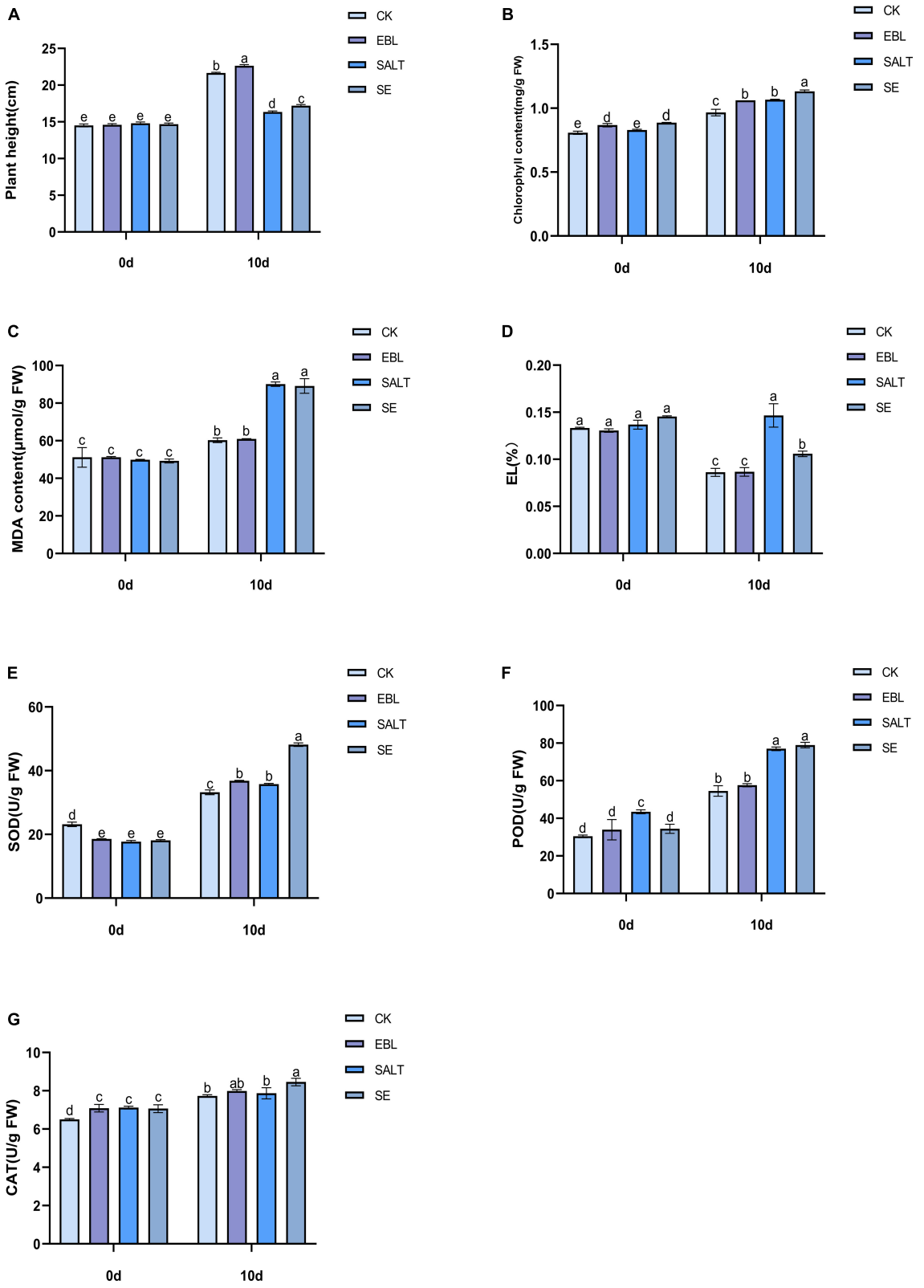

FIGURE 1
Effects of exogenous 24-epibrassinolide on growth and physiological characteristics of tall fescue under salt stress. **(A)** Plant height of tall fescue; **(B)** Chlorophyll content of tall fescue; **(C)** MDA content; **(D)** Electrolyte Leakage; **(E)** SOD activity; **(F)** POD activity; **(G)** CAT activity. Bars with different letters indicate significant difference at $P \leq 0.05$ (Duncan test).

10.3389/fpls.2022.976341

demonstrated that 24-epibrassinolide plays an important role in enhancing antioxidative enzyme activities of tall fescue in response to salt stress.

Transcriptome sequencing analysis and unigene annotation

The transcriptome sequencing obtained 129,866 unigenes after *de novo* assembly and de-redundancy. The total length, average length, N50 and GC content were 135,692,978 bp, 1,044 bp, 1,466 bp, and 48.89%, respectively (Supplementary Table 2). Among them, 19,111 unigenes with a length of 200–300 bp accounted for the largest number, and the number of unigenes with a length of 2,900-3,000 bp accounted for the least, with a total of 541. It is worth noting that there were 3,293 genes with length greater than or equal to 3,000 bp (Figure 2A). It can be seen from the expression stacking chart that the Fragments Per Kilobase of exon model per Million mapped fragments (FPKM) values between 1 and 10 in each group accounted for the most, and the number greater than 10 was the least (Figure 2B).

Unigenes were compared to seven functional databases for annotation, there were 85,000 in NR (65.45%), 76,023 in NT (58.54%), 58,513 in SwissProt (45.06%), 58,312 in KOG (44.90%), 61,897 in KEGG (47.66%), 61,289 in GO (47.19%) and 58,434 in Pfam (45.00%) (Figure 2C and Supplementary Table 3). We used the KEGG database to analyze pathway enrichment for all unigenes. As a result, 61,897 unigenes were annotated into five categories: cellular processes, environmental information processing, genetic information processing, metabolism, and organismal system. In this classification, genes were further divided into 19 functional pathways. Metabolic categories had the most types of enriched pathways, among which, carbohydrate metabolism accounts for the largest proportion except the global and overview maps. Genetic information processing was the second functional category with four subcategories. Although cellular processes and environmental information processing both have only one subclass, 2,479 and 3,288 single genes were enriched respectively (Figure 2D). In addition, the transcription factor families in which the unigenes belong were classified and counted. The results showed that the most genes belonged to the MYB family, followed by the bHLH family (Supplementary Table 4).

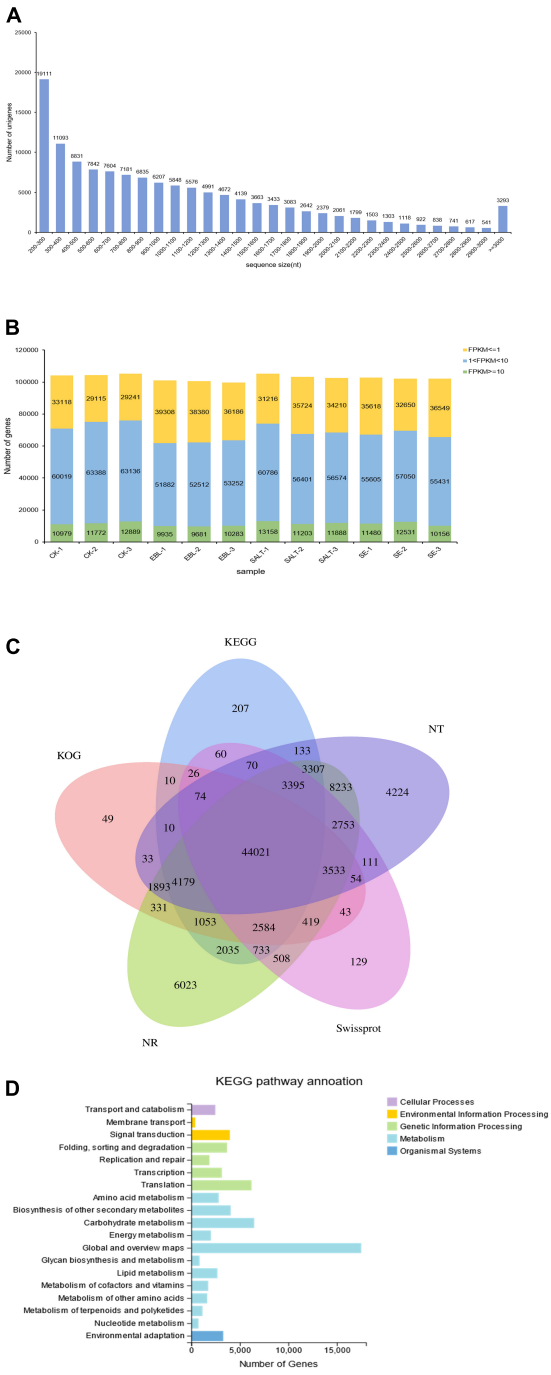

FIGURE 2
Overview of the tall fescue transcriptome dataset. **(A)** Unigene length distribution; **(B)** Number of genes in different FPKM intervals for each sample; **(C)** Venn diagram of KEGG, NT, NR, KOG, and Swissprot annotation results of the bermudagrass reference transcriptome; **(D)** Distribution and quantity statistics of KEGG functions.

Identification and gene ontology analysis of differentially expressed genes

We performed volcano plots for the differential gene expression of the four comparison groups. Compared with CK, EBL group had 6,618 genes up-regulated and 3,647 genes down-regulated, respectively. In the CK vs. SALT comparison, there were 13,830 different genes, including 7,968 up-regulated genes and 5,862 down-regulated genes. There were 10,537

differential genes in the groups of CK and SE, including 6,409 up-regulated genes and 4,128 down-regulated genes. In the SALT vs. SE comparison, 117 DEGs were obtained, containing 58 upregulated genes and 59 downregulated genes (**Figure 3**).

Based on the results, we selected the top 20 up-regulated and 20 down-regulated genes with the smallest Q-value in each comparison group for Gene Ontology (GO) analysis. According to GO annotation, differentially expressed genes (DEGs) are divided into three functional categories: molecular function (MF), cellular component (CC), and biological process (BP). And each functional category contains multiple levels of subcategories. In the CK vs. EBL comparison and the CK vs. SALT comparison, the most enriched GO term among the up-regulated genes were DNA-binding transcription factor activity in MF and protein-chromophore linkage in BP, respectively. The term with the highest number of down-regulated genes for both comparison groups was chloroplast in CC (**Figures 4A,B**). In the CK vs. SE comparison, chloroplast thylakoid membrane in CC was the most in up-regulated genes. Among down-regulated genes, carbohydrate metabolic process in BP and chloroplast in CC occupied the most by the same count (**Figure 4C**). In the SALT vs. SE comparison, the most abundant term in up-regulated genes was quinone binding in MF. The terms in down-regulated genes were actin filament depolymerization, sterol biosynthetic process in BP, actin cytoskeleton in CC, actin binding and oxidoreductase activity, acting on the CH-OH group of donors, NAD or NADP as acceptor in MF, respectively (**Figure 4D**).

Trend analysis of differentially expressed genes among different comparisons

A bidirectional clustering heatmap was created based on the 117 DEGs of SALT vs. SE comparison. DEGs with similar expression patterns were divided into multiple clusters using the k-means clustering method. Each cluster contained a heatmap and a trend graph. There were CL1355.Contig9, Unigene25288, Unigene5787, CL4441.Contig1, CL873.Contig36 in cluster 1 and the expression trends in the four groups were increased, and then decreased and finally increased again. There were 15 genes in cluster 2. Its trend was the same as cluster 1, but the fluctuation was smoother. Seven genes were in cluster 3 and the expression level of SALT was the highest among the four groups. There were 90 genes in cluster 4. It had the lowest gene expression among the four clusters, and the fluctuation of its trend was the smallest (**Figure 5** and **Supplementary Figure 2**).

Plant hormone signal transduction

Plant hormones play important roles in growth and development of plants. Here, genes involved in plant hormone signal transduction pathways were differentially expressed in EBL vs. SE comparison (**Figure 6**). Auxin is an important regulatory hormone in plants. Several components of auxin signal transduction pathway were down-regulated after SE treatment compared to EBL, including one auxin-responsive protein IAA (Aux/IAA), one SAUR family protein (SAUR). There were three DELLA proteins (DELLA) down-regulated in the gibberellin pathway. Similarly, the salicylic acid pathway involved in disease resistance also contains only down-regulated genes. There was an up-regulated Arabidopsis histidine-containing phosphotransfer protein (AHP), two down-regulated genes of two-component response regulator ARR-B family (B-ARR) and two-component response regulator ARR-A family (A-ARR) in the cytokinin transduction pathway. In the ethylene transduction pathway related to fruit ripening and senescence, genes were all up-regulated. Most genes were also up-regulated in the abscisic acid signaling pathway. For jasmonic acid, three jasmonate ZIM domain-containing protein (JAZ) were down-regulated and three transcription factor MYC2 (MYC2) were up-regulated after SE treatment. In the brassinosteroid pathway, both brassinosteroid insensitive 1-associated receptor kinase 1 (BAK1) and protein brassinosteroid insensitive 1 (BRI1) contain one up-regulated and one down-regulated gene, respectively. Compared with SALT, SE had up-regulated genes in auxin and cytokinin signal transduction pathways, which indicated that the application of 24-epibrassinolide could improve plant growth (**Supplementary Figure 3**).

Verification of differentially expressed genes

We selected eight DEGs for transcriptome sequencing validation (**Figure 7** and **Supplementary Figure 4**). Two genes were up-regulated in the three treated groups compared to the control group, and two genes were down-regulated in the three treated groups compared with the control group. Among the remaining four genes, two were expressed in the EBL and the SE, and the other two were expressed in the SALT or the SE. The expression levels of Unigene30391 and CL2028.Contig1 in the three treatment groups were higher than those of CK, and the expression levels of these two genes were the highest in EBL and SALT groups, respectively. CL1847.Contig5 and CL1052.Contig9 were both down-regulated in the three treatment groups, and the expression levels of these two genes were the lowest in EBL and SALT groups, respectively. Unigene4922 and Unigene7275 were only expressed in EBL and SE groups, and were significantly

higher than CK and SALT. The expression of CL1002.Contig34 was the largest in SALT group, SE was the same as CK, and EBL was slightly larger than CK. CL7400.Contig4 was expressed in both SALT and SE, and their expression levels were two times and one time higher than that of CK, respectively.

Discussion

In saline environments, plants develop multiple strategies at the physiological and molecular levels to mitigate the damage caused by salt stress. The results of this study showed that NaCl treatment inhibited the growth and physiology of tall fescue, while the addition of EBL could confer increased tolerance to salt stress. Under the influence of sodium chloride, the plant height and chlorophyll content of tall fescue decreased, while the MDA content and electrolyte leakage increased. These growth and physiological changes were improved when 24-epibrassinolide was used. We found that SOD and CAT activities of tall fescue increased under salt stress, which was consistent with the results of Xu et al. (2013). After adding EBL, the activity of the antioxidant enzyme system was enhanced to improve the resistance of plants to salt stress. Wu et al. (2017) also found that exogenous 24-epibrassinolide increased the chlorophyll content of perennial ryegrass, enhanced the activities of SOD and CAT, and decreased the EL and MDA content. Similarly, Alam et al. (2019) found that EBL reduced the electrolyte leakage and hydrogen peroxide content, as well as the accumulation of Na^+ of soybean. Moreover, Kolomeichuk et al. (2020) demonstrated that 24-epibrassinolide could increase peroxidase activity and improve the K^+/Na^+ ratio in potato leaves under NaCl treatment. These results suggest that 24-epibrassinolide may be an effective molecule for enhancing plant salt tolerance.

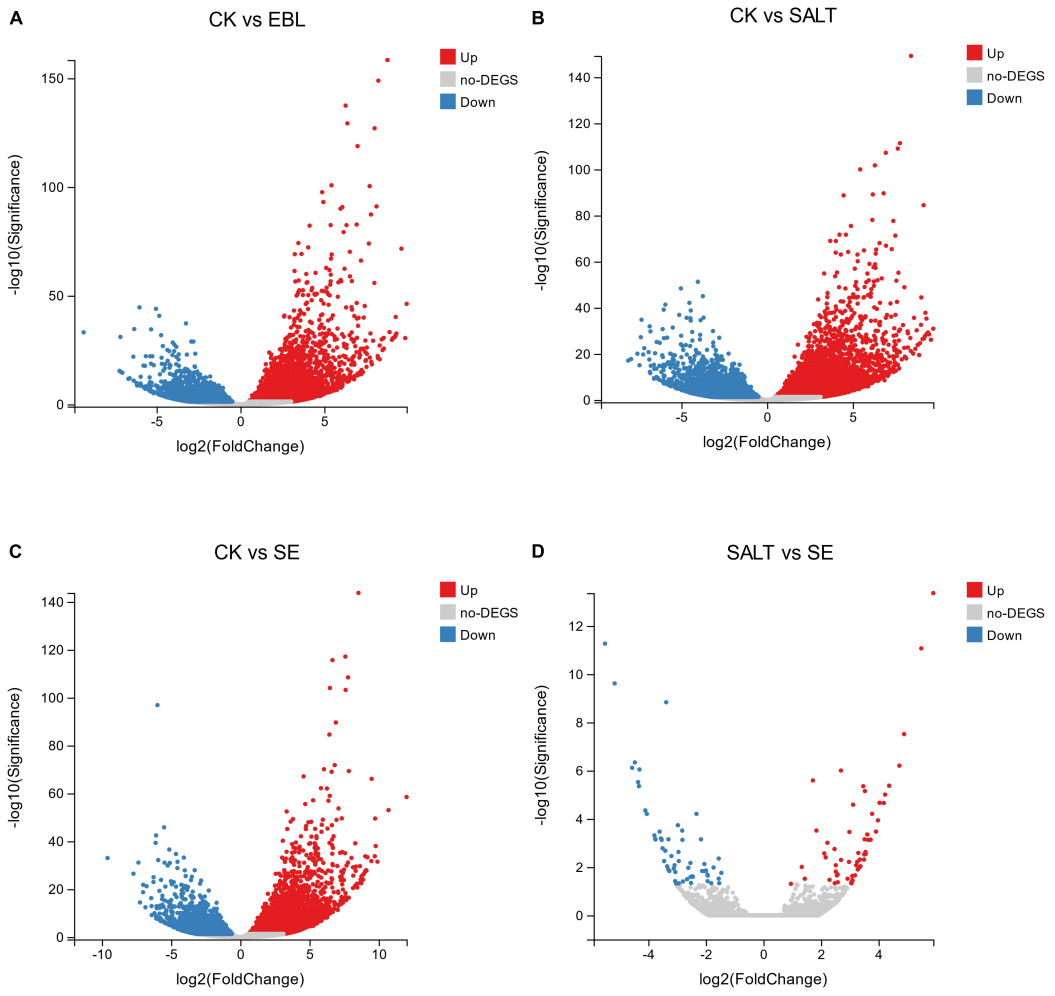

FIGURE 3
Differential genes between groups in volcano maps. **(A)** The distribution of differential genes between CK and EBL; **(B)** The distribution of differential genes between CK and SALT; **(C)** The distribution of differential genes between CK and SE; **(D)** The distribution of differential genes between SALT and SE. Up-regulated genes were shown in red and down-regulated genes were shown in blue.

10.3389/fpls.2022.976341

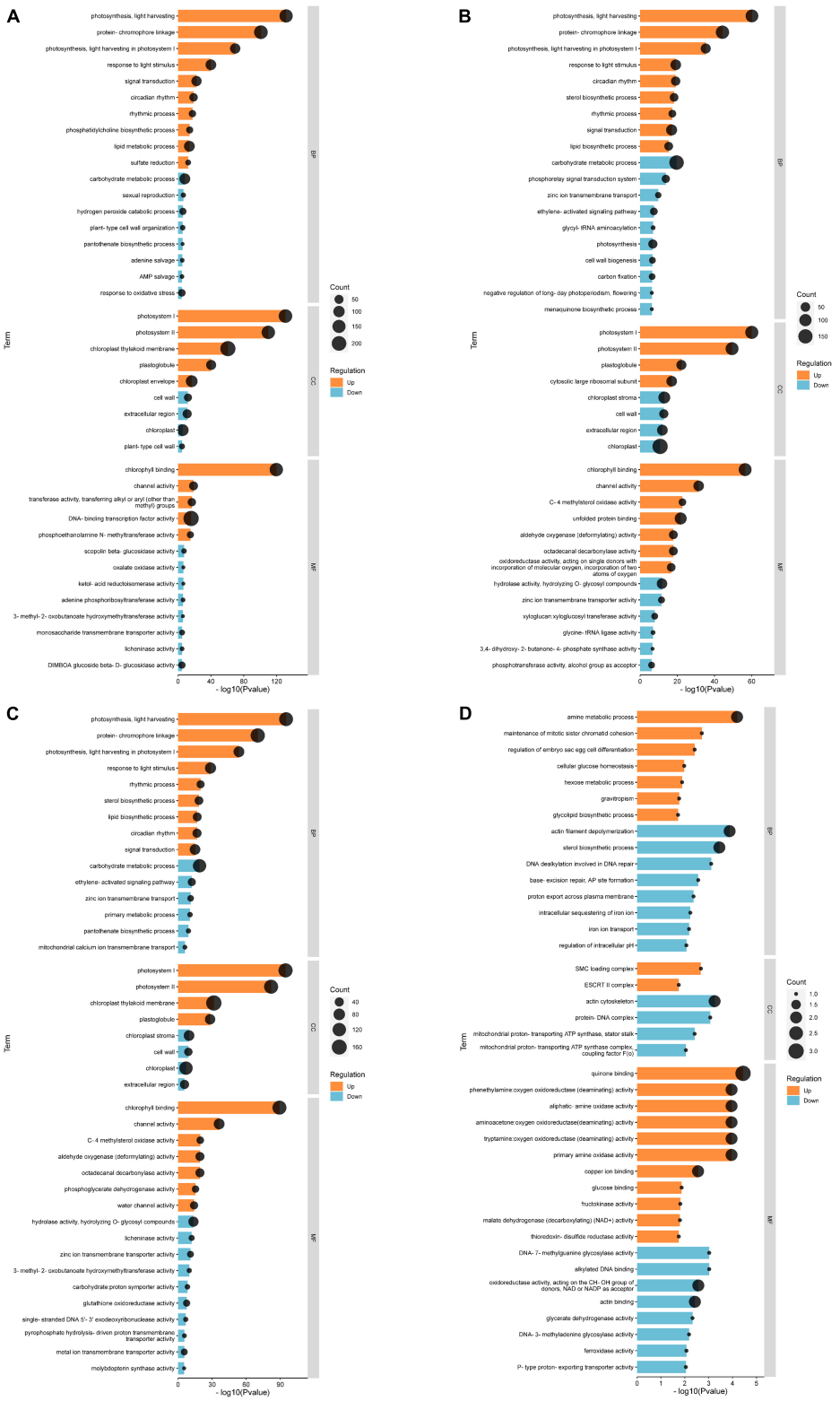

FIGURE 4

Gene ontology (GO) classification of genes with significant differences between groups. **(A)** GO classification of differential genes between CK and EBL; **(B)** GO classification of differential genes between CK and SALT; **(C)** GO classification of differential genes between CK and SE; **(D)** GO classification of differential genes between SALT and SE. The top 20 up-regulated genes between two groups were shown in orange and the top 20 down-regulated genes were shown in blue.

10.3389/fpls.2022.976341

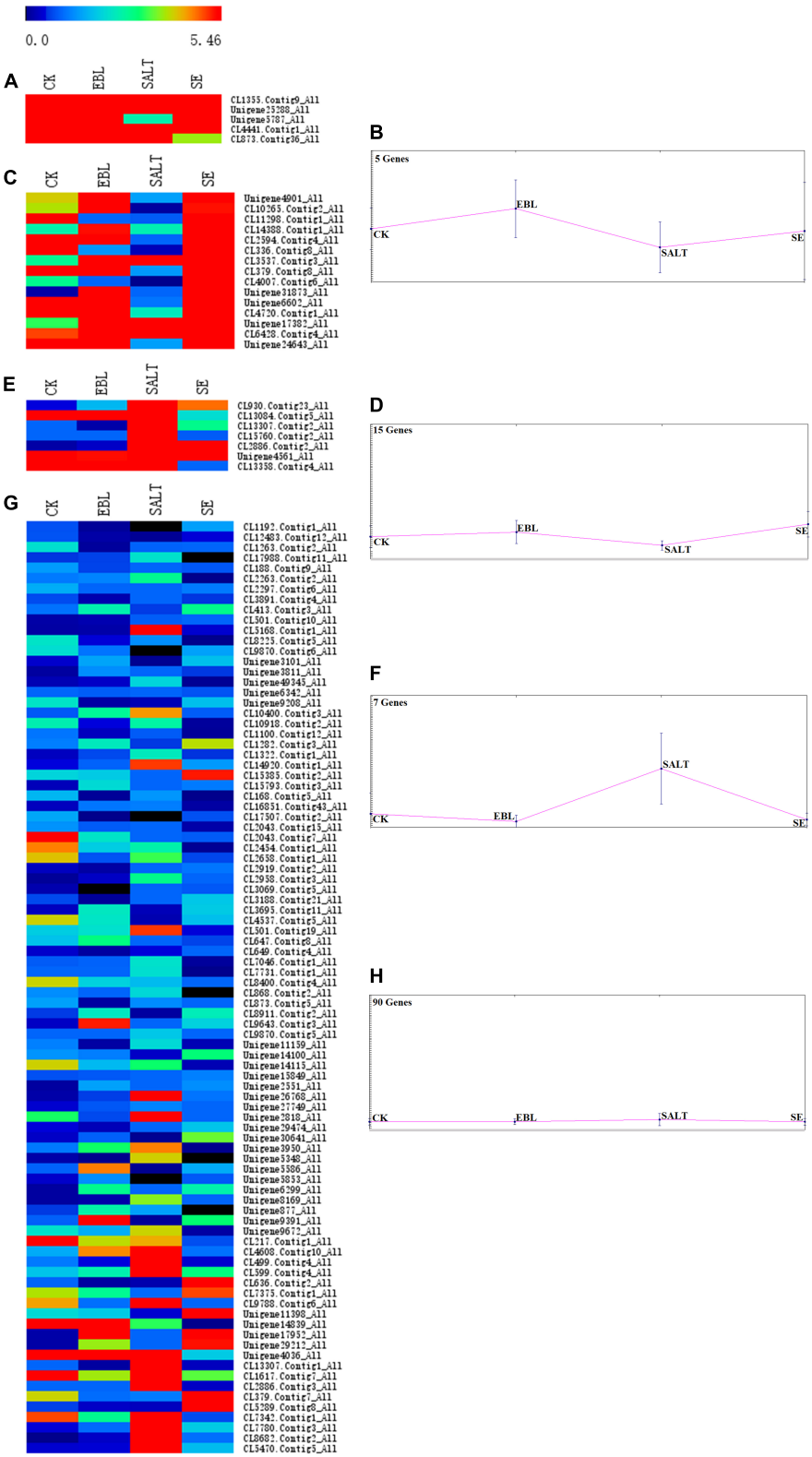

FIGURE 5
Trend analysis of DEG expression in four groups. **(A)** Heatmap of gene expression in cluster 1; **(B)** Trend graph of gene expression in cluster 1; **(C)** Heatmap of gene expression in cluster 2; **(D)** Trend graph of gene expression in cluster 2; **(E)** Heatmap of gene expression in cluster 3; **(F)** Trend graph of gene expression in cluster 3; **(G)** Heatmap of gene expression in cluster 4; **(H)** Trend graph of gene expression in cluster 4.

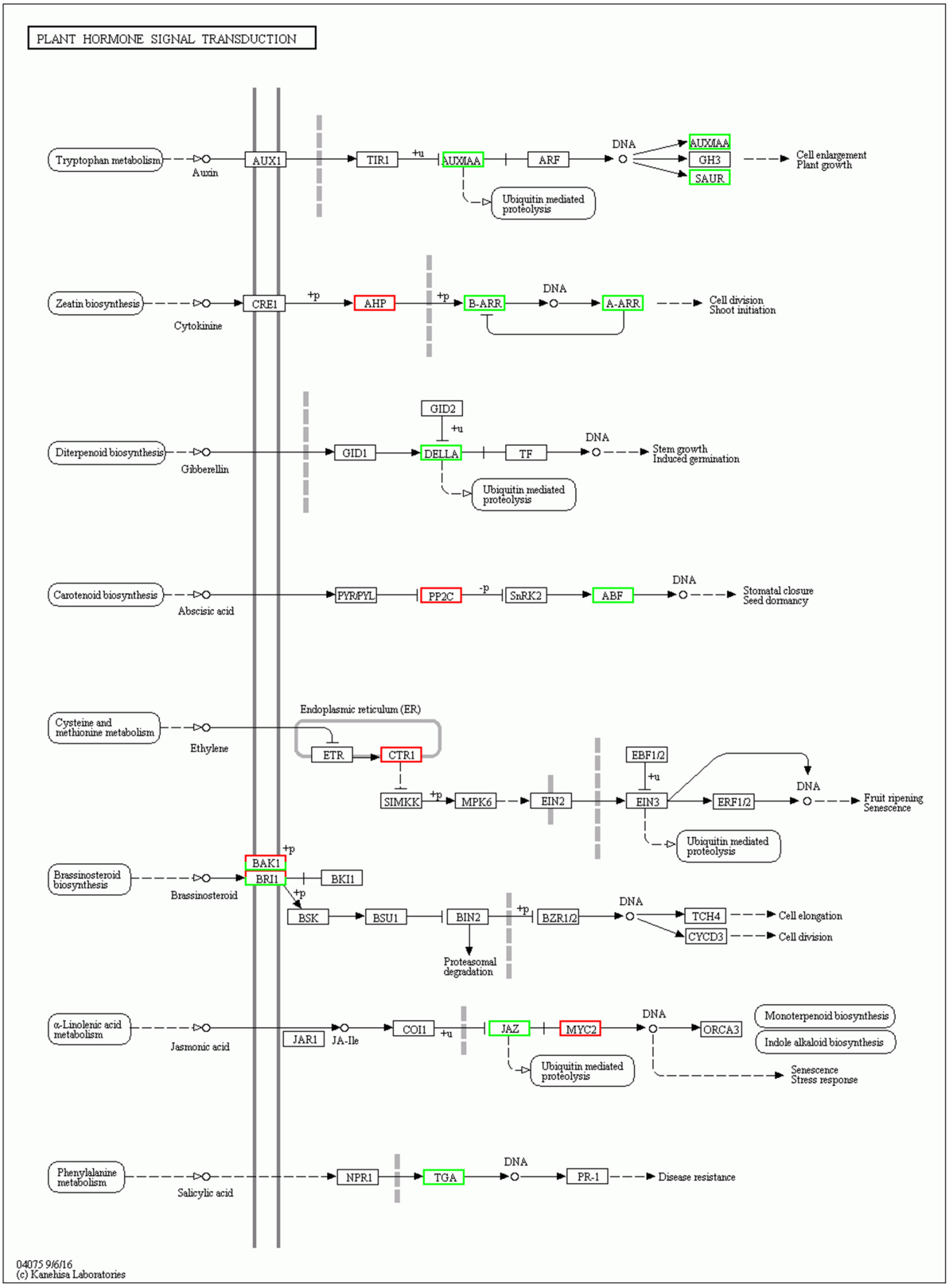

FIGURE 6
Plant hormone signal transduction in EBL vs. SE comparison. Up-regulated DEGs were indicated in red, down-regulated DEGs were indicated in green.

10.3389/fpls.2022.976341

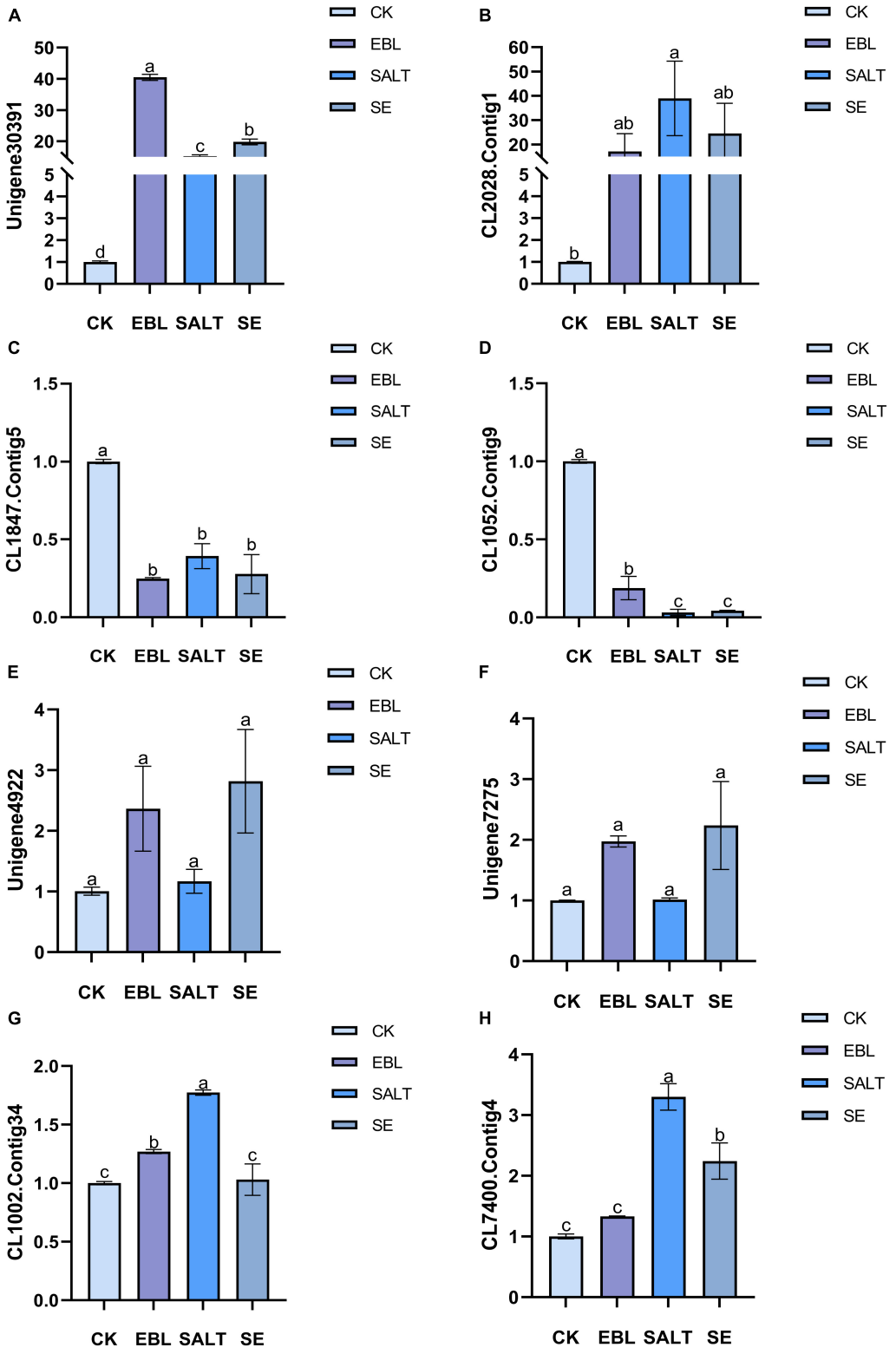

FIGURE 7

Quantitative real-time PCR (qRT-pCR) analysis of several differentially expressed genes in tall fescue. **(A)** Relative expression of Unigene30391; **(B)** Relative expression of CL2028.Contig1; **(C)** Relative expression of CL1847.Contig5; **(D)** Relative expression of CL1052.Contig9; **(E)** Relative expression of Unigene4922; **(F)** Relative expression of Unigene7275; **(G)** Relative expression of CL1002.Contig34; **(H)** Relative expression of CL7400.Contig4. Bars with different letters indicate significant difference at $P \leq 0.05$ (Duncan test).

In order to understand the response mechanism of 24-epibrassinolide in alleviating salt stress, DEGs were subjected to GO analysis. In the CK vs. SALT comparison (**Supplementary Table 5**), most DEGs were annotated to cellular anatomical entity (6,045) in cellular component, catalytic activity (4,429) and binding (4,423) in molecular function, cellular process (3,990) and metabolic process (3,613) in biological process. The results were accorded with the GO annotation results of differential genes in tall fescue after 24 h of salt treatment by Amombo et al. (2018). Interestingly, the top five annotation categories in the CK vs. EBL comparison (**Supplementary Table 5**) were the same as CK vs. SALT. We randomly selected several genes for validation, and these genes were up-regulated or down-regulated under salt or 24-epibrassinolide treatment compared to the control. The GO annotations of these genes in the molecular function were calcium ion binding, chlorophyll binding, DNA binding and ATP binding, respectively. In addition to salt stress, most of the molecular functional subcategories of GO analysis are binding under drought, heat and lead stress (Li et al., 2017; Shu et al., 2020; Liu et al., 2021; Ouertani et al., 2021). This suggests that binding-related genes play a significant role in plant resistance to various environmental stresses.

There are various signals and pathways in plants to enhance salt tolerance (Yang and Guo, 2018; Zelm et al., 2020). Salt stress induces ionic and osmotic stress, leading to an increase in cytoplasmic Ca^{2+} content, and then the SOS pathway is triggered to export excess Na^{+} to reduce salt toxicity (Zhao et al., 2021). In addition, the high-affinity potassium transporter (HKT1), the mitogen-activated protein kinases (MAPKs) and various plant hormones are also important anti-stress signals (Pan et al., 2011; Fujita et al., 2013; Zhang et al., 2013; Khan et al., 2019; Nolan et al., 2020; Zhou et al., 2020). In this study, the plant hormone signal transduction, MAPK signaling pathway-plant and plant-pathogen interaction were the most enriched signal transduction pathways in the signal transduction of DEGs. Salt stress is regulated by the interaction of multiple plant hormones, and auxin is a key mediator in this process (Ribba et al., 2020). Auxin is perceived by Transport Inhibitor Response 1 (TIR1), which ubiquitinates Aux/IAA. Then the inhibition of AUXIN RESPONSE FACTORS (ARFs) is released, and auxin-induced genes expression are activated (Leyser, 2018). The results showed that genes related with auxin were down-regulated after SE treatment compared to EBL. In addition, among the other three hormones related to plant growth, gibberellin genes were all down-regulated, most genes of cytokinins and half of brassinosteroids were also down-regulated. However, there were up-regulated genes in the ethylene and jasmonic acid pathways associated with senescence. Growth-related genes were reduced, while defense-related genes were increased. This may be a protective mechanism adopted by plants to resist the damage caused by external stress (He et al., 2022).

Most transcription factors such as MYB, WRKY, bHLH, and NAC play important roles in plant adaptation to salt stress (Baillo et al., 2019). Many MYB proteins have been implicated in salt tolerance. MYB74 and MYB20 can be induced and the interaction between MPK4 and MYB42 can be enhanced by NaCl treatment (Wang et al., 2021). Among the transcription factor families related to plant stress resistance, the bHLH family is the second largest family after the MYB family. bHLH is an indispensable factor in the salt tolerance of various plants (Sun et al., 2018). The top six transcription factors that we annotated in the TF database with the highest number were MYB, bHLH, AP2-EREBP, WRKY, FAR1, NAC. Moreover, the genes annotated to these six families were both up-regulated and down-regulated after NaCl and 24-epibrassinolide treatment, indicating that these transcription factors were actively involved in the salt response of tall fescue.

Conclusion

To better understand the effect of 24-epibrassinolide on the salt tolerance of tall fescue, we performed studies at the physiological and transcriptomic levels. Through RNA sequencing, a total of 129,866 unigenes were acquired in four groups of CK, EBL, SALT, and SE. These unigenes were annotated in seven functional databases. A large number of DEGs were obtained in different comparison groups. There were 10,265 and 13,830 DEGs in EBL and NaCl treatments compared with control, respectively. Most of them were annotated in metabolic process, binding, catalytic activity in GO database. Most of the DEGs were involved in plant signal transduction pathways, indicating that hormones actively mediated the salt response mechanism of tall fescue. At the physiological level, the plant height of tall fescue was significantly decreased and the level of membrane lipid peroxidation was increased under NaCl treatment. After the application of 24-epibrassinolide, the contents of MDA and EL in leaves were remarkably reduced, and the content of chlorophyll and the activities of antioxidant enzymes were enhanced. These results suggest that 24-epibrassinolide has non-negligible effects on the enhancement of plant salt tolerance.

Data availability statement

The data presented in the study are deposited in the China National Center repository, accession number PRJCA010198 (https://ngdc.cncb.ac.cn/bioproject/browse/PRJCA010198).

Author contributions

YC, JF, XY, and ZH conceived and designed the research. YC, YX, YG, YZ, and MC performed the experiments. YC analyzed the data and drafted

the manuscript. YC, JF, and AK revised the manuscript. All authors contributed to the article and approved the submitted version.

Funding

This study was supported by the Project of Forestry Science and Technology Innovation and Promotion of Jiangsu (Grant No. LYKJ [2021]09).

Acknowledgments

We thank the CAS Key Laboratory of Plant Germplasm Enhancement and Specialty Agriculture (Wuhan, China) for the seeds of Houndog 6 of this study.

Conflict of interest

ZH was employed by Hunan Tobacco Research Institute.

The remaining authors declare that the research was conducted in the absence of any commercial or financial relationships that could be construed as a potential conflict of interest.

Publisher's note

Supplementary material

The Supplementary Material for this article can be found online at: https://www.frontiersin.org/articles/10.3389/fpls.2022.976341/full#supplementary-material

SUPPLEMENTARY FIGURE 1
Growth of tall fescue after 10 days of 24-epibrassinolide and salt stress treatments.

SUPPLEMENTARY FIGURE 2
A bidirectional clustering heatmap of DEGs in the SALT vs. SE comparison.

SUPPLEMENTARY FIGURE 3
Plant hormone signal transduction in SALT vs. SE comparison.

SUPPLEMENTARY FIGURE 4
FPKM values of genes used for qRT-PCR analysis. **(A)** FPKM values of Unigene30391; **(B)** FPKM values of CL2028.Contig1; **(C)** FPKM values of CL1847.Contig5; **(D)** FPKM values of CL1052.Contig9; **(E)** FPKM values of Unigene4922; **(F)** FPKM values of Unigene7275; **(G)** FPKM values of CL1002.Contig34; **(H)** FPKM values of CL7400.Contig4.

References

Alam, P., Albalawi, T. H., Altalayan, F. H., Bakht, M. A., Ahanger, M. A., Raja, V., et al. (2019). 24-Epibrassinolide (EBR) confers tolerance against NaCl stress in soybean plants by up-regulating antioxidant system, ascorbate-glutathione cycle, and glyoxalase system. *Biomolecules* 9:640. doi: 10.3390/biom9110640

Amombo, E., Li, X. N., Wang, G. Y., An, S., Wang, W., and Fu, J. M. (2018). Comprehensive transcriptome profiling and identification of potential genes responsible for salt tolerance in tall fescue leaves under salinity stress. *Genes* 9:466. doi: 10.3390/genes9100466

Anders, S., and Huber, W. (2010). Differential expression analysis for sequence count data. *Genome Biol.* 11:R106. doi: 10.1186/gb-2010-11-10-r106

Anwar, A., Bai, L. Q., Miao, L., Liu, Y. M., Li, S. Z., Yu, X. C., et al. (2018). 24-Epibrassinolide ameliorates endogenous hormone levels to enhance low-temperature stress tolerance in cucumber seedlings. *Int. J. Mol. Sci.* 19:2497. doi: 10.3390/ijms19092497

Arora, P., Bhardwaj, R., and Kanwar, M. K. (2012). Effect of 24-epibrassinolide on growth, protein content and antioxidative defense system of *Brassica juncea* L. subjected to cobalt ion toxicity. *Acta Physiol. Plant.* 34, 2007–2017. doi: 10.1007/s11738-012-1002-2

Avalbaev, A., Yuldashev, R., Fedorova, K., Petrova, N., Fedina, E., Gilmanova, R., et al. (2021). 24-epibrassinolide-induced growth promotion of wheat seedlings is associated with changes in the proteome and tyrosine phosphoproteome. *Plant Biol.* 23, 456–463. doi: 10.1111/plb.13233

Baillo, E. H., Kimotho, R. N., Zhang, Z. B., and Xu, P. (2019). Transcription factors associated with abiotic and biotic stress tolerance and their potential for crops improvement. *Genes* 10:771.

Bajguz, A. (2000). Effect of brassinosteroids on nucleic acids and protein content in cultured cells of *Chlorella vulgaris*. *Plant Physiol. Biochem.* 38, 209–215. doi: 10.1016/S0981-9428(00)00733-6

Bhattarai, S., Fu, Y. B., Coulman, B., Tanino, K., Karunakaran, C., and Biligetu, B. (2021). Transcriptomic analysis of differentially expressed genes in leaves and roots of two alfalfa (*Medicago sativ*a L.) cultivars with different salt tolerance. *BMC Plant Biol.* 21:446. doi: 10.1186/s12870-021-03201-4

Cao, Y. J., Wei, Q., Liao, Y., Song, H. L., Li, X., Xiang, C. B., et al. (2009). Ectopic overexpression of AtHDG11 in tall fescue resulted in enhanced tolerance to drought and salt stress. *Plant Cell Rep.* 28, 579–588. doi: 10.1007/s00299-008-0659-x

Chen, Y. X., Chen, Y. S., Shi, C. M., Huang, Z. B., Zhang, Y., Li, S. K., et al. (2018). SOAPnuke: A MapReduce acceleration-supported software for integrated quality control and preprocessing of high-throughput sequencing data. *Gigascience* 7, 1–6. doi: 10.1093/gigascience/gix120

Fan, J. B., Hu, Z. R., Xie, Y., Chan, Z. L., Chen, K., Amombo, E., et al. (2015). Alleviation of cold damage to photosystem II and metabolisms by melatonin in bermudagrass. *Front. Plant Sci.* 6:925. doi: 10.3389/fpls.2015.00925

Feng, Q. J., Song, S. R., Yang, Y., Amee, M., Chen, L., and Xie, Y. (2021). Comparative physiological and metabolic analyzes of two Italian ryegrass (*Lolium multiflorum*) cultivars with contrasting salinity tolerance. *Physiol. Plant* 172, 1688–1699. doi: 10.1111/ppl.13374

Food and Agriculture Organization of the United Nations (2015). *Status of the world's soil resources (SWSR) – main report*. Available online at: http://www.fao.org/3/i5199e/i5199e.pdf (Accessed June 1, 2020)

Fujita, Y., Yoshida, T., and Yamaguchi-Shinozaki, K. (2013). Pivotal role of the AREB/ABF-SnRK2 pathway in ABRE-mediated transcription in response to osmotic stress in plants. *Physiol. Plant.* 147, 15–27. doi: 10.1111/j.1399-3054.2012.01635.x

Grabherr, M. G., Haas, B. J., Yassour, M., Levin, J. Z., Thompson, D. A., Amit, I., et al. (2011). Trinity: Reconstructing a full-length transcriptome without a genome from RNA-Seq data. *Nat. Biotechnol.* 29, 644–652. doi: 10.1038/nbt.1883

Hand, M. L., Cogan, N. O., Stewart, A. V., and Forster, J. W. (2010). Evolutionary history of tall fescue morphotypes inferred from molecular phylogenetics of the *Lolium-Festuca* species complex. *BMC Evol. Biol.* 10:303. doi: 10.1186/1471-2148-10-303

He, Z. H., Webster, S., and He, S. Y. (2022). Growth–defense trade-offs in plants. *Curr. Biol.* 32, R634–R639. doi: 10.1016/j.cub.2022.04.070

Hiscox, J., and Israelstam, G. (1979). A method for the extraction of chlorophyll from leaf tissue without maceration. *Can. J. Bot.* 57, 1332–1334. doi: 10.1139/b79-163

Hu, L. X., Li, H. Y., Pang, H. C., and Fu, J. M. (2012). Responses of antioxidant gene, protein and enzymes to salinity stress in two genotypes of perennial ryegrass (*Lolium perenne*) differing in salt tolerance. *J. Plant Physiol.* 169, 146–156. doi: 10.1016/j.jplph.2011.08.020

Khan, A., Kamran, M., Imran, M., Al-Harrasi, A., Al-Rawahi, A., Al-Amri, I., et al. (2019). Silicon and salicylic acid confer high-pH stress tolerance in tomato seedlings. *Sci. Rep.* 9:19788. doi: 10.1038/s41598-019-55651-4

Kim, H. S., Lee, B. Y., Won, E. J., Han, J., Hwang, D., Park, H. G., et al. (2015). Identification of xenobiotic biodegradation and metabolism-related genes in the copepod Tigriopus japonicus whole transcriptome analysis. *Mar. Genomics* 3, 207–208. doi: 10.1016/j.margen.2015.05.011

Kim, T. W., Guan, S. H., Sun, Y., Deng, Z. P., Tang, W. Q., Shang, J. X., et al. (2009). Brassinosteroid signal transduction from cell surface receptor kinases to nuclear transcription factors. *Nat. Cell Biol.* 11, 1254–1260. doi: 10.1038/ncb1970

Kolomeichuk, L. V., Efimova, M. V., Zlobin, I. E., Kreslavski, V. D., Murgan, O. K., Kovtun, I. S., et al. (2020). 24-Epibrassinolide alleviates the toxic effects of NaCl on photosynthetic processes in potato plants. *Photosynth Res.* 146, 151–163. doi: 10.1007/s11120-020-00708-z

Leyser, O. (2018). Auxin signaling. *Plant Physiol.* 176, 465–479. doi: 10.1104/pp.17.00765

Li, B., and Dewey, C. N. (2011). RSEM: Accurate transcript quantification from RNA-Seq data with or without a reference genome. *BMC Bioinformatics* 12:323. doi: 10.1186/1471-2105-12-323

Li, H. Y., Hu, T., Amombo, E., and Fu, J. M. (2017). Transcriptome profilings of two tall fescue (*Festuca arundinacea*) cultivars in response to lead (Pb) stress. *BMC Genomics* 18:145. doi: 10.1186/s12864-016-3479-3

Liu, F. W., Ali, T., and Liu, Z. (2021). Comparative transcriptomic analysis reveals the effects of drought on the biosynthesis of methyleugenol in *Asarum sieboldii* Miq. *Biomolecules* 11:1233. doi: 10.3390/biom11081233

Lou, Y. H., Zhao, P., Wang, D. L., Amombo, E., Sun, X., Wang, H., et al. (2017).). Germination, physiological responses and gene expression of tall fescue (*Festuca arundinacea* Schreb.) growing under Pb and Cd. *PLoS One* 12:e0169495. doi: 10.1371/journal.pone.0169495

Love, M. I., Huber, W., and Anders, S. (2014). Moderated estimation of fold change and dispersion for RNA-seq data with DESeq2. *Genome Biol.* 15:550. doi: 10.1186/s13059-014-0550-8

Miller, G., Suzuki, N., Ciftci-Yilmaz, S., and Mittler, R. (2010). Reactive oxygen species homeostasis and signalling during drought and salinity stresses. *Plant Cell Environ.* 33, 453–467. 02041.x doi: 10.1111/j.1365-3040.2009

Munns, R., and Gilliham, M. (2015). Salinity tolerance of crops – what is the cost? *New Phytol.* 208, 668–673. doi: 10.1111/nph.13519

Munns, R., and Tester, M. (2008). Mechanisms of salinity tolerance. *Annu. Rev. Plant Biol.* 59, 651–681. doi: 10.1146/annurev.arplant.59.032607.092911

Nolan, T. M., Vukašinoviíc, N., Liu, D., Russinova, E., and Yin, Y. (2020). Brassinosteroids: Multidimensional regulators of plant growth, development, and stress responses. *Plant Cell* 32, 295–318. doi: 10.1105/tpc.19.00335

Ouertani, R. H., Arasappan, D., Abid, G., Chikha, M. B., Jardak, R., Mahmoudi, M., et al. (2021). Transcriptomic analysis of salt-stress-responsive genes in barley roots and leaves. *Int. J. Mol. Sci.* 22:8155. doi: 10.3390/ijms22158155

Pan, J., Zhang, M., Kong, X., Xing, X., Liu, Y., Zhou, Y., et al. (2011). ZmMPK17, a novel maize group D MAP kinase gene, is involved in multiple stress responses. *Planta* 235, 661–676. doi: 10.1007/s00425-011-1510-0

Pertea, G., Huang, X., Liang, F., Antonescu, V., Sultana, R., Karamycheva, S., et al. (2003). TIGR gene indices clustering tools (TGICL): A software system for fast clustering of large EST datasets. *Bioinformatics* 19, 651–652. doi: 10.1093/bioinformatics/btg034

Pfaffl, M. W. (2001). A new mathematical model for relative quantification in real-time RT–PCR. *Nucleic Acids Res.* 29:e45. doi: 10.1093/nar/29.9.e45

Ribba, T., Garrido-Vargas, F., and O'Brien, J. A. (2020). Auxin-mediated responses under salt stress: From developmental regulation to biotechnological applications. *J. Exp. Bot.* 71, 3843–3853. doi: 10.1093/jxb/eraa241

Shen, X. Y., Wang, Z. L., Song, X. F., Xu, J. J., Jiang, C. Y., Zhao, Y. X., et al. (2014). Transcriptomic profiling revealed an important role of cell wall remodeling and ethylene signaling pathway during salt acclimation in *Arabidopsis*. *Plant Mol Biol.* 86, 303–317. doi: 10.1007/s11103-014-0230-9

Shi, H. T., Jiang, C., Ye, T. T., Tan, D. X., Reiter, R. J., Zhang, H., et al. (2015). Comparative physiological, metabolomic, and transcriptomic analyses reveal mechanisms of improved abiotic stress resistance in bermudagrass [*Cynodon dactylon* (L). Pers.] by exogenous melatonin. *J. Exp. Bot.* 66, 681–694. doi: 10.1093/jxb/eru373

Shu, B. S., Wu, Y. X., Qu, M. Q., Pu, X. H., Wu, Z. Z., and Lin, J. T. (2020). Comparative transcriptomic analyses revealed genes and pathways responsive to heat stress in *Diaphorina citri*. *Gene* 727:144246. doi: 10.1016/j.gene.2019.144246

Sun, X., Wang, Y., and Sui, N. (2018). Transcriptional regulation of bHLH during plant response to stress. *Biochem. Biophys. Res. Commun.* 503, 397–401. doi: 10.1016/j.bbrc.2018.07.123

Tanveer, M., Shahzad, B., Sharma, A., and Khan, E. A. (2019). 24-Epibrassinolide application in plants: An implication for improving drought stress tolerance in plants. *Plant Physiol. Biochem.* 135, 295–303. doi: 10.1016/j.plaphy.2018.12.013

Wang, G. Y., Bi, A. Y., Amombo, E., Li, H. Y., Zhang, L., Cheng, C., et al. (2017). Exogenous calcium enhances the photosystem II photochemistry response in salt stressed tall fescue. *Front. Plant. Sci.* 8:2032. doi: 10.3389/fpls.2017.02032

Wang, W. S., Zhao, X. Q., Li, M., Huang, L. Y., Xu, J. L., Zhang, F., et al. (2016). Complex molecular mechanisms underlying seedling salt tolerance in rice revealed by comparative transcriptome and metabolomic profiling. *J. Exp. Bot.* 67, 405–419. doi: 10.1093/jxb/erv476

Wang, X. P., Niu, Y. L., and Zheng, Y. (2021). Multiple functions of MYB transcription factors in abiotic stress responses. *Int. J. Mol. Sci.* 22:6125. doi: 10.3390/ijms22116125

Wang, Z. Y., Hopkins, A., Lawrence, R., Bell, J., and Scott, M. (2004). Field evaluation and risk assessment of transgenic tall fescue (*Festuca arundinacea*) plants. *Mol. Breed. Forage Turf* 11, 367–379. doi: 10.1007/1-4020-2591-2_32

Wu, W. L., Zhang, Q., Ervin, E. H., Yang, Z. P., and Zhang, X. Z. (2017). Physiological mechanism of enhancing salt stress tolerance of perennial ryegrass by 24-epibrassinolide. *Front. Plant Sci.* 8:1017. doi: 10.3389/fpls.2017.01017

Xu, R., Yamada, M., and Fujiyama, H. (2013). Lipid Peroxidation and Antioxidative Enzymes of Two Turfgrass Species Under Salinity Stress. *Pedosphere* 23, 213–222. doi: 10.1016/S1002-0160(13)60009-0

Yang, Y. Q., and Guo, Y. (2018). Unraveling salt stress signaling in plants. *J. Integr. Plant Biol.* 60, 796–804. doi: 10.1111/jipb.12689

Yu, Z. P., Duan, X. B., Luo, L., Dai, S. J., Ding, Z. J., and Xia, G. M. (2020). How plant hormones mediate salt stress responses. *Trends Plant Sci.* 25, 1117–1130. doi: 10.1016/j.tplants.2020.06.008

Zelm, E. V., Zhang, Y. X., and Testerink, C. (2020). Salt tolerance mechanisms of plants. *Annu. Rev. Plant Biol.* 71, 403–433. doi: 10.1146/annurev-arplant-050718-100005

Zhang, D., Jiang, S., Pan, J., Kong, X., Zhou, Y., Liu, Y., et al. (2013). The overexpression of a maize mitogen-activated protein kinase gene (ZmMPK5) confers salt stress tolerance and induces defence responses in tobacco. *Plant Biol.* 16, 558–570. doi: 10.1111/plb.12084

Zhao, S. S., Zhang, Q. K., Liu, M. Y., Zhou, H. P., Ma, C. L., and Wang, P. P. (2021). Regulation of plant responses to salt stress. *Int J Mol Sci.* 22:4609. doi: 10.3390/ijms22094609

Zhou, J. H., Li, Z. Y., Xiao, G. Q., Zhai, M. J., Pan, X. W., Huang, R. F., et al. (2020). CYP71D8L is a key regulator involved in growth and stress responses by mediating gibberellin homeostasis in rice. *J. Exp. Bot.* 71, 1160–1170. doi: 10.1093/jxb/erz491

Zhu, J. K. (2001). Plant salt tolerance. *Trends Plant Sci.* 6, 66–71. doi: 10.1016/S1360-1385(00)01838-0

frontiers | Frontiers in Plant Science

TYPE Original Research
PUBLISHED 23 September 2022
DOI 10.3389/fpls.2022.1007494

OPEN ACCESS

EDITED BY
Jin-Lin Zhang,
Lanzhou University, China

REVIEWED BY
Min Yu,
Foshan University, China
Mark A. Bernards,
Western University, Canada
Yanjun Guo,
Qingdao Agricultural University, China

*CORRESPONDENCE
Pei Wang
wangpei@swun.edu.cn

SPECIALTY SECTION
This article was submitted to Plant Abiotic Stress, a section of the journal Frontiers in Plant Science

RECEIVED 30 July 2022
ACCEPTED 05 September 2022
PUBLISHED 23 September 2022

CITATION
Liu X, Wang P, An Y, Wang C-M, Hao Y, Zhou Y, Zhou Q and Wang P (2022) Endodermal apoplastic barriers are linked to osmotic tolerance in meso-xerophytic grass *Elymus sibiricus*. *Front. Plant Sci.* 13:1007494. doi: 10.3389/fpls.2022.1007494

Endodermal apoplastic barriers are linked to osmotic tolerance in meso-xerophytic grass *Elymus sibiricus*

Xin Liu[1,2], Ping Wang[1], Yongping An[1], Chun-Mei Wang[3], Yanbo Hao[1], Yue Zhou[1], Qingping Zhou[1] and Pei Wang[1]*

[1]Sichuan Zoige Alpine Wetland Ecosystem National Observation and Research Station, Institute of Qinghai-Tibetan Plateau, Southwest Minzu University, Chengdu, China, [2]National Key Laboratory of Crop Genetic Improvement, Ministry of Agriculture Key Laboratory of Crop Ecophysiology and Farming System in the Middle Reaches of the Yangtze River, College of Plant Science and Technology, Huazhong Agricultural University, Wuhan, China, [3]Lanzhou Institute of Husbandry and Pharmaceutical Sciences, Chinese Academy of Agricultural Sciences, Lanzhou, China

Drought is the most serious adversity faced by agriculture and animal husbandry industries. One strategy that plants use to adapt to water deficits is modifying the root growth and architecture. Root endodermis has cell walls reinforced with apoplastic barriers formed by the Casparian strip (CS) and suberin lamellae (SL) deposits, regulates radial nutrient transport and protects the vascular cylinder from abiotic threats. *Elymus sibiricus* is an economically important meso-xerophytic forage grass, characterized by high nutritional quality and strong environmental adaptability. The purpose of this study was to evaluate the drought tolerance of *E. sibiricus* genotypes and investigate the root structural adaptation mechanism of drought-tolerant genotypes' responding to drought. Specifically, a drought tolerant (DT) and drought sensitive (DS) genotype were screened out from 52 *E. sibiricus* genotypes. DT showed less apoplastic bypass flow of water and solutes than DS under control conditions, as determined with a hydraulic conductivity measurement system and an apoplastic fluorescent tracer, specifically PTS trisodium-8-hydroxy-1,3,6-pyrenetrisulphonic acid (PTS). In addition, DT accumulated less Na, Mg, Mn, and Zn and more Ni, Cu, and Al than DS, regardless of osmotic stress. Further study showed more suberin deposition in DT than in DS, which could be induced by osmotic stress in both. Accordingly, the CS and SL were deposited closer to the root tip in DT than in DS. However, osmotic stress induced their deposition closer to the root tips in DS, while likely increasing the thickness of the CS and SL in DT. The stronger and earlier formation of endodermal barriers may determine the radial transport pathways of water and solutes, and contribute to balance growth and drought response in *E. sibiricus*. These results could help us better understand how altered endodermal apoplastic barriers in roots regulate water and mineral nutrient transport in plants that have adapted to drought environments. Moreover, the current findings will aid in improving future breeding programs to develop drought-tolerant grass or crop cultivars.

KEYWORDS
casparian strip, drought tolerance, *Elymus sibiricus*, endodermis, suberin

Introduction

Drought is the most serious abiotic stress that restricts agriculture and animal husbandry development. Drought stress reduces turgor pressure, disrupts ion homeostasis, damages cell membrane systems, and inhibits photosynthesis, among other effects. Furthermore, it not only impedes plant growth and metabolism at different stages, but also affects crop yields and quality (Reddy et al., 2004; Passioura, 2007). Global losses in crop production due to drought have totaled ~US $30 billion over the past decade. With the rapid growth of the global population, high-yield plants that use water more efficiently than their modern counterparts are urgently required (Gupta et al., 2020). *Elymus sibiricus* (Siberian wild rye) is an economically important perennial allotetraploid, meso-xerophytic and high-yield forage grass, native to northern Asia. It is palatable, nutrient-rich, and easily digestible, which are conducive to the growth and reproduction of domestic animals. This grass is widely used in natural grasslands and cultivated pastures on the Qinghai-Tibet Plateau owing to good forage quality, adaptability and excellent cold and drought tolerance (Ma et al., 2012; Liu et al., 2016; Xie et al., 2017). However, little is known about drought resistance strategies in this species.

A water deficit is the main cause of drought stress. Therefore, maintaining sufficient water absorption and preventing water loss in water-deficient environments enhance the drought resistance of plants. Plant roots are the first organs that sense the soil water status, and manage water deficiencies (Steudle, 2000). Root systems determine the capacity of a plant to access soil water, and their morphology and architecture can influence adaptation to water-limited conditions (Singh et al., 2010). According to the composite transport model, water and solutes are transported rapidly from the rhizodermis to xylem vessels in the stele *via* cell-to-cell (symplastic and transcellular) and apoplastic pathways (Kreszies et al., 2018). The key factors of water movement through the cell-to-cell pathway and the underlying mechanism have been investigated. For example, aquaporins contribute to water flux, and hence, function in drought tolerance (Lian et al., 2006; Chaumont and Tyerman, 2014; Grondin et al., 2016). Although root apoplastic barriers are theoretically important for plant adaptation to environmental stresses such as drought, little is known about their function and regulation.

The root apoplastic barriers comprise the Casparian strip (CS) and suberin lamellae (SL) of the endodermis and periderm and provide the main resistance to radial water transport *via* transcellular and apoplastic pathways in roots, which likely plays a crucial role in drought tolerance (Steudle, 2000; Kreszies et al., 2019; de Silva et al., 2021). The CS is the localized impregnation of a primary cell that longitudinally encircles an endodermal cell and might prevent the free apoplastic bypass flow (apoplastic pathway) of solutes in the extracellular spaces between the cortex and inner vasculature (Enstone et al., 2002; Geldner, 2013). The SL is deposited on the entire inner face of the cell wall adjacent to the plasma membrane, and it might be instrumental in preventing the movement of water and solutes from apoplasts directly into the endodermal protoplasts (Schreiber et al., 1999; Ranathunge et al., 2005; Martinka et al., 2012). The SL is polymerized based on polyaliphatic and polyaromatic domains. The aliphatic monomers are mainly ω-hydroxy fatty acids (ω-OH acids) and α,ω-dicarboxylic fatty acids (α,ω-diacids), with some primary alcohols and unsubstituted fatty acids, whereas the aromatic components are mainly ferulic and coumaric acids (Bernards, 2002; Pollard et al., 2008; Vishwanath et al., 2015). The CS is comprised of lignin or a lignin-like polymer (Geldner, 2013). It can also include aliphatic suberin in some species (Zeier and Schreiber, 1997), although histochemical staining and chemical analysis have shown that the CS is comprised only of a lignin-like polymer without suberin in *Arabidopsis* (Naseer et al., 2012).

The deposition of CS and SL not only changes throughout plant development but can also be modulated by abiotic stresses, such as drought (Barberon, 2017; Doblas et al., 2017; Campilho et al., 2020; de Silva et al., 2021). The SL is enhanced by osmotic stress in the seminal roots of barley (*Hordeum vulgare*) (Kreszies et al., 2019). Moreover, suberin deposition is induced under water-deficit conditions in grapevine (*Vitis riparia*) fine roots (Zhang et al., 2020). The *Arabidopsis esb1* (*enhanced suberin 1*) mutant has higher water-use efficiency and lower transpiration rates than the wild-type, and this is associated with enhanced suberin deposition and ectopic lignin in roots (Baxter et al., 2009). The SL acts as a powerful barrier that prevents the

uncontrolled backflow of water and solutes from the root to the medium and is important for *Arabidopsis* growth under drought and salt conditions (Wang et al., 2020a; de Silva et al., 2021). Natural variation in root suberization is associated with the local environment, especially edaphic water conditions, and the chemical composition, rather than only the amount of suberin, also plays a role in plant responses to drought and long-term adaptation to arid environments (Feng et al., 2022). Studies have also shown the role of the CS functions in the selective uptake of mineral nutrients and salinity tolerance of rice (*Oryza sativa*) and maize (*Zea mays*) (Krishnamurthy et al., 2011; Wang et al., 2019; Wang et al., 2022a; Wang et al., 2022b). Whereas the role of the CS as a barrier for water is poorly supported by functional evidence. Changes in root apoplastic barriers would alter water relationship and modulate drought tolerance in plants.

The total content and composition of suberin varies substantially between *Arabidopsis* and gramineous species, such as rice and barley. Various cultivars and growth conditions also contain different amounts of total suberin (Kreszies et al., 2018). Therefore, the study of root apoplastic barriers in gramineous grasses is necessary to understand the unique strategies used by grass and forage plants to adapt to environmental stress.

Here, we evaluated the drought tolerance of 52 *E. sibiricus* genotypes in seedlings. We identified drought tolerant (DT) and sensitive (DS) genotypes and compared the physiological, morphological, and ultrastructural responses of *E. sibiricus* with these genotypes under osmotic stress to elucidate the effects of root apoplastic barriers on drought tolerance. We also discuss whether differences in apoplastic barrier formation contribute to natural variations in drought tolerance between the two genotypes.

Materials and methods

Plant materials, growth conditions and treatments

Seeds from 52 wild *E. sibiricus* genotypes collected at the Sichuan Zoige Alpine Wetland Ecosystem National Observation and Research Station (Supplementary Table 1) were vernalized for 3 days in the dark at 4°C, then germinated on wet filter paper. The germinated seedlings were transferred to pots containing peat soil (Pindstrup, Mosebrug, Denmark) and watered compound fertilizer (N: P: K = 1:1:1) every 2 days. Ten-day-old seedlings were continuously watered or not (control) with distilled water for 8 days to evaluate the drought tolerance of germplasm resources. Seedlings were also transferred to aerated plastic boxes containing half-strength Hoagland solution (H353, Phyto TechLabs, Lenexa, KS, USA) for hydroculture. Thereafter, 28-day-old plants were placed in 0 (control) and 20% PEG 6000 (BioFroxx, Einhausen, Germany) with an osmotic potential of −1.38 MPa for 3 days, osmolality was determined using an OSMOMAT 3000-D osmometer (Gonotec GmbH., Berlin, Germany). Plants grown in PEG 6000 for 0, 3 and 24 h were assessed by real-time quantitative polymerase chain reaction (qRT-PCR). All plants were cultivated in a climatic chamber at day/night temperatures of 23°C/19°C under a light cycle of 16 h/8 h (light/dark), light intensity of 250 μmol $m^{-2}\cdot s^{-1}$, and relative humidity of ~ 60%.

Physiological evaluation of drought tolerance

Leaves were washed with distilled water and gently wiped. Chlorophyll fluorescence indexes including the initial fluorescence (Fo), maximum fluorescence under light (Fm'), maximum fluorescence under dark adaptation (Fm), difference between maximum fluorescence under light and minimum fluorescence (Fv'), difference between maximum fluorescence under dark adaptation and initial fluorescence (Fv), maximum photochemical efficiency of photosystem II in the dark-adapted state (Fv/Fm), electron transport rate (ETR), photochemical quenching coefficient (qP), and non-photochemical quenching coefficient (NPQ) were measured as described (Bhusal et al., 2021) using an Li-6800 portable photosynthetic instrument (LI-COR Biosciences Inc., Lincoln, NE USA). Chlorophyll contents were measured in alcohol and acetone as described by Zhang et al. (2022) using a CARY60 UV spectrophotometer (Agilent Technologies Inc., Santa Clara, CA, USA). Relative electric conductivity (REC; a.k.a. electrolyte leakage) was measured as described by Wang et al. (2020a) and membrane lipid peroxidation was assessed as malondialdehyde (MDA) contents using the thiobarbituric acid reaction as described by Niu et al. (2016).

Measurement of root hydraulic conductivity

Plants grown in 20% PEG 6000 were transferred back to half-strength Hoagland nutrient solution at least 1 h before measurements, based upon which hydrostatic hydraulic conductivity (Lp_r) was calculated as Lp_{hy}. The osmotic Lp_r (Lp_{os}) was measured by replacing the nutrient solution with 1/2 Hoagland solution containing 30 mM NaCl at least 1 h before measurements. Five independent biological replicates per experiment were evaluated.

The Lp_r (including Lp_{hy} and Lp_{os}) was measured using a high conductance flow meter (HFCM; Dynamax Inc., Houston, TX, USA) to determine the hydraulic conductance of the whole-plant water transport pathway. Samples were cut 4 cm above the basal root, and stumps were immediately connected to the HCFM that perfuses degassed water throughout the root system by applying pressure to a water-filled bladder within the

unit. The flow rate of water through the root was determined using the HCFM in transient mode, with flow measured under increasing pressure delivered by a nitrogen gas cylinder. The applied pressure was gradually increased from 6 to ~ 500 kPa over the course of ~ 1 min, and the flow rate was logged every 2 s using Dynamax software. A transient curve was constructed, then the Lp_r was calculated as:

$$Lp_r = Qv/P$$

where Qv is the volumetric flow rate ($kg{\cdot}s^{-1}$) and P is the applied pressure (MPa). The temperature was automatically recorded by the HCFM, and all conductance measurements were corrected to values at 25°C. Hydraulic conductance was calculated using a transient increase in pressure with simultaneous recording of volume flow and normalized by dividing conductance by the total surface areas of the root (Tsuda and Tyree, 2000; Rodríguez-Gamir et al., 2019).

Trisodium-8-hydroxy-1,3,6-pyrenetrisulphonic acid (PTS) analyses

Apoplastic bypass flow was analyzed using the water-soluble, fluorescent, and nontoxic tracer trisodium-8-hydroxy-1,3,6-pyrenetrisulphonic acid (PTS; Sigma-Aldrich Corp., St. Louis, MO, USA) that does not cross cell membranes or adhere to cell walls (Faiyue et al., 2010b; Krishnamurthy et al., 2011). Four-week-old plants were placed in 20% PEG 6000, 0.2 mM PTS (100 $mg{\cdot}L^{-1}$), and 0.2 mM PTS plus 20% PEG 6000 for 72 h, or normal half-strength Hoagland nutrient solution (control). Shoots were harvested and dried in an oven at 80°C for 72 h. Dry samples were immersed in 10 mL of distilled water for 2 h at 90°C. PTS florescence was analyzed at Λ_{ex} = 380 nm and Λ_{em} = 510 nm using a Varioskan LUX microplate reader (Thermo Fisher Scientific Inc., Waltham, MA, USA).

Elemental analyses of shoots

Plants were removed from the osmotic environment, washed with distilled water to remove surface salts. Then the shoots were harvested and dried at 80°C for 72 h. Ground dried samples (~ 0.5 g) were mixed with the internal standard indium and digested in a muffle furnace with 5 mL of concentrated nitric acid at 170°C for 4 h. The digest was cooled to room temperature and the acid was evaporated almost to dryness then diluted to a final volume of 25 mL with 18 MΩ water to extract ions. The contents of B, Na, Mg, K, Al, Ca, Mn, Fe, Ni, Cu and Zn were determined using a Thermo X series II, inductively coupled plasma mass spectrometer (ICP-MS; Thermo Fisher Scientific Inc.), as described by the manufacturer.

Root morphology and architecture

The roots of treated hydroponic plants were analyzed using a 12000XL scanner (Seiko Epson Corp., Tokyo, Japan), then images were analyzed using WinRHIZO2017 software (Regent Instruments, Sainte Foy, PQ, Canada) to obtain root parameters, namely total length, seminal root length and average diameter, surface area, forks, and fractal dimensions.

Histochemical detection of CS and SL

Seminal root materials were fixed in FAA (50% ethanol, 5% glacial acetic acid and 5% formaldehyde) and dehydrated in a graded ethanol series. Cross-sections were cut at 12%, 24%, 36%, 48%, and 60% of the total seminal root length from the tip, along the entire seminal root, using a Cryotome-H-E cryostat microtome (Thermo Fisher), to detect development of the CS and SL over the root length. Development of the CS was detected by staining with 0.1% (w/v) berberine hemisulfate for 1 h and with 0.5% (w/v) aniline blue for 0.5 h (Brundrett et al., 1988). The SL was stained with 0.01% (w/v) lipophilic Fluorol Yellow 088 (FY088; Sigma-Aldrich Corp.) for 0.5 h and with 0.5% (w/v) aniline blue for 0.5 h (slightly modified from Lux et al., 2005). Stained cross-sections were visualized using a DS-U3 epifluorescence microscope (Nikon Corp., Tokyo, Japan) with an ultraviolet filter set (excitation filter 361–389 nm, dichroic mirror 415 nm, barrier filter 430–490 nm) and photographed using a Nikon Eclipse camera at ISO 200 or 400 and 1–2 s exposure (Kreszies et al., 2018).

Chemical analysis of suberin in roots

Root tissues (~500 mg fresh weight per sample) were rinsed with deionized water and dried on paper towels. Suberin cannot be directly quantified due to being insoluble and having a complex structure. Samples were delipidated and depolymerized to release monomers, then derivatized using N, O Bis-trimethylsilyl-trifluoroacetamide as described by Jenkin and Molina (2015).

Suberin monomers were identified and quantified using an 8890-7000D gas chromatograph-mass spectrometer (GC-MS; Agilent Technologies) fitted with an HP-5MS capillary column (length, 30 m; i.d., 0.25 mm; film thickness, 0.25 µm). The injector was set at 250°C, the injected split ratio was 1:10 and helium was the carrier gas at a constant flow of 1.0 mL min^{-1}. The oven was initially set at 80°C for 2 min, increased by 15°C min^{-1} increments to 260°C, held for 10 min, then increased by 5°C min^{-1} increments to 320°C, and held for 24 min (total run time, 60 min). The temperature of the MS detector was 325°C, and the MS was set to a scan mode > 40–600 amu (electron

impact ionization). Four biological replicates per experiment were assessed.

qRT-PCR analysis

Total RNA was isolated using RNAiso Plus Mini Kits (Takara Bio Inc., Kusatsu, Japan). Complementary DNA was synthesized using RT OR-Easy TM II cDNA synthesis kits (Foregene, Chengdu, China). Supplementary Table 2 lists the primers that were designed using Primer Premier 6.0. Primer specificity was validated based on melting profiles. The qRT-PCR proceeded using a StepOne Plus RT-PCR System (Thermo Fisher Scientific Inc.) and SYBR Premix Ex Taq (Toyobo, Tokyo, Japan). Relative expression was normalized to that of the housekeeping gene DnaJ (encodes heat shock N-terminal domain-containing protein) based on the $2^{-\Delta\Delta Ct}$ method because this is the most stable internal gene in *E. sibiricus* under osmotic stress in qRT-PCR analyses (Zhang et al., 2019). All experiments included three technical and three biological replicates.

Statistical analyses

All results for traits in the evaluation of drought tolerance were converted into relative values to reduce inherent differences among different germplasm resources as:

$$trait\ relative\ value\ =\ Xs/Xc$$

where Xs and Xc represent drought stress and control, respectively (Zhang et al., 2022). The coefficient of variation for drought (CV_D) was calculated as:

$$CV_D = |CV_T - CV_C|/(CV_T + CV_C)/2$$

where CV_T and CV_C respectively represent the coefficients of variation (CV) of all tested materials under drought stress and control conditions. Principal component analysis was carried out using SPSS 20.0 (IBM Corp., Armonk, NY, USA). Correlations among traits were determined using Pearson correlation coefficients (Adler and Parmryd, 2010). Drought resistance (D) values for the drought tolerance capacity of each genotype were calculated using subordinate function analysis as described by Yan et al. (2020).

All other data were statistically analyzed by one-way analysis of variance (ANOVA) using SPSS 20.0. Values are shown as means ± standard deviation (SD). Significant differences between means were determined using Duncan multiple range tests. Values with $P< 0.05$ were considered statistically significant. Histograms and linear graphs were generated using Origin 2019 (OriginLab Corp., Northampton, MA, USA).

Results

Comprehensive evaluation of drought tolerance of *E. sibiricus* genotypes

Eight days after drought stress, 13 physiological traits associated with photosynthetic pigment contents, relative plasma membrane permeability, and chlorophyll fluorescence parameters were comprehensively assessed in the 52 *E. sibiricus* genotypes. These traits changed to varying degrees among the genotypes, and the CV_D of REC and Fv/Fm were > 1 (100%). This indicated that these two traits were the most representative and were highly sensitive in the drought tolerance evaluation. Except for Fo and Fm, the CV_D of the other 11 traits were all > 0.10 (10%) (Supplementary Table 3).

We then calculated the variance contribution of 11 traits (excluding Fo and Fm) using principal component analysis (PCA). The Eigen values of the top two principal components were > 1, and the cumulative variance contribution rate was 66.04% (Table 1). The Eigen value of the first principal component was 5.63 with a variance contribution rate of 51.18% (Table 1). Chlorophyll fluorescence parameters, including ΦPS II, NPQ, qP, Fv'/Fm', and Fv/Fm, as well as MDA, had the top six highest factor load capacities (Table 1). These six traits closely correlated ($P< 0.01$); MDA correlated positively with NPQ and negatively with the other four traits (Supplementary Figure 1). Chl a and Chl b had the top two highest factor load capacities in the second principal component (Table 1).

The relative drought tolerance reflected by the D values of the other 11 traits for each genotype were calculated according to the trait relative value (Supplementary Table 4), and ranked by subordinate function (Table 2). Three genotypes, B-12-9-1, I-1-5-46, and I-1-5-63, with D values > 0.95, were the most drought tolerant genotypes. The other three genotypes, I-1-5-2, I-1-5-3, and I-1-5-53, with D values< 0.20, were the most drought-sensitive genotypes (Table 1). We then selected I-1-5-46 and I-1-5-2 as the DT and DS genotypes for further analysis.

Radial transport of water and nutrients in roots during water deficits

According to the composite transport model, radial water transport in plant roots can occur *via* apoplastic, symplastic and transcellular pathways (Kim et al., 2018; Kreszies et al., 2020). The radial water flow in plant roots is usually measured as hydraulic conductivity (Lp_r in m s^{-1} MPa^{-1}). The hydrostatic Lp_r (Lp_{hy}) determines the water flow through both the apoplastic and cell-to-cell pathways, and the osmotic Lp_r (Lp_{os}) represents

TABLE 1 Variance contribution of the top five principal components and factor load capacity.

Traits	Principal component				
	1	2	3	4	5
Chl a	0.542	0.726	-0.126	0.183	-0.125
Chl b	0.465	0.762	0.038	0.304	-0.068
Car	0.666	0.364	-0.157	-0.466	0.125
REC	-0.344	0.295	0.845	-0.100	0.203
MDA	-0.845	0.026	0.113	0.265	-0.058
Fv/Fm	0.743	-0.368	0.080	0.216	-0.303
NPQ	-0.846	0.294	-0.165	0.030	0.058
ETR	0.612	-0.175	-0.109	0.323	0.684
qP	0.832	-0.117	0.324	-0.111	-0.111
ΦPSII	0.911	0.024	-0.012	-0.222	0.053
Fv'/Fm'	0.824	-0.197	0.182	0.268	-0.076
Eigen value	5.630	1.634	0.953	0.708	0.664
Variance contribution (%)	51.178	14.859	8.663	6.438	6.039
Cumulative contribution (%)	51.178	66.037	74.700	81.138	87.177

The data of the top five principal components were calculated based on the data shown in Supplementary Table 2. Car, carotenoid; Chl a, chlorophyll a; Chl b, chlorophyll b; ETR, electron transport rate, Fv/Fm, PS II maximum photochemical quantum yield; Fv'/Fm', PSII effective photochemistry quanta output; MDA, malondialdehyde content; NPC, non-photochemical quenching coefficient; qP, photochemical quenching coefficient; REC, relative conductivity rate; ΦPSII, quantum yield of PSII electron transport.

the water transport across the cell-to-cell pathway (Steudle, 2000; Kreszies et al., 2018). The ratios of Lp_{hy} to Lp_{os} indicate which pathway contributes more to the overall water transport across the root (Steudle and Peterson, 1998; Kreszies et al., 2018). Here, Lp_{hy} was higher in DS than in DT, whereas the trend of Lp_{os} was the opposite under non-stress conditions. Under osmotic stress, Lp_{hy} did not significantly differ between DS and DT, Lp_{os} was higher in DS than in DT, and Lp_{os} increased in DS but Lp_{hy} decreased in DT (Table 3). The ratio of Lp_{hy} to Lp_{os} was higher in control DS, but osmotic stress significantly decreased it to< 1 (Table 3).

The fluorescent dye, PTS, is a tracer for the apoplastic pathway translocation of solutes as it does not cross cell membranes or adhere to cell walls (Yeo et al., 1987; Faiyue et al., 2010b; Wang et al., 2020a). Therefore, we investigated the apoplastic bypass flow of solutes in *E. sibiricus* using this dye. In the absence of osmotic stress, the shoot PTS concentration was significantly higher in DS than in DT, indicating that DS possessed more apoplastic pathway radial transport of solutes than DT, which was consistent with the apoplastic transport of water (Table 3). Osmotic stress abolished apoplastic solute influx in both DT and DS (Figure 1).

We compared the mineral element profiles in shoots between DS and DT using ICP-MS. The concentrations of B, Na, Mg, K, Ca, Mn and Zn were significantly higher in DS than in DT under either control or osmotic stress conditions. However, the concentrations of Ni, Cu, and Al were lower in DS than in DT (Figure 2; Supplementary Table 5). Osmotic stress induced the accumulation of B, Mg, K, Ca, Mn, Fe, and Cu in shoots of DT and DS but increased the concentration of Ni and Al only in DT. Osmotic stress reduced Na accumulation in DT and Zn accumulation in DS (Figure 2; Supplementary Table 5).

Root morphology and anatomy

We investigated the effects of PEG-induced osmotic stress on the root morphology and architecture of DT and DS to determine why root radial transport of water and mineral nutrients differed between the genotypes (Figures 3A–G). The results showed that DT had a larger root surface area, more root forks, and a higher root fractal dimension than DS under control conditions (Figures 3E–G). Osmotic stress reduced the seminal root length in DS but not in DT (Figure 3C), and decreased total root length and root forks in DT, but not in DS (Figure 3A, F). The average diameter of seminal roots and the root fractal dimension were significantly higher in DT than in DS under osmotic stress (Figures 3D, G).

We assessed the development of CS and SL in roots by histochemical staining. Both the CS and SL were obvious in the endodermis, but not in the hypodermis, even at 60% of the total root length from the tip, under osmotic stress either in DT or DS (Supplementary Figure 2). Therefore, when grown

TABLE 2 Comprehensive evaluation through subordinate functions of 52 *Elymus sibiricus* genotypes.

	Subordinate function value												
ID	**Chl a**	**Chl b**	**Car**	**REC**	**MDA**	**Fv/Fm**	**NPQ**	**ETR**	**qP**	**ΦPSⅡ**	**Fv'/Fm'**	**D Values**	**Rank**
B-12-9-1	0.93	0.91	1.00	0.98	1.00	0.93	0.99	0.98	0.99	0.98	0.95	0.97	1
I-1-5-46	0.96	0.81	0.96	0.98	1.00	0.96	0.99	0.96	1.00	1.00	0.93	0.96	2
I-1-5-63	0.93	0.91	0.96	0.99	0.97	0.90	1.00	0.95	0.99	0.97	0.96	0.96	3
14-091	0.90	0.82	0.75	0.93	0.61	0.67	0.94	0.59	0.76	0.71	1.00	0.79	4
10-5	0.90	0.96	0.79	0.80	0.66	0.68	0.91	0.35	0.87	0.63	0.69	0.75	5
09-152	0.75	0.29	0.87	0.98	0.68	0.76	0.95	0.62	0.73	0.67	0.90	0.75	6
I-1-5-60	1.00	1.00	0.36	0.98	0.65	0.61	0.94	0.60	0.72	0.57	0.62	0.73	7
I-1-5-39	0.55	0.54	0.96	0.91	0.68	0.68	0.94	0.76	0.81	0.57	0.63	0.73	8
09-280	0.79	0.95	0.89	0.57	0.62	0.88	0.95	0.40	0.75	0.57	0.58	0.72	9
I-1-5-49	0.98	0.58	0.53	0.89	0.69	0.81	0.94	0.50	0.60	0.53	0.89	0.72	10
08-129	0.65	0.57	0.70	0.86	0.48	0.84	0.89	0.79	0.83	0.55	0.70	0.71	11
09-244	0.26	0.67	0.98	0.79	0.65	0.81	0.86	0.34	0.87	0.64	0.86	0.70	12
I-1-5-23	0.87	0.85	0.84	0.70	0.45	0.68	0.94	0.54	0.52	0.54	0.79	0.70	13
I-1-5-25	0.72	0.86	0.48	0.72	0.51	0.85	0.94	0.50	0.95	0.43	0.74	0.70	14
09-183	0.76	0.44	0.80	0.99	0.68	0.81	0.93	0.21	0.76	0.59	0.68	0.70	15
I-1-5-66	0.77	0.42	0.95	1.00	0.85	0.61	0.76	0.33	0.63	0.63	0.61	0.69	16
I-1-5-42	0.94	0.79	0.59	0.65	0.68	0.69	0.93	0.48	0.64	0.55	0.48	0.67	17
I-5-14	0.45	0.71	0.49	0.97	0.66	0.66	0.93	0.68	0.67	0.57	0.61	0.67	18
SWUN 2	0.54	0.49	0.97	0.48	0.82	0.68	0.88	0.80	0.61	0.55	0.52	0.67	19
09-055	0.20	0.26	0.71	0.93	0.62	0.85	0.94	0.62	0.66	0.64	0.89	0.67	20
I-1-5-45	0.61	1.00	0.53	0.24	0.67	0.68	0.86	0.68	0.68	0.55	0.76	0.66	21
I-1-5-61	0.43	0.86	0.35	0.52	0.65	0.73	0.77	0.83	0.68	0.55	0.87	0.66	22
11-14	0.52	0.30	0.85	0.62	0.57	0.61	0.94	0.88	0.69	0.64	0.58	0.65	23
09-089	0.94	0.91	0.84	0.51	0.60	0.13	0.65	0.40	0.83	0.63	0.62	0.64	24
I-1-5-67	0.32	0.37	0.56	0.82	0.68	0.57	0.94	0.70	0.84	0.62	0.64	0.64	25
I-1-4-12	0.32	0.65	0.51	0.77	0.53	1.00	0.94	0.17	0.87	0.51	0.78	0.64	26
14-16-2	0.39	0.32	0.95	0.87	0.62	0.67	0.92	0.37	0.70	0.62	0.60	0.64	27
I-1-5-50	0.29	0.23	0.54	0.92	0.69	0.75	0.85	0.64	0.80	0.62	0.70	0.64	28
I-5-2-9	0.91	0.64	0.49	0.51	0.60	0.61	0.72	0.49	0.68	0.58	0.78	0.64	29
I-1-5-30	0.63	0.42	0.52	0.88	0.67	0.66	0.87	0.65	0.64	0.51	0.55	0.64	30
I-1-5-21	0.07	0.50	0.68	0.84	0.45	0.62	0.95	1.00	0.61	0.45	0.78	0.63	31
I-1-4-1	0.60	0.62	0.35	0.63	0.48	0.75	0.93	0.68	0.61	0.48	0.80	0.63	32
09-149	0.14	0.22	0.69	0.91	0.64	0.35	0.92	0.79	0.76	0.61	0.65	0.61	33
09-083	0.55	0.35	0.61	0.37	0.61	0.65	0.94	0.34	0.83	0.59	0.83	0.61	34
09-124	0.48	0.78	0.57	0.30	0.66	0.33	0.93	0.35	0.83	0.72	0.61	0.60	35
I-1-5-18	0.21	0.25	0.57	0.80	0.62	0.68	0.88	0.43	0.74	0.64	0.73	0.60	36
I-1-5-29	0.25	0.33	0.22	0.90	0.56	0.78	0.87	0.69	0.61	0.52	0.69	0.58	37
I-1-5-71	0.04	0.45	0.56	0.53	0.85	0.56	0.92	0.26	0.86	0.58	0.65	0.57	38
14-694	0.56	0.55	0.74	0.00	0.44	0.56	0.89	0.31	0.95	0.69	0.57	0.57	39
I-1-5-41	0.04	0.00	0.20	0.65	0.54	0.79	0.92	0.73	0.90	0.49	0.95	0.56	40
I-1-5-20	0.11	0.20	0.37	0.69	0.64	0.87	0.94	0.32	0.69	0.59	0.78	0.56	41
I-1-5-59	0.11	0.03	0.19	0.97	0.69	0.72	0.95	0.53	0.77	0.52	0.70	0.56	42
I-1-3-3	0.29	0.15	0.34	0.27	0.57	0.85	0.94	0.73	0.86	0.40	0.74	0.56	43
B-12-13-2	0.22	0.38	0.66	0.76	0.38	0.78	0.85	0.51	0.68	0.41	0.49	0.56	44
I-1-5-28	0.58	0.35	0.44	0.41	0.49	0.74	0.94	0.26	0.70	0.50	0.69	0.55	45
I-1-5-40	0.15	0.12	0.78	0.37	0.67	0.69	0.95	0.52	0.65	0.55	0.56	0.55	46
I-1-6-2	0.09	0.30	0.11	0.62	0.47	0.66	0.95	0.80	0.69	0.59	0.72	0.55	47

(Continued)

TABLE 2 Continued

Subordinate function value

ID	Chl a	Chl b	Car	REC	MDA	Fv/Fm	NPQ	ETR	qP	ΦPSⅡ	Fv'/Fm'	D Values	Rank
09-071	0.09	0.21	0.08	0.98	0.55	0.81	0.86	0.21	0.84	0.55	0.75	0.54	48
I-1-5-58	0.00	0.04	0.43	1.00	0.69	0.69	0.94	0.37	0.53	0.58	0.36	0.51	49
I-1-5-53	0.21	0.31	0.13	0.37	0.28	0.16	0.00	0.13	0.20	0.00	0.25	0.19	50
I-1-5-3	0.08	0.22	0.09	0.64	0.07	0.00	0.16	0.06	0.19	0.04	0.00	0.14	51
I-1-5-2	0.06	0.19	0.00	0.60	0.00	0.07	0.19	0.00	0.00	0.12	0.03	0.11	52

Car, carotenoid; Chl a, chlorophyll a; Chl b, chlorophyll b; D values, drought resistance values; ETR, electron transport rate; Fm, maximal fluorescence; Fo, minimal fluorescence; Fv/Fm, PS II, maximum photochemical quantum yield; Fv'/Fm', PSII effective photochemistry quanta output; MDA, malondialdehyde content; NPC, non-photochemical quenching coefficient; qP, photochemical quenching coefficient; REC, relative conductivity rate; ΦPSII, quantum yield of PSII electron transport.

hydroponically, seminal roots of *E. sibiricus* did not develop an exodermis, even under osmotic stress.

No CS was found at 12% of the root length in control and osmotic-stressed plants of both genotypes (Figure 4) and at 24% of the root length in the control DS. The first appearance of a weak "dot-like" CS signal in the control DS was found at 36% of the root length, and at 48%, a fully-formed CS appeared in many endodermal cells in the control DS (Figure 4A). Of note, a fully-formed CS continuously lines the entire radial wall of an endodermal cell, rather than having an initial dot-like structure (Kreszies et al., 2019; Li et al., 2020). The DS did not develop a complete CS even at 60% of the root length under control conditions (Figure 4A). The osmotically stressed DS developed a complete CS from 24% of the root length (Figure 4B). A fully-formed CS appeared in some endodermal cells at 24% of the root length in DT, and the CS was well-developed at 60% of the root length, with no obvious difference in DT between control and water-deficient conditions (Figures 4C, D).

The developmental trend of the SL was very similar (Figure 5). The SL was not detectable at 12% of the root length in all plants. Patchy development of the SL was evident at 48% and 60% of the root length in the control DS (Figure 5A). The osmotically stressed DS had a patchy SL at 24% and 36%, and a well-developed SL at 48% and 60% of the root length. Very few endodermal cells without an SL were taken as passage cells (Figure 5B). A patchy SL was visible from 24%–48% along the main axis of the roots in control DT and detectable at 24%–36% of the root length in osmotically stressed DT. The SL was fully deposited at 48% and 60% of the root length in DT plants treated with PEG and was completely formed in control DT at 60% (Figures 5C, D).

Chemical analysis of suberin of *Elymus sibiricus* in response to osmotic stress

Suberin monomer contents were analyzed to further determine differences between DT and DS in terms of root apoplastic barriers under control and osmotic stress conditions. The monomer classes in *E. sibiricus* aliphatic suberin comprised unsubstituted fatty acids (UFAs), α,ω-dicarboxylic acids (DCAs), and ω-OH acids. The most abundant aliphatic suberin monomers were UFAs and ω-OH acids. The chain lengths of the aliphatic suberin monomers varied from C16 to C24. The aromatic suberin monomer in *E. sibiricus* root comprised a series of different substance classes, namely vanillin (VA), salicylic (SAs), coumaric (CAs), and ferulic (FeAs) acids, of which FeAs and CAs were the most abundant aromatic components (Figure 6A). Aromatic suberin accounted for 76%–83% of the total suberin content (Figure 6A), which is consistent with that in other Gramineae species, such as rice and barley (Kreszies et al., 2018).

The abundance of all suberin monomers was significantly higher in DT than in DS (Figures 6A, B). The total suberin

TABLE 3 Hydrostatic and osmotic hydraulic conductivity (Lp_r) in drought-tolerant (DT) and drought-sensitive (DS) genotypes grown under control or osmotic stress conditions.

Parameters	DS		DT	
	control	20% PEG	control	20% PEG
Hydrostatic Lp_r (Lp_{hy}) (10^{-8} m·s^{-1}·Mpa^{-1})	3.39 ± 1.60a	1.75 ± 0.5ab	1.56 ± 0.34b	0.92 ± 0.53b
Osmotic Lp_r (Lp_{os}) (10^{-8} m·s^{-1}·Mpa^{-1})	1.89 ± 0.51b	2.88 ± 0.53a	2.96 ± 0.27a	1.70 ± 0.69b
Hydrostatic/Osmotic (Lp_{hy}/Lp_{os})	1.89 ± 0.50a	0.62 ± 0.13b	0.53 ± 0.05b	0.61 ± 0.24b

Mean values of Lp_{hy} and Lp_{os} were calculated for the total root systems of individual plants. Results are given as mean with standard deviation (SD) of five independent replicates (n = 5). Different letters indicate significant differences at $P < 0.05$ based on one-way analysis of variance (ANOVA) (Fisher's Duncan test).

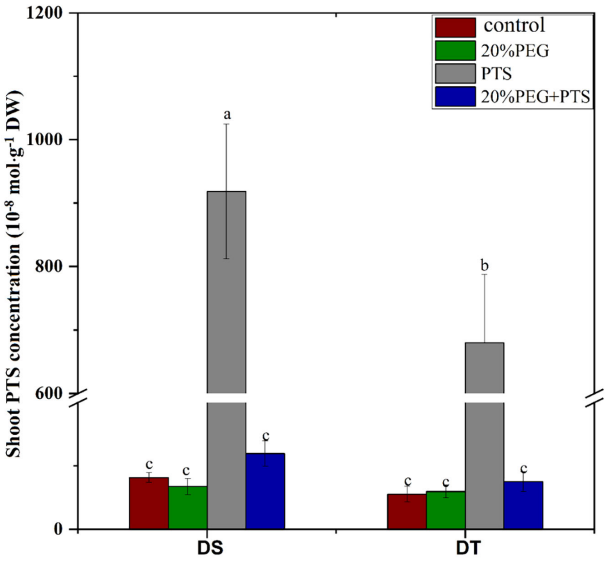

FIGURE 1
Trisodium-8-hydroxy-1,3,6-pyrenetrisulfonic acid (PTS) concentration in shoots of drought-tolerant (DT) and drought-sensitive (DS) genotypes grown under control or osmotic stress conditions. Plants were treated with 0.2 mM PTS or 0.2 mM PTS plus 20% (w/v) PEG 6000 for 72 h. Treatment without PTS was used as the negative control. Values are the mean ± standard deviation (SD) (n = 5). Different letters indicate significant differences at $P < 0.05$ based on one-way analysis of variance (ANOVA) (Fisher's Duncan test). DW, dry weight.

content was ~ 135% and 144% higher in DT than that in DS under control and osmotic stress conditions, respectively. Osmotic stress increased the suberin contents in DS and DT plants by ~ 35% and 41%, respectively, compared with controls (Figure 6C). Nevertheless, osmotic stress induction did not compensate for the lower suberin content in DS compared with DT (Figures 6A, B). Osmotic stress induced significant amounts of suberin, which closely corresponded with the histochemical staining results for SL in DS, but not in DT (Figure 5).

Expression of genes associated with apoplastic barriers

The relative expression of eight genes related to apoplastic barriers in roots were investigated by qRT-PCR. Among them, four each that were respectively associated with CS formation and suberin monomer synthesis comprised *MYB36*, *SHR1* (also regulates root suberization), *PER64*, and *CASP* (Naseer et al., 2012; Hosmani et al., 2013; Kamiya et al., 2015; Wang et al., 2020b; Wang et al., 2022a; Xu et al., 2022), and *MYB41*, *CYP86A1*, *KCS20*, and *FAR1* (Höfer et al., 2008; Lee et al., 2009; Domergue et al., 2010; Kosma et al., 2014; Shukla et al., 2021). Osmotic stress increased the expression of *PER64* in DS (24 h), downregulated that of *MYB36*, *SHR1*, and *CASP* to varying degrees in DS, and only slightly affected that of the four genes related to CS formation in DT (Figures 7A–D). Osmotic stress for 24 increased the expression of *KCS20* and *FAR1* and decreased that of *MYB41* in DS. Osmotic stress for 3 h downregulated transcription of the four genes associated with suberin synthesis in DS, whereas that for either 3 or 24 h induced their expression in DT (Figures 7E–H).

Discussion

Roots absorb water from soil, sense water deficits in dry soil, and transduce signals during water deficits. Water flow in roots, which is usually measured as Lp_r, varies according to growth conditions (Baxter et al., 2009; Wang et al., 2020a). Here, we selected drought-tolerant (I-1-5-46) and sensitive (I-1-5-2) *E. sibiricus* genotypes *via* a comprehensive evaluation and compared their differential root response mechanisms to drought. We found significantly lower overall water flow and lower apoplastic bypass flow of solutes, in DT, than in DS, in the absence of PEG 6000. Water and solutes were absorbed exclusively *via* the cell-to-cell pathway in response to osmotic stress (Table 3, Figure 1). The CS and SL are important barriers affecting apoplastic bypass flow of water and solutes in roots, and thus potentially play roles in abiotic stress tolerance, such as drought (Hose et al., 2001; Geldner, 2013; Wang et al., 2022a). In *Arabidopsis*, the *cyp86a1/horst* mutant, with a deficiency of aliphatic suberin, has increased Lp_{hy}, Lp_{os}, and Lp_{hy}/Lp_{os}, suggesting that aliphatic suberin plays a role in limiting water flow through the apoplastic and transcellular pathway

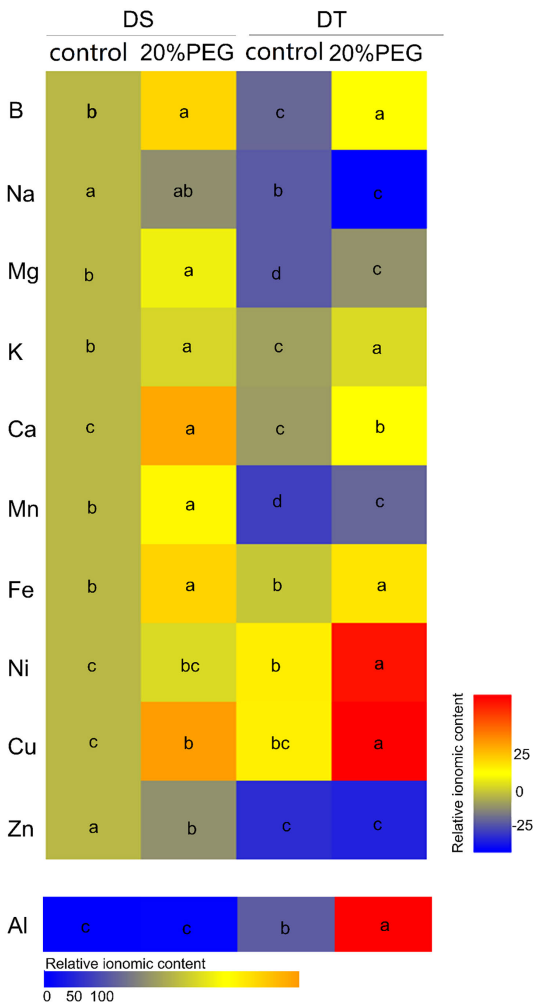

FIGURE 2
Mineral elemental accumulation in shoots of drought-tolerant (DT) and drought-sensitive (DS) genotypes grown under control or osmotic stress conditions. Mineral elemental concentrations were determined using inductively coupled plasma mass spectrometry (ICP-MS). Results are presented relative to the control DS values calculated from numeric values presented in Supplementary Table 5. Different letters indicate significant differences at $P < 0.05$ based on one-way analysis of variance (ANOVA) (Fisher's Duncan test).

(Ranathunge et al., 2011b). Most radial water uptake in barley occurs through weakly suberized younger roots (Ranathunge et al., 2017). Our histochemical, root hydraulic conductivity and PTS tracer findings precisely corresponded. The DT plants developed a CS and SL closer to the root tips and contained more abundant suberin monomer contents than DS in the absence of osmotic stress (Figures 4–6). The proportion of apoplastic bypass flow was higher in DS when endodermal barriers were not completely established. However, the deposition of barriers in the zone near the root tip largely blocked apoplastic water uptake, and the cell-to-cell pathway became the dominant transport route for root water uptake. A similar phenomenon has been found in barley (Kreszies et al., 2020). The Lp_{os} notably increased in DS in response to osmotic stress, which might be a compensation strategy associated with enhanced aquaporin activity and might represent an adaptative mechanism of *E. sibiricus* to ensure sufficient water uptake under osmotic stress. Water uptake *via* the cell-to-cell pathway mainly depends on plasma membrane aquaporins (Grondin et al., 2016). The contribution of this pathway to water uptake can be reversibly regulated by rapidly modulating the activity of aquaporins in barley roots (Kaneko et al., 2015). The decrease in Lp_{os} in osmotically stressed DT plants might be interpreted as thickened SL deposits blocking endodermal cell walls, thus reducing water uptake through transcellular pathways. Variations in suberin monomer arrangements and their microstructure in different cultivars might contribute to water movement in roots (Tao et al., 2017). More in-depth investigation into these aspects of cell physiology and ultrastructural observations are needed. Like water transport,

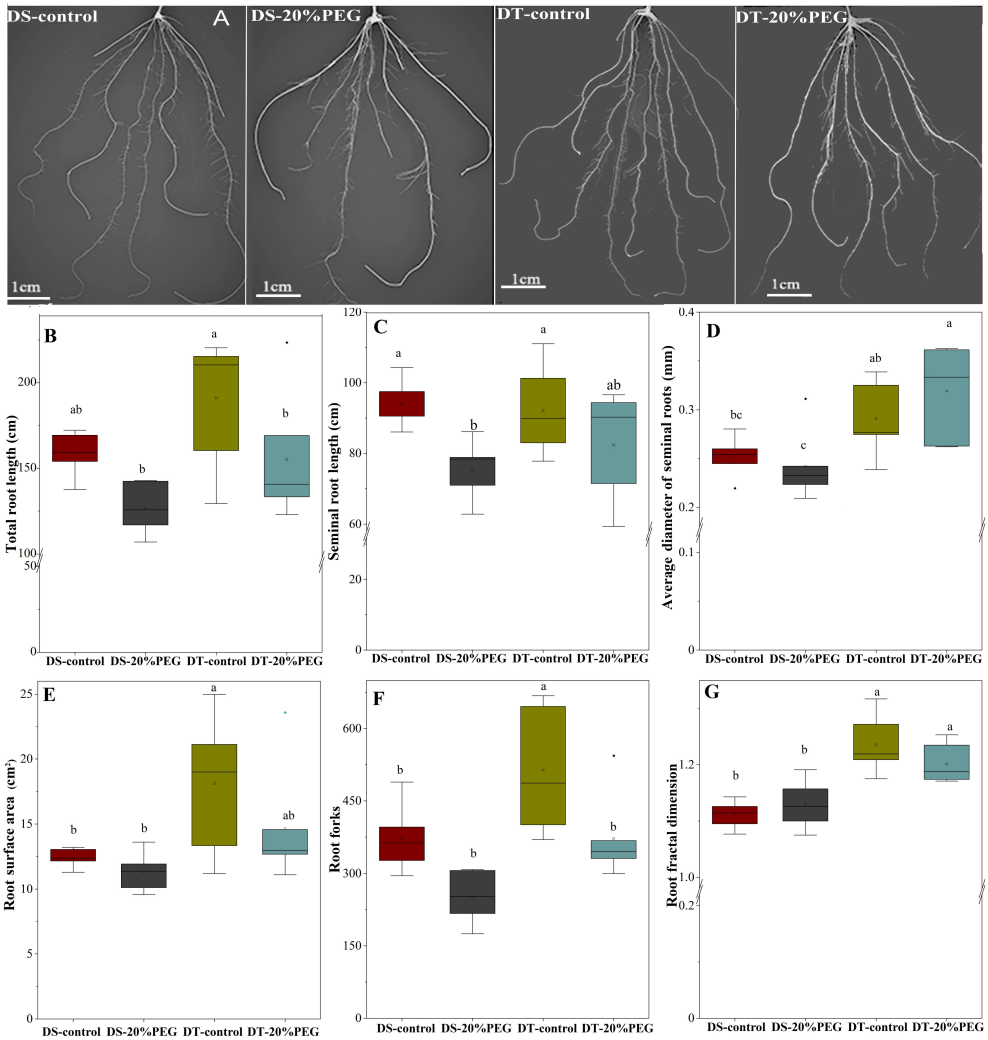

FIGURE 3
Root morphology and architecture of drought-tolerant (DT) and drought-sensitive (DS) genotypes grown under control or osmotic stress conditions. **(A)** Root images. **(B)** Total root length. **(C)** Seminal root length. **(D)** Average diameter of seminal roots. **(E)** Root surface area. **(F)** Root forks. **(G)** Root fractal dimension. All values represent the roots of each plant and are shown as mean with standard deviation (SD) of five independent replicates (n = 5). Different letters indicate significant differences at $P < 0.05$ based on one-way analysis of variance (ANOVA) (Fisher's Duncan test).

the radial transport of solutes in roots under osmotic stress relied on the cell-to-cell pathway. This was compatible with previous findings that PEG reduces bypass flow in rice (Yeo et al., 1999; Faiyue, 2010a).

Suberized cell walls in the endodermis/exodermis of roots form transport barriers to water and solutes (Peterson and Cholewa, 1998). In fact, suberization of the endodermis/exodermis is characterized by CS and SL deposition. The endodermis is not distinguished from the cortex before differentiation, whereas the exodermis is formed *via* specialization of the hypodermis (Barberon et al., 2016; Doblas et al., 2017). We found here that *E. sibiricus* did not develop an exodermis under normal conditions and even under osmotic stress (Supplementary Figure 2). This is consistent with the findings in *Arabidopsis* and barley but differ from that in other gramineous plants, such as rice, maize, and sheepgrass (*Leymus chinensis*), which develop a strong exodermis in response to stress (Schreiber et al., 2005; Kreszies et al., 2018; Kreszies et al., 2019; Li et al., 2020). *Elymus sibiricus* is currently the only known species among forage grasses that does not develop an exodermis, which might make it a good model for investigating endodermal barriers without interference from the outer parts of roots. A fraction of seminal roots in one wild barley accession (*Hordeum vulgare* spp. *spontaneum*) is induced to form a lignified and suberized exodermis in response to osmotic stress (Kreszies et al., 2018). Moreover, the wetland barley species,

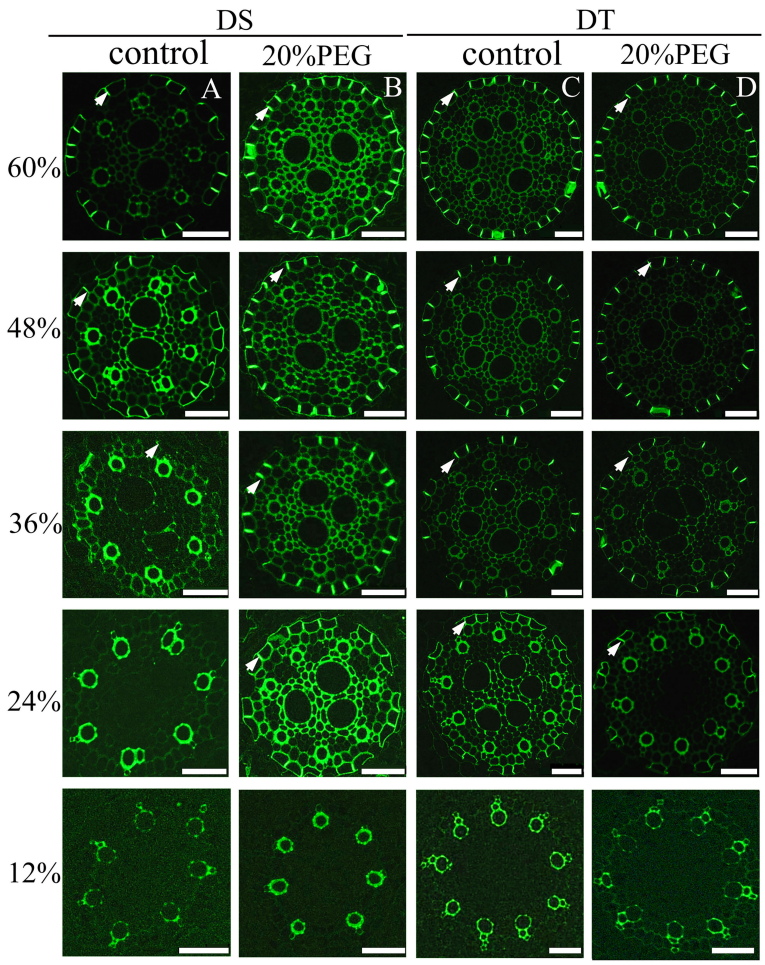

FIGURE 4
Fluorescence staining of Casparian strip (CS) in seminal roots of drought-tolerant (DT) and drought-sensitive (DS) genotypes grown under control or osmotic stress conditions. CS in seminal roots were stained with berberine hemisulfate for control DS **(A)**, osmotic-stressed DS **(B)**, control DT **(C)**, and osmotic-stressed DT **(D)**. Green fluorescent spots (white arrow) indicate the CS. Numbers on the vertical axis represent the distance from the tip as a percentage of the total root length (scale bars, 42.5 μm).

Hordeum marinum, generally forms and reinforces an exodermis to prevent radial oxygen loss when grown under stagnant conditions (Kotula et al., 2017). Whether *E. sibiricus* could form an exodermis in response to other stresses, such as salt, waterlogging, or cold, remains unknown. However, these grass plants that can survive and grow in such harsh environments for long periods might have better adaptive potential than their cultivated relatives.

Osmotic stress enhances suberization but not lignification in barley (Kreszies et al., 2018). Chronic drought increases root suberin content but does not alter its lamellar structure in *Arabidopsis* (de Silva et al., 2021). The induction or strengthening of apoplastic barriers is also very pronounced when rice is exposed to salinity (Krishnamurthy et al., 2009) or stagnant deoxygenated conditions (Ranathunge et al., 2011a). Moreover, natural variations in salt tolerance (Krishnamurthy et al., 2009; Krishnamurthy et al., 2011) and Cd accumulation (Qi et al., 2020) between rice cultivars have been attributed to differences in root apoplastic barriers. Here, the responses of the CS and SL to osmotic stress differed between genotypes of *E. sibiricus*, which is the first such finding in forage grasses. The suberin contents were higher under non-stressed conditions in DT, than in DS induced by osmotic stress. We speculated that the development of a precocious endodermal barrier under non-stress conditions, to cope with possible adverse environmental factors, might be an important survival strategy of DT plants. We found that osmotic stress induced the CS and SL of DS to form closer to root tips, whereas their development in DT was not obviously changed by water deficits (Figures 4, 5). However, osmotic stress indeed increased suberin contents in DT. Therefore, the reinforcement of suberization induced by osmotic stress in DT was likely manifested by an increase in the

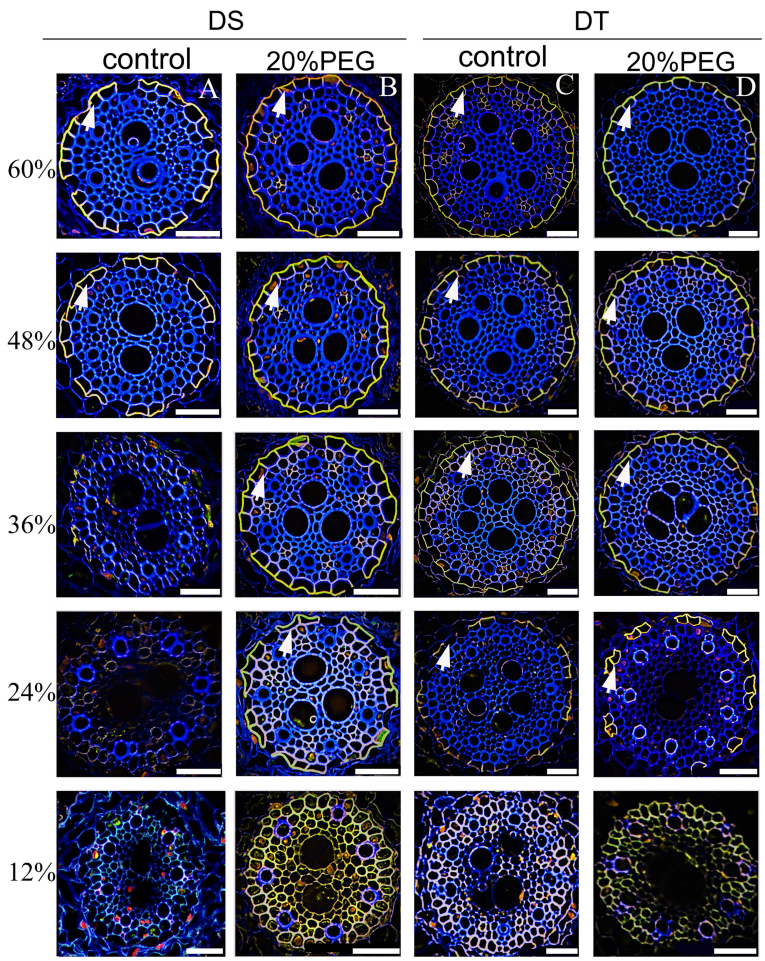

FIGURE 5
Fluorescence staining of suberin lamellae (SL) in seminal roots of drought-tolerant (DT) and drought-sensitive (DS) genotypes grown under control or osmotic stress conditions. The deposition of the SL in seminal roots was visualized by staining with Fluorol Yellow 088 for control DS **(A)**, osmotic-stressed DS **(B)**, control DS **(C)**, and osmotic-stressed DT **(D)**. The yellow fluorescent rings (white arrow) indicate the SL. Numbers on the vertical axis represent the distance from the tip as a percentage of the total root length (scale bars, 42.5 μm).

thickness of the SL. However, this notion requires further verification by transmission electron microscopy. Such thickening of the CS has also been identified in response to salt stress in several plant species (Karahara et al., 2004; Prathumyot and Ehara, 2010; Al Kharusi et al., 2019; Cui et al., 2021; Wang et al., 2022b). The establishment of apoplastic barriers in lateral roots provides another explanation for the gap between observations based on the SL in seminal roots and the total root suberin contents in DT. An auxin-induced process requires the local breaking and resealing of endodermal apoplastic barriers during lateral root emergence in *Arabidopsis* (Ursache et al., 2021). However, our qRT-PCR data did not correspond to the structure and composition results (Figure 7). Considering that root apoplastic barriers are both involved in root development and induced by stress responses, the expression of related genes in different zones of the root was very different (Wang et al., 2019). Further detailed investigation is needed to address this.

Although the CS and SL in the root endodermis have been described as tight barriers blocking the non-selective apoplastic transport of solutes and water (Geldner, 2013; Nawrath et al., 2013), the CS or SL might participate in the selective uptake of mineral elements in *Arabidopsis* and rice (Baxter et al., 2009; Barberon et al., 2016; Wang et al., 2019; Cohen et al., 2020; Wang et al., 2022). Suberization also shows nutrient-induced plasticity, and regulated by hormones such as abscisic acid, ethylene, and

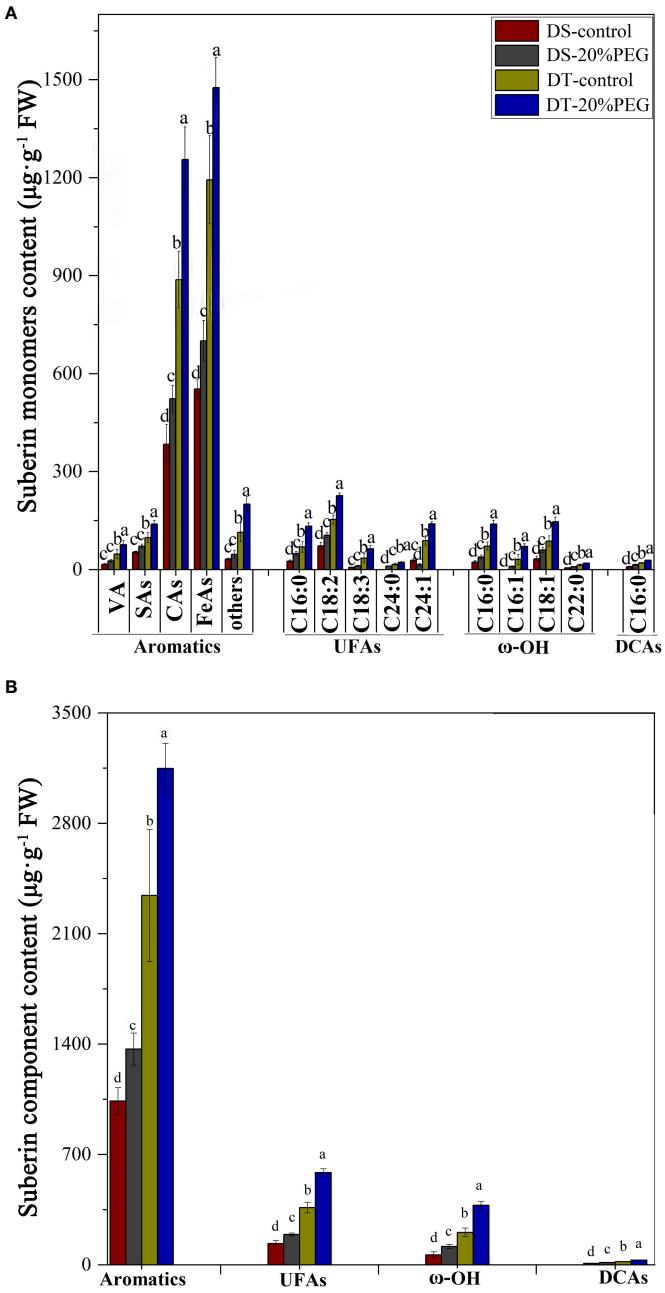

FIGURE 6
Amount of suberin in roots detected in drought-tolerant (DT) and drought-sensitive (DS) genotypes grown under control or osmotic stress conditions. **(A)** Amount of all detected monomers of suberin in roots. The substance classes of aromatic components include vanillin (VA), salicylic acids (SAs), coumaric acids (CAs), ferulic acids (FeAs), and others; the substance classes of aliphatic components included unsubstituted fatty acids (UFAs), ω-hydroxy acids (ω-OH), and α,ω-dicarboxylic acids (DCAs). **(B)** Amounts of major substance classes of suberin. Absolute amounts of suberin are shown as mean values in $\mu g \cdot g^{-1}$ fresh weight (FW) ± the standard deviation (SD) of four biological replicates (n = 4). Different letters indicate significant differences at $P < 0.05$ based on one-way analysis of variance (ANOVA) (Fisher's Duncan test).

auxin (Barberon et al., 2016; Ursache et al., 2021). Here, DT plants developed stronger apoplastic barriers and accumulated less Na, Mg, Mn, and Zn and more Ni, Cu, and Al than DS, regardless of osmotic stress (Figure 6). Whether this phenomenon is closely associated with the formation of the CS and SL remains unclear, but these results provide ideas for further investigation of the exact roles of apoplastic barriers in the selective uptake of mineral elements in grass plants.

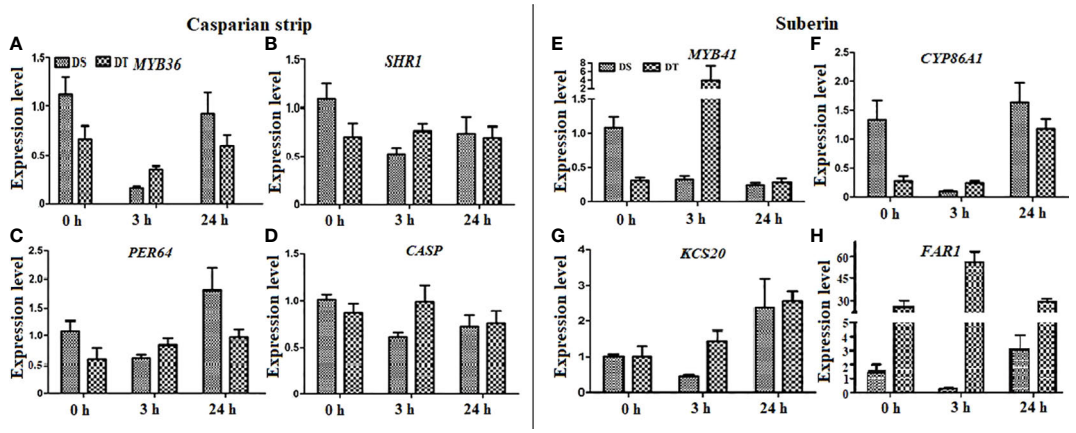

FIGURE 7
Expression levels of apoplastic barrier-related genes in drought-tolerant (DT) and drought-sensitive (DS) genotypes under osmotic stress conditions.Twenty-eight-day-old seedlings were subjected to 20% (w/v) PEG 6000 treatment for 0, 3, and 24 h. **(A–D)** Expression levels of Casparian strip-related genes. **(E–H)** Expression levels of suberin-related genes. *DnaJ* was used as a reference gene, and the relative expression levels of all genes were assessed using qRT-PCR. Values are mean ± standard deviation (SD) (n = 3).

Furthermore, the present study found that except for Na and Zn, most of the mineral elements accumulated more in leaves under osmotic stress conditions in both DT and DS (Figure 6), suggesting a potential role for endodermal barriers in preventing mineral nutrient reflux to the soil under osmotic stress.

Root morphology and architecture play a pivotal role in plant drought responses (Bengough et al., 2011; Kreszies et al., 2019). Our results suggested that reduced lateral root formation, rather than total seminal root length, differentiates DT from DS when adapting to a water deficit (Figure 3). This result differs from the findings of a comparative study of barley and wild barley, which showed that wild barley always had longer seminal roots, regardless of osmotic stress (Kreszies et al., 2020). Furthermore, longer and thicker seminal roots, more lateral roots, and more complex root systems developed in DT than in DS plants. This suggested a genetically fixed developmental trend and a stronger drought response strategy in DT to uptake water in deeper and wider soil areas. Although our experiments proceeded under artificial hydroponic conditions.

Conclusions

We identified DT and DS *E. sibiricus* genotypes among 52 genotypes based on an evaluation of drought tolerance. The root apoplastic bypass flow of water and solutes, as well as mineral nutrient accumulation differed between DT and DS. In addition, *E. sibiricus* roots did not form an exodermis, endodermal barriers (CS and SL) were more developed, and more suberin monomers were deposited in DT than DS plants. Osmotic stress induced the formation of barriers closer to the root tip in DS, but possibly increased their thickness in DT. Our results suggested that the establishment of a complete apoplastic barrier in the endodermis facilitates drought tolerance of *E. sibiricus*. Apoplastic barriers might also contribute to natural variations in drought tolerance between the studied genotypes. The beneficial traits of DT (I-1-5-46) could be selected for future breeding programs to develop more drought tolerant crops and forage.

Data availability statement

The original contributions presented in the study are included in the article/Supplementary Material. Further inquiries can be directed to the corresponding author.

Author contributions

PeW conceived and designed the experiments. QZ and PeW provided experimental materials and chemical reagents. XL, PiW, YA, YH, and YZ implemented experiments and analyzed data. PeW and XL drafted the manuscript. C-MW and PeW reviewed and improved the manuscript. All authors have read and approved the published version of the manuscript.

Funding

This study was supported by grants from the National Natural Science Foundation of China (31802122) and the Fundamental Research Funds for the Central Universities (ZYN2022018).

Acknowledgments

We thank Wahap Isac (Servicebio) for technical assistance with the histochemical detection of Casparian strips and suberin lamellae. We thank Editage (www.editage.cn) for English language editing.

Conflict of interest

The authors declare that the research was conducted in the absence of any commercial or financial relationships that could be construed as a potential conflict of interest.

Publisher's note

All claims expressed in this article are solely those of the authors and do not necessarily represent those of their affiliated organizations, or those of the publisher, the editors and the reviewers. Any product that may be evaluated in this article, or claim that may be made by its manufacturer, is not guaranteed or endorsed by the publisher.

Supplementary material

The Supplementary Material for this article can be found online at: https://www.frontiersin.org/articles/10.3389/fpls.2022.1007494/full#supplementary-material

References

Adler, J., and Parmryd, I. (2010). Quantifying colocalization by correlation: the Pearson correlation coefficient is superior to the mander's overlap coefficient. *Cytom. Part A.* 77, 733–742. doi: 10.1002/cyto.a.20896

Al Kharusi, L., Sunkar, R., Al-Yahyai, R., and Yaish, M. W. (2019). Comparative water relations of two contrasting date palm genotypes under salinity. *Int. J. Agron.* 2019, 4262013. doi: 10.1155/2019/4262013

Barberon, M. (2017). The endodermis as a checkpoint for nutrients. *New Phytol.* 213 (4), 1604–1610. doi: 10.1111/nph.14140

Barberon, M., Vermeer, J. E. M., Bellis, D. D., Wang, P., Naseer, S., Andersen, T. G., et al. (2016). Adaptation of root function by nutrient-induced plasticity of endodermal differentiation. *Cell.* 164, 447–459. doi: 10.1016/j.cell.2015.12.021

Baxter, I., Hosmani, P. S., Rus, A., Lahner, B., Borevitz, J. O., Muthukumar, B., et al. (2009). Root suberin forms an extracellular barrier that affects water relations and mineral nutrition in arabidopsis. *PloS Genet.* 5, e1000492. doi: 10.1371/journal.pgen.1000492

Bengough, A. G., McKenzie, B. M., Hallett, P. D., and Valentine, T. A. (2011). Root elongation, water stress, and mechanical impedance: a review of limiting stresses and beneficial root tip traits. *J. Exp. Bot.* 62, 59–68. doi: 10.1093/jxb/erq350

Bernards, M. A. (2002). Demystifying suberin. *Can. J. Bot.* 80 (3), 227–240. doi: 10.1139/b02-017

Bhusal, N., Lee, M., Lee, H., Adhikari, A., Han, A. R., Han, A., et al. (2021). Evaluation of morphological, physiological, and biochemical traits for assessing drought resistance in eleven tree species. *Sci. Total Environ.* 779, 146466. doi: 10.1016/j.scitotenv.2021.146466

Brundrett, M. C., Enstone, D. E., and Peterson, C. A. (1988). A berberine-aniline blue fluorescent staining procedure for suberin, lignin, and callose in plant tissue. *Protoplasma.* 146, 133–142. doi: 10.1007/BF01405922

Campilho, A., Nieminen, K., and Ragni, L. (2020). The development of the periderm: the final frontier between a plant and its environment. *Curr. Opin. Plant Biol.* 53, 10–14. doi: 10.1016/j.pbi.2019.08.008

Chaumont, F., and Tyerman, S. D. (2014). Aquaporins: highly regulated channels controlling plant water relations. *Plant Physiol.* 164, 1600–1618. doi: 10.1104/pp.113.233791

Cohen, H., Fedyuk, V., Wang, C., Wu, S., and Aharoni, A. (2020). Suberman regulates developmental suberization of the arabidopsis root endodermis. *Plant J.* 102, 431–447. doi: 10.1111/tpj.14711

Cui, B., Liu, R., Flowers, T. J., and Song, J. (2021). Casparian bands and suberin lamellae: Key targets for breeding salt tolerant crops? *Environ. Exp. Bot.* 191, 104600. doi: 10.1016/j.envexpbot.2021.104600

de Silva, N., Murmu, J., Chabot, D., Hubbard, K., Ryser, P., Molina, I., et al. (2021). Root suberin plays important roles in reducing water loss and sodium uptake in *Arabidopsis thaliana*. *Metabolites.* 11, 735. doi: 10.3390/metabo11110735

Doblas, V. G., Geldner, N., and Barberon, M. (2017). The endodermis, a tightly controlled barrier for nutrients. *Curr. Opin. Plant Biol.* 39, 136–143. doi: 10.1016/j.pbi.2017.06.010

Domergue, F., Vishwanath, S. J., Joubès, J., Ono, J., Lee, J. A., Bourdon, M., et al. (2010). Three arabidopsis fatty acyl-coenzyme a reductases, FAR1, FAR4, and FAR5, generate primary fatty alcohols associated with suberin deposition. *Plant Physiol.* 153 (4), 1539–1554. doi: 10.1104/pp.110.158238

Enstone, D. E., Peterson, C. A., and Ma, F. (2002). Root endodermis and exodermis: structure, function, and responses to the environment. *J. Plant Growth Regul.* 21, 335–351. doi: 10.1007/s00344-003-0002-2

Faiyue, B., Al-Azzawi, M. J., and Flowers, T. J. (2010b). The role of lateral roots in bypass flow in rice (*Oryza sativa* l.). *Plant Cell Environ.* 33 (5), 702–716. doi: 10.1111/j.1365-3040.2009.02078.x

Feng,, T., Wu, P., Gao, H., Kosma, D. K., Jenks, M. A., Lü, S., et al. (2022). Natural variation in root suberization is associated with local environment in Arabidopsis thaliana. *New Phytol, in press.* doi: 10.1111/nph.18341

Faiyue, B., Vijayalakshmi, C., Nawaz, S., Nagato, Y., Taketa, S., Ichii, M., et al. (2010a). Studies on sodium bypass flow in lateral rootless mutants *lrt1* and *lrt2*, and crown rootless mutant *crl1* of rice (*Oryza sativa* l.). *Plant Cell Environ.* 33 (5), 687–701. doi: 10.1111/j.1365-3040.2009.02077.x

Geldner, N. (2013). The endodermis. *Annu. Rev. Plant Biol.* 64, 531–558. doi: 10.1146/annurev-arplant-050312-120050

Grondin, A., Mauleon, R., Vadez, V., and Henry, A. (2016). Root aquaporins contribute to whole plant water fluxes under drought stress in rice (*Oryza sativa* l.). *Plant Cell Environ.* 39 (2), 347–365. doi: 10.1111/pce.12616

Gupta, A., Rico-Medina, A., and Caño-Delgado, A. I. (2020). The physiology of plant responses to drought. *Science.* 368, 266–269. doi: 10.1126/science.aaz7614

Höfer, R., Briesen, I., Beck, M., Pinot, F., Schreiber, L., and Franke, R. (2008). The arabidopsis cytochrome P450 *CYP86A1* encodes a fatty acid ω-hydroxylase involved in suberin monomer biosynthesis. *J. Exp. Bot.* 59 (9), 2347–2360. doi: 10.1093/jxb/ern101

Hose, E., Clarkson, D. T., Steudle, E., Schreiber, L., and Hartung, W. (2001). The exodermis: a variable apoplastic barrier. *J. Exp. Bot.* 52, 2245–2264. doi: 10.1093/jexbot/52.365.2245

Hosmani, P. S., Kamiya, T., Danku, J., Naseer, S., Geldner, N., Guerinot, M. L., et al. (2013). Dirigent domain-containing protein is part of the machinery required for formation of the lignin-based casparian strip in the root. *Proc. Natl. Acad. Sci. U.S.A.* 110, 14498–14503. doi: 10.1073/pnas.1308412110

Jenkin, S., and Molina, I. (2015). Isolation and compositional analysis of plant cuticle lipid polyester monomers. *J. Vis. Exp.* 105, e53386. doi: 10.3791/53386

Kamiya, T., Borghi, M., Wang, P., Danku, J. M., Kalmbach, L., Hosmani, P. S., et al. (2015). The MYB36 transcription factor orchestrates casparian strip formation. *Proc. Natl. Acad. Sci. U.S.A.* 112, 10533–10538. doi: 10.1073/pnas.1507691112

Kaneko, T., Horie, T., Nakahara, Y., Tsuji, N., Shibasaka, M., and Katsuhara, M. (2015). Dynamic regulation of the root hydraulic conductivity of barley plants in response to salinity/osmotic stress. *Plant Cell Physiol.* 56, 875–882. doi: 10.1093/pcp/pcv013

Karahara, I., Ikeda, A., Kondo, T., and Uetake, Y. (2004). Development of the casparian strip in primary roots of maize under salt stress. *Planta.* 219, 41–47. doi: 10.1007/s00425-004-1208-7

Kim, Y. X., Ranathunge, K., Lee, S., Lee, Y., Lee, D., and Sung, J. (2018). Composite transport model and water and solute transport across plant roots: an update. *Front. Plant Sci.* 9. doi: 10.3389/fpls.2018.00193

Kosma, D. K., Murmu, J., Razeq, F. M., Santos, P., Bourgault, R., Molina, I., et al. (2014). AtMYB41 activates ectopic suberin synthesis and assembly in multiple plant species and cell types. *Plant J.* 80 (2), 216–229. doi: 10.1111/tpj.12624

Kotula, L., Schreiber, L., Colmer, T. D., and Nakazono, M. (2017). Anatomical and biochemical characterisation of a barrier to radial O_2 loss in adventitious roots of two contrasting *Hordeum marinum* accessions. *Funct. Plant Biol.* 44, 845–857. doi: 10.1071/FP16327

Kreszies, T., Eggels, S., Kreszies, V., Osthoff, A., Shellakkutti, N., Baldauf, J. A., et al. (2020). Seminal roots of wild and cultivated barley differentially respond to osmotic stress in gene expression, suberization, and hydraulic conductivity. *Plant Cell Environ.* 43 (2), 344–357. doi: 10.1111/pce.13675

Kreszies, T., Schreiber, L., and Ranathunge, K. (2018). Suberized transport barriers in arabidopsis, barley and rice roots: from the model plant to crop species. *J. Plant Physiol.* 227, 75–83. doi: 10.1016/j.jplph.2018.02.002

Kreszies, T., Shellakkutti, N., Osthoff, A., Yu, P., Baldauf, J. A., Zeisler-Diehl, V. V., et al. (2019). Osmotic stress enhances suberization of apoplastic barriers in barley seminal roots: analysis of chemical, transcriptomic and physiological responses. *New Phytol.* 221 (1), 180–194. doi: 10.1111/nph.15351

Krishnamurthy, P., Ranathunge, K., Franke, R., Prakash, H. S., Schreiber, L., and Mathew, M. K. (2009). The role of root apoplastic transport barriers in salt tolerance of rice (*Oryza sativa* l.). *Planta.* 230, 119–134. doi: 10.1007/s00425-009-0930-6

Krishnamurthy, P., Ranathunge, K., Nayak, S., Schreiber, L., and Mathew, M. K. (2011). Root apoplastic barriers block na^+ transport to shoots in rice (*Oryza sativa* l.). *J. Exp. Bot.* 62 (12), 4215–4228. doi: 10.1093/jxb/err135

Lee, S. B., Jung, S. J., Go, Y. S., Kim, H. U., Kim, J. K., Cho, H. J., et al. (2009). Two arabidopsis β-ketoacyl CoA synthase genes, *KCS20* and *KCS2/DAISY*, are functionally redundant in cuticular wax and root suberin biosynthesis, but differentially controlled by osmotic stress. *Plant J.* 60 (3), 462–475. doi: 10.1111/j.1365-313X.2009.03973.x

Lian, H. L., Yu, X., Lane, D., Sun, W. N., Tang, Z. C., and Su, W. A. (2006). Upland rice and lowland rice exhibited different PIP expression under water deficit and ABA treatment. *Cell Res.* 16, 651–660. doi: 10.1038/sj.cr.7310068

Li, L., Pan, S., Melzer, R., and Fricke, W. (2020). Apoplastic barriers, aquaporin gene expression and root and cell hydraulic conductivity in phosphate-limited sheepgrass plants. *Physiol. Plant* 168 (1), 118–132. doi: 10.1111/ppl.12981

Liu, W., Zhang, Z., Chen, S., Ma, L., Wang, H., Dong, R., et al. (2016). Global transcriptome profiling analysis reveals insight into saliva-responsive genes in alfalfa. *Plant Cell Rep.* 35 (3), 561–571. doi: 10.1007/s00299-015-1903-9

Lux, A., Morita, S., Abe, J., and Ito, K. (2005). An improved method for clearing and staining free-hand sections and whole-mount samples. *Ann. Bot.* 96, 989–996. doi: 10.1093/aob/mci266

Ma, X., Chen, S. Y., Zhang, X. Q., Bai, S. Q., and Zhang, C. B. (2012). Assessment of worldwide genetic diversity of Siberian wildrye (*Elymus sibiricus* l.) germplasm based on gliadin analysis. *Molecules.* 17, 4424–4434. doi: 10.3390/molecules17044424

Martinka, M., Dolan, L., Pernas, M., Abe, J., and Lux, A. (2012). Endodermal cell-cell contact is required for the spatial control of casparian band development in *Arabidopsis thaliana*. *Ann. Bot.* 110, 361–371. doi: 10.1093/aob/mcs110

Naseer, S., Lee, Y., Lapierre, C., Franke, R., Nawrath, C., and Geldner, N. (2012). Casparian strip diffusion barrier in arabidopsis is made of a lignin polymer without suberin. *Proc. Natl. Acad. Sci. U.S.A.* 109, 10101–10106. doi: 10.1073/pnas.1205726109

Nawrath, C., Schreiber, L., Franke, R. B., Geldner, N., Reina-Pinto, J. J., and Kunst, L. (2013). Apoplastic diffusion barriers in arabidopsis. *Arabidopsis Book.* 11, e0167. doi: 10.1199/tab.0167

Niu, S. Q., Li, H. R., Paul, W., Aziz, M., Wang, S. M., Shi, H., et al. (2016). Induced growth promotion and higher salt tolerance in the halophyte grass *Puccinellia tenuiflora* by beneficial rhizobacteria. *Plant Soil.* 407 (1-2), 1–14. doi: 10.1007/s11104-015-2767-z

Passioura, J. (2007). The drought environment: physical, biological and agricultural perspectives. *J. Exp. Bot.* 58 (2), 113–117. doi: 10.1093/jxb/erl212

Peterson, C. A., and Cholewa, E. (1998). Structural modifications of the apoplast and their potential impact on ion uptake. (Proceeding of the German society of plant nutrition, Kiel, Germany). *Z. Pflanzenernahrung und Bodenkunde.* 161, 521–531. doi: 10.1093/insilicoplants/diab038

Pollard, M., Beisson, F., Li, Y., and Ohlrogge, J. B. (2008). Building lipid barriers: biosynthesis of cutin and suberin. *Trends Plant Sci.* 13, 236–246. doi: 10.1016/j.tplants.2008.03.003

Prathumyot, W., and Ehara, H. (2010). Identification of casparian strip in roots of *Metroxylon sagu*, a salt-resistant palm. *J. Plant Physiol.* 54, 91–97. doi: 10.11248/jsta.54.91

Qi, X., Tam, N. F., Li, W. C., and Ye, Z. (2020). The role of root apoplastic barriers in cadmium translocation and accumulation in cultivars of rice (*Oryza sativa* l.) with different cd-accumulating characteristics. *Environ. Pollut.* 264, 114736. doi: 10.1016/j.envpol.2020.114736

Ranathunge, K., Kim, Y. X., Wassmann, F., Kreszies, T., Zeisler, V., and Schreiber, L. (2017). The composite water and solute transport of barley (Hordeum vulgare) roots: effect of suberized barriers. *Ann. Bot.* 119, 629–643. doi: 10.1093/aob/mcw252

Ranathunge, K., Lin, J., Steudle, E., and Schreiber, L. (2011a). Stagnant deoxygenated growth enhances root suberization and lignifications, but differentially affects water and NaCl permeabilities in rice (*Oryza sativa* l.) roots. *Plant Cell Environ.* 34, 1223–1240. doi: 10.1111/j.1365-3040.2011.02318.x

Ranathunge, K., Schreiber, L., and Franke, R. (2011b). Suberin research in the genomics era–new interest for an old polymer. *Plant Sci.* 180, 399–413. doi: 10.1016/j.plantsci.2010.11.003

Ranathunge, K., Steudle, E., and Lafitte, R. (2005). A new precipitation technique provides evidence for the permeability of casparian bands to ions in young roots of corn (*Zea mays* l.) and rice (*Oryza sativa* l.). *Plant Cell Environ.* 28 (11), 1450–1462. doi: 10.1111/j.1365-3040.2005.01391.x

Reddy, A. R., Chaitanya, K. V., and Vivekanandan, M. (2004). Drought-induced responses of photosynthesis and antioxidant metabolism in higher plants. *J. Plant Physiol.* 161, 1189–1202. doi: 10.1016/j.jplph.2004.01.013

Rodríguez-Gamir, J., Xue, J., Clearwater, M. J., Meason, D. F., Clinton, P. W., and Domec, J. C. (2019). Aquaporin regulation in roots controls plant hydraulic conductance, stomatal conductance, and leaf water potential in pinus radiata under water stress. *Plant Cell Environ.* 42 (2), 717–729. doi: 10.1111/pce.13460

Schreiber, L., Franke, R., Hartmann, K. D., Ranathunge, K., and Steudle, E. (2005). The chemical composition of suberin in apoplastic barriers affects radial hydraulic conductivity differently in the roots of rice (*Oryza sativa* l. cv. IR64) and corn (*Zea mays* l. cv. helix). *J. Exp. Bot.* 56 (415), 1427–1436. doi: 10.1093/jxb/eri144

Schreiber, L., Hartmann, K., Skrabs, M., and Zeier, J. (1999). Apoplastic barriers in roots: chemical composition of endodermal and hypodermal cell walls. *J. Exp. Bot.* 50 (337), 1267–1280. doi: 10.1093/jexbot/50.337.1267

Shukla, V., Han, J. P., Cléard, F., Lefebvre-Legendre, L., Gully, K., Flis, P., et al. (2021). Suberin plasticity to developmental and exogenous cues is regulated by a set of MYB transcription factors. *P Natl. Acad. Sci.* 118 (39), e2101730011. doi: 10.1073/pnas.2101730118

Singh, V., Oosterom, E., Jordan, D., Messina, C., Cooper, M., and Hammer, G. (2010). Morphological and architectural development of root systems in sorghum and maize. *Plant Soil.* 333 (1), 287–299. doi: 10.1007/s11104-010-0343-0

Steudle, E. (2000). Water uptake by roots: effects of water deficit. *J. Exp. Bot.* 51, 1531–1542. doi: 10.1093/jexbot/51.350.1531

Steudle, E., and Peterson, C. A. (1998). How does water get through roots? *J. Exp. Bot.* 49, 775–788. doi: 10.1093/jexbot/49.322.775

Tao, Q., Jupa, R., Luo, J., Lux, A., Kováč, J., Wen, Y., et al. (2017). The apoplasmic pathway *via* the root apex and lateral roots contributes to cd hyperaccumulation in the hyperaccumulator *Sedum alfredii*. *J. Exp. Bot.* 68, 739–751. doi: 10.1093/jxb/erw453

Tsuda, M., and Tyree, M. T. (2000). Plant hydraulic conductance measured by the high pressure flow meter in crop plants. *J. Exp. Bot.* 51, 823–828. doi: 10.1093/jexbot/51.345.823

Ursache, R., Teixeira, C. D. J. V., Tendon, V. D., Gully, K., De Bellis, D., Schmid-Siegert, E., et al. (2021). GDSL-domain proteins have key roles in suberin polymerization and degradation. *Nat. Plants.* 7, 353–364. doi: 10.1038/s41477-021-00862-9

Vishwanath, S. J., Delude, C., Domergue, F., and Rowland, O. (2015). Suberin: biosynthesis, regulation, and polymer assembly of a protective extracellular barrier. *Plant Cell Rep.* 34 (4), 573–586. doi: 10.1007/s00299-014-1727-z

Wang, Y., Cao, Y., Liang, X., Zhuang, J., Wang, X., Qin, F., et al. (2022b). A dirigent family protein confers variation of casparian strip thickness and salt tolerance in maize. *Nat. Commun.* 13(1), 2222. doi: 10.1038/s41467-022-29809-0

Wang, P., Wang, C. M., Gao, L., Cui, Y. N., Yang, H. L., de Silva, N. D. G., et al. (2020a). Aliphatic suberin confers salt tolerance to arabidopsis by limiting na^+ influx, k^+ efflux and water backflow. *Plant Soil* 448, 603–620. doi: 10.1007/s11104-020-04464-w

Wang, C., Wang, H., Li, P., Li, H., Xu, C., Cohen, H., et al. (2020b). Developmental programs interact with abscisic acid to coordinate root suberization in arabidopsis. *Plant J.* 104 (1), 241–251. doi: 10.1111/tpj.14920

Wang, Z., Yamaji, N., Huang, S., Zhang, X., Shi, M., Fu, S., et al. (2019). OsCASP1 is required for casparian strip formation at endodermal cells of rice roots for selective uptake of mineral elements. *Plant Cell.* 31 (11), 2636–2648. doi: 10.1105/tpc.19.00296

Wang, Z., Zhang, B., Chen, Z., Wu, M., Chao, D., Wei, Q., et al. (2022a). Three OsMYB36 members redundantly regulate casparian strip formation at the root endodermis. *Plant Cell* 34(8):2948–2968. doi: 10.1093/plcell/koac140

Xie, W., Zhang, J., Zhao, X., Zhang, Z., and Wang, Y. (2017). Transcriptome profiling of *Elymus sibiricus*, an important forage grass in qinghai-Tibet plateau, reveals novel insights into candidate genes that potentially connected to seed shattering. *BMC Plant Biol.* 17 (1), 1–15. doi: 10.1186/s12870-017-1026-2

Xu, H., Liu, P., Wang, C., Wu, S., Dong, C., Lin, Q., et al. (2022). Transcriptional networks regulating suberin and lignin in endodermis link development and ABA response. *Plant Physiol. in press.* doi: 10.1093/plphys/kiac298

Yan, C., Song, S., Wang, W., Wang, C., Li, H., Wang, F., et al. (2020). Screening diverse soybean genotypes for drought tolerance by membership function value based on multiple traits and drought-tolerant coefficient of yield. *BMC Plant Biol.* 20, 321. doi: 10.1186/s12870-020-02519-9

Yeo, A. R., Flowers, S. A., Rao, G., Welfare, K., Senanayake, N., and Flowers, T. J. (1999). Silicon reduces sodium uptake in rice (*Oryza sativa* l.) in saline conditions and this is accounted for by a reduction in the transpirational bypass flow. *Plant Cell Environ.* 22, 559–565. doi: 10.1046/j.1365-3040.1999.00418.x

Yeo, A. R., Yeo, M. E., and Flowers, T. J. (1987). The contribution of an apoplastic pathway to sodium uptake by rice roots in saline conditions. *J. Exp. Bot.* 38, 1141–1153. doi: 10.1093/jxb/38.7.1141

Zeier, J., and Schreiber, L. (1997). Chemical composition of hypodermal and endodermal cell walls and xylem vessels isolated from *Clivia miniata* (identification of the biopolymers lignin and suberin). *Plant Physiol.* 113, 1223–1231. doi: 10.1104/pp.113.4.1223

Zhang, M. X., Bai, R., Nan, M., Ren, W., Wang, C. M., Shabala, S., et al. (2022). Evaluation of salt tolerance of oat cultivars and the mechanism of adaptation to salinity. *J. Plant Physiol.* 273, 153708. doi: 10.1016/j.jplph.2022.153708

Zhang, L., Merlin, I., Pascal, S., Bert, P. F., Domergue, F., and Gambetta, G. A. (2020). Drought activates MYB41 orthologs and induces suberization of grapevine fine roots. *Plant Direct.* 4, e0027. doi: 10.1002/pld3.278

Zhang, J., Xie, W., Yu, X., Zhang, Z., Zhao, Y., Wang, N., et al. (2019). Selection of suitable reference genes for RT-qPCR gene expression analysis in Siberian wild rye (*Elymus sibiricus*) under different experimental conditions. *Genes.* 10 (6), 451. doi: 10.3390/genes10060451

frontiers | Frontiers in Plant Science

TYPE Original Research
PUBLISHED 23 September 2022
DOI 10.3389/fpls.2022.982715

OPEN ACCESS

EDITED BY
Kehua Wang,
China Agricultural University, China

REVIEWED BY
Yi Han,
Anhui Agricultural University, China
Zhanqi Wang,
Huzhou University, China

*CORRESPONDENCE
Liebao Han
hanliebao@163.com

SPECIALTY SECTION
This article was submitted to Plant Abiotic Stress, a section of the journal Frontiers in Plant Science

RECEIVED 30 June 2022
ACCEPTED 29 August 2022
PUBLISHED 23 September 2022

CITATION
Li Y, Wang M, Guo T, Li S, Teng K, Dong D, Liu Z, Jia C, Chao Y and Han L (2022) Overexpression of *abscisic acid-insensitive gene ABI4* from *Medicago truncatula*, which could interact with ABA2, improved plant cold tolerance mediated by ABA signaling.
Front. Plant Sci. 13:982715.
doi: 10.3389/fpls.2022.982715

Overexpression of *abscisic acid-insensitive gene ABI4* from *Medicago truncatula*, which could interact with ABA2, improved plant cold tolerance mediated by ABA signaling

Yinruizhi Li[1], Mengdi Wang[1], Tao Guo[2], Shuwen Li[1], Ke Teng[3], Di Dong[1], Zhuocheng Liu[1], Chenyan Jia[4], Yuehui Chao[1] and Liebao Han[1]*

[1]Turfgrass Research Institute, College of Grassland Science, Beijing Forestry University, Beijing, China, [2]Chongqing Key Laboratory of Germplasm Innovation and Utilization of Native Plants, Chongqing Landscape and Gardening Research Institute, Chongqing, China, [3]Beijing Research and Development Center for Grass and Environment, Beijing Academy of Agriculture and Forestry Sciences, Beijing, China, [4]Inner Mongolia Mengcao Ecological Environment (Group) Co., Ltd., Hohhot, China

ABI4 is considered an important transcription factor with multiple regulatory functions involved in many biological events. However, its role in abiotic stresses, especially low-temperature-induced stress, is poorly understood. In this study, the *MtABI4* gene was derived from *M. truncatula*, a widely used forage grass. Analysis of subcellular localization indicated that ABI4 was localized in the nucleus. Identification of expression characteristics showed that *ABI4* was involved in the regulatory mechanisms of multiple hormones and could be induced by the low temperature. IP-MS assay revealed that MtABI4 protein could interact with xanthoxin dehydrogenase protein (ABA2). The two-hybrid yeast assay and the biomolecular fluorescence complementarity assay further supported this finding. Expression analysis demonstrated that overexpression of *MtABI4* induced an increase in *ABA2* gene expression both in *M. truncatula* and *Arabidopsis*, which in turn increased the ABA level in transgenic plants. In addition, the transgenic lines with the overexpression of *MtABI4* exhibited enhanced tolerance to low temperature, including lower malondialdehyde content, electrical conductivity, and cell membrane permeability, compared with the wide-type lines after being cultivated for 5 days in 4°C. Gene expression and enzyme activities of the antioxidant system assay revealed the increased activities of SOD, CAT, MDHAR, and GR, and higher ASA/DHA ratio and GSH/GSSG ratio in transgenic lines. Additionally, overexpression of *ABI4* also induced the expression of members of the Inducer of CBF expression genes (ICEs)-C-repeat binding transcription factor genes(CBFs)-Cold regulated genes (CORs) low-temperature response module. In summary, under low-temperature conditions, overexpression of *ABI4* could

enhance the content of endogenous ABA in plants through interactions with ABA2, which in turn reduced low-temperature damage in plants. This provides a new perspective for further understanding the molecular regulatory mechanism of plant response to low temperature and the improvement of plant cold tolerance.

KEYWORDS

ABI4, Medicago truncatula, cold tolerance, xanthoxin dehydrogenase, ABA

Introduction

abi4 abscisic acid-insensitive 4 was originally named after a series of ABA-insensitive mutants identified through a forward genetic screen (Finkelstein, 1994). In recent years, *ABI4* has been recognized as a core transcription factor with multiple regulatory functions, which is involved in many important biological events. For example, *ABI4* was associated with seed germination and seedling morphogenesis. The expression of *ABI4* gradually decreased with seed germination and seedling morphology (Shkolnik-Inbar and Bar-Zvi, 2011). Accordingly, overexpression of *ABI4* exacerbated the ABA-induced inhibition of seed germination in *Arabidopsis* (Finkelstein et al., 2011). *ABI4* also played some significant function in plastid/mitochondrial reverse signaling, especially acting as a downstream target of the *GUN1* in mediating the PGE pathway regulating plastid (Sun et al., 2011). Moreover, ABI4 was also involved in sugar signaling. Some studies showed that *ABI4* regulates the expression of the sugar-responsive gene by binding to CE1-like motif elements in the promoter region, such as the *ADP-glucose pyrophosphorylase large subunit ApL3* in the starch synthesis pathway and *precipitate branching enzyme SBE2.2* in the starch synthesis pathway (Bossi et al., 2009). *ABI4* affects lateral root production. *abi4* mutants increase lateral root density and length compared to the wild type, while their overexpression reduced lateral root production (Shkolnik-Inbar and Bar-Zvi, 2010).

Additionally, reactive oxygen species (ROS) are also involved in the ABI4-mediated reverse signaling pathway (León et al., 2012). Overall, ABI4 plays an integral role in plant growth, development, and response to adversity. Although in recent years studies have led to a certain understanding of the function of ABI4, its role remains incomplete, such as its regulatory mechanism in the low-temperature response.

Plant cold tolerance is a complex trait controlled by multiple genes, such as *COR*, *ICE*, *CBF*, and *GPAT*, which all play an important role in plant response to low-temperature stress and in improving cold tolerance (Zhu et al., 2019; Tang et al., 2020). In plants, the most widely studied low-temperature response signaling pathway is the CBF/DREB1 signaling pathway with the main upstream and downstream modules Inducer of CBF expression genes (ICEs)-C-repeat binding transcription factor genes (CBF)/DREB1s-Cold regulated genes (CORs). ICE1 binds to the promoter region of the *CBF* gene to activate the expression, thereby mediating cold tolerance in plants (Chinnusamy et al., 2007). Low-temperature signals do not directly regulate *ICE1* gene transcription, but the *E3 ligase HOS1* (*high osmotic expression1*) is involved in ICE1 ubiquitination and degradation via the 26S protease pathway, thereby affecting ICE1 protein stability (Shi et al., 2015). The activity of OST1 kinase (*open stomata1*) was found to be rapidly induced by low temperature, and ICE1 and activated OST1 interacted to phosphorylate ICE1 protein and improve its binding capacity to the *CBF3* promoter region and ICE1 stability (Ding et al., 2019), and it was also found that OST1 phosphorylated BTF3L and BTF3 and promoted their interaction with CBF (Ding et al., 2018). The Jas domains of JAZ1 and JAZ4 interacted with the C-terminal of the ICE1 protein and inhibited ICE1 activity in *A. mimosa*. When exposed to low-temperature stress, JAZ proteins were degraded by increased JA content activating JA signaling, thereby relieving the inhibitory effect of ICE1 by JAZ and improving low-temperature tolerance (Hu et al., 2013).

Low temperature triggers the change in the activity and content of hormones in plants, which in turn influence the metabolic processes of plant growth. Abscisic acid (ABA) as a natural hormone defending against the abiotic stresses, plays an important role in stresses such as low temperatures (Jiang and Zhang, 2002). There is a significant increase in ABA content in leaves of *Arabidopsis* and rice at low temperatures (Eremina et al., 2016). In addition, ABA reduces the water content of plants and promotes the accumulation of soluble sugars and total phenolic content, thus improving the cold resistance of plants (Yang et al., 2016). The first hormone found to be associated with cold resistance was gibberellin (GA), and studies have found that the expression of *CRT/DRE* transcription-related genes is associated with GAs. For example, studies on the relationship between *CBF1* and gibberellin have revealed that constitutive expression of *CBF1* reduces gibberellin activity (Chen et al., 2007). Salicylic acid (SA) content increases significantly under low-temperature conditions and is detrimental to plant growth if the xconcentration of SA is too high, while low concentrations of SA promote cell expansion

and growth (Klessig et al., 2018). Jasmonic acid (JA), a very important plant signaling molecule, can mediate the expression of those resistance genes, and JA interacts with CBF to regulate downstream cold-responsive genes, thereby enhancing cold tolerance in plants (Hu et al., 2017). Additionally, the increased JA content improves CAT, SOD, and APX activities, thereby enhancing plant cold tolerance (Campos et al., 2019).

There are fewer reports on the function of *ABI4* in the low-temperature response. Only one recent study was reviewed, showing that MdABI4 crosstalked jasmonic and abscisic acid signaling to regulate cold tolerance in apples (An et al., 2022). On the other hand, as a model plant of the legume family (Stacey et al., 2006), it is of great importance to investigate the low-temperature stress response genes of *M. truncatula* for exploring its cold tolerance mechanism and improving the cold tolerance ability, in agricultural production. It also has important implications for the study of other legumes. Therefore, in this study, the function and regulatory mechanisms of *MtABI4* in response to low temperature was characterized, aiming to lay the foundation for rapid breeding of cold-tolerance forage varieties of *M. truncatula* by means of genetic engineering.

Results

Molecular characterization and subcellular localization of MtABI4

Sequence analysis indicated that *MtABI4* possessed a complete coding region of 1,011 bp, encoding a polypeptide chain containing 336 amino acids with a predicted molecular weight of 37.8 kD. MtABI4 protein contained an AP2 DNA-binding domain, belonging to the AP2 superfamily (**Supplementary Figures 1A,B**). Homology and phylogenetic analysis showed that MtABI4 was more closely related to ABI4 from *Trifolium pratense*, and ABI4 with high homology from ten species all had three motifs and an AP2 domain (**Figure 1A**). SignalP predicted that MtABI4 had no signal peptide, and subcellular localization prediction showed that MtABI4 was an extracellular protein (**Supplementary Figures 1C,D**).

By observing the expression of an ABI4-GFP fusion protein in tobacco leaves, we found that ABI4 was localized in the nucleus, which was inconsistent with our previous prediction (**Figure 1B**).

MtABI4 gene responds to multiple hormones

To analyze the regulation mechanism of *MtABI4*, the upstream sequence of the gene, which was 2,000 bp in length, was obtained. Cis-acting elements analysis showed that the motifs enriched in the promoter region of *MtABI4* were widely involved in the abscisic acid responsiveness, anaerobic induction, auxin responsiveness, the MeJA-responsiveness, endosperm expression, low-temperature responsiveness, zein metabolism regulation, gibberellin-responsiveness, defense and stress responsiveness, salicylic acid responsiveness, and light response (**Figure 2A**), indicating that this gene may play a multifunctional role in response to multiple hormones and stress.

Based on this, wild-type plants were sprayed with the corresponding hormones and plant tissues were collected at different time points for analysis of the *MtABI4* gene response to these hormones. Quantitative fluorescence analysis indicated that the expression of *ABI4* was down-regulated under the treatment of IAA, 6-BA, GA, MEJA, and SA (**Figures 2C–G**). The difference was that *ABI4* had a rebound at 6 h under the treatment of 6-BA, and returned to the initial level at 12 h under the treatment of GA and IAA. In contrast to them, the expression level of *ABI4* showed an increasing trend under ABA treatment, with a down-regulation at 1 h and a peak at 9 h (**Figure 2H**). This would suggest that *ABI4* is indeed involved in the regulatory mechanisms of these hormones. In addition, tissue-specific expression analysis showed that the ABI4 gene possessed the highest expression in leaves, followed by fruits, and the lowest expression in seeds (**Figure 2B**).

MtABI4 improved the cold tolerance of the over-expressed transgenic plants

Considering that the promoter region of the *ABI4* gene contains a low-temperature element, the transgenic lines, and the wild type was incubated at 4°C for 5 days to investigate the role of the *ABI4* gene in the low-temperature response. Phenotypic observations showed that the plants all exhibited some degree of wilting, with the wild-type plants showing darker leaf color after low-temperature treatment (**Figure 3A**). The results of chloroplast pigment content measurements showed that chlorophyll a, chlorophyll b, chlorophyll, and carotenoids were slightly lower in the transgenic lines than in WT, but there were no significant changes in chloroplast pigment content in the individual lines, before and after the low-temperature treatment (**Figure 3B**). WT exhibited higher anthocyanin content than the transgenic strain after low-temperature treatment (**Figure 3C**). The wild-type and transgenic lines did not show significant differences in electrolytic leakage, membrane permeability, and malondialdehyde content before the low-temperature treatment, however, these indicators in WT showed a significant increase and were much greater than in the transgenic lines, after the low-temperature treatment (**Figures 3D,E**). These results suggested that the transgenic plants accumulated less anthocyanin and suffered less cell membrane damage under low-temperature conditions.

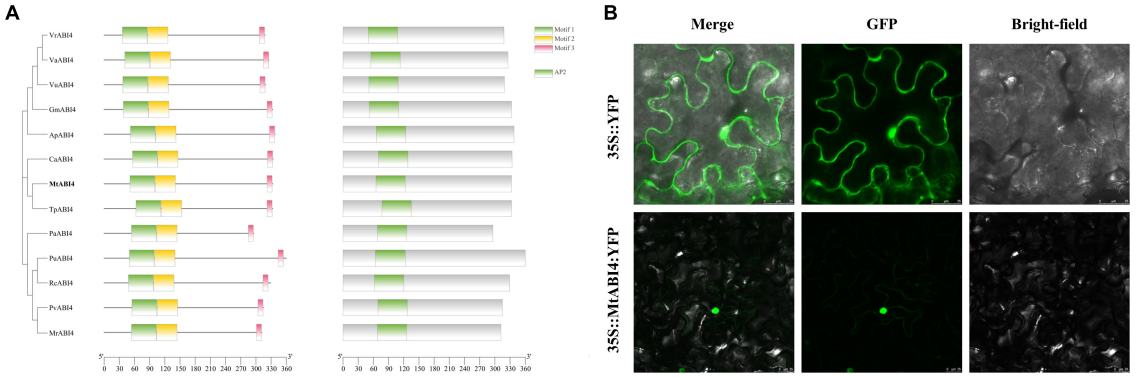

FIGURE 1
Phylogenetic tree, motif analysis, protein structural domains, and the subcellular localization of ABI4. In **(A)** different color blocks represent different motifs and structural domains. The scale bar represents the length of the amino acid sequence. **(B)** Represents the subcellular localization of ABI4.

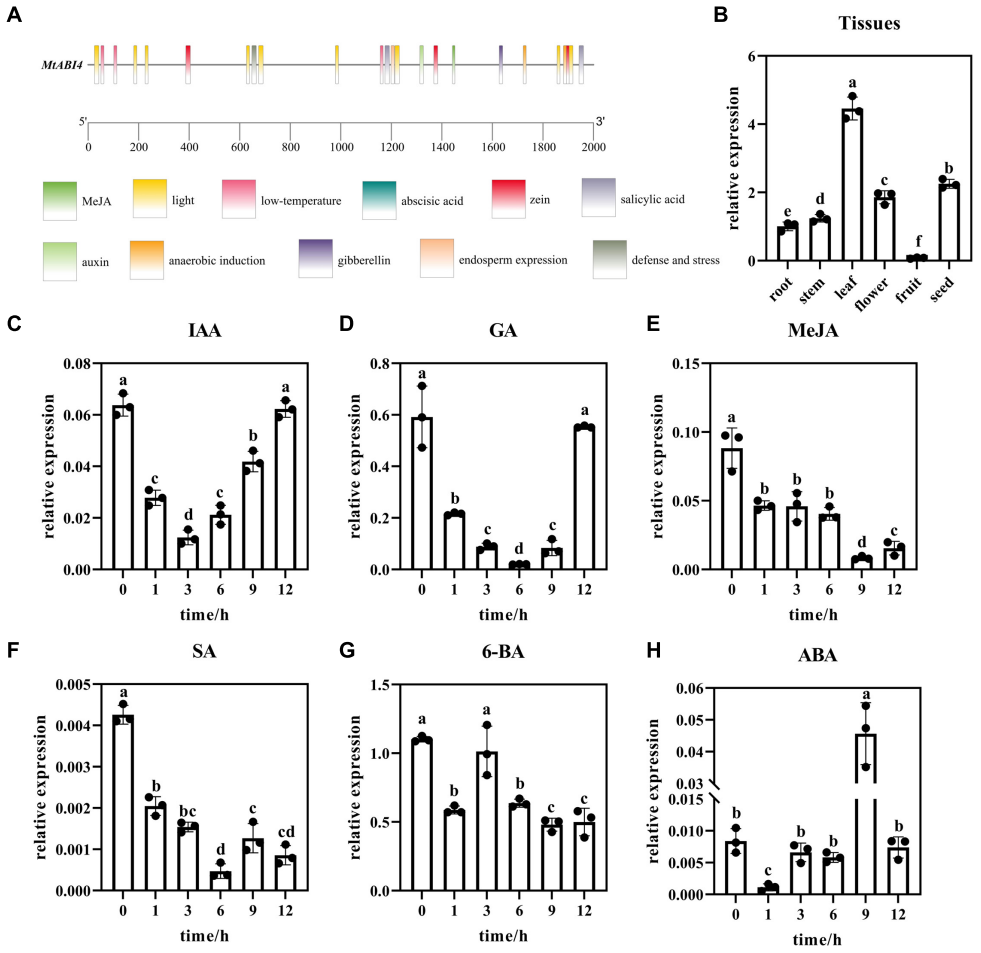

FIGURE 2
Cis-acting elements analysis and the expression patterns of *MtABI4* by qRT-PCR analysis. In graph panel **(A)**, different color blocks represent different cis-acting elements. The scale bar represents the length of the base sequence. Panel **(B)** represents the expression of *ABI4* in different tissues. Different letters in graphs indicate significant differences at $p \leq 0.05$. Panels **(C–H)** represents the expression of *ABI4* at different time points in response to IAA, GA, MeJA, SA, 6-BA, and ABA, respectively. The values are means ± SD ($n = 3$).

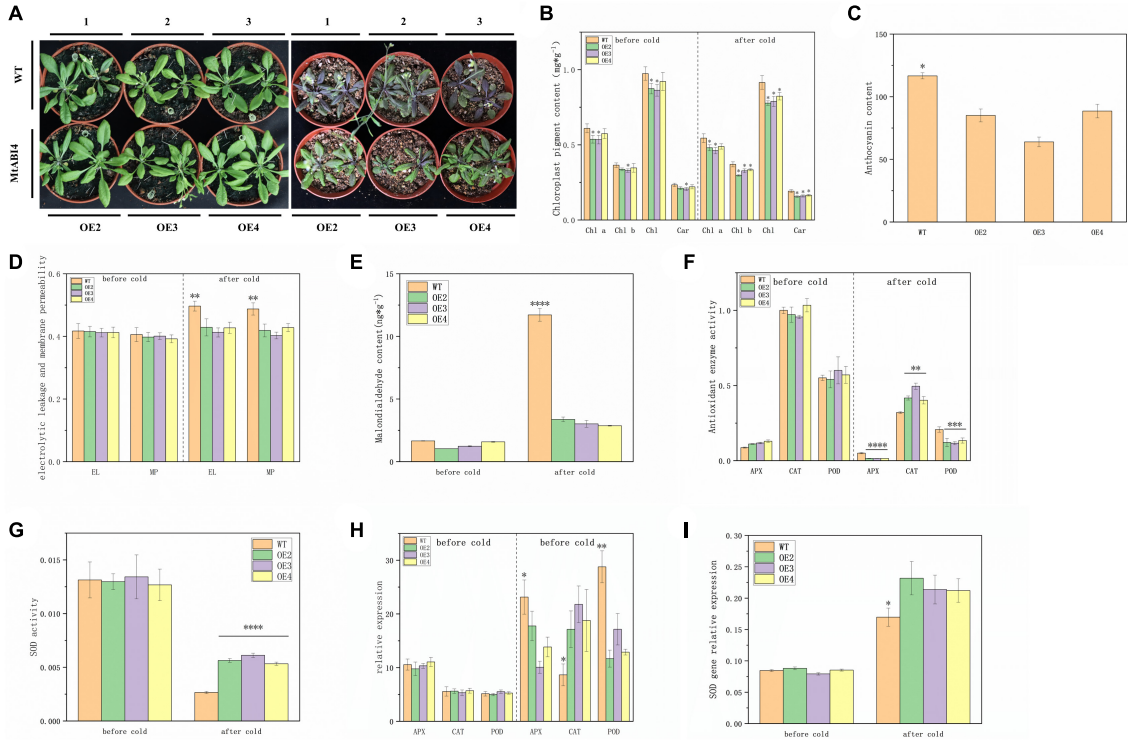

FIGURE 3
Plant growth status, physiological characteristics, and the expression of antioxidant enzyme genes at low temperatures. Panel **(A)** represents the growth condition of wild-type and transgenic plants before the low-temperature treatment and after the 5-day low-temperature treatment. Panels **(B–E)** represents the content of chloroplast pigments, anthocyanin, electrolytic leakage, membrane permeability, and malondialdehyde. Panels **(F,G)** represent the activity of APX, CAT, POD, and SOD. Panels **(H,I)** represent the expression of these antioxidant enzyme genes. The values are means ± SD (n = 3). *, in graphs, indicates significant differences in the means at $p < 0.05$ between each level in transgenic lines and WT plants, and **, ***, and ****, in graphs, indicate significant differences in the means at $p < 0.01$, $p < 0.001$, and $p < 0.0001$, respectively.

Analysis of antioxidant enzyme activities showed that there were no significant differences in APX, CAT, POD, and SOD contents between wild-type and transgenic lines before low-temperature treatment. These antioxidant enzyme activities decreased after low-temperature treatment, in both WT and transgenic lines. Among them, APX and POD activities were significantly lower in the transgenic lines than in the wild type, but the opposite was true for CAT and SOD (Figures 3F,G). The expression of the antioxidant enzyme genes also showed a similar profile to the enzyme activity, the only difference being that the expression of these genes showed an overall upregulation after low-temperature treatment (Figures 3H,I). These results suggested that overexpression of the ABI4 gene under low-temperature conditions affected gene expression and enzyme activity of these antioxidant enzymes.

As a major part of the non-enzymatic antioxidant system, the ASA-GSH cycle played an important role in the scavenging of reactive oxygen species and resistance to stresses in plants (Nahar et al., 2015). Corresponding compound content analysis indicated that the transgenic plants contained lower ASA and DHA, but higher ASA/DHA (Figures 4A–C). GSH, GSSG, and GSH/GSSG also exhibited similar trends (Figures 4D–F). This would suggest that there are lower levels of oxidation in transgenic plants. Meanwhile, the activities of MDHAR and GR in transgenic lines demonstrated a significant enhancement over those in WT, while the activity of DHAR showed no significant difference (Figures 4G–I). The expression of the *DHAR1* in transgenic plants was significantly upregulated compared to the WT, but there were no significant differences in MDHAR4 and GR1 (Figures 4J–L).

MtABI4 can affect the expression of the Inducer of CBF expression genes-C-repeat binding transcription factor genes-cold regulated genes module and some other low-temperature responsive genes

To further explore the regulation pattern of the *ABI4* response pathway to low temperature, the expression pattern of related genes was identified. The results showed that

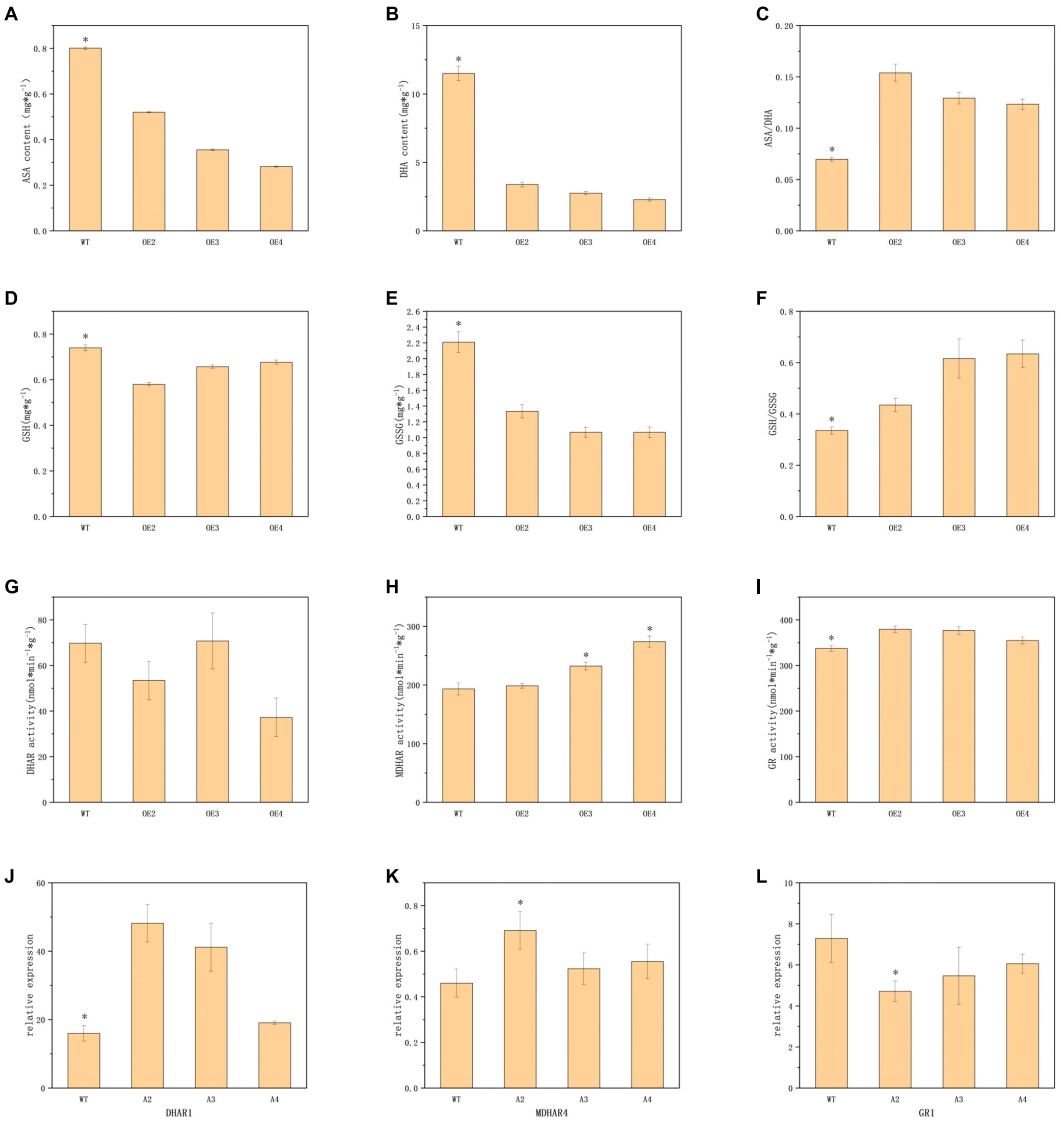

FIGURE 4
Determination of indicators related to non-enzymatic antioxidant systems. Panels **(A,B,D,E)** represents the content of ASA, DHA, GSH, and GSSG in turn. Panel **(C,F)** represents the ASA/DHA and GSH/GSSG ratio, respectively. Panels **(G–I)** represents the activities of DHAR, MDHAR, and GR. Panels **(J–L)** represents the relative expression of *DHAR1*, *MDHAR4*, and *GR1*. The values are means ± SD (n = 3). *, in graphs, indicates significant differences in the means at $p < 0.05$ between each level in transgenic lines and WT plants.

under room temperature conditions, the expression of *COR413*, *ICE1*, and *OST1* was significantly lower in transgenic plants than in WT, while the opposite was true for *CBF1*, *CBF2*, *CBF3*, and *CBF4* (Figures 5A–G). The expression of *RAV1* did not exhibit significant differences between the transgenic plants and WT (Figure 5H). This suggested that *MtABI4* can affect the expression of the COR-CBF-ICE module and *OST1*, however, the effect on RAV1 was not significant.

After low-temperature treatment, there was a significant increase in the expression of *COR413*, *CBF4*, *ICE1*, and *OST1* in all lines, compared to those before low-temperature treatment (Figures 5A,E,F,G). Among them, the expression of *COR413* and *OST1* was significantly higher in transgenic plants than in WT, in contrast to before treatment. In addition, the expression of *ICE1* remained higher in WT, and the expression of *CBF4* remained higher in transgenic plants. The expression of the remaining genes, including *CBF1*, *CBF2*, and *RAV1* was down-regulated both in the transgenic plants and WT after low-temperature treatment (Figures 5B,C,H). Among them, the transgenic plants exhibited a significantly higher expression of *CBF1* and *CBF2* than WT, while the expression of *RAV1* was higher in WT. This indicated that the roles of the COR-CBF-ICE module and *OST1* and *RAV1* in the molecular response

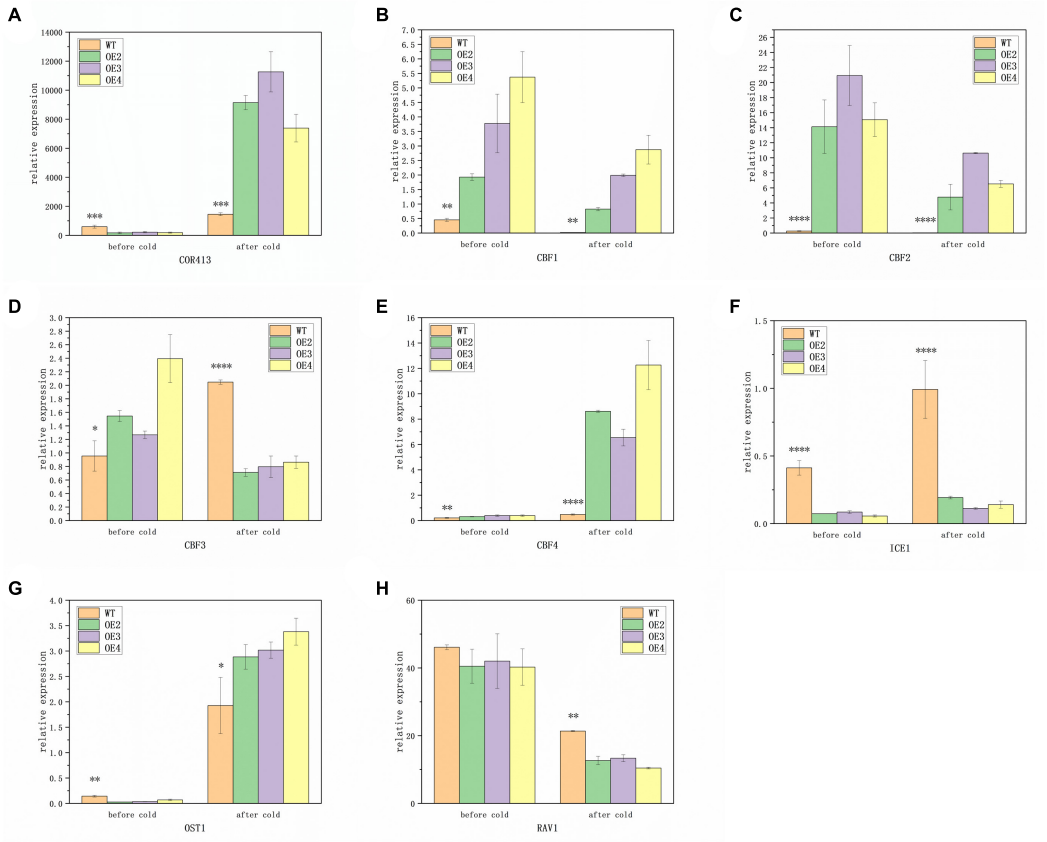

FIGURE 5
Expression patterns of genes responsive to low temperatures. **(A–H)** Represent the expression levels of *COR413*, *CBF1-4*, *ICE1*, *OST1*, and *RAV1*, in turn, under low temperatures. The values are means ± SD (n = 3). *, in graphs, indicates significant differences in the means at $p < 0.05$ between each level in transgenic lines and WT plants, and **, ***, and ****, in graphs, indicate significant differences in the means at $p < 0.01$, $p < 0.001$, and $p < 0.0001$, respectively.

mechanisms induced by low temperature were somewhat altered under the influence of overexpressed *ABI4* genes.

MtABI4 directly interacts with MtABA2 protein and promotes the expression of the *ABA2* gene, which in turn increases abscisic acid content in transgenic plants

To screen for candidate proteins that might interact with MtABI4 protein, we purified ABI4-3flag fusion proteins transiently expressed in the wild-type callus of *Medicago* using flag magnetic beads. SDS-page electrophoretic analysis of the purified products showed that some candidate target proteins were obtained (**Figure 6A**). Mass spectrometry analysis showed that 145 target proteins were collected (**Figure 6B**), including a xanthoxin dehydrogenase gene (*ABA2*), considered a key role in abscisic acid biosynthesis (González-Guzmán et al., 2002). Further, the yeast two-hybrid assay revealed that only the mixture of yeast, containing pGADT7-*ABA2* and pGBKT7-*ABI4*, respectively, could be capable of normal growth and turn blue in SD medium lacking the four amino acids, while the other controls could not (**Figure 6C**). Bimolecular fluorescence complementation (BIFC) assay indicated that GFP fluorescence in nuclear was observed only in *Tobacco* cells co-transformed with *ABI4*-^{N}YFP and *ABA2*-^{C}YFP (**Figure 6D**). Together, these results demonstrated that MtABI4 could directly interact with MtABA2 protein *in vivo*. In addition, the ABA2 protein was also located in the nucleus (**Figure 6E**).

To further explore the regulatory pattern of *ABI4* on *ABA2*, the expression of *ABA2* in previously transfected callus and transgenic *Arabidopsis* was characterized by qRT-PCR. The results showed that the expression of *MtABA2* and *AtABA2* was up-regulated under the induction of *MtABI4* (**Figures 6F,G**). It suggested that over-expression of *MtABI4* could promote the expression of the *ABA2* gene both in *M. truncatula* callus and transgenic *Arabidopsis*. Meanwhile, the ABA content also increased in the transgenic *Arabidopsis* (**Figure 6H**). Previous studies showed that the main function of *ABA2* is to catalyze

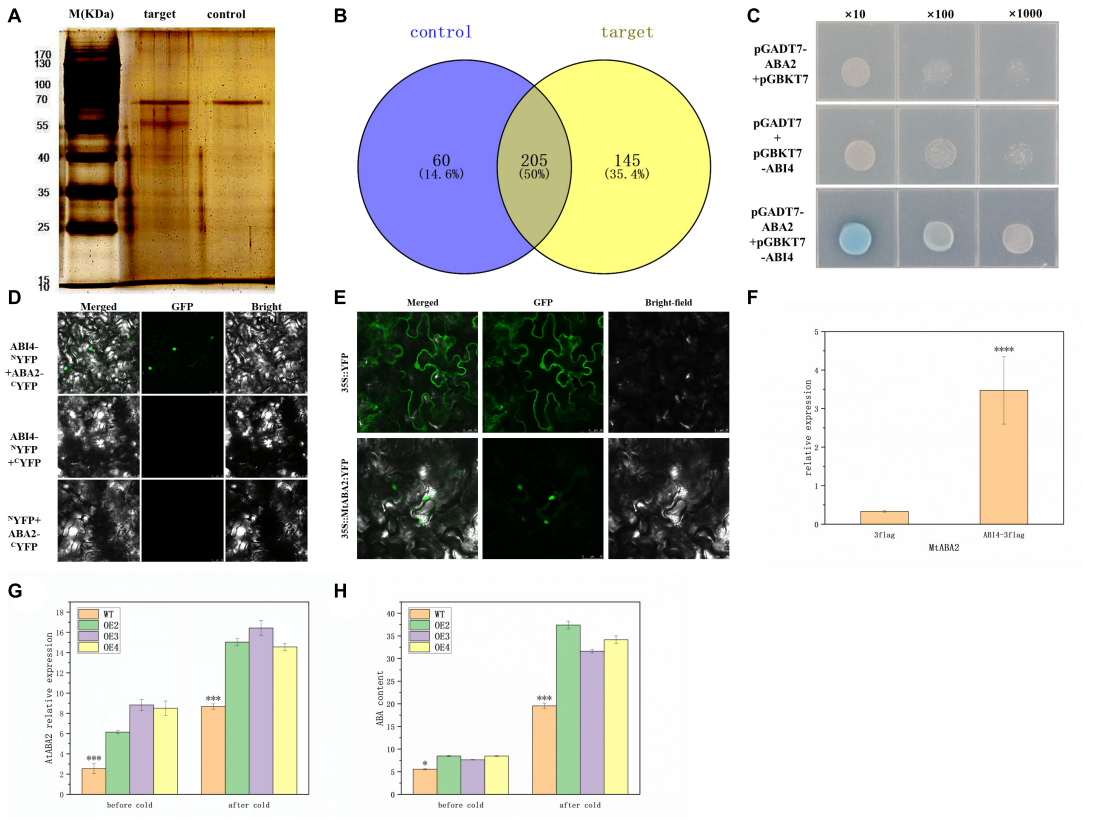

FIGURE 6
IP-MS, Y2H, BIFC, the expression level of ABA2, and ABA content. **(A)** Represents the results of the SDS-page electrophoretic. **(B)** Represents the intersection of the target and control mass spectrometry data. **(C)** Represents the growth of yeast in the Y2H analysis. **(D)** Represents the fluorescence observed in the BIFC analysis. **(E)** Represents the subcellular location of ABA2. **(F,G)** Represent ABA2 expression levels in *M. truncatula* callus, and in transgenic *Arabidopsis* before and after low-temperature treatment. **(H)** Represents the ABA level in the plant before and after the low-temperature treatment. *, in graphs, indicates significant differences in the means at $p < 0.05$ between each level in transgenic lines and WT plants, and ***, ****, in graphs, indicates significant differences in the means at $p < 0.001$ and $p < 0.0001$, respectively.

the conversion of xanthoxin to Abscisic Aldehyde which was confirmed as one of the last steps of the major ABA biosynthetic pathway (González-Guzmán et al., 2002). In conclusion, this was evidence that *MtABI4* could increase the ABA content in the transgenic *Arabidopsis* through the upregulated expression of *ABA2*. Furthermore, the overexpression of *MtABI4* also enhanced the expression of *ABA2* and improved the ABA biosynthesis of the plants, under low-temperature conditions (**Figures 6G,H**).

Discussion

ABI4 gene plays an integral role in plant growth and development and response to adversity. In this study, we found that the protein sequence of MtABI4 contains three elements and an AP2 structural domain, which is highly conserved with homologous proteins in other closely related legumes. This demonstrated that it was representative of investigating the function of the *MtABI4* gene from *Medicago truncatula*, a kind of model plant (Stacey et al., 2006), which could provide a reference for studying the function of homologous genes in other legumes. The MtABI4 protein was localized in the nucleus, and although this was inconsistent with our previous predictions, it was consistent with the localization of homologous proteins in *Arabidopsis* (Gregorio et al., 2014). This also confirms the accuracy of our results. It is important to note that YFP and GFP fluorescence have very close excitation light bands. To better avoid background interference, we chose the excitation band of GFP to observe the fluorescence of the YFP protein.

Analysis of the promoter sequence of the *ABI4* gene and hormone-induced expression analysis showed that the *ABI4* gene was able to respond to a variety of hormones, including IAA, 6-BA, GA, MeJA, SA, and ABA, which are thought to be associated with plant growth and development and stress response (Kazan, 2013; Colebrook et al., 2014). Several previous studies have suggested that *ABI4*, as a downstream of *DES1*,

is involved in the ABA response in Arabidopsis (Zhou et al., 2021). ABA stabilizes the ABI4 protein, while GA promotes its degradation (Shu et al., 2016). This also coincides with our results that *MtABI4* was down-regulated under the treatment of GA, but up-regulated under the treatment of ABA. In addition, *ABI4* expression is induced by cytokinin (CTK) but inhibited by IAA (Shkolnik-Inbar and Bar-Zvi, 2010). Notably, our results indicated that although the expression of *ABI4* showed a similar decrease in the IAA treatment, it showed a decrease followed by an increase under the 6-BA treatment rather than a simple increase. This may be because the response of *ABI4* to CTK is phased in a temporal gradient. Moreover, SA and MeJA induced the expression of *PtrWRKY18* and *PtrWRKY35*, and overexpression of *PtrWRKY18* and *PtrWRKY35* down-regulated the expression of *ABI4* (Guo et al., 2020). It is reasonable to speculate that the inhibition of *ABI4* by SA and MeJA in this study may also be mediated by *WRKY18* and *WRKY35*. In summary, *ABI4* is widely involved in the molecular response mechanisms of manyp lant hormones and may play a pivotal role in hormone synergy.

In addition, we also discovered a low-temperature response element in the promoter region of *ABI4*. After the low-temperature treatment, the transgenic plants accumulated less anthocyanin and suffered less cell membrane damage. Synthesis and accumulation of anthocyanins are employed to contribute to plant resistance to low-temperature stress. For example, as previously reported, the cold tolerance of the *Hedera helix* increases as the total sugar and anthocyanin content of the leaves increases (Parker, 1962). Wild-type *Arabidopsis* plants are significantly more freeze-resistant than the four cold-sensitive mutants that do not synthesize anthocyanins (McKown et al., 1996). The northern ecotype *Populus trichocarpa* is more susceptible to surviving the winter than the southern ecotype due to its ability to accumulate more anthocyanins during the progressively shorter photoperiod (Chalker-Scott, 1999). This means that the transgenic plants in this study are insensitive to low temperatures and do not require the accumulation of large amounts of anthocyanin to respond dramatically to low temperatures, as the wild type does. Further, no significant differences in gene expression and enzyme activities of the four antioxidant enzymes appeared in transgenic plants and WT before the low-temperature treatment, different from the situation in low-temperature conditions. This suggests that *ABI4* may not act directly on these antioxidant enzyme genes, but indirectly affects their performance at low temperatures. After low-temperature treatment, overexpression of *ABI4* promoted the gene expression and enzyme activity of CAT and SOD but inhibited those of APX and POD. Numerous studies have suggested that gene expression and enzyme activity of SOD and CAT are positively correlated with plant cold tolerance (Gao et al., 2009; Zhang et al., 2018, 2021). This is also consistent with our results. In contrast, the significantly lower APX and POD enzyme activities in transgenic plants than in WT may be due to the insensitivity of the transgenic plants to low temperatures. This is worth exploring further in the future. In addition, the activities of antioxidant enzymes in plants are in chronological order, with a trend of increasing and then decreasing with the duration of low-temperature treatment (Ahmad et al., 2010). This may account for the significant decrease in antioxidant enzyme activity in both transgenic plants and WT after up to 5 days of cold treatment.

ICE1 is the initial step in the ICE-CBF-COR signaling pathway, which plays a critical regulatory role in the low-temperature signaling pathway that involves multiple transcription factors (Stockinger et al., 1997). *TaICE1a* and *TaICE1d* were induced by cold treatment in wheat (Guo et al., 2019). Our results are also consistent with this, but the regulatory role of *MtABI4* on the expression of *ICE1* is more likely to be a repressor. And overexpression of *MdABI4* is capable of upregulating the *MdCBF1*, *MdCBF2*, *MdCBF3*, and *MdCOR47* in apple calli (An et al., 2022). Cold acclimation induces freezing tolerance in two chrysanthemums species by increasing *COR413* expression (Chen et al., 2014). Interestingly, except for those genes with the expression pattern consistent with previous results, *ABI4* acted as an inhibitor of *COR413* expression at room temperature but induced it at low temperature, whereas *CBF3* expression displayed the opposite trend. This "switch-like" regulation of *CBF3* and *COR413* by *ABI4* under low-temperature induction deserves further investigation. It has been shown that *COR* can only be activated to produce cold-regulated proteins only under certain conditions, such as low temperature and short sunlight, thus improving cold tolerance in plants (Jia et al., 2016). Under normal temperature, the HOS15-HD2C complex binds to the CORs promoter and represses expression by inducing CORs chromatin deacetylation. HOS15 enhances the binding of CBFs to the CORs promoter by activating the E3 ligase CUL4 (CULLIN4) for ubiquitinated degradation of HD2C under low-temperature stress (Park et al., 2015). It is reasonable to assume that *ABI4* may also play a similar role to that of *HOS15* in the regulation of *COR413* and *CBF3*. Apart from this, several studies have suggested that *RAV1* and *OST1* are also actively involved in adaption to cold stress in plants. For instance, *VaRAV1* may promote plant cold tolerance in grapevine cells via improving cell membrane stability and inducing the expression of genes involved in plant cell wall composition (Ren et al., 2021). At low temperatures, OST1 can be activated to phosphorylate ICE1, leading to its higher stability and transcriptional activity (Ding et al., 2015). In our results, their regulatory effects by *ABI4* also displayed a similar pattern to that of *CBF3* and *COR413*, which may be a new perspective to explore how *ABI4* and these cold-inducible genes are mutually regulated and act together in the process of plant low-temperature response.

ABA2 involved in the final step of the ABA biosynthetic pathway plays a vital role in the regulation of endogenous ABA levels in plants (González-Guzmán et al., 2002). It has been

shown that the Aba2-2 mutant has lower levels of endogenous ABA than the wild type (Nambara et al., 1998). This exactly complements our results that the elevation of *ABA2* expression levels caused by *ABI4* overexpression was accompanied by an increase in ABA content. ABA is an important signaling factor for stressful low temperatures and has a protective function for the microtubule structure of cells, and plants under low-temperature stress accumulate ABA in large quantities and rapidly to perform a protective function (Lang et al., 1994). The foliar application of exogenous ABA increased the endogenous ABA content of the leaves and improved the tolerance of the crop to low temperatures (Hongtao et al., 2017). Under low-temperature conditions, exogenous ABA can increase the content of proline, soluble sugar, and soluble protein in rice leaves, effectively increase SOD and CAT activities, reduce Malondialdehyde (MDA) accumulation and enhance cold tolerance of rice. Another more direct strategy adopted in our study was to promote the expression of *ABA2* and enhance the accumulation of endogenous ABA, through the overexpression of *ABI4*, thus improving the cold tolerance of plants.

Conclusion

MtABI4 protein was localized in the cell nucleus and could be induced by multiple hormones, including IAA, GA, MeJA, SA, 6-BA, and ABA. Moreover, MtABI4 could directly interact with MtABA2 protein and promotes the expression of the *ABA2* gene, which in turn increases abscisic acid content in transgenic plants. At low temperatures, the high accumulation of ABA in transgenic plants led to increased SOD, CAT, MDHAR and GR activity, a lower MDA level, a higher ASA/DHA ratio and GSH/GSSG ratio, and reduced anthocyanin content, thus providing some protection against low-temperature damage and leaf color deepening in plants. In addition, overexpression of *ABI4* also induced the expression of members of the ICEs-CBFs-CORs low-temperature response module. These factors combined to improve the cold tolerance of *ABI4* overexpression plants (**Figure 7**). This study provides a new insight into the mechanisms of ABA-mediated regulation of plant cold tolerance and offers a molecular theoretical basis for plant cold tolerance improvement.

Materials and methods

Plant materials, growth conditions, and treatments

The seeds of *M. truncatula* (R108), *Arabidopsis thaliana*, and *Nicotiana benthamiana*, and plant expression vector 3302Y, 3302-3flag, and *Agrobacterium tumefaciens* EHA105 strain used in this study were preserved in the laboratory of turfgrass science and management of Beijing forestry university. These seeds were vernalized for three days at 4°C and then germinated on the sterile filter paper for about one week. The seedlings were transferred to a vegetative soil matrix (peat: vermiculite = 1:1). *Medicago* and *Nicotiana* were cultivated in the greenhouse under the condition of a 16 h light/8 h dark cycle at 26°C/24°C, and *Arabidopsis* were under a 16 h light/8 h dark cycle at 23°C/21°C. After two months of cultivation, *Medicago* with similar growth was selected and sprayed with 10 μmol/L IAA, 10 μmol/L 6-BA, 10 μmol/L GA3, 10 μmol/L ABA, 10 μmol/L MeJA, and 0.5 mmol/L SA (Guo et al., 2020), respectively, and the plant tissues were collected at 0, 1, 3, 6, 9, and 12 h for temporal expression analysis.

Gene cloning and bioinformatics analysis

Total RNA was extracted from well-grown leaves of *M. truncatula*, and then reverse transcribed into cDNA by using the PrimeScript RT reagent Kit with gDNA Eraser from TAKARA. Using cDNA as a template and ABI4-CLONE-F, and ABI4-CLONE-R (**Supplementary Table 1**) as primers, the CDS of this gene was obtained by RT-PCR. And then it was attached to the pMD19-T clone vector from TAKARA, named as ABI4-pMD19-T vector, and was preserved in DH5α *E. coli* from TAKARA for further analysis.

DNAMAN 6.0 was used to analyze the sequence of *MtABI4* and predict the encoded amino acid sequence. Blast homology comparison was performed on the NCBI website. ABI4 homologous proteins in different species were mapped into evolutionary trees by MEGA 5.0. MEME website[1] was used for motif analysis. The results above were visualized via TBtools (Chen Chengjie, Guangzhou, Guangdong, China). SignalP 4.1 Server website[2] and Softberry website[3] were used to predict signal peptide cleavage sites and subcellular localization, respectively.

Subcellular localization and spatio-temporal expression analysis

Using the ABI4-pMD19-T vector as a template and ABI4-3302y-F, ABI4-3302y-R (**Supplementary Table 1**) as primers, the 35S:*MtABI4*:*YFP* expression vector was constructed by PCR and was turned into EHA105 *A. tumefaciens* for analysis of subcellular localization. The qualified bacterial solution above was injected into the young tender leaves of *Nicotiana*

1 https://meme-suite.org/meme/tools/meme
2 http://www.cbs.dtu.dk/services/SignalP/
3 http://www.softberry.com/

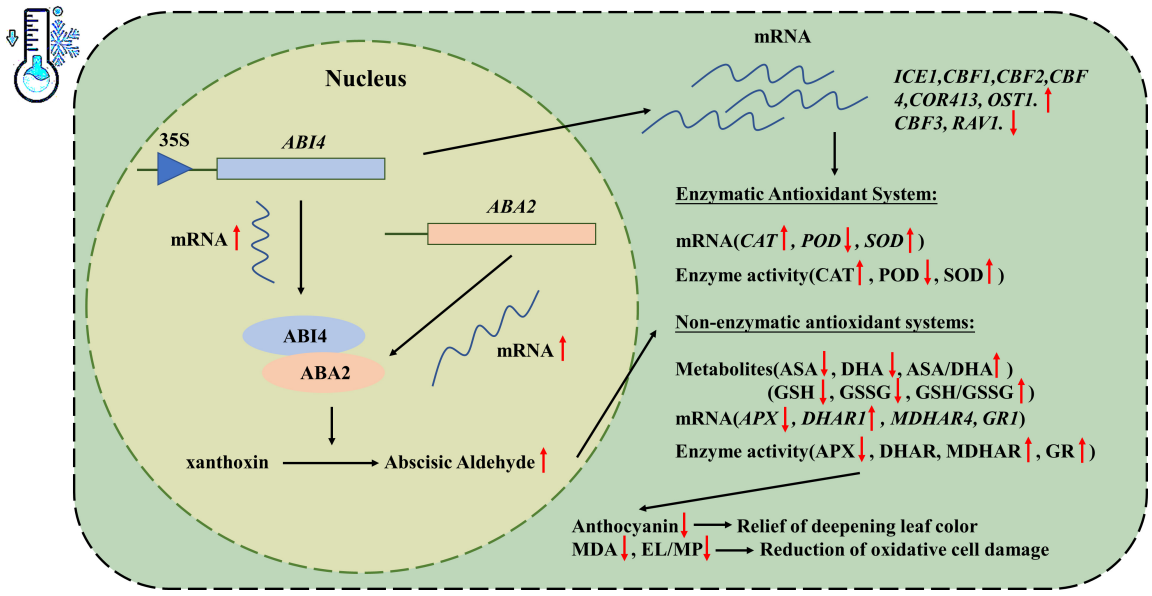

FIGURE 7
Putative regulatory mechanisms of *MtABI4*.

benthamiana. After 48 h of dark culture, the infected leaves were observed with LEICA SP-8 confocal microscope to determine the localization of the ABI4 protein. The localization of ABA2 protein was analyzed by the same methods.

The root, stem, leaf, flower, seeds, and pods of wild-type *M. truncatula* were collected and stored at −80°C after quick freezing with liquid nitrogen for further analysis of spatial differential expression. Total RNA of these tissues was extracted and then transcribed into cDNA as a template for quantitative fluorescence detection. Using ABI4-RT-F, ABI4-RT-R (**Supplementary Table 1**) as primers and the *MtActin* gene as the internal reference, real-time fluorescence quantitative analysis of the *MtABI4* gene was completed by the CFX Connect RT-PCR system. The reaction conditions were as follows: 95°C for 10 min;95°C 15 s, 60°C 1 min, 40 cycles. And the relative expression of *ABI4* was determined by the $2^{-\Delta\Delta CT}$ method (Guo et al., 2020). All samples were processed with three biological replicates. Temporal expression analysis of *MtABI4* adopted the same method mentioned above. The primers used were shown in the **Supplementary Table 1**.

Generation and identification of transgenic plants

The 35S:*MtABI4:YFP* expression vector was transformed into *Arabidopsis* plants by the floral dip method (Guo et al., 2020). Positive transgenic plants were screened by spraying 60 mg·L^{-1} glyphosate and then identified by PCR and RT-PCR. T3 generation transgenic lines were cultivated for further treatment and analysis. See **Supplementary Table 1** for the primers used.

Chlorophyll content

The chlorophyll content was determined using 95% ethanol as described in the previous report (Teng et al., 2021). Total chlorophyll, Chl a, Chl b, and carotenoid contents were calculated based on the absorbance recorded. All the samples were replicated three times.

Anthocyanin content

The anthocyanin content was determined using 10 mL 1% methanol hydrochloride solution (pH = 0–2). After shaking at 30°C for 5 h, the absorbance at 530 nm was measured.

Electrolyte leakage and cell membrane permeability

0.1 g plant sample in 25 mL distilled water was shaken for 24 h at room temperature. The electrolyte leakage of supernatant (EL1) was measured. After boiling water bath for 30 min, the electrolyte leakage of supernatant (EL2) was measured. The electrolyte leakage of distilled water (EL0) with the same shaking and boiling was also measured as a control. The electrolyte leakage of samples was calculated as

EL1/EL2, and the cell membrane permeability was calculated as (EL1- EL0)/(EL2- EL0).

Antioxidant enzyme activity and malondialdehyde content

SOD activity was measured by photoreduction with nitrogen blue tetrazolium (NBT). 3.4 mL of the reaction mix and 0.3 mL of 20 μmol L^{-1} riboflavin solution were added to 100 μL of the enzyme solution and then mix well, with no enzyme solution shaded with tin foil as control. The tubes were placed under a 4,000 l× lamp for 20–30 min and the OD values were measured at 560 nm.

POD activity was measured by guaiacol colorimetric assay. The reaction solution, containing 1 mL of phosphate buffer with 50 mmol L^{-1} pH 7.0, 0.95 mL of 0.2%guaiacol, 1 mL of 0.3% H_2O_2, and 50 μL of enzyme solution was added to a spectrophotometer cup (1 cm radius) and then mix well with no enzyme solution as a control. The kinetic OD values were measured at 470 nm in one minute. The Time interval was 5 s.

CAT activity was measured by UV spectrophotometry. 2.9 mL of the reaction solution, containing 20 mmol L^{-1} H_2O_2 solutions was added to 100 μL of enzyme solution and mix well. Distilled water was used as a blank control, the kinetic OD values were measured at 240 nm in one minute. The time interval was 5 s.

APX activity was measured by ascorbic acid colorimetric assay. The reaction solution, containing 2.82 mL of phosphate buffer with 50 mmol L^{-1} pH 7.0, 30 mL of 50 mmol L^{-1} ascorbic acid, 30 μL of 10 mmol L^{-1} EDTA, and 100 μL of enzyme solution was added to a spectrophotometer cup (1 cm radius) and then mix well with no enzyme solution as a control. The kinetic OD values were measured at 290 nm in one minute. The time interval was 5 s.

MDA content was measured by the thiobarbituric acid (TBA) reduction method. 1 mL of the enzyme solution, mixed with 2 mL TBA in a 5 mL centrifugal tube was boiled for 30 min. The tubes were then rapidly transferred to an ice bath for cooling to abort the reaction. After centrifugation at 10,000 *g* for 10 min, the supernatant was taken and the absorbance values at 600 and 532 nm were measured. All the samples above were replicated three times.

Determination of indicators related to non-enzymatic antioxidant systems

The content of ASA, DHA, GSH, and GSSG and the activities of DHAR, MDHAR, and GR was measured by the corresponding kits (No.G0201F, G0202F, G0206F, G0207F, G0212F, G0213F, and G0209F in turn) from GERUISI-BIO (Suzhou, China).

Abscisic acid content

ABA content were determined by high-performance liquid chromatography (Lu et al., 2010).

Immunoprecipitation, coupled with mass spectrometry

The entire experimental procedure for the Immunoprecipitation-mass spectrometry (IP-MS) analysis was referenced from the previous method with some modifications (Cao and Yan, 2016). Wild-type callus of *M. truncatula* was obtained via plant tissue culture. The ABI4-3302-3FLAG expression vector, constructed in a similar way to the aforementioned vectors, was transformed into callus by an Agrobacterium-mediated method for transient expression of ABI4 protein. In addition, the 3302-3FLAG expression vector was also transformed into the callus as a control.

After three days of dark incubation, the total protein of the callus was extracted by grinding in PBS buffer (pH = 7.4). The protein samples were purified using BeyoMag^{TM} Anti-Flag Magnetic Beads (Beyotime, China). The end products obtained by elution were subjected to electrophoretic analysis using 10% SDS-PAGE gel. When bands were observed on the silver-stained gel treated with the Fast Silver Stain Kit (Beyotime, China), the gel block was sent to Bio for mass spectrometry analysis (Biomarker, China). The candidate proteins that interacted with the target protein were obtained by subtracting the protein in the control group from the experimental group results.

Yeast two-hybrid

pGADT7-*ABA2* and pGBKT7-*ABI4* expression vectors were constructed by a similar method above and transformed into Y187 and yeast two-hybrid (Y2H) yeast strains in turn. The mixture of these two kinds of yeast was cultivated in SD solid medium lacking Leu, Trp, His, and Ade, supplemented with 40 μg ml^{-1} X-α-gal and 125 ng ml^{-1} Aureobasidin A, for 3–5 days at 29.5°C. Moreover, they matched with the yeast strains containing pGADT7or pGBKT7 empty vector and were cultivated under the same conditions as controls.

Bimolecular fluorescence complementation

ABI4-^{N}YFP and *ABA2*-^{C}YFP expression vectors were constructed by a method similar to those described above and transformed into *Agrobacterium tumefaciens* EHA105 strain. These fluids were injected into tobacco leaves by a method similar to subcellular localization. The mixture of strains

containing *ABI4*-^{N}YFP and *ABA2*-^{C}YFP was the treatment group and these two strains were mixed with those containing the ^{N}YFP or ^{C}YFP empty vectors, separately, as controls. GFP fluorescence in *tobacco* cells was observed with LEICA SP-8 confocal microscope, after 2 days of dark incubation.

Statistical analysis

Data were analyzed by SPSS 15.0, Excel 2020, GraphPad Prism 9.0, and Origin 2022. All data were presented as the mean ± SD (n = 3).

Data availability statement

The original contributions presented in this study are included in the article/**Supplementary material**, further inquiries can be directed to the corresponding author.

Author contributions

YL proposed ideas and designed the experiments and wrote the manuscript. YL, SL, and MW completed the experiments. YL, TG, and KT analyzed the experimental data. DD, ZL, and YC proposed key opinions that cannot be ignored. LH and CJ played a guiding role in the whole work process. All authors read and reached an agreement with the final manuscript.

Funding

This work is supported by the Fundamental Research Funds for the Central Universities (Grant No. 2021ZY84), the National Natural Science Foundation of China (Grant No. 31971770), the Performance Incentive and Guidance Special Project of Scientific Research Institution, Chongqing Science and Technology Committee, and the Special Support for Chongqing Postdoctoral Research Project. All of them provide funding for the entire research effort, which is used for material maintenance, reagents, data collection, labor costs and so on.

Conflict of interest

CJ was employed by Inner Mongolia Mengcao Ecological Environment (Group) Co., Ltd., Hohhot, China.

The remaining authors declare that the research was conducted in the absence of any commercial or financial relationships that could be construed as a potential conflict of interest.

Publisher's note

Supplementary material

The Supplementary Material for this article can be found online at: https://www.frontiersin.org/articles/10.3389/fpls.2022.982715/full#supplementary-material

SUPPLEMENTARY FIGURE 1
Bioinformatic analysis of *MtABI4*.

References

Ahmad, P., Jaleel, C. A., Salem, M. A., Nabi, G., and Sharma, S. (2010). Roles of enzymatic and nonenzymatic antioxidants in plants during abiotic stress. *Crit. Rev. Biotechnol.* 30, 161–175. doi: 10.3109/07388550903524243

An, J. P., Xu, R. R., Liu, X., Su, L., Yang, K., Wang, X. F., et al. (2022). Abscisic acid insensitive 4 interacts with ice1 and jaz proteins to regulate aba signaling-mediated cold tolerance in apple. *J. Exp. Bot.* 73, 980–997. doi: 10.1093/jxb/erab433

Bossi, F., Cordoba, E., Dupré, P., Mendoza, M. S., Román, C. S., and León, P. (2009). The Arabidopsis aba-insensitive (abi) 4 factor acts as a central transcription activator of the expression of its own gene, and for the induction of abi5 and sbe2.2 genes during sugar signaling. *Plant J.* 59, 359–374. doi: 10.1111/j.1365-313X.2009.03877.x

Campos, C. N., Ávila, R. G., de Souza, K. R. D., Azevedo, L. M., and Alves, J. D. (2019). Melatonin reduces oxidative stress and promotes drought tolerance in young *Coffea arabica* l. *Plants Agric. Water Manag.* 211, 37–47. doi: 10.1016/j.agwat.2018.09.025

Cao, X., and Yan, J. (2016). Identification of associated proteins by immunoprecipitation and mass spectrometry analysis. *Methods Mol. Biol.* 1407, 131–139. doi: 10.1007/978-1-4939-3480-5_10

Chalker-Scott, L. (1999). Environmental significance of anthocyanins in plant stress responses. *Photochem. Photobiol.* 70, 1–9.

Chen, I., Lee, S., Pan, S., and Hsieh, H. (2007). Gasa4, a ga-stimulated gene, participates in light signaling in *Arabidopsis*. *Plant Sci.* 172, 1062–1071. doi: 10.1016/j.plantsci.2007.03.012

Chen, Y., Jiang, J., Chang, Q., Gu, C., Song, A., Chen, S., et al. (2014). Cold acclimation induces freezing tolerance via antioxidative enzymes, proline metabolism and gene expression changes in two *Chrysanthemum* species. *Mol. Biol. Rep.* 41, 815–822. doi: 10.1007/s11033-013-2921-8

Chinnusamy, V., Zhu, J., and Zhu, J. (2007). Cold stress regulation of gene expression in plants. *Trends Plant Sci.* 12, 444–451. doi: 10.1016/j.tplants.2007.07.002

Colebrook, E. H., Thomas, S. G., Phillips, A. L., and Hedden, P. (2014). The role of gibberellin signalling in plant responses to abiotic stress. *J. Exp. Biol.* 217, 67–75. doi: 10.1242/jeb.089938

Ding, Y., Jia, Y., Shi, Y., Zhang, X., Song, C., Gong, Z., et al. (2018). Ost1-mediated btf3l phosphorylation positively regulates cbfs during plant cold responses. *Embo J.* 37:e98228. doi: 10.15252/embj.201798228

Ding, Y., Li, H., Zhang, X., Xie, Q., Gong, Z., and Yang, S. (2015). Ost1 kinase modulates freezing tolerance by enhancing ice1 stability in *Arabidopsis*. *Dev. Cell* 32, 278–289. doi: 10.1016/j.devcel.2014.12.023

Ding, Y., Shi, Y., and Yang, S. (2019). Advances and challenges in uncovering cold tolerance regulatory mechanisms in plants. *New Phytol.* 222, 1690–1704. doi: 10.1111/nph.15696

Eremina, M., Rozhon, W., and Poppenberger, B. (2016). Hormonal control of cold stress responses in plants. *Cell. Mol. Life Sci.* 73, 797–810. doi: 10.1007/s00018-015-2089-6

Finkelstein, R. R. (1994). Mutations at two new *Arabidopsis* aba response loci are similar to the abi3 mutations. *Plant J.* 5, 765–771. doi: 10.1046/j.1365-313X.1994.5060765.x

Finkelstein, R., Lynch, T., Reeves, W., Petitfils, M., and Mostachetti, M. (2011). Accumulation of the transcription factor aba-insensitive (abi)4 is tightly regulated post-transcriptionally. *J. Exp. Bot.* 62, 3971–3979. doi: 10.1093/jxb/err093

Gao, J. J., Qin, A. G., and Yu, X. C. (2009). Effects of grafting on cucumber leaf sod and cat gene expression and activities under low temperature stress. *Chin. J. Appl. Ecol.* 20, 213–217.

González-Guzmán, M., Apostolova, N., Bellés, J. M., Barrero, J. M., Piqueras, P., Ponce, M. R., et al. (2002). The short-chain alcohol dehydrogenase aba2 catalyzes the conversion of xanthoxin to abscisic aldehyde. *Plant Cell* 14, 1833–1846. doi: 10.1105/tpc.002477

Gregorio, J., Hernández-Bernal, A. F., Cordoba, E., and León, P. (2014). Characterization of evolutionarily conserved motifs involved in activity and regulation of the aba-insensitive (abi) 4 transcription factor. *Mol. Plant* 7, 422–436. doi: 10.1093/mp/sst132

Guo, J., Ren, Y., Tang, Z., Shi, W., and Zhou, M. (2019). Characterization and expression profiling of the ice-cbf-cor genes in wheat. *Peerj* 7:e8190. doi: 10.7717/peerj.8190

Guo, T., Wang, S., Li, Y., Yuan, J., Xu, L., Zhang, T., et al. (2020). Expression of a ngatha1 gene from *Medicago truncatula* delays flowering time and enhances stress tolerance. *Int. J. Mol. Sci.* 21:2384. doi: 10.3390/ijms21072384

Hongtao, X., Tongtong, W., Dianfeng, Z., Lizhi, W., Yanjiang, F., Yu, L., et al. (2017). Aba pretreatment enhances the chilling tolerance of a chilling-sensitive rice cultivar. *Braz. J. Bot.* 40, 853–860. doi: 10.1007/s40415-017-0409-9

Hu, Y., Jiang, L., Wang, F., and Yu, D. (2013). Jasmonate regulates the inducer of cbf expression–c-repeat binding factor/dre binding factor1 cascade and freezing tolerance in *Arabidopsis*. *Plant Cell* 25, 2907–2924. doi: 10.1105/tpc.113.112631

Hu, Y., Jiang, Y., Han, X., Wang, H., Pan, J., and Yu, D. (2017). Jasmonate regulates leaf senescence and tolerance to cold stress: Crosstalk with other phytohormones. *J. Exp. Bot.* 68, 1361–1369. doi: 10.1093/jxb/erx004

Jia, Y., Ding, Y., Shi, Y., Zhang, X., Gong, Z., and Yang, S. (2016). The cbfs triple mutants reveal the essential functions of cbfs in cold acclimation and allow the definition of cbf regulons in *Arabidopsis*. *New Phytol.* 212, 345–353. doi: 10.1111/nph.14088

Jiang, M., and Zhang, J. (2002). Involvement of plasma-membrane nadph oxidase in abscisic acid- and water stress-induced antioxidant defense in leaves of maize seedlings. *Planta* 215, 1022–1030. doi: 10.1007/s00425-002-0829-y

Kazan, K. (2013). Auxin and the integration of environmental signals into plant root development. *Ann. Bot.* 112, 1655–1665. doi: 10.1093/aob/mct229

Klessig, D. F., Choi, H. W., and Dempsey, D. A. (2018). Systemic acquired resistance and salicylic acid: Past, present, and future. *Mol. Plant Microbe Interact.* 31, 871–888. doi: 10.1094/MPMI-03-18-0067-CR

Lang, V., Mantyla, E., Welin, B., Sundberg, B., and Palva, E. T. (1994). Alterations in water status, endogenous abscisic acid content, and expression of rab18 gene during the development of freezing tolerance in *Arabidopsis thaliana*. *Plant Physiol.* 104, 1341–1349. doi: 10.1104/pp.104.4.1341

León, P., Gregorio, J., and Cordoba, E. (2012). Abi4 and its role in chloroplast retrograde communication. *Front. Plant Sci.* 3:304. doi: 10.3389/fpls.2012.00304

Lu, Q., Chen, L., Lu, M., Chen, G., and Zhang, L. (2010). Extraction and analysis of auxins in plants using dispersive liquid-liquid microextraction followed by high-performance liquid chromatography with fluorescence detection. *J. Agric. Food Chem.* 58, 2763–2770. doi: 10.1021/jf903274z

McKown, R., Kuroki, G., and Warren, G. (1996). Cold responses of *Arabidopsis* mutants impaired in freezing tolerance. *J. Exp. Bot.* 47, 1919–1925. doi: 10.1093/jxb/47.12.1919

Nahar, K., Hasanuzzaman, M., Alam, M., and Fujita, M. (2015). Exogenous spermidine alleviates low temperature injury in mung bean (Vigna *radiata* l.) Seedlings by modulating ascorbate-glutathione and glyoxalase pathway. *Int. J. Mol. Sci.* 16, 30117–30132. doi: 10.3390/ijms161226220

Nambara, E. H. U. S., Kawaide, H., Kamiya, Y., and Naito, S. (1998). Characterization of an *Arabidopsis thaliana* mutant that has a defect in aba accumulation: Aba-dependent and aba-independent accumulation of free amino acids during dehydration. *Plant Cell Physiol.* 39, 853–858. doi: 10.1093/oxfordjournals.pcp.a029444

Park, S., Lee, C. M., Doherty, C. J., Gilmour, S. J., Kim, Y., and Thomashow, M. F. (2015). Regulation of the *Arabidopsis* cbf regulon by a complex low-temperature regulatory network. *Plant J.* 82, 193–207. doi: 10.1111/tpj.12796

Parker, J. (1962). Relationships among cold hardiness, water-soluble protein, anthocyanins, & free sugars in hedera helix l. *Plant Physiol.* 37, 809–813. doi: 10.1104/pp.37.6.809

Ren, C., Li, H., Wang, Z., Dai, Z., Lecourieux, F., Kuang, Y., et al. (2021). Characterization of chromatin accessibility and gene expression upon cold stress reveals that the rav1 transcription factor functions in cold response in *Vitis amurensis*. *Plant Cell Physiol.* 62, 1615–1629. doi: 10.1093/pcp/pcab115

Shi, Y., Ding, Y., and Yang, S. (2015). Cold signal transduction and its interplay with phytohormones during cold acclimation. *Plant Cell Physiol.* 56, 7–15. doi: 10.1093/pcp/pcu115

Shkolnik-Inbar, D., and Bar-Zvi, D. (2010). Abi4 mediates abscisic acid and cytokinin inhibition of lateral root formation by reducing polar auxin transport in *Arabidopsis*. *Plant Cell* 22, 3560–3573. doi: 10.1105/tpc.110.074641

Shkolnik-Inbar, D., and Bar-Zvi, D. (2011). Expression of abscisic acid insensitive 4 (abi4) in developing arabidopsis seedlings. *Plant Signal Behav.* 6, 694–696. doi: 10.4161/psb.6.5.14978

Shu, K., Chen, Q., Wu, Y., Liu, R., Zhang, H., Wang, P., et al. (2016). Abi4 mediates antagonistic effects of abscisic acid and gibberellins at transcript and protein levels. *Plant J.* 85, 348–361. doi: 10.1111/tpj.13109

Stacey, G., Libault, M., Brechenmacher, L., Wan, J., and May, G. D. (2006). Genetics and functional genomics of legume nodulation. *Curr. Opin. Plant Biol.* 9, 110–121. doi: 10.1016/j.pbi.2006.01.005

Stockinger, E. J., Gilmour, S. J., and Thomashow, M. F. (1997). *Arabidopsis thaliana* cbf1 encodes an ap2 domain-containing transcriptional activator that binds to the c-repeat/dre, a cis-acting dna regulatory element that stimulates transcription in response to low temperature and water deficit. *Proc. Natl. Acad. Sci. U. S. A.* 3:1035. doi: 10.1073/pnas.94.3.1035

Sun, X., Feng, P., Xu, X., Guo, H., Ma, J., Chi, W., et al. (2011). A chloroplast envelope-bound phd transcription factor mediates chloroplast signals to the nucleus. *Nat. Commun.* 2:477. doi: 10.1038/ncomms1486

Tang, K., Zhao, L., Ren, Y., Yang, S., Zhu, J. K., and Zhao, C. (2020). The transcription factor ice1 functions in cold stress response by binding to the promoters of cbf and cor genes. *J. Integr. Plant Biol.* 62, 258–263. doi: 10.1111/jipb.12918

Teng, K., Tan, P., Guan, J., Dong, D., Liu, L., Guo, Y., et al. (2021). Functional characterization of the chlorophyll b reductase gene nyc1 associated with chlorophyll degradation and photosynthesis in *Zoysia japonica*. *Environ. Exp. Bot.* 191:104607. doi: 10.1016/j.envexpbot.2021.104607

Yang, Y., Yao, N., Jia, Z. K., Duan, J., Chen, F. J., Sang, Z. Y., et al. (2016). Effect of exogenous abscisic acid on cold acclimation in two magnolia species. *Biol. Plant.* 60, 555–562. doi: 10.1007/s10535-016-0623-5

Zhang, G., Ding, Q., and Wei, B. (2021). Genome-wide identification of superoxide dismutase gene families and their expression patterns under low-temperature, salt and osmotic stresses in watermelon and melon. *3 Biotech* 11:194. doi: 10.1007/s13205-021-02726-7

Zhang, Y., Ji, H., Yu, J., and Zhang, Z. (2018). Effect of cold and heat shock treatment on the color development of mature green tomatoes and the roles of their antioxidant enzymes. *Food Bioprocess Technol.* 11, 705–709. doi: 10.1007/s11947-017-2053-6

Zhou, M., Zhang, J., Shen, J., Zhou, H., Zhao, D., Gotor, C., et al. (2021). Hydrogen sulfide-linked persulfidation of abi4 controls aba responses through the transactivation of mapkkk18 in *Arabidopsis*. *Mol. Plant* 14, 921–936. doi: 10.1016/j.molp.2021.03.007

Zhu, T., Wu, S., Zhang, D., Li, Z., Xie, K., An, X., et al. (2019). Genome-wide analysis of maize gpat gene family and cytological characterization and breeding application of zmms33/zmgpat6 gene. *Theor. Appl. Genet.* 132, 2137–2154. doi: 10.1007/s00122-019-03343-y

frontiers | Frontiers in Plant Science

TYPE Original Research
PUBLISHED 30 September 2022
DOI 10.3389/fpls.2022.971999

OPEN ACCESS

EDITED BY
Jin-Lin Zhang,
Lanzhou University, China

REVIEWED BY
Xiaojun Nie,
Northwest A&F University, China
Liang Chen,
University of Chinese Academy of Sciences, China

*CORRESPONDENCE
Minqiang Tang
tangminqiang@hainanu.edu.cn
Li Liao
liaoli@hainanu.edu.cn
Zhiyong Wang
wangzhiyong@hainanu.edu.cn

†These authors have contributed equally to this work

SPECIALTY SECTION
This article was submitted to Plant Abiotic Stress, a section of the journal Frontiers in Plant Science

RECEIVED 17 June 2022
ACCEPTED 25 August 2022
PUBLISHED 30 September 2022

CITATION
Hu X, Hao J-S, Pan L, Xu T, Ren L-Z, Chen Y, Tang M-Q, Liao L and Wang Z-Y (2022) Genome-wide analysis of tandem duplicated genes and their expression under salt stress in seashore paspalum. *Front. Plant Sci.* 13:971999. doi: 10.3389/fpls.2022.971999

Genome-wide analysis of tandem duplicated genes and their expression under salt stress in seashore paspalum

Xu Hu[1,2†], Jiangshan Hao[1,3†], Ling Pan[2], Tao Xu[1,2], Longzhou Ren[1,2], Yu Chen[4], Minqiang Tang[2*], Li Liao[1*] and Zhiyong Wang[2*]

[1]College of Tropical Crops, Hainan University, Haikou, China, [2]Key Laboratory of Genetics and Germplasm Innovation of Tropical Special Forest Trees and Ornamental Plants, Ministry of Education, College of Forestry, Hainan University, Haikou, China, [3]School of Agriculture, Jinhua Polytechnic, Jinhua, China, [4]College of Agro-Grassland Science, Nanjing Agricultural University, Nanjing, China

Seashore paspalum (*Paspalum vaginatum*) is a halophytic, warm-season grass which is closely related to various grain crops. Gene duplication plays an important role in plant evolution, conferring significant plant adaptation at the genomic level. Here, we identified 2,542 tandem duplicated genes (TDGs) in the *P. vaginatum* genome and estimated the divergence time of pairs of TDGs based on synonymous substitution rates (Ks). Expression of *P. vaginatum* TDGs resulted in enrichment in many GO terms and KEGG pathways when compared to four other closely-related species. The GO terms included: "ion transmembrane transporter activity," "anion transmembrane transporter activity" and "cation transmembrane transport," and KEGG pathways included "ABC transport." RNA-seq analysis of TDGs showed tissue-specific expression under salt stress, and we speculated that *P. vaginatum* leaves became adapted to salt stress in the earlier whole-genome duplication (WGD; ~83.3 million years ago; Ma), whereas the entire *P. vaginatum* plant acquired a large number of TDGs related to salt stress in the second WGD (~23.3Ma). These results can be used as a reference resource to accelerate salt-resistance research in other grasses and crops.

KEYWORDS

abiotic stress, salt, seashore paspalum, tandem duplicated genes, transcriptome

Introduction

High salinity is a major abiotic environmental stress that is reported to be responsible for reductions in plant growth and crop production worldwide (Roy et al., 2014; Kumari et al., 2015). The production of salt-tolerant crops is potentially a cost-effective approach to provide improved growth in saline soils (Rasheed et al., 2022). It is therefore of critical interest to unravel the salt-resistance mechanisms of halophytes and transfer these, if

possible, to glycophytes (Kumari et al., 2015). Seashore paspalum (*Paspalum vaginatum* Sw.) is a halophytic, warm-season, perennial grass that has been utilized as turf for almost 100 years, especially in coastal and salt-affected regions across the world (Wu et al., 2018; Qi et al., 2019). *P. vaginatum* is one of the most saline-tolerant turfgrass species (Liu et al., 2011; Uddin et al., 2012; Spiekerman and Devos, 2020) and, as it is closely related to some of the world's most important grain crops, including maize, sorghum and millet (Qi et al., 2019), may provide a gateway for cereal crop improvements in salt resistance.

Gene duplication is a fundamental process in genome evolution (Holland, 1999; Paterson et al., 2010), and can result from whole-genome duplication, tandem duplication, duplication mediated by transposable elements, segmental duplication, and/or retroduplication (Panchy et al., 2016; Guo et al., 2019; Qiao et al., 2019). Tandem duplication refers to the generation of tandem arrays consisting of identical sequences in close genomic proximity. This occurs due to unequal chromosomal recombination, a widespread phenomenon in plant genomes which plays significant evolutionary roles including in adaptation to changing environments (Cannon et al., 2004; Yu et al., 2015). Tandem duplication events have been implicated in various plant traits such as stress resistance and membrane function in arabidopsis and rice (Rizzon et al., 2006), disease resistance in Solanaceae and Brassicaceae species (Leister, 2004), signal transduction in legumes (Bellieny-Rabelo et al., 2013) and glucosinolate biosynthesis diversification in the mustard family (Hofberger et al., 2013).

However, little is known about tandem duplicated genes (TDGs) and their possible contributions to the genome evolution of salt-stress resistance in *P. vaginatum*. Here, we report a comprehensive study of genome-wide TDGs present in the genome of *P. vaginatum* and surmise their evolutionary contributions. The functions of the TDGs were proposed using GO and KEGG enrichment analyses. The use of RNA-seq data made it feasible to identify TDGs that respond to salt stress in various tissues. Our findings can provide further insights into *P. vaginatum* evolution, particularly in relation to salt resistance. In addition, this genetic resource might also be useful for salt resistance research into other grasses and crops.

Materials and methods

Data sources

Protein sequence and General Feature Format (GFF) files of *Oryza sativa*, *Setaria italica*, *Sorghum bicolor*, and *Zea mays* were downloaded from EnsemblPlants.[1] We obtained a chromosome-level reference genome of diploid cultivated *P. vaginatum*: The reference genome size was 517.98 million bases (Mb), including 28,712 codable proteins. For genes with multiple transcripts, the longest transcript was selected for subsequent analysis.

TDG analysis

TDGs were mainly identified based on protein sequences and the GFF file. Firstly, BLASTP (Altschul et al., 1997; settings: E < 1e−10; first 10 matches) was performed with protein sequences to search for all potential homologous gene pairs within each genome. Secondly, the blast results were analyzed in MCScanX (Wang et al., 2012) using a modified MCScan algorithm. Thirdly, duplicated gene pairs were identified using the downstream analysis tool (duplicate_gene_classifier) which is incorporated into the MCScanX package. Finally, duplicated gene pairs with code 3 (representing TDGs) were extracted. The non-synonymous (Ka) and synonymous substitution (Ks) frequencies of duplicated genes were calculated using ParaAT (Zhang et al., 2012), which was further used to compute the approximate dates of duplication and divergence events using the formula $T = Ks/2\lambda$, assuming a clocklike rate (λ) of 1.5 synonymous substitutions per 10^{-8} years (Yang et al., 2020; Wang et al., 2021b) for *P. vaginatum*. Moreover, the Ka/Ks ratio was also employed to show the selection pressure for the duplicated genes.

GO term and KEGG pathway enrichment analyses

Based on the annotation information[2] (Huerta-Cepas et al., 2017), TDGs from *P. vaginatum* were analyzed for GO term and KEGG pathway functional enrichment using the R package clusterProfiler (Wu et al., 2021). "Rich factor" is the ratio of the number of differentially-expressed genes annotated in a term (or pathway) to the number of all genes annotated in this term (or pathway).

Identification and sequence analysis of the ABC gene family

The Hidden Markov Model (HMM) profile of the ABC domain (PF00664, PF00005, PF01061, PF02470 and PF01458) from the Pfam database[3] (Mistry et al., 2021) was utilized to identify the ABC members in *P. vaginatum* by using the HMMER software (Mistry et al., 2013)(settings: E < 1e−10), and redundant sequences were removed manually. Additionally, all obtained ABC protein sequences were analyzed online using the CDD website[4]

1 http://plants.ensembl.org/index.html

2 http://eggnog-mapper.embl.de/

3 http://pfam.xfam.org/

4 https://www.ncbi.nlm.nih.gov/cdd

(Marchler-Bauer et al., 2017) to verify conserved ABC domains. The members of the *P. vaginatum* ABC family were named according to chromosomal position. The number of amino acids, theoretical molecular weight (MW), and theoretical isoelectric point (pI) of the ABC family were obtained from the ExPASy web resource[5] (Gasteiger et al., 2003). In order to explore the phylogenetic relationships of *P. vaginatum* ABC-family genes, data from 105 ABC proteins of *O. sativa* were downloaded for multiple sequence alignment using MAFFT (Rozewicki et al., 2019), and multiple sequences were trimmed using TBtools (Chen et al., 2020). Phylogenetic trees (ML) were constructed using IQ-TREE (Minh et al., 2020) (settings: -m MFP -bb 1000 -alrt 1000) and generated using iTol online tools[6] (Letunic and Bork, 2021).

RNA-seq and bioinformatics analysis

The *P. vaginatum* salt-resistant ecotypes USA17-18 were analyzed by RNA-seq. For the RNA-seq experiments, similar stolons were cultivated in plastic pots under typical conditions. Two-month-old plants were treated with 400 mM NaCl or water as a control for 8, 12, 24, or 48 h or 5 days before harvesting tissues. Total RNAs were isolated from leaves with three biological replicates at each stress stage. RNA-seq and *de novo* assembly Paired-end sequencing of cDNA libraries were performed using the HiSeq 2000 platform (Supplementary Table 10). Clean reads were aligned to the reference genome using HISAT2 (Kim et al., 2015). FPKM (fragments per kilobase per million mapped reads) was used to estimate the expression levels of individual genes (Supplementary Table 11). Differentially expressed genes (DEGs) were determined using the R package DESeq2 (Love et al., 2014) with a false discovery rate (FDR) of ≤ 0.05 and $|\log_2 FC| \geq 1$ used as the threshold to determine statistically significant differences in gene expression. To determine whether these genes were tissue-specific to leaves or roots, gene expression patterns were compared in both transcriptomic data of control and treatment plants. Tissue-specifically expressed genes and co-expressed genes were defined based on the following rules: If the gene appeared up-regulated at least four times in one tissue but less than (or equal to) one time in another tissue, we considered it to be a tissue-specifically expressed gene; if the gene appeared up-regulated at least seven times in both tissues, it was considered to be a co-expressed gene.

5 https://web.expasy.org/protparam/

6 https://itol.embl.de/

Results

Identification and genomic distribution of TDGs

The *P. vaginatum* genome sequence consists of 517.98 Mb of DNA sequence and 28,712 protein coding genes. A total of 2,542 TDGs (8.85% of the gene set) were identified in the *P. vaginatum* genome, with a higher frequency than *O. sativa* (7.78%) and *Z. mays* (4.74%) but lower frequency than *S. italica* (11.55%) and *S. bicolor* (10.82%) (Supplementary Table 1). In addition, the distribution of TDGs was not uniform across chromosomes (Figure 1A): The most, 428, TDGs (16.84% of total TDGs), were located on chromosome 1

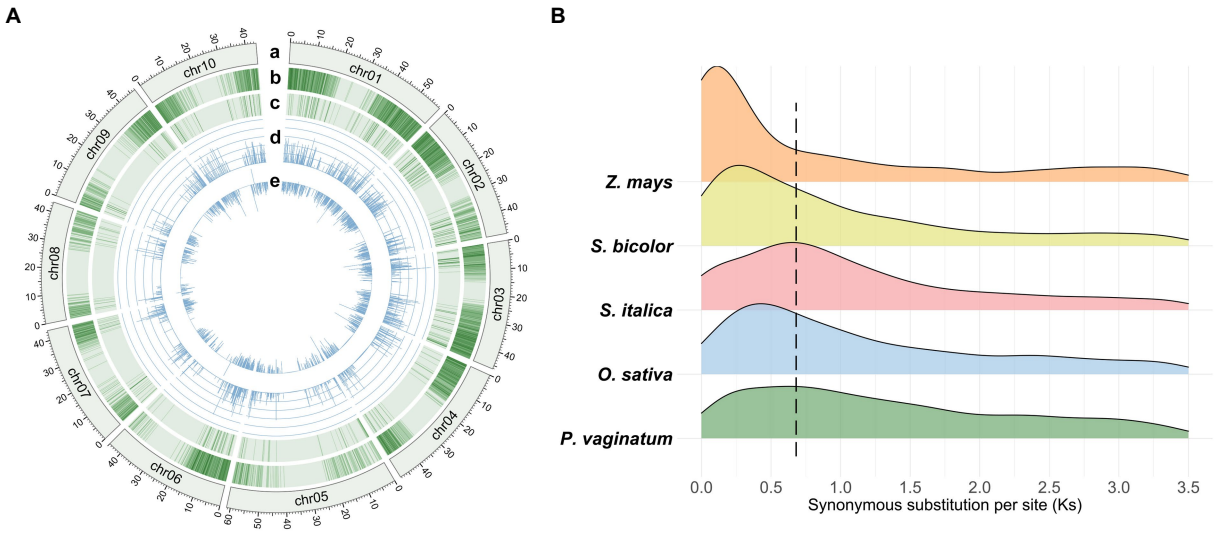

FIGURE 1
Overview of the *Paspalum vaginatum* genome and comparison of Ks. **(A)** Tracks from outer (a) to inner (e) rings indicate the following: (a) Chromosome size with units in Mb; (b) density of genes; (c) density of TDGs; (d) Ks of TDG pairs; (e) Ka/Ks values of TDG pairs and normalization by log2 (Ka/Ks). **(B)** Distribution of Ks calculated by TDG pairs between study species.

(chr01); the least, 134 (5.27% of the total TDGs) on chromosome 8 (chr08) (Supplementary Table 2). The synonymous substitution rates (Ks) in the TDG pairs were calculated for 1,581 gene pairs, and the distribution of Ks showed a single peak value ranging from 0.6 to 0.7 (Figure 1B; Supplementary Table 3). To infer the speciation occurrence time of *P. vaginatum*, the T = Ks/2λ method was used. Results indicated an estimated time of approximately 20.0–23.3 Ma, suggesting that *P. vaginatum* and *S. italica* might have shared common whole-genome duplicates. Ka/Ks values were then used to determine possible selection pressure between individual genes in a pair. The Ka/Ks values for *P. vaginatum* TDGs showed that there were few TDG pairs with Ka/Ks values much greater than 1, with most TDG pairs having Ka/Ks values much less than 1 (Supplementary Table 3), suggesting that most TDGs were under negative selection and that only a small number were under positive selection.

The number of TDGs in the same tandem cluster ranged from two to nine with the longest tandem clusters found with "UDP-glycosyltransferase" and "GRAS domain" (Table 1). We focused on TDGs with more than six genes in the same cluster and their functions (Supplementary Table 4). The majority of these long TDG clusters were found to be associated with salt resistance after reviewed evidence and included: "UDP-glycosyltransferase," "GRAS domain," "Auxin responsive protein," "Cytochrome P450," "FCS-type zinc-finger," "Dirigent protein," "BTB/POZ domain," "Expansin, cellulose-binding-like domain," "Glutathione S-transferase," "RING-type zinc-finger" and "FAD-linked oxidoreductase" (Table 1).

TABLE 1 TDGs with more than six genes in the same cluster and their functions.

The number of TDGs in the same cluster	Chr	Description	Reviewed evidence
9	chr03	UDP-glycosyltransferase	Li et al. (2017); Wang et al. (2021a)
	chr05	GRAS domain	Wang et al. (2020); Zhang et al. (2020)
8	chr02	Auxin responsive protein	Bouzroud et al. (2018); Kang et al. (2018)
7	chr02	UDP-glucosyl transferase	Wang et al. (2021a,c)
	chr03	Cytochrome P450	Magwanga et al. (2019); Krishnamurthy et al. (2020)
	chr06	FCS-type zinc-finger	Qin et al. (2021)
	chr06	HIPP	--
	chr06	Dirigent protein	Wang et al. (2022)
6	chr01	BTB/POZ domain	Wan et al. (2019)
	chr01	Expansin, cellulose-binding-like domain	Chen et al. (2017)
	chr03	Nucleotide-diphospho-sugar transferase	-
	chr03	Glutathione S-transferase	Xu et al. (2015); Yang et al. (2019)
	chr04	RING-type zinc-finger	Jung et al. (2013); Agarwal and Khurana (2020)
	chr10	FAD-linked oxidoreductase	Zhao et al. (2021); Wu et al. (2022)

The TDGs in *Paspalum vaginatum* contribute to adaptability, according to enrichment analyses

To gain insights into the biological processes necessary for the adaptation to the environment, the 2,542 TDGs in *P. vaginatum* were analyzed for GO enrichment. The set of TDGs was involved in 177 significant biological processes. The maximum Rich Factor was 0.75 (with xyloglucan biosynthesis), followed by 0.70 (with cellular response to high light intensity; Figure 2B; Supplementary Table 5). Then, a comparative analysis of four grass species (*O. sativa*, *S. italica*, *S. bicolor*, and *Z. mays*) with *P. vaginatum* was performed. Based on the GO terms, the *P. vaginatum* TDGs were found to be enriched in 62 unique GO terms compared with other analyzed species (Figure 2A). These GO terms included "cellular response to light intensity," "cellular response to UV" and "cellular response to heat" etc. (Figure 2C), which are related to adaptation to tropical climates. Other enriched GO terms included "ion transmembrane transporter activity," "anion transmembrane transporter activity" and "cation transmembrane transport" etc. (Figure 2C), which might be associated with adaptation to a saline environment.

KEGG pathway analysis provides classifications that are valuable for studying the complex biological functions of genes. Therefore, KEGG enrichment analysis was also performed on TDGs of the studied species. The results showed that TDGs in *P. vaginatum* were significantly enriched in 34 pathways (Figure 3B; Supplementary Table 6). The pathways enriched with the top three numbers of TDGs were "Phenylpropanoid biosynthesis," "MAPK signaling pathway" and "Metabolism of xenobiotics by cytochrome P450." In comparison to the other four species, *P. vaginatum* had six unique pathways (Figures 3A,C), five of which were related to KEGG pathway Metabolism ("Prodigiosin biosynthesis," "Tropane, piperidine and pyridine alkaloid biosynthesis," "Caprolactam degradation," "Nitrogen metabolism," "Biosynthesis of unsaturated fatty acids"), and one of which was related to Environmental Information Processing ("ABC transporters").

TDGs were tissue-specific under salt stress

Time-ordered, comparative, transcriptome analyses were performed, which focused on the expression of TDGs under salt stress. A total of 302 TDGs were identified as having up-regulated expression in response to salt stress (Supplementary Table 7), of

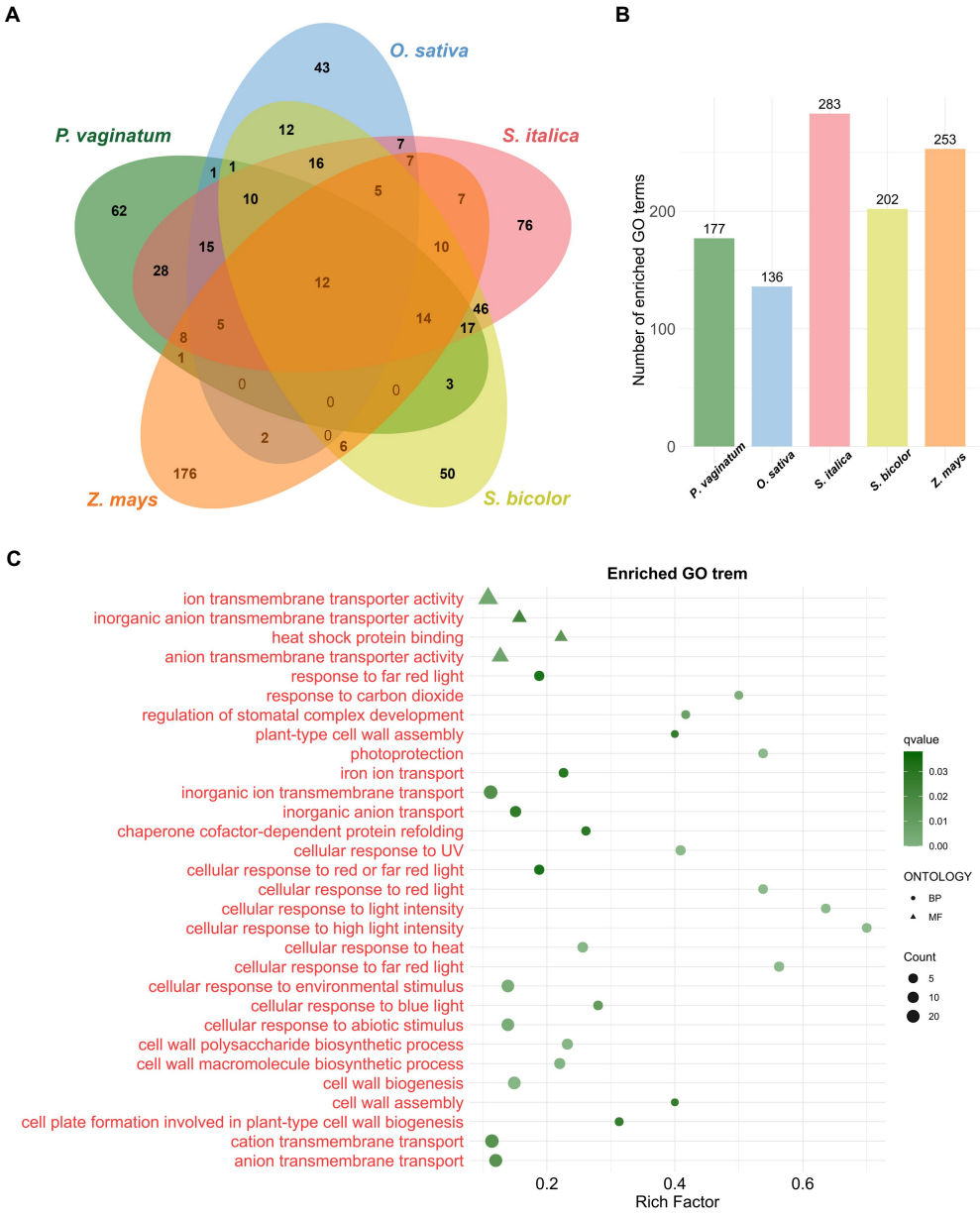

FIGURE 2
GO enrichment analysis of TDGs. **(A)** The venn diagram represents the shared and unique enriched GO terms among five species. **(B)** The size of enriched GO terms in each species. **(C)** The bubble diagram shows 30 significantly enriched GO terms. The terms in red are unique to *P. vaginatum* compared to the other four species.

which 48 were specifically expressed in leaves (Figure 4A); 116 were specifically expressed in roots (Figure 4B), and 138 were co-expressed in both roots and leaves (Figure 4C). These genes were annotated according to the NR, Swissprot and Pfam databases, and then literature searches were conducted to confirm whether their functions were related to salt resistance. It was found that most TDGs appeared to respond to salt stress. Some of these genes had been annotated as "Uncharacterized protein" (Supplementary Table 7), and it can be speculated that these genes also play an important role in the adaptation of *P. vaginatum* to salt stress. Even in the same gene family, some family members were expressed only in leaves but others in roots, such as "Cytochrome P450," "UDP glycosyltransferase" and "Multicopper oxidase family" etc.

The frequencies of synonymous substitution (Ks) were calculated to estimate the age of duplication events. There were similar peaks (~0.7) among the tissue-specifically expressed TDGs and the TDGs in whole genome. However, there was another peak (~2.5) with only tissue-specifically-expressed TDGs in leaves (Figure 4D), which included the gene functions for "Cation transporter," "Sulfate transporter," and "UDP-glycosyltransferase" etc. (Table 2).

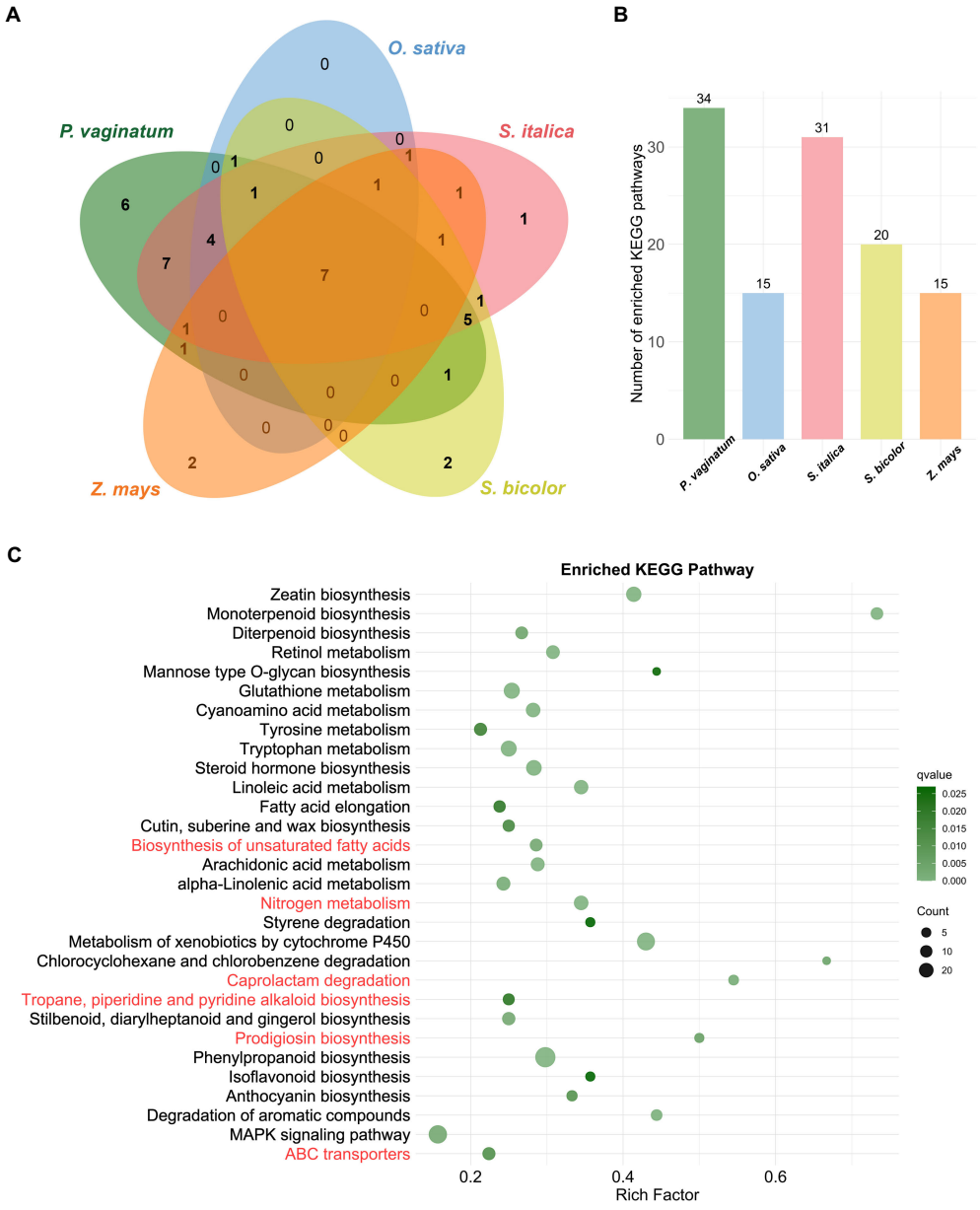

FIGURE 3
KEGG enrichment analysis of TDGs. **(A)** The venn diagram represents the shared and unique enriched KEGG pathways among five species. **(B)** The size of enriched KEGG pathways in each species. **(C)** The bubble diagram shows 30 significantly enriched KEGG pathways. The pathways in red are unique to *P. vaginatum* compared to the other four species.

Analysis of ABC gene family in *Paspalum vaginatum*

A total of 131 *P. vaginatum* ABC protein sequences were identified. To further understand the relationship between the ABC family genes, full-length protein sequences of *P. vaginatum* and *O. sativa* ABC proteins were aligned to construct a phylogenetic tree. The result showed that the ABC genes of these two species can be divided into eight subfamilies (Supplementary Figure 1). The ABC family genes in *P. vaginatum* were denoted as *PvABCA1-PvABCA6*, *PvABCB1-PvABCB33*, *PvABCC1-PvABCC17*, *PvABCD1-PvABCD5*, *PvABCE1-PvABCE4*, *PvABCF1-PvABCF9*, *PvABCG1-PvABCG45*, and *PvABCI1-PvABCI12*, according to their chromosomal location (Figure 5). Among these subfamilies, PvABCG had the largest number of members with 45 genes; PvABCB was the second largest subgroup, containing 33 genes; and the smallest subgroup was PvABCE, containing only 4 genes. Molecular masses ranged

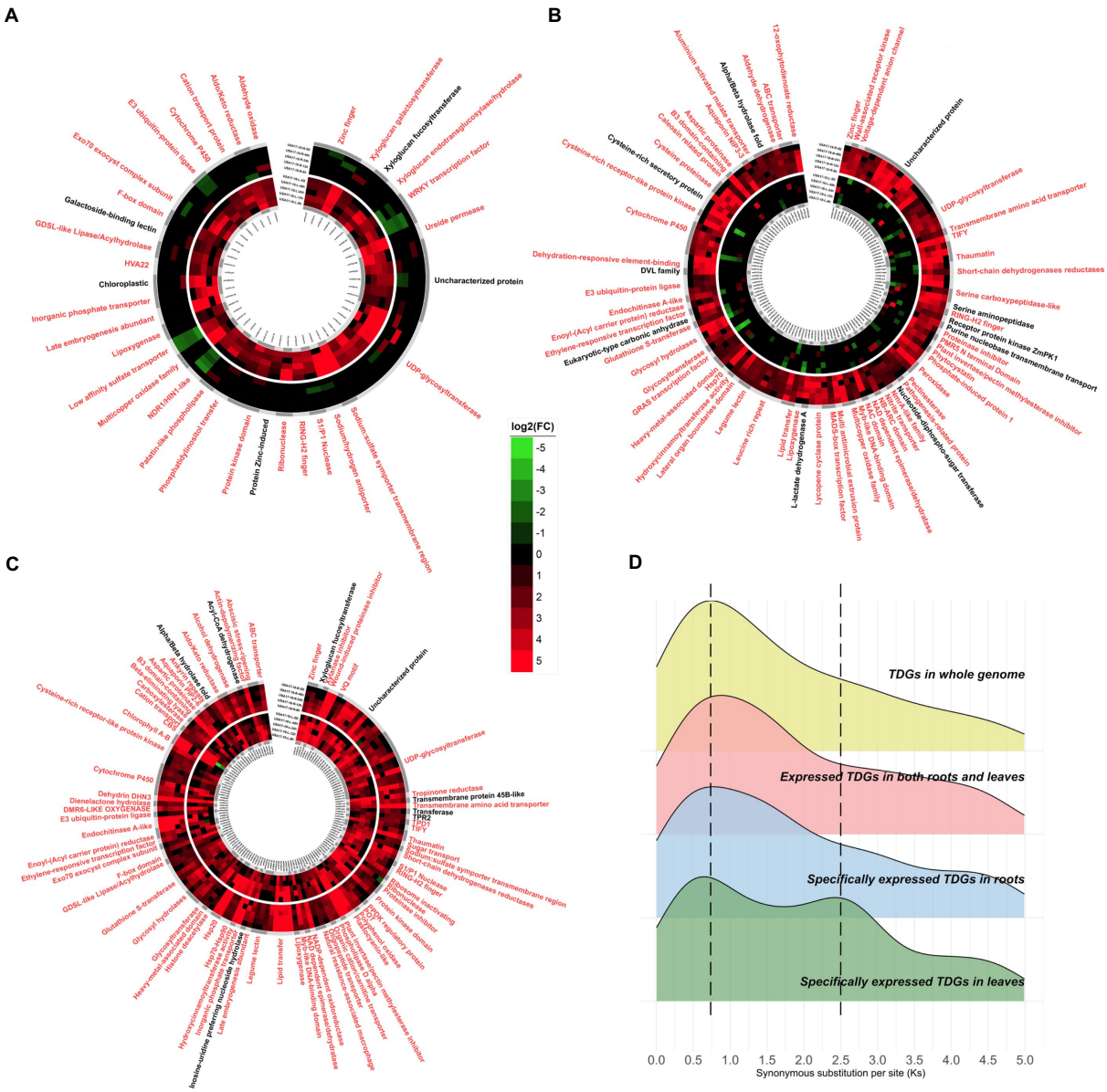

FIGURE 4
Tissue-specific expression of TDGs under salt stress. **(A)** Specifically expressed TDGs in leaves. Genes related to salt resistance with reviewed evidence were marked in red. **(B)** Specifically expressed TDGs in roots. **(C)** Expressed TDGs in both roots and leaves. **(D)** Distribution of Ks with different specific expression TDGs.

from 15.81 kDa to 596.82 kDa and pIs ranged from 4.81 to 9.87 (Supplementary Table 8).

To better understand the biological functions of the ABC family genes, the combined *P. vaginatum* transcriptome under salt stress was analyzed for expression patterns. As shown in Figure 5, the *PvABCs* exhibited different expression levels under salt stress. *PvABCB14* and *PvABCB15*, identified as TDGs, were highly upregulated in roots, whereas *PvABCC8* and *PvABCC9*, also identified as TDGs, were highly upregulated in leaves under salt stress. Many *PvABCs* were not differentially expressed.

Discussion

Long-tandem clusters in *Paspalum vaginatum* are strongly associated with abiotic stress

With long-tandem clusters (more than six genes in the same cluster), chromosomes 3 and 6 had the largest numbers of long clusters (four and three, respectively). A total of 14 long-tandem clusters (containing 97 TDGs) were found to be associated with abiotic stress, with 12 specifically associated with salt stress (Table 1).

TABLE 2 Specifically expressed TDGs in leaves with Ks of about 2.5.

Gene 1	Gene 2	Ka	Ks	Ka/Ks	Description
emOS121.100	emOS121.99	0.34	2.32	0.15	Galactoside-binding lectin
emFS28.27	emFS28.24	0.53	2.32	0.23	Uncharacterized protein
emOS169.431	emOS169.432	0.54	2.34	0.23	Protein Zinc-induced
emOS80.43	emOS80.44	0.53	2.43	0.22	E3 ubiquitin-protein ligase
emOS55.84.1	emOS55.83	0.46	2.49	0.18	Low affinity sulfate transporter
emFS4.55	emFS4.54	0.48	2.54	0.19	Cation transport protein
emFS28.24	emFS28.23	0.41	2.65	0.15	Uncharacterized protein
emFS26.201	emFS26.202	0.50	2.67	0.19	UDP-glycosyltransferase
emOS99.330	emOS99.331	0.26	2.84	0.09	Zinc finger
emOS56.23	emOS56.24	0.57	2.91	0.20	NDR1/HIN1-like
emOS36.477	emOS36.478	0.49	2.93	0.17	Xyloglucan fucosyltransferase
emOS55.83	emOS55.82	0.24	2.99	0.08	Low affinity sulfate transporter

Two clusters in particular (with nine and eight genes in each cluster) with function "UDP-glucosyl transferase" were of particular interest. Further research showed that "UDP-glucosyl transferase" can be associated with elevated antioxidant enzyme activity and reduced production of reactive oxygen species, which could control the oxidative burst under stress situations (Wang et al., 2021a). In the present study, many "UDP-glucosyl transferase" genes were identified resulting from tandem-duplication events, which have enriched the antioxidant capacity of *P. vaginatum*.

The unique GO terms and KEGG pathways of TDGs in *Paspalum vaginatum* seem to indicate contributions to salt tolerance

GO and KEGG enrichment analyses were used to determine the possible roles of TDGs in *P. vaginatum*, and were also compared in four related species (*O. sativa*, *S. italica*, *S. bicolor* and *Z. mays*). It was discovered that *P. vaginatum* TDGs were associated with some unique GO terms (such as "ion transmembrane transporter activity," "anion transmembrane transporter activity" and "cation transmembrane transport"). These GO terms indicate functions promoting osmoregulation, for example by accumulating compatible solutes to avoid osmotic stress caused by salinity (Kumari et al., 2015; Rahman et al., 2021). *P. vaginatum* TDGs were also found to be associated with some unique KEGG pathways, and one being "ABC transport." ABC transporters belong to a large protein family that utilize the energy released by ATP hydrolysis to transport a wide range of substrates across biological membranes. ABC transporters are involved in diverse cellular processes such as biotic and abiotic stress responses through plant hormone transport, ion transport, lipid transport and redox homeostasis (Do et al., 2018; Dahuja et al., 2021). In the present study, 131 ABC transporter genes were identified in *P. vaginatum*, with 13 (40%) of the 33 genes identified being TDGs. PvABCB was the second largest subgroup in the ABC transporter family and contained the most TDGs. *PvABCB14* and *PvABCB15*, identified from TDGs, were highly upregulated in roots, which might have an important role in enhancing the salt resistance of *P. vaginatum*.

The evolution of roots and leaves in response to salt stress

With transcriptome expression available at multiple time points under salt stress, *P. vaginatum* TDGs were divided into those with leaf-specific expression (48 TDGs), root-specific expression (116 TDGs), or co-expression in both leaves and roots (138 TDGs). Compared to leaves, roots had more TDGs in response to salt stress, possibly indicating that roots are more important than leaves in adapting to saline environments. Interestingly, when Ks was calculated for tissue-specifically expressed TDGs and compared with that for TDGs in whole genome, a similar peak (~0.7) was found, whereas another peak (~2.5) was found only in tissue-specifically expressed TDGs in leaves. Therefore, it was speculated that leaves became adapted to salt stress in an earlier whole genome duplication event (WGD; ~83.3 million years ago; Ma), whereas the entire *P. vaginatum* plant acquired a large number of TDGs related to salt stress in a second WGD (~23.3 Ma). Annotations of these expressed TDGs were found from multiple databases and it was found that most were related to salt stress. We therefore speculate that expressed TDGs annotated as "Uncharacterized protein" also contribute to salt resistance in *P. vaginatum*, and these genes could serve as potential and novel genes related to salt resistance.

Subfunctionalization of tandem duplicated pairs

Duplicate genes can diverge in function, representing a potential source of response mechanisms to survive stressful environments (Zou et al., 2009; Arsovski et al., 2015) and the TDGs in *P. vaginatum* have shown functional divergence. For example, emFS26.201 and emFS26.202 are tandem duplicated pairs (annotated as "UDP-glycosyltransferase"), but emFS26.201 has leaf-specific expression while emFS26.202 has root-specific expression under salt stress. As another example, from TDGs in the same tandem cluster, emOS168.286, emOS168.288, emOS168.289, and emOS168.290 (annotated as "Peroxidase"), only emOS168.290 responds to salt stress

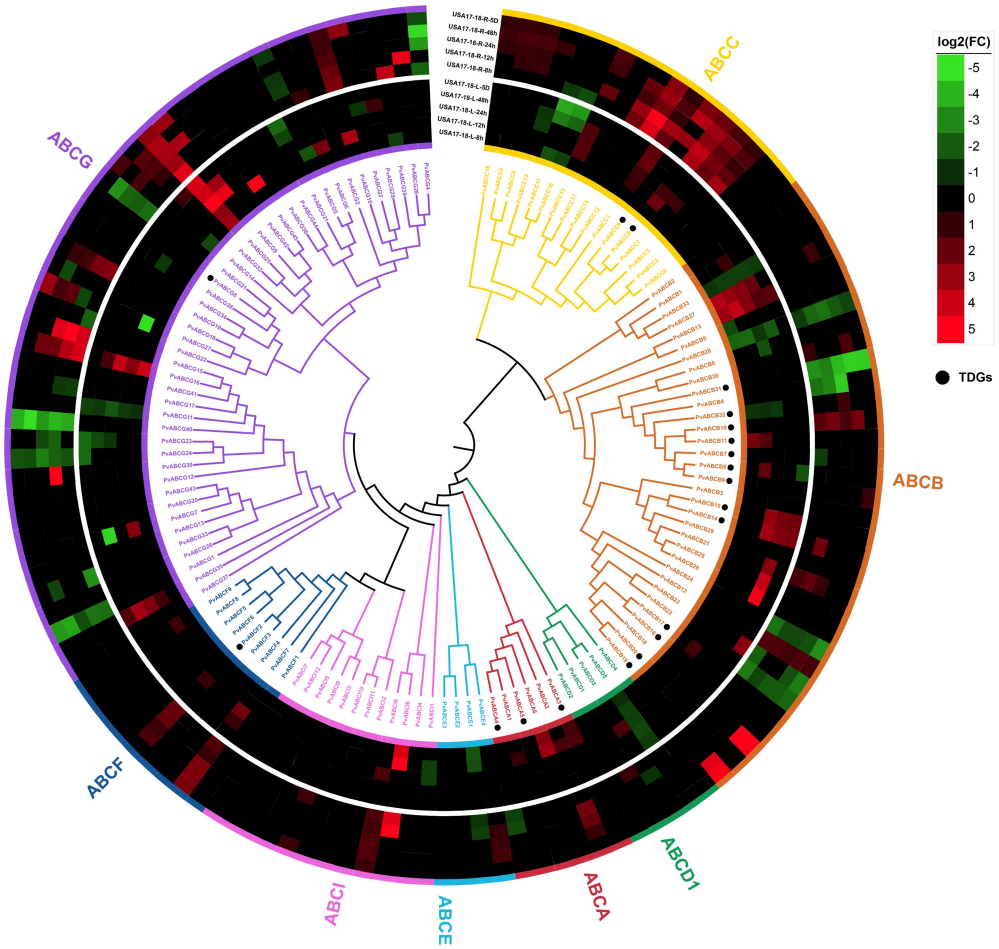

FIGURE 5
Phylogenetic tree of ABC transporter proteins from *P. vaginatum*. Eight subfamilies are highlighted in different colors. The genes marked with black dots represent TDGs. Heatmap shows transcriptome expression under salt stress.

(Supplementary Table 9). A total of 302 TDGs were identified in response to salt stress, and these TDGs were part of tandem clusters comprising 623 TDGs (Supplementary Table 9). In other words, nearly half of these duplicate lineages retain stress responsiveness.

The role of TDGs in evolution and adaptation

Evolutionary innovation is often built on variations from redundant genetic materials generated by gene duplication, and tandem duplication represents a potential source for such innovation (Arsovski et al., 2015; Guo et al., 2019). Previous studies have shown that: TDGs have driven diversification of the protein modifier SUMO in angiosperms (Hammoudi et al., 2016); TDGs have driven the divergent evolution of caffeine and crocin biosynthetic pathways in *Gardenia jasminoides* (Xu et al., 2020); TDGs are involved in defense and pollinator attraction in *Tectona grandis* (Zhao et al., 2019); and lastly that TDGs are significantly enriched in resistance-related pathways and more abundant in retrotransposon-related genes in *Cajanus cajan* (Liu et al., 2021). In this study, we identified TDGs in the *P. vaginatum* and found that TDGs of *P. vaginatum* were enriched in many unique GO terms and KEGG pathways which were associated with resistance, especially salt resistance. The TDGs associated with response to salt stress were identified by transcriptome analyses at multiple time points. This study provides insights into the roles of tandem duplications in the evolution and adaptation of *P. vaginatum* and lays the foundation for the genomics-based breeding of other grasses.

Data availability statement

The datasets presented in this study can be found in online repositories. The names of the repository/repositories and accession number(s) can be found in the article/Supplementary material. RNA-Seq data obtained have been uploaded to the National Center

for Biotechnology Information (https://www.ncbi.nlm.nih.gov/) and can be accessed with accession number PRJNA874860.

Author contributions

XH and J-SH contributed equally to this work performed data analyses, and wrote the manuscript. Z-YW and LL conceived and managed the project. MQ-T and YC designed the experiments. TX and L-ZR identified genes related to salt resistance through literature search. LP interpreted the results and revised the manuscript. All authors contributed to the article and approved the submitted version.

Funding

This work was supported by the National Natural Science Foundation of China (No.32060409), Key scientific research projects of colleges and universities in Hainan Province (No. Hnky2019ZD-3), the Construction of World First Class Discipline of Hainan University (No.RZZX201905), and National Project on Sci-Tec Foundation Resources Survey (2017FY100600).

Conflict of interest

The authors declare that the research was conducted in the absence of any commercial or financial relationships that could be construed as a potential conflict of interest.

Publisher's note

All claims expressed in this article are solely those of the authors and do not necessarily represent those of their affiliated organizations, or those of the publisher, the editors and the reviewers. Any product that may be evaluated in this article, or claim that may be made by its manufacturer, is not guaranteed or endorsed by the publisher.

Supplementary material

The Supplementary material for this article can be found online at: https://www.frontiersin.org/articles/10.3389/fpls.2022.971999/full#supplementary-material

SUPPLEMENTARY FIGURE 1
Phylogenetic tree of ABC transporter proteins from *P. vaginatum and O. sativa*. Eight subfamilies are highlighted in different colors.

SUPPLEMENTARY TABLE 1
Statistics of TDGs in *P. vaginatum* and other studied species.

SUPPLEMENTARY TABLE 2
Number of TDGs in chromosome of *P. vaginatum* genome.

SUPPLEMENTARY TABLE 3
Calculation of synonymous and nonsynonymous substitutions per site of TDG pairs.

SUPPLEMENTARY TABLE 4
TDGs with more than six genes in the same cluster and their functions.

SUPPLEMENTARY TABLE 5
GO enrichment results of TDGs in *P. vaginatum*.

SUPPLEMENTARY TABLE 6
KEGG enrichment results of TDGs in *P. vaginatum*.

SUPPLEMENTARY TABLE 7
TDGs which response to salt stress in *P. vaginatum*.

SUPPLEMENTARY TABLE 8
Basic information about the ABC transporter gene family in *P. vaginatum*.

SUPPLEMENTARY TABLE 9
Information of tandem clusters containing 302 tissue-specific TDGs.

SUPPLEMENTARY TABLE 10
Quality control of RNA-seq.

SUPPLEMENTARY TABLE 11
Expression (FPKM) of genes in *P. vaginatum* under salt stress.

References

Agarwal, P., and Khurana, P. (2020). TaZnF, a C3HC4 type RING zinc finger protein from *Triticum aestivum* is involved in dehydration and salinity stress. *J. Plant Biochem. Biotechnol.* 29, 395–406. doi: 10.1007/s13562-019-00546-8

Altschul, S. F., Madden, T. L., Schaffer, A. A., Zhang, J., Zhang, Z., Miller, W., et al. (1997). Gapped BLAST and PSI-BLAST: a new generation of protein database search programs. *Nucleic Acids Res.* 25, 3389–3402. doi: 10.1093/nar/25.17.3389

Arsovski, A. A., Pradinuk, J., Guo, X. Q., Wang, S., and Adams, K. L. (2015). Evolution of Cis-regulatory elements and regulatory networks in duplicated genes of *Arabidopsis*. *Plant Physiol.* 169, 2982–2991. doi: 10.1104/pp.15.00717

Bellieny-Rabelo, D., Oliveira, A. E., and Venancio, T. M. (2013). Impact of whole-genome and tandem duplications in the expansion and functional diversification of the F-box family in legumes (Fabaceae). *PLoS One* 8:e55127. doi: 10.1371/journal.pone.0055127

Bouzroud, S., Gouiaa, S., Hu, N., Bernadac, A., Mila, I., Bendaou, N., et al. (2018). Auxin response factors (ARFs) are potential mediators of auxin action in tomato response to biotic and abiotic stress (*Solanum lycopersicum*). *PLoS One* 13:e0193517. doi: 10.1371/journal.pone.0193517

Cannon, S. B., Mitra, A., Baumgarten, A., Young, N. D., and May, G. (2004). The roles of segmental and tandem gene duplication in the evolution of large gene families in *Arabidopsis thaliana*. *BMC Plant Biol.* 4:10. doi: 10.1186/1471-2229-4-10

Chen, C. J., Chen, H., Zhang, Y., Thomas, H. R., Frank, M. H., He, Y. H., et al. (2020). TBtools: an integrative toolkit developed for interactive analyses of big biological data. *Mol. Plant* 13, 1194–1202. doi: 10.1016/j.molp.2020.06.009

Chen, Y. H., Han, Y. Y., Kong, X. Z., Kang, H. H., Ren, Y. Q., and Wang, W. (2017). Ectopic expression of wheat expansin gene TaEXPA2 improved the salt tolerance of transgenic tobacco by regulating Na+/K+ and antioxidant competence. *Physiol. Plant.* 159, 161–177. doi: 10.1111/ppl.12492

Dahuja, A., Kumar, R. R., Sakhare, A., Watts, A., Singh, B., Goswami, S., et al. (2021). Role of ATP-binding cassette transporters in maintaining plant homeostasis under abiotic and biotic stresses. *Physiol. Plant.* 171, 785–801. doi: 10.1111/ppl.13302

Do, T. H. T., Martinoia, E., and Lee, Y. (2018). Functions of ABC transporters in plant growth and development. *Curr. Opin. Plant Biol.* 41, 32–38. doi: 10.1016/j.pbi.2017.08.003

Gasteiger, E., Gattiker, A., Hoogland, C., Ivanyi, I., Appel, R. D., and Bairoch, A. (2003). ExPASy: the proteomics server for in-depth protein knowledge and analysis. *Nucleic Acids Res.* 31, 3784–3788. doi: 10.1093/nar/gkg563

Guo, H., Jiao, Y., Tan, X., Wang, X., Huang, X., Jin, H., et al. (2019). Gene duplication and genetic innovation in cereal genomes. *Genome Res.* 29, 261–269. doi: 10.1101/gr.237511.118

Hammoudi, V., Vlachakis, G., Schranz, M. E., and van den Burg, H. A. (2016). Whole-genome duplications followed by tandem duplications drive diversification of the protein modifier SUMO in angiosperms. *New Phytol.* 211, 172–185. doi: 10.1111/nph.13911

Hofberger, J. A., Lyons, E., Edger, P. P., Chris Pires, J., and Eric Schranz, M. (2013). Whole genome and tandem duplicate retention facilitated glucosinolate pathway diversification in the mustard family. *Genome Biol. Evol.* 5, 2155–2173. doi: 10.1093/gbe/evt162

Holland, P. W. (1999). Gene duplication: past, present and future. *Semin. Cell Dev. Biol.* 10, 541–547. doi: 10.1006/scdb.1999.0335

Huerta-Cepas, J., Forslund, K., Coelho, L. P., Szklarczyk, D., Jensen, L. J., von Mering, C., et al. (2017). Fast genome-wide functional annotation through orthology assignment by egg NOG-mapper. *Mol. Biol. Evol.* 34, 2115–2122. doi: 10.1093/molbev/msx148

Jung, Y. J., Lee, I. H., Nou, I. S., Lee, K. D., Rashotte, A. M., and Kang, K. K. (2013). BrRZFP1 a *Brassica rapa* C3HC4-type RING zinc finger protein involved in cold, salt and dehydration stress. *Plant Biol.* 15, 274–283. doi: 10.1111/j.1438-8677.2012.00631.x

Kang, C., He, S. Z., Zhai, H., Li, R. J., Zhao, N., and Liu, Q. C. (2018). A sweetpotato auxin response factor gene (IbARF5) is involved in carotenoid biosynthesis and salt and drought tolerance in transgenic *Arabidopsis*. *Front. Plant Sci.* 9:1307. doi: 10.3389/fpls.2018.01307

Kim, D., Langmead, B., and Salzberg, S. L. (2015). HISAT: a fast spliced aligner with low memory requirements. *Nat. Methods* 12, 357–360. doi: 10.1038/nmeth.3317

Krishnamurthy, P., Vishal, B., Ho, W. J., Lok, F. C. J., Lee, F. S. M., and Kumar, P. P. (2020). Regulation of a cytochrome P450 gene CYP94B1 by WRKY33 transcription factor controls Apoplastic barrier formation in roots to confer salt tolerance. *Plant Physiol.* 184, 2199–2215. doi: 10.1104/pp.20.01054

Kumari, A., Das, P., Parida, A. K., and Agarwal, P. K. (2015). Proteomics, metabolomics, and ionomics perspectives of salinity tolerance in halophytes. *Front. Plant Sci.* 6:537. doi: 10.3389/fpls.2015.00537

Leister, D. (2004). Tandem and segmental gene duplication and recombination in the evolution of plant disease resistance gene. *Trends Genet.* 20, 116–122. doi: 10.1016/j.tig.2004.01.007

Letunic, I., and Bork, P. (2021). Interactive tree of life (iTOL) v5: an online tool for phylogenetic tree display and annotation. *Nucleic Acids Res.* 49, W293–W296. doi: 10.1093/nar/gkab301

Li, P., Li, Y. J., Zhang, F. J., Zhang, G. Z., Jiang, X. Y., Yu, H. M., et al. (2017). The *Arabidopsis* UDP-glycosyltransferases UGT79B2 and UGT79B3, contribute to cold, salt and drought stress tolerance via modulating anthocyanin accumulation. *Plant J.* 89, 85–103. doi: 10.1111/tpj.13324

Liu, L. M., Du, H. M., Wang, K., Huang, B. R., and Wang, Z. L. (2011). Differential photosynthetic responses to salinity stress between two perennial grass species contrasting in salinity tolerance. *HortScience* 46, 311–316. doi: 10.21273/Hortsci.46.2.311

Liu, C., Wu, Y. H., Liu, Y. X., Yang, L. Y., Dong, R. S., Jiang, L. Y., et al. (2021). Genome-wide analysis of tandem duplicated genes and their contribution to stress resistance in pigeonpea (*Cajanus cajan*). *Genomics* 113, 728–735. doi: 10.1016/j.ygeno.2020.10.003

Love, M. I., Huber, W., and Anders, S. (2014). Moderated estimation of fold change and dispersion for RNA-seq data with DESeq2. *Genome Biol.* 15:550. doi: 10.1186/s13059-014-0550-8

Magwanga, R. O., Lu, P., Kirungu, J. N., Dong, Q., Cai, X. Y., Zhou, Z. L., et al. (2019). Knockdown of cytochrome P450 genes Gh_D07G1197 and Gh_A13G2057 on chromosomes D07 and A13 reveals their putative role in enhancing drought and salt stress tolerance in *Gossypium hirsutum*. *Genes (Basel)* 10:226. doi: 10.3390/genes10030226

Marchler-Bauer, A., Bo, Y., Han, L., He, J., Lanczycki, C. J., Lu, S., et al. (2017). CDD/SPARCLE: functional classification of proteins via subfamily domain architectures. *Nucleic Acids Res.* 45, D200–D203. doi: 10.1093/nar/gkw1129

Minh, B. Q., Schmidt, H. A., Chernomor, O., Schrempf, D., Woodhams, M. D., von Haeseler, A., et al. (2020). IQ-TREE 2: new models and efficient methods for phylogenetic inference in the genomic era. *Mol. Biol. Evol.* 37, 1530–1534. doi: 10.1093/molbev/msaa015

Mistry, J., Chuguransky, S., Williams, L., Qureshi, M., Salazar, G. A., Sonnhammer, E. L. L., et al. (2021). Pfam: the protein families database in 2021. *Nucleic Acids Res.* 49, D412–D419. doi: 10.1093/nar/gkaa913

Mistry, J., Finn, R. D., Eddy, S. R., Bateman, A., and Punta, M. (2013). Challenges in homology search: HMMER3 and convergent evolution of coiled-coil regions. *Nucleic Acids Res.* 41:e121. doi: 10.1093/nar/gkt263

Panchy, N., Lehti-Shiu, M., and Shiu, S. H. (2016). Evolution of gene duplication in plants. *Plant Physiol.* 171, 2294–2316. doi: 10.1104/pp.16.00523

Paterson, A. H., Freeling, M., Tang, H., and Wang, X. (2010). Insights from the comparison of plant genome sequences. *Annu. Rev. Plant Biol.* 61, 349–372. doi: 10.1146/annurev-arplant-042809-112235

Qi, P., Eudy, D., Schnable, J. C., Schmutz, J., Raymer, P. L., and Devos, K. M. (2019). High density genetic maps of seashore paspalum using genotyping-by-sequencing and their relationship to the sorghum bicolor genome. *Sci. Rep.* 9:12183. doi: 10.1038/s41598-019-48257-3

Qiao, X., Li, Q. H., Yin, H., Qi, K. J., Li, L. T., Wang, R. Z., et al. (2019). Gene duplication and evolution in recurring polyploidization-diploidization cycles in plants. *Genome Biol.* 20:38. doi: 10.1186/s13059-019-1650-2

Qin, Y. X., Cui, S. F., Cui, P., Zhang, B., and Quan, X. Y. (2021). TaFLZ2D enhances salinity stress tolerance via superior ability for ionic stress tolerance and ROS detoxification. *Plant Physiol. Biochem.* 168, 516–525. doi: 10.1016/j.plaphy.2021.11.014

Rahman, M. M., Mostofa, M. G., Keya, S. S., Siddiqui, M. N., Ansary, M. M. U., Das, A. K., et al. (2021). Adaptive mechanisms of halophytes and their potential in improving salinity tolerance in plants. *Int. J. Mol. Sci.* 22:10733. doi: 10.3390/ijms221910733

Rasheed, A., Li, H., Nawaz, M., Mahmood, A., Hassan, M. U., Shah, A. N., et al. (2022). Molecular tools, potential frontiers for enhancing salinity tolerance in rice: A critical review and future prospective. *Front. Plant Sci.* 13. doi: 10.3389/fpls.2022.966749

Rizzon, C., Ponger, L., and Gaut, B. S. (2006). Striking similarities in the genomic distribution of tandemly arrayed genes in *Arabidopsis* and rice. *PLoS Comput. Biol.* 2:e115. doi: 10.1371/journal.pcbi.0020115

Roy, S. J., Negrao, S., and Tester, M. (2014). Salt resistant crop plants. *Curr. Opin. Biotechnol.* 26, 115–124. doi: 10.1016/j.copbio.2013.12.004

Rozewicki, J., Li, S. L., Amada, K. M., Standley, D. M., and Katoh, K. (2019). MAFFT-DASH: integrated protein sequence and structural alignment. *Nucleic Acids Res.* 47, W5–W10. doi: 10.1093/nar/gkz342

Spiekerman, J. J., and Devos, K. M. (2020). The halophyte seashore paspalum uses adaxial leaf papillae for sodium sequestration. *Plant Physiol.* 184, 2107–2119. doi: 10.1104/pp.20.00796

Uddin, M. K., Juraimi, A. S., Ismail, M. R., Hossain, M. A., Othman, R., and Rahim, A. A. (2012). Physiological and growth responses of six Turfgrass species relative to salinity tolerance. *Sci. World J* 2012:905468. doi: 10.1100/2012/905468

Wan, X., Peng, L., Xiong, J., Li, X. Y., Wang, J. M., Li, X. F., et al. (2019). AtSIBP1, a novel BTB domain-containing protein, positively regulates salt signaling in *Arabidopsis thaliana*. *Plants Basel* 8:573. doi: 10.3390/plants8120573

Wang, Y. Y., Cao, Y. B., Liang, X. Y., Zhuang, J. H., Wang, X. F., Qin, F., et al. (2022). A dirigent family protein confers variation of casparian strip thickness and salt tolerance in maize. *Nat. Commun.* 13:2222. doi: 10.1038/s41467-022-29809-0

Wang, Y., Chen, F., Ma, Y., Zhang, T., Sun, P., Lan, M., et al. (2021b). An ancient whole-genome duplication event and its contribution to flavor compounds in the tea plant (*Camellia sinensis*). *Hortic Res.* 8:176. doi: 10.1038/s41438-021-00613-z

Wang, Z. B., Li, H., Wei, Z. P., Sun, H. R., He, Y., Gao, J., et al. (2021c). Overexpression of UDP-glycosyltransferase genes enhanced aluminum tolerance through disrupting cell wall polysaccharide components in soybean. *Plant Soil* 469, 135–147. doi: 10.1007/s11104-021-05157-8

Wang, T., Ma, Y. Q., Huang, X. X., Mu, T. J., Li, Y. J., Li, X. K., et al. (2021a). Overexpression of OsUGT3 enhances drought and salt tolerance through modulating ABA synthesis and scavenging ROS in rice. *Environ. Exp. Bot.* 192:104653. doi: 10.1016/j.envexpbot.2021.104653

Wang, Y., Tang, H., Debarry, J. D., Tan, X., Li, J., Wang, X., et al. (2012). MCScanX: a toolkit for detection and evolutionary analysis of gene synteny and collinearity. *Nucleic Acids Res.* 40:e49. doi: 10.1093/nar/gkr1293

Wang, T. T., Yu, T. F., Fu, J. D., Su, H. G., Chen, J., Zhou, Y. B., et al. (2020). Genome-wide analysis of the GRAS gene family and functional identification of GmGRAS37 in drought and salt tolerance. *Front. Plant Sci.* 11:604690. doi: 10.3389/fpls.2020.604690

Wu, T., Hu, E., Xu, S., Chen, M., Guo, P., Dai, Z., et al. (2021). clusterProfiler 4.0: a universal enrichment tool for interpreting omics data. *Innovations* 2:100141. doi: 10.1016/j.xinn.2021.100141

Wu, J. Q., Liu, W. K., Jahan, M. S., Shu, S., Sun, J., and Guo, S. R. (2022). Characterization of polyamine oxidase genes in cucumber and roles of CsPAO3 in response to salt stress. *Environ. Exp. Bot.* 194:104696. doi: 10.1016/j.envexpbot.2021.104696

Wu, X. L., Shi, H. F., and Guo, Z. F. (2018). Overexpression of a NF-YC gene results in enhanced drought and salt tolerance in transgenic seashore paspalum. *Front. Plant Sci.* 9:1355. doi: 10.3389/fpls.2018.01355

Xu, Z., Pu, X., Gao, R., Demurtas, O. C., Fleck, S. J., Richter, M., et al. (2020). Tandem gene duplications drive divergent evolution of caffeine and crocin biosynthetic pathways in plants. *BMC Biol.* 18:63. doi: 10.1186/s12915-020-00795-3

Xu, J., Xing, X. J., Tian, Y. S., Peng, R. H., Xue, Y., Zhao, W., et al. (2015). Transgenic *Arabidopsis* plants expressing tomato glutathione S-Transferase showed enhanced resistance to salt and drought stress. *PLoS One* 10:e0136960. doi: 10.1371/journal.pone.0136960

Yang, Q., Liu, Y. J., and Zeng, Q. Y. (2019). Overexpression of three orthologous glutathione S-transferases from populus increased salt and drought resistance in *Arabidopsis*. *Biochem. Syst. Ecol.* 83, 57–61. doi: 10.1016/j.bse.2019.01.001

Yang, F. S., Nie, S., Liu, H., Shi, T. L., Tian, X. C., Zhou, S. S., et al. (2020). Chromosome-level genome assembly of a parent species of widely cultivated azaleas. *Nat. Commun.* 11:5269. doi: 10.1038/s41467-020-18771-4

Yu, J., Ke, T., Tehrim, S., Sun, F., Liao, B., and Hua, W. (2015). PTGBase: an integrated database to study tandem duplicated genes in plants. *Database (Oxford)* 2015:bav017. doi: 10.1093/database/bav017

Zhang, S., Li, X. W., Fan, S. D., Zhou, L. J., and Wang, Y. (2020). Overexpression of HcSCL13, a Halostachys caspica GRAS transcription factor, enhances plant growth and salt stress tolerance in transgenic *Arabidopsis*. *Plant Physiol. Biochem.* 151, 243–254. doi: 10.1016/j.plaphy.2020.03.020

Zhang, Z., Xiao, J. F., Wu, J. Y., Zhang, H. Y., Liu, G. M., Wang, X. M., et al. (2012). ParaAT: a parallel tool for constructing multiple protein-coding DNA alignments. *Biochem. Biophys. Res. Commun.* 419, 779–781. doi: 10.1016/j.bbrc.2012.02.101

Zhao, D., Hamilton, J. P., Bhat, W. W., Johnson, S. R., Godden, G. T., Kinser, T. J., et al. (2019). A chromosomal-scale genome assembly of Tectona grandis reveals the importance of tandem gene duplication and enables discovery of genes in natural product biosynthetic pathways. *Gigascience* 8:giz005. doi: 10.1093/gigascience/giz005

Zhao, Y., Li, X., Zhang, Z. X., Pan, W. J., Li, S. N., Xing, Y., et al. (2021). GmGPDH12, a mitochondrial FAD-GPDH from soybean, increases salt and osmotic stress resistance by modulating redox state and respiration. *Crop J.* 9, 79–94. doi: 10.1016/j.cj.2020.05.008

Zou, C., Lehti-Shiu, M. D., Thomashow, M., and Shiu, S. H. (2009). Evolution of stress-regulated gene expression in duplicate genes of *Arabidopsis thaliana*. *PLoS Genet.* 5:e1000581. doi: 10.1371/journal.pgen.1000581

frontiers | Frontiers in Plant Science

TYPE Original Research
PUBLISHED 30 September 2022
DOI 10.3389/fpls.2022.1001206

OPEN ACCESS

EDITED BY
Jing Zhang,
Nanjing Agricultural University, China

REVIEWED BY
Ke Teng,
Beijing Academy of Agricultural and Forestry Sciences, China
Gang Nie,
Sichuan Agricultural University, China

*CORRESPONDENCE
Ruicai Long
longruicai@caas.cn
Mingna Li
limingna@caas.cn

SPECIALTY SECTION
This article was submitted to Plant Abiotic Stress, a section of the journal Frontiers in Plant Science

RECEIVED 23 July 2022
ACCEPTED 23 August 2022
PUBLISHED 30 September 2022

CITATION
Yu A, Jiang X, Sun Y, Hu Q, Zhu X, Kang J, Chen L, Liu L, Hao L, Yang Q, Long R and Li M (2022) Genome-wide identification, characterization, and expression analysis of UDP-glycosyltransferase genes associated with secondary metabolism in alfalfa (*Medicago sativa* L.). *Front. Plant Sci.* 13:1001206. doi: 10.3389/fpls.2022.1001206

Genome-wide identification, characterization, and expression analysis of UDP-glycosyltransferase genes associated with secondary metabolism in alfalfa (*Medicago sativa* L.)

Andong Yu[1,2], Xueqian Jiang[1], Yan Sun[2], Qiannan Hu[2], Xiaoxi Zhu[1], Junmei Kang[1], Lin Chen[1], Lin Liu[3], Linfeng Hao[3], Qingchuan Yang[1], Ruicai Long[1]* and Mingna Li[1]*

[1]Institute of Animal Sciences, Chinese Academy of Agricultural Sciences, Beijing, China, [2]College of Grassland Science and Technology, China Agricultural University, Beijing, China, [3]Bayannur Institute of Agricultural and Animal Husbandry Sciences, Inner Mongolia, China

Uridine diphosphate glycosyltransferases (UGTs) are enzymes that catalyze glycosylation modifications and play an essential role in regulating plant metabolism. Alfalfa (*Medicago sativa* L.) is the most important legume in the world due to its high yields and protein content; however, the *UGT* genes in alfalfa have not yet been studied. Identifying *UGT* genes with metabolic roles in alfalfa is essential for identifying and modifying genetic traits that are relevant to yield and quality. In this study, 90 of the 239 *UGT* genes identified from the alfalfa "Zhongmu No. 1" genome database were found to be related to secondary metabolism, and a series of gene family characterization analyses were conducted on each. The results demonstrated that all 90 *UGT* genes were unevenly distributed on eight chromosomes with few introns and that tandem duplications were the crucial driving force expanding the UGT family in alfalfa. Notably, the 90 *UGT* genes can be clustered into ten evolutionary groups which contain specific PSPG motifs, and genes in these ten groups have specific tissue expressions. This suggests that the *UGT* genes in each group could have similar glycosylation roles corresponding to analogous secondary metabolites in alfalfa. Additionally, multiple *cis*-acting elements found in *MsUGT* promoter regions, such as phytohormone and flavonoids, indicate that 90 *UGT* members could be induced by these features, which are also related to secondary metabolism. Therefore, our study identified 90 UGT members inten evolutionary groups that are likely

related to glycosylation modifications with secondary metabolites in alfalfa. These findings help uncover pivotal regulatory mechanisms associated with secondary metabolism in plant yield and quality and contribute to genetic modification and breeding in alfalfa and other plant species.

KEYWORDS

Medicago sativa, UDP glycosyltransferase, secondary metabolism, flavonoids, terpenoids, phylogenetic analysis

Introduction

Glycosyltransferases (GTs) are enzymes that utilize activated glycosyl donors as substrates to regulate biochemical properties and subcellular localization by catalyzing the glycosylation reactions of molecules such as proteins, lipids, plant hormones, and phenylpropane compounds (Song et al., 2018; Speeckaert et al., 2020). In plants, glycosylation can preserve the diversity of small molecular compounds and plays an important role in regulating biological processes such as seed germination, growth, flowering, fruiting, and senescence (Li H. et al., 2020; Wu et al., 2020). The GT family 1 (GT1), which is referred to as UDP glycosyltransferase (UGT), mainly catalyzes UDP sugar transfer to specific receptors, such as proteins, nucleic acids, antibiotics, alkaloids, and plant hormones, and is the largest glycosyltransferase gene family in the plant kingdom (Zhang et al., 2020).

UGT is ubiquitous existed in both unicellular algae, where it has a simple structure, and higher plants, where it has a complicated structure (Rehman et al., 2018; Song et al., 2018). The first plant UGT family gene, *Bronze1*, which encodes a UGT enzyme that can synthesize flavonoid glycosides and regulate the accumulation of melanin in maize (*Zea mays*) seeds, was identified by Barbara McClintock in 1977 when she was studying the genetic traits of transposons in maize (Dooner and Nelson, 1977). Currently, many UGT gene families have been identified in several crops and plant species at the whole genome-wide level, such as wheat (*Triticum aestivum*) (He et al., 2018), soybean (*Glycine max)* (Yano et al., 2018), rice (*Oryza sativa*) (Dong et al., 2020), and *Arabidopsis thaliana* (Chen T. T. et al., 2020). Meanwhile, the sophisticated roles of plant hormone regulation, biotic and abiotic stress adaptation, yield and quality enhancement, and secondary metabolism adjustment, that UGTs played, have also been highlighted (Mohnike et al., 2021; Kurze et al., 2022; Wang et al., 2022; Zhang et al., 2022).

For instance, UGTs such as UGT84B1 and UGT76F1 in *Arabidopsis* (Aoi et al., 2020; Chen L. et al., 2020), CsUGT85A53 in *Camellia sinensis* (Jing et al., 2020), UGT76C2 in *Arabidopsis* (Li Y. et al., 2020), and the promoter of *SbUGT* in poplar (*Scutellaria barbata*) (Li et al., 2019), reportedly participate in regulating the glycosylation modifications of auxin (IAA), abscisic acid (ABA), and cytokinin (CK), respectively, controlling the growth and development of the roots, flowering, and root buds, respectively. Furthermore, UGTs such as AtUGT71C3 can compromise the excessive defense response of *Arabidopsis* by regulating the steady state of MeSA and SA (Chen et al., 2019), while the down-regulation of *CsUGT91Q2* decreased the scavenging capacity of reactive oxygen species and caused sensitivity to low-temperature stress (Zhao et al., 2020). Moreover, UGTs such as GhUGT103, GhUGT105 (Xiao et al., 2019), and OsUGT83A1 (Dong et al., 2020) were involved in regulating fiber development in upland cotton (*Gossypium hirsutum* L.) and grain size in rice, and have been considered important traits of grain yield.

In particular, UGTs such as UGT79B2 and UGT79B3 in *Arabidopsis* (Li et al., 2017), ZmUFGT2 (UGT78D2) in maize (Li et al., 2018), and UGT87A1 in *Carex rigescens* (Zhang K. et al., 2021), are involved in secondary metabolism *via* the glycosylation of flavonoids, which are a kind of natural polyphenolic secondary metabolite with antioxidant and free radical scavenging functions in different tissues (Rojas Rodas et al., 2014; Huo et al., 2021). Additionally, these UGTs can catalyze glycosylation reactions from anthocyanins, kaemferol, and quercetin to the corresponding glycosides *in vivo*. Decreasing the expression of *CsUGT91Q2* resulted in the decrease of neroli glycoside and caused sensitivity to low-temperature stress (Zhao et al., 2020), indicating that UGT acts on glycosylation terpenoids, which are the largest category of secondary metabolites (with more than 40,000 structures) and have several biological functions such as anti-tumor, antibacterial, hypoglycemic and economic value due to their flavor, tastants, and colorants (Chan et al., 2016; Kurze et al., 2022). Moreover, studies have demonstrated that the soyasaponins of soybean (Yano et al., 2018) and rebaudioside A (Reb A) of *Stevia rebaudiana* (Kim et al., 2019) can be converted by UGT91H9 and UGT76G1 respectively, leading to better taste and higher quality. Generally, the glycosylation modification functions that plant UGTs have on various secondary metabolites can generate active molecules that are involved in several processes related to biological regulation (Rehman et al., 2018; Yu et al., 2022). Therefore, studying the

functions of UGTs involved in secondary metabolism is essential for identifying and modifying genetic traits highly relevant to crop yield and quality production.

There is a highly conserved plant secondary product glycosyltransferase box (PSPG) composed of 44 amino acids at the C-terminal of the UGT gene family protein (Cheng et al., 2019). A previous study proposed that the whole folding and core region of UGT proteins in plants are conserved since the C-terminal domain of UGT proteins mostly recognizes the same or similar glycosyl donors, and the N-terminal domain recognizes specific receptors (Nair et al., 2020). This indicates that the PSPG motif is an important binding region that can recognize the UDP sugar donor of uridine, which contributes to glycosylating specific secondary metabolites in plants (Cheng et al., 2019). While the evolutionary relationships of the UGT gene family members are related and have similar exon and intron numbers and sequence characteristics (Xiao et al., 2019), 122, 148, 184, and 128 *UGT* genes have been identified in *Arabidopsis*, maize, grape (*Vitis vinifera* L.) and soybean, respectively, using the PSPG motif (Rehman et al., 2018). This suggests that UGTs have certain specificity in different plant species. For example, after comparing the amino acid sequences encoded by five *UGT* genes related to terpenoid glycosylation in *Panax notoginseng*, the positions of 17 amino acids were found to be highly conservative, while the other positions vary (Wang et al., 2020). Therefore, it is necessary to identify and characterize the specific UGT gene family in certain plant species before investigating the UGTs involved in secondary metabolic regulation.

Alfalfa (*Medicago sativa* L.) is the most important and widespread legume plant worldwide and is prized for its high protein content, nutritional quality, yield, and environmental adaptability (Barros et al., 2019; Shen et al., 2020). Studying the molecular regulatory role of *UGT* genes in alfalfa is important for improving its yield and quality through genetic engineering. However, few studies have researched *UGT* genes in alfalfa, and the biological role of UGTs associated with secondary metabolism has not been understood until now. Recently, the genome sequence data of the autotetraploid plant alfalfa has been gradually completed (Chen H. et al., 2020; Shen et al., 2020; Long et al., 2022), providing valuable genomic information and making it possible to identify and research the function of the UGT gene family in alfalfa at the genome-wide level. In this study, we performed a systematic genome-wide analysis to identify UGT family genes in alfalfa and screened 90 of them for their association with secondary metabolism. These 90 *UGT* genes were then clustered into ten phylogenetic groups, and their evolutionary relationship, conserved motif, chromosomal distribution, gene structure, *cis*-acting elements, intra- and inter-species collinearity, and tissue expression patterns were analyzed. This study aimed to identify the UGT gene family in alfalfa involved in secondary metabolism at the genome-wide level and clarify their gene and protein molecular characteristics, evolutionary relationship, and major induced factors. The results provide comprehensive genetic information and outline the molecular features of *UGT* genes related to secondary metabolism in alfalfa.

Materials and methods

Plant materials and treatments

Alfalfa (*Medicago sativa* L. cv. Zhongmu-1) seeds preserved in our lab were used as the plant material. Alfalfa seeds were germinated on filter paper immersed with ultrapure water in a petri dish in a growth chamber (GXZ-500, Jiangnan, China) 16 h light (1,200–1,250 μmol m^{-2} s^{-1}) at 25°C and 8 h darkness at 20°C. After 7 days of germination, the seedlings were transferred to a plastic cuboid container (25 cm × 20 cm × 7.5 cm) with 1/2 Hoagland nutrient solution under controlled conditions. For the transcriptional expression assay, the 4-week-old Hoagland solution was used to culture alfalfa seedlings under identical growth conditions. Samples were obtained from seven sections, including the new leaves (NL), the mature leaves (ML), the first real leaves (FL), and the stems of each 1/3 position from top to bottom: upper stems (US), middle stems (MS) and bottom stems (BS), and root, with three biological replicates for each (Ma et al., 2021).

Identification and sequence analysis of *UGT* genes in alfalfa

The *M. sativa* "Zhongmu No. 1" genome information (Shen et al., 2020) was downloaded from the figshare website[1]. UGT protein sequences of *Arabidopsis* were retrieved from the P450 database[2]. Alfalfa *UGT* genes were confirmed using the local BLAST with a cutoff E-value of 1.0 × 10^{-10} and TBtools software (Huazhong Agricultural University, Wuhan, China) (Chen C. et al., 2020). The UGT protein sequences of alfalfa were aligned using the Hidden Markov Model (HMM) model on the Pfam online website[3] (Finn et al., 2014). The UDPGT domain (PF00201) was used to identify UGT members in the Pfam database[4] (Finn et al., 2014).

UGT proteins identified in alfalfa were annotated in the eggNOG-Mapper database[5] functional annotation enrichment (Huerta-Cepas et al., 2019). UGT proteins involved in secondary metabolism were considered by the Pathway Name and

1 https://figshare.com/articles/dataset/Medicago_sativa_genome_and_annotation_files/12623960
2 http://www.p450.kvl.dk/UGT.shtml
3 http://hmmer.org/
4 https://www.ebi.ac.uk/Tools/pfa/pfamscan/
5 http://eggnog-mapper.embl.de/

Description in the KEGG Pathway Database[6] (Antonov et al., 2010), including metabolic pathways (K01115), glucosinolate biosynthesis (K11280), biosynthesis of various plant secondary metabolites (K21371), monoterpenoid biosynthesis (K21373, K21374), anthocyanin biosynthesis (K12930, K12938, K17193), zeatin biosynthesis (K13493, K13494, K13495, K13496), and phenylpropanoid biosynthesis (K12356).

Phylogenetic analysis and comparison of *MsUGT* genes

Basic physical and chemical characteristics, including the sequence start position, sequence end position, length, molecular weight, isoelectric point, and Grand average of hydropathicity (GRAVY) of *UGT* genes in alfalfa, which were screened by KEGG functional enrichment, were obtained from the ExPASy website[7] (Gasteiger et al., 2003). Subcellular localization prediction was performed by WoLF PSORT[8] (Horton et al., 2007).

Divergent UGT protein sequences were removed from the identified sequences after alignment with MEGA 11 software. The phylogenetic tree was built using MEGA11 software (Tamura et al., 2021) with UGT protein sequences from alfalfa, *Arabidopsis*, and maize by the neighbor-joining (NJ) method (bootstrap values for 1,000 replicates) and was visualized using the Evolview website[9]. UGT proteins in alfalfa were classified according to the 14 reported evolutionary groups in *Arabidopsis* (A-N) and the other three new groups found in maize (O-Q). The conserved PSPG motif, composed of 44 amino acids in each UGT phylogenetic group, was analyzed using MEME software[10] (Bailey et al., 2009).

Chromosomal location and structural characterization analysis of *MsUGT* genes

Information on the chromosomal location of *UGT* genes was retrieved and generated by TBtools. Ten motifs with lengths of 15–50 amino acids in UGT proteins from alfalfa were identified using the online MEME Suite (see text footnote 10) (Bailey et al., 2009). The MAST file was obtained from the MEME website, and the Newick tree string was visualized in TBtools. The exon and intron structures of *MsUGT* genes were analyzed using TBtools software, inputting gene annotation GFF files and Newick tree string.

6 https://www.genome.jp/kegg/pathway.html
7 https://web.expasy.org/compute_pi/
8 https://wolfpsort.hgc.jp/
9 http://www.evolgenius.info/evolview/
10 https://meme-suite.org/meme/tools/meme

Analysis of *cis*-acting elements of *MsUGT* genes

The promoter regions of *MsUGT* genes (2,000 bp sequence upstream of the DNA genome sequences) were obtained from the *M. sativa* genome database. PlantCARE database[11] was used to predict the *cis*-acting elements (Lescot et al., 2002). The results containing promoter information and the phylogenetic evolution of the UGT gene family in alfalfa were visualized using TBtools software.

Gene duplication pattern and collinearity analysis of *MsUGT* genes

The identification of gene duplication patterns in *MsUGT* genes was performed using multiple collinear scanning toolkits (MCScanX) with an E-value set to 10^{-5}. The syntenic relationship between *MsUGT* genes and *UGT* genes from *Medicago truncatula*, *Arabidopsis thaliana*, *Oryza sativa*, and *Glycine max* were determined using the Dual Synteny Plotter function in the TBtools software. The necessary genome sequence was obtained from the BioMart Ensemble plants database[12].

Tissue differential expression analysis of *MsUGT* genes in each evolutionary group

Total plant RNA was extracted using the total RNA Extraction kit (Shanghai Promega Biological Products, China), according to the manufacturer's instructions. Complementary DNA was generated with reverse transcriptase (TaKaRa, Beijing, China) at 42°C for 2 min, then at 37°C for 15 min, and finally at 85°C for 5 s. Quantitative real-time PCR (qRT-PCR) was conducted with 2 × EasyTaq® PCR SuperMix (+ dye) (TransGen Biotech, Beijing, China), according to the manufacturer's instructions, on the CFX96 Touch™ RT-PCR system (BioRad, Los Angeles, CA, United States). Three technical repeats were performed for each sample. The specific primer sequences of *MsUGT* genes for qRT-PCR determination are provided in **Supplementary Table 1**. The *Ms-ACTIN* gene was used as an internal control (**Supplementary Table 1**). The relative transcriptional expressions of each gene were analyzed based on the $2^{-\Delta\Delta Ct}$ method (Livak and Schmittgen, 2001). SPSS 20 software was used to process the experimental data by the analysis of variance (ANOVA). The least significant difference method (LSD, $P < 0.05$ level) was used for statistical

11 https://bioinformatics.psb.ugent.be/webtools/plantcare/html/
12 https://plants.ensembl.org/index.html

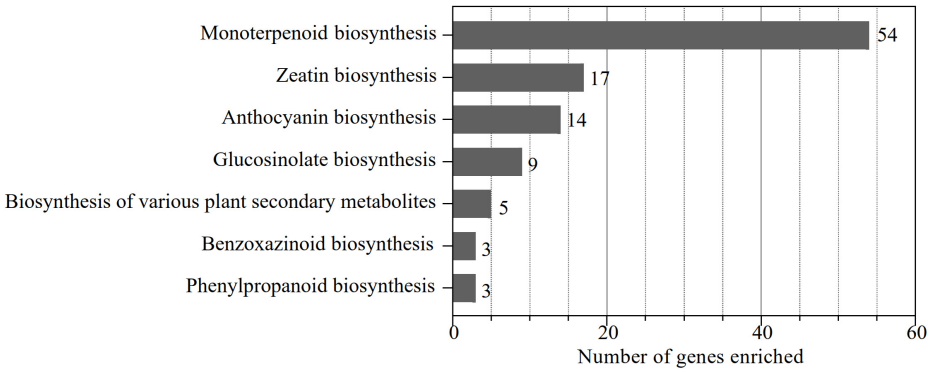

FIGURE 1
Number of *UGT* genes involved in secondary metabolism-related pathways. The KO identifiers (called K numbers) we considered associated with the secondary metabolism network are displayed: monoterpenoid biosynthesis (K21373, K21374), zeatin biosynthesis (K13493, K13494, K13495, K13496), anthocyanin biosynthesis (K12930, K12938, K17193), glucosinolate biosynthesis (K11280), biosynthesis of various plant secondary metabolites (K21371), phenylpropanoid biosynthesis (K12356), and benzoxazinoid biosynthesis (K13227).

testing (Ma et al., 2016). The results were completed and presented using Graphpad Prism 8.

Results

Identification and secondary metabolism pathway enrichments of *UGT* genes in alfalfa

To identify the UGT gene family in alfalfa, a local blast analysis was conducted on "Zhongmu No. 1" protein sequences using 122 UGT protein sequences from *Arabidopsis*. In total, 239 putative UGTs containing the UDPGT domain (PF00201) in alfalfa were obtained and were named according to their chromosomal location. In addition, these 239 *UGT* genes were enriched to KEGG pathways corresponding to the eggNOG-Mapper database (**Figure 1**). The results demonstrated that 90 genes were enriched in the functional pathways of monoterpenoid biosynthesis (54), zeatin biosynthesis (17), anthocyanin biosynthesis (14), glucosinolate biosynthesis (9), biosynthesis of various plant secondary metabolites (5), benzoxazinoid biosynthesis (3), and phenylpropanoid biosynthesis (3) (**Figure 1**), which are considered the pathways associated with secondary metabolism. This indicates that monoterpenoid biosynthesis is the dominant pathway associated with *UGT* genes in alfalfa, while zeatin biosynthesis, anthocyanin biosynthesis, and glucosinolate biosynthesis are the main functional pathways of enriched *UGT* genes. Therefore, based on these screening results, we analyzed the molecular characteristics, phylogenetic relationships, chromosomal localization, structural characterization, conserved motifs, *cis*-acting elements, intra- and interspecies collinearity, and expression pattern of these 90 UGT members to represent *UGT* genes related to secondary metabolism in alfalfa.

Molecular characteristics of UGT members associated with secondary metabolism in alfalfa

To characterize the 90 UGTs in alfalfa screened above, the basic molecular characteristics of the proteins were analyzed. The gene name, gene ID based on the "Zhongmu No. 1" database, the start and end point, the number of amino acids, molecular weight (Mw), isoelectric point (pI), and GRAVY of each gene are displayed in **Supplementary Table 2**. The amino acid length of MsUGTs varied among the 90 proteins, from 82 to 1,683 amino acids. The theoretical pI and Mw ranged from 4.94 to 8.86 and from 9,097.77 Da to 188,543.37 Da, respectively. Analysis of predicting subcellular localization found that 47 MsUGT members were localized in the chloroplast; 27 and 9 MsUGTs were distributed in the cytoplasm and nucleus, respectively; while a small number of MsUGT proteins were widely located in the mitochondria (2), extracell (1), peroxisome (1) and plasma membrane (1). These results provide an integrative view of the molecular characteristics of these 90 UGT members.

Phylogenetic analysis of UGT members associated with secondary metabolism in alfalfa

To better understand the evolutionary relationship of the 90 *UGT* genes associated with secondary metabolism, phylogenetic analysis was conducted based on the amino acid sequence similarity and topological structure (**Figure 2**). The results

demonstrated that the 90 UGT proteins were classified into ten different evolutionary groups (Figure 2A). The four groups with the largest numbers were G, L, A, and D, with 33, 14, 10, and 10 UGT members, respectively; the three groups with the fewest UGT proteins were groups F, H, and P, with 2, 3 and 3, respectively; and none were found in groups B, C, I, K, M, N, and Q in alfalfa. Moreover, ten phylogenetic groups of the *MsUGT* genes were further distinguished by the symbolic PSPG motif (Figure 2B). While the PSPG boxes were presented in each phylogenetic group, the PSPG sequences in different groups were not completely identical (Figure 2B). Twenty-two and 32 amino acid residues of PSPG motifs were fully conserved in groups D, J, and L and in groups H and P, respectively. Additionally, 16 amino acid residues were the same in these sequences, and groups A, E, F, G, and O had low sequence similarity with other groups, though they were conservative within the group.

Chromosomal location and structural characterization of UGTs associated with secondary metabolism in alfalfa

To explore the genomic distribution of alfalfa *UGT* genes, the chromosomal location of *MsUGT* genes was investigated based on the genome annotation database (Figure 3 and Supplementary Table 3). As shown in Figure 3, 88 UGTs were unevenly distributed across eight chromosomes, and two UGTs were identified in the scaffolds. Twenty *UGTs* were distributed on chromosome 6, and 19, 14, and 14 *UGTs* were distributed on chromosomes 5, 4, and 3. Notably, 23 gene pairs were involved in tandem duplications covering 39 *UGT* genes, which were clustered into seven alfalfa chromosomes (Figure 3).

Analysis of the gene structure and motifs was constructed with the phylogenetic tree (Figure 4A). Gene structure analysis demonstrated that the intron numbers of *UGT* genes associated with secondary metabolism ranged from 0 to 23 (Figure 4B). Most *UGT* genes contained 0–2 introns, *MsUGT74* had 23 (the most), and 26 genes (*MsUGT29*, *30*, *31*, *44*, *56*, *57*, *60*, *61*, *62*, *64*, *67*, *68*, *72*, *73*, *79*, *86*, *93*, *107*, *110*, *132*, *180*, *181*, *182*, *183*, *216*, and *235*) lacked introns (Table 1). We also identified ten motifs with 15–50 amino acids (Figure 4C and Supplementary Table 4). Most UGT proteins contained 6–10 conserved motifs, and UGT proteins of the same branch had similar conserved motif composition and sorting order, suggesting that MsUGT proteins in the same group could share similar functions.

Analysis of *cis*-acting elements of *UGT* genes associated with secondary metabolism in alfalfa

To better investigate the characteristics of *UGT* promoters, the *cis*-acting elements were analyzed (Figure 5 and Supplementary Table 5). The results demonstrated that the *cis*-acting elements of promoter regions of the UGT gene family were classified into five categories, including light responsiveness, plant hormone response, resistant response, promoter core elements (TATA-box), and common *cis*-acting element (CAAT-box). Except for the promoter core elements and common cis-acting elements, the number of light-responsive elements was the largest, with 2,676. Phytohormone-responsive elements were primarily related to GA, MeJA, IAA, ABA, and SA, and data for three abiotic stress response elements such as drought, low temperature, and salt stress, are displayed in detail (Figure 5). *MsUGTs* contained 11 flavonoid biosynthesis-related elements due to the potential involvement of *MsUGT* genes in secondary metabolism. Overall, the *cis*-element analysis indicated that *UGT* genes could respond to different kinds of metabolic processes.

Gene duplication and collinearity analysis of *UGT* genes associated with secondary metabolism in alfalfa

To explore the collinearity of the MsUGT gene family between and across species, we constructed syntenic maps of *MsUGT* genes with those in *M. truncatula* and three other model plants of *Arabidopsis thaliana*, *Glycine max,* and *Oryza sativa* (Figure 6 and Supplementary Table 6). A segmental duplication event was identified from *MsUGTs* (*MsUGT4*/*MsUGT182*), which was distributed on chromosomes 1 and 7 (Figure 6A). A total of 118 corresponding orthologs were identified, including 55, 16, 45, and 2 genes from *M. truncatula*, *Arabidopsis*, soybean, and rice, respectively (Figure 6B). These genes were unevenly distributed on eight chromosomes in alfalfa, while chr3 and chr5 identified more collinear genes than the others. These results indicate that *MsUGT* genes displayed different numbers of syntenic lines with four species, while most paralogous *MsUGTs* pairs could have variable expression patterns.

Tissue differential expression analysis of *UGT* genes associated with secondary metabolism in alfalfa

To investigate the tissue expression profiles of the 90 *UGT* gene members associated with secondary metabolism in alfalfa, we performed a transcriptional expression analysis of one representative gene from each evolutionary group (Figure 7 and Supplementary Table 7). The results demonstrated that the expression of *MsUGT28*, *MsUGT54,* and *MsUGT79* from groups A, H, and P have similar tissue expression profiles and were highest in the leaves and lowest in the roots (Figure 7A and Supplementary Table 7). *MsUGT28* expression in leaves was significantly higher than in the roots and

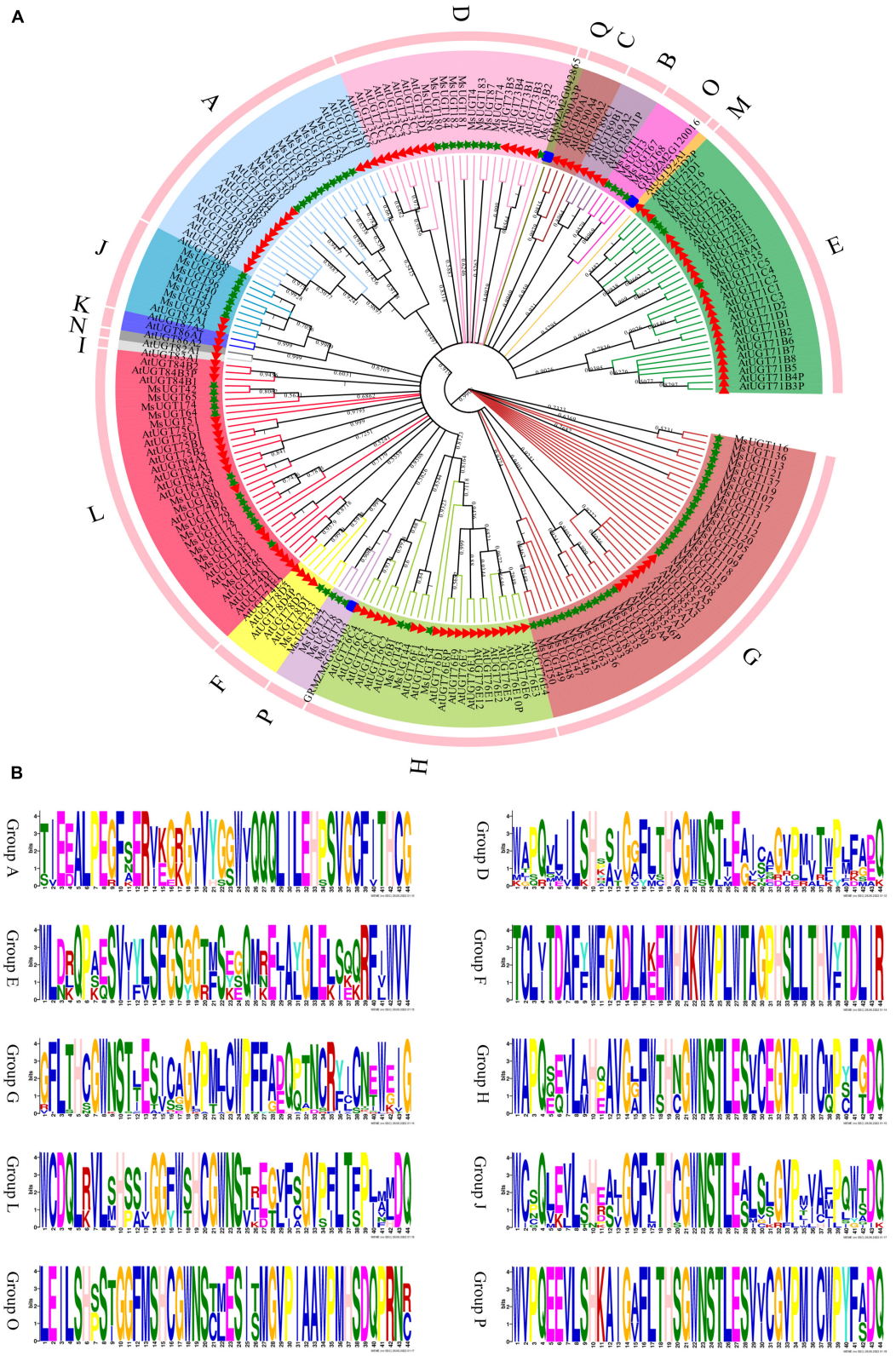

FIGURE 2
Phylogenetic and PSPG box analyses of MsUGT proteins associated with secondary metabolism in alfalfa. **(A)** The phylogenetic tree is generated by the NJ method with 1,000 repeats from the sequences of *Arabidopsis thaliana*, *Zea mays*, and *M. sativa*. **(B)** The PSPG motif of each phylogenetic group is shown.

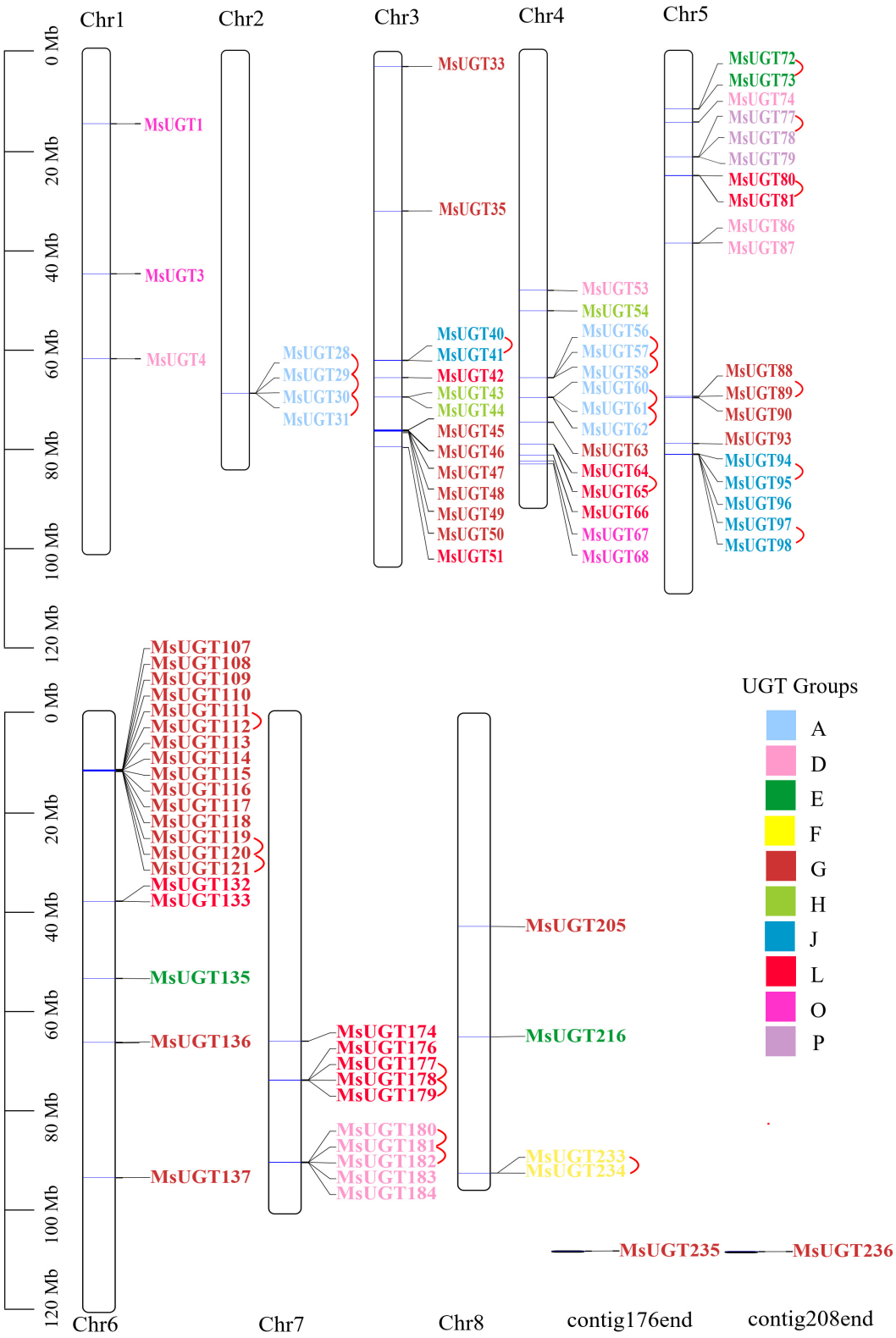

FIGURE 3
Chromosomal location and tandem duplication event analyses of *MsUGT* genes associated with secondary metabolism in alfalfa. The tandem duplicated gene pairs are connected by red lines. Each phylogenetic group is indicated by the same color used in the evolutionary tree in Figure 2A.

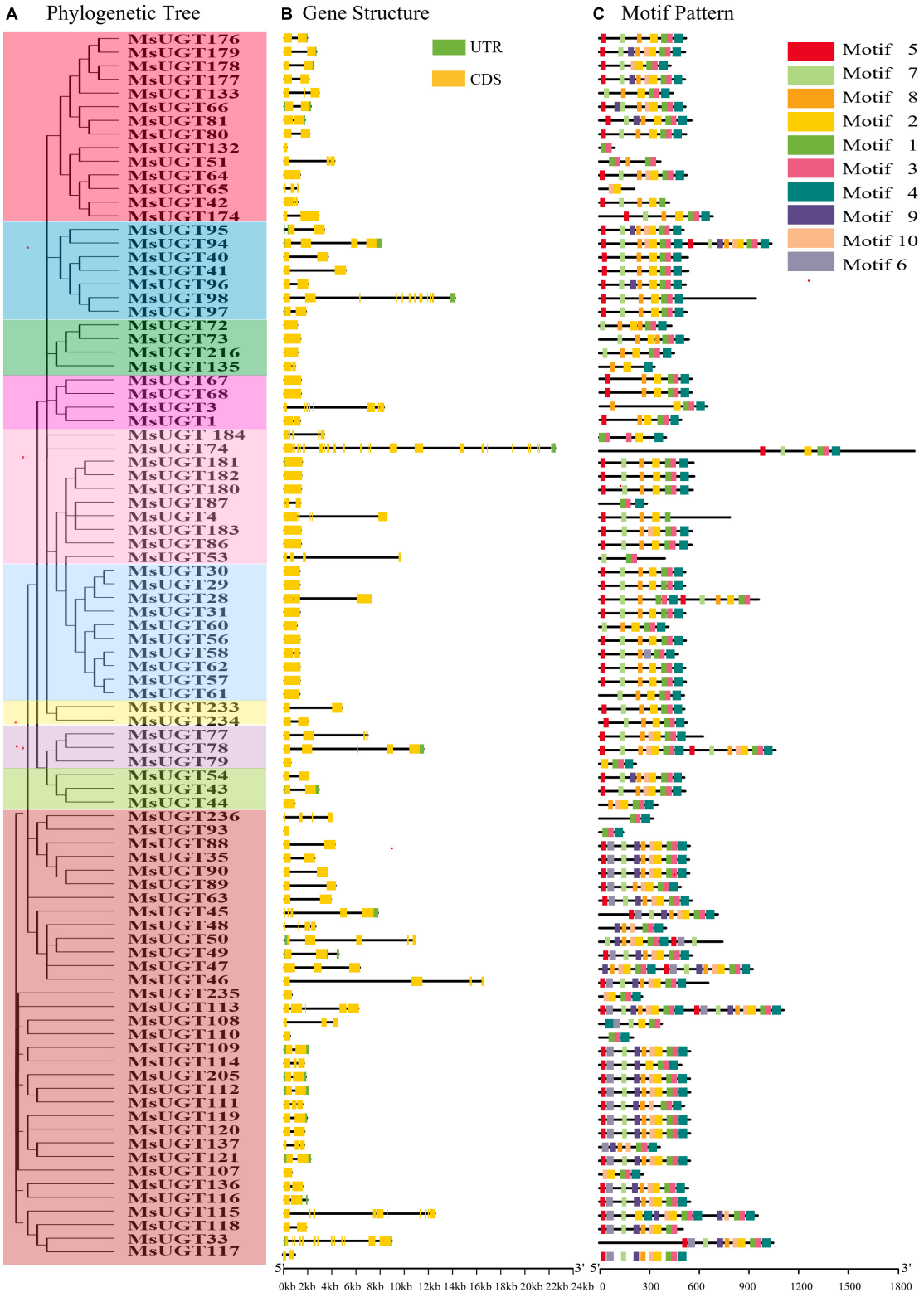

FIGURE 4
The phylogenetic relationship, exon-intron structure, and conservative motif analysis of 90 *UGT* genes associated with secondary metabolism in alfalfa. **(A)** The phylogenetic tree of 90 MsUGTs was constructed by the NJ method with 1,000 repeats. **(B)** The exon-intron structure analysis of 90 *UGT* genes was represented in detail. **(C)** The conservative motif analysis of 90 MsUGTs was predicted. Each phylogenetic group is indicated by the same color used in the evolutionary tree in **Figure 2A**.

TABLE 1 Number of *MsUGT* genes in each group according to number of introns.

Group	No. of introns										Total
	0	1	2	3	4	7	9	10	12	23	
A	8	1	1	-	-	-	-	-	-	-	10
D	5	1	1	-	2	-	-	-	-	1	10
E	3	1	-	-	-	-	-	-	-	-	4
F	-	2	-	-	-	-	-	-	-	-	2
G	4	16	5	3	3	-	1		1	-	33
H	1	2	-	-	-	-	-	-	-	-	3
J	-	5	-	1	-	-	-	1	-	-	7
L	2	8	4	-	-	-	-	-	-	-	14
O	2	1	-	-	-	1	-	-	-	-	4
P	1	-	-	1	1	-	-	-	-	-	3
Total	26	37	11	5	6	1	1	1	1	1	90

"-" represents absent.

stems, and the highest expression occurred in NL, reaching 43.52; the expression of *MsUGT79* was similar to that of *MsUGT28*, while its highest expression level appeared in NL, reaching 86.02, and its expression in three stem tissues also reached 17.21, 27.74 and 31.71; the expression level of *MsUGT54* reached 27.03, 5.64, and 4.80 in FL, NL, and ML, respectively, which was significantly higher than in the stems and roots.

The expression of *MsUGT86*, *MsUGT72*, *MsUGT94,* and *MsUGT67* from groups D, E, J, and O in the roots reached 273.23, 250.60, 21.58, and 30.89, respectively, which was higher than in other tissues. Of these, the expression of *MsUGT86* in three stem tissues from the bottom to the top was the lowest, and the expression in the leaves exceeded that in the stems, reaching 24.59, 12.27, and 48.53, respectively. The tissue expression patterns of *MsUGT72*, *MsUGT94,* and *MsUGT67* in FL were 53.79, 12.02, and 10.52, which was significantly higher than in other leaves and stems.

However, some *UGT* genes in each evolutionary group showed specific tissue expression profiles, such as *UGT88*, *UGT233*, and *UGT80* from groups G, F, and L, respectively. The expression of *MsUGT88* in group G exceeded 30 in both the stems and leaves, which was much higher than in the roots. The expression of *MsUGT233* in group F showed the highest expression in FL and BS, with 63.86 and 72.9, respectively, while MS was 20.48, which was significantly higher than in NL, ML, US, and root tissues. The expression of *MsUGT80* in group L was the highest in US, 18.86, and decreased from NL and MS, BS, root, ML, and FL. In summary, *MsUGT28* in group A, *MsUGT54* in group H, and *MsUGT79* in group P had the highest expression in leaves; *MsUGT233* in group F, *MsUGT88* in group E, and *MsUGT80* in group L had the highest expression in stem tissues; *MsUGT86* in group D, *MsUGT72* in group E, *MsUGT94* in group J, and *MsUGT67* in group O had the highest expression in the roots. These results demonstrate that *MsUGT* genes related to secondary metabolism could function in the full plant, and that *MsUGT* genes in each evolutionary group had tissue-specific expression profiles.

Discussion

Alfalfa is the most important legume in the world due to its high yield, high quality, and environmental adaptability, while the glycosylation reactions catalyzed by UGTs are necessary for maintaining and enhancing metabolic homeostasis by regulating flavonoids, terpenoids, lignin, and other metabolites. Accordingly, identifying and characterizing the *UGT* genes involved in secondary metabolism is important for improving yield, quality, and stress tolerance traits in alfalfa. In this study, 90 *UGT* genes associated with secondary metabolism screened by KEGG pathway functional enrichment were identified in alfalfa. They were classified into ten evolutionary groups, and their basic molecular characteristics, evolutionary genetic information, gene structure, motif conservation, promoter region function prediction, intra- and inter-species collinearity, and expression patterns were analyzed. Based on these results, their basic molecular features, genetic evolution properties related to secondary metabolism, and *cis*-element analysis were assessed.

In our study, *MsUGT* genes associated with secondary metabolism had similar conservative motifs and gene structures, demonstrating that the number of genes containing 0–2 introns adds up to 74 and accounts for 82.2% to the 90 members. The gene structures were similar to the results of previous studies of *UGT* genes in upland cotton (Xiao et al., 2019), *Arabidopsis* (Wu et al., 2020), and pomelo (*Citrus grandis*) (Wu et al., 2020). Of the 36 UGT members of upland cotton (Xiao et al., 2019), 17 and 19 genes contained one and two introns, respectively, while approximately 50% of the genes encoding glycosyltransferase in *Arabidopsis* and pomelo had no introns, most remaining *UGTs* contained one or two introns, and few genes contained multiple introns (Wu et al., 2020). The motif sequences of UGT members in groups with evolutionary relationships were similar, indicating that similarities in the motif location and gene structure of *MsUGTs* in the same subfamily sustained the phylogenetic classification of MsUGTs.

Our data also demonstrated that of the identified 90 *UGT* genes, 23 tandem duplications primarily occurred on chromosomes 2, 4, 5, 6, and 7, and one segmental duplication occurred on chromosomes 1 and 7. It is speculated that the variation in the number of UGT family members can be influenced by gene duplication

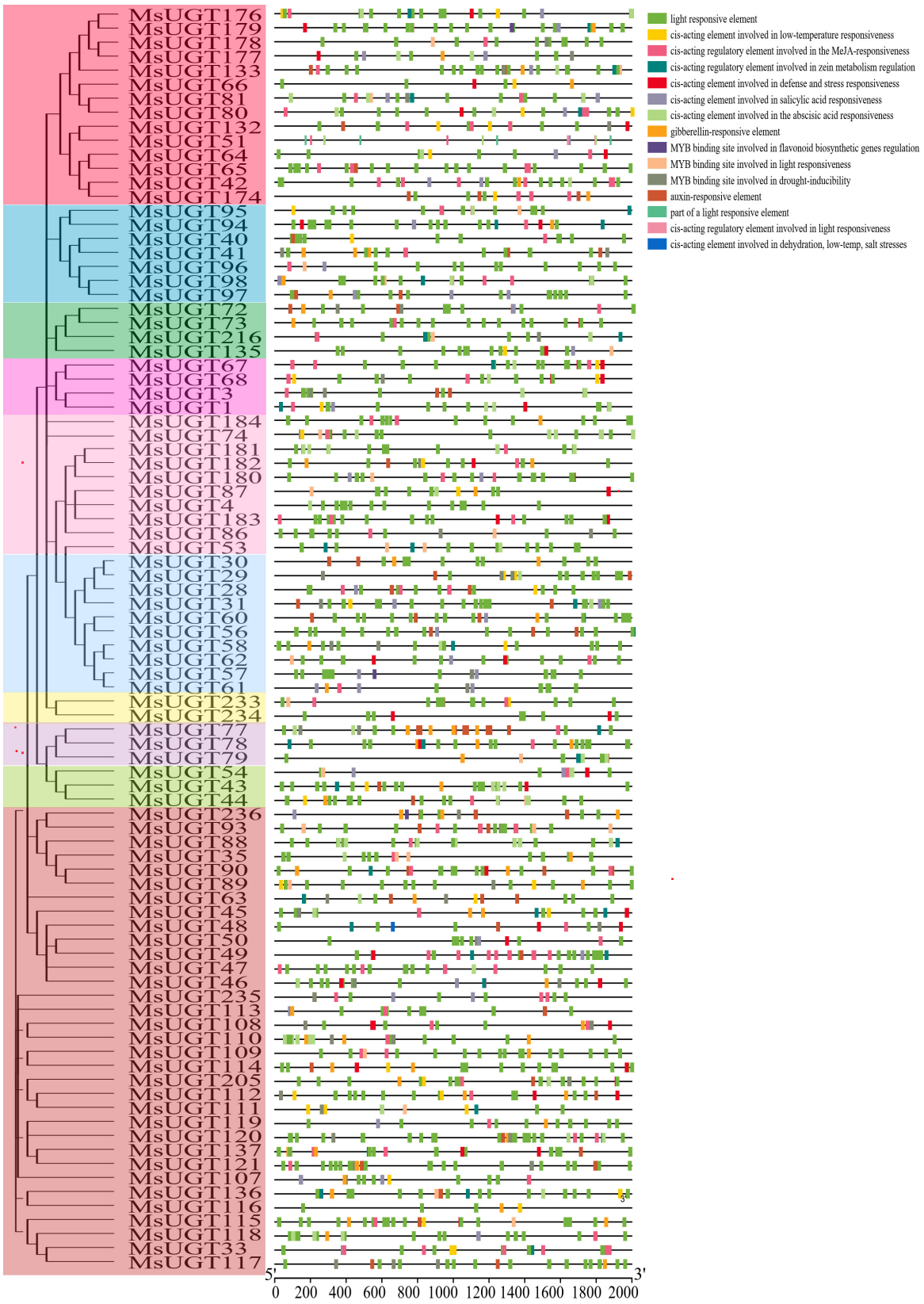

FIGURE 5
Cis-acting elements analysis in the promoter region of *UGT* genes associated with secondary metabolism in alfalfa. Each phylogenetic group is indicated by the same color used in the evolutionary tree in **Figure 2A**.

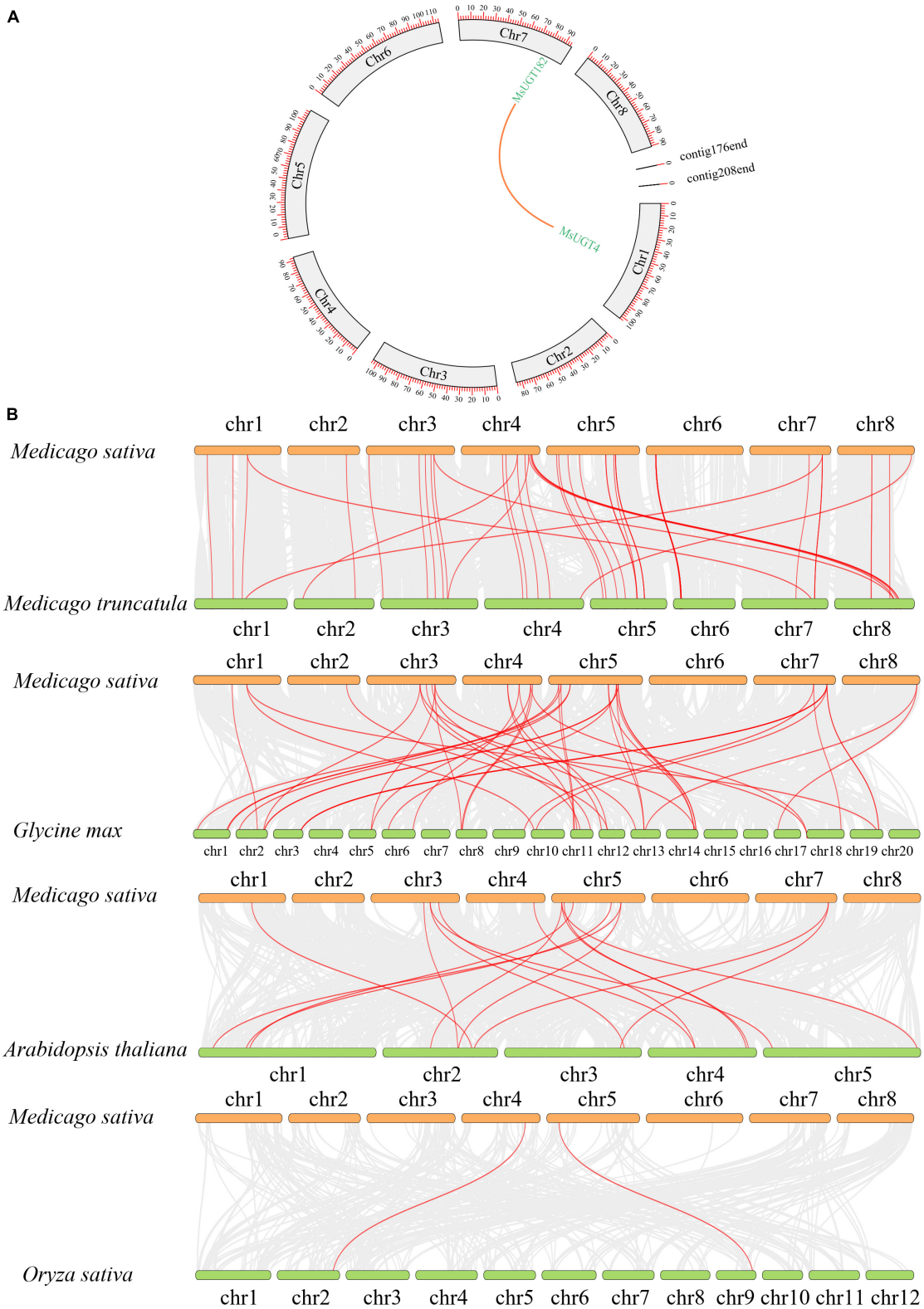

FIGURE 6
MsUGT gene duplications in the genomes between and within species. **(A)** The duplicated event is a collinearity block in the alfalfa genome, and the segmental duplication between *MsUGT4* and *MsUGT182* is drawn with an orange line. **(B)** The collinear blocks of *UGT* genes between *M. sativa* and *M. truncatula*, *Glycine max*, *Arabidopsis thaliana,* and *Oryza sativa,* respectively, are indicated by red lines.

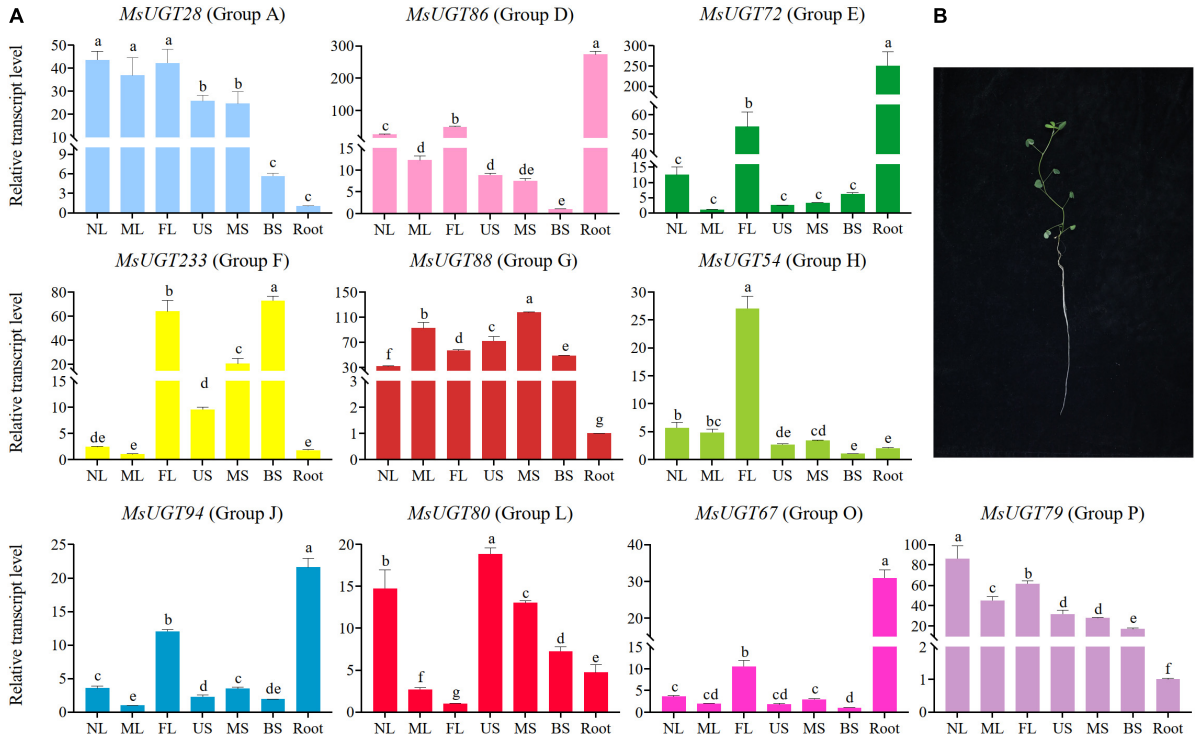

FIGURE 7
Transcriptional expression analysis of Ms*UGT* genes of 10 groups in seven different tissues. **(A)** Genes of *MsUGT28*, *86*, *72*, *233*, *88*, *54*, *94*, *80*, *67*, and *79* were selected from groups A, D, E, F, G, H, J, L, O, and P, respectively. The gene expression represented in each evolutionary group is shown with the same color as the phylogenetic tree in **Figure 2A**. **(B)** Tissues are harvested for transcriptional expression. NL, new leaves; ML, mature leaves; FL, the first real leaves; US, Upper stems; MS, middle stems; BS, bottom stems; Root.

events (Zhang H. et al., 2021). The tandem and segmental duplications of the genome provided more gene copies for generating novel gene functions and expanding gene families in alfalfa. However, compared with the seven segmental duplications in sacred lotus *(Nelumbo nucifera)* (Li H. et al., 2020), 24 gene segmental duplication events in cassava (*Manihot esculenta* Crantz) (Wu et al., 2021), and 28 segmental duplications in *Broussonetia papyrifera* (Wang et al., 2021), alfalfa has fewer segmental duplication genes and only one pair of highly homologous genes involving *MsUGT4* and *MsUGT182*. This indicates that tandem duplication events are more crucial than segmental duplications for *MsUGT* expansion. Furthermore, compared with the 16 and 2 corresponding orthologs identified in *Arabidopsis* and rice, the number of corresponding orthologs in *M. truncatula* and soybean was higher (36 and 40), demonstrating that UGT families could be related to the evolution of dicots but not monocots, and that whole genome duplication events could have contributed more to the evolution of species within the same family (Zhang H. et al., 2021).

The 90 *UGT* genes were clustered into ten evolutionary groups after confirming the UGT gene families in *Arabidopsis* and maize. Of them, ten genes (*MsUGT4*, *53*, *74*, *86*, *87*, *180*, *181*, *182*, *183*, and *184*) were identified in group D in alfalfa, which has been confirmed to catalyze terpenes and flavonoids; four UGTs (*MsUGT72*, *73*, *135*, and *216*) were identified in group E, which catalyzes phenylpropanoids (Song et al., 2019). For example, the UGT 72 family in group E has been shown to glycosylate two classes of phenylpropanoids (monolignols and flavonoids) (Speeckaert et al., 2022). Moreover, PSPG has been highlighted to play a critical role in regulating secondary plant metabolites (Zhang et al., 2018; Wang et al., 2020), and the PSPG analysis performed on the 90 MsUGT proteins in all ten evolutionary groups demonstrated that each evolutionary group had PSPG box in alfalfa. Accordingly, positions 1 (W), 4 (Q), 10 (H), 14 (G), 16 (F), 19–24 (HCGWNS), 27 (E), 32 (G), 34 (P), 39 (P), 43 (E/D) and 44 (Q) were highly conserved in MsUGT members in group D, J, and L, which indicate that crucial amino acids act on triterpenoids in *Panax notoginseng* (Wang et al., 2020). Therefore, differences in the glycosylation reactions of secondary metabolites among the evolutionary groups and the specificities in PSPG motif analyses further verified the involvement of these 90 *UGT* genes in secondary metabolic biosynthesis.

Our analysis demonstrated that ten *UGT* genes from each group showed different expression patterns in alfalfa tissues. Some MsUGT members were preferentially expressed in tissues as the stem, root, or leaves, which could be related to the higher accumulation of flavonoids and terpenoids. For instance, *MsUGTs* in groups A, H, and P, and *UGT* genes in groups D, E, J, and O have higher expression in leaves and root tissues, respectively, which is where flavone glucuronides primarily accumulate (Adiji et al., 2021). The highest expression levels of *MsUGT233*, *MsUGT88*, and *MsUGT80* were in BS, MS, and US, respectively, which are responsible for the glycosylation of the secondary metabolite lignin (Lin et al., 2016). This indicates that the expression of *UGTs* associated with secondary metabolism could differ widely from the specific active sites of glycosylation actions.

A remarkable amount of phytohormone response elements were obtained in the promoter regions of the 90 Ms*UGT* genes, suggesting that glycosylation reactions could be induced by these phytohormones. Plant hormones play an important role in responding to various stresses and normal growth and developmental progress (Tian et al., 2017; Radojicic et al., 2018; Shu et al., 2018). UGTs, such as UGT84A2 (Zhang et al., 2017), UGT75B1 (Chen T. T. et al., 2020) and UGT76D1 (Huang et al., 2018) in *Arabidopsis* could participate in the glycosylation of IAA, ABA, and SA, respectively, and regulate flowering, stress resistance, and systemic acquired immunity. However, recent studies have proposed that plant hormones could complete their functional role connected with some secondary metabolites by the UGTs. For example, GSA1 in rice had glycosyltransferase activity on flavonoids and lignitol monomers, indirectly affecting flavonoid-mediated auxin polar transport and the expression of related genes (Dong et al., 2020). Therefore, this might be an important line of UGT research in future studies.

In this study, eleven flavonoid response elements were identified in the promoter element, indicating that some UGTs in alfalfa could also be induced by flavonoids. Flavonoids are multifunctional secondary metabolites that are important for plants and human health, which can effectively delay antioxidation and anti-inflammatory effects in the human body (Yin et al., 2017a). A previous study demonstrated that CsUGT75L12 in tea plants can transfer sugar molecules to the C7 hydroxyl group of flavonoids, catalyzing the generation of flavonoid 7-*O*-glycosides (Dai et al., 2017); Plant secondary metabolites can be coupled with hormones to play an important role in responding to growth and developmental processes (Dong et al., 2020). The final step in the biosynthesis of particular flavonoids was glycosylation modifications by UGTs, while changes in the bioactivity, stability, and solubility of flavonoid compounds could ultimately affect the quality, yield, and adaptation of legumes to environmental changes (Yin et al., 2017a,b).

Conclusion

In this study, we identified 239 *MsUGT* genes from the alfalfa genome and further screened 90 of them that are involved in secondary metabolic pathways. The basic molecular characteristics, motifs, gene structure, and duplication events of the 90 *MsUGT* genes were assayed and demonstrated. The genetic evolution properties, including group classifications and PSPG motifs related to secondary metabolism, were analyzed. Tissue differential expression analysis revealed the tissue-specific expression patterns of *MsUGT* genes in each evolutionary group. *Cis*-elements analysis of the promoter regions predicted that UGTs could be induced by various phytohormones and flavonoids. Therefore, our study provides comprehensive genetic information and molecular features of the *UGT* genes associated with secondary metabolism in alfalfa, which helps reveal some of the regulatory mechanisms associated with secondary metabolites that can improve yield and quality in alfalfa and other plant species.

Data availability statement

The datasets presented in this study can be found in online repositories. The names of the repository/repositories and accession number(s) can be found in the article/**Supplementary material**.

Author contributions

AY and XZ collected plant materials. AY and XJ performed the experiment. AY, XJ, LL, and LH analyzed the data. AY, XJ, and QH processed the figures and tables. YS, RL, and ML conceived and designed the experiment. AY, RL, and ML wrote the manuscript. AY, JK, LC, QY, RL, and ML revised and finalized the manuscript. All authors have read and approved the final manuscript.

Funding

This work was supported by Key project of Science and technology vitalize Mongolia action (grant no. NMKJXM202110-5), China Agriculture Research System of MOF and MARA, China (grant no. CARS-34), and Agricultural Science and Technology Innovation Program, China (grant no. ASTIP-IAS14).

Conflict of interest

The authors declare that the research was conducted in the absence of any commercial or financial relationships that could be construed as a potential conflict of interest.

Publisher's note

All claims expressed in this article are solely those of the authors and do not necessarily represent those of their affiliated organizations, or those of the publisher, the editors and the reviewers. Any product that may be evaluated in this article, or claim that may be made by its manufacturer, is not guaranteed or endorsed by the publisher.

Supplementary material

The Supplementary Material for this article can be found online at: https://www.frontiersin.org/articles/10.3389/fpls.2022.1001206/full#supplementary-material

References

Adiji, O. A., Docampo-Palacios, M. L., Alvarez-Hernandez, A., Pasinetti, G. M., Wang, X., and Dixon, R. A. (2021). UGT84F9 is the major flavonoid UDP-glucuronosyltransferase in *Medicago truncatula*. *Plant Physiol.* 185, 1617–1637. doi: 10.1093/plphys/kiab016

Antonov, A. V., Schmidt, E. E., Dietmann, S., Krestyaninova, M., and Hermjakob, H. (2010). R spider: a network-based analysis of gene lists by combining signaling and metabolic pathways from Reactome and KEGG databases. *Nucleic Acids Res.* 38, W78–W83. doi: 10.1093/nar/gkq482

Aoi, Y., Hira, H., Hayakawa, Y., Liu, H., Fukui, K., Dai, X., et al. (2020). UDP-glucosyltransferase UGT84B1 regulates the levels of indole-3-acetic acid and phenylacetic acid in *Arabidopsis*. *Biochem. Biophys. Res. Commun.* 532, 244–250. doi: 10.1016/j.bbrc.2020.08.026

Bailey, T. L., Boden, M., Buske, F. A., Frith, M., Grant, C. E., Clementi, L., et al. (2009). MEME SUITE: Tools for motif discovery and searching. *Nucleic Acids Res.* 37, W202–W208.

Barros, J., Temple, S., and Dixon, R. A. (2019). Development and commercialization of reduced lignin alfalfa. *Curr. Opin. Biotechnol.* 56, 48–54.

Chan, W. K., Tan, L. T., Chan, K. G., Lee, L. H., and Goh, B. H. (2016). Nerolidol: A sesquiterpene alcohol with multi-faceted pharmacological and biological activities. *Molecules* 21:529

Chen, L., Wang, W. S., Wang, T., Meng, X. F., Chen, T. T., Huang, X. X., et al. (2019). Methyl salicylate glucosylation regulates plant defense signaling and systemic acquired resistance. *Plant Physiol.* 180, 2167–2181.

Chen, T. T., Liu, F. F., Xiao, D. W., Jiang, X. Y., Li, P., Zhao, S. M., et al. (2020). The *Arabidopsis* UDP-glycosyltransferase75B1, conjugates abscisic acid and affects plant response to abiotic stresses. *Plant Mol. Biol.* 102, 389–401. doi: 10.1007/s11103-019-00953-4

Chen, L., Huang, X. X., Li, Y. J., and Hou, B. K. (2020). Glycosyltransferase UGT76F1 is involved in the temperature-mediated petiole elongation and the BR-mediated hypocotyl growth in *Arabidopsis*. *Plant Signal. Behav.* 15:1777377. doi: 10.1080/15592324.2020.1777377

Chen, H., Zeng, Y., Yang, Y., Huang, L., Tang, B., Zhang, H., et al. (2020). Allele-aware chromosome-level genome assembly and efficient transgene-free genome editing for the autotetraploid cultivated alfalfa. *Nat. Commun.* 11:2494. doi: 10.1038/s41467-020-16338-x

Chen, C., Chen, H., Zhang, Y., Thomas, H. R., Frank, M. H., He, Y., et al. (2020). TBtools: An integrative toolkit developed for interactive analyses of big biological data. *Mol. Plant* 13, 1194–1202. doi: 10.1016/j.molp.2020.06.009

Cheng, Y., Zhang, J., Shao, Y., Xu, Y., Ge, H., Yu, B., et al. (2019). Enzyme-catalyzed glycosylation of curcumin and its analogues by glycosyltransferases from *Bacillus subtilis* ATCC 6633. *Catalysts* 9:734.

Dai, X., Zhuang, J., Wu, Y., Wang, P., Zhao, G., Liu, Y., et al. (2017). Identification of a Flavonoid Glucosyltransferase Involved in 7-OH Site Glycosylation in Tea plants (*Camellia sinensis*). *Sci. Rep.* 7:5926. doi: 10.1038/s41598-017-06453-z

Dong, N. Q., Sun, Y., Guo, T., Shi, C. L., Zhang, Y. M., Kan, Y., et al. (2020). UDP-glucosyltransferase regulates grain size and abiotic stress tolerance associated with metabolic flux redirection in rice. *Nat. Commun.* 11:2629. doi: 10.1038/s41467-020-16403-5

Dooner, H. K., and Nelson, O. E. (1977). Controlling element-induced alterations in UDPglucose: flavonoid glucosyltransferase, the enzyme specified by the bronze locus in maize. *Proc. Natl. Acad. Sci. U.S.A.* 74, 5623–5627. doi: 10.1073/pnas.74.12.5623

Finn, R. D., Bateman, A., Clements, J., Coggill, P., Eberhardt, R. Y., Eddy, S. R., et al. (2014). Pfam: The protein families database. *Nucleic Acids Res.* 42, D222–D230.

Gasteiger, E., Gattiker, A., Hoogland, C., Ivanyi, I., Appel, R. D., and Bairoch, A. (2003). ExPASy: The proteomics server for in-depth protein knowledge and analysis. *Nucleic Acids Res.* 31, 3784–3788. doi: 10.1093/nar/gkg563

He, Y., Ahmad, D., Zhang, X., Zhang, Y., Wu, L., Jiang, P., et al. (2018). Genome-wide analysis of family-1 UDP glycosyltransferases (UGT) and identification of UGT genes for FHB resistance in wheat (*Triticum aestivum* L.). *BMC Plant Biol.* 18:67. doi: 10.1186/s12870-018-1286-5

Horton, P., Park, K. J., Obayashi, T., Fujita, N., Harada, H., Adams-Collier, C. J., et al. (2007). WoLF PSORT: Protein localization predictor. *Nucleic Acids Res.* 35, W585–W587.

Huang, X. X., Zhu, G. Q., Liu, Q., Chen, L., Li, Y. J., and Hou, B. K. (2018). Modulation of Plant Salicylic Acid-Associated Immune Responses via Glycosylation of Dihydroxybenzoic Acids. *Plant Physiol.* 176, 3103–3119. doi: 10.1104/pp.17.01530

Huerta-Cepas, J., Szklarczyk, D., Heller, D., Hernandez-Plaza, A., Forslund, S. K., Cook, H., et al. (2019). eggNOG 5.0: A hierarchical, functionally and phylogenetically annotated orthology resource based on 5090 organisms and 2502 viruses. *Nucleic Acids Res.* 47, D309–D314. doi: 10.1093/nar/gky1085

Huo, K., Chen, Y., Sui, L., Wang, Y., Fu, Y., Pei, X., et al. (2021). Transient expression and enzymatic assay identified uridine-diphosphate glucosyltransferases related to flavonoid glycosylation in *Vernonia amygdalina* leaves. *Ind. Crops Prod.* 172:114005.

Jing, T., Zhang, N., Gao, T., Wu, Y., Zhao, M., Jin, J., et al. (2020). UGT85A53 promotes flowering via mediating abscisic acid glucosylation and FLC transcription in *Camellia sinensis*. *J. Exp. Bot.* 71, 7018–7029. doi: 10.1093/jxb/eraa373

Kim, M. J., Zheng, J., Liao, M. H., and Jang, I. C. (2019). Overexpression of SrUGT76G1 in Stevia alters major steviol glycosides composition towards improved quality. *Plant Biotechnol. J.* 17, 1037–1047. doi: 10.1111/pbi.13035

Kurze, E., Wust, M., Liao, J., Mcgraphery, K., Hoffmann, T., Song, C., et al. (2022). Structure-function relationship of terpenoid glycosyltransferases from plants. *Nat. Prod. Rep.* 39, 389–409. doi: 10.1039/d1np00038a

Lescot, M., Déhais, P., Thijs, G., Marchal, K., Moreau, Y., Van, P. Y., et al. (2002). PlantCARE, a database of plant cis-acting regulatory elements and a portal to tools for in silico analysis of promoter sequences. *Nucleic Acids Res.* 30, 325–327. doi: 10.1093/nar/30.1.325

Li, H., Yang, X., Lu, M., Chen, J., and Shi, T. (2020). Gene expression and evolution of Family-1 UDP-glycosyltransferases—insights from an aquatic flowering plant (sacred lotus). *Aquat. Bot.* 166:103270.

Li, Y., Liu, F., Li, P., Wang, T., Zheng, C., and Hou, B. (2020). An *Arabidopsis* Cytokinin-modifying glycosyltransferase UGT76C2 improves drought and salt tolerance in rice. *Front Plant Sci* 11:560696. doi: 10.3389/fpls.2020.560696

Li, P., Li, Y. J., Zhang, F. J., Zhang, G. Z., Jiang, X. Y., Yu, H. M., et al. (2017). The *Arabidopsis* UDP-glycosyltransferases UGT79B2 and UGT79B3, contribute to cold, salt and drought stress tolerance via modulating anthocyanin accumulation. *Plant J.* 89, 85–103. doi: 10.1111/tpj.13324

Li, W., Zhai, L., Strauss, S. H., Yer, H., Merewitz, E., Chen, J., et al. (2019). transgenic reduction of cytokinin levels in roots inhibits root-sprouting in *Populus*. *Plant Physiol.* 180, 1788–1792.

Li, Y. J., Li, P., Wang, T., Zhang, F. J., Huang, X. X., and Hou, B. K. (2018). The maize secondary metabolism glycosyltransferase UFGT2 modifies flavonols and contributes to plant acclimation to abiotic stresses. *Ann. Bot.* 122, 1203–1217. doi: 10.1093/aob/mcy123

Lin, J. S., Huang, X. X., Li, Q., Cao, Y., Bao, Y., Meng, X. F., et al. (2016). UDP-glycosyltransferase 72B1 catalyzes the glucose conjugation of monolignols and is essential for the normal cell wall lignification in *Arabidopsis thaliana*. *Plant J.* 88, 26–42. doi: 10.1111/tpj.13229

Livak, K. J., and Schmittgen, T. D. (2001). Analysis of relative gene expression data using real-time quantitative PCR and the $2-\Delta\Delta CT$ method. *Methods* 25, 402–408.

Long, R., Zhang, F., Zhang, Z., Li, M., Chen, L., Wang, X., et al. (2022). Genome assembly of alfalfa cultivar zhongmu-4 and identification of SNPs associated with agronomic traits. *Genomics Proteomics Bioinformatics* 13, S1672–S1229. doi: 10.1016/j.gpb.2022.01.002

Ma, D., Liu, B., Ge, L., Weng, Y., Cao, X., Liu, F., et al. (2021). Identification and characterization of regulatory pathways involved in early flowering in the new leaves of alfalfa (*Medicago sativa* L.) by transcriptome analysis. *BMC Plant Biol.* 21:8. doi: 10.1186/s12870-020-02775-9

Ma, X., Xu, Q., Meyer, W. A., and Huang, B. (2016). Hormone regulation of rhizome development in tall fescue (*Festuca arundinacea*) associated with proteomic changes controlling respiratory and amino acid metabolism. *Ann. Bot.* 118, 481–494. doi: 10.1093/aob/mcw120

Mohnike, L., Rekhter, D., Huang, W., Feussner, K., Tian, H., Herrfurth, C., et al. (2021). The glycosyltransferase UGT76B1 modulates N-hydroxy-pipecolic acid homeostasis and plant immunity. *Plant Cell* 33, 735–749.

Nair, P. C., Chau, N., Mckinnon, R. A., and Miners, J. O. (2020). Arginine-259 of UGT2B7 Confers UDP-Sugar Selectivity. *Mol. Pharmacol.* 98, 710–718. doi: 10.1124/molpharm.120.000104

Radojicic, A., Li, X., and Zhang, Y. (2018). Salicylic Acid: A double-edged sword for programed cell death in plants. *Front. Plant Sci.* 9:1133. doi: 10.3389/fpls.2018.01133

Rehman, H. M., Nawaz, M. A., Shah, Z. H., Ludwig-Muller, J., Chung, G., Ahmad, M. Q., et al. (2018). Comparative genomic and transcriptomic analyses of Family-1 UDP glycosyltransferase in three *Brassica* species and *Arabidopsis* indicates stress-responsive regulation. *Sci. Rep.* 8:1875. doi: 10.1038/s41598-018-19535-3

Rojas Rodas, F., Rodriguez, T. O., Murai, Y., Iwashina, T., Sugawara, S., Suzuki, M., et al. (2014). Linkage mapping, molecular cloning and functional analysis of soybean gene Fg2 encoding flavonol 3-O-glucoside (1 –> 6) rhamnosyltransferase. *Plant Mol. Biol.* 84, 287–300. doi: 10.1007/s11103-013-0133-1

Shen, C., Du, H., Chen, Z., Lu, H., Zhu, F., Chen, H., et al. (2020). The chromosome-level genome sequence of the autotetraploid alfalfa and resequencing of core germplasms provide genomic resources for alfalfa research. *Mol. Plant* 13, 1250–1261. doi: 10.1016/j.molp.2020.07.003

Shu, K., Zhou, W., Chen, F., Luo, X., and Yang, W. (2018). Abscisic acid and gibberellins antagonistically mediate plant development and abiotic stress responses. *Front. Plant Sci.* 9:416. doi: 10.3389/fpls.2018.00416

Song, C., Hartl, K., Mcgraphery, K., Hoffmann, T., and Schwab, W. (2018). Attractive but Toxic: Emerging roles of glycosidically bound volatiles and glycosyltransferases involved in their formation. *Mol. Plant* 11, 1225–1236. doi: 10.1016/j.molp.2018.09.001

Song, Z., Niu, L., Yang, Q., Dong, B., Wang, L., Dong, M., et al. (2019). Genome-wide identification and characterization of UGT family in pigeonpea (*Cajanus cajan*) and expression analysis in abiotic stress. *Trees* 33, 987–1002.

Speeckaert, N., Adamou, N. M., Hassane, H. A., Baldacci-Cresp, F., Mol, A., Goeminne, G., et al. (2020). Characterization of the UDP-glycosyltransferase UGT72 Family in poplar and identification of genes involved in the glycosylation of monolignols. *Int. J. Mol. Sci.* 21:5018. doi: 10.3390/ijms21145018

Speeckaert, N., El Jaziri, M., Baucher, M., and Behr, M. (2022). UGT72, a Major glycosyltransferase family for flavonoid and monolignol homeostasis in plants. *Biology (Basel)* 11:441. doi: 10.3390/biology11030441

Tamura, K., Stecher, G., and Kumar, S. (2021). MEGA11: Molecular evolutionary genetics analysis Version 11. *Mol. Biol. Evol.* 38, 3022–3027. doi: 10.1093/molbev/msab120

Tian, H., Lv, B., Ding, T., Bai, M., and Ding, Z. (2017). Auxin-BR interaction regulates plant growth and development. *Front. Plant Sci.* 8:2256. doi: 10.3389/fpls.2017.02256

Wang, D., Wang, J., Shi, Y., Li, R., Fan, F., Huang, Y., et al. (2020). Elucidation of the complete biosynthetic pathway of the main triterpene glycosylation products of *Panax* notoginseng using a synthetic biology platform. *Metab. Eng.* 61, 131–140. doi: 10.1016/j.ymben.2020.05.007

Wang, F., Su, Y., Chen, N., and Shen, S. (2021). Genome-wide analysis of the UGT gene family and identification of flavonoids in *Broussonetia papyrifera*. *Molecules* 26:3449. doi: 10.3390/molecules26113449

Wang, X., Wang, J., Cui, H., Yang, W., Yu, B., Zhang, C., et al. (2022). The UDP-glycosyltransferase MtUGT84A1 regulates anthocyanin accumulation and plant growth via JA signaling in *Medicago truncatula*. *Environ. Exp. Bot.* 201:104972.

Wu, B., Liu, X., Xu, K., and Zhang, B. (2020). Genome-wide characterization, evolution and expression profiling of UDP-glycosyltransferase family in pomelo (*Citrus grandis*) fruit. *BMC Plant Biol.* 20:459. doi: 10.1186/s12870-020-02655-2

Wu, C., Dai, J., Chen, Z., Tie, W., Yan, Y., Yang, H., et al. (2021). Comprehensive analysis and expression profiles of cassava UDP-glycosyltransferases (UGT) family reveal their involvement in development and stress responses in cassava. *Genomics* 113, 3415–3429. doi: 10.1016/j.ygeno.2021.08.004

Xiao, X., Lu, Q., Liu, R., Gong, J., Gong, W., Liu, A., et al. (2019). Genome-wide characterization of the UDP-glycosyltransferase gene family in upland cotton. *3 Biotech* 9:453. doi: 10.1007/s13205-019-1984-1

Yano, R., Takagi, K., Tochigi, S., Fujisawa, Y., Nomura, Y., Tsuchinaga, H., et al. (2018). Isolation and characterization of the Soybean Sg-3 gene that is involved in genetic variation in sugar chain composition at the C-3 position in soyasaponins. *Plant Cell Physiol.* 59, 792–805. doi: 10.1093/pcp/pcy019

Yin, Q., Shen, G., Chang, Z., Tang, Y., Gao, H., and Pang, Y. (2017a). Involvement of three putative glucosyltransferases from the UGT72 family in flavonol glucoside/rhamnoside biosynthesis in *Lotus japonicus* seeds. *J. Exp. Bot.* 68, 597–612.

Yin, Q., Shen, G., Di, S., Fan, C., Chang, Z., and Pang, Y. (2017b). Genome-wide identification and functional characterization of UDP-glucosyltransferase genes involved in flavonoid biosynthesis in Glycine max. *Plant Cell Physiol.* 58, 1558–1572.

Yu, A. D., Liu, L., Long, R. C., Kang, J. M., Chen, C., Yang, Q. Q., et al. (2022). Function and application prospect of plant UDP-glycosyltransferase(UGT). *Plant Physiol. J.* 58, 631–642.

Zhang, G. Z., Jin, S. H., Li, P., Jiang, X. Y., Li, Y. J., and Hou, B. K. (2017). Ectopic expression of UGT84A2 delayed flowering by indole-3-butyric acid-mediated transcriptional repression of ARF6 and ARF8 genes in Arabidopsis. *Plant Cell Rep.* 36, 1995–2006. doi: 10.1007/s00299-017-2225-x

Zhang, H., Liu, X., Wang, X., Sun, M., Song, R., Mao, P., et al. (2021). Genome-wide identification of GRAS gene family and Their Responses to Abiotic Stress in *Medicago sativa*. *Int. J. Mol. Sci.* 22:7729. doi: 10.3390/ijms22147729

Zhang, K., Sun, Y., Li, M., and Long, R. (2021). CrUGT87A1, a UDP-sugar glycosyltransferases (UGTs) gene from Carex rigescens, increases salt tolerance by accumulating flavonoids for antioxidation in Arabidopsis thaliana. *Plant Physiol. Biochem.* 159, 28–36. doi: 10.1016/j.plaphy.2020.12.006

Zhang, P., Zhang, Z., Zhang, L., Wang, J., and Wu, C. (2020). Glycosyltransferase GT1 family: Phylogenetic distribution, substrates coverage, and representative structural features. *Comput. Struct. Biotechnol. J.* 18, 1383–1390. doi: 10.1016/j.csbj.2020.06.003

Zhang, Y., Guo, W., Chen, L., Shen, X., Yang, H., Fang, Y., et al. (2022). CRISPR/Cas9-Mediated targeted mutagenesis of GmUGT enhanced soybean resistance against leaf-chewing insects through flavonoids biosynthesis. *Front. Plant Sci.* 13:802716. doi: 10.3389/fpls.2022.802716

Zhang, Z., Zhuo, X., Yan, X., and Zhang, Q. (2018). Comparative genomic and transcriptomic analyses of family-1 UDP glycosyltransferase in *Prunus Mume*. *Int. J. Mol. Sci.* 19:3382. doi: 10.3390/ijms19113382

Zhao, M., Zhang, N., Gao, T., Jin, J., Jing, T., Wang, J., et al. (2020). Sesquiterpene glucosylation mediated by glucosyltransferase UGT91Q2 is involved in the modulation of cold stress tolerance in tea plants. *New Phytol.* 226, 362–372. doi: 10.1111/nph.16364

frontiers | Frontiers in Plant Science

TYPE Original Research
PUBLISHED 03 October 2022
DOI 10.3389/fpls.2022.1008550

OPEN ACCESS

EDITED BY
Jing Zhang,
Nanjing Agricultural University, China

REVIEWED BY
Yanfu Bai,
Sichuan Agricultural University, China
Jing Meiling,
Qinghai Nationalities University, China

*CORRESPONDENCE
Ying Liu
liuying_yanhong@sina.com

SPECIALTY SECTION
This article was submitted to Plant Abiotic Stress, a section of the journal Frontiers in Plant Science

RECEIVED 31 July 2022
ACCEPTED 07 September 2022
PUBLISHED 03 October 2022

CITATION
Liu Y (2022) Grazing rest during spring regreening period promotes the ecological restoration of degraded alpine meadow vegetation through enhanced plant photosynthesis and respiration. *Front. Plant Sci.* 13:1008550. doi: 10.3389/fpls.2022.1008550

Grazing rest during spring regreening period promotes the ecological restoration of degraded alpine meadow vegetation through enhanced plant photosynthesis and respiration

Ying Liu*

Qinghai Academy of Animal Husbandry and Veterinary Sciences, Qinghai Provincial Key Laboratory of Adaptive Management on Alpine Grassland, Key Laboratory of Superior Forage Germplasm in the Qinghai–Tibetan Plateau, Qinghai University, Xining, China

Grazing rest during the spring regreening period is the most economical and feasible measure for the ecological restoration of degraded alpine meadows and has been widely popularized and applied in China. The aim of the present study was to undertake a comparative analysis of the effects of grazing rest on the ecological restoration of degraded alpine meadows by plant photosynthesis and respiration. Coverage, height, ground biomass, belowground biomass of degraded alpine meadow vegetation, net photosynthetic rate, stomatal conductance, transpiration rate, intercellular CO_2 concentration, chlorophyll fluorescence parameters, relative chlorophyll content, respiration rate, metabolite content, leaf relative water content, and related mineral element content of the dominant grass *Elymus nutans* Griseb. were measured in degraded alpine grassland with different grazing rest years. The results show that grazing rest during the spring regreening period promoted the ecological restoration of degraded alpine meadows by enhancing the photosynthesis and respiration of the dominant grass *E. nutans* Griseb. Grazing rest enhanced photosynthesis in dominant grass by increasing metabolites related to the Calvin cycle, chlorophyll content, leaf relative water content, and related mineral element content. Grazing at rest enhanced the respiration of dominant grass by increasing metabolites related to the TCA cycle, leaf relative water content, and related mineral element content. This positive effect gradually became stable with increasing years of grazing rest. Our results provide a fundamental basis for the popularization and application of grazing rest during the spring regreening period on degraded Tibetan Plateau grasslands.

KEYWORDS

photosynthesis, Calvin cycle, respiration, TCA cycle, grazing rest during spring regreening period

Introduction

The Qinghai–Tibet Plateau is a sensitive and ecologically fragile zone of global climate change. Because of global climate change and human activities, alpine grasslands on the Qinghai–Tibet Plateau continue to degrade, and the structure and function of the ecosystem are seriously disturbed (Fan et al., 2010). Overgrazing is the main reason for the degradation of alpine grasslands (Zimmer et al., 2010; Ash et al., 2011; Selemani et al., 2013; Li et al., 2016; Shang et al., 2017); therefore, short-term grazing rest has become an effective way to control degraded grasslands and perform natural restoration (Wu et al., 2017). The forage spring regreening period refers to the stage at which plants end their dormant state and begin to recover with an increase in temperature and moisture conditions after forage overwintering. This is the most important stage for the initial growth of grassland vegetation in a year (Zhang et al., 2011). Consequently, the implementation of grazing rest during the spring regreening period is an effective approach for the natural restoration and rational utilization of degraded grasslands. How grazing rest during the spring regreening period promotes the restoration of degraded grasslands remains a research hotspot (Mavromihalis et al., 2013; Li et al., 2017; Fedrigo et al., 2018). The answer to this scientific question can not only fill in the mechanism of the significant restoration of degraded grassland by grazing rest during spring regreening period but also provide a strong theoretical basis for the promotion of grazing rest during spring regreening period measures and further provide guidance for grassland management policies in China.

Carbon assimilation and utilization by plants play an important role in the restoration of degraded alpine grassland vegetation, and the main processes of carbon metabolism are photosynthesis and respiration (Liu et al., 2008; Chamizo et al., 2021). Photosynthesis and respiration are also sensitive processes in response to environmental changes (Martínkov et al., 2021; Crous et al., 2022). These can directly reflect the growth status of grassland plants (Chen et al., 2005). Zhao et al. (2009) and Zheng et al. (2011) reported that overgrazing significantly reduces the photosynthetic and transpiration rates of forage plants, and chlorophyll fluorescence parameters are appropriate for detecting the effect of environmental factors (Simkó et al., 2020). Chlorophyll is essential for plant photosynthesis. Livestock grazing can affect the chlorophyll content in steppe plants of Tuva (Zvereva, 2004). Plant respiration refers to the process by which plants absorb O_2 or release CO_2 per unit time, which provides most of the energy required for plant life activities (Noguchi and Yoshida, 2008). Shen et al. (2013) reported that grazing affects the respiration rate of grassland plants. In addition, photosynthesis and respiration are inseparable from water and mineral elements—for example, nitrogen (N), phosphorus (P), and potassium (K) are essential elements in photosynthesis and respiration (Brooks, 1986; Nobuyuki et al., 2008; Zhang et al., 2017). Magnesium (Mg)-containing chelatase is the first enzyme in the chlorophyll biosynthetic pathway (Rissler et al., 2002). Copper (Cu) is vital for photosynthetic and respiratory electron transport processes and other cellular redox reactions (Biswas et al., 2013), and manganese (Mn) is an essential component of chloroplasts (Anja and Sébastien, 2018). However, there is a dearth of information regarding the reasons underlying this grazing rest-induced effect on forage photosynthesis and respiration. Metabolomics is an emerging approach in the post-genome era, which can comprehensively analyze the changes in metabolite content in plants and their dynamic responses to exogenous environmental factors (Ning et al., 2013). Therefore, this approach is a good choice to explore the response mechanism of photosynthesis and respiration processes to grazing rest.

The objectives of this study were (a) to identify the effects on the physiological characteristics of degraded alpine meadow vegetation after varying years of grazing rest during the spring regreening period and (b) to determine how priming of forage with grazing rest during the spring regreening period affects photosynthesis and respiration in a dominant grass (*E. nutans* Griseb.) for the degraded alpine meadow vegetation.

Materials and methods

Plant materials and treatments

The study site is located in Wariga Village, Mole Town, Qilian County, Qinghai Province, with a geographical location of 37°56′ N, 100°13′ E and an altitude of 3,650 m mainly containing alpine meadow soil. The grassland is a typical alpine meadow vegetation. The main species were *Kobresia pygmaea*, *Kobresia humilis*, *E.*

nutans Griseb., and *Poa crymophila*. A relatively uniform natural alpine meadow was selected as the test area, with 24 hm^2 as the treatment area and the other 6 hm^2 as the control. The grassland utilization patterns were winter and spring pastures. The grassland degradation level in the experimental area was moderate (*i.e.*, the proportion of edible grass in the grassland was 5–15%). The mean value of the treatment area was divided into four parts. Grazing rest was implemented during the green-up period from 2015, 2016, 2017, and 2018 (the green-up period was from May 10 to July 10): treatment 1, grazing rest during the green-up period for 1 year (2018); treatment 2, grazing rest during the green-up period for 2 years (2017 and 2018); treatment 3, grazing rest during the green-up period for 3 years (2016, 2017, and 2018); and treatment 4, grazing rest during the green-up period for 4 years (2015, 2016, 2017, and 2018). The control area was free grazing according to local traditional (with moderately severe grazing intensity and utilization rate of forage grass above 50%). The control and treatment areas were three replicates, each with 2 hm^2. The total grassland coverage, ground biomass, belowground biomass and height, photosynthetic characteristics, chlorophyll fluorescence parameters, respiration rate, relative chlorophyll content, and leaf relative water content of the dominant species' leaves were measured at nine representative points in each replicate, and the indices were measured in August 2018. Based on the preliminary test results of our research group, the dominant species selected in this study was *E. nutans* Griseb.

Quantitative characteristics of alpine meadow

A quadrate method was used to determine the quantitative characteristics of grassland vegetation, and the quadrate area was 50 cm × 50 cm. The specific method was as follows: the total coverage of vegetation in the quadrate was evaluated by visual measurement. A steel tape was used to select three plants of *E. nutans* Griseb. in each square to measure the natural plant height, which was calculated as the average plant height of the dominant herbage species in the quadrate. All plants in the quadrate square on the ground were cut, put in an envelope bag, and brought to the laboratory to be dried to constant weight at 75°C. Their dry weight was the ground biomass. Five samples (0–15 cm) of the plant underground root system were taken from the quadrate with a root drill (inner diameter: 5 cm) and dried to constant weight after being washed with clean water, which was converted into the belowground biomass of vegetation in the quadrate.

Leaf water and chlorophyll contents

Ten representative *E. nutans* plants were selected, of which the leaves were cut and weighed as fresh weight and then brought to the laboratory for drying to a constant weight at 75°C. The dry weight was obtained, and the leaf water content was calculated. Relative chlorophyll content was measured using a chlorophyll meter (SPAD-502).

Photosynthesis and respiration parameters

The photosynthetic characteristics, chlorophyll fluorescence parameters, and respiration rate of *Elymus nutans* were measured using li-COR 6400XT (LI-COR, Lincoln, NE). The photosynthetic characteristics included the net photosynthetic rate (Pn), transpiration rate (Tr), intercellular CO_2 concentration (Ci), stomatal conductance (Gs), respiration rate (R), and fluorescence parameters. The chlorophyll fluorescence parameters included photochemical quantum efficiency (Fv/Fm), (Fv′/Fm′), actual photochemical quantum efficiency (φPSII), photochemical quenching coefficient (qP), and electron transfer rate (ETR). After being induced by natural light for 1.5–2 h, an open air path was adopted. According to the average temperature of 09:00–12:00 during the measurement period, the temperature of the measuring chamber (T-block) was set to 25°C, and the flow rate was 500 mol S^{-1}. After the gas exchange parameters were measured, the light source was closed. The leaves were maintained in the dark for 30 min for adaptation before measuring the minimum (F0) and maximum (Fm) fluorescence.

Metabolite content analysis

Representative and healthy two-leaf pots from each treatment replicate were selected as the six replicates for metabolite content analysis. Fresh leaves (0.1 g) were collected from each replicate (pot) for each treatment, immediately frozen in liquid nitrogen, and stored at −80°C for subsequent analysis. The extraction protocol used was modified from that described by Du et al. (2012). The frozen leaves were ground to a fine powder with liquid N_2, and then 100 mg of the powdered leaves was weighed in a 2-ml centrifuge tube. Then, 750 µl of methanol, 250 µl of chloroform, and 100 µl of aqueous chlorphenylalanine solution (3 mg ml^{-1}, as the internal standard solution) were added to the tube, and the solution was extracted at 60 Hz for 5 min in an ultrasonic water bath. The extraction solution was centrifuged at 12,000 × *g* for 10 min at 4°C, and then 400 µl of the polar phase was decanted and dried in a Centrivap benchtop centrifugal vacuum concentrator (Labconco, Kansas City, MI, USA). The dried polar phase was incubated for 90 min at 37°C with 100 µl methoxyamine hydrochloride (20 mg ml^{-1}) in pyridine and then incubated with 100 µl bis (trimethylsilyl) trifluoroacetamide for 1 h at 70°C. After methoximation and trimethylsilylation, the extracts were analyzed according to Du et al. (2013) using a gas chromatograph–mass spectrometer (TurboMass-Autosystem XL;

PerkinElmer, Waltham, MA, USA). The metabolites detected were identified using the Turbomass 4.1.1 software (PerkinElmer) coupled with commercially available compound libraries: NIST 2005 (PerkinElmer, Waltham, MS) and Wiley 7.0 (John Wiley & Sons, Hoboken, NJ).

Mineral element content analysis

Fresh and healthy leaves were dried at 60°C until a constant weight was achieved. The dried leaves were ground, and 1 g of powdered sample was weighed. Then, the weighed particulates were digested with a mixture of H_2SO_4 and H_2O_2 for further N and P determination. Total N was analyzed using a Kjeltec 2300 analyzer (Foss Tecator AB, Hoeganaes, Sweden), and the vanadium molybdate yellow colorimetric method was used to determine the total leaf P content.

The powdered samples (1 g) were placed in a silica crucible for K, Mg, Cu, and Mn determination (25 ml). The silica crucible was heated at 550°C for 3 h, and 2 ml of double-distilled water was added when the silica crucible was cooled. Then, 10 ml of 6.00 mol/L muriatic acid was added to the silica crucible at 25°C and was heated again until dry. Subsequently, 5 ml of 6.00 mol L^{-1} muriatic acid was added to the silica crucible and then dissolved in double-distilled water up to 50.00 ml for further determination of K, Mg, Cu, and Mn. The blank control group was subjected to the same procedure. K, Mg, Cu, and Mn were determined using an atomic absorption spectrophotometer (SOLAAR, Thermo Elemental) at 766.5, 285.2, 324.8, and 279.5 nm, respectively. The detection limits (micrograms per milliliter) of the four elements were 0.2474, 0.1650, 0.0633 and 0.0306. The instruments were calibrated using standard solutions (0.20–100 μg ml^{-1}) for the above-mentioned elements.

Statistical analysis

Data were preliminarily sorted and statistically analyzed using Excel 2010, and an independent sample *t*-test was conducted using SPSS 20.0, with a significance level of 0.05. Plot analysis was performed using Sigma Plot 12.5, and correlation analysis was conducted using R language.

Results

Effects of grazing rest during the spring regreening period on the quantitative characteristics of degraded alpine meadow vegetation

The quantitative characteristics of degraded alpine meadow vegetation included coverage, height, ground biomass, and belowground biomass. In this study, grazing rest during the spring regreening period significantly increased the coverage, height, ground biomass, and belowground biomass of degraded alpine meadow vegetation compared with the control (Figure 1). The coverage significantly increased from grazing rest during the spring regreening period of 1 year. There was no significant difference in coverage between grazing rests for one to four years. The height was significantly increased from grazing rest during the spring regreening period for 2 years, but then it decreased for grazing rest for 3 or 4 years. There was no significant difference in height between grazing rests for 3 and 4 years. The ground biomass significantly increased from grazing rest during the spring regreening period for 1 year and then approached the peak level for grazing for the remaining 2 years. The ground biomass did not differ significantly between grazing rests for 3 and 4 years. The belowground biomass significantly increased from grazing rest during the spring regreening period for 1 year but then decreased for grazing rest for 3 or 4 years. The belowground biomass did not differ significantly between grazing rests for 3 and 4 years.

Effects of grazing rest during the spring regreening period on the photosynthesis of degraded alpine meadow vegetation's dominant grass *E. nutans* Griseb.

All photosynthetic characteristics were significantly increased by grazing rest during the spring regreening period for several years compared with the control (Figure 2). The Pn, Cond, and Tr approached peak levels for grazing for the remaining 2 years. The Ci significantly increased for grazing rest during the spring regreening period of 2, 3, or 4 years, and there was no significant difference between them.

All chlorophyll fluorescence parameters were significantly increased by grazing rest during the spring regreening period for several years compared with the control (Figure 2). The maximal quantum yield of PSII (Fv/Fm) was not significantly different between grazing rests for 1, 2, 3, or 4 years. The photochemical efficiency of PSII in the light (Fv′/Fm′), actual photochemical quantum efficiency (φPS II), and ETR tended to increase first and then decrease. The photochemical quenching coefficient (qP) approached a peak level for grazing rest of 3 or 4 years.

The Calvin cycle is an important photosynthetic process. In this study, there were eight metabolites associated with this cycle, which were significantly changed by grazing rest during the spring regreening period for several years (Figure 3). The contents of all eight metabolites were significantly increased by grazing rest during the spring regreening period for 2, 3, and 4 years compared with the control, and the value of log_2FC reached a maximum at grazing rest for 2 years.

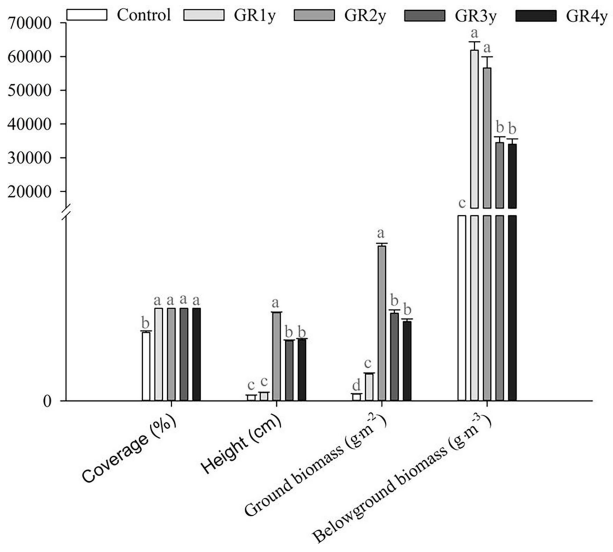

FIGURE 1
Effect of grazing rest during the spring regreening period on the quantity characteristics of the degraded alpine meadow vegetation. Bars represent SEs. Common letters above columns indicate no significant difference at $P = .05$. GR 1y, GR 2y, GR 3y, and GR 4y mean grazing rest for 1, 2, 3, and 4 years, respectively.

Effects of grazing rest during the spring regreening period on the chlorophyll synthesis of degraded alpine meadow vegetation's dominant grass *E. nutans* Griseb.

Grazing rest during the spring regreening period significantly increased the relative chlorophyll content for several years compared with the control (Figure 4A). The relative chlorophyll content approached the peak level for grazing for the remaining 2 years, and there was no significant difference between grazing rest for 3 or 4 years. There were two metabolites associated with the chlorophyll synthesis pathway, which were significantly changed by grazing rest during the spring regreening period (Figure 4B). The contents of the two metabolites were significantly increased by grazing rest for 1, 2, 3, and 4 years compared with the control, and the value of $\log_2$FC reached a maximum after 2 years of grazing rest.

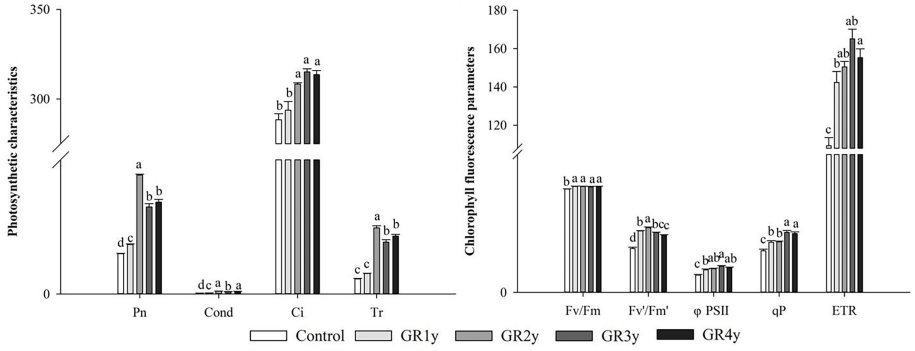

FIGURE 2
Effect of grazing rest during the spring regreening period on the photosynthesis of the dominant grass *Elymus nutans* Griseb of the degraded alpine meadow vegetation. Bars represent SEs. Common letters above columns indicate no significant difference at $P = .05$. GR 1y, GR 2y, GR 3y, and GR 4y mean grazing rest for 1, 2, 3, and 4 years, respectively.

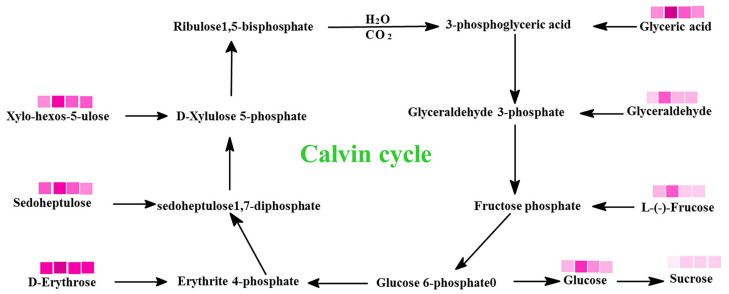

Metabolite names	CAS ID	Log_2FC (1 y/control)	Log_2FC (2 y/control)	Log_2FC (3 y/control)	Log_2FC (4 y/control)
Glyceraldehyde	56-82-6	0.07	0.33**	0.20*	0.11*
Glyceric acid	503-66-2	0.28*	0.62**	0.35*	0.29*
D-Erythrose	583-50-6	0.51*	0.67**	0.56*	0.54*
Xylo-hexos-5-ulose	62108-13-8	0.28*	0.56**	0.36*	0.32*
Sedoheptulose	74978-26-0	0.35*	0.57**	0.34*	0.29*
Sucrose	57-50-1	0.02	0.10**	0.08*	0.07*
L-(-)-Frucose	117307-13-8	0.11*	0.35**	0.08*	0.09*
Glucose	50-99-7	0.13*	0.40**	0.23**	0.14*

FIGURE 3
Effect of grazing rest during the spring regreening period on the Calvin cycle of the dominant grass *Elymus nutans* Griseb of the degraded alpine meadow vegetation. FC, fold change of relative content; *significant difference at $P = .05$; **significant difference at $P = .01$ represent log_2FC ≤0.7, ≤0.6, ≤0.5, ≤0.4, ≤0.3, ≤0.2, ≤0.1, and ≤0.05, respectively.

Effects of grazing rest during the spring regreening period on the respiration of degraded alpine meadow vegetation's dominant grass *E. nutans* Griseb.

The respiration rate first increased gradually to the highest levels and then reduced owing to grazing rest during the spring regreening period, with the peak at grazing rest for 2 years. The TCA cycle is a critical link in the entire respiration process (Figure 5A). We found six metabolites, the contents of which significantly increased in this cycle caused by grazing rest during the spring regreening period for several years compared with the control (Figure 5B). The value of log_2FC decreased after the peak at grazing rest for 2 years, and there was no significant difference between grazing rest for 3 and 4 years.

Effects of grazing rest during the spring regreening period on the leaf water and mineral contents of degraded alpine meadow vegetation's dominant grass *E. nutans* Griseb.

Grazing rest during the spring regreening period significantly increased the leaf relative water content in all rest periods. The leaf water content was not significantly different

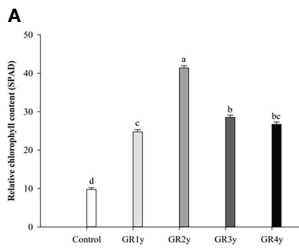

B

Glutamic acid → Porphobilinogen → Chlorophyllide → Phytol → Chlorophyll A

Metabolite names	CAS ID	Log_2FC (1 y/control)	Log_2FC (2 y/control)	Log_2FC (3 y/control)	Log_2FC (4 y/control)
L-Glutamic acid	56-86-0	0.49*	0.82**	0.71**	0.63**
Phytol	150-86-7	0.27*	0.62**	0.55**	0.41**

FIGURE 4
Effect of grazing rest during the spring regreening period on chlorophyll synthesis of degraded alpine meadows vegetation dominant grass Elymus nutans Griseb. **(A)** Effect of grazing rest during the spring regreening period on relative chlorophyll content of *Elymus nutans* Griseb. **(B)** Effect of grazing rest during the spring regreening period on metabolite contents in chlorophyll synthesis pathway of Elymus nutans Griseb. Bars represent SEs. Common letters above columns indicate no significant difference at $P = .05$. FC means fold change of relative content. * indicate significant difference at $P = .05$. ** indicate significant difference at $P = .01$. GR 1y, GR 2y, GR 3y and GR 4y mean grazing rest for 1 year, 2 years, 3 years and 4 years respectively represent log_2FC ≤0.7, ≤0.6, ≤0.5, ≤0.4, ≤0.3, ≤0.2, ≤0.1, and ≤0.05, respectively.

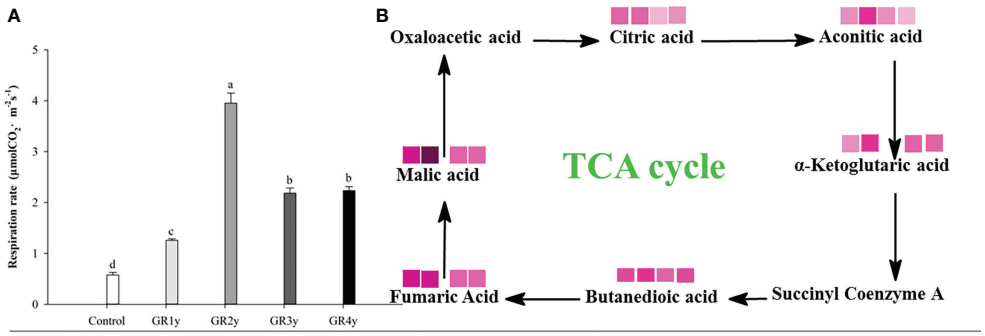

Metabolite names	CAS ID	Log_2FC (1 y/control)	Log_2FC (2 y/control)	Log_2FC (3 y/control)	Log_2FC (4 y/control)
Butanedioic acid	110-15-6	0.41*	0.57**	0.39*	0.48*
Fumaric acid	110-17-8	0.67**	0.67**	0.35*	0.32*
Malic acid	97-67-6	0.63**	0.83**	0.38*	0.39*
Aconitic acid	499-12-7	0.23*	0.56**	0.22*	0.12*
Citric acid	77-92-9	0.31**	0.37**	0.19*	0.24*
α-Ketoglutaric acid	328-50-7	0.21*	0.54**	0.32**	0.37**

FIGURE 5
Effect of grazing rest during the spring regreening period on respiration of degraded alpine meadows vegetation dominant grass Elymus nutans Griseb. **(A)** Effect of grazing rest during the spring regreening period on respiration rate of *Elymus nutans* Griseb. **(B)** Effect of grazing rest during the spring regreening period on metabolite contents in TCA Cycle of Elymus nutans Griseb. Bars represent SEs. Common letters above columns indicate no significant difference at $P = .05$. FC means fold change of relative content. * indicate significant difference at $P = .05$. ** indicate significant difference at $P = .01$. GR 1y, GR 2y, GR 3y and GR 4y mean grazing rest for 1 year, 2 years, 3 years and 4 years respectively. represent Log2FC ≤0.7, ≤0.6, ≤0.5, ≤0.4, ≤0.3, ≤0.2, ≤0.1 and ≤0.05 respectively. represent log2FC ≤0.7, ≤0.6, ≤0.5, ≤0.4, ≤0.3, ≤0.2, ≤0.1, and ≤0.05, respectively.

between grazing rests for 1 to 4 years (Figure 6). The macro elements (N, P, and K) showed the same variation tendency that increased first and approached the peak at grazing rest for 2 years and then decreased. There was no significant difference between grazing rest for 3 and 4 years. Mg showed an increasing trend year by year and was significantly increased by grazing rest for 2, 3, and 4 years. The Cu content of grass leaves significantly increased by grazing rest during the spring regreening period,

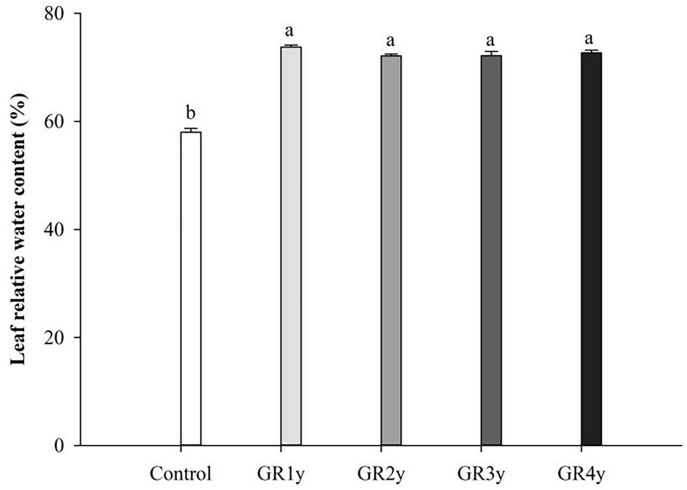

FIGURE 6
Effect of grazing rest during the spring regreening period on the leaf water content of the degraded alpine meadow vegetation. Bars represent SEs. Common letters above columns indicate no significant difference at $P = .05$. GR 1y, GR 2y, GR 3y, and GR 4y mean grazing rest for 1, 2, 3, and 4 years, respectively.

and there was no difference between the years of grazing rest. Grazing rest during the spring regreening period significantly increased the Mn content of the leaves. The Mn content under grazing rest for 2, 3, and 4 years was more than 1 year, and under the latter 3 years, the content tended to be stable (Figure 7).

Correlation analysis of vegetation quantitative characteristics, photosynthetic characteristics, respiratory characteristics, and key influencing factors of degraded alpine meadows

In this study, all indicators of degraded alpine grassland vegetation were significantly correlated with each other ($P < 0.05$). The correlation coefficients between aboveground biomass and Pn, height and Pn, aboveground biomass and respiration rate, and height and respiration rate were 0.89, 0.91, 0.83, and 0.80, respectively (Figure 8). This indicated that the restoration of degraded meadow vegetation by grazing rest during the spring regreening period was significantly correlated with photosynthesis and respiration. Cond, α-ketoglutaric acid, Tr, sucrose, glutamic acid, phytol, and N were highly correlated with Pn, except vegetation quantitative characteristics. In addition, the correlation coefficient between Fv′/Fm′ and erythrose was 0.82. These indicated that the key factors for increased photosynthesis were the supply of reactants involved in the Calvin cycle and the synthesis of chlorophyll. Meanwhile, glyceric acid, α-ketoglutaric acid, glucose, and aconitic acid were highly correlated with respiration rate, except vegetation quantitative characteristics. This suggests that the increase in respiration was due to an increase in the direct reactant content of the TCA cycle.

Discussion

Effects of grazing rest during the spring regreening period on the quantitative characteristics of degraded alpine meadow vegetation

Scholars generally agree that grazing rest can improve the vegetation growth of degraded grasslands (Zimmer et al., 2010; Ash et al., 2011; Selemani et al., 2013; Wu et al., 2017). In our study, grazing rest significantly increased the coverage, height, ground biomass, and belowground biomass of the degraded alpine meadow vegetation. Zhao et al. (2016) obtained a similar result in that grazing exclusion enhances plant height, total cover, aboveground biomass, and belowground biomass in the alpine steppe, alpine meadow, and swamp meadow. Bai et al. (2015); Qin et al. (2021), and Chen et al. (2007) also reported that grazing significantly decreases the aboveground biomass of the Inner Mongolia temperate steppe. Bai et al. (2015) indicated that grazing reduces root production. The most important reasons for the improvement of degraded grassland vegetation during grazing rest are to avoid trampling and feeding by livestock and to change the grassland ecosystem environment (Zhao et al., 2016). In addition, the improvement in vegetation quantitative characteristics gradually stabilized with the increase in rest years, which might be caused by the gradual adaptation to the environment without trampling and feeding by livestock. In order to understand the reason why the grazing rest during the

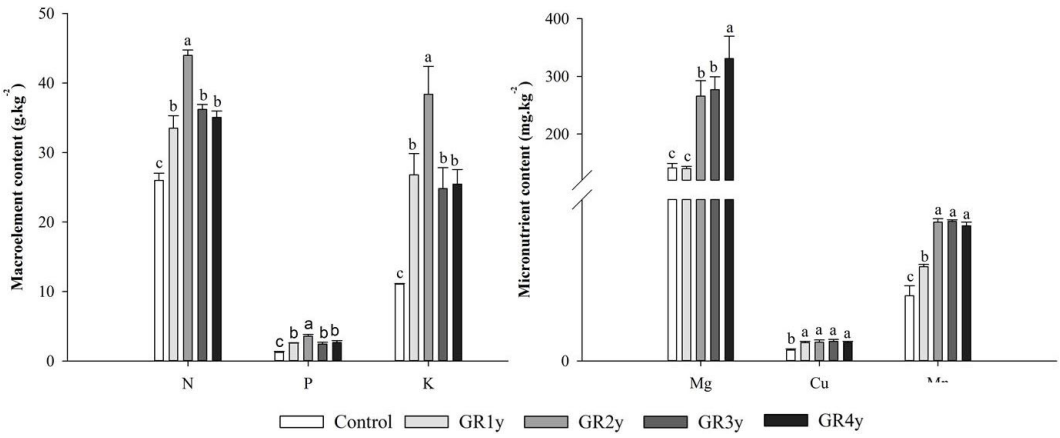

FIGURE 7
Effect of grazing rest during the spring regreening period on the mineral element content of the degraded alpine meadow vegetation. Bars represent SEs. Common letters above columns indicate no significant difference at $P = .05$. GR 1y, GR 2y, GR 3y, and GR 4y mean grazing rest for 1, 2, 3, and 4 years, respectively.

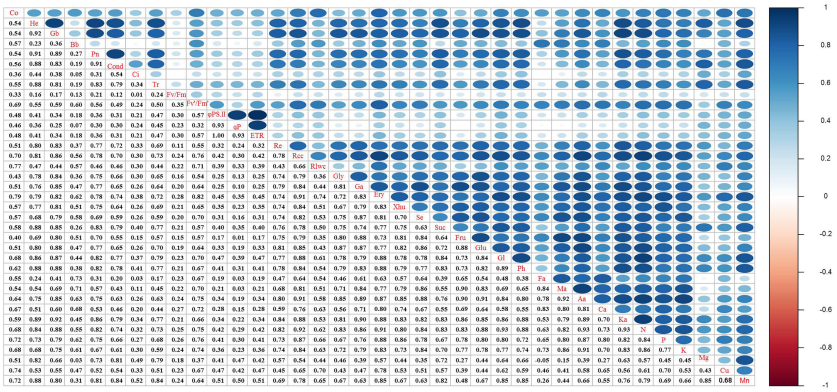

FIGURE 8
Effects of grazing rest during the spring regreening period on quantitative characteristics of degraded alpine meadow vegetation. Pn, Net photosynthetic rate; Cond, Stomatal conductance; Ci, Intercellular CO_2 concentration; Tr, Transpiration rate; Fv/Fm, Photochemical quantum efficiency; Fv′/Fm′, Effective photochemical quantum efficiency; φPSII, Actual photochemical quantum efficiency; qP, Photochemical quenching coefficient; ETR, Electron transfer rate; Re, Respiratory rate; Co, Coverage; He, Height; Gb, Ground biomass; Bb, Belowground biomass; Rcc, Relative chlorophyll content; Rlwc, Relative leaf water content; Gly, DL-Glyceraldehyde; Ga, Glyceric acid; Ery, D-Erythrose; Xhu, Xylo-hexos-5-ulose; Se, Sedoheptulose; Suc, Sucrose; Fru, Frucose; Glu, Glucose; Gl, Glutamic acid; Ph, Phytol; Ba, Butanedioic acid; Fa, Fumaric acid; Ma, Malic acid; Aa, Aconitic acid; Ca, Citric acid; Ka, α-Ketoglutaric acid.

spring regreening period promoted the restoration of the degraded alpine meadow vegetation, the photosynthesis and respiration processes were explored in this study. The correlation analysis showed that the quantitative characteristics of the alpine meadow vegetation were significantly correlated with the parameters of photosynthesis and respiration.

Effects of grazing rest during the spring regreening period on the photosynthesis of degraded alpine meadow vegetation's dominant grass *E. nutans* Griseb.

The photosynthesis of grass leaves is the primary determinant of carbohydrate sources for plant growth and development (Ellsworth et al., 2004). Our results show that all photosynthetic functions (Pn, Cond, Tr, and Ci) in *E. nutans* were significantly increased by grazing rest. Several researchers have obtained similar results. They found that overgrazing by livestock dramatically restricts leaf photosynthetic capacity and function (such as Pn, Cond, Tr, and Ci) under field conditions (Chen et al., 2005; Zhao et al., 2009; Zheng et al., 2011; Shen et al., 2013; Ren et al., 2017). Chlorophyll fluorescence parameters are highly sensitive to changes in external environmental conditions and can be used to evaluate the effects of external disturbances on plants (Maxwell and Johnson, 2000). Wang et al. (2022) found that chlorophyll fluorescence shows a good correlation with grassland productivity. Our results show that all chlorophyll fluorescence parameters (Fv/Fm, Fv′/Fm′, φPS II, ETR, and qP) of *E. nutans* were significantly increased by grazing rest. Zhang et al. (2022) obtained similar results in that the regulation of chlorophyll fluorescence is constrained under grazing. In addition, Li et al. (2018) found that Fv/Fm, φPSII, and qP are not significantly changed by grazing for 1 year. This may be caused by different climates, grassland types, and dominant grasses. Weng and Lai (2005) and Wang et al. (2022) found that the chlorophyll fluorescence parameters are decreased by heat and drought tolerance. These results indicate that the increase in chlorophyll fluorescence parameters caused by grazing rest resulted from the elimination of grazing stress. However, there have been no detailed reports on why grazing rest promotes photosynthesis in herbage. By using metabolomic techniques, our study demonstrated that grazing rest significantly promoted the Calvin cycle in herbage. We found that the levels of eight metabolites related to the Calvin cycle significantly increased under grazing rest, and sucrose and erythrose had a higher correlation with related parameters of photosynthesis among the eight enriched metabolites. At present, the relationship between grazing rest and the Calvin cycle has not been reported.

Moreover, the photosynthetic responses in different grazing rest years were compared in this study. We found that all photosynthetic functions and chlorophyll fluorescence parameters significantly increased first and then gradually stabilized. These results might be caused by the similar pattern of changes in the eight metabolites in the Calvin cycle, chlorophyll content, leaf relative water content, and mineral element content. Chlorophyll, a photosynthetic pigment, plays an important role in the absorption and utilization of light energy by green plants. Chlorophyll content is closely related to the level of plant photosynthesis. Many other researchers have reported similar results in that grazing rest induces more

chlorophyll than grazing (Thomas, 2012; Ren et al., 2017). Furthermore, we used metabolomics techniques and found that the increased chlorophyll content resulted from the increased levels of glutamic acid and phytol, which are metabolites related to chlorophyll biosynthesis, and the correlation coefficient between glutamic acid and relative chlorophyll content was 0.87. However, this may result from the decrease in plant leaf water and soil water contents after grazing disturbance, leading to some degradation of chlorophyll in forage leaves (Sohrabi et al., 2017). In this study, not only was leaf relative water content absolutely increased by grazing rest but also the N, Mg, and Cu contents in leaves. N and Mg are essential elements for chlorophyll biosynthesis (Rissler et al., 2002; Eckhardt et al., 2004). The Cu supply significantly increases the Chl-a concentration (Biswas et al., 2013). In addition to promoting chlorophyll biosynthesis, mineral elements play important roles in other photosynthetic processes. Nobuyuki et al. (2008) pointed out that N, P, and K deficiencies significantly decrease photosynthesis and RuBP carboxylase–oxygenase activity in rice (*Oryza sativa*) plants. Tanwar et al. (2013) indicated that phosphate application significantly increases photosynthesis and stomatal conductance in bell pepper (*Capsicum annuum*). Mn is indispensable for water splitting during photosynthesis (Eisenhut et al., 2018). Our results show that the N, P, K, Mg, Cu, and Mn contents were significantly increased by grazing rest. Yin and Lu (2013) obtained a similar result; *Leymus chinensis* displays increasing leaf N and P concentrations over time after grazing exclusion. Harrison et al. (2010) stated that grazing may affect photosynthesis as a consequence of changes in leaf water status, nitrogen content, and photosynthetic enzymes. Moreover, the variation trends of mineral elements and leaf relative water content with grazing rest years are consistent with the variation trends of the parameters related to underground biomass and photosynthesis. Therefore, it was reasonable to infer that grazing rest could enhance the grass absorption of mineral elements and water by increasing the underground biomass of herbage, thereby promoting chlorophyll biosynthesis and photosynthesis.

Effects of grazing rest during the spring regreening period on the respiration of degraded alpine meadow vegetation's dominant grass *E. nutans* Griseb.

Plant respiration is a basic process of plant physiological metabolism that provides energy for plant life activities (Noguchi and Yoshida, 2008). Respiration and photosynthesis cooperate closely in plant energy metabolism (Archontoulis et al., 2012). Similar to the net photosynthetic rate, the respiration rate of the degraded alpine meadows vegetation's dominant grass *E. nutans* Griseb. significantly increased by grazing rest during the spring regreening period. There are very few reports on the effects of grazing rest or grazing on plant leaf respiration rate. Shen et al. (2013) indicated that the dark respiration rate of *Gentiana straminea* in un-grazed regimes is higher than that in grazed regimes under ambient conditions. Furthermore, we used metabolomics to determine which metabolic process of respiration responds to grazing rest, and the results show that six key metabolites in the TCA cycle were significantly enriched and that aconitic acid and ketoglutaric acid had a higher correlation with respiration rate among the six enriched metabolites. In addition, a significant increase in respiration factors was also detected owing to grazing rest in this study. Water is necessary for respiration (Galmes et al., 2007). The rate of respiration is lower in P-deficient plants than in P-fertilized plants (Bahar et al., 2018). K enhances the respiration of *Nicotiana tabacum* by increasing the O_2 uptake (Wakhloo and Ruppenthal, 1989). Copper oxidase is involved in the reduction of oxygen molecules in plants and has significant effects on plant respiration (Patterson, 2013). Mn increases the respiration intensity of plants and regulates redox processes (Hsieh, 2011). This may be because grazing rest could enhance the respiration of the degraded alpine meadow vegetation's dominant grass *E. nutans* Griseb.

Conclusion

Grazing rest during the spring regreening period promoted the ecological restoration of degraded alpine meadows by enhancing the photosynthesis and respiration of the dominant grass *E. nutans* Griseb. Grazing rest enhanced photosynthesis in dominant grass by increasing the metabolites related to the Calvin cycle, chlorophyll content, leaf relative water content, and related mineral element content. Grazing rest also enhanced the respiration of dominant grass by increasing the metabolites related to the TCA cycle, leaf relative water content, and related mineral element content.

Data availability statement

The data analyzed in this study is subject to the following licenses/restrictions: according to state policies, requests to access these datasets should be directed to YL, liuying_yanhong@sina.com.

Author contributions

The author confirms being the sole contributor of this work and has approved it for publication.

Funding

This research was supported by the National Natural Science Foundation of China (U21A20241) and the Key Laboratory Project of Qinghai Province, China (2020-ZJ-Y03).

Acknowledgments

The author would like to thank Yushou Ma and Shixiong Li for providing the experimental field, and Wenhui Liu for providing the instruments facility. The author is grateful to all editors and reviewers for their valuable suggestions on the manuscript.

Conflict of interest

The author declares that the research was conducted in the absence of any commercial or financial relationships that could be construed as a potential conflict of interest.

Publisher's note

All claims expressed in this article are solely those of the authors and do not necessarily represent those of their affiliated organizations, or those of the publisher, the editors and the reviewers. Any product that may be evaluated in this article, or claim that may be made by its manufacturer, is not guaranteed or endorsed by the publisher.

References

Anja, K. L., and Sébastien, T. (2018). Importing manganese into the chloroplast: many membranes to cross. *Mol. Plant* 11, S1674205218302405. doi: 10.1016/j.molp.2018.07.006

Archontoulis, S. V., Yin, X., Vos, J., Danalatos, N. G., and Struik, P. C. (2012). Leaf photosynthesis and respiration of three bioenergy crops in relation to temperature and leaf nitrogen: how conserved are biochemical model parameters among crop species? *J. Exp. Bot.* 63 (2), 895–911. doi: 10.1093/jxb/err321

Ash, A. J., Corfield, J. P., Mcivor, J. G., and Ksiksi, T. S. (2011). Grazing management intropical savannas: utilization and rest strategies to manipulate rangeland condition. *Rangeland Ecol. Manage.* 64 (3), 223–239. doi: 10.2111/REM-D-09-00111.1

Bahar, N., Gauthier, P., O'Sullivan, O. S., Thomas, B., Evans, J. R., and Atkin, O. K. (2018). Phosphorus deficiency alters scaling relationships between leaf gas exchange and associated traits in a wide range of contrasting *Eucalyptus* species. *Funct. Plant Biol.* 45 (8), 813–826. doi: 10.1071/FP17134

Bai, W., Fang, Y., Zhou, M., Xie, T., Li, L., Zhang, W. H., et al. (2015). Heavily intensified grazing reduces root production in an inner Mongolia temperate steppe. *Agriculture Ecosyst. Environ.* 200, 143–150. doi: 10.1016/j.agee.2014.11.015

Biswas, H., Bandyopadhyay, D., and Waite, A. (2013). Copper addition helps alleviate iron stress in a coastal diatom: Response of *Chaetoceros gracilis* from the bay of bengal to experimental Cu and fe addition. *Mar. Chem.* 157 (20), 224–232. doi: 10.1016/j.marchem.2013.10.006

Brooks, A. (1986). Effects of phosphorus nutrition on ribulose-1,5-bisphosphate carboxylase activation, photosynthetic quantum yield and amounts of some calvin-cycle metabolites in spinach leaves. *Funct. Plant Biol.* 13 (2), 221–237. doi: 10.1071/PP9860221

Chamizo, S., Rodriguez-Caballero, E., Moro, M. J., and Cantón, Y. (2021). Non-rainfall water inputs: A key water source for biocrust carbon fixation. *Sci. Total Environ.* 792, 148299. doi: 10.1016/j.scitotenv.2021.148299

Chen, S. P., Bai, Y. F., Lin, G. H., Liang, Y., and Han, X. G. (2005). Effects of grazing on photosynthetic characteristics of major steppe species in the xilin river basin, inner Mongolia, China. *Photosynthetica* 43 (4), 559–565. doi: 10.1007/s11099-005-0088-9

Chen, Y., Lee, G., Lee, P., and Oikawa, T. (2007). Model analysis of grazing effect on above-ground biomass and above-ground net primary production of a Mongolian grassland ecosystem. *J. Hydrology* 333 (1), 155–164. doi: 10.1016/j.jhydrol.2006.07.019

Crous, K. Y., Uddling, J., and Kauwe, M. (2022). Temperature responses of photosynthesis and respiration in evergreen trees from boreal to tropical latitudes. *New Phytol.* 234, 353–374. doi: 10.1111/nph.17951

Du, H., Wang, Z., Yu, W., and Huang, B. (2012). Metabolic responses of hybrid bermudagrass to short-term and long-term drought stress. *J. Am. Soc. Hortic. Sci. Am. Soc. Hortic. Sci.* 137 (6), 411–420. doi: 10.21273/JASHS.137.6.411

Du, H., Zhou, P., and Huang, B. (2013). Antioxidant enzymatic activities and gene expression associated with heat tolerance in a cool-season perennial grass species. *Environ. Exp. Bot.* 87, 159–166. doi: 10.1016/j.envexpbot.2012.09.009

Eckhardt, U., Grimm, B. H., and Rtensteiner, S. (2004). Recent advances in chlorophyll biosynthesis and breakdown in higher plants. *Plant Mol. Biol.* 56 (1), 1–14. doi: 10.1007/s11103-004-2331-3

Eisenhut, M., Weber, A., Leister, D., Schneider, A., Hoecker, N., Schmidt, S. B., et al. (2018). The plastid envelope chloroplasr manganese transporter1 is essential for manganese homeostasis in *Arabidopsis*. *Mol. Plant* 11 (7), 955–969. doi: 10.1016/j.molp.2018.04.008

Ellsworth, D. S., Reich, P. B., Naumburg, E. S., Koch, G. W., Kubiske, M. E., and Smith, S. D. (2004). Photosynthesis, carboxylation and leaf nitrogen responses of 16 species to elevated pCO2 across four free air CO2 enrichment experiments in forest, grassland and desert. *Global Change Biol.* 10 (12), 2121–2138. doi: 10.1111/j.1365-2486.2004.00867.x

Fan, J. W., Shao, Q. Q., Liu, J. Y., Wang, J. B., Harris, W., Chen, Z. Q., et al. (2010). Assessment of effects of climate change and grazing activity on grassland yield in the three rivers headwaters region of qinghai–Tibet plateau, China. *Environ. Monit. Assess.* 170 (1), 571–584. doi: 10.1007/s10661-009-1258-1

Fedrigo, J. K., Ataide, P. F., Azambuja Filho, J., Oliveira, L. V., Jaurena, M., Laca, E. A., et al. (2018). Temporary grazing exclusion promotes rapid recovery of species richness and productivity in a long-term overgrazed Campos grassland. *Restor. Ecol.* 26 (4), 677–685. doi: 10.1111/rec.12635

Galmes, J., Ribas-Carbo, M., Medrano, H., and Flexas, J. (2007). Response of leaf respiration to water stress in Mediterranean species with different growth forms. *J. Arid Environments* 68 (2), 206–222. doi: 10.1016/j.jaridenv.2006.05.005

Harrison, M. T., Kelman, W. M., Moore, A. D., and Evans, J. R. (2010). Grazing winter wheat relieves plant water stress and transiently enhances photosynthesis. *Funct. Plant Biol.* 37 (8), 726–736. doi: 10.1071/FP10040

Hsieh, S. I. (2011). *Metal-responsive proteomes: Copper, iron, zinc, and manganese micronutrient deficiency in chlamydomonas reinhardtii[D]* (Los Angeles: University of California).

Li, W., Cao, W., Wang, J., Li, X., Xu, C., and Shi, S. (2017). Effects of grazing regime on vegetation structure, productivity, soil quality, carbon and nitrogen storage of alpine meadow on the qinghai-Tibetan plateau. *Ecol. Engeering* 98 (Complete), 123–133. doi: 10.1016/j.ecoleng.2016.10.026

Li, X., Huang, Q., Xue, M. I., Bai, Y., Zhang, M., and Li, X. (2018). Grazing every month minimizes size but boosts photosynthesis in stipa grandis in the steppe of inner Mongolia, China. *J. Arid Land* 10, 4, 11. doi: 10.1007/s40333-018-0011-4

Li, X., Perry, G., and Brierley, G. J. (2016). "Grassland ecosystems of the yellow river source zone: degradation and restoration[C]," in *Landscape and ecosystem diversity, dynamics and management in the yellow river source zone* (Switzerland, Springer International Publishing), 137–165.

Liu, X., Duan, S., Li, A., Xu, N., Cai, Z., and Hu, Z. (2008). Effects of organic carbon sources on growth, photosynthesis, and respiration of *Phaeodactylum tricornutum*. *J. Appl. Phycology* 21, 239–246. doi: 10.1007/s10811-008-9355-z

Martínkov, J., Hajek, T., Adamec, L., and Klimešová, J. (2021). Growth, root respiration and photosynthesis of a root-sprouting short-lived herb after severe biomass removal. *Flora* 284, 151915. doi: 10.1016/j.flora.2021.151915

Mavromihalis, J. A., Dorrough, J., Clark, S. G., Turner, V., and Moxham, C. (2013). Manipulating livestock grazing to enhance native plant diversity and cover in native grasslands. *Rangeland J.* 35 (1), 95–108. doi: 10.1071/RJ12074

Maxwell, K., and Johnson, G. N. (2000). Chlorophyll fluorescence–a practical guide. *J. Exp. Bot.* 51 (345), 659–668. doi: 10.1093/jexbot/51.345.659

Ning, Z., Lu, C., Zhang, Y., Zhao, S., Liu, B., Xu, X., et al. (2013). Application of plant metabonomics in quality assessment for large-scale production of traditional Chinese medicine. *Planta Med.* 79 (11), 897–908. doi: 10.1055/s-0032-1328656

Nobuyuki, K., Hitoshi, S., and Shigemi, A. (2008). Effects of nitrogen, phosphorus and potassium deficiencies on photosynthesis and RuBP carboxylase-oxygenase activities in rice plants. *Japanese J. Crop Sci.* 48 (3), 378–384. doi: 10.1626/jcs.48.378

Noguchi, K., and Yoshida, K. (2008). Interaction between photosynthesis and respiration in illuminated leaves. *Mitochondrion* 8 (1), 87–99. doi: 10.1016/j.mito.2007.09.003

Patterson, E. (2013). *Analyzing genetic response mechanisms associated with copper homeostasis in populus trichocarpa using a bioinformatics approach[D]* (Fort Collins, Colorado State University).

Qin, Q., Xu, D., Hou, L., Shen, B., and Xin, X. (2021). Comparing vegetation indices from sentinel-2 and landsat 8 under different vegetation gradients based on a controlled grazing experiment. *Ecol. Indic.* 133, 108363. doi: 10.1016/j.ecolind.2021.108363

Ren, W., Hu, N., Hou, X., Zhang, J., Guo, H., Liu, Z., et al. (2017). Long-term overgrazing-induced memory decreases photosynthesis of clonal offspring in a perennial grassland plant. *Front. Plant Sci.* 8, 419. doi: 10.3389/fpls.2017.00419

Rissler, H. M., Collakova, E., DellaPenna, D., and Pogson, W. (2002). Chlorophyll biosynthesis. expression of a second chllgene of magnesium chelatase in *Arabidopsis* supports only limited chlorophyll synthesis. *Plant Physiol.* 128 (2), 770–779. doi: 10.1104/pp.010625

Selemani, I. S., Eik, L. O., Holand, Ø., Ådnøy Mtengeti, T E., and Mushi, D. (2013). The effects of a deferred grazing system on rangeland vegetation in a north-western, semi-arid region of Tanzania. *Afr. J. Range Forage Sci.* 30 (3), 141–148. doi: 10.2989/10220119.2013.827739

Shang, Z. H., Cao, J. J., Guo, R. Y., Henkin, Z., Ding, L. M., Long, R. J., et al. (2017). Effect of enclosure on soil carbon, nitrogen and phosphorus of alpine desert rangeland. *Land Degradation Dev.* 28 (4), 1166–1177. doi: 10.1002/ldr.2283

Shen, H., Wang, S., and Tang, Y. (2013). Grazing alters warming effects on leaf photosynthesis and respiration in *Gentiana straminea*, an alpine forb species. *J. Plant Ecol.* 6 (5), 418–427. doi: 10.1093/jpe/rtt010

Simkó, A., Gáspár, G. S., Kiss, L., Makleit, P., and Veres, S. (2020). Evaluation of nitrogen nutrition in diminishing water deficiency at different growth stages of maize by chlorophyll fluorescence parameters. *Plants* 9 (6), 676–692. doi: 10.3390/plants9060676

Sohrabi, S., Ebadi, A., Jalali, S., and Salami, S. A. (2017). Enhanced values of various physiological traits and VvNACI, gene expression showing better salinity stress tolenrance in some grapevine cultivars as well as rootstocks. *Scientia Horticulture* 225, 317–326. doi: 10.1016/j.scienta.2017.06.025

Tanwar, A., Aggarwal, A., Kadian, N., and Gupta, A. (2013). Arbuscular mycorrhizal inoculation and super phosphate application influence plant growth and yield of *Capsicum annuum*. *J. Soil Sci. Plant Nutr.* 13 (1), 55–66. doi: 10.4067/S0718-95162013005000006

Thomas, A. D. (2012). Impact of grazing intensity on seasonal variations in soil organic carbon and soil CO2 efflux in two semiarid grasslands in southern Botswana. *Philos. Trans. R. Soc. London. Ser. B Biol. Sci.* 367, 3076–3086. doi: 10.1098/rstb.2012.0102

Wakhloo, J. L., and Ruppenthal, H. (1989). Respiration in developing leaves in relation to vertical profiles in concentration of potassium in shoots of *Nicotiana tabacum*. *J. Plant Physiol.* 135 (4), 501–504. doi: 10.1016/S0176-1617(89)80111-7

Wang, X., Pan, S., Pan, N., and Pan, P. (2022). Grassland productivity response to droughts in northern China monitored by satellite-based solar-induced chlorophyll fluorescence. *Sci. Total Environ.* 830, 154550. doi: 10.1016/j.scitotenv.2022.154550

Weng, J. H., and Lai, M. F. (2005). Estimating heat tolerance among plant species by two chlorophyll fluorescence parameters. *Photosynthetica* 43 (3), 439–444. doi: 10.1007/s11099-005-0070-6

Wu, G. L., Dong, W., Yu, L., Ding, L. M., and Liu, Z. H. (2017). Warm-season grazing benefits species diversity conservation. *Land Degradation Dev.* 28 (4), 1311–1319. doi: 10.1002/ldr.2536

Yin, J., and Lu, X. (2013). "Opposite responses in leaf n and p concentrations and resorption of two dominant grass species along a 30-yr temperate steppe restoration chronosequence[C]," in *Esa convention*. (Minneapolis: ResearchGate).

Zhang, Z., Gong, J., Shi, J., Li, X., Song, L., Zhang, W., et al. (2022). Multiple herbivory pressures lead to different carbon assimilation and allocation strategies: Evidence from a perennial grass in a typical steppe in northern China. *Agriculture Ecosyst. Environ.* 326, 107776. doi: 10.1016/j.agee.2021.107776

Zhang, R. Z., Huang, D., Wang, K., Zhang, Y. J., and Wang, C. J. (2011). Effect of mowing and grazing on ramet emergence of, leymus racemosus, in the inner Mongolia steppe during the spring regreening period. *Afr. J. Biotechnol.* 10 (10), 2216–2222. doi: 10.1186/1472-6750-11-24

Zhang, G., Johkan, M., Hohjo, M., Tsukagoshi, S., and Maruo, T. (2017). Plant growth and photosynthesis response to low potassium conditions in three lettuce (*Lactuca sativa*) types. *Horticulture J.* 86 (2), 229–237. doi: 10.2503/hortj.OKD-008

Zhao, W., Chen, S. P., and Lin, H. G.H. (2009). Effects of long-term grazing on the morphological and functional traits of *Leymus chinensis* in the semiarid grassland of inner Mongolia, China. *Ecol. Res.* 24, 99–108. doi: 10.1007/s11284-008-0486-0

Zhao, J., Li, X., Li, R., Tian, L., and Zhang, T. (2016). Effect of grazing exclusion on ecosystem respiration among three different alpine grasslands on the central Tibetan plateau. *Ecol. Eng.* 94, 599–607. doi: 10.1016/j.ecoleng.2016.06.112

Zheng, S. X., Lan, Z. C., Li, W. H., Shao, R. X., Shan, Y. M., Wan, H. W., et al. (2011). Differential responses of plant functional trait to grazing between two contrasting dominant C3 and C4 species in a typical steppe of inner Mongolia, China. *Plant Soil* 340, 141–155. doi: 10.1007/s11104-010-0369-3

Zimmer, H. C., Turner, V. B., Mavromihalis, J., Dorrough, J., and Moxham, C. (2010). Forb responses to grazing and rest management in a critically endangered Australian native grassland ecosystem. *Rangeland J.* 32 (2), 187–195. doi: 10.1071/RJ09069

Zvereva, G. K. (2004). Comparative assessment of the effects of livestock grazing and periodic cutting on steppe plants of tuva. *Russian J. Ecol.* 35 (6), 364–368. doi: 10.1023/B:RUSE.0000046971.38759.ab

frontiers | Frontiers in Plant Science

TYPE Original Research
PUBLISHED 03 October 2022
DOI 10.3389/fpls.2022.985603

OPEN ACCESS

EDITED BY
Maofeng Chai,
Qingdao Agricultural University,
Qingdao, China

REVIEWED BY
Xiao Ma,
Sichuan Agricultural University,
China
Guoan Shen,
Chinese Academy of Medical Sciences and
Peking Union Medical College, China

*CORRESPONDENCE
Junjie Wang
jjw62@163.com
Yan Zhao
zhaoyannmg@imau.edu.cn

SPECIALTY SECTION
This article was submitted to
Plant Abiotic Stress,
a section of the journal
Frontiers in Plant Science

RECEIVED 04 July 2022
ACCEPTED 26 August 2022
PUBLISHED 03 October 2022

CITATION
Zhou X, Li X, Zhang X, Yin D, Wang J and Zhao Y (2022) Construction of a high-density genetic map and localization of grazing-tolerant QTLs in *Medicago falcata* L.. *Front. Plant Sci.* 13:985603.
doi: 10.3389/fpls.2022.985603

Construction of a high-density genetic map and localization of grazing-tolerant QTLs in *Medicago falcata* L.

Xinyue Zhou, Xiaojie Li, Xiaoming Zhang, Dabao Yin, Junjie Wang* and Yan Zhao*

Key Laboratory of Grassland Resources (IMAU), Key Laboratory of Forage Cultivation, Processing and High Efficient Utilization, College of Grassland, Resource and Environmental Science, Ministry of Education, Ministry of Agriculture, Inner Mongolia Agricultural University, Hohhot, China

Background: Using genomic DNA from 79 F1 plants resulted from a crossing between parents with strong and weak grazing tolerance in *Medicago falcata* L., we generated an *EcoRI* restriction site-associated DNA (RAD) sequencing library. After sequencing and assembly, a high-density genetic map with high-quality SNP markers was constructed, with a total length of 1312.238cM and an average density of 0.844 SNP/cM.

Methods: The phenotypic traits of 79 F1 families were observed and the QTLS of 6 traits were analyzed by interval mapping.

Results: Sixty three QTLs were identified for seven traits with LOD values from 3 to 6 and the contribution rates from 15% to 30%. Among the 63 QTLs, 17 were for natural shoot height, 12 for rhizome Length, 10 for Shoot canopy diameter, 9 for Basal plant diameter, 6 for stem number, 5 for absolute shoot height, and 4 for rhizome width. These QTLs were concentrated on LG2, LG4, LG5, LG7, and LG8. LG6 had only 6 QTLs. According to the results of QTL mapping, comparison of reference genomes, and functional annotation, 10 candidate genes that may be related to grazing tolerance were screened. qRT-PCR analysis showed that two candidate genes (LOC11412291 and LOC11440209) may be the key genes related to grazing tolerance of *M. falcata*.

Conclusion: The identified trait-associated QTLs and candidate genes in this study will provide a solid foundation for future molecular breeding for enhanced grazing-tolerance in *M. falcata*.

KEYWORDS

***Medicago falcata* L., grazing tolerance, genetic linkage mapping, QTLs, high-density**

Introduction

Medicago falcata L. is a perennial legume in the *Medicago* genus (Wang et al., 2006, 2016). Distributed mainly in alpine regions such as Russia, Mongolia, and China's East Central Inner Mongolia and Xinjiang. *Medicago falcata* has a strong tolerance to cold, drought, and grazing, and can grow in marginal soil with wide adaptability (Shi et al., 2019; Zhou et al., 2021).

Because of these application values, *M. falcata* is widely used for grassland improvement, artificial range setup, and sand prevention (Popp et al., 2000). Improving grazing tolerance in cultivated alfalfa is a common goal worldwide in alfalfa breeding. In this regard, the values of *M. falcata* are well accepted for alfalfa breeding (Pecetti et al., 2008). In *M. falcata*, many traits, such as rhizome length, stem number, and shoot canopy diameter, are quantitative traits. It is practical to locate these traits in the *M. falcata* genome by using QTL analysis (McCord et al., 2014). The development and application of single nucleotide polymorphism (SNP) and the emergence of restriction site-associated DNA sequencing (RAD-Seq) technology pave the way for rapid development of SNPs and subsequent QTL analysis in non-model species, such as *M. falcata* (Li and Brummer, 2012; Kang et al., 2014). RAD-Seq is a new, yet powerful technology, which allows quick identification of millions of SNPs in a mapping population at low cost (Kumar et al., 2009; José et al., 2017; Yermekbayev et al., 2020). With RAD-Seq, we are able to generate a large number of SNPs, construct a genetic linkage map, and perform QTL analysis in *M. falcata*. Yin (2021) studied genetic diversity of *Elymus dahuricus* was analyzed by RAD-Seq sequencing. The results showed that the phenotypic clustering results were consistent with RAD sequencing results for about 50% of the materials within two years, indicating that phenotypic classification results and molecular sequencing results were mutually confirmed and well matched. For example, (Zhang et al., 2020) used single nucleotide polymorphism (SNP) markers to construct a high-density linkage map of alfalfa. QTL mapping for yield-related traits was carried out. Cui (2020) used 460 SNP markers to construct the genetic linkage map of alfalfa and *M. falcata*, and conducted QTL mapping for alfalfa agronomic traits. Liu (2012) constructed a genetic linkage map of tetraploid alfalfa using 51 RAPD markers and mapped QTL for 16 important agronomic traits. Liu (2017) constructed alfalfa genetic linkage map by using 176 SSR polymorphism markers and 960 SNP markers, and conducted QTL mapping for 19 related traits, such as alfalfa yield. Up to date, numerous studies have demonstrated the phenotypic features related to grazing tolerance, established the evaluation methodologies and metrics for grazing tolerance in *M. falcata*, and proven the unique advantages of *M. falcata* in the improvement of grazing tolerance in cultivated alfalfa. Wang et al. (2013) proved the reliability of optimal sequence analysis in *M. falcata* grazing tolerance, and through morphological index analysis showed that in the Hulunbuir native *M. falcata*, plant individuals with large projection area, great plant height, significant plants diameters stem number, long root depth and significant root diameters had strong grazing tolerance. Wang (2015) studied the grazing tolerance in Hulunbuir native *M. falcata*, cloned and analyzed some grazing tolerance-related genes (Jiang et al., 2022). Based on RAD-seq, the genetic linkage map and QTL mapping of *Medicago sativa* L. flowering stage traits were constructed, and 7 candidate genes related to flowering stage were screened out. However, there are no reports on the construction of genetic linkage map of *M. falcata*, QTL studies on grazing tolerance traits of *M. falcata,* and candidate gene screening (Luciano et al., 2021).

In this study, we chose two *M. falcata* parents with contrasting grazing tolerance, crossed the two parents, and generated a mapping population. Using RAD-seq technique, SNPS were identified, the first genetic linkage map was constructed, and QTL sites related to grazing tolerance were analyzed. Ten candidate genes related to grazing tolerance were screened out, and two of them were presumed to be key genes. The linkage map constructed and the QTL candidate genes identified for grazing tolerance will provide valuable information for future molecular mechanism studies and lay a solid foundation for improving grazing tolerance of alfalfa.

Materials and methods

Materials and population generation

Two native *M. falcata* genotypes (MF200401 and MF200402) from Hulunbuir, Inner Mongolia, China, were chosen as the parents for genetic crossing, and they were tetraploid plants. MF200401, which has high grazing tolerance, was used as the maternal parent, whereas MF200402, which has low grazing tolerance, was used as the paternal parent. Individual plants with contrasting grazing tolerance phenotypes were manually pollinated to generate an F1 population of 79 plants. From 2016 to 2018, we observed the agronomic traits related to grazing tolerance of *M. falcata* F1 population at grassland station of Hulunbuir Ewenki Autonomous Banner (119°07′ E latitude 49°01′ N latitude) and experimental base of Inner Mongolia Agricultural University, and focused on the identification and evaluation of grazing tolerance.

Trait definition and analysis

In this study, we focused on the following important traits: shoot height, basal plant diameter, stem number, shoot canopy diameter, rhizome length, and rhizome width. Each trait was measured with the following description:

Shoot height (cm): We measured the natural height and the absolute height. Natural height was measured as the height of shoot from the ground to the highest point of the shoot under natural growing status. Absolute height was measured as the height of shoot from the ground to the highest point of the shoot when the shoot was pulled and stretched straight.

Shoot basal diameter (cm): The diameter of the cluster below the first node was measured.

Stem number: Total number of shoots in a plant cluster.

Shoot canopy diameter (cm): The shoot canopy diameter was approximated by measuring the diameter of the shadow cast by the shoot canopy on the ground when the sun was on the top of the plant at noon.

Rhizome length (cm) and rhizome width(cm): The length and the diameter of the crown of each cluster of plants were measured.

DNA extraction

From the crossing population, 79 individuals were selected randomly to construct the genetic map. Genomic DNA of the 79 F1 individuals and two parents, MF200401 and MF200402, was extracted from young leaves using the Plant Genomic DNA Extraction Kit (DP305, TianGen, Beijing, China) following the manufacturer's instructions.

RAD library construction and sequencing

About 1 μg of genomic DNA was digested with *EcoRI*, followed by ligation of Solexa P1 Adapter (common adapter with EcoRI end), fragmentation, gel recovery of 300–700 bp fragments, end-filling of A, ligation of Solexa P2 Adapter (adapter with barcode). The individual samples were pooled together, purified, and PCR amplified with P1 and P2 primers for 18 cycles. The 300–700-bp amplicons were further gel purified and the quality was checked using Agilent 2100 Bioanalyzer and then sequenced using the Illumina HiSeq 2500 platform at BGI (Shenzhen, China).

Sequencing data analysis

In order to ensure the accuracy of subsequent information analysis, the original sequence was quality-filtered and compared to the reference genome for analysis by BWA software. Sequence data were analyzed using customized Perl scripts from BGI-Shenzhen (Shenzhen, China). Raw reads were cleaned up by removing the adapters, index sequences, and low-quality reads. RAD markers were developed using the clean data. SNPs markers were examined using the GATK[1] program. Reads from each individual were clustered into tag reads by sequence similarity (allowing five mismatches, at most, between any two reads within each tag reads cluster) and clusters with <3 or >100 reads were discarded. All the SNPs had total support reads ≥ 5, and for heterozygous SNPs, the inferior base depth was ≥3.

SNP detection and map construction

All SNPs markers used for genetic linkage map construction were filtered using the following criteria: (1) ratio of confidence levels to quality depth ≥ 2; (2) *p*-values from the Fisher's exact test ≤ 60; (3) RMS mapping quality values ≥ 40; (4) all markers were tested by Chi-square test ($p < 0.01$).

Genetic linkage maps were generated using JoinMap version 4.1. A logarithm of the odds (LOD) score between 2 and 20 was set to cluster linkage groups. The regression mapping was used as the mapping algorithm, and the genetic distances were calculated based on Kosambi's mapping function. All SNPs were clustered on 8 linkage groups (LGs). The location and distance between each SNP were calculated based on multipoint analysis.

QTLs analysis

QTL analysis was performed using MapQTL version 6.0 software based on the parental maps and phenotype data from 79 individual plants. QTLs were detected using interval mapping initially, and the mapping algorithm was a mixed model. Then multiple QTL mapping (MQM) was performed to detect additional QTLs that might be masked by the major QTLs. After a 1,000 permutation test, a LOD threshold of 3 was set to find significant QTLs at the 95% confidence level. The ranges above the LOD threshold of 3 were identified as QTL intervals. Markers located at or flanked with the peak LOD value of a QTL were recognized as QTL-associated markers.

Screening and analysis of candidate genes

Medicago falcata L. CV. Hulunbuir was selected as plant material to detect the expression of candidate genes. Choose the particle satiated *M. falcata*, with sandpaper, break hard real-time, in Petri dish culture to sprout, the germination of seeds in sterile culture in the soil and put to cultivate in artificial climate chamber, during the cultivation for long sunshine condition (16 h light/8 h) of the dark, day/night temperature 18°C to 26°C, well ventilated, and regular watering. When growth to the flowering period, choose three plants that grow better and the peak of flowering period simulated cutting processing, *M. falcata* cutting stubble height is 15 cm, respectively dealing with 3, 5, and 7 days, each point in time selecting a suitable amount of leaf and stem tissue in 2 ml centrifuge tube, and one not to cut processing plant as a control, sampling at the same time, the liquid nitrogen frozen. Total RNA was extracted according to the FastPure Plant Total RNA Isolation Kit (Vazyme, China), and biological replicates were performed three times. The quality of RNA was determined by electrophoresis of a 1% (w/v), agarose gel. First-strand cDNA was synthesized from 2 μg total RNA using the TransScript First-Strand cDNA Synthesis SuperMix Kit (TransGen, China). qRT-PCR was performed by SYBR green Super Mix and CFX96 Real-Time PCR Detection System (Bio-Rad, Hercules, CA, United States). Gene-specifc primers used for qRT-PCR were designed using Oligo 7.0. The expression level of *MfActin* was used as the internal control, the relative expression levels of candidate genes were calculated according to the $2^{-\Delta\Delta CT}$ method, and three independent biological replicates were used for each sample.

1 https://www.broadinstitute.org/GATK/

Results

Establish mapping groups

In this study, two alfalfa populations with extreme differences in grazing tolerance traits were selected as materials, and the parents with the greatest differences in important grazing tolerance-related traits such as regeneration rate, number of branches, and root neck depth into the soil were selected for intra-species one-to-one single sexual crosses to obtain two F1 populations, which could be asexually propagated and could be used as permanent mapping populations, and a population with 79 single plants was selected as the mapping population after hybrid testing and identification (Figure 1).

Analysis of variance of morphological index data observed after grazing

The morphological and physiological characteristics related to grazing tolerance of *M. falcata* were studied systematically. Five phenotypic traits directly affecting the formation of grazing tolerance of *M. falcata* and two phenotypic traits indirectly involved in the formation of grazing tolerance were identified, which revealed the morphological mechanism and physiological basis of grazing tolerance of *M. falcata*. Two genotypic population materials with significant differences in grazing tolerance were identified and screened (one was MF200401 material with high grazing tolerance, and one is MF200402 material with low grazing resistance; Table 1).

Polymorphism selection

In this study, a total of 1,412,614 high-quality polymorphic SNP loci were screened based on the RAD data of the parents. Based on the SNP detection results, the polymorphic SNPs between parents were screened (Table 2). For the F1 population, heterozygous loci with polymorphisms between parents (lm × ll, nn × np, ab × cd, ef × eg, hk × hk types) were screened (Table 3). Filter out loci with missing parental information. The marker loci with >10% deletion rate in the offspring population were filtered out, i.e., for single polymorphic loci, at least 90% of the samples have a definite genotype. After filtering to obtain parental polymorphic loci meeting the filtering 5,191 parental polymorphic loci were filtered, and the results were imported into JoinMap 4.1 software for further.

Biased segregation filtering In progenies

The offspring were genotyped according to the parental marker types obtained from the screening, and the obtained markers were tested by Chi-square test (significance level $\alpha = 0.01$) to remove the segregating markers (e.g., F2 population aa, ab, bb). The expected probability ratio of F2 population aa, ab, and bb genotypes is 1:2:1, and a significant deviation from this ratio is considered as a marker bias, the bias markers will affect the map

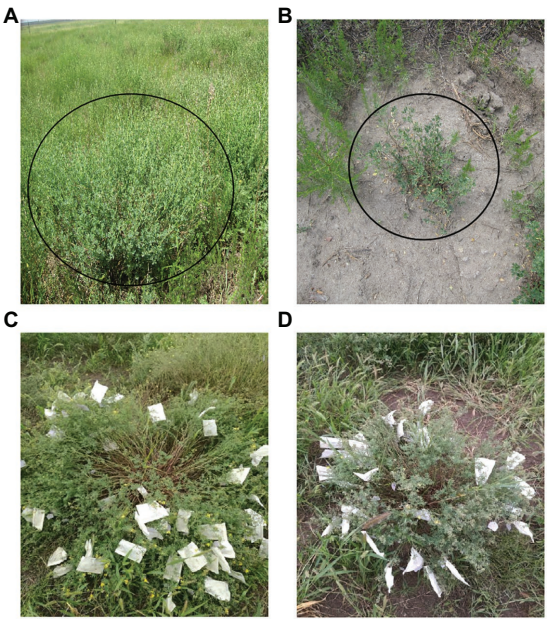

FIGURE 1
(A) Plants with high grazing tolerance were selected under continuous high-intensity grazing in Ewenki Autonomous Banner (119° 07′ E Latitude 49° 01′ N Latitude), Hulunbuir, China, and named (MF200401); **(B)** Plants with low grazing tolerance were selected under continuous high-intensity grazing in Ewenki Autonomous Banner (119° 07′E Latitude 49° 01/N Latitude), Hulunbuir, China, and named (MF200402); **(C)** Orthologous population; hybrid parent 1; 79 F1 populations obtained by crossing grazing-tolerant material (MF200401) with poorly grazing-tolerant material (MF200402); **(D)** Reverse cross population; hybrid parent 2; 54 F1 populations obtained by crossing grazing-tolerant material (MF200401) with poorly grazing-tolerant material (MF200402).

TABLE 1 Analysis of variance of phenotypic traits observed in F1 population of two sites in 3years was conducted.

	Non-grazing plant	The grazing resistance is high	The grazing resistance is low
Plant individuals with large projection area(cm^2)	5897.66a	3754.98a	1600.87a
Basal plant diameter(cm)	5.71c	11.73a	8.29b
Absolute shoot height(cm)	79.44a	63.98b	47.76a
Natural shoot height (cm)	77.20a	60.90b	44.36c
Stem number(a)	72.30a	62.14b	22.43c
Rhizome length(cm)	4.56b	4.19a	2.45c
Rhizome width(cm)	2.01a	2.84a	2.05a

There were significant differences between the morphological indexes of high grazing tolerance and low grazing tolerance, which indicated that continuous grazing had significant effects on the morphological characteristics of plants, and was beneficial to the expression of differences in grazing tolerance. Different letters indicate significant difference ($P < 0.05$).

10.3389/fpls.2022.985603

construction results and QTL localization, and the majority of the literature on the treatment of biased segregation, using the Chi-square test. The threshold value for segregation was set at 0.1, and the abnormal genotypes were filtered out according to the segregating genotypes of the offspring of different populations. The results were compiled into the Joinmap4.1 input file format for genetic mapping (Table 4).

Construction of genetic linkage map

Based on logarithm of the odds (LOD) values (2 < LOD < 20), 1,756 SNPs were used to generate the genetic linkage map using JoinMap version 4.1. The regression mapping was used as the mapping algorithm, and the genetic distances were calculated based on Kosambi's mapping function. These mapped SNPs were clustered in 8 linkage groups (LGs). The total length of the consensus map was 1312.238 cM with the average distance about 0.844 cM between markers. The distribution of SNPs in each LG and the genetic distances were summarized in Table 4 From the results in Table 4, LG4 and LG8 had the most SNPs, while LG6 had the least SNPs. LG8 had the smallest average genetic distance between SNPs, while LG6 had the largest average genetic distance of 1.69 cM. The largest gap between two SNPs (22.482 cM) was found in LG3. All SNPs were loaded to Joinmap4.1 and a genetic map was generated as shown in Figure 2.

Co-linear analysis of genetic map and physical map

From the collinearity analysis results, the collinearity results of genetic map and physical map were not very good, but the trend of most markers was consistent. Marker was evenly distributed on the genome.

Analysis of grazing tolerance QTLs

QTLs were detected using the interval mapping method in the MapQTL6 software. A total of 63 QTLs were identified for six grazing tolerance-associated traits (Table 5). Among them, 12 QTLs were related to rhizome length, which contributed for 16.9%–28.3% variance; 4 QTLs for rhizome width, contributing for 17.7%–20.3%; 10 QTLs for shoot canopy diameter, contributing for 16.7%–26%; 9 QTLs for basal plant diameter, contributing for 16.6%–27.4%; 6 QTLs for stem number, contributing for 16.5%–22.3%; 5 QTLs for absolute shoot height, contributing for 16.8–20.7%; and 17 QTLs for natural shoot height, contributing for 16.5%–24.4%. These QTLs were mainly distributed on LG2, LG4, LG5, LG7, and LG8. LG6 had the least QTLs. The LOD values were between 3 and 6 and the contribution was between 15% and 30%. There were no markers that had significantly high contribution (greater than 60%).

TABLE 2 The results of mutation detection and analysis by high-throughput sequencing showed that summary of SNPs in individual samples.

Sample_ ID	Total	Homo	Hete	Homo_ rate(%)	Hete_ rate(%)
H01	629,785	570,191	59,594	90.54	9.46
H02	524,816	494,067	30,749	94.14	5.86
H04	562,791	523,745	39,046	93.06	6.94
H10	658,919	581,161	77,758	88.2	11.8
H11	671,246	590,520	80,726	87.97	12.03
H12	639,810	575,487	64,323	89.95	10.05
H13	611,792	558,902	52,890	91.35	8.65
H14	610,369	558,251	52,118	91.46	8.54
H15	590,379	544,253	46,126	92.19	7.81
H16	599,237	549,814	49,423	91.75	8.25
H17	560,188	521,924	38,264	93.17	6.83
H18	346,826	336,690	10,136	97.08	2.92
H19	628,386	569,464	58,922	90.62	9.38
H20	709,345	578,355	130,990	81.53	18.47
H21	706,928	583,209	123,719	82.5	17.5
H22	716,673	556,186	160,487	77.61	22.39
H24	538,661	504,281	34,380	93.62	6.38
H25	482,521	456,552	25,969	94.62	5.38
H26	603,447	553,801	49,646	91.77	8.23
H27	542,397	506,108	36,289	93.31	6.69
H29	528,781	495,772	33,009	93.76	6.24
H30	639,210	574,955	64,255	89.95	10.05
H31	699,137	579,127	120,010	82.83	17.17
H32	683,180	583,133	100,047	85.36	14.64
H33	467,812	443,643	24,169	94.83	5.17
H34	374,120	361,015	13,105	96.5	3.5
H36	437,006	417,590	19,416	95.56	4.44
H37	544,192	507,617	36,575	93.28	6.72
H38	451,103	429,651	21,452	95.24	4.76
H39	697,647	581,017	116,630	83.28	16.72
H43	543,351	507,551	35,800	93.41	6.59
H44	643,833	579,401	64,432	89.99	10.01
H45	538,746	503,634	35,112	93.48	6.52
H47	563,069	519,805	43,264	92.32	7.68
H48	508,906	477,803	31,103	93.89	6.11
H49	279,432	273,067	6,365	97.72	2.28
H50	359,469	347,522	11,947	96.68	3.32
H51	569,924	526,554	43,370	92.39	7.61
H52	716,452	547,454	168,998	76.41	23.59
H53	640,006	574,547	65,459	89.77	10.23
H54	685,413	591,110	94,303	86.24	13.76
H55	579,611	535,577	44,034	92.4	7.6
H56	584,826	537,408	47,418	91.89	8.11
H58	619,020	563,143	55,877	90.97	9.03
H59	691,599	588,375	103,224	85.07	14.93
H61	706,157	578,625	127,532	81.94	18.06
H62	713,247	563,881	149,366	79.06	20.94
H63	714,794	560,315	154,479	78.39	21.61

(Continued)

TABLE 2 (Continued)

Sample_ ID	Total	Homo	Hete	Homo_ rate(%)	Hete_ rate(%)
H64	683,965	582,759	101,206	85.2	14.8
H65	618,592	558,140	60,452	90.23	9.77
H66	525,975	491,979	33,996	93.54	6.46
H67	550,167	511,867	38,300	93.04	6.96
H68	664,101	578,075	86,026	87.05	12.95
H69	595,697	544,149	51,548	91.35	8.65
H71	640,511	573,262	67,249	89.5	10.5
H72	628,274	559,643	68,631	89.08	10.92
H73	676,475	576,695	99,780	85.25	14.75
H74	581,103	529,890	51,213	91.19	8.81
H75	624,013	562,901	61,112	90.21	9.79
H76	603,548	546,388	57,160	90.53	9.47
H77	560,243	515,244	44,999	91.97	8.03
H78	639,971	566,110	73,861	88.46	11.54
H79	589,320	536,058	53,262	90.96	9.04
H80	179,512	176,698	2,814	98.43	1.57
H81	502,366	470,751	31,615	93.71	6.29
H83	505,541	473,952	31,589	93.75	6.25
H84	558,170	518,611	39,559	92.91	7.09
H85	706,562	578,636	127,926	81.89	18.11
H86	682,101	581,144	100,957	85.2	14.8
H87	700,590	581,675	118,915	83.03	16.97
H88	702,105	577,375	124,730	82.23	17.77
H89	707,803	581,006	126,797	82.09	17.91
H90	679,030	588,952	90,078	86.73	13.27
H92	696,768	584,581	112,187	83.9	16.1
H93	712,176	565,509	146,667	79.41	20.59
H94	677,064	587,480	89,584	86.77	13.23
H95	706,589	576,568	130,021	81.6	18.4
H96	592,612	540,033	52,579	91.13	8.87
H97	475,846	450,240	25,606	94.62	5.38
P1	696,915	548,925	147,990	78.76	21.24
P2	715,699	486,454	229,245	67.97	32.03

Homo is the number of homozygous SNPs. Hete is the number of heterozygous SNPs. Homo rate and Hete rate are the rate of homozygous and heterozygous SNPs in total SNPS, respectively. It was noted that the Homo rate and Hete rate in individual F1 samples varied greatly. The lowest Hete rate (samples H80) was only 1.57%, whereas the highest (sample H52) was 23.59%.

From the results in Table 5 and Figure 3, we identified 12 significant QTLs for the rhizome length in LG1, LG2, LG3, LG4, LG5, LG6, and LG8. The LOD values for the 12 QTLs were between 3.02 and 5.41 and the contribution ranged from 16.9% to 28.3%. The QTL with maximal LOD value was located in LG5, while the QTL with the minimal LOD was in LG3. Similarly, from the results in Table 6 and Figure 4, we identified four significant QTLs for the rhizome width in LG1 and LG4. The LOD values for the four QTLs were from 3.18 to 3.69 and the contribution ranged from 17.7 to 20.3%. From the results in Table 6 and Figure 5, we identified 10 significant QTLs for the shoot canopy diameter in LG3, LG4, LG6, LG7, and LG8. The LOD values for the QTLs were from 3.06 to 5.03 and the contribution ranged from 16.7% to 26%. From the results in Table 6 and Figure 6, we identified nine significant QTLs for the basal plant diameter in LG1, LG2, LG3, LG4, LG5, and LG8. The LOD values for the QTLs were from 3.04 to 5.35 and the contribution ranged from 16.6 to 27.4%. From the results in Table 6 and Figure 7, we identified 6 significant QTLs for the stem number in LG2, LG4, LG5, LG7, and LG8. The LOD values for the QTLs were from 3.02 to 4.21 and the contribution ranged from 16.5% to 22.3%. From the results in Table 6 and Figure 8, we identified five significant QTLs for the absolute shoot height inLG4, LG6, LG7, and LG8. The LOD values for the QTLs were from 3.08 to 3.87 and the contribution ranged from 16.8% to 20.7%. From the results in Table 6 and Figure 9, we identified 17 significant QTLs for the natural shoot height in LG1, LG2, LG3, LG4, LG5, LG6, and LG7. The LOD values for the QTLs were from 3.02 to 4.67 and the contribution ranged from 16.5% to 24.4%. The QTL with maximal LOD value was located in LG6 while the QTL with the minimal LOD was in LG2.

For each trait, the corresponding QTL map was shown in Figures 4–10.

Screening and identification of candidate genes for grazing tolerance

According to all the QTL ranges of grazing tolerance, we searched for genes in NCBI alfalfa genome database (CM001217.2), LG1 contained a total of 34 genes, LG2 obtained 35 genes, LG3 obtained 16 genes, LG4 found 30 genes, LG5 obtained 35 genes. Ten genes were obtained by LG6, 26 genes were obtained by LG7, and 29 genes were obtained by LG8. All the intervals contained 215 genes. Further analysis of gene annotation information was conducted to screen out 8 candidate genes that might be related to grazing tolerance, including genes related to MYB gene family, GRAS gene family, CAM gene family, etc. (Table 7).

The 10 candidate genes of *M. falcata* were verified by qRT-PCR. The results showed that the relative expression of LOC11422027 and LOC11429100 genes decreased continuously under different days of simulated cutting stress. The relative expression of LOC11442911 genes showed a trend of first increasing and then decreasing, and the relative expression of LOC25498220, LOC25493394, LOC11414942, LOC25487134, and LOC11409053 genes showed a trend of first decreasing and then increasing. The relative changes of LOC11412291 and LOC11440209 showed a trend of continuous up-regulation (Figure 10).

Discussion

RAD-seq analysis

Genetic map or genetic linkage map refers to the relative location and genetic distance of a gene or molecular marker on a

10.3389/fpls.2022.985603

TABLE 3 Type of markers.

Parent genotype	Marker type explanation	F1	F2/BC/DH/RIL	Progeny genotypes		
				F1	F2	DH/RIL
aa × bb	Both parents have different homozygous loci		√		aa, ab, bb	aa, bb
lm × ll	Parent 1 is heterozygous whereas parent 2 is homozygous	√		ll, lm		
nn × np	Parent 1 is homozygous whereas parent 2 is heterozygous	√		nn, np		
ab × cd	Both parents are heterozygous (four alleles)	√		ac, ad, bc, bd		
ef × eg	Both parents are heterozygous (three alleles)	√		ee, eg, ef, fg		
hk × hk	Both parents are heterozygous (two alleles)	√		hh, hk, kk		

TABLE 4 Summary of polymorphic types in F1 progenies.

Gene_type	Count	Rate (%)
hkxhk	115,902	45.52
nnxnp	107,427	42.2
lmxll	30,388	11.94
efxeg	876	0.34
abxcd	2	0

The number of gene type hkxhk was 115,902, with a ratio of 45.52%. The number of gene type abxcd was 2, with a ratio of 0.

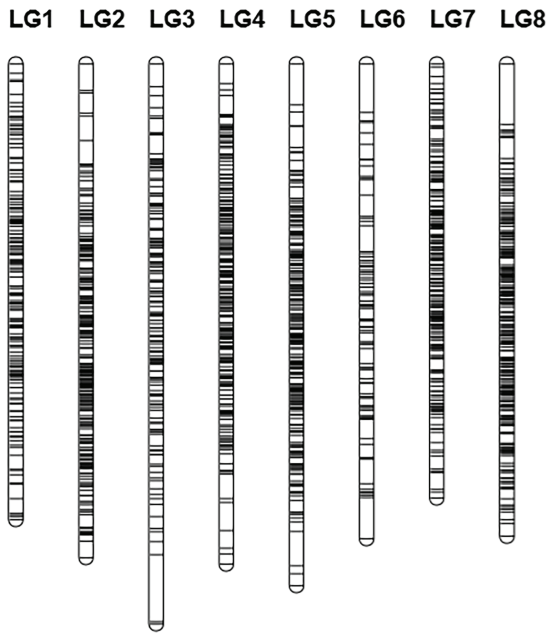

FIGURE 2
Genetic linkage map.

chromosome, which is different from the real distance in a physical map (Meng et al., 2015; Yagi et al., 2017; Lv et al., 2021). Genetic distance in a genetic map is calculated from the recombination rate of genes or markers. For instance, 1% of recombination rate corresponds to approximately 1 cM (centimorgan). The farther two loci are located, the higher probability a recombination will occur or the higher the recombination rate. A recombination of 50% means the two loci are located in two different linkage groups. That is to say, the maximal value of a recombination rate is 50%. Normally, one chromosome is one linkage group. However, if a chromosome is very long, it is possible to consider different arms of a chromosome as different linkage groups. The genetic distance does not always correspond to a fixed physical distance. For example, in species with a high LD value, 1 cM corresponds to a slightly larger chromosomal fragment. Even in the same species, different chromosomal regions may be different. For instance, in the centromere region, 1 cM corresponds to a slightly larger chromosomal fragment (Chen, 2018). A high standard linkage map requires an average genetic distance of 20 cM for genetic markers on a chromosome. The distance between genetic markers for a QTL locus should be 10–20 cM or less (Zhang, 2020). The currently constructed genetic linkage maps for diploid and tetraploid alfalfa and the QTL marker analyses of important traits symbolize the successful application of genetic improvement and molecular breeding technologies in alfalfa (Musial et al., 2006, 2007a,b; Robins and Brummer, 2010; Han et al., 2011; Qiang et al., 2015).

In recent years, with the rapid development of molecular biology, different new molecular marker technologies have been developed. SNP markers are the third-generation molecular markers. Due to its high density, high representativeness, high genetic stability, and easy detection, SNPs markers are widely used in genetic map construction in various species (Han et al., 2012; Pandey et al., 2017a,b). The restriction-site-associated DNA sequencing (RAD-seq) technology is a high throughput sequencing approach, which greatly reduces the complexity of complex genomes and rapidly identifies genome-wide high-density SNPs (Feng et al., 2020). For species lacking reference genomes, RAD-seq overcomes the limitation of a known genome sequence yet obtains large scale of SNPs markers. Reducing the genome complexity means reducing cost, thus RAD-seq is especially useful in population-level studies. In classical SNP analysis, when SNPs are identified, researchers need to design specific primers to genotype individual samples. However, for RAD-seq, this genotypic information is acquired simultaneously with the identification of SNPs. For species with reference genome sequences, the analysis of RAD-seq is simple and novel SNPs can be identified. Therefore, RAD-seq is a new approach to develop thousands of SNPs markers with low cost. It has been applied in multiple model and non-model plant species. Recently, researchers in the United States performed RNA-seq in 27 tetraploid and diploid

10.3389/fpls.2022.985603

TABLE 5 Results of QTL analysis from MapQTL6.

Trait	LG	Marker	Genetic distance (cM)	LOD	Contribution	Variance
Rhizome length	LG1	chr01_38977492	17.791	3.96	21.6	3.5
Rhizome length	LG1	chr01_38977519	17.929	4	21.8	3.5
Rhizome length	LG1	chr01_49110666	52.667	3.33	18.5	3.7
Rhizome length	LG1	chr01_4358824	94.374	4.78	25.4	3.4
Rhizome length	LG2	chr02_33256187	91.592	3.79	20.8	3.6
Rhizome length	LG6	chr06_3,615,590	112.904	3.03	17	3.3
Rhizome length	LG3	chr03_52697857	99.213	3.02	16.9	3.7
Rhizome length	LG4	chr04_45597769	127.674	3.12	17.4	3.7
Rhizome length	LG5	chr05_2131072	45.917	4.3	23.2	3.5
Rhizome length	LG5	chr05_3552366	46.626	5.41	28.3	3.2
Rhizome length	LG5	chr05_19559480	47.644	4.54	24.3	3.4
Rhizome length	LG8	chr08_9113282	56.893	3.41	18.9	3.7
Rhizome width	LG1	chr01_31131329	31.713	3.18	17.7	4.1
Rhizome width	LG1	chr01_31131332	31.713	3.24	18	4.1
Rhizome width	LG4	chr04_41435859	104.077	3.69	20.3	4.2
Rhizome width	LG4	chr04_18684136	104.707	3.52	19.4	4.2
Shoot canopy diameter	LG3	chr03_41784690	123.518	3.48	18.8	4.4
Shoot canopy diameter	LG4	chr04_50640951	117.62	3.06	16.7	4.5
Shoot canopy diameter	LG4	chr04_44959724	130.772	3.08	16.8	4.4
Shoot canopy diameter	LG6	chr06_24417495	37.652	3.33	18	4.3
Shoot canopy diameter	LG6	chr06_24417492	38.385	3.45	18.7	4.3
Shoot canopy diameter	LG6	chr06_8922282	38.939	3.45	18.7	4.1
Shoot canopy diameter	LG7	chr07_19256232	109.977	3.24	17.6	4.1
Shoot canopy diameter	LG8	chr08_16836275	60.222	3.58	19.3	4.2
Shoot canopy diameter	LG8	chr08_45317023	79.991	5.03	26	4.5
Shoot canopy diameter	LG8	chr08_8707992	80.031	3.36	18.2	4.4
Basal plant diameter	LG1	chr01_9917547	28.147	3.72	19.9	3.9
Basal plant diameter	LG2	chr02_4,417,521	84.524	3.24	17.6	4.1
Basal plant diameter	LG3	chr03_3184173	72.861	3.32	18	3.8
Basal plant diameter	LG4	chr04_23915754	86.789	5.35	27.4	4.3
Basal plant diameter	LG5	chr05_19136470	74.044	3.41	18.4	4.5
Basal plant diameter	LG5	chr05_19136429	76.756	3.18	17.3	4.3
Basal plant diameter	LG5	chr05_30967460	105.104	3.04	16.6	4.4
Basal plant diameter	LG8	chr08_8707992	80.031	3.32	18	4.4
Basal plant diameter	LG8	chr08_39307386	110.976	3.29	17.9	4.5
Stem number	LG2	chr02_11379759	84.524	4.21	22.3	4.3
Stem number	LG2	chr02_1782496	101.021	3.02	16.5	4.5
Stem number	LG4	chr04_1508899	62.807	3.07	16.8	4.5
Stem number	LG5	chr05_19136470	74.044	3.73	20	4.5
Stem number	LG7	chr07_1459167	98.102	3.56	19.2	3.9
Stem number	LG8	chr08_31605867	104.467	3.23	17.5	3.9
Absolute shoot height	LG6	chr06_22628780	118.818	3.71	19.9	4.5
Absolute shoot height	LG4	chr04_38,356,528	67.464	3.09	16.9	3.9
Absolute shoot height	LG7	chr07_34279538	92.741	3.08	16.8	4.3
Absolute shoot height	LG7	chr07_41091044	97.692	3.18	17.3	4.4
Absolute shoot height	LG8	chr08_42256225	141.879	3.87	20.7	4.3
Natural shoot height	LG1	chr01_49069297	150.782	3.54	19.1	4.4
Natural shoot height	LG1	chr01_49069365	152.757	3.57	19.2	4.4
Natural shoot height	LG2	chr02_21299826	63.993	3.46	18.7	4.5
Natural shoot height	LG2	chr02_30508990	78.382	3.83	20.5	4.1

(Continued)

TABLE 5 (Continued)

Trait	LG	Marker	Genetic distance (cM)	LOD	Contribution	Variance
Natural shoot height	LG2	chr02_38488687	121.387	3.02	16.5	4.3
Natural shoot height	LG2	chr02_38488685	121.475	3.02	16.5	4.3
Natural shoot height	LG2	chr02_7830781	134.138	3.83	20.5	4.4
Natural shoot height	LG2	chr02_38488729	135.291	3.88	20.7	4.3
Natural shoot height	LG3	chr03_27746993	93.877	4.07	21.6	4.1
Natural shoot height	LG4	chr04_36296510	87.645	3.26	17.7	4.3
Natural shoot height	LG5	chr05_39467311	57.638	3.5	18.9	4.3
Natural shoot height	LG5	chr05_19559628	64.596	3.33	18.1	4.5
Natural shoot height	LG5	chr05_20722800	120.884	3.04	16.6	4.0
Natural shoot height	LG5	chr05_20722779	120.884	3.03	16.6	4.0
Natural shoot height	LG6	chr06_32997819	67.553	4.67	24.4	4.3
Natural shoot height	LG7	chr07_7933121	63.778	3.03	16.6	4.5
Natural shoot height	LG7	chr07_5607731	85.279	3.39	18.4	4.3

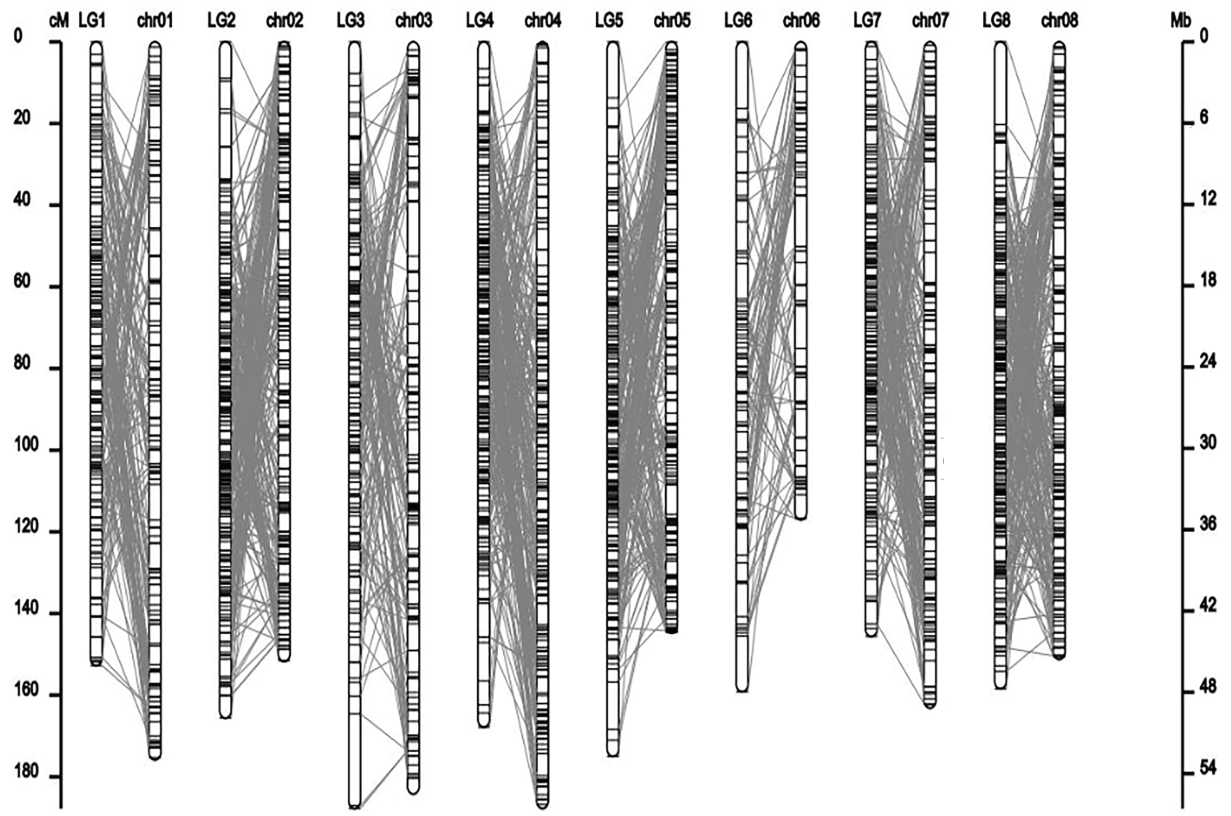

FIGURE 3
Collinearity analysis of genetic linkage map and physical map.

alfalfa genotypes. They identified 14,000 specific genes and 9 million SNPs and the construction of genetic linkage map and related QTL analysis are still in progress (Li et al., 2012, 2014; Fukuda et al., 2019; Wang L. et al., 2020). Using RAD-seq technology to detect SNP markers can obtain more polymorphic sites than Super GBS sequencing technology, and construct a higher density linkage map. Cui (2020) by using Super GBS sequencing technology, only obtained 460 SNP labeled in the Figure 11. Liu et al. (2017) obtained 4,346 SNP markers by RAD-sequence analysis. Wu et al. (2014) used RAD-seq technology to develop 3,804 pairs of new DNA markers, including SNPS and Indels, and combined with 1,230 SSR markers to construct a high-density genetic linkage map. Zhang et al. (2019)

used the SNPs obtained by RAD-seq technology to construct a high-density genetic linkage map, including 4,346 SNP markers and 119 simple sequence repeat (SSR) markers. In this study, 79 individuals from the F1 population were used as the mapping population, and the RAD-seq technology was used for database construction and sequencing. To construct a high-density genetic map of alfalfa RAD-seq. Finally, a high-density genetic linkage map containing 8 linkage groups and 1,756 markers was obtained, with a total map distance of 1312.238 cM and an average density of 0.844 cM. The marker density of RAD-Seq map constructed by RAD-seq technology has been greatly improved, the resolution of QTL mapping has been improved, the length of QTL interval has been shortened, and the value of determining causal loci to improve the traits of interest has been improved. Therefore, RAD-seq technology was applied in this study to develop molecular markers for alfalfa mapping population.

In this study, the genetic linkage map and the physical map were drawn simultaneously using the progeny separation information and sequencing information. The average coverage distance of the genetic map was 164.03 cM, while the average coverage distance of the physical map was 46.43 Mb. It can be seen from the results that there are some differences between different mapping methods, and the positions of some markers on the genetic map and the physical map are inconsistent. Many plants, such as wheat and alfalfa, also have the phenomenon that the genetic and physical distances between markers on linkage groups are not consistent, mainly because the physical and genetic distances between markers in the repressed and active regions of chromosome recombination are not consistent (Zhao et al., 2017; Jiang et al., 2022). After the map construction, using bioinformatics analysis software for the above markers genome distribution of statistical genetic map and genome position corresponding to the relationship between genetic and physical location linear system such as high quality, and the accuracy of assessment to ensure map all indicators show that the research of *M. falcata* genetic linkage map construction with high quality and accuracy. These maps will be helpful for QTL mapping and marker-assisted selection (MAS) of alfalfa in the future.

TABLE 6 Summary of genetic linkage map and distances.

Linkage group	SNPs number	Total genetic distance (cM)	Average genetic distance (cM)	Maximal gap (cM)
LG1	185	152.757	0.826	5.007
LG2	270	165.619	0.613	8.929
LG3	168	187.773	1.118	22.482
LG4	278	167.839	0.604	9.385
LG5	257	175.018	0.681	13.727
LG6	94	159.18	1.693	16.311
LG7	225	145.62	0.647	5.492
LG8	279	158.432	0.568	20.264
Total	1756	1312.238	0.844	22.482

Grazing tolerance-associated QTL traits

QTLs are widely used in model plants and field crops, especially the important agronomic traits. QTL localization is to

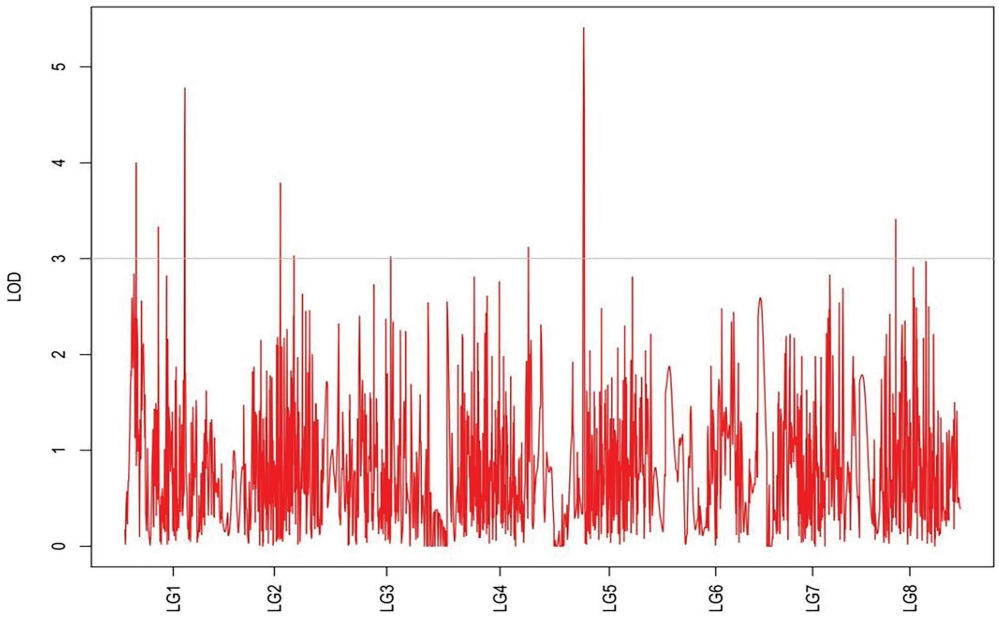

FIGURE 4
MapQTL localization of the rhizome length trait.

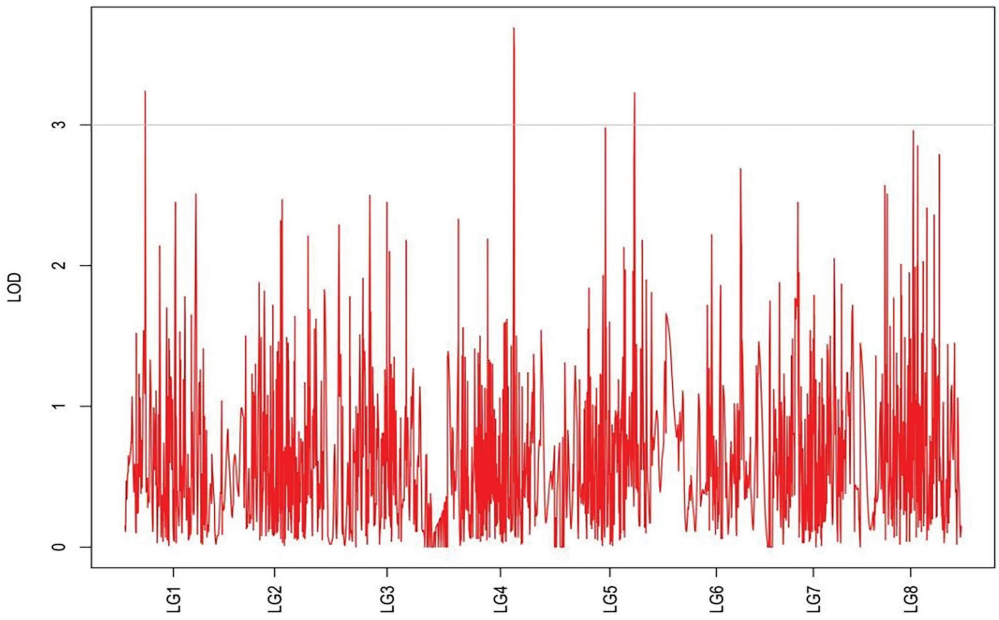

FIGURE 5
MapQTL localization of the rhizome width trait.

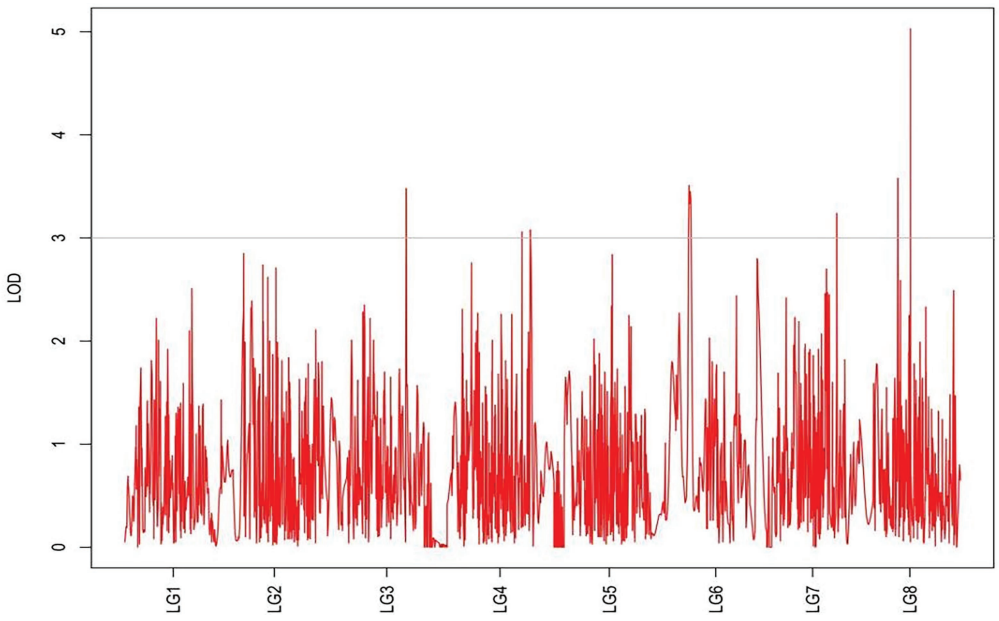

FIGURE 6
MapQTL localization of the shoot canopy diameter trait.

link specific traits with molecular makers on a genetic linkage map (Robins et al., 2007; Liu et al., 2014; Liu, 2016; Zhang, 2016). Using QTL mapping, some critical traits, such as yield (Wang L. et al., 2020) and cold tolerance (Chutimanitsakun et al., 2011; Shimoyama et al., 2020), have been linked to corresponding QTLs. Due to the practical values of QTL mapping in alfalfa, (Liu et al., 2017) located 19 QTL loci that are associated with agronomic traits in alfalfa. Zhang et al. (2020) detected 28 QTLs related to the important trait, flowering time. He (2016) constructed a genetic map and detected two QTLs associated with flowering time and leaf type in alfalfa. Tu (2011) identified 11 QTLs in *M. truncatula*. However, QTL analysis of agronomic traits in *M. falcata* is still in

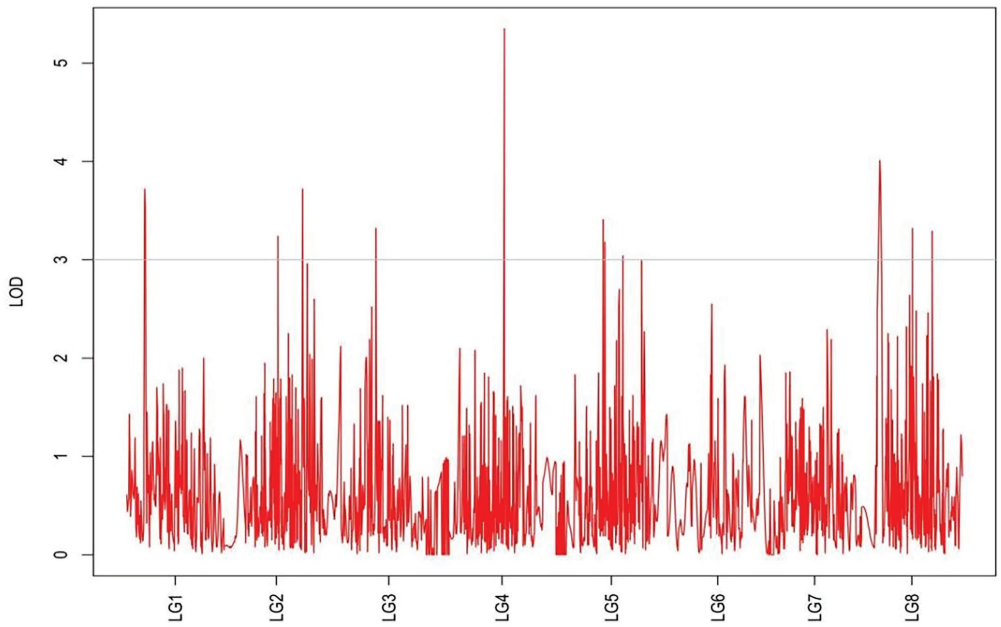

FIGURE 7
MapQTL localization of the basal plant diameter trait.

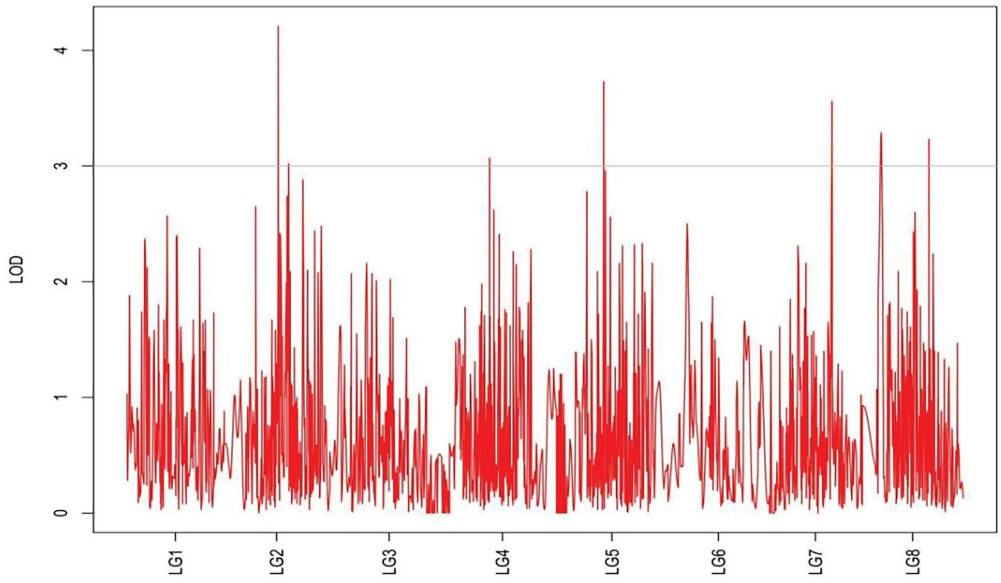

FIGURE 8
MapQTL localization of the stem number trait.

its preliminary stage. The success of QTL mapping in alfalfa and *M. truncatula* set a solid foundation for *M. falcata* studies.

In this study, we constructed a high-density genetic map in *M. falcata* and performed a QTL analysis for important grazing tolerance traits using interval mapping. Overall, we detected 63 QTLs for 6 grazing tolerance traits. These QTLs are distributed on eight LGs. Identification and location of the QTLs will aid in gene discovery, molecular marker-assisted selection, cloning, and regulation studies of quantitative trait-associated genes in *M. falcata*. These studies will eventually help improving and breeding the grazing tolerance varieties in *M. falcata*.

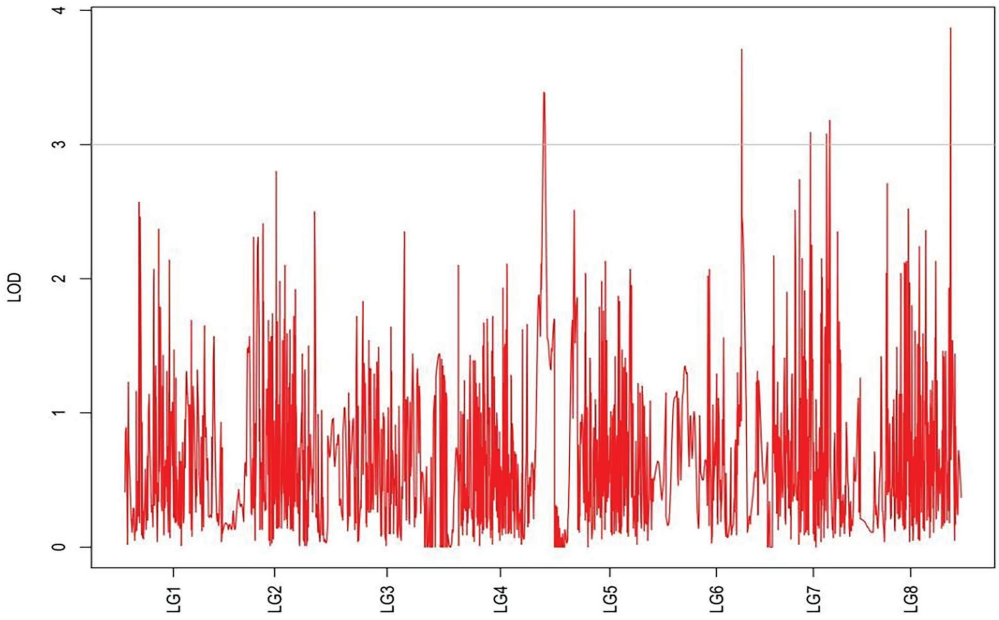

FIGURE 9
MapQTL localization of the absolute shoot height trait.

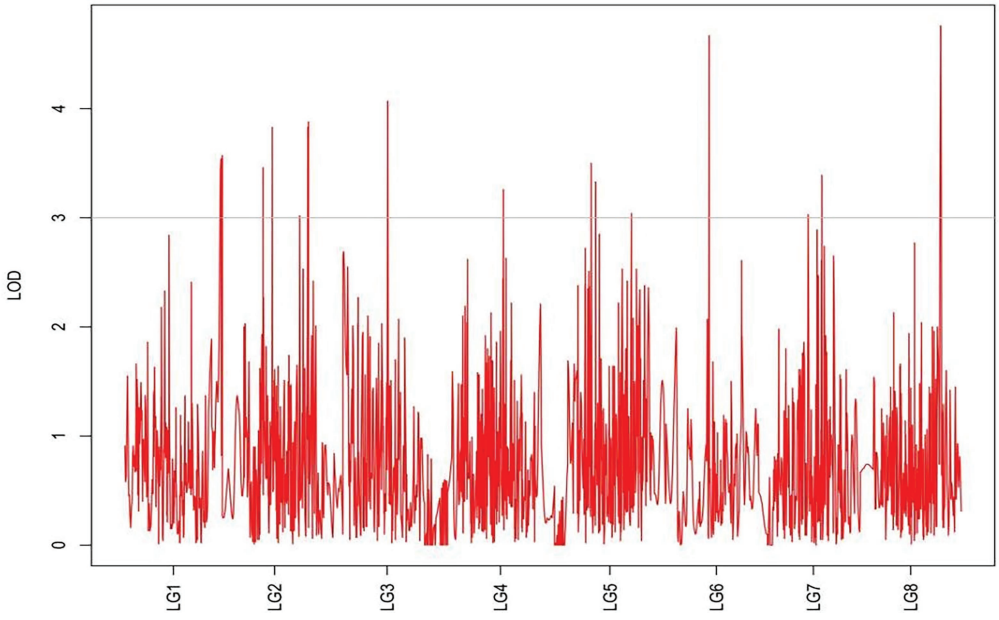

FIGURE 10
MapQTL localization of the natural shoot height trait.

Analysis of candidate genes for grazing tolerance traits

Previous QTL mapping studies on alfalfa mainly focused on flowering traits (Zhang et al., 2019, 2020). Although QTL mapping and RNA-seq integration have been applied to identify candidate genes in rice (*Oryza sativa* L.), maize (*Zea mays* L.), soybean (Glycine max), and other crops (Kuang et al., 2020; Lei et al., 2020; Han et al., 2022), but these methods have not been used to discover grazing tolerance trait genes in *M. falcata*.

In this study, 10 candidate genes that may be related to grazing tolerance were screened based on QTL mapping results, comparison

TABLE 7 Screening results of candidate genes related to grazing tolerance.

LG	Gene ID	Gene description	Position (bp)	Character
LG4	LOC11422027	Scarecrow-like protein 14	23,915,589–23,918,205	Shoot canopy diameter
LG4	LOC11440209	Transcription factor TCP15	44,959,722–44,961,035	Shoot canopy diameter
LG8	LOC11429100	Gibberellin 20 oxidase 3	39,307,107–39,307,609	Basal plant diameter
LG7	LOC25498220	Ethylene-responsive transcription factor-like protein At4g13040	19,256,208–19,256,385	Shoot canopy diameter
LG4	LOC25493394	chlorophyll a-b binding protein AB80, chloroplastic	38,356,528–38,357,582	Absolute shoot height
LG6	LOC11414942	Calmodulin-7	8,920,707–8,928,256	Shoot canopy diameter
LG2	LOC25487134	Solanesyl diphosphate synthase 1	30,508,874–30,509,001	Natural shoot height
LG4	LOC11409053	Cell wall/vacuolar inhibitor of fructosidase 1	50,640,870–50,641,400	Shoot canopy diameter
LG6	LOC11412291	Transcription factor MYB30	3,615,590–3,617,827	Rhizome length
LG2	LOC11442911	Pathogenesis-related genes transcriptional activator PTI5	4,417,521–4,418,430	Basal plant diameter

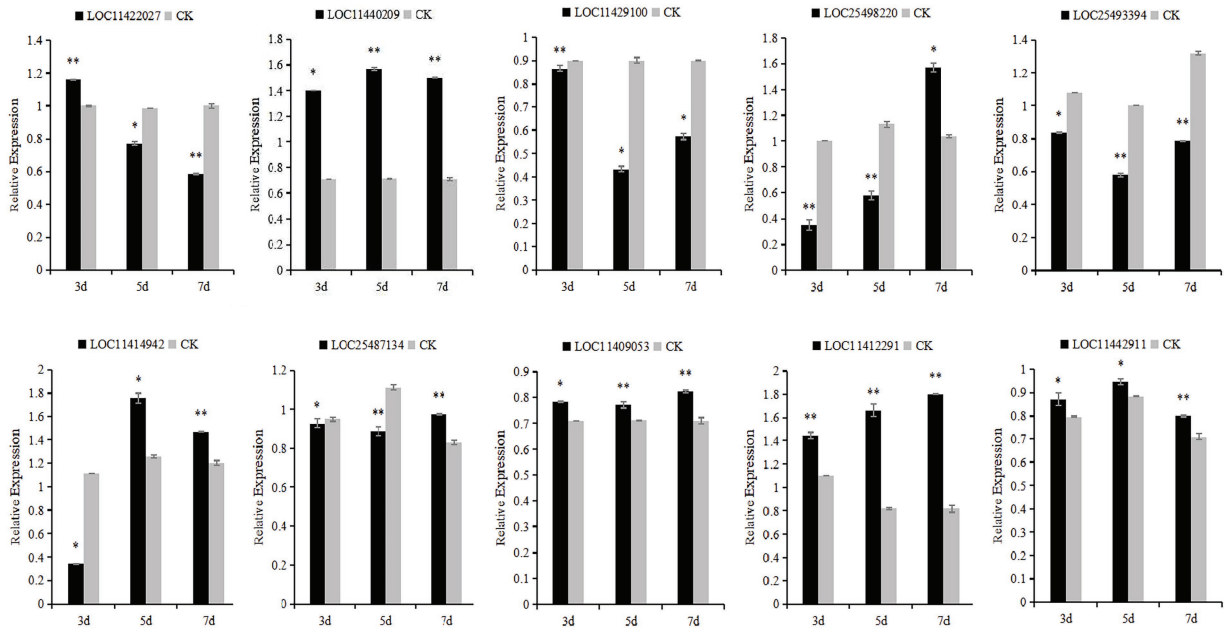

FIGURE 11
Relative expression levels of *Medicago falcata* after simulated cutting for 3, 5, and 7days. Asterisks indicate significant differences as determined by ANOVA (*p<0.05, **p<0.01).

of reference genomes, and functional annotation information. Among these candidate genes, LOC11422027 was located in Chr04.23915589–23918205. It is annotated as Scarecrow-like protein 14, which has been reported to be a multifunctional regulator involved in plant growth, photosynthesis, tolerance to photooxidative stress, and aging (Chen et al., 2014). The candidate gene LOC11429100 was located in LOC11429100 and was annotated as Gibberellin 20 oxidase 3, which is a key enzyme in GA biosynthesis (Yan et al., 2014). The candidate gene LOC25498220 was located in Chr07.19256208–19256385 and annotated as At4g13040 in Ethylene responsive transcription factor-like protein. At4g13040(referred herein as Apetala 2 family protein involved in SA-mediated disease defense 1—APD1) is an important regulator for SA-mediated plant defense (Mrunmay et al., 2014). In Chr04.38356528–38357582, LOC25493394 has an opposite pattern: A-B binding protein AB80, chloroplastic, (Gerardo et al., 1992) showed that chlorophyll A/B binding protein AB80 can promote chloroplast synthesis of coenzymes and improve the utilization of light energy in pea. The candidate gene LOC11414942 located in Chr06.8920707–8928256 was annotated as calmodulin-7, Recent studies further indicate that CAM7 is also an integral part of multiple signaling pathways including hormone, immunity, and stress (Zeb et al., 2019). Solanesyl diphosphate synthase 1 (SPS1) is the key enzyme in solanesol, a LOC25487134 gene located in Chr02.30508874–30509001 biosynthesis. Their studies in tobacco show that SPS1 significantly increased leaf growth, in tobacco, and in leaves content (Yan et al., 2020). LOC11409053 gene located in Chr04.50640870–50641400, Studies have shown that the Cell wall/vacuolar inhibitor of fructosidase 1 regulates ABA response and salt how in Arabidopsis (Yang et al., 2020). The candidate gene LOC11440209 located in

Chr04.44959722–44961035 was annotated as the transcription factor TCP15, TCP15 are required for an efficient elongation response to auxin, most likely by regulating a subset of auxin-inducible genes related to cell expansion (Luciav et al., 2020). The candidate gene LOC11412291 was located in Chr06.3615590–3617827, which was annotated as the transcription factor MYB30. Some studies have reported that MYB30 is necessary for root growth regulation during defense responses and can regulate the synthesis of Arabidopsis wax powder. Epidermal wax powder plays an important role in plant resistance to diseases and insect pests and reduction of ultraviolet radiation (Raffaele et al., 2006; Kaho et al., 2018). Some studies have shown that the deeper the root is buried in the soil, the higher the grazing tolerance of alfalfa (Wang et al., 2013). The candidate gene LOC11442911 was located in Chr02.4417521-4418430 and was annotated as pathogen-related genes transcriptional activator PTI5. The ERF family transcription factor Pti5 belongs to a member of the ERF subfamily in the AP2/ERF family. Wang Y. et al. (2020) showed that Pti5 transcription factor plays a regulatory role in disease resistance and fruit ripening in tomato. qRT-PCR was used to analyze the relative expression levels of these 10 candidate genes through simulated grazing tolerance cutting test. We found that the relative expression levels of LOC11412291 and LOC11440209 were significantly up-regulated with the increase of cutting days. Therefore, we predicted that *M. falcata* faced with abiotic stress (cutting or grazing). LOC11412291 and LOC11440209 genes may have certain regulatory functions, which can be used as key candidate genes related to grazing tolerance.

Conclusion

In this study, using RAD-seq technology, we sequenced 79 F1 individuals from a cross between a high (MF200401) and a low (MF200402) grazing tolerance *M. falcata* parent. After cleaning up reads and mapping to reference genome, we obtained 1756 high-quality SNPs and constructed a high-density genetic linkage map. These SNPs were located in 8 LGs with a consensus total length of 1312.238 cM and average distance of 0.844 cM between markers. Based on 6 phenotypic traits and linkage analysis, 63 QTLs associated with grazing tolerance traits were detected. Among them, 17 QTLs were associated with natural shoot height; 12 QTLs were related to rhizome length; 10 QTLs corresponded to shoot canopy diameter; 9 QTLs for basal plant diameter; 6 QTLs for stem number; 5 QTLs for absolute shoot height and 4 QTLs for rhizome width. Ten candidate genes that might be related to grazing tolerance were screened by QTL mapping and annotation information, and two key candidate genes (LOC11412291 and LOC11440209) were screened by qRT-PCR through simulated cutting test, and their functions could be further verified in *M. falcata*. The results presented in this study provide valuable information for breeding grazing tolerant alfalfa and *M. falcata*.

Data availability statement

The data presented in the study are deposited in the NCBI repository, accession numbers: PRJNA795270 and PRJNA795570.

Author contributions

XZho, XL, and DY assembled sequences and analyzed the data. XZho and XL wrote the manuscript. XZho collected the plant material. YZ and JW conceived the research and revised the manuscript. All authors contributed to the article and approved the submitted version.

Funding

This work was supported by grants from the National Natural Science Foundation of China (no. 31560662 and 32160326) and Inner Mongolia Autonomous Region Science and Technology Project (no. 2020GG0176).

Conflict of interest

The authors declare that the research was conducted in the absence of any commercial or financial relationships that could be construed as a potential conflict of interest.

Publisher's note

References

Chen, Y. M. (2018). *Construction of SNP linkage map and QTL mapping for flower color traits of Photophthora blight resistance in anther palm*. Hainan University, China.

Chen, K., Li, H., Chen, Y., Zheng, Q., Li, B., and Li, Z. (2014). *TaSCL14*, a novel wheat (*Triticum aestivum* L.) GRAS gene, regulates plant growth,photosynthesis, tolerance to photooxidative stress, and senescence. *J. Genet. Genomics* 42, 21–32. doi: 10.1016/j.jgg.2014.11.002

Chutimanitsakun, Y., Nipper, R. W., CuestaMarcos, A., Cistué, L., Corey, A., and Filichkina, T. (2011). Construction and application for QTL analysis of a restriction site associated DNA (RAD) linkage map in barley. *BMC Genomics* 12:4. doi: 10.1186/1471-2164-12-4

Cui, L. L. (2020). *Hybrid analysis of alfalfa and Medicago falcata L. and construction of SNP marker genetic map*. Chinese Academy of Agricultural Sciences, China.

Feng, J., Zhao, S., Li, M., Zhang, C., Qu, H., Li, Q., et al. (2020). Genome-wide genetic diversity detection and population structure analysis in sweetpotato(*Ipomoeabatatas*)using RAD-seq. *Genomics* 112, 1978–1987. doi: 10.1016/j.ygeno.2019.11.010

Fukuda, S., Nagano, Y., Matsuguma, K., Lshimoto, K., Hiehata, N., and Yamamoto, T. (2019). Construction of a high-density linkage map for bronze loquat using RAD-Seq. *Sci. Hortic.* 251, 59–64. doi: 10.1016/j.scienta.2019.02.065

Gerardo, A., Enrique, G., Mireya, S., Patricio, G., Luis, H., and June, S. (1992). Characterization of DNA sequences that mediate nuclear protein binding to the regulatory region of the *Pisum safiwum* (pea) chlorophyl a/b binding protein gene *AB80*: identification of a repeated heptamer motif. *Plant J.* 2, 301–309.

Han, Y. H., Dong-Man, K., and Monteros, M. J. (2012). High-resolution melting analysis for SNP genotyping and mapping in tetraploid alfalfa. *Mol. Breed.* 29, 489–501. doi: 10.1007/s11032-011-9566-x

Han, Y., Yun, K., Ivone, T.-J., Foo, C., Christopher, D., and Patrickx, Z. (2011). Genome-wide SNP discovery in tetraploid alfalfa using 454 sequencing and high resolution melting analysis. *BMC Genomics* 12, 350–360. doi: 10.1186/1471-2164-12-350

Han, Q., Zhu, Q., Shen, Y., Lee, M., Lübberstedt, T., and Zhao, G. (2022). QTL mapping low-temperature germination ability in the maize IBM Syn10 DH population. *Plants* 11:214. doi: 10.3390/plants11020214

He, F. (2016). *Construction of genetic map and QTL mapping for flowering and leaf type traits in Medicago sativa L.* Shihezi University, China.

Jiang, X. Q., Yang, T. H., Zhang, F., Yang, X. J., Yang, C. F., and He, F. (2022). RAD-Seq-based high-density linkage maps construction and quantitative trait loci mapping of flowering time trait in alfalfa (*Medicago sativa* L.). *Front. Plant Sci.* 13:899681. doi: 10.3389/fpls.2022.899681

José, D. R., Da Silva, N., Liu, S., Fábio, P., Caio Augusto, P., Priscilla Marqui, S. V., et al. (2017). Large-scale SNP discovery and construction of a high density genetic map of Colossoma macropomum through genotyping-by-sequencing. *Sci. Rep.* 7:46112. doi: 10.1038/srep46112

Kaho, M., Hiromasa, M., Tomotaka, I., Takamasa, S., Mika, N., and Satomi, S. (2018). MYB30 links ROS signaling, root cell elongation, and plant immune responses. *PNAS* 115, E4710–E4719. doi: 10.1073/pnas.1804233115

Kang, J. M., Zhang, T. J., Wang, M. Y., Zhang, Y., and Yang, Q. C. (2014). Research progress and application of QTL and whole genome selection in alfalfa. *Acta Pratacul. Sin.* 23, 304–312. doi: 10.11686/cyxb20140636

Kuang, C. H., Zhao, X. F., Yang, K., Zhang, Z. P., Ding, L., Pu, Z. E., et al. (2020). Mapping and characterization of major QTL for spike traits in common wheat. *Physiol. Mol. Biol. Plants* 26, 1295–1307. doi: 10.1007/s12298-020-00823-0

Kumar, P., Gupta, V. K., Misra, A. K., Modi, D. R., and Pandey, B. K. (2009). Potential of molecular markers in plant biotechnology. *Plant Omics.* 2, 141–162. doi: 10.1201/9780429505676-23

Lei, L., Zheng, H., Bi, Y., Yang, L., Liu, H., Wang, J., et al. (2020). Identification of a major qtl and candidate gene analysis of salt tolerance at the bud burst stage in rice (*Oryza sativa* L.) using QTL-Seq and RNA-Seq. *Rice* 13, 1–14. doi: 10.1186/s12284-020-00416-1

Li, X., Acharya, A., Farmer, A. D., Crow, J. A., Bharti, A. K., Kramer, R. S., et al. (2012). Prevalence of single nucleotide polymorphism among 27 diverse alfalfa genotypes as assessed by transcriptome sequencing. *BMC Genomics* 13:568. doi: 10.1186/1471-2164-13-568

Li, X., and Brummer, E. C. (2012). Applied genetic sand genomics in alfalfa breeding. *Agronomy* 2, 40–61. doi: 10.3390/agronomy2010040

Li, X., Han, Y., Wei, Y., Acharya, A., Farmer, A. D., Ho, J., et al. (2014). Development of an alfalfa SNP array and its use to evaluate patterns of population structure and linkage disequilibrium. *PLoS One* 9:e84329. doi: 10.1371/journal.pone.0084329

Liu, S. N. (2012). *Construction of genetic map and gene mapping of important agronomic traits in alfalfa*. Inner Mongolia University, China,.

Liu, S. R. (2016). *Construction of a high-density genetic linkage map and QTL mapping for leaf litter traits in citrus*. Huazhong Agricultural University, China.

Liu, F. Q. (2017). *Construction of genetic map and QTL mapping of important agronomic traits in alfalfa*. Harbin Normal University, China.

Liu, C. Q., Gao, P., and Luan, F. S. (2014). Construction of genetic map and QTL analysis of fruit related traits in watermelon. *Sci. Agric. Sin.* 47, 2814–2829. doi: 10.3864/j.issn.0578-1752.2014.14.012

Liu, N. X., Li, M., Hu, X. B., Ma, Q. B., Mu, Y. H., Tan, Z. Y., et al. (2017). Construction of high-density genetic map and QTL mapping of yield-related and two quality traits in soybean RILs population by RAD-sequencing. *BMC Genomics* 18:466. doi: 10.1186/s12864-017-3854-8

Luciano, P., Philippe, B., Sabrina, D., Paola, L., Paolo, A., and Bernadette, J. (2021). QTL analysis for grazing tolerance, autumn dormancy and growth habit offers prospects for marker-assistedselection in lucerne. *Euphytica* 217:1, –11. doi: 10.1007/s10681-021-02897-7

Luciav, F., Victoria, G., Federicod, A., Ivanal, V., and Danielh, G. (2020). Class I TCP proteins TCP14 and TCP15 are required for elongation and gene expression responses to auxin. *Plant Mol. Biol.* 105, 147–159. doi: 10.1007/s11103-020-01075-y

Lv, D. Y., Zhang, C. L., Yv, R., Yao, J. X., Wu, J. H., Song, X. P., et al. (2021). Utilization of a wheat 50K SNP microarray-derived high-density genetic map for QTL mapping of plant height and grain traits in wheat. *Plan. Theory* 10:1167. doi: 10.3390/PLANTS10061167

McCord, P., Gordon, V., Saha, G., Hellinga, J., Vandemark, G., and Larsen, R. (2014). Detection of QTL for forage yield, lodging resistance and springvigor traits in alfalfa (*Medicago sativa* L.). *Euphytica* 200, 269–279. doi: 10.1007/s10681-014-1160-y

Meng, L., Li, H. H., Zhang, L. Y., and Wang, J. K. (2015). QTL IciMapping: integrated software for genetic linkage map construction and quantitativetrait locus mapping in biparental populations. *Crop J.* 3, 269–283. doi: 10.1016/j.cj.2015.01.001

Mrunmay, K., Swadhin, S., Janesh, K., Subaran, S., Nidhi, S., Lipika, B., et al. (2014). The *Arabidopsis thaliana At4g13040* gene, a unique member of the AP2/EREBP family, is a positive regulator for salicylic acid accumulation and basal defense against bacterial pathogens. *J. Plant Physiol.* 171, 860–867. doi: 10.1016/j.jplph.2013.12.015

Musial, J. M., Lowe, K. F., Mackie, J. M., Aitken, K. S., and Lrwin, J. A. G. (2006). DNA markers linked to yield,yield components,and morphological traits in autotetraploid lucerne (*Medicago sativa* L.). *Aust. J. Agr. Res.* 57, 801–810. doi: 10.1071/AR05390

Musial, J. M., Mackie, J. M., Armour, D. J., Phan, H. T. T., Ellwood, S. E., Aitken, K. S., et al. (2007a). Identification of QTL for reaction to three races of colletotric humtrifolii and further analysis of inheritance of resistance in auto tetraploid lucerne. *Theor. Appl. Genet.* 114, 1417–1426. doi: 10.1007/s00122-007-0527-z

Musial, J. M., Mackie, J. M., Armour, D. J., Phan, H. T. T., Ellwood, S. E., Aitken, K. S., et al. (2007b). Identification of QTL for resistance and susceptibility to Stagonospora meliloti in auto tetraploid lucerne. *Theor. Appl. Genet.* 114, 1427–1435. doi: 10.1007/s00122-007-0528-y

Pandey, M. K., Agarwal, G., Kale, S. M., Clevenger, J., Nayak, S. N., and Sriswathi, M. (2017a). Development and evaluation of a high density genotyping "*Axiom_Arachis*" array with 58K SNPs for accelerating genetics and breeding in groundnut. *Sci. Rep.* 7:40577. doi: 10.1038/srep40577

Pandey, M. K., Khan, A. W., Singh, V. K., Vishwakarma, M. K., Shasidhar, Y., Kumar, V., et al. (2017b). QTL-seq approach identified genomic regions and diagnostic markers for rust and late leaf spot resistance in groundnut (*Arachis hypogaea* L.). *Plant Biotechnol. J.* 15, 927–941. doi: 10.1111/pbi.12686

Pecetti, L., Roman, M., De Rosa, L., and Piano, E. (2008). Selection of grazing-tolerant lucerne cultivars. *Grass Forage Sci.* 63, 360–368. doi: 10.1111/j.1365-2494.2008.00640.x

Popp, J., McCaughey, W., Cohen, R., McAllister, T., and Majak, W. (2000). Enhancing pasture productivity with alfalfa: A review. *Can. J. Plant Sci.* 80, 513–519. doi: 10.4141/P99-049

Qiang, H., Chen, Z. H., Zhang, Z. L., Wang, X. M., Gao, H. W., and Wang, Z. (2015). Molecular diversity and population structure of a world wide collection of cultivated tetraploid alfalfa(*Medicago sativa* subsp.*sativa* L.).Germplasm as revealed by microsatellite markers. *PLoS One* 10:e0124592. doi: 10.1371/journal.pone.0124592

Raffaele, S., Rivas, S., and Roby, D. (2006). An essential role for salicylic acid in *AtMYB30*-mediatedcontrol of the hypersensitive cell death program in *Arabidopsis*. *FEBS Lett.* 580, 3498–3504. doi: 10.1016/j.febslet.2006.05.027

Robins, J. G., Bquchan, G. R., and Brummer, E. C. (2007). Genetic mapping forage yield,plant height,and regrow that multiple harvests in tetraploid alfalfa(*Medicago sativa* L.). *Crop. Sci.* 47, 11–18. doi: 10.2135/cropsci2006.07.0447

Robins, J. G., and Brummer, E. C. (2010). QTL underlying self-fertility in tetraploid alfalfa. *Crop. Sci.* 50, 143–149. doi: 10.2135/cropsci2009.02.0104

Shi, H. F., He, S. J., He, X. Y., Lu, S. Y., and Guo, Z. F. (2019). An eukaryotic elongation factor 2 from *Medicago falcata* (MfEF2) confers cold tolerance. *BMC Plant Biol.* 19, 218–230. doi: 10.1186/s12870-019-1826-7

Shimoyama, N., Johnson, M., Beaumont, A., and Schläppi, M. (2020). Multiple cold tolerance trait phenotyping reveals shared quantitative trait loci in *Oryza sativa*. *Rice* 13, 57–17. doi: 10.1186/s12284-020-00414-3

Tu, D. P. (2011). *Construction of genetic map and QTL mapping of some agronomic traits in Medicago truncatula by SSR markers*. Yangzhou University, China.

Wang, D. (2015). *Cloning and genetic transformation of alfalfa tolerance related genes in tobacco*. Inner Mongolia: Inner Mongolia Agricultural University.

Wang, L., Conteh, B., Fang, L., Xia, Q., and Nian, H. (2020). QTL mapping for soybean (*Glycine max* L.) leaf chlorophyll-content traits in a genotyped RIL population by using RAD-seq based high-density linkage map. *BMC Genomics* 21:739. doi: 10.1186/s12864-020-07150-4

Wang, Y., Feng, G. D., Zhang, Z., Liu, Y., Ma, Y. L., Wang, Y. Y., et al. (2020). Overexpression of Pti4, Pti5, and Pti6 in tomato promote plant defense and fruit ripening. *Plant. Sci.* 302:110702. doi: 10.1016/j.plantsci.2020.110702

Wang, M. T., Jiang, L. H., Bada, L. H., Lv, S. J., and Wang, J. J. (2013). Application of optimal sequence analysis method in evaluation of grazing tolerance of *Medicago falcata* L. *Grassland Prata* 25, 51–56. doi: 10.3969/j.issn.2095-5952.2013.02.013

Wang, J. J., Lv, S. J., Wang, M. T., Wang, D., Bada, L. H., Jiang, L. H., et al. (2006). Morphological mechanism of grazing tolerance of alfalfa at individual level. *Grassland J.* 24, 35–41. doi: 10.11733/j.issn.1007-0435.2016.01.005

Wang, J. J., Zhao, Y., Ray, L., and Song, M. Z. (2016). Transcriptome responses in alfalfa associated with tolerance to intensive animal grazing. *Sci. Rep.* 6:19438. doi: 10.1038/srep19438

Wu, K., Liu, H. Y., Yang, M. M., Ye, T., Ma, H. H., Wu, W. X., et al. (2014). High density genetic map construction and QTLs analysis of grain yield-related traits in sesame(*Sesamum indicum* L.)basedon RAD-Seq. *BMC Plant Biol.* 14:274. doi: 10.1186/s12870-014-0274-7

Yagi, M., Shirasawa, K., Waki, T., Kume, T., Isobe, S., Tanase, K., et al. (2017). Construction of an SSR and RAD marker-based genetic linkage map for carnation (*Dianthus caryophyllus* L.). *Plant Mol. Biol. Rep.* 35, 110–117. doi: 10.1007/s11105-016-1010-2

Yan, N., Gai, X., Xue, L., Du, Y., Shi, J., and Liu, Y. (2020). Effects of *NtSPS1* overexpression on Solanesol content, plant growth, photosynthesis, and Metabolome of *Nicotiana tabacum*. *Plan. Theory* 9:518. doi: 10.3390/plants9040518

Yan, C., Yan, Z., Wang, Y., Yan, X., and Han, Y. (2014). Tudor-SN, a component of stress granules, regulates growth under salt stress by modulating *GA20ox3* mRNA levels in *Arabidopsis*. *J. Exp. Bot.* 65, 5933–5944. doi: 10.1093/jxb/eru334

Yang, W., Chen, S., Cheng, Y., Zhang, N., Ma, Y., Wang, W., et al. (2020). Cell wall/vacuolar inhibitor of fructosidase 1 regulates ABA response and salt tolerance in *Arabidopsis*. *Plant Signal. Behav.* 15:e1744293. doi: 10.1080/15592324.2020.1744293

Yermekbayev, K., GriffithsS, M., Chhetry, M., Leverington-Waite, M., Orford, S., Amalova, A., et al. (2020). Construction of a genetic map of RILs derived from wheat(T. aestivum L.) varieties pamyati azieva×paragon using high-throughput SNP genotyping platform KASP—kompetitive allele specific PCR. *Russ. J. Genet.* 56, 1090–1098. doi: 10.1134/S102279542009015X

Yin, T. T. (2021). *Analysis of phenotypic characters and Gentic diversity based on RAD-Seq sequencing of the Germplasm resources of Elymus*. Xinjiang Agricultural University, China.

Zeb, Q., Wang, X., Hou, C., Zhang, X., Dong, M., Zhang, S., et al. (2019). The interaction of CaM7 and CNGC14 regulates root hair growth in *Arabidopsis*. *J. Integr. Plant Biol.* 62, 887–896. doi: 10.1111/jipb.12890

Zhang, Z. D. (2016). *Optimization of high density genetic map and QTL mapping of important traits in jujube*. Beijing Forestry University, China.

Zhang, M. F. (2020). *Construction of high density molecular linkage map and QTL mapping for important traits such as starch content in tetraploid potato*. Inner Mongolia Agricultural University, China.

Zhang, F., Kang, J. M., Long, R. C., Yu, L. X., Sun, Y., Wang, Z., et al. (2020). Construction of high density genetic link age map and mapping quantitative trait loci(QTL)for flowering time in autotetraploid alfalfa(*Medicago sativa*L.)using genotyping by sequencing. *Plant Genome* 13:e20045. doi: 10.1002/tpg2.20045

Zhang, F., Kang, J. M., Long, R. C., Yu, L. X., Wang, Z., Zhao, Z. X., et al. (2019). High-density linkage map construction and mapping QTL for yield and yield components in auto tetraploid alfalfa using RAD-seq. *BMC Plant Biol.* 19:165. doi: 10.1186/s12870-019-1770-6

Zhao, L. B., Li, Z., Qu, J. P., Yu, Y., Lu, L., and Peng, Z. S. (2017). Novel fluorescent sequence-related amplified polymorphism(FSRAP) markers for the construction of a genetic linkage map of wheat(*Triticum aestivum* L.). *Genetika* 49, 1081–1093. doi: 10.2298/GENSR1703081Z

Zhou, X. Y., Han, H. J., Liu, Y. F., Qiu, R., and Zhao, Y. (2021). Research progress of *Medicago falcata* L. *Grassland Pratacul.* 33, 01–05. doi: 10.3969/j.issn.2095-5952.2021.02.002

frontiers | Frontiers in Plant Science

TYPE Original Research
PUBLISHED 03 October 2022
DOI 10.3389/fpls.2022.979956

OPEN ACCESS

EDITED BY
Jin-Lin Zhang,
Lanzhou University, China

REVIEWED BY
Bhaskar Gupta,
Government General Degree College, India
Juncheng Wang,
Gansu Agricultural University, China

*CORRESPONDENCE
Juying Wu
wujuying@grass-env.com
Qiang Guo
guoqiang@grass-env.com

SPECIALTY SECTION
This article was submitted to Plant Abiotic Stress, a section of the journal Frontiers in Plant Science

RECEIVED 28 June 2022
ACCEPTED 15 August 2022
PUBLISHED 03 October 2022

CITATION
Li C, Mur LAJ, Wang Q, Hou X, Zhao C, Chen Z, Wu J and Guo Q (2022) ROS scavenging and ion homeostasis is required for the adaptation of halophyte *Karelinia caspia* to high salinity. *Front. Plant Sci.* 13:979956. 10.3389/fpls.2022.979956

ROS scavenging and ion homeostasis is required for the adaptation of halophyte *Karelinia caspia* to high salinity

Cui Li[1], Luis A.J. Mur[2,3], Qinghai Wang[1], Xincun Hou[1], Chunqiao Zhao[1], Zhimin Chen[4], Juying Wu[1]* and Qiang Guo[1]*

[1]Institute of Grassland, Flowers and Ecology, Beijing Academy of Agriculture and Forestry Sciences, Beijing, China, [2]Institute of Biological, Environmental and Rural Sciences, Aberystwyth University, Aberystwyth, United Kingdom, [3]College of Software, Shanxi Agricultural University, Taigu, China, [4]College of Horticulture and Landscape, Tianjin Agricultural University, Tianjin, China

The halophyte *Karelinia caspia* has not only fodder and medical value but also can remediate saline-alkali soils. Our previous study showed that salt-secreting by salt glands is one of main adaptive strategies of *K. caspia* under high salinity. However, ROS scavenging, ion homeostasis, and photosynthetic characteristics responses to high salinity remain unclear in *K. caspia*. Here, physio-biochemical responses and gene expression associated with ROS scavenging and ions transport were tested in *K. caspia* subjected to 100–400mM NaCl for 7 days. Results showed that both antioxidant enzymes (SOD, APX) activities and non-enzymatic antioxidants (chlorogenic acid, α-tocopherol, flavonoids, polyamines) contents were significantly enhanced, accompanied by up-regulating the related enzyme and non-enzymatic antioxidant synthesis gene (*KcCu/Zn-SOD*, *KcAPX6*, *KcHCT, KcHPT1*, *Kcγ-TMT, KcF3H*, *KcSAMS* and *KcSMS*) expression with increasing concentrations of NaCl. These responses are beneficial for removing excess ROS to maintain a stable level of H_2O_2 and O_2^- without lipid peroxidation in the *K. caspia* response to high salt. Meanwhile, up-regulating expression of *KcSOS1/2/3, KcNHX1,* and *KcAVP* was linked to Na^+ compartmentalization into vacuoles or excretion through salt glands in *K. caspia*. Notably, salt can improve the function of PSII that facilitate net photosynthetic rates, which is helpful to growing normally in high saline. Overall, the findings suggested that ROS scavenging systems and Na^+/K^+ transport synergistically contributed to redox equilibrium, ion homeostasis, and the enhancement of PSII function, thereby conferring high salt tolerance.

KEYWORDS

halophyte, *Karelinia caspia*, ion homeostasis, antioxidant activity, photosynthesis, salt stress

Introduction

Soil salinization has become one of the most severe global environmental problems. It covers almost 7% of agricultural land on earth and predictions suggest that the continuous expansion of salinization may lead to a loss of 50% agricultural land by 2050 (Wang et al.,

2003). Most of crops are glycophytes, and have a low tolerance threshold for salinity (Ismail and Horie, 2017). However, halophytes are evolved the adaptive mechanism to complete life cycle in high salt environments more than 200 mM NaCl (Flowers and Colmer, 2008). Therefore, underlying the mechanisms of halophytes to adapt to salt stress could be important in breeding salt-tolerance crops (Guo et al., 2020).

Unlike crops, halophytes utilize not only organic osmotic substances but also inorganic osmolytes for osmotic adjustment (Sanadhya et al., 2015). Zeng et al. (2015) reported that inorganic ions may play more important roles than organic compounds in NaCl-induced osmotic adjustment in *Halostachys caspica*. The contribution of Na^+ to osmotic potential was up to 60% in halophyte *Solanum chilense* (Gharbi et al., 2017), which is mainly achieved by sequestration of Na^+ into the vacuole. Tonoplast Na^+/H^+ antiporters *NHX* and *AVP* mediated Na^+ movement in the vacuole (Liu et al., 2012; Toranj et al., 2020), Meanwhile, halophytes secreted excess Na^+ by salt glands, and the rate of salt secretion increased with the increasing salinity (Sanadhya et al., 2015). In *K. caspia, KcSOS1* silenced-lines disrupted the Na^+ transport, then decreased Na^+ secretion rates (Guo et al., 2020). These findings imply that *SOS1* mediated the Na^+ efflux in leaves, and may be the main regulator in salt secretion to maintain Na^+ homeostasis (Shi et al., 2002). Thus, regionalization of excess Na^+ into vacuoles or excretion reduced the concentration of Na^+ in the cytoplasm and maintained the balance of ions by regulating ion channel genes. Controlled uptake and compartmentalization of Na^+ enhanced the tolerance of halophytes to salinity (Flowers and Colmer, 2008). Besides, salinity induces the production of excess reactive oxygen species (ROS), including H_2O_2 and O_2^- in plants (Hernández et al., 2001). SOD has been considered the first defense against oxidative stress by dismutating O_2^- to H_2O_2, and antioxidant enzymes like CAT, and POD catalyzed the H_2O_2 into water and oxygen, to reduce damage by ROS (Bose et al., 2014). Further research demonstrated that overexpression of antioxidant enzyme genes such as *CAT* and *POD* regulated H_2O_2 homeostasis and improved the tolerance to salt stress (Zhou et al., 2018; Jin et al., 2019). Apart from the role of antioxidant enzymes in ROS scavenging, secondary metabolities such as chlorogenic acid, flavonoids, tocopherols, and polyamines play critical roles in the antioxidant mechanism (Guo et al., 2022). For example, Jin and Daniell (2014) reported that the overexpression of *γ-TMT* increased the content of α-tocopherol, then decreased the production of ROS, thus improving the tolerance of tobacco to salinity. Chlorogenic acid accumulation in *Lonicera japonica* suppressed the ROS content under salt treatments (Yan et al., 2017). Similarly, flavonoids were increased when exposed to salinity, and the accumulation of flavonoids effectively scavenged the hydroxyl radicals induced by salinity (Ismail et al., 2016). Above findings indicated that halophytes resist salt stress by regulating ionic homeostasis as well as ROS. However, most of previous studies only focused on ROS homeostasis or ion homeostasis (Al-Shamsi et al., 2020; Tran et al., 2020). The mechanism by which ROS and ion homeostasis combined to withstand salt stress remains unclear. In this study, we comprehensively explored the mechanisms of salt tolerance from ROS homeostasis, ion homeostasis, as well as osmotic adjustment. This was important to reveal the tolerance mechanism of halophytes to salinity.

Karelinia caspia is a recretohalophyte, perennial herb Asteraceae mainly distributed in semi-desert areas and desert grassland in Northwestern China, it is a pioneer species for improving saline-alkali and desertified soil, and it is also an important forage species for livestock in desert grassland (Wang et al., 2013). Previous studies have shown that *KcSOS1* mediates the excretion of Na^+ by salt glands (Guo et al., 2020), and *NHX1* mediates the Na^+ regionalization into vacuoles (Liu et al., 2012), thereby maintaining the ion homeostasis. Other adaptive mechanisms such as plant growth, osmotic adjustment, ionic homeostasis, ROS regulation of *K. caspia* to high saline stress need to be explored. Herein, we investigated the adaptation mechanisms of *K. caspia* by measuring plant growth, chlorophyll fluorescence, ion distribution, osmoregulation, enzymatic and non-enzymatic antioxidant components, and releted gene expression. This finding would provide valuable information for the remediation of *K. caspia* used in saline-alkali soil and the development of salt-resistant crop breeding.

Materials and methods

Plant material and experiment conditions

Seeds of *K. caspia* were collected from the experimental field at the College of Grassland and Environment Sciences of Xinjiang Agricultural University. Seeds were germinated in a 2:1 mixture of peat and sand under ambient conditions [temperature: 25°C/18°C (day/night), photoperiod: 16 h/8 h (day/night), relative humidity: 60%, photosynthetically active radiation: 300 μmol m^{-2} s^{-1}]. They were watered with Hoagland nutrient solution (Guo et al., 2017). After 6 weeks, the seedlings were transplanted to an opaque plastic culture tank (10*20 cm; hight*diameter) containing nutrient solutions. After 1 week of acclimation, seedlings were treated with solutions supplemented with 0, 100, 200, 300, and 400 mM NaCl. The salinity of the nutrient solutions was increased gradually by adding 100 mM NaCl per day until the designed concentrations were attained. Each treatment was repeated three times, and every replicate had two seedlings. Solutions were renewed every 3 days to maintain a stable concentration of NaCl. The duration of NaCl treatment was 7 days.

Measurement of growth parameters

Plant growth parameters such as relative growth rate (RGR), relative water content (RWC), and salinity tolerance index (STI) were measured in the experiment. The relative growth rate was calculated using the formula (Martínez et al., 2005). ; W_f is the

final dry weight, and W_i is the initial dry weights, Δt is the time of treatment. Relative water content was calculated using the formula (Aymen et al., 2016). Salinity tolerance index was calculated using the formula (Panda et al., 2019).

$$\mathrm{STI}(\%) = \frac{\text{Dry biomass of treated plant}}{\text{Dry biomass of control}} \times 100.$$

$$\mathrm{RGR} = \frac{\ln Wf - \ln Wi}{\Delta t}$$

Measurement of photosynthetic pigments, chlorophyll fluorescence and gas exchange parameters

Chlorophylls (Chl a and b) and total chlorophyll content were measured according to the method of Dere et al. (1998). The absorbance was measured at 470 nm, 645 nm, and 663 nm for chlorophylls calculation.

Chlorophyll fluorescence parameters were determined by the Handy PEA analyzer (Hansatech, United Kingdom). Firstly, leaf was covered by a leaf clip for 30 min for dark adaption, then opened the leaf clip and measured chlorophyll fluorescence by exposing the leaf to a 2 s saturating light pulse of 3,500 μmol photons m^{-2} s^{-1}. The parameters were calculated according to the protocol provided by the manufacturer. Thirty replicates were measured for every treatment.

Gas exchange in leaves was measured using a CIRAS-3 portable photosynthesis system (PP System, United States). The reference CO_2 concentration was maintained at 400 μmol·mol^{-1}, and photon flux density was set at 300 μmol m^{-2} s^{-1}. Gas exchange measurements were taken in the artificial climate chamber; five leaves were measured for every treatment.

Determination of cations concentration

Mineral ion content was measured according to the method of Rangani et al. (2018). Firstly, fresh leaves were dried at 60°C for 72 h and then ground into powder. The samples were dissolved in HNO_3 and $HClO_4$ mixture (4:1) and digested using microwave acid digestion. The extraction was filtered with a 0.45 μm filter, and then it was used to measure ions by inductively coupled plasma-optical emission spectrometry (ICP-OES; Agilent, United States).

Measurement of soluble sugars and proline

The content of soluble sugars was measured by the anthrone method (Watanabe et al., 2000). The absorption was measured at 620 nm. Proline content was measured according to the method of Bates et al. (1973). Fresh leaves were homogenized with 3% sulfosalicylic acid and then centrifuged at 14,000 g for 10 min. The mixture consisting of leaf extract, glacial acetic acid, and acid-ninhydrin was incubated at 100°C for 30 min, then added toluene and aspirated the upper solution. The absorption was measured at 520 nm.

Measurement of osmotic potential and relative contribution of inorganic and organic solutions

Osmotic potential (Ψs) and relative contribution of organic and inorganic solutes for osmotic adjustment were measured by the method of Silveira et al. (2009). Fresh leaves were homogenized with pestle mortar and centrifuged at 10,000 g for 10 min at 4°C. Then the supernatant was used to detect osmolality using a vapor pressure osmometer (Gonotec, German). The osmotic potential was calculated with the van't Hoff equation $\Psi s = -nRT$, where n is the osmolarity of solutions, R is the gas constant, and T is the absolute temperature. The relative contribution (RC) of organic and inorganic solutes to the osmotic potential was estimated as % the osmolality (Silva et al., 2010).

$$\mathrm{RC} = \frac{\text{Solute concentration}\left(\text{mmol / kg water tissue}\right)}{\text{Osmolality}\left(\text{mmol / kg solvent}\right)}.$$

Determination of lipid peroxidation, antioxidant enzyme and non-enzymatic antioxidants

To indicate lipid peroxidation, malondialdehyde (MDA) levels were measured according to the method of Cakmak and Marschner (1992) with slight modification. Fresh leaves (0.5 g) was ground into homogenization with 0.5% trichloroacetic acid (TCA), then centrifuged the homogenous at 15,000 g at 4°C for 10 min. The supernatant was collected and 0.6% thiobarbituric acid (v/v) was added and transferred to new tube. The tubes were heated at 95°C for 15 min, and quickly cooled in an ice bath. The absorbance at 450 nm, 532 nm, and 600 nm was measured by spectrophotometer (Persee, China).

Determination of H_2O_2 and O_2^-

The level of H_2O_2 in leaves was measured by examining the absorbance of the titanium peroxide complex at 415 nm according to the method of Hu et al. (2020). Fresh leaves (0.1 g) were ground into a homogenous slurry with 1 mL acetone, then centrifuged at 8,000 g at 4°C for 10 min. The supernatant was collected (v/v) and 5% titanium sulfate solution and ammonia water added. This was centrifuged at 4000 g, at 25°C for 10 min and pellet collected. The

pellets were dissolved in 2 mM sulfuric acid and the absorbance measured at 415 nm. Superoxide can react with hydroxylamine hydrochloride to form red azo compounds, and and so O_2- levels were calculated by measuring the absorbance at 530 nm as described by Yang et al. (2011).

Nitroblue tetrazolium (NBT) and 3,3-diaminobenzidine (DAB) staining was used to detect O_2^- and H_2O_2 *in situ*. NBT staining was carried out by the method of Fryer et al. (2002). The third leaf was dipped in NBT solution, under vacuum for 20 min, and then left to stand at room temperature for 1 h. After this, the leaf is decolorized in 95% ethanol solution. To detect H_2O_2, the third expanded leaf was used and wholly immersed in DAB solution, incubated for 8 h, then placed in 95% ethanol to decolorize (Thordal-Christensen et al., 2002).

Measurement of antioxidative enzyme activities and non-enzymatic antioxidants

To determine antioxidant enzyme activities and the levels of non-enzymatic antioxidants, fresh leaves (0.5 g) were ground into powder with liquid nitrogen and mortar and pestle. The activity of superoxide dismutase (SOD, EC 1.15.1.1), peroxidases (POD, EC 1.11.1.7) was measured using the method described by Guo et al., (2017). Ascorbate peroxidase (APX, EC 1.11.1.11) was measured by the decreased absorbance at 290 nm for 1 min (Nakano and Asada, 1981). Glutathione reductase (GR, EC 1.6.4.2) activity was calculated by measuring the absorbance of NADPH at 340 nm (Foyer et al., 1991). The reduced ascorbate (AsA) content and total ascorbate (AsA + DHA) were measured following the method of Gillespie and Ainsworth, (2007). Glutathione content including reduced (GSH) and total glutathione (GSH + GSSG) was measured according to Anderson (1985). Flavonoid contents were measured by the method of Jia et al., (1999).

α-tocopherol content was measured following the method of Zhang et al., (2020). Fresh leaves (0.5 g) were homogenized with a solution containing methanol and chloroform (2:1) and the extract was filtered with a 0.22 μm filter. High performance liquid chromatography (HPLC) was used with a C_{18} column (250*4.6 nm, 5 μm). The mobile phase consisted of 95% methanol and 5% isopropanol, and α-tocopherol was detected at 280 nm. Concentrations were calculated by a standard curve of α-tocopherol.

Chlorogenic acid content was assayed according to the method (Yan et al., 2016). Dry leaf powder (1 g) was homogenized in 30 mL 70% methanol and ultrasonic extraction for 30 min. The extraction was centrifuged for 10 min at 10,000 g. The assay was performed in high performance liquid chromatography (HPLC) with a C_{18} column (250*4.6 nm, 5 μm). The mobile phase was acetonitrile (13%) and 0.3% phosphoric acid (87%). Chlorogenic acids were detected at 327 nm, and their concentrations were determined using a standard curve of known concentrations of chlorogenic acid.

Fresh leaves were collected for the measurement of polyamines (spermine and spermidine). Fresh leaves (0.5 g) was grounded into power, homogenized with 1% perchloric acid and incubated for 1 h, centrifuged at 15000 g for 20 min. Then 200 μL saturated Na_2CO_3 and 400 μL dansyl chloride was added to the supernatant, and incubated overnight. Finally, the organic phase was extracted into 500 μL toluene and filtered with 0.22 μm filter. Spermine and spermidine levels were measured by HPLC as described by Marcé et al. (1995).

Gene expression assay

After 7 days of salinity treatments, leaves was collected for RNA extractions and gene expression assessments. RNA was extracted using the plant RNA Extraction Kit (TaKaRa, 9,769), then 1 μg RNA was reverse-transcribed to cDNA using Prime Script RT reagent Kit (TaKaRa, RR820A). qRT-PCR was carried out by CFX Connect real-time system (BioRad, United States) using a SYBR PCR mix (TaKaRa, RR420A). Thermal cycling conditions were 95°C for 30s, followed by 40 cycles of 95°C for 5 s, 60°C for 30s. The primer sequences of oftarget genes are listed in Supplementary Table S1. Gene expression was calculated using the formula $2^{-\Delta\Delta CT}$ and *KcActin* was used as the reference gene (Guo et al., 2020).

Statistical analyses

Data were presented as mean ± standard deviation (SD). One-way ANOVA was performed with Duncan's multiple range test ($p \leq 0.05$) using software SPSS22. There were 30 replicates for chlorophyll fluorescence parameters, five replicates for gas exchange parameters, and three replicates for all the other parameters. The correlation matrix was performed using Origin 2021.

Results

Effects of salinity on plant growth parameters, chlorophyll fluorescence, and photosynthetic efficiency

The effects of salt stress on the growth, chlorophyll fluorescence and photosynthetic efficiency were determined in *K. caspia*. No salt toxicity symptoms were observed in *K. caspia* after 7 days of NaCl treatment (Figure 1). In *K. caspia*, there was significant increase in shoot and root dry weight in 100 mM NaCl treatment. Similarly, the relative growth rate and salinity tolerance index increased by 7.2 and 24.76% under 100 mM NaCl, respectively. Both RGR and STI showed no significant difference in 200 to 400 mM NaCl treatments compared with controls. RWC was maintained at the same level among all treatments (Figure 1).

Compared to controls, the levels of the photosynthetic pigments such as Chla, Chlb, total chlorophyll, and Chl a/b ratio exhibited no significant differences (Table 1). To assess the effects of salinity on the photosynthetic function, chlorophyll fluorescence was measured using Handy PEA analyzer. The

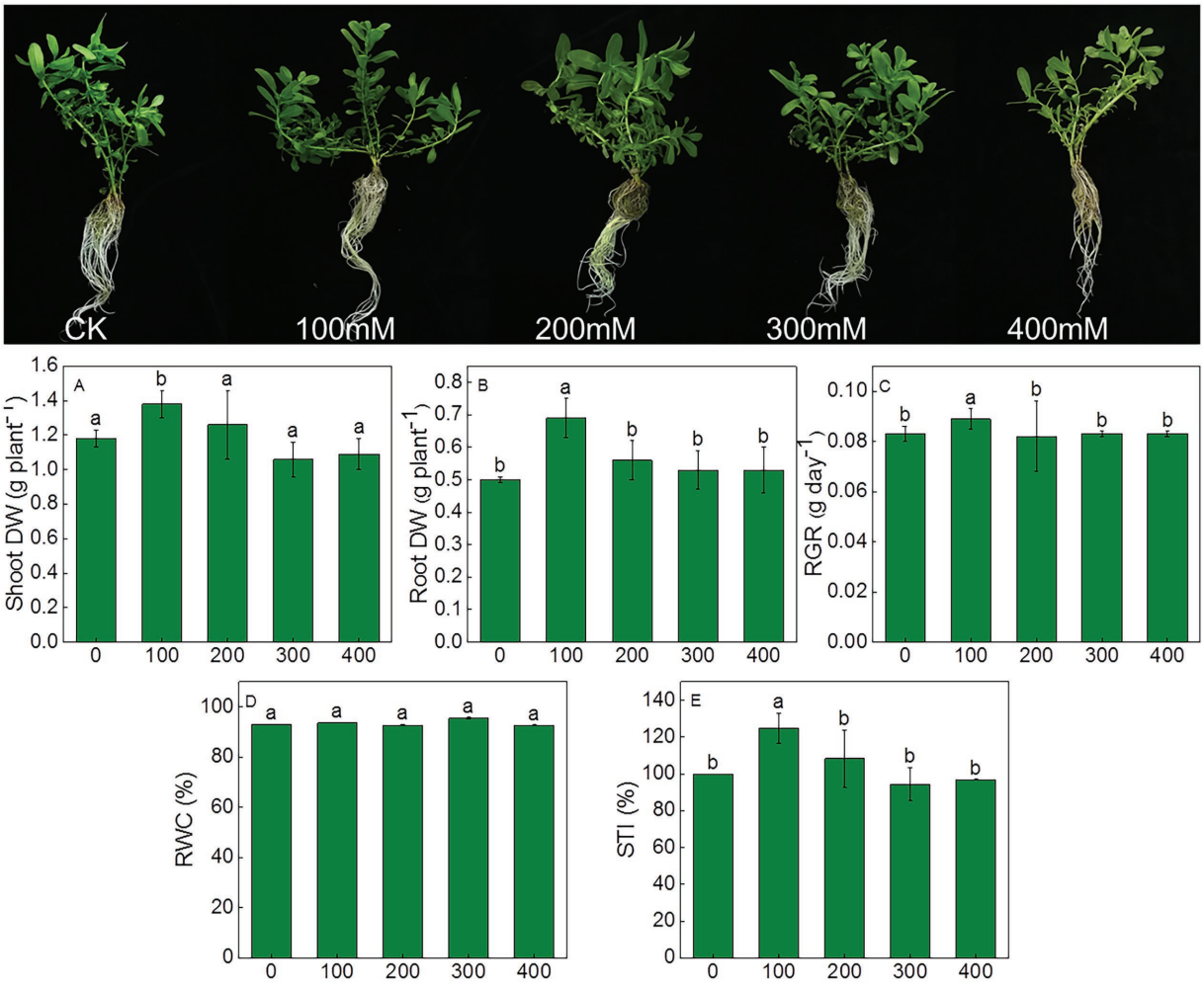

FIGURE 1
Morphological characteristics and changes in growth parameters of *Karelinia caspia* after 7 days of NaCl (mM) treatment. Different letters indicate significant difference at $p<0.05$.

derived parameters provided information concerning the structure and function of PSII. The maximum quantum yield of PSII (F_v/F_m) increased significantly in treatments from 200 to 400 mM NaCl. There was no significant difference in ABS/CS_m under salinity compared with control. TR_0/CS_m increased significantly under 400 mM NaCl treatment, and ET_0/CS_m increased significantly under the 300 and 400 mM NaCl treatments. The increase of ET_0/CS_m and RE_0/CS_m suggested elevated electron transport and increased efficiency of PSI. As compared to control, DI_0/CS_m decreased in NaCl treatments, especially in 300 and 400 mM NaCl treatment, decreasing by 21.9 and 32.4% compared with control. There was no significant difference in PI_{abs} under NaCl treatment from 100 to 300 mM compared with control, but it increased significantly under 400 mM NaCl treatment (Table 2).

Net photosynthetic rate (Pn) was significantly higher than the control under salt treatments, and they increased by 1.6, 1.9, 1.4, and 0.6 fold, respectively, from 100 to 400 mM NaCl (Table 3). Similarly, water use efficiency (WUE) was also increased significantly in saline treatments compared with control, and it was 3.6, 5.6, 6.4, and 3.9 fold that of the control, respectively, under salt treatments. However, stomatal conductance (gs) and transpiration (E) were all decreased as compared to the control, especially in 400 mM NaCl, stomatal conductance and transpiration decreased by 75.7 and 58.2%, respectively, (Table 3).

Ion accumulation and distribution of *Karelinia Caspia* in response to salinity

To understand how salinity effected the accumulation and distribution of nutrients in plants, K^+, Na^+, Ca^{2+}, Mg^{2+}, Zn^{2+}, and Fe^{2+} contents in roots, shoots, and leaves of *K. caspia* were measured after 7 days. The results showed that the content of Na^+ in roots, shoots, and leaves were significantly and positively

TABLE 1 The level of photosynthetic pigments responses to salinity in *Karelinia caspia*.

NaCl treatment (mmol L^{-1})	Chla (mg g^{-1}FW)	Chlb (mg g^{-1}FW)	Chl(a + b) (mg g^{-1}FW)	Chl a/b
0	0.21 ± 0.02a	0.13 ± 0.01a	0.34 ± 0.03a	1.65 ± 0.12a
100	0.27 ± 0.01a	0.15 ± 0.00a	0.42 ± 0.01a	1.70 ± 0.08a
200	0.22 ± 0.01a	0.13 ± 0.02a	0.35 ± 0.02a	1.79 ± 0.09a
300	0.26 ± 0.05a	0.14 ± 0.07a	0.40 ± 0.07a	1.80 ± 0.02a
400	0.21 ± 0.00a	0.12 ± 0.01a	0.33 ± 0.01a	1.79 ± 0.07a

Different letters indicate significant difference at $p < 0.05$.

TABLE 2 The changes of Chlorophyll fluorescence parameters in response to salinity in *Karelinia caspia*.

NaCl treatment (mmol L^{-1})	Chlorophyll fluorescence parameters					
	F_v/F_m	PI abs	Abs/CS_m	TRo/CS_m	ETo/CS_m	DIo/CS_m
0	0.71 ± 0.01c	0.25 ± 0.07b	1261.47 ± 49.36a	882.05 ± 43.89a	130.77 ± 18.50c	363.07 ± 22.84a
100	0.74 ± 0.01bc	0.27 ± 0.05b	1236.20 ± 74.99a	941.91 ± 43.73a	147.80 ± 15.87bc	334.57 ± 19.08a
200	0.75 ± 0.01b	0.45 ± 0.09b	1134.87 ± 57.50a	851.13 ± 42.13a	149.80 ± 18.70bc	326.60 ± 26.35a
300	0.76 ± 0.01b	0.39 ± 0.08b	1352.60 ± 42.14a	939.57 ± 23.00ab	192.50 ± 17.63b	283.73 ± 21.67b
400	0.80 ± 0.01a	0.95 ± 0.13a	1184.83 ± 36.30a	1018.03 ± 27.07b	274.83 ± 21.49a	245.27 ± 15.61b

Different letters indicate significant difference at $p < 0.05$.

TABLE 3 Effects of different salinity on photosynthetic parameters in *Karelinia caspia*.

NaCl treatment (mmol L^{-1})	Pn (μmol m^{-2} s^{-1})	gs (mmol m^{-2} s^{-1})	E (mmol m^{-2} s^{-1})	WUE
0	1.04 ± 0.07d	149.20 ± 6.98a	3.14 ± 0.12a	0.32 ± 0.02c
100	2.60 ± 0.30a	69.00 ± 4.70b	2.29 ± 0.12b	1.16 ± 0.11b
200	3.0 ± 0.12a	47.80 ± 1.39c	1.67 ± 0.06c	1.80 ± 0.09a
300	2.48 ± 0.08b	38.40 ± 3.75c	1.27 ± 0.12d	2.04 ± 0.22a
400	1.64 ± 0.09c	36.20 ± 2.60c	1.31 ± 0.08d	1.26 ± 0.07b

Different letters indicate significant difference at $p < 0.05$.

correlated with NaCl treatment concentration. Na^+ content increased significantly in roots, shoots, and leaves compared to the control. With the 400 mM NaCl treatment, Na^+ content was 48.2, 36.9, and 29.3 times that of the control in roots, shoots, and leaves of *K. caspia,* respectively (Figure 2A). However, the contents of K^+, Ca^{2+}, Mg^{2+}, Zn^{2+}, and Fe^{2+} were all decreased in roots, shoots, and leaves compared to the control except Zn^{2+} in leaves (Figures 2B–E). The content of Zn^{2+} in NaCl treatments was maintained at the same level as control (Figure 2F). Although ions content decreased compared with control, the content of K^+, Ca^{2+}, Mg^{2+}, Zn^{2+}, and Fe^{2+} had no significant difference among the treatments except in the root content of K^+ and Ca^{2+} with 100 mM NaCl treatment. The K^+/Na^+ ratio was also maintained at the same level among all NaCl treatments. Correlation analysis showed that the content of Na^+ in leaves was positively correlated with Na^+ in roots and stems, but negatively correlated with Ca^{2+}, Fe^{2+} and Mg^{2+}. Similarly, the content of Na^+ in roots was negatively correlated with Ca^{2+}, Fe^{2+}, K^+, and Mg^{2+} (Figure 3A). These results indicated that *K. caspia* accumulated a large amount of Na^+, and meanwhile maintained the homeostasis of other ions under salt treatment.

Relative contributions of organic and inorganic solutes to osmotic adjustment

In *K. caspia*, the soluble sugars increased progressively with NaCl treatments. There were significant differences with 300 and 400 mM NaCl treatments as compared to control (Figure 4A). In *K. caspia,* there was a significant increase under all treatments compared with control. The level of proline increased by 1.5, 1.5, 7.1, and 10.4 fold, respectively, in 100, 200, 300, and 400 mM NaCl treatments as compared to control (Figure 4B).

In *K. caspia*, the osmotic potential of leaves decreased with the increasing salinity, and the values of osmotic potential were −0.97, −1.48, −2.05, −2.51, and −2.74 MPa, respectively, in control and NaCl treatments from 100 to 400 mM. Our results suggested that the contribution of organic solutes in control was higher than that in NaCl treatments. However, the contributions of inorganic solutes were higher in NaCl treated plants than in control plants. Amongst the organic osmolytes, soluble sugars contributed 0.15–0.29% to osmotic adjustment, and proline had a very negligible contribution (0.01–0.04%) (Figure 4C). Among inorganic osmolytes, the contribution of K^+ towards osmotic adjustment in

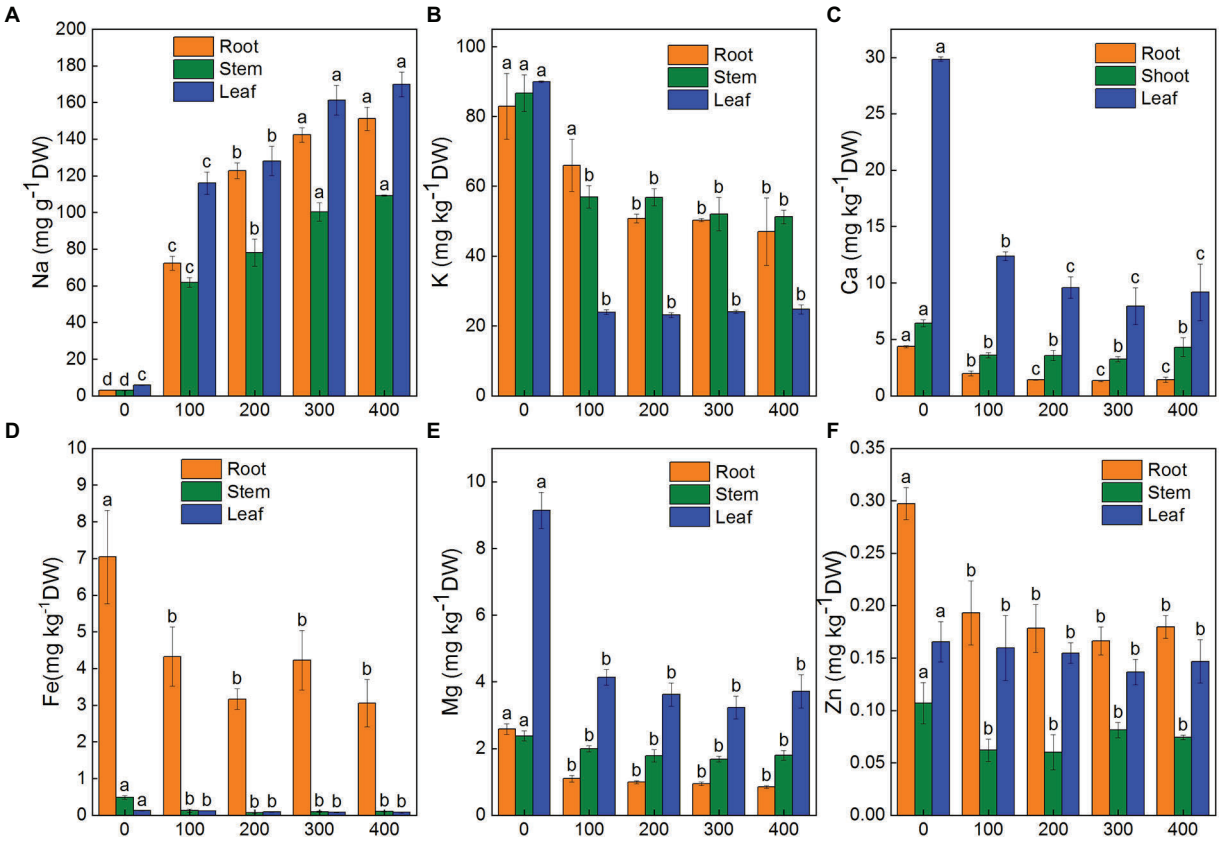

FIGURE 2
Effects of NaCl treatment (100, 200, 300, and 400 mM) on ions content in roots, stems and leaves of *Karelinia caspia*. **(A)** Na^+, **(B)** K^+, **(C)** Ca^{2+}, **(D)** Fe^{2+}, **(E)** Mg^{2+}, **(F)** Zn^{2+}. Different letters indicate significant difference at $p < 0.05$

control was 44.2%, and the contribution of Na^+ was only 4.8% in control. However, relative contributions of Na^+ to osmotic adjustment were 52.3 to 57.6% under salt treatments, and the contribution of K^+ was 4.4 to 7.0% (Figure 4D). These results showed that Na^+ acted as the main osmotic solute for osmotic regulation under salt stress.

Effects of salinity on H_2O_2 accumulation, lipid peroxidation, antioxidant enzyme activity and non-enzymatic antioxidants

To investigate salinity-induced oxidative stress, O_2^-, H_2O_2, MDA, antioxidant enzyme activity, and content of non-enzymatic antioxidants were examined under salinity. Our results showed that the content of O_2^-, H_2O_2, and MDA decreased under salinity, but no significant differences were observed between the NaCl treatments and the control (Figures 5A–C). Under salinity, NBT staining and DAB staining have no significant difference with control (Figures 5D–E).

The activity of antioxidant enzymes showed different trends under NaCl treatments. SOD activity remained unchanged in 100 mM NaCl treatment, but it increased significantly under treatment from 200 to 400 mM compared with control. SOD activity increased by 42.0, 35.1, and 38.4%, respectively, in 200, 300, and 400 mM treatments, and there was no significant difference between treatments (Figure 6A). APX activity increased by 56.3, 74.5, 84.4 and 64.5%, respectively, in the treatment from 100 to 400 mM NaCl compared with control. However, no significant differences were observed between treatments (Figure 6B). Compared to control, POD activity remained unchanged in 100 mM treatments but decreased sharply by 63.1, 60.3 and 74.6% in 200, 300, and 400 mM treatments (Figure 6C). GR activity remained unchanged in all treatments compared with control (Figure 6D).

In *K. caspia*, the content of α-tocopherol significantly increased under treatments as compared to control, and it increased by 29.8–50.4% in NaCl treatments, but there were no significant differences between treatments (Figure 6E). The content of chlorogenic and flavonoids were all increased with salinity. The content of chlorogenic significantly increased in 200, 300, and 400 mM NaCl treatments by 46.6, 46.2 and 56.0%, respectively (Figure 6F). The flavonoids were found to be increased significantly in 300 and 400 mM NaCl treated plants as compared to control, and increased by 1.4 and 1.3 folds, respectively (Figure 6G). Spermine content significantly increased under salinity, and it increased by 2.7, 11.4, 3.1 and 2.2 folds,

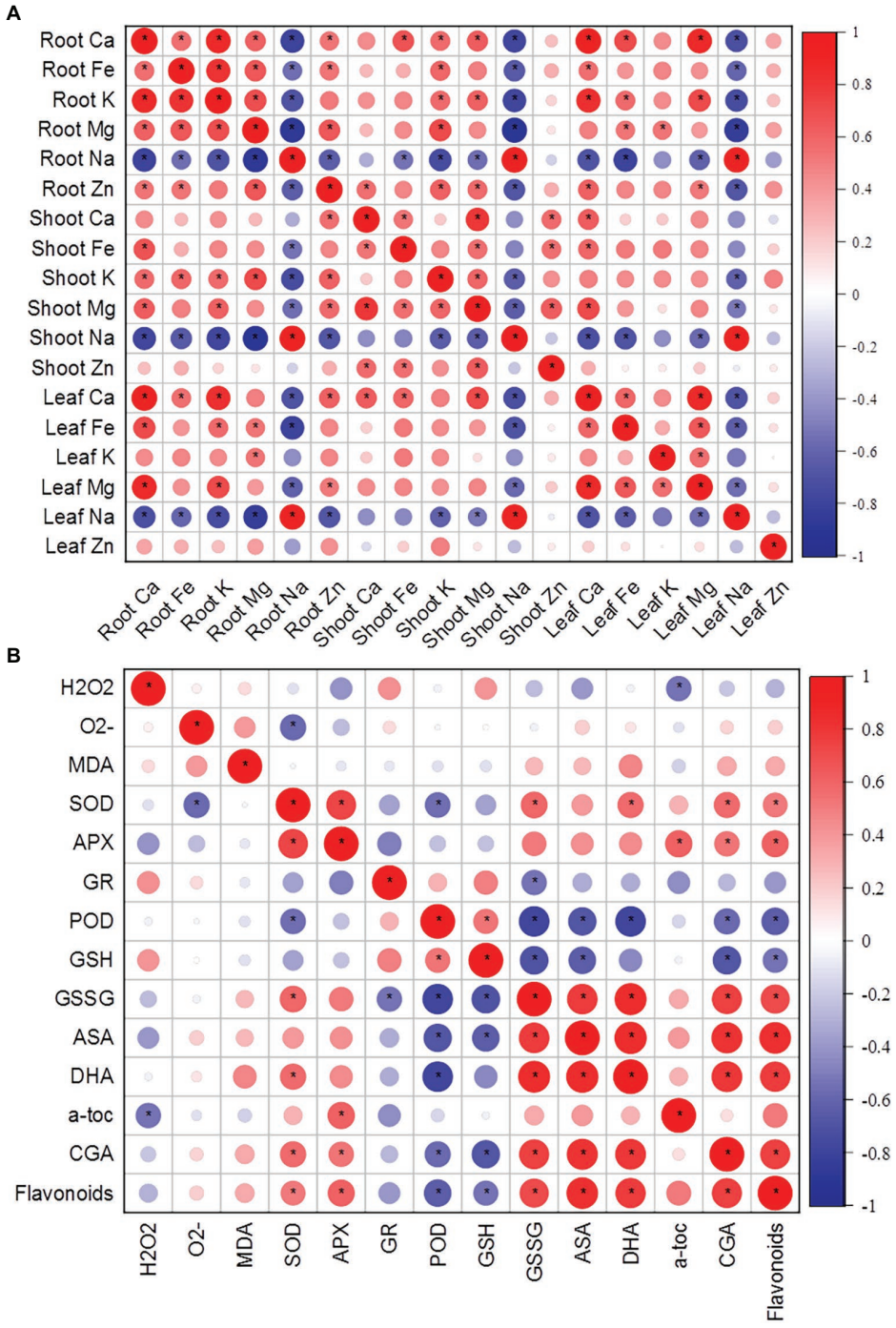

FIGURE 3
(A) Correlation matrix of various ions in roots, shoots, and leaves of *K. caspia*. **(B)** Correlation matrix between antioxidative components (antioxidant enzymes, non-enzymatic antioxidants) and stress indicators (O_2^-, H_2O_2, MDA). Asterisks indicate significant difference at $p<0.05$.

respectively, under the NaCl treatment from 100 to 400 mM (Figure 6H). Spermidine content was maintained at the same level as controls under salinity of 100 and 200 mM NaCl treatment, but increased by 16.7 and 17.8% under 300 and 400 mM treatment, respectively (Figure 6I). Correlation analysis between anti-oxidative components and oxidative stress indicators showed that SOD had a negative correlation with O_2^-, and positive correlation with chlorogenic acid and flavonoids. H_2O_2 exhibited a negative correlation with α-tocopherol (Figure 4B).

In *K. caspia*, the levels of total glutathione (GSH + GSSG) increased with the increasing NaCl concentrations. From a position

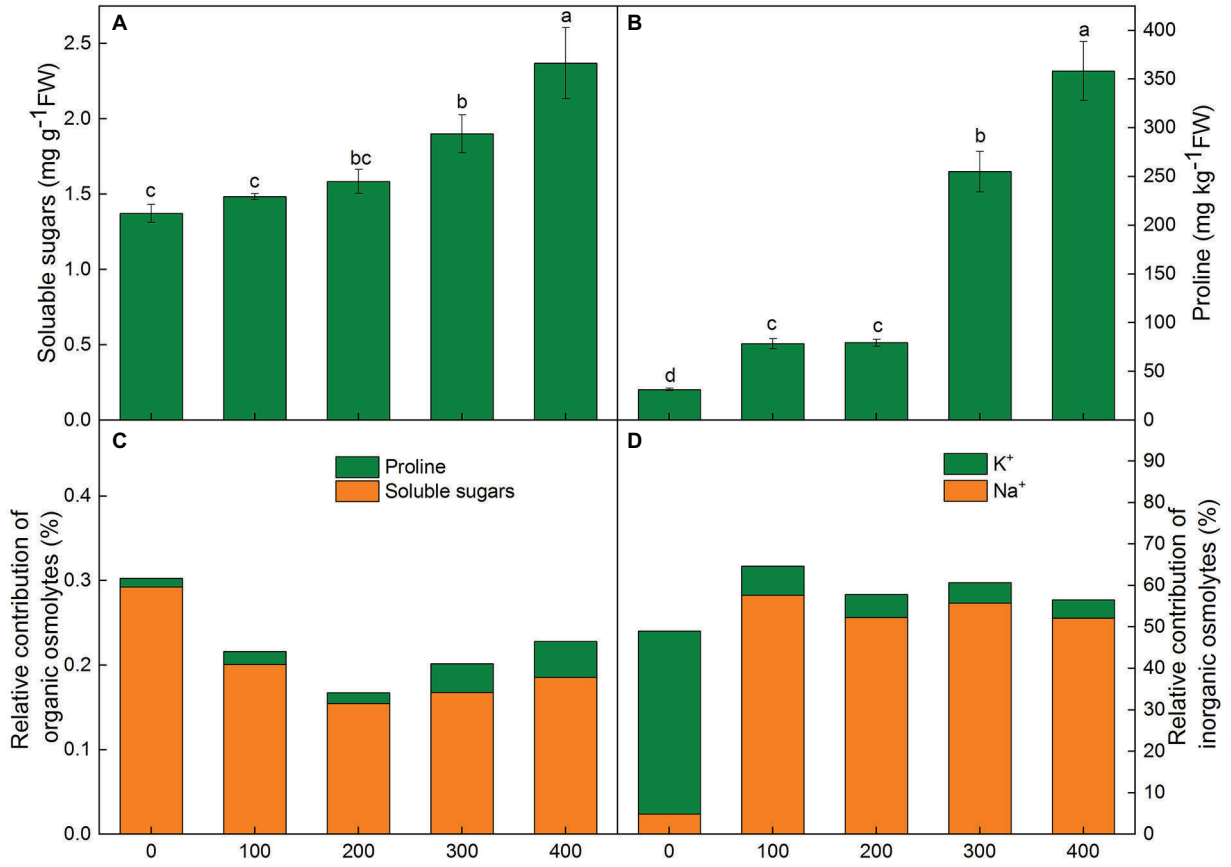

FIGURE 4
Changes of soluble sugars**(A)**, proline **(B)**, relative contribution of organic **(C)** and inorganic **(D)** solutes for osmotic adjustment in *Karelinia caspia* under salinity (mM NaCl) treatment (100, 200, 300, and 400 mM). Different letters indicate significant difference at $p < 0.05$.

of no significant difference with 100 mM NaCl treatments, total glutathione levels were significantly higher than control in 200–400 mM NaCl treatments. The levels of total glutathione increased by 35.1, 39.7 and 58.4% in 200, 300, and 400 mM NaCl treatments, compared to control, respectively (Supplementary Figure S2A). Although the GSH level decreased in the treatments compared with the control, there was no significant difference between treatments (Supplementary Figure S2B). The level of GSSG increased with the increasing NaCl treatment, and it was 1.9, 2.4, 2.5, and 3.1 fold that of the control, respectively, under 100, 200, 300, and 400 mM NaCl treatments (Supplementary Figure S2C). The ratio of reduced and oxidized glutathione decreased with salinity as compared to control, but there was no difference between treatments (Supplementary Figure S2D).

The level of total ascorbate (AsA + DHA) remained unchanged in 100 mM NaCl treatment but was 1.5, 1.7, and 2.0 fold greater than control in 200, 300, and 400 mM NaCl treatments, respectively (Supplementary Figure S2E). The level of AsA showed no difference in 100 mM treatment as compared to control, but it increased by 47.6, 88.2 and 92.0%, respectively, in 200, 300, and 400 mM treatments (Supplementary Figure S2F). The trend of DHA content was the same as that of the total ascorbate and reduced ascorbate. The level of DHA in 100 mM treatment was the same as control, but it increased by 49.3, 67.3 and 101.0%, respectively, in 200, 300, and 400 mM NaCl treatments (Supplementary Figure S2G). The level of total ascorbate increased by 48.8, 72.8 and 106.0%, respectively, in NaCl treatments from 200 to 400 mM. The AsA/DHA ratio was maintained at the same level in control and NaCl treatments (Supplementary Figure S2H). These results showed that ascorbate-glutathione cycle was likely to aid in maintaining the cellular redox status in *K. caspia* under salinity.

Expression level of transporters, antioxidant enzyme genes and genes related to antioxidant synthesis and signal pathway

After 7 days of salt treatment, the expression of *SOS1/2/3* genes in leaves was significantly up-regulated. Compared with the control, the *SOS1* gene was up-regulated by 3.7–6.6 times, and the expression level was highest under 200 mM NaCl treatment. The expression of the *SOS2* gene increased with NaCl treatment concentration, and the expression level was

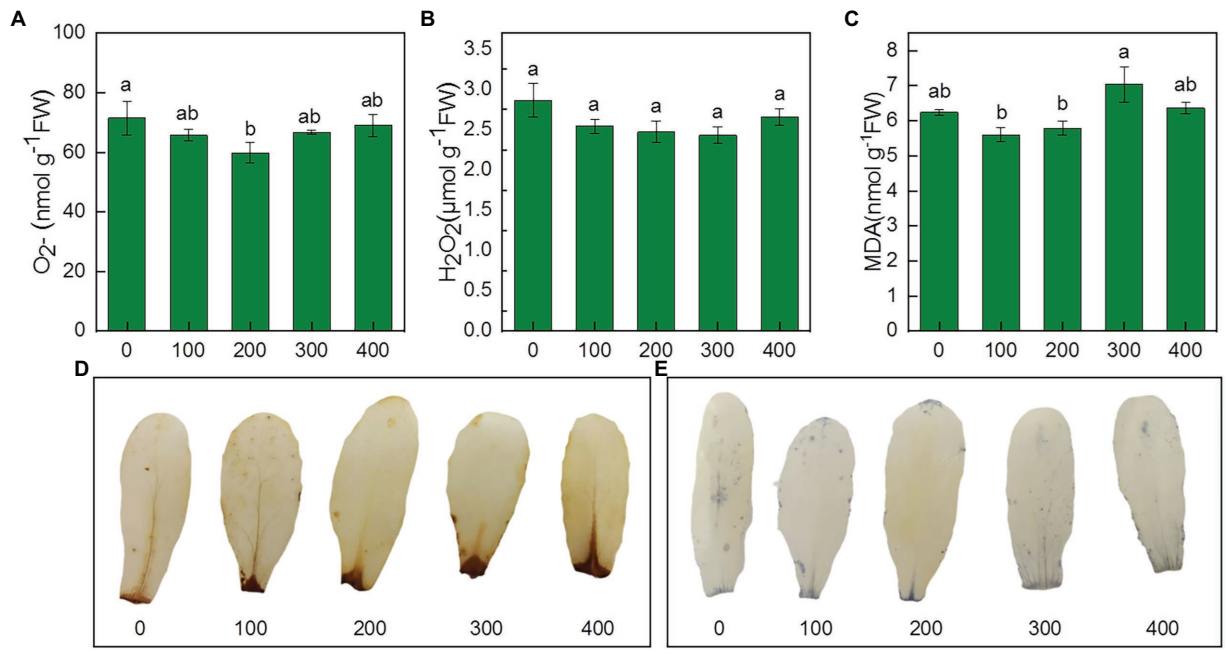

FIGURE 5
Effects of NaCl treatment (100, 200, 300, and 400 mM) on O_2^{-}、H_2O_2 and MDA of *Karelinia caspia*. **(A)** O_2^{-}, **(B)** H_2O_2, **(C)** MDA, **(D)** DAB staining for H_2O_2, **(E)** NBT staining for O_2^{-} Different letters indicate significant difference at $p < 0.05$.

up-regulated by 2.5 fold under 400 mM treatment. The *SOS3* gene was up-regulated by 2.1–5.0 fold under salinity. Similar patterns were also observed in *CAX* and *AVP* genes. The expression of *AVP* and *CAX* genes in leaves were up-regulated by 3.2–4.9 fold and 1.7–4.7 fold, respectively, under salinity (Figure 7).

Antioxidant enzyme genes and non-enzymatic antioxidant synthesis-related genes were all up-regulated in the leaves of *K. caspia* under salinity. The expression of *Cu/Zn SOD* was up-regulated by 1.6–2.6 fold, and it reached the highest value under 300 mM NaCl treatment. Similarly, the expression of *APX6* was also up-regulated under the 300 mM NaCl treatment. The expression of *HPT1* and *γ-TMT* was up-regulated by 1.2–1.4 and 1.4–2.1 fold, respectively, under salinity. The expression levels of *HCT* and *F3H* were up-regulated by 6.7 and 5.6 fold under 100 mM NaCl treatment, respectively (Supplementary Figure S3). The expression of *SAMS* increased significantly under salinity, and it increased by 5.1, 2.9, 3.8, and 3.1 fold under the treatments from 100 to 300 mM NaCl, respectively. The expression of *SMS* increased 2.5, 3.8, 2.9 and 2.5 fold under 100, 200, 300 and 400 mM NaCl treatment, respectively. MAPK cascade pathway related genes (*MEKK1* , *MKK2* , *MPK4/6*) were all increased under salinity. The expression of the four genes were up-regulated by 2.1–6.3, 1.2–6.1, 1.4–2.8 and 0.5–1.2 fold under NaCl treatments, respectively (Supplementary Figure S4). These results showed that salinity induced the up-regulated expression of kinase pathway, ions channels and antioxidant-related genes, which regulated the salt tolerance of *K. caspia*.

Discussion

Ion homeostasis and water maintenance under salt stress

Halophytes face the multiple challenges under salt stress, including ion toxicity and nutrient deficiencies (Acosta-Motos et al., 2017; Isayenkov and Maathuis, 2019). Halophytes can absorb Na^+ and transport it to the aerial part, and finally localized Na^+ into the vacuole to enhance tolerance to salt stress. In *K. caspia*, the concentration of Na^+ in roots, stems, and leaves under salt treatments were all significantly higher than that in control, and the Na^+ concentration in leaves was higher than that in roots and stems, which confirmed that *K. caspia* would uptake and accumulate more Na^+ in leaves (Matinzadeh et al., 2019). Our results also demonstrate that a large number of Na^+ was effectively sequestered into vacuoles, contributing to the osmotic adjustment of cytoplasm and maintaining the absorption of water and essential macronutrients (Rahman et al., 2019), then the relative water content of leaves was maintained at a steady level between control and NaCl treatments in *K. caspia*. In addition, scanning electron microscope results showed that the density of salt glands increased with the increase of NaCl treatment concentration. Especially in 300 and 400 mM NaCl treatments, the density of salt glands significantly increased as compared to control (Supplementary Figure S1), which indicated that salt secretion through salt glands is also an important strategy for *K. caspia* to cope with high salt stress.

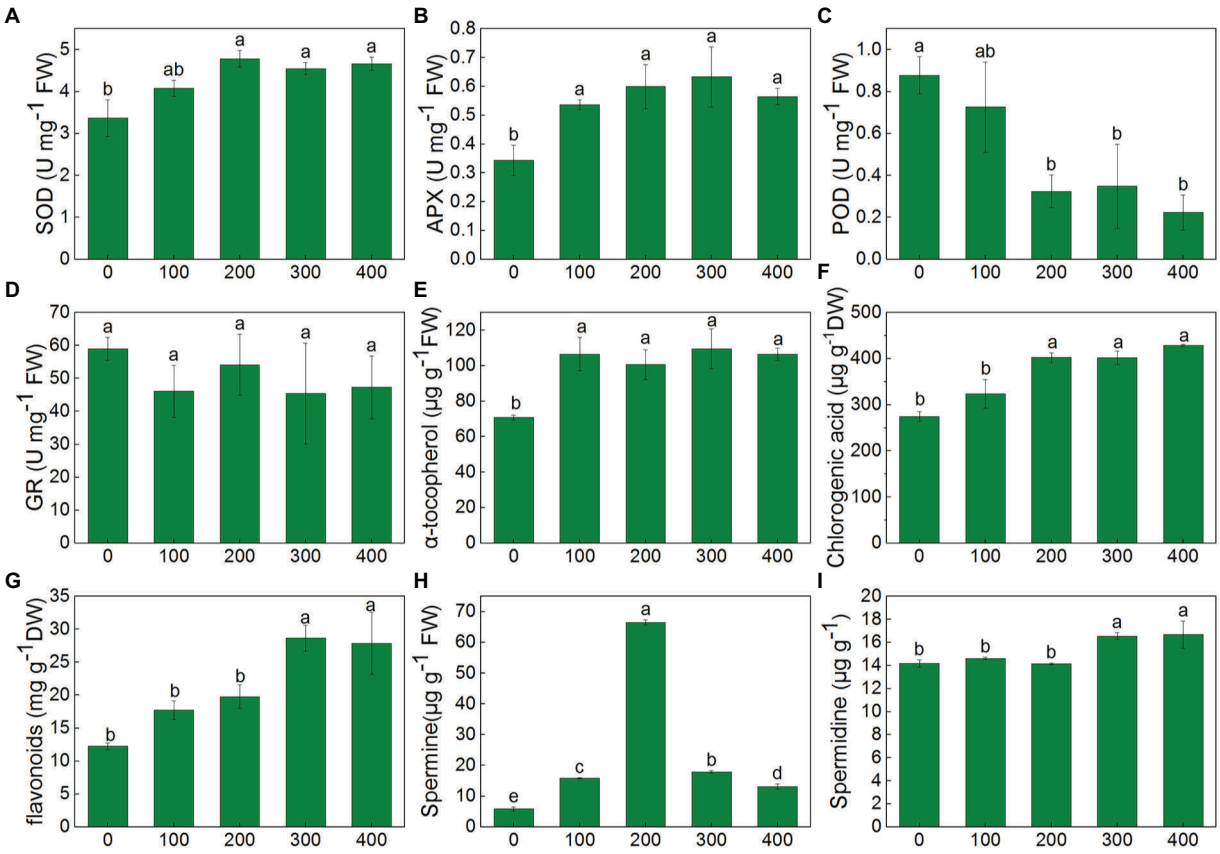

FIGURE 6
Changes of antioxidant enzymes and non-enzymatic antioxidants of *K. caspia* in response to NaCl treatment (100, 200, 300, and 400 mM). **(A)** SOD, **(B)** APX, **(C)** POD, **(D)** GR, **(E)** α-tocopherol, **(F)** chlorogenic acid, **(G)** flavonoids, **(H)** spermine, **(I)** spermidine Different letters indicate significant difference at $p < 0.05$.

The above results were further confirmed by the expression analysis of related genes of *K. caspia* under salinity. Salt overly sensitive (SOS) pathway, which comprises *SOS1*, *SOS2*, and *SOS3* genes, was an important pathway regulating Na^+ homeostasis. *SOS1* was activated by the complex of *SOS2* and *SOS3* under salinity (Shah et al., 2021). Our previous research showed that *KcSOS1* functions in extruding Na^+ from the cytoplasm of secretory cells to the exterior (Guo et al., 2020). In this study, the expression of *SOS1/2/3* were all up-regulated in the leaves of *K. caspia*, which further demonstrated that salinity activated the SOS pathway to expel excess Na^+ from leaves through the salt glands. The *NHX1*, tonoplast Na^+/H^+ antiporter, functions in transporting Na^+ to vacuoles (Rauf et al., 2014). *NHX1* was up-regulated both in leaves and roots of *K. caspia* under salinity, showing that Na^+ was transferred into vacuole, and then accumulated higher Na^+ in roots and leaves under salinity. The driving force of antiporters was created by H^+-pyrophosphatase pumps, and is encoded by *AVP* gene. Gaxiola et al. (2001) reported that overexpression of *AVP* enhanced the tolerance to salinity by supplying H^+ for *NHX1*-mediated Na^+/H^+ exchange, then contributing to the Na^+ sequestration into the vacuoles. In this study, the *AVP* was up-regulated 4.9 fold, which confirmed that the *AVP* and *NHX1* combined to regulate the Na^+ transportation to vacuoles. The regionalization of Na^+ to vacuoles and the secretion of salt through salt glands jointly resisted the toxicity of Na^+ to plants, thus ensuring the normal growth of plants.

Maintaining the homeostasis of Na^+ and other ions is essential for plant metabolism. Potassium is the most abundant cation in plant cells and plays an essential role in enzyme activation, protein synthesis, membrane potential, ion homeostasis, and many other physiological processes (Chérel, 2004). There is a competitive relationship between Na^+ and K^+. Na^+ enters cells through K^+ channels and non-selective cation channels. The increase of Na^+ is accompanied by the decrease in K^+ (Rahman et al., 2019; Bueno et al., 2020). So, the concentration of K^+ is 15 times that of Na^+ in control, however, the concentration of K^+ is only 0.2 times Na^+ in leaves under salinity. Although K^+ was significantly decreased in saline treatments compared with control in *K. caspia*, the concentration of K^+ was maintained at a steady level among all treatments both in roots and leaves, and the K^+/Na^+ ratio also remained in a stable state in the roots, stems, and leaves. Further, *NHX1* was up-regulated in saline treatments. Bassil et al. (2011) reported that *NHX1* also mediates K^+/H^+ exchange to accumulate

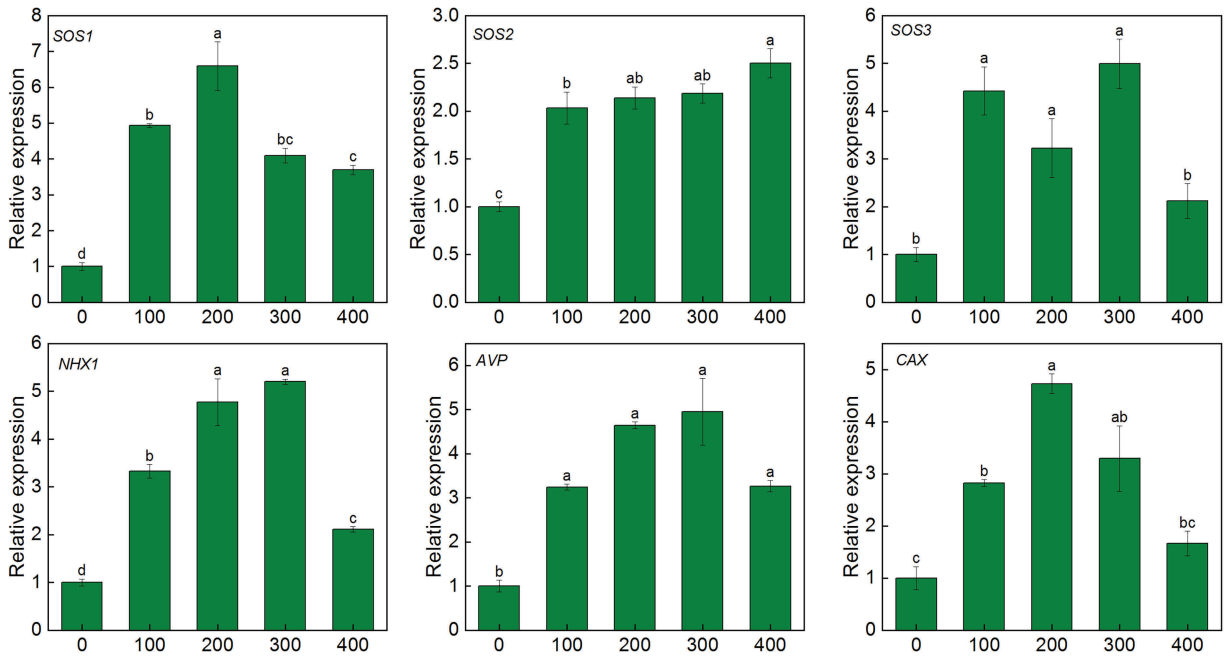

FIGURE 7
Expression level of ion transport-related genes in leaves of *K. caspia* under NaCl treatment (100, 200, 300, and 400 mM). salt overly sensitive 1/2/3(*SOS1/2/3*), tonoplast Na^+/H^+ antiporter1 (*NHX1*), vacuolar H^+-pyrophosphatase pump (*AVP*), Ca^{2+}/H^+ exchanger (*CAX*).Different letters indicate significant difference at $p < 0.05$.

K^+ in the vacuoles. Ca^{2+} and Mg^{2+} had no significant difference among salt treatments, and the concentration of both in leaves was significantly higher than that in stems and roots. The results indicated the Na^+ sequestration in vacuoles reduced antagonistic effects to other ions, allowing other ions to be transported upward from roots. The trace elements Zn^{2+} and Fe^{2+} were all in a stable state among treatments. Our findings suggest that ion homeostasis is an important mechanism for the normal growth of *K. caspia* under high saline conditions.

Osmotic adjustment of organic and inorganic substances under high salinity

Osmotic adjustment is an important physiological adaptation strategy against salt stress. Plants maintain water absorption by increasing osmolytes to reduce osmotic potential and maintain swelling pressure (Lu et al., 2021). In our study, the osmotic potential of *K. caspia* decreased significantly when exposed to salinity, and RWC was maintained at the same level between control and salinity. These results indicated that *K. caspia* has an effective osmotic adjustment mechanism. Low molecular compounds like proline and soluble sugars are considered important osmolytes (Parida et al., 2016). Our results showed that the content of proline increased significantly with the increase of salinity, but the content of proline was only 358 μg g^{-1}, and the contribution rate was low. This suggested that proline was not the major osmotic substance in *K. caspia*, as also seen in *Halogeton glomeratus* (Lu et al., 2021). Soluble sugars increase significantly under the treatments of 300 and 400 mM NaCl, and their contribution to osmotic adjustment was higher than proline. However, Na^+ accumulated significantly in *K. caspia*, and its contribution rate for osmotic adjustment was up to 57.6%, suggesting that Na^+ may be the main osmolytes in *K. caspia*. In agreement with our results, inorganic substances were the major osmolytes have been reported in other halophytes like *Solanum chilense* and *Chenopodium quinoa* (Hariadi et al., 2010; Gharbi et al., 2017). Rana et al. (2015) suggested that the synthesis of organic substances is energy-consuming, and the energy consumption of Na^+ transport is much lower than that of organic substances. This would be especially the case for halophytes, where the high concentration of Na^+ in the soil is passively absorbed into plants. Thus, halophytes rely on Na^+ as a "cheap osmoticum" to maintain cell turgor pressure (Zhao et al., 2020).

Integrity of photosynthetic system II maintained the photosynthetic efficiency under high salinity

Photosynthetic pigments are essential determinants of photosynthetic capacity. Chlorophyll a and chlorophyll b are important components of photosynthetic system II. In our present study, the content of Chl a, Chl b, and the ratio of Chl a/b were all higher or equal to the control under salinity in *K. caspia*, which indicated that the chlorophyllase activity was

unaffected by salinity. The integrity of chloroplasts in *K.caspia* enhanced the tolerance toward salt stress (Maršálová et al., 2016). These results contrast with the reports of the decreased chlorophyll under salinity in other halophytes (Al Hassan et al., 2017; Al-Shamsi et al., 2020). Chlorophyll a fluorescence parameters are regarded as important tools for analyzing the functionality of photosystems under salt stress. The F_v/F_m is a sensitive indicator of photo-inhibition of PSII under stress (Chowaniec and Rola, 2022). In *K. caspia*, F_v/F_m increased in salt treatments compared with control, indicating that salinity promoted the photosynthetic efficiency of PSII. Consistent with our result, F_v/F_m increased under salinity in *Arthrocnemum macrostachyum* (Redondo-Gómez et al., 2010). PI_{abs} presents the performance index on an absorption basis, and ABS/CS_m represents the light energy absorbed per unit cross-sectional area (Kumar et al., 2020b). In *K. caspia*, PI_{abs} increased significantly compared with control, especially in 300 and 400 mM NaCl treatments. However ABS/CS_m was maintained at the same level as control. So our results showed that salinity did not affect the light-harvesting, and enhanced the light-absorbing performance of PSII. ET_0/CS_m and RE_0/CS_m represent the electron transfer efficiencies of PSII and PSI, respectively, and DI_0/CS_m represents heat dissipation. In *K. caspia*, the electron transfer efficiency of PSII and PSI were all increased, while heat dissipation was decreased. The above results demonstrated that salinity did not cause damage to PSII, and further activated the activity of PSII by enhancing the efficiency of light-harvesting and electron transfer. This was further demonstrated by the increased net photosynthetic efficiency under salinity in *K. caspia*.

The net photosynthetic rate (Pn) increased under salinity in *K. caspia*. Similar results were also reported in halophyte *Atriplex portulacoides* and *Sarcocornia fruticose* (Redondo-Gómez et al., 2006). The improvement in the net photosynthetic rate may be attributed to the effective storage of Na^+ in the vacuole and salt exclusion by the salt gland, which protected chloroplasts (Benzarti et al., 2014). This is also confirmed by the unaffected chlorophyll content and the increased F_v/F_m in *K. caspia* under salt stress. In *K. caspia*, water use efficiency increased, stomatal conductance, and transpiration decreased under salinity. Similar results were also reported in halophyte *Achras sapots*(Rahman et al., 2019). Plants reduce stomatal conductance by closing stomata to reduce water loss due to transpiration. In halophytes, salt stress induces a decrease in stomatal conductance and transpiration rate, and thus improves water use efficiency as a strategy for water conservation (Panda et al., 2019).

ROS scavenging through a combination of antioxidant enzymes and non-enzymatic antioxidants

It has been reported that salt stress induces excess ROS production, and ROS accumulation induces lipid oxidation, oxidative malfunction of protein and DNA (Chang et al., 2012). Furthermore, it also generates aldehyde substances like MDA that is considered an indicator of oxidative stress (Luna et al., 2000). In our study, O_2^-, H_2O_2 and MDA all exhibited no significant difference between control and NaCl treatments, and DAB and NBT staining also verified this result, indicating an effective antioxidative mechanism in *K. caspia*. Plants scavenge ROS and maintain ROS homeostasis through a regulation mechanism comprising antioxidant enzymes and non-enzymatic antioxidants (Al Kharusi et al., 2019). SOD is considered the primary enzyme to defend against oxidative stress and catalyzes the dissimulation of O_2^- to H_2O_2 and O_2 (Bose et al., 2014). In *K. caspia*, SOD increased significantly under high salinity (200-400 mM). Correlation analysis showed that SOD had a negative correlation with O_2^-, and the expression level of *Cu/Zn SOD* gene increased with the increase of NaCl treatment, indicating that salinity induced the expression of *Zn-Cu SOD* of *K. caspia*, then the increased SOD activity regulated the proper level of O_2^-. So, O_2^- was maintained at a steady state when exposed to salt stress. APX, POD, and GR were key enzymes scavenging H_2O_2 (Shigeoka et al., 2002). In *K.caspia*, APX activity was significantly increased, and the expression level of *KcAPX6* also increased when exposed to salinity, demonstrating that APX plays an important role in H_2O_2 scavenging. POD activity decreased in salinity, but GR appeared stable under salinity. The activity of antioxidant enzymes are different in other halophytes when exposed to salinity (Yu et al., 2011). Our results showed that SOD and APX were the key antioxidative enzymes participating in ROS scavenging in *K. caspia*.

Non-enzymatic antioxidants play an important role in scavenging ROS and avoiding antioxidant damage. In our study, non-enzymatic antioxidants such as ascorbic, glutathione, α-tocopherol, chlorogenic acid, and flavonoids were measured. Ascorbate and glutathione scavenge H_2O_2 and maintain cellular redox status through the ascorbate-glutathione cycle (Foyer and Noctor, 2005). In *K. caspia*, the level of AsA, DHA, and AsA + DHA were all increased significantly when exposed to salinity from 200 to 400 mM NaCl. AsA has a vital role in maintaining APX activity for detoxication of H_2O_2 (Rangani et al., 2018), this is verified by increasing APX activity under saline treatment in *K. caspia*. The higher AsA level and APX activity in *K. caspia* contributed to their increased antioxidant capacity and tolerance to salinity. Furthermore, AsA/DHA ratio was maintained at the same level in NaCl treated plants of *K. caspia*. The steady ratio of AsA/DHA maintains the appropriate redox of the cell to mitigate the salt-induced oxidative stress. Unlike ascorbate, reduced glutathione(GSH) levels were significantly decreased as compared to control in NaCl treatments, but the level of GSH remained in a stable state under salinity. The lower GSH signifies the high rate of conversation of GSH into the production of GSSG, and the higher GSSG level helps maintain a steady level of GR activity (Panda et al., 2021). Although the GSH/GSSG decreased in NaCl treatment compared with control, the ratio of GSH/GSSG was maintained at the same level among NaCl treatments. Our results suggested that GSH and AsA, through the ascorbate-glutathione cycle, maintained the cellular redox status in *K. caspia* under salinity.

α-tocopherol is a lipid-soluble antioxidant best known for its ability to scavenge ROS. In *K. caspia*, the level of α-tocopherol significantly increased under salinity. Furthermore, expression of the genes *Kcγ-TMT* and *KcHPT1*, the key synthase genes for α-tocopherol, were significantly up-regulated under salt treatment. Studies have shown that overexpression of *Kcγ-TMT* and *KcHPT1* can increase the content of tocopherols in plants, thereby enhancing the salt tolerance of plants (Jin and Daniell, 2014). α-tocopherolis synthesized in the chloroplast, and it cooperates with ascorbic and glutathione to effectively scavenge and quench various free radicals, then maintain the homeostasis of ROS. This can helps protect photosystem II from damage caused by stress (Czarnocka and Karpiński, 2018; Kumar et al., 2020a). In *K. caspia*, α-tocopherol may maintain the integrity of the photosystem II by scavenging ROS, thereby improving the salt tolerance of *K. caspia*.

Chlorogenic acid and flavonoid belong to polyphenols, which are natural non-enzymatic antioxidants in plants (Sullivan and Michael, 2009). In *K. caspia*, the content of chlorogenic and flovanoids increased significantly under salinity from 200 to 400 mM and 300–400 mM respectively, and chlorogenic acid synthase *KcHCT* and flavonoid synthase *KcF3H* were all up-regulated under salinity. Other researchers have reported similar results. For example, salinity induced high expression of *HCT* in *Hibiscus cannabinus* (Chowdhury et al., 2012). Polyphenols such as chlorogenic acid and flavonoids accumulated in lettuces under salt stress (Sgherri et al., 2017). In many medical plants, phenolic compounds contribute to the trapping of free radicals (Bistgani et al., 2019). The increase of polyphenols enhanced the antioxidant activity, to protecting the plant from the damage of lipid peroxidation as indicated by the MDA levels. In line with this, the exogenous application of chlorogenic acid can alleviate the toxic effect of salt stress on plants (Zhang et al., 2021). So, in *K. caspia*, high salinity induced the production of chlorogenic acid and flavonoids, conferring the tolerance of *K. caspia* to salinity.

Polyamines (spermine, spermidine and putrescine) are aliphatic polycations that participate in the response to environmental stress (Liu et al., 2020). The accumulation of spermine was considered an important indicator of salt tolerance in plants (Simon-Sarkadi et al., 2007). Exogenous addition of polyamines or overexpression of polyamine synthesis genes could improve plant tolerance to abiotic stress (Zhang et al., 2015; He et al., 2019). Spermine also acts as signaling molecules to activate antioxidant enzyme activity or directly scavenge reactive oxygen species to regulate the homeostasis of ROS in plants (Tanou et al., 2014; Seifi and Shelp, 2019). In our experiment, the content of spermine was significantly increased under salinity, and the key associated biosynthetic enzymes such as *KcSMS* and *KcSAMS* were all up-regulated. This indicated that salinity induced the accumulation of polyamines in *K. caspia,* to enhanced the tolerance to salt stress. Elevated spermine is also an important osmoprotectant against salt stress (Paul and Roychoudhury, 2016). Furthermore, spermine may be involved in the excretion process and regulate ions fluxes through salt gland (Ben Hassine et al., 2009). Malliarakis et al. (2015) also reported that polyamine could restore PSII efficiency by interacting with PSII thylakoid proteins. So, elevated could regulate plant tolerance to salt stress by multiple regulatory pathways.

Signal transduction under salt stress in *Karelinia Caspia*

Plants produced a large amount of ROS when exposed to abiotic stress which can inhibit plant development or lead to plant death (Anjum et al., 2015). However, low level of ROS also has been considered as the key players of stress signaling in plants. It has been reported that H_2O_2 acted as a signaling molecular activated protein kinases or transcription factors, thereby activating the expression of related genes to resist abiotic stress (Hossain et al., 2015; Mansoor et al., 2022). In our experiment, the content of H_2O_2 in *K. caspia* was in a steady state at a low level under salinity, which indicated that H_2O_2 may played important role as a signaling molecule in response to salt stress.

The mitogen-activated protein kinase (MAPK) cascade is a universal signal transduction module and involved in stress-related pathways (Singh and Jwa, 2013), and *MEKK1, MKK2, MPK4/6* was activated by salt stress. In *K. caspia*, *KcMEKK1*, *KcMKK2*, *KcMPK4* and *KcMPK6* had the same expression patterns under different concentration of salt stress, and they were all up-regulated by salinity. It is reported that *MPK4* and *MPK6* has an important role in salt stress signaling (Ichimura et al., 2000). Völz et al. (2022) showed that ROS homeostasis was mediated by *MPK4*, and *mpk4* mutant showed accumulation of hydrogen peroxide (Völz et al., 2018). *MPK4* may also be involved in photosynthetic electron transport and chloroplast ROS metabolism. Yu et al. (2010) reported that *MPK6* phosphorylates *SOS1*, and further participated the regulation of Na^+ homeostasis. Activation of the protein kinase pathway enhanced plant tolerance to salt stress by regulating downstream defense responses. Taken together our data suggested roles for antioxidants, osmolytes, ion homeostasis and signal crosstalk in *K. caspia* subjected to salt stress. To ease comprehension these are illustrated schematically in Figure 8.

Conclusion

This study described mechanisms of salt tolerance in halophyte *K. caspia.* The results showed that the optimal growth condition is 100 mM NaCl treatment. The content of Na^+ in roots, stems and leaves of *K. caspia* increased significantly under salinity. Na^+ was compartmentalized into vacuoles and acted as the main osmotic adjustment substance to maintain the water balance of *K. caspia* under salinity. The excessive Na^+ was excreted through the salt glands, and the salt stress increases the number

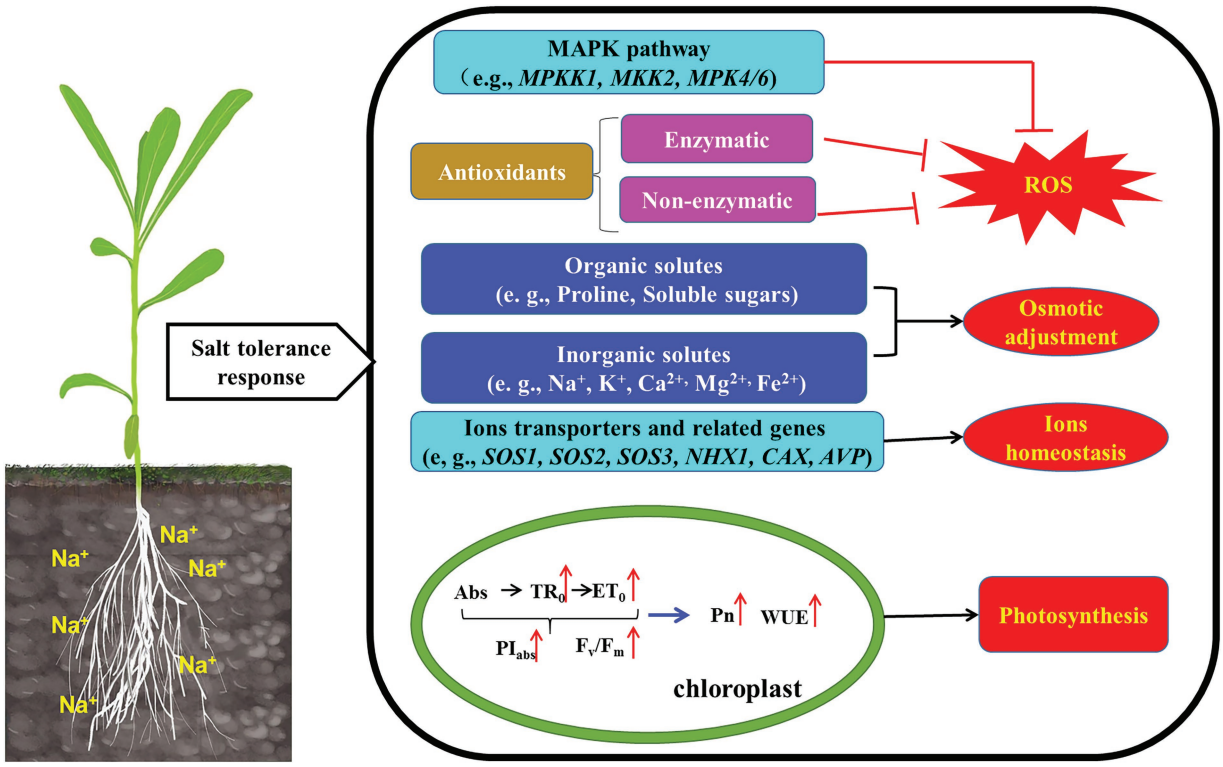

FIGURE 8
Schematic model illustrated that the mechanism of *K. caspia* resisted salt stress by regulating ROS homeostasis, osmotic balance, ion homeostasis, and photosynthesis. (1) The expression of MAPK pathway genes (*MEKK1-MKK2-MPK4/6*) were up-regulated, which crosstalk to ROS scavenging. (2) Antioxidant enzyme (SOD, APX) activity increased to reduce the excess ROS. The accumulation of α-tocopherol, chlorogenic acid, flavonoids and polyamines also scavenge ROS. Antioxidant enzyme and non-enzymatic antioxidants combined to maintain ROS homeostasis. (3) Accumulating organic solutes (soluble sugars, proline, polyamines) contributed to osmotic adjustment. (4) The up-regulated *SOS2* activated the transporter activity of *SOS1* and *CAX* in the plasma membrane, and extruded Na^+ into the apoplast and sequestrate Ca^{2+} into the vacuoles, and the *NHX1* was also activated to sequestrate Na^+ into the vacuoles. The accumulation of Na^+ in vacuoles contributed to osmotic adjustment. (5) Increased chlorophyll fluorescence parameters enhanced photosynthesis efficiency and water use efficiency, then maintained the normal growth of *K. caspia*.

of salt glands. The antioxidant enzymes (SOD, APX) and non-enzymatic antioxidants (α-tocopherol, chlorogenic acid, flavonoids, polyamines) combined to regulate the ROS homeostasis. So, the contents of H_2O_2, O_2-, and MDA can be maintained at appropriate levels under salt treatments. Salinity improved the performance of PSII. Meanwhile, the net photosynthetic rate and water use efficiency were all increased. Therefore, *K. caspia* can grow normally under high saline stress, through the combined action of ions regulation mechanism and, antioxidant defense systems, the higher tolerance index make *K. caspia* a suitable candidate for exploring saline-alkali tolerant resources and the restoration of saline-alkali land.

Data availability statement

The original contributions presented in the study are included in the article/Supplementary materials; further inquiries can be directed to the corresponding authors.

Author contributions

QG and JW designed the research. CL, QW, XH, CZ, and ZC performed the experiments. CL and QG analyzed the data. CL wrote the manuscript. QG, JW, and LM edited and revised the manuscript. All authors contributed to the article and approved the submitted version.

Funding

This study was funded by the Young Project of Beijing Academy of Agriculture and Forestry Sciences (QNJJ202221), Innovative Project of Beijing Academy of Agriculture and Forestry Sciences (KJCX20220407), National Natural Science Foundation of China (31601991), Biotechnology and Biological Sciences Research Council (BBSRC, United Kingdom) "A China–UK consortium to reduce environmental pollution with novel grass varieties" (BB/M027945/1).

Conflict of interest

The authors declare that the research was conducted in the absence of any commercial or financial relationships that could be construed as a potential conflict of interest.

Publisher's note

All claims expressed in this article are solely those of the authors and do not necessarily represent those of their affiliated organizations, or those of the publisher, the editors and the reviewers. Any product that may be evaluated in this article, or claim that may be made by its manufacturer, is not guaranteed or endorsed by the publisher.

Supplementary material

The Supplementary material for this article can be found online at: https://www.frontiersin.org/articles/10.3389/fpls.2022.979956/full#supplementary-material

References

Acosta-Motos, J., Ortuño, M., Bernal-Vicente, A., Diaz-Vivancos, P., Sanchez-Blanco, M., and Hernandez, J. (2017). Plant responses to salt stress: adaptive mechanisms. *Agronomy* 7:18. doi: 10.3390/agronomy7010018

Al Hassan, M., Chaura, J., Donat-Torres, M. P., Boscaiu, M., and Vicente, O. (2017). Antioxidant responses under salinity and drought in three closely related wild monocots with different ecological optima. *Aob Plants.* 9:plx009. doi: 10.1093/aobpla/plx009

Al Kharusi, L., Al Yahyai, R., and Yaish, M. W. (2019). Antioxidant response to salinity in salt-tolerant and salt-susceptible cultivars of date palm. *Agriculture* 9:8. doi: 10.3390/agriculture9010008

Al-Shamsi, N., Hussain, M. I., and El-Keblawy, A. (2020). Physiological responses of the xerohalophyte *Suaeda vermiculata* to salinity in its hyper-arid environment. *Flora* 273, 151705. doi: 10.1016/j.flora.2020.151705

Anderson, M. E. (1985). Determination of glutathione and glutathione disulfide in biological samples. *Method. Enzymol.* 113, 548–555. doi: 10.1016/S0076-6879(85)13073-9

Anjum, N., Sofo, A., Scopa, A., Roychoudhury, A., Gill, S. S., Iqbal, M., et al. (2015). Lipids and proteins—major targets of oxidative modifications in abiotic stressed plants. *Environ. Sci. Pollut. Res.* 22, 4099–4121. doi: 10.1007/s11356-014-3917-1

Aymen, S., Morena, G., Vincenzo, L., Laura, P., Lorenza, B., Abderrazak, S., et al. (2016). Salt tolerance of the halophyte Limonium delicatulum is more associated with antioxidant enzyme activities than phenolic compounds. *Funct. Plant Biol.* 43:607. doi: 10.1071/FP15284

Bassil, E., Tajima, H., Liang, Y., Ohto, M., Ushijima, K., Nakano, R., et al. (2011). The arabidopsis Na+/H+ antiporters NHX1 and NHX2 control vacuolar pH and K^+ homeostasis to regulate growth, flower development, and reproduction. *Plant Cell* 23, 3482–3497. doi: 10.1105/tpc.111.089581

Bates, L. S., Waldren, R. P., and Teare, I. D. (1973). Rapid determination of free proline for water-stress studies. *Plant Soil* 39, 205–207. doi: 10.1007/BF00018060

Ben Hassine, A., Ghanem, M. E., Bouzid, S., and Lutts, S. (2009). Abscisic acid has contrasting effects on salt excretion and polyamine concentrations of an inland and a coastal population of the Mediterranean xero-halophyte species *Atriplex halimus*. *Ann. Bot.* 104, 925–936. doi: 10.1093/aob/mcp174

Benzarti, M., Rejeb, K. B., Messedi, D., Mna, A. B., Hessini, K., Ksontini, M., et al. (2014). Effect of high salinity on *Atriplex portulacoides*: growth, leaf water relations and solute accumulation in relation with osmotic adjustment. *S. Afr. J. Bot.* 95, 70–77. doi: 10.1016/j.sajb.2014.08.009

Bistgani, Z. E., Hashemi, M., Dacosta, M., Craker, L., Maggi, F., and Morshedloo, M. R. (2019). Effect of salinity stress on the physiological characteristics, phenolic compounds and antioxidant activity of *Thymus vulgaris* L. and *thymus daenensis* Celak. *Ind. Crop Prod.* 135, 311–320. doi: 10.1016/j.indcrop.2019.04.055

Bose, J., Rodrigo-Moreno, A., and Shabala, S. (2014). ROS homeostasis in halophytes in the context of salinity stress tolerance. *J. Exp. Bot.* 65, 1241–1257. doi: 10.1093/jxb/ert430

Bueno, M., Lendínez, M. L., Calero, J., and Del Pilar Cordovilla, M. (2020). Salinity responses of three halophytes from inland saltmarshes of Jaén (southern Spain). *Flora* 266, 151589. doi: 10.1016/j.flora.2020.151589

Cakmak, I., and Marschner, H. (1992). Magnesium deficiency and high light intensity enhance activities of superoxide dismutase, ascorbate peroxidase, and glutathione reductase in bean leaves. *Plant Physiol.* 98, 1222–1227. doi: 10.1104/pp.98.4.1222

Chang, I., Cheng, K., Huang, P., Lin, Y., Cheng, L., and Cheng, T. (2012). Oxidative stress in greater duckweed (*Spirodela polyrhiza*) caused by long-term NaCl exposure. *Acta Physiol. Plant.* 34, 1165–1176. doi: 10.1007/s11738-011-0913-7

Chérel, I. (2004). Regulation of K^+ channel activities in plants: from physiological to molecular aspects. *J. Exp. Bot.* 55, 337–351. doi: 10.1093/jxb/erh028

Chowaniec, K., and Rola, K. (2022). Evaluation of the importance of ionic and osmotic components of salt stress on the photosynthetic efficiency of epiphytic lichens. *Physiol. Mol. Biol. Plants* 28, 107–121. doi: 10.1007/s12298-022-01134-2

Chowdhury, E. M., Bo, S. C., Sang, U. P., Lim, H. S., and Bae, H. (2012). Transcriptional analysis of hydroxycinnamoyl transferase (HCT) in various tissues of *Hibiscus cannabinus* in response to abiotic stress conditions. *Plant Omics.* 12, 305–313. doi: 10.1186/1471-2229-12-63

Czarnocka, W., and Karpiński, S. (2018). Friend or foe? Reactive oxygen species production, scavenging and signaling in plant response to environmental stresses. *Free Radical Bio. Med.* 122, 4–20. doi: 10.1016/j.freeradbiomed.2018.01.011

Dere, S., Gunes, T., and Sivaci, R. (1998). Spectrophotometric determination of chlorophyll-a, b and total carotenoid contents of some algae species using different solvents. *Botany* 22, 13–18.

Flowers, T. J., and Colmer, T. D. (2008). Salinity tolerance in halophytes. *New Phytol.* 179, 945–963. doi: 10.1111/j.1469-8137.2008.02531.x

Foyer, C., Lelandais, M., Galap, C., and Kunert, K. J. (1991). Effects of elevated cytosolic glutathione reductase activity on the cellular glutathione pool and photosynthesis in leaves under normal and stress conditions. *Plant Physiol.* 97, 863–872. doi: 10.1104/pp.97.3.863

Foyer, H. C., and Noctor, G. (2005). Redox homeostasis and antioxidant signaling: a metabolic interface between stress perception and physiological responses. *Plant Cell* 17, 1866–1875. doi: 10.1105/tpc.105.033589

Fryer, M. J., Oxborough, K., Mullineaux, P. M., and Baker, N. R. (2002). Imaging of photo-oxidative stress responses in leaves. *J. Exp. Bot.* 53, 1249–1254. doi: 10.1093/jexbot/53.372.1249

Gaxiola, R. A., Li, J., Undurraga, S., Dang, L. M., Allen, G. J., Alper, S. L., et al. (2001). Drought- and salt-tolerant plants result from overexpression of the AVP1 H+-pump. *Proc. Natl. Acad. Sci.* 98, 11444–11449. doi: 10.1073/pnas.191389398

Gharbi, E., Martínez, J., Benahmed, H., Hichri, I., Dobrev, P. I., Motyka, V., et al. (2017). Phytohormone profiling in relation to osmotic adjustment in NaCl-treated plants of the halophyte tomato wild relative species *Solanum chilense* comparatively to the cultivated glycophyte Solanum lycopersicum. *Plant Sci.* 258, 77–89. doi: 10.1016/j.plantsci.2017.02.006

Gillespie, K. M., and Ainsworth, E. A. (2007). Measurement of reduced, oxidized and total ascorbate content in plants. *Nat. Protoc.* 2, 871–874. doi: 10.1038/nprot.2007.101

Guo, Q., Han, J. W., Li, C., Hou, X. C., Zhao, C. Q., Wang, Q. H., et al. (2022). Defining key metabolic roles in osmotic adjustment and ROS homeostasis in the recretohalophyte Karelinia caspia under salt stress. *Physiol Plantarum.* 174. doi: 10.1111/ppl.13663

Guo, Q., Meng, L., Han, J., Mao, P., Tian, X., Zheng, M., et al. (2020). SOS1 is a key systemic regulator of salt secretion and K_+/Na^+ homeostasis in the recretohalophyte *Karelinia caspia*. *Environ. Exp. Bot.* 177:104098. doi: 10.1016/j.envexpbot.2020.104098

Guo, Q., Meng, L., Zhang, Y., Mao, P., Tian, X., Li, S., et al. (2017). Antioxidative systems, metal ion homeostasis and cadmium distribution in Iris lactea exposed to cadmium stress. *Ecotoxicol. Environ. Saf.* 139, 50–55. doi: 10.1016/j.ecoenv.2016.12.013

Hariadi, Y., Marandon, K., Tian, Y., Jacobsen, S. E., and Shabala, S. (2010). Ionic and osmotic relations in quinoa (*Chenopodium quinoa* Willd.) plants grown at various salinity levels. *J. Exp. Bot.* 62, 185–193. doi: 10.1093/jxb/erq257

He, M. W., Wang, Y., Wu, J. Q., Shu, S., Sun, J., and Guo, S. R. (2019). Isolation and characterization of S-Adenosylmethionine synthase gene from cucumber and responsive to abiotic stress. *Plant Physiol. Biochem.* 141, 431–445. doi: 10.1016/j.plaphy.2019.06.006

Hernández, J. A., Ferrer, M. A., Jiménez, A., Barceló, A. R., and Sevilla, F. (2001). Antioxidant systems and $O_2{-}/H_2O_2$ production in the apoplast of pea leaves. Its relation with salt-induced necrotic lesions in minor veins. *Plant Physiol.* 127, 817–831. doi: 10.1104/pp.010188

Hossain, M. A., Bhattacharjee, S., Armin, S. M., Qian, P., Xin, W., Li, H. Y., et al. (2015). Hydrogen peroxide priming modulates abiotic oxidative stress tolerance: insights from ROS detoxification and scavenging. *Front. Plant Sci.* 6:420. doi: 10.3389/fpls.2015.00420

Hu, Y., Siddiqui, M. H., Li, C., Jiang, L., Zhang, H., and Zhao, X. (2020). Polyamine metabolism, photorespiration, and excitation energy allocation in photosystem II are potentially regulatory hubs in poplar adaptation to soil nitrogen availability. *Front. Plant Sci.* 11:01271. doi: 10.3389/fpls.2020.01271

Ichimura, K., Mizoguchi, T., Yoshida, R., Yuasa, T., and Shinozaki, K. (2000). Various abiotic stresses rapidly activate arabidopsis MAP kinases AtMPK4 and AtMPK6. *Plant J.* 24, 655–665. doi: 10.1046/j.1365-313x.2000.00913.x

Isayenkov, S. V., and Maathuis, F. J. M. (2019). Plant salinity stress: many unanswered questions remain. *Front. Plant Sci.* 10:00080. doi: 10.3389/fpls.2019.00080

Ismail, H., Dragišic Maksimovic, J., Maksimovic, V., Shabala, L., Ivanovic, B. D., Tian, Y., et al. (2016). Rutin, a flavonoid with antioxidant activity, improves plant salinity tolerance by regulating K^+ retention and Na^+ exclusion from leaf mesophyll in quinoa and broad beans. *Funct. Plant Biol.* 43, 75–86. doi: 10.1071/FP15312

Ismail, A. M., and Horie, T. (2017). Genomics, physiology, and molecular breeding approaches for improving salt tolerance. *Annu. Rev. Plant Biol.* 68, 405–434. doi: 10.1146/annurev-arplant-042916-040936

Jia, Z., Tang, M., and Wu, J. (1999). The determination of flavonoid contents in mulberry and their scavenging effects on superoxide radicals. *Food Chem.* 64, 555–559. doi: 10.1016/S0308-8146(98)00102-2

Jin, S., and Daniell, H. (2014). Expression of γ-tocopherol methyltransferase in chloroplasts results in massive proliferation of the inner envelope membrane and decreases susceptibility to salt and metal-induced oxidative stresses by reducing reactive oxygen species. *Plant Biotechnol. J.* 12, 1274–1285. doi: 10.1111/pbi.12224

Jin, T., Sun, Y., Zhao, R., Shan, Z., and Li, Y. (2019). Overexpression of peroxidase gene GsPRX9 confers salt tolerance in soybean. *Int. J. Mol. Sci.* 20, 3745. doi: 10.3390/ijms20153745

Kumar, A., Prasad, A., Sedlářová, M., Ksas, B., Havaux, M., and Pospíšil, P. (2020a). Interplay between antioxidants in response to photooxidative stress in Arabidopsis. *Free Radical Bio Med.* 160, 894–907. doi: 10.1016/j.freeradbiomed.2020.08.027

Kumar, D., Singh, H., Raj, S., and Soni, V. (2020b). Chlorophyll a fluorescence kinetics of mung bean (*Vigna radiata* L.) grown under artificial continuous light. *Biochem. Biophys. Rep.* 24:100813. doi: 10.1016/j.bbrep.2020.100813

Liu, J. L., Yang, R. C., Jian, N., Wei, L., Ye, L. L., Wang, R. H., et al. (2020). Putrescine metabolism modulates the biphasic effects of brassinosteroids on canola and arabidopsis salt tolerance. *Plant Cell Environ.* 43, 1348–1359. doi: 10.1111/pce.13757

Liu, L., Zeng, Y., Pan, X., and Zhang, F. (2012). Isolation, molecular characterization, and functional analysis of the vacuolar Na+/H+ antiporter genes from the halophyte *Karelinia caspica*. *Mol. Biol. Rep.* 39, 7193–7202. doi: 10.1007/s11033-012-1551-x

Lu, Y., Zhang, B., Li, L., Zeng, F., and Li, X. (2021). Negative effects of long-term exposure to salinity, drought, and combined stresses on halophyte *Halogeton glomeratus*. *Physio.l Plantarum.* 173, 2307–2322. doi: 10.1111/ppl.13581

Luna, C., Garcia Seffini, L., Arias, C., Taleisnik, E., and Taleisnik, E. (2000). Oxidative stress indicators as selection tools for salt tolerance in Chloris gayana. *Plant Breed.* 119, 341–345. doi: 10.1046/j.1439-0523.2000.00504.x

Malliarakis, D., Tsiavos, T., Ioannidis, N. E., and Kotzabasis, K. (2015). Spermine and lutein quench chlorophyll fluorescence in isolated PSII antenna complexes. *J. Plant Physiol.* 183, 108–113. doi: 10.1016/j.jplph.2015.06.006

Mansoor, S., Ali Wani, O., Lone, J. K., Manhas, S., Kour, N., Alam, P., et al. (2022). Reactive oxygen species in plants: from source to sink. *Antioxidants.* 11, 225. doi: 10.3390/antiox11020225

Marcé, M., Brown, D. S., Capell, T., Figueras, X., and Tiburcio, A. F. (1995). Rapid high-performance liquid chromatographic method for the quantitation of polyamines as their dansyl derivatives: application to plant and animal tissues. *J. Chromatogr. B Biomed. Sci. Appl.* 666, 329–335. doi: 10.1016/0378-4347(94)00586-T

Maršálová, L., Vítámvás, P., Hynek, R., Prášil, I. T., and Kosová, K. (2016). Proteomic response of *Hordeum vulgare cv. Tadmor* and *Hordeum marinum* to salinity stress: similarities and differences between a glycophyte and a halophyte. *Front. Plant Sci.* 7, 3562. doi: 10.3389/fpls.2016.01154

Martínez, J., Kinet, J., Bajji, M., and Lutts, S. (2005). NaCl alleviates polyethylene glycol-induced water stress in the halophyte species *Atriplex halimus* L. *J. Exp. Bot.* 56, 2421–2431. doi: 10.1093/jxb/eri235

Matinzadeh, Z., Akhani, H., Abedi, M., and Palacio, S. (2019). The elemental composition of halophytes correlates with key morphological adaptations and taxonomic groups. *Plant Physiol. Biochem.* 141, 259–278. doi: 10.1016/j.plaphy.2019.05.023

Nakano, Y., and Asada, K. K. U. U. (1981). Hydrogen peroxide is scavenged by ascorbate-specific peroxidase in spinach chloroplasts. *Plant Cell Physiol.* 22, 867–880. doi: 10.1093/oxfordjournals.pcp.a076232

Panda, A., Rangani, J., and Kumar Parida, A. (2019). Cross talk between ROS homeostasis and antioxidative machinery contributes to salt tolerance of the xero-halophyte *Haloxylon salicornicum*. *Environ. Exp. Bot.* 166, 103799. doi: 10.1016/j.envexpbot.2019.103799

Panda, A., Rangani, J., and Parida, A. K. (2021). Physiological and metabolic adjustments in the xero-halophyte *Haloxylon salicornicum* conferring drought tolerance. *Physiol. Plant.* 172, 1189–1211. doi: 10.1111/ppl.13351

Parida, A. K., Veerabathini, S. K., Kumari, A., and Agarwal, P. K. (2016). Physiological, anatomical and metabolic implications of salt tolerance in the halophyte *salvadora persica* under hydroponic culture condition. *Front. Plant Sci.* 7, 105695. doi: 10.3389/fpls.2016.00351

Paul, S., and Roychoudhury, A. (2016). Seed priming with spermine ameliorates salinity stress in the germinated seedlings of two rice cultivars differing in their level of salt tolerance. *Trop. Plant Res.* 3, 616–633. doi: 10.22271/tpr.2016.v3.i3.082

Rahman, M. M., Mostofa, M. G., Rahman, M. A., Miah, M. G., Saha, S. R., Karim, M. A., et al. (2019). Insight into salt tolerance mechanisms of the halophyte *Achras sapota*: an important fruit tree for agriculture in coastal areas. *Protoplasma* 256, 181–191. doi: 10.1007/s00709-018-1289-y

Rana, M., Matthew, , and Gilliham, (2015). Salinity tolerance of crops - what is the cost? *New Phytol.* 208, 668–673. doi: 10.1111/nph.13519

Rangani, J., Panda, A., Patel, M., and Parida, A. K. (2018). Regulation of ROS through proficient modulations of antioxidative defense system maintains the structural and functional integrity of photosynthetic apparatus and confers drought tolerance in the facultative halophyte *Salvadora persica* L. *J. Photochem. Photobiol. B* 189, 214–233. doi: 10.1016/j.jphotobiol.2018.10.021

Rauf, M., Shahzad, K., Ali, R., Ahmad, M., Habib, I., Mansoor, S., et al. (2014). Cloning and characterization of Na+/H+ antiporter (*LfNHX1*) gene from a halophyte grass *Leptochloa fusca* for drought and salt tolerance. *Mol. Biol. Rep.* 41, 1669–1682. doi: 10.1007/s11033-013-3015-3

Redondo-Gómez, S., Mateos-Naranjo, E., Figueroa, M. E., and Davy, A. J. (2010). Salt stimulation of growth and photosynthesis in an extreme halophyte, *Arthrocnemum macrostachyum*. *Plant Biol.* 12, 79–87. doi: 10.1111/j.1438-8677.2009.00207.x

Redondo-Gómez, S., Wharmby, C., Castillo, J. M., Mateos-Naranjo, E., Luque, C. J., De Cires, A., et al. (2006). Growth and photosynthetic responses to salinity in an extreme halophyte, *Sarcocornia fruticosa*. *Physiol. Plant.* 128, 116–124. doi: 10.1111/j.1399-3054.2006.00719.x

Sanadhya, P., Agarwal, P., and Agarwal, P. K. (2015). Ion homeostasis in a salt-secreting halophytic grass. *Aob Plants.* 7, plv055. doi: 10.1093/aobpla/plv055

Seifi, H. S., and Shelp, B. J. (2019). Spermine differentially refines plant defense responses against biotic and abiotic stresses. *Front. Plant Sci.* 10:117. doi: 10.3389/fpls.2019.00117

Sgherri, C., Pérez-López, U., Micaelli, F., Miranda-Apodaca, J., Mena-Petite, A., Muñoz-Rueda, A., et al. (2017). Elevated CO_2 and salinity are responsible for phenolics-enrichment in two differently pigmented lettuces. *Plant Physiol. Biochem.* 115, 269–278. doi: 10.1016/j.plaphy.2017.04.006

Shah, W. H., Rasool, A., Saleem, S., Mushtaq, N. U., Tahir, I., Hakeem, K. R., et al. (2021). Understanding the integrated pathways and mechanisms of transporters, protein kinases, and transcription factors in plants under salt stress. *Int. J. Genom.* 2021, 1–16. doi: 10.1155/2021/5578727

Shi, H., Quintero, F. J., Pardo, J. M., and Zhu, J. (2002). The putative plasma membrane Na^+/H^+ antiporter *SOS1* controls long-distance Na^+ transport in plants. *Plant Cell* 14, 465–477. doi: 10.1105/tpc.010371

Shigeoka, S., Ishikawa, T., Tamoi, M., Miyagawa, Y., Takeda, T., Yabuta, Y., et al. (2002). Regulation and function of ascorbate peroxidase isoenzymes. *J. Exp. Bot.* 53, 1305–1319. doi: 10.1093/jexbot/53.372.1305

Silva, E. N., Ferreira-Silva, S. L., Viégas, R. A., and Silveira, J. A. G. (2010). The role of organic and inorganic solutes in the osmotic adjustment of drought-stressed Jatropha curcas plants. *Environ. Exp. Bot.* 69, 279–285. doi: 10.1016/j.envexpbot.2010.05.001

Silveira, J. A. G., Araújo, S. A. M., Lima, J. P. M. S., and Viégas, R. A. (2009). Roots and leaves display contrasting osmotic adjustment mechanisms in response to NaCl-

salinity in *Atriplex nummularia*. *Environ. Exp. Bot.* 66, 1–8. doi: 10.1016/j.envexpbot.2008.12.015

Simon-Sarkadi, L., Kocsy, G., Sebestyén, Z., and Galiba, G. (2007). Deletions of chromosome 5A affect free amino acid and polyamine levels in wheat subjected to salt stress. *Environ. Exp. Bot.* 60, 193–201. doi: 10.1016/j.envexpbot.2006.10.002

Singh, R., and Jwa, N. S. (2013). The rice MAPKK-MAPK interactome: the biological significance of MAPK components in hormone signal transduction. *Plant Cell Rep.* 32, 923–931. doi: 10.1007/s00299-013-1437-y

Sullivan, M., and Michael, L. (2009). A novel red clover hydroxycinnamoyl transferase has enzymatic activities consistent with a role in phaselic acid biosynthesis. *Plant Physiol.* 150, 1866–1879. doi: 10.1104/pp.109.136689

Tanou, G., Ziogas, V., Belghazi, M., Christou, A., and Molassiotis, A. (2014). (2014). Polyamines reprogram oxidative and nitrosative status and the proteome of citrus plants exposed to salinity stress. *Plant Cell Environ.* 37, 864–885. doi: 10.1111/pce.12204

Thordal-Christensen, H., Zhang, Z., Wei, Y., and Collinge, D. B. (2002). Subcellular localization of H_2O_2 in plants. H_2O_2 accumulation in papillae and hypersensitive response during the barley-powdery mildew interaction. *Plant J.* 11, 1187–1194. doi: 10.1046/j.1365-313X.1997.11061187.x

Toranj, S., Aliabad, K. K., Abbaspour, H., and Saeedpour, A. (2020). Effect of salt stress on the genes expression of the vacuolar H+ −pyrophosphatase and Na+/H+ antiporter in Rubia tinctorum. *Mol. Biol. Rep.* 47, 235–245. doi: 10.1007/s11033-019-05124-8

Tran, D. Q., Konishi, A., Cushman, J. C., Morokuma, M., Toyota, M., and Agarie, S. (2020). Ion accumulation and expression of ion homeostasis-related genes associated with halophilism, NaCl-promoted growth in a halophyte Mesembryanthemum *crystallinum L. Plant Prod. Sci.* 23, 91–102. doi: 10.1080/1343943X.2019.1647788

Völz, R., Harris, W., Hirt, H., and Lee, Y. H. (2022). ROS homeostasis mediated by MPK4 and SUMM2 determines synergid cell death. *Nat. Commun.* 13, 1746. doi: 10.1038/s41467-022-29373-7

Völz, R., Kim, S. K., Mi, J., Mariappan, K. G., Guo, X., Bigeard, J., et al. (2018). The Trihelix transcription factor GT2-like 1 (GTL1) promotes salicylic acid metabolism, and regulates bacterial-triggered immunity. *PLoS Genet.* 14:e1007708. doi: 10.1371/journal.pgen.1007708

Wang, C., Jia-Qiang, L., Shengyu, L., Donglei, M., Zaynulla, R., and Jie, Z. (2013). Morphological characteristics of Carelinia caspica nebkhas in the oasis desert ecotone in cele, Xinjiang, China. *J. Desert Res.* 33, 981–989.

Wang, W., Vinocur, B., and Altman, A. (2003). Plant responses to drought, salinity and extreme temperatures: towards genetic engineering for stress tolerance. *Planta* 218, 1–14. doi: 10.1007/s00425-003-1105-5

Watanabe, S., Kojima, K., Ide, Y., and Sasaki, S. (2000). Effects of saline and osmotic stress on proline and sugar accumulation in *Populus euphratica* in vitro. *Plant Cell Tiss. Org.* 63, 199–206. doi: 10.1023/A:1010619503680

Yan, K., Cui, M., Zhao, S., Chen, X., and Tang, X. (2016). Salinity stress is beneficial to the accumulation of chlorogenic acids in honeysuckle (*Lonicera japonica* Thunb.). Front. *Plant Sci.* 7:1563. doi: 10.3389/fpls.2016.01563

Yan, K., Zhao, S., Bian, L., and Chen, X. (2017). Saline stress enhanced accumulation of leaf phenolics in honeysuckle (*Lonicera japonica* Thunb.) without induction of oxidative stress. Plant Physiol. *Biochemist* 112, 326–334. doi: 10.1016/j.plaphy.2017.01.020

Yang, H., Wu, F., and Cheng, J. (2011). Reduced chilling injury in cucumber by nitric oxide and the antioxidant response. *Food Chem.* 127, 1237–1242. doi: 10.1016/j.foodchem.2011.02.011

Yu, J., Chen, S., Zhao, Q., Wang, T., Yang, C., Diaz, C., et al. (2011). Physiological and proteomic analysis of salinity tolerance in *Puccinellia tenuiflora*. *J. Proteome Res.* 10, 3852–3870. doi: 10.1021/pr101102p

Yu, L. J., Nie, J. N., Cao, C. Y., Jin, Y. K., Yan, M., Wang, F. Z., et al. (2010). Phosphatidic acid mediates salt stress response by regulation of *MPK6* in *Arabidopsis thaliana*. *New Phytol.* 188, 762–773. doi: 10.1111/j.1469-8137.2010.03422.x

Zeng, Y., Li, L., Yang, R., Yi, X., and Zhang, B. (2015). Contribution and distribution of inorganic ions and organic compounds to the osmotic adjustment in *Halostachys caspica* response to salt stress. *Sci. Rep.* 5, 13639. doi: 10.1038/srep13639

Zhang, L., Luo, Y., Liu, B., Zhang, L., Zhang, W., Chen, R., et al. (2020). Overexpression of the maize γ-tocopherol methyltransferase gene (ZmTMT) increases α-tocopherol content in transgenic arabidopsis and maize seeds. *Transgenic Res.* 29, 95–104. doi: 10.1007/s11248-019-00180-z

Zhang, L., Miras-Moreno, B., Yildiztugay, E., Ozfidan-Konakci, C., Arikan, B., Elbasan, F., et al. (2021). Metabolomics and physiological insights into the ability of exogenously applied chlorogenic acid and hesperidin to modulate salt stress in lettuce distinctively. *Molecules* 26, 6291. doi: 10.3390/molecules26206291

Zhang, Y., Zhang, H., Zou, Z. R., Liu, Y., and Hu, X. H. (2015). Deciphering the protective role of spermidine against saline–alkaline stress at physiological and proteomic levels in tomato. *Phytochemistry* 110, 13–21. doi: 10.1016/j.phytochem.2014.12.021

Zhao, C., Zhang, H., and Song, C. (2020). Mechanisms of plant responses and adaptation to soil salinity. *The Innovation.* 1, 41. doi: 10.1016/j.xinn.2020.100017

Zhou, Y., Liu, C., Tang, D., Yan, L., Wang, D., Yang, Y., et al. (2018). The receptor-like cytoplasmic kinase STRK1 phosphorylates and activates CatC, thereby regulating H_2O_2 homeostasis and improving salt tolerance in rice. *Plant Cell* 30, 1100–1118. doi: 10.1105/tpc.17.01000

frontiers | Frontiers in Plant Science

TYPE Original Research
PUBLISHED 06 October 2022
DOI 10.3389/fpls.2022.979883

OPEN ACCESS

EDITED BY
Sridev Mohapatra,
Birla Institute of Technology and Science, India

REVIEWED BY
Joelle Sasse Schlaepfer,
University of Zurich, Switzerland
Binod Bihari Sahu,
National Institute of Technology, India

*CORRESPONDENCE
Jin-Lin Zhang
jlzhang@lzu.edu.cn
Xiang-Wen Fang
fangxw@lzu.edu.cn

SPECIALTY SECTION
This article was submitted to Plant Abiotic Stress, a section of the journal Frontiers in Plant Science

RECEIVED 28 June 2022
ACCEPTED 09 September 2022
PUBLISHED 06 October 2022

CITATION
Wang Q, Ou E-L, Wang P-C, Chen Y, Wang Z-Y, Wang Z-W, Fang X-W and Zhang J-L (2022) *Bacillus amyloliquefaciens GB03* augmented tall fescue growth by regulating phytohormone and nutrient homeostasis under nitrogen deficiency. *Front. Plant Sci.* 13:979883. doi: 10.3389/fpls.2022.979883

Bacillus amyloliquefaciens GB03 augmented tall fescue growth by regulating phytohormone and nutrient homeostasis under nitrogen deficiency

Qian Wang[1,2], Er-Ling Ou[2], Pu-Chang Wang[3], Ying Chen[2], Zi-Yuan Wang[2], Zhi-Wei Wang[2], Xiang-Wen Fang[1*] and Jin-Lin Zhang[4*]

[1]State Key Laboratory of Herbage Improvement and Grassland Agro-ecosystems, College of Ecology, Lanzhou University, Lanzhou, China, [2]Guizhou Institute of Prataculture, Guizhou Academy of Agricultural Sciences, Guiyang, China, [3]School of Life Sciences, Guizhou Normal University, Guiyang, China, [4]State Key Laboratory of Herbage Improvement and Grassland Agro-ecosystems, College of Pastoral Agriculture Science and Technology, Lanzhou University, Lanzhou, China

Nitrogen is an important nutrient for plant growth and development. Soil microorganisms have been used to curb the imbalance between the limited content of natural environmental nitrogen and the pollution caused by increasing nitrogen fertilizer use in ecologically fragile areas. *Bacillus amyloliquefaciens* GB03 has been shown to confer growth promotion and abiotic stress tolerance in *Arabidopsis thaliana*. This study provided a new insight into the role of the plant growth-promoting rhizobacterium *B. amyloliquefaciens* GB03 as an initiator of defense against nitrogen deficiency in non-leguminous grass tall fescue (*Festuca arundinacea*). Two-week-old seedlings of tall fescue were grown with or without GB03 for 4 weeks under total nitrogen (3.75 mM NO_3^-) or low nitrogen (0.25 mM NO_3^-) treatment. Growth parameters, chlorophyll content, endogenous total nitrogen, total phosphorus content, and phytohormone content, including those of auxin indole-3-acetic acid, cytokinin, gibberellic acid, and abscisic acid, were determined at the time of harvest. Tall fescue grown in GB03-inoculated soil was more robust than the non-inoculated controls with respect to plant height, root length, plant biomass, chlorophyll concentration, and nutrient (total nitrogen and total phosphorus) contents under total nitrogen treatment. GB03 increased indole acetic acid content by 24.7%, whereas decreased cytokinin and abscisic acid contents by 28.4% and 26.9%, respectively, under a total nitrogen level. Remarkably, GB03 increased indole acetic acid content by more than 80% and inhibited abscisic acid production by nearly 70% under a low nitrogen level. These results showed, for the first time, that GB03 played a crucial role in mediating NO_3^-dependent regulation of tall fescue growth and

development, especially revealing the mechanism of soil bacteria improve resistance to nitrogen deficiency stress in non-nitrogen-fixing species.

KEYWORDS

Bacillus amyloliquefaciens GB03, plant growth promotion, nitrogen deficiency, phytohormone, nutrient, tall fescue

Introduction

In southwest China, cold-season turf grasses have received more attention owing to their longer green period. Tall fescue (*Festuca arundinacea*) belongs to the family Poaceae, subfamily Pooideae, tribe Poeae, and is a major cool-season turf grass and forage species worldwide. Additionally, because of its rapid growth, wide adaptability, strong regeneration, and long green period, it plays an important role in water and soil conservation, environmental protection, and ecological restoration (Yang et al., 2013; Tang et al., 2015). In previous studies, we collected several tall fescues from various lacations for cross-breeding. After years of comprehensive evaluation of drought, heat resistance, and production performance, we finally selected a new national forage grass variety "Qiancao No. 1" (registration number: 299) with superior indicators. Nevertheless, consistent with other species of tall fescue, the cultivation and seed production of "Qiancao No. 1" strongly depended on nitrogen fertilizers.

Nitrogen (N), an important nutrient for plant growth and development, is both the main structural material constituting plant organisms (Amtmann and Armengaud, 2009) and a key catalyst in various plant physiological and metabolic processes (Orsel et al., 2006). Nitrogen is absorbed from the soil either in inorganic forms, such as nitrate or ammonium, or in organic forms, mostly as free amino acids (Vance, 2001; Miller and Cramer, 2004). However, nitrate is the major form absorbed, and its availability can fluctuate markedly, both spatially and temporally, especially in ecologically fragile areas (Liu and Wang, 2012; Zhao and Ma, 2014). Application of a nitrogen fertilizer in the soil can effectively increase the yield of plant and crop, while increasing nitrogen fertilizer use severely causes environmental pollution (Foyer and Ferrario, 1994; Nosengo, 2003), particularly in aquatic ecosystems (Pretty, 2008; Robertson and Vitousek, 2009) and the atmosphere (Davidson, 2009; Smith et al., 2012). Therefore, it is extremely important to find a new method for solving the contradiction between the limited effectiveness of natural environmental nitrogen and environmental pollution due to increased fertilizer use.

In terrestrial ecosystems, plants are producers and soil microorganisms are decomposers. Producers release photosynthetic products into the soil in the form of root secretions and plant residues, supplying soil microbial energy and carbon sources. On the other hand, soil microorganisms convert organic nutrients into inorganic nutrients, contributing to plant absorption and utilization (Marschnera and Timonen, 2005). Plant rhizosphere soil contains large numbers of microorganisms that play important roles in organic matter decomposition, nutrient recycling, and plant nutrient utilization. Some plant growth-promoting rhizobacteria (PGPR) can promote plant growth, prevent disease, and increase crop yield (Schippers et al., 1987; Kloepper, 1992). Therefore, these bacteria have been widely applied in agriculture to increase seed emergence, improve plant weight and crop yield, promote efficient uptake and utilization of nutrients, and enhance disease resistance (Zhang et al., 2008a; Zhang et al., 2008b; Paré et al., 2011).

Bacillus subtilis GB03, now renamed as *Bacillus amyloliquefaciens* GB03, is a commercially available PGPR strain that can be introduced into the soil at the time of planting *via* seed coating (Choi et al., 2014). Since the mid-1990s, researchers had focused on the biotic stress control by GB03 firstly. Raupach and Kloepper (1998) found that GB03 enhanced the biological control of multiple cucumber pathogens. In *Arabidopsis thaliana*, many researchers provide new insight into the role of GB03 as an elicitor of defense responses (Pieterse et al., 2002; Ryu et al., 2004, Ryu et al., 2005; Rudrappa et al., 2010). In tomato (*Solanum lycopersicum*), the results of the present study suggested that integrated control of Fusarium crown and root rot could be achieved by combining the use of PGPR strains GB03 with plant disease inducers or conventional fungicides (Myresiotis et al., 2011). In the following, many studies had been conducted on composition analysis of the release, mechanism of action, and signal transduction pathways of GB03. Ryu et al. (2003) pointed out that GB03 could release volatile organic compounds (VOCs), devoid of classic phytohormones, which were capable of promoting plant growth. These VOCs also activated the differential expression of approximately 600 transcripts related to cell wall modifications, primary and secondary metabolism, stress responses, and hormone regulation (Zhang et al., 2007). Among these VOCs, methyl jasmonate, methyl salicylate, 2,3-butanediol, and acetoin had been found to trigger induced

systemic resistance (ISR) and protect plants against pathogenesis to increase the plant growth (Ryu et al., 2004, Ryu et al., 2005). Studies had also shown the potential of GB03 to control iron acquisition and light energy conversion and emphasize the sophisticated integration of microbial signaling in photosynthetic regulation (Zhang et al., 2008a; Zhang et al., 2009). Similar results had also been reported in cassava (*Manihot esculenta*), an important agricultural crop, in which iron accumulation was increased, and growth promotion and photosynthetic efficiency improvement were observed in greenhouse-grown plants exposed to GB03 (Freitas et al., 2015). In addition, GB03 augmented plant tolerance to salt and osmotic stresses by regulating tissue-specific expression of Na^+ transporter to decrease Na^+ uptake and accumulation and increasing osmoprotectant accumulation in many species (Zhang et al., 2008b; Zhang et al., 2010; Han et al., 2014a; Han et al., 2014b; Niu et al., 2016; Han et al., 2017).

Recently, it has been observed that bacterial volatile components can serve as agents for triggering growth promotion through many pathways. However, the ability of PGPR to induce nitrogen assimilation *via* established operational mechanisms in non-leguminous species, particularly the role of PGPR *B. amyloliquefaciens* strain GB03 in regulating gramineous plant growth and development, has not been reported. In this study, we reported a novel mechanism in which the bacterial strain GB03 augmented tall fescue growth by increasing the chlorophyll and nutrient contents and regulating the nitrogen-dependent homeostasis of phytohormones. We also proposed a new paradigm for PGPR to mediate nitrogen deficiency adaptation in non-nitrogen-fixing gramineous plants.

Materials and methods

Bacterial culture

PGPR strain *Bacillus amyloliquefaciens* GB03 was streaked onto Luria broth (LB) agar plates and incubated at 28°C for 24 h without light. PGPR cells were harvested from LB agar plates using double-distilled water (DDW) to yield 10^9 colony-forming units (CFU) mL^{-1}, as determined by optical density and serial dilutions with plate counts (Zhang et al., 2007; Zhang et al., 2008b).

Plant materials and treatments

Seeds of tall fescue (*Festuca arundinacea*) were obtained from our breeding line 'Qiancao No. 1' and were surface sterilized with 5% (v/v) bleacher followed by 70% ethanol and washed five times with sterile water, then germinated at 25°C on moist filter paper for 2 days. Uniform seedlings were transplanted to plastic pots (diameter 10 cm, five seedlings per pot) containing autoclave-sterilized vermiculite. Six pots in one pallet (the pallet length 50 cm, width 25 cm, and depth 5 cm, we arranged eight pallets totally) were filled with Hoagland nutrient solution containing 1.25 mM KNO_3, 0.25 mM KH_2PO_4, 0.5 mM $MgSO_4{\cdot}7H_2O$, 1.25 mM $Ca(NO_3)_2{\cdot}4H_2O$, 11.6 μM H_3BO_3, 4.6 μM $MnCl_2{\cdot}4H_2O$, 0.19 μM $ZnSO_4{\cdot}7H_2O$, 0.08 μM $CuSO_4{\cdot}5H_2O$, 0.12 μM $Na_2MoO_4{\cdot}2H_2O$, and 10 μM Fe(III)-EDTA. Nutrient solutions were renewed every 3 days. Seedlings were grown in the greenhouse under a daily photoperiod of 16/8 h (light/dark) with a light intensity of 230–300 μmol $m^{-2}{\cdot}s^{-1}$, temperature of 25°C ± 2°C/23°C ± 2°C (day/night), and relative humidity of 60 ± 5%.

Two-week-old seedlings were treated under the following conditions: (i) total nitrogen (TN-3.75 mM NO_3^-): seedlings were grown in Hoagland nutrient solution and (ii) low nitrogen (LN-0.25 mM NO_3^-): seedlings were subjected to 0.25 mM NO_3^- (Hoagland nutrient solution was deprived of KNO_3 and $Ca(NO_3)_2{\cdot}4H_2O$; 1.25 mM KNO_3 was substituted with 0.25 mM KNO_3 and 1 mM KCl, while 1.25 mM $Ca(NO_3)_2{\cdot}4H_2O$ was substituted with 1.25 mM $CaCl_2$). After 4 days, the seedlings were inoculated directly into the vermiculite with 1 ml bacterial suspension or 1 ml DDW as a control, for another 4 weeks (the bacterial suspension or sterile water was supplemented every week).

Plant biomass and physiological index measurements

Seven-week-old plants were removed from their pots, and their roots were rinsed with water to remove attached vermiculite. Plant height and root length were measured using a ruler. Thirty independent plants were measured for each treatment. Shoots and roots were separated and blotted, fresh weights (FW) were acquired immediately, and samples were dried in an oven at 70°C for 3 days to determine dry weights (DW). Eight independent biological replicates were used for each treatment.

The chlorophyll content was estimated according to the method of Porra et al. (1989). Fresh leaf samples were crushed thoroughly with 80% acetone in the dark and centrifuged at 9,000 g for 10 min at 4°C. The supernatant was collected, and absorbance was measured at 645 and 663 nm using a UV spectrophotometer (UV-2700, Unico Inc., Shanghai, China). Chlorophyll a, chlorophyll b, and total chlorophyll contents were estimated using the equations of Porra et al. (1989). Eight independent biological replicates were used for each treatment.

Determination of total nitrogen and total phosphorus

Plant total nitrogen and total phosphorus contents were analyzed in the dried samples. Total nitrogen content was

determined using semimicro-Kjeldahl digestion and distillation (Nelson and Sommers, 1980). Total phosphorus content was determined using the vanadomolybdate yellow method (Jackson, 1959). Eight independent biological replicates were used for each treatment.

Indole-3-acetic acid, cytokinin, gibberellic acid, and abscisic acid measurements

Auxin indole-3-acetic acid (IAA), cytokinin (CK), gibberellic acid (GA), and abscisic acid (ABA) were determined using enzyme-linked immunosorbent assay (ELISA). In brief, according to the instructions of IAA, CK, GA, and ABA ELISA kits (Mibio, Shanghai, China), we extracted the phytohormone and measured the absorbance (OD value) at 450 nm using a microplate reader (BioTek Inc., USA). Each sample was assayed in three independent biological replicates, and each biological replicate was assayed in three technical replicates. Finally, the IAA, CK, GA, and ABA contents were calculated according to the standard liquid concentration.

Statistical analysis

Statistical analyses were performed using 16.0 (SPSS Inc., Chicago, IL, USA). Duncan's multiple-range test was used to detect significant differences between the means at a significance level of $p < 0.05$.

Results

GB03 promoted tall fescue growth under various nitrogen levels

The GB03-exposed plants were greener than water control, and this phenotype was more pronounced under LN conditions, because the part of foliage showed yellow under LN without GB03 (Figure 1). Compared with TN treatment, LN stress reduced plant height by 21.3% but promoted root length dramatically by 83.8% without GB03 (Figures 2A, B). The PGPR strain GB03 enhanced plant height by 14% and 29.7% under TN and LN treatments, respectively, compared with the non-inoculated controls (Figure 2A). Root length increased by 13.2% under TN treatment, whereas it decreased by 34.8% under LN stress with the addition of GB03 (Figure 2B). Compared with TN, LN reduced shoot FW and DW by more than 50% (Figures 2C, D) but had no effect on root biomass without GB03 (Figures 2E, F). GB03 increased biomass in both the shoots (FW by 37.6%, DW by 41.8%) and roots (FW by 68.5%, DW by 62%) under TN treatment; meanwhile, the biomass of shoots (FW by 32.9%, DW by 29%) and roots (FW by 28.4%, DW by 29.2%) was improved under LN stress, although the latter was not statistically significant (Figures 2C–F).

GB03 enhanced nutrient accumulation in tall fescue under various nitrogen levels

Compared with the TN treatment, LN stress significantly decreased the shoot total nitrogen content by 30.8% without GB03; however, compared with water control, GB03 improved the shoot total nitrogen content by 7% under TN conditions, and the magnitude of increase under LN conditions (by 14.5%) was twice than under TN (Figure 3A). Consistent with that seen for the shoot, LN stress also reduced the root total nitrogen content by 39.4% compared with TN treatment without GB03; however, the root total nitrogen was enhanced by GB03 exposure under TN treatment (Figure 3B). On the other hand, phosphorus showed different changes from nitrogen under various treatments. First, the NO_3^- supply from 3.75 to 0.25 mM had no effect on total phosphorus content in neither shoot nor root without GB03, whereas plants with GB03 exposure had improved total phosphorus content in shoot under TN (by 16.5%) and LN (8.7%) treatments (Figure 3C). Root total phosphorus content was maintained at a steady level under various treatments (Figure 3D).

GB03 increased chlorophyll content in tall fescue under various nitrogen levels

Compared with the TN treatment, LN stress reduced the chlorophyll a content (by 18.5%) and the total chlorophyll content (by 15.5%) but had no effect on the chlorophyll b content without GB03 (Table 1). Nevertheless, regardless of TN treatment or LN stress, chlorophyll a, chlorophyll b, and total chlorophyll content increased by nearly 30% with GB03, compared with the water control (Table 1).

GB03 regulated pyhormone contents in tall fescue under various nitrogen levels

In non-GB03-exposured plants, LN stress reduced IAA and CK contents by 55.1% and 64.5%, respectively (Figures 4A, B), while it had no effect on GA content (Figure 4C) compared with TN treatment. On the contrary, ABA content was increased by 37.5% by LN stress versus TN treatment (Figure 4D). With GB03 exposure for 4 weeks, an increase in IAA content was observed under TN by 24.7% and under LN by 81.8% (Figure 4A). In contrast to IAA, the CK and ABA contents

10.3389/fpls.2022.979883

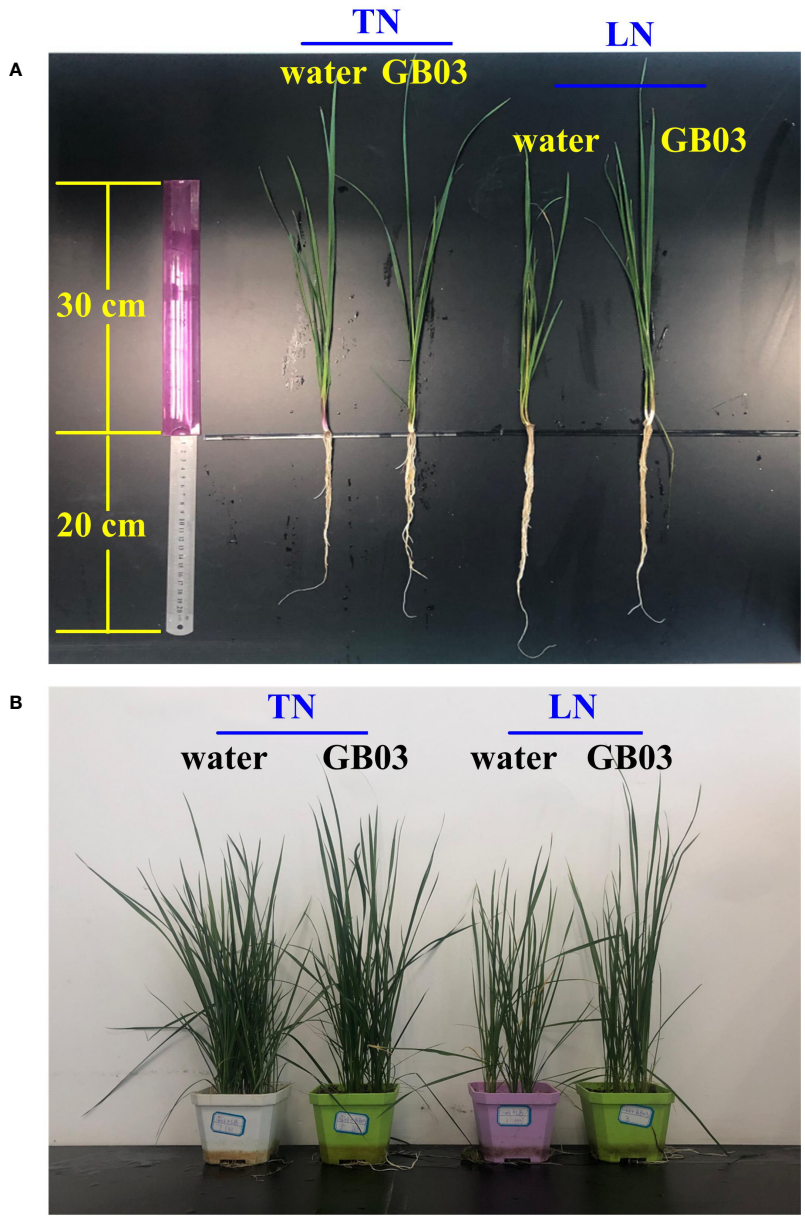

FIGURE 1
Effects of GB03 on tall fescue phenotype. **(A)** Individual plant and **(B)** one pot of plant (containing five seedlings) were photographed from different parallel treatments, including the total nitrogen level (TN-3.75 mM NO_3^-) and the low nitrogen level (LN-0.25 mM NO_3^-) with GB03, respectively, and the water treatment as control.

were reduced with GB03 exposure both under TN and LN treatments, and the decreasing degree of ABA content in the latter (nearly 70%) was larger than that in the former (no more than 30%) (Figures 4B, D). On the other hand, although NO_3^- levels had no effect on GA content in tall fescue without GB03, GA content responses varied with different NO_3^- concentrations under GB03 compared with the water control. GA increased by 98% under TN and decreased by 65% under LN (Figure 4C).

Discussion

B. amyloliquefaciens GB03 enhanced tall fescue growth under nitrogen deficiency stress

B. amyloliquefaciens GB03, as a PGPR strain, promoted plant growth in many plant species, including *Arabidopsis*

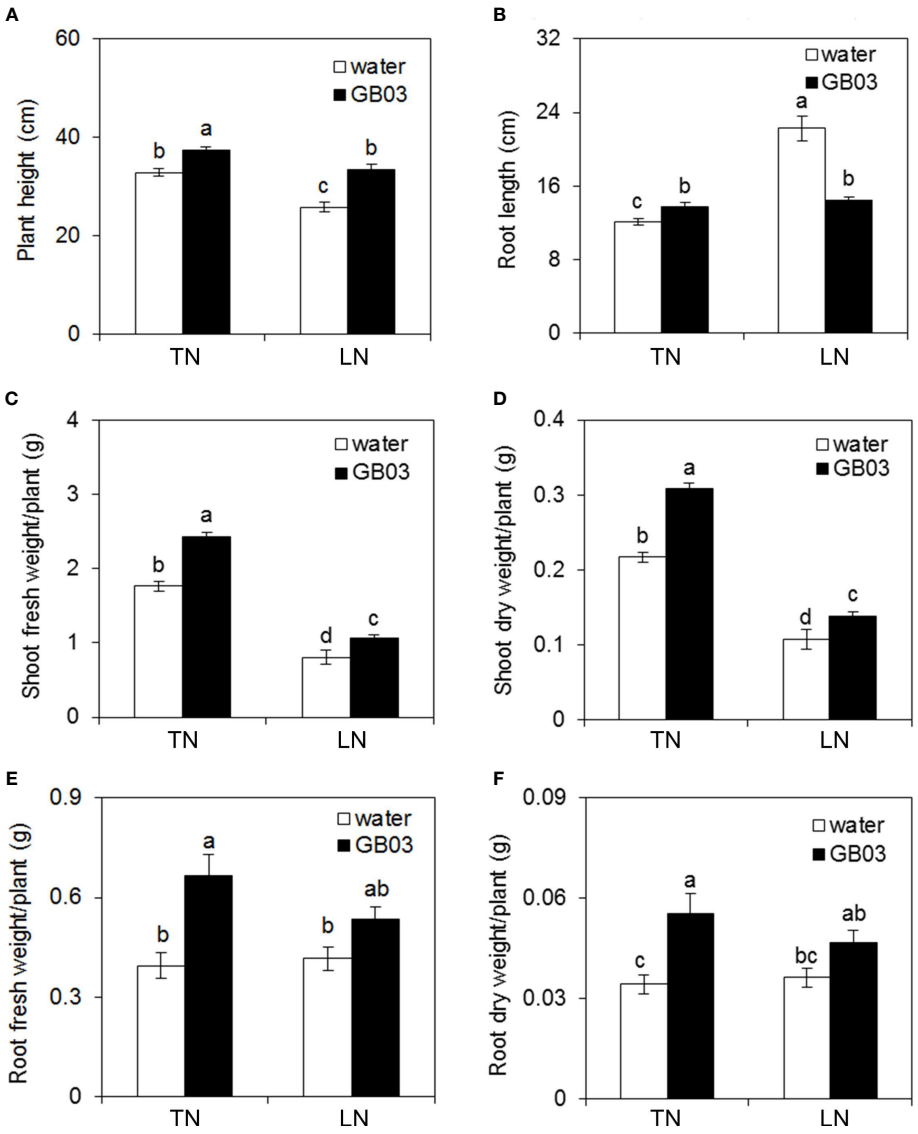

FIGURE 2
Effects of GB03 on tall fescue growth under various concentrations of NO_3^-. **(A)** Plant height, **(B)** root length, **(C)** shoot fresh weight, **(D)** shoot dry weight, **(E)** root fresh weight, and **(F)** root dry weight. Values are means ± SE (A and B n = 30; C-F n = 8), and bars indicate SE. Columns with different letters indicate significant differences at $p < 0.05$ (Duncan's test).

thaliana (Ryu et al., 2003; Zhang et al., 2008a; Xie et al., 2009; Paré et al., 2011), wheat (*Triticum aestivum*) (Zhang et al., 2014), alfalfa (*Medicago sativa*) (Han et al., 2014a), white clover (*Trifolium repens*) (Han et al., 2014b), cassava (*Manihot esculenta*) (Freitas et al., 2015), *Puccinellia tenuiflora* (Niu et al., 2016), and *Codonopsis pilosula* (Han et al., 2017). The growth promotion of tall fescue by *B. amyloliquefaciens* GB03 inoculation in the soil evaluated in our study was consistent with the above reports (Figure 1). Here, in order to prove that the growth promotion of GB03 had a certain strain specificity, we chose *Escherichia coli* strain DH5α as positive control at the initial growth experiment, finding that DH5a failed to augment growth with respect to plant height, root length, shoot and root FW, and DW regardless of TN or LN treatment (Figure S1, Table S1). Contrary to DH5α, compared with water control, the plant height, root length, and shoot and root FW and DW increased to varying degrees with GB03 TN conditions (Figure 2). In addition, inducible plant growth promotion mediated by GB03 had also been observed under some conditions, including salinity stress (Zhang et al., 2008b; Zhang et al., 2014; Han et al., 2014a; Han et al., 2014b; Niu et al., 2016; Han et al., 2017), iron deficiency (Zhang et al., 2009; Freitas et al., 2015), and

10.3389/fpls.2022.979883

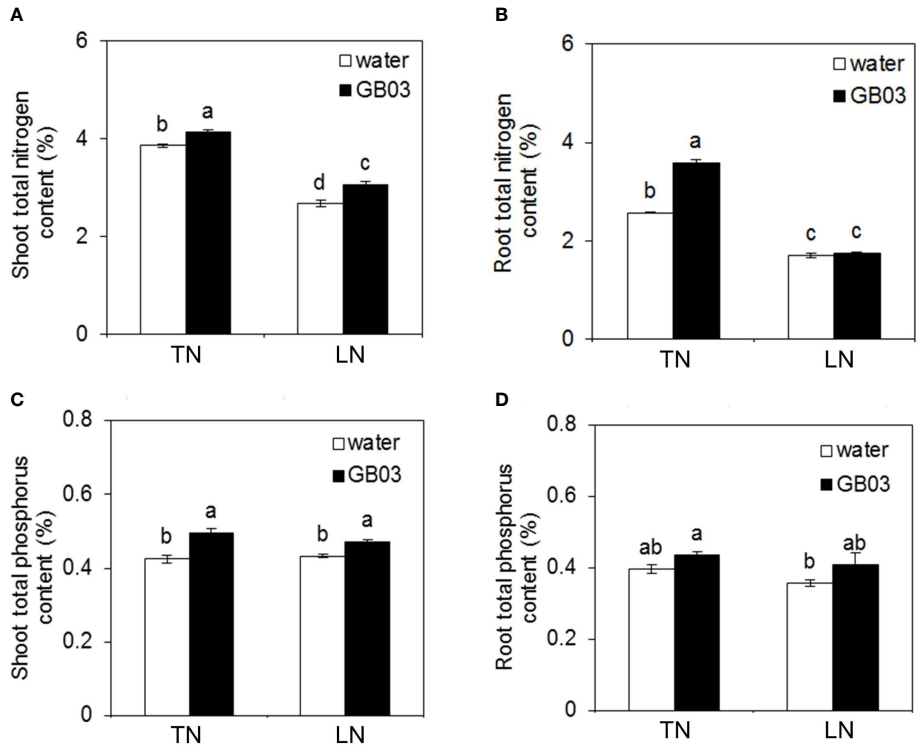

FIGURE 3
Effects of GB03 on N and P in tall fescue under various concentrations of NO_3^-. **(A)** Shoot total nitrogen content, **(B)** root total nitrogen content, **(C)** shoot total phosphorus content, and **(D)** root total phosphorus content. Values are means ± SE (n = 8), and bars indicate SE. Columns with different letters indicate significant differences at $p < 0.05$ (Duncan's test).

osmotic stress (Zhang et al., 2010), which could ultimately enhance plant stress resistance. However, the ability of GB03 to improve plant adaptability to nitrogen deficiency has not been previously reported. In the present study, the shoot FW and DW of tall fescue decreased by more than 50% from TN to LN without GB03 treatment (Figures 2C, D), and the shoot total nitrogen content also decreased by 30.8% (Figure 3A), indicating that nitrogen deficiency dramatically hindered shoot biomass accumulation in plants. When *B. amyloliquefaciens* GB03 was inoculated into the soil, the plant height and shoot FW and DW of tall fescue were increased under both TN and LN conditions; remarkably, the latter was twice as much as the former (Figures 2A, C, D). This was in line with the changes in shoot total nitrogen content, which was also elevated by GB03 and increased under LN, twice that of TN, compared with the water control (Figure 3A). The results presented here suggested that GB03 could regulate the distribution of nitrogen and improve the nitrogen deficiency resistance of grass by enhancing the accumulation of shoot total nitrogen. In addition, GB03 promoted shoot growth, possibly because it could enhance the accumulation of shoot total phosphorus, another essential macronutrient for plant growth and development (Figure 3C). A similar study pointed out that GB03 could improve *A. thaliana* salt tolerance by regulating the tissue-specific expression of genes to accumulate the less toxic Na^+ (Zhang et al., 2008b). Although our study also found that the growth-

TABLE 1 The chlorophyll *a*, *b* and total chlorophyll concentrations in tall fescue.

Treatments	Chlorophyll *a*(mg g^{-1} FW)	Chlorophyll *b*(mg g^{-1} FW)	Total chlorophyll(mg g^{-1} FW)
TN	1.08 ± 0.04^{b}	0.34 ± 0.01^{bc}	1.42 ± 0.07^{b}
TN + GB03	1.36 ± 0.02^{a}	0.44 ± 0.02^{a}	1.80 ± 0.02^{a}
LN	0.88 ± 0.02^{c}	0.33 ± 0.02^{c}	1.20 ± 0.03^{c}
LN + GB03	1.17 ± 0.06^{ab}	0.40 ± 0.01^{ab}	1.57 ± 0.06^{ab}

The treatments were total nitrogen (TN), total nitrogen with soil bacteria GB03 (TN + GB03), low nitrogen stress (LN), and low nitrogen stress with soil bacteria GB03 (LN + GB03). Values are means ± SE (n = 8). The different letters indicate significant differences at $p < 0.05$ (Duncan's test).

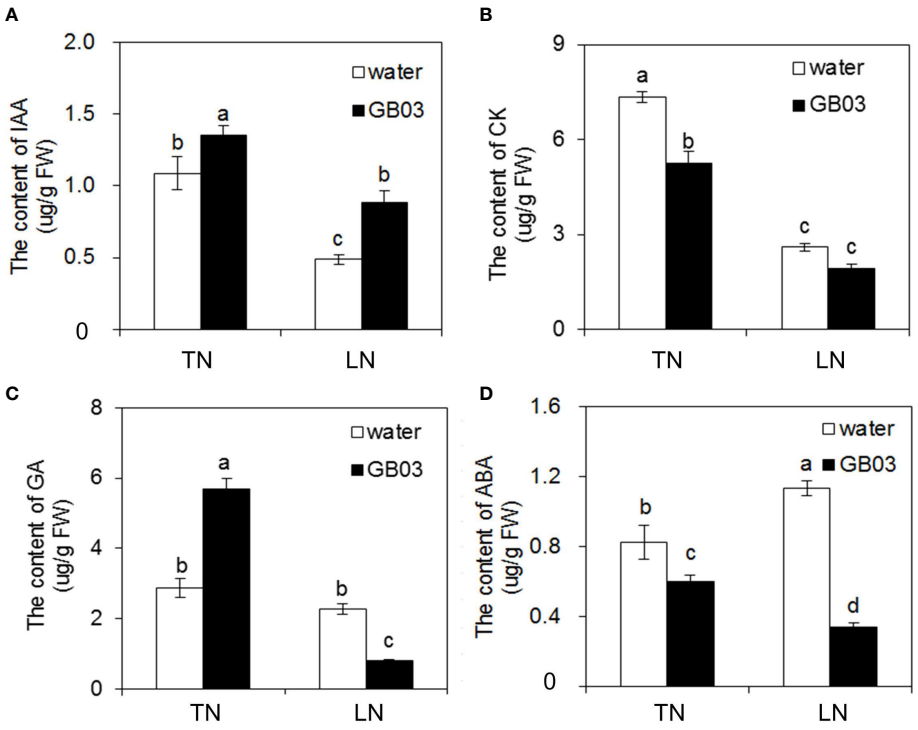

FIGURE 4
Effects of GB03 on phytohormone content in tall fescue under various concentrations of NO_3^-. **(A)** Indole-3-acetic acid (IAA) content, **(B)** cytokinin (CK) content, **(C)** gibberellic acid (GA) content, and **(D)** abscisic acid (ABA) content. Values are means ± SE (n = 9), and bars indicate SE. Columns with different letters indicate significant differences at $p < 0.05$ (Duncan's test).

promoting effect of GB03 under nitrogen deficiency was related to the improvement of nutrient accumulation at the physiological level, the transporters involved in this process require further in-depth research. Intriguingly, unlike GB03 which promoted root growth under TN conditions, it had no effect on root FW and DW under LN conditions (Figures 2E, F), and root total nitrogen and phosphorus content did not change between the water control and GB03 treatments (Figures 3B, D). In these contexts, the growth-promoting effect of GB03 was different for the two nitrogen levels: under TN conditions, GB03 promoted tall fescue growth not only by enhancing nutrient (nitrogen and phosphorus) accumulation in the shoot but also by facilitating nitrogen uptake in the root; under LN conditions, GB03 preferentially promoted nutrient (nitrogen and phosphorus) accumulation in the shoot, rather than root uptake, to resist nitrogen deficiency stress. This functional difference may be due to GB03-induced genes, encoding nutrient transporters, for which expression was NO_3^-dependent.

B. amyloliquefaciens GB03 also affects photosynthesis to varying degrees in plants. Photosynthesis converts light energy into chemical energy in the form of energy-rich sugar. The sugars produced serve not only as carbon and energy sources but also as pivotal signaling molecules for plant growth, development, and stress responses (Zhang et al., 2008a). In cassava, improved photosynthetic efficiency by increasing iron accumulation had been observed in greenhouse-grown plants exposed to GB03 (Freitas et al., 2015). In *Arabidopsis*, the potential of GB03 to control iron acquisition in plants and emphasize the sophisticated integration of microbial signaling in photosynthetic regulation were demonstrated (Zhang et al., 2009). GB03 enhanced the photosynthetic capacity of *Arabidopsis* by improving the efficiency of the conversion of light energy, as well as by enhancing the photosynthetic apparatus (including increase in photosynthetic efficiency and chlorophyll content) (Zhang et al., 2008a) Consistent with GB03 improving salt resistance by directly and indirectly regulating plant chlorophyll content (Han et al., 2014a; Han et al., 2014b; Han et al., 2017), in addition to improving the accumulation of nutrient, GB03 augmented tolerance to nitrogen deficiency stress by enhancing tall fescue photosynthetic capacity, as evidenced by increasing chlorophyll content (Table 1). This result at the physiological level was in accordance with a study at the molecular level, where the mining of microarray data identified several GB03-induced photosynthetic genes, such as chlorophyll a/b binding protein 165/180 (CAB2) and RuBisCO subunit binding proteins (Zhang et al., 2007).

B. amyloliquefaciens GB03 regulated nitrogen-dependent phytohormone levels in tall fescue

Phytohormones were originally defined as a group of naturally occurring organic substances that influence plant growth and development at low concentrations (Kiba et al., 2011). In addition, phytohormones have been linked to various environmental responses to salt, drought, light, temperature, and nutrients (Zhu, 2002; Halliday et al., 2009; Patel and Franklin, 2009; Argueso et al., 2009). Auxin (IAA) is an important hormone that modulates numerous physiological processes in plants, contributing to their growth and development (Teale et al., 2006; Benjamins and Scheres, 2008; Vanneste and Friml, 2009). Auxin is mainly synthesized in the shoot and performs shoot-to-root phloem transport (Ljung et al., 2005). Modification in auxin content under various N treatments had been studied in many species, including wheat (*Triticum aestivum*) (Chen et al., 1998), soybean (*Glycine max*) (Caba et al., 2000), pineapple (*Ananas comosus*) (Tamaki and Mercier, 2007), maize (*Zea mays*) (Liu et al., 2010) and *A. thaliana* (Krouk et al., 2010). In each case, auxin seemed to be translocated from shoot to root was stimulated by a decrease in NO_3^- supply. Therefore, it has long been a candidate for mediating nitrogen signals from shoot to root because of its basipetal transport and regulation of root growth and development (Forde, 2002; Jiang and Feldman, 2003; Fukaki and Tasaka, 2009). In *A. thaliana*, NRT1.1 favored basipetal transport of auxin in lateral roots, thus preventing auxin accumulation at the lateral root tip, which slowed the outgrowth and elongation of lateral roots in the absence of NO_3^- (Krouk et al., 2010). In maize, there was a significant negative correlation between nitrate concentrations and IAA levels in the roots, and the primary root closest to the root tip (10 cm from the root tip) was the main zone in which the IAA level responded sensitively to nitrate supply, whereas primary root length showed a positive correlation with IAA content in roots (Tian et al., 2008). In these contexts, we proposed the mode for interaction between nitrogen and phytohormones in the regulation of tall fescue growth under the different NO_3^- treatments (Figures 5A, B). LN firstly stimulated the transport of auxin from shoot to root, and NRT1.1 favored the basipetal transport of auxin in lateral roots, leading to auxin being accumulated in the primary root tip (Figure 5B), which promoted the growth of the primary root, while it inhibited the growth and development of the lateral root (Figure 2B). Inhibition of lateral root growth and development further hindered NO_3^- uptake by roots, resulting in the decrease in root total nitrogen content (Figure 3B). NRT1.5 had been identified as an essential transporter in NO_3^- long-distance transport from root to shoot in the xylem (Lin et al., 2008; Chen et al., 2012); its transport ability was weakened caused by its encoding gene *NRT1.5* being downregulated by LN in tall fescue root (these data were unpublished), decreasing the shoot total nitrogen content (Figure 3A). *B. amyloliquefaciens* GB03, as a PGPR, increased the IAA content under both TN and LN treatments (Figure 4A), indicating that GB03 induced IAA biosynthesis in tall fescue. GB03 induced IAA biosynthesis *via* a tryptophan-dependent pathway which was elucidated by transcript profiles. It was found that the transcripts of three nitrilases (which catalyze the terminal step in the tryptophan-dependent IAA pathway) were upregulated and transcripts of putative auxin efflux carriers were downregulated by GB03 exposure (Zhang et al., 2007). Additionally, auxin accumulation decreased in leaves and increased in roots with GB03 exposure, which was revealed in a transgenic DR5::GUS *Arabidopsis* line, suggesting that GB03 activated the basipetal transport of auxin in the shoot (Zhang et al., 2007). Here, based on the above, our model showed the role of GB03 in promoting tall fescue growth under different nitrogen levels (Figures 5C, D). Firstly, GB03 enhanced auxin biosynthesis in aerial regions and improved basipetal transport in the shoot; the amplification of IAA contents under LN conditions (increased by 81.8%) was much higher than under TN conditions (increased by 24.7%) (Figures 5C, D), which might be contributed to the GB03 dramatically induced tissue-specific gene expression of auxin-regulated genes under LN treatment. In addition, NRT1.5-mediated NO_3^- long-distance transport was enhanced by GB03 regardless of TN or LN condition (these data were unpublished), increasing shoot total nitrogen content (Figure 3A) and shoot biomass (Figures 2C, D). However, it should be noted that GB03 had different effects on root growth under different NO_3^- treatments. Under TN with GB03 treatment, the augments of root length and biomass were due to the increase in auxin biosynthesis and transport by GB03 and accumulation of auxin in both primary and later roots (Figure 5C). Under LN with GB03 treatment, despite the root biomass having had no change caused by auxin basipetal transport by NRT1.1 in later root (Figure 5D), GB03 effectively alleviated primary root elongation at a low nitrogen level (Figure 2B).

In addition, CK also controls various developmental processes in plants, such as cell division, senescence, gene expression, and nutritional signalings (Schmülling et al., 1997; Takei et al., 2002). CK is also well known for its ability to stimulate cell division and differentiation in the shoot (Kakimoto, 2003), and its level has frequently been found to correlate positively with the nitrogen status of the plant (Samuelson and Larsson, 1993; Wagner and Beck, 1993; Takei et al., 2001; Kiba et al., 2011). Moreover, it was well documented that nitrate induced cytokinin biosynthesis in roots, which was then transported from roots to shoots for systemic regulation (Sakakibara et al., 2006; Poitout et al., 2018). In our model, firstly LN hindered cytokinin biosynthesis in tall fescue root (Figure 5B), reducing the CK content (Figure 4B) and shoot growth (Figures 2A, C, D). Furthermore, CK also has a regulatory role in root architecture development, which has an

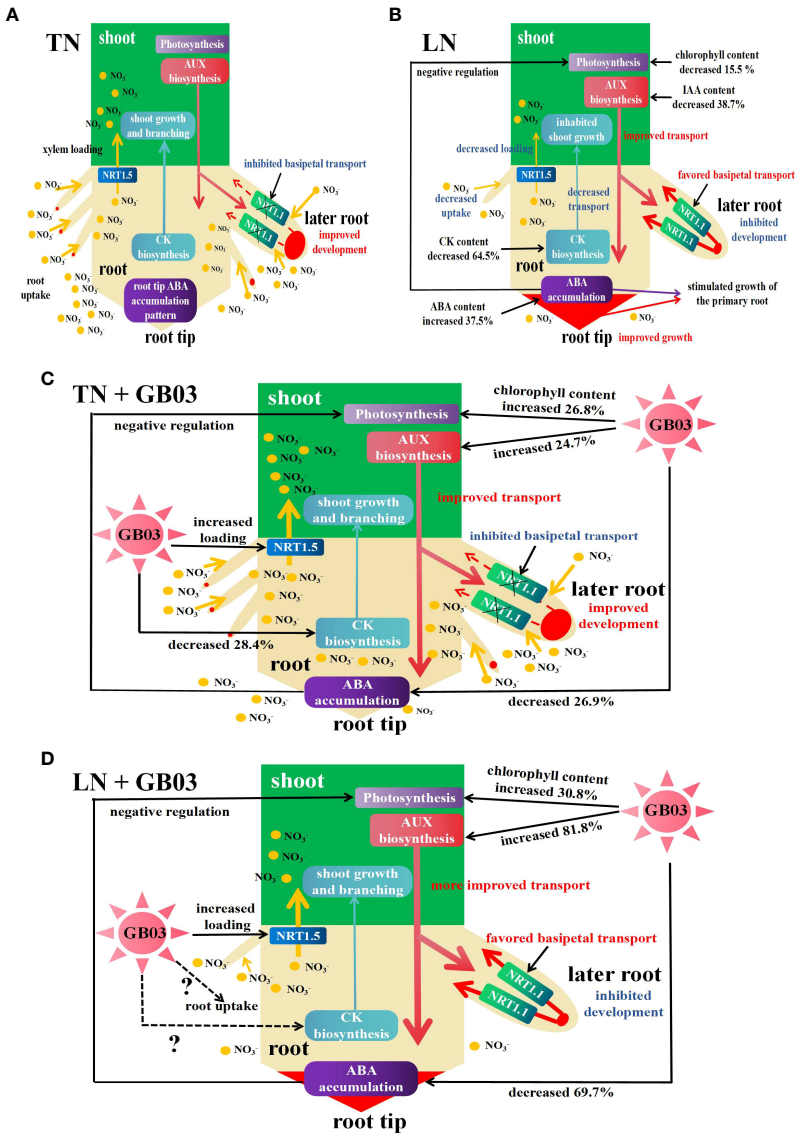

FIGURE 5
Schematic model for the interaction between nitrogen and phytohormones (auxin AUX, cytokinin CK, and abscisic acid ABA) in the regulation of tall fescue growth under different NO_3^- treatments with or without GB03. **(A)** Under TN conditions, AUX was synthesized in the shoot and then was basipetally transported into the root, the NRT1.1 basipetal transport of AUX in lateral roots was inhibited, and AUX was accumulated in the later root tip, triggering the growth and development of later root and uptake of NO_3^-; CK was synthesized in the root and then was apically transported into the shoot, along with NO_3^- loading by NRT1,5 from root to shoot, contributing to the shoot growth and branching; and NO_3^- regulated the primary root growth *via* regulation of ABA accumulation in the root tip. **(B)** Under LN conditions, AUX translocated from shoot to root was stimulated by a decrease in NO_3^- supply, along with NRT1.1 favoring basipetal transport of AUX in lateral roots, enhancing the accumulation of AUX in the primary root tip, which promoted the growth of the primary root versus inhibited the growth and development of the lateral root and impaired NO_3^- uptake; the root biomass was decreased; CK biosynthesis and apical transport, as well as NO_3^- loading by NRT1,5, were weakened by a decrease in NO_3^- supply, and the shoot growth was inhibited; and root tip ABA accumulation was augmented to simulate growth of the primary root and impaired photosynthesis in shoot. **(C)** Under TN conditions, GB03 enhanced the AUX biosynthesis and basipetal transport in the shoot, and the NRT1.1 basipetal transport of AUX in lateral roots was inhibited, and AUX was accumulated in the later root tip, increasing the growth and development of later root and uptake of NO_3^-; CK content was decreased by GB03 which might contribute to stimulate NO_3^- uptake by root, because of CK which had a negative regulation of nitrogen uptake-related genes; and the root tip ABA accumulation was decreased by GB03, which hindered the primary growth regulated by ABA. The abovementioned contributed to the increase in root biomass. Meanwhile, the reduction of ABA caused by GB03 negatively regulated photosynthesis, and GB03 enhanced chlorophyll content and NO_3^- loading in the xylem, and the shoot growth was promoted. **(D)** Under LN conditions, the dual function of GB03 increased AUX biosynthesis and LN stimulated AUX basipetal transport in the shoot, leading to more AUX being accumulated in the root. However, the strong decrease in ABA accumulation caused by GB03 blocked the growth of primary root; this effect was greater than AUX accumulation which was induced by NRT1.1 basipetal transport in lateral roots. Finally, GB03 effectively alleviated primary root elongation at a low nitrogen level. Meanwhile, GB03 preferentially augmented shoot growth by improving photosynthesis and shoot total nitrogen content to resist low nitrogen stress.

opposing effect on shoots and roots. For example, CK stimulated leaf expansion but inhibited root growth in tobacco (*Nicotiana tabacum*) (Werner et al., 2001) and the inhibitory effects of exogenous CK on lateral root formation (Laplaze et al., 2007). However, the cytokinin-dependent systemic N-signaling was required for responses to nitrate-rich supply, while another important element identified as part of this systemic N signal in roots under N deficiency was small signaling C-TERMINALLY ENCODED PEPTIDES (CEPs) (Tabata et al., 2014; Ohkubo et al., 2017; Vega et al., 2019). Ryu et al. (2003) found a role for the cytokinin-signaling pathway in growth promotion by GB03. In microarray experiments, the differential expression of the enzyme involved in cytokinin biosynthesis was observed between GB03 exposure and the control (Zhang et al., 2007). Additionally, microarray analyses had demonstrated that CK negatively regulated nitrogen uptake-related genes (Liu et al., 1999; Orsel et al., 2004; Li et al., 2006; Lin et al., 2008). In our work, CK content was decreased by GB03 compared with the water control under TN (Figure 4B); on the contrary, root total nitrogen content was increased under the same treatment (Figure 3B). Therefore, the reduction in CK content caused by GB03 may have promoted nitrogen uptake in the root, which finally contributed to enhance root and shoot growth (Figure 5C). Similarly, it had been reported that CK negatively regulated other nutrient acquisition-related genes in *Arabidopsis*, such as high-affinity phosphate transporter genes (Martin et al., 2000; Sakakibara et al., 2006), consistent with our result that the root total phosphorus content was increased by 10% under TN with GB03 compared to water control (Figure 3D). Interestingly, GB03 had no effect on CK content compared with the water control under LN conditions (Figure 4B), nor did it affect nitrogen content (Figure 3B) or root biomass (Figures 2E, F). In this context, they proposed that the role of GB03 promoted tall fescue growth by regulating CK which was nitrogen-dependent (Figures 5C, D). We also observed that the effect of auxin on root architecture was greater than that of CK.

In recent years, a connection between other phytohormone (including gibberellic acid (GA), brassinosteroid (BR), and jasmonate) and nitrate responses had been proposed using transcriptome approaches (Canales et al., 2014; Gaudinier et al., 2018; Varala et al., 2018). To date, nitrate and GA had been found to be associated with the modulation of flowering time (Gras et al., 2018), but not with shoot growth and root morphological development. In our study, NO_3^- levels had no effect on GA content in tall fescue without GB03; however, compared with water control, it showed diverse arrays of GA content responses to different NO_3^- concentrations with GB03 (Figure 4C). In microarray experiments, two gibberellin-responsive proteins and an enzyme involved in gibberellin biosynthesis were identified as differentially expressed by GB03 in *A. thaliana* (Zhang et al., 2007). Consistent with this result, GA content in tall fescue was increased by exposure to GB03 under TN treatment but decreased under LN treatment (Figure 4C). Nevertheless, early in the 19th century, to probe the mechanism underlying PGPR strain GB03 to enhance plant growth, it was tested against a series of *A. thaliana* mutants defective in specific regulatory pathways, and it was observed that enhanced total leaf surface area resulted from exposure to GB03 both for *Arabidopsis thaliana* WTs (Col-0, C-24, and Wassilewskija) and gibberellic acid-insensitive *gai2* mutants (Ryu et al., 2003). Taken together, we initially negated the essential involvement of the gibberellic acid-signaling pathway in the activation of growth promotion and tolerance of nitrogen starvation by GB03 in tall fescue.

Different from IAA, CK, and GA, ABA is generally known as a stress hormone involved in abiotic and biotic stress responses (Kiba et al., 2011). The results presented here showed that ABA content increased by 37.5% under nitrogen deficiency (Figure 4D). It was found that the primary root lengths of two *Arabidopsis* ABA-insensitive mutants *abi4-1* and *abi4-2* were both shorter than that of the wild type under 0.1 mM KNO_3; in contrast, no prominent differences had been observed between mutants and WT among various high KNO_3 concentrations (1, 10, and 50 mM), indicating the role of ABA in simulating primary root growth under low NO_3^- supply (Signora et al., 2001). Ondzighi-Assoume et al. (2016) revealed a root tip ABA accumulation pattern and demonstrated a mechanism for nitrate-mediated root growth *via* regulation of ABA accumulation in the primary root tip. As shown in our model, the root length of tall fescue was increased by 83.8% under LN, removing the effect of apical accumulation of auxin; the increase in ABA content also contributed it (Figure 5). Mining microarray data revealed a cluster of ABA-synthesized and ABA-responsive genes that were downregulated in *A. thaliana* upon exposure to GB03 (Zhang et al., 2008a). Consistent with the transcriptional reduction, ABA content was decreased by exposure to GB03 in our study (Figure 4D). This reduction in tissue accumulation of ABA fully explained the results presented here, in that the growth of tall fescue was enhanced by GB03, even under nitrogen deficiency stress (Figures 1, 2). Simultaneously, it explained well why GB03 could effectively alleviate primary root elongation at a low nitrogen level. The large decrease in ABA accumulation greatly inhibited primary root growth in the apical region, despite showing the relatively high accumulation of auxin at the same time (Figure 5D). Ristova et al. (2016) combinatorial experiments with auxin, cytokinin, ABA, and nitrate showed that ABA was the main stimulus shaping root system architecture. As a consequence, the inhibitory effect of ABA on root elongation was greater than the promoting effect of IAA under LN with GB03. In addition, the reduced ABA level was also necessary for GB03-enhanced plant photosynthetic activity (Zhang et al., 2008a). Photosynthesis converted light energy into chemical energy in the form of

energy-rich sugar molecules; conversely, elevated sugar levels in plant induced storage processes and conferred feedback inhibition of photosynthesis (Rook et al., 2001; Moore et al., 2003; Rolland et al., 2006). Hexokinases were evolutionarily conserved glucose sensors in eukaryotes (Rolland et al., 2006). Studies using *Arabidopsis* mutants defective in hexokinase-dependent sugar signaling indicated that GB03 augmented photosynthesis by repressing hexokinase-dependent, rather than hexokinase-independent, sugar signaling. Glucose signaling largely overlapped with ABA signal transduction, as revealed by the fact that *Arabidopsis* ABA synthesis mutant *aba* and ABA-insensitive mutant *abi* were also, to varying degrees, sugar-sensing mutants (Smeekens, 2000; Rolland et al., 2006). Therefore, the reduction in ABA levels (Figure 4D) indirectly explained the improved chlorophyll concentration (Table 1), which could serve as one of the parameters for enhancing tall fescue photosynthetic capacity, in GB03-exposed plants (Figures 5C, D).

Tall fescue has strong adaptability to temperature and soil conditions, so it is widely used in turf grass planting in China, including Zhejiang, northern regions of Jiangxi, Hunan, Hubei, Jiangsu, Shanghai, Anhui, Shandong, Henan, Hebei, Shanxi, Beijing, Tianjin, and other places (Chen and Zhu, 2006). Nitrogen fertilizer is the most required nutrient for turfgrass, which can effectively improve turfgrass quality and yield. With the steady increase in nitrogen fertilizer application, the problem of low nitrogen fertilizer utilization rate has attracted more and more attention. According to relevant data, China accounts for one-third of the global chemical fertilizer application; the average nitrogen fertilizer utilization rate is only 27%–28%, or even lower, and the loss rate of nitrogen fertilizer application is 45% (Zhang, 2019). Therefore, it is imperative to improve the utilization efficiency of nitrogen fertilizer. Soil microorganisms usually increase nitrogen utilization in plants, especially in legumes. However, the mechanism of their action in grasses is still lacking. Our study showed, for the first time, that the soil bacteria GB03 played a crucial role in mediating the nitrogen-dependent regulation of tall fescue growth and development by facilitating photosynthesis, nutrient accumulation, and phytohormone homeostasis at the physiological level, although the underlying cellular and molecular mechanisms of action remain unclear. Therefore, the cell size and morphology as well as tall fescue genome from various tissues under different treatments will be needed, which can more systematically illuminate the mechanism of growth-promoting and stress resistance by soil bacteria.

Data availability statement

The raw data supporting the conclusions of this article will be made available by the authors, without undue reservation.

Author contributions

QW designed the project, performed experiments, collected data, analyzed results, and wrote up the study. E-LO performed experiments, collected data, and analyzed results. YC performed experiments and collected data. Z-YW performed experiments. Z-WW collected data. P-CW analyzed the results and revised this paper. X-WF designed the project and analyzed the results. J-LZ designed the project, analyzed results, and wrote up the study. All authors contributed to the article and approved the submitted version.

Funding

This research was supported by the National Nature Science Foundation of China (31802128), the Qian Academy of Agricultural Sciences post-subsidy of the National Nature Science Foundation (qiannongkeyuanguojihoubuzhu[2021]25), the Guizhou Province Science and Technology Planning Project (qiankehejichu[2020]1Z027), the Guizhou Province Hundred-level talent Project (qiankehepingtairencai-GCC[2022]022-1), and the Qian Academy of Agricultural Sciences post-subsidy of the National Nature Science Foundation (qiannongkeyuanguojihoubuzhu[2021]13).

Conflict of interest

The authors declare that the research was conducted in the absence of any commercial or financial relationships that could be construed as a potential conflict of interest.

Publisher's note

Supplementary material

The Supplementary Material for this article can be found online at: https://www.frontiersin.org/articles/10.3389/fpls.2022.979883/full#supplementary-material

SUPPLEMENTARY FIGURE 1
Effects of DH5α and GB03 on tall fescue phenotype. **(A)** Individual plant and **(B)** one pot of plant (containing five seedlings) were photographed from different parallel treatments, including the total nitrogen level (TN-

3.75 mM NO_3^-) and the low nitrogen level (LN-0.25 mM NO_3^-) with DH5α or GB03, respectively, and the water treatment as control.

SUPPLEMENTARY TABLE 1
Effects of DH5α and GB03 on tall fescue growth under various concentrations of NO_3^-. The treatments were: total nitrogen (TN), total nitrogen with *E. coli* DH5α (TN + DH5α), total nitrogen with soil bacteria GB03 (TN + GB03), low nitrogen stress (LN), low nitrogen stress with *E. coli* DH5α (LN + DH5α) and low nitrogen stress with soil bacteria GB03 (LN + GB03). Values are means ± SE (n = 8). The different letters indicate significant differences at $p < 0.05$ (Duncan's test).

References

Amtmann, A., and Armengaud, P. (2009). Effects of n, p, K and s on metabolism: new knowledge gained from multi-level analysis. *Curr. Opin. Plant Biol.* 12, 275–283. doi: 10.1016/j.pbi.2009.04.014

Argueso, C. T., Ferreira, F. J., and Kieber, J. J. (2009). Environmental perception avenues: the interaction of cytokinin and environmental response pathways. *Plant Cell Environ.* 32, 1147–1160. doi: 10.1111/j.1365-3040.2009.01940.x

Benjamins, R., and Scheres, B. (2008). Auxin: the looping star in plant development. *Annu. Rev. Plant Biol.* 59, 443–465. doi: 10.1146/annurev.arplant.58.032806.103805

Caba, J. M., Centeno, M. L., Fernández, B., Gresshoff, P. M., and Ligero, F. (2000). Inoculation and nitrate alter phytohormone levels in soybean roots: differences between a supernodulating mutant and the wild type. *Planta* 211, 98–104. doi: 10.1007/s004250000265

Canales, J., Moyano, T. C., Villarroel, E., and Gutiérrez, R. A. (2014). Systems analysis of transcriptome data provides new hypotheses about *Arabidopsis* root response to nitrate treatments. *Front. Plant Sci.* 5. doi: 10.3389/fpls.2014.00022

Chen, J. G., Cheng, S., Cao, W., and Zhou, X. (1998). Involvement of endogenous plant hormones in the effect of mixed nitrogen source on growth and tillering of wheat. *J. Plant Nutr.* 21, 87–97. doi: 10.1080/01904169809365385

Chen, C.-Z., Lv, X.–F., Li., J.–Y., Yi., H.–Y., and Gong., J. M. (2012). Arabidopsis NRT1.5 is another essential component in the regulation of nitrate reallocation and stress tolerance. *Plant Physiol.* 159, 1582–1590. doi: 10.1104/pp.112.199257

Chen, X. F., and Zhu, X. F. (2006). Discussion on seeding technique of tall fescue turf. *Shanghai Agricul. Sci. Technol.* 2, 94. doi: 10.3969/j.issn.1001-0106.2006.02.083

Choi, S.-K., Jeong, H., Kloepper, J. W., and Ryu, C.-M. (2014). Genome sequence of *Bacillus amyloliquefaciens* GB03, an active ingredient of the first commercial biological control product. *Genome. Announc.* 2, e01092–e01014. doi: 10.1128/genomea.01092-14

Davidson, E. A. (2009). The contribution of manure and fertilizer nitrogen to atmospheric nitrous oxide since 1860. *Nat. Geosci.* 2, 659–662. doi: 10.1038/ngeo608

Forde, B. G. (2002). Local and long-range signaling pathways regulating plant responses to nitrate. *Annu. Rev. Plant Biol.* 53, 203–224. doi: 10.1146/annurev.arplant.53.100301.135256

Foyer, C. H., and Ferrario, S. (1994). Modulation of carbon and nitrogen metabolism in transgenic plants with a view to improved biomass production. *Biochem. Soc Trans.* 22, 909–915. doi: 10.1042/bst0220909

Freitas, M. A., Medeiros, F. H. V., Carvalho, S. P., Guilherme, L. R. G., Teixeira, W. D., Zhang, H. M., et al. (2015). Augmenting iron accumulation in cassava by the beneficial soil bacterium *Bacillus subtilis* (GB03). *Front. Plant Sci.* 6. doi: 10.3389/fpls.2015.00596

Fukaki, H., and Tasaka, M. (2009). Hormone interactions during lateral root formation. *Plant Mol. Biol.* 69, 437–449. doi: 10.1007/s11103-008-9417-2

Gaudinier, A., Rodriguez-Medina, J., Zhang, L., Olson, A., Liseron- Monfils, C., Bågman, A.-M., et al. (2018). Transcriptional regulation of nitrogen-associated metabolism and growth. *Nature* 563, 259–264. doi: 10.1038/s41586-018-0656-3

Gras, D. E., Vidal, E. A., Undurraga, S. F., Riveras, E., Moreno, S., Dominguez-Figueroa, J., et al. (2018). SMZ/SNZ and gibberellin signaling are required for nitrate-elicited delay of flowering time in *Arabidopsis thaliana*. *J. Exp. Bot.* 69, 619–631. doi: 10.1093/jxb/erx423

Halliday, K. J., Martinez-Garcia, J. F., and Josse, E.-M. (2009). Integration of light and auxin signaling. *Cold Spring Harb. Perspect. Biol.* 1, a001586. doi: 10.1101/cshperspect.a001586

Han, Q. Q., Jia, T. T., Lü, X. P., Li, H. R., Li, J., Zhao, Q., et al. (2014a). Effect of *Bacillus subtilis* GB03 on salt tolerance of alfalfa (*Medicago sativa*). *Plant Physiol. J.* 50, 1423–1428. doi: 10.13592/j.cnki.ppj.2014.0214

Han, Q. Q., Lü, X. P., Bai, J. P., Qiao, Y., Paré, P. W., Wang, S. M., et al. (2014b). Beneficial soil bacterium *Bacillus subtilis* (GB03) augments salt tolerance of white clover. *Front. Plant Sci.* 5. doi: 10.3389/fpls.2014.00525

Han, Q. Q., Wu, Y. N., Gao, H. J., Xu, R., Paré, P. W., Shi, H. Z., et al. (2017). Improved salt tolerance of medicinal plant *Codonopsis pilosula* by *Bacillus amyloliquefaciens* GB03. *Acta Physiol. Plant* 39, 35. doi: 10.1007/s11738-016-2325-1

Jackson, M. L. (1959). Soil chemical analysis. *J. Plant Nutr. Soil Sc.* 85, 251–252. doi: 10.1002/jpln.19590850311

Jiang, K., and Feldman, L. J. (2003). Root meristem establishment and maintenance: the role of auxin. *J. Plant Growth Regul.* 21, 432–440. doi: 10.1007/s00344-002-0037-9

Kakimoto, T. (2003). Perception and signal transduction of cytokinins. *Annu. Rev. Plant Biol.* 54, 605–627. doi: 10.1146/annurev.arplant.54.031902.134802

Kiba, T., Kudo, T., Kojima, M., and Sakakibara, H. (2011). Hormonal control of nitrogen acquisition: roles of auxin, abscisic acid, and cytokinin. *J. Exp. Bot.* 62, 1399–1409. doi: 10.1093/jxb/erq410

Kloepper, J. W. (1992). *Plant growth-promoting rhizobacteria as biological control agents*. New York: Marcel Dekker Inc.

Krouk, G., Lacombe, B., Bielach, A., Perrine-Walker, F., Malinska, K., Mounier, E., et al. (2010). Nitrate-regulated auxin transport by NRT1.1 defines a mechanism for nutrient sensing in plants. *Dev. Cell* 18, 927–937. doi: 10.1016/j.devcel.2010.05.008

Laplaze, L., Benkova, E., Casimiro, I., Maes, L., Vanneste, S., Swarup, R., et al. (2007). Cytokinins act directly on lateral root founder cells to inhibit root initiation. *Plant Cell* 19, 3889–3900. doi: 10.1104/PP.106.091223

Li, W. B., Wang, Y., Okamoto, M., Crawford, N. M., Siddiqi, M. Y., Glass, A. D. M., et al. (2006). Dissection of the AtNRT2.1:AtNRT2.2 inducible high-affinity nitrate transporter gene cluster. *Plant Physiol* 143, 425–33. doi: 10.1104/PP.106.091223

Lin, S.-H., Kuo, H.-F., Canivenc, G., Lin, C.-S., Lepetit, M., Hsu, P.-K., et al. (2008). Mutation of the *Arabidopsis NRT1.5* nitrate transporter causes defective root-to-shoot nitrate transport. *Plant Cell* 20, 2514–2528. doi: 10.2307/25224353

Liu, K.-H., Huang, C.-Y., and Tsay, Y.-F. (1999). CHL1 is a dual-affinity nitrate transporter of arabidopsis involved in multiple phases of nitrate uptake. *Plant Cell* 11, 865–874. doi: 10.2307/3870820

Liu, W.-X., and Wang, G. (2012). N and p stoichiometry of plant and soil on slope direction gradient of sub-alpine meadows. *J. Lanzhou Univ.* 48, 70–75. doi: 10.3969/j.issn.0455-2059.2012.03.012

Liu, J., Xia, A., Lei, C., Chen, F., Bao, J., Yuan, L., et al. (2010). Auxin transport in maize roots in response to localized nitrate supply. *Ann. Bot.* 106, 1019–1026. doi: 10.1093/aob/mcq202

Ljung, K., Hull, A. K., Celenza, J., Yamada, M., Estelle, M., Normanly, J., et al. (2005). Site and regulation of auxin biosynthesis in arabidopsis roots. *Plant Cell* 17, 1090–1104. doi: 10.1105/tpc.104.029272

Marschnera, P., and Timonen, S. (2005). Interactions between plant species and mycorrhizal colonization on the bacterial community composition in the rhizosphere. *App. Soil Ecol.* 28, 23–36. doi: 10.1016/j.apsoil.2004.06.007

Martin, A. C., del Pozo, J. C., Iglesias, J., Rubio, V., Solano, R., de la Peña, A., et al. (2000). Influence of cytokinins on the expression of phosphate starvation responsive genes in *Arabidopsis*. *Plant J.* 24, 559–567. doi: 10.1046/j.1365-313x.2000.00893.x

Miller, A. J., and Cramer, M. D. (2004). Root nitrogen acquisition and assimilation. *Plant Soil* 274, 1–36. doi: 10.1007/s11104-004-0965-1

Moore, B., Zhou, L., Rolland, F., Hall, Q., Cheng, W.-H., Liu, Y.-X., et al. (2003). Role of the *Arabidopsis* glucose sensor HXK1 in nutrient, light, and hormonal signaling. *Science* 300, 332–336. doi: 10.1126/science.1080585

Myresiotis, C. K., Karaoglanidis, G. S., Vryzas, Z., and Papadopoulou-Mourkidou, E. (2011). Evaluation of plant-growth-promoting rhizobacteria, acibenzolar-*S*-methyl and hymexazol for integrated control of fusarium crown and root rot on tomato. *Pest Manage. Sci.* 68, 404–411. doi: 10.1002/ps.2277

Nelson, D. W., and Sommers, L. E. (1980). Total nitrogen analysis of soil and plant tissues. *J. Assoc. Offic. Anal. Chem.* 63, 770–778. doi: 10.1093/jaoac/63.4.770

Niu, S.-Q., Li, H.-R., Paré, P. W., Aziz, M., Wang, S.-M., Shi, H.-Z., et al. (2016). Induced growth promotion and higher salt tolerance in the halophyte grass *Puccinellia tenuiflora* by beneficial rhizobacteria. *Plant Soil* 407, 217–230. doi: 10.1007/s11104-015-2767-z

Nosengo, N. (2003). Fertilized to death. *Nature* 425, 894–895. doi: 10.1038/425894A

Ohkubo, Y., Tanaka, M., Tabata, R., Ogawa-Ohnishi, M., and Matsubayashi, Y. (2017). Shoot-to-root mobile polypeptides involved in systemic regulation of nitrogen acquisition. *Nat. Plants* 3, 1–6. doi: 10.1038/nplants.2017.29

Ondzighi-Assoume, C. A., Chakraborty, S., and Harris, J. M. (2016). Environmental nitrate stimulates abscisic acid accumulation in *Arabidopsis* root tips by releasing it from inactive stores. *Plant Cell* 28, 729–745. doi: 10.1105/tpc.15.00946

Orsel, M., Chopin, F., Leleu, O., Smith, S. J., Krapp, A., Daniel-Vedele, F., et al. (2006). Characterization of a two-component high-affinity nitrate uptake system in arabidopsis. physiology and protein-protein interaction. *Plant Physiol.* 142, 1304–1317. doi: 10.1104/pp.106.085209

Orsel, M., Eulenburg, K., Krapp, A., and Daniel-Vedele, F. (2004). Disruption of the nitrate transporter genes *AtNRT2.1* and *AtNRT2.2* restricts growth at low external nitrate concentration. *Planta* 219, 714–721. doi: 10.1007/s00425-004-1266-x

Paré, P. W., Zhang, H.-M., Aziz, M., Xie, X.-T., Kim, M.-S., Shen, X., et al. (2011). Beneficial rhizobacteria induce plant growth: mapping signaling networks in *Arabidopsis*. *Soil Biol. Biochem.* 23, 403–412. doi: 10.1007/978-3-642-14512-4_15

Patel, D., and Franklin, K. A. (2009). Temperature-regulation of plant architecture. *Plant Signal. Behav.* 4, 577–579. doi: 10.4161/psb.4.7.8849

Pieterse, C. M. J., Van Wees, S. C. M., Ton, J., Van Pelt, J. A., and Van Loon, L. C. (2002). Signalling in rhizobacteria-induced systemic resistance in *Arabidopsis thaliana*. *Plant Biol.* 4, 535–544. doi: 10.1055/s-2002-35441

Poitout, A., Ruffel, S., Novak, O., Lacombe, B., Crabos, A., Krouk, G., et al. (2018). Responses to systemic nitrogen signaling in arabidopsis roots involve trans-zeatin in shoots. *Plant Cell* 30, 1243–1257. doi: 10.1105/tpc.18.00011

Porra, R. J., Thompson, W. A., and Kriendemann, P. E. (1989). Determination of accurate extinction coefficients and simultaneous equations for assaying chlorophyll a and b extracted with four different solvents:verification of the concentration of chlorophyll standards by atomic absorption spectroscopy. *Biochim. Biophys.Acta.* 975, 384–394. doi: 10.1016/S0005-2728(89)80347-0

Pretty, J. (2008). Agricultural sustainability: concepts, principles and evidence. *Phil. Trans. R. Soc. B.* 363, 447–65. doi: 10.1098/rstb.2007.2163

Raupach, G. S., and Kloepper, J. W. (1998). Mixtures of plant growth-promoting rhizobacteria enhance biological control of multiple cucumber pathogens. *Phytopathology* 88, 1158–1164. doi: 10.1094/PHYTO.1998.88.11.1158

Ristova, D., Carré, C., Pervent, M., Medici, A., Kim, G. J., Scalia, D., et al. (2016). Combinatorial interaction network of transcriptomic and phenotypic responses to nitrogen and hormones in the *Arabidopsis thaliana* root. *Sci. Signal.* 9, 1–11. doi: 10.1126/scisignal.aaf2768

Robertson, G. P., and Vitousek, P. (2009). Nitrogen in agriculture: balancing the cost of an essential resource. *Annu. Rev. Environ. Rosour.* 34, 97–125. doi: 10.1146/annurev.environ.032108.105046

Rolland, F., Baena-Gonzalez, E., and Sheen, J. (2006). Sugar sensing and signaling in plants: conserved and novel mechanisms. *Annu. Rev. Plant Biol.* 57, 675–709. doi: 10.1146/ annurev.arplant.57.032905.105441

Rook, F., Corke, F., Card, R., Munz, G., Smith, C., and Bevan, M. W. (2001). Impaired sucrose-induction mutants reveal the modulation of sugar-induced starch biosynthetic gene expression by abscisic acid signaling. *Plant J.* 26, 421–433. doi: 10.1046/j.1365-313x.2001.2641043.x

Rudrappa, T., Biedrzycki, M. L., Kunjeti, S. G., Donofrio, N. M., Czymmek, K. J., Paré, P. W., et al. (2010). The rhizobacterial elicitor acetoin induces systemic resistance in arabidopsis thaliana. *Commun. Integr. Biol.* 3, 130–138. doi: 10.2307/4281635

Ryu, C.-M., Farag, M. A., Hu, C.-H., Reddy, M. S., Wei, H.-X., Paré, P. W., et al. (2004). Bacterial volatiles promote growth in *Arabidopsis*. *Plant Physiol.* 134, 1017–26. doi: 10.2307/4281635

Ryu, C.-M., Farag, M. A., Hu, C.-H., Reddy, M. S., Wei, H.-X., Paré, P. W., et al. (2003). Bacterial volatiles promote growth in *Arabidopsis*. *Proc. Natl. Acad. Sci. U.S.A.* 100, 4927–4932. doi: 10.1073/pnas.0730845100

Ryu, C.-M., Farag, M. A., Paré, P. W., and Kloepper, J. W. (2005). Invisible signals from the underground: bacterial volatiles elicit plant growth promotion and induce systemic resistance. *Plant Pathol. J.* 21, 7–12. doi: 10.5423/PPJ.2005.21.1.007

Sakakibara, H., Takei, K., and Hirose, N. (2006). Interactions between nitrogen and cytokinin in the regulation of metabolism and development. *Trends Plant Sci.* 11, 440–448. doi: 10.1016/j.tplants.2006.07.004

Samuelson, M. E., and Larsson, C. M. (1993). Nitrate regulation of zeatin riboside levels in barley roots: effects of inhibitors of n-assimilation and comparison with ammonium. *Plant Sci.* 93, 77–84. doi: 10.1016/0168-9452(93)90036-Y

Schippers, B. A., Bakker, A. W., and Bakker, P. A. H. M. (1987). Interactions of deleterious and beneficial rhizosphere microorganisms and the effect of cropping practices. *Annu. Rev. Phytopathol.* 25, 339–358. doi: 10.1146/annurev.py.25.090187.002011

Schmülling, T., Schäfer, S., and and Ramanov, G. (1997). Cytokinins as regulators of gene expression. *Physiol. Plant* 100, 505–519. doi: 10.1034/j.1399-3054.1997.1000312.x

Signora, L., De Smet, I., Foyer, C. H., and Zhang, H. M. (2001). ABA plays a central role in mediating the regulatory effects of nitrate on root branching in *Arabidopsis*. *Plant J.* 28, 655–662. doi: 10.1046/j.1365-313x.2001.01185.x

Smeekens, S. (2000). Sugar-induced signal transduction in plants. *Annu. Rev. Plant Physiol. Plant Mol. Biol.* 51, 49–81. doi: 10.1146/annurev.arplant.51.1.49

Smith, K. A., Mosier, A. R., Crutzen, P. J., and Winiwarter, W. (2012). The role of N_2O derived from crop-based biofuels, and from agriculture in general, in earth's climate. *Phil. Trans. R. Soc B* 367, 1169–1174. doi: 10.1098/rstb.2011.0313

Tabata, R., Sumida, K., Yoshii, T., Ohyama, K., Shinohara, H., and Matsubayashi, Y. (2014). Perception of root-derived peptides by shoot LRR-RKs mediates systemic n-demand signaling. *Science* 346, 343–346. doi: 10.1126/science.1257800

Takei, K., Sakakibara, H., Taniguchi, M., and Sugiyama, T. (2001). Nitrogen-dependent accumulation of cytokinins in root and the translocation to leaf: implication of cytokinin species that induces gene expression of maize response regulator. *Plant Cell Physiol.* 42, 85–93. doi: 10.1093/pcp/pce009

Takei, K., Takahashi, T., Sugiyama, T., Yamaya, T., and Sakakibara, H. (2002). Multiple routes communicating nitrogen availability from roots to shoots: a signal transduction pathway mediated by cytokinin. *J. Exp. Bot.* 53, 971–977. doi: 10.1093/jexbot/53.370.971

Tamaki, V., and Mercier, H. (2007). Cytokinins and auxin communicate nitrogen availability as long-distance signal molecules in pineapple (*Ananas comosus*). *J. Plant Physiol.* 164, 1543–1547. doi: 10.1016/j.jplph.2007.01.010

Tang, X.-M., Wang, Y., Ma, D.-W., Cheng, H.-Y., Yang, H., Dai, Y., et al. (2015). Analysis of DNA methylation of tall fescue in response to drought based on methylation-sensitive amplification polymorphism (MSAP). *Acta Prataculturae Sin.* 24, 164–173. doi: 10.11686/cyxb20150420

Teale, W. D., Paponov, I. A., and Palme, K. (2006). Auxin in action: signalling, transport and the control of plant growth and development. *Nat. Rev. Mol. Cell Biol.* 7, 847–859. doi: 10.1038/nrm2020

Tian, Q.-Y., Chen, F.-J., Liu, J.-X., Zhang, F.-S., and Mi, G.-H. (2008). Inhibition of maize root growth by high nitrate supply is correlated with reduced IAA levels in roots. *J. Plant Physiol.* 165, 942–951. doi: 10.1016/j.jplph.2007.02.011

Vance, C. P. (2001). Symbiotic nitrogen fixation and phosphorus acquisition. plant nutrition in a world of declining renewable resources. *Plant Physiol.* 127, 390–397. doi: 10.2307/4280097

Vanneste, S., and Friml, J. (2009). Auxin: a trigger for change in plant development. *Cell* 136, 1005–1016. doi: 10.1016/j.cell.2009.03.001

Varala, K., Marshall-Colo´ n, A., Cirrone, J., Brooks, M. D., Pasquino, A. V., Le´ ran, S., et al. (2018). Temporal transcriptional logic of dynamic regulatory networks underlying nitrogen signaling and use in plants. *Proc. Natl. Acad. Sci. U.S.A.* 115, 6494–6499. doi: 10.1073/pnas.1721487115

Vega, A., O'Brien, J. A., and Gutiérrez, R. A. (2019). Nitrate and hormonal signaling crosstalk for plant growth and development. *Curr. Opin. Plant Biol.* 52, 155–163. doi: 10.1016/j.pbi.2019.10.001

Wagner, B. M., and Beck, E. (1993). Cytokinins in the perennial herb *Urtica dioica* l. as influenced by its nitrogen status. *Planta* 190, 511–518. doi: 10.1007/bf00224790

Werner, T., Motyk, V., Strnad, M., and Schmülling, T. (2001). Regulation of plant growth by cytokinin. *Proc. Natl. Acad. Sci. U.S.A.* 98, 10487–10492. doi: 10.1073/pnas.171304098

Xie, X.-T., Zhang, H.-M., and Paré, P. W. (2009). Sustained growth promotion in arabidopsis with long-term exposure to the beneficial soil bacterium *Bacillus subtilis* (GB03). *Plant Signal. Behav.* 4, 948–953. doi: 10.4161/psb.4.10.9709

Yang, P.-Y., He, Y.-L., and Wu, Y. M. (2013). Advances in genetic engineering of tall fescue resilience. *Pratacultural Sci.* 30, 1968–1972. doi: 10.11829\j.issn.1001-0629.2012-0534

Zhang, S. (2019). *Effects of exogenous nitrogen and potassium on the growth and nutrients uptake of festuca arundinacea. [master's thesis]* (Shandong: Liaochen University).

Zhang, J.-L., Aziz, M., Qiao, Y., Han, Q.-Q., Li, J., Wang, Y.-Q., et al. (2014). Soil microbe *Bacillus subtilis* (GB03) induces biomass accumulation and salt tolerance

with lower sodium accumulation in wheat. *Crop Pasture Sci.* 65, 423–427. doi: 10.1071/cp13456

Zhang, H.-M., Kim, M.-S., Krishnamachari, V., Payton, P., Sun, Y., Grimson, M., et al. (2007). Rhizobacterial volatile emissions regulate auxin homeostasis and cell expansion in *Arabidopsis*. *Planta* 226, 839–851. doi: 10.1007/s00425-007-0530-2

Zhang, H.-M., Kim, M.-S., Sun, Y., Dowd, S. E., Shi, H.-Z., and Paré, P. W. (2008b). Soil bacteria confer plant salt tolerance by tissue-specific regulation of the sodium transporter *HKT1*. *Mol. Plant Microbe Interac.* 21, 737–744. doi: 10.1094/mpmi-21-6-0737

Zhang, H.-M., Murzello, C., Sun, Y., Kim, M.-S., Xie, X.-T., Jeter, R. M., et al. (2010). Choline and osmotic-stress tolerance induced in *Arabidopsis* by the soil microbe *bacillus subtilis* (GB03). *Mol. Plant Microbe Interac.* 23, 1097–1104. doi: 10.1094/mpmi-23-8-1097

Zhang, H.-M., Sun, Y., Xie, X.-T., Kim, M.-S., Dowd, S. E., and Paré, P. W. (2009). A soil bacterium regulates plant acquisition of iron *via* deficiency-inducible mechanisms. *Plant J.* 58, 568–577. doi: 10.1111/j.1365-313x.2009.03803.x

Zhang, H.-M., Xie, X.-T., Kim, M.-S., Kornyeyev, D. A., Holaday, S., and Paré, P. W. (2008a). Soil bacteria augment *Arabidopsis* photosynthesis by decreasing glucose sensing and abscisic acid levels in planta. *Plant J.* 56, 264–273. doi: 10.1111/j.1365-313x.2008.03593.x

Zhao, M.-Z., and Ma, J.-Z. (2014). Distribution characteristics and source analysis of nitrate in different types of the soil in arid areas. *J. Lanzhou Univ.* 50, 424–430. doi: 10.13885/j.issn.0455-2059.2014.03.020

Zhu, J.-K. (2002). Salt and drought stress signal transduction in plants. *Annu. Rev. Plant Biol.* 53, 247–273. doi: 10.1146/annurev.arplant.53.091401.143329

frontiers | Frontiers in Plant Science

TYPE Original Research
PUBLISHED 06 October 2022
DOI 10.3389/fpls.2022.947882

OPEN ACCESS

EDITED BY
Jin-Lin Zhang,
Lanzhou University, China

REVIEWED BY
Muhammad Ahsan Farooq,
Zhejiang University, China
Lei Wang,
State Key Laboratory of Desert and Oasis Ecology, (CAS), China
Peiman Zandi,
Yibin University, China

*CORRESPONDENCE
Wensheng Liu
Liuwsairr@163.com
Wenbin Zeng
6722507@qq.com

SPECIALTY SECTION
This article was submitted to Plant Abiotic Stress, a section of the journal Frontiers in Plant Science

RECEIVED 19 May 2022
ACCEPTED 05 September 2022
PUBLISHED 06 October 2022

CITATION
Kuang X, Wang W, Hu J, Liu W and Zeng W (2022) Subcellular distribution and chemical forms of manganese in *Daucus carota* in relation to its tolerance. *Front. Plant Sci.* 13:947882. doi: 10.3389/fpls.2022.947882

Subcellular distribution and chemical forms of manganese in *Daucus carota* in relation to its tolerance

Xueshao Kuang, Wumin Wang, Jiayao Hu, Wensheng Liu* and Wenbin Zeng*

College of Life Science and Technology, Central South University of Forestry and Technology, Changsha, China

Daucus carota is a biennial herb of the Umbelliferae family, which is a candidate plant for the phytoremediation of Mn pollution. To reveal the mechanism of this plant to adapt to Mn stress, plant growth, anatomical structure, Mn accumulation characteristic, Mn subcellular distribution, and chemical forms of *D. carota* under six Mn^{2+} concentrations by pot culture experiments were studied. The results showed that with the rising Mn concentrations, the total dry weight and leaf area of *D. carota* increased firstly and then decreased, while the specific leaf area increased. The thickness of the main vein, upper epidermis, and lower epidermis; the thickness of the palisade tissue; and the thickness of the spongy tissue of the leaves increased firstly and then decreased. The Mn content in the aboveground and underground parts of *D. carota* increased, and the values of the bioconcentration factor (BCF) and translocation factor (TF) were higher than 1. The Mn existing in the cell wall and soluble components accounted for the largest proportion, and the proportion of Mn in the cell wall increased with increasing concentrations of Mn. In addition, Mn mainly existed in ethanol extraction state, deionized water extraction state, and sodium chloride extraction state. The results showed that *D. carota* could alleviate the damage caused by high manganese concentration by storing most of manganese in the cell wall and vacuole and existing in the form of low-activity state.

KEYWORDS

***Daucus carota*, Mn accumulation, anatomical structure, subcellular distribution, chemical forms**

Introduction

Manganese (Mn) is one of the essential trace elements for plant growth, which is involved in photosynthesis, while overdose of Mn in plants would interfere with the absorption and utilization of other mineral elements, influence energy metabolism, depress photosynthetic rates, and lead to oxidative stress (Fernando & Lynch, 2015; Tavanti et al., 2020), which would inhibit plant growth and development and even endanger human health through the food chain (Yao et al., 2012). In the field ecosystems, human activities such as mining, metallurgy, and illegal sewage discharge lead to Mn pollution in soil. It was reported that manganese toxicity is one of the main toxic factors inhibiting the crop growth in acid soil in China, and it is an urgent task to control the pollution (Xu et al., 2009; Huang et al., 2019; Xiao et al., 2019). Among various controlling technologies, phytoremediation is the one with low cost, wide range of adaptation, small impact on the original environment, and long-lasting governance effect (Bhaduri and Fulekar, 2012; Gallego et al., 2012; Tavanti et al., 2020). The premise of this technology is to screen plants with high heavy metal tolerance and high economic value (Huang et al., 2018; Wu et al., 2018). Therefore, screening plants with tolerance to heavy metals and revealing their tolerance mechanism is the key step for the remediation of contaminated soil by phytoremediation technology.

Morphological and microstructure changes can directly and comprehensively reflect the resistance of plants to environmental stress (Daud et al., 2009). Under stress, plant morphology would make some protective compensation responses to adapt to gradual or sudden changes of the environment (Elleuch et al., 2013). It was reported that low concentrations of Mn treatment can stimulate the activity of certain enzymes and promote plant growth (Mou et al., 2011), and high concentrations of the Mn treatment would cause plant biomass reduction (Yao et al., 2012). For example, the dry weight of roots, stems, and leaves of *Macleaya cordata* under low Mn treatment was significantly higher than that of the control (0 μM of Mn) (Pan et al., 2019b). The root growth of *Broussonetia papyrifera* increased firstly and then decreased with the increasing Mn concentration (Huang et al., 2019). Leaves are the main organs of photosynthesis and transpiration for plants; its structural characteristics reflect the adaptation of plants to the environment (Tian et al., 2014). For example, under high concentrations of Mn stress, the thickness of leaf palisade tissue and sponge tissue of *Populus cathayana* decreased significantly, indicating that mesophyll was seriously damaged under Mn stress (Lei et al., 2007).

In heavy metal-contaminated soils, plants cope with the potential heavy metal stress in different ways. Some plant species adopt an exclusion strategy to avoid the excessive uptake and transport of metal ions. In contrast, other plant species can take up large amounts of metals by roots and transport them to the shoots. The difference in the absorption and accumulation of Mn by different plants reflects its strategy. For example, the Mn content in plant tissues *Phytolacca acinosa* (Xue et al., 2004), *Alyxia rubricalis* (Marques et al., 2009), and *Polygonum lapathifolium* (Liu et al., 2016) was high and increased with the increasing Mn treatment concentration.

Subcellular distribution and chemical forms of heavy metal were associated with metal tolerance and detoxification in plants. In order to survive in Mn-contaminated soil, plants have evolved various strategies for Mn detoxification, including metal exclusion, binding of Mn to the cell wall, restriction of Mn accumulation in sensitive tissues/organelles, and sequestration in vacuoles. At the cellular and tissue levels, heavy metals are mainly distributed in the cell wall and vacuole, isolating them from metabolically active areas such as cytoplasm, mitochondria, and chloroplasts, so as to maintain the smooth progress of normal physiological metabolism (Wang et al., 2015). For example, the Mn content of the cell wall and vacuole in *Phytolacca americana* (Dou et al., 2009) and *Vitis vinifera* (Yao et al., 2012) was the highest, which illustrated that compartmentalization plays an important role in tolerant plants (Li et al., 2018).

The chemical form approach quantifies the metal fates within cells by sequentially extracting metals with different chemical solutions (Jiang et al., 2021). Although these chemical phases are operationally defined, studies have provided clear evidence that heavy metals in inorganic form and water-soluble form migrate more readily than metals binding to pectates, phosphates, and oxalates, and these forms have stronger negative effects on plant cells. The organic compounds secreted by plants can not only activate the heavy metals in the soil but also form stable metal chelates with them, reduce their toxicity to plant tissues, and control the absorption and migration of heavy metals (Daud et al., 2009). Most of the heavy metal ions absorbed by plants will be transformed into different chemical forms, and the chemical form is directly related to the migration ability, activity, and toxicity of heavy metals in plants. For example, Wang et al. (2007) found that deionized water-extracted Mn is the main form of occurrence in the roots, stems, and leaves of *Polygonum hydropiper*, which is conducive to the transportation and accumulation of Mn to the aboveground parts of plants. In the mining area, Mn in the leaves, stems, and roots of *Xanthium strumarium* mainly exists in the form of pectinate and protein binding state (21.88%~55.43%), phosphate (9.21%~39.29%), and Mn oxalate (3.20%~22.19%), while heavy metals in the form of phosphate and oxalate are mainly stored in plant cell walls and vacuoles, and heavy metals combined with pectin and protein are mainly stored in vacuoles (Pan et al., 2019a). This may be one of the reasons that plants can resist high Mn stress.

Daucus carota is a biennial herb of carrot belonging to Umbelliferae. It has the characteristics of large biomass, beautiful plant type, wide ecological adaptability, fast growth rate, and strong stress resistance. A field investigation showed that this plant is widely distributed in Xiangtan Mn Mine Wasteland and can flower and bear fruit normally, indicating

that the plant has strong Mn tolerance (Wu et al., 2019). At present, the related research of *D. carota* mainly focused on biological activity (Li et al., 2012) and plant response under cadmium and copper stress (Wu et al., 2006; Ke et al., 2007; Dong et al., 2009). However, there are few studies on the tolerance and mechanism of *D. carota* under Mn stress, which limited the application of this plant in Mn pollution control. In order to reveal the response and tolerance mechanism of *D. carota* to manganese stress, this study analyzes the growth characteristics, leaf anatomical structure, Mn accumulation ability, subcellular components, and chemical morphological characteristics of *D. carota* under Mn stress. The aim of this study is to address the following questions. (1) Are there variations in Mn accumulation under different Mn exposure conditions? (2) Are these variations associated with Mn subcellular distribution, chemical forms? The aim is to provide a theoretical basis for the application of *D. carota* in the remediation of a manganese-polluted environment. Characterization of mechanisms involved in Mn accumulation and detoxification will provide a basis for further screening or engineering Mn-tolerant plants.

Materials and methods

Seed collection

Field investigations showed that *D. carota* in the Xiangtan Mn Mine area of Hunan Province (112°85′E, 27°97′N) distributes widely, grows well, and sets many fruits in this area. In October 2019, about 100 *D. carota* plant individuals were randomly selected and mature fruits were collected and taken back to the laboratory by paper bag. After natural drying, they were stored at room temperature. The concentration of Mn in the soil in this area is about 52,319.25 $mg \cdot kg^{-1}$.

Plant cultivation under controlled conditions

In May 2020, plump and uniform-size seeds were selected and sown in a sterilized sand dish and placed in an artificial climate incubator with a light intensity of 5,000 lx, a temperature of (25 ± 1)°C, a photoperiod of 12 h/12 h (day/night), and a relative humidity of 70%. When the seedlings grew to 4~6 cm in height, 1/2 concentration of Hoagland nutrient solution was applied. When the seedlings grew to 8~10 cm in height, seedlings with the same height were transplanted to the plastic pots (20 cm in diameter, 14 cm in height) containing fine sand and perlite (1:1). During the culture period, deionized water was added every day to maintain the growth substrate moist, and Hoagland nutrient solution was applied every 5 days. According to our preliminary experiments, the highest concentration of *D. carota* tolerant to Mn is 20,000 $\mu mol \cdot l^{-1}$. Therefore, according to the method of Pan et al. (2019), six Mn concentration treatments were set (0 (CK), 1,000, 5,000, 10,000, 15,000, 20,000 $\mu mol \cdot l^{-1}$) by using $MnCl_2 \cdot 4H_2O$. After the seedlings were transplanted to the pots for 2 weeks, six concentrations of Mn solutions were added into the pots. Twenty pots per treatment were set, and 120 pots were set in total.

Determination of growth indicators

On the 30th day after carrying out the Mn treatment, 10 individuals were randomly selected in each treatment. A vernier caliper with an accuracy of 0.1 mm was used to measure the plant height and taproot length, respectively. Then, the plants were washed with deionized water. After the plants were dried, the root morphology was measured with an Epson scanner (expression 11,000 xl, Japan). The root surface area, root volume, root diameter, and fibrous root number were scanned and analyzed by WinRHIZO image analysis software (2013e, Regent Instruments Inc., Canada). The leaf area was measured with the same method. Finally, the plant individuals were put in the oven, scalded at 95°C for 10 min, and baked at 65°C to constant weight, and the dry weight was weighed. The specific leaf area (SLA, the ratio of leaf area and leaf dry weight) was also calculated.

Determination of leaf anatomical structure

After 30 days of Mn treatment, 20 mature leaves were selected from each treatment, and anatomical structures were studied by using the paraffin section method. The size of the cut was controlled to 5 mm × 5 mm and placed in FFA fixative solution (70% ethanol: formaldehyde: glacial acetic acid = 90:5:5), sealed and stored in a brown glass bottle, and stored at 4°C for later use. The fixed and preserved leaves were pumped again, and the leaves were selected for ethanol gradient dehydration (85% ethanol, 95% ethanol, and absolute ethanol), made transparent in xylene, and embedded after soaking in wax. A digital microscope (Motic Images Advanced 3.0) was used to observe and take pictures. Digitizer Image Measurement software was used to measure leaf thickness, upper epidermis thickness, lower epidermis thickness, palisade tissue thickness, sponge tissue thickness, and other related data. The ratio of palisade tissue thickness and spongy tissue thickness and the tightness of organizational structure (the ratio of palisade tissue thickness and blade thickness) were calculated.

Determination of Mn content

The content of Mn in the aboveground and underground parts of *D. carota* was determined by atomic absorption

spectrometry (Yao et al., 2012). After 30 days of stress, the whole plant was harvested and divided into two parts: the aboveground part and the underground part, cleaned with distilled water and dried to constant weight. After being ground and burned, the ash content was dissolved with HCl. Finally, the content of Mn was determined using an atomic absorption spectrophotometer (AA-7000, Shimadzu, Japan). The bioconcentration factor (BCF, the ratio of total Mn content of plant samples and matrix heavy metal content) and transport factor (TF, the ratio of aboveground Mn content and underground Mn content) were also calculated.

Subcellular distribution of Mn

The subcellular components of Mn were determined by differential centrifugation according to the improved method of Pan et al. (2019). Three grams of fresh plant samples was chosen and mixed with 9 ml subcellular extract (0.25 mmol·l^{-1} sucrose, 50 mmol·l^{-1} Tris–HCl buffer (pH 7.5), 1 mmol·l^{-1} dithioerythritol) and was ground into homogenate on ice bath. Then, they were transferred to a centrifuge tube and centrifuged at 300 r·min^{-1} for 5 min. The sediment was the cell wall component (F1). Then, the supernatant was centrifuged at 2,000 r·min^{-1} for 20 min, and the sediment was chloroplast and cell nuclear components (F2). In addition, the supernatant was centrifuged at 10,000 r·min^{-1} for 20 min, the residue was the mitochondrial component (F3), and the supernatant was the ribosomal component (F4, soluble component). The obtained components were transferred to a porcelain crucible without damage and dried to constant weight at 70°C. Then, the mixed acid HNO_3–$HClO_4$ (5:3, v/v) was added on the hot plate and boiled until the residue is completely dissolved and becomes a powder. Finally, it was fully dissolved, rinsed, and filtered with deionized water; the volume in a 25-ml volumetric flask was fixed and diluted to an appropriate multiple; and an atomic absorption spectrophotometer (AA-7000, Shimadzu, Japan) was used to determine the Mn content in the sample.

Determination of Mn chemical speciation

The chemical forms of Mn in plants were extracted using a sequence of different extractants as the method of Pan et al. (2019): (1) 80% ethanol, extracting inorganic Mn giving priority to nitrate/nitrite, chloride, and aminophenol manganese; (2) deionized water (d-H_2O), extracting water-soluble Mn–organic acid complexes and $Mn(H_2PO_4)_7$; (3) 1 M NaCl, extracting pectates and protein-integrated Mn; (4) 2% acetic acid (HAC), extracting undissolved manganese phosphate including $Mn_2(HPO_4)_7$ and $Mn_2(PO4)_7$ and other Mn–phosphate complexes; (5) 0.6 M HCl, extracting manganese oxalate; (6) Mn in residues.

Three grams of fresh plant samples was taken, mixed with 20 ml extractant (80% ethanol, 1 mol·L^{-1} sodium chloride, 2% acetic acid, 0.6 mol·l^{-1} hydrochloric acid), and ground into a homogenate, then transferred to a centrifuge tube, shaken at 25°C for 22 h, and centrifuged at 5,000 r·min^{-1} for 10 min. After pouring out the supernatant, 10 ml of the same extractant was continuously added, shaken for 2 h, and centrifuged for 10 min, and the supernatant was combined. The supernatant was respectively inorganic Mn, water-soluble organic acid Mn, pectate and protein-bound Mn, Mn phosphate, and oxalate Mn, and finally precipitates as residual state. Various chemical forms were transferred into a porcelain crucible without damage and dried at 70°C to a constant weight. Then, HNO_3–$HClO_4$ (3:1) mixed acid was added, heated, and digested on a hot plate until it became an off-white solid. Finally, 10% HNO_3 was used to dissolve, wash, filter, and fix the volume, and the content of Mn was determined using an atomic absorption spectrophotometer.

Statistical analysis

The data of each index were expressed as "mean ± standard deviation". SPSS 19.0 statistical software was used to conduct one-way ANOVA on the measured data, and the least significant difference method (LSD method) was used to make multiple comparisons of the significance of the difference between different treatments for each indicator.

Results

Effect of Mn stress on plant biomass

With the increasing Mn concentrations, the dry weight of aboveground and underground parts of *D. carota* plants increased firstly and then decreased, reaching the maximum at 1,000 μM (Table 1), and the root-to-shoot ratio decreased. The aboveground height, aboveground dry weight, underground length, underground dry weight, and root-to-shoot ratio reached the highest value at 1,000 μM and reached the lowest value at 20,000 μM. Compared with the control, these values at 1,000 μM increased by 20.35%, 8.36%, 22.29%, 36.77%, and 11.76%, and reduced by 27.89%, 60.23%, 62.14%, 82.06%, and 52.94%, respectively.

As the concentration of Mn increased, the root surface area, root volume, average root diameter, and fibrous root number of *D. carota* increased firstly and then decreased (Table 2). All of these values (the root surface area, root volume, average root diameter, and fibrous root number) reached the maximum under 1,000 μM Mn treatment, and compared with the control, it increased by 31.56%, 14.40%, 27.64%, and 31.70%, respectively (Table 2).

The leaf area of *D. carota* increased firstly and then decreased with the increase in Mn treatment concentration (Figure 1A), and the leaf area of 1,000 μM of Mn treatment

10.3389/fpls.2022.947882

TABLE 1 Effects of manganese stress on plant growth of *D. carota*.

Treatment (μmol·L-1)	Aboveground height (cm)	Underground length (cm)	Aboveground dry weight (mg/plant)	Underground dry weight (mg/plant)	Root-shoot ratio
0	32.23±2.65 b	30.85±1.51 a	6.55±0.73 b	2.23±0.20 b	0.34±0.05 ab
1000	38.79±1.58 a	33.43±1.98 a	8.01±0.34 a	3.05±0.39 a	0.38±0.06 a
5000	30.57±1.84 b	26.86±2.13 b	5.86±0.21 c	1.74±0.30 c	0.30±0.04 b
10000	27.30±0.91 c	22.23±1.29 c	3.78±0.16 d	0.94±0.08 d	0.25±0.03 b
15000	25.37±1.16 cd	16.73±1.71 d	2.87±0.22 e	0.58±0.02 de	0.20±0.01 bc
20000	23.24±1.42 d	12.27±0.92 e	2.48±0.27 e	0.40±0.01 e	0.16±0.02 c

Values are the mean ± S.D. (n=5). Values with different letters within the same column indicate significant differences at the $P < 0.05$ level between concentrations according to LSD test. The same as below.

reached the maximum. As shown in Figure 1B, the specific leaf area of *D. carota* generally showed an upward trend with the increase in concentration.

Anatomical structure

As Mn concentrations increased, the thickness of the main vein, the thickness of the upper epidermis, and the thickness of the lower epidermis of *D. carota* increased firstly and then decreased, while the leaf thickness decreased (Table 3; Figure 2). The thickness of the upper and lower epidermis and the main vein reached the maximum value under the treatment of 5,000 μM of Mn, and the minimum value was reached at 20,000 μM.

The thickness of sponge tissue reached the maximum at 5,000 μM and then decreased with the increase in Mn stress concentration. The thickness and tightness of the tissue structure of the *D. carota* fence reached the maximum value at 1,000 μM Mn treatment then decreased with the increase in Mn concentrations (Table 4; Figure 3).

Mn accumulation

The Mn content in the aboveground and underground parts of *D. carota* increased with the increase in Mn concentration (Figure 4A). The content of the aboveground and underground parts of *D. carota* showed a linear cumulative trend with the rising Mn concentrations (for aboveground parts: $y = 0.8993x + 929.49$, $R^2 = 0.9574$; for underground parts: $y = 0.5716x + 379.15$, $R^2 = 0.9276$). When the Mn concentration attained to 20,000 μM, both the Mn content in the aboveground part and underground part reached the maximum, which were 16,948.37 and 13,210.33 mg·kg^{-1}, respectively. The Mn content in the aboveground part of *D. carota* was higher than that in the underground part under different concentrations of Mn treatment. When the Mn treatment concentration ranged in 10,000~2,000 μM, the Mn content of the aboveground part of *D. carota* can reach over 10,000 mg·kg^{-1}.

As the Mn concentration increased, the bioconcentration factor of *D. carota* decreased, and the least value was 11.92 (Figure 4B). The transport coefficients (TF) increased firstly and then decreased, and all of the values were greater than 1. When the Mn concentration was 10,000 μM, the transport coefficient was the highest, which was 2.65 (Figure 4C).

Subcellular distribution of Mn

The content of Mn in cell wall components, chloroplast and nucleus components, mitochondrial components, and ribosome components of the aboveground part of *D. carota* increased with the increase in Mn treatment concentration (Figures 5A–D); the correlation coefficients were 0.862, 0.991, 0.912, and 0.985, respectively ($P < 0.05$). In the subcellular components of the aboveground part of *D. carota*, the cell wall component has the highest Mn content, followed by ribosomal component, chloroplast and nuclear component, and mitochondrial

TABLE 2 Effects of manganese stress on root characteristics of *D. carota*.

Treatment (μmol·L-1)	Root surface area (cm^2)	Root volume (cm^3)	Average root diameter (mm)	Root tip number
0	61.53±2.22 b	0.89±0.07 b	0.48±0.02 b	1164.00±75.44 b
1000	80.94±5.63 a	1.14±0.02 a	0.55±0.02 a	1533.00±81.66 a
5000	53.22±1.44 c	0.70±0.02 c	0.43±0.04 c	1093.67±62.04 b
10000	32.11±2.43 d	0.46±0.03 d	0.36±0.02 d	744.67±50.00 c
15000	16.49±1.15 e	0.29±0.02 de	0.33±0.01 e	331.33±20.84 d
20000	12.45±0.48 e	0.17±0.01 e	0.30±0.01 f	126.33±8.33 e

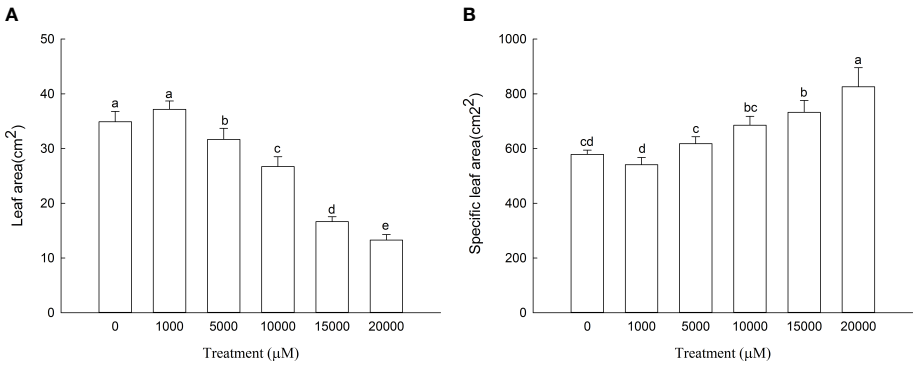

FIGURE 1
Leaf area **(A)** and specific leaf area **(B)** of *D carota* under Mn stress. Data points and error bars represent mean and S.D. (n = 3). Values with different letters indicate significant differences at the $P < 0.05$ level between different Mn concentrations according to the LSD test.

TABLE 3 The effects of Mn treatments on epidermal tissue and main vein structure in *D. carota*.

Treatment (μmol·L-1)	TE (μm)	TUE (μm)	TLE (μm)	TMV (μm)
0	119.79±1.76 a	10.50±0.76 bc	7.72±0.67 ab	169.24±10.04 ab
1000	106.20±2.32 b	11.25±0.65 b	7.44±0.57 b	162.37±3.57 b
5000	102.45±4.30 b	13.76±0.26 a	8.64±0.69 a	174.47±4.51 a
10000	100.40±4.58 b	8.75±0.14 c	7.33±0.52 c	149.24±3.16 c
15000	90.31±2.44 c	7.99±0.85 c	6.86±0.12 c	145.37±3.49 c
20000	95.75±7.35 c	7.21±0.32 c	6.63±0.26 c	142.54±3.06 c

TE, the leaf thickness; TUE, the thickness of the upper epidermis; TLE, the thickness of the lower epidermis; TMV, the thickness of the main vein.

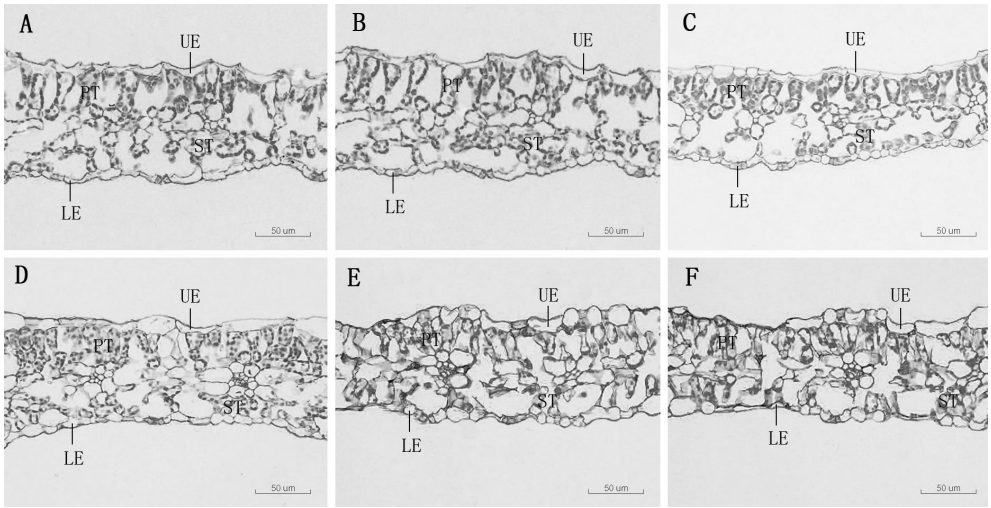

FIGURE 2
Leaf transverse anatomical structure of *D. carota* under Mn treatments **(A–F)**, UE, upper epidermis, LE, lower epidermis, PT, palisade tissue, ST, spongy tissue. **(A)** mdash;CK, **(B)** 1,000 μM, **(C)** 5,000 μM, **(D)** 10,000 μM, **(E)** 15,000 μM, **(F)** 20,000 μM.

TABLE 4 The effects of excess Mn treatments on mesophyll tissue structure in *D. carota*.

Treatment (μmol·L-1)	TP (μm)	TS (μm)	RPS	CTR
0	35.01±2.77 b	37.55±0.30 c	0.93±0.07 a	0.29±0.02 bc
1000	45.49±6.83 a	68.13±10.23 ab	0.69±0.19 b	0.43±0.06 a
5000	39.43±1.43 ab	69.20±5.43 a	0.57±0.06 b	0.38±0.03 ab
10000	32.30±2.92 b	59.43±5.05 b	0.55±0.10 bc	0.32±0.03 b
15000	21.09±2.21 c	56.33±3.46 b	0.38±0.05 c	0.23±0.02 c
20000	16.85±2.33 c	45.37±2.65 c	0.37±0.05 c	0.18±0.04 c

TP, the thickness of palisade tissue; TS, The thickness of sponge tissue; RPS, The ratio of palisade tissue/ spongy tissue; CTR, cell tense ratio.

component; the contents of Mn in the cell wall and ribosome components accounted for 73.38%~86.24% of the total. Under the treatment of 20,000 μM Mn, the Mn content of each subcellular component reached the highest value; the values were 640.51, 164.59, 56.43, and 244.12 mg·kg^{-1}, respectively (Figure 6A).

The content of Mn in cell wall components, chloroplast and nucleus components, mitochondrial components, and ribosome components in the underground part of *D. carota* increased with the increase in Mn treatment concentration; the correlation coefficients were 0.987, 0.950, 0.982, and 0.974, respectively ($P < 0.05$, Figures 5A–D). Among the subcellular components in the underground part of *D. carota*, the cell wall component has the highest Mn concentration, followed by the ribosomal component, chloroplast and nucleus component, and mitochondrial component which has the lowest content. The Mn content of cell wall components, chloroplast and cell nuclear components, ribosomal components, and ribosomal components all reached the maximum under the treatment of 20,000 μM Mn; they were 501.10, 127.56, 71.06, and 241.264 mg·kg^{-1}, respectively (Figure 6B).

Chemical forms of Mn

The Mn content in each chemical form of the aboveground part of *D. carota* is positively correlated with the Mn concentration; the correlation coefficients of ethanol, deionized water, sodium chloride, acetic acid, hydrochloric acid, and residual extracted Mn were 0.955, 0.987, 0.943, 0.910, 0.912, and 0.987, respectively ($P < 0.05$, Figures 7A–F). Its Mn content reached the maximum under 20,000 μM Mn treatment, which are 321.40, 505.98, 320.62, 214.67, 182.34, and 81.14 mg·kg^{-1}, respectively. The proportion distribution trend of the chemical forms of Mn in the aerial parts is deionized water extraction state > sodium chloride extraction state > ethanol extraction state > acetic acid extraction state > hydrochloric acid extraction state > residual state (Figure 8A).

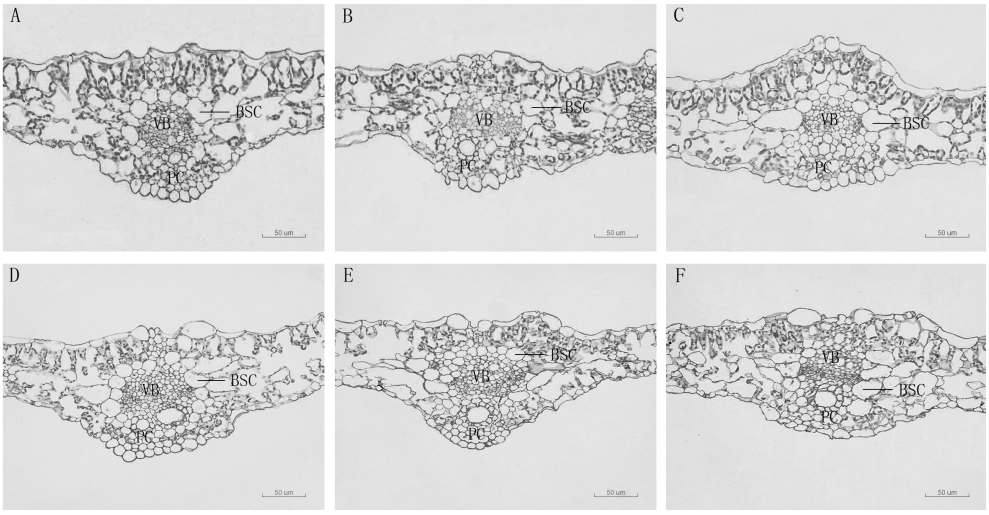

FIGURE 3
Leaf vein transverse anatomical structure of leaf blade of *D. carota* under Mn treatments **(A–F)**. BSC: bundle sheath cells, V, vascular bundle, C, pachycorn cells. **(A)** CK, **(B)** 1,000 μM, **(C)** 5,000 μM, **(D)** 10,000 μM, **(E)** 15,000 μM, **(F)** 20,000 μM.

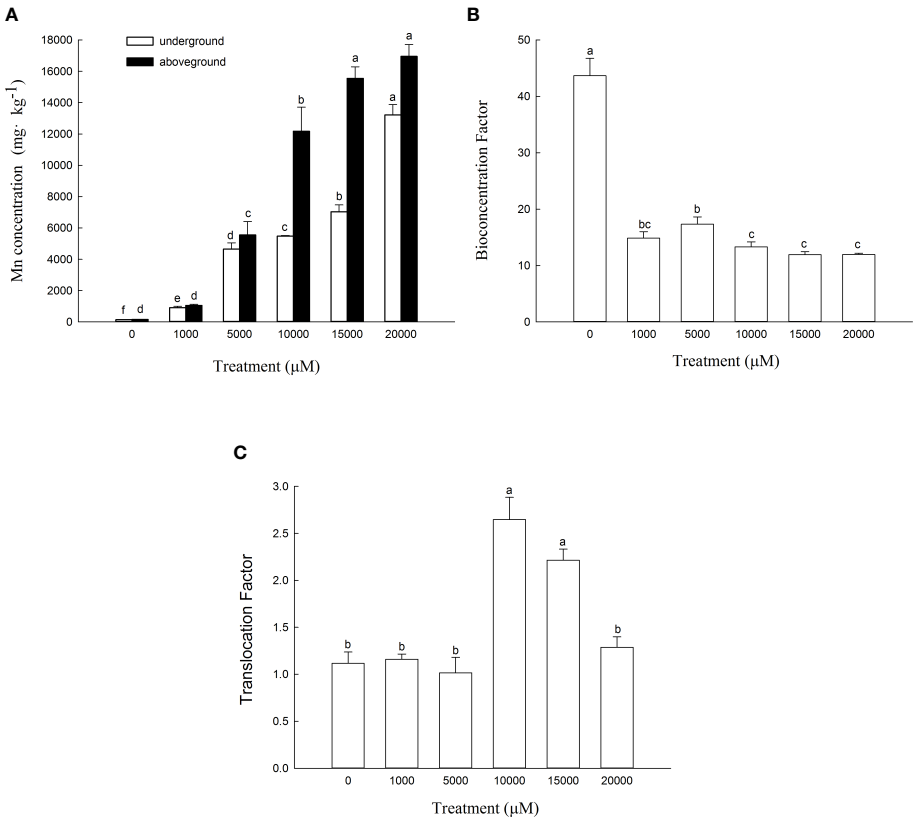

FIGURE 4
Mn concentrations in aboveground and underground parts **(A)**, bioconcentration factor (BCF) **(B)** and translocation factor (TF) **(C)** of D. carota under Mn stress. Data points and error bars represent mean and S.D. (n = 3). Values with different letters in the same parts of the plant indicate significant differences at the $p < 0.05$ level between different Mn concentrations according to the LSD test.

The Mn content in each chemical form in the underground part of *D. carota* is positively correlated with the Mn concentration; the correlation coefficients of ethanol, deionized water, sodium chloride, acetic acid, hydrochloric acid, and residual extracted Mn were 0.992, 0.931, 0.996, 0.993, 0.997, and 0.982, respectively ($P < 0.05$, Figures 6A–F). Its Mn content reached the maximum under 20,000 μM of Mn treatment; the values were 277.38, 373.40, 249.03, 209.17, 112.10, and 39.87 $mg \cdot kg^{-1}$, respectively. The content of Mn in the underground part of *D. carota* was lower than that in the aboveground part. The proportion distribution trend of the chemical forms of Mn in the underground part is deionized water extraction state > ethanol extraction state > sodium chloride extraction state > acetic acid extraction state > hydrochloric acid extraction state > residual state (Figure 8B).

Discussion

The present study showed that *D. carota* can live normally under a high Mn concentration environment. This plant had high Mn accumulation ability. The content of Mn in cell wall components and soluble components of *D. carota* was the largest part. Mn mainly existed in the form of ethanol extraction, deionized water extraction, and sodium chloride extraction.

Effects of Mn stress on plant growth

Biomass reflects the growth status of plants and is an important index to determine plant tolerance and the potential for phytoremediation (Xu et al., 2018). In this study, the dry weight of the aboveground part and underground part of *D. carota* increased firstly and then decreased with the increase in Mn concentration. This is consistent with the results of that of *Dianthus carthusianorum* (Załecka and Wierzbicka, 2002) and *Medicago sativa* (Cao et al., 2019) under Mn stress. It showed that low promotion and high suppression are a common phenomenon for Mn to the growth of plants.

The root system is the first organ that is exposed to environmental stress, and plants can adapt to the stress by adjusting the growth and metabolism of the root system.

10.3389/fpls.2022.947882

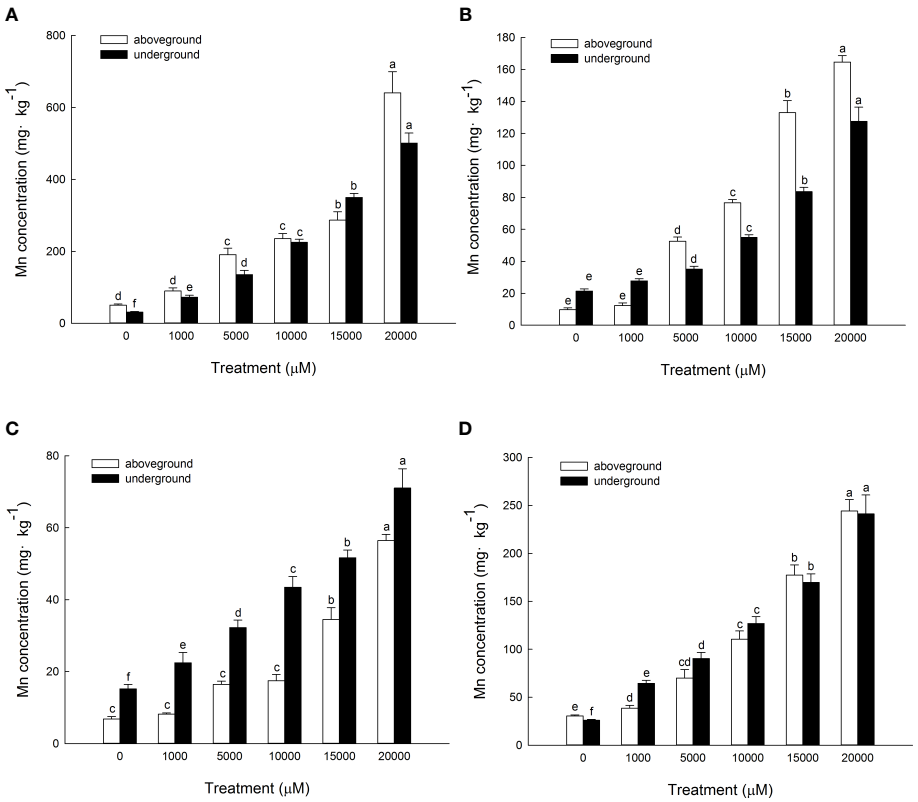

FIGURE 5
Concentrations of Mn in different subcellular compartments in *D carota* aboveground and underground under Mn stress (mg kg^{-1} FW) [**(A)** cell wall; **(B)** chloroplasts and cell nuclei; **(C)** mitochondria; **(D)** ribosomes)]. Data points and error bars represent mean and S.D. (n = 3). Values with different letters in the same parts of the plant indicate significant differences at the $p < 0.05$ level between different Mn concentrations according to the LSD test.

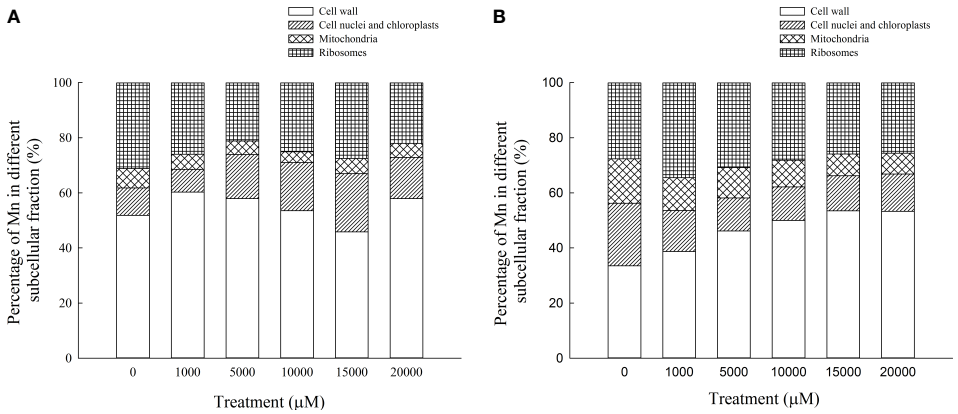

FIGURE 6
Percentages of subcellular distribution of Mn in aboveground part **(A)** and underground part **(B)** of *D carota* under different Mn treatments.

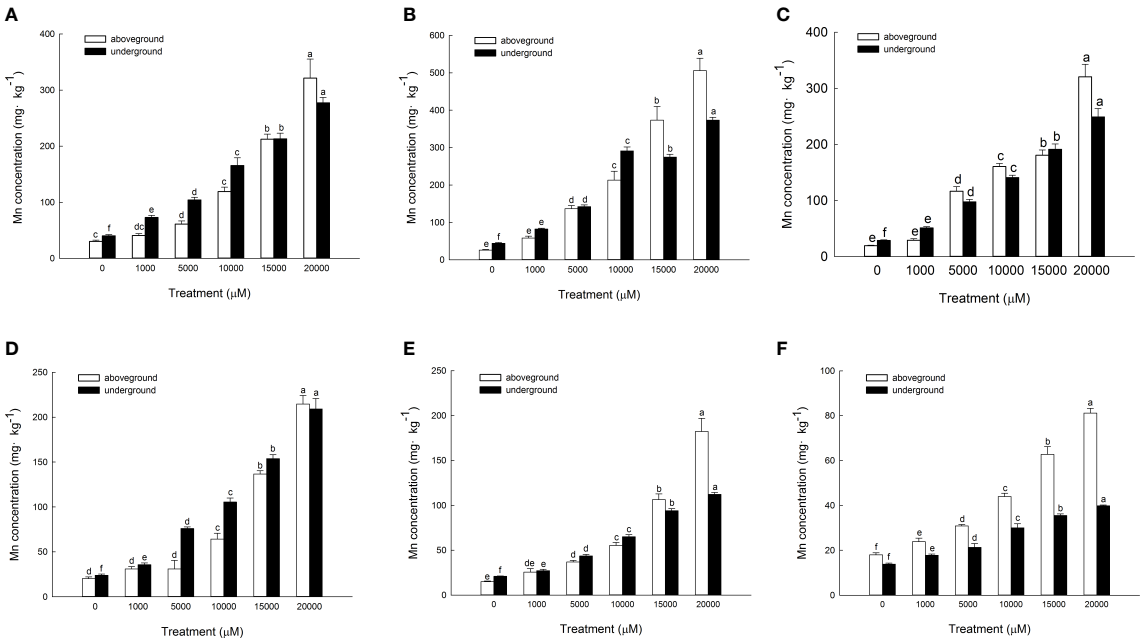

FIGURE 7
Concentrations of different Mn chemical forms in *D carota* aboveground and underground under Mn stress (mg kg^{-1} FW) [**(A)** 80% ethanol; **(B)** deionized H_2O; **(C)** 1 M NaCl; **(D)** 2% HAc; **(E)** 0.6 M HCl; **(F)** residue]. Data points and error bars represent mean and S.D. (n = 3). Values with different letters in the same parts of the plant indicate significant differences at the $p < 0.05$ level between different Mn concentrations according to the LSD test.

Because the root surface area, root volume, average root diameter, and number of fibrous roots are all indicators that reflect the growth and development of plant roots, it is important to study these indicators. This study showed that under the treatment of 1,000 μM of Mn concentration, the root surface area, root area, average root diameter, and number of fibrous roots of *D. carota* were all significantly higher than other treatments and the control, which illustrated that low concentrations of Mn can promote plant roots. This is consistent with the findings of Liu et al. (2010) on *Polygonum perfoliatum*.

Leaves are important organs for plants to photosynthesize and produce organic matter. The reduction in leaf area will

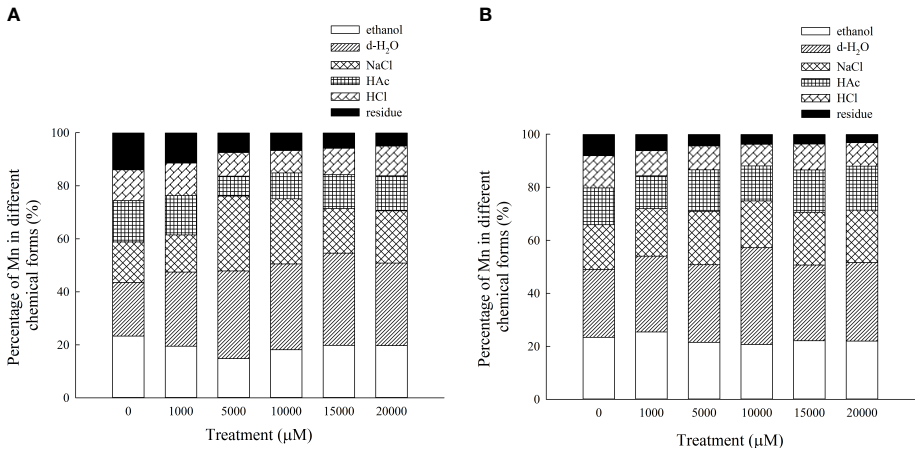

FIGURE 8
Percentages of different Mn chemical forms in aboveground part **(A)** and underground part **(B)** of *D carota* under different Mn treatments.

directly affect the accumulation of plant biomass. The specific leaf area can reflect the ability of plants to obtain environmental resources; the smaller the specific leaf area, the stronger the plant's ability to obtain water, nutrients, light, and carbon (Donovan et al., 2011). The present study showed that with the increase in Mn concentration, the leaf area of *D. carota* increased first and then decreased; this is consistent with the results of Xiao et al. (2020), which showed that the phenomenon of low leaf area and high inhibition is common. The specific leaf area of *D. carota* increased with the increase in Mn concentration; it is consistent with the results of Xiao et al. (2020) on *Cleome viscosa* under Mn stress and Wang et al. (2016) on *Cinnamomum camphora* under NaCl stress. The results showed that the ability of *D. carota* to obtain resources became weaker with the increase in Mn stress.

Effects of Mn stress on anatomical structure

The leaf anatomical structure is closely related to the adaptability of plants to the stress environment. In this study, under a high concentration of Mn stress, the thickness of the leaf epidermis and the main vein of *D. carota* decreased, the palisade tissue became thinner, the sponge tissue became thicker, and the ratio of palisade tissue/spongy tissue decreased. It showed that under Mn treatment, plants will change their key morphological characteristics in order to adapt to adverse stress. This is consistent with the results of Lei et al. (2007) and Zambrosi et al. (2016), which illustrated that high concentrations of Mn stress reduced the thickness of palisade tissue and sponge tissue of the leaves of *Populus cathayana* and *Saccharum officinarum*. The reason lies in the high concentration of Mn hurt the plants, which would cause leaves to lose water and become thinner. The inhibition to plant growth when Mn reaches the threshold for toxicity in leaves is associated with the occurrence of oxidative stress due to an increased production of reactive oxygen species (ROS) in leaf tissues (Zambrosi et al., 2016).

Effects of Mn accumulation characteristics

Mn accumulation ability reflects the strategy for plants to adapt to Mn stress; it is also the important index for screening phytoremediation plants. Normal concentrations of manganese in plant dry matter fall within the range of 20–500 mg/g and occasionally exceed 1,000 mg/g in plants on normal soils (Reeves and Baker, 2000). In this study, the maximum value of Mn concentrations in plants is 16,948 mg kg^{-1}. It indicated that *D. carota* has a strong accumulation ability on Mn. The enrichment coefficient (BCF) and transport coefficient (TF) can reflect the enrichment capacity of plants for heavy metals, and the BCF and TF of *D. carota* were both greater than 1; it showed that *D. carota* has high Mn absorption and transport ability under laboratory conditions. Compared with other plants, such as *Macleaya cordata* (Pan et al., 2019b) and *Broussonetia papyrifera* (Huang et al., 2019), *D. carota* had higher values of BCF and TF, which further illustrated that *D. carota* had a great application potential to phytoremediation of soil environment by Mn pollution.

Subcellular distribution of Mn

The subcellular distribution of heavy metals has important effects on the accumulation, migration, and detoxification of heavy metals in plants (Qiu et al., 2011). Plants would endure the toxicity of heavy metals through cell compartmentalization, bind excess metal ions to the cell wall, or separate them in vacuoles (Gallego et al., 2012). In this study, the percentage of Mn in the cell wall components of the aboveground and underground parts of *D. carota* was the largest, which accounted for 45.83% ~60.26% of the total. This is consistent with the results of *Polygonum hydropiper* (Wang et al., 2007) and *Cleome viscosa* (Xiao et al., 2020). The cell wall was the first barrier against metals in plant cells and could bind a large number of metal ions and avoid transmembrane transport and migration of these ions into cells, thereby reducing the concentration of metal ions in the protoplasm, protecting plants from poison. The cell wall, which is mainly composed of cellulose, hemicellulose, lignin, pectin, a large number of functional proteins, and a small number of aromatic compounds, can store metal ions and prevent them from being transported across the cytomembrane.

The results of this study showed that the contents of Mn in the cell wall and ribosome components accounted for 73.38% ~86.24% of the total, which illustrated that the soluble components of *D. carota* contained much more Mn than the chloroplast, nuclear components, and mitochondrial components. This is consistent with the results of *Xanthium strumarium* (Pan et al., 2019a) and *Polygonum hydropiper* (Wang et al., 2008). The reasons are that 95% of the volume of mature cells are vacuoles and the soluble components of cells are mainly composed of vacuoles. Therefore, the vacuole is the second largest place for storing Mn in *D. carotas* besides the cell wall. When the amount of heavy metals stored in the cell wall reached saturation, they would enter the protoplast through the cell membrane; most of them were transported to vacuoles and bound to their compounds, and heavy metal ions undergo fixation through compartmentalization, avoiding excessive accumulation of heavy metals in cell membranes and organelles, thereby protecting the cytoplasm from damage. The soluble fraction, which is mainly composed of vacuoles, acts as the secondary site of preferential Mn binding in the plant (Guan et al., 2018). Heavy metal ions would be transported to vacuoles when the cell wall becomes overwhelmed. Thus, vacuoles can act as a main

"sequestration zone" to accumulate excess Mn in spinaches and provide further protection against toxicity for organelles.

Subcellular localization can help with the understanding of the mechanisms of heavy metal accumulation, transport, and detoxification in plants. After uptake by the plants, heavy metal detoxification is achieved by chelation and sequestration by organo-ligands at a subcellular level. The function of vacuoles in metal compartmentalization and the affinity of cell walls for heavy metals play an important role in metal detoxification and tolerance of plants.

Chemical forms of Mn

The chemical form of Mn is one of the most important mechanisms to understand the accumulation and detoxification of Mn for plants (Lu et al., 2013), because it directly reflected the activity, toxicity, and migration ability of Mn. Mn in inorganic forms (extracted with ethanol) and in water-soluble forms (extracted with H_2O) had the highest activity, followed by pectates and protein-bound Mn (extracted with NaCl) and undissolved Mn phosphates (extracted with HAc), and the Mn oxalate (extracted with HCl) and residues had the lowest activity. The migration ability and toxicity of Mn extracted by ethanol and deionized water (mainly in the free state or in the form of heavy metals combined with organic acids and water-soluble substances) are much stronger than those extracted by sodium chloride (mainly heavy metals combined with pectin and protein), acetic acid, and hydrochloric acid (mainly phosphate and oxalic acid heavy metals with low solubility). In this study, Mn in the aboveground part of *D. carota* mainly existed in the form of deionized water, sodium chloride, and ethanol extract. Moreover, Mn in the underground part mainly existed in the form of deionized water, ethanol extract, and sodium chloride. Mn in *D. carota* plants mainly existed in the form of water-soluble organic acid salts; it is conducive to the detoxification and upward transportation of Mn. Most of the heavy metals combined with pectin and protein are mainly isolated in vacuoles; it further showed that the aboveground part of *D. carota* detoxifies mainly by forming soluble Mn organic acid salts and accumulating in vacuoles. The same phenomenon also appeared in the study of *Polygonum hydropiper*, and *Phytolacca acinosa* (Xue et al., 2011) under Mn stress (Wang et al., 2008). With the increase in Mn concentration, the content of Mn oxalate in *D. carota* plants did not change significantly; it showed that oxalic acid accumulation may be a common characteristic of *D. carota*, which illustrated that oxalic acid was the main organic acid for detoxification of Mn accumulation in plant leaves. Different chemical forms of heavy metals are closely related to different biological functions, which have distinct bioavailability and toxicities. Water-soluble Mn in the inorganic form (extracted by 80% ethanol) and the organic form (extracted by deionized water) migrate more easily and are more toxic to plant cells than pectate and protein-integrated Mn (1 M NaCl extractable Mn), insoluble Mn phosphate complexes (2% HAC extractable Mn), and Mn oxalate (0.6 M HCl extractable Mn) with little or no toxicity to plants.

Conclusions

In summary, the present study indicated that low concentrations of Mn treatment (0~1,000 μM) can promote the growth of *D. carota*, while high concentrations of Mn treatment (above 1,000 μM) can inhibit the growth. The Mn content in the aboveground and underground parts of *D. carota* were high and increased with the rising Mn concentrations. The content of Mn in cell wall components and soluble components was the largest part. In terms of chemical form, Mn mainly existed in the form of ethanol extraction, deionized water extraction, and sodium chloride extraction. It is concluded that Mn existed in the cell wall and soluble components as water-soluble organic acids and Mn oxalate, which might be an important Mn tolerance and detoxification mechanism for this plant. This study is still at a preliminary stage; further studies are needed to examine Mn storage sites and Mn abundance in the cells of plant tissue using promising techniques such as scanning electron microscopy (SEM) and energy-dispersive X-ray fluorescence spectrometry (EDX).

Data availability statement

The original contributions presented in the study are included in the article/supplementary material. Further inquiries can be directed to the corresponding authors.

Author contributions

WL designed this research. XK, WW and WZ analysed the data and wrote the manuscript. XK and JH performed the pot culture experiments. All authors contributed to the article and approved the submitted version.

Funding

This study is supported by the National Natural Science Foundation of China (grant number 42177018) and the Hunan Provincial Natural Science Fund (2021JJ31147).

Conflict of interest

The authors declare that the research was conducted in the absence of any commercial or financial relationships that could be construed as a potential conflict of interest.

Publisher's note

References

Bhaduri, A. M., and Fulekar, M. (2012). Antioxidant enzyme responses of plants to heavy metal stress. *Rev. Environ. Sci. Bio/Techn.* 11, 55–69. doi: 10.1007/s11157-011-9251-x

Cao, J., Li, X., and Wan, L. (2019). Effects of manganese stress on physiological and growth characteristics of alfalfa. *Chin. J. Grassland* 41, 15–22. doi: 10.16742/j.zgcdxb.20190048

Daud, M. K., Variatha, M. T., Ali, S., Najeeba, U., Jamil, M., Hayat, Y., et al. (2009). Cadmium-induced ultramorphological and physiological changes in leaves of two transgenic cotton cultivars and their wild relative. *J. Hazardous Materials* 168, 614–625. doi: 10.1016/j.jhazmat.2009.02.069

Dong, L., Zhao, X., Zhang, S., Zhang, Y., Liang, N., and Zhao, Y. (2009). The difference of plants accumulating heavy metal in polluted soil. *Chin. J. Soil Sci.* 40 4, 374–377. doi: 10.19336/j.cnki.trtb.2009.02.037

Donovan, L. A., Maherali, H., Caruso, C. M., Huber, H., and Kroon, H. (2011). The evolution of the worldwide leaf economics spectrum. *Trends Ecol. Evol.* 26, 88–95. doi: 10.1016/j.tree.2010.11.011

Dou, C. M., Fu, X. P., Chen, X. C., Shi, J. Y., and Chen, Y. X. (2009). Accumulation and detoxification of manganese in hyperaccumulator *Phytolacca americana*. *Plant Biol.* 11, 664–670. doi: 10.1111/j.1438-8677.2008.00163.x

Elleuch, A., Chaâbene, Z., Grubb, D. C., Drira, N., Mejdoub, H., and Khemakhem, B. (2013). Morphological and biochemical behavior of fenugreek (Trigonella foenum-graecum) under copper stress. *Ecotoxicol. Environ. Saf.* 98, 46–53. doi: 10.1016/j.ecoenv.2013.09.028

Fernando, D. R., and Lynch, J. P. (2015). Manganese phytotoxicity: New light on an old problem. *Ann. Bot.* 116, 313–319. doi: 10.1093/aob/mcv111

Gallego, S. M., Pena, L. B., Barcia, R. A., Azpilicueta, C. E., Iannone, M. F., Rosales, E. P., et al. (2012). Unravelling cadmium toxicity and tolerance in plants: insight into regulatory mechanisms. *Environ. Exp. Bot.* 83, 33–46. doi: 10.1016/j.envexpbot.2012.04.006

Guan, M., Zhang, H., Pan, W., Jin, C., and Lin, X. (2018). Sulfide alleviates cadmium toxicity in Arabidopsis, plants by altering the chemical form and the subcellular distribution of cadmium. *Sci. Total Environ.* 627, 663–670. doi: 10.1016/j.scitotenv.2018.01.245

Huang, M., Huang, M., Zhang, J., Quan, G., and Guo, J. (2018). Review on current research and utilization status of hyperaccumulation plants for heavy metal contaminated soils and the phytoremediation application prospect of invasive plants. *Ecol. Sci.* 37, 194–203. doi: 10.14108/j.cnki.1008-8873.2018.03.026

Huang, H., Zhao, Y., Xu, Z., Zhang, W., and Jiang, K. (2019). Physiological responses of *Broussonetia papyrifera* to manganese stress, a candidate plant for phytoremediation. *Ecotoxicol. Environ. Saf.* 181, 18–25. doi: 10.1016/j.ecoenv.2019.05.063

Jiang, Y., Han, J., Xue, W., Wang, J., Wang, B., Liu, L., et al. (2021). Overexpression of SmZIP plays important roles in Cd accumulation and translocation, subcellular distribution, and chemical forms in transgenic tobacco under Cd stress. *Ecotoxicol. Environ. Saf.* 214, 112097. doi: 10.1016/j.ecoenv.2021.112097

Ke, W. S., Xiong, Z. T., Xie, M. J., Xiong, S. L., Huang, H., and Li, M. J. (2007). Differences in Cu resistance and accumulation of elsholtzia haichouensis sun and daucus carota l. populations from Cu mine sites and uncontaminated sites. *Chin. J. Environ. Eng.* 1, 94–100. doi: 1673-9108(2007)05-0094-07

Lei, Y., Chen, K., Tian, X., Korpelainen, H., and Li, C. (2007). Effect of Mn toxicity on morphological and physiological changes in two *Populus cathayana* populations originating from different habitats. *Trees* 21, 569–580. doi: 10.1007/s00468-007-0152-0

Li, J. T., Gurajala, H. K., Wu, L. H., van der Ent, A., Qiu, R. L., Baker, A. J., et al. (2018). Hyperaccumulator plants from China: A synthesis of the current state of knowledge. *Environ. Sci. Technol.* 52, 11980–11994. doi: 10.1021/acs.est.8b01060

Li, M., Shao, L., Xu, L., Cheng, W., Gao, H., and Ding, Q. (2012). Study on constituents and biological activity of volatile oil from umbels of daucus carota Linn. *J. Chin. Cereals Oils Assoc.* 27, 112–115. doi: 1003-0174(2012) 09-0112-04

Liu, P., Tang, X., Gong, C., and Xu, G. (2010). Manganese tolerance and accumulation in six Mn hyperaccumulators or accumulators. *Plant Soil* 335, 385–395. doi: 10.1007/s11104-010-0427-x

Liu, K., Yu, F., Chen, M., Zhou, Z., Chen, C., Li, M. S., et al. (2016). A newly found manganese hyperaccumulator-polygonum lapathifolium Linn. *Int. J. phytoremediation* 18, 348–353. doi: 10.1080/15226514.2015.1109589

Lu, Z., Liu, Z., Song, Z., Zhang, C., and Sun, D. (2013). Subcellular distribution and chemical forms of cd and the synthesis of phytochelatins (PCs) in different barley genotypes. *J. Agro-Environ. Sci.* 32, 2125–2131. doi: 10.11654/jaes.2013.11.004

Marques, A. P. G. C., Rangel, A. O. S. S., and Castro, P. M. L. (2009). Remediation of heavy metal contaminated soils: Phytoremediation as a potentially promising clean-up technology. *Crit. Rev. Environ. Sci. Technol.* 39, 622–654. doi: 10.1080/10643380701798272

Mou, D., Yao, Y., Yang, Y., Zhang, Y., Tian, C., and Achal, V. (2011). Plant high tolerance to excess manganese related with root growth, manganese distribution and antioxidative enzyme activity in three grape cultivars. *Ecotoxicol. Environ. Saf.* 74, 776–786. doi: 10.1016/j.ecoenv.2010.10.040

Pan, G., Yan, W. D., Zhang, H. P., Xiao, Z. H., Li, X. H., Liu, W. S., et al. (2019a). Subcellular distribution and chemical forms involved in manganese accumulation and detoxification for xanthium strumarium l. *Chemosphere* 237, 124531. doi: 10.1016/j.chemosphere.2019.124531

Pan, G., Zhang, H., Liu, W., and Liu, P. (2019b). Integrative study of subcellular distribution, chemical forms, and physiological responses for understanding manganese tolerance in the herb macleaya cordata (papaveraceae). *Ecotoxicol. Environ. Saf.* 181, 455–462. doi: 10.1016/j.ecoenv.2019.06.040

Qiu, Q., Wang, Y. T., Yang, Z. Y., and Yuan, J. G. (2011). Effects of phosphorus supplied in soil on subcellular distribution and chemical forms of cad-miumin two Chinese flowering cabbage (Brassica parachinensis L.) cultivars differ in gincadmium accumulation. *Food Chem.Toxicol.* 49, 2260–2267. doi: 10.1016/j.fct.2011.06.024

Reeves, R. D., and Baker, A. J. M. (2000). "Metal-accumulating plants," in *Phytoremediation of toxic metals: Using plants to clean up the environment*. Eds. I. Raskin and B. D. Ensley (New York: John Wiley and Sons), pp 193–pp 229.

Tavanti, R. F. R., David Queiroz, G., Caroline Da Rocha Silva, A., Moya Peres, W., Pereira Paixão, A., Galindo, F. S., et al. (2020). Changes in photosynthesis and antioxidant metabolism of cotton (*Gossypium hirsutum* l.) plants in response to manganese stress. *Arch. Agron. Soil Sci.* 66, 743–762. doi: 10.1080/03650340.2019.1637857

Tian, C., Zhang, Y., Wang, K., and Zhang, W. (2014). The anatomical structure responses in alfalfa to salinity-alkalinity stress of $NaHCO_3$. *Acta Prataculturae Sin.* 23, 133–142. doi: 10.11686/cyxb20140515

Wang, H., Tang, S. M., Liao, X. J., and Cao, Q. M. (2008). Physiological and molecular mechanisms of Mn uptake by hyperaccumulating plant polygonum hydropiper (Polygonaceae). *Acta Bot. Yunnanica* 30, 489–495. doi: 10.3724/SP.J·1143.2008.07265

Wang, H., Tang, S., Liao, X., Cao, Q., Yang, A., and Wang, T. (2007). A new manganese-hyperaccumulator: *Polygonum hydropiper* l. *Ecol. Environ.* 2007, 830–834. doi: 10.16258/j.cnki.1674-5906.2007.03.025

Wang, J., Wang, S., Jianmin, Y., Zhang, J., Zhang, L., You, Y., et al. (2016). Physiological response of *Cinnamomum camphora* seedlings to NaCl stress. *Sci. Soil Water Conserv.* 14, 82–89. doi: 10.16843 /j. sswc.2016.05.011

Wang, Y., Shen, H., Xu, L., Zhu, X., Li, C., Zhang, W., et al. (2015). Transport, ultrastructural localization, and distribution of chemical forms of lead in radish (Raphanus sativus L.). *Front. Plant Sci.* 6:293. doi: 10.3389/fpls.2015.00293

Wu, M., Luo, Q., Zhao, Y., Long, Y., Liu, S., and Pan, Y. (2018). Physiological and biochemical mechanisms preventing cd toxicity in the new hyperaccumulator abelmoschus manihot. *J. Plant Growth Regul.* 37, 709–718. doi: 10.1007/s00344-017-9765-8

Wu, Y., Wan, Y. H., and Xie, M. J. (2006). The MDA accumulation in two daucus carota l. populations under copper stress. *J. Hubei Univ. (Natural Science)* 28, 313–316. doi: 1000-2375(2006) 03-0313-04

Wu, Y., Yang, C., Xin, H. L., Xiao, Z., Kuang, X., and Liu, W. (2019). Effects of stress growth, physiological and biochemical characteristics of *Daucus carota* seedling. *Northern Horticult.* (10), 23–30. doi: 10.11937/bfyy.20183569

Xiao, Z., Li, X., Pan, G., Wu, Y., Yang, C., Kuang, X., et al. (2019). Effects of manganese stress on seed germination, and seedling physiological and biochemical characteristics of cleome viscosa. *Acta Prataculturae Sin.* 28, 75–84. doi: 10.11686/cyxb2019041

Xiao, Z., Pan, G., Li, X., Kuang, X., and Liu, W. (2020). Effects of exogenous manganese on its plant growth, subcellular distribution, chemical forms, physiological and biochemical traits in cleome viscosa l. *Ecotoxicol. Environ. Saf.* 198, 110696. doi: 10.1016/j.ecoenv.2020.110696

Xue, S., Chen, Y., Reeves, R. D., Baker, A. J., Lin, Q., and Fernando, D. R. (2004). Manganese uptake and accumulation by the hyperaccumulator plant phytolacca acinosa roxb. (Phytolaccaceae). *Environ. pollut.* 131, 393–399. doi: 10.1016/j.envpol.2004.03.011

Xue, S. G., Wang, J., Liu, H., Lei, J., and Liu, F. H. (2011). Physiological response of phytolacca acinosa to manganese stress by FTIR spectroscopy. *J. Cent. South Univ. (Science Technology)* 42, 1852–1857. doi: 1672–7207(2011)07–1852–06

Xu, X., Shi, J., Chen, X., Chen, Y., and Hu, T. (2009). Chemical forms of manganese in the leaves of manganese hyperaccumulator phytolacca acinosa roxb. (Phytolaccaceae). *Plant Soil* 318, 197–204. doi: 10.1007/s11104-008-9829-4

Xu, Y. M., Wang, C. Q., Wu, J. X., Zhang, W. J., Wang, X. C., Cuizhen, C., et al. (2018). Effects of Mn^{2+} and Pb^{2+} on seed germination and seedling growth of *Elymus nutans*. *Acta Prataculturae Sin.* 27, 194–200. doi: 10.11686/cyxb2017387

Yao, Y., Xu, G., Mou, D., Wang, J., and Ma, J. (2012). Subcellular Mn compartation, anatomic and biochemical changes of two grape varieties in response to excess manganese. *Chemosphere* 89, 150–157. doi: 10.1016/j.chemosphere.2012.05.030

Załecka, R., and Wierzbicka, M. (2002). The adaptation of dianthus carthusianorum L.(Caryophyllaceae) to growth on a zinc–lead heap in southern Poland. *Plant Soil* 246, 249–257. doi: 10.1023/A:1020612930364

Zambrosi, F. C. B., Mesquita, G. L., Marchiori, P. E. R., Tanaka, F. A. O., Machado, E. C., and Ribeiro, R. V. (2016). Anatomical and physiological bases of sugarcane tolerance to manganese toxicity. *Environ. Exp. Bot.* 132, 100–112. doi: 10.1016/j.envexpbot.2016.08.011

frontiers | Frontiers in Plant Science

TYPE Original Research
PUBLISHED 13 October 2022
DOI 10.3389/fpls.2022.921824

OPEN ACCESS

EDITED BY
Sergey Shabala,
University of Tasmania, Australia

REVIEWED BY
Damian Joseph Allen,
Purdue University, United States
Reza Shafiei,
University of Dundee, United Kingdom

*CORRESPONDENCE
Zhiyong Chen
zhiyongchen@hunau.edu.cn
Meijuan Duan
duanmeijuan@163.com

SPECIALTY SECTION
This article was submitted to Plant Abiotic Stress, a section of the journal Frontiers in Plant Science

RECEIVED 16 April 2022
ACCEPTED 29 August 2022
PUBLISHED 13 October 2022

CITATION
Zheng C, Yi Z, Xiao L, Sun G, Li M, Xue S, Peng X, Duan M and Chen Z (2022) The performance of *Miscanthus* hybrids in saline-alkaline soil. *Front. Plant Sci.* 13:921824. doi: 10.3389/fpls.2022.921824

The performance of *Miscanthus* hybrids in saline-alkaline soil

Cheng Zheng[1], Zili Yi[2,3], Liang Xiao[2,3], Guorong Sun[4], Meng Li[2,3], Shuai Xue[2,3], Xiaoying Peng[2], Meijuan Duan[1]* and Zhiyong Chen[2,3]*

[1]College of Agronomy, Hunan Agricultural University, Changsha, China, [2]College of Bioscience and Biotechnology, Hunan Agricultural University, Changsha, Hunan, China, [3]Hunan Engineering Laboratory of Miscanthus Ecological Application Technology, Hunan Agricultural University, Changsha, Hunan, China, [4]Binzhou Polytechnic, Binzhou, Shandong, China

Cultivating the dedicated biomass crop *Miscanthus* on marginal land is a sustainable means of avoiding competition with food crops for arable land. A large proportion of global marginal land is saline–alkaline; however, little is known about the performance of *Miscanthus* in saline-alkaline soil. In this study, *Miscanthus* × *giganteus* and ten other *Miscanthus* hybrids grown in the Yellow River Delta were exposed to low and saline–alkaline soils during the 2016–2018 growing season to evaluate the agronomic traits, biomass quality and the potential productive index of eleven *Miscanthus* genotypes. Plant biomass, plant height, and tiller number significantly decreased in high saline–alkaline soil. In particular, the average plant biomass of ten *Miscanthus* hybrids in low saline–alkaline soil in 2017 and 2018 were 0.21 and 2.25 kg per plant, respectively, and in high saline-alkaline soil were 0.13 and 0.65 kg per plant, respectively. Cell wall, cellulose, and nitrogen content of all genotypes significantly decreased in high saline–alkaline soil, while hemicellulose, ash, sodium, potassium, magnesium, and calcium content significantly increased. However, high saline–alkaline soil had no observable impact on lignin content of *Miscanthus* biomass. The effect of high saline-alkaline on biomass quality parameters could provide important information for the application of *Miscanthus* biomass in saline-alkaline soil. The selected genotypes (A5) could be considered as breeding materials in saline-alkaline soil.

KEYWORDS

***Miscanthus*, saline-alkaline soil, agronomic traits, biomass quality, bioenergy**

Introduction

Miscanthus is a perennial rhizomatous giant C4 grass currently being developed for the production of lignocellulosic biomass as a fossil fuel replacement and as an eco-industrial crop (Acharya et al., 2018; Zhang et al., 2020; Sen and Baidurah, 2021). The cultivation of *Miscanthus* on marginal land for biomass production would contribute to food security and the efficient use of land resources (Clifton-Brown and Lewandowski, 2002; Tang et al., 2010; Xue et al., 2016; Wagner et al., 2019). Saline–alkaline stress is one

of the most common abiotic stresses affecting crops in diverse geographical locations, and the incidence of soil salinity is increasing worldwide (Dendooven et al., 2010). In China, the potential area of saline–alkaline soil planted *Miscanthus* is approximately 2.49 million hectare (Xue et al., 2016). Recent studies show that *Miscanthus* can improve saline–alkaline soil conditions and biodiversity (Pidlisnyuk et al., 2014; Xu et al., 2021). Thus, *Miscanthus* species are considered a non-food crop with a high potential for sustainable production on saline–alkaline soil.

Currently, only one clone, *Miscanthus* × *giganteus* is grown commercially (Xue et al., 2016). However, the capacity of *M.* × *giganteus* to saline-alkaline tolerance still need be improved (Stavridou et al., 2017). In addition, *M.* × *giganteus*, as a triploid infertile clone, cannot be directly established *via* seeds, which hinders its widespread application (Xue et al., 2016). Therefore, the development of new varieties with high saline–alkaline stress tolerance is urgently needed. The two key goals of *Miscanthus* breeding are high plant biomass and superior biomass quality, to meet the requirements of industrial-scale production on saline-alkaline soil. Unlike most crops produced for food, all the above-ground part of *Miscanthus* was harvested, plants grown in saline–alkaline soil are exposed to osmotic stress, ion toxicity, and high pH (Deinlein et al., 2014; Xue et al., 2016). In terms of *Miscanthus*, the plant biomass of *Miscanthus* is significantly reduced at the seedling stage under high salt conditions (Sun et al., 2014; Stavridou et al., 2017). Seventy genotypes of *Miscanthus* were investigated for salt tolerance in the greenhouse, finding that a good alternative for breeding purposes was the diploid species *M. sinensis* (Chen et al., 2017). However, *Miscanthus* as a perennial plant is important to investigate the effect of saline-alkaline on the plant biomass in the field. In addition, genotypes with saline-alkaline tolerance in the field have been developed by interspecific crossing (Zheng et al., 2021). However, whether these genotypes can adapt to higher saline-alkaline soil remains unknown. Moreover, the effect of high saline-alkaline soil on agronomic traits (plant biomass, plant height, stem diameter, tiller number) need be investigated.

Saline–alkaline conditions negatively impact not only plant biomass, but also cell wall biosynthesis (Oliveira et al., 2020) and composition (Birgit and Hartmut, 2000). The main component of *Miscanthus* biomass is the cell wall, which impacts the degradation and transformation of its biomass. For example, high cellulose and hemicellulose contents of *Miscanthus* enhance the yield of fermentative sugars, which are used for bioethanol production (Sekar et al., 2016). The efficiency of converting cell wall polysaccharides into fermentative sugars is determined by the content of lignin and the extent of cross-linking within lignin polymers (Gong et al., 2011; Jagtap et al., 2013; Li et al., 2014). In addition, the contents of ash and ash elements negatively affect power generation (Fu et al., 2014; Masto et al., 2015). Previous studies showed that drought and cold stresses after cell wall composition in *Miscanthus* by decreasing cellulose and substantially increasing hemicellulose, while having little effect on lignin content (Domon et al., 2013; Tim et al., 2016a). Recently, a transcriptomic study showed that cell wall- and ion transportation-related genes were differentially expressed under saline–alkaline stress conditions (Wang et al., 2019). In *Miscanthus*, the ash content of plant biomass increased under saline stress at the seedling stage (Stavridou et al., 2017). However, the effect of high saline-alkaline soil on cell wall components and ash content of *Miscanthus* biomass have so far been sparsely investigated. Moreover, combining plant biomass and quality traits in saline-alkaline soil to investigate the performance of *Miscanthus* would help breeder to develop the new varieties adaptability to saline-alkaline soil.

In this study, we therefore analyzed the agronomic traits and biomass quality of 10 high-biomass *Miscanthus* genotypes grown in Yellow River Delta, China, and *Miscanthus* × *giganteus*, a commercial variety (control) (Muylle et al., 2015). The aims of this study were: (i) investigating the effect of high saline-alkaline on agronomic and biomass quality traits (cell wall, cellulose, hemicellulose, lignin, ash and elemental content); and (ii) combining plant biomass and quality traits to assess the adaptability of these genotypes to saline-alkaline soil.

Materials and methods

Plant materials

Eleven *Miscanthus* genotypes were used in this study. Ten of these genotypes were *Miscanthus* hybrids (Y2, Y5, Y11, Y14, Y20, Y21, Y37, Y39, Y44, and A5). Y2, Y5, Y11, Y14, Y21, Y37, Y39, and Y44 selected from 216 *Miscanthus* genotypes in the Yellow River Delta in low saline-alkaline soil during the 2014–2016 growing season, by compared with the biomass yield of *M.* × *giganteus* (data no shown). The 216 *Miscanthus* genotypes derived from the open pollinating offspring of *M. sinensis*, *M. lutarioriparius*, and *M. sinensis* × *M. lutarioriparius* (**Supplementary Table 1**). Thus, Y2, Y5, Y11, Y14, Y21, Y37, Y39, and Y44 derived from different females. A5 with high biomass yield in the Yellow River delta derived from *M. sinensis* (♀, number: B0605) and *M. lutarioriparius* (♂, number: A0107) (Zheng et al., 2021). *M.* × *giganteus*, as a commercial variety, was used as a control, due to its wide adaptability and high biomass yield (Xue et al., 2016). All genotypes used in this study were obtained from the *Miscanthus* germplasm resource nursery in Binzhou, Shandong province, China (37°25′ N, 117°59′ E). Rhizomes were extracted from the soil, and cut into approximately 300-g pieces, each with two or three buds.

Individual rhizome pieces were packaged in air-tight bags to prevent water loss during transportation to the experimental site.

Experimental site and climatic conditions

The experimental site was located in Beihai, Shandong province, China, at the saline–alkaline experimental unit of Hunan Agricultural University (37°38′N, 118°07′E). Two kinds of soil were identified at the experiment site. The physical and chemical properties of these soils are summarized in Table 1. According to the definition of saline–alkaline soil outlined by the United States Department of Agriculture based on the criteria of electrical conductivity (EC; > 4 $dS.m^{-1}$) and pH (> 8.5), soil at the study site was considered as low saline–alkaline under experiment I (EC = 9.04; pH = 2.59). Because the soil EC and pH values in experiment II were higher than those in experiment I, the experiment II soil was defined as high saline–alkaline soil (Table 1). Cotton could be cultivated in experiment I but not in experiment II. The distance between experiment I and II was approximately 300 m. Rainfall and temperature data throughout the experiment were collected by a local meteorological station (Figure 1). Rainfall in 2016, 2017, and 2018 was 439.6, 414.0, and 599.0 mm, respectively.

Experiment design

Randomized block design was used in both locations, with five rhizomes per genotype in each of the three blocks. Before transplantation, 0.2-m deep furrows were prepared in the field, and rhizomes were placed at the bottom of the furrows, with an inter-rhizome distance of 1 m and row-to-row spacing of 1 m, to obtain a final planting density of 1 rhizome m^{-2}. On June 6, 2016, the furrows were filled with soil, and the soil surface was flattened to retain moisture and facilitate soil–rhizome adhesion. To avoid border effects, a supplementary row of A5 rhizomes was planted all the around the experimental site. In addition, to mitigate the edge effect with the neighboring hybrid, ridges were formed between blocks. The areas of location I and location II were both 216 m^2.

TABLE 1 Physical and chemical features of the soil at the experimental site (the saline–alkaline experimental unit of Hunan Agricultural University, 38°37′N, 118°07′E).

Items	Low saline-alkaline soil (experiment I)	High saline-alkaline soil (experiment II)
pH	9.04	9.62
Electrical conductivity (dS/m)	2.59	12.92
Organic matter (g/kg)	12.12	9.45
Total phosphorus (g/kg)	0.80	0.47
Total nitrogen (g/kg)	2.01	2.02
Total potassium (g/kg)	18.38	24.09
Available phosphorus (mg/kg)	6.10	4.00
Available nitrogen (mg/kg)	48.64	110.89
Available potassium (mg/kg)	338.64	86.61

Management practices

To ensure good root contact with the soil and facilitate seedling emergence, the rhizomes were watered immediately after planting. No irrigation was conducted. In the follow-up experiment. No fertilizer was applied throughout the experiment. Weeds were controlled three times each year by machine hoeing. All plants were survival and overwinter, however, no plant performance data were collected in the first year, because plants of the same genotype showed non-homogenous performance, with only a few tillers per plant.

Agronomic trait evaluation

Major agronomic traits, including plant biomass, plant height, tiller number and stem diameter, were determined at the end of the second and third growing seasons (on December 8th, 2017 and December 12th, 2018, respectively). The eleven *Miscanthus* genotypes flowered, and stems and leaves of these genotypes were yellow in December. All tillers of each plant were harvested using a Stihl clearing saw (Stihl, Germany) mounted with a steel cutting blade, which was dried to constant weight at 80°C, and plant biomass was weighed. Plant height was measured from the soil surface to the highest point of the last fully expanded leaf. The stem number per plant was measured, as described previously (Zub et al., 2011). To determine the tiller number per plant, only tillers reaching at least 60% of the plant height were counted. To determine the stem diameter, the diameter of a few stems per plant was measured at a height of 5 cm above the soil surface, and the average value was calculated. The above measurements were repeated five times.

Cellulose, hemicellulose and lignin content measurement

Subsamples were collected from random locations within eleven *Miscanthus* genotype windrows in the low and high saline-alkaline soil after the measured agronomic traits. Gravimetric measurements of neutral detergent fiber (NDF), acid detergent fiber (ADF) and acid detergent lignin (ADL) were determined by using the Van Soest method (Van Soest, 1967). NDF, a measure of cell wall content, is the residue left after

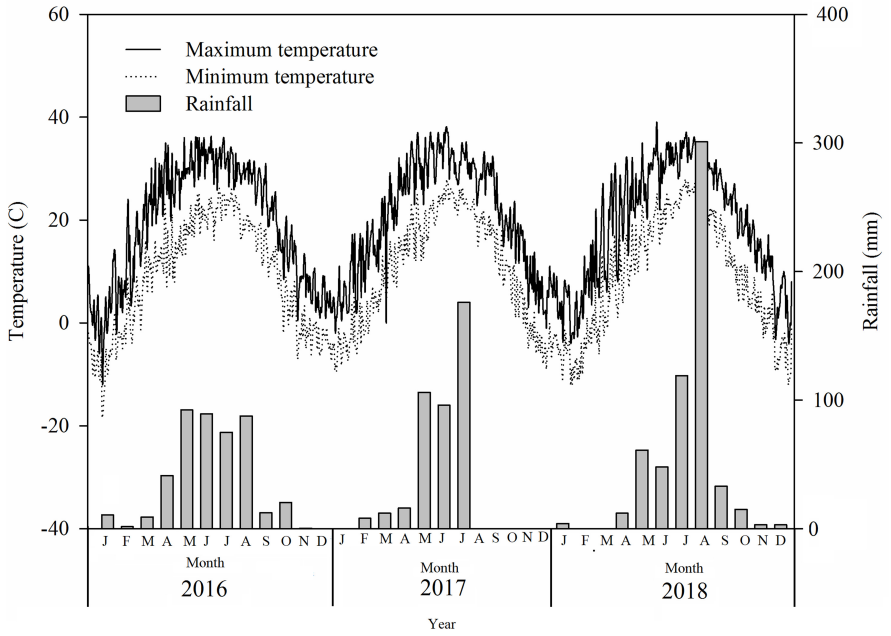

FIGURE 1
Rainfall and temperature in the experimental sites in 2016, 2017, and 2018.

refluxing for 1 h in a neutral buffered detergent solution. ADF is a measure of cellulose and lignin, the residue remaining after refluxing the samples in a solution of cetyltrimethylammonium bromide (CTAB) in 2 M sulfuric acid. ADL was measured by treating ADF with 72% sulfuric acid to solubilise the cellulose to determine crude lignin (Allison et al., 2011). The cellulose, hemicellulose and lignin contents of samples were estimated using the following three equations:

$$\text{Cellulose content} = \text{ADF} - \text{ADL} \quad (1)$$

$$\text{Hemicellulose content} = \text{NDF} - \text{ADF} \quad (2)$$

$$\text{Lignin content} = \text{ADL} \quad (3)$$

Ash content of plant biomass

The ash content of samples was determined as a percentage of dry matter (%DM) in accordance with the British Standard method (CEN/TS14775: 2004).

Elemental content of plant biomass

The contents of various elements, including nitrogen (N), phosphorus (P), sodium (Na), potassium (K), calcium (Ca) and magnesium (Mg), in plant biomass were determined. nitrogen analyses were carried out using the Kjeldahl method. Vanadium-molybdenum yellow colorimetry was used to determine the P content. To determine Na, K, Mg, and Ca contents, 0.5 g of dried biomass of each sample was dissolved in 8 ml of HNO_3 (65%). Then, 4 ml of H_2O_2 was added to the reaction to remove color. Samples were then digested in a microwave at 150°C and 24.16 bar for 40 min. The digested samples were filtered through Whatman filter paper and subjected to inductively coupled plasma-optical emission spectrometry (ICP-OES) to determine the content of various elements (Vista Pro; Varian Inc., Palo Alto, CA, USA).

Statistical analysis

Analysis of variance (ANOVA) was performed to determine the significance of genotype, location, year and interaction. To analyze agronomic and quality traits, genotype and location were set as fixed factors. Agronomic traits were analyzed using Model I, as shown below. Because biomass quality traits were measured only in 2018, these were measured using model II.

$$\text{Model I}: Y_{ijkl} = u + G_i + L_j + Y_k + B_l + (GL)_{ij} + (GY)_{ik} + (LY)_{jk} + (GLY)_{ijk} + e_{ijkl} \quad (4)$$

$$\text{Model II}: Y_{ijl} = u + G_i + L_i + B_l + (GL)_{ij} + e_{ijl} \quad (5)$$

Where Y_{ijkl} and Y_{ijl} are the response variables; u is the grand mean; G_i is the genotype effect; L_j is the location effect; Y_k is the year effect; B_l is the block effect;

$(GL)_{ij}$ represents the genotype × location interaction; $(GY)_{ik}$ represents the genotype × year interaction; $(LY)_{jk}$ represents the location × year interaction; $(GLY)_{ijk}$ represents the genotype × location × year interaction; and e_{ijkl} and e_{ijl} represent the residual error.

To identify significant genotypic differences within low or high saline-alkaline treatment, multiple comparison analyses were performed using Duncan's multiple range test. Significant differences in agronomic traits and biomass composition between the two groups of genotypes in low and high saline-alkaline soil treatments were evaluated using unpaired two-sample *t*-tests at $P < 0.05$.

In addition, The K^+/Na^+ ratio in relation to plant biomass and biomass quality-related variables were conducted by regression analysis (SPSS 19.0, USA).

Results

Agronomic traits of *Miscanthus* in low and high saline–alkaline soil

High saline–alkaline stress was found to have a significant ($P < 0.05$) impact on plant biomass, plant height, tiller number and stem diameter (Figures 2, 3 and Table 2). Mean plant biomass in low saline–alkaline soil was 0.60 and 2.19 kg per plant in 2017 and 2018, respectively. On average, high saline–alkaline stress conditions in this experiment significantly ($P < 0.01$) reduced plant biomass by 80% in 2017 (0.12 kg per plant) and 90% in 2018 (0.20 kg per plant). Mean plant height of all genotypes was significantly ($P < 0.01$) reduced by 44 and 160 cm in 2017 and 2018, respectively. Additionally, mean plant height was lower in high saline–alkaline soil than in low saline–alkaline soil in both years (191 vs. 235 cm in 2017; 167 vs. 327 cm in 2018). Similar results were observed for tiller number. Stem diameter was significantly ($P < 0.01$) influenced by high saline–alkaline conditions. Stem diameters of Y21, Y37 and A5 genotypes were significantly ($P < 0.01$) reduced under high saline–alkaline soil conditions. Genotype-location interactions had a significant impact on agronomic traits, expect stem diameter. In 2018, both A5 and Y39 genotypes showed relatively high yields (3.6 and 4.3 kg per plant, respectively) in low saline-alkaline soil; however, in high saline–alkaline stress, the yield of A5 (0.41 kg per plant) was considerably higher than that of Y39 (0.18 kg per plant). In addition, year–location interaction had a significant ($P < 0.01$) impact on plant biomass.

Cell wall, cellulose, hemicellulose and lignin contents of *Miscanthus* genotypes in low and high saline–alkaline soils

High saline–alkaline stress had a significant ($P < 0.05$) effect on most of the biomass quality traits of *Miscanthus* genotypes, including cell wall, cellulose and hemicellulose content (Table 3). Mean cell wall and cellulose contents of all 11 genotypes in high saline–alkaline soil (74.53 and 34.51%, respectively) were lower than those in low saline–alkaline soil (77.56 and 39.54%, respectively), which was a

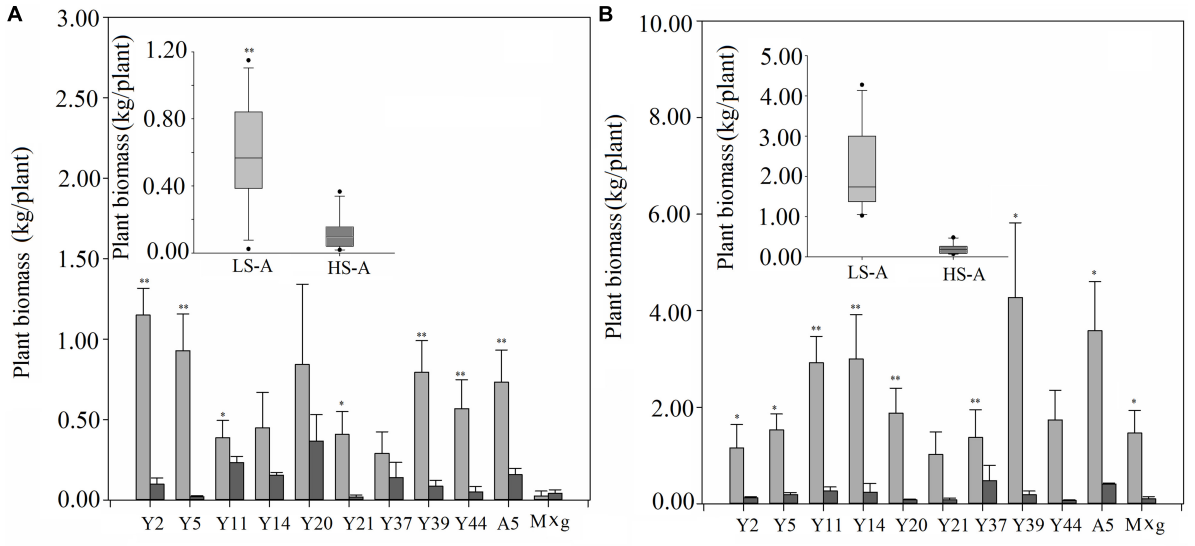

FIGURE 2
Plant biomass under low saline–alkaline soil (LS-A) (the light bars) and high saline-alkaline soil (HS-A) (the dark bars), of 11 genotypes of *Miscanthus* in 2017 **(A)** and 2018 **(B)**. Significance is denoted by $^*P < 0.05$ and $^{**}P < 0.01$.

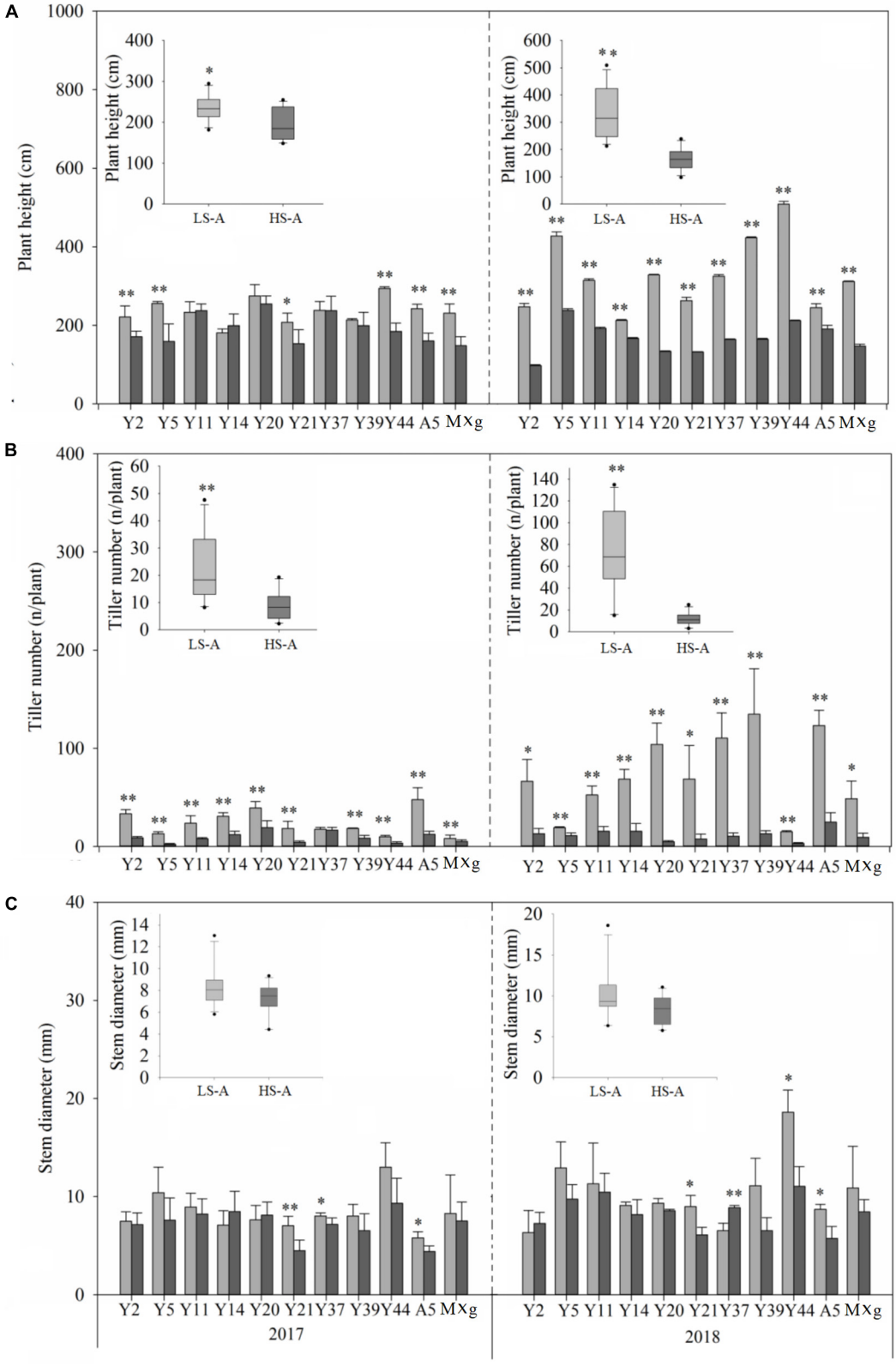

FIGURE 3
(A) Plant height, **(B)** tiller number, and **(C)** stem diameter of 11 genotypes of *Miscanthus* grown in low saline–alkaline soil (LS-A) (the light bars) and high saline–alkaline soil (HS-A) (the dark bars). Significance is denoted by $^{*}P < 0.05$ and $^{**}P < 0.01$.

TABLE 2 Significance of effect of genotype (G), location (L), year (Y), genotype × location (G × L), genotype × year (G × Y), location × year (L × Y), genotype × location × year (G × L × Y) on plant biomass, plant height, tiller number and stem diameter (model I).

Variance	Plant biomass	Plant height	Tiller number	Stem diameter
G	**	**	**	**
L	**	**	**	**
Y	**	**	**	**
G × L	**	**	**	NS
G × Y	**	**	**	NS
L × Y	**	**	**	**
G × L × Y	**	**	**	NS

Block (B) showed NS, with no shown in table. NS, no significance; **$P < 0.01$.

TABLE 3 Significance of effect of genotype (G), location (L), year (Y), genotype × location (G × L) on quality (model II).

Variance	G	E	G × L
Cell wall	*	*	NS
Hemicellulose	NS	*	NS
Cellulose	NS	*	**
Lignin	NS	NS	NS
Ash	**	**	NS
Nitrogen	*	**	**
Sodium	NS	NS	**
Potassium	NS	NS	**
Magnesium	NS	**	**
Calcium	NS	NS	**
Phosphorus	NS	NS	**

Block (B) showed NS, with no shown in table. NS, no significance; *$P < 0.05$; **$P < 0.01$.

significant difference ($P < 0.05$; 3.03 and 5.03%, respectively) (Figures 4A,C). In particular, the cell wall and cellulose contents of Y5, Y14, Y37 and *M.* × *giganteus* in high saline–alkaline soil were significantly ($P < 0.05$) lower than those in low saline–alkaline soil. In low saline-alkaline, the cell wall of *M.* × *giganteus* was 11. 40% higher than mean cell wall content (88.90 vs. 77.50%). In high saline-alkaline, although the cell wall of *M.* × *giganteus* was 3.13% higher than mean cell wall content (77.66 vs. 74.53%), the cell wall of Y2 was highest (82.33%) (Figures 4A,C). Similarity, the cellulose content of *M.* × *giganteus* was 10.79% higher than mean cellulose content in low saline-alkaline soil (50.33 vs. 39.54%). In high saline-alkaline soil, the cellulose content of Y39 was highest (40.22%). Interestingly, the mean hemicellulose content across all genotypes was significantly decreased by 3.68% in low compared with high saline–alkaline soil (27.10 vs. 30.78%) (Figure 4B). The mean hemicellulose of ten genotypes were 2.04 and 3.23% higher than that *M.* × *giganteus* in high and low saline-alkaline soil, respectively (30.96 vs. 28.92% and 27.66 vs. 21.43%). In addition, the hemicellulose contents of Y14 and *M.* × *giganteus* under high saline–alkaline conditions were significantly ($P < 0.05$) higher than that under low saline–alkaline conditions (Figure 4B). Genotype, high saline–alkaline soil conditions and location–genotype interactions had no observable impact on lignin content (Table 3). However, the mean lignin content of *M.* × *giganteus* in low and high saline-alkaline was the highest (14.40%) (Figure 4D).

Ash and elemental contents of *Miscanthus* under low and high saline–alkaline conditions

Higher saline–alkaline stress significantly ($P < 0.01$) and consistently increased the ash content of *Miscanthus*, while genotype–location interaction had no significant effect on this trait (Table 3). The mean ash content of all genotypes in high saline–alkaline soil was significantly higher than that in low saline–alkaline soil (5.50 vs. 4.06%); this was particularly evident in the ash content of Y14 (7.14 vs. 5.93%), Y20 (4.25 vs. 2.94%), Y39 (6.37 vs. 5.04%), A5 (6.50 vs. 5.26%) and *M.* × *giganteus* (3.77 vs. 1.64%) (Figure 5).

The mean nitrogen (N), phosphorus (P), sodium (Na), potassium (K), calcium (Ca), and magnesium (Mg) contents of all genotypes and each individual genotype in low and high saline-alkaline soil are shown in Figure 6. Saline–alkaline soil level had a significant ($P < 0.01$) impact on nitrogen and magnesium contents (Table 3). The mean nitrogen content across all genotypes was significantly ($P < 0.05$) higher in low saline–alkaline soil than in high saline–alkaline soil (0.82vs. 0.59 g/kg) (Figure 6). Furthermore, except Y44 and *M.* × *giganteus*, all genotypes showed lower nitrogen content in high saline–alkaline soil than in low saline–alkaline soil. By contrast, the sodium and magnesium contents across all genotypes were significantly ($P < 0.05$) elevated in high saline–alkaline soil compared with low saline–alkaline soil. In particular, the average magnesium content across all genotypes in high saline–alkaline soil was more than eight-fold higher than that in low saline–alkaline soil (2.77 vs. 0.33 g/kg). Although the mean potassium, calcium and phosphorus contents across all genotypes were greater in high saline-alkaline soil compared with low saline–alkaline soil, none of these differences were significant.

K^+/Na^+ ratio in relation to yield and quality-related variables

The K^+/Na^+ ratio of various genotypes was analyzed in relation to their plant biomass and quality-related variables by linear regression analysis. Among all variables tested, only tiller number showed a significant linear relationship with the K^+/Na^+ ratio ($R = 0.445$, $P = 0.036$) (Figure 7).

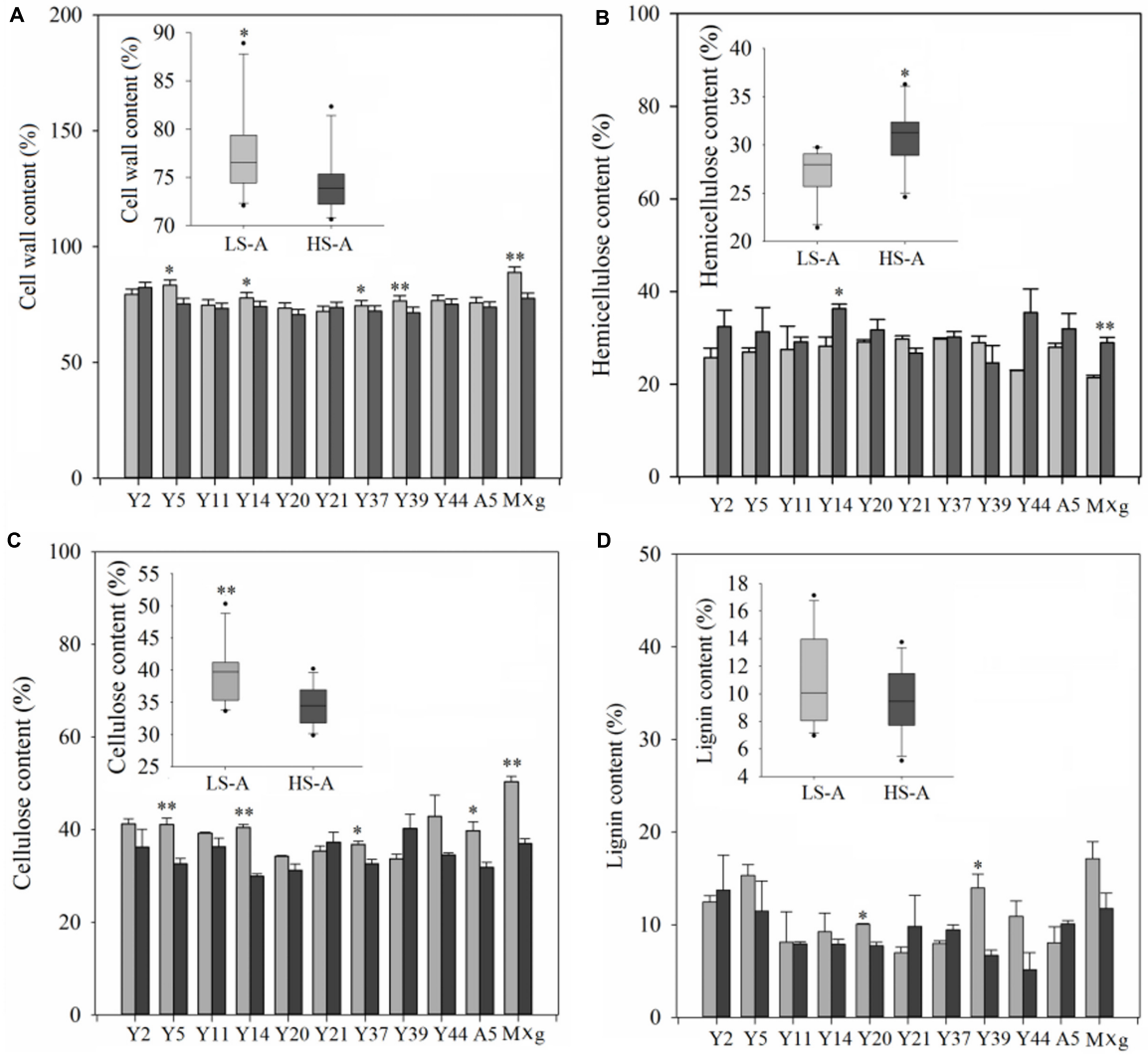

FIGURE 4
(A) Lignocellulose content, **(B)** hemicellulose content, **(C)** cellulose content, and **(D)** lignin content of 11 genotypes of *Miscanthus* grown in low saline–alkaline soil (LS-A) (the light bars) and high saline–alkaline soil (HS-A) (the dark bars). Significance is denoted by $^{*}P < 0.05$ and $^{**}P < 0.01$.

Discussion

High saline–alkaline soil influences agronomic traits

Agronomic traits of *Miscanthus*, including plant biomass, plant height, tiller number and stem diameter, were analyzed in this study to evaluate its potential as a bioenergy crop (Atienza et al., 2003; Liu et al., 2021). Plant biomass, as directly harvested trait, was significantly reduced in high saline–alkaline soil, which was consistent with the results of other bioenergy crops such as switchgrass (Liu et al., 2014; Zhang et al., 2021). The plant biomass of *M.* × *giganteus* was previously found to be reduced by 56% at 5–15 dS m^{-1} EC under high salinity stress (Stavridou et al., 2017). However, in the current study, plant biomass in high saline–alkaline soil (12.92 dS m^{-1}) was 10-fold lower than that in low saline–alkaline soil (2.59 dS m^{-1}). A possibility could explain that an effect of saline–alkaline stress on *Miscanthus* agronomic traits may be stronger than that of salinity or alkalinity alone. High photosynthesis and efficient water use still maintain biomass yield under alone salinity stress (Yan et al., 2015). However, under alkaline stress, the H^+ content of apoplast is vital for the maintenance of plasma membrane potential, which regulates cell growth (Yang et al., 2021). High pH value may have an adverse effect on the H^+ content of apoplast. However, the alkaline stress response of *Miscanthus* remains unknown. The conjecture needs to be confirmed.

In addition, the conclusion of Stavridou report was based on the salt tolerance in the seedling phase, when plant height and stem diameter mainly contributed to plant biomass.

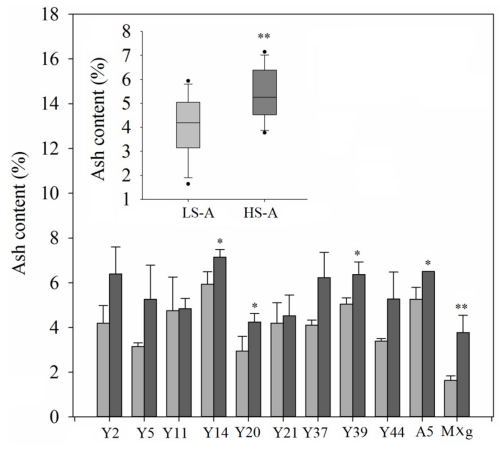

FIGURE 5
Ash content of 11 genotypes of *Miscanthus* grown in low saline–alkaline soil (LS-A) (the light bars) and high saline-alkaline soil (HS-A) (the dark bars). Significance is denoted by $^{*}P < 0.05$ and $^{**}P < 0.01$.

Interestingly, we found that tiller number was more sensitive than plant height and stem diameter. Moreover, no significant difference stem diameter between low saline-alkaline soil and high saline-alkaline soil was observed. The reason may be that may be that stem diameter is less affected by the location. Previous study showed that the location had no significant impacts on stem diameter (Jeżowski et al., 2011). However, the investigation of *Miscanthus* in the field is still necessary for breeding new varieties with saline-alkaline tolerance.

High saline–alkaline soil changes the cell wall compositions and ash content

Cell wall components, including cellulose, hemicellulose and lignin, constitute most of the *Miscanthus* biomass (Schäfer et al., 2018). The cell wall composition of *Miscanthus* varies with environment (Lewandowski et al., 2003; Jensen et al., 2017). In the current study, the cell wall content of *Miscanthus* biomass was reduced by high saline–alkaline stress, whereas the ash content increased, consistent with the findings in switchgrass (Liu et al., 2014). Moreover, results obtained in this study under high salinity stress were similar to those obtained previously (Stavridou et al., 2017). With saline-alkali stress, ash and lignin content of switchgrass biomass increased, and cellulose and hemicelluloses content of switchgrass biomass decreased (Liu and Wu, 2014). In the study, the hemicellulose content of *Miscanthus* was significantly higher in high saline–alkaline than in low saline–alkaline soil, while the lignin content of *Miscanthus* showed no significant difference between low and high saline-alkaline conditions. Under drought stress, hemicellulose content of *Miscanthus* also increased (Tim et al., 2016a), suggesting that adjustment of cell wall components to saline–alkaline and drought stress may be similar. An increase in the relative proportion of hemicellulose content, along with a decrease in the relative proportion of cellulose content, may therefore enable the plant cell walls to uphold their structural rigidity without compromising plasticity under high saline–alkaline conditions (Gall et al., 2015). This may explain the results of the current study. Interestingly, the lignin content of *Miscanthus* showed no significant difference between low and high saline–alkaline conditions, which should be studied in the future study. Although the soil EC and pH between location I and location II were mainly different, other differences (available nutrients) also existed, which may be explain why the cell wall changes observed in this study differed from those in other studies.

The ash content of *Miscanthus* was substantially higher in high saline–alkaline soil than in low saline–alkaline soil; similar results were observed by Stavridou et al. (2017). The ash of biomass combustion has a low melting point and is easy to adhere to the wall of furnace and superheater (Baxter et al., 2012). Furthermore, elements, released from ash in the combustion chamber, can be corrosive and can cause slagging and fouling (Lewandowski and Kicherer, 1997; Tim et al., 2016b). In addition, although we tried to make sure that all environmental factors, except for soil saline-alkaline, were similar. The soil nutrition was still different, which may be have impacts on elemental content of biomass. In the near future study, the effect of the elemental content of soil on elemental content of biomass will be investigated.

Implications of the current results for breeding saline–alkaline stress tolerant *Miscanthus* varieties

Although optimizing the establishment of *Miscanthus* on saline–alkaline soil may improve its adaptability, breeding new varieties grown on saline–alkaline soil is still a priority (Clifton-Brown et al., 2019; Zheng et al., 2021). Screening for saline–alkaline tolerance in genotypes selected from natural germplasm resources or developed by interspecific hybridization may address this pressing need (Zheng et al., 2021). *Miscanthus* species exhibit wide variation in saline stress tolerance (Chen et al., 2017), and screening for saline–alkaline stress tolerant genotypes from germplasm resources is possible (Zheng et al., 2019). These genotypes could be used directly for breeding new varieties.

Currently, production of bioethanol for *Miscanthus* biomass feedstocks, were initially identified as the most promising value chains (Hessini et al., 2019; Moll et al., 2020). We identified that *Miscanthus* genotypes A5 was significantly superior to *M.* × *giganteus* in low or high saline-alkaline soil, which are therefore promising genotypes for breeding saline–alkaline

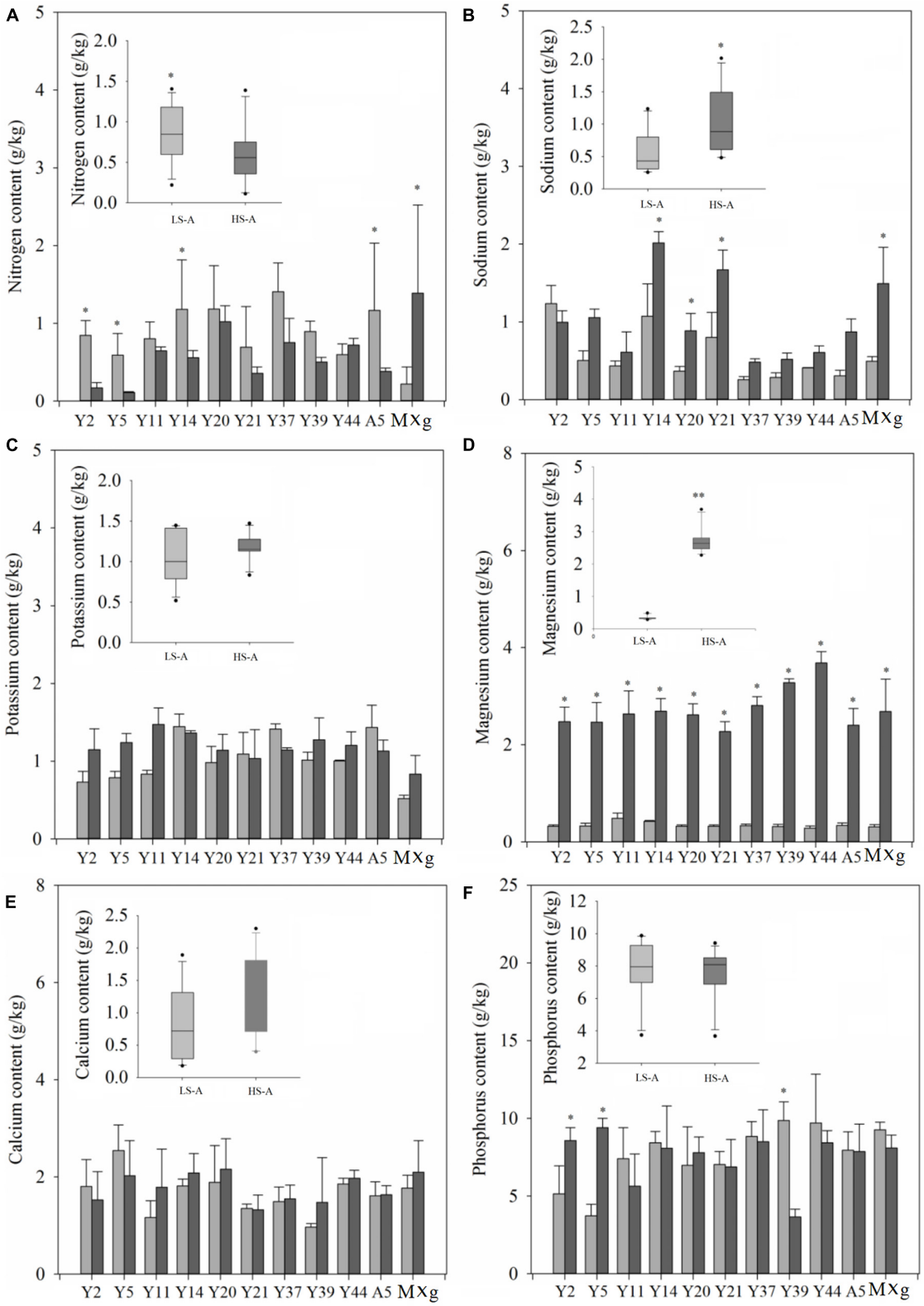

FIGURE 6
The nitrogen **(A)**, sodium **(B)**, potassium **(C)**, magnesium **(D)**, calcium **(E)**, and phosphorus **(F)** content of 11 genotypes of *Miscanthus* grown in low saline–alkaline soil (LS-A) (the light bars) and high saline–alkaline soil (HS-A) (the dark bars). Significance is denoted by $^{*}P < 0.05$ and $^{**}P < 0.01$.

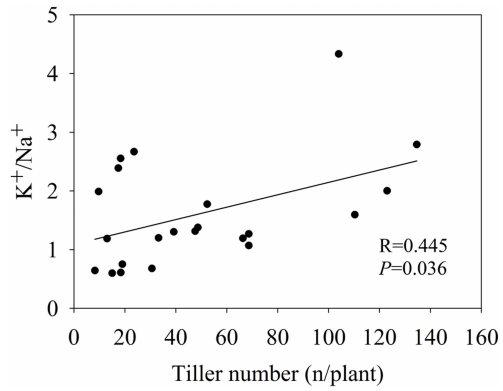

FIGURE 7
The linear relationship between tiller number and K^+/Na^+.

tolerant varieties. Although the plant biomass of the three genotypes in saline–alkaline soil was higher than that of *M.* × *giganteus*, their biomass quality still needs be improved for the production of bioethanol. In this study, the biomass quality of *M.* × *giganteus* was better than that of the other 10 genotypes assayed, owing to low lignin content contributing to biomass conservation. Therefore, it is important that how to improve biomass quality and reduce lignin content.

Cell wall quality traits is determined by many polygenic traits (Ragauskas et al., 2014; Van der Cruijsen et al., 2021). The highly diverse *Miscanthus* germplasm is an attractive resource for the selection of genotypes with desirable cell wall properties (Yong, 2012; Zhao et al., 2014). In the current study, among various *Miscanthus* species, *M. lutarioriparius* showed relatively better biomass quality, which could be used for the production of bioethanol, with cellulose and hemicellulose contents more than 80%, and lignin content less than 12% (Zheng et al., 2019). In the future, backcross could be used to improve the biomass quality, and the biomass quality traits of *M. lutarioriparius* may be introduced into hybrids with high yielding potential in saline–alkaline soil (Zheng et al., 2022). Meanwhile, high saline-alkaline soil had significant impacts on biomass quality traits, which may be negatively influences biomass conversion. Homogeneous biomass feedstocks help control production parameters. Thus, In the breeding process, the genotype, that biomass quality traits are not sensitive to environment, should be noticed.

In addition, analysis of biomass yield traits such as plant biomass, plant height and tiller number is an effective, but not an efficient, method for evaluating the saline–alkaline stress tolerance of *Miscanthus*, because its agronomically relevant traits can be evaluated in a representative matter only after a growth period of at least 2–3 years (Lewandowski et al., 2016). Thus, this is a time-consuming and laborious process. However, salt tolerance-related molecular markers are not yet available. We found that the tiller number of *Miscanthus* was significantly ($P < 0.001$) influenced by high saline–alkaline soil. Moreover, the K^+/Na^+ ratio of aboveground biomass, one of the most important physiological indicators used to estimate plant salt tolerance (Wu et al., 2013; Płażek et al., 2014; Chen et al., 2017), was significantly ($P = 0.036$) correlated with tiller number, implying that a preliminary comparison of yield potential can be made on the basis of K^+/Na^+ ratio. In addition, a previous study indicated that several salt tolerant *Miscanthus* species at the seedling stage showed relatively high K^+/Na^+ ratios in the shoots under salt stress conditions (Sun et al., 2014; Chen et al., 2017). Therefore, utilization of the K^+/Na^+ ratio of aboveground biomass, as an indicator of saline–alkaline stress tolerance, may speed up the breeding of *Miscanthus* genotypes suitable for cultivation in saline–alkaline soil.

Conclusion

Although *M.* × *giganteus* is a widely used commercial variety, its saline–alkaline tolerance is only moderate. In this study, we demonstrated that the detrimental effects of high saline–alkaline stress on plant biomass, plant height and tiller number are significant. Owing to its high saline–alkaline tolerance and biomass quality, the plant biomass of A5 was significantly higher than that of *M.* × *giganteus* in 2018, under low and high saline-alkaline, which are therefore promising genotypes for breeding saline–alkaline tolerant varieties. However, the biomass quality of A5 still need be improved, example for high ash content. In future studies, *Miscanthus* genotypes should be propagated to investigate and confirm plant biomass improvements in multiple saline–alkaline environments. Moreover, we found that the effects of high saline–alkaline soil on *Miscanthus* biomass quality traits were significant, with decreases in cell wall, cellulose, and nitrogen content, and increases in hemicellulose, ash, sodium, potassium, magnesium, and calcium content. No significant difference in lignin content of *Miscanthus* grown in low and high saline-alkaline soil was observed. These results provide a basis for optimizing the industrial utility of *Miscanthus* biomass. However, the effects of saline–alkaline soil on saccharification potential of *Miscanthus* biomass remains poorly investigated. Thus, in further studies, the impact of saline–alkaline soil on industrial production of *Miscanthus* should be investigated.

Data availability statement

The original contributions presented in this study are included in the article/**Supplementary material**, further inquiries can be directed to the corresponding authors.

Author contributions

CZ and ZY conceived and designed the experiments. CZ analyzed the data and wrote the manuscript. LX, GS, ML,

SX, and XP conducted the experiments. MD and ZC executed the projects and provided the funding. All authors contributed to the article and approved the submitted version.

Funding

This study was supported financially by the Foundation for the Construction of Innovative Hunan (grant numbers: 2019RS1051, 2019NK2011, and 2019NK2021), the Hunan Science and Technology Talents Support Project (2019TJ-Q08), International Cooperation Key Project of Science and Technology Bureau of Changsha (kq1901031), and National Natural Science Foundation of China (32000260).

Conflict of interest

The authors declare that the research was conducted in the absence of any commercial or financial relationships that could be construed as a potential conflict of interest.

Publisher's note

All claims expressed in this article are solely those of the authors and do not necessarily represent those of their affiliated organizations, or those of the publisher, the editors and the reviewers. Any product that may be evaluated in this article, or claim that may be made by its manufacturer, is not guaranteed or endorsed by the publisher.

Supplementary material

The Supplementary Material for this article can be found online at: https://www.frontiersin.org/articles/10.3389/fpls.2022.921824/full#supplementary-material

References

Acharya, M., Burner, D. M., Ashworth, A. J., Fritschi, F. B., and Adams, T. C. (2018). Growth rates of giant *Miscanthus* (*Miscanthus* × *giganteus*) and giant reed (*Arundo donax*) in a low-input system in Arkansas, USA. *Ann. Bot.* 9, 2371–2384. doi: 10.4236/ajps.2018.912172

Allison, G. G., Morris, C., Clifton-Brown, J., Lister, S. J., and Donnison, I. S. (2011). Genotypic variation in cell wall composition in a diverse set of 244 accessions of *Miscanthus*. *Biomass Bioenergy* 35, 4740–4747. doi: 10.1016/j.biombioe.2011.10.008

Atienza, S. G., Satovic, Z., Petersen, K. K., Dolstra, O., and Martín, A. (2003). Identification of QTLs influencing combustion quality in *Miscanthus sinensis* Anderss. II. Chlorine and potassium content. *Theor. Appl. Genet.* 107, 857–863. doi: 10.1007/s00122-003-1218-z

Baxter, X. C., Darvell, L. I., Jones, J. M., Barraclough, T., Yates, N. E., and Shield, I. (2012). Study of *Miscanthus*× *giganteus* ash composition – variation with agronomy and assessment method. *Fuel* 95, 50–62. doi: 10.1016/j.fuel.2011.12.025

Birgit, D., and Hartmut, G. (2000). Cell wall adaptations to multiple environmental stresses in maize roots. *J. Exp. Bot.* 51, 595–603. doi: 10.1093/jexbot/51.344.595

Chen, C. L., Schoot, H., Dehghan, S., Kamei, C., and Linden, C. (2017). Genetic diversity of salt tolerance in *Miscanthus*. *Front. Plant Sci.* 8:187. doi: 10.3389/fpls.2017.00187

Clifton-Brown, J., Schwarz, K. U., Awty-Carroll, D., Iurato, A., and Robson, P. (2019). Breeding strategies to improve *Miscanthus* as a sustainable source of biomass for bioenergy and biorenewable products. *Agron. J.* 9:673. doi: 10.3390/agronomy9110673

Clifton-Brown, J. C., and Lewandowski, I. (2002). Screening *Miscanthus* genotypes in field trials to optimise biomass yield and quality in southern Germany. *Eur. J. Agron.* 16, 97–110. doi: 10.1016/S1161-0301(01)00120-4

Deinlein, U., Stephan, A. B., Horie, T., Luo, W., and Schroeder, J. I. (2014). Plant salt-tolerance mechanisms. *Trends Plant Sci.* 19, 371–379. doi: 10.1016/j.tplants.2014.02.001

Dendooven, L., Alcántara-Hernández, R. J., Valenzuela-Encinas, C., Luna-Guido, M., Perez-Guevara, F., and Marsch, R. (2010). Dynamics of carbon and nitrogen in an extreme alkaline saline soil: A review. *Soil Boil. Biochem.* 42, 865–877. doi: 10.1016/j.soilbio.2010.02.014

Domon, J. M., Ba Ldwin, L., Acket, S., Caudeville, E., Arnoult, S., and Zub, H. (2013). Cell wall compositional modifications of *Miscanthus* ecotypes in response to cold acclimation. *Phytochemistry* 85, 51–61. doi: 10.1016/j.phytochem.2012.09.001

Fu, Z. H., Wang, B., Sun, G. Z., Li, W., and Liu, L. (2014). Regression analysis between ash content and ultimate analysis indexes for bio-fuels from the biomass power plant. *Adv. Mater. Res.* 884–885, 507–511.

Gall, H., Philippe, F., Domon, J. M., Gillet, F., Pelloux, J., and Rayon, C. (2015). Cell wall metabolism in response to abiotic stress. *Plants* 4, 112–166. doi: 10.3390/plants4010112

Gong, D., Holtman, K. M., Franqui-Espiet, D., Orts, W. J., and Zhao, R. (2011). Development of an integrated pretreatment fractionation process for fermentable sugars and lignin: Application to almond (*Prunus dulcis*) shell. *Biomass Bioenergy* 35, 4435–4441. doi: 10.1016/j.biombioe.2011.08.022

Hessini, K., Issaoui, K., Ferchichi, S., Saif, T., Abdelly, C., Siddique, K., et al. (2019). Interactive effects of salinity and nitrogen forms on plant growth, photosynthesis and osmotic adjustment in maize. *Plant Physiol. Biochem.* 139, 171–178. doi: 10.1016/j.plaphy.2019.03.005

Jagtap, S. S., Dhiman, S. S., Kim, T. S., Li, J., Lee, J. K., and Kang, Y. C. (2013). Enzymatic hydrolysis of aspen biomass into fermentable sugars by using lignocellulases from *Armillaria gemina*. *Bioresour. Technol.* 133, 307–314. doi: 10.1016/j.biortech.2013.01.118

Jensen, E., Robson, P., Farrar, K., Jones, S. T., Clifton-Brown, J., Payne, R., et al. (2017). Towards *Miscanthus* combustion quality improvement: The role of flowering and senescence. *GCB Bioenergy* 9, 891–908. doi: 10.1111/GCBB.12391

Jeżowski, S., Głowacka, K., and Kaczmarek, Z. (2011). Variation on biomass yield and morphological traits of energy grasses from the genus *Miscanthus* during the first years of crop establishment. *Biomass Bioenergy* 35, 814–821.

Lewandowski, I., Clifton-Brown, J., Trindade, L. M., van der Linden, G. C., Schwarz, K. U., Müller-Sämann, K., et al. (2016). Progress on optimizing *Miscanthus* biomass production for the European bioeconomy: Results of the EU FP7 project OPTIMISC. *Front. Plant Sci.* 7:1620. doi: 10.3389/fpls.2016.01620

Lewandowski, I., and Kicherer, A. (1997). Combustion quality of biomass: Practical relevance and experiments to modify the biomass quality of *Miscanthus*× *giganteus*. *Eur. J. Agron.* 6, 163–177. doi: 10.1016/S1161-0301(96)02044-8

Lewandowski, I., Scurlock, J., Lindvall, E., and Christou, M. (2003). The development and current status of perennial rhizomatous grasses as energy crops in the US and Europe. *Biomass Bioenergy* 25, 335–361. doi: 10.1016/S0961-9534(03)00030-8

Li, M., Feng, S., Wu, L., Li, Y., Fan, C., Zhang, R., et al. (2014). Sugar-rich sweet sorghum is distinctively affected by wall polymer features for biomass digestibility and ethanol fermentation in bagasse. *Bioresour. Technol.* 167, 14–23. doi: 10.1016/j.biortech.2014.04.086

Liu, J., Zhang, W., Long, S., and Zhao, C. (2021). Maintenance of cell wall integrity under high salinity. *Int. J. Mol. Sci.* 22:3260. doi: 10.3390/ijms22063260

Liu, J. L., and Wu, N. (2014). Biomass production of switchgrass in saline-alkali land. *Adv. Mater. Res.* 1008–1009, 93–96.

Liu, X. J. A., Fike, J. H., Galbraith, J. M., and Fike, W. B. (2014). Switchgrass response to cutting frequency and biosolids amendment: Biomass yield, feedstock quality, and theoretical ethanol yield. *Bioenergy Res.* 7, 1191–1200. doi: 10.1007/s12155-014-9454-4

Masto, R. E., Sarkar, E., George, J., Jyoti, K., Dutta, P., and Ram, L. C. (2015). PAHs and potentially toxic elements in the fly ash and bed ash of biomass fired power plants. *Fuel Process Technol.* 132, 139–152. doi: 10.1016/j.fuproc.2014.12.036

Moll, L., Wever, C., Völkering, G., and Pude, R. (2020). Increase of *Miscanthus* cultivation with new roles in materials production—a review. *Agronomy* 10:308. doi: 10.3390/agronomy10020308

Muylle, H., Hulle, S. V., Vliegher, A. D., Baert, J., Van Bockstaele, E., and Roldán-Ruiz, I. (2015). Yield and energy balance of annual and perennial lignocellulosic crops for bio-refinery use: A 4-year field experiment in Belgium. *Eur. J. Agron.* 63, 62–70. doi: 10.1016/j.eja.2014.11.001

Oliveira, D. M. D., Mota, T. R., Salatta, F. V., Sinzker, R. C., Končitíková, R., Kopečný, D., et al. (2020). Cell wall remodeling under salt stress: Insights into changes in polysaccharides, feruloylation, lignification, and phenolic metabolism in maize. *Plant Cell Environ.* 43, 2172–2191. doi: 10.1111/pce.13805

Pidlisnyuk, V., Stefanovska, T., Lewis, E. E., Erickson, L. E., and Davis, L. C. (2014). *Miscanthus* as a productive biofuel crop for phytoremediation. *Crit. Rev. Plant Sci.* 33, 1–19. doi: 10.1080/07352689.2014.847616

Płażek, A., Dubert, F., Kościelniak, J., Tatrzańska, M., Maciejewski, M., Gondek, K., et al. (2014). Tolerance of *Miscanthus× giganteus* to salinity depends on initial weight of rhizomes as well as high accumulation of potassium and proline in leaves. *Ind. Crop Prod.* 52, 278–285. doi: 10.1016/j.indcrop.2013.10.041

Ragauskas, A. J., Beckham, G. T., Biddy, M. J., Chandra, R., Chen, F., Davis, M. F., et al. (2014). Lignin valorization: Improving lignin processing in the biorefinery. *Science* 344:1246843. doi: 10.1126/science.1246843

Schäfer, J., Sattler, M., Iqbal, Y., Lewandowski, I., and Bunzel, M. (2018). Characterization of *Miscanthus* cell wall polymers. *GCB Bioenergy* 11, 191–205. doi: 10.1111/gcbb.12538

Sekar, R., Shin, H. D., and Dichristina, T. J. (2016). Direct conversion of cellulose and hemicellulose to fermentable sugars by a microbially-driven fenton reaction. *Bioresour. Technol.* 218, 1133–1139. doi: 10.1016/j.biortech.2016.07.087

Sen, K. Y., and Baidurah, S. (2021). Renewable biomass feedstocks for production of sustainable biodegradable polymer. *Curr. Opin. Green Sust.* 27:100412. doi: 10.1016/j.cogsc.2020.100412

Stavridou, E., Hastings, A., Webster, R. J., and Robson, P. (2017). The impact of soil salinity on the yield, composition and physiology of the bioenergy grass *Miscanthus×giganteus*. *GCB Bioenergy* 9, 92–104. doi: 10.1111/gcbb.12351

Sun, Q., Yamada, T., and Takano, T. (2014). Salinity effects on germination, growth, photosynthesis, and ion accumulation in wild *Miscanthus sinensis* Anderss. populations. *Crop Sci.* 54, 2760–2771. doi: 10.2135/cropsci2013.09.0636

Tang, Y., Xie, J. S., and Geng, S. (2010). Marginal land-based biomass energy production in China. *J. Integr. Plant Biol.* 52, 112–121. doi: 10.1111/j.1744-7909.2010.00903.x

Tim, V., Huxley, L. M., Hawkins, S., Sembiring, E. H., Farrar, K., Dolstra, O., et al. (2016a). Impact of drought stress on growth and quality of *Miscanthus* for biofuel production. *GCB Bioenergy* 9, 770–782. doi: 10.1111/gcbb.12382

Tim, V., Kiesel, A., Iqbal, Y., and Muylle, H. (2016b). Evaluation of *Miscanthus sinensis* biomass quality as feedstock for conversion into different bioenergy products. *GCB Bioenergy* 9, 176–190. doi: 10.1111/gcbb.12355

Van der Cruijsen, K., Al Hassan, M., van Erven, G., Dolstra, O., and Trindade, L. M. (2021). Breeding targets to improve biomass quality in *Miscanthus*. *Molecules* 26:254. doi: 10.3390/molecules26020254

Van Soest, P. J. (1967). Development of a comprehensive system of feed analyses and its application to forages. *J. Anim. Sci.* 26, 119–128. doi: 10.2527/jas1967.261119x

Wagner, M., Mangold, A., Lask, J., Petig, E., Kiesel, A., and Lewandowski, I. (2019). Economic and environmental performance of *Miscanthus* cultivated on marginal land for biogas production. *GCB Bioenergy* 11, 34–49. doi: 10.1111/gcbb.12567

Wang, Q., Kan, L., Lin, C., Song, Z., Tao, C. T., Sang, T., et al. (2019). Transcriptomic evaluation of *Miscanthus* photosynthetic traits to salinity stress. *Biomass Bioenergy* 125, 123–130. doi: 10.1016/j.biombioe.2019.03.005

Wu, D., Shen, Q., Cai, S., Chen, Z. H., Fei, D., and Zhang, G. (2013). Ionomic responses and correlations between elements and metabolites under salt stress in wild and cultivated barley. *Plant Cell Physiol.* 54, 1976–1988. doi: 10.1093/pcp/pct134

Xu, Y., Zheng, C., Liang, L., Yi, Z. L., and Xue, S. (2021). Quantitative assessment of the potential for soil improvement by planting *Miscanthus* on saline-alkaline soil and the underlying microbial mechanism. *GCB Bioenergy* 13, 1191–1205. doi: 10.1111/gcbb.12845

Xue, S., Lewandowski, I., Wang, X., and Yi, Z. (2016). Assessment of the production potentials of *Miscanthus* on marginal land in China. *Renew. Sust. Energy Rev.* 54, 932–943. doi: 10.1016/j.rser.2015.10.040

Yan, J., Zhu, C., Liu, W., Luo, F., Mi, J., Ren, Y., et al. (2015). High photosynthetic rate and water use efficiency of *Miscanthus lutarioriparius* characterize an energy crop in the semiarid temperate region. *GCB Bioenergy* 7, 207–218. doi: 10.1111/gcbb.12118

Yang, Z., Lin, W., Tang, W., Takahashi, K., and Kinoshita, T. (2021). TMK-based cell surface auxin signaling activates cell wall acidification in *Arabidopsis*. *Nature*. 599. doi: 10.21203/rs.3.rs-203621/v1

Yong, Y. (2012). *Comparsion of biomass chemical composition among Miscanthus germplasms*. Ph.D. thesis. Hunan: Hunan Agricultural University.

Zhang, B., Hastings, A., Clifton-Brown, J., Jiang, D., and Faaij, A. (2020). Modeled spatial assessment of biomass productivity and technical potential of *Miscanthus×giganteus*, *Panicum virgatum* l. and *Jatropha* on marginal land in China. *GCB Bioenergy* 12, 328–345. doi: 10.1111/gcbb.12673

Zhang, P., Duo, T., Wang, F., Zhang, X., Yang, Z., and Hu, G. (2021). De novo transcriptome in roots of switchgrass (*Panicum virgatum* L.) reveals gene expression dynamic and act network under alkaline salt stress. *BMC Genomics* 22:82. doi: 10.1186/s12864-021-07368-w

Zhao, H., Li, Q., He, J., Yu, J., Yang, J., Liu, C., et al. (2014). Genotypic variation of cell wall composition and its conversion efficiency in *Miscanthus sinensis*, a potential biomass feedstock crop in China. *GCB Bioenergy* 6, 768–776. doi: 10.1111/gcbb.12115

Zheng, C., Iqbal, Y., Labonte, N., Sun, G., and Xiao, L. (2019). Performance of switchgrass and *Miscanthus* genotypes on marginal land in the Yellow River Delta. *Ind. Crops Prod.* 141:111773. doi: 10.1016/j.indcrop.2019.111773

Zheng, C., Xiao, L., Iqbal, Y., Sun, G., Feng, H., Liu, F., et al. (2022). *Miscanthus* interspecific hybrids exceed the biomass yield and quality of their parents in the saline–alkaline Yellow River delta. *Food Energy Secur.* 11:e347. doi: 10.1002/fes3.347

Zheng, C., Xue, S., Xiao, L., Iqbal, Y., Sun, G. R., Duan, M. J., et al. (2021). "Two-steps" seed-derived plugs as an effective propagation method for the establishment of *Miscanthus* in saline–alkaline soil. *GCB Bioenergy* 13, 955–966. doi: 10.1111/gcbb.12820

Zub, H. W., Arnoult, S., and Brancourt-Hulmel, M. (2011). Key traits for biomass production identified in different *Miscanthus* species at two harvest dates. *Biomass Bioenergy* 35, 637–651. doi: 10.1016/j.biombioe.2010.10.020

frontiers | Frontiers in Plant Science

TYPE Original Research
PUBLISHED 07 November 2022
DOI 10.3389/fpls.2022.958029

OPEN ACCESS

EDITED BY
Jin-Lin Zhang,
Lanzhou University, China

REVIEWED BY
Yugo Lima-Melo,
Federal University of Rio Grande do Sul, Brazil
Vadim Volkov,
London Metropolitan University, United Kingdom
Lili Zhuang,
Nanjing Agricultural University, China

*CORRESPONDENCE
Xiaojun Yu
yuxj@gsau.edu.cn

SPECIALTY SECTION
This article was submitted to Plant Abiotic Stress, a section of the journal Frontiers in Plant Science

RECEIVED 31 May 2022
ACCEPTED 17 October 2022
PUBLISHED 07 November 2022

CITATION
Li Y, Yu X and Ma K (2022) Physiological effects of γ-aminobutyric acid application on cold tolerance in *Medicago ruthenica*. *Front. Plant Sci.* 13:958029. doi: 10.3389/fpls.2022.958029

Physiological effects of γ-aminobutyric acid application on cold tolerance in *Medicago ruthenica*

Ying Li, Xiaojun Yu* and Kaikai Ma

Key Laboratory of Grassland Ecosystem, Ministry of Education, Sino-U.S. Center for Grassland Ecosystem Sustainability, College of Grassland Science, Gansu Agricultural University, Lanzhou, China

Low temperatures in the seedling stage during early spring limit *Medicago ruthenica* germination and seedling growth. Elucidating the physiological mechanism of γ-aminobutyric acid (GABA)-regulated cold tolerance in *M. ruthenica* could provide a reference for alleviating the harmful effects of low temperatures on legumes in alpine meadows. The regulatory effects of GABA on *M. ruthenica* physiological parameters were explored by simulating the ground temperatures in the alpine meadow area of Tianzhu, China, in early May (2 h at 7°C; 6 h at 15°C; 4 h at 12°C; 2 h at 7°C; 10 h at 3°C). Our results showed that 15 mmol/l GABA was the optimal spray concentration to promote growth in the aboveground and belowground parts and increase the fresh and dry weights of seedlings. At this concentration, GABA enhanced the activities of catalase, peroxidase, superoxide dismutase, and ascorbate peroxidase; increased the osmotic balance; and inhibited the production of harmful substances in the cells under low-temperature conditions. GABA also regulated the tissue structure of leaves, increased the cell tense ratio, maintained photochemical activity, increased the amount of light energy to the photochemical reaction center, and improved the photosynthetic rate. Furthermore, exogenous GABA application increased the endogenous GABA content by promoting GABA synthesis in the early stages of low-temperature stress but mainly participated in low-temperature stress mitigation *via* GABA degradation in the late stages. Our results show that GABA can improve the cold tolerance of *M. ruthenica* by promoting endogenous GABA metabolism, protecting the membrane system, and improving the leaf structure.

KEYWORDS

low temperature, GABA, antioxidation, photosynthesis, metabolism, leaf structure

Introduction

Medicago ruthenica is a perennial herb with high crude protein content, good palatability, ecological width, and strong resistance to environmental and biological stressors (Yin et al., 2021). *M. ruthenica* is superior to *Medicago sativa* in terms of soil nutrient utilization and is more suitable for low-input cropping systems (Campbell et al., 1997). *M. ruthenica* mainly exists in Mongolia, Korea, and typical steppe and sandy steppe habitats in the low-temperature and cold temperate zones of northern China (Hao and Shi, 2006). Due to its good cold tolerance, *M. ruthenica* has the potential to be produced in the cold areas of China. Furthermore, it plays an important role in improving natural grassland, building artificial grassland, and improving the contradiction between grass and livestock (Xie et al., 2021). The alpine region lacks suitable legume species because of climate and environment problems; thus, *M. ruthenica* is an ideal species for natural grassland reseeding and artificial grassland planting in this region.

M. ruthenica is generally planted in early May each year in the alpine area of north China. Since the alpine grassland may suffer from prolonged low-temperature stress during sowing in early spring, it is preferable; moreover, it also affects plant yield and overwintering of *M. ruthenica*. In the Tianzhu Alpine Meadow in China, the average temperature in May has not exceeded 8°C in the last 30 years (Tong et al., 2021). Although *M. ruthenica* is cold-resistant, triggering antioxidant defenses when exposed to cold stress, plant defenses may be insufficient to mitigate extreme cold damage. Thus, additional substances may be needed to normalize plant growth at low temperatures. In recent years, the application of exogenous chemicals has become a common way to improve plant resistance. Exogenous chemical application has several ideal characteristics, such as economic viability, environmental safety, simple operation, strong applicability, and high effectiveness (Wang et al., 2021). Therefore, applying exogenous substances to improve the cold tolerance of *M. ruthenica* may be an effective approach for improving the utilization value of herbage.

γ-Aminobutyric acid (GABA) is a four-carbon, non-protein, free amino acid. Previous studies have focused on GABA as an inhibitory neurotransmitter in vertebrates to reduce the incidence of cardiovascular diseases (Xu et al., 2008). Later, GABA was used to regulate plant growth and development (Roberts, 2007; Beuve et al., 2004), especially under stress. GABA has been proven to effectively alleviate seed germination delay and growth retardation of plants under abiotic stress (Cheng et al., 2018), improving plant resistance. Most previous investigations on the regulatory effects of GABA have focused on salt stress (Kalhor et al., 2018), drought stress (Yong et al., 2017), and high-temperature stress (Liu et al., 2019). The alleviating effect of GABA on low-temperature stress has been observed in some fruits, vegetables, and crops, such as peach (*Prunus persica*) (Bustamante et al., 2016), wheat (*Triticum aestivum*) (Malekzadeh et al., 2012), and watermelon (*Citrullus lanatus*) (Palma et al., 2019); however, the effect of exogenous GABA application on *M. ruthenica* cold tolerance has not been reported.

In this study, we investigated the effects of the exogenous application of different GABA concentrations on the growth of *M. ruthenica* seedlings under low-temperature stress. The physiological mechanism of low-temperature regulation by GABA was evaluated by assessing changes in the antioxidant system, osmotic regulation system, photosynthetic fluorescence system, endogenous GABA metabolism, and leaf anatomical structure. Our findings will provide a reference for alleviating the harmful effects of low-temperature on legumes in alpine meadows.

Materials and methods

Plant material and growth conditions

M. ruthenica specimens were collected in Ningxian County, Gansu Province (35°33′N, 107°49′E, altitude 1,220 m), in 2015, planted in Huangyang Town in 2016, and harvested at the forage test station of Gansu Agricultural University, Huangyang Town, Wuwei City, Gansu Province (37°30′N, 103°15′E, altitude 1,660 m), in September 2018. *M. ruthenica* seeds were sown in containers (upper diameter 9.5 cm, lower diameter 5.0 cm, and height 10.5 cm) filled with vermiculite and distilled water, and all containers were randomly placed in the growth chambers (25/20°C (day/night), 70% relative humidity, and light for 12 h per day) for 7 days of germination. Plants were fertilized weekly with half-strength Hoagland's nutrient solution (Hoagland and Arnon, 1950). Plants were transferred to light incubators after 1-month establishment in the growth chambers. The environmental conditions of light incubators were maintained at day/night temperatures of 25°C/20°C, 70% relative humidity, light for 12 h per day, and luminous flux density of 400 μ mol/m^2·s. Plants were maintained in those conditions for 3 days before spraying GABA.

Experimental design

The experiment comprised two parts: the GABA concentration screening test and the GABA regulation experiment. Six GABA spraying concentrations were used for the screening test, 0 (distilled water spraying, CK), 1, 5, 10, 15, and 20 mmol/l, respectively, with six repetitions per treatment. The low-temperature cycle was set to simulate the ground temperature at the forage experimental station of Gansu Agricultural University in early May (2 h at 7°C; 6 h at 15°C; 4 h at 12°C; 2 h at 7°C; 10 h at 3°C). The first three low-temperature cycling intervals were illuminated for 12 h per day,

and the last two low-temperature intervals were set in darkness. The optimum GABA spraying concentration for promoting the growth of *M. ruthenica* was determined by measuring the growth indexes of plants. After the optimal GABA concentration was determined, four treatment groups were set up for the GABA regulation experiment: (1) leaves sprayed with distilled water + normal temperature (N); (2) leaves sprayed with 15 mmol/l GABA + normal temperature (NG); (3) leaves sprayed with distilled water + low-temperature stress (L); (4) leaves sprayed with 15 mmol/l GABA + low-temperature stress (LG). The normal-temperature culture conditions were 25°C (12 h per day)/20°C (12 h night); the low-temperature culture conditions were the same as those used in the GABA concentration screening test. Ten hydroponic boxes were set up for each treatment, six plastic bowls were placed in each hydroponic box, and each plastic bowl contained eight seedlings.

Experimental methods

The leaves of *M. ruthenica* were sprayed with GABA on their abaxial and adaxial surfaces at 9:00 every morning. *M. ruthenica* seedlings were then put into the light incubator (25°C/20°C, 12 h/12 h, 12 h light/day) for 3 days and continuously sprayed for 3 days. On the fourth day, the seedlings were placed in an incubator that simulated the low temperatures of the Tianzhu Alpine meadow and exposed to light for 12 h/day. For the GABA concentration screening experiment, the seedlings were cultured for 15 days. The GABA regulation experiment seedlings were cultured for 35 days, and the physiological and photosynthetic indexes were measured at 0, 7, 14, 21, 28, and 35 days.

Measurement of seedling growth index

On the day before low-temperature stress exposure, 30 seedlings were randomly selected from each treatment. The plant height (H1) of *M. ruthenica* was measured with a ruler and marked. At the end of the low-temperature stress exposure, the plant height (H2) was measured, and the plant height growth rate was calculated using the following formula. The root length and stem diameter were measured using a vernier caliper (mm); the leaf area was measured using a portable leaf area meter (Model: CI-203, CID Bio-Science, Inc., Camas, WA, USA). Five seedlings were randomly collected from each treatment and divided into aboveground and belowground parts. The fresh weight was measured using an analytical balance, and then the plant parts were dried in an oven at 105°C for 30 min, followed by 75°C until reaching a constant dry weight.

$$\text{Plant height growth rate} = (H_2 - H_1)/H_1 \times 100\,\%$$

Measurement of relative electrical conductivity

Referring to the study of Zhang et al. (2020), leaves in the same position were collected and placed in a 10-ml centrifuge tube filled with ultrapure water for 15 h. The conductivity (EC) was measured using a conductance instrument (EC-TDS-NaCl-°C, Hanna Instruments, China). The tissue was inactivated by boiling for 25 min, and the conductivity (EC1) was measured again when the solution cooled to room temperature. The relative electrical conductivity (REC) was calculated as (EC/EC1) × 100.

Measurement of oxidative damage

We referred to the methods of Li (2000) to measure the following indicators; malondialdehyde (MDA) content was determined by thiobarbituric acid colorimetry: 2 ml supernatant was mixed with 2 ml 2-thiobarbituric acid, incubated in a boiling water bath for 30 min, the absorbance measured at 450, 532, and 600 nm. The superoxide anion (O_2^-) production rate was measured using the hydroxyl ammonia oxidation method: 0.5 ml supernatant was mixed with 0.5 ml phosphate-buffered saline (PBS, pH 7.8) and 1 ml of 10 mmol/l hydroxylamine hydrochloride in a centrifuge tube for 1 h at 25°C, then added to the reaction solution (1 ml of 17 mmol/l *p*-aminobenzene sulphonic acid and 1 ml of 7 mmol/l α-naphthylamine). The absorbance of the aqueous phase was determined at 530 nm. Hydrogen peroxide (H_2O_2) content was determined by potassium iodide–iodine spectrophotometry: 0.5 ml supernatant was added to 0.5 ml of 10 mmol/l potassium phosphate and 1 ml of 1 mol/l potassium iodide, and the absorbance was measured at 390 nm. An ultraviolet spectrophotometer (Q-6, Shanghai Metash Instruments, China) was used for all absorbance measurements.

Referring to the method of Li (2016), 2 mmol/l NBT was stained in 20 mmol/l PBS (pH 6.8) for 12 h, followed by ethanol decolorization and rinsing with deionized water, resulting in blue staining of O_2^-. The leaves were stained with 0.1% (w/v) 3-diaminobenzidine (DAB; pH 3.8) for 24 h, decolorized with ethanol, and rinsed with deionized water, resulting in reddish-brown staining of H_2O_2.

Measurement of antioxidant enzyme levels

We referred to the methods of Li (2000) to measure the following indicators. Catalase (CAT) activity was determined using the ultraviolet absorption method: 0.1 ml supernatant and 2.9 ml CAT reaction solution (100 ml of 0.15 mol/l PBS with pH

7.0 and 0.1546 ml of 30% H_2O_2) were mixed. Absorbance was recorded every 40 s at 240 nm. Peroxidase (POD) activity was determined using the guaiacol method: 40 µl supernatant and 3 ml POD reaction solution (50 ml of 0.2 mol/l PBS with pH 6.0, 28 µl guaiacol, and 19 µl of 30% H_2O_2) were mixed, and absorbance was recorded every 40 s at 470 nm. Superoxide dismutase (SOD) activity was determined *via* nitroblue tetrazole (NBT) reduction: 40 µl supernatant was mixed with 3 ml SOD reaction solution (162 ml of 14.5 mmol/l methionine, 26 ml of 3 mmol/l EDTA-Na_2, 6 ml of 2.25 mmol/l nitroblue tetrazolium, and 6 ml of 60 µmol/l riboflavin). To assay ascorbate peroxidase (APX) activity, 0.1 ml of enzyme solution and 2.9 ml of APX reaction solution (2.60 ml of 0.05 mol/l PBS with pH 7.0 [containing 0.1 mmol/l EDTA-Na_2], 0.15 ml of 5 mmol/l ascorbic acid, and 0.15 ml of 20 mmol/l H_2O_2) were mixed, and change in absorbance was measured at 470 nm after 40 s.

Measurement of osmotic substance content

According to the method of Li (2000), the free proline (Pro), soluble sugar (SS), and soluble protein (SP) contents were determined. The free Pro content was determined by the acid ninhydrin colorimetric method: 0.5 g fresh sample was ground into a test tube with 5 ml of 3% sulfosalicylic acid and extracted for 10 min in boiling water. The supernatant (2 ml) and reaction solution (2 ml glacial acetic acid and 2 ml acidic ninhydrin) were put in boiling water for 30 min, 4 ml toluene was added to the mixture, and absorbance was measured at 520 nm. The SS content was determined by anthrone colorimetry: 0.1 g fresh sample was ground into a test tube with 5 ml distilled water and extracted for 30 min in boiling water. The supernatant (0.5 ml) was mixed with 1.5 ml distilled water and absorbance was measured at 630 nm. The SP content was determined by Coomassie Brilliant Blue G-250 staining: 1 ml supernatant was mixed with 5 ml Coomassie Brilliant Blue G-250 solution, and absorbance was measured at 595 nm.

Measurement of photosynthetic parameters and photosynthetic pigments

The net photosynthetic rate (Pn), transpiration rate (Tr), stomatal conductance (Gs), and intercellular CO_2 concentration (Ci) of leaves were measured from 9:00 to 11:30 using a Li-6400XT photosynthetic apparatus (LI-COR Biosciences, Lincoln, NE, USA). The determination light intensity was 400 $\mu mol \cdot m^{-2} \cdot s^{-1}$, the equipment's leaf compartment was 3 cm^2, and the CO_2 concentration was set to 370 $\mu mol \cdot mol^{-1}$. The temperature setting of the leaf compartment was consistent with the temperature of seedlings in low- and normal-temperature incubators under the measured time. A fresh sample of the sixth leaf (0.1 g) was immersed in anhydrous ethanol and placed under dark conditions for 24 h. The absorbance of the supernatant was measured at wavelengths of 665, 649, and 470 nm. Then, we used the following formula to calculate the chlorophyll a, chlorophyll b, and carotene contents (Arnon, 1949).

$$\text{Chlorophyll a concentration} = 13.95\ A665 - 6.88\ A649$$

$$\text{Chlorophyll b concentration} = 24.96\ A649 - 7.32\ A665$$

$$\text{Carotenoid concentration} = (1000\ A470 - 2.05\ Ca - 114.8\ Cb)/245$$

$$\text{Chlorophyll content} = (\text{pigment concentration} \times \text{volume of extract})/\text{fresh weight of sample}$$

Measurement of chlorophyll fluorescence coefficient

According to the method of Zhang (2019a), the following fluorescence parameters were determined. The sixth fully developed leaf was measured from 9:00 to 11:00 using a portable modulated chlorophyll fluorescence instrument (PAM-2100, WALZ, Germany). The initial fluorescence (F0) was determined after 20 min of dark acclimation, and the maximum fluorescence (Fm) was determined by irradiation saturation pulse (2,800.0 $\mu mol \cdot m^{-2} \cdot s^{-1}$). The steady-state fluorescence (Ft) under light adaptation was measured by switching on the endogenous photochemical light (600.0 $\mu mol \cdot m^{-2} \cdot s^{-1}$) for 5 min, and the maximum fluorescence (Fm′) under light adaptation was measured by switching on the saturation pulse (2,800.0 $\mu mol \cdot m^{-2} \cdot s^{-1}$) at 20-s intervals. Fluorescence parameters and leaf light energy distribution were determined according to the following formulas.

$$\text{Potential photochemical efficiency (Fv/F0)} = (Fm - F0)/F0$$

$$\text{Maximal photochemical efficiency (Fv/Fm)} = (Fm - F0)/Fm$$

$$\text{Photochemical quantum yield (ΦPSII)} = (Fm' - Ft)/Fm'$$

$$\text{Photochemical quenching coefficient (qP)} = (Fm' - Ft)/(Fm' - F0)$$

$$\text{Non-photochemical quenching coefficient (NPQ)} = (Fm - Fm')/Fm'$$

$$\text{Photochemical electron transfer rate (ETR)} = \Phi PSII \times PAR \times 0.50 \times 0.84$$

We determined the light energy distribution of the leaf, including the dissipation part of antenna [D = 1 − (Fm′ − F0′)/Fm′], the photochemical reaction part [P = qP × (Fm′ − F0′)/Fm′], the dissipation part of the reaction center [E = (1 − qP) × (Fm′ − F0′)/Fm′], and the excitation energy distribution imbalance between photosystem (PS)II and PSI: β/α − 1 = (Fm′ − F0)/(Fm′ − Fs)− 1.

Measurement of endogenous GABA metabolism

The endogenous GABA content and glutamic acid decarboxylase (GAD) activity were determined using the Suzhou Coming test box method, and aminobutyrate transaminase (GABA-T) activity was determined *via* the Ruixin biological ELISA test box method (Yong et al., 2017).

Measurement of the anatomical structure

The anatomical structure of plant leaves was determined according to the method of Zhang (2019b). Briefly, the sample was fixed in formalin–aceto–alcohol solution for more than 24 h. We used different gradients of alcohol for dehydration: 75% alcohol for 4 h, 85% alcohol for 2 h, 90% alcohol for 2 h, 95% alcohol for 1 h, anhydrous alcohol I for 30 min, anhydrous alcohol II for 30 min, alcohol benzene for 5–10 min, xylene I for 5–10 min, xylene II for 5–10 min, paraffin I for 1 h at 65°C, paraffin II for 1 h at 65°C, and paraffin III for 1 h at 65°C. The wax block was embedded and trimmed. Finally, the repaired wax block was cut into 4-μm pieces by a paraffin slicer, and the tissue was stained by ferro red–solid green staining and sealed. The leaf samples were observed on a light microscope (ECLIPSE Ci-L, Nikon, Japan). The thickness of leaf (LT), thickness of mesophyll (TM), thickness of upper epidermis (TUE), thickness of lower epidermis (TLE), thickness of palisade tissue (TPT), and thickness of sponge tissue (TST) were measured using Image-Pro Plus 6.0 analysis software. The palisade ratio, cell tense ratio, and spongy ratio were calculated using the following formulas.

$$\text{Palisade ratio} = TPT/TST$$

$$\text{Cell tense ratio (CTR)} = TPT/LT \times 100\,\%$$

$$\text{Spongy ratio (SR)} = TST/LT \times 100\,\%$$

Data analysis and graphics

Microsoft Excel 2010 was used for data sorting. Values are presented as the mean ± standard error. IBM SPSS Statistics 26 software was used for variance analysis of the measured data, and Duncan's new complex range method was used for multiple comparisons. The difference was considered statistically significant when $P< 0.05$. All images were created using Origin 2019.

Results

Effects of different GABA concentrations on the seedling growth index

Figure 1 shows that the growth index first increased and then decreased with the increase in GABA concentration. The spraying concentration of 1–10 mmol/l GABA increased the growth indicators, such as the plant height growth rate, root length, stem diameters, leaf area, and dry weights; however, the difference was not significant compared with the increase obtained *via* the distilled water spraying treatment (control). The plant height growth rate in the 15- and 20-mmol/l GABA spraying treatments significantly increased by 102.39% and 94.91%, respectively, compared with the distilled water spraying treatment (Figure 1A). The GABA spray concentration of 15 mmol/l significantly promoted root elongation, increasing the root length by 11.28% compared with the control roots. The 20-mmol/l GABA spray concentration had an inhibitory effect on root length (Figure 1B). The stem diameters were largest in the 10-mmol/l GABA spraying treatment and the 15-mmol/l treatment, which were respectively 10.83% and 7.68% larger than the control (Figure 1C). The GABA spraying treatments did not significantly affect the leaf area (Figure 1D). The GABA spray concentration of 15 mmol/l increased the fresh and dry weights of seedlings by varying degrees (Figures 1E–H).

By measuring and calculating the height growth rate, root length, stem diameter, leaf area, and fresh and dry weights of *M. ruthenica* seedlings sprayed with different GABA concentrations, we concluded that the spray concentration of 15 mmol/l GABA was the optimal concentration to attenuate the effects of low-temperature stress on *M. ruthenica* growth.

Effects of GABA on the phenotypic and oxidative damages of seedlings

Pre-spraying with GABA (LG) alleviated the effect of leaf wilting and poor growth caused by low temperatures (Figure 2). On days 21, 28, and 35 of the low-temperature treatment, the

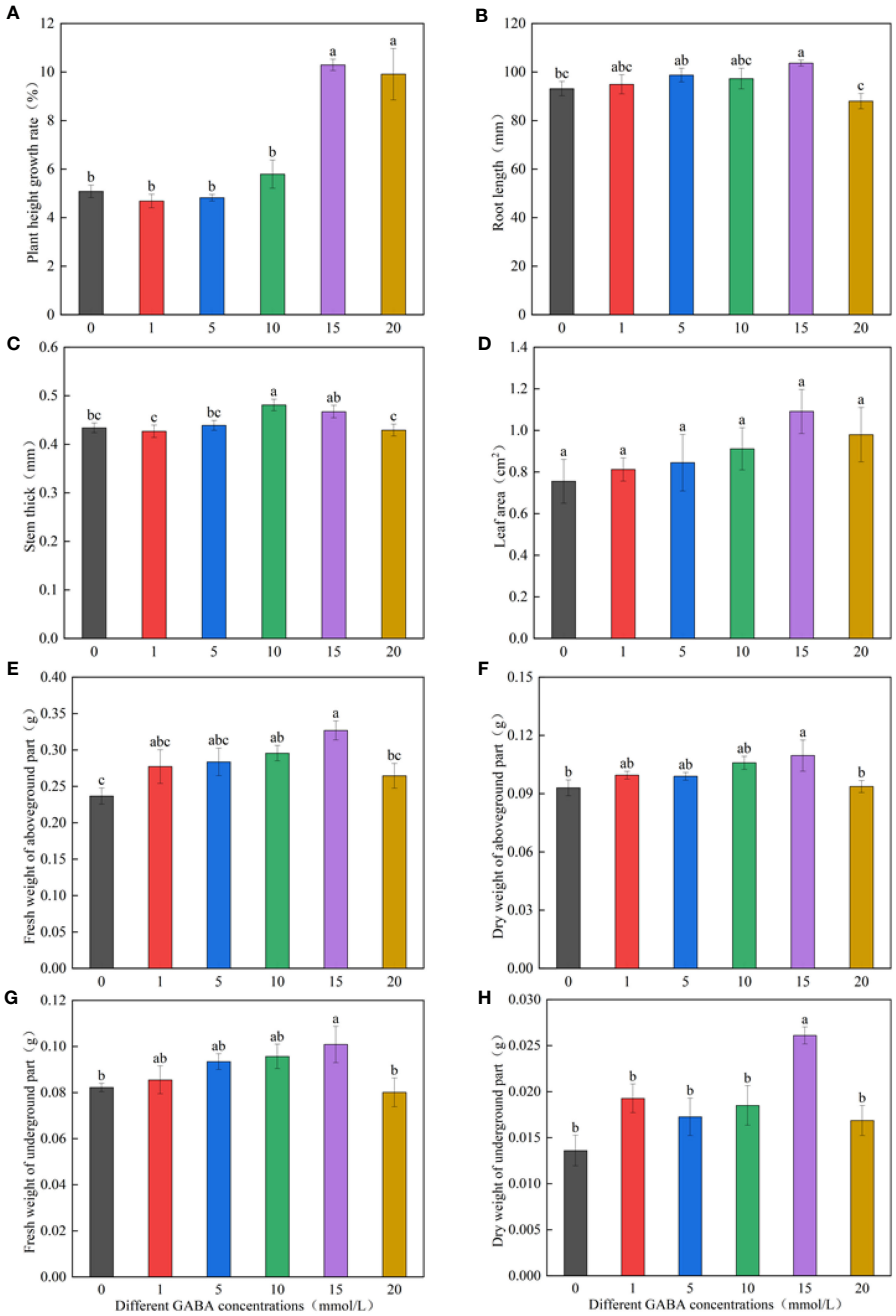

FIGURE 1
Effects of different GABA concentrations on seedling growth indexes. The growth temperature of seedlings is low-temperature in Figure **(A-H)**. Different lowercase letters indicate significant differences between treatments ($P< 0.05$).

REC of LG significantly decreased by 16.81%, 30.44%, and 18.61%, respectively, compared with the L treatment (Figure 3A). On days 14 and 35 of low-temperature treatment, the MDA content of LG significantly decreased by 47.76% and 28.6%, respectively, compared with L (Figure 3B). On day 28, exogenous GABA alleviated the increase in the O_2^- production. On day 35, the O_2^- production rate of the LG was 12.43% lower than that of the L treatment (Figure 3C). The H_2O_2 content of LG significantly decreased by 26.08%, 24.23%, and 7.29% than L on days 14, 21, and 35, respectively (Figure 3D).

The NBT staining degree in the LG treatment was lighter than that in the L treatment, and there were fewer stained parts. Thus, GABA application alleviated the excessive O_2^- accumulation at low temperatures (Figure 3E). The

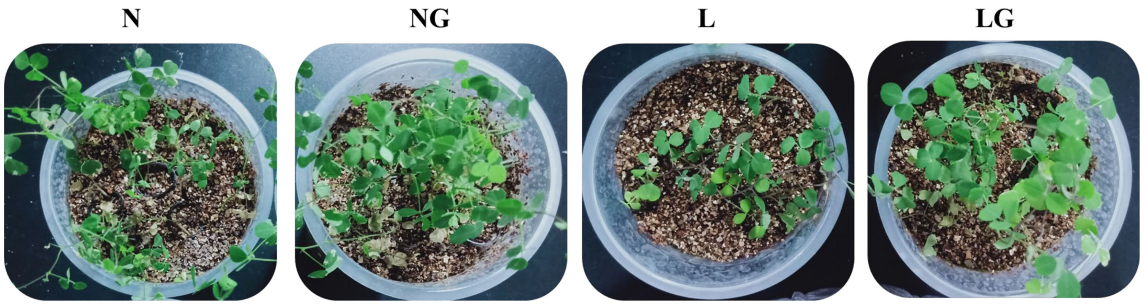

FIGURE 2
Effect of GABA spraying on the phenotypic characteristics of *M. ruthenica* seedlings under normal- and low-temperature treatments. N, leaves sprayed with distilled water + normal temperature (25°C/20°C); NG, leaves sprayed with 15 mmol/l GABA + normal temperature; L, leaves sprayed with distilled water + low-temperature stress (2 h at 7°C; 6 h at 15°C; 4 h at 12°C; 2 h at 7°C; 10 h at 3°C); LG, leaves sprayed with 15 mmol/l GABA + low-temperature stress.

accumulation of H_2O_2 in seedlings was visualized by DAB staining. Fewer leaves were stained brown in LG than in L, indicating that GABA reduced the massive accumulation of H_2O_2 in seedlings under low-temperature stress (Figure 3F).

Effects of GABA on antioxidant characteristics

On day 21, GABA effectively enhanced CAT activity at normal temperatures (NG) and low temperatures (LG), and the CAT activity was highest in the LG treatment (Figure 4A). There was no significant difference in POD activity between N and NG. On days 21 and 28 of the low-temperature treatment, the POD activity of LG seedlings was significantly higher (18.91% and 24.08%, respectively) than that of L seedlings, and the enzyme activity showed a downward trend on the 35th day (Figure 4B). GABA spraying increased the SOD activity at normal and low temperatures. The activity of SOD was significantly higher (27.16%) in the NG treatment than in N. At low temperatures, GABA increased SOD enzyme activity by 35.81%, 32.45%, and 29.24% compared with that of L treatment on days 7, 28, and 35, respectively (Figure 4C). Compared with the N and L treatments, GABA spraying enhanced APX activity under both normal- and low-temperature conditions on days 28 and 35, and the activity showed a trend of LG > L > NG > N (Figure 4D).

Effects of GABA on osmotic substance in seedlings

From the day 14 to day 35, the proline content of NG treatment was higher than that of N; however, the difference was not significant. At low temperature, pre-spraying GABA could increase proline content, which was significantly increased by 11.25% and 43.28% compared with L treatment on day 14 and day 35 (Table 1). The SS content in the N and NG treatments decreased from day 7 and then increased on day 35. The SS content in the L and LG treatments significantly increased from days 7 to 28 and decreased on day 35. The SS content in the LG treatment was highest on day 21, reaching 2.36 times that in the L treatment in the same period (Table 1). The SP content in LG was 18.85% and 31.08% higher than that in L on days 28 and 35, respectively (Table 1).

Effects of GABA on photosynthetic parameters and photosynthetic pigments of seedlings

The Pn of LG seedlings increased by 95.2% compared with L treatment seedlings on day 35 (Figure 5A). No significant differences in Tr, Gs, and Pn were observed between N and NG treatments. The Tr value in the LG treatment was 2.35, 2.06, and 2.65 times that in the L treatment on days 21, 28, and 35, respectively. The Tr of L and LG treatment decreased on days 0–28, and the Gs in the LG treatment was 54.39% higher than that in the L treatment on day 35 (Figures 5B, C). The Ci values in the L and LG treatments were higher than those in the N and NG treatments, and the Ci value was significantly lower (28.29%) in LG than in L on days 28 and 35 (Figure 5D).

The chlorophyll a, b and carotenoid contents decreased under low-temperature stress (Figure 6). Moreover, spraying GABA significantly increased the chlorophyll a and carotenoid contents at low temperatures but had no significant effect on the content of chlorophyll b. The chlorophyll a and carotenoid in LG were 18.48% and 31.07% higher than in L, respectively. The photosynthetic pigment contents were similar between N and NG treatments.

Effects of GABA on chlorophyll fluorescence parameters

Fv/F0, Fv/Fm, ΦPSII, qP, and ETR decreased and NPQ increased with increasing time in the low-temperature stress

treatments (Figure 7). Compared with L, Fv/F0 in LG significantly increased by 52.46%–72.45%, and Fv/Fm in LG significantly increased by 15.94%–30.09% on days 14–35 (Figures 7A, B). From days 21 to 35, the ΦPSII in the LG treatment increased by 6.62%–20.53%, and the qP significantly increased by 9.93%–23.43% compared with those in the L treatment (Figures 7C, D). NPQ was significantly higher in the low-temperature treatments. From day 7, the increase of NPQ in LG was much less than that in L. The NPQ was 18.79% lower in LG seedlings than in L seedlings on day 35 (Figure 7E). GABA also promoted increases in ETR, which were 20.05%, 32.69%, and 23.72% higher in LG than in L on days 14, 28, and 35, respectively (Figure 7F).

Effects of GABA on absorbed light energy distribution in leaves

As the number of low-temperature stress days increased, the distribution of absorbed light energy to the dissipation part of the antenna (D) and photochemical reaction part (E) increased, whereas that to the dissipation part of the reaction center (P)

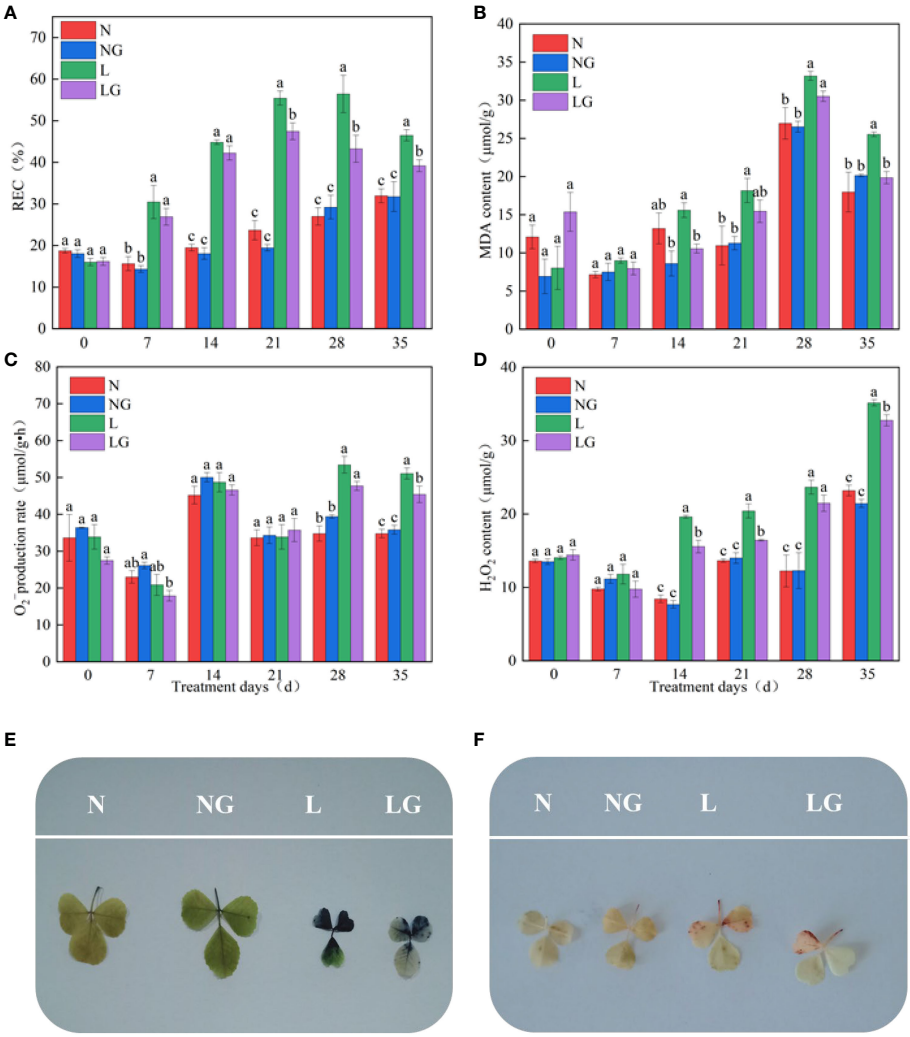

FIGURE 3
Effect of GABA spraying on oxidative damage parameters in *M. ruthenica* seedlings on different treatment days. **(A)** Relative electric conductivity (REC) content in leaves; **(B)** malondialdehyde (MDA) content in leaves; **(C)** superoxide anion (O_2^-) generation rate in leaves; **(D)** hydrogen peroxide (H_2O_2) content in leaves; **(E)** visualization results of superoxide anion (O_2^-); **(F)** visualization results of hydrogen peroxide (H_2O_2). N, the plant pretreated with distilled water and grown at normal temperature. NG, the plant pretreated with GABA and grown at normal temperature. L, the plant pretreated with distilled water and grown at low temperature. LG, the plant pretreated with GABA and grown at low temperature. Different lowercase letters indicate significant differences between N, NG, L, and LG on the same treatment day ($P< 0.05$).

10.3389/fpls.2022.958029

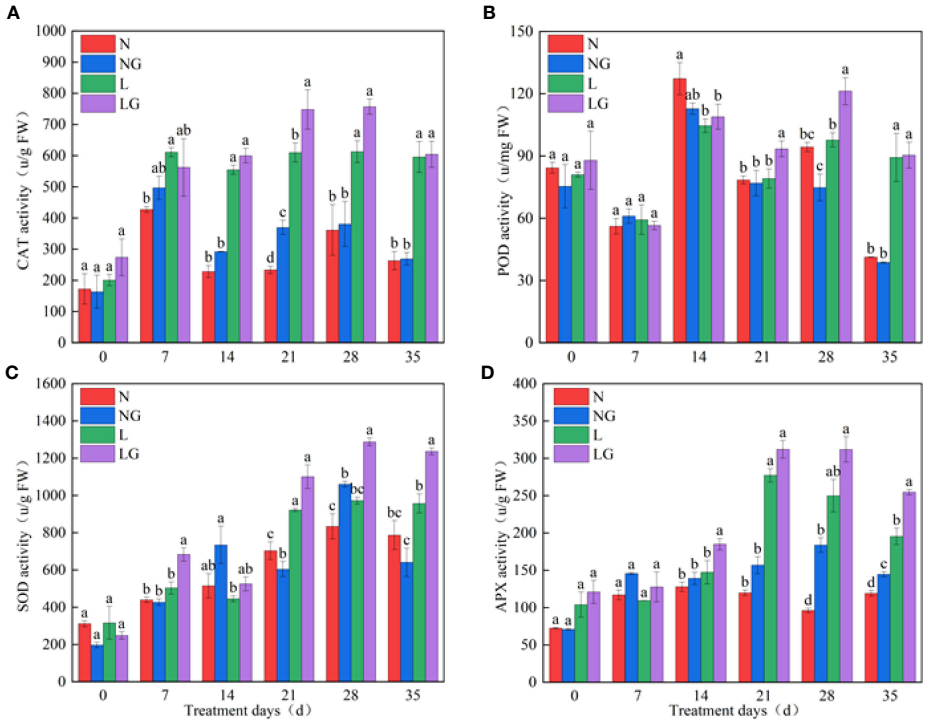

FIGURE 4
Effect of GABA spraying on antioxidant enzyme activity in *M. ruthenica* seedlings on different treatment days. **(A)** Catalase (CAT) activity in leaves; **(B)** peroxidase (POD) activity in leaves; **(C)** superoxide dismutase (SOD) activity in leaves; **(D)** ascorbate peroxidase (APX) activity in leaves. N, the plant pretreated with distilled water and grown at normal temperature. NG, the plant pretreated with GABA and grown at normal temperature. L, the plant pretreated with distilled water and grown at low temperature. LG, the plant pretreated with GABA and grown at low temperature. Different lowercase letters indicate significant differences between N, NG, L, and LG on the same treatment day ($P < 0.05$).

TABLE 1 Effects of GABA spraying on osmoprotectants in *M. ruthenica* seedlings on different treatment days.

Osmoprotectants	Treatments	Treatment days (d)					
		0	7	14	21	28	35
Pro (μg/g)	N	17.02 ± 1.02a	10.28 ± 0.26b	14.65 ± 1.52c	5.45 ± 1.62b	17.33 ± 2.94b	17.50 ± 1.23c
	NG	15.37 ± 3.04a	7.89 ± 1.29b	15.10 ± 0.61c	6.10 ± 2.68b	23.46 ± 4.13b	19.88 ± 4.07c
	L	12.88 ± 0.67a	145.52 ± 9.00a	272.27 ± 10.71b	53.13 ± 0.16a	192.55 ± 19.15a	133.85 ± 17.14b
	LG	15.54 ± 1.46a	286.92 ± 22.79a	302.89 ± 9.56a	63.26 ± 0.44a	226.57 ± 17.07a	191.78 ± 14.93a
SS (mg/g)	N	5.10 ± 0.22a	2.70 ± 0.27b	4.09 ± 0.43b	4.31 ± 0.75c	2.09 ± 0.14b	8.11 ± 0.65c
	NG	4.78 ± 0.61a	2.22 ± 0.41b	3.58 ± 0.26b	5.49 ± 0.49c	3.15 ± 0.80b	10.90 ± 0.66b
	L	4.34 ± 0.33a	7.06 ± 0.91a	24.96 ± 1.11a	16.91 ± 1.72b	33.00 ± 0.42a	17.45 ± 0.44a
	LG	6.27 ± 0.96a	7.46 ± 0.58a	23.43 ± 0.94a	39.98 ± 0.05a	35.02 ± 0.43a	17.86 ± 0.49a
SP (mg/g)	N	29.27 ± 3.76a	23.97 ± 0.88a	37.23 ± 2.88a	29.22 ± 0.6a	33.86 ± 1.99a	43.27 ± 3.01b
	NG	30.30 ± 1.85a	27.48 ± 0.57a	37.78 ± 1.26a	30.07 ± 1.44a	29.23 ± 0.94bc	50.51 ± 9.71ab
	L	31.04 ± 3.31a	25.68 ± 0.59ab	30.47 ± 1.04b	26.42 ± 1.32a	25.15 ± 0.45c	53.32 ± 10.02ab
	LG	35.83 ± 2.40a	19.72 ± 2.30b	29.78 ± 0.89b	28.18 ± 0.85a	29.89 ± 0.33ab	69.89 ± 4.01a

The contents of proline (Pro), soluble sugar (SS), and soluble protein (SP) in the four treatments of N, NG, L, and LG were measured on days 0, 7, 14, 21, 28, and 35. The first four lines represent the changes in Pro under different treatments, the middle four lines represent the changes in SS, and the last four lines represent the changes in SP. Under the same measurement indexes, different lowercase letters indicate the significant differences among N, NG, L, and LG on the same treatment days ($P < 0.05$).

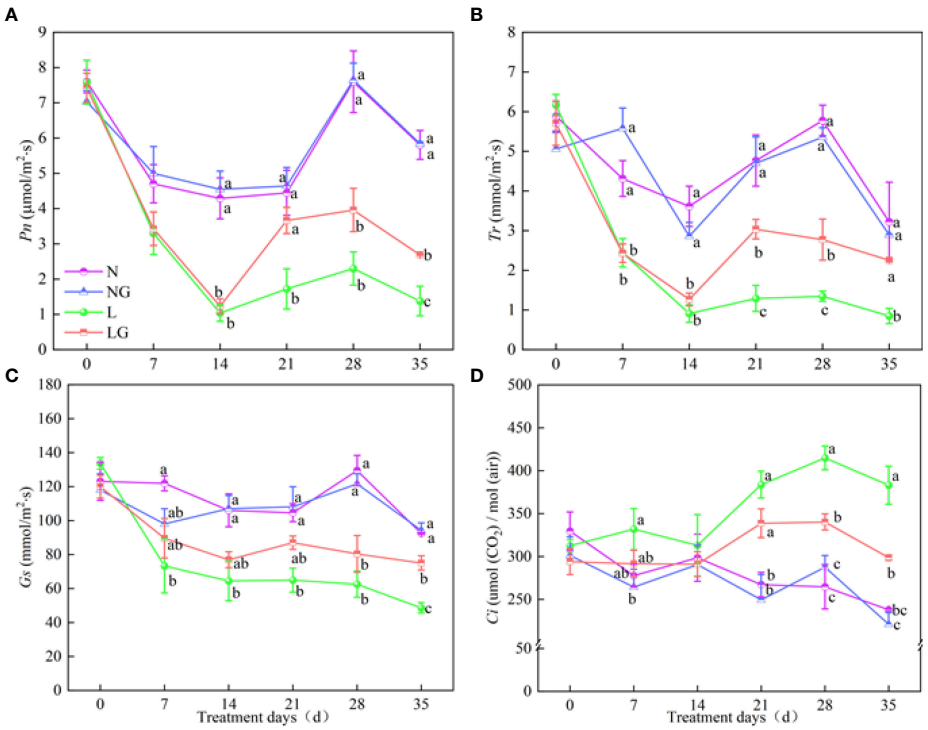

FIGURE 5
Effects of GABA spraying on photosynthetic parameters in *M. ruthenica* seedlings on different treatment days. **(A)** The net photosynthetic rate (Pn) in leaves; **(B)** transpiration rate (Tr) in leaves; **(C)** stomatal conductance (Gs) in leaves; **(D)** intercellular carbon dioxide concentration (Ci) in leaves. N, the plant pretreated with distilled water and grown at normal temperature. NG, the plant pretreated with GABA and grown at normal temperature. L, the plant pretreated with distilled water and grown at low temperature. LG, the plant pretreated with GABA and grown at low temperature. Different lowercase letters indicate significant differences between N, NG, L, and LG on the same treatment day ($P < 0.05$). Those not marked with letters under the same treatment day indicate that there is no significant difference between treatments.

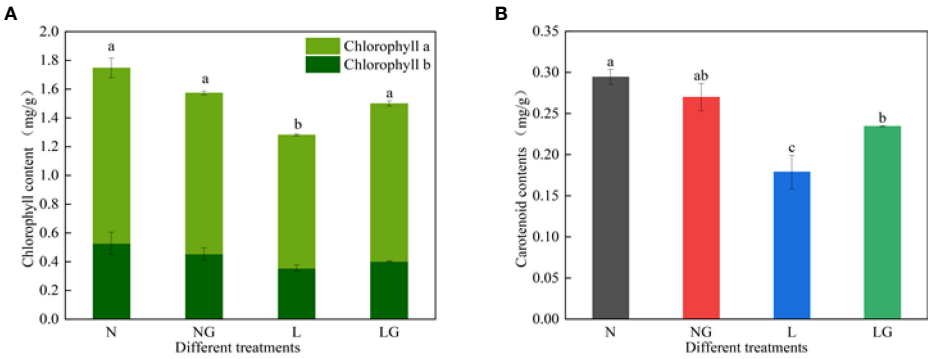

FIGURE 6
Effects of GABA spraying on photosynthetic pigment contents in *M. ruthenica* seedlings at normal and low temperatures. **(A)** Chlorophyll a and chlorophyll b content in leaves; **(B)** carotenoid content in leaves. N, the plant pretreated with distilled water and grown at normal temperature. NG, the plant pretreated with GABA and grown at normal temperature. L, the plant pretreated with distilled water and grown at low temperature. LG, the plant pretreated with GABA and grown at low temperature. Different lowercase letters indicate significant differences between treatments ($P < 0.05$).

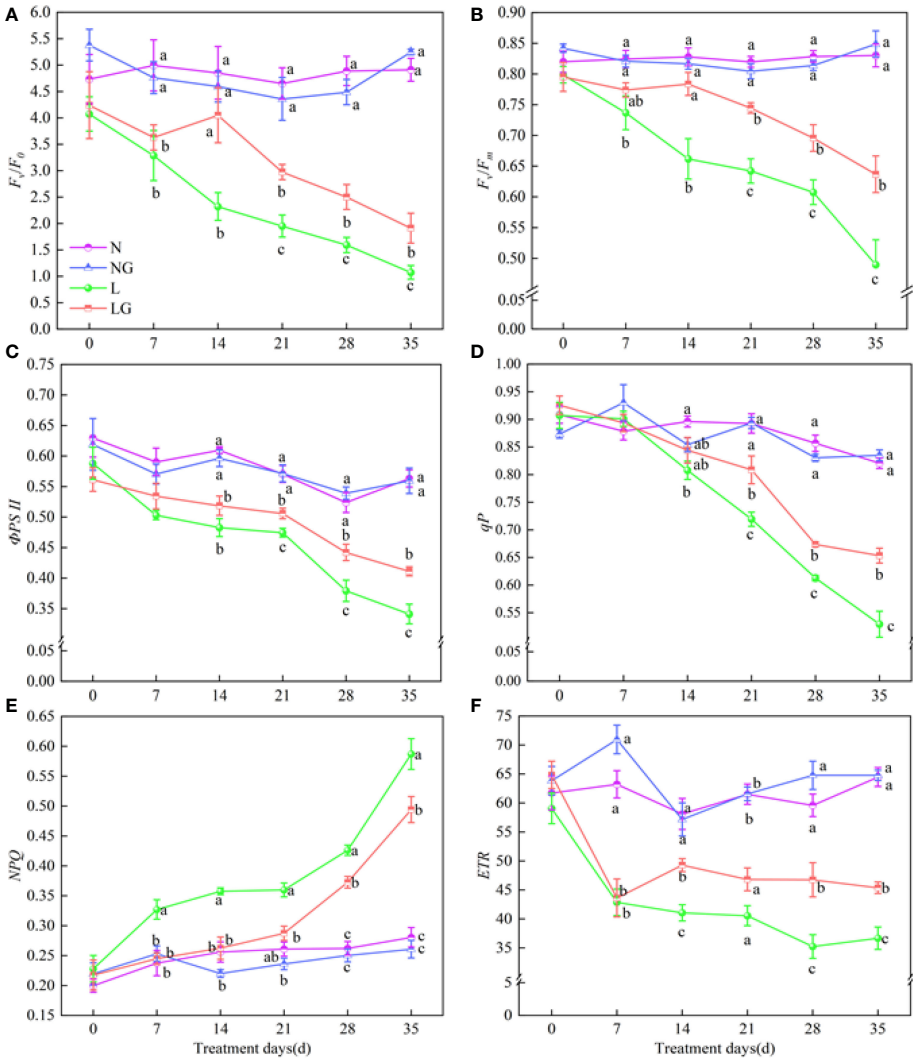

FIGURE 7
Effects of GABA spraying on the chlorophyll fluorescence parameters of seedlings on different treatment days. **(A)** Potential photochemical efficiency (Fv/F0) in leaves; **(B)** maximal photochemical efficiency (Fv/Fm) in leaves; **(C)** photochemical quantum yield (ΦPSII) in leaves; **(D)** photochemical quenching coefficient (qP) in leaves; **(E)** non-photochemical quenching coefficient (NPQ) in leaves; **(F)** photochemical electron transfer rate (ETR) in leaves. N, the plant pretreated with distilled water and grown at normal temperature. NG, the plant pretreated with GABA and grown at normal temperature. L, the plant pretreated with distilled water and grown at low temperature. LG, the plant pretreated with GABA and grown at low temperature. Different lowercase letters indicate significant differences between N, NG, L, and LG on the same treatment day ($P< 0.05$). Those not marked with letters under the same treatment day indicate that there is no significant difference between treatments.

continuously decreased (Figure S1). On day 35, the distribution of absorbed light energy to D and E was 41.85% and 36.82% lower in LG than in L, respectively, and the distribution to P was 27.08% higher in LG than in L, indicating that GABA spraying alleviated the energy dissipation at low temperatures (Figures S1A-C). β/α-1 continuously increased, showing a large energy imbalance between PSII and PSI at low temperatures. GABA alleviated this phenomenon, reducing β/α-1 in LG by 23.71%, 34.63%, 76.13%, 48.48%, and 27.54% compared with L on days 2, 14, 28, and 35, respectively (Figure S1D).

Effects of GABA on the leaf anatomical structure

The leaves thickened irregularly at low temperatures. The LT in the L treatment was significantly higher than that in the N and NG treatments. Compared with L, the LG treatment significantly reduced the LT and mesophyll thickness at 14, 28, and 35 days (Table 2). The lower epidermis thickness of LG seedlings was significantly decreased by 27.51% and 23.16% on days 14 and 28, respectively, but GABA did not significantly affect the upper

10.3389/fpls.2022.958029

epidermis thickness (Table 2). Low temperatures also increased the TPT and TST. With continuous low-temperature stress, the arrangement of palisade tissue changed from compact to loose. On days 14, 28, and 35, the palisade tissue thickness was 29.65%, 10.59%, and 10.94% lower in LG than in L, respectively, and the sponge tissue thickness decreased by 35.19%, 28.95%, and 37.16%, respectively (Figures S2, S3, Table 2). The leaf palisade ratio and CTR gradually decreased as the low-temperature exposure time progressed, and the SR increased. GABA effectively alleviated the CTR decline caused by low temperature. Compared with the L treatment, the palisade ratio in LG increased significantly by 24.19% and the SR decreased by 13.45% after the low-temperature treatment (Figure S2, Table 2).

Effects of GABA on endogenous GABA metabolism in seedlings

As the number of treatment days increased, the endogenous GABA content of seedlings increased under low temperatures

TABLE 2 Effects of GABA spraying on the anatomical structure of leaves of seedlings at low temperatures.

Treatment days (d)	Different treatments	LT (μm)	TM (μm)	TUE (μm)	TLE (μm)	TPT (μm)	TST (μm)	TPT/TST	CTR (%)	SR (%)
7	N	120.10 ± 1.60ab	92.77 ± 3.14a	18.98 ± 1.30a	13.98 ± 1.70b	51.73 ± 1.80a	40.83 ± 1.26a	1.27 ± 0.04a	43.15 ± 1.86a	34.01 ± 1.01a
	NG	115.01 ± 2.03b	84.93 ± 3.67ab	14.54 ± 1.09b	15.35 ± 0.21b	46.67 ± 0.72b	39.81 ± 2.80a	1.19 ± 0.07ab	40.60 ± 0.61a	34.58 ± 2.22a
	L	122.18 ± 2.71ab	80.46 ± 5.16b	18.68 ± 0.75a	20.09 ± 1.18a	41.16 ± 1.51c	41.95 ± 2.60a	1.00 ± 0.07c	33.79 ± 1.65b	34.33 ± 1.98a
	LG	124.20 ± 2.67a	88.11 ± 1.15ab	17.37 ± 0.78ab	17.33 ± 0.67ab	44.28 ± 0.99bc	42.82 ± 1.70a	1.04 ± 0.04bc	35.71 ± 0.99b	34.54 ± 1.60a
14	N	97.20 ± 1.33c	67.66 ± 2.30b	16.19 ± 0.70b	16.97 ± 1.13b	37.12 ± 0.96c	33.49 ± 2.33c	1.14 ± 0.10ab	38.26 ± 1.44a	34.43 ± 2.24ab
	NG	141.57 ± 0.78a	101.09 ± 2.95a	20.80 ± 0.96a	21.20 ± 0.92a	55.26 ± 1.69a	44.99 ± 2.28b	1.24 ± 0.07a	39.03 ± 1.17a	31.75 ± 1.44b
	L	138.73 ± 3.47a	104.44 ± 5.12a	18.31 ± 0.65ab	17.15 ± 0.74b	47.09 ± 1.67b	54.21 ± 2.87a	0.87 ± 0.03b	34.09 ± 1.80a	39.23 ± 2.59a
	LG	107.00 ± 3.25b	74.83 ± 3.51b	19.51 ± 0.83a	13.45 ± 0.68c	36.32 ± 1.54c	40.10 ± 3.72bc	0.95 ± 0.12b	34.10 ± 1.98a	37.26 ± 2.65ab
21	N	83.80 ± 1.29c	55.99 ± 1.87c	15.04 ± 0.87a	13.17 ± 1.44a	28.95 ± 2.12a	36.21 ± 2.83b	0.88 ± 0.10a	36.89 ± 2.20a	43.16 ± 3.12a
	NG	88.35 ± 1.91b	65.50 ± 0.70b	15.58 ± 2.18a	9.40 ± 1.00a	30.97 ± 1.10a	34.88 ± 0.55b	0.89 ± 0.04a	35.16 ± 1.64a	39.58 ± 1.29a
	L	112.71 ± 3.03a	82.60 ± 2.69a	16.26 ± 1.41a	13.96 ± 1.71a	32.01 ± 1.47a	50.30 ± 2.80a	0.64 ± 0.04b	28.43 ± 1.26b	44.64 ± 2.39a
	LG	110.55 ± 1.13a	78.48 ± 1.15a	17.68 ± 1.42a	14.07 ± 2.15a	29.26 ± 0.78a	51.57 ± 2.27a	0.57 ± 0.04b	26.49 ± 0.87b	46.69 ± 2.19a
28	N	81.27 ± 2.16d	52.12 ± 2.13c	11.78 ± 1.06b	13.61 ± 0.52ab	32.05 ± 0.77c	25.63 ± 2.40c	1.31 ± 0.15a	31.08 ± 0.41b	31.59 ± 2.99a
	NG	92.07 ± 3.34c	69.58 ± 4.64b	11.18 ± 0.65b	8.17 ± 0.40c	32.23 ± 0.62c	30.59 ± 1.16bc	1.06 ± 0.04ab	33.62 ± 0.60a	33.26 ± 0.82a
	L	125.41 ± 1.58a	87.90 ± 2.31a	22.05 ± 0.99a	15.05 ± 0.76a	42.17 ± 1.02a	44.50 ± 1.97a	0.95 ± 0.02b	33.62 ± 0.60b	35.44 ± 1.26a
	LG	113.91 ± 2.11b	73.99 ± 1.53b	20.40 ± 0.80a	12.22 ± 0.57b	38.13 ± 1.83b	34.51 ± 0.49b	1.11 ± 0.05 ab	32.99 ± 2.12b	30.35 ± 0.83a
35	N	79.54 ± 1.00c	65.21 ± 4.76bc	17.76 ± 0.92a	14.07 ± 1.09a	27.96 ± 1.64b	29.28 ± 0.61c	0.95 ± 0.05a	35.23 ± 2.33a	36.86 ± 1.19b
	NG	76.48 ± 2.98c	56.72 ± 4.01c	14.86 ± 0.66ab	10.57 ± 1.08a	26.37 ± 1.79b	29.33 ± 2.07c	0.91 ± 0.05a	34.35 ± 1.24a	38.20 ± 1.82b
	L	129.88 ± 0.72a	105.21 ± 1.12a	15.26 ± 1.32ab	13.91 ± 0.99a	36.41 ± 0.66a	59.15 ± 2.10a	0.62 ± 0.03c	28.05 ± 0.65b	45.55 ± 1.61a
	LG	107.33 ± 3.35b	70.83 ± 2.86b	14.10 ± 1.25b	14.19 ± 1.47a	32.82 ± 1.21a	43.03 ± 1.36b	0.77 ± 0.04b	30.79 ± 1.92ab	40.15 ± 1.11b

LT, leaf thickness; TM, thickness of mesophyll; TUE, thickness of upper epidermis; TLE, thickness of lower epidermis; TPT, thickness of palisade tissue, TST, thickness of sponge tissue; TPT/TST, palisade ratio; CTR, cell tense ratio, and SR, spongy ratio. Different lowercase letters indicate that there are significant differences among N, NG, L, and LG on the same treatment days and the same indexes ($P < 0.05$).

(Figure 8). The endogenous GABA content was highest in LG and was significantly higher (24.81%) than in L on day 28 (Figure 8A). GABA spraying also affected the seedling GAD. The GAD activity was highest in LG and was significantly higher (49.04%) than in L on day 21. After day 21, GAD activity began to decrease and was 24.16% lower in LG than in L on day 35 (Figure 8B). The GABA-T activity significantly increased in LG on the 14th day of low temperature and was 19.57%, 29.66%, and 28.66% higher than in L on days 21, 28, and 35 (Figure 8C).

Discussion

Low-temperature stress can cause lipid membrane damage, physiological metabolism disorder, and cell structure destruction in plants (Liu et al., 2018). Higher conductivity and MDA content are markers of oxidative stress and reduced membrane stability and integrity. Our results showed that the electrical conductivity and MDA content increased as the low-temperature exposure time progressed, which reflects an increase in electrolyte leakage and cell membrane damage. GABA inhibits MDA formation during lipid oxidation (Deng et al., 2010), effectively protecting the membrane system (Li et al., 2016). GABA had a protective effect on the membrane in this study, delaying increases in relative conductivity and MDA content at low temperatures. Excessive reactive oxygen species (ROS) production can cause oxidative damage in plants under long-term stress (Mignolet-Spruyt et al., 2016), resulting in H_2O_2 and O_2^- accumulation. Leaf staining showed that H_2O_2 and O_2^- contents in leaves increased under low-temperature conditions. However, GABA attenuated the increases in H_2O_2 and O_2^-, showing that GABA plays an important role in resisting oxidative damage. However, whether GABA can directly eliminate ROS is worth further discussion. Currently, no studies have confirmed that GABA directly removes ROS. The effect on ROS reduction observed in this study may be ascribed to the activation of some physiological mechanism by GABA to regulate the ROS removal process. We hypothesize that GABA may alleviate low-temperature stress by triggering antioxidant mechanisms. In this study, the activities of CAT, POD, SOD, and APX first increased and then decreased as the number of low-temperature days increased. The addition of GABA prevented reductions in antioxidant enzyme activities, enabling these enzymes to effectively remove ROS and protect cell membranes from damage. Our findings show that GABA enhances the cold tolerance of *M. ruthenica* by regulating the antioxidant system. The same conclusion was also reached in a study on wheat plants under salt stress (Li et al., 2016).

Plants usually rapidly synthesize and accumulate small molecular solutes (such as proline and soluble protein) to reduce water potential in plants and regulate osmotic pressure imbalance caused by environmental stress. In this study, the content of SS, Pro, and SP in seedlings at low temperature was higher than that at normal temperature. Exogenous GABA could be directly used as osmotic protectant or improve the osmotic adjustment ability of plants by increasing the content of soluble protein and proline to alleviate the damage caused by stress (Seifikalhor et al., 2019). In this study, the GABA treatment increased the free proline, soluble sugar, and soluble protein contents. This may be that exogenous GABA could improve the osmotic regulation ability of cells by increasing the content of osmotic substances, which can ensure the relatively normal growth of plants (Sikder et al., 2020). It may also be that GABA increases the contents of osmotic substances by upregulating enzymes related to the synthesis of these substances, such as Pro and trehalose, improving the growth of plant leaves under stress (Priya et al., 2019).

Photosynthesis is essential for plant growth and development. Stress will cause excessive light energy, resulting in light stress and excessive ROS production, damaging the

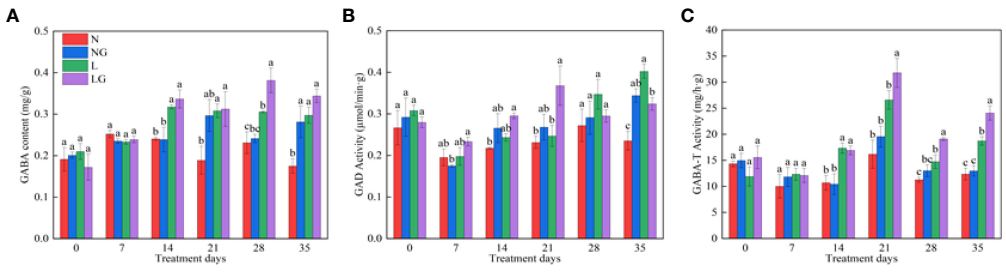

FIGURE 8
Effects of GABA spraying on the endogenous GABA metabolism of seedlings on different treatment days. **(A)** The endogenous γ-aminobutyric acid (GABA) content in leaves; **(B)** glutamic acid decarboxylase (GAD) activity in leaves; **(C)** aminobutyrate transaminase (GABA-T) activity in leaves. N, the plant pretreated with distilled water and grown at normal temperature. NG, the plant pretreated with GABA and grown at normal temperature. L, the plant pretreated with distilled water and grown at low-temperature. LG, the plant pretreated with GABA and grown at low-temperature.

photosynthetic mechanism, and hindering plant growth. The results reveal that the Gs and Tr decreased, indicating physiological activity and slower transpiration metabolism of plants at low temperature. In this study, Pn decreased and Ci increased at low temperature, which is related to the low temperature affecting the transport of CO_2 to chloroplasts and inhibiting the normal progress of the Calvin–Benson–Bassham cycle. Low temperature may reduce the activity of enzymes involved in the Calvin–Benson–Bassham cycle, and there was no CO_2 restriction (Tang, 2021). Thus, why could GABA improve the photosynthetic capacity of *M. ruthenica* at low temperatures? We speculate that adding GABA maintains the photosynthetic capacity of plants under stress by reducing plant water loss and increasing the transpiration rate under stress (Xu et al., 2021). GABA may also slow down the reduction rate of enzyme activity to maintain the photosynthesis, increase the excess light energy, and alleviate the reduction of the photosynthetic rate. In the growth diagram of this study, GABA alleviated the stunted growth of seedlings under low temperatures, which is related to the fact that GABA participates in the regulation of the photosynthetic system, protecting the photosynthetic mechanisms of seedlings under low temperatures and improving photosynthetic capacity. Chlorophyll content directly reflects the adaptation potential of plants to environmental changes (Wan et al., 2008). Carotenoid content can affect the absorption and utilization of light energy by plants (Fracheboud et al., 2004). In this study, both chlorophyll and carotenoid contents were reduced at low temperatures, indicating that stress may stimulate chlorophyll degradation, inhibit chlorophyll synthesis, or disorganize chloroplast tissue *via* photooxidation (Camejo et al., 2006). GABA may improve light utilization by increasing or decreasing photosynthetic pigment contents. Our results showed that the addition of GABA prevented decreases in chlorophyll a and carotenoid contents at low temperatures, indicating that GABA alleviates the rapid degradation of photosynthetic pigments. GABA may protect the pigments by reducing the excessive accumulation of chlorophyll a and chlorophyll precursors and maintaining the integrity of the chloroplast membrane structure (Xiang et al., 2016).

PSII is a major component of the photosynthetic electron transport chain and plays a key role in light energy conversion and electron transfer (Li et al., 2018). In this study, the chlorophyll fluorescence parameters related to the integrity of PSII changed at low temperatures, as Fv/F0, Fv/Fm, ΦPSII, qP, and ETR decreased. These changes signify the damages to the PSII complex. GABA alleviated these effects, suggesting that GABA contributes to maintaining photosynthetic electron transfer, enhancing the activity of the photosynthetic reaction center, protecting PSII from damage, and increasing the absorption of light energy. In this study, a large amount of light energy was dissipated at low temperatures, and the energy used in the photochemical reaction center gradually decreased, indicating that low-temperature stress created an imbalance of energy in leaves, limiting the photochemical reaction capabilities of seedlings. GABA effectively attenuated the massive dissipation of plant light energy, promoted the distribution of light energy to the photochemical reaction center by redistributing leaf light energy, reduced the amount of heat energy dissipation, limited the excitation energy distribution imbalance between PSII and PSI, strengthened leaf photosynthesis, and improved the survival ability of plants under stress.

Leaf structure is an important index to evaluate the cold tolerance of plants. Under normal circumstances, the leaves of plants are thin, which is conducive to photosynthesis. Photosynthesis is weakened under stress; to carry out normal CO_2 assimilation, the leaf structure changes. We found that the thickness of leaf significantly increased under low-temperature stress. This change may occur because small and thick leaves can adapt to stress by improving water storage and retention capacity. However, if the thickness of the leaf increases to a certain extent, the CO_2 exchange capacity may be affected. Exogenous GABA application improved the leaf structure and prevented leaf thickening, not only enhancing the exchange and transportation capacity of CO_2 and H_2O but also protecting the leaf structure at low temperatures (Shi, 2016). The arrangement and the thickness of palisade tissue and sponge tissue reflect the adaptability of plants to the environment. We observed an increase in the thicknesses of palisade tissue and sponge tissue at low temperatures, particularly the sponge tissue, which is very unfavorable for leaf water retention. If the leaf structure of plants remains in this condition for an extended period, the photosynthesis and phenotypic characteristics of plants will be affected. The results of this study showed that adding GABA slowed down the overdevelopment of sponge tissue to maintain a reasonable proportion and improved the cell tense ratio, indicating that GABA can prevent the loose structure of plant leaves and weaken the negative effects of membrane lipid peroxidation and reduce photosynthesis at low temperatures. Considering that there are few studies on the effects of GABA on forage leaf structural characteristics, the results of this study will provide a reference for using GABA to improve leaf cell structures under stress.

The glutamic acid decarboxylation pathway is one of the important pathways of GABA metabolism. At low temperature, the synthesis of glutamine in plants is blocked, the synthesis of protein is reduced, and the transformation of glutamic acid to GABA in plants is increased under the action of glutamic acid decarboxylase (GAD) (Shi et al., 2007). Therefore, this study showed that the endogenous GABA content of the two groups of seedlings increased under low-temperature treatment, and the content of seedlings sprayed with GABA increased more significantly, indicating that spraying GABA on leaves could promote the transformation

of glutamate into more GABA content. GABA accumulation and utilization result from the balanced regulation of its synthesis and degradation. When GABA accumulates, GABA-T plays an important role in the GABA degradation pathway. The substrate generated in this process participates in the tricarboxylic acid cycle of plants, which can enhance stress resistance (Ji, 2020). This study showed that the activity of GABA-T was weak and the GAD and GABA contents were high in the early stage of stress (0–14 days), indicating that the GABA synthesis pathway was active, and GABA played a positive feedback regulation role in endogenous GABA synthesis. During the middle stage of stress (21 days), the GAD activity and GABA-T activity in the LG treatment simultaneously increased, and the GABA content was also high, indicating that GABA accumulated to a certain extent at this time. In the later stage of stress (28–35 days), the GAD activity in LG decreased. The plant accelerates the degradation of GABA by enhancing the activity of GABA-T, resulting in the consumption of more GABA at low temperatures and the provision of higher ATP, promoting the tricarboxylic acid cycle, reducing the damage caused by low-temperature, and endowing plants with higher resistance (Fait et al., 2008; Podlešáková et al., 2019).

Therefore, we proposed that exogenous GABA alleviates the slim growth of *M. ruthenica* seedlings under low-temperature and enhances the cold tolerance, which is closely related to the antioxidant system, photosynthetic regulation system, light energy distribution, and leaf anatomical structure of plants. GABA could effectively remove ROS, reduce membrane system damage, improve cell osmotic regulation ability, and alleviate low-temperature injury. Moreover, the endogenous metabolism of GABA also plays a positive role in alleviating the low-temperature injury, accelerating the synthesis of GABA substances and providing substrates for the TCA cycle. Interestingly, in our study, GABA improved the growth of plants under low temperatures but did not significantly affect plants during the normal temperature treatment. This might be because GABA alleviates the low temperatures suffered by plants *via* the regulation of physiological mechanisms rather than providing only nitrogen sources.

Conclusion

Our experimental results demonstrate that GABA can reduce the degree of membrane system damage by enhancing antioxidant enzyme activity, increasing the contents of osmotic substances, and reducing the relative conductivity, MDA content, and ROS generation at low temperatures. GABA increases the light energy used in the photosynthetic reaction center by increasing the photosynthetic rate and the activity of PSII in the photochemical reaction center. GABA protects leaf structures from cold damage by reducing the thickness of leaf, increasing the palisade ratio, and reducing the spongy ratio. GABA participates in low-temperature remission by regulating GABA synthesis in the early stress stage and GABA degradation in the later stress stage (Figure 9). Therefore, we believe that GABA is an effective chemical agent to alleviate low-temperature stress in plants. If GABA is applied to alpine meadow forages, it is expected to provoke a stress-priming response in plants before exposure to cold in early spring.

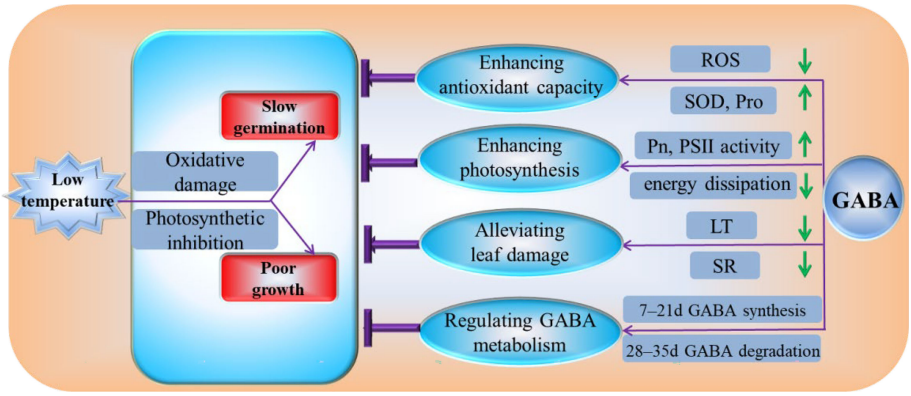

FIGURE 9
Physiological mechanism by which GABA regulates the cold tolerance of *M. ruthenica* under low-temperature conditions. ROS, reactive oxygen species; SOD, superoxide dismutase activity; Pro, the free proline; Pn, the net photosynthetic rate; PSII, photosystem II; LT, the thickness of leaf; SR, spongy ratio; GABA, γ-aminobutyric acid.

Data availability statement

The original contributions presented in the study are included in the article/Supplementary Material. Further inquiries can be directed to the corresponding author.

Author contributions

YL and XY conceived and designed the experiment. YL and KM conducted the experiment. YL analyzed the data and wrote the manuscript. XY revised the manuscript. All the authors read and approved the final manuscript.

Funding

This research was funded by the Industrial Support Project of Universities in Gansu Province (No. 2022CYZC-50).

Acknowledgments

The authors would like to thank NES for the English language review.

Conflict of interest

The authors declare that the research was conducted in the absence of any commercial or financial relationships that could be construed as a potential conflict of interest.

Publisher's note

All claims expressed in this article are solely those of the authors and do not necessarily represent those of their affiliated organizations, or those of the publisher, the editors and the reviewers. Any product that may be evaluated in this article, or claim that may be made by its manufacturer, is not guaranteed or endorsed by the publisher.

Supplementary material

The Supplementary Material for this article can be found online at: https://www.frontiersin.org/articles/10.3389/fpls.2022.958029/full#supplementary-material

References

Arnon, D. L. (1949). Copper enzymes in isolated chloroplasts, polyphenol oxidase in *Brta vulgaris*. *Plant Physiol.* 24, 1–15. doi: 10.1104/pp.24.1.1

Beuve, N., Rispail, N., Laine, P., Cliquetet, J. B., and Deunff, E. L. (2004). Putative role of γ-aminobutyric acid (GABA) as a long distance signal in upregulation of nitrate uptake in *Brassica napus* l. *Plant Cell Environ.* 27, 1035–1046. doi: 10.1111/j.1365-3040.2004.01208.x

Bustamante, C. A., Monti, L. L., Julieta, G., Federico, S., Gabriel, V., and Budde, C. O. (2016). Differential metabolic rearrangements after cold storage are correlated with chilling injury resistance of peach fruits. *Front. Plant Sci.* 7. doi: 10.3389/fpls.2016.01478

Camejo, D., Ana, J., Juan José, A., Walfredo, T., Juana María, G., and Francisca, S. (2006). Changes in photosynthetic parameters and antioxidant activities following heat-shock treatment in tomato plants. *Funct. Plant Biol.* 33, 177–187. doi: 10.1071/FP05067

Campbell, T. A., Bao, G., and Xia, Z. L. (1997). Agronomic evaluation of *Medicago ruthenica* collected in inner Mongolia. *Crop Sci.* 37, 599–604. doi: 10.2135/cropsci1997.0011183X003700020048x

Cheng, B., Li, Z., Liang., L., Cao, Y., Zeng, W., Zhang, X., et al. (2018). The γ-aminobutyric acid (GABA) alleviates salt stress damage during seeds germination of white clover associated with Na^+/K^+ transportation, dehydrins accumulation, and stress-related genes expression in white clover. *Int. J. Mol. Sci.* 19, 2520. doi: 10.3390/ijms19092520

Deng, Y., Xu, L. J., Zeng, X., Li, Z., Qin, B., and He, N. (2010). New perspective of GABA as an inhibitor of formation of advanced lipoxidation end-products: it's interaction with malondiadehyde. *J. Biomed. Nanotechnol.* 6, 318–324. doi: 10.1166/jbn.2010.1130

Fait, A., Fromm, H., Walter, D., Galili, G., and Fernie, A. R. (2008). Highway or byway: the metabolic role of the GABA shunt in plants. *Trends. Plant Sci.* 13, 14–19. doi: 10.1016/j.tplants.2007.10.005

Fracheboud, Y., Jompuk, C., Ribaut, J. M., Stamp, P., and Leipner, J. (2004). Genetic analysis of cold-tolerance of photosynthesis in maize. *Plant Mol. Biol.* 56, 241–253. doi: 10.1007/s11103-004-3353-6

Hao, J. H., and Shi, F. L. (2006). Study on drought resistance of *Melilotoides ruthenica* accessions. *Chin. J. Grassland.* 28, 39–43.

Hoagland, C. R., and Arnon, D. I. (1950). The solution culture method for growing plants without soil. *California Agr. Expt. Circ.* 347, 1–32. doi: 10.1016/S0140-6736(00)73482-9

Ji, J. (2020). *Regulatory roles of γ-aminobutyric acid (GABA) in growth and acclimation in poplar under salt stress* (Beijing: Chinese Academy of Forestry), 17–19. doi: 10.27625/d.cnki.gzlky.2020.000037

Kalhor, M. S., Sasan, A., Seif, M., Asayesh, E. J., Bernard, F., and Hassani, B. (2018). Title: Enhanced salt tolerance and photosynthetic performance: Implication of γ-amino butyric acid application in salt-exposed lettuce (*Lactuca sativa* l.) plants. *Plant Physiol. Bioch.* 130, 157. doi: 10.1016/j.plaphy.2018.07.003

Li, H. S. (2000). *Principles and techniques of plant physiological biochemical experiment* (Beijing: Higher Education Press), 164–258.

Li, L., Gu, W., Li, J., Li, C., Xie, T., Qu, D., et al. (2018). Exogenously applied spermidine alleviates photosynthetic inhibition under drought stress in maize (*Zea mays* l.) seedlings associated with changes in endogenous polyamines and phytohormones. *Plant Physiol. Bioch.* 129, 35–55. doi: 10.1016/j.plaphy.2018.05.017

Liu, T., Liu, Z., Li, Z., Peng, Y., and He, L. (2019). Regulation of heat shock factor pathways by γ-aminobutyric acid (GABA) associated with thermotolerance of *creeping bentgrass*. *Int. J. Mol. Sci.* 20, 4713. doi: 10.3390/ijms20194713

Liu, X. M., Zhou, Y. L., Xiao, J. M., and Bao, F. (2018). Effects of chilling on the structure, function and development of chloroplasts. *Front. Plant Sci.* 9. doi: 10.3389/fpls.2018.01715

Li, Z., Yu, J. J., Peng, Y., and Huang, B. R. (2016). Metabolic pathways regulated by γ-aminobutyric acid (GABA) contributing to heat tolerance in *creeping bentgrass* (*Agrostis stolonifera*). *Sci. Rep-UK.* 6, 30338. doi: 10.1038/srep30338

Malekzadeh, P., Khara, J., and Haidari, R. (2012). Effect of exogenous gama-aminobutyric acid on physiological tolerance of wheat seedlings exposed to chilling stress. *Iranian J. Plant Physiol.* 3, 611–617.

Mignolet-Spruyt, L., Xu, E., Idnheimo, N., Hoeberichts, F. A., Mühlenbock, P., Brosché, M., et al. (2016). Spreading the news: Subcellular and organellar reactive oxygen species production and signalling. *J. Exp. Bot.* 67, 3831–3844. doi: 10.1093/jxb/erw080

Palma, F., Carvajal, F., Jiménez-Muñoz, R., Pulido, A., Jamilena, M., and Garrido, D. (2019). Exogenous γ-aminobutyric acid treatment improves the cold tolerance of zucchini fruit during postharvest storage. *Plant Physiol. Bioch.* 136, 188–195. doi: 10.1016/j.plaphy.2019.01.023

Podlešáková, K., Ugena, L., Spíchal, L., Doleal, K., and Diego, N. D. (2019). Phytohormones and polyamines regulate plant stress responses by altering GABA pathway. *N. Biotechnol.* 48, 53–65. doi: 10.1016/j.nbt.2018.07.003

Priya, M., Sharma, L., Kaur, R., Bindumadhava, H., and Nayyar, H. (2019). GABA (γ-aminobutyric acid), as a thermo-protectant, to improve the reproductive function of heat-stressed mungbean plants. *Sci. Rep-UK.* 9, 1–14. doi: 10.1038/s41598-019-44163-w

Roberts, M. R. (2007). Does GABA act as a signal in plants? Hints from molecular studies. *Plant Signal Behav.* 2, 408–409. doi: 10.4161/psb.2.5.4335

Seifikalhor, M., Aliniaeifard, S., Hassani, B., Niknam, V., and Lastochkina, O. (2019). Diverse role of γ-aminobutyric acid in dynamic plant cell responses. *Plant Cell Rep.* 38, 847–867. doi: 10.1007/s00299-019-02396-z

Shi, L. L. (2016). *Leaf anatomical structure and drought resistance of ammopiptanthus mongolicus and ammopiptanthus nanus* (Lanzhou: Gansu Agricultural University), 3–4.

Shi, Z., Shi, S. Q., Zhong, C. F., Yao, H. J., and Gao, R. F. (2007). The roles of γ-aminobutyric acid on physiology and regulation under stress in plants. *Life Sci. Res.* 11, 57–61.

Sikder, R. K., Wang, X., Zhang, H., Gui, H., and Song, M. (2020). Nitrogen enhances salt tolerance by modulating the antioxidant defense system and osmoregulation substance content in *gossypium hirsutum*. *Plants* 9, 450. doi: 10.3390/plants9040450

Tang, C. N. (2021). *Physiological and molecular mechanism of strigolactones regulated chilling stress tolerance in pepper* (Lanzhou: Gansu Agricultural University), 3–4.

Tong, Y. S., Yu, X. J., Xu, C. L., Wang, P. B., Song, J. C., Li, Z., et al. (2021). Effects of sowing date on forage yield and quality of seven oat varieties in tianzhu alpine region. *Acta Agrestia Sin*. 29, 1094–1106. doi: 10.11733/j.issn.1007-0435.2021.05.027

Wang, W., Wang, X., Huang, M., Cai, J., and Jiang, D. (2021). Alleviation of field low-temperature stress in winter wheat by exogenous application of salicylic acid. *J. Plant Growth. Regul.* 40, 811–823. doi: 10.1007/s00344-020-10144-x

Wan, H. W., Yang, Y., Bai, S. Q., Xu, Y. H., and Bai, Y. F. (2008). Variations in leaf functional traits of six species along a nitrogen addition gradient in *Leymus chinensis* steppe in inner Mongolia. *Chin. J. Plant Ecol.* 32, 611–621. doi: 10.3773/j.issn.1005-264x.2008.03.010

Xiang, L. X., Hu, L. P., Xu, W. N., Zhen, A., Zhang, L., Hu, X. H., et al. (2016). Exogenous γ-aminobutyric acid improves the structure and function of photosystemII in muskmelon seedlings exposed to salinity-alkalinity stress. *PloS One* 11, e0164847. doi: 10.1371/journal.pone.0164847

Xie, J., Mao, J., Li, Z., Liang, C., and Shen, Y. (2021). Complete chloroplast genome of a high-quality forage in north China, *Medicago ruthenica* (Fabaceae: Trifolieae). *Mitochondrial DNA Part B*. 6, 29–30. doi: 10.1080/23802359.2020.1845578

Xu, B., Long, Y., Feng, X., Zhu, X., and Gilliham, M. (2021). GABA signalling modulates stomatal opening to enhance plant water use efficiency and drought resilience. *Nat. Commun.* 12, 1–13. doi: 10.1038/s41467-021-21694-3

Xu, Y., Xu, M. Y., and Li, X. (2008). Modulation of γ-aminobutyric acid on painful sense in central nervous system of morphine-dependent rats. *Neurosci. Bull.* 24, 278–282. doi: 10.1007/s12264-008-0227-y

Yin, M., Zhang, S. Z., Du, X., Mateo, R. G., Guo, W., Li, A., et al. (2021). Genomic analysis of *Medicago ruthenica* provides insights into its tolerance to abiotic stress and demographic history. *Mol. Ecol. Resour*. 21, 1641–1657. doi: 10.1111/1755-0998.13363

Yong, B., Xie, H., Li, Z., Li, Y. P., Zhang, Y., Nie, G., et al. (2017). Exogenous application of GABA improves PEG-induced drought tolerance positively associated with GABA-shunt, polyamines, and proline metabolismin white clover. *Front. Physiol.* 8. doi: 10.3389/fphys.2017.01107

Zhang, C. M. (2019a). *Physiological and molecular mechanisms of response to drought stress in different drought-resistant alfalfa (Medicago sativa l.) varieties)* (Lanzhou, Gansu: Gansu Agricultural University).

Zhang, P. (2019b). *Effects of post-harvest cracking on different treatments of fresh jujube* (Changsha, Hunan: Central South University of Forestry and Technology).

Zhang, Q., Liu, Y., Yu, Q., and Ma. Y. and Yang, D. (2020). Physiological changes associated with enhanced cold resistance during maize (*Zea mays*) germination and seedling growth in response to exogenous calcium. *Crop Pasture. Sci.* 71, 529–538. doi: 10.1071/CP19510

frontiers | Frontiers in Plant Science

TYPE Original Research
PUBLISHED 08 November 2022
DOI 10.3389/fpls.2022.970496

OPEN ACCESS

EDITED BY
Jin-Lin Zhang,
Lanzhou University, China

REVIEWED BY
Farah Deeba,
Council of Scientific and Industrial Research (CSIR), India
Zhipeng Liu,
Lanzhou University, China

*CORRESPONDENCE
Xin-Rong Ma
maxr@cib.ac.cn

SPECIALTY SECTION
This article was submitted to Plant Abiotic Stress, a section of the journal Frontiers in Plant Science

RECEIVED 16 June 2022
ACCEPTED 12 October 2022
PUBLISHED 08 November 2022

CITATION
Li X-Y, Wang Y, Hou X-Y, Chen Y, Li C-X and Ma X-R (2022) Flexible response and rapid recovery strategies of the plateau forage *Poa crymophila* to cold and drought.
Front. Plant Sci. 13:970496.
doi: 10.3389/fpls.2022.970496

Flexible response and rapid recovery strategies of the plateau forage *Poa crymophila* to cold and drought

Xin-Yu Li[1,2,3], Yan Wang[1], Xin-Yi Hou[1,2], Yan Chen[1,2], Cai-Xia Li[1] and Xin-Rong Ma[1]*

[1]Chinese Academy of Sciences, Innovation Academy for Seed Design, Chengdu Institute of Biology, Chengdu, Sichuan, China, [2]University of Chinese Academy of Sciences, Beijing, China, [3]College of Life Sciences, Sichuan University, Chengdu, Sichuan, China

Cold and drought stress are the two most severe abiotic stresses in alpine regions. *Poa crymophila* is widely grown in the Qinghai–Tibet Plateau with strong tolerance. Here, by profiling gene expression patterns and metabolomics-associated transcriptomics co-expression network, the acclimation of *Poa crymophila* to the two stresses was characterized. (1) The genes and metabolites with stress tolerance were induced by cold and drought, while those related with growth were inhibited, and most of them were restored faster after stresses disappeared. In particular, the genes for the photosynthesis system had strong resilience. (2) Additionally, cold and drought activated hypoxia and UV-B adaptation genes, indicating long-term life on the plateau could produce special adaptations. (3) Phenolamines, polyamines, and amino acids, especially N′,N″,N‴-*p*-coumaroyl-cinnamoyl-caffeoyl spermidine, putrescine, and arginine, play key roles in harsh environments. Flexible response and quick recovery are strategies for adaptation to drought and cold in *P. crymophila*, accounting for its robust tolerance and resilience. In this study, we presented a comprehensive stress response profile of *P. crymophila* and provided many candidate genes or metabolites for future forage improvement.

KEYWORDS

***Poa crymophila*, transcriptome-associated metabolome, cold and drought stresses, photosynthetic system, nitrogen transport, polyamine and phenolamide**

Introduction

The cold and arid alpine conditions are the important and governing factors limiting the productivity of grasslands on the Qinghai–Tibet Plateau. The coldest period (November to February) of the Qinghai–Tibet Plateau has a monthly average temperature as low as −20°C~−10°C, and the lowest temperature can reach −30°C

(data from China Meteorological Administration, http://data.cma.cn/). On the other hand, precipitation in most parts of the Qinghai–Tibet Plateau is scarce, and precipitation from November to February is even less than 20 mm. Observations from 1980 to 2015 showed a significant increase in the arid area of the Qinghai–Tibet Plateau (Shao et al., 2018). Global climate change exacerbates the occurrence of extreme weather, severely affects vegetation growth, and limits the productivity of prairies.

Poa crymophila is a perennial forage species in alpine meadows and grasslands (Shen et al., 2019). Also, the variety *P. crymophila* Qinghai is widely distributed in wet grassland, alpine grassland, forest edges, hillsides, valleys, and beaches at an altitude of 2,150~4,800 m in the Qinghai–Tibet Plateau, including Qinghai, Tibet, and Sichuan provinces, China. After more than 30 years of selection, cultivation, and domestication, the variety was approved by the National Grass Variety Approval Committee in December 2003 (variety registration number 261). This variety not only survives the winter safely at a low temperature even of −36°C with a wintering rate of over 95%, but its well-developed root system is mostly concentrated in the soil layer of 10–18 cm, with a cylindrical root sheath structure that facilitates water absorption from moist sand. It has been cultivated as forage with high tolerance to cold and drought stresses (Zhou et al., 2010; Hua et al., 2019). Therefore, *P. crymophila* is an excellent material for exploring the molecular mechanisms of cold and drought tolerance in the alpine region.

Transcriptome analysis can reveal the mechanism of plant adaptation to stress at the transcriptional level and explore the function of pivotal genes. Weighted gene co-expression network analysis (WGCNA) is an efficient and powerful method for constructing a co-expression network and digging into core genes. In this way, four pivotal genes of *CAD*, *POD*, *CCoAMT*, and *CML* were found in strawberries (*Fragaria nilgerrensis*) under cold stress, which has the key function of controlling high cold resistance (Liu et al., 2021a). Similarly, by comparing with the transcriptome of cold-tolerant and cold-sensitive varieties of Chinese prickly ash (*Zanthoxylum bungeanum* Maxim), the top 150 hub genes were identified and the mechanism of cold stress was discussed (Tian et al., 2021). Furthermore, module preservation analysis (MPA) was developed from the WGCNA algorithm to eliminate irrelevant expression differences and focus on the most variable and relevant unigenes. MPA was used to analyze the molecular mechanism of *Arabidopsis* heterosis by comparing the transcriptomes of ecotypes Col-0, Per-1, and their F1 hybrids, revealing that differentially expressed genes involved in photosynthesis and cell division pathways were the main factors for heterosis (Liu et al., 2021b).

Plant secondary metabolites also play an important role in stress response. For instance, proline could help plant cells maintain redox balance under normal and stressful conditions (Per et al., 2017). Increases in arginine and polyamines were associated with preventing H_2O_2 from oxidative stress on the plasma membrane (Hassan and Mohamed, 2019). Phenamides, also commonly known as hydroxycinnamamides (HCAAs), can act as products of polyamine catabolism or as a storage form of polyamines and phenolics, and have specific functions in plant development and environmental adaptation. Some of them, like di-feruloylputrescine, di-feruloylspermidine, and ferulic acid tyramide, were found in the seeds of rice and maize and participated in plant growth by depleting themselves to maintain polyamine levels (Luo et al., 2009). Phenamines are suitable substrates for peroxidases, and they also favor the scavenging of hydrogen peroxide (Groppa et al., 2008); the stress tolerance mainly depends on the antioxidant activity. It was discovered that a special phenamine, *N′*,*N″*,*N‴*-*p*-coumaroyl-cinnamoyl-caffeoyl spermidine, can participate in scavenging phenanthrene to protect *Salix viminalis* from poison (Xia et al., 2021).

We reanalyzed previous RT-qPCR-validated transcriptome data combined with metabolome data to explore the source of *P. crymophila's* robust tolerance to cold and drought. Although many stress-related metabolites and coding genes were found, the regulatory network and factors are still not fully understood. Metabolome-associated transcriptome analysis could further reveal stress resilience mechanisms. Our previous research found that a series of stress tolerance-related metabolites such as phenylpropanoids and carbohydrates, and genes like *MYB* and *CCR*, were found in *P. crymophila* under drought and low-temperature stress (Wang et al., 2021b). In this study, using the advantage of the sophisticated implements of WGCNA and MPA, we further combined the metabolome and transcriptome to deeply explore regulatory networks and reveal the adaptive mechanism of *P. crymophila* to low temperature and drought in an alpine environment.

Methods

Material treatments and phenotype analysis

The plants of *Poa crymophila* Keng cv. Qinghai were prepared as the procedure by Wang et al. (2021b). The seeds were planted in plastic pots and grew in a greenhouse for 2 months. Before treatments, plants were transferred to a growth chamber (22/16°C, photoperiod 14 h, at a relative humidity of 60% and an irradiance of 200 mmol·m^{-2} s^{-1}) for 2 weeks. The plants grew at 22/16°C and were well-watered as in the control group (CK). For cold treatment, the plants were transferred to another −5°C growth chamber for 24 h (Cold). They were then returned to normal conditions for 48 h of recovery (ReCold). As to drought treatment, the plants were deprived of water for 10 days as part of the drought stress group (Drought) and then rewatered for recovery for 48 h (ReDrought). Three replicates were collected from each sampling point (CK, Cold, Drought, ReCold, and ReDrought), with each replicate containing at least

50 plants. Samples were frozen in liquid nitrogen and stored at −80°C.

The growth state and photosynthetic rate were collected at CK, Cold, Drought, ReCold, and ReDrought time points. The photosynthetic rate was measured using a portable photosynthetic fluorescence measurement system (GFS-3000) with a 3010-standard measuring head and a 3055 leaf chamber fluorometer (Walz, Germany). The measurements were taken from at least four pot plants.

To demonstrate the robust cold tolerance of *P. crymophila*, the cool-season forage perennial ryegrass (*Lolium perenne* cv. Mathilde) with strong cold adaptation was planted at the same time with the same method. *P. crymophila* and *L. perenne* were stressed for 24 h at −5°C and −12°C, recovered for 48 h, and their growth states and photosynthetic rate were compared.

Leaves are not only the main site of photosynthesis but also an important part of sensing adverse conditions. Leaves can directly reflect the growth state of plants. Therefore, we chose leaves as the research material to explore plant stress responses. RNA was extracted and sequenced using an Illumina HiSeqTM 2000 (Illumina) at BGI (Shenzhen, China). The sequencing results with quantitative real-time (qRT)-PCR verification were deposited to the Sequence Read Archive database (http://www.ncbi.nlm.nih.gov/Traces/sra/, accession number: SRX2725266). A widely targeted metabolome was completed by Wuhan Metware Biotechnology Co. Ltd. (Wuhan, China). The results were putatively annotated by the self-built database Metware Database (MWDB; Wuhan Metware Biotechnology Co. Ltd., Wuhan, China). These transcriptome and metabolome data were obtained from preliminary work (Wang et al., 2021b).

Data filtering, assessment, and differential expression analysis

Based on the terms of the fragments per kilobase of exon model per million (FPKM), the expression levels of unigenes were calculated by RSEM software (RNA-Seq by Expectation Maximization) (Li & Dewey, 2011). The correlation between samples was represented by the square of the Pearson coefficient, and the results were used to reflect the reliability of the experiment and the rationality of sample selection. Statistical parameters such as standard deviation, mean, and coefficient of variation (CV) were used to characterize the expression of unigenes. To filter genes with low expression and poor consistency, genes with an average FPKM < 10 and coefficient of variation (CV) value of biological replicates of > 1 at all samples were discarded. For evaluating the result of data filtering, principal component analysis (PCA) was performed using the PCA OmicShare online tools (https://www.omicshare.com/tools/Home/Soft/pca). The data were normalized by *Z*-core before performing PCA to eliminate the influence of genes with abnormally high and low expression levels.

Based on the unigenes count number, the parameters of expression differences were obtained by R package DESeq2 (Love et al., 2014). The threshold of DEG was set to $|\log_2 FC| \geq 1$ and false discovery rate (FDR) to <0.05.

Gene expression pattern and functional enrichment analysis

The expression data were divided into two groups based on the stress types: the cold-related group, which included three sampling points of CK, Cold, and ReCold, and the drought-related group, which included three sampling points of CK, Drought, and ReDrought. The two groups shared the same CK. For profiling the unigene expression pattern upon stress and recovery, the R package TCseq was applied (Jun and Gu, 2021). The expressive pattern of the cold and drought treatment groups was respectively profiled by adopting the "cm" (cmeans) algorithm, setting the *k*-value to "8", and standardizing it as "True".

Based on the annotation of the Gene Ontology (GO) and Kyoto Encyclopedia of Genes (KEGG) databases, the selected unigene list was subjected to the online functional enrichment tools (https://www.omicshare.com/tools/Home/Soft/getsoft). Because there is no reference genome for *Poa crymophila*, all unigenes with biological repeat stable expression and high quality were used as the background gene files for the KEGG and GO enrichment analyses.

Consensus module analysis

For comparing similar features between responses to cold and drought stresses, module preservation and consensus module analysis were performed. Genes with similar functions and shared stress responses can be mined using highly correlated gene modules.

Module preservation analysis was performed between the individually constructed gene co-expression networks of cold- and drought-related datasets with a parameter of 200 nPermutations. The permutation test defines the preservation degree of modules in the two networks by providing Z summary values that summarize the preservation statistics based on density and connectivity. Zsummary > 10 represented strong preservation, 10 < Zsummary < 2 represented moderate to weak preservation, and Zsummary < 2 represented no preservation. By using blockwiseConsensusModules in the R package WGCNA (Zhang, B. & Horvath, 2005), the conserved gene co-expression networks affected together by cold and drought stresses were detected. Based on the conserved preservation results, the consensus co-expression network between cold and drought datasets was constructed, and the dynamic tree-cutting method was implemented with the following parameters: maxBlockSize of 15,000, power value of 10, deepSplit level 2,

minModuleSize of 30, and mergeCutHeight of 0.25. The co-expression network of each group of core-conserved genes is detected by correlation coefficient (k_{ME}) to evaluate the value of the module member of each gene. The important metabolic pathways that core genes are involved in were visualized through GO functional annotation.

Transcriptome-associated widely targeted metabolome analysis

WGCNA, the R package, was implemented for constructing the gene co-expression network. The unigenes were from RNA-Seq data of 15 samples (five sampling points × three replicates) and divided into two groups: the cold-related group (CK, Cold, ReCold) and the drought-related group (CK, Drought, ReDrought) as individual datasets. By setting the maxBlockSize value of 15,000 (both), and the soft threshold power β-value of 18 (cold) and 10 (drought) for balancing intramodule connectivity (Supplementary Figure S1) and intermodule independence in different co-expression network, the correlation matrix by cold- and drought-related datasets was transformed into an adjacency matrix, respectively. By using the dissimilarity measure approach, the corresponding topological overlap matrix (TOM) was transited from the two adjacency matrixes. Hierarchical clustering trees were constructed based on TOM similarity for module detection, and each module calculated the relationship with the differential metabolites. Depending on the relationship and *p*-value, the closely related metabolites of each module can be obtained.

According to the annotation of GO, Swissprot, and other databases, the scope of transcriptome analysis was further narrowed, and stress tolerance-related modules and key core genes were identified. The eigenvalues, k_{ME}, that measure the correlation between each gene and eigengenes of modules, were used to evaluate the core genes of modules. The unigenes with k_{ME} >0.9 and $p < 0.001$ can be used as core genes representing the expression tendency of modules. Based on all edges of nodes calculated from WGCNA, the co-expression networks were constructed using Cytoscape v3.5.1 (Shannon et al., 2003).

Results

The phenotype under low-temperature and drought stress

We subjected *P. crymophila* to low-temperature stress at −5°C and −12°C, as well as drought stress for 10 days after water was cut off, before recovering for 48 h. Simultaneously, *L. perenne* was treated at the same low temperature to compare the frost resistance of *P. crymophila*. The results showed that the growth of *P. crymophila* and *L. perenne* was inhibited under a low temperature of −5°C, and their photosynthetic efficiency also decreased significantly. However, after 48 h of recovery, the plant can completely recover and the photosynthetic index reaches the control level (Figures 1, 2). Furthermore, under low-temperature stress of −12°C, *P. crymophila* survived after freezing, and its growth gradually recovered after 48 h, with the net photosynthetic rate returning. Regardless, *L. perenne* was damaged by frost at −12°C to death (Figure 3).

Ten-day drought stress has little impact on *P. crymophila*, and its growth status and photosynthetic rate have quickly returned to normal after 48 h of rehydration (Figure 4).

Low-temperature- and drought-responsive transcriptome

A Pearson correlation analysis indicated that the three biological replicates of each treatment showed highly consistent transcriptome profiles (R^2 = 0.8192–0.9906, Supplementary Figure S2). Based on previous research, further focus should be on core differentially expressed genes, with low-expressed and poorly consistent genes being excluded. Genes with an average FPKM of <10 and a CV of biological replicates of > 1 were discarded at all sampling points, leaving 14,380 genes. All of them exhibited high consistency between biological replicates and apparent partitions between different treatments (Supplementary Figure S3; Supplementary Table S1-1).

A total of 4,577 nonredundant DEGs from the cold-related group were identified (Supplementary Figure S4A; Supplementary Table S1-2), including 2,599 DEGs (1,679 upregulated, 920 downregulated) in Cold *vs.* CK, 1,983 DEGs (1,202 upregulated, 781 downregulated) in ReCold *vs.* CK, and 2,662 DEGs (1,153 upregulated, 1,509 downregulated) in ReCold *vs*. Cold. In total, 5,129 nonredundant DEGs were obtained from the drought-related group (Supplementary Figure S4B), including 2,032 DEGs (933 upregulated, 1,099 downregulated) in Drought *vs*. CK, 2,623 (1,434 upregulated, 1,189 downregulated) in ReDrought *vs.* CK, and 3,087 DEGs (1,838 upregulated, 1,249 downregulated) in Redrought *vs*. Drought.

Gene expression pattern and function analysis

In order to explore the mechanism of cold and drought stress adaptation, gene expression pattern analysis was performed. As a result, 4,577 cold-responsive DEGs and 5,129 drought-responsive DEGs were all clustered into eight expression patterns, clusters 1~8 (Figure 5; Supplementary Table S2). The expression of DEGs in cluster 1 was decreased by stress and then recovered to the control level after stress removal. Cluster 2 was downregulated and then recovered only slightly. Cluster 3 was reduced and difficult to recover. Cluster 4

10.3389/fpls.2022.970496

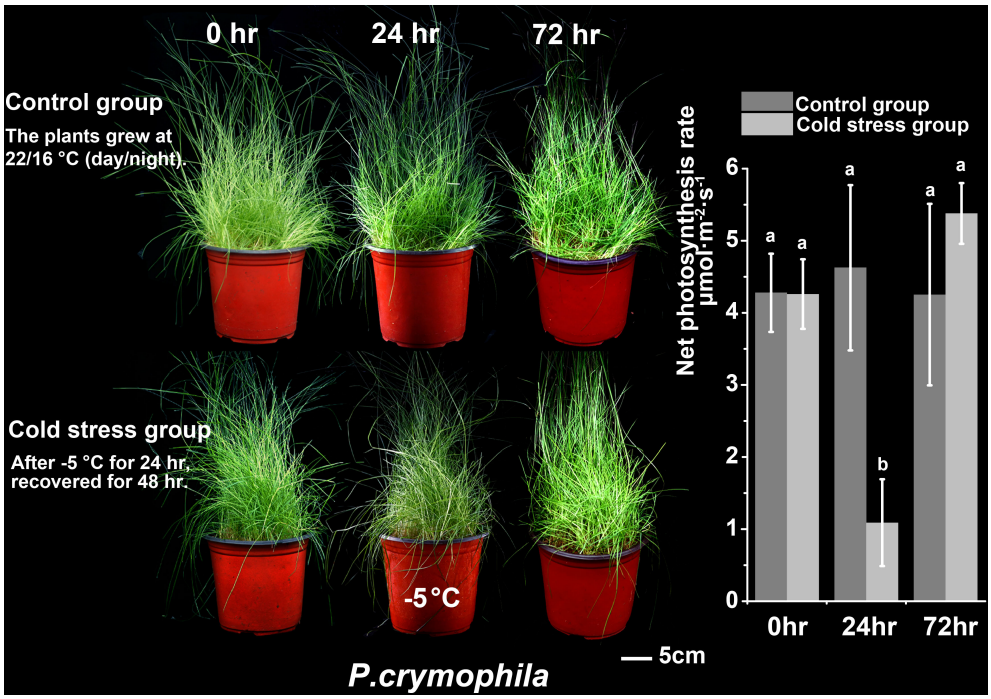

FIGURE 1
The cold stress (–5°C) and recovery of *P. crymophila*.

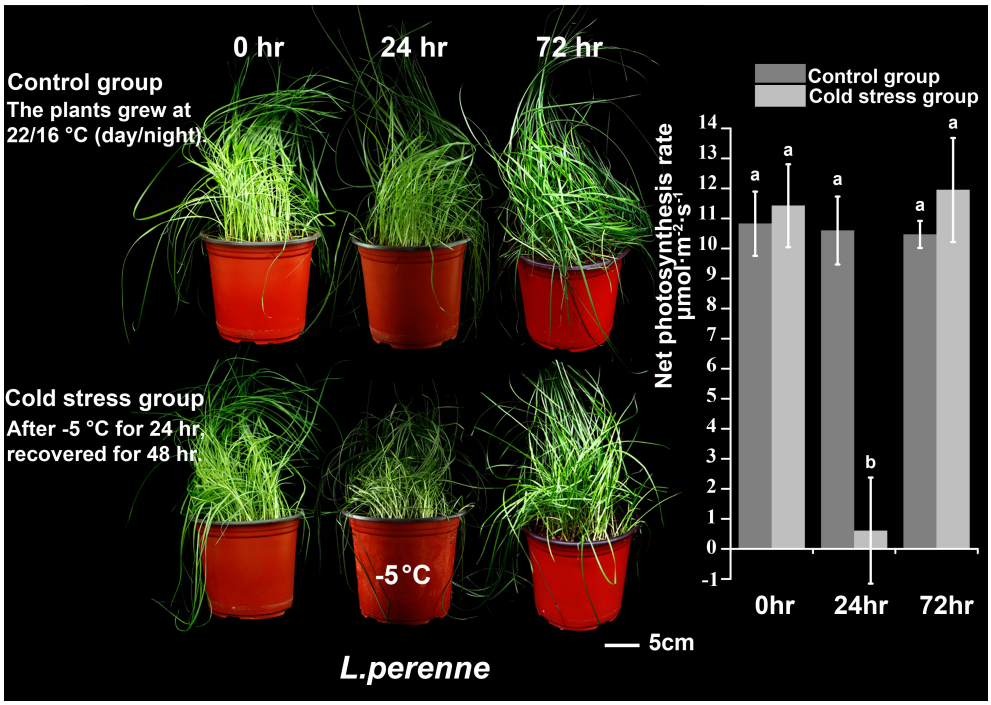

FIGURE 2
The cold stress (–5°C) and recovery of *L. perenne*.

10.3389/fpls.2022.970496

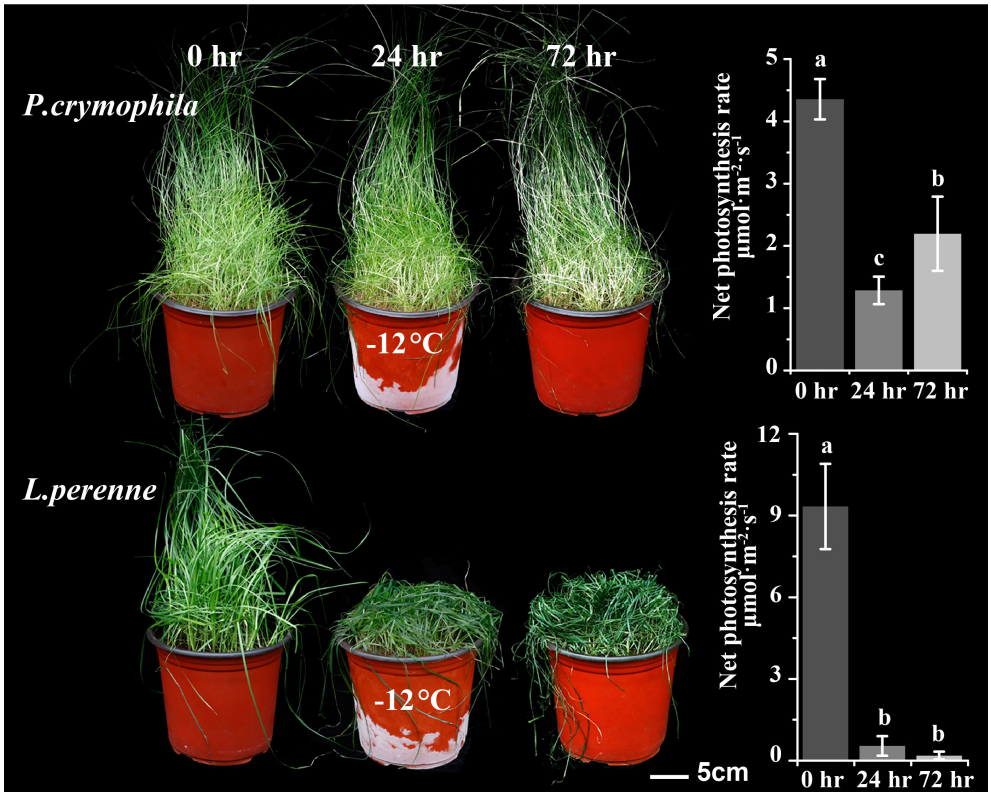

FIGURE 3
The cold stress (–12°C) and recovery of *P. crymophila* and *L. perenne*.

was unchanged under stress but downregulated during recovery. Cluster 5 was stress-induced and quickly returned to normal levels. Cluster 6 was induced only during recovery. Cluster 7 was induced by stress and consistently upregulated during recovery. Cluster 8 was stress-induced and recovered slightly but not to control levels. Based on the functional analysis of GO annotations, the different clusters were involved in different processes (Table 1). Most abiotic stress response genes were found in clusters 5, 7, and 8, while clusters 1, 2, and 3 were mainly related to plant growth. Clusters 4 and 6 had a specific response that was only down- or upregulated after the stress disappeared, with the former being associated with negative effects on plants and the latter with the photosynthetic system and other positive effects.

Consensus co-expression network between cold and drought

To find the similar and strongly correlated responses and genes under the cold and drought stresses, the consensus co-expression network between both of them was constructed using MPA analysis. The results were represented by consensus modules (CMs), indicating the clusters of co-expressed genes. As a result, 14,342 genes were assigned to 31 non-grey CMs (Figure 6B; Supplementary Table S3-1).

The conservation of co-expression networks with each other was assessed using permutation tests (Figure 6A). By projecting the drought-related transcriptome dataset onto the cold-related network, 12 out of 31 modules were strongly preserved ($Z_{summary} > 10$) and 11 modules exhibited weak to moderate preservation ($10 > Z_{summary} > 2$). A total of 23 out of 31 modules were at least weakly preserved in drought compared with cold stress (Supplementary Table S4). These results suggested that some similar and conserved transcriptional architecture dynamically regulated by cold and drought may exist in *P. crymophila* (Figure 6C).

Among those preserved modules, some genes with similar responses to both cold and drought stress were discovered. Abiotic stress response genes *LTI6B* and *LTI65* and transcription factors *NAC67* and *DREB1B* were downregulated and then recovered to the control level. While growth-related *PKS3*, *ARF17*, and *APC7* were suppressed by stress, their expression levels were completely or partially restored after the stress disappeared. In addition, as the members of the NRT1/PTR family are involved in nitrogen transport in plants, the

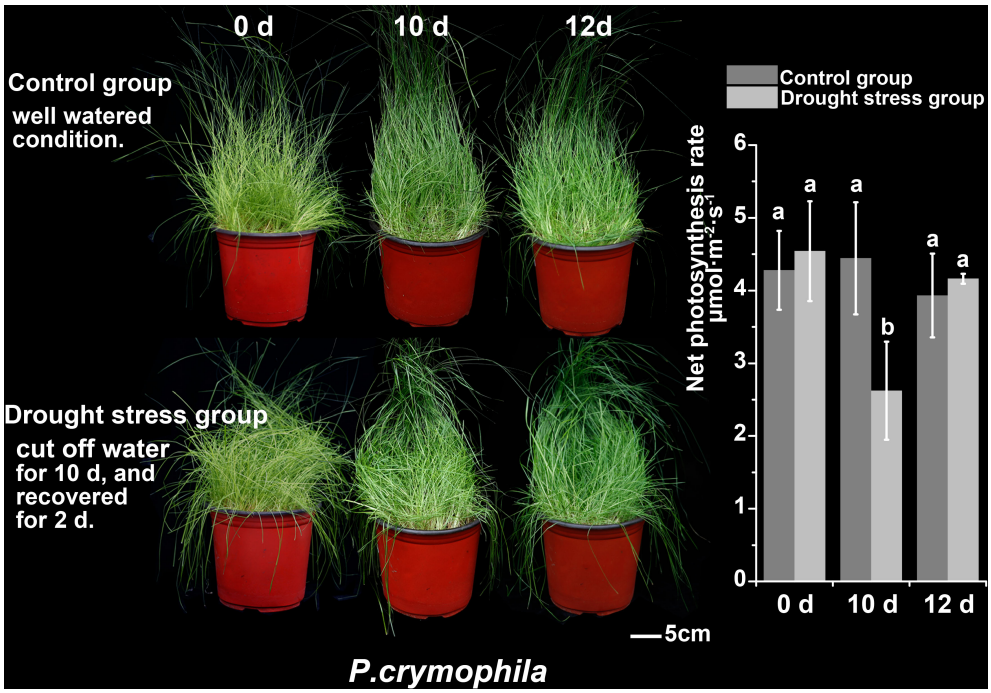

FIGURE 4
The drought stress and recovery of *P. crymophila*.

members of *NRT1.1* rapidly recovered after being inhibited by stress, while the *NRT1.3* genes, on the contrary, rapidly decreased after being activated by stresses, and *NRT1.4*s showed significant upregulation during plant recovery. These genes had similar response patterns in response to the two stresses and participated in important biological functions, which may account for the general strategies for cold and drought response.

Additionally, based on thresholds (k_{ME} in cold set or drought set > 0.9 and $p < 0.001$), a total of 3,859 core genes were submitted to GO enrichment analysis (Supplementary Table S3-2). Moreover, the results showed that these genes were significantly enriched in photosynthetic pigments (chloroplasts and carotenoids) and were found in the chloroplast stroma, thylakoid, and envelope (Table 2). Of them, CYP97A3, CYP97C1, CHLD, etc., were only significantly upregulated during the recovery process (Figures 6D, E). Furthermore, 34 enzyme genes involved in chlorophyll and carotenoid synthesis were found (Figure 7). Most of them had similar responses that were slightly inhibited by stress and recovered quickly after the stress disappeared. Only CHYB responded differently under the two stressors. Cold stress upregulated their expression but drought inhibited them. Moreover, we also found 31 genes encoding photosystem proteins, such as *LHCs*, *PSIs*, and *PSIIs*, play important roles in photosynthesis. Both *LHCs* and *PSIs* were inhibited by cold and drought stress, especially under drought stress. They were also able to return to normal levels after the stress disappeared. Although *PSIIs* responded differently to stress, most were upregulated during the recovery process.

Transcriptome-associated metabolome co-expression network

The association analysis of transcriptome and metabolome was performed by WGCNA. Based on the correlation between transcriptome and metabolome at different sampling points, unigenes can be divided into several modules (Supplementary Figures S5, S6). Genes in the same module may have similar features or highly interrelated functions. Through analyzing the key modules, their highly related metabolites also can be found. In this way, we can better understand the response of *P. crymophila* to cold and drought stress.

In cold-related datasets (CK, Cold, and ReCold), 14,376 genes were divided into 25 cold-related modules (CMEs) (Supplementary Figure S5; Supplementary Table S5-1). Among these CMEs (Supplementary Figure S5), only the 1,563 unigenes in CME-blue responded positively to cold stress and had the coldest acclimation-related genes, such as *COR413PM1*, *ICY*, *LTI6B*, *CAD1*, *CML16*, etc. (Figure 8A). Based on the threshold of k_{ME} ≥0.9, a total of 525 core unigenes were identified from the 1,563 unigenes in CME-blue.

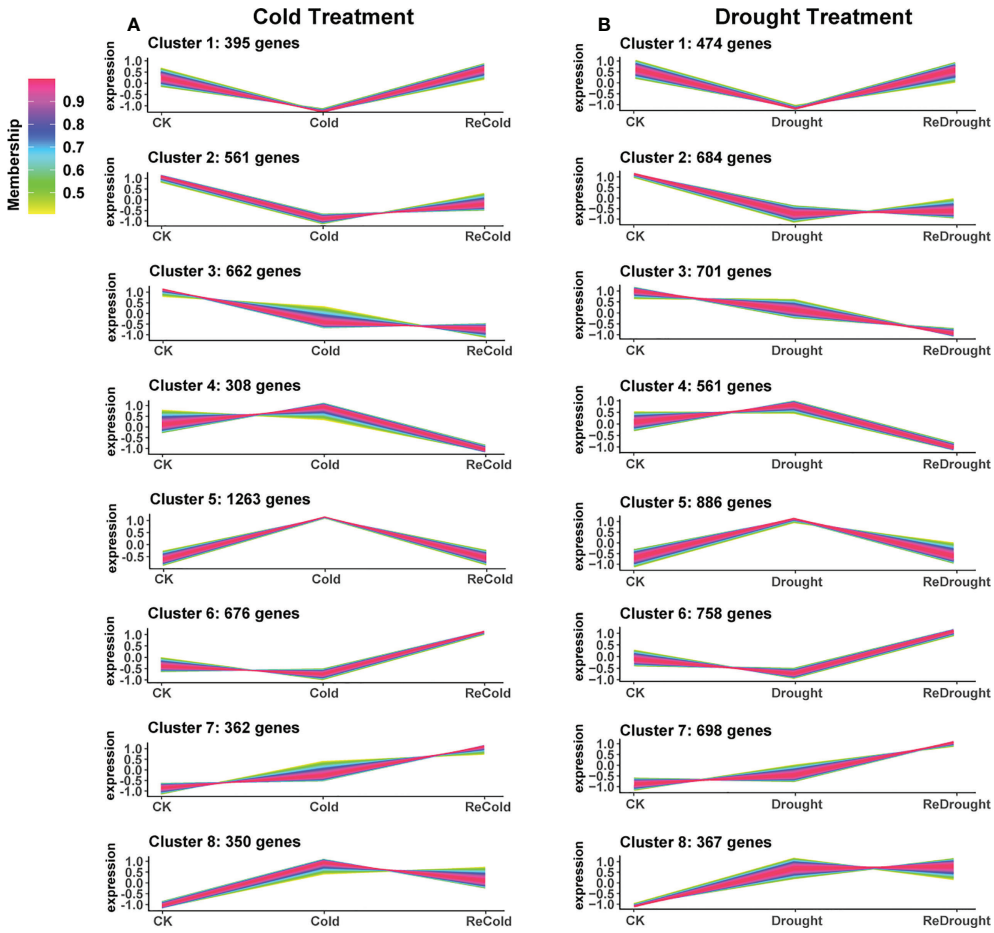

FIGURE 5
The expression patterns of differentially expressed genes. **(A)** Cold stress. **(B)** Drought stress. The vertical axis represents the relative level of the gene, and the line color represents the model fit.

These core unigenes respond to cold and are involved in lipid metabolism and response to water deficiency, abscisic acid, UV-B, etc. (Figure 8C). In addition, a total of 33 transcription factors like *NAC67* (*CL14612.Contig2_DB*), *DREB1As* (*CL7116.Contig8_DB*, *Unigene43646_DB*), *DREB1B* (*CL26928.Contig10_DB*), and *HSFC1B* (*CL6331.Contig3_DB*) with important regulatory functions were located in the core of CME-blue. Therein, *NAC67* (*CL14612.Contig2_DB*) increased from 67 to 1,793 by cold and then recovered to 146 (Figure 8B). Therefore, CME-blue may play a crucial role in cold stress tolerance, and its associated metabolites can be inferred to have similar tolerant functions.

These 25 CMEs had a different relationship with 213 metabolites with significant changes (Supplementary Figure S7; Supplementary Table S6-1). Based on |Correlation|>0.8, $p < 0.05$, 195 metabolites highly related to CME-blue were identified (Supplementary Figure S7; Supplementary Table S6-1). In the 90 metabolites with positive correlation, there are 27 lipid compounds (LysoPC 16:1, 9-HOTrE, 14,15-dehydrocrepenynic acid, etc.), 12 flavones (C-hexosyl-chrysin *O*-feruloylhexoside, afzelechin, phloretin, etc.), eight amino acids and derivatives (arginine, asparagine, homocysteine, glutathione oxidized, etc.), six carbohydrates (D-glucose 6-phosphate, glucose-1-phosphate, D-fructose 6-phosphate, etc.), five nucleotide and derivates (hypoxanthine, uridine 5′-monophosphate, hypoxanthine-9-β-D-arabinofuranoside, etc.), five organic acids (azelaic acid, γ-aminobutyric acid, creatine, etc.), and others (nandrolone, azadiradione, dehydrovomifoliol, etc.). In addition, 105 negatively correlated metabolites contained 45 flavonoids, 16 phenylpropanoids, 15 organic acids and derivatives, and others. Among them, syringetin, baicalin, isorhamnetin 3-*O*-neohesperidoside, and isorhamnetin *O*-acetyl-hexoside were the most inhibited.

In addition to our previous findings of sugars, flavonoids, phospholipids, etc. (Wang et al., 2021b), it is worth noting that amino-related metabolism was also affected by stress. For instance, the content of γ-aminobutyric acid increased from

TABLE 1 The gene functions of different patterns in response to cold or drought.

Cluster	Expression pattern	Cold stress		Drought stress	
		Function	Representative genes	Function	Representative genes
1	Decreased and then recovered to control level	Water, glycerol, carbohydrate, nitrogen transport; anther morphogenesis; plant epidermis development	NRT1.1, RCAA, PIP1-2, CHLP, LHCA4	Nitrogen transport; photosynthesis; photosynthetic electron transport chain; oligopeptide transport	NRT1.1, MT2C, PSBT, PSAF, CAO
2	Decreased and then recovered, but only slightly	Auxin polar transport; flower morphogenesis; pollen–pistil interaction; regulation of protein ubiquitination	ABCB21, D3, COL6, RPT2, PAO	Malate transmembrane transport; protein deacetylation; regulation of root morphogenesis; callose deposition in cell wall	RPT2, PSY, CML10, ASG4
3	Decreased and difficult to recover	Meristems transition from vegetative to reproductive stages; photoperiodism; circadian rhythm; protein modification; seed dormancy; seedling development process	UBC28, FH7, FH20, DI19-1, HSC-2, CSN1	Regulation of biological process (nitrogen compound, nucleobase-containing compound, metabolic process, nucleic acid-templated transcription)	UBC28, AGL19, ARR2, IAA1, IAA6, IAA10
4	Decreased only during recovery	Histone H2B ubiquitination; negative regulation of developmental process (flower, post-embryonic and other developments)	UBC15, UBC2, MADS22, SPA4, SIZ1	Superoxide anion generation; purine nucleobase catabolic process; multiple biological processes	PP2C30, CIPK14, XDH, MCSU3, MADS22
5	Increased and then rapidly returned to normal levels	Cold acclimation; polyamine; carbohydrate biosynthetic process; regulation of response to osmotic stress	COR410, LEA14-A, NAC67, LTI6B, NRT1.3, DREB1H	Response to desiccation; L-proline biosynthetic process; carbohydrate homeostasis; stomatal movement	LEA14-A, NAC67, P5CS, CAT2, NRT1.3, COR413P
6	Increased only during recovery	Lipid, carbohydrate derivative, nitrogen compound, and vitamin metabolic process; monosaccharide transport; photosystem II assembly; plastid organization	LHBC, CAB1, CAB8, PETE, WHAB1.6, LHCA4	Photosynthesis (light harvesting); chlorophyll and carotenoid biosynthetic process; terpenoid, phospholipid, polysaccharide organonitrogen biosynthetic process	LHBC, CAB1, CAB8, PETE, LHC, RCABP89
7	Consistently increased	Photosynthesis (light capture and dark reactions); ammonia assimilation cycle; isopentenyl diphosphate; organonitrogen compound metabolism	RCABP89, LHBC, CAB1, CAB1B, GAD	Photosystem assembly; protein targeting to chloroplast; other chloroplast organization processes	PSBS, GAPC2, CAB1, TGA4, WHAB1.6
8	Increased and then recovered slightly, but not to control levels	Response to UV-B, karrikin, disaccharide, red light; nicotinamide nucleotide and inositol phosphate metabolism	HY5, UGT73C5, PSBS, PAP2	Similar to cluster 7	GAPC, SODCP, CAB7, UVR8

1.72×10^6 to 5.8×10^6 under cold stress and reached 6.09×10^6 after the stress disappeared. The gene expression of the γ-aminobutyric synthetic rate-limiting enzyme GADs (CL2552.Contig1_DB,CL2552. Contig5_DB, CL2552.Contig6_DB, and CL2552.Contig7_DB) was significantly increased by cold. Moreover, we also found that low-temperature stress activated the metabolism of polyamine and phenolamide (Figure 9A). The key enzymes catalyzing the synthesis of putrescine were largely induced by cold, like *ADC1s* encoding arginine decarboxylase (ID: CL4914.Contig2_DB, CL4914.Contig3_DB) and *PAO2s* encoding polyamine oxidase (CL7418.Contig1_DB, CL12207.Contig1_DB). As a result, the content of putrescine accumulated massively. In a previous study, we found that some phenylpropanoids responded strongly to cold stress. Together with polyamines, they can be catalyzed into phenolamides by *N*-hydroxycinnamoyltransferase. It is worth noting that several phenolamides changed significantly in content under cold. Only *N*′,*N*′′,*N*′′′-*p*-coumaroyl-cinnamoyl-caffeoyl spermidine accumulated rapidly under stress, while *N*′-*p*-coumaroyl agmatine, *N*′-*p*-coumaroyl putrescine, and *N*′-feruloyl putrescine decreased sharply (Figure 9A). Interestingly, all of them gradually recovered to normal levels after the stress disappeared. The changes in these amino compounds also suggested their potential functions and importance in stress tolerance.

According to the conserved domain HXXXD, some putative *N*-hydroxycinnamoyltransferases were identified (Figure 9A). Combined with the annotation of the database, these enzymes are divided into spermidine hydroxycinnamoyltransferase, omega-hydroxypalmitate *O*-feruloyltransferase, hydroxycinnamoyl-CoA: shikimate/quinate hydroxycinnamoyltransferase, and agmatine coumaroyltransferase. Their encoding genes responded differently to cold, suggesting that the expressions of these genes affected the contents of phenolamine.

In drought-related datasets (CK, Drought, and ReDrought), 14,346 unigenes were clustered into 32 drought-related modules (DMEs) (Supplementary Figure S6; Supplementary Table S5-2). According to the annotation, most genes responsive to drought and ABA were present in DME-blue (Supplementary Figure S6), such as *ADH1*, *LEA14-A*, *P5CS*, and *SAPK4* (Figures 10A, B). The 853 hub genes were the core of 4,086 genes in DME-blue and were involved in cell wall biosynthesis, nitrogen transport, hypoxia, UV-B response, and other biological processes (Figure 10C). In the core

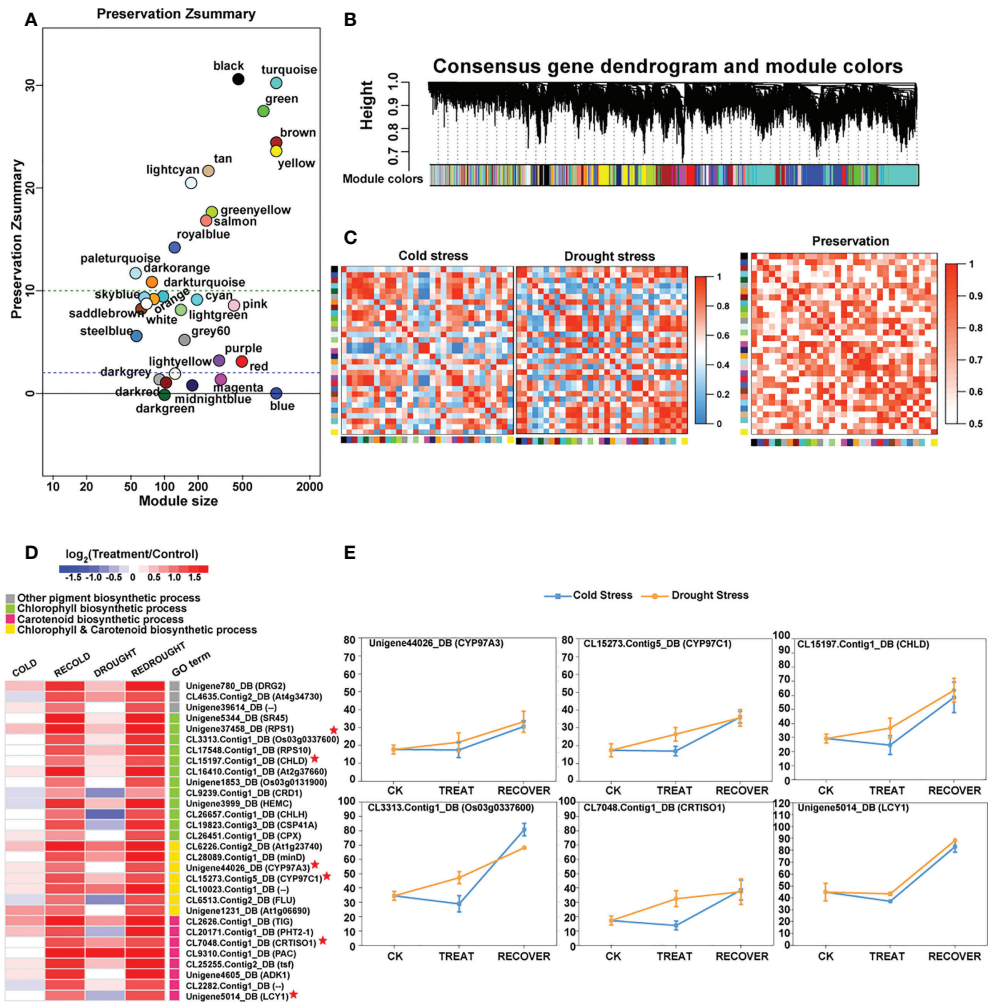

FIGURE 6
The preservation of consensus modules (CMs) and the functions of CM core genes. **(A)** The preservation results of CMs. The vertical axis represents the *Z*-score, and the horizontal axis denotes the module size. **(B)** Hierarchical cluster dendrogram showing consensus gene co-expression modules. In the dendrogram, each leaf represents one gene, and each module below the dendrogram is labeled with one color. **(C)** Heat maps of eigengene networks showing the relationships among CMs in cold and drought stress. The preservation heat map shows the preservation network, defined as one minus the absolute difference of the eigengene networks in both sets, and the barplot depicts the mean preservation of adjacency for each of the eigengenes to all other eigengenes. **(D)** The expression profile of the important core genes. In the heat map, color intensity represents the coefficients calculated by expression pattern analysis, and different GO terms are represented by different colors. Some genes marked with red stars as the characterization of each GO term show expression trends in line graphs. **(E)** The line graphs of some function genes with a star mark related to photosynthetic pigment biosynthesis. Drought stress is represented by a yellow line, and cold stress is shown by a blue line. The horizontal axis denotes the sampling points, and the vertical coordinates reflect the gene expression level (FPKM value).

genes, a total of 25 transcription factors were identified, and most of them were from the bZIP family (GBF3, GBF4, TGA2, TGA3, TRAB1, and DPBF3). HSFC1B (CL6331.Contig3_DB) was induced to express and was silenced after the stress disappeared.

These 32 DMEs showed different relationships with the 203 metabolites whose contents changed under drought (Supplementary Figure S8; Supplementary Table S6-2). A total of 195 metabolites remained highly correlated with DME-blue. Among the 59 metabolites positively correlated (Supplementary Figure S8; Supplementary Table S6-2) were 19 flavonoids (luteolin *O*-hexosyl-*O*-pentoside, luteolin 6-C-hexoside, 8-C-hexosyl-*O*-hexoside, *O*-methylnaringenin-C-pentoside, etc.), nine carbohydrates (D-glucose 6-phosphate, glucose-1-phosphate, sucrose, etc.), six amino acids and derivatives (proline, L-homocitrulline, D-erythro-sphinganine, etc.), four organic acids (L-malic acid, *p*-coumaroyl quinic acid *O*-glucuronic acid, anisic acid *O*-feruloyl hexoside, etc.), and others (coixol, phytocassane C, dulcitol, etc.). In the 136 metabolites with a high negative correlation, there were 66 flavonoids (isosakuranetin, baicalin, prunetin, acacetin, etc.), 16 lipids (LysoPC 20:4, LysoPC 18:0,

10.3389/fpls.2022.970496

TABLE 2 The GO functions of the core genes in consensus modules between cold and drought.

ID	Description	Nonredundant DEGs	FDR	Cold stress		Drought stress	
				DEG number	Main expression patterns	DEG number	Main expression patterns
GO:0006779	Porphyrin-containing compound biosynthetic process	31	5.07E−05	26	Cluster 6 (20)	29	Cluster 7 (17)
GO:0033014	Tetrapyrrole biosynthetic process	31	8.81E−05	26	Cluster 6 (20)	29	Cluster 7 (17)
GO:0019288	Isopentenyl diphosphate biosynthetic process, methylerythritol 4-phosphate pathway	41	5.01E−06	37	Cluster 6 (31)	39	Cluster 7 (22)
GO:0009240	Isopentenyl diphosphate biosynthetic process	41	5.01E−06	37	Cluster 6 (31)	39	Cluster 7 (22)
GO:0046490	Isopentenyl diphosphate metabolic process	41	5.01E−06	37	Cluster 6 (31)	39	Cluster 7 (22)
GO:0046148	Pigment biosynthetic process	48	3.08E−06	39	Cluster 6 (28)	43	Cluster 7 (21)
GO:0009658	Chloroplast organization	40	9.44E−05	34	Cluster 6 (26)	39	Cluster 7 (20)
GO:0019682	Glyceraldehyde-3-phosphate metabolic process	57	5.01E−06	48	Cluster 6 (38)	54	Cluster 7 (28)
GO:0042440	Pigment metabolic process	54	8.10E−06	43	Cluster 6 (28)	49	Cluster 7 (23)
GO:0008299	Isoprenoid biosynthetic process	57	5.01E−06	46	Cluster 6 (37)	53	Cluster 7 (24)
GO:0006720	Isoprenoid metabolic process	59	5.97E−06	40	Cluster 6 (30)	45	Cluster 7 (21)
GO:0009532	Plastid stroma	118	1.99E−09	92	Cluster 6 (62)	114	Cluster 7 (57)
GO:0009570	Chloroplast stroma	115	2.35E−09	90	Cluster 6 (60)	111	Cluster 7 (55)
GO:0009579	Thylakoid	85	7.76E−06	65	Cluster 6 (47)	83	Cluster 7 (42)
GO:0009941	Chloroplast envelope	93	6.03E−05	75	Cluster 6 (46)	91	Cluster 7 (40)
GO:0009526	Plastid envelope	94	8.02E−05	76	Cluster 6 (46)	92	Cluster 7 (41)
GO:0044435	Plastid part	184	5.73E−09	141	Cluster 6 (92)	178	Cluster 7 (85)
GO:0044434	Chloroplast part	181	9.36E−09	139	Cluster 6 (90)	175	Cluster 7 (83)
GO:0009507	Chloroplast	300	8.39E−07	221	Cluster 6 (134)	282	Cluster 7 (116)
GO:0009536	Plastid	396	8.65E−06	298	Cluster 6 (160)	356	Cluster 7 (132)

LysoPC 18:1, LysoPE 18:2, etc.), 12 organic acids (3-*O*-*p*-coumaroyl shikimic acid, 5-*O*-*p*-coumaroyl shikimic acid, 4-hydroxybenzaldehyde, etc.), 11 phenylpropanoids (3-hydroxy-4-methoxycinnamic acid, ferulic acid, caffeate, *p*-coumaric acid, etc.), and others (lumichrome, L-ascorbate, L-dencichin, *N*-lauryldiethanolamine, 1-methylguanidine, etc.).

Similarly, amino compound metabolisms, especially amino acid and polyamine metabolisms, were affected by drought stress. *P5CSs* and *PROC*, the enzymes that catalyze proline synthesis, were upregulated, and the abundance of some *P5CSs* surged up to 116 times (Figure 9B). As a result, the L-proline content increased from 7.85×10^6 to 57.5×10^6. The metabolic enzymes OAT, ARGAH1, ADC1, etc., linked proline to other amino acids, and polyamine metabolism was slightly regulated by the stress (Figure 9B). In the metabolic pathways, arginine, agmatine, and putrescine increased, and only ornithine decreased. Therein, the content of putrescine increased dramatically from 1.3×10^6 to 3.24×10^6. As an important part of amino compounds, the content of phenolamides also fluctuated under drought stress. Among the three phenolamides

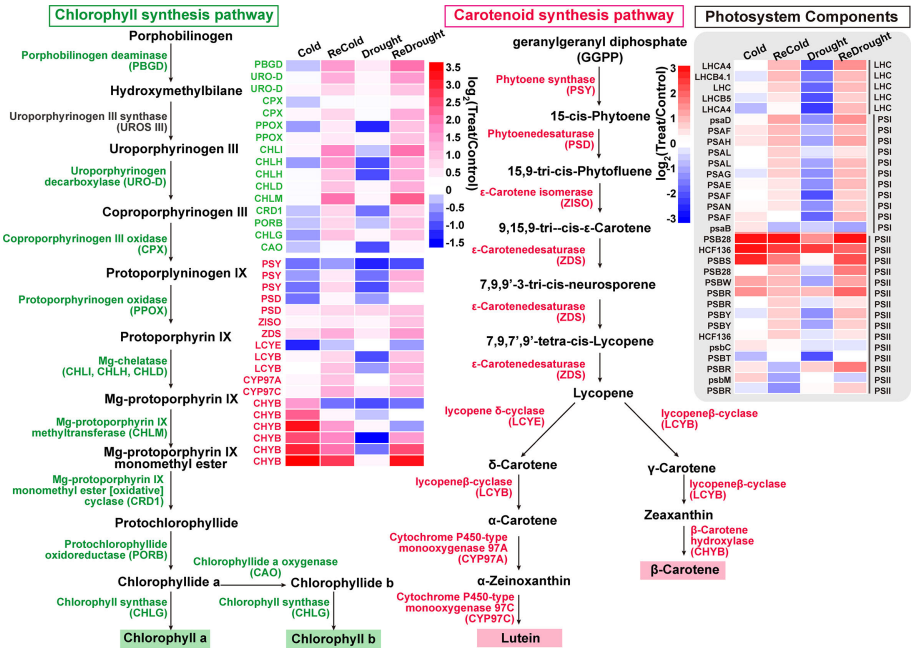

FIGURE 7
The components of photosynthetic pigment biosynthesis and photosystem. The expression changes of genes are denoted by heat maps, and the color intensity represents the expression level.

with significant changes, *N*-hexosyl-*p*-coumaroyl putrescin and *N*-feruloyl spermidine accumulated rapidly, while *N*-*p*-coumaroyl agmatine was dramatically consumed (Figure 9B).

Discussion

Potential environmental adaptation strategies

Previously, we found that compounds such as carbohydrates, flavonoids, and phenylpropane and genes involved in their synthesis and regulation, like *CCR*s, *MYB*s, *LEA*s, etc., were induced by low temperature and drought in *P. crymophila*. In addition, the accumulation of schisandrin and flavonoids in the phenylpropanoid pathway probably acted as potential stress-resistant substances to improve the tolerance of plants to stresses (Wang et al., 2021b). In this study, by analyzing gene expression patterns and comprehensively correlating metabolomic and transcriptomic results, more details of *P. crymophila's* responses to cold and drought were revealed, leading to a deeper understanding of its adaptation strategies to alpine environments.

Stresses induced the expression of stress-tolerant genes, inhibited growth-related genes, and most of them quickly returned to normal levels after the stress disappeared. Many crucial genes in a positive response to low temperature and drought stress showed flexible resilience, such as *ABFs*, *CORs*, *CBF/DREBs*, *ALDHs*, *LEA14-A*, etc. Those stress-repressed but quickly recovered genes were mostly related to water, glycerol, carbohydrate, and nitrogen transmembrane transport and other processes. Regardless of the positive or negative response of genes, the rapid recovery of the expressions after the stress disappears is the strong resilience of *P. crymophila* to stresses (Figure 11).

In addition, some gene expressions were altered significantly only after the stress was removed. For example, the genes involved in the negative regulation of growth and superoxide anion generation were downregulated after the stress disappeared, while a large number of genes related to photosynthetic pigment synthesis and photosystem composition were rapidly activated. These changes can help plants quickly return to normal growth. These responsive traits also reflected the robust tolerance of *P. crymophila* to cold and drought stresses.

As downstream of regulatory genes, metabolic genes and related metabolites also contribute to plant tolerance. Based on the transcriptome-associated metabolome analysis, we found genes involved in nitrate transport and amino compound metabolism and corresponding amino compounds such as amino acids, polyamines, and phenylamines may also play important roles in supporting robust tolerance in *P. crymophila*.

10.3389/fpls.2022.970496

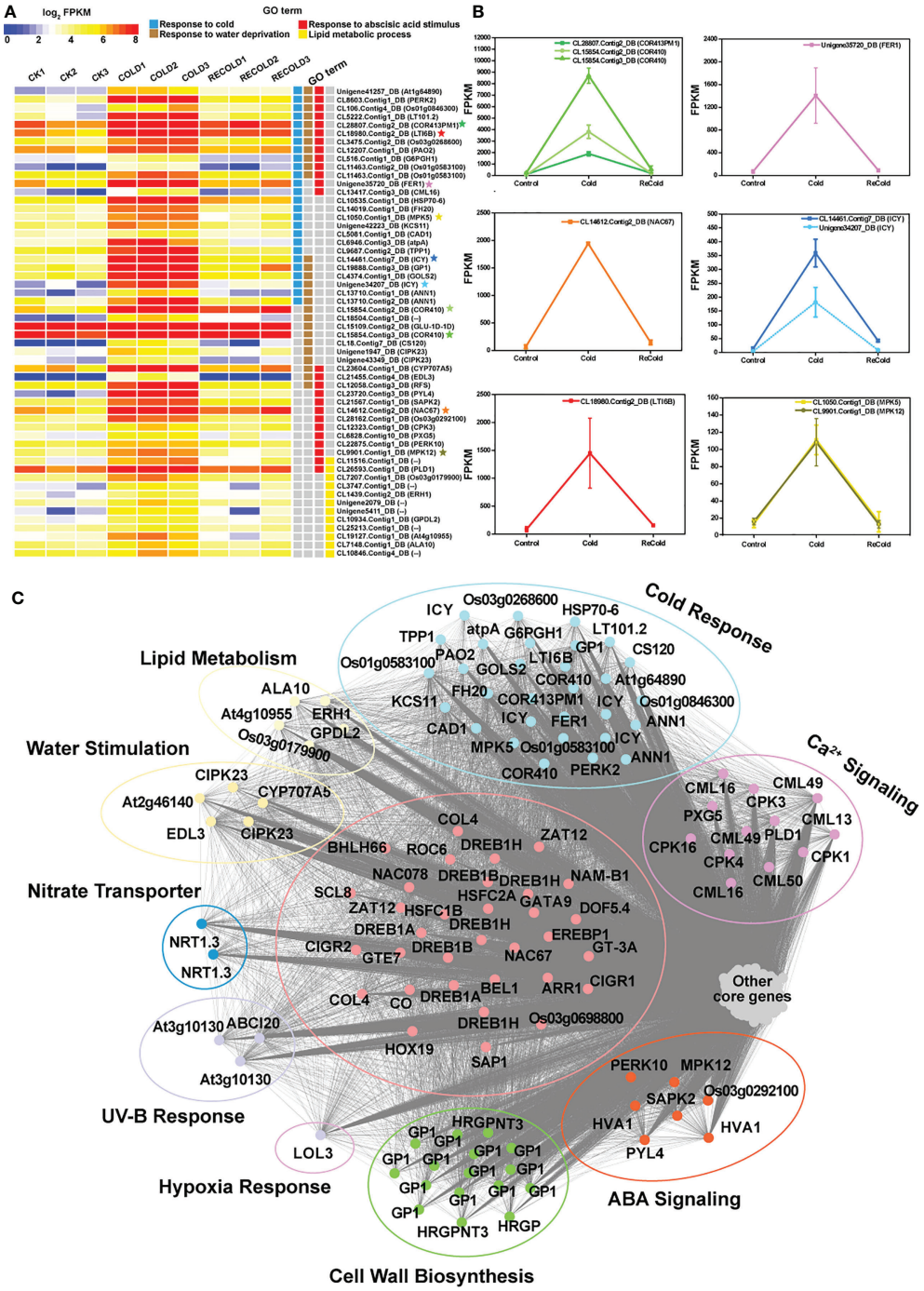

FIGURE 8
The expression patterns and functions of CMEblue core genes under cold. **(A)** Expression profiles of the representative CMEblue genes (Supplementary Figure S3). In the heat map, each gene has three stages and three repetitions. Color intensity represents the expression level, and different GO terms are represented by four columns with different colors. Some genes marked with stars as the characterization of GO term show expression trends in line graphs. **(B)** The line graphs of some function genes with a star mark related to the cold stress response. The horizontal axis denotes the sampling points, and the vertical coordinate reflects the gene expression level (FPKM value). **(C)** Different functions of CMEblue hub genes. The edges represent potential relationships between genes, and the thicker the line, the stronger the correlation.

10.3389/fpls.2022.970496

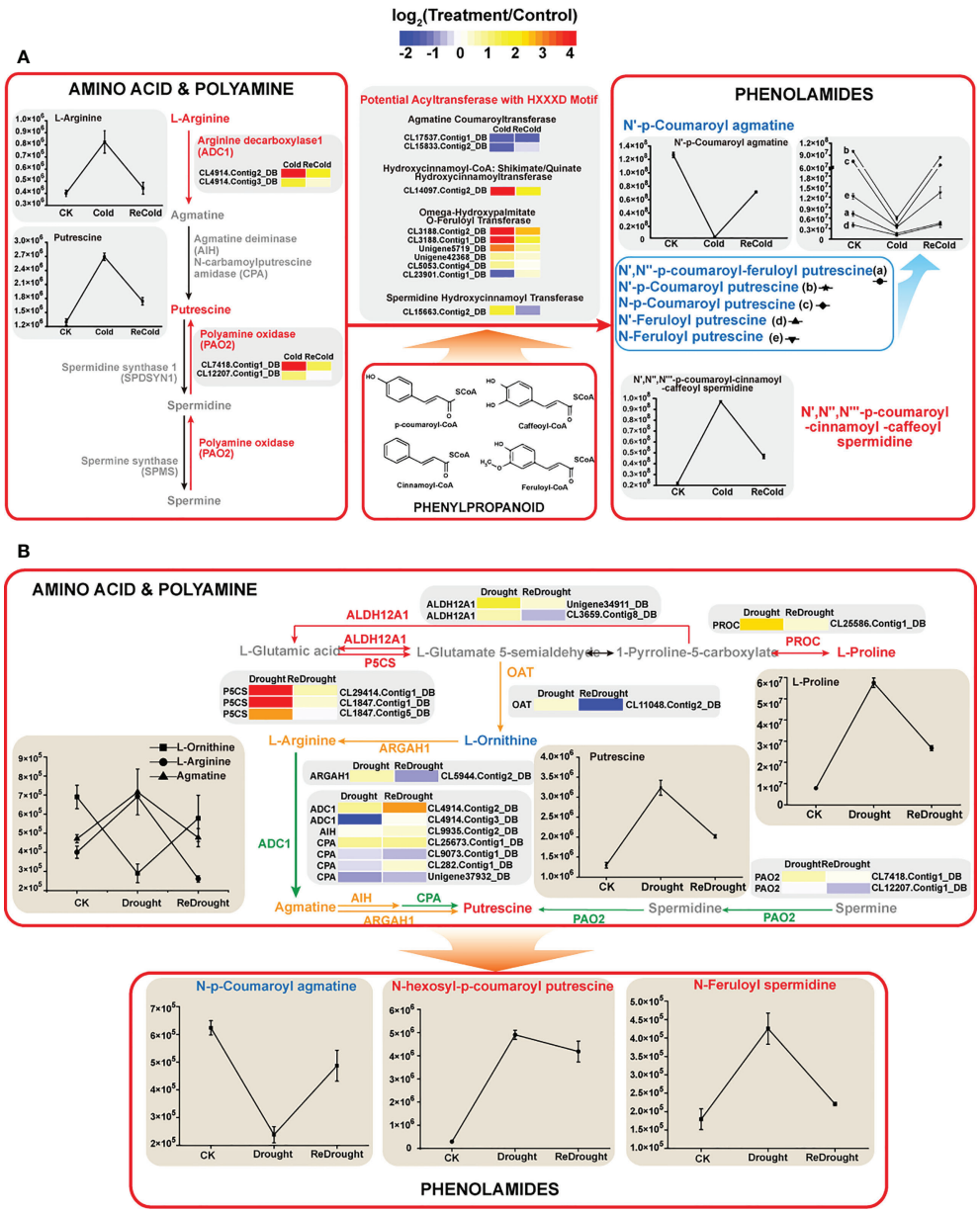

FIGURE 9
Amino compound metabolism under cold or drought stresses. **(A)** Cold stress. **(B)** Drought stress. The expression changes of genes are denoted by heat maps, and the color intensity represents the expression level. The fluctuant contents of metabolites are represented by line charts. Red arrows and labels: genes or metabolites significantly upregulated; yellow arrows and labels: genes or metabolites moderately upregulated; green arrow and label: gene members with up- or downregulated changes. ALDH12A1, delta-1-pyrroline-5-carboxylate dehydrogenase 12A1; P5CS, delta-1-pyrroline-5-carboxylate synthase; PROC, pyrroline-5-carboxylate reductase; OAT, ornithine aminotransferase; ARGAH1, arginase; ADC, arginine decarboxylase; AIH, agmatine deiminase; CPA, *N*-carbamoylputrescine amidase; PAO_2, polyamine oxidase 2.

Ca^{2+} signaling, ROS scavenging system, and core transcription factor responses

Ca^{2+} and reactive oxygen species (ROS) can act as chemical and electrical signals involved in signal transductions responding to various stresses (Wang et al., 2021a). In *P. crymophila*, we found many genes encoded calcium-related proteins that respond to cold stress, such as Ca^{2+} channel protein ACA, calcium-binding protein CMLs, and kinase CPKs. Only a few genes encoded ROS-scavenging enzymes that responded to drought stress, such as iron superoxide dismutases (FeSODs), manganese superoxide dismutases (MnSODs), catalases (CATs), and ascorbate peroxidases (APXs).

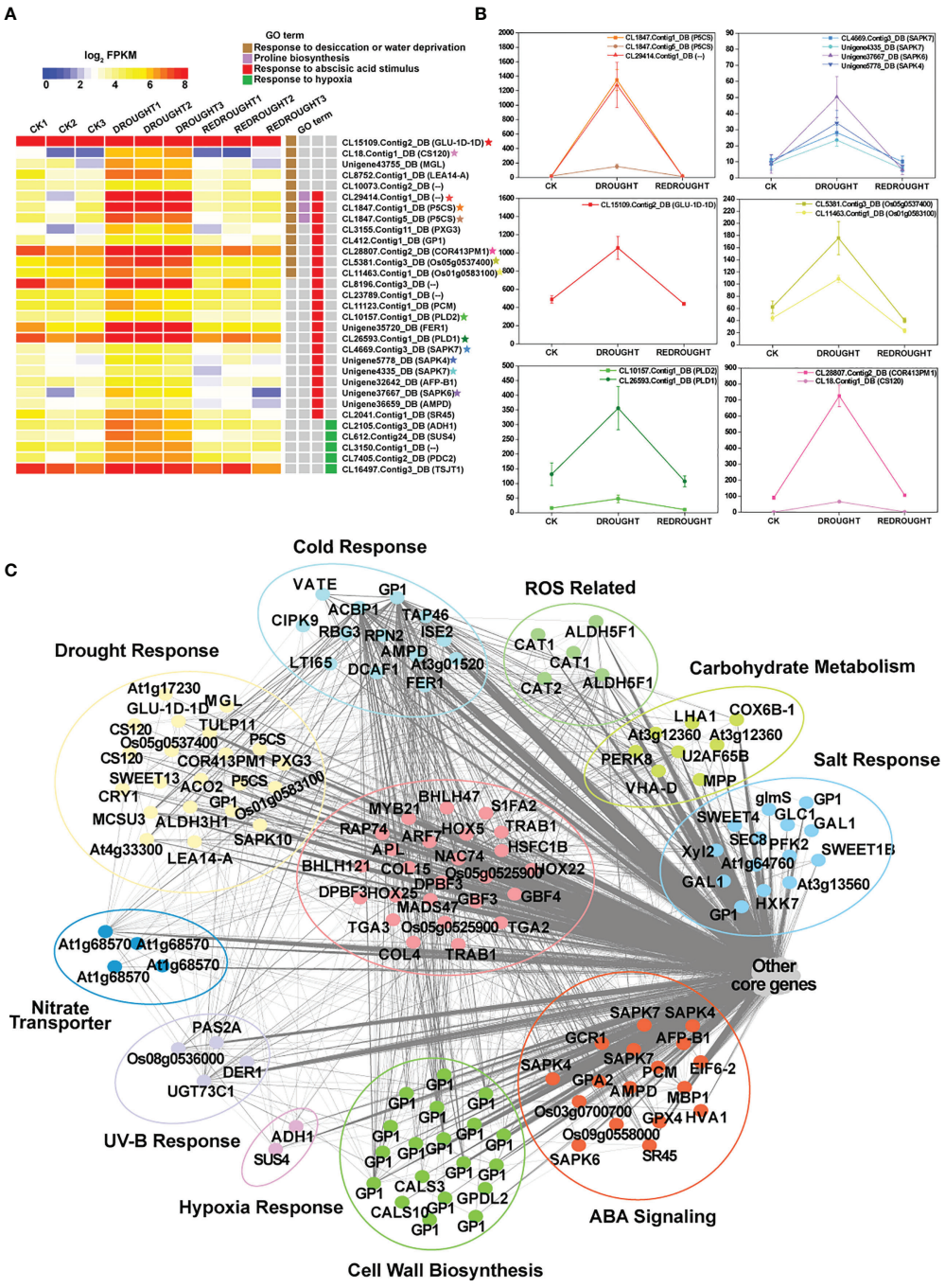

FIGURE 10
The function, expression pattern, and network of DMEblue hub genes under drought. **(A)** Expression profiles of the representative DMEblue genes (Supplementary Figure S4). Some genes marked with stars as the characterization of GO term show expression trends in line graphs. **(B)** The line graphs of some function genes with a star mark related to the drought stress response. The horizontal axis denotes the sampling points, and the vertical coordinates reflect the gene expression level (FPKM value). **(C)** Different functions of DMEblue hub genes.

Ca^{2+} is a key signal in the cold response network of plant cells (Guo et al., 2018). The tetraploid cold-tolerant strawberry has a higher expression level of the calcium channel protein so as to ensure the normal transmission of cold stress signals with the fluctuation of calcium ion concentration (Liu et al., 2021a). Calcium-binding protein senses the temperature variation through the change of intracellular calcium level, decodes it as a stress signal, and transmits it downstream as a master switch to

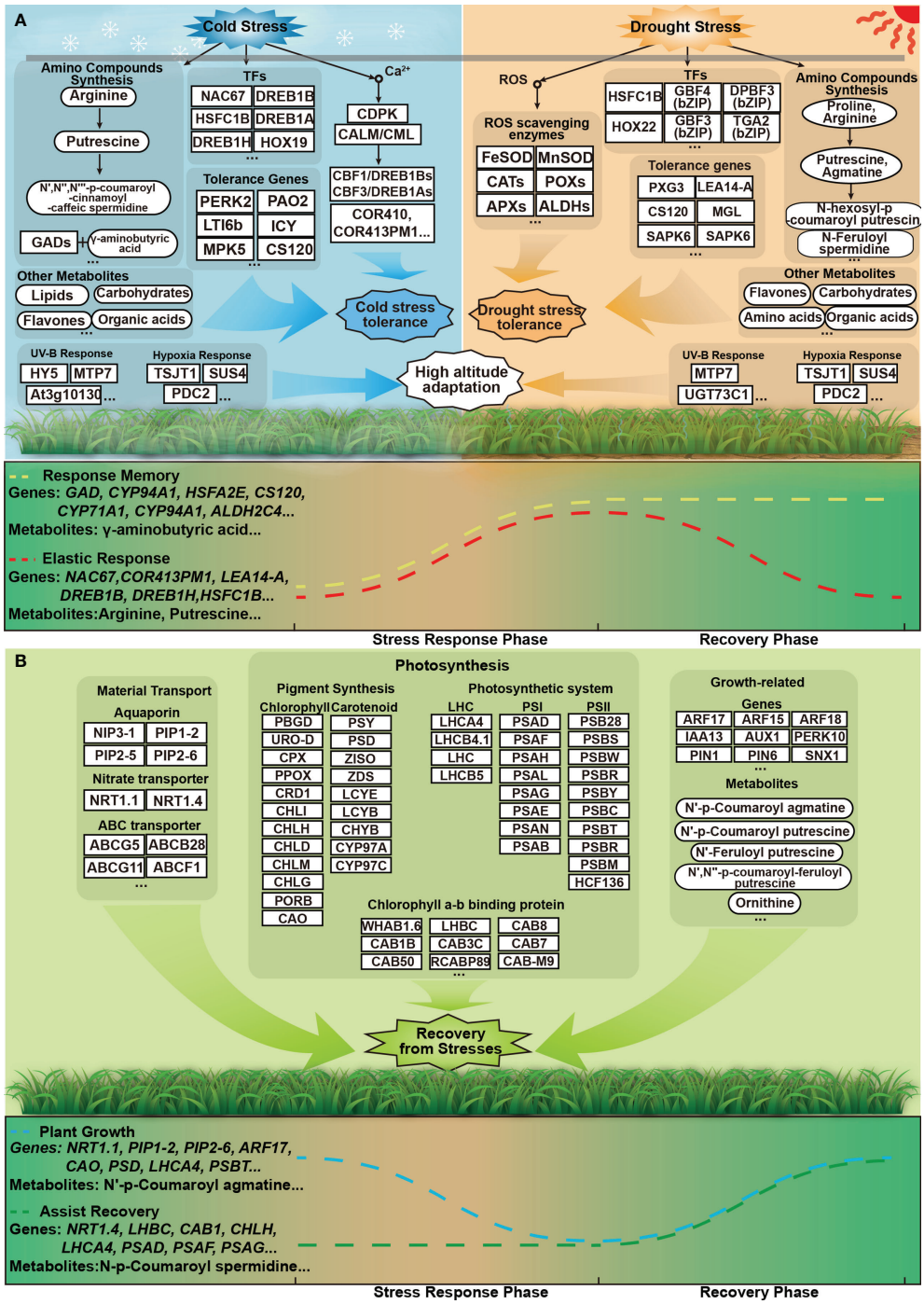

FIGURE 11
Flexible answer and quick recovery models of *P. crymophila* under cold and drought stresses. **(A)** The stress-adaptive strategies of the induced genes and metabolites. In the stress stage, a large number of response genes are rapidly expressed. Most of these genes and metabolites can be recovered from stress, and some of them are difficult to recover. **(B)** The stress-adaptive strategies of the repressed and unchanged genes and metabolites under adversity. These genes and metabolites involved in material transport, photosynthesis, and plant growth can rapidly restore or improve after stress disappears.

control various stress genes (Mahajan and Tuteja, 2005). Therefore, *P. crymophila* may rely on calcium-related proteins to utilize calcium ions as cold stress signals to regulate the expression of downstream stress-responsive genes such as *CBFs* and *CORs* and finally produce physiological and biochemical responses of cold stress defense such as cell wall reinforcement, hypersensitive response, and stomatal closure (Liu et al., 2021a).

ROS can act as a drought stress signal to affect the expression of the downstream genes. However, it also could produce severe negative effects, such as protein denaturation, nucleic acid mutations, and cell damage (Chen and Yang, 2020). Therefore, the ability to scavenge ROS and hydroxyl radicals is an important part of drought tolerance. The SODs are the first line of defense to scavenge O_2^- (Mittler et al., 2004). FeSOD and MnSOD are located separately in chloroplasts and mitochondria, and both can catalyze cytotoxic superoxide anion radicals to generate H_2O_2 (Mylona et al., 2007). Furthermore, the H_2O_2 is detoxified by the H_2O_2 scavenging enzyme group, including CATs, POXs, and APXs, thereby efficiently completing the removal of ROS. These enzymes of the ROS scavenging system protect cells from damage and ensure normal life under stress, which is also the strategy of *P. crymophila* drought adaptation.

The stress signals induced active expression of massive transcription factors, such as *DREBs* under low-temperature stress and *bZIPs* under drought stress. Transcription factors *RAP2-10*, *NAC67*, *HSFC1B*, *HOX22*, *DREB1B*, and *COL4* exhibited similar responses under both stresses, suggesting that their functions under low-temperature and drought stresses are overlapping. Small changes in transcription factors can cause large differences in downstream gene expression. However, *NAC67*, one of the NAC family members, soared rapidly when subjected to both stress and recovered rapidly after the stress disappeared. In rice, the expression of *Os07g12340* (*ONAC067*) was increased with low temperature (Fang et al., 2008; Takasaki et al., 2010). In addition, *EcNAC67* also responded to drought in finger millet (*Eleusine coracana* L.) (Rahman et al., 2016). These transcription factors, especially those located at the core of co-expression networks, may be an important source of plant tolerance.

Rapid recovery of the photosynthetic system and plateau-specific cross-adaptive genes

Through consensus analysis, we found that the rapid recovery of the photosynthetic system may be the source of resilience. The expression of genes related to the photosynthetic system, such as photosynthetic pigment synthesis, photosystem proteins, etc., increased rapidly after the stress disappeared. The photosynthetic system is an important source of materials and energy and can also be used as a key indicator to measure the impact of stresses. Stress could inhibit the photosynthetic rate and impair the absorption, transfer, and transformation of light energy in leaves, resulting in photoinhibition (Liu et al., 2019). Reportedly, the photosynthetic gene expressions and photosynthesis in maize were inhibited by drought and low-temperature stresses but can be recovered after drought stress disappeared, while it was difficult to recover and even withered after low-temperature stress (Guo et al., 2021). The sensitivity of the photosynthetic system results in low cold tolerance in maize.

Although cold and drought similarly repressed the expression of photosynthetic genes in *P. crymophila*, unlike other plants, these repressed genes can be rapidly recovered after the stress disappeared, even under freezing stress. Furthermore, during the recovery phase, more photosynthetic system genes were activated, and the plants remained green and vigorous in both severe cold and arid environments. In contrast to cold stress assaying, the cool-season forage perennial ryegrass cv. Mathilde, which has cold tolerance, can endure −5°C but was frozen to death when exposed to −12°C. However, *P. crymophila* can stand the chilling stress. All these characteristics of *P. crymophila* reflect its superior resilience.

Furthermore, we also found that both cold and drought activated the expression of genes that responded to UV-B and hypoxia. The expression of *SUS4*, *ADH1*, and *PDC2* was induced by hypoxia. In *sus4* mutants, root growth was retarded under hypoxia (Liu et al., 2017). ADH1 and PDC2 also play important roles in hypoxia stress response as important tolerant genes (Yang, 2014; Gravot et al., 2016). UVR8, RUP1, HY5, and UGT73C1 were identified as key players in UV-B response (Jiang et al., 2012; Lee, 2016) in *P. crymophila* under cold and drought stress. After experiencing a certain kind of adversity, the tolerance of plants to other stresses will also be improved, and this adaptation between different adversities is called cross-adaptation. Due to the special growth habitat of *P. crymophila*, it may have produced special cross-resistance consistent with the high-altitude environment. Similar features were found in the high-altitude perennial *Arabis alpine*, which is more tolerant to UV-B-induced oxidative stress than its relative *Arabidopsis thaliana* (Ozgur et al., 2021). Therefore, this particular cross-adaptation is the result of long-term growth at high altitudes. Through the initial perception of abiotic stresses such as low temperature and drought, genes related to hypoxia and UV-B were stimulated, thereby allowing *P. crymophila* to adapt to complex and harsh high-altitude conditions.

Nitrate transport and amino compound metabolism

Genes involved in nitrate transport and amino compound metabolism were also affected by cold and drought stresses. The

transport of nitrate and nitrogen compounds is mainly through NRT1/PTR family proteins (Wang et al., 2012). The stresses mainly affect the expression of NRT1.1, NRT1.3, and NRT1.4 genes. After the stresses disappeared, the expressions of NRT1.1s (stress-inhibited expression) and NRT1.3s (stress-promoted expression) rapidly recovered, and NRT1.4s increased rapidly. The root-specific NRT1.1s is a dual-affinity transporter involved in soil nitrate uptake and auxin transport (Fang et al., 2021), which suggested that NRT1.1 is associated with the growth of plants. NRT1.3s are highly expressed in flowers, leaves, and stems. These genes are involved in nitrogen transport, polyamine metabolism, and chlorophyll synthesis (Tong et al., 2016). The petiole-specific NRT1.4s was shown to be a low-affinity nitrate transporter. The different responses of the three transporter genes may be related to the metabolic changes of amino compounds under stress, which confer *P. crymophila* with strong adaptability to low temperatures and drought.

Amino acids and polyamines are common and important amino compounds in plants with a variety of important biological functions, including abiotic stress responses. Phenolamines are also increasingly important as functional amino compounds for plants to adapt to adversity, and their functions are closely related to polyamines and amino acids (Macoy et al., 2015). It is of great significance to study the functions of amino acids, polyamines, and phenolamines in plant growth and development and stress.

Changes in the expression of metabolism-related genes affect the anabolism of small molecules. Cold-induced expression of arginine decarboxylase gene (*ADC1*) promoted the synthesis of putrescine, doubling its content in *P. crymophila*. Reportedly, after exposure to cold stress, ADC1 was uniquely enhanced, and exogenous application of putrescine or overexpression of the ADC1 gene could improve potato cold tolerance (Kou et al., 2018). Furthermore, as putrescine accumulated, arginine levels not only did not drop but nearly tripled. Exogenous application of arginine reduced peroxidase activity, malondialdehyde content, and electrolyte leakage and enabled tomato to relieve plant frostbite, but treatment with arginase inhibitors aggravated the damage (Zhang et al., 2010). Thus, arginine accumulation can impart a higher cold tolerance to plants. Furthermore, coumaroyl, feruloyl, caffeoyl, etc. can be added to polyamines to form different phenolamines by BAHD acyltransferases. Under freezing stress, only the content of *N*′,*N*′′,*N*′′′-*p*-coumaroyl-cinnamoyl-caffeic spermidine significantly increased fivefold, which suggested that this particular phenolamine may be closely related to tolerance to abiotic stress. Currently only found in *Salix viminalis*, this special spermidine contributes to the nonspecific protection of plants after phenanthrene treatment (Xia et al., 2021). In addition, some phenolamines like *N*′-*p*-coumaroyl agmatine, *N*′-*p*-coumaroyl putrescine, and *N*′-feruloyl putrescine decreased after low-temperature stress. Some of them were detected during the germination and growth of rice seeds, which are related to growth (Park et al., 2009). As the stress subsided, the abovementioned gene expression levels and small molecule content quickly returned to normal. Therefore, the rapid response and recovery of polyamine and phenolamide metabolism are also important sources of cold tolerance in *P. crymophila*. On another front, after the low temperature disappeared, γ-aminobutyric acid (GABA) and its synthase gene GADs remained at high levels, which may be related to the formation of cold domestication in plants. GABA plays an important role in the cold domestication of mulberry, spinach (*Spinacia oleracea*) (Yoon et al., 2017), barley, and wheat (Mazzucotelli et al., 2006).

The effects of drought stress on amino compound metabolism can be traced back to proline. The abundance of *P5CS*, encoding a key enzyme that catalyzes the synthesis of proline, increased by more than 100 times under drought, and the content of proline also increased by nearly eight times. Proline as an efficient osmotic regulator can improve plant tolerance to drought and play an important role in stress (Per et al., 2017). Ornithine and arginine cannot only participate in plant polyamine metabolism but also improve plant tolerance to drought and salt stress (Anwar et al., 2018; Hussein et al., 2019). When exposed to drought, the content of arginine increased in *P. crymophila*, while ornithine decreased. It is speculated that part of ornithine was used for the synthesis of proline (Díaz et al., 2005). Regarding polyamines, the contents of agmatine and putrescine accumulated. Both of them play an important role in improving plant drought tolerance (Juzoń et al., 2017). In addition, the changes and functions of phenolamine are also worthy of attention. Different from low-temperature stress, drought accumulated the content of *N*-hexosyl-*p*-coumaroyl putrescin and *N*-feruloyl spermidine, and their functions in plants have not yet been reported. These special metabolites are speculated to be drought-tolerant substances in plants, which deserve further verification in the future.

Although there were massive differences in amino compound metabolism under cold and drought stresses, some commonalities could also be found. Arginine and putrescine were abundantly accumulated, while *N*-*p*-coumaroyl agmatine was consumed, which indicated their functions were crossed under low-temperature and drought stress. Taken together, these results suggested that the metabolism of amino acids, polyamines, and phenolamides contributes to plant adaptation to stressful environments.

Interestingly, some neural-related metabolites were detected, such as serotonin, melatonin, and acetylcholine (ACh). Although these compounds did not change significantly under stress, it is

speculated that their responses probably be as fast and transient as in animals, resulting in no significant changes being detected. Plant neurobiology is an emerging field of research, which shows the roles of nerve signal substances in various plant processes, including environmental stress adaptation (Michmizos and Hilioti, 2019).

Conclusion

Poa crymophila cv. Qinghai is a forage species grown on the Qinghai–Tibet Plateau, and its special environment has given it a strong and special adaptation to quickly cope with cold and drought, as well as the ability to quickly recover its growth after the stresses have been removed. We previously mainly identified genes involved in the phenylpropanoid pathway, as well as secondary metabolites such as schisandrin, small sugars, and flavone. In this study, further in-depth analysis and clustering of gene expression patterns revealed that pathways such as Ca^{2+} signaling (*ACA*, *CML*, *CPK*, etc.), ROS scavenging system (*SOD*, *CAT*, *APX*, etc.), core transcription factors (*DREB1H*, *NAC67*, *HSFC1B*, etc.), nitrate transport and amino compound metabolism (*NRT1.3*, *PAO2*, *ADC*, etc.), as well as photosynthesis-related genes, respond fast and flexibly to stress. Meanwhile, amino acids (arginine, asparagine, proline, L-homocitrulline, etc.), lipids (LysoPC 16:1, 9-HOTrE, LysoPC 20:4, LysoPC 18:0, etc.), organic acids (azelaic acid, γ-aminobutyric acid, L-Malic acid, etc.), and other compounds (nandrolone, azadiradione, coixol, phytocassane C, dulcitol, etc.) actively respond to stresses. The flexible response of a large number of genes and metabolites under stress, and the rapid recovery after stress relief, endows *P. crymophila* with robust cold and drought tolerance.

Data availability statement

The original contributions presented in the study are included in the article/Supplementary Material. Further inquiries can be directed to the corresponding author.

Author contributions

X-RM and X-YL conceived this study, designed the experimental plan, analyzed data, and drafted and revised the manuscript. YW designed the experimental plan and participated in data analyses. X-YH, YC, and C-XL participated in sample preparation, treating, collecting, and total RNA extracts. All authors contributed to the article and approved the submitted version.

Funding

This work was supported by the Key Research and Development Program of Sichuan, China (Grant No.2019YFN0017) and the National Natural Science Foundation of China (Grant No.31502003).

Conflict of interest

The authors declare that the research was conducted in the absence of any commercial or financial relationships that could be construed as a potential conflict of interest.

Publisher's note

All claims expressed in this article are solely those of the authors and do not necessarily represent those of their affiliated organizations, or those of the publisher, the editors and the reviewers. Any product that may be evaluated in this article, or claim that may be made by its manufacturer, is not guaranteed or endorsed by the publisher.

Supplementary material

The Supplementary Material for this article can be found online at: https://www.frontiersin.org/articles/10.3389/fpls.2022.970496/full#supplementary-material

SUPPLEMENTARY FIGURE 1
Analysis of network topology for various soft-thresholding powers. **(A)** cold related co-expression network; **(B)** drought related co-expression network.

SUPPLEMENTARY FIGURE 2
Pearson's correlation coefficient between samples.

SUPPLEMENTARY FIGURE 3
The 2D and 3D PCA results of all unigenes and filtered unigenes. **(A, B)** The 2D PCA results of all unigenes and filtered unigenes, respectively; **(C, D)** The 3D PCA results of all unigenes and filtered unigenes, respectively; **(A, C)** reflects the expression profiles of unigenes before filtered, and **(B, D)** shows the expression of filtered unigenes. In the legend, CK represents control group; **(C)** denotes cold stress group; **(D)** represents drought stress group; RC represents cold recovery group; RD denotes drought recovery group. The axes represents the dimension reduction axis, and the number represents the percentage interpretation rate of the axis.

SUPPLEMENTARY FIGURE 4
The Venn diagrams of differential expressed genes. **(A)** Cold stress dataset; **(B)** Drought stress dataset.

SUPPLEMENTARY FIGURE 5
Cold related weighted gene co-expression network. **(A)** Clustering dendrogram of genes, with dissimilarity based on topological overlap, together with assigned module colors; **(B)** Visualization of the eigengene

network representing the relationships among the modules and the content of D-glucose-6phosphate; **(C)** Visualizing the gene network using a heatmap plot.

SUPPLEMENTARY FIGURE 6
Drought related weighted gene co-expression network. **(A)** Clustering dendrogram of genes; **(B)** Visualization of the eigengene network; **(C)** Visualizing the gene network using a heatmap plot.

SUPPLEMENTARY FIGURE 7
Correlations between cold-responsive metabolites and different modules. The relationship from negative to positive is represented by the color from blue to red.

SUPPLEMENTARY FIGURE 8
Correlations between drought-responsive metabolites and different modules. The relationship from negative to positive is represented by the color from blue to red.

SUPPLEMENTARY TABLE 1
Gene expressions of P. crymophila and expression differences

SUPPLEMENTARY TABLE 2
Gene Expression Clusters.

SUPPLEMENTARY TABLE 3
The results of consensus analysis.

SUPPLEMENTARY TABLE 4
The results of module preservation analysis.

SUPPLEMENTARY TABLE 5
The results of cold and drought co-expression network.

SUPPLEMENTARY TABLE 6
The association results between differential metabolomes and co-expression networks.

References

Anwar, A., She, M., Wang, K., Riaz, B., and Ye, X. (2018). Biological roles of ornithine aminotransferase (OAT) in plant stress tolerance: Present progress and future perspectives. *Int. J. Mol. Sci.* 19, 3681. doi: 10.3390/ijms19113681

Chen, Q., and Yang, G. (2020). Signal function studies of ROS, especially RBOH-dependent ROS, in plant growth, development and environmental stress. *J. Plant Growth Regul.* 39, 157–171. doi: 10.1007/s00344-019-09971-4

Díaz, P., Borsani, O., Márquez, A., and Monza, J. (2005). Osmotically induced proline accumulation in lotus corniculatus leaves is affected by light and nitrogen source. *Plant Growth Regulation.* 46, 223–232. doi: 10.1007/s10725-005-0860-7

Fang, X. Z., Fang, S. Q., Ye, Z. Q., Liu, D., Zhao, K. L., and Jin, C. W. (2021). NRT1.1 dual-affinity nitrate Transport/Signalling and its roles in plant abiotic stress resistance. *Front. Plant science.* 12, 715694. doi: 10.3389/fpls.2021.715694

Fang, Y., You, J., Xie, K., Xie, W., and Xiong, L. (2008). Systematic sequence analysis and identification of tissue-specific or stress-responsive genes of NAC transcription factor family in rice. *Mol. Genet. Genomics* 280, 547–563. doi: 10.1007/s00438-008-0386-6

Gravot, A., Richard, G., Lime, T., Lemarié, S., Jubault, M., Lariagon, C., et al. (2016). Hypoxia response in arabidopsis roots infected by plasmodiophora brassicae supports the development of clubroot. *BMC Plant Biol.* 16, 251. doi: 10.1186/s12870-016-0941-y

Groppa, M. D., Rosales, E. P., Iannone, M. F., and Benavides, M. P. (2008). Nitric oxide, polyamines and cd-induced phytotoxicity in wheat roots. *Phytochemistry.* 69, 2609–2615. doi: 10.1016/j.phytochem.2008.07.016

Guo, Q., Li, X., Niu, L., Jameson, P. E., and Zhou, W. (2021). Transcription-associated metabolomic adjustments in maize occur during combined drought and cold stress. *Plant Physiol.* 186, 677–695. doi: 10.1093/plphys/kiab050

Guo, X., Liu, D., and Chong, K. (2018). Cold signaling in plants: Insights into mechanisms and regulation. *J. Integr. Plant Biol.* 60, 745–756. doi: 10.1111/jipb.12706

Hassan, A. M., and Mohamed, H. E. (2019). L-arginine pretreatment enhances drought resistance of sunflower (Helianthus annuus l.) plants by increase in polyamines content. *J. Plant Growth Regul.* 38, 600–605. doi: 10.1007/s00344-018-9873-0

Hua, Q., Yu, Y., Dong, S., Li, S., Shen, H., Han, Y., et al. (2019). Leaf spectral responses of poa crymophila to nitrogen deposition and climate change on qinghai-Tibetan plateau. *Agricult. Ecosyst. Environment.* 284, 106598. doi: 10.1016/j.agee.2019.106598

Hussein, H. A., Mekki, B. B., El-Sadek, M. E. A., and El Lateef, E. E. (2019). Effect of l-ornithine application on improving drought tolerance in sugar beet plants. *Heliyon.* 5, e02631. doi: 10.1016/j.heliyon.2019.e02631

Jiang, L., Wang, Y., Li, Q.-F., Björn, L. O., He, J.-X., and Li, S.-S. (2012). Arabidopsis STO/BBX24 negatively regulates UV-b signaling by interacting with COP1 and repressing HY5 transcriptional activity. *Cell Res.* 22, 1046–1057. doi: 10.1038/cr.2012.34

Jun, M., and Gu, L. (2021) *TCseq: Time course sequencing data analysis*. Available at: http://www.bioconductor.org/packages/release/bioc/html/TCseq.html (Accessed August 2021).

Juzoń, K., Czyczyło-Mysza, I., Marcińska, I., Dziurka, M., Waligórski, P., and Skrzypek, E. (2017). Polyamines in yellow lupin (Lupinus luteus L.) tolerance to soil drought. *Acta Physiologiae Plantarum.* 39, 202. doi: 10.1007/s11738-017-2500-z

Kou, S., Chen, L., Tu, W., Scossa, F., Wang, Y., Liu, J., et al. (2018). The arginine decarboxylase gene ADC1, associated to the putrescine pathway, plays an important role in potato cold-acclimated freezing tolerance as revealed by transcriptome and metabolome analyses. *Plant J. Cell Mol. Biol.* 96, 1283–1298. doi: 10.1111/tpj.14126

Lee, J.-H. (2016). UV-B signal transduction pathway in arabidopsis. *J. Plant Biol.* 59, 223–230. doi: 10.1007/s12374-016-0155-8

Li, B., and Dewey, C. N. (2011). RSEM: accurate transcript quantification from RNA-seq data with or without a reference genome. *BMC Bioinf.* 12, 323. doi: 10.1186/1471-2105-12-323

Liu, W., He, G., and Deng, X. W. (2021b). Biological pathway expression complementation contributes to biomass heterosis in arabidopsis. *Proc. Natl. Acad. Sci.* 118, e2023278118. doi: 10.1073/pnas.2023278118

Liu, J., Li, J., and Fu, C. (2021a). Comparative physiology and transcriptome analysis reveals the regulatory mechanism of genome duplication enhancing cold resistance in fragaria nilgerrensis. *Environ. Exp. Botany.* 188, 104509. doi: 10.1016/j.envexpbot.2021.104509

Liu, B., Sun, L., Ma, L., and Hao, F.-S. (2017). Both AtrbohD and AtrbohF are essential for mediating responses to oxygen deficiency in arabidopsis. *Plant Cell Rep.* 36, 947–957. doi: 10.1007/s00299-017-2128-x

Liu, W., Zheng, C., Chen, J., Qiu, J., Huang, Z., Wang, Q., et al. (2019). Cold acclimation improves photosynthesis by regulating the ascorbate–glutathione cycle in chloroplasts of kandelia obovata. *J. For. Res.* 30, 755–765. doi: 10.1007/s11676-018-0791-6

Love, M. I., Huber, W., and Anders, S. (2014).). Moderated estimation of fold change and dispersion for RNA-seq data with DESeq2. *Genome Biol.* 15, 550. doi: 10.1186/s13059-014-0550-8

Luo, J., Fuell, C., Parr, A., Hill, L., Bailey, P., Elliott, K., et al. (2009). A novel polyamine acyltransferase responsible for the accumulation of spermidine conjugates in *Arabidopsis* seed. *Plant Cell.* 21, 318–333. doi: 10.1105/tpc.108.063511

Macoy, D. M., Kim, W.-Y., Lee, S. Y., and Kim, M. G. (2015). Biosynthesis, physiology, and functions of hydroxycinnamic acid amides in plants. *Plant Biotechnol. Rep.* 9, 269–278. doi: 10.1007/s11816-015-0368-1

Mahajan, S., and Tuteja, N. (2005). Cold, salinity and drought stresses: An overview. *Arch. Biochem. biophys.* 444, 139–158. doi: 10.1016/j.abb.2005.10.018

Mazzucotelli, E., Tartari, A., Cattivelli, L., and Forlani, G. (2006). Metabolism of γ-aminobutyric acid during cold acclimation and freezing and its relationship to frost tolerance in barley and wheat. *J. Exp. Bot.* 57, 3755–3766. doi: 10.1093/jxb/erl141

Michmizos, D., and Hilioti, Z. (2019). A roadmap towards a functional paradigm for learning & memory in plants. *J. Plant Physiol.* 232, 209–215. doi: 10.1016/j.jplph.2018.11.002

Mittler, R., Vanderauwera, S., Gollery, M., and Van Breusegem, F. (2004). Reactive oxygen gene network of plants. *Trends Plant Sci.* 9, 490–498. doi: 10.1016/j.tplants.2004.08.009

Mylona, P. V., Polidoros, A. N., and Scandalios, J. G. (2007). Antioxidant gene responses to ROS-generating xenobiotics in developing and germinated scutella of maize. *J. Exp. Bot.* 58, 1301–1312. doi: 10.1093/jxb/erl292

Ozgur, R., Uzilday, B., Yalcinkaya, T., Akyol, T. Y., Yildirim, H., and Turkan, I. (2021). Differential responses of the scavenging systems for reactive oxygen species (ROS) and reactive carbonyl species (RCS) to UV-b irradiation in arabidopsis thaliana and its high altitude perennial relative arabis alpina. *Photochemical photobiological sciences: Off. J. Eur. Photochem. Assoc. Eur. Soc. Photobiol.* 20, 889–901. doi: 10.1007/s43630-021-00067-1

Park, S., Kang, K., Kim, Y. S., and Back, K. (2009). Endosperm-specific expression of tyramine n-hydroxycinnamoyltransferase and tyrosine decarboxylase from a single self-processing polypeptide produces high levels of tyramine derivatives in rice seeds. *Biotechnol. Let.* 31, 911–915. doi: 10.1007/s10529-009-9951-2

Per, T. S., Khan, N. A., Reddy, P. S., Masood, A., Hasanuzzaman, M., Khan, M. I. R., et al. (2017). Approaches in modulating proline metabolism in plants for salt and drought stress tolerance: Phytohormones, mineral nutrients and transgenics. *Plant Physiol. Biochem.* 115, 126–140. doi: 10.1016/j.plaphy.2017.03.018

Rahman, H., Ramanathan, V., Nallathambi, J., Duraialagaraja, S., and Muthurajan, R. (2016). Over-expression of a NAC 67 transcription factor from finger millet (Eleusine coracana l.) confers tolerance against salinity and drought stress in rice. *BMC Biotechnol.* 16, 35. doi: 10.1186/s12896-016-0261-1

Shannon, P., Markiel, A., Ozier, O., Baliga, N. S., Wang, J. T., Ramage, D., et al. (2003). Cytoscape: A software environment for integrated models of biomolecular interaction networks. *Genome Res.* 13, 2498–2504. doi: 10.1101/gr.1239303

Shao, D., Chen, S., Tan, X., and Gu, W. (2018). Drought characteristics over China during 1980–2015. *Int. J. Climatol.* 38, 3532–3545. doi: 10.1002/joc.5515

Shen, H., Dong, S., Li, S., Xiao, J., Han, Y., Yang, M., et al. (2019). Grazing enhances plant photosynthetic capacity by altering soil nitrogen in alpine grasslands on the qinghai-Tibetan plateau. *Agricult. Ecosyst. Environment.* 280, 161–168. doi: 10.1016/j.agee.2019.04.029

Takasaki, H., Maruyama, K., Kidokoro, S., Ito, Y., Fujita, Y., Shinozaki, K., et al. (2010). The abiotic stress-responsive NAC-type transcription factor OsNAC5 regulates stress-inducible genes and stress tolerance in rice. *Mol. Genet. Genomics* 284, 173–183. doi: 10.1007/s00438-010-0557-0

Tian, J., Ma, Y., Tian, L., Huang, C., Chen, M., and Wei, A. (2021). Comparative physiology and transcriptome response patterns in cold-tolerant and cold-sensitive varieties of zanthoxylum bungeanum maxim. *Ind. Crops Products.* 167, 113562. doi: 10.1016/j.indcrop.2021.113562

Tong, W., Imai, A., Tabata, R., Shigenobu, S., Yamaguchi, K., Yamada, M., et al. (2016). Polyamine resistance is increased by mutations in a nitrate transporter gene NRT1.3 (AtNPF6.4) in arabidopsis thaliana. *Front. Plant Sci.* 7, 834. doi: 10.3389/fpls.2016.00834

Wang, Y.-Y., Hsu, P.-K., and Tsay, Y.-F. (2012). Uptake, allocation and signaling of nitrate. *Trends Plant science.* 17, 458–467. doi: 10.1016/j.tplants.2012.04.006

Wang, Y., Li, X. Y., Li, C. X., He, Y., Hou, X. Y., and Ma, X. R. (2021b). The regulation of adaptation to cold and drought stresses in poa crymophila keng revealed by integrative transcriptomics and metabolomics analysis. *Front. Plant science.* 12, 631117. doi: 10.3389/fpls.2021.631117

Wang, L., Sadeghnezhad, E., Guan, P., and Gong, P. (2021a). Review: Microtubules monitor calcium and reactive oxygen species signatures in signal transduction. *Plant science: an Int. J. Exp. Plant Biol.* 304, 110589. doi: 10.1016/j.plantsci.2020.110589

Xia, L., Xiaodong, M., Yunhe, C., Junxiang, L., Junzhu, Z., Feifei, Z., et al. (2021). Transcriptomic and metabolomic insights into the adaptive response of salix viminalis to phenanthrene. *Chemosphere* 262, 127573. doi: 10.1016/j.chemosphere.2020.127573

Yang, C.-Y. (2014). Hydrogen peroxide controls transcriptional responses of ERF73/HRE1 and ADH1 *via* modulation of ethylene signaling during hypoxic stress. *Planta.* 239, 877–885. doi: 10.1007/s00425-013-2020-z

Yoon, Y.-E., Kuppusamy, S., Cho, K. M., Kim, P. J., Kwack, Y.-B., and Lee, Y. B. (2017). Influence of cold stress on contents of soluble sugars, vitamin c and free amino acids including gamma-aminobutyric acid (GABA) in spinach (Spinacia oleracea). *Food Chem.* 215, 185–192. doi: 10.1016/j.foodchem.2016.07.167

Zhang, B., and Horvath, S. (2005). A general framework for weighted gene co-expression network analysis. *Stat. Appl. Genet. Mol. Biol.* 4, 1–37. doi: 10.2202/1544-6115.1128

Zhang, X., Shen, L., Li, F., Zhang, Y., Meng, D., and Sheng, J. (2010). Up-regulating arginase contributes to amelioration of chilling stress and the antioxidant system in cherry tomato fruits. *J. Sci. Food Agricult.* 90, 2195–2202. doi: 10.1002/jsfa.4070

Zhou, W.-s., Wu, N., and Bao, W.-k. (2010). Growth and potential reproduction of poa crymophila in response to season precipitation shortage in the Eastern Tibetan plateau, China. *Russian J. Ecol.* 41, 147–152. doi: 10.1134/S1067413610020062

frontiers | Frontiers in Plant Science

TYPE Original Research
PUBLISHED 20 December 2022
DOI 10.3389/fpls.2022.968965

OPEN ACCESS

EDITED BY
Jing Zhang,
Nanjing Agricultural University, China

REVIEWED BY
Fuai Sun,
University of California, Davis, United States
Jin-Lin Zhang,
Lanzhou University, China

*CORRESPONDENCE
Guowen Cui
cuigw603@126.com
Xiujie Yin
yinxiujie@126.com

SPECIALTY SECTION
This article was submitted to Plant Abiotic Stress, a section of the journal Frontiers in Plant Science

RECEIVED 14 June 2022
ACCEPTED 23 November 2022
PUBLISHED 20 December 2022

CITATION
Zhang X, Jiang J, Ma Z, Yang Y, Meng L, Xie F, Cui G and Yin X (2022) Cloning of *TaeRF1* gene from Caucasian clover and its functional analysis responding to low-temperature stress. *Front. Plant Sci.* 13:968965. doi: 10.3389/fpls.2022.968965

Cloning of *TaeRF1* gene from Caucasian clover and its functional analysis responding to low-temperature stress

Xiaomeng Zhang, Jingwen Jiang, Zewang Ma, Yupeng Yang, Lingdong Meng, Fuchun Xie, Guowen Cui* and Xiujie Yin*

College of Animal Science and Technology, Northeast Agricultural University, Harbin, China

Low temperature (LT) is an important threat to the normal growth of plants. In this study, based on the full-length transcriptome sequencing results, the cold resistance genes were cloned from Caucasian clover with strong cold resistance. We cloned the CDS of *TaeRF1*, which is 1311 bp in length and encodes 436 amino acids. The molecular weight of the protein is 48.97 kDa, which had no transmembrane structure, and its isoelectric point (pI) was 5.42. We predicted the structure of *TaeRF1* and found 29 phosphorylation sites. Subcellular localization showed that *TaeRF1* was localized and expressed in cell membrane and chloroplasts. The *TaeRF1* gene was induced by stress due to cold, salt, alkali and drought and its expression level was higher in roots and it was more sensitive to LT. Analysis of transgenic A. thaliana plants before and after LT treatment showed that the *TaeRF1* gene enhanced the removal of excess H_2O_2, and increased the activity of antioxidant enzymes, thus improving the plant's ability to resist stress. Additionally, the OE lines showed increased cold tolerance by upregulating the transcription level of cold-responsive genes (*CBF1*, *CBF2*, *COR15B*, *COR47*, *ICE1*, and *RD29A*). This study demonstrates that *TaeRF1* is actively involved in the responses of plants to LT stress. We also provide a theoretical basis for breeding and a potential mechanism underlying the responses of Caucasian clover to abiotic stress.

KEYWORDS

Caucasian clover, *TaeRF1*, overexpression, low-temperature stress, antioxidant enzyme

Introduction

The normal growth and development of plants are severely limited by various abiotic stresses in nature (Julia and Claudia, 2012), among which low temperature (LT) is an important threat to the normal growth of plants and adversely affects their survival and reproduction (Min et al., 2020). LT stress causes dehydration of plant cells and tissues,

changes in membrane lipids, production of reactive oxygen species (ROS), and degradation of some necessary macromolecules, such as polysaccharides, lipids, photosynthetic pigments, enzymes and nucleic acids (Kazemi-Shahandashti and Maali-Amiri, 2018), LT stress can decrease the rate of photosynthetic rate and the performance of antioxidant defense systems and can also cause imbalances in osmotic regulation and active oxygen metabolism (Andreas Theocharis et al., 2012). Plants have evolved different mechanisms to handle LT stress during the historical evolution process (Zhang et al, 2016; Zhang et al., 2021). Among them, the ICE1-CBF-COR signaling pathway related to cold acclimation in A.thaliana is considered to be the main pathway that endows plants with LT resistance. C-repeat/dehydration response element binding factors (CBF/DREB) are critical transcription factors that actively regulate the expression of downstream cold-responsive (COR) genes during cold stress (Stockinger et al., 1997). Cold-induced CBF genes specificity identification combined with the existed in the promoter of conservative C-repeat/dehydration response motif (CRT/DRE, CCGAC), thereby rapidly inducing the expression of CBF and stimulating the expression of cold response (COR) gene (Jaglo et al., 1998; Thomashow, 2010). COR encodes hydrophilic peptides that stabilize the plasma membrane and enhance cold resistance in plants (Gilmour et al., 1998). ICE1 (CBF expression inducer 1) is a major regulator of the expression of C-repeat binding factors (CBFs) and CORs, and plays a role in inducing CBFs expression through specific binding CBF promoters (CANNTG) at LT (Chinnusamy et al., 2003; Wang et al., 2022). Numerous genes are involved in plant cold resistance, but the identification of gene function to date is limited. More genes that affect cold resistance are still needed to guide the molecular breeding of cold-resistant crops, and using conventional breeding strategies to improve cold resistance is a challenging task.

Eukaryotic releasing factor 1 (eRF1) is a kind of translation terminator protein that combines termination codons and ribosomes, and protein synthesis is terminated when the translating ribosome encounters one of UAA, UAG or UGA (Brown et al., 2015; Kurilla et al., 2020). In eukaryotes, termination of mRNA translation is the final step in protein biosynthesis, and this process is controlled by three factors: polypeptide chain releasing factor eRF1 and eukaryotic releasing factor 3 (eRF3), and ribosomal cycling factor ABCE1 (Urakov et al., 2017). In previous studies, A. thaliana eRF1 proteins encoding genes (EeRF1-1, eRF1-2 and eRF1-3) have been functionally validated in mutant S. cerevisiae strains (Chapman and Brown, 2004). eRF1 is involved in the translation termination of specific cysteine glutamolysins in the endosperm of rice and plays a role in the conversion of glutamolysin mRNA into nascent polypeptides (Elakhdar et al., 2019), a process that leads to decreased glutaminolysis protein levels in rice (Ushijima et al., 2011). The expression of eRF1 is tightly controlled because its concentration determines the termination efficiency and frequency of translation read-through, and the protein recognizes termination signals and promotes the hydrolysis of peptidyl-tRNA ester bonds (Polina et al., 2013, Denis et al., 2018; Lashkevich et al., 2020). Histological analysis revealed a reduced cell height, ectopic lignification of some bast sieve cells and bundle-forming layer regions, enhanced lignification of interbundle fibers, and altered cell division in bundle-forming tufts, most of which were disorganized with enlarged laminae, demonstrating that eRF1 affects cell elongation and radial division in Arabidopsis (Anne Petsch et al., 2005). The role of eRF1 in other plants has yet to be investigated.

Caucasian clover *(Trifolium ambiguum* M. Bieb.) is a perennial leguminous plant with a long crown, relatively low growth and multiple branches with deep roots (Zhang et al., 2019). It is also the only perennial leguminous clover species with underground root tillers and strong clonal growth *via* rhizomes (Taylar and Smith, 1997). This species originates in the cold climates of the Russian Caucasus Mountains, eastern Turkey and northern Iran (Barneby et al., 1965) and has strong cold resistance, flooding resistance, drought resistance and grazing tolerance (Brummer and Moore, 2000). Our research group previously used RNA-Seq and PacBio high-throughput sequencing technology to sequence the Caucasian clover transcriptome (Yin et al., 2020). In this study, we analyzed the expression pattern of the *TaeRF1* gene in Caucasian clover for the first time, and speculated that it unctions under some abiotic stresses. The *TaeRF1* gene in Caucasian clover was herein cloned and bioinformatically analyzed. The trans-*TaeRF1* gene was then inserted into *A. thaliana via* an Agrobacterium-mediated method, and physiological indicators under LT stress were measured to assess gene function. This study revealed the genes that confer the LT tolerance of Caucasian clover, thereby providing a theoretical basis and technical support for the further selection and breeding of excellent forage grasses and laying the foundation for the molecular breeding of Caucasian clover.

Materials and methods

Plant materials and treatments

Caucasian clover (*Trifolium ambiguum* Bieb.) was provided by the College of Animal Science and Technology at Northeastern Agricultural University, while Ben's tobacco (*Nicotiana benthamiana*) and Colombian wild-type (WT) Arabidopsis were obtained from Wuhan Boyuan Biotechnology Co. Caucasian clover was cultured at 26°C under a 12 h photoperiod, and seedlings aged 28 days (d) were subjected to 4°C, 150 mmol/L NaCl, 150 mmol/L $NaHCO_3$ and 15% PEG-6000. The roots, stems and leaves of each stressed Caucasian clover plant were harvested after 0 (CK), 3, 6, 12, 24 and 48 h of treatment. Three biological replicates were performed per treatment.

Cloning and expression analysis of the *TaeRF1* gene

The total RNA was extracted from Caucasian clover leaves using an Ultrapure RNA Kit (ComWin Biotech Corporation, Beijing, China). The cDNA template for reverse transcription PCR was synthesized using HiScript II Reverse Transcriptase (Vazyme, Nanjing, China). The primers used for cloning were designed by Primer 5 for cloning *TaeRF1* based on the results of transcriptome sequencing (Table S1). PCR amplification was performed using 2×Phanta® Max Master Mix (Vazyme Biotech Co.) from Caucasian clover cDNA as a template. The amplified PCR products were detected by 1% agarose gel electrophoresis, and the target gene fragment was recovered by a Vazyme FastPure Gel DNA Extraction Mini Kit. The obtained 1311 bp full-length fragment was cloned into a 5minTM TA/Blunt-Zero Cloning vector (Vazyme Biotech Co.) and then subjected to DNA sequencing. Real-time fluorescence quantification was performed with cDNA as the template (Table S1). The qRT-PCR analysis was performed using ChanQ Universal SYBR qPCR Master Mix Kit, and relative gene expression levels were calculated by the $2^{-\Delta\Delta}$Ct method. Using AtActin as the internal reference, specific primers (Table S1) were used for qPCR analysis of key genes responding to LT stress (*AtCBF1*, *AtCBF2*, *AtCOR15B*, *AtICE1*, *AtRD29A* and *AtCOR47*).

Bioinformatic analysis of the *TaeRF1* sequence

BLAST was used to search for homologous sequences of *TaeRF1*. DNAMAN was used for multiple alignment of amino acid sequences. To investigate the evolutionary relationships between *TaeRF1* in Caucasian clover and other species, phylogenetic analysis was performed with MEGA 5 based on the maximum likelihood method. The physicochemical properties (including molecular weight, pI) and instability coefficient) of the *TaeRF1* amino acid sequence were analyzed using ProtParam software. The transmembrane structural domain of *TaeRF1* was predicted using the transmembrane prediction server TMHM, and its secondary structure was analyzed using Predict Protein online software. Protein tertiary structures were predicted using the SWISS-MODEL online site. Protein structural domain analysis of the *TaeRF1* gene of Caucasian clover was performed using the MEME online website. *TaeRF1* protein phosphorylation sites were predicted using the NetPhos 3.1 website. The Protscale online website was used to analyze the hydrophilicity of the *TaeRF1* protein, and *TaeRF1* signaling peptides were predicted using Signal P 4.1. Subcellular localization analysis of the *TaeRF1* amino acid sequence was performed using the Predict Protein online website.

Construction of vectors

The plasmid of DH5α bacterial solution with correct sequencing was used as the template, and the overexpression and transient expression primers (Table S1) containing protective bases and enzyme cutting sites were used for PCR amplification, and the inserted fragment was obtained after gel recovery. pBWA(V)BS-ccdB plasmids were linearized by double digestion with Bsa I and Eco31 I. Overexpression expression vector were obtained by recombination of the inserted fragments and vectors. pCAMBIA1300-35S-sGFP plasmids were linearized by double digestion with BamHI and SacI. And instantaneous expression vectors were obtained by recombination of the respective inserted fragments and vector. The vectors were transferred into Escherichia coli DH5α for culture, and the single colony was selected for PCR detection and sequence alignment to determine the correct. The plasmid with correct sequencing results was transformed into Agrobacterium EHA105 by freeze-thaw method, and then screened on the double-resistant YEB medium containing kanamycin and rifampicin. After 60 h culture, the single colony was selected and verified by PCR to determine the correct.

Subcellular localization analysis of *TaeRF1*

The tobacco seeds were seeded in a mixture of vermiculite and nutrient soil. After the seeds germinated, each seedling was transplanted to a separate pot and watered daily for 1 month. The agrobacterium solution containing the transient expression vector was taken out of the -80°C, and the YEB liquid medium containing Kan and Lif was shaken to turbidity. The bacterial solution was centrifuged, discarded the supernatant and cleaned twice with a working solution (0.5 mol/L MES, 100 mmol/L acetyleugenone, 1 mol/L MgCl). The concentration was measured and diluted to OD600 = 0.2, then injected into the back of Nicotiana benthamiana tobacco leaves (avoiding the main vein) with a 1 mL syringe. The infected leaf tissue was obtained under dark conditions for 48 h, and the cellular localization of *TaeRF1*: GFP fusion protein was determined by laser microscope.

Generation of transgenic Arabidopsis plants overexpressing *TaeRF1*

The floral dip method was employed to transfer the *TaeRF1* gene into Colombia-0. After harvesting the seeds, all seeds were grown on MS medium containing glyphosate. The surviving plants were transplanted into the soil for further cultivation. Glyphosate was sprayed again for screening and PCR detection of transgenic plants, and T0 Arabidopsis plants were obtained. Three transgenic

lines were selected from the successfully identified eleven transgenic lines for planting and seed harvesting. T1-transformed *TaeRF1* overexpressed Arabidopsis plants were obtained after seed germination screening and PCR detection.

Phenotypic identification

WT and transgenic Arabidopsis seeds were soaked in 75% ethanol for 1 min, sterilized with 10% NaClO for 10 min, and rinsed with sterile water 6 times. They were then germinated on 1/2 MS media at 23°C and 4°C. Changes in germination were measured. The 1/2 solid MS medium is composed of MS powder (2.22 g/L), sucrose (15 g/L), and agar powder (4.25 g/L) and the pH is 5.8. The protrusion of the radicle was considered the standard for the germination of seeds. After germination, the plants were moved to the incubator, and the root lengths of the 14d seedlings were measured. The petri dishes were stored vertically. To investigate the cold tolerance of transgenic lines, the seedlings were transplanted into soil and vermiculite, and the 30d plants were subjected to LT stress at 4°C. After treatment, the expression analysis of the cold-responsive genes was analyzed in leaf samples. The experiments were repeated three times.

Physiological measurements

WT and transgenic Arabidopsis thaliana were cultured for different times (0, 24 and 72 h) under normal conditions and LT conditions, and the physiological indexes of plant leaves were measured. For the enzyme activity assays, SOD, POD and CAT kit (Keming, Suzhou, China) were used to measure the activity of superoxide dismutase (SOD), catalase (CAT) and peroxidase (POD). The index measurement method and calculation method refer to the manual. Malondialdehyde (MDA) content was determined by the thiobarbituric acid method, and proline (Pro) content was determined by the acid ninhydrin method.

Statistical analyses

Data statistics and chart making are through Excel and Origin. SPSS software and Duncan multiple comparisons were used to analyze the differences.

Results

Cloning and phylogenetic analysis of the *TaeRF1*

Total RNA of Caucasian clover was extracted, the quality of RNA was detected by Agarose gel electrophoresis (1% Agarose), and it showed bright and clear 18S and 28S bands (Figure S1A). The RNA was reversely transcribed into cDNA, and the quality was verified by PCR using reference primers (Table S1, Figure S1B). Specific primers were designed to clone *TaeRF1* CDS based on transcriptome data (Table S1). RT-PCR was used to amplify CDS of *TaeRF1* (Figure S1C), the amplified product was cloned into pCE2 TA/Blunt Zero vector and transferred to DH5α. Sequencing results showed that the CDS length of *TaeRF1* was 1311 bp, encoding 436 amino acids, and the nucleotide sequence and amino acid series were obtained (Table S2). The amino acid sequence of *TaeRF1* was uploaded to SMART website for domain prediction, and the results showed that *TaeRF1* contained an eRF1 domain between residues 4 and 140 (Figure 1A).

The *TaeRF1* protein sequence was subjected to a BLAST search using the NCBI protein website, and the results revealed high similarity to other eRF proteins. The amino acid sequence of the protein from Caucasian clover was aligned to those of its homologs in other organisms, and the phylogenetic tree was constructed by MEGA 5 (Figure 1B). (*Medicago truncatula* RHN52517.1, XP 013452837.1), peanut (*Arachis Hypogaea* RYR56863.1), soybean (*Glycine Max* XP 006587430.1), wild soybean (*Glycine Soja* RZB62078.1, KRH38906.1), Arachis ipaensis (XP 016203317.1, XP 016203315.1), pinto bean (*Spatholobus suberectus* TKY44911.1), kidney bean (*Phaseolus vulgaris* XP 007152574.1), cowpea (*Vigna angularis* XP 017440033.1), *Mucuna pruriens* (*Mucuna pruriens* RDX60945.1), lupin (*Lupinus angustifolius* XP 019436781.1), and chickpea (*Cicer arietinum* XP 012567217.1), with similarities of 97.94%, 95.41%, 96.09%, 96.55%, 95.64%, 95.63%, 95.17%, 94.95%, 94.94%, 94.02% and 98.62%, respectively. The amino acid sequences were compared by DNAMAN and we label the eRF domain in the graph (Figure 1C). The *TaeRF1* gene was highly homologous to those from chickpea and *Medicago truncatula*, suggesting that the three genes are closely evolutionarily related and have similar functions.

Physicochemical properties of the *TaeRF1* protein

The amino acid sequence of *TaeRF1* was analyzed by ProtParam. *TaeRF1* was shown to have a molecular formula of C_{2172} H_{3411} N_{593} O_{672} S_{12}, a molecular weight of 48.97 kDa, and a theoretical pI of 5.42. The *TaeRF1* protein was mostly comprised of Leu residues (9.2%), and Trp and Cys residues accounted for the lowest percentage (both 0.7%). The protein contained 62 negatively charged residues and 53 positively charged residues. The protein was considered stable (stability coefficient 29.55), and the lipid index was 81.40.

To further analyze the *TaeRF1* protein, PredictProtein was used to predict its structure. The secondary structure of the

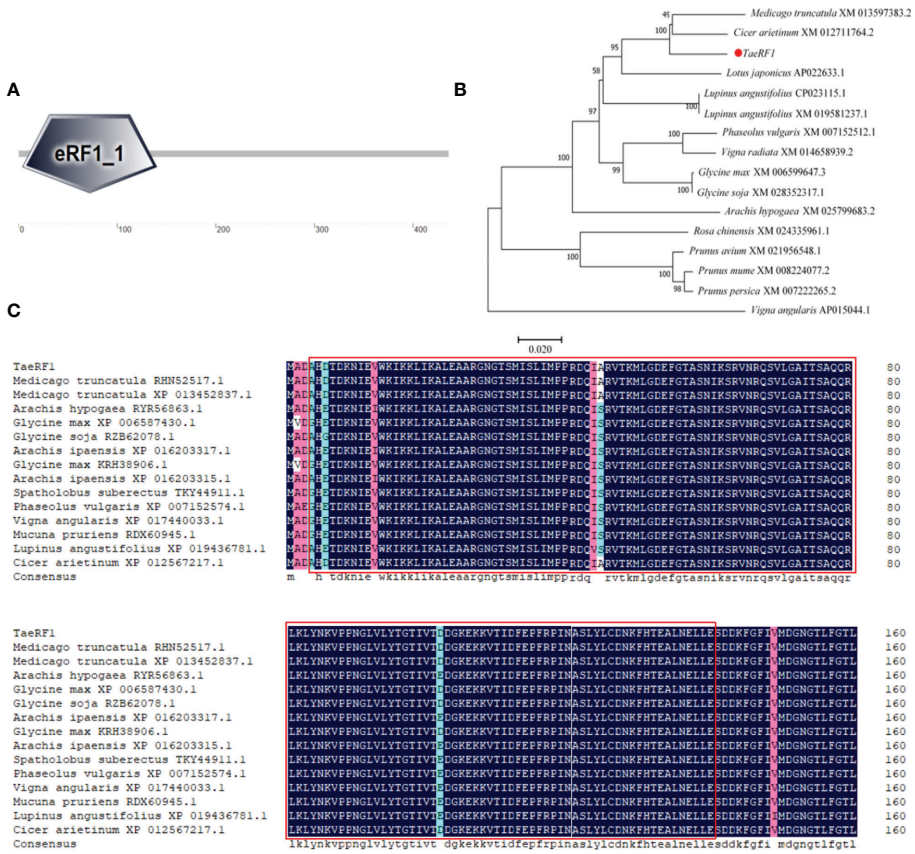

FIGURE 1
Cloning and multiple sequence alignment of *TaeRF1* homologous proteins. **(A)** SMART domain analysis of the *TaeRF1* gene. **(B)** Phylogenetic analysis of the *TaeRF1* gene in Caucasian clover. **(C)** Multiple sequence alignment of the eRF proteins. The color-coding indicates sequence similarity, with blue indicating the highest sequence similarity, pink indicating lower similarity, and cyan indicating the lowest similarity. The predicted conserved motifs of the eRF proteins are labeled as red square.

TaeRF1 protein was shown to comprise α-helices, β-extended strands and an irregular coil (Figure S2A). Among these features, irregular coil accounted for 46.56% of the protein, while α-helices and β-extended strands accounted for 35.55% and 17.89%, respectively. Swiss model predicted the tertiary structure of *TaeRF1* protein (Figure S2B).

The phosphorylation sites of the *TaeRF1* protein were predicted by NetPhos 3.1 website, revealing a total of 29 phosphorylation sites (Figure S3A), including 6 tyrosine phosphorylation sites, 7 threonine phosphorylation sites and 16 serine phosphorylation sites. The Protscale website was used to analyze the hydrophilicity and hydrophobicity of the *TaeRF1* protein (Figure S3B). The results revealed that most of the amino acids had negative values, and many negative amino acids have strong hydrophilic properties. Therefore, it can be inferred that *TaeRF1* is a hydrophilic protein. The trans-membrane domain of *TaeRF1* protein was predicted (S3C) by TMHMM online website, and the results showed that *TaeRF1* protein did not contain transmembrane domain (Figure S3C).

Signal P 4.1 was used to predict the signaling peptides of *TaeRF1*, yielding Max. Y and mean S values of 0.061 and 0.170, respectively. The fact that both of these values were less than 0.5 indicated that the *TaeRF1* protein had no signaling peptide cleavage sites and thus contained no signaling peptide sequences (Figure S3D).

Subcellular localization analysis

The localization of the protein encoded by the *TaeRF1* gene was therefore analyzed using the Predict Protein online website. The results suggested localization in the cytoplasm. To further assess the subcellular localization of *TaeRF1*, pCAMBIA1300-35S-sGFP plasmids were digested with BamHI and SacI, and the vectors were linearized. The target fragment was amplified with transient-expression primers, and the tobacco transient expression vector pCAMBIA1300-35S-sGFP-*TaeRF1* was obtained after recombination. The resulting tobacco transient expression vector

construct was transformed into Agrobacterium EHA105, and the transformed cells were injected into tobacco. The transient expression of *TaeRF1* in *Nicotiana benthamiana* was observed by confocal laser microscopy, revealing expression in the cell membrane and chloroplasts (Figure 2).

Analysis of the *TaeRF1* gene expression pattern

QRT-PCR was used to detect the relative expression of the *TaeRF1* in roots, stems and leaves of Caucasian clover at different time points under LT, salt, alkaline and drought stress (Figure 3). The results revealed altered expression levels of *TaeRF1* changed in response to different stress treatments and at different time points. The variation in gene expression under the four stresses, salt (NaCl), alkalinity ($NaHCO_3$), LT (4°C) and drought (15% PEG-6000), indicated that the gene responded to these four stresses.

Under LT stress, the expression level of *TaeRF1* gene was significantly increased, and the expression level was the lowest at 3 h and the highest at 48 h ($p< 0.05$). Stem expression of the *TaeRF1* gene was not obvious; the expression level was the highest at 6 h and the lowest at 12 h under stress, and the expression levels were significantly higher at these time points than at 0 h ($p< 0.05$). The expression level of the *TaeRF1* gene in leaves fluctuated, with the lowest expression observed at 3 h and the highest expression at 24 h ($p< 0.05$).

The expression level of *TaeRF1* gene in roots under 150 mmol/L NaCl stress increased firstly and then decreased, and reached the highest at 24 h ($p< 0.05$). The expression level of *TaeRF1* in the stems of the treated plants was significantly lower than that in the stems of CK plants ($p< 0.05$). The expression level of the *TaeRF1* gene in leaves was affected by salt stress: the highest value was observed at 6 h under stress and the lowest at 48 h, and the expression levels at 12 and 48 h were lower than that at 0 h ($p< 0.05$).

The expression of the *TaeRF1* gene in roots was affected under alkaline stress, initially exhibiting a decreasing trend, followed by an increase and then another decrease. The highest expression levels were observed at 3 h, while the lowest levels were observed at 48 h, and the levels were lower at 24 and 48 h than at 0 h. The expression levels at all other time points were higher than at 0 h ($p< 0.05$). The expression of *TaeRF1* in leaves was more obviously altered, initially showing an increasing trend, followed by a decrease. The highest expression level was observed at 6 h under stress, while the lowest levels were observed at 48 h under stress. The expression levels at 24 h and 48 h points were lower than that at 0 h. The expression levels at 24 h did not significantly differ from that at 0 h, while the levels at all other time points did significantly differ from that at 0 h ($p< 0.05$).

The expression of *TaeRF1* gene in the root under 15% PEG-6000 simulated drought stress was significantly higher than that in CK group at 6 h, and the lowest expression level was at 12 h

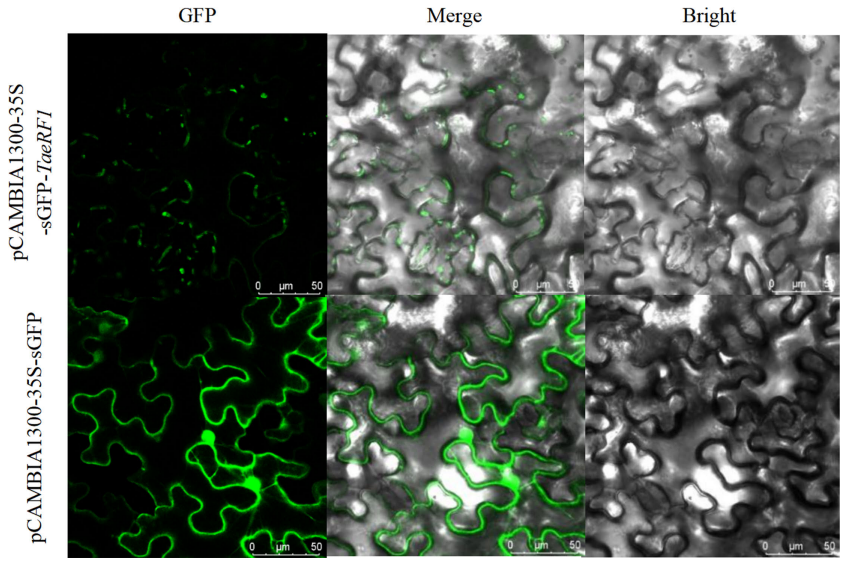

FIGURE 2
Subcellular localization of *TaeRF1*. Bright: bright-field; GFP: GFP Green fluorescent signal; Merged: merged images. Scale bar, 50 mm.

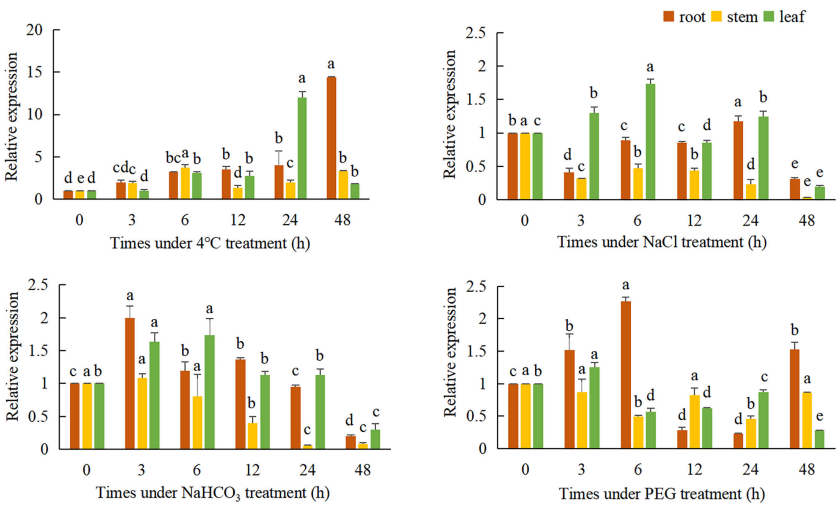

FIGURE 3
Expression of *TaeRF1* at various stress levels. Different characters on the error line represent a difference at a level of P<0.05 between the treatments. Different letters means significant difference at the 0.05 level.

and 24 h ($p< 0.05$). The expression of the *TaeRF1* gene in stems and leaves was not clear and showed a fluctuating trend.

Generation and selection of *TaeRF1*-overexpressing transgenic A. thaliana plant lines

pBWA(V)BS-ccdB plasmids were linearized by double digestion with Bsa I and Eco31 I. The target gene was linked to the vector and introduced into agrobacterium tumefaciens receptive state. The transformed recombinant plasmid was identified by bacterial liquid PCR. A fragment of approximately 1300 bp was obtained, which was basically the same size as the *TaeRF1* gene (Figure S4A). Arabidopsis flowers were infected three times by Agrobacterium tumefaciens containing the target gene (Figure S4B). The mature seeds were collected and placed on petri dishes containing herbicides for culture. The surviving plants were transplanted into the soil for further culture, and herbicide was sprayed again for screening (Figure S4C). Eleven transgenic lines overexpressing *TaeRF1* were obtained, among which OE-1, OE-2 and OE-3 were significantly expressed (Figure S4D). Positive Arabidopsis plants were transplanted into soil for further culture until seeds were harvested (Figure S4E).

Overexpression of *TaeRF1* in Arabidopsis improves tolerance to LT stress

The germination experiment can explore the adaptation of *TaeRF1* to LT stress. WT and transgenic Arabidopsis seeds were planted on MS medium, and the germination rates was recorded at 23°C and 4°C. Under normal temperature (23°C), the germination rates of the transgenic seeds were similar to that of WT seeds. However, after moving to normal temperature (23°C) after LT (4°C) stress, seed germination of both the WT and the transgenic lines was inhibited (Figure 4A). The germination rates of transgenic seeds at 24 and 72 h were significantly higher than that of the WT (Figures 4B, C), and the root length and fresh weight after LT treatment were measured. At 23°C, the root length of transgenic seedlings was not much different from WT. Root length increased slowly at 4°C, but the difference was not significant, indicating that *TaeRF1* overexpression had a less obvious effect on root growth under low-temperature stress (Figures 4D, E). We measured the fresh weight and found that under LT treatment, the fresh weight of *TaeRF1*-overexpressing plants was significantly higher than that of WT, indicating that LT seriously affected the biomass of the plants (Figure 4F). Therefore, *TaeRF1* overexpression enhanced LT tolerance in transgenic seedlings.

Functional verification of *TaeRF1*-overexpressing A. thaliana in response to LT stress

We performed a LT stress (4°C) assay on 30 d plants of WT and transgenic plants to further characterize the phenotype of the transgenic lines. After 1 day of cold treatment at 4°C, the leaves of the plants turned dark green. After 3 d of being exposed to 4°C, transgenic plants showed mild wilting but grew well, while the WT plants showed obvious wilting and slow growth (Figure 5A). The effects of LT on plants can be further understood by

10.3389/fpls.2022.968965

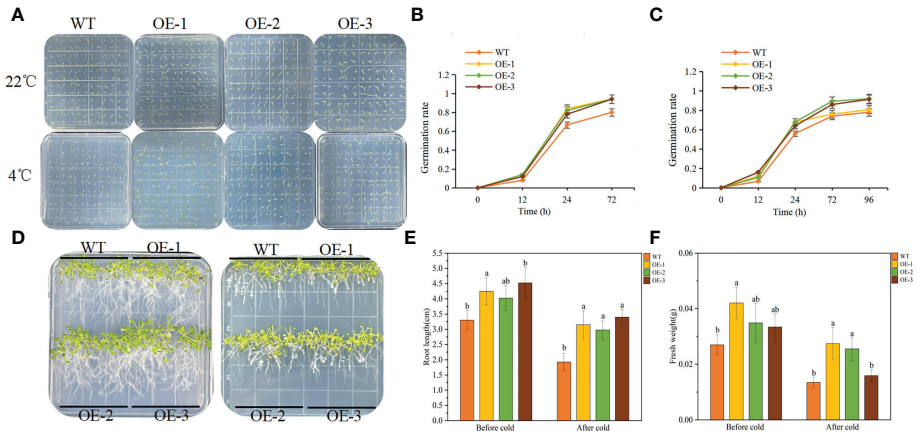

FIGURE 4
Overexpression of *TaeRF1* in Arabidopsis improved cold tolerance. Seed germination phenotype **(A)** and germination rate **(B-C)** of transgenic Arabidopsis lines overexpressing *TaeRF1* under LT stress. After 3 d of vernalization, one group was incubated at 22°C for 3 d (D left), and the other group was incubated at 4°C for 7 d (D right) and then moved to 22°C for 3 d. After that, the petri dishes were placed vertically. The root lengths and fresh weights of the 14-d-old seedlings were measured **(E–F)**. Different lowercase letters indicate that different plants showed a significant difference under the same stress ($p< 0.05$).

measuring plant physiological indexes, the SOD, POD, CAT, MDA and Pro contents in plants were measured. There was no significant difference between transgenic and WT lines under normal conditions, but almost all plants were affected to some extent under LT stress condition.

Under LT stress, the SOD content in WT and transgenic plants overexpressing *TaeRF1* tended to be upregulated (Figure 5B). After 3 d of stress, the SOD content in transgenic plants was higher than that in the WT plants, and the difference was significant ($p< 0.05$). After 3 d of stress, the POD content in transgenic plants overexpressing *TaeRF1* was higher than that in WT plants (Figure 5C). The CAT content in transgenic and WT plants first increased and then decreased (Figure 5D), but changes in the CAT content in transgenic plants were not significant ($p< 0.05$). Under LT stress, the MDA content of WT increased compared with CK group (P< 0.05). The content of MDA in OE-2 increased continuously, the content of MDA in CK group was the lowest, and the content of MDA in OE-2 group was the highest after 3 d of stress treatment (P< 0.05). MDA content of OE-1 and OE-3 decreased firstly and then increased ($p< 0.05$). Under the same stress time, the content of MDA in CK group was the highest (Figure 5E). Under LT stress, Pro content of Arabidopsis and WT showed a trend of first increasing and then decreasing (Figure 5F). After LT stress for 3 d, the Pro content of transgenic plants was significantly higher ($p< 0.05$).

TaeRF1 activates the expression of LT stress-responsive genes

We further analyzed the expression of LT responsive genes in Arabidopsis by qRT-PCR, such as *AtCBF1* and *AtCBF2* and their associated genes, including *AtCOR15B*, *AtICE1*, *AtCOR47* and *AtRD29A* (Table S1). The results showed that under normal conditions, there was no significant difference in the expression levels of 6 LT response genes between WT and overexpressed plants. After LT treatment, the expression level of six genes in overexpressed lines was significantly higher than that of WT, indicating that *TaeRF1* positively regulates the expression of corresponding genes in LT and can improve the cold tolerance of transgenic Arabidopsis (Figures 6A–F).

Discussion

As a naturally stress-resistant species, the Caucasian clover represents an important resource for studying the resistance mechanisms and forage breeding. In this study, eRF1 gene was successfully cloned from the third-generation full-length transcriptome data of Caucasian clover. After cloning CDS, the sequencing results were consistent with the predicted results, and the gene was named TaeRF1. The full-length CDS of *TaeRF1* was determined to be 1311 bp, encoding 436 amino acids. SMART domain analysis showed that the *TaeRF1* gene has an eRF1 domain, which showed that the *TaeRF1*gene belongs to the eRF1 family. Phylogenetic tree analysis and multiple sequence alignment between the gene in Caucasian clover and homologs in other organisms showed that *TaeRF1* is highly homologous to eRF1 in *M. truncatula* and chickpea, which are also in the legume family. Analysis of the *TaeRF1* gene expression pattern showed that *TaeRF1* participates in the responses to several stresses such as cold, salinity, alkalinity, and drought. The roots of plants subjected to LT stress exhibited

10.3389/fpls.2022.968965

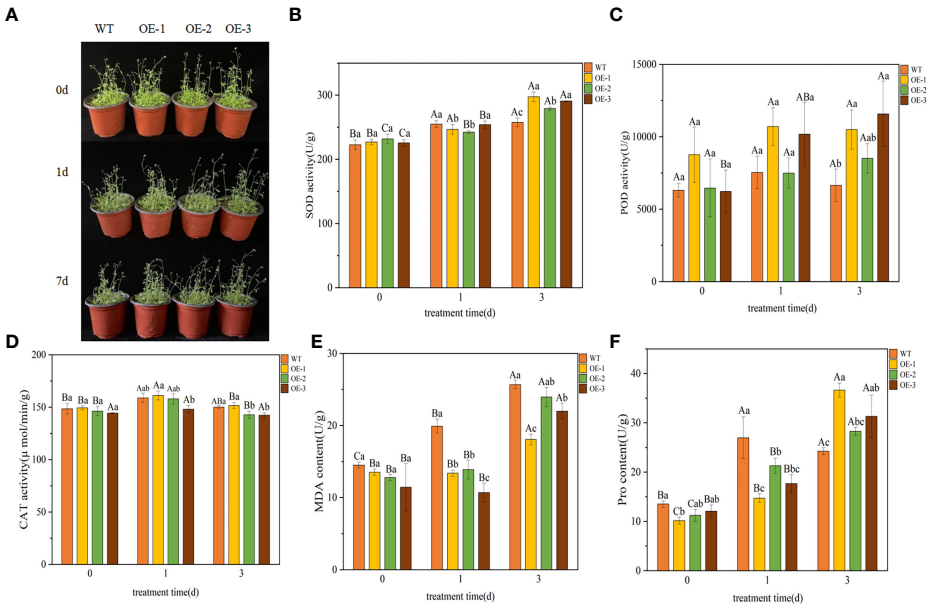

FIGURE 5
Functional verification of *TaeRF1*-overexpressing Arabidopsis under LT stress. Comparisons of phenotypes **(A)** and SOD, POD, CAT, MDA and Pro activities **(B-F)** between WT and transgenic *A. thaliana* under LT stress. The data are shown as the mean ± SD of three biological replicates. Different capital letters indicate that the same plant showed a significant difference on different stress days ($p < 0.05$); different lowercase letters indicate that different plants showed a significant difference under the same stress ($p < 0.05$).

significantly increased *TaeRF1* gene expression, indicating that this gene may be involved in the response of plants to LT stress and that *TaeRF1* may perform functions in the root.

LT can prohibit plant growth, development, survival and productivity and is the most severe stress that limits normal plant growth (Mishra et al., 2018). In response to complex environmental changes, plants have evolved different signaling mechanisms to cope with stress. LT causes the accumulation of ROS, such as singlet oxygen, hydrogen peroxide and superoxide radicals, which can lead to cellular oxidative stress, a major factor

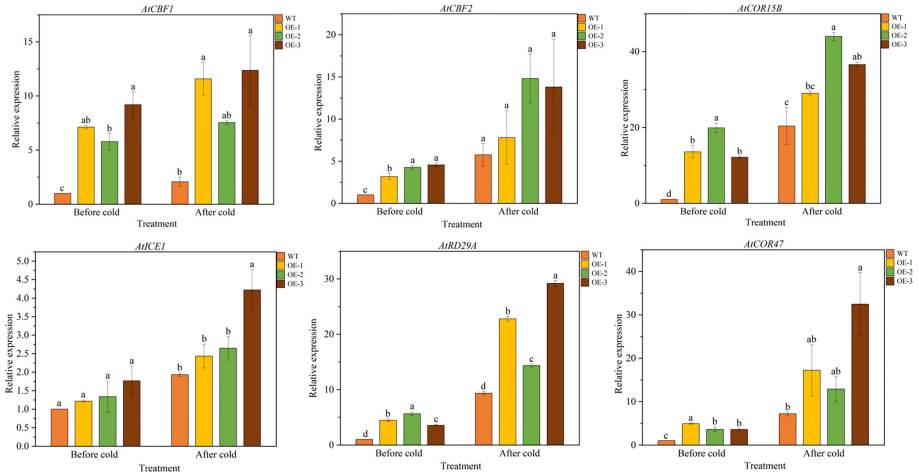

FIGURE 6
Expression patterns of cold-responsive genes in WT and *TaeRF1*-overexpressing Arabidopsis lines under cold stress treatment. Expression profiles of cold-responsive genes, including *AtCBF1*, *AtCBF2*, *AtCOR15B*, *AtICE1*, *AtRD29A* and *AtCOR47*. Different letters means significant difference at the 0.05 level.

underlying the damage caused by LT (Gómez et al., 2019). To scavenge ROS and reduce oxidative damage, plants have developed an effective defense system consisting of several antioxidant enzymes, such as catalase, ascorbate peroxidase, superoxide dismutase and peroxidase (Bai, 2019). Usually, upon the exposure of plants to abiotic stress, tolerant cells activate enzymatic antioxidant systems to remove ROS and protect the cells (Yu, 2020). At 48 h of LT stress, the relative expression of the *TaeRF1* gene significantly peaked in the roots and was 14.38-fold higher than that in the control plants, and its expression tended to increase. At 24 h of stress, the relative expression was more pronounced in the leaves, indicating that this gene can respond to LT stress. Caucasian clover grows in the extremely cold Caucasus Mountain region and therefore has a certain degree of cold tolerance and can overwinter. The high *TaeRF1* gene expression in the roots indicates that the roots play a positive role in resisting damage caused by LT. Moreover, ROS may be produced in leaf cells over periods of prolonged stress, resulting in increases in the levels of various peroxidases to eliminate ROS, thus increasing the cold tolerance of Caucasian clover.

Under adverse stress conditions, most plants accumulate large amounts of ROS, which damage the plant membrane system (Hu et al., 2010; Feng et al., 2014; Peng et al., 2019). The balance of intracellular ROS production and clearance can protect plants from stress damage. In plant cells, the SOD enzyme can eliminate ROS, functioning to eliminate and convert O_2^- into H_2O_2 to limit plant cell damage (Wang, S. Q. et al., 2019; Lin et al., 2019). When WT plants were stressed for 1 day, SOD was used to eliminate O_2^- and thereby prevent the excess accumulation of ROS. However, the SOD content was reduced after 3 d of stress in the WT plants, and the SOD activity decreased, while the SOD content in the transgenic plants overexpressing *TaeRF1* continued to increase, indicating that ROS was eliminated continuously under stress conditions and that plant cell damage was mitigated (Wang, Y. et al., 2019). At 3 d of LT stress, the SOD content was the highest in the OE-1 plants, and the SOD contents in the OE-1, OE-2 and OE-3 plants were significantly different from that in the WT plants ($p< 0.05$). In conclusion, the overexpression of *TaeRF1* may affect the SOD content under stress, thereby reducing plant damage; the *TaeRF1* gene can increase the SOD content under conditions of LT stress. These results also support the hypothesis that *TaeRF1* enhances stress tolerance by promoting the production of plant protective enzymes (Li et al., 2008).

Because excessive H_2O_2 is harmful to plant cells, POD is also indispensable for the protective enzyme system in plants, as it can degrade the generated H_2O_2 to limit damage to the membrane system (Sun et al., 2019, Surisa Phornvillay et al., 2019; Wang, M. et al., 2019). The result demonstrates that LT stress increased the POD content in the transgenic plants overexpressing *TaeRF1* to a certain extent. Compared with the WT plants, the transgenic plants had some certain resistance to LT stress. The *TaeRF1* gene may have a certain impact on the POD content under LT stress (Hao et al., 2018). Nearly all aerobic cells contain CAT, which functions similarly to POD, as it can degrade excessive H_2O_2 in plant tissues into oxygen and water, thereby reducing ROS accumulation in plant tissues (Han et al., 2020; Sun et al., 2020) and maintaining the integrity of the plant cell structure. To protect the plant cell membrane system, the browning of plant tissues and the aging of cells are delayed (Zhang et al., 2017). Under LT stress, the CAT contents in the WT and transgenic plants first increased and then decreased. After 1 day of stress, the contents in the OE-1 and OE-2 plants were comparable to that in the OE-3 plants, while the contents in the WT, OE-1, OE-2 and OE-3 plants were significantly different after 3 d of stress ($P<0.05$). Therefore, the enhanced antioxidant capacity of overexpressing *TaeRF1* in Arabidopsis can alleviate the damage of plants under LT stress.

LT can damage plants in many ways. The MDA content can reflect the degree of damage to the cell membrane, which is the first structure that is destroyed upon exposure to LT. MDA is a product of lipid peroxidation caused by ROS, which can inhibit the activity of protective enzymes and thus aggravate membrane lipid peroxidation (Liu et al., 2014; Sha et al., 2011; Wu et al., 2012). Studies have shown that the MDA content reflects the degree of damage to plant tissues under stress (Ning et al., 2021). The lower MDA content in transgenic plants under LT stress indicated less membrane damage than WT. The overexpression of TaeRF1 has a protective membrane integrity under LT stress. The amino acid Pro exists in a free state in plants. Under stress conditions such as drought, LT and salinity, Pro accumulates in large quantities in most plants. In addition to being an osmotic regulatory substance in the plant cytoplasm, Pro can stabilize the structures of biological macromolecules, reduce the acidity of plant cells and remove toxic ammonia (Polturak et al., 2018; Yan et al., 2019). In addition, Pro can regulate the ROS balance in plants and ensure balance in the cytoplasm. The membrane integrity and cold tolerance of plants are important, and Pro is a key factor underlying cold tolerance because it regulates osmotic pressure (Savoi et al., 2016; Zhao et al., 2019). Therefore, changes in Pro metabolism play an important role in improving the LT adaptability of plants. The Pro content in plants reflects their stress tolerance to a certain extent, and stronger LT tolerance is correlated with higher Pro accumulation (Wang, 2019). Under LT stress, the Pro content in WT plants was increased more than that of *TaeRF1*-overexpressing plants after 1 day of stress and decreased after 3 d of stress, while the Pro content in the transgenic plants continued to increase under stress, and the Pro contents of OE-1, OE-2 and OE-3 plants were significantly different from those in the WT plants after 3 d of stress ($P< 0.05$). These results indicate that the *TaeRF1* gene may resist the adverse effects of LT stress by increasing the Pro content.

The most classical plant response to cold stress is the ICE-CBF-COR regulatory pathway (Chinnusamy et al., 2007; Hwarari et al., 2022). This study quantitatively analyzed the expression levels of the CBF-dependent pathway, and their downstream cold stress responsive genes *AtCOR15B* and *AtCOR47*. We found that *TaeRF1* upregulates overexpressed Arabidopsis cold response genes. These experimental results were consistent with current expectations and similar to those of other studies (Dong et al., 2021; Yin et al., 2021). Therefore, we predicted that TaeRF1 likely enhances cold tolerance *via* the CBF-dependent pathway in Arabidopsis.

In this study, we cloned the *TaeRF1* gene from Caucasian clover, performed bioinformatics analyses to understand the genetic information, and analyzed the evolutionary relationships among multiple species. *TaeRF1* was transferred into Colombian Arabidopsis, and transgenic Arabidopsis plants overexpressing *TaeRF1* were successfully obtained. Physiological indicators were measured to assess the possible functions of the *TaeRF1* gene, and we speculated that *TaeRF1* was highly responsive to cold stress. The overexpression of *TaeRF1* in response to abiotic stress could regulate antioxidant enzyme activity in plants. In subsequent experiments, the gene can be transformed into Caucasian clover to obtain overexpression plants, and measurements can be performed to better understand its functions.

Conclusions

In this study, the *TaeRF1* gene was screened and cloned based on the full-length transcriptome sequencing results of third-generation Caucasian clover plants. The expression of *TaeRF1* was significantly induced in response to LT stress. Overexpression of *TaeRF1* significantly enhanced LT resistance, and could better reduce the accumulation of ROS under cold stress in Arabidopsis thaliana. *TaeRF1* mediates cold signal transduction by increasing the transcription level of stress-responsive genes, thereby improving transgenic plant tolerance to cold stress. These results indicate that *TaeRF1* plays an active regulatory role in the responses of plants to LT stress. At the same time, *TaMYC2* in Caucasian clover can also increase the activity of antioxidant enzymes in plants, and increase the expression of ROS scavenging related genes and stress response genes under LT and drought stress, thereby enhancing the response ability of transgenic plants to stress (Zhao et al., 2022). Taken together, these findings provide further insights into the properties of *TaeRF1* protein and how it protects plants at low temperatures, and provide references for clover breeding.

Data availability statement

The datasets presented in this study can be found in online repositories. The nucleotide sequence TaeRF1 can be found at GenBank with the accession number OQ000837. Further inquiries should be directed to the corresponding author.

Author contributions

GC and XY conceived and designed the experiments; XZ and JJ performed the experiments; YY, ZM, LM, and FX analyzed the data; and XZ and JJ wrote the manuscript. All authors contributed to the article and approved the submitted version.

Funding

This work was supported by the Natural Science Foundation of Heilongjiang Province of China (LH2021C040), the National Natural Science Foundation of China (31802120) and Academic Backbone Fund Project of Northeast Agricultural University. The funders did not design the experiment or draft and revise the manuscript.

Conflict of interest

The authors declare that the research was conducted in the absence of any commercial or financial relationships that could be construed as a potential conflict of interest.

Publisher's note

Supplementary material

The Supplementary Material for this article can be found online at: https://www.frontiersin.org/articles/10.3389/fpls.2022.968965/full#supplementary-material

References

Bai, J. (2019). *Physiological response and DNA methylation of brassica napus under low temperature stress* (Gansu Agricultural University).

Barneby, R. C., Davis, P. H., Edmondson, J. R., Hill, R. R., and Tan, K. (1965). Flora of Turkey and the East Aegean islands. *Q. Rev. Biol.* 35 (1), 103–104. doi: 10.2307/2806060

Brown, A., Shao, S., Murray, J., Hegde, R. S., and Ramakrishnan, V. (2015). Structural basis for stop codon recognition in eukaryotes. *Nature* 524 (7566), 493–496. doi: 10.1038/nature14896

Brummer, E. C., and Moore, K. J. (2000). Persistence of perennial cool-season grass and legume cultivars under continuous grazing by beef cattle. *Agron. J.* 92 (3), 466–471. doi: 10.2134/agronj2000.923466x

Chapman, B., and Brown, C. (2004). Translation termination in arabidopsis thaliana: Characterisation of three versions of release factor 1. *Gene* 341, 219–225. doi: 10.1016/j.gene.2004.06.053

Chinnusamy, V., Ohta, M., Kanrar, S., Lee, B. H., Hong, X., Agarwal, M., et al. (2003). ICE1: a regulator of cold-induced transcriptome and freezing tolerance in arabidopsis. *Genes Dev.* 17 (8), 1043–1054. doi: 10.1101/gad.1077503

Chinnusamy, V., Zhu, J., and Zhu, J. K. (2007). Cold stress regulation of gene expression in plants. *Trends Plant Sci.* 12, 444–451. doi: 10.1016/j.tplants.2007.07.002

Denis, C. L., Richardson, R., Park, S., Zhang, C., Wen, X., Laue, T. M., et al. (2018). Defining the protein complexome of translation termination factor eRF1: Identification of four novel eRF1-containing complexes that range from 20s to 57s in size. *Proteins* 86 (2), 177–191. doi: 10.1002/prot.25422

Dong, J., Cao, L., Zhang, X. Y., Zhang, W. H., Yang, T., Zhang, J. Z., et al. (2021). An R2R3-MYB transcription factor *RmMYB108* responds to chilling stress of Rosa multiflora and conferred cold tolerance of arabidopsis. *Front. Plant Sci.* 12. doi: 10.3389/fpls.2021.696919

Elakhdar, A., Ushijima, T., Fukuda, M., Yamashiro, N., Kawagoe, Y., and Kumamaru, T. (2019). Eukaryotic peptide chain release factor 1 participates in translation termination of specific cysteine-poor prolamines in rice endosperm. *Plant Sci.* 281, 223–231. doi: 10.1016/j.plantsci.2018.12.006

Feng, Y. N., Zhang, M., Guo, Q. F., Wang, G., Gong, J. F., Xu, Y., et al. (2014). Manipulation of monoubiquitin improves chilling tolerance in transgenic tobacco (*Nicotiana tabacum*). *Plant Physiol. Biochem.* 75 (1), 138–144. doi: 10.1016/j.plaphy.2013.11.003

Gilmour, S. J., Zarka, D. G., Stockinger, E. J., Salazar, M. P., Houghton, J. M., and Thomashow, M. F. (1998). Low temperature regulation of the arabidopsis CBF family of AP2 transcriptional activators as an early step in cold-induced COR gene expression. *Plant J.* 16 (4), 433–442. doi: 10.1046/j.1365-313x

Gómez, R., Vicino, P., Néstor, C., and Lodeyro, A. F. (2019). Manipulation of oxidative stress responses as a strategy to generate stress-tolerant crops. from damage to signaling to tolerance. *Crit. Rev. Biotechnol.* 39 (5), 693–708. doi: 10.1080/07388551.2019.1597829

Han, D., Han, J., Yang, G., Wang, S., Xu, T., and Li, W. (2020). An ERF transcription factor gene from malus baccata (L.) borkh, *MbERF11*, affects cold and salt stress tolerance in arabidopsis. *Forests* 11 (5), 514–529. doi: 10.3390/f11050514

Hao, Y. Q., Lu, G. Q., Wang, L. H., Wang, C. L., Guo, H. M., Li, Y. F., et al. (2018). Overexpression of *AmDUF1517* enhanced tolerance to salinity, drought, and cold stress in transgenic cotton. *J. Integr. Agric.* 17 (10), 2204–2214. doi: 10.1016/S2095-3119(17)61897-5

Hu, X. L., Liu, L. X., Xiao, B. L., Li, D. P., Xing, X., Kong, X. P., et al. (2010). Enhanced tolerance to low temperature in tobacco by over-expression of a new maize protein phosphatase 2C, *ZmPP2C2*. *J. Plant Physiol.* 167 (15), 1307–1315. doi: 10.1016/j.jplph.2010.04.014

Hwarari, D., Guan, Y., Ahmad, B., Movahedi, A., Min, T., Hao, Z., et al. (2022). ICE-CBF-COR signaling cascade and its regulation in plants responding to cold stress. *Int. J. Mol. Sci.* 23 (3), 1549. doi: 10.3390/ijms23031549

Jaglo, K. R., Gilmour, S. J., Zarka, D. G., Schabenberger, O., and Thomashow, M. F. (1998). Arabidopsis CBF1 overexpression induces COR genes and enhances freezing tolerance. *ence* 280 (5360), 104–106. doi: 10.1126/science.280.5360.104

Julia, K., and Claudia, J. (2012). Drought, salt, and temperature stress-induced metabolic rearrangements and regulatory networks. *J. Exp. Bot.* 63 (4), 251–261. doi: 10.1093/jxb/err460

Kazemi-Shahandashti, S.-S., and Maali-Amiri, R. (2018). Global insights of protein responses to cold stress in plants: Signaling, defence, and degradation. *J. Plant Physiol.* 226, 123–135. doi: 10.1016/j.jplph.2018.03.022

Kurilla, A., Szke, A., Auber, A., Káldi., K., and Silhavy, D. (2020). Expression of the translation termination factor eRF1 is autoregulated by translational readthrough and 3'UTR intron-mediated nmd in neurospora crassa. *FEBS Lett.* 594 (21), 3504–3517. doi: 10.1002/1873-3468.13918

Lashkevich, K. A., Shlyk, V. I., Kushchenko, A. S., Gladyshev, V. N., and Dmitriev, S. E. (2020). Ctels: a cell-free system for the analysis of translation termination rate. *Biomolecules* 10 (6), 911. doi: 10.3390/biom10060911

Lin, K. H., Sei, S. C., Su, Y. H., and Chiang, C. M. (2019). Overexpression of the arabidopsis and winter squash superoxide dismutase genes enhances chilling tolerance *Via* aba-sensitive transcriptional regulation in transgenic arabidopsis. *Plant Signaling Behav.* 14 (12), 1685728. doi: 10.1080/15592324.2019.1685728

Liu, Y., Wang, L., Jiang, S., Pan, J., Cai, G., and Li, D. (2014). Group 5 LEA protein, ZmLEA5C, enhance tolerance to osmotic and low temperature stresses in transgenic tobacco and yeast[J]. *Plant Physiol. Biochem.* 84, 22–31.

Li, G. W., Zhang, M. H., Cai, W. M., Sun, W. N., and Su, W. A. (2008). Characterization of OsPIP2;7, a water channel protein in rice. *Plant Cell Physiol.* 49 (12), 8–1851. doi: 10.1093/pcp/pcn166

Min, X. Y., Liu, Z. P., Wang, Y. R., and Liu, W. X. (2020). Comparative transcriptomic analysis provides insights into the coordinated mechanisms of leaves and roots response to cold stress in common vetch. *Ind. Crops Prod.* 158 (3), 321–334. doi: 10.1016/j.indcrop.2020.112949

Mishra, K. B., Mishra, A., Kubásek, J., Urban, O., Heyer, A. G., and Govindjee, (2018). Low temperature induced modulation of photosynthetic induction in non-acclimated and cold-acclimated arabidopsis thaliana: Chlorophyll a fluorescence and gas-exchange measurements. *Photosyn. Res.* 139 (1), 123–143. doi: 10.1007/s11120-018-0588-7

Ning, Y. A., Bo, L. A., Py, A., Xia, C. A., Hui, L. A., Wei, W. A., et al. (2021). Molecular cloning, characterization and expression analysis of *Cbpldδ* gene from chorispora bungeana in low temperature. *Cryobiology* 98, 119–126. doi: 10.1016/j.cryobiol.2020.11.016

Peng, L. N., Xu, Y. Q., Wang, X., and Feng, X. (2019). Overexpression of paralogues of the wheat expansin gene *TaEXPA8* improves low-temperature tolerance in arabidopsis. *Plant Biol.* 21 (6), 1119–1131. doi: 10.1111/plb.13018

Petsch, K. A., Mylnel, J., and Botella, R. J. (2005). Cosuppression of eukaryotic release factor 1-1 in arabidopsis affects cell elongation and radial cell division. *Plant Physiol.* 139 (1), 115–126. doi: 10.1104/pp.105.062695

Phornvillay, S., Pongprasert, N., Wongs-Aree, C., Uthairatanakij, A., and Srilaong, V. (2019). Exogenous putrescine treatment delays chilling injury in okra pod (*Abelmoschus esculentus*) stored at low storage temperature. *Sci. Hortic.* 256, 108550–108557. doi: 10.1016/j.scienta.2019.108550

Polina, K., Alexander, G., Boris, E., Anna, K., Ludmila, F., and Elena, A. (2013). Two-step model of stop codon recognition by eukaryotic release factor eRF1.[J]. *Nucleic Acids Res.* 41 (8).

Polturak, G., Heinig, U., Grossman, N., Battat, M., Leshkowitz, D., Malitsky, S., et al. (2018). Transcriptome and metabolic profiling provides insights into betalain biosynthesis and evolution in mirabilis jalapa. *Mol. Plant* 11 (1), 189–204. doi: 10.1016/j.molp.2017.12.002

Savoi, S., Wong, D., Arapitsas, P., Miculan, M., Bucchetti, B., and Peterlunger, E. (2016). Transcriptome and metabolite profiling reveals that prolonged drought modulates the phenylpropanoid and terpenoid pathway in white grapes (Vitis vinifera l.). *BMC Plant Biol.* 16 (1), 67–74. doi: 10.1186/s12870-016-0760-1

Sha, Y., Tang, X. F., Ma, N. N., Wang, L. Y., and Meng, Q. W. (2011). Heterology expression of the sweet pepper CBF3 gene confers elevated tolerance to chilling stress in transgenic tobacco. *J. Plant Physiol.* 168 (15), 1804–1812. doi: 10.1016/j.jplph.2011.05.017

Stockinger, E. J., Gilmour, S. J., and Thomashow, M. F. (1997). Arabidopsis thaliana CBF1 encodes an AP2 domain-containing transcriptional activator that binds to the c-repeat/DRE, a cis-acting DNA regulatory element that stimulates transcription in response to low temperature and water deficit. *Proc. Natl. Acad. Sci. U.S.A.* 94, 1035–1040. doi: 10.1073/pnas.94.3.1035

Sun, Y., He, Y., Irfan, A. R., Liu, X., and Yang, D. (2020). Exogenous brassinolide enhances the growth and cold resistance of maize (*Zea mays* l.) seedlings under chilling stress. *Agronomy* 10 (4), 488–498. doi: 10.3390/agronomy10040488

Sun, X., Zhu, Z., Zhang, L., Fang, L., Zhang, J., and Wang, Q. (2019). Overexpression of ethylene response factors *VaERF080* and *VaERF087* from vitis amurensis enhances cold tolerance in arabidopsis. *Sci. Hortic.* 243, 320–326. doi: 10.1016/j.scienta.2018.08.055

Taylar, N. L., and Smith, R. R. (1997). Kura clover (*Trifolium ambiguum* m. b.) breeding, culture, and utilization. *Adv. Agron.* 63.08 (1998), 153–178. doi: 10.1016/S0065-2113(08)60243-6

Theocharis, A., Clément, C., and Ait Barka, E. (2012). Physiological and molecular changes in plants grown at low temperatures. *Planta* 235 (6), 1091–1105. doi: 10.1007/s00425-012-1641-y

Thomashow, M. F. (2010). Molecular basis of plant cold Acclimation:Insights gained from studying the CBF cold response pathway. *Plant Physiol.* 154 (2), 571–577. doi: 10.1104/pp.110.161794

Urakov, V. N., Mitkevich, O. V., Safenkova, I. V., and Ter-Avanesyan, M. D. (2017). Ribosome-bound Pub1 modulates stop codon decoding during translation termination in yeast. *FEBS J.* 284 (12), 1914–1930. doi: 10.1111/febs.14099

Ushijima, T., Matsusaka, H., Jikuya, H., Ogawa, M., and Kumamaru, T. (2011). Genetic analysis of cysteine-poor prolamin polypeptides reduced in the endosperm of the rice Esp1 mutant. *Plant Sci.* 181 (2), 125–131. doi: 10.1016/j.plantsci.2011.04.011

Wang, Z. Y. (2019). Effects of low temperature on proline content of elderberry. *Jilin Agric.* 443 (2), 60. doi: 10.14025/j.cnki.jlny.2019.02.021

Wang, M., Dai, W., Du, J., Ming, R., Dahro, B., and Liu, J. (2019). *ERF109* of trifoliate orange (*Poncirus trifoliata* (L.) raf.) contributes to cold tolerance by directly regulating expression of Prx1 involved in antioxidative process. *Plant Biotechnol. J.* 17 (7), 1316–1332. doi: 10.1111/pbi.13056

Wang, Y., Liang, C., Meng, Z., Brestic., M., and Yang, X. H. (2019). Leveraging atriplex hortensis choline monooxygenase to improve chilling tolerance in cotton. *Environ. Exp. Bot.* 162, 364–373. doi: 10.1016/j.envexpbot.2019.03.012

Wang, X. P., Song, Q. P., Liu, Y., Brestic., M., and Yang, X. H. (2022). The network centered on ICEs play roles in plant cold tolerance, growth and development. *Planta* 255, 81. doi: 10.1007/s00425-022-03858-7

Wang, S. Q., Tang, J., Hu, K. D., Huang, Z. Q., Yang, F., and Zhang, H. Y. (2019). Antioxidative system in sweet potato rootis activated by low-temperature storage. *J. Sci. Food Agric.* 99 (8), 3824–3833. doi: 10.1002/jsfa.9604

Wu, L., Zhou, M., Shen, C., Jing, L., and Lin, J. (2012). Transgenic tobacco plants over expressing cold regulated protein *CbCOR15b* from capsella bursa-pastoris exhibit enhanced cold tolerance. *J. Plant Physiol.* 169 (14), 1408–1416. doi: 10.1016/j.jplph.2012.05.016

Yan, L., Shah, T., Cheng, Y., LÜ, Y., Zhang, X. K., and Zou, X. L. (2019). Physiological and molecular responses to cold stress in rapeseed (Brassica napus l.). *J. Integr. Agric.* 18 (12), 2742–2752. doi: 10.1016/S2095-3119(18)62147-1

Yin, X. J., Yi, K., Zhao, Y. H., Hu, Y., Li, X., He, T., et al. (2020). Revealing the full-length transcriptome of caucasian clover rhizome development. *BMC Plant Biol.* 20 (1), 429. doi: 10.1186/s12870-020-02637-4

Yin, F. L., Zeng, Y. L., Ji, J. Y., Wang, P. J., Zhang, Y. F., and Li, W. H. (2021). The halophyte halostachys caspica AP2/ERF transcription factor HcTOE3 positively regulates freezing tolerance in arabidopsis. *Front. Plant Sci.* 12. doi: 10.3389/fpls.2021.638788

Yu, P. H. (2020). *Researches on the mechanism and regulations underlying cold stress impaired early indica rice* (Chinese Academy of Agricultural Sciences).

Zhang, M. Y., Ren, Y. X., Li, X., Sun, B. Y., and Yin, X. J. (2019). Effect of IBA and NAA on *Trifolium ambiguum* seed germination and growth of creeping-root. *Pratac. Sci.* 36 (1), 93–100. doi: 10.11829/j.issn.1001-0629.2018-0219

Zhang, L., Ren, J., Li, T., Wang, A., and Tan, D. (2016). De novo transcriptome sequencing of cold-treated Kentucky bluegrass (Poa pratensis) and analysis of the genes involved in cold tolerance. *J. Hortic.* 3 (3), 1000182. doi: 10.4172/2376-0354.1000182

Zhang, Y. T., Zhang, M., Hu, H., Yang, J. J., Cui, J. B., and Xu, J. (2021). Cloning and cold-resistance analyses of *CfICE1* gene in cryptomeria fortunei. *Plant Physiol. Biochem.* 162, 456–467. doi: 10.1016/j.plaphy.2021.03.020

Zhang, Q. R., Zhuang, Y. H., Wen, Q. F., Liu, J. T., Ye, X. R., Chen, M. D., et al. (2017). Study on enzymatic characteristics of catalase (CAT) in luffa. *China Hortic. Abstr.* 33 (9), 1–3, 31.

Zhao, Y. H., Yang, Y. P., Jiang, J. W., Zhang, X. M., Ma, Z. W., Meng, L. D., et al. (2022). The Caucasian clover gene *TaMYC2* responds to abiotic stress and improves tolerance by increasing the activity of antioxidant enzymes. *Genes* 13 (2), 329. doi: 10.3390/genes13020329

Zhao, Y., Zhou, M., Xu, K., Li, J., and Yang, X. (2019). Integrated transcriptomics and metabolomics analyses provide insights into cold stress response in wheat. *Crop J.* 7 (6), 857–866. doi: 10.1016/j.cj.2019.09.002

Frontiers in
Plant Science

Cultivates the science of plant biology and its applications

The most cited plant science journal, which advances our understanding of plant biology for sustainable food security, functional ecosystems and human health.

Discover the latest Research Topics

See more →

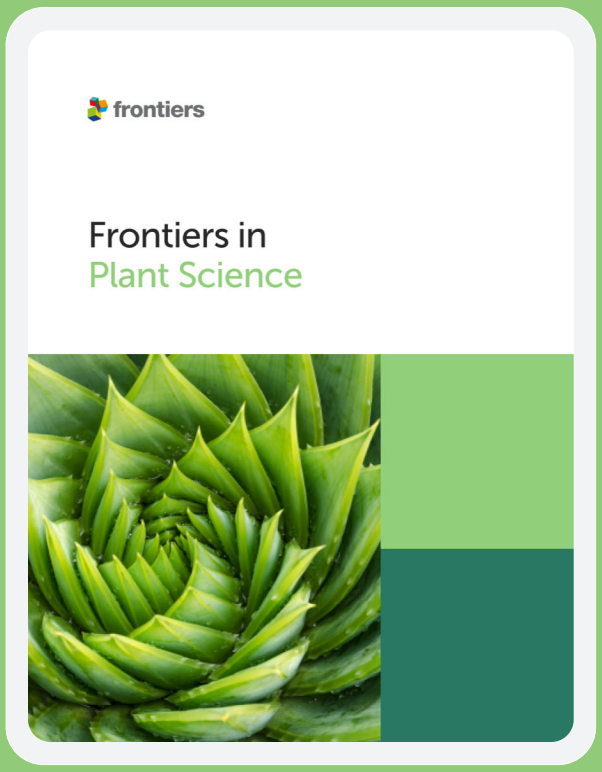

Frontiers

Avenue du Tribunal-Fédéral 34
1005 Lausanne, Switzerland
frontiersin.org

Contact us

+41 (0)21 510 17 00
frontiersin.org/about/contact